



Proceedings
PRO 130

Proceedings of the 5th Historic Mortars Conference



Edited by José Ignacio Álvarez, José María Fernández,
Íñigo Navarro, Adrián Durán, Rafael Sirera

RILEM Publications S.A.R.L.

5th Historic Mortars Conference

5th Historic Mortars Conference

19-21 June 2019
Pamplona, Spain

Edited by
José Ignacio Álvarez, José María Fernández,
Íñigo Navarro, Adrián Durán, Rafael Sirera

RILEM Publications S.A.R.L.

Published by RILEM Publications S.A.R.L.
4 avenue du Recteur Poincaré 75016 Paris - France
Tel : + 33 1 42 24 64 46 Fax : + 33 9 70 29 51 20
<http://www.rilem.net> E-mail: dg@rilem.net
© 2019 RILEM – Tous droits réservés.
ISBN: 978-2-35158-221-3
e-ISBN: 978-2-35158-222-0

Publisher's note: *this book has been produced from electronic files provided by the individual contributors. The publisher makes no representation, express or implied, with regard to the accuracy of the information contained in this book and cannot accept any legal responsibility or liability for any errors or omissions that may be made. All titles published by RILEM Publications are under copyright protection; said copyrights being the property of their respective holders. All Rights Reserved.*

No part of any book may be reproduced or transmitted in any form or by any means, graphic, electronic, or mechanical, including photocopying, recording, taping, or by any information storage or retrieval system, without the permission in writing from the publisher.

RILEM, The International Union of Laboratories and Experts in Construction Materials, Systems and Structures, is a non profit-making, non-governmental technical association whose vocation is to contribute to progress in the construction sciences, techniques and industries, essentially by means of the communication it fosters between research and practice. RILEM's activity therefore aims at developing the knowledge of properties of materials and performance of structures, at defining the means for their assessment in laboratory and service conditions and at unifying measurement and testing methods used with this objective.

RILEM was founded in 1947, and has a membership of over 900 in some 70 countries. It forms an institutional framework for co-operation by experts to:

- optimise and harmonise test methods for measuring properties and performance of building and civil engineering materials and structures under laboratory and service environments,
- prepare technical recommendations for testing methods,
- prepare state-of-the-art reports to identify further research needs,
- collaborate with national or international associations in realising these objectives.

RILEM members include the leading building research and testing laboratories around the world, industrial research, manufacturing and contracting interests, as well as a significant number of individual members from industry and universities. RILEM's focus is on construction materials and their use in building and civil engineering structures, covering all phases of the building process from manufacture to use and recycling of materials.

RILEM meets these objectives through the work of its technical committees. Symposia, workshops and seminars are organised to facilitate the exchange of information and dissemination of knowledge. RILEM's primary output consists of technical recommendations. RILEM also publishes the journal *Materials and Structures* which provides a further avenue for reporting the work of its committees. Many other publications, in the form of reports, monographs, symposia and workshop proceedings are produced.

RILEM Publications

The following list is presenting the global offer of RILEM Publications, sorted by series. Each publication is available in printed version and/or in online version.

RILEM PROCEEDINGS (PRO)

PRO 1: Durability of High Performance Concrete (ISBN: 2-912143-03-9); *Ed. H. Sommer*

PRO 2: Chloride Penetration into Concrete (ISBN: 2-912143-00-04);

Eds. L.-O. Nilsson and J.-P. Ollivier

PRO 3: Evaluation and Strengthening of Existing Masonry Structures (ISBN: 2-912143-02-0);

Eds. L. Binda and C. Modena

PRO 4: Concrete: From Material to Structure (ISBN: 2-912143-04-7); *Eds. J.-P. Bournazel and Y. Malier*

PRO 5: The Role of Admixtures in High Performance Concrete (ISBN: 2-912143-05-5);

Eds. J. G. Cabrera and R. Rivera-Villarreal

PRO 6: High Performance Fiber Reinforced Cement Composites - HPFRCC 3

(ISBN: 2-912143-06-3); *Eds. H. W. Reinhardt and A. E. Naaman*

PRO 7: 1st International RILEM Symposium on Self-Compacting Concrete (ISBN: 2-912143-09-8); *Eds. Å. Skarendahl and Ö. Petersson*

PRO 8: International RILEM Symposium on Timber Engineering (ISBN: 2-912143-10-1);

Ed. L. Boström

PRO 9: 2nd International RILEM Symposium on Adhesion between Polymers and Concrete

ISAP '99 (ISBN: 2-912143-11-X); *Eds. Y. Ohama and M. Puterman*

PRO 10: 3rd International RILEM Symposium on Durability of Building and Construction

Sealants (ISBN: 2-912143-13-6); *Eds. A. T. Wolf*

PRO 11: 4th International RILEM Conference on Reflective Cracking in Pavements

(ISBN: 2-912143-14-4); *Eds. A. O. Abd El Halim, D. A. Taylor and El H. H. Mohamed*

PRO 12: International RILEM Workshop on Historic Mortars: Characteristics and Tests

(ISBN: 2-912143-15-2); *Eds. P. Bartos, C. Groot and J. J. Hughes*

PRO 13: 2nd International RILEM Symposium on Hydration and Setting (ISBN: 2-912143-16-0); *Ed. A. Nonat*

PRO 14: Integrated Life-Cycle Design of Materials and Structures - ILCDES 2000

(ISBN: 951-758-408-3); (ISSN: 0356-9403); *Ed. S. Sarja*

PRO 15: Fifth RILEM Symposium on Fibre-Reinforced Concretes (FRC) - BEFIB'2000

(ISBN: 2-912143-18-7); *Eds. P. Rossi and G. Chanvillard*

PRO 16: Life Prediction and Management of Concrete Structures

(ISBN: 2-912143-19-5); *Ed. D. Naus*

PRO 17: Shrinkage of Concrete – Shrinkage 2000 (ISBN: 2-912143-20-9);

Eds. V. Baroghel-Bouny and P.-C. Aïtcin

PRO 18: Measurement and Interpretation of the On-Site Corrosion Rate (ISBN: 2-912143-21-7);

Eds. C. Andrade, C. Alonso, J. Fullea, J. Polimon and J. Rodriguez

PRO 19: Testing and Modelling the Chloride Ingress into Concrete (ISBN: 2-912143-22-5);

Eds. C. Andrade and J. Kropp

- PRO 20:** 1st International RILEM Workshop on Microbial Impacts on Building Materials (CD 02) (e-ISBN 978-2-35158-013-4); *Ed. M. Ribas Silva*
- PRO 21:** International RILEM Symposium on Connections between Steel and Concrete (ISBN: 2-912143-25-X); *Ed. R. Eligehausen*
- PRO 22:** International RILEM Symposium on Joints in Timber Structures (ISBN: 2-912143-28-4); *Eds. S. Aicher and H.-W. Reinhardt*
- PRO 23:** International RILEM Conference on Early Age Cracking in Cementitious Systems (ISBN: 2-912143-29-2); *Eds. K. Kovler and A. Bentur*
- PRO 24:** 2nd International RILEM Workshop on Frost Resistance of Concrete (ISBN: 2-912143-30-6); *Eds. M. J. Setzer, R. Auberg and H.-J. Keck*
- PRO 25:** International RILEM Workshop on Frost Damage in Concrete (ISBN: 2-912143-31-4); *Eds. D. J. Janssen, M. J. Setzer and M. B. Snyder*
- PRO 26:** International RILEM Workshop on On-Site Control and Evaluation of Masonry Structures (ISBN: 2-912143-34-9); *Eds. L. Binda and R. C. de Vekey*
- PRO 27:** International RILEM Symposium on Building Joint Sealants (CD03); *Ed. A. T. Wolf*
- PRO 28:** 6th International RILEM Symposium on Performance Testing and Evaluation of Bituminous Materials - PTEBM'03 (ISBN: 2-912143-35-7; e-ISBN: 978-2-912143-77-8); *Ed. M. N. Partl*
- PRO 29:** 2nd International RILEM Workshop on Life Prediction and Ageing Management of Concrete Structures (ISBN: 2-912143-36-5); *Ed. D. J. Naus*
- PRO 30:** 4th International RILEM Workshop on High Performance Fiber Reinforced Cement Composites - HPFRCC 4 (ISBN: 2-912143-37-3); *Eds. A. E. Naaman and H. W. Reinhardt*
- PRO 31:** International RILEM Workshop on Test and Design Methods for Steel Fibre Reinforced Concrete: Background and Experiences (ISBN: 2-912143-38-1); *Eds. B. Schnütgen and L. Vandewalle*
- PRO 32:** International Conference on Advances in Concrete and Structures 2 vol. (ISBN (set): 2-912143-41-1); *Eds. Ying-shu Yuan, Surendra P. Shah and Heng-lin Lü*
- PRO 33:** 3rd International Symposium on Self-Compacting Concrete (ISBN: 2-912143-42-X); *Eds. Ó. Wallevik and I. Nielsson*
- PRO 34:** International RILEM Conference on Microbial Impact on Building Materials (ISBN: 2-912143-43-8); *Ed. M. Ribas Silva*
- PRO 35:** International RILEM TC 186-ISA on Internal Sulfate Attack and Delayed Ettringite Formation (ISBN: 2-912143-44-6); *Eds. K. Scrivener and J. Skalny*
- PRO 36:** International RILEM Symposium on Concrete Science and Engineering – A Tribute to Arnon Bentur (ISBN: 2-912143-46-2); *Eds. K. Kovler, J. Marchand, S. Mindess and J. Weiss*
- PRO 37:** 5th International RILEM Conference on Cracking in Pavements – Mitigation, Risk Assessment and Prevention (ISBN: 2-912143-47-0); *Eds. C. Petit, I. Al-Qadi and A. Millien*
- PRO 38:** 3rd International RILEM Workshop on Testing and Modelling the Chloride Ingress into Concrete (ISBN: 2-912143-48-9); *Eds. C. Andrade and J. Kropp*
- PRO 39:** 6th International RILEM Symposium on Fibre-Reinforced Concretes - BEFIB 2004 (ISBN: 2-912143-51-9); *Eds. M. Di Prisco, R. Felicetti and G. A. Plizzari*
- PRO 40:** International RILEM Conference on the Use of Recycled Materials in Buildings and Structures (ISBN: 2-912143-52-7); *Eds. E. Vázquez, Ch. F. Hendriks and G. M. T. Janssen*
- PRO 41:** RILEM International Symposium on Environment-Conscious Materials and Systems for Sustainable Development (ISBN: 2-912143-55-1); *Eds. N. Kashino and Y. Ohama*

- PRO 42:** SCC'2005 - China: 1st International Symposium on Design, Performance and Use of Self-Consolidating Concrete (ISBN: 2-912143-61-6); *Eds. Zhiwu Yu, Caijun Shi, Kamal Henri Khayat and Youjun Xie*
- PRO 43:** International RILEM Workshop on Bonded Concrete Overlays (e-ISBN: 2-912143-83-7); *Eds. J. L. Granju and J. Silfwerbrand*
- PRO 44:** 2nd International RILEM Workshop on Microbial Impacts on Building Materials (CD11) (e-ISBN: 2-912143-84-5); *Ed. M. Ribas Silva*
- PRO 45:** 2nd International Symposium on Nanotechnology in Construction, Bilbao (ISBN: 2-912143-87-X); *Eds. Peter J. M. Bartos, Yolanda de Miguel and Antonio Porro*
- PRO 46:** ConcreteLife'06 - International RILEM-JCI Seminar on Concrete Durability and Service Life Planning: Curing, Crack Control, Performance in Harsh Environments (ISBN: 2-912143-89-6); *Ed. K. Kovler*
- PRO 47:** International RILEM Workshop on Performance Based Evaluation and Indicators for Concrete Durability (ISBN: 978-2-912143-95-2); *Eds. V. Baroghel-Bouny, C. Andrade, R. Torrent and K. Scrivener*
- PRO 48:** 1st International RILEM Symposium on Advances in Concrete through Science and Engineering (e-ISBN: 2-912143-92-6); *Eds. J. Weiss, K. Kovler, J. Marchand, and S. Mindess*
- PRO 49:** International RILEM Workshop on High Performance Fiber Reinforced Cementitious Composites in Structural Applications (ISBN: 2-912143-93-4); *Eds. G. Fischer and V.C. Li*
- PRO 50:** 1st International RILEM Symposium on Textile Reinforced Concrete (ISBN: 2-912143-97-7); *Eds. Josef Hegger, Wolfgang Brameshuber and Norbert Will*
- PRO 51:** 2nd International Symposium on Advances in Concrete through Science and Engineering (ISBN: 2-35158-003-6; e-ISBN: 2-35158-002-8); *Eds. J. Marchand, B. Bissonnette, R. Gagné, M. Jolin and F. Paradis*
- PRO 52:** Volume Changes of Hardening Concrete: Testing and Mitigation (ISBN: 2-35158-004-4; e-ISBN: 2-35158-005-2); *Eds. O. M. Jensen, P. Lura and K. Kovler*
- PRO 53:** High Performance Fiber Reinforced Cement Composites - HPRFRC5 (ISBN: 978-2-35158-046-2); *Eds. H. W. Reinhardt and A. E. Naaman*
- PRO 54:** 5th International RILEM Symposium on Self-Compacting Concrete (ISBN: 978-2-35158-047-9); *Eds. G. De Schutter and V. Boel*
- PRO 55:** International RILEM Symposium Photocatalysis, Environment and Construction Materials (ISBN: 978-2-35158-056-1); *Eds. P. Baglioni and L. Cassar*
- PRO56:** International RILEM Workshop on Integral Service Life Modelling of Concrete Structures (ISBN 978-2-35158-058-5); *Eds. R. M. Ferreira, J. Gulikers and C. Andrade*
- PRO57:** RILEM Workshop on Performance of cement-based materials in aggressive aqueous environments (e-ISBN: 978-2-35158-059-2); *Ed. N. De Belie*
- PRO58:** International RILEM Symposium on Concrete Modelling - CONMOD'08 (ISBN: 978-2-35158-060-8); *Eds. E. Schlangen and G. De Schutter*
- PRO 59:** International RILEM Conference on On Site Assessment of Concrete, Masonry and Timber Structures - SACoMaTiS 2008 (ISBN set: 978-2-35158-061-5); *Eds. L. Binda, M. di Prisco and R. Felicetti*
- PRO 60:** Seventh RILEM International Symposium on Fibre Reinforced Concrete: Design and Applications - BEFIB 2008 (ISBN: 978-2-35158-064-6); *Ed. R. Gettu*
- PRO 61:** 1st International Conference on Microstructure Related Durability of Cementitious Composites 2 vol., (ISBN: 978-2-35158-065-3); *Eds. W. Sun, K. van Breugel, C. Miao, G. Ye and H. Chen*

- PRO 62:** NSF/ RILEM Workshop: In-situ Evaluation of Historic Wood and Masonry Structures (e-ISBN: 978-2-35158-068-4); *Eds. B. Kasal, R. Anthony and M. Drdácý*
- PRO 63:** Concrete in Aggressive Aqueous Environments: Performance, Testing and Modelling, 2 vol., (ISBN: 978-2-35158-071-4); *Eds. M. G. Alexander and A. Bertron*
- PRO 64:** Long Term Performance of Cementitious Barriers and Reinforced Concrete in Nuclear Power Plants and Waste Management - NUCPERF 2009 (ISBN: 978-2-35158-072-1); *Eds. V. L'Hostis, R. Gens, C. Gallé*
- PRO 65:** Design Performance and Use of Self-consolidating Concrete - SCC'2009 (ISBN: 978-2-35158-073-8); *Eds. C. Shi, Z. Yu, K. H. Khayat and P. Yan*
- PRO 66:** 2nd International RILEM Workshop on Concrete Durability and Service Life Planning - ConcreteLife'09 (ISBN: 978-2-35158-074-5); *Ed. K. Kovler*
- PRO 67:** Repairs Mortars for Historic Masonry (e-ISBN: 978-2-35158-083-7); *Ed. C. Groot*
- PRO 68:** Proceedings of the 3rd International RILEM Symposium on 'Rheology of Cement Suspensions such as Fresh Concrete (ISBN 978-2-35158-091-2); *Eds. O. H. Wallevik, S. Kubens and S. Oesterheld*
- PRO 69:** 3rd International PhD Student Workshop on 'Modelling the Durability of Reinforced Concrete (ISBN: 978-2-35158-095-0); *Eds. R. M. Ferreira, J. Gulikers and C. Andrade*
- PRO 70:** 2nd International Conference on 'Service Life Design for Infrastructure' (ISBN set: 978-2-35158-096-7, e-ISBN: 978-2-35158-097-4); *Ed. K. van Breugel, G. Ye and Y. Yuan*
- PRO 71:** Advances in Civil Engineering Materials - The 50-year Teaching Anniversary of Prof. Sun Wei' (ISBN: 978-2-35158-098-1; e-ISBN: 978-2-35158-099-8); *Eds. C. Miao, G. Ye, and H. Chen*
- PRO 72:** First International Conference on 'Advances in Chemically-Activated Materials – CAM'2010' (2010), 264 pp, ISBN: 978-2-35158-101-8; e-ISBN: 978-2-35158-115-5, *Eds. Caijun Shi and Xiaodong Shen*
- PRO 73:** 2nd International Conference on 'Waste Engineering and Management - ICWEM 2010' (2010), 894 pp, ISBN: 978-2-35158-102-5; e-ISBN: 978-2-35158-103-2, *Eds. J. Zh. Xiao, Y. Zhang, M. S. Cheung and R. Chu*
- PRO 74:** International RILEM Conference on 'Use of Superabsorbent Polymers and Other New Additives in Concrete' (2010) 374 pp., ISBN: 978-2-35158-104-9; e-ISBN: 978-2-35158-105-6; *Eds. O.M. Jensen, M.T. Hasholt, and S. Laustsen*
- PRO 75:** International Conference on 'Material Science - 2nd ICTRC - Textile Reinforced Concrete - Theme 1' (2010) 436 pp., ISBN: 978-2-35158-106-3; e-ISBN: 978-2-35158-107-0; *Ed. W. Brameshuber*
- PRO 76:** International Conference on 'Material Science - HetMat - Modelling of Heterogeneous Materials - Theme 2' (2010) 255 pp., ISBN: 978-2-35158-108-7; e-ISBN: 978-2-35158-109-4; *Ed. W. Brameshuber*
- PRO 77:** International Conference on 'Material Science - AdIPoC - Additions Improving Properties of Concrete - Theme 3' (2010) 459 pp., ISBN: 978-2-35158-110-0; e-ISBN: 978-2-35158-111-7; *Ed. W. Brameshuber*
- PRO 78:** 2nd Historic Mortars Conference and RILEM TC 203-RHM Final Workshop – HMC2010 (2010) 1416 pp., e-ISBN: 978-2-35158-112-4; *Eds J. Válek, C. Groot, and J. J. Hughes*
- PRO 79:** International RILEM Conference on Advances in Construction Materials Through Science and Engineering (2011) 213 pp., e-ISBN: 978-2-35158-117-9; *Eds Christopher Leung and K.T. Wan*

PRO 80: 2nd International RILEM Conference on Concrete Spalling due to Fire Exposure (2011) 453 pp., ISBN: 978-2-35158-118-6, e-ISBN: 978-2-35158-119-3; *Eds E.A.B. Koenders and F. Dehn*

PRO 81: 2nd International RILEM Conference on Strain Hardening Cementitious Composites (SHCC2-Rio) (2011) 451 pp., ISBN: 978-2-35158-120-9, e-ISBN: 978-2-35158-121-6; *Eds R.D. Toledo Filho, F.A. Silva, E.A.B. Koenders and E.M.R. Fairbairn*

PRO 82: 2nd International RILEM Conference on Progress of Recycling in the Built Environment (2011) 507 pp., e-ISBN: 978-2-35158-122-3; *Eds V.M. John, E. Vazquez, S.C. Angulo and C. Ulsen*

PRO 83: 2nd International Conference on Microstructural-related Durability of Cementitious Composites (2012) 250 pp., ISBN: 978-2-35158-129-2; e-ISBN: 978-2-35158-123-0; *Eds G. Ye, K. van Breugel, W. Sun and C. Miao*

PRO 85: RILEM-JCI International Workshop on Crack Control of Mass Concrete and Related issues concerning Early-Age of Concrete Structures – ConCrack 3 – Control of Cracking in Concrete Structures 3 (2012) 237 pp., ISBN: 978-2-35158-125-4; e-ISBN: 978-2-35158-126-1; *Eds F. Toutlemonde and J.-M. Torrenti*

PRO 86: International Symposium on Life Cycle Assessment and Construction (2012) 414 pp., ISBN: 978-2-35158-127-8, e-ISBN: 978-2-35158-128-5; *Eds A. Ventura and C. de la Roche*

PRO 87: UHPFRC 2013 – RILEM-fib-AFGC International Symposium on Ultra-High Performance Fibre-Reinforced Concrete (2013), ISBN: 978-2-35158-130-8, e-ISBN: 978-2-35158-131-5; *Eds F. Toutlemonde*

PRO 88: 8th RILEM International Symposium on Fibre Reinforced Concrete (2012) 344 pp., ISBN: 978-2-35158-132-2, e-ISBN: 978-2-35158-133-9; *Eds Joaquim A.O. Barros*

PRO 89: RILEM International workshop on performance-based specification and control of concrete durability (2014) 678 pp, ISBN: 978-2-35158-135-3, e-ISBN: 978-2-35158-136-0; *Eds. D. Bjegović, H. Beushausen and M. Serdar*

PRO 90: 7th RILEM International Conference on Self-Compacting Concrete and of the 1st RILEM International Conference on Rheology and Processing of Construction Materials (2013) 396 pp, ISBN: 978-2-35158-137-7, e-ISBN: 978-2-35158-138-4; *Eds. Nicolas Roussel and Hela Bessaies-Bey*

PRO 91: CONMOD 2014 - RILEM International Symposium on Concrete Modelling (2014), ISBN: 978-2-35158-139-1; e-ISBN: 978-2-35158-140-7; *Eds. Kefei Li, Peiyu Yan and Rongwei Yang*

PRO 92: CAM 2014 - 2nd International Conference on advances in chemically-activated materials (2014) 392 pp., ISBN: 978-2-35158-141-4; e-ISBN: 978-2-35158-142-1; *Eds. Caijun Shi and Xiadong Shen*

PRO 93: SCC 2014 - 3rd International Symposium on Design, Performance and Use of Self-Consolidating Concrete (2014) 438 pp., ISBN: 978-2-35158-143-8; e-ISBN: 978-2-35158-144-5; *Eds. Caijun Shi, Zhihua Ou, Kamal H. Khayat*

PRO 94 (online version): HPFRCC-7 - 7th RILEM conference on High performance fiber reinforced cement composites (2015), e-ISBN: 978-2-35158-146-9; *Eds. H.W. Reinhardt, G.J. Parra-Montesinos, H. Garrecht*

PRO 95: International RILEM Conference on Application of superabsorbent polymers and other new admixtures in concrete construction (2014), ISBN: 978-2-35158-147-6; e-ISBN: 978-2-35158-148-3; *Eds. Viktor Mechtcherine, Christof Schroefl*

PRO 96 (online version): XIII DBMC: XIII International Conference on Durability of Building Materials and Components (2015), e-ISBN: 978-2-35158-149-0; *Eds. M. Quattrone, V.M. John*

- PRO 97:** SHCC3 – 3rd International RILEM Conference on Strain Hardening Cementitious Composites (2014), ISBN: 978-2-35158-150-6; e-ISBN: 978-2-35158-151-3; *Eds. E. Schlangen, M.G. Sierra Beltran, M. Lukovic, G. Ye*
- PRO 98:** FERRO-11 – 11th International Symposium on Ferrocement and 3rd ICTRC - International Conference on Textile Reinforced Concrete (2015), ISBN: 978-2-35158-152-0; e-ISBN: 978-2-35158-153-7; *Ed. W. Brameshuber*
- PRO 99 (online version):** ICBBM 2015 - 1st International Conference on Bio-Based Building Materials (2015), e-ISBN: 978-2-35158-154-4; *Eds. S. Amziane, M. Sonebi*
- PRO 100:** SCC16 - RILEM Self-Consolidating Concrete Conference (2016), ISBN: 978-2-35158-156-8; e-ISBN: 978-2-35158-157-5
- PRO 101 (online version):** III Progress of Recycling in the Built Environment (2015), e-ISBN: 978-2-35158-158-2; *Eds I. Martins, C. Ulsen and S. C. Angulo*
- PRO 102 (online version):** RILEM Conference on Microorganisms-Cementitious Materials Interactions (2016), e-ISBN: 978-2-35158-160-5; *Eds. Alexandra Bertron, Henk Jonkers, Virginie Wiktor*
- PRO 103 (online version):** ACESC'16 - Advances in Civil Engineering and Sustainable Construction (2016), e-ISBN: 978-2-35158-161-2
- PRO 104 (online version):** SSCS'2015 - Numerical Modeling - Strategies for Sustainable Concrete Structures (2015), e-ISBN: 978-2-35158-162-9
- PRO 105:** 1st International Conference on UHPC Materials and Structures (2016), ISBN: 978-2-35158-164-3, e-ISBN: 978-2-35158-165-0
- PRO 106:** AFGC-ACI-fib-RILEM International Conference on Ultra-High-Performance Fibre-Reinforced Concrete – UHPFRC 2017 (2017), ISBN: 978-2-35158-166-7, e-ISBN: 978-2-35158-167-4; *Eds. François Toutlemonde & Jacques Resplendino*
- PRO 107 (online version):** XIV DBMC – 14th International Conference on Durability of Building Materials and Components (2017), e-ISBN: 978-2-35158-159-9; *Eds. Geert De Schutter, Nele De Belie, Arnold Janssens, Nathan Van Den Bossche*
- PRO 108:** MSSCE 2016 - Innovation of Teaching in Materials and Structures (2016), ISBN: 978-2-35158-178-0, e-ISBN: 978-2-35158-179-7; *Ed. Per Goltermann*
- PRO 109 (2 volumes):** MSSCE 2016 - Service Life of Cement-Based Materials and Structures (2016), ISBN Vol. 1: 978-2-35158-170-4, Vol. 2: 978-2-35158-171-4, Set Vol. 1&2: 978-2-35158-172-8, e-ISBN : 978-2-35158-173-5; *Eds. Miguel Azenha, Ivan Gabrijel, Dirk Schlicke, Terje Kanstad and Ole Mejlhede Jensen*
- PRO 110:** MSSCE 2016 - Historical Masonry (2016), ISBN: 978-2-35158-178-0, e-ISBN: 978-2-35158-179-7; *Eds. Inge Rörig-Dalgaard and Ioannis Ioannou*
- PRO 111:** MSSCE 2016 - Electrochemistry in Civil Engineering (2016), ISBN: 978-2-35158-176-6, e-ISBN: 978-2-35158-177-3; *Ed. Lisbeth M. Ottosen*
- PRO 112:** MSSCE 2016 - Moisture in Materials and Structures (2016), ISBN: 978-2-35158-178-0, e-ISBN: 978-2-35158-179-7; *Eds. Kurt Kielsgaard Hansen, Carsten Rode and Lars-Olof Nilsson*
- PRO 113:** MSSCE 2016 - Concrete with Supplementary Cementitious Materials (2016), ISBN: 978-2-35158-178-0, e-ISBN: 978-2-35158-179-7; *Eds. Ole Mejlhede Jensen, Konstantin Kovler and Nele De Belie*
- PRO 114:** MSSCE 2016 - Frost Action in Concrete (2016), ISBN: 978-2-35158-182-7, e-ISBN: 978-2-35158-183-4; *Eds. Marianne Tange Hasholt, Katja Fridh and R. Doug Hooton*
- PRO 115:** MSSCE 2016 - Fresh Concrete (2016), ISBN: 978-2-35158-184-1, e-ISBN: 978-2-35158-185-8; *Eds. Lars N. Thrane, Claus Pade, Oldrich Svec and Nicolas Roussel*

- PRO 116:** BEFIB 2016 – 9th RILEM International Symposium on Fiber Reinforced Concrete (2016), ISBN: 978-2-35158-187-2, e-ISBN: 978-2-35158-186-5;
- PRO 117:** 3rd International RILEM Conference on Microstructure Related Durability of Cementitious Composites (2016), ISBN: 978-2-35158-188-9, e-ISBN: 978-2-35158-189-6; *Eds. Changwen Miao, Wei Sun, Jiaping Liu, Huisu Chen, Guang Ye and Klaas van Breugel*
- PRO 118 (4 volumes):** International Conference on Advances in Construction Materials and Systems (2017), ISBN Set: 978-2-35158-190-2, Vol. 1: 978-2-35158-193-3, Vol. 2: 978-2-35158-194-0, Vol. 3: ISBN:978-2-35158-195-7, Vol. 4: ISBN:978-2-35158-196-4, e-ISBN: 978-2-35158-191-9; *Ed. Manu Santhanam*
- PRO 119 (online version):** ICBBM 2017 - Second International RILEM Conference on Bio-based Building Materials, (2017), e-ISBN: 978-2-35158-192-6; *Ed. Sofiane Amziane*
- PRO 120 (2 volumes):** EAC-02 - 2nd International RILEM/COST Conference on Early Age Cracking and Serviceability in Cement-based Materials and Structures, (2017), Vol. 1: 978-2-35158-199-5, Vol. 2: 978-2-35158-200-8, Set: 978-2-35158-197-1, e-ISBN: 978-2-35158-198-8; *Eds. Stéphanie Staquet and Dimitrios Aggelis*
- PRO 121 (2 volumes):** SynerCrete18: Interdisciplinary Approaches for Cement-based Materials and Structural Concrete: Synergizing Expertise and Bridging Scales of Space and Time, (2018), Set: 978-2-35158-202-2, Vol.1: 978-2-35158-211-4, Vol.2: 978-2-35158-212-1, e-ISBN: 978-2-35158-203-9; *Ed. Miguel Azenha, Dirk Schlicke, Farid Benboudjema, Agnieszka Knoppik*
- PRO 122:** SCC'2018 China - Fourth International Symposium on Design, Performance and Use of Self-Consolidating Concrete, (2018), ISBN: 978-2-35158-204-6, e-ISBN: 978-2-35158-205-3
- PRO 123:** Final Conference of RILEM TC 253-MCI: Microorganisms-Cementitious Materials Interactions (2018), Set: 978-2-35158-207-7, Vol.1: 978-2-35158-209-1, Vol.2: 978-2-35158-210-7, e-ISBN: 978-2-35158-206-0; *Ed. Alexandra Bertron*
- PRO 124 (online version):** Fourth International Conference Progress of Recycling in the Built Environment (2018), e-ISBN: 978-2-35158-208-4; *Eds. Isabel M. Martins, Carina Ulsen, Yury Villagran*
- PRO 125 (online version):** SLD4 - 4th International Conference on Service Life Design for Infrastructures (2018), e-ISBN: 978-2-35158-213-8; *Eds. Guang Ye, Yong Yuan, Claudia Romero Rodriguez, Hongzhi Zhang, Branko Savija*
- PRO 126:** Workshop on Concrete Modelling and Material Behaviour in honor of Professor Klaas van Breugel (2018), ISBN: 978-2-35158-214-5, e-ISBN: 978-2-35158-215-2; *Ed. Guang Ye*
- PRO 127 (online version):** CONMOD2018 - Symposium on Concrete Modelling (2018), e-ISBN: 978-2-35158-216-9; *Eds. Erik Schlangen, Geert de Schutter, Branko Savija, Hongzhi Zhang, Claudia Romero Rodriguez*
- PRO 128:** SMSS2019 - International Conference on Sustainable Materials, Systems and Structures (2019), ISBN: 978-2-35158-217-6, e-ISBN: 978-2-35158-218-3;
- PRO 129:** 2nd International Conference on UHPC Materials and Structures (UHPC2018-China), ISBN: 978-2-35158-219-0, e-ISBN: 978-2-35158-220-6;

RILEM REPORTS (REP)

- Report 19:** Considerations for Use in Managing the Aging of Nuclear Power Plant Concrete Structures (ISBN: 2-912143-07-1); *Ed. D. J. Naus*
- Report 20:** Engineering and Transport Properties of the Interfacial Transition Zone in Cementitious Composites (ISBN: 2-912143-08-X); *Eds. M. G. Alexander, G. Arliguie, G. Ballivy, A. Bentur and J. Marchand*

- Report 21:** Durability of Building Sealants (ISBN: 2-912143-12-8); *Ed. A. T. Wolf*
- Report 22:** Sustainable Raw Materials - Construction and Demolition Waste (ISBN: 2-912143-17-9); *Eds. C. F. Hendriks and H. S. Pietersen*
- Report 23:** Self-Compacting Concrete state-of-the-art report (ISBN: 2-912143-23-3); *Eds. Å. Skarendahl and Ö. Petersson*
- Report 24:** Workability and Rheology of Fresh Concrete: Compendium of Tests (ISBN: 2-912143-32-2); *Eds. P. J. M. Bartos, M. Sonebi and A. K. Tamimi*
- Report 25:** Early Age Cracking in Cementitious Systems (ISBN: 2-912143-33-0); *Ed. A. Bentur*
- Report 26:** Towards Sustainable Roofing (Joint Committee CIB/RILEM) (CD 07) (e-ISBN 978-2-912143-65-5); *Eds. Thomas W. Hutchinson and Keith Roberts*
- Report 27:** Condition Assessment of Roofs (Joint Committee CIB/RILEM) (CD 08) (e-ISBN 978-2-912143-66-2); *Ed. CIB W 83/RILEM TC166-RMS*
- Report 28:** Final report of RILEM TC 167-COM ‘Characterisation of Old Mortars with Respect to Their Repair (ISBN: 978-2-912143-56-3); *Eds. C. Groot, G. Ashall and J. Hughes*
- Report 29:** Pavement Performance Prediction and Evaluation (PPPE): Interlaboratory Tests (e-ISBN: 2-912143-68-3); *Eds. M. Partl and H. Piber*
- Report 30:** Final Report of RILEM TC 198-URM ‘Use of Recycled Materials’ (ISBN: 2-912143-82-9; e-ISBN: 2-912143-69-1); *Eds. Ch. F. Hendriks, G. M. T. Janssen and E. Vázquez*
- Report 31:** Final Report of RILEM TC 185-ATC ‘Advanced testing of cement-based materials during setting and hardening’ (ISBN: 2-912143-81-0; e-ISBN: 2-912143-70-5); *Eds. H. W. Reinhardt and C. U. Grosse*
- Report 32:** Probabilistic Assessment of Existing Structures. A JCSS publication (ISBN 2-912143-24-1); *Ed. D. Diamantidis*
- Report 33:** State-of-the-Art Report of RILEM Technical Committee TC 184-IFE ‘Industrial Floors’ (ISBN 2-35158-006-0); *Ed. P. Seidler*
- Report 34:** Report of RILEM Technical Committee TC 147-FMB ‘Fracture mechanics applications to anchorage and bond’ Tension of Reinforced Concrete Prisms – Round Robin Analysis and Tests on Bond (e-ISBN 2-912143-91-8); *Eds. L. Elfgren and K. Noghabai*
- Report 35:** Final Report of RILEM Technical Committee TC 188-CSC ‘Casting of Self Compacting Concrete’ (ISBN 2-35158-001-X; e-ISBN: 2-912143-98-5); *Eds. Å. Skarendahl and P. Billberg*
- Report 36:** State-of-the-Art Report of RILEM Technical Committee TC 201-TRC ‘Textile Reinforced Concrete’ (ISBN 2-912143-99-3); *Ed. W. Brameshuber*
- Report 37:** State-of-the-Art Report of RILEM Technical Committee TC 192-ECM ‘Environment-conscious construction materials and systems’ (ISBN: 978-2-35158-053-0); *Eds. N. Kashino, D. Van Gemert and K. Imamoto*
- Report 38:** State-of-the-Art Report of RILEM Technical Committee TC 205-DSC ‘Durability of Self-Compacting Concrete’ (ISBN: 978-2-35158-048-6); *Eds. G. De Schutter and K. Audenaert*
- Report 39:** Final Report of RILEM Technical Committee TC 187-SOC ‘Experimental determination of the stress-crack opening curve for concrete in tension’ (ISBN 978-2-35158-049-3); *Ed. J. Planas*
- Report 40:** State-of-the-Art Report of RILEM Technical Committee TC 189-NEC ‘Non-Destructive Evaluation of the Penetrability and Thickness of the Concrete Cover’ (ISBN 978-2-35158-054-7); *Eds. R. Torrent and L. Fernández Luco*
- Report 41:** State-of-the-Art Report of RILEM Technical Committee TC 196-ICC ‘Internal Curing of Concrete’ (ISBN 978-2-35158-009-7); *Eds. K. Kovler and O. M. Jensen*

Report 42: ‘Acoustic Emission and Related Non-destructive Evaluation Techniques for Crack Detection and Damage Evaluation in Concrete’ - Final Report of RILEM Technical Committee 212-ACD (e-ISBN: 978-2-35158-100-1); *Ed. M. Ohtsu*

Report 45: Repair Mortars for Historic Masonry - State-of-the-Art Report of RILEM Technical Committee TC 203-RHM (e-ISBN: 978-2-35158-163-6); *Eds. Paul Maurenbrecher and Caspar Groot*

Report 46: Surface delamination of concrete industrial floors and other durability related aspects guide - Report of RILEM Technical Committee TC 268-SIF (e-ISBN: 978-2-35158-201-5); *Ed. Valérie Pollet*

Organizing Committee

Conference Chair

José Ignacio Álvarez (University of Navarra, Pamplona, Spain)

Members (University of Navarra, Pamplona, Spain)

José María Fernández

Íñigo Navarro

Adrián Durán

Rafael Sirera

Jesús Fidel González

Burcu Taşcı

Cristina Luzuriaga

Joan Puig

Max Renaud Petitjean

Alessandro Speziale

Scientific Committee

Alvarez, José Ignacio.
UNAV, Spain

Biçer-Şimşir, Beril. GCI,
USA

Bokan Bosiljkov,
Violeta. UL, Slovenia

Faria, Paulina. NOVA de
Lisboa, Portugal

Groot, Caspar. UDeft,
Netherlands

Gulotta, Davide. GCI, USA

Hughes, John. UWS, U.K.

Ioannou, Ioannis. UCY,
Cyprus

Maravelaki-Kalaitzaki,
Pagona-Noni. TUC, Greece

Martínez Ramírez, Sagrario,
IEM-CSIC, Spain

Pachta, Vasiliki. AUTH,
Greece

Papayianni, Ioanna. AUTH,
Greece

Pavia, Sara. TCD, Ireland

Rodríguez Navarro, Carlos.
UGR, Spain

Santos Silva, António.
LNEC, Portugal

Secco, Michele. UNIPD,
Italy

Starinieri, Vincenzo.
Sheffield Hallam University,
U.K.

Stefanidou, Maria. AUTH,
Greece

Theodoridou, Magdalini.
Cardiff University, U.K.

Valek, Jan. ASCR, Czech
Republic

Van Hees, Rob P.J. UDeft,
Netherlands

Veiga, Maria
Rosário. LNEC, Portugal

Velosa, Ana. University of
Aveiro, Portugal

Contents

PREFACE.....	1
TOPIC 1: EARTH-BASED PLASTERS AND MORTARS ON ARCHAEOLOGY AND HISTORIC CONSTRUCTIONS.....	3
Earth-based and current plasters: assessment of efficiency and contribution to indoor air quality.....	5
Tânia Santos, Maria Idália Gomes, Flávia Coelho, Paulina Faria	
Earth-based plasters: the influence of clay mineralogy	21
José Lima, Paulina Faria, António Santos Silva	
Rescuing the manufacturing process of traditional mortars present on XIX-century earthen buildings in Brazil	36
Andrea Cavicchioli, Isabela Ferreira Sodr� dos Santos, Jo�o Guilherme Kimura Moreira, Lucy Gomes Sant'Anna	
Assessment of adhesive strength of an earth plaster on different substrates through different methods	51
Paulina Faria, Jos� Lima, Jo�o Nabais, Vitor Silva	
Similar appearance of mortar and brick masses in Algiers Casbah houses during the Ottoman period (16th - early 18th centuries)	65
Semha Bernou, Tsouria Kassab, Rosa Bustamante, Francisco Fern�ndez	
Macroscopic high resolution techniques to the characterization the mortars structures in the S�-Cathedral's archaeological complex in Idanha-a-Velha (Portugal).....	80
Pablo Guerra-Garc�a, Jorge Mor�n de Pablos, Isabel S�nchez Ramos	
TOPIC 2: USE OF NANOTECHNOLOGY FOR HIGH PERFORMANCE MORTARS	93
Evaluation of the influence of nano-SiO₂ and nano-Al₂O₃ on the physico-mechanical properties and microstructure of calcareous clay.....	95
Eirini-Chrysanthi Tsardaka, Maria Stefanidou	
The use of nanoparticles to improve the performance of restoration mortars.....	108
Beatriz Men�ndez, Dita Frankeov�, Jos� Diaz, Radek �ev��k, Petra Macov�, Mouna Faiz, Zuzana Sl�zkov�	
Evaluation of SiO₂ nanoparticles as additive for lime mortars: changes in the microstructure and mechanical properties.....	121
Mar�a del Mar Barbero-Barrera, Aranzazu Sierra Fern�ndez, Duygu Ergenc , Luz Stella Gomez Villalba, Rafael Fort	
Enhancing clay mortars' properties	132
A. Karozou, M. Stefanidou	
Study of the role of different nanoparticles in lime pastes.....	144
Eirini-Chrysanthi Tsardaka, Maria Stefanidou	
Active photocatalytic-superhydrophobic coating with TiO₂/ZnO nano-heterostructures for lime mortars... 	155
Alessandro Speziale, Jes�s Fidel Gonz�lez-S�nchez, �nigo Navarro-Blasco, Jos� M. Fern�ndez, Jos� I. Alvarez	

TOPIC 3: GYPSUM-BASED PLASTERS AND MORTARS IN HISTORICAL CONSTRUCTIONS..... 169

Study of properties of gypsum plasters from Araripe’s Pole for application in restoration mortars 171
Fernanda Cavalcanti Ferreira, Jose Getulio Gomes de Sousa, Arnaldo Manoel Pereira Carneiro

Characterization of Gypsum Renders in the Paris Region and Determination of the Traditional Fabrication Process 186
Jean Ducasse-Lapeyrousse, Véronique Vergès-Belmin

The use of stucco-marble to restore veined polished limestone. The case of the pavement in the major sacristy of the Cathedral of Seville 201
Antonio González Portillo, Maria Teresa Freire

Stucco marble in the Portuguese architecture: first insights in mineralogical, physical and mechanical properties 211
Maria Teresa Freire, António Santos Silva, Maria do Rosário Veiga

Clay and gypsum mortars used during antiquity in Cyprus..... 226
Maria Philokyprou

Physical- mechanical comparison of the traditional gypsums from Albarracín and Pallars..... 237
David Osmar Batres Hernández, Antonia Navarro Ezquerro, Joan Ramon Rosell Amigó

Detailed studies of gypsum plasters from the Ishrat Khana Mausoleum in Samarkand, Uzbekistan 248
Steffen Laue

TOPIC 4: FUNCTIONAL MORTARS FOR THE CONSERVATION OF HISTORIC AND MODERN CULTURAL HERITAGE STRUCTURES..... 259

Use of natural zeolite aggregate in restoration lime renders..... 261
Martin Vyšvařil, Patrik Bayer, Tomáš Žižlavský, Pavla Rovnaníková

Fibre reinforced mortars for cultural heritage protection 273
Miloš Drdácý, Dagmar Michoinová

Comparative evaluation of the morphological and rheological characteristics of nanolime dispersions for the consolidation of architectural monuments..... 283
Anastasia Michalopoulou, Elisavet Michailidi, Evangelos Favvas, Noni-Pagona Maravelaki, Vassilis Kilikoglou, Ioannis Karatasios

Autogenic vs. autonomic self-healing process in conservation mortars with crystalline admixture 296
Maria Amenta, Matina Papaioannou, Marios S. Katsiotis, Dimitris Gournis, Vassilis Kilikoglou, Ioannis Karatasios

Addressing safety and durability requirements of architectural heritage by developing functional conservation mortars..... 307
Ioannis Karatasios, Zoi S. Metaxa, Stavros K. Kourkoulis, Nikolaos D. Alexopoulos, Vassilis Kilikoglou

Self- healing lime-based mortars using biological mechanisms and microvascular networks 319
Cristina De Nardi, Magdalini Theodoridou, Philip Sim, Michael Harbottle, Anthony D. Jefferson

Hydrophobized lime grouts prepared with microsilica and superplasticizers 330
Jesús Fidel González-Sánchez, Íñigo Navarro-Blasco, Adrián Duran, Rafael Sirera, José M. Fernández, José Ignacio Álvarez

Photoactive Fe-TiO₂ Lime Plasters for Building Protection	346
Chrysi Kapridaki, Nikolaos Xynidis, Nikolaos Xekoukoulotakis, Nikolaos Kallithrakas-Kontos, Noni Maravelaki	
Lime-based rendering mortars with photocatalytic and hydrophobic agents: assessment of the water repellency and biocide effect	359
Jesús Fidel González-Sánchez, Burcu Taşçı, Guillermo Martínez de Tejada, José M. Fernández, Íñigo Navarro-Blasco, José Ignacio Alvarez	
SRG, Steel Reinforced Grout for strengthening masonry structures: from tests to applications	373
Paolo Casadei, Paolo Girardello	
TOPIC 5: CHARACTERIZATION OF HISTORIC MORTARS AND MASONRY STRUCTURES. SAMPLING AND TEST METHODS.....	383
Calcite or quartz powder as aggregate of Roman plasters (Lombardy, Italy)	385
Roberto Bugini, Luisa Folli	
Analytical and chromatic characterization of the interior walls finishes in the Batlló House of Gaudí in Barcelona. A surprising discovery	396
Àgueda Serra, Joan Casadevall	
Roman mortars of floor substrates and walls from Arroyo de la Dehesa de Velasco site: petrographic and mineralogical characterization	410
Ainhoa Alonso-Olazabal, Luis Ángel Ortega, M ^a Cruz Zuluaga, Graciela Ponce, Javier Jiménez Echevarría, Carmen Alonso Fernández	
Provenance study of raw materials used for lime making at Prague Castle during medieval times	424
Petr Kozlovcev, Jan Válek, Olga Skružná	
Interpretation of scientific data derived from analytical techniques used in the characterization of Roman mortars	439
Duygu Ergenç, Rafael Fort, Nevin Aly, Olivier Henry, Sayed Hemedá	
Petrography of Historic Mortar Materials: Polarising Light Microscopy as a Method for Characterising Lime-Based Mortars	453
Kristin Balksten, Bo Nitz, John J. Hughes, Jan-Erik Lindqvist	
Roman vs. medieval crushed brick lime mortars: A comparative study	468
Martin Schidlowski, Tobias Bader, Anja Diekamp	
A map is worth a thousand pictures: Using FTIR-imaging to analyze petrographic thin sections of historical and experimental mortar.....	482
Anthony J. Baragona, Marta Anghelone, Johannes Weber	
Characterisation of concrete structures along the Reschen frontier, South Tyrol, Italy	495
Tobias Bader, Anja Diekamp	
Chemical, mineralogical and hydraulic characteristics of Roman mortars in Turkey.....	506
Burcu Taşçı, Hasan Böke	
506	
DB-HERITAGE: A database of mortars composition and characteristics.....	516
António Santos Silva, Rodrigo Giollo, Maria João Correia, Maria do Rosário Veiga, Paulina Faria	
Algarve vernacular architecture facade ornaments: chemical and mineralogical characterization	529
Marta Santos, António Santos Silva, Rosário Veiga	

Characterisation methodology for lime based materials – A case study of the Rajagopuram of Pundarikaksha temple in Tamil Nadu, India	544
Divya Rani and Manu Santhanam	
Sampling cataloging methodology procedures for the conservation of historical colours in urban landscapes	555
Isolina Díaz-Ramos, Jorge Manzano Cabrera	
Mineralogical characterization of historical cement-based mortars from Rupnik military fortification line	565
Petra Štukovnik, Janez Peter Grom, Marjan Marinšek, Violeta Bokan Bosiljkov	
TOPIC 6: HISTORIC PRODUCTION, PROCESSING AND APPLICATION OF MORTARS, RENDERS AND GROUTS. LIME TECHNOLOGIES.....	577
Warm applied Mortar (WAM) – An insight into the historical technique of “Heiße Speis” and its use for renders	579
Robert Wacha, Farkas Pintér	
Blast furnace slag in historic mortars of Bergslagen, Sweden	585
Jan Erik Lindqvist, Kristin Balksten, Birgit Fredrich	
Composition and Technology of the 17th Century Stucco Decorations at Červená Lhota Castle in the Southern Bohemia	596
Jan Válek, Olga Skružná, Petr Kozlovce, Dita Frankeová, Petra Mácová, Alberto Viani, Ivana Kumpová	
Hot applied lime mortar – assessment of a traditional technique used in modern restoration	614
Thomas Köberle, Matthias Zöttl, Alexander Fenzke, Heiner Siedel	
Preliminary research on potential raw material sources for dolomitic lime mortars at St. John’s convent at Müstair, Switzerland	628
Giovanni Cavallo, Marta Caroselli, Albert Jornet, Patrick Cassitti	
A Mortar Maker’s guide to evolving mortar specifications in 18th and 19th C France and England and their implications today	642
Lucie Fusade	
TOPIC 7: MORTARS IN ARCHAEOLOGICAL SITES. CONSTRUCTION HISTORY. ARCHAEOOMETRY.....	653
Characterization and durability analysis of coral stones in a marine environment.....	655
Swathy Manohar, Manu Santhanam	
Technical analysis on materials and characteristics of mortar-based compounds in Roman and Late antique Aquileia (Udine, Italy). A preliminary report of the results	665
Simone Dilaria, Michele Secco, Jacopo Bonetto, Gilberto Artioli	
Fernandina old Wall of Lisbon – Characterization towards its preservation	681
Leandro Gomes, Paulina Faria, Vitor Silva, António Santos Silva	
M.N.I.A.R. techniques of macroscopic characterization from the colorimetry and chromatographies analysis applied to the mortars in the archaeological site of Los Hitos (Arisgotas, Toledo, Spain).....	695
Pablo Guerra-García, Jorge Morín de Pablos, Isabel Sánchez Ramos	

Analysis of mortar samples from the Church of the Saints Sergius and Bacchus at Umm as-Surab (Jordan).....	713
Piero Gilento, Cecilia Pesce, Giovanni Pesce	
Characterisation of Roman Mortar from the Archaeological Site of <i>Mirobriga</i>	727
Alvin Sern Hao Chua, Cristina Galacho, Patrícia Moita, José Carlos Quaresma	
Insights into Carolingian construction techniques – results from archaeological and mineralogical studies at Müstair Monastery, Grisons, Switzerland	743
Marta Caroselli, Christine Bläuer, Patrick Cassitti, Giovanni Cavallo, Irka Hajdas, Sophie Hueglin, Hans Neukom, Albert Jornet	
Animal, Vegetable or Mineral? Characterising shell-lime, maerl-lime and limestone-lime mortar evidence from the Late Norse and Medieval site of Tuquoy, Orkney	758
Mark Thacker, John Hughes, Nic Odling	
TOPIC 8: DATING OF HISTORIC MORTARS.....	779
An Ecology of Castle Construction: geoarchaeology, archaeobotany & radiocarbon analysis in the ecotone of Lochindorb Castle	781
Mark Thacker	
Characterization of historic mortars: techniques used to establish a construction chronology. Case study: “Aragoneses’ Mill” as it belongs to popular architectural heritage.....	800
Esther Moreno Fernández, Javier Pinilla Melo, Francisco González Yunta, Alberto Sepulcre Aguilar, Ignacio Lombillo Vozmediano, Yosbel Boffill Orama	
TOPIC 9: NATURAL AND ROMAN CEMENT MORTARS.....	817
From marlstone to rotary kilns – the early development of Portland cements in Central Europe	819
Farkas Pintér, Christophe Gosselin, Thomas Köberle, István Vidovszky, Johannes Weber	
European natural cements - their key technical properties under standardised conditions	833
David Hughes, Johannes Weber, Vincenzo Starinieri, Farkas Pinter, Christophe Gosselin, Steven Feldman, Cecilia Pesce	
Restoration techniques using 1930’s Portland cements at Porte de l’Est in the Roman city-wall of Aventicum, Switzerland	848
Christophe Gosselin, Noé Terrapon	
Drying Shrinkage of Historic Portland Cements: Factors to be Considered for Successful Repair.....	862
Simeon Wilkie, Thomas Dyer	
Repairs to Historic Concrete Pavement at Jacob Riis Park Utilizing Natural, Roman and Portland Cements	877
Michael P. Edison	
Methodology of identification of natural and historic Portland cements. Application and study in mortars of Madrid and Barcelona.....	886
Cristina Mayo Corrochano, Judith Ramírez-Casas, David Sanz Arauz, Antonia Navarro Ezquerra, Juan Ramon Rosell Amigo	
The use of mortars in Palau Güell by Antoni Gaudi	901
Ricardo Gomez-Val, Judith Ramirez-Casas, Antonia Navarro-Ezquerra	

When Portland cement meets natural cement.....	914
Elisabeth Marie-Victoire, Myriam Bouichou	

TOPIC 10: CONSERVATION ISSUES CONCERNING MORTARS, PLASTERS, RENDERS AND GROUTS. DIAGNOSIS. DECAY AND DAMAGE MECHANISMS. CASE STUDIES..... 929

Decorative renders simulating stone of middle 20th century in the region of Lisbon	931
Maria do Rosário Veiga, António Santos Silva, Cláudia Martinho, Paulina Faria	

The analysis of the proportion of mortar for Japanese roof tile (Ibushikawara) in Taiwan by applying of Taguchi Method	944
Mei-Tsu Hsu, Bing-Sheng Yu	

Evolution of mortars composition and characteristics during the 20th century– Study of Portuguese buildings awarded with Architecture Valmor Prize	959
Luís Almeida, António Santos Silva, José Mirão, Maria do Rosário Veiga	

Practical application of lime-pozzolan mortars to damp masonry	973
Dita Frankeová, Dana Janotová, Zuzana Slížková	

The use of dolomitic lime in mortar samples from a 15th-century buttress of York Minster (York, UK)	986
Cecilia Pesce, Alick Leslie, Alison Henry, John David, Giovanni Pesce	

The Restoration of the church of Our Lady of the Assumption, Dauis, Bohol, Philippines	997
Jim Franklin O. Kalaw, Raul Y. Naguit Jr	

Digital image analysis as basis for the evaluation of repair mortars in architectural conservation	1008
C. Kaiser, L. Oetinger, R. Killian	

TOPIC 11: PRESERVATION. CONSOLIDATION MATERIALS AND TECHNIQUES. DEVELOPMENT OF NEW PRODUCTS. PREVENTIVE CONSERVATION 1021

Frost resistance of reproduced mosaic mortars	1023
Pavla Bauerová, Pavel Reiterman, Eva Vejmelková, Martin Keppert	

Preliminary results on the use of ammonium phosphate solutions for the consolidation of lime-based mortars	1032
Enrico Sassoni, Cesare Pizzigatti, Elisa Franzoni	

Comparative study of ethyl silicate versus acrylic resin consolidation of wall painting with high water and salts contents: a case study at the Chapter Hall of Chartres cathedral.....	1040
Laura Normand, Stéphanie Duchêne, Véronique Vergès-Belmin, Claire Dandrel, David Giovannacci, Witold Nowik	

Comparative analysis of permeability values of traditional aerial lime mortars for preventive conservation	1056
Ana González-Serrano, Reyes Rodríguez-García, Esther Ontiveros-Ortega	

Challenges and strategies of preventive conservation in places of worship – Church of Nossa Senhora de Guadalupe case study	1068
Alexandra Marco, Manuela Pintado, Patrícia R. Moreira, Eduarda Vieira	

TOPIC 12: REPAIR MORTARS AND GROUTS. REQUIREMENTS AND DESIGN. COMPATIBILITY ISSUES. DURABILITY AND EFFECTIVENESS. REPAIR MORTARS: ADEQUACY OF TESTING PROCEDURES.....	1085
Effects of natural zeolite addition to lime based render layers for restoration of historical buildings	1087
Marina Aškračić, Dimitrije Zakić, Aleksandar Savić, Ljiljana Miličić	
Use of ultrafine mafic rocks for the enhancement of carbonation reaction in lime renders	1099
Loucas Kyriakou, Ioannis Rigopoulos, Ioannis Ioannou	
Microstructure of lime pastes with the addition of vegetable oils	1112
Cristiana Nunes, Alberto Viani, Kateřina Mlsnová, Dita Frankeová, Petra Mácová	
Improvements to Water, Salt-Scaling and Freeze-Thaw Resistances of Historic Mortar Replication Mixes.....	1125
Michael P. Edison, Chad Lausberg	
Formulated lime mortars as a sustainable practice for Built Heritage conservation in Mexico.....	1142
Marlene Sámano Chong	
The impact of elevated temperatures on the properties of lime-based mortars	1156
Vasiliki Pachta, Sofia Triantafyllaki, Maria Stefanidou	
Characterization and compatibility assessment of commercial stone repair mortars.....	1166
Barbara Lubelli, Timo G. Nijland, Rob P.J. van Hees	
Impact of aggregates on fresh mortars' properties	1180
Ana Rita Santos, Maria do Rosário Veiga, António Santos Silva, Jorge de Brito	
NHL-based plasters and renders – Assessing the influence of mixing method on workability and hardened mortar properties.....	1195
Frowin Ruegenberg, Martin Schidlowski, Tobias Bader, Anja Diekamp	
Lime-based grouts for architectural surface repair. Comparison of their performance by using laboratory and field test methods.....	1215
Vasiliki Pachta, Ioanna Papayianni, Thomas Spyriiotis	
Evaluation of the fresh state properties of lime-based grouts through inter-laboratory comparative testing	1225
Vasiliki Pachta, Davide Gulotta, Jan Valek, Ioanna Papayianni	
Lime-pozzolan injection grouts with ovalbumin and ethanol added as water-reducing agents: grout design and assessment of the mineralogical evolution	1238
Chiara Pasian, Michele Secco, Francesca Piqué, Gilberto Artioli, Sharon Cather	
Limestone-filled, hydraulic-lime mortars for historic and traditional fabrics	1251
Marwa Aly, Sara Pavía	
Comparing the moisture permeability of limecrete and concrete floor slabs	1267
Grace A. Phillips, Kevin Briggs, Iain McCaig, Richard J. Ball	
Impact of guar gum and chitosan ethers on physico-mechanical properties and durability of natural hydraulic lime mortars.....	1279
Tomáš Žižlavský, Martin Vyšvařil, Patrik Bayer, Pavla Rovnaníková	

Diethyl oxalate-based microgrouts in calcium carbonate systems: formulation, field testing and mineralogical characterization	1291
J. Herrick Porter, C. Pasian, M. Secco, M. Salameh, N. Debono	
Influence of the substrate on the mechanical characteristics of the applied mortars.....	1306
Isabel Torres, Dora Silveira, Inês Flores-Colen, Rafael Pinto, Gina Matias	
Lime Based Mortars. Relationships between Composition Parameters and Mechanical Strength.....	1316
Ioanna Papayianni, Dimitris Papadimitriou	
Investigating differences in the performance of lime-based mortars	1325
Ioanna Papayianni, Vasiliki Pachta, Emmanouela Berberidou, Maria Kalogirou	
A grout and mortar system for fine cracks and shallow surface fills in Carrara marble.....	1333
Andrew Thorn	
Evaluation of the rheological behaviour of a natural additive of vegetal origin in restoration lime mortars as an ecological and sustainable alternative	1346
N. Guasch-Ferré, M.R. Veiga, T. Díaz Gonçalves, M. T. Doménech-Carbó, J.L. Prada, X. Mas i Barberà, M.P. de Luxán Gómez del Campillo	
The initial reactions of lime-pozzolan pastes for conservation of masonry	1361
Tuğçe Büşra Su, Richard J Ball, Juliana Calabria Holley	
Efficiency of field test methods for evaluation of non-structural injection grouts in Slovenian conservation practice.....	1374
Andreja Padovnik, Violeta Bokan Bosiljkov	

Preface

It is my pleasure to write this preface on the occasion of the 5th Historic Mortars Conference and to welcome you to Pamplona, and, in particular, to the University of Navarra. The HMC series reaches a good number and takes us the opportunity to look back, remembering the previous editions in Lisbon, Prague, Glasgow and Santorini. I would like to thank the effort and underline the success of my colleagues who were at the head of the previous editions: Rosário Veiga - who had the intuition and good judgment of promoting the first edition -, Jan Válek, John Hughes and Ioanna Papayianni. Without forgetting Caspar Groot, who, as former chairman of successive RILEM Committees on historic and repair mortars, encouraged and contributed to the success of the previous events.

Thanks to the effort of all of them and their respective teams, we can confirm that HMC's are fully consolidated as a one-of-a kind forum to deal with historic mortars, renders and grouts, the variety of their compositions and raw materials, diverse methodologies of study, archeological sites, dating, preservation, durability, obtaining of repair materials and testing methods, consolidation, and even the upgrade of the repair mortars by nano-technology.

This HMC 2019 gathers 140 scientific and technical high-levelled contributions of participants from the five continents with a wide range of topics that enrich the final outcome of the event. The profitable exchange between the science advances and the practice taking place during the Conference is supported by contributions focused on a more theoretical scientific point of view combined with those works more oriented towards real applications, including case studies, assessment of the state of conservation of some ancient materials or monitoring of the effectiveness of some rehabilitation procedures and repair materials.

The old Kingdom of Navarre offers you a thriving, avant-garde community with a great natural and cultural diversity. In good connection with the framework of the Conference, the preservation and restoration of the Built Heritage is made reality in Navarra. The institution Príncipe de Viana of the Government of Navarra takes care of the vast Architectural Heritage, part of which is ascribed to the Way of Saint James, which passes through these lands.

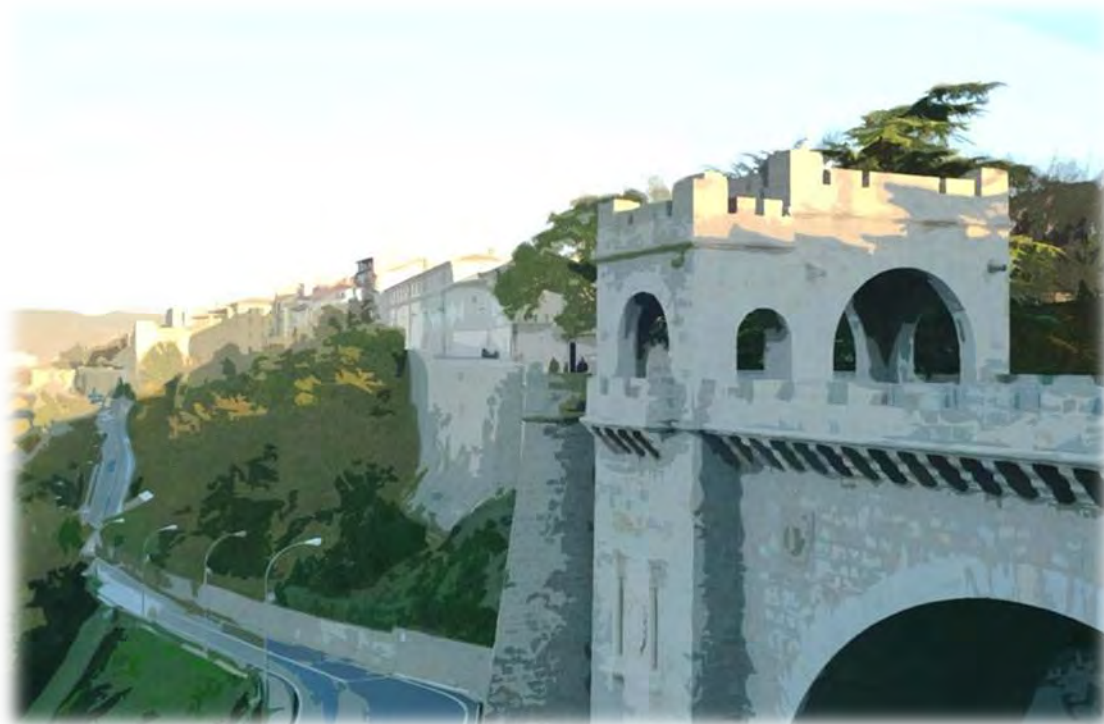
I take for granted that the University of Navarra, is a venue where the great eagernesses devoted to this conference bear fruit. I must thank many people who have made this event possible: those responsible for the University itself, the sponsors for their invaluable help and my colleagues of the Department of Chemistry who have cooperated in the organization.

Finally, the success of this HMC 2019 stems from the know-how and competence of these people below that are gratefully acknowledged: the members of the Scientific Committee for their intense work and constructive criticism of all the submitted contributions, Prof. Antonia Moropoulou for delivering such a remarkable inaugural lecture, Leopoldo Gil Cornet for being an unbeatable guide to observe good practices of restoration, the chairpersons and, of course, all the speakers and participants.

Prof. José Ignacio Álvarez

Chairman 5th HMC 2019

Topic 1: Earth-based plasters and mortars on archaeology and historic constructions



Earth-based and current plasters: assessment of efficiency and contribution to indoor air quality

Tânia Santos¹, Maria Idália Gomes², Flávia Coelho³, Paulina Faria⁴

(1) CERIS and Dep. Civil Engineering, ISEL, Polytechnic Institute of Lisbon, tr.santos@campus.fct.unl.pt

(2) Dep. Civil Engineering, ISEL, Polytechnic Institute of Lisbon, idaliagomes@dec.isel.pt

(3) Dep. Civil Engineering, FCT, NOVA University of Lisbon Institution, fh.coelho@campus.fct.unl.pt

(4) CERIS and Dep. Civil Engineering, FCT, NOVA University of Lisbon Institution, paulina.faria@fct.unl.pt

Abstract

Indoor air quality is very important for comfort but also for buildings inhabitant's health, since poor indoor air quality can lead to adverse health effects, like allergies and chronic diseases such as asthma. Therefore it is considered that is extremely important to understand if plasters have the ability to capture indoor pollutants and contribute to the regulation of indoor air quality. In the present study, five different plasters are analysed to compare the behaviour of earth-based plasters with commonly used plasters. Before assessing the contribution of plasters to the capture of pollutants, it is necessary to characterize the m. It is possible to conclude that the addition of air lime to an earth plastering mortar decrease mechanical strength and hygroscopic capacity. Earth plasters show high sorption and desorption capacity when compared to commonly used plasters, such as cement and gypsum-based. The lower sorption capacity of plasters with current binders may induce a lower air pollutants capture capacity but that still needs to be tested.

Introduction

World Health Organization (WHO) estimates that 3.8 million annual causes of death are attributed to indoor air pollution from buildings [1]. Indoor air quality (IAQ) is very important for comfort but also for health of buildings inhabitants, since poor IAQ can have a high impact in health, comfort, well-being and cognitive performance of building occupants. Particularly long term exposure of building occupants to a poor quality indoor air can produce various symptoms in the buildings occupants, like fatigue, eye irritation, headaches, dizziness, skin irritation, chronic problems, among others [2]. It is important to emphasize that people spend much of their time inside buildings. Currently, around 50 % of the world's population lives in cities and about 80 – 90 % of their lives is spent inside the buildings (home, work and leisure) [3-5]. For this reason, the IAQ is a major issue not only for new construction but also for the conservation of old buildings. Therefore, it is necessary to consider the materials that are used inside the buildings and, above all, analyse its contribution to improve IAQ.

There is a lot of tradition on cement-based construction around the world; cement is the second most consumed substance in the world by weight [2] and widely used in interior finishes, such as cement plastering mortars. However, it is known that about 900 kg of CO₂ are emitted into the atmosphere during the production of 1 ton of cement [2]. Given these facts, whenever possible, it is very important to use environmentally friendly building materials – ecological, sustainable, with lower CO₂ emissions – and materials that may also contribute to improve IAQ of buildings.

Earthen mortars present several advantages: the raw material is natural, non-toxic, low costly, involving low CO₂ emissions to be applied as a building material, with low embodied energy, reusable (when not chemically stabilized). Through the hygroscopic capacity of clays, earth plasters have a high capacity to adsorb and release water vapour, contributing to balance indoor relative humidity (RH) and temperature, promoting the comfort of the occupants and indoor air quality [6-15]. The interest of the scientific community by earth plasters has emerged in the last decade. But earth plasters characteristics are not often tested in comparison with common plasters. With regard to earth plasters pollutants absorption capacity, no study has yet been carried out to prove this capability. However, there are already some advances in this area regarding cement mortars [2].

In order to improve IAQ, it is extremely important to understand the relationship between indoor air pollutants and the ability of a plaster system, based on mortars, to capture these pollutants and contribute to the regulation of temperature, RH and, consequently, IAQ. Before understanding the contribution of plasters to pollutants capture, it is necessary to characterize them physically and mechanically. In consequence, in the present study the physical and mechanical characteristics of three earth-based plastering mortars are evaluated – a pre-mixed earth plastering mortar, a laboratory formulated earth mortar and a pre-mixed earth-air lime plastering mortar–, in comparison to two pre-mixed plastering mortars commonly used in Portugal, one based on hemi-hydrated gypsum and the other on cement. Mortars are characterized in the fresh and hardened states, in terms of bulk density, mechanical strength, capillary, drying, sorption and desorption.

Materials and methods

Characterization of materials

In the present study five different plastering mortars are analysed: a pre-mixed earth mortar with natural fibres (T_E), produced by Embarro; an earth mortar formulated in laboratory (T_AP), with a red clayish earth (RCE), fine (FS) and (CS) coarse sands; a pre-mixed earth-air lime mortar (T+CL), produced by Aldeias de Pedra company; a pre-mixed cement mortar (C) – RHP Manual Interior –, produced by Secil Argamassas company; and a pre-mixed gypsum mortar including a finishing coat (G) – Project 2010 and Massa de Acabamento –, produced by Sival company.

The T_E mortar is composed by a clayish earth, from Algarve region, fine sand with particle size distribution of 0 – 2 mm and straw fibres cut with less than 10 mm in length. Other researchers analysed a similar pre-mixed earth mortar from the same producer and concluded that this mortar was produced with an ilitic clay [16-18]. The proportions of each constituent of this mortar are not exactly known. The T_AP mortar was formulated in laboratory conditions and was produced with volumetric ratio of 1:3:1.5 and mass ratio of 1:3.04:1.78 (RCE:FS:CS). The T+CL mortar is composed with yellow clayish earth (YCE), provided by Sorgila, coarse sand (CS), limestone powder (LP) and an addition of air lime putty (ALP). The exact proportions of each constituent are not known. The same happens with cement (C) and gypsum-based (G) mortars, since these are already marketed as pre-mixed.

The loose bulk density of the materials were analysed by EN 1097-3 [19], taking an average of three specimens of each material and can be seen in Table 1.

Table 1. Loose bulk density of the materials

Material	Loose bulk density [kg/dm ³]
Pre-mixed earth mortar (T_E)	1.40 ± 0.01
Red clayish earth (RCE)	1.36 ± 0.01
Yellow clayish earth (YCE)	1.20 ± 0.00
Limestone powder (LP)	1.37 ± 0.02
Fine sand (FS)	1.38 ± 0.00
Coarse sand (CS)	1.61 ± 0.00
Pre-mixed cement mortar (C)	1.50 ± 0.00
Pre-mixed gypsum mortar (G)	0.81 ± 0.01

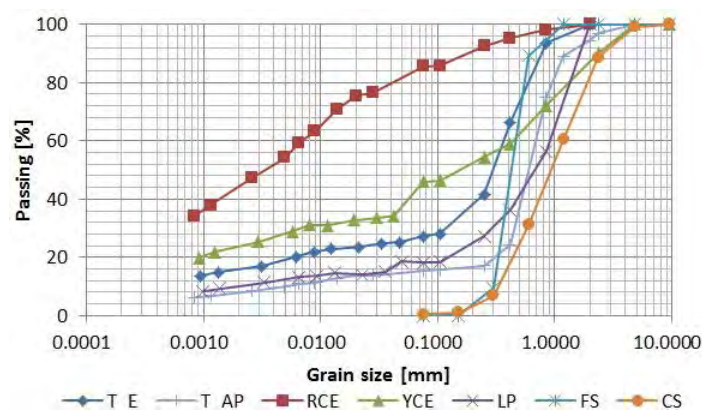


Figure 1. Particle size distribution of the materials (T_E, RCE, YCE and LP by wet method and sedimentation, and by dry method for FS and CS) and T_AP mortar.

Particle size distribution of the materials were performed by EN 1015-1 [20]. The wet method was used for the clayish earths (RCE and YCE), pre-mixed earth mortar product (T_E) and limestone powder (LP). The dry method was used for fine and coarse sands (FS and CS). To complement the particle size distribution of RCE, YCE, T_E and LP materials, since these materials presents particles lower than 0.075 mm, the sedimentation was also analysed,

according to LNEC specification E196 [21]. From the particle size distribution of the materials present on T_AP mortar (RCE, FS and CS) it was possible to determine its particle size distribution. The results are shown in Figure 1. According to the producer's indication, the cement-based mortar present particle size lower than 1.2 mm, by EN 1015-1 [20].

Mortars and specimens

The pre-mixed earth, earth with air lime putty and cement mortars (T_E, T+CL and C) were produced only by addition of the water content indicated by each producer (15 %, 20 % and 14 %, respectively). Due to lack of indication from the producers, for T_AP and G mortars a water content was defined (10 % and 43 %, respectively) by an experienced craftsman to assure good workability.

In order to reproduce, as much as possible, the method carried out on construction site, all mortars were produced using a mixer blade (Figure 2a). Dry materials were placed in a bucket and the water was slowly added. An initial mixture of 8 minutes was carried out; after this period, the mortar that adhered to the bucket edges was removed and added to the remaining mortar, followed by a further 3 minutes of mixing (Figure 2Figure 2a). This was considered time enough for the mortars to be homogeneous. The T+CL mortar was produced the day before of their specimens were moulded. The remaining mortars were produced the same day of moulding. For each plastering mortar different types of specimens were produced in metallic moulds: six prismatic specimens with 40 mm x 40 mm x 160 mm (Figure 2b and Figure 2c), moulded in two layers mechanically compacted with 20 strokes each and manually levelled; three planar specimens with 200 mm x 500 mm x 15 mm (Figure 3), manually compacted and levelled.



Figure 2. Production of the T_E mortar (a), prismatic specimens of T_AP and T+CL in the metallic moulds (b) and prismatic specimens of C mortar (c).



Figure 3. Finishing of planar specimen of T_AP plaster (a) and planar specimens of T+CL plaster (b) and planar specimens of G plaster (c).

The gypsum finishing coat was only applied, with 1 mm of thickness, to the G planar specimens. Only the prismatic specimens were demoulded when dried, after at least 7 days. All specimens were placed in laboratory conditions at 20 ± 2 °C and 65 ± 5 % prior to the characterization tests. The age of the specimens of each plastering mortar for each characterization test can be observed in Table 2. A longer aging of T+CL mortar was justified by the fact of being the only mortar with slow reaction due to carbonation. For this reason, the mechanical strength was only assessed after 4 months. Unstabilised earth mortars (T_E and T_AP) harden just by drying. Cement-based (C) and gypsum-based (G) mortars are known by their fast hardening reactions. Therefore these mortars were tested for strength after 2 months.

Table 2. Age of mortar specimens for each characterization test

Characterization test	Age of specimens mortars (in days)				
	T_E	T_AP	T+CL	C	G
Dry bulk density	28	41	111	40	33
Flexural and compressive strength	54	68	138	67	60
Capillary absorption	56	75	146	109	68
Drying	61	75	153	116	75
Sorption and desorption	118	124	194	138	131

Methods

There is no specific standardization for earthen mortars, except the German standard DIN 18947 [22], which refers to some European standard tests for masonry mortars and complementary ones. Due to the fragility of earth mortars in the presence of water and low mechanical strength, these mortars present constraints more stringent than cement or gypsum-based mortars. For this reason, some adjustments were necessary to be made on the test procedures. In order to obtain comparable results, the adjustments made to test the earthen mortars were also carried out for testing the remaining mortars.

Fresh state

All mortars were characterized in fresh state by flow table consistency, according to EN 1015-3 [23] and by wet bulk density, according to EN 1015-6 [24]. The results are the average of two measurements for each mortar.

Dry bulk density and strengths

Six prismatic specimens of each mortar were used to evaluate the dry bulk density and flexural and compressive strengths. The dry bulk density was geometrically determined by the ratio between the dry mass and the volume of each specimen, provided by an electronic digital scale with 0.001 g of precision and a digital calliper, according to the DIN 18947 [22] and EN 1015-10 [25]. The flexural and compressive strengths were determined by DIN 18947 [22] and EN 1015-11 [26], using a Zwick Rowell Z050 equipment, with load cells of 2 kN and

velocity of 0.2 mm/min for flexural strength and 50 kN and velocity of 0.7 mm/min for compressive strength.

Capillary absorption and drying

The capillary absorption of the mortars were evaluated according to EN 15801 [27] and EN 1015-18 [28]. Six cubic specimens with 40 mm x 40 mm x 40 mm were used, for each type of mortar. These specimens were cut from the prismatic specimens with a circular saw. The specimens were prepared according to the procedure used by Gomes et al. [29] for earth mortars: the lateral faces of the cubic specimens were waterproofed with a mixture of 50% of beeswax and 50% of pitch blond (mass proportions); the bottom face was covered with a cotton cloth; the specimens were placed in partial immersion, on a layer of 1 – 2 mm of water, on a saturated damp cloth with 5 mm of thickness, inside a box with a lid, which was only opened for weighing the specimens, to limit evaporation from the specimens. The test was carried out in controlled environment conditions of $20 \pm 2^\circ\text{C}$ temperature and $65 \pm 5\%$ RH.

The weight gain of the specimens over time was recorded. With these results the absorption curve of each mortar (the average of six specimens) was obtained with the amount of water absorbed per unit area (kg/m^2) as a function of the square root of the time ($\text{s}^{1/2}$). The capillary absorption test ended when the difference of the mass of water absorbed by the specimens between two successive weightings in 24 hours did not exceed 1 % [27]. The capillary water absorption coefficient (AC, in $\text{kg}/(\text{m}^2 \cdot \text{s}^{1/2})$) is the slope of the linear section of the absorption curve and was calculated by linear regression using at least 5 successive aligned points [27].

For the drying test, according to EN 16322 [30], the same specimens used for the capillary absorption test were used. The drying test began immediately after the capillary test. The specimens were maintained under controlled environment conditions of $20 \pm 2^\circ\text{C}$ and $65 \pm 5\%$ with only the top face exposed to the air, so that drying only occurs through that surface. The drying curve of the first phase of each mortar (the average of six specimens) was obtained with the amount of evaporated water (kg/m^2) – measured by periodical weightings – as function of the time (s). With this curve the drying rate in the first phase (D1, in $\text{kg}/\text{m}^2 \cdot \text{h}$) and the drying index (ID, dimensionless) [30] were determined. For determination of the drying rate of the second phase (D2, in $\text{kg}/\text{m}^2 \cdot \text{h}^{1/2}$), the drying curve obtained with the amount of evaporated water as a function of the square root of the time ($\text{s}^{1/2}$) was plotted.

Sorption and desorption

The sorption and desorption of the plasters were determined with three planar specimens in the metallic moulds of each plaster, according to DIN 18947 [22]. Therefore, only one face of the specimens was exposed. Initially the specimens were placed in the climatic chamber at 23°C and 50 % RH for 24 hours, until constant mass (less than 2 % of variation). Then, the RH inside the climatic chamber was increased to 80 % (maintaining the temperature at 23°C),

starting the sorption phase of the plasters. The water vapour gain by the plasters, in g/m^2 , was determined after 1, 3, 6, 12 and 24 hours, by weighing of the specimens using an electronic digital scale with 0.1 g of precision. Although DIN 18947 [22] reported a weighting in the first 30 min (0.5 hours), this was not performed, once this period (between the first 30 min until 1 hour) was considered too short to stabilize the climatic chamber and with negative influence on the test results at 1 hour of test. The DIN 18947 [22] also defines that the test ends after 12 hours. However, in this study the evaluation of the sorption was held up to 24 hours [10, 31, 32].

Although DIN 18947 [22] only requests the analysis of the sorption capacity of plasters, it was also considered important to evaluate their water vapour desorption capacity [10, 31, 32]. For that the reverse process was used. After 24 hours, the RH was changed to 50 % and the decrease of water vapour content on the plasters specimens, also in g/m^2 , was evaluated at the same defined periods of time (from 1 up to 24 hours).

Results and discussion

Fresh state

The flow table consistency and wet bulk density of the mortars are presented in Table 3.

Table 3. Flow table consistency and wet bulk density of the mortars

Mortar	Flow table consistency [mm]	Wet bulk density [kg/dm^3]	Water/dry components ratio [-]
T_E	125 ± 8	2.03 ± 0.02	0.1
T_AP	136 ± 19	1.56 ± 0.06	0.1
T+CL	153 ± 1	1.99 ± 0.02	0.2
C	138 ± 14	1.90 ± 0.00	0.1
G	-	1.58 ± 0.05	0.4

For earth mortars, DIN 18947 [22] defines that the flow table consistency should be 175 ± 5 mm and the wet bulk density should be higher than 1.2 kg/dm^3 . Earthen mortars, but also the remaining mortars, fulfilled the wet bulk density defined by DIN 18947 [22]. However, the flow table consistency was not accomplished for any mortars. The non-compliance is related to the water content used in the mortars mixture. For the earth mortars it was chosen to obtain a good workability, defined by the craftsman, with the aim of resembling the reality on a working site. The added water was the minimum to achieve good workability. The water content used on C mortar was the indicated by the producer. The flow table consistency of the G mortar was not evaluated due to the wall effect: the mortar in the fresh state was clinging to the truncated conical mould used in the test, being impossible to perform the test.

Dry bulk density and strengths

Figure 4 reports the dry bulk density, flexural and compressive strength of the mortars. In general, earth mortars (T_E, T_AP and T+CL) present similar dry bulk density. The C mortar presents bulk density similar to earthen mortars and the G mortar present lower bulk density. These results can be justified by the bulk density of each material: all the materials presents similar loose bulk density (Table 1), with the exception of the gypsum material, which has the lowest loose bulk density and, consequently, lower dry bulk density.

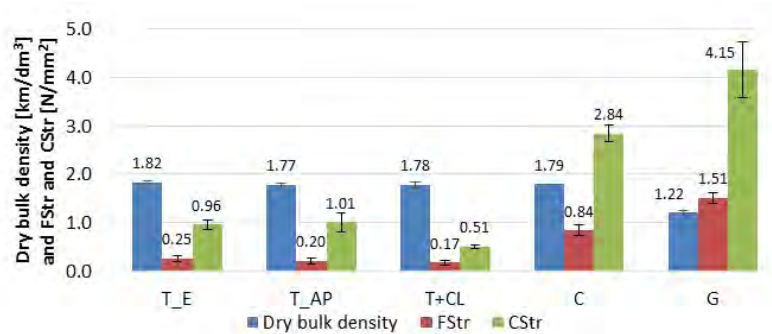


Figure 4. Dry bulk density and flexural (FStr) and compressive (CStr) strengths of the mortars.

Flexural and compressive strength of T+CL mortar were performed after 138 days – much aged in comparison to the remaining mortars (Table 2). Nevertheless, by Figure 4 it can be concluded that T+CL mortar present lower strengths, even when comparing with earth mortars without addition of any type of binder. This means that, in this case, the addition of air lime does not improve the mechanical strength of the mortar. One possibility for this result is if the carbonation reaction of the air lime has not been completed yet. Nevertheless, Santos et al. [17] concluded also that the addition of 5 % of air lime decreased the mechanical strength of an earth mortar. Another study performed by Gomes et al. [29] have shown similar results with air lime additions up to 15 %. In these studies the justification given was that low amounts of lime interrupts the clay matrix connection, without creating a lime network strong enough to replace those clay connections. Although the content of air lime in the T+CL mortar is not known, the same phenomena may have happened.

The earthen mortars present lower mechanical strength compared to cement and gypsum mortars – which present values confirmed by previous studies: in a study with ancient gypsum-based plasters from the 18th – 20th centuries, Freire et al. [33] obtained compressive strength of 1.02 – 4.27 N/mm²; Brás et al. [34], for cement mortar with CEM II B-L 32.5 N cement, obtained flexural strength of 5.2 N/mm² and compressive strength of 24.4 N/mm², at 28 days of age; Bogas et al. [35] analysed cement mortars with CEM I 42.5 R cement and obtained flexural strength of 6.7 N/mm² and compressive strength of 41.9 N/mm², at 28 days of age.

Veiga et al. [36] defined general requirements concerning some characteristics of plastering mortars for application on old buildings: flexural strength of 0.2 – 0.7 N/mm² and

compressive strength of 0.4 – 2.5 N/mm². Unlike cement and gypsum mortars, earth mortars meet the flexural and compressive strength requirements and can be applied to repair old buildings. The EN 998-1 [37] defined different classes for compressive strength for plastering mortars: CSI for 0.4 – 2.5 N/mm²; CSII for 1.5 – 5.0 N/mm²; CSIII for 3.5 – 7.5 N/mm² and CSIV for ≥ 6 N/mm². The earth mortars analysed in the present study (T_E, T_AP and T+CL) can be classified as CSI and the cement mortar as CSII. The EN 13279 [38] defines that gypsum plasters must meet at least a flexural strength of 1 – 2 N/mm² and a compressive strength of 2 – 6 N/mm². The gypsum mortar analysed in the present study meets the minimum values defined by EN 13279 [38].

Capillary absorption and drying

Observing the capillary absorption curves of each mortar presented in Figure 5a it is possible to conclude that T+CL and C mortars have very similar behaviour. Similar values for capillary water absorption coefficient, 0.10 and 0.12 kg/(m².s^{1/2}), and also similar values in respect to the total quantity of water absorbed per unit area, 9.09 and 9.11 kg/m² (Figure 5b), are presented for T+CL and C, respectively. The capillary water absorption coefficients (AC) are shown in Table 4 and it can be concluded that:

- T_E mortar presents slower capillary water absorption (Figure 5a) and, therefore, lower capillary coefficient; therefore, this mortar presents a good behaviour in a first contact with water. Nevertheless, it did not reach an asymptotic value; at the end of the test, this mortar was still absorbing water by capillarity. The behaviour of this mortar can be justified by the type of clayish earth, which may block the water ingress, slowing its absorption. This mortar seems to indicate water-repellence. To the authors knowledge water repellents were not added or at least that information was omitted by the producer.
- T_AP mortar presents high initial capillarity water absorption (Figure 5a), which is confirmed by the higher capillary coefficient when compared to the other mortars. This mortar presents the worst behaviour when subjected to the action of water by capillary absorption. This mortar also showed to be very sensitive to water and, after 210 minutes, mass loss occurred; for this reason the capillary test stopped before the remaining mortars.
- T+CL mortar present lower capillary water absorption in relation to the remaining earth mortars (T_E and T_AP). It seems that lime blocks the behaviour of clay. This behaviour, between clay and cement or lime, is documented and studied by Gomes et al. [39]. The researchers refer that clay has a different behaviour when it is mixed with lime – this binder acts as blocker of the clay structure, inhibiting the characteristics of the clay.
- Current pre-mixed mortars (C and G) have the same initial capillary water absorption behaviour – present the same slope of the linear section of the absorption curve (Figure 5a); the AC confirms this behaviour. Nonetheless, the G mortar has a greater capacity to

absorb high amount of water by capillarity, with water absorbed per unit area of 14.8 kg/m^2 (Figure 5b). The higher capillary water absorption of the G mortar may be related to the higher fineness of the material and, possibly, higher porosity and pore size distribution [33]. In the present study, these conclusions cannot be established since porosity and pore size distribution could not be analysed yet. C and T+CL mortars present similar capillary water absorption behaviour, with similar capillary coefficient and asymptotic value.

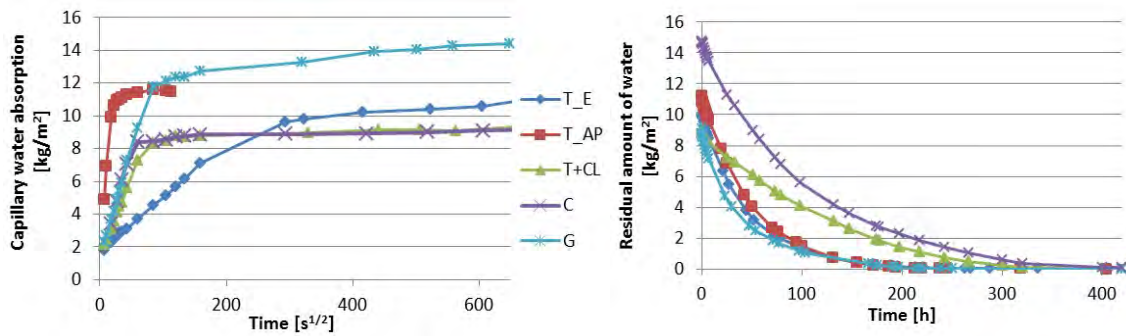


Figure 5. Capillary absorption (a) and drying (b) curves.

The drying curves allowing determining the first drying phase of each mortar can be observed in Figure 5b. The drying rates of first (D1) and second (D2) phases, and the drying index (ID) (at 420 hours approximately) are presented in Table 4.

Table 4. Capillary water absorption coefficient, drying rate of first and second phase and drying index

Mortar	AC [kg/m ² .s ^{1/2}]	D1 [kg/m ² .h]	D2 [kg/m ² .h ^{1/2}]	ID [-]
T_E	0.03 ± 0.00	0.15 ± 0.01	1.11 ± 0.05	0.11 ± 0.01
T_AP	0.41 ± 0.06	0.15 ± 0.00	1.15 ± 0.03	0.12 ± 0.00
T+CL	0.10 ± 0.01	0.05 ± 0.00	0.44 ± 0.03	0.25 ± 0.03
C	0.12 ± 0.00	0.17 ± 0.01	1.03 ± 0.07	0.11 ± 0.03
G	0.14 ± 0.01	0.11 ± 0.01	0.91 ± 0.06	0.24 ± 0.01

AC – Capillary water absorption coefficient; D1 –Drying rate in the first phase;
D2 – Drying rate in the second phase; ID – Drying Index.

It is possible to conclude that:

- The T_E, T_AP and C mortars present similar drying behaviour and this is confirmed by drying rates and drying indexes. In global terms they present adequate drying, since they present high drying rate – ensuring fast initial drying – and low drying index – ensuring total drying capacity – in comparison with the remaining mortars.
- The T+CL mortar presents the worst drying behaviour, with low drying rates and high drying index. This behaviour may be justified by the presence of lime, which seems to contribute to significantly increase the capillary suction and decrease the drying capacity [39].

- G mortar presents the highest amount of water absorbed per unit area; so it is also the mortar that has more water to evaporate at the beginning of the test. Although it has a higher water content to evaporate, presents similar drying behaviour when compared to T_E, T_AP and C mortars; this is confirmed by drying rates results.

Sorption and desorption

Figure 6 presents the results of the sorption and desorption of the plasters. In this figure the limits of sorption classes (WSI, WSII and WSIII) defined by DIN 18947 [22] are also presented. For earth plasters, DIN 18947 [22] defines three sorption classes: WSI for sorption ≥ 35 g/m²; WSII for ≥ 47.5 g/m²; WSIII for ≥ 60 g/m², after 12 hours.

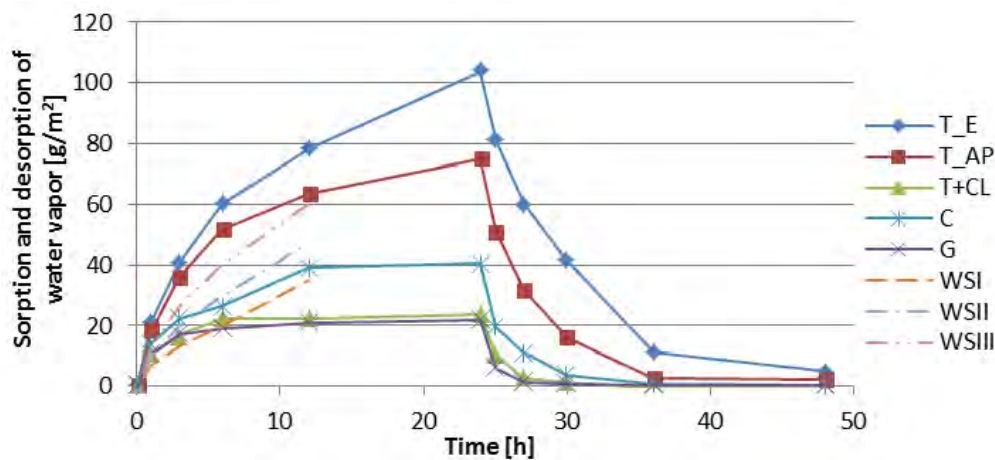


Figure 6. Sorption and desorption curves and sorption limits (WSI, WSII and WSIII) defined by DIN 18947 [22].

The results show that the earth plasters present significantly higher sorption and desorption capacity in comparison to all the plasters with common binders. The T_E and T_AP plasters can be classified in WSIII class, by DIN 18947 [22], since their sorption is higher than 60 g/m² of water vapour after 12 hours. The T_E plaster presents the higher sorption capacity having adsorbed about 104 g/m² after 24 hours. Despite the good water vapour sorption capacity demonstrated by the T_AP plaster, it only absorbs about 76 g/m² during the test. By observing the sorption curves (Figure 6), it is possible to conclude that T_E and T_AP plasters could adsorb a higher amount of water vapour since the sorption curves still show a growing trend at 24 hours. The high sorption capacity demonstrated by the T_E plaster may be related to the type of clay present in the plaster and/or the addition of natural fibres, since fibres increase the hygroscopicity of earth plasters [11].

By Figure 6 it is also possible to conclude that the addition of air lime decreases the sorption capacity of earth plasters. The T+CL plaster only adsorbed about 24 g/m² of water vapour during the 24 hours of the test. The low water vapour sorption capacity of this plaster may be related to the addition of air lime, but also to the type of clay used. Analysing DIN 18947 [22], the T+CL is impossible to classify, since at 12 hours this plaster presents a sorption lower than the limit for the lower class (WSI ≥ 35 g/m²). Unlike earth plasters without

mineral binders, the T+CL plaster presents stable adsorption behaviour after 6 hours of testing. It seems that lime blocks the behaviour of clayish particles, as previously mentioned.

The C and G plasters present lower sorption capacity in comparison with unstabilized earth plasters (T_E and T_AP). The sorption capacity of the C plaster is 40 g/m². The G and T+CL plasters present similar sorption behaviour.

Relative to desorption, all plasters present a good behaviour, having desorbed almost the entire water vapour that adsorbed. The T_E and T_AP plasters desorb a little less water vapour than they adsorbed, after 24 hours – they would probably reach the same initial values if there were more time to perform the test, since they show a downward trend. After performing the desorption test the remaining plasters present similar water vapour content in relation to 0 hours. This means that these plasters (T+CL, C and G) desorbed all the vapour water they have adsorbed in a similar period of time.

Conclusion

There are known complaints and discomfort felt by the occupants of the buildings which, through scientific evidence, are related, not only but also, with the building materials used indoors. It is increasingly important to be aware of the influence that building materials have on the health and comfort of inhabitants. Therefore, it is extremely important to study hygienic and human toxicological aspects, in order to ensure the existence of healthy, pleasant and comfortable environments. The INDEEd project intend to help answering these questions by attempting to quantify possible improvements that may be beneficial to indoor air quality presented by different types of earth-based plasters compared to other plasters commonly used in Portugal, based on gypsum and cement mortars.

It was verified, in the present study, that earthen mortars present lower mechanical strength when compared to mortars with current mineral binders (gypsum and cement). Also the addition of air lime to earth mortars seems to decrease their mechanical strength. On the other hand, it has been demonstrated that unstabilized earth plasters presents a high capacity of sorption and desorption, validating their ability to regulate RH and temperature. Therefore unstabilized earth plasters contribute to indoor comfort and, perhaps, the ability to capture indoor pollutants may be related with their sorption capacity. This capacity is being studied in the INDEEd project and will be reported in future work.

Acknowledgements

Acknowledgments are due to Aldeias de Pedra, Embarro, Secil Argamassas and Sival Companies for providing the materials and pre-mixed mortars. This study was funded by the Portuguese Foundation for Science and Technology through project INDEEd – Indoor air quality regulation through the usage of eco-efficient mortars (SAICT/23349/2016), by Operational Programme Competitiveness and Internationalization (COMPETE 2020) and by

FEDER funds through the Regional Operational Programs of Lisbon and of Center (Lisbon 2020, Center 2020).

References

1. WHO (2018) News release: 9 out of 10 people worldwide breathe polluted air. <http://www.who.int/airpollution/en/>. Accessed 08 June 2018
2. Krejcirikova B, Kolarik J, Wargocki P (2018) The effects of cement-based and cement-ash-based mortar slabs on indoor air quality. *Build Environ.* 135:213–223. doi: 10.1016/j.buildenv.2018.03.011
3. Ginja J, Borrego C, Coutinho M et al (2012) Indoor air quality in Portuguese housing (in Portuguese). In: CINCOS'12 - Congress of Innovation on Sustainable Construction, 20-22 September, Aveiro, Portugal
4. Maskell D, da Silva CF, Mower K (2017) Bio-based plaster for improved indoor air quality. In: 2nd International Conference on Bio-Based Materials and 1st Conference on ECOlogical valorization of GRANular and Fibrous materials, 21-23 June, Clermont-Ferran, France
5. Crump D, Dengel A, Swainson M (2009) Indoor air quality in highly energy efficient homes: A review. IHS BRE Press. ISBN: 978-1-84806-104-0
6. Minke G (2006) Building with earth. Design and Technology of a Sustainable Architecture. WITpress, Berlin. ISBN-13: 978-3-7643-7477-8
7. Cagnon H, Aubert JE, Coutand M et al (2014) Hygrothermal properties of earth bricks. *Energ Buildings.* 80:208–217. doi: 10.1016/j.enbuild.2014.05.024
8. Emiroğlu M, Yalama A, Erdoğan Y (2015) Performance of ready-mixed clay plasters produced with different clay/sand ratios. *Appl Clay Sci.* 115:221–229. doi: 10.1016/j.clay.2015.08.005
9. Melià P, Ruggieri G, Sabbadini S et al (2014) Environmental impacts of natural and conventional building materials: a case study on earth plasters. *J Clean Prod.* 80:179–186. doi: 10.1016/j.jclepro.2014.05.073
10. Lima J, Faria P, Santos Silva A (2016) Earthen plasters based on illitic soils from barrocal region of Algarve: Contributions for building performance and sustainability. *Key Eng Mater.* 678:64–77. doi: 10.4028/www.scientific.net/KEM.678.64
11. Ashour T, Georg H, Wu W (2011) An experimental investigation on equilibrium moisture

- content of earth plaster with natural reinforcement fibres for straw bale buildings. *Appl Therm Eng.* 31:293–303. doi: 10.1016/j.applthermaleng.2010.09.009
12. Liuzzi S, Stefanizzi P (2015) Experimental investigation on lightweight and lime stabilized earth composites. *Key Eng Mater.* 666:31–45. doi: 10.4028/www.scientific.net/KEM.666.31
 13. Randazzo L, Montana G, Hein A et al (2016) Moisture absorption, thermal conductivity and noise mitigation of clay based plasters: The influence of mineralogical and textural characteristics. *Appl Clay Sci.* 132–133:498–507. doi: 10.1016/j.clay.2016.07.021
 14. Bruno AW, Gallipoli D, Perlot C et al (2017) Effect of stabilisation on mechanical properties, moisture buffering and water durability of hypercompacted earth. *Constr Build Mater.* 149:733–740. doi: 10.1016/j.conbuildmat.2017.05.182
 15. Maskell D, Thomson A, Walker P et al (2018) Determination of optimal plaster thickness for moisture buffering of indoor air. *Build Environ.* 130:143–150. doi: 10.1016/j.buildenv.2017.11.045
 16. Faria P, Santos T, Aubert JE (2016) Experimental Characterization of an Earth Eco-Efficient Plastering Mortar. *J Mater Civil Eng.* 28:04015085. doi: 10.1061/(ASCE)MT.1943-5533.0001363
 17. Santos T, Nunes L, Faria P (2017) Production of eco-efficient earth-based plasters: Influence of composition on physical performance and bio-susceptibility. *J Clean Prod.* 167:55–67. doi: 10.1016/j.jclepro.2017.08.131
 18. Santos T, Faria P, Silva V (2019) Can an earth plaster be efficient when applied on different masonries?. *J Build Eng.* 23:314–323. doi: 10.1016/j.job.2019.02.011
 19. EN 1097-3 (1998) Tests for mechanical and physical properties of aggregates, Part 3: Determination of loose bulk density and voids. CEN, Brussels
 20. EN 1015-1 (1998/2006) Methods of test for mortar for masonry, Part 1: Determination of particle size distribution (by sieve analysis). CEN, Brussels
 21. E196 (1966) Particle size analysis (by dry sieving and sedimentation) (in Portuguese). LNEC, Lisbon
 22. DIN 18947 (2013) Earth plasters – Terms and definitions, requirements, test methods (in German). DIN, Berlin
 23. EN 1015-3 (1999/2004/2006) Methods of test for mortars for masonry, Part 3: Determination of consistency of fresh mortars. CEN, Brussels

24. EN 1015-6 (1998) Methods of test for mortars for masonry, Part 6: Determination of bulk density of fresh mortars. CEN, Brussels
25. EN 1015-10 (1999/2006) Methods of test for mortars for masonry, Part 10: Determination of dry bulk density of hardened mortar. CEN, Brussels
26. EN 1015-11 (1999) Methods of test for mortars for masonry, Part 11: Determination of flexural and compressive strength of hardened mortar. CEN, Brussels
27. EN 15801 (2009) Conservation of cultural property, Test methods, Determination of water absorption by capillarity. CEN, Brussels
28. EN 1015-18 (2002) Methods of test for mortars for masonry, Part 18: Determination of water absorption coefficient due to capillary action of hardened mortar. CEN, Brussels
29. Gomes MI, Faria P, Gonçalves TD (2016) Earth-based mortars for repair and protection of rammed earth walls. Stabilization with mineral binders and fibers. *J Clean Prod.* 172:2401–2414. doi: 10.1016/j.jclepro.2017.11.170
30. EN 16322 (2013) Conservation of Cultural Heritage, Test methods, Determination of drying properties. CEN, Brussels
31. Lima J, Faria P (2016) Eco-efficient earthen plasters: The influence of the addition of natural fibers, in: Figueiro R, Rana S (ed) *Natural Fibres: Advances in Science and Technology Towards Industrial Applications*. RILEM Bookseries, Springer Netherlands, 12:315–327. doi: 10.1007/978-94-017-7515-1_24
32. Faria P, Lima J (2018) Earth plasters (in Portuguese). *Cadernos de Construção com Terra* 3. ARGUMENTUM, Lisbon. ISBN: 978-989-8885-04-3
33. Freire MT, Veiga MR, Santos Silva A et al (2019) Studies in ancient gypsum based plasters towards their repair: Physical and mechanical properties. *Constr Build Mater.* 202:319–331. doi: 10.1016/j.conbuildmat.2018.12.214
34. Brás A, Leal M, Faria P (2013) Cement-cork mortars for thermal bridges correction. Comparison with cement-EPS mortars performance. *Constr Build Mater.* 49:315–327. doi: 10.1016/j.conbuildmat.2013.08.006
35. Bogas JA, Carriço A, Pereira MFC (2019) Mechanical characterization of thermal activated low-carbon recycled cement mortars. *J Clean Prod.* 218:377–389. doi: 10.1016/j.jclepro.2019.01.325
36. Veiga MR, Fragata A, Velosa AL et al (2010) Lime-based mortars: Viability for use as substitution renders in historical buildings. *Int J Archit Herit.* 4:177–195. doi:

10.1080/15583050902914678

37. EN 998-1 (2010) Specification for mortar for masonry, Part 1: Rendering and plastering mortar. CEN, Brussels
38. EN 13279-1 (2008) Gypsum binders and gypsum plasters, Part 1: Definitions and requirements. CEN, Brussels
39. Gomes MI, Gonçalves TD, Faria P (2016) Hydric behaviour of earth materials and the effects of their stabilization with cement or lime: a study on repair mortars for historical rammed earth structures. *J Mater Civil Eng.* 28(7):04016041. doi: 10.1061/(ASCE)MT.1943-5533.0001536

Earth-based plasters: the influence of clay mineralogy

José Lima¹, Paulina Faria², António Santos Silva³

(1) Faculty of Architecture, University of Lisbon, email: jose.lima.ferreira@gmail.com

(2) CERIS and Dep. Civil Engineering, FCT, NOVA University of Lisbon, email: paulina.faria@fct.unl.pt

(3) Dep. Materials, National Laboratory for Civil Engineering, Lisbon, email: ssilva@lnec.pt

Abstract

Earth-based mortars have been used all over the world since ancient times, in an extensive range of building types, from vernacular architecture to monuments. Plastering is one of the most common current applications of earth-based mortars, as for earthen-building conservation or contemporary architecture. Raw earth is a very diverse natural raw material, and clay minerals play a key role on plaster properties, being responsible for its setting process and the capability of balancing the indoor hygrometric conditions of buildings, which have strong benefits on energy saving for comfort and health of inhabitants and building conservation. For this study three mortars were produced with different clayish earths to assess the influence of clay mineralogy. Mortars characterizations confirmed that clay mineralogy drives important plaster properties, like vapour adsorption, drying shrinkage, and also have significant influence on mechanical resistance, dry abrasion and thermal conductivity. Within the studied mortars illitic clayish earth stands out as more adequate for earth-base plasters, with balanced linear drying shrinkage, mechanical resistance, dry abrasion and vapour adsorption.

Keywords:

clayish earth, montmorillonitic clay, kaolinitic clay, illitic clay, mortar, shrinkage, hygroscopicity

Introduction

Earth-based mortar were probably the first type of mortars to be used by humankind when ancestors mixed excavated earth with water to fill the space between wood branches used to build shelters. Henceforth earth-based mortars have been used all over the world, as masonry layering mortar or as wall, ceiling and floor protective or decorative coatings, in an extensive range of building types, from vernacular architecture to monuments.

Each earth is a natural raw material characterized by its own and unique properties, due to its diverse composition comprising certain types and content ratios of clay, silt, sand and gravel. Therefore, earth-based mortars properties are highly dependent on the type of earth used. Nowadays plastering is one of the main applications of earth-based mortars, for which

raw earth is disaggregated and sieved, to eliminate gravel. If the content of clay present is too high, sand (or other artificial aggregate with similar particle size distribution) has to be added in order to control shrinkage. For this purpose a recurrent proportion between the fine particles of earth (clay and silt) and sand is 1:3 in volume, with water addition of 20-30 % in weight of the dry components.

Clay minerals play a key role in this type of mortars being responsible for its setting process, associated only with drying unless a binder is added for stabilization, and when used for plastering, its contribution to equilibrium of indoor hygrometric conditions due to clay minerals high hygroscopicity. Montmorillonitic clays are known for having very high hygroscopicity but also very high shrinkage. Kaolinitic clays, at the other end, are known for having the opposite: low shrinkage but also low hygroscopicity. Illitic clays normally present average conditions, with a compromise between shrinkage and hygroscopicity. Although these effects are referred in the literature [1, 2], they were not yet quantified when the clays are used to produce plasters, as well as its influence on plasters strength and durability.

Earth-based mortars have specific characteristics in comparison with conventional binder mortars, such as cement-based and lime-based mortars. To the authors knowledge the only standard specifically dedicated to define requirements, classification and test procedures for earth mortar is the German standard DIN 18947 [33], which was followed in the present study. For testing this DIN standard remits to several parts of EN 1015 standards that will be referred further ahead.

This study aims to assess the influence of different clays on the properties of earth-based plasters. For that purpose three mortars were produced with three different clayish earths, each one presenting a clay with prevalence of a specific clay mineral, namely a montmorillonitic clay, a kaolinitic clay and an illitic clay. All mortars were formulated considering the same volumetric ratio of clayish earth and siliceous sand. Mortar mixing and fresh state characterization, as well as sample preparation and hardened state characterization were performed, and are presented in this study. Results are compared between the different clay earth-based plasters and with results obtained with other plasters, from previous studies. The influence of each of the clays is highlighted in terms of advantages and drawbacks for eco-efficient plasters applications.

Materials and methods

Materials

The three types of clayish earth used to prepare the mortars assessed in this study were extracted from three different locations in Portugal where the predominate clay minerals were assessed in previous studies. The illitic clayish earth (E) was extracted from a clay quarry located in the east part of Algarve region, in southern Portugal, and was previously studied and used by the authors in previous campaigns [4, 5]. This sector of Algarve

sedimentary basin presents a high concentration of reddish soils with a mineralogy dominated by the illite clay mineral [66, 7]. After open air drying the raw earth was mechanically grinded to pass in a 2 mm sieve. The kaolinitic clay (K) was supplied by Mibal mining company and was quarried from Barqueiros deposit located near Barcelos city, northwestern region of Portugal. This sedimentary deposit is characterized by the presence of highly concentrated kaolinitic layers, showing extremely fine grain, and colour variations from high whiteness to shades of yellow [88, 9]. The raw material was supplied in powder form grinded to pass in a 30 μm sieve. The montmorillonitic clayish earth (B) was extracted from Serra de Dentro region in Porto Santo Island, Madeira archipelago, where small size deposits of greenish-yellowish bentonite clay occur derived to submarine alteration process of pyroclastic volcanic rock of trachyte composition [1010]. After open air drying the raw earth was mechanically grinded to pass in a 2 mm sieve. The sand used for the formulation of all mortars assessed in this study, labelled sand S, is a siliceous unwashed sand extracted from a quarry located in Santiago do Cacém, near Setubal city, southwest part of Portugal.

Methods

Mineralogical characterization

The mineralogical characterization of the three clayish materials used in the present study was confirmed through X-ray diffraction analysis (XRD), complemented by thermogravimetric and differential thermal analysis (TG-DTG). XRD was obtained with a Phillips PW3710 X-ray diffractometer using Fe-filtered Co K α radiation, with 35 kV and 45 mA, speed of 0.05 $^{\circ}$ /s, from 3 to 74 $^{\circ}$ 2 θ . The crystalline phases present were identified by comparison with the International Centre for Diffraction Data Powder Diffraction Files (ICDD PDF). The TG-DTG tests were performed in a Netzsch STA 449 F1 analyzer, under nitrogen atmosphere, with heating rate of 10 $^{\circ}$ C/min, from room temperature to 1000 $^{\circ}$ C.

Loose bulk density and particle size distribution

The bulk density of the clayish materials and the sand was determined based on EN 1097-3 [11]. The particle size distribution of the sand S was analysed by dry sieving, according to standard EN 1015-1 [1212].

Mortars formulation and fresh state characterization

The three earth-based mortars were formulated considering the same volumetric proportions of clayish earth and siliceous sand, respectively 1:3. For each mortar one of the previous mentioned clayish earth types was used, namely illitic clayish earth for mortar labelled E1S3, kaolinitic clay for mortar labelled K1S3, and montmorillonitic clay for mortar labelled B1S3.

The standard DIN 18947 [33] was followed for preparing and mixing the mortars, as well as for fresh state characterization. The mortars E1S3 and K1S3 were prepared with the

minimum amount of water needed to ensure adequate workability and compliance with the flow table consistency defined in the DIN 18947 (175 ± 5 mm). To prepare mortar B1S3, due to thixotropic behaviour of the montmorillonitic clay, the amount of water used was just the minimum to guarantee adequate workability. Although presenting flow table consistency under the minimum limit defined in the DIN 18947 [3], the workability of the mortar was considered excellent. The mortars formulation is registered in Table 1, in terms of both volumetric and weight percentages of clayish earth, sand and water contents. Wet density, determined by EN 1015-6 [1313] and flow table consistency, assessed according to EN 1015-3 standard [1414], were also registered.

Table 1. Composition and fresh state mortars characterization.

Mortar	Volumetric ratios					Weight ratios					Density (c) [kg/m ³]	Consistency (d) [mm]
	E	K	B	S	Water (a)	E	K	B	S	Water (b)		
	[%]	[%]	[%]	[%]	[%]	[%]	[%]	[%]	[%]	[%]		
E1S3	25.0	0.0	0.0	75.0	19.6	21.6	0.0	0.0	78.4	12.8	2130.7	173.2
K1S3	0.0	25.0	0.0	75.0	22.3	0.0	7.6	0.0	92.4	17.2	2028.0	170.4
B1S3	0.0	0.0	25.0	75.0	31.3	0.0	0.0	18.3	81.7	21.3	1957.8	165.2

E – Illitic clayish earth (muscovite); K – Kaolinitic clay; B – Montmorillonitic clay (bentonite); S – siliceous unwashed sand. Notes: (a) – percentage of volume added, considering the total volume of clayish earth and sand; (b) – percentage of mass added, considering the total mass of clayish earth and sand; (c) – fresh state density; (d) – flow table consistency

Samples preparation and hardened state characterization

Samples preparation and hardened state characterization of the mortars also followed the DIN 18947 [3], as well as EN 1015 standards [15-17], EN 14146 standard [1818] and test procedures currently used by the research team. The mortars were assessed in terms of linear drying shrinkage [3], dry bulk density [15], dynamic modulus of elasticity [1818], flexural and compressive strength [1616], adhesive strength [1717], dry abrasion resistance [33], as well as thermal conductivity, performed with a Heat Transfer Analyzer ISOMET 2104 with a 60 mm diameter contact probe API 210412 with a measurement range of 0.3 to 2.0 W/(mK).

Prismatic samples of 160 mm x 40 mm x 40 mm were prepared, in metallic moulds, for testing each mortar regarding linear drying shrinkage, dry bulk density, dynamic modulus of elasticity, and flexural and compressive strength, allowing six assessments for each test. Adhesive strength and dry abrasion resistance were assessed on samples of 20 mm plaster layer applied over hollow bricks, with a surface of approximately 295 mm x 195 mm, allowing respectively three and four tests per sample. For testing thermal conductivity six circular samples of 90 mm diameter and 20 mm thickness were used.

Dynamic vapour adsorption and desorption

For the dynamic adsorption and desorption test DIN 18947 [3] define that three planar samples, with a surface area of 1000 cm² (500 mm x 200 mm) and a thickness of 15 mm, should be prepared for each mortar. Each sample was prepared in a metallic mould, and kept on it during testing, to guarantee that vapour adsorption and desorption would occur only in the top exposed surface of the samples.

The samples were stabilized in a climatic chamber at 50 % relative humidity (RH) and 23 °C. After the stabilization of the samples the climatic chamber condition was set to 80 % RH for the adsorption test phase. The samples were weighted at time intervals defined on the standard, respectively: 0, 1, 3, 6 and 12 h. The adsorption test was extended till 24 h, beyond the 12 h interval defined in the standard, in order to achieve a more comprehensive understanding of the adsorption behaviour of the samples. After 24 h the samples were weighted and the condition of the chamber was changed back to 50 % RH, forcing the samples to a desorption phase, that was assessed with the same time interval protocol during another period of 24 h.

Results and discussion

Mineralogical composition

Table 2 summarizes the mineralogical composition of the earthen materials assessed by XRD, which confirms a mineralogical composition dominated respectively by illite (earth E), kaolinite (clay K) and montmorillonite (earth B). It should be noted that in clayish earth E, quartz is also a predominant compound while dolomite and kaolinite are also detected in medium proportions, along with small amounts of an iron oxide (hematite). In clay K, apart from kaolinite predominance, small amounts of illite, quartz, hematite and feldspar were also detected. In montmorillonitic clayish earth B, feldspar was also detected in medium proportion.

Table 2. Mineralogical composition of the clayish earths assessed by XRD

Crystalline compounds	Clayish materials		
	E	K	B
Magnesiohornblende ($\text{Ca}_2[\text{Mg}_4(\text{Al}, \text{Fe}^{+++})]\text{Si}_7\text{AlO}_{22}(\text{OH})_2$)	–	–	tr
Dolomite ($\text{CaMg}(\text{CO}_3)_2$)	+ / ++	–	–
Feldspar ($(\text{K}, \text{Na}, \text{Ca})\text{AlSi}_3\text{O}_8$)	?	+	++
Gibbsite ($\text{Al}(\text{OH})_3$)	–	tr	–
Hematite (Fe_2O_3)	+	+	–
Kaolinite ($\text{Al}_2\text{Si}_2\text{O}_5(\text{OH})_4$)	+ / ++	+++	–
Montmorillonite ($(\text{Na}, \text{Ca})_{0,3}(\text{Al}, \text{Mg})_2\text{Si}_4\text{O}_{10}(\text{OH})_2 \cdot n(\text{H}_2\text{O})$)	–	–	++ / +++
Muscovite/illite ($\text{KAl}_2\text{Si}_3\text{AlO}_{10}(\text{OH})_2$)	++ / +++	+	–
Quartz (SiO_2)	++ / +++	+	–

+++ high proportion (predominant compound); ++ medium proportion; + low proportion;
tr - traces; – undetected; ? doubts in presence

Figure 1 presents the TG-DTG curves of the three clayish earths. The TG-DTG curves agree with the mineralogical composition obtained (Table 2), showing characteristic weight losses patterns for the clay types assessed.

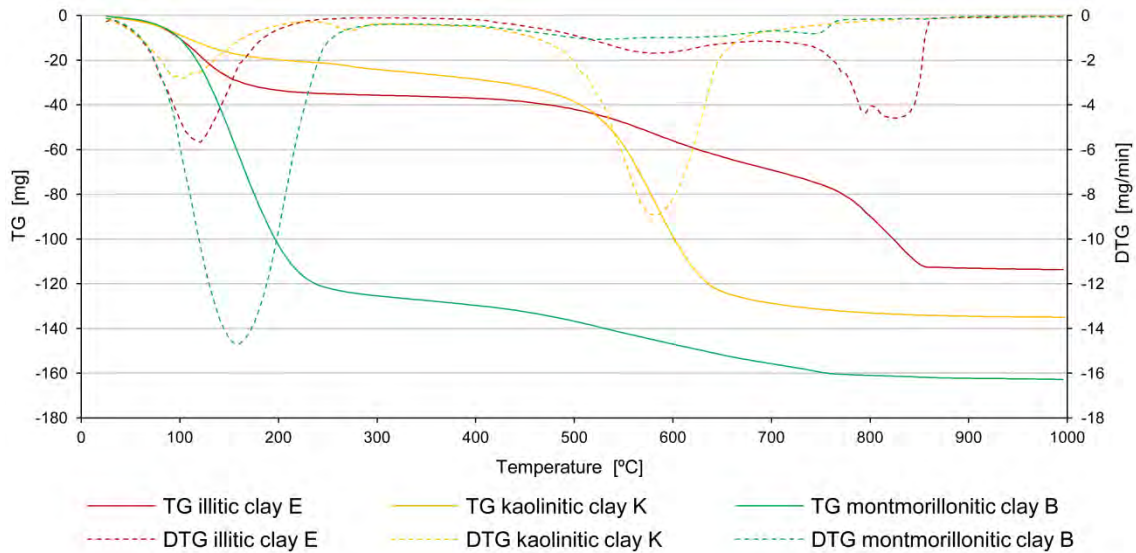


Figure 1. Thermogravimetric curves (TG) and Derivative thermogravimetric curve (DTG)

The first important weight loss occur at relatively low temperature, till 200 °C for illitic clayish earth E and kaolinitic clay K and till 250 °C for montmorillonitic clayish earth B, corresponding to the release of free or sorbed water [1919]. The second weight loss phase occurs at mid-range temperature, from 400 to 650 °C for illitic clayish earth E and kaolinitic clay K, and continuing until 750 °C for montmorillonitic clayish earth B, corresponding to loss of bounded water or dissociation of hydroxyls from the lattice, inducing its amorphization [1919]. At high temperature, from 750 to 850 °C, occurs the final breakdown of the residual clay lattice and eventual formation of new mineral and/or glass phases [1919]. For illitic clay E that happens along with decarbonation of dolomite present in this earthen material in medium proportion.

Loose bulk density and particle size distribution

The loose bulk density of the three clayish materials reflects its origin. The illitic clayish earth (E) and montmorillonitic clayish earth (B), both corresponding to excavated natural soils (mechanically grinded to pass in a 2 mm sieve), respectively show a loose bulk density of 1317 kg/m³ and 1066 kg/m³, denoting balanced composition of clay, silt and sand. The kaolinitic clay (K), quarried in a clay pit (supplied in powder form grinded to pass in a 30 µm sieve), presents a loose bulk density of 393 kg/m³, in accordance to the declared high concentration of clay [8].

The sand S, used for the formulation of all the mortars, presented a loose bulk density of 1592 kg/m³, and Figure 2 presents its particle size distribution, analyzed by dry sieving according to standard EN 1015-1 [1212].

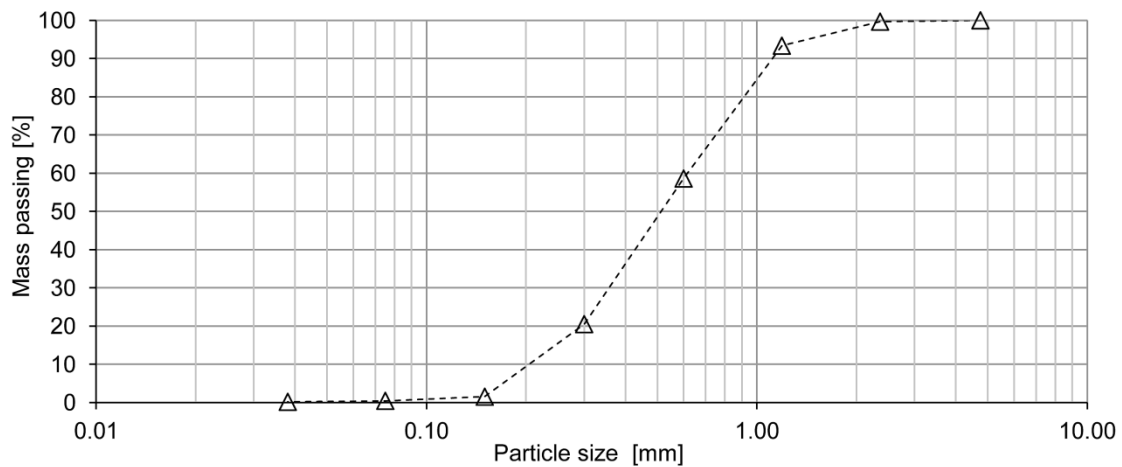


Figure 2. Particle size distribution curve of sand S by dry sieving.

Hardened state characterization

Linear drying shrinkage

Mortars linear drying shrinkage was assessed on the prismatic samples as well as on the planar samples. The results obtained on both type of samples reflect mortars clayish earth mineralogy and are presented in Figure 3A. Kaolinitic mortar K1S3 present the lowest shrinkage (0.38 % for prismatic samples) while montmorillonitic mortar B1S3 shows the highest shrinkage, almost ten times higher (3.30 % for prismatic samples). Illitic mortar E1S3 presents an intermediate shrinkage value, although relatively low and closer to kaolinitic mortar (0.85 % for prismatic samples). The correlation between linear drying shrinkage of prismatic and planar samples (Figure 3B) reveal that both type of samples shows similar shrinkage behaviour, but should be noted that for low shrinkage mortars, like K1S3, the difference between shrinkage of these type of samples can be significant (mortar K1S3 presents a ratio of 73.4 %).

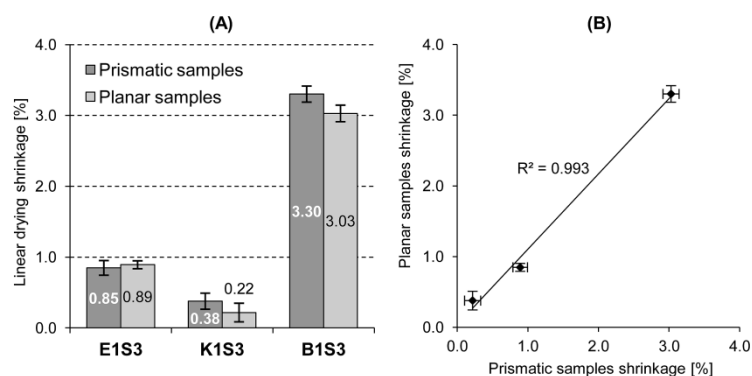


Figure 3. (A) Linear drying shrinkage assessed in prismatic and planar samples; (B) Prismatic samples shrinkage vs. planar samples shrinkage.

Figure 4 presents the samples of 20 mm plaster layer applied over hollow bricks. The occurrence of plaster cracking is significant on montmorillonitic mortar B1S3, rare on illitic mortar E1S3 and absent on kaolinitic mortar K1S3, which is in accordance with the results of the linear drying shrinkage test and also reflects each mortars clayish earth mineralogy.



Figure 4. Samples of 20 mm plaster layer applied over hollow bricks: E1S3 - Illitic mortar; K1S3 - Kaolinitic mortar; B1S3 - Montmorillonitic mortar.

Dry bulk density and thermal conductivity

Figure 5A presents the results of dry bulk density and thermal conductivity tests. The illitic mortar E1S3 presents the higher bulk density, which falls within density class 2.0 as defined in DIN 18947 [3], and is similar to results obtained by the authors in previous campaigns [4, 5] and other researchers that also study not stabilized illitic mortars [2020, 21]. The kaolinitic and montmorillonitic mortars, K1S3 and B1S3, present similar values of bulk density, which are slightly lower than E1S3, falling within density class 1.8 of the standard previously mentioned, and are also in the interval range of the results assessed by other authors that also studied mortars with similar composition and mineralogy [2222, 23]. In a previous campaign, that studied mortars formulated with different ratios of clayish earth and siliceous sand [44], the authors found a correlation between bulk density and drying shrinkage. That correlation is not clearly present in this study results (Figure 5B) which emphasise the influence of clay mineralogy in earth-based plasters properties.

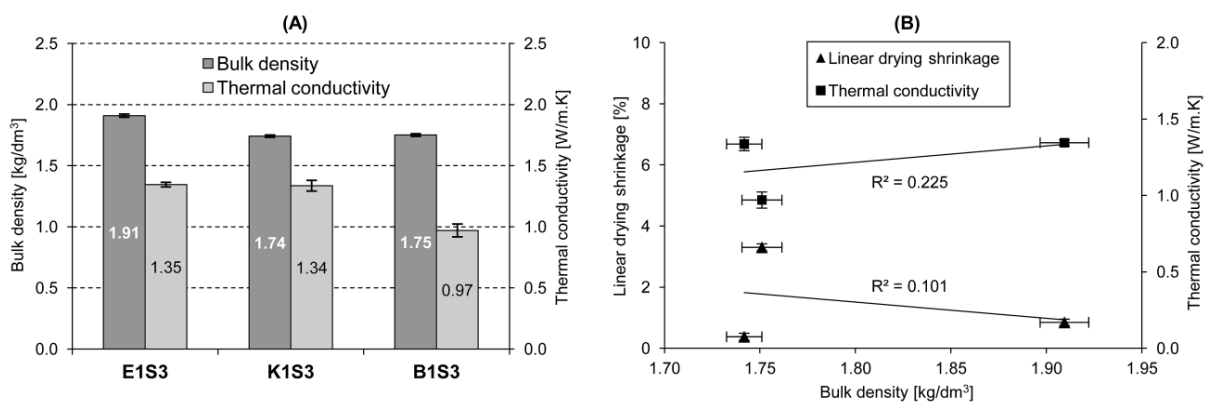


Figure 5. (A) Bulk density and thermal conductivity; (B) Bulk density vs. linear drying shrinkage and vs. thermal conductivity.

Regarding thermal conductivity the illitic and kaolinitic mortars, E1S3 and K1S3, present almost equal results, which are within the same range of the results found in other studies [44, 5, 23]. In comparison the montmorillonitic mortar B1S3 shows a relatively lower thermal conductivity (less 27 %) although with similar dry bulk density of mortar K1S3. These results make evident that thermal conductivity also do not follow the trend of bulk density results (Figure 5B), which is in contradiction to the correlation found by the authors in previous campaigns [4, 5] and by other researchers in the field [2020, 24], once again highlighting the influence of clay mineralogy in earth-based plasters performance.

Compressive, flexural and adhesive strength, and dynamic modulus of elasticity

Figure 6A shows the results of compressive, flexural and adhesive strength along with dynamic modulus of elasticity. Illitic mortar E1S3 obtained the higher values of compressive and flexural strength, however not achieving (even by a small difference) the minimum values of mechanical resistance defined in the resistance class S-I of the DIN 18947 [3] (compressive strength ≥ 1.0 MPa and flexural strength ≥ 0.3 MPa). The kaolinitic and montmorillonitic mortars, K1S3 and B1S3, obtained significantly lower compressive and flexural strengths, the latter presenting slightly higher values.

Only mortar E1S3 achieve the minimum values of adhesion strength defined in the resistance class S-I of the DIN 18947 [33] (≥ 0.05 MPa). Again mortars K1S3 and B1S3 show significantly lower adhesion strength, in this case, the latter presents the lowest value. Adhesion strength, like linear drying shrinkage, is an extremely important property for plastering mortars and, once more, these results highlight the influence of clay.

The results of dynamic modulus of elasticity show that Illitic mortar E1S3 have the higher value, montmorillonitic mortar B1S3 the lowest and kaolinitic mortar K1S3 an intermediate value. When correlating dynamic modulus of elasticity with compressive, flexural and adhesive strength (Figure 6B) no significant concordance is observed for compressive or flexural strength, differently from what is usually considered for earthen materials, as mentioned by other authors [23] and some standards [2525]. Nevertheless a strong correlation is evidenced between dynamic modulus of elasticity and adhesive strength ($R^2=0.901$), but since this tendency is not followed by any other results of the tests performed in this study, neither by the ratios of clayish earth and sand present in mortars formulations (Table 1), it seems likely it may be driven also by clay mineralogy.

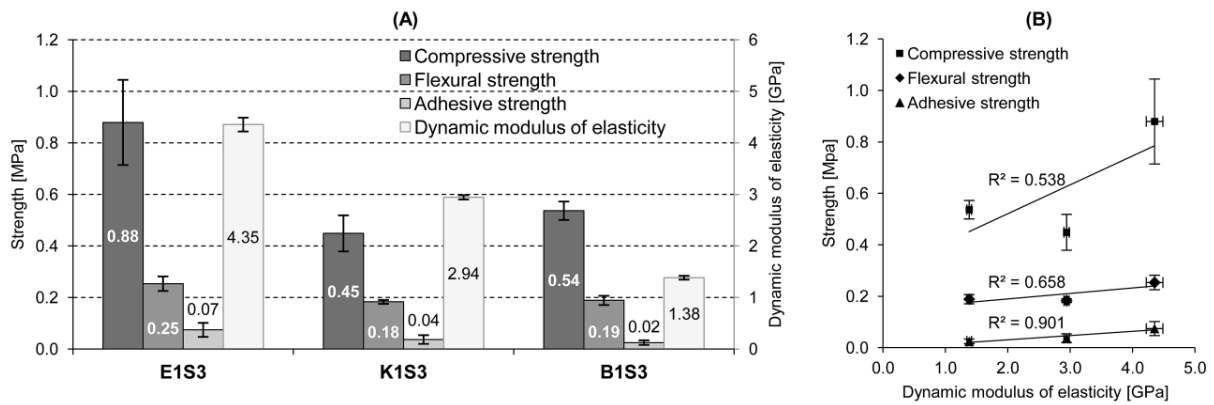


Figure 6. (A) Compressive, flexural and adhesive strength and dynamic modulus of elasticity; (B) Dynamic modulus of elasticity vs. compressive, flexural and adhesive strength.

Dry abrasion resistance

Figure 7 presents the mortars sample surface aspect after dry abrasion test. According to DIN 18947 [33] abrasion test results are expressed by the mass loss by the samples during test, and are presented in Figure 8A. It can be observed that illitic mortar E1S3 is significantly more resistant to dry abrasion than the other two mortars and, kaolinitic mortar K1S3 is by far the less resistant.

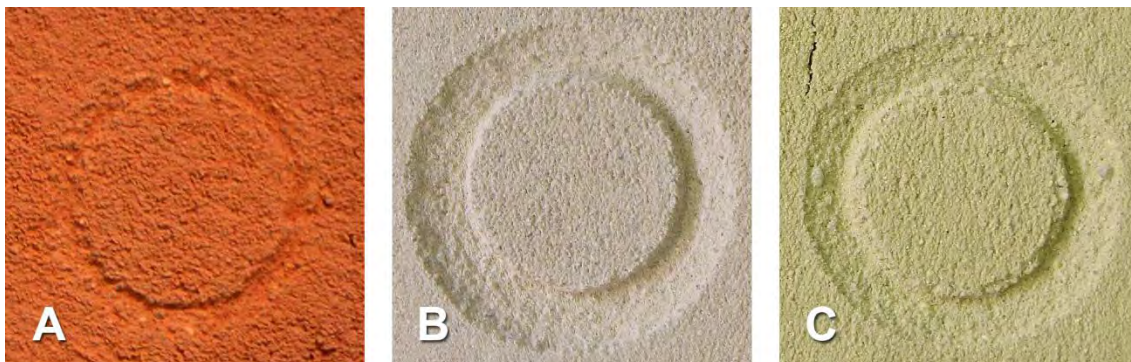


Figure 7. Aspect of dry abrasion over samples of 20 mm plaster layer applied over hollow bricks: (A) - Illitic mortar; (B) - Kaolinitic mortar; (C) - Montmorillonitic mortar.

Till some extent, a negative correlation between dry abrasion resistance and mortar mechanical strength is observed (Figure 8B). This negative concordance is particularly evident regarding dry abrasion and compressive strength ($R^2=0.957$), being also strong with flexural strength ($R^2=0.894$) and less significant with adhesive strength. In real world applications plaster abrasion resistance is one of the properties of utmost importance directly influencing plaster lifecycle. These results seem to indicate that, as previously mentioned for mechanical strength, clay mineralogy is a key factor also for dry abrasion resistance.

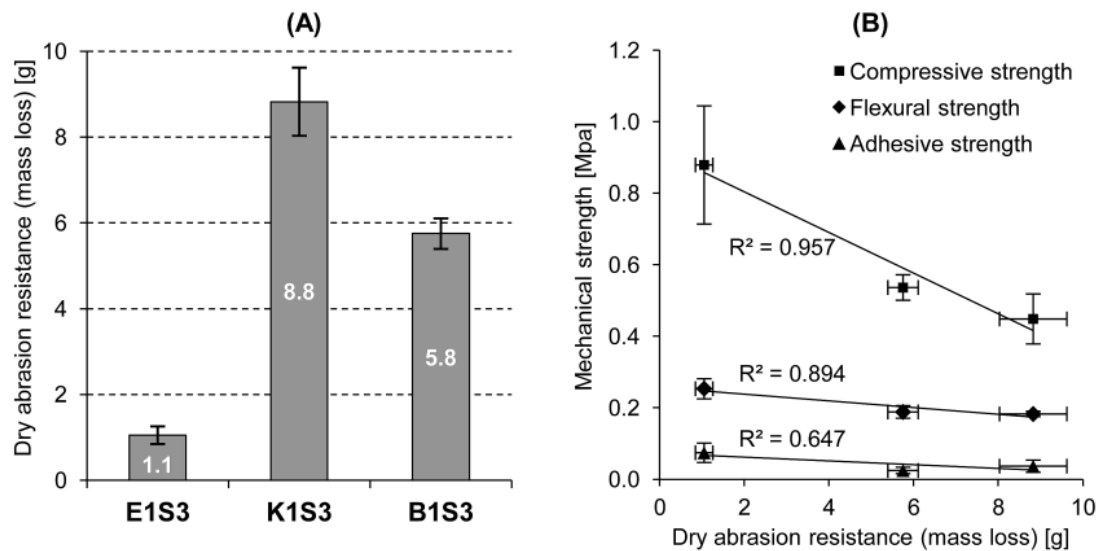


Figure 8. (A) Dry abrasion resistance (mass loss); (B) Dry abrasion resistance (mass loss) vs. compressive, flexural and adhesive strength.

Dynamic vapour adsorption and desorption

Plasters vapour adsorption and desorption capacity is of utmost importance since it allows the plasters to act as a moisture buffer, passively contributing to balance the RH of the indoor environment of buildings and, therefore, with benefits for energy saving and sensitive materials conservation, as well as promoting comfort and health of inhabitants.

The results of the dynamic vapour adsorption and desorption test are presented in Figure 9 along with the limits of the three adsorption classes defined in DIN 18947 [3]. The montmorillonitic plaster B1S3 shows a very high adsorption and desorption capacity, achieving a significant vapour adsorption of 110 g/m² after 12h, which is almost the double of class WS-III (≥ 60 g/m²). In comparison, illitic plaster E1S3 presents lower values although still presenting a high adsorption and desorption capacity, slightly above the same class WS-III. In turn kaolinitic plaster K1S3 obtained the lowest adsorption and desorption capacity, with an adsorption after 12h near class WS-I (≥ 35 g/m²).

These results clearly show that vapour adsorption and desorption of earth-based plaster is significantly driven by clay mineralogy, reflecting the high hygroscopicity of montmorillonite clay mineral, the low hygroscopicity of kaolinite and the intermediate behaviour of illite. Nevertheless it should be noted that vapour adsorption and desorption is also dependent on the mortars clay contents. Although the data of the present study do not allow to analyse this correlation, that was demonstrated in previous study that specifically address the correlation between illitic mortars with diverse clay contents and its adsorption capacity [44]

Although having significantly diverse vapour adsorption capacity, in terms of adsorption and desorption pattern the three plasters show similar dynamic behaviour. However it should be noted that montmorillonitic plaster B1S3 and illitic plaster E1S3 present some desorption hysteresis, both with a similar value of 8 %. Similar hysteresis effect was found in previous

studies comprising illitic mortars [4, 5]. In the present study kaolinitic plaster K1S3 do not present any hysteresis effect.

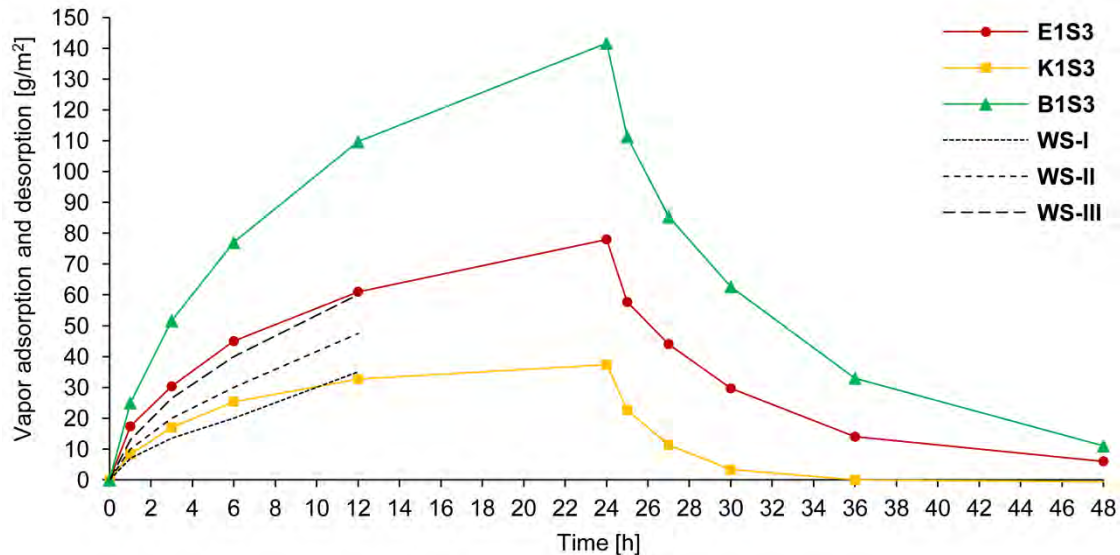


Figure 9. Vapour adsorption and desorption of plasters and vapour adsorption classes defined in DIN 18947 [3] (WS-I, WS-II and WS-III).

A remark should be made to highlight the significance of vapour adsorption and desorption capacity of earth-based plasters and its contribution to passively balancing the RH of the indoor environment of buildings. Considering a small building compartment with floor dimensions of 3 m x 3 m, with a ceiling height of 3 m (with a window of 1 m² and a door of 2 m²), having walls and ceiling coated with the illitic plaster E1S3, with 15 mm thickness, if a indoor RH variation occurs, from 50 to 80 %, than a plaster adsorption capacity of almost 2 kg of vapour is expected after 6h.

Conclusions

It is possible to conclude that clay mineralogy play a key role in the properties of the earth-based plasters assessed in this study. It clearly drives vapour adsorption and desorption capacity, linear dry shrinkage and shrinkage cracking, and also have significant influence on mechanical resistance, dry abrasion and thermal conductivity, although with less obvious interpretation.

Among the studied mortars the illitic clayish earth stands out as more adequate to produce earth-base plasters, presenting an advantageous balance between plaster key properties, like linear drying shrinkage, mechanical resistance, dry abrasion and vapour adsorption and desorption.

In order to allow a more comprehensive knowledge of the role clay mineralogy may have in the performance of earth-based plasters more research is needed regarding its influence in

plasters porosity, vapour permeability, as well as the study of eventual interaction of clay minerals with different types of sand, with diverse particle size and mineralogy.

Efforts should also be made to better understand what drives the hysteresis effect presented by some earth-based plasters. The desorption delay of plaster can generate a lag effect between consecutive cycles of adsorption and desorption, which, over a certain period of time, may lead to the decrease of adsorption and desorption capacity of the plaster, or even to its full moisture saturation.

Acknowledgments

The authors acknowledge the support of Fundação para a Ciência e Tecnologia (FCT), Portugal for funding José Lima's scholarship (SFRH/BD/119703/2016), as well as the research project PTDC/EPH-PAT/4684/2014: DB-Heritage - Database of building materials with historical and heritage interest. The authors also acknowledge the EMBARRO company for providing the illitic clayish earth and MIBAL mining company for providing the kaolin clay for this study.

References

1. Murray H (2007) Applied Clay Mineralogy: Occurrences, Processing and Application of Kaolins, Bentonites, Palygorskite-Sepiolite, and Common Clays (Vol. 2). Amsterdam: Elsevier. ISBN: 978-0-444-51701-2.
2. Bergaya F, Lagaly G (Eds.) (2013) Handbook of Clay Science – Part A: Fundamentals (Vol. 5). Amsterdam: Elsevier. ISBN: 978-0-08-099364-5.
3. DIN 18947 (2013) Earth plasters – Terms and definitions, requirements, test methods (in German). DIN Deutsches Institut für Normung, Berlin.
4. Lima J, Faria P, Santos-Silva A (2016) Earthen Plasters Based on Illitic Soils from Barrocal Region of Algarve: Contributions for Building Performance and Sustainability. Key Eng, 678, 64–77. DOI: 10.4028/www.scientific.net/KEM.678.64
5. Lima J & Faria P (2016) Eco-Efficient Earthen Plasters: The Influence of the Addition of Natural Fibers. In Fangueiro R & Rana S (Eds.) Natural Fibres: Advances in Science and Technology Towards Industrial Applications (Vol. 12, pp. 315–327). Dordrecht: Springer Netherlands. DOI: 10.1007/978-94-017-7515-1_24
6. Manuppella G, Moreira J, Grade J, Moura A (1985) Contribuição para o conhecimento das características das argilas do Algarve. Porto: Estudos, Notas e Trabalhos do Serviço de Fomento Mineiro e Laboratório da D.G.G.M. Tomo 27, p.59-75.

7. Trindade M, Rocha F, Dias M, Prudêncio M (2013) Mineralogy and grain-size distribution of clay-rich rock units of the Algarve Basin (South Portugal). *Clay Minerals*, 48(1), 59–83. DOI: 10.1180/claymin.2013.048.1.04
8. MIBAL (2005) Kaolin MIB-A product data sheet. Mibal Minas de Barqueiros S.A. Available at: <https://www.mibal.pt/>
9. Santos I, Costa C, Quintela A, Terroso D, Ferraz E, Rocha F, et al. (2014) Mineralogical composition of sedimentary and residual kaolin deposits from Portugal. *Comunicações Geológicas*, 101(Especial I), 195–197.
10. Cordeiro N, Silva J, Gomes C, Rocha F (2010) Bentonite from Porto Santo Island, Madeira archipelago: surface properties studied by inverse gas chromatography. *Clay Minerals*, 45(1), 77–86. DOI: 10.1180/claymin.2010.045.1.77
11. EN 1097-3: 1998 - Tests for Mechanical and Physical Properties of Aggregates - Part 3: Determination of Loose Bulk Density and Voids. CEN - European Committee For Standardization.
12. EN 1015-1: 1998 - Methods of test for mortar for masonry; Part 1: Determination of particle size distribution (by sieve analysis). Brussels: CEN – European Committee for Standardization.
13. EN 1015-6: 1998. Methods of Test for Mortar for Masonry. Part 6: Determination of Bulk Density of Fresh Mortar. CEN - European Committee For Standardization.
14. EN 1015-3: 1999 - Methods of test for mortar for masonry; Part 3: Determination of consistence of fresh mortar (by flow table). Brussels: CEN – European Committee for Standardization.
15. EN 1015-10: 1999 - Methods of test for masonry; Part 10: Determination of dry bulk density of hardened mortar. Brussels: CEN – European Committee for Standardization.
16. EN 1015-11: 1999 - Methods of test for masonry; Part 11: Determination of flexural and compressive strength of hardened mortar. Brussels: CEN – European Committee for Standardization.
17. EN 1015-12: 2000 - Methods of test for mortar for masonry; Part 12: Determination of adhesive strength of hardened rendering and plastering mortars on substrates. Brussels: CEN – European Committee for Standardization.
18. EN 14146: 2004 CEN, 2004. Natural Stone Test Methods. Determination of the Dynamic Modulus of Elasticity (By Measuring the Fundamental Resonance Frequency). CEN, Brussels.

19. Bernal S, Juenger M, Ke X, Matthes W, Lothenbach B, De Belie N, Provis J (2017) Characterization of supplementary cementitious materials by thermal analysis. *Materials and Structures*, 50(1). DOI: 10.1617/s11527-016-0909-2
20. Santos T, Nunes L, Faria P (2017) Production of eco-efficient earth-based plasters: influence of composition on physical performance and bio-susceptibility. *Journal of Cleaner Production*, 167, 55-67. DOI:10.1016/j.jclepro.2017.08.131
21. Santos T, Faria P, Silva V (2019) Can an earth plaster be efficient when applied on different masonries? *Journal of Building Engineering*, 23, 314–323. DOI: 10.1016/j.jobbe.2019.02.011
22. Delinière R, Aubert J E, Rojat F, Gasc-Barbier, M (2014) Physical, mineralogical and mechanical characterization of ready-mixed clay plaster. *Building and Environment*, 80, 11–17. DOI: 10.1016/j.buildenv.2014.05.012
23. Gomes M I, Faria P, Gonçalves T D (2018) Earth-based mortars for repair and protection of rammed earth walls. Stabilization with mineral binders and fibers. *Journal of Cleaner Production*, 172, 2401–2414. DOI: 10.1016/j.jclepro.2017.11.170
24. Laborel-Préneron A, Magniont C, Aubert J-E (2018) Hygrothermal properties of unfired earth bricks: Effect of barley straw, hemp shiv and corn cob addition. *Energy and Buildings*, 178, 265–278. DOI: 10.1016/j.enbuild.2018.08.021
25. NZS 4297:1998 Engineering design of earth buildings (Specific Design). NZS – New Zealand Standards.

Rescuing the manufacturing process of traditional mortars present on XIX-century earthen buildings in Brazil

Andrea Cavicchioli¹, Isabela Ferreira Sodr  dos Santos², Jo o Guilherme Kimura Moreira³,

Lucy Gomes Sant'Anna⁴

(1) School of Arts, Sciences and Humanities, University of S o Paulo, Brazil, andrecav@usp.br

(2) Institute of Chemistry, University of S o Paulo, Brazil, isafsodre@gmail.com

(3) School of Arts, Sciences and Humanities, University of S o Paulo, Brazil, joaogkmoreira@gmail.com

(4) School of Arts, Sciences and Humanities and Institute of Energy and Environment, University of S o Paulo, Brazil, lsantann@usp.br

Abstract

The present paper deals with the issue of earthen surface finishes used on earthen buildings in a territory of southeast Brazil that is historically linked with the first economic coffee cycle (XIX century), i.e., the basin of the *Para ba do Sul* river. The aim was to draw a picture of the different solutions adopted in the conception of such materials in terms of composition in different historical moments. The research was based on the assembly of a bank of samples and their physical and chemical characterisation by thermal analysis, FTIR, XRF and MEV-EDS. The results obtained show that the earlier layers present on the building surfaces are most likely made of clayish earth without significant addition of any other material, such as lime, organic substances or vegetable fibres. Coarser texture than the typical local soils is preferred, a solution that were obtained by searching less weathered soils. In two cases of original mortars, a low percentage of lime (less than 5% in weight) was recorded: one single farmhouse and a luxurious urban palace. Later layers overlapping the earlier ones denote the adoption of more industrialised raw materials, with increasing amounts of lime and the likely addition of sand.

Introduction

Traditional earthen architecture techniques such as of wattle-and-daub, rammed earth and adobe were the usual approach to building in inland Brazil up to the end of the XIX century [1-2]. An exceptionally wide, rich and well preserved ensemble of edifications in which all these techniques can simultaneously be found is encountered in the upper to medium basin of the *Para ba do Sul* river, located in the north-east area of the state of S o Paulo (Figure 1) [3-4]. This district, currently referred to as “Historical Valley of S o Paulo” (*Vale Hist rico Paulista*), beheld the introduction of coffee plantation in Brazil and staged the first economic cycle associated with this culture, between 1820 and 1880. On account of this, during this period, local landowners accumulated enormous fortunes and were responsible for the expansion of local villages and the construction of sumptuous urban and rural manors

(Figure 1), many of which still survive as a legacy of exceptional value. This heritage, today distributed in a territory that comprises six municipalities (Figure 1), is at risk of disappearing and demands suitable preservation policies. In turn, these policies depend on the support of research actions, encompassing a detailed characterisation of the composition of materials.

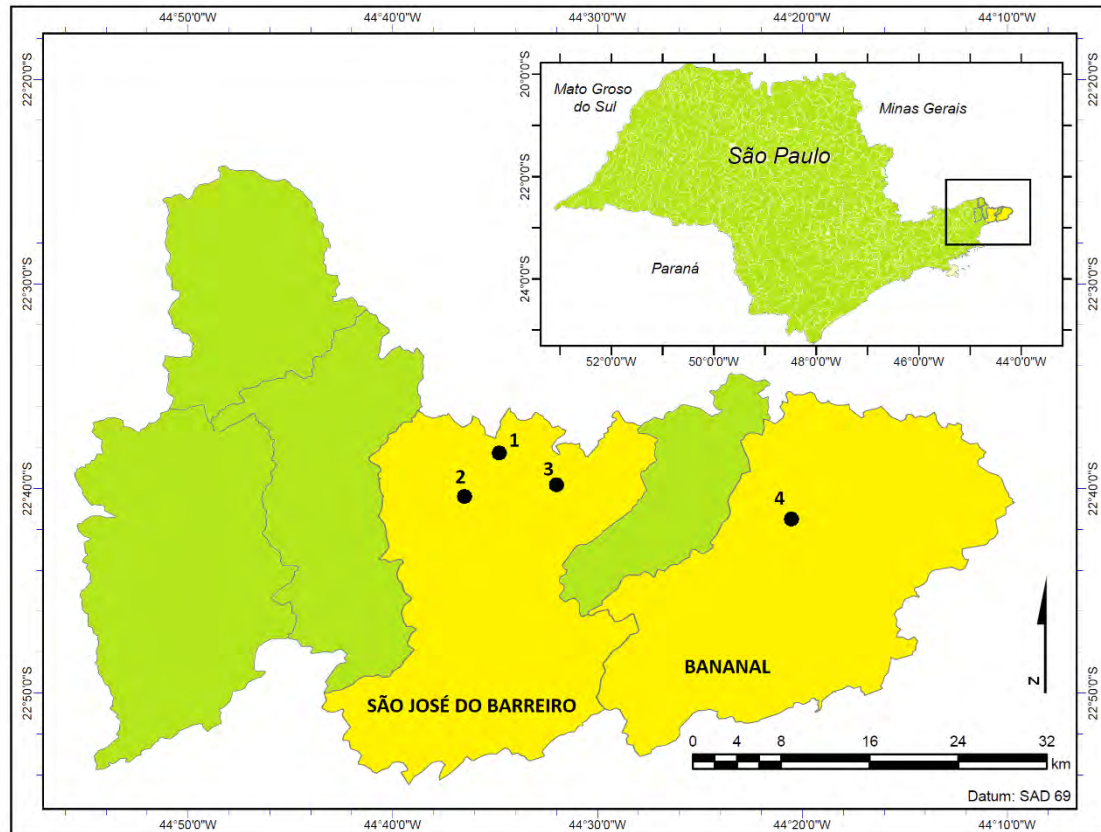


Figure 1. Map of the study area with the location of the edifications studied in this work. 1: town of São José do Barreiro; 2: Farmhouse *São Miguel*; 3: Farmhouse *Catadupa* (photo on the left); 4: town of Bananal (photo on the right)

In previous studies [3], the process behind the manufacture of the structural elements was approached, but the investigation did not include the mortars used to protect and decorate the earthen walls nor has ever been attempted, to date. On the other hand, the characterisation of such materials is important for three orders of reasons that encompass historical, conservation and environmental sustainability issues. Firstly, enlightening the traditional process of mortar manufacture can provide useful information on the state-of-art of the know-how on building practices of a population or a community at a specific time and

location (not always easily available in written records), as well as on commercial routes, movements of social groups and knowledge exchanges. Secondly, conservation and restoration heavily rely on sound information on physical and chemical composition of materials, their properties and the way they interact with their surroundings – an issue that is particularly important for earthen buildings for which the compatibility between the earthen structure and the coating mortar is crucial [5]. Finally, revaluing traditional forms of producing building materials, hence also mortars, might help promoting processes involving least consumption of energy, which has been pointed out, by many, as an important task towards eco-efficient materials and sustainable use of natural resources [6]. In the present paper, the issue of mortar manufacture in the Historical Valley of São Paulo in the XIX century is dealt with through the characterisation of surface finishes used on adobe, rammed earth and wattle-and-daub walls of historical buildings still existing in two of its largest municipalities.

Materials and methods

This study was based on the physical and chemical analysis of eight mortar samples (Figure 2) collected from the indoor or outdoor surface of five historical buildings located in the rural and urban areas of the municipalities of São Jose do Barreiro and Bananal, as summarised in Table 1. It should be noted that, in this paper, the conventional distinction between “plaster” and “render” for mortar coatings on external or internal walls was not adopted because there is no recorded evidence that different techniques were employed for producing indoor and outdoor finishes in the specific historical and cultural context of the construction of the buildings investigated in this work. Furthermore, in Portuguese this linguistic difference does not exist, the word *argamassa* being customary in both situations even in technical books of the XIX century [7].

A group of samples were collected from single-layer coatings which were certainly (sample 563) or likely (samples 524, 525 and 544) original. The other group included samples collected from coatings that exhibited two layers, whose bottom one was always predominant and uniform, whereas the top was either uniform (561) or encountered in isolated patches (501 – in this case, the former was considered original and the latter presumed to be a later restoration).

After collection, fragments of samples that featured the macroscopic characteristics (colour and texture) of the predominant mortar were dried at low temperature (38 °C) for 48h and then analysed using the techniques and protocols illustrated in the following subsections.

Colour and texture

Whole samples were characterized for colour and texture. Colours were described by visual comparison with the Munsell soil colour charts [8]. Standard charts (e.g. [8]) were used for estimating the relative proportion of rock fragments (> 2mm). The size of rock fragments

was estimated by measuring the particles judged to represent their maximum size, as in [9]. Texture of fine earth (particles < 2mm) was determined using a Microtrac Bluewave particle size analyser: results were classified according to the Soil Survey Division Staff of the US Department of Agriculture [10] and Embrapa [11].



Figure 2. Fragments of the mortars studied in this work

Table 1. Sample identification

Sample code	Building name	Building location	Building wall technique	Indoor/outdoor	Layer	Uniformity
500	Farmhouse <i>São Miguel</i>	Rural area of São José do Barreiro	Adobe	Indoor	Bottom	Uniform
501	Farmhouse <i>São Miguel</i>	Rural area of São José do Barreiro	Adobe	Indoor	Top	Isolated patch
524	Old hospital <i>Santa Casa</i>	Urban area of Bananal	Adobe	Indoor	Single	Uniform
525	Old hospital <i>Santa Casa</i>	Urban area of Bananal	Rammed earth	Indoor	Single	Uniform
544	Farmhouse <i>Catadupa</i>	Rural area of São José do Barreiro	Adobe	Indoor	Single	Uniform
560	Residence house	Urban area of São José do Barreiro	Wattle and daub	Outdoor	Bottom	Uniform
561	Residence house	Urban area of São José do Barreiro	Wattle and daub	Outdoor	Top	Uniform
563	Manor house <i>Aguar Valim</i>	Urban area of Bananal	Wattle and daub	Render	Single	Uniform

Scanning electron microscopy-Energy dispersive spectroscopy

The surface of whole fragments was covered with a thin film of platinum and analysed in a Scanning Electron Microscope (SEM) FEI model Quanta 650 FEG, equipped with Energy-Dispersive X-ray Spectroscopy (EDS) operated at low vacuum and 20 kV.

X-ray fluorescence, Fourier transform infrared spectroscopy and thermogravimetric analysis

To carry out X-ray fluorescence (XRF), attenuated total reflection Fourier transform infrared spectroscopy (ATR-FTIR) and thermogravimetric analysis (TGA), a separate fragment of approximately 5g was finely ground in order to obtain particles of diameter smaller than 75 μm .

Elemental analysis for Si, Al, Ca, Fe Ti, Na and K was performed by X-ray fluorescence, in triplicate, on tablets (7 mm diameter, 1 mm thickness) prepared by compressing 500 mg of slightly wet powder in a mechanical manually-operated device (the tablets were subsequently dried up at room temperature). For the analysis, a portable Tracer III Spectrometer (Bruker) was used. The equipment was operated in the bench-top mode at tube voltage and current of 15 kV and 25 μA and with an acquisition time of 120 s (under internal vacuum and without any excitation filter). The quantitative results were obtained on the basis of the calibration for soil, ceramics and mud rocks provided by Bruker. The results used in the discussion correspond to the average of the triplicate analysis of each sample.

ATR-FTIR spectra were obtained on a Bruker Optics ALPHA FTIR spectrometer, equipped with KBr optics and DTGS detector in the ATR module (diamond crystal, single reflection mode). The spectra were recorded with 4 cm^{-1} resolution. TGA was carried out by a TA Instruments Q500 thermogravimetric analyser, typically with 10 mg samples, from ambient temperature up to 950 $^{\circ}\text{C}$, at a heating speed of 10 $^{\circ}\text{C}/\text{min}$.

Results and discussion

Samples exhibit colours ranging from pink (one sample) to yellow (two samples), though the majority was identified as brownish yellow, a fact that immediately suggest the use of soil as an important raw material for the manufacture of all mortars. In a previous study [1], the colours of the same area had been classified mainly in the 5YR and 10YR ranges, therefore the predominance of colours centred in a specific hue area (10YR) indicates that, to a certain extent, soils were selected to produce mortars. To a macroscopic inspection, the samples did not reveal vegetable fibres, at least as a systematic component (although sporadic pieces were encountered) and a very minor presence of rock fragments larger than 2 mm, as detailed in Table 2.

Table 2. Sample characterisation (Colour: predominant sample colour according to the Munsell chart; Rock fragments: percentage proportion of particles larger than 2 mm [10-11])

Sample code	Colour	Rock fragm.	Texture
500	10YR 6/6 Brownish yellow	1%	Sandy loam
501	7.5YR 7/3 Pink	1%	Sand
524	10YR 6/6 Brownish yellow	3%	Loamy sand
525	10YR 6/8 Brownish yellow	1%	Loamy sand
544	10YR 6/8 Brownish yellow	3%	Loamy sand
560	10YR 6/6 Brownish yellow	3%	Loamy sand
561	10YR 7/6 Yellow	1%	Loamy sand
563	10YR 8/6 Yellow	<1%	Sandy loam

The texture ranges from sand (one sample) to sandy loam (two samples), with the majority of them falling into the loamy sand category, thus diverting from the most common texture of local soils, classified as loam [1].

The FTIR spectra of all samples, shown in Figure 3, display the presence of bands characteristic of silicate compounds (asymmetric stretching Si-O-Si at 1164, 1097 and 1030 cm^{-1} ; asymmetric stretching Al-O-Si at 1007 cm^{-1} ; symmetric stretching Si-O-Si at 796, 779 and 692 cm^{-1} ; symmetric stretching Si-O-Al at 532 cm^{-1} and Si-O-Si bending at 466 cm^{-1}) [12-14]. In particular, the peaks at 3620 and 3694 cm^{-1} (Al-O-H stretching of structural hydroxyl groups, octahedral), 3450 and 3439 cm^{-1} (related to water adsorbed on the surface of the clay) and 913 cm^{-1} (Al-Al-OH bending of inner OH groups) are all typical of kaolinite [13-15]. This confirms that the main raw material used for their manufacture is soil. It should be noted that, from previous studies, the main minerals found in local soils are quartz, feldspars, amphiboles, phyllosilicates (chlorite, mica, illite-smectite interstratified, and kaolinite) and oxides (goethite and hematite) [3]. The FTIR spectra are compatible with the presence of such minerals, although their specific bands cannot be distinguished and, therefore, their individual presence cannot be confirmed.

These soils are typically very low in Ca and Mg carbonates and this fact helps confirming that no lime was employed in the manufacture of mortar 500, since the FTIR does not exhibit the typical bands in the vicinities of 1400 (asymmetric stretching), 870 (out-of-plane bend) and 710 (in-plane bend) cm^{-1} . This result (confirmed in the TGA curve by the absence of any significant mass loss above 500 °C, Table 2) is in line with the observation that lime was rarely detected in the earthen structures built in the valley of the *Paraíba do Sul* river during the XIX century [16], mainly because of the absence of substantial local natural sources, which would have implied in cumbersome transportation from distant seaside locations. Similar results are observed in three other historical mortars: one of a residential house in the urban area of the same municipality (sample 560, Figure 3) and two of the old hospital of Bananal (samples 524 and 525, Figure 3). Yet, the carbonate bands are observed in samples of materials that are likely to be original of the XIX century: 544 in São Jose do Barreiro and 563 in Bananal (Figure 3), though with a rather small percentage of CaCO_3 , the weight

proportion of which can be calculated from the TGA curves (Figure 4) as being 4.7 and 3.5 %, respectively. The particularly low temperature at which CaCO_3 decomposes in these samples is described by Chiari et al. [17] and Shoal et al. [18] and can be attributed to the crystals imperfections which, in turn, result from the rapid carbonation of the lime exposed to atmospheric CO_2 .

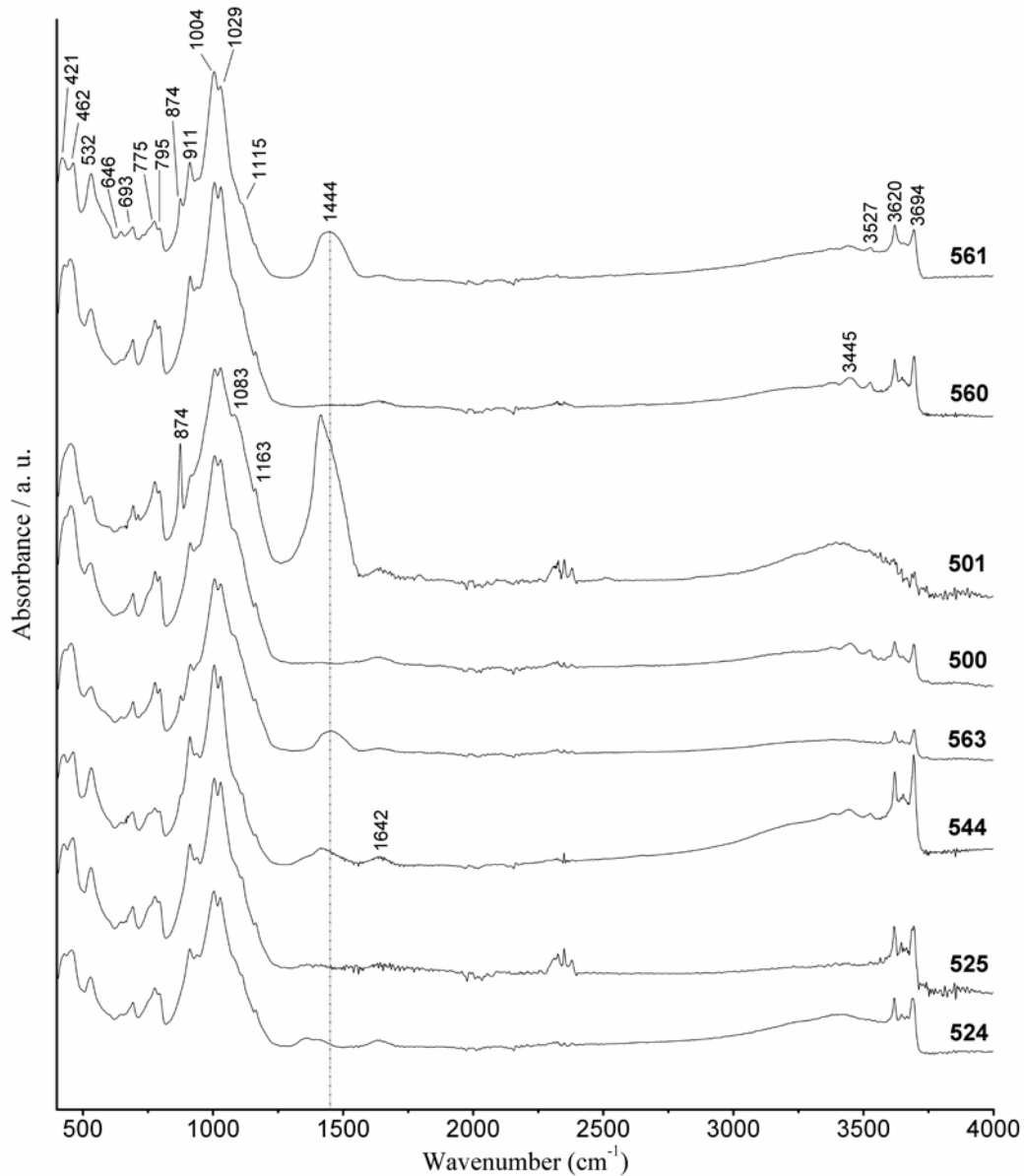


Figure 3. ATR-FTIR spectra

The presence and quantity of kaolinite is confirmed in all (likely) original mortar both by its typical FTIR features and by the mass loss in the 350-500 °C interval in the TGA curves (Figure 4), associated with its transformation to metakaolinite by dihydroxylation, as revised by Redfern [19].

Sample 501 is clearly a later coating and exhibits larger amounts of CaCO_3 (Figure 3) with approximately 8% of CaCO_3 (Figure 4). In addition, sample 501 does not display the typical

kaolinite bands nor the mass loss associated with the dehydroxilation process. This result suggests that in the case of sample 501 a smaller proportion of natural soil – hence of clay – was used in the manufacture of this mortar. In sample 561 the features of sample 560 (same house) are maintained, but with the difference of the presence of CaCO_3 (8%). This fact suggests that the two layers were prepared using the same raw material but with the addition, in the case of the most external coating, of CaO , possibly in order to provide the mortar exposed to the effect of rain with extra strength (samples 560 and 561 correspond to the only finish collected from an outdoor wall surface).

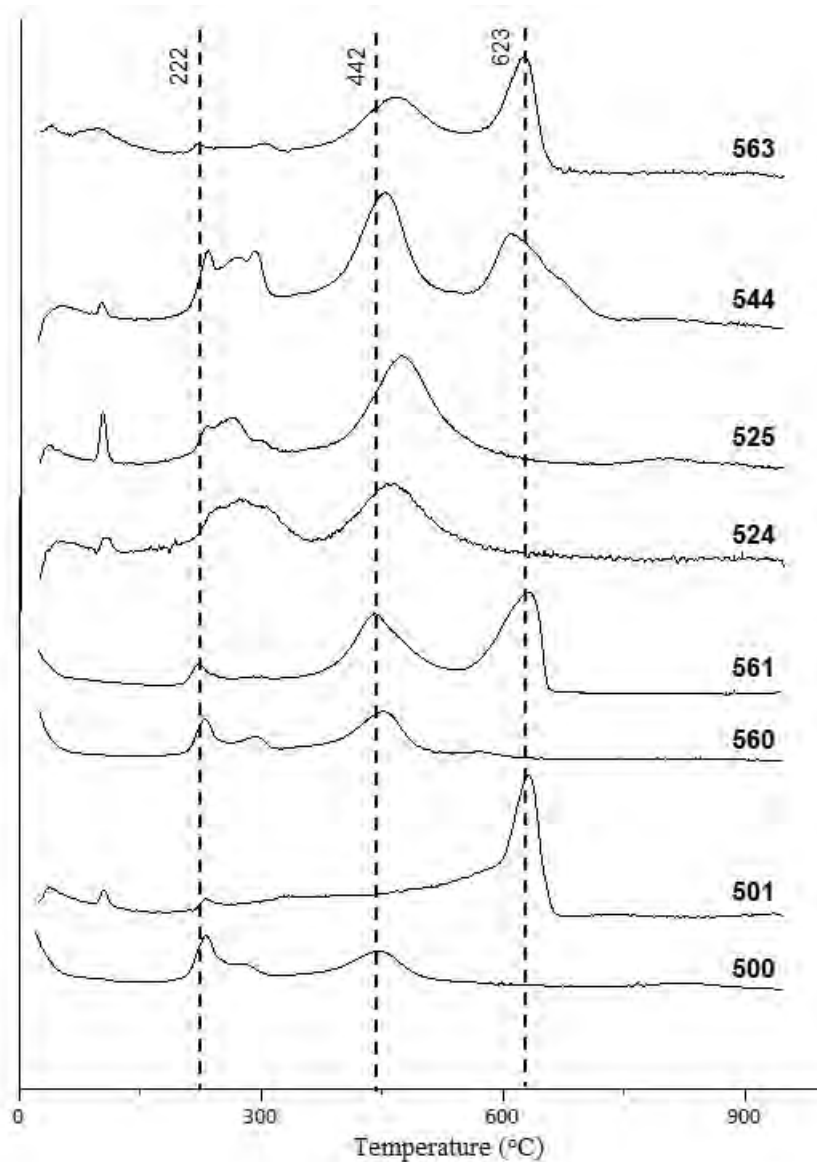


Figure 4. TGA differential curves

There is an interesting difference between the original sample 500 and the later coating 501 as far as the aggregate phase is concerned. The MEV-EDS images of Figure 5 show that there are at least two types of minerals associated with the larger particles. The particles highlighted as 1 correspond to Ca and Na rich aluminosilicates, possibly plagioclase

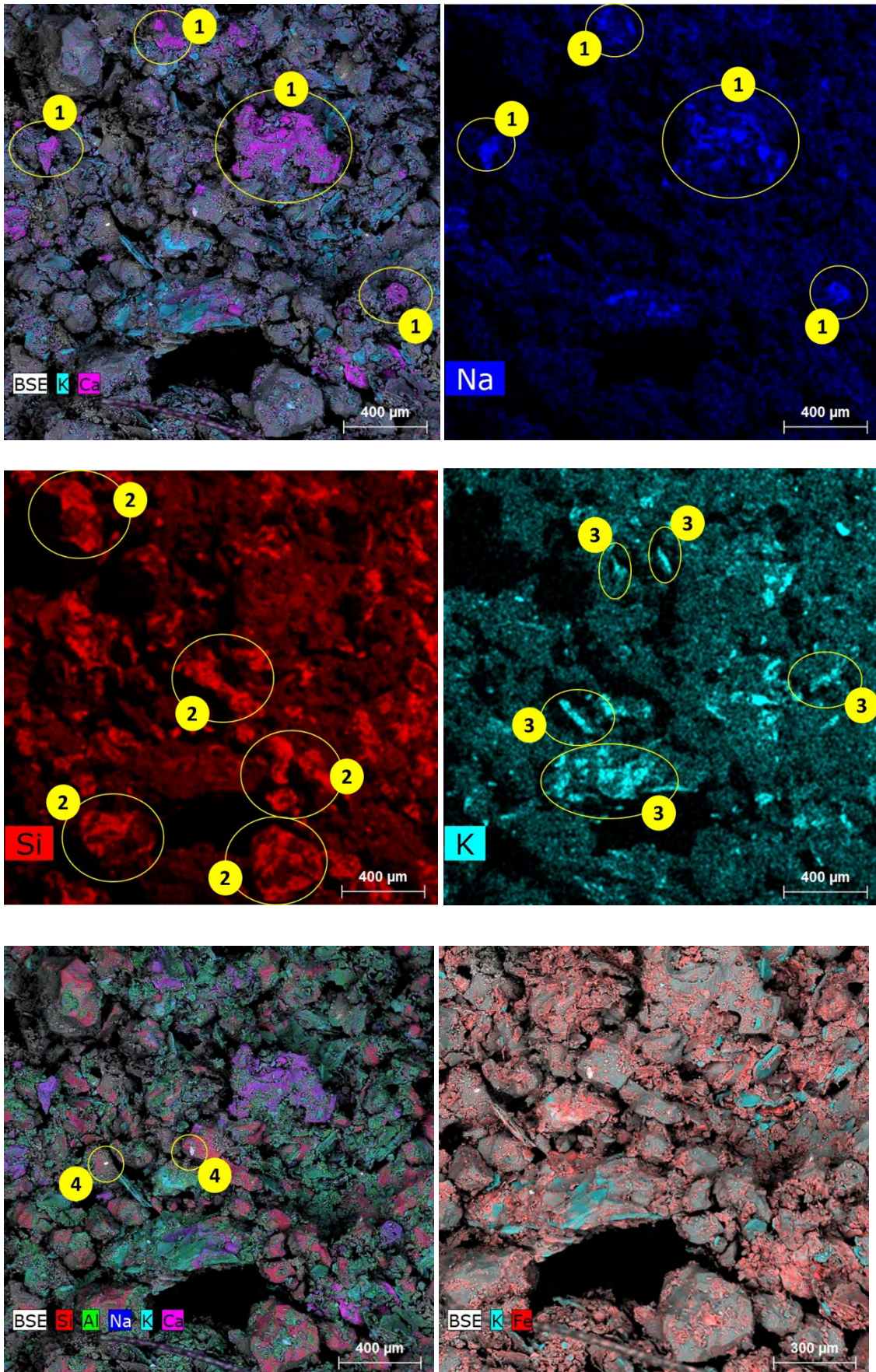


Figure 5. MEV-EDS images of sample 500

feldspars, whereas particles pointed out as 2 are Si-rich Al-poor minerals, clearly corresponding to quartz. The presence of plagioclase containing Ca indicates a soil at an intermediate stage of weathering [20]. Furthermore, the images highlight the presence of mica (circles 3 in Figure 5), which at a higher magnification (not shown) exhibited signs of incomplete weathering. Finally, in the analysed fragment, two points (identified as 4) with abundance of Zr were detected, a fact that together with the other observations suggests a soil formed from an original rock containing zircon, which is quite common in the substrate of the study area [20]. Therefore, it seems that in the manufacture of mortar 500, a natural soil, derived from granitic-gneissic rocks and only partially weathered (and, therefore, somewhat rich in rock material) was used in order to obtain the desired texture (sandy loam, Table 2), thus without adjustment by mixing with sand. It should also be noted that in the MEV-EDS images, iron is clearly concentrated in the fine fraction and, therefore, its concentration can be used as a proxy for clay content.

On the base of such rationale, samples were compared in terms of their elemental composition (Table 3 and Figures 6-7). The concentration of Ca, clearly, reflects the content of CaCO₃ as highlighted in the FTIR spectra and the TGA curves since the natural amount of Ca in the local soils is less than 1%, thus with the largest amounts of this element in samples 501, 561, 563 and 544. The content of Ca is to a good extent anti-correlated with that of Fe, suggesting that the addition of soil earth to the mortar formulation decreased with the increase of lime, which is compatible with the switching of the agglutination role from clay to CaCO₃ particles. Sample 525 is the major outlier in this correlation due to an unexpected low Fe concentration.

Table 3. XRF results in terms of relative proportion (in mass) of major elements

Sample	Si	Al	Ca	Fe	K	Ti
500	2.9 10 ¹	7.3	4.0 10 ⁻¹	3.8	1.2	4.4 10 ⁻¹
501	2.3 10 ¹	2.6	8.5	1.2	1.0	1.4 10 ⁻¹
524	2.8 10 ¹	7.1	4.1 10 ⁻¹	3.9	1.2	4.4 10 ⁻¹
525	2.8 10 ¹	7.4	5.0 10 ⁻¹	2.5	1.7	3.6 10 ⁻¹
544	2.6 10 ¹	7.3	2.4	3.5	2.1	4.2 10 ⁻¹
560	2.8 10 ¹	7.4	5.2 10 ⁻¹	3.6	1.1	3.9 10 ⁻¹
561	2.4 10 ¹	8.8	4.1	1.8	3.1	1.7 10 ⁻¹
563	3.0 10 ¹	5.6	3.0	2.2	1.4	2.9 10 ⁻¹

A high Si/Al ratio is indicative of the presence of quartz and can be associated with the intentional addition of sand aiming at correcting the material texture. While samples 500, 524, 525, 560 and, to a lesser extent, 561 exhibit a similar value at around 3.5-4.0, samples 501 and 563 clearly display ratios (8.8 and 5.4, respectively) that suggest that the formulation was adjusted with the introduction of sand in order to obtain a sandier texture (86% of sand in both cases, being the highest of all the samples). The positive correlation with the concentration of Ca is explained by the fact that choosing to use lime as

agglutination agent was consistent with the option of an adoption of a larger proportion of aggregate. Sample 561 reveals the use of a rather large proportion of lime on a conventional clayish soil, confirming that this external outdoor mortar is merely a modification of the bottom layer of the same wall simply obtained by adding lime.

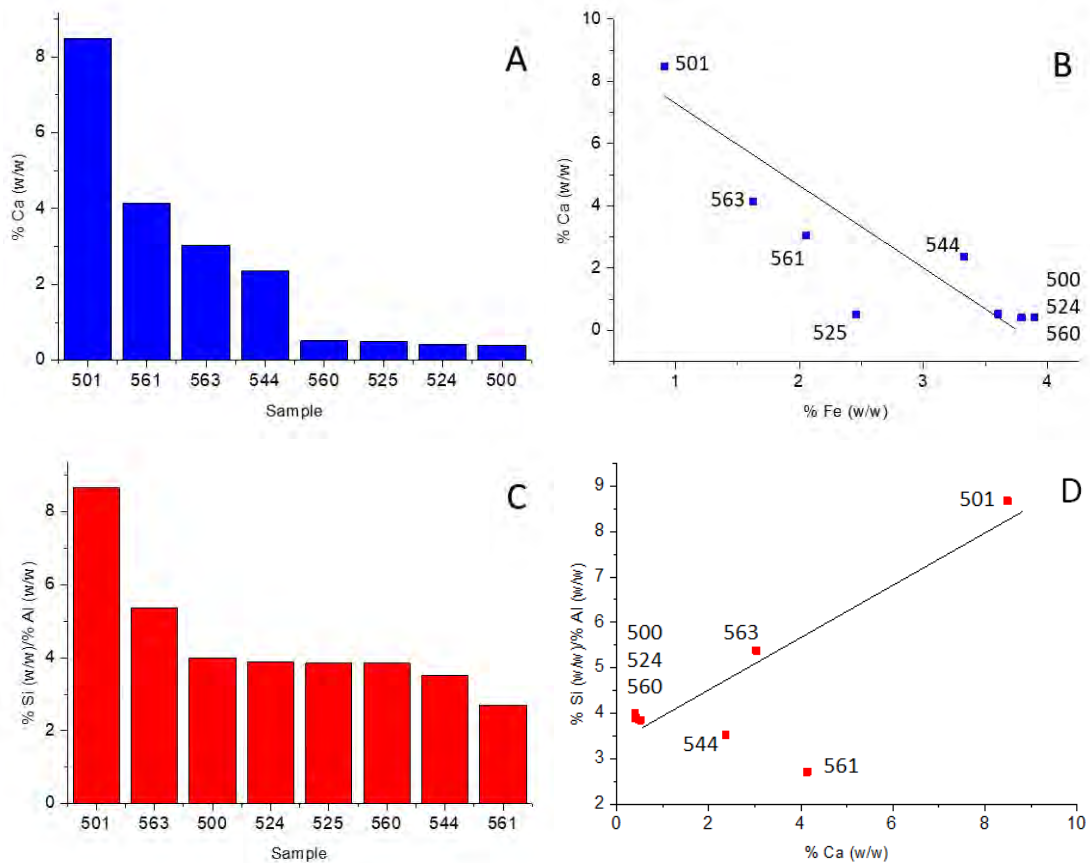


Figure 6. Comparison of mortar samples in terms of elemental composition. A: % content of Ca (w/w); B: correlation between the content of Ca and Fe; C: Si/Al ratios; D: correlation between Si/Al ratio and Ca content

A convenient summary of the situations observed with the eight samples can be drawn on the bases of Figure 7 that illustrates the distribution of the samples in terms of the concentration of Al, Fe and K that are typically elements associated with soil minerals. Samples 500, 524 and 560 are clustered together and possibly represent characteristic original mortars based on the use of soil without adjustment with lime nor sand (though, possibly selectively chosen among less weathered soils in order to guarantee adequate texture without losing agglutination properties). On the other extreme, 501 sample is the poorest in Al, K and Fe and correspond to a certainly later material made with significant alteration of the original soil, with addition of lime and sand. Mortar 563 is original and can be regarded as a pioneer attempt towards a new technology at a time (approximately 1860) in which the use of lime is not yet established but is employed in special occasions (as it is the case of the manor house of the rich family *Aguiar Valim* in the centre of Bananal). Sample 561 (standing out for its content of Al and K) is a mortar still bound to use of soil as main raw material but with the addition of lime adopted to minimise the effect of rain erosion on an outdoor wall; sample 544 being the case of an original indoor mortar attempting in the

same direction, but with a lower content of CaO. Clearly, sample 525 does not differ significantly from the main cluster of original mortars apart from a particularly low level of Fe, possibly simply resulting from the use of a soil with unusually low Fe content.

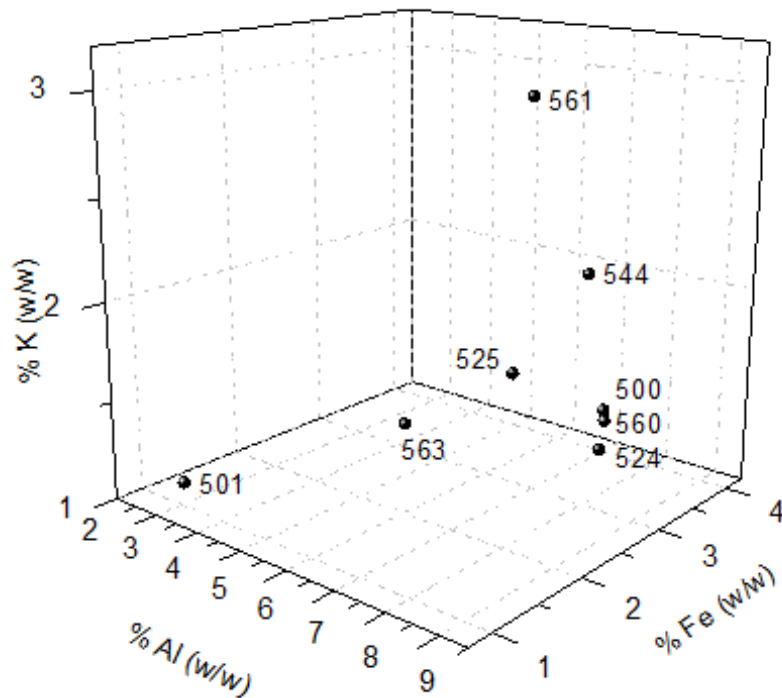


Figure 7. Clustering of samples in a tridimensional space on the basis of their concentration of elements typical of soil (Al, K and Fe).

One final remark concerns the possible presence of organic matter. Although in the FTIR spectra the very weak band observed at ca. 1634 cm^{-1} can in principle indicate the presence of organic molecules [21] (stretching vibrations of C=O bonds from carboxylic acid anions) the absence of other bands characteristic of organic compounds suggest that this band are likely due to adsorbed water in inorganic material (H-O-H bending) [13, 22-23]. This could also explain the mass loss observed in the majority of samples in the $200\text{-}350\text{ }^{\circ}\text{C}$ interval, but this issue is to investigated into detail in future works.

Conclusions

The mortar samples investigated in this work and collected from the surface of earthen historical buildings in the basin of the *Paraíba do Sul* river, XIX century, can be divided into three groups. The first and largest one comprises original (or likely-to-be) layers that are made only by soil, without the addition of lime or of sand. However, their sandier character, with respect to the majority of local soils, suggests that the raw material was probably obtained from less weathered soil sources, as confirmed by the MEV-EDS analysis of one of the samples.

The second group is represented by mortars that exhibit both addition of lime and sand to the soil: one of the samples is certainly original and shows that in specifically important constructions newer technological solution were already been employed, though probably at a later historical stage when the introduction of locally unavailable raw materials (like lime) was less problematic. The other sample is certainly a later layer and is representative of the path that the production of mortars would take by the end of the XIX century, with the gradual loss in the use of earth in their manufacture. Finally, the third group of samples encompass situations in which lime starts to appear in the formulation of mortars, still with an important presence of soil in the composition, possibly aiming at less vulnerable coatings, especially in outdoor situations.

These findings certainly require further investigations to improve their scientific confidence, both by broadening the number of objects under study and by including other analytical techniques (e.g. XRD analysis) or data handling strategies (e.g. statistical analysis, spectra deconvolution).

Acknowledgements

The São Paulo State Research Foundation (FAPESP), Projects N. 2017/03071-7 and 2017/16477-1.

References

1. Vasconcellos S (1979) *Arquitetura no Brasil – Sistemas construtivos*. Universidade Federal de Minas Gerais, Belo Horizonte
2. Kanan MI (2009) The mediterranean Portuguese influence in the Brazilian earth-building tradition: a valuable heritage to research. In: *Mediterra*, Villanovaforru, 2009. http://www.revistaamericapatrimonio.org/the_mediterranean_portugues.pdf. Accessed 21 April 2016
3. Cavicchioli A, Santana LG, Perroni MS (2018) Enlightening the use of materials and techniques in earthen architecture in southeast Brazil during the first coffee cycle (19th century). *J Cult Herit* 31:208-214
4. Fazio AT, Cavicchioli A, Penna DSA et al (2015). Towards a better comprehension of biodeterioration in earthen architecture: study off ungi colonisation on historic wall surfaces in Brazil. *J Cult Herit* 16:934-938
5. Gomes MI, Faria P, Gonçalves TD (2018) Earth-based mortars for repair and protection of rammed earth walls. Stabilisation with mineral binders and fibers. *J Clean Prod* 172:2401-2414

6. Lima J, Faria P, Silva AS (2016) Earthen Plasters Based on Illitic Soils from Barrocal Region of Algarve: Contributions for Building Performance and Sustainability. *Key Eng Mat* 678:64-77
7. de Rainville C (1880) *Vinhola brasileiro novo manual pratico do engenheiro, architecto, pedreiro, carpinteiro, marceneiro e serralheiro*. Laemmert, Rio de Janeiro
8. [Munsell Color (2000) *Munsell Soil Color Charts*. Munsell Color, Grand Rapids
9. Swann DH, Fisher RW, Walters MJ (1959), Visual estimates of grain size distribution in some Chester sandstones. *Illinois State Geological Survey Circular* 280
10. Soil Survey Division Staff (1993) *Soil survey manual*. Soil Conservation Service. US Department of Agriculture Handbook 18
11. Embrapa (1979) *Manual de métodos de análise de solo*. Serviço Nacional de Levantamento e Conservação de Solo, Rio de Janeiro
12. Bertoluzza A, Fagnano C, Morelli MA et al (1982) Raman and infrared spectra on silica gel evolving toward glass. *J Non-Cryst Solids* 48(1):117-128
13. Saikia BJ, Parthasarathy G (2010) Fourier transform infrared spectroscopic characterization of kaolinite from Assam and Meghalaya. Northeastern India. *J Mod Phys* 1(04):206.
14. Lee W, Van Deventer J (2003) Use of infrared spectroscopy to study geopolymerization of heterogeneous amorphous aluminosilicates. *Langmuir* 19(21):8726-8734.
15. Panda AK, Mishra BG, Mishra DK et al (2010) Effect of sulphuric acid treatment on the physico-chemical characteristics of kaolin clay. *Colloid Surface A* 363(1-3):98-104
16. Lemos C (1999) *Casa Paulista*. EDUSP, São Paulo
17. Chiari G, Santarelli ML, Torracca G (1992) Caratterizzazione delle malte antiche mediante l'analisi dei campioni non frazionati. *Materiali e strutture* 2(3):111-137
18. Shoval S, Gaft M, Beck P et al (1993) Thermal behaviour of limestone and monocrySTALLINE calcite tempers during firing and their use in ancient vessels. *J Therm Anal* 40:263-273
19. Redfern SAT (1987) The kinetics of dehydroxylation of kaolinite. *Clay Miner* 22:447-456
20. Perrotta MM, Salvador ED, Lopes RC et al (2005) *Mapa Geológico do Estado de São Paulo, escala 1:750.000, Programa Geologia do Brasil*. Companhia de Pesquisa de Recursos Minerais, São Paulo
21. Ellerbrock R, Gerke H (2004) Characterizing organic matter of soil aggregate coatings and biopores by Fourier transform infrared spectroscopy. *Eur J Soil Sci* 55(2):219-228.

22. Russell J (1979) Infrared spectroscopy of ferrihydrite: evidence for the presence of structural hydroxyl groups. *Clay Miner* 14(2):109-114.
23. Mendelovici E, Villalba R, Sagarzazu A et al (1995) The 1640 cm⁻¹ infrared band, monitor for the gain and thermal stability of water produced in ground kaolinites. *Clay Miner* 30(4):307-313

Assessment of adhesive strength of an earth plaster on different substrates through different methods

Paulina Faria¹, José Lima², João Nabais³, Vitor Silva³

(1) CERIS and Dep. Civil Engineering, FCT, NOVA University of Lisbon, paulina.faria@fct.unl.pt

(2) Faculty of Architecture, University of Lisbon, jose.lima.ferreira@gmail.com

(3) Dep. Civil Engineering, FCT, NOVA University of Lisbon, p110260@campus.fct.unl.pt, vmd.silva@fct.unl.pt

Abstract

The adhesion capacity of an earthen mortar is one of the most important properties for plastering. This paper aims to assess the influence of two different substrates, namely adobe and hollow fired clay bricks, in the adhesive strength of an earth plastering mortar formulated in laboratory, through tensile and shear tests methods. The substrates are prepared differently, with and without prior application of a clay grout. The test samples were produced also differently, by cutting while fresh, cutting after hardening and directly sample moulding. Tests were performed in two different relative humidity environments: 65% and 95%. The results are compared, evaluating the influence of the different parameters, and with results of other plasters. The earth plaster presented a good performance regarding adhesion on both substrates studied, being advantageous the preparation of the support with a clay grout. The cutting procedure of the samples influences the test results being the fresh mortar cut less harmful. The relative humidity increment has a negative effect on the adhesion capacity but even a high percentage does not compromise the stability of the plaster. The shear test proved to be a valid instrument when specific pull-off equipment is not available.

Introduction

In recent years earthen mortars and plasters have been calling the attention of the building community not only because they are ecological, reversible, compatible with historic masonries such as earth-based or rubble stone, but also because they can be efficient even when applied on current contemporary masonries [1, 2, 3]. Particularly, the contribution earthen plasters can give to relative humidity indoor equilibrium, based on the high hygroscopicity of clays, classifies them as passive technologies to achieve indoor comfort [4]. Nevertheless, the knowledge on the application of earthen plasters was almost lost in developed countries and is being re-gained in the last years [5,6].

One of the aspects that is fundamental for plastering earthen or mineral binder-based mortars is the adhesive strength on substrates, which is the capacity of the plaster to resist to normal and tangential tensions at the interface with the support. It depends mainly on the following physical phenomena: the matrix mortar penetration in the support pores and

the surface connections anchoring the mortar to support roughness. The higher the roughness, the higher the contact area. Therefore, the porous structure of the support and its roughness are fundamental to adhesion. Nevertheless, the porosity of the support should not be too high to avoid excessive mortar matrix absorption that can weaken the layer of mortar in direct contact with the support (Figure 1).

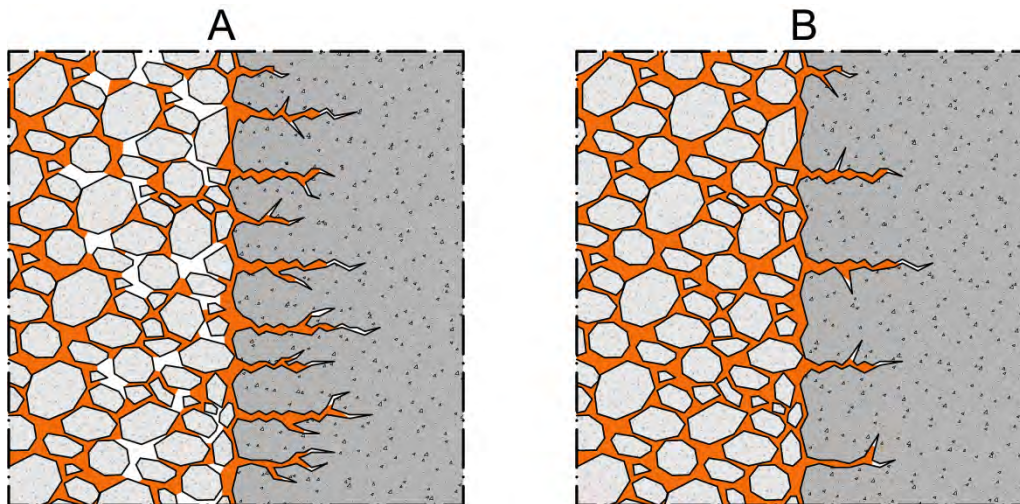


Figure 1. Schematic representation of a mortar applied to a more (A) or less porous (B) support

Furthermore, as a complex mechanism, adhesion is also affected by in service factors [7], such as the type of support where the mortar is applied and their cleanliness or preparation, the mortar formulation and thickness of application, the hygrothermal conditions when the application is performed.

A traditional way of improving the adhesion of a plaster is to perform support preparation with the application of a grout or slurry that can increase roughness of too smooth surfaces and control mortar matrix absorption, acting as a primer to the plaster system application. For earthen plasters Deliniere et al [5] applied earthen plasters on a concrete support with and without the previous application of a water-clay slurry or grout (*barbotine*) by brush. In this study the grout application increased the adhesive strength results by pull-off test based on EN 1015-12 [8] and all the mortars surpassed the minimal limit of DIN 18947 [9].

For earth mortars the bonding depends mainly on the clay content. An earth plaster with very high clay content will crack and loose adhesion, while a plaster with a too low clay content will have a weak bond to the support [10]. In fact, the thickness of a plaster (and of each plaster layer) is also important because it is directly proportional to the adhesive action due to gravity.

The influence of hygrothermal conditions on the adhesion of an earth plaster is due to the high hygroscopicity of clays. When in contact with liquid water, clays acquire plastic properties which, from a certain extent, may compromise the plaster hardened state stability. For earth mortars the DIN 18947 [9] defines that the test can only be performed after the specimens are at least 7 days at 23 ± 2 °C and 50 ± 5 % relative humidity (RH).

The DIN 18947 [9] defines the assessment of adhesive strength of earth plasters to a support based on the EN 1015-12 [8] test procedure. However, there are problems to assess the adhesion by EN 1015-12 standard [8] test procedure even for air lime-based plasters and renders [11]. In fact this test is generally performed on plaster samples that are cut on *in situ* plasters or, in laboratory, on a plaster specimen applied on a support. In the laboratory, that support can be a concrete small slab, a brick or a ceramic tile. The cut of the sample is generally performed when the plaster specimen is hardened; that is always the case *in situ*. The cut should penetrate few millimetres on the support itself. After the cut, a metallic device with circular area (Figure 2A) is glued to the sample ensuring complete contact. The pull-off can be applied through it. The pull-off can be applied by a pull-off test equipment (Figure 2B) or even by a tensile test equipment. The rupture can occur: in the thickness of the sample - cohesive rupture (Figure 2C) - meaning that the adhesive strength is higher than the registered value; by the contact surface between the mortar and the support - adhesive rupture - registering the adhesive strength; by the support, meaning that the adhesive strength is higher than the registered value [8]. In this last case it also means that the plaster is stronger than the support, what can be a problem for architectural heritage conservation, considering that the plaster should be there to protect the support and not imposing extra tensions. Both the type of rupture and the adhesive strength, that is obtained by the quotient of the maximum force and the contact area, are registered.



Figure 2. Pull-off test: A - Metallic devices glued to the plaster specimens; B – Pull-off equipment perpendicular to the specimen being tested; C – specimen after cohesive rupture

For low strength plastering mortars the samples cutting process, inflicting some level of vibration, can damage the sample and turn it unusable. Therefore, in laboratory sometimes the cut is performed manually while the plastering mortar applied on the support is still fresh [8], without cutting the support. The difference is that, in this case, as the cut does not penetrate in the support, the rupture hardly will happen in that element, therefore eventually misleading conclusion regarding absence of cohesive rupture.

The characterization of adhesive strength of plasters by a tensile test can be argued because the application of a force perpendicular to the support may not be the best way to simulate adhesive tension of that plaster. Delinière et al [5] suggest that a shear test should be more appropriate. Shear tests are not standardised and different studies used diverse equipment to perform it. Stolz and Masuero [12] used what they called an adhesive meter specifically

developed. Hamard et al [10] assessed the adhesion of earthen plasters by a simple shear test that can be performed easily *in situ*. Vertical earth plaster samples with 50 mm x 40 mm x 20 mm are applied on a support or cut with those dimensions after drying. A simple device, as described in Hamard et al [10], is placed with good contact with the sample top and avoiding contact with the wall to reduce friction. The device is successively loaded with 250 g weigh with 10 s intervals. The total mass that produces the sample rupture from the support is registered. For masonry walls, there should be samples on the masonry units but also samples on both the masonry joints and units. Earth plaster samples on which rupture do not occur when loaded with a force of 20 N (approximately 2 kg) are considered adequate [10].

The DIN 18947 [9] considers the adhesive strength, together with the flexural and compressive strengths, to mechanically classify earth mortars (Table 1).

Table 1. Mechanical classes of earth plasters defined by DIN 18947 [9]

Mechanical class	Compressive str. [N/mm²]	Flexural str. [N/mm²]	Adhesive str. [N/mm²]
SI	≥ 1.0	≥ 0.3	≥ 0.05
SII	≥ 1.5	≥ 0.7	≥ 0.10

Rohen and Ziegert [13] consider that earth plasters should present minimum adhesive strength of 0.03 N/mm² but that values of 0.15 N/mm² are common. In fact, Faria et al [6] for a ready-mixed earth plaster formulated with an illitic clay from Algarve Barrocal, Portugal, obtained adhesive strength of 0.15±0.03 N/mm².

Therefore, this study intends to give a contribution on how to assess adhesion of earthen plasters to a masonry, namely comparing the influence of tensile and shear testing procedures, on two different substrates - adobe and hollow fired clay bricks - , prepared differently, with application of a clay slurry previous to the plastering or just water spray, with the test samples produced differently, by cutting while fresh, cutting after hardening and directly sample moulding with aimed test dimensions, and in equilibrium on two different RH environments: 65% and 95%.

Materials, mortar and samples

The clayish earth was excavated in an Algarve Barrocal quarry, south Portugal. It was grinded to reduce clods and sieved to remove coarse particles. The earth used is composed by sand, silt and clay. The latter is mainly illitic and has been characterized by Lima et al. [4]. As the earth clay content is high, additional siliceous sand was used to prepare the earth mortar. The dry particle size distribution of the grinded earth and the sand, determined based on EN 1015-1 [14], are presented in Figure 3. The sand presents higher content of particles between 0.25 and 1 mm in comparison with the earth, that in turn presents a higher content on fines and a more homogeneous distribution of particles.

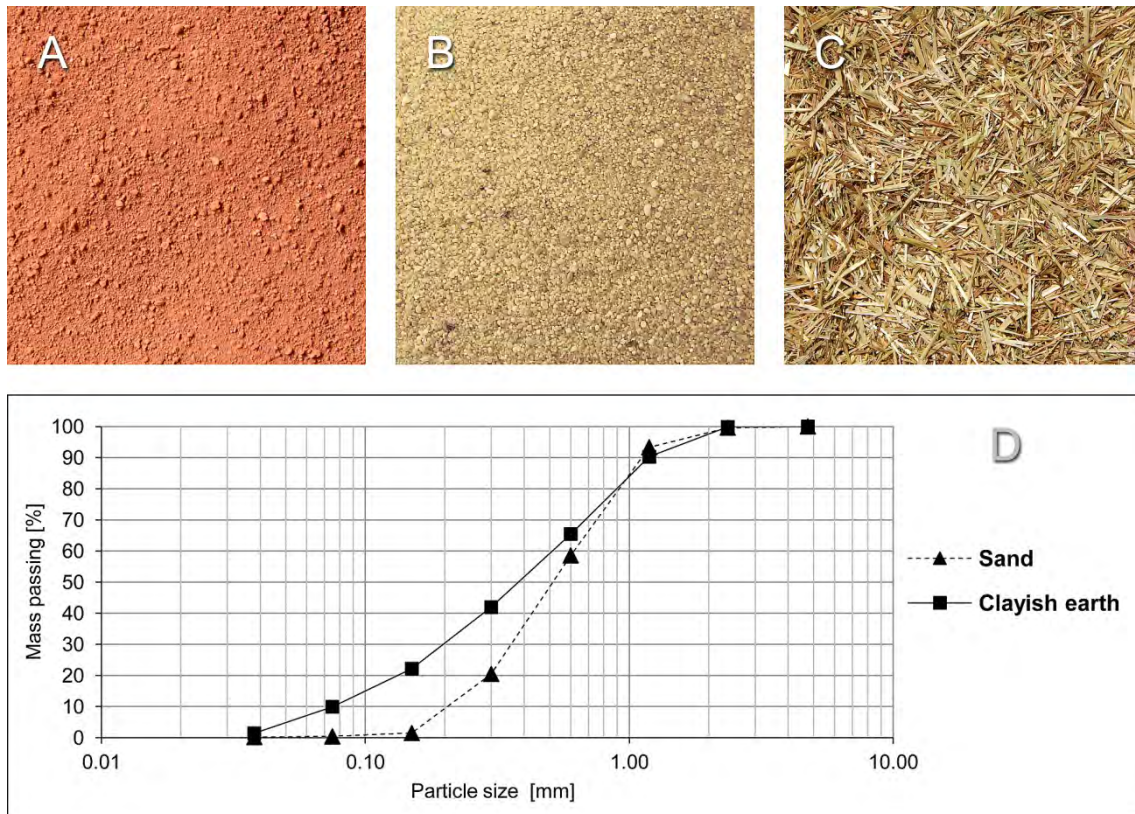


Figure 3. Clayish earth (A), sand (B), oat fibres (C) and dry particle size distribution of the sand and clayish earth (D) used in the mortar formulation.

Oat fibres were also used for the mortar formulation. The loose bulk density of all the materials was determined based on EN 1097-3 [15] (average and standard deviation of six tests) and is presented in Table 2.

Table 2. Loose bulk density of mortar materials and water absorption coefficient under low pressure of supports

	Loose bulk density [kg/m ³]			AC [kg/(m ² .min ^{0.5})]	
	Earth	Sand	Fibres	Brick	Adobe
Average	1317.0	1591.8	62.5	0.82	0.45
Stand. Dev.	1.8	0.6	4.9	0.06	0.08

It can be observed that the sand bulk density is higher than the one of the earth, which may be explained by lower content on silica grains of the latter, while the bulk density of the fibres is, as expected, very low. The high standard deviation of the fibres was justified by the fact that the test is performed without compaction and, therefore, the position of the fibres produces different voids. Santos et al. [16] also achieved a similar bulk density of 70 kg/m³ for oat fibres.

The supports for the plaster were ceramic fired hollow brick, with 30 cm x 20 cm x 7 cm, and adobe, with 30 cm x 15 cm x 7 cm, representing a nowadays prevailing support and an earthen one. Both materials water absorption under low pressure was determined by Karsten tube test after 60 minutes, based on LNEC Fe Pa 39 [17] and EN 16302 [18], and

results are presented in Table 2. Water absorption coefficient of the brick is higher in comparison with adobe.

The mortar was formulated with a volumetric proportion of 1:3 (clayish earth:sand) adding 5% (of total weight of earth and sand) of fibers. Based on the loose bulk density, it corresponds to 1:3.6:0.01 mass proportion of earth:sand:fibers. The mortar preparation was performed based on the DIN 18947 [9]. A previously defined amount of water of 12.8% (of total weight of earth and sand) that ensure good workability of the mortar [4] was placed in the mechanical mixer recipient and the solid components were added during the first 30 seconds of mixing. A mechanical mixing went on for 30 seconds and the mortar rested for 5 minutes, after which it was mechanical mixed again for 30 seconds more.

Prismatic samples with 40 mm x 40 mm x 160 mm were produced in metallic moulds, with two layers compacted in sequence. The excess of mortar was removed and the surface regularized.

Plaster samples with 2 cm thickness were produced over both brick and adobe surfaces, with 30 cm x 20 cm and 30 cm x 15 cm, respectively, after water spraying or the application with a brush of a clayish grout made with 1:1 mass proportion of the earth and water. The support materials were placed inside a frame mould with height 2 cm higher than the supports. To simulate and homogenize the mortar projection energy to the support, the mortar was dropped vertically from a height of 70 cm. The excess of mortar was removed and samples were regularized. In some cases the mortar did not plastered all the support but only the moulds of adhesion test specimens that were specifically placed on the support surface, depending on the test procedure (see test procedure for adhesion tests).

After moulded all the samples were kept for one month in a conditioned room at $23\pm 2^{\circ}\text{C}$ and $65\pm 5\%$ RH before being tested.

Test procedures

General characterization of the mortar

The mortar was characterized for common properties both in the fresh and hardened state. In the fresh state flow table consistency was performed based on EN 1015-3 [19] and bulk density was assessed following EN 1015-6 [20].

In the hardened state the mortar was tested for bulk density by the geometrical methods defined by EN 1015-10/A1 [21] and for dynamic modulus of elasticity (E_d) based on EN 14146 [22] using a Zeus Resonance Meter ZMR 001, with its own software, that calculates E_d based on the geometry and mass of the sample, gravitational acceleration and longitudinal resonance frequency.

Based on EN 1015-11 [23] the flexural and compressive tests were performed with a Zwick/Rowell Z050 equipment, with load cells of 2 kN, a speed of 0.2 mm/min and a 3 point bending test for flexural, with 100 mm between the supports, and a 50 kN load cell, 0.7 mm/min speed and a compressive area of 40 mm x 40 mm for compression. Six samples were tested for each property.

Pull-off test

The pull-off test was performed based on EN 1015-12 [8] with the mortar samples in equilibrium at 65±5 % RH and 90±5 % RH, with previous sprayed water or clayish grout application and different specimen preparation. A PosiTest AT-M equipment, a pull-off equipment specific for low strength, was used with circular metallic pieces with 50 mm diameter. For the application of the circular pieces three different types of specimens were produced and tested: cylindrical specimens cut when the plaster sample on the support was hardened (hardened cut HC); cylindrical specimens cut with a metallic cylinder tube when the plaster sample was fresh (fresh cut FC) and cylindrical specimens that were directly moulded using a cylindrical plastic mould placed on the support instead of plastering the all support surface (direct moulding DM). The equipment was manually and slowly and gently operated so that the rupture occurred after 20-60 seconds. The adhesion strength was obtained dividing the rupture force by the contact area of the sample cut section, in N/mm². Nevertheless, the glued area is always measured and if the contact was not total, the real adhesive strength is corrected dividing the metallic piece area by the real contact area. The type of rupture is also registered. Results are an average of 5 tests.

Shear adhesion test

The shear adhesion test was performed in the laboratory following the methodology defined by Hamard et al. [10] and described previously, with a simple device specifically made (Figure 4A). The 50 mm x 40 mm x 20 mm samples were cut on the hardened plaster or directly moulded, both on the brick. Maritime plywood pieces were used for moulding the latter samples without using any demoulding agent and some problems occurred for demoulding due to adherence of the mortar to the plywood.

The hollow bricks surface (one of the supports) have grooves aligned with the length dimension. The samples were tested vertically aligned with that direction.

All the samples are measured and the average of two measurements of each dimension is considered. The device has a weight of 500 g, corresponding to the first test load. All the applied weights of 250 g are calibrated in a precision scale of 0.001 g. The device is placed in direct and complete contact with the top surface of a plaster sample, without eccentricity and minimizing friction with the support, applying shear tension. After 10 s with the first load from the device, 250 g are applied and the sequence is repeated until the rupture of the sample (Figure 4B). When the rupture occurs (Figure 4C), the total weight is registered and

the shear strength (N/mm^2) is calculated by the quotient of the total weight multiplied by the acceleration due to gravity ($9,807 \text{ m}/\text{s}^2$) and the samples area of contact with the support (mm^2). Results are an average of at least 5 tests.

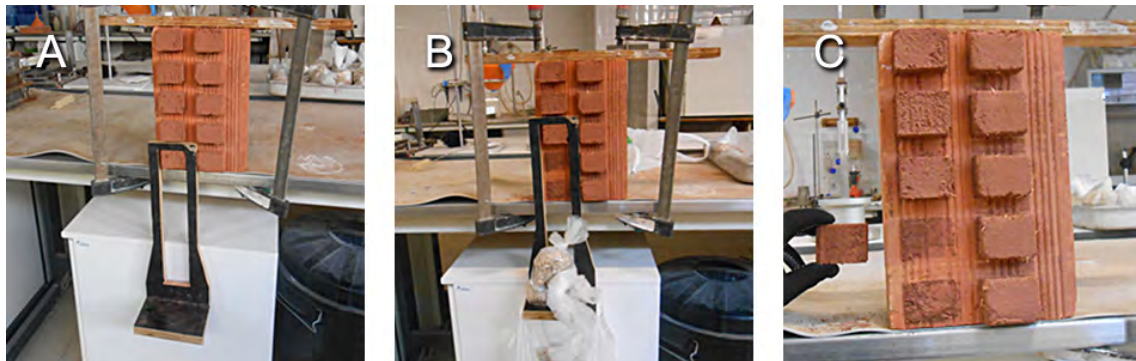


Figure 4. Shear adhesion test on moulded samples: (A) application load device on a sample; (B) successive 250 g loads applied on the device; (C) a moulded samples after rupture.

Results and discussion

Fresh and hardened state characterization of the mortar

Flow table consistency of the mortar was 176 ± 1.5 mm. The result is within the range of 175 ± 5 mm defined by DIN 18947 [9]. Fresh state bulk density had an average value of $2.06 \text{ kg}/\text{dm}^3$, which is higher than the minimal of $1,2 \text{ kg}/\text{dm}^3$ defined by DIN 18947 [9]. Nevertheless, the value is comparable with the ones of Delinière et al. [5] that for two ready-mixed mortars and three laboratory formulated ones presented results of 2.0 - $2.1 \text{ kg}/\text{dm}^3$. The results are also within the range of the ready-mixed earth plaster produced with an illitic earth from the same quarry tested by Faria et al. [6] that registered $2.03 \text{ kg}/\text{dm}^3$ and $2.11 \text{ kg}/\text{dm}^3$, respectively when the mortar was mixed on site and in the laboratory. Santos et al. [16] when testing a ready-mixed earth mortar and a formulated mortar with oat fibres obtained a similar bulk density of $2.00 \text{ kg}/\text{dm}^3$ as well as Gracia-Vera et al. [24] that registered $2.06 \text{ kg}/\text{dm}^3$ and $2.05 \text{ kg}/\text{dm}^3$ for two earthen plasters based in two different raw earths.

Hardened state bulk density (average and standard deviation) was $1.97 \pm 0.01 \text{ kg}/\text{dm}^3$. Based on DIN 18947 [9] the mortar is classified in class 2 (between 1.81 and $2.00 \text{ kg}/\text{dm}^3$). This result is similar to other studies. Delinière et al [5] for both ready-mixed and formulated earth mortars registered bulk densities of 1.7 - $1,8 \text{ kg}/\text{dm}^3$, Lima and Faria [25] when testing illitic earth plasters achieved bulk densities between $1.91 \text{ kg}/\text{dm}^3$, $1.66 \text{ kg}/\text{dm}^3$, respectively without and with addition of oat or typha, while Garcia-Vera et al. [24] achieved $1.83 \text{ kg}/\text{dm}^3$ and $1.81 \text{ kg}/\text{dm}^3$, respectively for red and yellow plasters, although with a much higher standard deviation. The bulk density of the present study mortar is also higher than the one of the ready-mixed mortar tested by Faria et al. [6] that registered $1.77 \text{ kg}/\text{dm}^3$ and the ready-mixed mortar and the oat fibres formulated mortar tested by Santos et al. [16] with $1.77 \text{ kg}/\text{dm}^3$ and $1.72 \text{ kg}/\text{dm}^3$, respectively.

Mortar dynamic elasticity modulus (E_d), flexural and compressive strengths results are presented in Table 3.

Table 3. Dynamic modulus of elasticity, flexural and compressive strength of mortar

Property	N/mm ²
E_d	4231±86
Flexural str.	0.24±0.02
Compressive str.	0.81±0.22

The flexural and compressive results are consistently lower in comparison to the ready-mixed earth mortar characterized by Faria et al. [6] produced with clayish earth from the same quarry, using similar test procedures, that registered 0.3 N/mm² and 1.1 N/mm², respectively. That was inverse to what was expected by the higher bulk density of the mortar tested in the present study. Nevertheless, E_d of the present study is higher than the one of Faria et al. [6], in agreement with that higher bulk density. Results of the present study are also lower than the ones of Delinière et al. [5] that achieved for five earth mortars flexural strength results of 0.49-0.69 N/mm² and for compressive strength between 1.3-2.1 N/mm². Nevertheless, the compressive and flexural strength are similar to the ones obtained by Lima et al. [4] for a mortar with clayish earth from the same quarry but without fibers, respectively 0.25 N/mm² and 0.88 N/mm², and respectively slightly lower than the results of Lima and Faria [25] for the same mortar but with addition of oat fibers, respectively 0.23 N/mm² and 0.67 N/mm², and slightly higher with addition of typha fiber-wool, that registered 0.31 N/mm² and 1.02 N/mm². When comparing with the present study, García-Vera et al. [24] testing both a red and a yellow earth mortars registered similar compressive strength results at 95% RH (0.8 N/mm² and 0.7 N/mm², respectively) and higher values when testing at 60% RH (1.0 N/mm² and 1.2 N/mm², respectively), showing that the ambience test conditions may have a more significant influence than the type of earth.

Adhesion strength and type of rupture

Table 4 presents the type of rupture (adhesive or cohesive) and Table 5 presents the results of pull-off adhesion strength, while Table 6 presents the results of shear adhesion test.

The ready-mixed mortar tested by Faria et al. [6] presented a pull-off mainly adhesive rupture on samples applied on hollow brick after water spraying, cut after hardening and tested by the same type of equipment, with adhesion strength of 0.15 N/mm² that is higher than the result of the present study. Nevertheless, using the same test procedure, Lima and Faria [25] registered adhesive strength of 0.09 N/mm² for the tested earth plaster with oat fibres addition, 0.11 N/mm² for similar plaster but with typha fibres and 0.07 N/mm² for the same plaster without fibres, results that are in the same range as the one registered in the present study for the same test conditions. Comparing the results of Delinière et al. [5] that applied the earth plasters on concrete panels and tested samples cut when the mortar was fresh, after water brushing (0.06-0.08 N/mm²) and after applying a water-earth grout (0.11-

0.14 N/mm²), it can be seen that the influence of the preparation was more significant possibly due to the concrete substrate.

Table 4. Pull-off adhesion rupture depending on the specimen preparation

Rupture	Fresh.cut	Hard.cut	Moulded	Global
	Number/%	Number/%	Number/%	Number/%
Cohesive	11/55	11/55	7/35	29/48
Adhesive	9/45	9/45	13/65	31/52
Total	20/100	20/100	20/100	60/100

Table 5. Pull-off adhesion of the mortar depending on the test procedure

Support	RH (%)	Preparation	Specimen	Adhesion str. (N/mm ²)
Brick	65	Water	FC	0.13±0.01
			HC	0.09±0.01
			DM	0.14±0.02
		Grout	FC	0.13±0.00
			HC	0.12±0.01
			DM	0.14±0.02
90	Water	HC	0.08±0.00	
	Grout	HC	0.09±0.01	
Adobe	65	Water	FC	0.13±0.01
			HC	0.11±0.01
			DM	0.15±0.01
		Grout	FC	0.14±0.01
			HC	0.13±0.01
			DM	0.15±0.01
	90	Water	HC	0.08±0.01
		Grout	HC	0.08±0.00

Notation: FC – fresh cut; HC – hardened cut; DM – direct moulding

Table 6. Shear adhesion of the mortar depending on the test procedure

Support	Preparation	Specimen	Adhesion str. (N/mm ²)
Brick	Water	HC	0.04±0.01
		DM	0.04±0.00
	Grout	HC	0.05±0.00
		DM	0.04±0.00
Adobe	Water	HC	0.05±0.00
		DM	0.01±0.00
	Grout	HC	0.05±0.01
		DM	0.03±0.01

Notation: FC – fresh cut; HC – hardened cut; DM – direct moulding

By the results obtained, it is not possible to mechanically classify the earth plaster based on the DIN 18947 [9] not because of the pull-off test results, that for a common RH environment of 65% present a minimum strength of 0.09 N/mm², but because the flexural and compressive strengths does not achieve the minimum values for class SI (Table1).

Nevertheless, particularly the flexural strength is very close to the lower limit of SI class and, associated with the good values of adhesion, that is very positive for compatible plastering mortars.

The good results of the pull-off test may be partially justified by the equipment that was used – not a conventional pull-off for mortars but one more used for paint systems adhesion assessment. The adhesion was slightly higher to the adobe than to the brick. The testing at a high RH reduces adhesive strength but do not jeopardize adhesion of the plaster when comparing to the DIN 18947 [9] requirements. The previous application of the grout has a positive effect on adhesion in comparison with just the water spray, corroborating results of Delinière et al. [5]. The direct moulding of the samples (without cut) has also a positive effect on the adhesion and rupture is mainly adhesive, being the hardened cut the sampling method with the more negative effect. Nevertheless, the cut methods have a higher percentage of cohesive rupture meaning that the adhesion to the support is higher than the registered values. Although the hardened cut method is the only one that can be performed to assess adhesion on existent plasters, the fresh cut method seems to be the easier to be performed in the laboratory and even in situ when new plasters or experimental samples of plasters are being applied.

The shear test presented significantly lower adhesion strength in comparison with the pull-off test. Nevertheless, in comparison with the adhesive strength obtained by Hamard et al. [10], that registered maximum values of 0.047 N/mm², 0.029 N/mm² and 0.028 N/mm² when testing three earthen plasters on a cob wall, it can be supposed that results obtained by the described shear test should not be quantitatively compared with the ones of pull-off. Therefore, more studies are needed using this test procedure so that more results can be compared.

Particular attention has to be taken on demoulding and cutting the samples of the dry mortar. Therefore, in following test campaigns, particularly when considering this shear test method, the moulding and the cutting must be optimized. For the time being the test is a good possibility for comparison between small samples for hypothesis of replacement plasters and renders tested on a real building, when a mechanical equipment is not available. It was easily performed on both brick and adobe supports and, as the pull-off test, the grout application has also positive effect on adhesion strength. In following experimental campaigns the test should be performed with the brick longest dimension oriented horizontally in order to assess the influence of the brick surface grooves, that in the present study were vertically oriented, therefore aligned with the shear force.

Conclusions

Results show that an earth plaster even without high compressive strength can perform well in terms of shrinkage and present efficient performance regarding adhesion on both substrates studied (brick and adobe). The preliminary preparation of the support with a clay

grout/slurry is advantageous to adhesion performance, regardless of the testing methods. The cutting and moulding/demoulding procedure of the samples influences the test results. The relative humidity increment has a negative effect, decreasing the adhesion capacity, but even a high percentage does not compromise the stability of the plaster adhesion. The shear test proved to be a valid instrument mainly to compare experimental mortar samples that are being tested *in situ* for repair intervention when a pull-off device is not available. For testing existent plasters *in situ* the harden cut pull-off test is less destructive than the shear test (because the latter implies the removal of adjacent areas of the plaster sample) and is the only that can assess cohesive rupture by the support, assessing compatibility between the plaster and the support. For laboratory testing the pull-off test with previously fresh cut samples seems to be the most appropriate.

It is possible that similar conclusions can be enlarged to similar low strength plasters, such as air lime-based ones.

References

1. Melià P, Ruggieri G, Sabbadini S et al (2014) Environmental impacts of natural and conventional building materials: a case study on earth plasters. *J Clean Prod* 80:179-186
2. Faria P, Lima J (2018) *Earthen plasters* (in Portuguese). Argumentum, Lisbon
3. Santos T, Faria P, Silva V (2019) Can an earth plaster be efficient when applied on different masonries? *J Build Eng* 23:314-323
4. Lima J, Faria P, Santos Silva A (2016) Earthen plasters based on illitic soils from Barrocal region of Algarve: Contributions for building performance and sustainability. *Key Eng Mat* 678:64-77
5. Delinière R, Aubert JE, Rojat F et al (2014) Physical, mineralogical and mechanical characterization of ready-mixed clay plaster. *Build Environ* 80:11-17
6. Faria P, Santos T, Aubert JE (2016) Experimental characterization of an earth eco-efficient plastering mortar. *J Mater Civil Eng* 28(1):04015085
7. Matos Silva C, Flores-Colen I, Gaspar S (2013) Numerical analysis of renders' adhesion using an interface model. *Constr Build Mater* 38:292-305
8. EN 1015-12 (2016) *Methods of test for mortar for masonry. Part 12: Determination of adhesive strength of hardened rendering and plastering mortars on substrates*. CEN, Brussels
9. DIN 18947 (2013) *Earth plasters – Terms and definitions, requirements, test methods* (in German). DIN, Berlin

10. Hamard E, Morel JC, Salgado F et al (2013) A procedure to assess the suitability of plaster to protect vernacular earthen architecture. *J Cult Herit* 14(2):109-115
11. Airaghi C, Botteon D, Canziani G et al (2014) EN 1015-11 and EN 1015-12: Proposal to update procedures for lime products. 9th International Masonry Conference, Guimarães.
12. Stolz C, Masuero A (2012) Influence of the real contact area of rendering mortars on shear strength adhesion (in Portuguese). 4^o Congresso Português de Argamassas e ETICS, Coimbra.
13. Röhlen E, Ziegert C (2011) *Earth building practice*. Beuth Verlag GmbH, Berlin
14. EN 1015-1 (1998) *Methods of test for mortar for masonry. Part 1: Determination of particle size distribution (by sieve analysis)*. CEN, Brussels
15. EN 1097-3 (1998) *Tests for mechanical and physical properties of aggregates. Part 3: Determination of loose bulk density and voids*. CEN, Brussels.
16. Santos T, Nunes L, Faria P (2017) Production of eco-efficient earth-based plasters: Influence of composition on physical performance and bio-susceptibility. *J Clean Prod* 167:55-67
17. LNEC FE Pa 39 (2002) *Wall coatings. Test of water absorption under low pressure (in Portuguese)*. LNEC, Lisbon
18. EN 16302 (2013) *Conservation of cultural heritage. Test methods. Measurement of water absorption by pipe method*. CEN, Brussels
19. EN 1015-3 (1999) *Methods of test for mortar for masonry. Part 3: Determination of consistence of fresh mortar (by flow table)*. CEN, Brussels
20. EN 1015-6 (1999) *Methods of test for mortar for masonry. Part 6: Determination of bulk density of fresh mortar*. CEN, Brussels
21. EN 1015-10 (1999) *Methods of test for mortar for masonry. Part 10: Determination of dry bulk density of hardened mortar /A1*. CEN, Brussels
22. EN 14146 (2004) *Natural stone test methods. Determination of the dynamic modulus of elasticity (by measuring the fundamental resonance frequency)*. CEN, Brussels
23. EN 1015-11 (1999) *Methods of test for mortar for masonry. Part 11: Determination of flexural and compressive strength of hardened mortar*. CEN, Brussels
24. García-Vera V, Lanzón M (2018) Physical-chemical study, characterisation and use of image analysis to assess the durability of earthen plasters exposed to rain water and acid rain. *Constr Build Mater* 187:708-717

25. Lima J, Faria P (2016) Eco-efficient earthen plasters. The influence of the addition of natural fibers. *Natural Fibres: Advances in Science and Technology Towards Industrial Applications. From Science to Markets*. R. Figueiro, S. Rana (Eds.). Springer, RILEM Book Series 12:315-327

Similar appearance of mortar and brick masses in Algiers Casbah houses during the Ottoman period (16th - early 18th centuries)

Semha Bernou¹, Tsouria Kassab¹, Rosa Bustamante², Francisco Fernández²

(1) Polytechnic School of Architecture and Urbanism (EPAU-Algiers), semha.bernou@gmail.com, tsouriakassab@yahoo.fr

(2) Universidad Politécnica de Madrid (UPM), rosa.bustamante@upm.es, francisco.fernandezm@upm.es

Abstract

The mixture of traditional mortars used in the houses of the Algiers Casbah during the Ottoman period (16th-early 18th centuries) has a similar appearance to the bricks mass. Grains of fired crushed ceramics of 5 mm or more, pebbles from sedimentary stones, shale, remains of nummulite limestone from the Algerian Atlas, and ashes from the lime calcination can be found in the mixture. The mortar joints were applied to the mixed masonry walls in layers that were thicker than or equally thick to the rows of bricks, whereas in the floors they are layered in thick beds interspersed with bricks until reaching 30-40 cm. Unhydrated lime lumps are encountered due to the artisanal mixing with limited water amounts to maintain a compact mortar. The Reddish colour of these earth-based mortars stems from the use of quartz, sand with illite, hematite and other components detected by XRD, EDXRF and DTA tests carried out on material samples. In light of this study, it is concluded that the Roman tradition of using lime and fired crushed ceramics is maintained in the earth-based mortars of the Ottoman period; knowing that their appearance is similar to the bricks one can argue that the bricks look like a baked mortar.

1. Introduction

The Casbah of Algiers is located within the current capital's bay at 120 m above sea level. Endowed with a Permanent Safeguarding and Presentation Plan that occupies a surface of 105 ha, it is divided administratively in six residential neighbourhoods, where great mosques, markets, public baths, historical houses and a citadel are amongst its most important buildings (Figure 1). The urban growth of the Medina was based on hydrographic units; each one was autonomous in terms of rainwater drainage system, which indicates its size by the end of the Arab-Berber period (950-1516). The Ottoman occupation took advantage of this urban layout (1516-1830) and strengthened the fortifications system upgrading thus Algiers, from a medieval marginal city to a Mediterranean capital [1].

Subsequently during the French colonization, the historic centre Casbah suffered a transformation process through the enlargement of its main streets, which led to the demolition and replacement of the traditional facades lining the roads [2]. Considering that building materials used in the conservation of the Casbah must be compatible with the

existing ones [3], this study provides information about the construction techniques and materials implied during the Ottoman period. It consists of analysing the traditional mortars and bricks used in the houses that did not undergo transformations and are therefore considered original and authentic.

2. Constructive systems of the traditional Casbah house

The traditional house is usually introverted according to the Muslim culture principles, with a chicane entrance to the patio where the water-well is located [4, 5]. The rooms are organized around a central courtyard on two floors, with lattice windows and doors opening to a gallery of arcades supported by stone columns and a terrace overlooking the Mediterranean Sea (Figure 3). However, this stepped design adjusting to the site topography was altered by the French vertical densification (1830-1962).

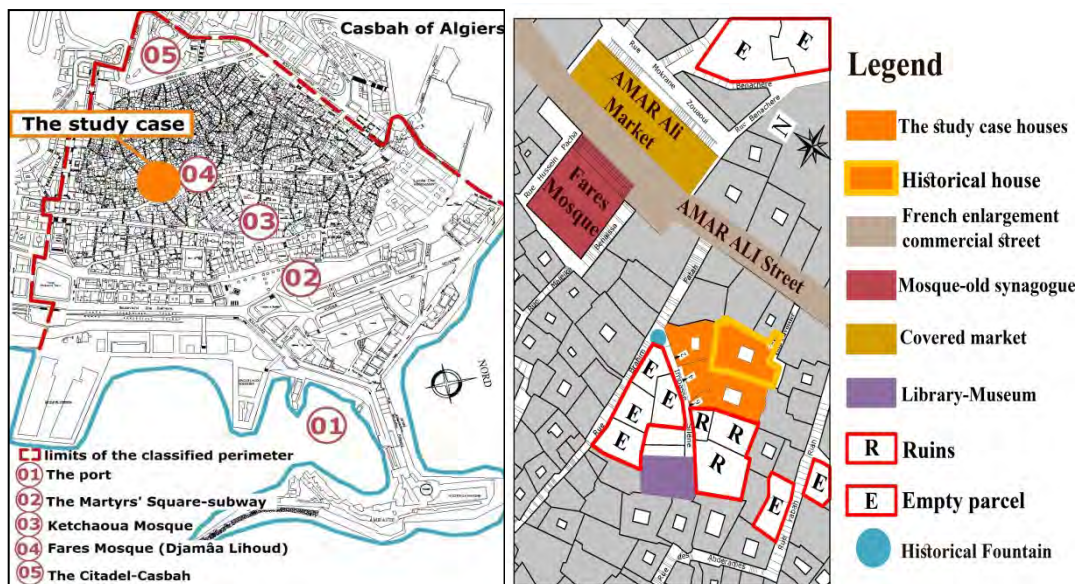


Figure 1. Left, the Casbah of Algiers. Right, location of the study case houses.

2.1 Masonry walls, ceilings and floors

The materials used in the construction of the Casbah houses came from the nearby environment notably the quarries of Bâb el Oued Faubourg later known as Jaubert extraction site during the French period (Figure 2), except for the ceramic wall tiles that were imported from Tunis, Italy, Spain and Netherlands [6]. The thickness of the walls varies 40-90 cm; they were made of bricks or mixed masonries (*opus mixtum*), adding rubbles or blue stones, with the bricks arranged horizontally or to 45° (*opus spicatum*) and the mortars applied in broad layers like to the brick's thickness.

In the masonry construction work, besides the discharge arcs, round logs of Barbary Thuja (*tetraclinis articulata*) are inserted every 0.80-1.20m to reinforce the bearing walls against seismic solicitations [7], also acting like wall ties. Usually, the roofing systems of 30-100 cm in section, consists of large earthen and lime-based mortar layers inserted with brick beds,

arranged on top of wooden sheathing supported by Thuja logs. Sometimes, calcareous stones of less density were used instead of the bricks, the same constructive system can be found in the terraces. In Turkey, the use of pumice stone in earthen mortars to lighten and mitigate the heat flow in the covering systems of the 13th century is a known masonry practice [8].



Figure 2. Left: Plan of Algiers and its surroundings in 1808 by BOUTIN. Right: Lime Kiln of the Faubourg Bab el Oued in 1838 by Adolphe OTTH (BNF-Gallica archives).

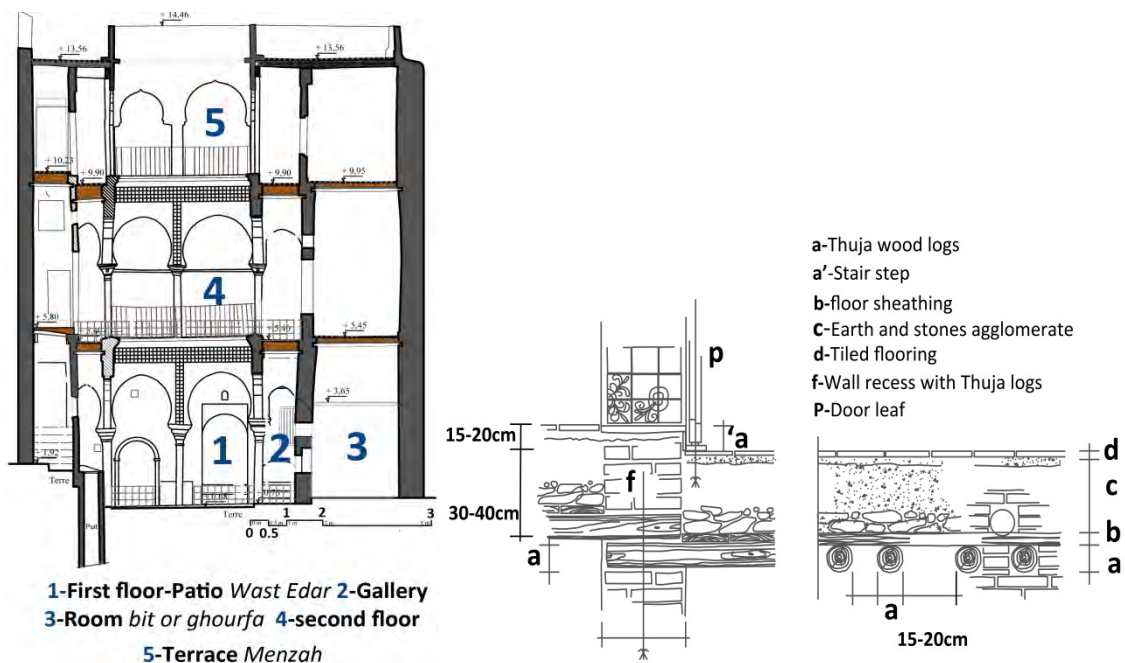


Figure 3. Left: Cross-section of a traditional house (Ali PACHA Agency). Right: Constructive system of ceilings/floors [9].

2.2 Mortars and bricks

The masonry mortars are generally of reddish or earth tones, with big rubbles of fired crushed ceramics (size 2mm-1.5 cm) in and sedimentary detritus from the Algerian Atlas, nummulite limestones remains, shale and ash. The mortars containing lime nodules and

brick dust, or grains are known as *Khorasan* mortar in Turkey, *Surkhi* in India and are called *Cocciopesto* in ancient Rome [10, 11]. Fragments of recycled waste pottery and sometimes bones are found in the bedding mortar masses (Figure 4). The granulometry is variable, thin sand has a maximum size of 4 mm and pebbles of 5 mm or more. The presence of non-hydrated lime lumps is due to the artisanal mixing of the mortars, but especially to mixing a reduced amount of water maintaining an almost dry consistency and possibly using formwork panels during the mass application and hardening.

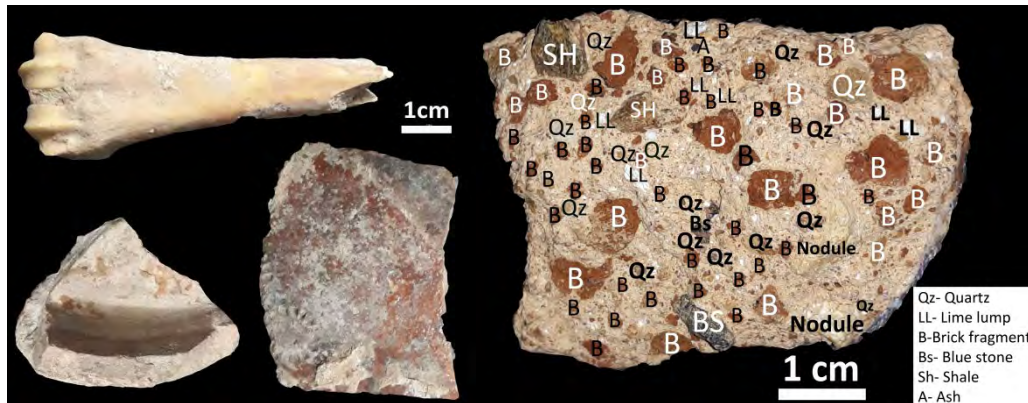


Figure 4. Left: Fragments of waste pottery, ceramic and bones added to the bedding mortar masses. Right: Microscopic characterization of sample M4.6.E1b, an elevation mortar.

On the other hand, brick dimensions are 25x12 cm; usually their thickness is less than 4cm. According to a previous research about mortars in the Citadel of Algiers and a Casbah house, the ratio between the lime binder and aggregates in mortar joints is one volume of lime per two of sand (1: 1.5 - 2), and one volume of crushed bricks, adding organic additives like olive oil and eggs in the walls rendering mixtures [12]. Generally, waste bricks and tiles are used to increase the mixture volume and to get a pozzolanic mortar with the finest grains [13].

3. Materials and methods

3.1 Sampling materials

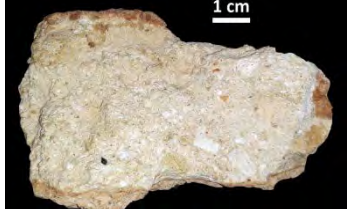
Four attached houses under current restoration works define our study area. They form an interlocked cluster located in the lower Casbah (Figure 1), on a commercial street resulting from a French enlargement of the medina's organic fabric, near an old synagogue converted into a mosque, a market hall and a historical fountain, their entrance is on a dead-end street. The corpus presents different states of conservation: a well-preserved martyr house (related to the Algerian revolution against the French occupation) and three partially collapse ones, due to the 2003 earthquake and a bombing incident during the colonization. Nine samples were collected composed of five bricks and four mortar fragments from various parts and levels of the houses. They were located on the data sheet below (Figure 5).

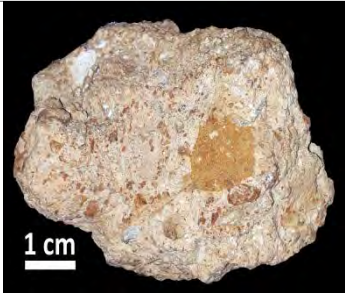
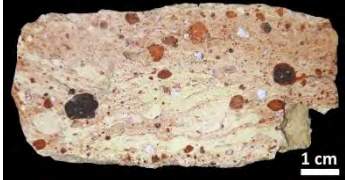
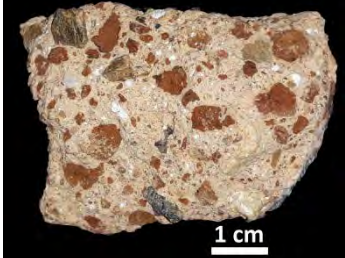
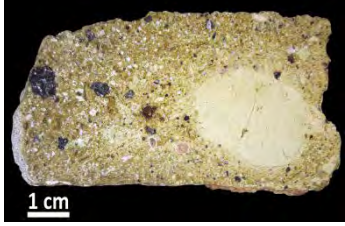


Figure 5. Data sheet of the house layout and the collected samples position

Non-destructive sampling protocol was carefully applied on bearing walls (main facade, inner partitions) and floors [14] from seriously damaged areas. Due to the lack of historical documentation and archives access, it is difficult to determine the construction date of the houses and the possible transformation phases they went through with accuracy, but the period is generally between the middle of 16th to early 18th centuries.

Table 1. Samples visual aspect and their location inside the construction.

House	Sample code	Material	Situation	Visual aspect
3 Imp Lavoisier	M1.3.E4a	Brick	 <p>Terrace Ceiling</p>	
3 Imp Lavoisier	M1.3.E4b	Mortar		
2 Imp Silène	M2.2.E8a	Brick	 <p>Bearing wall</p>	

House	Sample code	Material	Situation	Visual aspect
2 Imp Silène	M2.2.E23a	Mortar	 Inner Partition wall	
4 Imp Silène	M3.4.E19a	Brick	 Bearing neighbouring wall	
4 Imp Silène	M3.4.E20b	Mortar		
6 Imp Silène	M4.6.E1a	Brick	 Elevation wall	
6 Imp Silène	M4.6.E1b	Mortar		
6 Imp Silène	M4.6.E20a	Brick	 Bearing wall	

3.2 Experimental methods

All samples were analysed and examined to determine the components, their dimensions, physical and chemical properties. For this purpose, different analytical techniques were applied in the characterisation the Casbah houses materials, among which X-ray diffraction (XRD) to identify the mineralogical composition, using a Siemens/Bruker D5000 instrument (40 kV, 40 mA), with a step of 0.03° and 4 s/step, from 10° to 80° in 2θ for the bricks. In the mortars, the X-Ray analysis was taken for the 2θ range of 4° to 100° to detect possible clay

minerals. The chemical composition of the bricks and mortars was determined by Energy-dispersive X-ray fluorescence spectrometry (EDXRF) using the S2 PUMA device on pressed pellets. Differential thermal (DTA) and Thermogravimetric analysis (TG) were realized in order to assess the samples hydraulic properties by examining the weight loss at certain temperatures using SDT-Q600 TA Instrument (RT to 900°C, at heating rate of 20°C/min, in air flow: 100 mL/min). Chromaticity analysis was conducted on both mortars and bricks by means of an 8 mm Portable Digital Colorimeter and the Munsell rock and soil colour chart. Preliminarily, the initial step of these procedures consisted of a visual assessment of the samples with the naked eye and via Dino light Edge digital microscope 1.3-5 MP resolution, observing their texture and shape, aggregates consistency and size, especially the organic particles that can sustain damage or crumble before and during the tests.

4. Results and discussion

4.1 Visual analysis and chromaticity of the samples

In order to obtain prior qualitative information about the properties of the mortar and brick samples, macroscopic analysis was performed to determine the bonding agent and aggregates type. According to the visual aspect, texture and colour of the bricks under study, three main groups are distinguished (Table 2): yellow, red and pale olive.

Table 2. Chromaticity analysis results.

Sample code	Material	Colorimeter measures			Munsell chart
		L	a	b	
-	-				-
M1.3.E4a	Brick	65.542	4.283	14.714	2.5Y 8/2 pale yellow
M1.3.E4b	Mortar	59.432	6.056	14.183	2.5Y 9/2 very pale yellow
M2.2.E8a	Brick	53.192	14.106	19.141	5YR 6/4 light reddish brown- interior
		52.152	5.508	12.084	2.5Y 8/3 pale Brown- brick's exterior
M2.2.E23a	Mortar	54.181	10.031	16.409	10YR 7/3 very pale brown-Mortar
M3.4.E19a	Brick	52.071	14.670	19.782	7.5yr 7/4 pink-brick's interior
		43.994	13.642	17.669	5YR 5/4 reddish brown-clay spreads
M3.4.E20b	Mortar	46.371	10.334	17.846	7.5 YR 6/4 light brown
M4.6.E1a	Brick	54.740	10.853	17.039	5yr 6/4 light reddish brown
M4.6.E1b	Mortar	51.110	9.724	16.267	10YR 7/4 very pale brown
		40.353	11.787	16.579	5YR 4/4 reddish Brown-Clay nodule
M4.6.E20a	Brick	34.844	2.921	13.731	5Y 6/3 pale olive-brick's interior
		65.151	3.730	20.041	10YR 6/4 light yellowish brown-exterior

The first group comprises sample M1.3.E4a made with a yellowish *impasto*, homogeneous and rich in medium to fine grains of quartz (size <1mm) and very occasionally crushed brick ballasts. The second group contains three heterogeneous samples (M2.2.E8a, M3.4.E19a and M4.6.E1a), varying from pale to reddish brown (Figure 6). Generally, the red coloured bricks

have a high iron contents while white or yellow colours are due to the high lime contents [15], which suggests a higher firing temperature. A white outer layer covers the brown-red matrix of the brick sample M2.2.E8a that contains medium to coarse quartz (size 1-3mm), shale and fired brick grains, while wavy yellow layers of clay spreads are packed in the paste matrix of sample M4.6.E1a, including an abundant quantity of crushed ceramic fragments (size 1-5mm). On the contrary, the presence of angular and rounded crystals of quartz in translucent pink or grey color is observed in large amounts compared to the crushed brick, in sample M3.4.E19a.

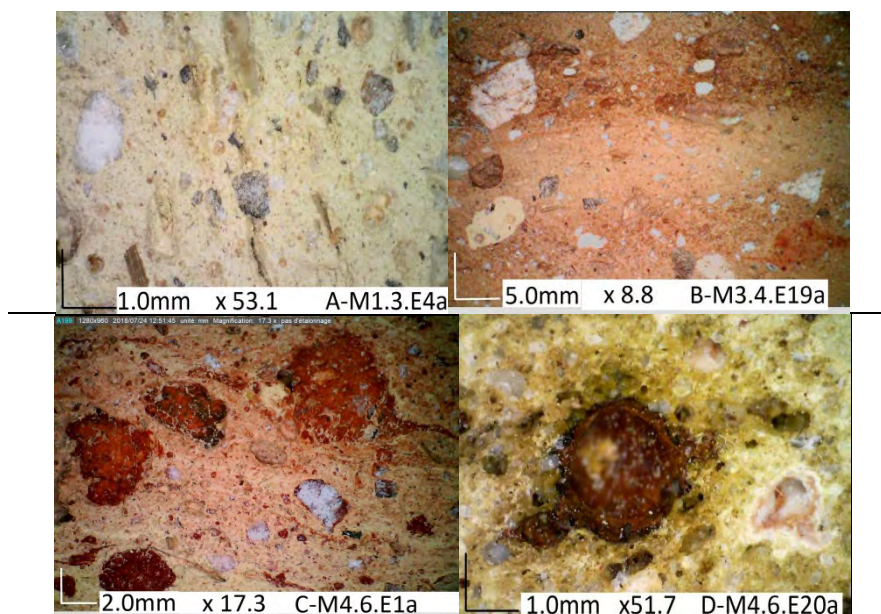


Figure 6. Macroscopic aspect of bricks. M1.3.E4a: yellow *impasto* with quartz grains. M3.4.E19a: yellow and red layers of clay with quartz, pebbles, shale and crushed ceramics. C-M4.6.E1a: Fired crushed ceramic fragments with dark reaction rings and quartz. D-M4.6.E20a: Fired crushed brick fragment in a pale olive paste showing dark reaction ring.

The last group includes sample M4.6.E20a, collected from one of the oldest parts of the house at the bottom of a neighbouring wall. This brick is pale olive with a yellow lump of the original clay matrix; this grain has dark reaction rings at the interface with the clayey matrix (Table 1), there are also quartz sand and dark fired crushed ceramics of medium to coarse size reaching 2 cm. On the other hand, the mortar specimens present similar aspects. Observed by the naked eye, they are all composed mainly of sand, lime, large visible crushed ceramic fragments used as coarse material additives and accessory minerals like quartz (Figure 7). Based on the colour of patina, the mortars are divided in two groups. Sample M1.3.E4b stands out from the other mixtures with its very pale yellow binder. The matrix has a very refined texture including rounded unhydrated lime lumps not exceeding 6mm in size, and small amounts of crushed ceramic fragments (size<0.5mm), while ash and fine-grained aggregates of quartz are found very occasionally, when compared to the other samples. It is noteworthy that another layer of brown reddish mortar was applied on top of this roof filling mixture to prepare the floor tiling (Figures 3, 7).

The second group contains samples M2.2.E23a, M3.4.E20b and M4.6.E1b, where the binders are reddish to pale brown and present different quantities and variation in the types of aggregates, their size and shapes. The occurrence of sand grains, quartz and pebbles particles, sub-rounded fired crushed ceramics (size 0.5-3mm), and unhydrated lime lumps (size 0.5-4mm) is found in sample M2.2.E23a. Evident ballast of brick of 1.2mm in length is observable with no reaction rings and a good cohesive aspect with the pale brown matrix. Sample M3.4.E20b shows crystals of quartz, shale (size 4-8mm) and crushed ceramic fragments engrossed in a reddish matrix ranging from clay to sand.

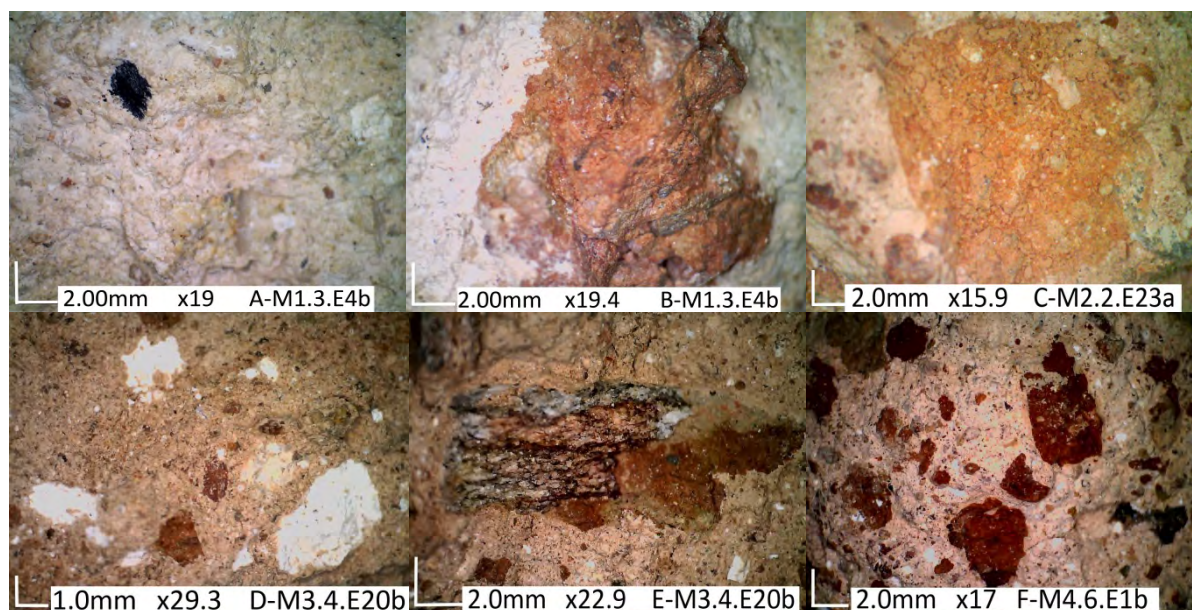


Figure 7. Visual aspects of the mortars. A-M1.3.E4b: yellow *patina* with quartz grains, lime lumps and ash. B-M1.3.E4b: layer of reddish bedding mortar covering the filling mixture. C-M2.2.e23a: coarse crushed brick fragment in a brown mortar matrix. D-M3.4.E20b: medium lime lumps and fine to coarse fired brick clasts, E-M3.4.E20b: shale and crushed brick fragment. F-M4.6.E1b: fine-grained quartz and lime nodules, subangular brick clasts.

Sub-angular and Rounded lime masses appear in large amounts up to 4mm in length, indicating that the lime was dry-slaked using a small amount of water. The shale and blue stones are extracted in-situ according to their abundance during the earth and foundation works of the house. Differently from the other samples, M4.6.E1b has rather an important quantity of sub-angular crushed bricks in medium to coarse size (1-8mm), in addition to quartz, blue stone and ash. Boundary reactions are observed at the interface between these particles and the binder. In roman times, the coating lime mortars used in water related structures or buildings located in areas with high humidity contained pozzolanic material like crushed ceramics, tiles and pottery fragments [16]. This specimen was collected from the exterior façade, highly exposed to climate conditions.

4.2 Mineralogical and chemical composition of the samples

This visual examination was contrasted with data from X-ray diffraction analysis on both mortar and brick samples whose main components are indicated in Table 3.

The XRD patterns of the bricks indicate that quartz and calcite are the main dominant components of the matrix, with the presence of feldspars and plagioclase (Albite and Anorthite) in small amounts, phyllosilicates (muscovite) as accessory minerals. The yellow and red bricks are mineralogically different.

Table 3. Results of XRD analysis

Sample	Qz	Cal	Ms	He	S	Fs				Gh	Di	β-c	CM		Ah
						Ab	An	Mc	A				K	I	
M1.3.E4a	+++	++	-	±	-	±	±	-	-	+	+	-	-	-	-
M1.3.E4b	+	+++	-	-	-	-	-	-	-	-	-	-	-	±	-
M2.2.E8a	+++	++	±	+	-	±	-	±	-	+	+	-	-	-	-
M2.2.E23a	+++	+++	±	-	-	±	-	±	-	-	-	-	±	-	-
M3.4.E19a	+++	++	±	-	-	±	-	±	-	-	-	-	-	-	-
M3.4.E20b	+++	++	±	-	±	±	-	-	±	-	-	±	±	-	-
M4.6.E1a	+++	++	-	+	-	-	-	-	±	-	+	-	-	-	-
M4.6.E1b	+++	++	+	±	-	+	-	+	-	-	-	-	-	-	-
M4.6.E20a	+++	++	-	-	-	-	-	-	±	-	+	-	-	-	-

Qz=Quartz, cal=Calcite, Ms=Muscovite, He=Hematite, Fs=Feldspar (Ab=Albite, An=Anorthoclase, Mc=Microcline, A=Anorthite), Gh=Gehlenite, Di=Diopside, β-c=Cristobalite beta, CM= Clay minerals (K=Kaolinite, I=Illite), S= Siderite, Ah= Anhydrite.

+++ Very abundant, ++ abundant, + present, ± scarce, - not detected.

The presence of calcium silicate diopside can explain the yellowish color of the first group (M1.3.E4a), suggesting the existence of carbonate, which inhibits the development of iron oxides, they were presumably made from calcareous kaolinic or illitic clays. The second group (M2.2.E8a, M3.4.E19a and M4.6.E1a) has hematite providing the red color of the bricks (Figure 8). Indeed, the formation of iron oxides by recrystallization during the decomposition of the phyllosilicates demonstrates that these bricks were fired around 850°C. Calcite peaks are detected in all samples showing that the firing temperature of the bricks is between 700 and 900°C. The Gehlenite is usually formed from 800°C; it appears in samples M1.3.E4a and M2.2.E8a. The feldspar evolved into Anorthite in samples M4.6.E1a and M4.6.E20.

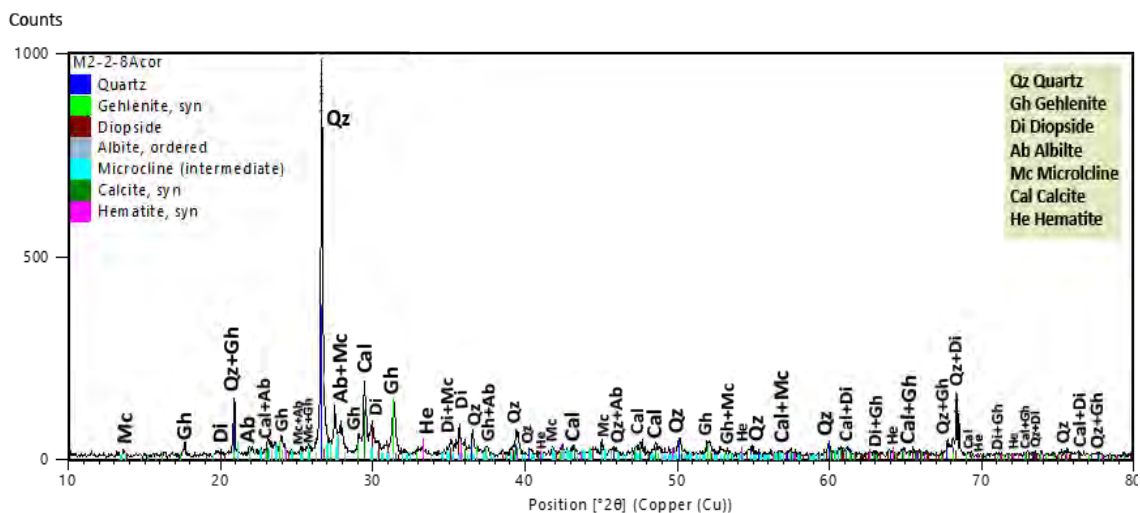


Figure 8. XRD pattern of brick sample M2.2.E8a.

The mineralogical composition of the mortar samples includes multiple crystalline phases. The most present minerals are calcite, quartz, feldspar, plagioclase and phyllosilicates such as kaolinite in samples M2.2.E23a and M3.4.E20b, while illite peaks characterize only sample M1.3.E4b. The latter portrayed a vitreous amorphous phase that is evident by the increasing slope observed at the range $2\theta = 10^\circ\text{--}20^\circ$ (Figure 9).

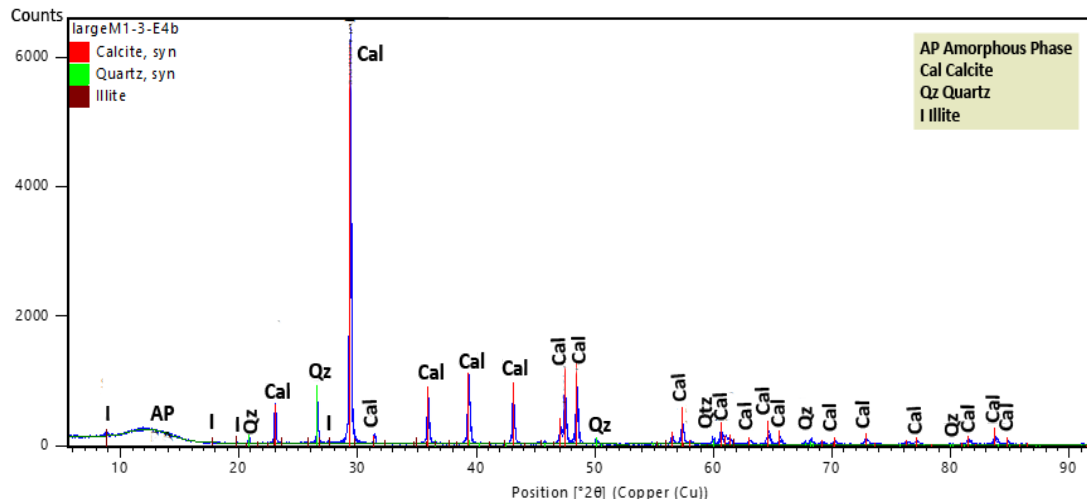


Figure 9. XRD pattern of mortar sample M1-3-E4b (ceiling).

Furthermore, the existence of Muscovite and Albite, likely due to the use of fired crushed ceramic fragments as pozzolanic additives, was found in almost all the samples apart from M1.3.E4b that was extracted from the ceiling of the last level in the house. Other components, such as Hematite was encountered in the reddish mixture of specimen M4.6.E1b, whereas the embedded anhydrite and siderite in M3.4.E20b stems probably from the clay minerals of the soil.

Meanwhile, oxide concentration has been obtained in the samples by XRF analysis and results are indicated in Table 4. Only the results of the M1.3.E4a and M4.6.E1a brick samples are reliable because magnesium oxide has not been detected in the others. In any case, these results would correspond to the use slacked hydrated air lime. The high amount of Fe_2O_3 in sample M4.6.E1a confirms the presence of hematite in red bricks.

Table 4. Oxide concentration in the samples (Wt. %) by XRF analysis

Sample	MgO	Al ₂ O ₃	SiO ₂	P ₂ O ₅	SO ₃	K ₂ O	CaO	TiO ₂	Fe ₂ O ₃
M1.3.E4a	0.48	12.37	52.79	0.41	0.71	0.92	26.25	0.45	5.23
M1.3.E4b	-	1.79	13.79	0.59	0.2	0.21	79.52	0.17	2.67
M2.2.E8a	-	11.11	49.45	0.92	0.3	2.65	25.11	0.78	8.86
M2.2.E23a	-	10.02	46.87	0.65	0.52	2.2	28.73	0.68	9.04
M3.4.E19a	-	7.84	46.12	0.46	0.66	1.86	30.58	0.86	10.44
M3.4.E20b	-	13.9	48.22	0.55	0.15	2.53	21.36	0.97	11.46
M4.6.E1a	0.3	11.84	52.76	0.69	0.72	2.19	18.03	0.96	11.13
M4.6.E1b	-	11.63	48.16	0.65	0.19	2.53	24.71	0.96	10.03
M4.6.E20a	-	7.87	49.35	0.73	-	1.91	29.36	0.73	9.04

4.3 Differential thermal and Thermogravimetric tests (DTA-TG)

In order to evaluate the hydraulic properties of mortar samples, TG/DTA tests were carried out. For this purpose, percentages of weight loss between RT (Room Temperature) and 120°C maybe due to humidity or to the dehydration of the sample. The weight losses between 650 and 800°C can be attributed to the decarbonization of the limestone. It is observed that the (CO₂/H₂O) ratio of the samples is lower than 10 [17]. According to this ratio in Table 5, two groups were identified; the first one contains sample M1.3.E4b, while the second includes samples M2.2.E23a, M3.4.E20b and M4.6.E1b with a close (CO₂/H₂O) ratio and better hydraulic properties compared to the first group.

Table 5. TG/DTA analysis results in mortars

Sample code	H ₂ O (%)	CO ₂ (%)	CO ₂ / H ₂ O
M1.3.E4b	0.76	4.07	5.53
M2.2.E23a	2.82	6.16	2.18
M3.4.E20b	2.38	6.16	2.58
M4.6.E1b	2.78	6.76	2.43

Results of Differential thermal (DTA) and Thermogravimetric analysis (TG) show the decomposition of calcium carbonate CaCO₃ (calcite phase) at 650° and conversion of quartz alpha to quartz beta at 577.23°C in bricks (Figure 10), determining their firing temperature at approximately 800-900°C. On the other hand, it is known that the same kilns were used for lime slacking and baking the bricks.

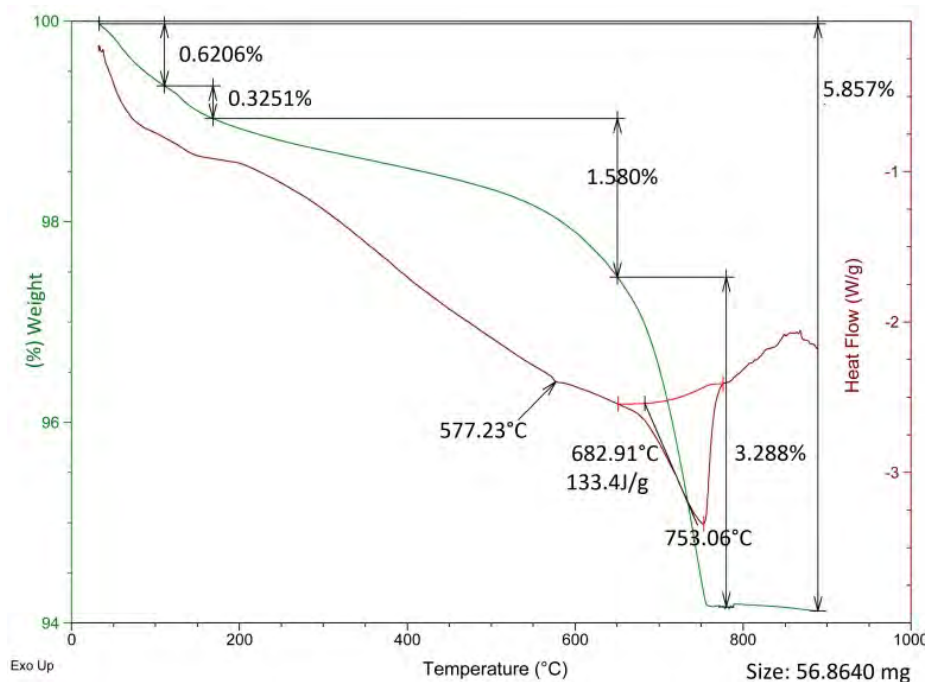


Figure 10. Thermal degradation curve of brick sample M2-2-8a

5. Conclusion

In this research, representative samples of mortars and bricks from the traditional houses of Algiers Casbah were investigated, allowing the following results:

a) The macro-scale analysis by microscopy and visual investigation of mortar and brick samples, has demonstrated its efficiency in observing the mass and particularly the heterogeneous granulometry of the crushed ceramics. Also, the size and distribution of the organic material, presenting overall a good compactness by the absence of interface cracks between the large clasts and matrix of fine grains, which is important for the constructive study.

b) The DRX results have shown that the mortars and bricks are composed mostly of calcite, quartz and other components from the soil in which the sand has been collected. Anhydrite was encountered in mortar M3-4-E20b extracted from an inner partition-bearing wall of a room that was not altered; while traces of illite were observed in floor mortar M1-3-E4b, which confirms the presence of unburned clay material.

c) This study classifies the mortar joint in the Casbah houses as “lime based mortar”, composed mainly by siliceous aggregates and calcitic slaked lime binder. The aggregate include quartz, pebbles, combined with shale or blue stone, occasionally ash and brick fragments as coarse additives (Muscovite). In addition to feldspars and phyllosilicates, three of the four mortar samples analyzed in this paper, present kaolinite, but it has not been detected in the bricks probably due to their firing treatment.

d) The fundamental difference in the mineralogical composition between bricks and mortars is that the former has diopside, anorthite or gehlenite, but the latter do not.

e) The brick samples M4-6-E1a (elevation) and M4-6-E20a (room) present the same major components except that the first one have hematite; they could have the same age, but their firing in oxidizing atmosphere may have produce the whitish appearance in the first sample and the unidentified amorphous materials in the second.

f) In some bricks, the outer white layer hypothetically may come from the lime beds used in the kilns used for baking and drying the bricks or may have formed during the firing process in the same kilns. However, the presence of calcite in all of them has been confirmed in the tests.

g) Artisanal kneading and mixing may have led to the disparity and heterogeneity in the clay matrix, forming layers or lumps of raw materials. In general, the firing temperatures of the bricks did not exceed 900 °C.

h) The use of lime and crushed ceramics as pozzolanic additives in the mortars and bricks, confirm their similar appearance and that the masons prepared similar mixtures for both of them.

i) Finally, the obtained data could be useful to produce compatible repair mortars in the restoration and consolidation works of the masonry in the Casbah of Algiers upon further investigation.

Acknowledgment

The authors would like to express their gratitude to National Agency of safeguarded sectors ANSS-Algiers for allowing the samples collecting and providing required assistance, the Algerian Ministry of culture for authorizing their transportation to Spain. We also acknowledge Ali PACHA Agency the restoration project manager in our study case and their junior architect DJIDI Smail for their valuable contribution, by supplying the architectural surveys and the technical information in situ. We also thank Khadidja GUELLIL from the research and development center CRD-Sonatrach.

References

1. Boulefaa ET, Kassab T (2018) Relief Morphology and Urban Hydrography as Historic Sources: Algiers in the Beginning of the Ottoman Period. *International Journal of Historical Archaeology*. doi: 10.1007/s10761-018-0459-0
2. Piaton C, Lochard T (2017) Architectures et propriétaires algérois, 1830-1870. In: IREMAM (ed) *Propriété et société en Algérie contemporaine. Quelles approches?*. Aix-en-Provence. doi: 10.4000/books.iremam.3686.
3. Algerian Ministry of culture (2011) Plan for the safeguarding and enhancement of the Safeguarded Sector of the Casbah of Algiers-PPMVSS, regulatory requirements. Non-published.
4. Missoum S (2003) *Alger à l'époque ottomane, la médina et la maison traditionnelle*. INAS, Alger.
5. Disli G (2014) Sustainability of Historic Building Systems: Anatolian Sejuk and Ottoman Hospitals. *APT International Bulletin of the Association for Preservation Technology Vol. XLV*, 4:45-51.
6. National center of Studies and Applied researches in Town planning CNERU (2007), Plan for the safeguarding and enhancement of the Safeguarded Sector of the Casbah of Algiers-PPMVSS, Manual of architectural, architectonic and constructive typologies. Non-published.
7. Novelli VI, D'Ayala D, Makhloufi N, Benouar D, Zekagh A (2005) A procedure for the identification of the seismic vulnerability at territorial scale. Application to the Casbah of Algiers. *Bull Earthquake Eng*. doi: DOI 10.1007/s10518-014-9666-1.

8. Önge Y (1995) Anadolu'da XII-XIII. yüzyıl Türk hamamları, Vakıflar Genel Müdürlüğü, Ankara.
9. Ravéreau A (1989) La Casbah d'Alger, et le site créa la ville. Sindbad, Paris.
10. Oguz C, Turker F, Kockal NU (2014) Construction Materials Used in the Historical Roman Era Bath in Myra. The scientific World Journal. doi.org/10.1155/2014/536105
11. Böke H, Akkurt S, Ipekoğlu B, Uğurlu E (2006) Characteristics of brick used as aggregate in historic brick-lime mortars and plasters. Cement and Concrete Research. doi: 10.1016/j.cemconres.2006.03.011
12. Mahindad Abderrahim N, Hamiane M (2016) Characterization of mortars from the Ottoman period in Algiers (Algeria) through their physical and chemical properties, International Journal of Physical Sciences. doi: 10.5897/IJPS2016.4505.
13. Binic H, Akcan M, Aksogan O and Resatoglu R (2017) Physico-chemical and mineralogical study of ancient mortars used in Harran area (Turkey). Advances in Concrete Construction Vol. 5: 639-658. doi: 10.12989/acc.2017.5.6.639.
14. CEN (2012) EN 16085 Conservation of Cultural property. Methodology for sampling from materials of cultural property. General rules.
15. El-Midany AA, Mahmoud HM (2015) Mineralogical, physical and chemical characteristics of historic brick-made structures. Miner Petrol. doi: 10.1007/s00710-015-0406-2.
16. Elsen J (2006) Microscopy of historic mortars—a review. Cement and Concrete Research. doi: 10.1016/j.cemconres.2005.12.006
17. Moropoulou A, Bakolas A, Bisbikou K (2000) Investigation of the technology of historic mortars. Journal of Cultural Heritage 1: 45–58.

Macroscopic high resolution techniques to the characterization the mortars structures in the Sé-Cathedral's archaeological complex in Idanha-a-Velha (Portugal)

Pablo Guerra-García¹, Jorge Morín de Pablos², Isabel Sánchez Ramos³

(1) Universidad Politécnica de Madrid, p.guerra.garcia@gmail.com

(2) Auditores de Energía y Medio Ambiente SA, jmorin@audema.com

(3) Institute of Archaeology, University College London, i.sanchez@ucl.ac.uk

Abstract

The archaeological site of *Santa Maria's Sé-Cathedral* is located in the parish of Idanha-a-Velha (Portugal). Roman *municipium* in High Imperial Era, when structures dated to the First and Second Centuries AD are documented, it appears that this city was known as *Ciuitas Igaeditanorum* and developed a reputation along the Fourth Century AD. as a new Episcopal See. In this moment a Christian cult building was erected from another one in an earlier structure. This last building persists even in Islamic Period, at the same time that another new Mozarabic structure that was added to the complex at the end of the Ninth Century. Given the presence of numerous phases of occupation and therefore, a several techniques and materials construction, archaeological direction decided to analyze some constructive elements like mortars present in joints, coatings and plasters of different rooms. Different macroscopic techniques were developed using high resolution images taken from, combined with the use of software that analyze the data obtained from colorimetries test and the spectral analysis from the mortars cross sections. Relevant results have been obtained in relation to the quantitative characterization and the composition of each mortar.

Introduction

The building known as *Santa Maria's Sé-Cathedral* has several structures overlapping each other, which respond to the long occupation of the settlement over the centuries. Along this time, building materials and areas were amortized [1]. In this respect structures from Roman Era was documented outside the liturgical building, the epicentre of the archaeological area of *Paço dos Bispos*. Meanwhile walls and foundations of different chronologies coexist beneath the foundations. The importance of the bishopric mentioned as *Egitania* by written sources is supported by the well-done manufactures, especially in the works of quarry with the presence of capitals and high quality ornaments. On the contrary manufactures of worse quality are appreciated, especially in coatings where the work seems as simples plasters of mud pressed and mixed with fine aggregates. Both work qualities should not be in relation with a chronological period, but maybe could be in relation to a constructive moment in which, either due to lack of resources or due to lack of knowledge, builders and bricklayers did not take care in finishes.



Figure 1. Location of the *Paço dos Bispos* site in the town of *Idanha-a-Velha* (Portugal), where the *Sé-Catedral* is located. Source: GoogleMaps.

The interest to analyze the mortars of this archaeological settlement comes from the need to improve the knowledge of the rural enclaves that have suffered changes throughout the history as *Medina Albalat* Islamic Period settlement (Romangordo, Cáceres), or *Los Hitos* archaeological complex (Arisgotas-Organza, Toledo) [2]. In relation with the mortar analysis, it has been carried out a simple method based on taking high resolution photographs and in the processing of images through software's that were designed for biomedicine and technical works. The use of this software allows to develop simple granulometries of the cross sections without chemical products that could affect the original material.

Methodology and samples

Sampled and proceeded

The sampling phase followed standard procedures in respect of extraction, which was carried out by manual means. According with the sampling process, rules established by the *RILEM* organization and the published recommendations in *Practical Sampling of Historical Mortars* were followed. In our case, extraction and stored were developed using appropriate tools (little chisel and spatula) as guidelines indicates [3]. Although the procedure is similar to archaeological works in terms of collection and documentation (graphic and photographic), some actions require a minimum knowledge about treatment and handling (plastered and painting layers, whitewashed walls...) [4].



Figure 2. Detail of some sampling points, inside the exterior (north façade) of the building.

After choose the areas of analysis, and once the extraction points was selected, outside layers of mortars were removed with a spatula, in order to eliminate organic components and other materials that could alter the test. The samples selection was chosen by the archaeological direction in relation with the structures and the chronological sequence of the complex, choosing structures from the beginning of the foundation to the latest phase of occupation. Afterwards the bagging of the samples was carried out using the appropriate instruments, as explained in some of the studies consulted [5].

Once in the laboratory, the samples were processed in order to facilitate both the macroscopic visualization and the subsequent preparation of the test-tube and the thin sections. As in the previous phase there are precedents referring to the standard guidelines for the preparation of this test-tubes [6].

The manufacture of the test-tube consists in cutting the samples through a diamond disk or cutting edge to achieve the shape of a cube with dimensions of between 1 and 2 cm each side. The cuts were carried out with a radial with hydraulic pump and dry mechanical cuts. Finally in the surfaces was developed a polishing treatment with blade disc between 600 and 1800 grain-fine. Thanks to this process a polished planes were generated, in which the lime matrix, the aggregates, the ceramic additions and other components were perceptible clearly. This procedure has also been carried out recently in the development of a mortars catalogue for a doctoral thesis [7].



Figure 3. Sequence of preparing the IV8 sample.

In this process neither chemical product nor organic products such as waxes or resins has been applied. The cleaning of the samples was done at first, by dry mechanical cleaning in order to avoid the loss of organic components (pigmentation, additives). Finally, a cleaning with distilled water was applied. The process of cleaning could be done with samples that kept enough consistency and samples that had the enough thickness to allow the following tests. Acronym of the samples was IV, followed by an increasing numbering.

Macroscopic Characterization

The macroscopic characterization consists in the visual analysis of an object or element through optical magnification with reflected light. In our case a characterization of raw and polished samples has been developed after a photographic treatment of the pictures. This helps in the way of make the view clear of the components such as aggregates, or main characteristics like microstratigraphy. The photographic processing have a long history in the field of research with examples based on raw materials [8] or even on thin sections of mortars [9].

In this way one of the most interesting works was developed in the Church of *Santa María* in Évora (Portugal) by the team of the University of Évora and the *Laboratório Nacional de Engenharia Civil de Lisboa*. The samples of mortar were analyzed by means of a stereomicroscope, being able to specify the kind of aggregates as well as lime nodules and other additions [10].

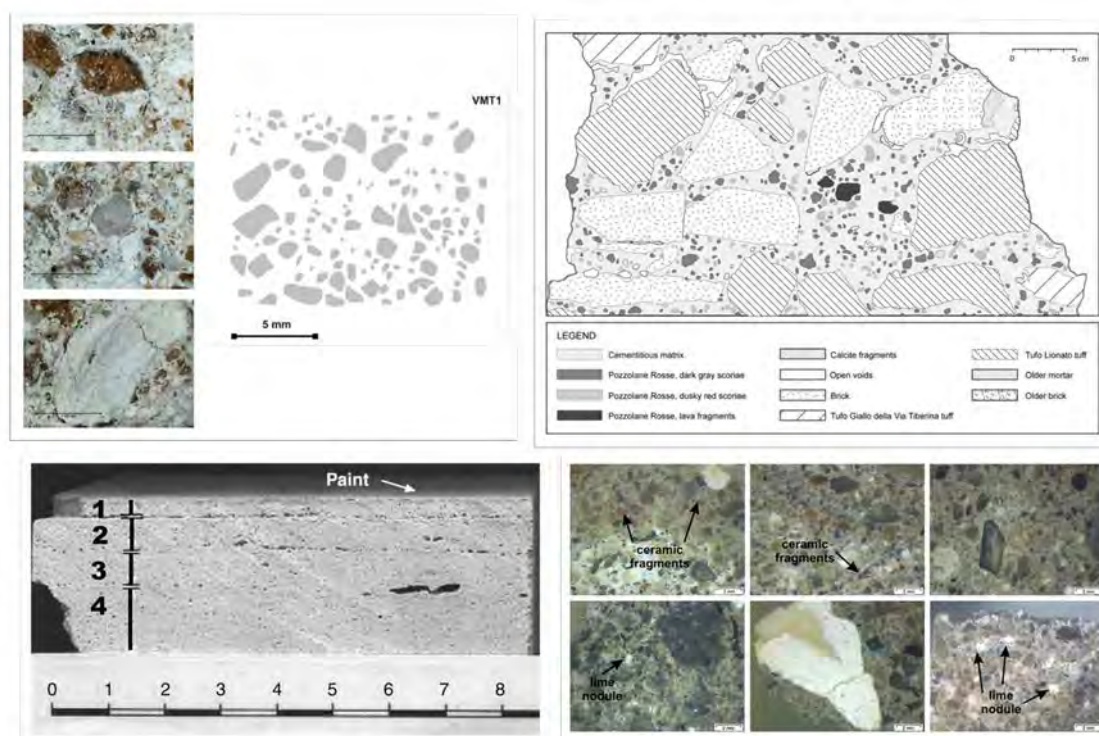


Figure 4. Different works based on the macroscopic characterization, from left to right and from top to bottom: Roman villa of Villamanta (Community of Madrid, Spain) [11], Market of Trajan in Rome (Italy) [12], Church of San Manuel and San Benito (Community of Madrid, Spain) [13] and Church of Santa María (Évora, Portugal) [14].

Once the test-tubes were prepared, a characterization was developed by means of a binocular lens or stereomicroscope, by which the primary components of the mortars were identified (aggregates, decorations, additives, microstratigraphy, intrusions). There are many advantages with the observation through binocular lenses: a real and detailed view of the materials without disturbing elements; testing the components and their distribution on the matrix, their geometric configuration; and even the superficial organic and inorganic pathologies. In this respect the preparation of the samples in cubes with polished surfaces was fundamental in order to differentiate the elements inside the mortar, as indicated above. There are bibliographic references where have used macroscopy as method of characterization, for example in Portugal too, as is the case of macroscopic studies in Évora [15], in the Pamplona Cathedral [16], or in *Volubilis* Roman settlement (Morocco), where mortars were tested through a simple macroscopy [17].

Secondly, a granulometric analysis was developed. This procedure, which also has a wide research background, analyzes the distribution of the components in the mortar and its vectorization: in short, its distribution in the area inside the mixture. Knowing the metric quantification obtained from the aggregates allows to determine the selection of the components in the mixture: the size of pottery and ceramic grains, the presence of bigger/smaller sand, graves, bones... Also this method is useful to know if the mortar was made carefully (well-done selection of aggregates with homogeneous average size) or was made neglected (aggregates with irregular selection and heterogeneous average size). These results allows to distinguish one hand from another in relation with the aggregates in the

manufacturing process. Highlights in the bibliography consulted the work of Ricciardi, who develops granulometries in mortars of Medieval Age, obtaining interesting results thanks to the comparison of the dimensions of aggregates, combining with Differential Thermal Analysis [18].

Samples

The total number of mortars sampled was 8. From 1 to 5 were taken from inside of Sé-Cathedral, while 6, 7 and 8 samples were taken from the outside. Below in the table showing the description of the sampling-points:

Table 1. List of samples taken and the location.

Sample	Location
IV1	Interior of the church. Column base joint.
IV2	Interior of the church. Joint of the main chapel and triumphal arch.
IV3	Interior of the church. Joint of masonry of the main chapel.
IV4	Interior of the church. Plastering of masonry of the main chapel.
IV5	Interior of the church. Plastering of the north wall.
IV6	Exterior of the church. Plastering of a rendered basin with brick.
IV7	Exterior of the church. Joint of rendered basin with brick.
IV8	Exterior of the church. Plastering of open hall to the west.

Computers and software

Taking into account that the objective of this article the definition of the equipment and the software used is very relevant, especially because they were chosen in order to obtain the best results without any kind of chemical or physical tests. For this study we used a *Motic* binocular magnifier, model SMZ-140 series; a stereomicroscope *Marés Carton* with double light source and 400 magnifications; and a Veho USB microscope, model VMS-004 of 20x400 magnification and lighting of eight LED's focus. For the scale, a calibrated micrometric lens coupled into the binocular loupe was used. The microscopic documentation was developed with a petrographic microscope *AXIO Scope A1* with Zeiss lens.

The software used were VEHO 1.3 for the previous visualization and selection of the main components; for the treatment of pictures taken, GIMP 2.8.0 and ImageJ 1.51 j8; for the basic characterization, IMP Scope 1.65 (8a) and Micam 1.6; and finally, for the measurements and granulometries, JMicrovision 1.2.7, Digimizer 5.3.5 and again ImageJ 1.51 j8. All of them were used following a methodology designed previously.

Results

Regarding the macroscopic characterization the results can be summarized in the following table:

Table 2. Granulometric results.

Sample	Binder	Aggregates	Granulometry	Distribution	Raymond Classification
IV1	Lime	Siliceous	Fine-medium	Reg./Iso	Subcirc./Subang.
IV2	Lime	Siliceous/ceramics	Medium-coarse	Irreg./Pseu.	Subang./Ang.
IV3	Lime	Siliceous/ceramics	Medium-coarse	Irreg./Pseu.	Subang./Ang.
IV4	Lime	Siliceous	Fine	Reg./Iso	Subcirc./Subang.
IV5	Lime	Siliceous	Very fine	Reg./Iso	Circ./subcirc.
IV6	Clay	Siliceous	Medium	Reg./Iso	Subang./Ang.
IV7	Lime	Siliceous	Fine	Reg./Iso	Subcirc./Subang.
IV8	Clay	Siliceous	Medium	Reg./Iso	Subang./Ang.

The basic analysis of the components was carried out thanks to Micam and IMP Scope software, doing a first view of the different mortars and identifying, for example, the presence of lime nodules, quartz, feldspar and micas grains, ceramic aggregates and main characteristics of binder (colour and texture, irregular distribution, chemical reaction rims).

The results obtained through macroscopic test offer us the main components of mortars (aggregates and binders in appearance), as well as a previous granulometry, distribution of the aggregates and the geometric perimeter shape of these according to the Raymond classification. This qualification system establish a parameters in relation to the geometric shape of the grain (circular, angular, subangular or subcircular) [19]. These parameters are defining an hypothetical manufacture of the mortars, establishing two different groups in Idanha-a-Velha: a) mortars with a lime binder, of which two more subgroups are differentiated, with ceramic aggregate, or without him; b) plasters whose binder is a kneaded clay mixed with siliceous aggregate that react as a coarse coating. High-resolution images were taken and processed with Veho software. After that the same software chose of frames and calibrated the pictures between 1 mm and 500 microns. Subsequently, the samples were analyzed with binocular and stereomicroscope, once the most relevant elements were chosen.

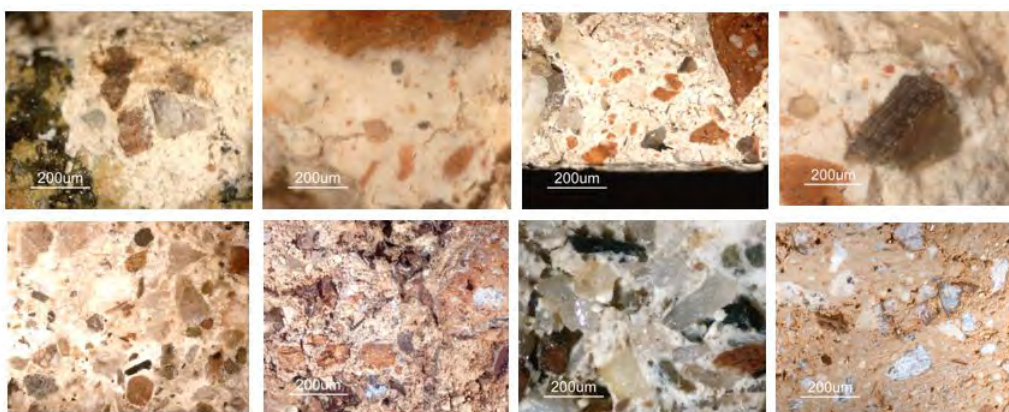


Figure 5. From left to right, and from top to bottom, microphotographs of the analyzed samples of *Sé-Cathedral*, where the difference between the mortars and the plasters is well appreciated.

The treatment of the photographs taken was developed to improve the identification of the components. Although there are many software's and programs that could enhance the visual of RGB channels, such as Photoshop or Illustrator, in our case both Gimp and ImageJ in order to analyse saturations, lighting and contrast. This phase enable a better visualization of the grains edges and allows easily the granulometry with JMicrovision and Digimizer programs. This software, designed for biomedical and biology work, has been used for testing the spectral range of the mortar components from a sequence of images taken in high resolution (between 10 and 25 MG in size per snapshot). This process was developed in cross sections of the mortars, either through thin sections, or raw samples [20]. Minimum requirements must be demanded in order to proceed correctly: photographic serial shot must cover all the surface of the sample; artificial light must be used; and, if possible, perfectly polished surfaces. This last feature could be optional, although if the samples are not polished properly, shadows could be generated in the pictures and difficult the work with the software.

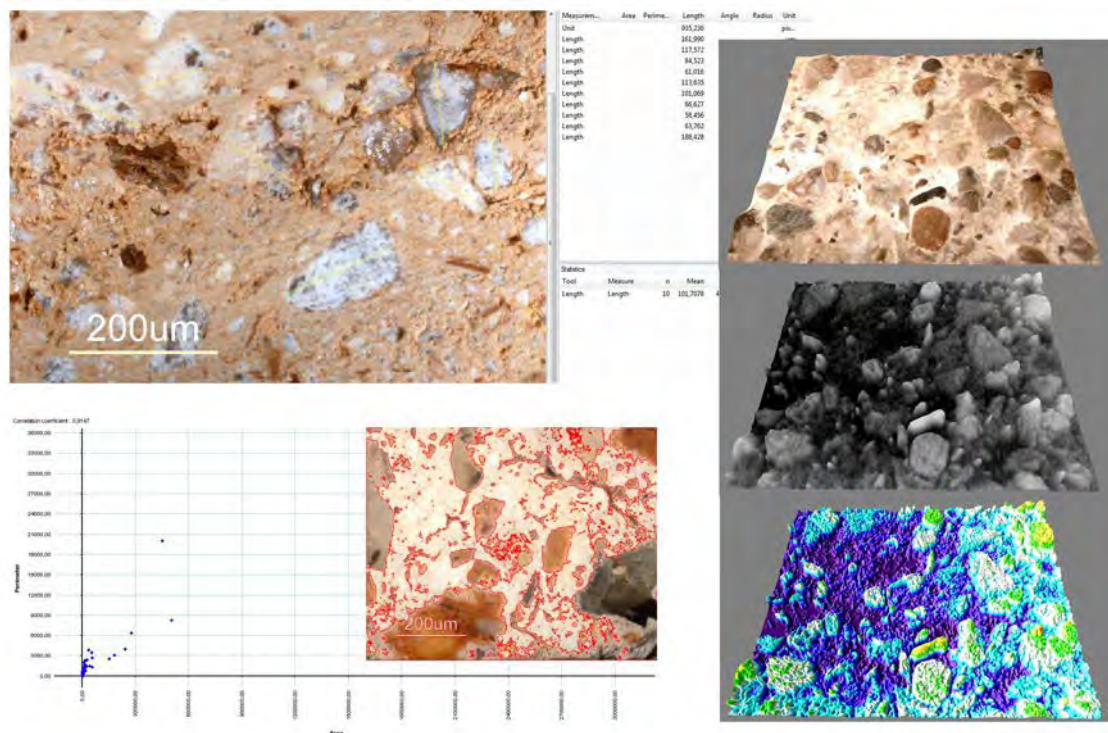


Figure 6. Characterization phases of the Idanha-a-Velha mortars. On the left, absolute granulometries obtained with Digimizer and JMicrovision. On the right side, 3D surface scanning with thermal and gray with ImageJ.

With this methodology we obtained a visual prognosis that can allows to work with samples photographs taken before. Thus, for example, ImageJ software allows a surface scan of mortars, documenting reliefs and height from outside layer with differences from mortar surface (zero value). In this 3D view all the components are documented and differentiated by its colour range (huge, saturation, gray scale), methodology applied in rock art studies [21]. Once the scan has been obtained it allows to work with the 3D model generated and it is possible to create layers from the chromatographic analysis (gradient, thermal, spectral,

red, gray and blue channels, etc.). This process is in the forefront of research in the field of Optics and Biomedical research [22].

Regarding the quantitative results, JMicrovision software allows to calibrate the images. In the *Santa Maria's Sé-Cathedral* samples they had already been calibrated previously by the Veho and Micam software. With JMicrovision we can develop quantifications, measurements, accounting in relation with the chromatic scales, or vectored granulometries too. These last ones allow to generate scales of colour variation in an area that researcher can choose himself, for example could be a painted surface, or a building level based with organic resources. The research become easier in the way to distinguish between different granulometries in the same sample, as well as to create different graphs of area-perimeter average from each grain of a visible section of the mortar.

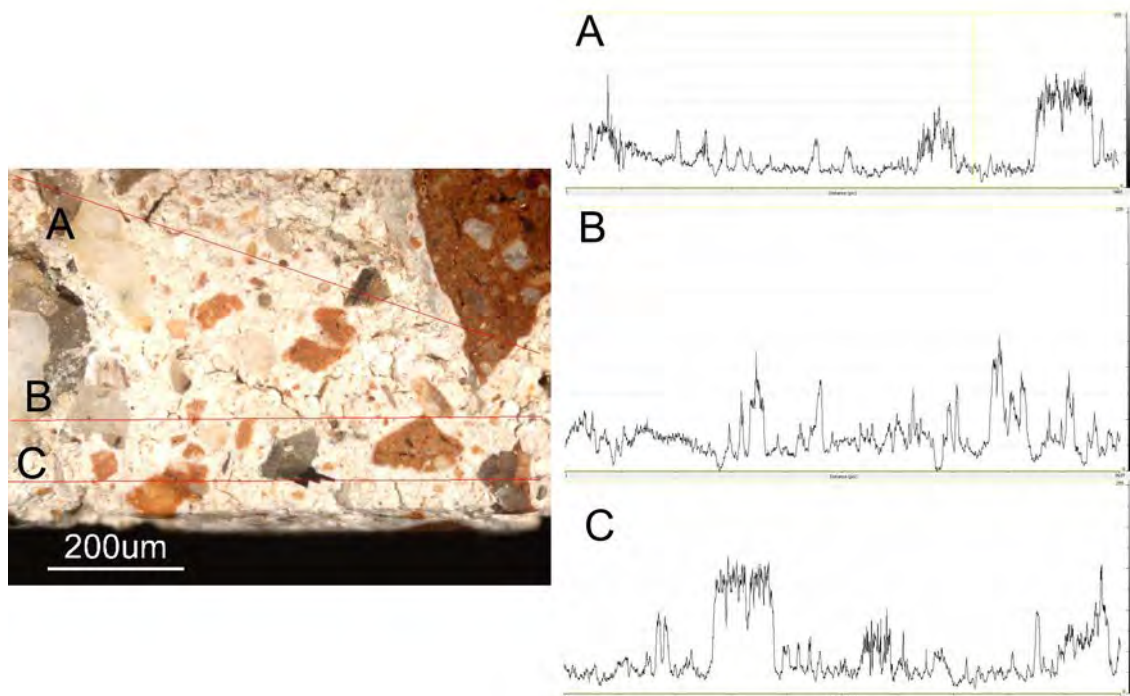


Figure 7. Detail of a linear granulometry from the IV2 sample, where the variation of the colour values shows a granulometric differences between the larger (vectors A and C) and smaller size (vector B) aggregates.

As a result of the combination of these software tools, also with the use of high definition microphotographs, progress has also been achieved in the advancement of new characterization processes. As a consequence today we are capable to distinguish mortars with plasters because the spectral microphotographs obtained shows as the difference between textures of both manufactories (especially thermal and spectral views). So in Idanha-a-Velha there are also elements in mortars that could be shown like the different percentage of aggregates with homogeneous/heterogeneous sizes, average or mortars inside the main building with respect to mortars from the outside.

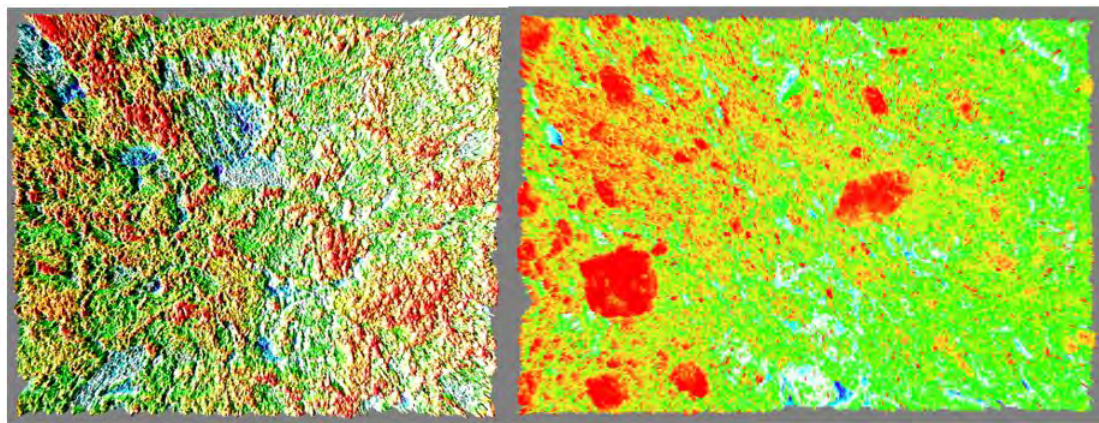


Figure 8. Comparison of two samples of Idanha-a-Velha, where on the left microphotograph is a lime mortar, while on the right a clay plaster is presented. In both cases, a surface scanner and a thermal spectral treatment have been developed.

Hydraulic mortars with the presence of ceramic aggregates were a different case, and nowadays we are still working about this. We do not know exactly why this aggregate appears in some samples, maybe casually because the application of mortar did not require any kind of hydraulic lime (non industrial structures, rooms, liturgical halls). This possibility has been ruled out because *cocciopesto*/brick crushed and ceramic pieces are shown in several samples and with considerable size, as shown in the 3D scans and colour analyses.

Conclusion

The use of software applications for the characterization of historical mortars documented from *Santa María's Sé-Cathedral*, has been the first step of this project. This phase is the first link in a series of research works that have been undertaken and are still ongoing in the framework of the *IdaVe Project*, focused on the archaeological knowledge about urban and architecture planning of the city in Roman Period, and Islamic Era. As indicated before, the area and the different buildings suffered several structural modifications, both in the space allocation and in the use of resources and materials. Because of that the implementation of this kind of procedures and methodologies of analyses allow us to progress forward in the understanding the architectural evolution [23].

The use of macroscopic techniques should be understood as a first step, but not the last, to improve the knowledge of the mortars [24]. In the way to know the components, granulometries and even pathologies could support the application before of analytical techniques, especially those that characterize the chemical and mineralogical composition. Better results could be obtained if we are capable to combine high resolution photographs with computer software that improve, on the one hand, the visual perception of mortars applying photogrammetric and 3D techniques, and on the other hand, obtaining data quantifiable about its composition based on the spectral chromatographic analysis. In short it is the application of new technologies in a field as Archaeological and Architectural Heritage, and that has much to improve.

Regarding the results in Idanha-a-Velha, it should be noted that the IV5 sample shows characteristics of Roman Age manufacturing in which typical mortars present fine/medium aggregates with homogeneous lime matrix. In most cases of the mortars analyzed we have documented mixtures close to be from Medieval Age, with medium/thickness aggregates and heterogeneous and heavy lime matrix. In only two cases plasters with clay compacted has been documented, interpreted as Medieval mixtures poorly finished. Outside coating and finishes use to be finer than the rest so in mortars came from inside the building joints shows siliceous fine aggregates and lime matrix without organic addition. Apparently better resources were used for masonries of the *Sé-Cathedral* and low quality resources were used for structures from outside, probably in relation with different phases of occupation. This hypothesis only would be reaffirmed with more complete analyzes and incorporating results in terms of mineralogical or chemical characterization.

Acknowledgements

Our most sincere gratitude to the staff of the *Istituto per la Conservazione e la Valorizzazione del Beni Culturale*, agency belonging to the *Consiglio Nazionale delle Ricerche* in Florence (Italy), where the sample preparation techniques were developed for the first time and where the visualizations were made too. Specifically, we thank Dr. Fabio Fratini for all his help and courtesy.

References

1. Sánchez Ramos, I, Morín de Pablos J (2015) El grupo episcopal de Egitania (Idanha-a-Velha, Portugal). *Actas del Encuentro de Arqueología del Suroeste Peninsular*, 7. Aroche, Portugal.
2. Guerra García, P, Guilotte, S. (2018) Argamasas y emplastos del yacimiento de Medina Albalat (Romangordo, Cáceres). Trabajo inédito.
3. Hughes J, Callebaut, K (2000) Practical sampling of historical mortars. En Bartos, P, Groot, C, y Hughes, JJ (eds.) *Proceedings of the RILEM International Workshop Historic Mortars: characteristics and tests*: 17–26.
4. Doebley, CE, Spitzer, DS (1996) Guidelines and standards for testing historic mortars. En Kelly, SJ (ed.) *Standards for preservation and rehabilitation*. American Society for Testing Materials: 285-293.
5. Mertens, G, Elsen, J, Brulet, R et al (2009) Quantitative composition of ancient mortars from the Notre Dame Cathedral in Tournai (Belgium). *Conférence: Euroseminar on Microscopy Applied to Building Materials (EMABM)*, Porto. *Materials Characterization*, A, 60, 7: 580-585.

6. Alonso Rodríguez, FC (2002) Ensayos físicos de caracterización y comportamiento de materiales. En Gisbert Aguilar, P (ed. y coord.) I Jornadas de Caracterización y Restauración de Materiales Pétreos en Arquitectura, Escultura y Restauración, I: 149-169.
7. Guerra García, P (2018) Un catálogo de argamasas históricas. Revista electronica ReCoPar, 13, 53-72.
8. Arpin, TL, Mallol, C, Goldberg, P (2002) Short contribution: a new method of analyzing and documenting micromorphological thin sections using flatbed scanners: applications in geoarchaeological studies. *Geoarchaeology*, 3: 305-313.
9. Miriello D, Bloise A, Crisci Gino M et al (2011): Characterisation of archaeological mortars and plasters from Kyme (Turkey). *Journal of Archaeological Science*, A, 38, 4: 794-804.
10. Adriano, P, Santos Silva, A, Veiga, R et al (2009) Microscopic characterisation of old mortars from the Santa Maria Church in Évora. *Materials Characterization*, 60: 610-620.
11. Guerra G9arcía, P (2017) Caracterización macroscópica de morteros romanos de tipo ind825ustrial en Villamanta (Madrid). Primeros datos. *European Scientific Journal*, 13 (25). DOI 10.19044/esj.2017.v13n35p1
12. Jackson MD, Logan, JM, Scheetz Barry, E et al (2009): Assessment of material characteristics of ancient concretes, Grande Aula, Markets of Trajan, Rome. *Journal of Archaeological Science A*, 36, 11: 2481-2492.
13. Varas, MJ, Álvarez de Buergo, M, Pérez-Montserrat, E et al (2008): Decay of the restoration renders mortar of the church of San Manuel and San Benito, Madrid, Spain. Results from optical and electron microscopy. *Materials Characterization*, 59: 1531-1540.
14. Adriano, P, Santos Silva, A, Veiga, R et al. (2009) Microscopic characterisation of old mortars from the Santa Maria Church in Évora”. *Materials Characterization*, 60: 610-620.
15. Adriano, P, Santos Silva, A (2006) Caracterização de argamassas antigas da Igreja de Santa Maria de Évora- Sé Catedral de Évora”. En Relatório, LNEC 59/06, NMM. Lisboa.
16. Álvarez Galindo, JI, Navarro, I, García Casado, PJ (2000) Thermal, mineralogical and chemical studies of the mortars used in the cathedral of Pamplona (Spain). *Thermochimica Acta*, 365: 177-187.
17. Antonelli, F, Lazzarini, L, Cancelliere, S et al (2009) Volubilis (Meknes, Morocco): Archaeometric study of the white and coloured marbles imported in the Roman age. *Journal of Cultural Heritage*, 10: 116-123.
18. Ricciardi, MP, Lezzerini, M, Carò, F et al (2007) Microtextural and microchemical studies of hydraulic ancient mortars: Two analytical approaches to understand pre-industrial technology processes. *Journal of Cultural Heritage*, 8, 4: 350-360.

19. Pecchioni, E, Fratini, F, Cantisani, E (2008) *Le malte antiche e moderne: tra tradizione ed innovazione*. Pàtron Editore, Bologna.
20. Prendes Rubiera, N (2006) El tratamiento digital de imágenes como una herramienta de evaluación y análisis en la restauración del Patrimonio Arquitectónico. *Revista ReCoPar*, 1.
21. Acevedo, A, Franco, N (2012) Aplicación Dstretch-ImageJ a imágenes digitales del arte rupestre de Patagonia (Argentina). *Comechingonia Virtual, Revista Electrónica de Arqueología*, 6, 2: 152-175.
22. Castañeda, R, Piedrahita Quintero, P, García Sucerquia, J (2015) Procesamiento y cómputo de imágenes para holografía digital con ImageJ. *Óptica Pura y Aplicada*, 48, 2: 11-18.
23. Sánchez Ramos, I, Morin de Pablos, J (2014) *Idanha-a-Velha. Portugal. El episcopio de Egítania en época Tardoantigua*. Audema S.A.: Madrid.
24. Guerra García, P, Heras Martínez, C, Bastida Ramírez, A (2016) Técnicas constructivas y estructuras microestratigráficas en elementos industriales de carácter hidráulico documentados en el yacimiento romano de La Magdalena (Alcalá de Henares, Madrid). *Zona Arqueológica, Especial Vides, Monumenta, Veterum. Madrid y su entorno en época romana*, I: 468-476.

Topic 2: Use of nanotechnology for high performance mortars



Evaluation of the influence of nano-SiO₂ and nano-Al₂O₃ on the physico-mechanical properties and microstructure of calcareous clay

Eirini-Chrysanthi Tsardaka¹, Maria Stefanidou¹

(1) Laboratory of Building Materials, School of Civil Engineering, Aristotle University of Thessaloniki, Greece, extsardaka@gmail.com, stefan@civil.auth.gr

Abstract

The incorporation of nano-silica (NS) and nano-alumina (NA) in calcareous clay binder gave significant results, concerning the physico-mechanical properties and microstructure of the system. Two different proportions of nanoparticles were tested, 1.5wt% and 3.0wt%, in order to evaluate their degree of influence. Each nanoparticle modified the system, due to its different mechanism of action. NS seemed to stabilise calcareous clay specimens. The positive capillarity influence was the most important benefit. Calcareous clay with incorporated NS was the only system that completed the water capillary absorption test without collapse. On the other hand, NA did not benefit the physico-mechanical properties significantly in time, but maintained a low volume change. This limited volume change was not sufficient to emerge NA-composite as a favored system.

Introduction

From the beginning of construction history, clay had a starring role in building systems. Since early Neolithic age, clay has been one of the basic construction materials, due to its abundance, availability and ease of application. Clay was used either as a primary structural building material or, more often, as a binding material for joining and covering wooden skeletons and masonry [1-4]. Clay has been used in plasters and joining mortars, either alone or combined with other binders, such as aerial lime and pozzolan. Nowadays, it is still used as an intervention material for the conservation and restoration of historic constructions. As a binder, however, clay has certain disadvantages [1] [4]. The main issues are its low mechanical properties and its low resistance to humidity. Humid conditions may cause collapse of clay due to the high water absorption capacity and dimensional changes associated with clay swelling and shrinking.

Over the last decades, nanoparticles have been studied for their influence on the properties of building materials. Particularly, the addition of NS and NA in cement based systems [5], lime based systems [6], hydraulic systems [7-9] and clay-lime binders [10] has been studied, focusing on physico-mechanical properties and microstructure modifications. Previous studies have shown that the beneficial effect of NS relies on the pozzolanic action (“can act as nucleation agent” [11]) and the filling of the microstructure [5, 11]. NS increases

compressive strength and reduces open porosity in time and NA works favorably as filler. The NA nanoparticles effect in traditional binding systems depends on the content of the binder. Mechanical properties of lime-pozzolan binder were hampered, whilst compressive strength of lime-metakaolin binder was enhanced [8]. Furthermore, the pore size distribution of lime-pozzolan binders was negatively affected by NA addition and the proportion of pores, with size above 200 μ m, increased at 90 days [7]. Nevertheless, NA incorporation in traditional binding systems and cement-based systems did not significantly modify the w/b ratio [10, 12].

The contribution of nanoparticles addition in clay and soil had a positive impact in these systems [13]. After the incorporation of 1.0 to 5.0wt% nano-silica with lime [14], the addition of 10-20wt% colloidal silica in clay [15] and 0.1wt% NA in clay [16], an increase of mechanical properties of soils has been recorded. According to these reports, siliceous soils and clays were benefited after the addition of nanoparticles, at the optimum percentages of the investigations results.

So far, NS benefits steadily the properties of binding systems over time, from traditional binders to cement [4]. On the other hand, NA acts as filler in cement but seems to have a controversial role in hydraulic traditional binders. NA lime-pozzolan composites presented hindered properties, while NA-lime metakaolin composites resulted in improved mechanical properties [8]. The purpose of the present work is to evaluate the effect of adding NS and NA in clay binder with high total calcium oxide content, from the Greek island of Creta. Nanoparticles were incorporated in calcareous clay in proportions 1.5% and 3.0% by mass of binder. Physico-mechanical properties were studied in order to determine whether nanoparticles affect positively the clay structure. Compressive strength and open porosity were recorded up to 365 days. Capillarity was determined at early age and after a year, and volume changes were recorded up to 45 days. Specimens were observed with SEM-EDS at 120 days, in order to verify the modifications in microstructure.

Experimental

Materials and Methods

Calcareous clay from the island of Creta was dried and sieved and particles below 2mm were used. The content of calcareous clay in metal oxides is given in Table 1, measured with Atomic Absorption Spectrometry (AAS), AAnalyst 4400, Perkin Elmer. Loss of Ignition was measured by using 1 g of binder and oven heat up to 1000°C. Nano-silica (0.014 μ m) and nano-alumina (<50nm, according to TEM results) were supplied from Sigma-Aldrich.

Table 1. Chemical composition (wt%) and specific gravity of calcareous clay

	Na ₂ O	K ₂ O	CaO	MgO	Fe ₂ O ₃	Al ₂ O ₃	SiO ₂	L.I.%	Sp. Gravity g/cm ³
Clay	0.94	1.08	34.70	1.71	3.91	9.32	25.58	22.76	2.281

Compressive strength of the produced specimens was measured at 90, 120 and 365 days using a Technik ToniNorm device (according to EN196-3) and the rate of the applied load was 0.2 kN/s. Open porosity of specimens was determined at 90, 120 and 365 days according to standard RILEM CPC 11.3 method based on water absorption under vacuum, using heptane instead of water to avoid specimen collapse during measurement. Capillarity test was performed at 90 and 365 days according to EN 1015-18.

A balance Kern PCB 4000-2 (max capacity 4000±0.01g) was used to weight the binders and an analytical balance B204-S/FACT of Mettler Toledo (max. capacity 220.0 ±0.0001g) was used to weight nano-particles. Microstructure was observed at 120 days with Scanning Electron Microscopy (SEM-EDS) using a Jeol JSM-6390LV, Oxford Instruments. For the preparation of suspensions of nano-particles in water, the ultrasound embodied in the Mastersizer 2000, Hydro2000 MU of Malvern Instruments was used.

Preparation of binding systems

Nanoparticles were weighted and added in pre-weighted water in proportions of 1.5% and 3.0% by mass of binder (wt%). To disperse nanoparticles in water, suspensions were ultrasonicated for 30 minutes. Subsequently, the suspension was directly added to the binder and the mixture was homogenized under mechanical stirring. The demand of water increased when 3.0wt% of nanoparticles were added. It was decided to maintain standard consistency of the binding systems (Vicat test). Clay pastes were cast in prismatic moulds (25x25x50 mm and 25x25x100mm). Right after demolding, specimens were cured in dry conditions (25°C ±1, RH ~75%) until tested. Table 2 summarizes the w/b ratio as well as the nano-particle content of binding systems keeping the clay content constant, in all cases.

Table 2. Content of reference system and calcareous clay modified with nanoparticles.

Acronym	W/B	NS (wt%)	NA (wt%)	Vicat (mm)
E	0.42	-	-	15.5
Es	0.42	1.5	-	15.1
Ea	0.42	-	1.5	15.6
Es3	0.60	3.0	-	16.0
Ea3	0.50	-	3.0	15.0

Results and Discussion

Compressive strength

Table 3 and Figure 1 present the compressive strength (MPa) of binders at 90, 120 and 365 days. Compressive strength was derived from the mean value of eight measurements. The positive or negative influence of the addition of nanoparticles is provided in Figure 2, by demonstrating the percent variation of compressive strength. Nano-modified binders are compared with the reference sample and the variation is given as a comparing factor. For the calculation of the values, the equation used was: $(N-R)*100/R$, where N is the

compressive strength value from nano-modified specimen (Es, Ea, Es3, Ea3) and R the value of reference specimen (E). Negative percentages show a negative impact due to a reduction in compressive strength and positive percentages imply a benefited system.

Table 3. Compressive strength (MPa) of reference system and nano-modified systems over time. Mean values of eight specimens and standard deviation of values.

Compressive strength (MPa)			
Acronym	90 days	120 days	365 days
E	2.263 ±1.108	3.176 ±0.892	3.271 ±0.916
Es	2.903 ±0.377	3.731 ±0.624	4.092 ±1.135
Ea	2.600 ±0.202	2.238 ±0.984	2.451 ±0.576
Es3	3.225 ±0.861	3.280 ±0.760	3.380 ±0.817
Ea3	3.320 ±0.193	2.248 ±0.219	2.189 ±0.420

Compressive strength was benefited by both nanoparticles, NS and NA, at 90 days. In fact, binders with NA nanoparticles presented significant increase in compressive strength, by 42.5% and 46.7% respectively for Ea and Ea3. This increase probably relies on the action of NA as filler. However, this behaviour was not preserved. As the specimens were drying, the behaviour of compressive strength changed. At 120 and 365 days, Ea3 provided lower values of compressive strength, as compared to the reference. Additionally, Ea at 120 and 365 days does not show significant differences, as compared to the reference.

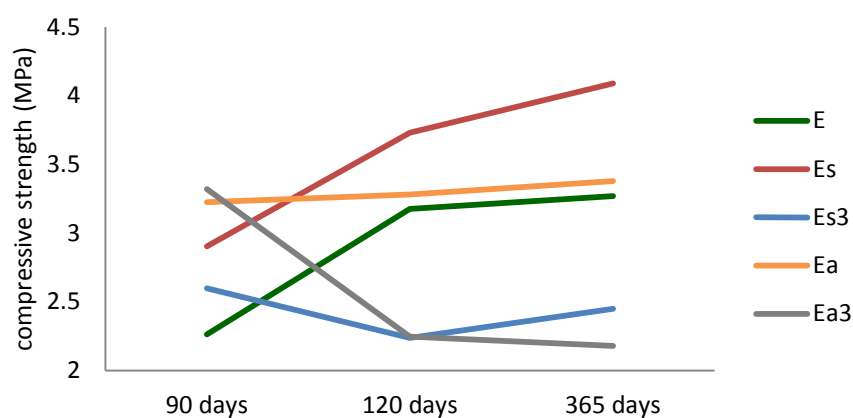


Figure 1. Evolution of compressive strength (MPa) of nano-modified calcareous clay, over time.

Even if Es3 and Ea3 display encouraging results at 90 days, the amount of 3.0wt% nanoparticle in the system leads to opposite results, over time. Considering the economic side, the latter constitutes an advantage. Still, this evidence might be connected to the curing of specimens. In other hydraulic traditional binding systems, where the water quantity was kept stable in all pastes, the increase in the proportion of NS resulted in increased compressive strength [6] [8].

NS presents a constant benefit in the compressive strength of the calcareous clay systems (Es in Figure1), as it enhances this property by 28%, 17% and 25%, with time (Figure 2). So, NS contributes to the improvement of the mechanical properties of calcareous clay over

time, when the proportion of NS is low. When nanoparticles quantity increases (in Es3), the water demand increases too (Table 2). The latter is responsible for the hampered compressive strength of clay. The proportion 1.5wt% NS does not affect the water demand and proves out to be a “tolerable” quantity for the specific w/b ratio and consistency of clay pastes.

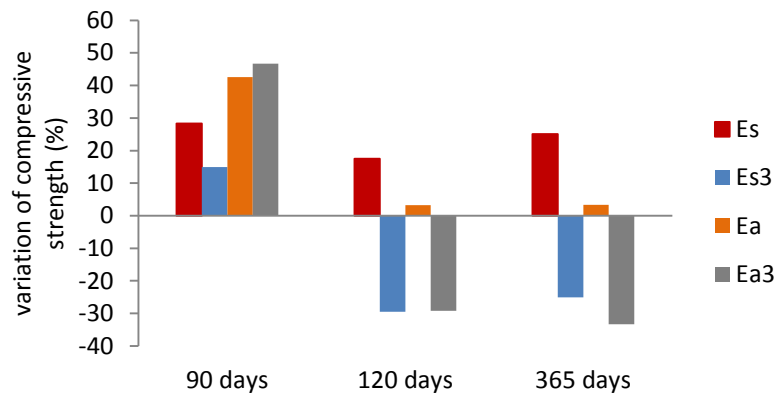


Figure 2. Variation of compressive strength (%) of nano-modified calcareous clay, in respect to the reference.

Open porosity (RILEM CPC 11.3)

It has been demonstrated that NS enhances the early age properties (compressive strength and porosity), when it is used in traditional binders, such as lime mortars [6], lime-clay [10] and lime-pozzolan binding systems [7]. Accordingly, NS seems to have diminished the connected open pores of clay at 90 days. NA had also a positive effect, by reducing porosity of clay at that age. Mixtures Es and Ea presented a decrease of open porosity by 35.41% and 19.90% respectively (Figure3).

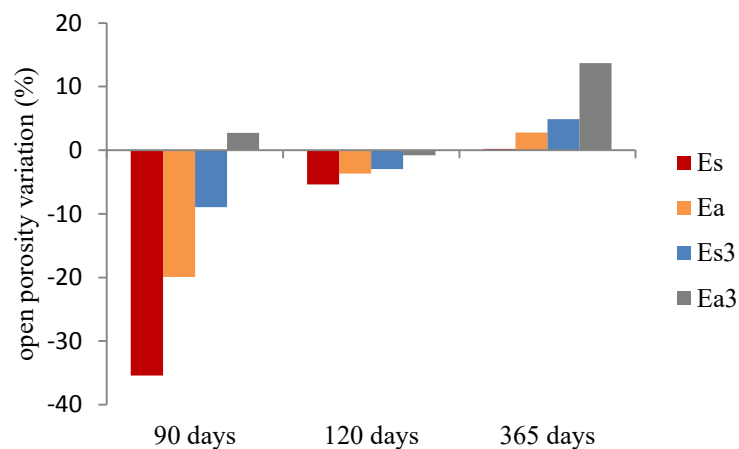


Figure 3. Open porosity variation (%) of nano-modified calcareous clay systems, with respect to the reference.

At 120 days, the open porosity was not notably varied in nano-modified systems. At 365 days, Es, Es3 and Ea systems present porosity values close to the reference. After 90 days, the proportion 3wt% NA seems to affect negatively the open porosity of clay, which comes to an agreement with compressive strength results, probably due to the formation of shrinkage cracks.

Open porosity (Table 4) shows that both nanoparticles have a filling effect in the structure of clay, meanwhile the proportion used should be taken into consideration. The amount of 1.5% NS or NA is a satisfactory percentage to contribute positively in the reduction of the early age porosity in clay with high total calcium oxide content. This property is not favoured in time, but only at 90 and 120 days measurements.

Table 4. Open porosity (%) of reference system and nano-modified systems

Open porosity (%)			
Acronym	90 days	120 days	365 days
E	26.97	25.20	24.36
Es	17.42	20.52	24.41
Ea	21.60	24.28	25.03
Es3	24.55	24.45	25.20
Ea3	27.7	25.00	27.60

Open porosity and compressive strength of Ea are complementary. At 90 days compressive strength is enhanced and open porosity is reduced. After 120 days and when specimens were completely dried, these properties were alike the reference sample, which means that the filling contribution of NA is intensive at early age. On the contrary, NS maintains its contribution to compressive strength over time, even when open porosity is no longer favored probably due to crack formation. The presence of NS in calcareous clay seems to benefit mechanical properties in clay systems and this was observed throughout 365 days.

Capillary water absorption

Capillary water absorption is one of the most important properties of traditional binders and its determination is particularly critical in specific applications, requiring additional protection from water penetration. Also, this test discloses the connection of porosity and voids in the structure. The capillary voids of the structure can be affected by the water quantity added during sample preparation, the compaction of the material in the molds and the curing regime. Capillarity was measured at 90 days (Figure 4).

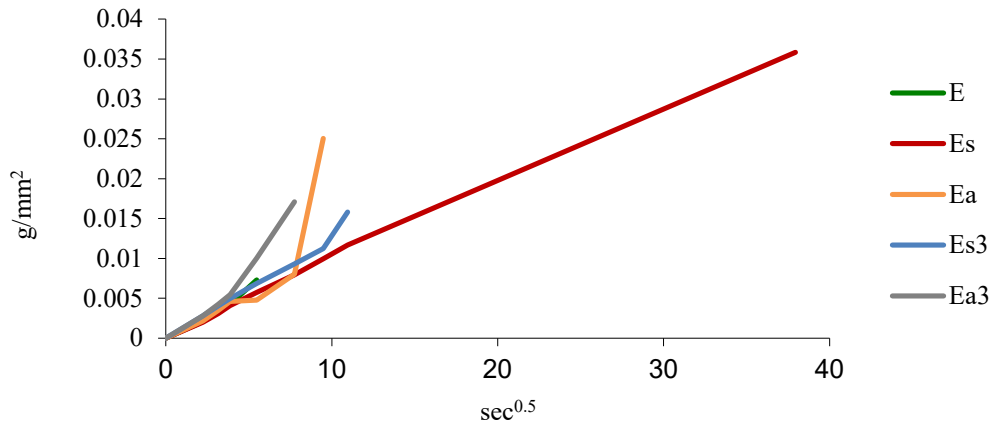


Figure 4. Influence of nanoparticles on capillarity of nano-modified calcareous clay at 90 days.

Clay systems behaved differently, according to the nanoparticle added. As long as the water penetrated, from the bottom to the top of the specimen, all specimens except Es, gradually collapsed. Calcareous clay (E) collapsed at 30 minutes, Ea and Ea3 at 60 and 90 minutes respectively and Es3 collapsed at 120 minutes (Figure 5). The adequacy of 1.5wt% NS is also shown through this test. Clay was stabilised and presented acceptable values of capillarity. The higher w/b ratio of Ea3 and Es3 definitely affected these results, as the increased water quantity lead to many more capillary voids, after water evaporation.

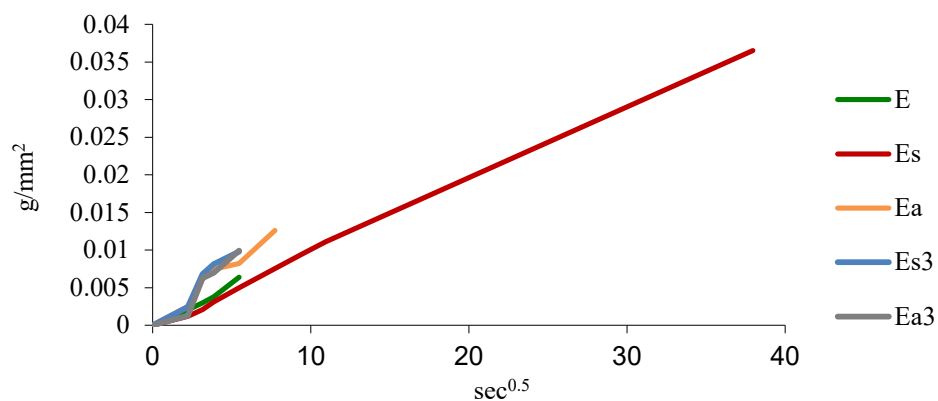


Figure 5. Influence of nano-particles on capillarity of nano-modified calcareous clay at 365 days.

NA contributed to the mechanical properties of clay at 90 days, but could not reduce penetrability during water impregnation. Contrary, it seems that NS managed to minimise capillary voids of clay, probably by making the structure denser than the reference.

The same behaviour in clay systems was also observed at 365 days, when E, Ea, Ea3 and Es3 specimens collapse before 60 minutes (Figure 5). Es specimens completed the test and yielded alike capillarity with 90 days results. The structure of Es remained stable and hindered water impregnation until 365 days. Along with compressive strength results, capillarity test proves the stabilization of calcareous clay by NS 1.5wt%.

Volume change

Volume change of specimens was determined by measuring the dimensions of representative specimens of all systems. After demolding, the samples were maintained in dry conditions, in a climatic chamber (RH 75%, $25\pm 1^\circ\text{C}$) and their dimensions were measured daily. Figure 6 shows the volume change of specimens up to 45 days. Negative volume change implies shrinkage of the specimens. The intensive shrinkage of the first seven days was owing to the drying of clay.

Clay specimens with NA presented less shrinkage than the reference, so NA acted positively concerning volume change. The shrinkage of Ea specimens was hardly modified comparing to the reference (Figure 6). Specimens Ea3 presented clearly less shrinkage, which was attributed to the filling effect of NA. It seems that after drying, the structure of specimens had enough pores and capillary voids to allow air penetration.

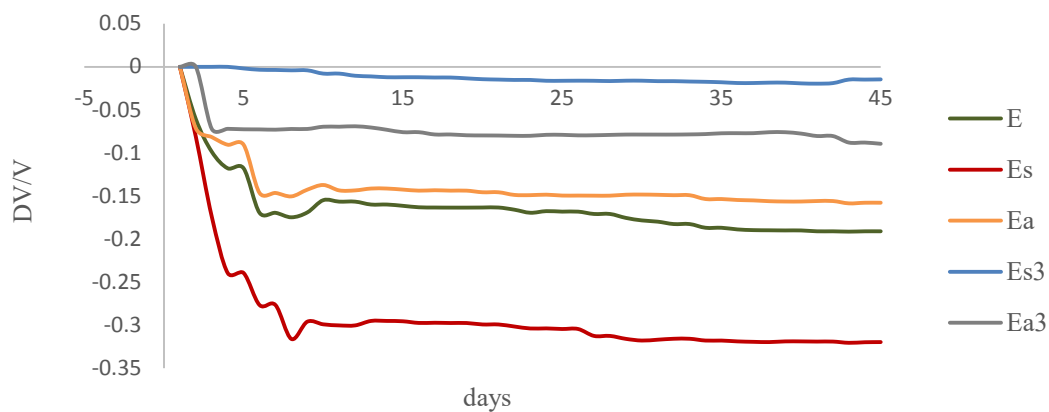


Figure 6. Volume change of binders from demolding up to 45 days.

Sample Es3 presents the most stable behaviour, by maintaining volume stability. This was surprising as the composition contained rather high amount of water ($W/B=0.6$). On the contrary, Es displayed high shrinkage, approximately 100% higher than the reference sample. Further analysis and repetition of the test is required to check the results.

SEM observation

The microstructure of nano-modified specimens was evaluated in comparison to the reference system. Figure 7 pictures calcareous clay microstructure (E), obtained from SEM-EDS instrumentation, at 120 days. The loose structure of the clay is attributed to pores of different size and capillary voids. Spectrum 1 is the elemental analysis of total area of the image and Spectra 2-4 are spot measurements. The ratio $\text{Ca/Si-Al}=2/1$ of clay is given by EDS analysis.

In microstructure of Es, the pores have different distribution and they are of smaller size, comparing to E system (Figure 8). Absence of many cracks and discontinuous areas display a

more homogeneous microstructure. This complies with the higher compressive strength and capillarity test results, which prove the stabilisation of calcareous clay by NS 1.5wt%.

Figure 9 is a representative SEM image of Ea. Areas of denser structure with higher silicon-aluminum content (Spectrum 2-4) and looser areas of higher calcium content (Spectrum 5) were revealed during the observation. Pores of different size are present in the structure.

The increase of nano-particles proportion boosted certain phenomena in the pastes. The structure of Es3 samples presented a rigid and inhomogeneous structure. Plus, small different texture areas were observed in Es3. These areas consist of a dense core with amorphous loosen structure around the core. In Figure 10, a representative dense area with inhomogeneous surface and texture is shown. The dense core consists mainly of silicon areas (Spectrum 1). Detected areas rich in calcium content found close to these cores (Ca/Si: 7/1, Spectrum 2). The loose areas around the core had micro-cracks and ratio Ca/Si: 2/1 (Spectrum 3). The increase of NS content lead to modifications of microstructure, due to the shaping of these silicious cores that caused the micro-cracks. Finally, it seems that the increasing of NS proportion resulted in certain micro-cracks around the cores, but also hard and dense areas were created. In traditional binders so far, the addition of NS lead to the shaping of such areas that appear denser and are accompanied by cracks and homogenous structure around.

In Figure 11 the microstructure of Ea3 specimen is shown. The texture was loose and inhomogeneous. The microstructure has thick areas within voids that look like large capillary voids rather than porosity. Most probably, these canals were created while specimens were drying. Certain areas of the specimen have been filled with NA and turned to robust parts of material and other areas were devoid of nanoparticles. Although the latter is a negative effect for the microstructure, it might explain the stable behavior of Ea and Ea3 pastes during volume change tests. These large void cavities show that microstructure did not shrink during drying. Specimens Ea3 retained the initial volume in macro-observation. At the same time, large voids worked against capillarity, as they allowed water permeability.

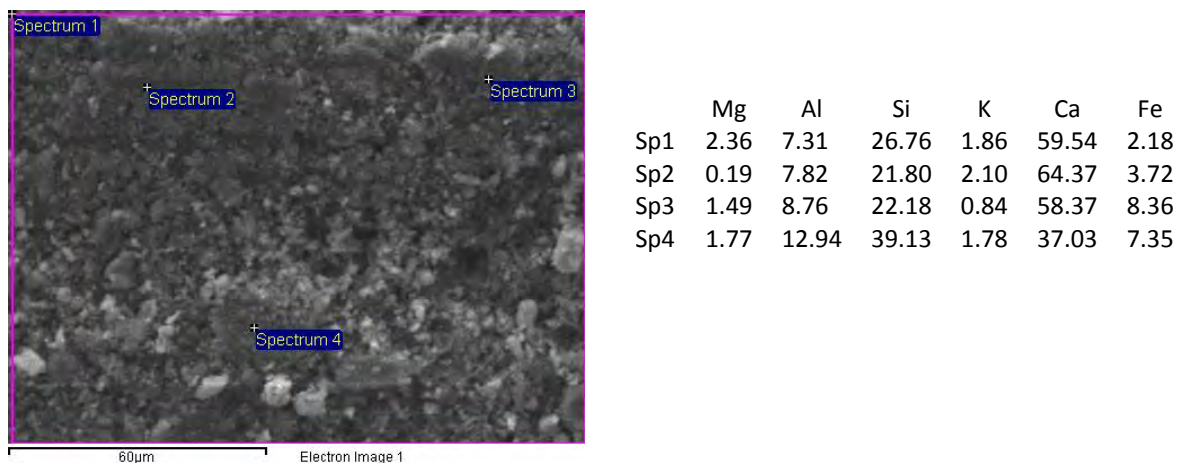
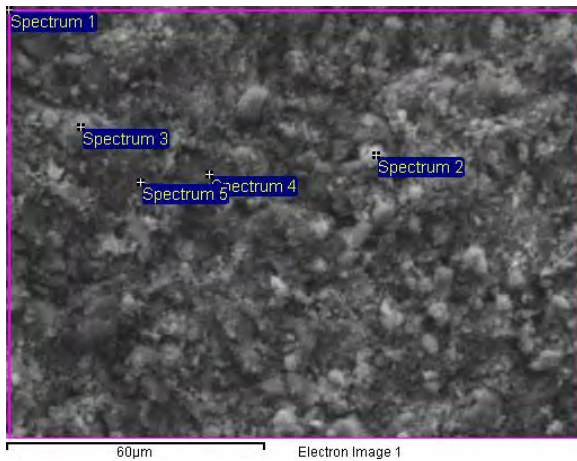
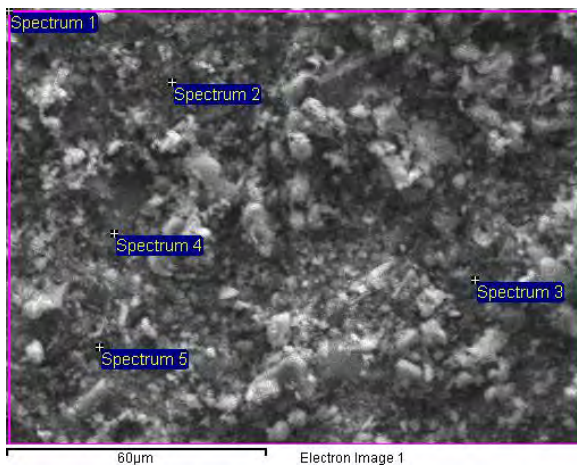


Figure 7. SEM image of calcareous clay (E) and elemental analysis by EDS.



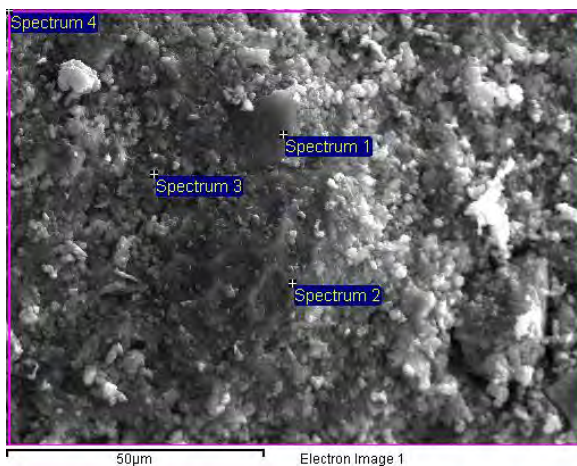
	Mg	Al	Si	K	Ca	Fe
Sp1	3.41	8.25	34.94	1.84	45.79	5.77
Sp2	0.64	5.17	18.90	0.11	73.05	2.13
Sp3	1.01	8.07	28.45	1.65	51.72	9.10
Sp4	3.27	6.97	40.35	1.36	44.15	3.90
Sp5	3.24	7.54	36.73	1.02	41.98	9.50

Figure 8. SEM image of calcareous clay with 1.5wt% NS (Es) and elemental analysis by EDS.



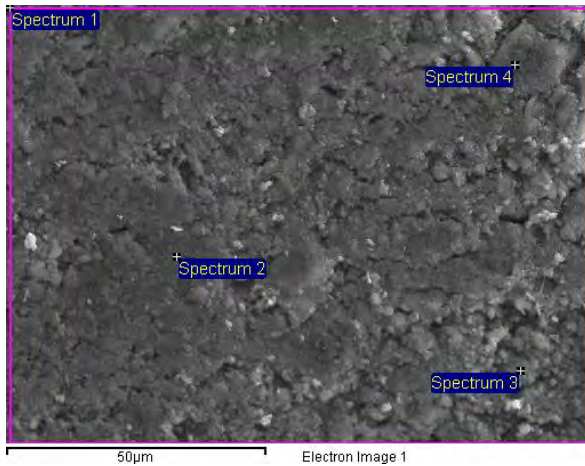
	Mg	Al	Si	K	Ca	Fe
Sp 1	1.99	9.41	32.28	2.02	47.87	6.43
Sp 2	3.69	17.79	45.20	1.32	26.55	5.45
Sp 3	1.39	0.86	83.99	0.14	6.94	6.68
Sp 4	3.23	6.35	66.59	1.52	19.95	2.36
Sp 5	5.87	9.87	24.29	2.17	53.79	4.02

Figure 9. SEM image of calcareous clay with 1.5wt% NA (Ea) and elemental analysis by EDS.



	Mg	Al	Si	K	Ca	Fe
Sp 1	0.91	5.01	62.30	0.53	27.79	3.47
Sp 2	1.57	3.68	12.41	0.85	77.54	3.96
Sp 3	1.67	5.68	29.11	1.46	58.41	3.68
Sp 4	2.00	5.07	32.07	1.93	53.82	5.10

Figure 10. SEM image of calcareous clay with 3.0wt% NS (Es3) and elemental analysis by EDS.



	Mg	Al	Si	K	Ca	Fe
Sp1	1.62	10.94	23.33	1.86	55.77	6.48
Sp2	2.03	11.14	32.79	2.70	43.03	8.30
Sp3	2.79	10.82	21.96	2.73	54.18	7.53
Sp4	1.48	15.58	72.48	2.33	5.06	3.07

Figure 11. SEM image of calcareous clay with 3.0wt% NA (Ea3) and elemental analysis by EDS.

Conclusion

After the comparative study of calcareous clay pastes with incorporated nanoparticles, certain advantages and disadvantages resulted from the evaluation of properties.

As for the pros, they are easily observed in strength development and capillarity over and microstructure at 120 days. The 90 days compressive strength, which seems to be representative for the nature of clay, was benefited from both nanoparticles, NS and NA, at 1.5wt% and 3.0wt%. In long term compressive strength evolution, Es was the only steadily improved system up to 365 days. Open porosity is also favored by nanoparticles addition. Especially at 90 days, NS offers a reduction of porosity by one third (~34%). This is an important factor that shows stabilization of the clay at 90 days. Capillary water absorption results validated the stabilization of clay at 90 and 365 days, by 1.5wt% NS addition. Es was the only system that completed the test without collapse at 90 days. When the test was repeated at 365 days, the systems had alike behavior. This means that stabilization of the clay by NS was preserved from early to later age. SEM observation explained the behavior of improved Es system. Microstructure of clay became more homogeneous than the reference, with better distribution and smaller pores size. As a consequence, open porosity and capillary water absorption were improved and compressive strength was enhanced.

The disadvantages that were indicated in this work are related to the water demand and volume change of the specimens with 3.0wt% nanoparticles content. The increased proportion of nanoparticles caused augmented water demand for both, Es3 and Ea3. The water to binder ratio increased significantly and might have influenced all tested properties. More specific, the increase of water demand is connected to the hampered open porosity and the negatively modified microstructure of systems with 3.0wt% nanoparticles. Also, the homogeneous distribution of a high amount of nanoparticles could not be efficiently achieved.

This study displays that low amount of NS can stabilize calcareous clay-based materials. Thus, application field of nanoparticles could be enlarged, in favor of conservation purposes.

References

1. Wright JRH (2005) Ancient Building Technology. Vol 2: Materials. Main series: Technology and Change in History. Leiden: Brill, Boston
2. Papayianni I (2004) Design of Compatible Repair Materials for the Restoration of Monuments. *Int J Restor* 10:623-636
3. Hughes JJ (2012) RILEM TC 203-RHM: Repair mortars for historic masonry. The role of mortar in masonry: an introduction to requirements for the design of repair mortars. *Mat Struct* 45:1287-1294
4. Warren J (1999) Conservation of earth structures. Butterworth - Heinemann, Oxford
5. Sanchez F, Sobolev K (2010) Nanotechnology in concrete- a review. *Con Build Mat* 24:2060–2071
6. Duran A, Navarro-Blasco I, Fernández JM, Alvarez JI (2014) Long-term mechanical resistance and durability of air lime mortars with large additions of nanosilica. *Con Build Mat* 58:147–158
7. Tsardaka EC, Pavlidou E, Stefanidou M (2018) The Role of Nanoparticles on the Durability of Lime-Pozzolan Binding System. *Solid State Phenomena* 286:119-132 (doi:10.4028/www.scientific.net/SSP.286.119)
8. Stefanidou M, Pavlidou E, Tsardaka EC (2017) Influence of nano-silica and nano-alumina in lime-pozzolan and lime-metakaolin binders. *Mat Today: Proceedings* 4:6908-6922
9. Stefanidou M, Tsardaka EC, Pavlidou E (2016) Influence of combined nano-particles in traditional binding systems, 4th Historic Mortars Conference (HMC 2016), Proceedings, October 10-12, Santorini, Greece
10. Tsardaka EC, Skevi L, Stefanidou M (2018) The role of nano- Al_2O_3 in traditional binders, Proceedings: 10th International Symposium on the Conservation of Monuments in the Mediterranean Basin, 20-22 September 2017, Athens, Greece
11. Dirak S, Srirama D (2015) A review of stabilization of expansive soils by using nanomaterials. In :50th Indian Geotechnological Conference , Pune, Maharashtra, India
12. Gowda R, Narendra H, Nagabushan BM, Rangappa D, Prabhakara R (2017) Investigation of nano-alumina on the effect of durability and microstructural properties of the cement mortar. *Mat Tod: Proceedings* 4:12191–12197

13. Huang Y, Wang L (2016) Experimental studies on nanomaterials for soil improvement: A review. *Env Earth Sc* 75(497)
14. Ghasabkolaei N, Choobbasti AJ, Roshan N, Ghasemi SE (2017) Geotechnical properties of the soils modified with nanomaterials: A comprehensive review. *Arc Civil Mechan Eng.* 17:639-650
15. Persoff P, Apps J, Moridis G, Whang JM (1999) Effect of dilution and contaminants on sand grouted with colloidal silica. *J Geotechn Geoenviron Eng* 125(6):461–469
16. M.R. Taha, O.M.E. Taha, Influence of nanomaterial on the expansive and shrinkage soil behavior, *Journal of Nanoparticle Research* 14 (1190) (2012).

The use of nanoparticles to improve the performance of restoration mortars

Beatriz Menéndez¹, Dita Frankeová², José Díaz¹, Radek Ševčík², Petra Macová², Mouna Faiz¹,

Zuzana Slížková²

(1) Geosciences and Environment Cergy, Cergy-Pontoise University (France), beatriz.menendez@u-cergy.fr; iqijosediaz@gmail.com; faiz.mouna@gmail.com

(2) Institute of Theoretical and Applied Mechanics of the Czech Academy of Sciences, frankeova@itam.cas.cz; sevcik@itam.cas.cz; macova@itam.cas.cz; slizkova@itam.cas.cz

Abstract

The work presented here corresponds to some preliminary results of a project whose goal is to study the effects of nanoparticles on the characteristics and performance of lime mortar. As a starting point, a commercial lime mortar was used to produce a set of test specimens to which SiO₂ nanoparticles were added in quantities ranging from 1 to 7 wt%. The mortar specimens were stored at 25°C in 35% relative humidity for a period of four months to allow for carbonation, and were then tested. Conclusions have not yet been completely established, but it seems that the physical and mechanical properties of the modified mortars are significantly affected both by the quantity of nanoparticles added as well as by the procedure with which the nanoparticles are incorporated during mortar preparation. Further studies are still necessary.

Introduction

The term restoration mortars designates a group of products used to repair masonry. They can be used to rebuild damaged or missing parts of buildings, monuments or sculptures, as well as to make replicas of architectonic or sculptural elements of high cultural value that will be placed in buildings or museums to ensure their protection. To guarantee a performant restoration, it is important to assure the compatibility between the mortar and the substratum materials in order to avoid potential damages. The use of nanoparticles in different industries, including cultural heritage conservation and restoration, is growing rapidly because of their unique chemical and physical properties [1]. It has been shown that nanoparticles may improve the physical and mechanical properties of mortars, together, in some cases, with the preservation of the substrate [2].

The application of nanoparticles to the conservation of stone cultural heritage objects began at the beginning of this century, principally with cleaning, consolidation, water repellent, antimicrobial and anti-graffiti applications [1]. Several applications of nanoparticles in cultural heritage conservation can be found in the book edited by Hosseini and Karapanagiotis in 2017 [3]. Nowadays, the use of nanoparticles is widespread in the building

industry [4], including in cultural heritage repair mortars [5-9]. However, only a limited number of works have dealt with the application of nanoparticles in mortars used to reconstruct missed parts of buildings. The nanoparticles most employed in cement based materials are composed of SiO₂ and TiO₂ [10]. SiO₂ is employed because of its low cost and pozzolanic properties. Mesdes et al [10] have reported the results of various studies on the addition of SiO₂ nanoparticles to cement based mixes. They concluded that SiO₂ nanoparticles increase the compressive strength of mortars, even though in some cases this increase reaches a maximum with a certain quantity of particles, and then decreases with higher concentrations. Porosity, on the other hand, follows a contrary behaviour, and some studies have shown that permeability, at least up to a nanoparticle content of 3%, behaves in a similar way. The changes produced by the addition of nanoparticles include a decrease in the carbonation rate as well as altered microstructural properties. These changes are caused by a pozzolanic reaction as reflected in thermogravimetric measurements [11].

Greco et al [12] have tested different SiO₂ and Fe₂O₃ nanoparticle concentrations in concretes with Portland cement for the restoration of historical and contemporary buildings, and they found an increase in mechanical strength, water resistance and elastic modulus, with pozzolanic reactions occurring between the nanoparticles and the portlandite.

Another study on the influence of the addition of nanoparticles to cementitious repair mortars was conducted by Haruehansapong et al (2017) [13]. Among other properties, they investigated the effect of SiO₂ nanoparticles of various sizes on drying shrinkage. They observed that in mortars containing 10% nanoparticles, cracking is more prevalent when the nanoparticle size is 12 nm or 20 nm than when the size is 40 nm.

The mixing procedure itself, for cement/lime based mortars and nanomaterials, plays a crucial role, and it has been shown that due to the nanoparticles' high surface area, the amount of water used should be increased in order to maintain good mortar workability, [14].

Next we present some preliminary results of a collaboration project between the Institute of Theoretical and Applied Mechanics of the Czech Academy of Sciences and the Geosciences and Environment laboratory of the University of Cergy-Pontoise. These results concern the influence of using nanosilica particles to a commercial repair mortar mixture. The goal of the research was to study the impact of silica nanoparticles on the mineralogical composition, microstructure and therefore the material properties of the mortar mixture.

Materials and methods

Mortar preparation

The commercial repair mortar Artopierre TM, produced by the Parexlanko company (France), was selected for the preparation of the samples used in this study. This mixture has already been characterised in a previous paper [15]. It is a complex mixture composed of an

aerial lime (CL binder, 70% in volume) with hydraulic, mineral and organic additives, mineral pigments, and calcareous and siliceous aggregates with a grain size of up to 1.5 mm. An optical image of Artopierre mortar without the addition of nanosilica is depicted in Fig 1. This mortar is commonly used in the restoration of monuments built with carbonate stones [15].

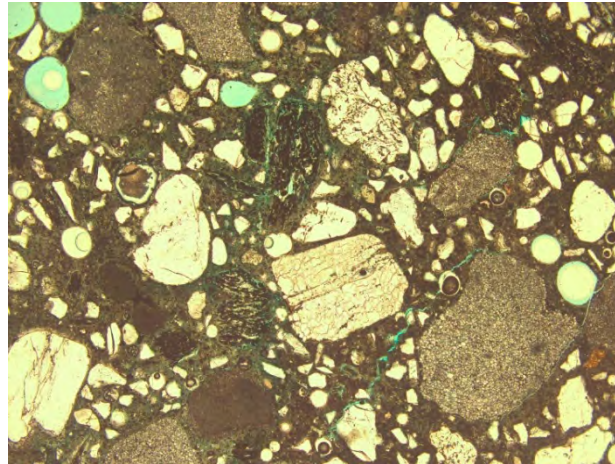


Figure 1. Optical transmission micrograph of Artopierre mortar. Image width is 4 mm.

The mineral aggregates in the raw material consist mainly of vermiculite, a phyllosilicate with Mg, Al and Fe. The aggregate granulometry is uniformly distributed between 0.2 mm and 1.25 mm.

Silica nanoparticles (SiO_2 , Sigma-Aldrich), with an average particle size of 14 nm, were used as the additive. The mortars tested contain various quantities of SiO_2 nanoparticles: 1, 2, 3, 5, and 7 wt%. The nanoparticles were dispersed in water in an ultrasound bath to avoid agglomeration and assure good particle dispersion in the mortar. A paste was mixed by hand for three minutes and then placed in a standard cast 4 cm x 4 cm x 16 cm in size. The water/solid ratio increases with the quantity of nanoparticles as shown in Fig 2. Fresh mortar specimens were covered with a plastic film for seven days and then air-dried. The samples were tested after a period of four months in the laboratory at 25°C and 35% relative humidity.

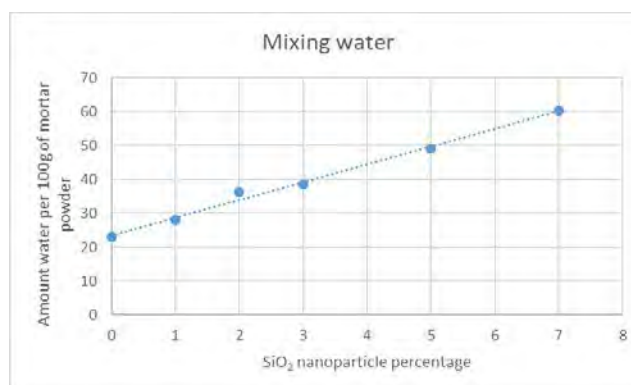


Figure 2. The quantities of mixing water used for mortars of various nanoparticle concentrations

Employed methods

Thermogravimetric analysis (TGA/DTG) tests were performed on two sets of mortar samples. The mortars were gently crushed in a porcelain bowl, and the finest fraction, containing grains below 0.063 mm in size, was used for a thermal analysis. The thermal analysis was carried out on the SDT Q600 instrument (TA Instruments) in the range of temperatures between 25-1000°C. For the analysis, volumes of about 20 mg in mass were placed in ceramic pans and heated in an N₂ atmosphere at a rate of 20°C per minute.

X-ray powder diffraction patterns were recorded on an X'Pert3Powder X-ray Diffractometer from Malvern Panalytical. The anode material used was Cu, K-Alpha1 wavelength 1.5405980 Å, K-Alpha2 wavelength 1.5444260 Å, and the divergence slit was fixed at 1.52 mm. No monochromator was used. 2θ scan range goes from 3° to 80° with a scan step size of 0.0167113 and 4608 points. The scan type was continuous, and the time per step was 55.245 s. Tension was set to 45 kV, and the Current to 40 mA.

The qualitative phase analysis was conducted using HighScore Plus software.

Fourier transform infrared (FTIR) spectroscopy measurements were performed on grinded samples (with grains below 0.063 mm in size) using the iZ10 external module of the Nicolet iN10 spectrometer (Thermo Scientific) equipped with a DTGS detector, a KBr beamsplitter and an ATR accessory with a diamond crystal. The spectra were collected in the range 4000–525 cm⁻¹ at 4 cm⁻¹ spectral resolution.

Open porosity and apparent density were obtained using the triple weight procedure, completely saturating the samples in water under a vacuum following the NF P94-410-3 standard (2001) [16]. The pore size distribution of the samples was measured with a Micromeritics AutoPore IV. The measured pore sizes ranged from 500 μm to 0.005 μm.

Dynamic water vapour sorption curves were measured with the Vsorp system from ProUmid. The moisture sorption analysis investigated the hygroscopic properties of the mortars.

Young modulus and Poisson's coefficient were calculated from acoustics P and S velocities.

The durability of the mortars was determined by accelerated ageing tests. Two different kind of tests were performed; frozen/thaw and salt crystallization tests. As the results of both tests were very similar, only the salt crystallization results are shown. The salt crystallization test was conducted according to the procedure described in the EN-12370 [17] standard, with a total immersion period of two hours in a decahydrate sodium sulphate 14% wt. solution, a drying period of at least 16 hours at 60°C, and a cooling period. The weight was measured at the end of each drying period, and pictures were taken after each cycle.

Results

Thermogravimetric analysis (TGA/DTG)

The results of the TGA/DTG measurements are shown in Figure 3. All the samples showed a calcium carbonate decomposition peak in the interval between 500°C to 850°C. Mass loss between 70°C and 150°C corresponds to the dehydration of calcium silicate hydrates coming from larnite hydration or even from a pozzolanic reaction between the calcium hydroxide and the silica. In the thermal interval 150°C – 500°C, the release of water bound in other hydrates took place. Table 1 shows that the total carbonate content decreased in samples containing higher additions of nanosilica. Such behaviour indicates that the higher amount of nanosilica introduced into the testing samples may favour pozzolanic reaction.

Table 1. Detected weight losses and CaCO₃ content at selected intervals for samples measured with TGA/DTG.

Sample	Weight loss (% wt)			Content (% wt.)
	70-500°C	500-700°C	700-850°C	CaCO ₃
AR	5.1	1.7	25.7	62.1
AR 1	5.6	5.7	22.6	64.3
AR 2	5.1	7.2	22.1	66.5
AR 3	5.2	7.9	20.7	65.0
AR 5	6.7	13.0	14.8	63.3
AR 7	7.0	13.9	10.4	55.2

Another effect of nanosilica addition was found by means of DTG analysis, as depicted in Figure 3 (at right).

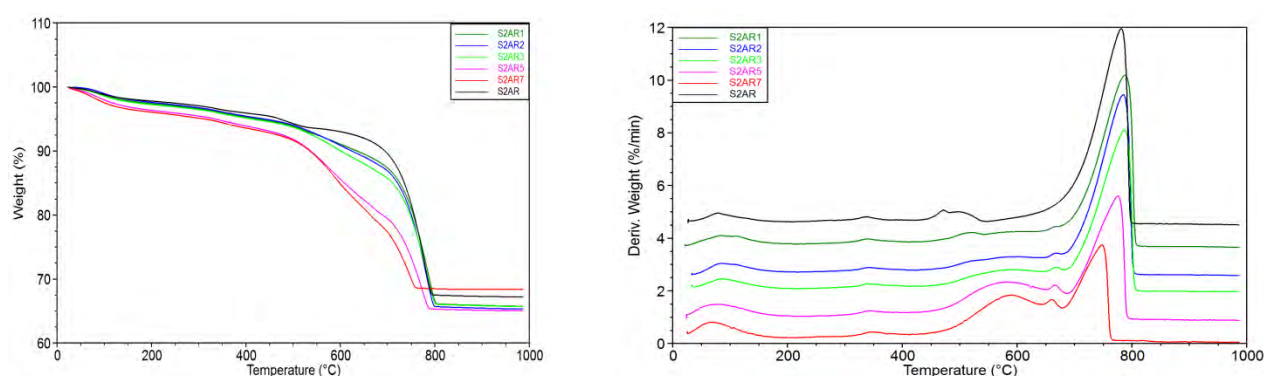


Figure 3. TGA (left) and DTG (right) curves for the studied samples.

With the higher amount of added nanosilica, broad bands in the temperature range from 500°C to 700°C began to appear, especially for samples with the highest amount of nanosilica AR5 and AR7. It has been described that such broadening may appear due to the formation of metastable CaCO₃ polymorphs (vaterite, aragonite) and/or the formation of

CaCO₃ with crystal defects, or as a result of the crystallization of smaller particles [18-19]. For the higher silica content, the formation of calcite, the most stable CaCO₃ polymorph under Earth-surface conditions, seems to be reduced, as is visible from the DTG curves in Figure 3 and XRPD patterns showed in Figure 4. The weight contents of the phases decomposed in the ranges of 500 to 700°C and 700 to 800°C are summarized in Table 1.

X-ray powder diffraction

The XRPD pattern (Figure 4) shows the amorphous nature of SiO₂ nanoparticles.

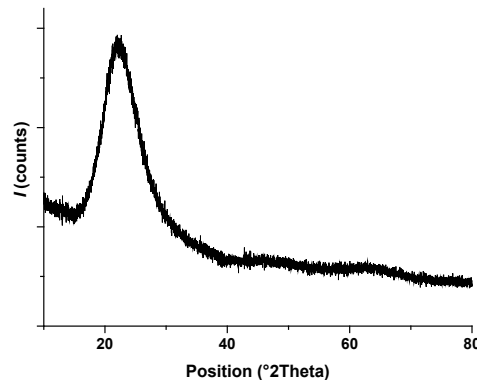


Figure 4. X-Ray diffraction diagram of employed SiO₂ nanoparticles. Peak height is approx. 2000 counts.

XRPD measurements (Figure 5) confirmed the presence of minor amounts of vaterite in all the samples. Aragonite was also detected in the samples, and it seems that with a higher amount of added nanosilica its concentration was slightly higher (Figure 6). The lower formation of metastable modifications of CaCO₃ in samples with a higher amount of calcite, detected with TGA/DTG, is detectable in the XRPD patterns as well (Figure 5). The XRPD measurements also revealed the presence of calcium silicates.

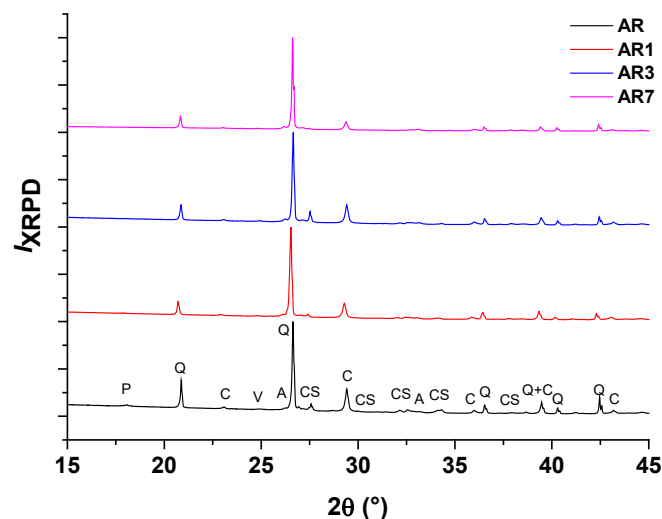


Figure 5. Selected XRPD diffraction patterns for the test samples. Maximum peak heights are approx. 200000 counts for all mortars. The main Bragg peaks for phases are indicated (P = portlandite, Q = quartz, CS = calcium silicates, V= vaterite, C = calcite, A = aragonite).

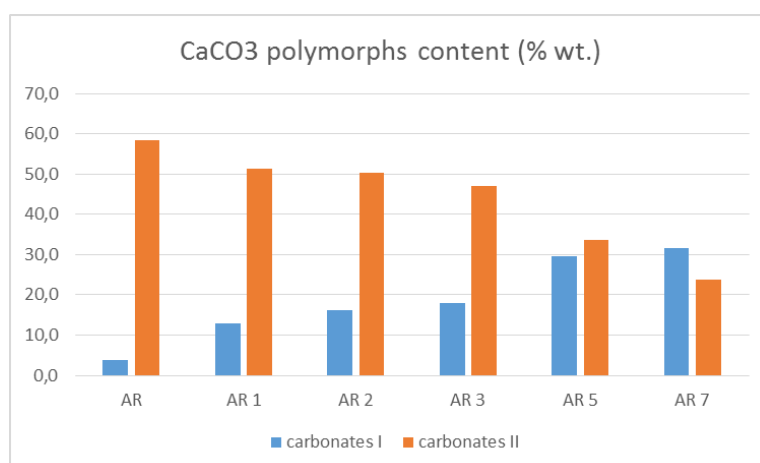


Figure 6. Representation of individual CaCO₃ polymorphs. Carbonates I – metastable modifications, carbonates II – calcite.

Fourier-transform infrared spectroscopy (FTIR)

The presence of calcite, vaterite and aragonite was also confirmed with ATR-FTIR measurements (Figure7). The peaks with highest intensity, corresponding to aragonite and calcite, were found in samples AR7 and AR, respectively, which is in agreement with the XRPD results. The characteristic peak for portlandite (3641 cm⁻¹) appeared mainly in the spectrum for the AR sample. Small portlandite peaks were also observed in samples AR1, AR2, and AR3 (in order from highest to lowest intensity), indicating incomplete carbonation. Peaks in the spectral range ~1290–900 cm⁻¹ and at ~800 cm⁻¹, correspond to SiO₂ from aggregates or SiO₂ nanoparticles. These bands are more intense in samples containing higher concentrations of nanosilica.

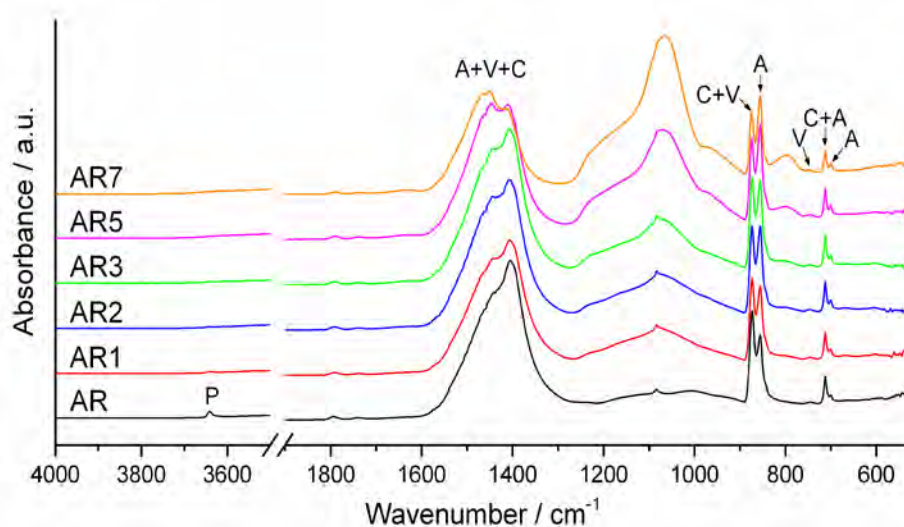


Figure 7. ATR-FTIR spectra of the samples. The peaks of calcite (C), vaterite (V), aragonite (A) and portlandite (P) are indicated.

The low intensity peak at 1738 cm^{-1} , present in all the spectra, could be attributed to C=O vibration, originating from organic additives. It is well known that the presence of organic additives may promote the formation of metastable CaCO_3 polymorphs. As the consequence of the presence of organic additives in the Artopierre repair mortar, vaterite and aragonite formed in all the test samples. The presence of vaterite was very low in the samples, but in the case of aragonite, the occurrence of this CaCO_3 polymorphs increased when greater amounts of nanosilica were added. It can be speculated that such aragonite could have also formed as a result of the decomposition of e.g. CSH phase.

Physical and mechanical properties

Open porosity and apparent density values are shown in Table 2.

Table 2. The open porosity and grain density of the studied mortars.

Sample	Open porosity (%)	Real density (kg/m^3)	Apparent density (kg/m^3)
AR	41.1	2614	1540
AR1	41.8	2620	1525
AR2	41.7	2611	1524
AR3	42.7	2606	1493
AR5	45.0	2584	1420
AR7	54.9	2522	1138

It is clearly visible that porosity increased with the additions of nanosilica. The two highest nanosilica additions in particular significantly affected the porosity value. In comparison to the AR sample, the porosity of AR7 was found to be 14% higher. The opposite trend was found in the case of apparent density. For samples AR-AR2, the changes are negligible, but in the samples with nanosilica content at 5 and 7 wt%, the mineral density began to change.

Pore size distribution curves representing the calculated pore size diameters of the mixtures are plotted in Figure 8. The presented results correspond to nanoparticle contents of 1 and 2.5 wt%.

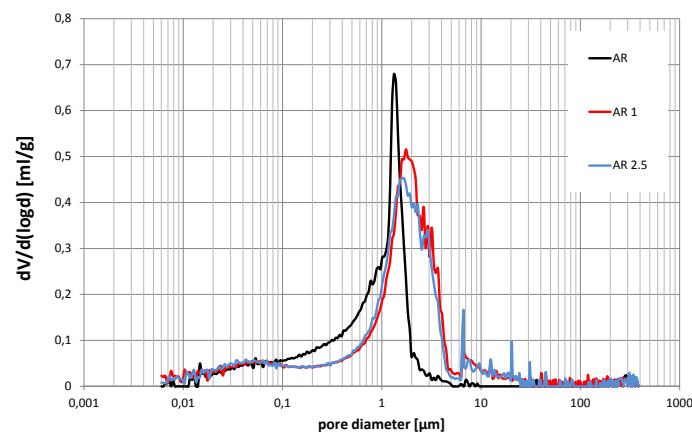


Figure 8. Pore size distribution of 28-day-old mortar samples with and without nanoparticles.

Water absorption investigation based on “the drop test” (Fig 9) shows that in all the samples water droplets penetrate faster when compared to the reference mortar, and that the water droplet absorption time decreases with an increase in the amount of nanoparticles added.

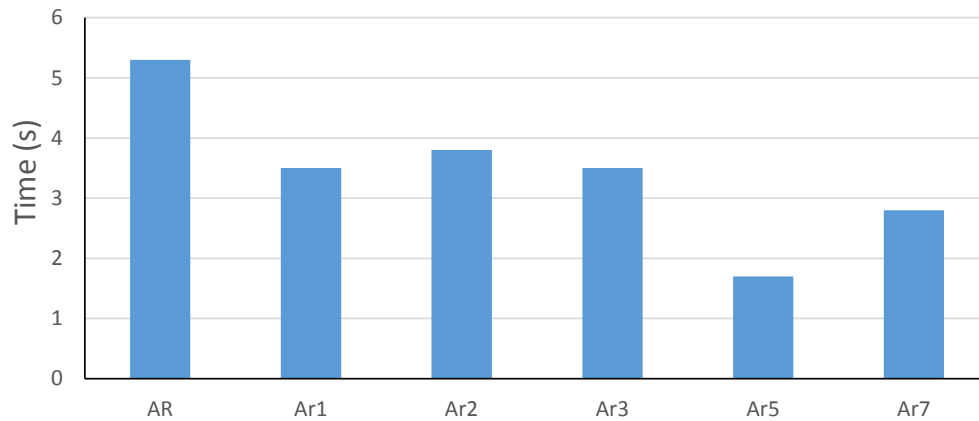


Figure 9. Water droplet absorption time for each mortar sample.

This finding corresponds to the presence of larger pores that were detected in the samples modified with nanoparticles. As can be seen from the pore size distribution curves for the 28-day-old mortars (Figure 8), the higher amount of nanoparticles (introduced into the mortars using a larger amount of mixing water) shifted the pore sizes of these mortars to larger diameters. Within larger pores, water moves faster by capillary transport.

The dynamic vapour water absorption results (Figure 10) show an increase in water vapour absorption as a function of SiO₂ nanoparticle content.

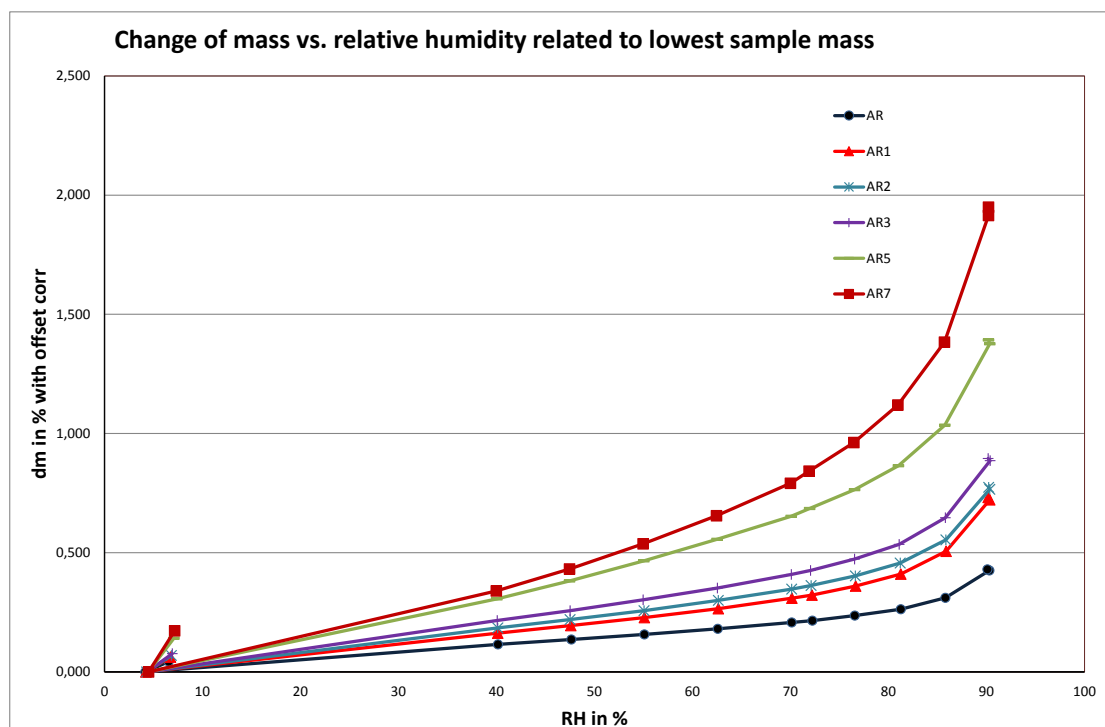


Figure 10. Water vapour absorption of samples as a function of relative humidity.

Mechanical properties

Young modulus, related to elasticity, significantly decreases with the amount of added nanoparticles. The obtained results (Tab. 3) are in agreement with the above findings on the increase in porosity of the mortars. The tendency of Poisson's coefficient, related to volume deformation, is less clear.

Table 3. Mechanical properties of the studied mortars.

Sample	Dynamic Young Modulus (MPa)	Dynamic Poisson's coefficient
S2 AR	2945	0.204
S2 AR1	2397	0.218
S2 AR2	2373	0.197
S2 AR3	1907	0.175
S2 AR5	1302	0.206
S2 AR7	402	0.175

Salt Crystallization tests

After the testing procedure, the mortar samples containing nanoparticles were more affected by salt than the sample without any addition of nanoparticles. In Figure 11 we can observe the evolution of sample weights over a period of 10 cycles. After ten cycles the samples were destroyed, and it was no longer possible to continue the tests.

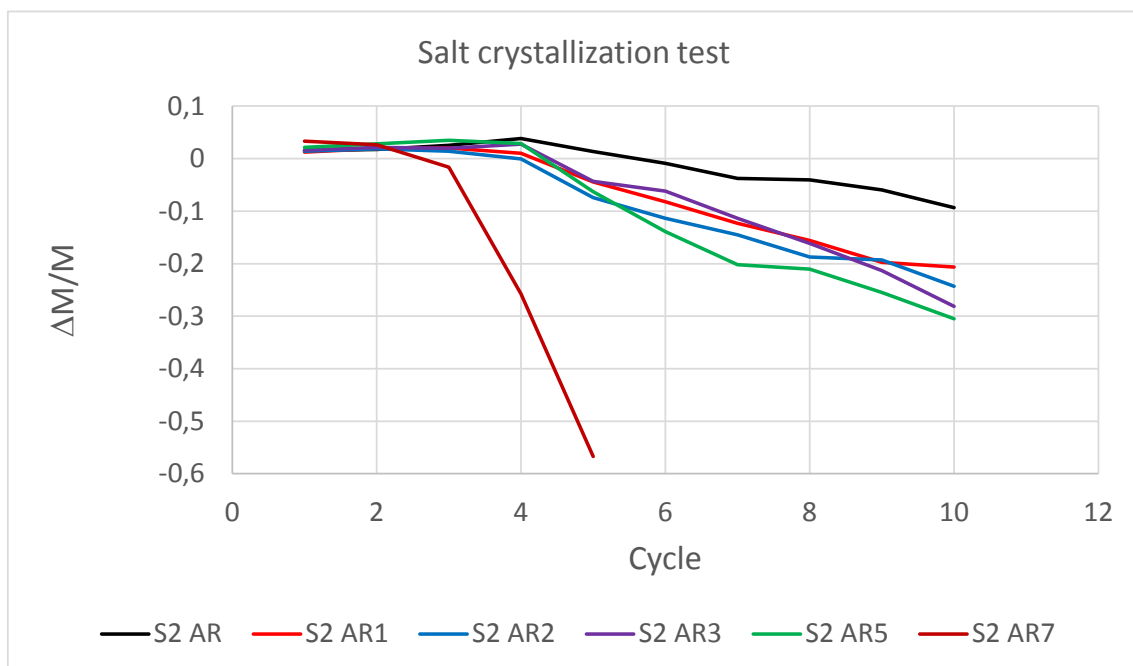


Figure 11. Weight variation of mortar samples during salt crystallization test.

Discussion and conclusion

In this paper we have presented some results concerning the physical and mineralogical effects of the addition of SiO₂ nanoparticles to a commercial restoration mortar. The results obtained are not the ones we expected. We expected to see an increase in the mechanical strength of the samples, but instead we observed a decrease. There was an increase in porosity that induced an increase in water transfer properties. These variations also induced a lower durability in the samples containing nanoparticles during the artificial ageing test.

Several explanations can be given for the unexpected results. For example, the fact that we did not use a superplasticizer and/or that we did not know the exact details on all the various additives contained in the original mortar mix.

We found that the microstructure, porosity and mechanical properties of the hardened mortars were affected more by the amount of mixing water used than by the amount of nanoparticles added. The crucial tasks for the next phase of this research are selection of a suitable method of mixing nanoparticles into the mortar and optimization of the mixing water quantity.

Acknowledgments

This research was supported by the Barrande exchange program between Czech Republic and France; on the Czech side under the project 8J18FR019 “Nanomaterials for cultural heritage conservation”, supported by the Ministry of Education, Youth and Sports of the Czech Republic, as part of the program Mobility 7AMB18FR.

References

1. Sierra-Fernandez A, Gomez-Villalba L S, Rabanal M E, Fort R (2017) New nanomaterials for applications in conservation and restoration of stony materials: A review. *Materiales de Construcción*. 67 (325), e107. doi: 10.3989/mc.2017.07616
2. Cavazos J-S, González G, Kharissova O V, Ortega B, Peña L, Osorio M, Garza-Castañón M (2017) Effect of Nanoparticles on Mechanical Properties of Cement-Sand Mortar Applications. *Advances in Chemical Engineering and Science* 07(03):270-276, doi: 10.4236/aces.2017.73020
3. Hosseini M, Karapanagiotis I (Eds.) (2018) *Advanced Materials for the Conservation of Stone*. Springer International Publishing, 332p, doi: 10.1007/978-3-319-72260-3, eBook ISBN 978-3-319-72260-3
4. Alsaffar K A (2014) Review of the Use of Nanotechnology in Construction Industry. *International Journal of Engineering Research and Development* 8 (10): 67-70. ISSN: 2278-067X, p-ISSN: 2278-800X

5. Senffa L, Hotza D, Repette W L, Ferreira V M, Labrincha J A (2010) Mortars with nano-SiO₂ and micro-SiO₂ investigated by experimental design, *Construction and Building Materials* 24: 1432–1437 doi: 10.1016/j.conbuildmat.2010.01.012
6. Maravelaki N, Lionakis E, Kapridaki C, Agioutantis Z, Verganelaki A, Perdikatsis V (2012). Characterization of hydraulic mortars containing nano-titania for restoration applications. 12th Int. Congress on the Deterioration and Conservation of Stone, New York, USA
7. Stefanidou M (2013) Nano-modified lime pozzolana pastes. *Romanian Journal of Materials* 43(3): 246-250
8. Fernandez J M, Duran A, Navarro-Blasco I, Lanas J, Sirera R, Alvarez J I (2013) Influence of nanosilica and polycarboxylate ether superplasticizer on the performance of lime mortars. *Cement and Concrete Res* 43: 12-24. Doi: 10.1016/j.cemconres.2012.10.007
9. Theodoridou M, Kyriakou L, Ioannou I (2014) Salt crystallization resistance of nano-modified repair mortars. 3th Int. Conference on Salt Weathering of Building and Stone Sculptures. Brussels, Belgium
10. Mendes T M, Hotza D, Repette W L (2015) Nanoparticles in cement based materials: A review. *Reviews on Advanced Materials Science*. 40: 89-96
11. Collepardi M, Olagot J J O, Troli R, Skarp U (2002). Influence of Amorphous Colloidal Silica on the Properties of Self-Compacting Concretes. International Conference, Challenges in Concrete Construction- Innovations and Developments in Concrete Materials and Construction, Dundee, UK
12. Greco E, Ciliberto E, Damiano Verdura P, Lo Giudice E, Navarra (2016) Nanoparticle-based concretes for the restoration of historical and contemporary buildings: a new way for CO₂ reduction in architecture. *Applied Physics A* 122:524 doi: 10.1007/s00339-016-0056-1
13. Haruehansapong S, Pungern T, Chucheepsakul S (2017) Effect of Nanosilica Particle Size on the Water Permeability, Abrasion Resistance, Drying Shrinkage, and Repair Work Properties of Cement Mortar Containing Nano-SiO₂ *Advances in Materials Science and Engineering*, Article ID 4213690, 11 p doi: 10.1155/2017/4213690
14. Lucas S S, Ferreira V M, Aguiar J L B (2013) Incorporation of titanium dioxide nanoparticles in mortars — Influence of microstructure in the hardened state properties and photocatalytic activity. *Cement and Concrete Research* 43: 112-120 doi: 10.1016/j.cemconres.2012.09.007
15. Lopez-Arce P, Tagnit-Hammou M, Menendez B, Mertz J-D, Kaci A (2016). Durability of stone-repair mortars used in historic buildings from Paris. *Materials and Structures* 49 (12): 5097–5115 doi: 10.1617/s11527-016-0846-0

16. NF P94-410-3 (2001) Roches - Essais pour déterminer les propriétés physiques des roches
17. EN 12370 (1999) Natural stone test methods. Determination of resistance to salt crystallisation.
18. Sauman Z. (1971) Carbonization of porous concrete and its main binding components, Cement and Concrete Research 1(6): 645-662
19. Villain G, Thiery M, Platret G (2007) Measurement methods of carbonation profiles in concrete: Thermogravimetry, chemical analysis and gammadensimetry. Cement and Concrete Research 37(8):1182-1192 doi:10.1016/j.cemconres.2007.04.015)
20. Bläuer Ch, Franzen Ch, Vergès-Belmin V (2012) Simple field tests in stone conservation. 12th International Congress on the Deterioration and Conservation of Stone, Columbia University, New York, USA

Evaluation of SiO₂ nanoparticles as additive for lime mortars: changes in the microstructure and mechanical properties

María del Mar Barbero-Barrera¹, Aranzazu Sierra Fernández², Duygu Ergenc², Luz Stella

Gomez Villalba², Rafael Fort²

(1) *Universidad Politécnica de Madrid, mar.barbero@upm.es*

(2) *Instituto de Geociencias (CSIC, UCM), arsierra@ucm.es; duyguerg@ucm.es; luzgomez@geo.ucm.es; rafael.fort@csic.es*

Abstract

The use of additions, such as ceramic materials (crushed or finely ground bricks), with pozzolanic activity in lime-based mortars and plasters is an old practice in the field of construction. The reason is attributed to the pozzolanic reaction of these materials with the lime in the presence of water to generate different hydration products (aluminosilicates), which can contribute to enhance its strength and behaviour. Moreover, in recent times, nanoparticles (NPs) have been considered as a potential addition to boost the reactions in calcium hydroxide from mortars. Among different NPs, SiO₂ NPs is considered a promising additive due to its action as nanofiller. In this research, effects induced by the addition of commercial nanosilica to aerial lime mortars containing different aggregates (standard siliceous sand and crushed and ground Roman ceramic) were studied. Specifically, the microstructural modifications produced by the presence of ceramic aggregates and nanoparticles into the lime-based mortars were studied related to the hydric properties and mechanical performance.

Introduction

Lime had been the most important binder used in historic masonry construction. The feasibility of the raw material in the Iberian Peninsula justified their use since ancient times. The main type of carbonate rock used as raw material was the one of high purity; However, in some regions, hydraulic (commonly slightly or moderate hydraulic) lime was employed [1].

The lack of hydraulic performance of the binder involved the addition of different types of inorganic materials with pozzolanic activity. These pozzolanic materials are expected to play a key role on the enhancement of certain properties or even induce special performances in lime-based mortars, such as an increase of mortar strength [2]. The reason is attributed to the pozzolanic reaction, of these additions, with the lime in the presence of water to produce different hydration products (aluminosilicates), which are able to provide filling effect and contributing to the strength gain of the mortars and plasters [2, 3]. Among different types of pozzolanic additions, natural rocks mainly coming from volcanic origin

were used in areas where they were available [3]. However, in the absence of these types of materials, which provide a high content of amorphous compounds, with a high content of silica or aluminosilicates, they were replaced by other pozzolanic additions such as ceramic powder (crushed or finely ground bricks) [4, 5]. In this regard, the influence of calcination parameters of the ceramics, such as time and temperature, play an important role in the final properties of the blends [6]. Thus, in order to get pozzolanic properties, ceramics were widely fired at a relatively low calcination temperature, at about 800°C depending on the type of clay mineral [5, 7, 8]. The calcination provoked a chemical disequilibrium in the medium as a result of reactions which favour phase transformations. These chemical reactions modify the crystallinity degree and affect stability of mineral phases. From this interaction, pozzolanic meta-stable or amorphous nature substances (aluminosilicates) are achieved. In fact, according to the research work carried out by Böke et al [5], bricks used for the preparation of hydraulic mortars needed to be selected among the ones with higher amount of clays and calcinated at temperatures sufficiently low (commonly under 800 °C), to prevent the formation of mineral phases such as mullite or cristobalite [5]. In any case, depending of the calcination temperature, different mineral reactions and products could occur.

Furthermore, different studies had been focused on investigating the effect of using brick dust in the physico-chemical and mechanical properties of mortars [9, 10]. From these studies, it was concluded that the presence of ground brick modifies significantly the pore size distribution of the mortars, and consequently altered their compressive strength [9, 10]. This is produced by the dilution effect and generation of additional C-S-H gel from reaction of bricks with calcium hydroxide [10]. Moreover, the reduction of the alkali-silica reaction expansion is another important modification derived from the use of ground bricks as a pozzolanic material in mortars [11].

On the other hand, the application of nanoparticles (NPs) in the field of mortar technology for improving their performance had been the focus of recent research [12]. Their physical and chemical properties, mainly their high-surface area and reactivity, may modify the mechanical properties and, consequently the durability of the mortars [13, 14]. Indeed, since the pozzolanic activity may increase with the reduction of size fraction of the particles [15], different research had been specially focused in the use of silica nanoparticles (SiO₂ NPs) into lime mortars [13, 14, 16, 17]. In general terms, the use of SiO₂ NPs can generate microstructural modifications into mortars due to its action as nanofiller in the lime-based binding, which enhance their compressive strength and durability [16, 17].

This research deals with the effects that the addition of commercial nanosilica induces in aerial lime mortars containing different aggregates (standard siliceous sand and crushed and ground Roman ceramic). A special focus was thus set in studying the influence of the presence of ceramic aggregates and nanoparticles on the pore structure of lime-based mortars and, consequently its effect on their hydric and mechanical performance.

Materials and method

Materials

The composition of mortars was defined by the characterization of Roman ones coming from the Complutum archaeological Site (Alcalá de Henares, Madrid, Spain) [18]. Lime putty, which was used as binder, had maturation time of four years. It was composed of a 59 % of $\text{Ca}(\text{OH})_2$, 26 % of CaCO_3 and 15 % of water content. Moreover, the bulk density of the lime putty was 1326 kg/m^3 and was supplied by Proiescon S.L. (Madrid, Spain).

EN-196-1: 2006 Standard siliceous sand CEN-NORMSAND was used as aggregate. This sand is characterized by a high silica composition (99 % of SiO_2 in weight).

Furthermore, ceramic aggregates were collected from the original bricks and tiles of the Complutum archaeological site. These materials were crushing and grinding up to achieve different grain sizes, in order to reproduce the grain size distribution of the Complutum Roman mortars. The chemical analysis of raw materials taken on ceramic fragments showed that they were mainly composed by 53 % of SiO_2 and 19.9 % of Al_2O_3 , in percentage by weight. Additionally, in lesser amounts these materials also contained 7.1 % of MgO , 6.6 % of Fe_2O_3 , 4.6 % of K_2O , 0.7 % of Na_2O , and 0.8 % of TiO_2 .

Finally, an aqueous colloidal solution of nanosilica (30 % dry residue), which is distributed under the trade name of NanoEstel[®], was used in this research. The SiO_2 NPs presented spherical shapes with a quite uniform particle size of about $20 \pm 5 \text{ nm}$.

Sample Preparation

Two types of mortars were prepared: one with lime putty and sand, and named as M1, and another type with the additional use of ceramic aggregates and called M2. The M1 mortars were made by using a dosage ratio by volume of 1:3 (lime putty: sand). Whereas the proportion of M2 were carried out following the data obtained from the characterization of Roman mortars from Complutum [18]. Thus, a dosage ratio of 1:2:1:0.5, by volume, which corresponded to lime: sand: ceramic fragment: ceramic dust, was used for reference M2-type mortars.

When nanoparticles were added, they were introduced in a volume ratio of 0.5: 1 by volume (nanoparticles:binder). This percentage followed the recommendation of Rosato et al. [19]. Thereby, based on the addition of the ceramic aggregates and the SiO_2 nanoparticles four types of mortars were prepared, two control samples (M1-C and M2-C), only composed of lime, sand and ceramic aggregates (dust and fragments), and another two in which the effect of nanosilica addition was analysed and called as M1- SiO_2 and M2- SiO_2 . The constituents of mortars and the content of each sample is showed in Table 1.

Regarding the sample preparation and curing, solid compounds (sand and ceramic aggregates) were firstly homogenized, mixed, and added to the lime putty. Afterwards, the required amount of mixing water was added while continuing mixing. This water to binder ratio (lime water: lime putty) was fixed into 0.2 ratio. Finally, the SiO₂ nanoparticles were added into the blend and mixed with them. The workability of the fresh mortars was comprised between 140 and 160 mm, being slightly increased with the presence of the aqueous colloidal solution of nanosilica into the blend (Table 1).

Table 1. Mix proportions of mortars by volume, as well as their flow value

Sample	Binder	Sand	Ceramic Fragment	Ceramic Dust (<125µm)	SiO ₂ NPs	Water/Binder Ratio	Flow Diameter (mm) *
M1-C	1	3	-	-	-	0.2	143
M1-SiO ₂	1	3	-	-	0.5	0.2	153
M2-C	1	2	1	0.5	-	0.2	142
M2- SiO ₂	1	2	1	0.5	0.5	0.2	155

* Values obtained by standard flow table test (EN 1015-3:2000).

Finally, the blends were casted into 40 x 40 x 40 mm³ cubic silicon moulds and compacted. The moulds were transferred to a temperature and humidity-controlled room for 7 days, in both cases, with 90 % of relative humidity and 25 ± 3 °C. Specimens were demolded after 7 days, and then were cured under controlled conditions in a ventilated chamber at around 50 % of relative humidity (RH), 25 ± 3°C, and under a carbon dioxide (CO₂) concentration over 700 ± 100 ppm. They were kept in these conditions up to the tests at 120 days of curing time.

In all tests, at least three samples were used for every composition, to ensure the statistical significance and reproducibility of results.

Characterization

Mineralogical composition

The mineralogical composition of mortar specimens was studied at 120 days of curing time by X-ray diffraction (XRD), employing a Panalytical X'Pert MPD diffractometer, and employing a CuK α radiation ($\lambda = 1.54 \text{ \AA}$) source, in Bragg-Brentano geometry. The measurement conditions were: 2 θ : 4-80° scan range, 2 θ = 0.03 step size, 1 sec/step time measurement and operating at 45 kV and 40 mA.

Microstructure

The different mortar samples were analyzed through an environmental scanning electron microscope coupled with an energy dispersive X-ray detector (ESEM-EDS) (FEI QUANTA 200,

OXFORD INSTRUMENTS Analytical-Inca). Moreover, the microstructure and porosity of the different mortars were also investigated with Brunauer-Emmet-Teller (BET) method (Micromeritics Tristar 3000 Analyzer), in both cases after 120 days of curing. The N₂ sorption isotherms were obtained at 77.35 K under continuous adsorption conditions. Moreover, the Barret-Joyner-Halenda (BJH) method [20] was applied to accurately analyze the distribution of pore size. High purity nitrogen gas (>99.99 %) was used in all measurements.

Hydric performance

Open porosity and bulk density were determined following the standard EN 1936:2007.

Compressive strength

The compressive strength of the mortar samples was measured at 120 days of curing time following the EN 1015-11. An autotest-200/10-SW for 2kN was used at a constant rate of 0.01 N/m².s.

Results and discussion

Mineralogical phases of mortars

Figure 1 shows the XRD patterns obtained on the surface of the different mortars, after 120 days of curing. Overall, the XRD patterns for all samples showed peaks corresponding to the presence of portlandite and calcite coming from the binder and quartz from aggregates (Figure 1a and 1b). The presence of hematite was also detected in the M2 mortars (Figure 1b) due to the presence of ferromagnesian minerals including phyllosilicates from raw materials. Most of these minerals deposit fragments, which react producing oxidation to finally precipitate hematite from the Roman tiles and bricks used as aggregates. These minerals cause a red coloration in these samples.

Moreover, as expected, according to the XRD patterns the carbonation process was not complete after 120 days of curing time. The analysis showed thus the presence of uncarbonated portlandite in all mortars (Figure 1). However, noticeable differences in the degree of carbonation reaction associated to the presence of ceramic aggregates and the incorporation of nanoparticles in the samples could be established. Indeed, the addition of the ceramic aggregates (M2-C and M2-SiO₂) enhanced the carbonation process when compared to the samples without them (Figure 1). Furthermore, it should be highlighted that when SiO₂ nanoparticles were introduced, an increased carbonation rate was detected as well, but only in the surface of both types of mortars. It could be due to the water retention capacity of the ceramic aggregates and nanoparticles compared to the silica sand which favoured the conditions for a higher carbonation degree and hydraulic activity.

This agreed to the fact that it was possible to notice the presence of hydrated forms in the M2-SiO₂ samples. The formation of these hydration products, such as C-S-H gels is expected

as a result of the reaction of silicate and aluminate ions with Ca^{2+} ions [2, 21]. Contrary to this, on M1-SiO₂, it was not possible to detect the formation of hydrated phases. However, it is worth noting that probably because its amount could be under the detection limit of this analytical technique (3-5 %) [22].

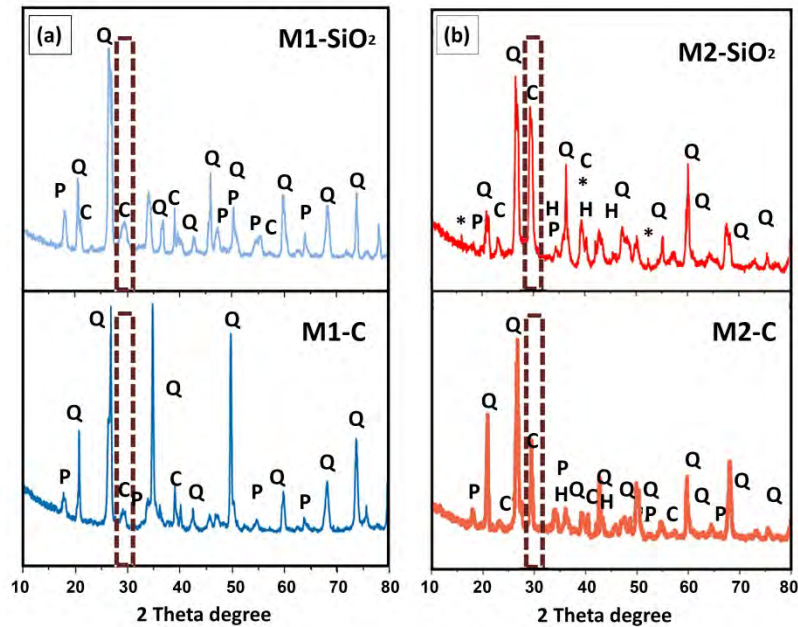


Figure 1. XRD patterns of external surface of mortars, after 120 days of curing. C= Calcite; P=Portlandite; Q= Quartz; H= Hematite; *= C-S-H phases. The main peak of calcite is marked.

Moreover, a great decrease of $\text{Ca}(\text{OH})_2$ was detected in M2 samples in comparison with M1 type mortars. This could be not only representative of an increased carbonation rate but also an advanced hydration process with the consequent consumption of portlandite in the large amount of pozzolanic additions.

Microstructure

An ESEM microtextural analysis was carried out for the different mortar samples (Figure 2). A high porous surface with the presence of cracks was observed in the mortars M1 (Figure 2a), contrary to the filler effect of ceramic aggregates which induced a greater compactness (Figure 2b). These results agreed to previous studies [23] in which was stated that whereas the channel type pores are formed next to sand aggregate in the mortars without ceramic, the use of ceramics generated pores in the binder when kneading water was evaporated.

Moreover, compared to the control samples (Figure 2a and 2c), the presence of SiO₂ NPs in the mortars generated smooth and compact surfaces (Figure 2b and 2d), as possible consequence of C-S-H and C-A-S-H gel generation in these samples. It should be highlighted that the addition of SiO₂ NPs also resulted in the generation of various visible microcracks on the surface of the samples attributed to the shrinkage (Figure 2 bi and di), related to the volumetric changes of samples [24].

Figure 3 shows the BET results (BET-surface area, pore size and pore volume) for the different samples. The measurements of BET-surface area showed that the incorporation of SiO₂ NPs as well as ceramic aggregates induced an increased value of surface area in lime-based mortars, being of around 40 % higher for the M1-SiO₂ NPs compared to M1-C, and 98 % higher for the M2-SiO₂ samples in comparison by M2-C.

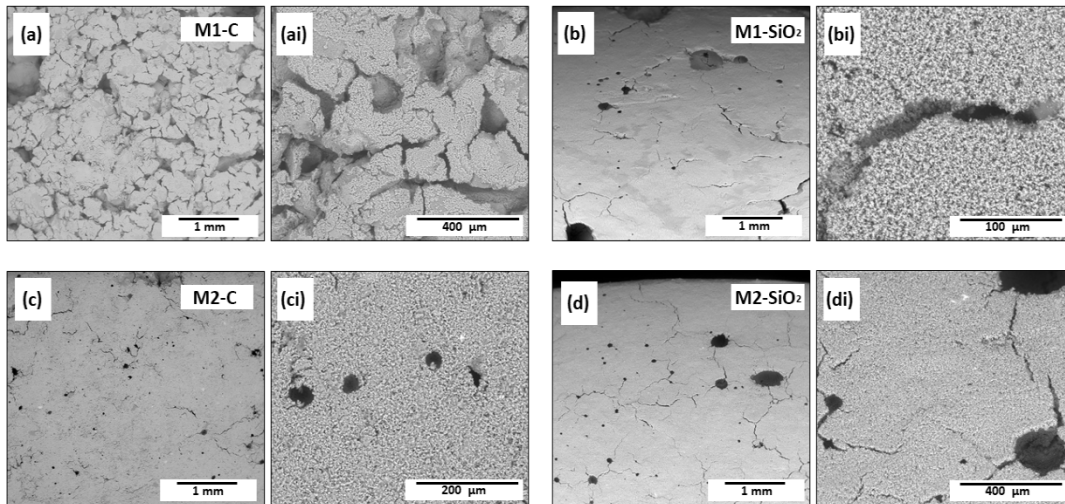


Figure 2. ESEM images of the four types of mortars, after 120 days of curing time. (a and ai): M1-C; (b and b1): M1-SiO₂; (c and ci): M2-C; (d and di) M2-SiO₂.

To note the different presence of fissures in the mortars, depending on their composition.

Besides, an important increased surface area value of ~115 % for the M2-C compared with the M1-C sample was also detected (Figure 3a). As expected, the surface area and pore volume were in similar trend. On one side, it can be explained by the ceramic dust dispersed around the binder as well as by two phenomena: the microcracking, which was detected by ESEM (Figure 2), due to shrinkage, occurred during drying and carbonation [24, 25]; and/or the widening of the gel pores which was occurred during formation of the hydrated phases (C-S-H and C-A-S-H). The widening was the result of the volumetric changes of the crystals when those mentioned phases were partially carbonated [26].

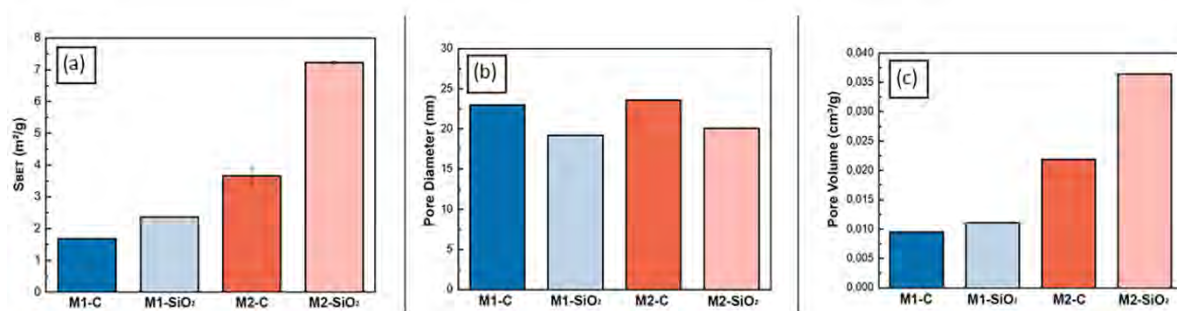


Figure 3. BET results of the mortar samples after 120 days of curing time. (a) surface area; (b) pore diameter; (c) pore volume

On the other hand, the pore diameters were smaller in the presence of NPs (Figure 3b), since the transformation of portlandite into calcium carbonate filled the largest pores.

Hydric properties and Compressive strength

The analysis of the pore system showed that the presence of ceramics and SiO₂ NPs induced a higher open porosity, with an increase of around 64 % and 89 % for M2-C and M2-SiO₂ samples, respectively, in comparison with M1-C sample (Table 2). The presence of pozzolanic material (crushed and ground ceramics) used as aggregates in M2-type mortars, had high capillary properties and increased surface area (Figure 3). Thereby, their presence into mortars can enhance the mortar's water absorption [27, 28]. Moreover, the appearance of microcracking in these samples (Figure 2) could also induce the increase in open porosity.

On the other hand, the bulk density of the different mortars decreased when the ceramic aggregates and SiO₂ NPs were added (Table 2). In this regard, it should be mentioned that no healthy data could be recorded in M1-SiO₂ because the samples were seriously damaged during the measurements. The high volume of microcracks detected in these samples did not allow performing the measurements. Taking this into account, the bulk densities were in the following order: M1-C > M2-C > M2-SiO₂, which is in accordance with the pore volume and surface area detected by BET.

Furthermore, the compressive strength was in agreement with their bulk density [29]. As can be seen in Table 2, contrary to previous studies [30, 31] mortar with ceramic aggregate (M2-C) showed less compressive strength than its pair (M1-C), although the increase in open porosity was in the same trend. Besides, the addition of SiO₂ NPs into the M2 provoked a sharp loss of cohesion in its structure which was coherent with the increase of its pore volume. Previous studies have also shown how the stability of the hydrated phases is also crucial to achieve strength [17]. In this way, the detrimental mechanical properties detected in these samples could be induced by the presence of highly reactive pozzolanic additions, which may not provide enough strength development to the mortars due to the phase modifications. In any case, the loss of compressive strength by the increase of surface area could be related to the excess of initial water in the blends, and continuously formed microcracks after the transformation of unstable hydrated phases and portlandite.

Table 2. Open porosity, density and compressive strength of mortar samples

Sample	Open Porosity (%)	Density (kg/m ³)	Compressive Strength (MPa)
M1-C	19.39 ± 0.07	1867.26	0.87
M1-SiO ₂	-	-	-
M2-C	31.82 ± 0.03	1663.94	0.74
M2- SiO ₂	36.58 ± 0.34	1489.37	0.55

Conclusions

The present research evaluated the effects of ceramic aggregates and SiO₂ NPs in the hydric and mechanical performance of lime-based mortars. To summarize, the following results could be obtained from this study:

- Incorporation of pozzolanic materials (Roman ceramics and nanosilica) into the mortars increased the carbonation degree on their surfaces. It was also detected the formation of hydrated phases in these mortars.
- Important variations of the microstructure have been found in all mortars, as a consequence of the presence of pozzolanic materials. Thereby, smooth and compact surfaces were observed with the latter. However, a great amount of microcracks was detected over the surface of the mortars with NPs, especially, in the case of M2. These mortars presented also the highest surface area and pore volume attributed to the hydration of hydraulic phases of hydrated calcium aluminosilicates and silicates generated in these samples.
- The presence of Roman ceramics and nanosilica induced a higher open porosity and a lower density value. The use of NPs could thus enhance the water absorption in lime-based mortars. Moreover, a decreased compressive strength was detected after 120 curing days when the pozzolanic additions were used in the mortars. This detrimental strength development detected in these mortars could be due to the deficient stability of the produced hydrated phases and/or the presence of microcracks detected in these samples.

Acknowledgement

This study was financially supported by the CLIMORTEC BIA2014-53911-R project coming from the Ministerio de Ciencia, Innovación y Universidades as well as TOP Heritage P2018/NMT-4372 Project, both of the Comunidad de Madrid.

References

1. Barbero-Barrera MM (2012) Mejora del comportamiento térmico de los morteros de cal aditivados y su empleo en la rehabilitación de inmuebles. UPM PhD Thesis. Available at: <http://oa.upm.es/10612/>
2. Arizzi A, Cultrone G (2012) Aerial lime-based mortars blended with a pozzolanic additive and different admixtures: A mineralogical, textural and physical-mechanical study. *Constr Build Mater* 135-143
3. Massazza F (2004) Pozzolana and pozzolanic cements in: Hewlett P (ed) *Lea's chemistry of cement and concrete*. Elsevier Science
4. Baronio G, Binda L, Lombardini N (1997) The role of brick pebbles and dust in conglomerates based on hydrated lime and crushed bricks. *Constr Build Mater* 1: 33-40
5. Böke H, Akkurt S, Ipekoglu B, Ugurlu E (2006) Characteristics of brick used as aggregate in historic brick-lime mortars and plasters. *Cement Concrete Res* 36. 1115-1122.

6. Fernandez R, Martirena F, Scrivener KL (2011) The origin of the pozzolanic activity of calcined clay minerals: A comparison between kaolinite, illite and montmorillonite. *Cement Concrete Res* 113-122.
7. Wild S, Khatib JM, O'Farrell M (1997) Sulphate resistance of mortar, containing ground brick clay calcined at different temperatures. *Cement Concrete Res* 27: 697– 709
8. González Cortina M, Villanueva Domínguez L (2002) Morteros hidráulicos de cal y chamota. *Mater Constr* 266: 65-76.
9. Wong Chee Lum, Mo Kim Hung, Poh Yap Soon, Alengaram UJ, Ling TC (2018) Potential use of brick waste as alternate concrete-making materials: A review. *J Clean Prod* 226-239.
10. O'Farrell M, Wild S, Sabir BB (2001) Pore size distribution and compressive strength of waste clay brick mortar. *Cement Concrete Comp* 23: 81-91.
11. Turanli L, Bektas F, Monteiro PJM (2003) Use of ground clay brick as a pozzolanic material to reduce the alkali-silica reaction. *Cement Concrete Res* 33: 1539-1542.
12. Sierra-Fernandez A, Gomez-Villalba LS, Rabanal ME, Fort R (2017) New nanomaterials for applications in conservation and restorations of stony materials: A review. *Mater Constr.* 67(325): e107
13. Li LG, Zhu J, Huang ZH, Kwan AKH, Li LJ (2017) Combined effects of micro-silica and nano-silica on durability of mortar. *Constr Build Mat* 157: 337-347.
14. Stefanidou M, Chrysanthi TE, Pavlidou E (2017) Influence of nano-silica and nano-alumina in lime-pozzolan and lime-metakaolin binders, *Mater Today Proceed* 4:6908-6922.
15. Ranganath RV, Bhattacharjee B, Krishnamoorthy S (1998) Influence of size fraction of ponded ash on its pozzolanic activity. *Cement Concrete Res* 28: 749-761.
16. Alvarez JI, Fernández JM, Navarro-Blasco I, Duran A, Sirera R (2013) Microstructural consequences of nanosilica addition on aerial lime binding materials: Influence of different drying conditions. *Mater Charac* 80:36-49.
17. Nunes C, Slížková Z, Stefanidou M, Němeček J (2016) Microstructure of lime and lime-pozzolana pastes with nanosilica, *Cement Concrete Res* 83: 152-163.
18. Ergenç D (2017) Roman mortars used in the archaeological sites in Spain and Turkey: a comparative study and the design of repair mortars. UPM PhD Thesis.
19. Rosato L, Stefanidou M, Milazzo G, Fernández F, Livreri P, Muratore N, Terranova LM (2017) Study and evaluation of nano-structured cellulose fibers as additive for restoration of historical mortars and plasters. *Mater Today Proceed* 4: 6954-6965.

20. Barret EP, Joyner LG, Halenda PP (1951) The determination of pore volume and area distribution in Porous Substances I. Computation from Nitrogen Isotherms. *J Am Chem Soc* 73: 373-380.
21. Arandigoyen M, Bicer-Simsir B, Alvarez-Galindo JI, Lange DA (2006) Variation of microstructure with carbonation in lime and blended pastes. *Appl Surf Sci* 252: 7562-7571.
22. Arizzi A, Martinez-Huerta G, Sebastián-Pardo E, Cultrone G (2015) Mineralogical, textural and physical-mechanical study of hydraulic lime mortars cured under different moisture conditions. *Mater Constr* 6:318.
23. Ergenç D, Gomez-Villalba LS, Fort R (2018) Crystal development during carbonation of lime-based mortars in different environmental conditions, *Materials Characterization*, <https://doi.org/10.1016/j.matchar.2018.05.043>
24. Lawrence M, Mays T, Rigby S, Walker P, D' Ayala D (2007) Effects of carbonation on the pore-structure of non-hydraulic lime mortars. *Cem Concr Res.* 37: 1059-1069.
25. Arandigoyen M, Bicer-Simsir B, Alvarez-Galindo JI, Lange DA (2006) Variation of microstructure with carbonation in lime and blended pastes. *Appl Surf Sci* 252: 7562-7571.
26. Morandea A, Thierry M, Dangla P (2014) Investigation of the carbonation mechanism of CH and C-S-H in terms of kinetics, microstructure changes and moisture properties, *Cement and Concrete Research* 56: 153 - 170. [10.1016/j.cemconres.2013.11.015](https://doi.org/10.1016/j.cemconres.2013.11.015)
27. Silva J, De Brito J, Veiga R (2008) Fine ceramics replacing cement in mortars Partial replacement of cement with fine ceramics in rendering mortars. *Mater Struct* 41: 1333-1344.
28. Chen J, Poon CS (2009) Photocatalytic activity of titanium dioxide modified concrete materials-Influence if utilizing recycled glass cullet as aggregates. *J Environ Manage* 90: 3436-3442.
29. Cultrone G, Sebastián E, Ortega Huerta M (2005) Forced and natural carbonation of lime-based mortars with and without additives mineralogical and textural changes. *Cement Concrete Res* 35: 2278-2289.
30. Ergenç D, Fort R, Santos Silva A, Veiga R, Sanz Arauz D (2018) The effects of DiloCarB as carbonation accelerator on the properties of lime mortars. *Mater Struct* 51: 10.
31. Ergenç D, Fort R (2018) Accelerating carbonation in lime-based mortar in high CO₂ environments. *Construction and Building Materials* 188: 314–325. <https://doi.org/10.1016/j.conbuildmat.2018.08.125>

Enhancing clay mortars' properties

A. Karozou^{1*}, M. Stefanidou¹

(1) School of Civil Engineering, Aristotle University of Thessaloniki, akarozou@gmail.com, stefan@civil.auth.gr

Abstract

In an effort to find ways to improve the inherent weaknesses of clay-based materials in an efficient and compatible way, this study examines the effect of metakaolin and nanoparticles on the properties of clay mortars. The clay binder used (which is rich in lime by nature) was partially replaced by 10 and 20% w/w of metakaolin, while nanoparticles were also used as to act synergistically on the properties of the mortars. The nanoparticles used as additives were a combination of nano-silica and nano-alumina in percentage of 1 and 0.5% w/w of binder respectively. All specimens were cured in air conditions at 25°C, while the experiments were conducted after a curing period of 28 days. The fresh and hardened properties of these mixtures are reported, including workability, compressive and flexural strength, capillary absorption, volume stability and porosity, while all the samples were examined microscopically. The results indicate the positive effect in terms of microstructure for the case of 10% metakaolin replacement with a 13.72% improvement in volume loss, while the use of nanoparticles also contributed to the stabilization of clay mortars. The slow hardening effect of metakaolin on cement mortars, was also reported in the case of clay mortars as far as the mechanical test results are concerned. The compatibility of the materials used was on the benefit of their properties.

Introduction

Earthen structures are part of the human civilization for more than 10.000 years. Even nowadays, around 30% of the world population dwells in earthen buildings. As far as third world countries are concerned, however, this percentage is increased to about 50% of the population [1, 2]. Besides being already a part of human cultures and societies, earthen constructions can serve as an alternative solution to reduce greenhouse gas emissions due to their low embodied energy [3]. The low energy required for the preparation, transportation and handling of earthen materials, compared to others usually used, as well as being a local abundant material that can be easily found and used immediately on the construction site, earth is considered an energy efficient material. Because of those aspects, the cost of construction can decrease significantly, while, as a reusable material, the cost of preservation can be further reduced [4, 5]. So, as a material of low carbon footprint, recyclable, inexpensive and easy to use, earth is being reconsidered as a pertinent material for modern and vernacular construction methods.

However, earthen materials present several drawbacks that need to be faced as to become commercialized and render regulations for their use. Low mechanical strength and poor resistance to water penetration are the main reasons for the limited application in modern construction [6, 7]. Moreover, the tendency to crack during drying and the high shrinkage earthen materials possess, make the structure significantly vulnerable. Thus, these issues need to be dealt with for the use of earth in construction to be reverted [8, 9]. The durability and low seismic response of earthen structures are also two other aspects that need to be considered, since they are highly susceptible to weathering and even to low seismic forces [10, 11]. Hence, various studies have been conducted as to encounter the brittle behavior of earthen materials and enhance their physical and mechanical properties [12, 14].

To face the vulnerability of clay-based materials numerous methods were established throughout the centuries. Various agents have been used as additives and stabilizers, while protective coatings were also a common practice [15]. The use of additives and stabilizers can alter certain aspects as to manage shrinkage, enhance mechanical characteristics and obtain water-proof abilities. Traditionally, the mechanical and physical properties of earthen materials were enhanced using animal, mineral and plant products, natural fibers and lime [5, 13]. Each of these additives acted with a different mechanism as to improve physical and mechanical abilities.

Nowadays, nanotechnology has created a new opening in material science as far as constructional engineering is concerned. Nano-agents are applied both inside the matrix and as coatings, as to augment physical and mechanical properties, while the opportunity of forming advanced nano polymer composites, is offering great advances in modern science. Durability of structures can be improved drastically, since nanoparticles can alter the materials' pore structure [16, 17]. The nanoparticles that mostly find practice in engineering are nano silica, nano clays, nano-calcium, nano-titanium oxide (TiO_2), nano-iron (Fe_2O_3) and nano-alumina (Al_2O_3). Additionally, in relation to improve surface properties these nano-sized particles were combined with organic components as to increase surface roughness, while reducing surface free energy, thus achieving super hydrophobic materials. Each agent used, prevents from deterioration in different ways of action [17, 18]. Numerous studies examine the effect of such agents as additives, however, most of these projects refer to cement or lime-based mortars instead of soil-based ones [19-21]. Other methods used to improve mechanical resistance and durability in soil materials is the stabilization with addition of Portland cement or lime [22]. However, besides the positive effects it carries, Portland cement presents drawbacks in terms of sustainability and compatibility, while it increases porosity and sorptivity [23]. Instead, the use of lime, has been widely studied, since it is considered a more compatible material for soil stabilization providing a more sufficient solution [23, 24]. Other binders such as fly ashes, silica fume and ground granulated blast-furnace slag have been also studied with encouraging results which require further research [25, 26].

Metakaolin is a material with pozzolanic behavior that is obtained by the calcination of kaolinitic clay at temperatures ranging between 500 °C and 800 °C. It is mainly used as a replacement of cement and lime, as well as a geopolymer precursor [27-29]. The high lime content of the present clay could react with the metakaolin thus improving the system. The high strength and the increased durability metakaolin grants, makes it ideal for mortar and concrete manufacture [26]. However, this stands true for cement products and has not been tested further in materials such as clays. The positive effect of metakaolin in reducing shrinkage is also an aspect that led to the use of metakaolin in clay mortar composition in this research [30]. The enhancement in compressive strength has been also proven in air lime mortars and renders manufactured for restoration of adobe buildings [31]. Moreover, nano particles as previously mentioned, are used as supplementary materials to improve permeability and strength. The nano particles due to their small particle size and therefore to their large surface area, facilitate the mechanisms necessary to produce a dense matrix [25].

Materials and techniques

Specimen preparation

In this study clay mortars were manufactured with metakaolin (MK) replacement of clay binder. Clay was partially replaced at a percentage of 10% (MK10) and 20% (MK20) w/w of metakaolin. Moreover, two more compositions were held with addition of nanoparticles and 0% (SA) and 10% MK replacement (MKSA). In all cases, the used clay coming from the area of Crete was rich in calcium oxide and consisted, besides aluminum compounds and quartz, of calcite (CaCO_3) and gypsum (CaSO_4) in small percentages. In Figure 1, the particle size distribution of Cretan clay used, is presented. It seems that particles 2-500 μm prevail in the mass. The specific gravity of dry clay is 1.96 g/cm^3 . In this study, the clay was sieved to have a grain diameter of less than 0.5 mm. The color determination of dry material using Munsell charts is 5Y 7/1, light grey. The specific gravity of metakaolin is 2.44 g/cm^3 , while its particle size analysis is presented in Figure 2 below. The sand used for the mortars was river sand of silica composition, with similar color than that of the clay, and with grains size between 0-4mm. The mixture proportions of the mortars by mass were 1:2.5 (binder: aggregate ratio), and the goal was to reach workability of $15\pm 1\text{cm}$ as tested by flow table test (EN 1015-3:1999). The tests in hardened state were performed 28 days after the manufacture of the mortars.

The nanoparticles used were silica (silica fumed, amorphous, powder 0.014 μm) and alumina (aluminum oxide, nanopowder <50 nm particle size) at 1 and 0.5% w/w of binder respectively and were provided by Sigma Aldrich. The addition of the nanoparticles inside the matrix was held after being subjected to stirring by ultrasounds for 30 minutes. Previously to stirring, the nanoparticles were dispersed with a small amount of pre-weight water, as to avoid agglomeration. The chemical analysis of the clay and metakaolin used is

listed in Table 1. In total the compositions designed were the ones listed in Table 2, with the reference one recorded as A. The increased amount of water needed for the compositions containing nanoparticles is obvious. The specimens created were of 4 × 4 × 16 cm rectangular shape for each series of mortars.

Table 1. Chemical composition of clay of Crete and metakaolin (% w.t.)

Sample	Na ₂ O	K ₂ O	CaO	MgO	Fe ₂ O ₃	Al ₂ O ₃	SiO ₂	LoI	Cl ⁻	NO ₃ ⁻	SO ₄ ²⁻
Clay	0.94	2.09	25.33	7.48	6.52	13.03	30.87	13.74	0.01	0.01	0.21
Metakaolin	1.02	0.70	1.61	0.08	1.54	53.47	39.06	1.62	<0.01	<0.01	0.02

Table 2. Mixtures and water to binder ratios

Mixtures	w/b
A	0.65
MK10	0.69
MK20	0.65
SA	0.71
MKSA	0.78

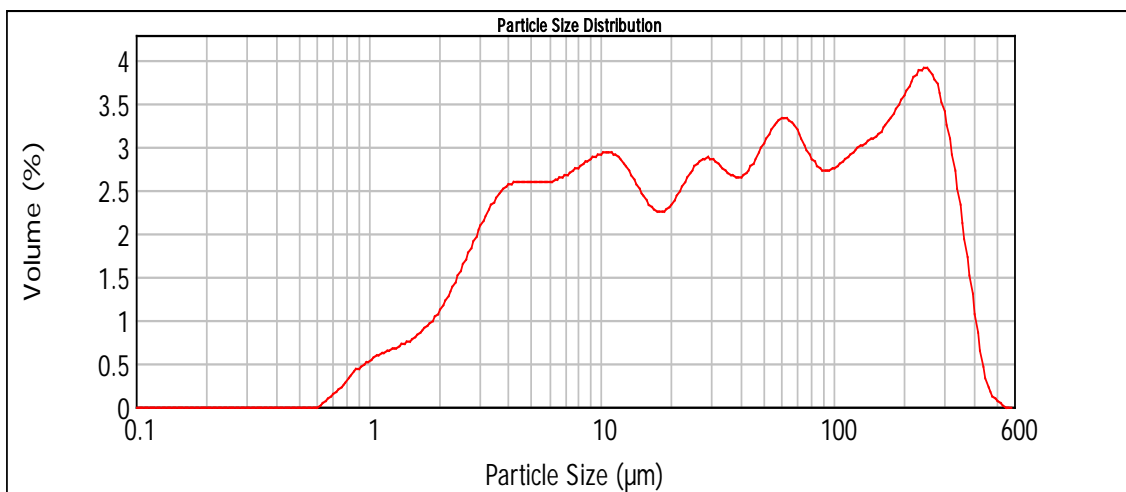


Figure 1. Particle size of Cretan clay used.

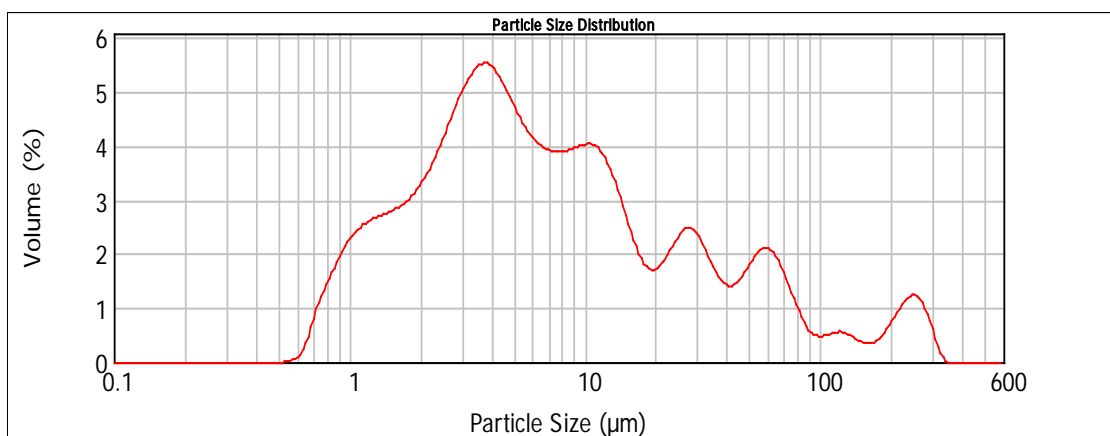


Figure 2. Particle size of metakaolin used.

Tests performed

The purpose of this study was to determine ways of improving the physical and mechanical properties of clay mortars. As to test the behavior of the samples against water penetration various tests were performed. Capillary absorption and porosity tests were performed according to UNI EN 15801:2010 and RILEM CPC11.3 respectively. It is noted, that porosity test was conducted using heptane instead of water, due to the inability of the specific material to withstand water contact. The capillary test was conducted for all samples at 28 days, while porosity results were recorded at 28- and 90-days period after manufacture. Moreover, as to test the ability to remove water as fast as they absorb it, the drying procedure was also measured (EN 16322:2013). The procedure followed for the drying test was as a reverse capillary test, while the values were recorded for 40 days for each sample. Furthermore, water absorption through Karsten tube penetration test (CSTLI7500-TQC) was examined. The test was conducted after the completion of 90 days. Karsten tubes were applied onto the surface of the samples using plasticine and the tubes were filled with 2 ml of water. The duration of the test was ten (10) minutes for each sample, while the values of the water absorbed were recorded every 30 seconds. Apart from the physical properties tested, the mechanical properties of the samples were examined as well. Compressive strength tests were conducted after the completion of 28 and 90 days for all specimens (A, MK10, MK20, SA, MKSA).

Volume stability was also of interest and indirectly the shrinkage tendency of the samples was also measured. The specimens were preserved at a chamber of constant conditions of temperature and humidity ($20^{\circ}\text{C}\pm 2$ & 65% RH) and the values of the volume loss were recorded until the completion of 28 days. Ageing tests were performed to test the durability, for samples A, MK10 and MK20 as to determine the most favorable results of MK replacement. The tests started 90 days after the samples manufacture. Thus, freeze-thaw and wet-dry deterioration cycles were conducted. The total number of the cycles performed were fifty, unless the samples were destroyed before that time. The total mass loss of the samples was recorded at the end of each deterioration test.

Moreover, all samples were examined to detect alterations on their surface, cracking and roughness. To do so, stereoscopic observation using microscope LEICA WILD M10 and microscopic examination by SEM (JEOL840A JSM) were used. In all cases the reference composition samples were untreated (recorded as A) and were examined for comparison reasons.

Experimental results

The physical and mechanical properties of the samples for the above-mentioned periods of time are listed at Table 3 below. In Table 4 the reaction of the reference samples and the ones with metakaolin replacement without addition of nanoparticles, under weathering conditions are recorded. The experimental results showed the positive effect of the addition

of nanoparticles mainly in terms of physical properties. Moreover, the development of early compressive strength and the low volume loss indicated the positive influence of nanoparticles in terms of mechanical properties as well. Regarding the mortars with metakaolin replacement, it is noted that no replacement percentage enhanced the structure significantly. A significant drop of flexural strength values of metakaolin mixtures are presented in all ages tested, yet the slight increase from 28 to 90 days in both cases is considered a positive aspect. The increase in compressive strength from 28 to 90 days, however, of MK10 samples by 95.5%, compared to the 63.2% of MK20 samples and the 95% of the reference ones, point out a potential benefit through time.

Overall, MK10 specimens performed similarly to the reference samples A, showing some beneficial aspects in terms of physical characteristics, such as the water penetration and the drying index, I_s . It can be stated that the higher replacement content of metakaolin does not act favorably in clay matrix. High porosity values and low mechanical strength both in early age and after 90 days, support that statement. Moreover, the higher mass loss of the MK20 samples that undertook the ageing cycles (Table 4), also points out the less favorable action of metakaolin in such a replacement ratio.

Table 3. Physical and mechanical properties of the samples

Mixtures	Porosity (28d) (%)	Porosity (90d) (%)	Capillary coefficient ($\text{g}/\text{cm}^2 \cdot \text{min}^{1/2}$)	I_s	Water penetration (ml/min)	Volume loss (%)	σ_{com} (28d) (MPa)	σ_{com} (90d) (MPa)	σ_f (28d) (MPa)	σ_f (90d) (MPa)
A	16.47	17.64	2.67	0.299	0.530	3.34	0.82	1.60	0.73	0.54
MK10	17.43	17.86	2.94	0.150	0.209	3.75	0.67	1.31	0.01	0.02
MK20	20.70	19.16	3.27	0.205	0.430	3.53	0.68	1.11	0.04	0.01
SA	17.26	18.47	2.81	0.090	0.213	1.30	1.19	1.26	0.52	0.65
MKSA	20.94	21.06	4.64	0.064	0.287	3.09	0.34	0.78	0.34	0.44

Table 4. Mass loss after the completion of the fifty weathering cycles

Mixtures	Mass loss (%) Wet-dry	Mass loss (%) Freeze-thaw
A	2.56	1.16
MK10	3.06	2.61
MK20	4.32	3.24

From Table 3 it can be seen that despite the porosity decrease in samples containing MK10% and the reduced water penetration, the compressive and the flexural strength were reduced. Further increase of metakaolin influences negatively both physical and mechanical properties in all ages tested. The role of nanoparticles seems to be important in stabilizing the volume and increasing the early strength which is important for the vulnerable nature of clay materials.

Therefore, by the first results that were conducted at 28 days, the compositions with the use of nanoparticles were decided to be tested for 10% metakaolin replacement only. The effective action of nanoparticles in clay matrix is observed mainly in the low shrinkage value and in early development of compressive strength.

The results of the capillary absorption test indicated the similar behavior of SA samples with those of the reference A. In Figure 3 it is noted, that through the conduction of this experiment, almost every specimen followed a similar absorption pattern with that of the reference samples. The samples that seemed to differ were the ones with metakaolin at 10% replacement and the addition of nanosilica and nanoalumina. This fact could be explained, in accordance with the high porosity results, due to a possible agglomeration of nanoparticles and metakaolin that could not be distributed evenly inside the clay matrix. However, as it can be detected both from Figure 4 and Table 3, the drying procedure of the samples indicate the high liquid conductivity of the samples MKSA at the first two days. The low value of I_s for MKSA samples is translated as a low resistance against drying, meaning an unhindered flow of inner water to the surface of the materials. It is further noted that the reference and MK20 mortars acted as low liquid conductivity materials judging by the short first drying phase.

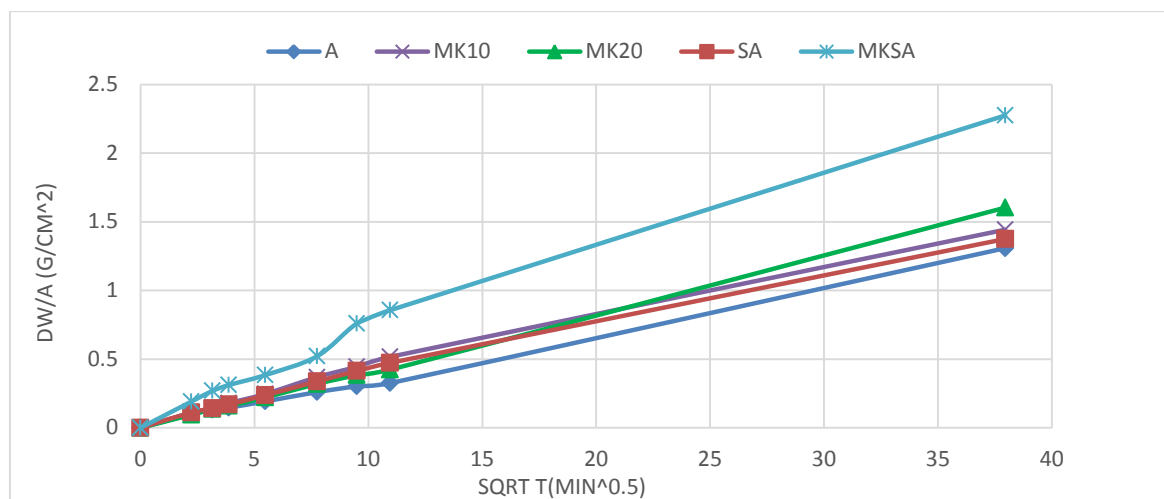


Figure 3. Capillary absorption of specimens at 28 days.

The results of water penetration through Karsten tubes show that all samples had a better performance compared to the reference sample. Furthermore, mortars MK10 and SA presented the lowest water intake, fact that seems to be consistent among the results of capillary and Karsten tube test.

As previously mentioned, the volume stability of the nanomodified mortars SA was proven by the shrinkage measurement values, indicating a comparatively low volume loss. Beneficial was also the role of nanomodified metakaolin mortars (MKSA) in volume stability, despite the highest water to binder ratio and porosity value. The increased porosity values after the completion of 90 days was observed for all samples as expected, justified by the compressive tests results, apart from the samples with the replacement percentage of

metakaolin by 20%. The MK20 samples presented a 19.78% decrease in porosity value from 28 to 90 days, not affecting, however, positively the compressive test results.

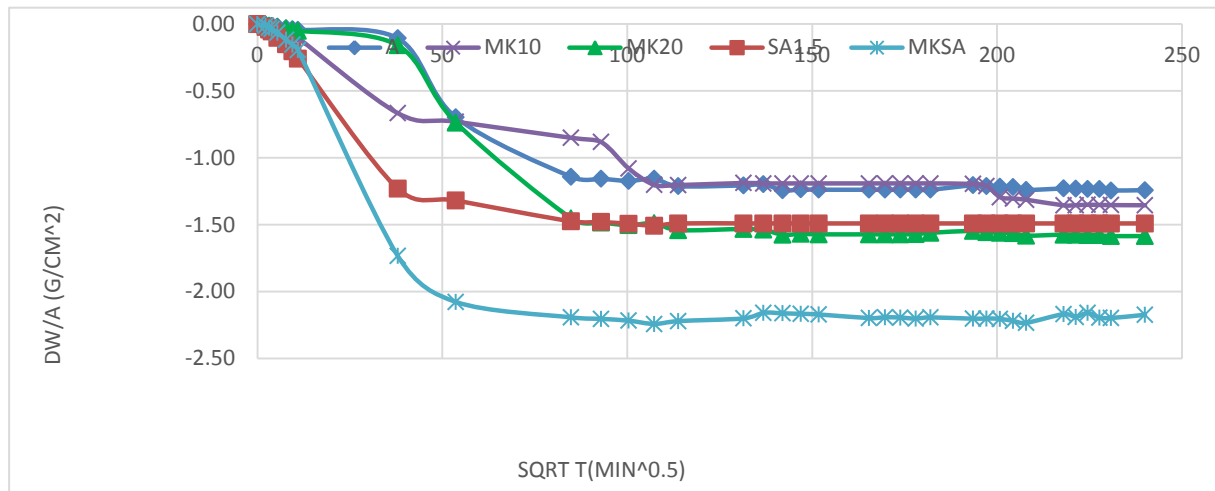


Figure 4. Drying procedure of the samples.

Through the microscopic observation of the samples the high porosity values of the samples MK20 are justified due to the existence of the large pores that can be detected on their surface (Figure 5). Similar porous surfaces were detected stereoscopically for all samples with metakaolin replacement, along with shrinkage cracks. This case also stands for reference samples A, as well as for the nanomodified specimens SA.

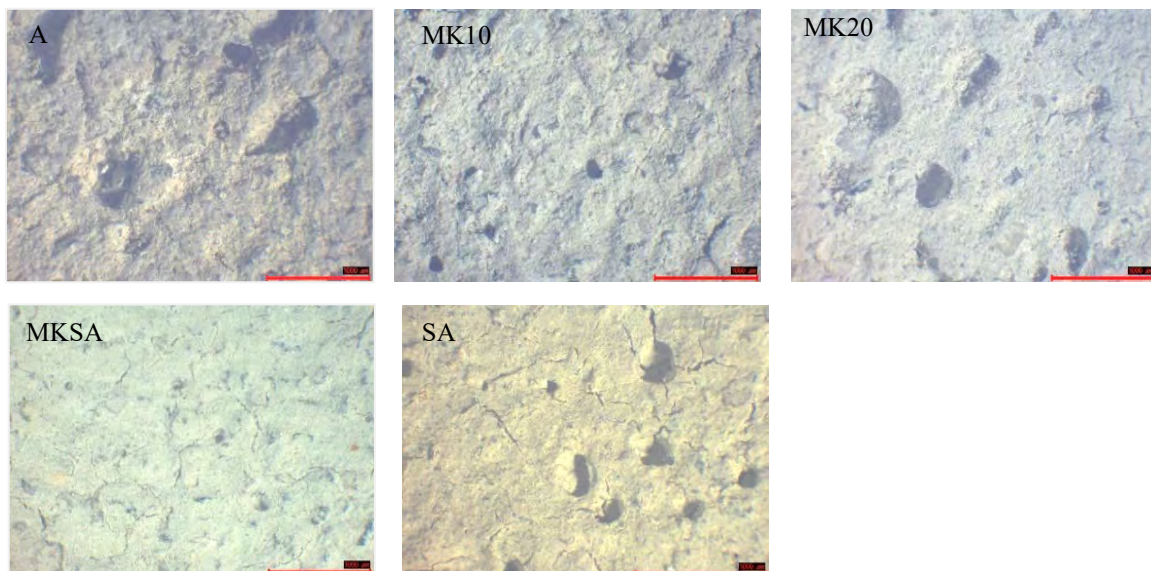


Figure 5. Stereoscopic images of the specimens (scale-1000 μ m).

As can be observed through microscopic examination by SEM (JEOL840A JSM) equipped with EDS device, the addition of metakaolin at 10% has caused a better coherence between the clay matrix and the aggregates, compared to the MK20 samples (Figure 6). In specimens with metakaolin with 20% replacement, white calcium agglomeration spots were detected, explaining perhaps their inadequate behavior, due to the non-reactive calcium. The non-modified samples A presented a loose crystal structure, while the formation of a crystal

network was observed in case of MKSA samples. This concentrated crystal network may explain their inability to withstand the experimental tests, due to a possible agglomeration of the nanoparticles. The combination of metakaolin with nano particles of silica and alumina seemed to have a disadvantageous role, probably because of the excessive amount of nanoalumina contained both in metakaolin and the nanoparticles that were added. A needle like crystal formation was also seen in case of samples modified with nanosilica and nanoalumina SA, showing a denser structure than the other mixtures with a better cohesiveness of the mortar.

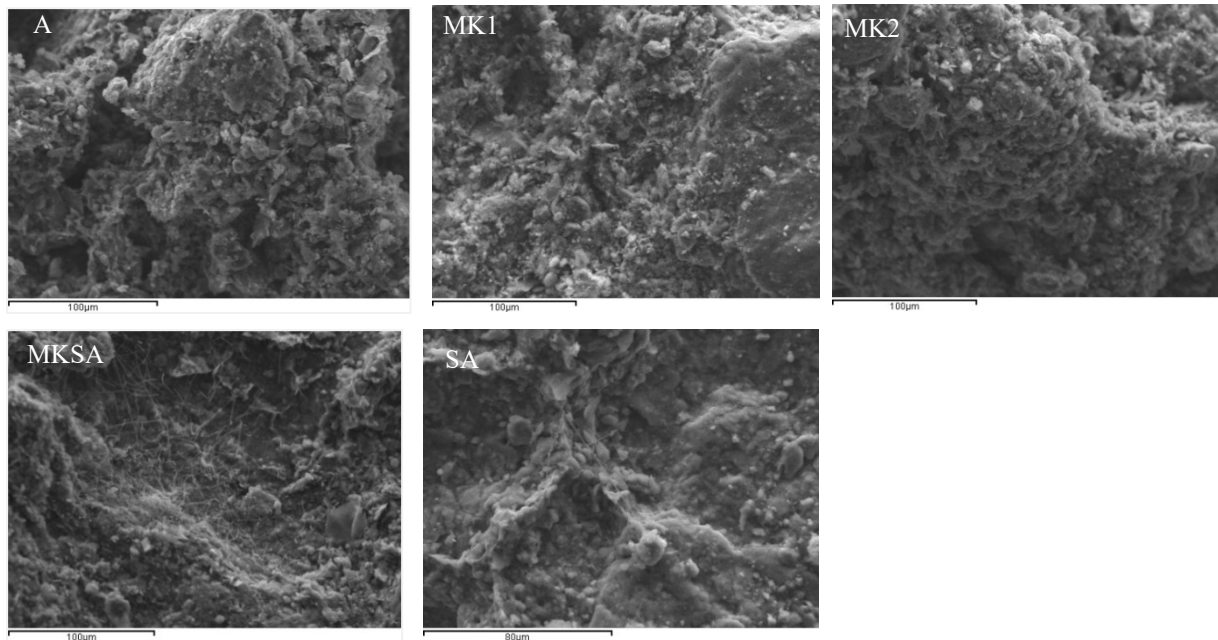


Figure 6. SEM images of the specimens (scale-100µm for A, MK10, MK20, MKSA and 80µm for SA).

Conclusions

In an effort to combine metakaolin with clay binders, various compositions of clay mortars were created. The replacement of clay by metakaolin at 10% and 20%w.w., as well as the use of nanoparticles as additives at 1%w.w. for nanosilica and 0.5%w.w. for nanoalumina were examined. The use of metakaolin in the clay matrix resulted in lower compressive strength with no significant volume stabilization rate. However, the positive effect of metakaolin at certain physical properties, such as water penetration, renders it as a promising replacement agent. Perhaps, different curing conditions could assist the development of a more compact inner structure and could conduct better experimental results.

The use of nanoparticles on the other hand, has been proven beneficial both for physical and mechanical properties. The different effects of the nanomodified samples SA on the various properties examined, can be detected in Table 3, showing an overall positive influence. The early strength development, as well as the significant volume stability makes the use of nanoparticles in the clay matrix desirable. When, however, nanoparticles were combined

with metakaolin, the results differed considerably. The high capillary absorption and porosity values together with the negative effect on shrinkage and compressive strength, could be explained by the information taken from SEM images due to the agglomeration of the nanoparticles.

In total, different curing conditions, alternative values of replacement percentages of metakaolin, as well as varying addition of nanoparticles (for instance nano calcium instead of nanoalumina) could be proven beneficial and so further research is encouraged to be conducted.

Acknowledgements

Author Karozou A. would like to thank the General Secretariat for Research and Technology (GSRT) and the Hellenic Foundation for Research and Innovation (HFRI) for founding the research through the scholarship foundation program for PhD candidates.

References

1. Berge B, (2009) *The Ecology of Building Materials*. Elsevier Ltd, Oxford
2. Niroumand H, Zain MFM, Jamil M, Niroumand S, (2013) Earth Architecture from Ancient until Today. *Procedia - Social and Behavioral Sciences* 89: 222–225
3. Fabbri A, Morel JC, (2016) *Earthen materials and constructions. Nonconventional and Vernacular Construction Materials*. doi: 10.1016/B978-0-08-100038-0.00010-X
4. Sharma V, Vinayak HK, Marwaha BM, (2015) Enhancing compressive strength of soil using natural fibers. *Construction and Building Materials*. doi: 10.1016/j.conbuildmat.2015.05.065
5. Minke G, (2006) *Building with Earth Design and Technology of a Sustainable Architecture*. Birkhäuser – Publishers for Architecture, Basel · Berlin · Boston
6. Aubert JE, Fabbri A, Morel JC, Maillard P, (2013) An earth block with a compressive strength higher than 45 MPa! *Construction and Building Materials* 47: 366–369
7. Nakamatsu J, Kim S, Ayarza J, Ramirez E, Elgegren M, Aguilar R, (2017) Eco-friendly modification of earthen construction with carrageenan: Water durability and mechanical assessment. *Construction and Building Materials*. doi: 10.1016/j.conbuildmat.2017.02.062
8. Kanema JM, Eid J, Taibi S, (2016) Shrinkage of earth concrete amended with recycled aggregates and superplasticizer: Impact on mechanical properties and cracks. *Materials and Design* 109: 378–389

9. Sameh SH, (2014) Promoting earth architecture as a sustainable construction technique in Egypt. *Journal of Cleaner Production* 65: 362–373
10. Pacheco-Torgal F, Jalali S, (2012) Earth construction: Lessons from the past for future eco-efficient construction. *Construction and Building Materials* 29: 512–519
11. Miccoli L, Muller U, Fontana P, (2014) Mechanical behaviour of earthen materials: A comparison between earth block masonry, rammed earth and cob. *Construction and Building Materials*. doi: 10.1016/j.conbuildmat.2014.03.009
12. Ciancio D, Beckett CTS, Carraro JAH, (2014) Optimum lime content identification for lime-stabilised rammed earth. *Construction and Building Materials* 53: 59–65
13. Alam I, Naseer A, Shah AA, (2015) Economical stabilization of clay for earth buildings construction in rainy and flood prone areas. *Construction and Building Materials* 77: 154–159
14. Galán-Marín C, Rivera-Gómez C, Petric J, (2010) Clay-based composite stabilized with natural polymer and fibre. *Construction and Building Materials* 24: 1462–1468
15. Laborel-Preneron A, Aubert JE, Magniont C, Tribout C, Bertron A, (2016) Plant aggregates and fibers in earth construction materials: A review. *Construction and Building Materials* 111: 719–734
16. Matziaris K, Stefanidou M, Karagiannis G, (2011) Impregnation and superhydrophobicity of coated porous low-fired clay building materials. *Progress in Organic Coatings* 72: 181–192
17. Scarfato P, Di Maio L, Fariello ML, Russo P, Incarnato L, (2012) Preparation and evaluation of polymer/clay nanocomposite surface treatments for concrete durability enhancement. *Cement and Concrete Composites* 34: 297–305
18. Woo RSC, Zhu H, Chow MMK, Leung CKY, Kim JK, (2008) Barrier performance of silane-clay nanocomposite coatings on concrete structure. *Composites Science and Technology* 68: 2828–2836
19. Jia L, Shi C, Pan X, Zhang J, Wu L, (2016) Effects of inorganic surface treatment on water permeability of cement-based materials. *Cement and Concrete Composites* 67: 85–92
20. Morsy MS, Alsayed SH, Aqel M, (2010) Effect of Nano-clay on Mechanical Properties and Microstructure of Ordinary Portland Cement Mortar. *International Journal of Civil & Environmental Engineering IJCEE-IJENS* 10: 23–27
21. Norhasri MSM, Hamidah MS, Fadzil AM, (2017) Applications of using nano material in concrete: A review. *Construction and Building Materials* 133: 91–97

22. Gallipoli D, Bruno AW, Perlot C, Mendes J, (2017) A geotechnical perspective of raw earth building. *Acta Geotechnica*. doi: 10.1007/s11440-016-0521-1
23. Gomes MI, Gonçalves TD, Faria P, (2016) Hydric Behavior of Earth Materials and the Effects of Their Stabilization with Cement or Lime: Study on Repair Mortars for Historical Rammed Earth Structures. 1–11
24. Eires R, Camões A, Jalali S, (2017) Enhancing water resistance of earthen buildings with quicklime and oil. *Journal of Cleaner Production* 142: 3281–3292
25. Morsy MS, Al-Salloum YA, Abbas H, Alsayed SH, (2012) Behavior of blended cement mortars containing nano-metakaolin at elevated temperatures. *Construction and Building Materials* 35: 900–905
26. Siddique R, Klaus J, (2009) Influence of metakaolin on the properties of mortar and concrete: A review. *Applied Clay Science* 43: 392–400
27. Rocha T da S, Dias DP, França FCC, Guerra RR de S, Marques LR da C de O, (2018) Metakaolin-based geopolymer mortars with different alkaline activators (Na⁺ and K⁺). *Construction and Building Materials* 178: 453–461
28. Nunes C, Mácová P, Frankeová D, Ševčík R, Viani A, (2018) Influence of linseed oil on the microstructure and composition of lime and lime-metakaolin pastes after a long curing time. *Construction and Building Materials* 189: 787–796
29. Bignozzi MC, Manzi S, Lancellotti I, Kamseu E, Barbieri L, Leonelli C, (2013) Mix-design and characterization of alkali activated materials based on metakaolin and ladle slag. *Applied Clay Science* 73: 78–85
30. Khatib JM, (2008) Metakaolin concrete at a low water to binder ratio. *Construction and Building Materials* 22: 1691–1700
31. Andrejkovičová S, Alves C, Velosa A, Rocha F, (2015) Bentonite as a natural additive for lime and lime-metakaolin mortars used for restoration of adobe buildings. *Cement and Concrete Composites* 60: 99–110

Study of the role of different nanoparticles in lime pastes

Eirini-Chrysanthi Tsardaka¹, Maria Stefanidou¹

(1) Laboratory of Building Materials, School of Civil Engineering, Aristotle University of Thessaloniki, Greece, extsardaka@gmail.com, stefan@civil.auth.gr

Abstract

This study is an effort to evaluate the contribution of different nanoparticles in the properties of lime pastes. The use of nano-silica (NS), nano-alumina (NA) and nano-calcium oxide (NC) can contribute differently in physico-mechanical properties and microstructure. Nanoparticles enhance compressive strength and open porosity, whilst do not affect significantly the capillarity. Compressive strength at 28 days was improved by 52.4% and 90%, when 3% NS and 3% NA was incorporated, respectively. NC leads to denser structure, according to SEM observation. Moreover, it was proved that the different mechanisms of nanoparticles' action lead to different carbonation degrees of nano-modified hydrated lime. The observation of microstructure clarified the physico-mechanical results and revealed nano-scale differences in lime pastes.

Introduction

The incorporation of nano-silica (NS) and nano-alumina (NA) in building materials has been extensively studied the last decades. The utilization of such nanoparticles in cement and traditional binders has brought up certain advantages and disadvantages. The main benefit seems to be the contribution of nanoparticles to mechanical properties especially at early ages and microstructure. Singh et al. revised that the addition of NS increased the production of calcium hydroxide and early age compressive strength of cement pastes, as well as “dense and compact microstructure was achieved” [1]. Nunes et al. indicated that lime pastes with NS had denser structure in respect to the reference [2]. Sharma et al. showed that the capillary porosity of cementitious system was reduced by the addition of small proportion of colloidal silica [3]. Yu et al. concluded that NS “compensated the retardation of cement hydration” when high proportions of superplasticizer were used [4]. Certain drawbacks are related to water demand increase and effective dispersion. It has been proved that the water to binder ratio can be handled by using superplasticizers [5-6] and dispersion issues can be treated with ultrasonication [7-8] and pH handling solutions [9].

In different binding systems, the incorporation of NS and NA has shown the possible connection between the type of nanoparticle and the chemical content of the binding system [10-12]. On the other hand, nano-lime (NC) has been connected to healing properties in cement-lime mortars and porosity reduction in cement pastes [13]. Furthermore, the combination of NC along with NA in lime- pozzolan binders yielded durability against wet-dry, sea water and sodium sulfate cycles [10].

Lime is a critical and basic binder that is used along with other binders or alone for several applications, from restoration to advanced materials [14-15]. The evaluation of the behaviour of different nanoparticles in aerial lime could result to useful conclusions, concerning the applicability of nanoparticles in lime and the changes that can cause to its properties. For that reason, lime pastes with NS, NA, and NC and combination of the nanoparticles were prepared and tested. The study highlighted the benefited physico-mechanical properties and the modification of microstructure. Also, the recording of carbonation degree and calcium hydroxide content by DTA-TGA revealed that NS modifies the proportions of these compounds.

Experimental

Materials and Methods

Hydrated lime was coded as CL90 according to EN 459-1. Nano-silica (SiO_2 , particle size $0.007\mu\text{m}$), nano-alumina (Al_2O_3 , particle size $<50\text{nm}$) and nano-calcium oxide (CaO , particle size $<160\text{nm}$) were supplied from Sigma-Aldrich. A balance Kern PCB 4000-2 (max capacity $4000\pm 0.01\text{g}$) was used to weight the binders and an analytical balance B204-S/FACT of Mettler Toledo (max. capacity $220.0 \pm 0.0001\text{g}$) was used to weight nanoparticles of silica, alumina and calcium oxide. A mechanical stirrer was used to mix the materials and produce the pastes.

Compressive strength of lime specimens was measured at 28 and 90 days using a Technik ToniNorm device (according to EN 196-3). Open porosity was measured according to standard RILEM CPC 11.3 method based on water absorption under vacuum. Capillary water absorption test was performed at 28 days according to EN 1015-18 and microstructure observation was made at 90 days, using SEM-EDS instrumentation, Jeol JSM-6390LV, Scanning Electron Microscope, Oxford Instruments. Calcium carbonate content and calcium hydroxide content as % by mass were determined using SDT 2960 TA Instruments, Simultaneous DTA-TG, under N_2 atmosphere over heat up to 1000°C . The determination of volume change (%) of specimens was performed by measuring the dimensions (height, length, width in mm) of specimens that were cured in climatic chamber ($25^\circ\text{C} \pm 1$, RH $\sim 75\%$). The ultrasonication of the nanoparticles' suspension was performed by Mastersizer 2000, Hydro 2000 MU, Malvern Instruments.

Preparation of binding systems

Suspensions of silica and alumina nanoparticles were prepared by adding nanoparticles in water and ultrasonicate for 30 minutes. NC was added in water without ultrasonication. Proportions of 1.5% and 3.0% by mass of binder (wt%) were prepared for NS and NA, while NC was tested only at 1.5wt%. In combined systems 1.5wt% of total nanoparticles amount was used. The prepared suspension was added in the binder and the mixture was homogenized with mechanical stirrer. Lime pastes were cast in moulds to be shaped as

prisms 25x25x50 mm and 25x25x100mm in size. The composition of binding systems is given in Table 1. The reference hydrated lime paste was prepared with standard consistency (EN 450-1, Vicat 15±1mm) and 1 kg of hydrated lime was added in 670mL water, for the required consistency. It was decided to maintain water quantity ($w/b=0.67$) of the systems stable, so a poly-carboxylate superplasticizer was used to avoid consistency deviation when nanoparticles were incorporated. All specimens were demolded and cured in dry conditions ($25^{\circ}\text{C} \pm 1$, RH $\sim 75\%$) in a climatic chamber.

Table 1. Composition of hydrated lime pastes.

Acronym	SP(wt%)	NS (wt%)	NA (wt%)	NC (%wt)	Vicat (mm)
L	-	-	-	-	15
LNS	1.5	1.5	-	-	15
LNS3	2.0	3.0	-	-	15.5
LNSC	1.5	0.75	-	0.75	15
LNA	-	-	1.5	-	16
LNA3	1.0	-	3.0	-	15
LNAC	1.0	-	0.75	0.75	15
LNC	1.0	-	-	1.5	15

Results and Discussion

Compressive strength

Figure 1 shows compressive strength evolution of hydrated lime pastes at 28 and 90 days. Figure 2 demonstrates the variation of compressive strength values of nano-modified systems comparing to reference lime paste. For the calculation of the variation values, the following equation was used: $(N-R)*100/R$, where N is the compressive strength value from nano-modified specimen and R the value of reference specimen (L). Improved compressive strength is exhibited when systems present positive variation. Contrary, negative values in Figure 2 imply hindered the development compressive strength.

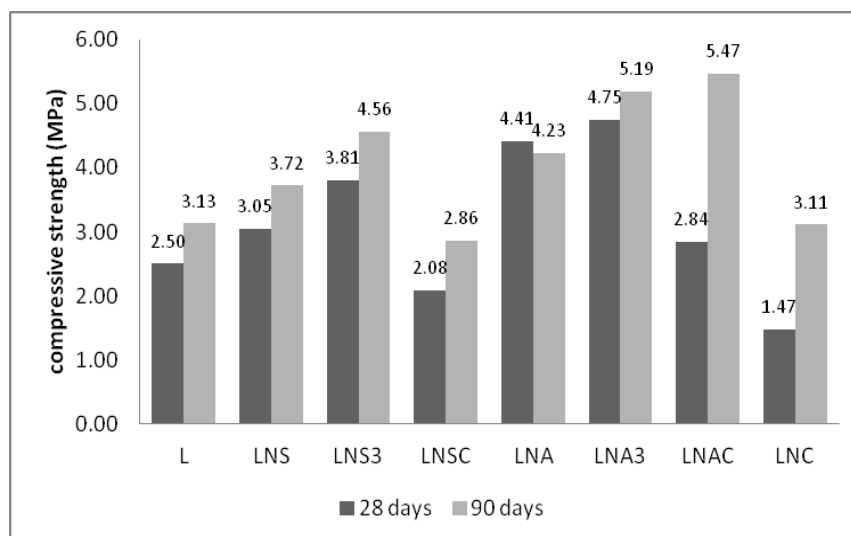


Figure 1. Compressive strength values (MPa) of nano-modified hydrated lime systems.

Despite the fact that lime pastes were cured in a climatic chamber, they retained moisture approximately up to 28 days. This phenomenon was more intense at the LNC specimens and probably influenced the physico-mechanical results.

The increased compressive strength after the addition of NS complies with literature reports [2, 3, 16]. The test proved that NS had positive action in lime systems. The contribution of NS in lime systems relies on filling action of the structure and also, relies on the interaction of NS with portlandite, forming C-S-H compounds [2, 17]. LNS and LNS3 specimens presented positive variation by 22.0% and 52.4% at 28 days respectively. It has been demonstrated that bigger proportions of NS (by mass of binder) can benefit lime systems [18]. Though, this study aims to evaluate additions of low proportions of nanoparticles. The combination of NS with NC added in lime pastes hindered the increase of compressive strength (Figure 2).

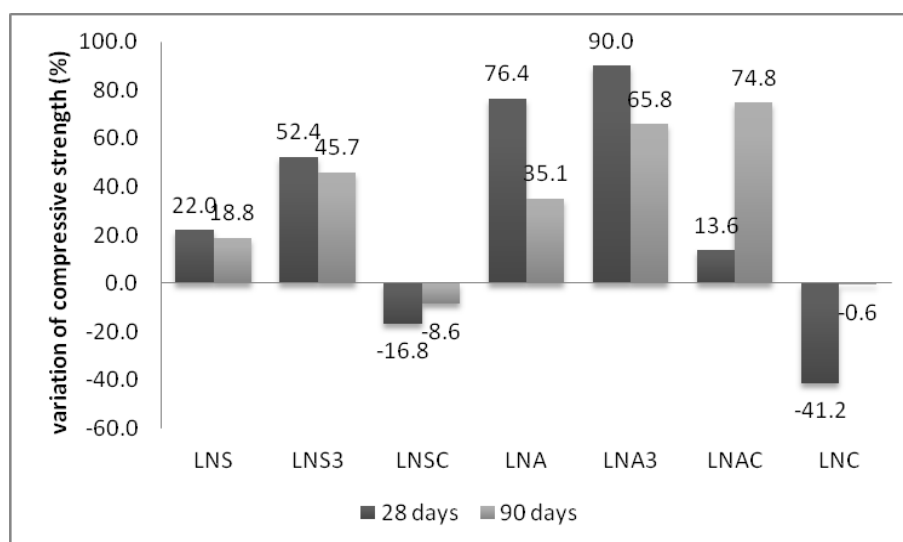


Figure 2. Variation of compressive strength (%) of nano-modified hydrated lime systems, in respect to the reference.

Lime pastes were benefited by NA addition. The positive effect is given by the increased compressive strength values of LNA, LNA3 and LNAC (Figure 1). The filler action of NA seems to have benefited lime pastes even in low proportions, 1.5wt% and 3.0wt%.

The development rate of the compression strength was intense during the first 28 days. Compressive strength of LNA and LNA3 at 28 days was increased by 76.4% and 90.0% respectively. At 90 days, compressive strength enhancement of LNA and LNA3 was 35.1% and 65.8%, in respect to the reference.

LNAC showed greater increase of compressive strength at 90 days than at 28 days. The latter indicates that probably, the system is boosted by two different mechanisms. The first is the filling effect that is ought to NA addition and is favoring the system at early age. The second might be attributed to reactions taking place during carbonation. LNC alone hindered drying of specimens and as a result compressive strength delayed to yield. In fact, LNC at 28 days had significantly lower values of compressive strength than reference.

Open porosity (RILEM CPC 11.3)

The variation of open porosity is shown in Figure 3. For the calculation of the values, the equation used was: $(N-R)*100/R$, where N is the open porosity value of nano-modified specimen and R the value of reference specimen (L).

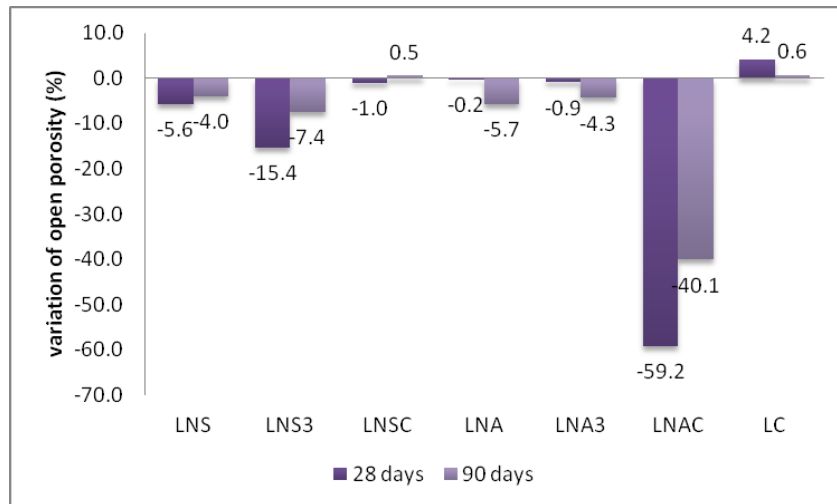


Figure 3. Open porosity variation (%) of nano-modified hydrated lime systems, in respect to the reference.

NS and NA decreased open porosity, at 90 days decrease was by 4.0% and 5.7% in respect to the reference. When nanoparticles proportion increased, open porosity was further reduced in the case of NS. Lime pastes with NS 3.0wt% (LNS3 specimens) presented a reduction of open porosity by 15.4%. Most probably the porosity reduction is related to pores size modification [3]. On the other hand, the addition of NA 3.0wt% (LNA3 specimens) did not modify the open porosity of the pastes more than the addition of NA 1.5wt%. So, the latter should be investigated in time to prove the stability of the system.

The drying delay of the LNC specimens affected open porosity, in the same way as mentioned in compressive strength. NC slightly increased open porosity. Additionally, NC along with NS presented alike behavior both at 28 and 90 days.

On the other hand, the combination of NA and NC (1.5wt% total content of nanoparticles) was sufficient to modify open porosity of hydrated lime pastes considerably. The reduction of porosity reached 59.2% and 40.1% at 28 and 90 days, respectively. This combination of nanoparticles acted very positively in physico-mechanical properties of lime.

Thermogravimetric analysis (DTA-TG)

The carbonation of hydrated lime is the main mechanism that offers strength in lime pastes. The quantification of calcite can contribute to the evaluation of the nanoparticles' action. Figure 4 presents the content of calcite (CaCO_3) and calcium hydroxide (Ca(OH)_2) wt% of lime pastes. Sample L presents the calcite content of pure lime pastes at 28 days. Nano-silica addition reduced calcite and calcium hydroxide content, regardless the proportion added by

mass of binder, comparing to the reference samples. The remaining percentage of calcium content of LNS and LNS3 pastes has not been recorded by DTA. This is probably attributed to the participation of calcium to C-S-H compounds.

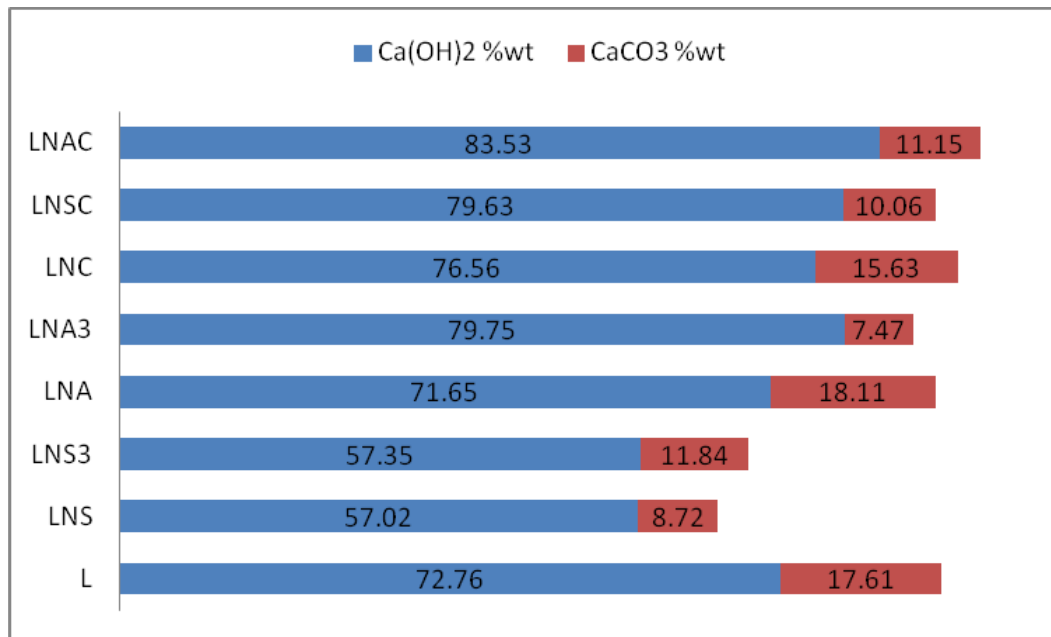


Figure 4. Calcite and calcium hydroxide content wt% of nano-modified hydrated lime systems, in respect to the reference at 28 days.

Regardless the percentage of NS added in lime pastes, the calcite and the calcium hydroxide content do not differ significantly. That shows that NS acts in lime pastes even in low proportions (1.5%wt.). Nevertheless, the rest of the systems have alike or higher content of calcium hydroxide and less calcite than reference. This enforces the conclusion that NA and NC acted as fillers in the lime pastes, and that lead to denser structure. Additionally, the highly increased compressive strength of LNA, LNA3 and LNAC cannot be attributed to carbonation increase, that is the main mechanism of lime pastes strength development. In fact, the compressive strength of LNA, LNA3 and LNAC is contributed to the filling effect of nanoparticles. The increased calcium hydroxide content could also be connected to the delay of drying of the specimens up to 28 days.

Capillary water absorption

Capillarity was recorded at 28 days and is displayed in Figure 5. All pastes present very similar behavior and maintain low values of water absorption. LNS specimens had slightly smaller water absorption. This means that capillary voids dimensions have been modified and NS 1.5 wt% can favor this property. Larger percentage of NS did not support this phenomenon, which is probably connected to the microstructure of the systems.

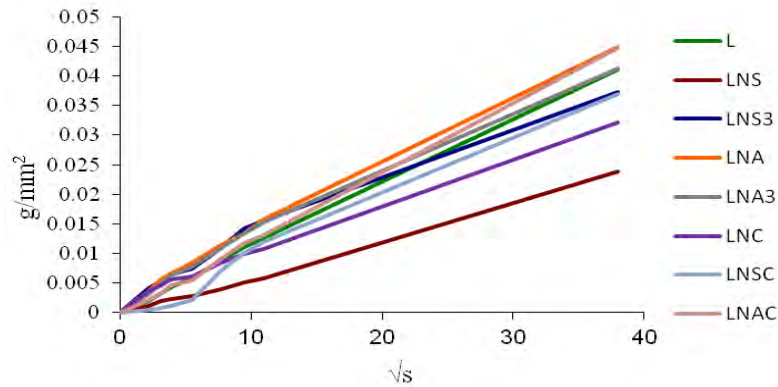


Figure 5. Capillary water absorption evolution of lime pastes at 28 days.

Volume change

The daily recording of lime pastes' dimensions displayed early volume change of specimens and after that stable behavior in time, as shown in Figure 6. After demolding at 7 days, lime pastes showed shrinkage deformations increase only for few days. Then the volume was approximately stabilized and within a week (at 15th day) all the systems show stable volume. All nano-modified systems had similar shrinkage degree compared to the L pastes. LNS demonstrated the smallest volume change and LNAC specimens presented the highest shrinkage of all pastes. High increase in shrinkage of the LNAC specimens can be due to great reduction of porosity. It is important to be mentioned that NA and NC alone did not behave in similar way as the samples where nanoparticles were combined.

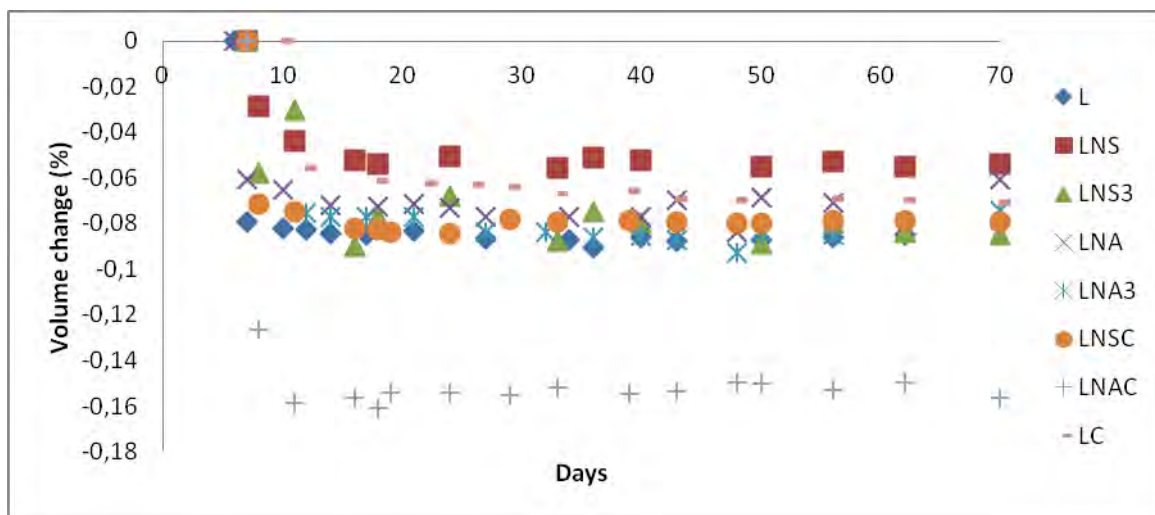


Figure 6. Volume change of lime pastes.

Microstructure observation

The observation of nano-modified lime pastes by SEM revealed the characteristics of their microstructure. Figure 7 shows the microstructures under two different magnification. The addition of NS seems to have modified the pore size of hardened lime paste and also formed certain areas of denser structure and micro-cracks around them (Figure 7a).

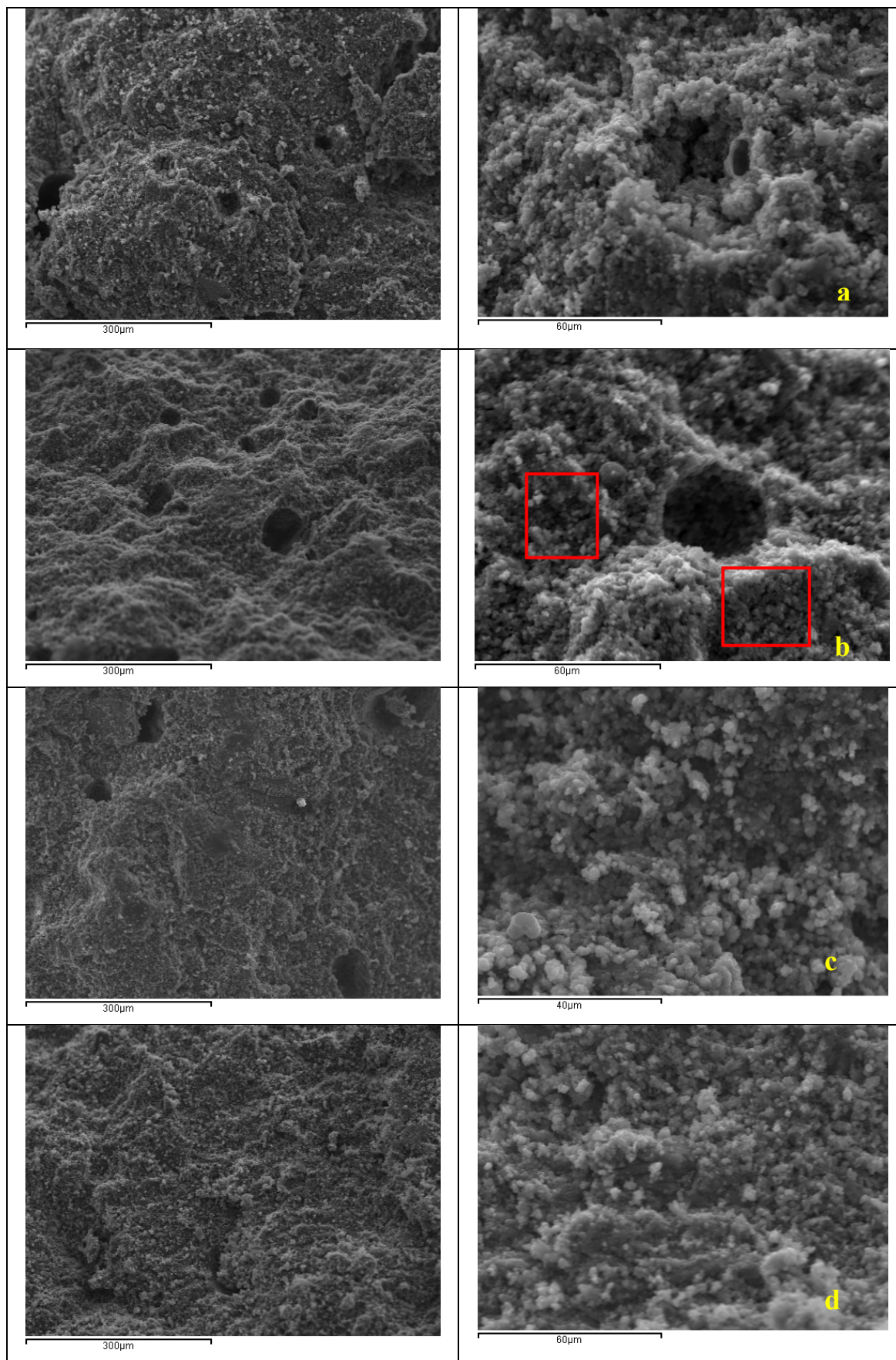


Figure 7. SEM micrographs of nano-modified lime pastes a) LNS3, b) LNA3, c) LNAC d) LNC at 90 days at different magnification

Most probably, few cracks were formed probably due to drying in areas that were found with high silica content and present compact nucleus. The addition of NA did not seem to modify significantly the microstructure of lime, yet large pores were observed. Large capillaries were absent, but small cracks were observed (Figure 7b) and seemed to have made the microstructure more susceptible to water absorption in capillarity test.

The combination of NA and NC has made the microstructure of lime denser, as is shown in Figures 7c. It seems that, in the case where a combination of nanoparticles was used, these particles acted as filler and also, as an agent that caused “blooming of the structure” that gave a more coherent and homogeneous appearance.

The addition of NC acted differently than NS and NA so far. In NC modified pastes the filling of the pores with extra calcium hydroxide was observed (Figure 7d).

Conclusions

Nano-silica acted positively in lime pastes even in small proportions and displayed a stable system with improved microstructure. The formation of C-S-H compounds that was implied by DTA-TG determination offered improved compressive strength and capillarity, along with stable microstructure.

Nano-alumina that acted as filler, managed to contribute extensively in all tested properties of lime pastes, as filling mechanism proved to have a positive influence.

Impressive results were obtained by the combination of NA and NC, whilst NS along with NC lead to weak system. LNAC system was benefited by two different mechanisms of action from two different nanoparticles. NA offers filling of the structure from early age and NC leads to a denser microstructure. This combination triggered compressive strength, open porosity results and microstructure. Lime pastes were unaffected by NS-NC addition, except from compressive strength that was slightly reduced.

This study concluded that different nanoparticles can offer significant advantages in hydrated lime pastes. Each type of nanoparticles contributed in the microstructure of lime pastes in a different way. NS offered stability, NA offered filling effect and NC offered dense structure. Moreover, it has been demonstrated that combining specific types of nanoparticles can offer double advantages in the systems. As a result, it can be concluded that small nanoparticle proportions can offer important and determinant properties in lime pastes. If the advantages of each combination will be taken into consideration and after further study of the durability, they could improve the inherent weaknesses of lime, thus increasing its application fields.

References

1. Singh LP, Karade SR, Bhattacharyya SK, Yousuf MM, Ahalawat S (2013) Beneficial role of nanosilica in cement based materials – A review. *Con Build Mat.* 47:1069-1077
2. Nunes C, Zliskova Z, Stefanidou M, Nemejeck J (2016) Microstructure of lime and lime-pozzolana pastes with nanosilica. *Cem Con Res.* 83:152–163
3. Sharma U, Singh LP, Zhan B, Poon CS (2019) Effect of particle size of nanosilica on microstructure of C-S-H and its impact on mechanical strength. *Cem Con Comp.* doi: 10.1016/j.cemconcomp.2019.01.007
4. Yu R, Spiesz P, Brouwers HJH (2014) Effect of nano-silica on the hydration and microstructure development of Ultra-High Performance Concrete (UHPC) with a low binder amount. *Con Build Mat.* 65:140–150
5. Fernández JM, Duran A, Navarro-Blasco I, Lanas J, Sirera R, Alvarez JI (2013) Influence of nanosilica and a polycarboxylate ether superplasticizer on the performance of lime mortars. *Cem Con Res.* 43:12–24
6. Papo A, Piani L (2004) Effect of various superplasticizers on the rheological properties of Portland cement pastes, *Cem Con Res.* 34:2097-2101
7. Jafari V, Allahverdi A, Vafei M (2014) Ultrasound-assisted synthesis of colloidal nanosilica from silica fume: effect of sonication time on the properties of product, *Powder Technol.* 25:1571–1577.
8. Mandzy N, Grulke E, Druffel T (2005) Breakage of TiO₂ agglomerates in electrostatically stabilized aqueous dispersions. *Powder Technol.* 160:121–126
9. Tsardaka EC, Stefanidou M (2019) Application of an alternative way of silica fume dispersion in cement pastes without ultrasonication. *Cem Con Res* 115:59–69
10. Tsardaka EC, Pavlidou E, Stefanidou M (2019) The Role of Nanoparticles on the Durability of Lime-Pozzolan Binding System. *Sol St Phenom* 286:119-132 (doi:10.4028/www.scientific.net/SSP.286.119)
11. Stefanidou M, Tsardaka EC, Pavlidou E (2017) Influence of nano-silica and nano-alumina in lime-pozzolan and lime-metakaolin binders. *Mat Today: Proceedings* 4:6908–6922
12. Tsardaka EC, Skevi L, Stefanidou M (2017) The role of nano-Al₂O₃ in traditional binders. 10th International Symposium on the Conservation of Monuments in the Mediterranean Basin. *Natural and Anthropogenic Hazards and Sustainable Preservation.* Springer 27:267-272 (doi:978-3-319-78093-1_27)
13. Stefanidou M, Tsardaka EC, Tsampali E (2018) The role of nano-particles in self-healing process of cementitious materials. *SynerCrete'18 International Conference on*

Interdisciplinary Approaches for Cement-based Materials and Structural Concrete, 24-26 October 2018, Funchal, Madeira Island, Portugal

14. Barbero-Barrera M, Maldonado-Ramos L, Van Balen K, García-Santos A, Neila-González FJ (2014) Lime render layers: An overview of their properties. *J Cult Herit* 15:326-330
15. Prošek Z, Nezerka V, Hluček R, Trejbal J, Tesárek P, Karra'a G (2019) Role of lime, fly ash, and slag in cement pastes containing recycled concrete fines. *Con Build Mat* 201:702-714
16. Theodoridou M, Charalambous E, Maravelaki-Kalaitzaki P, Ioannou I (2016) Amelioration of crushed brick - lime composites using nano-additives. *Cem Con Comp* 68:77-87
17. Sanchez F, Sobolev K (2010) Nanotechnology in concrete- a review, *Con Build Mat* 24:2060–2071
18. Duran A, Navarro-Blasco I, Fernández JM, Alvarez JI (2014) Long-term mechanical resistance and durability of air lime mortars with large additions of nanosilica. *Con Build Mat* 58:147–158

Active photocatalytic-superhydrophobic coating with TiO₂/ZnO nano-heterostructures for lime mortars

Alessandro Speziale¹, Jesús Fidel González-Sánchez¹, Íñigo Navarro-Blasco¹, José M.

Fernández¹, José I. Alvarez¹

(1) Heritage, Materials & Environment (MIMED) research group, Department of Chemistry, University of Navarra, mimed@unav.es, aspeziale@alumni.unav.es, jgonzalez.65@alumni.unav.es, inavarro@unav.es, jmfdez@unav.es, jalvarez@unav.es

Abstract

Active coatings to be applied onto hardened surfaces of lime rendering and masonry mortars and stones of the Built Heritage were developed. Nano-heterostructures of TiO₂/ZnO (50:50 and 10:90) were obtained by Flame Spray Pyrolysis as photocatalytic agents with expanded sensitivity towards solar light, instead of the restricted UV dependence of the pure TiO₂ or ZnO. A superhydrophobic medium was simultaneously prepared and photocatalytic nanoparticles were added to obtain the coatings. The active products were expected to prevent the water absorption of the substrates and the subsequent degradation effects as well as to allow the stones and mortars to act as self-cleaning materials, reducing the dirt deposition and the biological colonization. Dispersions were applied onto the surface of lime mortars and siliceous stone. Measurements of the photocatalytic oxidation activity of the coatings were carried out by means of the NO degradation, showing a very good efficiency of the nanoparticles even at long term tests (values of NO oxidation of ca. 35%). Water contact angle assessment evidenced a strong hydrophobization of the treated surfaces, with WCA values higher than 140°. The results proved the synergistic effect of these coatings with respect to the durability of the treated substrates, giving rise to a promising way of preventive conservation for building materials of the Cultural Heritage.

Introduction

In terms of preventive conservation, the use of water-repellent and biocide materials can be useful for keeping clean and safe Built Heritage for long time [1,2]. Active coatings could be applied onto the building materials (pre-existent and new repair components as well) to prevent the water access, the accumulation of dirt deposits and the biological colonization [3-5].

The obtaining of compatible coatings would be then of the utmost importance, presenting the following advantages: i) Water repellent surfaces would hinder the water uptake minimizing the subsequent decay processes; ii) for coating combining water repellent agents and photocatalysts, also self-cleaning surfaces could be obtained due to the synergistic effect between the photocatalytic oxidation (PCO) of the dirt compounds and the

hydrophobicity of the surface that would difficult the anchorage of the stains and would facilitate the removal of the PCO by-products; and iii) finally, biological colonization would be reduced or even avoided by breaking the bonds between microorganisms and substrates by PCO.

While TiO_2 is a recognized photocatalyst that can oxidize dirt components by PCO, it is only efficient under UV illumination [6-8]. In this work nano-heterostructures of TiO_2/ZnO (50:50 and 10:90) were obtained by Flame Spray Pyrolysis as new photocatalytic agents sensitive towards the visible light spectrum. New coatings were thus designed combining stable dispersions of these nanoparticles with a water repellent admixture (superhydrophobic agent). The coatings were also prepared by adding dispersing agents, superplasticizers, which can avoid the agglomeration of the photocatalytic nanoparticles that is supposed to increase their activity [9]. These new dispersions used as coatings were applied onto sandstone and lime mortar. The study of modified stones and mortars with waterproofing, biocidal and self-cleaning features would be of interest for possible application in preventive conservation of historic buildings. Waterproofing measurements and self-cleaning tests were performed, and photocatalytic activity was also measured through NO_x abatement studies.

Experimental section

Materials

Two different heterostructures of $\text{TiO}_2\text{-ZnO}$ (50:50 and 10:90) were studied as powder compounds and used to prepare different synergistic superhydrophobic (SPHB) and photocatalytic dispersions further applied as active coatings onto lime mortar and sandstone, as representative building materials of the Cultural Heritage. Nanoparticles of $\text{TiO}_2\text{-ZnO}$ were synthesized by Lurederra Technological Center by FSP. Previously to their incorporation, nanoparticles were calcined in order to remove all possible nitrogen compounds residual from the synthesis of the nanoparticles.

Calcitic air lime mortars were prepared by mixing 18.3% calcitic air lime supplied by Cal Industrial S.A. (Calinsa Navarra), classified as CL-90 by European regulations and 81.7% standardized siliceous sand (supplied by IETCC) later shaped into cylindrical samples of 3 cm diameter and finally cut around 1 cm high. Rectangular prisms of 5x5x3 cm were obtained for siliceous stone.

Two of the applied coatings were used both in air lime mortar and siliceous stone as dispersions 1% w/v of photocatalyst 50:50 and 1 % w/v photocatalyst 50:50 with a superhydrophobic agent, respectively. While the first dispersion only contains the photocatalyst (pH=5), the second one with superhydrophobic agent (as prepared by Lurederra) consists in an alcoholic solution including photocatalyst. The later was used as a

primary dispersion for preparing modified dispersions. The first one was used as control with the aim of proving the PCO efficiency of the new photocatalysts.

Methods

Photocatalyst characterization

Particle size (BET, Table 1), mineralogical composition (XRD, Figure 1) and morphology (TEM, Figure 2) of the two heterostructures were characterized and results are shown below. Heterostructures showed a nanometric size and a mineralogical composition according to the structure between the two main components (TiO₂ and ZnO).

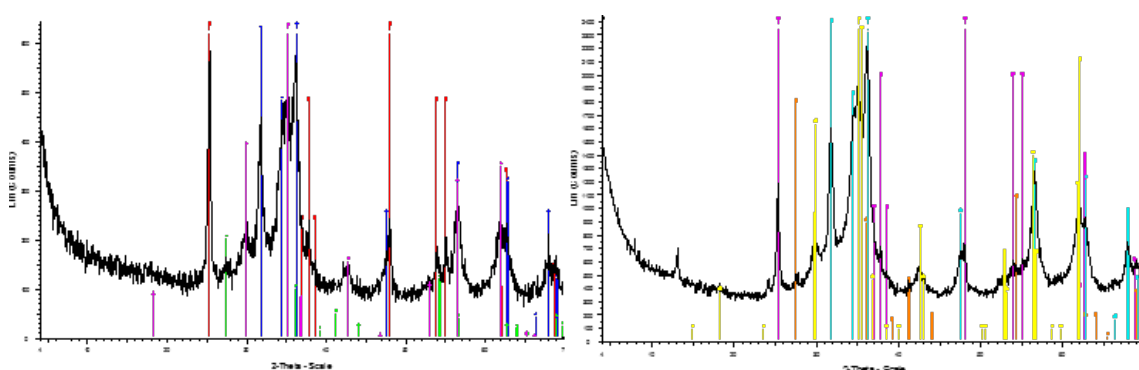


Figure 1. X-ray diffraction patterns corresponding to TiO₂/ZnO 50:50 and TiO₂/ZnO 10:90 samples.

Table 1. BET specific surface area and size of the nano-heterostructures.

Sample	BET (m ² /g)	Estimated size (nm)
TiO ₂ /ZnO (50:50)	84.8	15
TiO ₂ /ZnO (10:90)	79.7	19

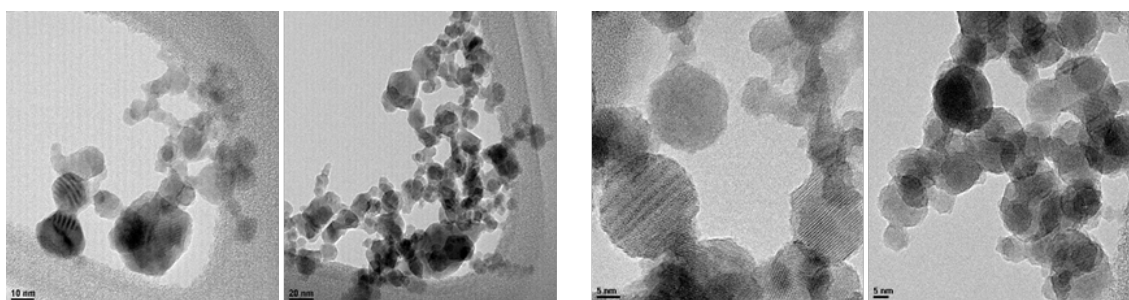


Figure 2. TEM micrographs (Left: TiO₂/ZnO 50:50; right: TiO₂/ZnO 10:90), showing a mixed morphology between the spherical one of TiO₂ and the elliptical one of ZnO.

Preparation and characterization of superhydrophobic and photocatalytic dispersions

Alcoholic superhydrophobic solutions containing photocatalytic nanoparticles TiO₂/ZnO 50:50 and TiO₂/ZnO 10:90 (1 weight % with respect to the total volume of solution) were the basic media for the preparation of several dispersions using superplasticizers. Active

dispersing agents polynaphtalenesulfonate (PNS), polycarboxylate ether (PCE), melamine sulfonate (MEL) and polyacrylate (PA) were added in 1% with respect to the photocatalyst. Table 2 collects a summary of the composition of the dispersions.

Table 2. Composition of the active coatings

COATING NAME	COMPOSITION
P	Photocatalyst 50:50 TiO ₂ /ZnO in a 1% (w/v) dispersion
SPHB	SPHB dispersion + 50:50 TiO ₂ /ZnO 1%
PCE-50	SPHB dispersion + 50:50 TiO ₂ /ZnO 1% + PCE
PNS-50	SPHB dispersion + 50:50 TiO ₂ /ZnO 1% + PNS
PA-50	SPHB dispersion + 50:50 TiO ₂ /ZnO 1% + PA
MEL-50	SPHB dispersion + 50:50 TiO ₂ /ZnO 1% + M
PCE-10	SPHB dispersion + 10:90 TiO ₂ /ZnO 1% + PCE
PNS-10	SPHB dispersion + 10:90 TiO ₂ /ZnO 1% + PNS
PA-10	SPHB dispersion + 10:90 TiO ₂ /ZnO 1% + PA
MEL-10	SPHB dispersion + 10:90 TiO ₂ /ZnO 1% + M

Particle size distribution measurements of these dispersions were carried out by means of Malvern Mastersizer laser diffractometer equipment.

Application of the dispersions on different building materials

The as-prepared dispersions were applied onto siliceous stone samples and air lime mortars by simple deposition using a pipette, pouring 1 mL in order to cover the whole surface and leaving the sample drying for 24 hours under lab conditions.

Photocatalytic studies: NO_x oxidation

The photocatalytic activity of the nanoparticles was studied in a laminar-flow reactor (ISO 22197-1 [10]), under UV, solar and visible radiation, using a cut-off filter for the last one. The initial concentration of NO was fixed to 500 ppb and concentrations of NO and NO₂ were determined by using a chemiluminescence detector (Environnement AC32M) at a 3.0 L·min⁻¹ flow.

The photocatalytic effect of the coatings applied onto air lime mortars and sandstone was also studied under UV and solar conditions following the same experimental conditions. Active nanoparticle powders were tested for 5 hours. Since the initial trials proved that the values of NO_x abatement were constant, the test time was then reduced to 30 min for the coatings.

Samples were subjected to an accelerated ageing process in a climatic chamber, according to the steps depicted in Table 3. After that, photocatalytic activity of the samples was again measured to establish the durability of the active coatings.

Table 3. Characteristics of the cycle of accelerated weathering

Cycle duration	Step	Temperature (°C)	Relative Humidity (%)	Rain	UV Light	Time (min)
24 h	1	35	30	No	Yes	160
	2	12	80	Yes	No	160
	3	20	50	No	No	160
	4	12	60	No	No	160
	5	35	30	No	Yes	160
	6	12	80	Yes	No	160
	7	35	30	No	Yes	160
	8	20	50	No	No	160
	9	12	60	No	No	160

Hydrophobicity studies

Using a video-based optical contact angle measuring instrument (OCA 15EC Dataphysics), the static water contact angle (WCA) of the treated surface of the samples was registered. Droplets of 5 μ L deionized water were poured and monitored during 10 s, in order to achieve reliable data [9, 11].

Self-cleaning test

First, 1 mL of a 10^{-3} M Rhodamine B solution was poured on top of three different samples of sandstone and lime mortar: non-treated sample (Control), dispersion of 1 % photocatalyst TiO_2/ZnO 50:50 heterostructure (Photocatalyst), dispersion of both 1% TiO_2/ZnO 50:50 photocatalyst and superhydrophobic agent (SPHB). One minute after the application the samples were moved vertically and left for 1 hour, and photos were taken.

In the second part of the test 1 mL of the previously prepared Rhodamine B solution was poured on the six samples that remained in horizontal position. Meanwhile, a UV lamp was placed about 30 cm on top of the sample. The light was set on and photos were taken at times 0, 10, 15, 30, 45, 60, 75, 90, 120, 300, 480 min and 24 h.

Results and discussion

Characterization of PSD of superhydrophobic-photocatalytic dispersions

Figure 3 shows the particle size distribution (PSD) of dispersions with nano-heterostructures TiO_2/ZnO 50:50. Control 1 corresponds to dispersion with just the photocatalyst, showing a unimodal PSD, with a maximum at 18 μ m. When this dispersion was modified upon the

addition of SPHB agent, nanoparticles tended to agglomerate, yielding a maximum at around 60 μm (Control 2).

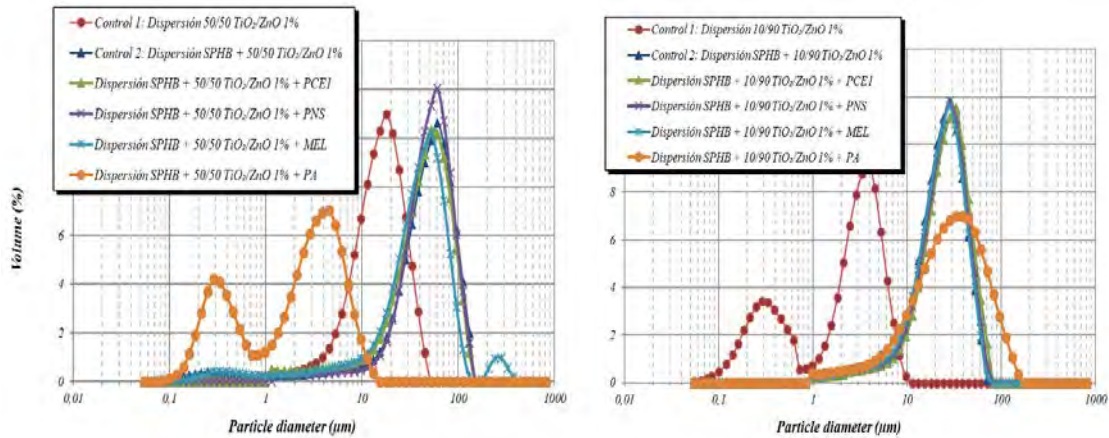


Figure 3. Particle size of the superhydrophobic-photocatalytic dispersions.

Superplasticizers were also added with the aim of preventing nanoparticles from agglomeration. PNS did not show any efficiency in reducing the size of the agglomerates, whereas very slight improvements could be detected for PCE1 and MEL polymeric superplasticizers. Maybe the dosage of these SPs should be modified to reach an effective dispersion of nanoparticles.

The only exception was the dispersion with PA, which showed a bimodal PSD with maximum values at 0.3 μm and 3.9 μm .

As for the PSD of nano-heterostructures TiO_2/ZnO 10:90 (Figure 3, right), the dispersion of just photocatalyst depicted lower size of agglomerates than that of the TiO_2/ZnO 50:50 and a bimodal distribution with two maximums at 0.3 and 4 μm . The presence of the SPHB agent caused the agglomeration of the nanoparticles, although a smaller particle diameter, of around 30 μm , was obtained compared with the TiO_2/ZnO 50:50 dispersion.

PCE 1, PNS and MEL superplasticizers hardly modified the PSD, whereas PA did not perform as well as in the case of the TiO_2/ZnO 50:50 dispersions.

Photocatalytic performance

Photocatalytic activity of ZnO and TiO₂ powder nano-heterostructures

The photocatalytic activity of the original nanoparticles in powder was studied and compared with pure TiO_2 and pure ZnO nanoparticles (Figure 4 and Figure 5). With respect to pure ZnO, the newly synthesized heterostructures improved their activity and increased both the NO and NO_x abatements. As compared with pure TiO_2 , the NO abatement of the two heterostructures was slightly lower although NO_x removal was higher. This was ascribed to the higher NO_2 release provoked by the TiO_2 action.

As main conclusion, the nano-heterostructures evidenced outstanding photocatalytic activity, yielding better NO_x removal rates than those of pure semiconductor oxides like ZnO or TiO₂. TiO₂/ZnO 10:90 seems to be a little more efficient than TiO₂/ZnO 50:50.

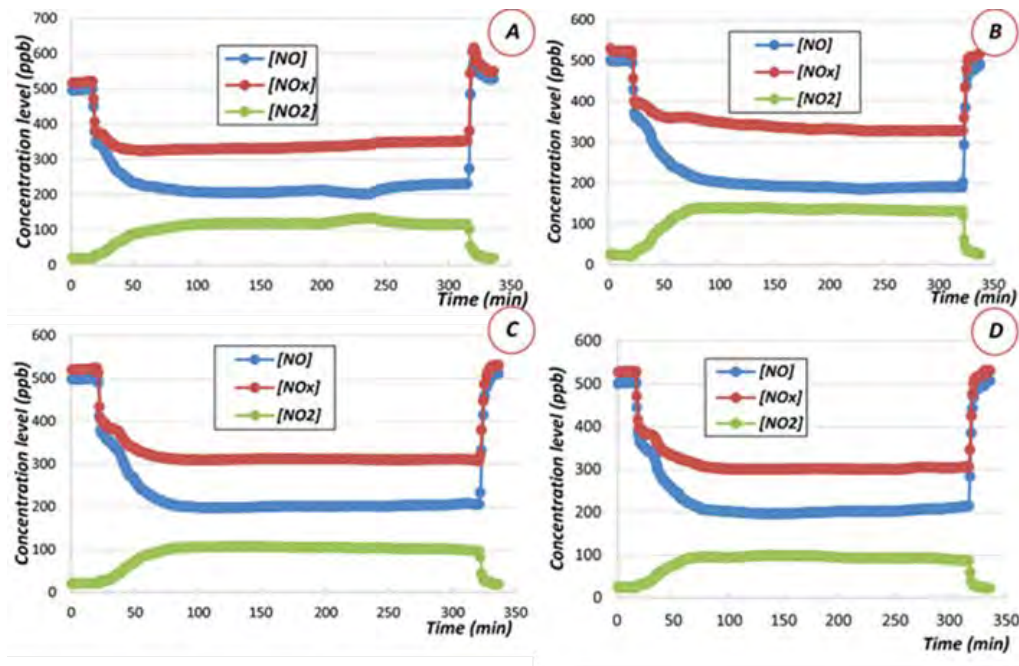


Figure 4. Profiles of NO, NO₂ and NO_x abatements for ZnO (a), TiO₂ (b) and the heterostructures TiO₂/ZnO 50:50 (c) and 10:90 (d).

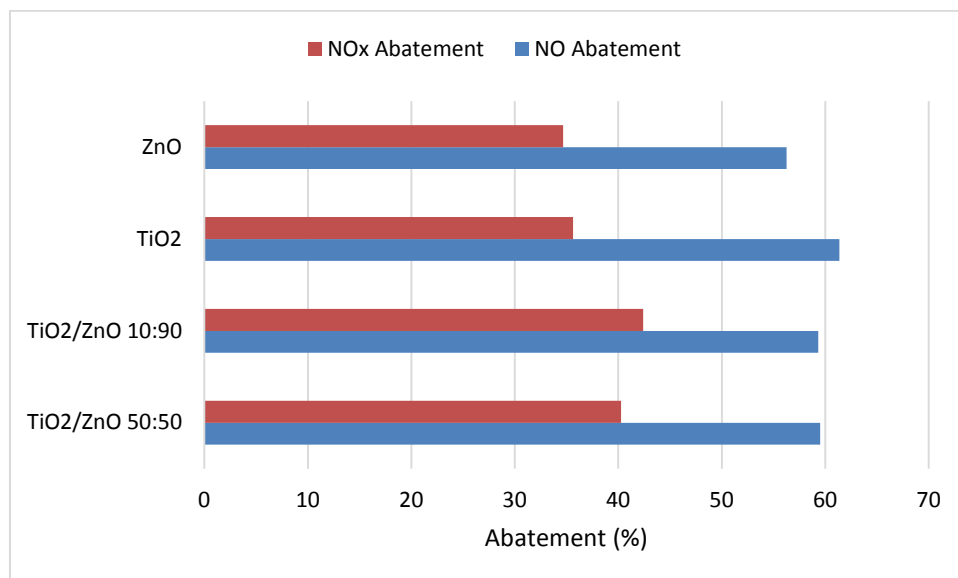


Figure 5. NO abatement values of TiO₂, ZnO and the two heterostructures.

Photocatalytic activity of the coatings with nano-heterostructure TiO₂/ZnO 50:50.

After applying the active coatings onto sandstone, results showed that the presence of the photocatalyst increased the activity under both UV and solar radiation (Figure 6) as compared with the non-treated specimens. When the coatings were prepared with SPHB

agent, the photocatalytic activity underwent a decrease, suggesting a certain degree of undesirable interaction. This finding could be ascribed to the blockage of active sites of the photocatalyst or to the absence of the necessary water for the PCO due to the hydrophobic environment caused by the SPHB admixture.

For the coating including SFHB and photocatalyst, the sandstone treated samples showed the highest efficiency in NO removal under UV illumination, whereas under solar light illumination were the lime mortar samples. The observed decrease in NO removal from UV to solar light illumination is ascribed to the different quantum efficiency between the UV and solar photons.

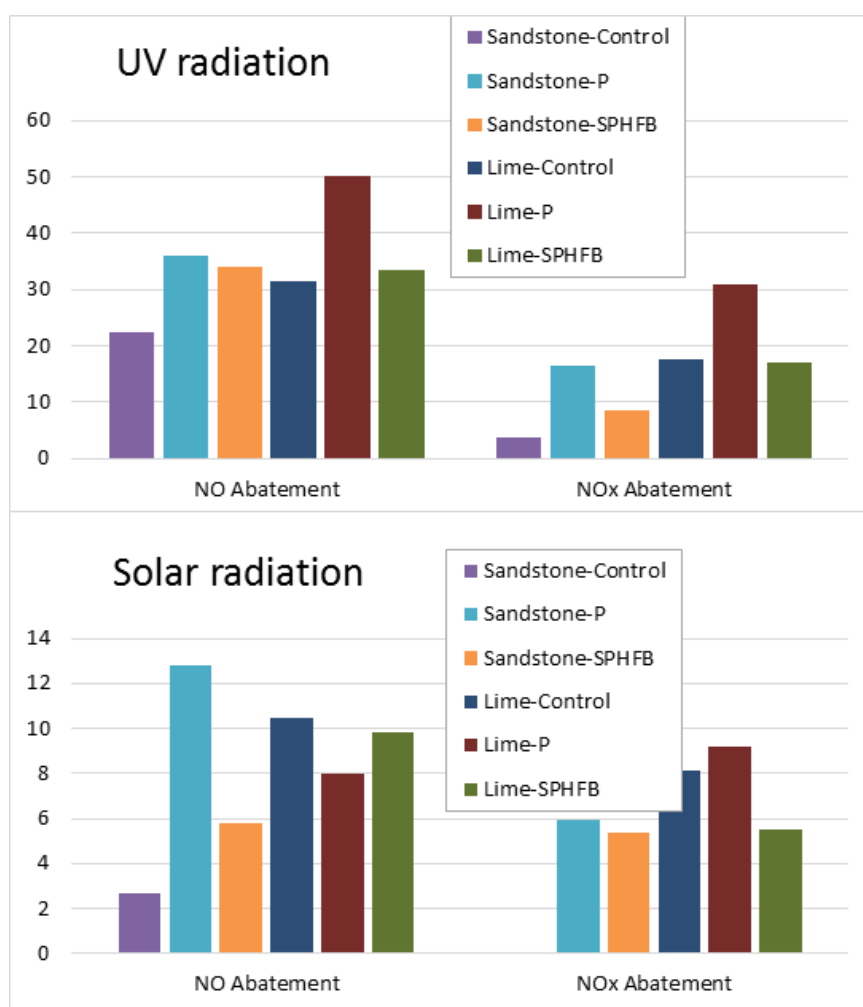


Figure 6. NO and NOx abatement of different samples treated with active coatings: non-treated sample (Control), only heterostructured photocatalyst TiO₂/ZnO 50:50 in a 1% (w/v) dispersion (P); and a dispersion containing both photocatalyst and superhydrophobic agent (SPHB).

Generally speaking, the higher activity of the lime samples (control and treated samples as well) can be explained owing to the occurrence of secondary reactions (mainly NO disproportionation) due to the highly alkaline medium of the mortar.

Effect of the superplasticizers: photocatalytic activity of the coatings with nano-heterostructures TiO₂/ZnO 10:90 and 50:50 including dispersing agents

A comparison between the samples treated with coatings modified with SPs was carried out to ascertain the influence of the dispersing agents on the photocatalytic performance of the coatings. Figure 7 collects the results, being the control a sample of raw material with no coating applied.

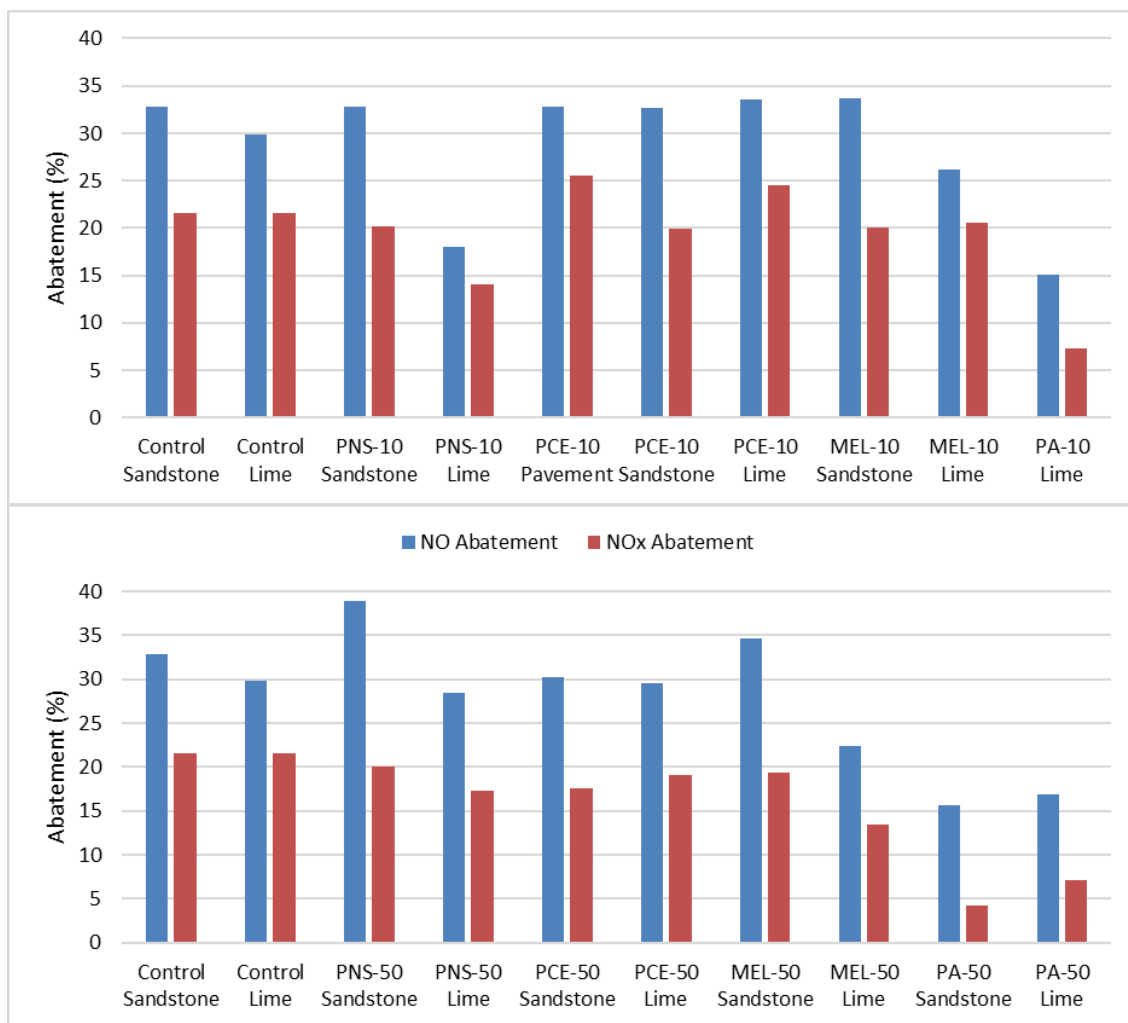


Figure 7. Effect of the different dispersing agents: NO and NO_x abatement of the coatings prepared with TiO₂/ZnO 10:90 (top) and 50:50 (bottom) photocatalysts.

The majority of the samples showed NO_x abatements higher than 25%. On one hand, treated sandstone samples showed similar results and all of them improved the NO and NO_x abatements with respect to the control. The results of lime samples were not uniform and only the treatment with PCE-10 showed a higher NO_x abatement than that of the control. It should be noted that MEL and PNS additives work well with coating applied to the siliceous stone but not with the coatings applied to lime mortar. It has to be in mind that the active surface of the stone (15 cm²) is more than twice of that of the mortar (7 cm²).

The most interesting samples in terms of PCO efficiency were subjected to accelerated weathering in a climatic chamber following the cycles described in the Experimental section. Then, the results of NO_x abatement were again recorded and showed in Figure 8. It can be observed that climatic ageing caused a decrease in the photocatalytic activity, but samples still yielded NO_x abatements higher than 20%, involving a reasonable durability of the active coatings.

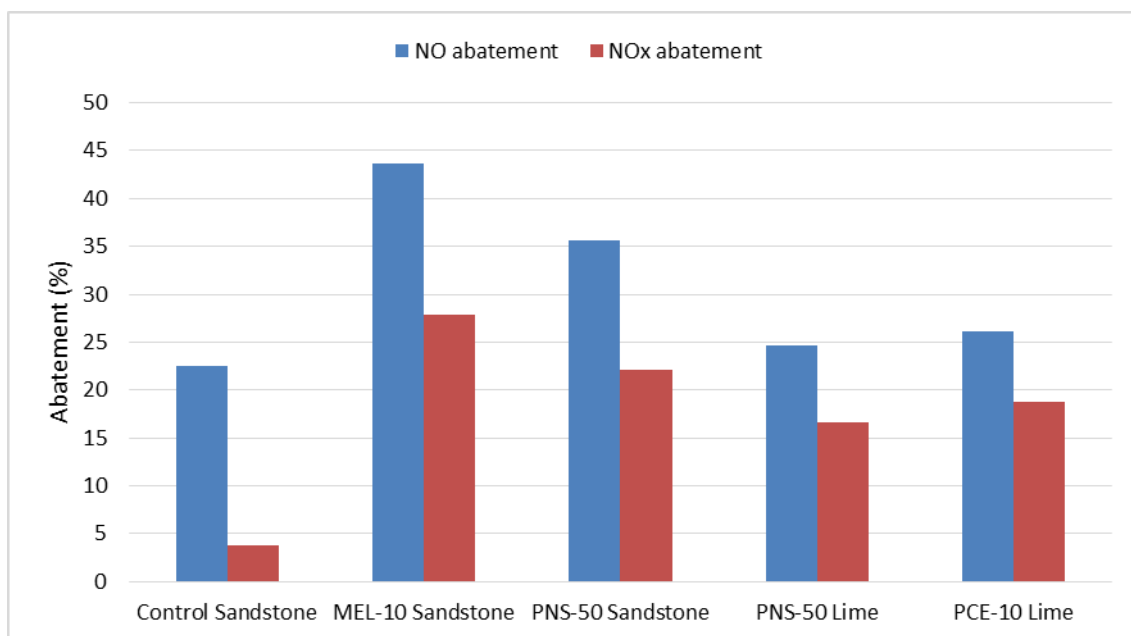


Figure 8. NO and NO_x abatement of the samples with better results after accelerate weathering treatment.

Waterproofing studies

The majority of the treated samples were seen to have WCA higher than 100°, suggesting a high efficiency of the SPHB agent and a good compatibility with the photocatalytic additives (Table 4).

Table 4. Water contact angle of the samples treated with TiO₂/ZnO 10:90 photocatalyst.

Sample	Θ	Partial Absorption of the drop of water
Lime-Control	< 10	Yes
Lime-MEL	82.9	No
Lime-PA	129.6	Yes
Lime-PCE	131.7	No
Lime-PNS	87.3	No
Sandstone-Control	11.5	Yes
Sandstone-MEL	142.6	No
Sandstone-PA	119.5	Yes
Sandstone-PCE	131.7	No
Sandstone-PNS	131.7	No

The presence of the SPs was not detrimental for the hydrophobization of the surfaces of the treated stones and mortars, with the exception of the coatings bearing melamine sulfonate and polynaphthalene sulfonate applied onto air lime mortars. This result might be explained as a consequence of the dosage and compatibility of the SP with the strong alkaline lime medium. Also, it should be noticed that both substrates treated with PA-bearing coating showed a tendency to absorb the water drop over the time. Maybe the PA creates strong hydrogen bonds with the water drop, jeopardizing the hydrophobic protection of the coatings.

Self-cleaning tests

SP-free coatings were applied onto sandstone and lime mortars to assess the self-cleaning ability of the photocatalyst and of the SPHB-photocatalyst coatings. In this test, the objective was to identify if the coating was able to efficiently degrade the organic dye deposited on the surface of the sample, as represented below (Figure 9 and Figure 10). Samples were observed along the time. Results gathered at different times are represented in Table 5, being the levels of degradation at naked eye: 0 no degradation, 1 slight degradation, 2 sharp degradation and 3 total degradation.

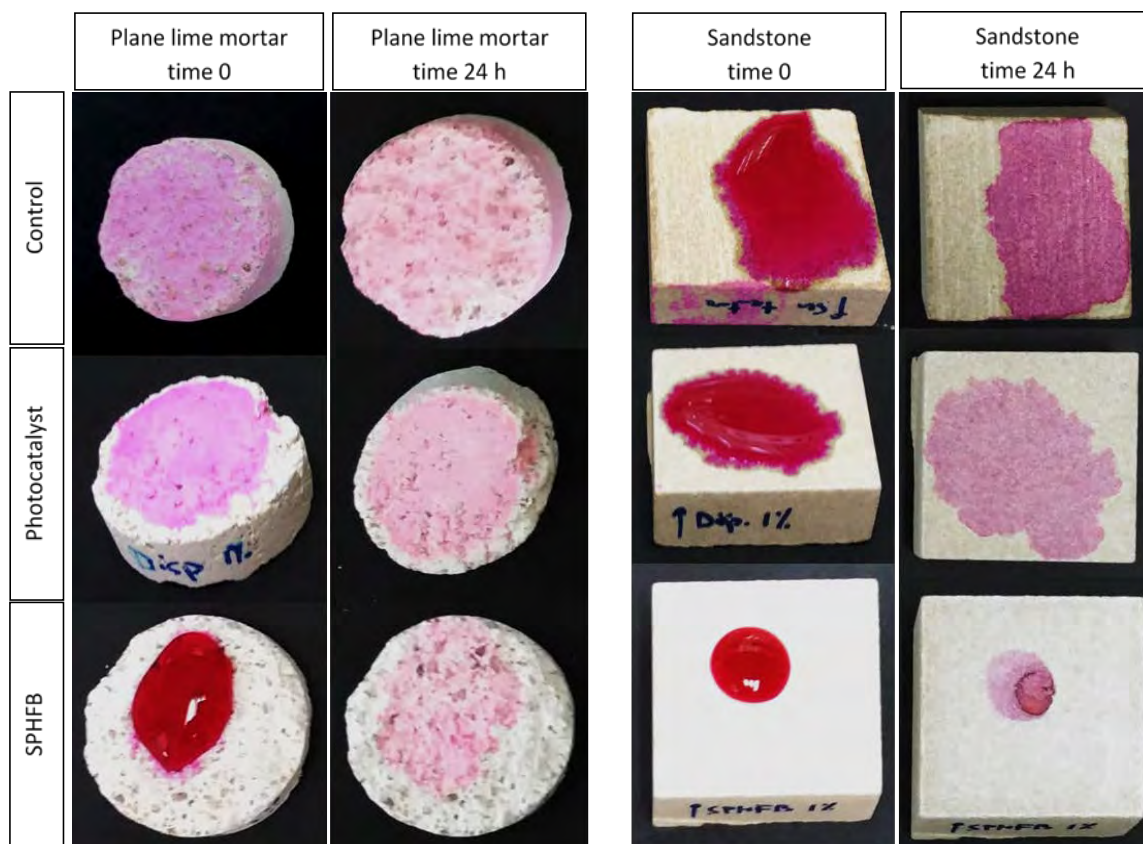


Figure 9. Results of the photocatalytic self-cleaning test at time 0 and 24h for lime mortar and siliceous stone samples. White coloring in Sandstone at time 0 is due to the light source.

Results showed that the non-treated specimens were fully affected by the dye deposition, with a large degree of dye penetration from the surface to the inner part of the substrate. After 24 hours, the stain provoked by the dye was evident, showing, if any, negligible degradation of the dye (0 value in Table 5).

Table 5. Degradation levels for the photocatalytic self-cleaning test.

Degradation level	Time (min)	0	10	15	30	45	60	75	90	120	300	480	1440
	Lime-Control	0	0	0	0	0	0	0	0	0	0	0	0
Lime-Photocatalyst	0	0	0	0	1	1	1	1	1	1	1	1	2
Lime-SPHB	0	0	0	0	0	0	1	1	1	1	1	2	2
Stone-Control	0	0	0	0	0	0	0	0	0	0	0	0	0
Stone-Photocatalyst	0	0	0	0	0	1	1	1	1	1	1	1	2
Stone-SPHB	0	0	0	0	0	0	0	0	1	1	1	2	2

The coating applied with photocatalyst was much more efficient in reducing the intensity of the colour of the dye's stain. This is a clear evidence of the positive action of the photocatalytic additive. Finally, the coating including both photocatalyst and SPHB agent showed a synergistic and positive effect on the dye degradation: on one hand, the superhydrophobicity hindered the adsorption and penetration of the dye, as can be observed in the photographs at time 0; and, on the other hand, photocatalyst was able to oxidize the pigment along the time.

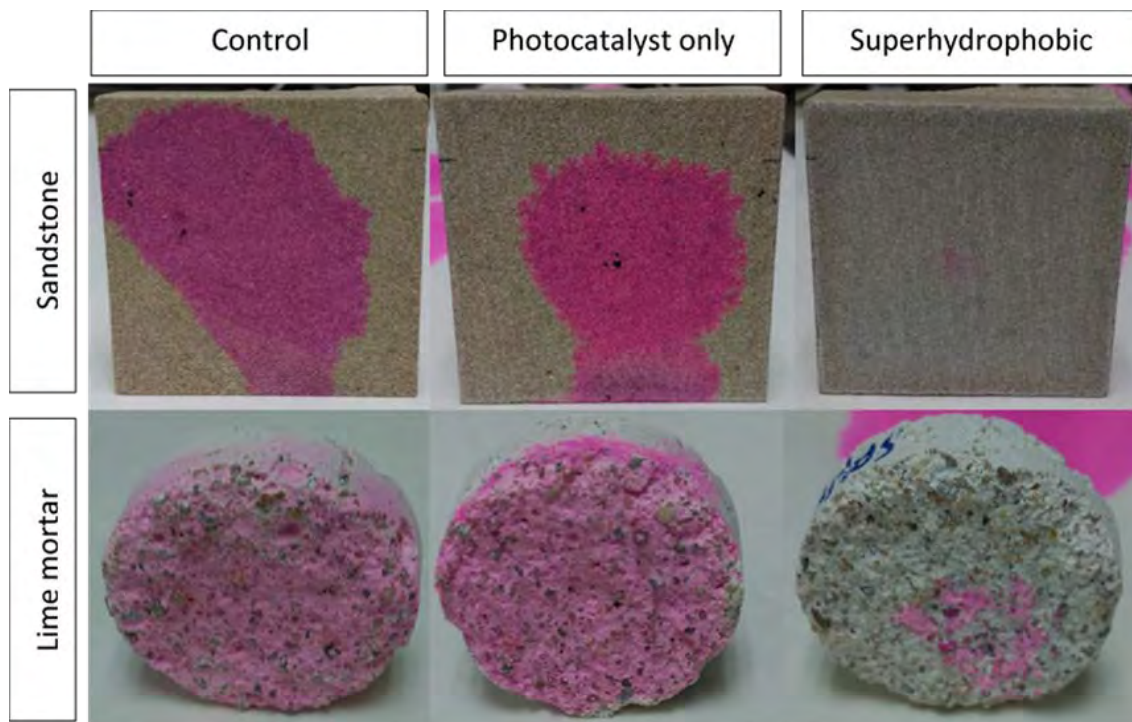


Figure 10. Results of the self-cleaning test for samples in vertical position: dye was deposited onto lime mortar and siliceous stone samples for one minute in horizontal position and then moved to vertical position.

The self-cleaning ability was also measured for these materials placed in vertical position. As expected, the superhydrophobic effect is extremely important for preventing the dye from being absorbed and thus retained. As shown in Figure 10, the dye is practically not retained for samples with SPHB agent.

Conclusions

New coatings with self-cleaning and superhydrophobic abilities have been prepared and applied onto air lime mortar and siliceous stone. The objective of these coatings was to obtain modified stones and mortars with waterproofing, biocidal and self-cleaning features that would be of interest for application in preventive conservation of historic buildings. The coatings have been obtained combining stable dispersions of nano-heterostructures of TiO₂/ZnO (50:50 and 10:90) and a water repellent admixture (superhydrophobic agent). These new photocatalytic agents were seen to be sensitive towards the visible light spectrum.

In addition, dispersing agents, superplasticizers, were also in some cases added with the purpose of avoiding the agglomeration of the photocatalytic nanoparticles to increase their activity.

Photocatalytic activity of the treated specimens was seen to increase due to the active coatings. Combination of photocatalyst with SPHB agent slightly reduced the activity of the former. NO abatement measurements were favoured in the case of air lime mortars most probably ascribed to the highly alkaline pH.

Self-cleaning tests showed a positive synergistic effect between photocatalyst and SPHB agent, reducing the dye adsorption and absorption and degrading the organic pigment by photocatalytic oxidation.

Concerning the use of SPs, most interesting results were obtained for the dispersions of melamine sulphonate with TiO₂/ZnO 10:90 on sandstone and polycarboxylate ether applied onto lime mortar, in both superhydrophobic and photocatalytic activities.

Despite having good particle size, dispersions with PA did not provide good results of NO_x abatement and this finding has been correlated with the concentration of the polymeric additive.

The future perspectives require water vapor permeability measurements to be carried out later on in order to understand the real behavior of the coating once applied to Architectural Heritage materials. Optimization of some dosages of the admixtures should be also envisaged.

Acknowledgments

Funded by MINECO under Project MAT2015-70728-P, and by the Government of Navarra under grant number Exp. 0011-1383-2018-000005, project PC065 RECURBAN. A. Speziale is a Research Training Program student and J.F. González-Sánchez thanks the Friends of the University of Navarra, Inc., for a pre-doctoral grant.

References

1. Quagliarini E et al. Smart surfaces for architectural heritage: preliminary results about the application of TiO₂-based coatings on travertine. *J Cult Herit* 2012; 13:204-9.
2. Quagliarini E et al. Self-cleaning materials on architectural heritage: compatibility of photo-induced hydrophilicity of TiO₂ coatings on stone surfaces. *J Cult Herit* 2013;14:1-7
3. Brimblecombe P, Grossi CM. Aesthetic thresholds and blackening of stone buildings. *Sci Total Environ* 2005;349:175-89
4. Maro D et al. Aerosol dry deposition in the urban environment: Assessment of deposition velocity on building facades. *J Aerosol Sci* 2014;69:113-31
5. Camuffo D. Dry Deposition of Airborne Particulate Matter: Mechanisms and Effects. In: *Microclimate for Cultural Heritage*, Boston: Elsevier; 2014, p. 283-346
6. Sugrañez R, Alvarez JI et al. Enhanced photocatalytic degradation of NO_x gases by regulating the microstructure of mortar cement modified with titanium dioxide. *Build Environ* 2013 11;69:55-63.
7. Folli A et al. TiO₂ photocatalysis in cementitious systems: Insights into self-cleaning and depollution chemistry. *Cem Concr Res* 2012;42:539-48
8. Pérez-Nicolás M, Navarro-Blasco I, Fernández JM, Alvarez JI. Atmospheric NO_x removal: study of cement mortars with iron- and vanadium-doped TiO₂ as visible light-sensitive photocatalysts. *Constr Build Mater* 2017;149:257-271
9. M. Pérez-Nicolás, J. Plank, D. Ruiz-Izuriaga, I. Navarro-Blasco, J.M. Fernández, J.I. Alvarez, Photocatalytically active coatings for cement and air lime mortars: Enhancement of the activity by incorporation of superplasticizers, *Construction and Building Materials* 162 (2018) 628–648.
10. ISO 22197-1 Fine Ceramics (Advanced Ceramics, Advanced Technical Ceramics). Test Method for Air Purification Performance of Semiconducting Photocatalytic Materials. Part 1: Removal of Nitric Oxide, 2007.
11. M. Fronzia, M. H. N. Assadib, D. A. H. Hanaorc, Theoretical insights into the hydrophobicity of low index CeO₂ surfaces, *Applied science surface* 478 (2019) 68-74.

Topic 3: Gypsum-based plasters and mortars in historical constructions



Study of properties of gypsum plasters from Araripe's Pole for application in restoration mortars

Fernanda Cavalcanti Ferreira¹, Jose Getulio Gomes de Sousa², Arnaldo Manoel Pereira

Carneiro¹

(1) Federal University of Pernambuco, fernandacavalcantif@gmail.com, ampc@ufpe.br

(2) Federal University of San Francisco Valley, jose.getulio@univasf.edu.br

Abstract

Gypsum plaster is the earliest binder known. It has been extensively used for indoor masonry coatings. Brazilian northeast has abundance and quality of the gypsum raw material, especially in Araripe's Pole. In this context, it is verified that the gypsum plaster ($\text{CaSO}_4 \cdot 0.5\text{H}_2\text{O}$ without admixture and additions) from the Araripe's Pole can be an excellent option for execution and repairing of historical coatings. In order to know in detail the material and understand the relation between the way of production of the gypsum plaster and its influence in the characteristics of these materials, the relationship between gypsum plaster production control characterized by the size of the company and gypsum plaster properties was evaluated. The experimental program was divided into analysis of characterization of gypsum plaster and evaluation of bond strength of coatings executed with these materials. Six samples of gypsum plaster were collected from different producers in the region. It was verified that the samples have high quality and, regardless of the manufacturer, present satisfactory performances. This is explained by the characteristics of the raw material present in the region, allowing its use in restoration mortars.

Introduction

Gypsum plaster is the earliest binder known. Findings reveal that this material was already used for the manufacture of containers and plasters for decorative purposes around 9000 BC [28]. The presence of gypsum plaster in historic masonry is verified in various periods [25].

The gypsum plaster is obtained by mechanical and physico-chemical processes, which may involve manual ore withdrawal, crushing, sieving, silage, calcination, thermal stabilization in silos, grinding and bagging [12]. It is through dehydration of the gypsum ore as a function of temperature and pressure that the following phases are formed: hemihydrate ($\text{CaSO}_4 \cdot 0.5\text{H}_2\text{O}$), anhydrite I (CaSO_4), anhydrite II (CaSO_4) and anhydrite III ($\text{CaSO}_4 \cdot \xi \text{H}_2\text{O}$).

The influence of type of ore, production control related to the type of furnace, temperature and calcination time, type and concentration of admixture, impurities, particle size, water/gypsum plaster ratio (w/g), mixing time, among others, influence the type and quality of the gypsum plaster obtained [3, 16, 17, 18, 19, 29, 30, 34, 36].

The application of gypsum plaster ($\text{CaSO}_4 \cdot 0.5\text{H}_2\text{O}$) in construction occurs by the hydration of the material in powder by a chemical and physical phenomenon, which produces a homogeneous paste that quickly acquires plasticity and solidifies until its hardening, when the material acquires mechanical resistance, returning to its stable form of dihydrate ($\text{CaSO}_4 \cdot 2\text{H}_2\text{O}$) [27]. Characteristics of workability, setting time and dimensional variation of the pastes are observed during the hydration of the gypsum plaster.

The Northeast region of Brazil has an advantage in relation to others around the world, since it presents abundance and quality of gypsum ore, especially in the Gypsum's Pole in Araripe, in which it is produced gypsum plaster by companies of different sizes and production control [24]. In Brazil, at the pace of production in 2014, it is estimated that there are gypsum ore reserves for more than a century of exploration [22].

In this country, the gypsum plaster is usually supplied and sold in powder form, obtained from the calcination of the gypsum ore without admixture and additions. It means the powder is mostly composed by calcium sulfate hemihydrate ($\text{CaSO}_4 \cdot 0.5\text{H}_2\text{O}$), as well as anhydrite and impurities. For its application, it is mixed with water and, optionally, admixture can be added.

In the context of the conservation and restoration of ancient buildings, finding appropriate and scientifically proven solutions for the rehabilitation of traditional historical coatings has fundamental importance [25]. In this field, the use of gypsum plaster in restoration mortars is common. In order to use this material, there is a need for physical and mechanical characterization. One of the most important requirements for historic masonry mortars is bond strength, followed by mechanical strength and deformability and elasticity [35].

The gypsum plaster sold of the Gypsum's Pole in Araripe can be an excellent option for the execution and repairing of historical coatings due to its high quality. In order to know in detail the material and understand the relation between the form of production of the gypsum plasters and its influence in the characteristics of these materials, the relationship between gypsum plaster production control was evaluated through the evaluation of the characteristics of the producing company and properties of the gypsum plaster.

The experimental program of the study was divided into a characterization study of six gypsum plasters, by means of technological, chemical, physical and microstructural tests in the anhydrous, fresh and hardened states, and an evaluation of the bond strength of coatings made with paste.

Materials and methods

The study was divided into 3 stages: I – Obtainment of gypsum plaster samples; II - Characterization of gypsum plaster samples; III - Evaluation of coatings.

Obtainment of gypsum plaster samples

The study began with the collection of six gypsum plaster samples (in powder, without admixture and additions - $\text{CaSO}_4 \cdot 0.5\text{H}_2\text{O}$) for coating, provided by different manufacturers/merchants in the Gypsum's Pole in Araripe, Pernambuco, Brazil. The samples were collected from different cities and companies with different sizes, distributed between the cities of Araripina and Ouricuri. Table 1 shows the encoding of samples as well as the city of origin.

Table 1. Coding and origin of gypsum plaster samples

Plaster coding	City of origin	Sizes of companies	Time of operation	Type of calcination furnace
GA	Ouricuri – PE	1 to 10 employees	6 to 10 years	<i>Barriga quente</i> (hot belly)*
GB	Ouricuri – PE	-	11 to 20 years	<i>Barriga quente</i> (hot belly)
GC	Araripina – PE	31 to 60 employees	11 to 20 years	<i>Barriga quente</i> (hot belly)
GD	Araripina – PE	-	11 to 20 years	-
GE	Araripina – PE	Over 100 employees	11 to 20 years	-
GF	Araripina – PE	-	11 to 20 years	-

*Horizontal rotary cylinder in indirect burning steel that works by batch (non-continuous).

Characterization of gypsum plaster samples

The characterization and evaluation of the gypsum plasters samples in the anhydrous, fresh and hardened conditions was performed by the methods described in Table 2. For the study of the pastes in the fresh and hardened states, a water/gypsum plaster ratio (w/g) of 0.8 was used, which is a value commonly used in practice in civil works. Figure 1 shows some tests on the anhydrous, fresh and hardened states samples.

Table 2. Characterization tests for plaster

State	Characteristic/property analyzed	Method
Anhydrous	Particle size	NBR 12127 [4]
	Mineralogical composition	X-ray diffraction (XRD)
	Mineralogical characterization by mass variation of the material as a function of temperature	Thermal analysis (TGA and DTA)
	Chemical analysis	NBR 12130 [7]
Fresh	Setting time	NBR 12128 [5]
Hardened	Hardness	NBR 12129 [6]
	Compressive strength	NBR 12129 [6]



Figure 1. Gypsum plaster tests: a. Grain size tests: sequence of sieves and retained material; b. setting time using the Vicat apparatus; c. Hardness; d. compressive strength.

For determination of hardness, a universal EMIC test machine was used, applying indirect contact loading between the machine and the specimen through a metal sphere with a diameter of 9.5 mm. A load of 50 N was applied for 2 seconds. Then, this load was increased to 500 N during 15 s. This process was applied to the lower molding faces and to two other opposing lateral faces chosen from all the specimens, that is, 3 faces. The ball produces an impression on the surface of the specimen, which must have a measured depth. NBR 12129 [6] highlights that the value adopted for the series should be the average of the three results obtained, except when one of the individual values diverges more than 15% from the mean, being excluded from the depth calculation. If more than one diverges, the test must be remade. The hardness value (N/mm^2) is calculated by the division the load applied (N) by the product of π , diameter of the sphere (mm) and average of the depth (mm).

Evaluation of coatings

The performance of the gypsum plaster as a finished product, that is, as coating, by means of the bond strength was evaluated through NBR 13528 [10] at 28 days. The gypsum plaster samples were mixed with water and the obtained paste was applied to ceramic bricks, considering the situations with and without pre-wetting of the base since the revoked NBR 13867 [11] guides the wetting before application of the paste.

Results and discussion

Grain size

The grain size test of gypsum plaster has fundamental importance, since grain size is one of the properties that shows the best applications for the material [20]. The grain size has influence on several other properties such as unit weight, setting time, normal consistency,

hardness, bond and compressive strength. Figure 2 shows the grain size curves of the samples studied.

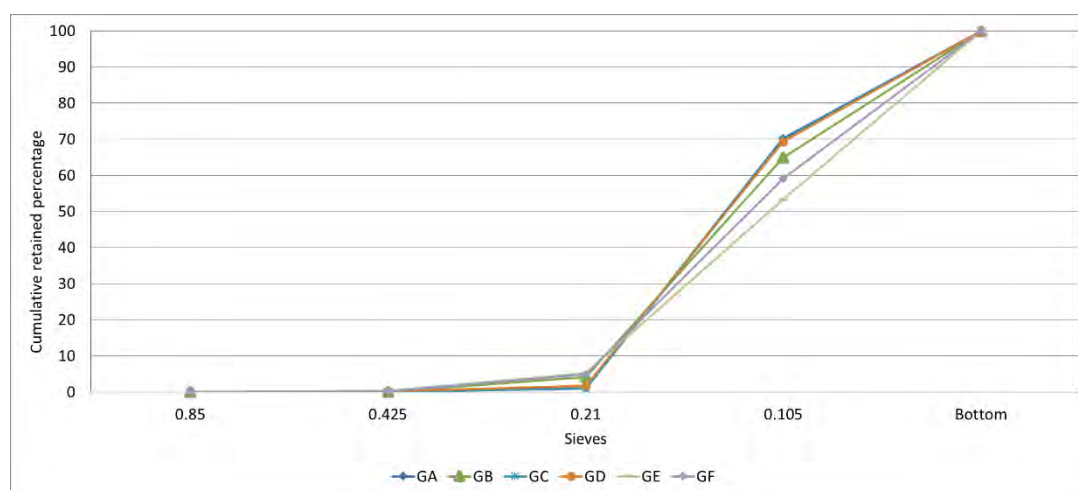


Figure 2. Grain size curves of gypsum plaster.

NBR 13207 [9] requests that gypsum plaster must have at least 90% of material passing on the sieve with opening of 0.21 mm for use in coating. Therefore, all the samples are in compliance.

It can be seen that the samples with the highest content of material retained in the sieve with opening of 0,105 mm are GA, GB, GC and GD (60 to 69%). The GE sample has a higher content of fines, explained by the greater amount retained in the bottom (more than 44%) and also retains approximately 50% in the sieve with opening of 0.105 mm. However, it presents more than 5% of material retained in the sieve with opening of 0.21 mm, being the sample that presents the highest content of material retained in this sieve when compared to the others. The GF sample is in an intermediate situation, presenting around 55% retained in the sieve with opening of 0.105 mm and 40% in the bottom.

X-ray diffraction

Figures 3 and 4 present X-ray diffractograms of the studied samples. GB and GC plasters were selected for an initial analysis and, due to their similarity, the X-ray diffraction test of the others was not performed. The raw material of these samples was obtained in the same region.

It is noticed that the samples present crystalline phases, with well defined peaks of the present minerals. The diffractograms show that gypsum plaster is predominantly composed of bassanite, a composition of $\text{CaSO}_4 \cdot 0.5\text{H}_2\text{O}$. Peaks relative to anhydrite (CaSO_4) and impurities such as quartz, alunite, muscovite and halite were also found.

The highest peaks for bassanite are found at $2\theta = 14.67^\circ$, 25.72° , 29.79° and 31.79° , corresponding to planes (200), (220), (400) and (204), respectively. In addition, lower intensity peaks attributed to bassanite can be observed in $2\theta = 42.24^\circ$, 49.18° , 52.92° , 54.09°

e 55.11° regarding the plans (422), (424), (207), (604) and (620), respectively [13, 31, 33]. Some peaks at approximately $2\theta = 25.33^\circ$, 31.10° , 38.60° , 40.70° , 48.80° and 56.00° are attributed to anhydrite.

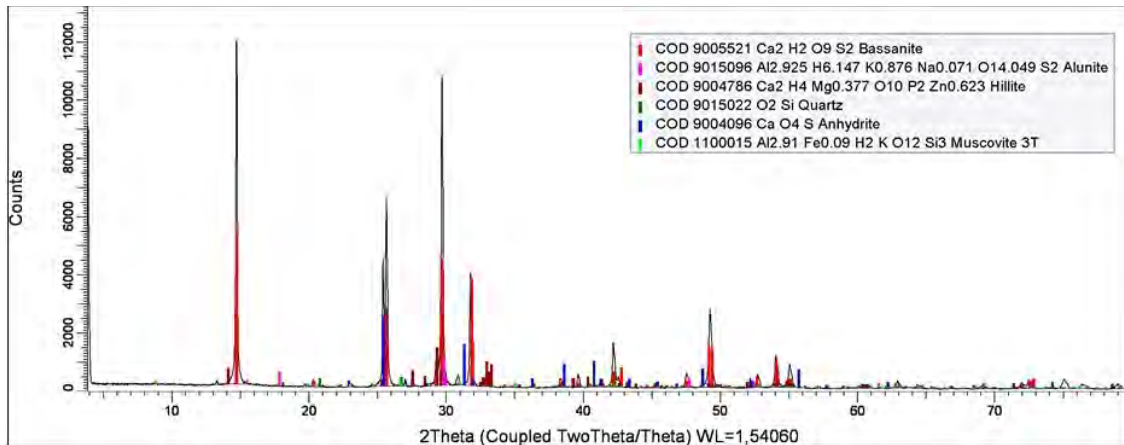


Figure 3. X-ray diffractogram of GB gypsum plaster.

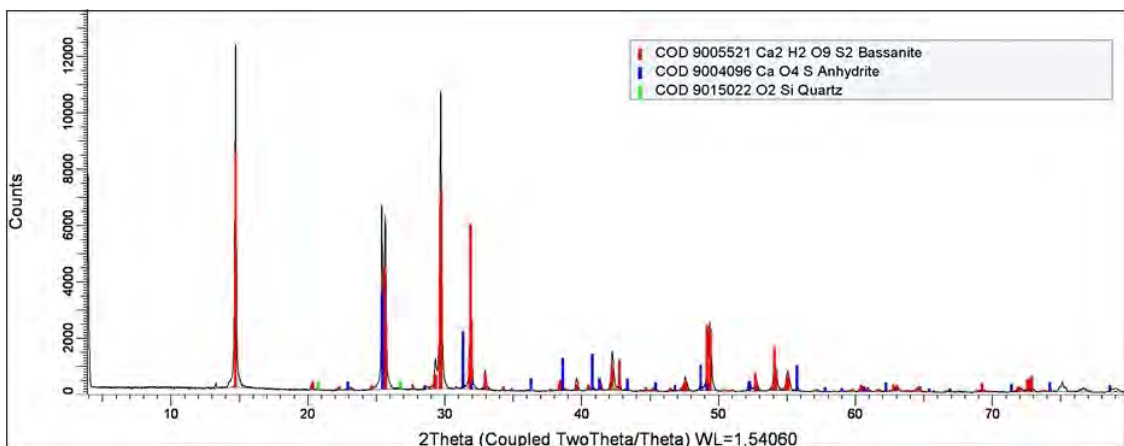


Figure 4. X-ray diffraction of GC gypsum plaster.

The bassanite and anhydrite in the diffractograms individualize different hydration conditions of the compounds related to the elimination of combined/bound water molecules in the gypsum ore calcination process to obtain gypsum plaster in the Arape region, which, depending on temperature, can generate 3 different types of anhydrite (III, II and I).

Thermogravimetric analysis

Figures 5 and 6 present the thermogravimetric analysis (TGA) and differential thermal analysis (DTA) curves of gypsum plaster studied. GB and GC samples were selected for an initial analysis and, due to the similarity between them, the thermal tests of the others were not performed.

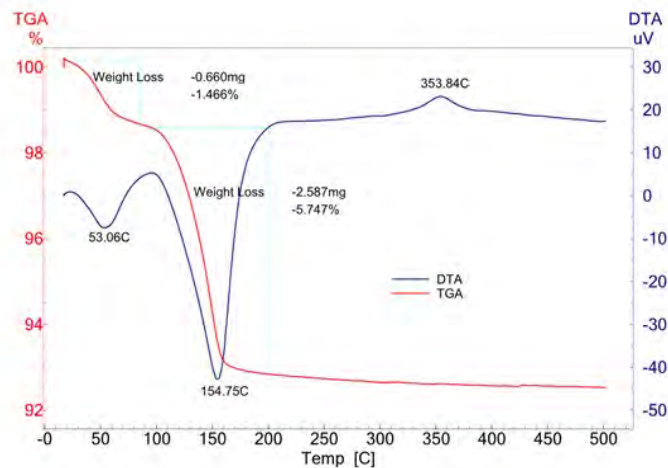


Figure 5. TGA and DTA curves of GB gypsum plaster.

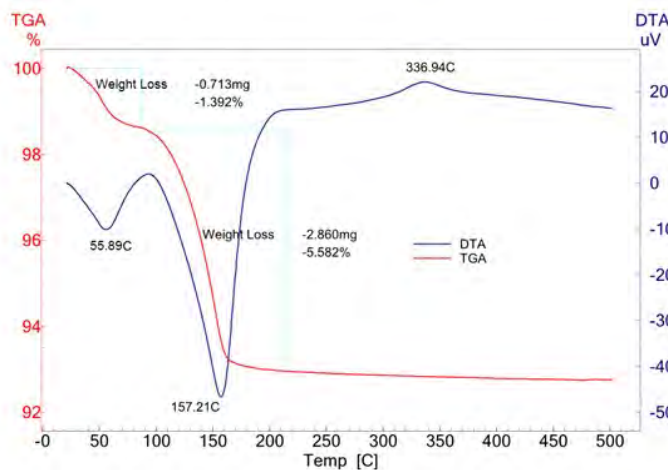


Figure 6. TGA and DTA curves of GC gypsum plaster.

The TGA curve shows the loss of mass of the material when subjected to controlled temperature programming. The DTA curve shows the events that occur through the derivative of the TGA curve. The great necessity of the DTA happens because an event can occur without mass loss, for instance alteration of the polymorph. It is observed the similarity of the curves regarding the values of mass loss, behaviour and reaction temperatures.

Three events can be verified by the DTA curve. The first is around 50 °C, where there is free water loss and it is an endothermic reaction. The second happens around 150 °C, where there is loss of water of crystallization. It is an endothermic reaction, where the hemihydrate ($\text{CaSO}_4 \cdot 0.5\text{H}_2\text{O}$) loses 0.5 molecule of water transforming into anhydrite III (CaSO_4). The mass loss of the sample, close to 6%, is justified stoichiometrically by the reaction ($\text{CaSO}_4 \cdot 0.5\text{H}_2\text{O} + \text{heat} \rightarrow \text{CaSO}_4 + 0.5\text{H}_2\text{O}$), where the half-molecule of water represents 6.2% of the mass. As the material is not composed only by hemihydrate, the value obtained is not exact. The third event is between 330 and 360°C, where the exothermic reaction of transformation of

anhydrite III (soluble) into anhydrite II (insoluble) occurs. No variation of mass was confirmed by the TGA curve, only change of the polymorph.

The obtained curves are typical of thermal analyzes of hemihydrate. It was not verified the presence of events characteristic of the presence of other compounds. This factor demonstrates the quality of the material.

Chemical analysis

The chemical analysis of the GA and GC samples of gypsum plasters (calcined gypsum powder without admixture and addition) was performed following the specifications of NBR 12130 [7], as shown in Table 3.

Table 3. Results of chemical analysis of gypsum plaster

Determinations	%	
	GA	GC
Free water	1.00	0.90
Crystallization Water	5.69	5.40
Insoluble Residue in hydrochloric acid (RI + SiO ₂)	0.73	0.41
Sesquioxides (R ₂ O ₃)	0.43	0.23
Calcium oxide (CaO)	37.8	38.2
Magnesium oxide (MgO)	0.43	0.11
Sulfuric anhydride (SO ₃)	53.1	54.10
Carbon dioxide (CO ₂)	0.69	0.34

From the data in Table 3, the high purity of the gypsum plaster was verified, as evidenced by the calcium oxide contents, close to 38%, and sulfuric anhydride, of 53.1 and 54.1%, for samples GA and GC, respectively, both oxides of hemidrate and anhydrite composition. This is attributed to the high purity of the raw material, since few companies in the region of the Araripe's Pole exert control of gypsum production [24].

Setting time

The initial and final setting times of the gypsum plaster were obtained by the method exposed in NBR 12128 [5] for pastes with w/g ratio of 0.8 and are presented in Figure 7.

According to NBR 13207 [9], a gypsum plaster paste for coating without admixture should have an initial and final setting time of at least 10 and 35 minutes, respectively, for dosed pastes of normal consistency. For the w/g ratio used, the initial setting time varied between 23.82 and 35.38 minutes; and the final setting time varied between 32 and 47 minutes. The setting times obtained are consistent and sufficient for handling in a mortar for restoration.

The differences in the setting times are due to differences in the raw material, the calcination process and the particle size. John and Cincotto [27] mention the influence of the mixing procedure on the setting time and the hardening of samples from the same raw

material and calcination conditions. Due to non-uniformity in the calcination process of the gypsum ore for formation of the hemihydrate, there may be the formation of the anhydrites III, II and I, which present different reactivities, influencing the setting time.

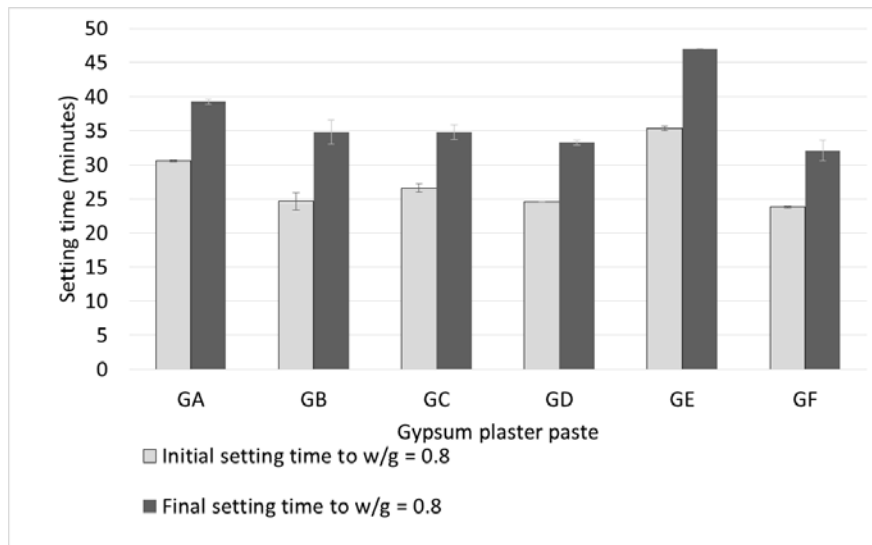


Figure 7. Initial and final setting time of the paste with w/g of 0.8.

Hardness

According to Dias and Cincotto [23], the importance of determining the hardness is justified by the need to evaluate the mechanical qualities of the coating and its ability to receive finishes such as special paints or glued components. For Ribeiro [32], it aims to assess the resistance to permanent deformation directly related to the atoms bonding strength in each sample separately.

The values of the hardness tests [6] of samples are shown in Figure 8.

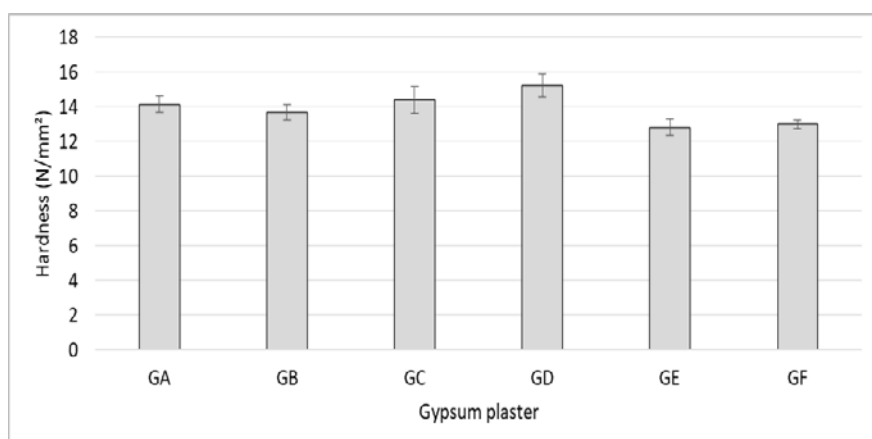


Figure 8. Hardness of plasters for w/g ratio of 0.8.

According to NBR 13207 [9], gypsum plaster for civil construction must have a hardness higher than or equal to 20 N/mm², when dosed with w/g obtained in the test of normal consistency, which is a value lower than 0.8. It is important to note that the increase in w/g

decreases stiffness and increases the deformation capacity of the material [24]. The values obtained are consistent for use in coating.

From the Tukey's test, by means of which the sample is confronted in pairs to verify statistically significant differences, it can be verified that most of the values found were similar to each other regardless of their raw material, grain size and calcination process. That is, the performance of different samples is similar.

Compressive strength

The compressive strength values are shown in Figure 9. The values obtained for dosed pastes with w/g ratio of 0.8 is between 5.38 and 6.89 MPa. The previous edition of NBR 13207 [8] required a minimum compressive strength of 8.40 MPa for a gypsum plaster produced with a w/g ratio of normal consistency. The values of compressive strength found are satisfactory for application in restoration mortars.

Veiga [35], in her studies on historic masonry, found compressive strength for gypsum mortars (1:0.15 being gypsum plaster: siliceous aggregate) of 3.5 MPa. Standard ASTM C 28-92 [2] establishes that plaster gypsum for masonry applications should have a compressive strength higher than 2.8 MPa for mortars with sand or perlite and 2.2 MPa for those with vermiculite.

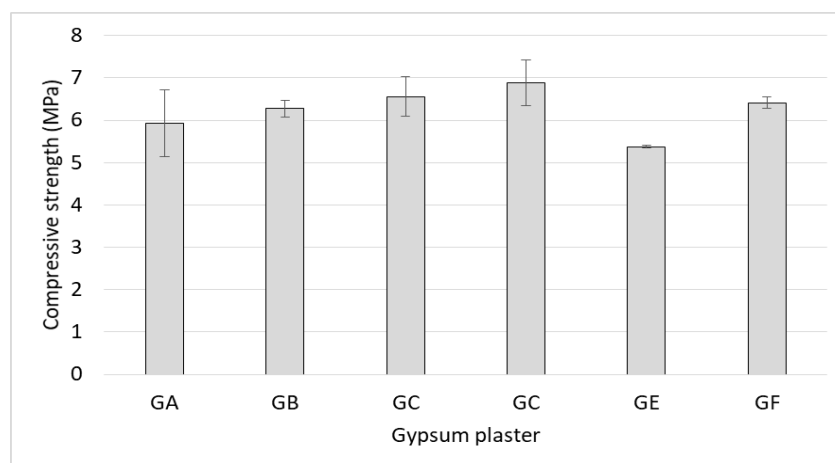


Figure 9. Compressive strength of plasters for w/g ratio of 0.8.

Figure 12 shows that the compressive strengths exhibit differences among them even though produced from pastes with the same w/g ratio, although they have similar workability. This behaviour was also reported by Bardella [14] and this difference is explained by the specific characteristics of the material in addition to the possibility of variation inherent to the test.

However, when performing the analysis using statistical tools (Tukey's test), there are no statistically significant differences between them in the compressive strength group. That is, the performance of different samples is similar.

Karni and Karni [29] claim that resistance is a result of the following factors: the quality of material (plaster and admixtures); the w/g ratio; the age of the product and the storage conditions of the product, also during hardening.

Bond strength

The bond strength results of the coatings tested according to NBR 13528 [10] are found in Table 4.

Table 4. Bond strength of coatings performed with and without pre-wetting of the base

Gypsum plaster	Bond strength (MPa)	
	Without base pre-wetting	Based on the pre-wetting
GA	0.27 ± 0.17	0.26 ± 0.15
GB	0.37 ± 0.14	0.23 ± 0.09
GC	0.54 ± 0.17	0.34 ± 0.12
GD	0.58 ± 0.13	0.22 ± 0.12
GE	0.51 ± 0.14	0.39 ± 0.10
GF	0.21 ± 0.11	0.37 ± 0.13

It is observed that the bond of the coatings, regardless of the base treatment and gypsum plaster sample, reaches the minimum value requested by NBR 13207 [9] of 0.2 MPa. According to the criteria of BS EN 13279-1 [15], the bond strength of the plaster must be equal to or higher than 0.1 MPa. The ruptures in the test occurred mainly in the substrate/coating interface, that is, they were ruptures of adhesive and non-cohesive nature.

According to Barbosa et al. (2004) apud Bardella [14], the characteristics of the application surface of the pastes have a significant influence on the bond strength of the coatings, since a more permeable material provides a more resistant microanchorage with greater penetration of the paste in the pores.

The face of the ceramic bricks used as the substrate for gypsum plaster coatings presents a glazed face, once it is made of red ceramics obtained by burning, reducing the permeability of the ceramic substrate and the microanchorage [14]. In addition, the pre-wetting indicated by NBR 13867 [11] reduces the suction capacity of the substrate, resulting in a reduction of material that penetrates the base pores, which would ensure mechanical anchoring.

However, even in these situations, the coating presented satisfactory bond, which basis the orientation of the use of this material for repairing of historical coatings. Bond is one of the

properties of great importance in these applications. The bond results of the coating are consistent with others authors [1, 21, 23, 26].

In order to evaluate the influence of gypsum plaster manufacturers on bond strength, a Tukey test was performed, which shows that, in general, there are no statistically significant differences for most of the values found. An evaluation was also made to verify if there is a statistically significant difference between the types of treatment: without pre-wetting and with pre-wetting of the base. For most of the results obtained, it is observed that there is difference between the two types of treatment. Therefore, it is not recommended the use of pre-wetting of the base in order to guarantee higher levels of bonding.

Conclusions

From the study, it was possible to study in detail the gypsum plasters produced in the Gypsum's Pole in Araripe, Brazil, especially the properties necessary for their use in mortars for restoration. It was verified that the gypsum plasters (calcined gypsum without admixtures and additions - $\text{CaSO}_4 \cdot 0.5\text{H}_2\text{O}$) have high quality, presenting high purity. The forms of production control and the size of the manufacturers in the Pole are different, but the quality of the resulting material and the performance was satisfactory and similar. This is explained by the characteristics of the raw material (gypsum ore) in the region.

In restorations of historical constructions, there must be guaranteed the high quality of materials used, given the high value of the construction. Therefore, due to the high quality of the obtained product, in terms of mechanical properties and purity, it is recommended the use of gypsum plaster produced in the Araripe's Gypsum Pole in restoration mortars.

Acknowledgement

The authors thank UNIVASF, UFPE and IPT for the support in conducting the tests.

References

1. Almeida YKR (2014) **Estudo de resistência de aderência de revestimento executados com pasta de gesso, considerando diferentes substratos**. 75 p. Trabalho de Conclusão de Curso (Graduação em Engenharia Civil) - Fundação Universidade Federal Vale do São Francisco
2. American Society for Testing and Materials. ASTM C 28-92 (1992): Standard specification for gypsum plasters. Pennsylvania
3. Antunes RPN, John VM (2000) Influência da cal hidratada nas pastas de gesso endurecidas. In: Encontro Nacional de Tecnologia do Ambiente Construído, VIII, 2000, Salvador/BA. Anais do VIII Encontro Nacional de Tecnologia do Ambiente Construído. Salvador: ANTAC, 2000

4. Associação Brasileira de Normas Técnicas. NBR 12127 (2017): Gesso para construção: Determinação das propriedades físicas do pó. Rio de Janeiro, 6p
5. _____. NBR 12128 (2017) Gesso para construção: Determinação das propriedades físicas da pasta. Rio de Janeiro. 5p
6. _____. NBR 12129 (2017) Gesso para construção: Determinação das propriedades mecânicas. Rio de Janeiro, 6p
7. _____. NBR 12130 (2017) Gesso para construção - Determinação da água livre e de cristalização e teores de óxido de cálcio e anidrido sulfúrico. Rio de Janeiro, 4 p
8. _____. NBR 13207 (1994) Gesso para construção civil - Requisitos. Rio de Janeiro, 3p
9. _____. NBR 13207 (2017) Gesso para construção civil - Requisitos. Rio de Janeiro, 2017. 3p
10. _____. NBR 13528 (2010) Revestimento de paredes de argamassas inorgânicas: Determinação da resistência de aderência à tração. Rio de Janeiro, 15p
11. _____. **NBR 13867 (1997)** Revestimento interno de paredes e tetos com pasta de gesso - Materiais, preparo, aplicação e acabamento. Rio de Janeiro
12. Baltar CAM, Bastos FF, Luz AB (2005) Gipsita. In: Adao Benvindo da Luz; Fernando Antonio Freitas Lins. (Org.). Rochas & Minerais Industriais. 1ed. Rio de Janeiro: CETEM, v. 1 c21, p. 449-470
13. Barbosa AA, Ferraz AV, Santos GA (2014) Caracterização química, mecânica e morfológica do gesso obtido do pólo do Araripe. Cerâmica (São Paulo. Impresso), v. 60, p. 501-508
14. Bardella OS (2011) **Análise das Propriedades de Pastas de Gesso de Construção Reciclado**. Universidade Estadual de Campinas. Campinas. Tese (Doutorado). 235 p
15. British Standard European Norm. **BS EN 13279-1 (2008)** Gypsum binders and gypsum plasters. Definitions and requirements. Bruxelas
16. Camarini G, Pimentel LL, SÁ NHR (2011) Assessment of the material loss in walls renderings with b-hemihydrate paste, Applied Mechanics Materials. 71–78 1242–1245
17. Camarini G, Pinto MCC, De Moura AG, MANZO NR (2016) Effect of citric acid on properties of recycled gypsum plaster to building componentes. Construction and Building Materials 124, 383–390.
18. Caufin B, Papo A (1983) Rheological testing methods for gypsum plaster pastes. RILEM materials and structures 95:315–321.

19. Clifton JR (1973) Some aspects of the setting and hardening of gypsum plaster. NBS Technical Note 755
20. Costa JEB (2013) **Análise comparativa entre as propriedades do gesso obtido de rejeito da produção de sal e gessos comerciais.** Dissertação (mestrado). Universidade Federal do Rio Grande do Norte. 79 p
21. Delgado CB, Pires Sobrinho CWA (1997) Revestimentos de gesso (pasta e argamassa) determinação das propriedades mecânicas. II Simpósio Brasileiro de Tecnologia das Argamassas. Anais... Salvador – BA, 11 p
22. Departamento Nacional De Produção Mineral (DNPM) (2015) Sumário Mineral 2015. Brasília: DNPM, 146 p
23. Dias AMN, Cincotto MA (1995) **Revestimento à Base de Gesso de Construção.** São Paulo: EPUSP. Boletim Técnico PCC n. 142
24. Ferreira FC (2017) Estudo de caracterização do gesso para revestimento produzido no Polo Gesseiro do Araripe. Dissertação (mestrado). Universidade Federal de Pernambuco. Recife. 199 p
25. Freire MT, Veiga MR, Silva AS, Brito J (2012) RESTAURO DE ESTUQUES ANTIGOS COM PRODUTOS COMPATÍVEIS. Jornadas LNEC. LNEC. 2012. 12 p
26. Hincapie AM, Oliveira CTA, Takeashi MS, Cincotto MA, Selmo SMS (1997) Revestimento de gesso liso-Avaliação da aderência e dureza superficial, sobre diversos substratos. Gypsum Fair, 97. Olinda, PE, p. 119-126
27. John VM, Cincotto MA (2007) Gesso de Construção Civil. In: ISAIA, G. C.. Materiais de Construção Civil. São Paulo: IBRACON. Cap. 22.2, p. 727-760
28. Kanno WM (2009) Propriedades mecânicas do gesso de alto desempenho. 130f. Tese de Doutorado - Universidade de São Paulo, São Carlos
29. Karni J, Karni E (1995) Gypsum in Construction: origin and properties. Materials and Structures, v. 28, n. 176, p.92-100
30. Lewry AJ, Williamson J (1994) The setting of gypsum plaster - Part II - The development of microstructure and strength, Journal of Material Science, 29 5524– 5528
31. Nascimento AF (2014) Aproveitamento do resíduo de gesso de construções como material alternativo para revestimento. Recife. 87 p. Dissertação (mestrado). Associação Instituto de Tecnologia de Pernambuco, Recife
32. Ribeiro AS (2011) Estudo e otimização do processo de produção de gesso reciclado a partir de resíduos da construção civil. 321 p. Tese (Doutorado) – Universidade Federal de Pernambuco, Recife

33. Silva MGS (2010) Desenvolvimento de compósitos à base de gesso e pó de fibras de coco. Dissertação (mestrado). Universidade Federal de Sergipe. Sergipe. 84 p
34. Tydlitát V, Tesárek P, Cerný R (2008) Effects of the type of calorimeter and the use of plasticizers and hydrophobizers on the measured hydration heat development of fgd gypsum. *Journal of Thermal Analysis and Calorimetry*, Vol. 91, 791–796
35. Veiga MR (2012) Argamassas de alvenarias históricas. Funções e características. CIREA 2012. Lisboa. Pp. 17-27. ISBN: 978-989-20-3080-7
36. Ye Q, Guan B, Lou W, Yang L, Kong B (2011) Effect of particle size distribution on the hydration and compressive strength development of α -calcium sulfate hemihydrate paste. *Powder Technology*, 207, p. 208–214

Characterization of Gypsum Renders in the Paris Region and Determination of the Traditional Fabrication Process

Jean Ducasse-Lapeyrusse^{1,2*}, Véronique Vergès-Belmin²

(1) *Cercle des Partenaires du Patrimoine,*

(2) *Laboratoire de Recherche des Monuments Historiques, Centre de Recherche sur la Conservation (CRC, USR 3224)*

* *Contact author : jean.ducasselapeyrusse@gmail.com, jean.ducasse-lapeyrusse@culture.gouv.fr*

Abstract

This study aims to characterize traditional gypsum renders to understand their traditional fabrication process. A large sampling campaign covering the historical region of Paris and all building typologies from the 16th century to the early 20th century was conducted. The cross-sections of renders were first observed with the naked eye and then under the microscope to characterize the number, thickness, and granular typology of their layers. X-ray diffraction analysis and mercury intrusion porosimetry were performed on each render layer and the proportion of each crystallized phase was estimated using the Rietveld method. Calcite and quartz contents vary from building to building and even between two layers in a single render. On average, however, their content is low and gypsum appears to be the main and often the only component. Usually, only calcined gypsum is used to make renders, especially for the most prestigious urban monuments. For these types of buildings the renders are made up of several layers. These layers are applied successively and prepared with a single coarse plaster powder sieved at different grain sizes and mixed at specific water ratios.

Introduction

Gypsum renders are omnipresent in the Paris region. Used since the Middle Ages, they were widely employed in all building typologies including farms, stables, castles, churches, apartment buildings, and Paris' "hôtels particuliers", etc. Gypsum used outdoors is more common than generally accepted [1-3] and can have remarkable physico-mechanical properties [4]. With the proper knowledge of application rules, gypsum renders can have very good durability: some of them have endured hundreds of years. The technological evolution that began in the mid-19th century induced the disappearance of traditional materials and as a consequence the plasterers' know-how died out. Old buildings in France are currently renovated with mortars made out of gypsum, lime, and sand, a type of mixture developed in the 1980s. Following the same approach as for many other places in Europe, a study on the materiality of traditional renders, and more specifically gypsum renders, appears fundamental [5,6].

This historic heritage must be further investigated to formally recognize its historical and architectural values and its remarkable performance. In order to achieve this objective, a research program was launched in 2015, combining the efforts of various organizations. Two interconnected projects were conducted: a PhD thesis in the history of architecture [7], wherein 121 gypsum renders were collected, and a physico-chemical characterization of those renders, conducted by the *Cercle des Partenaires du Patrimoine* (CPP), an association sponsored by private companies. Both studies were performed with the help of the French Ministry of Culture, in the Laboratoire de recherche des monuments historiques.

Traditional renders in the Paris region are made using gypsum, which is abundant in the local subsoil and originating from Tertiary terrains. Traditional kilns - the so-called “fours culée”- but also other types of kilns used in the past produced a plaster where various calcium sulphate phases coexisted due to the heterogeneous temperature inside the kilns (Figure 1).

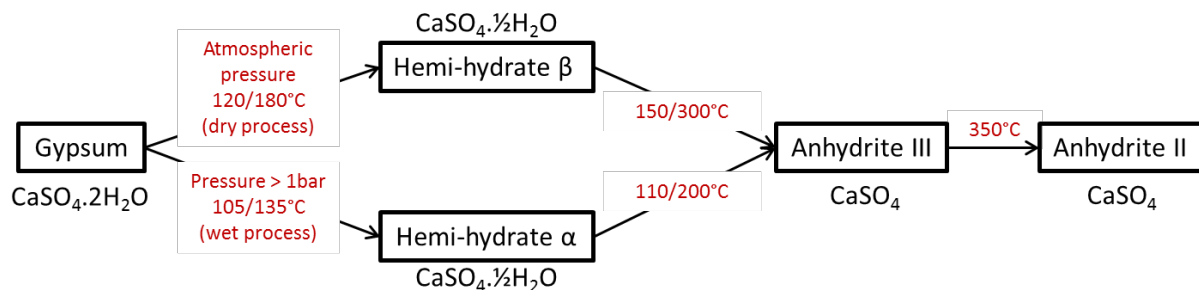
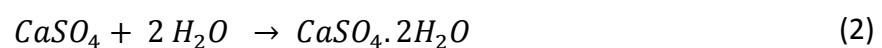
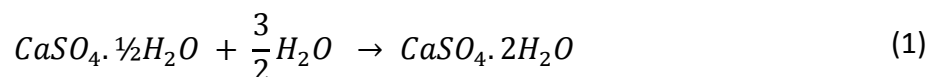


Figure 1: Calcium sulphate phases obtain by gypsum calcination at different temperatures.

The products obtained by gypsum calcination react with water and recover their initial degree of hydration, reconstituting gypsum. The hemihydrate and anhydrite hydration reactions follow the equations bellow:



Materials and methods

Corpus

The corpus consists of render samples collected from buildings constructed in a period of time ranging from the 16th to the early 20th century in the Paris region. The collecting area had a radius of 70 kilometers around Paris. The sampling campaign focused on buildings whose renders could be dated with the help of land registers, historical investigations, etc. [8]. Some buildings were visited, documented and their renders sampled without necessarily being analyzed in the laboratory. The table below (Table 1) summarizes the number of buildings, renders and coats documented and the part also analyzed in laboratory. Further information, including historical, environmental architectural and analytical details on the buildings studied can be found in the PhD thesis [7] and analytical reports [9].

Table 4: Number of buildings, renders and coats simply documented and analyzed.

	Buildings	Renders	Coats
Visited and documented	60	121	237
Analysed	33	56	126

The sampling is done with an angle grinder or with a hammer and a chisel. Each sample (area: 10x10cm² on average) includes all the render coats, and thus reaches the support. The sampled render is dry cut to make a cross-section showing the entire render stratigraphy, thus allowing the measurement of the overall render thickness, the number of constitutive coats, and their thickness and color.

Visual analysis

The measurement of each coat thickness and of the grain sizes is performed with a stereoscopic-microscope Leica Wild M 10. This visual analysis allows a partial identification of the grains. For further information about the grain compositions, thin sections and polished cross sections are prepared on a selection of coats, and are observed with optical microscopy respectively in transmitted and reflected light using a digital microscope 3D type Keyence VHX 5000.

X-ray diffraction (XRD)

For each coat, a representative part of approximately 3 cm³ is crushed into a powder passing through 100µm sieve. An X-ray diffraction analysis (Bruker D8 Advance diffractometer, Co anode, LinxEye Super Speed detector) is performed on the powder to obtain the mineralogical composition. The standard conditions are as follows: 40 kV, 40 mA, angular area covered 2θ from 5 to 64°, acquisition time 1 second, step width 0.02°. The diffractograms are interpreted by comparison with the JCPDS database diffractograms, section 1 to 83. Quantification of identified crystalline phases in each render layer is estimated using a Rietveld refinement applied on each diffractogram (program TOPAS, Bruker).

Mercury Intrusion Porosimetry

On a selection of coats, a 1 cm³ sample is cut and dried at 40°C until it reaches a constant weight (when over a period of 24 hours it shows a deviation equal to or less than 0.1% of its mass). If the coat contains aggregates, only the matrix is sampled. Mercury Intrusion Porosimetry (MIP) is performed on the samples using an Autopore IV 9500 porosimeter, controlled by the software AutoPore IV version 1.07.

Calculation of the water to powder ratio

The water/powder ratio (W/P) used during the mixing determinates the final porosity of a gypsum plaster. With pure hemihydrate, the W/P stoichiometric ratio should be equal to 0.186 for the transformation of a hemi-hydrate powder into gypsum. In reality, to obtain a suitable rheology for practical use, the W/P ratio must be much higher in the fresh plaster paste. The volume occupied by this residual water in the fresh plaster paste is considered to be exactly equal to the porous space volume of the material in its final state, i.e. once set and after the evaporation of the residual water [10]. Considering this hypothesis, it becomes possible, if the final porosity of an individual render coat is known, to estimate the W/P ratio of its original water/ powder mixture.

A part of the water used during the mixing reacts with the hemihydrate ($W_{\text{Stoichiometric}}$). The other part, the residual water (W_{Residual}), creates the void volume after evaporation:

$$W = W_{\text{Stoichiometric}} + W_{\text{Residual}} = 1.5 \times P \times \frac{M_{\text{H}_2\text{O}}}{M_{\text{CaSO}_4 \cdot \frac{1}{2}\text{H}_2\text{O}}} + V_{\text{Void}} \times \rho_{\text{H}_2\text{O}} \quad (2)$$

W and **P** are respectively the masses of water and plaster powder (hemihydrate) used during the mixing (g). $W_{\text{Stoichiometric}}$ is the mass of the water (g), reacting with the hemihydrate. W_{Residual} is the mass of the residual water (g). $M_{\text{H}_2\text{O}}$, and $M_{\text{CaSO}_4 \cdot \frac{1}{2}\text{H}_2\text{O}}$ are respectively the molar masses of the water and hemihydrate (g/mol). V_{Void} is the void volume (mL) and $\rho_{\text{H}_2\text{O}}$ is the water density (g/mL).

The void volume can be express from the porosity and the solid volume:

$$\varphi = \frac{V_{\text{Void}}}{V_{\text{Void}} + V_{\text{Solid}}} \quad \text{then} \quad V_{\text{Void}} = \frac{\varphi}{1 - \varphi} \times V_{\text{Solid}} \quad (3)$$

φ is the porosity (%), V_{Void} , is the void volume (mL) and V_{Solid} , is the solid volume, (mL).

The solid volume in a gypsum plaster, after setting, corresponds to the volume of the gypsum crystals formed by the hemihydrate hydration:

$$V_{\text{Solid}} = P \times \frac{M_{\text{CaSO}_4 \cdot 2\text{H}_2\text{O}}}{M_{\text{CaSO}_4 \cdot \frac{1}{2}\text{H}_2\text{O}}} \times \frac{1}{\rho_{\text{CaSO}_4 \cdot 2\text{H}_2\text{O}}} \quad (4)$$

V_{Solid} is the solid volume, (mL) and **P** is the mass of plaster powder (hemihydrate) used during the mixing (g). $M_{\text{CaSO}_4 \cdot 2\text{H}_2\text{O}}$ and $M_{\text{CaSO}_4 \cdot \frac{1}{2}\text{H}_2\text{O}}$ are respectively the molar masses of gypsum and hemihydrate. $\rho_{\text{CaSO}_4 \cdot 2\text{H}_2\text{O}}$ is the gypsum density (g/mL).

With equation (3) and (4), equation (1) becomes:

$$W = 1.5 \frac{M_{H_2O}}{M_{CaSO_4 \cdot \frac{1}{2}H_2O}} \times P + \frac{\varphi}{1 - \varphi} \times P \times \frac{M_{CaSO_4 \cdot 2H_2O}}{M_{CaSO_4 \cdot \frac{1}{2}H_2O}} \times \frac{1}{\rho_{CaSO_4 \cdot 2H_2O}} \times \rho_{H_2O} \quad (5)$$

The mixing ratio W/P can be deduced from the porosity, according to equation (6):

$$\frac{W}{P} = \frac{1.5 \times M_{H_2O}}{M_{CaSO_4 \cdot \frac{1}{2}H_2O}} + \frac{\varphi}{1 - \varphi} \times \frac{M_{CaSO_4 \cdot 2H_2O} \times \rho_{H_2O}}{M_{CaSO_4 \cdot \frac{1}{2}H_2O} \times \rho_{CaSO_4 \cdot 2H_2O}} = 0.186 + \frac{\varphi}{1 - \varphi} \times 0.511 \quad (6)$$

W and **P** are respectively the masses of water and plaster powder (hemihydrate) used during the mixing (g). M_{H_2O} , $M_{CaSO_4 \cdot \frac{1}{2}H_2O}$ and $M_{CaSO_4 \cdot 2H_2O}$ are respectively the molar masses of water (18.02 g/mol), hemihydrate (145.15 g/mol) and gypsum (172.17 g/mol). φ is the porosity (%). ρ_{H_2O} and $\rho_{CaSO_4 \cdot 2H_2O}$ are respectively the water density (1.00 g/mL) and the gypsum density (2.32 g/mL).

Equation (6) is used to estimate the W/P ratio of the coat samples thanks to the accessible porosity obtain by Mercury Intrusion Porosimetry. On a construction site, the plaster powder is not only composed of hemihydrate but also contains anhydrite and impurities (mainly calcite). The formula is not accurate if the plaster powder contains a significant quantity of aggregates. Nevertheless, reconstitutions of traditional renders [11] show that the actual water/powder ratio used is close to the estimated theoretical water/hemihydrate ratio with a ± 0.05 absolute precision.

Results and discussion

Stratigraphy

The observation of the layers, their position in the render, their thickness and the grain size of their inclusions inside, allows a categorization of coats: 9% of the layers correspond to a leveling coat, i.e. a layer directly applied on an irregular support (rubble or brick masonry/timber-framed wall) in order to equalize the surface. 39% of the layers are scratch coats, which are quite thick (1-6 cm) and usually contain grains up to 10 mm large. 44% of the layers are finishing coats, i.e. the final and therefore superficial coats of the render. This kind of layer is generally much finer than the scratch coat; it contains small grains (diameter <5mm); the following Figures 2 and 3 illustrate a typical render stratigraphy and the coat types.

A large variety of renders can be observed in the Paris region. The numbers of coats, their grain sizes, color, and surface treatments vary, but certain render typologies are often encountered. A number of render typologies have been identified. Their distribution according to their main characteristics is proposed below (Figure 4).



Figure 2: Cross section with different coat types. Render sampled from the building “Hôtel Amelot de Bisseuil”, Paris, France (1660).

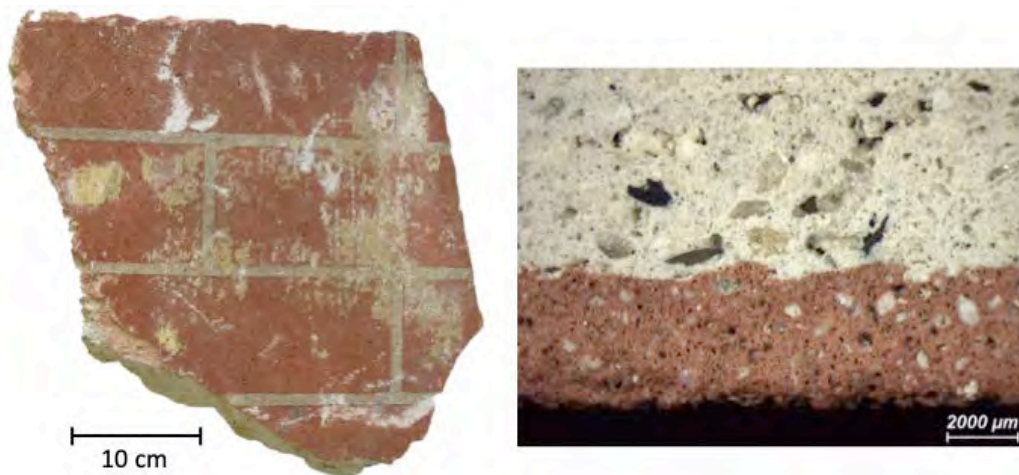


Figure 3: “False brick” render and cross section observed under microscope at the interface scratch coat/finishing coat (left) and on the finishing coat imitating brick (right). Building 1 rue Royale, Versailles, (1743).

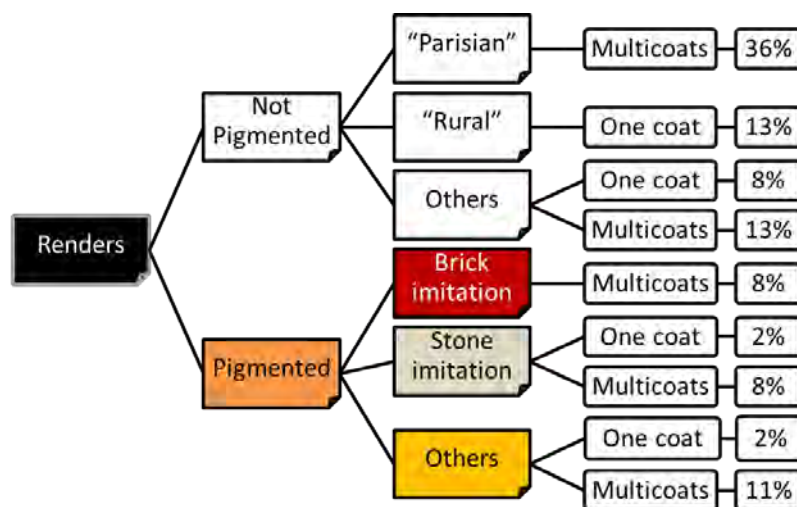


Figure 4: Typology distribution of the analyzed renders

The render category “Not pigmented/Others” gathers together various typologies. The application date of these renders is estimated to be later than 1850. They illustrate the technical evolution at the time. Some finishing coats have textured surfaces to create decorative patterns, and other ones are covered with one or more very thin white coats.

A frequently encountered render typology is the so-called “*Parisian render*” (36% of the collected renders). This consists of at least 2 non-pigmented coats: a scratch coat, and a finishing coat. The scratch coat systematically contains coarser grains than the finishing coat, the grain size of which is less than 0.5mm. The finishing coat has a smooth surface, which is obtained by a specific action on the coat surface while it is still not set completely: the coat is “coupé” (“cut”) with the sharp side of the Berthelée trowel. The *Parisian render* is found on urban or prestigious buildings (castles, mansions, hôtel particuliers, etc.).

Another typical group, which we called “*Rural render*” (13% of the collected renders), has also been identified. This kind of render is composed of a single coat without any pigmentation and containing coarse grains (essentially underburnt gypsum and remnants of coal). This kind of render is applied on modest rural buildings such as farms.

Coats composition

The XRD coupled with the Rietveld refinement allow the mineral composition of each coat to be determined. Gypsum is the main component. 90% of the coats analyzed contain less than 3% quartz. Calcite and, for some renders, dolomite and quartz, are also identified. Out of 126 analyzed coats, only 10% of the coats have a gypsum content lower than 80%, the median gypsum content being almost 89.7% (Figure 5). Two thirds of the coats have calcite contents lower than 5%. The same tendency is observed with the dolomite content (Figure 6) but calcite and dolomite contents do not seem to be correlated: some coats are rich in calcite and dolomite (more than 10%), some are rich only in calcite or dolomite, and other ones have a low calcite content and no detectable dolomite (Figure 7).

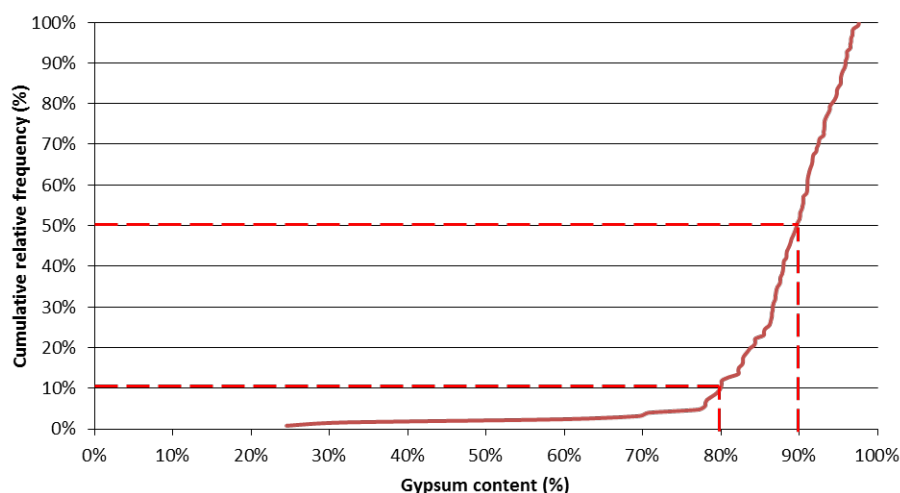


Figure 5: Cumulative relative frequency of analyzed coats as a function of their gypsum content.

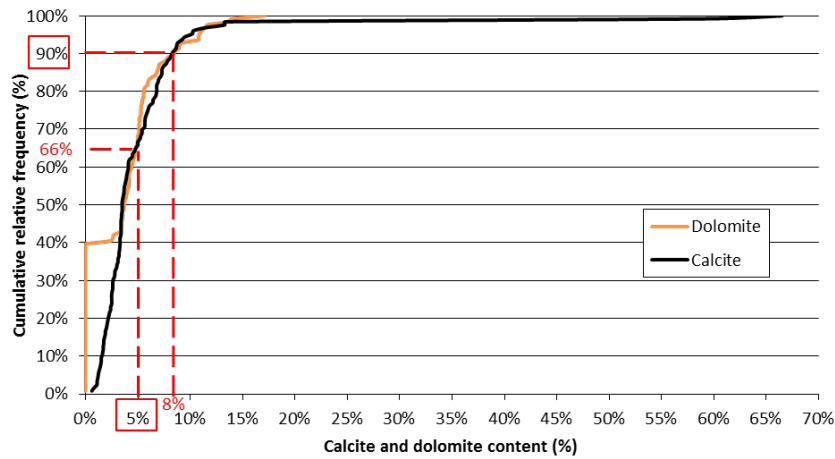


Figure 6: Cumulative relative frequency of analyzed coats as a function of their calcite and dolomite content.

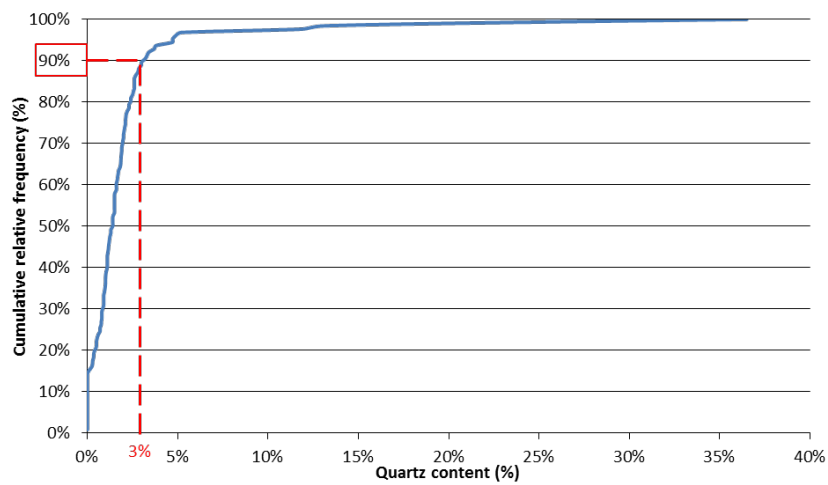


Figure 7: Cumulative relative frequency of analysed coats as a function of their quartz content.

The coats with high dolomite content (> 10%) are all localized in the southwest of Paris (Figure 8).

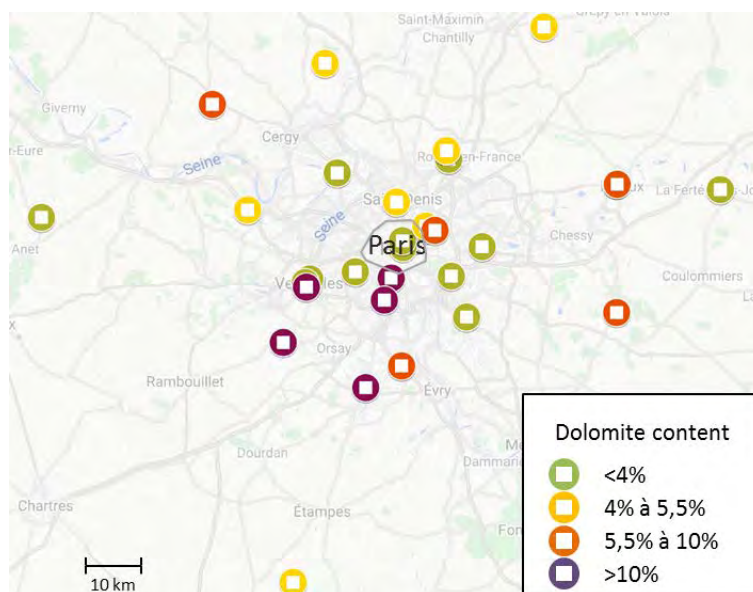


Figure 8: Buildings location. The color codes refer to the coat having the highest dolomite content in the considered render.

Nature of the grains

The coats are composed of a matrix containing diverse grains. Their size ranges from 10 μm to several centimeters. Various observation techniques, associated with XRD and SEM-EDS analyses allow the following grain types to be identified: remnants of combustible materials from the kiln (coal or coke), fragments of gypsum rock (underburnt gypsum), aggregates of several millimeters which may contain calcite, dolomite, and or quartz, originating from a deliberate or accidental addition, sub-millimeter grains (calcite, anhydrite II, quartz) and other unidentified grains. The most common grain type is a fragment of gypsum monocystals or microcrystalline aggregates originating from an incomplete calcination of the gypsum rock during the hemihydrate (plaster powder) manufacturing process (Figure 9). Remnants of combustible materials used in the kiln are also usually found in all the coats (Figure 10). Significant quantities of aggregates like gravels or silica sand are found in less than 6% of the coats.

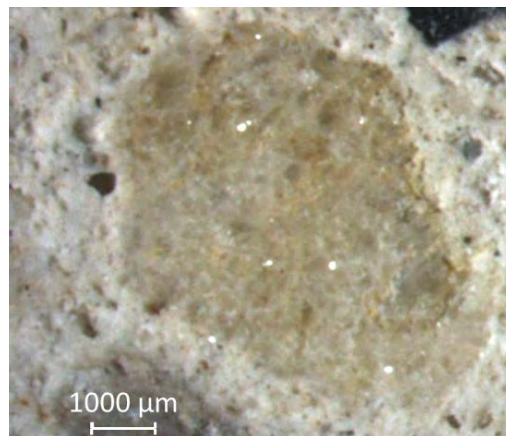


Figure 9: Microscope observation of a gypsum rock fragment (saccharoid gypsum) in the scratch coat of the “Hôtel Amelot de Bisseuil”, Paris, France (1660).



Figure 10: Microscope observation of a coal fragment (black grain on the left) and a gypsum rock fragment (white grain on the right) in the scratch coat of the "Séminaire Saint Rémy", Meaux, 1776

Dolomite grains found in the coats in the south-west of Paris appear as very fine rounded grains dispersed into the coats (Figure 11).

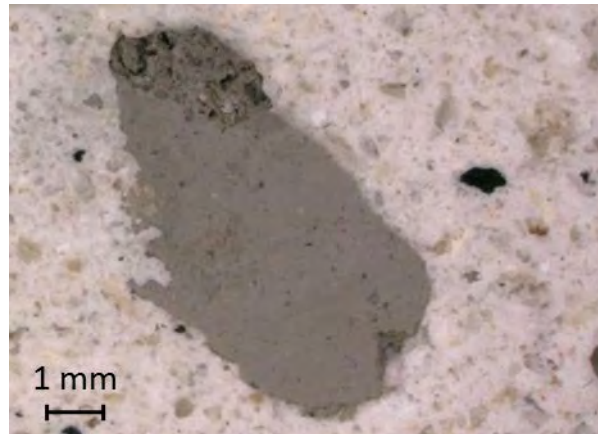


Figure 11: Microscope observation of a dolomite grain in the scratch coat of the “Moulin de Claye”, Saint Rémy-lès-Chevreuse (1930).

The nature of the smaller grains could be identified on a late 19th century render by observation of thin sections (Figure 12) under a polarizing microscope. Micritic calcite grains and quartz hundreds of micrometers large could be observed. Anhydrite III and hemihydrate are not found in the analyzed coats, most probably because they react very easily with water to form gypsum. Thanks to its high birefringence, anhydrite II grains could be easily distinguished from other phases, even though only few were present in the coat. This feature is interesting, as anhydrite II is known to transform very slowly into gypsum [12, 13]. Its presence in a 19th century render proves that it may still not have reacted after more than one hundred years of outdoors exposure.

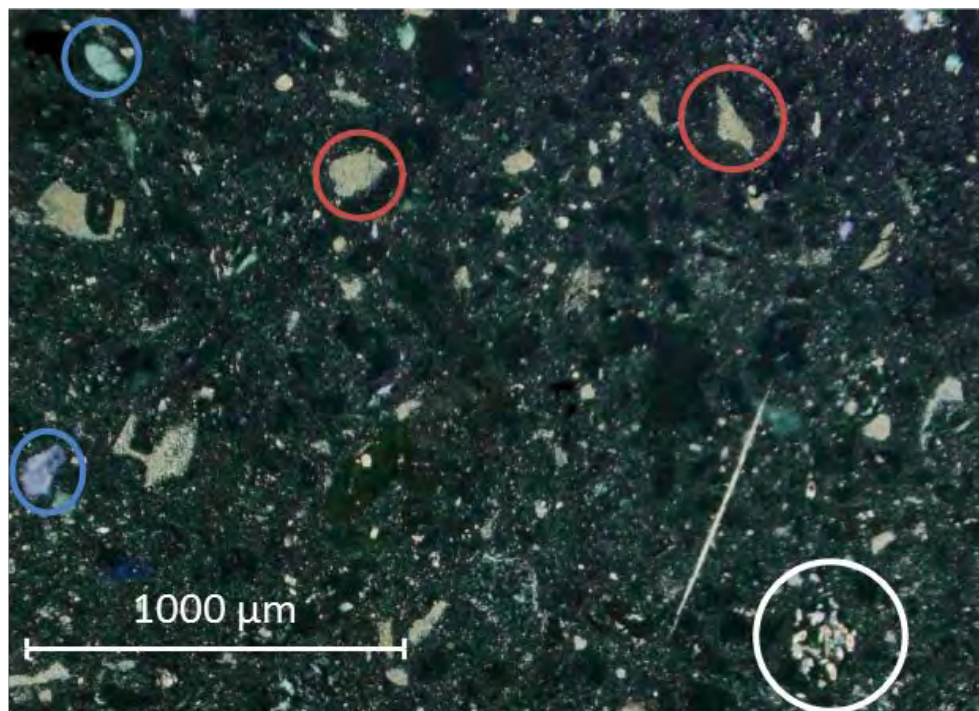


Figure 12: Observation under polarised light / crossed nicols of the finishing coat of the “Théâtre de la Renaissance », Paris, 1873. Quartz (blue circles), micritic calcite (red circles) and anhydrite II (white circle) can be observed.

Porous network

Mercury Intrusion Porosimetry allows the estimation of the accessible porosity and the pore size distribution. In all coats analysed with this technique, the pore size distribution is unimodal: the major part of the mercury penetrates in the sample by pores with closely grouped opening sizes (Figure 13). This threshold radius ranges to 0.6 μm to 1.90 μm depending on the coat. The accessible porosity ranges from 30 to 49 vol% according to the coat type.

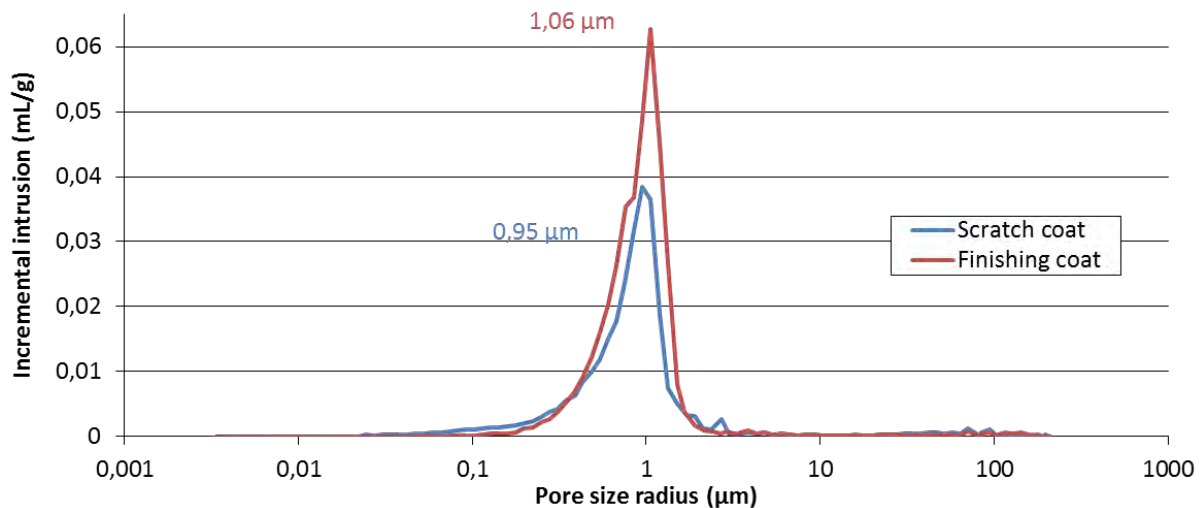


Figure 13: Pore size distribution and threshold radius of scratch and finishing coats from “Hôtel Amelot de Bisseuil”, Paris, 1660.

Table 2 summarizes the information obtained on the porous network of each tested coat. The theoretical water/hemi-hydrate ratio calculated on the basis of accessible porosity is also presented.

The threshold radius does not appear to be connected to the accessible porosity. The average accessible porosity is not significantly different between the two types of coats.

The average threshold radius in the scratch coat is 0.20 bigger than the average threshold radius in the finishing coat but this difference does not appear to be significant, and more MIP should be performed on old render to observe a clear tendency. The threshold radius remains around 1 μm whatever the type of coat and its porosity.

The calculated W/P ratio ranges from 0.41 to 0.67. This is quite low with respect to the W/P ratios advised nowadays in France for commercial plaster powders without any additives: for instance, the “*Plâtre Gros de Construction*”, mainly composed of hemihydrate β and anhydrite II is usually mixed with a minimal W/P ratio of around 0.7 in order to obtain a suitable workability without any additives.

Table 2: Pore characteristics of coats and estimation of the mixing ratio

Building-Façade-Render	Type of coat	Accessible porosity (vol %)	Theoretical mixing ratio (water / hemihydrate)	Threshold radius (µm)
HAH-F1-EZ2	Finishing coat	47	0.63	1.06
	Scratch coat	40	0.52	0.95
	Leveling coat	42	0.56	0.84
	Molding	48	0.66	1.19
TR-F1-E3A	Finishing coat	34	0.45	0.60
	Scratch coat	41	0.54	1.33
V1R-F1-E1	Finishing coat	36	0.47	1.05
	Scratch coat	30	0.41	0.84
FHUV-F1-E1	Finishing coat	45	0.60	0.68
	Scratch coat	38	0.50	1.07
FSJ-F2-E1	Finishing coat	36	0.47	1.69
	Scratch coat	39	0.51	1.51
MBS-F2-E3J	Finishing coat	49	0.67	1.68
	Scratch coat	46	0.62	1.68
ASTM-F1-E1	Finishing coat	34	0.45	0.85
	Scratch coat	46	0.61	1.89
HPC-F1-E3	Finishing coat (coat 1)	35	0.46	1.07
	Scratch coat (coat 2)	41	0.54	0.95
	Scratch coat (coat 3)	35	0.46	1.51
	Leveling coat (coat 4)	40	0.53	1.51
Total	Average	40	0.53	1.20
	Standard deviation	5	0.8	0.38
Finishing coat	Average	39	0.53	1.08
	Standard deviation	6	0.9	0.41
Scratch coat	Average	40	0.53	1.28
	Standard deviation	5	0.7	0.39

Discussion and Conclusion

Unlike the ready-to-use mixtures of gypsum plaster, lime and sand (the so-called “*Mortiers Plâtre et Chaux*”) proposed today for the replacement of traditional gypsum renders, lime and sand were not significant components of the traditional gypsum renders made before 1850. Despite the fact that gypsum renders in the Paris region have an important diversity, gypsum appears to be the major component for almost all the sampled renders (the median gypsum content is 89.7%).

Calcite content is not necessarily a proof of lime use. The major part of the calcite content most probably originates from the gypsum rock itself or from unintentional addition during the fabrication process. The gypsum rocks in the Paris Basin subsoil naturally contain calcite up to 10% depending on the quarry site and the stratum.

The grains present in traditional renders are generally not composed of quartz sand, but rather, mainly of underburnt gypsum due to the uneven calcination of the gypsum rock in traditional kilns. The extraction, calcination, and crushing on the ground (traditionally with a wooden staff) to make the plaster powder can also contribute to the incorporation of impurities such as calcite, dolomite, or quartz. However, in most coats having a calcite or dolomite content higher than ten percent, which represent around 12% of the analyzed coats, a small quantity of calcite or dolomite grains was probably voluntarily added in order to reduce the price of the raw material. Coat compositions show that this potential addition does not exceed 10% of the mineral content in the coat. The presence of dolomite seems to be specific to a particular area in the south west of Paris. Local practices and local raw materials may account for this particularity. Deliberate addition of silica sand or gravel appears to be limited as they are found in less than 6% of the coats. The aggregates represent more than 15% of the coat weight in only two of them (23% and 37%). In comparison, the aggregates represent 35% of the coat in today's prescriptions that follow the French standard relative to renders (NF DTU 26.1) [14].

The low porosity of certain coats tends to indicate the use of retarders or water reducers during the mixing phase. In fact, we could identify gum arabic in some of the renders [9]. Some render samples were exposed during a long time to liquid water. An orange substance migrates and concentrates on the sample surface. Fourier-Transform InfraRed spectroscopy (FTIR) was performed on the orange substance and the spectrum was compared to the laboratory reference spectra database (results not shown). Gypsum and gum Arabic appear to be the more likely components present. Gum arabic is known as a water reducer [15], but these components are usually difficult to identify due to their very low concentration - typically less than 1% - in the mixtures [15-17].

Our conclusions – drawn on the basis of analyses made on a limited number of coats - may not be considered as representative of the situation in Ile-de France. However, this study is the only one published to date that includes a scientific approach, an archive documentation, and an architecture analysis on gypsum render in the Paris region. Although the most durable renders can be overrepresented and give a false representation of historical practices, these results confirm that renders composed almost exclusively of gypsum can withstand the test of time. Traditional know-how, beginning with gypsum powder fabrication and ending with the implementation techniques mastered by the plasterer, appears to create remarkably durable renders.

Acknowledgments

This research was supported by the founding of Parex Group and Pradeau Morin through the association of the Cercle des Partenaires du Patrimoine. The corpus sampling and the historical researches were made in partnership with Tiffanie Le Dantec through her PhD thesis work [7].

References

1. Middendorf B, Knöfel D (1993) Gypsum and lime mortars of historic German brick buildings: analytical results as well as requirements for adapted restoration material. NATO-CCMS Pilot Study Conserv Hist Brick Struct Proc 6th Expert Meet Williamsbg 28-31 Oct 1992 35–37
2. Franzoni E, Sandrolini F, Baldazzi L (2010) Characterization of gypsum-selenite plasters from historic buildings in the Emilia-Romagna region (Italy). s.n, pp 157–164
3. Mileto C, Vegas F, La Spina V (2011) Is Gypsum External Rendering Possible? The Use of Gypsum Mortar for Rendering Historic Façades of Valencia's City Centre. In: Advanced Materials Research. Trans Tech Publ, pp 1301–1304
4. Middendorf B (2002) Physico-mechanical and microstructural characteristics of historic and restoration mortars based on gypsum: current knowledge and perspective. Geol Soc Lond Spec Publ 205:165–176
5. La Spina V, Mileto C, Vegas F (2013) The historical renderings of Valencia (Spain): An experimental study. J Cult Herit 14:S44–S51. <https://doi.org/10.1016/j.culher.2012.11.011>
6. La Spina V, Fratini F, Cantisani E, et al (2014) The ancient gypsum mortars of the historical façades in the city center of Valencia (Spain). Period Mineral Vol 82 3 Dec 2013 82:443
7. Le Dantec T (2019) Les façades enduites au plâtre d'Île-de-France. Le déclin du plâtre extérieur, du XVIIe au XXe siècle. PhD Thesis in history, history of art and archeology. Laboratoire de recherche de l'École nationale supérieure d'Architecture de Versailles, Université de Versailles-Saint-Quentin-en-Yvelines
8. Le Dantec T (2016) Gypsum external renders of Paris: history and fabrication. In: Further Studies in the History of Construction: the Proceedings of the Third Annual Conference of the Constructin History Society. Lulu. com, p 59
9. Ducasse-Lapeyrusse J, Le Dantec T, Vergès-Belmin V (2019) Caractérisation d'enduits en plâtre datant du XVIIème au XXème siècle, provenant de nombre d'édifices d'Île de France. Laboratoire de Recherche des Monuments Historiques, Cercle des Partenaires du Patrimoine
10. Sanahuja J (2008) Influence of structural morphology on the mechanical properties of building materials : applications to gypsum and cement pastes. PhD thesis, Ecole des Ponts ParisTech

11. Ducasse-Lapeyrusse J, Vergès-Belmin V Essais de vieillissement artificiel sur une sélection d'enduits extérieurs à base de plâtre ou de chaux. Laboratoire de Recherche des Monuments Historiques, Cercle des Partenaires du Patrimoine
12. Murat M, El Hajjouji A, Comel C (1987) Investigation on some factors affecting the reactivity of synthetic orthorhombic anhydrite with water. I. role of foreign cations in solution. *Cem Concr Res* 17:633–639. [https://doi.org/10.1016/0008-8846\(87\)90136-0](https://doi.org/10.1016/0008-8846(87)90136-0)
13. Sievert T, Wolter A, Singh NB (2005) Hydration of anhydrite of gypsum (CaSO₄.II) in a ball mill. *Cem Concr Res* 35:623–630. <https://doi.org/10.1016/j.cemconres.2004.02.010>
14. NF DTU 26.1 P1-1 (2008) Travaux de bâtiment - Travaux d'enduits de mortiers
15. Alsadi S, Combe EC, Cheng Y-S (1996) Properties of gypsum with the addition of gum arabic and calcium hydroxide. *J Prosthet Dent* 76:530–534. [https://doi.org/10.1016/S0022-3913\(96\)90013-X](https://doi.org/10.1016/S0022-3913(96)90013-X)
16. Singh NB, Middendorf B (2007) Calcium sulphate hemihydrate hydration leading to gypsum crystallization. *Prog Cryst Growth Charact Mater* 53:57–77. <https://doi.org/10.1016/j.pcrysgrow.2007.01.002>
17. Nohier M (1986) Construire en plâtre. Editions L'Harmattan

The use of stucco-marble to restore veined polished limestone. The case of the pavement in the major sacristy of the Cathedral of Seville

Antonio González Portillo¹, Maria Teresa Freire²

(1) Freelance restorer, Seville, Spain, toniogp@gmail.com

(2) CERIS and Materials Department of LNEC - National Laboratory for Civil Engineering, Lisbon, Portugal, mtfreire@lnec.pt

Abstract

This paper shows the methodology and the results of the intervention of restoration of the pavement of the major sacristy of the Cathedral of Seville. The pavement dates from the beginning of the 19th century and is made of polished white and black paving stones of marble and red slabs of limestone.

This difference between the types of materials was translated into uneven resistance to wear, leading to a faster decay of limestone. The result is now inappropriate, both from the aesthetical and the security of the users' point of view. In fact, the main reason to carry out this restoration was to avoid people stumbling on the largest holes that exist in the slabs of limestone, subjected to daily pedestrian trafficking in one of the most visited monuments in Spain.

Due to the abrasion caused by the large influx of people, it was necessary to re-integrate the lost volume and at the same time preserve the veined morphology and colours of the limestone, despite the abrasion actions through time.

It was decided to use the traditional technique of stucco-marble, also known as “scagliola”, since it allows achieving a marble-like finish of a great aesthetic quality. At the same time, depending on the type of plaster chosen, surfaces with a great resistance to abrasion, similar to the stone, can be obtained.

One year after the intervention, the reintegrated materials maintain quite a remarkable appearance, conserving a very similar brightness to that of the slabs of limestone which have been restored, in spite of the abrasion derived from continued pedestrian trafficking.

Introduction

The main purpose of this paper is to show a real intervention of restoration in a stone pavement using the traditional technique of stucco marble, a gypsum based plaster prepared with water, animal glue and pigments. The theoretical proposal for this restoration was conceived and directed by the heritage restoration company Artyco SL, from Spain, and

the execution was carried out by the restorers Antonio González Portillo, one of the authors of this paper, and Pepa Parra Granell.

So far, only one study has been found on the use of this technique to restore marble and it was focused on the application to skirting boards [1]. Nevertheless it is more common to find information or notice of the use of stucco marble in the restoration of old pieces made already with this technique [2-5].

Stucco marble was mainly used and developed in the Baroque period. It is known by its remarkable mechanical resistance and stone-like appearance, mainly due to the polishing operations and application of organic coatings to the external surface. These coatings are usually hydrophobic and promote the protection of the surface against the action of wear and condensation moisture, without reducing the water vapour permeability of the underneath material [1, 3].

The pavement of the major sacristy of the Cathedral of Seville is composed of two types of paving stones: white and dark grey marble and red limestone (Figure 1). The different resistance to wear between marble and limestone is due to their distinct geological formation: the first is a metamorphic rock where calcite crystals form a compact microstructure, while the second is a sedimentary rock, composed of calcium carbonate with fossil fragments, more porous and sensitive to water or mechanical actions. In this case, the limestone slabs suffered from spalling, a pathology that lead to significant losses of material along time. The result is now inappropriate, both from the aesthetical and the security of the users' point of view. In fact, large holes with more than 1-2 cm depth already exist in some of the paving stones and were the main reason to carry out this intervention.



Figure 1. Major sacristy of the Cathedral of Seville: general view of the stone pavement

The selection of the methodology had to take into account that this is a pavement subjected to intensive daily pedestrian trafficking in one of the most visited monuments of Spain. Sometimes it is possible to see the reintegration of lost pieces of marble or limestones with resins, like polyester or epoxy [6, 7], products with very different chemical, physical and aesthetical properties, whose application is frequently irreversible due to their very high mechanical adhesion to the substrate. It can also cause severe damages to the original pavement due to lack of porosity and high thermal expansion.

On the contrary, besides being a natural mineral based non-toxic material, with more chemical affinity, stucco marble is a porous material, allowing the circulation of water vapour between the substrate and the environment, reducing the risk of the intervention.

Like in many other situations, in this case the restorer was contacted to solve the problem in a short time. The aim was to obtain a surface with the same aspect of the original stone (including veins) and with abrasion resistance similar to it. The promising results obtained with some laboratory formulations previously studied [1] and the endless versatility of colours and veins that can be achieved with stucco marble, allowed concluding that it could be a suitable technique to be used in this case. However, the materials used have to be further studied and several physical (capillary water absorption, water vapour permeability, and thermal and moisture expansion coefficients) and mechanical properties need to be quantified.

Restoration process

The intervention of restoration of the limestone slabs of the major Sacristy of the Cathedral of Seville was carried out in November of 2017.

Pathologies of the pavement. Selection criteria for restoration

The first step was the analysis of the areas that needed to be restored. The quantity of damaged stones was very large in the total of the pavement, so, the criterion that helped deciding which had to be restored in first place was based on those that represented a real danger of stumbling to the users: they had large holes and loss of material corresponding to one, or more centimetres in depth, leading to levelling irregularities between the damaged slabs of limestone and the adjacent slabs of marble (Figure 2). A total of sixteen pieces, two of them with total loss of the surface, were selected.



Figure 2. Detail of one damaged paving stone: the red line shows the part to be restored with stucco marble

Cleaning

The pavement was very dirty, mainly with remains of waxes of the liturgical acts that occur several times a year in the Cathedral. The choice and the rigorous implementation of the

cleaning process are paramount issues for the success of the intervention, as they will influence the adhesion of the restoration material.

It was decided to clean also all the damaged points with less than one centimetre (which would not be covered with stucco). By doing so, a profound cleaning, that could damage the volume reintegrations that were going to be made, will be avoided in the future.

After vacuum the dust with a vacuum cleaner, the holes in the damaged limestone were cleaned with hot steam, using a steam cleaner. This operation was followed by the direct application of an aqueous solution of surfactant at 5% in the pavement, and mechanical cleaning with nylon brushes. As some parts of the holes were still not clean enough, paper pulp soaked in a saturated solution of ammonium bicarbonate in water was applied (Figure 3) and covered with plastic for two hours, to avoid evaporation. After that, the pulp was removed and the stone slabs were cleaned again mechanically with brushes.

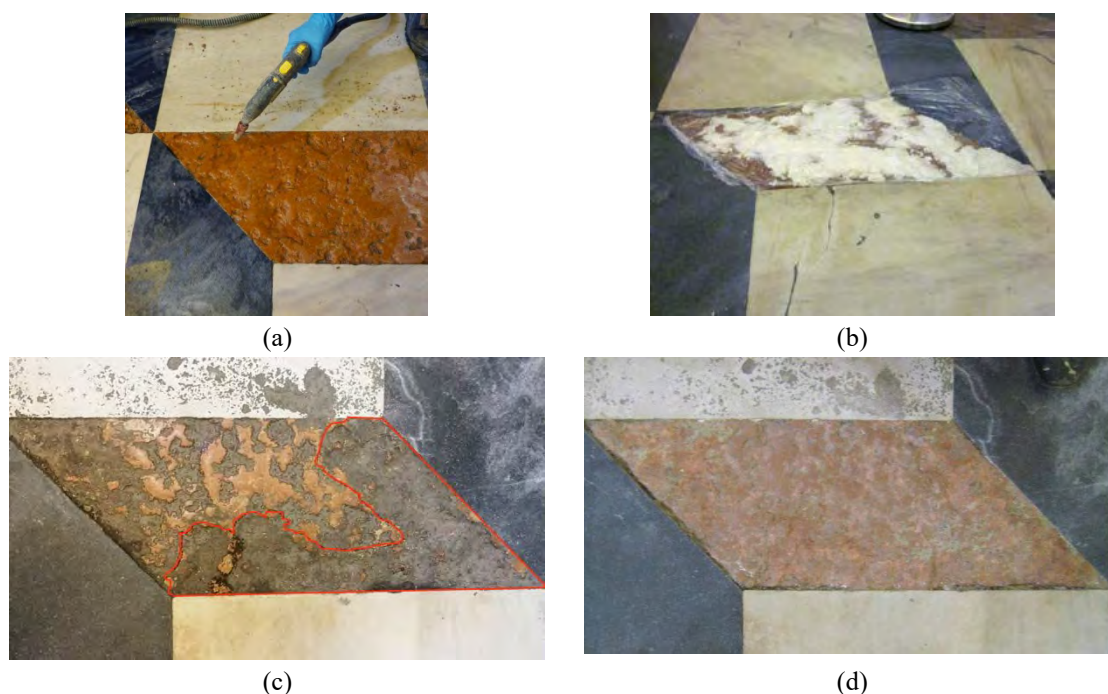


Figure 3. Cleaning of the paving stones: (a) using the steam cleaner; (b) application of paper pulp with ammonium bicarbonate; (c) stone slab before cleaning; (d) the same slab after cleaning

A new poultice of paper pulp was applied only with deionised water. In this case, it was important to leave the paper on the surface of the stone until the water was completely evaporated, to guarantee that all traces of ammonium bicarbonate were out of the stone.

Once all the slabs of limestone and their holes were cleaned, the shape of their edges was clearer. Because of that, it was decided to fill the holes in the proximity of the joints with lime mortar so that the joints and the edges were respected (Figure 4). This mortar has two functions: it serves as volume filler to prevent the stucco marble paste from occupying the space of the original shape of the adjacent slabs and/or the space of the joints; it absorbs part of the compression movements derived from the pavement as it is less resistant than the stone slabs and avoids a direct contact between them.

Preparation and application of the stucco pastes

Before the preparation of the stucco marble pastes, it was necessary to study the morphology, colours and veins of the original stone to be restored. After several trials, two different recipes were established, according to the two general tonalities of colour of the red limestone (Figure 5).

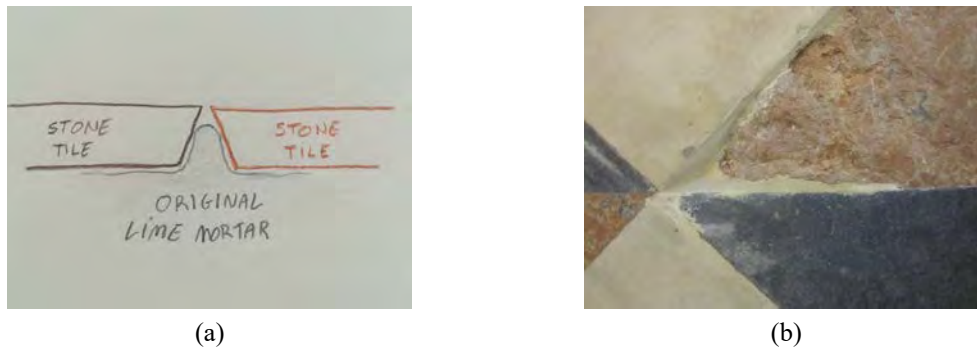


Figure 4. Restoration of the joints: (a) section of the shape of the slabs on the edges; (b) detail of one of the fillings with lime mortar

Afterwards, it was necessary to trace the contours of the damaged paving stones in order to have a clear idea of the quantity and the shape of the surface of stucco marble to be applied in the holes.

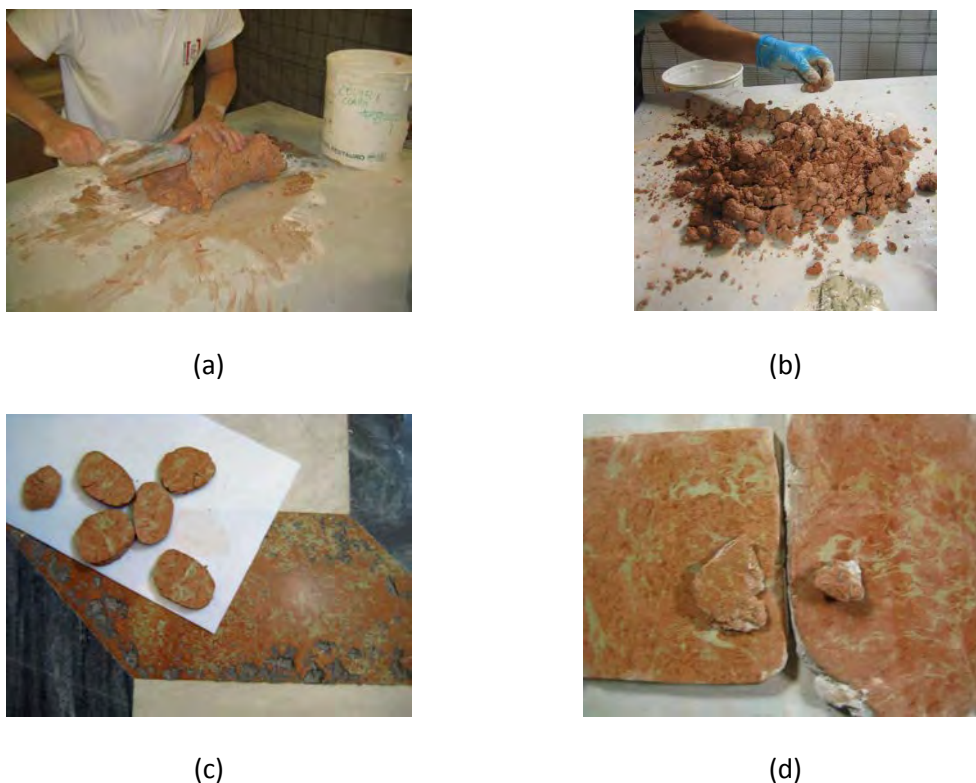


Figure 5. Preparation of stucco marble pastes: (a) mixing the gypsum plaster with the kneading water; (b) selecting different colours to obtain a similar esthetical effect; (c) final mixes before curing; (d) two pieces of limestone above the two recipes of stucco marble selected

The manufacturing of stucco marble begins with the kneading of a fine plaster using a blend of water, animal glue, pigment and a small portion of lime putty (that acts as preservative due to the animal glue). The material selected for this work was an extra hard commercial gypsum plaster with a Brinell hardness $>5.000 \text{ kg/cm}^2$. No additional information was given by the producer.

Once the stucco marble paste was prepared, the first step consisted in the application of a grout (Figure 6a) constituted by a fluid paste of the same stucco, to make a bonding interface, improving the adhesion to the limestone. Afterwards, a layer of the same stucco paste mixed with siliceous gravel was applied, which worked as compression filler (Figure 6b). This mix was carefully compacted by hand.



Figure 6. Application of the preparation layers: (a) stucco grout; (b) stucco mixed with gravel.

The layer of stucco marble with all the different colours and veins, previously moulded on a table to fit the shape of the corresponding stone slab, was finally applied (Figure 7a). This last layer was compacted following the traditional way of application of stucco marble, using a trowel to hit the surface in order to improve the bonding to the preparation layers (Figure 7b).



Figure 7. Application of the final layer: (a) fitting the previously moulded stucco marble paste; (b) compacting the surface with a trowel.

Once the paste was fixed to the damaged area of the slab, the excess of material was cut until levelling it with the adjacent slabs (Figure 8a) and the edges were redefined (Figure 8b). This step revealed the morphology of the veins and the tonalities of the interior of the paste.

Finally, the gypsum was left for curing. Once it was completely hardened, the next process was the polishing of the surface using wet sandpapers. Between each reference of sandpaper, it was necessary to apply a layer of the same stucco in a very fluid consistency, for covering all the small holes caused by air bubbles in the paste. The aim is to achieve a homogeneous smooth surface without visible pores. They were used different grains of grit sandpapers (from 120 to 2000) (Figure 9). After the last sandpaper, it was cleaned and left to dry completely.



(a)



(b)

Figure 8. (a) Cutting the excess of paste from the surface; (b) redefining the edges



(a)



(b)

Figure 2. Finishing of the surface: (a) polishing using different wet sandpapers; (b) application of fluid pastes to fill the pores that still prevail

The last step of the stucco marble application process consists of another polishing operation and the protection of the external surface against moisture [8, 9]. In this case, first it was applied crude linseed oil which was left for one day in contact with the surface, until saturation of the porosity of the paste, followed by a mixture of bees wax with a little portion of carnauba wax (Figure 10).



(a)



(b)

Figure 10. Protection of the external surface: (a) application of a mixture of waxes; (b) final polishing of the surface

Evaluation of the intervention

After a year of intensive use, the restored surfaces maintain a remarkable brightness, similar to that of the red limestone (Figure 11), showing that the resistance to abrasion of the stucco marble applied is adequate for this type of intervention. However, some marks can be observed on the surface of the stucco, like scratches, but they are also present on the natural stone (Figure 11d).

Concerning the paving stones with some loss of material (less than a centimetre in depth, which were not covered with stucco), despite having been cleaned during the restoration works, they have already a similar (dirty) appearance, with a negative aesthetical impact to the whole (Figure 11b and c). In future interventions of the same type, consideration should be given to the restoration of all the stone slabs with visible signs of degradation. It can be a controversial option because a significant area of the pavement would probably not have the original surface exposed. However, it is an option that should be taken into account, as it would help preserving the original materials underneath.

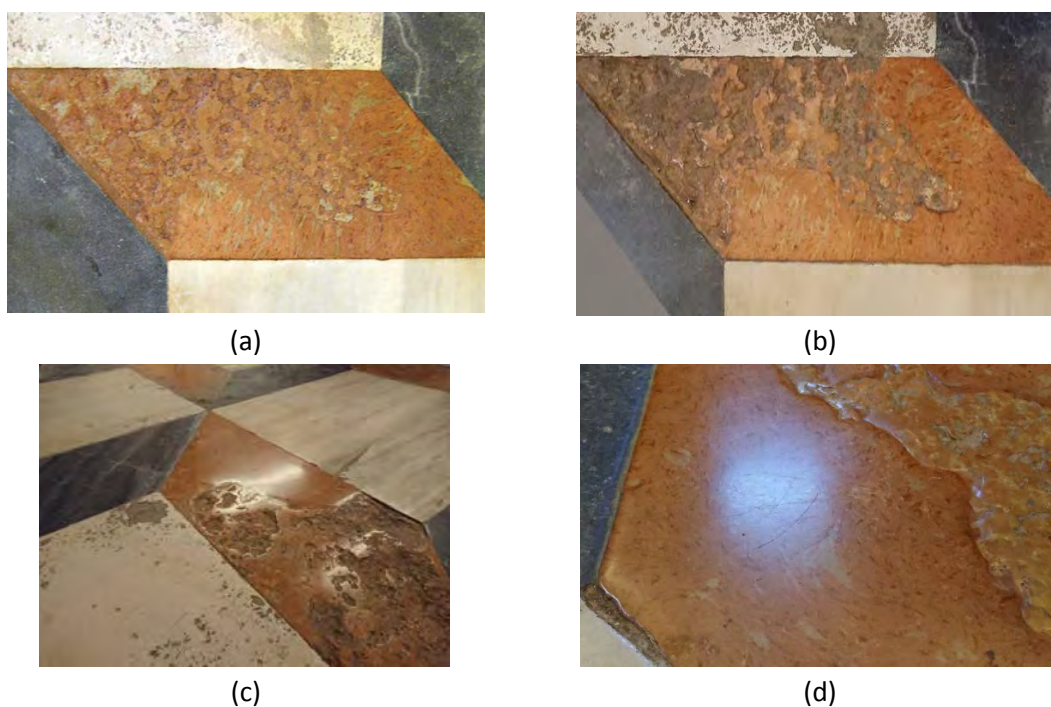


Figure 11. Evaluation of the intervention after one year: (a) stone slab just after restoration; (b) the same slab after a year of use; (c) stone partly restored, where the dirtiness on the unrestored holes is visible; (d) surfaces of the stone and of the reintegrated parts in stucco with some visible scratches

Conclusions. Future investigations

The materials used in this intervention have proved to be appropriate so far; however, it is still necessary to keep their behaviour monitored for a longer period of time, in order to detect the appearance of any possible changes in their properties.

Anyway, these results are already very promising and it would be interesting to carry out a research, based on the plaster pastes used in this work, in order to quantify their main properties (porosity, capillary water absorption, water vapour permeability, thermal and moisture expansion coefficients, dynamic modulus of elasticity, flexural and compressive strength, resistance to abrasion, hardness, etc.) and respective adequacy for this type of application. In fact, some requirements, like the resistance to abrasion or to the action of water, are predictably more demanding in a pavement than in a vertical surface, due to the continuous pedestrian traffic and the permanent contact with moisture and dissolution products coming from the ground, which are entrained and mobilized through the materials.

Some analytical studies have discovered that, in old decorations of stucco marble, the mechanical properties were higher than those found in common gypsum plasters, being even comparable to those of stone, or concrete, in some cases [10, 11]. It is pointed out that the reason for that is probably the use of a multiphase gypsum plaster as binder, with considerable amounts of anhydrite II, instead of a common hemi-hydrate plaster: anhydrite II needs less kneading water to achieve the same consistency as hemi-hydrate pastes, producing much more compact micro structures, with less porosity and better resistance [12, 13]. Nowadays, in stucco marble formulations it is more common to use alpha hemi-hydrate gypsum plaster because it is easier to find in the market and easier to work with. Besides, it has many characteristics in common with anhydrite II based plasters, namely most of the physical and mechanical properties [14].

So, the use of the traditional technique of stucco marble can be a very promising solution to be used by the restorers in multiple applications, like the possibility to use it in the restoration of interior stone pavements, so common in the European architectural heritage, or in restorations with different pathologies, that need materials more resistant to mechanical requirements and/or to water, both in liquid or in vapour phases.

References

1. Martinez Fuentes R (2003) El estuco. Técnica, conservación y restauración. Aplicación a la reintegración del mármol. PhD thesis. Universidad Politécnica de Valencia, Spain (in Spanish)
2. Reithmeir C (1995) Scagliola or stucco marble: restoration of the altars in the church of Lichtenfels, Bavaria. *Trans Built Environ* 15:213–223
3. Wittenburg C, Berner M, Weber J, et al (1999) Baroque Artificial Marble - Environmental Impacts, Degradation and Protection, ENVIART, Contract N° ENV 4-CT95-0103, Protection and conservation of European cultural heritage. Research Report N° 9
4. Wouters J, Van Bos M, Lamens K, (2000) Baroque stucco marble decorations. I. Preparation of laboratory replicas and establishment of criteria for analytical evaluation of organic materials. *Stud Conserv* 45(2):106–116

5. Wouters J, Van Boos M, Lamens K (2000) Baroque stucco marble decorations. II. Composition and degradation of the organic materials in historical samples and implication for their conservation. *Stud Conserv* 45(3):169–179
6. Mas i Barberà X (2006) Estudio y caracterización de morteros compuestos, para su aplicación en intervenciones de sellados, reposiciones y réplicas, de elementos pétreos escultórico-ornamentales. doi: 10.4995/Thesis/10251/1941
7. Kröner S, Mas i Barberà X, T, Doménech-Carbó M (2008) Evaluation of the efficiency of resin bound mortars in the ambit of stone restoration. *ARCHÉ* 3:173–178
8. Massinelli A M (1997) Scagliola. L'arte della pietra di luna. Editalia, Roma (in Italian)
9. Zecchini A (1997) Arte della scagliola sul Lario. L'intarsio e il finto marmo raccontato dagli ultimi artigiani della Valle Intelvi. Hoelpli, Milan
10. Freire T, Santos Silva A, Veiga M R, de Brito J (2016) The 19th century revivalisms in the Portuguese architecture: Characterization of the interior plaster coatings of Monserrate Palace in Sintra. In: I Papayianni, M Stefanidou, V Pachta (Eds.), Proc. 4th Hist. Mortars Conf. HMC2016, Santorini, Greece: 187–194
11. Freire M T, Santos Silva A, Veiga M R, de Brito J, Schluetter F (2016) Natural or artificial? Multi-analytical study of a scagliola from Estoi Palace simulating imperial red porphyry. *Microscopy and Microanalysis*, 22(6): 1281-1303. doi: 10.1017/S1431927616011909
12. Freire M T, Santos Silva A, Veiga M R, de Brito J (2019) Studies in ancient gypsum based plasters towards their repair: Mineralogy and microstructure. *Constr Build Mater* 196: 512-529. doi: 10.1016/j.conbuildmat.2018.11.037.
13. Freire M T, Veiga M R, Santos Silva A, de Brito J (2019) Studies in ancient gypsum based plasters towards their repair: Physical and mechanical properties. *Constr Build Mater* 202: 319-331. doi: 10.1016/j.conbuildmat.2018.12.214.
14. Wirsching F (2005) Calcium sulfate. *Ullmann's Encyclopedia of Industrial Chemistry*. Wiley-VCH Verlag GmbH & Co. KGaA: 1-33.

Stucco marble in the Portuguese architecture: first insights in mineralogical, physical and mechanical properties

Maria Teresa Freire¹, António Santos Silva¹, Maria do Rosário Veiga²

(1) Materials Department, National Laboratory for Civil Engineering, Lisbon, Portugal, mtfreire@lnec.pt, mtfreire@gmail.com, ssilva@lnec.pt

(2) Buildings Department, National Laboratory for Civil Engineering, Lisbon, Portugal, rveiga@lnec.pt

Abstract

The magnitude of the presence of stucco marble in the Portuguese architecture is still not known and studies addressing the characterisation of the materials used to produce its complex coloured pastes are almost inexistent.

In this paper, the results of the mineralogical, physical, and mechanical analysis of twelve samples belonging to five case studies are presented and discussed. Gypsum is the main constituent, but anhydrite is also present in most samples in higher quantities than those found in common gypsum based plasters. A multiphase gypsum plaster was used as binder, possibly to improve the mechanical properties of the hardened pastes. However, in the case of stucco marble, the grinding and polishing operations of the surfaces used to obtain an aesthetical appearance similar to the natural stone have also a major influence in the main properties of the final materials.

The dynamic moduli of elasticity results are extremely high in the samples incorporating anhydrite and the capillary water absorption is almost inexistent. On the contrary, the samples without anhydrite have low absorption values but show absorption curves according to gypsum based plasters.

The results obtained constitute the first approach to the knowledge of ancient stucco marble coatings in Portugal and intend to contribute to the future development of compatible restoration products.

Introduction

Stucco marble is a very complex man-made decorative technique. It has its origin in the Italian *scagliola*, an inlay work of coloured stucco pastes and was extensively used in the baroque period in central and southern Europe to imitate marble stone, being often referred to as “Baroque artificial marble” [1]. According to the literature, the materials used consisted mainly of a mixture of calcined gypsum, pigments and water with animal glue [2-4]. The glue had the function of retarding the setting of gypsum and enhancing its hardness, while keeping it easier to polish [5].

In spite of being representative of an important period of the European decorative arts, the only known characterisation studies of ancient samples of these materials are those made in the scope of the European research project ENVIART [1], in the late 1990's, and the resulting publications [5-7], being a little explored field of study. The magnitude of the use of stucco marble in the Portuguese architecture is still not known, partly due to the difficulty in distinguishing this material from real stone and from *stucco lustro*, another decorative technique used to imitate stone materials, based on lime plaster and painting [2]. The correct identification of stucco marble and the knowledge of the original materials used to perform it are essential for the definition of adequate conservation and restoration procedures, based on the principles of authenticity, minimum intervention and use of compatible materials and constitute the main objectives of this research work.

Several examples of the use of stucco marble in buildings in Portugal from the 18th to the 20th century have been identified so far and samples were collected. A multi-analytical study comprehending the determination of the mineralogical composition using X-ray diffraction (XRD), optical microscopy observations of the samples and of its stratigraphy, capillary absorption and dynamic modulus of elasticity was performed.

The results showed that gypsum (calcium sulphate dihydrate) is the main constituent. Anhydrite (calcium sulphate) was also found in most part of the samples though in less quantity, with the exception of one sample, where it is the main constituent. It was also possible to conclude that the quality of the gypsum raw material used is remarkable. Only in two samples the presence of quartz was detected in higher amounts, probably used as aggregate, an issue that still needs to be clarified. The mechanical characterisation showed very high values of dynamic modulus of elasticity, much higher than those of common ancient gypsum based plasters [8], and the capillary absorption had the opposite trend, being almost inexistent in the samples with anhydrite. Similar results had already been observed in previous studies of two samples that intended to simulate stone and it was concluded that anhydrite, obtained from gypsum calcination at higher temperatures, was intentionally used in the binder to produce materials with improved physical and mechanical performance [9,10].

In this paper the characterisation results of twelve samples of stucco marble belonging to five case studies are presented and discussed. A relationship between composition, techniques of application and the intended performance of the materials is established.

Experimental work

Materials

The samples of stucco marble were collected directly on site (e.g. IP1, IP2 and IP3), or resulted from previous detachments. Their identification and description is presented in Table 1 and some images are shown in Figure 1. The assignment of two case studies to the

18th century was made based on the dating of other decorative campaigns that took place in those buildings, but no documents specifically referring to the stucco work are known so far.

Table 1. Identification and description of the samples analysed

Period (century)	Case study /Localization	Sample	Description*/State of conservation/Thickness
18 th (?)	<i>Paulistas</i> church/Lisbon	IP1	Wall coating from the church - Yellow, with purple veins/Surface mostly eroded/4.5-5.5 mm
		IP2	Wall coating from the church - Brick coloured, with black, yellow and orange veins/Surface with some erosion/5-6 mm
		IP3	Wall coating from the sacristy - Light grey with yellow and bordeaux coloured veins/Surface in very good condition/6-8mm
18 th (?)	<i>S. João Novo</i> church/Oporto	ISJ1	Wall coating from the church - Salmon coloured with dark pink and black veins/Surface with loss of bightness/3-3.6 mm
		ISJ2	Wall coating from the church- Brick to orange with black and bordeaux coloured veins/Surface with convex deformation and cracks due to salts crystallisation/3.5-3.8 mm
		ISJ3	Wall coating from the presbitery - Dark pink (almost red) with dark, yellow and light pink veins/Surface in good condition with only partial loss of bightness/5-6 mm
		ISJ4	Wall coating from the same wall as ISJ3 – Light salmon with pink, yellow and purple veins/Surface in quite good condition/3 mm
19 th	<i>Clérigos</i> church/Oporto	IC1	Ceiling coating - Brick to orange with black and bordeaux coloured veins(very similar to ISJ2)/Surface slightly convex, with gloss in the non scratched parts/2.4-2.7 mm
		IC3	Wall coating, close to the ceiling - Dark pink (almost red) with bordeaux, yellow and light pink veins/Surface very eroded, with slight loss of material in some places/4.2-4.9 mm
		IC4	Wall coating close to the ceiling - Dark coloured with some white spots/Surface fairly eroded and almost without bright areas/2.5-3 mm
20 th (until 1940)	Theater-Circus/Braga	TCB1	Coating of a column - Orange with brown, dark and yellow veins (probably not corresponding to the original colours (Figure 1))/Surface with some scratches, but still bright/10-12 mm
	Secondary School/Beja	LB1	Coating of a pilaster - Very light salmon, beige and white with black veins/Surface in very good condition/3.2-3.6 mm

* The colours indicated refer to the finished surfaces at present and might have changed by the yellowing of the finishing products applied (e.g. oils), as it appears to be the case of sample TCB1

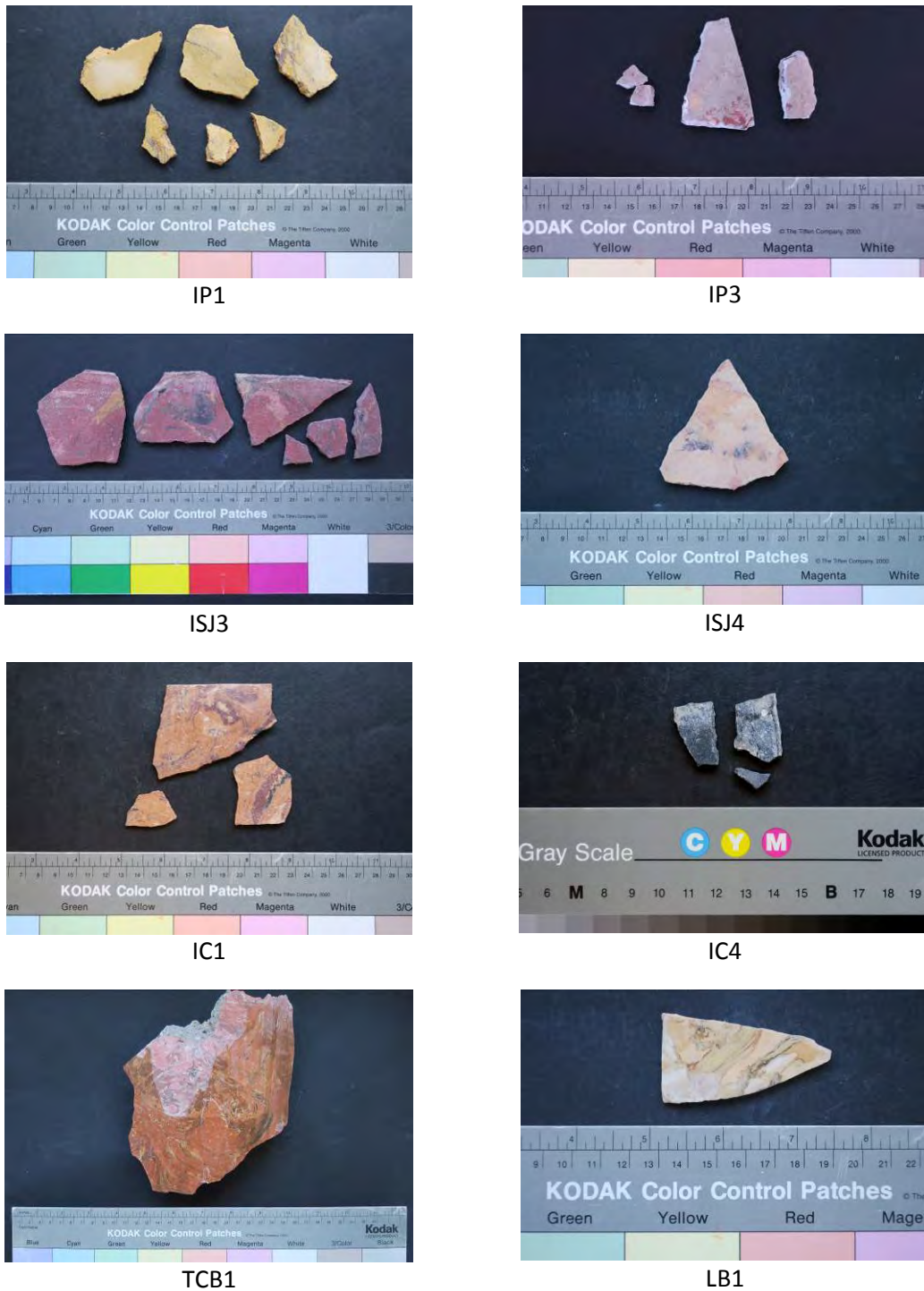


Figure 1. Stucco marble samples collected in Portuguese buildings dated from 18th to 20th centuries

Experimental data

The analytical characterisation started with a photographic recording, sometimes assisted by an Olympus SZH stereo-zoom microscope equipped with a video camera Olympus DP20, especially in the observation of the polished surfaces.

X-ray diffraction analysis (XRD) was performed to determine the mineralogical composition of the binder and other possible crystalline constituents from the pigments and the

aggregates. A Philips X'Pert diffractometer with Fe filtered cobalt $K\alpha$ radiation ($\lambda=1.7903 \text{ \AA}$), operating at 35kV and 45 mA was used. Powder diffraction data were collected in the range 3° - 74° (2θ) in steps of 0.05° with 1 second measuring time per step. The samples were previously ground and sieved until all powder particles passed through a sieve of $106 \mu\text{m}$. Afterwards they were deposited on a XRD sample holder, using the back-loaded process. The X'Pert Quantify© software was used to collect the data and the diffractograms were analysed with a X'Pert HighScore© software using the XRD cards from the International Centre for Diffraction Data Powder Diffraction Files (ICDD PDF).

The water absorption tests were performed using a capillary absorption by contact method developed for irregular and/or friable samples (Figure 2) [11]. The area of absorption was determined using CAD software applied to the contour of the surfaces. The samples were weighed at predefined time intervals, until 24 h. Then, they are taken out of the baskets, polyethylene film was applied to all faces except the face where the drying would take place (the same as for the absorption) and weighed again at predefined time intervals until achieving constant weight.

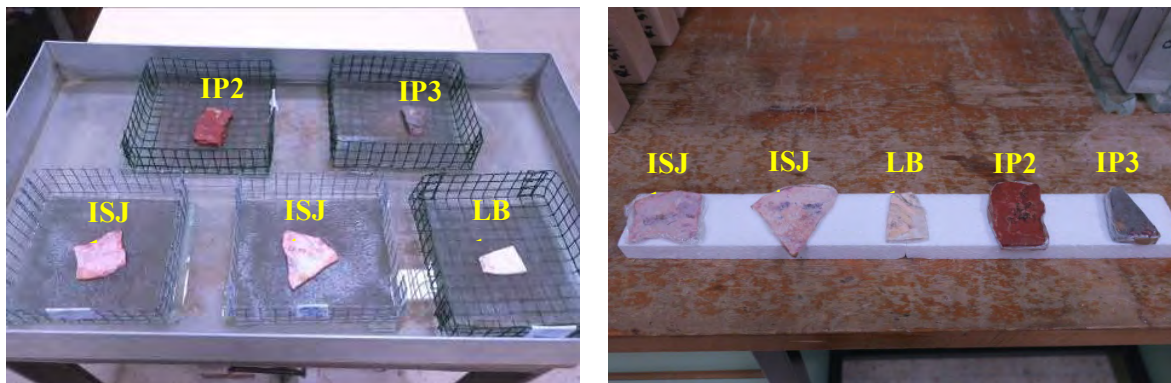


Figure 2. Determination of the capillary water absorption by contact and drying behaviour of the samples

The bulk density values were obtained by weighing and calculating the volume of the samples (area of the surface x thickness).

The dynamic modulus of elasticity (DME) was determined using the method based on the measurement of the ultrasonic pulse velocity (UPV), e.g., the velocity of high frequency sound waves passing through the material, allowing the calculation of elastic parameters [12].

Special exponential probes with pointed ends were used to provide good and precisely located contact with the samples surfaces. The "Steinkamp Ultrasonic Tester BP-7" equipment and the "WinUltraSonic/BP-7" software were used. The UPV was measured at the surface (indirect method - superficial transmission).

Results and Discussion

Visual observation of the samples

The visual observation of the samples gave a series of clues, namely related to the state of conservation and the way pigments were used to produce the desired colours. In Figure 3 images of the surfaces of some samples obtained with the stereo-zoom microscope are shown.

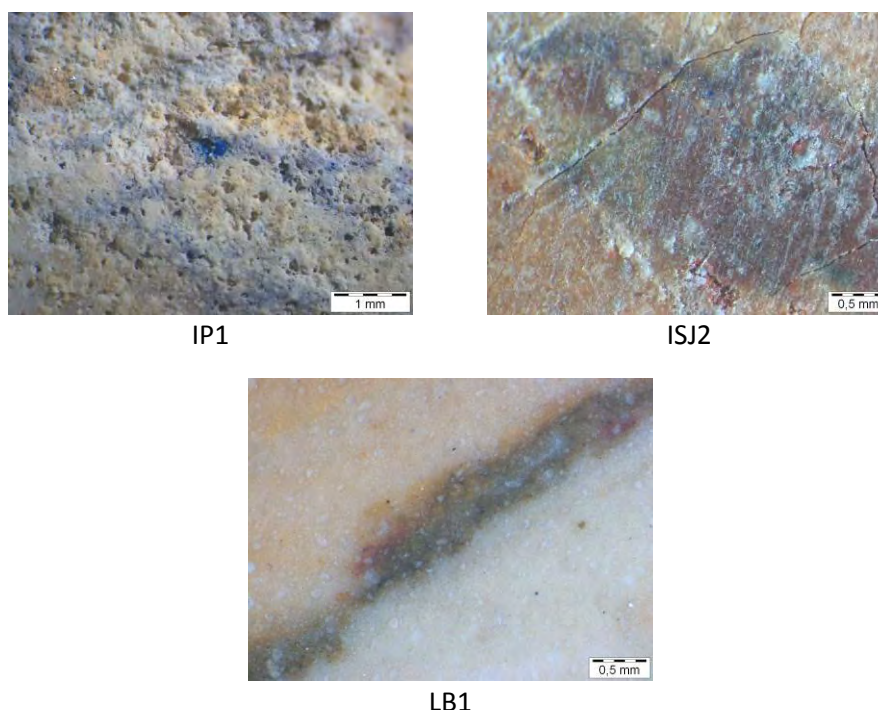


Figure 3. Stereo-zoom microscope images of the surfaces of samples IP1, ISJ2 and LB1, showing different states of conservation

The observation of the cross-section polished surfaces (Figure 4) revealed high porosity of IP1's paste, caused by partial dissolution of the material, in agreement with the extensive exposure to moisture. On the contrary, LB1 has a very dense matrix, with much lower porosity, while ISJ2 shows some macro porosity, but not very significant. This macro pores seem to result from the dissolution of some of the larger crystal grains observed in the matrix and in some of them the deposition of soluble salts is visible.

The pigments were also clearly observed in most of the samples. The purple veins of sample IP1 result from the use of a blue pigment, probably ultramarine blue. Its exact composition will help to have more certainty about the dating of the samples, due to the differences between the natural (lapis lazuli, used until the first quarter of the 19th century) and the synthetic pigment. Dark blue grains were also observed in the Bordeaux coloured veins of ISJ2 and of many other samples. The grey colour of sample IP3 was obtained through the

addition of a black pigment to the white plaster; its larger grains are very perceptible both at the surface and in the matrix.

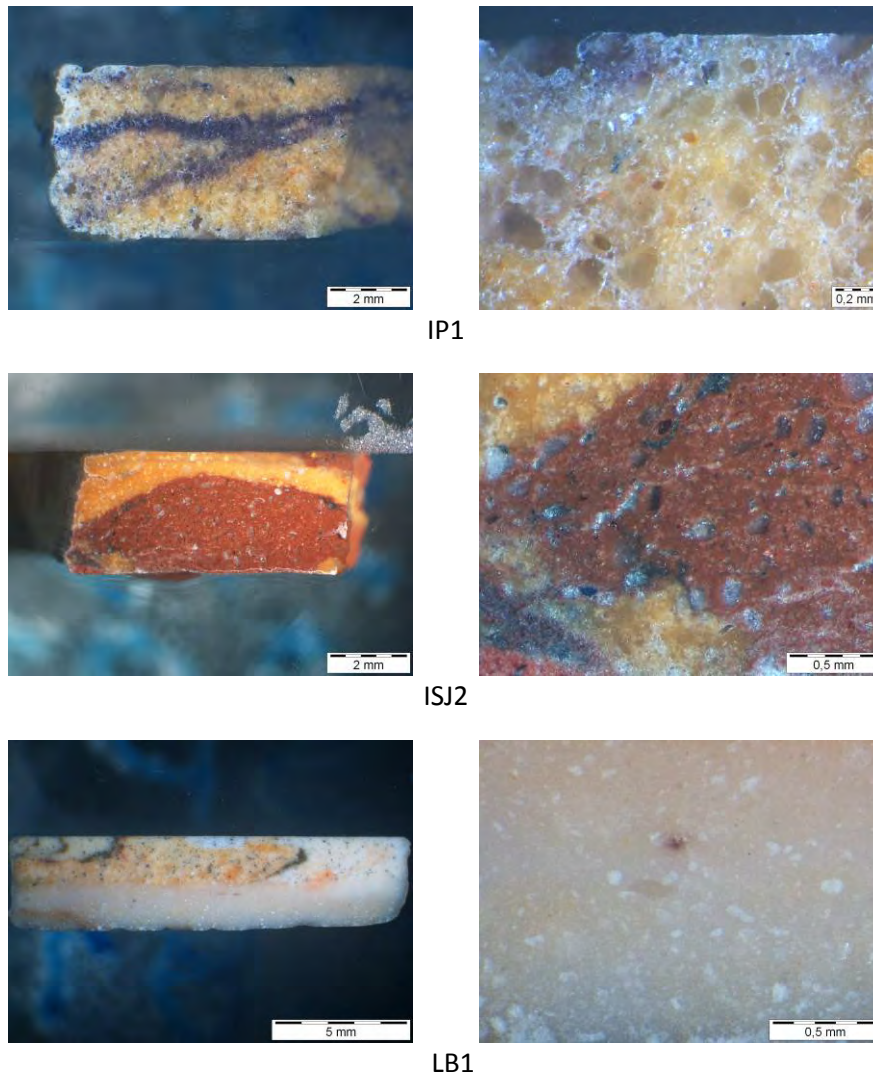


Figure 4. Cross-section polished surfaces of samples IP1, ISJ2 and LB1, showing the stratigraphy and the porosity of the matrixes

Another important detail that was possible to see in samples with fracture and detachment of the surface of the stucco marble is the difference between the compactness and orientation of the last micrometres of the plaster (forming a layered structure) and in depth (Figure 5). Similar observations have been made in samples of Baroque stucco marble of a Polish chapel using SEM [1], attesting the importance of the procedures of repeated grinding and polishing the surface, often referred in the literature [2-4]. During the execution of these procedures, the holes appearing at the surface are filled with a low consistency mixture of gypsum and glue. Turco [4] states that “in the imitation of marble what counts the most is the superficial appearance and gypsum plaster is the binder that allows obtaining the most perfect results”.



Figure 5. Sample IP3: image showing the difference between the texture of the plaster in the bulk and closer to/at the surface

Mineralogical analysis using XRD

The mineralogical analysis using XRD allowed identifying the crystalline compounds present, namely the binder and some pigments. The results showed that gypsum is the main constituent, except in sample LB1, where anhydrite exists in higher quantity, a compound also present in the majority of the samples (Table 2).

Table 2. Mineralogical composition determined by XRD analysis

Samples	Identified crystalline compounds*				
	Gypsum	Anhydrite	Calcite	Quartz	Others
IP1	++++	-	trc	trc	-
IP2	+++ /++++	trc	trc/+	trc	Hematite (trc)
IP3	++++	?	-	-	-
ISJ1	+++ /++++	+	-	-	-
ISJ2	+++ /++++	+	-	trc	-
ISJ3	++++	+	-	trc	Graphite?
ISJ4	++++	trc+?	-	-	-
IC1	+++ /++++	+	-	?	-
IC3	+++ /++++	trc	trc	+	-
IC4	+++	++	-	+	Graphite (trc)
TCB1	+++	++ /+++	-	trc	-
LB1	++	+++	-	-	-

* Notation used in XRD peak analysis: ++++ very high proportion (predominant compound); +++ high proportion; ++ medium proportion; + weak proportion; trc - traces; "-" not detected

With the exception of the samples from *Paulistas* church and one sample from *Clérigos* church (IC3), the presence of anhydrite was detected in higher quantities than usually observed in common ancient gypsum plaster coatings [13].

Similar results were obtained in a previous study of two samples of stucco marble [9, 10]. It was concluded that the presence of this anhydrous phase, obtained by calcination of the gypsum rock at higher temperatures, was intentional, indicating that multiphase gypsum plaster was used as binder. The aim was to improve even more the mechanical strength of the corresponding materials, as anhydrite needs less kneading water (increasing mechanical characteristics).

In samples IP1, IP2, IP3 and IC3 the almost absence of anhydrite means that lower temperatures of calcination were used and that the binder was calcium sulphate hemihydrate (the β type). This phase needs more kneading water, leading to more porous materials.

Another feature important to highlight is the quality of the gypsum used. Only in samples IC3 and IC4 quartz is clearly detected, which could be either an impurity of the raw material, or an intentional addition. Considering that the quality of the gypsum plaster used to produce stucco marble is one of the paramount issues referred in the literature [2, 3], quartz was most probably added as aggregate. Further analyses are needed to confirm this hypothesis.

One final remark to highlight is that no reference to the detection of anhydrite in stucco marble samples has been found in the literature so far.

Capillary water absorption and drying

The capillary water absorption and the drying behaviour were evaluated in five samples and the results are presented in Table 3 and in Figure 6.

Table 3 - Capillary water absorption results

Sample. Test specimen	Weight (g)	Absorption area (mm ²)	Coefficient of absorption at 5 min (kg/m ² min ^{1/2})
IP2.1	16.72	2056	0.18
IP3.1	11.66	945	0.32
ISJ1.1	13.25	1958	0.00
ISJ4	13.28	2200	0.00
LB1	7.36	1049	0.00

During the 24h of the procedure, only samples IP2 and IP3 behaved according to common gypsum plasters. Even though, the coefficients of absorption at 5 minutes are low and more approximate to the values obtained for thin-layer plasters [8]. The main reason for the distinct behaviour of these two samples must be the intrinsic higher porosity they have due to the binder used in their production (calcium-sulphate hemihydrate), a feature already explained in the previous section. The influence of the state of conservation of the surfaces, very good in the case of sample IP3, and the application of products to increase their gloss and brightness, like oils and waxes, were not enough to completely hinder the water absorption.

The drying behaviour of samples IP2 and IP3 showed that they also lose water easily and recover their weight.

Concerning the other three samples, only LB1 showed some absorption, but still not significant. After drying it was perceptible certain erosion on part of its surface, which was probably the cause for the absorption observed. This means that the surface did not resist

much to the action of water; yet, the matrix is so compact that the water uptake is negligible.

ISJ1 and ISJ4 had similar behaviour to the two samples of stucco marble previously studied [8, 9], showing practically no water absorption.

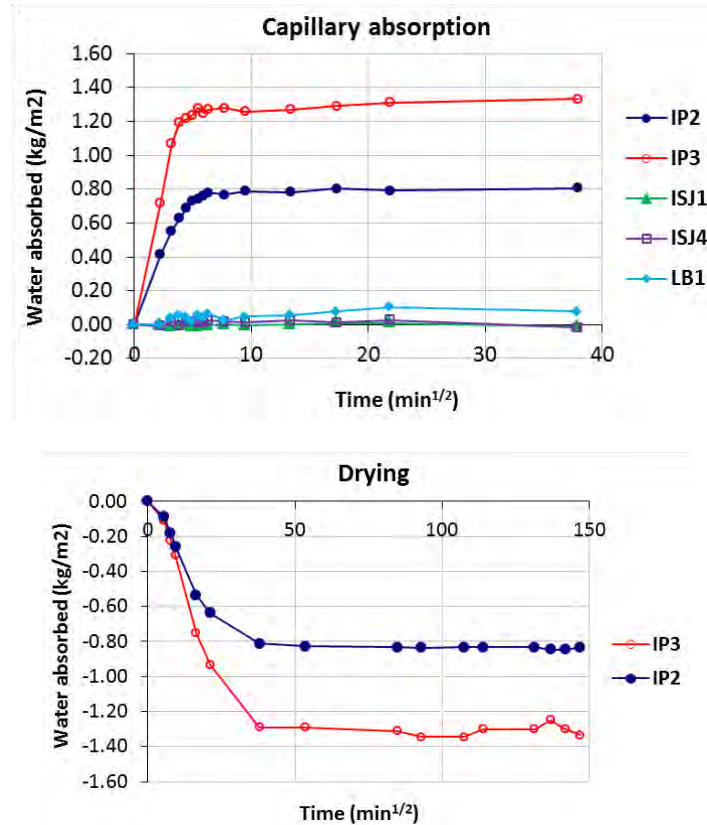


Figure 6. Capillary water absorption and drying curves

Dynamic modulus of elasticity

The dynamic modulus of elasticity was determined according to the equation:

$$DME = v^2 \rho K$$

where:

DME - Dynamic modulus of elasticity

v - Velocity of the ultrasound waves through the material (inverse of the slope of the respective curve, Figure 7)

ρ - Bulk density

K - Constant that depends of the coefficient of Poisson (φ):

$$K = \frac{(1 + \varphi)(1 - 2\varphi)}{(1 - \varphi)}$$

For mortars, when the coefficient of Poisson is not exactly known, it is assumed the approximate value of 0.2, which was the case in this work.

The test specimens used for the determination of the UPV had a minimum of 60 mm length, in order to allow measurements at five different distances (minimum) from the origin, where the transmission probe is located, and obtain feasible results (Figure 7).

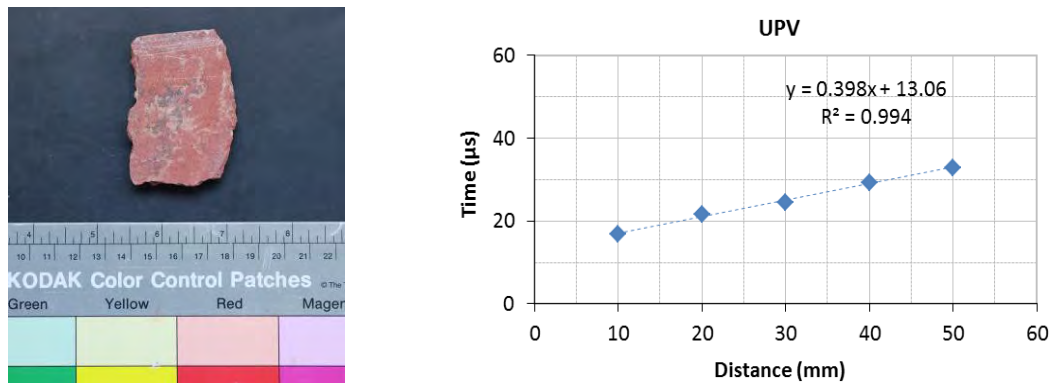


Figure 7. Determination of the UPV in sample IP2: image of the test specimen used (IP2.1) and graphical representation of the results

Table 4 shows the results of the bulk density, ultrasonic pulse velocity and the calculation of the dynamic modulus of elasticity.

Table 4. Dynamic modulus of elasticity results

Sample	Bulk density (kg/m ³)	Ultrasonic pulse velocity (m/s)	Dynamic modulus of elasticity
IP1	1262	*	*
IP2	1419	2513	8065
IP3	1765	*	*
ISJ1	2011	2950	15750
ISJ4	2040	3108	17740
LB1	2008	3683	24520
TCB1	1857	1563	4090

* Not determined due to insufficient size of the test specimens

With the exception of samples IP1 and IP2, whose bulk density is lower (an expected result, considering their long exposure to moisture and partial dissolution), the values of bulk density are much higher than those of ancient gypsum plasters and the same can be said about the dynamic modulus of elasticity. However, they are both in accordance with the results of two stucco marble samples analysed in previous studies [8].

The few values found in the literature for this type of materials vary between 6090 and 18620 MPa [8, 13]. In spite of having been determined by the resonance frequency method, they are also much higher than what is usually obtained for a gypsum plaster prepared with

β -hemihydrate using the same method [14]. However, no references are made to the gypsum phases present.

In the case of the samples analysed in this study, the explanation for such high values must be in the use of multiphase plasters, with high contents of anhydrite.

Middendorf and Knöfel [15] tested mixtures of 80 % β -hemihydrate and 20 % anhydrite and obtained values of dynamic modulus of elasticity between 11060 and 12780 MPa, closer to those of samples ISJ1 and ISJ4. Nevertheless, sample LB1 is still much above, with values only comparable to gypsum plasters prepared with α -hemihydrate (22000 MPa [16] and 1 MPa [15]). In the cross-section polished surfaces observations with stereo-zoom microscope sample LB1 had the most compact matrix (Figure 4), in accordance with the highest result of dynamic modulus of elasticity of all samples.

The value found for sample IP2 is still high, though it is only about half of samples ISJ1 and ISJ4, and one third of sample LB1. This result is in agreement with its bulk density and with the fact of having been prepared with β -hemihydrate. In the case of sample TCB1, the determination of the UPV could have been influenced by micro cracks, as it does not correspond to the state of conservation and compactness visually observed, neither to the measured density.

In fact, the indirect method used in the determination of the dynamic modulus of elasticity is influenced by the state of conservation of the material close to the surface as it is based on superficial transmission. In the case of stucco marble, if the state of conservation is good, this is precisely where the material is more compact (Figure 5) and the highest results are expected.

Conclusions

In this paper the results of mineralogical, physical and mechanical properties of a set of twelve samples of stucco marble, comprehending a period of two centuries (18th to 20th), are presented and discussed.

The samples presented different states of conservation. A detailed visual observation with the stereo-zoom microscope showed that some had only superficial degradation, with impact on aesthetical appearance (loss of brightness, scratches). However, the few with long time exposure to moisture and/or salt loaded walls, showed more severe damages, like partial dissolution of the matrix, deformation and cracks.

The mineralogical analysis using XRD confirmed that the binder used was obtained from high quality raw gypsum. In most of the cases anhydrite is present in significant quantities, meaning that higher temperatures of calcination were used to obtain a multiphase gypsum plaster. This is not a commonly observed feature in ordinary ancient gypsum based plasters, indicating that such procedure was intentional. In fact, the use of a multiphase gypsum

plaster leads to more resistant, less porous hardened materials, as it needs less kneading water. The more anhydrite it has, the more accentuated are all these characteristics. So, the preparation of the gypsum to be used in the production of stucco marble was not only limited to the choice of high purity raw materials but also to special calcination conditions, in order to get as close as possible to the properties of the material that was intended to imitate, and not only to the aesthetical appearance.

This aesthetical appearance was achieved with the final preparation of the surface, which enhanced the compactness of the material, attested by visual observation of some of the samples analysed and by the extremely high results of ultrasonic pulse velocity obtained by the indirect method (which is related with the transmission through superficial layers).

Aggregates were not commonly used in the stucco marble coatings. Only quartz was detected in higher amounts in two samples but further analyses are needed to clarify its role.

The capillary water absorption tests showed that the application of certain products, like oils and waxes, to increase the gloss and brightness of the surfaces after drying, contribute to give a certain resistance to the action of water. However, this capacity is limited; the absorption is also related to the porosity of the material, where the phase of the gypsum used as binder (β -hemihydrate or multiphase plaster with significant amounts of anhydrite) is of major influence.

The higher compactness, lower porosity and much higher mechanical properties of these materials compared to those of the common gypsum-based plaster is attributed to the use of high quality raw materials and higher calcination temperatures, in order to obtain multiphase gypsum plasters. The use of animal glue in the kneading water and the addition of pigments, can also contribute to enhance the referred characteristics.

Further analysis of this set of samples are needed, namely SEM-EDS observations and determination of the organic compounds still present, in order to have a more complete information about the original mixes used. Other samples of stucco marble are still available to perform the multi-analytical characterisation. The compilation and analyses of all the results obtained will contribute to provide a solid support for the development of compatible restoration products, the final aim of this research work.

Acknowledgements

The authors would like to thank the Foundation for Science and Technology (FCT, Portugal) for the financial support within Maria Teresa Freire's post-doc scholarship (SFRH/BPD/121034/2016) and the Research Project DB Heritage – Database of construction materials with historical and heritage interest (PTDC/EPH-PAT/4684/2014). They also acknowledge Marco Aurélio, conservator and restorer of gypsum-based plasters for the supply of many of the samples analysed in this study.

References

1. Wittenburg C, Berner M, Weber J, et al (1999) Baroque Artificial Marble - Environmental Impacts, Degradation and Protection, ENVIART, Contract N^o ENV 4-CT95-0103, Protection and conservation of European cultural heritage. Research Report N^o 9.
2. Arcolao C (1998) *Le ricette del restauro*, 2nd ed. Marsilio Editore, Venezia
3. Beard G (1983) *Stucco and Decorative Plasterwork in Europe*. Thames and Hudson, London
4. Turco T (2008) *Il Gesso. Lavorazione, Trasformazione, Impieghi*, Seconda ed. Editore Ulrico Hoepli, Milano
5. Kozłowski R, Wittenburg C, Zeunert A (2000) Stucco marble in the Dukes Chapel in Krzeszów, Poland - Microclimate and degradation mechanisms. *Int Zeitschrift für Bauinstandsetz und Baudenkmalpfl* 6(4):463–480
6. Wouters J, Van Boos M, Lamens K (2000) Baroque stucco marble decorations. II. Composition and degradation of the organic materials in historical samples and implication for their conservation. *Stud Conserv* 45(3):169–179
7. Wouters J, Van Bos M, Lamens K (2000) Baroque Stucco Marble Decorations. I. Preparation of Laboratory Replicas and Establishment of Criteria for Analytical Evaluation of Organic Materials. *Stud Conserv* 45(2):106–116
8. Freire MT, Veiga MR, Santos Silva A, Brito J de (2019) Studies in ancient gypsum based plasters towards their repair: Physical and mechanical properties. *Constr Build Mater* 202:319–331
9. Freire MT, Santos Silva A, Veiga MR, Brito J de, Schluetter F (2016) Natural or Artificial? Multi-Analytical Study of a Scagliola from Estoi Palace Simulating Imperial Red Porphyry. *Microsc Microanal* 22(6):1281–1303
10. Freire T, Silva AS, Veiga MR, Brito J de (2016) The 19th century revivalisms in the Portuguese architecture: Characterization of the interior plaster coatings of Monserrate Palace in Sintra. In: Papayianni I, Stefanidou M, Pachta V (eds) *Proc. 4th Hist. Mortars Conf. HMC2016*. Santorini, pp 187–194
11. Veiga MR, Magalhães A, Bosiljkov V (2004) Capillarity tests on historic mortar samples extracted from site. Methodology and compared results. 13th Int. Brick Block Mason. Conf
12. (2007) NP EN 12504-4:2007 - Ensaios de betão nas estruturas. Parte 4: Determinação da velocidade de propagação dos ultra-sons.

13. Freire MT, Santos Silva A, Veiga MR, Brito J de (2019) Studies in ancient gypsum based plasters towards their repair: Mineralogy and microstructure. *Constr Build Mater* 196:512–529
14. Freire MT (2016) Restoration of ancient Portuguese interior plaster coatings: Characterization and development of compatible gypsum-based products. PhD Thesis, Instituto Superior Técnico, University of Lisbon
15. Middendorf B, Knöfel D (1998) Gypsum and lime mortars of historic german brick buildings. In: Baer NS, Fitz S, Livingston RA (eds) *Conserv. Hist. Brick Struct.* Donhead Publications, Ltd., pp 197–208
16. Dalui SK, Roychowdhury M, Phani KK (1996) Ultrasonic evaluation of gypsum plaster. *J Mater Sci* 31(5):1261–1263

Clay and gypsum mortars used during antiquity in Cyprus

Maria Philokyprou

University of Cyprus, mphiloky@ucy.ac.cy

Abstract

Clay and gypsum constitute two of the most ancient, and at the same time, the most friable types of mortar used in architecture in Cyprus, as well as in other East Mediterranean countries. When used as plaster, they were most commonly placed over adobes due to their compatibility with such edifices, whereas clay was diachronically used as the main binding material between stones and adobes. The very simple methodology required for the preparation of clay and gypsum mortar made them perfect ecological materials. The research presented in this paper derived from a PhD thesis, as well as research programmes financed by the Research Promotion Foundation of Cyprus and the University of Cyprus. The results show the close relationship between the raw materials used, and the geology of the immediate environment of each settlement. On the other hand, the rather limited use of gypsum in the architecture of the island during the first periods of antiquity remains without explanation. Despite its limited use during these periods, gypsum was used more widely during the medieval time, as well as in the vernacular architecture of the 19th-20th century.

Introduction - Methodology

Clay and gypsum constitute two of the primary building materials used as mortars throughout antiquity in Cyprus until the last centuries, as well as in many other countries especially in the Mediterranean area. They were used alone, or in combination as binding materials and plasters in the construction of stone and adobe walls, as well as for the construction of floors and roofs [1, 2].

This paper presents the results of a holistic investigation regarding the different mortars and plasters used during the earliest periods of antiquity in Cyprus. Comparisons to similar mortars used in the vernacular architecture of the 19th-20th century are also presented at the end of the paper. The first part of the investigation was carried out in the framework of a PhD thesis on prehistoric building materials [1] and the second part was carried out in the context of research programmes founded by the Research Promotion Foundation of Cyprus and the University of Cyprus.

The detailed research on prehistoric mortars and plasters, involved the bibliographic investigation of prehistoric settlements, the on-site observation of several archaeological locations, as well as microscopic and laboratory analyses of a large number of samples collected from various prehistoric sites of the island and vernacular structures for comparison reasons. More specifically a large number of samples of mortars and plasters

were selected from Neolithic, Chalcolithic and Bronze Age settlements such as Khirokitia, Kalavassos-Tenta, Marki-Alonia, Alambra-Mouttes, Kissonerga-Mosphilia, Maroni-Vournes, Kalavassos-Ayios Dhimitrios, Kition-Kathari, Kouklia-Palepaphos, Alassa-Paliotaverna. Samples were put under many laboratory tests such as chemical, mineral (XRD) and petrographic analysis, as well as examination under a scanning electron microscope, in order to investigate the microstructure of the samples and the method of their preparation [1].

Clay used as a mortar and plaster

General Remarks

Earth, always readily available in nature and within the vicinity of the various settlements, was the basic raw material used for the preparation of mortars and plasters for the construction of circular, as well as rectangular dwellings during the prehistoric period. Earth was used as mortar and plaster in stone and adobe walls, as plaster for the construction roofs and as a coating for the construction of floors.

The wide use of clay as a mortar between stones and adobes during the prehistoric period, can be linked to the geology of the island (abundance of raw materials – clay and calcitic soils), as well as to the very simple preparation procedure. Before the clay was prepared as mortar, the raw material (soil with some clay content) was collected from neighbouring areas around the settlements. The process of soil selection and preparation for the manufacture of clay mortar is similar to that of the preparation of adobes. Sometimes clay mortar was prepared by mixing different types of soil, so that the end product had the proper amount of clay and sand. Initially, any large stones found in the soil were removed and the required amount of water was added, as well as ingredients such as straw or reeds to improve the adhesion of the plaster. In some cases, other additives such as ash or small pebbles were added during the preparation of clay mortar. The mixture was left for two or three days to mature and ferment, before its use as mortar or plaster [1].

In situ observations and bibliographic information

The bibliographic and in situ research showed that clay was diachronically the main material used as a binder between rubble stones (Figure 1) and ashlar (Figure 2), as well as between adobes (Figure 2). It was mixed with small stones to fill the space between the two external faces (shells) of rubble and ashlar stones (Figure 2), as well as between the successive layers of stones and adobes. The thickness of the mortar between the successive layers of adobes was about 1-3 cm. An interesting aesthetic result derives from the use of a different colour of clay as a binding material in adobe walls in Khirokitia, Marki-Alonia, Alambra-Mouttes, Maroni-Vournes (Figure 2) and Hala Sultan Tekke, when compared to the colour of the adobes themselves. This was probably not intentional, as these structures were then plastered.



Figure 1. Clay mortar between rubble walls in Khirokitia and Kalavassos-*Ayios Dhimitrios*



Figure 2. Clay mortar used between ashlar blocks in the Late Bronze Age Settlement of Hala Soultan Tekke and between adobes in the Late Bronze Age settlement of Maroni-*Vournes*

Clay was also used as a plaster on rubble and adobe walls from the Neolithic period (Figure 3) onwards for structural and aesthetic reasons [3]. There are also some rare bibliographic references for the existence of plaster over ashlar in Enkomi [4] and Kition [5], but the plaster found on these ashlar surfaces may be related to later phases of Late Bronze Age buildings being reused. Plasters were often laid in a considerable thickness [3] of up to 7 cm (Enkomi) [4] or even 10 cm (Lemba) [6], in two or more thin successive coats for structural reasons in order to avoid them collapsing under their own weight. The final thin coating of finer ingredients was often applied over a coarser base layer. The coarser layer contributed to the better adhesion of the coating to the structure of the wall, especially in the case of adobes. The plastering was most probably carried out by hand and the smoothing of the finished surface was achieved with the help of a stone tool. The final smoothing results in a better aesthetic outcome and also serves to fill any voids in the plaster. A variety of colours can be observed in the clay used as plaster, dependent on the provenance of the raw material used, such as red (Enkomi), white (*Alambra-Mouttes*) or yellowish (*Morphou-Toumba tou Skourou*).

In some cases, the adobe superstructure was placed in a recess of about 3 cm from the vertical face of the ashlar blocks that constitute the base of the structure. According to the excavator of the site of Kition, this recess served to better support the clay plaster to be laid

above the adobes [5]. A similar solution was followed in the structures of Enkomi [4]. The final appearance of some plaster surfaces laid above adobes is of special interest. Specifically, in *Maa-Palaiokastro* some adobe walls have an external layer of plaster that has the appearance of ashlars [7].



Figure 3. Clay plasters from the Neolithic settlement of Khirokitia and the Middle Bronze Age settlement of *Alambra-Mouttes*

In the lower part of the vertical walls, where they met the horizontal floors, a series of small rounded stones (pebbles) were sometimes laid to ease the curvature of the wall plaster [8] (Khirokitia), which continued as floor coating. The floor coating often constituted of two or three successive layers of a considerable thickness of up to 25 cm (*Kalavassos-Tenta*) [9] according to the duration or lifespan of the structures. A fine-grained coating was often laid over one or two coarser substrates, often placed above a base layer of flat stones (Figure 4). Floors were sometimes compressed in order to achieve a compact final surface. There are also cases where the floor coating was laid on the physical rocks without any previous substructure of stones. In the floor plasters, a variety of additives were recognised by the excavators such as pebbles, ash, straw, grass, fossils and charcoal (*Enkomi*, *Cap-Andreas-Kastros*, *Lemba-Lakkous*).

The horizontal roofs of the structures (circular and rectangular) were constructed with the use of successive layers of earth laid above the layers of timber and braches. A part of a horizontal roof found burned and collapsed on the floor of a dwelling in Khirokitia gives us information about the structure of the horizontal layers of earth placed above the roof timber structure. Actually, three successive layers were observed, with the first layer put in place, then left to dry and solidify before the next layer was placed on top and so on. This can be verified by the clear separation between the different layers of clay. In the clay layers, straw was observed [8, 10]. Some of the pieces have a curved finish that seems to correspond to the ceiling joint with the wall. In some pieces of a roof revealed during the excavation of the Chalcolithic settlement of *Kissonerga-Mosphilia*, remains of reeds were recognised [11]. The roofs needed constant conservation and renewal and thus new layers of earth were placed diachronically in order to safeguard the structure and extend its lifespan.



Figure 4. Plaster floors from the Neolithic settlement of Khirokitia and the Late Bronze Age settlement of Kalavassos- *Ayios Dhimitrios*

Laboratory analysis

The samples selected were initially observed in the laboratory under a stereoscope and thin sections of each specimen were prepared after vacuum impregnation with an epoxy resin. Thin sections were observed under a petrographic microscope for the mineralogical characterization of the samples. Further scientific analysis included chemical analysis for the identification of the main and accessory chemical elements in the form of oxides and mineral analyses using X-ray diffraction in order to investigate the mineral phases. For the detailed observation and examination of the microstructure of a smaller number of samples in the micron particle size, a scanning electron microscope (SEM) equipped with a microanalyzer (EDS) was employed.

The chemical and mineralogical analyses of various prehistoric samples of clay mortars have shown that their manufacture involved the use of soil with a high content of calcite (30% to 40%), as well as a significantly high content of silicon oxide (10% to 20% or higher) and a relatively significant proportion of aluminium oxide (2% to 5% or higher: 7.45% to 10%). The XRD analysis showed that aluminium and silicon oxides seem to have come from clay minerals (montmorillonite, kaolinite, nontronite, etc.), which give the clay its cohesive properties.

The chemical analysis of plasters selected from two different layers showed a more calcitic composition in the external layer compared to the base layer (Table 1). More specifically in a number of samples from the Neolithic settlement of Khirokitia, the base layer has about 14.4% to 21.52% SiO_2 compared to the external layer which has a more calcitic composition (35%) and less SiO_2 (6.7-12.9%).

The laboratory analysis of some of the clay based plasters derived from Kalavassos-*Tenta* showed the presence of small quantities of gypsum (Table 2). The existence of gypsum in the settlement's clay based plasters can be attributed to the use of soil from the immediate surroundings consisting of gypsum and covered by secondary deposits of lime and gypsum compositions [9]. Another peculiarity revealed in the clay based plasters from the Neolithic settlement of Khirokitia, through the XRD analysis, is the existence of a high percentage of

strontium (sulphate celestite – Table 1). This mineral is quite rare on the island and is mainly found in the geological strata of the area near the Neolithic settlement of Khirokitia. The examination of thin sections of clay based samples under the petrographic microscope and the detailed observation under SEM showed the presence of clay minerals as well as calcite (Figure 5).

Table 1. Chemical analysis of two wall plasters with successive layers from Khirokitia (base layers: KH.8A, KH.13A and upper layers: KH.8B, KH.13B)

Sample	KH.8A	KH.8B	KH.13A	KH.13B
SiO ₂	6.71	14.41	12.95	21.52
Al ₂ O ₃	1.68	2.74	132	4.33
Fe ₂ O ₃	0.75	1.50	0.70	2.42
MgO	0.74	1.08	0.48	1.27
CaO	35.62	33.22	34.90	33.35
Na ₂ O	-----	0.05	-----	0.32
K ₂ O	0.19	0.34	0.17	0.64
MnO	0.06	006	0.03	0.06
SrO	15.17	1066	11.43	2.36
SO ₃	10.22	7.38	8.67	1.82
L.I.	29.12	28.32	28.95	31.65
Total	100.26%	99.76%	99.60%	99.74%

Table 2. Chemical analysis of clay plasters from Kalavassos-Tenta

Sample	KT.6	KT.9	KT.10	KT.21	KT.24
SiO ₂	22.45	16.44	15.79	18.23	19.54
Al ₂ O ₃	5.40	3.70	3.70	3.69	3.95
Fe ₂ O ₃	3.06	2.49	1.85	2.35	2.20
MgO	2.87	2.47	2.30	3.16	3.22
CaO	26.37	37.20	37.92	36.86	34.98
Na ₂ O	0.95	0.59	0.26	0.46	0.46
K ₂ O	0.86	0.36	0.36	0.56	0.66
MnO	0.08	0.05	0.04	0.06	0.05
SO ₃	12.56	4.34	6.09	0.56	0.73
C.W.	8.46	5.74	3.74	-	-
L.I.	16.5	26.67	27.89	34.43	33.97
Total	99.56%	100.05%	99.94%	100.36%	99.76%

From the above, it is obvious that the manufacture of clay based plaster was achieved using local soils (or a combination of two in order to achieve the proper amount of clay) readily available in the immediate environment of the settlements. Sometimes the use of havara (i.e. surficial calcareous deposit) and crushed kafkala (i.e. hard limestone crust) was recognised. The detailed investigation of samples under the stereoscope, has shown that

various plant residues were added into the mixture for the preparation of clay mortar, including straw and broken stalks (Khirokitia, Kalavastos-*Tenta*), traces of grass and other plant residues, or reeds and seaweed in coastal settlements (Maa-*Palaiokastros*). The most common addition was straw, a material that can be also found in similar plasters of more recent periods.

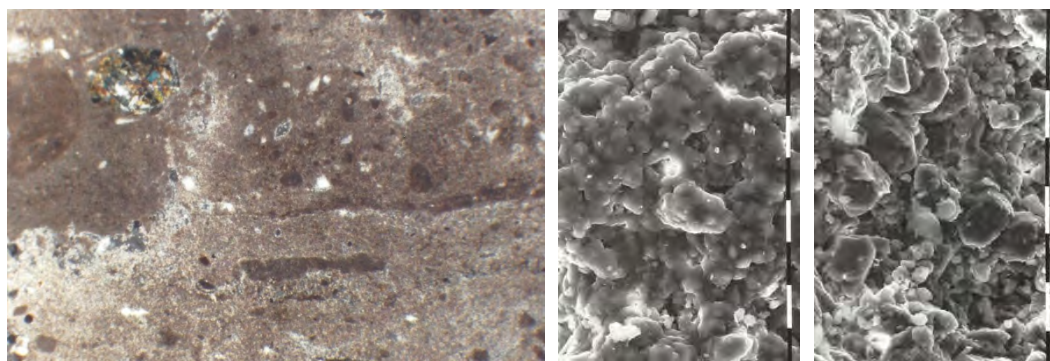


Figure 5. Clay plaster from a wall in Khirokitia. Thin section and photos from SEM

Gypsum mortars

General Remarks

Gypsum mortars have been used in Cyprus since the prehistoric period and are employed mainly as plaster. For the preparation of gypsum plasters, natural gypsum rocks were first selected from the natural deposits around the settlements and then heated in trenches or kilns that were constructed for this purpose [1]. During calcination, the natural rock undergoes a chemical change, and when crushed into a powder and mixed with water, creates a paste that can be easily worked. For the preparation of gypsum plaster the required temperature is below 200°C (100°C -190°C), much lower than the required temperature for the calcination of calcitic rocks used for the preparation of lime [12, 13]. Thus, gypsum was more easily manufactured with the use of less amount of wood. This made gypsum an environmentally friendly material. Gypsum plasters have some limitations in use as they are very sensitive to moisture and water and get solid very quickly during their application. If the mixture is heated at a higher temperature, the microstructure of the final product is different and at the same time acquires better qualities and strength [12].

In situ observations and bibliographic information

Gypsum has a more limited use compared to clay and lime mortars, despite the very notable deposits of this type of rock on the island [12]. It was found to be used mainly in the Neolithic settlement of Kalavastos-*Tenta*. During this period, gypsum was used as a plaster coating for walls and floors, either separately or in combination with other materials (soil, lime). In the Neolithic settlement of Kalavastos-*Tenta*, the walls were usually coated with a thin whitish plaster layer laid on a base of friable clay plaster [1]. The insertion of an exterior

layer with a better appearance laid above a coarser one is a technique that was also followed in other periods of antiquity and even in recent years [1].

Later on, gypsum was found to have a limited use in a number of settlements of the Late Bronze Age such as Kalavassos-*Ayios Dhimitrios* and Maroni-*Vournes*. In these cases, it was found to have been used in special applications in certain parts of the buildings, showing a good knowledge of its properties [12]. It was mainly found at places adjacent to timber elements such as door frames, serving as an intermediate material between the wood and the stone wall (i.e. as a material for fastening wooden elements). It was also used for fastening timber posts or pithos containers onto the floors of storage areas [12].

Laboratory analyses

The laboratory procedure followed for the examination of gypsum samples was the same with the procedure mentioned above followed for the examination of clay mortars. The chemical and mineralogical analyses of a number of samples collected from the Neolithic settlement of Kalavassos-*Tenta*, have shown that some of the plasters used in this settlement were of gypsum composition, sometimes in combination with calcitic material. The petrographic analysis has shown that in some of the Kalavassos-*Tenta* gypsum samples the binder material was gypsum, as gypsum crystals surround the grains of other materials (Figure 6) that act as aggregates (calcite, clay etc. Examination under an SEM revealed that the microstructure of Neolithic gypsum plasters is different from the microcrystallines of the natural gypsum rocks [13]. At the same time the Neolithic crystals differ from the needle-like structure of the common gypsum plasters. This can be attributed to the heating procedure, as well as to the age of the samples (Figure 6).

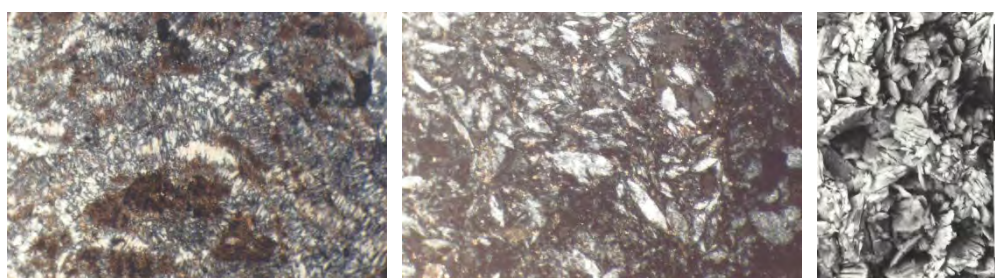


Figure 6. Gypsum plasters from Kalavassos-*Tenta*. Thin Sections and photo from SEM

The examination of samples of gypsum plasters selected from Late Bronze Age sites revealed the existence of well-shaped rounded or elongated crystals (Figure 7) that are also different from contemporary gypsum plasters and show some similarities with other historic gypsum plasters [1, 13].). In some cases gypsum seems to have been also used as an aggregate (Figure 7). In his publication, Middenforf [14] describes similar historic gypsum mortars, and connects the appearance of large, rounded gypsum crystals to the long-term, accumulated crystallisation process induced by wet and dry cycles during weathering processes. In order to investigate the method of preparation of the gypsum mortars under investigation, a procedure described by Strahan [15] was followed. According to this method, the XRD

diagram can help towards the distinction between the final gypsum product of calcination and the natural rock. In order to duplicate the preferred orientation of the gypsum crystals the samples are mixed with acetone on a quartz plate. The three major gypsum XRD peaks were compared and more specifically the first one was compared to the two others. The first peak was lower than the two others in the prehistoric plasters examined, leading to the conclusion – according to the Strahan theory – that the sample had overcome calcination [1, 12, 13].

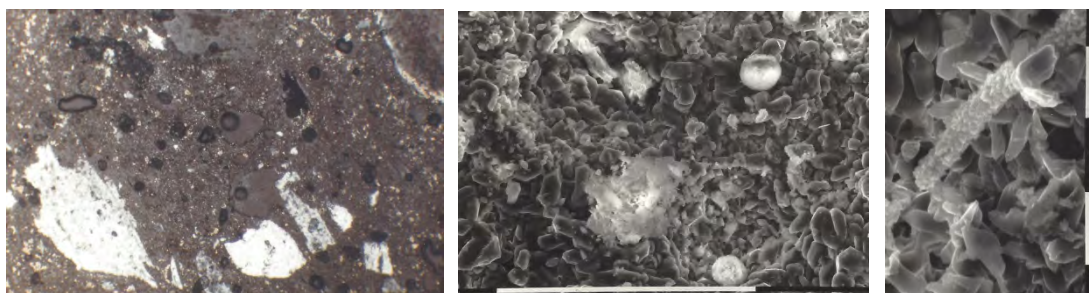


Figure 7. Gypsum plasters from Kalavassos-Ayios Dhmitrios. Thin section and photos from SEM

Discussion and Conclusions

From the above research, it is clear that during the prehistoric period, there was a selective use of the most suitable raw materials in each case for the preparation of mortars, which implies a clear understanding of the capabilities and properties of each material. There was always a selection of the most suitable clay soil for mortars and as a covering material for ceilings, as well as of gypsum rocks for the manufacture of gypsum plasters. At the same time, there was a great knowledge of the different properties of each mortar and plaster. Thus, the most appropriate mortar was selected to be used in each case. Clay was mainly used as mortar between stones and adobes due to the ease of preparation, as well as the compatibility to the raw material used for the manufacture of the adobes, whereas the use of gypsum was restricted in cases of fastening timber elements with stone etc [16].

The investigation showed that in prehistoric architecture, there was always an effort to satisfy the various functional needs and to solve the various constructional problems, using the most economic materials and the simplest techniques. Thus, preference was given to clay as a bonding mortar due to the easier and more economical means of preparation without the use of fuel. The geophysical resources, as well as the climatic conditions of the island, played an important role in the creation of the built environment. The abundance of clay soil in the areas around the settlements resulted in the extensive use of this material as a bonding mortar.

It is also remarkable that in the vernacular architecture of the 19th -20th century, the same traditional techniques for the manufacturing of mortars and plasters have been followed, underlining the fact that prehistoric people managed to solve basic structural problems very early on, following simple and economical solutions. In the vernacular architecture, the most

common mortar between stone and adobe walls was clay mixed with straw. There was also a limited use of gypsum and lime. Clay based plaster prepared in the same way as the mortar, but with the addition of more water, was employed to plaster the faces of walls, especially those of adobes. The plaster was usually prepared a few days before being used to allow the fermentation of the straw and improve its adhesion properties [17-19]. Frequently even more water was added to clay and used as a clay-washed layer to smooth the external surface of the wall.

Later, in the last centuries clay based plasters were replaced by gypsum plasters. Numerous gypsum furnaces have been located in parts of the island where gypsum plasters were prepared. Nevertheless, gypsum could not adhere to the adobe walls easily and so timber pegs were driven into the walls prior to plastering. These pegs served to connect the adobes and the gypsum plaster, with very good results. Many interior and exterior walls had their facades white-washed with white-soil (calcareous soil called *asprochoma* or *asprogi*), which was later substituted with a solution of lime (called *asvestogala*). In the interiors, the walls were covered with a coat of gypsum about 1 cm thick which was subsequently white-washed every year with a very thin coat of the same material [17].

The research showed that throughout antiquity and even in the vernacular architecture of the last two centuries, the climatic conditions of the island, its geology and geomorphology have played a very important role in the selection and use of building materials and especially mortars and plasters. The island has many deposits of suitable clay, calcitic soils and gypsum, which were the main raw materials used for the preparation of mortars and plasters.

As this paper has indicated, the use of the same mortars and plasters on the island since the prehistoric period onwards can be attributed to the simplicity and efficiency of these materials and techniques, as well as to the environmental and climatic conditions of the island, which led to the use of readily available materials and the following of functional solutions that could satisfy the same needs and requirement for domestic dwellings diachronically.

References

1. Philokyprou M (1998) *Building Materials and Structures in Ancient Cypriot Architecture* (Unpublished PhD thesis, University of Cyprus).
2. Philokyprou M (1998) Building Materials and Methods employed in Prehistoric and Traditional Architecture in Cyprus. *Ethnography of European Traditional Cultures, Arts, Crafts of Heritage*. Athens, 150-164.
3. Le Brun A (1981) Un Site Néolithique Précéramique en Chypre. Cap Andreas-Kastros, Paris.

4. Dikaios P (1969) *Enkomi. Excavations 1948-58. The Architectural Remains 3*, Mainz am Rhein.
5. Karageorghis V, Demas M (1985), *Excavations at Kition V. The Pre-Phoenician Levels, I-II*, Department of Antiquities, Nicosia.
6. Peltenbrgh EJ (1985) *Lemba Archaeological Project, Cyprus. I. Excavations at Lemba-Lakkous 1976-83 (Sima LXX:1)*, Goteborg.
7. Karageorghis V, Demas M (1988) *Excavations at Maa-Palaeokastro 1979-86*. Nicosia.
8. Le Brun A (1984) *Fouilles Récent à Khirokitia (Chypre) 1977-1981*, Paris
9. Todd I (1987) *Vasilikos Valley Project 6. Excavations at Kalavastos-Tenta (Sima LXXI:6)*, Goterberg.
10. Le Brun A (1994) *Fouilles Récent a Khirokitia (Chypre) 1988-91*, Paris.
11. Thomas G (1995) *Prehistoric Cypriot Mud Buildings and their Impact on the Formation of Archaeological Sites* (PhD Thesis, University of Edinburgh).
12. Philokyrou M (2012) The Beginnings of Pyrotechnology in Cyprus. *International Journal of Architectural Heritage* (Taylor and Francis), Vol. 6, Issue 2, pp.172-199.
13. Kingery WD, Vandiver PB, Prickett M (1988) The Beginnings of Pyrotechnology, Part II: Production and use of lime and gypsum plaster in the Pre- Pottery Neolithic Near East. *Journal of Field Archaeology* 15, 219-244.
14. Middendorf B (2002) Physico-chemical and microstructural characteristics of historic and restoration mortars bases on gypsum: Current knowledge and perspective. In *Natural stone, weathering phenomena, conservation strategies and case studies*, eds., Siegesmund S, Weiss T, Vollbrecht, 165–176, London, UK: Geological Society.
15. Shrahan DK (1991) Naturally deposited versus intentionally applied gypsum on archaeological materials from Harappa, Pakistan. *Journal of the Field Archeology* 18. 527–530.
16. Wright GRH (1992) *Ancient Building in Cyprus*, E.J. Brill, Leiden.
17. Papacharalambous G (2001) *The Cyprus Vernacular Dwelling*, Nicosia
18. Sinos S (1976) *An Overview of the Vernacular Architecture of Cyprus*, Athens.
19. Ionas I (1988) *La Maison Rurale de Chypre. Aspects et Techniques de Construction*, Nicosie.

Physical- mechanical comparison of the traditional gypsums from Albarracín and Pallars

David Osmar Batres Hernández¹, Antonia Navarro Ezquerra¹, Joan Ramon Rosell Amigó¹

(1) *Escuela Politécnica Superior de Edificación de Barcelona, ing_davbat@hotmail.com, antonia.navarro@upc.edu, joan.ramon.rosell@upc.edu*

Introduction

In 2016, the CEG Association (Center d'estudis del Guix) visited the region of Pallars with the intention of making a traditional kiln with the autochthonous stone found in the area and then to obtain a traditional plaster product from it. Once the traditional kiln was built and the processes of calcination and crushing of the stone were finished, approximately half a ton of traditional plaster was obtained, which was stored in bags of 25 kilograms each.

In the year 2017, it was decided to carry out the physical-mechanical characterization from the traditional gypsum product obtained in the region of Pallars. Furthermore, looking for a point of comparison, it was decided to carry out also the physical-mechanical characterization of the traditional gypsum of Albarracín. The last one, probably is the only traditional gypsum which is commercialized in Spain.

As a result of this, the question arises as to whether the traditional plaster of Pallars has sufficient physical and mechanical properties to be able to compete with the traditional commercial plaster of Albarracín.

Previous Knowledge

Gypsum is a natural mineral that is chemically composed from calcium sulphate and water ($\text{CaSO}_4 \cdot 2\text{H}_2\text{O}$). This stone is light in weight but tough in hardness, does not make effervescence with acids and generally presents colors such as: white, ashen, yellow, brown, gray and if it contains ferric oxide, it is presented in reddish white. Likewise, it is known by the name of plaster to the product that results from cooking and crushing the mineral gypsum, while the homogeneous mixture of this product with water is called plaster paste. This paste has the property of hardening through the setting process, thus becoming calcium sulphate dihydrate once again [1].

Traditional gypsum is defined as the product of calcination of calcium sulphate dihydrate ($\text{CaSO}_4 \cdot 2\text{H}_2\text{O}$) in traditional kilns, a process which has the following characteristics [2, 3]:

- During cooking, there is no temperature control inside the oven.
- Cooking is not homogeneous, but multiphase. Depending on the size of the stone and the exposure to heat, all the phases of calcium sulphate can be found in the product.

- There is no selection or purification process in the raw material.

Generally, traditional gypsum kilns have square floor plan and assembled with three walls attached by an embankment. Among them, the gypsum stone is placed in the form of a vault in a descending manner (meaning that the larger stones should be placed at the bottom and the little ones are above), with the objective that the dehydration or firing of the stone is as equitable as possible [4]. Under the vault formed by the gypsum stone itself is located the area where the fuel that feeds the kiln is located. This combustible is constituted by wood, branches or charcoal.

Materials and Test Methods

Materials

In order to evaluate the human and material resources, like time, labor and cost that were necessary for the elaboration of traditional gypsum, the CEG Association carried out the elaboration of a traditional oven in Pallars Sobirá located in Lerida in the year 2016 (Figure 1)

The raw material was extracted with the help of a backhoe excavator and the brigade of the town hall of Senterada. All the rocks from the extraction were placed in the kiln and formed part of the firing, as all the extracted material should form a homogenous mixture.

The kiln was assembled in the same place where the extraction was made, taking advantage of the hole left by the cut with the backhoe. For the creation of this traditional kiln, two side walls were built and one in the center, above them, the gypsum stone was placed in the form of a vault, leaving two holes in the lower part for the placement of the fuel. A plant called "boj" was used as fuel, in addition to wood, material, which was extracted from the same mountain where the gypsum stone was.

When the firing of the material was completed, a plastic layer was placed on top of the extinguished furnace and allowed it to cool. Months later, the brigade returned to crush the product obtained from the firing and store it in bags of 25kg, obtaining 20 bags of traditional plaster in total.



Figure 1. Pictures of the elaboration of the traditional oven in Pallars by the CEG brigade

At present, in Albarracín there is the only one kind of kiln able to create a satisfactory traditional plaster. This kiln is created in form of a vault with gypsum stone from two nearby quarries. This gypsum stones contains silica and clay impurities [5].

The plaster made in Albarracín, is a handmade product that has two different presentations depending on its color: a red color or a grayish color. It is a product backed up for years by its precedence in the coatings and waterproofing of the facades in Albarracín. The extraction of the stone in Albarracín or its mountain it is made with machinery from the existing quarries of gypsum and the selection procedure is manual. Once the product is powdered, it is packed in paper bags. The color of the material is indicated on the bag and a stamp is added as guaranty that the product was created by a trusted artisan [6] (Figure 2).

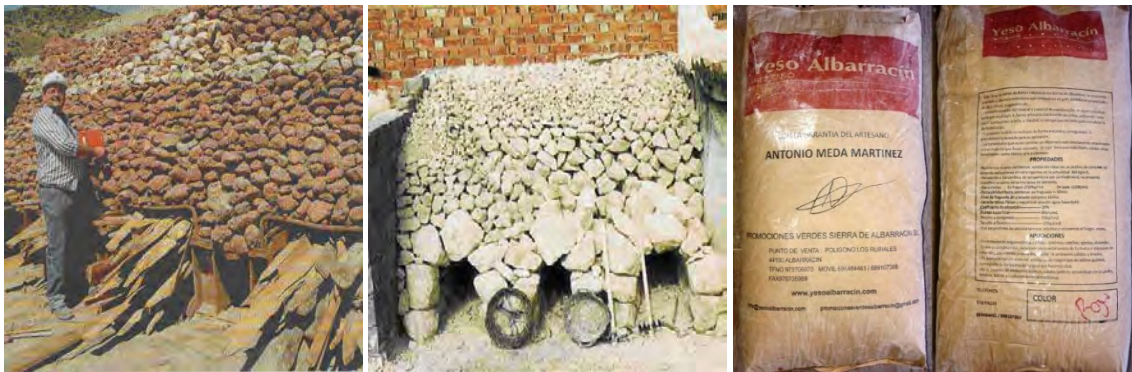


Figure 2. Pictures of ovens and plaster made in Albarracín

Dosages

Considering that the experimental plaster of the Pallars will be compared with the plaster of Albarracín, the technical file of the plaster of Albarracín was taken into account to find the correct dosages of the plaster of the Pallars.

This technical sheet marks the values of water/gypsum ratio (W/G) between 0.34- 0.40. It was also decided to choose relatively close W/G values from the technical sheet, from 0.30 to 0.45, to experiment with the two types of gypsum and to make some mixtures and so to be able to observe the behavior of the material with these amounts of water (Table 1).

Once the tests had been carried out, it was concluded that the W/G ratios suitable for working with both materials are as follows: $W/G = 0.34$, $W/G = 0.37$ and $W/G = 0.40$.

Table 1. Water/gypsum test with Pallars's and Albarracín gypsum.

W/G Ratio	Gypsum (g)	Water (mL)	Pallars Gypsum	Albarracín Gypsum
0.30	50.00	15.00		
0.34	50.00	17.00		
0.37	50.00	18.50		
0.40	50.00	20.00		
0.45	50.00	22.50		

Sample Preparations

There were made rectangular prism- shaped specimens, both with traditional gypsums (Pallars and Albarracín) for the tests. All of them were design following the Spanish standard UNE-EN 13279-2 [7] using metal molds with measurements of 4x4x16cm and following the dosages of water and plaster previously provided. Additionally, it was taken into account, two different mixing times: one and three minutes.

A total of 18 test pieces were made, three pieces for each W/G ratio, as well as for each mixing time. (Figure 3).



Figure 3. Preparation of test pieces for the mechanical tests according to the Standard Norm UNE-EN 13279-2.

Hardened Mortar

All the test specimens were allowed to set for seven days, before tensile load and compression load tests were carried out, furthermore the specifications of the UNE-EN 13279-2 standard were followed all the time [7]. The mechanical press used in mechanical tests is Wykeham Farrance brand with a maximum load of 5000 kg. The porosity test procedure followed the Spanish standard norm UNE-EN 1015-10: 2000 [8], while the coefficient of capillary absorption and desorption of the hardened gypsum followed the standard UNE-EN 1925: 1999 [9] which refers to the natural stone.

All the test pieces showed many similarities between Albarracín and Pallars plasters. However, different variations could be observed due to the different water / gypsum ratios and the established mixing times.

Table 2. Pallars's gypsum results at a mixing time of one minute.

	W/G	D. & Porosity			Mechanical Resistances		Water Mobility		
	Water/ Gypsum Ratio	Apparent Density	Relative Density	Porosity	T Flexión	T comp	c.A.C	Se	Coef. evaporación
		g/cm ³	g/cm ³	%	MPa	MPa	ΔKg/m ² /Vh	%	%
Pallars 1 min	0.34	1.54	2.52	39.00	1.39	3.70	20.06	8.79	2.08
	0.37	1.48	2.53	41.50	1.08	2.44	27.11	8.23	1.59
	0.40	1.42	2.51	43.27	0.81	1.91	25.17	5.66	1.62

Table 3. Albarracín gypsum results at a mixing time of one minute.

	W/G	D. & Porosity			Mechanical Resistances		Water Mobility		
	Water/ Gypsum Ratio	Apparent Density	Relative Density	Porosity	T Flexión	T comp	c.A.C	Se	Coef. evaporación
		g/cm ³	g/cm ³	%	MPa	MPa	ΔKg/m ² /Vh	%	%
Albarracín 1 min	0.34	1.46	2.38	38.77	0.91	1.89	19.31	5.68	1.52
	0.37	1.41	2.33	39.37	1.03	1.98	20.58	7.25	1.38
	0.40	1.37	2.33	41.20	1.01	1.95	21.55	12.39	1.55

Table 4. Pallars's gypsum results at a mixing time of three minutes.

Pallars 3 min	W/G	D. & Porosity			Mechanical Resistances		Water Mobility		
	Water/ Gypsum Ratio	Apparent Density	Relative Density	Porosity	T Flexión	T comp	c.A.C	Se	Coef. evaporación
		g/cm ³	g/cm ³	%	MPa	MPa	$\Delta\text{Kg/m}^2/\text{vh}$	%	%
	0.34	1.39	2.54	45.13	1.88	6.51	19.87	14.53	1.54
	0.37	1.44	2.56	43.67	2.56	6.64	19.30	15.17	1.40
	0.40	1.44	2.55	43.37	2.29	7.08	18.59	14.21	1.56

Table 5. Albarracín gypsum results at a mixing time of three minutes.

Albarracín 3 min	W/G	D. & Porosity			Mechanical Resistances		Water Mobility		
	Water/ Gypsum Ratio	Apparent Density	Relative Density	Porosity	T Flexión	T comp	c.A.C	Se	Coef. evaporación
		g/cm ³	g/cm ³	%	MPa	MPa	$\Delta\text{Kg/m}^2/\text{vh}$	%	%
	0.34	1.46	2.47	40.63	1.43	3.04	20.79	10.65	2.16
	0.37	1.46	2.46	40.53	1.21	2.53	21.58	9.22	1.81
	0.40	1.40	2.49	43.93	1.06	2.04	28.09	6.64	1.80

Results and Discussion

Densities and Porosities

The summary of the necessary parameters (apparent density and relative density) to calculate the percentage of porosity for Albarracín gypsum, as for Pallars at its different water/ gypsum ratios are noted in Tables 2-5.

It is observed, in all cases, that the relative density is much higher than the apparent density, being logical since the relative density refers to the compact mass without pores.

Nevertheless, it is evident the relation that exist between the quantity of water in the piece and the time of kneading to form the porous network of the piece. In such way that, in a short mixing time (1 min), the greater the amount of water added to the piece, the greater the porosity created in it is. This happens, since the mixing time to which it is exposed is sufficient for the gypsum paste to absorb the particles of water needed to work, but

insufficient to be able to evaporate the excess of water. On the other hand, in a longer mixing time (3 minutes), the greater the amount of water in the piece, the smaller the network of pores that is formed, as there is enough time to be able to evaporate the excess water found in the piece.

This means that, having two mixtures with the same amount of water but mixed at different times (one and three minutes), as result, it will end up with a different porosity.

Mechanical Properties

The factors that can affect the mechanical resistance of the gypsum can be many and it is difficult to establish a relation between the properties of this, because they do not influence equally in all cases.

The values of the tension and compression strength of our samples are established in Tables 2-5. In these tables, it can be observed that in average, the highest results for the tensile load are found in the Pallars gypsum at a mixing time of three minutes; while the lowest results are found in Albarracín gypsum at a mixing time of one minute. Furthermore, comparing all the results from both gypsums, the highest result is found in the ratio water/ gypsum= 0.37 at a mixing time of three minutes of the Pallars gypsum, while the lowest result is found in the ratio water/ gypsum= 0.40 of the Pallars gypsum as well, but at a mixing time of one minute, with a difference of 68.35%.

On the other hand, the values obtained from the compression load are found linked to those of the tensile load. In average, the samples with the highest resistance to compression load correspond to those made with the Pallars gypsum at a mixing time of three minutes, with the load values from 6.51 MPa to 7.08 MPa. Meanwhile, the samples with the lowest compression resistance correspond to those made up with the Albarracín gypsum at a mixing time of one minute, with load values from 1.89 MPa to 1.95 MPa.

Comparing the highest results (Pallars gypsum), against the lowest ones (Albarracín gypsum), we found a difference of up to 73.30%.

Water Transport

The purpose of the water characterization of our gypsum is to evaluate the ability to capture or lose water, in liquid or vapor form. This is of great interest in order to be able to assess the behavior of the material in front of the alteration.

The values obtained from the coefficients of capillary water transport and water desorption for both gypsums are summarized in Tables 2-5. In the absorption by capillarity, the results that we found are very similar to each other, the difference is that for Pallars gypsum the highest values were recorded in the mixing time of one minute, while, for Albarracín gypsum, the highest values are found in the mixing time of three minutes.

On the other hand, it is clearly demonstrated that porosity influences the water absorption. In the graphs (Figures 4-5) we observed that the porosity increases according to the amount of water added and in turn the capillary coefficient increases according to the percentage of porosity.

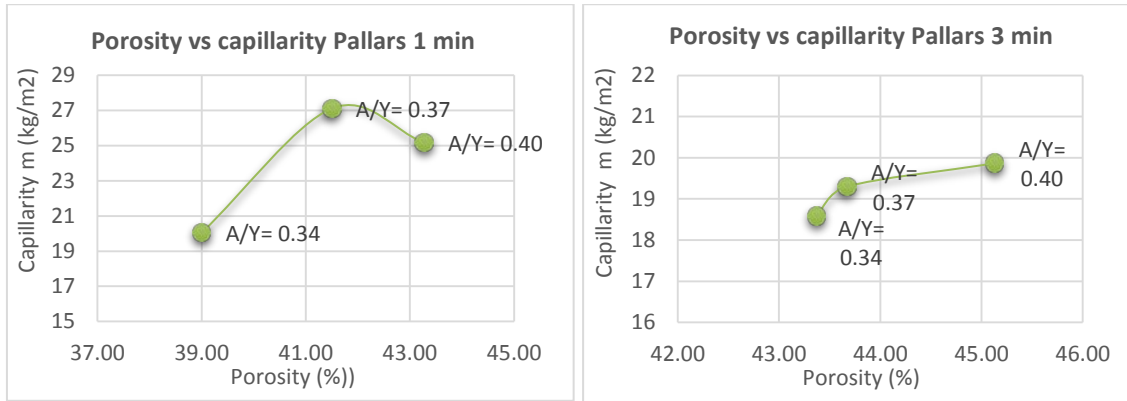


Figure 4. Pallars's gypsum graphics "Porosity vs capillary water transport" in a mixing time 1 and 3 minutes.

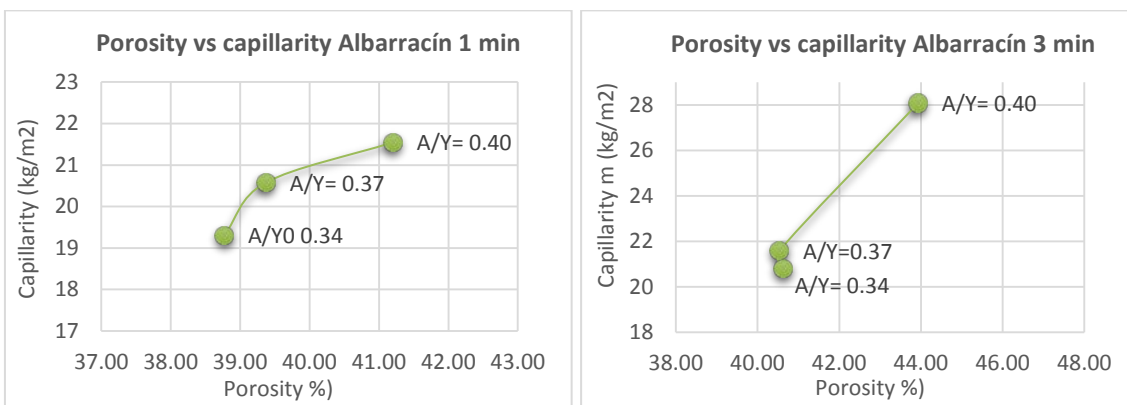


Figure 5. Albarracín gypsum graphics "Porosity vs capillary water transport" in a mixing time 1 and 3 minutes.

Likewise, in the desorption of water, the variations that happen in the loss of liquid of a material depend on the porous network from the same one. The values obtained from the test (Tables 2-5) refer to the percentages of the total water that remained in the piece at the end of a certain time.

In the graphs (Figures 6-7), we observe that the porosity that exists in the Pallars pieces at a mixing times of one and three minutes, as well as the Albarracín samples at a mixing time of 3 minutes, grow as the W/ G ratio used increases, and at the same time, the percentage of water found in the piece at the end of the desorption test decreases. This is easy to deduce with our porosity values, as they indicate the percentage of existing pores that go from the outside to the inside of the piece, and these in turn, allow a better ventilation in the sample and simpler evaporation of water.

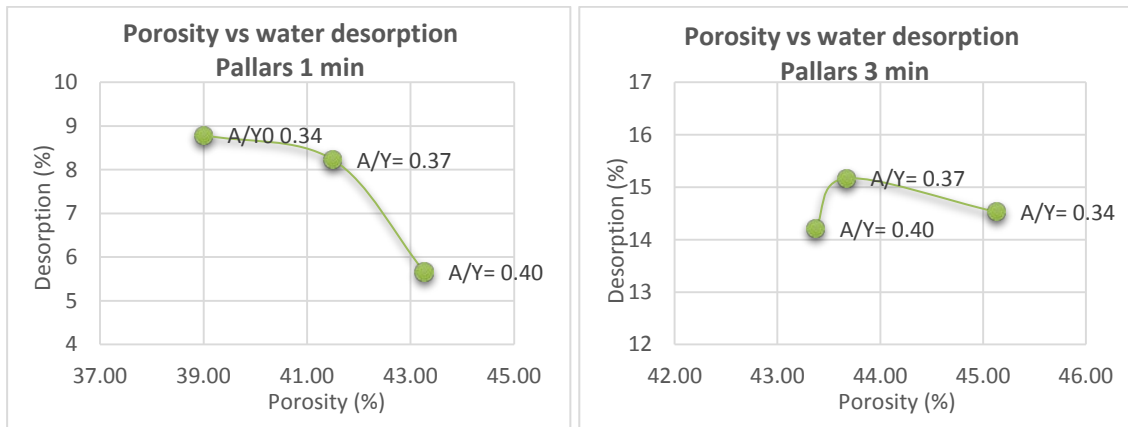


Figure 6. Pallars's gypsum graphics "Porosity vs water desorption" in a mixing time 1 and 3 minutes.

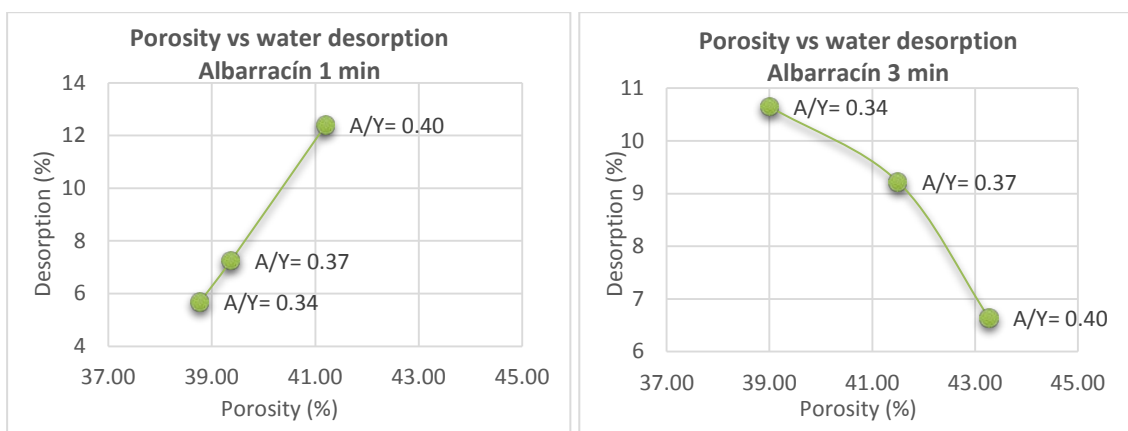


Figure 7. Albarracín gypsum graphics "Porosity vs water desorption" in a mixing time 1 and 3 minutes.

In the graph (Figure 7) referring to Albarracín plaster at a mixing time of one minute, it is observed that the porosity vs desorption curve behaves completely different from the others, being the opposite of them. On the one hand, like all other samples (test pieces of Pallars at a mixing times of 1 and 3 minutes and test pieces of Albarracín at a mixing time of 3 minutes), the greater the amount of water used in the W/G ratio, the greater the percentage of porosity found; but, the greater the percentage of existing pores, the greater the percentage of water retained in the sample, concluding that the evaporation rate was slower.

Conclusions

The aim of the study was to compare some of the physic-mechanical characteristics of the Albarracín gypsum and Pallars gypsum. Thus, based on the results obtained in the tests that were carried out, the following conclusions are presented.

There are many similarities in the results obtained in the two types of plaster, presenting some notable differences in the kneading times.

Despite the similarities in the results obtained, in the mechanical tests of tensile load and compression load, the Pallars gypsum proved to be more resistant than Albarracín gypsum. In addition, the highest values could be found at higher mixing time.

The porosity test confirmed the hypotheses about the relation between the number and size of pores with the water/gypsum ratio, in conjunction with the mixing time. On one side, the percentage of porosity will be higher, the greater the excess of liquid is in the plaster during the drying and setting process, since this excess at the moment of evaporation will form air bubbles. On the other hand, the network of pores will also be higher if there is an insufficiency of liquid, since the plaster will absorb all the water leaving empty spaces.

Therefore, big percentages of porosity can be found in low water/gypsum ratios at high kneading time, as well as high water/gypsum ratios at short kneading times.

Finally, from the results and graphs of the water transport tests, it is concluded that the two types of gypsum absorb water through their capillaries at a high speed. In addition, as expected, the absorption and desorption properties are related to the percentage of porosity that exists in the samples.

Given that no excessive differences were found between the qualities of the Pallars gypsum and Albarracín gypsum, it is deduced that the mineral found in Pallars could be suitable for use in construction; however, this would require a broader study that includes the composition of the material.

References

1. L Villanueva Dominguez and A García Santos (2001) *Manual del yeso*. Madrid.
2. R F Rubio Domene (2006) "El material de yeso: Comportamiento y conservación."
3. L Novo (8ª edición) "*El yeso en la construcción*"
4. D Sanz Arauz (2007) "Hornos tradicionales de yeso para construcción," *RECOPAR*, no. 5.
5. D Sanz (2009) "Análisis del yeso empleado en revestimientos exteriores mediante técnicas geológicas"
6. Promociones Verdes Sierra de Albarracín SL "Yeso Albarracín. Mil años de historia, mil años de futuro." <http://www.yesoalbarracin.com/index.html>.
7. AENOR (2006) "Norma española UNE- EN 13279-2: Yesos de construcción y conglomerantes a base de yeso para la construcción. Parte 2: Metodos de ensayo."
8. AENOR (2000) "Norma española UNE-EN 1015-10:2000. Metodos de ensayo de los morteros para albañilería. Parte 10: Determinación de la densidad aparente en seco del mortero endurecido."

9. AENOR (1999) “Norma española UNE-EN 1925: Métodos de ensayo para piedra natural. Determinación del coeficiente de absorción de agua por capilaridad.”

Detailed studies of gypsum plasters from the Ishrat Khana Mausoleum in Samarkand, Uzbekistan

Steffen Laue

University of Applied Sciences Potsdam, Germany, st.laue@fh-potsdam.de

Abstract

The Ishrat Khana mausoleum was constructed in 1464 and is today a ruined protected monument. Badly damaged by two earthquakes and then left to decompose over more than one hundred years, the Ishrat Khana mausoleum was investigated to create an appropriate conservation concept for the materials and decorating surfaces.

In this study, the historic plasters and stucco applications are analysed in detail by using polarizing microscopy and SEM/EDX of thin sections.

All original materials contain gypsum as a binder, some plaster contain lime in addition. Aggregates are quartz, feldspar, mica, carbonates, and soil fragments, which frequently contain calcite (marl). Different binder/aggregate ratios enable a varied application of this building material in Ishrat Khana. This type of historic gypsum mortar is called *Ganch* in Central Asia.

Introduction

The Ishrat Khana mausoleum (Figure 1 and 2) is a prominent ruined protected monument in Samarkand, Uzbekistan, and was erected in 1464 to bury the royal wives of the Timurid ruling dynasty – more details of the history are given by [1]. The mausoleum consists of brick masonry with decorative surfaces like wall paintings and glazed bricks. Badly damaged by two earthquakes in 1860 and 1903 and then left to decompose over more than one hundred years, the Ishrat Khana mausoleum offers a fascinating opportunity to undertake a direct study of the building materials and structural details revealed. Some remains of the original rich interior decoration are also retained, like wall paintings in kundal technique and polychrome stucco [2].

During a research project between 2009 and 2014 the building materials and wall paintings were investigated extensively to prepare an appropriate conservation concept for the structure, materials and decorating surfaces [3], [4].

In Ishrat Khana all kind of plasters, joint mortars and stuccos are made of a white-beige coloured mortar material containing gypsum as a binder. Generally, this type of historic mortar is called *ganch* in Central Asia [4], [5]. First investigations of the *ganch* materials in Ishrat Khana are described in [3]. In this paper additional detailed studies on selected *ganch*

samples from Ishrat Khana are presented to document and understand the composition and structures of the ganch material.



Figure 1. Mausoleum Ishrat Khana in 2013, front view.

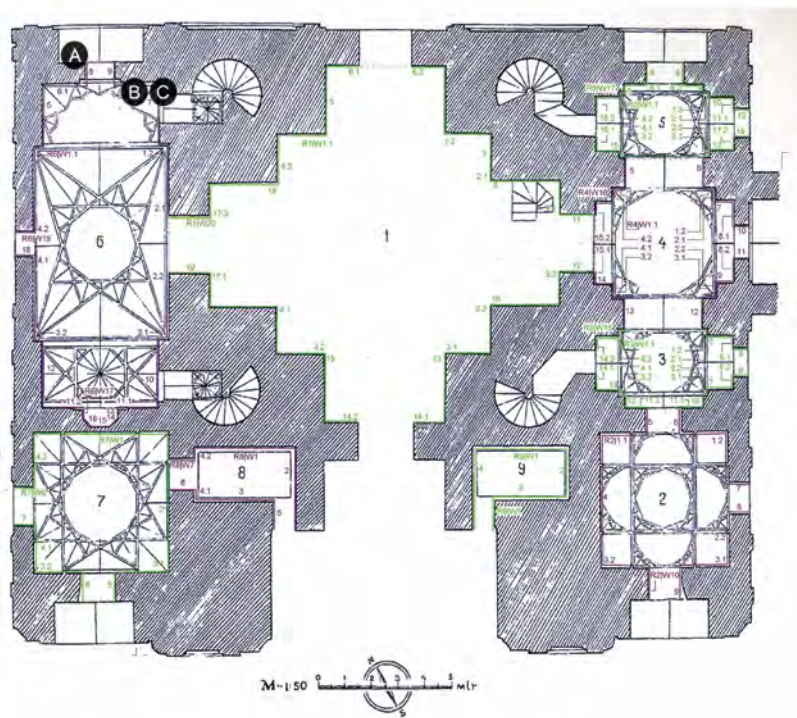


Figure 2: Ground plan of the mausoleum Ishrat Khana and sample locations, later modified [1]

Samples

In Ishrat Khana *ganch* was used as plasters, levelling coats, joint mortars, relief plasters and stuccos [3], for definitions see [6]. In this paper, the investigation of three representative samples of a levelling coat (A), a plaster (B) and a relief plaster (C) are presented in detail.

Plaster A is used as a multi-layered coat between two brick layers to compensate for irregularities in the masonry and is located in the northern entrance area to room 6 in 2 m height (Figure 2 and 3).



Figure 3: Plaster A, sample location, entrance area to room 6

Plaster B is a plaster at the northern wall inside of room 6 in 1.30 m height. Plaster C was used as a relief plaster to mould a haunch to the cornice in 2.50 m height. On top of plaster C partly a whitewash is present, on which probably wall paintings were existent before decomposition (Figure 4).

Analytical methods

The combination of the investigation of thin sections by polarizing microscopy and SEM/EDX gives evidence to the composition and structure of the plasters.

Thin sections which had been impregnated with blue coloured resins were prepared to study the structure, binder and aggregates of the plasters by polarizing microscopy (PLM, BX51 Olympus) in transmitted light, with the capability of microphotography.

After the preparation of polished thin sections, the elemental composition of the binder and aggregates were investigated with a scanning electron microscopy (SEM) using a Jeol (JSM-6510) equipped with a link energy-dispersive X-ray (EDX) microanalytical system (Oxford Instruments with Inca 1.0 software).

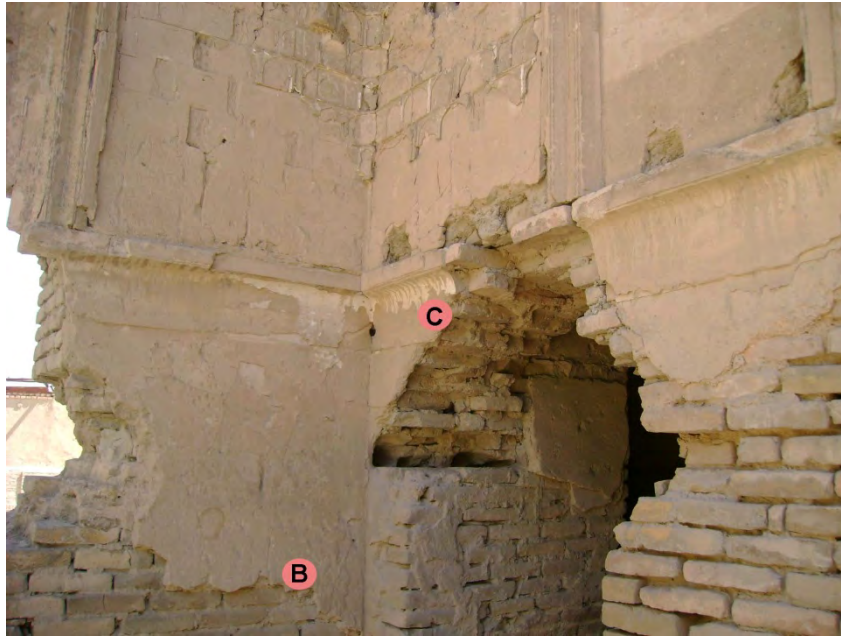


Figure 4: sample locations of the plasters B and C in the western corner of room 6

Results

Plaster A – levelling coat

In Figure 5, 6 and 7 the structure and mineral composition of plaster A are demonstrated by PLM and SEM/EDX of thin sections. The plaster show a heterogeneous structure with gypsum as the binder and aggregates of different sizes composed mainly of quartz, sodium and potassium feldspars, carbonates (calcite and less dolomite), soil fragments and less mica, titanite [CaTiSiO₅] and celestine [SrSO₄]. The optical properties like birefringence of the brownish micas indicate that the micas are biotites. Soil fragments consist of clay minerals, quartz, feldspar, micas and carbonates and can be named as marl, which is defined as a mixture of silicates and carbonates.

Figure 7 shows a detail of a marl aggregate and the distribution of elemental composition measured by elemental mapping using SEM/EDX. The compositions can be interpreted that silicate minerals consist of quartz, feldspars, clay minerals and micas whereas the carbonate is calcite. But the investigation of other soil fragments in plaster A by SEM/EDX demonstrates that there are also existing soil fragments without calcite which has to be called adobe fragments.

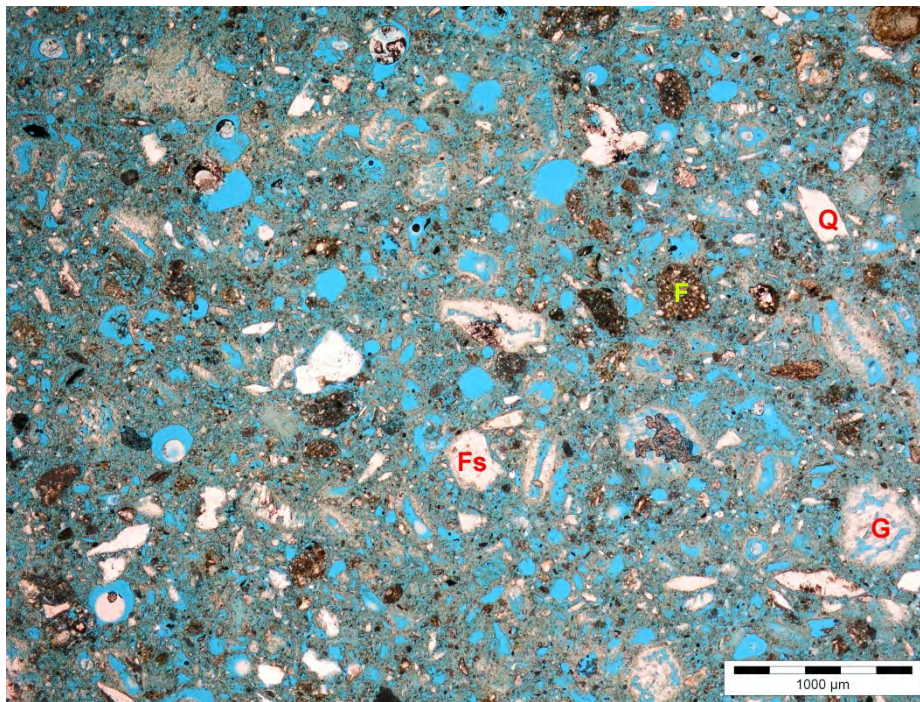


Figure 5: Thin section of plaster A under plane-polarized light, the binder is gypsum, partly recrystallized (G), aggregates are quartz (Q), feldspars (Fs) and soil fragments (F)

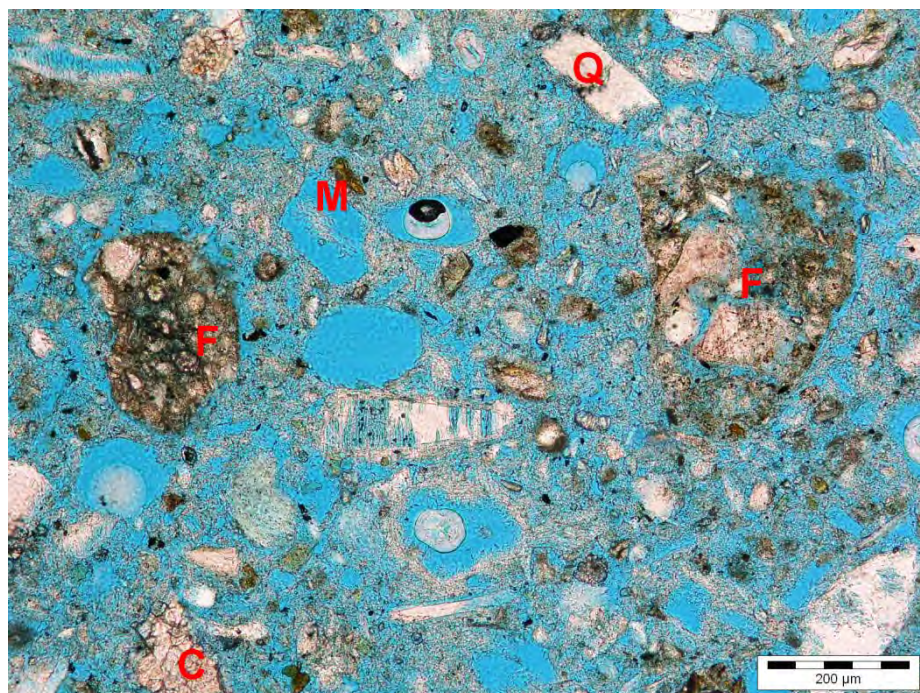


Figure 6: Thin section of plaster A under plane-polarized light, the binder is gypsum, aggregates are quartz (Q), soil fragments (F), coarse grained calcite (C) and brown micas (M)

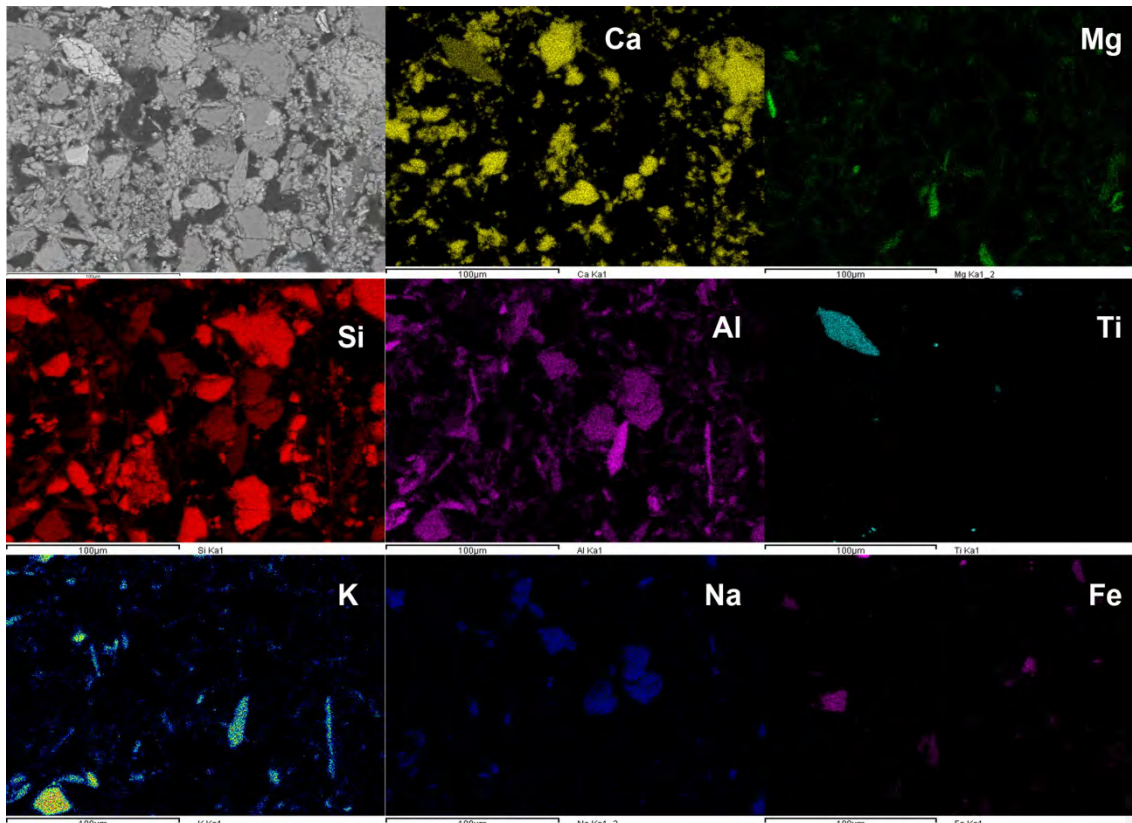


Figure 7: Detail of a marl fragment as aggregate in plaster A, thin section analysed by SEM/EDX, SEM backscatter image top left, elemental composition by EDX mapping

Plaster B – plaster of an inside wall

In Figure 8 and 9 the structure and mineral composition of plaster B is presented by PLM of thin sections. The overall binder is gypsum, but some parts of the plaster show a slightly brownish colour. These areas are characterized by a higher content of carbonates showing high birefringence by using PLM under crossed polarized light. SEM/EDX analyses proved that calcite is present in the brownish areas together with gypsum. The mineral composition together with the texture indicates that lime was added to the binder gypsum in the brownish areas of plaster B, but the addition is heterogeneously distributed (see Figure 8)

Concerning the aggregates in plaster B, nearly the same minerals as in plaster A can be detected: quartz, feldspars, carbonates (calcite and dolomite), soil fragments and less mica, titanite and celestine.

But in contrast to plaster A, in plaster B up to 0.5 cm in size large dark brown fragments consisting of fine grained dolomite (SEM/EDX) can be detected that contribute as well as calcite to the slightly brownish colour of plaster B.

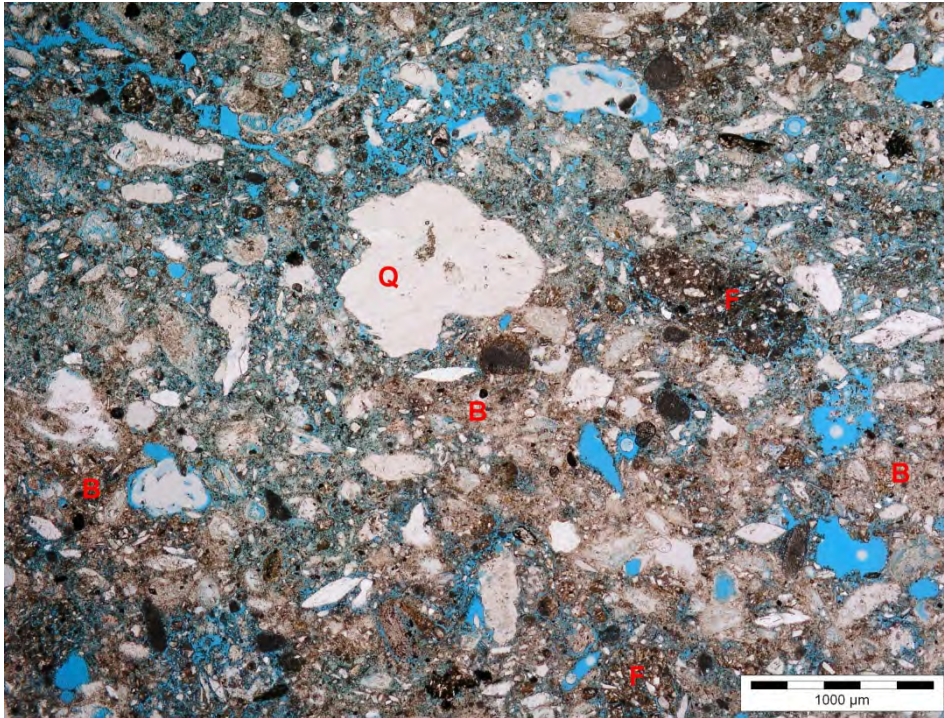


Figure 8: Thin section of plaster B under plane-polarized light, the overall binder is gypsum, brownish areas (B) contain calcite, further aggregates are quartz (Q) and soil fragments (F) besides feldspar and mica

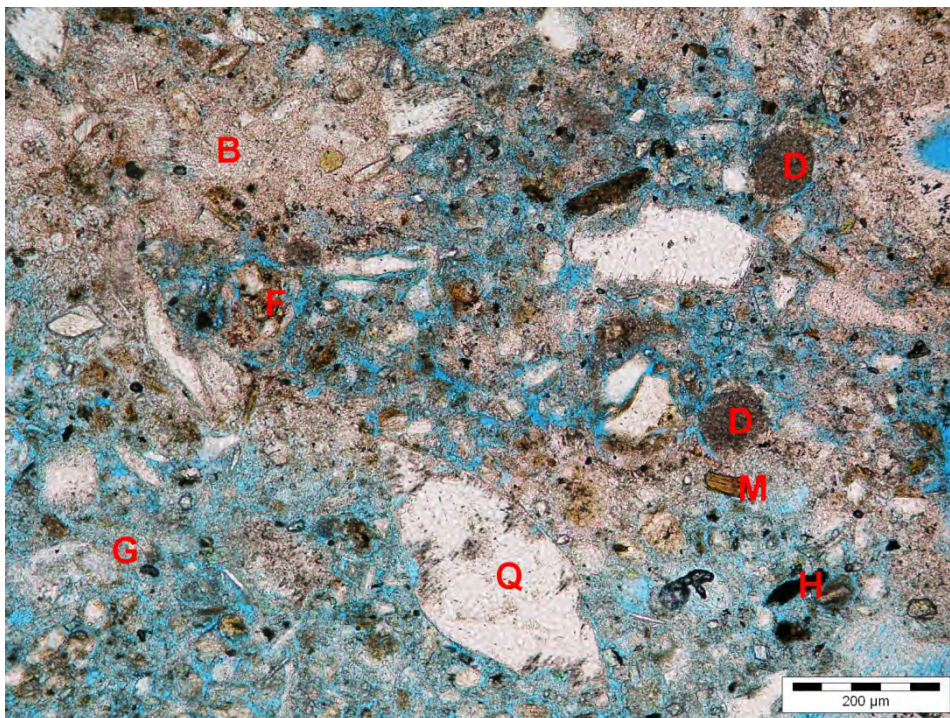


Figure 9: Thin section of plaster B in more detail under plane-polarized light, brownish areas (B) contain additional lime in contrast to light areas where only gypsum (G) is present as a binder, aggregates are quartz (Q), micas (M), dolomite (D), soil fragment (F), H = remains of charcoal

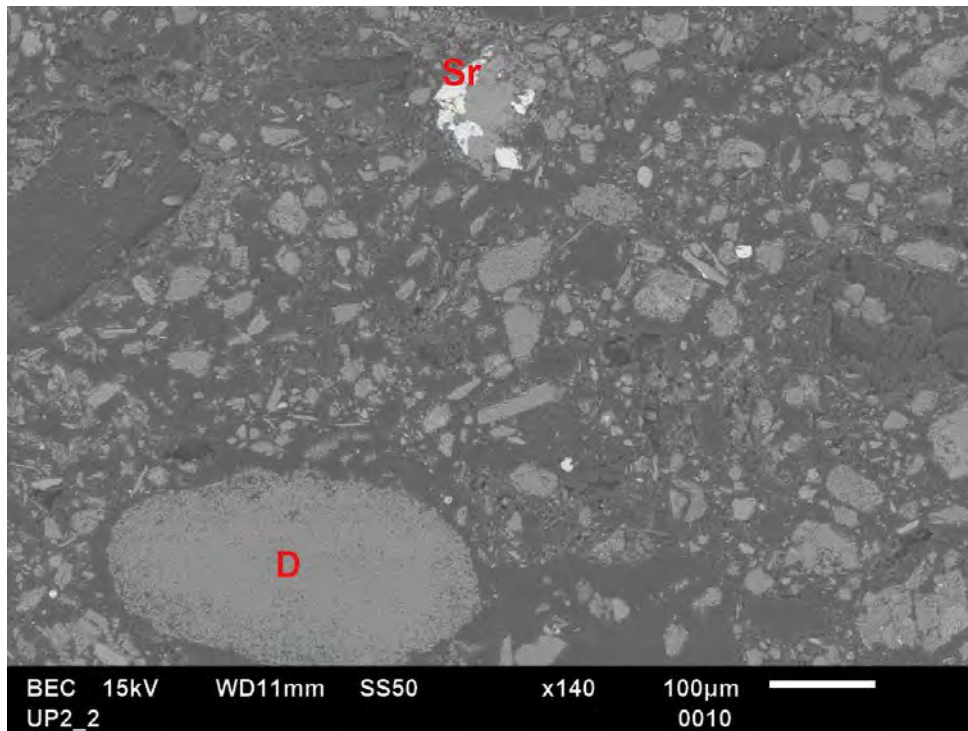


Figure 10: SEM backscattered image of plaster B, a rounded carbonate aggregate consist of dolomite (D), above a limestone aggregate with light celestine (SrSO_4)

Plaster C – relief plaster

The relief plaster was used to mould a haunch to the cornice at the eastern wall in room 6. On top of plaster C a whitewash is present, on which probably wall paintings were existent before decomposition. Today, the whitewash is partly still existent (see Figure 4) and consists of gypsum as the binder and small sharp-edged quartz as aggregates (Figure 11).

In Figure 11 and 12 the structure and mineral composition of plaster C is illustrated by PLM of thin sections. The binder is gypsum and nearly the same aggregates as in plaster A can be detected: quartz, sodium and potassium feldspars, carbonates, soil fragments, mica and less titanite and celestine. But in contrast to plaster A and B, the relief plaster contains, conspicuously, a higher content of micas (Figure 12).

Soil fragments in plaster C – just as in plaster A and B – contain fine- and coarse grained carbonates, quartz, feldspar, clay minerals and micas. One example of a soil fragment is shown in Figure 13 investigated by SEM/EDX. EDX analyses indicate that the elemental composition of the grey bedded minerals refer to the clay mineral montmorillonite whereas the light inclusions consist of calcite (Figure 13).

Because of the mixtures of carbonates and silicates, this soil fragment can be addressed as marl.

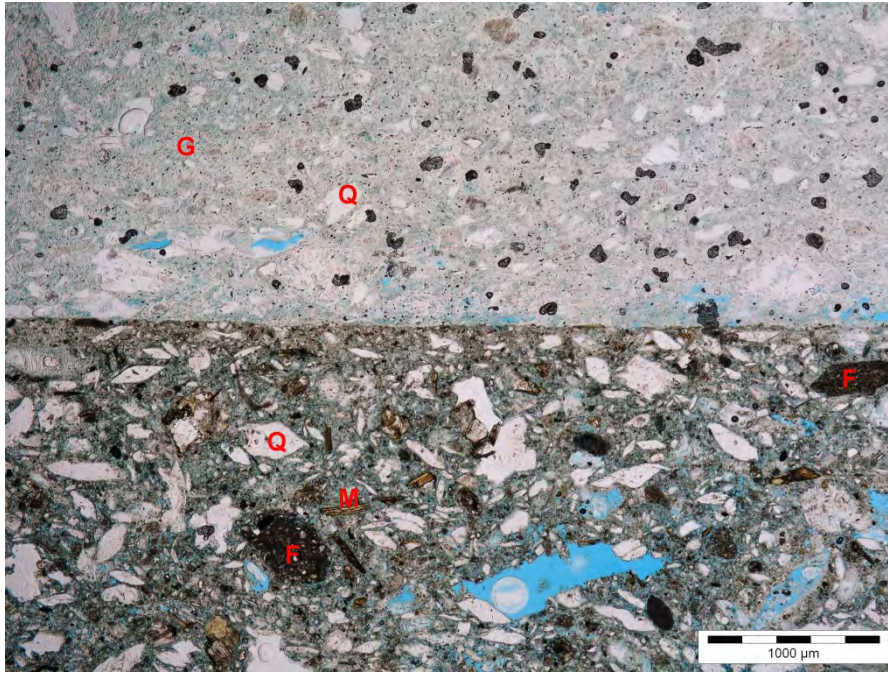


Figure 11: Thin section of relief plaster C (below) and the whitewash above under plane-polarized light, in both the binder is gypsum, aggregates are quartz (Q), soil fragments (F) and micas (M)

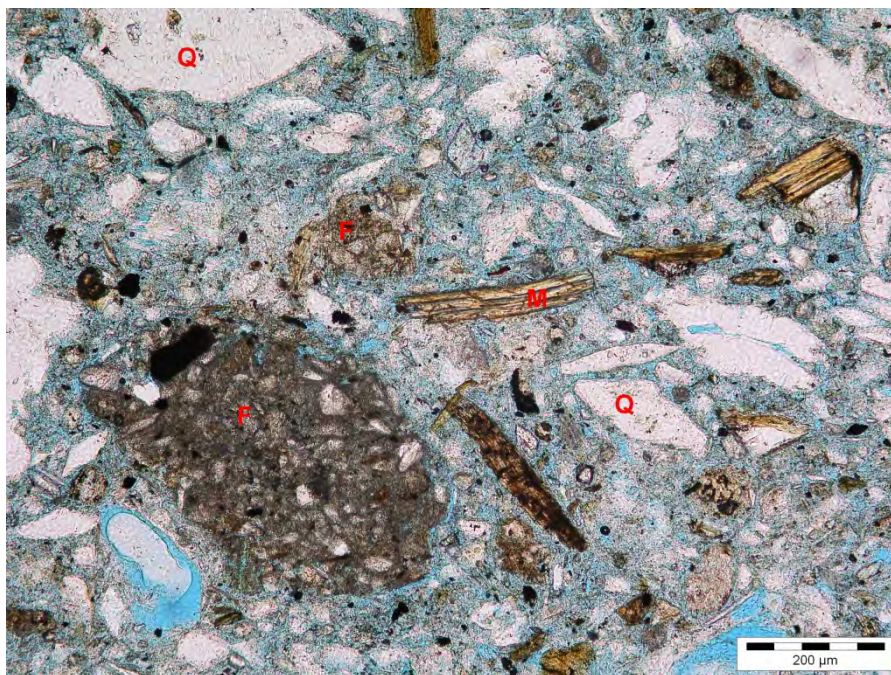


Figure 12: Detail of figure 13, thin section of relief plaster C under plane-polarized light, the binder is gypsum, aggregates are quartz (Q), soil fragments (F), and here frequently micas (M)

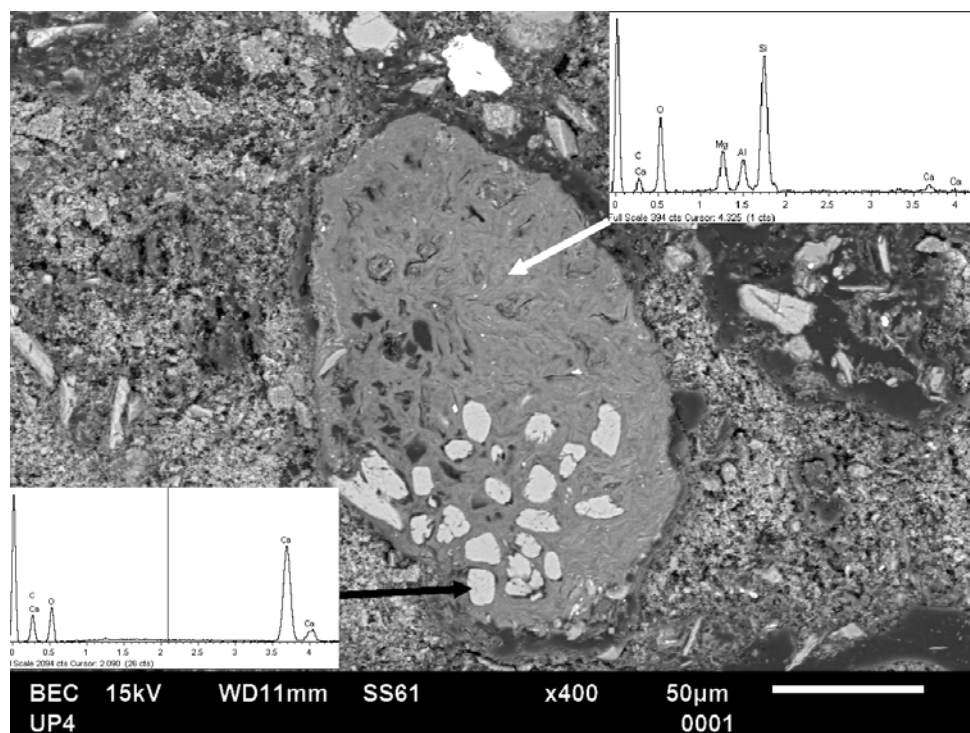


Figure 13: SEM backscattered image of a soil fragment, EDX measurements indicate clay minerals (probably montmorillonite) and calcite (bright spots)

Conclusion

In the mausoleum Ishrat Khana all original plasterwork like plaster, levelling coats and relief plaster are made of nearly the same material, but in different proportions of binder and aggregates.

The detailed investigation of thin-sections by PLM and SEM/EDX demonstrate that gypsum is the predominant binder, only some plasters contain additionally lime as binding material, e.g. plaster B.

Aggregates consist of quartz, sodium and potassium feldspars, carbonates (calcite and dolomite), soil fragments (marls and adobe) and less mica, titanite and celestine.

The examination of the samples demonstrates the use of a broad variation of aggregates depending on the application of the plaster. The relief plaster C contain a somewhat higher content of micas whereas the indoor plaster B is characterized by a higher amount of carbonates which lead to a more brownish colour of the plaster. Thus, different binder/aggregate ratios and compositions enable a varied application of this building material in Ishrat Khana.

It can be concluded that the historical construction workers knew the material Ganch very well. They variegated the binder/aggregation ratios to use the same ground material for different purposes. In literature [3, 5] it is mentioned that partly organic additives were

appended to the plasters, which could not yet identified in the samples of Ishrat Khana, probably because of the low content and the alteration of the organic materials.

Acknowledgements

This study was developed within the project “Ishrat Khana” financed by the German Foreign Office, the German Academic Exchange Service, the Gerda Henkel Foundation and the Volkswagen Foundation. The author is thankful to the University of Potsdam, Institute for Earth and Environmental Science for using SEM/EDX, special thanks to Uwe Altenberger and Christina Günter. Further, the author wishes to thank the following colleagues for very good collaborations and helpful discussions during the field work in Samarkand: Martina Abri, Christiane Kaiser, Khabibilla Kamilov, Shukrullo Kamilov, Pamela Kleinmann, Abdukabil Tulaganov and Sven Wallasch.

References

1. Pugachenkova GA (1963) Íschrát –Kaneh and Ak-Saray, two timurid mausoleums in Samarkand. *Ars Orientalis*: 177–189
2. Brandenburg D (1972) Samarkand. Studien zur islamischen Baukunst in Uzbekistan (Zentralasien). Berlin
3. Laue S, Kamilov S (2016) Ganch as historical building material in the Mausoleum Ishrat Khana, Samarkand, Uzbekistan. Proceedings of the 4th Historic Mortars Conference, 10 -12 October 2016, Santorini, Greece: 104–110
4. Laue S, Kleinmann P (2018) Ganch as Historical Building Material and the Kundal Wall Painting Technique in the Mausoleum Ishrat Khana, Samarkand, Uzbekistan. In: Krist G, Zhang L (ed) *Archaeology and Conservation along the Silk Road, Conference 2016 Postprints*, Böhlau Verlag Wien Köln Weimar: 49–62.
5. Vinner AV (1953): Materials and techniques of ornamental paintings. Gosudarstvenoe Izdatel'stvo, Iskusstvo, Moskau [Russ.]
6. Weyer A, Picazo, PR, Pop D, Cassar JA, Özköse A, Vallet JM, Srša I (2015) *EwaGlos European Illustrated Glossary of Conservation terms for Wall painting and Architectural Surfaces*. Michael Imhof, Petersberg
7. Birstein VJ (1975) On the technology of Central Asia wall paintings: the problem of binding media. *Studies in Conservation* 20: 8–19

Topic 4: Functional mortars for the conservation of historic and modern cultural heritage structures



Use of natural zeolite aggregate in restoration lime renders

Martin Vyšvařil¹, Patrik Bayer¹, Tomáš Žížlavský¹, Pavla Rovnaníková¹

(1) Brno University of Technology, Faculty of Civil Engineering, Veveří 331/95, 602 00 Brno, Czech Republic, vysvaril.m@fce.vutbr.cz

Abstract

Natural zeolites have been used with limes already in the Roman times and its perspectives of effective use as a pozzolanic additive to lime or cement composites were studied by a number of authors. The use of zeolitic materials for the production of lightweight aggregates in concrete is already known. However, the application of natural zeolite as an aggregate in lime renders (suitable for restoration and conservation) has not been investigated yet. In this study, the utilization of natural zeolite as lightweight aggregate in lime renders and natural hydraulic lime renders has been investigated therefore. The results revealed improved strengths of air lime renders with zeolite despite the fact, that the renders showed higher total porosity and water absorption than those with quartz aggregate. Increased porosity of renders resulted in improvement of their frost resistance and salt crystallization resistance. The analyzed renders with natural zeolite aggregate have a very good potential for practical applications because their properties are significantly enhanced, as compared with the common lime renders with quartz aggregate.

Introduction

The increasing attention for restoration and conservation of historical construction and a more elevated environmental sensitivity (reduction of CO₂ emissions in atmosphere) has re-awakened the interest for lime-based binders. Lime renders are not suitable for use in the moist environment because of their non-hydraulic properties and low frost resistance. The use of renders with hydraulic properties is therefore often preferred for renovation purposes. Significant change of material characteristics of air lime renders can be achieved by addition of pozzolanic admixtures or aggregates with pozzolanic properties. Porous pozzolan active aggregate can be used to prepare lightweight non-hydrophobic remedial renders with a high ability to salt accumulation from masonry and enhanced water vapor permeability. These renders facilitate easy moisture transport to the plaster surface. The use of zeolitic materials for the production of lightweight aggregates in concrete is already known [1, 2, 3]. However, the application of natural zeolite (NZ) as an aggregate in lime renders (suitable for restoration and conservation) has not been examined yet. Barnat-Hunek et al. used coarse (0.5–2 mm) natural zeolite in hydrophobized cement-lime renders to accumulation of sufficient amount of salt and ice [4]. E. Ferraz et al. investigated the behaviour of synthetic coarse and fine zeolite pellets incorporated in air lime–metakaolin renders for repairing ancient masonry [5]. They concluded that the zeolite pellets slow the

carbonation process of renders and improve the mechanical properties of renders due to the formation of fan-shaped clusters of aragonites. Some researchers used fine natural zeolites in lime renders as a partial replacement of lime [6, 7]. Zeolitic additions were effective in reducing the porosity and shrinkage of the hardened renders. Lime–zeolite renders hardened in humid environment exhibited higher frost resistance and they were stable in water in contrast to lime renders.

The main aim of this study was to evaluate the behaviour of NZ incorporated as an aggregate in air lime mortars and natural hydraulic lime mortars to be used as restoration renders. The properties of mortars with natural zeolite aggregate are compared with the properties of common lime mortars with pure quartz sand.

Materials and methodology

Commercial hydrated lime CL 90-S (Carmeuse Czech Republic, Ltd.) and natural hydraulic lime (NHL 3.5, Zement- und Kalkwerke Otterbein GmbH & Co. KG, DE) were used as binders. Natural zeolite (the fine fraction 0/2 mm from ACRE, Ltd., CZ, with loose bulk density of 1020 kg m⁻³) and pure quartz sand (the fine fraction 0/2 mm from Filtrační písky, Ltd., Chlum u Doks, CZ, with loose bulk density of 1670 kg m⁻³) were used as aggregates. Pozzolanic activity of the natural zeolite (NZ) determined by the Chapelle test was 409.2 mg Ca(OH)₂/g after 1 d treatment and 646.2 mg Ca(OH)₂/g after 5 d treatment. The chemical composition of all raw materials is given in Table 1.

Table 1. Chemical composition of initial materials (mass%)

	SiO ₂	Al ₂ O ₃	Fe ₂ O ₃	CaO	MgO	K ₂ O	Na ₂ O	P ₂ O ₅	TiO ₂	SO ₃	L.O.I.
Lime	0.92	0.71	0.39	68.09	1.33	0.48	0.11	0.05	0.10	0.19	27.94
NHL	12.76	4.12	1.47	59.87	2.79	1.13	0.09	0.15	0.05	0.15	15.28
Quartz sand	98.50	0.38	0.15	0.01	0.03	0.09	0.01	0.04	0.09	0.02	0.12
Zeolite	67.46	11.73	1.37	2.84	0.73	3.02	0.50	0.03	0.17	0.01	11.57

The phase compositions obtained by the X-ray diffraction analysis are presented in Table 2. The granulometry of aggregates and binders, and the image of NZ from scanning electron microscope (SEM) is shown in Figure 1. Since fine ground NZ is often used in cement mixtures to suppression of alkali silica reaction (ASR) [8, 9], it is not expected that the NZ, described in this paper, would underlie the ASR, and therefore no investigation to determine the ASR of this aggregate has been done.

Render mixtures were prepared using the correct amount of water required to obtain normal consistency and a good workability of the renders (160 ± 5 mm; measured by the

flow table test). The proportioning of the render mixtures is given in Table 3. The composition of render mixtures considers constant binder:aggregate volume ratio of 1:1.15 based on a practical point of view and historical traditions. Fresh mixtures were cast into prismatic moulds of size 40 × 40 × 160 mm. Standard conditions of sample storage were 22 ± 2 °C and relative humidity of 50 ± 5%.

Table 2. Phase composition of initial materials (mass%)

Mineral	Lime	NHL	Quartz sand	Zeolite
Albite	–	–	–	2.6
Aluminate	–	2.7	–	–
Larnite	–	22.5	–	–
Biotite	–	–	–	1.9
Brownmillerite	–	1.4	–	–
Brucite	0.5	–	–	–
Calcite	1.8	6.2	–	–
Clinoptilolite	–	–	–	50.5
Cristobalite	–	–	–	9.3
Illite	–	–	–	2.0
Microcline	–	–	0.4	–
Portlandite	97.1	41.3	–	–
Quartz	–	–	97.9	3.4
Staurolite	–	–	1.1	–
Amorphous phases	–	25.1	–	30.2

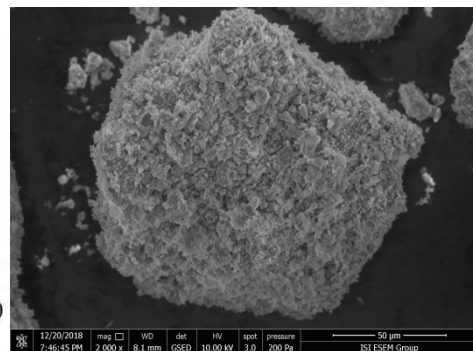
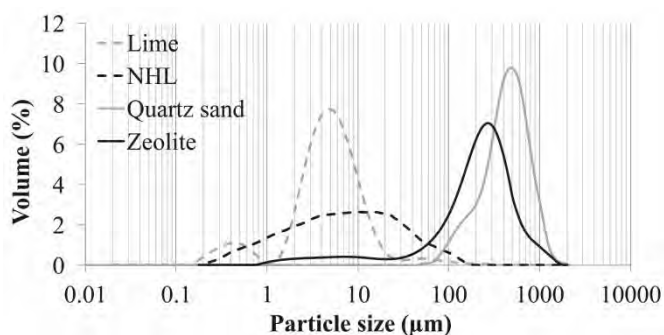


Figure 1. Particle size distribution of initial materials and SEM image of NZ aggregate.

The bulk density, the flexural and compressive strengths were determined after 28, 56 and 90 curing days. Flexural strengths of the samples were determined using a standard three-point-bending test and compressive strengths were measured according to EN 1015-11. The water absorption of renders was measured according to EN 13755 after curing times of 28 d. Six render specimens at least were used to conduct each of the mentioned tests. The porosity of the specimens was assessed using a mercury intrusion porosimetry. Detailed microstructure images were taken via a scanning electron microscope (SEM). Frost resistance tests were carried out according to modified Czech standard ČSN 722452. The

samples were tested after 28 curing days. The total test required 15 freeze-thaw cycles. One cycle consisted of 6 h freezing at $-20\text{ }^{\circ}\text{C}$ and 12 h thawing in a desiccator at constant relative humidity of 98 % and temperature of $20\text{ }^{\circ}\text{C}$. The frost resistance coefficient D_f was determined as the ratio of flexural strength of specimens subjected to 15 freeze-thaw cycles to the flexural strength of reference specimens that did not undergo the frost resistance test. The carbonation rate and the content of water in renders were observed using a differential thermal analysis (DTA) in combination with a thermogravimetric analysis (TG). The transport of liquid water in the studied materials was characterized by the water absorption coefficient, sorptivity and the liquid water diffusivity. The dried samples were firstly provided with epoxy resin on all circumferential sides. The front surface of the 40×40 mm samples was contacted with the distilled water reservoir. Subsequently, a change in sample weight over time was observed and recorded. The absorption coefficient for water A was calculated from the slope of the straight line of cumulative water weight increments in the sample at square root of time. Water sorption S ($\text{m s}^{-1/2}$) was determined using Equation (1)

$$A = S \times \rho_w, \quad (1)$$

where ρ_w is the density of water (kg m^{-3}). The liquid water diffusivity κ was calculated according to Equation (2) [10]

$$\kappa \approx \left(\frac{A}{w_{sat} - w_0} \right)^2, \quad (2)$$

where w_{sat} is the moisture saturated in a sample (kg m^{-3}) and w_0 is the initial moisture in a sample (kg m^{-3}).

The following solutions were used to determine the salt crystallization resistance of renders: 10% Na_2SO_4 , 3% NaCl and 3% KNO_3 . The dried samples were immersed in the solutions for 7 h and then dried for 16.5 h at $60\text{ }^{\circ}\text{C}$, after 30minutes standing at ambient temperature, the samples were weighed. The process was performed in the number of 10 cycles or till the partial disintegration of the samples. The procedure was performed according to the relevant European standard EN 12370. The state of the test specimens was monitored photographically.

Table 3. Composition of render mixtures

Mixture	Lime (g)	NHL 3.5 (g)	Quartz sand (g)	Zeolite (g)	H ₂ O (mL)
L-Q	100	–	400	–	120
L-NZ	100	–	–	246	153
NHL-Q	–	100	340	–	75
NHL-N	–	100	–	208	115

Results and discussion

Mechanical properties

The bulk densities of renders with NZ were 25% lower compared to the bulk densities of renders with quartz sand (Figure 2) due to the differences in loose bulk densities of the aggregates. The NZ samples decreased the bulk density even at 90 d because of the higher water content in the samples and their still unfinished drying. In the samples with quartz sand, a carbonation took effect causing the slight increase in bulk density.

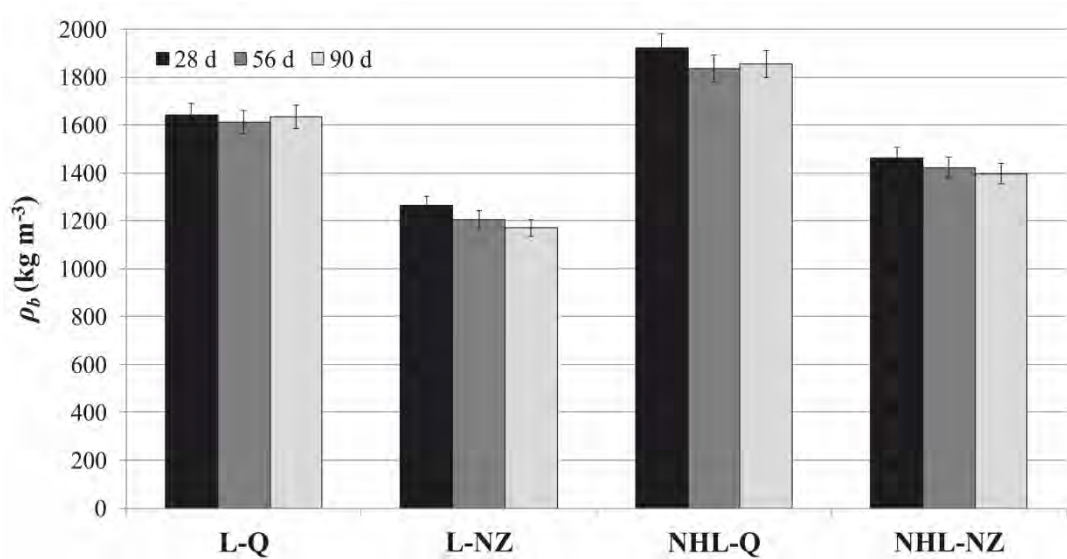


Figure 2. Bulk density of renders over time.

The flexural and compressive strengths of renders increased with curing time because of render hardening (Figure 3).

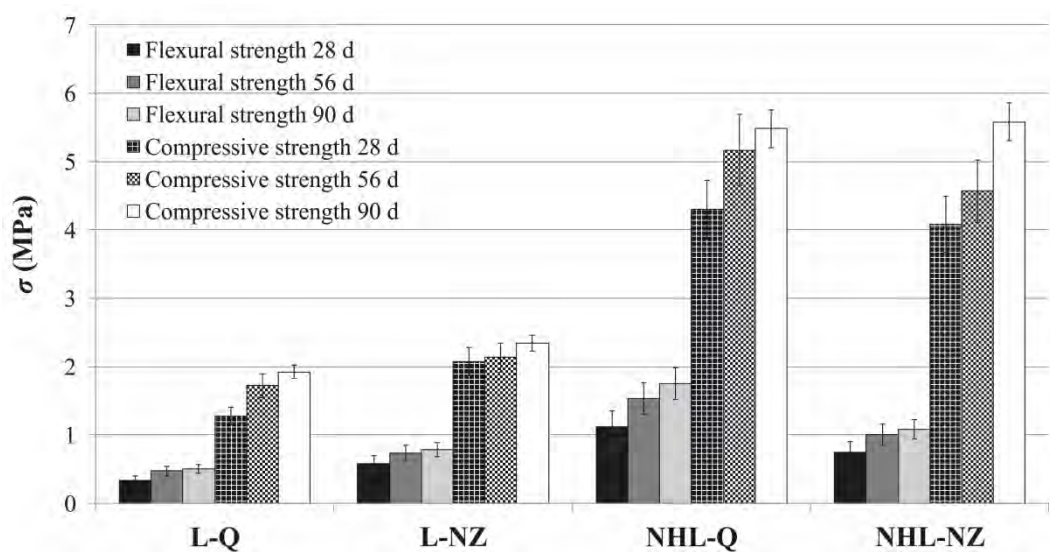


Figure 3. Flexural and compressive strength of renders over time.

The use of natural zeolite aggregate resulted in slightly improved mechanical properties of the hydrated lime renders (L) despite the higher amount of mixing water required for the same fresh render consistency. It is in accordance with a literature [5] but the reason for this improvement does not seem to be in the formation of aragonite clusters, as the literature claims (SEM images did not record the typical structures of aragonite), but more likely in the pozzolanic reaction of the natural zeolite (proven by SEM and TG/DTA). On the other hand, the natural zeolite has not shown the higher strength in NHL renders. This may be caused by a large amount of mixing water required for the production of NHL-NZ render (50% more than of NHL-Q) and a lower amount of calcium hydroxide available in NHL renders to the pozzolanic reaction of the natural zeolite aggregate. In these renders, a lower percentage of pozzolan will probably react and increase mechanical strengths. In order to establish the mechanical requirements of the specimens to be used in restoration works, the EN 998-2 presents the minimum strength for each class of mortar. At 90 days, NHL-Q and NHL-NZ renders are M 5 (render with at least 5 N mm² of the compressive strength). L renders fulfil the conditions for M 1 class.

Carbonation rate

The content of water (free and bonded summarily), portlandite, and calcite in the renders were studied using differential thermal analysis in combination with thermogravimetry (DTA/TG). The difference in percentage representation of water, portlandite, and calcite in the renders is shown in Table 4. The amount of water dramatically rose with using the NZ aggregate; after 90 days, the NZ renders still contained over 14% of water. The lower content of portlandite in the renders with NZ was due to its depletion by the pozzolanic reaction. The slower decrement of portlandite and the faster accrual of calcite in the L-NZ compared to the L-Q render suggests that the carbonation of the components (CSH) originating from the NZ pozzolanic reaction proceeded [11]. Carbonation is slower in the NHL-NZ render due to the lower content portlandite.

Table 4. Results of DTA/TG analysis in studied renders (mass %)

Mixture	H ₂ O 28 d	H ₂ O 56 d	H ₂ O 90 d	Ca(OH) ₂ 28 d	Ca(OH) ₂ 56 d	Ca(OH) ₂ 90 d	CaCO ₃ 28 d	CaCO ₃ 56 d	CaCO ₃ 90 d
L-Q	0.29	0.27	0.24	13.79	12.12	10.83	5.47	7.42	8.45
L-NZ	24.19	18.58	14.36	11.57	11.32	11.15	3.57	5.23	7.23
NHL-Q	5.67	1.85	1.79	8.63	8.35	7.27	3.10	5.21	8.05
NHL-NZ	20.23	19.63	15.31	6.37	6.35	5.70	4.45	5.37	6.04

Pore structure

The results of cumulative pore volume determination for the render samples are graphically compared in Figure 4. The renders with quartz sand contained mainly large capillary pores with radii around 1 µm, which is typical of lime renders. These renders were evidently less porous than the renders with NZ (see Table 5). The L-Q render contained also more pores

larger than 1 μm . The use of NZ as an aggregate caused dramatic growth in porosity and it markedly changed the pore size distribution in the renders. These renders included a significantly higher proportion of pores with a diameter greater than 1 μm . The L-NZ render was characterized by an unprecedented number of pores with a diameter of about 10 μm , their presence was caused by the high amount of mixing water used in the production of this render.

In the renders with NZ, a second growth of cumulative pore volume is present in an area of pore diameter between 0.01 and 0.1 μm . The presence of NZ resulted in the development of these smaller pores normally formed by the network of hydrated calcium silicates (CSH). This is another confirmation of the pozzolanic reaction of the natural zeolite aggregate in lime renders.

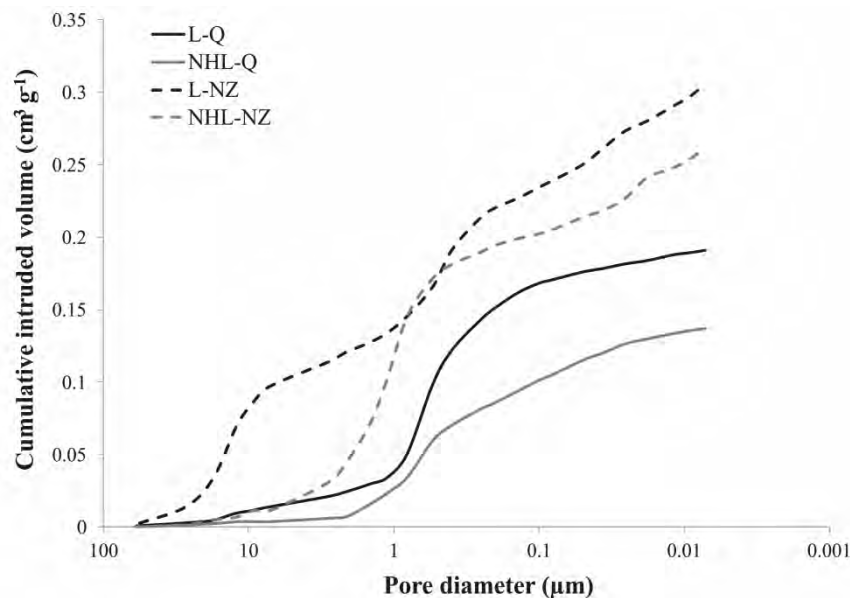


Figure 4. Cumulative pore volume in renders at 28 days.

The total porosity of renders (Table 5) expectantly increased with using of the NZ and water absorption of renders grew hand-in-hand with the increasing total porosity.

Table 5. Total porosity, frost resistance coefficient (D_f) and liquid water transport parameters of renders

Mixture	Total porosity (%)	D_f (-)	Water absorption (%)	A ($\text{kg m}^2 \text{s}^{-1/2}$)	κ ($\text{mm}^2 \text{s}^{-1}$)	S ($\text{mm s}^{-1/2}$)
L-Q	32.2	0.15	14.7	0.1938	1.799	0.194
L-NZ	37.7	0.22	35.8	0.2950	2.457	0.296
NHL-Q	26.1	0.29	12.2	0.1308	0.941	0.131
NHL-NZ	33.2	0.24	32.3	0.3287	2.971	0.329

Liquid water transport

Capillary liquid water transport in the renders was measured applying sorption experiments. The results achieved are given in Table 5 and Figure 5. The renders with NZ aggregate showed higher ability of liquid water transport compared to the renders with quartz aggregate. Water absorption coefficient (A), liquid water diffusivity (κ), and sorptivity (S) of NHL render were dramatically enhanced by using the NZ aggregate. The difference is caused by the high number of pores with a diameter around $1\ \mu\text{m}$ in the NHL-NZ render. Although the L-Q render contained a large number of pores with a diameter of about $10\ \mu\text{m}$, the capillary water action was slower, which was reflected by lower A , κ , and S values. Too large pores in the render structure slow down the capillary water action. The water, rising through the capillary, cannot pass through the pore with a large diameter, because the pore height can be larger than the capillary suction. However, the transport of moisture proceeds by water evaporation in the pore and diffusion to the opposite wall where the water vapor condensates again and in the liquid state, rises through the capillaries further upward. Additionally, some of these large pores could be closed and therefore did not participate in the capillary water action.

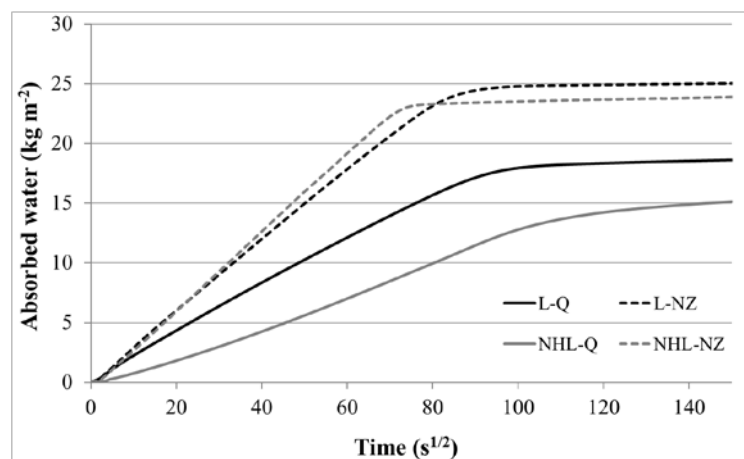


Figure 5. Cumulative mass of capillary water action versus time for studied renders.

Durability of renders

Frost resistance

All of the renders did not meet the standard criterion of $D_f > 0.75$ (table 5). The result obtained for the lime render with quartz sand (L-Q) was worse than the one obtained for the L-NZ render; this was caused by higher total porosity and higher content of large pores in the L-NZ render. Higher total porosity and large pores in the render allow a trouble-free expansion of the ice during its crystallization and reduce a tension on the pore wall and the risk of cracks formation. A lower D_f value for the NHL-NZ render compared to the NHL-Q can be caused by the absence of large pores with a diameter of about $10\ \mu\text{m}$ and a large amount of free and physically bound water in the cavities and channels of NZ structures.

Salt crystallization resistance

The state of the test specimens after 10 cycles of salts crystallization is given in Table 6. The sequence of the decay cycle is stated for the samples that have broken down earlier.

Table 6. State of renders in salt crystallization resistance tests (10 cycles)

Type of solution	L-Q	L-NZ	NHL-Q	NHL-NZ
10% Na ₂ SO ₄	Breakdown at the 6 th cycle	Breakdown at the 9 th cycle	Breakdown at the 4 th cycle	Breakdown at the 7 th cycle
3% NaCl	Intact	Breakdown at the 8 th cycle	Intact	Breakdown at the 8 th cycle
3% NH ₄ NO ₃	Intact	Intact	Breakdown at the 10 th cycle	Breakdown at the 10 th cycle

The table shows that the renders with NZ are not resistant to crystallization of sodium chloride. All render samples were also broken down after several crystallization cycles of sodium sulfate, where gypsum with high molar volume is likely to occur. The NHL renders break down in the sodium sulphate solution earlier due to the presence of the aluminate phase and the formation of bulkily ettringite breaking the structure of the render. The use of NZ as aggregate slightly improves the resistance of renders to crystallization of sodium sulphate. A detailed study of the NZ impact on the render's resistance to salts crystallization, including XRD, XRF, and SEM EDX analyses, is beyond the scope of this paper and will be part of the separate forthcoming publication.



L-Q after 6 cycles of Na₂SO₄ crystallization

L-NZ after 9 cycles of Na₂SO₄ crystallization

Figure 6. Images of fractured render samples during the sodium sulfate crystallisation test.

Microstructure

The microstructure of render samples was determined at 28 curing days by SEM. Micrographs of renders L-Q and L-NZ are present in Figures 7 and 8.

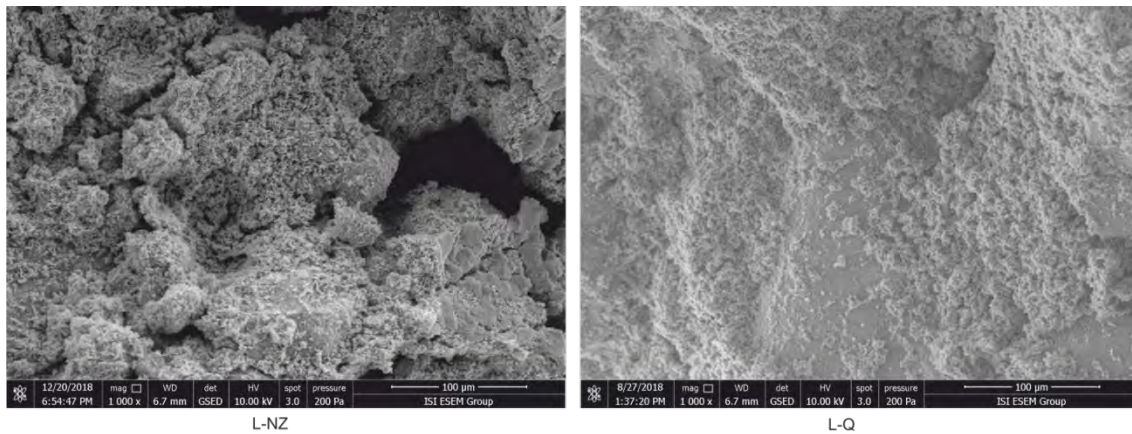


Figure 7. SEM overview of microstructure of L-Q and L-NZ render samples

The L-NZ render was markedly more porous with existence of different types of phases. The calcite and portlandite crystals were identified in matrix of the L-Q sample. The aggregate grains in L-NZ render was covered by typical amorphous structure of CSH gel; which proved the pozzolanic properties of NZ.

Ferraz et al. [5] reported the formation of acicular elongated crystals of aragonite in lime mortars when using 5 wt.% of coarse synthetic zeolite pellets. Probably because of the low content of Mg^{2+} ions in the NZ, used in this work, crystalline neoplasms belonging to aragonite were not detected in the microstructure of NZ renders. According to Taylor [12], $CaCO_3$ precipitates as aragonite rather than calcite in presence of Mg^{2+} ions.

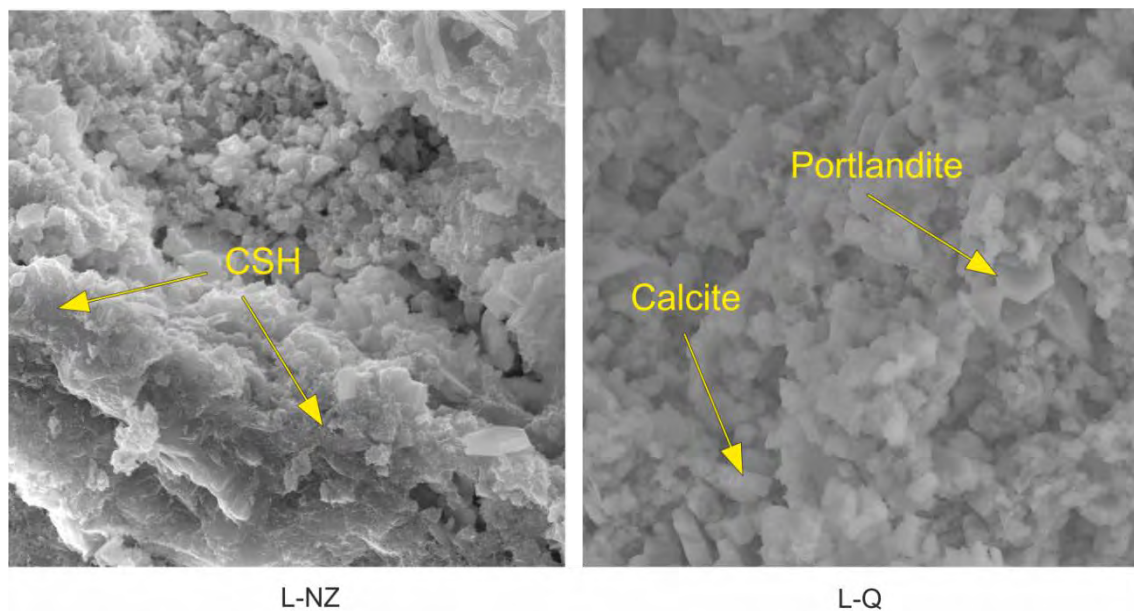


Figure 8. Detailed SEM images (magnification 10 000 ×) of L-Q and L-NZ render samples.

Conclusion

This paper has focused on the effect of fine natural zeolite (NZ) aggregate on the mechanical properties, microstructure, durability and liquid water transport in air lime renders and natural hydraulic lime (NHL) renders. It has been observed that the replacement of quartz

sand by natural zeolite causes a slightly strength enhancement of air lime renders despite the higher amount of mixing water required for the same fresh consistency. The natural zeolite does not positively affect the strengths of NHL renders due to the lower amount of calcium hydroxide available in NHL renders to the pozzolanic reaction. The NZ significantly affects the pore size distribution in the renders by the formation of large pores with radius comprised between 1 and 20 μm and also medium capillary pores formed by the network of calcium silicate hydrates. The usage of NZ as an aggregate increases the open porosity of renders resulted in improvement of their frost resistance and higher ability of liquid water transport through the render. The NZ slightly improves the resistance of renders to crystallization of sodium sulfate, but its utilization is not suitable on chlorides contaminated masonry. On the basis of Chapelle test, TG-DTA analysis, SEM microscopy, and porosity evaluation of lime renders, it was confirmed that applied NZ exhibits the pozzolanic activity. The capability of the used NZ to utilization in lime and NHL renders was thus concluded. Improving the properties of renders using NZ is a good prerequisite for its use in practice.

Acknowledgement

The work has been achieved with the financial support from the GA ČR research project No. 18-07332S and from the Ministry of Education, Youth and Sports under the „National Sustainability Programme I“ – the project No. LO1408 „AdMaS UP – Advanced Materials, Structures and Technologies“.

References

1. Ghourchian S et al (2013) An investigation on the use of zeolite aggregates for internal curing of concrete. *Constr Build Mater* 40:135–144
2. Kiliñarslan Ş (2011) The effect of zeolite amount on the physical and mechanical properties of concrete. *Int J Phys Sci* 6:3041–3046
3. Karakurt C, Kurama H, Topçu IB (2010) Utilization of natural zeolite in aerated concrete production. *Cem Concr Comp* 32:1–8
4. Barnat-Hunek D, Siddique R, Klimek B, Franus M (2017) The use of zeolite, lightweight aggregate and boiler slag in restoration renders. *Constr Build Mater* 142: 162–174
5. Ferraz E et al (2014) Synthetic zeolite pellets incorporated to air lime–metakaolin renders: Mechanical properties. *Constr Build Mater* 69:243–252
6. Pavlik V, Užáková M (2016) Effect of curing conditions on the properties of lime, lime–metakaolin and lime–zeolite renders. *Constr Build Mater* 102:14–25

7. Liguori B, Caputo D, Iucolano F (2015) Fiber-reinforced lime-based renders: Effect of zeolite addition. *Constr Build Mater* 77:455–460
8. Feng N, Hao T (1998) Mechanism of natural zeolite powder in preventing alkali-silica reaction in concrete. *Adv Cem Res* 10:101–108
9. Sujjavanich S, Wongtanasarasin C, Kongkachuichay P (2017) Effect of synthetic and natural zeolite on ASR expansion. *Engineering Journal* 21:269–278
10. Kumaran MK (1999) Moisture diffusivity of building materials from water absorption measurements. *J Therm Envelope Build Sci* 22:349–355
11. Papadakis VG, Fardis MN (1989) A reaction engineering approach to the problem of concrete carbonation. *AIChE Journal* 35:1639–1650
12. Taylor HFW (1997) *Cement Chemistry*. Thomas Telford Publishing, London

Fibre reinforced mortars for cultural heritage protection

Miloš Drdácý¹, Dagmar Michoinová²

(1) Institute of Theoretical and Applied Mechanics of the Czech Academy of Sciences, Prague, drdacky@itam.cas.cz

(2) National Heritage Institute in Prague, michoinova.dagmar@npu.cz

Abstract

The adding of natural fibres to mortar mixtures is arguably the most important ancient technology applied the world over for its ability to improve performance. Even though modern synthetic fibrous materials are replacing historical ones, natural fibres may still be a competitive option by virtue of their ecological and economic qualities. The paper presents selected results of comprehensive investigations into the behaviour of lime mortars modified with natural and synthetic fibres and fibrous particles. It summarizes technical data for fibre reinforced mixtures made of lime matrix, sand and natural fibres (goat and horse hair), fibrous particles (sawdust and grain husks), as well as polypropylene fibres. Observations are presented regarding the impact the fibres have on the physical characteristics of the resulting matured mortars. The results of mechanical tests illustrate the degree to which fibres influence mortar strength. A positive effect on tensile strength is documented in an example where such mortars are applied as reinforcing layers to low-strength masonry. The effects of weathering were also tested on small uncovered areas of plaster layers applied to burnt clay roof tiles exposed to one year in an outdoor environment.

Introduction

In historical architecture – either designed by architects or built by master masons or even laymen in vernacular architecture – mortars modified with the addition of natural fibres or fibrous particles were very common in Europe and beyond. Fibres were added to the mortar mixtures solely on the basis of long-term experience, and a builder was able to estimate the necessary dosage according to the effects desired.

The positive effects of fibres on a brittle matrix have motivated scientists and engineers to conduct research on the behaviour of fibre-modified quasi-brittle composites. For decades research in the field has been concentrated mainly on mortars with cement based binders, and several mortar producers have introduced such mixtures modified with synthetic fibres onto the market [1]. At the turn of the millennium very little scientific knowledge existed on the behaviour of natural fibres in mortars with a purely lime-based matrix [2]. At that time the authors carried out an experimental study on pure lime mortars with fibres, and found beneficial effects on the reduction of shrinkage macro-cracks [3].

Recently, research into lime based mortars modified with fibres has intensified. The focus has been on fibre characterisation [4], [5], and the use of new synthetic fibres as well as natural fibres extracted from plants using innovative technologies [6], [7]. Applying inorganic fibres to lime mortars has also been tested, including in the restoration of heritage objects [8]. The most modern approach aims to optimize the relation between the characteristics of the fibres and those of the matrix, especially during the crack development stage [9], [10]. The results are outstanding.

Materials

Our investigation focused on the performance of historical materials and their replicas. Therefore, mortars based on a lime binder and mostly reinforced with natural fibres were studied.

Fibres

Horse and goat fibres represented the animal hair, and they were complemented with synthetic polypropylene fibres. In many historical mortars hair was replaced with lamellar particles, e.g. straw or other plant fibres. In the described study, sawdust and husks were used. For the sake of comparison, all fibres and lamellae had the same length of 12 mm. Regarding model similarity, the aspect ratio parameter would be more suitable for the purpose of comparative testing, but it is impossible to maintain this parameter constant considering the variety of natural fibrous particles.

Table 1. Fibre and lamellar particle characteristics.

Fibre or particle	Abbr.	Legth (mm)	Equiv. diameter (μm)	Flexural strength (MPa)	Modulus of elasticity (GPa)	Elongation at failure (%)	Moisture (%)
PP fibre CRACKSTOP	PP	12	18	70-200	3.5	5-40	negligible
goat hair	Ko	12	30-100	110-230	6.2-7.7	2-29	negligible
horse hair	Ku	12	50-140	110-200	3.9-5.1	4.5-32	negligible
husk	Pl	2-3	max. 540	unknown	unknown	unknown	7.5
sawdust	Pi	2-3	max. 1180	unknown	unknown	unknown	12

The mechanical characteristics of animal fibres had not been published before the experiments started; therefore it was decided to test them using a non-standard method. Animal hair is so short that it is not possible to fix it in grips usually used for the testing of fibres. Moreover, the cross section of animal fibres is not regular and changes along the length, which causes twisting of the fibres during loading. Therefore a specific fixture was used for the testing, and an optical method was developed for measuring fibre deformations. White marks were made on the fibres, and their positions were recorded before incremental loading began. Then at each loading step the positions of the marks

changed, and this was recorded as a new reference. In this way the deformation that occurred during the course of loading was evaluated [4]. Polypropylene fibres have known characteristics given by their producer. The material characteristics of the reinforcing additives are given in Table 1.

Mortar

The matrix is based on a very pure calcium hydrate (air lime) of the following average chemical composition: CaO – 72 %; MgO – 0,6 %; CO₂ – 2,5 %; SiO₂ + non-soluble particles – 0,85 %; hydrate water – 22 %. The basic mixture is filled with a natural siliceous sand of the following granulometric data: above 2,5 mm – 0 %; 2 mm – 7 %; 1 mm – 23 %; 0,5 mm – 31 %; 0,25 mm – 17 %; under 0,25 mm – 5 %. Humidity max 1 %, specific gravity 1480 kg/m³. Drinking water from the public distribution net was used in amounts from 0,30 (in most cases) to 0,43 l/kg.

The reinforcing plaster used in the adobe masonry test was prepared using an optimised mixture designed by Přinosil [9]. The weight portions are the following: 0,750 g of hydrated air lime powder CL90, 0,250 g of metakaolin L05, 1,840 g of silica sand (0-0,1 mm), 1,154 g of silica sand (0,1-0,3 mm), 1,200 mL of water, 0,024 g plasticizer and 0,059 g of polypropylene fibres 12 mm long. This mortar has been developed for optimum behaviour taking into account the maximum bridging effect across micro-cracks balanced with pullout resistance.

Test specimens

All test specimens were made from an identical basic dry mixture which was then modified by the addition of fibres. The basic mixture was composed of binder and sand in the volumetric ratio of 1:1, which ensures the creation of cracks in the early stages of mortar setting. The specific gravity of the dry mixture was 1000 kg/m³. The dose of fibres, measured in percentage of the total mass of the mortar mixture, varied according to Table 2. The variation was adopted with the aim of confirming the optimum dosage recommended in literature.

A minimum of five prismatic specimens of standard dimensions of 40 mm × 40 mm × 200 mm were made for each series of material composition. The samples were cast in moulds with sides provided with a separator, cured in laboratory conditions for 2 days, then taken out of the form and cured for another 90 days before the first tests started (ČSN EN 1015-2, T 21±2°C, RH 50±5%).

For the weather resistance tests the mortar, after being mixed and left to mature for about one hour, was placed on a wet ceramic porous roof tile and its surface was tightened with a plastering trowel. The specimens hardened in laboratory conditions, and when they were dry (approximately after one week), they were exposed to exterior climatic activity for a year.

The reinforcing plaster mortar was applied on an adobe brick wall built using adobe mortar for the masonry joints.

Table 2. Fibre dosage and resulting mortar strength of 1:1 volume ratio composition mortar.

Fibres or fibrous particles	Test series marking	Dose of fibres in mass %	Flexural strength in MPa	Compression strength in MPa	Flexural modulus of elasticity in MPa
polypropylene	PP0.1	0.1	0.48	2.35	2033
	PP0.3	0.3	0.58	2.13	2024
	PP0.5	0.5	-	-	-
goat hair	Ko0.1	0.1	0.75	3.16	2933
	Ko0.2	0.2	0.65	2.72	2898
	Ko0.4	0.4	0.25	2.39	2312
horse hair	KO.1	0.1	0.75	2.68	3031
	KO.2	0.2	0.52	2.18	2413
	KO.4	0.4	0.62	1.94	2249
sawdust	Pi2	2	0.58	1.62	2150
	Pi4	4	0.31	0.95	1043
	Pi6	6	0.36	1.38	1347
husk	PI2	2	-	1.02	-
	PI4	4	-	-	-
	PI6	6	0.30	1.15	1204
plain mortar	C	0	0.40	3.98	1839
polypropylene	plaster		4.04	10.24	1200

Test results

The mechanical test results are discussed in detail in [3], (they were performed according to the ČSN EN 1015-11 Standard). For this contribution the protective and sustainability effects were the focus of interest. However, for the sake of the reader's comfort, let us mention that the flexural (tension) strength tests were carried out on standard beams in a four point bending configuration which also enabled determination of deformability (modulus of elasticity). The compression tests were carried out on cubes 40 mm × 40 mm × 40 mm. The results show that even after 90 days the carbonation was not complete and much lower than the carbonation of plain mortar, which was further demonstrated using phenolphthalein tests. The cumulative results are presented in Table 2.

The flexural strengths were positively affected by the addition of animal hair as well as PP fibres. The animal hair almost doubled the flexural strength in the lowest dosage of 0,1% of the total mass of the mortar mixture. A greater amount of hair however results in a decrease in the positive strengthening effect. On the other hand, an increased addition of PP fibres apparently increases the reinforcing effect. The compression strength of the mortars containing fibres was lower than that of the plain mortar, however, in this case the results are significantly influenced by incomplete carbonation across the specimens.

Water absorption of mortars

Water absorption of the mortars was determined as an increase in mass of the testing specimen after its gradual wetting. It is evaluated as the ratio of the mass increase after full saturation to the mass of a dry specimen

$$N_m = (m_n - m_s) \cdot m_s^{-1} \cdot 100$$

where N_m is water absorption as a percentage of mass, m_n and m_s are the mass (in g) of water-saturated and dry mortars respectively. Water absorption was tested on cubes of 40 x 40 x 40 mm³ after water-uptake rate measurements. The specimens were placed in a container into which water was added at a rate of 2/5 of the specimen height each hour. The specimens were totally immersed in water during the experiments. The mass increments were evaluated every 24 hours up to full saturation. The result is presented in Table 3.

Table 3. Water absorption and porosity of mortars.

Test specimen	Water absorption in %	Open porosity in %	Closed porosity in %	Ratio of open to closed porosity
PP0.1	16.54	16.5	18.5	0.9
PP0.3	17.62	17.6	10.8	1.6
PP0.5	-	-	-	-
Ko0.1	17.67	17.7	21.5	0.8
Ko0.2	16.92	16.9	22.0	0.8
Ko0.4	15.69	15.7	22.9	0.7
K0.1	17.43	17.4	21.8	0.9
K0.2	18.3	18.3	20.9	0.9
K0.4	18.15	18.2	21.0	0.9
Pi2	17.34	17.3	21.1	0.8
Pi4	20.78	20.8	22.4	0.9
Pi6	21.91	21.9	23.4	0.9
PI2	18.93	18.9	22.4	0.8
PI4	18.02	18.0	23.2	0.8
PI6	-	-	-	-
C	19.29	19.3	20.2	0.96

Ratio of open to closed porosity

Water absorption also determines the volume of pores not open for water uptake in a fully saturated specimen. From the experimental results it follows that, for the mortars filled with goat hair, the closed porosity increases with the increase in the amount of fibres. This may be influenced by a certain hydrophobic effect of organic compounds released from the hair. A phenomenon similar to this decrease in water absorption is also observed in the lower carbonation rate of the mortars containing goat hair [1]. No other trends were observed — Table 3.

Weather resistance of mortars with fibres

The effect of fibres on weathering damage was assessed by visual observation only. It was documented by means of photography and a description of the defects and damage.

Goat hair

After one year of exposure, this mortar showed practically no visible degradation. On the specimens containing 0.1 % and 0.2 % hair, shrinkage cracks were more visible. This demonstrates how the addition of fibres influences the volumetric stability of mortars. The shrinkage cracks did not occur with the 0.4 % addition of this hair. In fact, goat hair exhibited the best effect on minimizing shrinkage macro-cracks and aging defects. Figure 1a.

Horse hair

The mortar with the addition of horse hair exhibited similar effects, however not as much as in the previous case. On the specimens with 0.1 % hair there are a few pronounced initial shrinkage cracks visible, while in the mortar containing 0.2 % hair, many smaller cracks appeared. Here also shrinkage cracks did not occur with the 0.4 % addition of hair, which prevented weathering damage. During the winter period the shrinkage cracks allowed for water inlets under the surface layer, and the mortar suffered frost damage — Figure 1b.

Polypropylene

Significant colour darkening was the visual effect most noticeable after one year of weathering for the mortars with PP fibres. On the other hand, this mortar survived without being strongly affected by defects or damage. Here also the higher percentage of fibres resulted in fewer shrinkage macro-cracks and a better resistance to weathering. However, it must be mentioned that at a higher percentage of fibres, namely 0.3 % and especially 0.6 % the workability was rather poor, and it was difficult to create a layer without stretched fibres visible on the surface. The character of the composite containing PP fibres is completely different from those mixed with gross fibres or fibrous particles.

Saw dust

The mortars mixed with sawdust showed the best aging properties. The tendency of the dosage impact was the same as for the animal fibres, i.e. for 2% and 4% only a slight increase in the occurrence of shrinkage cracks, and for 6% no apparent shrinkage or degradation cracks after a year of exposure to weathering — Figure 1c.

Plain lime mortar

The plain mortar layer detached from the tiles after one year of outdoor exposure. In fact, partial detachment was observed shortly after the hardening of the mortar, and complete

separation occurred after the winter period. However, the mortar floes separated by strong shrinkage cracks were rather compact in the areas between the cracks. Figure 1d.

Husk

The husk dosages above 2% caused an apparent loss of cohesion of the mortar layer after one year of weathering. The best results were achieved with the 2% husk addition.

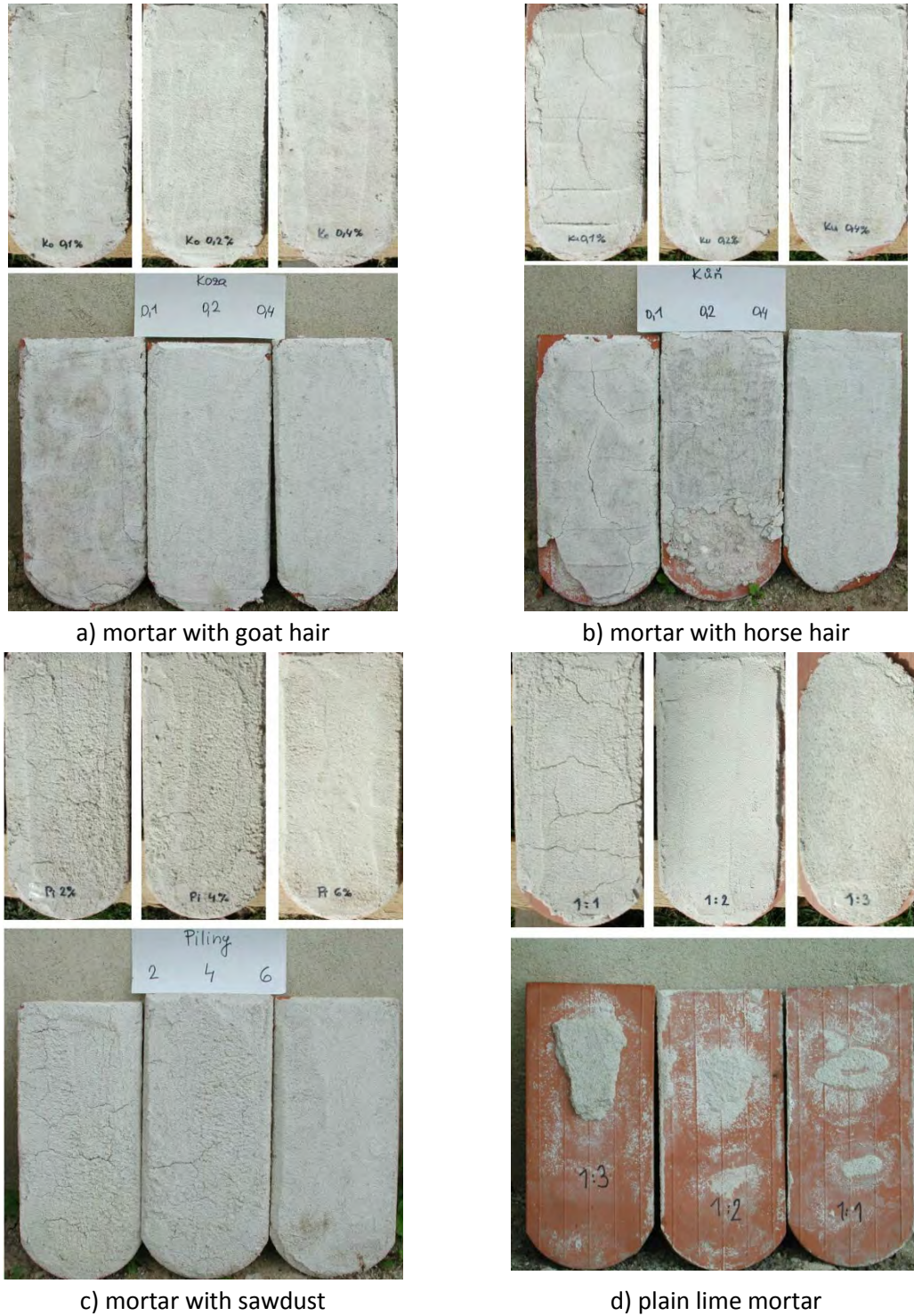


Figure 1. Damage patterns on mortars before and after one year of weather exposure.

Reinforcing plaster with fibres

The potential for the practical application of mortars containing fibres was tested in a short study on the reinforcing of adobe walls against out of plane bending frequently present at earthquake disasters [11]. A low adobe wall (750 x 960 x 115 mm³) rendered on the both sides with a fibre reinforced plaster 15mm thick was loaded with four-point out-of-plane bending - Figure 2.

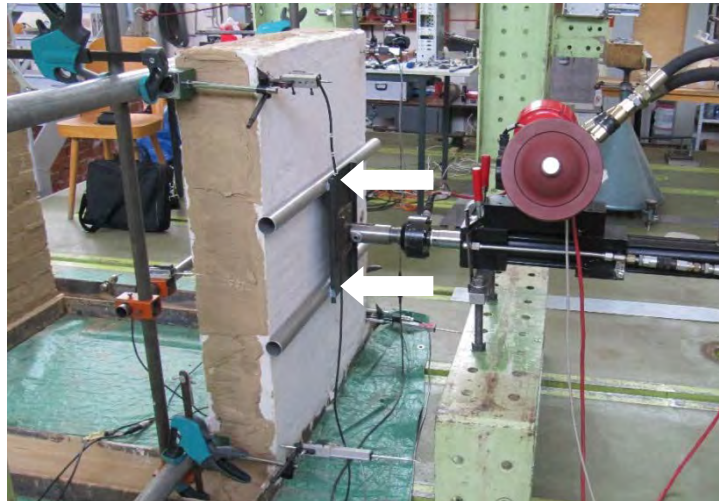


Figure 2. Test arrangement and loading of the adobe wall reinforced with plaster.

The effect is apparent in Figure 3, where the illustrative load displacement diagram shows the difference in load carrying capacity of an unreinforced masonry wall (1) and a wall (6) rendered with a high-strength fibre- reinforced lime mortar.

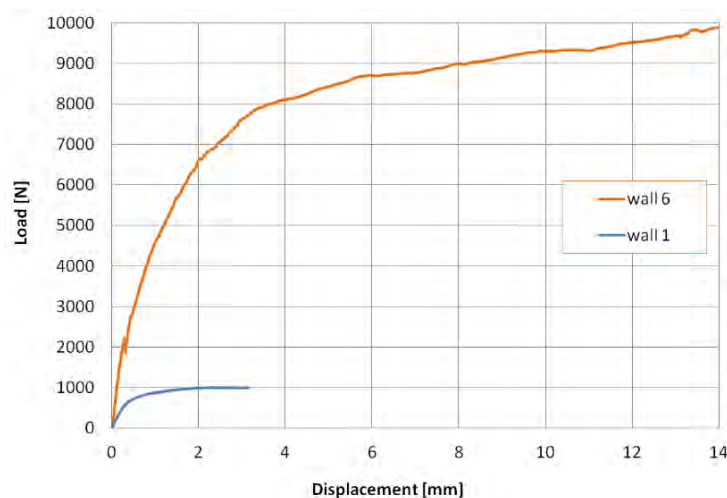


Figure 3. Load displacement behaviour of URM wall 1 and the lime render fibre-reinforced wall 6.

During bending tests, a substantial increase was observed in the maximum load, and in addition, full destruction of the wall was prevented or substantially delayed after it reached its ultimate load and after a significant crack pattern had developed.

Conclusion

The expected and rather well known positive effects of adding fibres to lime mortar on volumetric stability during setting and hardening were also observed on mortar layers applied onto a burnt clay substrate. This effect influences the durability of fibre modified mortars when exposed to the outdoor environment and weather activity. The prolonged life of mortars increases their protective and sustainability functions when applied on cultural heritage objects. Such mortars are suitable for details and structural elements heavily subjected to unfavourable and repeated weathering activity and loadings. For example, tile joints on roofs or cornices are candidates for the application of lime mortars with fibres. It is worth mentioning that traditional materials – animal hair, wood and plant particles – are sufficiently capable of playing such a role, even though they do not amend lime mortars in the best way from the mechanical behaviour point of view.

The behaviour of animal hair in the mortar matrix is significantly different from the behaviour of synthetic or steel fibres. Animal hair, due to its surface characteristics, separates from the matrix during setting and hardening, and is anchored in the mortar mostly due to the friction of the curved fibres and their crossings. Synthetic fibres remain fixed and are able to bridge cracks that develop during tension stress in the matrix.

Modern synthetic fibres, e.g. polypropylene fibres, enable better optimization of fibre modified lime based composites because they are regular, thinner, high-strength and relatively cheap. Modified lime mortar composites with matrices ensuring proper anchoring of such strong fibres exhibit much higher mechanical strength and can be used for reinforcing low-strength masonries, e.g. adobe walls.

The results presented here indicate that further investigation into the behaviour of traditional mortars reinforced with natural fibres would be worthwhile.

Acknowledgement

This contribution to the HMC Conference has been supported by the Interreg CE project ProteCHt2save and the institutional grant RVO 68378297 which is cordially acknowledged. We thank Marek Eisler for proofreading the text.

References

1. Zollo, R.F.: Fiber-reinforced Concrete: an Overview after 30 Years of Development, Cement and Concrete Composites, 19, 1997, pp. 107-122.

2. Gibbons, P.: Preparation and Use of Lime Mortars, Historic Scotland Technical Advice Note 1, Historic Scotland, 1995.
3. Drdäcký M F, Michoinová D (2003) Lime mortars with natural fibres. In „Brittle Matrix Composites 7“ Proceedings of the 7th Int. Symposium (A M Brandt, V C Li, I H Marshall, eds.). Woodhead Publishing Ltd./Zturek Research Sci.Inst., Cambridge and Warsaw, 523-532
4. Drdäcký M, Jiroušek O, Slížková Z, Valach J and Vavřík D (2007) Hybrid testing of historic materials. In Experimental Analysis of Nano and Engineering Materials and Structures, Proc. of the 13th Int. Conf. on Experimental Mechanics (E Gdoutos,ed.), Alexandroupolis, Greece, 275-276
5. Přinosil M, Němeček J Mechanical properties of organic and synthetic PVA fibers. <https://docplayer.net/83574167-Mechanical-properties-of-organic-and-synthetic-pva-fibers.html>
6. Papayianni, M Stefanidou E Anastasiou (2008) Use of synthetic fibers in lime-based mortars. 1st National Congress on Building Materials and Components Technical Chamber of Greece, Athens 2008, 1885-1892
7. Stefanidou M, Papachristoforou M, Kesikidou, F (2016) Fibre-reinforced lime mortars. https://www.researchgate.net/publication/315698586_Fiber-reinforced_lime_mortars
8. Iucolano F, Liguori B, Colella C (2013) Fibre-reinforced lime-based mortars: A possible resource for ancient masonry restoration. Con. Build. Mat. doi:10.1016/j.conbuildmat.2012.09.050
9. Přinosil M. Multiscale testing, modeling and design of fiber-reinforced lime-based mortars. Doctoral Thesis, CTU in Prague, 2015, 169 p.
10. Přinosil M, Kabele P (2016) Mechanical Properties of Fiber Reinforced Lime-Based Mortars Evaluated from Four-Point Bending Test. Appl.Mech. and Mat. Vol. 821, pp 526-531.doi:10.4028/www.scientific.net/AMM.821.526
11. Drdäcký M, Urushadze Sh, Papadopoulou K (2016) Out-of-plane behavior of masonry walls with imperfect reinforced rendering. In Maka S, Duwal S. (ed.). International Conference on Earthquake Engineering and Post Disaster Reconstruction Planning. Conference proceedings. Part 1 Bhaktapur: Khwopa Engineering College & Khwopa College of Engineering, 314-322.

Comparative evaluation of the morphological and rheological characteristics of nanolime dispersions for the consolidation of architectural monuments

Anastasia Michalopoulou^{1,2}, Elisavet Michailidi¹, Evangelos Favvas¹, Noni-Pagona

Maravelaki¹, Vassilis Kilikoglou¹, Ioannis Karatasios¹

(1) Institute of Nanoscience and Nanotechnology, National Centre for Scientific Research “Demokritos” and School of Architecture, Technical University of Crete a.michalopoulou@inn.demokritos.gr

(2) School of Architecture, Technical University of Crete

Abstract

This paper focuses on the comparative evaluation of four different laboratory synthesized nanolime dispersions. The modification of the surface tension between the dispersion medium and nano-particles was realized by the addition of Triton –X100 (non-ionic surfactant) and the use of mixed polar dispersion mediums of 2-propanol and a) distilled water or b) an O₂ nano-bubbles (NBs) enriched aqueous dispersion medium. The morphological and mineralogical characterization of the nanoparticles produced was carried out by Scanning Electron Microscopy (SEM) and X-Ray Diffraction (XRD) analysis. The stability of the dispersions was determined by UV-VIS spectroscopy.

The evaluation of the consolidation effectiveness was focused on the penetration ability of the nanodispersions. The modification of the surface tension with the addition of the non-ionic surfactant and the use of a mixed polar dispersion medium led to the reduction of the nanoparticles size and the absence of aggregates. Also, the mixed use of 2-propanol and distilled water enriched with NBs of O₂ underlined that the relation between kinetic stability and the penetration ability of the nano-dispersions is not proportional.

Introduction

Consolidation of porous building materials such as natural stones, mortars and bricks holds a significant role in the field of the conservation of architectural heritage, since it promotes the re-adjustment of the internal cohesion of the decayed parts of the substrate and prevents the substrate from fast degradation due to prolonged impact of natural weathering phenomena [1-3]. The consolidation action of nanolime dispersions involves three main stages: a) penetration, b) deposition of Ca(OH)₂ nanoparticles inside the pores of the calcareous substrate and c) the subsequent carbonation of Ca(OH)₂ to calcium carbonate [4-5].

Compared to traditional limewater, nanolime dispersions present both chemical and mineralogical compatibility with the calcareous substrate, elevated percentage of active

component, [6-7] and enhanced reactivity of the active component (due to the particle size in the nano-scale) [8]. However, the application of nanolime dispersions is still characterized by specific disadvantages such as the phase separation between the $\text{Ca}(\text{OH})_2$ nanoparticles and the dispersion medium [9], presence of aggregation phenomena and the consequent poor penetration ability and the partial migration of the nanoparticles during the evaporation of the organic dispersion medium [7, 10]. The production of stable nanodispersions, without the presence of aggregation phenomena is currently based on the reduction of the surface tension between the $\text{Ca}(\text{OH})_2$ nanoparticles and the dispersion medium by either electrostatic stabilization (through the addition of a polar solvent) or steric stabilization (with the use of non-ionic surfactants) [8].

Aiming to contribute in this area, this study concerns the comparative evaluation of four $\text{Ca}(\text{OH})_2$ nanodispersions in terms of their rheological characteristics and the morphological characteristics of the $\text{Ca}(\text{OH})_2$ nanoparticles. The modification of the surface tension between the dispersion medium and nanoparticles was achieved by the addition of Triton X100 (non-ionic surfactant) and the use of mixed polar dispersion mediums of 2-propanol and a) distilled water [8] or b) an O_2 nano-bubbles (NBs) enriched aqueous dispersion medium [13]. The application of the four $\text{Ca}(\text{OH})_2$ nanodispersions on two different substrates (a natural sandstone and a calcareous mortar) was evaluated in terms of the penetration ability of the $\text{Ca}(\text{OH})_2$ nanodispersions and the morphological characterization of the deposited material.

Materials and Methods

Materials

The $\text{Ca}(\text{OH})_2$ nanoparticles were produced via the two main methodologies: a) bottom-up and b) top-down. For the synthesis of the $\text{Ca}(\text{OH})_2$ nanoparticles, the following materials were used: i) calcium chloride hydrated ($\text{CaCl}_2 \cdot \text{H}_2\text{O} \geq 99\%$, Sigma-Aldrich), ii) sodium hydroxide ($\text{NaOH} \geq 98\%$, Sigma-Aldrich), iii) 2-propanol ($\text{C}_3\text{H}_8\text{O} \geq 99.5\%$) (Sigma-Aldrich), as reagents, and iv) Triton-X 100 (Sigma-Aldrich) as surfactant. The polar dispersion medium was different for the four synthetic procedures, as presented in Table 1. Three types of dispersion medium were used: a) distilled water ($\text{Cd} = 1.7 \mu\text{S}$), b) 2-propanol and c) distilled water enriched with O_2 nanobubbles (NBs) of average dimension ca. 800 nm.

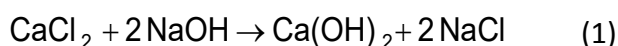
Table 1. Description of the experimental procedures of the four nanolime dispersions

Sample	Method	Dispersion medium
Exp01	Bottom-up	50 % Dist. water + 50 % 2-propanol
Exp02	Bottom-up	20 % Dist. water + 80 % 2-propanol
Exp03	Bottom-up	20 % O_2 NBs + 80 % 2-propanol
Exp04	Top-down	20 % Dist. water + 80 % 2-propanol

Synthesis of Ca(OH)₂ nanoparticles

Bottom-up methodology

The synthesis of the Ca(OH)₂ nanoparticles was based on the displacement reaction between calcium chloride CaCl₂ (0.3 mol/L) and sodium hydroxide NaOH (0.6 mol/L) in aqueous solution (bottom-up method). Following the relevant literature, 1 g of Triton X-100 was previously added to the calcium chloride aqueous solution [11]. The final products were calcium hydroxide nanoparticles Ca(OH)₂ and the water soluble sodium chloride NaCl (as by-product), according to the reaction:



NaOH was added drop by drop in the CaCl₂·H₂O solution. The temperature of both reactants and the final products solutions was maintained constant at 90 °C throughout the synthetic procedure, using a thermal bath, in order to reduce the dissolution of the newly formed calcium hydroxide in the aqueous dispersion medium. The synthetic procedure was implemented with the use of a special reactor providing inert atmospheric conditions (He).

At the end of the synthesis, the NaCl by-product was removed by continuous washings. At the final step of the experimental procedure, the aqueous dispersion medium was substituted with a mixed polar dispersion medium (as presented in Table 1).

An alternative approach was the replacement of the aqueous dispersion medium with distilled water enriched with nanobubbles of O₂. Nanobubbles are gaseous cavities (in the specific case of O₂) of nanometric size, presenting high stability, longevity and ability of adsorption mainly to hydrophobic surfaces [12-13]. In the specific case, due to the average size of the nanobubbles (800 nm) suspended in distilled water, they can be characterized as bulk nanobubbles [13]. The stability of the specific dispersion medium is attributed to the innovative method of production stable nanobubbles (gas phase) in the bulk aqueous phase. The design of the procedure is based on the phenomenon of cavitation and dissolution of the gas phase in the vortex zone through the flow/circulation of water and is implemented with the use of generator with particular characteristics [4,14-16].

Top-down methodology

According to relevant references for the top-down methodology [5],[9], approximately 2.2 g of laboratory produced lime putty by mixing 1.2:1 w/w water with (Ca(OH)₂), matured for three years (d=1.75 g/cm³), where dissolved in 200 ml of distilled water (Exp04) , under continuous stirring for 1.5 hours. The water content of the paste was taken into account, in order to produce a nanodispersion of a solid content of similar concentration (e.i. close to 1 wt%) with the other three nanodispersions (Exp01-03).

The addition of the non-ionic surfactant Triton X-100 ($C_{14}H_{22}O(C_2H_4O)_{10}$) was common in all four experimental procedure. The selection of the specific surfactant was based on its ability of being adsorbed on the surface of the $Ca(OH)_2$ nanoparticles, forming a steric barrier, thus, preventing the occurrence of aggregation phenomena between the $Ca(OH)_2$ nanoparticles. The optimum amount of the surfactant was selected following the relevant literature [11].

Preparation of substrates and application procedure

Two types of substrates were selected a) a porous sandstone, consisted of quartz, calcite and K-feldspar and b) a historic lime mortar. Cubic specimens ($3 \times 3 \times 3 \text{ cm}^3$) were cut off from larger blocks and dried at $60 \pm 5 \text{ }^\circ\text{C}$ to constant mass. Aiming to primarily investigate the effect of the alteration of the dispersion medium on the morphological and rheological characteristics of the dispersions, all four newly formed nanolime dispersions were applied drop to drop on the top face of the cubic specimens, by the use of a pipette and a brushstroke, allowing the nanolime dispersions to be fully absorbed between two consecutive applications (Figure 1). The nanolime dispersions were being placed under ultrasonic agitation throughout the application procedure. The application of the nanolime dispersion was completed after 10 consecutive applications. Upon consolidation completion, the samples were stored in a sheltered box for 28 days, under laboratory atmospheric conditions ($T = 20 \text{ }^\circ\text{C}$, $RH = 60\text{-}80 \%$).



Figure 1. Application procedure

Methods

Characterization of the nanolime dispersions

In all four samples, nanolime was dispersed by the use of ultrasonic agitation (UIP 1000 hdT Hielscher), in order to achieve disaggregation of any agglomerates formed.

The mineralogical characterization was implemented by X-ray powder diffraction (XRD), in a Siemens D-500 diffractometer, using the $Cu\text{-}K\alpha$ radiation ($\lambda = 1.5406 \text{ \AA}$) with a graphite monochromator in the diffraction beam, at 1.2 kW (40 kV, 30 mA). The diffractograms were collected in the range of $5\text{-}55^\circ 2\theta$ scale, with a step of

0.03 °/sec. All four samples were deposited on Si wafers adjusted on typical XRD holders and left to dry under laboratory conditions. The evaluation of the morphological characteristics of the nanoparticles was carried out primarily by Scanning Electron Microscope coupled with Energy Dispersive X-ray analyzer (SEM/EDX). SEM images were acquired in a FEI Quanta Inspect instrument operated at 25 kV. All specimens were deposited on carbon taped SEM-holders, left to dry under laboratory conditions and were gold-coated prior to examination.

The kinetic stability (KS) of all four nanolime dispersions was estimated by turbidity measurements, determining the absorbance at $\lambda = 600$ nm in respect to time (upon 4 hours) intervals by UV/VIS spectrometer (UV2100 Veluda). The turbidity of the dispersions is considered to be proportional to the absorbance at 600 nm, and its decrease over time is related with the occurrence of particle agglomeration and settling. The relative kinetic stability (KS %) is estimated according to the formula (2):

$$KS \% = \left\{ 1 - \frac{(A_o - A_t)}{A_t} \right\} \times 100 \quad (2)$$

Where A_o is the starting absorbance and A_t the t time interval [10].

Evaluation of the penetration ability of the nanolime dispersions

At the end of the 10th application, the penetration of the nanolime dispersions was estimated with the use of phenolphthalein test. In specific, 1 % phenolphthalein solution (60 % ethanol-40 % water) [7] was applied by spraying directly on the surface, indicating through the alteration of colour (from colourless to purple) the basic pH > 9.8 [7], and thus the penetration and deposition of the Ca(OH)₂ nanoparticles. The observation of the penetration of the nanolimes was also observed by the use of the stereomicroscope.

Results and Discussion

Characterization of the Ca(OH)₂ nanoparticles

Mineralogical characterization

The results of all nanolime dispersions were characterized by the presence of portlandite (Ca(OH)₂). In particular the presence of the major peaks 4,667 Å, 3,077 Å, 2,62 Å, 1,75 Å, and 1,64 Å [17], along with the sharpness of the peaks, led to the identification of portlandite particles with typical hexagonal crystal structure (Figure 2). A minor phase identified was calcite (CaCO₃) [18] (Figure 2).

The presence of calcite was related with the initiation of the carbonation process and could be connected with the aqueous part of the dispersion medium and the consequent

formation of a surface film on the $\text{Ca}(\text{OH})_2$, promoting the dissolution of CO_2 and thus the initiation of the carbonation reaction [5, 7, 19].

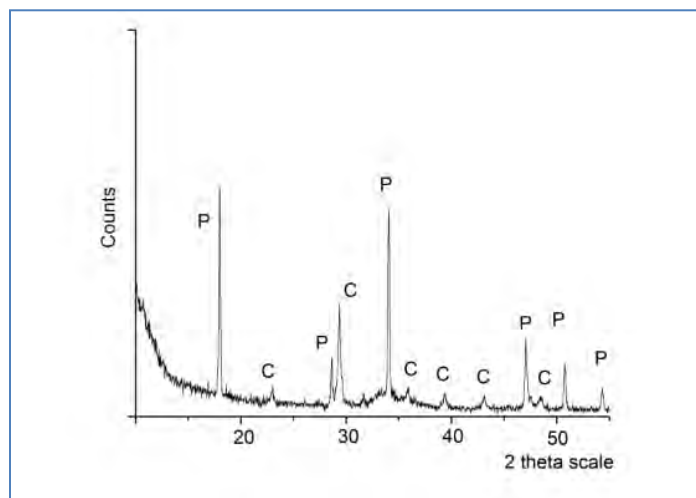


Figure 2. Representative X-ray diffraction pattern of the produced particles of the bottom-up methodology

Morphological characterization

The morphological characteristics of the newly formed nanoparticles produced following the bottom-up synthetic route, based on electron microscopy examination (SEM), are presented in Figures 3-4.

The use of mixed polar dispersion medium (1:1 distilled water and 2-propanol) (Exp01) resulted in the production of plate-like and of undetermined shape nanoparticles of $\text{Ca}(\text{OH})_2$ (Figure 3a). The dimensions of the nanoparticles vary between 180 -600 nm. Also, they presented a preferential alignment on the hexagon base.

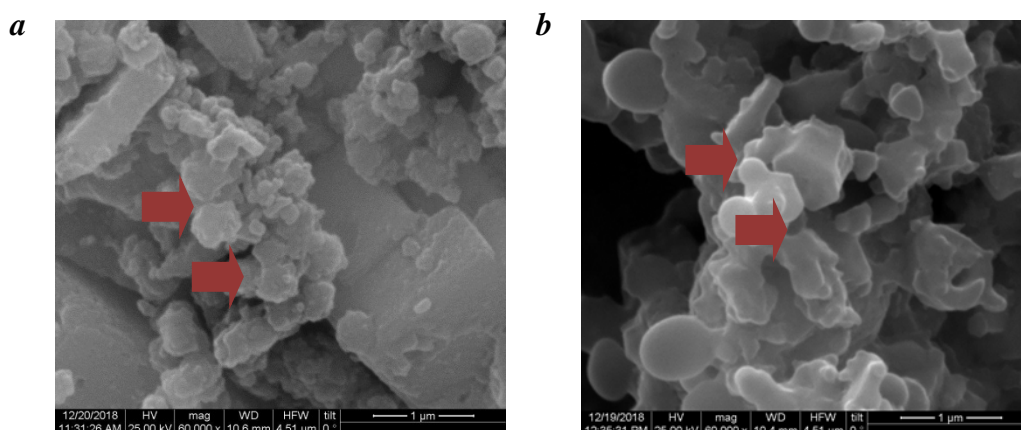


Figure 3. (a) Plate-like and of undetermined shape nanoparticles of $\text{Ca}(\text{OH})_2$ (Exp01); (b) Hexagonal, spherical and of undetermined angular shape nanoparticles of $\text{Ca}(\text{OH})_2$ (Exp02)

The increase of the amount of 2-propanol in the mixed polar dispersion medium (Exp02) resulted in the production of hexagonal, spherical and of undetermined shape nanoparticles

of $\text{Ca}(\text{OH})_2$ (Figure 3b). The dimensions of the nanoparticles vary between 200 -800 nm. The use of distilled water enriched with NBs of O_2 (Exp03) with the 2-propanol resulted in the production of hexagonal, spherical and angular nanoparticles of $\text{Ca}(\text{OH})_2$ (Figure 4a).

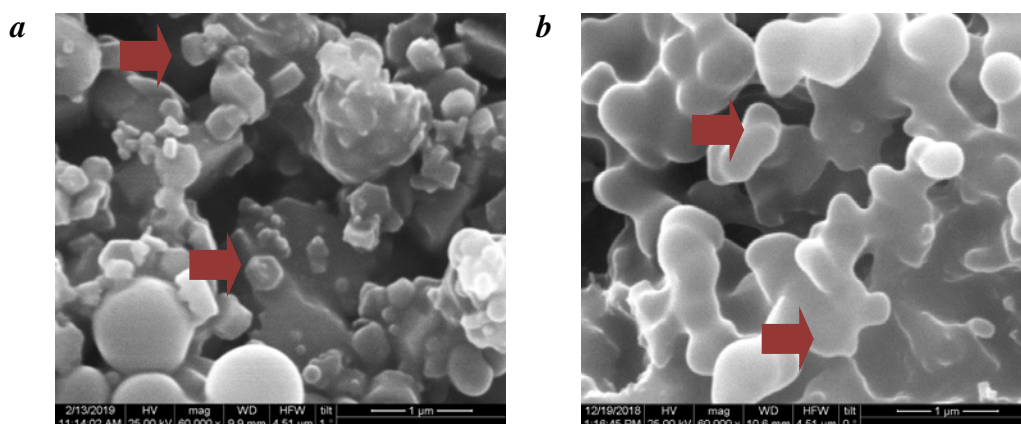


Figure 4. (a) Hexagonal, spherical and angular nanoparticles of $\text{Ca}(\text{OH})_2$ (Exp03); (b) Spherical and angular nanoparticles $\text{Ca}(\text{OH})_2$ and presence of aggregates (Exp04)

The nanoparticles were characterized by the variation in terms of size and shape, and their dimensions vary between 110 -450 nm. Whereas, the use of the same mixed polar dispersion medium following the top-down synthetic route (Exp04) resulted in the production of spherical and angular nanoparticles $\text{Ca}(\text{OH})_2$ and the presence of aggregates (Figure 4b). The dimensions of the nanoparticles vary between 100 -400 nm.

Stability of the nanolime dispersions

The relative kinetic stability of the four nanolime dispersions is presented in Figure 5.

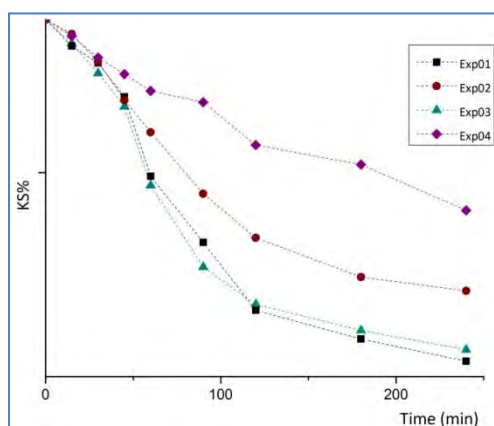


Figure 5. Relative kinetic stability of the four nanolime dispersions

Overall, the addition and increase of content of 2-propanol (Exp01, Exp02 compared to Exp03 and Exp04) proved to have a direct effect to the increase of the colloidal stability of the nanolime dispersions (Figure 5). According to the relevant literature [5, 20] the increase of the colloidal stability of the nanoparticles is caused by the adsorption of 2-propanol on their surface, creating a hydrophobic effect, thus reducing the dissolution of the nanoparticles and increasing their overall colloidal stability. Furthermore, the use of distilled

water enriched with O₂ NBs instead of water (Exp03) proved to cause a slight reduction of the colloidal stability of the dispersions. Finally, the nanolime dispersion produced via the top-down synthetic route (Exp04) proved to be more stable, when compared with the nanolime dispersions produced via the bottom –up synthetic route (Figure 5).

Evaluation of treatment effectiveness

Overall, the evaluation of the penetration ability of the four nanolime dispersions underlined the penetration of the dispersions inside the porous substrates of the sandstone, contrary to the poor and superficial penetration ability of the dispersions in the mortars (Figure 6).

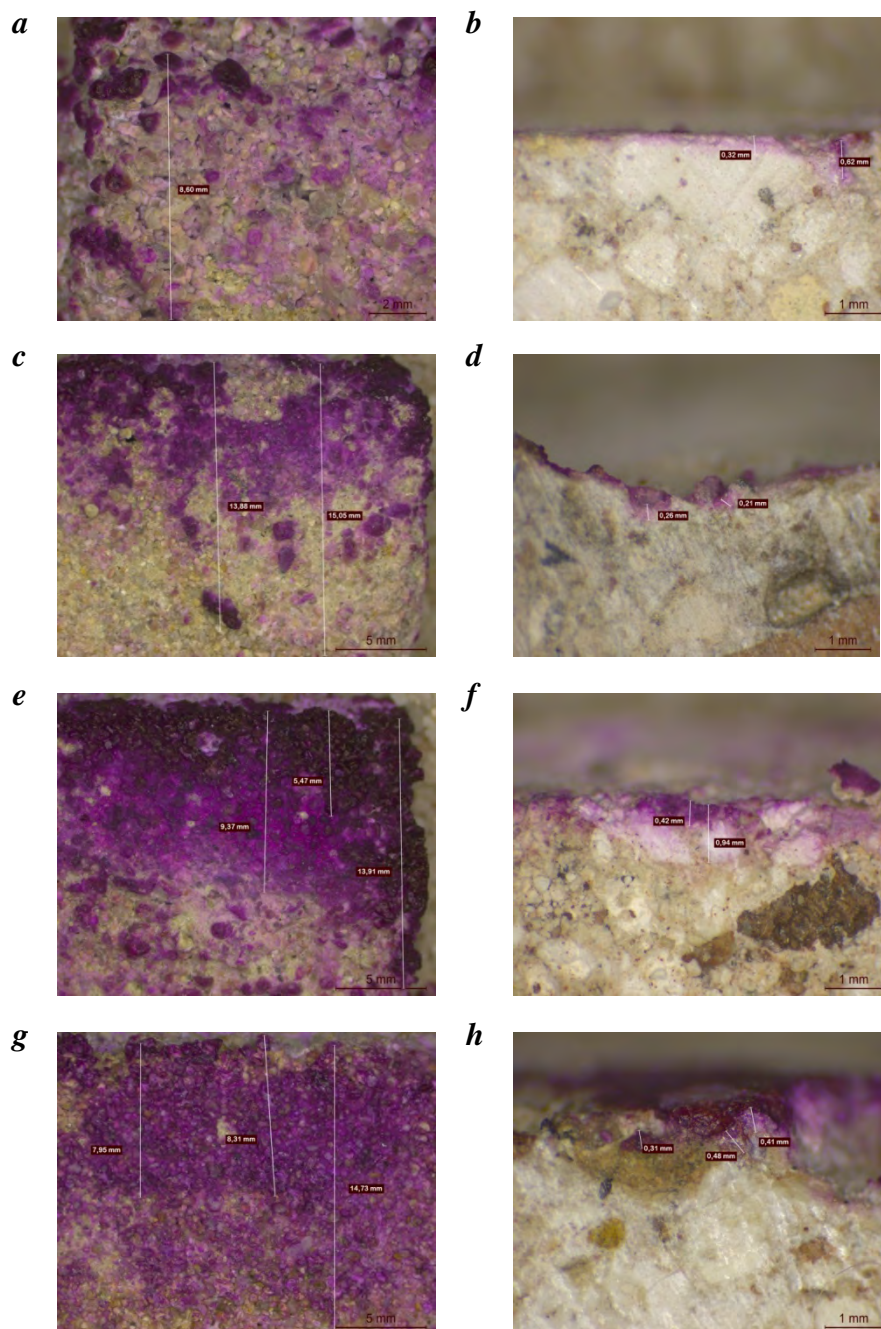


Figure 6. Evaluation of penetration ability on sandstone of a) Exp01, c) Exp02, e) Exp03 and g) Exp04 and on mortar b) Exp01, d) Exp02, f) Exp03 and h) Exp04

Exp01 and Exp03 presented an intense increase on the penetration ability inside both substrates (Figure 6a, 6b and 6e, 6f, respectively). In specific, in the case of sandstone, the extent of the penetration of the two dispersions varied from 13 to 35 mm, whereas in the case of mortar they penetrated up until 1mm. Exp02 and Exp04, presented a slight increase in the penetration ability inside the sandstone reaching the 15 mm, whereas the penetration ability inside the mortar remained up until 0,41 mm (Figure 6c, 6d and 6g, 6h, respectively).

It must be mentioned that in the case of Exp03, the $\text{Ca}(\text{OH})_2$ nano-dispersion proved to be characterized by low kinetic stability (Figure 5) and enhanced penetration ability into the porous substrate (Figure 6e). This underlined the fact that in the case of the use of 2-propanol and of distilled water enriched with NBs of O_2 , the relation between kinetic stability and the penetration ability of the nano-dispersions is not proportional.

The examination of the treated samples after 28 days was implemented by the use of SEM/EDX (Figure 7). Overall, the evaluation of the penetration ability of the four nanolime dispersions underlined the penetration of the dispersions inside the porous substrates of the sandstone, contrary to the poor penetration at the layers close to the surface, observed in the case of the mortar. The comparison between the untreated sandstone specimens (Figure 7a) to the four treated specimens (Figure 7b-e) underlined the precipitation and deposition of the $\text{Ca}(\text{OH})_2$ nanoparticles on the grains and the binding medium of the sandstone and inside the pores. Upon completion of the carbonation process, in all four cases the calcite crystals that were observed could be characterized by uniformity in size. In the cases of Exp01, Exp02 and Exp04, where mixed polar dispersion mediums (2-propanol and distilled water) were used, calcite crystals rhombohedral calcite crystals with scalenohedral terminations were identified (Figure 7b,c,e).

The use of the distilled water enriched with NBs of O_2 with the 2-propanol (Exp03) resulted in the production of calcite crystals of both tabular and rhombohedral with scalenohedral terminations [2, 21] (Figure 7d). In the case of the mortar specimens, the comparison between the untreated sample (Figure 7f) and the treated ones, revealed that the $\text{Ca}(\text{OH})_2$ nanoparticles were precipitated and deposited inside the pores of the surface layers. This is more evident in the cases of Exp02 and Exp03, where calcite crystals rhombohedral calcite crystals with scalenohedral terminations were identified (Figure 7g and 7h, respectively).

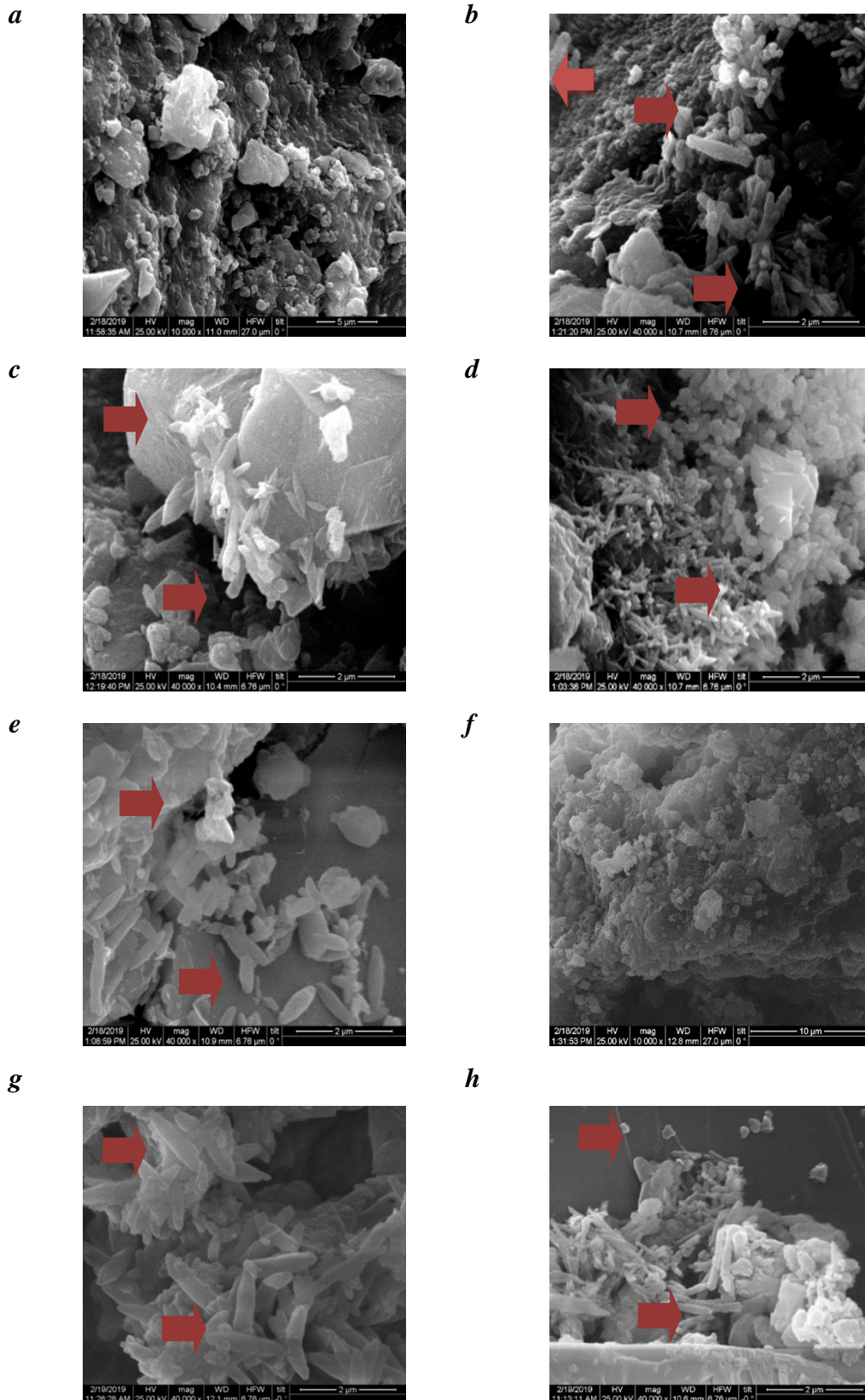


Figure 7. SEM observations of *sandstone* a) untreated and treated specimens with sandstone of b) Exp01, c) Exp02, d) Exp03 and e) Exp04 and of *mortar* f) untreated g) Exp02 and h) Exp03

Conclusions

The comparative evaluation of $\text{Ca}(\text{OH})_2$ nanodispersions synthesized with the bottom-up methodology and characterized by the use of different polar dispersion medium revealed the direct effect of the polar dispersion medium on the shape and size of the $\text{Ca}(\text{OH})_2$ nanoparticles. The use of 2-propanol resulted to the formation hexagonal, spherical and of undetermined shape nanoparticles of $\text{Ca}(\text{OH})_2$. The addition of 2-propanol resulted in the enhancement of the kinetic stability and consequently, the penetration ability of the nanodispersions. However, the size of the nanoparticles was slightly enhanced.

The use of distilled water enriched with NBs of O_2 resulted in an improvement in terms of the morphological characteristics of the $\text{Ca}(\text{OH})_2$ nanoparticles that is summarized on the production of hexagonal particles in the nano-scale and absence of aggregation phenomena. Although, this was not reflected in the reduced kinetic stability of the $\text{Ca}(\text{OH})_2$ nanodispersions, the nanodispersion presented enhanced penetration. This highlighted the fact that, in the specific case, the relation between kinetic stability and the penetration ability of the nanodispersions was not proportional.

In contrast, the use of the break-down methodology resulted in the production of micro-scale sized aggregates of nanoparticles of $\text{Ca}(\text{OH})_2$. The enhanced kinetic stability presented did not result in an enhanced penetration ability of the nanodispersions.

Overall, the use of distilled water enriched with NBs of O_2 proved to improve the morphological characteristics of the nanoparticles of $\text{Ca}(\text{OH})_2$, whereas the addition of 2-propanol proved to improve kinetic stability, and consequently the penetration ability of the nanodispersions. Finally, the application of nanodispersions of $\text{Ca}(\text{OH})_2$ turned out to be more efficient in the case of the porous sandstone, in contrast with the air lime mortar.

Acknowledgements

This research is co-financed by Greece and the European Union (European Social Fund- ESF) through the Operational Programme «Human Resources Development, Education and Lifelong Learning» in the context of the project “Strengthening Human Resources Research Potential via Doctorate Research” (MIS-5000432), implemented by the State Scholarships Foundation (IKY).



References

1. Karatasios I, Theoulakis P, Kalagri A, Sapalidis A, Kilikoglou V (2009) Evaluation of consolidation treatments of marly limestones used in archaeological monuments. *Constr and Build M* doi:10.1016/j.conbuildmat.2009.03.001
2. Arizzi A, Gomez-Villalba L S, Lopez-Arce P, Cultrone G, Fort R (2015) Lime mortar consolidation with nanostructured calcium hydroxide dispersions: the efficacy of different consolidating products for heritage conservation. *Eur J Mineral* doi: 10.1127/ejm/2015/0027-2437
3. Maravelaki-Kalaitzaki P, Kallithrakas-Kontos N, Agioutantis Z, Maurigiannakis S, Korakaki S (2008) A comparative study of porous limestones treated with silicon-based strengthening agents, *Progr in Org Coat* doi: 10.1016/j.porgcoat.2007.09.020
4. Michalopoulou A, Favvas EP, Mitropoulos AC, Maravelaki P, Kilikoglou V, Karatasios I (2018) A comparative evaluation of bottom-up and top-down methodologies for the synthesis of calcium hydroxide nanoparticles for the consolidation of architectural monuments. *Mat Tod: Proc* doi: 10.1016/j.matpr.2018.09.060
5. Rodriguez-Navarro C, Suzuki A, Ruiz-Agudo E (2013) Alcohol Dispersions of Calcium Hydroxide Nanoparticles for Stone Conservation. *Langm* doi: 10.1021/la4017728
6. Daehne A, Herm C (2013) Calcium hydroxide nanosols for the consolidation of porous Build. materials - results from EU-STONECORE, *Her Sci* doi: 10.1186/2050-7445-1-11
7. Borsoi G, Lubelli B, Van Hees R, Veiga R, Santos Silva A (2016) Understanding the transport of nanolime consolidants within Maastricht limestone *J of Cult Her* doi: 10.1016/j.culher.2015.07.014
8. Baglioni P, Chelazzi D, O'Brien P, Nanoscience for the Conservation of Works of Art, RCR Nanotechnology and Nanoscience N. 28, (Eds.) (2013) Royal society of Chemistry, Cambridge
9. Ambrosi M, Dei L, Giorgi R, Neto C, Baglioni P (2001) Colloidal Particles of $(Ca\ OH)_2$: Properties and Applications to Frescoes Restoration. *Langm* doi: 10.1021/la010269b
10. Borsoi G, Lubelli B, VanHees R, Veiga R, Santos Silva A, Colla L, Fedele L, Tomasin P (2016) Effect of solvent on nanolime transport within limestone: How to improve in-depth deposition. *Coll and surf A: Physicochem And Eng Asp* doi: 10.1016/j.culher.2015.07.014
11. Daniele V, Taglieri G (2012) Synthesis of $Ca(OH)_2$ Nanoparticles with the Addition of Triton X-100. Protective Treatments on Natural Stones: Preliminary Results. *J of Cult Her* doi:10.1016/j.culher.2016.06.010

12. Azevedo A, Etchepare R, Calgaroto S, Rubio J (2016) Aqueous dispersions of nanobubbles: Generation, properties and features. *Min Eng* doi: 10.1016/j.mineng.2016.05.0010892-6875
13. Kyzas Z, Bomis G, Kosheleva RI, Efthimiadou EK, Favvas EP, Kostoglou M, Mitropoulos AC (2018), Nanobubbles effect on heavy metal ions adsorption by activated carbon. *Chem. Eng J* doi: 10.1016/j.cej.2018.09.019
14. Mitropoulos AC, Stefanopoulos KL, Favvas EP, Vansant EF, Hankins N (2015) On the Formation of Nanobubbles in Vycor Porous Glass During Desorption of Halogenated Hydrocarbons. *Sc Rep* doi: 10.1038/srep10943
15. A. Mitropoulos, G. Bomis, European Patent 2995369A1 Mar (2016) Mar 2016
16. Favvas E, Mitropoulos A, Bomis G, Varoutoglou A, Kosheleva R, Michailidi E, Efthimiadou E, Hellenic Industrial Property Organisation (2017) Application for Patent (Submitted).
17. Nagai T, Ito T, Hattori T, Yamanaka T (2000), Compression mechanism and amorphization of portlandite. *Phys and Chem of Min* doi:10.1007/s002690000084
18. Antao SM, Hassan I (2010) Temperature dependence of the structural parameters in the transformation of aragonite. *The Can Min* doi: 10.3749/canmin.48.5.1225
19. Cizer O, Balen K, Elsen J, Van Gemert D (2012) Real-time investigation of reaction rate and mineral phase modification of lime carbonation. *Constr and Buil Mater* doi: 10.1016/j.conbuildmat.2012.04.036
20. Fratini E, Page MG, Giorgi R, Colfen H, Baglioni P, Deme B, Zemb T (2007) Competitive Surface Adsorption of Solvent Molecules and Compactness of Agglomeration in Calcium Hydroxide Nanoparticles. *Lang* doi: 10.1021/la062023i
21. Otero J, Starinieri V, Charola AE (2018) Nanolime for the consolidation of lime mortars: A comparison of three available products. *Constr and Build M* doi:10.1016/j.conbuildmat.2018.06.055

Autogenic vs. autonomic self-healing process in conservation mortars with crystalline admixture

Maria Amenta¹, Matina Papaioannou¹, Marios S. Katsiotis², Dimitris Gournis³, Vassilis

Kilikoglou¹, Ioannis Karatasios¹

(1) Institute of Nanoscience and Nanotechnology, N.C.S.R. Demokritos, Athens, Greece, m.amenta@inn.demokritos.gr, s.papaioannou@inn.demokritos.gr, v.kilikoglou@inn.demokritos.gr, i.karatasios@inn.demokritos.gr

(2) Group Engineering Technology, TITAN Cement Company S.A., Athens, Greece, m.katsiotis@titan.gr

(3) Department of Materials Science & Engineering, University of Ioannina, Ioannina, Greece, dgourni@cc.uoi.gr

Abstract

Self-healing mortars can serve as a promising solution for enhancing the efficiency of conservation interventions, extending their service life and safeguarding built heritage. In this study, the autogenic self-healing capacity of natural hydraulic lime mortars is contrasted with the autonomic self-healing capacity of the same mixture with the addition of a crystalline admixture (CA). The self-healing capacity of both mixtures was evaluated by water permeability and capillary absorption tests. Moreover, the reduction of crack width due to self-healing was measured by means of optical microscopy, while the secondary healing phases produced inside the cracks were characterized and quantified by XRD and SEM/EDS. It was found that secondary healing products in NHL mixtures were mainly composed by calcite, portlandite and CSH phases whereas the addition of the crystalline admixture resulted in additional formation of sodium silicate hydrates. In terms of performance, it is shown that both mixtures partially recovered their water tightness due to the autogenic phenomenon, whereas the formation of CA healing products inside the micro-crack resulted in the enhancement of the autogenic self-healing mechanism which leads to a further reduction of water permeability.

Introduction

The autogenous self-healing phenomenon in cement-based materials is a new field of research that aims at reducing the requirement of external maintenance interventions and at the same time decrease the overall energy footprint of the buildings through the autonomic healing of micro-cracks by secondary reaction products [1]. In self-healing mortars, micro-cracks can be repaired without any external intervention. This could contribute greatly to the longevity of historic structures [2] by hindering the degradation phenomena due to penetration of aqueous weathering solutions.

This is a significant aspect in the design of restoration mortars e.g. natural hydraulic lime (NHL) mortars that usually exhibit moderate hydraulicity and low mechanical strength. The

low strength may result in the formation of multiple micro-cracks due to shrinkage cracking in the binder matrix, even from the first days of their application. The most common degradation mechanisms that take place in masonry structures are related to the presence of water or aqueous solutions. Micro-cracks formed in the cement matrix can act as entry points for aqueous solutions, which results in the development of salt crystallization, biological degradation, freeze-thaw related damages and eventually reinforcement corrosion [3, 4]. Thus, the preventive repair of these micro-cracks could postpone the appearance of degradation phenomena and enhance the durability of the mortars.

In cement mortars, self-healing mechanism can take place autogenously [5, 6], however, the addition of admixtures that act as healing agents may further promote the self-healing efficiency of the material. In this context, crystalline admixtures are used mainly for waterproofing applications when they are mixed in cement mortar or concrete. Therefore, their use as self-healing agents could be promising, since these admixtures could promote the production of secondary healing products within cracks, contributing to the water tightness of the mortars [7]. This property is often mentioned in the literature as “self-sealing”, indicating that the recovered property is specifically the water tightness [8].

In this study, the autogenic self-healing capacity of natural hydraulic lime (NHL) mortars is contrasted with the self-healing capacity of the same mixture with the addition of a commercially available crystalline admixture (NHL-CA). The methodological approach followed in this study is dual, focused both on the assessment of the performance recovery of the mortar specimens after controlled damage has been inflicted, as well as on the boundary conditions of the self-healing mechanism (cracking age, curing time, crack opening etc.). Specifically, the sealing capacity was evaluated by water permeability and capillary absorption tests considering aspects of healing period duration.

Materials and Methods

Two natural hydraulic lime (St. Astier NHL5) mortar mixtures were prepared according to BS-EN196-1, with (NHL-P) and without (NHL) the addition of a crystalline agent (Penetron Admix). Standard sand [CEN 196-1] was added as aggregate in a cement/aggregate ratio 1:3 (w/w) (Table 1).

Table 1. Mixture composition and flow table values

	NHL5 (g)	Crystalline admixture (g)*	b/a	w/c	Flow value (cm)
NHL	450	-	1:3	0.5	16
NHL-CA	450	4.5 (1%)	1:3	0.5	16
pNHL	1800	-	-	0.45	16
pNHL-CA	1800	180 (1%)	-	0.45	16

*Penetron Admix

Moreover, a second set of mixtures (pNHL, pNHL-P) was prepared without the addition of sand. All mixtures were cured in a temperature and humidity controlled chamber ($95\pm 2\%$ RH, $20\pm 2^{\circ}\text{C}$) until the designated cracking age and were subsequently cured under water for 14 or 28 days healing period.

Healing capacity – Sealing

In this study, the healing capacity was focused on the sealing potential of the specimens. Specifically, this was performed by applying two separate methodologies. The first method was used to measure the effect of the crack closure on the reduction of the capillary absorption of the mortar specimens and was based on the modification of the EN 1015-18 standard. The second method was used to assess the decrease of water permeability through the crack thus assessing the self-healing efficiency of the mortars.

Absorption by capillary through the crack

Prismatic specimens ($40\times 40\times 160$ mm) of each mortar mixture ($n=3$) (NHL, NHL-CA) were fractured by three point bending tests after different curing periods (14 and 28 days), in order to examine the effect of the age of the specimen when damage occurs. The notched specimens were subjected to three point bending tests in an INSTRON 100kN compression machine. A continuous load ($100\ \mu\text{m}/\text{min}$) was applied to all specimens, allowing the crack opening of specimens up to $100\ \mu\text{m}$ after crack initiation. The crack opening was measured in real-time during the test by COD sensors attached to the specimen surface (Figure 1). The characteristics of the cracks produced, were further determined by means of optical microscopy.

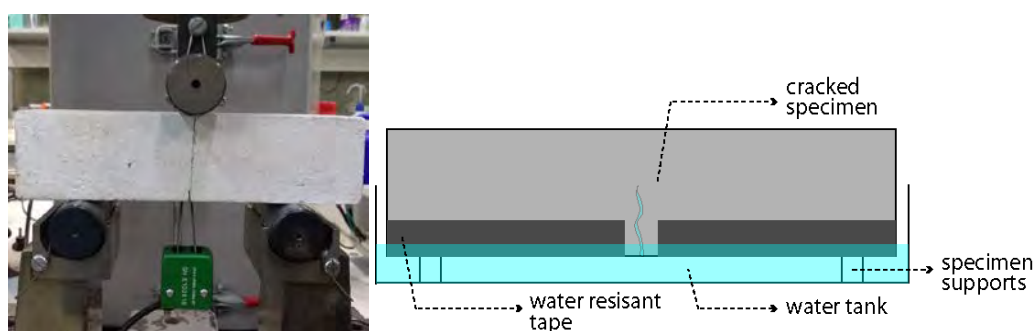


Figure 1. (Left) Crack control during 3-point bending test (left) and absorption by capillary through the crack test setup (right).

After cracking the specimens were immersed in water for an additional period of 14 or 28 days and then, water absorption by capillary through the crack was tested (Figure 1). Thus, the healing efficiency of the mixtures was assessed by the calculation of the absorption coefficient.

Water permeability

Similarly, cylindrical specimens of 135 mm diameter and 20 mm height were fractured in an INSTRON 100kN compression machine by Brazilian tensile stress. This fracture method results in a single crack along the two notches of the specimen (Figure 2). The characteristics of the produced cracks were also determined by means of optical microscopy. The cracked specimens were subsequently immersed in water and their water permeability was tested after 14 and 28 days. The decrease of the water flow due to the crack width reduction was measured for each mortar specimen and their healing efficiency was contrasted.

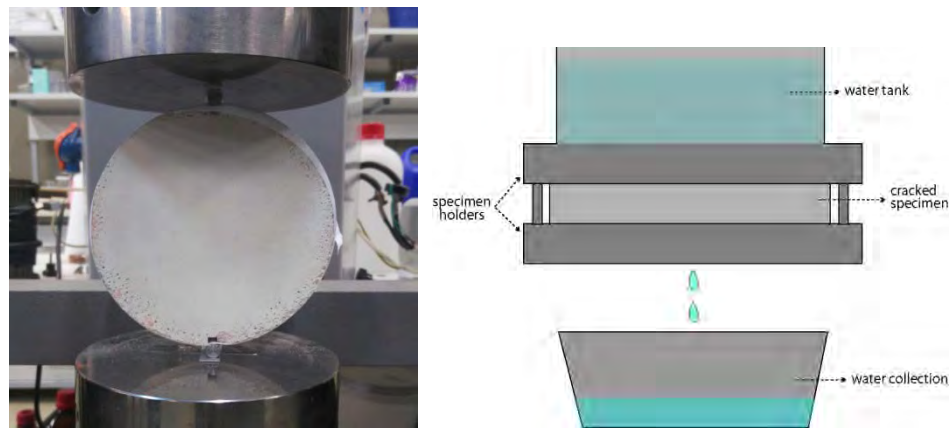


Figure 2. Splitting test of cylindrical specimens for water permeability measurements (left) and water permeability test setup (right).

Self-Healing mechanism - Characterization of healing products

In order to gain a better understanding of the self-healing mechanism, the characterization and quantification of healing products was performed following a separate experimental methodology. Prismatic specimens (40x40x160 mm) of each paste mixture (pNHL-P, pNHL,) were cut in parallel slices of 15 mm width after 28 days curing period (Figure 3). Subsequently the slices re-attached with each other, secured with rubber bands and cured under water, simulating the conditions of the self-healing mechanism taking place inside the cracks. After a subsequent 14 or 28 days healing period, the slices were separated and one slice was examined using Scanning Electron Microscopy (SEM) equipped with Energy Dispersive X-Ray Analysis (EDS), in order to examine the morphology, as well as the chemical composition of the secondary hydration products. Moreover, after the end of the healing period, the healing products were scraped off each slice and examined using X-ray diffraction (XRD) analysis in order to determine their composition after each healing period.

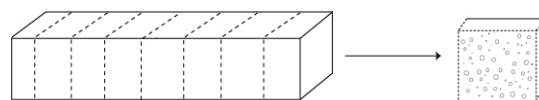


Figure 3. Specimen preparation for the characterization of healing products

Results

Self-Healing capacity – Sealing

Self-healing of cracked specimens was firstly examined at the stereomicroscope, through the observation of cracks before and after the designated healing period. The cracks were measured at two time intervals, i.e. after 14 and 28 days of healing under water. The detail of the observed cracks on the specimens surface in both NHL-CA and NHL control mixtures are shown in Figure 4. Evidently, the NHL-control specimens did not exhibit a measurable reduction of crack width due to autogenic self-healing (Figure 4). At the same time, NHL mixtures incorporating the crystalline admixture exhibited a high crack closure after 14 days of healing under water, which was also observed on the same specimen after 28 days.

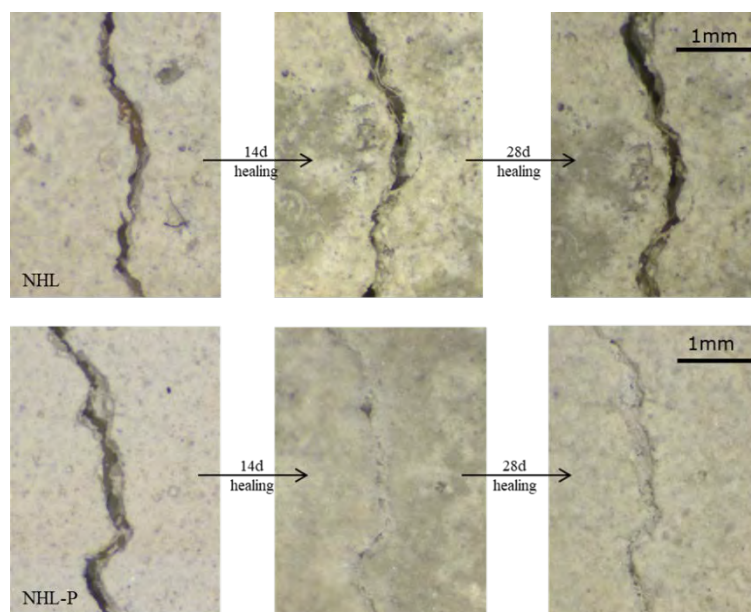


Figure 4. 200 µm crack healing observation at the stereomicroscope

Absorption by capillary through the crack

The capillary absorption measurements were carried out in cracked specimens, after 0, 14 and 28 days of healing. The absorption was reduced in both NHL-CA and control NHL specimens after 28 days of healing under water (Figure 5). More specifically, in NHL control specimens the reduction in water absorption is evident between 0 and 14 days, whereas additional curing period under water did not affect substantially its healing efficiency. At the same time, NHL-CA specimens exhibit lower initial water absorption (0 days) and a continuous reduction in water absorption after 14 and 28 days of healing. It is noteworthy that, after 28 days healing period, NHL-CA specimens showed overall lower water absorption coefficient, whereas the NHL control specimens exhibited a higher reduction of water absorption compared to their initial values.

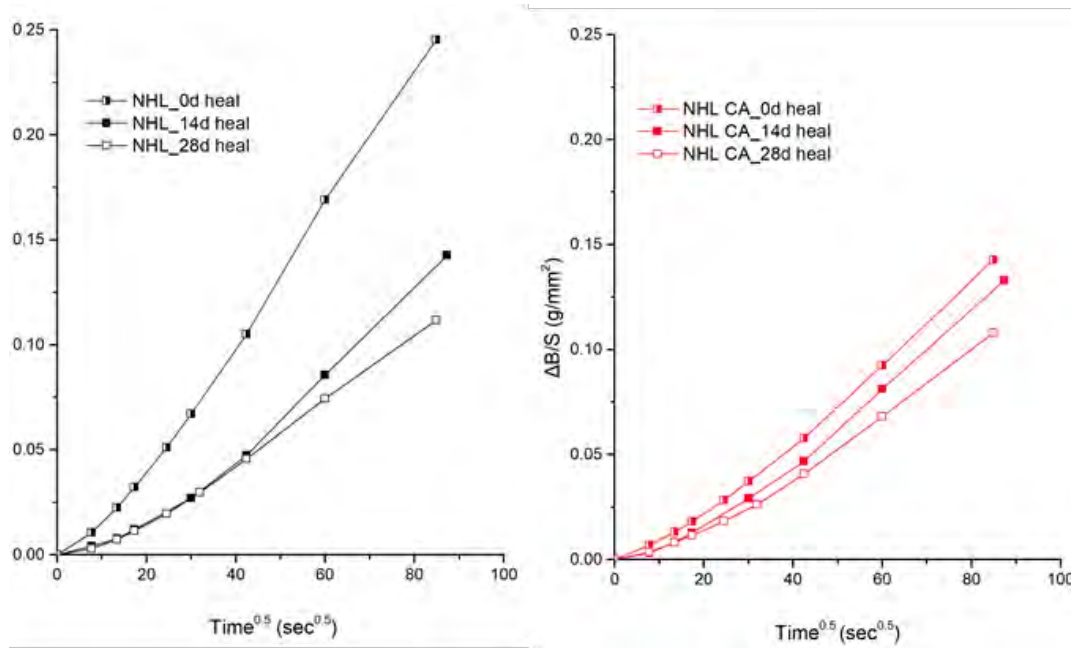


Figure 5. Water absorption by capillary through the crack after 0, 14 and 28 days healing period

Water permeability

Similar to the capillary absorption measurements, water permeability was measured after healing periods of 14 and 28 days. Figure 6 illustrates the flow of water passing through the cracked specimens after each healing period. Due to the autogenic self-healing capacity of NHL mortars, control specimens presented a 31% reduction in water flow between 14 and 28 days of healing. In the same manner, the crystalline admixture addition resulted in the enhancement of the autogenic phenomenon, reducing the water permeability by 78%.

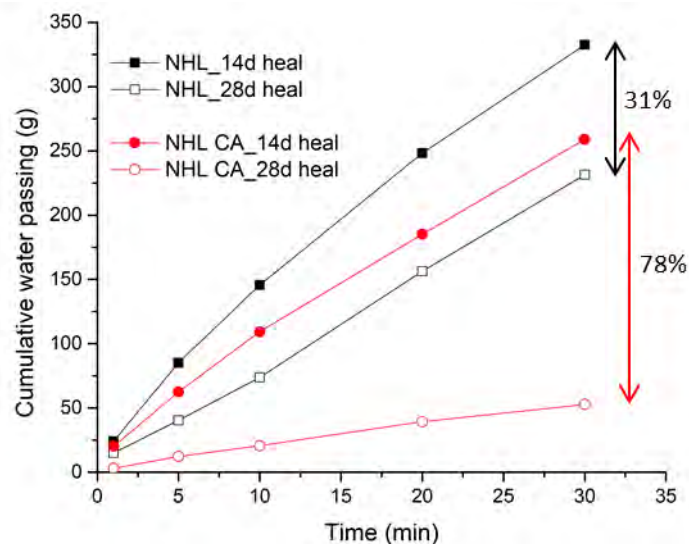


Figure 6. Cumulative water passing through the crack for the two mortar mixtures after 14 and 28 days healing period

Characterization of healing products

After the assessment of the water tightness recovery of the two mixtures, a deeper insight on the self-healing mechanism was attempted by combining microscopic and crystallographic techniques. The morphological characteristics of the healing products formed inside the cracks were examined using SEM combined with EDS analysis.

The evolution of the self-healing mechanism was examined by analysing the secondary healing products formed inside the cracks of the specimens cured for 14 or 28 days under water. In both mortar mixtures, irrespective of the addition of the CA, the presence of the autogenic healing mechanism products was profound. More specifically, well-formed portlandite crystals were abundant on the crack surface (Figures 7-8), as a result of the secondary hydration of the binder matrix alongside to CSH phases. Similarly, needle-like CSH phases were observed in all specimens, although their volume and density was higher in samples cured for 28 days under water (Figure 8).

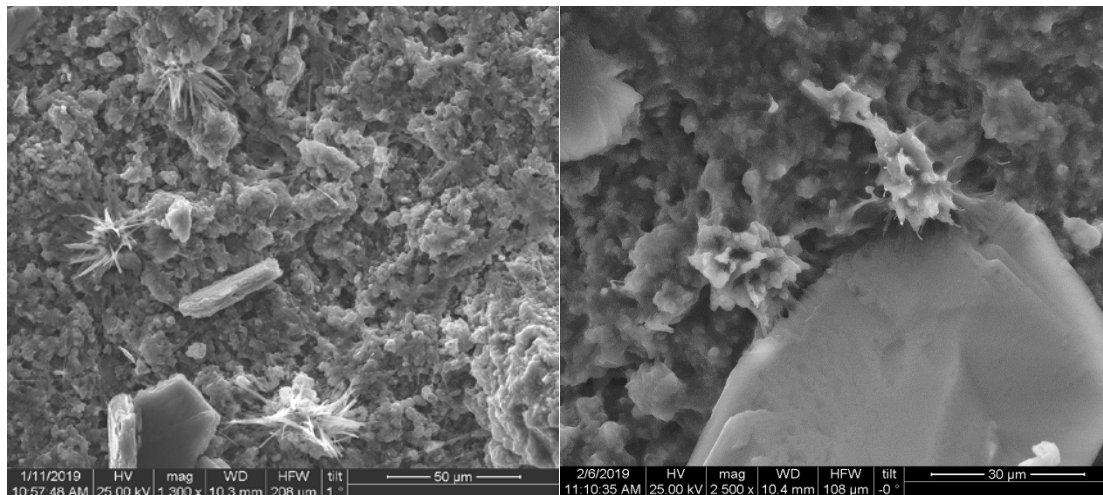


Figure 7. Portlandite crystals and needle-like CSH phases observed after 14 days healing period. NHL (left) and NHL-CA (right)

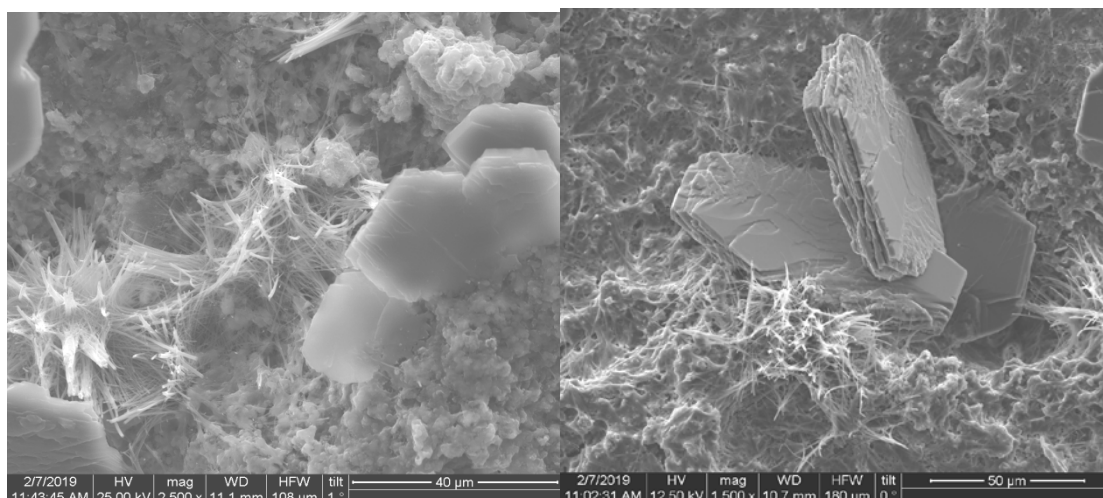


Figure 8. Portlandite crystals and needle-like CSH phases observed after 28 days healing period. NHL (left) and NHL-CA (right)

Regarding the NHL-CA mixtures, after 28 days of healing, the presence of dense Na-rich crystalline formations was observed (Figure 9). These phases, due to the presence of sodium in their composition, could be attributed to the CA. Moreover, the presence of scattered ettringite crystals was detected throughout the crack surface and its composition was verified by EDS (Figure 10).

XRD analysis also showed the presence of ettringite as an additional healing product in specimens incorporating the CA admixture (Figure 11). Moreover, the presence of portlandite and C-S-H phases were also corroborated by XRD analysis in both mixtures, since they are the main products of the autogenic self-healing mechanism. It is noteworthy that calcite was also detected by XRD analysis, which could be attributed mainly to the binder matrix of NHL mortars that is mainly composed of calcite. However, it could also derive from the carbonation of portlandite through the autogenic self-healing mechanism.

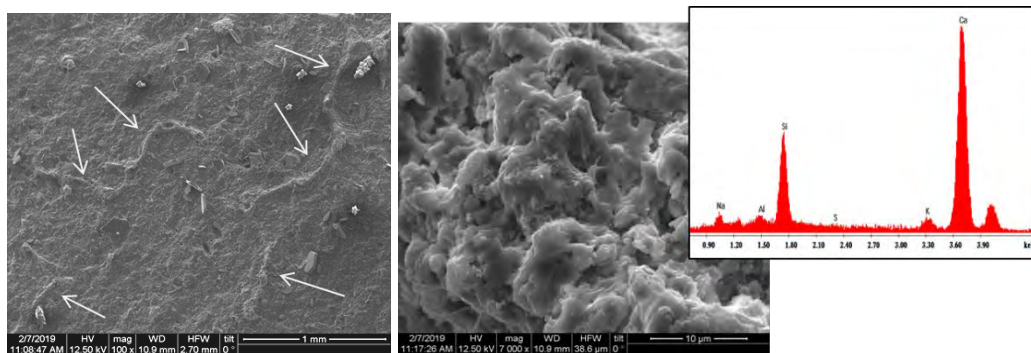


Figure 9. Crystalline formations observed in NHL-CA specimens after 28 days healing period

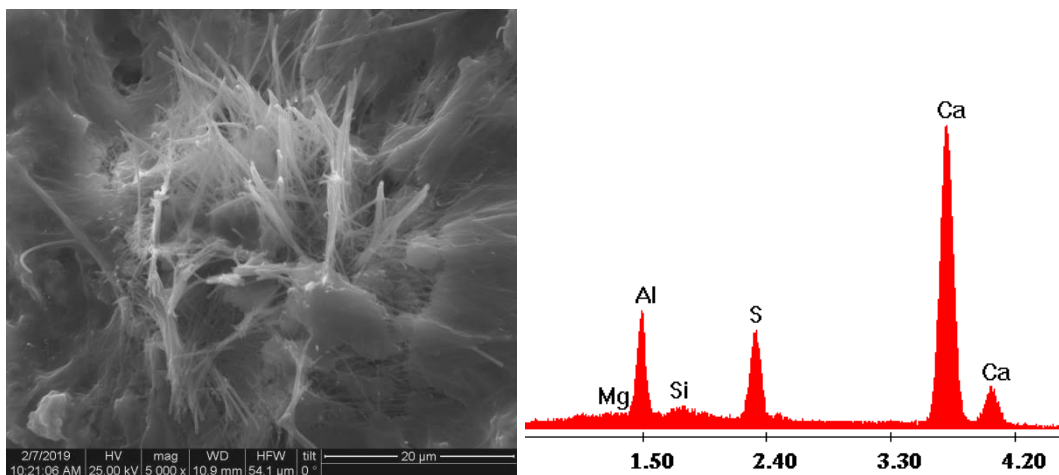


Figure 10. Ettringite crystals observed in NHL-CA specimens after 28 days healing period

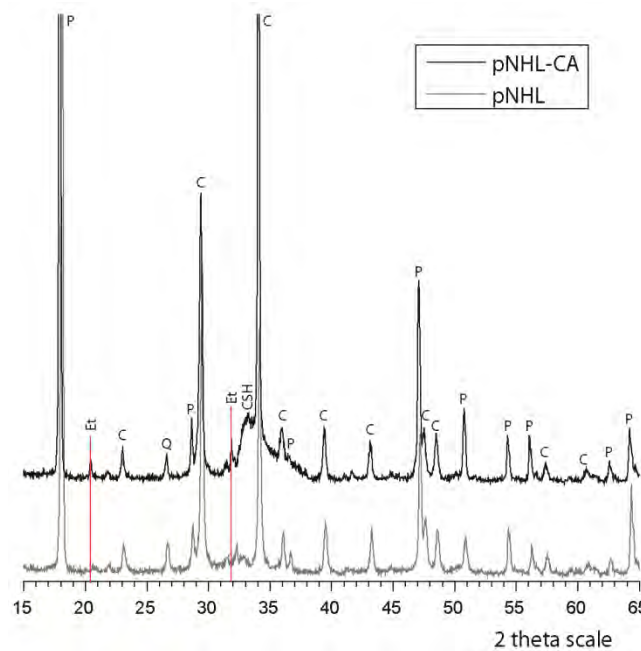


Figure 11. Diffractogram of the healing products produced in NHL-CA and control specimens after a 28 days healing period. [P: portlandite, C: Calcite, Q: Quartz, Et: Ettringite]

Discussion

Two different methodologies were employed in order to assess the self-healing capacity of NHL mortars related to their water tightness. The experimental results suggest that the addition of a crystalline admixture (CA) in NHL mortars improved the performance recovery of the damaged specimens, in terms of water permeability. This was additionally confirmed by scanning electron microscopy and X-ray diffraction analysis which suggest that the addition of a crystalline admixture led to the formation of additional healing phases on the crack surface. More specifically, the addition of the crystalline admixture led to reduction of water flow through the crack by 78%, compared to the control samples where the corresponding reduction was 31%.

Furthermore, the importance of the healing period duration is highlighted, as the results suggest that the healing efficiency of both mixtures is improved after 28 days of healing. Nevertheless, the impact of the autogenic self-healing phenomenon is more pronounced after 14 days of curing under water, whereas the addition of the CA contributes after 28 days of curing. The findings of this study are consistent with previous studies [9] on the autogenic self-healing phenomenon of NHL mortars, where it is shown that the hydration mechanism is more evident during the first 14 days of curing.

The results derived by the two methods employed also highlight the challenges related to the assessment of the self-healing capacity by quantifying the recovery of the mortars performance characteristics.

However, considering the wide variety of commercially available crystalline admixtures, further study is needed in order to better define their action mechanism and transport the findings of this study in the field.

Conclusions

In this study, the autonomic self-healing capacity of NHL mortars incorporating crystalline admixtures was compared with the autogenic-healing of NHL mortars. The results point out the favourable impact of the incorporation of crystalline admixtures in mortars used for restoration purposes, especially in the cases where there is a pressing need for water-resistant restoration mortars that can prevent or treat the appearance of degradation phenomena such as microcracks.

Moreover, it was shown that NHL mortars -due to their autogenic self-healing mechanism- have the ability to improve their water tightness, whereas the addition of a crystalline admixture may further enhance their self-healing capacity, especially in terms of water permeability.

Overall, the potential of further improving the autogenic self-healing capacity of restoration mortars was highlighted, while the exploitation of the results presented in this study could contribute to the enhancement of mortars durability in restoration interventions and the longevity of monuments.

Acknowledgements

This research was conducted within the framework of NCSR “Demokritos” Industrial Research Fellowship Program, funded from the Stavros Niarchos Foundation and TITAN Cement S.A..

This research has been co-financed by the European Union and Greece through the Operational Program Competitiveness, Entrepreneurship and Innovation, under the call RESEARCH – CREATE – INNOVATE (AKEISTHAI – Self-healing and self-sensing nano-composite conservation mortars - MIS 5031866).



References

1. Li V C, Sakulich A R, Reinhardt H W, and Schlangen E (2013) *Self-Healing Phenomena in Cement-Based Materials*. Dordrecht: Springer Netherlands
2. Lubelli B, Nijland TG, van Hees RPJ (2011) Self-healing of lime based mortars: microscopy observations of case studies. *Heron* 56(1/2): 75–91
3. Collepardi M (1990) Degradation and restoration of masonry walls of historical buildings. *Mater Struct* 23: 81–102
4. van Hees R P J, Binda L, Papayianni I, and Toumbakari E (2004) Characterisation and damage analysis of old mortars. *Mater Struct* 37: 644–648
5. Hearn N. (1998) Self-sealing, autogenous healing and continued hydration: What is the difference? *Mater Struct* 31: 563–567
6. Van Tittelboom K, Gruyaert E, Rahier H, and De Belie N (2012) Influence of mix composition on the extent of autogenous crack healing by continued hydration or calcium carbonate formation. *Constr Build Mater* 37:349–359
7. Ferrara L, Krelani V, and Moretti F On the use of crystalline admixtures in cement based construction materials: from porosity reducers to promoters of self healing. *Smart Mater Struct* 25: 084002
8. Roig-Flores M, Pirritano F, Serna P, and Ferrara L (2016) Effect of crystalline admixtures on the self-healing capability of early-age concrete studied by means of permeability and crack closing tests. *Constr Build Mater* 114: 447–457
9. Amenta M, Karatasios I, Maravelaki P, and Kilikoglou V (2016) Monitoring of self-healing phenomena towards enhanced sustainability of historic mortars. *Appl Phys A* 122:554

Addressing safety and durability requirements of architectural heritage by developing functional conservation mortars

Ioannis Karatasios¹, Zoi S. Metaxa², Stavros K. Kourkoulis², Nikolaos D. Alexopoulos³, Vassilis Kilikoglou¹

(1) Institute of Nanoscience and Nanotechnology, N.C.S.R. Demokritos, Athens, Greece, i.karatasios@inn.demokritos.gr , v.kilikoglou@inn.demokritos.gr

(2) Laboratory of Strength and Materials, National Technical University of Athens, Athens, Greece, zmetaxa@central.ntua.gr , stakkour@central.ntua.gr

(3) Department of Financial and Management Engineering, University of the Aegean, Chios, Greece, nalexop@aegean.gr

Abstract

In this work the development of novel conservation mortars, reinforced at the nano-scale by the incorporation of carbon nanostructures was investigated. The above technology was tested for the first time in lime-pozzolan-cement ternary conservation mixtures, by incorporating multiwall carbon nanotubes (MWCNTs) in three different amounts: 0.05, 0.1 and 0.2 % wt. The electrical properties of the nanocomposites were studied. Additionally, their mechanical properties under compressive and flexural loading conditions were investigated, after curing for 28 days. The electrical resistance of the CNT-modified conservation mixtures was simultaneously recorded during monotonic compression tests and a correlation between mechanical loading and electrical measurements was established. The results clearly indicate the beneficial role of nano-reinforcement on the mechanical performance of nano-composite mixtures when compared to the reference ones. Moreover, the incorporation of CNTs modified the electrical performance of all the nanocomposites investigated, so as to follow the applied stress. Overall, this work highlights a new perspective on the design of conservation mortars, giving emphasis on the new functionalities and advantages that nanotechnology can provide to cultural heritage conservation.

Introduction

Today, the safety of historic buildings and the protection of people that works in or visits the monuments are two of the main requirements that define the framework for designing the interventions and selecting or developing restoration mortars that satisfy both conservation principles and structural stability requirements. The latter is of particular importance in the cases of listed buildings or rehabilitation and re-use of historic buildings. These requirements highlight the importance of enhancing durability and continuous monitoring of the load-bearing parts of the structure, especially in monuments located in areas with increased earthquake activity.

The development of carbon-based nanomaterials with exceptionally mechanical properties [1-3] and additional functionalities [4, 5] has opened a new field of research for the design and development of multifunctional conservation mortars. The incorporation of carbon nanostructures such as carbon nanotubes (CNTs) or graphene nanoplatelets (GnPs) [6] aims to enhance the crack-resistance of conservation mortars, increase their strength -especially in flexure-, increase the toughness of the mortars and thus reduce/limit the crack propagation and increase the service life of conservation interventions.

Besides strength properties, the incorporation of carbon nanostructures into the mortar's matrix creates a conductive network within their mass, which attributes to the mixture new functionalities, such as the ability to act as piezoresistive material. In that case, when the mortar is subjected to mechanical loadings the electrical resistance of the material is altered as well. Thus, the strain under static or dynamic conditions can be detected by measuring - continuous and remotely - the electrical properties of the nano-composite material. By considering an average cost of 150-200 euros per 100 g of CNTs and considering the low concentrations that are required (0.05 – 0.1 wt% of binder) in order to take advantage of their beneficial properties, the additional cost in the mortars production is very low.

To date, few studies have been conducted on examining the reinforcing effect of CNTs on pozzolan-cement matrices. Morsy et al. [7] were the first to investigate the effect of CNTs addition on the compressive strength of an ordinary Portland cement (OPC) matrix where 6 wt.% was substituted by metakaolin. The results showed a 11% increase in the compressive strength with the addition of 0.02 wt.% of cement CNTs. Following, Tokarev et al. [8] examined the effect of single walled CNTs at a gypsum matrix containing either 3% OPC, or 5% silica fume or 1% metakaolin. It was found that the 7d compressive strength of the matrix is increased by up to 85% when 3% cement and 0.002% of CNTs are used. More recently, El-Gamal et al. [9] studied separately the effect of CNTs, nano-silica and nano-metakaolin on the mechanical properties of a high sulphate resistance cement. They found that all three can be used to improve the compressive strength of the cementitious matrix when used at optimum concentrations. Unfortunately, they didn't study their effects combined.

To the best of our knowledge, besides the work of Faria et al. [10] the effect of multiwall carbon nanotubes addition on a lime-pozzolan-cement matrix specifically designed to be used in historic buildings' conservation and protection hasn't been performed heretofore.

Based on the above context, this work studies the potential of incorporating multiwall carbon nanotubes (MWCNTs) in ternary conservation mixtures aiming to investigate their feasibility in reinforcing the lime-pozzolan-cement matrix and providing piezoresistive properties. Thus, acting as a "material embedded sensor" that could provide real time and continuous monitoring of mechanical loads and damage initiation at nano-/micro- scale. Considering that lime-based hydraulic binders exhibit completely different microstructure and mechanical properties from cement mixtures, this initial step is essential for developing

further new types of functional conservation mixtures that could be used as bedding, joining, or grouting applications.

Methodology

Materials and mix proportions

In this study, Type I Portland cement (OPC) (Titan Cements S.A.), lime powder (CaO-Hellas) and a highly reactive pozzolan, i.e. metakaolin (Dalkafoukis S.A.) were used for preparing the ternary mixtures. Multi-walled carbon nanotubes (MWCNTs) having an average diameter of 9.5 nm and an average length of 1.5 μm were provided by Nanocyl S.A. (Figure 1). The nanotubes were dispersed in a superplasticizer provided by Sika S.A. (ViscoCrete[®] 5500 HP). The mix proportions of the mixtures studied are presented in Table 1. No sand or any other aggregate were used in the mixtures, in order to study exclusively the properties of the binder matrix.

Since C-based nanomaterials are typically provided in a powder form, they form agglomerates due to the Van der Waals forces developed. Therefore, in order to achieve homogeneous distribution within the binder matrix it is necessary to disperse them in a liquid medium, so as to fully take advantage of their nano-scale properties. In this study, the MWCNTs were dispersed in the mixing water incorporating the superplasticizer at a concentration of 0.4 wt% of water, under sonication for two sets of 30 mins.

Table 1. Mix proportion of nanomodified ternary mixtures.

Mixture	Lime powder wt%	Metakaoline wt%	Cement wt%	w/c *	CNTs wt%**
LMCR	40	40	20	0.7	0
LMC05	40	40	20	0.7	0.05
LMC1	40	40	20	0.7	0.1
LMC2	40	40	20	0.7	0.2

* including 0.4 wt % of superplasticizer; ** based on the dry weight of the binder

The nanocomposite mixtures were prepared by mixing the binding materials with the CNT/suspensions according to the ASTM C305, using a standard mixer. The nanocomposites prepared had a water to binder ratio of w/c=0.7 by weight, adding 0.4 % wt of superplasticizer in the water amount (Table 1). The addition of superplasticizer helped to overcome the modification of consistency due to the addition of carbon nano-materials (more stiff texture), resulting a uniform flow value (15.5 - 16.0 cm) for all mixtures. After mixing, the materials were placed into 20×20×80 mm prismatic molds, compacted in two layers on a jolting table (similar to the procedure described in EN 196-1) and finally, placed in a curing chamber (95±2 %RH, 21±2 °C) until demolding (one day). Following, they were cured in the same chamber until testing.

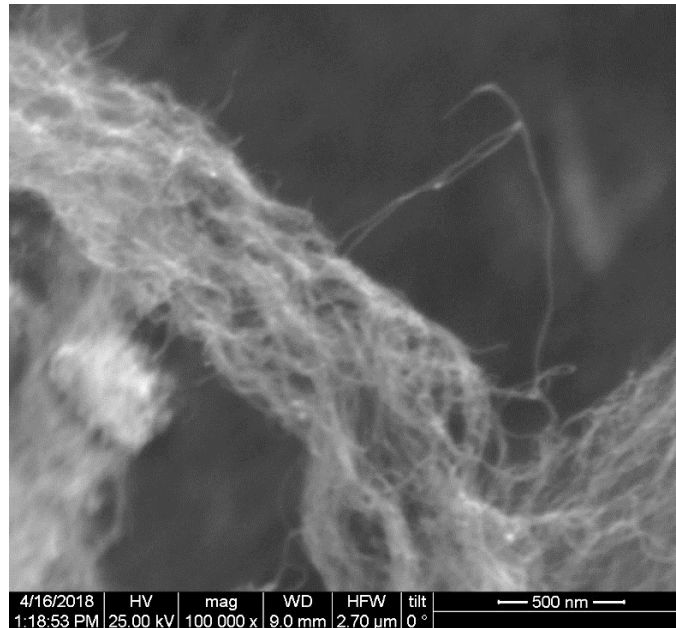


Figure 1. SEM photomicrograph of the CNTs in the solid state, prior to incorporation in the ternary mixtures.

Testing methods

The microstructure development of the CNTs-modified mixtures were studied in fractured sections under scanning electron microscope (SEM), while open porosity and water absorption coefficient have been determined by slightly modifying the procedures described in EN 1936:1999 and EN 1015-18:2002 standards respectively (in terms of specimens dimensions). Porosity values were used as an indication for the microstructural differences that may be resulted by adding a nano-materials into the binder matrix, while together with water absorption values were used for the interpretation of electric resistance and piezoresistivity results.

The mechanical properties of ternary mixtures under compressive and flexural loading conditions were measured, after curing for 28 days. Three-point bending tests at the age of 28 days were conducted to study the performance of the conservation nanocomposites under flexure. An Instron loading frame (capacity 100 kN) was used. The experiments were performed under displacement control conditions, at a constant rate of 100 μm/min. The compressive strength of the conservation nanocomposites was also determined at the age of 28 days using the same Instron loading frame. The experiments were performed under displacement control conditions, at a constant rate of 150 μm/min. The load and crosshead displacement data were recorded and stored during both tests.

Additionally, the electrical properties of the nanocomposites were studied using the 4-wire method. The four-wire method was used to measure the electrical resistance of the nanocomposites. Immediately after casting, four stainless steel mesh electrodes were placed inside the wet specimens making sure that they covered the entire cross-section of the samples. The distance between the outer and inner electrodes was 15 mm while the respective distance between the inner electrodes was 30 mm, Figure 2. A Keysight

multimeter was used for the four wire ohm measurements. The electrical resistance was continuously recorded for a total period of 30 minutes. The average resistance values were calculated from the data of the last five minutes of the measurement. All the specimens were measured at the age of 7-days after they were fully covered with plastic wrap to maintain their moisture.

Finally, a correlation between mechanical loading and electrical measurements was established. The piezoresistive behavior of the produced nanocomposites under monotonic compression, at a constant crosshead displacement rate of 150 $\mu\text{m}/\text{min}$, was studied, by simultaneously recording the crosshead displacement and force from the loading frame in conjunction with the electrical resistance from the multimeter using the aforesaid four wire method. Prior testing the samples were oven dried at 80°C for 3 days to eliminate any discrepancies caused due to electric polarization effects. A correlation between mechanical loading and electrical measurements was established by analyzing the test results.

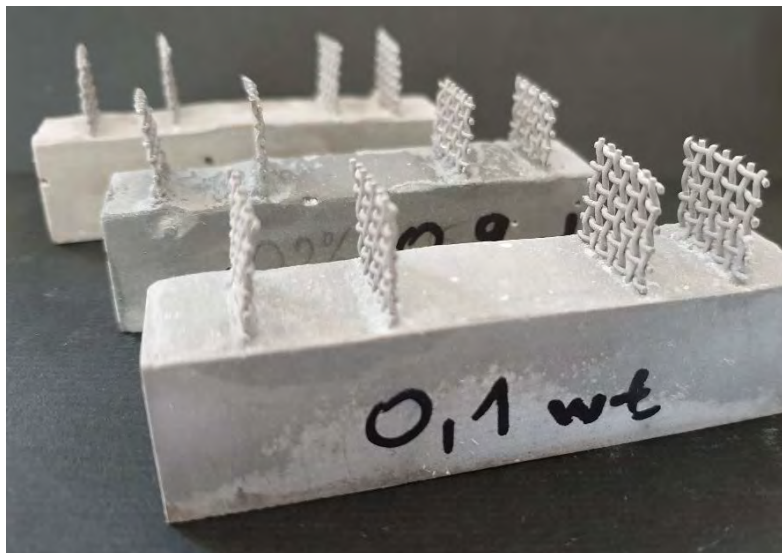


Figure 2. The prismatic specimens of nanommodified mixtures used for measuring the electrical resistance and piezoresistivity at monotonic compression.

Results and discussion

Microstructural characterization

Microstructure examination of the ternary mixtures in SEM (Figure 3) revealed that the methodology selected for the dispersion of CNTs into the binder matrix had resulted a uniform result without obvious conglomerations. This is depicted in Figure 3b, where the addition of 0.2 wt% CNTs is smoothly incorporated, allowing the marginal determination of CNTs.

Although the incorporation of CNTs into the ternary mixtures resulted in a very similar microstructure in terms of open porosity values (around 55%) the water absorption coefficient presents considerable fluctuations (Table 2). These variations are attributed to

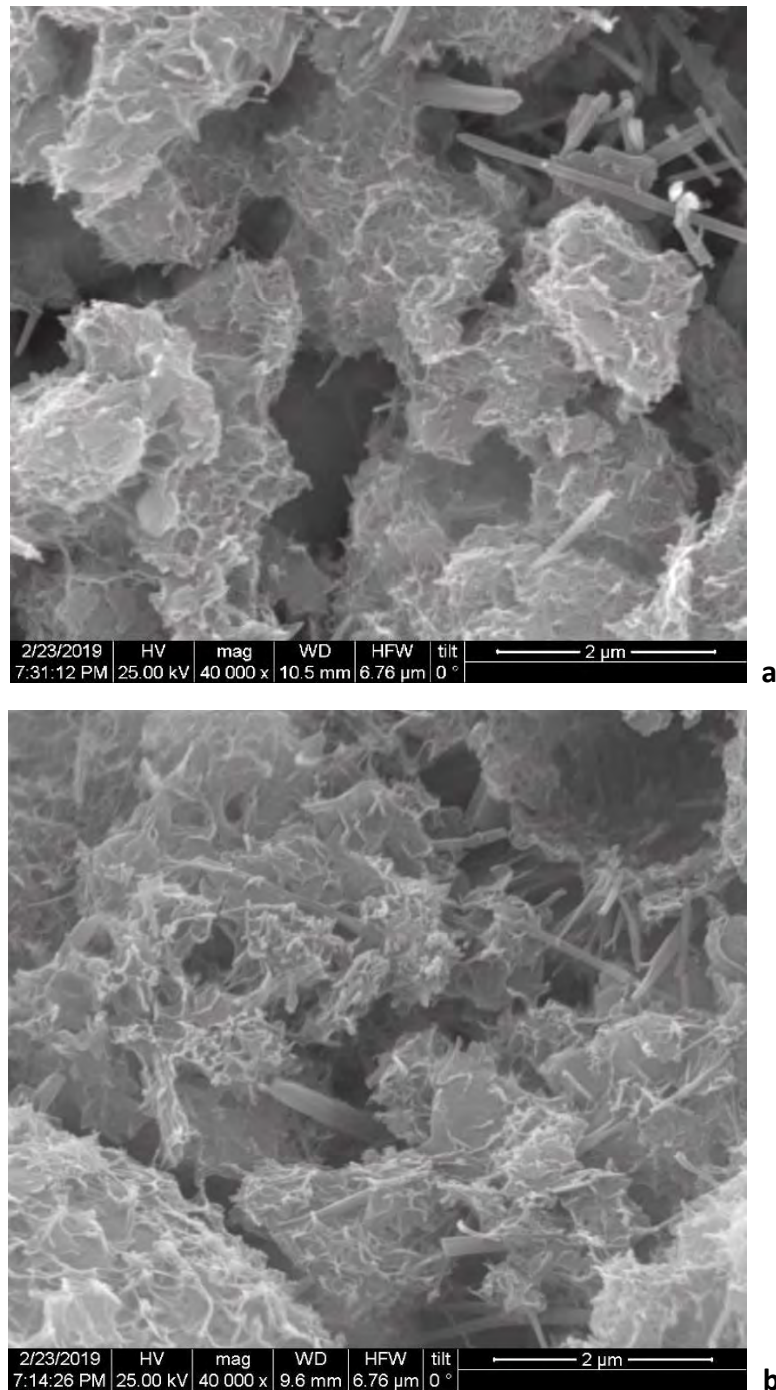


Figure 3. SEM photomicrographs of the binder matrix formed during setting in the reference mixture (a) and the LMC2 mixture, containing 0.2 wt% CNTs (b). The curved fibrous formations in the lower picture – having very similar morphology to the C-S-H hydration products – are attributed to CNTs. These are absent in the upper picture that depicts the hydrated matrix at the same magnification.

the different pores size formed during setting due to the different content and dispersion results of CNTs. The resulted differences could be further attributed to the action of superplasticizer, which forms a thin layer around the cement and CNTs particles and thus hinders their agglomeration due to the Van der Waals forces. The space formed between cement particles is partially filled or increased by CNTs, thus resulting into pores with different pore diameter. It should be noted that open porosity values presented in Table 2 are referred to ternary mixtures without aggregates.

Table 2. Physical properties and water absorption values of CNTs modified ternary mixtures.

mixture	real density (g/cm ³)	apparent density pa (g/cm ³)	porosity %	water abs. coefficient (g/m ² *s ^{1/2})
LMCR	2.76	1.24	54.9	3.3
LMC05	2.73	1.23	54.9	4.8
LMC1	2.73	1.26	54.2	2.9
LMC2	2.71	1.25	53.9	3.9

Electric resistance

The electric resistance measurements of water saturated mixtures, proved the beneficial role of carbon nano-structures (CNTs) towards the formation of a conductive network, even in the case where the pores are filled in by a conductive pore solution. The incorporation of CNTs resulted in a four times reduction of the resistance values, while the small differences between the different mixtures indicates the potential for tailoring and optimizing the electric properties of nano-modified ternary mixtures using very low CNTs concentrations. Moreover, the differentiation between resistance values of water-saturated and dry specimens provides an additional ability of those mixtures, that of humidity or water content indicator.

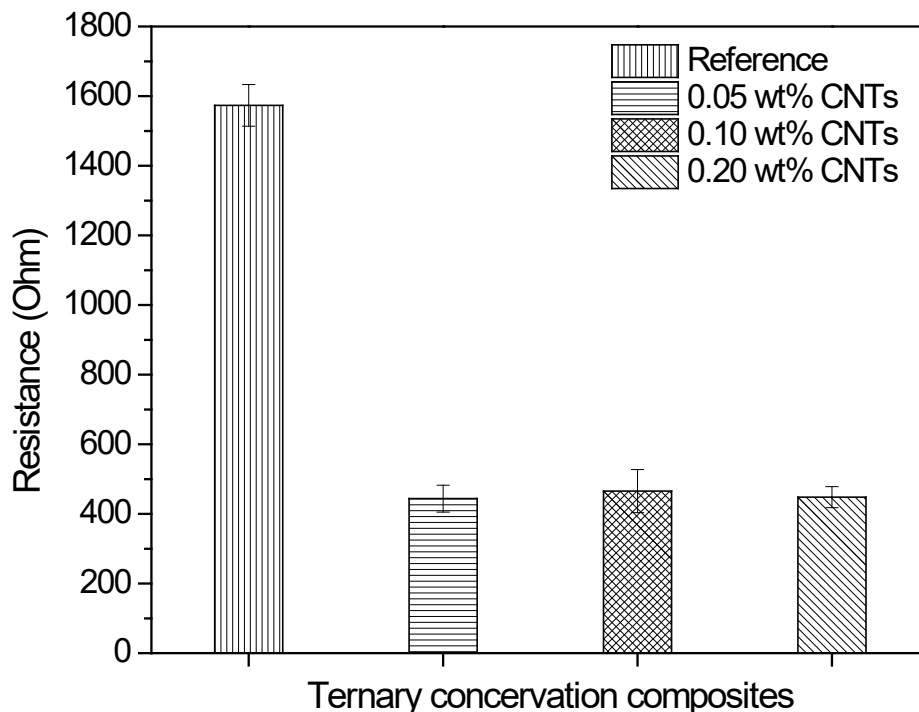
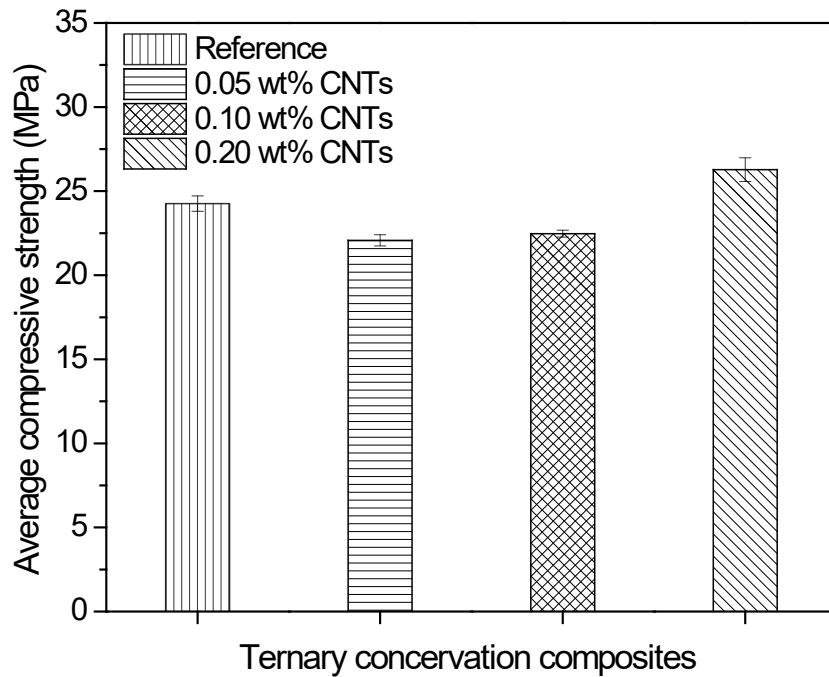


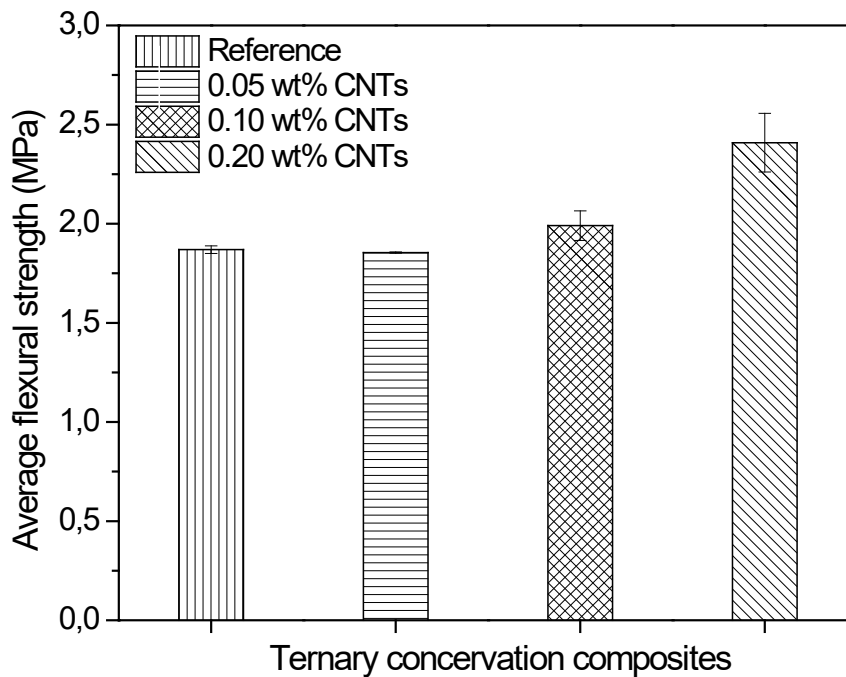
Figure 4. Electrical properties of water saturated ternary mixtures after 7 days setting/hydration time.

Mechanical properties and piezoresistivity

The incorporation of CNTs into the ternary mixtures altered their mechanical properties (Figure 5), resulting a small decrease of compressive strength values at 28 days, for CNTs concentrations below 0.1 wt% (LMC05 and LMC1 mixtures).



a



b

Figure 5. Compressive (a) and flexural (b) strength properties of nano-modified ternary mixtures, after 28 days setting/hydration time.

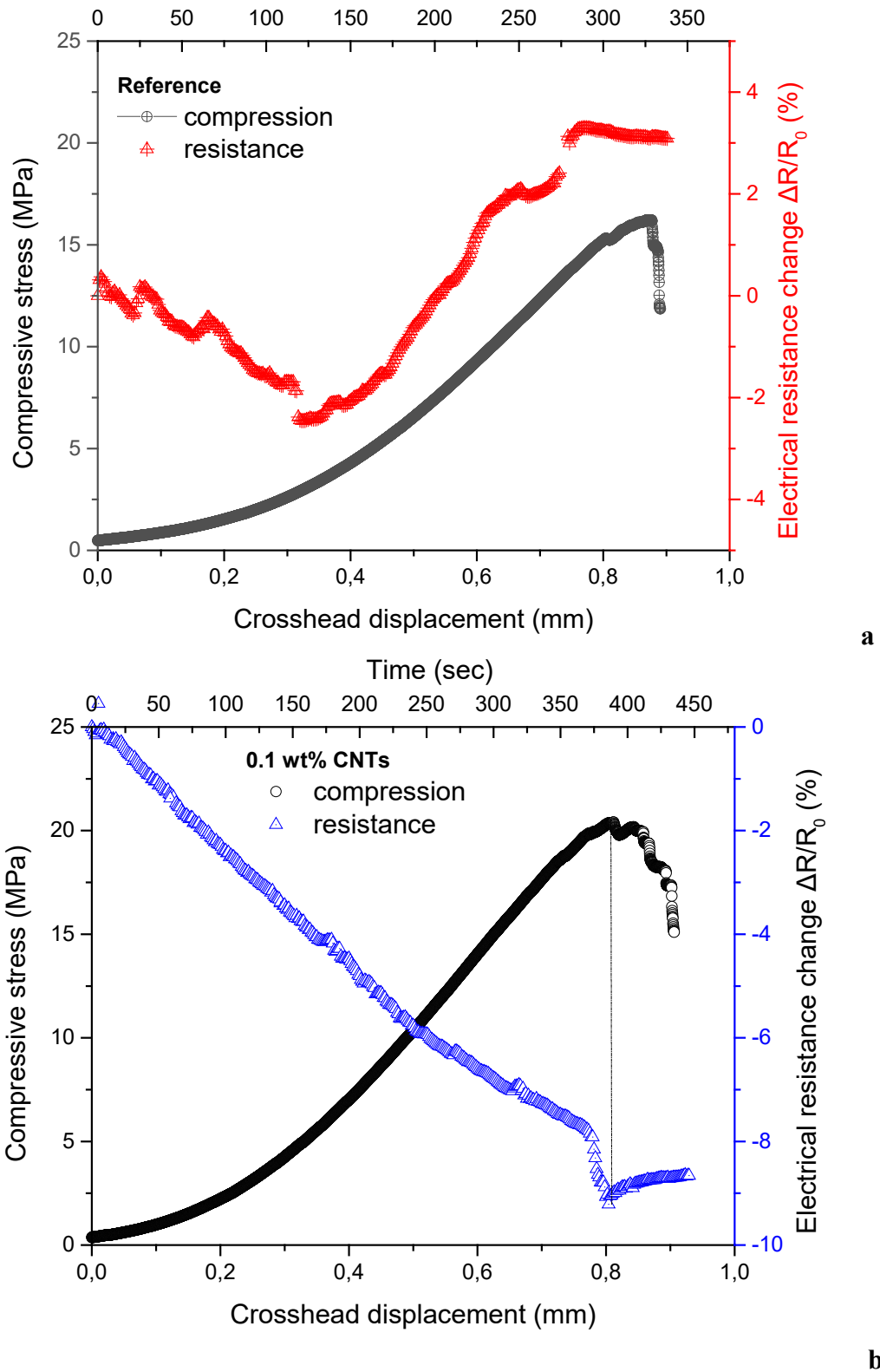


Figure 6. Representative graphs of the piezoresistive response of two ternary mixtures, i.e. LMC2 (a) and LMC2 (b) during monotonic compression, after 28 days setting/hydration time.

In contrast, at concentration of 0.2 wt% the compressive strength slightly increases. The above strength alterations could be related to the microstructural differences already observed in water absorption coefficient values (Table 2), i.e. the formation of pores with

different diameter. The later should be attributed to the distraction created during the mixing process and the different packing resulted in the nano- and micro- scale into the binder matrix [11,12]. In contrast, in the case of flexural strength (Figure 5b) the addition of CNTs has no negative effect. The 0.05 wt% load of CNTs exhibit the same flexural strength with the reference one, while 0.1 and 0.2 wt% CNTs mixtures result in higher strength values.

In the case of piezoresistivity (Figure 6), the resistance of the reference mixture recorded during monotonic compression indicates an irregular behaviour that is divided in two parts (Figure 6a). The first part presents a decrease of resistance up to almost the 30% of the maximum load, which is attributed to the initial compaction of the binder mass and therefore to lower density. The second part that describes the elastic-to-plastic deformation is characterized by an increase of the resistance values. This behaviour could be related to the formation of nano-, micro- cracks within the binder that introduce various types of insulation zones, which finally results in the resistance increase.

In contrast, the incorporation of CNTs (Figure 6b) creates a uniform conductive network that takes advantage of the compaction/deformation of the binder matrix during compression. Thus, the resistance graph is continuously linear, following a decreasing trend. Moreover, it is observed that the resistance follows the crack initiation at maximum load by forming a step followed by increased values (change of slope). The same behaviour was recorded for all mixtures. However, LMC2 exhibits the better example for comparing the effect of CNTs on the formation of a conductive network that attributes to the ternary mixtures the piezo-resistive properties.

Conclusions

- Based on SEM and porosity results, the methodology selected for the dispersion of CNTs into the binder matrix had resulted a uniform distribution, without obvious conglomerations.
- The incorporation of CNTs between 0.05 to 0.2 wt% of the binder mass resulted into very similar microstructure in terms of open porosity values (around 55%). However, better study of pore-size distribution is required (e.g. by mercury porosimetry), since the water absorption coefficient presents considerable fluctuations.
- The incorporation of CNTs resulted in a four times reduction of the resistance values, while the small differences between the different mixtures indicates the potential of tailoring and optimizing the electric properties of nano-modified ternary mixtures using very low CNTs concentrations.

- The differentiation between resistance values of water-saturated and dry specimens could provide an additional ability of C-modified mixtures, that of humidity or water content indicator.
- The incorporation of CNTs creates a uniform conductive network that takes advantage of the compaction/deformation of the binder matrix during compression, providing a linear response to external load.

Overall, the experimental results presented in this study indicates that CNTs modified ternary mixtures could be successfully designed and optimized in order to provide enhanced mechanical performance and simultaneous piezoresistive response to external loads.

Thus, carbon nano-modified conservation mixtures could be successfully implemented in conservation mixtures, acting as a material embedded sensor that could provide real time and continuous monitoring of mechanical loads and damage initiation at nano-/micro- scale.

Acknowledgements

This research has been co-financed by the European Union and Greece through the Operational Program Competitiveness, Entrepreneurship and Innovation, under the call RESEARCH – CREATE – INNOVATE (AKEISTHAI – Self-healing and self-sensing nano-composite conservation mortars - MIS 5031866).



References

1. Yu M -F, Lourie O, Dyer M J , Moloni K, Kelly T F, Ruoff R S (2000) Strength and breaking mechanism of multiwalled carbon nanotubes under tensile load, Science 287:637-640
2. Belytschko T, Xiao S P, Schatz G C, Ruoff R S (2002) Atomistic simulations of nanotube fracture, Phys Rev B 65:235430
3. Tserpes K I, Papanikos P (2005) Finite element modeling of single-walled carbon nanotubes, Compos Part B 36:468-477
4. Dharap P, Li Z, Nagarajaiah S, Barrera E V (2004) Nanotube film based on single-wall carbon nanotubes for strain sensing. Nanotechnology 15:379-382
5. Tomblor T W, Zhou C, Alexseyev L, Kong J, Dai H, Liu L, Jayanthi C S, Tang M, Wu S-Y (2000) Reversible electromechanical characteristics of carbon nanotubes under local-probe manipulation, Nature 405:769-772

6. Liew K.M., Kai M.F., Zhang L.W (2016) Carbon nanotube reinforced cementitious composites: An overview. *Composites: Part A* 91:301-323
7. Morcy M S, Alsayed S H, Aquel M (2011) Hybrid effect of carbon nanotube and nano-clay on physico-mechanical properties of cement mortar, *Constr Build Mater* 25:145-149
8. Tokarev Y, Ginchitsky E, Sychugov S, Krutikov V, Yakovlev G, Buryanov A, Senkov S (2017) Modification of gypsum binders by using carbon nanotubes and mineral additives, *Proc Eng* 172:1116-1168
9. El-Gamal S M A, Hashem F S , Amin M S (2017) Influence of carbon nanotubes, nanosilica and nanometakaolin on some morphological-mechanical properties of oil well cement pastes subjected to elevated water curing temperature and regular room air curing temperature, *Constr Build Mater* 146:531-546
10. Faria P., Duarte P., Barbosa D., Ferreira I (2017) New composite of natural hydraulic lime mortar with graphene oxide. *Constr Build Mat* 156:1150-1157
11. Konsta-Gdoutos M.S., Danoglidis P., Falara M., Nitodas S (2017) Fresh and mechanical properties, and strain sensing of nanomodified cement mortars: The effects of MWCNT aspect ratio, density and functionalization. *Cem Concr Compos* 82:137-151
12. Mohsen M.O., Al-Nuaimi N., Abu Al-Rub R.K., Senouci A., Bani-Hani K.A (2016) Effect of mixing duration on flexural strength of multi walled carbon nanotubes cementitious composites. *Constr Build Mat* 126:586-598

Self- healing lime-based mortars using biological mechanisms and microvascular networks

Cristina De Nardi¹, Magdalini Theodoridou¹, Philip Sim¹, Michael Harbottle¹, Anthony D.

Jefferson¹

(1) School of Engineering, Cardiff University, denardic@cardiff.ac.uk, theodoridou2@cardiff.ac.uk, SimPJ@cardiff.ac.uk, harbottlem@cardiff.ac.uk, jeffersonad@cardiff.ac.uk

Abstract

This study investigates the innovative application of calcite biomineralisation using specifically designed microvascular networks (MVNs) for the development of self-healing lime-based mortars to be used in both historic and contemporary structures. Four series of laboratory hydraulic lime-based mortar specimens were produced. The first comprised lime and aggregates only, while in the second, empty 3D printed MVNs were added. A MVN is a system of small diameter channels, able to break when damage occurs and release the hosted healing component. In the third series, *Sporosarcina pasteurii* were added to the mortar during mixing, while nutrient solution was stored in the MVNs. In order to better evaluate the efficiency of the MVNs with a non-biological healing agent, the fourth series MVNs were again included, this time containing sodium silicate. Damage was induced 14 days after casting by means of three-point bending loading in displacement control. All specimens were then stored in an incubator for five days of healing. Following the healing stage, the specimens were re-tested to determine the level of restored performance. The results showed the potential of the MVNs and the biological self-healing mechanism to restore efficiently the flexural strength of the lime-based mortars when damage occurred.

Introduction

Since the pre-historical times, lime-based mortars have been widely used in the construction of buildings (e.g. ancient Egyptian constructions [1], Roman Empire architecture [2]).

In recent years, lime has been considered one of the principle binders for the production of repair materials in the restoration of heritage structures due to its compatibility with the substrate, its chemical purity [3], and its autogenous self-healing properties [4]- [5]. Self-healing materials could repair damage all by themselves similarly to what happens in biological systems, as well as in the human body. Several studies have investigated healing mechanisms concrete, where two main categories are used; the autogenous and autonomous healing [6]. As defined in the RILEM technical committee 221-SHC “autogenous is the process of self-healing triggered without the need of any external operation, while autonomous is developed by adding engineered admixture for healing purposes” [7]. While an increasing research activity has been focused on self-healing cement-based composites in

the last decade, little attention has yet been paid to the investigation of similar phenomena in lime-based mortar [8] [9]- [10].

In this work an innovative combination of two different techniques – a biological mechanism using bacteria and a 3D printed mini-vascular network - for developing autonomous self-healing lime-based mortars has been investigated.

Microbial calcite precipitation has been explored for healing or consolidating porous materials, such as soil [11] building stone [12]- [13]- [14]- [15]- [16] and concrete [17]. The potential for biological healing has led to the technique being considered as part of a new class of self-healing construction materials [18]. Biological self-healing would incorporate techniques similar to those discussed above, but be able to sense damage or deterioration and adapt or repair themselves to restore their original properties or limit further deterioration [19]. The opportunities in cementless materials, such as lime-based mortars, for biological self-healing are considerable due to their bioreceptivity and suitability for biomineralisation, as well as the extent to which such materials are in use worldwide. Furthermore, the healing product of such mechanisms, i.e. calcium carbonate, is compatible with the nature of lime-based mortars and most of the substrate porous materials typically found in historic masonry structures.

Mimicking the vascular structure of the human body, the vascular approach allows healing agents to be delivered to damage sites within a specimen. The vascular approach consists of a single set, or network, of hollow pipes, placed inside the specimen upon casting; the healing agent is supplied externally - pumped under pressure for few cycles of healing - or stored inside the vascular pipes. Dry [20] first studied the use of vascular system and cyanoacrylate as healing agents to reduce the cracks, while reducing the permeability in cementitious matrices. Furthermore, Joseph et al. [19] similarly to that investigated in polymeric materials by White et al [21], studied the effect of adhesive-filled glass tubes, highlighting the good potential of a low-viscosity glue.

The 3D printed mini vascular networks MVNs herein used is a system of small hollow channels - made of polylactic acid (PLA), a biopolymer produced from non-toxic renewable resources - able to break when damage occurs and release the hosted components required for healing. Previous studies conducted by Joseph et al [19] demonstrated that if the fracture surfaces of the tubes used to store the adhesive is not well exposed to the atmosphere, the capillary attractive force is not enough to allow the coming out of the liquid. Thus, the MVNs are designed to create interconnected channels, that prevent the suction of the liquid hosted inside.

The effect of a solution of sodium silicate (SS), stored in the MVNs, was also evaluated for the sake of comparison as it's widely used as healing agents [22]- [23]- [24].

All the samples were tested under three-point flexural bending and results given in terms of load against crack mouth opening displacement (CMOD) [25]. The healing efficiency (η_{eff}) was estimated as the ratio of the recovered ultimate strength over the initial capacity.

Materials and Methodology

Table 1 describes the four series of specimens employed in the experimental programme. The first series acted as a reference, comprised only lime mortar. The second series was also a reference, and comprised lime mortar containing empty MVNs. MVNs were used as delivery mechanisms in the third and fourth series, delivering nutrients to feed bacteria, and sodium silicate, respectively.

Table 1. Laboratory lime-based samples

Sample Code	Lime+Aggregates+Water	Bacteria	MVNs	Nutrients	SS
R1	+	-	-	-	-
R2	+	-	+	-	-
B	+	+	+	+	-
S	+	-	+	-	+

Three 40x40x160 mm prisms were prepared for each series employing a natural hydraulic lime mortar (NHL 3.5) with the binder to aggregate ratio 1:3. Fine aggregates were employed according to the BS EN 13139:2002 Standard [26]. The water/binder ratio in the fresh mixtures was kept constant at 0.75. For three days after casting the prisms were kept in the moulds covered with a damp Hessian sheet. After this, the specimens were demoulded and stored at a constant room temperature (ca. 20°C) in a sealed container covered with a damp Hessian cloth to provide high relative humidity values (>90%) and promote hydration.

The MVNs were made of white PLA (Verbatim wire spool, 1.75 mm diameter), manufactured at 190 °C using a 3D printer (WASP 2040 Turbo2), 0.25 mm nozzle and layer height 0.06 mm, single wall thickness 0.25 mm. Flat ribs (5 mm space) were designed along the ligaments of the MVNs in order to increase the bond properties.

In Figure 1 the shape and dimensions of the 3D printed MVNs are depicted, as well as their position in the lime-based mortar specimens (the bases are just functional to the printing process).

Sporosarcina pasteurii, a highly ureolytic, aerobic bacterium was used to bring about microbially induced calcite precipitation in the laboratory lime-based mixtures. Stock cultures of the bacterium were used to inoculate liquid growth medium containing per litre of deionised water 13 g of nutrient broth (Oxoid CM001), autoclaved at 120 °C for 15 minutes, and 10 g of urea added with a sterile syringe filter (0.2 µm). The flasks were incubated at 30°C and 150 rpm overnight and used to inoculate liquid growth medium in

new flasks aiming at an optical density of 0.9-1.2 measured at a wavelength of 600 nm (equivalent to $10^7 - 10^8$ cells/ml).

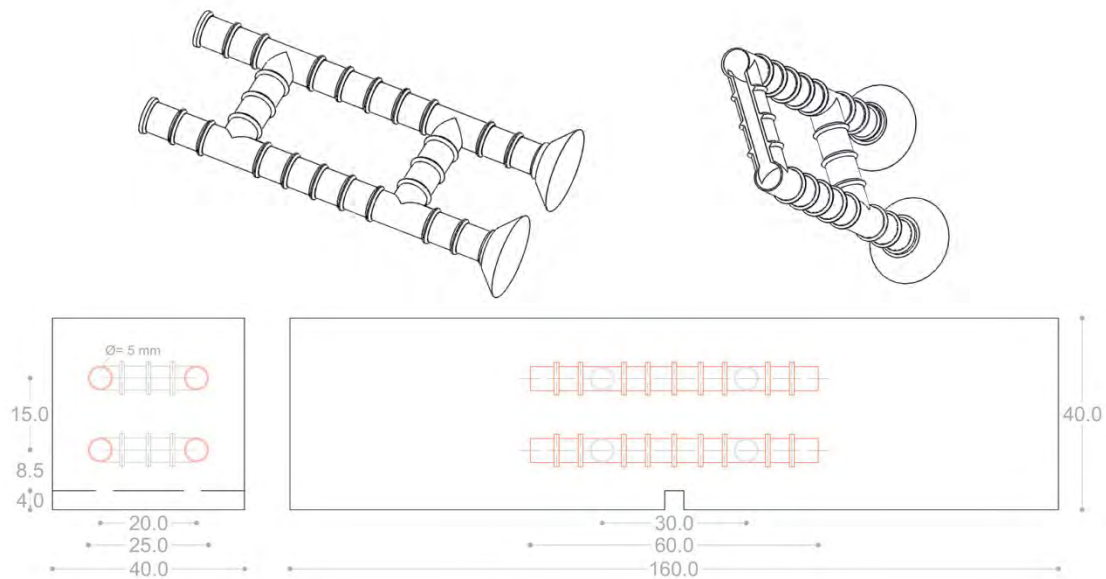


Figure 1. MVNs design and their position in a lime mortar specimen

Cells were centrifuged at 3200 rpm for 20 mins and washed in sterile phosphate buffered solution (PBS: 8 g NaCl, 1.42 g Na₂HPO₄, 0.24 g KH₂PO₄ per litre of deionised water).

The final bacteria suspension (113 ml) was added to a 9.8 kg mixture of lime mortar, requiring 1.55 l of water. The actual amount of water added to the mixture was reduced by the amount of bacteria suspension available (113 ml).

The nutrient solution (i.e. cementation medium) used for the microbial induction of calcium carbonate precipitation contained per litre of deionised water: 3 g Oxoid, 2.12 g NaHCO₃, 22.053 g CaCl₂H₂O (autoclaved as previously) and 20 g urea and 10 g NH₄Cl added through a 0.2µm sterile syringe filter.

The 3D printed ladders were sterilised in 'Virkon' aqueous solution (10 g/L). The nutrient solution was then inserted in the ladder through a sterile syringe and the ladders were sealed with silicone. When casting the specimens, the position of the ladders was the same as shown on Figure 1.

For the sake of comparison, a liquid solution of sodium silicate (Fischer Chemical), with SiO₂/Na₂O ratio equal to 2:1 was also injected in the MVNs. The idea was that, similarly to what happens in concrete, the sodium silicate might react with the calcium hydroxide, forming calcium-silica-hydrate (C-S-H) gel [27].

The experimental program including five steps, is shown in Figure 2.

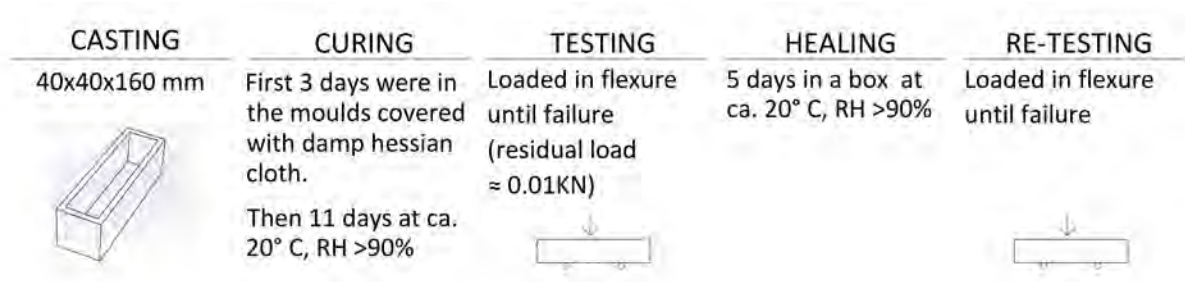


Figure 3. Experimental program for studying self-healing of lime-based mortars

After 14 days all specimens were subjected to three-point bend testing (Figure 3) in order to damage the specimens and activate the healing mechanism. Specimens were then re-tested in flexure until failure after three days of further curing. Three-point bend tests were carried out in displacement control with a rate equal to 0.0001 mm/s. In order to induce the crack, samples were pre-notched with a notch depth of 5 mm. Tests were carried out for each notched mortar specimen, by using a servo-hydraulic universal machine with a load cell capacity of 100 kN. The Crack Mouth Opening Displacement (CMOD) mode was used through a clip-on extensometer.



Figure 3. Testing arrangement on notched beams

The strength recovery depends on the flexural strength, a measurement of the residual strength at the time of healing is initiated and the strength after healing has occurred. This is represented by the healing efficacy (η_{eff}) in equation 1.1 and it's illustrated in Figure 4 [27].

$$\eta_{eff} = \frac{\sigma_c^{healed} - \sigma_c^{damaged}}{\sigma_c^{undamaged} - \sigma_c^{damaged}} \times 100 \quad (1.1)$$

Where σ_c^{healed} is the flexural strength of the material after damage and healing, $\sigma_c^{damaged}$ is the residual flexural strength of the material after damage and before the healing stage, $\sigma_c^{undamaged}$ is the flexural strength of the undamaged material.

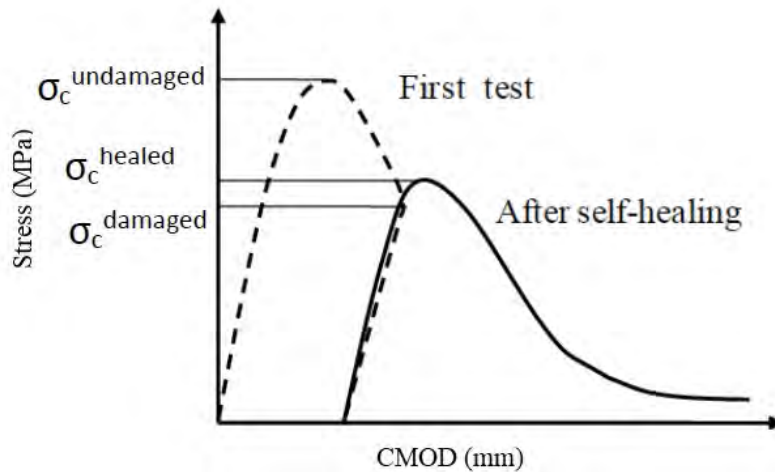


Figure 4. Schematic Stress- CMOD graph before and after healing after [27].

Results and discussion

Table 2 summarises the mechanical behaviour of all specimens subjected to three-point bend tests before and after healing. The average values for the flexural strengths, defined as above are reported in Table 2, with the standard deviations included in brackets. Based on the aforementioned values, the healing efficacy (η_{eff}) calculated using equation 1.1 are given in Table 2.

Table 2. Flexural strength before and after healing

	Before healing		After healing	η_{eff}
	$\sigma_c^{\text{undamaged}}$ (MPa)	$\sigma_c^{\text{damaged}}$ (MPa)	σ_c^{healed} (MPa)	
R1(reference without MVNs)	0.362 (7%)	0.085 (34%)	n/a	n/a
R2 (reference with empty MVNs)	0.235 (13%)	0.036 (37%)	0.039 (38%)	1%
B (bacteria + MVNs with nutrients)	0.208 (15%)	0.046 (16%)	0.094 (16%)	29%
S (MVNs with sodium silicate)	0.119 (20%)	0.030 (20%)	0.163 (3%)	150%

The presence of the MVNs influences the flexural strength of the lime-based mortars in the undamaged conditions; the reference samples with empty MVNs embedded in their structure (R2) show an average flexural strength about 35% less than the reference samples without MVNs (R1). The initial strength of the mortars with MVNs (R2) seems to decrease further when the MVNs are filled with sodium silicate (S); it is possible that the sodium silicate has modified the properties of the MVN material and this issue is being explored in an on-going investigation. This doesn't seem to be the case when the MVNs are filled with nutrient solution (B). The latter could be partly related to the absence of sodium silicate and

to the positive effect of the bacteria cells in the matrix which have the ability to act as nucleation sites for precipitation [28].

After the healing phase, all R1 specimens failed when setting up the three-point bend test, when the extensometer was attached, implying that they had almost zero strength. In the case of the reference samples where empty MVNs were added (R2), the healing efficiency was considered negligible (1%), indicating that the MVNs helped to hold the prisms together but that no autogenic healing of the lime mortar occurred in the time available. The mechanical performance of the samples with bacteria in the matrix and MVNs with nutrients solution (B) was notably restored, based on the calculated healing efficacy index η_{eff} (29%).

The efficiency of the MVNs to act as the storage space for healing agents in lime-based mortars was further confirmed with the use of MVNs with sodium silicate (S). Despite the fact that the presence of MVNs seems to have reduced the initial flexural strength of the mortars, it enhanced the deformation capacity of the tested mortar specimens, when compared to the brittle behaviour of the R1 reference samples without MVNs (Figure 4). Furthermore, the MVNs proved to respond to damage efficiently, as breakage and prompt release of the healing agent was observed macroscopically, resulting in the complete remediation of the mortars mechanical performance in the case of the S series of mortars where sodium silicate was inserted in the MCNs (Figure 5). It should be noted that the latter can be considered of great importance for the long-term performance of the studied lime-based mortars, which are commonly considered as sacrificial materials in masonry structures.

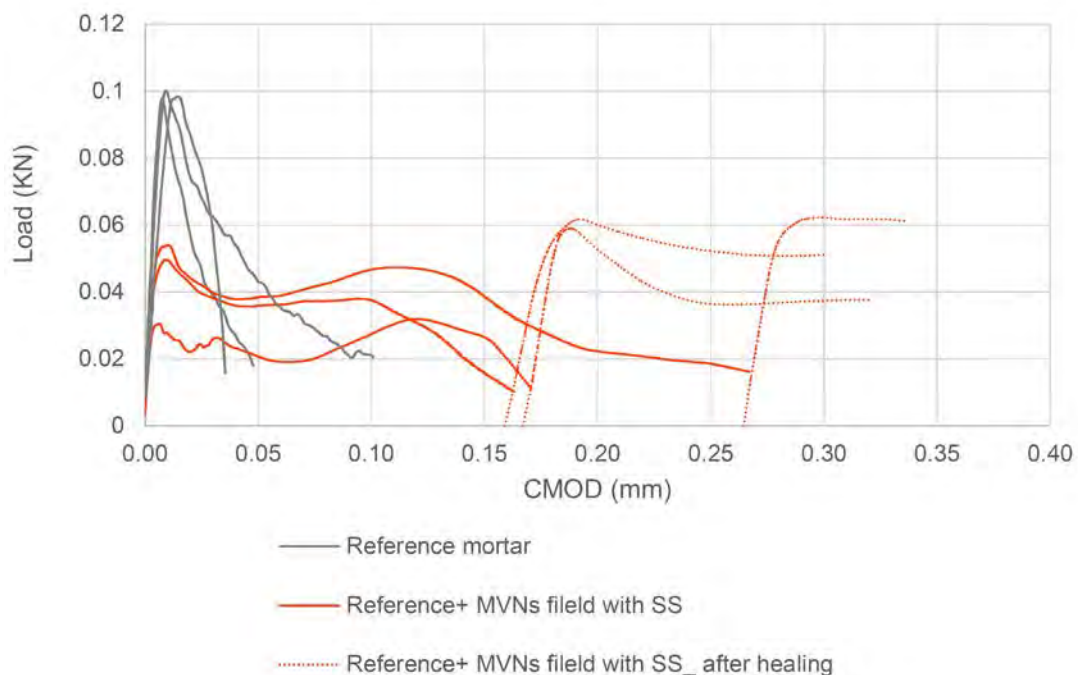


Figure 5. Load – CMOD diagram of samples with MVNs filled with sodium silicate (S) compared to the reference samples (R1).

In Figure 6 the response of the specimens with bacteria and MVNs filled with nutrients (B) is compared with that of the control specimens (R1). In the undamaged condition, the flexural moduli of the mixture B specimens, determined from the slopes of the linear parts of the Load-CMOD curves, are similar to the ones of the control specimens. Moreover, the residual strengths of the two sets of specimens are relatively close (7%), as may be seen from Fig 6 (mixture B). After the healing phase, the loading moduli of the mixture B specimens are significantly less than the intact flexural moduli and yet the response shows a significant strength increase. The exact reason for this apparent inconsistency between the post-healed strength and flexural modulus is as yet unknown but it is possible that this response was influenced by unbroken strands of the MVN material.

Figure 6. Load – CMOD diagram of samples with bacteria and MVNs filled with nutrients (B) compared to the reference samples (R1).

Conclusions

In this research the behaviour of an innovative self-healing system has been investigated for applications in lime-based mortars. It involved the use of newly designed 3D printed mini-vascular networks (MVNs), which were filled with healing components: (i) nutrients in the case where bacteria were added to the matrix and (ii) sodium silicate for better investigating the function of the designed MVNs. In this paper, the evaluation of the performance of the studied systems was assessed through a specifically designed three-point bend test. The results before and after the healing stage were evaluated, and the performance of the mortars with MVNs and the applied biological mechanism were compared to the reference samples.

The main conclusions are following:

- The system of interconnected channels, called mini-vascular networks (MVNs), provides an effective reservoir of healing agent that flows into cracks under capillary action. Thus, MVNs ligaments break and release the healing agent, thereby healing the crack. The presence of the MVNs seem to act as a reinforcement, but actually affects the flexural strength.
- The application of the selected bacteria (*Sporosarcina pasteurii*) and nutrients seems to be appropriate for partly restoring the performance of lime-based mortars; the estimated flexural strength after damage and healing was increased and the healing efficacy value was positive, yet at a level that would not alter significantly the microstructure and breathability of the material. Furthermore, the fact that the healing product of the studied biological mechanism is calcite, strengthens its compatibility with the nature of the lime mortars and of the typical substrate porous materials found in historic masonry (e.g. natural building stones).

Overall, the ability of the proposed self-healing system to heal damage in lime-based mortars can be vital for the longevity of valuable heritage structures, as well as for reducing the maintenance costs of buildings. Hence, the outcomes of this research can be considered as a measure taken in the future to contribute to the global efforts for decreasing the energy consumption in the construction sector.

References

1. Boynton RS (1980) Chemistry and Technology of Lime and Limestone New York John Wiley & Sons.
2. Cowan H (1977) The master builders: a history of structural and environmental design from ancient Egypt to the nineteenth century New York Willey & Sons.
3. U. M. Concrete (1966) Specification for lime and its uses in plastering, stucco, National Lime Association Unit Masonry and Concrete Washington DC.
4. Anderegg F (1942) Autogeneous healing in mortars containing lime ASTM Bulletin.
5. Nijland T, Larbi J, van Hees R J L B (2007) Self healing phenomena in concretes and masonry mortars: a microscopic study in Proceedings of the First International Conference on Self Healing Materials Noordwijk aan Zee The Netherlands.
6. Jonkers J (2007) Self Healing Concrete: A biological Approach, in Self Healing Materials. An alternative Approach to 20 Centuries of Materials Springer Series in Materials Science.
7. R. T. Committee (2017) State-of-the-Art Report of RILEM Technical Committee 221-SCH Springer.

8. Lubelli B, Nijlan T G, van Hees R P J (2011) Simulation of self-healing of dolomitic lime mortar in 13th Euroseminar on Microscopy Applied to Building Materials Ljubljana Slovenia.
9. De Nardi C, Cecchi A, Ferrara L, Benedetti A, Cristofori D (2017) Effect of age and level of damage on the autogenous healing of lime Composites part B 124:144-157.
10. De Nardi C, Bullo S, Ferrara L, Ronchin L, Vavasori A (2017) Effectiveness of crystalline admixtures and lime/cement coated granules in engineered self-healing capacity of lime mortars Materials and Structures 50: 190-202.
11. Harbottle MJ, Al-Tabbaa A (2008) Degradation of 2-chlorobenzoic acid in stabilised/solidified soil systems International Biodeterioration & Biodegradation 61 2:173-181.
12. Le Métayer-Levrela G, Castaniera G, Oriol J, Floubière J, Perthuisot P (1999) Applications of bacterial carbonatogenesis to the protection and regeneration of limestones in buildings and historic patrimony Sedimentary Geology 14:25-34.
13. Tiano P, Cantisani E, Cantisani, Sutherland I, Paget J M (2006) Biomediated reinforcement of weathered calcareous stones 7 1:49:55.
14. Jroundi F, Gómez-Suaga P, Jimenez-Lopez C, González-Muñoz MT, Fernandez-Vivas MA, (2012) Stone-isolated carbonatogenic bacteria as inoculants in bioconsolidation treatments for historical limestone Science of the Total Environment 425:89-98.
15. Dhami N K, Reddy M S, Mukherjee A (2013) Application of calcifying bacteria for remediation of stones and cultural heritages Review Arctile Frontiers in Microbiology 5 Article 304
16. Perito B, Marvasi M, Barabesi C, Mastromei G, Bracci S, Vendrell M, Tiano P (2014) A Bacillus subtilis cell fraction (BCF) inducing calcium carbonate precipitation: Biotechnological perspectives for monumental stone reinforcement Journal of Cultural Heritage 15: 345-351.
17. Van Tittelboom K, De Belie N, De Muynck W (2010) Use of bacteria to repair cracks in concrete Cem Concr Res 40: 157-166.
18. Theodoridou M, Harbottle M J (2018), Preventing deterioration of construction geo-materials; the new concept of biological self-healing for porous building stone Geophysical Research Abstracts 20 EGU2018-13831.
19. Joseph C, Jefferson A, Isaacs B, Lark R, Gardner R (2010) Experimental investigation of adhesive-based self-healing of cementitious materials Magazine of Concrete Research 62 11:831–843.

20. Dry C (1994) Matrix cracking repair and filling using active and passive modes for smart timed release of chemicals from fibers into cement matrices *Smart Mater Struct* 3 2: 118.
21. White S, Sottos N, Geubelle P (2001) Autonomic healing of polymer composites *Nature* 409:794–797.
22. Formia A, Terranova S, Antonaci P, Tulliani M, Pugno M (2015) Setup of extruded cementitious hollow tubes ascontaining/releasing devices in self-healing systems *Material* 8 4: 1897-1923.
23. Giannaros P, Al-Tabaa A, Kanellopoulos A (2016) Sealing of cracks in cement usingmicroencapsulated sodium silicate *Smart Mater Struct* 25.
24. Suganya D, Vignesh K, Rajapreethi C (2016) Novel Technique of Sodium Silicate in Healing of Concrete *IJSRD - International Journal for Scientific Research & Development* 4 3:142-145.
25. Ferrara L, Krelani V, Carsana M (2014) A “fracture testing” based approach to assess crack healing of concrete with and without crystalline admixtures *Construction and Building Materials* 68: 535-551.
26. Standard B. E. 13139:2013 Aggregates for mortar.
27. Homma D, Mihashi H, Nishiwaki T (2009) Self-healing capability of fibre reinforced cementitious composites’ *Journal of Advanced Concrete Technology* 7 2:217–228.
28. Phillips AJ Gerlach R, Lauchnor E, Mitchell AC, Cunningham AB, Spangler L (2013) Engineered applications of ureolytic biomineralization: a review *Biofouling* 29 6:715–733.

Hydrophobized lime grouts prepared with microsilica and superplasticizers

Jesús Fidel González-Sánchez¹, Íñigo Navarro-Blasco¹, Adrián Duran¹, Rafael Sirera¹, José M. Fernández¹, José Ignacio Álvarez¹

(1) MIMED Research Group, Chemistry Department, University of Navarra, mimed@unav.es, jgonzalez.65@alumni.unav.es, inavarro@unav.es, adrianduran@unav.es, rsirera@unav.es, jmfdez@unav.es, jalvarez@unav.es

Abstract

This work reports the obtaining of lime-based grouts as repairing materials. Microsilica was added as pozzolanic additive to enhance the compressive strength of the hardened grouts. Sodium oleate, as water repellent admixture, and different superplasticizers (SPs) were also incorporated to reduce the water absorption and to enhance the injectability of the grouts. Polycarboxylate ether (PCE), polynaphthalene sulfonate (PNS), melamine sulfonate (MMS) and polyacrylic acid (PA) were tested as SPs. Regarding the fluidity of the grouts, PCE was seen to improve the injectability, followed by PNS, MMS and PA. However, PCE addition was also accompanied by a severe delay in the setting time. The other three superplasticizers did not provoke significant delays in the hardening of the samples. The water contact angle underwent an increase pointing to an effective hydrophobization of the surface as a consequence of the water repellent admixture. The combination with PCE was the most effective in keeping the water repellency in comparison with the control sample (lime grout + oleate). MMS yielded high compressive strengths and durability of the mortars, in the face of freezing-thawing cycles, was enhanced.

Keywords: Lime Superplasticizers; Microsilica; Repellent

Introduction

Filling or injection mortars, specially designed for cavity repair and masonry defects, must flow properly in a fresh state and combine strength and durability [1-5]. However, in most cases, available information is limited to the effect of a single additive, without considering the possible joint or even synergistic effect of the most interesting combinations of two or more additives and/or pozzolanic additions [6,7]. One work has been recently published raising the combination of a pozzolanic addition with some superplasticizing additives, evidencing very good and hopeful results [8]. The simultaneous combinations of two or more additives and/or additions in lime mortars have not been previously investigated by the scientific community and the study of these synergies offers very interesting possibilities of scientific-technical progress.

For the preparation of lime mortars, the bibliography has detailed the possibility of increasing resistance, shortening setting times and allowing hardening - even if the access of the CO₂ is difficult - by including pozzolanic additions to mixtures. Metakaolin has been one of the most classic pozzolans studied, but also nanosilica has been the target of some research works [9-12]. There are previous papers that study the compatibility of some of the combinations between nanosilica with polycarboxylate ethers-type superplasticizers. As a matter of fact there have been no studies of compatibility with other superplasticizers of the same type and different molecular weight or with other SPs common in the chemistry of the binders – cement mainly – such as polynaphthalene sulfonate (PNS), melamine sulfonate (MMS) and polyacrylic acid (PA). All these chemical compounds are mixing water reducers and improve workability. They present important advantages to be used in injection and filling mortars. Little is known about the activity or compatibility between these admixtures and water repellent agents, compounds that reduce the water absorption by capillarity (including oleates and stearates). The use of these water repellents is very important to minimise the water inlet to mortars, and these combinations between air lime + pozzolan + water repellent agent + superplasticizer could result in a range of mortars of enormous usefulness in the restoration of the Built Heritage, particularly for the obtaining of grouts.

Therefore, the objective of this work is to determine the behavior and compatibility in lime mortars/grouts of different combinations of additives and mineral additions, in order to optimize the mixtures and thus to obtain new mortars that could serve for the restoration of the Architectural Heritage. The following combinations will be studied: calcitic air lime with pozzolanic addition (Microsilica), superplasticizers (Polycarboxylate ether (PCE1), polynaphthalene sulfonate (PNS), melamine sulfonate (MMS) and polyacrylic acid (PA) and a Water repellent (Sodium Oleate (O)).

Materials and methods

Preparation of the mortar. Mixing proportions

The weight proportions of the mortars were: 25% slaked calcitic lime supplied by Cal Industrial S.A. (Calinsa Navarra), classified as CL-90 by European regulations, 75% calcareous sand (Class AF-T -0/1-C sand, supplied by HOPASA Group). In addition, when necessary, the following components were added with respect to lime: 20% mineral pozzolan (Microsilica, supplied by ULMEN Europa), 0.5% water repeller (sodium oleate, provided by ADI-CENTER) and superplasticizer added in two different dosages 0.5% and 1% (PCE1, BASF's Melflux commercial product; melamine sulfonate, BASF's Melment F10; polynaphthalene sulfonate, marketed as Conplast SP340 Fa of FOSROC International and polyacrylic acid, of Sigma-Aldrich). The mixing water was established by 31%, resulting from an adjustment of the water demand of the control mortar (additives/admixtures-free) to obtain a fluidity – as measured in the flow table test – around 185 mm.

For the preparation of the pastes, lime and the required amount of calcitic sand (limestone aggregate) were blended for 5 min using a solid-admixtures mixer BL-8-CA (Lleal, S.A., Spain). Afterwards, the necessary water and superplasticizers were then added and mixed for 90 s at low speed and adjusted according to UNE-EN 196-1 [13], in a Proeti ETI 26.0072 (Proeti, Madrid, Spain) mixer.

Mortar samples were moulded in prismatic 40 × 40 × 160 mm, stored at 20 °C and 60% RH and demoulded 7 days later. Different curing times were considered: 7, 28, 91, 182 and 365 days. In order to make the results representative, three replicates of the mortars were tested at each curing time.

Fresh-state tests

The tests of the mortars at plastic state started with the slump measurements, which were recorded after 15 strokes of the flow table, 1 per second according to the indications of the standard UNE-EN 1015-3.

Then the period of workability of the material was determined according to standard UNE-EN 1015-9 [15]. Every 15 minutes a probe was slowly introduced, scoring the weight. When this weight was higher than 1500 g, the assay was finished.

All these experiments were carried out by triplicate and the depicted values are an average value of all the recorded measurements.

Hardened-state tests

Regarding the hardened state study, prismatic specimens with dimensions of 160 x40x40 mm were prepared in Proeti C00901966 moulds. For the filling and compaction the standard UNE-EN 196-1 was carried out to perform the filling in two layers and using to compact each layer an automatic compactor (IBERTEST iB32-045E-1), eliminating the air bubbles present in the mixture. Finally, the excess of mass was eliminated with a rule. The prepared grouts were cured at 20° C and 60% RH and demoulded 7 days later.

The mechanical resistances were measured at 28, 91, 182 and 365 days, to observe possible modifications over time. For all these measurements, 3 specimens were tested, in order to obtain representative values. For the compressive strength tests, a compression breaking device Proeti ETI 26.0052 was used at a breaking speed 5-50 KP · s⁻¹ with a time interval between 30 and 90 seconds.

In hardened specimens different characterization methods were performed. For thermal analysis, a simultaneous TG-sDTA 851 Mettler Toledo thermoanalyzer device (Schwerzenbach, Switzerland) was used under the following experimental conditions: alumina crucibles, temperature range from 25 to 1000 °C, and a heating rate of 10 °C·min⁻¹ under static air atmosphere.

The porous structure of the material was studied by Mercury Intrusion Porosimetry (MIP), using a Micromeritics AutoPore IV 9500 equipment with a pressure range of 0.0015-207 MPa, which automatically recorded the pressure, pore diameter and volume of mercury intrusion.

For the durability studies, prismatic samples (prepared and cured for 28 days as described before) were tested to assess the durability. Hardened grouts were subjected to Frost resistance, which was determined by means of freezing-thawing cycles. The cycles consisted of water immersion of the samples for 24 h and subsequently freezing at -10 °C for 24 h. For these experiments, a CARAVELL 521-102 freezer was used.

The evaluation of the hydrophobicity of the sample was carried out with a measuring instrument of the contact angle OCA 15EC Dataphysics. In this way it was possible to determine the contact angle of a drop of water deposited on the surface of the sample, and the time for the absorption of the same by the material.

Results and discussion

Mortar Properties in Fresh

Bulk density

Comparing the results, the fresh grout of plain lime (Lime in Figures) is denser than the control samples obtained by combination of Lime-Oleate (L-O) and Lime-Microsilica-Oleate (L-M-O), as shown in the Figure 1.

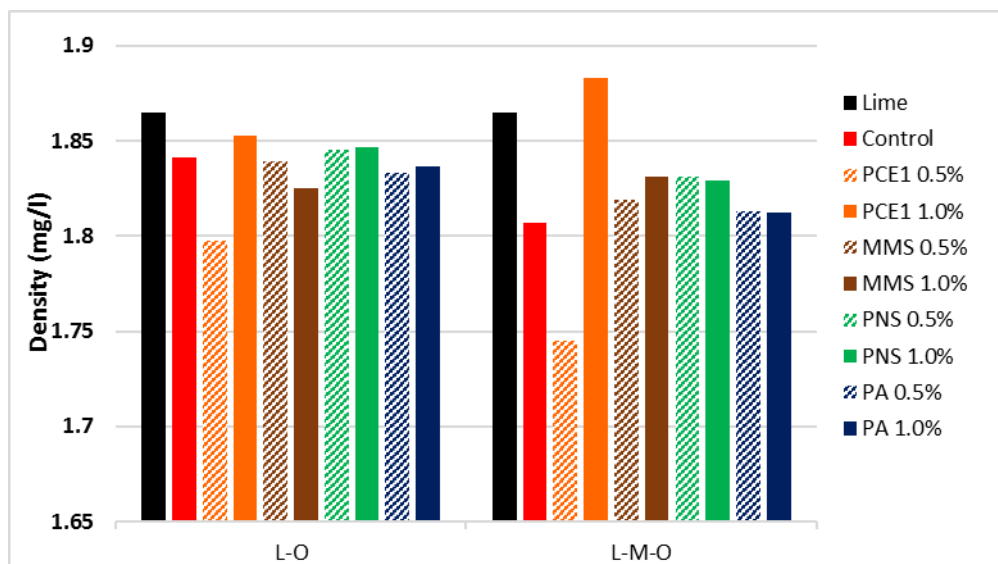


Figure 1. Density of the different mixtures

However, by adding the different superplasticizers, as shown in Figure 1, there are changes in the density of all bulks. In the case of PCE1 in the Lime-Oleate (L-O) and Lime-Microsilica-Oleate (L-M-O) mixture, the density values decreased when a dosage of 0.5% of SP was

added, while increased when the SP dosage was 1%. When using PCE1 in the L-M-O mixture, the density is the lowest with the 0.5% dose and is the highest with 1% dose. When using MMS in the L-O mixture, the density decreased for 1% dose, and increased for the others. When PNS is used in each mixture with both percentages, bulk density raised. As for the PA, the density was very similar to SP-free mixtures (Control) in all the cases.

Air content

The experimental values of air content of the fresh pastes were also determined and collected in the Figure 2. Although values underwent small variations, there is a general trend showing an increase in the air content in all the samples when any of the additives was incorporated to the lime. The presence of the polymer PCE1 exerted an influence on the density and air-entrained values. PCE1 increased the air-entrained during the mixing process when was added in 0.5%, thus reducing the density (Figure 1). Conversely, the incorporation of the other superplasticizers gave rise to lower levels of air content, thus achieving comparatively denser packing systems, but in all cases the percentage of air content are greater than the pure lime. The excess in the air-entrained together with the low density of the fresh paste could involve a porosity increase after the hardening of the sample, as will be discussed below.

This performance (increasing in entrained air and a parallel density reduction) may be ascribed to the tensioactive character of the admixtures. The SPs, as well as the water repellent agents, are characterized by a dual molecule, showing a non-polar part area and also a polar segment. During the mixing process, these admixtures can be distributed at the interface area between the aqueous phase and the air, stabilizing air bubbles and giving rise to the observed values.

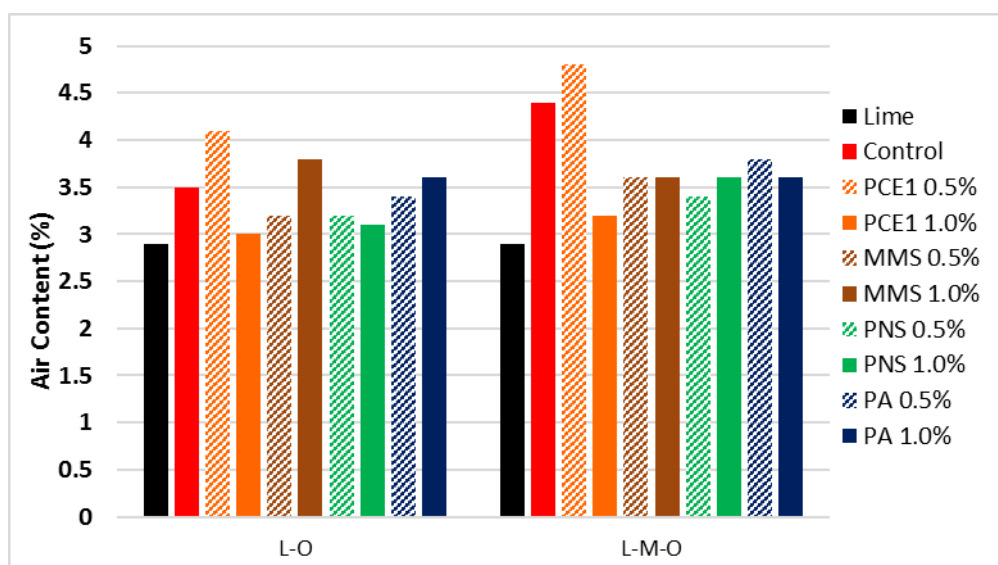


Figure 2. Air content in the different mixtures

Fluidity and workability (open time)

The fluidity was studied for the L-O and L-M-O mixtures, with and without the presence of superplasticizer. The Figure 3 shows how the fluidity of the lime grouts is affected after mixing with a water repellent agent and with a pozzolan. As it can see the L-O mixture showed a lower fluidity, while the presence of the pozzolanic addition (M) resulted in a fluidity increase. This finding can be explained as a consequence of the spherical shape of the microsilica that increases spread by allowing the lubrication of the fresh grout. The value of the L-O mix was seen to be very similar to the one of the pure lime.

Figure 3 depicts the spread values of fresh grouts with superplasticizer. The Polyacrylic Acid (PA) 1% decreases the fluidity as compared with the value of the control mix. The lowest dosage (0.5%) gave rise to a value very similar to that of the pure lime. When incorporating PNS the spread value increased in all cases with both dosages, depicting a very similar behavior to the one observed when MMS was used. After the addition of PCE1 at any dosage, the fluidity of the mixture dramatically increased, exceeding the value of 300 mm, resulting in a high-fluidity mixture. The efficiency of polycarboxylate ether derivatives has been mentioned in the literature in lime and cement systems, and is supported on the strong effect of the steric hindrance (more effective) of these additives compared with the electrostatic repulsions (less efficient).

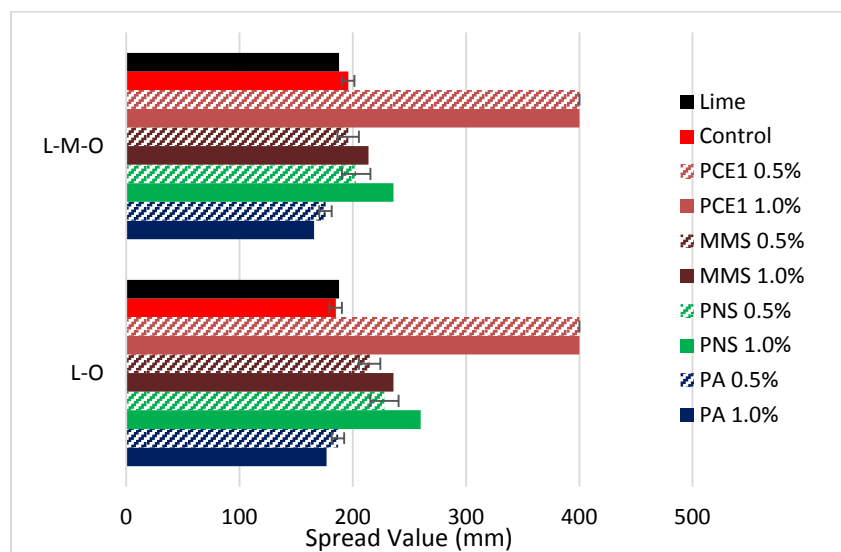


Figure 3. Fluidity of the different mixes

The workability of the different mixtures is gathered in the Figure 4. The addition of the sodium oleate accelerates the setting time of the sample, while – surprisingly- the pozzolanic agents delayed it.

The workability suffered substantial changes when the SPs were added to L-M-O grouts. The setting time with PCE1 is so high that this grouts would not be able to be used in practical applications. For all mixtures (L-O, and L-M-O) the addition of SP (except PCE1) considerably

shortened the setting time. This finding could be also helpful to achieve a workability improvement but without a delay in the setting time. In all cases the use of a 0.5% dosage was better than the use of 1% (except when PA is used).

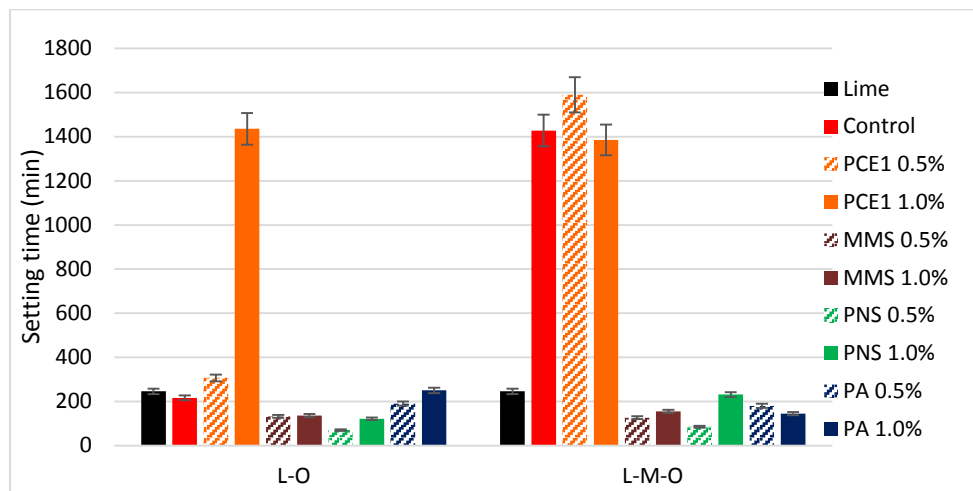


Figure 4. Workability of the different mixes

Hardened-state Properties

Compressive Strength

Carbonation has a significant influence in the hardening process along time in lime-based systems. The mechanical strengths increase over time due to the carbonation process, resulting in the formation of CaCO_3 . Accordingly, on average, the highest values of compressive strength were obtained at long-term curing times, usually after 365 curing days (Figure 5 and 6).

For the control mix L-O at 365 curing days, without the addition of the SPs, its compressive strength was lower than that of the plain lime mortars (1.5 MPa) which could be ascribed to the interference of the sodium oleate with the lime carbonation process, as will be discussed below.

For samples with 0.5% SP at 365 curing days, samples exhibited higher compressive strength than the plain lime mortars (except in the case of PA). When a dosage 0.5% PCE1 is used in the L-O mixture, after 365 curing days, the mechanical strength was the highest (Figure 5).

When 1% SP is used, mechanical strengths increased at 365 curing days in all mixes except in the L-O mixture with PA (Figure 6). In the case of MMS strength underwent a clear increase and exhibited the highest compressive strength after 365 curing days. With respect to PA in all cases the compressive strength decreased and the use of this superplasticizer provides the lowest compressive strengths.

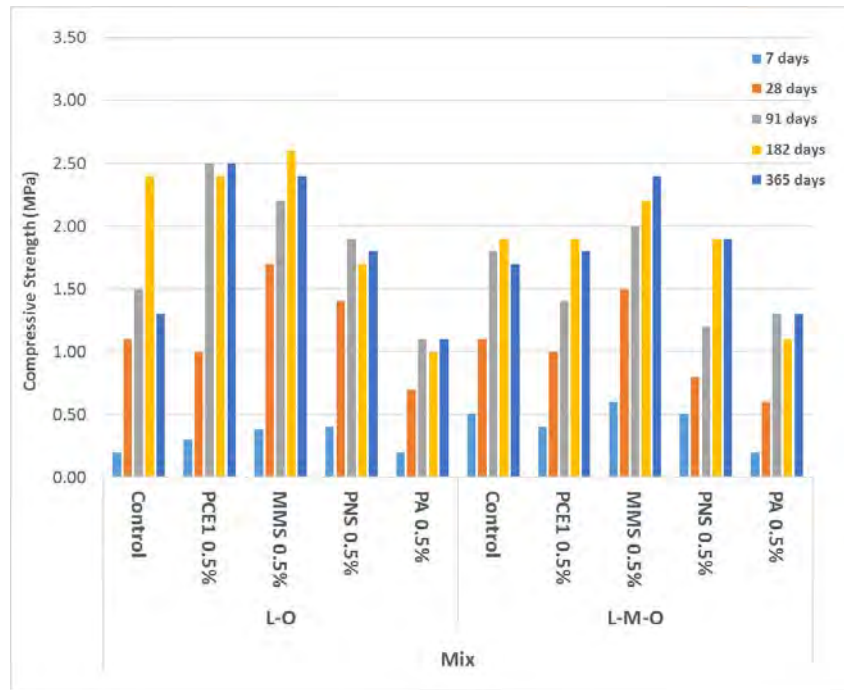


Figure 5. Compressive strength in the Hardened Mortars at different times (mixtures with 0.5% of superplasticizer)

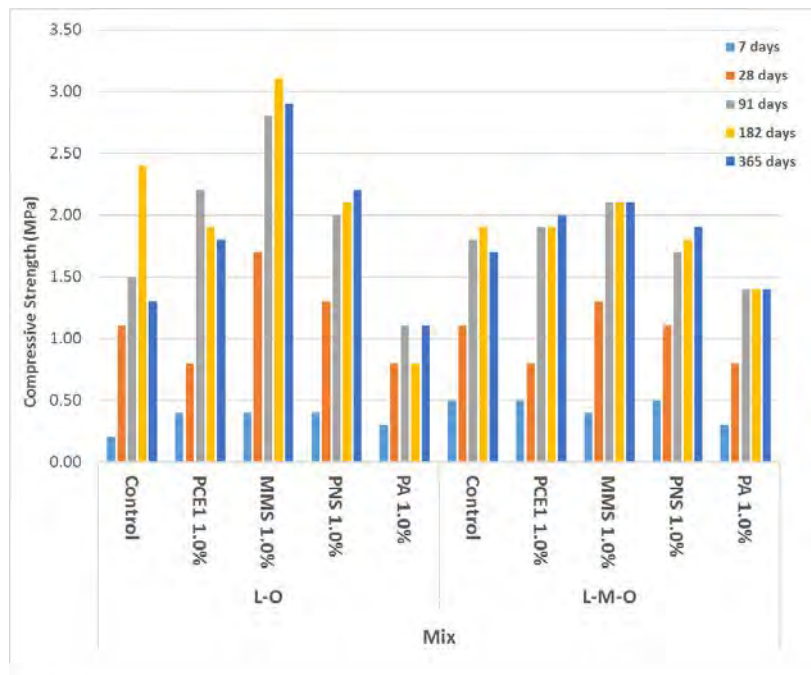


Figure 6. Compressive strengths at different times (mixtures with 1.0% of superplasticizer).

TG-DTA

The rate of carbonation and the pozzolanic reaction at the different curing times were followed by TG-DTA analyses. Previous works also correlated the structure of the materials with the TG measurements. Figures 7 depicts the percentages of $\text{Ca}(\text{OH})_2$ and CaCO_3

calculated from TG weight loss due to dehydroxylation of portlandite at ca. 450°C, and weight loss owing to the calcite decomposition at ca. 800°C.

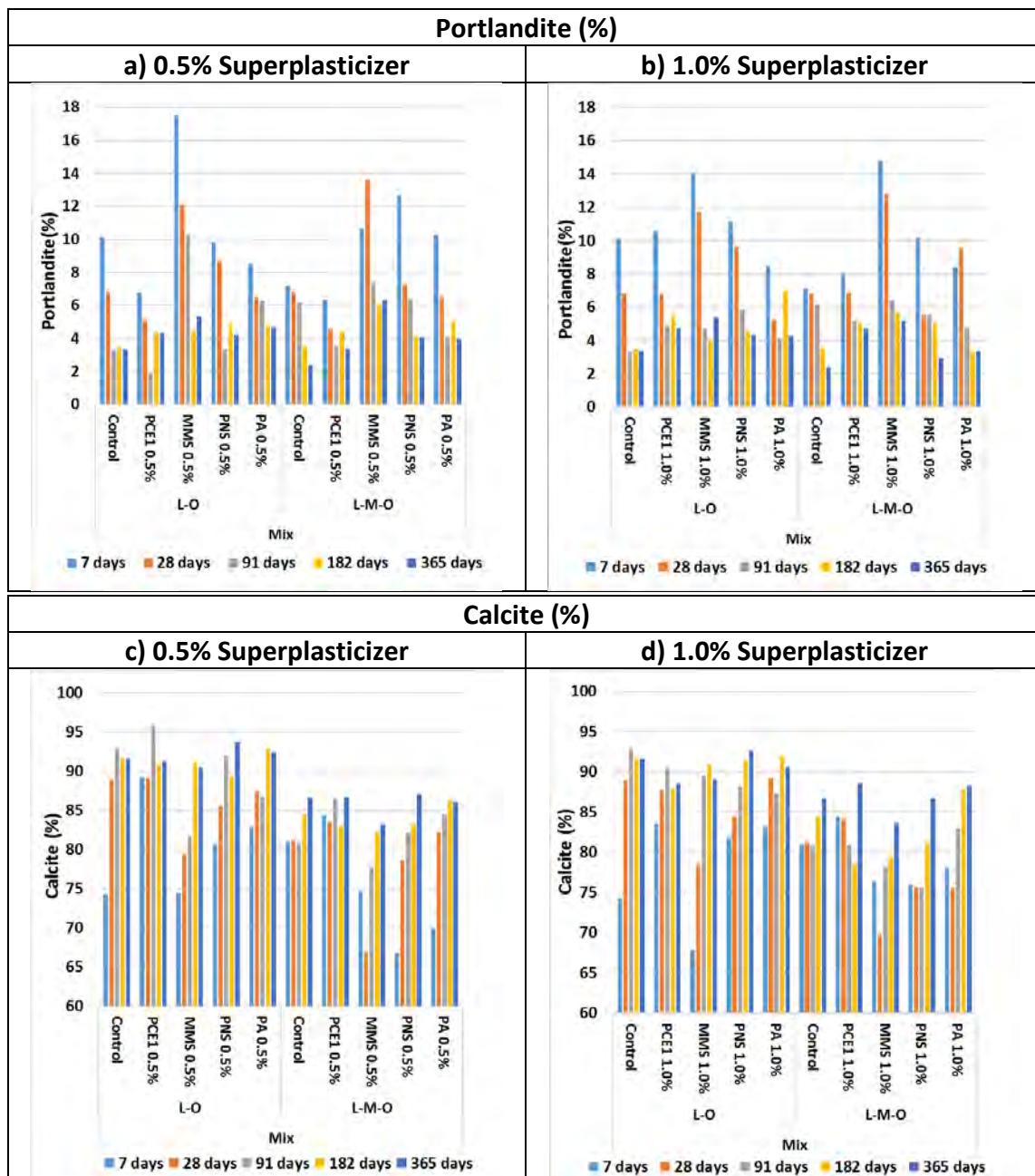


Figure 7. Percentages of Portlandite ($\text{Ca}(\text{OH})_2$) and Calcite (CaCO_3) of grouts at different curing times.

The degree of carbonation was helpful to understand these results: the presence of the different SPs clearly hindered the carbonation as confirmed by the thermal studies. The quantitative values obtained by TG (Figure 7) showed that the presence of any superplasticizer's doses yielded comparatively higher content in $\text{Ca}(\text{OH})_2$. Comparing the control samples of L-O and L-M-O, a reduction in $\text{Ca}(\text{OH})_2$ was observed due to the presence of microsilica because a pozzolanic reaction between the lime and the microsilica could be expected (Figure 7a and 7b). When PNS was used in L-O and L-M-O mixtures both at 0.5%

and 1%, the amount of calcite increased, thus suggesting that this SP did not interfere with the carbonation of the lime grout (Figure 7c and 7d).

Porosity measurements

Pore size distribution measurements (Figure 8) carried out by MIP showed that the addition of the pozzolanic additive reduced porosity about 1 μm in diameter due to: (i) the filling effect of the microsilica; and (ii) the pozzolanic reaction. In addition, the small capillary pores attributed to the formation of C-S-H increased (see the range pores between 0.1 and 0.01 μm). The reduction of larger pores explains the increase in mechanical resistances as a result of the presence of microsilica.

In the case of the L-O mixture (Figure 8A and 8B) with SP, the presence of PCE1 gave rise to a drop in the amount of pores about 1 μm , but, it permits the appearance of pores in the range of 6 to 11 microns. In the case of L-M-O mixture plus SPs (Figure 8C and 8D) the behavior was very similar without the presence of them, except in the case of the PCE1 where there is amount reduction of pores about 1 μm .

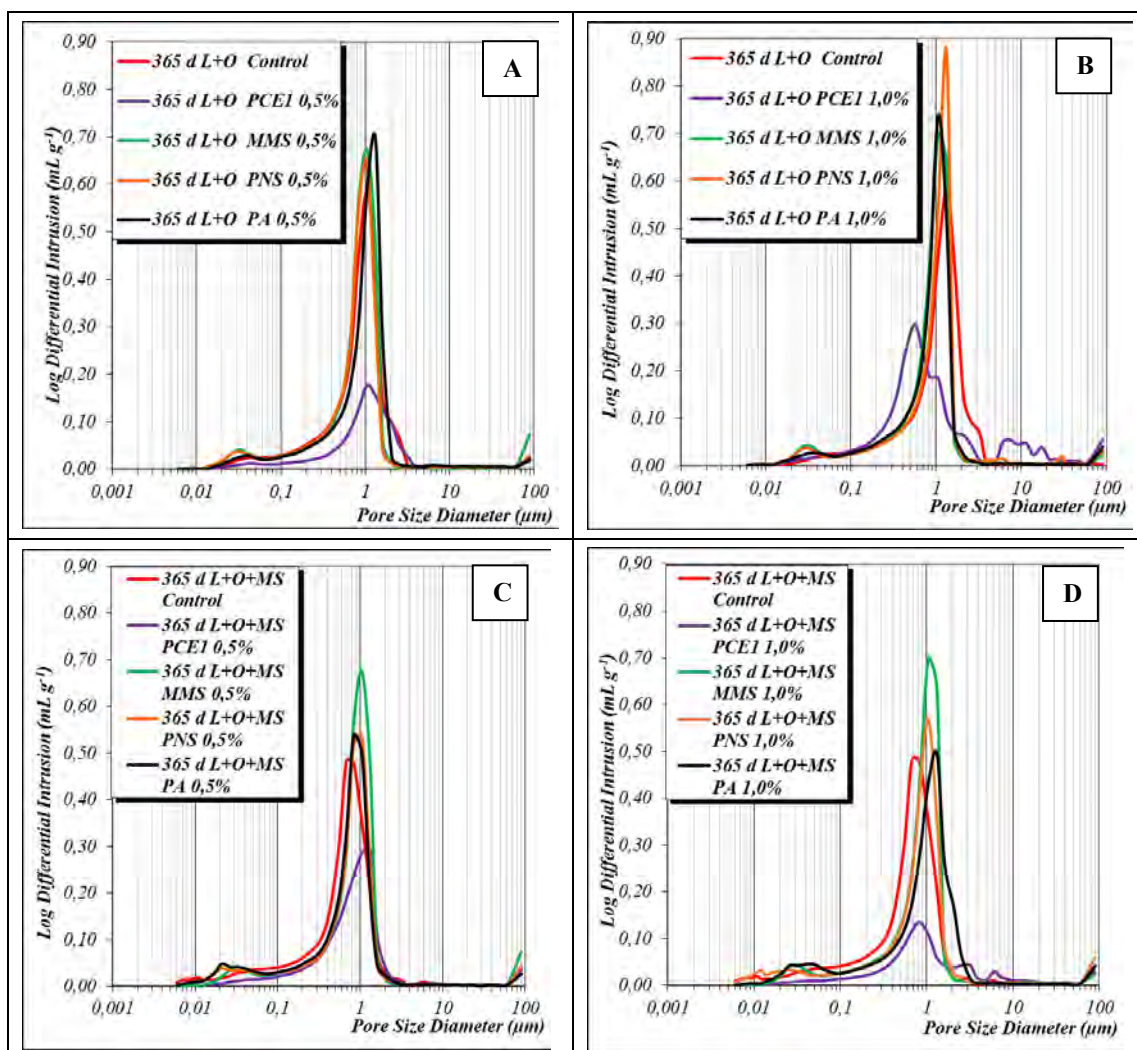


Figure 8. Pore size distributions of different samples after 365 days of curing.

Freezing-thawing

The plain grouts subjected to frost resistance test (freezing-thawing (F–T) cycles) underwent serious decay leading to the total destruction of the sample after just one cycle (Fig. 9).



Figure 9. Pure air lime grouts subjected to one freezing-thawing cycle

Fitting itself to a dosage-response pattern, the incorporation of sodium oleate clearly enhanced the F-T durability of the grouts. It can be observed (Figure 10A) that L-O control sample can endure up to 18 F–T cycles displaying serious decay only in the last cycle. However F-T endurance provided by the pozzolanic admixture included in lime mortars with the incorporation of microsilica changed this behaviour: the sample of L-M-O control showed serious decay after just two cycles (Figure 10A). This behavior could be explained as a consequence of the interaction between microsilica and sodium oleate. The SP addition involved different performance and some of grouts withstood more F-T cycles. The decrease in the mean pore size hindered the absorption of liquid water, preventing its later freezing and expansion damage, and consequently, increasing the durability of this type of grouts.

The increase in the percentage of SP did not enhance the F-T resistance of the samples. However, each one of the superplasticizer imparts a different performance. All the superplasticizers in the case of the samples of L-O, decreased the durability of the samples and in the case of the mixture of L-M-O, SPs were helpful to improve the durability. PNS yielded the worst results in terms of F-T endurance, whereas 0.5% of PCE1 enhanced the durability in the sample of L-M-O. For all the conditions, the durability of mixtures containing MMS was rather high.

Hydrophobicity

The static water contact angle (WCA) and the water absorption time (i.e., the vanishing time of the water drop after its deposition, water drop lifespan, of interest for very porous substrates) were measured for the different grouts. Samples were cured for 365 days. The results are shown in the Table 1.

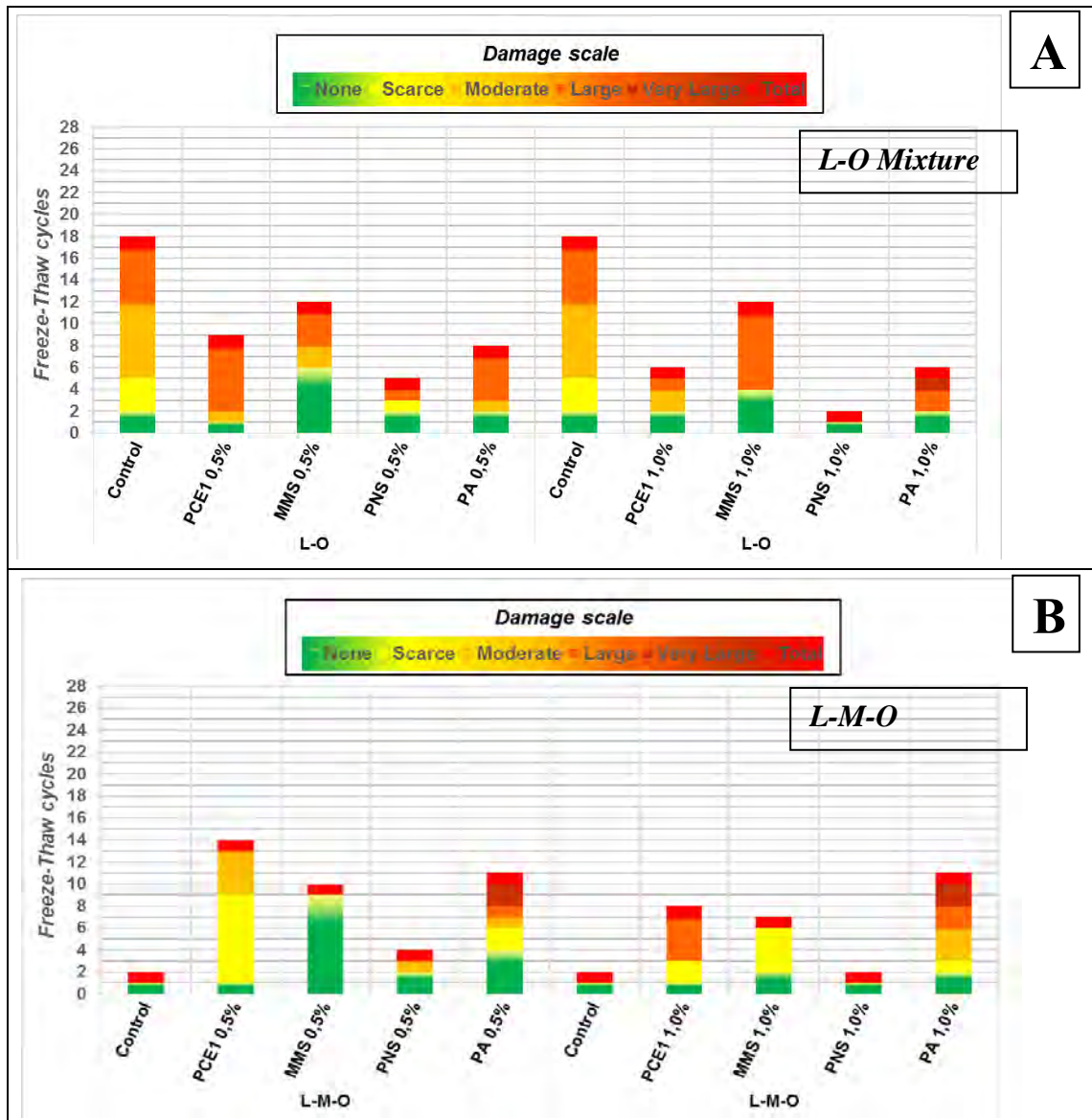


Figure 10. Alteration degrees of grouts after freeze-thaw cycles.

Table 1: Contact angle Measurement Results

Mixture	Contact angle	Full Absorption of the drop of Water and disappearance in short time interval
Lime + Oleate	75.0	No
Lime + Oleate + Microsilica	59.2	No
Lime + Oleate + PCE1 1%	66.8	No
Lime + Oleate + MMS 1%	53.5	No
Lime + Oleate + PNS 1%	29.4	Yes
Lime + Oleate + P.A. 1%	58.2	No
Lime + Oleate + Microsilica + PCE1 1%	95.1	No
Lime + Oleate + Microsilica + MMS 1%	30.2	Yes
Lime + Oleate + Microsilica + PNS 1%	29.6	Yes
Lime + Oleate + Microsilica + P.A. 1%	13.7	Yes

The mixture with the best hydrorepellency was the one with Lime + Oleate + Microsilica + PCE1 1%, due to: (i) the lowest total porosity of this grout among the all tested; (ii) PCE1 does not interfere with the oleate water-repellent activity, resulting in two highly compatible additives. The most hydrophilic mixture was the Lime + Oleate + PNS 1%, which raises the hypothesis - to be confirmed - of a chemical interaction between PNS and sodium oleate, in such a way that the water repellent action of the oleate drops, increasing the rate of water absorption. It should be noted that the hydrorepellency in all mixes was a superficial phenomenon, due to the tensioactive characteristics of sodium oleate. The hydrophobic part was exposed on the surface (air phase) during the mixing process with aqueous dispersion. However, in internal fragments of the samples, it was not possible to measure the WCA as a consequence of a dramatic reduction of the hydrophobicity (the water drop disappeared immediately absorbed by the sample), indicating that the hydrophobization took place mainly at a superficial level.

Summary of results

In Table 2 all results are summarized, numbering and giving a grade in each test to from 1 to 4, where the number 1 refers to the sample that shows a result similar to that of a common lime grout and the number 4 represents an improvement in the tested mix. It has been considered improvement, for the injection grouts studied, and always within reasonable limits, an improvement in fluidity (workability), a shortening of the setting time (usually high for lime-based materials), an increase in the compressive strength developed, a porosity reduction and a hydrophobic surface that generates water repellency to minimise absorption and prevent deterioration and F-T endurance.

Table 2. Summary of the results of the tests carried out, both fresh and hardened to the mortars studied

Mixture	Property						
	Fluidity	Setting Time	Compressive Strength	Porosity	Freezing-thawing	Water contact Angle	Global Qualitative Rating
Lime	1	1	1	1	1	1	6
Lime + Oleate	1	3	1	1	3	4	13
Lime + Oleate + Microsilica	2	1	2	2	1	2	10
Lime + Oleate + PCE1 0.5%	4	2	4	4	2	3	19
Lime + Oleate + MMS 0.5%	2	3	4	2	2	3	16
Lime + Oleate + PNS 0.5%	2	4	3	2	2	2	15
Lime + Oleate + P.A. 0.5%	1	1	1	2	2	3	10
Lime + Oleate + PCE1 1%	4	1	2	4	2	3	16
Lime + Oleate + MMS 1%	2	3	4	2	2	3	16
Lime + Oleate + PNS 1%	3	4	3	1	1	2	14
Lime + Oleate + P.A. 1%	1	1	1	2	2	3	10
Lime + Oleate + Microsilica + PCE1 0.5%	4	1	1	3	2	4	15
Lime + Oleate + Microsilica + MMS 0.5%	2	3	3	2	2	2	14
Lime + Oleate + Microsilica + PNS 0.5%	3	4	2	1	2	2	14

Mixture	Property						
	Fluidity	Setting Time	Compressive Strength	Porosity	Freezing-thawing	Water contact Angle	Global Qualitative Rating
Lime + Oleate + Microsilica + P.A. 0.5%	2	2	1	1	2	2	10
Lime + Oleate + Microsilica + PCE1 1%	4	1	2	4	2	4	17
Lime + Oleate + Microsilica + MMS 1%	2	3	2	2	2	2	13
Lime + Oleate + Microsilica + PNS 1%	3	2	2	1	2	2	12
Lime + Oleate + Microsilica + P.A. 1%	1	3	1	1	2	2	10

As it can be seen, the mixture that showed similar value to that of the plain lime grout was Lime + Oleate + Microsilica + PA (in both percentages 0.5% and 1%), while the mixture Lime + Oleate + PCE1 0.5% is the one showing the most favorable changes in all characteristics studied, being the mixture with the greatest compressive strength, best fluidity, lowest porosity and also was the samples with the highest hydrophobicity. In addition, the workability of this mixture improves with respect to control without superplasticizer.

Conclusions

Through this study with a scientific and technical point of view was able to determine the behavior and the compatibility existing in lime-based grouts and mortars with various combinations of additives and mineral additions. This paper describes the behavior of the different mixtures between calcitic aerial lime, pozzolanic additions, superplasticizers and water-repellent agents. The results are favorable for using some of these grouts in the restoration of Architectural Heritage, resulting in the best mix of Lime + Oleate + PCE1 0.5% that improves the properties of a plain lime grout. Adjustment of the dosages of the superplasticizers should be carried out depending on the desired injectability.

Acknowledgments

Work funded by the Project MAT2015-70728-P of the Ministry of Economy and Competitiveness. J.F. González-Sánchez thanks the Association of Friends of the University of Navarra for a pre-doctoral fellowship.

References

1. S. Andrejkovičová CA, Velosa A, Rocha F (2015) Bentonite as a natural additive for lime and lime – metakaolin mortars used for restoration of adobe buildings, *Cement and Concrete Composites*, 60: 99-110

2. Pozo-Antonio JS (2015) Evolution of mechanical properties and drying shrinkage in lime-based and lime cement-based mortars with pure limestone aggregate, *Construction and Building Materials*, 77: 472-478
3. Silva BA, Ferreira Pinto AP, Gomes A (2014), Influence of natural hydraulic lime content on the properties of aerial lime-based mortars, *Construction and Building Materials*, 72: 208-218
4. Rodríguez-Navarro C, Hansen E, Ginell WS (1998) Calcium Hydroxide Crystal Evolution upon aging of lime putty, *J. Am. Ceram. Soc.*, 81: 3032-3034
5. Conclusions of the Symposium (1990) "Mortars, cements and grouts used in the conservation of historic buildings", Rome, *Materials and Structures*, 23: 235
6. Navarro-Blasco I, Pérez-Nicolás M, Fernández JM, Duran A, Sirera R, Alvarez JI, (2014) Assessment of the interaction of polycarboxylate superplasticizers in hydrated lime pastures modified with Nanosilica or Metakaolin as Pozzolanic You reactivate, *Construction and Building Materials*, 73: 1-12
7. Fernández JM, Duran A, Navarro-Blasco I, Sirera R, Alvarez JI (2013), Influence of Nanosilica and a polycarboxylate ether Superplasticizer on the performance of lime mortars, *Cement and Concrete Research*, 43: 12-24
8. Duran A, González-Sánchez JF, Fernández JM, Sirera R, Navarro-Blasco I, Alvarez JI. Influence of Two Polymer-Based Superplasticizers (Poly-naphthalene Sulfonate, PNS, and Lignosulfonate, LS) on Compressive and Flexural Strength, Freeze-Thaw, and Sulphate Attack Resistance of Lime-Metakaolin Grouts. *Polymers* 2018; 10(8): 824.
9. Silva BA, Ferreira Pinto AP, Gomes A (2014) Influence of natural hydraulic lime content on the properties of aerial lime-based mortars, *Construction and Building Materials*, 72: 208-218
10. Nežerka. V, Slížková P, Tesárek T, et al. (2014) Comprehensive study on mechanical properties of lime-based pastes with additions of metakaolin and brick dust, *Cement and concrete Research*, 64: 17-29
11. Arizzi A. Cultrone, G. (2012) Aerial Lime-based mortars blended with a pozzolanic additive and different admixtures: a mineralogical, textural and physical – mechanical study. *Constr. Build. Mater.*, 31: 135 – 143
12. Duran A, Navarro-Blasco I, Fernández JM, Alvarez JI (2014) Long-term mechanical resistance and durability of air lime mortars with large additions of Nanosilica. *Construction and Building Materials* 58: 147-158
13. UNE-EN 196-1, cement test Method. Part 1: Determination of mechanical resistances, 2005.

14. UNE-EN 1015-3, Methods of testing mortars for masonry. Part 3: Determination of fresh mortar consistency (by shaking table), 2000.
15. UNE-EN 1015-9, Methods of testing mortars for masonry. Part 9: Determination of the period of workability and open time of fresh mortar, 2000.

Photoactive Fe-TiO₂ Lime Plasters for Building Protection

Chrysi Kapridaki^{1*}, Nikolaos Xynidis¹, Nikolaos Xekoukoulotakis², Nikolaos Kallithrakas-

Kontos³, Noni Maravelaki^{1**}

(1) School of Architectural Engineering, Technical University of Crete, Akrotiri University Campus, 73100 Chania, Crete, Greece, ckapridaki@gmail.com, xn1983@hotmail.com, pmaravelaki@isc.tuc.gr

(2) School of Environmental Engineering, Technical University of Crete, Akrotiri University Campus, 73100 Chania, Crete, Greece, nikos.xekoukoulotaki@enveng.tuc.gr

(3) School of Mineral Resources Engineering, Technical University of Crete, Akrotiri University Campus, 73100 Chania, Crete, Greece, kalli@mred.tuc.gr

Abstract

TiO₂ and Fe-doped TiO₂ nanoparticles, containing Fe concentrations of 0.05, 0.10 and 1.00% w/w) were synthesized through a simple sol-gel method. FTIR, XRD, XPS and XANES analyses of the Fe-doped TiO₂ nanoparticles revealed the predominant presence of anatase crystalline form, as well as the incorporation of the Fe³⁺ ions into the crystal lattice of TiO₂. The photocatalytic assessment of the Fe-doped TiO₂ nanoparticles indicated that the low Fe content TiO₂ nanoparticles (0.05 and 0.1 w/w %), have a positive effect on the photocatalytic degradation of Methyl Orange under the visible radiation. Moreover, FTIR monitoring of lime pastes enriched with Fe-doped TiO₂, revealed that an enhancement of carbonation occurred for the undoped TiO₂ and 0.05Fe doped TiO₂. Therefore, the doping of TiO₂ with Fe at low concentration up to 0.05% w/w resulted as the best performed both, from the photocatalytic point of view in protecting the architectural surfaces from the pollutant deposition and, in enhancing the carbonation process.

Introduction

The excessive environmental pollution along with the climatic changes impose the use of resistant construction materials that can maintain the architectural facades intact by the harmful impact of the pollutants. Addressing the problem of the decay of the external facades from the influence of the pollution, plasters and coatings possessing self-cleaning ability, hydrophobicity, water vapor permeability and appropriate mechanical properties were proposed [1-3]. In the construction sector, nano-TiO₂ is recognized as an effective admixture incorporating in coatings, paints, plasters, mortars, in the cement industry, etc. Research has shown that TiO₂ can contribute to the abatement of pollutants and to enhancement of fundamental processes in the mortar curing, such as carbonation and hydration [1-3]. The beneficial effects of TiO₂ are mainly attributed to its photo-activation under the UV irradiation that allows electrons from the valence band to move in the conduction band, thus generating holes that successively react with the surrounding water and oxygen molecules to yield free radicals. The latter, attack the pollutants and decompose

them in CO₂ and H₂O under several reactions that will be promoted by the factors, such as the lack of recombination electron/hole system, the humidity etc. improved by shifting the semiconductor performance towards higher wavelengths, such as the visible light and imparting to the additive TiO₂ specific features when incorporated within blends of construction materials [4]. Innovative solutions, intensively investigated so far, refer to research activities mainly motivated by the efficient activation of TiO₂ under visible light. Therefore, significant studies and examples of well-performed building materials exhibiting multi-purpose aspects mainly due to the effective combination of TiO₂ with capable dopants were proposed, accordingly [4, 5].

Our research is addressed towards the improvement of photocatalytic activity of TiO₂ with dopants. Having studied specific features of lime mortars, such as the flexibility, workability, water-retention and evaporation, strength, freeze-thaw and salt-decay resistance, autogenous self-healing, the adopted scenario presented here, included lime as binder and the activation of the admixture TiO₂ iron (Fe) doping [1, 4]. The choice of Fe is based on a multi-criterial decision taking into account: (a) its presence in the construction materials and the induced compatibility in terms of physico-chemical and mechanical properties, (b) the low cost and occurrence in a number of compounds, (c) the colour of ochre that could provide in the coatings, (d) its capability to be embedded into the TiO₂ crystalline structure due to the similar radii of Ti⁴⁺ (0.68 Å) and Fe³⁺ (0.68 Å), and finally (e) the enhancement of the TiO₂ photocatalytic activity, as Fe³⁺ ions play a crucial role to this procedure, functioning as hole and electron scavengers [4-7].

The effect of Fe nanoparticles on the enhancement of the TiO₂ photoactivation and the influence of specific parameters, such as the type of iron compounds, concentration, microstructural and morphological characteristics, along with the way of the Fe embedded within the TiO₂ and lime matrix, were thoroughly studied. Furthermore, TiO₂ nanoparticles and TiO₂ Fe-doped nanoparticles were added to pastes containing air lime and were evaluated as promoters of carbonation. Therefore, the rate of carbonation of Ca(OH)₂ paste with TiO₂ undoped and Fe-doped catalysts was investigated and correlated with the results obtained from the degradation of the Methyl Orange (MO).

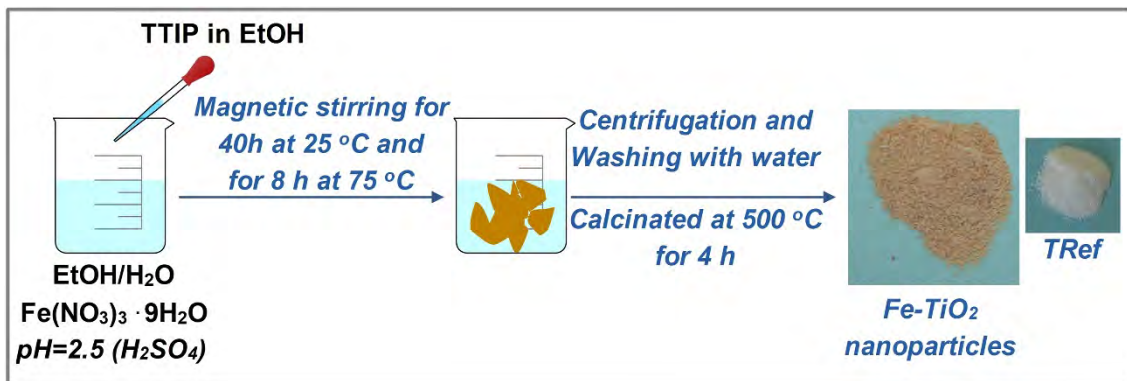
Experimental part

Preparation of Fe-doped TiO₂ nanoparticles

The photoactive Fe-doped nanoparticles were prepared by combining the sol-gel technique with thermal treatment [6, 7]. Titanium (IV) isopropoxide (TTIP, Sigma Aldrich) was used as precursor for the TiO₂ nanoparticles and Iron (III) nitrate nonahydrate (Fe(NO₃)₃ · 9H₂O, Panreac) as Fe⁺³ dopant. Ethanol (EtOH, Sigma Aldrich, 99%) and deionized water were used as solvents, while sulphuric acid (H₂SO₄, Panreac) was used as catalyst. Overall, three differed Fe-doped nanoparticles were synthesized which varied in the % amount of Fe⁺³. The doped synthesized TiO₂ nanoparticles were denoted as §FeT, where the symbol § indicates

the % (w/w) of Fe with respect to the TiO₂ (0.05FeT, 0.1FeT, 1FeT). For comparison purposes, undoped TiO₂ nanoparticles were also produced (TRef).

Scheme 1 illustrates briefly the experimental process used in this study. Specific care was undertaken in order to use a simple and non-laborious experimental procedure guaranteeing the incorporation of Fe³⁺ into the TiO₂ matrix and the production of anatase crystals under calcination consummating the minimum required energy. The molar ratio of the TTIP/H₂O/EtOH was 0.03/2.3/1.56.



Scheme 1. The experimental procedure of the incorporation of Fe-ions within the TiO₂ matrix first and further their incorporation into the lime paste.

Synthesis of the Photoactive Fe-TiO₂ Lime Plasters

The evaluation of the Fe-TiO₂ concerns the mixing with commercial calcium hydroxide (L: Lime, Fluka, > 96%) for monitoring the evolution of hardening through carbonation. For comparative purposes pastes with pure lime were also taken into consideration. The pastes prepared with lime contained 3% (w/w) of the various Fe-doped TiO₂. The ratio of water to binder was calculated 0.7 for all the mixes. The five synthesized pastes, which were casted into ceramic tubes with dimensions of 3 cm in diameter and 3 cm in height, can be fallen into the following categories:

- (a) three pastes incorporating the various Fe-doped TiO₂ nanoparticles, denoted as L§FeT, where § denotes the %Fe (L0.05FeT, L0.1FeT, L1FeT),
- (b) one paste containing the TRef nanoparticles (LTRef), and
- (c) one paste without addition of nanoparticles (LBlank)

The above pastes were being kept both in a curing chamber for setting, at RH = 65 ± 3 % and T = 20 ± 2 °C (19 h per day) and under sun irradiation (5 h per day) for 45 days.

Characterization of the Photoactive Fe-doped TiO₂ nanoparticles

All the analysed samples with the techniques that followed were in the form of powders. Fourier Transform Infrared Spectroscopy (FTIR) was used for the characterization of the

chemical bonds of the synthesized TiO₂ nanoparticles. The absorption spectra were collected from a Perkin-Elmer 1000 spectrometer in the range of 400-4000 cm⁻¹. The crystalline phases of the photoactive TiO₂ nanoparticles were identified through the X-Ray Diffraction patterns recorded on Burker D8 Advance diffractometer, operated at 35 kV and 35 mA with Cu K α radiation with a nickel filter at a scan rate of 2° min⁻¹ and a Bruker Lynx Eye strip silicon detector. The photoemission experiments (XPS) were carried out in an ultra-high vacuum system (UHV) which consists of a fast entry specimen assembly, a sample preparation and an analysis chamber. The base pressure in both chambers was 1×10⁻⁹ mbar. Unmonochromatized AlK α line at 1486.6 eV and an analyzer pass energy of 97 eV, giving a full width at half maximum (FWHM) of 1.7 eV for the Au 4f_{7/2} peak, were used in all XPS measurements. The XANES measurements were performed at the IAEA XRF beamline in Elettra Sincrotrone, Trieste, Italy [8], with Ring energy 2.0 GeV and Ring current 220 mA. XANES spectrometry was performed in an Ultra-high vacuum chamber (pressure 8.7e-9 mbar) at Total reflection X-ray fluorescence geometry, with a Silicon Drift Detector (SDD), nominal resolution of 131 eV (at Mn-K α). Spectra step 0.2-2 eV (depending on the energy), 2 repetitions, 5 s/step. The diffuse reflectance spectra (DRS) of the photoactive TiO₂ nanoparticles were obtained using a UV-Vis Perkin-Elmer Lambda 35 spectrophotometer equipped with an integrating sphere Labsphere RSA-PE-20. The band gaps were calculated from the obtained Tauc plots.

Assessment of the Photocatalytic Activity of the nanoparticles

The photocatalytic efficiency of the TiO₂ nanoparticles was assessed by monitoring the degradation of the methyl orange compound (MO, Fluka), at room temperature, under simulated Solar irradiation. A solar radiation simulator (Newport, model 96000) along with a 150-W xenon ozone-free lamp, was utilized for the simulation of the solar radiation. In a typical experiment, the powdered photocatalysts were dispersed in an aqueous solution MO (5 ppm). For all the experiments carried out, the final concentration of the nanoparticles into the MO solution was equal to 0.8 g L⁻¹. The methodology followed was explained in detail in previously published work [9].

Evaluation of the carbonation process of the photoactive Fe-TiO₂ Lime Plasters

The evolution of the carbonation process of the designed plasters was monitored at pre-set time periods, of 5, 10, 15, 28 and 45 days. The examined samples were immersed in acetone after sampling, so that the carbonation reaction to be interrupted, and before their analysis they were dried at 70 °C for 30 h. The samples were examined by FTIR analysis.

Results and Discussion

Characterization of the photoactive Fe-doped TiO₂ nanoparticles

Figure 1 reports the FTIR spectra of the modified photocatalytic nanoparticles along the spectrum of the undoped samples for comparison purposes. The obtained spectra exhibited vibrations attributed to the Ti-O, Fe-O, C-O, C-H and O-H bonds, but most importantly the peaks at 2920 cm⁻¹ and 2850 cm⁻¹, which are evident in all the spectra except for the 0.10FeT and in a minor intensity in the 0.05FeT, originate from the CH₂ and CH₃ of TTIP [10]. The presence of -CH₂ and -CH₃ evidenced the partial hydrolysis of TTIP; the latter, further influences the amount of the active TiO₂ in the powders. On the other hand, the wide band ranging from 400 to 900 cm⁻¹, observed in all of the FTIR spectra, assigned to the chemical bonds of Ti-O, Ti-O-Ti and Fe-O mainly evidenced the hydrolysis of TTIP and the formation of TiO₂ nanoparticles [11]. Comparing the Fe-doped TiO₂ spectra with the TRef spectrum, the observed changes in the intensity and the redshift of the band 400-900 cm⁻¹ can be ascribed to the new-formed Fe/TiO₂ system [12, 13]. Finally, the intense absorption of the spectral region 3000–3500 cm⁻¹ is related to the chemical bond O-H of the hydroxyl groups of the TiO₂ surface. These OH groups in combination with the absorbed water (peak at 1630 cm⁻¹) may positively contribute to the photocatalytic activity of the TiO₂ nanoparticles, functioning as electron/hole scavengers [14].

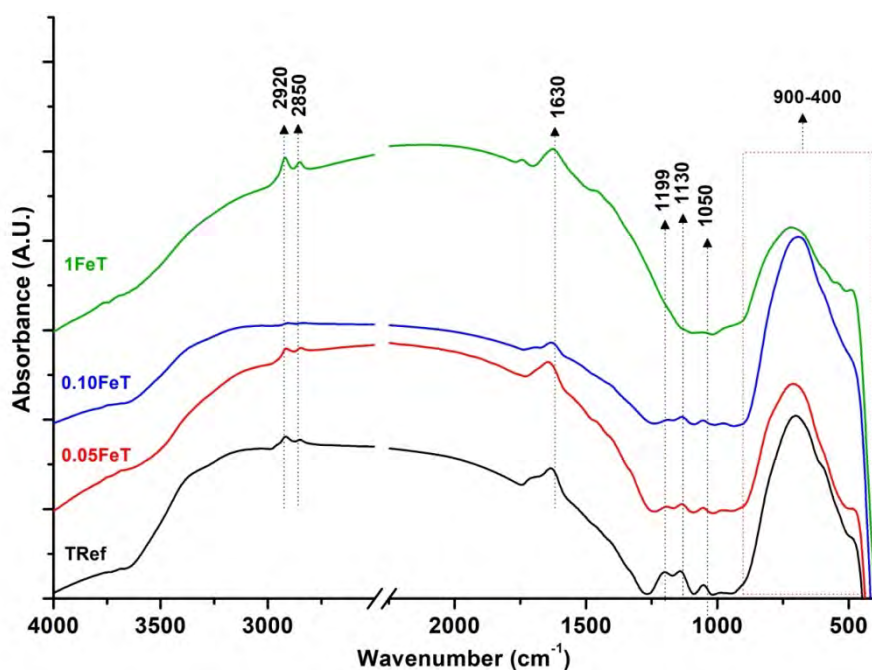


Figure 1. FTIR spectra of the synthesized photoactive Fe-doped TiO₂ nanoparticles along with the TRef sample.

The XRD results of the Fe-doped synthesized nanoparticles presented in Figure 2, revealed that the major crystalline phase of TiO₂ is anatase (25.3°, 37.8° and 47.9°) accompanied with the secondary phase of brookite (31.2°) [11, 15]. No diffraction peaks corresponding to Fe, such as secondary Fe₂O₃ phases, are detected most probably due to both the homogeneous distribution of Fe³⁺ into the titania host lattice, replacing the Ti⁴⁺ ions, and the low quantity of Fe [4, 6, 16, 17]. The crystallite size of the undoped and iron-doped TiO₂ samples, determined by the Debye-Scherrer equation using XRD data, ranged between 10-13 nm.

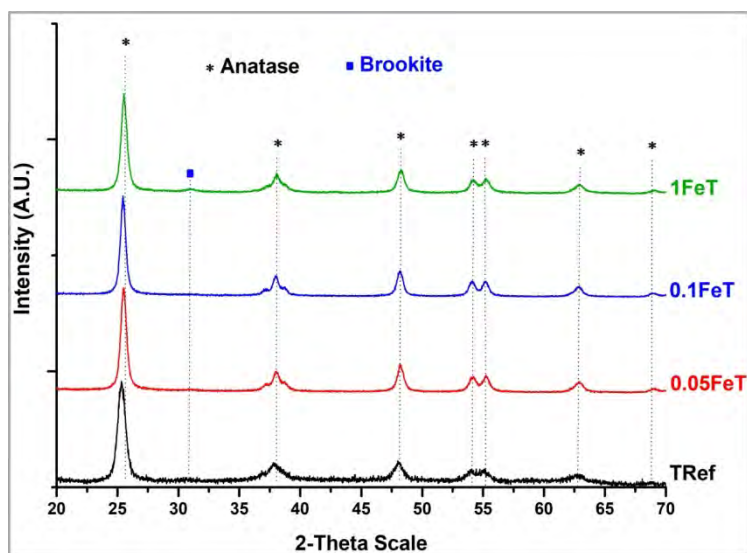


Figure 2. XRD patterns of the synthesized photoactive Fe-doped TiO₂ nanoparticles along with the TRef sample.

The band gaps of the TiO₂ and Fe-TiO₂ nanoparticles were calculated from the diffuse reflectance spectra using the Tauc plots, according to the methodology in [9]. The band gap of the Fe-doped powders reduced from 3.13 eV observed in the TRef to 3.06, 2.95 and 2.64 eV for 0.05FeT, 0.1FeT and 1FeT, respectively. As expected a clear relationship exists between energy band reduction and Fe increase.

In order to gain further insights into the crystal lattice of the synthesized TiO₂ nanoparticles, XPS analysis was performed. Figure 3 illustrates the obtained XPS results of Fe-doped and TRef nanoparticles. In the Ti 2p core level spectra of all the nanoparticles, the doublet appeared at 459 eV and 465 eV, evidenced that the oxidation state of titanium is Ti⁴⁺ [18]. The peaks of O 1s at 531 eV are attributed to TiO₂; the shifting to higher energy is related to the presence of OH groups on TiO₂ surface and to the oxygen from the iron doping [19, 20]. This observation is in accordance with the FTIR results indicating the presence of the hydroxyl bonds and Fe-O bonds. By comparing the peaks of Ti 2p and O 1s of the Fe-doped samples with the TRef, no shifting of the peaks in the doped samples occurred, but only a widening as a function of the Fe-doped increase. These results may be related to a Fe ion embedment into the crystal lattice without inducing any chemical interaction [20]. As it has been already mentioned, the replacement of Ti⁴⁺ ions from Fe³⁺ can be achieved due to their similar radii and electronegativity.

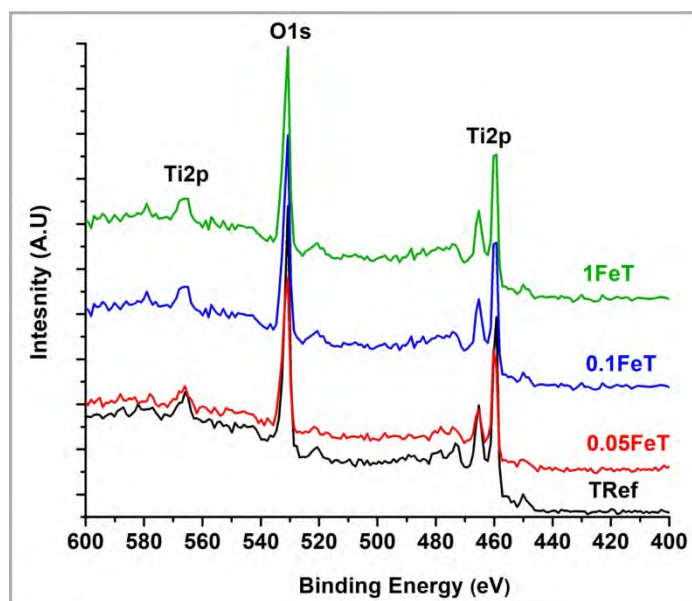


Figure 3. Wide-survey XPS spectra (a) and high resolution XPS spectra of Ti 2p (b), O 1s (c) and Fe 2p (d, e, f) of the TRef and Fe-doped nanoparticles.

The oxidation state of both Ti and Fe was further established through the study of the Ti K-edge and Fe K-edge XANES spectra depicted in Figure 4. For comparison purposes, the Ti K-edge spectra of the commercial TiO₂-P25 (80% Anatase and 20% Rutile) and a metal foil of Ti are shown in Figure 4. Firstly, the Ti K-edge spectra presented in Figure 4 pointed out that the TRef and Fe-doped nanoparticles exhibit similar features in both pre-edge and post-edge areas. Specifically, in the pre-edge area, three distinguished peaks at 4967, 4970 and 4973 eV, labelled as A1, A2 and A3 respectively, are observed. These three pre-peaks derived from the hybridization of p and d orbitals of the Ti and its surrounding atoms [21]. The shoulder B obtained in all of the spectra is associated with the 1s to 4p transition, while the peak C corresponds to the p atomic orbitals [21].

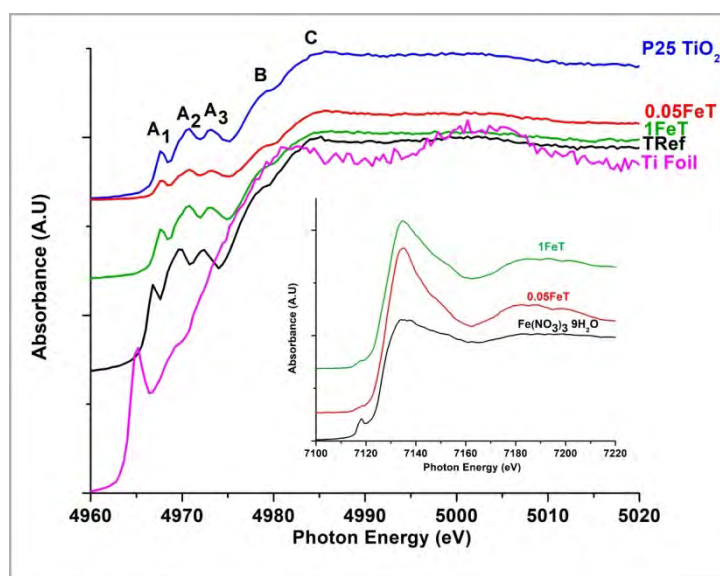


Figure 4. Ti K-edge (a) and Fe K-edge (b) XANES spectra for TRef, 0.05FeT, 0.1FeT and 1FeT nanoparticles. XANES spectra of Ti foil, TiO₂-P25 and Fe(NO₃)₃·9H₂O were used as references.

The inset of Figure 4 demonstrates the K-edge XANES spectra of the Fe-doped nanoparticles along with the spectrum of $\text{Fe}(\text{NO}_3)_3 \cdot 9\text{H}_2\text{O}$ for comparative purposes. The pre-edge peak assigned to 7117 eV is connected with the forbidden transition from 1s to 2d which eventually is partially allowed because of the interactions between of the d orbitals of the metal with the p orbitals of its surrounding oxygen atoms [22]. The strong band at 7134 eV observed in all the samples is ascribed to the 1s to 4p transition, thus confirming the existence of Fe as Fe^{3+} [22]. From Figure 3b, it is clearly revealed that these two main peaks (7117 and 7134 eV) of the nanoparticles are fully coincided with the peaks of the $\text{Fe}(\text{NO}_3)_3 \cdot 9\text{H}_2\text{O}$ further confirming the oxidation state (Fe^{3+}) of the Fe in the doped TiO_2 nanoparticles. The XANES results are in accordance with the results of XRD and XPS referring to the formation of octahedron TiO_2 phase (Ti^{4+}) and the incorporation of Fe as Fe^{3+} into this anatase crystal lattice.

Further supporting to this statement derived from the decrease of the band gaps attributed to overlapping of the Fe-3d, Ti-3d and O-2p orbitals originating from the Fe incorporation into the TiO_2 crystal lattice. This reduction in TiO_2 energy gap definitely enables the visible light to be absorbed [14]. In addition, the embedment of Fe into the TiO_2 structure induces a distinguishable change to the colour of the nanoparticles from white to light brown (Scheme 1). It should be also noted here that the Fe^{3+} ions into the TiO_2 crystals can function as trapping sites which further support the separation of the photogenerated hole and electron pairs improving the photocatalytic activity of the nanoparticles into the visible region [6].

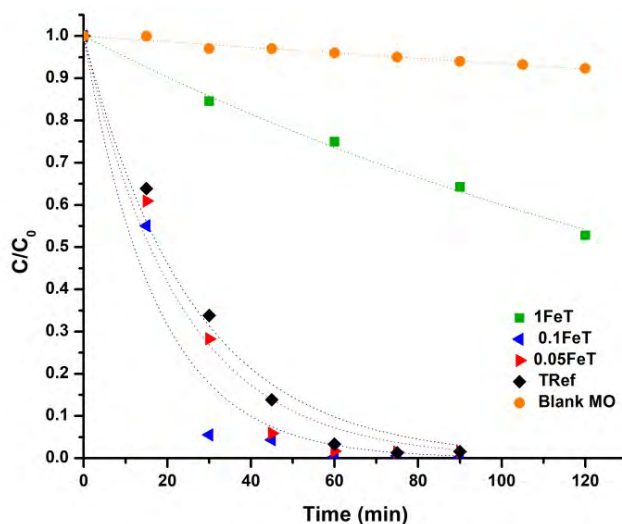


Figure 5. Photocatalytic efficiency of the synthesized nanoparticles.

The photocatalytic activity of all of the synthesized TiO_2 nanoparticles was evaluated by monitoring the degradation of MO under solar radiation (Figure 4). It can be seen from the plots of the Figure 4 that the photochemical degradation of MO (Blank MO) is negligible. Comparing the photocatalytic efficiency of the nanoparticles, the lowest activity was clearly recorded for 1FeT, while the maximum activity was derived from the 0.1FeT nanoparticles. As it has been already mentioned, the analyses of the nanoparticles through the XRD, XPS

and XANES techniques elucidated that the Fe exists in Fe³⁺ oxidation state and it has been successfully incorporated into the TiO₂ crystal. Therefore, the photocatalytic results revealed that the Fe ions into the nanoparticles in the lowest concentration (0.05%) slightly improved the photocatalysis compared to the undoped sample, whereas the 0.1FeT remarkably enhanced it, evidencing the Fe 0.1% as the optimal concentration.

It is well known that the enhancement of the Fe-doped TiO₂ photocatalytic activity under visible light is due to, both the restriction of the hole-electron recombination and, the photogeneration of additional new electrons in the TiO₂ conduction band [23]. However, it should be mentioned that the beneficial role of the Fe³⁺ ions as hole and electron scavengers can be achieved up to an optimum Fe concentration, beyond this value the Fe³⁺ ions act as recombination centers, inducing decline of the photocatalytic activity [23, 24]. An example sustaining this statement derives in our case from the synthesized 1FeT nanoparticles, which present a remarkable reduction of the photocatalytic activity compared to 0.05FeT and 0.1FeT, because of this reverse function of the Fe³⁺ ions (see Figure 5).

Assessment of the Carbonation process of the plasters

The assessment of the evolution of plasters carbonation was performed through the FTIR analysis of the spectra obtained at 5, 10, 15, 28 and 45 days of curing and the results are depicted in Figure 6.

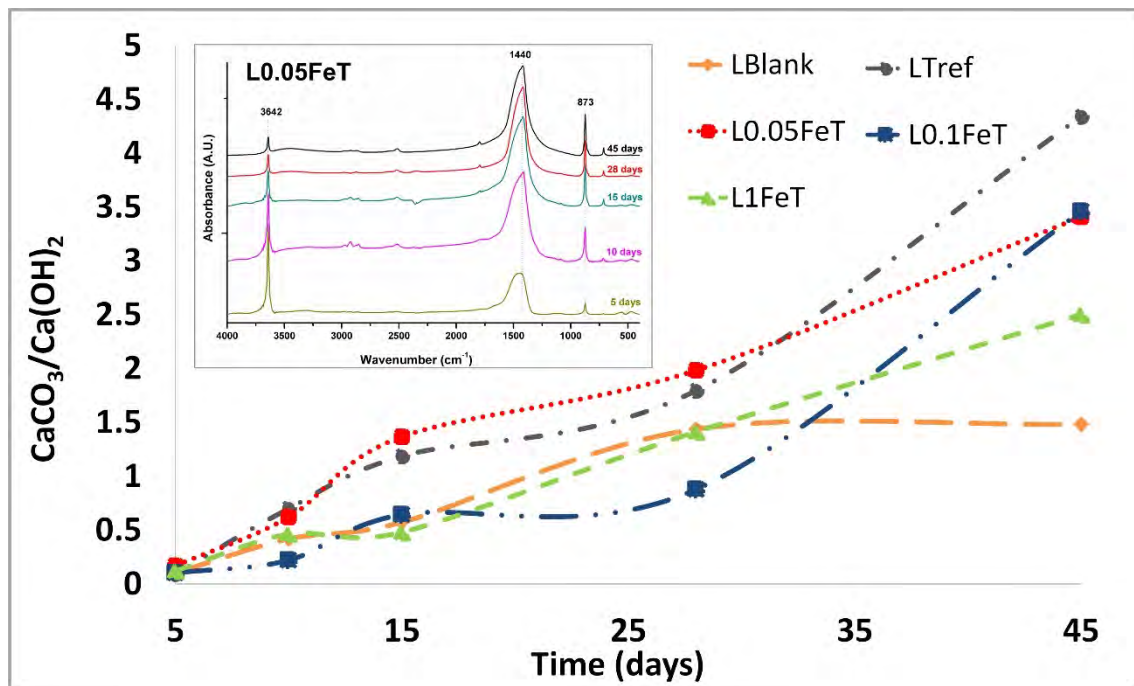


Figure 6. Evolution of the carbonation process of the pastes; in inset the FTIR spectra of L0.05FeT as a function of the curing time.

The evaluation of the carbonation process was obtained by monitoring the ratio of the intensity of the height of peaks corresponding to the neo-formed calcite (873 cm⁻¹) and the

portlandite peak located at 3642 cm^{-1} versus established curing time of the Lime plasters (see inset of Figure 6). The peak of calcite was increasing, whereas the peak of $\text{Ca}(\text{OH})_2$ was reducing over curing time. In the inset of Figure 6 indicative FTIR spectra of the best performed L0.05FeT for specific curing time are displayed, showing the evolution of carbonation over time by decreasing the portlandite and increasing the calcite peaks.

An increasing carbonation was recorded for the reference sample (LTref), which is a lime paste with undoped TiO_2 , comparing to the pure lime paste (LBlank), once again demonstrating the beneficial effect of the TiO_2 addition in the carbonation of lime mortars [1, 3]. As far as the iron doped samples is concerned, only the L0.05FeT and for the 28 days of curing enhanced the carbonation more than the pure TiO_2 . In 45 days of curing the L0.05FeT sample performed similarly to L0.1FeT, but both were less effective than the pure TiO_2 . The sample L1FeT with the highest iron showed a negligible effect on the carbonation of lime pastes up to 28 days of curing, whereas the carbonation increased in 45 days, but to a lesser degree than that observed in the other doped samples.

It was expected that the best photocatalyst of the MO degradation 0.1FeT to enhance similarly the carbonation of lime pastes. However, the analytical results presented here demonstrated that carbonation was retarded in L0.1FeT. In an attempt to explain this behaviour it should be taken into account that carbonation is a dynamic multiparametric process depending on the microstructure, humidity, temperature, CO_2 flow and diffusivity in samples [25]. It is very reasonable to assume that a dense carbonated layer formed on the surface of lime paste with the CO_2 produced by the best photocatalyst, prevented CO_2 diffusivity and, therefore, the carbonation was retarded. On the other hand, the other effective photocatalyst 0.05FeT, which decomposed the MO in a very similar rate to the pure TiO_2 , increased slightly the carbonation of the lime paste comparing to pure TiO_2 up to 28 days; then exhibited a reduced carbonation rate most probably attributed to decreasing CO_2 diffusion [26]. Generally, the increase in iron doping of TiO_2 might block active sites in lime pastes and this was reflected into lowering the carbonation conversion. Work is in progress to study microstructural characteristics of the pastes in order to elucidate these results.

Conclusions

In the present work, Fe-doped TiO_2 nanoparticles were designed aiming to be used as additives in lime plasters. The doped TiO_2 nanoparticles were synthesized through a simple sol-gel process combining thermal treatment. Three different concentrations of Fe (0.05, 0.1 and 1 % w/w) were embedded into TiO_2 nanoparticles, with the aim of determining the optimum concentration of photocatalyst. FTIR, XRD, XPS and XANES analyses confirmed not only the presence of the octahedron structure of TiO_2 (Ti^{4+}) in anatase crystalline phase, but also the incorporation of Fe^{3+} into the TiO_2 crystal lattice. Concerning the MO decomposition, the Fe doping in low concentrations (0.05 and 0.1 % w/w) was beneficial to the reactivity of the synthesized TiO_2 nanoparticles under the visible radiation compared to the undoped nanoparticles. Most importantly, the 0.05FeT additive in lime pastes enhanced the

carbonation process up to 28 days of curing. However, in 45 days, all the iron doped lime pastes exhibited lower carbonation conversion than the undoped TiO₂, but greater than the pure lime. Taking into account the photocatalytic activity of iron doped TiO₂ in low Fe content it can be suggested this use for both increasing the carbonation in early stages and abating harmful pollutants.

Acknowledgements

The authors would like to thank the Elettra Sincrotrone staff for their excellent and scientific and technical support for XANES measurements as well as the International Atomic Energy Agency (IAEA) for the scientific and financial support of the project 18262, “Experiments with Synchrotron Radiation for Modern Environmental and Industrial Applications”. The authors also acknowledge Mrs Olga Orfanou from Centre of Research and Technology Hellas (CE.R.T.H.) in performing the BET measurements. The XPS analysis was carried out in the Surface Science Laboratory at the Institute of Chemical Engineering and High Temperature Chemical Processes, Foundation of Research and Technology Hellas (ICEHT-FORTH).

References

1. Maravelaki-Kalaitzaki P, Agioutantis Z, Lionakis E et al (2013) Physico-chemical and mechanical characterization of hydraulic mortars containing nano-titania for restoration applications. *Cem Concr Compos* 36:33–41
2. Pozo-Antonio J S & Dionísio A (2017) Physical-mechanical properties of mortars with addition of TiO₂ nanoparticles *Constr Build Mater* 148:261–272
3. Karatasios I, Katsiotis M, Likodimos V et al. (2010) Photo-induced carbonation of lime-TiO₂ mortars. *Appl Catal B Environ* 95:78–86
4. Pérez-Nicolás M, Navarro-Blasco I, Fernández J M et al (2017) Atmospheric NO_x removal: Study of cement mortars with iron- and vanadium-doped TiO₂ as visible light-sensitive photocatalysts. *Constr Build Mater* 149:257–271
5. Lucas S (2017) Influence of operating parameters and ion doping on the photocatalytic activity of mortars containing titanium dioxide nanoparticles. *Mater Today Proc* 4:11588–11593
6. Pawar S H, Meena S S, Delekar S D et al (2012) Structural refinement and photocatalytic activity of Fe-doped anatase TiO₂ nanoparticles. *Appl Surf Sci* 263:536–545
7. Vijayan P, Mahendiran C, Suresh C et al (2009) Photocatalytic activity of iron doped nanocrystalline titania for the oxidative degradation of 2,4,6-trichlorophenol. *Catal Today* 141: 220–224

8. Karydas A G, Czyzycki M, Leani J J et al (2018) An IAEA multi-technique X-ray spectrometry endstation at Elettra Sincrotrone Trieste: Benchmarking results and interdisciplinary applications. *J Synchrotron Radiat* 25:189–203.
9. Kapridaki C, Pinho L, Mosquera M J et al (2014) Producing photoactive, transparent and hydrophobic SiO₂-crystalline TiO₂ nanocomposites at ambient conditions with application as self-cleaning coatings. *Appl Catal B Environ* 156–157:416–427.
10. Velasco M J, Rubio F, Rubio J et al (1999) Hydrolysis of titanium tetrabutoxide study by FT-IR spectroscopy *Spectrosc. Lett* 32:289–304
11. Castro C A, Centeno A & Giraldo S A (2011) Iron promotion of the TiO₂ photosensitization process towards the photocatalytic oxidation of azo dyes under solar-simulated light irradiation. *Mater Chem Phys* 129:1176–1183
12. Marami M B, Farahmandjou M & Khoshnevisan B (2018) Sol–Gel Synthesis of Fe-Doped TiO₂ Nanocrystals. *J. Electron. Mater.* 47:3741–3748
13. Cheng H H, Chen S S, Yang S Y et al (2018) Sol-Gel hydrothermal synthesis and visible light photocatalytic degradation performance of Fe/N codoped TiO₂ catalysts. *Materials (Basel)*. 11:939
14. Ali T, Tripathi P, Azam A et al. (2017) Photocatalytic performance of Fe-doped TiO₂ nanoparticles under visible-light irradiation. *Mater Res Express* 4
15. Xie Y, Heo S H, Yoo S H et al (2010) Synthesis and photocatalytic activity of anatase TiO₂ nanoparticles-coated carbon nanotubes. *Nanoscale Res Lett* 5:603–607
16. Elghniji K, Atyaoui A, Livraghi S et al (2012) Synthesis and characterization of Fe³⁺ doped TiO₂ nanoparticles and films and their performance for photocurrent response under UV illumination. *J Alloys Compd* 541:421–427
17. Lei X F, Zhang Z N, Wu Z X et al (2017) Synthesis and characterization of Fe, N and C tri-doped polymorphic TiO₂ and the visible light photocatalytic reduction of Cr(VI). *Sep Purif Technol* 174:66–74
18. Butler E B, Chen C C, Hung Y T et al (2016) Effect of Fe-doped TiO₂ photocatalysts on the degradation of acid orange 7. *Integr Ferroelectr* 168:1–9
19. Abidov A, Allabergenov B, Lee J et al (2013) X-Ray Photoelectron Spectroscopy Characterization of Fe Doped TiO₂ Photocatalyst. *Int J Mater Mech Manuf* 1:294–296
20. Cris M, Răileanua M, Drăgana N et al (2015) Sol-gel iron-doped TiO₂ nanopowders with photocatalytic activity. *Appl Catal A Gen* 504:130–142
21. Wang D, Liu L, Sun X et al (2015) Observation of lithiation-induced structural variations in TiO₂ nanotube arrays by X-ray absorption fine structure. *J Mater Chem A* 3:412–419

22. Huang C H, Paul Wang H, Wang J et al (2009) In situ XANES studies of TiO₂/Fe₃O₄@C during photocatalytic degradation of trichloroethylene. Nucl Instruments Methods Phys Res Sect A 619:98–101
23. Yu J, Xiang Q, & Zhou M (2009) Preparation, characterization and visible-light-driven photocatalytic activity of Fe-doped titania nanorods and first-principles study for electronic structures. Appl Catal B Environ 90:595–602
24. Tong T, Zhang J, Tian B et al (2008) Preparation of Fe³⁺-doped TiO₂ catalysts by controlled hydrolysis of titanium alkoxide and study on their photocatalytic activity for methyl orange degradation. J Hazard Mater 155:572–579
25. Nuño, M.; Pesce et al (2015) Environmental performance of nano-structured Ca(OH)₂/TiO₂ photocatalytic coatings for buildings. Build. Environ. 92: 734-742.
26. German Montes-Hernandez, Alejandro Fernandez-Martinez et al (2008) Textural properties of synthetic nano-calcite produced by hydrothermal carbonation of calcium hydroxide. J Cryst Growth 310:2946-2953.

Lime-based rendering mortars with photocatalytic and hydrophobic agents: assessment of the water repellency and biocide effect

Jesús Fidel González-Sánchez¹, Burcu Taşci², Guillermo Martínez de Tejada³, José M.

Fernández¹, Íñigo Navarro-Blasco¹, José Ignacio Alvarez¹

(1) MIMED Research Group, Chemistry Department, University of Navarra, mimed@unav.es, jgonzalez.65@alumni.unav.es, jmfdez@unav.es, inavarro@unav.es, jalvarez@unav.es

(2) Department of Architecture, Izmir Katip Çelebi University, burcutasci@iyte.edu.tr

(3) Microbiology and Parasitology Department, School of Medicine, University of Navarra, gmartinez@unav.es

Summary

Different rendering mortars were prepared by mixing air lime and air lime-pozzolanic nanosilica with TiO₂ and sodium oleate as, respectively, photocatalytic and water repellent agents, added in bulk. The aim of the work was to design and obtain new rendering mortars with improved durability focusing in the reduction of the water absorption of these materials and in their self-cleaning and biocide effect. To achieve a better distribution of the TiO₂ particles, which was expected to enhance their efficiency, different dispersing agents were also incorporated to the fresh mixtures. Four diverse polycarboxylate ethers superplasticizers and a poly-naphthalene-sulfonate were tested. Workability and fluidity of the fresh rendering mortars were determined to guarantee the applicability of the final products. Water contact angle was monitored with the aim of assessing the hydrophobicity of the mortars lent by the water repeller. The biocide effect was studied by means of the culture of a strain of *Pseudomonas fluorescens*. The colonization of the mortars' surface was analyzed by determining the number of colonies forming units (CFU) after several days subjecting the samples to suitable T and RH conditions. At the same time, the surface of the mortars was irradiated with solar light to activate the photocatalyst. Results showed the efficiency of the sodium oleate in reducing the water uptake of the rendering mortars. Good compatibility between the water repellent agent, the pozzolanic additive and some of the polycarboxylate superplasticizers was observed. The presence of the photocatalyst was found to be very effective in preventing microbiological colonization.

Keywords: Lime Superplasticizers; Titania; Biocide

Introduction

Scientists are nowadays facing major challenges in air pollution. One remaining challenge is to study ways of decomposing dirt caused by the organic species deposited on the building surfaces, which are responsible for the deterioration of building materials.

It should be noted that the deposition of atmospheric particles, aerosols or even the irreversible formation of black crusts - deposits of carbon particles, often sulphated - and, in general, deposits of hydrocarbon compounds, as well as the appearance of biological colonization, cause aesthetic problems to the historic building. It is also a way to initiate irreversible alterations in building materials especially stone and mortar [2]

In addition, the presence of these deposits causes high maintenance costs, eliminating them through laser ablation processes or sandblasting, which can be harmful for the historic material [3].

Photocatalysts incorporated to historic building materials can be an interesting solution to provide lower maintenance and cleaning costs by reducing surface soiling destroying organic products through a photocatalytic oxidation reaction [1]. There are different photocatalyst additives of great importance. Among them, TiO₂ stands out clearly. These additives, usually semiconductors based on oxides of the transition elements, through the action of light (for TiO₂ in the ultraviolet spectrum, UV), allow the chemical decomposition / oxidation of pollutants and deposits of organic matter [4]. In addition, these additives show biocidal efficiency by avoiding biological colonization on mortars such as algae, lichens or cyanobacteria [5]. Photocatalysts break the bonds between microorganisms and substrates (stone or mortar).

The TiO₂ photocatalysts have been investigated extensively for the killing or growth inhibition of bacteria [5-7]. Most works have been done by using a fine TiO₂ powder and a strong UV light. A little work has been reported in the use of TiO₂ nanoparticle aqueous solutions coated on substrates [8,9]. Recently, nanosized (<100 nm) TiO₂ particles have attracted a lot of activity from many researchers [10]. These nanometer-sized TiO₂ particles exhibit many special properties due to the fact that the small TiO₂ particles offer a very large surface area.

One of the drawbacks of these photocatalysts is related to the photo-induced superhydrophilicity, which could lead to the formation of water film on the surface of the renders. The uptake of water would result in severe decay processes. The addition of a water repellent agent is aimed to minimize this problem. Furthermore, in order to synergistically improve the self-cleaning and biocidal activity of the new lime-based renders, the water repellent is also expected to hinder the anchorage of microorganisms and dirt due to the superficial hydrophobicity.

In the current research work, nano-particles of photocatalytic additives (titania) in bulk were applied. Different samples were prepared with diverse superplasticizers, SPs. The use of different polycarboxylate-based superplasticizers (PCE1, PNS, 52IPEG, 23APEG and 45PC6) prevented nano-particles from agglomeration. These SPs were added to optimize the distribution of the photocatalysts improving the remotion of dirt and biological deposits. Also, water repellents were used to minimize water entry ways to lime-based mortars.

The as-obtained lime-based rendering mortars could be useful for the preservation of the Built Heritage as materials with self-cleaning and biocidal capacities. They will help to significantly reduce the maintenance and cleaning costs by preventing damage of the use of chemicals or abrasive agents in restoration works.

Materials and methods

Preparation of the mortar.

The weight proportions of the mortars were: 25% slaked calcitic lime supplied by Cal Industrial S.A. (Calinsa Navarra), classified as CL-90 by European regulations; 75% calcareous sand (Class AF-T -0/1-C sand, supplied by HORMASA Group). In addition, when necessary, the following components were added with respect to lime: 20% mineral pozzolan (nanosilica, supplied by ULMEN Europa); 0.5% water repellent agent (sodium oleate, provided by ADI-CENTER); 2.5% of nano-particles of bare TiO₂ (Aeroxide P25, Evonik) as photocatalyst; 0.5% or 1.0% of five superplasticizers were also used: three different polycarboxylate-based polymers (52IPEG is based on the copolymerization via free radical from acrylic acid and isoprenyl ω -hydroxy polyethylene glycol macromonomers; 23APEG contains α -allyl- ω -methoxy poly(ethylene glycol) macromonomers containing 23 ethylene oxide units and an equimolar amount of maleic anhydride; 45PC6 is composed of methacrylic acid and the macromonomer ω -methoxy poly(ethylene glycol) methacrylate ester with 45 ethylene oxide units at a molar ratio of 6:1) these SPs have been used and characterized in a previous work [14]. Additionally, two commercial superplasticizers (PCE1, Melflux's BASF commercial product PNS, Melcret® 500F, BASF Construction Polymers, Trostberg/Germany,) were also employed.

The mixing water was fixed at 28%, resulting from an adjustment of the water demand of the control mortar (additives/admixtures-free) to obtain a slump of ca. 160 mm as measured in the flow table test.

For the preparation of the pastes, lime and the required amount of calcitic sand (limestone aggregate) were blended for 5 min using a solid-admixtures mixer BL-8-CA (Lleal, S.A., Spain). Afterwards, the necessary water and superplasticizers were then added and mixed for 90 s at low speed and adjusted according to UNE-EN 196-1 [13], in a Proeti ETI 26.0072 (Proeti, Madrid, Spain) mixer.

Afterwards, mortars were cast in cylindrical moulds (36 mm height and 40 mm diameter) and demoulded 7 days later, stored at 20 °C and 60% RH. Different curing times were considered: 28 and 91 days. In order to make the results representative, three replicates of the mortars were tested at each curing time. Afterwards the samples were cut into three discs to have replicates during the test.

Fresh-state tests

The tests of the mortars at plastic state started with the slump measurements, which were recorded after 15 strokes of the flow table, 1 per second according to the indications of the standard UNE-EN 1015-3.

Then the period of workability of the material was determined according to standard UNE-EN 1015-9. Every 15 minutes a probe was slowly introduced, monitoring the weight until this weight was higher than 1500 g.

All these experiments were carried out by triplicate and the depicted values are an average value of all the recorded measurements.

Hardened-state tests

The mechanical resistances were measured at 28 and 91 days, to observe possible modifications over time. For all these measurements, 3 specimens were tested, in order to obtain representative values. For the compressive strength tests, a compression breaking device Proeti ETI 26.0052 was used at a breaking speed $5-50 \text{ KP} \cdot \text{s}^{-1}$ with a time interval between 30 and 90 seconds.

Hydrophobicity: water contact angle

The evaluation of the hydrophobicity of the sample was carried out with a measuring instrument of the contact angle OCA 15EC Dataphysics. In this way it was possible to determine the contact angle of a drop of water deposited on the surface of the sample, and the time for the absorption of the same by the material.

Photocatalytic activity: NO abatement

Photocatalytic activity was studied in a flow-through experiment that has been adapted from an ISO standard method [13]. In this experiment the photocatalytic oxidation of nitric oxide was continuously monitored and used as an indicator of the photocatalytic activity. Experimental conditions were $50 \pm 10\%$ RH and 25 ± 2 °C. The cylindrical photoreactor (height 12 cm; diameter 14 cm) was fed by a 500 ppb NO stream. Concentrations of NO and NO₂ were determined by a chemiluminescence detector (Environment AC32M) at a $0.78 \text{ L} \cdot \text{min}^{-1}$ flow. Experiments were carried out for discs of the samples prepared as above explained (height 1 cm; diameter 4 cm). The total exposed area of the discs was 25.14 cm^2 . UV illumination (Osram Ultravitalux 300 W) was irradiated.

Biocidal study

To develop this experiment, an environmental strain of *Pseudomonas fluorescens* was used. Fresh cultures were obtained from stocks at -80°C stored in 10% skimmed milk and

propagated on plates of Luria Bertani culture medium (LB-agar). Bacterial growth in liquid medium was performed in LB broth in an oven at 37°C and with orbital shaking (180 rpm). To prepare the bacterial inoculum, fresh cells were first obtained on an LB-agar plate grown for 18 hours. With these cells, a suspension was prepared which was adjusted with sterile saline solution (0.9% NaCl in distilled water) to an optical density of 0.04 to 600 nm, equivalent to 5×10^7 colony forming units (CFU) / mL, approximately. On the day of the experiment, the cylinders were hydrated for 2 hours in LB and then each cylinder was inoculated on its upper surface with 200 μ L (microliters) of the suspension, equivalent to 1×10^6 CFU / mL (i.e., one million CFU), approximately. After incubation in the chamber for 5 days at 37°C, the upper surface of the cylinders was scraped homogeneously with a sterile spatula and the material was resuspended in 1 mL of sterile saline. The amount of material peeled off the cylinders (mg) was determined by weighing the tube before and after placing the material from the cylinder therein. After vigorously homogenizing this suspension in a mechanical agitator, the number of bacteria present in the suspension was determined by viable count. For this, successive dilutions of the suspension were made in tubes containing sterile saline and 50 μ L were transferred to LB-agar plates which were incubated at 37°C for 48 hours.

Results and discussion

Fluidity and workability (open time)

The fluidity was studied for every mixture, with and without the presence of superplasticizer. Figure 1 shows how the fluidity of the lime grouts is affected after mixing with a water-repellent agent and with a pozzolan, both causing a fluidity reduction. As it can be seen the L-O mixture showed a lower fluidity than that of the plain lime mortar, and the presence of the pozzolanic addition (nanosilica) also resulted in a sharper fluidity decrease. In the mixture L-O after the addition of 23 APEG and 45 PC6 at 1.0% the fluidity of the mixture dramatically increased, exceeding the value of 300 mm, resulting in a high-fluidity mixture. In the mixtures with other SPs at any dosage the behaviour was very similar between them.

The workability of the different mixtures is depicted in Figure 2. Compared with plain lime mortars, the addition of the sodium oleate accelerated the setting time of the sample, while – unexpectedly- the addition of the pozzolanic agent delayed it.

The workability suffered substantial changes when the SPs were added to the mortars. The setting time with 23 APEG 1.0% is so high that some practical problems could be expected making thus necessary a strict mixing water adjustment. For all mixtures (L-O, and L-M-O) the addition of SP (except PCE1) considerably increased the setting time.

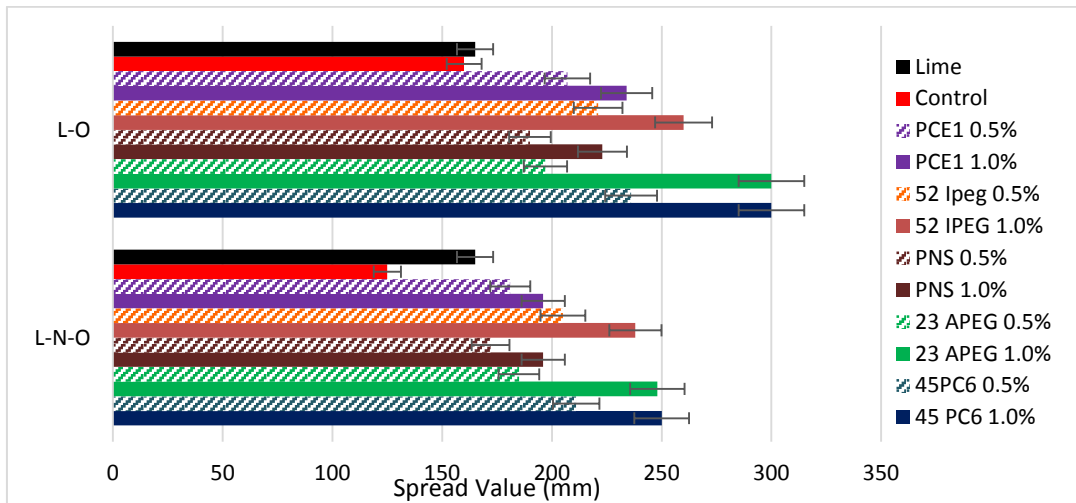


Figure 1. Fluidity of the different mixes

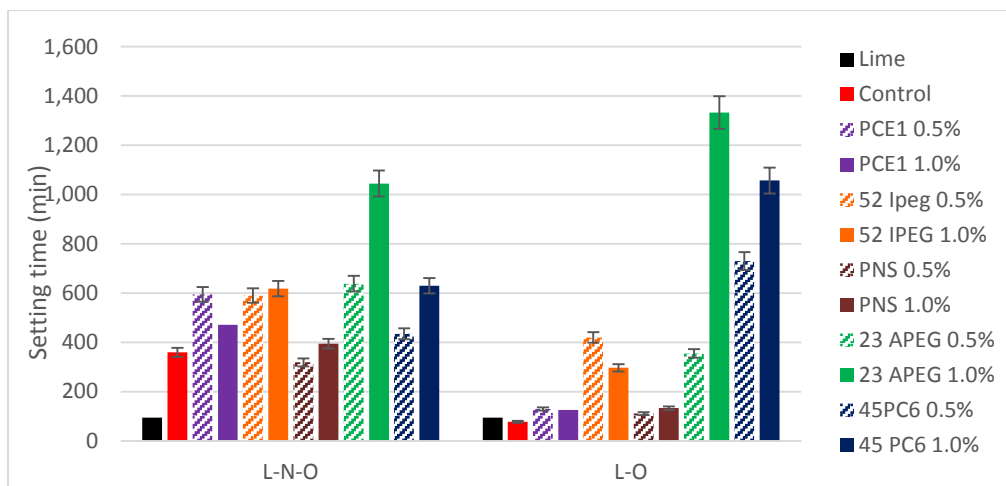


Figure 2. Workability of the different mixes

Compressive Strengths

The mechanical strengths increase over time due to the carbonation process, resulting in the formation of CaCO_3 . Accordingly, on average, the highest values of compressive strength were obtained at long-term curing times, usually after 91 curing days (Figure 3 and 4). For the control mix L-O at 91 curing days, without the addition of the SPs, its compressive strength was highest in comparison with the other mixtures.

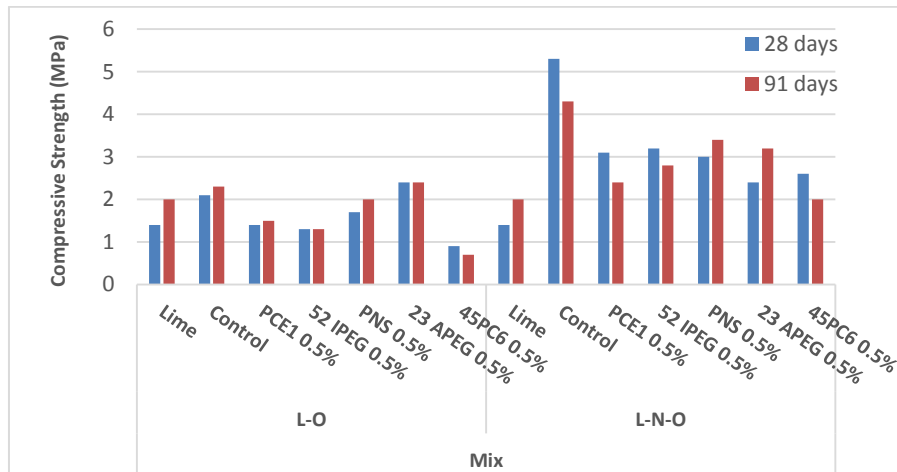


Figure 3. Compressive strength in the Hardened Mortars at different curing times (mixtures with 0.5% of superplasticizer)

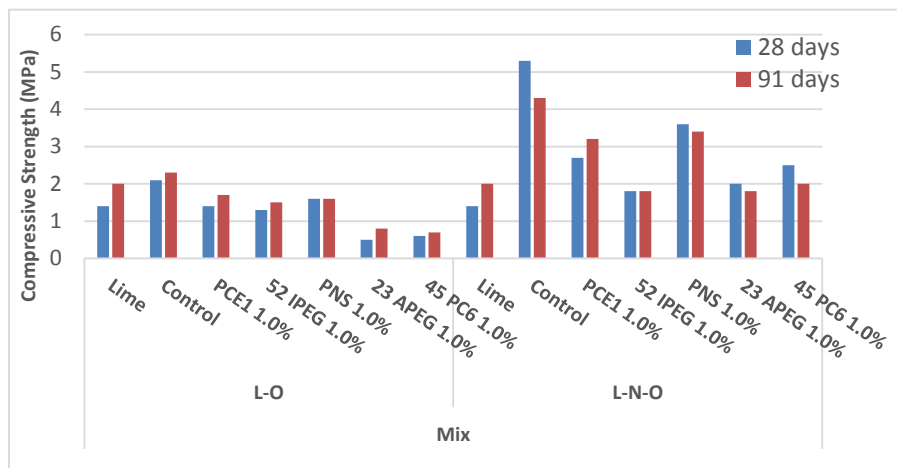


Figure 4. Compressive strengths at different curing times (mixtures with 1.0% of superplasticizer).

Hydrophobicity

The static water contact angle (WCA) and the water absorption time (i.e., the vanishing time of the water drop after its deposition, water drop lifespan, of interest for very porous substrates) were measured for the different grouts. The results are shown in Table 1.

In most samples water is fully absorbed after a certain period of time, as could be foreseen due to the very porous characteristics of the mortars' substrate. However it should be noted that, unlike a plain lime mortar, the WCA was able to be measured in all samples, thus indicating the water repellency brought about by the sodium oleate. In the curing time of 28 days the sample with excellent properties of water repellence is Lime + Oleate + Nanosilica +45PC6 1.0%+ TiO₂ and in 91 curing days is Lime + Oleate + Nanosilica +45PC6 1.0%+ TiO₂ this is because the drop was kept in the surface and the angle contact was higher than in the other samples.

Table 1. Water contact angle results

Mixture	Contact angle		Full Absorption of the water drop and disappearance in a short-time interval	
	28 days	91 days	28 days	91 days
Lime + TiO ₂	-	-	Yes	Yes
Lime + Oleate+ TiO ₂	26	23	Yes	Yes
Lime + Nanosilica+ TiO ₂	29	32	Yes	Yes
Lime + Oleate + Nanosilica+ TiO ₂	24	21	Yes	Yes
Lime + Oleate + PCE1 0.5%+ TiO ₂	31	33	Yes	Yes
Lime + Oleate + PCE1 1.0%+ TiO ₂	34	33	No	Yes
Lime + Oleate + 52IPEG 0.5%+ TiO ₂	25	44	Yes	No
Lime + Oleate + 52IPEG 1.0%+ TiO ₂	21	35	Yes	Yes
Lime + Oleate + PNS 0.5%+ TiO ₂	22	27	Yes	Yes
Lime + Oleate + PNS 1%+ TiO ₂	25	26	Yes	Yes
Lime + Oleate + 23APEG 0.5%+ TiO ₂	37	17	No	Yes
Lime + Oleate + 23APEG 1.0%+ TiO ₂	30	24	Yes	Yes
Lime + Oleate + 45PC6 0.5%+ TiO ₂	23	20	Yes	Yes
Lime + Oleate + 45PC6 1.0%+ TiO ₂	40	30	Yes	Yes
Lime + Oleate + Nanosilica +PCE1 0.5%	14	33	Yes	Yes
Lime + Oleate + Nanosilica + PCE1 1.0%+ TiO ₂	44	28	Yes	Yes
Lime + Oleate + Nanosilica + 52IPEG 0.5%+ TiO ₂	22	26	Yes	Yes
Lime + Oleate + Nanosilica +52IPEG 1.0%+ TiO ₂	28	23	Yes	Yes
Lime + Oleate + Nanosilica +PNS 0.5%+ TiO ₂	9	17	Yes	Yes
Lime + Oleate + Nanosilica +PNS 1.0%+ TiO ₂	21	24	Yes	Yes
Lime + Oleate + Nanosilica +23APEG 0.5%+ TiO ₂	44	42	No	Yes
Lime + Oleate + Nanosilica +23APEG 1.0%+ TiO ₂	40	42	Yes	Yes
Lime + Oleate + Nanosilica +45PC6 0.5%+ TiO ₂	16	20	Yes	Yes
Lime + Oleate + Nanosilica +45PC6 1.0%+ TiO ₂	46	28	No	Yes

Photocatalytic activity (NO abatement)

In the current research work, photocatalytic efficiency of lime-based mortars was investigated as a measurement to estimate the potential self-cleaning performance. Photocatalytic studies were carried out to assess the effect of TiO₂, nanosilica, oleate, and different types and percentages of superplasticizers in limes-based mortars that had a

different hardening time (28 and 91 days). The profiles of NO, NO₂ and NO_x abatement measurements over time were obtained according to these studies (Figure 5). All samples showed similar behaviour in three periods of NO profile: in the absence of UV radiation (10 min), under UV radiation (30 min) and during the last 10 min when the UV radiation was off. First, the concentration of NO was kept constant. In the second stage, the decrease in NO concentration attained its maximum value and became constant. This was the consequence of the NO oxidation that took place due to a photocatalytic process on the surface of TiO₂ active sites. In the last stage, the NO concentration returned to its beginning value. For the NO_x profile, the same behaviour was observed. The NO₂ (by-product of the NO oxidation) gas profile increased under UV radiation similar to previous studies on lime-based photocatalytic mortars.

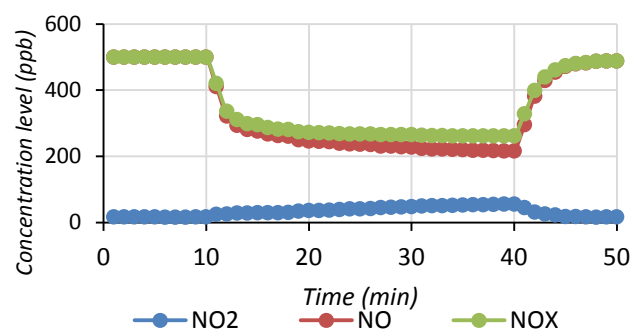


Figure 5. Profiles of NO, NO₂ and NO_x abatements for mortar with 1 % percentage of 45PC6 superplasticizer and nanosilica-free (91 days hardening)

Results revealed that presence of TiO₂ in lime-based mortars helped to better remove NO. Generally speaking, the presence of superplasticizers improved the NO reduction under UV irradiation. In this way it could be said that the different SPs enhanced the self-cleaning process. As shown in Figure 6, the percentage of the NO removal was commonly higher in SP-bearing samples after 91 curing days. Some contradictory values of NO abatement with some superplasticizers were observed for 28-days aged samples. The rates of NO removal were lower than that of control sample. 28 curing days might not be enough for lime-based mortars to show the PCO efficiency (Figure 6).

Samples with 0.5 % SPs after 28 days of curing showed similar efficiency of NO reduction (values of 43-50 %), except 23APEG that showed the lowest value (38 %). When samples with 1.0 % SPs were tested, the NO removal rates of PCE1 and 45PC6 yielded 47 % and 46%, respectively, but the rest of superplasticizers presented lower values (35-39 %) than that of the control sample.

After 91 days of curing (samples with 0.5% SP), the NO abatement values were increased for all samples with SP in comparison with control sample (NS-free samples). For samples with NS the presence of SPs improved the NO abatement (except for 52IPEG sample).

In the mixture L+ NS+ O samples with 0.5 % percentage SPs with 28 days hardening time, the range of remotion was 42-46 % in all superplasticizers except for PNS (34 %). Then at 91

hardening days, values were similar in PCE1, PNS, 23APEG and 45PC6 superplasticizers (43-46 %); in this case, value of 52IPEG was measured lower than control sample. With 1 % percentage of SPs in the same mixture, for the 28 days hardening time, all samples except for 52IPEG had the similar reduction values of 36-43 %. 52IPEG showed the same value with control sample. For 91 days, PCE1, 23APEG and 45PC6 presented the best values between 45 %, 48 % and 51 %, respectively. The other superplasticizers showed lower values than control sample.

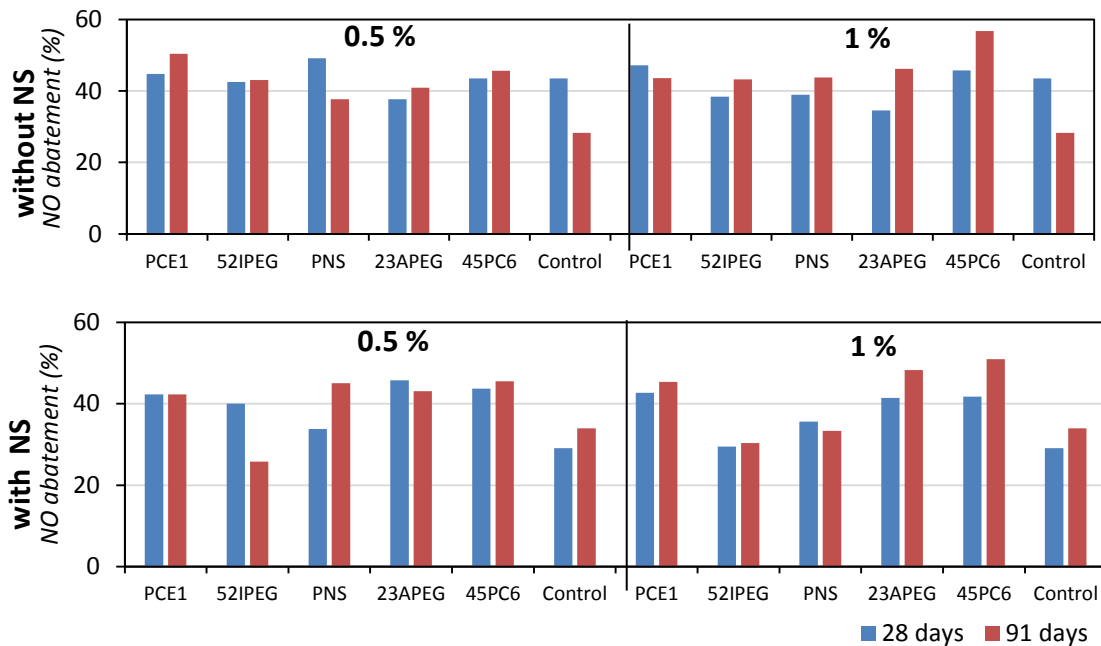


Figure 6. Percentages of NO abatement

Superplasticizers, mainly 45PC6 and PCE1, reduced the agglomeration of the nanoparticles of the photocatalytic additive and increased the potential self-cleaning characteristic of samples after 91 curing days. 45PC6 superplasticizer (1 %) with and without nanosilica exhibited a very remarkable NO removal rate (51 % and 57 %). It could be said that the efficiency of 45PC6 superplasticizer without nanosilica was better than the one with nanosilica when it was compared with control samples, probably as a consequence of the pozzolanic reaction that gave rise to the formation of a denser microstructure with a pore size reduction. These results were similar to the previous works dealing with the NO_x abatement in lime-based systems.

Biocidal study

Once the photocatalytic studies were made, the samples were submitted to a biocidal study, and the results are gathered in Table 2.

Table 2. Results of biocidal study

Name of Sample	Photographs of the bacterial colonies form after peeling off the cylinder.	Pseudomonas Fluorescens presence
Lime		YES
Lime + Oleate		YES
Lime + Oleate + Nanosilica		YES
Lime + Oleate + Nanosilica+ TiO ₂ Lime + Oleate + Nanosilica+ TiO ₂ +PCE1 0.5% Lime + Oleate + Nanosilica+ TiO ₂ +52IPEG 0.5% Lime + Oleate + Nanosilica+ TiO ₂ +PNS 0.5% Lime + Oleate + Nanosilica+ TiO ₂ + 23APEG 0.5% Lime + Oleate + Nanosilica+ TiO ₂ +45PC6 0.5% Lime + Oleate + Nanosilica+ TiO ₂ +PCE1 0.5% Lime + Oleate + Nanosilica+ TiO ₂ +52IPEG 1.0% Lime + Oleate + Nanosilica+ TiO ₂ +PNS 1.0% Lime + Oleate + Nanosilica+ TiO ₂ + 23APEG 1.0% Lime + Oleate + Nanosilica+ TiO ₂ +45PC6 1.0%		The behavior was the same in every TiO ₂ -bearing sample: the growing of <i>Pseudomonas Fluorescens</i> was fully inhibited

As can be seen in Table 2, the growing of *Pseudomonas Fluorescens* was noticeable in control lime-based rendering mortar and decreased (less CFU) for renders composed of nanosilica and oleate. Maybe the hydrophobicity of the surface hampered the microbiological colonization. No appearance of bacterial colonies was observed in all the samples that contain titanium dioxide in the mortar's formulation.

From these results it was not possible to establish the influence of the superplasticizer on the biocidal effect in the samples, since all TiO₂-bearing samples totally hindered the bacterial colonization. Further studies will intend to increase the number of colonies in each sample and controlling the microbiological growth over time.

Conclusions

The study on these new lime-based rendering mortars with TiO₂ focused on the efficiency of self-cleaning (measured as photocatalytic efficiency) and biocidal capacities of these renders to be used for the preservation of the Built Heritage.

To this aim, TiO₂, a water repellent agent, a pozzolanic additive and superplasticizers were combined with calcitic air lime. Compatibility between the admixtures and enhancement of different properties were assessed. Render mortars were seen to efficiently remove *Pseudomonas Fluorescens* proving the biocidal ability in comparison with plain lime-based renders. Hydrophobicity of the samples was generally increased, minimizing the detrimental effect of water uptake- Superplasticizers seemed to increase the photocatalytic efficiency (NO abatement) preventing TiO₂ particles from agglomeration, but all the renders showed photocatalytic activity and thus a potential self-cleaning capacity which might significantly reduce the maintenance and cleaning costs by preventing damage of the use of chemicals or abrasive agents in restoration works.

According to the results obtained in fluidity and workability time tests, the composition of these renders should be optimized for the real application of these mortars. The best mix with the highest water repellency was Lime + Oleate + Nanosilica + 45PC6 1.0% + TiO₂, as it showed the greatest WCA after 91 curing days.

Acknowledgment

Work funded by the Project MAT2015-70728-P of the Ministry of Economy and Competitiveness. J.F. González-Sánchez thanks the Association of Friends of the University of Navarra for a pre-doctoral fellowship.

References

1. Pinho, L, Rojas, M, & Mosquera, MJ (2015). Ag-SiO₂-TiO₂ nanocomposite coatings with enhanced photoactivity for self-cleaning application on building materials. *Applied Catalysis B: Environmental*. <https://doi.org/10.1016/j.apcatb.2014.10.002>.
2. Pozo-Antonio, J. S., & Dionísio, A. (2017). Self-cleaning property of mortars with TiO₂ addition using real diesel exhaust soot. *Journal of Cleaner Production*. <https://doi.org/10.1016/j.jclepro.2017.05.202>.
3. Munafò P, Goffredo GB, Quagliarini E (2015), TiO₂-based nanocoatings for preserving architectural stone surfaces: An overview, *Construction and Building Materials*, 84: 201-218
4. Pérez-Nicolás M, Balbuena J, Cruz-Yusta M, Sánchez L, Navarro-Blasco I, Fernández JM, Alvarez JI (2015), Photocatalytic NO_x abatement by calcium aluminate cements modified with TiO₂ : improved NO₂ conversion, *Cem Concr Res* 70: 67-76
5. Pinho L, Rojas M, Mosquera MJ (2015), Ag-SiO₂-TiO₂ nanocomposite coatings with enhanced photoactivity for self-cleaning application on building materials, *Applied Catalysis B: Environmental*, 178: 144-154.
6. Sunada K, Watanabe T & Hashimoto K (2003). Bactericidal activity of copper-deposited TiO₂ thin film under weak UV light illumination. *Environmental Science and Technology*. <https://doi.org/10.1021/es034106g>
7. Jacoby WA, Maness PC, Wolfrum EJ, et al. (1998). Mineralization of bacterial cell mass on a photocatalytic surface in air. *Environmental Science and Technology*. <https://doi.org/10.1021/es980036f8>.
8. Linkous, CA, Carter, GJ, et al. (2000). Photocatalytic inhibition of algae growth using TiO₂, WO₃, and cocatalyst modifications. *Environmental Science and Technology*. <https://doi.org/10.1021/es001080>
9. Sunada K, Kikuchi Y, Hashimoto K & Fujishima A. (1998). Bactericidal and detoxification effects of TiO₂ thin film photocatalysts. *Environmental Science and Technology*. <https://doi.org/10.1021/es970860o>
10. Wolfrum, EJ, Huang, J, et al. (2002). Photocatalytic oxidation of bacteria, bacterial and fungal spores, and model biofilm components to carbon dioxide on titanium dioxide-coated surfaces. *Environmental Science and Technology*. <https://doi.org/10.1021/es011423j>

11. European Committee for Standardization UNE-EN 459-1:2011(2011) Building lime Part 1: Definition, specification and conformity criteria, CEN, Brussels
12. Navarro-Blasco I, Pérez-Nicolás M, Fernández JM, Duran A, Sirera R, Alvarez JI (2014) Assessment of the interaction of polycarboxylate superplasticizers in hydrated lime pastes modified with nanosilica or metakaolin as pozzolanic reactives *Constr. Build. Mater.*, 73, pp. 1-12,
13. ISO 22197-1 (2007). Test Method for Air Purification Performance of Semiconducting Photocatalytic Materials. Part 1: Removal of Nitric Oxide, International Organization for Standardization.
14. Pérez-Nicolás M *et al.* (2018), Photocatalytically active coatings for cement and air lime mortars: Enhancement of the activity by incorporation of superplasticizers. *Construction and Building Materials*. 162, 628–648.

SRG, Steel Reinforced Grout for strengthening masonry structures: from tests to applications

Paolo Casadei¹, Paolo Girardello¹

(1) Strengthening Division, Kerakoll Spa, Sassuolo (MO), Italy, paolo.casadei@kerakoll.com, paolo.girardello@kerakoll.com

Introduction

Recent seismic events in Italy (L'Aquila 2009, Emilia 2012, center Italy 2017) have shown the vulnerability of masonry structures. Most of the existing building inventory in Europe were designed without taking into account seismic loads and/or have not undertaken any major refurbishment. Till 20 years ago, and in many cases still today, engineers and architects, when intervening on existing structures, were forced to interrupt the use of a structure because available technologies were very invasive and most important among all, were forcing to long times of construction connected to the large use of reinforced concrete, heavy steel plate bonding and section enlargement, the only technologies available to improve the structural performance of any type of building. FRP and SRG systems became more widespread thanks to their excellent strength to weight ratio and relatively ease and rapid installation times compared to the above well-established techniques.

Material properties

Galvanized steel fiber sheet

SRGs are made of fine ultra-high tensile galvanized steel filaments, twisted to form cords and tailored similarly to unidirectional fiber sheets (carbon, aramid or glass), see Figure 1, in order to be easily installed on site with the manual lay-up technique.



Figure 1. Galvanized Steel fiber sheet

Filaments and cords are manufactured according to ISO/DIS 17832 standard which describes manufacturing techniques and reference parameters. Typical properties of filaments and cords are reported in Table 1.

Table 1. Properties of filaments and cords

Material	Tensile strength ksi [MPa]	Elastic modulus ksi [MPa]	A _s in ² [mm ²]	ε [-]
Wire	420.61 [2900]	29732.73 [205000]	0.1668e-3 [0.1076]	
Cord 3x2	406.11 [2800]	27557.17 [190000]	0.8339e-3 [0.538]	> 1.50%

The twisting of the filaments allows some mechanical interlock between the cords and the matrix, and may induce an overall ductile behavior upon stretching because of the unwinding of the three twisted cords around the two linear ones and yielding in the upper part of the curve as reported in Figure 2.

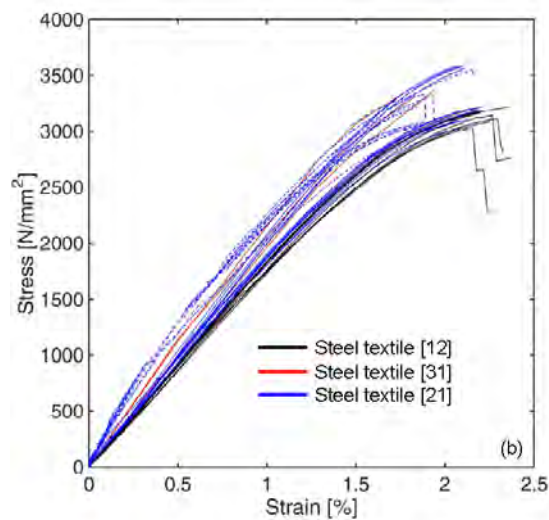


Figure 2. Stress-strain tensile response curves of dry textile

The cords are galvanized making the material free of any corrosion and suitable for different kind of environmental exposure depending on the matrix chosen. Zinc coating is governed by EN 10244-2 and typical mass of zinc is greater than 15.97g/m² (0.523 oz./ft²). In Figure 3 is reported a SEM image of the filament magnified 40x times to determine thickness as well as mineralogy of the zinc coating for quality control purposes.

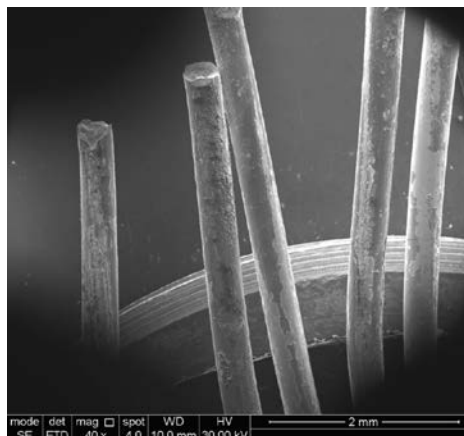


Figure 3. SEM image of the single filament

Current standards require that the SRG system shall resist till 3000hrs under complete immersion in ocean water as per ASTM D 1141-98 and ASTM C 581-03. Steel fiber sheets are available in four different densities based upon the spacing with the cords. Lower densities, which include 1.57 and 3.19 cords per cm (4 and 8 cords per inch), are the one suitable for mineral matrices while higher densities, 4.72 and 7.09 cords per cm (12 and 18 cords per inch), can be installed only with epoxy matrices, see Figure 4.

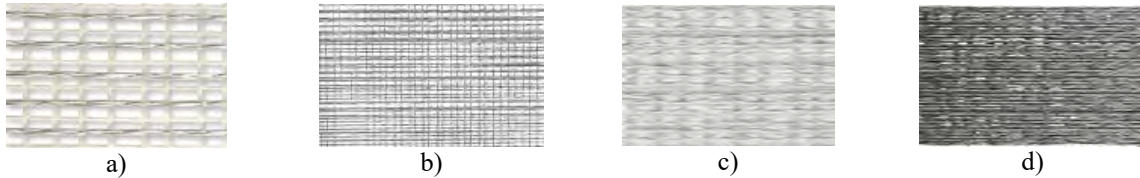


Figure 4. Four different densities of steel fiber, cords per inch: a) 4, b) 8, c) 12 and d) 18

SRG presents several advantages respect to traditional FRP composites systems: being made of high strength steel cords, makes them have a considerable shear strength when cords are subjected to stresses perpendicular to their development, not present in other types of fiber. This property makes them particularly attractive for column wrapping and also for easily realizing mechanical anchors/spikes, prohibitive with typical FRP strengthening solutions. Simply cutting the mesh on which cords are glued, allows to directly anchor the end of an SRG strip, see Figure 5, or realize single and double side spikes for containing masonry wall expansion when subjected to combined axial and bending actions.



Figure 5. Double side spikes for anchoring

Hydraulic Lime and Cement based matrices

The choice of the matrix is based upon the type of substrate where bonding the composite material, being either an hydraulic lime based matrix when strengthening masonry structures. Table 2 reports typical mechanical properties of mineral matrices. The hydraulic lime based matrix is particularly well suited to provide reinforcement of masonry structures in which the all-natural origin of its components guarantees compatibility, perfect adhesion, porosity, hygroscopicity and breathability.

Table 2. Mechanical properties of mineral matrix

Material	Compressive strength ksi [MPa]	Flexural tensile strength ksi [MPa]	Modulus of elasticity ksi [MPa]	Adhesive bond ksi [MPa]
GeoCalce F Antisismico	2.18 [15]	0.73 [5]	1338.70 [9230]	0.12 [0.8]

Table 3. Summary of experimental test results (% increase with respect to un-strengthened specimen)

Single lap shear tests	60% (4 cords per inch), 30% (8 cords per inch) of the tensile strength of the fibers
Masonry walls (diagonal compressive test)	from 230% to 527% (SRG)
Vaults (asymmetric load at the quarter of span, load)	355% (extrados SRG)
U-shape masonry wall (shaking table test, peak ground acceleration)	520% (SRG ties)

Structural behaviour and research studies on SRG

Several research studies have been carried out on SRG systems in the last fifteen years and a great input has been given since 2009 when the L'Aquila earthquake showed how masonry structures and in particular those made of rubble masonry could not be successfully retrofitted with traditional FRP composite systems.

Small scale specimens

The SRG-to-substrate bond performance is of primary importance for the effectiveness of externally bonded reinforcements. A number of experimental tests were carried out on specimens manufactured by applying an SRG strip to the substrate (clay brick, brickwork prism, natural stone block), with single-lap schemes. The SRG bond behavior was investigated on clay brick substrates. The load rate did not have any influence on the peak load because for long (> 150 mm, >5.91 inch) bonded lengths rupture of the fibers occurred with low density steel fibers (4 cords per inch).

Masonry medium-large scale specimens

On masonry were performed diagonal compressive tests on three leaf masonry and clay bricks with an increase of the shear resistance more than 3 times the sample unreinforced. The shaking table tests, on natural scale U-shape masonry wall retrofitted with SRG strips, have allowed a significant improvement of the out-of-plane seismic capacity of masonry wall and may be an effective alternative to traditional strengthening devices. In the experimental campaign the maximum Peak Ground Acceleration was 0.29g for the unreinforced wall (failure by overturning) and 1.51g for the wall retrofitted with SRG (damage without collapse). Excellent performance has been experienced also on tests on arches and vaults

both on-site as well as in the laboratory retrofitted at the extrados and intrados with SRG installed with hydraulic-lime-mortars. If FRPs have also demonstrated excellent performance with respect to un-reinforced arches, the greater ductility and ease of installation, jointly with the much easier installation/anchoring of strip's end makes SRG the winning solution in this type of application.

Case studies

The following case studies represents, among many, typical SRG applications on seismic upgrade and strengthening on masonry and reinforced concrete structures performed in Italy in the past 5 years. Two case studies are of buildings, which suffered the L'Aquila earthquake, that stroke in central Italy in 2009, characterized by a variety of structural applications. The remaining case study of historic building represents one of the most significant and prestigious structures in the south of Italy, Caserta's Royal Palace, where SRG have been implemented after a sophisticated finite element modeling. In all cases, higher compatibility with substrates, vapor permeability, ease and speed of installation associated with lower cost of intervention without compromising structural performance so far guaranteed by epoxy matrices, made SRG the only possible solution to be adopted by engineers and appreciated by contractors and owners.

Ciolina-Ciampella Palace - L'Aquila

Ciolina-Ciampella palace located in L'Aquila city center was severely damaged by the 6th of April 2009 earthquake (Figure 6).



Figure 6. Ciolina-Ciambella Palace – L'Aquila

It was built during the XVII century and after the 1915 earthquake (Avezzano) some metallic ties were inserted and a part of original wooden roof had been replaced by a stiff roof made by steel and reinforced concrete beams on the top of masonry. The building reported severe damage both in the structural elements (walls, vaults and roofs) that in the artistic heritage (frescoes, stucco and stone elements). The façade along Umberto street manifested a visible outward overturning and most of the vaults collapsed such as a big portion of wooden roof and the molding on the top of the walls. The aim of the project was to reach the appropriate level of seismic safety in compliance with the restoration and conservation rules of Italian

Ministry of Cultural Heritage. The design of interventions started from the damage survey and from the identification of the activated collapse mechanisms. To improve the integrity of the structures, the connection wall-to-wall and wall-to-floor was obtained installing typical steel ties. The survey of the horizontal elements allowed recognizing four different types of vaults: stone vaults, brick vaults with 2 different thickness 5 cm and 12 cm and no structural vaults realized with wooden frame. Structural vaults (stone and brick with hydraulic lime) were retrofitted using ultra-high tensile galvanized steel filaments installed with hydraulic lime based matrix (NHL 3.5) at the extrados. This solution guarantees the restoration of compromised structural continuity and the improvement of the bearing capacity of the vaults thanks to the presence of an element able to absorb tensile stresses, without increasing dead loads. The choice of the inorganic matrix has been adopted to ensure compatibility with the existing substrate in terms of breathability, porosity and hygroscopicity required from the Cultural Heritage Authority in case of frescoes at the intrados (Figure 7).



Figure 7. SRG extrados strengthening

Historic Building - L'Aquila

The building block located in L'Aquila near via Roma within the city center, represents a typical aggregate of ancient building present in the Italian historical centers. The vertical bearing structures are of considerable thickness but made with irregular stone of various sizes, irregularly arranged and jointed with a mortar of poor quality, which does not ensure effective cohesion of the units, even in case of heritage buildings. Another vulnerability element is represented by the building constructive evolutions which shows an articulated construction, as often happens in the historical buildings. For example: the wrong use of reinforced concrete, in particular the replacement of wooden trusses in the roofs and the substitution of timber floor with reinforced concrete trusses or reinforced concrete slabs. The survey of the damage highlighted numerous problems: collapse of vaults and of parts of the wooden roof, overturning of masonry, diagonal cracks on the masonry walls. The proposed interventions combined the conservation aspects with the seismic safety upgrade of the structures. Interventions are summarized as described below:

- local dismantling and rebuilding (“scuci-cuci”) to restore the wall continuity;

- strengthening of building portions by means of bond beams reinforced with interposition in joints of galvanized steel fiber sheet strips and pure natural hydraulic NHL 3,5 lime mortar. The reinforced-masonry beams were included at different heights of the masonry walls;
- the masonry vaults were repaired and reinforced with unidirectional galvanized steel fiber sheet. The anchorage at the ends of the strip was performed by rolling the ends of the steel fibers and insert them into the holes on the masonry walls and injected with fluid hydraulic lime based mortar to anchor the sheets (Figure 8).



Figure 8. Ring beams reinforced with interposition in bed-joints of galvanized steel fiber strips

Caserta's Royal Palace, Bagni della Regina vault - Caserta

The Royal Palace at Caserta and its park, inserted as one of the 50 Italian UNESCO World Heritage Sites in 1997. Commissioned by Charles III of Bourbon in the XVII century, Luigi Vanvitelli planned this palace. The strengthening intervention, here described, regards the vaults of the “Bagni della regina Carolina”. It was a delicate intervention on a high historic structural element that has required diagnostic investigations, FEM modelling and minimally invasive strengthening solutions. The SRG technology adopted has ensured greater compatibility, low invasiveness, reversibility and durability in compliance with the Guidelines for the assessment and mitigation of seismic risk of cultural heritage (Italian Ministry of Cultural Heritage). The non-destructive diagnostic campaign had foreseen accurate 3D laser scanner survey to define geometries, cracks and deformation pattern. In the second step, Finite Element Methodology using structural analysis software was used to understand structural behavior and the causes of the cracks pattern. The output results from FEM analysis showed strength enhancement required due to increase the dead loads on the structure and for seismic behavior. To strengthen the vault, the project required design and use of externally bonded steel reinforced grout reinforcement (SRG) as per CNR DT 200 R1/2013 (Italian guidelines) were used to strength the element. The strengthening intervention had foreseen accuracy and engineering of all the steps from the preparation of the support to the installation of SRG (Figure 9):

- remove plaster only in the strips where SRG was applied;
- drill holes in the position of spikes;

- apply SRG system with ultra-high tensile galvanized steel filaments and hydraulic lime based matrix;
- insert spikes realized with the same fibres;
- inject fluid hydraulic lime mortar from the center of the spikes.



Figure 9. Intrados strengthening of vaults

Conclusions

Since 2004 when the use of high strength steel fiber sheets in civil engineering has begun, several research investigations have been carried out in order to study their mechanical properties and their effectiveness as external bonded reinforcement in civil engineering applications. The advantage of installing steel fibers using mineral mortars instead of organic matrices, allows SRG to become very versatile thanks to their compatibility and ease of installation. The comprehensive and systematic review of the experimental investigations and case histories carried out so far on masonry structures retrofitted with SRG, demonstrates their effectiveness, cost efficiency and reliability. SRG have proven to increase the load-carrying capacity of structural members subjected to tensile and dynamic stresses for which they may not withstand current design loads, safeguarding against deterioration, and enhancing their ductility with respect to more traditional retrofitting techniques such as the most know FRPs. Research studies, as well as in-situ applications, in the last decade have proven with no doubts that this new family of composite materials can be included, with no reserves, among the variety of composite materials used for structural strengthening, and when installed with inorganic matrices, provide better response and, at the same time, be easily designed with existing calculation design approaches already tested for more validated materials.

References

1. Casadei P and Agneloni E Advance composites applications on historical structures in Italy: Case studies and future developments 6th International Conference on Structural Analysis of Historical Construction – Preserving Safety and Significance, Bath, United Kingdom, July 2-4, 2008, ISBN Vol.2:978-0-415-48107-6.
2. Casadei P and Agneloni E Case Studies on Advanced Composite Materials for Civil Engineering and Architectural Applications Structural Engineering International, vol.21, 3/ 2011, 271-278.
3. Borri A, Casadei P, Castori G, Hammond J. Strengthening of brick masonry arches with externally bonded steel reinforced composites. *J Compos Constr* 2009;13(6):468-475.
4. Casadei P, Nanni A, Alkhrdaji T, Thomas J. Performance of Double-T prestressed concrete beams strengthened with Steel Reinforced Polymer. *Adv Struct Eng* 2005;8(4):427-442.
5. Casadei P, Nanni A, Alkhrdaji T. Steel-Reinforced Polymer: an innovative and promising material for strengthening the infrastructures. *Concr Eng Int* 2005;9(1):54-56.
6. De Santis S, de Felice G. Tensile behaviour of mortar-based composites for externally bonded reinforcement systems. *Compos Part B: Eng*, 2015;68:401-413.
7. De Santis S, de Felice G, Napoli A, Realfonzo R Strengthening of Structures with Steel Reinforced Polymers: A state-of-the-art review. *Compos Part B: Eng*, 2016; 104:87-110
8. De Santis S., Casadei P., De Canio G., de Felice G., Malena M., Mongelli M., Roselli I. Seismic performance of masonry walls retrofitted with steel reinforced grout. *Earthquake Engineering and Structural Dynamics*, 2016;45(2):229-251. DOI: 10.1002/eqe.2625.
9. De Santis S., Casadei P., de Felice G. Tests on the bond performance of mortar based strengthening systems on masonry substrates. *Proc. Int. Conf. IMC'14 - 9th International Masonry Conference (Guimarães, Portugal, 7-9 July 2014)*. ISBN: 978-972-8692-85-8.
10. Faella C, Napoli A, Realfonzo R. Seismic behaviour of RC beam-column joints strengthened with steel fiber composite materials. In: *Proceedings of XVI Convegno ANIDIS, L'Aquila, 2015 (in Italian)*.
11. Napoli A, Realfonzo R, Casadei P. Rinforzo a flessione di solette in c.a. con sistemi in SFRP/SFRM. In: *Proceedings of XX Congresso CTE, Milano, Italy, 2014 (in Italian)*.
12. Napoli A, Realfonzo R, Petracca M, Candeloro F, Camata G, Casadei P. Flexural strengthening of RC slabs with SRP/SRG: an experimental-numerical comparison. In: *Proceedings of ACE 2015, Vietri sul Mare, Salerno, Italy, 2015*.

13. Napoli A, Realfonzo R. Compressive behavior of concrete confined by SRP wraps. *Construction and Building Materials* 2016 (in press).
14. Napoli A, Perri F, Realfonzo R, Ruiz Pinilla, JG. Seismic performance of RC columns strengthened with SFRP systems: experimental study. In: *Proceedings of FRPRCS-11*, Guimarães, Portugal, 2013.

Topic 5: Characterization of historic mortars and masonry structures. Sampling and test methods



Calcite or quartz powder as aggregate of Roman plasters (Lombardy, Italy)

Roberto Bugini¹, Luisa Folli¹

(1) CNR – Istituto Conservazione Beni Culturali, Milan (Italy). bugini@icvbc.cnr.it

Abstract

The aggregate of finish coats of Roman plasters was studied on samples coming from archaeological excavations of Lombardy. Two kinds of aggregate, made of calcite or quartz crystals, are pointed out through microscopic analyses. The origin and provenance of the raw materials are also compared with samples taken in different stone outcrops or loose deposits.

Introduction

The plasters of the Roman sites of Lombardy (Northern Italy) were made, as in the whole Roman world, of superimposed coats of mortar: a render coat, a finish coat, a painted coat. The aggregate, or “filler”, is a main component of a mortar, together with the binder and the water, it should be a test to discriminate these types of mortar. Normally the aggregate is composed by inorganic material such as: sand, crushed stone, potsherd, pozzolana. The most significant disparities, in Roman plaster of Lombardy, are present in the aggregates of finish coats: the features of two particular kinds of aggregate (marble-calcite powder, quartz powder) were investigated on mineralogical basis. In order to recognize the provenance of calcite, a comparison was made with samples coming from marbles and veined stones of Italy and other Mediterranean countries. At the same time a comparison was made with samples coming from loose deposits of Quaternary to recognize the provenance of quartz.

Materials and methods

Plaster samples, coming from different archaeological sites of the present-day territory of Lombardy, were cut from surface to interior to highlight the sequence of coats. Some thin sections were arranged, starting from the transverse cut, to the observation by optical microscopy (Nikon Eclipse E400 Pol - Nikon Pol objectives). Besides, X-ray diffractions on powders were performed on each coat of the plasters and on the samples examined for comparison (PANalytical X'Pert PRO MPD).

The archaeological sites (Table 1) are mainly located in Milan (1st - 4th centuries CE) and in Brescia province (1st - 2nd centuries CE).

Table 1. Sites in Lombardy

Archaeological sites	Aggregate of finish coats (chronol.)
Milan, <i>hall</i> via Broletto [1]	Calcite (late 3 rd century)
Milan, <i>domus</i> piazza Fontana [2]	Quartz (early 1 st c.) or Qz+silicates (mid 1 st c.)
Milan, <i>domus</i> piazza Meda [3]	Quartz (mid 1 st or early 4 th c.)
Milan, <i>domus</i> via Correnti [4]	Qz+silicates (1 st c.) or Qz+limestone (2 nd c.)
Milan, <i>palatium</i> via Brisa [5]	Potsherd (early 4 th century)
Mi, <i>palatium</i> via St Maria Porta [5]	Quartz (2 nd century)
Mi, <i>palatium</i> Monastero Magg.[6]	Quartz+silicate or Calcite (3 rd c.)
Gropello C.* St Spirito, <i>domus</i> [7]	Calcite (first half 1 st century)
Brescia, republican sanctuary [8]	Dolomite+limestone (early 1 st c. BCE)
Brescia, <i>domus</i> via Trieste [9]	Calcite (mid 1 st century)
Brescia, baths pzza Foro [10]	Dolomite (early or late 1 st century)
Cividate C.**, Theatre-Amphit. [11]	Calcite (1 st century)
Cividate C., <i>domus</i> via Palazzo [11]	Calcite (early 1 st century)
Breno**, sanctuary of Minerva [12]	Calcite (1 st century)
Sirmione**, "Grotte Catullo" [13]	Limestone+calcite (2 nd century)
Calvatone***, rubbish (pit) [14]	Calcite or limestone or potsherd (2 nd c.)

*Pavia province, **Brescia province;*** Cremona province – Chronology is approximate

Results - Aggregate features

Plasters show a relative uniformity as regard to the composition of the render coats: mainly a mix of quartz and silicate clasts. The mineralogical analyses pointed out, on the contrary, a significant variation in the composition of the aggregate of the finish coats: quartz and silicate clasts; quartz, silicate and carbonate clasts; dolomite or limestone powder; potsherd; marble (calcite) powder; quartz powder. In particular, it is crucial to consider the aggregates made of calcite or quartz powder, both prepared by means of mechanical crushing. The first one is mainly present in Brescia province, the second one in Milan.

Comparison with Latin Authors

A comparison between the archaeological artefacts and the data reported by Latin Authors, writing about architecture and stone materials, puts on view a rather divergent situation.

Vitruvius mentioned different kinds of plaster coats in his treatise [15]: a render coat (aggregate made of sand - *harenatum*), a finish coat (aggregate made of marble powder - *marmoratum*), a painted coat (support of pigments - *pictura*). About the aggregate, the Author listed: sand (sand pit, river bed, gravel, sea-shore - 2,4), marble powder (lumps of shining flakes, splinters - 7,6), pozzolana (from the region of Baia - 2,6) or potsherd (sieved - 2,5). Pliny, in his encyclopaedia of natural sciences [16], reported the different coats (*harenatum* and *marmoratum*) together with aggregates made of sand (pit, river, sea - 36,175), of potsherd (36,175) or of marble powder (36,175).

The authentic Roman practice, as revealed from artefacts of Lombardy, shows a similar sequence of coats, but the aggregates are more heterogeneous: river sand (quartz, silicates,

carbonates), potsherd, dolomite or limestone (carbonate sedimentary rock) powder, marble (calcite) powder, quartz powder.

Discussion

The discussion will be focused upon the aggregates made of calcite or quartz: two particular kinds of aggregate used in different locations and for a long period of time (1st - 4th centuries). An accurate refinement about the chronology must be necessary in order to explain the meaning of the modification or of the persistence of the aggregate composition during the decades and the centuries. At the present time, the great majority of Roman plasters lies in rubbish, put together one another, so preventing from a significant dating to the artefacts.

Discussion 1 - Calcite

The calcite aggregates [17-24] show two different types of clasts:

- i) poly-crystalline (size 0.5 - 3.5 mm), sub-rounded boundaries; each clast contains only few calcite crystals ranging from 0.1 to 2.0 mm and often showing polysynthetic twinning;
- ii) single crystal (size up to 5 mm), euhedral, clear, unit extinction, angular boundaries according to the calcite rhombohedral cleavage; twinning lamellae are lacking (Figure 1).



Figure 1 (left) - Single calcite crystals (finish coat of plaster Cividate C., *domus*)
Optical microscopy on transverse thin section – XPL



Figure 2 (right) - Calcite vein in limestone (Giallo Antico, Northern Tunisia)

The term “calcite” is a modern term (from the Latin *Calx-calcis*, meaning “calcium carbonate” or “lime”) and it was unknown to Latin Authors. Pliny [16] reports some “marbles”, obviously ignoring the mineralogical composition: white marble (*marmor candidum*), quarried in the greek islands (Cyclades, Lesvos, Thasos) or dark veined marble quarried near Athens (Hymittus) or *marmor lunense*, quarried in Apuanian Alps (Tuscany) and named from the near harbour town of *Luna* (36, 4-54). About the origin of the calcite used as aggregate, Vitruvius [15] enumerates: “the marble”, “the lumps containing transparent grains like salt and this kind when crushed and ground is extremely serviceable

in stucco works” and “the splinters thrown down by the marble workers” (7,6). Pliny [16] is less detailed on this subject: the “*marmoratum*” is reported as the finish coat of plasters, but the occurrence of the raw materials is ignored (36,176-177).

In order to detect the origin of calcite crystals, samples of Lombard, Italian and Mediterranean marbles, were analysed and compared. The samples were mechanically crushed to an appropriate grain size.

On the basis of this comparison, polycrystalline clasts (i) obtained by the mechanical crushing of fine to coarse grained marble (Table 2) show the same features of calcite clasts used in the aggregate. The hypothesis on the origin of calcite clasts as by-product of the work of stone material, is the most valuable and it is also suggested by the excerpts from Vitruvius’ book [15] mentioned above (7,6).

Table 2. Marbles for comparison

Marble (location)	Marble features (grain-size)
Candoglia (Verbano, Italy)	pink to white marble (coarse)
Ornavasso (Verbano)	pink to grey grey marble (coarse)
Crevoladòssola (Verbano)	brown veined marble (coarse)
Veza d’Oglio (Sondrio, Italy)	white marble (coarse)
Torano (Carrara, Tuscany, ITA)	white marble (fine)
Gioia (Carrara, Tuscany, ITA)	white marble (fine)
Spilia (Pendeli, Attica, Greece)	white marble (fine)
Kesariani (Himittus, Attica, Greece)	black veined greyish marble (medium)
Chorodakia (Paros, Cyclades, GR)	white marble (fine)
Apollonas (Naxos, Cyclades, GR)	white marble (coarse)
Moria (Lesvos, Greece)	grey marble (fine)
Aliko (Thasos, Greece)	white marble (medium)
İscehisar (Afyon, Turkey)	purple veined marble (fine)
Belevi (Selçuk, İzmir, Turkey)	white marble (fine)
Kapıkırı (Lake Bafa, Muğla, Turkey)	white marble (fine)

Samples of coarse grained calcite veins [25], present in stones of Lombardy, Italy and other Mediterranean countries, were also crushed, analysed and compared. Coarse single crystals (ii) obtained by the crushing of calcite veins (fibrous or drusy spar showing an increasing crystal size away from the substrate - Table 3) show the same features of single crystals of the aggregate. At the same time, it is possible to exclude the provenance of these crystals from the crushing of coarse grained Alpine marbles (Candoglia, Crévola, Veza): the comparison shows very different features.

The provenance of coarse single crystals from calcite veins is an interesting issue and the hypothesis of the use of by-products is always effective. Thick calcite veins were harmful in a dressed block, so they were discarded and removed by the quarrymen and rapidly converted into an useful by-product. An example to support this hypothesis was found in the Roman villa of Sirmione, called “Grotte di Catullo” and located in a narrow peninsula on the southern bank of lake Garda (eastern Lombardy): calcite crystals used as plaster aggregate,

observed through microscopy on thin section, show the same features (radial-fibrous calcite, unit-extinguishing) of the calcite veins spread in the marly-limestone, called “Scaglia Lombarda” (Cretaceous), forming the bedrock of the Sirmione peninsula and employed (thick slabs) to make the masonries of the same Roman villa.

Table 3. Coarse calcite veins for comparison

Lithotype	Provenance
Black limestone (white veins)	“Calcare Varenna” (Triassic, Lombardy)
Red limestone (white veins)	“Rosso Ammonitico” (Jurassic, Venetia)
Grey marly-limestone (white veins)	“Calcari Mt Antola” (Cretaceous, Ligurian)
Reddish marly-limestone (white v.)	“Scaglia Lombarda” (Cretaceous, Lombardy)
Brown Alabaster (travertine)	“Alabastro di Albino” (Pleistocene, Lombardy)
White marble (coarse vein)	Gioia (Carrara, Tuscany)
Giallo Antico limestone (white vein)	Chemtou (Jendouba, Tunisia)
White marble (coarse vein)	Chorodakia (Paros)
White marble (coarse vein)	Apollonas (Naxos)
White marble (coarse vein)	Moria (Lesvos)
Grey marble (coarse vein)	Kesariani (Hymittus)
Settebasi meta-conglomerate (white vein)	Tris Boukes (Skyros, Sporades, Greece)
Breccia corallina limestone (white vein)	Vezirhan (Bilecik, Turkey)
Pavonazetto marble (coarse v.)	İscehisar (Afyon)

Therefore, this hypothesis about the provenance, is suitable for other stone materials containing coarse calcite veins as white or “coloured” marbles (Figure 2), largely used by the Romans for architectural and decorative purpose (Table 3).

Discussion 2 - Quartz

The aggregates made of quartz [23,26,27] show two different kinds of clasts:

- (i) poly-crystalline (size 0.1 -2.2 mm), opaque, undulose extinction, regular-shape, medium sphericity and angular to rounded boundaries;
- (ii) single crystal (size 0.1 – 0.2 mm), clear, unit extinction, irregular shape, low sphericity and angular boundaries (Figure 3).

This kind of aggregate was totally ignored by Latin Authors. The term “quartzum” was introduced by Georgius Agricola [28] (book 6, p.118) in the middle of 16th century. Agricola also explained: «The greek name for “quartz” comes from its close resemblance to ice (κρύσταλλος) and the Latins have translated the Greek name into their own language and call it “crystallus”». Strabo [29](15.1.67) in the 1st century BCE and Claudius Aelianus [30](15.8) in the 3rd century CE wrote about “κρύσταλλος” or “rock-crystal” coming from India. Pliny [16] wrote on the “cristallum” (rock-crystal) “formed of moisture from the sky falling as pure snow” (37, 23-29), accurately describing the features (“formed with exagonal faces”) and the provenance (Alps, Asia Minor, Cyprus, India etc.). Pliny [16] used also the term “silex” (36, 16-170), but referring to a black hard stone useful for paving and identified

with the volcanic rocks (tephrite-leucite lava, Pleistocene) of the “Vulcano laziale” (northern Latium, Viterbo and Rome provinces). The term “crystallus”, meaning rock-crystal, was also used by Curtius Rufus [31] (3.3.8) and Statius [32] (1.2.126) in the 1st century CE. Later this term was employed by Isidore [33] (16, 12-13) and also Del Riccio [34] (chap. 120 and 125) used the Italian translation “Cristallo”. All these Authors described this transparent material as useful to make containers of liquids as cup or vessel.



Figure 3 (left) - Single quartz crystals (finish coat of plaster - Milan, p.zza Fontana) -Optical microscopy on transverse thin section - XPL



Figure 4 (right) - White quartz pebbles (river Mäggia deposit - Canton Ticino, CH)

In order to detect the origin of quartz clasts, fluvial and glacio-fluvial deposits were sampled, choosing areas of western Lombardy because of the prevalence of metamorphic rocks (made of quartz and silicates) of the pre-Permian Basement and the scarcity of carbonate ones in the same area.

Table 4. Sands for comparison

Location (province)	Feature of deposit (Quaternary)
Mouth of Mäggia (Locarno, CH)	Clast-matrix supported gravels (fluvial)
Mid course of Ticino (Turbigo, MI)	Clast-matrix supported gravels (fluvial)
Torba (Castelseprio, Varese)	Clast supported gravels (glacio-fluvial)
Asnago (Cantù, Como)	Matrix supp. gravels (glacio-fluvial)

To compare the single quartz crystals, some milky-white pebbles, made only of quartz [35,36] and widely occurring along the river courses in western Lombardy [37,38], were sampled and analysed (Figure 4). Further comparisons were made using quartz pebbles spread along the river courses of northern Apennine [39]. The samples were mechanically crushed to an appropriate grain size.

Table 5. Quartz pebbles for comparison

Location (province)	Feature of deposit (Quaternary)
Mouth of Mäggia (Locarno, CH)	Clast supported gravels and sands
Mid course Ticino (Turbigo, MI)	Clast supported gravels, sands and silt
Low course Adda (Lodi)	Clast supported gravels, sands and silt
Low course Sècchia (Sassuolo, MO)	Gravels, sands and locally blocks
Low course Tièpido (Gorzano, MO)	Gravels, sands and locally blocks
Low course Panaro (Vignola, MO)	Gravels, sands and locally blocks

On the basis of these comparisons, poly-crystalline clasts (i) match the clasts of the fluvial or glacio-fluvial deposits; single crystals (ii) match the crystals of crushed quartz pebbles.

Poly-crystalline quartz (i) of fluvial deposits shows undulose extinction, high sphericity and sub-rounded boundaries; these clasts are associated with single crystals finer in size. Poly-crystalline quartz of glacio-fluvial deposit shows the same features, but crystals show low sphericity and sub-angular boundaries. Quartz clasts are always mixed with plagioclase, potash feldspar, micas and other minerals as chlorite, serpentine or dolomite according to the geology of the basin. This kind of loose material match the features reported by Vitruvius [15] about the sand suitable for mortar aggregate: “makes a noise when rubbed in the hand” and “if a white garment is not soiled and no dirt adheres to it” (2,4). Moreover, a poly-crystalline quartz aggregate was usually employed in render coats of the whole plasters examined in the archaeological sites of Lombardy.

Quartz crystals (ii) coming from crushed pebbles (Figure 5) are clear, unit-extinguishing, irregular shaped (Figure 6) and match the single crystals of quartz used in the aggregates.



Figure 5 (left) - Quartz crystals in a quartz pebble (river Muggia)
Optical microscopy on thin section - XPL



Figure 6 (right) - Quartz clasts obtained through the crushing of a quartz pebble

This material is totally lacking in quotations of Latin texts, but also a mere distinction between quartz and calcite was impossible without a mineralogical skill, especially if quartz and calcite are in the form of smooth pieces (Figure 7).

Veins, lenses, nodules of massive quartz are present in metamorphic rocks, as gneiss and paragneiss, widely diffused in the outcrops of Pre-Permian Basement, located in the Alpine range (Northern Lombardy). The dismantling, through weathering agents, of these rocks generates irregular blocks, then converted in pebbles during the transport and piled up, together with gravels and sands, along the river courses. The occurrence of the quartz pebbles suggests the hypothesis of their contextual excavation with sands, according to the coincidence of the sedimentation areas. Smaller pebbles, with similar crystal features and coming from quartz veins of Tertiary sandstones, also occur in the fluvial deposits of Apennine rivers, but their location was too far to consider an employ in Roman cities of Lombard territory.



Figure 7 - Pebbles (maximum size 4 cm) of quartz (above) and of calcite (below)

Conclusion

Some Roman plasters of Lombardy are made of two superimposed coats which feature a finish coat constituted by crushed material such as aggregate and lime as binder. This crushed material features a different mineralogical composition, roughly according to the geographic location: marble (calcite) powder (East Lombardy) or quartz powder (Milan). The aggregates contain poly-crystalline clasts or single crystals. The origin of poly-crystalline clasts is ascribable to: (i) crushing of a calcite marble (calcite); (ii) natural loose deposit (quartz and silicate sand) of river courses based on metamorphic rocks (North-western Lombardy). The origin of single crystals is ascribable to: (iii) crushing of coarse grained calcite veins spread in limestone, sandstone and sometimes in marble; (iv) crushing of milky-white quartz pebbles occurring in deposits of river courses based on metamorphic rocks (North-western Lombardy). The usage of quartz as aggregate instead of calcite (the kind of aggregate reported by Latin Authors) is probably due to a misunderstanding caused by the absence of mineralogical skill of the Roman plaster makers: a rounded element of quartz may be easily mistaken for white marble; calcite and quartz crystals, obtained by crushing, show similar macroscopic features. Therefore, the use of quartz powder could be an unintentional surrogate of the calcite powder, related to the sediments locally available, rather than a deliberate choice of another raw material.

References

1. Pagani C (2014) Una testimonianza di pittura celebrativa nell'area di via Broletto a Milan. In: 11th AIPMA Colloquium 2010. Akademie der Wissenschaften, Wien
2. Ceresa Mori A, Pagani C (2010) Gli intonaci dipinti dello scavo di piazza Fontana a Milan. In: 10th AIPMA Colloquium 2007. L'Orientale Università, Napoli

3. Pagani C, Cavalli R (2013) Milan piazza Meda - corso Matteotti. In: Notiziario 2010-11. Soprintendenza Beni Archeologici Lombardia, Milan
4. Ceresa Mori A (2004) L'anfiteatro di Milan e il suo quartiere. Skira, Milan
5. Folli L, Bugini R (2017) Milan via Brisa - Le malte. In: Fedeli AM, Pagani C (eds) L'area archeologica di via Brisa. Quaderni Museo Archeologico, Milan
6. Blockley P, Cecchini N, Pagani C (2012) L'area archeologica del Monastero Maggiore di Milan. Quaderni Museo Archeologico, Milan
7. Pagani C (2018) Personal communication
8. Bugini R, Folli L (2014) Materiali da costruzione e metodologie di messa in opera nel Santuario repubblicano di Brescia. In: Rossi F (ed) Un luogo per gli dei. All'insegna del Giglio, Firenze
9. Mariani E (1996) Contributo preliminare sugli affreschi ritrovati in via Trieste. In: Rossi F (ed) Carta Archeologica Lombarda - Brescia la città. Panini, Modena
10. Mariani E (1996) Contributo preliminare sugli affreschi ritrovati sotto il palazzo Martinengo Cesaresco. In: Rossi F (ed) Carta Archeologica Lombarda - Brescia la città. Panini, Modena
11. Mariotti V (2004) Il teatro e l'anfiteatro di Cividate Camuno. All'insegna del Giglio, Firenze
12. Mariani E (2010) La decorazione pittorica del vano 1. In: Rossi F (ed) Il Santuario di Minerva a Breno. Edizioni ET, Milan
13. Roffia E, Bugini R, Biondelli D, Folli L (2005) Le pitture murali della villa romana "Grotte di Catullo". In: Convegno Scienza e Beni Culturali. Arcadia Ricerche, Venezia.
14. Mariani E (1997) Calvatone romana: un pozzo ed il suo contesto - Intonaci. Quaderni di ACME 29:185-204
15. Vitruvius (1931) De Architectura, Granger F (ed). Harward University Press, Cambridge
16. Pliny the Elder (1962) Naturalis Historia, Eichholz DE (ed). Harward University Press, Cambridge
17. Bianchetti PL, Campisi M, Gratziu C, Melucco A (1990) La calcite spatca dell'intonaco romano. In: Convegno Scienza e Beni Culturali. Libreria Progetto, Padova.
18. Béarat H (1996) Chemical and mineralogical analyses of Gallo-Roman wall painting from Dietikon. Archaeometry 38:81-95

19. Béarat H, Fuchs M, Maggetti M, Paunier (1997) Roman wall painting - Materials, techniques, analysis and conservation. Fribourg University, Fribourg
20. Bugini R, Folli L (1999) Il marmor degli intonaci romani (I): provenienza della materia prima. Quinta giornata Scienze Terra - Archeometria. Patron, Bologna
21. Bugini R, Folli L (2000) Il marmor degli intonaci romani (II): sperimentazione con aggregati preparati artificialmente. Bollettino Accademia Gioenia Scienze Naturali 33:157-164
22. Baraldi P, Bonazzi A, Giorani N, Paccagnella F, Tannini P (2006) Analytical characterization of Roman plaster of the domus Farini in Modena. Archaeometry 48:481-500
23. Bugini R, Folli L (2013) Critères pour la comparaison des enduits peints romains de la Lombardie. Archéosciences 37:41-50
24. Leone G, De Vita A, Magnani A, Rossi C (2016) Thermal and petrographic characterization of Herculaneum wall. Archaeometry 59:747-757
25. Flügel E (2010) Microfacies on carbonate rocks. Springer, Berlin
26. Bugini R, Folli L (2011) Monomineralic aggregates in mortars: examples from Lombardy. 10th ICAM Applied Mineralogy, Broekmans M (ed). Trondheim 85-92
27. Bugini R, Folli L, Biondelli D (2013) Grain morphology of aggregates in Roman plasters. 14th EMABM Microscopy on Building Materials. Danish Technological Institute, Helsingor 25-28
28. Georgius Agricola (1955) De natura fossilium, Bandy MC, Bandy JA (eds). Geological Society of America, New York
29. Strabo (1917) Geographica, Jones HL (ed). Harward University Press, Cambridge
30. Claudius Aelianus (1959) De Natura Animalium, Scolfield AF (ed). Harward University Press, Cambridge
31. Curtius Rufus (1908) Historiae Alexandri Magni, Hedicke E (ed), Teubner, Leipzig
32. Statius (2000) Silvae, Canali L (ed). Armando Dadò, Locarno
33. Isidore of Seville (2004) Etymologiarum sive originum, Valastro Canale A (ed). Utet, Torino
34. Del Riccio A (1996) Istoria delle pietre, Gnoli R, Sironi A (eds). Umberto Allemandi, Torino
35. Robin PYF (1979) Theory of metamorphic segregation and related processes. Geochimica et Cosmochimica Acta 43:1587-1600
36. Rykart R (1995) Quarz Monographie. Ott, Thun

37. Carta Geologica della Lombardia (1990), Montrasio A (ed). Istituto Poligrafico, Roma.

38. Carta Geologica d'Italia - Progetto CARG, sheet 75 – Como

www.isprambiente.gov.it/it/carte-geologiche-e-geotematiche

39. Carta Geologica d'Italia - Progetto CARG, sheet 219 - Sassuolo

www.isprambiente.gov.it/it/carte-geologiche-e-geotematiche

Analytical and chromatic characterization of the interior walls finishes in the Batlló House of Gaudí in Barcelona. A surprising discovery

Àgueda Serra¹, Joan Casadevall¹

(1) Gabinet del Color S.L., (technical consultancy firm focused on chromatic and materials analyses of the historic architecture, Barcelona), gabinet@gabinetdelcolor.com

Abstract

It is well known that Modernism implemented and promoted the decorative arts in architecture. In Barcelona, chief town of the avant-garde in the bend from XIX to XX centuries, the use of coloured lime stucco in the interior and exterior coatings of buildings was very prolific. This paper presents the outcome of our chromatic study of the interior walls of Gaudí House “Casa Batlló”, built in 1904 at the Pg. de Gràcia boulevard. We have inferred not only the materials and colours of finishing but also the execution technique, which was innovative and involved a high degree of difficulty.

The systematic study of the interiors of the Casa Batlló's noble floor through different analytical techniques has revealed the modernist finishes, serving as a basis for its restoration process. The main rooms have been inspected and documented, and micro-samples have been extracted ‘in situ’ to verify the presence of original coatings. The combination of several analytical techniques carried out in different laboratories, together with the deep knowledge of the artisan techniques of the stucco, the sgraffito and the ironing of the lime-stucco from master artisans, have led to outstanding results presented here in a novel way.

Introduction

Gabinet del Color is a technical consultancy firm formed by architects, restorers, historians and technical architects, that is focused on chromatic and materials analyses of the historic architectures in different towns [2, 3]. Its operational basis is located in Barcelona, where more than 12000 historic facades have been analysed [6, 9]. One of them is the Gaudi House “Casa Batlló” in the Pg. de Gràcia Boulevard, discussed hereafter (Figure 1).

The “Casa Batlló” is a building designed by the architect Antoni Gaudí that was built in 1904 to be the residence of the Batlló family, in the centre of Barcelona (Figure 2). It involved a completely innovative formal and architectonic language that has become afterwards one of the paradigms of the Modernism as well as a UNESCO world heritage monument.

At present, it is a museum-house and many apartments in different floors can be visited, hence allowing to infer how it could be to live in such a unique environment. Gaudí defined and controlled finishing of all the architectonic and decorative elements where usage of

applied arts could have a fundamental role [1]. The team of “Gabinet del Color” has been analysing the materials and finishes chromatisms from different elements sampled during the last 6 years, such as the chimneys of the rooftop, inside and outside railings, interior carpentry and finally the inner coatings of the apartments.



Figure 1. Barcelona's views of Pg. de Gràcia boulevard, where the Casa Batlló is situated. The maps above with the red points are the Gabinet's Database of the façades that have been studied through more than 30 years in Barcelona. Figure 2. The façade of Gaudí's Casa Batlló.

This paper focuses on the characterization of the finishes of the walls' coatings of noble rooms of such lodgement (see Figures 3 to 6) in order to verify if they are still preserved and to evaluate its eventual restoration. It should be reminded that the “Casa Batlló” was affected by two major interventions, in 1954 (when Modernism was much less appreciated than today) and in the period 1989-1995, when some floors of the building were recovered for exhibition purposes (some neighbours are still living in other floors). Presently, the walls and roofs of the noble stage of the “Casa Batlló” are decorated by acrylic repaints. Hence, one could question what was hidden beneath the paintings and establish its genuineness. Hereafter, we present the surprising result of the analyses made in the noble floors of the “Casa Batlló”.



Figure 3. Picture from 1927 of the main living room, compared with the present view (©Casa Batlló).



Figure 4. Main living room and detail of the finishing of the coatings.



Figure 5. Dining room and detail of the finishing of the coatings.



Figure 6. Fireplace room and detail of the finishing of the coatings.

Samples

The study carried out includes all lounges of the noble floor, the former residence of the Batlló's owners. At present, these lounges are repainted imitating the famous "trencadís" of Antoni Gaudí, but they are in fact the result of repaints and maintenance operations performed during the last 50 years. Our aims were to infer how the walls and ceilings were originally achieved in 1904, and in which rooms that original finishing is still preserved and, hence, deserves a deep restoration to recover it [4]. The stuccoes had been documented through historical and technological analysis of traditional local practice combined with applied research in situ and in the lab, as well as with the background knowledge. The Methodology used for the analysis of interior coatings can be divided in two types of samples: Non-destructive and Destructive samples.

Non-Destructive Samples

We have analysed samples of this type from careful stripping of the paints superimposed in small pieces of walls and ceilings in previously selected points according to their potential information, in order to establish the nature of the underlying [7]. Up to 35 tests have been retained in strategic points. We performed the stripping in local areas selected because the historic finishing was probably preserved, or in points where some repairs should be made, in order to compare repaints and mortars. They were carried out mechanically using paint-stripping gels, by carefully removing the superimposed paints up to reach the original lime stucco finish. The size of those samplings rises from 10x10 cm up to 15x20 cm (Figure 7a).

The stripping allowed inferring that some of the noble living rooms keep the original lime stuccoes that presumably cover the stays (Figure 7b). This procedure has helped to settle the finishing technique and has provided one of the first surprises. The stuccoes were hot-ironed and besides, they preserve the incision of the punch that profiles the famous Gaudi “trencadís” along all the walls and ceilings, a finishing that fragments the flat surfaces by means of an outline that modulates small pieces that form a mosaic (like broken tiles). The observation of these stripping samples reveals that the “trencadís” is placed at the same level as the whole stucco (Figure 7c).



Figures 7a, 7b and 7c. Selective samples showing the different layers along the interventions.

We have built up some test samples of traditional lime mortar trowel and hot-ironed finished [5, 7] (Figs. 8a to 8c), to be used as a reference pattern to controtype the original finishing detected in Casa Batlló. In this way, we could perform some tests of surface stripping and basically, to check the presence of organic products which are usually applied to pressed and ironed finishing like the studied ones [7, 8].



Figures 8a, 8b and 8c. Making up of coloured stucco palettes with chromatic controtype.

As a non-destructive technique, infrared reflectography was also used to study the underlying layers of the pictorial layers without the need to extract samples. The coatings were examined with a monochrome camera with both Ultraviolet (UV) and Infrared (IR) filters. After different attempts at different wavelengths and placing different tone filters, it was concluded that overlay acrylic paint did not allow to see the lower layers. (Figure 9a to 9c).



Figures 9a, 9b and 9c. Examination of samples with infrared camera and different color filters.

Destructive samplings

Following the in-situ stripping, and once assessed the potential of the original mortars preserved, we proceed to extract small, unaltered and representative samples. All the coating thickness is kept, to allow implementation of different analytical techniques. Up to 16 samples have been extracted from coloured lime mortars (Figure 10 and 11).



Figure 10. Detail of a sample extracted off the walls' coating in the main room of the Casa Batlló.

Figure 11. Collection of the samples extracted in different points of the main floor.

Extractions were performed with escarpment and hammer, as well as portable drill with one-piece hammer core cutter, to extract coating thickness [2, 9], all of them referenced and located (Figure 12).

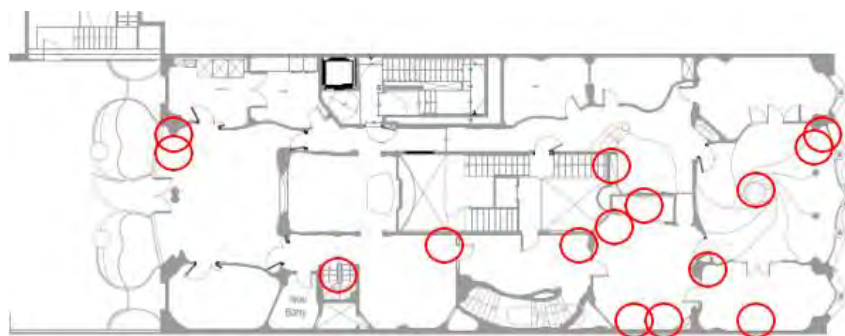


Figure 12. Location of the samples extracted from lounges in the noble floor

Analysis and characterization methodology

Architectonic and organoleptic examination.

A combination of analytical techniques has been designed to achieve as much information as possible [3]. Firstly, the different rooms in the noble floor have been studied, bearing in mind the architectonic modifications of the building during more than 100 years, by establishing the best points to perform stripping tests followed by micro-samples extraction. Afterwards, various complementary analytical techniques have been applied to the wall finishing, starting with an organoleptic examination that recognizes features of the material (finishing, chromatism, texture) which serve as a filter for the subsequent precise analyses.

Stratigraphic examination and binocular microscopy with chromatic analysis.

A stratigraphic analysis is performed with binocular lens and incident lighting observation of the extracted samples, in cross sections to show the composing strata. The chromatic analysis consists of duplication of the colour observed in the lime mortar paste, mixed with pigments and sand starting from the original pigment identification. The reference system used is the ACC International code, the same as the Barcelona Colour Chart [2, 9]. We used a stereoscopic microscope with digital camera Leica S8 Apochromatic. The original chromatisms have been deduced from chromatic patterns referenced and duplicated in a physical pattern.

Analytical techniques.

The combination of analytical techniques and magnified lens observation of studied samples has resulted in the determination of their chemical nature, morphology and compounds [3]. Even though we deal with lime inorganic mortars, the assumption that the stuccoes could be hot-ironed finished has been verified by looking for organic compounds in the historic superficial strata. The techniques employed were:

-Optical Microscopy with polarized, incident and transmitted light, halogen light and UV light (OM). -Fourier Transform Infrared Spectroscopy (FTIR). -Gas Chromatography and Mass-Spectrometry (GC-MS). -Scanning Electron Microscopy (SEM) with X-Ray Dispersion Spectrometry (EDX) -Raman Micro-Spectroscopy. -X-ray diffraction (DRX).

Results and discussion

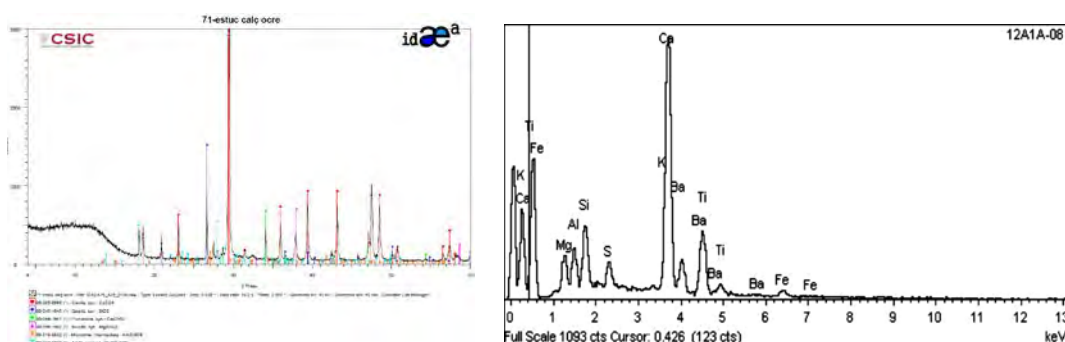
In this section we describe outstanding results obtained in the most relevant rooms that still have the original finishing underlying.

Coating of the walls.

The vertical walls and ceilings show continued finishing corresponding to a high-quality lime-mortar stucco, with pure white lime (in this case magnesium lime) and marble sand and marble powder as a well selected arid (of 0.5 mm) on top of a clay-rich rendering, to provide hydraulicity (Figs. 13a and 13b). All this lime stucco was coloured wholesale with different mineral pigments depending on the lounge and the wished chromatism in each room. The dining room, westward oriented, displays a stucco dyed with ocher iron oxide (Figs. 14a and 14b), whereas the main living room, eastward oriented and opened to the Passeig de Gràcia was pigmented with ultramarine blue and barium white (Figs. 15a and 15b). The Fireplace room holds a lime stucco dyed with natural iron oxides, like hematite. All of them are very good shape stuccoes, with well cohesive strata and showing an execution technique typical of a stucco master. It should be emphasized how meritorious is that this coating remains continued along walls and ceilings, despite the continual presence of sinuous shapes.



Figures 13a and 13b. Wall presently painted, and coloured lime stucco section.



Figures 14a and 14b. X-ray Diffraction and X-ray Spectroscopy of the mass of the ocher lime mortar.

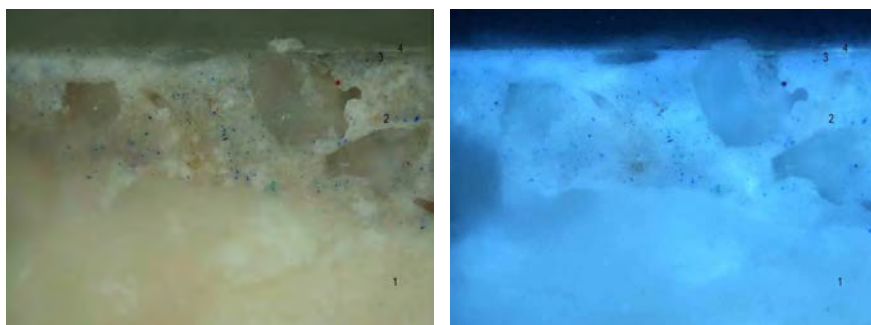


Figure 15a and 15b. OM Cross section (10X/0,30) with incident light and UV light of the coloured stucco, where it is perceived: 1-white base stucco; 2-lime mortar with blue pigment; 3-finishing layer hot-ironed; 4-acrylic paint overlaid.

The private space of the Sacristy has a green trowel finished stucco (Figs. 16a and 16b) and, besides ultramarine blue pigment, it incorporates a curious green pigment. An elementary analysis by SEM-EDX (Figure 17a) has revealed its silicon nature, and the Raman analysis also relates the green pigment with a silicate rather than with a usual pigment in the paint layers (like green chrome or copper acetates detected in other samples studied). Therefore, we conclude that it consists of a micronized glass of green tonality, intended to achieve a more sparkling effect, which has never been documented through the extended-path analyses of lime coloured coatings (Figs. 17b, 18a and 18b).

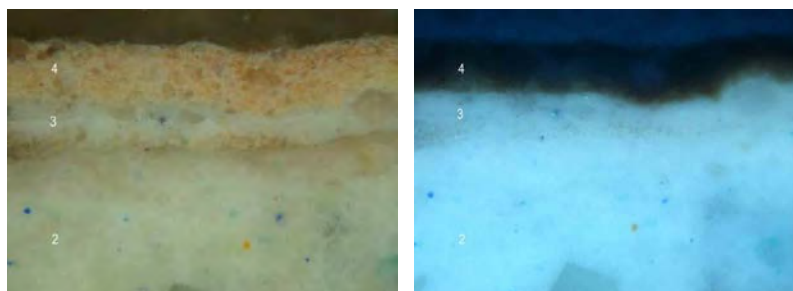


Figure 16a. Stratigraphic cross section of the wall's coating: 2.-original lime and blue and green pigment's stucco; 3-superimposed white primer layer; 4-current finish ocher painted. Figure 16b. Same as before, with UV light for organic compounds.

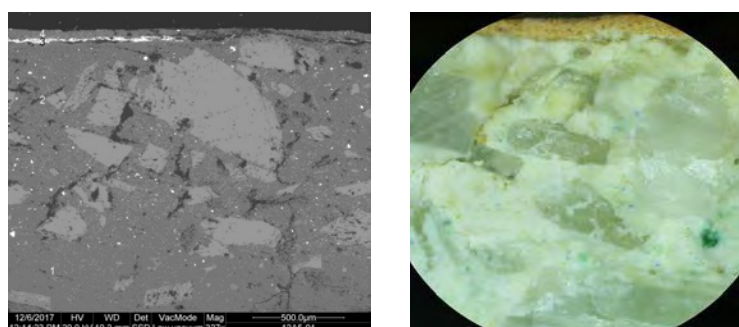


Figure 17a. Same sample as before, SEM observation, where the light points correspond with pure silicon. Figure 17b. OM at 80X of the same sample: lime stucco with blue pigment micro-nodules and presence of green pigment.

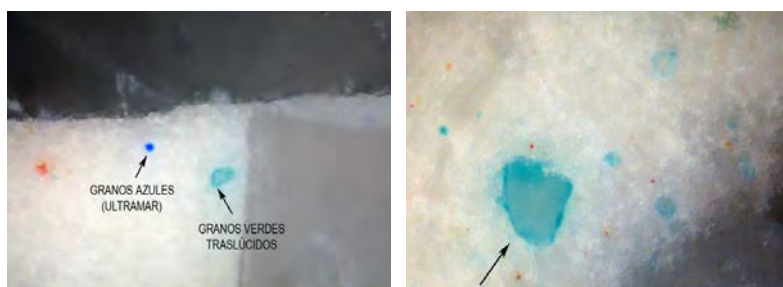


Figure 18a. OM with presence of known blue pigment and presence of green particles based on silicon. Figure 18b. OM at 80X of the translucent silicon green.

“Trencadís” sgraffito hot-ironed finished

The original finishing that mimics the “trencaadís” technique and shapes its irregular quartering consists of a trowel finish stucco over which traditional soapy inks are applied, basically to carry out hot-ironed stuccoes [5]. Following the traditional recipe, the procedure consists of a mixture of soap flakes dissolved in water that is taken to boiling and is further mixed with some lime putty and water. In this procedure, the soapy inks coloured with pigments are applied on the stucco which is hot-ironed over its surface. Hence, the stucco achieves a very soft finishing, similar to marble (Figure 19). In the Casa Batlló the analyses detected traces related to soap and wax in the extract with solvents got from the coloured layers (Figs. 21a and 21b) thus confirming our hypothesis. These inks were dyed with natural pigments, and presumably they had no uniform colour, but were multitone with alveolar shapes.



Figure 19. Hot-ironed stucco’s technique, applying a hot iron tool over the surface of the lime mortar, that ends up by giving a shiny and smooth result, as shown in the pictures.

After this first finishing hot-ironed, the stucco master performed some sgraffito [5] by setting some grooves of 3,6 x 0,9 mm simulating the joints of the “trencaadís” to mimic (Figs. 20a and 20b). These grooves were filled of white lime, cleaning the edges which had been ironed before and configuring at the end the white lines observed over the coloured bottom of walls and ceilings. To finish it was given a final waxing.

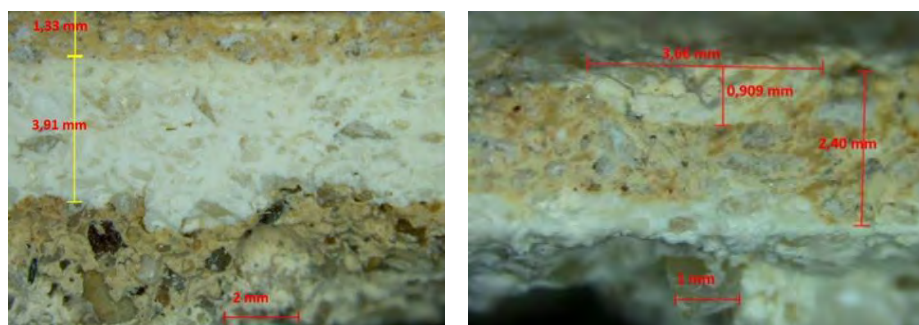


Figure 20a. OM cross section of the sgraffito at 10X: Layers of rendering, first layer and coloured finish layer.

Figure 20b. Idem previous at 20 X, in detail the notches of 3.6 x 0.9 mm.

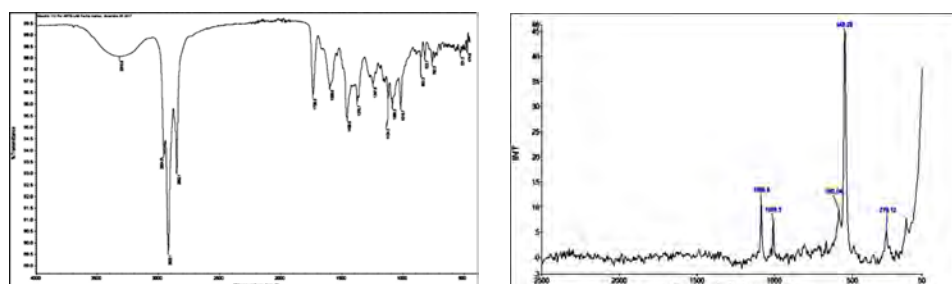


Figure 21a. FTIR spectroscopy of the organic compounds. Figure 21b. Raman spectroscopy for detecting soaps and pigments.

This reported technique of ironed finishing needs a high expertise and involves high execution difficulties. Therefore, this discovery has allowed not only to recover the original finishing of the Casa Batlló but also to evidence the high degree of exigency of Antoni Gaudí towards the artisan masters working there. In this case, they implemented lime stuccoes of very high level and hardness that have lasted to this day, hidden behind repaint layers.

Golden finishes

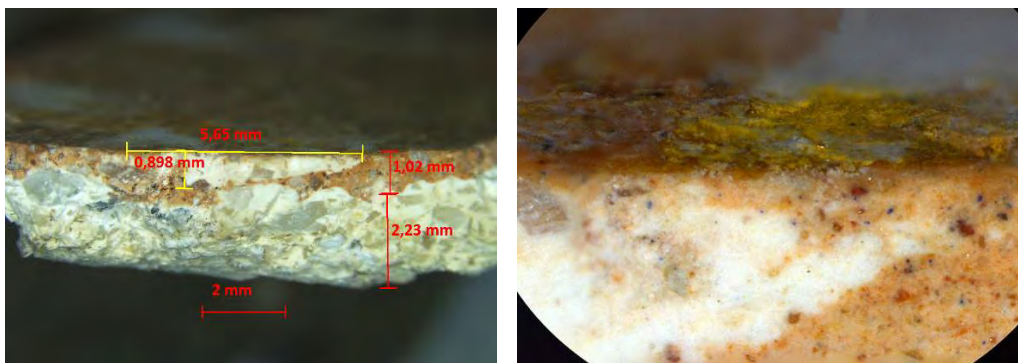
If the stucco application technique described before is already a high difficulty work, in the Hall of the Fireplace the “trencadís” is even more surprising. Whereas in the outside rooms a “trencadís” of bright colours and with a white joint was mimic, in this room darker tones of ceramic colours were retained, including the excellence of gold in the joints (Figure 22a). In this room, in parts behind the heating appeared some gypsum mortars repaint with purpurin, probably coming from repairs between 1960 and 1990, which we used as a comparative pattern with the original finishing (Figure 22b).

In this case, the soapy coloured inks previously reported were applied, hot-ironed with a dominant clay tone. Firstly, the “trencadís” joints were sgraffito with the lime mortar still tender and were filled out with white stucco inlayed in the groove left by the sgraffito tool. Remarkably, in this case these white joints (Figure 23a) were goldened with fine gold leaf (Figs. 22c and 23b). To end up, a general polish was made.

As it is shown in the Figures 24a to 26b, the golden leaf is detected in the different analyses that have been done and it is a very high-quality gold that still remains below the repainted.



Figure 22a. Current paint. Figure 22b. Extraction of micro-samples. Figure 22c. Detail of the golden leaf appeared in the selective stripping.



Figures 23a and 23b. Stucco with sgraffito's joint at 10X i 80X: white joint, golden leaf and red lime mortar.

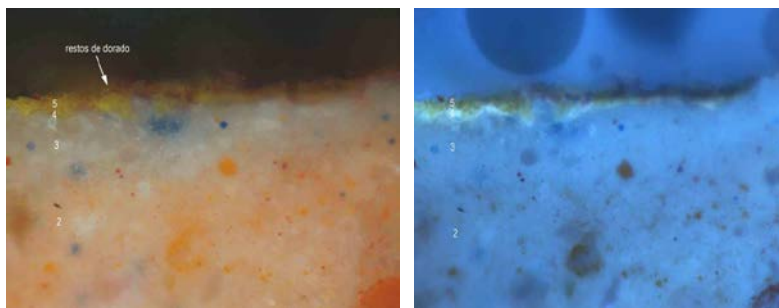


Figure 24a. Cross section= 2: lime mortar and red pigment; 3: Lime mortar of the joint; 4: primer layer; 5: golden leaf. Figure 24b. Idem before with UV light for detecting organic compounds and the nature of the gold.

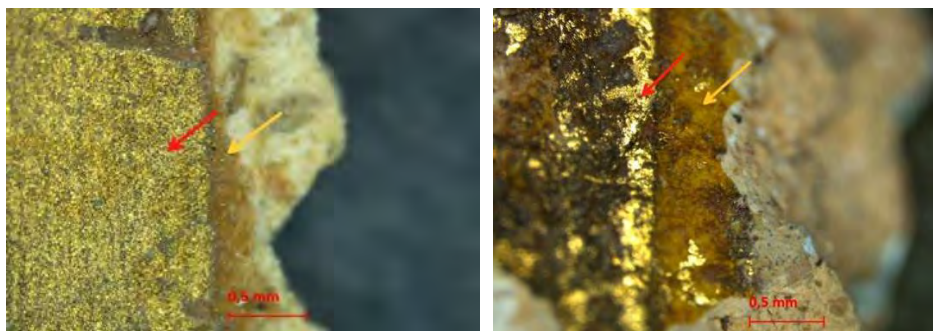


Figure 25a. Microphotography of the glitter layer from the repainted area. Figure 25b. Microphotography of the real gold leaf under the glitter of the repaint.

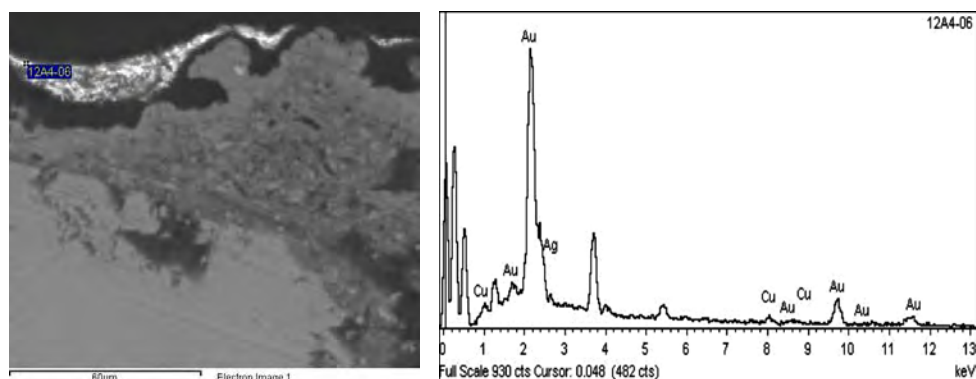


Figure 26a. Spectroscopy of the ocher lime mortar's mass. Figure 26b. Elemental composition of the golden leaf: 92,71 % Gold (Au)/ 3,30 % Silver (Ag)/ 3,39 % Copper (Cu).

Finishing chromatisms

The results of the analytics previously reported should be complemented with determination of the chromatic patterns of the different rooms studied and provide the specific colour range for each ambience.

In “Gabinet del Color” we are specialized in determining the stuccoes colours and lime mortars of historical architecture [6, 9]. We use a methodology consisting of controtyping of colours of the dyed historic mortars compared to test samples based on lime mortar and various dosages of sand and pigment over which some chromatic parameters have been fixed [2, 9]. Depending on the texture and finishing technique, they can be assimilated to a colour code referred in the international system ACC, that allows its duplication either in restoring mortars or in chromatic reintegration with painted finishing (Table 1).

We have been able to establish the chromatic patterns in the main rooms of the noble floor of the Casa Batlló (Figure 27 a-d), from the chromatic deduction by binocular observations of the coloured stuccoes, combined with the analytic detection of the different pigments used to colour them and together with the colour references inferred in the selective stripping performed, considering also the dominant multitone chromatism in the backdrop and in the “trencadís” joint.

Table 1. Chromatic references of the main rooms studied, determining the dominants colours and the colour of the joints. *Colours in Acoat Colour Codification.

Chamber	Colour 1*	Colour 2*	Colour 3*	Fig.
Dining Room	F2.15.75	F2.10.80	F2.06.84	27a
Living Room	S7.05.75	QN.02.78	F2.06.84	27b
Fireplace Room	D2.30.50	D6.25.65	Gold leaf	27c
Sacristy	K2.09.79	L0.04.78	F2.06.84	27d



Figure 27a. Chromatic pattern of the Dining Room. Figure 27b. Living Room's chromatic pattern. Figure 27c. Fireplace Room's chromatic pattern. Figure 27d. Chromatic pattern of the Sacristy.

Conclusions

The conclusion of this study is that in this Barcelona bourgeois house Casa Batlló, Gaudí exalted the creative modernist movement, designing for the walls and interior ceilings some imitations of its famous “trencadís” made with coloured lime stucco, and later finishing it with hot iron. Unlike the known “trencadís” made with glazed ceramics, where the outline arises arbitrarily, in our case the designed elements are the lines that give rise to a mesh that is the one that takes center stage

These previous studies have allowed the careful restoration of the noble rooms. The restoration has consisted on stripping the overlaid paintings and the application of nutrients based on waxes and soaps to recover the textures and chromatisms finished by Antoni Gaudí (Figure 28 and 29).

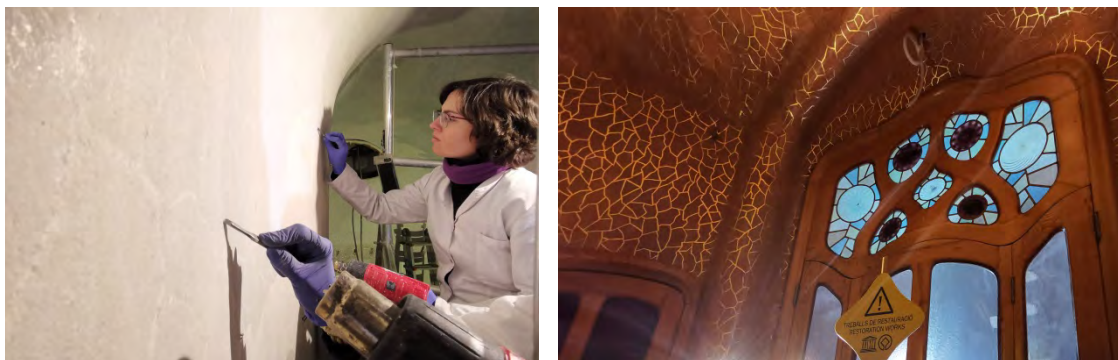


Figure 28. Restoration works, stripping the paints and recovering the original coloured lime stuccoes and their sgraffitos. Figure 29. Fireplace Room already restored, with the original finishes recovered.

Acknowledgments

We want to thank the laboratories involved, as the X-Ray Laboratory of the Institute of Environmental Assessment and Water Research (IDAEA) from CSIC, the Centre of Conservation-Restoration of the Generalitat de Catalunya-CRBMC, the Arte-Lab Laboratory in Madrid, and our own Laboratory of the Gabinet del Color. We would also thank Ana Atance from Inmobiliaria Casa Batlló and Josep Gallart, geophysicist and clairvoyant mind.

References

1. Flores, C. (1982) Gaudí, Jujol y el Modernismo Catalán. Aguilar, Barcelona.
2. Casadevall, J (1993) Els Colors de l'Eixample. Ajuntament de Barcelona, Barcelona.
3. Casadevall, J (1998) Caracterización de revestimientos tradicionales. Informes de la Construcción 450. Instituto Eduardo Torroja, Madrid.
4. Torsello, B P, Musso, S F (2003) Tecniche di restauro. Utet (Torino)
5. Martín, M et al. (1998) Guía Práctica de la Cal y el Estuco. Escuela de los Oficios (León)
6. Lecerf, G (2014) Modalites de la couleur & de la coloration urbaines, Joan Casadevall à Barcelone. Le coloris comme expérience poétique. L'Harmattan (Paris)
7. Casadevall, J (2003) La reversibilità e la compatibilità dei prodotti industriali sugli intonaci tradizionali, In: La reversibilità nel restauro, Atti del Convegno di Studi Bressanone 1-4 luglio 2003. Edizione Arcadia Ricerche (Venezia).
8. Matteini, M, Moles, A (1989) La chimica nel restauro; i materiali dell'arte pittorica. Nardini Editore (Firenze).
9. Serra, À, Casadevall, J. (2016). Chromatic analysis applied to heritage architecture of a large town: Barcelona. E-conservation journal. doi: 10.18236/econser5.201704

Roman mortars of floor substrates and walls from Arroyo de la Dehesa de Velasco site: petrographic and mineralogical characterization

Ainhoa Alonso-Olazabal¹, Luis Ángel Ortega¹, M^a Cruz Zuluaga¹, Graciela Ponce¹, Javier

Jiménez Echevarría², Carmen Alonso Fernández²

(1) University of Basque Country UPV/EHU, ainhoa.alonso@ehu.es, luis.ortega@ehu.es, mcruz.zuluaga@ehu.es, graciela.ponce@ehu.es

(2) Cronos S.C. Arqueología y Patrimonio, jj@cronossc.es, ca@cronossc.es

Abstract

Wall and floor mortars a public building from Arroyo de la Dehesa de Velasco site (Burgo de Osma, Soria, Spain) has been characterised. The site of the early Roman Imperial Period is related to a bath complex integrated into the settlement around the city of *Uxama Argaela*. Optical microscopy and X-ray diffraction techniques were used to characterise the mineralogical composition of floor and wall mortars. Generally, mortar samples are sandy siliceous nature with a lime binder matrix. Floor and wall mortars display a multi-layer structure with siliceous sand aggregates and lime. Compositionally the multilayer mortars exhibit very similar aggregates and some walls display a *cocciopesto* layer to prevent damage due to humidity. Roman standardised techniques were used for both floor and wall constructions.

Introduction

Since ancient times mortars have been used in construction and historically their composition varies largely both geographically and during different time periods [1-3]. During Roman period the technical guidelines for the construction of walls and floors for different purposes were described. Vitruvius and Pliny the Elder described many aspects of building construction [4, 5]. Besides Vitruvius explained the recipes for wall and floor constructions, consisting usually a mixing of lime and aggregates. Romans used lime or gypsum and aggregates (volcanic ash, siliceous sand, crushed marble, crushed bricks, organic materials, etc) as basic materials [6] and these recipes were the key function in Roman architecture. Mortars of the different structures varied according to whether primary function or finishing were being applied.

Roman ancient authors suggested multilayer substrates and good layer compaction to enhance the durability of the mortars. The nature and volume of the aggregates and binder nature in multilayers substrates can be miscellaneous related to the local geologic lithologies -raw materials- and to ability of artisans [7-10]. The identification of aggregates mineralogy and the textural features (morphology, aggregates distribution, porosity, aggregate volume,

binder/aggregate ratio) [11, 12] of multilayers substrates by standard petrography indicate building technology issues, construction distinctions of the main rooms, private and public spaces and inferences about social grading. The mortars of this Roman context, nowadays concealed, provide several compositional and technological data to understand the used technique of the construction of floors and walls.

The studied archaeological site of Arroyo de la Dehesa de Velasco (Burgo de Osma, Soria) is situated in surrounding of the roman city of *Uxama Argaela*. This site was discovered during the construction of the Duero motorway between Burgo de Osma and Santiuste. The city of *Uxama Argaela* is located in the plain of the medium-high course of the Duero River, at the confluence of the Ucero and Abión Rivers. It was located on one of the great Celtiberian cities and the later romanization promoted some very significant building transformations, mainly those of public character [13-15]. During the Low Empire period several villas outskirts were constructed and the city preserved its urban characteristics and functions until the end of Late Antiquity [16, 17]. According to archaeological data the discovered site was related to a bath complex, possibly for public use. Archaeological evidence of the excavation works provides a relative chronology for the first building structure related to baths on the early Roman Imperial Period. The coatings of stucco and their pictorial elements are noteworthy and the pictorial style, imitating marble in baseboards and with figures on the rest of the wall, date the building to the 2nd century AD.

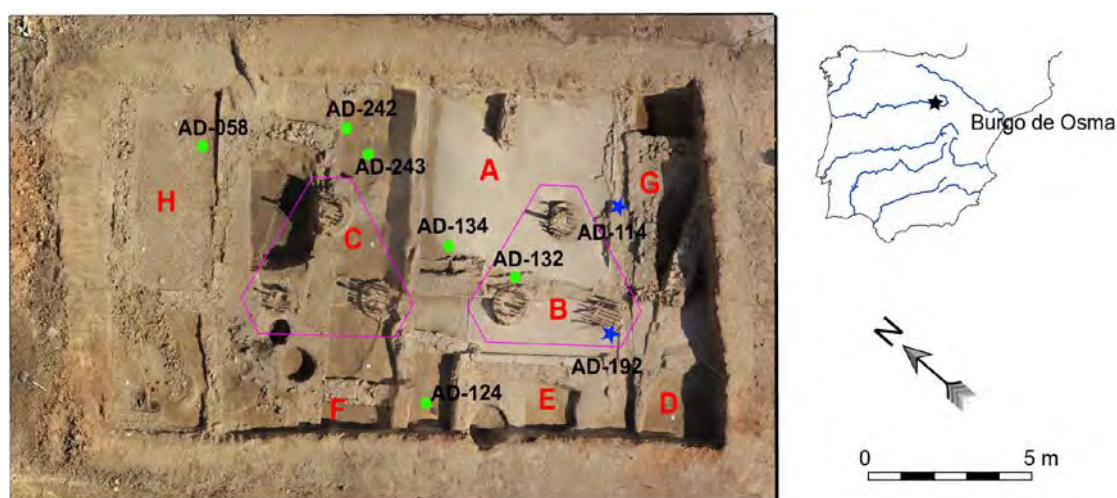


Figure 1. The excavation plan of Arroyo de la Dehesa de Velasco site (Burgo de Osma, Soria, Spain) with the location of the samples and labelled rooms. The green circles correspond to wall mortar samples and blue stars to floor mortar samples

The aim of this study is focused on the characterization of the wall of floor mortars of the main rooms of the site of Arroyo de la Dehesa de Velasco, by means of the analysis of the mineralogy and texture of the mortar-based materials. This investigation provides new data on raw materials composition and the construction techniques.

Materials and methods

Materials

Eight mortars were sampled from the structural supports of floor and walls of the different rooms of the Arroyo de la Dehesa de Velasco archaeological site. The description of the samples is indicated in Table 1 and its location is shown in Figure 1. Two mortars from floor structures and six mortars from walls are sampled. The layers that compose the mortars are labelled from the outermost layer (layer 0, L0) to the innermost layer (L5).

Methods

The mortars were studied in situ (structural support, mortar types, pictorial surface and pictorial techniques) and after the cleaning, the samples were cut to observe macroscopic features of the layers profile by a stereomicroscope at the laboratory. The petrographic analysis was carried out on thin sections using a polarised light microscopy with a Nikon Eclipse LV100pol equipped with a DSF-11 digital camera and DSL-2 control unit. Seventeen thin sections were obtained to determine its mineralogy and texture.

The mineralogical composition of the binder fraction was evaluated. The binder was separated by a settling extraction procedure described by [18]. The mortar sample was crumbled up manually and disaggregated in pH=8 water by means of an ultrasonic bath and the suspended fraction is extracted from the topmost dissolution to obtain the coarse fraction of the binder (<20 microns). The mineralogy of the extracted fraction was performed by X-ray diffraction (XRD) analysis in a powder sample using a Philips X'Pert diffractometer (Malvern PANalytical, Almelo, The Netherlands) equipped with a monochromatic Cu- α 1 X-radiation obtained at 40 kV and 20 mA. The data collection on the powder sample was performed by a continuous scan in the range 5 to 70 °2 θ at an acquisition rate of 0.02° per second [20]. The interpretation of diffraction patterns and semi-quantitative calculation were performed with X'Pert HighScore Plus 3.0 software (Malvern PANalytical, Almelo, The Netherlands).

Results and discussion

Macroscopic observations

The macroscopic stratigraphy and the characteristics of the floor and wall mortars are resumed in Table 1. Studied floor mortars are extremely different in mineralogical terms and structure. The sample AD-192 exhibits a complete support structure with visible three layers. An outermost thin lime layer and the other two layers thickness were become thicker towards the soil substrate. Below in the innermost layer, only moulds of hand-size pebbles were observed. The mortar AD-114 exhibit a unique brownish layer (see Table 1).

Table 1. Stratigraphy and macroscopic features of the sampled mortars from different rooms

Sample	Room Type	Layers (L) Thickness (cm)	Colour	Photographs
AD114	A Floor	L1 (1.5)	Brownish	
AD192	B Floor	L0 (0.1) L1 (5.5) L2 (4-6) L3 ?	Whitish rose Greyish Whitish	
AD132	A Wall	L0 L1 (1.5) L2 (2)	Whitish Whitish yellow Whitish orange	
AD134	A Collapsed wall	L0 (0,2) L1 (2) L2 (2)	Whitish Whitish Whitish	
AD242	C Wall	L1 (4) L2 (2) L3 (2,5) L4 (2)	Whitish rose Reddish Whitish rose Brownish	

Table 1 (Continued). Stratigraphy and macroscopic features of the sampled mortars from different rooms

Sample	Room Type	Layers (L) Thickness (cm)	Colour	Photographs
AD243	C Collapsed wall	L0 (0.2) L1 (2) L2 (2.5)	Whitish orange Whitish orange Whitish orange	
AD124	E Wall	L0 (0.1) L1 (2) L2 (2-2.5) L3 (1-2) L4 (1-1.5) L5 (1) L6 (1)	Whitish Greyish Reddish Creamy Creamywhitish Whitish Brown	
AD058	H Wall	L0 (0.1) L1 (1.5) L2 (2.5)	Whitish Creamy greyish White reddish	

The macroscopic structure of the AD-192 mortar displays a complete structure of opus signinum type floors. The outermost very thin layer (<1 mm) is whitish-cream and corresponds to a lime nature layer. Immediately below, there is a greyish-whitish layer of 5.5 cm thick with oriented crushed limestone fragments in the upper part of the layer. Mortar is based on lime and aggregates in a proportion from 1:2. Limestone aggregates of angular shape and homogeneous size (1-2 cm) compose this layer. The innermost layer of 4 to 6 cm thick corresponds to a whitish mortar composed by rounded aggregates from riverine sands (1-3 cm). This inner layer exhibits binder-aggregate ratio of 2:1. Between these layers chips of wood have observed, probably used to increase the stability of layers but also could be remains of wooden rammers that used for compaction [19]. Below, a preparatory layer composed by large round pebbles up to 12 cm is observed.

However, the AD114 floor substrate displays one layer. This mortar corresponds to a brownish coloured external layer of 1 – 2.5cm thick composed by clay-sandy aggregates mixed with lime binder with lumps (1 - 3mm) and occasionally larger lumps are observed (7 mm).

Respects to wall mortars, two types are observed: (i) multilayer mortars with four or five layers and (ii) two-layers mortars (Table 1). Over these layers a thin layer (<1 mm) can be observed corresponding to the outermost layer sometimes with pictorial figures.

Multilayer construction technology is observed in samples AD-242 and AD-124 see Table 1. Sample AD124 displays six layers including the mural painting layer. The outermost layer L0 corresponds to a thin layer of < 1mm of whitish colour of lime well held to the next. The L1 layer correspond to a whitish in colour mortar of 2 cm thick composed by 2 - 5mm siliceous sandy aggregates with scarce fragments of tiles and lumps of lime. The L2 layer is a reddish layer of 2 – 2.5cm thick with large amount of tile fragments ranging from 1 to 5 mm in grain size providing the distinctive red colour. Occasionally siliceous aggregates of fine grain size are present. The L3 layer of whitish-creamy colour exhibits abundant and heterogeneous grain-size aggregates of siliceous nature. The thickness of the layer varies between 1 to 2cm thick. The L4 layer correspond to a whitish mortar of 2 cm thick exhibiting a larger binder/aggregates ratio than previous layers. The aggregate grain size is preferentially lower than <4 mm and lime lumps are frequent. The innermost L5 layer corresponds to a brownish clay mortar. The sample AD242 exhibit similar structures and features but the innermost layer couldn't be recovered. This sample shows a clayed brownish mortar joined laterally to the main layers.

The second group of wall-mortar or two-layer- mortars include the samples AD-058, AD-132, AD-134, AD-243 (Table 1). These samples have an external paint layer based on lime and is well adhered to next layer (L0).

The L1 and L2 layers are composed mainly by subrounded and rounded aggregates of silica and rock fragments (quartz and quartzites), minor amount of subangular limestone fragments and arenites (see Table 1). These mortars exhibit similar layer thickness sequences (1.5-2 cm) and composition (sandy siliceous, lime and lumps); although diminishing on thickness towards the exterior is observed. In some samples vegetable fibres, probably straw, are observed. The addition of straw is generally associated to the inner layers to give cohesion to a rendering [19]. Although, both layers show aggregates of similar nature, layers are distinguished according the grain size, the distribution of aggregates and the presence (L2) or absence (L1) of vegetable fibres. The presence of straw lead to larger porosity and more cohesive character to the L2 inner layer.

Polarized optical microscopy

Petrographic study of the two floor mortars shows different mineralogical composition (see Table 2) and texture (Figure 2). The multilayer floor mortar mineralogy corresponds to subangular-angular limestones fragments bearing layer and followed by a layer with very rounded siliceous aggregates in a lime matrix. A high proportion of aggregates for the outmost layer and higher proportion of binder for innermost layers are observed. Natural aggregates are recognized: different types of limestones (nodulous limestone, milialids

limestone, bioclastic mudstone, recrystallized limestone) and these aggregates generally do not exhibit reaction zones with the binder. The texture of the layer exhibits a discontinuous grain size distribution with the presence of larger grains together with a finer fraction. The innermost layer display centimetric very rounded quartz and quartzite aggregates, with high sphericity and some arenites, limestones. Vegetable fibres are observed and lime lumps are also common. They vary in size and generally do not observe reaction zones no retraction crack indicating a slow reaction of lime with water. The binder matrix is a micritic carbonate with scarce siliceous inclusions. The nature of the aggregates suggest that local raw material associated to fluvial sands of Duero River tributaries, tertiary sands and Cretaceous limestone used for the construction of these mortars [20].

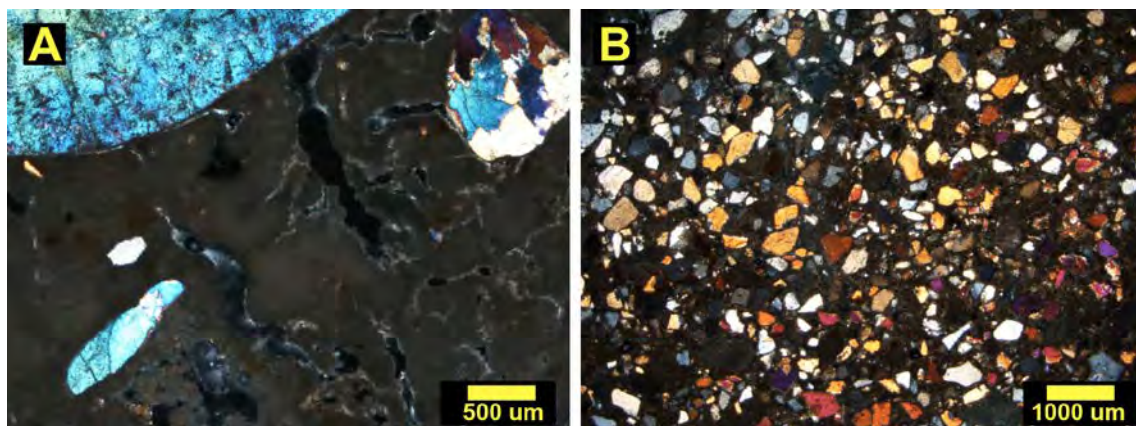


Figure 2. Petrographic observation of floor mortars (crossed polars). A) AD-192 mortar with scarce quartz inclusions in binder. B) Quartz aggregates and lumps in the AD-114 mortar

Instead, the sample AD-114 exhibits a clearly singular mineralogical composition with subangular quartz aggregates and binder. The aggregates of quartz show homogeneous grain size distribution about 0,25mm with a binder/aggregate ratio less than one. The study of the matrix reveals a clay component that coloured the mortar in brown. Lime lump with similar grain size that quartz aggregates are also observed, the lime nodules display micritic appearance. The binder mineralogy characterised by XRD indicate the occurrence of kaolinite with some illite and others phyllosilicates.

Petrographic study wall mortars shows similarity in the aggregate mineralogical composition in all layers. The mortar L0, outermost layer shows a micrite- binder with angular aggregates of calcite. Sometimes sporadic lumps, quartz and recrystallized limestone fragment are also observed (Figure 3). The aggregate: binder ratio of the external layers is generally less than one and it was well held to the inner layer. This layer can be considered as a *marmolina* layer [21, 22].

The transition with the next layer is always continuous and strongly adhered. The inner layer is characterised by medium size to coarse sand-sized aggregates (<1 – 2 mm). The common aggregate nature is: quartz, quartzite, potassium feldspar, sandstone, fossiliferous limestone, bioclastic mudstone, recrystallized limestone and bivalve fossils of angular to sub-rounded shape. They generally show a bimodal grain size distribution and the larger

Sample	Layer (L)	Mean Aggregate size (mm)	Wentworth size class	Max. Aggr. size (mm)	Aggregates	Ceramic fragments	Sorting	Observation
AD114	L1	0.240	Medium sand	0.6	Clay, Cal, Qz	-	WS	Clay-sand
AD192	L1	9	Small pebbles	12	Qz, limst, foss, micr, limst	-	MS	Limestone, bio-mudstone
	L2	2	Medium pebbles	16	Qz, Qzt	-	PS	Fluvial Sand
AD132	L0	0.25	Fine sand	1	Micr, Cal, tile	-	PS	Size gradation from up to down good adherence of layers
	L1a	0.6	Coarse sand	3	Qz, Qzt, limst, L, foss	-	VPS	
	L2	0.8-1	Coarse sand	5	Qz, Qzt, fsp, limst, L, foss	-	MS	
AD134	L0	0.3	Fine sand	2	Micr, Cal, limst	-	VPS	Size gradation. Lumps larger and richer in L1 than in L2
	L1	0.6	Medium sand	3	Qz, Qzt, fsp, aren, Cal, limst	-	MS	
	L2	0.6	Small pebbles	4	Qz, Qzt, fsp, aren, Cal, limst	poor	MS	
AD242	L0	0.3	Fine sand	1.5	Micr, Cal,		VPS	Pozzolanic material occurrence, dust of tiles and tile fragments. Bad cohesion
	L1a	1	Fine sand	2	Qz, Cal		MS	
	L1b	0.6	Medium sand	1.5	Qz, Qzt, aren, limst, rlimst		PS	
	L2	1.2	Coarse sand	5	T, Qz,	rich	PS	
	L3	0.2	Fine-medium s		Qz, Qzt, Qz, Cal, T	poor	VP	
	L4	0.11	Very fine s	2	Clay, Qz, T, foss		MS	
	L0	0.3	Medium sand	1.5	Micr, Cal, Qz		VPS	
AD243	L1	0.4	Fine sand	2	Qz, fsp, Qzt, L		WS	Well compacted, homogeneous mortar
	L2	1	Medium-coarse	4	Qz, Qzt, Fsp, limst, L		PS	
	L0	0.3	Silt	1	Micr, Cal,		PS	
AD124	L1.1	0.3	Medium sand	2-3	Qz, Qzt, Cal, T p	powder	PS	Pozzolanic material occurrence tiles powder and fragments. Good cohesion and adherence
	L1.2	0.6	Coarse sand	2	T p, T, qz, qzt, limst	rich	MS	
	L2	0.6	Coarse sand	3	Qz, Qzt, Fsp, L, limst, cal		PS	
	L3	0.7	Coarse sand	3	Tiles, Qz, Qzt, L,	rich	MS	
	L4	1	v. coarse sand	5	Qz, Qzt, limst, Cal, L		VPS	
AD058	L5	0.4	Medium sand	5	Qzt, clay, qz, limst, T, L	very poor	PS	Very homogeneous in mineralogy. Larger lumps in L1 and horizontal porosity at inner layers
	L0	0.3	Medium sand	1	Micr, Cal, Qz		PS	
	L1	0.4	Medium sand	2.5	Qz, Qzt, Fsp, L		PS	
L2	0.7	Coarse sand	2.5	Qz, Qzt, Fsp, L, limst		MS		

Table 2. Petrographic characteristics of the thin section of mortars.

Abbreviations: Qz, quartz; Qtz, quartzite; Cal, calcite; foss, fossils; micr, micrite; limst, limestone; L, lumps; rlimst, recrystallized limestone; Fsp, potassium feldspar; aren, sandstone; T, tile; Tp, Tile powder. VPS, very poorly sorted; PS, poorly sorted; MS, moderately sorted; WS, well sorted; VPS, very poorly sorted.

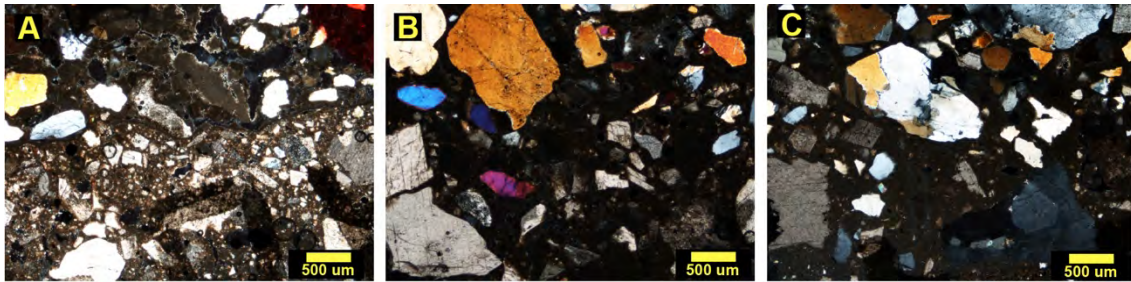


Figure 3. Petrographic observations (crossed polars) of marmolina layers. A) sample AD-124 with a:b > 1. B) sample AD-134 with a:b < 1. C) sample AD-243 a:b < 1

aggregates (Wentworth scale: coarse sands, granules and small pebble clast) tend to be sub-rounded, and the smaller aggregates, subangular.

The multilayer samples with more than four layers (AD-124 and AD-242 samples) are composed by siliceous nature aggregates (quartz and quartzites), the grain size corresponds to fine sand to coarse sand, with a low sphericity and subangular-subrounded aggregates prevail. The layers of the mortar display generally an alternating disposition of worse sorted to better sorted aggregate distribution (Figure 4). The binder matrix corresponds to a greyish micritic carbonate with small lumps. The lumps do not show any cracking. The reddish layer with ceramic fragments or crushes bricks (cocciopesto) display variable grain size from 1 to 5mm in a cryptocrystalline brownish matrix with very fine sand grainsize quartz. The addition of ceramic and ceramic powder reduces the permeability and increase the mechanical strength providing a hydraulic character to the mortar [19]. The aggregate binder ratio is generally about 1:1. The inner layers of the multilayer mortar have the similar matrix composition with larger grain size and rounder morphology. No voids or detachments are observed between layers contacts so they exhibit a strong adhesion. The innermost clay-sand mortar would be the base layer which was joined to the stone.

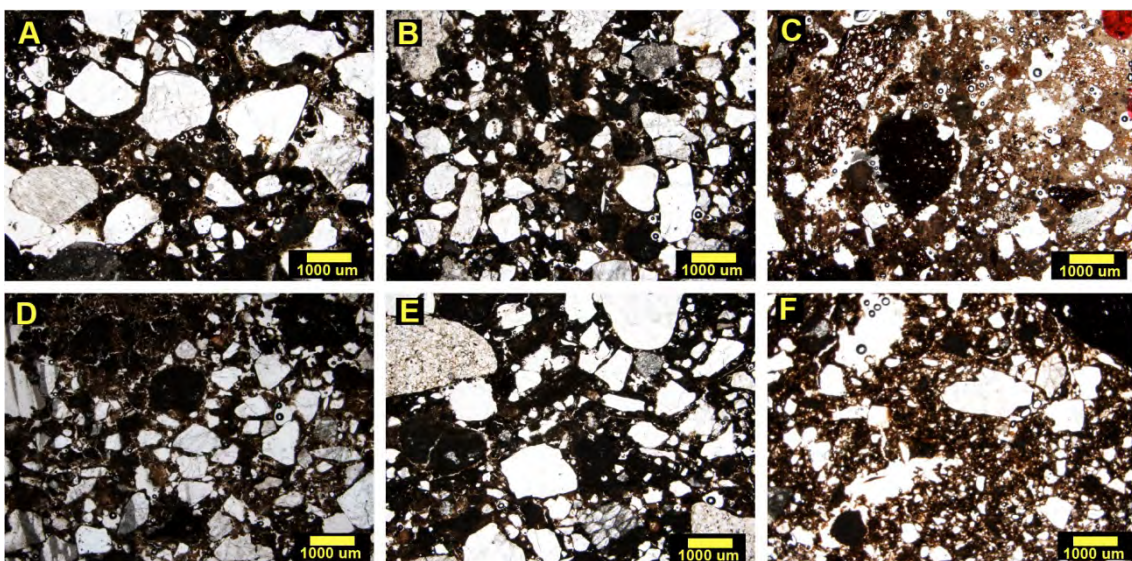


Figure 4. Petrographic observations (plain polars) of the multilayer wall mortar AD-124. A) Poorly sorted aggregates of the L1. B) Aggregated disposition of the L1.2. C) cocciopesto L2. D) Aggregates and lumps of L3. E) Poorly sorted aggregates of the L4. F) Clayed layer L5

Concerning to two-layers wall mortars exhibit the same aggregate siliceous mineralogy as multilayers mortars but do not exhibit bricks fragment layer (*cocciopesto* layer) (Figure 5). The layers are distinguished based on aggregate grain size and sorting. Generally, we clearly distinguish two layers below the outermost L0 layer. The quartz and quartzite represent the most prevailing aggregate type of the mortars. Both layers are distinguished by the grain size and the sorting of the aggregates. Medium sand to coarse sand size with a low sphericity and subangular-sub-rounded aggregates prevail and the aggregate size is smaller than previously described multilayer mortars.

The larger grain size sub-rounded aggregates are prevalent in the inner layers. AD-058 and AD-132 mortars were nowadays bad adhered to the underlying layer because meteorization processes induced by the larger porosity. Pieces of straw or sticks were added to the matrix of the lower layers increasing the cohesion among the components of the mortars. Besides larger quartz aggregates can be observed in the contact zone of the layers, increasing the roughness of both layers limit. Both additions increase the contact area between both layers promoting the adherence [19, 23]. The occurrence of wide range of grain size aggregates (poorly sorted) need minor quantity of binder in the mortar mixture and the shrinking phenomena are reduced [24].

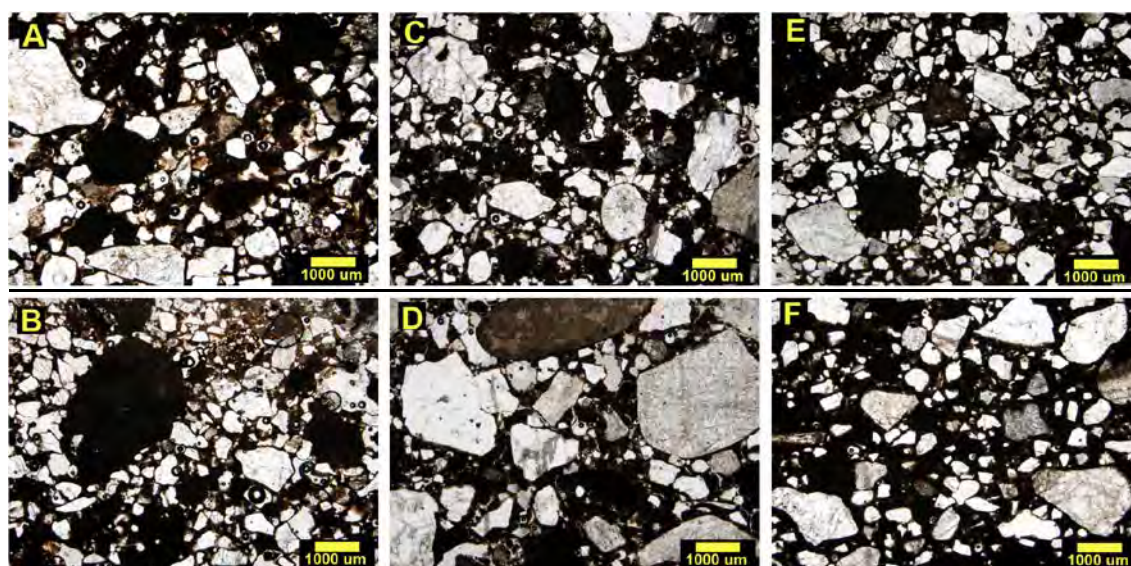


Figure 5. Petrographic observations (plain polars) of the two layer wall mortars. A) L1 layer of the AD-058 mortar. B) L2 layer of the AD-058 mortar. C) L1 layer of the AD-132 sample. D) L2 layer of the AD-132 sample. E) L1 layer of the mortar AD-134. F) L2 layer of the mortar AD-134

X-Ray Diffraction (XRD)

Mineralogical composition data of the samples is shown in the Table 3. XRD data indicates that calcite, quartz, phyllosilicates and illite compose mainly the binder fraction. Most of the samples display the kaolinite occurrence, moreover, only some layers of the multilayer mortars exhibit kaolinite mineral (see Table 3).

Kaolinite phase have been described in Oligocene age sediments where the site is geologically located [25]. The kaolinite presence in the binder fraction can suggest the usage of Oligocene sediments composed by a mix of sands and clays to make the mortars, or the kaolinite can come from the alteration of feldspar aggregates or can be intentionally added by craftsman. Nevertheless feldspars aggregates do not display alteration features to clay minerals and besides, no feldspar is noticed in XRD mineralogy. Kaolinite improves the hydraulic properties and durability, and in fact, nowadays a kaolinite quarry is located near the site, but the kaolinite is not the dominant mineral in binder XRD mineralogy. The most reasonable option would be the alternating usage of Oligocene age kaolinite bearing sands and Quaternary age riverside sands. The use of different age sands for the constructions of layers could explain the XRD data of the multilayer.

Table 3. Mineralogical composition of the binder (<20 micron fraction) in order of decreasing relative abundance

Sample	Room	Type	Layers (L)	Mineralogy
AD114	A	Floor	L1	Cal, Qz, Illt, Kln
AD192	B	Floor	L1	Cal, Qz
			L2	Cal, Qz
AD132	A	Wall	L1	Cal, Qz
AD134	A	Collapsed wall		Cal, Kln, Qz
AD242	C	Wall	L1	Cal, Qz
			L2	Cal, Kln, Illt, Qz
			L3	Cal, Kln, Illt, Qz
AD243	C	Collapsed wall	L2	Cal, Qz
AD124	E	Wall	L0	Cal, Kln, Illt, Qz
			L1	Cal, Illt, Qz
			L2	Cal, Illt, Kln, Qz
			L3	Cal, Illt, Kln, Qz
			L4	Cal, Qz
AD058	H	Wall	L5	Cal, Illt, Kln, Qz
			L2	Cal, Kln, Illt, Qz

Abbreviations: Qz-quartz, Cal-calcite, Kln-kaolinite, Illt- illite

Concerning to raw materials source, mortars were manufactured from locally available materials of similar mineralogical and lithological characteristics. The Oligocene and Quaternary age sands of the site surrounding exhibit a great variability. In fact, rounded fluvial siliceous sands from Abi3n River can be consistent with the used aggregates as well as with the previously described kaolinite bearing sands. The analysis of Oligocene and Palaeocene materials located near the site is complex because the monotony of detrital facies, the scarcity of fossil record and the lack of continuity of outcrops of many lithologic unities. Different types of limestone fragments are also used as aggregate, and are consistent with the surrounding Cretaceous lithologies, probably the raw material of the lime. Bioclastic limestone fragments with miliolids are highly compatible with the Hortizuelas and Hontoria del Pinar limestone formation [20].

Conclusions

The wall and floor structures of Arroyo de la Dehesa de Velasco site are good enough to maintain the decorative elements of their walls and floor. The floor and wall mortar data highlight the traditional constructive techniques following ancient recipes. The multilayer supports are an important clue on the durability of the wall structures of the site.

The floor structure corresponds to a *signinum* type floor structure constructed on three layers with a lime external layer. The wall mortars display two types of structures. Some of them are multilayers of four or five substrate layers and the other type displays two layers mortars. Among the floor mortars, AD-114 sample is made of a mixture of clay, lime and aggregate. This last mortar does not follow ancient technological approaches. Multilayer mortars have been constructed for valuable zone or important buildings.

Wall mortars and floor mortar display a thin *marmolina* layer. Multilayers mortars of more than four layers display a crushed tiles layer (a *cocciopesto* layer) can be distinguished in the intermediate mortar layer. The *cocciopesto* layer increase the resistance to humidity. The remaining two layers wall mortars exhibit features of the most common *opus arenatum* in overall Roman constructions. In this building, the craftsmen followed classical architecture rules for wall and floor mortars.

The mortars for the construction of the Arroyo de la Dehesa de Velasco building were manufactured from locally available raw material sources of similar mineralogical and lithological characteristics.

References

1. Furlan V, Bissegger P (1975) Les mortiers anciens, Histoire et essais d'analyse scientifique. Rev Suiss d'art et archaéol 32:2-14
2. Martinet G, Deloye FX, Golvin JC (1992) Caractérisation des mortiers pharaoniques du temple d'Amon à Karnak. Bull Liasons Lab Ponts et Chaussées 181:39-45
3. Middendorf B, Knöfel D (1998) Characterization of historic mortars from buildings in Germany and Netherlands. In: Baer NS, Fitz S, Livinstong R (ed), Conservation of historic brick structures, Donhead Publ. Ltd
4. Vitruvius Pollio M (1826) The Architecture, translated by Gwilt J, Priestly and Weale, London
5. Pliny (1857) The Natural History, translated by Bostock J and Riley HT, Bohm HG, London
6. Stefanidou M, Papayianni I (2005) The role of aggregates on the structure and properties of lime mortars. Cem and Concr Res 27:914-919

7. Leone G, De Vita A, Magnani A et al (2017) Thermal and petrographic characterization of Herculaneum Wall Plasters. *Archaeom* 59:747-761
8. Puertas F, Blanco-Varela MT, Palomo A, et al (1994) Decay of Roman and repair mortars in mosaics from Italica, Spain. *Sci. Total Environ.* 153:123-131
9. Pachta V, Stefanidou M (2018) Technology of multilayer mortars applied in ancient floor mosaic substrates. *J Archaeol Sci Rep* 20:683-691
10. Ontiveros Ortega E, Rodriguez Gutierrez O, Navarro Martinez AD (2016) Mineralogical and physicalchemical characterisation of Roman mortars used for monumental substructures on the Hill of San Antonio, in the Roman city of Itálica (prov. Baetica, Santiponce, Seville, Spain). *J Archaeol Sci Rep* 7: 205-223
11. Neville AM (1995) *Properties of concrete*. Longman, Harlow
12. Mehta PK (1986) *Concrete, structure, properties and materials*. Prentice-Hall, NJ
13. García Merino C (1995) Uxama I. Campañas de 1976 y 1978. La casa de la Cantera, la casa del Sectile y del Tambor. *Excav. Arqueol. España*, Madrid
14. García Merino C (1999) Urbanización y ordenación del territorio en Uxama Argaela. Mesa redonda. *Emergência e desenvolvimento das cidades romanas no norte da Península Ibérica*, Porto
15. García Merino C (1975) Población y poblamiento en Hispania romana. *El Conventus Cluniensis. Estud Roman I*
16. García Merino C (2000) Las raíces históricas de la sede episcopal oxoniense. Aproximación a la etapa tardo-antigua de Uxama. *Primera semana de Estudios históricos de la Diócesis de Osma (Soria)*. Univ Alfonso VIII, Diput Soria, Soria
17. Dohijo E (2011a) Evolución y transformación urbana de las ciudades del Alto Valle del Duero durante la Antigüedad Tardía. *Espacios urbanos en el occidente mediterráneo (S. VI-VIII)*
18. Ortega LA, Zuluaga MC, Alonso-Olazabal A et al (2012) Historic lime-mortar 14C dating of Santa María la Real (Zarautz, northern Spain): extraction of suitable grain size for reliable 14C dating. *Radiocarbon* 54:23-36
19. Stefanidou M, Papayianni I, Pachta V (2012) Evaluation of inclusions in mortars of different historical periods from Greek monuments, *Archaeom* 54:737-751
20. Ruíz Fernández de la Lopa V, Valverde Hernández, M (1991) Memoria Mapa Geológico 1:50.000 n. 377 Burgo de Osma. IGME
21. Elsen J (2006) Microscopy of historic mortars: a review. *Cem Concr Res* 36:1416-1424

22. Piovesan R, Siddall R, Mazzoli C et al (2011) The temple of Venus (Pompeii): a study of the pigments and painting techniques. *J Archaeol Sci* 38:2633-2643
23. Stolz CM, Masuero AB, Pagnussat DT et al (2016) Influence of substrate texture on the tensile and shear strength of rendering mortars. *Constr Build Mater* 128:298-307
24. Nogueira R, Ferreira Pinto AP, Gomes A (2018) Design and behavior of traditional lime-based plasters and renders. Review and critical appraisal of strengths and weaknesses. *Cem and Concr* 89:192-204
25. Valverde Hernández, M (1991) Memoria Mapa Geológico 1:50.000 n. 378 Quintana Redonda. IGME

Provenance study of raw materials used for lime making at Prague Castle during medieval times

Petr Kozlovcev¹, Jan Válek¹, Olga Skružná¹

(1) Institute of Theoretical and Applied Mechanics of the Czech Academy of Sciences, Prosecká 809/76, 190 00 Praha 9-Prosek, Czech Republic, kozlovcev@itam.cas.cz, valek@itam.cas.cz, skruzna@itam.cas.cz

Abstract

A number of historic mortars sampled from archaeological finds at Prague Castle area were compared in order to study the provenance of raw materials used for lime production in the Middle Ages. These mortar samples contained a considerable amount of lime particles that could have been related to the original raw material. It was possible to identify some of these particles as relicts of several limestone members from the Prague surroundings.

Historic mortar samples were processed by several analytical techniques. Polarized light microscopy (PLM) and scanning electron microscopy with energy dispersive spectrometer (SEM-EDS) were used to determine petrographic characteristic and mineralogical composition of the present particles. It was possible to analyse these particles in more detail by SEM-EDS and to semi-quantitatively characterise their chemical composition. Based on these results, it was possible to compare collected limestone samples from historic localities and currently active quarries near Prague.

The fragments of limestone material in the studied historic mortars originated mostly from the Prague Basin, Palaeozoic geological unit located close Prague agglomeration. This sedimentary basin composed various types of limestone, most of them of an industrial and constructional importance. The most represented limestone particles were possible to classify as Příklad, Radotín, Slivenec, Dvorce-Prokop and Zlíchov limestone. Moreover, the degree of hydraulic properties of historic binders was comparable with the selected limestone members from the Prague Basin (e.g. Dvorce-Prokop or Zlíchov limestone).

Introduction

During the archaeological excavations at Prague Castle, that have been under way for a hundred years, a number of mortar samples from various building elements have been collected and stored in depositories. In this unique archaeological complex there is also a great variety of stone masonry, mortars, renders, floor layers, wooden constructions and ceramics preserved and still accessible as they have been kept permanently uncovered for further studies. The archaeological findings were covered up with a concrete slab that nowadays forms the 3rd courtyard of Prague castle in 1929. The environment of this site is monitored and a various specialised research is carried out in order to ensure its optimal conservation.

This research deals with the properties of mortars from Prague Castle and it especially focuses on analyses with regard to the raw material provenance of the binder used in the medieval times. The origin of raw materials can be related to the availability of minerals resources and geological structure in the particular area near Prague, which is considerably diverse. Close Barrandian Area, especially the central part of the basin – the Prague Basin (or Prague Synform), is a dominant source of limestone material. Presence of various lithostratigraphic limestone members (Upper Silurian-Middle Devonian) is typical for this area. The variation in mineralogical, chemical and physical characteristics of individual limestone members can help to identify and distinguish them from each other. The analytical study focused on the Middle Ages as other information sources (archival data) that typically help to identify the lime production raw materials do not exist or are very limited for this period. In this case, the analytical procedure can be the only possibility to link the binder (building) and the resource (locality) and thus also to contribute to the interpretation of building history of the past. This study was performed by using polarized light microscopy and scanning electron microscopy [1]. The results obtained from the historic mortar analysis were used for identification of used raw materials. Microscopic character of mortars from the Prague Castle complex was studied earlier by Zeman et al. [2]. However, this research focused on a petrographic character of mortars but not on analyses of limestone fragments and their provenance.

Summary of the development of the Prague Castle complex

According to the archaeological evidence, the area of Prague Castle was first inhabited during the Neolithic period. The first written references are associated with the reign time of the Premyslid family and building of the Church of Our Lady – one of the first stone and lime construction built in 870 AD [3]. The building activities of Prague Castle and the whole Prague area were further developed during the pre-Romanesque and Romanesque periods and culminated in the middle of the 14th century under the rule of the Czech King and Emperor of the Holy Roman Empire, Charles IV [4]. These latter construction works were already in Gothic building style. The improvement of the Prague Castle area continued under the rule of the Jagiellons in the 15th century [5]. Next major rebuilding of the castle was carried out by Empress Maria Theresa in the second half of the 18th century [4]. After the World War I, the castle became the seat of the first president of the Czechoslovak Republic. The architectural adaptation of New Royal Palace and the gardens to this new use was carefully carried out by the Slovenian architect Jože Plečnik [6]. In this period also the main St Vitus Cathedral was finally completed. Further renovations continued under Plečnik's successor Pavel Janák in 1936 [4].

Archaeological research at Prague Castle

The area of Prague Castle has been an object of archaeological research since the 19th century [5]. These works were also connected with the completion of St. Vitus Cathedral and the repair of St. George Church [6]. So far the most extensive systematic research was

realized in the years 1925 to 1929 during the rebuilding works and the adaptation of Prague Castle as the seat of the first president of the Czechoslovak Republic. The first real idea of the oldest appearance of Prague Castle was based on these archaeological works [5]. After 1945 several construction works were carried out in the area of the castle during which the archaeological research continued. The Church of Our Lady was discovered by archaeological excavations in the years 1950 to 1951 [3]. Archaeological studies are still ongoing today.

Sampling sites

The mortar samples were collected during archaeological excavations in the Prague Castle complex. Several mortar samples were obtained from the Church of Our Lady. Additional mortar samples were obtained from the area under the current St. George square, which were archaeologically dated to the 10th century. A relatively large set of mortars was sampled in the area under the 3rd courtyard of Prague Castle from remains of the church referred to as St. Bartolomeo. Samples were also collected from various buildings of Old Priory house that is dated to the 11th or 12th century. Some mortar samples were obtained from the floor of St. Vitus rotunda (10th century) and the Romanesque curtain wall from the mid-12th century.

The studied samples are listed in Table 1. The sampling sites of the Church of Our Lady (A) and the Church of St. Bartolomeo (B) are shown in Figure 1.

Table 1. The list of studied mortars sampled in the Prague Castle complex.

Sampling site	Sample identification	Approximate datation	Short description of the sampled material
Church of Our Lady	PM 1-20	9 th and 11 th century	Fragments of mortar from foundations and masonry mortar, tomb plaster
Building fragments from St. George square	PH 1-11	10 th century	Daub mortar from a wattle (woven lattice of wooden rods) structure
Buildings of Old Priory house	PHA 1-27	11 th or 12 th century	Masonry mortar, fireplace, floor layers
Rotunda of St. Vitus	MPHBP1	10 th century	Mortar from floor layer
Church of St. Bartholomeo	PH 17-34	11-12 th century	Bedding mortar, foundation masonry mortar

Methodology

The first approach of the provenance research was based on a search and subsequent analysis of unburnt or partially burnt limestone fragments in the mortars. Based on their petrographic and mineralogical characteristics, it was possible to classify them and compare them with the potential limestone sources. This study was primarily performed by polarized

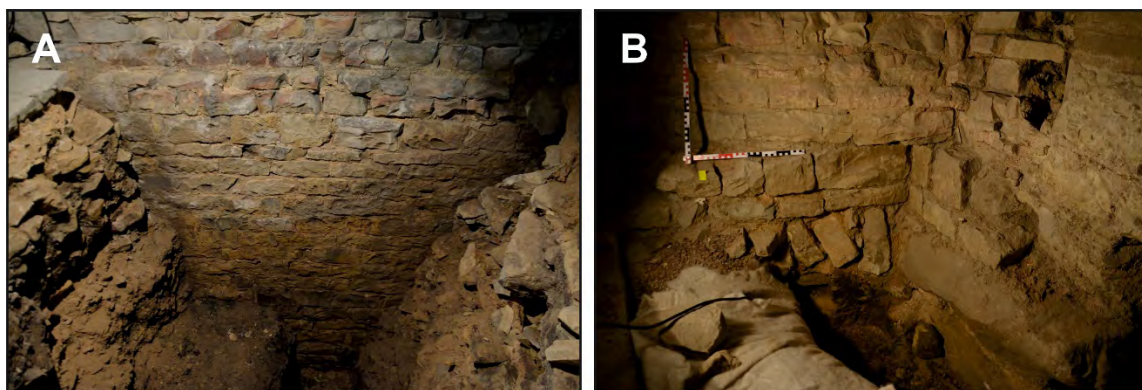


Figure 1. The exterior apse wall of the eastern part of the Church of Our Lady (A) and the interior south wall of the Church of St. Bartholomeo (B). Prague Castle, 2018.

light microscopy (PLM) and supplemented by scanning electron microscopy with energy dispersive spectrometer (SEM-EDS).

The second approach was based on micro-chemical analysis of fine-grained calcitic binder (mortar matrix) by SEM-EDS. According to the results of chemical composition, the cementation index (CI) was calculated [7]. It was used to describe the hydraulic properties of the studied binders. Based on CI it was possible to compare the obtained results with the chemical analyses and hydraulic properties of available limestone raw materials from the Prague Basin.

The mortars were cut with a saw and impregnated under vacuum with an epoxy resin. Polished thin-sections app. 35 μm thick were produced from them. They were studied using a polarising light microscope (PLM) Olympus BX53M equipped with a digital camera Olympus DP27. The samples were observed in a plain polarised light (PPL) and a crossed polarised light (CPL). Scanning electron microscopy (SEM-EDS) was performed by using Tescan MIRA II LMU, with an energy-dispersive analytical system (Bruker AXS) on the carbon coated thin-sections.

Mineralogical and petrographic characteristics of the partially burnt and unburnt limestone particles were described according the Folk [8] and Dunham [9] classifications. Both systems subdivide limestones primarily on the basis of matrix content.

Cementation index (CI) is influenced by the presence of oxides (SiO_2 , Al_2O_3 , Fe_2O_3) and their proportion to the carbonates (CaO and MgO). According to this index, binders can be classified as non-hydraulic, feebly hydraulic, moderately hydraulic, eminently hydraulic and natural cements, as presented in Table 2.

Table 2. Classification systems of hydraulic properties according cementation index (CI).

Hydraulic character	Cementation index (CI)
Feebly hydraulic	0.3–0.5
Moderately hydraulic	0.5–0.7
Eminently hydraulic	0.7–1.1
Natural cement	>1.1

Geology of the Prague area

The bedrock of the Prague area is characterized by a diversity of geological structures. Exploration of limestone and production of raw materials for lime is historically concentrated in the Prague Basin (Prague Synform). It is the most important geological unit situated southwest from the centre of Prague (Figure 2). It is a rift-like depression [10] filled with Lower Palaeozoic unmetamorphosed marine deposits [11].

The lithology of the Prague Basin is characterised by the presence various sediments. Siliciclastic members were typical for the Ordovician period, deposition of shales was dominant in the Lower Silurian and sedimentation of various limestone types was common in the Lower/Middle Devonian eras (Table 3) [12].

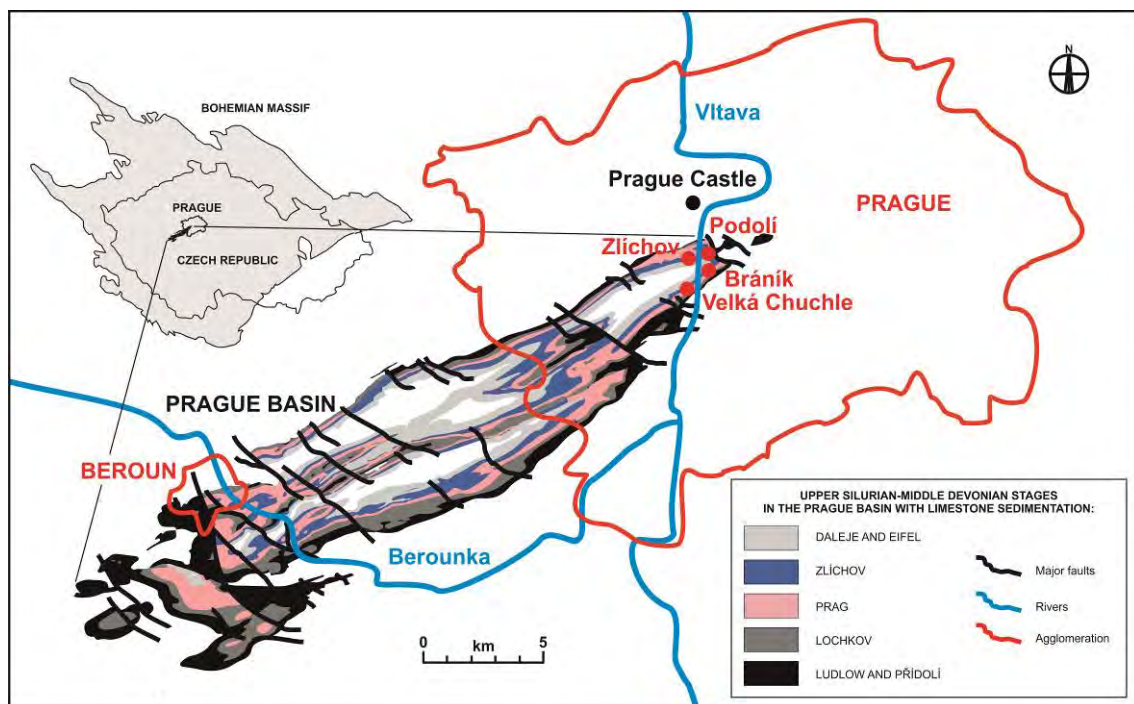


Figure 2. Geological scheme of the Palaeozoic sedimentary formations in the Prague Basin.

Besides Prague Basin, other geological units are located in Prague surroundings. The biggest is the Czech Cretaceous Basin in the north. This geological structure is filled with Late Cretaceous sediments - siliciclastic siltstones and sandstones are the most common [14]. This stone material was not used for lime production but as a common building stone [15]. The younger tertiary and quaternary sediments reaching Prague surroundings do not have any significant limestone layers usable for lime production.

Due to the geological diversity of this area, there is a number of lower Palaeozoic limestone types with a variable mineralogical and chemical composition. Their geographical distribution also considerably varies within the Prague Basin. The intensity of mining and subsequent processing of these natural resources has differed throughout the past.

Unfortunately, there is insufficient evidence about the specific positions of historic quarries of these raw materials. Occasionally, we know locations defined as local names which correspond to the later quarries, which were however much larger and probably replaced the mediaeval explorations. Because there is a lack of written records from the Middle Ages, it is possible to derive used limestone raw materials only from material analysis of mortars from relevant historic monuments and the geological structure of the Prague area.

Table 3. Simplified stratigraphical record of the Prague Basin (Upper Silurian-Middle Devonian) with most important limestone types (classification according Folk [8] and Dunham [9]).

Era	Stage	Limestone type	Basic limestone characteristics
MIDDLE DEVONIAN	EIFEL	Choteč lm.	Fine-grained packstone and wackstone, with layers of clayed shales [12, 13].
LOWER DEVONIAN	DALEJ	Suchomasty lm.	Bioclastic material accumulations in shallow parts of the basin [10, 13].
		Třebotov lm.	Pelagic fine-grained limestones (nodular mudstone and wackstone [9, 12].
	ZLÍCHOV	Zlíčov lm.	Uniform gray-coloured limestones (mudstones or wackstones [12, 13].
	PRAG	Dvorce-Prokop lm.	Deep-water basinal facies of micritic limestones (mudstones or wackstones [10].
		Loděnice lm.	Mottled (gray and red) limestones with layers of shales [8, 13].
		Řeporyje lm.	Red-colored and fine-grained limestone types [8, 12].
		Slivenec lm.	Crystalline and calcite-rich limestones [12].
		Koněprusy lm.	Shallow reef calcite-rich limestone types, grainstones and boundstones [9, 13].
	LOCHKOV	Radotín lm.	Dark-coloured micritic limestones deposited in deep parts of the basin [12].
		Kosoř lm.	
Kotýs lm.		Poor or relatively calcite-rich limestones with layers of shales [11].	
UPPER SILURIAN	PŘÍDOLÍ	Přídolí lm.	Various biomicritic and biodetritic limestones [8, 10].
	LUDLOW	Kopanina lm.	

Results

Basic character of the studied mortars

The studied samples had a heterogeneous character in the sense of their function in building as presented in Table 1. All the studied samples were prepared as two-component mortars comprising of aggregate and binder, no pozzolanic additives were found. However, some fragments of building stone, pieces of wood, charcoal, burnt ceramic particles as accessorial or minor components were presented.

Typically, there were fine-grained quartz grains corresponding to alluvial sandstone used as an aggregate. Some accessories such as feldspar, biotite, muscovite or rutile were also

presented. The aggregate was mostly half-shaped with small cracks. Clusters of inorganic material were also identified. They were composed of a mixture of siliceous dust and silicate isotropic matrix. They probably originated during the binder processing. Relicts of ceramics (bricks), dust and Al-rich components were also detected. Unburnt or partially burnt fragments of limestone raw material were the most important mortar components for the provenance study. Besides the limestone material, fragments of other rocks such as opuka stone have been identified.

The binder was a calcium-rich material with an admixture of other non-carbonate components. Depending on the content of these oxides (SiO_2 , Al_2O_3 , Fe_2O_3), the binder was assumed to achieve a certain degree of hydraulicity that was expressed by the cementation index (CI). This is based on a presumption that the hydraulic oxides originated from the raw material (limestone) and reacted with CaO and MgO during the calcination to form various mineral phases. This presumption idealised and it is valid only for certain types of limestone burnt under optimal conditions.

Specific components were binder related particles [1]. Most of these particles existed in the form of lime lumps (imperfectly processed well burnt lime binder) but other binder-derived particles were discovered. The most relevant for the provenance studies were the partially burnt (underburnt) and unburnt fragments.

Analysis and identification of limestone fragments

The determination of the provenance was based on a detail petrographic and structural analysis using PLM and SEM-EDS of the limestone fragments present in mortars. In addition to the classical structural properties of rocks, the determination of the bioclastic material has proven to be very important. This material was formed mostly of microscopic relicts and bioclastic fragments. Depending on the characteristics of these particles it was possible to determine the stratigraphic position corresponding to the limestone fragments. The characteristics of individually studied limestone fragments are presented in Table 4.

Samples of Slivenec lm. (Figure 3A) were characterised by specific crystalline structure (Figure 3B). This structure is unique within the Prague Basin and thus allows for differentiation of this type from the other limestones.

For samples of Dvorce-Prokop lm., a fine grained micritic matrix with isolated sparitic zones was typical (Figure 4A and B). This limestone type is usually rich in bioclastic material and shales relicts. Characteristic is especially presence tentaculite shales (*Styliolina* sp.), which were identified in limestone fragments in studied mortar sample PHA 3b-s (Figure 4A) and also in comparative limestone material from the historic quarry in Prague-Bráník (Figure 4B).

For fragments of Zlíčov lm., presence of sparitic veins filed in calcite material, which occurs in several generations, was typical (Figure 5A and B). This limestone type was also characteristic by a low presence of bioclasts and large zones of sparitic cements.

Table 4. The list of samples containing underburnt and unburnt rock fragments and their determined characteristics along with the assumed stratigraphic positions of these rocks types.

Sample	Material character	Characteristics of raw materials present in mortar sample	Typical characteristics of specific rock type	Stratigraphy (Stage or Formation)	Limestone (Lm.) or rock type
PHA 6	Masonry mortar	Fine-grained micritic limestone (mudstone). Gray or dark gray color, occasional presence of bioclasts (ostracoda).	Fine-grained micritic matrix (dark grey color) with bitumenous content and ostracoda relicts.	Přídolí stage (Upper Silurian) or Lochkov stage (Lower Devonian)	Přídolí lm. or Kotýs lm.
PH 1SL	Masonry mortar	Fine-grained micritic limestone (mudstone). Presence of organic material (dark color) and cherts (SiO ₂), relicts of (ostracoda and radiolaria).	Fine-grained micritic matrix with typical dark coloured organic pellets, often cherts and bioclasts relicts.	Lochkov stage (Lower Devonian)	Radotín lm. or Kosoř lm.
PH 6	Underburnt limestone found within bedding mortar				
PAH 3b-m	Masonry mortar	Sedimentary limestone with a crystalline structure (the result of recrystallization). Presence of crinoidea.	Cristalline structure and presence of transformed relicts of crinoidea shells.	Prag stage (Lower Devonian)	Slivenec lm.
MPHBP1	Floor mortar				
PM 5	Foundation mortar				
PHA 3b-s	Masonry mortar	Fine-grained micritic limestone (mudstone or wackestone). Dark gray or green color, often bioclast relicts (tentaculites <i>Styliolina</i> sp., ostracoda, bivalva or brachiopoda).	Micritic matrix with typical grey or green colour, presence of characteristic tentacullite shells (<i>Styliolina</i> sp. and <i>Nowakia</i> sp.)	Prag stage (Lower Devonian)	Dvorce-Prokop lm.
PM 15					
PM 17					
PH 5	Partially burnt limestone found within bedding mortar	Fine or moderately-grained limestone (sparitic wackestone). Light grey color and often calcitic veins.	Light grey sparitic matrix, presence of calcitic veins (often several generation).	Zlíčov stage (Lower Devonian)	Zlíčov lm.

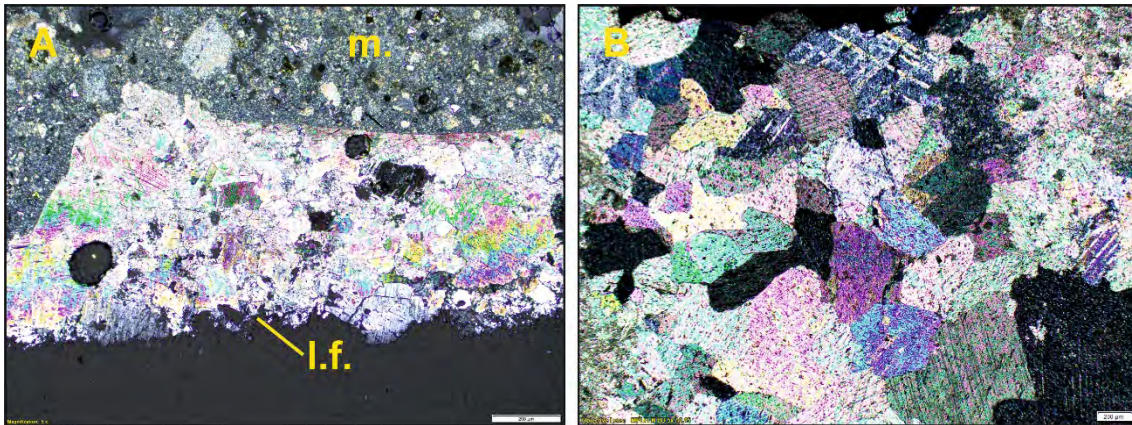


Figure 3. A. Microscopic character of the Slivenec lm. fragment (l.f.) found in the MPHBP1 sample with a fine grained mortar matrix (m.). B. Microscopic structure of the Slivenec lm. from the Radotín-Špička quarry. Both in CPL.

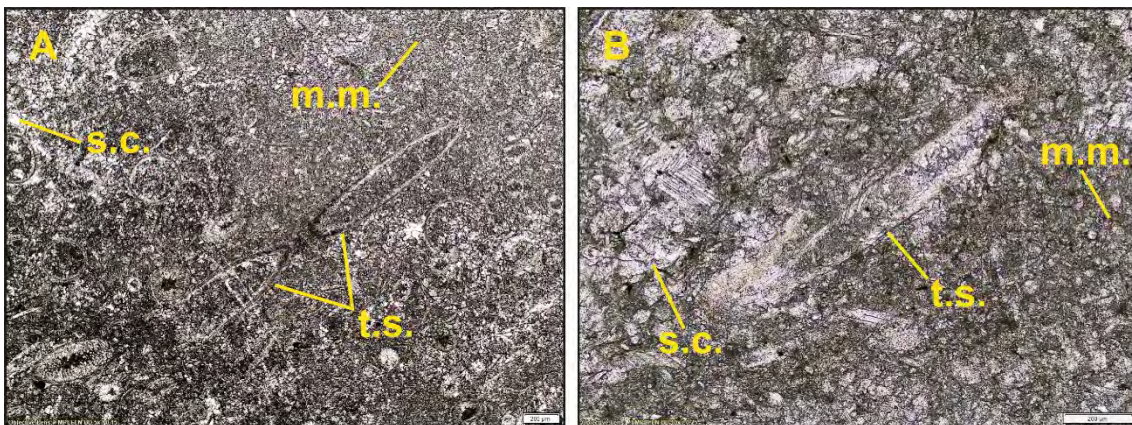


Figure 4. A. Microscopic character of the Dvorce-Prokop lm. fragment found in the sample PHA 3b-s. B. Example of microscopic structure of the Dvorce-Prokop lm. from the historic quarry in Prague-Bráník with marked micritic matrix (m.m.), sparitic cement (s.c.) and tentaculite shales (*Styliolina* sp.) (t.s.). Both in PPL.

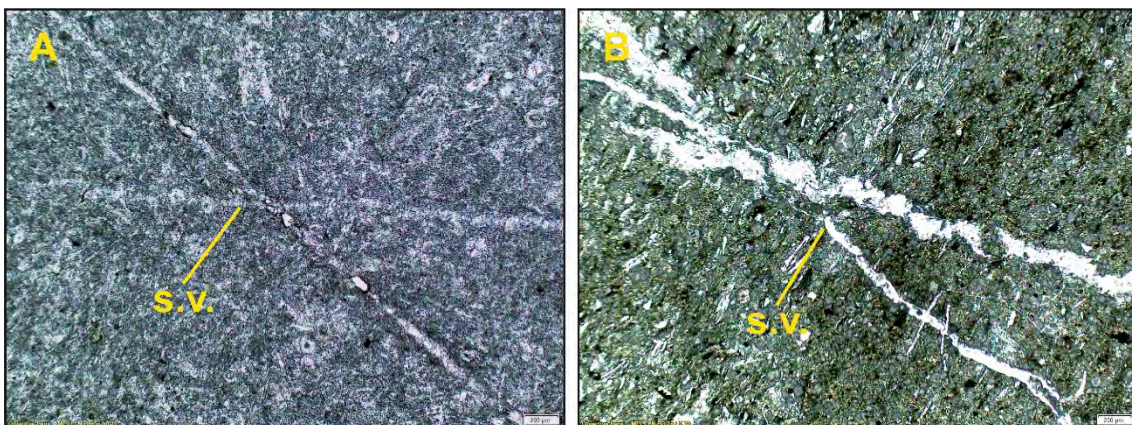


Figure 5. A. Microscopic character of the Zlíčov lm. fragment found in the sample PH 5. B with marked sparitic veins (s.v.). Example of microscopic structure of the Zlíčov lm. from the historic quarry in the Prokop Valley in Prague. Both in PPL.

Hydraulic properties of studied mortar samples

Determination of hydraulic properties was based on the chemical composition of the fine-grained calcitic binder (matrix) present in mortar samples quantified by SEM-EDS (micro-chemical analyses), see Figure 6 and Table 5. The resulting hydraulic properties were derived from the chemical composition and classified by CI. The usefulness of the chemical composition characteristics for the determination of provenance of raw materials is commented further in the discussion chapter.

Discussion

The studied samples differ in chemical composition and properties of their binding matrix. According to the cementation index (CI), a wide range of hydraulic properties (from non-hydraulic to eminent hydraulic) was determined.

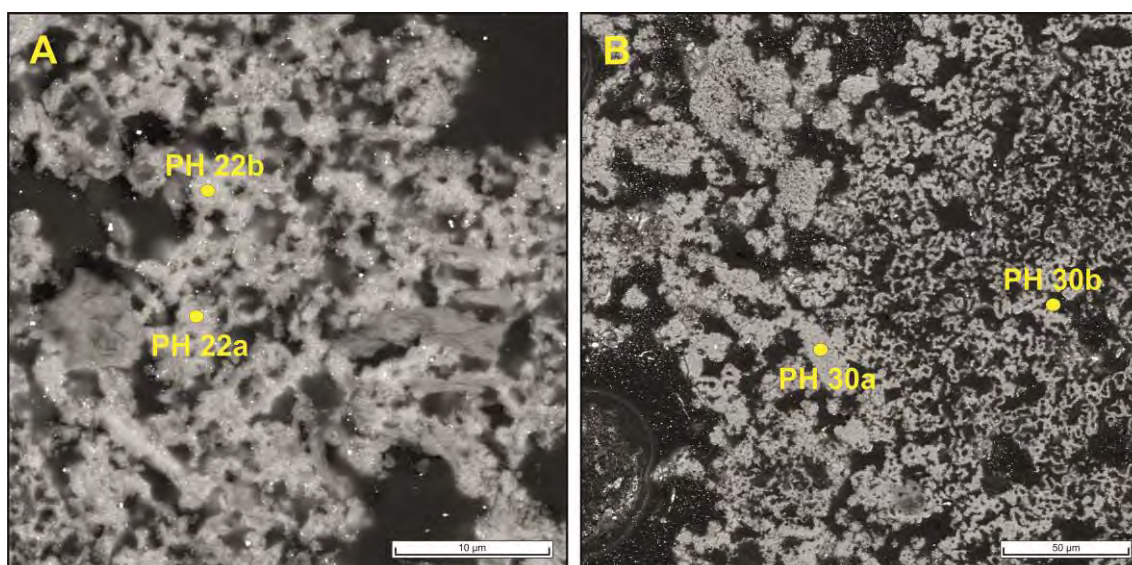


Figure 6. Character of the fine-grained mortar matrix observed in SEM with BSE detector (samples PH 22 – A and PH 30 – B), with marked positions of the micro-chemical analyses.

This comparison showed Choteč, Třebotov and especially Silivenec limestone as potentially relevant sources of non-hydraulic or feebly hydraulic binders. Use of Koněprusy and Loděnice limestone, that would also fit these categories based on their chemistry is less probable due to their location in the central part of the Prague Basin.

Historical exploitation of Kotýs, Kosoř, Radotín, Řeporyje and especially Dvorce-Prokop and Zlíchov limestone can be also expected with a great probability, eventually also Kopanina and Přídolí limestone. These limestone types correspond to the characteristics identified by the analysis - chemical composition and a relevant degree of hydraulicity. Moreover, they occur in the northwest part of the Prague Basin which is conveniently close to Prague Castle.

Table 5. Selected micro-chemical analyses of the mortars from Prague castle complex performed by SEM-EDS (proportional wt.-%) and their classification based on the cementation index CI: A – air lime (0–0.3), F – feebly hydraulic lime (0.3–0.5), M – moderately hydraulic lime (0.5–0.7), E – eminently hydraulic lime (0.7–1.1).

Sample	CaO	SiO ₂	Al ₂ O ₃	MgO	Na ₂ O	K ₂ O	SO ₃	FeO	CI	Hydraulicity
PM 4a	77.33	13.23	7.22	0.28		1.93			0.58	M
PM 4b	86.43	6.36	3.69	0.24	0.28	1.74			0.25	F
PM 4c	87.79	6.63	3.47	0.17	0.06	1.65			0.25	F
PHA 4a	82.66	12.21	2.95	0.74		0.39			0.45	F
PHA 4b	73.53	16.39	5.02	1.29	0.11	0.62	0.17	2.3	0.70	E
MPHBP1a	72.62	16.64	6.71	0.66	0.62	1.65	0.33		0.73	E
MPHBP1c	88.27	7.76	2.77	0.36	0.19	0.65			0.28	F
MPHBP1b	83.59	10.66	3.39	0.27		1.31			0.40	F
PH 22a	86.99	8.75	2.25	0.82		0.29	0.53	0.38	0.31	F
PH 22b	91.33	5.08	2.04	0.87			0.67		0.18	A
PH 30a	98.65	1.01	0.10	0.24					0.03	A
PH 30b	97.89	1.22	0.34	0.46					0.04	A

For the comparison between hydraulic properties of the studied samples and the raw materials from the Prague surroundings the analytical data were taken from unpublished exploratory reports, which were summarized in literature [16] (Table 6).

However, it is necessary to evaluate hydraulic properties of the studied mortars and raw materials according CI cautiously. It is not possible to determine the provenance of material used for lime production merely on the basis of its hydraulic properties due to a considerable variability of the local limestone (Table 6). Achieved hydraulicity can be used primarily as supplementary data for further analyses (e.g. based on petrography). Moreover, CI can be used for an identification of the technological provenience.

In a relatively significant number of samples, a mixture of binder related particles with a considerably different chemical composition was identified. This can be explained by a natural variation of the quarried limestone strata or by mixing of different limestone sources. The latter point seems to be more probable considering that some of the hydraulic binder related particles were underburnt but the surrounding matrix consisted of low amount of hydraulic oxides, i.e. could be classified as air lime. Therefore, it was not uncommon to produce mortar from a mixture of limes made of limestones of different local origin. The analysis did not distinguish if this was an intentional use or at which part of the procedure this intermixing occurred. It could have been during the stone collection before or

after the burning phase. The latter would suggest a certain empirical understanding and perhaps even an intentional use.

Table 6: Hydraulic properties (derived from CI and CaCO₃ content) of selected limestone types from the Prague Basin [16].

Limestone type	Studied localities	Range of CaCO ₃ (% wt.)	Range of CI (-)	Range of hydraulicity	The most common hydraulicity
Choteč	3	89.9–96.4	0–0.3	A–F	A
Třebotov	5	62.3–96.1	0.1–1.7	A–E	F
Zlíchov	7	55.4–83.6	0.6–1.0	M–E	M
Dvorce-Prokop Lm.	8	77.6–92.7	0.3–1.2	F–E	M
Řeporyje	8	77.0–90.3	0.3–0.6	F–M	M
Loděnice	6	77.2–92.7	0.1–0.4	A–F	F
Slivenec	8	84.6–95.9	0–0.4	A–F	A
Koněprusy	10	87.5–98.5	0–0.2	A	A
Kotýs	6	77.3–90.5	0.3–0.5	F–M	M
Kosoř	3	74.1–89.6	0.3–0.4	F–M	M
Radotín	4	69.6–83.6	0.3–1.2	F–E	M
Přídolí	5	47.7–72.9	0.9–3.8	M–E	E
Kopanina	4	34.4–76.6	1.1–5.5	M–E	E

Explanatory: hydraulic properties according CI: A – air lime (0–0.3), F – feebly hydraulic lime (0.3–0.5), M – moderately hydraulic lime (0.5–0.7), E – eminently hydraulic lime (0.7–1.1).

During the Middle Ages, the Vltava River was the main transport route for building materials. Limestone was transported downstream to the central part of Prague, where it was further processed in local kilns [17]. Depending on the location of the mentioned rock types in the Prague Basin the assumed origin of the limestone fragments found in the studied samples can be verified with a certain probability based on accessibility. Lower Palaeozoic limestone members are common on both banks of the Vltava River (in today's Prague districts Braník, Podolí, Zlíchov and Malá Chuchle). In this areas, significant rock formations of Upper Silurian (Kopanina and Přídolí limestone) and Lower Devonian (Kotýs, Kosoř, Radotín, Dvorce-Prokop, Zlíchov, Třebotov and Choteč limestone) exist and have been uncovered. Moreover, quarrying in Braník district in accumulation of Dvorce-Prokop limestone is mentioned in historical literature [18].

The fragments of limestone with crystalline structure (samples MPHBP1 and PH3b-m) also probably come from the Prague Basin. The reason is the presence of bioclasts relicts (crinoids) in sample PH 3b-m, which are typical for Slivenec limestone. It can be mentioned, that transport of raw materials from other potential sources of crystalline limestone would

be more difficult and therefore it also seems less probable and for lime production unnecessary.

The fragments of opuka stone cannot be considered as a material suitable for lime production because of their chemical composition and low CaCO₃ content.

Conclusion

Based on the microscopic studies of the mortars from the Prague Castle complex petrographic characteristics, mineralogical and chemical composition of present underburnt and unburnt limestone fragments and lime-based matrix were determined.

Some of the limestone fragments probably belong to the Upper Silurian Přídolí limestone and/or Lower Devonian Kotýs, Radotín or Kosoř, Slivenec, Dvorce-Prokop and Zlíchov limestone. A wide range of hydraulic properties (from non-hydraulic to eminent hydraulic) was determined based on the cementation index. The mixture of various binders can be explained by the use of different kinds of raw materials at the same time. The hydraulic properties of the historic binders was comparable with the potential hydraulicity of the local limestones including Choteč, Třebotov or Slivenec limestone (non-hydraulic), Kotýs, Kosoř, Radotín, Řeporyje, Dvorce-Prokop and Zlíchov limestone (feebly or moderate hydraulic) and Kopanina and Přídolí limestone (eminently hydraulic).

Due to the lack of written records from the Middle Ages and poor evidence of local raw materials used at Prague Castle, there was necessary to analyse historic mortar samples and to compare determined limestone fragments with currently available raw materials. However, the entire process was difficult due to the absence of the original lime kilns and the complete extraction of the historic quarries that had been quarried over the centuries.

The chemical composition and cementation index alone are not sufficient provenance markers in the case of the Prague Basin due to its complexity. However, they case serve as indicators of the use of various raw materials and are highly relevant additional parameters to the provenance study. The great geological variability of Prague surroundings and occurrence of many lithostratigraphic members (with different composition and properties) provides a further research challenges for future.

Acknowledgement

The research was carried out with the support of the Czech Ministry of Culture as a contribution to a project DG16P02H012 – Lime materials for restoration and conservation of authentic elements of historic structures.

References

1. Elsen J (2006) Microscopy of historic mortars – a review. *Cement and Concrete Research* 36, 1416-1424.
2. Zeman A, Válek J, Frolík J, Langrová A, Růžičková E (2008) Petrographical and mineralogical characterisation of mortars in our Lady Church from Prague Castle, 1st Historical Mortar Conference, Lisbon, Portugal.
3. Borkovský I (1953) Kostel Panny Marie na Pražském hradě, PA XLIV, 129–200
4. Berglund BR (2017) *Castle and Cathedral in Modern Prague*. Central European University Press, Budapest.
5. Frolík J, Maříková-Kubková J, Růžičková E, Zeman A (2000) *Nejstarší sakrální architektura Pražského hradu*. Peres, Praha
6. Frolík J, Smetámka Z (1997) *Archeologie na Pražském hradě*. Paseka, Praha.
7. Eckel E (2005) *Cements, limes and plasters. A facsimile of the 3rd ed.*, Donhead Publishing, Dorset
8. Folk RL (1959) Practical petrographic classification of limestones. *AAPG Bulletin* 43(1): 1–38.
9. Dunham RJ (1962) Classification of carbonate rocks according to depositional textures. *Mem. Am. Assoc. Pet. Geol.* 1: 108–121.
10. Havlíček V (1981) Development of a linear sedimentary depression exemplified by the Prague Basin (Ordovician – Middle Devonian, Barrandian, Central Bohemia). *Sb. Geol. Věd, G 35*: 7–48
11. Chlupáč I, Havlíček V, Kříž J, Kukul Z, Štorch P (1998) *Palaeozoic of the Barrandian (Cambrian to Devonian)*. Czech Geological Survey, Prague
12. Chlupáč I, Kukul Z (1988) Possible global events and the stratigraphy of the Palaeozoic of the Barrandian (Cambrian-Middle Devonian, Czechoslovakia). *Sb. Geol. Věd, 43*: 83–146
13. Kříž J (1999) *Geologické památky Prahy*. Český geologický ústav, Praha
14. Malkovský M (1975) Paleogeography of the Miocene of the Bohemian Massif. *Věst. ÚÚG, 50*: 27–31
15. Příklad R, Příkladová J, Racek M, Weishauptová Z, Kreislová K (2017) Decay mechanism of indoor porous opuka stone: a case study from the main altar located in the St. Vitus Cathedral, Prague. *Environmental Earth Sciences* 76.

16. Kozlovcev P, Příklad R (2013) Re-evaluation of Lower Paleozoic limestones from the Prague Basin (Barrandian area, Czech Republic) as a raw material for production of natural hydraulic lime and/or natural cement. 12th SGA Biennial Meeting, Uppsala, Sweden.
17. Holec F (1961) Branické vápencové lomy. Časopis Společnosti přátel starožitností, 69: 204–212
18. Zeno F (1770) Beschreibung des bei Prag von dem Wissehrader Tore gelegenen Kalksteinbruches, mit seinen Seeeversteinerungenun anderen Fossilien. Neue physikalische Belustigungen 2: 362–420.

Interpretation of scientific data derived from analytical techniques used in the characterization of Roman mortars

Duygu Ergenç¹, Rafael Fort¹, Nevin Aly², Olivier Henry³, Sayed Hemed⁴

(1) Institute of Geosciences (CSIC-UCM), Spain, duyguerg@ucm.es; rafael.fort@csic.es

(2) Suez University, Faculty of Petroleum and Mining Engineering, Science and Mathematical Engineering Department, Egypt, Nevin.Aly@suezuniv.edu.eg

(3) Ecole Normale Supérieure, AOROC, France, olivierhenry@gmail.com

(4) Cairo University, Faculty of Archaeology, Archaeological Conservation Department, Egypt, sayed.hemeda@cu.edu.eg

Abstract

Mortars made by lime and pozzolans were a standout amongst the most critical contribution of Romans to the architectural history. Roman lime mortars have been exceptionally renowned for their quality and durability which generally relied upon the resources utilized in Roman domains. A comprehensive examination of this past technology leads us to better conservation practice and more sustainable construction.

To have a broader perspective this research was carried out in different Roman provinces. This paper aims at presenting the characteristics of Roman mortars from three archaeological sites in Spain (Mérida), Egypt (Alexandria) and Turkey (Labraunda). Characterization was carried out through polarized optical microscopy (POM), X-ray diffraction (XRD), thermal analysis and differential scanning calorimetry (TGA-DSC), scanning electron microscopy coupled with energy-dispersive X-ray spectroscopy (SEM-EDS), X-ray fluorescence (XRF), Fourier Transform Infrared spectroscopy (FT-IR).

The central focus of the study is to understand the usefulness of the analytical methods which give clue about the construction technology, selection of raw materials according to the function and conservation state of mortars. We will also discuss to what extent we can find answers concerning aggregates, natural and inorganic additives and their effect on shrinkage, the manufacture of lime, the effects of environmental conditions and the interaction between adjacent building materials.

Introduction

The characterization of materials provides a basis to compare current and future conservation states. It is important to determine the most suitable intervention technique and materials for the restoration of archaeological and historic sites. Defining intervention procedures includes rigorously documenting the original materials and identifying decay mechanisms and factors [1]. In addition to stone and brick, which are common in historic constructions, historic mortars are crucial for evaluating the structural performance of

masonry. For proper restoration and conservation efforts, it is necessary to have detailed information about the masonry's components, composition, and behaviour under weathering conditions.

Roman concrete edifices that are still standing today are impressive for their durability. In accordance with today's sustainable construction goals, their durability can improve our knowledge of construction techniques and materials. Roman mortars have been characterized chemically, physically and mineralogically, which help us to understand the provenance, technological changes, and chronology of the building at archaeological sites as well as prepare mortars for restoration [2-6]. Archaeological conservation projects bring together experts from different areas such as archaeology, conservation, geology, chemistry, architecture, and history. Every discipline has its own approach and it is essential they recognize other areas' contributions to archaeological heritage. It is important to know which techniques are effective yet affordable.

Various analytical methods have been used for mortar characterization [7]; however, not all produced equally-reliable results that can be applied to restoration efforts, for instance using acid to separate binder and aggregate [8,9] and subsequent sieve analysis to obtain the granulometry of the aggregates [10]. This technique has unreliable results if the mortar has carbonic or derived rocks. Because the reaction products are acid soluble [11], this is a poor means of assessing the mortar's original ratio of binder, aggregate, and additive.

Whether characterizing mortars for archeometric research or conservation and restoration, the main interest is determining the nature of the binder (air lime, hydraulic lime, Portland cement) as well as the mineralogy, morphology, size, and porosity of the aggregate. The elements responsible for physical performance are the most informative about long-term durability. Previous research has shown that Roman builders preferred non-hydraulic lime binder [12,13] and hydraulicity was provided by adding highly reactive silica and alumina aggregates, which cause pozzolanic reactions that resulted in strong bonding [14,15]. Roman mason also started to use volcanic origin aggregates, ceramic fragments and dust as artificial pozzolanic material in a wider geographic area [16].

This study summarizes the characteristics of Roman mortar from three archaeological sites and highlights the usefulness of common characterization techniques.

Materials

Roman mortars were collected from constructions dated to the first and fourth centuries AD at three archaeological sites inform around the Mediterranean basin.

The Roman city Augusta Emerita (Figure 1a) was founded in 25 BC [17]. It has been a UNESCO World Heritage site since 1993. Geologically, it is located in the Central Iberian Zone (Spain), which includes clastic meta-sedimentary rocks and rarely, carbonate rocks. Igneous

rocks, both intrusive and extrusive, are present near the site [18]. Mortar samples were collected from aqueduct San Lazaro, snow well, Amphitheatre, Temple of Diana and others.

The site of Labraunda (Figure 1b) is located in southwestern Turkey, in the ancient region of Caria, some 16 km northwest of the ancient city of Mylasa (modern Milas) [19]. The site became particularly famous in the Late Classical period for housing the sanctuary of Zeus Labraundos, the tutelary divinity of the Hekatomnid Dynasts/Satraps. This sacred place was established on the southern slope of the Latmos range, known for its unique augen micaschist gneiss formation, surrounded by phyllite, metaquartzite, metasandstone, marble and slate [20]. The site was occupied from the early Bronze Age to middle Byzantine times. Mortar samples were collected from buildings Andron A and C, Hypostile, East, South and Tetraconch Bath, pool (*Natatio*).

The site Kom El-Dikka (Alexandria, Egypt) (Figure 1c) has undergone large scale excavations since the 1950s. The site is an entire Roman city that dates from the second to the seventh century AD. The site is built mainly from limestone [21], calcarenite, and aeolianite rocks, in addition to bricks that were used to construct the third-century baths [22]. Mortar samples were taken from the buildings Sahareg and Alhaman, which are thought to have been constructed in the first or second century. Later interventions are possible, as in the auditorium [21].



Figure 1. Archaeological sites (a) Augusta Emerita (b) Labraunda (c) Kom El-Dikka

Analytical Methods

Thin sections were prepared in order to investigate the surface and core of the mortars. Polarised light optical microscopy (POM) was conducted on an Olympus BX51 petrographic microscope fitted with an Olympus DP12 digital camera.

Gold-coated mortar small mortar fragments were analysed with scanning electron microscopy together with energy dispersive X-Ray spectroscopy (SEM/EDS). The SEM JEOL JSM 6400 was fitted with an Oxford-Link Pentafet EDS analyser. The VP-SEM-EDS analyses were carried out using a Hitachi™ S3700N SEM coupled to a Bruker™ XFlash 5010 SDD EDS Detector®. The samples were analysed at an accelerating voltage of 20 kV and at low vacuum (40 Pa). The images were acquired in the backscattered mode.

Bruker D8 Advance X-ray diffractometer fitted with a copper anode tube and PC-ADP diffraction software. X-ray diffraction (XRD) patterns were acquired operating at 40 kV and 30 mA at 2θ angles of 2–68° with a 0.020-step scan, a speed of 2° per minute, CuKα radiation

and a graphite monochromator. The powder fraction (<63 µm) of the mortar samples were analysed.

Thermal analysis (TG-DSC) was performed with a TA Instruments SDT-Q600, DSC Q-200 and General V4.1C DuPont 2000 thermogravimetric analyser, respectively, in a nitrogen ambient at 10 °C/min heating rate. For the X-Ray Florescence (XRF) analyses, samples were ground and pressed into a wafer. The analyses were conducted with a PHILIPS Magix Pro (PW-2440) spectrometer with 4 kW X-Ray Generator. Micro Fourier transform infrared spectroscopy (µ-FTIR) Bruker ALPHA (with reflection, transmission, and ATR module) was used with ground samples.

Results and Discussion

Most samples were cream and light brown color binders with small aggregates. Samples from Augusta Emerita mortars had high cohesion. Mortars from Labraunda had less cohesion. Mortars from Kom El-Dikka were whitish to cream with medium consistency.

Traditional methods were used for mortar characterization, which are preferred for making qualitative identifications of mortar components [6, 23]. In samples from Augusta Emerita, there were rock fragments (diorite, metagranite, quartzite, slate and monzogranite). The minerals were mainly quartz and feldspar. Ceramic fragments, which were rarely used, were seen in mortar and the rims around the aggregate were diagnostic of pozzolanic reactions (Figure 2a) [24]. Microscopic observation of Labraunda mortars revealed highly angular augen gneiss, mica schist, and marble rock fragments embedded in the micrite size calcitic mass. Aggregate distribution was poor to medium. Mica sheets detached from schistic rock fragments were dispersed into the binder (Figure 2b). In the mortar sample from the wall in Alhaman wall at Kom El-Dikka, there was high dissolution and recrystallization in the matrix. The binder had a micro-cryptocrystalline appearance (<4 µm) with significant irregular porosity and fissures (> 15%). There were also organic and fossil fragments (Figure 2c). Unlike in Augusta Emerita mortars, ceramic fragments were abundant in Labraunda and Kom El-Dikka mortars. Unlike samples from other sites, Kom El-Dikka mortars had oolitic fossiliferous limestone fragments, which were added as aggregate or remained as uncalcinated fragments during fossiliferous limestone calcination. The edges of carbonate rocks were not well defined but well integrated because of dissolution and re-precipitation. Gradually increasing the temperature during carbonation partially burns the core. Lime lumps were common in Augusta Emerita mortars but rare in Labraunda mortars. Both were quicklimes with undefined edges which ended the process of lime cycle later on. This could be due to a lack of water during lime slaking and/or hot lime mixing.

Hydraulicity could not be precisely measured with petrography but it could be inferred based on the presence of reaction rims around the particles, revealing the outcome of reactions between amorphous silica, aluminosilicates, and alkaline binder [23, 25].

Interfacial transition zones (ITZs) around the ceramic aggregates (Figure 2a) and organic fragment (Figure 2c) were detected with POM.

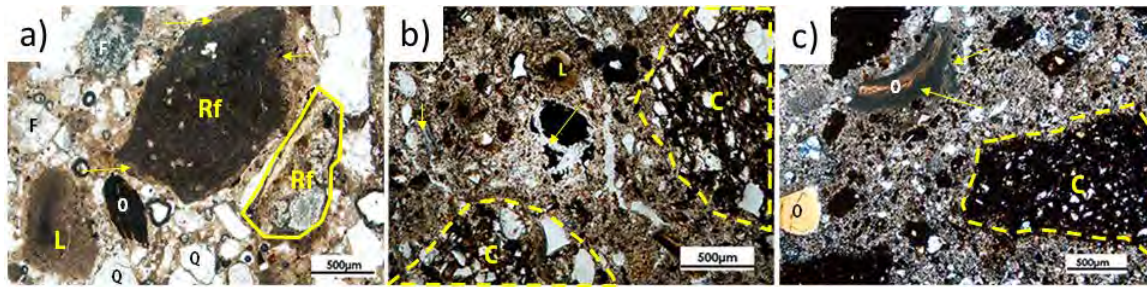


Figure 2. Thin section images of mortar samples from a) the Snow well in Augusta Emerita b) the *Natatio* at Labraunda c) the Alhaman in Kom El-Dikka

POM revealed samples' binder type, crystallinity state, granulometry, shape, mineralogy of aggregates and decay types [25]. Digital image analysis made it possible to identify binder to aggregate ratios and grain size distribution from representative thin sections. These ratios have usually been estimated from wet chemical analysis [26, 27]. Accurate result estimates strongly depend on the absence of carbonic aggregates, as in the Labraunda and Kom El-Dikka mortars. Soluble pozzolanic reaction products and organic additives are dispersed in the binder, which created confusion about the binder ratio in the Augusta Emerita and Labraunda mortars. There was still confusion about hydraulicity when the characterization was done only on the so-called binder.

In recent years, interest in SEM/EDS has been increased because it requires a small size of sample and provides valuable microstructural information [28]. In mortar characterization, SEM has been used to detect the C-S-H phases and carbonate crystals. Carbonate crystals in historic mortars have mostly appeared in nondescript shapes. It can be difficult to differentiate the crystals by shape due to the numerous dissolutions variable velocities of (re)carbonation processes, and different environmental conditions. These factors could lead to different polymorphs and/or morphologies [29].

Hence EDS, the chemical analysis, is necessary to provide an accurate morphological descriptions and identify the relationships of mortar constituents. The measurement method could use spots, areas or lines. However, elemental detection has not been highly reliable in polycrystalline materials such as mortars because adjacent or subjacent crystals can affect measurement. Analysis of some materials might require an additional step in sample preparation to allow for high-quality SEM data, which was often the case with mortar samples. Although the mortar was sufficiently oven-dried, due to its high porosity, it immediately grabbed humidity. This decreased focus sometimes made the SEM/EDS analysis difficult. Coating the material with graphite, gold and chrome inhibited the electrical conducting (charging) improved the signal coming from secondary electrons. This was required to acquire a high-quality image to use in evaluating morphology; however, it was misleading for quantification for EDS analysis [28].

Roman mortar is more common than mortar from other periods and larger samples are usually available. However, in cases such as wall paintings, only small samples are available so coating may not be practical. ESEM can be used to examine mortar samples without any covering. Generally crystals cannot be seen; however, in good conditions in samples without humidity crystals are clearly visible at higher magnifications. For example dispersed ceramic dust and mica crystals throughout the binder were seen under POM (Figure 2b). As seen in Figure 3b, the C-S-H gels and fibrous crystals, similar to those detected in nautical Roman concretes [30], were present due to pozzolanic reactions. ESEM-EDS analysis showed that the Labraunda mortar binder was composed of calcite, silicates, and magnesite (Figure 3b) and same was revealed at Augusta Emerita (Figure 3c). Nevertheless, one question is still unanswered: was the binder derived from pure calcitic limestone/marble or with dolomite inclusions? EDS analysis on lime lumps could give more accurate results [2]; however, no lumps could be detected in the samples. It was previously reported that EDS was only capable of detecting the presence of Ca in lime binder and Al and Si in crushed bricks but not in the ITZs between them [31]. In fact, similarities between the mechanisms of Roman mortar and rocks, which are the product of the tectonic uplifts, have been shown by microscopic analyses. These studies apply principles from geosciences to archaeological material [32].

In the beginning of the characterization of a material, the researcher mostly knows what to search for, based on knowledge of its appearance, location and function. The presence of portlandite plates (Figure 3a) indicates the incomplete re-carbonation. This is unexpected in a mortar sample from structures built during the Roman period. Is it possible for a binder to remain -un-carbonated after more than two millennia? The answer is affirmative, if the necessary conditions for carbonation (CO_2 , RH, T, pH, ion concentration, etc.) have not been created by one of the re-carbonation processes. Past interventions increased the dissolution of binder and the recrystallization process can be interrupted due to the high amount of gypsum, which was detected by other analyses.

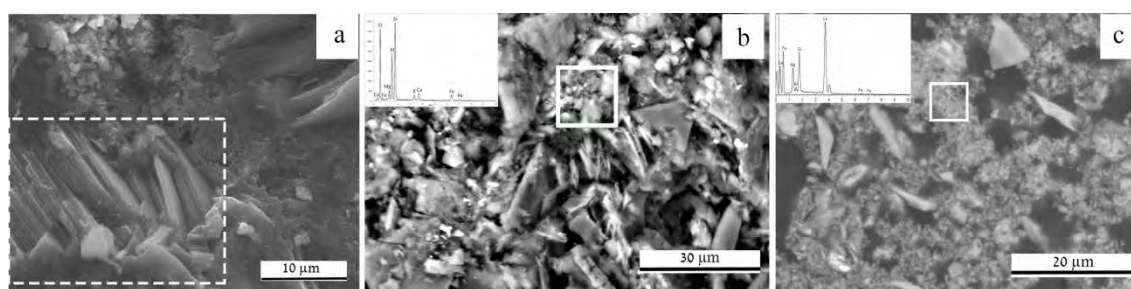


Figure 3. a) SEM image of mortar sample from the Alhama at Kom El-Dikka (portlandite plates are marked) and b) ESEM image of mortar sample from the *Natatio* at Labraunda ESEM image of mortar sample from Snow Well at Augusta Emerita (EDS are from the square from the binder)

Table 1. Examples of the main major elements of the samples

%	The Snow Well at Augusta Emerita	The Natatio at Labraunda	The Alhaman at Kom El-Dikka
SiO ₂	47.45	58.14	28.56
Al ₂ O ₃	6.64	17.68	5.57
Fe ₂ O ₃	4.17	5.24	3.84
MgO	5.49	2.34	-
CaO	15.75	4.65	31.84

XRF has been widely used in provenance studies because it identifies trace elements which are signatures of the rocks and minerals. In Roman mortars, XRF has been used to study chemical composition; aggregates [33], whole samples [34,35], lime lumps [36, 37] and the reaction between lime and ceramics [38].

XRD was used to detect mineral phases. In the mortars from Kom El-Dikka, gypsum peaks were detected (7.56, 4.28 Å). It was confirmed with POM examinations and SEM-EDS. The actinolite peak in XRD patterns of Augusta Emerita mortars agreed with the microscopic observations of a pale green/brown amphibole mineral from igneous and metamorphic rocks (e.g. granodiorite, metagranite). The presence of this mineral explained the higher MgO in the XRF analysis (Table 1). Besides, ESEM-EDS analysis on the binder supported (Figure 3c). In Labraunda mortars magnesite, which could have come from the ceramic dust, did not appear in XRD; however, its presence was shown with XRF and SEM/EDS. XRD did not detect it because it was less than 5% of the total sample. The complexity of the juxtaposition of several phases reduced the potential of XRD as the main distinctive tool for studying Roman mortars. One approach is to separate the binder and whole mortar from the aggregate before analysis, which clarifies the nature of the binder [26,39]. Nevertheless, in Roman mortars, which have high consistency, definite mechanical separation is not possible in most cases. XRD could analyze crystalline materials including binder phases, alteration products, C-S-H crystals and amorphous humps [40].

It has not been a straightforward task to understand the source of hydraulicity in Roman mortars. POM, XRD, XRF provide useful information, but the most useful method is thermogravimetric (TG) analysis. Weight losses in TG quantify carbonate and hydraulic phases [41, 42]. Two Labraunda mortar samples (Figure 4a, b) had similar D/TG profile even though one is from the first or second century AD and the other is a repair mortar from an older intervention in the Andron A building, dated to the Hellenistic period. A sample from the *Natatio* was collected after recent excavations. There was no previous intervention, the collected sample was original and according to other findings the building was from Roman times. As seen in Figure 4a, the sample lost its main weight below 200°C. A loss below 120°C indicates hygroscopic water, which could indicate porous aggregate (e.g. ceramic fragments). Additionally, clay minerals decomposed between 580–640°C; and CaCO₃ decomposition was unclear [43]. The sample from the Andron building which was thought to be a repair mortar from previous interventions, had a similar thermograph without

carbonate decomposition weight losses (Figure 4b). These results suggest the binder leaching. High pozzolan use in *Natatio* sample caused leaching of the binder; its solubility increased with ceramic dust and could not be recrystallized in high RH. In the second sample, attenuated alkali levels and degradation were caused by clinker. When the hydrated phases were lighter, the pore solution reached the equilibrium with the decalcification in [44]. Macroscopic observations of the samples provided other clues to complete the interpretation.

Figure 4c displays the mortar sample from the Snow Well at Augusta Emerita. Weight losses of 200- 400 °C were attributed to the inflaming of organic substance and at 600- 900 °C to decarboxylation [3,48,49,50]. The Kom El-Dikka sample (Figure 4d) showed weight losses associated with gypsum (120-200 °C) and Ca(OH)₂ lost its chemically bound water between 350 and 550 °C due to dehydroxylation. Weight losses between 200 and 600 °C were ascribed to the loss of chemically bound water of hydrated phases (CSAH and/or CSH) [45] which indicated the hydraulic nature of the mortar. Other compounds (e.g. organics, Ca(OH)₂, Mg(OH)₂ Mg₅(CO₃)₄(OH)₂·4H₂O, etc.) could have decomposed in the same temperature range [46,47]. Additional carbonate decomposed at lower temperatures due to the presence of salts. Weight loss after 800 °C was due to re-carbonation or carbonate aggregate. The results agree with those obtained by POM, XRD and SEM (Figure 2).

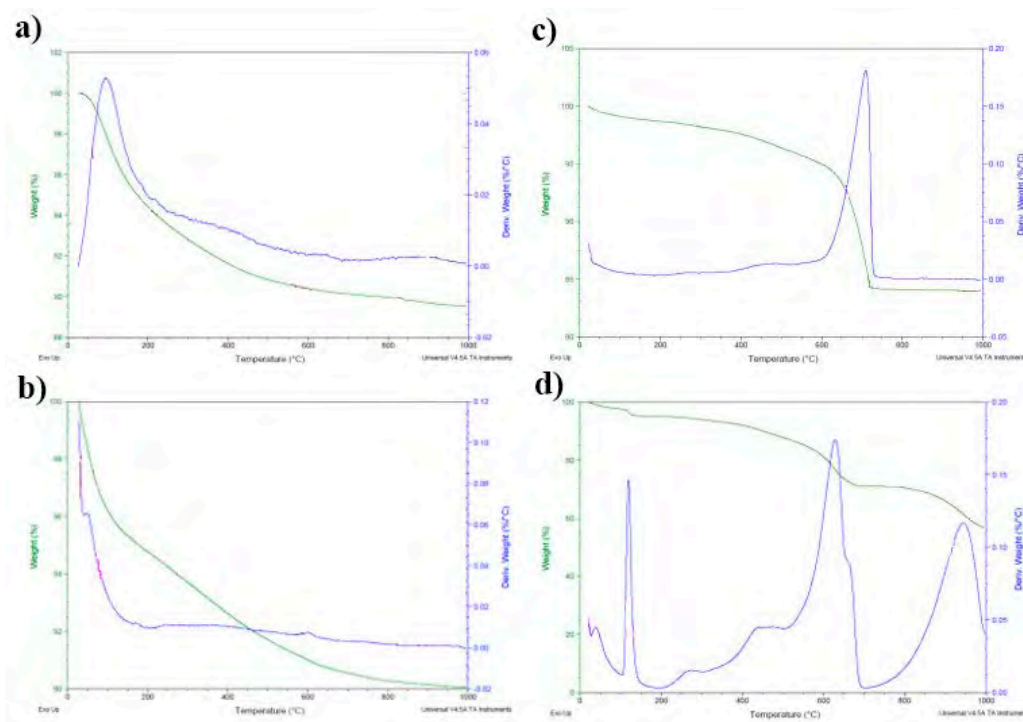


Figure 4. Thermographs of a) Labraunda mortar from the *Natatio*, b) repair mortar from the building Andron A c) Augusta Emerita mortar from the Snow Well d) Kom El-Dikka mortar from the Sahareg

FT-IR has been useful in detecting organic additives and previous chemical interventions [51]; however, the former was not detected by our measurements. Microbiological activity led to the enzymatic decomposition of the primary organic compounds in the samples,

which did not enable us to measure organics [52]. Clays from ceramic dust were recorded. As seen in Figure 5 the FTIR spectra have stretching OH bands (ν_1 and ν_3) of the H₂O molecules around $\sim 3380\text{ cm}^{-1}$ and $\sim 1003.05\text{ cm}^{-1}$ (Si–O–Al bending [51]), $\sim 1639.47\text{ cm}^{-1}$ (illite [53]) $\sim 670.50\text{ cm}^{-1}$ (quartz or montmorillonite), $\sim 421.54\text{ cm}^{-1}$ (Si–O bending), which could be attributed to silicate minerals from ceramic fragments (Figure 5a) and clinker (Figure 5b). The FT-IR spectrum of the Roman mortar was expected to have lime binder and it showed mainly the band vibrations of C–O stretching (874 and 1430 cm^{-1}), C–O bending (409 cm^{-1} , 712 cm^{-1} , 705 cm^{-1}). The Si–O–Si band peaked at 1032 cm^{-1} , and finally, the Al–O–H bands and $\nu_3\text{ SiO}_4^{4-}$ at 914 cm^{-1} and 938 cm^{-1} [51] silica sand grains SiO_2 at 1031 cm^{-1} (Si–O stretching) and 470 cm^{-1} (Si–O bending). For the quantitative IR study, polymorph type, orientation, and particle size were the main factors. The first two were negligible for the analysis of inorganic constituents and the third could be reduced by well grinding [54].

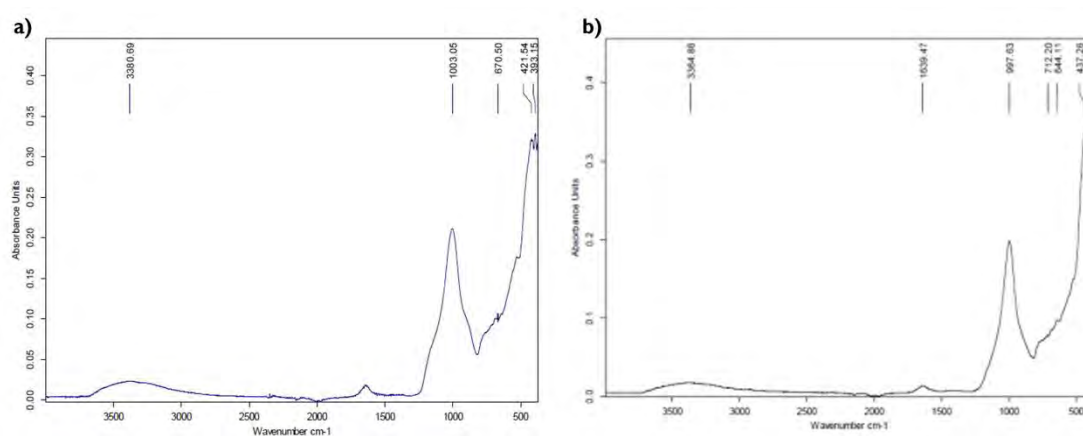


Figure 5. FTIR spectra of Labraunda mortars from a) *Natatio* b) the Andron building

Conclusions

This article has discussed the efficiency of widely-used analytical techniques and presented examples of Roman mortar samples from same period collected at the sites Augusta Emerita, Labraunda and Kom El-Dikka. Although the samples had a similar macroscopic appearance, there were clear differences in microstructure. The pore and crystal network of Roman mortar undergo many dissolution-recrystallization cycles due to weathering agents before and after burial. In addition, it is often difficult to understand the source of the alteration. Any previous intervention such as cleaning or consolidation which is documented in the archaeological excavation reports may assist to the forensic study.

This study shows that no single technique can define Roman mortars. Multiple techniques are complementary. Debating the efficiency of techniques might help to save time and money in multidisciplinary projects. An analytical procedure is necessary, starting from an adequate selection of samples and macroscopic descriptions. Microscopic techniques (optical and electron) are fundamental in Roman mortar characterization and to define which aggregate type of TGA-DSC is vital to determine the degree of hydraulicity as well as the chemical analyses, which provide information on the possible origin of the raw materials.

XRD and FT-IR is considered are valuable complementary techniques. The original Roman and intervention mortars showed similarities in TGA, XRD, FTIR. Distinctive techniques such as POM and SEM will be done in the future.

Acknowledgements

This research has been financed by CLIMORTEC project (BIA2014-53911-R) of Spanish Ministry of Science, Innovation and Universities and by Geomateriales 2 (S2013/MIT-2914) and TOP Heritage-CM (P2018/NMT4372) of Community of Madrid. The authors would like to thank to Miguel Alba and Pedro Dámaso Sánchez Barrero from the Consortium of the Monumental City of Mérida for providing convenience in sampling.

References

1. Hughes JJ (2017) Ineducable us: the applications and contexts of microscopy used for the characterisation of historic building materials, RILEM Technical Letters 2: 136-144 DOI: <http://dx.doi.org/10.21809/rilemtechlett.2017.52>
2. Crupi V, Galli G, La Russa M F, Longo F, Maisano G, Majolino D, Malagodi M, Pezzino A, Ricca M, Rossi B, Ruffolo SA , Venuti V (2015) Multi-technique investigation of Roman decorated plasters from Villa dei Quintili (Rome, Italy). *Applied Surface Science*, 349, pp 924-930.
3. Cardoso I, Macedo M F, Vermeulen F, Corsi C, Santos Silva A, Rosado L, Candeias A , Miraõ J (2014) A Multidisciplinary Approach to the Study of Archaeological Mortars from the Town of Ammaia in the Roman Province of Lusitania (Portugal). *Archaeometry*, 56, 1–24.
4. Belfiore C M, Fichera G V, La Russa MF, Pezzino A, Ruffolo S A, Galli G , Barca D (2015) Multidisciplinary approach for the archaeometric study of pozzolanic aggregate in roman mortars: the case of villa dei quintili (Rome, Italy), *Archaeometry* 57, 2 pp. 269–296, doi: 10.1111/arcm.12085
5. Goins E (2000) A new protocol for the analysis of Historic Cementitious Materials: Interim Report in PRO 12: International RILEM Workshop on Historic Mortars: Characteristics and Tests, RILEM Publications, p. 71,
6. Elsen, J. Mertens, G. Degryse, P. & Waelkens, M. (2005) Conservation of Ancient Mortars at Sagalassos-Turkey. International RILEM Workshop on Repair Mortars for Historic Masonry (pp. 94-98). RILEM Publications Pro 67.
7. P. Hauková, D. Frankeová and Z. Slížková (2019) Characterisation of Historic Mortars for Conservation Diagnosis Thailand in: *Historic Mortars Advances in Research and Practical Conservation*, John J. Hughes, Jan Válek Caspar J. W. P. Groot (eds.), Springer <https://doi.org/10.1007/978-3-319-91606-4>

8. Alvarez JI, Martín A, García Casado PJ, Navarro I, Zornoza A (1999). Methodology and validation of a HCl acid attack for the characterisation of ancient mortars. *Cement and Concrete Research*, 29, 1061–1065.
9. Casadio F, Chiari G, Simon S (2005) Evaluation of binder/aggregate ratios in archaeological lime mortars with carbonate aggregate: a comparative assessment of chemical, mechanical and microscopic approaches. *Archaeometry* 47(4): 671–89.
10. Pavia S and Caro S (2006) Lime mortars for masonry repair: Analytical science and laboratory testing versus practical experience. In: *Proceedings of International Seminar Theory and Practice in Conservation- a tribute to Cesare Brandi*. Eds. J. Delgado Rodrigues, J. M. Mimoso. LNEC, Lisboa, pp. 493-500.
11. Farci A, Floris D, Meloni P (2005) Water permeability vs. porosity in samples of Roman mortars. *Journal of Cultural Heritage* 6
12. Hamey LA, Hamey JA (1990) *The Roman Engineers*. Published in cooperation with Cambridge University Press. Lerner Publications Co.
13. Siddall R (2011) From kitchen to bathhouse: the use of waste ceramics as pozzolanic additives in Roman mortars. In Å. Ringbom, & R. L. Hohlfelder (Eds.), *Building Roma aeterna: current research on Roman mortar and concrete*. The Finnish Society of Sciences and Letters, 128, 152-168.
14. Rodríguez-Navarro C (2004) Binders in historical buildings: Traditional lime in conservation. *Seminario SEM 09*, 91-112.
15. Mertens G, Snellings R, Van Balen K, Bicer-Simsir B, Verlooy P, Elsen J (2009) Pozzolanic reactions of common natural zeolites with lime and parameters affecting their reactivity. *Cement and Concrete Research* 39: 233–240.
16. Stefanidou M (2016) Use of natural pozzolans with lime for producing repair mortars. *Environmental Earth Sciences*, 75, 758.
17. Alba M (2005) Evolución y final de los espacios romanos emeritenses a la luz de los datos arqueológicos en Augusta Emerita: Territorios, Espacios, Imágenes y Gentes en Lusitania Romana, *Monografías Emeritenses* 8, 207-253.
18. Mota-López MI, Fort R, Álvarez de Buergo M, Pizzo A, Maderuelo-Sanz R, Meneses-Rodríguez J M & Ergenç D (2016) Characterization of concrete from Roman buildings for public spectacles in Emerita Augusta (Mérida, Spain). *Archaeological and Anthropological Sciences*, 1-16.
19. Henry O (2012) Le Sanctuaire de Labraunda. Historique, état des lieux et perspectives de recherche, *Anatolia Antiqua* XX, 227-260]

20. Ergenç D, Fort R (2016) Characterization of Roman mortars of Nysa in the ancient Caria, Turkey. Proceedings of the 4th Historic Mortars Conference HMC2016 10th-12th October 2016, Santorini, Greece Ed. I. Papayianni, M. Stefanidou, V. Pachta, Aristotle University of Thessaloniki, ISBN: 978-960-99922-3-7
21. Hamed S (2013) Laser Induced Breakdown Spectroscopy and other Analytical Techniques Applied on Construction Materials at Kom El-Dikka, Alexandria, Egypt, Mediterranean Archaeology and Archaeometry, Vol. 13, No 2, pp. 103-119
22. Theodore V (2001) Alexandria, City of the Western Mind, Free Press, New York
23. Elsen J, Van Balen K, Mertens G (2012) Hydraulicity in Historic Lime Mortars: A Review. in: Válek J., Hughes J., Groot C. (eds) Historic Mortars. RILEM Bookseries, vol 7. Springer, Dordrecht
24. Ergenç D, Fort R (2017) Preliminary investigation of repair mortars for the Temple of Diana, Mérida, Ge-Conservación, nº 11, ISSN: 1989-8568, pp 42-49
25. Elsen J (2006) Microscopy of historic mortars – a review. Cement and Concrete Research 36 pp 1416-1424
26. Middendorf B, Hughes JJ, Callebaut K (2005) Investigative methods for the characterisation of historic mortars—Part 2: Chemical characterisation. Materials and Structures 38(8): 771-780. doi:10.1007/BF02479290
27. Ingham J P (2013) Geomaterials Under the Microscope. 8 - Mortar, plaster, and render. Boston: Academic Press.
28. Stefanidou M, Pavlidou E (2018) Scanning Mortars to Understand the Past and Plan the Future for the Maintenance of Monuments, Scanning, <https://doi.org/10.1155/2018/7838502>
29. Ergenç D, Gómez-Villalba LS, Fort R (2018) Crystal development during carbonation of lime-based mortars in different environmental conditions, Materials Characterization, <https://doi.org/10.1016/j.matchar.2018.05.043>
30. Jackson MD, Chae S, Mulcahy S R, Meral Ç, Taylor R, Li P, Emwas A-HM, Moon J, Yoon S, Vola G, Wenk H R, Monteiro PJM (2013) Unlocking the secrets of Al-tobermorite in Roman seawater concrete. American Mineralogist, 98: 1669–1687.
31. Nežerka V, Slížková Z, Tesárek P, Plachý T, Frankeová D, Petráňová V (2014) Comprehensive study on mechanical properties of lime-based pastes with additions of metakaolin and brick dust. Cement and Concrete Research, 64, 17-29.
32. Vanorio T, Kanitpanyacharoen W (2015) Rock physics of fibrous rocks akin to Roman concrete explains uplifts at Campi Flegrei Caldera, Science. 2015 Aug 7; 349(6248):617-21. doi: 10.1126/science.aab1292. Epub 2015 Jul 9.

33. Lancaster L, Sotilli G, Marra F, Ventura G (2011) Provenancing of lightweight volcanic stones used in ancient Roman concrete vaulting: Evidence from Rome. *Archaeometry*, 53: 707–727.
34. Miriello D, Bloise A, Crisci GM, Apollaro C, La Marca A (2011) Characterisation of archaeological mortars and plasters from kyme (Turkey). *Journal of Archaeological Science*, 38:794-804.
35. Crisci G M, Franzini M, Lezzerini M, Mannoni T, Riccardi MP (2004) Ancient mortars and their binder. *Periodico di Mineralogia*, 73: 259-268.
36. De Luca R, Miriello D, Pecci A, Domínguez Bella S, Bernal Casasola D, Cottica D, Crisci G M (2014) Mortars and plasters from the “Garum Workshop” at Pompei (Italy): An archeometric study. VIII Congresso Nazionale di Archeometria Scienze e Beni Culturali
37. Cantisani E, Cecchi A, Chiaverini I, Fratini F, Manganafelli del Fà C, Pecchioni E, Rescic S (2002) The binder of the «Roman Concrete» of the Ponte di Augusto at Narni (Italy). *Periodico di Mineralogia*, 71:113-123.
38. Theodoridou M, Ioannou I, Philokyrou M (2013) New evidence of early use of artificial pozzolanic material in mortars. *Journal of Archaeological Science*, 40: 3263-3269.
39. Santos Silva, A. Paiva, M. Ricardo, J. Salta, M. Monteiro, A. M. Candeias, A. E. 2006a. Characterisation of roman mortars from the archaeological site of Troia. *Materials Science Forum*, 514, 1643-1647.
40. Gliozzo, E. Dalconi, M. C. Cruciani, G. & Turbanti Memmi, I. 2009. Application of the Rietveld method for the investigation of mortars: a case study on the archaeological site of Thamusida (Morocco). *European Journal of Mineralogy*, 21, 457-465.
41. Moropoulou, A. Bakolas, A. Bisbikou, K. 2000b. Investigation of the technology of historic mortars, *Journal of Cultural Heritage*, vol. 1 pp 45-58.
42. Moropoulou, A. Bakolas, A. Moundoulas, P. Aggelakopoulou, E. & Anagnostopoulou, S. 2005. Strength development and lime reaction in mortars for repairing historic masonries. *Cement and Concrete Composites*, 27, 289-294.
43. Bonazza A, Ciantelli C, Sardella, Pecchioni E, Favoni O, Natali I, Sabbioni C (2013) Characterization of hydraulic mortars from archaeological complexes in Petra. *Periodico di Mineralogia*, 82(2), pp. 459-475.
44. Yang H, Che Y, Leng F (2018) Calcium leaching behaviour of cementitious materials in hydrochloric acid solution, *Science Scientific Reports* 8:8806, DOI:10.1038/s41598-018-27255-x
45. Silva DA, Wenk HR, Monteiro PJM (2005) Comparative investigation of mortars from Roman Coliseum and cistern. *Thermochimica Acta*. 438: 35-40.

46. Maravelaki-Kalaitzaki P, Bakolas A, Moropoulou A (2003) Physico-chemical study of Cretan ancient mortars. *Cement and Concrete Research*, Volume 33:651–661.
47. Biscontin G, Birelli M P, Zendri E (2002) Characterization of binders employed in the manufacture of Venetian historical mortars. *Journal of Cultural Heritage*: 3, 31–37.
48. Lawrence R (2006). A Study of carbonation in nonhydraulic lime mortars, PhD Dissertation, Bath: University of Bath
49. Genestar C, Pons C, Más A (2006) Analytical characterisation of ancient mortars from the archaeological Roman city of Pollentia (Balearic Islands, Spain). *Analytica Chimica Acta*, Volumen 557, p. 373–379.
50. Izzo F, Arizzi A, Cappelletti P, Cultrone G, De Bonis A, Germinario C, Graziano S F, Grifa C, Guarino V, Mercurio M, Morra V, Langella A (2016) The art of building in the Roman period (89 B.C. – 79 A.D.): Mortars, plasters and mosaic floors from ancient Stabiae (Naples, Italy). *Construction and Building Materials*, vol 117, 129-143.
51. Ergenç D, La Russa MF, Ruffolo SA, Fort R, Sánchez Montes AL (2018) Characterization of the wall paintings in La Casa de los Grifos of Roman city Complutum, *The European Physical Journal Plus*, “New Challenges in the Scientific Applications to Cultural Heritage” edited by M. Fedi, L. Liccioli, et al. 133: 355, <https://doi.org/10.1140/epjp/i2018-12223-7>
52. Siedel H, Wendler E, Ullrich B (2019) Historic Renders and Their Weathering at the Temple Wat Mahathat, UNESCO World Heritage Site of Ayutthaya, Thailand In John J. Hughes, Jan Válek Caspar J. W. P. Groot (eds.), *Historic Mortars Advances in Research and Practical Conservation*, Springer <https://doi.org/10.1007/978-3-319-91606-4>
53. Rodica-Mariana et al (2016) Ceramic Materials Based on Clay Minerals in Cultural Heritage Study <http://dx.doi.org/10.5772/61633>
54. Ugurlu Sagin E, Boke H, Aras N, Yalcin S (2011) Determination of CaCO₃ and SiO₂ content in the binders of historic lime mortars, *Materials and Structures* (2012) 45:841–849 DOI 10.1617/s11527-011-9802-1

Petrography of Historic Mortar Materials: Polarising Light Microscopy as a Method for Characterising Lime-Based Mortars

Kristin Balksten¹, Bo Nitz², John J. Hughes³, Jan-Erik Lindqvist⁴

(1) Conservation, Campus Gotland – Uppsala University, Sweden, kristin.balksten@konstvet.uu.se

(2) Bo Nitz, Visby, bonitz@hotmail.se

(3) University of the West of Scotland, john.hughes@uws.ac.uk

(4) RISE Research Institutes of Sweden, janerik.lindqvist@ri.se

Abstract

In studying historic, repair and restoration mortars comprised of lime-based material there is an analytical method that answers more questions than any other; transmitted (and reflected) polarised light microscopy (PLM). The present study is based on thin-section analysis of historic and restoration mortars made by the authors in Sweden and Scotland since the 1980's, previous research [1, 2, 3, 4] and petrographic atlases [5, 6, 7, 8]. This paper is written to be a pedagogically useful complement to previous work.

We present a selection of microphotographs to show the variety of questions that the method can give answers to, such as, in the study of:

- lime binder; source materials, hydraulicity, slaking methods, lime lumps, cracking characteristics
- aggregates; grading, mineralogy/lithology and texture
- additives; inorganic pozzolanic materials and organic materials
- paint layers; different binders, pigments, thicknesses
- pore structure; durability, vapour transport and capillarity
- craftsmanship; various application and working techniques

The aim of this paper is to contribute with more illustrations of reference materials and to illustrate the usefulness of Polarising Light Microscopy as a method for characterising lime-based mortars and to review the most significant analyses parameters.

Keywords: Petrography, thin sections, lime mortar, polarisation light microscopy, optical microscopy

Introduction

When a lime mortar as well as all other materials is to be analysed, the analysis method to be utilised can be determined, to some extent by the questions asked in an investigation. A lime mortar can be analysed to identify its components, its pore structure or parameters related to compatibility with its substrate, or other mortars. Sometimes you want to determine its material properties, sometimes you want to identify why decay or damage has

occurred, and sometimes you want to see if a newly produced lime mortar, applied during conservation, is in line (i.e. similar, with an authentic composition) with the historic lime mortar. Sometimes you just want to understand a historic lime mortar, based on its origin and age. All these questions can normally be answered by one superior method; thin section analysis using Polarising Light Microscopy, utilising either reflected or transmitted light.

When starting to use the method it is of great value to have access to colleagues with great experience as well as to a reference material. In Sweden there is for example, thanks to an initiative of one of the authors, Bo Nitz, a collection of thin sections made since the 1940's are now accessible for research at the museum archive on Gotland. This paper has the aim to share some of the knowledge and provide, hopefully, inspiration to use the method. The aim is also to provide and make a reference photo material available to more users to widen the usefulness of the method, because of this the paper includes many figures.

A very brief historic review

The thin section technique was developed by geologists in the middle of the 19th century [9], in order to allow for easier study of rocks and the determination of their mineral make up. Around 1920 the technique began to be utilised on construction materials, such as concrete and mortar. In the 1960's the advent of fluorescence microscopy allowed for the study of crack formation, cavities and porous structures. Today the technique is utilised on a very wide variety of materials, in addition to mineral/inorganic construction materials.

Principle of application

The idea of grinding samples very thin is to enable light to pass through its constituent materials. The optical qualities of the constituents can be taken advantage of to identify them, and studied in order to perform structural and textural analysis, in particular using polarization filtering. There are many excellent descriptions of the sample preparation method available, and reviews of application in geological and construction applications [1, 5, 7].

Compared to many geological applications, to enable thin section preparation of brittle materials such as concrete and mortars, usually the samples *must* be stabilized by imbedding in and impregnation of porosity with epoxy resin. By imbedding, the sample can be ground down to 20-30 μm , which is the most common range of thickness. However, when performing analysis of mortar binders, 15-17 μm is preferred by some workers.

On a thicker object glass, the sample is glued after drying and impregnation procedures. When the sample is attached to the object glass it is then ground to the desired thickness. Thereafter a cover glass is glued on the sample for two reasons: protection and optical reasons. If the cover glass is omitted, this allows the sample to be polished for reflected light analysis and also for characterisation using electron microscopy, and other instrumental methods where reflectance is required.

To increase the contrast between constituent phases and allow for their identification, optical filters are commonly used, mainly polarization filters, placed as shown below. A polarization filter is placed above and below the sample in the light beam passage.

What can be analysed

With mineral-based construction materials such as bedding mortar, render and pointing mortars etc., it is of interest to analyse the composition of aggregate, binders and admixtures. The texture of mortar is also of interest, in particular the pore structure, as pores have a great influence on the material characteristics. The development of the hydration of binder (when studying hydraulic mortars) as well as the interaction of mixed binder systems can be analysed in, addition to the degree of carbonation. When damage has occurred, its manifestation and its cause can be studied. Regarding aggregate quality, petrographic studies may be performed, embracing grain size distribution and shape factor analysis. Porosity, or the air void system, is of great interest as it has a great impact on the durability of the mortar, as well as a relation to the rheology of the materials.

Regarding historical lime mortars, the same parameters are of interest but apart from that;

- The binder/aggregate ratio; how binder- enriched is the mortar?
- What additives (pozzolanic or others) were used?
- What kind of aggregate was used? Where was it from and was it sieved/controlled in some way?
- What quality of air void structure can be determined? What does that tell us about mixing and application?
- In addition, there are textural and compositional parameters that can be analysed that tell us about the technology of lime sourcing, calcination and mortar preparation, by answering, for example:
 - How was the lime slaked (to putty or hot)? The occurrence of lime inclusions tells us that mortar probably was hot-mixed.
 - What is the origin of the lime (provenance of source carbonate)? Analysis of the texture and composition tells us the type of carbonate source material.
 - What is the degree of lime burning? Are there lumps of un-burnt or partially burnt limestone in the mortar? Unburnt material also provides direct information on sources of carbonate used for burning.
- Are there lime lumps with information on the slaking technique?
- Does slag material occur and what does it tell us about production processes?

Some qualities can be measured but *a great part of the quality of the examination is built on the experience of the microscope user*. The technique provides a good overview of the materials' general condition and structural qualities. If quantification is desired regarding characterisation in addition to the microscope analysis, some chemical analysis can help, such as determination of acid soluble silicon which may show possible hydraulic qualities. Thermo-gravimetric analysis will show relation of hydroxide/carbonate in case un-carbonated lime is believed to remain in the mortar. Electron microscopy combined with EDS elemental analyses is also commonly performed on uncovered polished thin sections and blocks.

Examples of thin section analyses

The composition and microstructure of the samples discussed were analysed using thin sections in polarization and fluorescence microscopy. Quantitative analysis was performed according to methods described in [4]. The method is illustrated below by a selection of microphotographs that show a variety of features related to questions and problems that the method can give answers to, such as, in the study of:

Lime binder

Historic lime mortars are often characteristic of their location, both geographically and chronologically. Medieval lime mortar often contain visible lime lumps and small amounts of sand compared to, for example, 18th century mortars which may contain a variety of different additives and more aggregate compared with older mortars. In order to fully interpret historic mortar, one often needs access to a reference material that extends over time and space, made of the same type of binder and aggregate as before and with the same manufacturing processes as before. Below are presented a selection of examples of petrographic characteristics of lime mortars, showing how they can differ. Here one can distinguish slaking methods, storage of lime, hydraulicity, lime lumps, shrinkage cracks, recrystallization and more.

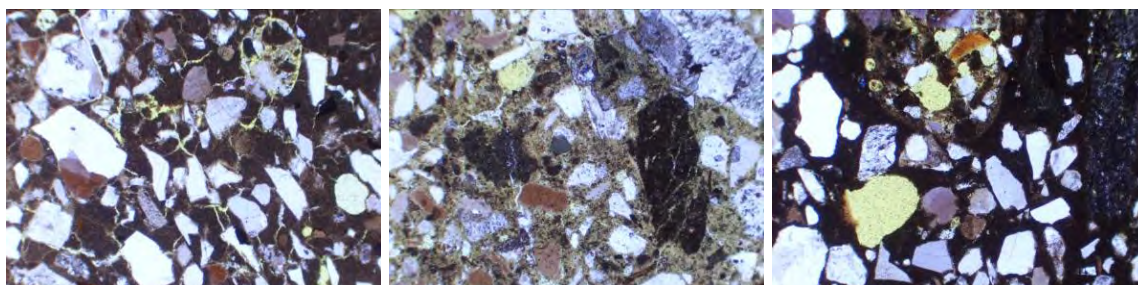


Figure 1. Three mortars made from the same sand and mixing ratio; 1:1 by volume. Wet slaked lime from different Silurian (1) and Ordovician (2-3) lime stone from 1) Hall Gotland, 2) Marieby Jämtland and 3) Näversjöberg Jämtland. In historic mortars very local lime can often be found. As we have burned and produced several local lime binders in Sweden in the 21st century we can now produce reference materials for comparing to historic mortars. Width of each image covers 2.65 mm. Illustration: Kristin Balksten [10, 11].

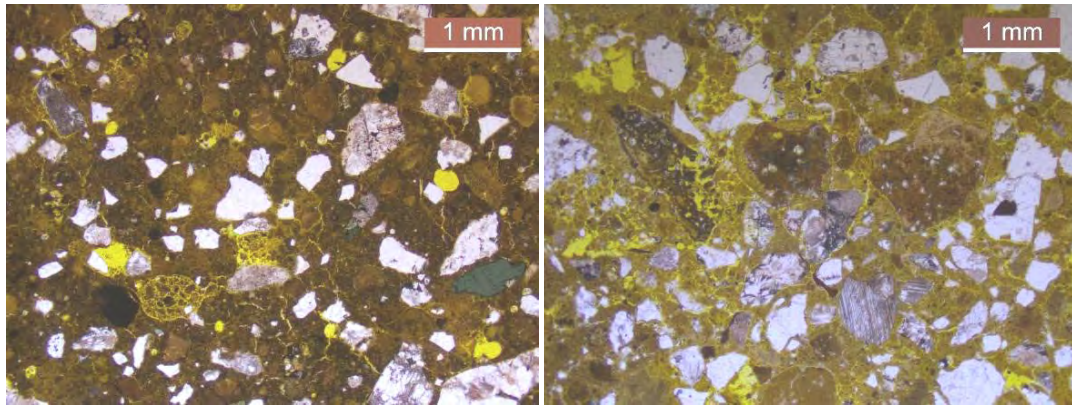


Figure 2. A very white fat lime putty (left) and a greyish lean lime putty (made of feebly hydraulic lime) (right), stored in the ground for 200 years, mixed with sand 3:2 in volume. In the grey lime putty mortar, lime lumps were not possible to still be mixed or activated, after 200 years, as they are in the white lime putty. For the grey putty the lime lumps (upper mid part of image) represent a kind of lumps often seen in wet slaked sub-hydraulic mortars and they have become part of the ballast rather than as an active binder. Illustration: Kristin Balksten [13, 14].

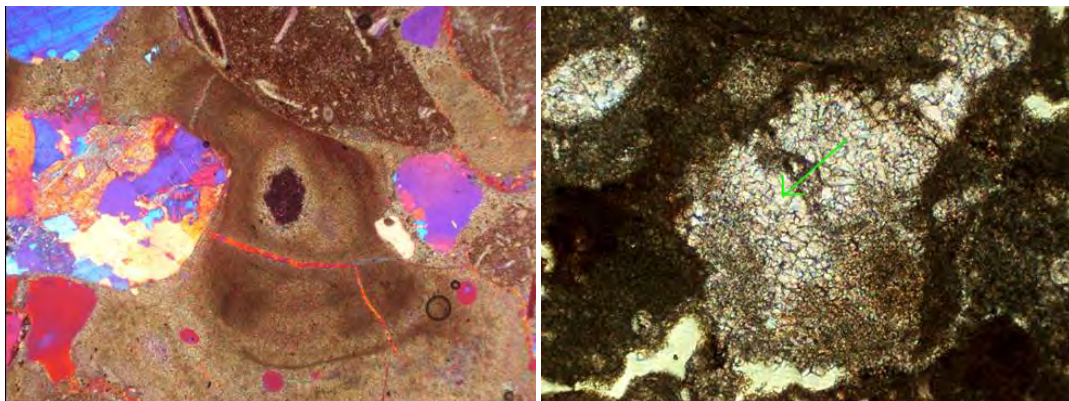


Figure 3. To left: Above is an example of lime use with partially burnt lime. The dark area in the centre of the picture is lime that is not burned. All lime in a shaft or lime kiln was not burned, so limestone lumps remained after quenching. The image covers 4.7 x 3.1 mm.

To right: The lime concrete sample above is dated to 7000 BC. It is from a floor found during excavations of several cultural layers under what is considered Jericho. The lime has been dissolved and recrystallised in a way that made it very dense. The strength has been measured at approx. 70 MPa, which the floor was not near as new. The green arrow shows large calcite crystals that have been formed for a long time. 1.0 x 0.6 mm.

Illustrations: Bo Nitz.

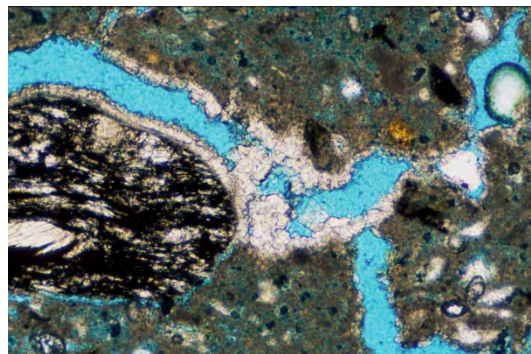


Figure 4. 16th Century lime mortar from Gylen Castle, Island of Kerrera, Inner Hebrides, Scotland. Example of secondary calcite crystallisation in pores. Image width 2mm. Illustration: John Hughes.

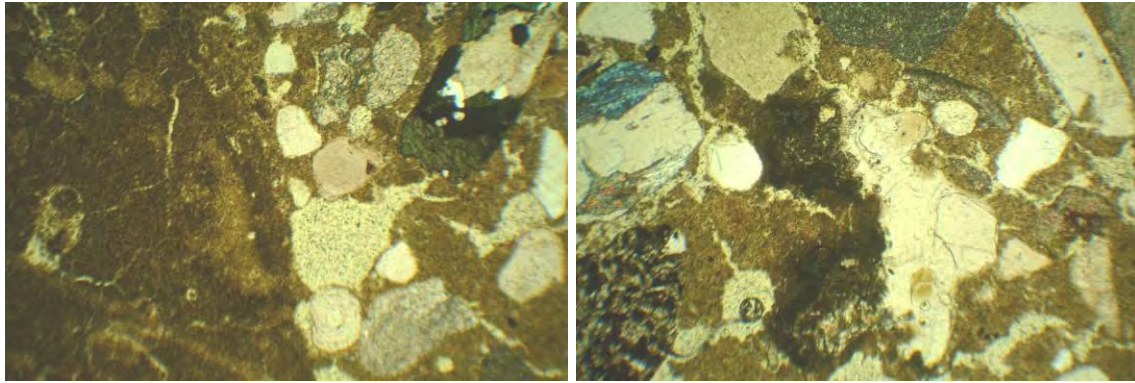


Figure 5. 19th century lime render from Visby showing the characteristic lime putty made from the fat Silurian lime of Gotland. In the putty there is often un-mixed lime lump (to the left), air voids and micro cracks (both pale yellow). Width of the image covers 2.65 mm. Illustration Kristin Balksten [14].

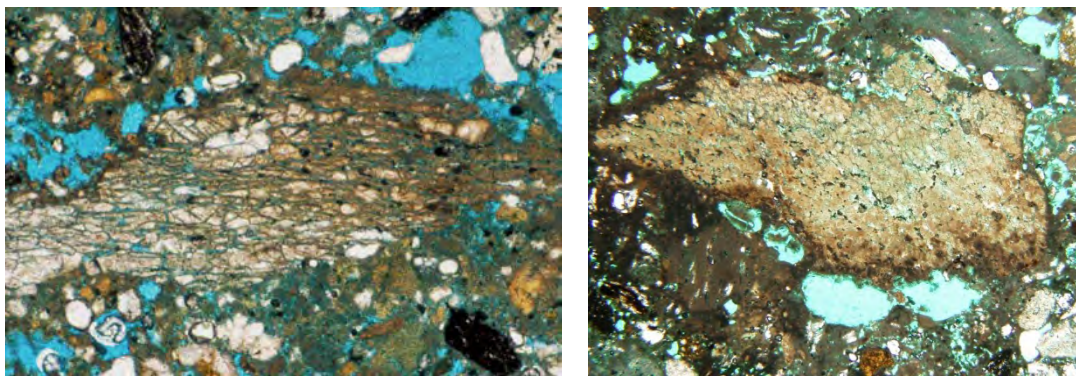


Figure 6. 16th Century lime mortar from Gylen Castle, Island of Kerrera, Inner Hebrides, Scotland. Left: main fragment is a partially burnt mildly schistose medium grained marble, grading to right to material texture merging with the main binder of the mortar. Uncalcined lithology shows separation of grains perhaps relating to processing of the lime. Right: lime inclusion with remnant pseudomorph texture of the marble, with notable intra-granular porosity, possible due to shrinkage during hydration and carbonation. Images 5 mm width, both PPL. Illustration: John Hughes.

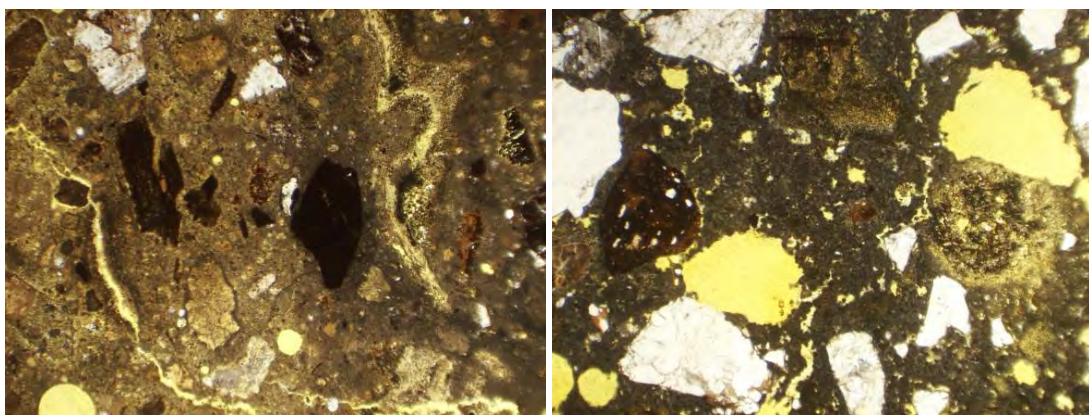


Figure 7. Extremely lime rich historic mortars made from hydraulic lime, from two medieval church ruins in Sunne and Hassela, Sweden. The sample from Sunne (left) shows a mortar almost without sand, containing many lime lumps of different character, some air pores and micro cracks. The sample from Hassela (right) show a grainy lime with large lime crystals in the putty, lime lumps of hydraulic lime, air pores and micro cracks. The width of each sample covers 4.5 mm. Illustration: Kristin Balksten [10, 15].



Figure 8. Gypsum plaster from 18th century Drottningholm Theatre, seen in three different scales. The width is equivalent to 4.5, 0.9 and 0.225 mm in the pictures above. The sample is a gypsum plaster with very fine ballast in size 0-0.5 mm with a large amount of stone flour. The render is very rich in binder and has a mixing ratio of about 1: 0.25-1: 0.5 between gypsum and stone flour. The surface of the render is covered by a lime paint layer with a layer thickness of 0.05-0.1 mm, which means that it is made with a thicker lime paint about 1: 2 in volume ratio between lime paste and water. When the lime paint and gypsum plaster meet, the difference between the lime's fine-grained structure and the needle-shaped plaster is clearly visible. Illustration: Kristin Balksten.

Aggregates

The sand can vary greatly in historic mortars as well as in modern repair mortars. The sand is often obtained locally and this means great variation in mineral composition, grain size distribution, grain shape and colour. It all affects the appearance of the mortar, mixing ratio, workability, etc. Among the ballast, other characteristic mineral grains can also be detected such as fossils and sea shells. Sometimes the hydraulic particles of the lime have already hardened and then these are also functioning as ballast grains, see under the previous heading.

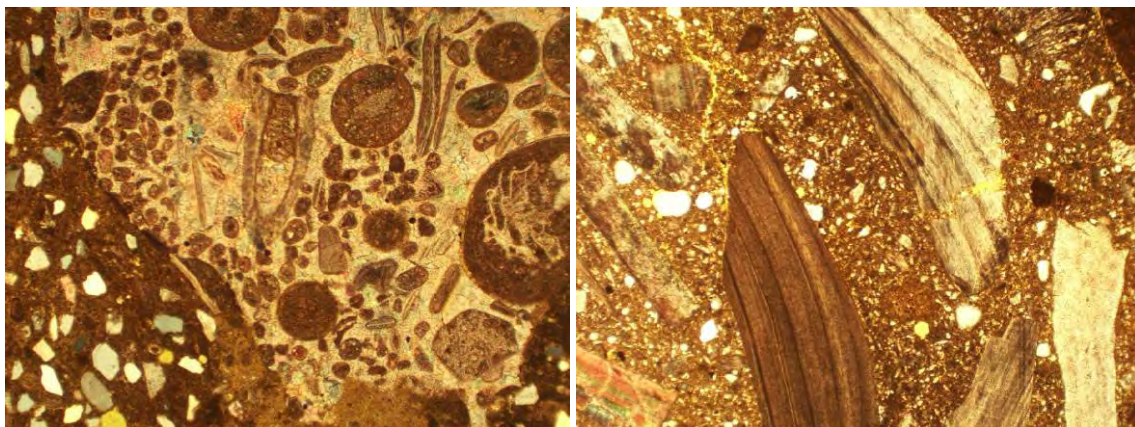


Figure 9. Among aggregates both fossils and sea shells can be found. Fossils can often be seen on Gotland where the sand can contain local Silurian limestone. The sea shells can often be found on the Swedish west coast where shell banks from the ice age have been used in historic mortars. The width of each sample is equivalent to 4.5 mm. Illustration: Kristin Balksten.

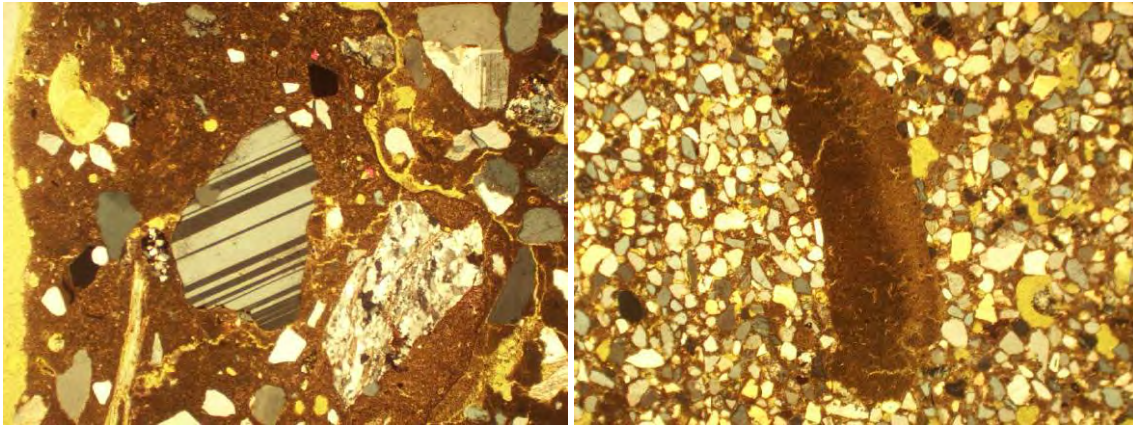


Figure 10. Difference in mineralogy, shape of the grains and sand curve is illustrated by samples with a medieval lime mortar and a 19th century lime mortar. The width of each sample is equivalent to 4.5 mm. Illustration: Kristin Balksten.

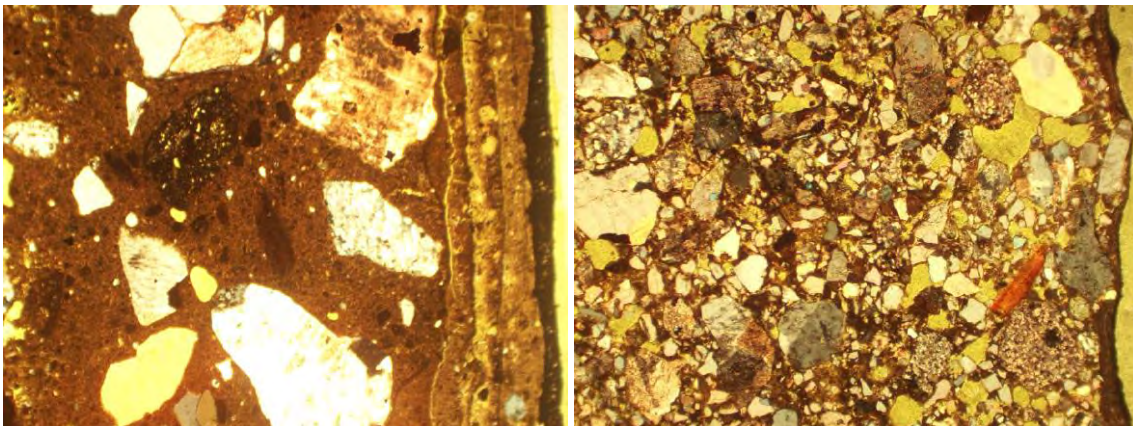


Figure 11. Difference in mineralogy, sand curve and hence, mixing ratio is illustrated by samples from Älvros church by a mortar from 1740 and a mortar from 2000. Here the difference in thickness of historic and modern lime wash can also be compared. The width of each sample is equivalent to 4.5 mm. Illustration: Kristin Balksten.

Additives

A number of different types of additives are known in old mortars throughout history. It is all from air-pore-forming additives, hydraulic additives, reinforcing fibres to additives that affect the aesthetic appearance. For example, traces of organic fibres can often be found. For example, the following have been found by the authors over the years; wood fibers from lime bin and tools, char coal pieces from lime burning, straw or hemp shivs for reinforcement / insulation, animal hair for reinforcement [2]. Among hydraulic additives, besides the puzzolan, there are also other locally produced particles such as slag [16], crushed bricks, ash of alum shale etc. Most of these additives affect the properties and appearance of the mortars in some aspect. Many additives can also be seen with the naked eye.

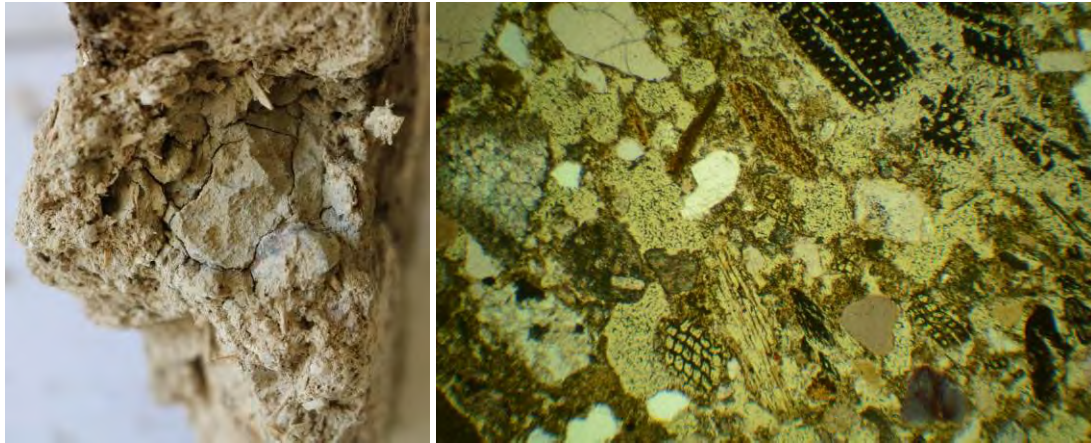


Figure 12. Clay mortars with organic fibers in an early 19th century render on a wooden house in Visby. Often it is of great importance to compare the mortar sample with the thin section to be able to make a correct interpretation. The width of the sample covers 2.65 mm. Illustration: Kristin Balksten [14].

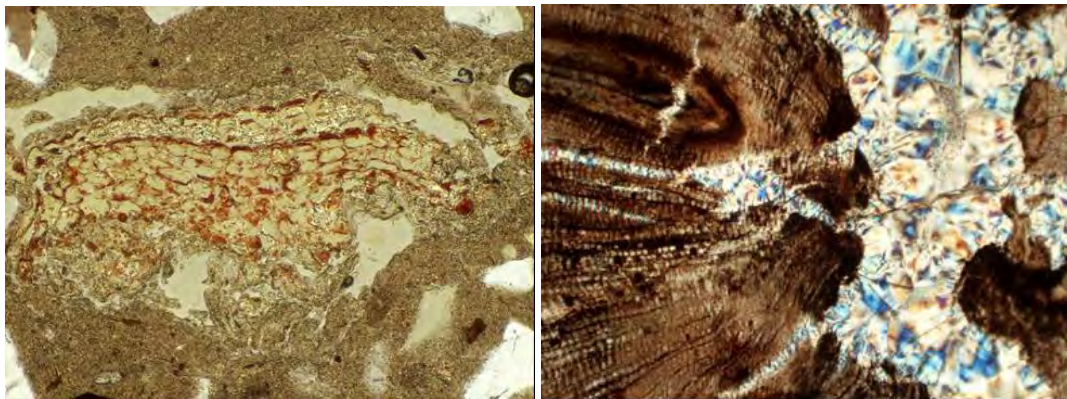


Figure 13. The left picture shows an approximately 120 year old sample. Brown rings are visible in the middle of the picture. There are wood cells in a wood chip that surely come from a scouring board or other tool. The image covers 1.0 x 0.6 mm. The right picture shows a section of a silicon fossil of a tree branch from Arizona, ca. 200 million years. Silicate formation is thought to come from volcanic ash that covered the forest and by the rain dissolved and impregnated the wood. The small brown rings in rows are wood cells. 4.8 x 3.1 mm. Illustration: Bo Nitz.

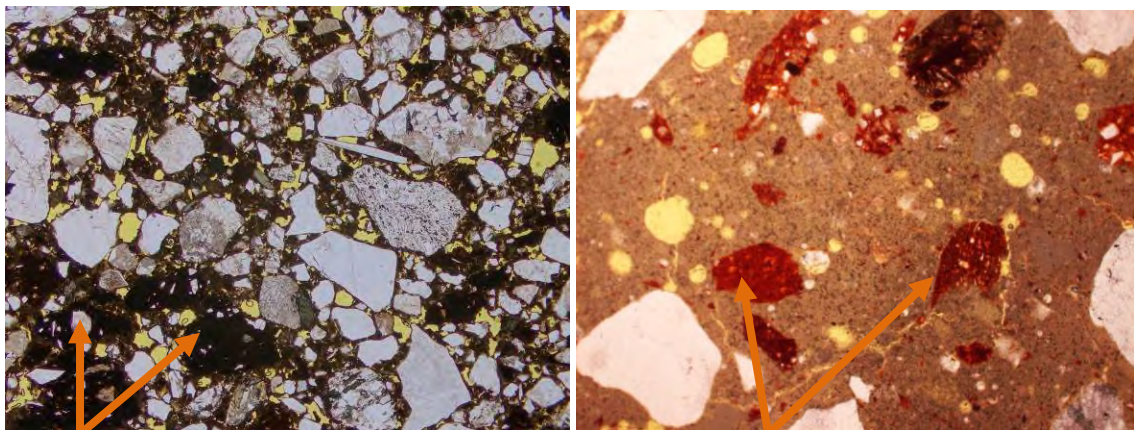


Figure 14. Crushed red bricks (see arrow) can often be found in mortars for renders or pointing. Here it is illustrated by a modern NHL3,5-mortar made for the re-rendering of Stockholm royal castle and a historic render on När church. In both samples it is mainly there for aesthetic reasons as the aggregate is visible due to the surface working method and the render is left without lime wash. Illustration: Kristin Balksten.

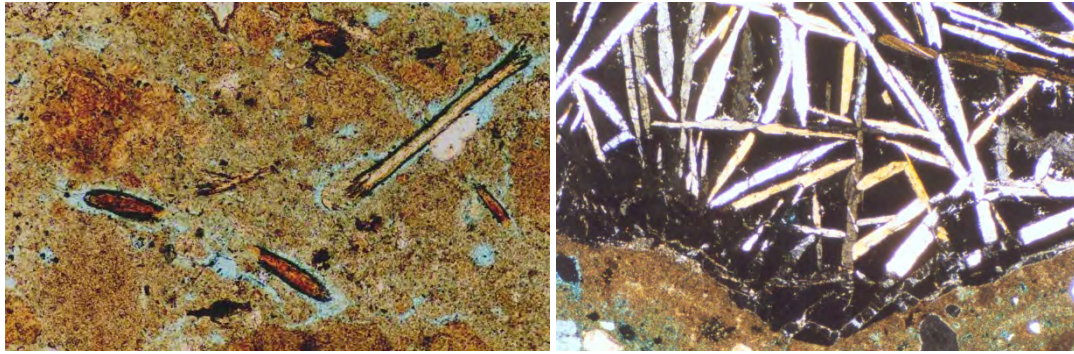


Figure 15. Examples of additives, deliberate and possibly not deliberate. Left, Lime plaster from ‘Old Auchentroig’, 1702, Buchlyvie, Stirlingshire, Scotland. Lime rich, low content of aggregate, with inclusion of animal hair as a tensile improver in the plaster. Image 2mm width, PPL. Right : Lime mortar, Charlestown, Fif Scotland, 1810, glass-spinaflex slag. Image 5mm width, XPL. Illustration: John Hughes.

Paint layers

On the surface of renders and plasters there are often paint layers. These can consist of different binders and different pigments [7]. The layers can be applied in many coats and with different consistency. Medieval lime paint is often seen as a few thick layers compared to modern lime paint that was applied in many thin coats. Also, paint layers containing ballast or organic binders are commonly used. Sometimes one can see that the lime in the lime paint is of the same type as the binder in the mortar, sometimes it is made by a completely different kind of lime.

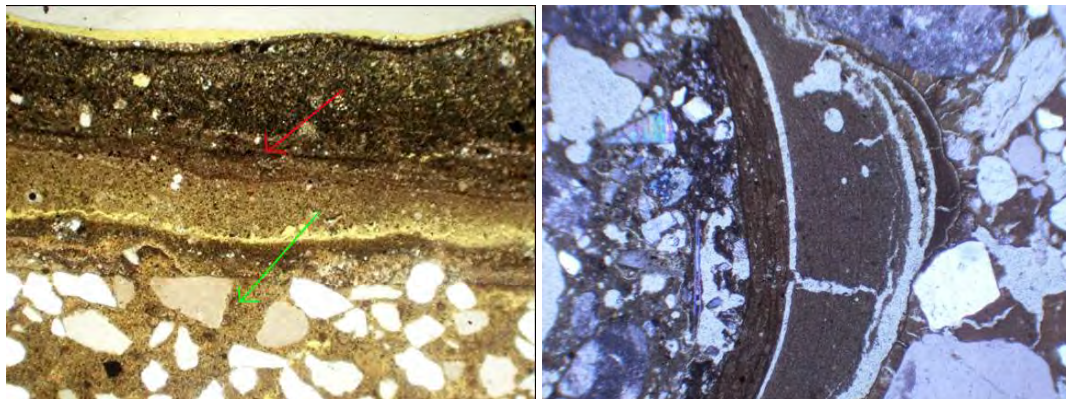


Figure 16. To the left: The sample above is from a French defense plant in Madagascar. The wall is made of bricks that have been plastered and decalcified. The green arrow points out the plaster and the red decolour. 4.8 x 3.1 mm. Illustration: Bo Nitz. To the right: Many layers of lime render, covered with two lime wash layers (each in many applications) and another two layers of lime renders. 4.8 x 3.1 mm. Illustration: Kristin Balksten.

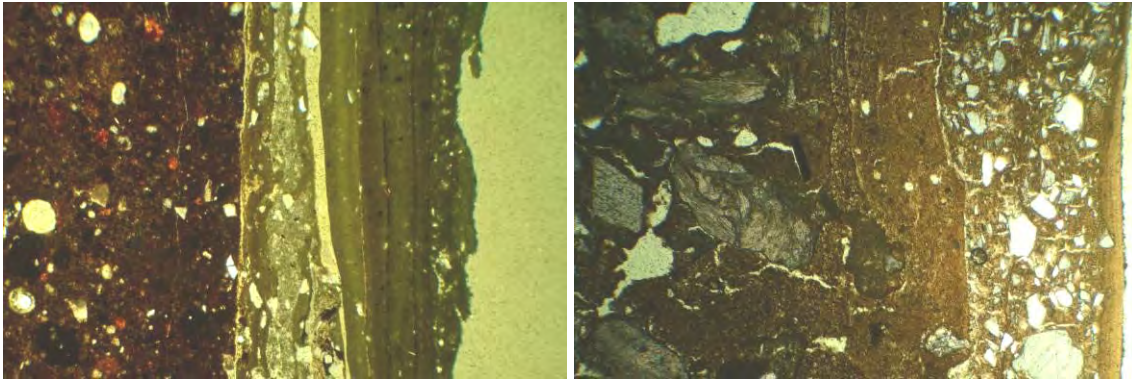


Figure 17. Mortars covered with a variation of paint layers; oil paint, lime wash, lime wash containing dolomite, and tempera. Also, adhesion between layers and compatibility can be considered from this kind of thin section analysis. The width of each sample is equivalent to 2.65 mm. Illustration: Kristin Balksten.

Pore structure

The pore structure is often of interest as we want to understand the durability of a lime mortar [17, 18, 19]. In thin sections we can distinguish air pores and capillary pores. Instead, to study gel pores, SEM is recommended as a microscopy method. The pore structure can also be collapsed, i.e. the air pores are interconnected and this can often be studied as a result of incorrect mixing conditions and application, see under next heading.

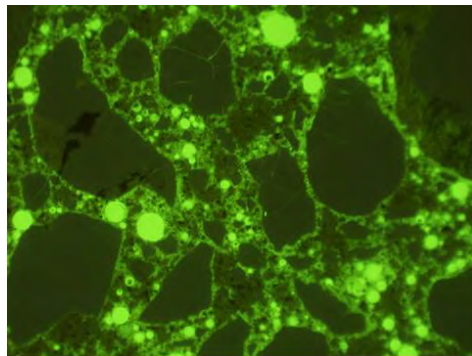


Figure 18. As mentioned, the pore structure is important for the function of use. A fluorescence photograph of a structure where the large dark green fields are aggregate, the speckled paste and the light green dots are air voids. Using this technique, the spacing factor, size and amount can be calculated. 4.8 x 3.1 mm. Illustration: Bo Nitz.

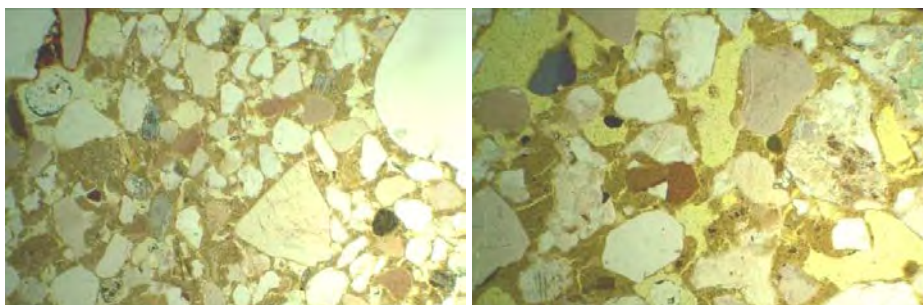


Figure 19. With fluorescent epoxy is used for preparing the thin section samples the air pores and capillary pores is clearly visible as light yellow in the photos. In these two samples the pores are connected with capillary pores, but only the example to the right has a collapsed pore system as the amount of binder is less than what it needs to fill up the sand. The width of each sample is equivalent to 2.65 mm. Illustration: Kristin Balksten.

Craftsmanship and working techniques

Using thin section for analysing results due to craftsmanship can verify and illustrate what is known already by skilled craftsmen [19, 20, 21]. The consistency of the mortar due to mixing ratio, water content and the suction capacity of the substrate can be verified. The knowledge can be useful i.e. damage investigations due to poor craftsmanship or poorly mixed mortar [19].

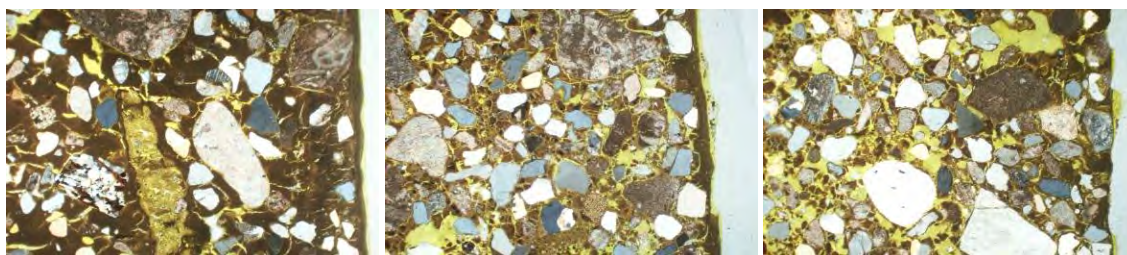


Figure 20. Mixing ratio 1:1, 1:2 and 1:3 by volume made from the same wet slaked lime putty and sand. All samples were worked on in the correct semi-dry consistency working all micro cracks together. On the surface there is lime wash. The 1:3-mortar has an open irregular pore structure and it is not compact enough to be frost resistant. The width of the sample show 4.5 mm. Illustration: Kristin Balksten [18, 19].

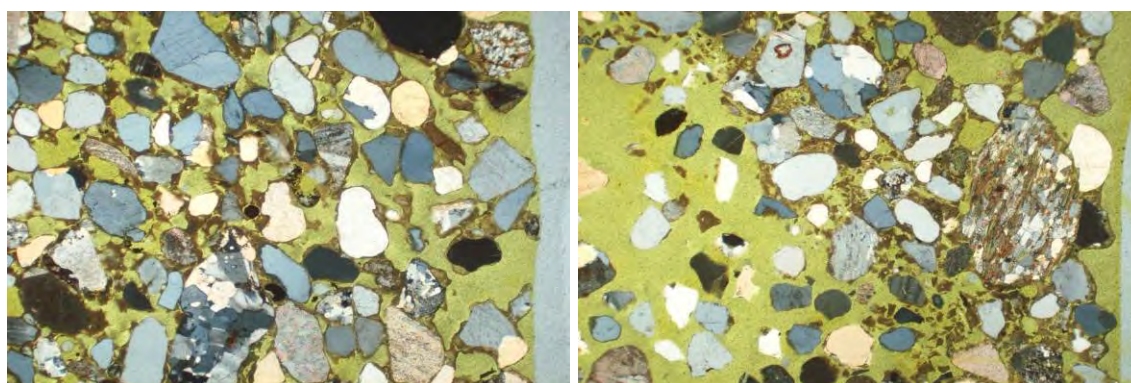


Figure 21. Mixing ratio 1:3 by volume, made of dry slaked lime and sand. The samples illustrate two surfaces made from the same mortars on the same substrate, worked on in different range of drying; left sample is worked on in the correct semi-dry consistency while the right sample is worked on in a too wet consistency. As the render was worked on too early a big void was created just under the surface (yellow). It is also clear that the mixing ratio for this specific lime to this sand has to be different if the mortar should receive a pore structure with frost resistance. The surface of the sample is to the right. The width of the sample show 4.5 mm.

Illustration: Kristin Balksten [18, 19].

Discussion and conclusions

Analysis of historical mortar and lime-based mortars with thin sections, provides a great deal of information with a single analysis. The method is quick and simple, it requires no complicated equipment, but it requires experience in the analyst, often with specialised training. In Sweden, and to a lesser extent in Scotland, it has become a frequently used method to analyse;

- historic lime mortars for their source of knowledge,
- repair mortars to create sustainable, compatible and authentic repairs

- damage to and problems with failing recent restorations

Where further information about the mortars is desirable, the thin section analysis often provides information about what is interesting to study further. Combined with other material analyses; chemical analyses, SEM, XRD and other methods that show density, porosity, capillarity, permeability etc., one can obtain a very clear and pedagogical picture of how the lime mortar works. If there is also a reference material that other more time-consuming analyses have been carried out on, allowing for some calibration of observation from known composition, texture etc., then thin section analysis can often be used as the only analysis method to provide all the information that is requested.

Notes on contributors

Bo Nitz has made thin section analyses since 1987. He has studied a wide range of samples, from historic mortars to modern cementitious materials at Cementa Research, Maxit and Weber. Jan Erik Lindqvist is a senior researcher at RISE, Research Institutes of Sweden. He has made thin section analysis since the 1970's studying a wide range of mortars based on lime and cement, both historic and modern. John Hughes first looked at a thin section in 1986, as a student at Edinburgh University, and began analysing historic mortar materials in 1996 at the University of Paisley. Kristin Balksten has made thin section analyses since 2002, with guidance from Bo Nitz, Jan-Erik Lindqvist and Thorborg von Konow. She has studied Swedish lime mortars; both historic mortars and newly produced restoration mortars from traditionally produced lime from all over Sweden.

References

1. Elsen J (2005) Microscopy of historic mortars – a review. *Cement and Concrete Research* 36 (2006) 1416-1424.
2. Blaeuer C, Kueng A (2007) Examples of microscopic analysis of historic mortars by means of polarising light microscopy of dispersions and thin sections. *Materials Characterization* 58(11):1199-1207
3. Middendorf B, Hughes J J, Callebaut K, Banonio G (2005) Investigative methods for the characterisation of historic mortars. Part 1: Mineralogical characterization. *Materials and Structures* 38(8):761-769
4. Lindqvist JE, Sandström M (2000) Quantitative analysis of historical mortars using optical microscopy. *Materials and Structures* vol 33, 612-617.
5. MacKenzie W S & Adams A E (1994) A color atlas of rocks and minerals in thin section. Halsted Press, New York

6. Larbi JA, van Hees RPJ (2000) A microscopical method for characterisation of original composition and constituents of (historical) mortars. TNO Report 2000-BT-MK-R0081.
7. Ingham J (2010) Geomaterials under the Microscope A Colour Guide; building stone, roofing slate, aggregate, concrete, mortar, plaster, bricks, ceramics, and bituminous mixtures. Manson Publishing Ltd, London
8. Karin Kraus (2015) Historische Mörtel im Dünnschliff. IFS Bericht, vol 48, 91 pp.
9. N.Worley (2009), Henry Clifton Sorby (1826-1908) & the development of thin section petrography in Sheffield, in: P.S. Quinn (Ed.), Interpreting silent artefacts; Petrographic approaches to Archaeological Ceramics. Archaeopress, 1-9
10. Balksten K & Mebus U (2012) Bruk av ruiner. Fornsalens förlag, Visby. Available at: <http://urn.kb.se/resolve?urn=urn:nbn:se:uu:diva-220106>
11. Balksten K, Persson C and Eriksson J (2019) Lime burning tradition in a field kiln of the Jämtland model in Sweden. In: Hughes, J. J., Válek, J. & Groot, C.J.W.P. (red.) (2019). Historic Mortars Advances in Research and Practical Conservation. Cham: Springer International Publishing
12. Ytterberg N, Balksten K (2016) Trade and use of building lime – early 19th-century lime barrels from an excavation in Uddevalla, Bohuslän. In: Meta historiskarkeologisk tidskrift, Historiskarkeologiska föreningen, Uppsala
13. Balksten K, Lindqvist J-E (2016) Two-hundred year old lime putty from barrels found in the ground explaining the character of fat historic mortar. In: Proceedings of 4th Historic Mortars Conference HMC-2016, Santorini, Greece
14. Nygren S, Balksten, K (2019) Reveterade hus i Visby. In: Balksten, K, Strandberg-de Bruijn (2019) Hampakalk – Tilläggsisolering på reveterade trähus och saltskadat tegelmurverk. Project report. Lund: LTH
15. Balksten K (2010) Understanding historic mortar and their variations – a condition for performing restorations with traditional materials. In: Proceedings of 2nd Historic Mortars Conference HMC-2010, Prague, Czech Republic.
16. Lindqvist J E, Balksten K, Friedrich B (2019) Blast furnace slag in historic mortars of Bergslagen, Sweden. Submitted to HMC2019, University of Navarra, Pamplona
17. Konow T von (1997) Restaurering och reparation med puts- och murbruk. PhD Thesis, Åbo akademi, Åbo
18. Carlsson T (1995) Luftporstrukturens inverkan på egenskaperna hos puts- och murbruk. Lic-avh. LTH, Lund. Available at: <http://lup.lub.lu.se/record/1273299>

19. Balksten K (2007) Traditional lime mortar and plaster: reconstruction with emphasis on durability. PhD Thesis, Chalmers, Gothenburg. Available at: <http://urn.kb.se/resolve?urn=urn:nbn:se:uu:diva-220119>
20. Balksten K, Klasén K (2005) The influence of craftsmanship on the inner structures of lime plasters. In: Proceedings of the International RILEM Workshop Repair Mortars for Historic Masonry. University of Technology, Delft
21. Jornet A et al (2005) Lime mortar for renders; is there a relationship between finishing technique and properties? Preliminary results. In: Proceedings of the International RILEM Workshop Repair Mortars for Historic Masonry. University of Technology, Delft

Roman vs. medieval crushed brick lime mortars: A comparative study

Martin Schidlowski¹, Tobias Bader¹, Anja Diekamp¹

(1) Unit of Material Technology, University of Innsbruck, Martin.Schidlowski@uibk.ac.at, Tobias.Bader@uibk.ac.at, Anja.Diekamp@uibk.ac.at

Abstract

A detailed material description of medieval crushed brick lime mortars from the Alpine region has not yet been performed. The present study focuses on the mineralogical characterization of mortars of this type in comparison to Roman age mortars. The samples were studied by polarized light microscopy, SEM-EDS, XRPD and TG-DTG in order to assess material characteristics.

First results of petrographic investigations revealed that the medieval as well as the Roman binders are inhomogeneous concerning their colour and structure, which is attributed to differences in the chemical composition of the binders, transformation of binder phases over time and a varying extent of alteration. Calcite, aragonite, lizardite and brucite as well as C-S-H phases and M-S-H phases were identified as components of the binder. The STA results indicated a hydraulic character of the mortars most likely resulting from a pozzolanic reaction between the slaked lime and the crushed bricks. The frequent occurrence of Mg-bearing phases, such as lizardite, brucite and M-S-H phases, suggests the widespread use of dolomitic lime as raw material for the binder production. Based on the results obtained, most of the samples can be classified as hydraulic dolomitic lime mortars.

Introduction

One factor for the centuries-long existence of relics of the Roman Empire was the building material *opus caementitium*, which is widely regarded as the predecessor of today's concrete. The material was, quite similar to today's concrete, based on a mixture of a binder, aggregates such as gravel and sand and water [1]. The binder was composed of slaked lime and volcanic ash, the so-called pozzolana. The reaction of lime with pozzolana and water is also called the pozzolanic reaction. In this reaction, strength-building mineral phases containing chemically combined water are formed [2].

Volcanic ash as a pozzolan was first used by the Greeks 500-300 AD [3]. Later, instead of volcanic ash, the Romans used more and more crushed bricks as additives to achieve similar results [4]. As the Roman Empire expanded, the knowledge of the use of pozzolanic additives was spread over many regions of Western and Southern Europe. For this reason, during the time of the Roman Empire, a largely uniform composition of mortar is found throughout

Europe [5]. This knowledge was largely lost with the collapse of the Roman Empire, starting around the 5th century AD.

Examples indicating that this technique was also used during the Middle Ages are so far limited to the Mediterranean area [6, 7]. In recent years it has become apparent that binders with pozzolanic additives in the form of crushed bricks were also used in the Alpine region in the Middle Ages [8]. A detailed characterization of the medieval crushed brick mortars occurring in the Alpine region has not yet been performed. In the present study samples of objects in South Tyrol and East Tyrol containing variable amounts of crushed bricks were examined. In order to make comparisons with focus on material characteristics (e.g. mineral phases, amount of brick, hydraulic character), Roman age mortars were characterized using the same analytical techniques.

Materials and analytical techniques

In total, 21 mortar samples from six Roman and five medieval objects in West Germany, East Tyrol and Northern Italy were analyzed. An overview is given in Table 1. Exemplary images of the samples are given in Figure 1. The Roman ones can be dated back to the early 2nd until late 4th century AD and were taken from residential buildings or thermal bath buildings [9]. The medieval samples can be dated back to the 13th until 16th century and origin from water cisterns [10].



Figure 1. Exemplary mortar samples from Colonia Ulpia Traiana (top left), the Roman museum Schwarzenacker (top right), Bruneck Castle (bottom left) and Sabiona Monastery (bottom right).

Table 1. Overview of the analyzed samples.

	Sample	Object	Location	Description	Age
	CUT1	Colonia Ulpia Traiana	Xanten, North Rhine-Westphalia	Opus signinum from the caldarium of the “Große Thermen”	circa AD 125
	SA1	Roman museum Schwarzenacker	Homburg, Saarland	Opus signinum, presumably from a craftsman’s house or a pottery	Possibly before AD 275/276
	VB1	Roman Villa Borg	Perl, Saarland	Floor screed from the frigidarium of the so-called “Villa Rustica”	Transition 2 nd /3 rd century AD
Roman	CA1-CA3	Archaeological park Cambodunum	Kempton, Bavaria	Opus signinum from the caldarium of the “Kleine Thermen”	2 nd half of the 2 nd century AD
	CA4A-CA4C	Archaeological park Cambodunum	Kempton, Bavaria	Opus caementitium from the caldarium of the “Kleine Thermen”	2 nd half of the 2 nd century AD
	CA5-CA7	Archaeological park Cambodunum	Kempton, Bavaria	Floor screed (non-heated) from a residential building	2 nd half of the 2 nd century AD
	VA1	Via Appia	Latium	Floor screed from a thermal bath building	AD 300-310
	MCA1	Aguntum	Dölsach, East Tyrol	Masonry mortar	Probably 1 st century AD
Medieval	SB1	Bruneck Castle	Bruneck, South Tyrol	Cistern mortar from the “Brunnenhaus”	Probably 16 th century
	KLS1-KLS2	Sabiona Monastery	Klausen, South Tyrol	Cistern mortar	medieval, undated
	HG1	Castle ruins Hochgalsaun	Kastellbell, South Tyrol	Cistern mortar	1329
	LB1-LB2	Laimburg	Pfatten, South Tyrol	Cistern mortar	2 nd half of the 13 th century
	BH1	Heinfels Castle	Heinfels, East Tyrol	Cistern mortar	medieval, undated

Thin sections of the mentioned samples were analyzed by polarized light microscopy with an Axio Imager.A2m Zeiss petrographic microscope. The focus of the petrographic analysis was on the description of the binder and the microstructure of the mortar.

To correlate the microstructural characteristics with chemical information and to examine the microstructure of the mortars in more detail based on material contrasts in the micron range, a Fei Company Quanta 200 3D scanning electron microscope (SEM) was used. The

semi-quantitative chemical analysis of selected binder areas was performed using an energy-dispersive X-ray spectrometer (EDS).

With the help of the ImageJ image processing program the brick fragments in the thin sections were measured and their percentage of the total sample as well as the fine proportion (<1 mm²) was calculated.

The qualitative mineralogical analysis of the binder using X-ray powder diffraction (XRPD) was carried out on the so-called binder-enriched fraction. This fraction was gained by carefully crushing samples (to prevent brick fragments and components of the aggregate from being crushed) and subsequently sieving off the fraction smaller than 63 microns. This fraction was analyzed with the Panalytical Empyrean X-ray diffractometer (Cu K-alpha = 1,54 Å, 5-70 °2θ, step size 0.013°, step time 1 s).

The hydraulic properties and the character of the binders were determined with thermogravimetric analyses (TG-DTG) by measuring the weight loss due to chemically bound water of hydraulic products between 200 and 600 °C, and the weight loss due to the carbon dioxide content of the carbonated lime between 600 and 1000 °C by using a Netzsch STA 449 F5 Jupiter (25-1000 °C, 10 °C/min heating rate, under air atmosphere).

Results and discussion

Microstructural characterization

The investigated binders are extremely heterogeneous with respect to their color. The color spectrum ranges from different shades of gray to brown shades. Lighter and darker, sometimes diffuse, "cloudy" areas, which indicate the hydraulic character of the binder [8], can be distinguished (Figure 2). Descriptions of the heterogeneity and variability of the binder of historic mortars are also found in the literature [11, 12, 13].

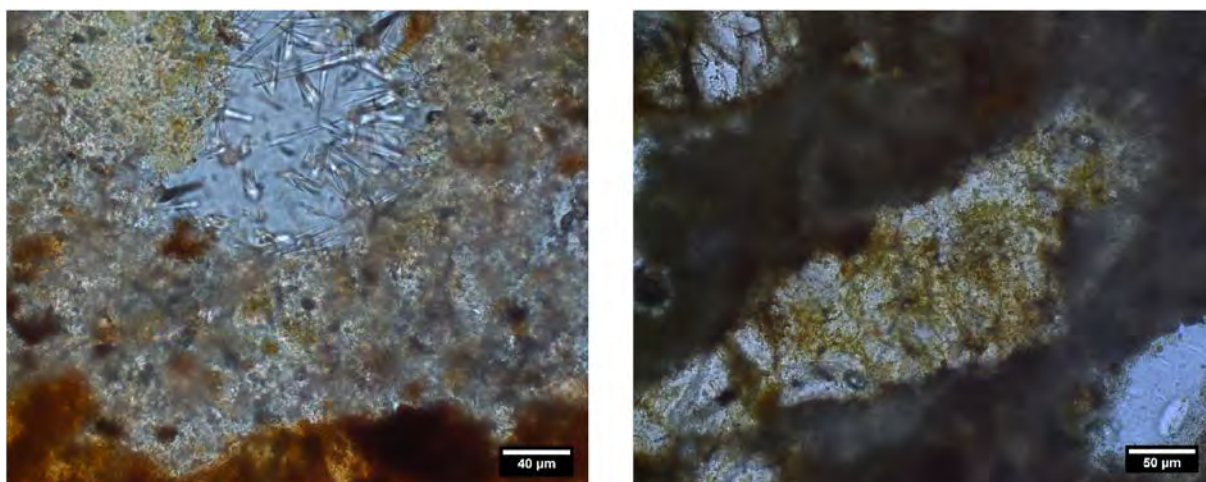


Figure 2. "Cloudy" structures around a pore filled with needles in sample VB1 (left). Polarizing microscope image, parallel polarizers. Diffuse dark areas at the edge of a pore of sample CA4B (right). Polarizing microscope image, parallel polarizers.

In order to correlate the different color levels of the binder observed by petrographic microscope images with its chemical composition, additional investigations on thin sections were made by SEM-EDS. It was found that mostly different contents of calcium or magnesium are responsible for the observed differences in the coloring. This can be clearly recognized by the sample CUT1. The slightly brownish areas in the polarizing microscope image appear brighter in the SEM image (Figure 3), which is due to a higher amount of calcium. The gray areas have a darker color in the SEM image and thus a higher content of the lighter element magnesium.

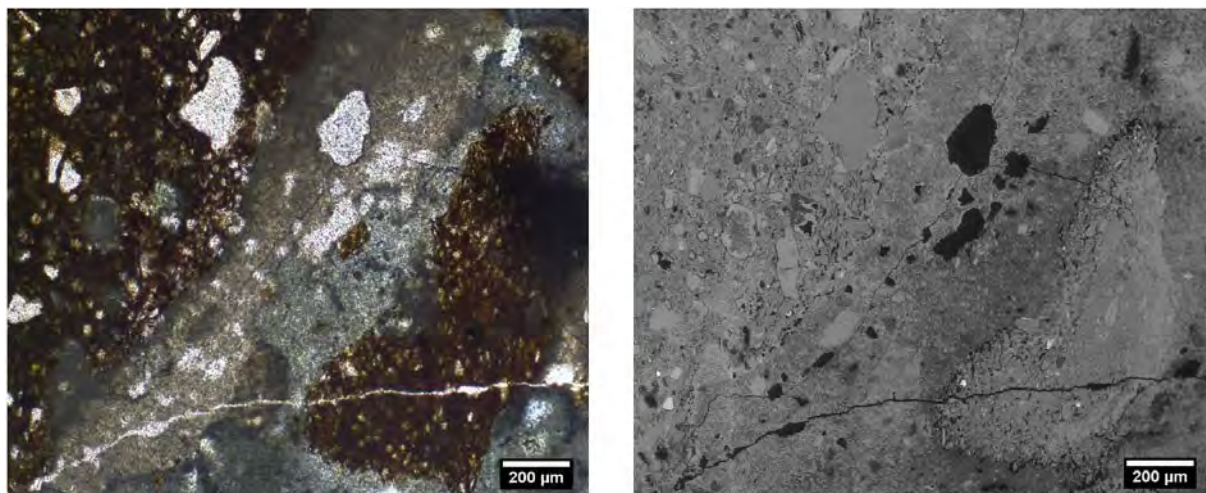


Figure 3. Inhomogeneous binder between brick fragments (very dark brown) in the sample CUT1 (left). Polarizing microscope image, parallel polarizers. Area of the left image (right). SEM image.

The samples differ with respect to the amount of aggregates. The crushed brick fragments are not counted among the aggregates, although depending on their size they can act like classic aggregates. Especially the larger pieces of brick can affect the deformability and the weight of the mortar and bring air into the binder to obtain a more efficient carbonation [4, 14]. The function of the finer grain fractions is to react pozzolanically with the quick lime in the binder to result in a hydraulic character of the binder [4]. An estimation of the ratio of aggregate to binder and crushed bricks was made on the thin sections. The percentage of aggregates ranges from 0% (Bruneck Castle) up to 50% (some samples from Cambodunum). Since no indications for reaction rims at the interface of aggregates and binder were found on the polarizing microscope, the aggregates were not investigated further.

The analyses with the ImageJ image processing program were used to characterize the brick fragments. First, the diameter of the largest brick fragments was measured (Table 2). In the Roman period samples, it varies from 3 mm to 20 mm. The brick fragments of the medieval samples are 2 mm to 10 mm in size. Thresholded areas were used to calculate the percentage of brick fragments in the total sample (Figure 4). It ranges between 4% (BH1) and 47% (CUT1, SA1). On average the bricks amount to 30% in the Roman period samples and to 23% in the medieval samples. Furthermore, the fine proportion ($<1 \text{ mm}^2$) was determined. The results were classified in the categories low ($<3\%$), medium (3-6%) and high ($>6\%$). The determined fine fraction is largely constant within individual samples but varies greatly

(between 0.9 and 8.6%) between the samples. Due to the relatively low number of samples per object, these average values are only to be seen as a rough estimate.

Table 2. Data generated by means of image processing for the characterization of the crushed bricks.

	Sample	Max. diameter (mm)	Brick proportion (%)	Fine proportion (<1mm ²)
Roman	CUT1	11	47	low
	SA1	13	47	medium
	VB1	6	43	high
	CA1	4	5	low
	CA2	5	30	medium
	CA3	6	16	low
	CA4A	20	34	low
	CA4B	8	36	low
	CA4C	4	27	low
	CA5	4	23	high
	CA6	13	37	low
	CA7	5	34	medium
	VA1	3	9	medium
	MCA1	6	30	medium
	Medieval	SB1	5	39
KLS1		5	39	high
KLS2		4	27	medium
HG1		2	11	high
LB1		10	21	low
LB2		5	17	low
BH1		4	4	low

Chemical and mineralogical characterization of the binder

Based on XRPD analyses, the mineral constituents of the binder-enriched fraction were determined (Table 3). Calcite is the dominant phase in the binder of the Roman period mortars. In some samples, aragonite appears, but only in small quantities. Two samples (CUT1, MCA1) contain lizardite ((Mg,Al)₃[(Si,Fe)₂O₅]OH₄). Quartz is the dominant aggregate. Besides that, cristobalite, feldspar (microcline or albite), carbonates (calcite or dolomite) were identified in most samples. VA1 is the only mortar which contains pyroxene.

Calcite is also in the medieval binders the dominant phase. A special case is the sample BH1, which has only a very low content of calcite and no further binder phases. Aragonite occurs in five samples in low quantities. The sample KLS2 has brucite in the binder. Two diffractograms (SB1 and KLS2) show a broad peak at 10-12 °2θ, which is difficult to assign. The existence of a calcium- and aluminum-containing hydroxide (e.g. hydrocalumite) is

regarded as potential binder phase. Quartz is by far the most common aggregate. Besides that, feldspars (microcline or albite) and carbonates (calcite or dolomite) are present in all samples. With the exception of sample SB1, all samples show evidence of phyllosilicates (muscovite or clinocllore). In the samples SB1, KLS1 and KLS2 hematite is found. KLS1 is the only sample with significant proportions of gypsum, which is believed to have been formed as a result of atmospheric pollution by SO₃.

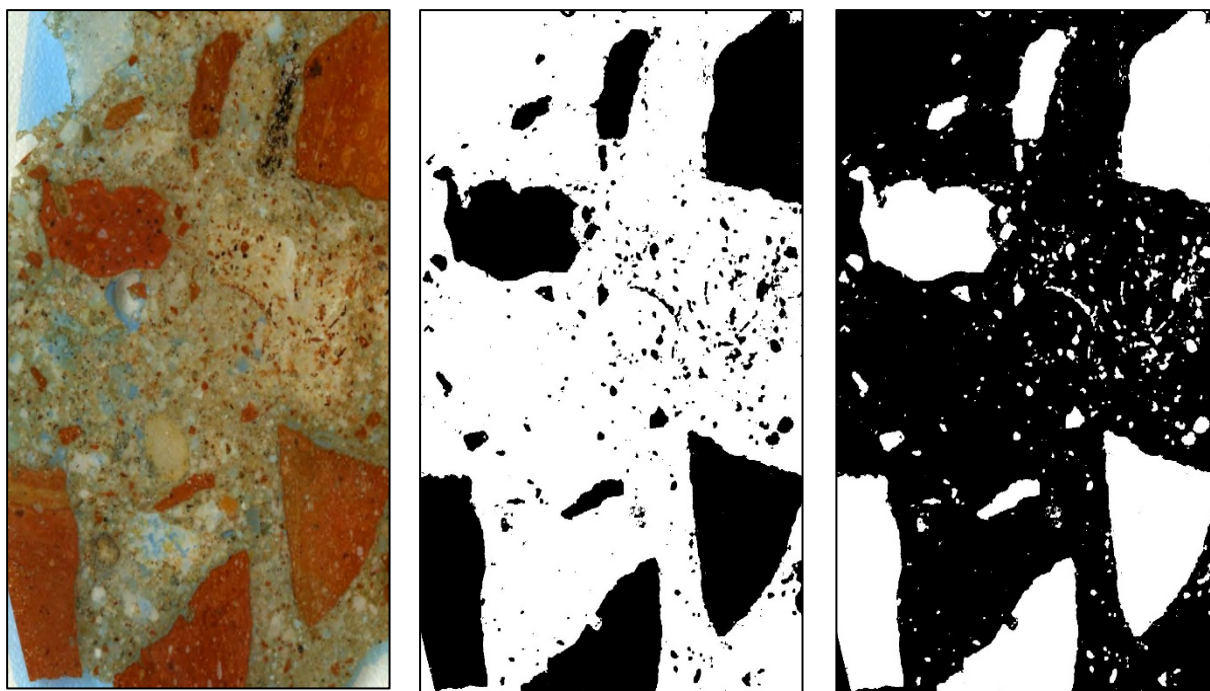


Figure 4. Section of the thin section of sample CA2 (left), brick fragments marked in black (center), binder marked in black (right). Image width approx. 17 mm.

Furthermore, in some Roman and medieval diffractograms there are indications on poorly crystalline, respectively, amorphous calcium silicate hydrates (C-S-H phases) and magnesium silicate hydrates (M-S-H phases) in the form of broad, diffuse peaks and elevated backgrounds. The same samples show high contents of magnesium (up to 33% MgO) in EDS analysis, although in some of them no magnesium-containing binder phases could be detected by means of XRPD. This is a strong indication of M-S-H phases.

The presence of lizardite or other M-S-H phases in the binder of historic mortars is also found in the literature [15]. For a more detailed analysis of a Mg-rich binder, binder areas in fragments of CUT1 were investigated by SEM-EDS. The obtained results show that these areas are highly enriched in magnesium and silicon (Figure 5). The Mg/Si ratio is greater than 1, which may indicate M-S-H phases such as serpentine or the serpentine precursor lizardite [16,17]. This means that the lizardite identified in the binder-enriched fraction by means of XRPD can be assigned to the binder. The high magnesium content in the binder indicates dolomitic lime as a raw material. Between the Mg content of quicklime and the brick dust, a similar reaction to the pozzolanic reaction has most likely occurred. Secondary formation originating from C-S-H phases through aqueous, Mg rich solutions can be excluded due to the differences in silicate structure and ionic radii [15].

Table 3. Mineralogical composition of the binder-enriched fraction.

	Sample	Composition
Roman	CUT1	Cal +++, Qz ++, Lz ++, Mc +, Ab ?
	SA1	Cal +++, Qz ++, Mc +, Ab ?
	VB1	Cal +++, Qz +++, Arg ++, Dol +, Mc +
	CA1	Cal +++, Qz ++, Dol +, Arg +
	CA2	Cal +++, Qz ++, Dol +, Mk ?, Ab ?, Arg ?
	CA3	Cal +++, Qz +++, Dol +, Mc +, Ab ?, Crs ?
	CA4A	Cal +++, Qz ++, Dol +, Mc ?, Ab ?, Crs ?
	CA4B	Cal +++, Qz ++, Mc +, Ab ?, Dol ?, Crs ?
	CA4C	Cal +++, Qz ++, Dol +, Ab ?, Crs ?
	CA5	Cal +++, Qz ++, Dol +, Mc ?, Ab ?
	CA6	Cal +++, Qz ++, Dol +, Mc ?, Ab ?
	CA7	Cal +++, Qz ++, Dol ?, Mc ?, Crs ?
	VA1	Cal +++, Qz +, Px +
	MCA1	Cal +++, Qz ++, Dol +, Arg +, Lz +, Ill ?
Medieval	SB1	Cal +++, Qz ++, Mc +, Hm +, Arg +, Hc ?
	KLS1	Cal +++, Qz +++, Mc ++, Gy ++, Hm +, Dol ?, Ms ?
	KLS2	Cal +++, Qz +++, Mc +, Arg +, Hm +, Brc+, Dol ?, Hc ?, Ms ?
	HG1	Cal +++, Qz ++, Ab +, Dol +, Ms +, Mc ?
	LB1	Qz +++, Cal ++, Ab +, Mc +, Arg +, Ms +, Clc +, Dol ?
	LB2	Qz +++, Cal ++, Ab +, Mc+, Ms +, Dol +, Arg ?, Clc ?
	BH1	Qz +++, Ab ++, Ms +, Cal +, Clc +, Arg ?

Ab: albite, Arg: aragonite, Brc: brucite, Cal: calcite, Clc: clinocllore, Crs: cristobalite, Dol: dolomite, Gy: gypsum, Hc: hydrocalumite, Hm: hematite, Ill: illite, Lz: lizardite, Mc: microcline, Ms: muscovite, Px: pyroxene, Qz: quartz. Based on the peak intensities, the individual fractions were quantified according to the following system [11]: +++ present, dominant; ++ present; + traces; ? possibly present.

Results of STA provide important parameters for the characterization of the binders. The evaluation of the DTA-TG curves according to Bakolas et al. (1998) is shown in Table 4. The weight loss at temperatures below 120 °C is due to the loss of adsorbed (physically bound) water. In the range of 120-200 °C, the weight loss is due to the loss of water from hydrated salts (e.g. gypsum). In the interval of 200-600 °C the weight loss corresponds to the loss of hydraulic (chemically bound) water. The weight loss between 600-1000 °C is due to the loss of CO₂ during the decomposition of carbonates. From this value, the CaCO₃ content of the binder-enriched fraction can be calculated. The CO₂/H₂O ratio gives important hints on the hydraulic nature of the binder [6]. The CO₂/H₂O ratio of the analyzed mortars ranges between 0.7 and 6.8. None of the samples has a value above 7.5, as would be typical for a pure lime mortar [18].

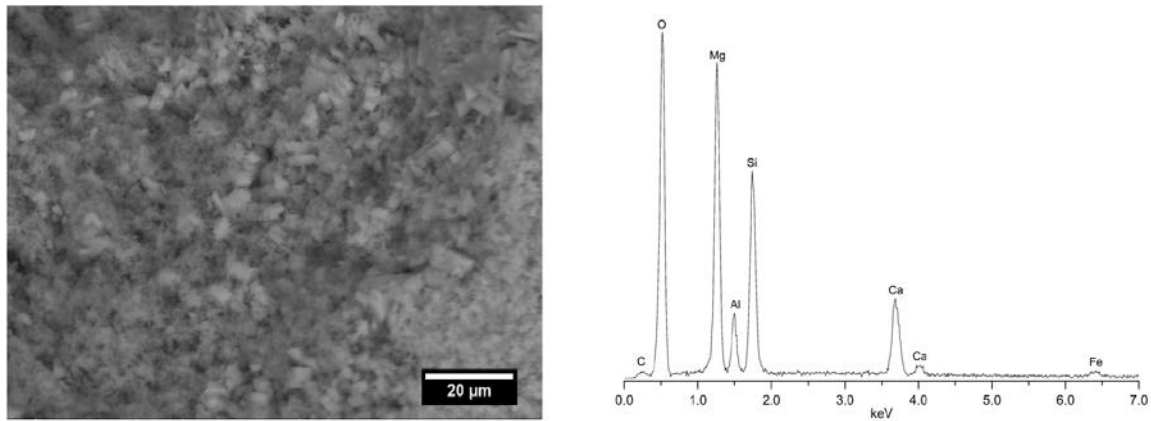


Figure 5. SEM image of a fragment of sample CUT1 (left). Corresponding spectrum of EDS measurement (right).

Table 4. Results of the simultaneous thermal analysis.

	Sample	Mass loss (%) per temperature interval (°C)					CO ₂ /H ₂ O	Weight% CaCO ₃
		25-120	120-200	200-600	600-1000	Total		
Roman	CUT1	1.45	0.82	5.34	16.28	23.89	3.04	37.0
	SA1	1.57	1.20	5.03	25.04	32.84	4.98	57.0
	VB1	2.75	1.67	3.86	18.71	26.99	4.85	42.6
	CA1	1.55	0.81	4.16	28.31	34.83	6.81	64.4
	CA2	1.36	1.06	5.28	21.71	29.41	4.11	49.4
	CA3	2.17	1.12	4.30	18.25	25.84	4.24	41.5
	CA4A	1.72	0.79	3.55	24.07	30.13	6.78	54.7
	CA4B	1.39	0.55	3.49	23.69	29.12	6.79	53.9
	CA4C	1.38	0.85	3.31	22.56	28.10	6.82	51.3
	CA5	3.16	2.06	4.71	17.67	27.60	3.75	40.2
	CA6	2.59	1.66	4.45	20.61	29.31	4.63	46.9
	CA7	2.28	1.66	4.79	18.39	27.12	3.84	41.8
	VA1	2.50	3.47	6.96	14.47	27.40	2.08	32.9
	MCA1	2.42	1.84	5.64	12.82	22.72	2.27	29.2
Medieval	SB1	4.10	2.89	10.42	13.14	30.55	1.26	29.9
	KLS1	2.35	2.81	6.48	9.90	21.54	1.53	22.5
	KLS2	2.85	3.16	12.50	8.15	26.66	0.65	18.5
	HG1	1.60	1.09	6.02	20.47	29.18	3.40	46.6
	LB1	2.29	1.14	5.18	8.59	17.20	1.66	19.5
	LB2	2.34	1.11	6.25	7.57	17.27	1.21	17.2
	BH1	2.73	1.20	4.30	4.96	13.19	1.15	11.3

A graphical evaluation of some STA results from Table 4 is shown in Figure 6. Comparative values for the classification into different categories were graphically presented as well [18]. The 21 mortar samples examined were divided into four different groups:

- Nine samples (CUT1, SA1, VB1, CA2, CA3, CA5, CA6, CA7, HG1) are in the category of artificial pozzolanic mortars, of which only one is medieval (HG1). The calcium carbonate contents range between 37.0 and 57.0%. None of the samples shows high levels of magnesium or aluminum in the binder. It is probable that in these mortars a pozzolanic reaction has taken place, which has shifted its chemistry into the field of artificial pozzolanic mortars.
- Four samples from Cambodunum (CA1, CA4A, CA4B, CA4C) are in the category of hydraulic lime mortars. The reason for their assignment to this category is the CO₂/H₂O ratio. High calcium carbonate contents (51.3 to 64.4%) compared to the previous category and only small amounts of brick dust determine the character of these mortars. EDS analyzes showed that the levels of calcium within the binder vary, but on average are higher than in all other samples.
- Two samples (SB1, KLS2) are in the category of natural pozzolanic mortars. They are characterized by a very high content of hydraulic water (10.4 and 12.5%). The samples are the only ones in which hydrocalumite was detected. In addition, the evaluation of the XRPD data and the DTG curves showed the presence of brucite, which is also hydrous. Binder ranges are found in both samples in which the magnesium content exceeds the calcium content.
- Six samples (VA1, MCA1, KLS1, LB1, LB2, BH1) are also in the category of natural pozzolanic mortars or close to it. The levels of hydraulic water in these samples would be in the category of artificial pozzolanic mortars. The reason for the low CO₂/H₂O ratio is the low level of calcium carbonate in these binders. In the samples MCA1, KLS1, LB1, LB2 and BH1, the magnesium contents exceed the calcium contents in all binder ranges investigated by EDS. VA1 is a special case because the aluminum content in the binder exceeds that of calcium.

From the obtained results the following comments regarding the categorization can be drawn:

- The system used by Moropoulou et al. (2005) [18] to evaluate STA results was considered for the categorization of mortars with a calcium-rich character of the binder. Once this is magnesia-rich or aluminum-rich, there are problems in assigning to these categories.
- Despite the utmost care in sample preparation, the binder-enriched fraction of some samples contains appreciable amounts of ground up, mostly SiO₂-rich aggregates. The CO₂ content or the CO₂/H₂O ratio is shifted to lower values, which is why the chemistry of the samples may be shifted as well.

- Historic crushed brick mortars can't always be classified in distinct categories in terms of their chemistry due to the heterogeneity in the composition and the different production.
- Small differences in the semi-quantitative mineralogical composition may occur due to different states of alteration of the objects [12, 13].

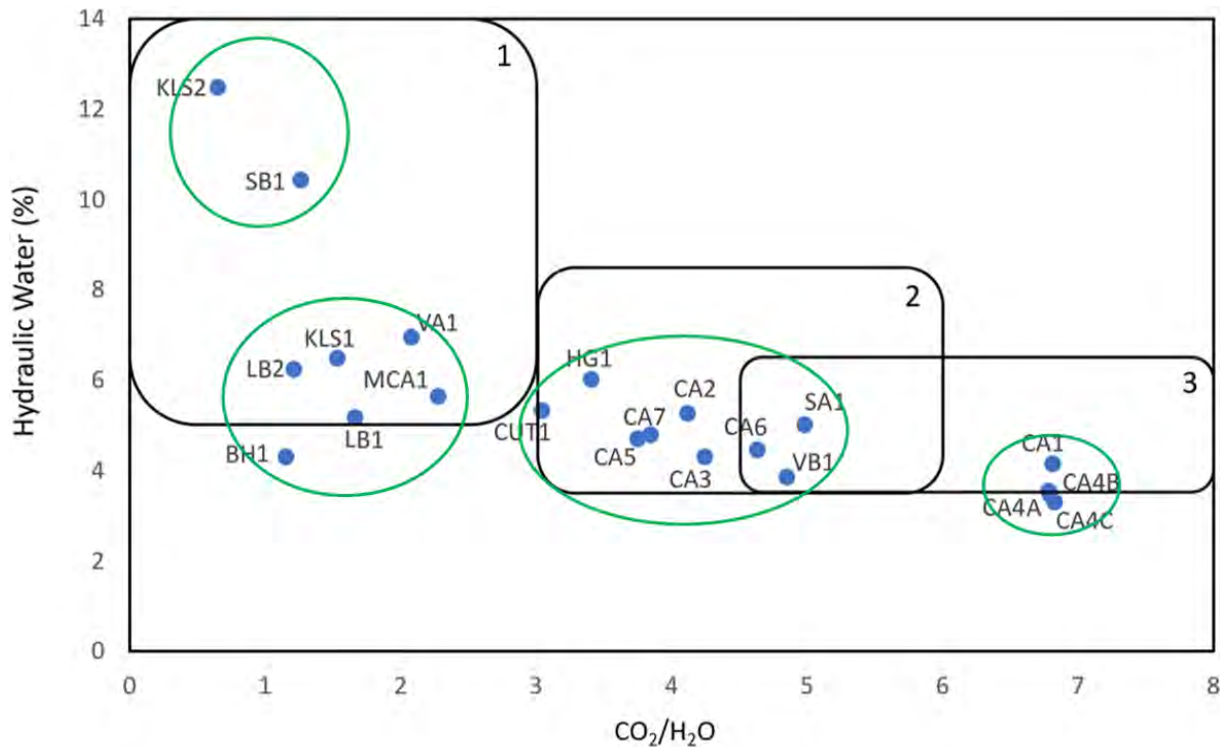


Figure 6. Hydraulic Water (%) against $\text{CO}_2/\text{H}_2\text{O}$ ratio. Different categories (1-3) as suggested by Moropoulou et al. (2005) [18]. 1: mortars with natural pozzolana. 2: mortars with artificial pozzolana. 3: hydraulic lime mortars. Framed in green are the four categories into which the examined mortars were classified according to chemical parameters.

From the STA results, it can be concluded that all investigated binders have a hydraulic character. According to Cardiano et al. (2008) [19], the estimation of the hydraulic character by the $\text{CO}_2/\text{H}_2\text{O}$ ratio can be problematic if mica is included in the mortar. This is the case in samples MCA1, KLS1, KLS2, HG1, LB1, LB2 and BH1, but only in traces. The character of these samples can still be described as hydraulic. The phenomena of the diffuse, "cloudy" structures observed in the polarization microscope in some samples also indicate a hydraulic character of the binder. They are discussed in more detail at Diekamp et al. (2012) and Diekamp (2014) [20, 8].

If magnesium phases have been detected in the binder of a mortar, which indicates the use of dolomite or dolomitic lime as raw material, it can be characterized as hydraulic dolomite lime mortar instead of hydraulic lime mortar. The widespread distribution of dolomitic lime mortar has only recently become the subject of research.

Conclusions

In the present study it was shown that historic crushed brick mortars were used at least locally as cistern mortars in the Alpine region during the Middle Ages, although this knowledge was long thought to be lost.

The investigated medieval and Roman mortars are extremely heterogeneous with respect to the color and structure of the binder. The main reasons for that are a different chemical composition, transformation of the binder over the centuries and a different state of alteration. The proportion of the brick fragments in the medieval mortars is slightly lower than in the Roman ones. The finer fractions seem to serve as pozzolanically active components to affect the hydraulic character of the binder. The large brick fragments act rather like classic aggregates.

Calcite is the main constituent of the binder in all medieval and Roman mortars. Furthermore, aragonite, lizardite and brucite were identified as constituents of the binder, with brucite only in small amounts in medieval times. Lizardite was only detected in Roman samples and is thought to have formed from Mg-rich quicklime and brick dust in the course of a reaction similar to the pozzolanic reaction. XRPD as well as STA analyses give strong indications on C-S-H phases and M-S-H phases in the binder.

All investigated mortars have a hydraulic character. The Roman samples can be classified, with two exceptions, according to categories presented in the literature, as artificial pozzolanic mortars or hydraulic lime mortars (in the case of little brick dust in the binder). The medieval ones, with one exception, can't be assigned to these two categories. This fact can be attributed to high levels of hydraulic water due to the appearance of hydrous mineral phases and a magnesium- or aluminum-rich character of the binder. If magnesium phases are present in the binder, the mortars can be classified as hydraulic dolomitic lime mortars.

Acknowledgements

The authors would like to thank Hannes Lehar, Tim Rekelhoff, Martin Mittermair and Martin Auer for purchasing the samples.

References

1. Locher FW (2000) Zement - Grundlagen der Herstellung und Verwendung. Verlag Bau und Technik, Düsseldorf
2. Massaza F (1998) Pozzalana and Pozzolanitic Cements. In: Hewlett PC (ed) Lea's chemistry of cement and concrete, 3rd edn. Butterworth Heinemann, Oxford
3. Idorn MG (1997) Concrete progress from Antiquity to the third millenium. Telford, London

4. Baronio G, Binda L & Lombardini N (1997) The role of brick pebbles and dust in conglomerates based on hydrated lime and crushed bricks. *Constr Build Mater* 11:33-40
5. Genestar C, Palou J & Pons P (2008) Thermal study of historic mortars from Mallorca. In: *Proceedings of the HMC, Historic Mortars Conference, 24th-26th September 2008, Lisbon*
6. Bakolas A, Biscontin G, Moropoulou A & Zendri E (1998) Characterization of structural byzantine mortars by thermogravimetric analysis. *Thermochim Acta* 321(1-2):151-160
7. Moropoulou A, Çakmak AS, Biscontin G, Bakolas A & Zendri E (2002) Advanced Byzantine cement based composites resisting earthquake stresses: The crushed brick/lime mortars of Justinian's Hagia Sophia. *Constr Build Mater* 16(8):543-552
8. Diekamp A (2014) *Bindemitteluntersuchungen an historischen Putzen und Mörteln aus Tirol und Südtirol*. Dissertation University of Innsbruck
9. Lehar H, private communication
10. Rekelhoff T, private communication
11. Middendorf B, Hughes JJ, Callebaut K, Baronio G & Papayianni I (2005) Investigative methods for the characterisation of historic mortars – Part 1: Mineralogical characterisation. *Mater Struct* 38:771-780
12. Elsen J, van Balen K & Mertens G (2012) Hydraulicity in historic lime mortars: a review. In: Valek J, Hughes JJ, Groot CJWP (eds) *Historic Mortars*. Springer Netherlands
13. Miriello D, Bloise A, Crisci GM, Apollaro C & La Marca A (2011) Characterisation of archaeological mortars and plasters from kyme (Turkey). *J Archaeolog Sci* 38:794-804
14. Velosa A, Coroado J, Veiga M & Rocha F (2007) Characterisation of Roman mortars from Conimbriga with respect to their repair. *Mater Charact* 58:1208-1216
15. Sabbioni C, Bonazza A & Zappia G (2002) Damage on hydraulic mortars: the Venice Arsenal. *J Cult Herit* 3:83-88
16. Lothenbach B, Nied D, L'Hôpital E, Achiedo G & Dauzères A (2015) Magnesium and calcium silicate hydrates. *Cem Concr Res* 77:60-68
17. Nied D, Enemark-Rasmussen K, L'Hôpital E, Skibsted J & Lothenbach B (2016) Properties of magnesium silicate hydrates (M-S-H). *Cem Concr Res* 79:323-332
18. Moropoulou A, Bakolas A & Anagnostopoulou S (2005) Composite materials in ancient structures. *Cem Concr Compos* 27:295-300
19. Cardiano P, Sergi S, De Stefano C, Ioppolo S & Piraino PJ (2008) Investigations on ancient mortars from the basilian monastery of Fragalà. *J Therm Anal Calorim* 91:477-485

20. Diekamp A, Stalder R, Konzett J & Mirwald PW (2012) Lime Mortar with Natural Hydraulic Components: Characterisation of Reaction Rims with FTIR Imaging in ATR-Mode. In: Valek J, Hughes JJ, Groot CJWP (eds) Historic Mortars. Springer Netherlands

A map is worth a thousand pictures: Using FTIR-imaging to analyze petrographic thin sections of historical and experimental mortar

Anthony J. Baragona¹, Marta Anghelone², Johannes Weber¹

(1) Institute for Art and Technology/ Conservation Science, University of Applied Arts, Vienna

Salzgries 14/1, Vienna, Austria A-1013, anthony.baragona@uni-ak.ac.at

(2) Institute for Conservation, University of Applied Arts, Vienna

Salzgries 14/1, Vienna, Austria A-1013, marta.anghelone@uni-ak.ac.at

Abstract

This contribution describes analyzing polished petrographic thin sections of mortar by means of a succession of image-based analytical techniques, starting with optical microscopy, moving to scanning electron microscopy combined with energy dispersive X-ray spectroscopy and culminating with FTIR imaging combined with image analysis software. The use of thin sections preserves the most important features of a mortar: the spatial relationships and context between a mortar's micro-features, which are imperative to understanding the materials and techniques employed by an artisan in producing the mortar, as well as alteration phenomena that have taken place since.

This approach is illustrated here by its application to a number of mortars from Roman antiquity as well as experimental mortars, all of which consist of an air-lime binder mixed with a reactive aggregate - either ceramic or volcanic pozzolan. Long-term chemical changes make direct correlation between experimental and historical mortars a challenge, but the technique did produce both qualitative and quantifiable results that otherwise could not have been achieved without the destruction of the sample.

Keywords: FTIR-imaging, mortar characterization, microscopy, pozzolanic mortar, C(A)SH

1. Introduction

A wide variety of analytical methods are available to researchers when choosing an investigative path for examining historical mortar. Traditional analysis focuses on chemical dissolution methods, the most thorough of which were codified by a team of the most experienced researchers at RILEM in 2004 [1]. These techniques have a number of significant advantages: they are fast and inexpensive to perform and utilize common laboratory equipment, they produce clearly quantifiable results, and because of the previous two reasons, a large body of data exists for comparison of results. However, they include

significant disadvantages as well, all of which they share with methods that employ thermogravimetric techniques. Firstly, they destroy the mortar sample precluding further analysis. Secondly, mechanical and chemical separation of a mortar's binder and aggregate is often difficult to impossible to perform adequately [2]. This especially in the case of the highly altered, historical lime-pozzolan mortars presented herein where it is unclear if very fine pozzolan is behaving as an aggregate or binder portion or conversely, if large lime lumps are behaving more as aggregates than binder, despite their chemistry. Finally and perhaps most importantly, chemical and thermal dissolution deletes any information that could be gained from observing the mortar's microstructure [2].

In ancient pozzolanic mortars, microstructural data such as the spatial relationships between mortar constituents, quantity and shapes of macro-porosity and cracking, and the morphology and density of relic lime clasts (lime lumps), reactive silicate aggregate and/or degradation products hold the key to understanding the "life story" of the mortar. This story includes the production of the binder material, the selection of aggregate, the production and application of mortar and subsequent physical and chemical changes that occur both during its service life and as an archaeological remnant [3]. Of primary interest in these types of mortars is how they form a cementing binder through the pozzolanic reaction, that is a reaction between calcium hydroxide and fine amorphous alumina-silicate material in the presence of water [4]. This is detectable by performing various types of microscopy on larger aggregates through the detection of reaction rings, areas that exhibit the mixing of calcium and silicate material. In ancient mortar it can be the case that the source of reactive silica is not immediately evident, thus underscoring the need of thorough microscopic analysis [5]. The degree to which an aggregate reacts gives insight into the qualities of a mortar, such as how strong could it become or in which applications could have it been used [5,6]. Physical and chemical changes over time such as the interaction between the alkaline binder and the aggregates effect a mortar's durability, an issue which is of interest to contemporary cementitious materials as well as historical [7]. This type of information is lost during chemical and thermal dissolution techniques that quantify chemical compounds independently of physical context.

This study focuses on number of mortars from Roman antiquity as well as experimental mortars produced in the laboratory and in the field intended to emulate such antique mortars. All of these mortars consist of an air-lime binder mixed with a reactive aggregate - either ceramic or volcanic pozzolan - and are from structural applications, such as *opus caementicium* or *signinum*. Comprehensive, image-based analysis was performed on high quality, polished (uncovered) petrographic thin sections, which allows for a sample to be examined successively by optical microscopy (OM), scanning electron microscopy combined with energy-dispersive X-ray spectroscopy (SEM-EDX) and Fourier transform infrared spectroscopy, here used in reflection mode to create spectral maps (FTIR). Performing all of these analyses on the same sample preparation eliminated the need to form correlations between separate analytical techniques, since, for example, EDX data can be drawn from an area that is visible in optical microscopy and via the SEM. Building upon the foundation

established by OM and SEM-EDX, FTIR-imaging was found to be particularly useful in illustrating binder matrix composition including degradation and hydration products, the latter of which are nearly impossible to conclusively identify by OM or SEM-EDX. FTIR has been widely applied to the study of inorganic materials in general since the mid 20th century [8] and for cementitious systems specifically ever since then [9-11]. Calcium alumina-silicate hydrates (C(A)SH), a group of minerals that form the main products of the pozzolanic reaction which give a mortar its strength and ability to set have likewise been well studied by FTIR generally on homogenous preparations of hydrated cement [12-14]. This database of FTIR spectra allowed the identification of C(A)SH and other reaction and degradation products within both the experimental and archaeological mortars. While both FTIR mapping (in ATR mode) and Raman spectral mapping have previously shown potential in identifying different regions of cement hydrates within mortar [15-17], Raman proved difficult to use on samples containing fine ceramic dust due to fluorescence of the clay minerals. FTIR-ATR FTIR-mapping showed great potential in studying the distribution of the formation and degradation products of pozzolanic lime mortar.

2. Experimental Set-up

The experiment consisted of the comprehensive image-based analysis of both experimental mortar and historical mortar, which allowed for the comparison between the two. Performing the analysis on experimental mortar of known provenance provided both a test control of the technique as well as a view of what the historical mortar could have looked like early in its development.

2.1 Production of the experimental mortar

Two sets of experimental mortar were produced in a controlled setting. Mortar was produced by the “hot slaked lime” technique [18]. Quicklime from a traditional lime kiln was mixed with both volcanic pozzolan (Terra Pozzolana Nera, Kremer Pigmente GmbH & Co. KG, Germany) and lab-fired ceramic from two types of clay (provided by Wienerberger GmbH, Austria) in the volumetric ratio of 1:2.5. The water to binder ratio varied dependent on workability, but was in the range of 1.5-2:1. This mortar was intended to emulate Roman-era, structural pozzolanic mortar. It was cast in large plates then cured and stored in a controlled environment with high humidity (sealed in plastic with excess moisture, equivalent to 100% Rh) previous to physical testing, per international concrete testing standards [19]. After physical testing, pieces of mortar were prepared as thin sections as described below.

2.2 The historical mortar samples

The experimental samples were compared to historical mortar samples from a number of Roman archeological sites. Examples of lime – volcanic pozzolan mortar from Ostia Antica, Italy and lime – ceramic pozzolan mortar from Vindobona (Vienna, Austria) and Školarice,

Slovenia are described in this work. With the exception of the samples from Ostia, all mortars would have experienced high exposure to humidity (for example in a Roman bath) during their service life before becoming archeological relics.

2.3 Sample Preparation

All mortar samples were prepared as polished petrographic thin sections, left uncovered to allow their analysis by detectors that use reflected light or lasers. Prior to thin sectioning, the samples were vacuum-impregnated with blue-dyed (EpoBlue from Buehler GmbH, Germany) epoxy resin (Araldite 2020 from Hunstman, USA), the blue dye allowing for the easy visual separation of porosity from clear minerals. The samples were mounted on glass slides and polished to approximately 35 μm in thickness. Samples prepared in this way could then be analyzed by transmitted and reflected light OM, as well as SEM-EDX and FTIR in reflected mode [3].

3. Analytical Procedure

In concept the analytical procedure is intended to move through the methods in the order listed below, but in practice there is often switching between these methods as new discoveries are made. This is particularly true when elemental (EDX) or molecular (FTIR) results contradict observations made by OM. Once an area of interest is positively identified, FTIR imaging can be calibrated to focus on find the distribution of that constituent through the sample area, e.g. the intensity of one of the IR bands that would indicate C(A)SH.

3.1 Optical Microscopy (OM)

As the first step, optical microscopy was used to identify possible areas of interest such as reaction rims, lime lumps and areas of binder alteration. The first microscope was a Nikon SMZ 1500 stereomicroscope (SM), with an 8x eyepiece, 1x lens, and the ability to zoom from 0.75-11.25x, for range of magnification from 6-90x. The second microscope was an Olympus BX40 polarizing light microscope (PLM) with a 10x eyepiece and 5, 10, 20, 50 and 100x objectives, for a range of magnification of 50-1000x. The incident and transmitted light sources are polarizable for this microscope. The stereomicroscope was most useful for studying the binder, with different densities most clearly visible in photomicrographs taken with plane polarized light in dark-field mode (PPL-DF) or incident light with white background (ILW). The PLM was used for mineral identification, especially with cross-polarized illumination (XPL), as well as to provide high detail of binder content crystallography, visible starting at magnifications around 200x. Both microscopes provided scaled images to serve as an underlying layer for the final parts of this procedure. With both microscopes, a Cannon EOS 600D DSL camera coupled with the EOS Utility software was used to capture photomicrographs.

3.2 Scanning electron microscopy - energy-dispersive X-ray spectroscopy (SEM-EDX)

After the identification of areas of interest through OM, SEM-EDX was used to make high magnification images and gain chemical information in the form of elemental or oxide analysis. Stoichiometric elemental analysis of areas of binder or the binder-aggregate interface (a “reaction rim”) can verify the presence of pozzolanic activity.

A FEG Quanta 250 Scanning Electron Microscope (FEI, U.S.A.) coupled with a Pegasus APEX Energy-Dispersive X-ray spectroscope (Ametek EDAX, U.S.A.) equipped with the Genesis SEM Quant software (SEM-EDX) was used. Images were generally taken in back-scattered electron mode (BSE) at 20 kV with a spot size of 4.0 nm. Thin sections were un-spattered and observed in low-vacuum mode. The SEM images can also be used as an underlying layer for a smaller scale, higher resolution FTIR-map based image.

3.3 Fourier-transform infrared spectroscopy imaging (FTIR)

The penultimate step, and final step of data collection is FTIR-imaging. An area tentatively identified in the previous steps of analysis can then be positively identified through the collection of FTIR spectra. Spectra are collected from selected mortar thin sections, which include target areas identified by OM and SEM-EDX. In the target areas spectra are evaluated, and FTIR bands characteristic of phenomena of interest, for example a reaction rim for C(A)SH minerals, are identified. By selecting the bands the software automatically displays the distribution of the intensity of such bands across the entirety of the image. A color scale from red (strong) to blue (absent) indicates the distribution of the selected bands, which corresponds to the distribution of chemical species. The FTIR images are then used to overlay the previous images (OM or SEM) creating a map for digital image analysis.

The device used was a Nicolet iN 10 MX Infrared Imaging Spectrometer (Thermo-Fischer Scientific, USA), with cooled MCT-A linear array detector, and interfaced with OMNIC Picta software. Spectra were collected in reflection mode, spectral range 4000-720 cm^{-1} , aperture 25 μm , with 8 cm^{-1} spectral resolution, and spatial resolution <10 μm . Ultra-fast mapping mode was used for mapping larger sections. The spectra were finally vector normalized and base-line corrected.

3.4 Digital Image Analysis

The resulting maps and images were then combined with digital editing software, in this case Adobe Photoshop®, although the editing is simple enough that it can be done with any of a variety of available freeware. The FTIR images are scaled and overlapped with images acquired by OM or SEM to create hybrid maps. These are able to provide a great deal of qualitative data regarding the nature of the mortar sample. Additionally, through pixel counting of the areas with highest intensity of selected characteristic FTIR bands in a specified area, quantitative comparison between two mortar samples was carried out. This

should be understood to be a *volumetric* quantitative comparison of mortar contents, which has the additional great benefit of showing *where* in the samples these contents occur, as contrasted to the *gravimetric* quantitative data found by thermo-gravimetric or chemical dissolution methods.

4. Results

4.1 Identifying reaction rims and hydrates in the binder matrix

The protocol described above was first used to search for reaction rims on individual aggregates, that once analyzed by FTIR should yield spectra that allow for the identification of C(A)SH resulting from the pozzolanic reaction. The molecules grouped together under the description of “C(A)SH” are relatively complex inorganic materials, but are identifiable in the mid- FTIR range by signature bands, which correspond to carbonates (CO₃; stretching around 1350 cm⁻¹ to 1500 cm⁻¹ assignable to both calcite and aragonite [15]) and to silicates (Si-O stretching between 1200 and 950 cm⁻¹ [8-14]). A wide range of hydrate species (X-OH) is also detectable, particularly in fresh, experimental mortar, the most important being a band at ca. 1660 cm⁻¹ indicating the interstitial bound (or “crystal”) water of C(A)SH [10-14].

Figure 1 shows the investigation of an ancient lime-ceramic mortar (*opus signinium*). Although it can be assumed that ceramic fines have reacted pozzolanically, a large piece of ceramic aggregate does not show any indication of reaction upon first inspection by OM. Examining the same aggregate by SEM reveals a border zone where the ceramic appears to be more dissolved than OM indicated. This border area was then investigated with EDX detecting a high amount of calcium, confirming that the chemical composition was ideal for reactivity. Finally, the presence of C(A)SH is confirmed by FTIR, where an image was created localizing carbonate and silicate at the border zone of the aggregate. While carbonate exists throughout the sample, the silicate band at ca. 1050 - 950 cm⁻¹ is detected only at the reaction rim indicating that it is a distinct type of silicate from those found within the ceramic body, and is likely co-molecular with the carbonate.

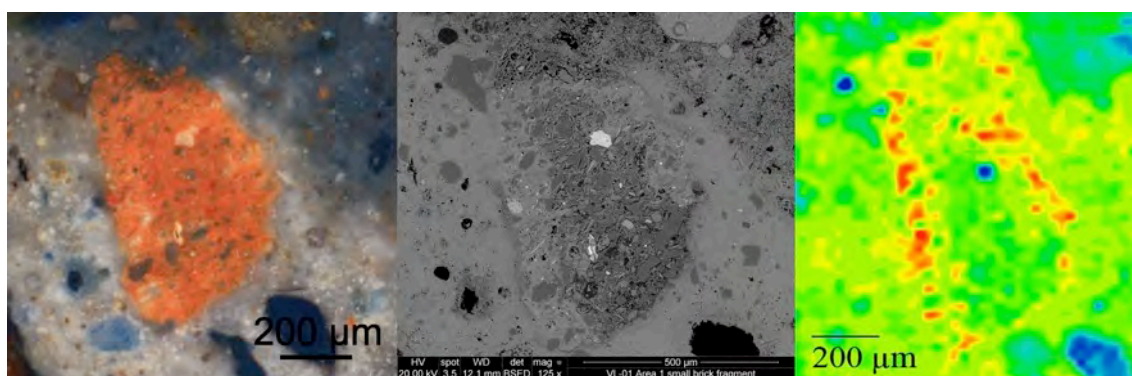


Figure 1. Left and Center: SM and SEM images of a ceramic aggregate; Right: FTIR image of the overlapping zones of carbonate and silicate. Scale: Red to Blue: 1.0-0.0. Roman hypocaust floor, Vindobona (Austria). (Previously Published in Weber & Baragona 2019 [3])

Figure 2 shows the same application of this protocol to the investigation of an ancient lime-pozzolana mortar (*opus caementicium*). While in this case, all types of investigation revealed that the rim area completely surrounding the glassy silicate aggregate to be predominately calcium carbonate, immediately outside of this ring, the surrounding binder area is rich in C(A)SH. What this indicates is that while the chemistry and mechanism for pozzolonic activity is similar between both mortar types, the place where the reaction takes place preferentially is somewhat different, in the aggregate's fine pore space in the ceramic example, in the binder matrix in the volcanic pozzolana example. This is shown on a larger scale in Figure 6.

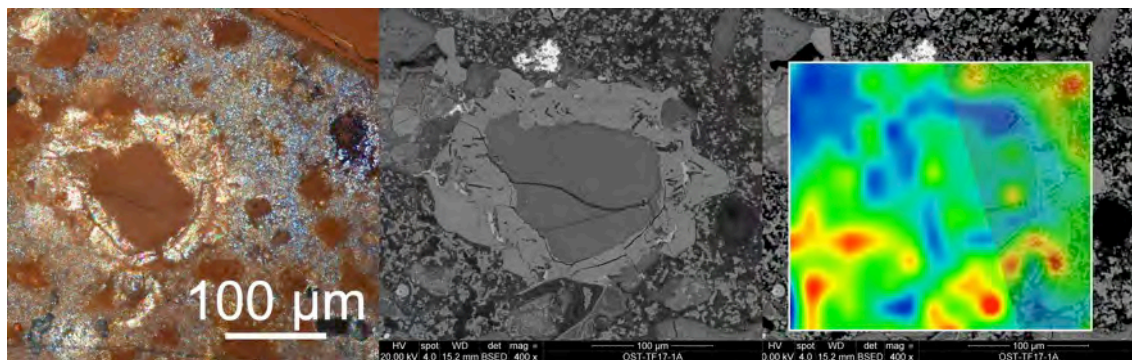


Figure 2. Left and Center: PLM and SEM images of a volcanic aggregate, surrounded by a dense ring of calcium carbonate; Right: FTIR map of the overlapping zones of carbonate and silicate (100%-50% opacity). Scale: Red to Blue: 1.0-0.0. *Opus caementicium*, Ostia Antica (Italy)

4.2 Application to experimental mortar

Applying this methodology to a larger scale provides both the opportunities to both visualize where in the sample the target materials occur, as well as extrapolate volumetric quantitative data. Figures 3 and 4 show this as applied to mortar created in a controlled setting, in which the materials used and in which proportions and the curing and aging environment are all known.

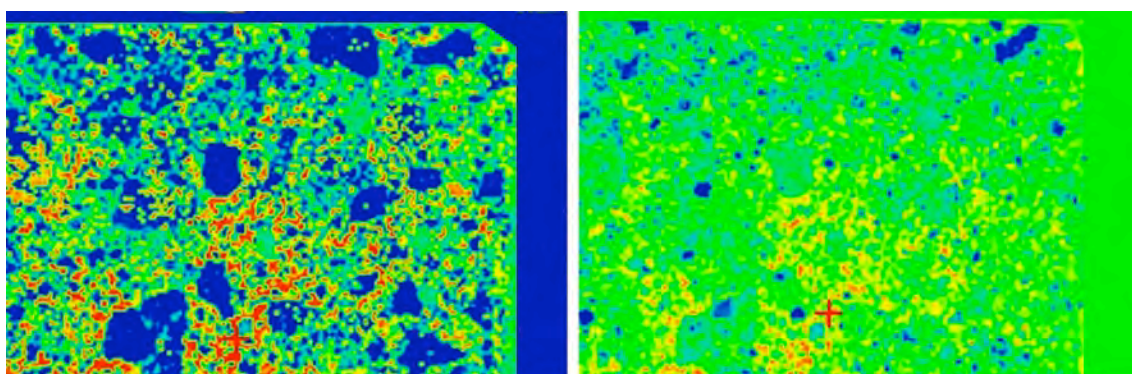


Figure 3 : Experimental Lime-Pozzolana Mortar. FTIR spectra associated with a reaction rim identified with SEM-EDX: Left image indicates highest density of the band, centered on 1663 cm^{-1} . Scale: Red to Blue: 4.0-0.0. Right image indicates the highest density of the band centered on 955 cm^{-1} . Scale: Red to Blue: 2.6-0.0.

Figure 3 shows FTIR images of an experimental lime-pozzolana mortar. Created by selecting a reaction rim previously discovered through OM and SEM-EDX, different bands associated with C(A)SH have been mapped. The top left image highlights the distribution of bound water (ca. 1720-1600 cm^{-1}). From the image it is visible that the bound water is mostly located in the interstitial matrix. The top right image shows the distribution of the silicate material most associated with C(A)SH, obtained by mapping the Si-O stretching band at 955 cm^{-1} [10,11,14]. This band is clearly in the same location within the binder matrix as the bound water shown in the other image. The results correspond well with C(A)SH at this particular location.

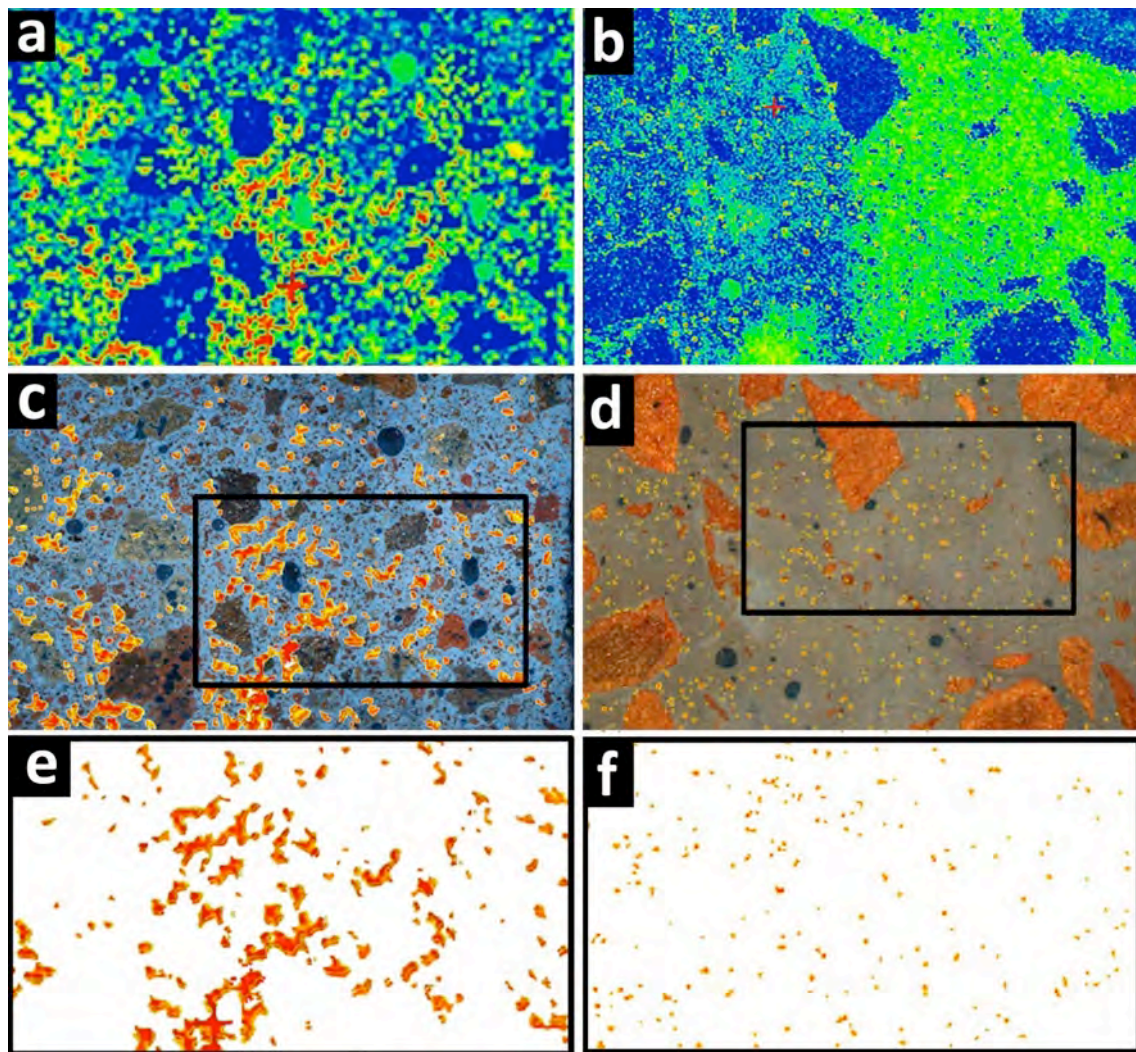


Figure 4: A comparison of two types of experimental mortar, with quantitative volumetric analysis provided by pixel-counting equivalent areas of the highest density of bound water of a FTIR maps overlaying scaled OM images. Scale (both): Red to Blue: 2.5-0.0. Area of black rectangle is 0.5 mm^2 . The pixel density of the left, lime-pozzolana mortar is 3.5 x that of the right, ceramic-lime mortar.

Figure 4 shows a further application of the proposed method, using the data acquired by the different techniques to compare two types of experimental mortar. A FTIR map at the same scale and with the same settings was made of an experimental lime-ceramic mortar that was produced at the same time and under the same conditions as the lime-pozzolana mortar shown in Figure 3. A C(A)SH-rich reaction rim that had been located by SEM-EDX was

selected so that the same bands could be mapped as on the previous mortar. It is immediately evident comparing the two maps side by side (Figure 4 a,b) that the pozzolana mortar (top left) has a greater density of the reaction products. In Figure 4 c and d, the colors (red and orange) related to the localization of the highest intensity of the band associated with bound water have been superimposed and scaled over OM images of both mortars, with a black box representing an area of 0.5 mm² around a selection of the binder matrix. Using pixel-counting software, it was determined that the area of the reactive products of the lime-pozzolana mortar was 3.5 times the area of the ceramic-lime mortar, shown more clearly in Figure 4 e and f. While this does not necessarily mean that gravimetric analysis would find 3.5 times the same difference, but it does provide an important point of comparison. Physical testing of prisms of each mortar showed that not only did the pozzolana mortar set more rapidly, but it achieved a higher final strength, which would correspond to a more reactive, denser mortar binder [20].

4.3 Application to historical/ archeological mortar

Figure 5 demonstrates the same technique, this time used to compare an archeological mortar (ca. 2nd century C.E.) and a restoration mortar (ca. 1930s) made using the same materials. Once again, images were created by overlapping the FTIR map of bound water (ca. 1720-1600 cm⁻¹) over an OM image and adjusting the scale.

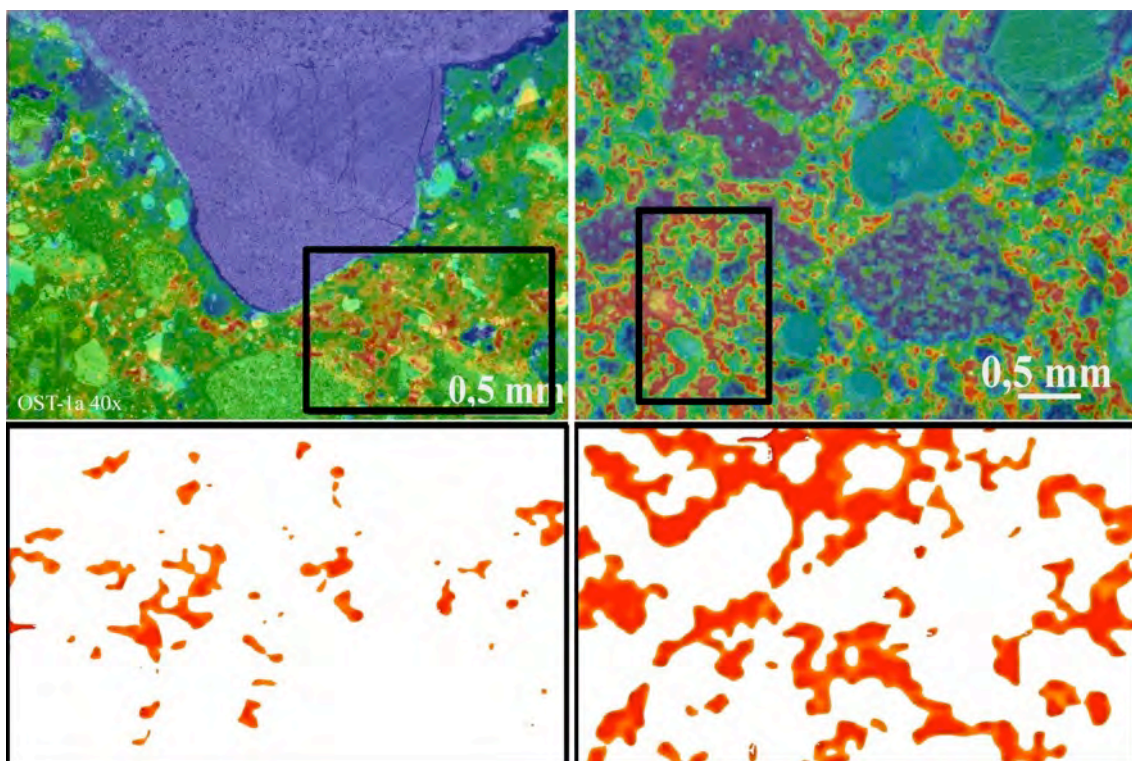


Figure 5: FTIR maps of the band corresponding to bound water (1720-1600 cm⁻¹) overlaying scaled OM images of lime-pozzolana mortar. Left: 2nd century C.E., Right: 1930's restoration. Ostia Antica (Italy). Area of black rectangle is 1.5 mm². The pixel density of the restoration mortar is 7.5 x that of archeological mortar. Scale (both): Red to Blue: 3.0-0.0.

The restoration mortar displays a much higher density of bound water, which demonstrates the degree to which the archeological mortar has altered over time, since C(A)SH tends to decompose into secondary calcium carbonate and silica gel resulting in less bound water. [3,5,6,21]. The restoration mortar, 1800 years younger, exhibits 7.5 times the bound water of the archeological mortar.

Following this protocol can additionally be used to make comparisons between historical mortars with different mortar formulations, such as the two shown in Figure 6.

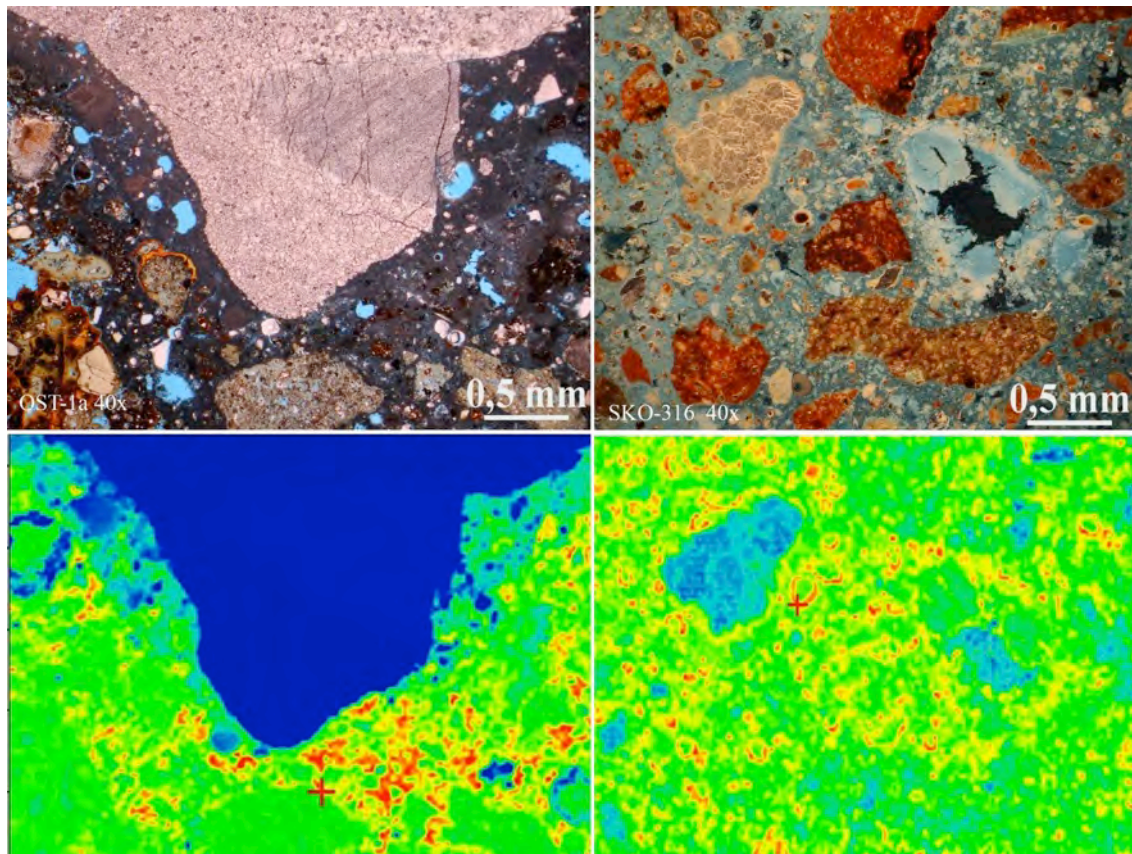


Figure 6: OM image (upper) and FTIR image (lower) of a lime-pozzolana mortar, 2nd century, Ostia Antica (Italy) (Left) and a lime-ceramic mortar, late Antique, Školarice, Slovenia (Right). Note differing locations and density of reaction products (red/orange in the FTIR maps) and clearly identifiable reaction rings in the right sample. Bands as described in text.

A binder density quantification comparison was not attempted in this case since the maps were generated selecting different bands, although both are associated with C(A)SH. The left side shows the OM and FTIR images of the archeological lime-pozzolana sample shown in Figure 5 before being overlapped, with the FTIR map generated by displaying the bound water ($1720-1600\text{ cm}^{-1}$) band. The right side shows OM and FTIR images of an archeological lime-ceramic mortar, with the FTIR image generated by displaying the density of the band associated with the semi-crystalline silica found in C(A)SH ($1050-950\text{ cm}^{-1}$)[11-14]. While an equivalent volumetric comparison cannot be made in this case, it can be stated that these are the locations of C(A)SH in both samples. Additionally, these images demonstrate on a wider scale what was illustrated in Figures 1 and 2, namely the position of C(A)SH relative to

the reactive aggregate. Whereas C(A)SH is dispersed throughout the binder matrix in the pozzolana sample, it is quite clearly highly concentrated in the rims of the aggregate in the ceramic sample. This further demonstrates the utility of this approach, in that it is able to both preserve and display not just the presence of mortar constituents, but also the spatial relationships between them.

5. Conclusions

One of the main advantages of comprehensive image-based analysis of historic mortar is its ability to provide information that would certainly be lost by thermal or chemical dissolution of the mortar sample. By the technique of combining and scaling FTIR images with OM and SEM images to create hybrid maps, it is possible to partially overcome one of the main limitations of image-based analysis – that it is difficult to use it to make quantitative analysis or a quantitative correlation between the physical performance of a material based on its contents. FTIR imaging visualized where these products could be found in the mortar within the context of the other mortar contents, e.g. near aggregate reaction rims, lime lumps, dispersed within the matrix etc., in other words, it created a “map” of the sample. Finally image-editing software was used to lay the FTIR data over either OM or SEM imagery at the same scale, producing a hybrid image that displayed chemical data over imagery allowing for correlative analysis. Pixel counting (the areas of the highest intensity of certain bands) allowed the quantification of chemical data over the surface area of the sample, and by comparing the same surface area of two different samples makes volumetric quantification between the samples possible, e.g. one sample exhibits a higher density of bound water per surface area than another. The results of comprehensive image-based analysis can then be correlated with physical attributes of a mortar in much the same way as physical and chemical dissolution techniques.

While pixel counting of these images analysis shows potential, the process still requires refinement. For example, further corrections could include using the data from this protocol to express each binder constituent as a percentage of the binder matrix, as well as percentage of the overall mortar surface area. Additional parallel physical testing can be used to form correlations with image-based analysis, for example nano-indentation of areas described by FTIR mapping [22]. Most of all, the continued use of this protocol would add an ever increasing database with which to analyze historic mortar.

Acknowledgements

Thanks to: Martin Mosser at The Wien Museum (Vindobona), Paolo Tomassini from the Centro Studi Pittura Romana Ostiense (CeSPRO) (Ostia Antica), and Katharina Zanier from The Institute for the Protection of Cultural Heritage of Slovenia (Školarice) for the provision of archeological material. Thanks to Gabriela Krist, University for Applied Arts, Vienna for access to the FTIR device and Valentina Pintus, Academy of Fine Arts, Vienna for her FTIR advice.

References

1. Middendorf B et al (2005) Investigative methods for the characterisation of historic mortars- Part 2: Chemical characterization. *Materials and Structures* 38:771-780
2. Elsen, J (2006) Microscopy of historic mortars — a review. *Cem Con Res* 36:8: 1416-1424
3. Weber J and Baragona A (2019) Microscopy brings it to light: Roman mortar technology studied by polarizing microscopy and SEM. Cavalieri M and Tomassini P (eds.), *La peinture murale antique : méthodes et apports d'une approche technique*, Bordeaux (Pictor collection) (in press)
4. Mehta P K (1987) Natural pozzolans: Supplementary cementing materials. *Proc, Int Symp on Advances in Concrete Technology* V M Malhotra, ed, CANMET, Athens, Greece, 407-430
5. Weber J et al (2015) Hydraulicity in Ancient Mortars: Its Origin and Alteration Phenomena. *Proc 15th Euroseminar on Microscopy Applied to Building Materials*, Delft, June 17-19, 2015. 147-156
6. Elsen J et al (2012) Hydraulicity in historic lime mortars: a review. *Historic Mortars*, Springer, Netherlands. 125-139
7. Katayama T (2011) So-called alkali-carbonate reaction - petrographic details of field concretes in Ontario. *13th Euroseminar on Microscopy Applied to Building Materials* 14-18 June 2011, Ljubljana, Slovenia
8. Nyquist A and Kagel R (1971) *Infrared Spectra of Organic Compounds*. Academic Press, London
9. Ghosh S N and Chatterje A K (1974) Absorption and reflection infrared spectra of major cement minerals, clinker, and cements. *J Mater Sci* 9:1577-1584
10. Hughes T L et al (1995) Determining cement composition by Fourier Transform Infrared Spectroscopy. *Adv Cem Based Mater* 2:91-104
11. Farcas F and Touzé P (2001) La spectrométrie infrarouge à transformée de Fourier (IRTF) Une méthode intéressante pour la caractérisation des ciments. *Bulletin des laboratoires des ponts et chaussées* - 230:77-88
12. Yu P et al (1999) Structure of calcium silicate hydrate (C-S-H): near, mid and far-infrared spectroscopy. *J Am Ceram Soc* 82:742-748

13. Hidalgo Lopez A et al (2008) Microstructural evolution of calcium aluminate cements hydration with silica fume and fly ash additions by SEM, and mid and near-infrared spectroscopy. *J Am Ceram Soc* 91:1258-1265
14. Horgnies et al (2013) Overview about the use of Fourier Transform Infrared spectroscopy to study cementitious materials. *Mater Charact* VI:251-262
15. Diekamp A (2014) Bindesmitteluntersuchungen an historischen Putzen und Mörteln aus Tirol und Südtirol. Dissertation University of Innsbruck
16. Dariz P & Schmid T (2017) Ferruginous phases in 19th century lime and cement mortars: A Raman microspectroscopic study. *Mater Charact* 129:9-17
17. Schmid T & Dariz P (2016) Chemical imaging of historical mortars by Raman microscopy. *Const Build Mater* 114:506-516
18. Valek J and Matas T (2012) Experimental Study of Hot Mixed Mortars in Comparison with Lime Putty and Hydrate Mortars. *Historic Mortars*, Springer, Netherlands. 269-281
19. ASTM C511-13, Standard Specification for Mixing Rooms, Moist Cabinets, Moist Rooms, and Water Storage Tanks Used in the Testing of Hydraulic Cements and Concretes, ASTM International, West Conshohocken, PA, 2013 *Note: Roughly equivalent to EN 197, EN 206.*
20. Baragona A (2019) Pozzolan-lime mortar: from antiquity to present: On the utility of experimental archeology and image-based analysis for understanding historical mortar. Dissertation University of Applied Arts Vienna (In preparation)
21. Pintér F et al (2011) Brick-Lime Mortars and Plasters of a Sixteenth Century Ottoman Bath from Budapest, Hungary. *Proc. of the 37th International Symposium on Archaeometry*, 12th-16th May 2008, Siena, Italy. Springer, Berlin Heidelberg, 293-298.
22. Nežerka et al (2015) Investigation of crushed brick-matrix interface in lime-based ancient mortar by microscopy and nanoindentation. *Cem Con Comp* 55:122-128

Characterisation of concrete structures along the Reschen frontier, South Tyrol, Italy

Tobias Bader¹, Anja Diekamp¹

(1) Unit of Material Technology, University of Innsbruck, tobias.bader@uibk.ac.at, anja.diekamp@uibk.ac.at

Abstract

In the years 1938 - 1942, an extensive system of fortification was built along the Reschen frontier, South Tyrol, Italy. The military fortification system comprises different concrete structures, which were subjected to natural weathering for more than eight decades. The present study deals with first results of the chemical-mineralogical characterisation of two concrete structures (bunker, anti-tank barrier). Polished thin sections of the near-surface parts were analysed by polarized light microscopy and scanning electron microscopy coupled with energy-dispersive X-ray spectroscopy in order to assess the material characteristics. The observed high binder to aggregate ratio in combination with sub-angular to angular shaped aggregate grains suggests the use of lean concrete for the construction of the fortification system. The current condition of the investigated concrete structures differs with regard to the position within the fortification system. The position of the anti-tank barrier within the high moor in combination with the climatic conditions of the Alps seem to have promoted deleterious chemical reactions between sulphate ions and components of the hardened cement paste. The knowledge on material characteristics (microstructure and individual components of concrete) and the current condition of the concrete structures is believed to be beneficial for the planning of maintenance works in the future.

Introduction

In the late 1930s, an extensive system of fortification was created along the Reschen frontier at the border triangle between Italy, Austria and Switzerland. The impressive concrete structures (bunkers and anti-tank barrier) were part of the Alpine Wall (Vallo Alpino del Littorio) and can nowadays be visited as architectural relics of the interwar period. The majority of the concrete structures are still preserved although being exposed to the harsh environment of the Alps for several decades. This circumstance is of interest for current investigations as it is generally believed that since 1930 the deterioration problems of concrete increased due to growing demand for higher strength at early ages that was achieved by increasing the fineness and the alite (C₃S) content of Portland cement (PC) [1,2]. However, the additional increase in water/cement ratio influences the characteristics of concrete with regard to porosity and permeability [2]. Currently, numerous studies investigated the deterioration mechanisms of concrete (e.g. [3-5]) and highlighted the effect of permeability on the progress of deterioration processes. The permeability, in turn, can be

either experimentally characterised or described by the material characteristics (microstructure and individual components of concrete).

The studies dealing with the retrospective examination of material characteristics of concrete structures from the end of the 19th and the beginning of the 20th century are limited (e.g. [6-10]). The majority of these studies have in common that they all highlighted the well-preserved condition of these structures. Distinct differences to modern PCs were observed with regard to the selection of raw materials (e.g. marlstone instead of artificially by-mixed raw materials), differences in the manufacturing process (e.g. vertical shaft kilns instead of rotary kilns) and composition of clinker minerals (specific phases such as $C_{12}A_7$ (mayenite)).

Recently, Pintér and Gosselin [9] pointed out that the coarse grain size of historical PC and the presumable application of a historical deactivation method seem to have influenced the material characteristics by inducing the formation of a high microporosity (capillary porosity). However, in contrast to concrete structures made of modern PC the relatively high capillary porosity is not apparently involved in any durability issues. Accordingly, the present study fits into the increasing interest in the durability of historic PC based structures by characterising concrete structures of the Reschen fortification system, which were subjected to natural weathering for more than eight decades.

In this paper, first results of the chemical-mineralogical characterisation of two concrete structures (anti-tank barrier, bunker) will be presented. The underlying investigations were carried out by employing the traditional methods polarising light microscopy (PLM) and scanning electron microscopy (SEM) coupled with energy-dispersive X-ray spectroscopy (EDS) [11,12]. The gained knowledge on material characteristics (microstructure and individual components of concrete) can be beneficial for both, the understanding of historic PC structures and the planning of maintenance work in the future. This is of growing interest because currently applied repair procedures are developed for modern structural concrete and do not consider conservation principles.

Concrete structures, sampling and methods

Concrete structures

The construction of the military fortification system at plateau Plamort, a high moor above the village of Reschen, South Tyrol, Italy, started in 1938 and was almost completed in the same year [13]. The system covers an area of about one km² at an altitude of about 2050 m [14]. It comprises a cavern system, barracks, bunkers, anti-tank barriers (so-called dragon's teeth) with a length of about 250 m and two anti-tank ditches, which were built into former peat pits (see Figure 1a). The anti-tank barriers are made of tree trunks, which were piled in the swampy ground and latter embedded in a concrete basement. The parts of the tree

trunks protruding from the basement (height up to 1.20 m) was covered with iron cones and completely encased in concrete (see Figure 1b) [15].

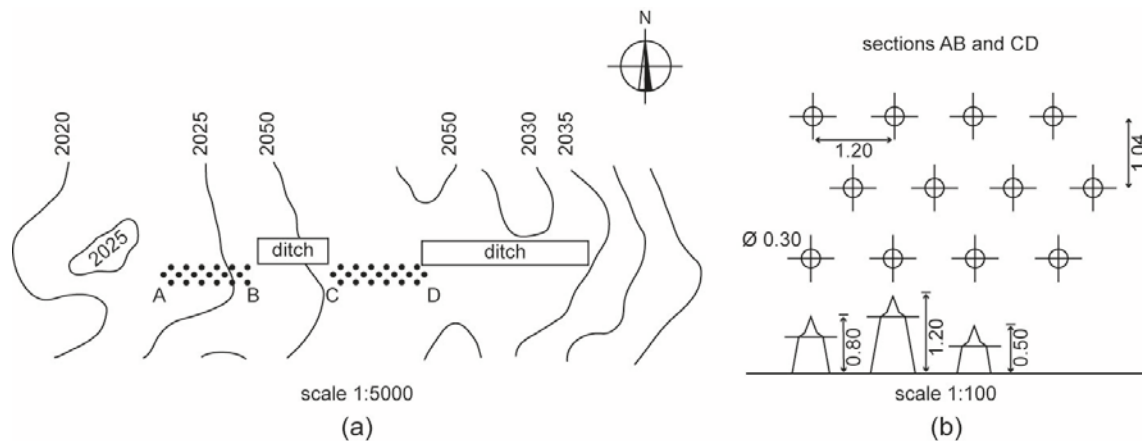


Figure 1: (a) schematic illustration of the anti-tank barriers and anti-tank ditches situated in the high moor at plateau Plamort and (b) detailed sketch of the individual anti-tank barriers. Values are given in meters (adapted from [15]).

The fortification was extended between 1940 and 1942 by building additional barracks and bunkers. From 1959 till 1962 all objectives were subjected to maintenance work and periodically controlled till 1998 [13]. Today, the fortification system is still preserved except for two structures, which are inexistent.

Sampling

For the characterisation of the concrete structures historic concrete samples were taken from one anti-tank barrier (1938) named sample ATB and one bunker (building phase 1940 - 1942) named sample B. The investigated specimens were located in the near-surface part of the concrete structures and were taken using hammer and chisel. Thin sections were cut out perpendicular to the surface of each specimen.

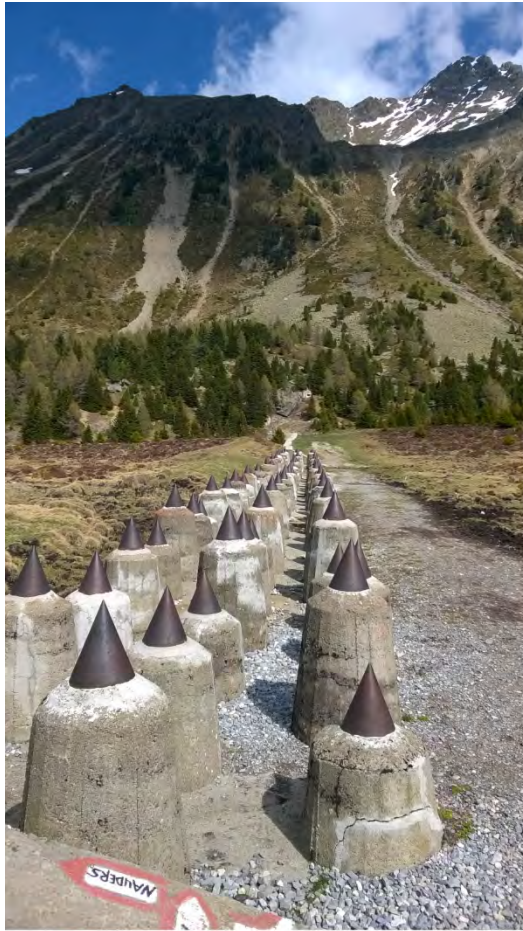
Methods

Polished thin sections were prepared and analysed by optical microscopy (Zeiss Axio Imager A2m) using reflected and polarised light. Additionally, specimens were investigated by scanning electron microscopy (FEI Quanta 3D 200i DualBeam) coupled with energy-dispersive X-ray spectrometer (EDAX Sapphire Si(Li)) in low vacuum mode using an acceleration voltage of 25 kV with a current of 1.2 nA.

Results and Discussion

Macroscopic description of investigated concrete structures

Photographs showing the investigated non-reinforced concrete structures in their current state are given in Figure 2a-c. The surface of the individual anti-tank barriers showed a beige



(a)



(b)



(c)

Figure 2: Photographs of the two investigated concrete structures: (a) anti-tank barriers located in the high moor of plateau Plamort, (b) deteriorated anti-tank barrier exposing tree trunk as well as iron cone fastening and (c) investigated bunker covered with residuals of bituminous surface protection.

colouration suggesting the superficial carbonation of the hydrated cement constituents [9]. Additionally, damage is visible in terms of mainly vertical and horizontal cracks. Most severe cracking occurred vertically leading in some cases to the splitting of anti-tank barriers exposing the underlying tree trunk and iron cone fastening. The roof of the investigated bunker is still partly covered with a bituminous layer.

Microscopic description of investigated concrete structures

Exemplary micrographs illustrating the microstructure in the near-surface area of both investigated samples are given in Figure 3a-d.

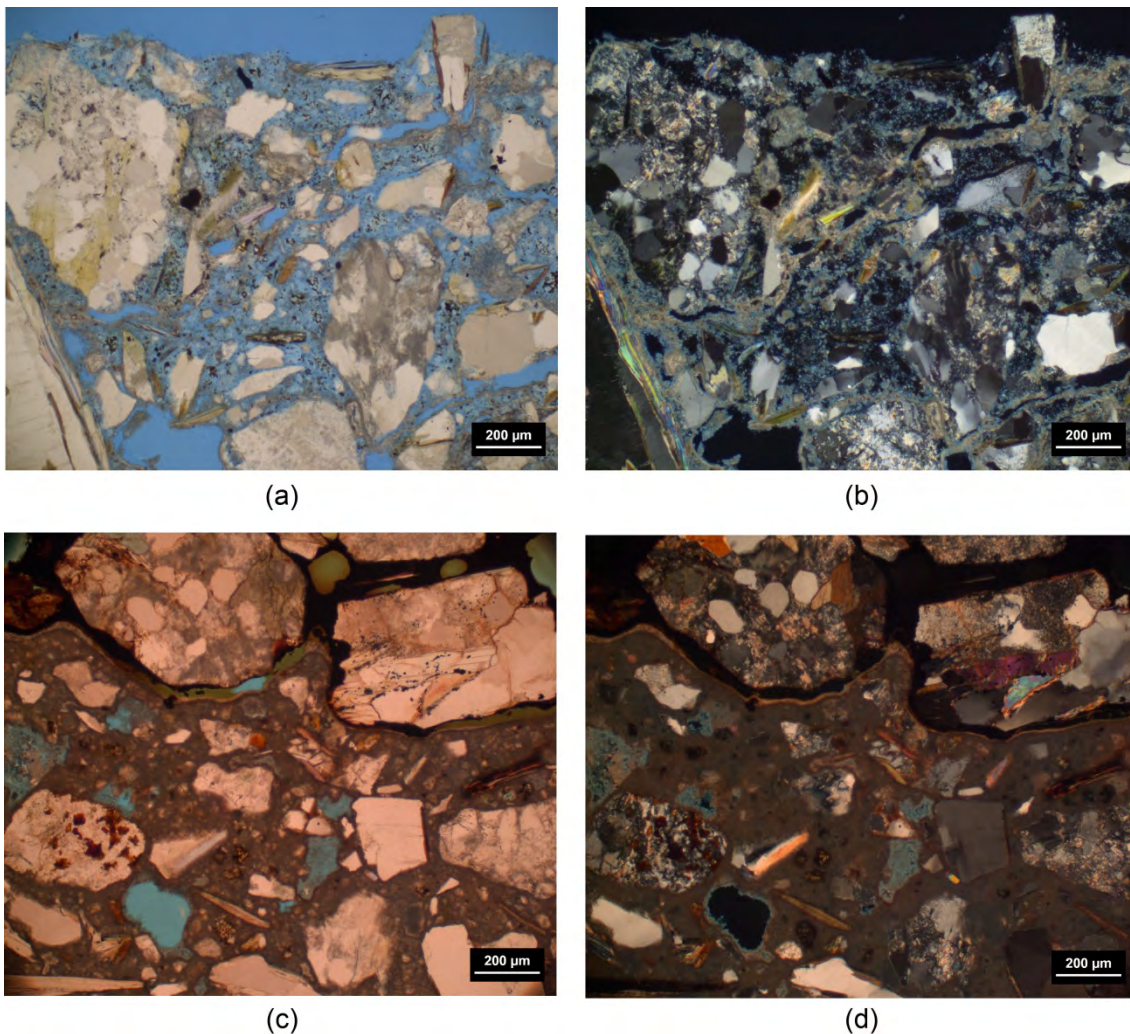


Figure 3: Exemplary micrographs of thin sections: (a) near-surface part of ATB showing a dark-brownish matrix with high content of aggregates as well as irregular formed voids (PPL), (b) same spot of sample ATB in XPL highlighting PCD, (c) near-surface part of B showing a dense dark-brownish matrix in contact with the above located bituminous mortar (PPL) and (d) same spot in XPL highlighting pore lining (calcite).

The micrographs are shown under plane-and cross polarized light (PPL, XPL) in order to make additional optical parameters (e.g. interference colour) visible. The matrix of both samples showed a brownish colour in PPL confirming the carbonation of the near-surface parts. The near-surface area of specimen ATB exhibited an evenly distributed mottled pattern of individual clusters of calcite (so-called 'popcorn calcite deposition' (PCD)) surrounded by a

matrix with elevated porosity. Additionally, individual aggregate grains sticking out the surface were observed. In case of specimen B, the near-surface area appeared dense and exhibited an overlying bituminous mortar containing aggregates, which are similar in size and shape as well as mineralogical composition to the underlying concrete.

The aggregate particles of both specimens are approximately well graded and exhibited a sub-angular to angular surface texture. The small grains showed predominantly an irregular shape, which changed with increasing grain size towards a flakier shape. The coarse aggregate with a maximum grain size of about 4 mm are predominantly composed of metamorphic rocks (mica schist, gneiss). The fine aggregate comprised mainly monomineralic grains such as strained quartz, biotite and plagioclase. Based on visual observations at several locations the estimated binder to aggregate (b/a) ratios of both concrete varied between 1:6 and 1:8.

In addition, both specimens contained various irregularly shaped voids up to 1.5 mm, which were frequently observed near the coarse aggregate grains. The pores are often lined by fine-grained calcite with characteristic high order interference colours under XPL (see Figure 3b and d). In sample ATB, some of the pores are filled with a mass of needle-like crystals. Additional SEM analysis revealed that these void fillings are composed of sections with either randomly oriented or well-ordered crystals with the latter occurring preferentially in oriented sheets. Moreover, sporadic clusters of granular calcium carbonate crystals (mostlikely PCD) were observed within the void fillings. Results of SEM-EDS investigation of the two different crystal morphologies are given in Figure 4a-d. The SEM-EDS analysis of both sections revealed similar elemental composition. Hence, the observed void fillings seem to consist of sulphate containing minerals such as thaumasite and ettringite.

Residual cement grains of both specimens exhibited an angular to sub-angular surface texture and varied in grain size with very large grains (>100 µm) being commonly observed. Their composition appeared inhomogeneous which represents in combination with the large grain sizes a characteristic feature of historical PCs [16,17]. Consistent with the carbonation of the hardened cement paste also unhydrated cement residuals seem to be affected by carbonation [18]. As consequence of exposure to carbon dioxide the original calcium silicate constituents of the residual anhydrous cement grains were transformed into decalcified Si-rich pseudomorphs of belite and alite. These pseudomorphs are surrounded by a finely crystalline matrix made of ferrite suggesting that ferrite is so far unaffected by carbonation. Exemplary results of SEM-EDS analysis of an unhydrated cement residual which was affected by carbonation are given Figure 5a and b.

The results currently obtained can be summarized as follows:

Both concrete structures are mostlikely made with similar mix design containing coarsely ground heterogeneous PC. The mix design is characterised by a high b/a ratio and sub-angular to angular aggregates grains of metamorphic origin. The amount and shape of aggregates suggests the use of lean concrete for the construction of the fortification system.

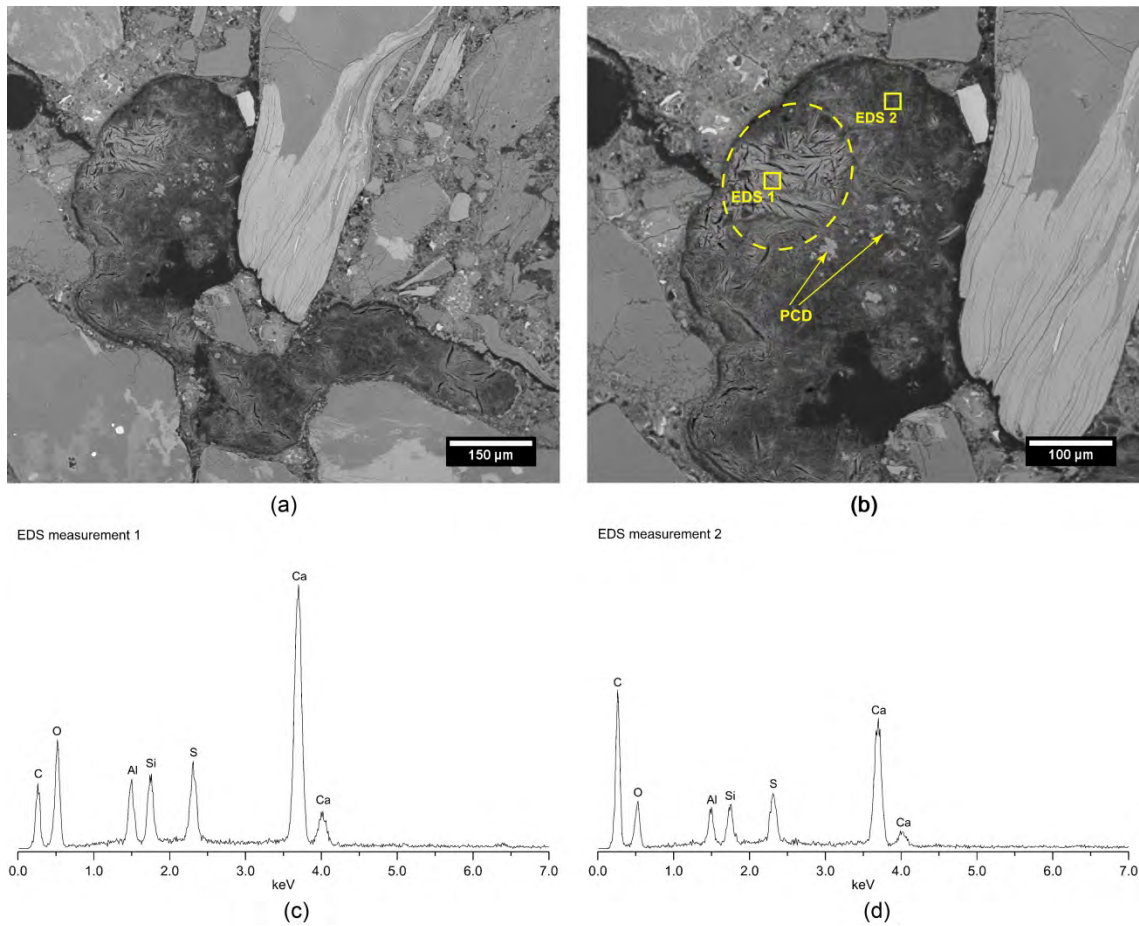


Figure 4: SEM-EDS analysis of specimen ATB: (a) void that is almost completely filled with a mass of needle-like crystals, (b) closer view of the same spot revealing crystals that are either randomly oriented or well-oriented (the latter is marked by oval). Additionally, clusters of granular calcium carbonate crystals (mostlikely PCD, marked by arrows) within the mass of needle-like crystals were observed. (c) EDS spectra of measurement 1 within well-ordered crystals and (d) EDS spectra of measurement 2 within randomly oriented crystals.

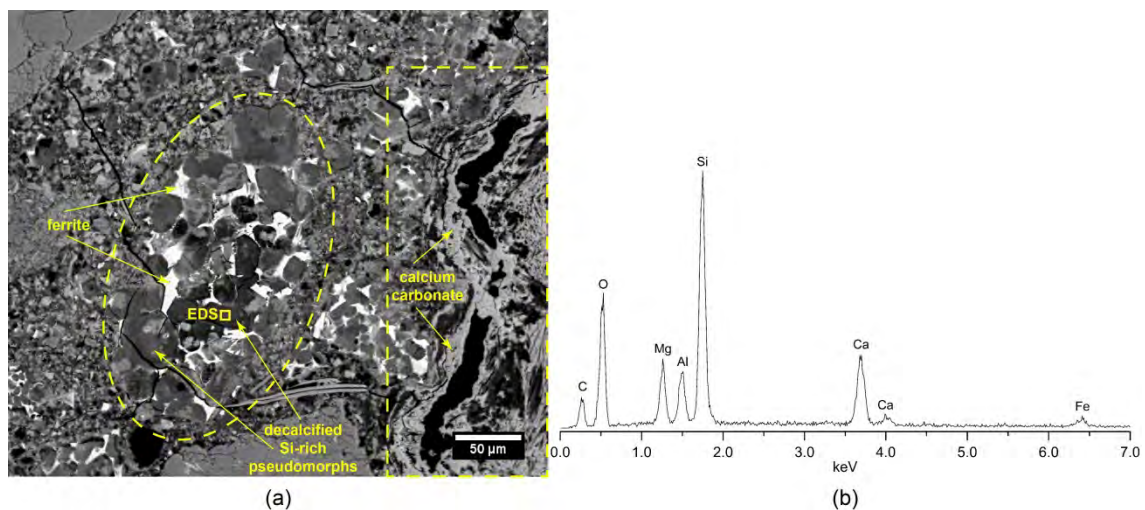


Figure 5: SEM-EDS analysis of specimen ATB: (a) residual cement grain (marked by oval) showing pseudomorphs of belite and alite that are surrounded by finely crystalline ferrite. Precipitation of calcium carbonate lining a crack can be seen on the right (marked by rectangular). (b) Exemplary EDS analysis of a pseudomorph of former calcium silicate constituent indicating the depletion in calcium.

The term lean concrete is used to describe normal PC-based concrete with low binder content [19]. The observed irregular shaped voids suggest difficulties in the workability of the fresh concrete mixture and/or the used compaction technique (tamping?). However, the two investigated concrete structure differ with regard to surface protection (structure B was additionally covered with a bituminous mortar) and their position in the fortification system, respectively. Concrete structure B is located hillside whereas concrete structure ATB is located in the high moor [13]. The above-mentioned difference in surface protection and position within the fortification system may have influenced the degradation of specimen ATB and specimen B, which is discussed in the following:

Generally, the near-surface part of both investigated concrete structures represents the alteration zone front, which is in permanent contact with the atmospheric environment. The observed decalcification of hydrates and residual cement grains of both investigated concrete structures is associated with chemical degradation due to carbonation resulting from exposition to carbon dioxide for more than 80 years of service life. Additionally, the microstructural observations of the near-surface part of specimen ATB suggest leaching and erosion of the original surface. Thus, the near-surface part of the structures became more porous which may have facilitated further degradation. The observed formation of sulphate containing minerals within voids requires according to Hagelia et al. [20] a reduction in the internal pH of concrete, the presence of sulphate and a wet and cool environment. Hence, the position within the high moor (sulphate source) in combination with carbonation, leaching and the climatic conditions of the Alps seem to have promoted the formation of deleterious sulphate containing minerals such as thaumasite. Additionally, the observed PCD texture is associated with various deterioration mechanisms which also include thaumasite formation [21].

In case of specimen B, the bituminous mortar layer seems to have reduced the ingress of water and, thus, mostlikely minimised the effect of leaching and freeze thaw scaling. Furthermore, as consequence of the position of the bunker within the fortification system at the adjacent hillside, the concrete structure may not be in contact with the high moor that is suspected to be the origin of sulphate ingress.

Conclusion

Within the present study, first results of the chemical-mineralogical characterisation of two concrete structures from the military fortification system along the Reschen frontier, South Tyrol, Italy, were presented. The investigated concrete structures are an anti-tank barrier located in the high moor of the plateau Plamort and a bunker situated at the adjacent hillside. The concrete structures were built between 1938 and 1942 and subjected to natural weathering for more than eight decades. Specimens were taken from the near-surface area and investigated by PLM and SEM-EDS in order to assess the material characteristics as well as the current condition. From the obtained results the following conclusions can be drawn:

- Both concrete structures are most likely made with similar mix design containing coarsely ground heterogeneous PC cement. The observed high binder to aggregate ratio (between 1:6 and 1:8) in combination with sub-angular to angular shaped aggregate grains suggests the use of lean concrete for the construction of the fortification system. The observed irregular shaped voids are attributed to difficulties in the workability of the fresh concrete mixture and/or the used compaction technique (tamping?).
- The position of the concrete structures within the fortification system and the application of surface protection seem to have influenced the current conditions of the individual structures. Both structures showed evidence of chemical degradation through carbonation. Consequently, calcium silicate hydrates were decomposed to calcium carbonate and silica-rich gels. The calcium silicate constituents of unhydrated cement grains were also converted into decalcified Si-rich pseudomorphs. Additionally, the voids of the anti-tank barrier were partially filled with sulphate containing minerals. It is postulated that the position within the high moor seems to be responsible for the ingress of sulphate. Thus, the wet and cool environment of plateau Plamort in combination with the decalcification of calcium silicate hydrates may have promoted the formation of deleterious minerals such as thaumasite. Based on the currently obtained results the use of sulphate resisting cement for future maintenance work is recommended.

Next steps comprise the collection of drilling cores in order to characterise the non-carbonated part of the structures with regard to chemical characteristics of hydration products and residual cement grains in order to gain insights into the technology of historic PC.

Acknowledgements

The authors are grateful for fruitful discussions with Farkas Pintér as well as his assistance in the course of the presented research work.

References

1. Mehta PK, Burrows RW (2001) Building durable structures in the 21st century. *Concr Int* 75:437-443
2. Aïtcin PC (2000) Cements of yesterday and today: concrete of tomorrow. *Cem Concr Res* 30:1349-1359
3. Basheer L, Kropp J, Cleland DJ (2001) Assessment of the durability of concrete from its permeation properties: a review. *Constr Build Mater* 15:93-103
4. Wang K, Jansen DC, Shah SP et al (1997) Permeability study of cracked concrete. *Cem Concr Res* 27:381-393

5. Ollivier J, Massat M (1992) Permeability and microstructure of concrete: a review of modelling. *Cem Concr Res* 22:503-514
6. Idorn G, Thaulow N (1983) Examination of 136 years old Portland cement concrete. *Cem Concr Res* 13:739-743
7. Rayment D (1986) The electron microprobe analysis of the C-S-H phases in a 136 year old cement paste. *Cem Concr Res* 16:341-344
8. Ando Y, Hirono S, Sawaki D et al (2014) Microscopy to evaluate the properties of cement and alterations in historic mortar/concrete of old Nobiru Port project, Northeast Japan. In: *Proceedings of 36th International Conference on Cement Microscopy*. Milan, Italy
9. Pintér F, Gosselin C (2018) The origin, composition and early age hydration mechanisms of Austrian natural Portland cement. *Cem Concr Res* 110:1-12
10. Blezard R (1984) A discussion of the paper “examination of 136 years old portland cement concrete” by GM Idorn and N. Thaulow, *Cem Concr Res* 14:154-156
11. Weber J, Köberle T, Pintér F (2019) Methods of Microscopy to Identify and Characterise Hydraulic Binders in Historic Mortars—A Methodological Approach. In: Hughes JJ, Válek J, Groot CJWP (ed) *Historic Mortars: Advances in Research and Practical Conservation*. Springer, Switzerland
12. Scrivener KL (2004) Backscattered electron imaging of cementitious microstructures: understanding and quantification, *Cem Concr Compos* 26:935-945
13. Urthaler J, Pozza A, Niederkofler C (2005) *Bunker*. Athesia, Bozen
14. IDM Südtirol-Alto Adige (2019) Fortification Alps Wall in Plamort. https://www.suedtirol.info/en/experience/Fortification-Alps-Wall-in-Plamort_activity_75311 Accessed 20 January 2019
15. Bernasconi A, Muran G (1999) *Le fortificazioni del Vallo Alpino: Littorio in Alto Adige*, Temi, Trento
16. Blezard RG (1998) The history of calcareous cements. In: Hewlett PC (ed) *Lea’s Chemistry of Cement and Concrete*, 4th edn. Elsevier, Oxford
17. Ingham J, *Geomaterials under the microscope: a colour guide* (2013), Manson Publishing, London
18. Shtepencko O, Hills C, Brough A, Thomas M (2006) The effect of carbon dioxide on β -dicalcium silicate and Portland cement. *Chem Eng J* 118:107-118
19. Trueb U (1985) Über Magerbeton. *Cem Bull* 53:1-6

20. Hagelia P, Sibbick R, Crammond N et al (2003) Thaumasite and secondary calcite in some Norwegian concretes, *Cem Concr Compos* 25:1131-1140
21. Hagelia P, Sibbick R, (2009) Thaumasite Sulfate Attack, Popcorn Calcite Deposition and acid attack in concrete stored at the «Blindtarmen» test site Oslo, from 1952 to 1982. *Mater Charact* 60:686-699

Chemical, mineralogical and hydraulic characteristics of Roman mortars in Turkey

Burcu Taşçı¹, Hasan Böke²

(1) Department of Architecture, Izmir Katip Çelebi University, burcutasci@iyte.edu.tr

(2) Department of Architectural Restoration, Izmir Institute of Technology, hasanboke@iyte.edu.tr

Abstract

In this study, chemical, mineralogical and hydraulic characteristics of binders of mortars, composed of fine siliceous aggregates and carbonated lime in some ancient Roman buildings, located Xanthos (Antalya), Patara (Antalya) and Tlos (Muğla) in Southern Turkey were investigated. Mineralogical compositions of binders were determined with X-Ray Diffractometer (XRD) and Fourier Transform Infrared Spectroscopy (FTIR) analysis. Chemical compositions and microstructures were determined with a Scanning Electron Microscope Coupled with X-Ray Energy Dispersive Spectrometry (SEM-EDS). Hydraulic properties of binders were identified by determining the weight losses between 200-600°C and 600-900°C by Thermogravimetric Analysis (TGA). The pozzolanic activity of the fine aggregates was determined by measuring the differences in electrical conductivity. Analysis results showed that binders of Roman mortars are composed of lime and pozzolanic fine aggregates. Due to the use of pozzolanic fine siliceous aggregates, mortars are hydraulic.

Introduction

In the construction history, Romans have an important role with the use of lime and pozzolanic aggregates in mortar production [1]. Pozzolanic aggregates composed of amorphous silicates and aluminates react with lime that gives hydraulic character and high strength to the mortar [2]. The mortars used in many Roman period structures are hydraulic since they were prepared by using natural pozzolans [3-7].

In Turkey, there are more than three hundred archaeological sites from Roman period that are witnesses of the ancient Roman time (Figure 1). In this study, chemical, mineralogical and hydraulic characteristics of binders of Roman mortars that are composed of fine siliceous aggregates and carbonated lime were determined. The mortars collected from Patara (Antalya), Tlos (Muğla) and Xanthos (Antalya), located in the Mediterranean region (Figure 1).

Patara, Tlos and Xanthos represent the most unique architectural example of the ancient Lycian Civilization in Turkey. Patara, located in Antalya, was the principal port of Lycia. It was one of the main ancient maritime and trade center of the eastern Mediterranean. Some significant finds at Patara are acropolis, baths, theatre, bouleuterion and light house [9].

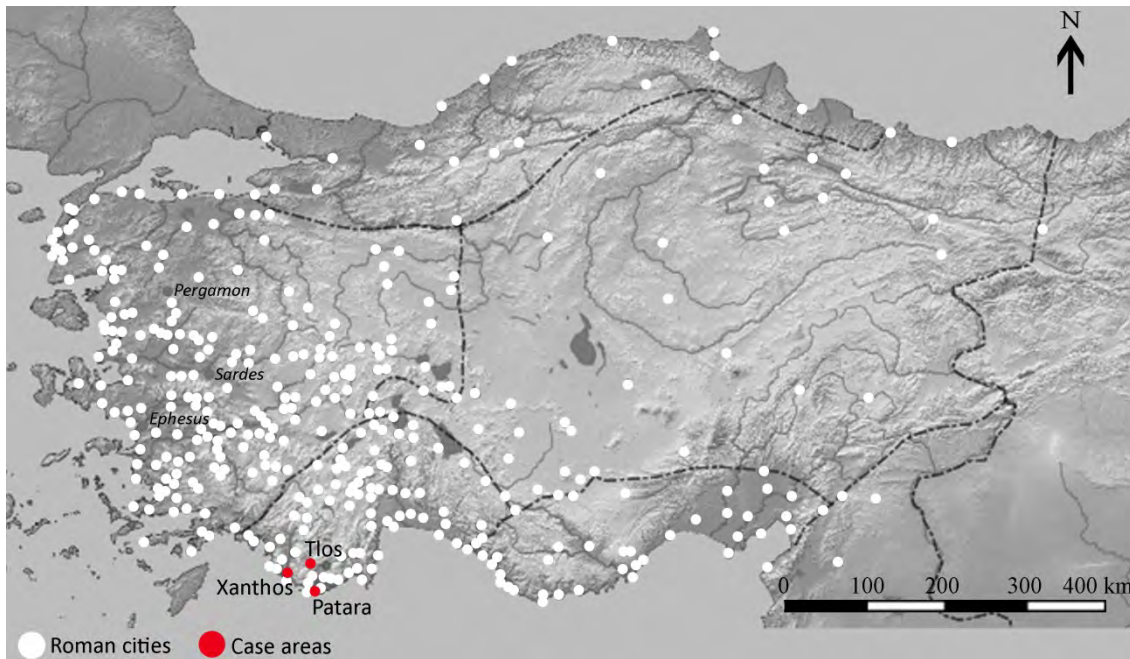


Figure 1. Archaeological sites of Roman period in Turkey and location of Patara, Tlos and Xanthos [8]



Figure 2. Theatre and tomb of Xanthos

Tlos, located in Muğla Province, is another important city in Lycia region. Recent archaeological investigations show that this area was settled long before the Late Bronze Age. Tlos had metropolis status in the Roman period. In 2009, Tlos was added to the UNESCO Temporary List of World Heritage. The rock-cut tombs, the stadium, the agora, the baths, the city basilica and the theatre are one of the outstanding examples of the city [10].

Xanthos, located in Antalya Province, was the capital of ancient Lycia (Figure 2). The site may have existed during the Bronze Age or during the first centuries of the Iron Age. It illustrates the continuity and combination of the Anatolian, Greek, Roman, and Byzantine civilizations. In 1998, Xanthos was added to the UNESCO List of World Heritage Site with ancient city of Letoon. The tombs, the theatre, the bath, the agora and the basilica are the most important architectural examples of the city [11].

Experimental Part

In this study, chemical, mineralogical and hydraulic characteristics of binders of Roman mortars that were collected from Patara, Tlos and Xanthos archaeological sites were investigated (Table 1). All samples were collected in accordance with the European Standard (UNI EN 16085) [12].

Table 1. Roman lime mortar samples from Patara, Tlos and Xanthos

Sample	Location	Building Type	Description
PG	Patara	Gate	Mortar from the rubble core of the ashlar masonry
PB	Patara	Bath	Mortar from the rubble core of the ashlar masonry
PT	Patara	Theatre	Mortar from the ashlar masonry
TB	Tlos	Bath	Mortar from the ashlar masonry
TS	Tlos	Stadium	Mortar from the ashlar masonry
TT	Tlos	Theatre	Mortar from the ashlar masonry
XA	Xanthos	Agora	Mortar from the rubble masonry
XB	Xanthos	Bath	Mortar from the rubble core of the ashlar masonry
XT	Xanthos	Theatre	Mortar from the rubble core of the ashlar masonry

Nine samples were entitled according to the name of ancient city they were taken from (P: Patara, T: Tlos, X: Xanthos) and the name of function of structure (A: Agora, B: Bath, G: Gate, S: Stadium, T: Theatre), respectively.

Mineralogical compositions of binders of mortars were determined with X-Ray Diffractometer (XRD) and Fourier Transform Infrared Spectroscopy (FTIR) analysis performed by Philips X-Pert Pro and by Spectrum BX II FTIR spectrometer (Perkin Elmer). For FTIR analysis, a few milligrams of standard mixtures and the powdered binders of the Roman mortar samples were dispersed in about 80 milligram of spectral grade potassium bromide (KBr) and pressed into pellets under 10 tons/cm² pressure. Their chemical compositions and microstructures were determined with a Scanning Electron Microscope Coupled with X-Ray Energy Dispersive Spectrometry (SEM-EDS) (Quanta 250FEG).

The hydraulic properties of the binders were evaluated at temperatures between 200 °C and 600 °C by determining its weight loss due to the loss of bound water of calcium silicate hydrates and calcium aluminate hydrates and weight loss due to carbon dioxide released during the decomposition of calcium carbonates at temperatures over 600 °C by using Shimadzu TGA-21.

Pozzolanic activity of fine aggregates (less than 53 μm size) were determined by measuring the differences in electrical conductivities (mS/cm) before and after addition of the samples into saturated calcium hydroxide solution [13].

Results and Discussion

General characteristics of the mortars

The Roman mortars were mainly composed of lime and natural aggregates. Density and porosity values of mortars were between 1.20-1.60 g/cm^3 and 39-53 % for Patara mortars, 1.80-1.90 g/cm^3 and 24-33 % for Tlos mortars and 1.50-1.93 g/cm^3 and 27-42 % for Xanthos mortars [14]. The lime/aggregate ratios were in the range of 3/2-5/2 in Patara mortars and 2/3-1 in Xanthos mortars [14]. They had similar raw material compositions and physical characteristics that have been found from the mortars used in some Roman structures in Italy, Spain and Turkey [15-21]. Also, SEM-EDS images showed that mortars were composed of binder which mainly includes carbonated lime, and small size of aggregates (Figure 3).

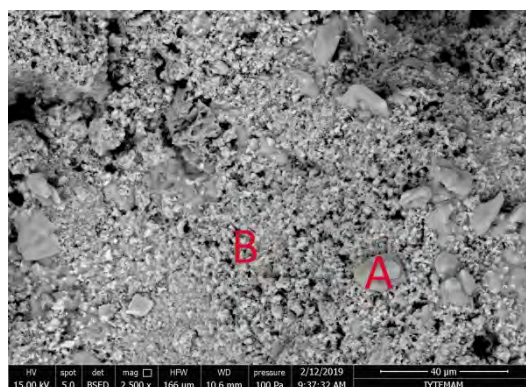


Figure 3. SEM images (2500x) of binder (B) and small size of aggregates (A) of the mortars

Mineralogical and chemical compositions of binders and fine aggregates

Mineralogical analysis carried out by XRD and FT-IR analysis showed that binders were mainly composed of calcite, quartz, hematite, dolomite, albite and anorthite minerals (Figure 4). The FTIR spectrum of the binders showed the characteristics of CaCO_3 bands at $\sim 1438 \text{ cm}^{-1}$ (C–O stretching), ~ 875 and $\sim 712 \text{ cm}^{-1}$ (C–O bending). The band at $\sim 1050 \text{ cm}^{-1}$ (Si–O stretching) and $\sim 470 \text{ cm}^{-1}$ (Si–O bending) could be attributed to siliceous materials. Also, the broad band from ~ 3250 to 3580 cm^{-1} (O–H stretching) was due to bound water (Figure 5). Chemical compositions of binders determined by SEM-EDS analysis indicated that they were mostly composed of high amount of CaO (61.0-85.1 %), SiO_2 (7.1-22.9 %) and moderate amount of Al_2O_3 (1.9-10.1 %), MgO (1.5-10.1 %) and low amount of Fe_2O_3 (0.00-3.9 %) and other compounds (0.00-2.8 %) (Figure 6). These results indicate that binders were composed of high amount of carbonated lime containing magnesium and aggregates composed of mainly silica, alumina and iron.

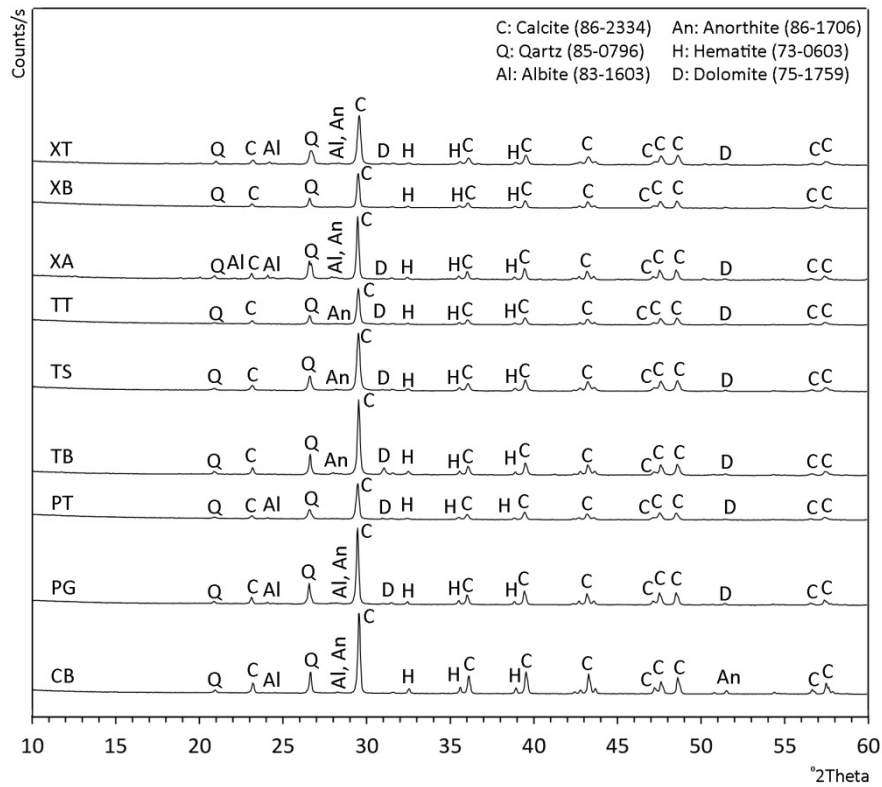


Figure 4. XRD patterns of binders

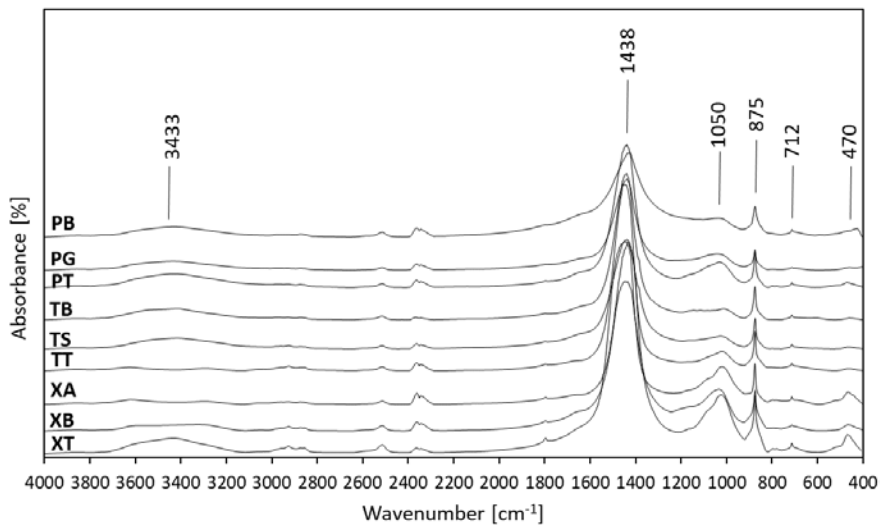


Figure 5. FTIR spectrum of binders

XRD analyses showed that aggregates were mainly composed of quartz, albite, muscovite, diopside and the diffuse band between 20-30 degrees for the amorphous silica. The results of the SEM-EDS analyses supported the XRD analysis. Analysis results indicated that aggregates were mainly composed of high amount of SiO₂ (56.0-89.6 %), moderate amount of Al₂O₃ (4.6-14.6 %), MgO (1.0-6.8 %), Fe₂O₃ (2.1-9.5 %) and low amount of CaO (1.0-7.0 %), P₂O₅ (0.00-4.1 %), K₂O (0.00-2.4 %) and other compounds (0.00-0.6 %).

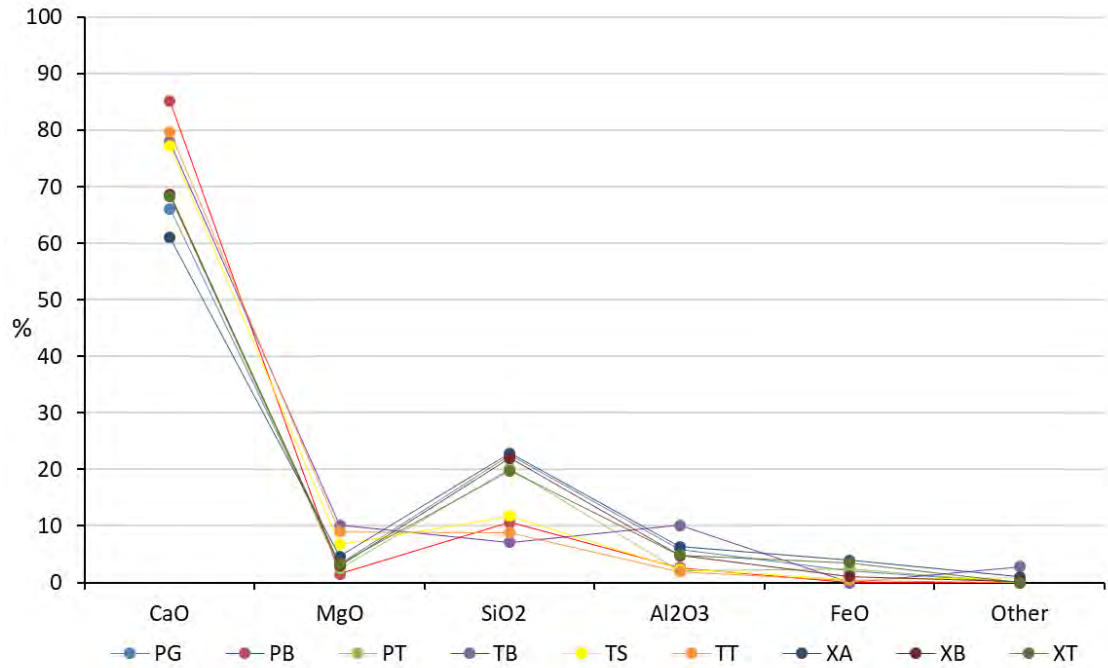


Figure 6. Chemical compositions of binders

Hydraulic Properties of Binders

The hydraulic properties of binders were determined by thermo gravimetric analyses (TGA). These analyses showed that the binders contained nearly 7% structurally bound water between 200 °C and 600 °C and 37% carbon dioxide over 600 °C (Figure 7). CO₂/H₂O ratios of binders ranged between 4.5-14.1 in Patara mortars, 4.1-6.0 in Tlos mortars and 5.2-6.1 in Xanthos mortars. According to these results, all mortars except for PB could be regarded as medium-hydraulic (Figure 8). The hydraulicity of the mortars could be explained by the use of pozzolanic aggregates.

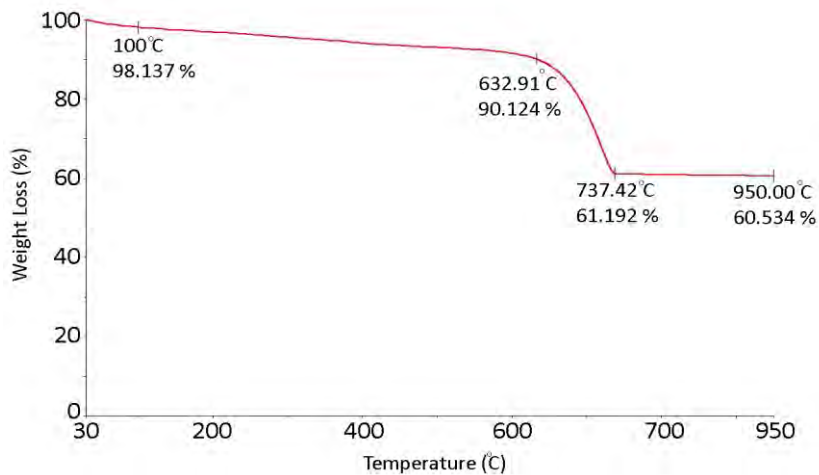


Figure 7. TGA spectra of binder (XT)

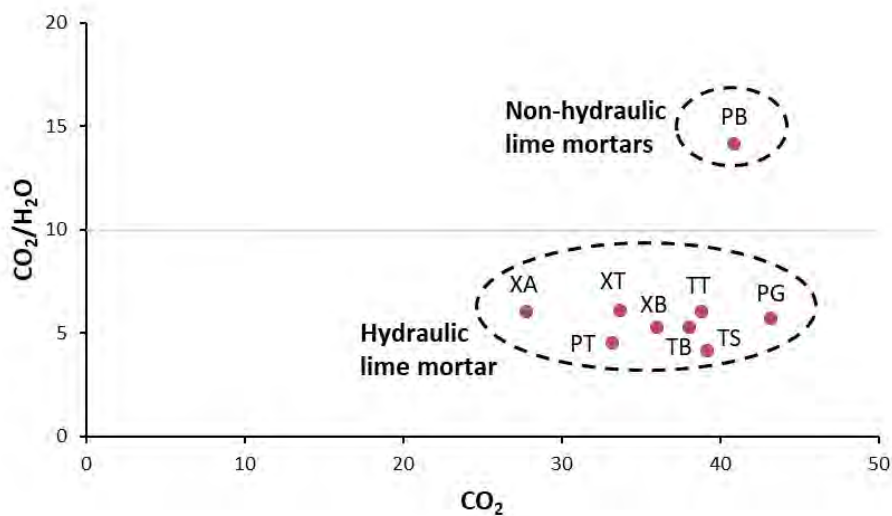


Figure 8. Hydraulic classification of mortars by CO₂/H₂O

In addition, hydraulic index (H.I.) calculated by SEM-EDS analysis of the binders was used to determine the hydraulic properties of mortars. Hydraulic index was defined according to the Boynton formula [22]. Hydraulic indexes of binders were between 0.2-0.4 for Patara, were between 0.1-0.2 for Tlos and were between 0.4-0.5 for Xanthos mortars (Figure 9). Results revealed that mortars from Patara and Xanthos were highly hydraulic except for PB which was weakly hydraulic, and mortars from Tlos were weakly hydraulic [23].

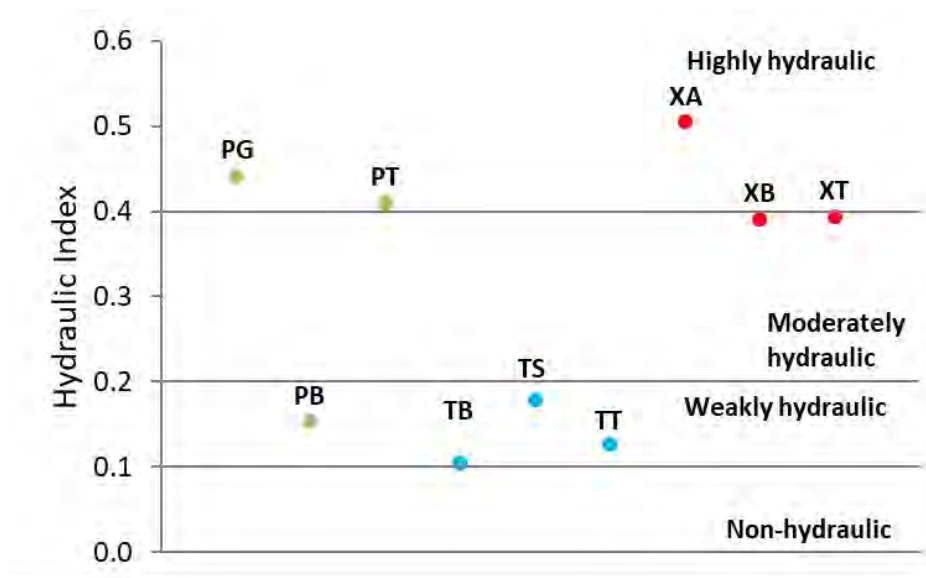


Figure 9. Hydraulic indexes of binders

The pozzolanic activity of fine aggregates was investigated by electrical conductivity measurements. Before and after the addition of aggregates into saturated calcium hydroxide solution, the high differences in electrical conductivity values of were observed (Table 2).

Table 2. Electrical conductivity measurements of fine aggregates

Sample Code	Electrical Conductivity (mS/cm)		Difference in Electrical Conductivity (mS/cm)
	Before	After	
PG	7.77	3.75	4.02
PB	7.69	0.87	6.83
PT	7.70	1.23	6.47
TB	7.78	1.34	6.44
TS	7.77	2.79	4.98
TT	7.75	1.09	6.66
XA	8.20	5.66	2.54
XB	7.82	3.67	4.15
XT	8.03	4.60	3.43

Electrical conductivity differences of fine aggregates ranged between 4.0-6.8 mS/cm in Patara mortars, between 4.9-6.6 mS/cm in Tlos mortars, and between 2.5-4.1 mS/cm in Xanthos mortars (Table 2). All these results indicated that the fine aggregates could be volcanic with pozzolanic amorphous silica which gave a hydraulic character to the mortar.

Conclusions

Lime mortars from Roman period buildings in Patara, Tlos and Xanthos are composed of high calcium lime and natural pozzolanic aggregates composed of mainly silica and alumina. The lime and aggregate ratios ranged between 2/3 – 5/2 by weight. Aggregates are mainly composed of quartz, albite, diopside and amorphous silica that may derived from the use of volcanic ash as pozzolan. They have good pozzolanicity since they were produced from raw materials of high silica content. They were mainly composed of a high amount of SiO₂, Al₂O₃ and moderate amount of Fe₂O₃, and CaO. The binder of the mortars composed of lime and fine aggregates have uniform structure. Binders of mortars are hydraulic due to the use of pozzolanic aggregates.

Acknowledgements

The authors would like to thank the researchers of the Centre for Materials Research at the Izmir Institute of Technology for XRD, SEM-EDS and TGA analyses for the experimental stage of this study.

References

1. Adam JP (2005) Roman building materials and techniques. (First published in 1937). Translated by Anthony Mathews. Routledge, London and New York.
2. Davey N (1961) A history of building materials. Phoenix House, London.

3. Mirieollo D, Barca D, Bloise A et al (2010) Characterisation of archaeological mortars from Pompeii (Campania, Italy) and identification of construction phases by compositional data analysis. *Journal of Archaeological Science* 37: 2207-2223.
4. Degryse P, Elsen J, Waelkens M (2002) Study of ancient mortars from Sagalassos (Turkey) in view of their conservation. *Cement and Concrete Research* 32: 1457-1463.
5. Leone G, De Vita A, Magnani A, Rossi C (2016) Characterization of archaeological mortars from Herculaneum. *Thermochimica Acta* 624: 86-94.
6. Massazza F, Pezzuoli M (1981) Some teachings of Roman concrete mortars. Proceedings of the ICCROM Symposium "Mortars, cements and grouts used in the conservation of historic buildings". Rome, November 3-6, 219–248.
7. Elsen J, Brutsaert A, Deckers M, Brulet R (2004) Microscopical study of ancient mortars from Tournai (Belgium). *Material Characterization* 53: 289–94.
8. Ligt L, Bintliff J, and Pobleme J (2017) *Cities of Roman Asia Minor*. Leiden University. <https://www.universiteitleiden.nl/en/research/researchprojects/humanities/cities-of-roman-asia-minor>. Accessed 10 February 2019.
9. Dündar E (2017) *Transport jars and stamped amphoras from Patara 7th to 1st centuries BC. The maritime trade of a harbor city in Lycia*. Ege Publications, İstanbul.
10. Tlos Excavations, <http://www.tloskazilari.com/en/antikent.htm>. Accessed 17 January 2019.
11. UNESCO, <http://whc.unesco.org/en/list/484>. Accessed 17 January 2019.
12. European Committee for Standardization (2012) UNI EN 16085 Conservation of cultural property-Methodology for sampling from materials of cultural property-General rules. Brussels, Belgium.
13. Luxán MP, Madruga F, Saavedra J (1989) Rapid evaluation of pozzolanic activity of natural products of conductivity measurement. *Cement Concrete Res* 19: 63-68.
14. Taşcı B, Böke H (2018) Properties of Roman lime mortars in ancient Lycia region. 2nd International Conference on Environment, Chemical Engineering & Materials (ECEM 2018), 22-24 June, Malta.
15. Aslan Ö, Böke H (2009) Properties of Roman bricks and mortars used in Serapis Temple in the city of Pergamon. *Material Characterization* 60: 995–1000.
16. Uğurlu Sağın, E (2012) *Characteristics of Roman mortars produced from natural and artificial pozzolans in Aigai and Nysa*. Ph.D. thesis, İzmir Institute of Technology, Turkey.

17. Sánchez-Moral S, Luque L, Cañaveras J.C et al (2005) Lime pozzolana mortars in Roman Catacombs: Composition, structures and restoration. *Cement and Concrete Research* 35 (8): 1555–1565.
18. Jackson M.D, Logan J.M, Scheetz B.E et al (2009) Assessment of material characteristics of ancient concretes, Grand Aula, Markets of Trajan, Rome. *Journal of Archaeological Science* 3: 2481-2492.
19. Uğurlu Sağın E, Böke H, Aras N, Yalçın Ş (2012) Determination of CaCO₃/SiO₂ content in the binders of historic lime mortars. *Materials and Structures* 45 (6): 841-849.
20. Benedetti D, Valetti S, Bontempi E et al (2004) Study of ancient mortars from the Roman Villa of Pollio Felice in Sorrento (Naples). *Applied Physics A* 79: 341-345.
21. Genestar C, Pons C, Más A (2006) Analytical Characterisation of ancient mortars from the Archaeological Roman city of Pollentia (Balearic Islands, Spain). *Analytica Chimica Acta* 557: 373-379.
22. Boynton RS (1980) *Chemistry and Technology of Lime and Limestone*. 2nd Edition. John Wiley & Sons, New York.
23. Vicat LJ (2003) *Mortars and Cements*. (First published in 1837). Donhead Publishing Ltd, Dorset.

DB-HERITAGE: A database of mortars composition and characteristics

António Santos Silva¹, Rodrigo Giollo¹, Maria João Correia¹, Maria do Rosário Veiga², Paulina

Faria³

(1) Materials Department, National Laboratory for Civil Engineering, Portugal, ssilva@lnec.pt, rgiollo@lnec.pt, mjmcorreia@lnec.pt

(2) Buildings Department, National Laboratory for Civil Engineering, Portugal, rveiga@lnec.pt

(3) CERIS and Civil Engineering Dep., FCT, NOVA University of Lisbon, Monte da Caparica, Portugal, mpr@fct.unl.pt

Abstract

Mortars are materials which are present in constructions from the antiquity to nowadays, being complex in terms of their constituents and microstructure, incorporating traditions and techniques related to the local knowledge. Furthermore, the mortar characteristics vary also with its role in the structure and the place and environment of use.

The knowledge of the mortars constituents, characteristics and behaviour in their specific service conditions is important for improving the materials history and for a better definition of conservation strategies. That knowledge, obtained by many different researchers and practitioners of the area, should be easily available for all the professionals who need it, both for further research and for direct use in the field.

This has been the background for the development of the DB-HERITAGE database project (<http://dbheritage.lnec.pt/>), which intends to build a repository for historical building materials, and a free-access IT-tool to collect the related data. This paper addresses specifically data from conservative interventions made on mortars applied on historic constructions. Additionally an overview of the database tools will be presented, exemplifying some of its outputs and potentialities related to historic mortars in different case studies in Portugal.

Keywords: Web database; building Heritage; mortar's composition, mortars' characteristics.

Introduction

Mortars are complex materials in terms of its constituents and microstructure, being in general influenced by local available raw materials, and also dependent of traditions and techniques that are used by the different countries and cultures. Similar to other materials, mortars have also had an evolution, which is closely linked to their roles and service environments, as well as to binders availability and production.

The study of mortars composition, their characteristics and behaviour in service conditions gives important information and data regarding their durability and history, which is necessary and important for materials improvement and for the definition of conservation strategies.

It is consensual that conservation and restoration in old buildings and monuments must respect the original materials, implying knowledge of the characteristics and functions of existing materials, as well as of their performance under service conditions [1]. Therefore, in the formulation of repair mortars, in addition to the characteristics of old mortars and substrates, the appropriate materials availability, the structure requirements and the exposure environment must be taken into account [2, 3]. The compatibility between materials will allow to maintain the old structure without causing harmful side effects, providing an effective protection. However, for this process to be successful, it is essential to record and preserve information on the characteristics of both old materials and those used in conservation and restoration interventions, as well as their positive or negative results.

That knowledge, obtained by many different researchers and practitioners of the area, should be easily available for all the professionals who need it, both for further research and for direct use in the field. In the last years there has been increasing global information on these topics, as well as on materials deterioration and ageing mechanisms.

This was, therefore, the framework for the creation of a digital infrastructure, designated DB-HERITAGE, to collect information on building materials with historical and heritage interest, and to provide different tools for documenting and preserving materials history, properties and performance. Mortars are one of the historical materials included in it, with a lot of information already collected.

This paper presents some of the potentialities available in this database (<http://dbheritage.lnec.pt/>), illustrated with some examples of mortars characteristics of Portuguese historic constructions.

DB-HERITAGE Database – General characteristics

The data which is being archived in the database consists of generic information on monuments/case studies, including reports, articles, photos and videos, historic overview of events (e.g. inspection, repair, conservation), including results of construction materials characterization by different analytical techniques, and the environmental characterization.

The user of the database can select specific monuments/case studies related data (e.g. generic information, historical events, material characterization) and access it according to different visualization options, including material type (e.g. mortar, stone, wood, etc.), and structure type (e.g. church, fort, palace, etc.) with option on filtering by case study designation (Figure 1).

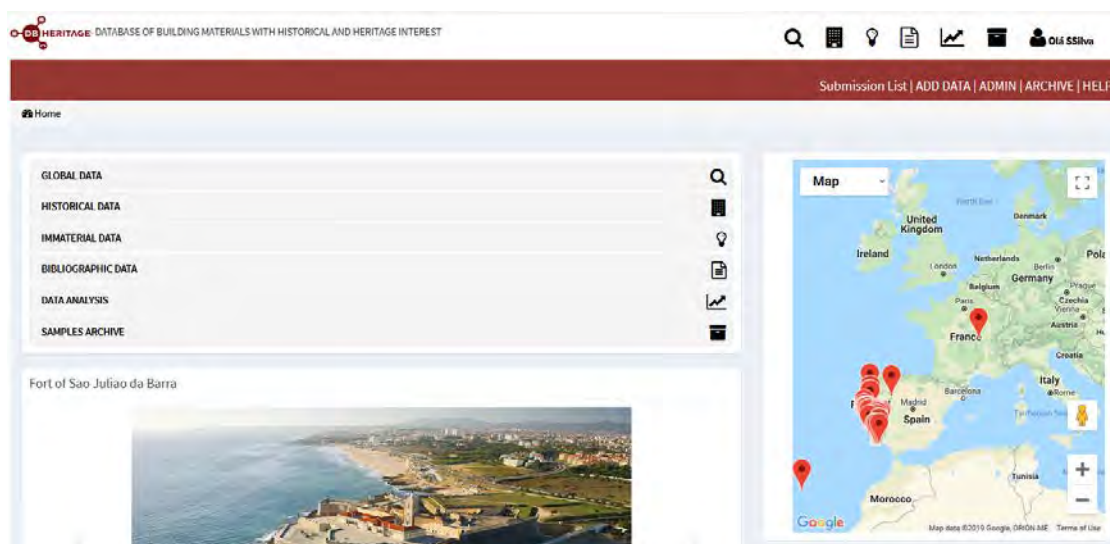


Figure 1. Data query options in DB-HERITAGE database; in the map it is possible to see the location of the available case studies

The data for a given monument is hierarchically grouped according to its elements (e.g. tower, bastion, etc.) and components (e.g. interior wall, floor, etc.) - Figure 2.

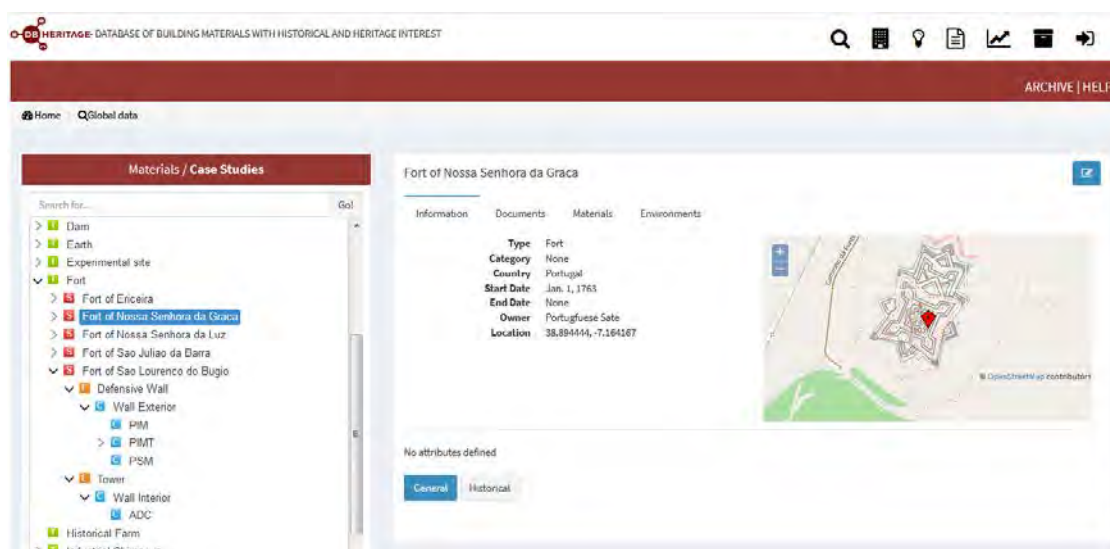


Figure 2. Example of a hierarchical schematization of a case study

Environmental characterization data, namely meteorological and air pollution information, or soil and water characteristics, can also be included. The user may access the environmental information registered in the region where the monument is located or access the local registers associated with a related element or component of that monument.

The characterization data of each material is also grouped according to its nature in chemical, mineralogical, microstructural, physical or mechanical issues.

The events on each case study are subdivided into inspection, maintenance, monitoring and conservation/repair interventions. Each of these listed actions and detailed information can

be accessed by the user. This information is synthesized in a dynamic framework that allows navigating to the materials characterization results by a given test method applied on a case study event.

The database provides the possibility of exporting data in different formats, and in the near future should allow data analysis, integrating some simplified analysis tools such as graphic representations and filters.

Historic mortars – Some features of the DB-HERITAGE database

To illustrate some of the functionalities of the database, examples of the characterization data of mortar samples from different case studies in Portugal are presented in the following sections.

Case studies

The Fort of São Julião da Barra (SJB), in Figure 3, is located on the right bank of the Tagus River, at the Point of São Gião. It is an example of military baroque architecture being the most complete military defense complex constructed to defend the port of Lisbon. It was operational in 1580 but its construction took nearly a century to complete. Throughout Spanish dominion (1580–1640) it was used as a state prison. Latter, in 1650, works were undertaken to increase the power of the defensive landside. In the early 19th century, during the French occupation, Napoleon military forces were installed in São Julião da Barra to combat the English fleet that blocked the entrance of the Tagus river. The latest military action involving the fortress took place in the context of the 1831 Portuguese civil wars. Two samples, taken by the Portuguese Directorate-General for Cultural Heritage, one from the filling mortar (SBJ-J) and another from a rendering mortar (SJB-R), both from south wall [4], were characterized in terms of material constituents.



Figure 3. Aerial view of Fort of São Julião da Barra

The Fortress of Nossa Senhora da Luz (NSL), in Figure 4, is currently classified as a building of public interest, being located on the right bank of Tagus River, in Cascais Municipality. It is considered to be representative of the architecture transition from the medieval castle model to the bulwark fortress [5]. Built in 1580, in the Philippine period, it includes an earlier structure, the *Santo António Tower*, also known as *Joanina Tower*, ordered to be built by D.

João II, in 1488, later transformed into a fortress with three Bastions, at the end of the 16th century, to reinforce the defense of the Bay of Cascais, constantly threatened by the English navy [6,7].

This fortress has a trace considered to be uncommon in Portuguese military architecture, a triangular plant with an interior courtyard that provides the connection between its three bastions and from where the stairs to the Joanina Tower and cisterns start. The two bastions face the sea from obtuse angles, while the third one forms an acute angle [6,7]. Due to the damages imposed by the Lisbon earthquake at 1755, part of the fortress and of the Joanina Tower have suffered important architectural transformations [5,6,7]. Currently, the fortress belongs to Cascais Municipality, and undergoes a process of recovery and revitalization with the purpose of implementing a museum space [7]. In 2012 a study was carried out on the characterization of the exterior and interior plasters of the fortress, aiming: (i) the in-situ evaluation of the state of conservation of the mortars; (ii) extraction of samples of the external and internal renders (labelled as NSL) for laboratory characterization.



Figure 4. Bulwark of Fortress Nossa Senhora da Luz

The Fort of Nossa Senhora da Graça (NSG), also known as Fort Count of Lippe (Figure 5), classified as National Heritage Site in 2010, and World Heritage Site by UNESCO in 2012, located in a mountain in the north of the town of Elvas, was built in the late 18th century ordered by King Joseph I of Portugal and by his minister, the Marquis of Pombal [8].

It is a masterwork of the 18th century military architecture, and is considered one of the greatest symbols of the bulwark fortresses of the world. The central structure is a 150 meters side quadrangle with pentagonal bastions at corners. Four ravelins cover the curtain wall, one of which constitutes the monumental entry. The central part of the bastioned structure features an octagonal stronghold with two floors and a parapet with gun ports. The fort's octagonal tower has two vaulted floors. The first floor features a cross plant and includes a chapel in one of the cross's arms. The second floor is divided in several compartments including gun ports, kitchens and wards. Below the stronghold, carved into the rock, there is a cistern. The stronghold is surmounted by de Governor's House, also

divided in two floors. In the external side, the structure is completed by a hornwork, a fifth ravelin and a wide dry moat [8,9].

As part of nomination by UNESCO, a conservation and restoration plan was implemented in 2015, involving a detailed characterization of materials used on fort's construction. For this, several render samples (named NSG) were collected and tested in laboratory. The conservation and restoration works of mortars were carried out with compatible repair materials, selected according to the physical-chemical characterization study and their degradation state [8].



Figure 5. Aerial view of Fort of Nossa Senhora da Graça [10]

Results of mortars characterization

The mortar samples were collected in elements that were considered representative of the environmental conditions in each case study. Their selection is in agreement with the methodology used by the National Laboratory for Civil Engineering (LNEC) to characterize mortars of ancient buildings and takes into account the importance of the different areas in terms of archaeological survey, techniques and materials. The characterization techniques used include: X-ray diffraction analysis (XRD), simultaneous thermogravimetric and differential thermal analysis (TGA-DTA), scanning electron microscopy with X-ray microanalysis (SEM/EDS), grain size analysis, wet chemical analysis, water absorption capillarity coefficient and compressive strength.

In the following sections examples of the results obtained will be presented showing some of the outputs generated by the database.

Figure 6 shows an example of an event, including its type, a brief description and the date. Two samples of S. Julião da Barra Fort, *SJB_J* from a masonry mortar and *SJB_R* from the external render are exemplified. A list of the test methods applied on a given sample is available in the database. The respective measurements can be accessed in the “details” column, or filtered by the method used. The tool also provides a search field and the possibility of exporting the concerned information in different formats.

Mortars characterization of Fort of Sao Juliao da Barra

Type: Inspection
Date: June 1, 2002
Description: Characterization of masonry mortar and external render samples from south facing defensive wall of the Sao Juliao da Barra Fort.

Show 10 entries CSV Excel PDF Search:

Element	Method	Material	Details
External Render SJB-R < South Defensive Wall < Fort of Sao Juliao da Barra	Microstructural analysis	Mortar:Mortar:Mortar	👁
External Render SJB-R < South Defensive Wall < Fort of Sao Juliao da Barra	Binder/Aggregate Ratio	Mortar:Mortar:Mortar	👁
External Render SJB-R < South Defensive Wall < Fort of Sao Juliao da Barra	Chemical analysis	Mortar:Mortar:Mortar	👁
External Render SJB-R < South Defensive Wall < Fort of Sao Juliao da Barra	Grain-size distribution (sand)	Mortar:Mortar:Mortar	👁
External Render SJB-R < South Defensive Wall < Fort of Sao Juliao da Barra	DTA/TG/DTG	Mortar:Mortar:Mortar	👁
External Render SJB-R < South Defensive Wall < Fort of Sao Juliao da Barra	XRD Composition	Mortar:Mortar:Mortar	👁
External Render SJB-R < South Defensive Wall < Fort of Sao Juliao da Barra	Macro Description	Mortar:Mortar:Mortar	👁
Masonry Mortar SJB-J < South Defensive Wall < Fort of Sao Juliao da Barra	Microstructural analysis	Mortar:Mortar:Mortar	👁
Masonry Mortar SJB-J < South Defensive Wall < Fort of Sao Juliao da Barra	Chemical analysis	Mortar:Mortar:Mortar	👁
Masonry Mortar SJB-J < South Defensive Wall < Fort of Sao Juliao da Barra	Binder/Aggregate Ratio	Mortar:Mortar:Mortar	👁

Showing 1 to 10 of 14 entries Previous 1 2 Next

Method Used

Binder/Aggregate Ratio Chemical analysis DTA/TG/DTG Grain-size distribution (sand) Macro Description Microstructural analysis XRD Composition

General Historical

Figure 6. List of the test-methods used for mortars characterization of Fort São Julião da Barra

Figure 7 gives an example of the microstructural analysis data related to the SJB-J sample. In the right hand column the user can select the associated information, which in this example includes several SEM images and an EDS spectrum. In the main frame, the elected image is detailed. This example concerns an aggregate/paste interface where a neoformation product on a quartz grain surface is visible.

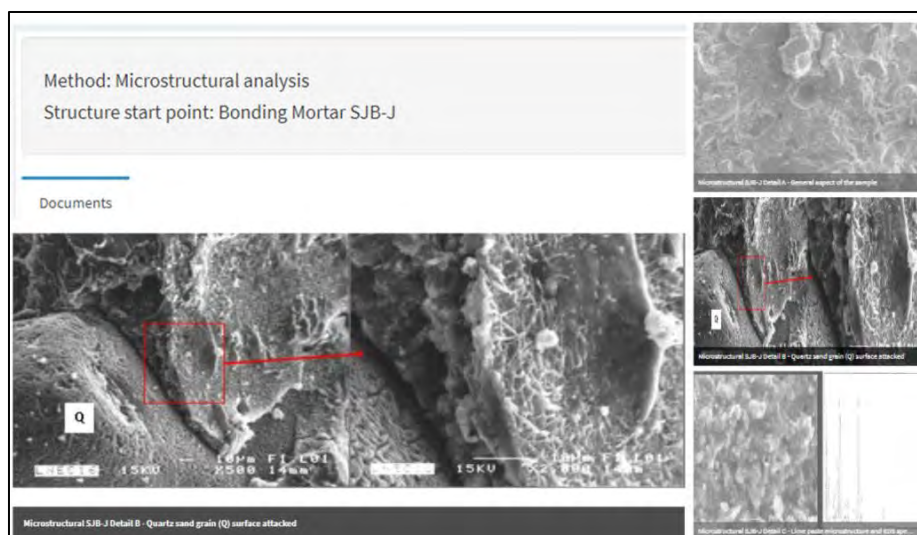


Figure 7. Example of the data regarding the microstructural characterization results of the SJB-J sample

The available information on the database allowed downloading the data included in the following tables of analysis.

XRD composition

Tables 1 to 3 summarize the XRD composition obtained for the analysed samples. The results show the analysis of two fractions: an overall fraction and a binder rich fraction. This allows obtaining deeper information on neoformation products formed, as well as on degradation products present in the mortars.

Table 1. XRD composition of mortar samples from SJB

Crystalline phases	SJB-R		SJB-J	
	Overall fraction	Binder rich fraction	Overall fraction	Binder rich fraction
Quartz	+++	+	+++	+ / ++
Feldspars	+ / ++	+	+ / ++	+
Mica	vtg	vtg	vtg	vtg
Kaolinite	vtg / +	vtg / +	vtg	vtg
Iron Oxide	vtg	vtg	vtg	vtg
Calcite	++ / +++	+++	++	++ / +++
Aragonite	vtg	vtg / +	vtg	vtg
Magnesite	?	vtg	?	vtg
Calcium Aluminate Hydrate and/or Chloroaluminate	-	-	vtg	+
Gypsum	-	-	vtg	vtg
Ettringite	-	-	vtg	+
Zeolite	vtg	vtg	vtg	vtg

Notation: +++ abundant; ++ present; + small amount; vtg traces; ? doubts in presence; - undetected

SJB samples: The rendering mortar, consisting essentially of sand minerals (quartz, feldspar, mica and kaolinite) and calcite, is characteristic of an air lime mortar with siliceous aggregates. The presence of magnesite and aragonite is attributed to the action of an environment rich in magnesium ions, such as seawater, that promotes the dissolution of calcite and its subsequent recrystallization in the form of aragonite and also cation exchange reactions between Ca^{2+} and Mg^{2+} in calcium carbonates to form magnesite. On the other hand, the masonry mortar sample presents also a mineralogical composition characteristic of an air lime mortar, although the proportion of calcite is lower than in the rendering mortar sample. The type of sand minerals identified in the masonry mortar is very similar to that of the render mortar sample. An interesting feature in both samples is the identification of a zeolite-type compound, with a composition similar to a hydrated sodium and calcium aluminosilicate, attributed to the development of pozzolanic reactions in these mortars of the calcium hydroxide of the air lime with some altered minerals present in the sand grains.

NSL samples: Mortars of Nossa Senhora da Luz Fort are relatively similar regarding the type of binder, which is a calcitic air lime, except NSL-BS5 sample that is a dolomitic lime, and possibly related to a restoration campaign. Also, the type of sand is similar, being siliceous. In samples of bulwarks (MP10 and MS9) and of the Torre Joanina (TJ1) some hydrated calcium aluminates (carbo and chloro) were identified, probably resulting from pozzolanic reactions between the aggregates and the lime, favored by the high moisture content in the

environment around this Fort. In another masonry mortar the presence of sodalite and cristobalite compounds was detected, attributed to the employed sands, that may explain the the hydrated calcium aluminates found in most of the NSL mortar samples.

Table 2. XRD composition of mortar samples (overall fractions) from NSL

Crystalline phases	NSL BN7	NSL BS5	NSL MP10	NSL MS9	NSL TJ1-E	NSL TJ1-I
Quartz	+++	+++	+++	+++	+++	+++
Feldspars	++/+++	++	+	+	++	+
Mica	vtg	?	vtg	?	vtg	vtg
Aragonite	vtg	vtg/+	?	vtg	-	-
Dolomite	vtg	+	-	-	-	-
Calcite	+++	+++	++/+++	+++	++/+++	++
Hydromagnesite	-	+	-	-	-	-
Goethite	-	vtg/+	-	-	-	-
Gypsum	-	-	vtg	-	-	-
Ettringite	-	-	-	-	-	vtg
Hematite	vtg	-	vtg	vtg	vtg	-
Monocarboaluminate	-	-	?	-	-	+
Halite	-	-	vtg	-	-	-
Chloroaluminate	-	-	vtg	vtg	vtg/+	+ / ++
Kaolinite	-	-	-	-	vtg	-

Notation: +++ abundant; ++ present; + small amount; vtg traces; ? doubts in presence; - undetected

Table 3. XRD composition of mortar samples (overall fractions) from NSG

Crystalline phases	NSG-1R	NSG-3RE	NSG-3RI	NSG-8RE	NSG-8RI	NSG-9RE	NSG-17R
Quartz	++/+++	+++	++	+++	+ / ++	++	++
Feldspars	++/+++	+++	++	++	++	++	+ / ++
Mica	+	+	Vtg	vtg	vtg	vtg/+	vtg/+
Clinochlore	-	-	-	-	vtg	vtg	-
Kaolinite	vtg	vtg/+	?	vtg	?	-	+
Amphiboles	+ / ++	vtg/+	+	vtg	+ / ++	vtg/+	++
Talc	vtg	vtg	Vtg	?	vtg	?	vtg
Calcite	++	+ / ++	++/+++	+ / ++	++	++	+ / ++
Dolomite	vtg	vtg	vtg	vtg	-	-	vtg
Calcium aluminate hydrate	?	?	vtg	vtg	? / vtg	vtg	vtg/+
Hydromagnesite	-	-	-	-	vtg	-	-
Magnesite	-	-	-	vtg	-	-	-

Notation: +++ abundant; ++ present; + small amount; vtg traces; ? doubts in presence; - undetected

NSG samples: The rendering mortars consist of air lime and sands, which appear to be from igneous and metamorphic rocks given the type of minerals present (quartz, feldspars, mica, amphibole, chlorite and talc). Lime is of dolomitic nature, since in the binder rich fraction hydromagnesite and magnesite compounds are always present. Some of the mortars present in their composition calcium aluminate hydrates, which are associated to the

reaction of certain alumina rich minerals of the aggregates (e.g. feldspars, mica) with the lime.

Binder/aggregate ratio

Table 4 presents the results of the binder/aggregate ratio (b/a) for the samples of the three case studies. The b/a values (weight ratios) obtained are very diversified, varying from 1:1 to 1:10, with an average of 1:3.5. This high variability, even within the same structure, suggests that the proportions binder/aggregate were not defined in advance. Apparently, the mixes were made in situ, probably according to workability, plasticity, bond, and in general the “hand” of the worker.

Table 4. Binder/aggregate weight ratios obtained for samples from SJB, NSL and NSG case studies

Case study	Element	Sample identification	Binder	Aggregate
SJB	South defensive wall	SJB-J	1	10
	South defensive wall	SJB-R	1	4
NSL	Wall interior of North bastion	NSL BN7	1	1
	Wall interior of South bastion	NSL BS5	1	2
	Wall interior of West defensive wall	NSL MP10	1	3
	Wall exterior of South defensive wall	NSL MS9	1	2
	Wall exterior of Joanina Tower	NSL TJ1-E	1	1
	Wall interior of Joanina Tower	NSL TJ1-I	1	2
NSG	Exterior stronghold	NSG-1R	1	3
	Powder magazine - exterior layer	NSG-3RE	1	6
	Powder magazine - internal layer	NSG-3RI	1	2
	Tunnel - external layer	NSG-8RE	1	4
	Tunnel - internal layer	NSG-8RI	1	2
	Counterscarp - external layer	NSG-9RE	1	5
	Interior of cistern	NSG-17R	1	6

Physical and mechanical characteristics

Due to difficulties found in the physical and mechanical characterization of some samples collected in the case studies, such as irregular shape, small size and low cohesion, standard test methods cannot be directly applied, and it is necessary to make use of adaptations of existing laboratory test methods and to validate the results. In this sense, LNEC has been developing and validating some test methods to evaluate the water absorption by capillarity, the drying capacity, the modulus of elasticity by ultrasound pulse velocity and the compressive strength.

The results obtained are evaluated by comparison with reference values. Thus, together with the other tests to which the samples are subjected, it is also possible to evaluate, from the point of view of their mechanical characteristics and behaviour to the water, the level of degradation of the building and its possible interventions needs.

The capillarity coefficient by contact (C_{cc}), the compressive strength by the confinement mortar method (S_{ccm}) and ultrasonic velocity to calculate the dynamic modulus of elasticity (E), determined for some mortar samples from the case studies, are presented in Table 5.

Table 5. Physical and mechanical results for some mortar samples from SJB, NSL and NSG case studies

Case study	Sample identification	C_{cc5} [Kg/(m ² .min ^{0.5})]	S_{ccm} [N/mm ²]	E [N/mm ²]
NSL	NSL BN7	0.45	0.26	2895
	NSL BS5	2.73	1.4	1380
	NSL MP10	1.26	2.9	2960
	NSL MS9	1.92	2.0	3530
	NSL TJ1-E	0.98	3.7	2870
	NSL TJ1-I	3.83	n.d.	2750
NSG	NSG-1R	0.3	1.6	n.d.
	NSG-3RE	0.9	4.0	n.d.
	NSG-8RE	2.2	n.d.	n.d.
	NSG-8RI	5.5	n.d.	n.d.
	NSG-9RE	1.3	1.1	n.d.
	NSG-17R	1.6	1.1	n.d.

n.d. – not determined

As shown, the values of physical and mechanical properties do not always present a good correlation with the values of binder/aggregate ratio. In fact the physical and mechanical characteristics of air lime mortars are related with their microstructure [11], which depends not only on the binder/aggregate ratio but mainly on the grain size distribution, nature and shape of the aggregate that condition the bond between the particles. The interrelation of matrix and aggregate define the pore structure, which greatly influence the carbonation rate, together with the environment conditions.

On the other hand, some inverse correlation can be found between compressive strength and capillary coefficient. For example, for NSL samples, with the exception of NSL BN7, the lowest C_{cc5} (0.98) corresponds to the highest S_{ccm} (3.7), while the highest C_{cc5} (2.73) is found for the sample with the lowest S_{ccm} (1.4). In fact both properties are influenced by the pore structure.

The formation of some hydraulic compounds, such as carbo and chloroaluminate, as found in NSL MP10 and NSL TJ1-E may also contribute for increased mechanical strength and reduced water absorption rate.

Besides the mortars characteristics of the case studies presented in this paper, the database contains complete information on various other building materials and heritage referential structures and will have its potential maximized as it receives new case studies and gains new functionalities. Therefore, their contribution to the preservation of the built heritage will also increase.

Conclusions

The study of materials of historical constructions, especially of mortars, allows obtaining very relevant information about the history of the monument itself, but also on the performance of the material in the exposure conditions to which it was subjected. This information, when used in contrast to the same or other similar monuments or case studies, facilitates the decision in terms of the materials and compositions to be used in conservation and restoration interventions.

The developed database of building materials allows collecting the existing dispersed information and its assessment to respond to the needs of the conservation of the built heritage. In addition to the information on the performance of materials, it is possible relating it with other data such as meteorological data. Bibliographical information about a particular case study is also freely available. Simultaneously, it potentiates research to fill some identified knowledge gaps. This tool will continue to be expanded and developed in order to be indexed and queried by WHERE, WHEN and WHAT on a European cloud (ARIADNEplus).

Acknowledgments

The authors acknowledge the support of Fundação para a Ciência e Tecnologia (FCT), Portugal, for funding the research project PTDC/EPH-PAT/4684/2014: DB-Heritage - Database of building materials with historical and heritage interest.

References

1. Veiga MR, Aguiar J, Santos Silva A, Carvalho F (2001) Methodologies for characterisation and repair of mortars of ancient buildings. Proceedings of the 3rd International Seminar Historical Constructions, Guimarães, Universidade do Minho, pp. 353-362.
2. Riccardi M, Lezzerini M, Caro F, Franzini M, Messoga B (2007) Microtextural and microchemical studies of hydraulic ancient mortars: Two analytical approaches to understand pre-industrial technology processes. *Journal of Cultural Heritage*. 8, pp. 350-360
3. Veiga MR (2012) Conservation of Historic Renders and Plasters: From Laboratory to Site. In: Válek J, Hughes J, Groot C (eds) *Historic Mortars*. RILEM Bookseries, vol 7. Springer, Dordrecht, pp 207-225.
4. Santos Silva A, Cruz T, Paiva MJ, Adriano P, Candeias A, Schiavon N, Mirão J (2011) Mineralogical and chemical characterization of historical mortars from military fortifications in Lisbon harbour (Portugal), *Environmental Earth Sciences*, 63 (7), 2011, pp. 1641-1650

5. Ramalho MM, Barro MF, Boiça J (2001) As fortificações marítimas da costa de Cascais, Quetzal, Cascais.
6. Website consulted: <http://www.patrimoniocultural.gov.pt/pt/>. Accessed 10 April 2019.
7. Veiga MR, Santos Silva A, Tavares M, Santos AR, Lampreia N (2013) Characterization of renders and plasters from a 16th Century Portuguese Military Structure: Chronology and durability. In *Restoration of Buildings and Monuments*, Vol. 19, n.4, 2013. pp. 223–238.
8. Santos Silva A, Santos AR, Veiga MR, Llera F (2016) Characterization of Mortars from the Fort of Nossa Senhora da Graça, Elvas (Portugal) to support the conservation of the monument. In: *HMC2016 - 4th Historic Mortars Conference*, Santorini, Greece, pp. 42-49. ISBN: 978-960-99922-3-7.
9. Guerra S (2008) O Forte de Nossa Senhora da Graça, *Monumentos*, n.º 28, pp. 44-51.
10. In situ Lda. (2015) Conservation Plan. Aerial view.
11. Santos AR, Veiga MR, Santos Silva A, Brito J, Alvarez JI (2018) Evolution of the microstructure of lime based mortars and influence on the mechanical behaviour: The role of the aggregates. *Construction and Building Materials*, Vol. 187, pp. 907–922.

Algarve vernacular architecture facade ornaments: chemical and mineralogical characterization

Marta Santos¹, António Santos Silva², Rosário Veiga³

(1) Faculty of Architecture University of Lisbon, Portugal, marta.rodrigues.santos@gmail.com

(2) Materials Department, National Laboratory for Civil Engineering, Portugal, ssilva@lnec.pt

(3) Buildings Department, National Laboratory for Civil Engineering, Portugal, rveiga@lnec.pt

Abstract

In Algarve, southern region of Portugal, vernacular architecture presents extensive facade decoration, characterized by the presence of coloured relief ornaments. These ornaments are mentioned in the literature as mainly made with air lime mortars and modelled through three modelling techniques, namely, in situ carving, cast moulding and run out moulding. This study aims to assess whether the different types of modelling techniques required specific mortars compositions, namely by, the use of specific binders, aggregate types and binder-aggregate ratios. For this purpose 27 samples were collected from four buildings from different historical periods, mid-18th century, early-20th century and mid-20th century, comprising different moulding techniques and iconographies. Results showed that all assessed samples were designed with air lime binder and siliceous aggregates, regardless from building date or modelling technique. Older mortars present relatively higher binder to aggregate ratios. The more recent samples from 20th century showed traces of calcium aluminium silicates, indicating probable addition of hydraulic binders, eventually related with the need of higher mechanical strength for the viability of cast moulding technique, predominant at the time.

Keywords: Algarve, vernacular architecture, facade ornaments, moulding techniques, mortars composition

Introduction

This study is part of an ongoing PhD research concerning the interpretation of historical exterior coatings in vernacular architecture of Algarve region (Southern of Portugal). Besides façade ornaments, these traditional coatings include lime washing paintings, skim coat renders, decorative mural paintings (fresco techniques) and sgraffito, which constitute the prevalent ornamental program of the facades of Algarve vernacular architecture.

The exterior mortar's ornaments, found in buildings dated from different historical periods, present extensive and diverse iconographies. Although several ancient ornament fragments were found in archaeological sites dated from the 11th to 13th centuries, and other erudite examples are dated from 18th century, the end of 19th century towards the first half of 20th

century is the period that these ornamental phenomena intensively spread through Algarve region and became more widely present in vernacular buildings facades. In last century, important alterations occurred on the elaboration techniques of the facade ornaments, comprising the extensive use of casting moulds, rather than in situ direct modelling, more common in previous centuries. These modified or improved techniques probably required an adaptation of mortar's composition due to the need of fluid mortars to allow cast moulding, rather than the compact mortars used for in situ modelling.

It is commonly accepted that this type of facade ornaments are made mainly with air lime mortars and aggregates specifically selected by craftsmen, considering their colour and grading, according to the desired aesthetic aspect of skim coatings or renders. Additions to the mortar mixture, such as natural fibres or ceramic materials with pozzolanic characteristics were used, when improvement of skim coating or render strength was required. Admixtures were also considered, like vegetal oils or animal fat or wax, in order to improve render waterproofing, water erosion resistance or deterioration by moisture [1, 2].

These facade ornaments comprise three different types of modelling techniques: in situ carving, cast moulding and run out moulding.

For in situ modelling craftsmen moulded, sculpted and carved a relieved mortar freshly-laid directly on the building facade.

Cast moulding, comprising a diverse range of moulds, made with flexible materials as wax, gelatine or silicone, or rigid materials as dry clay or gypsum. The moulds could have detachable parts that allow craftsmen to easily demould the ornaments. Natural fibres or ceramics materials could be added to the mixture to improve strength. High reliefs and large dimension ornaments could also be reinforced with structural metal elements, placed inside the ornament during casting, which will also help to fix the ornament to the facade, where in some cases complementary metal elements were previously fixed.

Run out moulding technique comprises the elaboration of ornaments characterized by presenting a continue section profile, such as pilasters, frieze, cornices and frames. This technique consists in running a profile mould directly through a mortar freshly-laid on the building facade, moulding the ornament in situ, or running the profile mould on a bench moulding the ornament, which after hardening is applied on the facade. The moulds used for this technique consist in metal sheet (zinc or brass), shaped as negative profile of the ornament and fixed to a wood frame, which helps to hold the mould and run it along the guiding elements. This technique requires a more consistent mortar than the previous mentioned cast moulding technique.

Some studies [1, 2] report that in situ carving was the most common technique until the improvement of casting technique occurred, comprising generalization of rigid moulds with detachable parts, enabling more complex and high relieve ornaments.

Apart from the moulding technique used, the facade ornaments of Algarve vernacular architecture present diverse finishing processes. The ornament can be painted with white or coloured lime wash, or its render can be left visible, finished as a sanded texture, or a matte or glossy surface.

This study aims to assess whether the different types of modelling techniques require specific mortar compositions, such as the use of specific binders, aggregate type and binder to aggregate ratio.

Case Studies

For this study six buildings were selected for sampling, from three different historical periods, namely, mid-18th century, early-20th century and mid-20th century, each comprising two buildings. Apart from building date, the criteria for selecting the three pairs of buildings comprised also the occurrence of similar ornament modelling techniques and identical ornament iconography. For the building selection eventual authorships and contractors relations were also considered.

The first building selected from mid-18th century was the Horta dos Cães tower at Convento de São Francisco's garner (labelled building A), dated back to 1740–1760, located at Faro town (Figure 1A). This building presents a unique decorative program conceived by Diogo Tavares e Ataíde (1711 – 1765), an architect and sculptor considered one of the most outstanding artistic personality of the Baroque of the Algarve region [3]. The second building selected from the same historical period was the Bívar Cúmano Villa (labelled building B), dated back to 1750–1760, located at Faro town (Figure 1B), also assigned to Diogo Tavares e Ataíde, presenting unique dolphins monsters figures, along with diverse geometric and vegetal ornaments that adorned the irrigation tank of that villa. These buildings present the moulding techniques of in situ carving and run out moulding.

Two buildings from the early-20th century were selected due to their similar ornamental program, composed of ribbons, flower mosaics and garland flower petals, and modelled by in situ carving and cast moulding techniques. One is the *Emídio Rolão* building (labelled building C), dated back to 1912–1914, located at Fuseta village (Figure 1C). The other building is *Marília* building (labelled building D), dated back to 1930 to 1932, and located at Faro town (Figure 1D). Both these buildings represent a profound transformation of the ornamental technique compared with the previously mentioned from the mid-18th century.

The two selected buildings from mid-20th century are both dated back to 1930-1950. One is located at Azinhal village and was labelled building E (Figure 1E) and the other is at Vista Real and was labelled building F (Figure 1F), both near Castro Marim town. These are two common examples of Algarve vernacular domestic architecture, comprising just ground floor with a simple architectural program, but with a not less important facade decoration. This type of vernacular buildings ornamentation is usually composed of colourful friezes, pilasters

and entrance door ornamental elements, as well as extensively decorated roof parapet, although in these examples the last mentioned is not present.

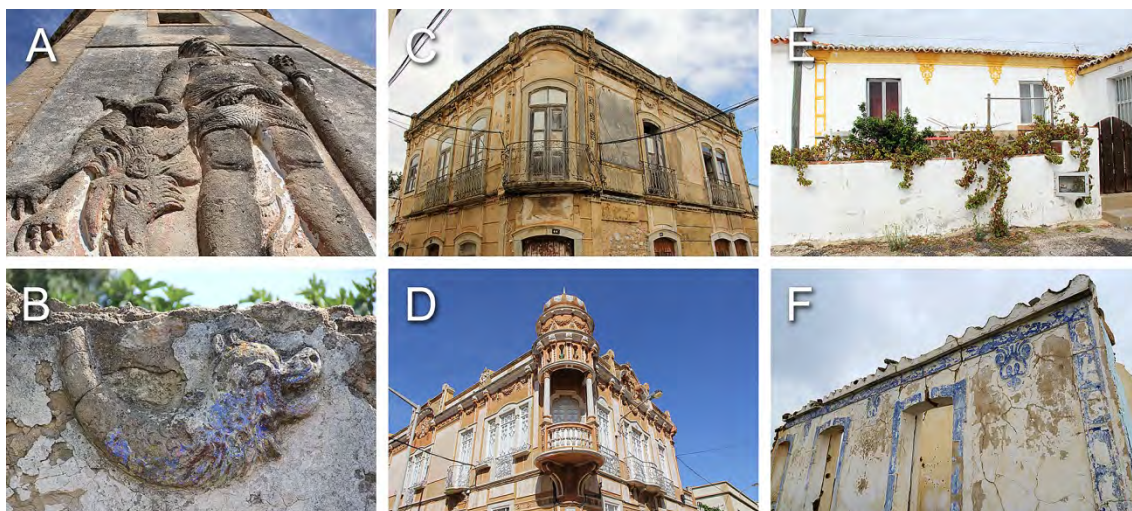


Figure 1. (A) *Horta dos Cães* tower at *Convento de São Francisco*'s garner (1740–1760) at Faro; (B) *Bívar Cúmano* Villa water tank facade (1750–1760) at Faro; (C) *Emídio Rolão* town house building (1912–1914) at Fuseta; (D) *Marília* town house building (1730–1732) at Faro; (E) Small house (1930–1950) at Azinhal village, near Castro Marim town; (F) Small house (1930–1950) at Vista Real, near Castro Marim town.

Materials and methods

Samples

Within the six selected buildings, due to administrative constraints, samples collection was only possible in the four buildings that are not presently in use, namely, building A, B, C and F, also presenting the most advanced state of degradation. The samples collection criteria intended to be representative firstly, of the most significant ornaments of the building, and secondly of the diversity in modelling techniques, such as in situ carving, cast and run out moulding. For this study a total of 26 samples were collected from the four mentioned buildings as listed in Table 1.

Methods

Visual and optical microscopy observation

The 26 collected samples were firstly visually analysed and photographically registered. Some particular aspects were observed and registered, such as the ornaments morphology, mortars visible layers and colour, presumable modelling technique and the presence of fibrous materials or other visible additives.

Microscopic observations were made on polished surfaces of the mortar samples. For these analyses, samples were dried for 12 h at 60 °C and then were impregnated under vacuum with an epoxy resin. Impregnated cross sections were polished and observed with an

Olympus SZH stereozoom microscope and an Olympus PMG3 optical microscope. Images were recorded with an Olympus DP-20 digital microscopy camera.

Table 1. Samples identification, ornament description and modelling technique.

Building	Sample	Description of ornament	Modelling technique
A	A01	Frieze of Hercules pedestal's	Run out moulding
	A03	Render	Mortar with single layer (with polychromy)
	A11	Hércules's stick	In situ carving
	A12	Pilaster (inner layer)	Mortar with single layer (with polychromy)
	A13	Pilaster	Mortar with single layer (with polychromy)
	A14	Hydra from Lerna of Hércules	In situ carving
	A15	Hércules's ankle	In situ carving
B	B02	Frieze	Run out moulding (with polychromy)
	B03	Dragon's tail	In situ carving (with polychromy)
	B04	Frieze	Run out moulding (with polychromy)
	B06	Frieze	Run out moulding (with polychromy)
	B07	Facade (inner layer)	Mortar with single layer
	B08	Frieze	Run out moulding (with polychromy)
	B09	Frieze	Run out moulding (with polychromy)
C	C01	Ribbon	In situ carving
	C02	Ribbon	In situ carving
	C03	Ribbon	In situ carving
	C06	Flower mosaic	Cast moulding
	C08	Garland flower petal	Cast moulding
	C09	Garland flower petal	Cast moulding
F	F03	Vegatalist ornament	In situ carving (with polychromy)
	F04	Vegatalist ornament	In situ carving (with polychromy)
	F05	Vegatalist ornament	In situ carving (with polychromy)
	F07	Geometric ornament (pilaster)	In situ carving (with polychromy)
	F09	Surface coating	Mortar with single layer (with polychromy)
	F13	Surface coating	Mortar with single layer (with polychromy)

Chemical and mineralogical characterization

The chemical and mineralogical characterization methodology carried out comprised complementary tests, which aim of identifying mortars characteristics (e.g. binder and aggregate) and the decay processes on the historical substrates. Samples were characterized through wet chemical analysis (WCA), X-ray diffraction analysis (XRD), thermogravimetric and differential thermal analysis (TGA-DTA) and scanning electron microscopy coupled with energy dispersive X-ray spectrometry (SEM-EDS).

The WCA tests were performed with the aim of defining the siliceous aggregate content and particle size distribution of the aggregates. Selected portions of samples were carefully disaggregated and then attacked with an aqueous solution of hydrochloric acid (1.2 M) to separate the siliceous aggregate (insoluble residue) from the binder. The insoluble residue was weighed and mechanically sieved to determine the particle size distribution of the siliceous aggregates.

The XRD tests were performed with a Phillips PW3710 X-ray diffractometer using Fe-filtered Co K α radiation, with 35 kV and 45 mA, speed of 0.05 °/s, from 3 to 74° 2 θ . The crystalline phases present were identified by comparison with the International Centre for Diffraction Data Powder Diffraction Files (ICDD PDF).

The TGA-DTA tests were carried out in a Setaram TGA 92 simultaneous thermal analysis system, under argon atmosphere (3 L/h). Samples were previously dried at 40 °C in a drying oven for 48 h. The thermal analysis was performed with heating rate of 10 °C/min, from room temperature to 1000 °C.

SEM-EDS analyses were performed to observe the microstructure and texture of the mortars, as well as to detect the presence of hydraulic binders, neo-formed products and soluble salts. Samples were sputtered with a gold film before being analysed in a Jeol JSM-6400 SEM, working at an acceleration voltage of 15 kV and coupled with an Oxford energy dispersive (EDS) X-ray spectrometer.

Samples selection for testing

Due to availability constraints of samples material, it was not possible to perform all tests in all of the 26 collected samples. The criteria to decide which tests should be carried out on each sample intended to increase the reliability of the results, by taking into account the maximum diversity of modelling techniques, historical periods and ornaments iconography.

Results and discussion

Visual and microscopic observations

The samples from the two buildings from 18th century (A and B) present similarities, concerning the mortar hardness and compactness, as well as the dimensions and colours of the aggregates. It is also possible to observe that most of the ornaments modelled by in situ carving technique are composed by one single mortar layer with the exterior surface smoothed by stiletos (Figure 2A). In the ornaments modelled by run out moulding it was possible to observe that they were made through the consecutive running of several layers of freshly-laid mortar, having a smoothed exterior surface. The coloured lime wash finishing was made over the hardened render (Figure 2B), probably in a different period of time, corresponding to a subsequent campaign, as mentioned in art history studies [4, 5].

In the Fuseta building (C) from the early-20th century, portions of a material with very distinctive greyish colour can be observed inside the samples mortar. Some fragments of an external finishing layer, very thin and with a yellowish colour, can be observed in parts of the samples, which may correspond to previous painting campaigns since ochre is the predominant colour of the building facade. Clear distinctive mortars are observed for the wall render layer and for the in situ carved ornament, with no evidence of any fixing inter layer mortar (Figure 2C, Figure 2D), confirming that the ornament was made in a freshly-laid

mortar. In these samples white lime nodules are also visible, in some cases with significant size (Figure 2E).

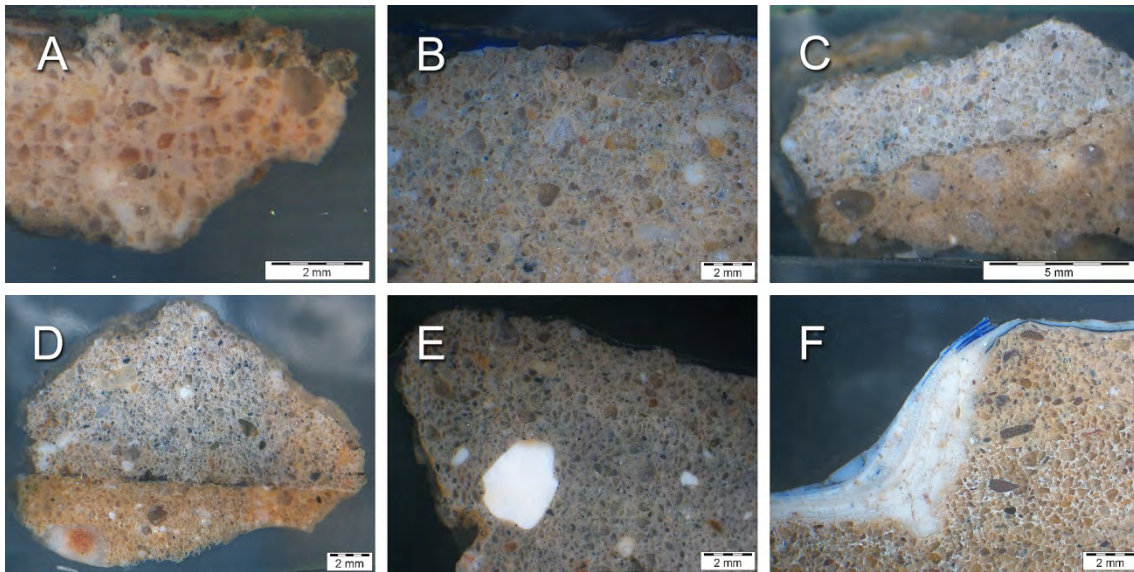


Figure 2. Images of microscopic observations of polished surfaces: (A) Sample A14; (B) Sample B03; (C) Sample C03; (D) Sample C06; (E) Sample C08; (F) Sample F03.

The ornaments of the Castro Marim building (F) from mid-20th century, moulded by in situ carving and run out moulding present a single and continuous layer forming the wall render and the ornament, with no evidence of any transition between them, suggesting they were made simultaneously. The ornaments were finished with coloured lime wash, presenting polychrome layers of greyish, greenish and bluish tones, applied over the hardened render (Figure 2F).

The information obtained by visual observation of the samples is summarized in Table 2 grouped by modelling technique and ornament type.

Chemical and mineralogical characterization

In order to ensure sample availability for future physical and mechanical characterization, the chemical and mineralogical characterization was performed just on six of the 26 samples collected, namely A11, B03, B04, B06, C03 and F03 samples. Table 3 presents the results of insoluble residue, with values varying from 62.4 % (samples A11) to 71.5 % (sample F03).

From the Insoluble residue of the six samples mentioned it was only possible to obtain material for particle size distribution curves (Figure 3) of samples B03, B04, B06 and F03. The obtained distribution curves show that all samples from building B have similar particle size distributions, characterized by the predominance of fine aggregates between 0.075 and 0.16 mm, whereas the sample from building F presents a coarser aggregate mostly ranging from 0.16 up to 0.63 mm.

Table 2. Visual observation of the ornament samples

Building data	Modelling technique and ornament type	Ornament description	Samples
(A) Horta dos Cães tower at Convento de São Francisco's garner (1740–1760) at Faro	Run out castmoulding, frieze	Exterior surface smoothed by the run out castmoulding. One single layer. Very stiff and compact. Finishing without pigment.	A01
	Mortar, facade and pilaster	Surface coating with single layer. Limewash and polychromy (yellowish).	A03 A12 A13
	In situ carving, stucco figures	Exterior surface seemed to be softened during modeling. One single layer. Finishing without pigment.	A11 A14 A15
(B) Bívar Cúmano Villa water tank facade (1750–1760) at Faro	In situ carving, stucco figures	Limewash and polychromy (bluish), painted in its dry state. Layer of the ornament is clearly different from the surface finishing.	B03
	Run out castmoulding, frieze	Limewash and polychromy (pinkish and yellowish), painted in its dry state. Black particles inside the mortar. Different layers, executed in fresh state, due to the run out cast moulding technique. Very compact.	B02 B04 B06 B08 B09
	Mortar with single layer, facade	Inner layer. Rough mortar.	B07
(C) Emídio Rolão town house building (1912–1914) at Fuseta	In situ carving, stucco ornaments (ribbon)	Clear differentiation between the layer of the surface finishing and the ornament. Grayish parts inside the mortar. Possible traces of a thin layer with polychromy (yellowish). Very fragile.	C01 C02 C03
	Cast moulding, stucco ornaments (flower)	Clear differentiation between the mortar of the surface finishing (yellowish) and the ornament (greyish). No traces of a thin layer of plaster between surface coating and precasted ornament. Less fragile than C01, C02 and C03.	C06 C08 C09
(F) Small house (1930–1950) at Vista Real, near Castro Marim town	In situ carving, stucco ornaments (vegetalist)	Ornaments moulded directly on the wall, with no different layer between surface coating and ornament. Limewash and polychromy (greyish, greenish and bluish), painted in its dry state.	F03 F04 F05
	In situ carving, stucco ornament (geometric)	Ornaments moulded directly on the wall, with no thin layer between mortars. Limewash and polychromy (greyish, greenish and bluish), painted in dry state.	F07
	Mortar with single layer, facade	Surface coating. Limewash and polychromy (greyish, greenish and bluish), painted in its dry state.	F09 F13

Table 3. Insoluble residue results

Samples	A11	B03	B04	B06	C03	F03
IR [%]	62.4	66.6	66.6	69.6	69.2	71.5

Notation: IR – Insoluble residue

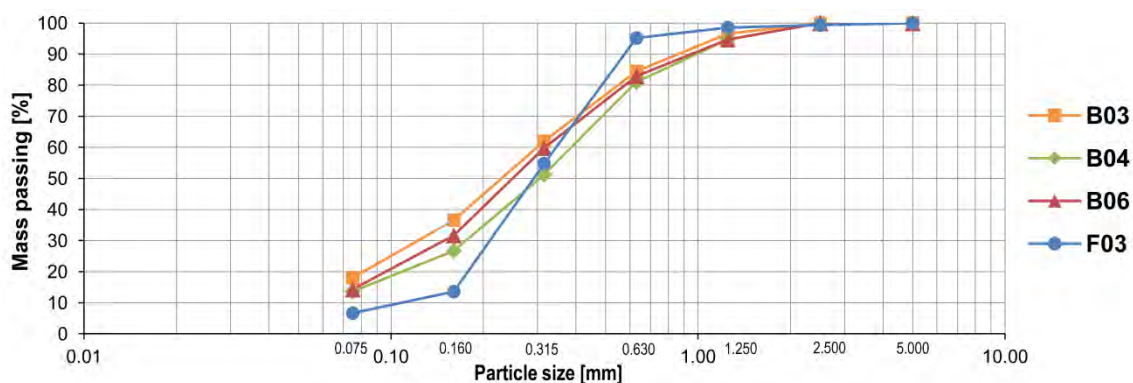


Figure 3. Particle size distribution curves of aggregates of samples B03, B04, B06 and F03

Table 4 summarizes the mineralogical composition of the six samples assessed by XRD. Quartz is predominant in all the samples, which, along with the low proportion of feldspar also in all of the samples, indicates the use of siliceous aggregates. In terms of binder, calcite is present in all of the samples, although in lower amount in samples C03 and F03. Sample C03 shows aragonite in low proportion, traces of gypsum and doubts regarding the presence of calcium silicates from Portland clinker. Sample F03 shows hydromagnesite, an indication of the use of a dolomitic lime, and traces of a calcium aluminium hydrate phase. It should also be noted that traces of vaterite were found in sample A11, along with traces of hematite, which was also found in samples B03 and B04.

Table 4. XRD mineralogical composition of samples A11, B03, B04, B06, C03 and F03.

Crystalline compounds	Samples					
	A11	B03	B04	B06	C03	F03
Quartz (SiO ₂)	+++	+++	+++	+++	+++	+++
Feldspars ((K,Na,Ca)AlSi ₃ O ₈)	+	+	+	+	+	+
Hematite (Fe ₂ O ₃)	tr	tr	tr/+	–	–	–
Hydromagnesite (4MgCO ₃ ·Mg(OH)2·4H ₂ O)	–	–	–	–	–	+
Calcite (CaCO ₃)	++	++	++	++	+ / ++	+ / ++
Vaterite (CaCO ₃)	tr	–	–	–	–	–
Aragonite (CaCO ₃)	–	–	–	–	+	–
Calcium aluminate hydrate (Ca ₂ Al(OH) ₇ ·6.5H ₂ O)	–	–	–	–	–	?
Gypsum (CaSO ₄ ·2H ₂ O)	–	–	?	–	tr	–
Ettringite (Ca ₆ Al ₂ (SO ₄) ₃ (OH) ₁₂ ·26(H ₂ O))	–	–	–	–	–	?
Portland clinker calcium silicates (C ₃ S, C ₂ S)	–	–	–	–	?	?

Notation: +++ high proportion (predominant compound); ++ medium proportion; + low proportion; tr - traces; ? possible presence; – undetected

Figure 4 presents the TG-DTG curves of the six samples selected for chemical and XRD analysis, which are in agreement with the mineralogical composition assessed by XRD (Table 4). Samples A11, B03, B04, and B06 present significant weight losses from 500 to 900 °C, a characteristic pattern related to calcite decarbonation, confirming that the ornament mortars were formulated with air lime, and in agreement with the fact of the buildings being dated from mid-18th century.

Samples C03 and F03, originating from building dated from early-20th century and mid-20th century, respectively, also show weight losses at mid-range to high temperature, although less intense than the previously mentioned samples, indicating that air lime was also used in these mortars formulation. However, sample C03 presents a more pronounced weight loss at relatively low temperature, till 200 °C. This weight loss corresponds to the release of free or adsorbed water and also to the dehydration of the gypsum detected by XRD, and eventually also to the dehydration of small quantities of ettringite and calcium aluminate hydrates [6], doubtfully detected in XRD. Further mass loss occurs progressively till the total decarbonation of calcite, although with a peak of the DTG curve approximately at 650 °C probably corresponding to aragonite. In sample F03, apart from the weight loss of calcite decomposition, it is also possible to notice two other temperature ranges, the first from 200 °C till 315 °C and the second immediately following, till 480 °C, corresponding to hydromagnesite decomposition [7].

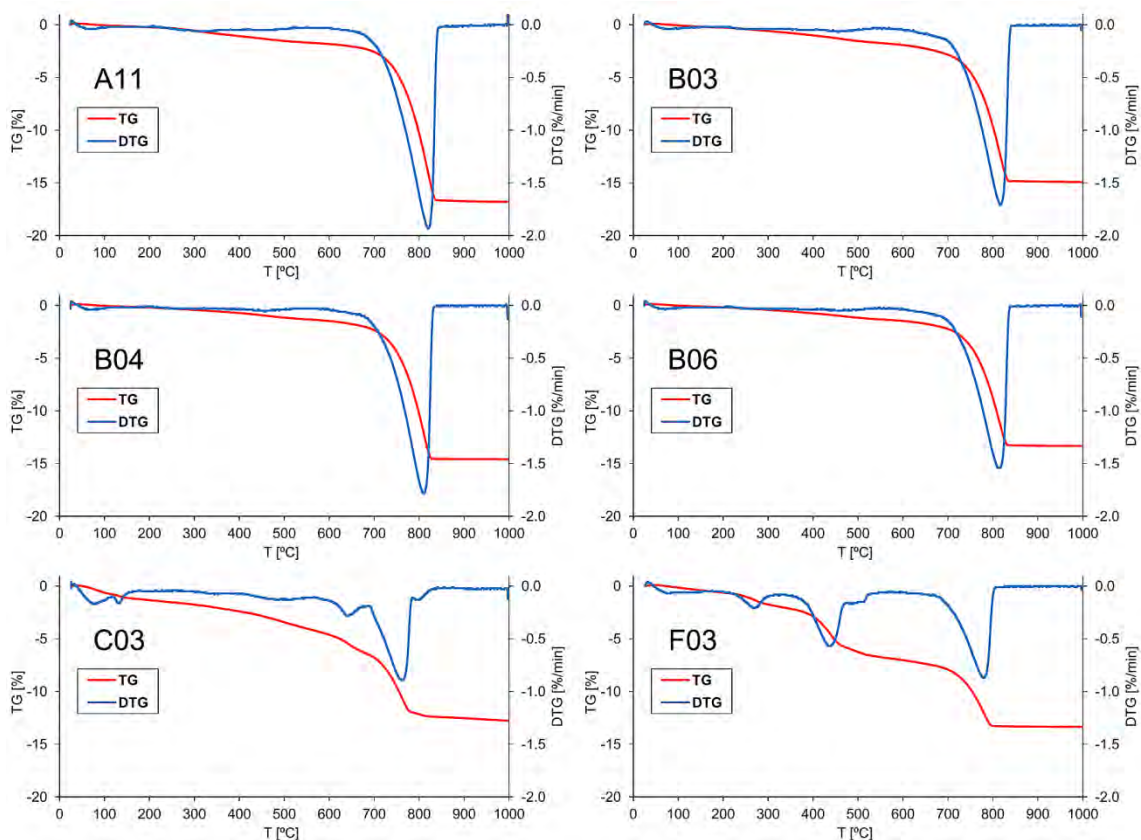


Figure 4. TG-DTG curves of samples A11, B03, B04, B06, C03 and F03

SEM-EDS analysis were made on polished and fractured surfaces. Due to availability constraints of samples material it was not possible to perform this analysis on samples from building A. The analysis of sample B06 (Figure 5) confirmed a calcitic lime binder and the employment of a siliceous sand, rich in quartz and with some feldspar particles. The analysis of lime nodules on sample C03 (Figure 6 and Figure 7) also confirms the use of a calcitic lime binder, along with the presence of gypsum on the sample outer paste layer, probably due to external sulphates contamination.

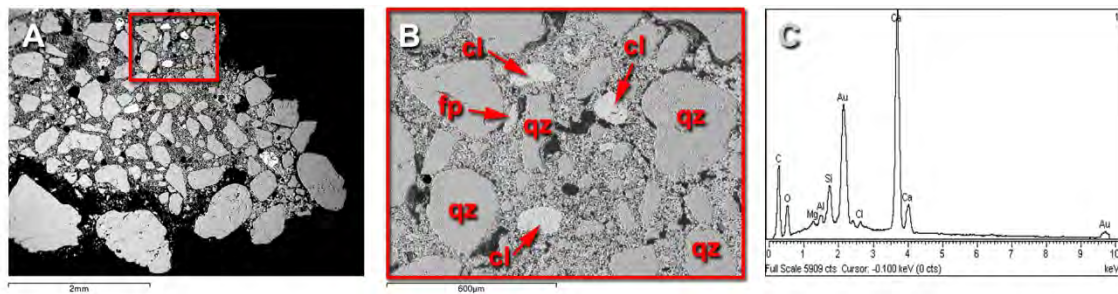


Figure 5. SEM/EDS analysis of sample B06: (A) general view of polished surface; (B) detail of the area marked in A showing quartz (qz) and feldspar (fp) aggregate grains and lime nodules (cl); (C) EDS spectrum of lime nodule in A

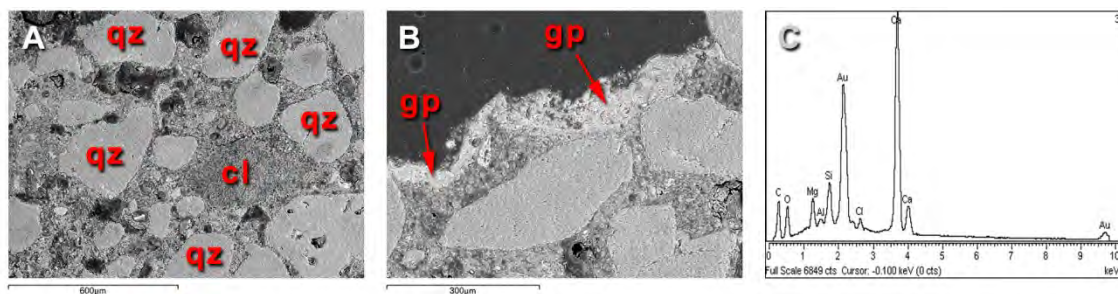


Figure 6. SEM/EDS analysis of sample C03 (polished surface): (A) general view where is visible the grains of the aggregate, mainly quartz (qz), and a lime nodule (cl); (B) detail external layers showing an outer layer rich in gypsum; (C) EDS spectrum of calcitic lime nodule

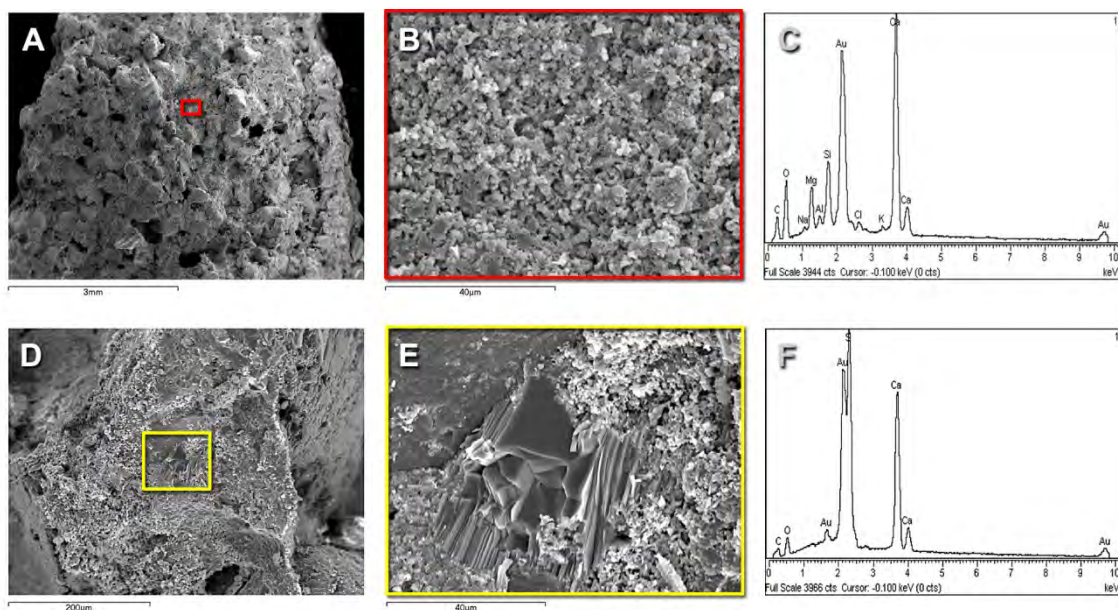


Figure 7. SEM/EDS analysis of sample C03 (fractured surface): (A) general view of the sample; (B) detail of the paste marked in A; (C) EDS spectrum of lime paste in B; (D) zone in the paste with gypsum; (E) close up view showing gypsum; (F) EDS spectrum of gypsum founded in E

The observation of sample C08 (Figure 8) also confirms a calcitic lime binder. In this sample some calcium aluminium silicates could be observed in the paste, probably due to the use of marly limestones in lime preparation. In fact, EDS analysis made in some lime nodules (Figure 8B and Figure 8D) indicate the presence of silicon, magnesium and, in some cases, also aluminium (Figure 8F). However, neither calcium silicates nor calcium aluminates normally associated to hydraulic binders were observed.

In the observation of sample F03 (Figure 9) some binder particles of a clinker silicate could be found, doubtfully detected in XRD. The fractured surface of this sample (Figure 10) confirms the use of a dolomitic lime in the binder paste showing the extensive presence of hydromagnesite.

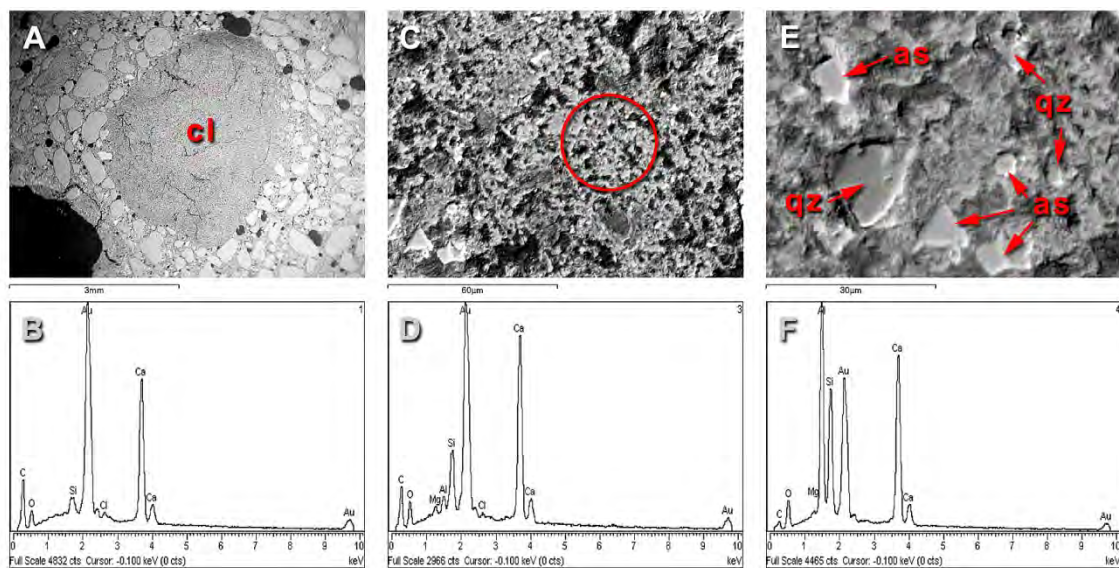


Figure 8. SEM/EDS analysis of sample C08 (polished surface): (A) General view showing the aggregates distribution and a lime nodule (cl); (B) EDS spectrum of the calcite nodule founded in A; (C) close up view showing the lime paste; (D) EDS spectrum of the binder zone marked in C; (E) details of the paste showing quartz aggregates (qz) and calcium aluminium silicates (as); (F) EDS spectrum of the calcium aluminium silicates founded in E

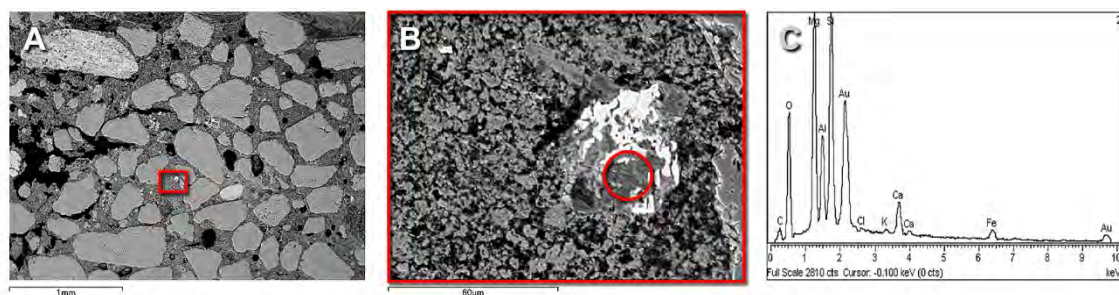


Figure 9. SEM/EDS analysis of sample F03 (polished surface): (A) general view showing aggregates and the porosity; (B) detail of the area marked in A with a particle of clinker silicate; (C) EDS spectrum of the clinker silicate marked in B

Table 5 presents the relative proportions of the samples mortar compositions, hydrated lime content and binder to aggregate weight ratio, calculated from the insoluble residue test from wet chemical analysis and the weight losses registered on TG-DTG analysis. It is possible to observe that older mortars, from mid-18th century samples (A11, B03, B04 and

B06), present relatively higher binder contents, having binder to aggregate weight ratio varying from 1:2.4 till 1:3.4. The samples from 20th century (C03 and F03) show lower binder concentration with ratios of 1:4.4 and 1:4.1. This may be related to the possibility the more recent mortars to having been formulated with addition of small quantity of hydraulic binders [8, 9], as partially identified in XRD and SEM-EDS analyses. The hydraulic binder induced mechanical strength and quick hardening eventually allowing a formulation with a lower binder to aggregate weight ratio to be employed.

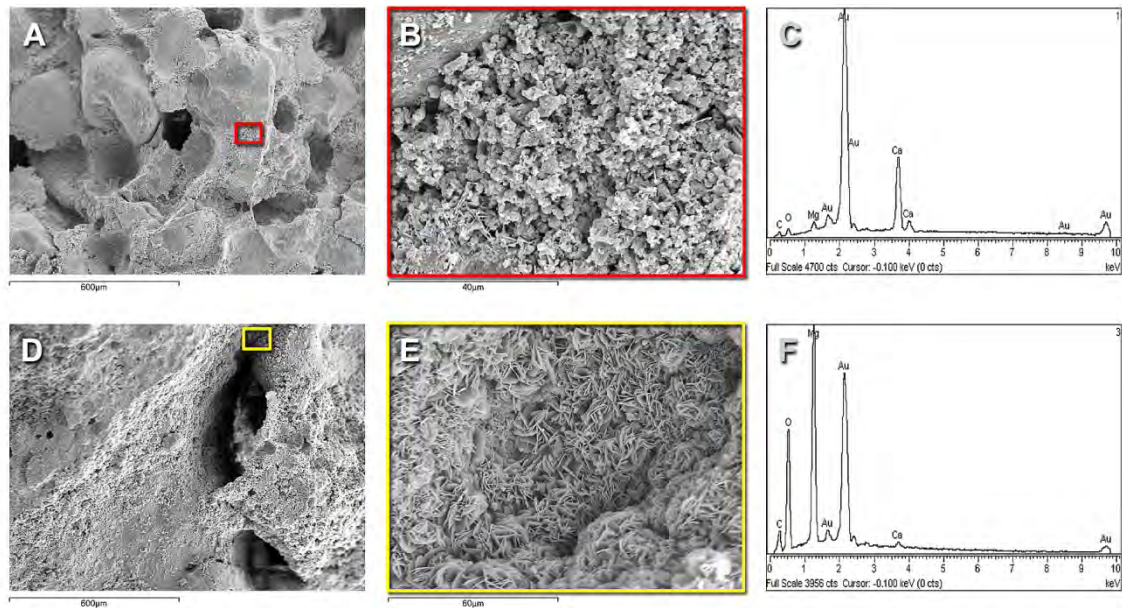


Figure 10. SEM/EDS analysis of sample F03 (fractured surface): (A) general sample view; (B) detail of the area marked in A corresponding to the lime paste; (C) EDS spectrum of the dolomitic lime binder paste; (D) aggregate interface showing hydromagnesite presence; (E) detail of the area marked in D showing hydromagnesite lamellar crystals; (F) EDS spectrum of hydromagnesite founded in E

Table 5. Mortars composition

samples	sample mortar composition			hydrated lime content		mortar formulation	
	Aggregate ¹ [%]	Calcite ² [%]	Magnesite ² [%]	calcitic [%]	dolomitic [%]	weight ratios binder aggregate	
A11	62.4	34.5	0.0	25.6	0.0	1.0	2.4
B03	66.6	30.3	0.0	22.4	0.0	1.0	3.0
B04	66.6	30.5	0.0	22.6	0.0	1.0	2.9
B06	69.6	27.6	0.0	20.4	0.0	1.0	3.4
C03	69.2	21.1	0.0	15.6	0.0	1.0	4.4
F03	71.5	15.4	4.3	0.0	17.6	1.0	4.1

(1) - Content obtained from the insoluble residue determination; (2) – Contents obtained from the TGA analysis

Conclusions

It is possible to conclude that all samples assessed in this study, regardless from building date or modelling technique, present air lime as main binder. More specifically all the studied mortars were formulated with calcitic lime, except for the sample from the newer building that contains dolomitic lime.

All sample mortars were formulated with siliceous aggregates, although some samples present scattered feldspar particles. Older mortars present relatively higher binder content, with mid-18th century mortars having a binder to aggregate weight ratio of 1:2.4, whereas 20th century mortars present a ratio of 1:4.4. This may be related to the fact that samples from 20th century buildings may contain small additions of hydraulic binders, probably to confer higher mechanical strength, an important property for viability of cast moulding technique that was becoming prevalent recently. This hypothesis needs to further be confirmed through future physical and mechanical characterization.

Acknowledgments

The authors acknowledge the support of Fundação para a Ciência e Tecnologia (FCT), Portugal for funding Marta Santos's scholarship (SFRH/BD/88732/2012), as well as the research project PTDC/EPH-PAT/4684/2014: DB-Heritage - Database of building materials with historical and heritage interest. The author also acknowledges Paula Menezes, Fátima Menezes and Dora Soares from the Materials Department and Dora Santos from the Buildings Department of LNEC for their support in the execution of the experimental work.

References

1. Lade K, Winkler A (1960) *Yeseria y estuco – revoques, enlucidos, moldeos, rabitz*. Barcelona: Editorial Gustavo Gili.
2. Garate-Rojas I (1999) *Artes de los Yesos. Yeserias e Estucos*. Madrid: Instituto Español de Arquitectura, MRRP, Universidad de Alcalá, Munilla-Lería.
3. Santana D (2018) *Diogo Tavares e Ataíde Arquitecto Algarvio (1711-1765)*. Lisboa: Edições Colibri.
4. Horta-Correia J (2010) *O Algarve em património*. Olhão: Gente Singular Editora.
5. Lameira F (1997) *Faro Edificações Notáveis*. Faro: Câmara Municipal de Faro, 2^a Edição.
6. Gabrovšek R, Vuk T, Kaučič V (2006) Evaluation of the Hydration of Portland Cement Containing Various Carbonates by Means of Thermal Analysis. *Acta Chimica Slovenica*, 2(53), 159–165.

7. Silva A S, Adriano P, Magalhães A, Pires J, Carvalho A, Cruz A J, Mirão J, Candeias A (2010) Characterization of Historical Mortars from Alentejo's Religious Buildings. *International Journal of Architectural Heritage*, 4(2), 138–154. DOI: 10.1080/15583050903046322
8. Segurado J E S, (n.d.) *Acabamentos das construções: estuques, pinturas*. 3ª edição, Bertrand (Portugal) and Francisco Alves (Brasil).
9. Füller J (n.d.) *Manual do formador e estucador*. 2ª edição, Lisboa: Livrarias Aillaud e Bertrand (Portugal) e Francisco Alves (Brasil).

Characterisation methodology for lime based materials – A case study of the Rajagopuram of Pundarikaksha temple in Tamil Nadu, India

Divya Rani¹ and Manu Santhanam¹

(1) *Indian Institute of Technology Madras, India, divyalino@gmail.com, manusanthanam@gmail.com*

Abstract

The focus of this paper is to discuss the methodology for characterization of lime based materials from historical monuments, with a view to their repair. The case study of the lime mortar samples collected from the grand entrance tower of the Pundarikaksha temple in the southern state of India, Tamil Nadu, is discussed. Most part of the monument is exposed masonry, and the historic mortar is observed to be identical throughout the structure. The historic lime binder is non-hydraulic in nature and the inert phases are mostly quartz and feldspar. Even though the aggregates are well graded, the mortar is highly porous. A methodology to determine the binder content, binder type and porosity and pore size distribution of the historic mortar and a few design aspects of the restoration mortar are discussed.

1. Introduction

India has a rich collection of historic buildings and most of these monuments are in need of immediate intervention. Several unsuccessful repair experiences in the past with incompatible materials have emphasised the need for adequate scientific analysis prior to any intervention. A comprehensive methodology of characterisation of historic mortars is established by the works of RILEM TC 167 [1]. In India, technical standards referring to historic building conservation have not been established yet. Hence, there is a great need for studies related to the materials used in this region. A methodology for characterisation of historic mortars is illustrated in a case study in this paper, which can be used for the assessment of other monuments of similar genesis.

The Pundarikaksha Perumal temple is located in Thiruvellarai, a village on the outskirts of Tiruchirappalli district in Tamil Nadu, India. The unfinished *Rajagopuram* (entrance tower-see Figure 1.a), which is the focus of this study, serves as the main entrance to the temple and has three tiers - two brick masonry tiers over a granite masonry base made of lime mortar. Above the second tier of brick masonry, a few courses of brickwork corresponding to an incomplete tier are present. In order to complete the historical structure to a seven tiered entrance tower, which is typical of *Dravidian* style of architecture prevalent in this region, an assessment of the existing structure was undertaken. Characterisation of the historic mortar

and design of a compatible repair mortar was deemed to be critical in ensuring a successful intervention and long-term durability of the structure.

Even though the understanding of physico-chemical and microstructural properties is critical to the holistic characterization of the historic mortar, the development of a suitable repair mortar requires specific knowledge of certain parameters. These critical parameters are decided mainly based on the function of the mortar in the building [2]. The other factors to be considered in the design are the environmental conditions, adherence to conservation philosophies, available craftsmanship and duration and cost of the project. For a bedding mortar, adhesion or bond strength to the building unit and deformability are considered more important than its compressive or tensile strength and weathering resistance. Aesthetic compatibility is least important as compared to all the other factors [2]. The deformability is a significant factor which depends upon the binder content of the mortar. The type of binder determines the hydraulicity and hence the stiffness of the mortar [3]. Bond strength is a parameter that depends upon the surface characteristics, pore structure and suction properties of the building unit [4]. The water retention and plasticity of the fresh mortar are important factors that affect bond strength, but are difficult to characterize in historic masonry. However, the shape and size of the constituent materials and the pore structure of the mortar gives an indication of the workmanship and production technology. Also, an increase in hydraulicity of the binder increases bond strength [5].

Several characterization techniques can be used for the identification of binder type and binder content in the mortar. The characterization was mostly based on traditional wet chemical analysis until 1980s [1]. A simple wet chemical analysis relies on acid dissolution/separation of the binder from the aggregate, and provides additional information on the acid-soluble binder and insoluble aggregate, using several other chemical reagents. However, this is not applicable if the aggregate is acid-soluble and hence the later schemes of characterization propose a petrographical analysis using thin sections. Ideally, a thin section analysis should precede the chemical analysis as this will clarify if the aggregate is soluble in acid and if the binder has soluble silica from hydraulic phases [6]. Thin section analysis using Optical Microscopy (OM) combined with X-ray diffraction (XRD) will give preliminary information on the type of binder and aggregate. The shape and size of aggregates, presence of hydrated salts and pozzolanic additions can also be identified. However, the main limitation of OM is that the spatial resolution is 1 μm at best and a much better resolution can be obtained by examining the samples using scanning electron microscopy (SEM). XRD can detect only crystalline compounds, and only when they are present in sufficient amounts - higher than 3 weight %. Thermogravimetric analysis (TGA) allows the detection of low crystalline phases that cannot be identified in XRD. It is also an accurate technique to qualitatively and quantitatively estimate the amount of hydrates and carbonates present in the binder [1, 6]. The total porosity of a mortar comprises of both open and closed pores, and these can be determined by several direct and indirect techniques. The durability and weathering resistance of the mortar depends on the

interconnected pores, while both open and closed pores influence the mechanical properties of the mortar [1, 7].

In the present study, a preliminary qualitative analysis was performed by OM and the binder to aggregate ratio was estimated by acid dissolution analysis. The mineralogical composition of the constituent phases was determined by XRD and TGA. The porosity and pore size distribution was qualitatively determined by SEM and quantitatively by Mercury Intrusion Porosimetry (MIP).

2. Sampling and characterisation methodology

A total of five representative samples were collected from different parts of the tower with a mortar chisel and labelled as TR1, TR2, TR3, TR4 and TR5. By visual examination, it could be indentified that the texture of the mortar was identical throughout the structure. A few non-structural cracks and missing units could be located in the structure. Five different locations were identified for sampling as shown in Figure 1. One sample was collected from the top tier which was already detached from the structure.



Figure 1: (a) - Front view of the entrance tower, (b) to (e) - sampling locations inside the tower, (f) – a detached sample from the top of the tower

The samples were suitably sawn to a thin slice and dried at 40 °C until the mass was constant, and this sample was impregnated with epoxy resin to prepare the thin sections. After the hardening of epoxy, the specimens were glued on to a glass slide and lapped and polished first on a coarse grinding wheel and then using a series of successively finer grade of diamond pastes to make a thin slice of about 30 µm. Another chunk of sample was gently ground with a rubber hammer and treated with 10% hydrochloric acid for 24 hr followed by filtration and weighing of the residue. The samples for XRD and TGA were powdered to a size less than 75 µm for separating the binder fraction. An X-ray diffractometer with Cu K α

radiation, step scan of 0.05/s, and between 5° and 75° 2 θ , was used. The diffraction patterns were analyzed by means of the X'Pert High Score Plus software. TGA was conducted on SDT 650 (of TA Instruments, USA) from 30 to 1000 °C, at a constant heating rate of 10 °C per minute in a nitrogen purged atmosphere. For SEM, the specimens were impregnated with epoxy, and were lapped and polished using a series of successively finer grade of diamond pastes. They were then coated with Au-Pd to prevent charging, and observed in backscatter mode along with Energy Dispersive Spectroscopy (EDS). The porosity and pore size distribution were quantified using Pascal 140-440 porosimeter from Thermo Scientific, by intruding mercury with an increase of pressure from vacuum to 400 Mpa. The samples were broken into small pieces of nearly 5 mm size and about 3 to 4 of such broken pieces were tested exposing a large surface area of the sample.

3. Results and discussion

3.1 Estimation of binder content

Optical microscopy study on thin sections was performed first in order to know the mineralogy of aggregates and characteristics of the binder. The images from transmitted light microscopy are shown in Figure 2 a-b. The mortar is composed of a heterogeneous mixture of small and large grains of quartz and feldspar aggregates and a fine grained matrix, which is fully carbonated. Significant amounts of fine grained quartz particles are also seen in the matrix. As the aggregates are non-calcareous, a quantitative analysis was not attempted to estimate the binder content, as this was performed by acid dissolution test. A qualitative analysis of other features of the mortar indicates that the aggregates are well graded. They are angular in shape, indicating that they were procured from local sources and are devoid of damage due to transportation and erosion. The presence of any pozzolanic additives like brick powder or organic fibers (hair, straw etc.) typical in historic mortars could not be identified. Presence of unmixed areas or lime lumps could be observed in some of the samples. These are part of the unburnt residue in the parent limestone or the original lime which was not mixed well while preparing the mortar [1].

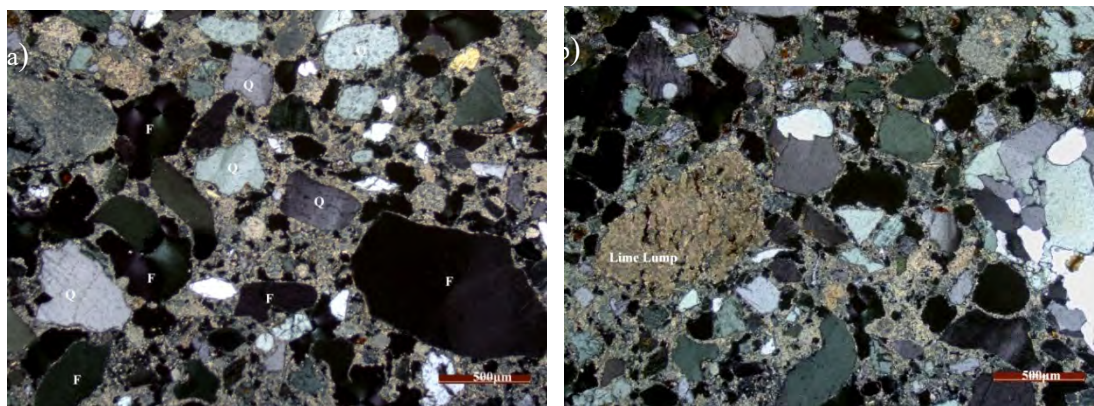


Figure 2. (a)- Images of transmitted light microscopy showing quartz (Q) and feldspar (F) aggregates and a carbonated matrix (b)- Micrograph showing the presence of lime lump

The binder to aggregate ratio was determined by acid dissolution test and is reported in Table 1. The value ranges from 1: 2.6 to 1: 4.4 by weight, and the average of all the five samples is 1: 3.7. Even though there exist a lot of controversies regarding the testing procedure [8], this is a basic test that is valid for a quick estimation of binder and aggregate content. For mortars containing carbonate aggregates and for a more specialized analysis, quantitative microscopy or other traditional wet chemical or micro analytical techniques like atomic absorption spectroscopy can be employed [1, 9].

Table 1. Binder to aggregate ratio of the mortar (by weight)

Sample ID	TR1	TR2	TR3	TR4	TR5
Binder to aggregate ratio	1: 2.6	1: 4.4	1: 3.8	1: 3.8	1: 4.0

3.2 Classification of binder

The binder classification or identification of the type of binder is an important pre-requisite for decisions concerning the selection of materials for restoration mortar [2]. The binder fraction was analysed by XRD and TGA to determine the hydraulicity and hence the binder type. The diffractogram data obtained from XRD is presented in Figure 3.

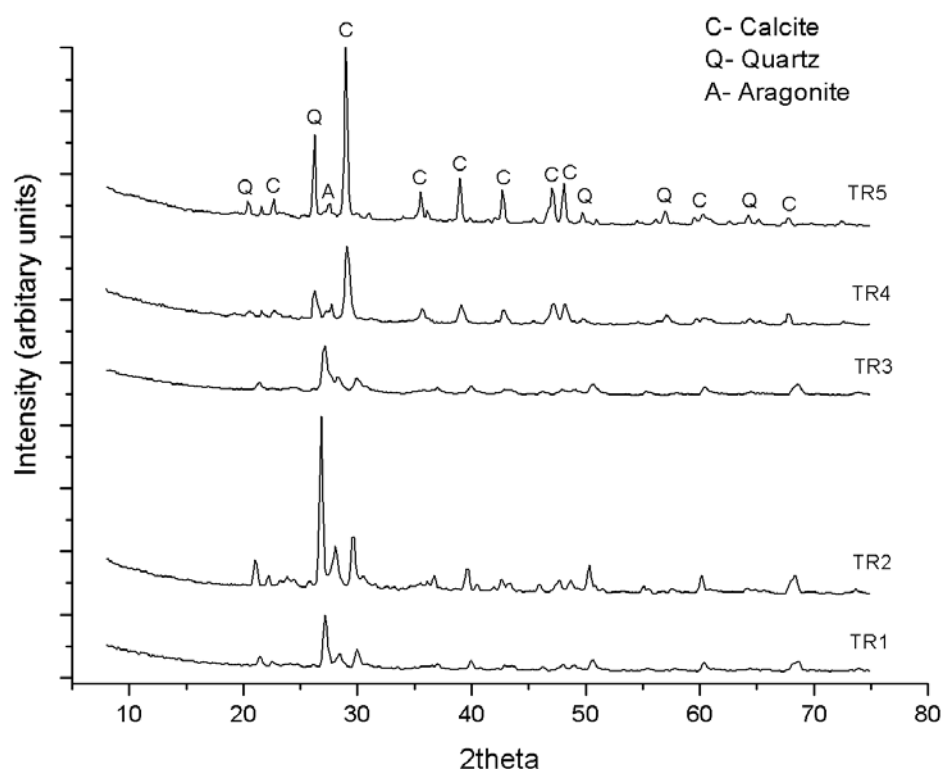


Figure 3: X-ray diffractogram of the historic mortar samples

The mineralogical composition is similar for all the samples analysed. The presence of calcite (CaCO_3) is evident in all the samples and other peaks contribute to the silicates present in aggregates which would have been ground to a size $< 75 \mu\text{m}$ and got mixed with the binder.

Presence of aragonite, which is another polymorph of calcite was observed in traces. There is an absence of any major hydraulic compound of calcium silicate or aluminate, indicating the binder to be composed of non-hydraulic lime.

The results of TGA/DTG analysis are presented in Table 2 in terms of weight loss at specific temperature ranges.

Table 2. TG-DTG weight losses as a function of temperature range (wt %)

Sample ID	< 120 °C	120-200 °C	200-600 °C	>600 °C	CO ₂ / bound H ₂ O
TR1	2.13	1.21	9.87	28.66	2.90
TR2	1.51	1.63	8.30	20.70	2.49
TR3	1.19	1.75	11.61	21.64	1.86
TR4	1.77	0.68	9.93	34.61	3.48

The weight loss below 120 °C is due to the loss of free water from the sample. The weight loss due to hydrated phases occurs at 120-200 °C, and this is very low in all the samples analysed. The presence of hydrated phases could not be identified in XRD and OM as well. The loss of structurally bound water takes place from 200-600 °C and it varies from 8.30 to 11.61% for the samples analysed in this study. The weight loss from decarbonation of calcite occurs beyond 600 °C and varies from 20.70 to 34.61%.

According to the widely accepted classification of Moropoulou [10], the mortars belong to the category of lime mortars with unaltered portlandite. Two representative thermograms are shown in Figure 4. The major weight loss at around 750 °C is due to the decarbonation reaction and the minor peak in TR4 at 480 °C is due to dehydroxylation of portlandite. The process of carbonation is slow and can take many years to complete depending upon the conditions at site. The low CO₂ concentration in the atmosphere and especially in the areas of high relative humidity can inhibit the carbonation reaction. In the case of thick masonry walls, the external portions get converted to carbonates and further diffusion of CO₂ deep into the wall occurs at a slower rate hindering the carbonation reaction [10].

In the present study, the tower is composed of three leaf masonry walls with the stones and bricks forming the outer leaves and lime, rubble, brickbats and gravel forming the infill. Also, since the mean monthly relative humidity at the site location is high (70-80%), these factors could have resulted in an incomplete carbonation of the lime binder. However, the presence of portlandite could not be observed in XRD.

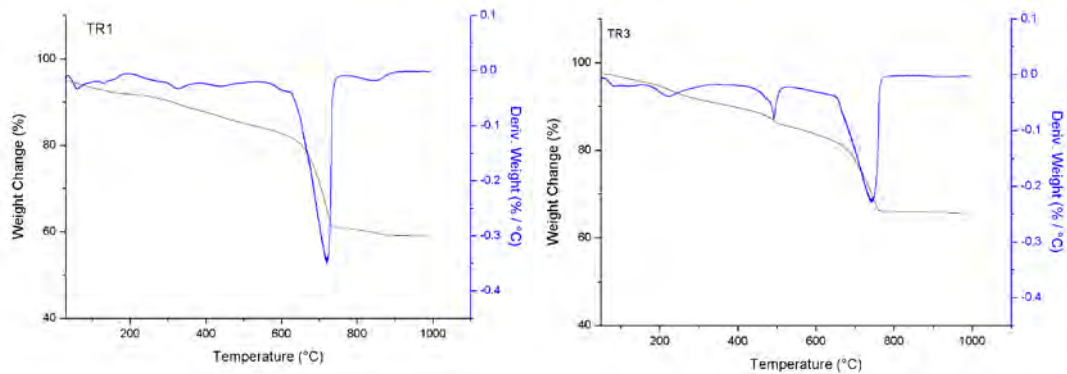


Figure 3: TG/DTG curves of the historic samples (TR1 is representative of TR2 and TR4)

3.3 Porosity and pore size distribution of mortar

In order to have a better understanding of the microstructure, all the samples were examined under SEM and EDS. A general view of the microstructure is shown in Figure 4 at low magnification (25x). The black regions in the image indicate porosity, and it can be seen that the mix is highly porous. Again, the aggregates are well graded and angular in shape indicating that they were procured locally, as observed in OM. A magnified image (500x) of the matrix is shown in Figure 5. The interconnectivity of the pores can be observed and the microanalysis indicates that the matrix is fully carbonated. The total porosity including the closed pores can be quantified by image analysis [2].

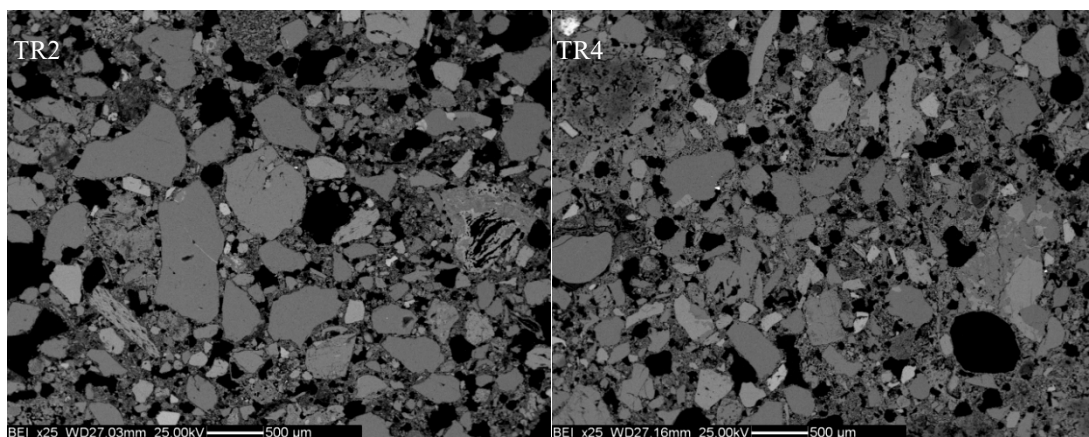


Figure 4. Micrograph of the lime mortar sample indicating numerous pores and different size and shape of aggregates

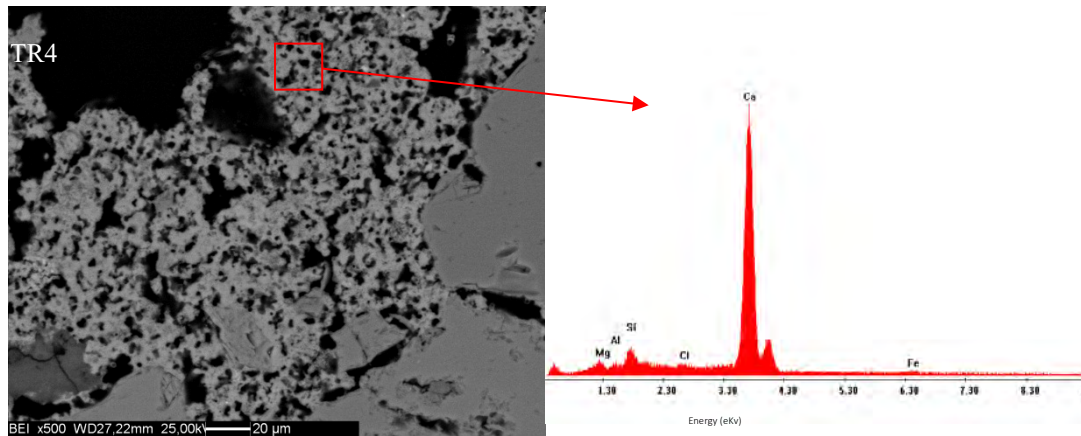


Figure 5. Micrograph showing interconnected pores and a carbonated matrix

For quantification of the porosity and pore size distribution, the samples were analysed by MIP. The results are shown in Figure 6. The total permeable porosity was around 35% - 45% which is comparable to the porosity of air lime mortars. Even though there are two maxima in the derivative curve at around 7.5 μm and 66 μm , indicating critical pore diameter, the mortars have a broad distribution of pore sizes. The presence of much larger ‘air’ pores is universally observed in historic mortars, indicating that the mortars have rarely been able to develop a dense microstructure [7]. The effect of the several weathering cycles that the mortars have undergone cannot be ignored. The larger size pores could be due to the possible leaching of the secondary minerals formed over the course of time due to weathering. However, as the host material is very porous and weak, the porosity of the repair mortar should be suitably matched to the existing material.

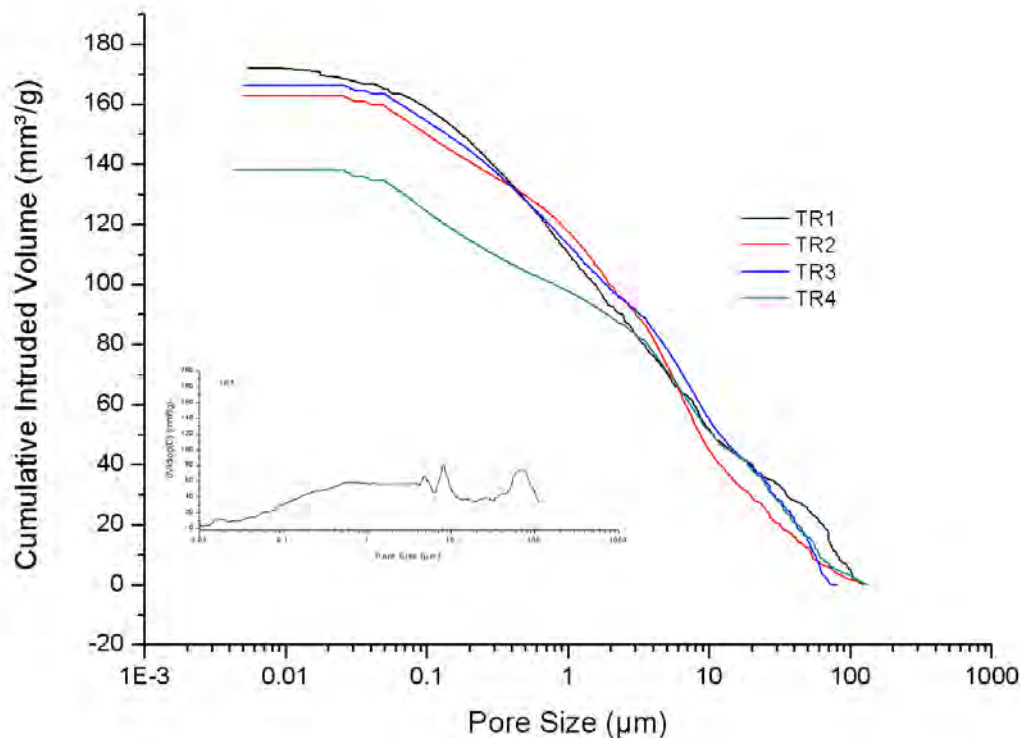


Figure 6. Cumulative and differential intrusion curve obtained from MIP analysis

4. Prescriptive versus Performance approach for design

A thorough understanding of the existing mortar and its relation to the historic masonry assembly is critical to establish the design parameters for a repair mortar. It is also essential to understand the current need for restoration of the building, and how well the mortar or masonry assembly is performing for the current service requirements and environment. Both prescriptive and performance based specifications are approved by ASTM C1713-12 [11], whichever better suits the requirements of the work. Prescriptive specifications would be arrived based on the characteristics of the original mortar such as the binder to aggregate ratio, binder and aggregate type, granulometry of aggregates and any additives present. Even though these parameters seem to be easy to arrive at by the direct characterisation of original mortar, there exist lot of complexities and variability in this approach. The performance characteristics of the repair materials, even though they match the original formulations, will be different from the historical material due to the differences in the quality of the materials and craftsmanship available today. The historic mortar is a multi-phase composite, consisting of both crystalline and amorphous phases, and the physico-chemical changes that it undergoes with time, leads to recrystallization of the existing minerals or formation of secondary minerals. The microstructure, especially the pore structure of the mortar, evolves with these changes. Hence, it is not possible to obtain the characteristics of the historic mortar as per its original design. Moreover, the prescriptive specifications are difficult to verify after repair. It is more effective to match the level of performance of a successfully performing masonry assembly by matching the properties of the repair mortar to the current host material. This can be achieved by arriving at suitable performance specifications for the repair mortar. The performance specifications for this particular study should be arrived from the lab-based experimental testing of non-hydraulic lime mortars considering the environmental exposure at the site (mainly temperature, relative humidity and accelerated wetting-drying cycles), followed by a pilot examination of repair mortar at the site. There is also scope for designing an improved performance of the repair mortar, in case of any structural distress in the historic masonry assembly. However, it is most critical to decide the parameters to be evaluated in a performance based specification. These have to be arrived at mainly based on the function of the mortar and the current state of distress in the building. For the present study, as indicated in the previous sections, the deformability and bond strength are two critical parameters in addition to compressive or tensile strengths, and weathering resistance. The permissible limits for these parameters can be achieved after a detailed analysis of the building units.

5. Conclusions

The existing scheme of characterisation of historic mortars is extensive and has to be suitably modified according to the purpose of characterisation. The present study discussed a general scheme of characterisation of historic mortars with a view to their repair. The historic mortar in the structure under investigation is characterised as a non-hydraulic lime

binder, with quartz and feldspar as aggregates. Presence of unaltered portlandite is identified from thermal analysis. The binder to aggregate ratio is 1: 3.7 (by weight) and the mix appears to be lean with increased porosity. The aggregates are well graded and angular in shape indicating that they were procured from local sources. The mortar has a broad distribution of pore sizes with a total porosity of about 40%. These results will help in identifying the suitable material and property requirements for a performance based design of reconstruction mortar.

Acknowledgements

This research work is a part of the feasibility study conducted by the National Centre for Safety of Heritage Structures (NCSHS) at Indian Institute of Technology, Madras for the Department of Hindu Religious and Charitable Endowments (HR&CE), Government of Tamil Nadu and Sri Pundarikaksha Perumal Rajagopura Thiruppani Committee (SPPRTC) which is currently involved in the reconstruction work.

References

1. Caspar Groot, Geoff Ashal, John Hughes (2010) Characterisation of old mortars with respect to their repair RILEM TC 167-COM: State-of-the-art report. RILEM publications.
2. Paul Maurenbrecher and Caspar Groot (2016) Repair mortars for historic masonry RILEM TC 203-RHM: State-of-the-art report. RILEM publications.
3. Forster AM (2004), How hydraulic lime binders work. Technical report published by Scottish Lime Centre Trust, Edinburgh.
4. Lawrence SJ and So L (1994) The influence of some factors on the tensile bond strength of masonry. Proceedings of the 10th International Brick/Block Masonry Conference, Calgary, July 1994, pp 929–38.
5. Barr S, McCarter WJ, Suryanto B (2015) Bond-strength performance of hydraulic lime and natural cement mortared sandstone masonry. *Construction and Building Materials* 84: 128-135
6. Sangeeta Bais, Manu Santhanam, Divya Rani (2018) Lime Manual for Conservation Works. National Centre for Safety of Heritage Structures. India. ISBN: 978-93-5300-526-9
7. Klisin'ska-Kopacz A, Renata Tis'lova, Grzegorz Adamski, Roman Kozłowski (2010) Pore structure of historic and repair Roman cement mortars to establish their compatibility. *Journal of Cultural Heritage* 11: 404–410
8. Alvarez JI, Martin A, Casado PJG, Navarro I, Zornoza A (1999) Methodology and validation of a hot hydrochloric acid attack for the characterisation of ancient mortars. *Cement and Concrete Research* 29: 1061-1065

9. Lindqvist JE, Sandsrrom M (2000) Quantitative analysis of historic mortars using optical microscopy. *Materials and Structures* 33: 612-617
10. Moropoulou A, Asterios Bakolas and Sophia Anagnostopoulou (2005) Composite materials in ancient structures. *Cement and Concrete Composites* 27: 295-300.
11. ASTM C1713-12 (2012) Standard specification for mortars for the Repair of Historic Masonry. American Society for Testing and Materials, United States.

Sampling cataloging methodology procedures for the conservation of historical colours in urban landscapes

Isolina Díaz-Ramos¹, Jorge Manzano Cabrera¹

(1) University of Las Palmas de Gran Canaria, isodiram@gmail.com; jmancab7@gmail.com

Abstract

Vernacular buildings from our historical centres are suffering the replacement of their original mortars, renders and colours with Portland cement and modern chemical binders. As a consequence, the important heritage value of authenticity is disappearing. Retaining this heritage value requires a fundamental framework for recording historic architectural finishes and a drive towards sustainable conservation practices to preserve and restore the historic landscape. The authors of this paper have developed a methodology for sampling architectural finishes in domestic buildings of neoclassical period in Las Palmas de Gran Canaria city (Spain). An interdisciplinary approach will be taken followed by sampling methods and practical colour research. Sampling will allow creating a map and a database of historic coloured mortars that can be used for decision-making by building surface restorers when selecting materials and pigments for the restoration of the historic aesthetic.

Introduction

The original colour palette of historic buildings has not received proper attention for a long time. A considerable number of original mortars, renders and colours have been removed over the last years, which means a terrible loss of information about original materials employed in vernacular building surfaces.

What are the initial steps to study the colour of urban landscapes? What do we know about the colour of a specific architectural style? These are the questions this paper attempted to answer.

In this study, we explain a preliminary method and describe an elementary mechanism of sampling historic buildings' mortars located in the city of Las Palmas de Gran Canaria, Spain.

This article includes a first part designed to give a brief overview of the historical context that involves our research. The following sections describe the method designed to extract and sample cataloging of historic mortars and renders. Results and discussion are outlined in the fourth paragraph and our conclusions are drawn in the final section.

The resulting database of historic mortars, how the ideas of materiality and polychrome of 19th century architects from San Fernando Academy interacted with the available materials

and contexts. This will contribute to the conservation of historical colours and further direct the choices of conservators working to restore heritage townscapes.

Arenales, the birth of a neighborhood

The end of the 19th century and beginning of the 20th were decisive in the history of the city of Las Palmas de Gran Canaria, Canary Islands, Spain. The ancient walls that surrounded the historical towns of Vegueta and Triana were a meaningful urban landmark of the city which were demolished in 1852 in order to enlarge the city beyond the city walls. The new neighbourhood named Arenales was urbanized (Figure 1).



Figure 1. Year 1883 city map of Las Palmas de Gran Canaria by López Echegarreta

Unlike Vegueta and Triana, a rectangular grid and a regular plot was followed in Arenales [1]. Another significant event was the construction of the new port 'Muelle de la Luz y Las Palmas'. Both developments introduced the island in the modern world. Figures 1 and 2 show our period of study and the rapid expansion of the city.



Figure 2. Las Palmas de Gran Canaria city in 1943

In 1787, the Royal Academy of Fine Arts was established in Madrid. As result of its foundation, architect and master builder professions were consolidated [10].

José A. López Echegarreta, Francisco de la Torre, Laureano Arroyo, Fernando Navarro and other architects of that time built under the precepts of neoclassical style. All of them were trained at the Royal Academy of Fine Arts and designed the new urban image of Arenales during the course of our research.

Domestic buildings of the period are mainly two-story with architectural features characterized by straight and high rectangular door and window frames on stonework; facades topped by balustrades or stone cornices [9], as well as high-quality design on iron-work balconies (Figure 3).



Figure 3. Neoclassical examples of urban architecture in Arenales neighbourhood

The main questions that the authors ask themselves are: How would it be to go for a walk through this new town under construction? Which were the colours of the new architectonic features? To answer these questions, nine buildings have been selected in order to analyse the original mortars and colour layers that formed part of the neoclassical style.

Method and selection of samples

Few researchers have undertaken colour analysis on the island of Gran Canaria. The city of Las Palmas de Gran Canaria had its first and only evaluation of the colours of its buildings in 1999 [7]. During the assessment, five architectural style typologies were identified across the

city: traditional, modernist, eclectic, rationalist and popular style. The sampling of building layers was used to produce a local commercial colour chart linked to different colour combinations according to architectural style. This was a useful exercise but the methodology is not sufficiently detailed within this study.

The method described in this research is simple and easy to replicate. Working procedures have been developed in four work phases: building selection, invitation to participate, sampling procedures and visual analysis of samples¹.

The study was carried out in the neighbourhood of Arenales in Las Palmas de Gran Canaria (Spain).

Local catalogues published by Las Palmas de Gran Canaria council were used in order to identify the buildings with aforementioned characteristics [2, 3]. These documents allowed the researchers to have a first access to the buildings that are protected and of interest for the study.

Four types of buildings were selected, which are described below:

- Ground floor dwellings on the corner (GC)
- Ground floor dwellings side attached² (GA)
- First floor dwelling on the corner (FC)
- First floor dwelling side attached (FA)

The purpose of the building selection was to get a general picture of the most representative neoclassical constructions from Arenales. A total of 26 buildings were initially chosen from the catalogues consulted.

An on-site evaluation was the second step of this work phase. It helped to establish the housing that had original features preserved in good condition. Only two of the selected dwellings had undergone changes in their appearance (31 and 45 Obispo Rabadán Street). As consequence of addition of new materials and the destruction of original mortars in former restorations, these two buildings were discounted.

During the on-site evaluation, other three buildings that were not on the catalogues were considered of interest. They were located in 35 Eusebio Navarro, 54 and 56 Obispo Rabadán Streets.

¹ Phases 1, 2 and 3 were performed during three months in Las Palmas de Gran Canaria city. Currently, phase 4 “Visual analysis of samples” is being carried out by the restorer Díaz-Ramos as part of the ‘Becas MAEC-AECID de Arte, Educación y Cultura’ 2018-2019 within the fellowship program of the Royal Spanish Academy in Rome.

² We use the term “side attached” to refer to buildings that are not on the corner but between other dwellings.

Postal invitation to participate was sent to the 27 final selected owners in Arenales. 20 of the chosen buildings were First floor side attached (FA); 3 houses were First floor on the corner (FC); 3 dwellings were Ground floor side attached (GA) and only 1 building was Ground floor on the corner (GC).

60% of the proprietors responded positively. Negative answers were produced because the building had recently been painted or owners were not interested (14%); no feedback was received in cases when buildings were uninhabited (26%).

A total of nine houses from five streets have been selected for further study. Building information data sheets were created for the selected buildings (Figure 4).

Ficha nº 1		M41
Datos generales Dirección: Calle Murga 41 Autor: Laureano Arroyo Fecha: 1909 (P) Ficha del catálogo general protección: ARQ 406	Descripción Inmueble de dos plantas situado entre medianeras. Alzado caracterizado por la disposición de huecos verticales enmarcados en cantería, al igual que los zócalos y cornisas. El fondo del muro está cubierto de pintura plástica color blanco. Las carpinterías de la planta superior se encuentran pintadas de blanco, mientras que las de la parte inferior están barnizadas. Balcón y ventanas pintadas con pintura de metales color plata. El edificio presenta continuidad con las viviendas que le siguen.	Estado de conservación Malo. Arietamiento de la parte superior del lienzo. Bicateración y lagunas de soporte producida por el hombre en la instalación de cableado y erosión con la consiguiente pérdida de materia. Cuarteado de la capa pictórica superficial, permitiendo observar la original a la cal. Suciedad superficial y grafiti.
	Localización 	 

Figure 4: General data sheet

General data sheet is composed of four sections. Firstly it offers general building information as the address, author, year of construction and the number given to the building in the local catalogues.

Second section provides a property description, focusing on the current colour of walls, wood and metalwork.

Paragraph called 'Location' shows a map with the studied buildings in blue. The one analysed on the sheet has a red spot.

The final section depicts the state of conservation of paints described in the second part, using the terminology outlined by Calvo et al [5].

Sampling procedures

An adaptation of Prime's method was used during the designation of extracted samples [11]. Specifically, samples were recorded as follows: First letter of the address; street number; feature; sample number: SCO44 - M 1 (Table 1).

Table 1. List of acronyms used in this work

Street name	Acronym	Feature	Acronym
Senador Castillo Olivares	SCO	Muro (wall)	M
Obispo Rabadán	OR	Puerta (door)	P
Murga	M	Ventana (window)	V
Canalejas	C	Herrajes (metal)	H
Eusebio Navarro	EN	Zócalo (plinth)	Z
		Decoración (ornament)	D

During sampling stage, efforts were made to minimize aesthetics effects on the wall surfaces by extraction procedure, as most of the dwellings were privately owned. The samples were taken from a hidden place to reduce any damage. Fissures on the walls were used to remove the mortars and coloured fragments in most of the cases.

Sampling methodology employed in Spanish cities as Granada [6] and Valencia [8] was not considered. Mentioned authors have used drill bit which extracts a sample of 30 mm diameter minimum. This instrumental can be very useful when buildings are abandoned. However, this method was declined in this study due to noticeable damage caused.

The tools employed to extract the fragments were a hammer, a chisel and a scalpel. An envelope to preserve the pieces with a written sample identification code (SIC) as well as labels and data sheets designed to the fieldwork were also required.

As shown in the Figure 5, sheet contains information about the samples' location and name. It is also appointed the removal date and the name of the technician who extracted the material. Dwellings on the corner were recorded in two data sheets, following the building elevation of every street, named 'a' or 'b' as in the example.

A total of 98 samples from nine dwellings were collected during the fieldworks. General fragments measured 100 mm x 100 mm square. All samples were carefully documented at the Royal Spanish Academy in Rome.



Figure 5: Data sheet of sampling extraction

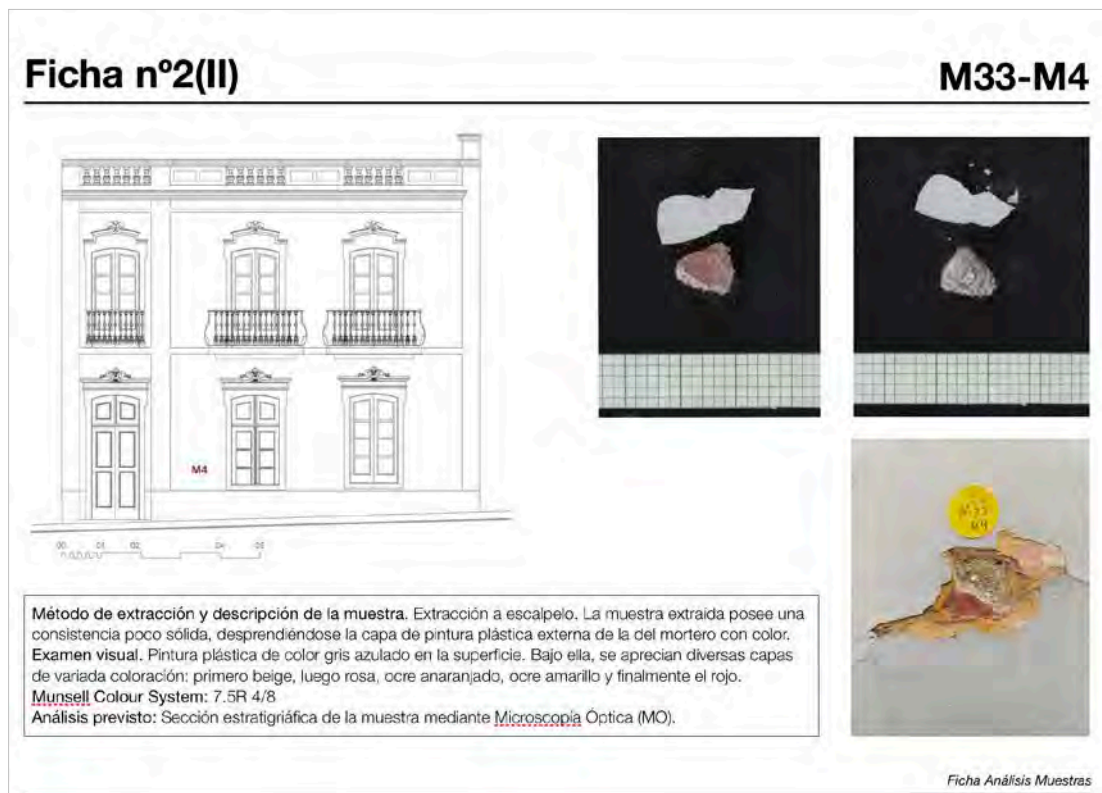


Figure 6: Data sheet designed for every sample

Figure 6 shows the data sheet designed for the analysis of the samples. It gives information about the procedures, tools of extraction and description of the sample. A visual analysis of the colour layers with its respective Munsell colour system assignation is also described. Final paragraph offers a suggestion to further chemical analysis.

Sampling analysis data sheet comprises also the scanned images of the sample [4], photography of the wall where the fragment was extracted and the piece placement in the building elevation.

Results and discussion

One of the main objectives of this work was to find a simple and replicable method of sampling and documenting mortars and renders of historic buildings.

Previous studies on similar subject employed a wide range of different laboratory analysis methods for original colour layers. As they attempted mainly to obtain information about the building original palette, the sampling methodology during on-site works was not described in sufficiently detail.

We pursue to have a collection of historic mortars in order to preserve them and obtain a sampling map of original building materials. Therefore, the accuracy description of work methodology is crucial. This procedure is a clear improvement on current sampling methods and is a useful tool for research on urban and historical coloured landscapes. It can be helpful, moreover, to conservators during the documentation of building colours.

It is important to note that two factors can significantly reduce the number of dwellings to study: the existing conservation state of buildings can differ from those showed on the catalogues, therefore it is essential the undertake on-site evaluation. Also, the possibilities of a refusal to participate in the duty by the owners as well as the inhabitation of dwellings are aspects to consider. Therefore, a big amount of buildings should be examined initially.

Figures 4, 5 and 6 show the data sheets required for every phase of the research. These have been designed fully compliant with international standards [12] and a number of previous sampling methods adopted by Prime [11], Collado [6] and García [8].

Figure 4 includes general information collected during the building selection and invitation to participate phases. Figure 5 shows the sheet to be completed during sampling procedure. Lastly, data sheet required during the sample visual analysis is shown in Figure 6. This contains information about the render, colour, structural aspect and apparent condition of the samples.

Although this is a small study undertaken locally, results can be generalized and applied to other historical towns and environments. The data sheets previously filed provide examples of essential information to consider when collecting coloured mortars.

Importantly, this method may help to explain why a rigorous documentation of architectural finishes is a significant tool in itself. It allows to create useful databases helping to retain the heritage value of authenticity, conserve the historic mortars and renders, and safeguard endangered historical components.

Conclusions

To sum up, this work provides a methodological framework for collecting, recording and analyzing historic architectural finishes.

Data sheets play an important role during sampling the historic aesthetics. They are very helpful and significant in every stage of the described work phases.

Future efforts will entail refining our sampling methodology and expanding the samples extraction in the city to the enlargement of the coloured database that will contribute in a further design of a map of colours.

Overall, the findings highlight the importance of the creation of detailed data in order to conserve the original mortars and colours of our historical environments. We hope that our research will provide a base for future studies on the conservation of historic mortars and renders.

Acknowledgements

We want to express our gratitude to the owners of the buildings who facilitated the study of their dwellings and the extraction of samples.

The authors wish to gratefully acknowledge the Royal Spanish Academy in Rome and Ernesto Borrelli by their support during the visual analysis of samples phase.

References

1. Alemán S (2008) Las Palmas de Gran Canaria: Ciudad y arquitectura (1830-1930). Las Palmas, Cabildo Insular de Gran Canaria
2. Ayuntamiento de Las Palmas de Gran Canaria, GEURSA (2018) Catálogo arquitectónico. Plan especial de protección entorno de la calle Perojo. Documento de ordenación. Ayuntamiento de Las Palmas de Gran Canaria, Las Palmas de Gran Canaria

3. Ayuntamiento de Las Palmas de Gran Canaria, GEURSA (2012) Catálogo municipal de protección - Catálogo de patrimonio arquitectónico. Vol. 4 & Vol. 5. Ayuntamiento de Las Palmas de Gran Canaria, Las Palmas de Gran Canaria
4. Borrelli E (2017) Un inusuale uso di uno scanner 2D per l'ottenimento di immagini ad alta risoluzione ed elevata profondità di campo di artefatti e oggetti tridimensionali. *Archeomatica* 1:14-20
5. Calvo A, García S, Macarrón M, et al (2018) Terminología básica de conservación y Restauración del Patrimonio Cultural. Universidad Complutense de Madrid: <http://eprints.ucm.es/46544/>. Accessed 3 February 2019
6. Collado F, Medina V, García A (2007) Metodología de estudio cromático de acabados arquitectónicos. Aplicación en la ciudad de Granada. Granada, Universidad de Granada
7. Fierro F (1999) Guía del color de Las Palmas de Gran Canaria. Ayuntamiento de Las Palmas de Gran Canaria, Las Palmas de Gran Canaria
8. García A, Llopis J, Masiá J et al (2012) El color de Valencia. Generalitat Valenciana, Valencia
9. Herrera A (1990) Arquitectura neoclásica en Gran Canaria. *Caja Insular de Ahorros* 185:21-29
10. Hernandez A (1990) Primeras propuestas del arquitecto Laureano Arroyo: una nueva interpretación de la arquitectura de uso privado. IX Coloquio de Historia Canario-Americana: 1205-1217
11. Prime BL (2011) Exterior architectural finishes in Puerto Rico: The painting tradition of Guayma's vernacular architecture (Master thesis) University of Pennsylvania, Philadelphia PA. https://repository.upenn.edu/hp_theses/164/. Accessed 3 February 2019
12. Technical Committee CEN/TC 346 (2010) Conservation of Cultural property - Methodology for sampling from materials of cultural property-General rules, prEN16085:2010(E)

Mineralogical characterization of historical cement-based mortars from Rupnik military fortification line

Petra Štukovnik¹, Janez Peter Grom², Marjan Marinšek³, Violeta Bokan Bosiljkov¹

(1) UL FGG Jamova ulica 2, 1000 Ljubljana, petra.stukovnik@fgg.uni-lj.si, violeta.bokan-bosiljkov@fgg.uni-lj.si

(2) UL FA Zoisova cesta 12, 1000 Ljubljana, Janez.Grom@fa.uni-lj.si

(3) UL FKKT Večna pot 113, 1000 Ljubljana, marjan.marinsek@fkkt.uni-lj.si

Abstract

The paper presents the results of cement-based mortars characterization that were taken from rendered layers of military bunkers in Rupnik Line. The Rupnik Line was conceived as part of the fortified defence system protecting the newly formed Rapallo border between the Kingdom of Italy and the Kingdom of Yugoslavia, established in 1920. The mortars are of different compositions and were aimed at protecting the massive concrete walls and slabs of the bunkers, as well as representing camouflage layer that enabled merging of the bunkers with the environment. Results of petrographic examination and microstructural and chemical analysis (SEM-EDS) of the samples confirmed that locally available carbonate sands with angular grains were used as an aggregate in the mortar. As a binder, pure Portland cement clinker or mixture of the cement and ground granulated blast furnace slag were used. The selection of the aggregate and binder type in particular mortar was based on the colour of the produced “artificial stone” that should be light grey (cement and dolomite aggregate) or greenish (cement, slag and limestone aggregate). The samples with the dolomite aggregate grains show the characteristic appearance of the ACR reaction, dedolomitisation of the aggregate grains and secondary calcite formation, along with the Mg-Al-Si phase formation.

Introduction

At the end of World War I in 1918, the nations of the former Austro-Hungarian Monarchy were facing disputes over irredentist claims, as they had been previously non-homogeneously included into the monarchy, and the territorial claims of large neighbouring nations. In relation to the study area – the initial western border between the Austro-Hungarian Monarchy and later of the Kingdom of Serbs, Croats and Slovenes (hereinafter: Kingdom of SHS), and the Kingdom of Italy –, the Kingdom of Italy, a member of the victorious Entente, which emerged from the conflict as a superpower, started to pursue its territorial pretensions by occupying the territory even during the cease-fire. After several unsuccessful attempts at redrafting the border at the Paris peace conference of 1919, the final agreement on the Rapallo Border was reached on 12 November 1920 [1].

Under the treaty, the Slovene ethnic territory was taken over by the Kingdom of Italy, including the islands of Srakane, Unije, Cres, Lošinj, Lastovo, Palagruža, and Zadar, while Italy officially recognised the Kingdom of SHS. For Italians, this agreement was better than the assurances Italy received in the London Pact. Italians were aware of this fact, as confirmed by the Italian negotiator of the Treaty of Rapallo, Count Carlo Sforza: “*It gave Italy an Alpine frontier as perfect as under the Roman Empire*” [2]. To establish the border on the ground, both sides agreed to form a commission, *Commisione Italo - S.H.S. per la delimitazine dei confini fra il Regno d'Italia e il Regno S.H.S.*, which convened for the first time in Ljubljana. In fact, after their second meeting, they started to demarcate the border on the ground, regardless of the disputes concerning the border in the mountains [3].

In its final form, the border stretched for 289 kilometres from the borders between the Kingdom of Italy, Austria and the Kingdom of Yugoslavia in the north to the gulf of Rijeka in the south. The fortification efforts to protect the newly formed border soon led to a systematic building approach from both countries. The Italians erected the Vallo Alpino, as the last stretch of their defence system protecting the northern borders all the way from Genova. The Yugoslavs established the Rupnik line defence system. Both nations used the basic logic of the doctrine adopted in the construction of the Maginot line. The new doctrine replaced the concepts of national defence in a specific zone using the system of fortified positions of the permanent fortification type [4]. To put it simply, both nations established sets of primary defence fortified positions in the valleys facing the Rapallo border and a main fortified defence positions, the secondary line, on hilltops above these valleys. Both systems were interdependent and connected in a complex unified defence line of enormous scales. In the case of the Rupnik line, smaller fortified structures or machine-gun nests formed the primary defences. Stronger infrastructure hosting large calibre artillery was positioned mostly as the secondary defence on the hilltops (Figure 1).



Figure 1: Hilltop bunker after construction.

The Municipality of Žiri (Figure 2) offers unique study-relevant conditions from the point of view of its spatial position, geomorphological characteristics, its landscape image, due to its historical significance owing to its geographical position and spatial attributes. From its definition in 1921 to the April War in 1941, the Rapallo Border ran partially along the border and partially in the area of the Municipality of Žiri as it is today. After Yugoslavia's

capitulation in April 1941, it was in the area of Žiri that the new German-Italian border turned from the Rapallo Border course eastward.

The fortified positions of the Rupnik Line in the system of connected machine-gun nests were positioned along the eastern slope of the hills of the Sovra River valley along the entire valley course, from its widening at Žiri in the north to the narrowed down crossing at the border with the Municipality of Logatec lying to the south. In the system of the first line of defence or the outpost position [5] along the eastern slopes, various fortified facilities, fortified machine-gun positions, and strongly fortified artillery positions were strategically placed. This first line of defence protected the expanded mouth of the SW Račeva valley, while the entire northern valley of the Sovra river downstream was defended, using the same logic as that in the valley south of the settlement.

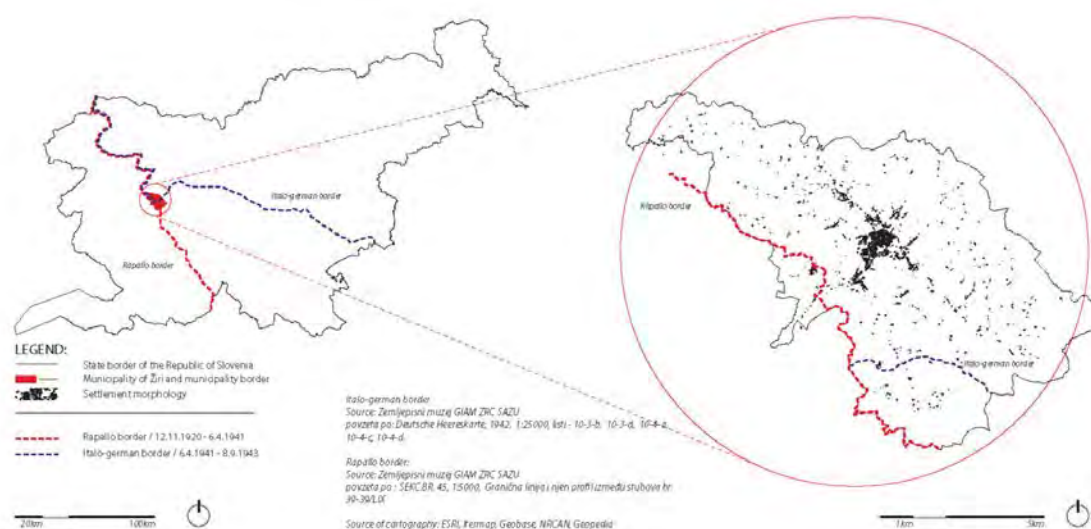


Figure 2: Position of Rupnik line.

In a research carried out by Grom J.P. in August 2018, the real scale of the Rupnik defence line in the municipality of Žiri was established, with additional 66 fortified positions discovered that had not yet been investigated before. This discovery is the source for a multitude of information to different research fields, spanning from historical, urban and architectural, to sociological and the field of construction technologies.

This paper presents the first results of the study aiming at revealing information about the composition of cement-based materials used to build the military bunkers and technologies applied. Besides reinforced concrete of very high quality that was used as the main construction material, special renders were applied to the massive concrete walls and slabs to protect the concrete from the environmental influences and to camouflage the fortified facilities as part of nearby natural environment.

Position of samples and test methods

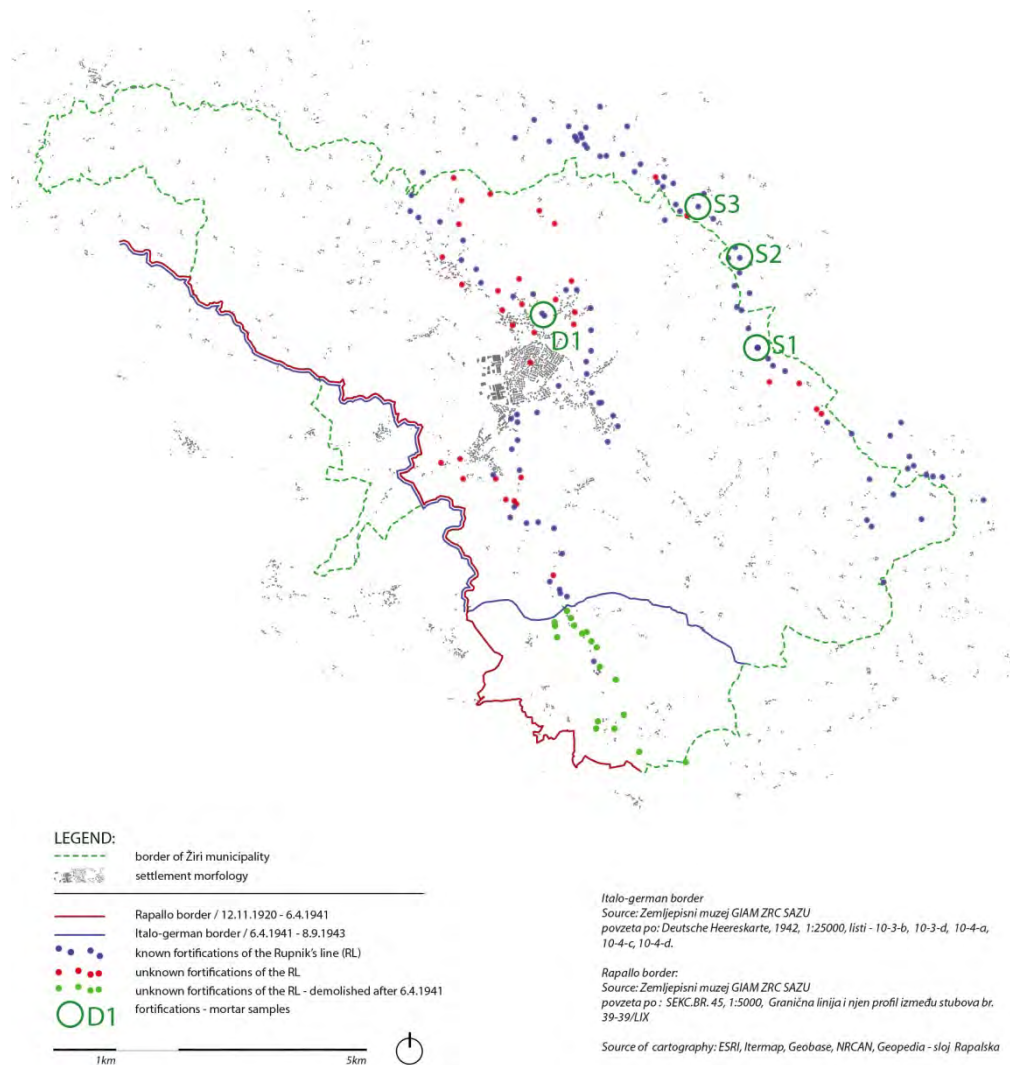


Figure 3: Position of sampled fortifications.

Four fortified positions were selected for the sampling of mortars (Figure 3 and Figure 4). The first one marked as D1 was part of the primary defence system in the valley where also the settlement of Žiri is situated (Figure 3). The other three marked as S1, S2 and S3 are all larger fortified positions intended to host both machine guns as well as artillery. As such they were part of the main defence system, the secondary line, and are positioned on a hilltop above Žiri (Figure 3). Airline distance between bunker D1 and bunkers S1 to S3 is approximately 2.7 kilometres. There is no visual connection between the two groups of bunkers, but bunkers S1 to S3 on the hilltop offered artillery coverage to the group of valley fortifications to which bunker D1 belongs.

Microstructural characterizations of the samples taken from the four bunkers (Figure 4) were first performed by optical microscopy (a polarizing optical microscope with transmitted light, Zeiss Axio Imager Z1). Thin sections (15-20 μm) were prepared from the mortar samples by following the instructions given in [6, 7]. Additionally, electron microscopy was

carried out using FE-SEM Zeiss Ultra Plus microscope equipped with EDS Oxford X-Max SDD 50 mm² 106 detector and INCA 4.14 5 X-ray microanalysis software.

Optical photomicrographs were also used to determine *aggregate: binder: pore volume ratios* of analysed samples, by using stereological expression $V=S$. Volume fraction of a composite material component can be estimated by areal fraction of the same component on any cross-section through the material under observation. Analysis was carried out via the following procedure proposed by Terry and Chilingar [8] and by using five different photomicrographs of a particular sample.



Figure 4: Bunkers that are subject of the study.

Microscopic observations

Results of the optical microscopy confirm that all samples are homogenous and that Portland cement clinker was used as the main binder.

Sample D1 (Figure 4), which was part of the primary defence system in the valley (Figure 3), is good representative of the used cement mortar. The *aggregate : binder : pore volume ratio* of the sample is 64:35:1. The aggregate particles are angular, with size ranging from some micrometres to 3 millimetres. The EDS analysis confirmed that the aggregate grains originate from dolomitic rocks. Detailed investigations by using microscopic techniques revealed the presence of dedolomitization process (Figure 5), as part of progressive alkali dolomite reaction (ACR). The ACR is visible as recrystallization areas inside the dolomite grains, for which change of initially bright colour of the dolomite crystals to the darker colour of recrystallization products is characteristic (Figure 5). Increased density of the binder (dark

necks), due to the formation of secondary calcite or “Ca halo” close to the dedolomitized grains, can also be observed in the micrographs of Figure 5 [9-11].

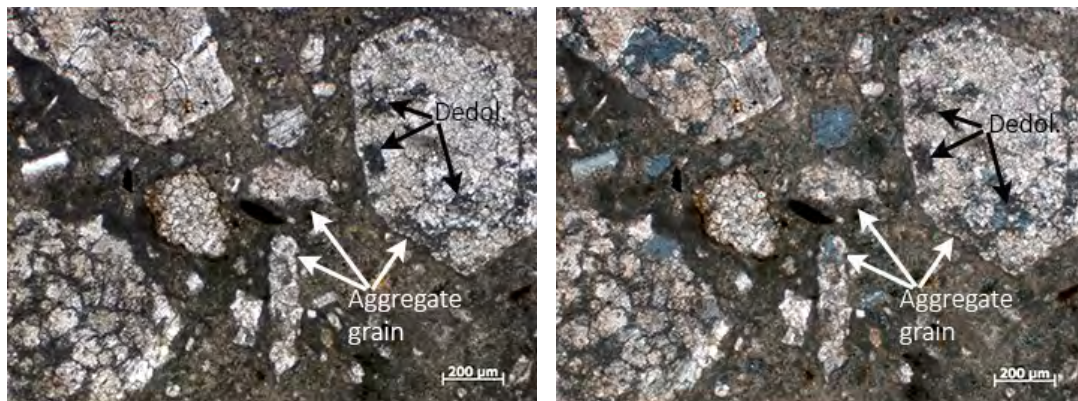


Figure 5: Sample D1 under optical microscope. Magnification 50x, PPT (left). Magnification 50x, XPT (right).

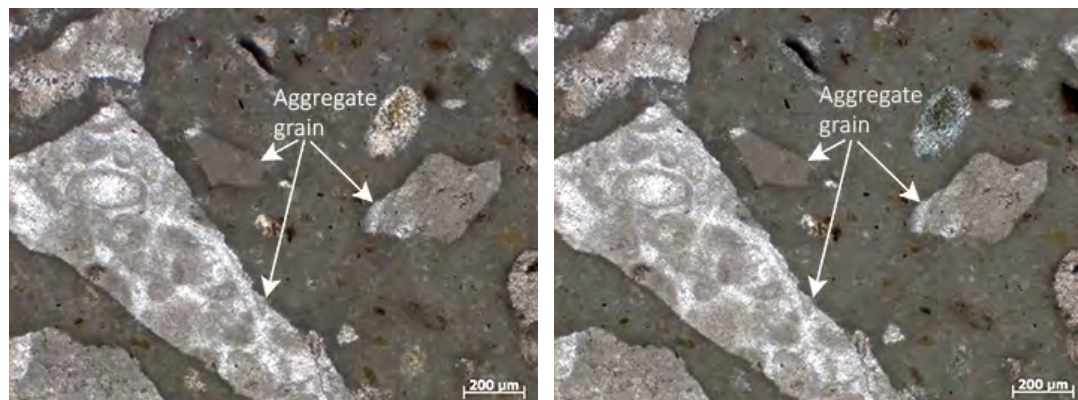


Figure 6: Sample S1 under optical microscope. Magnification 50x, PPT (left). Magnification 50x, XPT (right).

Sample S1 (Figure 4) is homogenous, with aggregate : binder : pore ratio equal to 64:35:1. The aggregate grains are angular with size ranging from a few micrometres to a few millimetres (Figure 6). The analyses by SEM and EDS confirmed that the source of the aggregate is limestone rock. Observed SiO₂ fragments, which are rare, could be part of ground granulated blast furnace slag added to the cement binder. This conclusion is also supported by the sample's colour, which is of greenish appearance, typical for the cement-based composites with the ground granulated blast furnace slag as supplementary binder. We also observed a few empty cracks in the sample.

The composition of sample S2 (Figure 4) is different from that of sample S1. The aggregate: binder : pore ratio is equal to 47:50:3, which indicates higher content of the cement binder in mortar S2. The source of the aggregate grains is dolomitic rock. The aggregate particles are angular, with the grain size distribution up to a few millimetres. Cracks were detected also in mortar S2, but the majority of them were filled with new phase. The detailed investigation confirmed the presence of amorphous phase rich in aluminium and sulphur ions (Figure 7). The source of sulphur ions could be gypsum from cement. Moreover, the process of dedolomitization was detected inside of some aggregate grains of sample S2, in

the form of typical myrmekitic texture, characterised by mixed but separated concentration of calcium and magnesium atoms.

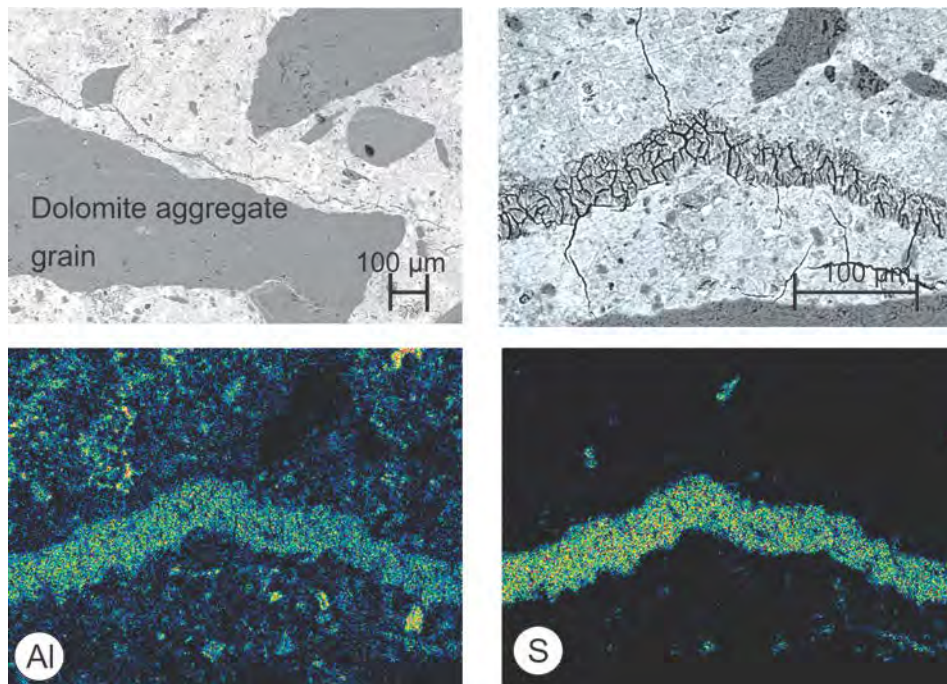


Figure 7: SEM and EDS analyses of Sample S2.

Two samples (S32 and S33) taken from the same bunker at position S3 (Figure 4) were finally analysed. Sample S32 is composed of two mortar layers that are clearly visible with naked eye. Sample S33 is a good representative of the mortar layer applied directly to the bunker's construction elements. Microscopic observation of sample S33 confirms that mortar is homogenous, with *aggregate: binder : pore ratio* of 68:30:2. The source of the aggregate is limestone rock. The appearance of the limestone grains (Figure 8) is the same as for sample S1 (Figure 6). The fragments of SiO₂ visible under optical microscope could be part of ground granulated blast furnace slag (Figure 8), which was used in order to obtain special greenish colour of the mortar.

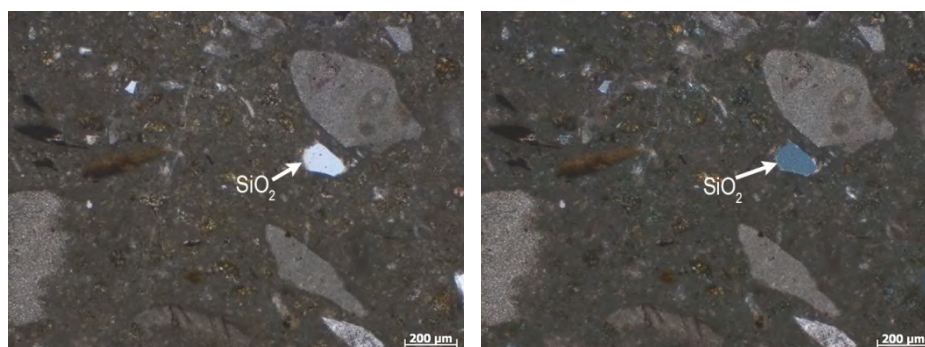


Figure 8: Sample S33 under optical microscope. Magnification 50x, PPT (left). Magnification 50x, XPT (right).

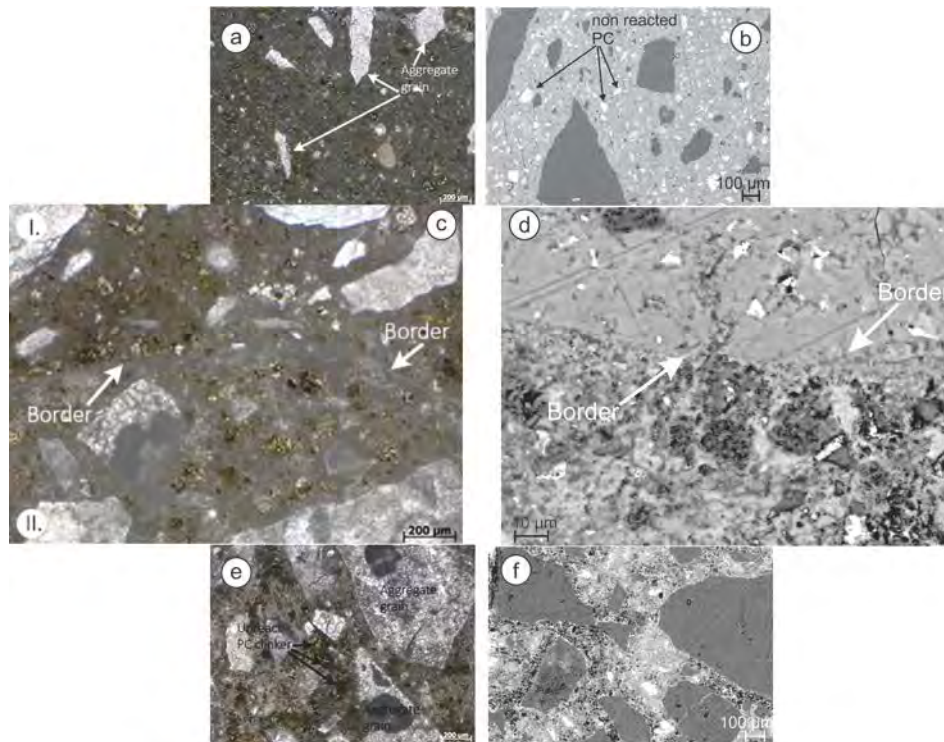


Figure 9: Sample 32. Layer I of sample S32 under optical microscope. Magnification 50x, PPT (a). Layer I of sample S32 under SEM (b). Border between layer I and layer II of sample S32 under optical microscope. Magnification 50x, PPT (c). Border between layer I and layer II of sample S32 under SEM (d). Layer II of sample S32 under optical microscope. Magnification 50x, PPT (e). Layer II of sample S32 under SEM (f).

Micrographs obtained when analysing sample S32 are shown in Figure 9. The sample consists of the two layers. The *aggregate: cement : pore ratio* of the upper layer mortar (marked I in Figure 9c) is equal to 20:78:2, which indicates unusually high content of the cement binder. Aggregate grains originate from dolomitic rock. They are angular in shape and with grain size ranging from some micrometres to 3 millimetres. The detailed investigation by SEM revealed the presence of high number of non-reacted PC clinker grains (Figure 9b).

The mortar used for the lower layer (marked II in Figure 9c) has similar composition as the mortar taken from bunker S2. Also the process of dedolomitization and other characteristic products of the ACR reaction are the same as for sample S2.

Discussion

In 1921, when the construction of military bunkers in the Rupnik Line started, steel reinforced concrete was still relatively new construction material. Therefore, the application of renders to the construction elements in order to protect them from environmental actions seems a logical decision that originates from the construction technology of that time. On the other hand, differently composed renders acting as camouflage could be the main motive for the renders' application. Military knowledge of hiding military structures by presenting them as part of local natural environment could also be used in case of the Rupnik line.

Mortar composition with the *binder : aggregate volume ratio* of 30-35:68-64, where the binder part represents the hydrated binder paste (cement + ground granulated blast furnace slag + water), and with the maximum aggregate grain size of 3 mm, can be designated as coarse mortar. This composition was prepared with limestone or dolomite aggregate, and applied to the construction elements of bunkers D1, S1 and S3. We believe that the main aim of slag addition was obtaining a special greenish colour in such mortars, which enables effective camouflage treatment of the bunkers. Mortar composition with the binder : aggregate volume ratio of 50:47 represents fine mortar composition, where only dolomite grains were used as the aggregate. It was applied as the only render of bunker S2 and as the lower layer of render S32 on bunker S3. Renders S2 and S32 contain several cracks. Larger drying shrinkage of the hydrated cement paste, due to the higher volume of the paste, and/or shrinkage, due to the dedolomitization process inside the dolomite grains, are plausible causes for the crack formation. In case of bunker S3, fine mortar S32 represents substratum of the shaped upper layer S32. In this layer, as much as 80 % of the volume is filled by the binder. Binder : aggregate ratio of 78:20 enables easy shaping of the layer in the form of relief surface. At the same time, many cement grains remained unhydrated, due to the lack of water available for the cement hydration. The relief surface is crisscrossed by black lines painted by bitumen. We believe that the surrounding natural environment was mimicked using a combination of shaped render and painted black lines. Moreover, alternation of relief patches with patches made of coarse mortar S33 prepared using the composite cement-slag binder which provides a greenish appearance of the surface most probably enables a perfect camouflage of fortified position S3 in the natural environment.

Composed Portland cement – ground granulated blast furnace slag binder was used only in combination with the limestone aggregate grains. Therefore, it can be concluded that special greenish colour of the coarse mortar was the main reason for the use of this combination of materials. In mortars with the dolomite aggregate grains only pure Portland cement was used as the binder. For these compositions, bright grey colour of the render's surface is typical, which matches the colours of typical carbonate rocks in the nearby natural environment.

However, for all compositions where dolomite grains were used as the aggregate, microstructural alteration typical for the alkali-carbonate reactions (ACR) were detected: dedolomitization inside the dolomite grains resulting in the formation of brucite and calcite, the formation of the secondary calcite or “carbonate halo” in the cement binder close to the dolomite grains, and the formation of amorphous phase rich in Mg and Al or/and Si ions [9]. The phase replaces part of the dolomite grain along its edge.

Conclusions

Four different fortification facilities from the Rupnik Line were selected for detailed microscopic characterization of renders applied to the reinforced concrete bunkers. Four samples (S1, S2, S32 and S33) are representatives of mortars that were used to make

renders on bunkers in the secondary defence system. Sample D1, on the other hand, represents the mortar used to build the primary defence system. Detailed observations confirmed that local carbonate rocks are the source of the used aggregates. The limestone aggregate was used to prepare mortars that were applied to bunkers S1 and S3. On the other hand, the dolomitic aggregate grains were used in mortars of the primary (sample D1) and secondary defence system (S2 and S3), as well as for the production of concrete [3]. In all the investigated samples, Portland cement clinker was used as the main binder, and in the sample with very high content of cement (the upper layer of sample S32), non-reacted clinker grains were often detected. The presence of supplementary cementitious material, ground granulated blast furnace slag, was detected only in samples with the limestone aggregates (S1 and S33). We may conclude that the slag was used to obtain special greenish colour of the rendered surfaces. Moreover, from the alternating application of different renders to the larger S3 fortification we can be quite sure that the main goal of the renders was to mimic the surrounding natural environment. This conclusion is also supported by the presence of turf on the bunkers D1 and S3. Therefore the colour of the mortar and shape of the rendered surfaces were the main characteristics needed. However, in addition to being used as camouflage, the mortars also protected the structural concrete from decay.

Acknowledgement

The authors acknowledge the financial support from the Slovenian Research Agency, through the research core funding No. P2-0185 and No. P1-0175, and research project No. J2-8194.

References

1. Mikša, P., Zorn, M., (2018), Rapalska meja : četrto stoletje obstoja in stoletje dediščine. in proceedings of Conference Nečakov zbornik : procesi, teme in dogodki iz 19. in 20. stoletja, AJLEC, K., BALKOVEC, Bojan, REPE, Božo (eds.)
2. Troha, N., (2001) Slovensko/jugoslovansko-italijanska meja. Zgodovina v šoli X
3. Grom, J., Štukovnik, Petra, (2018) Sektorska delitev obrambnih sistemov Rapalske meje in odkrivanje obsega sistema utrdb Rupnikove linije v prostoru. Igra Ustvarjalnosti - Creativity Game
4. Milan, R. (1937), Sistem savremene stalne fortifikacije. Ratnik sv.4. Beograd
5. Habernal, M., Čermak, L., Gregar, O., Markovič, Z. (2005), Rupnikova črta in druge jugoslovanske utrdbe iz obdobja 1926-1941. Češka Republika, Dvůr Králové nad Labem
6. Ingham, J. (2011), Geomaterials Under the Microscope., Mason Publishing London
7. St John Donald, A., Poole Alan, W., Sims, I. (1998), Concrete Petrography., Arnold and Meber of the Hodder Headline Group New York

8. Terry, R.D., Chilingar, George Varos, (1955) Summary of "Concerning some additional aids in studying sedimentary formations," by M. S. Shvetsov. *Journal of Sedimentary Research*
9. Štukovnik, P., Prinčič, T., Pejovnik, R.S., Bokan Bosiljkov, V., (2014) Alkali-carbonate reaction in concrete and its implications for a high rate of long-term compressive strength increase. *Construction and Building Materials*
10. Štukovnik, P., Marinšek, M., Mirtič, B., Bokan Bosiljkov, V., (2015) Influence of alkali carbonate reaction on compressive strength of mortars with air lime binder. *Construction and Building Materials*
11. Štukovnik, P., Marinšek, M., Bokan-Bosiljkov, V., (2013), Observation of reactions between dolomite aggregate grains and lime-based binder in lime mortars. in *proceedings of Conference Abstracts : 3rd Historic Mortars Conference : HMC 13 : Glasgow, 11-13 September 2013* Hughes, J.J. (eds.)

Topic 6: Historic production, processing and application of mortars, renders and grouts. Lime technologies



Warm applied Mortar (WAM) – An insight into the historical technique of “Heiße Speis” and its use for renders

Robert Wacha¹, Farkas Pintér²

(1) Information and Training Centre of Cultural Heritage Preservation, Federal Monuments Authority Austria, Kartäuserplatz 2, A-3001 Mauerbach, Austria, robert.wacha@bda.gv.at

(2) Scientific Laboratory, Federal Monuments Authority Austria, Arsenal 15/4, A-1030 Vienna, Austria, farkas.pinter@bda.gv.at

Abstract

The method of using dry slaked mortar while it is still hot or warm (warm applied mortar, WAM) originates mainly from an oral tradition amongst craftsmen in Austria, describing the method as “the hot matter” (“Heiße Speis” in German). For this purpose, mortar was not left to rest but used immediately after the mixing process and ongoing slaking reaction. To test this seemingly unconventional technique under field conditions quicklime and local river sand was dry slaked in boxes, mixed and used warm to render a chapel’s façade. During the application the “WAM” showed surprisingly good workability and good state of preservation even after harsh winters. Render samples from the test site were analysed after seven years of exposition. SEM images showed signs of a characteristic structure of shrinkage cracks. The paper shows the first results of practical tests of producing and working with warm applied mortar and the experience with this special technique.

Warm applied lime mortar in historical manuals and narratives

Aside some oral traditions amongst masons and renderers the technique of warm lime mortar is rarely reported in a few German manuscripts and manuals of the 18th and 19th century. As an example a German manual from 1755 [1] says that *„the lime being warm by slaking produces the best mortar that was used by folks very much...”* and *“Lime should not be stored for three or four years, but only the amount should be slaked which is required for the same day [...], the lime has also be used warm [...], the lime used for rendering and rendering has also be thrown on warm.”* On the contrary, other manuals strictly warn about the usage of warm lime mortar due to the expansive forces forming by the in situ slaking of quicklime particles on the façade. The manual *“Bürgerliche Baukunst “* from 1798 [2] clearly describes this phenomenon *„Sometimes it happens, that you use the lime and mix it to mortar just after it is slaked and that it is still warm”*. Gernrath writes in 1835 [3]: *„Fresh slaked lime is not as suitable for rendering as the one that was slaked a few days ago”*. Nevertheless, there are hints of traditional air lime mortars used in a warm state. This would also fit the common historical praxis of dry slaking where lime was directly slaked by using wet sand.

Furthermore, many applications of warm mortar simply occurred, because there was not sufficient time for the mortar to cool down when big façades were rendered and a large amount of material was needed.



Figure 1: Dry slaking of WAM in boxes (2009)

The definition of WAM

In our definition “WAM” (Warm Appplied Lime Mortar) refers to a historic technique that uses dry slaked (or so-called hot-mixed) mortar immediately after slaking without resting the mixture for hours/days and thus waiting until the complete slaking of quicklime takes place [4,5]. This means that the mortar is still warm when used for different applications (e.g. rendering). WAM is not referring to modern approaches to produce repair mortars by using fine quicklime powder. Due to the rapid exothermic reaction these mixes become hot (i.e. up to 100 °C) and therefore they are often called *hot or real hot lime mortars*. Furthermore, they have special properties compared to the material of the present study. WAM is simply a dry slaked mortar without the recommended resting time [5].

Application and field testing of WAM

An occasion to test this technique came up during a conservation project in Laussa, Upper Austria in 2009, where a baroque chapel was rendered with lime mortar by a local association without any preparations in one day. Up to 12 people worked at the same time, so dry slaking seemed to be a proper way to produce continuously large amounts of lime mortar.

Quicklime granulates, used for agricultural purposes with an average grain size of 0.5 to 1 cm, were filled together with local fluvial sand of carbonate origin in layers in large wooden boxes and sprinkled with water. As soon as the reaction reached its apex, the ingredients were mixed up and the façade was immediately rendered. The boxes were then filled up for the next charge (Figure 1). When the mortar was applied on the wall it was still warm with an estimated temperature of around 35 to 40°C. The mortar consisted of three volume parts of natural river sand and one volume part of granulated quicklime. The render was applied in 15 mm thickness in one layer by throwing it by trowels.

During the application the masons reported about a very good consistency and workability (Figure 2). The mortar was soft and “cosy” getting easily thrown off the trowel. It didn’t set faster as usual, although the renderers used sprinkling water to keep it formable. The method of continuous dry slaking, mixing and refilling the wooden boxes produced enough mortar to get the work done in a day. Next morning the crew came back to evaluate the surface and apply a final lime wash on it. The render set over night and although minute shrinkage cracks and a few expanding lime lumps were recognisable all over the surface, there was no significant damage to observe (Figure 3). Furthermore, the observation carried out seven years after the application showed only minor spallings on the surface, predominantly near to the footing zone of the chapel (Figure 4).



Figure 2: Rendering with warm mortar (2009)



Figure 3: Fresh WAM render with lime lump (2009)

Preliminary analysis of field samples

The façade of the chapel was sampled after seven years of exposition in order to get a visual evaluation of the render. The samples were embedded in epoxy resin, polished sections were prepared and analysed in the scanning electron microscope (Zeiss EVO MA 15).



Figure 4: The chapel in 2016, seven years after the application. Only minor damages are visible

Preliminary results show a characteristic crack pattern frequently observed in lime binders produced by the dry slaking process (Figure 5) [5]. The good bond between the finishing coat and the mortar layer (Figure 6) indicates not only good-quality craftsman

labour, but also suggests that the finishing coat protected well the exterior rendering. The first impressions clearly showed the nature of the samples; although the limited amount of water was significant, the rather dry consistency obviously did not damage the material or the surface. On the other hand, despite the less amount of water, large shrinkage cracks have formed, a phenomenon that can be led back to the general higher b/a ratios of dry slaked mortars [5, 6, 7]. Although the present experiment and research has not dealt with the investigation of physical and mechanical parameters (such as porosity, water uptake, strength, etc.), we assume, which is also suggested by other authors [4], that the apparently “weak” and porous microstructure rich in shrinkage cracks decreases the modulus of elasticity and thus led to a better performance of the material as a rendering mortar. Nevertheless, to get more insights into the fresh mortar properties, further test and analyses are needed.

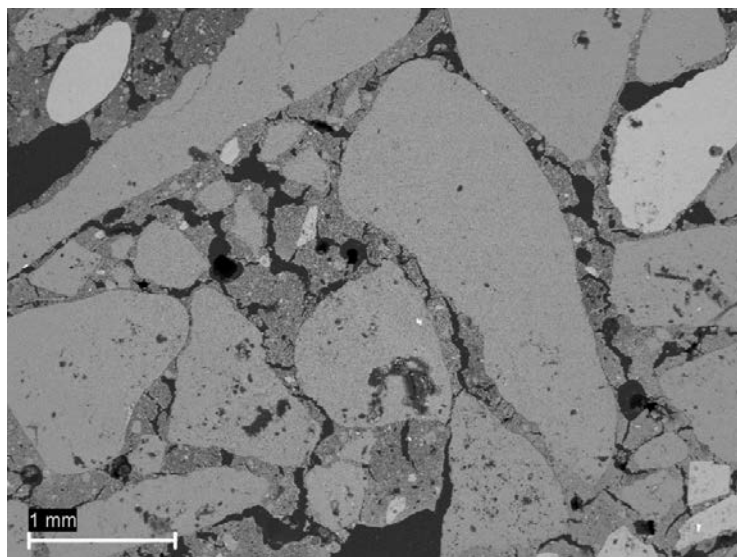


Figure 5: Shrinkage cracks in the matrix of the test mortar sample (SEM-BSE)

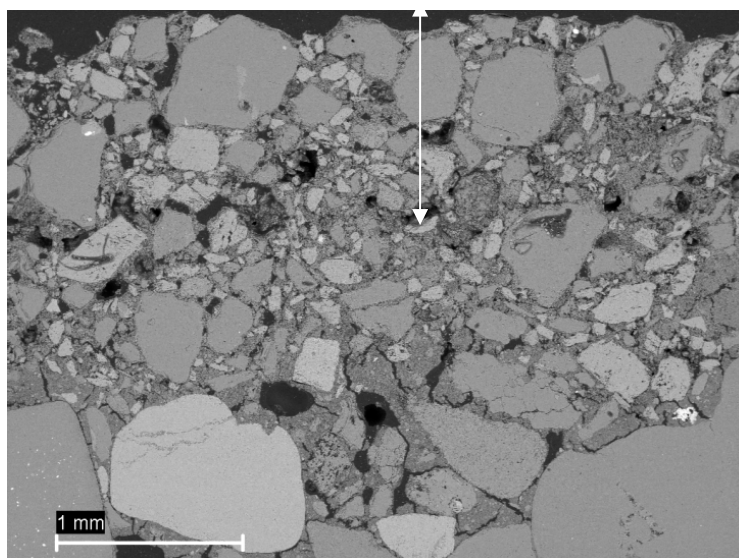


Figure 6: Finishing coat (arrow) at the top of the render layer (SEM-BSE)

Conclusions

Even in the past the technique of warm applied mortar was highly controversial. It seems plausible that the technique was frequently executed when restricted time was available for resting the mortar and large amount of quicklime was dry slacked. Also logistic problems such as the transportation of lime putty and/or the lack of lime pits could lead to the use of dry slaked and warm applied air lime mortars. Field tests proved that it is possible to use WAM for simple render works and even a “reactive” mortar is suitable for rough outdoor façades. In the forthcoming part of our project further applications of the material is planned (such as a mixes for stonewalls, more complex render works, etc.). Accompanying physical analyses and comparison with other air lime types (i.e. lime putty, basket lime, etc.) are also planned to get more insights into the fresh mortar properties of WAM.

Acknowledgements

The authors would like to thank to Thomas Köberle for his critical comments on the manuscript.

References

1. NN (1755) without title - in: Göttingische Anzeigen von gelehrten Sachen unter der Aufsicht der königl. Gesellschaft der Wissenschaften, J.F. Hager, Göttingen
2. Stieglitz C L (1796) Encyklopädie der bürgerlichen Baukunst; Ein Handbuch für Staatswirth, Baumeister und Landwirth: Kalk – Dritter Teil K-M; C. Fritsch, Leipzig
3. Gernrath J K (1835) Handbuch der Bauwissenschaften – zweite Ausgabe, L.W. Seibel, Brünn
4. Válek J, Matas T (2012) Experimental study of hot-mixed mortars in comparison with lime putty and hydrate mortars. In: Valek J, Hughes J, Groot C (eds) Historic Mortars, Characterisation, Assessment and Repair, Springer, London
5. Wacha R (2012) Die "Heiße Speis" im Pechgraben. Anwendung und Analyse zur historischen Technik des Heißkalkmörtels an der Sengtschmidkapelle in Laussa. In: Denkmalpflege in Oberösterreich 2010-2011, Jan Cemper-Kiesslich, Salzburg
6. Wacha R, Pintér F (2016) Lime slaking in baskets. Proc. of the 4th Historic Mortars Conference, Santorini, Greece
7. Alison H (2018) Hot-mixed mortars: the new lime revival. Context. <http://ihbconline.co.uk/context/154/32/#zoom=z>

Blast furnace slag in historic mortars of Bergslagen, Sweden

Jan Erik Lindqvist¹, Kristin Balksten², Birgit Fredrich¹

(1) RISE CBI, Ideon Lund, janerik.lindqvist@ri.se, birgit.fredrich@ri.se

(2) Conservation, Uppsala University, Campus Gotland, kristin.balksten@konstvet.uu.se

Abstract

Water cooled granulated blast furnace slag is today commonly used as a binder mixed with cement. Since the late 18th century blast furnace slag was used as an additive in bedding and pointing mortars of lime in the area of Bergslagen, the iron producing area in central Sweden. This type of mortars has not been documented and described previously in Sweden. The aim with the present project has been to document possible traditional use of slag in mortars in iron producing areas in Sweden and to see if it is possible to identify pozzolanic or hydraulic reactions. During the studied time period granulated blast furnace slag was invented, but this is not reflected in the studied material. The unsuitable chemical composition of the slag gave it a very low reactivity. As this study only included a small part of the production sites, it is still possible that some furnace produced slag with a composition that could give a better reactivity.

Keywords: slag mortar, slag cement, blast furnace slag, hydraulic additive, lime mortar

Introduction

The aim with the present project has been to document and understand possible traditional use of blast furnace slag (BF slag) in mortars in areas in Sweden with historic iron production, in this case the Bergslagen area in central Sweden. The studied time period reaches from when slag was first mentioned in the Swedish mortar literature in the mid-18th century and until the early 20th century when granulated blast furnace slag (GBF slag) was first used systematically as a binder together with lime or cement in Sweden. The project involves type of slag that was used and how it was treated prior to the application in mortars. This includes also if any pozzolanic/hydraulic reaction can be identified.

Water cooled GBF slag is today commonly used as a binder mixed with cement. This use of GBF slag was first described in 1862 by Emil Langens. Slag lime cement was first used in Germany in 1865 [1]. The GBF slag reacts and contributes to the hardening of the mortar. The chemical composition of the slag is important for its reactivity. A common requirement has been a value higher than 1 calculated according to:

$$\frac{(CaO + MgO + Al_2O_3)}{SiO_2} > 1$$

Historical use of slag mortars in Sweden according to literature

Already in the 18th century were researchers in Sweden experimenting with milled BF slag in lime mortars. Their results were not encouraging for this use [2]. Hermelin and Rinman concluded in 1773 that “Blast furnace slag do not contribute more to the hardening than clean good sand” [3]. Espling on the other hand mentions in 1784 that slag may be used to produce water resistant mortars were there was iron production [4]. This difference in view may reflect that the properties of the slag varied depending on the type of ore and how the process was run. Both Esplings opinion and the BF slag mortar research imply a tradition of BF slag in mortars at the time.

In Swedish building handbooks from 19th and 20th century slag cement and slag lime mortars are described as a material in use. Henström mentions 1869 that “meshed forgery slag is a cement, when added to a fat lime, which makes a mortar suitable for render or bedding mortar in non-moist places, and added a little hydraulic lime, making it the same for water mortar” [5].

In 1920 lime slag mortar was described as a certain type of mortar by Prof. Kreüger [6]:

“Of blast furnace slag and lime, one can produce slag cement. However, this method has not been used in our country for factory use, whereas it has often been produced by slag addition to lime mortar with considerably greater strength than air mortar. The blast furnace slag acts as a hydraulic additive, with the hydraulic properties appearing very weakly. The main constituents of the slag are: lime, clay soil, silicic acid, iron oxide and magnesia. For the slag being suitable for this purpose, certain relationships must be present between the amounts of the constituents. It has not been possible to find the most suitable proportions, but some chemical analyses, given in light of the strength tests performed, give some guidelines. The lime content of the slag should be greater than the silica content if basic slag is to be used. Acidic slag leaves poor results. The silica content should be at least twice as large as the sum of clay soil and iron oxide. The magnesium content should, if it exceeds 8 %, adversely affect the volume resistance. In addition to the chemical composition, the formation of the slag grains also influences the properties. In the granulation of the slag, a fully satisfactory cooling is required, which gives the grains a glassy structure. The slag then receives a lighter colour. If the cooling is not satisfactory, the grains become opaque and dark. The difference between glassy and opaque slag appears clearly in the microscope. Intermediate stages, i.e. mixture of glassy and translucent slag, also occur, and some proportion between the two types can produce good results. The way in which the two types of slag are affected is not fully resolved. At least there are different opinions. The

author has only wanted to find out through practical experiments that the slag, which has predominantly glassy structure, is the best additive to lime mortar” [6].

Kreüger was involved when the Stockholm City Hall was built in 1911-1923 where GBF slag mortars was used as masonry mortars in part of the construction. [8,9,10]. The early laboratory trials and tests have been discussed also in recent literature [11,12,13].

According to Kjellin and Hökerberg;

“...slag cement is made from granulated, finely ground blast furnace slag and lime. The slag is said to be acidic if it is relatively siliceous, otherwise, at a relatively large lime content, it is said to be basic, and it is the latter that is used for slag cement. Mixing ratios depend on the lime content of the slag, and depending on the same, the addition of lime hydrate varies from about 15-25% of the slag weight. The binding time is about one day, and the hardening is slow. Pressure strengths up to 150 to 200 kg/cm² can be obtained after 28 days, and after one year even up to 400 kg/cm² in the most favourable cases. Slag cement is economically advantageous to use, if only a lower degree of strength is required” [7].

There are some examples of forgery slag in historic mortars in Sweden. One such example is renders from the castle Mälsåker applied in 1670 contains iron in forgery slags that now can be seen as stains from iron oxide [14]. There was at the time a belief that the forgery slag made the mortar harden faster. In the stone walls surrounding the late 18th century mansion Gimo has black forgery slag been used as black pigment in masonry and jointing mortars.

The history of iron production in the Bergslagen area

The Bergslagen area has been a centre for iron production at least since 700 AD. The blast furnace technique has been used since the 12th century [15, 16]. There has been technology exchange with northern Europe from medieval times and onwards. From the mid-18th and through the 19th century the Bergslagen area was a region with research related to iron production. To some extent the same researchers were also involved in development of mortars for water constructions.

Slag as a building material in the Bergslagen area

In Bergslagen, the building tradition is clearly characterized by the iron industry. This is most clearly visible by the occurrence of the building blocks made of the slag in different formats. Both cast blocks and slag chips were used, which were used as building blocks. Both mansions and barns were built of slag blocks and chips. It is recognized as a glassy stone that varies in colour from black, green and blue (Figure 1).



Figure 1 left. BF slag mortars and masonry blocks of cast slag in forge shop at Flatenbergs hyttan. The repair above the door is made with pure lime mortar. Other parts of the building still have the original mortar. Figure 1 right. Example from Schisshyttan the ruin of a steel workshop constructed in 1763.



Figure 2 left. Slag stone with a glassy structure. Figure 2 right. A barn made of slag chips.



Figure 3 left. Cast slag blocks and slag mortar where the slag particles are rather big. Figure 3 right. A slag mortar with both sand and slag granulates.

Coarse crushed slag chips, cm to dm size, was often used in masonry in the Bergslagen area (Figure 2). There are some examples of houses where the walls are cast of a lime mix with or without slag. Masonry blocks cast of slag were commonly used in the area from the late 18th to early 20th century [17] (Figure 3, 4).

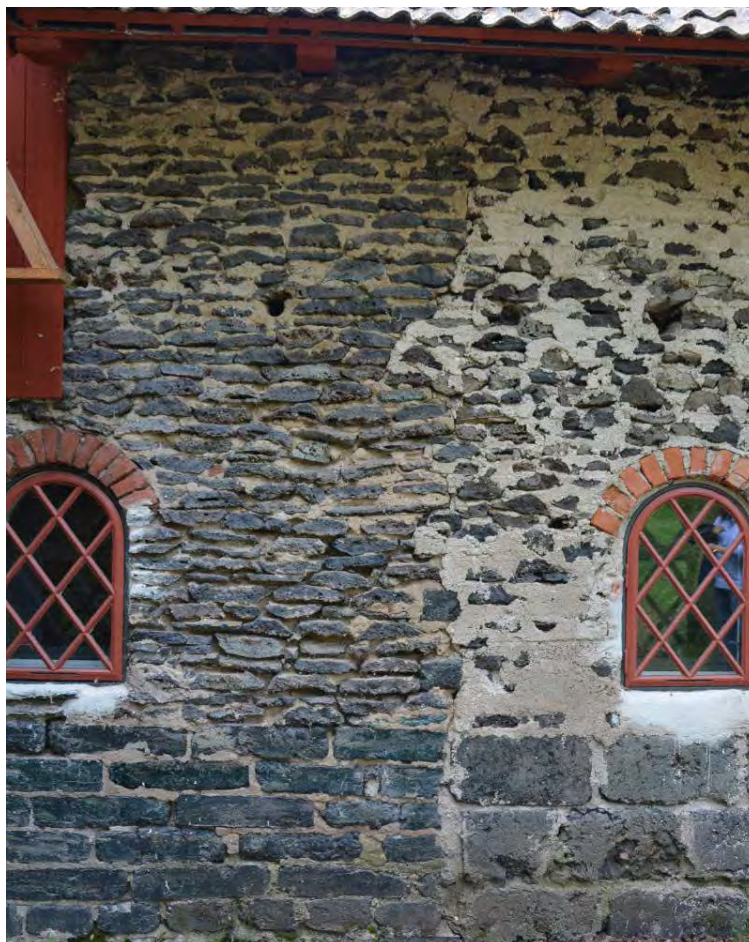


Figure 4. At the Unesco site of Engelsberg can buildings with different types of cast masonry slag blocks be studied.

Material sampling

The field work was performed in September 2016. Nine localities were visited and twenty-nine constructions were sampled. Thirteen samples were analysed in thin section and SEM/EDS. The analysed samples come from joint or masonry mortars with exception for one sample from a cast farm building at Mårdshyttan. The Norberg sample comes from a joint in the foundation to a mill in the village. The masonry was composed of cast slag blocks, core crushed slag chips, natural stone and bricks.

The studied area is a central part of Bergslagen. It was selected in order to cover the time span from mid-18th century to the early 20th century. The visited localities were mainly abandoned industrial sites that today have cultural protection. These include both preserved buildings and ruins. The industrial constructions were such as blast

furnaces, forge shops, office buildings and dwelling-houses. The sampled constructions were related to the iron production with exception for a cast farmhouse in Mårdshyttan. Schisshyttan was active from mid-17th to the early 20th century but today only ruins remain, mainly from the second half of the 18th century. At Skrikarhyttan occurs a ruin of a blast furnace from late 19th century. Pershyttan and the World heritage Engelsberg has a well preserved built industrial environment from the 19th and early 20th century. The village Norberg was a centre for the mining and steel activity in the area from medieval time. Norberg still has a well preserved historic centre.

Table 1. The sampled objects.

Locality	Construction	Time
Engelsberg; EB	Houses, foundations	18 th century to 1910
Flatenberg; FB	Industrial environment	1870
Mårdshyttan; MH	Cast slag lime house	19 th century
Norberg; NB	House foundation	18 th to 19 th century
Pershyttan; PH	Houses and furnace	1850-1900
Schisshyttan; SCH	Ruins of iron industry	1753-1800
Skrikarhyttan; SK	Slagg wall, industry ruin	19 th century

Method

The composition and microstructure of the samples were analysed using thin section technique in polarization and fluorescence microscopy. The quantitative analysis was done according to methods described by [18]. Mix proportions were calculated according to NT Build 370 [19] and Lindqvist et al. [20] based on point counting in light microscopy. Microchemistry was analysed using scanning electron microscopy with energy dispersive equipment for micro chemical analyses, SEM/EDS. The EDS results are given in weight percentages.

Results

Field observations

The use of BF slag in mortars was very common in this area during the studied time interval. Masonry and renders of the houses that are still in use are generally in good condition. The types of construction are given in table 1. The BF slag mortars are dark greyish to yellow brown and the slag can often be seen as green-grey glassy particles, see Figure 3.

Microscopical and micro chemical analysis

The character of the mortars varies. The properties of samples from different localities differ considerably. There are, in some cases, also significant variations between samples from the same locality.

The composition of the aggregate is, with some variation, depending on the geology in the area. The main constituents are quartz, feldspar, calcite and mica together with fragments of granite, porphyry and mafic rocks. In several samples occur skarn minerals. The maximum particle size of the aggregate in the different samples varies between the different samples from 1.5 to 10 mm. The shape varies from rounded to slightly angular, answering to natural fluvial respectively till deposits.

The BF slag in the samples is mainly glassy (Figure 2). The slag content varies in the analysed thin sections given as volume-% from Engelsberg 0.5 till 15 %, Norberg 35 % Pershyttan 30 %. The maximum particle size of the glassy slag is in the range 3 to 5 mm. There is slag foam with a max particle size of 2 to 6 mm (figure 3). Large glassy slag particles have both rounded and angular sides. Fine particles are often elongated and flaky. The shape of the slag particles show that they have been crushed. In some samples has the foam slag reacted and only a relict structure remains in the paste (figure 3). There are also a few examples of devitrified glassy BF slag that has textural relations implying reaction.

The analysed BF slag in each locality has its own chemical characteristics (Table 2). The magnesium content varies from 1 to 15 % while the iron content is generally low. The manganese content is fairly high in the slag of some samples. The highest is in EB5 with approximately 5 %. The composition of the Skrikhyttan sample differs as it contains both crystalline as well as glassy slag.

The color of the paste seen in the microscope varies from almost white to relatively strong colour. The micro chemical analyses of the lime paste in the mortars imply that there has been a contribution from hydraulic or pozzolanic reactions in some samples (Table 3). The maximum magnesium content in the paste is 4 %, with an exception for Skrikhyttan at 10-15 %. Lime lumps are common. It occurs often as relicts of marble or partly under-burned marble.

The content of air voids is in the range 1 to 25 % (EB1 to Sk1). The shape of the air voids varies from rounded to highly irregular. The variation in shape probably reflects the rheology of the fresh mortar. The capillary porosity of the paste assessed through fluorescence microscopy varies strongly between the analysed samples.

The mix proportions of binder aggregate and BF slag calculated from the point counting results varies from given in weight lime/aggregate/slag 100/45/85 (EB5) and 100/20/280 (NB1) and 100/75/215 (Ph4). But it may also be only a few percent BF slag.

Some of the samples are based on a lime cement mortar with a small amount of crushed glassy BF slag, lime/cement/aggregate/slag 65/35/415/5 (EB2).

Table 2. Results from the point counting. Values given as volume percentage.

	EB 1	EB 2	EB 5	FB 1	MH 1	NB 1	PH 2	Ph 4	Ph 6	Sk 1	Sk 2	Sch 2	Sch 4
Air	4	12	13	21	10	18	4	10	13	23	17	16	12
Agregate	47	51	7	45	57	4	13	17	56	34	12	54	28
Paste	47	34	15	30	31	36	50	42	29	21	27	26	55
Lumps	0	0	52	3	1.7	5	2	1	2	4	9	4	16
Slag	0.5	0.6	14	0	0	37	28	29	0	18	35	0	
Total	100	100	100	100	100	100	100	100	100	100	100	100	100
Points	442	513	443	431	363	402	433	406	399	369	518	453	436

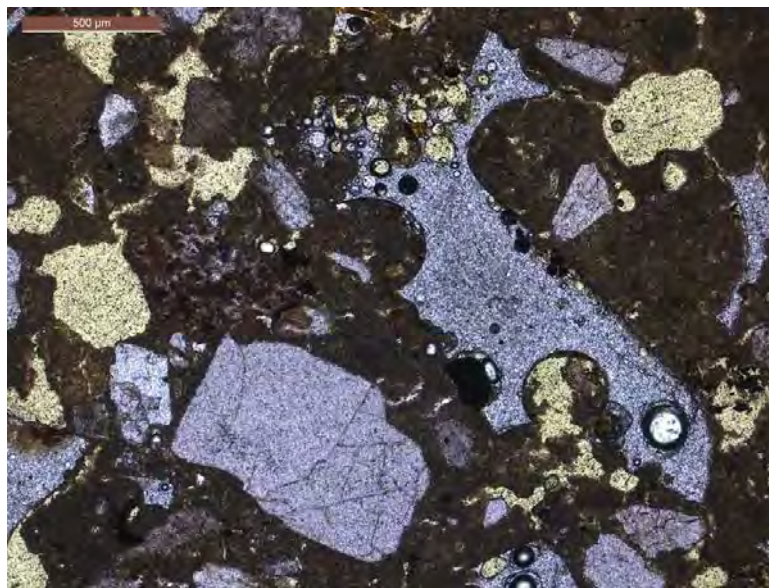


Figure 5. Glassy BF slag, sample EB5 from Engelsberg. Image taken in plain light.

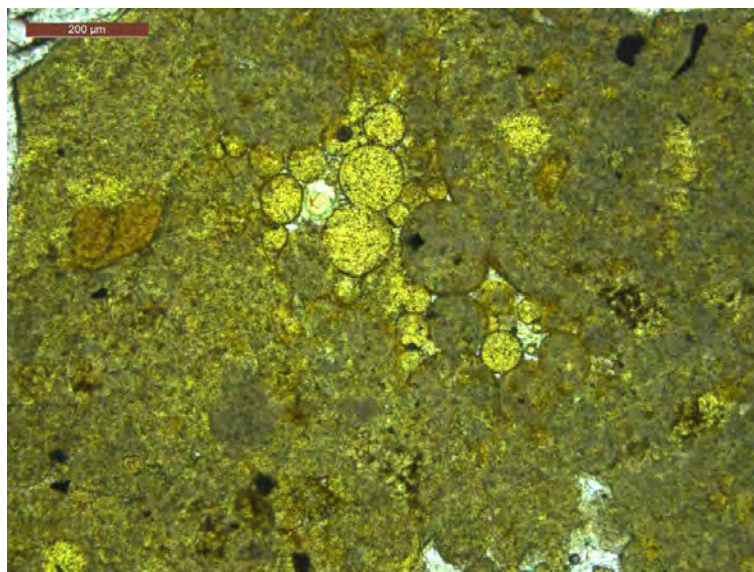


Figure 6. Reacted slag foam in sample PH2. Image taken in plain light.

Discussion

The results from both literature studies, field work and laboratory analyses confirm that there has been a local tradition with crushed BF slag mortars in the Bergslagen area during the studied time span. The mix proportions are similar to what was used in conventional mortars at the time [9, 11, 21].

The microscopical analyses of the slag used in the studied samples only show limited signs of reaction. The results from the micro chemical analyses show the (C+M+A)/S ratio in the slag is lower than 1 which imply that the BF slag used could only give a limited contribution to the hardening of the mortars (Table 3). The results agree with the view of the Swedish researchers in the late 18th early 19th century that the available BF slag gave little contribution to the hardening of the mortar.

Table 3. The Al/Ca and Si/Ca ratios of the lime paste together with calculated (C+M+A)/S ratios for the BF slag. An Si/Ca ratio higher than 0.25 indicates reaction.

Sample	Al/Ca	Si/Ca	(C+M+A)/S
EB4	0.03	0.14	0.7
NB1	0.01	0.06	0.67
Ph2	0.1	0.35	0.82
Ph4	0.05	0.28	0.85
Sch2	0.04	0.19	No slag
Sch4	0.05	0.28	No slag
Sk2	0.08	0.37	0.8

The influence of the chemical composition of the BF slag on its reactivity was not known at the beginning of the studied time period. The use of GBF slag as a binder was established in the second half of the 19th century. This development is however not reflected in the studied material.

The function of the BF slag was mainly as aggregate but they had easy access to aggregate so the idea was probably a contribution as a binder. It can however not be excluded that there exist localities where more active BF slag were produced.

Conclusion

The results show that BF slag was used in mortars in Bergslagen during the studied time period. This type of historic mortars has not been analysed in Sweden previously even though they were mentioned in masonry handbooks during the 19th and 20th centuries. The unsuitable chemical composition and the size distribution of the slag gave it a very low reactivity. The method for cooling the slag was too slow to produce a BF slag with high reactivity. As a result, the function of the slag was mainly as aggregate and it gave the mortars a characteristic appearance. During the studied time

period were GBF, granulated blast furnace, slag invented but this is not reflected in the studied material. As this study only included a small part of the production sites is it still possible that some furnace produced slag with a composition that gave better reactivity.

Acknowledgement

The field work was financed of Richerts Foundation which is kindly acknowledged. Prof Kerstin Barup is kindly acknowledged for the valuable assistance in selecting constructions to sample at the World Heritage Engelsberg.

References

1. Hewlett PC (1998) ed Leas's chemistry of cement and concrete. Arnold New York 1998, 1053 pp.
2. Pasch GE (1824) Berättelse om de vid Motala station anställde Murbruks-försök, inlämnad till Göta Canals Direktion år 1818 och 1822. Jernkontorets annaler. Stockholm.
3. Rinman S, Hermelin S (1773) Rön om cement. Kungliga Vetenskapsacademiens avhandlingar.
4. Espling O (1784) Mineraliskt användande i byggningskonsten kemisk – oeconomisk afhandling.
5. Henström A (1869) Praktisk handbok i landtbyggnads-konsten. Örebro: Beijer.
6. Kreüger H (Eds) (1920) De tekniska vetenskaperna: bibliotek för teknisk vetenskap och dess tillämpning på svensk industri och byggnadskonst. Avd. byggnadskonst, Bd 1, Byggnadsmaterialier. Stockholm: Bonnier.
7. Kjellin E, Hökerberg O (Eds) (1928) Byggnadskonsten, dess teori, juridik och praktik. Stockholm: Hökerberg.
8. Larsson R (2011). Secrets of the walls: a guide to Stockholm City Hall. Stockholm: Langenskiöld in association with History of Architecture, Royal Institute of Art. 20, In Sweidsh.
9. Eriksson J, Johansson S, Lindqvist JE (2016) Development of mortars in Sweden during the period 1800 to 1950. Eds I Papayianni, M Stefanidou, V Pachta. Proceedings of the 4th Historic Mortar Conference – HMC 2016.

10. Berggren K (2017) Kalkens hemligheter, teknik och historia. (In Swedish) Balkong Förlag Stockholm, 183 pp.
11. Eriksson J (2015) Bruk av kalk och sand. Licentiat thesis Gothenburg Studies in Conservation 34, 183 pp, abstract in English.
12. Johansson S (2006) Hydraulic lime mortars. In Swedish abstract in English. Studies in conservation 20, Acta Universitatis Gothenburgensis, pp 327.
13. Johansson S (2017) Hydrauliskt kalkbruk i Norden – från 1000-talet till nutid. <http://bksjab.se/media/docs/Slutrapport2-1-postdocBildHems1702.pdf>
14. Lindqvist JE, Sandin K, Sandström H, Sandström M, Schouenborg B, Sidmar E, Sundner B (1999) Gammal kalkputs - analys och utvärdering. Riksantikvarieämbetets förlag, Stockholm, 53 pp.
15. Bindler R, Segerström U, Pettersson-Jensen IM, Berg A, Hansson S, Holmström H, Olsson K, Renberg I (2011) Early medieval origins of iron mining and settlement in central Sweden: multiproxy analysis of sediment and peat records from the Norberg mining district. Journal of Archaeological Science, vol 38:2, 291-300.
16. Myrstener E, Lidberg W, Segerström U, Biester H, Damell D, Bindler R (2016) Was Moshyttan the earliest iron blast furnace in Sweden? The sediment record as an archeological toolbox. Journal of Archaeological Science: Reports Volume 5, Pages 35-44.
17. Gunnarsson AM (2016) Slaggsten och slagghus – unika kulturskatter. Balkong förlag Stockholm 216 pp.
18. Lindqvist JE, Sandström M (2000) Quantitative analysis of historical mortars using optical microscopy. Materials and Structures vol 33, 612-617.
19. NT Build 370 (1991) Mortar hardened: Cement content and aggregate binder ratio. Nordtest.
20. Lindqvist JE, Nijland T, von Konow T, Wester Plessner TS, Nyman P, Larbi J, van Hees R (2006) Analysis of mortars with additives. SP report 2005:32, 31 sid. <http://www.diva-portal.org/smash/record.jsf?pid=diva2%3A962322&dswid=-5955>
21. Lindqvist JE, Johansson S (2019) The Development of Binders and Mortars in Sweden. In: Hughes J., Válek J., Groot C. (eds) Historic Mortars. Springer, Cham.

Composition and Technology of the 17th Century Stucco Decorations at Červená Lhota Castle in the Southern Bohemia

Jan Válek¹, Olga Skružná¹, Petr KozlovceV¹, Dita Frankeová¹, Petra Mácová¹, Alberto

Viani¹, Ivana Kumpová¹

(1) The Czech Academy of Sciences, Institute of Theoretical and Applied Mechanics, valek@itam.cas.cz, skruzna@itam.cas.cz, kozlovcev@itam.cas.cz, frankeova@itam.cas.cz, macova@itam.cas.cz, viani@itam.cas.cz, kumpova@itam.cas.cz

Abstract

The stucco decoration from the Great Chamber of the castle Červená Lhota in the Southern Bohemia was surveyed and characterised as part of its planned conservation. The repair works that are still to be specified in detail should be based on a good knowledge of the original material and technique. The main focus was on the fruit pieces decorating the ribs of vaults. Altogether, over twenty mortar samples were collected from the vault bedding mortar, plaster, drawn elements and stuccos. Additionally, some pieces of fruits, that were loose and had to be temporarily removed, were studied macroscopically and by X-ray CT. Characterisation of binder, aggregate and additives was carried out using TA, acid attack, sieve analysis of unsolvable residue, XRD, FTIR and nL-MS. The characterisation led to understanding of the uses of various mortar mixes and determination of their recipes. A typical fruit piece was composed of an inner modelling core mortar made of lime-gypsum binder and a coarser aggregate covered with a 5–20 mm thick lime rich stucco layer containing calcitic air lime and fine siliceous sand. This stucco mortar was also used for modelling various small decorations - fine and thin shapes like leaves, cherries and grapes. These were attached to the main piece by a fine adhesive mortar made of lime and gypsum in various proportions. The use of gypsum and the differences in lime to gypsum ratio corresponded to a certain functional requirements (performances). This finding was a key parameter that contributed to the reconstruction of the original application technique and procedure. Qualitative analysis of animal proteins determined presence of collagen – an animal glue that was used to modify the setting of gypsum and which was also used in the final finish. The results are discussed as an example of a procedure that aims at a detailed replication of the original technique.

Keywords

Historic production, processing and application of mortars, renders and grouts, lime technologies, stucco decorations

Introduction

The rediscovery of the antique plaster formula by Giovanni da Udine in the early 16th century was followed by a widespread use of stucco for architectural decorations [1, 2]. Materially, stucco is a mortar that is typically composed of a mixture of lime and gypsum, the binding elements and sand, the filler. Stucco mortars have specific properties that allow to produce decorations with a high spatial plasticity. One of these specific properties is setting that can be modified by proportioning of two binding components and addition of organic substances, e.g. animal glue [3]. However, there are considerable differences between stuccos varying from site to site and artist to artist.

Building conservation tasks require knowledge of original materials and techniques in order to be able to maintain the values imbedded in them. This is also the case of the stucco decorations from Červená Lhota castle made by Innocenzo Cometa in 1674-1675 [4]. There are 17th century frescos painted by Giacomo Tencalla in the Great Chamber [4] that are currently being uncovered and conserved and this extends also to the stucco decorations, Figure 1. Along with the conservation works a detailed research is being carried out aiming at re-discovering the original mortar composition and the working techniques applied there.

Innocenzo Cometa (1651–1681) was the son of a more famous stuccoer Giovanni Bartolomeo Cometa (1620–1687) who was born in Arogno in Ticino but worked mainly in Austria, Bohemia and Saxony [4]. This transfer of building and artistic techniques from the northern Italy to the regions north of the Alps was typical for the Renaissance and Baroque periods and especially the Ticino region in Switzerland was a famous cradle of many recognised artists and craftsmen of that time [5, 6].



Figure 1. Stucco decorated vaulted ceiling of the Great Chamber at Červená Lhota castle at the stage of detailed surveying – a preparatory phase for uncovering the frescos and cleaning the coatings.

Samples and Methods

Samples

Altogether, over twenty mortar samples were collected from the bedding mortar, plaster, drawn elements and stuccos. Additional samples were also taken from the pieces of fruits that were loose and had to be temporarily removed, transferred to a workshop for cleaning, which also allowed their further detailed studies. The collected samples are listed in Table 1. The main focus was on the fruit pieces decorating the ribs of vaults as their partial reconstruction will be considered if there is enough information regarding their material composition and production techniques.

The characterisation of the binder, aggregate and additives was carried out using thermal analysis, acid attack, sieve analysis of the unsolvable residue, X-ray powder diffraction, Fourier transform infrared spectroscopy, nano-liquid chromatography-mass spectrometry.

Table 1. Studied stucco, plaster and mortar elements from Červená Lhota castle.

Construction and/or decorative element	Description	Sample identification (in bold – tested for organics)
Small decorations	Leaves, grapes and cherries	SCL 1, 2, 3, 4, 5, 8, 11, 12, 13
Fruit pieces	Inner modelling mortar	LCL 3, 4, 5, 6, 7, 8
	Outer stucco layer, app. 5–10 mm thick	SCL 9, 10, 14
Adhesive mortar I	Fine adhesive mortar	JCL 1, 2, 3
Adhesive mortar II	Coarse adhesive mortar	LCL 1, 2
First coat	Frist coat under the stucco decoration	MCL 1
Bead mould	Bead enriched moulding running along ribs	SCL 6, 15
Rib	Two L shape mortar profiles enclosing fruits and forming the rib at the cross-section of the barrel vault with the side lunettes.	SCL 7
Masonry mortars	Bedding mortars from the brick vault of the Great Chamber (MCL2) and the vault above the room next to it (MCL3).	MCL 2, 3
Older stucco decoration	Stucco decoration from the arcades, made after app. 1641.	SCL 16

The distinction between the different layers and materials presented in Table 1 is based on a preceding assessment, which is out of the scope of this paper. This is an assumption closely connected with the application technique that was used to build

the stucco. A verification or a contribution to the further clarification of this assumption was also part of this study.

Decorated mortar ribs were made at the cross-sections of the barrel vault with the side lunettes. One rib was composed of two parallel L-shaped mortar profiles that had a running bead mould next to them from their outer sides and a rich fruit decoration in between them, Figure 2.



Figure 2. Bottom part of a rib formed by two L shape mortar profiles enclosing the vase with the fruit. Transfers from the rib to the plain vaulted surfaces are decorated by a bead moulding.

Fruit pieces were composed of an inner modelling mortar and an outer stucco layer. It seems the fruit pieces (more than 20 different types) were mostly prepared on a working desk and then attached to the substrate formed by the hardened (stiffened) first coat. The pieces were glued to the substrate by app. ~5 mm thick layer of a relatively fast setting adhesive mortar II, Figure 3. Rarely, an iron nail was found placed in the centre of a fruit piece that helped to anchor the heavier pieces and/or those which were at the top of the vault (at this position the whole weight is to be borne by the tensile capacity of the adhesive mortar). An alternative approach, the use of a mould for modelling the same fruit shapes seems less probable so far. Small decorations were also prepared separately on a desk and then glued to the already well-set fruits by using the adhesive mortar I, Figure 4. It is possible that some smaller pieces and fruits were also modelled directly on the spot but probably only in the cases where it was convenient in terms of appearance and composition, and/or easiness of application. All stucco decorations had several historic layers of lime wash coating. The last two were applied by spraying covering entirely the original final finish.

Bedding mortars from the top parts of the brick vaults were sampled for comparative reasons, as well as, another stucco decoration made in the castle at an earlier date.

Based on the symbols depicted on the stucco it can be dated after 1641 when the castle changed its ownership [7], Figure 5.



Figure 3. Top part of a rib with some fruit pieces fallen out showing the first coat and the remains of the adhesive mortar II layer on sides and between the fruits. The scalpel points at the position of sample MCL1.



Figure 4. Detail of the fruit pieces (almonds, pomegranate, grapes and cherries) with small decorations (leaves, cups and other shapes) added for an enrichment.



Figure 5. Stucco decoration made at an earlier refurbishment phase of the castle.

Methods

X-ray CT

Selected fruit pieces with irregular shape and approximate dimensions up to $130 \times 80 \times 70$ mm were investigated tomographically using TORATOM (twinned orthogonal adjustable tomograph) device [8]. CT scan was performed with one pair X-Ray tube – detector, employing a microfocus reflective type X-ray tube (XWT-240-SE, X-Ray WorX, Germany) operating at micro-focus mode and an amorphous silicon (a-Si) CsI:Tl image sensor flat panel (XRD 1622 AP 14, Perkin Elmer, USA) with dimensions of $409,6 \times 409,6$ mm, pixel matrix of 2048×2048 and $200 \mu\text{m}$ pixel size. For each fruit piece a geometry adjustment of the focus-detector distance and focus-object distance was done in order to obtain the best possible resolution with regard to the size of the specimen and the detector area. In case of the fruit piece no. 118 discussed in the results part the projection magnification factor 4,21 was obtained, leading to the resolution of $47,51 \mu\text{m}$ per pixel in projections.

During the rotation of the specimen against the CT system 1800 X-ray images (projections) with an exposition time of 1200 ms were acquired. Preprocessing and corrections of obtained datasets was performed using on site developed software. Filtered back projection CT reconstruction module of VG Studio MAX 3.2 (Volume Graphics GmbH, Germany) was used to obtain 3D virtual models of the investigated specimens.

TA, XRD

Composition of mortars was characterised by a thermogravimetric analysis (TGA/DTG) and X-ray powder diffraction (XRD). All coatings were removed mechanically. The purged samples were gently crushed and sieved under 63 μm to enrich the binder portion. The instrument SDT Q600 (TA Instruments) was used to measure thermal behaviour between 25-1000°C for which a sample of app. 10 mg was heated at the rate of 20°C/min in air and/or in nitrogen atmosphere. Endothermic dehydration of gypsum occurs in two steps between 150°C and 250°C (steps can be overlapping) and endothermic decomposition of calcite is around 900°C, exact temperature depends on the crystallinity [9].

Before the XRD analysis an internal standard (NIST 676a corundum, 10 wt.%) was homogenized with the sample. Data were collected on a diffractometer D8 Bruker Advance pro (Cu K α radiation, 40kV and 40mA) with 0.01°C step size 2 θ and counting time 0.4 s/step. Crystalline and amorphous fractions were determined with combined Rietveld-RIR method.

MALDI-TOF, FTIR

Presence of organic compounds had been verified by mass spectrometry on the MALDI-TOF principle and Fourier transform infrared spectroscopy (FTIR). Infrared spectra of samples were collected with microscope iN10 (Thermo Scientific) equipped with ATR module in the spectral range 4000-525 cm^{-1} . Representative amount of sample was deposited on the diamond ATR crystal summing up 64 scans using resolution 4 cm^{-1} was measured. To verify the presence of proteins samples were cleaved by trypsin for 2 hours then re-cleaned and thickened on a reverse basis C18 (Zip Tip). The analysis was done by nanoliquid chromatography with mass spectrometry ESI-Q-TOF MaxisImpact. Proteins were identified by software Mascot 2.2.04 in database SwissProt, NCBIInr and MS/MS. The database contains proteins from microorganisms to mammals' proteins, methods doesn't allow to identify other organic compounds (oils, saccharides, DNA) [10].

Dissolution and sieve analysis

The proportion of insoluble residue (aggregate) was determined by dissolving the sample in 10 % solution of acetic acid. Samples containing gypsum had to be dissolved in boiling hydrochloric acid (1:3) for about 2 minutes [11]. After dissolution the aggregate was washed with distilled water several times. After cleaning, sieve analysis was carried out to describe the granulometry of aggregate and optical microscopy was used to specify its mineralogical composition.

Results

X-Ray Computed Tomography Model

The virtual CT models were assessed qualitatively, revealing the inner structure of the fruit pieces including the way of attachment of the small decorations, Figure 6.

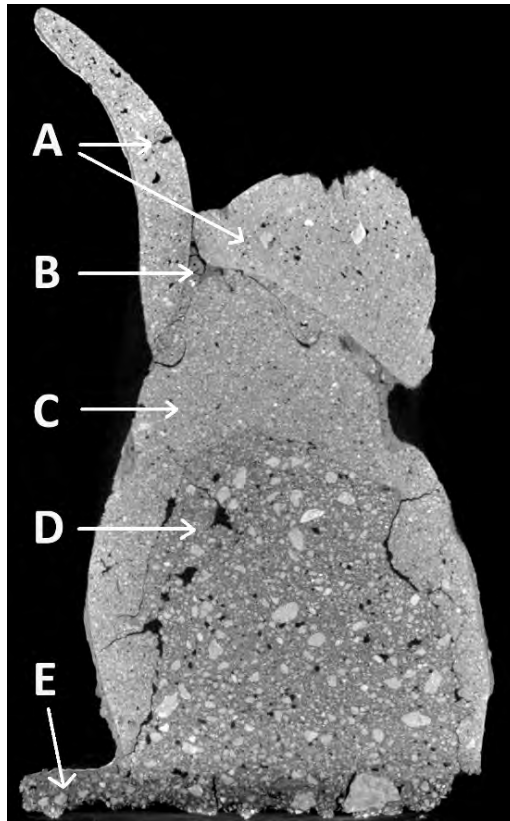


Figure 6. CT model cross section of the fruit piece No. 118. It shows the structure of stucco pieces including: A – small decorations, B – adhesive mortar I (fine), C – outer stucco layer, D – inner modelling mortar, E – adhesive mortar II (coarse).

The core of the fruit piece was made of the inner modelling mortar. It was heterogeneous containing visible pores, small voids, cracks between application layers and coarser aggregate with the size estimated up to ~8 mm. The core was roughly proportional to the kind of the modelled fruit. The spiky or tilted shapes had the corresponding shapes of the core etc.

The final surface was made from the outer stucco mortar, which was about 5 to 20 mm thick but locally varying depending on the complexity of the shape. The mortar was generally quite dense and homogeneous with only sporadically occurring larger particles and rounded pores that were typically under 1 mm in size. The outer stucco and inner modelling mortar contact interface was emphasised by occurrence of cracks between the layers and also by voids. Clearly visible were also shrinkage cracks within the stucco layer perpendicular to the surface. These cracks did not reach the surface;

they were probably closed during the surface treatment throughout the course of production.

The small decorations mortar appeared similar to the outer stucco one but it lacked the larger shrinkage cracks. The small decoration elements were attached to fruit pieces or to each other with the fine adhesive mortar I. This mortar adhered to both surfaces well and the bonding contact was much better than that of the one between the core and outer mortar, but some imperfections along the surface plains including also shrinkage cracks were observed too.

The adhesive mortar II was similar to the inner modelling mortar in structure as it also contained a filler of various particle sizes. The boundary between the modelling and adhesive mortars was very soft and the transition was not emphasised by cracks as it was in the cases of the other joints mentioned above. Slight differences in the colour shade indicated varying material density caused possibly by its nonhomogeneous composition.

Binder Composition

Thermal analysis was used to assess the binder and based on it the samples were divided into three types – A, B and C. Type A contains no or very small amount of gypsum (up to 2.5 wt.%) and its weight loss between 200–600°C is less than 3.5 wt.%. Samples with a higher weight loss in this interval (200–600°C) were labelled as type B. Type C is like A but contains gypsum in larger proportions. Representative TGA/DTG curves of individual binder type groups are shown in Figure 6.

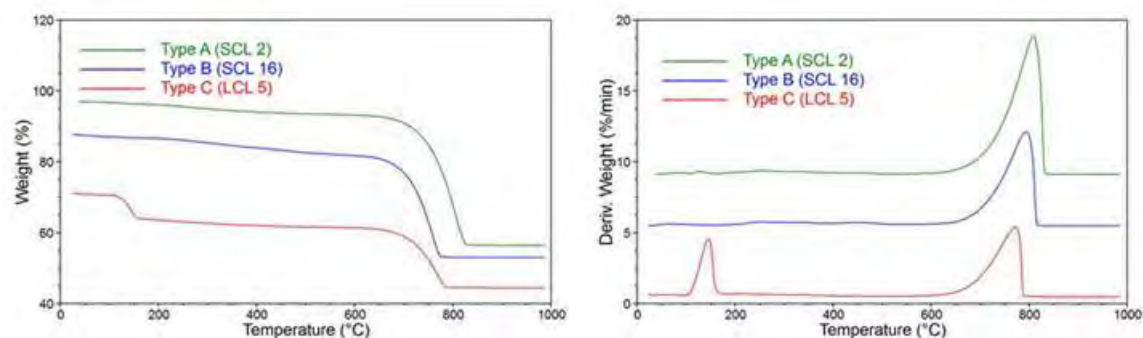


Figure 6. TGA (left) and DTG (right) curves of representatives of three categories of the binder enriched samples based on their thermal decomposition behaviour.

Weight proportions of gypsum ($\text{CaSO}_4 \cdot 2\text{H}_2\text{O}$) and lime (CaCO_3) were quantified based on the TG curve, Table 2.

Table 2. Proportions between lime and gypsum dehydrate based on TG.

		Category	CaCO ₃	CaSO ₄ ·2H ₂ O
Small decorations	SCL 2	A	83.4	2.4
	SCL 3	A	81.4	1.9
Fruit pieces – inner modelling mortar	LCL 3	C	38.4	30.0
	LCL 4	C	40.2	32.4
	LCL 5	C	38.2	32.9
	LCL 6	C	45.5	28.6
	LCL 7	C	33.6	41.4
Fruit pieces – outer stucco	SCL 9	A	75.5	1.4
Adhesive mortar I	JCL 1	C	42.5	39.0
	JCL 2	C	50.0	13.3
	JCL 3	C	20.7	72.4
Adhesive mortar II	LCL 1	C	42.3	40.0
	LCL 2	C	59.5	13.4
Bead mould	SCL 6	B	56.8	-
	SCL 15	B	63.0	1.9
Rib	SCL 7	B	61.2	-
First coat	MCL 1	B	42.2	-
Masonry mortar	MCL 2	A	70.9	-
	MCL 3	B	30.7	-
Older stucco	SCL 16	B	65.0	-

The analysed samples were not solely composed of binder but they also contained a certain amount of the finest fraction of aggregate. This amount was typically about 15 to 30 wt.% but exceptionally the TA results detected much higher contaminations, especially in samples MCL 1 and 3, where the higher weight loss between 200–600°C may be connected with the presence of a fine fraction. This was also confirmed by XRD-QPA analysis (Table 3) that determined the presence of quartz, albite, feldspar, mica and kaolinite.

Table 3. Mineralogical composition of samples analysed by XRD-QPA.

	Fruit pieces – inner mortar	Adhesive mortar I	Adhesive mortar II		First coat
Phase	LCL 7	JCL 3	LCL 1	LCL 2	MCL 1
Quartz	4.1	0.7	1.1	4.0	4.0
Calcite	29.4	19.1	37.4	53.5	35.7
Albite	1.9	0.7	2.3	3.7	13.9
K-Feldspar	1.7	0.2	0.1	1.8	2.4
Muscovite	0.7	0.4	0.5	0.8	4.5
Gypsum	41.2	66.7	38.7	13.7	-
Kaolinite	-	-	-	-	15.8
Chlorite	<0.2	-	-	-	-
Amorphous	20.4	13.0	19.8	22.5	23.6

The amounts of calcite determined by XRD-QPA were in proportion to the amounts of CaCO_3 determined by TA. However, XRD values were systematically lower and the difference with TA increased with the increasing amounts. The higher was this difference the higher was also the amorphous content suggesting that a certain amount of calcite/ CaCO_3 had not a fully developed crystallinity and was thus included under the amorphous phases.

Organic additives

Collagen proteins were identified in all analysed samples. Source of collagen is typically an animal glue which is traditionally used to modify the setting of gypsum (retard) and to influence its hardened performance [3]. In agreement with the expected, collagen was found in the lime-gypsum mortars, i.e. in the inner modelling mortar (LCL 5) and adhesive mortar II (LCL 1). However, collagen was also identified in the mortars without gypsum, like in the small decorations (SCL 2 - leaf, 3 -cherry), in the fruit piece outer stucco layer (SCL 5) and also in the older stucco decoration (SCL 16). Collagen was also confirmed only in the coating layers of the leaf (SCL 8) and the bead mould (SCL 6) samples. The analytical outcome confirmed a match of several protein chains which meant a higher reliability of the result.

An unsuccessful attempt to quantify the amount of collagen was carried by FTIR on five different samples (SCL 2, SCL 8, LCL 1, LCL 2, MCL 1), Figure 7. It seems that the amount of collagen in these samples was below the detection limit of this method, which is estimated to detect compounds above 5 wt.%.

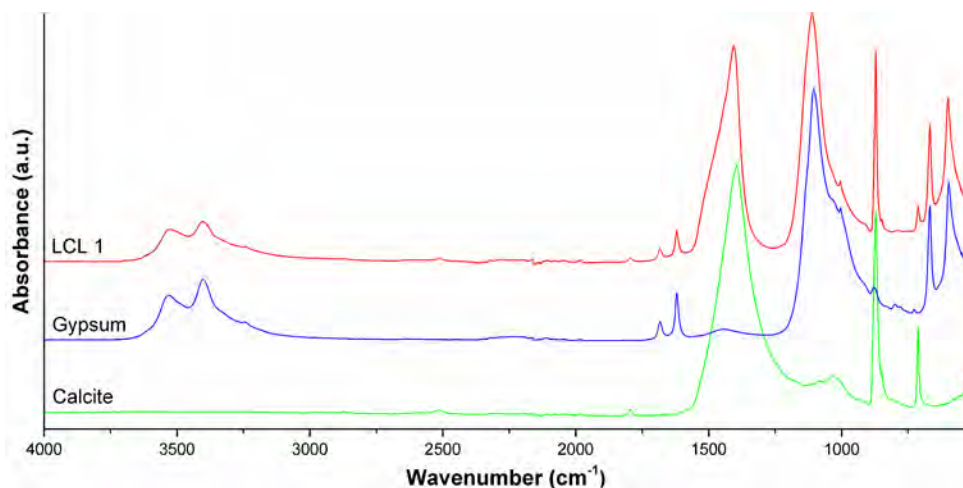


Figure 7. FTIR outputs showing the main compounds of the binder – gypsum and lime, sample LCL 1.

Mortar proportions and sand

Acid dissolution determined the amount of insoluble part and from this the binder to aggregate ratio was estimated, Table 4. The composition lime and gypsum proportions were based on the TA results. The following equations were used to calculate the

weight proportions of the sampled mortars (the amount of organic additives was neglected):

$$w_A = w_{IP}$$

$$w_{LP} = w_{SP} * \frac{74}{100} * w_{dry\ mass} * w_{CTA}$$

$$w_{PW} = w_{SP} * \frac{74}{100} * w_{CTA}$$

$$w_G = w_{SP} * \frac{145.15}{172.17} * w_{GTA}$$

Where:

w_A is mass fraction of aggregate in fresh mortar

w_{IP} is mass fraction of insoluble part

w_{PW} is mass fraction of lime powder in fresh mortar

w_{LP} is mass fraction of lime putty in fresh mortar

w_{SP} is mass fraction of soluble part

$w_{dry\ mass}$ is mass fraction of dry mass in lime putty (we used 0.5)

w_{CTA} is mass fraction of CaCO₃ in binder (sum of lime and gypsum) determined by thermal analysis

w_G is mass fraction of gypsum in fresh mortar

w_{GTA} is mass fraction of gypsum in binder (sum of lime and gypsum) determined by thermal analysis

Table 4. Acid dissolution results as weight ratios of aggregate and binder (slaked lime and gypsum).

	Sample	Insoluble part [wt.%] w_{IP}	Soluble part [wt.%] w_{SP}	Gauging ratio of sand : lime powder : gypsum ($w_A : w_{PW} : w_G$)	Gauging ratio of sand : lime putty : gypsum ($w_A : w_{LP} : w_G$)
Small decorations	SCL 2	50.9	49.1	1.4 : 1 : 0	0.7 : 1 : 0
	SCL 3-2	51.4	48.6	1.4 : 1 : 0	0.7 : 1 : 0
	SCL 4	35.3	64.7	0.7 : 1 : 0	0.4 : 1 : 0
	SCL 5	37.9	62.1	0.8 : 1 : 0	0.4 : 1 : 0
	SCL 8	44.0	56.0	1.1 : 1 : 0	0.5 : 1 : 0
Fruit pieces – inner mortar	LCL 3	66.2	33.8	4.7 : 1 : 0.9	2.4 : 1 : 0.4
	LCL 5	62.8	37.2	4.2 : 1 : 1.0	2.1 : 1 : 0.5
	LCL 6	62.1	37.9	3.6 : 1 : 0.7	1.8 : 1 : 0.4
Adhesive mortar II	LCL 2	58.0	42.0	2.7 : 1 : 0.3	1.4 : 1 : 0.1
Bead mould	SCL 15	74.9	25.1	4.0 : 1 : 0	2.0 : 1 : 0
Rib	SCL 7	70.0	30.0	3.1 : 1 : 0	1.6 : 1 : 0
First coat	MCL 1	76.4	23.6	4.4 : 1 : 0	2.2 : 1 : 0
Masonry mortars	MCL 2	77.1	22.9	4.5 : 1 : 0	2.3 : 1 : 0
	MCL 3	84.7	15.3	7.5 : 1 : 0	3.7 : 1 : 0

Mineralogy of the insoluble portions was assessed by OM and particle size distribution was determined by sieve analysis. Mineralogy was in agreement with the XRD results

(without carbonate components). Most of the sand samples consisted of quartz predominantly, less frequent were feldspars (albite and K-feldspar) and muscovite (Table 3). All studied samples contained fragments of orthogneiss. Increased proportion of feldspars (albite) and illite was typical in the samples MCL 1, 2 and 3 an. Observed minerals and aggregates were angular to rounded but some sharp-edged grains were also included. The studied sands had mostly light grey colour with red and orange tones. Exemptions were sands from masonry mortars (MCL 2 and 3). For sample MCL 2, brown-red colour is typical, sample MCL 3 is mostly light-red coloured.

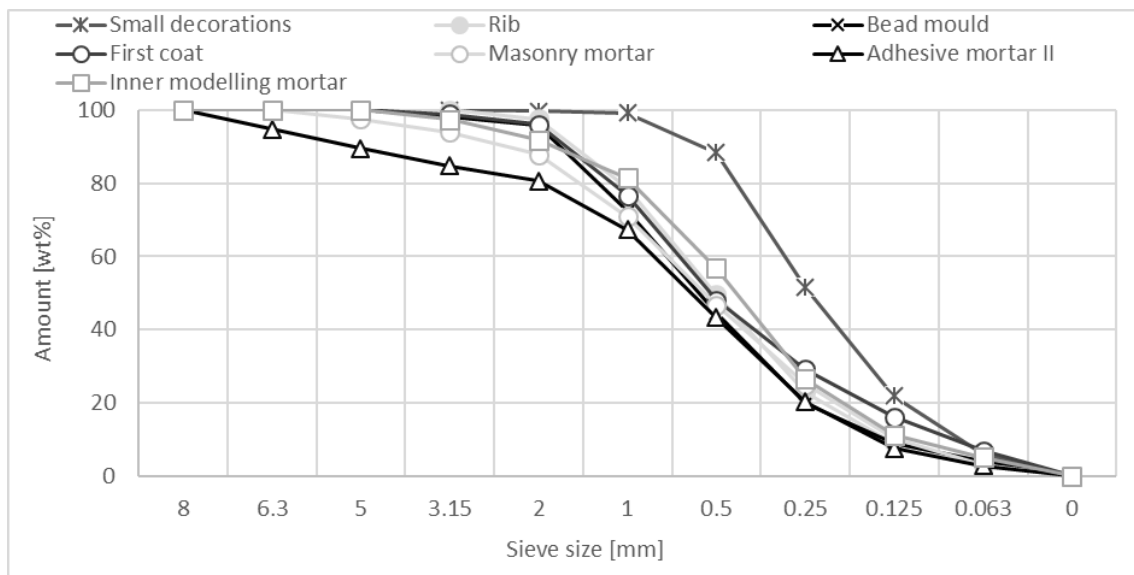


Figure 8. Particle size distribution of insoluble residue – examples of typical curves of the relevant sample groups.

The individual mortar groups differed in granulometry, especially in the maximum particle size. Small decorations (SCL 4, 5, 8) contained a very fine sand, max. grain size was about 1 mm, fine fraction (<63 μ m) varied from 5 – 10%. Sands of the rib (SCL 7) and the bead mould (SCL 15) samples had very similar grain size distributions, max. grain size was about 2 and 4 mm and the content of fine fraction was lower than 4%. The first coat (MCL 1) sample was similar to masonry mortars (MCL 2, 3) with its max. grain size about 4 and 6 mm but these sands significantly differed in the amount of fine fraction: 7% (MCL 1), 3% (MCL 2) and even 12% (MCL 3). The coarsest sand was from the adhesive mortar I sample (LCL 2), max. grain size was about 8 mm and fine fraction content was lower than 3%. The inner modelling mortars (LCL 3, 5, 6) differed slightly in their max. grain sizes (4 – 8 mm) but the grain size distribution and the fine fraction (about 5%) were very similar. Bulk densities were measured for three sand samples - SCL 8 1420 kg/m³, LCL 5 and 6 1560 kg/m³.

Discussion

The analyses confirmed that a mortar mixture with similar mixing proportions and properties was used for a particular layer or a part of decorative element. The mortar recipes thus corresponded to certain properties that were required from the mixture to serve the desired function. Understanding of this intended use and the specific behaviour can help to comprehend the historic application technique.

Lime-gypsum mixtures were used as the inner modelling mortar and both adhesive mortars due to their ability to set and harden fast. The TA, XRD and acid dissolution results showed that the mixing ratio of lime to gypsum and sand was relatively similar for all the analysed samples of the inner modelling mortars (taking into account the precision of gauging by volume at building site conditions). It seems that the mortar preparation formula was deliberately kept the same for the inner modelling mortar and was approximately 1 : 0.4–0.5 : 1.8–2.4 (lime putty : gypsum : sand) by mass. On the contrary, both adhesive mortars exhibited a higher variation in the proportion between lime and gypsum. A higher amount of gypsum would provide faster setting and stronger bond and this could have possibly been individually considered when the mixtures were prepared. To attach leaves and other small decorations rather small quantities of mortar would probably be prepared according to the actual work tasks and conditions. The aggregate was of a local origin. In all cases it was a siliceous sand with a similar mineralogical composition – quartz, feldspars and micas. It seems that the sand deposits with low clay content were preferred. The size of the grains was reduced by sieving according to the mortar application. The fresh properties were modified by the addition of animal glue diluted in water but its mass portion was not possible to quantify. It can be assumed that it was less than 5 wt.% which is the FTIR detection limit. A slightly higher amounts ~ 8 and 10.5 wt.% are mentioned in literature but only in connection with scagliola and painting base ground [3, 12].

The stucco mortar for small decorations and the outer stucco layer of fruits had a similar composition. This mortar was made only of lime and sand with approximate proportions 1 : 0.5 (lime putty : sand). The small amount of gypsum detected in some samples was most probably only an incidental contamination that occurred during mortar preparation. Sand was of the same quality as for the lime-gypsum mixtures and it was passed through a 1 mm sieve. Due to the lack of larger binder related particles, it seems that the binder was also passed through the same sieve.

Bead mould, rib and first coat mortars were composed of lime and sand without any addition of gypsum. The proportions ranged from 1 : 1.6 to 2.2 (lime putty : sand). They also contained sand with similar particle size distribution, grain shapes and mineralogy. However, the sand of the first coat sample MCL 1 contained a significantly higher amount of the fine fraction which also affected the colour of the mortar.

Bedding mortars from the two vaults (MCL 1 and 2) differed between each other by the mixing proportions and also by the quality of sand.

Animal glue was detected present not only in the mortars containing gypsum but also in the small decoration and bead moulding mortars. It was present also in the surface coating layers (samples SCL 8) suggesting that it was possibly used as a compound in the coating applied during the final finishing of surfaces.

The analyses have been carried out in order to re-discover the original mortar composition, technology of its production and the applied stucco techniques. The presented results show that it is possible to establish the main components of the mixes and their proportions. However, to reach this goal, each material must be characterised further from the technological point of view. For example, in the case of lime it is to specify its chemical composition and hydraulicity. Microscopy methods (optical and SEM-EDS) can be used to crosscheck the results of the other analytical methods and also to describe other specific features that can, to a certain extent, indicate the mortar production technology [13]. Of a particular interest are binder related particles, which applies, not only to lime but also to gypsum. Identification of provenance of the raw materials can help to their further understanding including also their processing technologies. Some research contributing to the above mentioned characterisation has been carried out but it is not part of this paper. The raw materials for lime production are assumed to be about 30 km north from the site, where there is a metamorphic limestone outcrop – marble with a high calcite content (above 95 wt.%). Similarly, also the sources of sand were traced locally. There are some deposits that correspond to the sand found in the analysed samples. Both of these two raw materials are accessible for sampling and can be used for an experimental replication of the studied mortars. The origin of gypsum is however less clear as there are no written records and natural gypsum does not occur in the vicinity of the site. The nearest potential deposits are south of Vienna about 220 km far from the castle.

In order to fulfil the aim of the re-discovering the original mortar composition and the working techniques applied there, the following key issues remain still open:

- provenance of gypsum and its burning temperature (production and processing technologies)
- effective use of gypsum with lime and animal glue
- processing of sand (depending on the available resources)
- processing of quicklime (dry or wet slaking, maturation)
- application techniques (production of lime-gypsum mortars with animal glue and their setting time, surface finishing techniques)

These open issues require a further analytical research. They can be also at least partially answered by building experiments, when adequate raw materials (matching the original ones) are acquired and processed by the contemporary historic production techniques. The resulting mortars are then assessed by the same analytical techniques as are used for the characterisation. This is actually the current stage of ongoing research where material experts work with practical conservators who have practical experience with the preparation and application of mortar, Figure 9.



Figure 9. Trial replicas of the fruit decoration made according to the analytical results. Lime binder was made from marble sampled at the original outcrop, burnt in a wood-fired kiln and processed by wet slaking following the historic procedures.

Concluding remarks

Stucco decoration from the Great Chamber of Červená Lhota castle was studied in order to design its optimal conservation procedure. Detailed survey and X-ray computer tomography of fruit pieces allowed categorisation of individual mortar groups and the analytical techniques confirmed that the mortars within one group had a similar composition. The main compounds – lime, gypsum, sand and collagen were identified and the original mixing formulas of lime to gypsum and sand were established. The composition of the stucco mortars had to be adjusted to meet practical requirements given by the particular application on site. Therefore, the relation between the properties of raw materials and their influence on performance can help to determine the optimal uses of the analytically rediscovered mortar formulas. The key issues to be answered in future by a following experimental programme should be related to the effects of animal glue and to the properties of gypsum calcined at low and high temperatures on a mortar mixture, namely on its setting time, plasticity, workability and hardening processes.

Acknowledgement

The research has been carried out with the support of the Czech Ministry of Culture as a contribution to a project DG16P02H012 – Lime materials for restoration and conservation of authentic elements of historic structures. The research interest was initiated by the restorers Zuzana Wichterlová and Jana Waisserová and underpinned by the site manager Tomáš Horyna.

References

1. Millar W (2010) Plastering plain and decorative. Re-edition, first published 1897, Taylor & Francis Ltd.
2. Beard G (1983) Stucco and Decorative Plasterwork in Europe. Thames & Hudson Ltd.
3. Elert K, Benavides-Reyes C, Cardell C (2019) Effect of animal glue on mineralogy, strength and weathering resistance of calcium sulfate-based composite materials. *Cement and Concrete composites* 96:274–283.
4. Mádl M (2013) Štukatéri v Čechách kolem Giacomma Tencally. Barokní nástěnná malba v českých zemích, Tencalla I. M. Mádl (ed), Artefactum, Praha.
5. Caroselli M, Cavallo G, Felici A, Luppichini S, Nicoli G, Aliverti L, Jean (2019) Gypsum in Ticinese stucco artworks of the 16-17th century: Use characteriaation, provenance and induced decay pheonomena. *Journal of Archaeological Science: Reports* 24:208–219.
6. Rampazzi L, Rizzo B, Colombo C, Conti C, Realini M, Bartoluci U, Colombini MP, Spiriti A, Facchin L (2008) The stucco decorations from St. Lorenzoin Laino: The materials and the techniques employed by the “Magistri Comanchini”. *Analytica Chimica Acta* 630: 91–100.
7. Teplý F (1935) Dějiny města Jindřichova Hradce. Vol. 1, issue 3, obec Hradecká, Jidřichův Hradec.
8. Fíla T, Kumpová I, Koudelka P, Zlámal P, Vavřík D, Jiroušek O, Jung A (2016) Dual-energy X-ray micro-CT imaging of hybrid Ni/Al open-cell foam. *Journal of Instrumentation* 11(01).
9. Földvári M (2011) Handbook of thermogravimetric system of minerals and its use in geological practice. Occasional Papers of the Geological Institute of Hungary, 213. Budapest.

10. Kuckova S, Cejnar P, Santrucek J, Hynek R (2018) Characterization of proteins in cultural heritage using MALDI-TOF and LC-MS/MS mass spectrometric technique. *Physical Sciences Reviews*.
11. Middendorf B, Hughes JJ, Callebaut K, Baronio G, Papayianni I (2005) Investigative methods for the characterisation of historic mortars - Part 2: Chemical characterisation. *Materials and Structures* 38, 771–780.
12. Salavessa E, Jalali S, Sousa LMO, Fernandes L, Duarte AM (2013) Historical plasterwork techniques inspire new formulations, *Constr. Build. Mater.* 48:858–867.
13. Elsen J (2006) Microscopy of historic mortars—a review. *Cement and Concrete Research*, 36-8:1416–1424.

Hot applied lime mortar – assessment of a traditional technique used in modern restoration

Thomas Köberle¹, Matthias Zötzl², Alexander Fenzke³, Heiner Siedel¹

(1) TU Dresden, Institute of Geotechnical Engineering, Dresden, Germany, thomas.koeberle@tu-dresden.de (corresponding author)

(2) Institut für Diagnostik und Konservierung an Denkmälern in Sachsen und Sachsen Anhalt e.V., Halle, Germany

(3) Freelance mason and restorer, Bad Marienberg, Germany

Abstract

Lime was one of the most important binder groups used for mortars in historic building activities and is often favoured in restoration work due to its mechanical and chemical compatibility to the historic structures. In the past, different methods of slaking were in use. One remarkable method is to slake and process the lime binder in one procedure. Thus, the heat development during slaking is part of the working process when the mortar is applied in this hot stage. The technique of hot applied mortar (HAM) is quite rare in use today. However, craftsmen assign unique properties to such hot applied mixtures, like better cohesion, fast setting and a slight expansion during the slaking process, which could prevent shrinkage. In addition, a higher initial strength and better salt resistance is postulated. This performance seems to be of interest for modern restoration work. To compare hot applied mortars with hot mixed mortars, which are normally used after they cooled down, test areas on a medieval wall from a monastery in Saxony were applied and evaluated during a one-year cycle. In addition, laboratory tests with the same mortar mixtures were conducted.

Introduction

Modern restoration work requires mortars which are compatible to the historic ones. Especially for pointing and render on outside walls or in salt contaminated areas a material is needed which gives enough strength to withstand climate and salt attack. Another demanding topic is building with uneven, often round boulders or construction of vaults in a short time. For that, mortars with fast strength development are wanted, otherwise progress in bedding is very slow because one has to wait till the mortar is strong enough to keep the next layer in place without collapsing. Often hydraulic systems are in use for such purposes, sometimes with the disadvantage that they contain cations that could lead to the formation of salt systems, which are harmful for the building. Modern restoration mortars with hydraulic additives show an

initial fast setting, what is needed, but develop to high mechanical strength, which is in the end not compatible anymore.

The latter leads to different thermal and hygric behaviour compared to the historic surrounding what as well could lead to damage in future. Thus, HAM might be an interesting alternative. Nowadays, the technique is not well established yet. There are just a few craftsmen who use it all over Europe. According to surveys in some European countries, for example Italy, Czech Republic and Scandinavia, it even seems to be unknown. A centre of practise is the United Kingdom and Germany, in minor Austria.

Although it is claimed by craftsmen that hot applied mortar (HAM [1], in German “Heißkalk”) is a technique which can be traced back to antiquity, namely to the work of Vitruv [2], this turned out to be a legend [3]. A first proven witness is the work of Lorient in 1774 [4]. He admixed powdered quicklime to a slaked lime mortar and used the resulting mixture in a warm state. Today, in hot lime technique applied by some craftsmen in Germany, powdered quicklime is used to prepare the mixture in a whole. The resulting temperature is higher compared to Lorient’s mixtures because of the highly reactive industrial fine powdered quicklime, which is not diluted by slaked lime. In the United Kingdom kibbled quicklime is more common. One reason is safety at work, because powdered quicklime always has the risk of airborne dust development which might harm the eyes of the worker. However, also in Germany, the selection of quicklime used is often limited by availability on the market.

The paper presents the results of a case study with different HAM mixtures in comparison to mortars which are hot mixed but applied after they cooled down, on salt contaminated historic stonework (see Figure 1) as well as accompanying laboratory tests.



Figure 1. Test wall in Buch, middle of Saxony/Germany

The test site and the test areas

The medieval Cistercian monastery in Buch, near Leisnig in the middle of Saxony/Germany, was founded in the late 12th century in a river sinuosity [5]. The monastic florescence of medieval time ended with reformation in 1527. In the following centuries, the monastery had a changeable utilisation, from education site for aristocrats to agricultural property. The last commercial use was as an agricultural production cooperative in the time of German Democratic Republic. Today just small parts of the former monastery buildings are left. They are maintained and used for cultural events by a non-profit association. From the beginning, the location, situated very close to a river, led to numerous flooding events. The most affecting one in the last decades was in 2002, when the whole area was nearly 2 m submerged.

All buildings on the convent area are made of rubble stone from nearby quarries. The stone is a highly welded ignimbrite (“porphyry”) from Permian time. All mortars are lime based with a remarkable magnesium content [6]. The walls, exposed to climate, show severe damages with losses of mortar and stone surfaces due to moisture and salt attack. The test area is a wall from the former main church of the monastery. This side was the exterior, towards the former covered cloister. Today the wall is completely free of render or harl but it is to assume that it was at least in medieval time, during the active period of the monastery, covered with a render. In some parts the wall shows deep gaps where the bedding mortar is eroded. In Figure 2 a small area of the wall is presented. The rubble stone of different size and shape dominates and joints are more or less filled with mortar. Some of the joints are 20 cm deep and up to 7 cm wide. With mortar made out of lime putty or with hot mixed mortar it is difficult to fill in one-step because the mortar runs out of the joints if not fixed with additional pieces of rock. With HAM, it is possible to fill these gaps in one-step, especially when a mixture with pumice or brick sand is used.

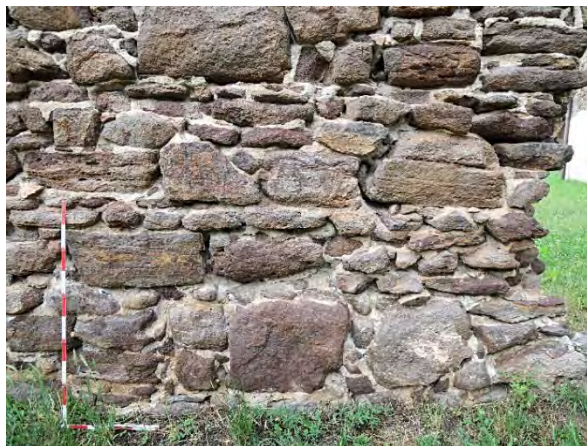


Figure 2. Part of the test wall with rubble stone of different size and shape and joints in parts deeply eroded

In Figure 3 a trial with a H3 mixture on a wall can be seen. The folding meter documents that the layer, which was applied at once, is 13 cm thick. It sticks to the wall and sets in less than a minute.



Figure 3. Hot applied mortar (HAM) in mixture H3, with pumice, allows a thick package of mortar applied in one step because of very fast setting

Materials and methods

For the experiments in laboratory and on test site, practical proven standard mixtures were used. Based on a sand/quicklime mixture (1) that was applied for laboratory tests as well as on the test areas, some parts of sand are occasionally replaced by brick sand (2) or pumice (3) for further laboratory tests. In Table 1 the three mixtures are given, either used hot, while slaking (with the abbreviation “H”) or cold, four weeks after hot mixing (named “C”).

Table 1. Three mixtures for hot application (H1-3) and for cold application after hot mixing (C1-3) in laboratory tests and for test areas

	sand	brick sand	pumice	quicklime	water
bulk density [g/cm ³]	1.35	1.07	0.93	0.87	
mixture	volume parts				
H1 or C1	5	-	-	1	2
H2 or C1	2.5	2.5	-	1	2
H3 or C1	2.5	-	2.5	1	2

All contents are given in parts per volume, what is common on construction site. The bulk density is also given, but it has to be accented that density was measured in an earth-moist condition, of course except this of quicklime. The sand substitutes accelerate the setting time and should lead to higher strength and additional salt resistance.

A local silicate sand with an aggregate size from 0 to 4 mm was used. The brick sand is a commercial available recycling product from brick production also with an aggregate size from 0 to 4 mm, the same with the natural pumice from Eifel/Germany. For binder a powdered quicklime (Schaefer Precal S30: CL90Q, R5, P1 according to DIN EN 459-1:2015-07 [7]) was used. The aggregates for the test areas were stored outside, so they contain the natural humidity. For laboratory samples the water content of the earth-moist aggregates was measured following standard DIN EN 1097-6:2013-09 [8] and then added to the dried substrate. Especially for laboratory work the adjustment of humidity in aggregates is essential. The setting time is mainly driven by the water content of the system [9]. In Table 2 the natural water contents of the earth-moist aggregates used on-site for the test areas are given.

Table 2. Water content of the earth-moist aggregates

substrate	water content [wt-%]
sand	5.2
brick sand	11.0
pumice	21.0



Figure 4. Wooden box covered with a thick plastic foil to prepare a hot mixed mortar in a sand-quicklime sandwich technique

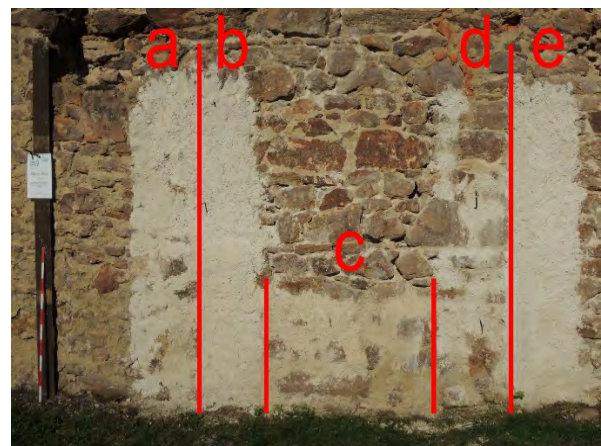


Figure 5. Test area at the historic wall with the applied mortar mixtures

In a first step, a batch of hot mixed lime was prepared for later “cold” application on the test area (4 weeks before the test started), see Figure 4. In a wooden box, sealed with a thick plastic foil, 5 parts per volume of sand and one part of quicklime were placed in layers. For this hot mixed mortar a more granular form of Precal S30 was used, a Precal 21S (R5, 10-50mm grain size). The sand was split in two volumes and the first was placed to the bottom of the box, then the lime was filled in and covered with the second part of sand. For slaking the batch, 2 parts per volume of water were added and then the box was covered with the foil to mature.

For HAM preparation – on site and the same for laboratory tests - first 2.5 volume parts of sand are measured in a heavy duty basket (normal baskets do not withstand the high temperature). Then quicklime is added and covered either with another 2.5 volume part of sand or (for additional laboratory tests) by brick sand or pumice. With a single paddle mixer the mass is quickly homogenised. In this state the first slaking reaction starts because of the earth-moist condition of the aggregates. After a first quick mix the water is added at once and mixing continues. The water content in this stage is very high so a liquid slurry is the result and mixing works without agglutination of aggregate and binder. Moreover, the maximum temperature of the system is reached in this stage: measured temperature was up to 80°C, what means a boiling slurry. Due to slaking and water uptake the mortar stiffens very quickly. Workability is reached within seconds, and after some minutes and in some cases even quicker the mass is consolidated and not workable anymore. The processing time is ruled by the mixture, water content, the temperature of ingredients and the stirring time. For this reason, especially when working with HAM on site with unknown sand and quicklime brands, foregoing tests to adjust water addition in a fixed stirring time, are essential. Time of workability in the given mixtures differs from 100 seconds to 30 hours, depending on the water content. For that a standardised mixture is essential to compare results [9].

In Figure 5 the test area is displayed. It was divided into 5 parts. The used mixtures (Table 1), the restoration intention and the respective surface treatment are given in Table 3.

Table 3. Mortar mixtures and intended surface of the different fields in the test area

Name	Mortar mixture	Restoration intention / surface treatment
a	H1	fill open joints and level the surface
b	H1	Close surface with a roughcast
c		Area is not topic of this publication
d	C1	fill open joints and level the surface
e	C1	Close surface with a roughcast

Prisms of standard size (4 x 4 x 16 cm) were prepared for all mixtures given in table 1 to measure the compressive strength development according to the standard DIN EN

1015-11 [10] (exception to standard: load was path-controlled: 2mm/min) after 7, 28, 90 and 360 days of storing in a constant climate of 20°C and 65% relative humidity. Moreover, prisms of the same dimension were prepared for testing the salt resistance of HAM mixtures H1, H2, and H3 after a 90 days storage in constant climate (see above). The detailed procedure for accelerated salt crystallization tests is given with the results below.

Safety instructions

For all who work with lime safety regulations are important to know (see compilation in [11]). First step is a documented risk assessment which covers all hazards on site, not only the work with lime. In case of working with quicklime special danger has to be pointed out. This is on one hand the risk of alkali burn, especially of the eyes and second incineration due to high temperature (approximately up to 80°C). For all this additional risk precaution has to be carefully worded. Help can be found in the safety data sheet which has to be offered by the supplier of the quicklime raw material according to REACH regulations. In case of working with powdered quicklime main focus has to be on protecting the eyes. For all work with quicklime in a powdered state special closed safety goggles, which protect against chemical splashing and the impact of airborne dust (for example according to ANSI Z87.1-2015 [12]) has to be worn. Contact lenses should not be worn when working with quicklime. Also nitrile gloves are recommended instead of leather gloves. In case of an accident with airborne dust that reaches the eye action of flushing the eye to remove the particles has to be started as soon as possible. A commercial available eye-cleaning solution would be most appropriate, but also water or even beer or milk is possible [13]. Most important is to react immediately with extensive rinsing before searching for the eye-cleaning solution or distilled water. Take note that because of extreme pain a first reflex is to close the eye. For rinsing it has to be opened as wide as possible, something what should be practiced by the user regularly.

Preliminary investigations and first evaluation of test areas

Preliminary investigations of wall masonry were undertaken to analyse the content of moisture and salinity. Follow-up examinations were carried out after a one-year cycle. For salt and moisture analysis, drill powder samples were taken on the test area (Figure 6) by a 12 mm spiral driller from different depths (0-2 cm from the surface for salt analysis; 0-2, 2-4, 4-15, 15-30 and 30-45 cm from the surface for moisture analysis) and at different heights, respectively (45/55, 135 and 200 cm above the ground). Moisture content was determined by weighing the humid powder and the oven dried one (105 °C). Determination of soluble contents of K^+ , Ca^{2+} , Mg^{2+} , SO_4^{2-} , Cl^- , and NO_3^- were carried out by photometrical analysis of water eluates from the drill powder

(HACH DR/2000); Na⁺ was determined by the HACH Sension 2-method. Salt efflorescence was analysed by X-ray diffraction (Siemens D5000).

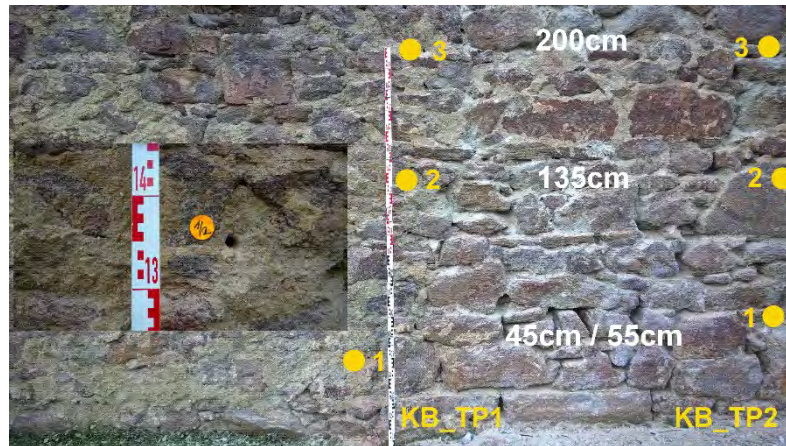


Figure 6. Test area at the historic wall with sampling points for salt and moisture investigations

In the base area between 45 cm and 55 cm above the ground, the depth profiles showed the highest values of moisture suggesting a high water saturation in the entire cross section (Figure 7 and 8). At a height of about 130 cm and 200 cm, the moisture decreases to lower contents. Conspicuously, some profiles show a slightly increased humidity near the surface due to hygroscopic salts. The salt analyses display a high salt contamination with sulphates and nitrates and low chloride values. XRD analyses performed on two efflorescence salt samples (taken at different heights) show gypsum as well as highly hygroscopic potassium nitrate and magnesium sulphate hydrates such as hexahydrate ($\text{MgSO}_4 \cdot 6 \text{H}_2\text{O}$) and epsomite ($\text{MgSO}_4 \cdot 7 \text{H}_2\text{O}$).

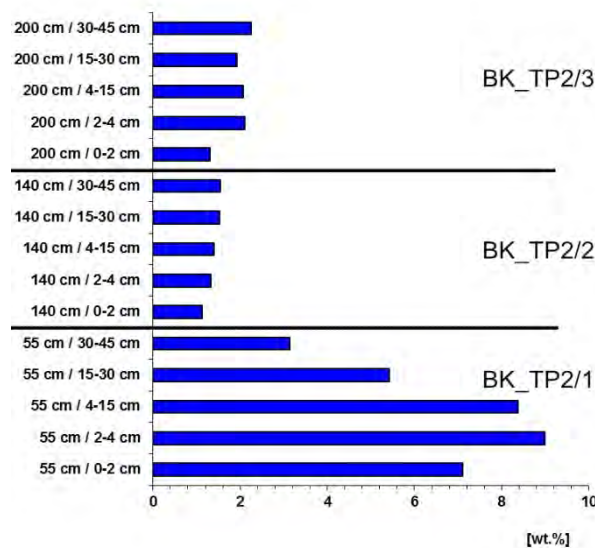


Figure 7. Moisture distribution in profile 1.

The damaging potential of magnesium sulphate hydrates is well-know from many other case studies in the region [6]. Thus, the selected wall with the test areas

represents a typical situation of moisture and salt loaded masonry, which offers the opportunity to evaluate HAM with respect to their durability.

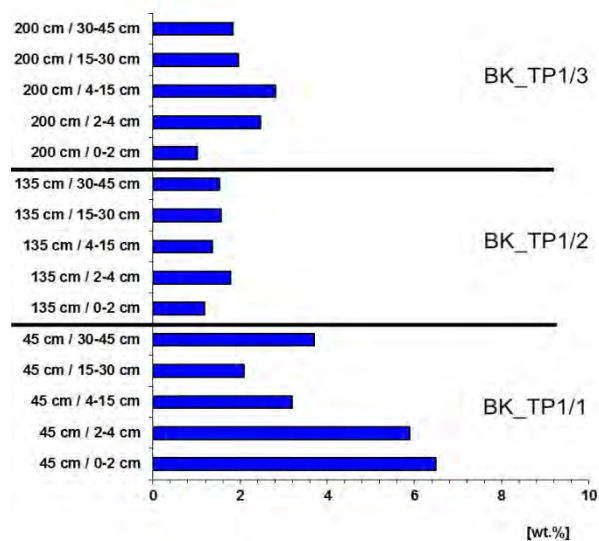


Figure 8. Moisture distribution in profile 2.

Table 4. Results of the chemical salt analyses in wt.-%

Sample /height level / Sample depth	Results of the chemical salt analyses in wt.-%						
	Ca ²⁺	Mg ²⁺	K ⁺	Na ⁺	SO ₄ ²⁻	Cl ⁻	NO ₃ ⁻
KB_TP1_1 / 45 cm / 0-2 cm	<0.01	0.195	0.413	0.057	0.53	0.03	0.40
KB_TP1_2/ 135 cm / 0-2 cm	0.25	0.092	0.297	0.064	0.46	0.12	1.78
KB_TP1_3/ 200 cm / 0-2 cm	0.08	0.129	0.036	0.023	0.46	0.06	1.14
KB_TP2_2/ 135 cm / 0-2 cm	<0.01	0.230	0.145	0.039	0.40	0.12	1.48
KB_TP2_3/ 200 cm / 0-2 cm	0.03	0.125	0.055	0.010	0.43	0.04	0.60

To compare the stability to moisture and salt influence of the HAM (mixture H1) and hot mixed, cold applied mortars (mixture C1), first follow-up examinations were performed after one year. Again, drill powder samples were taken at different height levels comparable to the preliminary investigation. As a result, an accumulation of damaging salts is observed in both HAM (H1) and hot mixed, cold applied (C1) mortar surfaces. Especially highly soluble niter (KNO₃) is enriched in mortar surfaces, whereas the other components show lower contents. Salt efflorescence was not determined on any surface. The surfaces of both HAM and hot mixed, cold applied mortars are visibly not affected by salt decay and show no serious damage or loss of material so far under the conditions described.

The brush test, a simple field test adopted from the field of stone conservation, where it is used to assess the intensity of granular disintegration of vertical stone surfaces, was performed in order to compare both mortars [14]. The test is not really suitable for rough surfaces with larger aggregates. However, taking into account possible errors, it offers a possibility of comparison. Thereafter, these comparative tests were

carried out on all test area at height levels from 60 cm to 70 cm and from 160 cm to 170 cm by brushing an area of 10 x 10 cm. The brushed material was collected and then evaluated gravimetrically. The areas sampled at the lower base area show relative intense sanding compared to those at higher level.

Conclusively, one year after application, the examined test areas with HAM (H1) and hot mixed, cold applied mortars (C1) show no significant differences in their weathering resistance yet. Further investigations shall follow up the development of the test areas in the next years.

Test on salt resistance

To evaluate the salt resistance of hot applied mortar in a short time period a laboratory test program with harsh conditions was planned and carried out. Mortar prisms of the mixtures H1, H2, and H3 were placed in plastic boxes, filled with 200 ml of salt solution. According to the test site findings, magnesium sulphate was chosen. For the test, solutions of 2.5 %, 5.0 %, and 10.0 % of a saturated brine were used. For all concentrations the results are comparable. In Figure 9 the test results after 60 days are demonstrated for the 2.5 % solution.

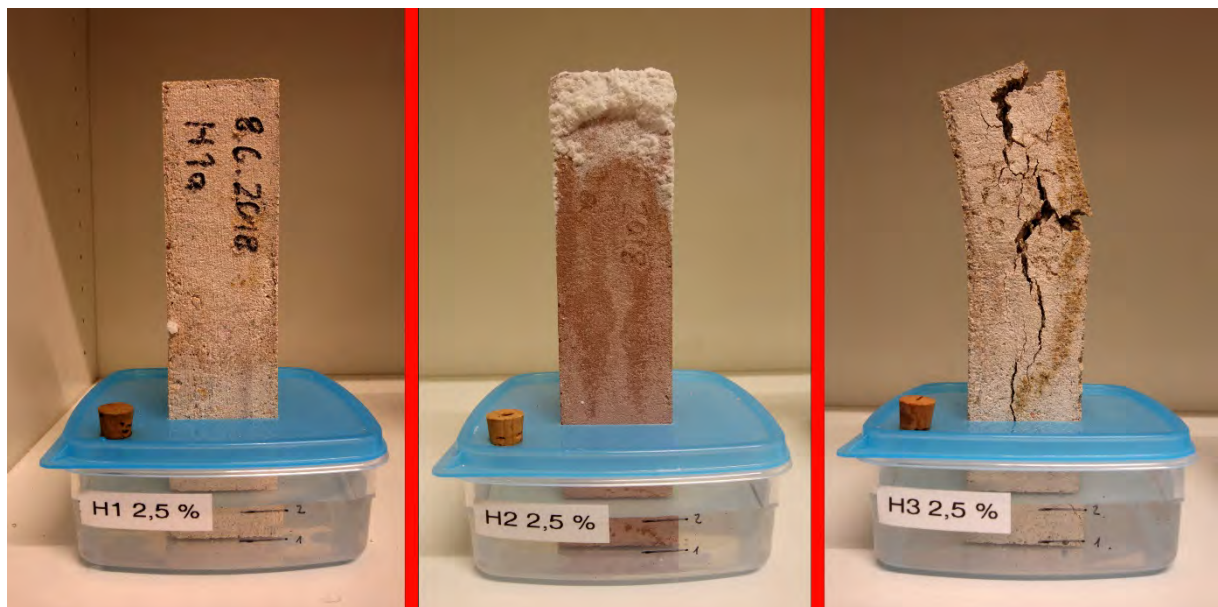


Figure 9. Mortar prisms of hot applied mortars with different mixtures in a 2.5% magnesium salt solution after 60 days

The salt solution evaporates on the surface of the prism. The boxes are covered with a plastic lid to prevent additional evaporation. The evaporated solution is refilled regularly with solution of the same concentration. Although the prisms are stored in a constant climate with 20°C and a humidity of 65% (+-5%, according to DIN EN 1015-11 [10]) they show different phenomena after 60 days. In mortar H1 no cracks or loss of the surface can be detected. It seems to be intact. In addition, efflorescence is nearly

absent. Mortar H2 has a big crust on the top of the prism but also no damage. On the contrary, mortar H3 shows no efflorescence, which is comparable to H1, but has the highest grade of decay. These phenomena can be compared with the water uptake and the evaporation rate and parallel with the salt enrichment. In figure 10 the water uptake and the sum of accumulated salt after 60 days are presented for every mixture.



Figure 10a+b: diagram with evaporated salt solution after 60 days and table with the accumulated salt content

In diagram 10a a linear progression of water uptake during the 60 days is visible. The small aberration from the regression line can be explained by imperfections during filling with salt solution. There is neither a fast uptake at the beginning nor a decelerated uptake towards the end of the experiment because of blocking the pores with salt efflorescence. Uptake of salt solution is lower in mixture H1 compared to mixture H3 with resulting different salt accumulation (Figure 10b). In the mortar mixture H3 8.0g of magnesium salt is accumulated, which means an average salt load of 2.1 wt-% in the mortar. The conclusion for practice of the salt experiment is, that the hot applied mortar can be adjusted to the needs of the craftsman. If a long lasting, durable mortar with a moderate water uptake is wanted, mixture H1 is to favour. If salts should be transported to the surface to be removed i.e. by brushing, mixture H2 is to recommend. If the mortar is used as a sacrificial render with highest performance in water uptake and best in salt accumulation, in a short period, mixture H3, also the “lightweight” under the compared mortars, is to prefer.

Test of compressive strength

The results of compressive strength tests on HAM mixtures in comparison to those of hot mixed mortars used cold are given in Figure 11. For each measurement three samples per mixture were tested, the average results of which are presented. The hot applied mortars H1-H3 are displayed in continuous lines, the hot mixed and cold applied ones in dashed lines. Values after 7 days storage could only be obtained for HAM mixtures. The same mixtures used cold (C1) were not set enough to be removed from the mould. If strength of 28 days is considered, one can see that HAM in all

mixtures (H1-3) shows higher values compared to the same mixture used cold. The same is evident for the measurement at 360 days.

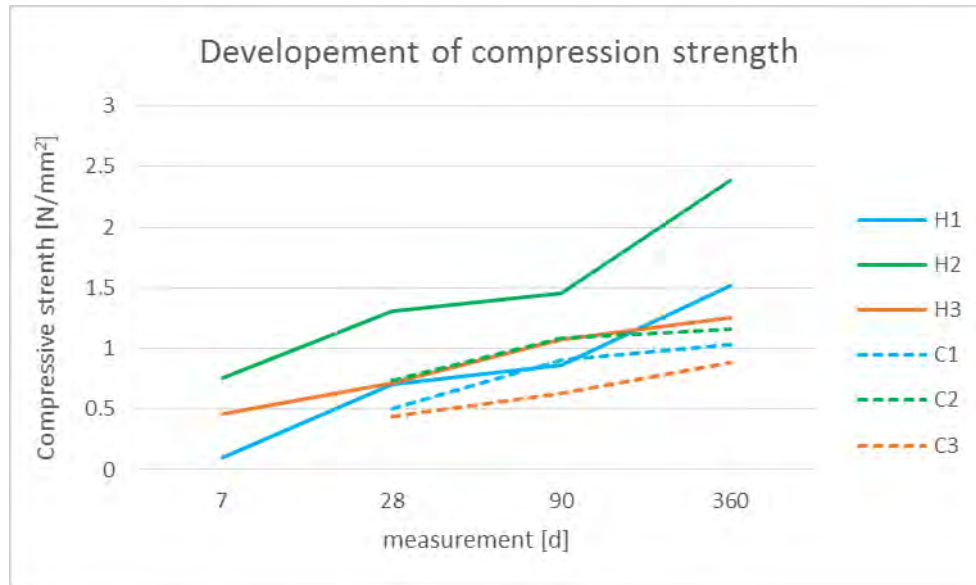


Figure 11. Diagram of compressive strength measurement of HAM and Hot-mixed mortars

As a conclusion of the compressive strength measurements, one can confirm the empirical observations of the craftsmen. HAM shows a much faster strength development and in the end is also stronger compared to the cold applied mixtures.

Conclusion

Hot applied mortar (HAM) is an alternative to hot mixed mortars, although they are both pure lime based mortars. The difference is in the slaking method and from that there are different properties. HAM offers an advantage with a good adhesion (see Figure 3), fast setting rate (see 7 days value in Figure 11) and slightly higher strength (see 360 days value in Figure 11). Especially the fast setting allows a more quick working progress when deep holes in a wall are to close or bedding with rubble stone in a wet environment has to be carried out. The higher strength develops especially at the beginning but is present also after one year. Compared to hydraulic systems compressive strength is moderate. This modern technique, by using powdered quicklime, offers an additional way to work with lime, for very special needs. Research to this technique is at the beginning and should be continued. Especially the admixture of porous aggregates and the water content should be in the focus.

Acknowledgment

The binder for the research project was kindly donated by SCHAEFER KALK GmbH & Co. KG / Dietz Germany (Sales Manager H.-G. Brendl). Thanks are due to the German Environmental Foundation for financially funding this study (Az 33877).

References

1. Abbreviation was coined by Dipl.-Ing. (FH) R. Wacha, Mauerbach/Austria.
2. Laube, A.-S. (2018): Studien zur „Heißkalktechnik“ auf Grundlage von Expertenbefragungen – not published module essay at the University of Fine Arts Dresden, pp 1-145.
3. Henke F. & Thiemann, L. (2014): Vitruv über Stuck und Putz – in: Firmitas et Splendor; Vitruv und die Techniken des Wanddekors, Studien aus dem Lehrstuhl für Restaurierung, Kunsttechnologie und Konservierung TU München, pp 13-125.
4. Lorient, A. J. (1774): Mémoire sur une découverte dans l'art des batir – Paris, De l'Imprimerie de M. Lambert, rue de la Harpe, près Saint Côme, pp 1-47.
5. Delang, S. (2006): Geschichtlicher Überblick - in: Das Zisterzienserkloster Buch, Arbeitshefte des Landesamtes für Denkmalpflege Sachsen, Sax Verlag Beucha, pp 7-17.
6. Siedel, H. (2013): Magnesium sulphate salts on monuments in Saxony (Germany): regional geological and environmental causes. Environ. Earth Sci, 69, pp 1249-1261.
7. DIN EN 459-1:2015-07: Building lime – Part 1: Definitions, specifications and conformity criteria; German version EN 459-1:2015.
8. DIN EN 1097-6:2013-09: Tests for mechanical and physical properties of aggregates – Part 7: Determination of the particle density of filler – Pycnometer method; German version EN 1097-7-2008.
9. Gschlecht, S. (2018): Der Erstarrungsprozess von Heißkalk-Frischmörteln – Erarbeitung eines Messverfahrens. Not published module essay at the University of Fine Arts Dresden, pp 1-71+54.
10. DIN EN 1015-11: 2007:05 -Methods of test for mortar for masonry –Part 11: Determination of flexural and compressive strength of hardened mortar;German version EN 1015-11:1999+A1:2006.
11. Artiz, R. (2018): Specifying hot-mixed lime mortar - Historic Environment Scotland technical paper, No 28, pp 16-17.
12. ANSI Z87.1-2015 - American National Standard for Occupational and Educational

Personal Eye and Face Protection Devices.

13. Schrage, N. (2016): Augenirritation und Augenverätzung - in: Verbrennungschirurgie, eds.: Lehnhardt, M.; Hartmann, B.; Reichert, B. Springer Berlin Hamburg, pp 307-321.
14. Bläuer, C.; Franzen, C.; Vergès-Belmin (2012): Simple field tests in stone conservation - in: Proceedings of the 12th international congress on the deterioration and conservation of stone, New York 22-26 October 2012, pp 1-9.

Preliminary research on potential raw material sources for dolomitic lime mortars at St. John's convent at Müstair, Switzerland

Giovanni Cavallo¹, Marta Caroselli¹, Albert Jornet¹, Patrick Cassitti²

(1) *University of Applied Sciences and Arts of Southern Switzerland (SUPSI), Institute of Materials and Constructions (IMC) giovanni.cavallo@supsi.ch, marta.caroselli@supsi.ch, albert.jornet@supsi.ch*

(2) *Foundation Pro Monastery of St. John, patrick.cassitti@muestair.ch*

Abstract

The Benedictine convent of St. John at Müstair (UNESCO world heritage site) in Grisons, Switzerland, preserves a huge amount of well-documented (dolomitic) archaeological mortar samples dated from the Carolingian to the Baroque Age (8th to 18th century). In the medieval period, the architecture of the Val Müstair and the surrounding regions was characterized by stone and mortar constructions. The geological overview of the area around the monastery indicates that dolomitic rocks are widely available and the production of lime was a common practice in the Müstair valley as demonstrated by the presence of mortar mixers, lime-kilns and local toponyms.

As part of an ongoing research project, the question about the potential source(s) of the raw materials for the production of the binder of the historic mortars was posed. The proposed research is based on the close relationship between the geological raw materials and the underburnt relics (lime lumps) found in the archaeological mortars.

Textural features and mineralogical composition were investigated by combining Polarizing Light Microscopy (PLM) and X-ray Powder Diffraction (XRPD) analysis.

Results indicate that the textural evidence (sometimes) retained by underburnt relics of dolomitic rocks cannot be used as possible criteria for provenance studies due to the high variability of dolomite crystal size, fabric and heterogeneity within the same group and at the scale of individual samples. However, the presence of silicate phases may suggest potential proxies.

1. Introduction

The monastic site of St. John in the Swiss canton of Grisons was founded in the last quarter of the 8th century. The complex then underwent significant changes, and most of the original complex was subsequently replaced by newer structures. Thanks to decades of archaeological research at the site, the construction history of the monastery is well-known [1]. Over the centuries, buildings were torn down and new

ones added, so that today the site preserves structures from across 12 centuries, dated from around 775 AD to the present. Since the beginning of research activities at the site in 1969, over 5000 mortar samples from all construction periods have been collected. This provides a unique basis for the study of historic mortar production and building techniques. Since 2017 the project “Mortar Technology and Construction History at Müstair Monastery”³ has been looking at these questions by applying an interdisciplinary approach to the study of the site, its mortar samples and construction history, as well as the region around it.

The ongoing research project offered the possibility for an in-depth study of the raw materials used for the design of the mixes used in mortar production through the centuries, focusing on the provenance of those used for lime production. There is evidence of the use of dolomitic lime in Carolingian mortars [2, 3] and painted Romanesque plasters [4]; in addition, the presence of dolomitic rock formations very close to the monastery sets ideal conditions for such research.

Provenance studies are based on the textural and mineralogical relationship between raw materials used for lime production and underburnt relics (lime inclusions or lime lumps) in archaeological mortars. Petrographic examination of lime inclusions in historic mortars from Scotland and Belgium [5] provided clues for the limestone provenance thanks to the presence of relics or pseudomorph textures of the original rock. In addition, underburnt fragments may also provide information about the hydraulicity of the lime as for the Notre-Dame Cathedral in Tournai, Belgium [6-7]. The use of marble for quicklime production used for the Leaning Tower of Pisa, Italy [8], is assumed on the basis of the close vicinity and availability of quarries, even if no textural and geochemical data support this evidence. The vicinity of limestone sources and the presence of a fragment of raw material in the thin section are the only (weak) arguments for demonstrating the provenance of ancient Indian lime [9]. The proximity of the limestone outcrop is the criterion for assessing the provenance of the carbonate raw materials used for the mortars and plasters of the Roman villa in ancient Stabiae in Naples, Italy [10]. The presence of tufa fragments in Roman mortars collected from several places in La Rioja, Spain [11] is advocated as possible raw material evidence for making lime. Finally, the provenance of raw materials for dolomitic and calcitic lime production in the post-Cistercian abbey in Kamieniec Ząbłowski (Poland) was inferred combining archival, historical, geological and petrographic evidence [12].

The aims of this manuscript are the following: i. to investigate the possibility to make a clear distinction between the diverse dolomitic rock groups outcropping in Müstair valley on the basis of their specific textural characteristics and fabric features; ii. to correlate the petrographic features of the raw materials with those of the lime

³ Financed by the Swiss National Fund, the Foundation Pro Monastery of St. John and the Biosfera Val Müstair.

inclusions found in the archaeological mortars; iii. to understand the role that accompanying minerals could play as distinctive (silicate) phases; iv. to identify toponyms referring to lime-burning activities in the Müstair valley and correlate them with potential quarrying sites.

2. Geographic and geological overview of the area

The Müstertal (Convent Valley) lies within the domain of the Austroalpine nappes, in the southeast of the Swiss canton of Grisons, in close proximity to the border with Italy (Figure 1). The valley is oriented approximately from west to east and is traversed by the Rom stream. Its most important tributaries are the streams Aua da Vau (which descends through the Val Vau), Muranzina (Val Muraunza) and the Valgarola (Val d’Avigna). The first two tributaries flow from the south and southwest, while the third comes from the north. Behind the Val Vau there is another valley easily accessible from the Müstair valley, the Val Mora, but the stream running through it, the Aua da Val Mora, empties northwards into the Inn river.

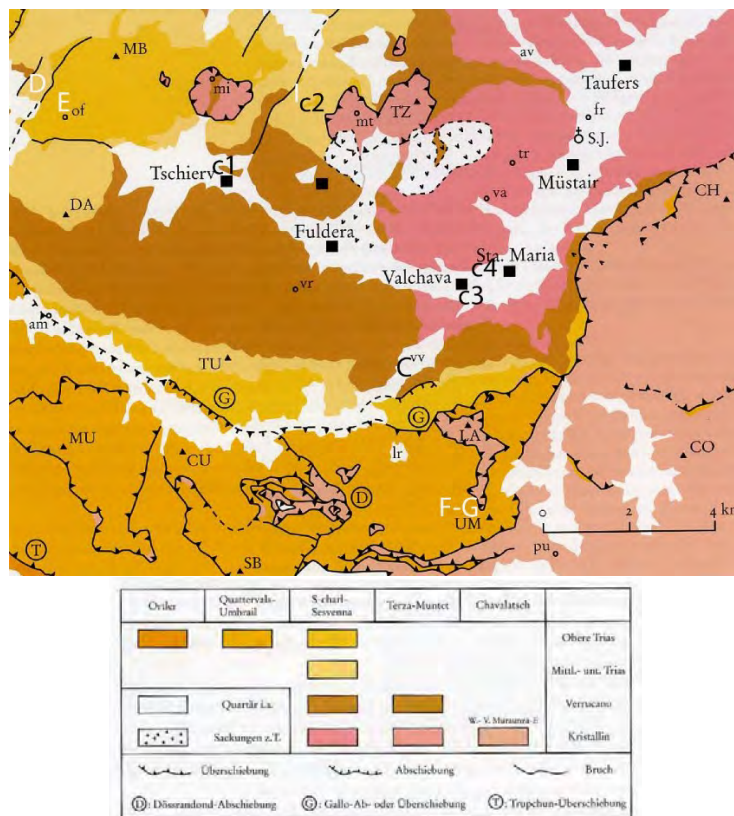


Figure 1. Schematic geological view of Müstair valley (by Trümpy, 2007). Capital letters from C to I indicate the geological sampling areas; c1-c4 notations the historical lime-kilns (CH Piz Chavalatsch; CO Piz Costainas; CU Cuclèr da Jon dad’Onsch; DA Piz Daint; LA Piz Lad; MB Munt da la Bescha; MU Piz Murtaröl; SB Piz Schumbraida; TU Piz Turettas; TZ Piz Terza/Urtirolaspitz; UM Piz Umbrail; am Alp Mora; av Val d’Avigna; fr Fradetssch; lr Lai da Rims; mi Minschuns; mt Muntet; of Ofenpass; pu Pass Umbrail; tr Taunter Ruinas; va Vallatscha; vr Val Ruina; vv Val vau. † S. J. St. John’s Monastery).

The area North of Val Mora, Val Vau and the lower Val Müstair basically is composed of Permo-Triassic sediments from the S-Charl-Nappe and their basement, the Sevenna

and Münstertal crystalline. The southern chain area concerning Piz Murtaröl, Piz Schumbraida, Piz Umbrail, Piz Chavalatsch, is characterized by several thrust nappes, the Quattervals and Umbrail nappes made of mainly dolomitic rocks and the Chavalatsch nappe made of crystalline rocks [13].

3. Materials and methods

Potential quarrying sites and historical locations of lime kilns were identified by studying the geological and topographical maps of the Swiss Federal office of Topography and then carrying out field surveys. The toponym “chalchera” in the official cadastral surveying plans was used as an indicator for the locations of historical lime kilns. In order to qualify as a potential quarrying site, dolomitic rock outcrops had to be easily accessible by path or road. The sites were then compared to the locations of potential quarrying sites, in order to determine methods of selection and transport of raw materials.

Samples of dolomitic rocks were collected in the southern and northern sector of Münstertal, corresponding to the Upper Austroalpine domain (*Engadiner Dolomiten*). The places where samples come from are reported in Figure 1 and a description is provided in Table 1, including the analytical techniques used.

Mortars of different periods were selected and their binders analysed in order to detect the nature of mineralogical phases correlated with dolomitic raw materials.

The binder of the archaeological mortars was separated by sieving. The samples were broken in a plastic bag using nipper pieces to avoid fine splinter of the aggregate. The crushed material was vibrated in a sieve series. The grain-size fraction <63 µm was chosen for all the samples, except the sample 6577 (fraction <45 µm).

The mineralogical analysis of the mortar binders and of geological samples was carried out using X-ray Powder Diffraction (XRPD). After grinding in an agate mortar, randomly oriented samples were prepared and deposited in the hollow of a Si monocrystal zero-background plate, supplied by Assing spa, Monterotondo, Italy. A Rigaku Miniflex system, operating in $\theta:2\theta$ mode was used; generator setting 30 kV, 10 mA, Cu anode (Cu $K\alpha = 1.5418 \text{ \AA}$), Ni filter, 2θ range 5-55°, step size 0.02°, scan speed 0.3 ° min⁻¹. Qualitative phase determination was carried out using the software QualX2.0 [14] and the correlated COD database [15].

Polarized Light Microscopy (PLM) on thin sections of (archaeological and geological samples; except sample C-04 which requires thin section preparation using staining techniques) was carried out for mineralogical and textural analysis; a Zeiss Axioskop 4.0 Polarizing Light Microscope (PLM) was used and micrographs were acquired with a digital camera, and processed with the software Axiovision (Zeiss, release 4.5.1).

Table 1. Geological and archaeological samples description

GEOLOGICAL SAMPLES					
ID	Location	Description	Notes	Analytical techniques	
				PLM	XRPD
C	Val Vau	Pebbles and gravels from the river bed deriving from the weathering of the southern dolomitic rock mountains	A (restored) lime-kiln is in the same area (Valchava; c3 in Figure 1)	✓	✓
D	Ofenpass	(Isolated) dolomitic rock outcrops	=	✓	✓
E		Dolomitic rocks associated with gypsum	=	✓	✓
F	Piz Umbrail	Slope detrital fragments	Dark dolomite	✓	✓
G		Individual samples taken from an outcropping area	Yellowish-brown dolomite	✓	✓
I	Lü village	Samples from layered sequences	Topographic sheet reports here a place called lime-kiln (<i>chalchera</i> ; c2 in Figure 1)	✓	✓
ARCHAEOLOGICAL SAMPLES					
ID	Location	Description	Notes	Analytical techniques	
				PLM	XRPD
6577	315, 11902	Carolingian mortars	Binder		✓
315, 11902			Mortar	✓	
8641		Ottonian mortars	Binder		✓
			Mortar	✓	
24351		Early Romanesque mortars	Binder		✓
24318, 24351			Mortar	✓	
13112		Late Romanesque mortars	Binder		✓
3340, 22570			Mortar	✓	
23604		Gothic mortars	Binder		✓
2137, 23276			Mortar	✓	

4. Results

4.1 X-ray powder Diffraction (XRPD)

4.1.1 Geological samples

Qualitative mineralogical analysis of dolomitic rock samples is reported in Table 2A. All of the samples are carbonate rocks composed of dolomite, generally with accompanying minerals.

According to the mineralogical analysis, the samples belonging to the D and I groups exhibit not negligible amount of quartz. This mineral is absent in the sample groups F and C (except sample C-03) and in traces in the group G. Group E is characterized by the presence of gypsum (Gp). Illite/muscovite (Illt/Ms) is a mineral always associated with the I sequence. It was also detected in the samples D-03 and G-01. Finally, barite (Brt) was identified in the sample G-02.

Table 2A. Qualitative mineralogical analysis of rock samples (*)

ID	Qualitative mineralogical analysis					
	Dol	Cal	Qz	Illt/Ms	Gp	Brt
C-01	+++					
C-02	+++					
C-03	+++		tr			
C-04	+++	+++				
C-06	+++					
D-01	+++		+			
D-02	+++		tr			
D-03	+++	+	+	+		
E-Dol	+++		tr		+	
F-01	+++					
F-02	+++					
G-01	+++		tr	+		
G-02	+++		tr			tr
I1-01	+++	tr	+	tr		
I1-02l	+++	tr	+	tr		
I1-02u	+++		+	+		
I1-03	+++	tr	+	tr		
I2-01	+++	tr	+	tr		
I2-02	+++	tr	+	tr		

(*) Notation used: +++ mineral in predominant relative amount; ++ subordinate; + accessory; tr trace; - absent or below the limit of detection. Mineral abbreviations as in Whitney and Evans [16].

4.1.2 Archaeological samples

Qualitative mineralogical analysis of the binder of the archaeological samples is reported in Table 2B. Results indicate that the binder of the samples 6577 and 24351 is dolomitic for the presence of hydromagnesite. The presence of amorphous phases (related with the formation of Mg-based products?) was detected in the samples 8641 and 23604. The remaining sample (13112) does not display any mineralogical phase related with the carbonation of dolomitic lime. The presence of clay minerals, quartz and dolomite is due to the fraction of aggregates that passed the sieve (grain size <63 µm). For the same reason, Fe-oxides (most probably both goethite and hematite, respectively Gth and Hem in Table 2B) were found as constituents of the sample 24351 (the binder of this sample is pale brown).

Table 2B. Qualitative mineralogical analysis of the binder of archaeological mortars (*)

ID	Qualitative mineralogical analysis								
	Cal	Qz	Dol	Illt/Ms	Chl	(H)Mgs	Gth	Hem	Amorphous
6577	++	+++		+		tr			
8641	+++	+	tr	tr	tr				✓
24351	+++	++	+	+	tr	tr	tr	tr	
13112	++	+++	tr	tr	tr				
23604	+	+++	+	tr	tr				✓

(*) Notation used: +++ mineral in predominant relative amount; ++ subordinate; + accessory; tr trace; - absent or below the limit of detection. Mineral abbreviations as in Whitney and Evans [12].

4.2 Polarizing Light Microscopy (PLM)

4.2.1 Geological samples

The petrography of the dolomite rock samples is reported in Table 3. The dolomitic rock texture was described according to their crystal boundary shapes, size and shape of dolomite crystals [17].

The petrographic examination of the dolomitic rocks analysed indicates the variability of the textural characteristics both between the different groups and within the individual group (Figure 2). In addition, there is evidence of textural variability at the scale of individual samples. The sequences I1 and I2 display very similar textural features. More promising is the presence of accompanying minerals scattered within the matrix such as Fe-oxides and/or in the form of void filling minerals.

Table 3. Petrographic analysis of dolomite rock samples

SAMPLE ID	MINERALOGY	TEXTURE AND OTHER FEATURES
C01-C06	Dolomite	Equigranular non planar dolomite with void filling planar-e dolomite crystals
C-02	Dolomite	very fine (peloidal) dolomite with non mimic replacement of bioclasts
C-03	Dolomite, quartz	very fine; matrix replaced by (inequigranular) non planar dolomite with void filling non planar dolomite and quartz crystals
D01-D02	Dolomite	fine; void filling non planar dolomite
D03	Dolomite	(equigranular) non planar
E-Dol	Dolomite, opaque minerals	very fine with replaced microcrystalline equigranular (planar-s) dolomite cement. (Inequigranular) non planar and planar-s void filling dolomite occurs. Presence of dark stylolites
F-01	Dolomite	(equigranular) non planar; presence of dark stylolites
F-02	Dolomite	very fine and microcrystalline with replaced inequigranular planar-s cement. Presence of dark stylolites
G-01	Dolomite; Fe-oxides	Microcrystalline, non planar; presence of dark microlaminations
G-02	Dolomite, quartz, (yellow) Fe-oxyhydroxides	(equigranular) non planar
I1-01, I1-02l, I1-02u, I1-03	Dolomite, quartz, illite/muscovite	microcrystalline (equigranular) with void filling
I2-01, I2-02		

4.2.2 Archaeological samples

The mortar analysis was focused on features of the lime lumps. The mortars of all the archaeological building phases are characterized by the presence of binder related particles (BRP) both overburnt, underburnt and lime lumps *sensu strictu* [7].

The Carolingian mortars show a large number of BRPs as underburnt fragments of dolomitic rocks that retain texture and unreacted minerals such as quartz (Figure 3a). These underburnt fragments commonly show reaction edges. Lime lumps *sensu strictu* sometimes display anisotropic rounded, radial phases with spherulitic textures 100-250 microns large (Figure 3b); under XPOL they show a roundish rosette-like shape with radial growth. These particular features may also be present as fractures or pores fillings. Their presence is quite common in dolomitic lime, and they can be interpreted as hydromagnesite or Mg-correlated phases [18]. In the fragments belonging to the Planta Tower (built during the Ottonian period) many lime lumps *sensu strictu*, and underburnt fragments were found; some of them are very rich in polycrystalline quartz (Figure 3c-c1).

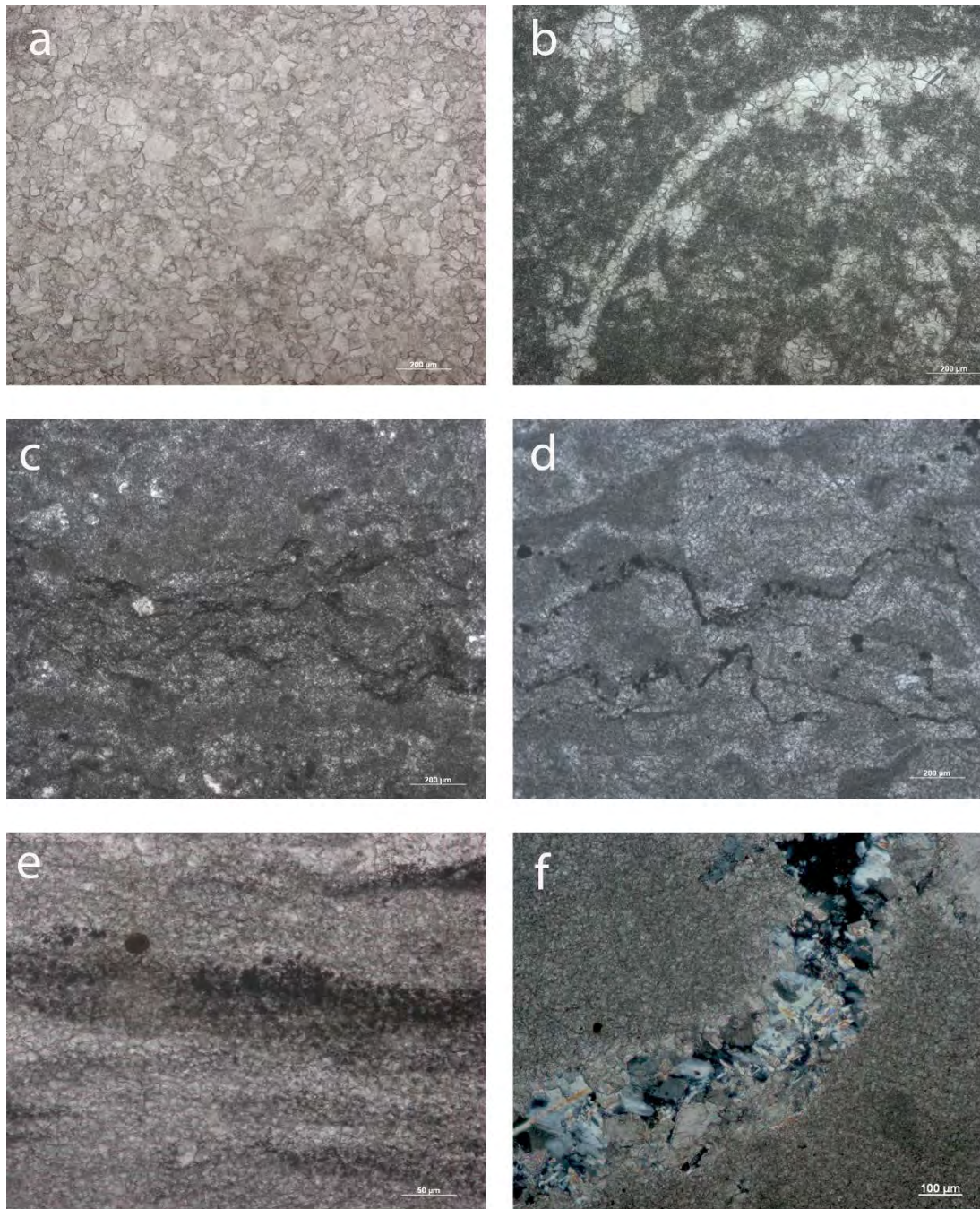


Figure 2. Micrographs of dolomitic rock samples. (a) sample C1; (b) sample C-02; (c) sample D-01; (d) sample E-dol; (e) sample G-01; (f) sample I-01 (all images are under XPOL, except 2a, PPL).

The building phases from the 11-12th centuries show two different type of mortars. In the first period (Early Romanesque) there are many overburnt fragments (Figure 3d) whilst the underburnt are very rare. Few lime lumps *sensu strictu* with melted siliceous phases can be distinguished (Figure 3e).

On the contrary, in the samples attributed to the Late Romanesque building phase, a large majority of underburnt fragments was found. Sometimes siliceous phases are visible within lime lumps, but it is not clear where they originate from (original raw materials or mixed with the binder during mortar preparation).

Similarly, in the Gothic samples, it is possible to distinguish different underburnt rock textures. Spherulite shaped crystals were formed within lumps, possibly related to high Mg amount in the raw material or to specific conservative conditions of the mortars.

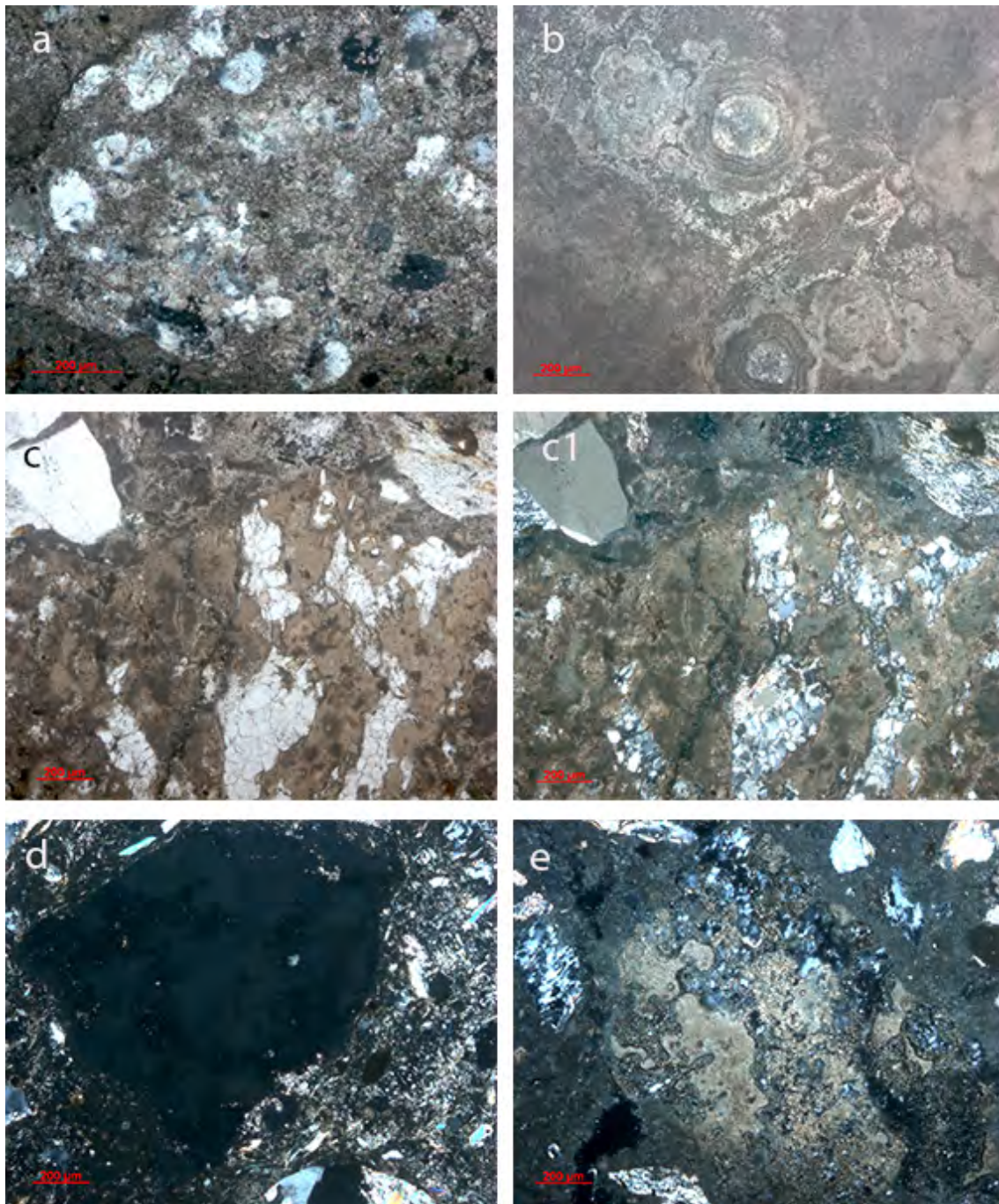


Figure 3. Micrographs of the binder of archaeological samples. a) underburnt rock fragment (XPOL); b) textural features related with the presence of hydromagnesite (XPOL); c-c1) lime lump with unreacted quartz (PPL and XPOL respectively); d) overburnt vitrified (amorphous) BRP, formed in the hottest areas of the kiln where the temperatures reached were sufficient to start melting the carbonate phases. Some quartz grains are clearly visible inside the lump matrix. –(XPOL); e) lime lump with partially melted siliceous phases.

4.3 Lime kiln locations in relation to potential quarrying sites

The toponym *chalchera* is found four times in the Val Müstair. Their location is shown in Figure 1. Site C1 (Prà Chalchera – Lime kiln meadow) lies in the village of Tschier, at the foot of a large scree slope below a dolomitic rock outcrop close to the pass dal Fuorn. C2 marks a dolomitic outcrop near the village of Lü with the name “crippel de la chalchera” – cliff of the lime-kiln. In two cases the “chalchera” toponyms (C3 and C4) are located in the bottom of the valley next to a water course, with no dolomitic outcrops nearby.

The geographic distribution of the toponym *chalchera*, which indicates the former presence of lime kilns, shows that they were erected close to the material sources, and that different ways of collecting carbonate rocks were used. Apart from rocky outcrops, from which stones had to be quarried, scree slopes and riverbeds were used as a source of dolomitic material. This has important implications for the provenancing of the materials, since dolomitic rocks collected from riverbeds could have originated from different sites along the river’s course. A batch of lime coming from a kiln and used in mortar production could therefore include materials from different sources.

The fact that the lime kilns were located close to the sources of material is economic, as lime has a smaller density than the carbonate minerals used in its production and is therefore easier to transport. The toponyms give no indication as to the age of the kilns; it is therefore not possible to say if the kiln sites were in contemporary use, or if the mode of collection of raw materials changed over time.

5. Discussion and conclusions

The lime binder of the mortar samples from the monastery of St. John from the different periods is composed of mineralogical phases characteristic of dolomitic binders with the exception of the archaeological sample of the Late Romanesque period. This confirms the strong relationship with the geological resources of the area.

The textural analysis of the dolomitic rock samples demonstrated that the same typological groups exhibit different textural characteristics. This is not only true for the lithological variability of pebbles and gravels collected in the Val Vau river bed but also for the remaining groups. In addition, the individual samples may show marked heterogeneity of the dolomite crystal size, morphology, boundary of the crystals, replacement of bioclasts, void filling minerals. Results clearly show that there is not a specific texture for each group. Therefore, the affinity between the textural features of the raw materials and that of the underburnt fragments in the lime lumps cannot be used as criterion for a univocal correlation.

More promising is the mineralogical composition of the samples analysed. The rocks belonging to the D and I groups show not negligible amounts of quartz in the form of void filling mineral. Unreacted quartz (and most probably mica muscovite) was detected in the sample from the Ottonian period suggesting the provenance from outcrops from the Early-Middle Triassic dolomite rock formation in the northern sector of Müstair valley. Quartz was also detected in underburnt fragments of the Carolingian and Early Romanesque period suggesting similar procurement areas. For the remaining archaeological mortars (Gothic and Late Romanesque), provenance cannot be inferred, even if quartz was found associated with lime lumps from the Romanesque period.

The analytical evidence finds additional motivation from the close vicinity of I outcrops with the local toponym indicating a lime-kiln near Lü village (c2 location in Figure 1).

A complementary approach using geochemistry of major, minor and trace elements also including Rare Earths Elements (REEs), both of the geological and archaeological samples using (Laser Ablation) ICP-MS, will be the next step of the research as suggested in other scientific research [19-21]. Finally, the petrographic application to raw materials sourcing will be further investigated including a major number of archaeological samples. Heating trials of dolomitic rocks will be carried out to control the modification induced during the technological process of dolomitic lime manufacturing.

References

1. Sennhauser HR, Courvoisier H-R (1996) Die Klosterbauten - eine Übersicht. In: Sennhauser HR (ed) Müstair, Kloster St. Johann. Bd. 1: Zur Klosteranlage. Vorklösterliche Befunde. Vdf, Zürich, pp. 15-65.
2. Caroselli M, Bläuer C, Cassitti P, Cavallo G, Hajdas I, Hueglin S, Neukom H, Jornet A (2019) Insights into Carolingian construction techniques – results from archaeological and mineralogical studies at Müstair Monastery, Grisons, Switzerland. Proceedings of HMC2019, Pamplona, Spain.
3. Martinucci C (2017) I frammenti di pittura murale carolingi del monastero di San Giovanni a Müstair. Materiali e tecnica esecutiva. Unpublished BA thesis, Supsi.
4. Leandri C (2018) I frammenti di intonaco dipinto romanico del monastero di Müstair (GR). Studio dei materiali e tecnica esecutiva. Unpublished BA thesis, Supsi.
5. Hughes J J, Leslie A B, Callebaut K (2001) The petrography of lime inclusions in historic lime based mortars. *Annales Geologiques des pays Helleniques*, Edition Speciale, Volume XXXIX, ISSN 1105-004, 359-364.

6. Elsen J, Mertens G, Van Balen K (2011) Raw materials used in ancient mortars from the Cathedral of Notre-Dame in Tournai (Belgium). *European Journal of Mineralogy*, 23, 871-882.
7. Elsen j (2006) Microscopy of historic mortars – a review. *Cement and concrete research*, 36, 1416-1424.
8. Franzini M, Leoni L, Lezzerini M, Sartori F (2000) The mortar of the “Leaning Tower of Pisa: the product of a medieval technique for preparing high-strength mortars. *European Journal of Mineralogy*, 12, 1151-1163.
9. Karanth R V, Krishnan K, Hegde T M (1986) Petrography of Ancient Indian Lime Plasters. *Journal of Archaeological Science*, 13, 543-551.
10. Izzo F, Arizzi A, Cappelletti P, Cultrone G, De Bonis A, Germinario C, Sossio F G, Grifa C, Guarino V, Mercurio M, Morra V, Langella A (2016) The art of building in the Roman period (89 B.C. – 79 A.D.): Mortars, plasters and mosaic floors from ancient *Stabiae* (Naples, Italy). *Construction and Building Materials*, 117, 129-143.
11. Pavía S, Caro S (2008) An investigation of Roman mortar technology through the petrographic analysis of archaeological material. *Construction and Building Materials*, 22, 1807-1811.
12. Bartz W, Kierczak J, Gąsior M, Wanat P (2017) Historical materials from the post-Cistercian abbey in Kamieniec Zabkowicki (southwestern Poland) – application of mineralogical methods for identification of source of raw materials. *Archaeological Anthropological Sciences* 9 279-291.
13. Trümpy R (2007) Zur Geologie des Münstertals (Val Müstair), 4 *Naturwissenschaftliche und technische Beiträge*, vdf AG ETH Zürich, pp 11-22.
14. Altomare A, Corriero N, Cuocci C, Falcicchio A, Moliterni A, Rizzi R (2015) QualX2.0: a qualitative phase analysis software using the freely available database POW_COD. *Journal of Applied Crystallography*, 48, 598-603.
15. Gražulis S, Chateigner D, Downs RT, Yokochi AF, Qiuirós M, Lutterotti L, Manakova E, Butkus J, Moeck P, Le Bail A (2009) Crystallography Open Database – an open-access collection of crystal structures. *Journal of Applied Crystallography*, 42(4), 726-729.
16. Whitney DL, Evans BW (2010) Abbreviations for names of rock-forming minerals. *American Mineralogist*, 95:185-187.
17. Sibley DF, Gregg JM (1987) Classification of dolomite rock textures. *Journal of Sedimentary Petrology*, 57 (6), 967-975.

18. Diekamp A, Jürgen K, Peter W M (2009) Magnesian lime mortars - identification of magnesium-phases in medieval mortars and plasters with imaging techniques. 12th Euroseminar on Microscopy Applied to Building Materials. Dortmund.
19. Miriello D, Barca D, Crisci GM, Barba L, Blancas J, Ortíz A, Pecci A, López Luján L (2011) Characterization and provenance of lime plasters from the Templo Mayor of Tenochtitlan. *Archaeometry* 53, 6, 1119-1141.
20. Ortega LA, Zuluaga MC, Alonso-Olazabal A, Insausti M, Ibáñez A (2008) Geochemical characterization of archaeological lime mortars: provenance inputs. *Archaeometry* 50, 3, 387-408.
21. Carran D A (2015) The characterisation of historic mortars with a focus on provenance. PhD dissertation, University of the West of Scotland, Paisley.

A Mortar Maker's guide to evolving mortar specifications in 18th and 19th C France and England and their implications today

Lucie Fusade

University of Oxford, School of Geography and the Environment, lucie.fusade@ouce.ox.ac.uk

Abstract

In France and England, the late 18th and early 19th centuries saw the publications of essential treaties on construction and building materials, such as “Cours d’Architecture” by Jacques-François Blondel (1777), “Traité sur l’Art de Bâtir” by Jean-Baptiste Rondelet (1803), George R. Burnell’s “Rudimentary Treatise on Limes, Cements, Mortars, etc.” (1850) and Valentin Biston’s “Manuel théorique et pratique du chaffournier” published (1836). In all of them, the way to burn lime is detailed along with methods to mix lime with sand, and recipes of a range of mortars are compared and given. It was a time of reflections and research on what constitutes a “good mortar” and how to improve it. Conservation practice is currently undergoing similar considerations and discussions. This work aims to explore the reflections and recommendations exposed in these treatises and guidance and how they could inform the choice of materials and the methods of mixing for the design of the conservation mortars used today, such as how to mix sand with fat lime and whether and when to add quicklime. By combining a detailed literature review of these treaties with knowledge of current mortars in conservation this work links history of construction and conservation science to help inform conservation decisions. These treatises reflect the evolution of thoughts and considerations on the composition of a good lime mortar at that time and show that many aspects, such as the quality and type of the burnt limestones, the sand, and especially how the mortar is mixed, are most important to obtain a good mortar. Conservation practice today could reflect those evolutions by adapting to the period of construction of the fabric being repaired and by being authentic about the methods and the overall type of mortar that was used at the time of the building.

1. Introduction

In the second part of the 18th century and early 19th century numerous architectural and technological developments were the opportunity for architects, theoreticians and engineers to engage with reflections and research on the nature of lime and the best methods to make mortars: what makes a mortar durable, which limestones to use, how to burn it, how to slake quicklime, when to add sand, etc. [1]. All of these with the aim to obtain the best possible mortar and a mortar as good as the Ancient one.

1756 – 1855 was indeed a time of experimentations and discussions to recreate the “hydraulic limes” of the Romans [2]. Important work was carried out by John Smeaton who wanted to develop a mortar that would survive in harsh salty and wet environment forced by the Eddystone Lighthouse in 1756 [3]. He was the first to understand that the hydraulicity of limes is due to their clay content [2]. Following this, in 1818, Louis Vicat was the first to come up with a classification of limes into five categories based on their clay content [2, 11].

This period also saw the publications of essential treaties on construction and building materials. Some of these treatises gave general principles on architectural styles, concepts and materials, such as the “Cours d’Architecture” (“Architectural Course”) by Jean-François Blondel, 1777 [5] and the “Traité sur l’Art de Bâtir” (“Treatise on the art of building”) by Jean-Baptiste Rondelet, 1802-1817 [6] and some were more specific such as de Raucourt’s “Traité sur l’Art de faire de bons mortiers et d’en bien diriger l’emploi ou Méthode générale pratique pour fabriquer en tous pays la chaux, les cimens et les mortiers” (“Treatise on the art of making a good mortar and of well directing its use or General practical method to make lime, cements and mortars in all countries”), 1828 [7], Valentin Biston’s “Manuel théorique et pratique du chaffournier” (“Theoretical and practical guidebook of the lime maker”), 1836 [8] and George R. Burnell’s “Rudimentary Treatise on Limes, Cements, Mortars, etc.”, 1850 [9]. In all of them, lime calcination is detailed along with methods to mix lime with sand. Recipes of a range of mortars are compared in order to find what compositions makes a good, or even, the best mortar.

Conservation practice is currently undergoing similar considerations and discussions about which lime to use and how to use it to obtain the best and most authentic lime mortars [10]. Nowadays a good mortar for repair and conservation could refer as one that is compatible with both with the existing masonry and the intended use of the mortar. Compatibility refers to the appropriateness of fit visually, physically and chemically [11]. In recent years for instance, experiments have been done to re-evaluate using quicklime, as it could be a more authentic method to make mortar and could produce a mortar with better durability, adhesion and workability [9,10]. The techniques of making and the compositions of lime mortars that are used today are directly inherited from both craftsmanship that remains through generations, and what documentary sources and archives can tell us [1].

Previous work exploring written sources and historical documents highlighted the importance of combining the usual analytical characterisation of original and historic mortars with the information these texts provide on the methods of burning lime or mixing the raw materials for instance [14]. Analytical characterisation can give information on the raw materials and is often used as a basis to replicate and use the composition for repair. However, the physical composition of mortars modifies over

time as they interact with the environment [15] so that accurate characterisation may not always be possible. Besides, it does not provide information about the reasons and the methods for the use of a material over another [14].

When it comes to designing and specifying conservation mortars it is interesting to understand what previous discussions have concluded in terms of what constitutes a good mortar, how to make a good mortar and what we could learn from these discussions. It is important that the knowledge of many centuries these treaties bring together inform what we know of mortars today and how we use them. There is indeed much to consider when designing a repair mortar. Therefore, this paper aims to explore what were the reflections and recommendations exposed in these treatises and guidance, especially on the type of lime, and how they could inform the choice of materials and the methods of mixing for the design of conservation mortars used today.

2. Historical sources

The corpus of written sources explored in this study focuses on France and England and mainly on discussions over the use, specification and mixing of air lime as conservation today is undergoing similar discussions. The written documents chosen are those of renowned architectural theoreticians or engineers in the late 18th and early 19th centuries. This work looks at five of them.

Jacques-François Blondel (1705-1774), published a series of Architectural Courses “Cours d’architecture civile” from 1771 to 1777 (finished by Pierre Patte) in six volumes, specifically called “Cours d’architecture ou traité de la décoration, distribution, construction des bâtiments” (“Architectural course on decoration, distribution, construction of buildings”). Volume 2 on “Construction: type and quality of stones and marbles” is of particular interest. Jean-Baptiste Rondelet (1743 – 1829), architectural theorist, wrote the “Traité théorique et pratique de l’Art de Bâtir” (“Theoretical and practical treatise on the art of building”) from 1830 to 1832, in seven volumes. In this paper, the second section dedicated to mortars is discussed. Antoine de Raucourt, engineer-colonel (1789-1841), wrote a very technical treatise in 1828 “Traité sur l’Art de faire de bons mortiers et d’en bien diriger l’emploi ou Méthode générale pratique pour fabriquer en tous pays la chaux, les cimens et les mortiers” (“Treatise on the art of making a good mortar and of well directing its use or General practical method to make lime, cements and mortars in all countries”). Chapters IV on the general composition of mortars, V on ancient mortars – and the second part on application and good use of it, and specifically Chapter X, give a very detailed account on what constitutes the best mortar, how to calcinate limestones, how to place the stones in the kiln, with wood to use, as well as how to apply mortar and mainly how to make hydraulic mortars. Valentin Biston published in 1836 the “Manuel théorique et

pratique du chaffournier” (“Theoretical and practical guidebook of the lime maker”) which focuses mainly on the types of lime kiln and the techniques of lime burning. The second part, on the composition of mortars, concrete and putty is of interest and gives an account and summary of other treatises. Finally, the architect and engineer George Rowden Burnell (1814-1868) wrote “Limes, Cements, Mortars, Concretes, Mastics, Plastering, etc” in 1850, a condensed treatise gathering “the knowledge and information dispersed through a numerous collection of authors” [9, p. iii]. All these documents relate the reflections and considerations on these architects and engineers while considering original sources.

Most of the written sources considered in this paper are from France, which, as Burnell suggests, could be partly explained by the “dislike to theory” of England, a “practical nation” [6, p. iii]. This study does not consider the work of Smeaton and Vicat as both authors focused on understanding the hydraulicity of limes rather than what makes a good mortar in consideration on ancient recipes and experimentations.

3. What makes a good mortar?

The aim of all of the treaties and guidebooks explored is to show how to perfect the making and compositions of lime mortars. Although most of them also consider cement and concrete this paper focuses on the air lime and feebly hydraulic based mortars as these are the compositions that brings discussions into conservation decisions today. In the late 18th and early 19th centuries, is a good mortar based on durability, on locally source materials, on ancient compositions? The following section explores what were the reflexions and recommendations exposed in these treatises and guides about the choice of materials, the methods of mixing and how to make the most efficient compositions.

3.1 Careful considerations of the raw materials

All treaties spend many pages detailing the choice of limestones and the best method to burn them and slake lime. In summary, Blondel and Rondelet both mention that the best limestones are dense, hard, white with fine homogeneous grain [5, 6], in the line of the concepts established by Vitruvius and Plini; concepts that will be changed over the following years as the understanding of hydraulic lime increases [2]. They all agree, and Biston especially points it out, that the way lime is slaked has great influence on the quality of mortar, mainly for hydraulic ones [8]. Rondelet for instance, suggests to divide the quicklime in small pieces to dissolve it quicker. Burnell follows from this, recommending that lime should be ground to powder with the exact amount of water necessary to reach this state in order to enable the more inactive particles to be able to absorb water more favourably, especially for hydraulic lime [9, p.66].

All emphasise the importance of the choice and quality of sand. Indeed, Rondelet explains the excellence of Roman mortar by the quality of the sand and lime they used. Biston also explains that the type of sand: calcitic, siliceous, granitic, etc. matters less than the fact that the sand should be pure. However, they seem to all agree on the use of mixed and fine sand [6, 8].

They all agree that the lime:sand ratio varies according to the quality of both the lime and the sand [5] and that the workmen should be able to judge this ratio by experience [7]. Blondel gives several suggestions of ratio according to the type of sand: for a sand from the ground: three parts for one part of lime; for a sand from a gully: two parts and one of lime; for a wet sand from river: two parts and one of lime with no added water; and for a dry river sand: two parts and one third of lime with necessary added water.

Overall, although they give clear explanations on the methods that should be followed to burn limestones and produce lime, the type and proportions of sand they all suggest varies depending on the purpose of the mortar [8] and the quality of the lime used.

3.2 How to make a “good mortar”? Importance of the methods of mixing

Across those written sources, a “good mortar” is defined as one that is quick to harden and durable. For Blondel for instance, it is one that unifies stones together and hardens shortly after having been used to make one body with the other materials of the masonry. It also should not shrink at drying and be water resistant. Blondel also clearly states that to make a good mortar three steps are necessary: lime should be slaked properly, sand should be of good quality and that while mixing, water should not be added as it slows down “the spirits of the mortar” (5, p. 190), meaning its ability to perform. There are then three ways of using lime to make a good mortar:

1. with lime that has just been slaked and in which is introduced sand or cement to be used straight away,
2. mixing sand or cement in a lime that has been very recently slaked,
3. using lime a few years after its slaking. This is similar to what conservation practice does nowadays, where at least one year-old lime putty are favoured as the aging of lime putty is recommended to be beneficial. Burnell also recommends that all limes, of any type, should be reduced to a paste before being mixed with the other ingredients.

For Rondelet, the more the mortar is mixed the better consistency it obtains and the quicker it hardens. The mixing method is the main way to succeed to make the best possible mortar in relation to the materials that are employed. He points out that workers and practitioners, such as masons, should be able to adjust the mixing

methods and compositions of mortars based on the materials available and the building type.

Burnell summarises the challenge of bringing scientific research and best-practice to making mortar: “in reality, mortar-making is a branch of practical chemistry [...] one which does not admit of the care and exactness of the laboratory. But the safety of a building often depends upon the perfection with which it is executed, and a great amount of scientific acquirements is necessary to insure that perfection. Yet architects and engineers almost invariably leave every operation connected with it to the most ignorant class of workmen” [9, p. 66]. The same challenges are faced nowadays in conservation.

In summary, the quality and technique of the method of mixing and whether water is added or not are the two main aspects of making a “good mortar”. However, a good mixing method is not always sufficient and these authors have explored new compositions.

3.3 Recommendations on improving ordinary mortars

The search for the “good mortar” also comes by improving ordinary mortars that are made of river sand and lime putty. This section reviews the evolving mortar specification from using non-hydraulic quicklime to hydraulic lime.

For Blondel following the recipes and methods of the Ancient is not a solution. That is why he suggests several types of mortars. The “*méthode Lorient*”, detailed by both Blondel and Rondelet, consists of mixing some quantity of quicklime, usually a quarter or a third and in powder, in an ordinary mortar made of lime and sand (one part slaked lime, three part aggregate, one part crushed brick for instance) or of lime and cement. This method would make mortar achieve considerable strength, quick hardening, as easy to use as a plaster and good at resisting water. Blondel recommends to quickly use this mortar to ensure the action of the quicklime happens only once used. In other words, he recommends to use it hot while the action is still happening. Indeed, the heat generated forces the humidity out and sort of cooks the material together, unifies and fixes them, giving a good adhesion between the lime and other building materials, especially with sand. The heat also seems to prevent any cracks and voids so that shrinkage is not to fear [5, p.199]. Rondelet also explains that the quicklime added absorbs water quickly. However if too much quicklime is used, its effects is too quick and the mortar cannot be used quickly enough and becomes like a powder. If too little quicklime is used, the effect is too slow so that the humidity stays in one place and it has the same disadvantages that an ordinary mortar [6, p.286]. Rondelet also points out that over time this mortar loses its advantage whereas an ordinary mortar keep gaining strength. It is a costly mortar as it requires twice the amount of lime and making the quicklime in powder is time consuming. Besides, for Rondelet, these

mortar types do not work for all masonry, but only for underwater masonry. However, for Rondelet, it is unlikely that this method of making mortar with two types of lime was used by the Roman as Pliny or Vitruvius would have mentioned it clearly, especially as quicklime requires some specific preparation [6, p.296].

Another method, “*méthode La Faye*”, is mentioned briefly by Rondelet and consists of mixing three parts of earthen sand and one part of lime to make a fat mortar [6, p.296]. Finally, the “*méthode de Morveu*” from 1774, again suggests burning the lime that has been slaked already: called a revived quicklime; with three part of fine sand, three parts of brick cement, two parts of lime putty and two parts of revived quicklime. According to Rondelet, following this method of revived quicklime seems to make the “*mortier Loriot*” easier and less dangerous to use, but doubt that this revived quicklime would be as good as the quicklime right from the oven [6, p.292].

Another way to make a mortar as good as the one from the Roman mentioned by Rondelet follows the Philibert Delorme’s recommendation of covering quicklime with sand and slowly watering it until the sand is saturated. This is a good mortar for building in water or humid environments, especially when the lime is used while still hot [6, p.303]. Interestingly Rondelet does not mention much the use of hydraulic lime, even though Vicat and Smeaton had already shown their experiments and prefer to refer to the way the ancients made their mortars.

After Vicat and Smeaton, guides and treatises by de Raucourt, Biston and Burnell tend to define a “good mortar” as a hydraulic-based one. Indeed, for de Raucourt, ordinary mortars, with no hydraulic base, are often very bad mortar and quickly weather when exposed to the environment [7, p.64]. De Raucourt recommends improving ordinary mortars by using a high amount of sand and quicklime mixed hot or cold with a hydraulic base. For him the main solution for a better mortar is a hydraulic mortar: “lime only gives results when mixed with a hydraulic basis” “true mortars are called hydraulic mortars” [7, p. 294]. He is clearly turned towards contemporary inventions and does not try to replicate Ancient mortars: “the excellence or antique mortars have often been highlighted, and ignoring their compositions has all the more been regretted, that moderns were persuaded that it was impossible to make mortar that would have their strength and durability. However, experiences have shown that Antic mortars are not all equally good; and that not all contains pozzolans” [7, p. 116].

Biston gives some suggestions of composition of improved ordinary mortars, all mainly hydraulic: Large mortar of lime and sand: 3 parts fine grain sand, 2 parts hydraulic lime; Fine mortar: 3 parts fine and dry sand, 2 parts lime well slaked and in putty: for ashlar masonry and repointing; Fine mortar: 2 parts of very fine sand, 1 part of quicklime slaked into a putty: for internal work; Basic mortar: mixing ordinary mortar and plaster in powder: this mortar is to be made when used [8, p. 186].

Improving mortar is therefore mainly based on the use of specific lime: part of quicklime in ordinary mortar, revived quicklime, hydraulic lime or on the choice of a precise ratio, based on the type of sand and function of the mortar. It is also interesting that from the late 19th century a good mortar has to be a hydraulic one. Some compositions of mortar suggested are interesting to understand, especially when it comes to analytical characterisation, but perhaps conservation practice today can learn more about mortar choices than compositions.

4. What can we learn for today's conservation practice and decisions?

The treaties studied in this paper reflect a quick evolution of thoughts, reflections and considerations over the late 18th and early 19th centuries. From Blondel who cites Philibert de L'Orme, Palladio, Plini and Vitruvius, where it is clear that not much have changed in centuries, considerations evolve to Biston and Burnells who mainly considers Smeaton and Vicat. In a few years a real shift occurred and different answers were given to the same questions: how to improve mortars? And what makes a good mortar?

Similar considerations are faced nowadays in trying to define what makes a good mortar and which lime should be used. Nowadays, the design of conservation mortar usually follows one of three main approaches [16]: the identical reproduction of the original historic mortar; the production of a new mortar mix based on the characteristics of the existing mortar, such as permeability and porosity; or the creation of a completely new mix, compatible with the existing masonry and designed for a specific conservation purpose. These approaches are a balance between always replicating Ancient mortars or only looking ahead at innovations, as it seems to be suggested by some of these authors.

Although today's definition of what makes a good mortar can be quite different - it is likely not a mortar that is quick to harden and durable - conservation practice can learn from these discussions and explorations.

Firstly, discussions, debates, experiments, agreeing and disagreeing with some methods and compositions are part of the process of understanding the materials and helping to make progress both scientifically and practically. These guidebooks show that there is not one manner to prepare conservation mortar, but that many aspects, such as the quality of the burnt limestones, the sand, and especially how the mortar is mixed, are most important to obtain a good mortar and should always be considered.

Secondly, the authors of these treaties did not try to replicate the ancient, i.e. Roman, mortars. They acknowledge what was good: great technical content and skills in mixing and choosing the right materials, but they knew the limitations and therefore were trying to improve it to respond to the contemporary needs. This idea is in a way

summarised by Burnell: “[the ancients] made mortar in one way, and doubtlessly that way was all that was practically necessary to secure the result then sought for – so we continue without examination in the track they beat for us. Our requirements are however very different” [9, p.iv] and he cites railways and general construction.

Finally, perhaps these treaties and guides can tell conservation practice more than a suggestion of compositions and technical recommendations. Indeed, the way these authors considered their buildings and the types of limes they used at that time can inform our conservation decisions for buildings of that time period. The evolution of thoughts and specifications that is clearly seen in those written sources, could guide conservation practice today into adapting to the period of construction of the fabric being repaired. Examining practices and ideas of a time period can affect our approach to maintaining a building.

For instance, the method of slaking quicklime and mixing with sand, and the compositions evolved and changed with new experiments, understanding of technology and availability of the materials. It is clear that after the experiences of Vicat and Smeaton, architectural treatises and engineer guides recommended more the use of hydraulic limes - and these buildings are now almost 200 years old, whereas before experiences on hydraulic limes, most treatises referred to ancient and medieval mortars. Therefore, the conservation mortars used, to be authentic, should reflect the craftsmanship of the time of construction. This could induce that all buildings that qualify as “historic” (i.e. usually pre-1919) cannot be conserved in the same way. We could argue that it is appropriate to use historic hydraulic lime and low hydraulic lime on buildings that used it initially, if it does not harm the masonry. Without matching the exact compositions of the original mortar in the walls, the specification could perhaps refer back to the general type, or tendency, or mortar that was used at this time and for this location.

5. Conclusions

This paper explored what were the reflections, recommendations and specifications suggested in these late 18th and early 19th centuries treatises and guidance, on the types of lime and sand recommended, the methods of mixing and the design of mortars, and considered how they could inform conservation practice and decisions today. These treatises reflect the evolution of thoughts and considerations on lime mortars at that time.

It is interesting to consider how they used quicklime with good outcomes in their ordinary mortar but also how it was quickly replaced by hydraulic lime. The emphasis on the increased use of hydraulic limes goes in the opposite direction from contemporary conservation recommendations and guidance.

When doing repair, conservation practice today could reflect those evolutions by adapting to the period of construction of the fabric being repaired and by being authentic about the methods and the overall type of mortar that was used at the time of the building. This means that to be authentic, considering practices and ideas of the time is also necessary. Therefore, when analysing historic mortar the craftsmanship of the time of construction should be considered and when designing conservation mortars the ideas and suggestions of the time of the building construction should be, to be authentic, reflected. When designing and considering a conservation mortar it is also essential to scientifically characterise the mortar in order to verify its physical and chemical compatibility with other materials, but reading historic texts provides a wider context.

6. References

1. Coutelas A (2009) *Le mortier de chaux*. Errance, Paris.
2. Sickels L B (1987) "Mortars in old buildings and in masonry conservation: A historical and practical treatise". Doctoral thesis, University of Edinburgh.
3. Smeaton J (1793) *A narrative of the building and a description of the construction of the Edystone lighthouse with stone: to which is subjoined, an appendix, giving some account of the lighthouse on the Spurn point, built upon a sand.*, 2nd ed. London.
4. Vicat L J (1818) *Recherches expérimentales sur les chaux de construction, les bétons et les mortiers ordinaires*. Goujon, Paris.
5. Blondel J-F (1777) *Cours d'architecture, ou Traité de la décoration, distribution et construction des bâtiments: contenant les leçons données en 1750 et les années suivantes*. Paris.
6. Rondelet J B (1803) *Traité théorique et pratique de l'art de bâtir*. L'auteur, Paris.
7. Colonel Raucourt de Charleville (1828) *Traité sur l'Art de faire de bons mortiers et d'en bien diriger l'emploi ou Méthode générale pratique pour fabriquer en tous pays la chaux, les cimens et les mortiers*. Librairie Scientifique et Industrielle De Malher et Cie, Paris.
8. Biston V (1836) *Manuel théorique et pratique du chauxfournier : contenant l'art de calciner la pierre à chaux et à plâtre, de composer toutes sortes de mortiers ordinaires et hydrauliques, cimens...* (2e édition, revue, corrigée et augmentée). Librairie encyclopédique de Roret, Paris.
9. Burnell G R (1850) *Rudimentary treatise on limes, cements, mortars, concretes, mastics, plastering, etc*. C. Lockwood & Son, London.

10. Henry A (2018) Hot-mixed mortars: the new lime revival. *Context, Institute Hist. Build. Conserv.*, vol. 154:30–33.
11. Schueremans L, Cizer Ö, Janssens E, Serré G, and Van Balen K (2011), Characterization of repair mortars for the assessment of their compatibility in restoration projects: Research and practice. *Constr. Build. Mater.* doi: 10.1016/j.conbuildmat.2011.01.008
12. Forster A (2004) Hot-Lime Mortars: A Current Perspective. *J. Archit. Conserv.* doi: 10.1080/01823328908726936
13. Artis R (2018), Specifying Hot-Mixed lime mortars - Technical Paper 28. <https://www.historicenvironment.scot/archives-and-research/publications/publication/?publicationId=ef85b75a-6a80-4247-95f2-a8780115daa2>
14. Marinowitz C, Neuwald-burg C, and Pfeifer M (2010) Historic Documents in Understanding and Evaluation of Historic Lime Mortars. 2nd Historic Mortar Conference HMC2010, Prague, pp. 267–274.
15. Leslie B A and Hughes J J (2002) Binder microstructure in lime mortars: implications for the interpretation of analysis results. *Q. J. Eng. Geol. Hydrogeol.* doi: 10.1144/1470-923601-27
16. Van Hees R (2012) RILEM TC 203-RHM: Repair mortars for historic masonry. *Mater. Struct.* doi: 10.1617/s11527-012-9917-z

**Topic 7: Mortars in archaeological sites.
Construction history. Archaeometry**



Characterization and durability analysis of coral stones in a marine environment

Swathy Manohar¹, Manu Santhanam¹

(1) Indian Institute of Technology Madras, India, swathymanohar@yahoo.com, manusanthanam@gmail.com

Abstract

This study reports the characterization of coral stones collected from a historic structure of 15th century from Southern India. The chemical composition, analysed using X-ray diffraction, revealed the presence of calcite and aragonite. The pore structure and porosity of the highly porous stone was determined using mercury Intrusion Porosimetry. The stones were then subjected to accelerated weathering tests in laboratory using immersion in sodium sulphate and sodium chloride solutions allowing dry-wet cycles. The mass loss was determined after each cycle, and microstructural characterization was carried out to see the modified pore distribution and porosity after the weathering cycles. It was found from the investigation that even though coral stones possess low compressive strength, they have extremely good performance with respect to durability. From the results, sodium chloride was found to be not a detrimental weathering agent for coral stones, whereas long-term exposure to sodium sulphate in heavy dosages caused slow but homogeneous kind of weathering. Hence, providing water repellent coatings is not a suggestive remedy for preventing further deterioration.

Introduction

Coral stones are a variety of porous limestones, common in historic masonry structures and are well known for their incomparable heat repelling ability and cladding applications. Use of the coral stones can be abundantly seen in the heritage buildings in the coastal settlements throughout the Indian Ocean, Arabian/Persian Gulf, Caribbean and the Red Sea.

Durability of any natural stone is often related to its strength; stones with high strengths are generally found as durable. But corresponding to the severity of exposure conditions and the chances of weathering, durability of the stone shall be rated based on the resistance of the stone to weathering [1]. Coral stones are also being used as aggregates in concrete, as coral sand concrete (CSC). It is reported that coral aggregates in concrete resulted in improved resistance to sulphate drying-wetting and chloride ion penetration and more rapid early strength development compared to river sand concrete. But CSC exhibits higher drying shrinkage and capillary water absorption [2]. Also, the use of coral filler in replacing cement clinker in Calcium sulpho-aluminate cements has been studied and reported that the replacement could provide similar compressive strength and better flexural strength [3]. The

performance of the coral stone as a masonry material is not yet reported with respect to durability.

Salt crystallization is identified as the most crucial mechanism for damage in historical masonry units. The mechanism and hence the damage patterns vary with different salts, most commonly - the highly deleterious sodium sulphate and the omnipresent sodium chloride. Sodium sulphate can sustain very high supersaturation before the nucleation of salt crystals inside the pores, which in turn induce high crystallization pressures on the pore walls [4]. When the stress acting on pore wall is higher than the strength of the material, damage starts. The case of sodium chloride is different, as it cannot sustain high supersaturation before nucleation. The case of high crystallization pressure on pore walls is therefore less, and hence the extent of deterioration will be much lesser with sodium chloride than with sodium sulphate. Another interesting fact is that crystallization pressure is larger in smaller pores [5,6]. In a smaller pore, the high supersaturation has to be balanced by the curvature and crystallization pressure. Whereas, in larger pores, which are enough to accommodate the growing crystal, supersaturation can be balanced by the curvature alone, where no generation of extra stresses occurs [7, 8].

Coral stones, being very porous, and mostly exposed to environments with more salts (as they were extensively used in structures where local availability from sea was a factor), there is a need to understand their behaviour in a salt-laden environment. On account of the weathering in ancient structures with age, it is essential to understand the properties of the material and performance with respect to durability prior to suggesting the protection/remedial measures in conservation. In the current study, coral stones are collected from a historical temple in Southern India, which was constructed in the 15th century. The porous white coral stones are characterised for mechanical properties and microstructural features. Salt weathering resistance of the stones is evaluated by performing accelerated salt weathering studies in laboratory.

Materials and Methods

Materials

Stones of coral were collected from the temple stockyard. From the collected samples, cube specimens of size 10 cm were properly cut to test mechanical properties, and cubes of 5 cm were cut to test salt weathering resistance by accelerated weathering test procedures.

Methods

Compressive strength of the material was tested on 10 cm coral stone cubes as per IS 1121 (2013). 6 cubes were tested, out of which 3 were from stones that looked least weathered or unweathered and 3 were from stones that looked weathered, and the average compressive

strength of 6 cubes was reported. Water sorptivity tests were conducted on 12 specimens, out of which 6 each were from the two categories as explained above.

The stone samples were characterized using X-ray diffraction technique to analyse the mineralogical composition. A Bruker Discover D8 power diffractometer was used with step scanning from 5° to 90° 2 θ with a count of 0.5 s/step. The diffractograms were then analysed using the software X'PERT HighScore Plus.

Porosity and pore structure were studied using Thermo Scientific 140-440 Pascal Mercury Intrusion Porosimeter instrument. Small samples of weighing than 1 g were chosen for this study, and mercury was intruded into the sample at high pressures. The pore structure details were obtained from the volume change (because of intrusion) of mercury.

Scanning Electron Microscopy (SEM) was used to obtain the morphological characteristics of the fractured surfaces of the samples. An Emcrafts GENESIS 2100 SEM device was used, which was also equipped with an energy dispersive X-Ray analysis (EDX) system, in order to identify the phases on the imaged surface.

Accelerated salt weathering tests were conducted as per RILEM Test V (a), 1992, on cube specimens of 5 cm. 6 specimens each were considered for the immersion wet- dry cycles, with both sodium sulfate solution and sodium chloride solution, and subjected to 15 cycles as per the recommendation.

Results and discussions

Compressive strength and water absorption

Compressive strength of the stone specimens was found to vary from 35 to 70 MPa with a standard deviation of 17.5 MPa and average strength of 58 MPa. The results revealed that there was no significant strength difference between the specimens that appeared intact and the ones that possessed light weathering. Figure 1 shows a typical failure of coral stone cube under compression. From the water sorptivity tests, the capillary porosity for the samples was found to be between 8.5% and 13.5%, with a coefficient of variation of 13.4%.



Figure 1. Failure of the coral stone cube under compression

X-ray diffraction

Samples for XRD were selected based on the visual degree of deterioration. Two sets of samples, one with minimal degree of weathering and the other with larger extent of deterioration (more porous and granular) were selected for XRD study. Major mineral components in both the samples were found as Aragonite, Magnesian Calcite and Calcite. Minor amounts of Halite (NaCl) were found in both samples, with marginally larger quantity in the highly weathered sample.

The X-ray diffractograms showing the peaks are shown in Figures 2 and 3 for lightly weathered and highly weathered samples respectively. No major mineralogical differences were observed among the different samples.

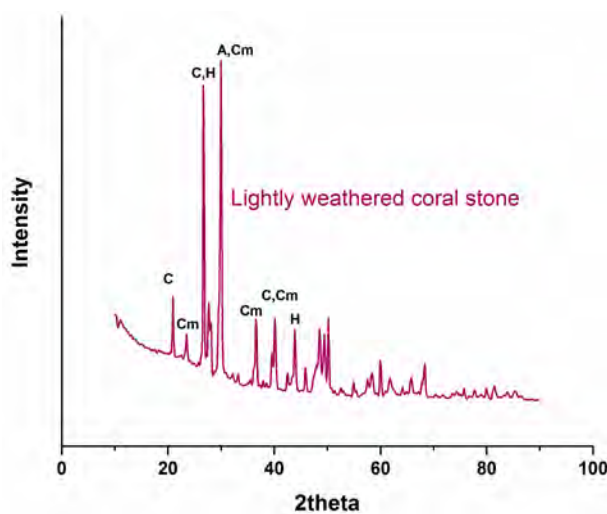


Figure 2. Diffractogram of lightly weathered coral stone sample

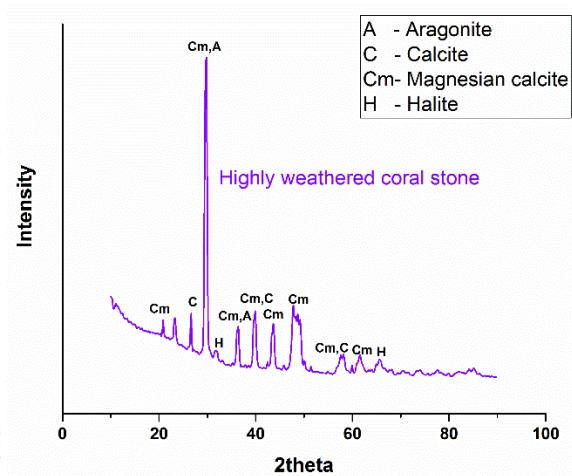


Figure 3. Diffractogram of highly weathered coral stone sample

Scanning Electron Microscopy

SEM images were taken at 500x and 2000x on the fractured surfaces of the samples. Grains of size >100 μm were observed distributed throughout. From EDS, these were identified as sand grains composed of Si and Mg oxides. Pore-lining and pore-filling Calcites were observed adjacent to these well-developed sand grains. Figure 4a shows the larger grains surrounded by the filling calcite and Figure 4b shows the Mg Calcite formation.

On observing each grain, there were no evident inter granular or intra granular cracks found. This points at the intact structure of the material without structural damage, though the quantification of porosity seen is important in determining the durability aspects.

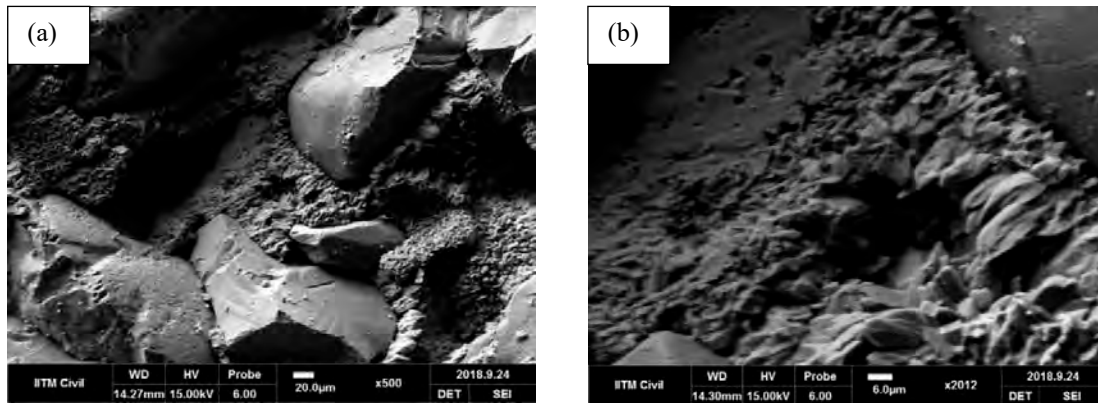


Figure 4. a) SEM image of coral stone at 500 X showing sand grains and pore filling Calcite b) SEM image at 2000X showing Magnesium Calcite formation

Accelerated salt weathering studies

The wet-dry weathering cycling was done as per RILEM Test V (a), 1992. The specimens were subjected to salt crystallization cycles, each cycle being of 24 hours. One cycle is defined as 2 hours of immersion in salt solution, 19 hours of drying at 60 °C and 3 hours of cooling at room temperature. The mass of the specimens was recorded by the end of every cycle and the specimens were observed for any visible changes. The normalized mass loss calculated with respect to initial mass of each specimen is shown in Figures 5 and 6, with the number of cycles on the Y-axis.

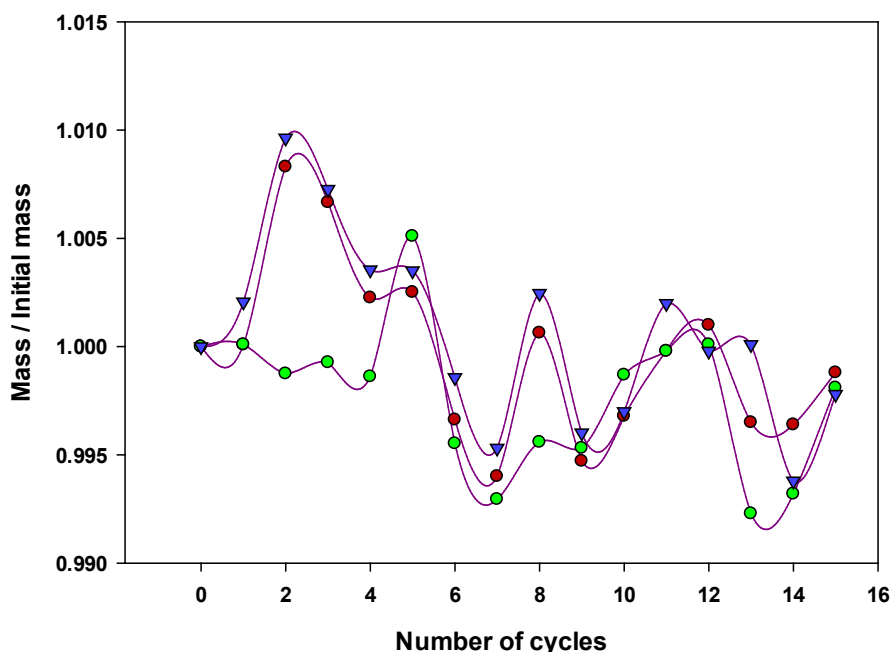


Figure 5. Mass loss of the specimens on salt weathering with sodium sulphate solution

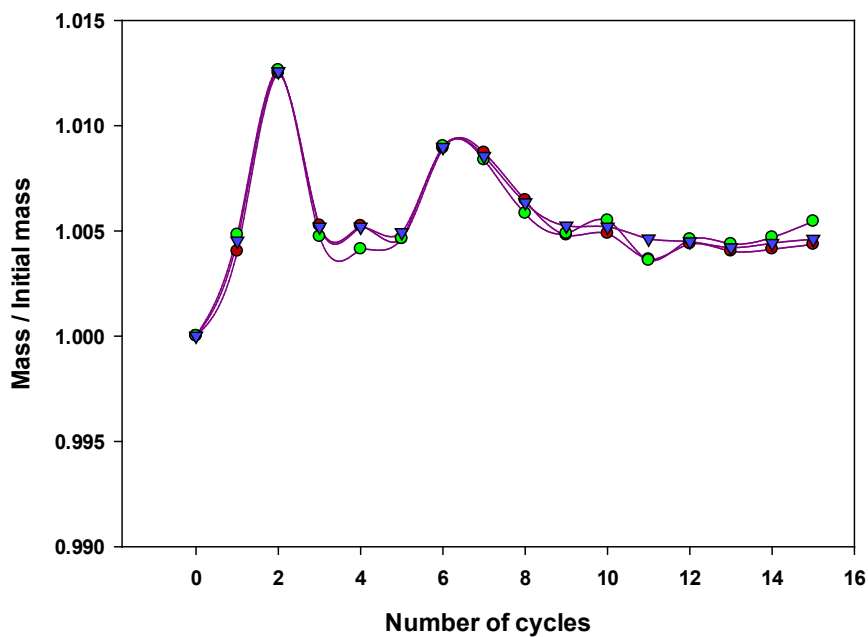


Figure 6. Mass loss of the specimens on salt weathering with sodium chloride solution

The procedure was carried out with two different salt solutions - 10% Na₂SO₄ solution and 15.6% NaCl, each tested with 3 identical specimens. Normally, prior to deterioration or mass loss, there would be a mass increase due to the salt deposition inside the matrix, followed by a period of either mass loss or gain due the competition between salt deposition and mass loss. This phase is expected to be overcome by the mass loss due to deterioration soon, say by 6-8 cycles. This pattern was consistent among the 3 different specimens tested in each category.

With sodium sulphate solution, very minute but negligible change in texture of the surface and decrease in sharpness of the corners were observed, whereas in sodium chloride exposure, no trace of degradation was observed. Mass gain due to salt deposition in the pores was prominent. In both cases and for all the tested specimens, the phase of continuous mass loss degradation is not reached in 15 cycles, which shows their high salt resistance.

Figure 7 shows the tested specimens prior to laboratory salt exposure and after 15 cycles. S1, S2, S3 represent samples subjected to sulphate weathering, and C1, C2, C3 represent those subjected to chloride weathering. No evident damage is observed visually also, despite the heavy and highly deleterious salt exposure. Compressive strengths of the cubes were determined after the salt crystallization cycles, and were found to vary from 35 MPa to 47 MPa, with an average compressive strength of 42 MPa.

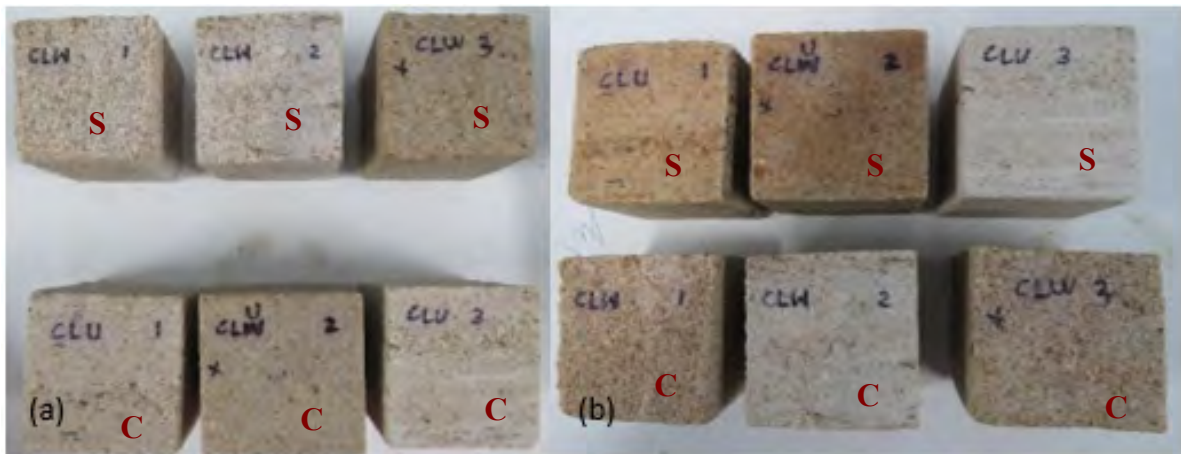


Figure 7. Specimens (a) before and (b) after salt weathering cycles

Mercury Intrusion Porosimetry

The pore structure parameters, namely critical pore diameter and total pore volume are found from the MIP plots for each sample. Critical pore size is the pore diameter that corresponds to the highest frequency of pore sizes, and is obtained as the peak in the differential intrusion curve. Systems that have finer pore sizes are expected to have lower values for both these parameters. Any deterioration (weathering or fire related damage) is expected to shift the pores towards coarser sizes.

The aged and naturally weathered coral stone sample was tested with MIP to analyse the pore structure and porosity. Then the artificially accelerated sample (weathered with sodium sulphate solution, as this was the one with a little noticeable deterioration) was also tested, to see the characteristic modification with respect to pore structure and pore distribution with artificial Na_2SO_4 weathering.

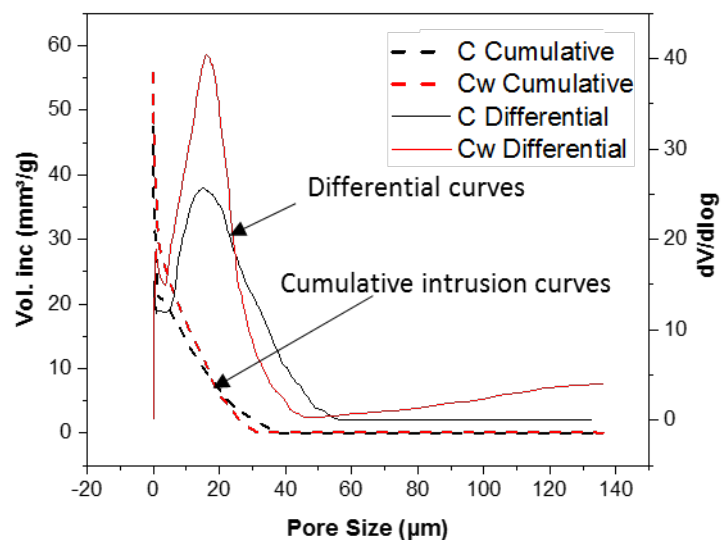


Figure 8. Curves from MIP data for natural coral stone sample in as received condition “C” and accelerated weathered sample “Cw”

Figure 8 shows the cumulative distribution curves and differential curve for the natural sample that is in as received condition- denoted as C, and the accelerated weathered sample denoted as Cw. The total porosity and bulk density have not shown any significant changes between the original sample and the accelerated weathered sample. This indicates the negligible effect of Na₂SO₄ salt weathering in the coral stones, which again proves the good salt resistance of the stone. The critical pore diameter, which is the pore size at peak of the differential curves, has moved slightly to the right, indicating a small increase in the most common size of pores in the tested sample. Since the right shift is very minute on weathering, the degree of deterioration at a microstructure level can be reported as minimal. The pore structure parameters of the two samples are shown in Table 1.

Table 1. Pore parameters of the samples from MIP data

Properties	Naturally aged coral stone	Accelerated weathered coral stone
Bulk density (g/cm ³)	3.24	2.89
Porosity by Hg intrusion (%)	17.45	17.86
Critical pore diameter (μm)	15.04	16.00

Table 2 shows the relative pore volumes in different size ranges. The results are similar for both the as received sample and accelerated weathered sample. Around 27% of total porosity consisted of pores between 10 and 100 μm, and more than 70% of total pores were greater than 1 μm. The chances of salt crystallization damage to happen in these macropores are low, because it is difficult to sustain high crystallization pressure in larger pores. Also, the increased strength of the grains adds to the reason for the damage-free behaviour.

Table 2. Pore size ranges for different samples

Pore diameter ranges (μm)	Relative volume fraction of pores (%)	
	Received as such sample	Accelerated salt weathered
100.0000-10.0000	26.92	27.47
10.0000-1.0000	21.18	29.16
1.0000-0.5000	9.85	8.81
0.5000-0.1000	11.3	11.99
0.1000-0.0500	5.22	4.46
0.0500-0.0100	13.28	9.07
0.0100-0.0050	11.31	4.02
0.0050-0.0010	0.94	4.76

Conclusions

The physical and microstructural properties of coral stone as a masonry unit were studied in this paper. The durability performance was evaluated with respect to the salt weathering resistance of the stones in the accelerated weathering procedure conducted in the laboratory. The compressive strength of the coral stones was found to be more than 50 MPa on average. X-ray diffraction studies showed Calcite, Mg calcite and Aragonite as the major mineral constituents. The capillary porosity was calculated from water sorptivity test, and was found to vary between 8.5 and 13.5%. Total porosity was calculated from MIP to be around 17%. Further, as more than 70% of the total pores were found to be close to the capillary pore range (greater than 0.1 μm), the chances for salt crystallization and further damage are low. In the smaller fraction of micro-porosity, even though crystallization pressures occur at higher supersaturations, the substantial strength of the grains would be able to resist the pressure and prevent any damage. The samples subjected to accelerated weathering tests with sodium sulphate and sodium chloride solution separately were found to possess impressive salt weathering resistance, as no noticeable damage could be seen after 15 cycles. SEM images also supported the uncracked microstructure of the centuries old samples. All the mechanical and microstructure studies conducted in the study point towards the high durability of coral stones in a salt exposed condition.

References

1. Winkler EM (1975) *Stone: Properties, Durability in Man's Environment*, 2nd Ed. Vienna, New York: Springer Verlag. doi: <https://doi.org/10.1007/978-3-7091-3819-9>
2. Cheng S, Shui Z, Sun T, Yu R, and Zhang G (2018) "Durability and microstructure of coral sand concrete incorporating supplementary cementitious materials." *Construction and Building Materials*, Elsevier Ltd, 171, 44–53. doi: 10.1016/j.conbuildmat.2018.03.082
3. Wang X, Shui Z, Yu R, Bao M, and Wang G (2017) "Effect of coral filler on the hydration and properties of calcium sulfoaluminate cement based materials." *Construction and Building Materials*, Elsevier Ltd, 150, 459–466. doi: 10.1016/j.conbuildmat.2017.05.194
4. Flatt RJ, Caruso F, Sanchez AMA, and Scherer GW (2014) "Chemo-mechanics of salt damage in stone." *Nature Communications*, Nature Publishing Group, 5, 1–5. doi: 10.1038/ncomms5823
5. Fitzner B (1988) Porosity properties of naturally or artificially weathered sandstones. In: Ciabach, J. (ed) *Vlth International Congress on Deterioration and Conservation of stone*, Torun, 236-245.
6. Tsui N, Flatt, RJ, and Scherer GW (2003) "Crystallization damage by sodium sulfate." *Journal of Cultural Heritage*, 4(2), 109–115. doi: 10.1016/S1296-2074(03)00022-0

7. Scherer GW (2004) "Stress from crystallization of salt." *Cement and Concrete Research*, 34(9), 1613–1624. doi: 10.1016/j.cemconres.2003.12.034
8. Angeli M, Benavente D, Bigas JP, Menéndez B, Hébert R, and David C (2008) "Modification of the porous network by salt crystallization in experimentally weathered sedimentary stones." *Materials and Structures*, 41(6), 1091–1108. doi: 10.1617/s11527-007-9308-z

Technical analysis on materials and characteristics of mortar-based compounds in Roman and Late antique Aquileia (Udine, Italy). A preliminary report of the results

Simone Dilaria¹, Michele Secco², Jacopo Bonetto³, Gilberto Artioli⁴

(1) University of Padova, Department of Cultural Heritage, simone.dilaria@phd.unipd.it

(2) University of Padova, Department of Civil, Environmental and Architectural Engineering (ICEA); Inter-departmental Research Center for the Study of Cement Materials and Hydraulic Binders (CIRCe), michele.secco@unipd.it

(3) University of Padova, Department of Cultural Heritage, jacopo.bonetto@unipd.it

(4) University of Padova, Inter-departmental Research Center for the Study of Cement Materials and Hydraulic Binders (CIRCe); Department of Geosciences, University of Padova, Italy, gilberto.artioli@unipd.it

Abstract

In the present paper we report the preliminary results of an ongoing research focused on the investigation of Roman mortars and concretes employed in Aquileia from Roman to Early Medieval Age (II century BC – VI century AD). More than 250 samples have been collected from buildings spread all over of the town, with different chronologies of construction and different functions. Material characterization was achieved throughout a multi-analytical approach comprising optical microscopy (OM), X-Ray powder diffraction (XRPD) and Scanning Electron Microscopy-Energy Dispersive microanalysis (SEM-EDS). Analytical data have been strictly crosschecked in relation with the chronology and purpose of the structure from which mortars have been collected from. The preliminary results we obtained are providing intriguing outcomes: we observed a high specialization on “recipes” in relation to the function of mortars and concretes, but also chronology of production appears to have an important role in the composition of mortar-based compounds. Such an extensive sampling is giving valuable insights to decipher the relations among crafts and artisans in ancient construction and decorative activities.

Introduction and state of art

The present project is part of a larger research promoted by the Department of Cultural Heritage and the Department of Geosciences of the University of Padova, aimed at the investigation of types and characteristics of mortars and concretes exploited in ancient times. In the wake of the recent impulse devoted on studies concerning the “Archaeology of Architecture”, “Archaeology of Construction” and “Archaeology of building materials”, the ancient Provincia Cisalpina, corresponding to the actual northern Italy, has become, in the last decades, a fertile territory for archaeological and archaeometric researches. The results of these studies are demonstrating how Roman architecture in Cisalpina deeply differs from centre-southern Italian constructive traditions, in terms of forms, materials and techniques employed by ancient crafts [1-3].

Nevertheless, specific analytical researches on mortar-based materials have not been carried out in such a way as it has been done for centre-southern Italy, where the cases of Rome and Pompeii remain emblematic terms of comparison for these definite topics [4]. On the other hand, an analytical approach for the study of mortars and concretes has been rarely undertaken for significant case studies in the Roman Cisalpina. Wall-paintings are surely the materials on which mayor part of the researches have been based on, even if a main focus was dedicated to the characterization of pictorial layers, more than the analysis of supporting mortars (tectorium). Lombardy [5], North-Eastern Italy [6, 7, 8] and, in the last years, Slovenia (Emona-Ljubljana) [9] are the regions on which the sampling has been carried out in a more exhaustive way in statistical terms, as, since the '90, more than 200 wall-paintings have been taken into exam.

On the other hand, no extensive analytical datasets are available for other typologies of mortar-based compounds. Exceptions are represented by analyses on a targeted sampling of structural mortars employed in specific contexts such as Padova [10], Ravenna [11], Desenzano (Brescia) [12], Milan [13], Susa, the ancient Segusium (Turin) [14, 15] and Mošnje (Slovenia) [16]. Finally, other types of mortar-based materials employed in antiquity, for instance the ones manufactured for flooring purposes, have been traditionally investigated in relation to restoration activities. Specific studies on mortar bedding screeds have been performed on Roman pavements of Montegrotto (Padua) [17] and Cremona [18].

In this scenario, Aquileia represents a perfect context for developing a research on mortars-based compounds which were, in the last years, only marginally investigated [1, 19]. During Roman times, Aquileia was one of the most prosperous towns of the Northern Italy and an important centre for the development of trends and practices in the field of art and architecture. After being established in 181 BC, the city become, during the Imperial age, a flourishing urban centre, as it was enriched by monumental buildings and highly prestigious private residences. In the IV century AD, it was considered by Ausonius (XI, 9, 4) one of the nine most important and extended cities of the ancient world, but in the 425 AD Aquileia collapsed under Attila's invasion and the town was progressively abandoned by the end of the V century [20]. All these different historical periods are represented by the buildings that modified the shape and the plan of the city.

In the last decade new impulse on excavations activities was promoted thanks to the contribution of Universities and private foundations such as Fondazione Aquileia, leading excavation, valorisation and preservation projects in several archaeological areas of the ancient town.

Along with archaeological excavations and restoration activities, the University of Padova promoted research projects focused on the analysis on building techniques [3], mosaic art [21] and pictorial culture [22] in Aquileia.

In the wake of this solid historic-archaeological background, these researches have established a fertile ground to fully immerse and contextualize the results of an analytical project focused on mortars-based materials characterization⁴.

Preliminary publications on this topic have revealed the potentialities of the exploitation of the single context approach in order to acquire a full and deep knowledge on characteristics of mortars and concretes employed along space and time in a determined area [23, 24, 25, 26, 27, 28]. The data in course of acquisition are providing new lymph for a thorough discussion on the issues related to competences and know-how of ancient crafts and artisans, their correlation with economic power of patronage, function of buildings and chronology of construction, in the framework of a realistic reconstruction of the history and economy of an ancient Roman town.

Investigation contexts and sampling

In order to crosscheck the characteristics of mortar-based materials employed in archaeological complexes with different chronology, social level and functional destination (i.e. private contexts, public buildings, defensive systems, suburban quarters etc.), a series of archaeological areas of the ancient city of Aquileia have been taken into exam (Figure 1).

Main contexts are represented by houses (*Domus of Tito Macro*, *Domus of Bestie Ferite* [29], *Domus at Stalla Violin* [30]) which life spans from the I century BC to the V century AD, along with periodic renovations activities that determined frequent reconstruction of floors, canalizations and wall structures; public buildings are represented by the theatre [31] and the amphitheatre [32], that were probably established during the early imperial age, and by the mayor Roman thermal complex of the city, the so-called *Thermae Felices Constantiniana*, which were probably built under the patronage of the Constantine family during the IV century AD [33]; defensive architecture has been considered, as the city walls were taken into exam along with their construction phases, ranging from the period of foundation of the city throughout reconstructions and modifications during Late Antiquity and Byzantine age [34]; Aquileia suburb was also examined by investigating of structures in a productive area in the immediate surrounding of the city [35].

More than 200 samples of mortars and concretes have been collected from the cited sites. Samples refer to a) foundations mortars (sometimes acquired by the direct sampling of core drillings); b) wall jointing mortars and wall core mortars; c) concrete vaults; d) floors and floor beddings (mosaic, concrete floors, brick floors, *opus sectile* floors, mortar floors); e) structural and revetment mortars of hydraulic systems (water tank, canalization conducts,

⁴ The current research has been supported by the Superintendence of Archaeology, Fine Arts and Landscape of Friuli Venezia Giulia and by research teams of the Universities currently involved in the annual archaeological excavations in the ancient city. In particular, we are grateful for the collaboration of the excavation directors of the investigated sites in Aquileia: Prof. J. Bonetto and Prof. M. Salvadori (Dep. of Cultural Heritage, University of Padova); prof. P. Basso (Dep. of Culture and Civilization, University of Verona); prof. D. Cottica (Dep. of Humanities, University Ca' Foscari of Venice); prof. M. Rubinich (Department of Humanistic Studies and Cultural Heritage, University of Udine).

piscinae)⁵. Apart from the mortar samples taken directly on site, more than 60 wall-painting fragments have been also analysed, mainly collected from the materials conserved in the deposits of the Archaeological Museum of Aquileia and usually recovered during excavations conducted in last century in different areas of Aquileia. Samples were taken from assemblages of well dated wall painting fragments which were already studied according to stylistic features [25, 28].

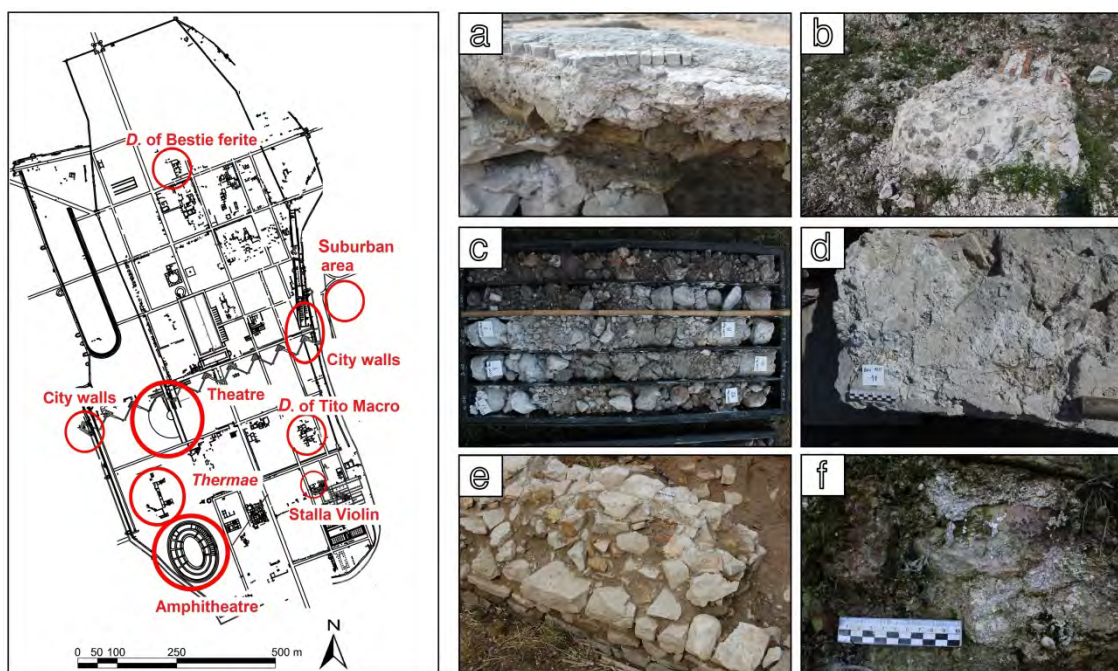


Figure 1. Aquileia. Plan of the investigated archaeological sites. a) mosaic bedding screed at *Domus* of Bestie ferite; b) collapsed vault of *Thermae Felices Constantinianae*; c) core drilling in theatre foundation platform; d) jointing mortars of the amphitheatre; e) wall of eastern fluvial bank; f) joint mortar with shell aggregates of Bizantine city walls.

Methodology

The collected samples have been analysed following a multi analytical approach. Firstly, all the samples have been described according to their macroscopic features (Figure 2). A preliminary petrographic study through optical microscopy (OM) was then performed on all the analysed samples following macroscopic and microstratigraphic procedures for mortar-based materials described in UNI Norm 11176:2006 “Cultural heritage - Petrographic description of a mortar”.

The study was performed both by optical microscopy (OM) on 30 µm thin sections, obtained by vacuum impregnating portions of the materials with epoxy resin and sectioning them transversally (Figure 3). Mineralogical quantitative phase analyses (QPA) were performed on a selection of representative samples through X-ray powder diffraction (XRPD). Then, QPA's were performed using the Rietveld method [36]. XRPD analyses on the sole binder fraction were performed after separation through the Cryo2Sonic 2.0 procedure [37] in order to

⁵ Mortar-based compounds from hydraulic structures are still under examination and they will be not discussed in the present paper.

properly define hydraulic phases on those samples showing pozzolanic properties after OM or XRPD bulk examinations. The determination of both crystalline and amorphous content was calculated by adding 20% wt. of ZnO to the powders as internal standard.

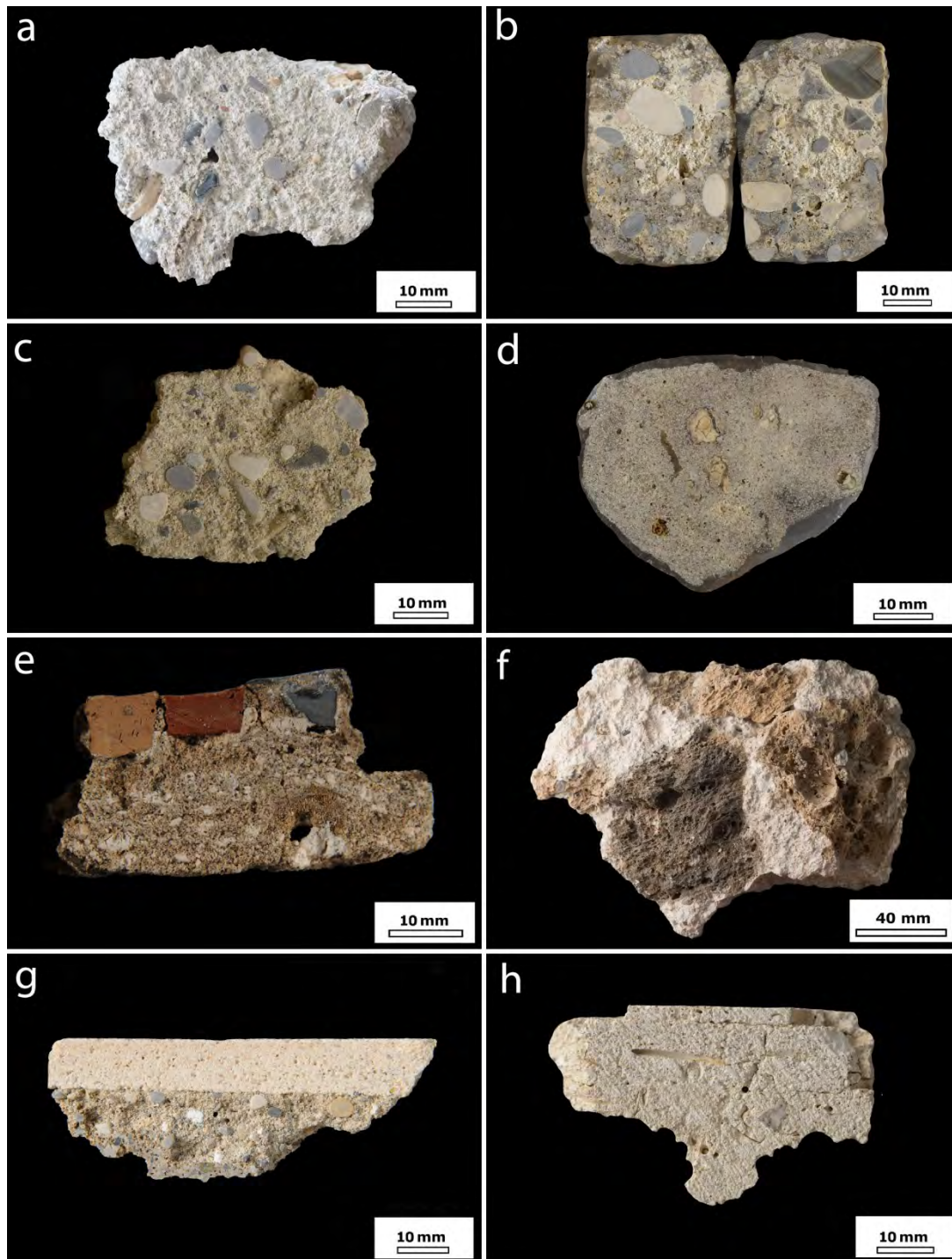


Figure 2. Macroscopic images of mortar-based compounds. a) sample from the theatre *opus caementicium* substructure (cross section); b) sample from the amphitheatre *opus caementicium* substructure (cross section after consolidation in epoxy resin); c) wall joint mortar from *Domus* of Tito Macro (cross section); d) wall joint mortar from *Domus* of Tito Macro (petrographic section after consolidation in epoxy resin); e) late antique floor bedding from *Domus* of Bestie Ferite (petrographic section); f) concrete vault from *Thermae Felices Constantianae*; g) IInd style wall painting from *Domus* of Bestie Ferite (cross section); IVth cen. AD wall painting from Teodorian complex (cross section).

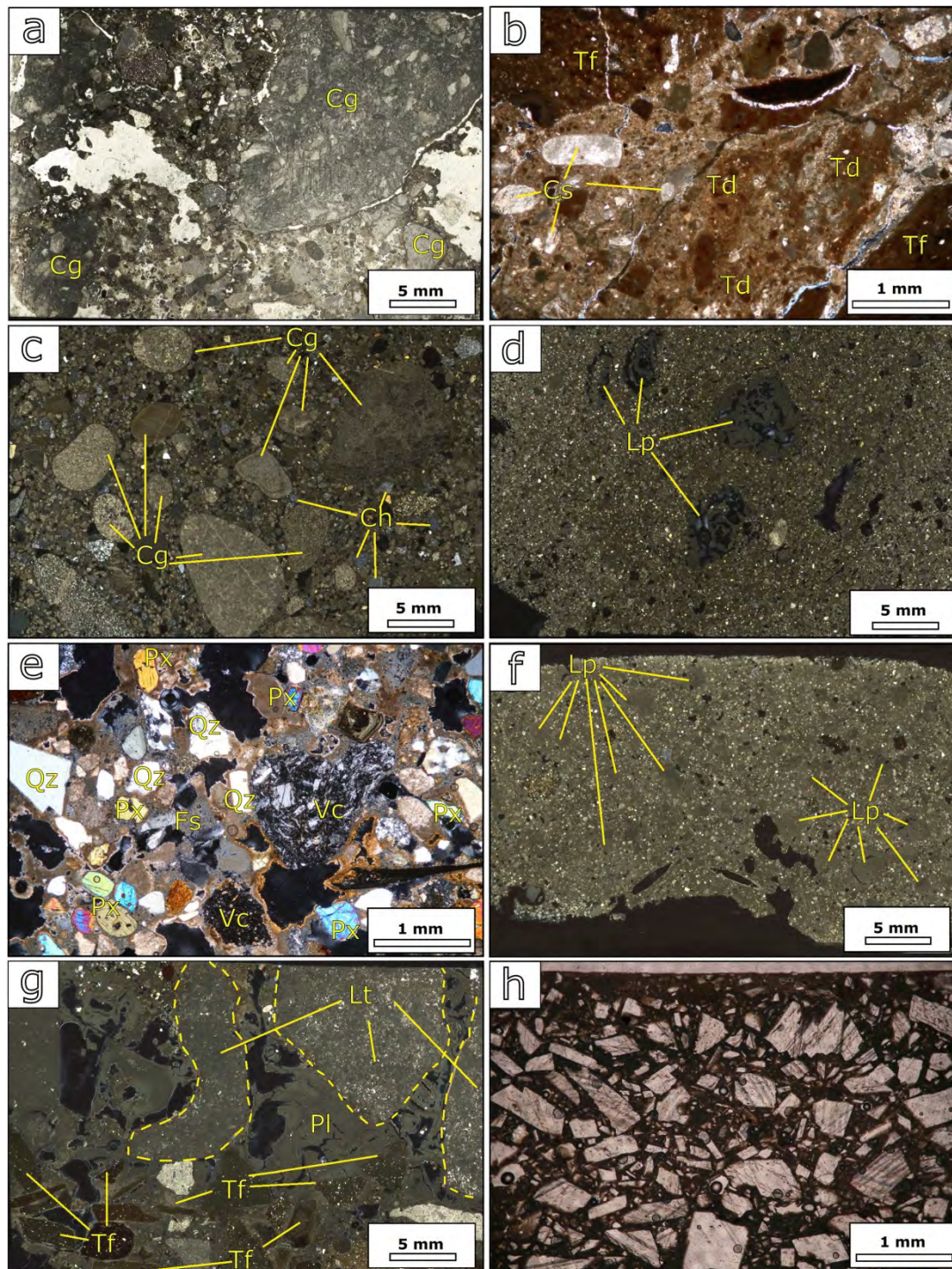


Figure 3. Petrographic analysis on thin section of mortar-based compounds. a) OM-TL-Pn, theatre mortar from platform foundational *opus caementicium* (Cg: carbonate gravel); b) OM-TL-Xn, *terracotta* dust (Td) and *terracotta* fragments (Tf) with secondary aliquots of carbonate sand (Cs) from the bottom *cocciopesto* layer of theatre platform foundation; c) OM-TL-Xn, square rubble masonry wall joint mortar (Cg: carbonate gravel; Ch: chert); d) OM-TL-Xn, brick wall joint mortar (Lp: lime lump); e) OM-TL-Xn, pyroxenes (Px) and volcanic (Vc) aggregates in a wall joint mortar, with subordinated feldspars (Fs) and quartz (Qz); f) OM-TL-Xn, Late Antique wall joint mortar with diffuse presence of lime lumps (Lp); g) cross section of I cen. AD mosaic bedding screed (Lt: limestone *tesserae*; Pl: lime-putty setting bed; Tf: *terracotta* fragments of the nucleus); h) OM-TL-Pn, Ist style wall painting, *intonachino* layer with diffuse euhedral spathic calcite. (OM: optical microscopy; TL: transmitted light; Xn: crossed nicols; Pn: parallel nicols)

Data were collected using a Bragg–Brentano θ – θ diffractometer (PANalytical X’Pert PRO, Co–K α radiation, 40kV and 40 mA) equipped with a real-time multiple strip (RTMS) detector

(X'Celerator by Panalytical). Divergence and anti-scattering slits, of 0.5° and 1° respectively, were mounted in the incident beam pathway. The pathway of the diffracted beam included a Ni filter, a Soller slit (0.04 rad) and an antiscatter blade (5 mm). Data acquisition was performed by operating a continuous scan in the range 3–80° 2 θ , with a virtual step scan of 0.02° 2 θ . Diffraction patterns were interpreted using the X'Pert HighScore Plus 3.0 software by PANalytical, qualitatively reconstructing mineral profiles of the compounds by comparison with PDF databases from the International Centre for Diffraction Data (ICDD). Then, QPAs were performed using the Rietveld method. Refinements were accomplished using the TOPAS software (version 4.1) by Bruker AXS. Finally, the thin section samples were microstructurally and micro chemically characterized by Scanning Electron Microscopy (SEM). A CamScan MX2500 scanning electron microscope was used, equipped with a LaB6 cathode and a four-quadrant solid state BSE detector for imaging. The analytical conditions were as follows: accelerating voltage 20 kV; filament current 1.80 A; emission current 20 μ A; aperture current 300 nA; working distance 20–30 mm. Furthermore, an EDAX–EDS energy-dispersive X-ray fluorescence spectrometer was used for chemical microanalysis, mounted with a Sapphire Detector composed of a LEAP+ Si(Li) crystal and a Super Ultra Thin Window.

Preliminary results

Even if the investigations on mortar-based samples are still ongoing, some preliminary results can be here outlined. The results showed high variability on mortar and concrete “recipes”, depending on their function in structures and chronology of production.

Foundations

Foundational mortars are mainly represented by samples collected from core drillings performed in the substructures of the theatre and amphitheatre of Aquileia, from the upper portion of ground platform of the *Thermae Felices Constantinianae*, and from a particular *opus caementicium* [38] foundation casting identified at the basis of the south-eastern part of the Republican city walls. Different “recipes” were employed in these structures. In both the theatre and amphitheatre platforms, the foundations were made with a > 3 m deep *opus caementicium* structure made of a mixture of lime, gravel and sand to which decimetre sized limestone fragments were added [38]. Petrographically (Figure 2, a-b; Figure 3, a), aggregate fraction is represented by carbonates and secondary silicates (chert, quartz) compatible with sands and gravels locally sourced from river bed deposits of Natiso/Torre and Isonzo [39].

SEM-EDS analysis clearly detected de-dolomitization of dolostone aggregates (Figure 4, a) and alkali-silica reactions of chert (Figure 4, b-c) in the mortars of the *opus caementicium* foundation of the theatre of Aquileia, which produced a diffuse silicate-magnesian gel in the matrix, deeply permeated with calcium of binder fraction [40]. Being absent *pozzolanae* of fictile fraction, it is possible that the use of salt water in the preparation of the mixture could have determined a highly alkaline pH in the compounds activating de-dolomitization and silica reaction of chert fragments [41]. Crystalline C-S-H of AFm phases have not been

detected after XRPD bulk analysis. At the base of the theatre foundation platform a layer of fine *cocciopesto* [38] was placed, probably to contrast rising ground water enhancing waterproofing properties and avoiding water infills (Figure 3, b).

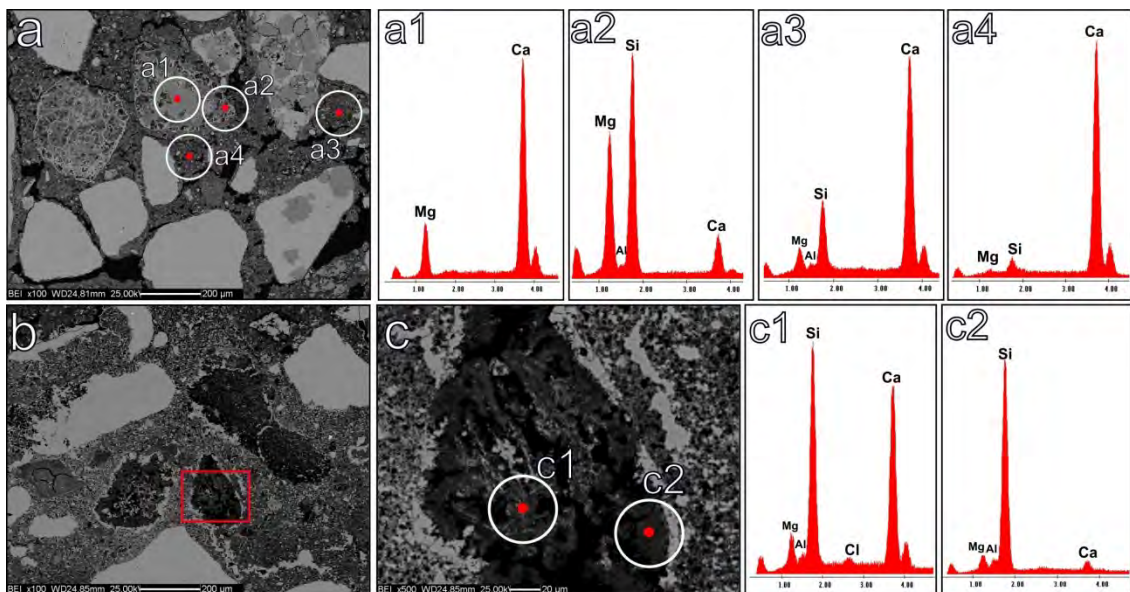


Figure 4. SEM-EDS of theatre *opus caementicium* foundations (BSE images). a) dolostone clasts with clear de-dolomitization phenomena; a1) EDS microanalysis of an un-altered dolostone relict; a2) EDS analysis of de-dolomitized dolostone interface with binder matrix; a3) EDS analysis of mortar matrix; a4) EDS microanalysis of nodules of pure carbonates in mortar matrix; b) altered chert fragments; c) highlighted area of the figure b; c1) EDS analysis of an highly altered portion of a chert fragment with Ca/Mg ions permeated from the matrix; c2) EDS analysis of a chert relict feebly altered.

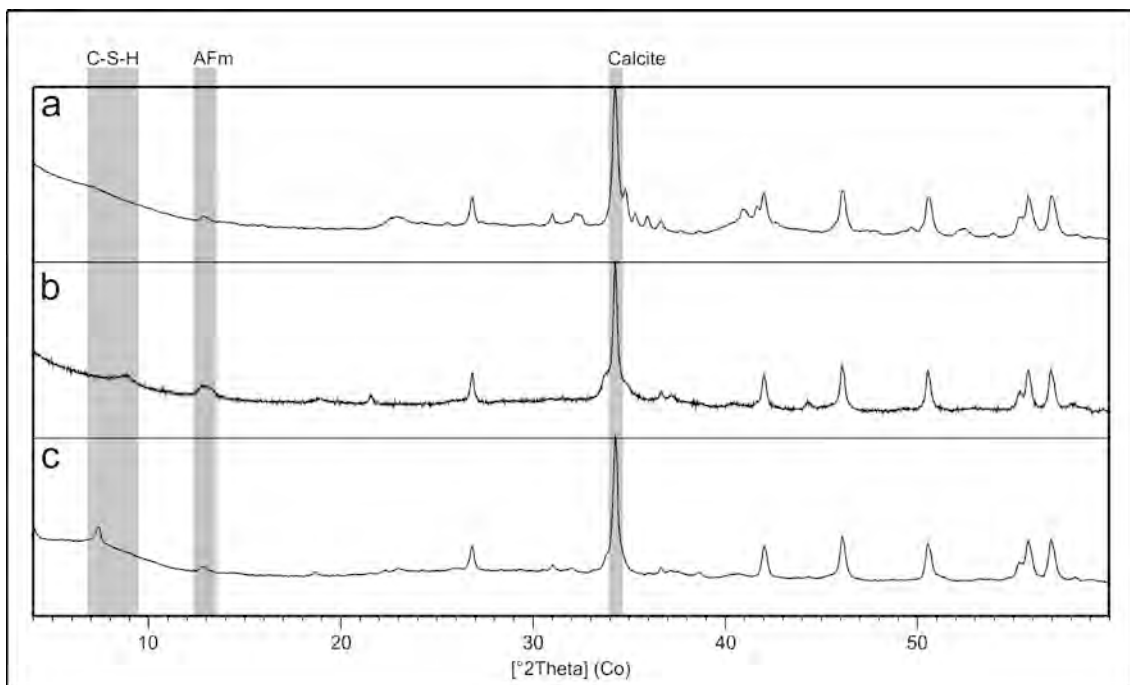


Figure 5. XRPD patterns of the binder fractions of selected hydraulic mortars, with highlighted the main diffraction peaks of the anthropogenic binding phases: a) theatre, *cocciopesto* mortar at the base of the foundation platform; b) *Thermae Felices Constantinianae*, coating mortar of a pool; c) Republican city walls, foundational concrete.

OM coupled with XRPD binder analyses demonstrated the presence of diffused *terracotta* dust in the foundational *cocciopesto* layer of the theatre, which determined the formation of moderate AFm hydrated phases (Figure 5, a).

Cocciopesto mortars with significant amounts of fine *terracotta* dust have been employed also in the foundations and several other structures of the *Thermae Felices Constantinianae*. Also in this case, XRPD binder fraction analyses showed the formation of AFm hydrates, indicating the occurrence of pozzolanic reaction processes (Figure 5, b).

From a petrographic point of view, also the *opus caementitium* structures in the foundations of Republican walls seem to be realized with the traditional mix of raw material defined above in relation to the theatre and amphitheatre foundations. However, the high strength and cohesion of this compound is an indication of relevant hydraulic reaction, as confirmed by the occurrence of Tobermorite 14A and AFm hydraulic phases in the binder fractions (Figure 5, c). The formation of hydrated phases appears to be due to the presence in the matrix of high silica aliquots responsible for the diffuse formation of pure C-S-H. Being absent clasts of volcanoclastic *pozzolanae* (as previously supposed [24]) or dusty *terracotta* fraction, it is probable that a cherty limestone could have been calcined in order to obtain a natural hydraulic lime, as supposed also in the case of the Ponte di Augusto in Narni [42]. Chert aggregate fraction added to the mortars could have been another secondary activator of the pozzolanic reaction [43], mainly if combined with salt water, as previously observed in relation with the theatre.

Wall structures

During the Republican and Proto-Imperial ages, walls in Aquileia were usually made with limestone or sandstone coursed square rubble masonry [3]. Jointing mortars were produced with lime mortars. The aggregate fraction is represented by dominant carbonate lithic particles, with secondary aliquots of chert and quartz and traces of sandstones, with binder/aggregate (B/A) ratios around 1:2 (Figure 2, c; Figure 3, c). In the case of brick walls [3], finer mortars produced mixing lime and well-graded carbonate/silicate sand were most commonly employed (Figure 2, d; Figure 3, d). Mineralogical analyses on bulk samples revealed calcite and dolomite as prevalent fraction, while feldspars and micas occur in modest amounts always < 5%. Amorphous and smectite phases are related mainly to clay inclusions which are present, in different aliquots, in all the compounds. Also in this case, in mayor part of the samples aggregate sands and gravels are locally sourced from river bed deposits of Natiso/Torre and Isonzo [39]. Only in a few occasion aggregates are not local. This is the case of two jointing mortar samples were aggregates are represented by abundant pyroxenes, volcanic clasts and feldspars (Figure 3, e). It is possible to assume that these non-local sands represent the reuse of ballast bags which originally reached Aquileia via fluvial or terrestrial routes.

In other occasions, mortars with high ratios of chert gravels were used in the walls of the Republican *Domus of Tito Macro*. The high oxidization of chert and carbonate aggregates, as well as the absence of dolomite fraction, indicate a possible provenance from paleo fluvial deposits, partially pedogenized, which should be located in the fluvial plain of the foothills area of Friuli region, northern of Aquileia⁶. The reason for the choice of these quarrying basins is still unclear.

It has been observed a progressive modification in “recipes” of jointing wall mortars, as revealed from the analysis of IV-V century AD city wall and housing structures. Late Antique mortar-based compounds present high lime binder fraction in B/A ratios of $\geq 1:1$, highly sorted carbonate aggregates and frequent lime lumps inclusions (Figure 3, f). The widespread praxis of spoliation and calcination of limestones and marbles during late antiquity, observed also in the case of Aquileia [3], could be addressed as a cause of the large availability of quicklime that could have determined this variation of “recipes”.

Finally, it has been observed the use of shells as aggregate fraction in the mortars of the Bizantine city defensive system. This characteristic appears to be common in Bizantine period: shell-rich mortars have been employed in the jointing mortars of city walls of Leptis Magna, but attestation of these practices traces back even to the Minoan period [44]. The presence of prevalent coastal shell species, probably coming from beach shoreline proximal area, demonstrates the substantial modification of sand quarry zones, probably as consequence of the loss of control of the inland territories north of Aquileia after barbarian invasions [20].

Vaults

Three samples of mortars from the vaults of the Late Antique *Thermae Felices Constantinianae* have been analysed. As widely documented in literature [45], lightweight *caementa* were employed as aggregate in order to reduce the weight of the vaults of *Thermae Felices Constantinianae*. In this context, lightweight *caementa* are constituted of three different species of volcanic tuff scoria which were surely imported (Figure 2, f), considering that there are no such formations in the Friulan territories and surrounding areas. Petro-chemical trace elements analyses will be performed for the determination of the provenance of these materials. The results will be compared with the volcanoclastic tuff and scoria petrochemical signature database of the Latial and Campanian volcanic formations [46, 47].

Floors and floor beddings

Floor bedding mortars refer mainly to mosaics and *opus sectile* bedding screeds. As recently published [23, 26], we observed that Late Republican and Proto-Imperial mosaic were realized over bedding screeds generally composed of two layers. The inner one, that can be

⁶ We are grateful for the advice to prof. A. Fontana, University of Padova.

associate with the Vitruvian *rudus* (VII, 1, 3), is made of a concrete with broken *terracotta* fragments composed of sole lime and centimeter sized *terracotta* fragments [38]; the outer layer, that can be associated with the *nucleus* (VII, 1, 3), is a *cocciopesto* mortar made of lime and millimeter-sized *terracotta* fragments [38]. In high-quality mosaics, *tesserae* were usually placed over a millimeter-thick layer of pure lime-putty [38] sometimes mixed with sparse spathic calcite (Figure 3, g). Even if not attested in ancient literature, this *stratum* has been already observed [48] and it was probably made to allow a more precise setting of the *tesserae* along during the mosaic production.

Opus sectile pavements were placed over thicker screeds made of *cocciopesto* mortars or concrete with broken *terracotta*. The presence of diffuse *terracotta* dust, observed via OM analyses, substantially distinguish mortar-based compound for *opus sectile* screeds from the mosaic bedding ones.

Also in this case, a variation along time of materials and “recipes” has been proved. If *opus sectile* construction traditions do not seem to be substantially modified along time, Late Antique mosaics bedding mortars in private contexts (houses) were frequently made over a single 2 cm thick layer of weakly cohesive/highly porous lime mortar (Figure 2, e). Aggregate fraction is constituted of moderately sorted carbonate sands, mixed with chert and quartz, while *terracotta* fraction appears to be absent. This clear downgrade in the quality and durability of mosaic foundations clearly reflects a progressive loss of crafts skills and economical power of customers during Late Antiquity [23, 26].

Wall paintings

Petro-mineralogical composition of wall-painting pictorial layers and *tectoria* has also been preliminary described elsewhere [25, 28]. Here we just recall the main features of these materials. In Ist to IVth style (II century BC to I century AD) wall-paintings, the *tectorium* consists of one up to two *intonachino* layers followed by 1 up to 4 inner *arriccio* and *rinzafo* layers (Figure 2, g). This sequence of *strata* recalls Vitruvian precepts for *opus albarium* (VII, 3, 6). *Intonachino* layers are always made with a bright, highly cohesive *stucco* mortar [38] composed of pure lime mixed with well-sorted and perfectly mixed euhedral clasts of spathic calcite and sporadic marble fragments (Figure 3, h). Layer thicknesses range from around 0.8 cm up to 1.5 cm. Mayor modifications in the *intonachino* composition were highlighted in relation to Middle and Late Imperial wall-painting samples. The upper layer appears to be a unique *stratum*, 0.1 up to 0.2 cm thick (Figure 2, h), composed of pure lime mixed with sporadic local carbonate/silicate fluvial sands, while spathic calcite and marble fragments are totally absent. As observed in relation with mosaics, this clear modification in wall-painting *tectorium* composition has been connected to a progressive loss of quality and prestige of pictorial art during Late Antiquity in Aquileia [25, 28].

Conclusions

This ongoing project is providing intriguing results in the field of the researches on mortar-based compounds used in antiquity. We observed a high specialization on “recipes” in relation to the function of mortars and concretes. Chronology appears to have an important role in the composition of mortar-based compounds. The analysis of the “recipes” could be pointed out as a way for dating Aquileia structures and buildings, supporting traditional dating methodologies based on stratigraphy and pottery chrono-typologies. Quarrying area are being analysed and variations in selections of raw materials will be discussed in relation with historical and economical background of Aquileia. The continue crosscheck of data obtained from such an extensive sampling is giving valuable insights for the deciphering of the relations among crafts and artisans in ancient construction and decorative activities. These considerations could be stressed as a way for renovating the discussion on the Art of Making in a crucial centre for the history of Roman *Cisalpina* as it was Aquileia.

Author contribution

Introduction: JB, GA; “State of Art” discussion: SD; Context of interest selection: SD, JB; Sampling: SD, JB; Analytical methodology: SD, MS, GA; Samples preparation and analysis: SD, MS; Data processing and interpretation: SD, JB; Conclusions: SD; Supervision: JB, GA; Writing: SD

References

1. Portulano B, Urban M (2001) *Materiali e tecniche murarie nel Basso e Medio Friuli in età romana*. Editreg, Trieste
2. Bacchetta A (2003) *Edilizia rurale romana. All’Insegna del Giglio*, Firenze
3. Previato C (2015) *Aquileia. Materiali, forme e sistemi costruttivi dall’età repubblicana alla tarda età imperiale*. Padova University Press, Padova
4. Pizzol L (2015/2016) *Archaeometric analyses of Roman Mortars in Italy: a historiographic review*. MA Thesis, Sup. Prof. J Bonetto, University of Padova
5. Bugini R, Folli L (2013) *Critères pour la comparaison des enduits peints romains de la Lombardie*. *ArcheoSciences*. <https://journals.openedition.org/archeosciences/3973>
6. Mazzocchin G A, Agnoli F, Mazzocchin S, Colpo I (2003) *Analysis of pigments from Roman wall paintings found in Vicenza*. *Talanta*. <https://www.sciencedirect.com/science/article/pii/S0039914003003230>
7. Mazzocchin G A, Agnoli F, Salvadori M (2004) *Roman age wall paintings found in Pordenone, Trieste and Montegrotto*. *Talanta*.

<https://www.sciencedirect.com/science/article/pii/S0039914004001845>

8. Mazzocchin G A, Del Favero M, Tasca G (2007) Analysis of pigments from Roman wall paintings found in the “Agro Centuriato” of Julia Concordia (Italy). *Anal. Chim.* <https://doi.org/10.1002/adic.200790075>
9. Gutman M, Lesar Kikelj M, Zupanek B, Kramar S (2016) Wall paintings from the Roman *Emona* (Ljubljana, Slovenia): characterization of mortar layers and pigments. *Archaeometry*. <https://doi.org/10.1111/arcm.12167>
10. Baccelle Scudeler L, De Vecchi G (2003) Tessitura e composizione degli aggregati presenti nella malta dell'*opus caementicium* nell'anfiteatro romano di Padova. In: Tosi G *Gli edifici per spettacoli nell'Italia romana*, 1, Quasar, Roma
11. Costa U, Gotti E, Tognon G (2000) Nota tecnica: malte prelevate da mura antiche dallo scavo della banca popolare di Ravenna. In: Quilici Gigli S, Quilici L (eds) *Fortificazioni antiche in Italia: età repubblicana*. L'Erma di Bretschneider, Roma
12. Bugini R, Folli L (2007) Le malte. In: Roffia E (ed) *Dalla villa romana all'abitato altomedievale*. Scavi archeologici in località Faustina - S. Cipriano a Desenzano. Edizioni ET Milano, Milano
13. Folli L, Bugini R (2016) Milano, via Brisa, scavi del 1959 (Via Brisa, 1959). Le malte. *Quaderni del Civico museo archeologico e del civico Gabinetto numismatico di Milano* 5:92-93
14. Grassi G, Stafferi L, Delorenzo R, Papotti L (1993) Calcestruzzi tardo-romani: le mura e le porte di Susa. In: Biscontin G, Mietto D (eds), *Calcestruzzi antichi e moderni: Storia, Cultura e Tecnologia*, Libreria Progetto, Padova
15. Sfrecola S (2015) Analisi archeometriche sulle malte murarie dell'antica Segusio. In: *Segusium, L'arco di Susa e i monumenti della propaganda imperiale in età augustea*. Graffio snc, Susa
16. Kramar S, Zalar V, Urosevic M et al (2011) Mineralogical and microstructural studies of mortars from the bath complex of the Roman *villa rustica* near Mošnje (Slovenia). *Material Characterization*. <https://doi.org/10.1016/j.matchar.2011.07.019>
17. Maritan L, Mazzoli C, Pompermaier A et al (2006) Le malte dei pavimenti di età imperiale del complesso di Via Neroniana (Montegrotto Terme - Padova): indagini preliminari. In: D'Amico C (ed) *Proceedings del Convegno Nazionale AIAr*. Pàtron, Bologna
18. Bugini R, Folli L, Portulano B, Roffia E (2012) The analytical approach to the Roman mosaics. A case study in Northern Italy. In: Sahin M (ed), *XI International Colloquium on Ancient Mosaic*. Ege Yayinlari, Istanbul

19. Portulano B, Bugini R, Folli L (2002) Caratteri stratigrafici di mosaici romani di Aquileia. In: Biscontin G, Driussi G (eds) *I mosaici. Cultura, Tecnologia, Conservazione*. Arcadia ricerche, Venezia
20. Ghedini F, Bueno M, Novello M eds (2009); *Moenibus et portu celeberrima*. Aquileia, storia di una città. Ist. Poligrafico dello Stato, Roma
21. Ghedini F, Bueno M, Novello M, Rinaldi F eds (2017), *I pavimenti romani di Aquileia. Contesti, tecniche, repertorio decorativo*. Padova University Press, Padova
22. Salvadori M, Scagliarini D eds (2015) *Tect 1. Un progetto per la conoscenza della pittura parietale romana nell'Italia settentrionale*. Padova University Press, Padova
23. Dilaria S, Addis A, Secco M et al (2016) Vitruvian recipes in Roman Aquileia (Italy): the floor bedding mortars of Bestie Ferite and Tito Macro *domus*. In: Papayianni I, Stefanidou M, Pachta V (eds) *Proceedings of the 4th Historic Mortars Conference*. Aristotle University of Thessaloniki, Thessaloniki
24. Bonetto J, Artioli G, Secco M, Addis A (2016), *L'uso delle polveri pozzolaniche nei grandi cantieri della Gallia Cisalpina in età romana repubblicana: i casi di Aquileia e Ravenna*. In: DeLaine J, Camporeale S, Pizzo A (eds) *Arqueología de la Construcción V. Man-made materials, engineering and infrastructure*. Consejo Superior de Investigaciones Científicas, Madrid
25. Salvadori M, Dilaria S, Sebastiani L (2017) *La ricerca archeometrica applicata allo studio della pittura parietale romana: il caso di Aquileia (UD)*. In: Portale E C, Galioto G (eds), *Scienza e archeologia. Un efficace connubio per la divulgazione della cultura scientifica*. Edizioni ETS, Pisa
26. Secco M, Dilaria S, Addis A et al (2018) *Evolution of the Vitruvian recipes over 500 years of floor making techniques: the case studies of Domus delle Bestie Ferite and Domus di Tito Macro (Aquileia, Italy)*. *Archaeometry*. <https://doi.org/10.1111/arcm.12305>
27. Dilaria S, Secco M (2018) *Analisi archeometriche sulle miscele leganti (malte e calcestruzzi)*. In: Basso P, *L'anfiteatro di Aquileia: nuovi dati da nuovi scavi*, SAP publication, Quingentole (Mantua)
28. Sebastiani L, Dilaria S, Salvadori M et al (2019) *Tectoria e pigmenti nella pittura medio-imperiale e tardoantica di Aquileia: uno studio archeometrico*. In: Salvadori M, Fagioli F, Sbrolli C (eds) *AIRPA I - Nuovi dati per la conoscenza della pittura parietale antica*. Edizioni Quasar, Roma.
29. Bueno M, Centola V, Ghiotto A R (2014) *Le domus dei fondi ex-Cossar e delle Bestie Ferite: due esempi di trasformazione delle case aquileiesi in età tardoantica*. *Aquileia Nostra LXXXIII-LXXXIV:171-181*

30. Tiussi C (2018) Aquileia: *Domus* e Palazzo episcopale. *Archeologia Viva* 190:64-55
31. Ghiotto A R, Berto S, Deiana R et al 2018, Il teatro romano di Aquileia: l'individuazione dell'edificio e lo scavo della cavea. FOLD&R.
<http://www.fastionline.org/docs/FOLDER-it-2018-404.pdf>
32. Basso P (2018) L'anfiteatro di Aquileia: nuovi dati da nuovi scavi. SAP, Quingentole (Manua)
33. Rubinich M (2014) Le Grandi Terme Costantiniane. *Aquileia Nostra*, LXXXIII-LXXXIV:97-117
34. Bonetto J (2004) Difendere Aquileia, città di frontiera. In: Cuscito G (ed) *Aquileia dalle origini alla costituzione del Ducato longobardo: topografia, urbanistica, edilizia pubblica*. Editreg, Trieste
35. Cottica D, Bertoldi F, Cameriere R et al (2017) Le attività di scavo e ricerca del Dipartimento di Studi Umanistici a Pompei ed Aquileia e gli studi paleobiologici sulla necropoli di piazza Corrubbio a Verona. In: Sperti L (ed), *Giornata dell'archeologia: scavi e ricerche del Dipartimento di Studi Umanistici*. Edizioni Ca' Foscari, Venezia
36. Rietveld H (1969) A profile refinement method for nuclear and magnetic structures. *J. Appl. Crystallogr.* <https://doi.org/10.1107/S0021889869006558>
37. Marzaioli F, Nonni S, Passariello I et al (2013) Accelerator mass spectrometry 14C dating of lime mortar: Methodological aspects and field study applications at CIRCE (Italy), *Nucl. Instr. and Meth.* <https://doi.org/10.1016/j.nimb.2012.09.006>
38. Ginouvès R, Martin R (1985) *Dictionnaire méthodique de l'architecture grecque et romaine, Tome I, Matériaux, techniques de construction, techniques et formes du décor*. Publications of the École Française de Rome, Rome.
39. Gazzi P, Zuffa G, Gandolfi G, Paganelli L (1973) Provenienza e dispersione litoranea delle sabbie delle spiagge adriatiche fra le foci dell'Isonzo e del Foglia: inquadramento regionale. *Memorie della Società Geologica Italiana* 12:1-37
40. Katayama T (2010) The so-called alkali-carbonate reaction (ACR). Its mineralogical and geochemical details, with special reference to ASR. *Cem Concr Res.* <https://www.sciencedirect.com/science/article/pii/S0008884609002737>
41. Karim M E, Jahangir A, Hoque S (2017) Effect of salinity of water in lime-fly ash treated sand. *International Journal of Geo-Engineering.* <https://doi.org/10.1186/s40703-017-0052-0>
42. Cantisani E, Cecchi A, Chiaverini I et al (2002) The binder of the «Roman Concrete» of the Ponte di Augusto at Narni (Italy). *Periodico di Mineralogia* 71:113-123

43. Pecchioni E, Fratini F, Cantisani E (2014) Atlante delle malte antiche in sezione sottile al microscopio ottico. Nardini editore, Firenze
44. Dilaria S (2017) Costruire ingegnosamente riutilizzando materiali poveri. L'impiego di conchiglie a fini edilizi ad Aquileia tra età repubblicana e tarda antichità. Reudar. <https://doi.org/10.21071/reudar.v1i0.10162>
45. Lancaster L C (2015) Innovative Vaulting in the architecture of the Roman Empire. 1st to 4th centuries CE. Cambridge University Press, Cambridge.
46. Marra F, D'Ambrosio E, Gaeta M, Mattei M (2016) Petrochemical identification and insights on chronological employment of the volcanic aggregates used in ancient Roman mortars. Archaeometry. <https://doi.org/10.1111/arcm.12154>
47. Lancaster L C, Sottili G, Marra F, Ventura G (2011) Provenance of lightweight volcanic stones used in ancient Roman concrete vaulting: evidence from Rome. Archaeometry. <https://doi.org/10.1111/j.1475-4754.2010.00565>
48. Moore R E M (1968) A newly observed *stratum* in Roman floor mosaics. Am. J. Arch. 72(1):57-68

Fernandina old Wall of Lisbon – Characterization towards its preservation

Leandro Gomes¹, Paulina Faria², Vitor Silva¹, António Santos Silva³

(1) Dept. of Civil Engineering, Faculty of Sciences and Technology – NOVA University of Lisbon, lf.gomes@campus.fct.unl.pt; vmd.silva@fct.unl.pt

(2) CERIS and Dept. of Civil Engineering, Faculty of Sciences and Technology – NOVA University of Lisbon, paulina.faria@fct.unl.pt

(3) Dept. of Materials, National Laboratory for Civil Engineering - Lisbon, ssilva@lnec.pt

Abstract

The Fernandina Wall of Lisbon started to be built in 1373 and had an extension of 4.69 km in the old city. This Wall in nowadays completely “emerged” and surrounded by the city. Several interventions mainly performed on old buildings confining with, or including, the Wall have been held in the last years. Nevertheless, so far there is a lack of information on the original materials and the ones applied in the history of interventions. Seven sections of the Wall were inspected, and the constitutive materials extracted from rammed earth, rubble stone and regular stone masonries to be characterized in laboratory. *In situ* non-destructive testing on two wall sections allowed to preliminary characterize original and more recent materials and start gathering results for a heritage database that will record data relating to the history, properties and performance of materials, aiming supporting future interventions.

Introduction

The historical and architectural Portuguese heritage is composed of several monuments, buildings and other structures that includes the Fernandina Wall, in Lisbon. The Wall construction intended to ensure the defense of the city due to intense and continuous growth because the Moorish Fence could no longer ensure the protection of the historical and commercial parishes that made part of the city in the 14th century. Built during the reign of king D. Fernando, in the second half of the 14th century, the Fernandina Wall construction began in 1373 and its completion was in 1375, although there are some documents that mentions that the full completion was in 1378 [1]. The general and original design of this Wall is composed by what is similar to two large circles that are involving the central circle where Moorish Fence is located [2]. It is composed by 76 towers and 35 entrances, with an extension of 4.69 km, having two main sections: East, limited between St. George’s Castle and Terreiro do Trigo Street, and West, starting also at the St. George’s Castle and finishing at Misericórdia Street (Figure 1).



Figure 1 – Lisbon’s city plan with Moura Wall in the central area, Fernandina’s Wall outlined [1] and surveyed sections: (1) – Jogo da Pêla Tower, (2) – Santana’s Street building, (3) – Independence Palace, (4) – Gil Vicente’s School, (5) – Rosa Palace, (6) – Bragança Terraces Residence, and (7) – Corpo Santo Hotel

The Fernandina Wall is nowadays completely “emerged” and surrounded by the city. Defining an area of 101 hectares around the 14th century city, nowadays there are elements of this structure, such as main walls, towers, small towers (in Portuguese known by “cubelos”), entrances and a few small doors (in Portuguese called “postigos”), integrated into conventional buildings, hotels, schools and other infrastructures. Those elements do not have the same material composition. In total and according to Vieira da Silva [1] 86.000 m³ of masonry are estimated in its construction. Its average height is 8 m and the thickness is between 1.75 and 2.00 m, according [2].

Several interventions mainly performed on old buildings confining with, or including, sections of the Wall have been held in the last years. Nevertheless, so far, there is a lack of information on the original materials and the ones applied in the history of interventions.

This paper presents the first results of an experimental campaign performed to overcome this lack in information, with an overview of the sections of the Wall inspected and where masonry and render mortar samples were extracted, with preliminary results of physical and mechanical *in situ* non-destructive tests.

Surveyed sections of the Fernandina Wall of Lisbon

Previous studies about the Fernandina’s Wall of Lisbon have not been centred in the materials characterization and on the identification of their building construction

techniques. In order to improve this kind of information several sectors of this Wall were inspected, being the description presented in the following sections.

Jogo da Pêla Tower

This Tower is one of the few remaining towers that composed this Wall (Figure 2). It is located very closed to Martim Moniz Square (Figure 1 (1)), and on the West section of the Wall. Its transversal dimensions are 6 m x 8 m with a height of 11.30 m. Figure 2 presents an example of the changes occurred in this Tower in last 70 years. In the past, shops and a factory have been installed there. In the last years, the annexed volumes had been demolished and a provisional coverage was placed by the Lisbon city council heritage, that has developed interventions of geological and archaeological nature [3-4] that helped this research.

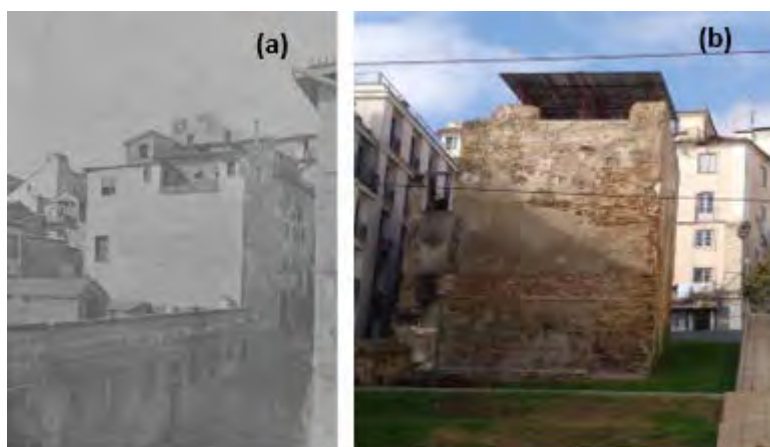


Figure 2 – Jogo da Pêla Tower: (a) in 1949 and (b) in 2019

On the top of the Tower there is a void, with about 2.5 m x 3 m, that is rendered, where some samples were extracted horizontally and vertically to know the stratigraphy of this rubble stone masonry. The visual analysis of the core samples extracted (Table 1) revealed that the inner nucleus of the tower is composed by a rubble limestone masonry with a lime mortar with red ceramic aggregates, apart from siliceous sand. Different limestone types could be observed (Table 1).

Tower at Santana's Street Building

This tower is located inside a building at Santana's Street 131-137 (Figures 1 (2) and 3). It is a small tower named "Norte do Mosteiro da Encarnação", which is part of the West section of the Wall, with dimensions of 8 m x 8 m and a height of about 11 m. The tower façade visible in the building (Figure 3 (b)) was built in rubble stone masonry and has regular stone masonry in the visible corner. A horizontal sample core was extracted at a height corresponding to the first floor of the building (Table 1).

The sample observation confirms the use of rubble stone technique. There is an intervention going on, with supervision of the Municipality, on the only private apartment with access to the top of the small tower.

Table 1 – Samples s extracted from surveyed sites

Wall section and sample code	Sample details		
1. Jogo da Pêla Tower - Inside JP_T1, JP_T2 and JP_T3	 Horizontal core: JP_T1	 Vertical core: JP_T2	 Vertical core: JP_T3
2. Santana's Street small tower CS_C	 Horizontal core: CS_C		
4. Gil Vicente School Wall - EGV_M1 Wall - EGV_M2 Small tower - EGV_C	 Horizontal core: EGV_M1	 Horizontal core: EGV_M2	 Horizontal core: EGV_M3
6. Bragança Terraces Residence Tower: TB_T1 and TB_T2 South Wall: TB_M1 and TB_M2	 Vertical core: TB_T1	 Vertical core: TB_T2	 Horizontal core: TB_M1
7. Corpo Santo Hotel João Bretão Tower: CSH_T1 and CSH_T2	 Vertical core: CSH_T1	 Vertical core: CSH_T2	

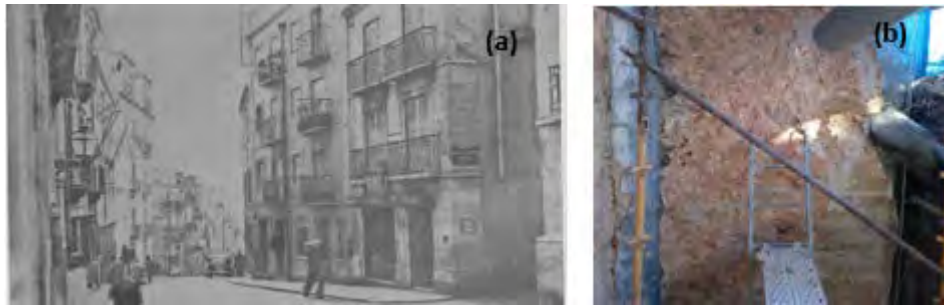


Figure 3 – (a) Santana's Street in 1949 [1] and (b) wall masonry of the tower inside the building

Independence Palace

This Palace is classified as a national Portuguese monument and is located at São Domingos Square (Figure 1 (3)) very close to the popular Rossio Square. Presently, it is the headquarters of Historical Society of the Independence of Portugal. In the back part of the palace there is a garden and a section of the Fernandina Wall with around 20 meters long (Figure 4). This wall section has been subjected to intensive weathering exposure and to several interventions, such as a staircase on its top and the repair with different mortars - Figure 4. Although it was not possible to extract any core sample from this section, the façade that is visible seems to be a rubble limestone masonry.



Figure 4 – Wall section at the north of Independence Palace garden: (a) general view and (b) detail of the wall

Gil Vicente's school

The walls of the garden of Gil Vicente's School presents one of the most protected and preserved sections of the Fernandina Wall, with a well preserved section of about 50 m, with small towers and large walls. Sited on the eastern section of the Fernandina Wall (Figure 1 (4)), it was the only surveyed site visited in the East section. The building techniques used includes stone masonry, mainly in the small towers base and corners, as well as rammed earth in other areas of the small towers (Figure 5 (a)) and on a Wall section that could be observed (Figure 5 (b)). It was possible to induce that the rammed earth was air lime stabilized because white friable nodules could be easily observed on the rammed earth surface, dispersed within the earthen matrix. The stabilization of rammed earth with air lime was a common technique on Portuguese defensive structures like castles and fortresses [5]. The rammed earth section presented a very eroded render with lack of cohesion that was falling, exposing the rammed earth technique (Figure 5 (b)).



Figure 5 – Gil Vicente’s School: (a) small tower with stone masonry corners and rammed earth and (b) rammed earth section of the Wall

Two samples were extracted, one from the wall and another from the small tower. The observation of these samples confirms that they are built with rammed earth technique. Also, an intervention held in 2016 [6] in the construction of a car parking in the opposite side of this Wall section confirms this technique.

Rosa Palace

This palace is located at the beginning of the western section of the Fernandina Wall, very closed to the St. George Castle (Figure 1 (5)). In this section it is possible to find some different construction characteristics, including the foundations on geological substrate and a tunnel excavated inside of the Wall. Figure 6 (a) shows a section of the Wall and Figure 6 (b) the palace façade facing south. Due to the masonry characteristics (a rubble stone masonry) it was not possible to extract core samples from Rosa Palace. The palace, with a very impressive area, will soon be transform into a historical hotel.

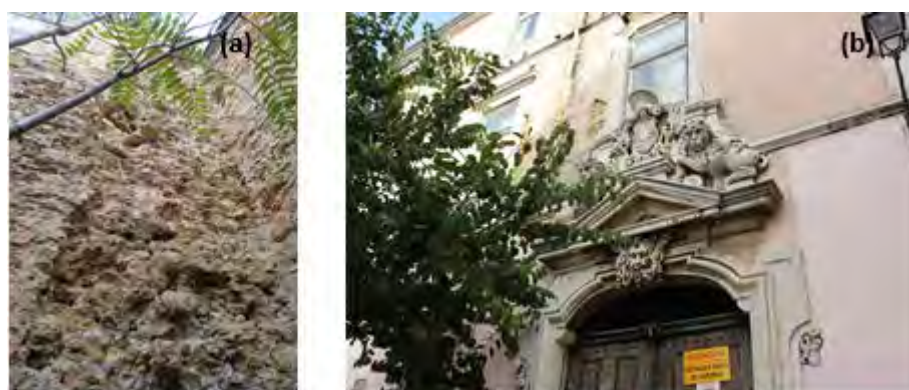


Figure 6 – Rosa Palace: (a) Wall section and (b) south façade of the palace

Bragança Terrace Residences

These residences belongs to an apartment complex designed by the famous Portuguese architect Siza Vieira, located in the old city centre of Lisbon, very closed to Cais do Sodré Square (Figure 1 (6)). This complex built in 2003 in the surrounding area of the old fortress, has one of the best places to see sections of the Wall in two distinct structures: main walls

(Figure 7 (a)) and one tower called “Conde Vimioso Tower” (Figure 7 (c)). The tower presents a base where the ground foundation is being exposed. The upper levels of the Tower present stone masonry. The Wall sector facing west is long (more than 20 m) and could not be accessed due to a building that is being retrofitted in its back. The Wall sector facing south (with about 10 m long) presents lack of cohesion, significant thickness lacunae (Figure 7 (b)), efflorescence’s and biological development. This is partially covered by the new buildings, being always in the shadow, and since the last couple of years it seems to have the rear surface waterproofed by construction works that have been performed in the adjacent building. Therefore, the microclimate of the Wall section has completely changed, being this part very damaged nowadays. There is also a low high remain of the Wall exposed to east and west with more than 10 m long. After the conclusion of the construction of this apartments complex, a replica of an original Wall sector was made following the continuity of the east-west exposed wall and the original plan of the Fernandina’s Wall, with more than 10 m long, using hydrated air lime-stabilized rammed earth technique [7] (Figure 7 (d)), and being also covered by the building. Two core samples were extracted vertically from the top of the tower and another two from the Wall sector facing south (Table 1). The tower seems to be mainly filled with rubble stone, including ceramic fragments and different types of limestones, namely Lisbon’s Miocene fossiliferous limestone. The wall samples observation confirmed that it was built with rammed earth technique.

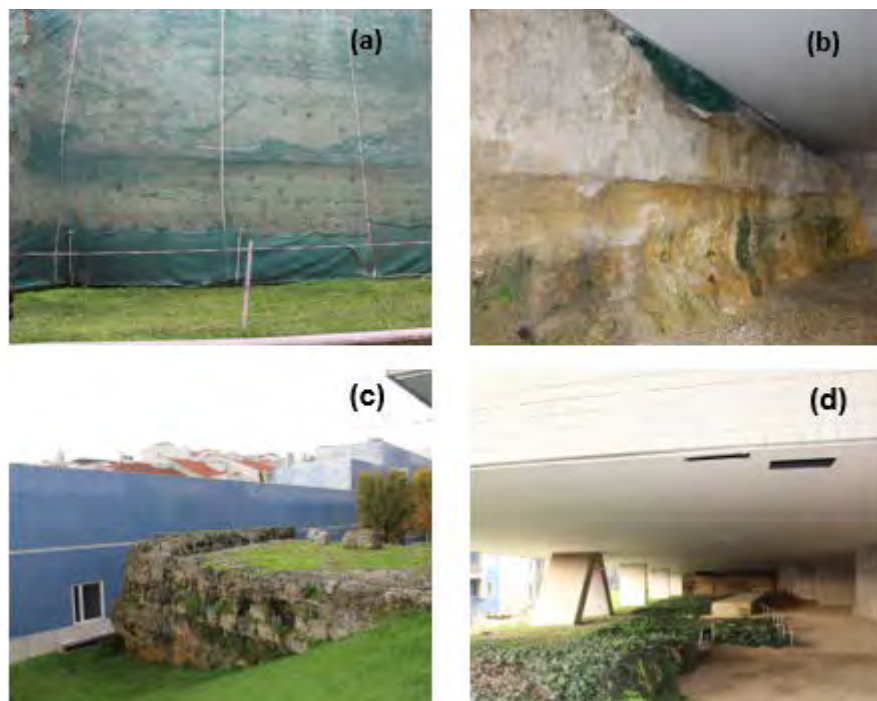


Figure 7 – Fernandina Wall in Bragança Terraces Residence: (a) rammed earth wall section facing West showing the holes of the originally used formwork; (b) rammed earth wall section exposed to south but presently under a building; (c) part of the tower with stone masonry; (d) remains of an old Wall section and its replica

Corpo Santo Hotel



Figure 8 – Corpo Santo Hotel: (a) João Bretão Tower and (b) nucleus of the tower

According to Vieira da Silva [2], this part of the city is lacking in studies about the Fernandina Wall. Nevertheless, when Corpo Santo Hotel start being built, an archaeological and restoration campaign was performed and important data was collected [8-9], having the Hotel won an international prize for this preservation. This part of the Wall was built to protect attacks from pirate ships entering the Tagus river (Figure 1 (7)). Nowadays, the hotel offers a large room where remains of the João Bretão Tower and a section of the adjacent Wall are visible (Figure 8). Two core samples were extracted from the top of João Bretão Tower. These samples allowed to observe the top layers of the rubble stone masonry walls of the tower.

***In situ* testing methods**

During the sampling campaign it was possible to perform some *in situ* testing in Jogo da Pêla Tower and in Bragança Terraces Residence.

Pendular sclerometer test

Pendular sclerometer was carried out according ASTM C805-08 standard [10]. This test consists on the register of a directly measured rebound value that pendulum causes in a contact with a vertical surface (Figure 9 (a)). To do this type of testing the equipment should be vertical and with a stable and firm position to be dropped through a spring producing an impact in the wall [11].

Martinet Baronnie – Sphere impact test

This test uses the Martinet Baronnie apparatus [12]. Consists on the application of a steel sphere with 50 mm of diameter causing an impact with the energy of 3 Joules [13]. This impact resistance is evaluated by measuring the diameter caused in the surface that is being considered and if there is cracking or not (Figure 9 (b)).

Karsten tubes – Water absorption test

The water absorption test under low pressure was performed based on EN 16302 standard [14] specific for cultural property materials, with Karsten graduated tubes with a scale of 0 to 4 ml of water capacity [11] (Figure 9 (c)).



Figure 9 – *In situ* tests: (a) Pendular sclerometer in Bragança Terraces Residence wall section facing south; (b) Sphere impact test at a wall facing East inside Jogo da Pela Tower and (c) Karsten tubes test at a wall section facing East at Bragança Terraces Residence

A defined area of water contacts with the test surface by the application of a waterproof plasticine. The water volume absorbed during short intervals of time is registered; in the present case, up to 30 min or when all the 4 ml were absorbed due to the type of porous materials in presence. Results are expressed by absorption curves [14].

Results and discussion

Surface hardness by pendular sclerometer

Figure 10 presents the pendular sclerometer results for the different analysed zones of the West, East and North walls of Jogo da Pêla Tower, and in Figure 11 the same for the East exposed Wall section base and replica in Bragança Terraces Residence, south exposed Wall section base, upper level and recently sample with render. The surface hardness values in Jogo da Pêla Tower revealed different trends, depending on the render zone tested, being the average values between 63-69 Vickers (Figure 10). For Bragança Terraces Residence, it can be observed that surface hardness of both original and replica of the East Wall section are quite similar - 56 Vickers. The same for base and upper level of South Wall section, with 70-73 Vickers, presenting the recently rendered sample a lower value (56 Vickers), inducing compatibility with the original Wall (Figure 11).

Although the Jogo da Pêla Tower sections were rendered rubble stone masonry, results are not significantly different from rammed earth wall sections of Bragança Terraces Residence. The results presented by [12] applied on earth plasters reveals average values between 35-45 Vickers.

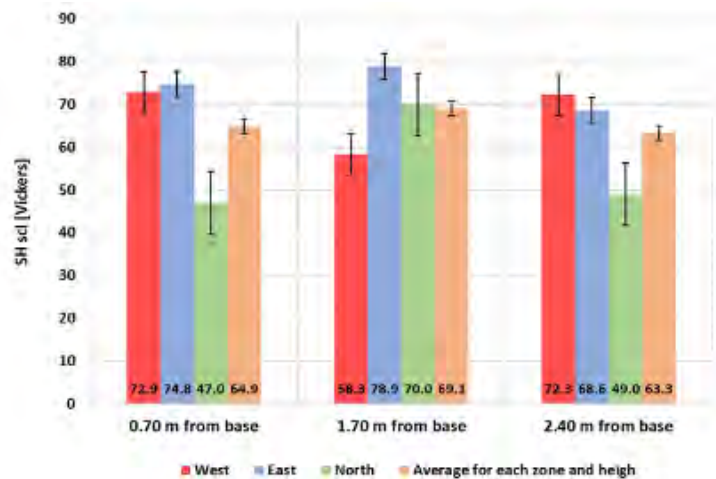


Figure 10 - Pendular sclerometer results in Jogo da Pêla Tower

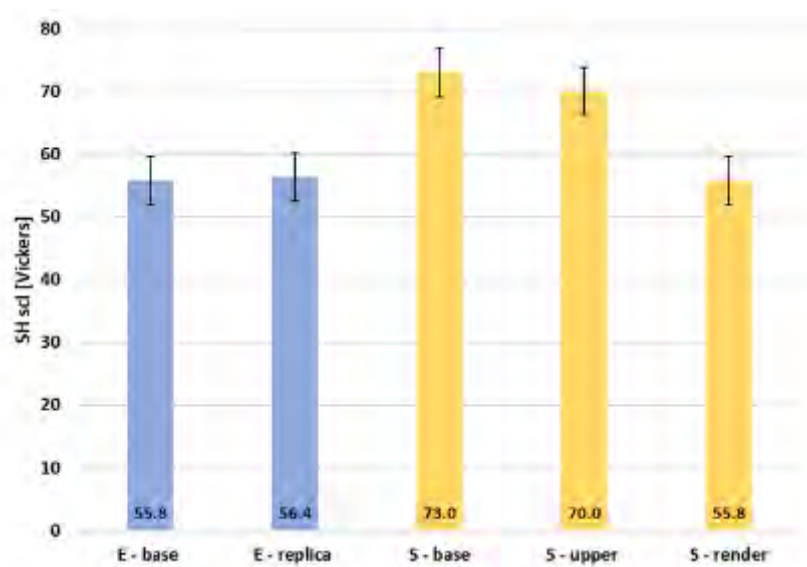


Figure 11 - Pendular sclerometer results in Bragança Terraces Residence

Sphere impact

The values of diameter of the concavity resulting from the sphere impact test, using the Martinet-Baronnie equipment, can be observed in Figure 12. At Bragança Terraces Residence it was only possible to test the lime-stabilized rammed earth replica, 20 cm and 60 cm from the ground, obtained 14.6 mm and 13.8 mm respectively. These values, unlike to the results presented by [12], that reveals larger diameters, between 18-21 mm, and lower mechanical resistance. In [13] Veiga et al. analysed by the same methods the surface hardness of two panels of different renders and obtained a sphere impact diameter of 15 mm and 12 mm for hydraulic lime and white cement, respectively.

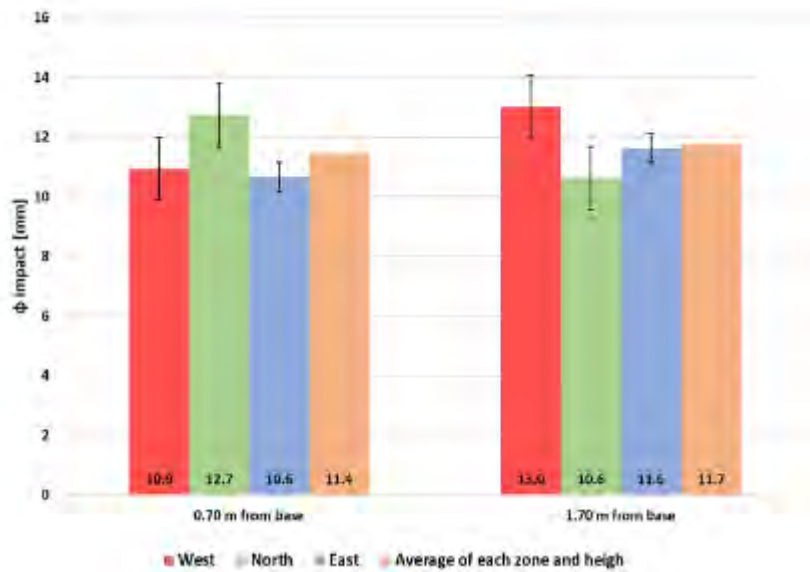


Figure 12 – Sphere impact results in Jogo da Pêla Tower

Water permeability under low pressure

Water absorption under low pressure by Karsten tubes was performed on two zones of the North and East walls of the interior hole in the Jogo da Pêla Tower. Zero absorption was registered after the 30 minutes test period, showing that the existing plaster blocked the water ingress. There is no data on the plaster formulation, application or eventual surface treatment; therefore, it was not possible to justify this behaviour.

Results for the water absorption are presented in Figure 13 for two different surfaces in Bragança Terraces Residence: south exposed original rammed earth wall and replica.

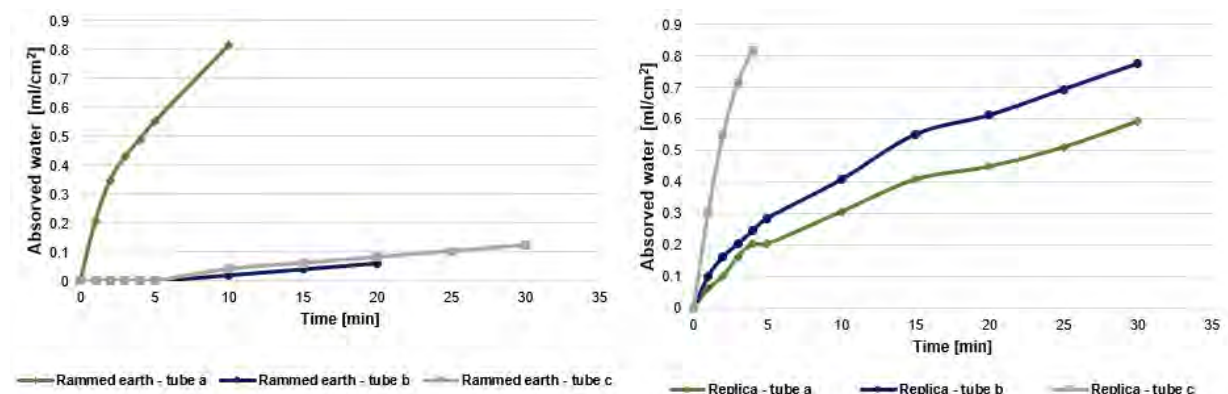


Figure 13 – Water absorption by three Karsten tubes at Bragança Terraces Residence: (a) south exposed rammed earth wall; (b) rammed earth replica

In both cases of Figure 13 two tubes register a low absorption with time and one tube a much faster absorption. There were no visible cracks but, in both cases, eventual microcracking may justify the behaviour of one of the tubes absorptions. For the other two tubes, the water absorption of the replica was faster in comparison with the original

rammed earth wall (Figure 13). Presently it is not known if the original rammed earth is lime stabilized and with which lime content; but the stabilization of the replica rammed earth seems to be high. Therefore, the faster water absorption of the replica may be justified by that lime stabilization that interrupts the clay lamella connections. Therefore, clay lamella seems to be more efficient on blocking the water migration in comparison to a lime stabilization of the rammed earth. Another possible reason for the slow absorption rate in the original rammed earth is that it may be partially saturated, due to rising water migration, the humid environment (under the building and without direct sunlight and with a waterproofing membrane located in their back. Tubes b and c for the old Wall section (Figure 13 (a)) revealed that the water absorption only started after a 6 or more minutes compared to similar tubes on the replica (Figure 13 (b)). The results in Figure 13 (a) could have been improved and made as in [15] which the water capillarity coefficient obtained for earth rammed material was performed during more time.

Conclusions

The inspection campaign made on several sections of the Fernandina's Wall of Lisbon have shown their different compositions, environments, exposure, maintenance and interventions carried on and needed. Fortunately, all those cases are being followed by experienced professionals of Lisbon Municipality and Portuguese Cultural Directorate what is a very good prognostic for the future. Furthermore, most of the private owners have now conscience of the cultural significance of the sections they are "guardians" and seem to be receptive to adequate interventions. This was very perceptible in the cases of the hotels (existent and in project), the private building with their small tower and the apartments complex. The later seems to be one of the most significant remains of rammed earth sections of the Wall and needing intervention soon. Public cases may have more problems for maintenance because of lack of financial support, such as the school and the Independence palace.

The *in situ* tests performed in the different sites proved to be rather adequate, being easy and quick to interpret, despite not having results for various materials in all visited sites the results obtained shows consistent values for the analysed material. The work will carry on with further *in situ* testing analysis and the chemical/mineralogical and physical testing on the extracted samples. These analyses can identify the components and the characteristics of original and more recent materials, such as mortars and stone masonry, and eventually help to localize their origin, preparation and application techniques. The gathered survey, namely of degradation of original and recent materials, and its causes, is expected to be useful to support decisions on future interventions, namely on the definition of repair mortars that need to be compatible and assure efficient conservation of sections that are being accessible of the old wall. The data will soon be available in DB-Heritage project database [16].

Acknowledgments

The authors wish to thank Manuela Leitão from Lisbon Municipality for all the support and fruitful informations, to Luís Almeida and Nuno Garcia for their collaboration in carrying out of the samples extraction. Acknowledgments are also due to Centro de Arqueologia de Lisboa, Direção Geral do Património Cultural and the owners for the possibility of inspecting and testing each surveyed section. The authors are very grateful to the DB-HERITAGE project (ref. PTDC/EPH-PAT/4684/2014) which supports this research.

References

1. Oliveira E (1887) Elementos para a História do Município de Lisboa. Câmara Municipal de Lisboa, Lisboa
2. Vieira da Silva A (1987) A Cerca Fernandina de Lisboa. Publicações Culturais da Câmara de Lisboa, Lisboa
3. Leitão, M (2014) As muralhas de Lisboa. Gabinete de Estudos Olisiponenses DMC/DPC/CML. Rossio – Estudos de Lisboa Nº 3
4. Brito, R (1998) Contribuição geológica para a recuperação da Torre do Jogo da Pêla (Muralha Fernandina de Lisboa). MSc Thesis, FC, Universidade de Lisboa
5. Cotrim Coradinho M (2018), Castelo de Paderne – Caracterização histórica e material. MSc thesis, FCT, Universidade NOVA de Lisboa.
6. Oliveira J, Manso C (2018) Intervenção Arqueológica – Parque de Estacionamento da Graça. Arqueologia e Património
7. Varandas J (2004) Terraços de Bragança: Construção em taipa de réplica da muralha fernandina de Lisboa. Pedra & Cal 24, pp. 26
8. Pedrosa F (2015) A torre de João Bretão na muralha Fernandina de Lisboa. Arquivo Municipal de Lisboa. Um acervo para a história II.
9. Rocha A (2015) A Muralha de D. Dinis e a Cidade de Lisboa. Fragmentos arqueológicos e evolução histórica. Lisboa: Museu do Dinheiro/Banco de Portugal
10. ASTM C805 (2008) Standard test method for rebound hammer of hardened concrete. ASTM Standards: United States
11. Faria P, Silva V, Jamu N, Dias I, Gomes I (2013) Evaluation of air lime and clayish earth mortars for earthen wall renders. Vernacular Heritage and Earthen Architecture Contributions for Sustainable Development, CRC Press/Taylor & Francis Group, pp. 407-413

12. Santos T, Faria P, Silva V (2019) Can an earth plaster be efficient when applied on different masonries? *Journal of Building Engineering* 23. pp. 314-323
13. Veiga M, Velosa A, Magalhães A (2009) Experimental applications of mortars with pozzolanic additions: Characterization and performance evaluation. *Constructions and Building Materials* 23, pp. 318-327
14. EN 16302 (2013) Conservation of Cultural heritage – Test methods: Measurement of water absorption by pipe method, CEN: Brussels
15. Faria P, Rocha M, Silva V, Pereira C (2012) The monitoring of rammed earth experimental walls and characterization of rammed earth samples. *RESTAPIA 2012 – International Conference on Rammed Earth Conservation*. Taylor & Francis Group, London, pp. 91-97
16. <http://dbheritage.lnec.pt/>

M.N.I.A.R. techniques of macroscopic characterization from the colorimetry and chromatographies analysis applied to the mortars in the archaeological site of Los Hitos (Arisgotas, Toledo, Spain)

Pablo Guerra-García¹, Jorge Morín de Pablos², Isabel Sánchez Ramos³

(1) *Universidad Politécnica de Madrid, p.guerra.garcia@gmail.com*

(2) *Audidores de Energía y Medio Ambiente SA, jmorin@audema.com*

(3) *Institute of Archaeology, University College London, i.sanchez@ucl.ac.uk*

Abstract

The archaeological settlement of Los Hitos is located in the village of Arisgotas (Toledo). Different chronological ecclesiastical occupations have been documented there: one, a palatial building of the 6th century AD; second, a Visigoth phase, with reuse of the palace and new church, from the 7th to the 8th centuries AD; and finally, an Andalusian farmstead, from the 9th to the 11th centuries. Mortars of different nature were identified in all chambers. Some samples were analysed following a methodology based on macroscopy (N.I.M.H.R., Non-intrusive Macroscopy with High Resolution). This process was divided in two procedures: one, a non-destructive sampling through microphotographs; and two, an extraction of samples for further processing. In both cases, an image treatment has been developed with professional biomedicine or geology programs (VehoCapture 1.3, Gimp 2.8, JMicrovision 1.2.7, Micam 1.6, among others) developing a three-dimensional surface maps and granulometries based on the high quality spectral analysis of sections. More than 2000 photographic microtomes of 400 magnifications have been taken with a portable magnifying binocular. The results have been documenting several phases of mortar application have been documented, identifying damage elements such as micro cracks, and documenting microstratigraphies in some cases too.

Introduction

The archaeological site of *Los Hitos*, that is located in the village of *Arisgotas (Orgaz, Toledo)*, is integrate by an ecclesiastical complex where different occupations phases, and it preserves some architectonical features that can be recognised in other late antique churches of the Region of Toledo, such as *Santa Maria de Melque* and *San Pedro de la Mata* (monasteries complexes founded between 7th to the 11th centuries), and even it share some aspects with other relevant monuments date in the early Middle Ages, such as *Santa Maria del Naranco* in Asturias (palace complex founded in 9th century) [1].

From the first archaeological excavations in the 70s', the architectural remains have been the most important elements to study [2]. In relation with the architecture, archaeologists

have highlighted the buttresses presents in the main floor of a tripartite building, complemented by other stays adjudged in the Andalusian period and later.

Regarding the complex, we emphasize the presence of three well differentiated spaces: a palatial space, tie to delayed occupation of 6th century; a Visigoth occupation, with the reuse of the palace attaching floors and one church, from 7th to the 8th century; and finally an Andalusian farmstead, re-arranging rooms and adding many others, from the 9th to the 11th centuries AD [3].



Figure 1. The archaeological settlement of *Los Hitos* located near *Arisgotas-Orgaz (Toledo)*. GoogleMaps.

Coating mortars are one of the most important elements, besides the funeral and ornamental components. Mortars, concretes and plasters of different types and invoices have been located in walls, masonries and buildings, sometimes with the manufacturing phases along the time, microstratigraphies and also pathologies. On the other hand, neither paintings nor pigments nor incised or excised plasters and decorations have been identified, something usual in this kind of ecclesiastical enclosure. However, a large number of additions on mortars have been identified, like organic material of various kinds, selected granulometries for outer layers that indicative work-careful in the execution or remnants of spatulate marks.

After evaluating the mortars state of conservation (mainly with *visu* characterization in site), and before the extensive occupational sequence of the site for centuries, the first option that has been considered was to analyse the different mixtures in relation with the archaeological data, covering all the chronological fields. There are no referents about mortars researching in this area nor in this geographical scope. So our results could be compared only with those obtained in the archaeological intervention. These analyses have consisted in a macroscopy *in situ* and in a second macroscopy in the laboratory with samples

taken, developing a series of high-resolution microphotographs treated with programs that can analyse the chromatic spectrums. Later on, the images have been analysed, obtaining data about the granulometries, the microstratigraphy or the basic composition of the mortars. Nowadays we are considering to develop mineralogical and chemical characterization to reinforce knowledge about the mortars of *Los Hitos*.



Figure 2. Aerial view of *Los Hitos* complex, after the present archaeological intervention developing by Jorge Morín de Pablos e Isabel Sánchez Ramos. Source: ABC Press.

Methodology and samples

Macroscopic Characterization

The whole investigation was developed with macroscopic methodology. The macroscopic characterization processes are based on the visual test of object and element enhanced with reflected light. Procedure is known for many years and main bibliography has been reviewed previously to this work [4]. Unlike other cases characterization of raw and polished samples were carried out [5], in this case the portable microscope tool obtain a sequence of ten micro photos-shots of a target selected. This generated a large collection of microphotographs (between 20 and 400 magnifications) through millimetre scale and a resolution higher than normal.

Thank with this process and this subsequent treatment of the images, it is possible to identify better components such as aggregates or document the microstratigraphy. These techniques of image processing also have bibliographic references in which there are raw materials and thin section testing of mortars [8]. Among the reviews consulted, highlight the research at the Cathedral of Florence by Giuseppe Musumarra and María Fichera, where microphotographs of mortars were taken [9].

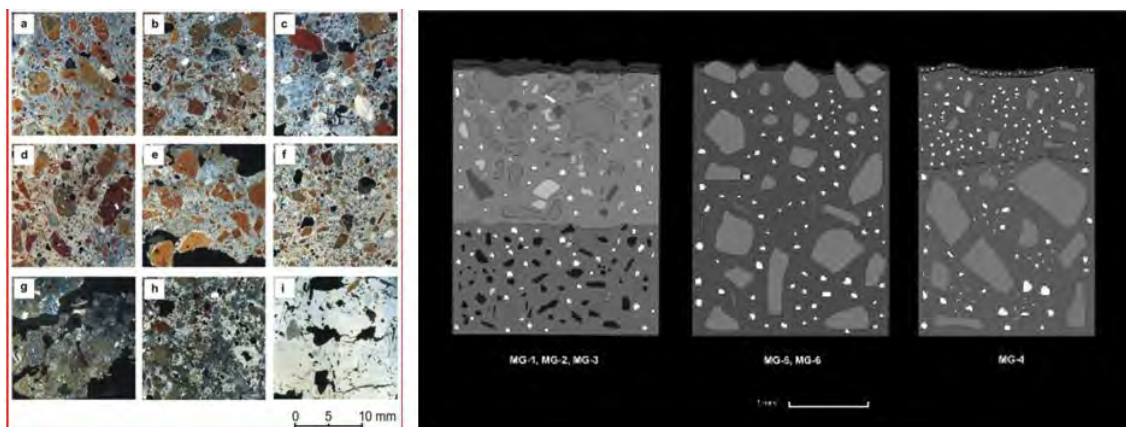


Figure 3. Two examples of researches using macroscopic characterization: at left, mortars of Roman city of *Kyme* (Turkey) [6]; at right, graphic documentation about mortars of Roman settlement of *La Magdalena* (Alcalá de Henares, Madrid) [7].

Macroscopy allows specifying the basic components of the mortar, its microstratigraphic distribution (if any) or the granulometry, as will be explained in succeeding paragraphs. The book *Geomaterials under the Microscope*, written by Jeremy Ingham, has been consulted. Here, variables of analysis of aggregates in mortars are established according to their distribution within the binder [10]. Both in the research of Ingham and in the of Elena Pecchioni, Fabio Fratini and Emma Cantisani, criteria for the classification of mortar aggregates have been agreed upon, according with the distribution and morphology of the aggregates. Among the criteria used, the *Raymond Classification* stands out to determine the type of aggregate used based on the geometric shape of them.

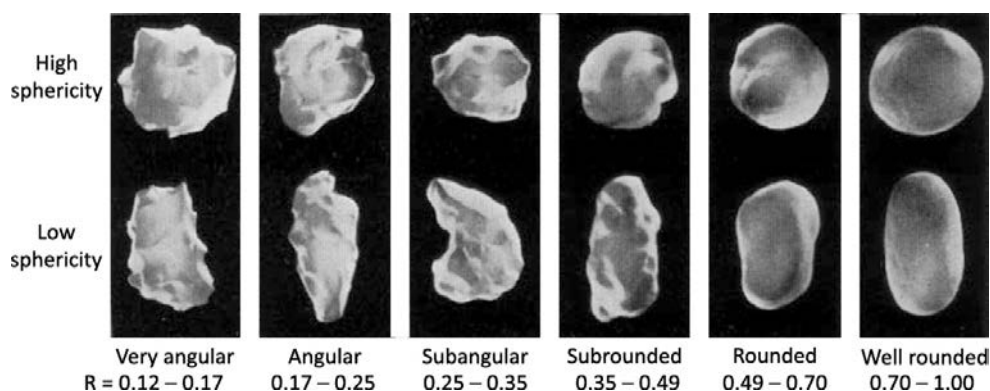


Figure 4. Aggregates classification developed by Raymond, cited by Pecchioni [11].

Once the targets shoots-macrophotographs were selected in all the buildings, *in situ* and in the samples taken from the masonries, a basic characterization was developed by means of a binocular lens or stereomicroscope. In this step primary components of the mortars were identified (main aggregates, decorations, additives, intrusions). There are many benefits doing a fist observation through binocular lenses, allowing a first directed and detailed monitoring of the materials, testing the components and their distribution too, their configuration and even the most superficial pathologies in cases. To that end, targets must be chosen in the way to preserve the integrity of the original masonry (in order to avoid

damage or loss of material), selecting areas unaltered by anthropic facts (graffiti, repairs, recent renovations, restorations) and points without organic components (roots, moss, lichens, nesting, residues, waste).

Secondly, a granulometric analysis was carried out. This procedure analyses the distribution of the components inside the mortar and its orientation in the area occupied within the mixture. Metric developed is in the way to the size of aggregates and to know its relation with the area occupied inside the mortar. These results facilitate to distinguish different hand-made labour in the production and applying of mortars, showing care in the factories or in the selection of the aggregates. In this way, researchers like Mertens use to apply software to highlight the aggregates and develop their metrics [12].

Data collection by microtomes (phase I)

Microtomes were taken over the masonries and the soils of *Los Hitos*, applying the focus directly without alteration of the original building and making photographic microtomes with a portable binocular loupe of 400 magnifications. These high-resolution shots were processed and calibrated the images, and finally stored them on a hard drive for treatment in the laboratory. The points were chosen according with the archaeological direction guideline, trying to include all the masonries from every chronological phase to compare the mortars at first and compare with the archaeological results too. Actually the archaeological team is continuing its investigations about the occupation sequence.

This monitoring of the samples has already been applied in other locations such as *Medina Albalat* (Romangordo, Cáceres), *La-Sé-Cathedral* of Idanha-a-Velha (Portugal) or in the Roman site of *La Magdalena* (Alcalá de Henares, Madrid) [13]. In all of them, high-resolution microphotographs were taken with minimal impact on the original walls, and then the images were processed. Previously, the sampling points should be chosen according to the objectives and the targets, the conservation of mortars and their morphological characteristics [14]. Finally, we proceeded to remove the outside layers of vegetation and organic remains that could modify the results, and the photographic sequence was developed with shots of between 10 and 25 megawatts each all. Neither in the checking nor in the sampling were damaged during the work.



Figure 5. Sampling-shoots microphotographs with a portable hardware.

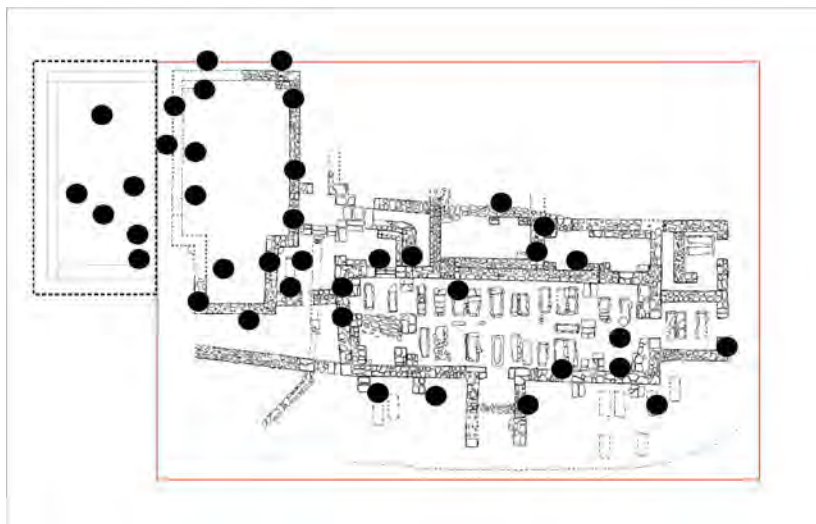


Figure 6. A view of a sampling point in the archaeological area.

A second phase consisted in the extraction of small samples of mortar in areas where deterioration has caused that pieces had been detached or were about to do so. The sampling was documented graphically and photographically, supplementing the previous phase of macroshoots *in situ*. During the extractions state of conservation of the archaeological elements has been respected, reducing the area of affection even though the sampling supposes a small alteration of masonries. Each sample has 50 grams, which is equivalent to approximately half a cubic decimetre. The sampling process is established by the international scientific community and accepted by different councils of materials certification like the *Réunion Internationale des Laboratoires et Experts des Matériaux*, R.I.L.E.M. [15], which establish suggestions and criteria improving the conservation of the samples, reducing the damage caused in original masonries and improving the knowledge about mortars and plasters [16].

The total number of macrophotographs amounted to almost 2000, between those taken in the archaeological site and those taken in the laboratory through the samples. The serial microphotographs were distributed along several points depending on the previous archaeological results, in such a way that all the masonries and the mortars preserved had a minimum of twenty high-resolution microphotographs. This would make it possible to distinguish the hand-made and compare the results with the archaeological conclusions. At the same a complete typology of the mortars in the archaeological settlement was made.

The north and south areas were not analysed because there include the access into the site and the limit of the archaeological intervention. However the sampling cover much more than the 95% of the archaeological area, which every year is expanded and could be increased the catalogue of samples.

Table 1. Abstract of macrophotographs developed (each one amounts *in situ* shoots and lab testing).

Zone	Built	Macrophotographs
Palace	East Outside	5
Palace	Inside	7
Palace	West Outside	8
Transept between the Palace and the church	Inside	11
Outside perimeter wall	West	3
Church	Inside	20

Instruments and software

This research combines both the results obtained and the methodology used. That is why the description of the equipment and the software is as important as the concluding thoughts at least. In this work we have used a *Motic* binocular magnifier, model SMZ-140 series; a stereomicroscope *Marés Carton* with double light and 400 magnification, and a *Veho* USB microscope, model VMS-004 of 20x400 magnification and lighting of eight LED's. For the scale, a calibrated micrometric lens coupled to the binocular loupe was used. A *Bresser* microscope with 5MP sensor and CMOS of 40x1400 magnifications has also been used.

Regarding the software used, both for displaying *in situ* and in the inspection of the samples in the laboratory, the VEHO 1.3 software has been used at 20 optical magnification; for the treatment of images was developed by GIMP 2.8.0 and ImageJ 1.51 j8; the basic characterization was achieved thanks to IMP Scope 1.65 (8a) and Micam 1.6; and finally, measurements and granulometries was implemented through JMicrovision 1.2.7, Digimizer 5.3.5, and ImageJ 1.51 j8 too.

Most of these softwares are based on the analysis of the colorimetries from images taken. Colorimetry is a science that studies the colour in the way to obtain a scale of numerical values. Through this semi quantitative method it is possible to get a measurement of the components, calculating the chromatic spectrum of one, two or multiple grains. In the same way could be made a rough estimation of areas and surfaces of a macrophotographic shoot, analysing the area occupied by a colour or the different ranges, the lime of a mortar or the ceramics aggregates among other materials. These techniques have different bibliography examples like the work of Saenko [17], in usefulness is supported thanks to specialized computer software like Metamorph or JMicrovision. In the next point we explain in detail the tests developed.

Chromatography test

In this work analytics developed is based on the chromatographic analysis in mortars with the following tests:

Graphical colorimetry based on variables of colour, saturation, hue and contrast: this test do an interpretation about the chromatic parameters of an image supported by colour variables of the RGB scale (difference between the higher and the lower value depending on the mortar). The software allows choosing other chromatic ranges, but by default these are the most suitable for the relation of components present in mortars (quartz, feldspars, micas, calcites, biotites, etc.). The ranges of value, hue and saturation have also been selected in relation with the binder and the densest aggregates like ceramics or bricks-crushed.

Linear and vertical granulometry by total saturation: the software chooses the points where happen increase-decrease saturation levels. This variable measures the cleanliness of the colour, based on the relation between saturation and cleanliness. In mortars if aggregates with similar mineralogical morphology have been mixed, graphic saturation use to keep the homogeneous appearance. On the other hand mixing materials and colours cause a non-homogeneous saturation graphic.

Random quantitative granulometry in area-perimeter ratio: this quantitative analysis is based on the statistical calculation of the area and the perimeter of each grain, chosen randomly, for its measurement and graphic representation with respect to metric relationship. This system allows establishing a real semiquantitative relationship between the aggregates of samples.

Estimate the area of the binder through discrimination of aggregates: this test discriminates the aggregates looking for the interface, establishing patterns of calculation of the area covered by the binder. In this way, in addition to get a visual reference, the relation between aggregate and binder has offered percentage quantification.

Results

The macroscopic analysis of the aggregates in mortars was developed through the Micam and IMP Scope software, visualizing the different mortars, identifying for example, the presence of lime nodules, siliceous and ceramic aggregates, different microstratigraphies, etc. Once the images taken have been treated, the objective was to achieve the identification of the main components. Gimp and ImageJ software have been used in this way, testing saturations, lighting and contrast, improving the edges of the grains and getting easily the execution of the granulometry with JMicrovision and Digimizer software.

As a result three kinds of mixtures have been determined at least:

Table 2. Detail of the results obtained through previous macroscopy.

Class	Sub-class (size of aggregates)	Used	A	C
I	Concrete	Load foundation	M/C	
II	Mortar	Grouts and coatings	M/S	X
III	Mortar	Plasters	F	X

A - Aggregates (S – small (0,3-0,5 mm.); M – medium (0,5-2 mm.); C – coarse (+ 2 mm)); C - Microstratigraphy

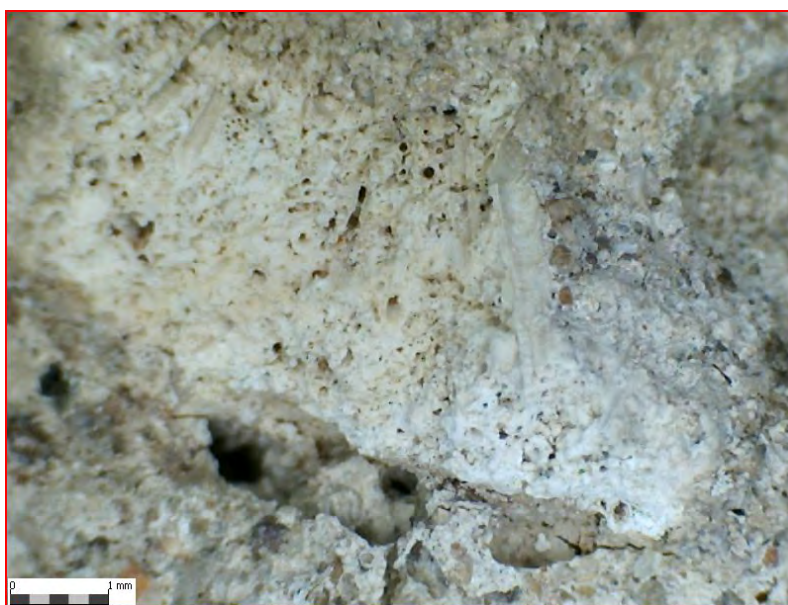


Figure 7. A detail of a bone fragment that clearly shows a spongy material.

In general, the mortars analysed present microstratigraphy, but only documented in isolated cases identified as coatings. The masonries do not present constructive layers, as they are masonries with an execution on time.

Samples from brick-joints and from the foundations mortars do not offer a clear stratigraphy, so this is not the case with the plasters where that have been identified in several mortars analysed. Bones animal remains (microvertebrates) have been identified and will be analysed in depth as soon as possible, as well as vegetable fibres.

On the other hand JMicrovison software allows calibrating microphotographs, obtaining quantifications and measurements too, accounting to chromatic scales. This software has made it possible to carry out all the colorimetry studies summarized in the following way and choosing some specific samples:

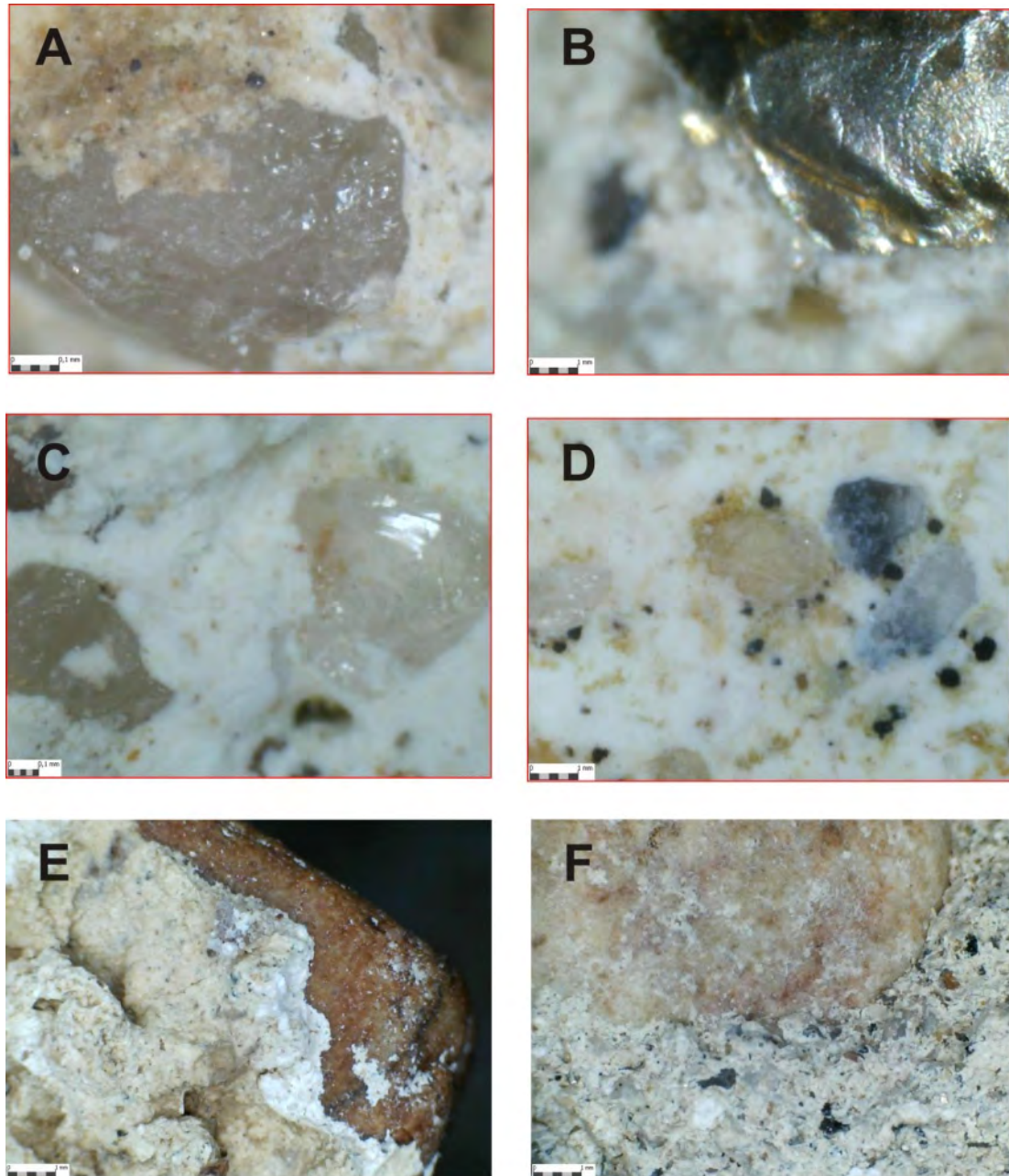


Figure 8. Different aggregates identified in the mortars of *Los Hitos*: A) Quartz in sample HIT3; B) Mica in sample HIT5; C) White and rose quartzes in sample HIT11; D) Small sizes aggregates with feldspar in sample HIT12; E) Piece of quartzite in sample HIT19; F) Sand and graves in concrete of simple HIT37.

Graphic colorimetry supported in variables of colour, saturation, hue and contrast.

In order to know the general values of the mortars according to the spectral ranges, a serial of samples have been chosen:

HIT1: The vectors indicate a chromatic variation in aggregates with changes in saturation within the usual values of mass-produced concretes. Saturation peaks in graphics indicate the presence of gravels with opaque colours unlike the high translucent quartz crystals.

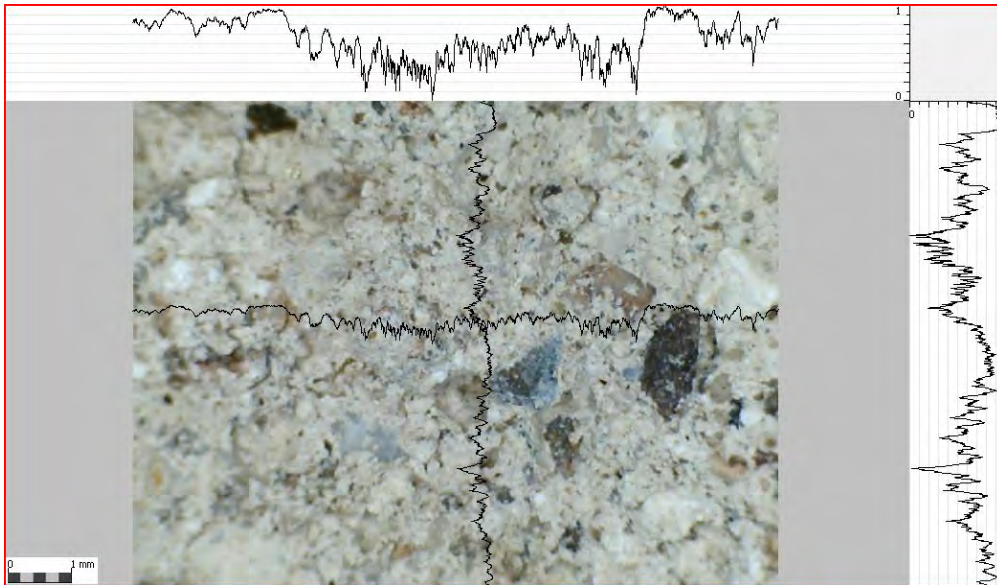


Figure 9. Colorimetry graphic of sample HIT1, showing saturation ratios where the presence of gravel is indicated through pronounced peaks.

HIT4. The vectors indicate a homogeneous chromatic variation, for the aggregates do not present chromatic variations that change the tones and the saturations ranges. As the graph on the right shows, the peaks respond to small crystals of quartz and mica, unlike the extremes, represented by the mortar interface and a large lime nodule.



Figure 10. Colorimetry graphic of sample HIT4 shows saturation and hue, while lime-nodules and quartzes change the results of graphic (high-low peaks).

Linear and vertical granulometry according with total saturation.

Using the example the samples HIT4 and HIT7, a random vector colorimetry was developed from outside to inside the mortar, according to the microstratigraphy, results corroborates that there are no changes inside the matrix with respect to the outer layer.

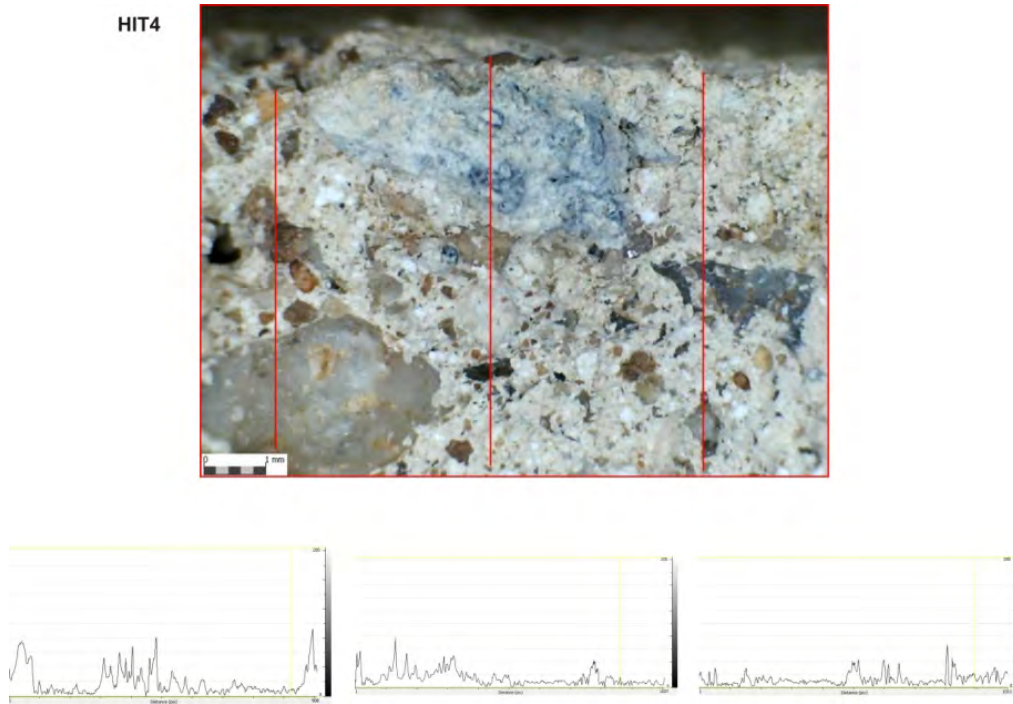


Figure 11. Graph of vector and vertical colorimetry analysis, in which three results are showing from three different vectors. Saturation peaks are produced by the presence of aggregates with high size in relation with the sands (maybe gravels or calcites).

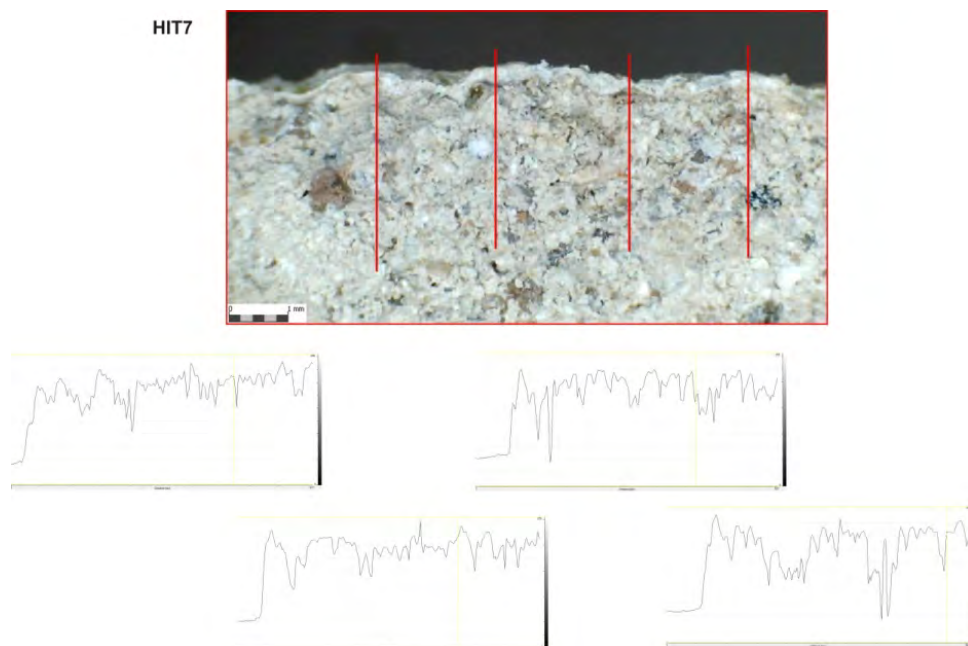


Figure 12. Vertical and random chromatographies of sample HIT7, where grey tones are showed in the graphics and the presence of carbonation hardness is reflected in a sudden drop of values.

In the case of the sample HIT7, corresponding with a level of flooring inside the building-palace, grey tones has been taken as references. Changes of peaks show aggregates of small size and minimal variations, as show the figure 12, considering that the sample has been taken from a microstratigraphic sequence inside the building-palace. The granulometry

based on grey range and vectors, determines a homogeneous coating execution. It is worth mentioning the recarbonation slab or carbonate hardness outside of the coating, marked in the graphics as a peak with a characteristic platform homogeneous line (coating fine-grained).

A quantitative granulometry size in relation to the area-perimeter

This analysis develop a rough calculation of the areas and the perimeters of each grain of aggregates, establishing a relation between the coefficients and therefore, determining a basic granulometry of the aggregates. In this work 70% of the samples have been selected to validate such results (percentage in relation with the sample could be tested), although in the present work different samples have been chosen to demonstrate the difference of the results, as show the figure 13. In graphics can be appreciated the range of values depending on the results and its usefulness.

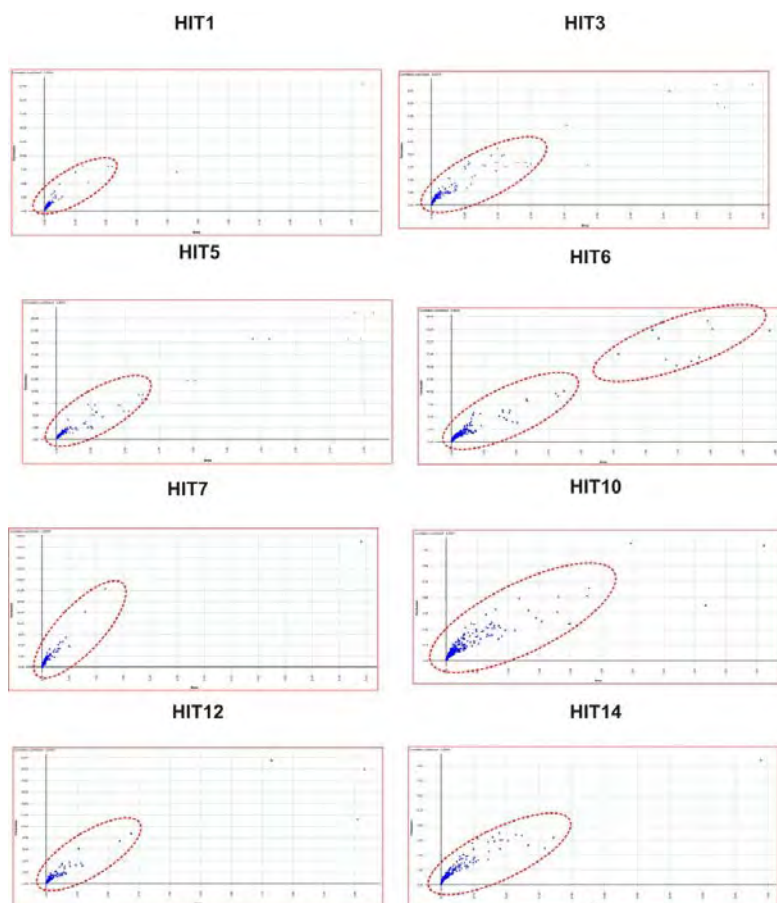


Figure 13. Granulometry graphics of area-perimeter range (randomly assigned in this case) to show the differences between samples HIT16 (with two groups of sizes), HIT10 (with a heterogeneous granulometry) and HIT5 (with a homogeneous granulometry).

If the results are closest to the value point 0, granulometry is more homogeneous with grains with similar relation area-perimeter. On the contrary, if the graph does not concentrate the measurements or subgroups are established, it shows heterogeneous sizes in grains:

Surface Scanning

Thanks to the ImageJ software and one of its plugging, scans in surface of the mortars have been developed (surface scan) in order to obtain thermal, spectral and gradient images, following a system of microphotogrammetry based on the analysis of the colours. Once the scan has been obtained, it is possible to interact with the 3D model and create selective layers from the chromatographic analysis (gradient, thermal, spectral, red, grey and blue channels, etc.). This way has already been developed in other projects [18], and stay at the forefront in Optical researches [19, 20]. In this work the most recent and visible results are shown, although still we continue studying and developing new images.

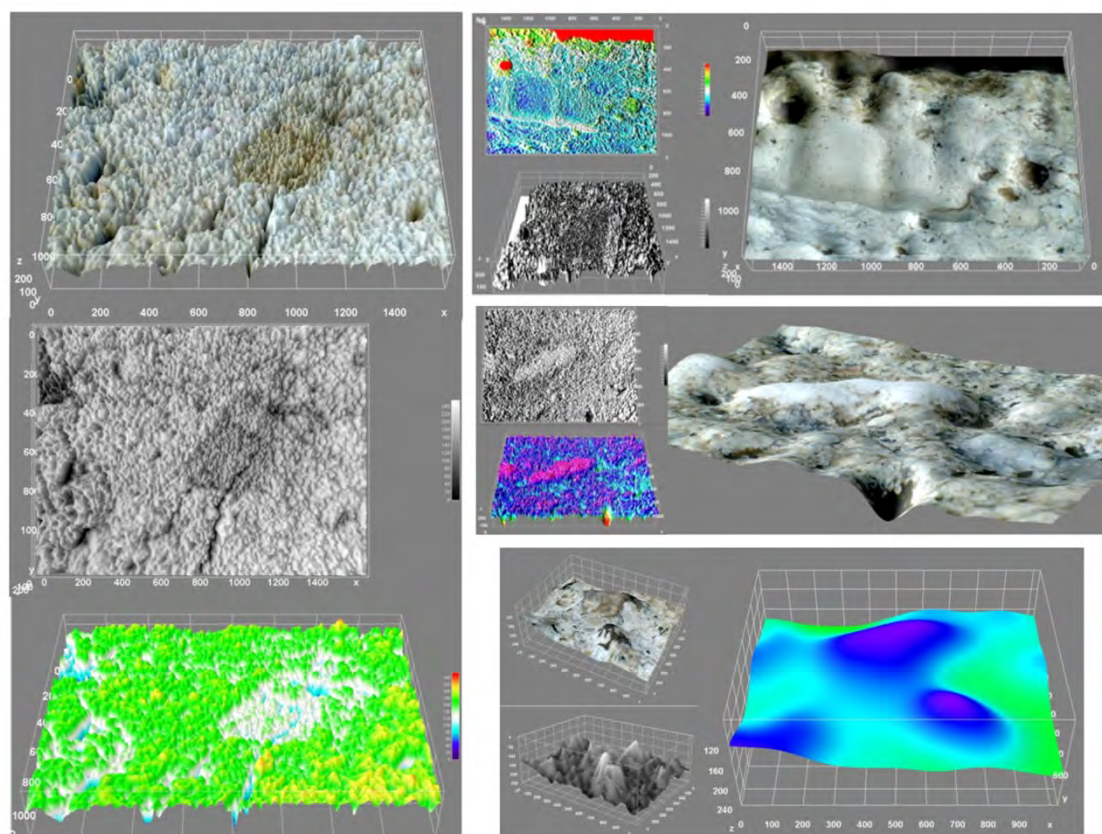


Figure 14. Images sequence (thermal, spectral and gradient of grey) in different samples analysed with this software (ImageJ).

This virtualization processes will be really helpful (as the virtualization technology in general) because provide to the researchers a first map to work, and could show elements in mortars including damage and deterioration (small breaks as figure 14 shows), pores or organic additions. The research of Architectural Heritage performed different tools and processes like point clouds or virtual reality to improve the characterization of techniques and materials [21, 22]. Actually we are working the methods over the mortars analyzed in *Los Hitos*, obtaining pictures aimed to improving the social knowledge of the mortars in museums, for example.

Conclusions

The quality ranges in the mortars can be established by the results obtained in this study. Actually, the samples from the construction of the building called "palace" hold a better qualitative than the other samples. Outside the main building, granulometry shows that mortars with characteristics close to mass-productions for load-bearing masonries (walls, abutments, pillars, etc.). Regarding the surrounding rooms, corridors and perimeter walls, different hand-made mortars were documented.

Regarding the aggregates, they are generally siliceous with quartz and micas as the most abundant, as well as quartzites and gravels of medium and high size in the concrete types. They emphasize the first ones, with a whitish coloration, and without hardly edges (this could interpreted as a good selection of material). Ceramic and brick-crushed aggregates are absent except in some samples, and this could be interpreted as a result of the process of firing the limestone's with clay impurities. In general, a good preparation of the aggregates is appreciated. The coatings stand out, with finer aggregates and regularly distributed throughout the lime matrix, documenting even spatulate marks process on the surface. Maybe the mortars were more liquefied in the phase of their application, with a lower dosage of aggregate than usual.

In relation with the types of mortars identified (by average size of the grain), they are represented:

- Mortars applied outside, presenting characteristics of plasters with finer and chosen dosages, without pigmentation but with refining marks (spatulate, chiselled, etc.). Microstratigraphic units have not documented. Some coatings samples present sections of square chiselling, maybe executed for the application of a second outer layer. The different stratigraphies analysed generally show, in the mortars, a medium-fine grain size with little aggregates squared.
- Foundation mortars (with sand), showing in general on all surfaces analysed but especially inside the palace and the church. They are mortars without hydraulic aggregate or similar addictions, and could perfectly correspond to *caementicia* Roman concrete. As a singularity, it is worth highlighting the average granulometry and it is apparently with regular distribution.
- Concrete (with gravel), present in most of the walls, pillars and load masonry. It highlights the presence of gravel, quartzite and lime nodules. These nodules correspond with the detachment of some quartzite grains. Due to the wear effect, the gravel crumbled from the mortar, creating medium sized cavities and pores. Usually these concretes are thought for the adhesion of coatings, with a thin layer of mortar inside that bond the outside finest plaster.

As figure 16 shows, where the central area corresponds with the palace and the left sides correspond with later expansion, mortars were documented in the palace and the church and coating, while concretes (with aggregates higher size average) were documented outside, pillars corridors and isolated rooms.

The results that have been presented in this essay have been obtained using a methodology based on the use of software applications and the treatment of microphotographs. There are precedents about the use these procedures separately, even combining mineralogical and chemical analysis, combining GIS techniques with mapping, and metrics analyses based on the treatment of images. The scope of these procedures is to establish pathology patterns, quantitative analysis, etc. Recent works also apply these techniques combined with software tools, such as SketchFab, Revit, photogrammetric techniques in archaeological areas and monuments.

However, the use of macroscopic techniques and colour spectrum analysis should be understood as a first step, but not the last, to improve the knowledge of mortars. Determining their components, granulometries and even pathologies, could improve the application of other analytical techniques, especially those that improve the chemical or mineralogical composition.



Figure 16. Distribution of the mortars documented in colours (mortars in red; concretes in yellow), and the relation between the situation and the complex.

Finally, and defending the use of 3d technology in *Los Hitos*, there is a notable increase of 3D techniques application to the Cultural Heritage. Its implementation in the methodological sequence does not need any demonstration. A good example is the different applications of software like ImageJ, used in this research with assiduity, or others as *Reality Capture* or

MeshLab, used also in other fields, such as Optics. In future, this will open a question whether this methodology suggested is useful, and if it would prove adequate to obtain new results.

References

1. Caballero, L, Latorre, JI, (1980) La iglesia y el monasterio visigodo de Santa María de Melque. Arqueología y arquitectura. San Pedro de la Mata (Toledo) y Santa Comba de Bande (Orense). EAE, 109: 501-516.
2. Maquedano Carrasco, B, (2002) Catálogo de relieves visigodos de Arisgotas (Orgaz, Toledo). Ayuntamiento de Orgaz.
3. Barroso Cabrera, R, Carrobles Santos, J, Morín de Pablos, J et al (2015) Los Hitos. Arisgotas (Orgaz, Toledo). De palacio a panteón visigodo. Ayuntamiento de Orgaz. Toledo.
4. Middendorf, B, Hughes, JJ, Callebaut, K et al (2005) Investigative methods for the characterisation of historic mortars. Part 1: Mineralogical characterisation. En: Materials and Structures, 38: 761-769.
5. Miriello, D y Crisci, GM (2006): Image analysis and flatbed scanners. A visual procedure in order to study the macro-porosity of the archaeological and historical mortars. En: Journal of Cultural Heritage, 7: 186-192.
6. Miriello D, Bloise A, Crisci Gino M et al (2011): Characterisation of archaeological mortars and plasters from Kyme (Turkey). Journal of Archaeological Science, A, 38, 4: 794-804.
7. Guerra García, P, Heras Martínez, C, Bastida Ramírez, A (2016) Técnicas constructivas y estructuras microestratigráficas en elementos industriales de carácter hidráulico documentados en el yacimiento romano de La Magdalena (Alcalá de Henares, Madrid). Zona Arqueológica, Especial Vides, Monumenta, Veterum. Madrid y su entorno en época romana, I: 468-476.
8. Prendes Rubiera, N (2006): El tratamiento digital de imágenes como una herramienta de evaluación y análisis en la restauración del patrimonio arquitectónico. Revista Electrónica ReCoPar, 1: 41-53.
9. Musumarra, G y Fichera, M (1998): Chemometrics and cultural Heritage. En: Chemometrics and Intelligent Laboratory Systems, 44: 363–372.
10. Ingham, J (2010): Geomaterials under the microscope. CRC Press: Manson
11. Pecchioni, E, Fratini, F, Cantisani, E (2008) Le malte antiche e moderne: tra tradizione ed innovazione. Pàtron Editore, Bologna.

12. Mertens, G, Elsen, J, Brulet, R et al (2009) Quantitative composition of ancient mortars from the Notre Dame Cathedral in Tournai (Belgium). *Conférence: Euroseminar on Microscopy Applied to Building Materials (EMABM)*, Porto. *Materials Characterization*, A, 60, 7: 580-585.
13. Guerra García, P, Guilotte, S (2018) Argamasas y emplastos del yacimiento de Medina Albalat (Romangordo, Cáceres). Trabajo inédito.
14. Guerra García, P (2018) Un catálogo de argamasas históricas. *Revista Electrónica ReCoPar*, 13: 53-72.
15. Hughes J, Callebaut, K (2000) Practical sampling of historical mortars. En Bartos, P, Groot, C, y Hughes, JJ (eds.) *Proceedings of the RILEM International Workshop Historic Mortars: characteristics and tests*: 17–26.
16. Elsen, J (2006) Microscopy of historic mortars: a review. En: *Cement and Concrete Research, Actas del X Euroseminar on Microscopy Applied to Building Materials*, June 21-25, 2005, University of Paisley, 36, 8:1416-1424.
17. Saenko, SW, Teyssier, J, Van der Marel, D et al (2013): Precise Colocalization of Interacting Structural and Pigmentary Elements Generates Extensive Colour Pattern Variation in Phelsuma Lizards. *BMC Biology*, 11: 105-127.
18. Acevedo, A, Franco, N (2012) Aplicación Dstretch-ImageJ a imágenes digitales del arte rupestre de Patagonia (Argentina). *Comechingonia Virtual, Revista Electrónica de Arqueología*, 6, 2: 152-175.
19. Castañeda, R, Piedrahita Quintero, P, García Sucerquia, J (2015) Procesamiento y cómputo de imágenes para holografía digital con ImageJ. *Óptica Pura y Aplicada*, 48, 2: 11-18.
20. Solá-Morales, P, Puche Fontanilles, JM, Macás Solá, JM et al (2017) Ensayos de nuevos análisis óptico-visuales para el estudio de estructuras arquitectónicas-patrimoniales. El uso de la reflectancia láser. En Roldán, L, Macías Solé, JM, Pizzo A y Rodríguez Gutierrez, O (eds.): *Modelos constructivos y urbanísticos de la arquitectura de Hispania Definición, evolución y difusión del periodo romano a la Antigüedad tardía*, 29: 77-88.
21. Puche Fontanilles, JM ; Macias Solé, JM, Toldrà Solé, JM et al (2017) Más allá de la métrica. Las nubes de puntos como expresión gráfica semántica. *EGA. Revista de Expression Grafica Arquitectónica*, 22, 31; 228-237.
22. Guerra García, P (2017) Caracterización macroscópica de morteros romanos de tipo industrial en Villamanta (Madrid). *Primeros datos. European Scientific Journal*, 13 (25). DOI 10.19044/esj.2017.v13n35p1

Analysis of mortar samples from the Church of the Saints Sergius and Bacchus at Umm as-Surab (Jordan)

Piero Gilento¹, Cecilia Pesce², Giovanni Pesce²

(1) University Paris 1 Panthéon-Sorbonne, UMR7041, ArScAn, France, piero.gilento@univ-paris1.fr (P.G.)

(2) Department of Architecture and Built Environment, Northumbria University, Newcastle upon Tyne, UK, cecilia.pesce@northumbria.ac.uk (C.P.), giovanni.pesce@northumbria.ac.uk (G.P.)

Abstract

This study presents the results of some XRD and SEM analyses carried out on mortar samples from the church of the SS. Sergius and Bacchus, in the village of Umm as-Surab, Northern Jordan. The analysis aimed at providing useful information on the building materials and technologies used in the construction of the church and adjacent rooms. Building archaeology methods and techniques were used to highlighting the complex stratigraphy of the remains and, in such context, the analyses allowed a detailed investigation of the differences between the various parts of the complex. Results suggest that during the Byzantine period mortars were produced using lime as a binder, whereas during the Islamic period mortars with decorative function were produced using a mixture of lime and gypsum as a binder. These information allow a more precise investigation of the chronology of the building and contributes to broaden our knowledge of the material culture in the Ḥawrān region.

Introduction

Northern Jordan has a complex system of ancient villages almost entirely built using basalt as a construction material which, thanks to particular historical, cultural, geological and environmental convergences, survived until today in fairly good conditions. This built landscape is located at the border between the steppe and the desert areas called Ḥawrān. This is an area that for centuries has been part of a network of important communication routes between the Mediterranean Sea and the Arabian Peninsula (Figure 1). Because of this, the area was the melting pot of various cultures such as Nabatean, Roman, Byzantine, Sassanid, and Islamic. In such rich cultural context, the architecture reflects the cultural variety and becomes a fundamental source of information not only of the local material culture but also for the study of the social and cultural phenomena behind some crucial historical changes that happened especially in the Late Antiquity and in the Middle Ages.

Because of the complexity of the built environment of the area, an archaeological approach was used to unlock the information contained in it. It is general knowledge that the most advanced archaeological approach to the historical development of buildings and structures is the Building Archaeology [1, 2]. This discipline applies the basic principles of horizontal

stratigraphy to the standing structures allowing the unravelling of the complex sequence of construction and demolition phases common to a large number of historic buildings. Such complex sequence is often difficult to identify because of the reuse of building materials and/or the continuity in the use of some construction techniques.

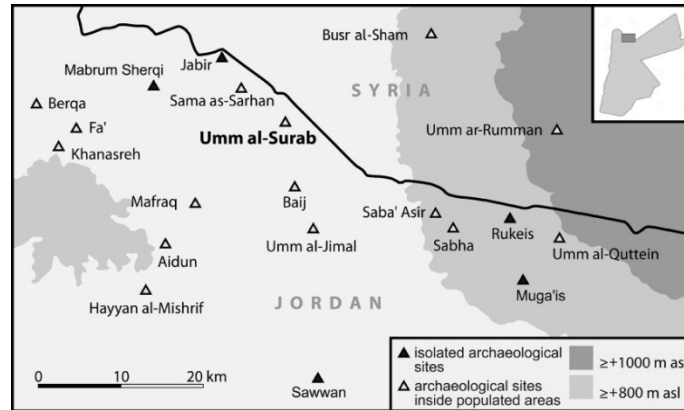


Figure 1. Localisation of the village of Umm as-Surab in the context of the Jordanian Hawrān. (from: Anastasio, Gilento, Parenti 2016 [3]).

The village of Umm as-Surab, in Northern Jordan, is a site of about 17 ha that lies about 13 km north-east from Mafrāq and 80 km north from Amman. In this village the building archaeology was applied to a religious complex, identified as Topographical Unit 28 (hereafter TU28), that includes the church of the Saints Sergius and Bacchus, founded in 489 AD, and some rooms adjacent to the north side of the religious building, interpreted as a monastery (Figure 2).



Figure 2. Aerial view of the village of Umm as-Surab with the localisation of TU28. Image by the Spanish Archaeological Mission in Jordan, flight 1978 (credit by Antonio Almagro).

The investigation is part of a wider research project on the building techniques used in the past centuries in the Mediterranean area (i.e. ACTECH project, G.A. 703829, founded by a Marie Skłodowska-Curie fellowship) and was focused on the characterisation and analysis of the mortars used in the religious complex. The research aimed at answering various research questions regarding the construction technologies and the history of the buildings. In particular, the investigation focused on the study of the bedding mortars in the church of the

two Saints and in the adjacent rooms with the aim to acquire useful information for an absolute chronology of the structures. A further aim was to broaden the knowledge on the historical use of the building materials in Jordanian Ḥawrān, which so far has only been studied in the nearby village of Umm al-Jimāl [4, 5]. This information will help creating chronologically organised typologies for the mortars at regional level, that can be used for both, dating and conservation purposes.

Historical-constructive evolution of the church of Saints Sergius and Bacchus

The first systematic study of the village of Umm as-Surab was carried out by the American scholar Howard Crosby Butler between 1904 and 1905 when, leading the Princeton Archaeological Expedition to Syria, he visited and recorded the entire area of southern Ḥawrān [6]. On that occasion a measured survey of the church of the Saints Sergius and Bacchus was carried out, together with a precious photographic shot of the interior.

In the 1980's the English researcher G.R.D. King carried out a new detailed survey of the village, producing a new plan of the church and a detailed architectural study of the complex, for which he suggested new interpretations [7]. Moreover, he identified other two apsidal buildings, only mentioned by Butler, which were definitively interpreted as churches.

The church of Saints Sergius and Bacchus has an east-west orientation and a basilica plan subdivided into three naves supporting galleries on both sides with Doric and Ionic columns. An apse 4 m deep, occupies the centre of the east side and is flanked to the north and south by two quadrangular rooms, respectively, the *prothesis* and *diachonicon*. A tower built above the *prothesis* in the north-eastern corner of the church, dominates the whole building and strongly marks out its overall appearance (Figure 3). Butler suggested that the tower was built together with the church in 489 AD and also highlighted some changes to the fabric of the building that date back to the Islamic era [6]. Subsequently, King confirmed that the church was subjected to important changes in the Islamic era and suggested that the tower and the wall closing the apse were part of an Islamic-era remodelling. According to this interpretation, the tower was probably used as a minaret and not as a bell tower [7].



Figure 3. The façade of the church of SS. Sergius and Bacchus (photo by Piero Gilento, 2017).

The stratigraphic analyses of the standing remains, carried out between 2009 and 2012, led to the identification of at least 7 construction phases as highlighted in Figure 4 and described in Table 1 [3, 8].



Figure 4. The seven building phases of TU28 (Anastasio, Gilento, Parenti 2016 [3])

Mortar analysis

To further investigate the above mentioned construction phases and provide an initial description of the construction materials and technologies used in the various phases, seven mortar samples were collected and sent to Northumbria University for chemical and mineralogical analysis. The samples included bedding and coating mortars from both, the church and the adjacent rooms. A list of samples is provided in Table 2 whereas the sampling points are highlighted in Figure 5. The sampling was based on the stratigraphic analysis of the different construction phases of the walls and of the buildings. Combination of the results of the archaeometric analyses with the results of the stratigraphic analysis allows us to obtain significant data associated to the historical evolution of the fabric.

Substantial modifications to the buildings were probably made after the Islamic conquest. These affected the entire volume of the complex and included the construction of the tower-minaret [9]. In the Islamic period, the church was transformed into a mosque with a high tower for the call to prayer. Significant evidence of this change in the cult are the wall closing

off the apse, a possible blocking of the western entrances, and the opening of a new entrance on the northern side of the apse via the courtyard [3, 9].

Table 1. List of the construction phases identified for the church of the SS Sergius and Bacchus.

Construction phase	Chronology	Characteristics
1	Late Roman / Early Byzantine	Prior the construction of the church, a previous structure existed. Its traces are still visible, especially in the northern court of the complex
2	Byzantine / Late Byzantine	The two main building elements (BE) of TU 28 were built: the church of the Saints Sergius and Bacchus (BE 1) and another building on the south-western corner (BE 2)
3		The northern court and part of the façade were renewed
4-5	Islamic	Significant modification to the church of the Saints Sergius and Bacchus: a large part of the north-eastern side of the church and the prothesis were demolished (or collapsed), and a tower (BE 4) was built
6	Modern	Several construction activities were carried out, corresponding to the Druze occupation
7	Contemporary	Recent conservation works were carried out by the Department of Antiquities

Table 2. List of the seven mortar samples analysed and related information.

Sample	Construction phase - Chronology	Feature
S_M_28_1	Phase 2 - Byzantine	Mortar between the two lintels of the door on the second level above room 9
S_M_28_3	Phase 3 - Late Byzantine / Islamic	Room 15, eastern door jamb
S_M_28_2	Phase 4-5 - Islamic	Room 15, east wall, mortar filling the joints
S_M_28_4		Mortar between the joints of the voisoirs of the pointed arch n.2 of the cistern in the court n. III
S_M_28_5		Plaster on the southern part of the arch n.3 of the cistern in the court n. III
S_M_28_6		Mortar in the central pillar of the staircase of the tower-minaret
S_M_28_7		Plaster on the exterior eastern wall of the tower-minaret



Figure 5. Plan of Topographical Unit 28 in yellow the church and in green the monastery and the localisation in red spots of the seven mortar samples (modified by Piero Gilento and Sara Peñalver Martín, 2018).

Materials and methods

The macroscopic characteristics of the samples were investigated by observing the samples as received and fresh fractures under a Leica S6 D stereomicroscope equipped with a Leica digital camera, at low magnification (i.e. 10x) using incident visible light.

Micro-morphological characterisation of the binder and aggregate in each sample was carried out using a Tescan Mira 3 Scanning Electron Microscope (SEM) in high vacuum mode, equipped with an Energy-Dispersive X-ray spectrometer (EDX) for elemental analysis. A fresh broken surface of each sample was observed. Prior to analysis, the surface was coated with a 5nm-thick Platinum layer.

Mineralogical characteristics of the mortars were investigated using the X-Ray Diffraction analysis (XRD). Each sample was grinded using an agate mortar and pestle and sieved to obtain a powder of <250 μm diameter particles. The samples were, then, analysed with a Siemens D5000 diffractometer with Cu- K_{α} radiation as X-ray source, $2-\theta$ range of 2-70 degrees with an increment of 0.02/step and scan speed of 1 sec/step, at 40 KV and 40 mA. Interpretation of diffractograms for qualitative analysis was carried out using the reference included in the EVA software database and in the RRUFF mineral database [10]. A quantitative analysis was carried out on sample SM-28-6, which was prepared as described above and subsequently mixed with 10%w/w of ZnO powder, used as internal standard. Quantification of compounds was performed through software Profex and the optimised fit was accepted when a value of $\chi^2 < 1.6$ was obtained [11].

Results and discussion

Macroscopic characteristics

At the optical microscope the samples showed very different characteristics (Figure 6).

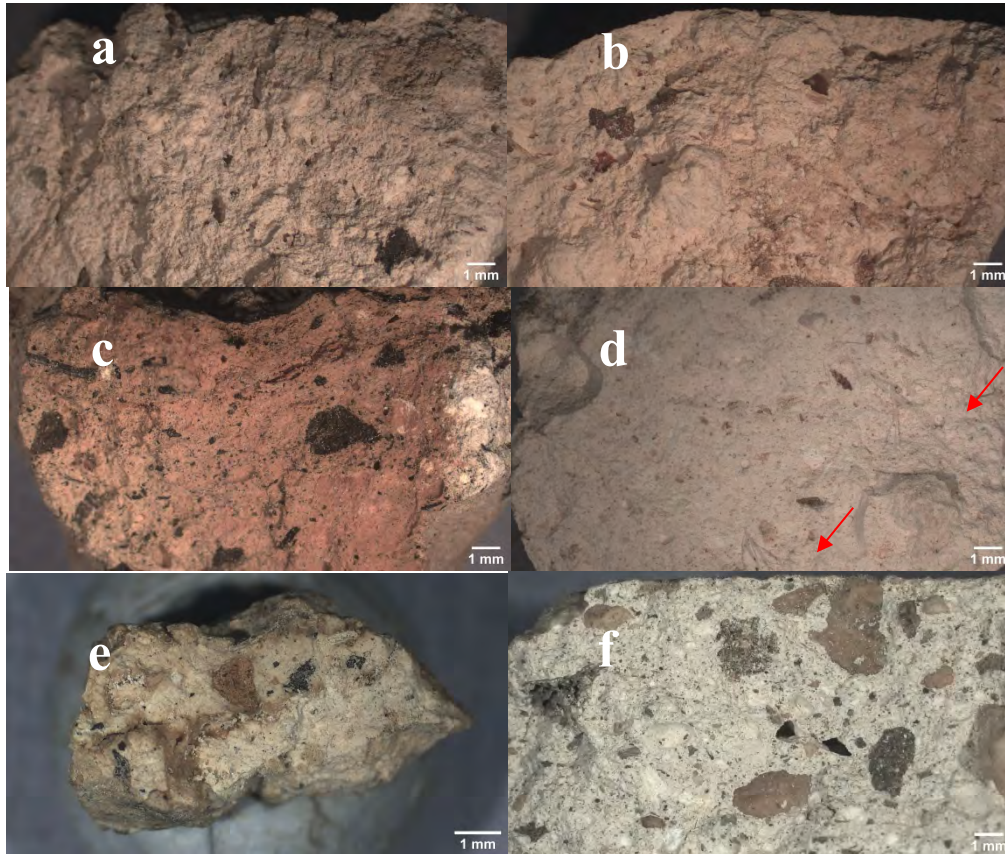


Figure 6. Stereomicroscope images of fresh surfaces of the samples SM-28-1 (a), SM-28-2 (b), SM-28-3 (c), SM-28-7 (d), SM-28-4 (e), and SM-28-6 (f).

Sample SM-28-1 (Figure 6a) exhibited a grey-brownish porous matrix. This appeared inhomogeneous, with white, grey and dull red ochre areas with no clear border between each other, suggesting that the mortar was produced with different mixtures, mixed together while still fresh. The natural aggregate is made of sub-rounded particles of ~ 1 mm \emptyset . Black particles with irregular shape and size from 0.1 mm to 1.5 mm \emptyset are visible. Sample SM-28-2 (Figure 6b) showed a more compact white matrix and sub-rounded aggregate with particles size between 0.1 mm and 1.5 mm. In Figure 6c a fresh fractured of the SM-28-3 is showed highlighting the red vivid matrix. At a higher magnification, it was observed that the matrix is homogeneous and that the red colour is not due to the addition of a specific pigment, but it is likely to be due to the binder itself, possibly because of the nature of the lime used in the mortar. Several charcoals particles of various size (0.1-2.5 mm \emptyset) were observed in the sample. Sample SM-28-7 (Figure 6d) showed a white compact matrix with very few aggregate particles with size between 0.1 mm and 0.5 mm. Red coloured fragments embedded in the sample showed the characteristics of a mortar sample, probably crushed

and reused as aggregate. Several organic fibres embedded in the mixture are highlighted by the red arrows in Figure 6d. Sample SM-28-4 (Figure 6e) showed a white-brownish matrix, sub-angular natural aggregate and sub-rounded particles, probably fragments of an older mortar that was crushed and reused as an aggregate. SM-28-6 (Figure 6f) showed a similar matrix to SM-28-4. The samples is characterised by sub-rounded aggregate particles of 0.1mm-3 mm \varnothing .

X-Ray Diffraction analyses

Results of the X-ray diffraction analysis are summarised in Table 3 where the main mineralogical phases are listed with the related estimated amount based on the relative peak height.

Table 3. Results of the X-Ray diffraction analysis with an estimation of the abundance of the mineralogical phases based on the relative peak height.

Sample	Calcite	Quartz	Gypsum	Halite	Aragonite
SM-28-1	+++	++	—	—	—
SM-28-2	+++	traces	+	+	—
SM-28-3	+++	+	+	+	—
SM-28-4	+++	+	—	+	—
SM-28-6	+++	+	—	traces	+
SM-28-7	+++	+	++	—	++

+++ = dominant; ++ = abundant; + = present; traces; — = absent

Calcite was the dominant crystalline phase in all samples, suggesting that all mortars were produced using lime as main binder. Gypsum was identified in samples SM-28-2, SM-28-3, and SM-28-7, either as binder and/or as aggregate. The presence of gypsum as binder might explain the more compact appearance previously observed at the stereomicroscope of these samples compared to sample SM-28-1 [12]. Quartz was found in samples SM-28-1, SM-28-3, SM-28-4 and SM-28-7, and only in traces in SM-28-2. The lack of quartz in the latter sample might support the hypothesis of use of gypsum as binder, since gypsum-containing mortars are characterised by a reduced shrinkage upon setting compared to lime-based mortar. Therefore the addition of aggregate to these mortars held no further benefit [13, 14]. Halite was found in samples SM-28-2, SM-28-3, and SM-28-4. This mineral is commonly associated with the presence of gypsum (although gypsum was not detected in all samples containing halite) [15]. Aragonite was found abundant in SM-28-7 and in traces in SM-28-6. Its formation could have been fostered by the high concentration of sulphates in the sample [16]. Results of the quantitative analysis on sample SM-28-6 are illustrated in Table 4.

Table 4. Amount of minerals found in sample SM-28-6 by XRD.

Mineral	%w/w	SD
Calcite	60	2
Quartz	2.63	0.28
Aragonite	11.62	0.73
Halite	0.16	0.13
Amorphous phase	25.6	2.4

The main mineral phase is calcite (60%) with subsequent aragonite (11.62%), quartz (2.63%) and halite (0.16%). A significant amount of amorphous phase has been identified, which can be due to various reasons such as a microcrystalline fraction and charcoal fragments.

SEM-EDX analyses

Results of the analyses with the SEM and EDX suggest a substantial presence of calcium carbonate. Other elements such as Si, Al, Mg, Na, Cl, Fe and K are also detected. In SM-28-1, point analysis on the binder shows a dominant signal of O, Ca and C, followed by Si, Mg, Al, K, Na, and traces of Fe, which might be accountable for the slight ochre colour of the binder. In the same sample, glassy inclusions made of almost exclusively Si and O were found embedded in the binder, along with silico-aluminates fragments. In SM-28-3 the several black fragments observed at the optical microscope (Figure 6c) were confirmed to be charcoal by both its microstructure (Figure 7) and by the EDX spectrum, which showed C as dominant element (Figure 8) [17]. Within the lime binder, sulphur-rich areas were found with micritic, aligned laminar crystals ascribable to gypsum [18].

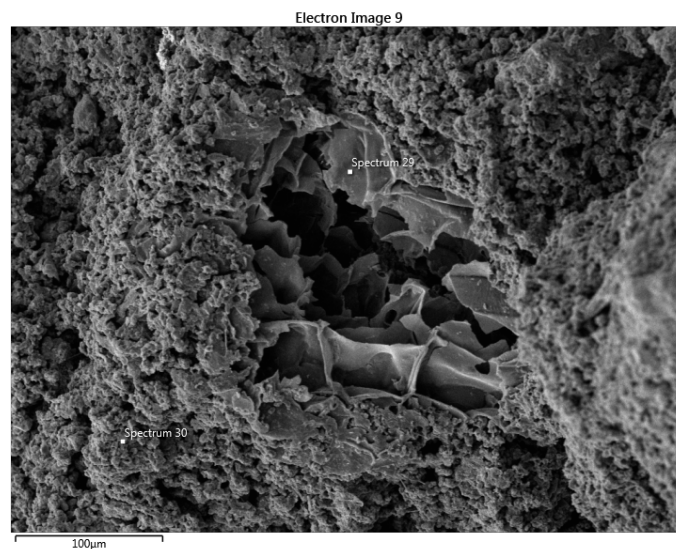


Figure 7. SEM image of a charcoal aggregate embedded in the carbonate-based binder of sample SM-28-3.

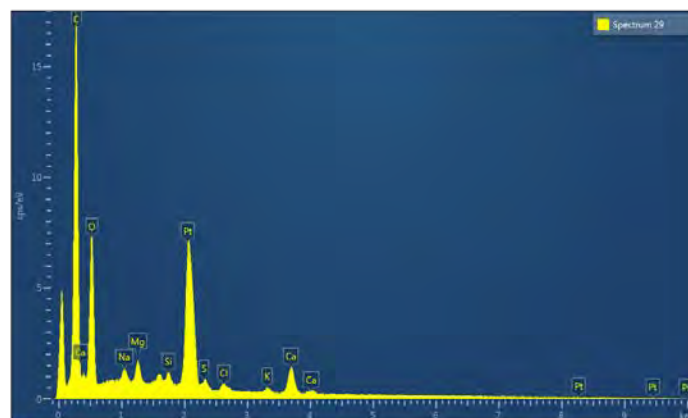


Figure 8. Point EDX measurement of a charcoal fragment in sample SM-28-3.

In samples SM-28-2 and SM-28-7 pseudo-prismatic gypsum crystals (1-10 μm sized) were found within the carbonate-based binder (Figure 9). Gypsum crystals were bigger than CaCO_3 crystals, most likely as a consequence of their higher susceptibility to dissolution and recrystallisation processes during long-term weathering, due to their higher solubility with respect to CaCO_3 [19].



Figure 9. SEM image of the binder in sample SM-28-2.

In sample SM-28-7, abundant acicular crystals embedded in the binder were found (Figure 10). Point EDX investigations on such crystals showed similar peaks to those of the surrounding binder, i.e. mainly O, C, and Ca, suggesting that these crystals are aragonite, a polymorph of CaCO_3 that can precipitate along with calcite in Mg^{2+} and SO_4^{2-} -rich solutions [16, 20].

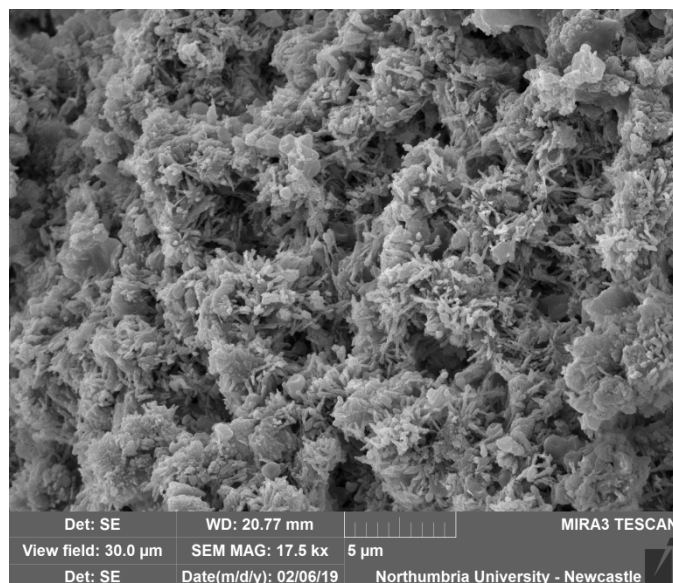


Figure 10. SEM image of the binder of sample SM-28-7. Needle-like crystals of aragonite are found within rombohedral calcite crystals.

Conclusions

Based on the results of both, the stratigraphic analysis and the laboratory analyses, the mortar samples described in this paper could be divided into 4 groups, detailed in Table 5.

Table 5. Clustering of samples with common characteristics.

Group	Sample	Phase-Period - Building Archaeology	Localisation	Binder colour	Gypsum	Type of aggregate	Organic fibers
I	SM-28-1	Byzantine	Mortar between the two lintels of the door on the second level above room 9.	Light brownish grey with darker spots	Absent	Sub-rounded silica-aluminates fragments (very abundant)	Absent
II	SM-28-3	Late Byzantine / Islamic	Room 15, right side of the doorframe.	Red	Present	Charcoals (dominant) and silica-aluminates fragments (abundant)	Absent
III	SM-28-2	Islamic	Room 15, wall east, pointing mortar.	White	Present	Sub-rounded silica-aluminates fragments (scarce)	Absent
	SM-28-7	Islamic	Plaster on the exterior eastern wall of the minaret.	White	Abundant	Sub-rounded silica-aluminates fragments and mortar fragments (both scarce)	Abundant
IV	SM-28-4	Islamic	Bedding mortar of the voissoirs of the pointed arch n.2 of the cistern in the court n. III	Light grey	Absent	Sub-rounded silica-aluminates fragments and mortar fragments (both abundant)	Absent
	SM-28-6	Islamic	Mortar in the central pillar of the staircase of the minaret.	Light grey	Absent	Rounded silica-aluminates fragments (very abundant)	Absent

Group I (sample SM-28-1), considering its provenance within the religious complex, can be defined as the most ancient of all analysed samples. It dates back to the byzantine period, during which the church and the adjacent rooms were built. The mortar is characterised by a lime-based binder with a high content of siliceous aggregate, as typical of the byzantine tradition [4, 21, 22]. Groups II and III include mortars produced in a later period and based on a mixture of lime and gypsum. In group II (SM-28-3), which dates back to the late byzantine/Islamic period, the mortar is part of a doorframe and is characterised by a red-coloured binder based on a mixture of lime, gypsum and abundant charcoal. Group III (SM-28-2, SM-28-7) dates back to the Islamic period and, considering the provenance of the sample (Table 2), the mortars had a decorative function that seems to be reflected by their composition. Both mortars, in fact, are characterised by a binder made of a mixture of lime and gypsum, and by a very low content of siliceous aggregate. Group IV (SM-28-4, SM-28-6) also dates back to the Islamic period. The mortars of this group have a structural function and are based on lime as a binder, with inclusions of siliceous sand and mortar fragments as aggregate.

Overall, these results provide an initial description of the materials and technologies used in the church of the Saints Sergius and Bacchus and adjacent rooms, in the village of Umm as-Surab (Northern Jordan). In particular, the analyses confirmed that the complex was built in various periods using a variety of materials, and, at the same time, provided an insight in the cultural and historical context in which the religious complex was built. The results suggest that during the Byzantine period mortars were produced exclusively using lime as a binder, whereas during the Islamic phases mortars with decorative function were produced using a mixture of lime and gypsum as a binder. These information allow a more precise investigation of the chronology of the building and contributes to broaden our knowledge of the material culture in the Ḥawrān region in the past centuries.

References

1. Boato A (2008) *L' Archeologia in Architettura*. Misurazioni, stratigrafie, datazioni, restauro. Marsilio, Venezia
2. Brogiolo GP, Cagnana A (2012) *Archeologia dell' Architettura*. Metodi e interpretazioni. All'Insegna del Giglio, Firenze
3. Anastasio S, Gilento P, Parenti R (2016) Ancient Buildings and Masonry Techniques in the Southern Hauran, Jordan. *Journal of Eastern Mediterranean Archeology and Heritage Studies* 4.4:299–320
4. Al-Bashaireh K (2016) Use of lightweight lime mortar in the construction of the west Church of Umm el-Jimal, Jordan: radiocarbon dating and characterization. *Radiocarbon* 58-3:583-598

5. Dunn E, Rapp G (2004) Characterization of Mortars and Pozzolanic Materials from Umm al-Jimal. *Studies in Conservation* 49-3:145-160
6. Butler HC (1909) *The Southern Haurân. Part 2 Southern Syria. Section A Ancient Architecture in Syria.* Princeton University Archaeological Expeditions to Syria in 1904–1905 and 1909 Publications 2. Brill, Leiden
7. King GRD (1983) Two Byzantine Churches in Northern Jordan and Their Re-Use in the Islamic Period. *Damaszener Mitteilungen* 1:111–136
8. Gilento P (2014) La Chiesa dei Santi Sergio e Bacco, Umm as-Surab (Giordania). Risultati storico-costruttivi dall'analisi archeologica degli elevati. *Arqueología de la Arquitectura* 11. doi: <http://dx.doi.org/10.3989/arq.arqt.2014.015>
9. Parenti R (2011) Minareti e campanili. *Arkos* 24:58–62
10. Lafuente B, Downs R T, Yang H, Stone N (2015) The power of databases: the RRUFF project. In: *Highlights in Mineralogical Crystallography*, T Armbruster and R M Danisi, eds. Berlin, Germany, W De Gruyter, pp 1–30
11. Döbelin N (2015) First Steps: Basic Refinement. PROFEX - Open Source XRD and Rietveld Refinement. http://profex.doebelin.org/?page_id=404. Accessed 1 Dec 2018
12. Ingham J (2013) *Geomaterials Under the Microscope. Mortar, plaster, and render.* Academic Press
13. Sánchez JA, Barrios J, Barrios A et al (1997) The shrinkage in lime mortars. *Materiales De Construcción* 47:17–28
14. Doleželová M, Krejsová j, Vimmrová A (2018) Influence of fine aggregate on some properties of gypsum mortars. *IOP Conf Ser Mater Sci Eng* 379
15. Boggs S (1987) *Principles of Sedimentology and Stratigraphy.* Pearson Prentice Hall
16. Bots P, Benning LG, Rickaby REM et al (2011) The role of SO₄ in the switch from calcite to aragonite seas. *Geology* 4:331–334
17. Kawiak T (1991) Gypsum Mortars from a Twelfth-Century Church in Wiślica, Poland. *Stud Conserv* 36:142–150
18. Bonny S, Jones B (2003) Microbes and mineral precipitation, Miette Hot Springs, Jasper National Park, Alberta, Canada. *Can J Earth Sci* 40:1483–1500
19. Middendorf B (2002) Physico-mechanical and microstructural characteristics of historic and restoration mortars based on gypsum: current knowledge and perspective. *Geol Soc* 205:165–176

20. Lubelli B, Nijland TG, Van Hees RPJ (2011) Self-healing of lime based mortars: Microscopy observations on case studies. *Heron* 56:81–97
21. Freidin C, Meir IA (2005) Byzantine mortars of the Negev Desert. *Constr Build Mater* 19:19–23
22. Bakolas A, Biscontin G, Moropoulou A et al (1998) Characterization of structural byzantine mortars by thermogravimetric analysis. *Thermochim. Acta* 321:151–160

Characterisation of Roman Mortar from the Archaeological Site of *Mirobriga*

Alvin Sern Hao Chua¹, Cristina Galacho¹, Patrícia Moita¹, José Carlos Quaresma²

(1) Universidade de Évora, m38414@alunos.uevora.pt, pcg@uevora.pt, pmoita@uevora.pt

(2) Universidade Nova de Lisboa, josecarlosquaresma@gmail.com

Abstract

Mirobriga is a Roman site located in the municipality of Santiago do Cacém, in Setúbal, a district in the southwest of Portugal. Mortar samples were collected from the domestic, commercial buildings, and public buildings from the site. The samples may be divided according to their function – filling, rendering, and plaster. The chemical, mineralogical, and microstructural characterisation of the samples was performed using a number of complementary techniques – stereomicroscopy, polarised light microscopy, chemical and granulometric analysis, thermogravimetric analysis (TGA), powder X-ray diffraction (XRD), and variable pressure scanning electron microscopy-energy dispersive spectrometry (SEM-EDS). The results show that in most of the samples, the aggregates consist of quartz sand, whilst the binder is lime-based. The exception, however, may be seen in the samples where stratigraphy is present. In such samples, the external layer of the mortar functions as a plaster, and both the aggregate and the binder consist of calcite. In addition, the majority of samples have a binder to aggregate ratio of 1 : 3. As a whole, the raw materials used for the production of the mortars may be said to be quite similar, and shows little difference between the filling and rendering mortars, though the aggregates of these two types of mortar are different from those functioning as plaster.

Keywords: *Mirobriga*, Roman mortars, SEM-EDS, XRD, TGA.

Introduction

Mirobriga is a Roman site located in the municipality of Santiago do Cacém, in Setúbal, a district in the southwest of Portugal. Situated on the western slope of the Grândola mountain range, the ruins of this Roman settlement are close to the present town of Santiago do Cacém. According to the archaeological evidence, the site was occupied as early as the Early / First Iron Age, i.e. the 8th / 9th century BC [1], prospered and was urbanised during the Roman period, i.e. between the 1st and 2nd centuries AD [1], and was abandoned either during the 3rd/4th century AD, the 5th century AD, or even as late as the first half of the 6th century AD [1, 2]. Archaeological excavations at *Mirobriga* have uncovered a variety of structures, which may be classified according to their function – public, domestic, and commercial. The public structures that have been excavated at the site include the *forum* and *thermae*, whereas the domestic buildings consist of several *domus*.

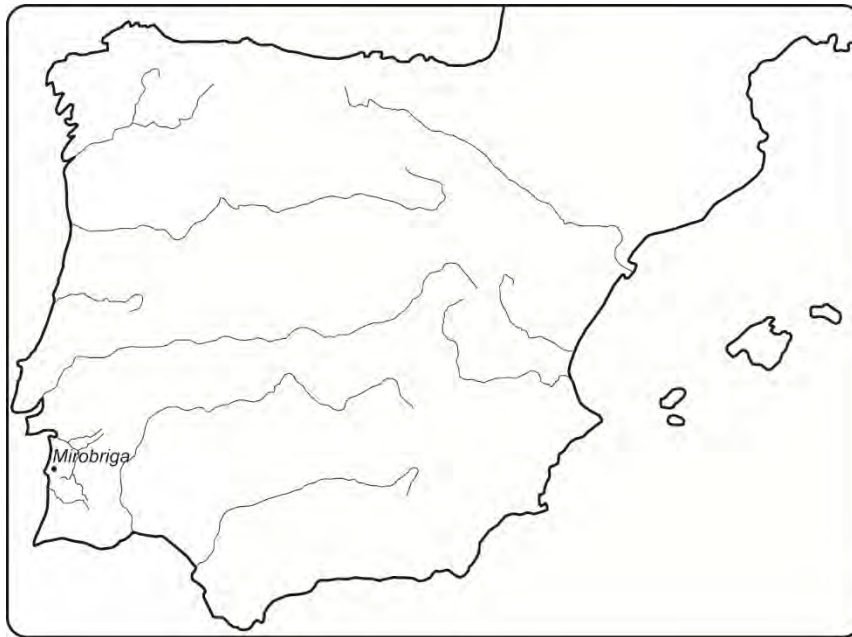


Figure 1. The location of *Mirobriga* in the Iberian Peninsula.

The commercial structures at the site include the *tabernae* and the *macellum*, which are currently the focus of a project entitled 'TabMir. Tabernae of Mirobriga, Chãos Salgados, Santiago do Cacém: A Study-Case on Roman and Late Antique Economy in Lusitania', which is directed by José Carlos Quaresma.



a. The Western *Thermae*



b. *Taberna* 1 (left) and 2 (right)



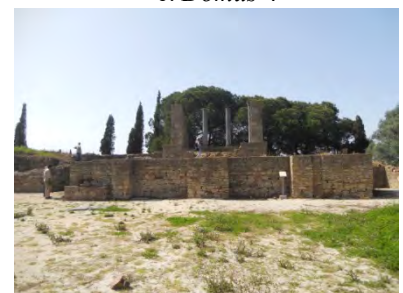
c. *Domus* 4



d. *Domus* 3



e. The *macellum* (*cryptoporticus*?)



f. The *forum* (temple podium)

Figure 2. The various archaeological structures at *Mirobriga*.

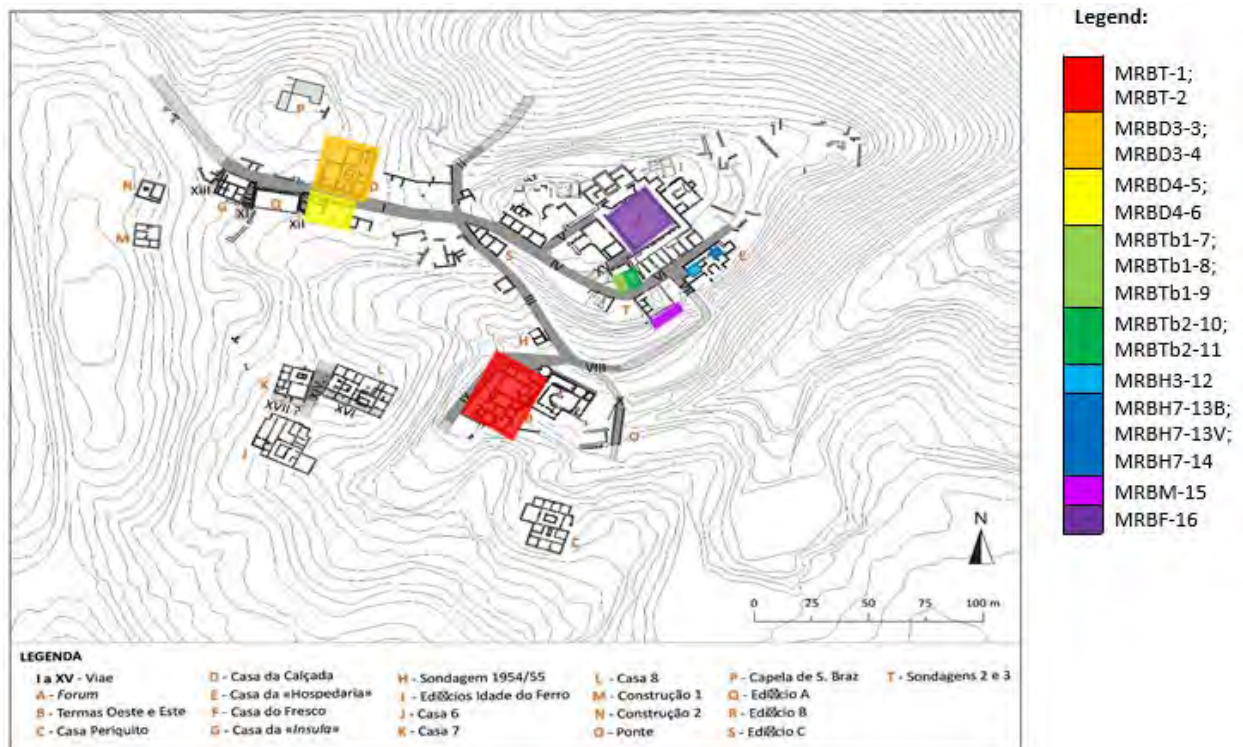
The aim of this study was to characterise the samples. This chemical, mineralogical, and microstructural characterisation of the samples was achieved using several complementary techniques.

Sampling Methodology

For the purpose of this study, a total of 17 mortar samples were collected from various structures at the site – one each from the *Macellum* (MRBM-15), and the *Forum* (MRBF-16); two each from the Western *Thermae* (MRBT-1, MRBT-2), *Domus* 3 (MRBD3-3, MRBD3-4), *Domus* 4 (MRBD4-5, MRBD4-6), and *Taberna* 2 (MRBTb2-10, MRBTb2-11); three from *Taberna* 1 (MRBTb1-7, MRBTb1-8, MRBTb1-9); and four from the ‘Hospedaria’ [one from Room 3 (MRBH3-12), and three from Room 7 (MRBH7-13B, MRBH7-13V, MRBH7-14)]. With the exception of two samples from Room 7 of the ‘Hospedaria’, which were taken from the depot, all of the samples were collected at the site. Additionally, the samples were classified either as rendering mortar, filling mortar, or plaster.

As a general rule, the samples were collected from areas where the mortar could be easily dislodged, so as to minimise the damage inflicted on the structures. When necessary, however, a hammer and chisel was used to dislodge the samples. In areas where restoration had been done in the past, *i.e.* the *thermae*, precaution was also taken so as to avoid collecting materials from the restoration material, *i.e.* cement. The samples were photographed before being placed in individual plastic bags.

Figure 3. Location of the mortar samples in the general plan of the site.



Characterisation Methodology

The samples were first photographed, and a preliminary visual assessment was made using the naked eye. A general description of the samples is provided in Table 1. After leaving the samples in an oven at 50 °C overnight, the samples were left to cool before being cleaned with a brush and chisel. The cleaned samples were observed under a stereo microscope (*Leica M205 C*, with a *Leica DFC290 HD* digital camera). The samples were then prepared according to the requirements of the individual techniques.

Polarised light microscopy was used for the visual identification of the aggregates within the samples, as well as their grain size and texture. A *Leica DM2500 P* polarising microscope was used to observe the finished thin sections, under both plane polarised light (PPL) and cross polarised light (XPL), and the images captured with a *Leica MC170 HD* digital camera.

Chemical analysis was used to determine the ratio between the soluble fraction and the insoluble residue of the samples, whereas granulometric analysis was used to quantify the size distribution of the grains in the insoluble residue, as well as to observe the composition and morphology of the insoluble residue. The samples were subjected to acid attack (10 g) with hydrochloric acid (HCl, concentration of 1:3 v/v %, 120 mL), in order to separate the soluble fraction and the insoluble residue. The latter was then sieved with a stainless steel sieve (ASTM E11, diameter of 100 mm x 40 mm, with the following mesh sizes: 4, 2, 1, 0.500, 0.250, 0.125, and 0.063 mm) for grain size analysis, and observed under a *Leica M205 C* stereo microscope.

Thermogravimetric Analysis (TGA) was used to quantify the amount of binder with a carbonate composition. In combination with the chemical analysis, TGA allowed the aggregate: carbonate: solubles ratio of the samples to be calculated. The powdered samples were analysed in a simultaneous thermal analyser, *STA 449 F3 Jupiter* under inert atmosphere (nitrogen – 70 ml/min.), with a uniform heating velocity of 10°C/min. from 40 to 1000 °C.

Powder X-Ray Diffraction (XRD) was used to determine the mineralogical composition of the samples. Both the global and fine fractions were analysed. The samples were analysed using an X-ray diffractometer, *Bruker AXS-D8 Advance*, with Cu-K α radiation ($\lambda = 0.1540598$ nm), under the following conditions: scanning between 3° and 75° (2 θ), scanning velocity of 0.05° 2 θ /s, accelerating voltage of 40 kV, and current intensity of 30 mA.

Scanning Electron Microscopy (SEM) was used for imaging purposes, whilst Energy Dispersive Spectroscopy (EDS), was used for elemental analysis, elemental mapping, and punctual analyses. A *Hitachi S-3700N* SEM coupled with a *Bruker XFlash 5010 SDD* detector was used for the sample analysis. The analysis samples were performed under low vacuum, *i.e.* 40 Pa, with a current of 20 kV. The spectra were plotted on an energy scale of 0-20 keV, with a spectral resolution of 129 eV at Mn K α .

Table 1. General description of the samples.

Sample	Structure	Location	Period	Function	Colour	Inclusions	Notes
MRBT-1	Western <i>Thermae</i>	Frigidarium; south wall; internal; from the upper part of the wall	Roman	E: Layer of 'powdered marble'	E: White	-	Two layers of mortar
				I: Rendering / 'sand mortar' for stucco	I: Beige	Lime lumps	
MRBT-2	Western <i>Thermae</i>	Frigidarium; north wall; internal; between marble skirting and wall	Roman	E: Rendering	E: Red	E: Lime lumps, ceramic fragments	Heterogeneous stratigraphy; external layer very fragile
				I: Filling	I: Beige	I: Lime lumps, stones	
MRBD3-3	<i>Domus</i> 3	North wall; external	Roman	Filling	Beige	Lime lumps, stones	
MRBD3-4	<i>Domus</i> 3	Stairs; external	Roman	Filling	Beige	Lime lumps	
MRBD4-5	<i>Domus</i> 4	Stairs from the street	Roman	Filling	Beige	Lime lumps	
MRBD4-6	<i>Domus</i> 4	North wall; internal	Roman	Filling	Beige	Lime lumps	
MRBTb1-7	<i>Taberna</i> 1	South wall; external; from the top of the wall	Roman	Filling (?)	Beige	Lime lumps, ceramic fragments	
MRBTb1-8	<i>Taberna</i> 1	East wall; internal, between Tb1 and Tb2; from the top of the wall	Roman	Filling (?)	Beige	Lime lumps, ceramic fragments	
MRBTb1-9	<i>Taberna</i> 1	North wall; internal, from the vertical face of the wall	Roman	Rendering (?)	Beige	Lime lumps	
MRBTb2-10	<i>Taberna</i> 2	East wall; external; adjacent to the street	Roman	Filling	Beige	Lime lumps	
MRBTb2-11	<i>Taberna</i> 2	Entrance	Roman	Filling	Beige	Lime lumps, ceramic fragments	
MRBH3-12	'Hospedaria', Room 3	North wall; internal; wall with paintings	Roman	E: Layer of 'powdered marble'	E: Orange, white	-	Heterogeneous stratigraphy; internal layer fragile; chromatic layer and two layers of mortar
				I: Rendering / 'sand mortar' for stucco	I: Beige	I: Lime lumps	
MRBH7-13B	'Hospedaria', Room 7	Northeast wall; internal	Roman	E: Layer of 'powdered marble'	E: White	-	From the depot; homogenous stratigraphy, chromatic layer, two layers of mortar
				I: Rendering / 'sand mortar' for stucco	I: Beige	I: Lime lumps	
MRBH7-13V	'Hospedaria', Room 7	Northeast wall; internal	Roman	E: Layer of 'powdered marble'	E: Red, white	-	From the depot; homogenous stratigraphy, chromatic layer, two layers of mortar
				I: Rendering / 'sand mortar' for stucco	I: Beige	I: Lime lumps, stones	
MRBH7-14	'Hospedaria', Room 7	South wall; internal	Roman	Rendering	Beige	Lime lumps	
MRBM-15	<i>Macellum</i>	Back of structure, <i>cryptoporticus</i> (?); internal (?)	Roman	Filling	Beige	Lime lumps	<i>Macellum</i> yet to be excavated
MRBF-16	<i>Forum</i>	Podium of the temple	Roman	E: Layer of 'powdered marble'	E: White	-	Two layers of mortar
				I: Rendering / 'sand mortar' for stucco	I: Beige	I: Lime lumps	

Results and Discussion

Stereo Microscopy

In general, the results of stereo microscopy show that there is little compositional difference. For the majority of the samples, the aggregate consists mainly of hyaline and milky quartz (some of the latter possibly being feldspars). The quartz grains may be described as uniform, and its roundness ranging from 'subangular' to 'well-rounded' (Figure 4.a.). Black minerals (later identified as ilmenite), and lime lumps (Figure 4.b.) were also visible in the samples. Nevertheless, MRBT-2 is noticeably different from the rest of the samples, due to its function. Ceramic fragments were observed in this sample (Figure 4.c.),

and the red colour of this layer is due to the addition of powdered bricks / ceramics in the binder. MRBT-1E, MRBH3-12E, MRBH7-13BE, MRBH7-13VE, and MRBF-16E are also different from the other samples, as these were the preparation layers on which paint was applied. Calcite crystals (Figure 4.d.) were observed in these samples.

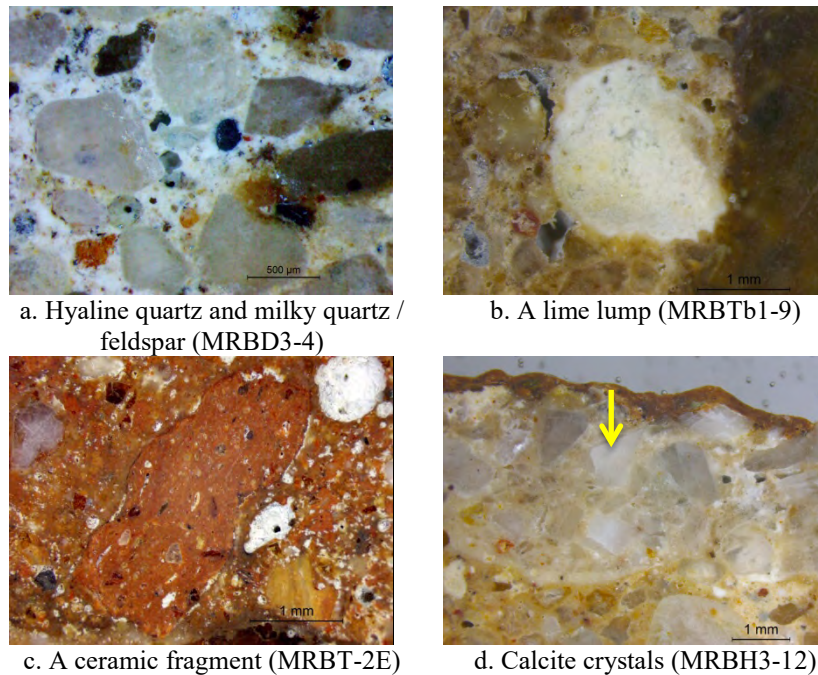


Figure 4. General aspects of the samples observed under the stereo microscope.

Polarised Light Microscopy

Polarised light microscopy shows that for the majority of the samples, quartz (Figure 5.a.) is the principal constituent of the aggregate. This mineral is present either as single grains, or as lithic fragments, *i.e.* quartzite, and the roundness of the grains ranges from ‘subangular’ to ‘well-rounded’. Feldspars (both K-feldspar and plagioclase) (Figures 5.b. and 5.c.) were also commonly found in the samples. Ilmenite was viewed under PPL, whilst tourmaline (Figure 5.d.) is present in many of the samples, albeit in small quantities, *i.e.* one or two grains. The exceptions to the rule are MRBT-1E, MRBH3-12E, MRBH7-13BE, MRBH7-13VE, and MRBF-16E, where large calcite grains (Figure 5.e.) were observed. The morphology of these grains may be described as ‘angular’ / euhedric.

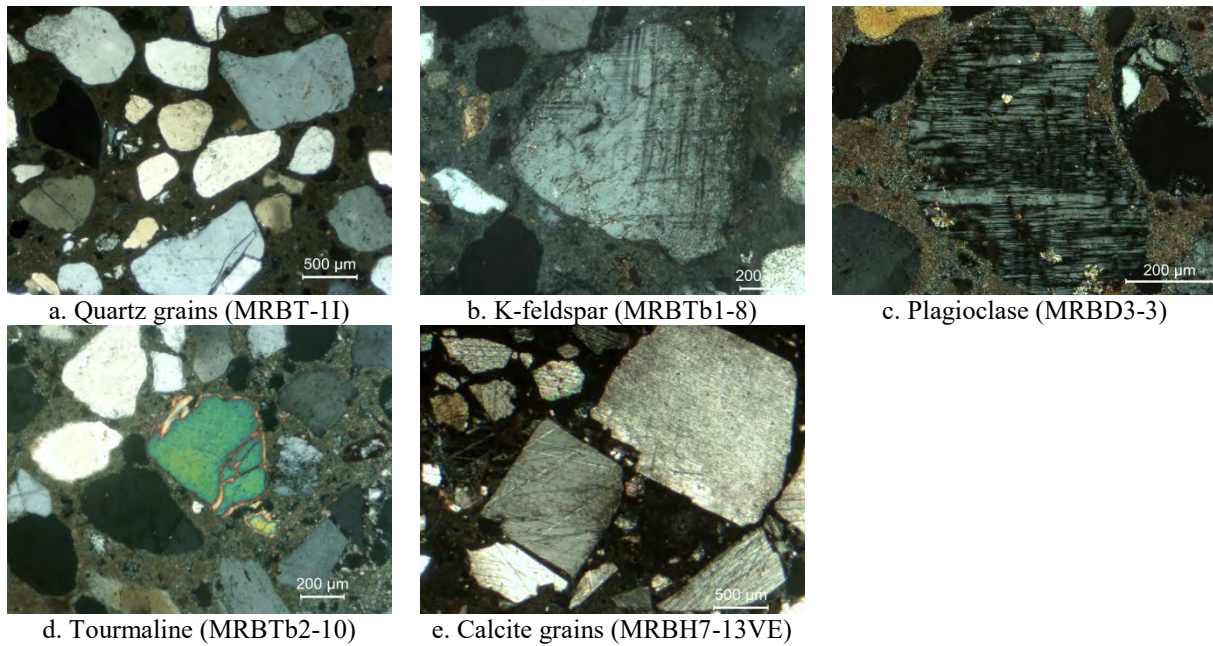


Figure 5. Observations under the polarising microscope in XPL.

Chemical and Granulometric Analysis

The amount of insoluble residue and soluble fraction (in percentage) of each sample is shown in Figure 6.

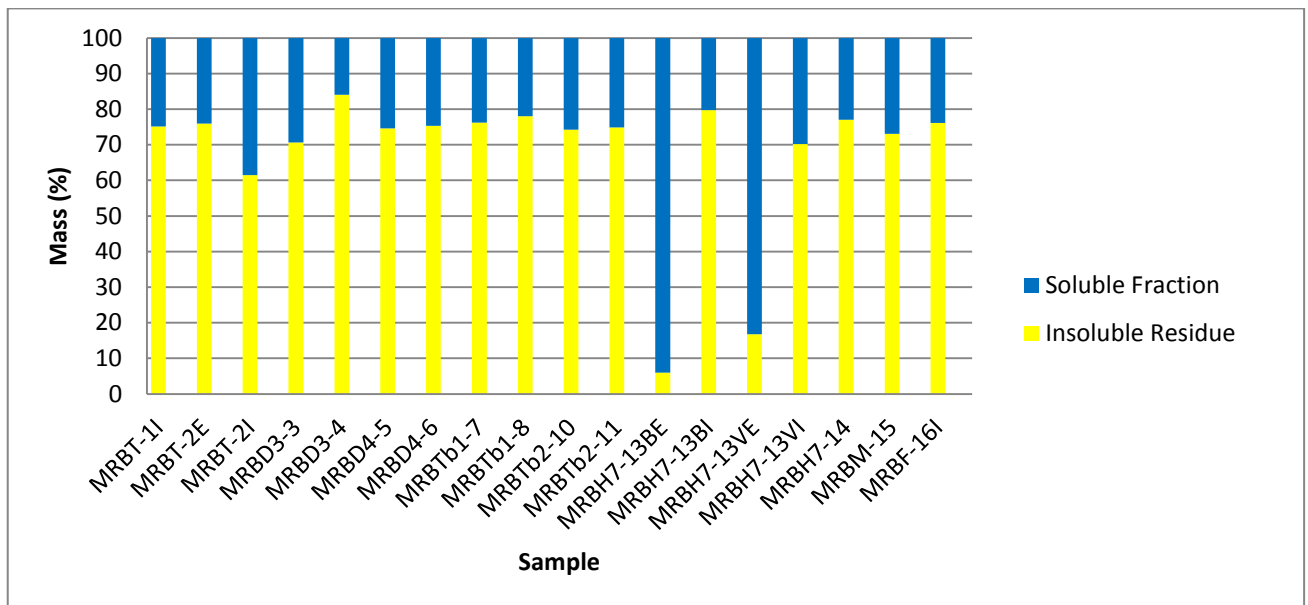


Figure 6. The insoluble residue and soluble fraction of the samples.

In all of the samples, apart from MRBH7-13BE and MRBH7-13VE, the amount of insoluble residue is higher than that of the soluble fraction, and ranges from 61.47% in MRBT-2I to 84.08% in MRBD3-4. The insoluble residue and the soluble fraction may be equated with the aggregate and binder respectively, and hence has been used for the calculation of the binder

to aggregate ratio. The results show that most of the samples respect Vitruvius' formula for mortar made with pit sand [3], which is 1 : 3.

The grain size distribution of the insoluble residue for each sample is shown in Figure 7. In terms of modality, all but one sample may be classified as unimodal. The predominant fraction for these samples is either 0.25 – 0.50 mm or 0.5 – 1.0 mm, the former being a 'fine fraction', whilst the latter a 'medium fraction', according to the designation provided by Coutinho [4]. MRBTb1-8 is the only sample that may be described as bimodal, having both 0.25 – 0.50 mm and 0.5 – 1.0 mm as its predominant fraction.

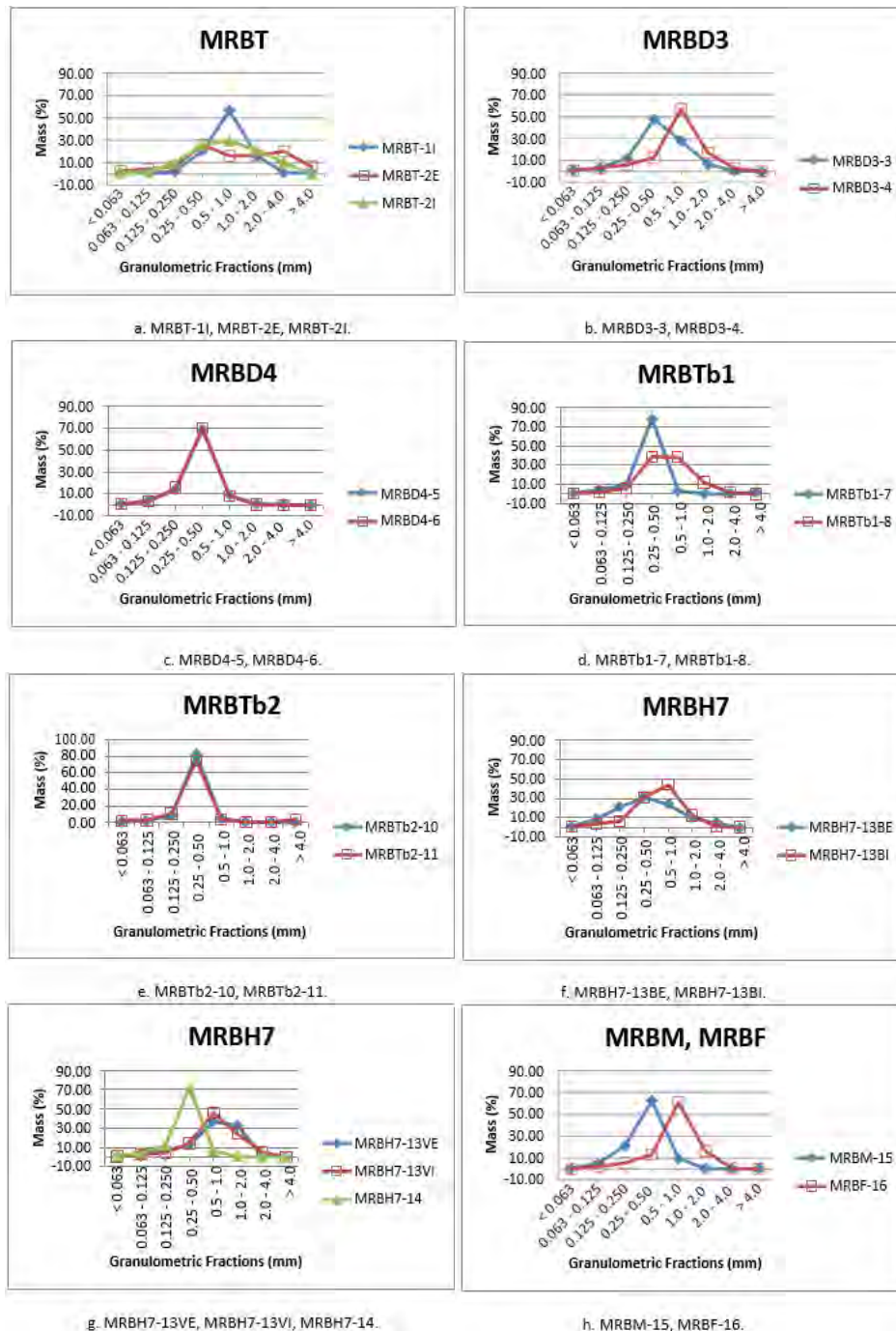


Figure 7. Grain size distribution of the insoluble residue

Observation of the insoluble residue under the stereo microscope shows that in the majority of samples, the bulk of the residue consists of quartz (both hyaline and milky) (Figure 8.a.). The roundness of these grains ranges from ‘subangular’ to ‘well-rounded’. In MRBT-2E, a significant amount of ceramic fragments was present in the residue (Figure 8.b.).

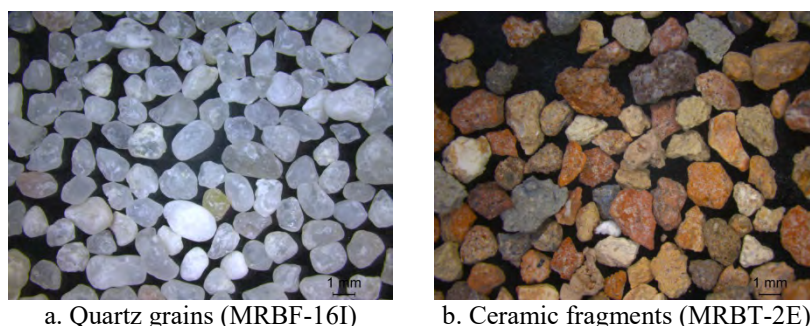


Figure 8. Examples of the insoluble residue observed under the stereo microscope.

Thermogravimetric Analysis

Table 2. shows the mass change (in percentage) of the samples during thermogravimetric analysis (TGA). The 40-120 °C, 200-600 °C, and 600-950 °C ranges corresponds to the change in mass attributed to the physically bound / absorbed water (also referred to as hygroscopic water), the structurally bound water (also referred to as chemically bound water or hydraulic water), and the decomposition of carbonates (more specifically the calcites) (resulting in the release of carbon dioxide) respectively [5, 6]. In the majority of samples, the peak of the DTG curves was registered between 700°C and 800°C, which lies within the temperature range in which calcite decomposes [7].

In Table 2, it may be observed that mass change in the 200-600 °C range (attributed to the structurally bound water) is low in the samples, the lowest being -0.66% (MRBF-16), and the highest being -2.53% (MRBH3-12I). On the contrary, the change in mass in the 600-950 °C (attributed to the calcite decomposition, during which carbon dioxide is released) varies between the samples, ranging from -3.52% in MRBD3-4 to -37.99% in MRBH7-13BE. In most of the samples, the carbon dioxide content may be described as ‘low’, *i.e.* < 10.00%. The rest of the samples may either be described as having a ‘medium’ (10–20 %) or ‘high’ (> 20%) proportion of calcite. MRBT-2I, MRBD4-6, and MRBTb1-9 belong to the former, whilst MRBH3-12E, MRBH13-BE, MRBH7-13VE, and MRBF-16E belong to the latter. The ‘high’ amount of calcite in the latter four samples was expected, as their aggregate consist mainly of this mineral.

Using the results from the TGA and the chemical analysis, a simplified composition of the samples, *i.e.* the insoluble residue (the aggregate), the calcium carbonate (the binder and the lime lumps), and the soluble fraction (possibly products of pozzolanic reaction), was calculated, according to the method proposed by Jedrzejewska [8]. This simplified composition is presented in Table 3.

Table 2. TGA mass change.

Sample	Mass Change (%)				
	40-120 °C	120-200 °C	200-600 °C	600-950 °C	Total
MRBT-1I	0.49	0.03	-0.74	-8.59	-8.81
MRBT-2E	-0.58	-0.99	-2.06	-4.33	-7.96
MRBT-2I	0.21	-0.03	-0.78	-15.16	-15.76
MRBD3-3	0.20	-0.02	-0.89	-9.52	-10.23
MRBD3-4	-0.16	-0.15	-0.76	-3.52	-4.59
MRBD4-5	-0.06	-0.28	-1.41	-7.76	-9.51
MRBD4-6	-0.36	-0.24	-2.01	-13.48	-16.09
MRBTb1-7	-0.11	-0.12	-0.82	-7.57	-8.62
MRBTb1-8	-0.19	-0.27	-1.36	-7.94	-9.76
MRBTb1-9	-0.17	-0.23	-2.07	-11.73	-14.20
MRBTb2-10	-0.11	-0.08	-1.14	-7.78	-9.11
MRBTb2-11	-0.24	-0.26	-1.27	-7.88	-9.65
MRBH3-12E	-0.03	-0.08	-1.69	-29.84	-31.64
MRBH3-12I	-0.41	-0.31	-2.53	-8.38	-11.63
MRBH7-13BE	-0.07	-0.12	-1.15	-37.99	-39.33
MRBH7-13BI	-0.27	-0.20	-1.41	-6.44	-8.32
MRBH7-13VE	-0.09	-0.12	-1.41	-32.32	-33.94
MRBH7-13VI	0.39	-0.12	-1.08	-9.99	-10.80
MRBH7-14	0.00	-0.07	-1.09	-7.89	-9.05
MRBM-15	-0.47	-0.37	-1.18	-4.43	-6.45
MRBF-16E	-0.41	-0.38	-1.80	-26.18	-28.77
MRBF-16I	-0.06	-0.15	-0.66	-7.96	-8.83

Table 3. The insoluble residue, the calcium carbonate, CaCO₃, the solubles, and the calcium hydroxide, Ca(OH)₂⁷.

Sample	Insoluble Residue (%)	Calcium Carbonate, CaCO ₃ (%)	Solubles (%)
MRBT-1I	75.17	19.54	5.29
MRBT-2E	75.95	9.85	14.20
MRBT-2I	61.47	34.48	4.05
MRBD3-3	70.64	21.65	7.71
MRBD3-4	84.08	8.01	7.91
MRBD4-5	74.61	17.65	7.74
MRBD4-6	75.29	30.66	-5.95
MRBTb1-7	76.26	17.21	6.53
MRBTb1-8	78.05	18.06	3.89
MRBTb1-9	-	26.68	-

⁷ The negative value of the solubles in MRBD4-6 may be due to the heterogeneity of the sample, *i.e.* that an area with less calcium carbonate was acquired for the chemical analysis, or one with more for the TGA.

MRBTb2-10	74.26	17.69	8.05
MRBTb2-11	74.89	17.92	7.19
MRBH3-12E	-	67.86	-
MRBH3-12I	-	19.06	-
MRBH7-13BE	5.98	86.40	7.62
MRBH7-13BI	79.69	14.65	5.66
MRBH7-13VE	16.76	73.50	9.74
MRBH7-13VI	70.18	22.72	7.10
MRBH7-14	77.06	17.94	5.00
MRBM-15	73.06	10.07	16.87
MRBF-16E	-	59.54	-
MRBF-16I	76.13	18.10	5.77

Powder X-Ray Diffraction

Table 4. shows the semi-quantitative results of the Powder X-Ray Diffraction (XRD) analysis on the global fractions, whereas those of the fine fractions are presented in Table 5.

Table 4. The semi-quantitative results of the XRD analysis (global fraction).

Sample	Mineral						
	Qz	Cal	Kfp	Pl	Micas	Dol	Arg
MRBT-1I	++++	+	++	+	++	-	-
MRBT-2E	+++	+	++	+	++	-	-
MRBT-2I	++++	+	++	-	++	+	-
MRBD3-3	++++	++	++	-	-	-	-
MRBD3-4	++++	+	++	-	-	-	+
MRBD4-5	+++	+	++	-	+++	-	-
MRBD4-6	++++	+	++	-	-	-	-
MRBTb1-7	++++	+	++	-	++	-	-
MRBTb1-8	++++	+	++	-	++	-	-
MRBTb1-9	++++	+	++	-	+	-	-
MRBTb2-10	++++	+	+	-	+	-	-
MRBTb2-11	++++	+	++	-	+	-	-
MRBH3-12E	++	++++	+	-	-	-	-
MRBH3-12I	++++	++	+	+	++	-	-
MRBH7-13BE	+	++++	++	+	-	++	-
MRBH7-13BI	++++	+	++	-	+	-	-
MRBH7-13VE	++	++++	+	-	-	-	-
MRBH7-13VI	++++	+	++	+	-	-	-
MRBH7-14	++++	+	+	-	-	-	-
MRBM-15	++++	+	++	-	+	-	-
MRBF-16E	++++	+++	+	-	-	-	-
MRBF-16I	++++	+	+	-	-	-	-

++++ (very high proportion / predominant mineral); +++ (high proportion); ++ (medium proportion); + (low proportion); - (undetected)

Table 5. The semi-quantitative results of the XRD analysis (fine fraction).

Sample	Mineral											
	Qz	Cal	Mg Cal	Kfs	Pl	Micas	Clays	Dol	Ilm	Tur	Arg	Gp
MRBT-1I	++	++++	++	++	+	-	-	tr.	-	+	-	?
MRBT-2E	+++	++	++	+	+	++	+	+	tr.	+	-	-
MRBT-2I	+	++++	++	+	-	-	++	+	tr.	+	-	-
MRBD3-3	++	+++	++	++	-	++	++	tr.	tr.	+	-	-
MRBD3-4	++	+++	++	++	+	-	++	tr.	+	+	++	-
MRBD4-6	++	++++	++	++	-	++	+	tr.	tr.	+	-	-
MRBTb1-7	++	+++	++	+	-	++	++	tr.	-	+	-	-
MRBTb1-8	++	++++	++	++	+	++	+	+	-	+	-	-
MRBTb2-10	++	+++	++	+	+	++	+++	tr.	-	-	-	-
MRBTb2-11	+++	+++	++	++	+	+	+	+	tr.	+	-	-
MRBH7-13BI	++	+++	++	++	-	++	++	+	tr.	+	-	-
MRBH7-13VI	++	++++	+++	++	+	-	++	tr.	+	+	-	-
MRBH7-14	+++	+++	++	++	+	++	+	tr.	-	+	-	-
MRBM-15	+++	+++	+	++	+	++	+	+	tr.	+	-	-
MRBF-16I	+	+++	++	++	tr.	++	+	+++	tr.	+	-	-

++++ (very high proportion / predominant mineral); +++ (high proportion); ++ (medium proportion); + (low proportion); tr. (traces); ? (uncertain); - (undetected)

In Table 4., it is clear that quartz is the predominant mineral in almost all of the samples. By contrast, calcite exists either in small or medium quantities in these samples. The inverse is true for MRBH3-12E, MRBH7-13BE, and MRBH7-13VE, where calcite is the predominant mineral, as expected, whereas quartz is present either in low or medium quantities. Feldspars were also detected in the samples. K-feldspar was detected in all of the samples (either in small or medium proportions), whilst plagioclase was found only in several of the samples. In addition, the presence of micas was detected in several samples, whilst dolomite was observed in two samples (MRBT-2I and MRBH7-13BE). Finally, aragonite was detected in MRBD3-4.

As the extremely intense peaks of quartz masked those of the other minerals in the samples, the fine fractions were also analysed. In Table 5., it is evident that the proportion of quartz was significantly reduced, thus allowing other minerals within the samples to be identified. The higher amount of binder present in the fine fractions is reflected in the increased proportion of calcite. Moreover, magnesium calcite was detected in the samples, though this mineral is present only in low or medium quantities (the exception being MRBH7-13VI, where a high proportion of magnesium calcite was observed). Micas and clay minerals were also present in most samples, either in low or medium proportions. Dolomite was detected in all samples, either in low amounts, or as traces. Ilmenite was found in most samples, though as traces, whilst tourmaline was detected in low quantities in all but one sample. Finally, aragonite was detected in MRBD3-4.

The presence of clay minerals and / or micas in the samples was detected with XRD. It has been noted, however, that the identification of these minerals with this technique is complicated due to two factors – firstly, these minerals usually occur in small quantities in the samples, meaning that they might either not stand out adequately, or be masked by the major components (this problem was mitigated by analysing the fine fraction of the samples); secondly, the peaks of these minerals occur within a narrow range, and may overlap one another, making it difficult to separate one from the other [9].

Variable Pressure Scanning Electron Microscopy-Energy Dispersive Spectrometry

From the SEM-EDS analysis, it was found that in all the samples (apart from MRBT-IE, MRBH3-12E, MRBH7-13BE, MRBH7-13VE, and MRBF-16E), the aggregate is of a siliceous nature (Figure 9.a.). In other words, the aggregate used for the production of these mortars was quartz (SiO_2) sand, as opposed to carbonate sand. The morphology of the quartz grains ranges from being ‘subangular’ to ‘well-rounded’. In many of the samples, grains containing aluminium (Al) and potassium (K), in conjunction with silicon (Si), were also seen. These were identified as K-feldspars (Figure 9.b.). Additionally, grains containing both titanium (Ti) and iron (Fe) were common, and were identified as ilmenites (Figures 10.a. and 10.b.). On the other hand, calcium (Ca) was found to be the main element of the aggregates in MRBT-IE, MRBH3-12E, MRBH7-13BE, MRBH7-13VE, and MRBF-16E (Figures 11.a. and 11.b.), and these grains are ‘angular’ / euhedric in shape. These aggregates were identified as calcite.

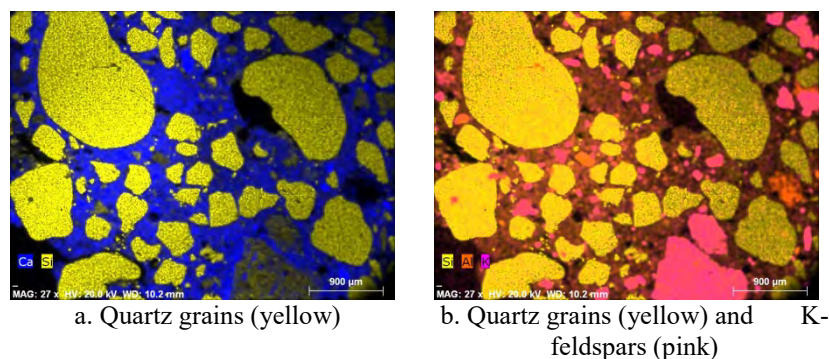


Figure 9. Elemental maps of MRBTb1-8.

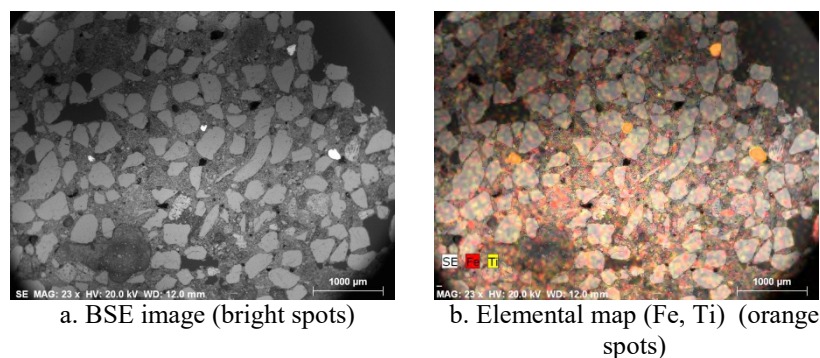


Figure 10. Ilmenites in MRBTb2-10.

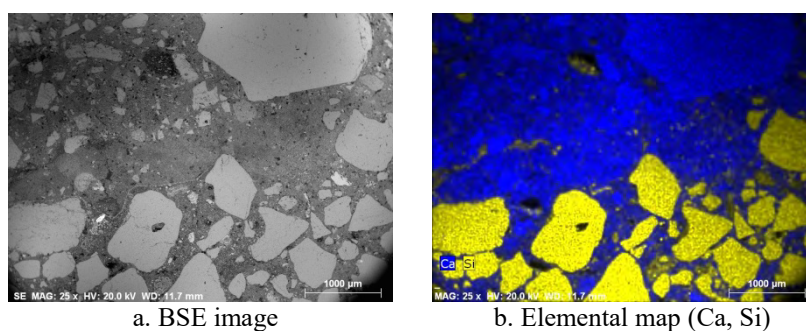


Figure 11. External and internal layers of MRBH7-13B.

Point analysis and elemental mapping were used to analyse the binder. The results of the point analysis suggest that, as a whole, the binder is of a heterogeneous nature. Point analyses performed on the lime lumps show that the limestone used contained little impurities. The elemental mapping of MRBT-1, MRBH3-12, MRBH7-13B, and MRBH7-13V suggest that there is a difference in the chemical composition of the binder in the different stratigraphic layers (Figures 12.a. and 12.b.). The elemental maps of these samples show that the binder in the external layers contains a lower amount of magnesium (Mg) than that in the internal layers, which suggest that limestone with fewer impurities may have been deliberately selected for the production of the former.

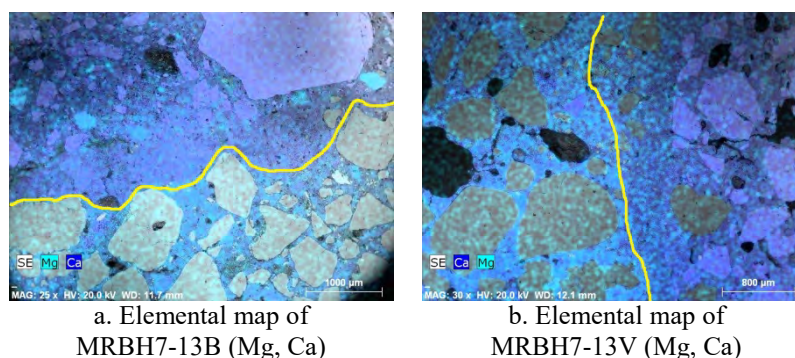


Figure 12. The difference between the external and internal layers.

Conclusion

The most striking aspect about the samples studied is their uniformity. No clear difference was observed between the filling and rendering mortars, in terms of chemical and mineralogical composition, as well as their microstructure. In addition, this uniformity would lend support to the archaeological results regarding the period of the buildings' construction, *i.e.* that they are contemporaneous, and were built between c. AD 50/75 and the first half of the 2nd century AD.

In terms of the composition of the mortars, it was found that in most of the samples, the aggregate consists mainly of quartz, and that these grains have a consistent morphology and size. The same may be said of the binder, in that they are chemically and mineralogically consistent in the majority of the samples.

Nevertheless, several samples, *i.e.* the plaster layers, were found to be markedly different. The aggregates in MRBT-IE, MRBH3-12E, MRBH7-13BE, MRBH7-13VE, and MRBF-16E were found to consist mainly of calcitic crystal grains, probably marble. Additionally, it may be said that the binder for these layers contain less impurities. These samples served as stucco layers on which paint was applied. MRBT-2E is also noticeably different due to the addition of ceramic fragments. Additionally, powdered bricks / ceramics were also mixed into the binder, causing it to have a reddish colour. These additives function as an artificial pozzolan in the mortar.

Acknowledgements

This project was made possible thanks to Dr. Manuela de Deus and the Direção Regional de Cultura do Alentejo, the Laboratório HERCULES/Universidade de Évora, and the ARCHMAT Consortium.

References

1. Slane KW, Biers WR, Biers JC & Soren D (1984) Mirobriga: The 1983 Season. *Muse* 17:38-63
2. Quaresma JC (2010) Changement et continuité: la romanisation à Chãos Salgados, Santiago do Cacém – Mirobriga? – (Portugal). In: Corsi C & Vermeulen F (eds) *Changing Landscapes: The Impact of Roman Towns in the Western Mediterranean: Proceedings of the International Colloquium, Castelo de Vide, Marvão, 15th-17th May, 2008*. Ante Quem, Bologna
3. Vitruvius, *The Ten Books on Architecture* [Morgan MH (trans)(1914) *Vitruvius' The Ten Books on Architecture*. Harvard University Press, Cambridge, Mass.]
4. Coutinho J de S (1999) *Materiais de construção I : agregados para argamassas e betões*. FEUP, Porto
5. Bakolas A, Biscontin G, Moropoulou A & Zendri E (1998) Characterization of structural byzantine mortars by thermogravimetric analysis. *Thermochim. Acta* 321:151-160
6. Moropoulou A, Bakolas A & Bisbikou K (1995) Characterization of ancient, byzantine and later historic mortars by thermal and X-ray diffraction techniques. *Thermochim. Acta* 269/270:779-795
7. Chiari G, Santarelli M & Torraca G (1992) Caratterizzazione delle malte antiche mediante l'analisi di campioni non frazionati. *Materiali e Strutture. Problemi di Conservazioni* 3:111-137
8. Jedrzejewska H (1960) Old Mortars in Poland: A New Method of Investigation. *Studies in Conservation* 5(4):132-138

9. Alvarez J, Navarro I, Martín A & Casado PG (2000) A study of the ancient mortars in the north tower of Pamplona's San Cernin church. *Cement and Concrete Research* 30:1413-1419

Insights into Carolingian construction techniques – results from archaeological and mineralogical studies at Müstair Monastery, Grisons, Switzerland

Marta Caroselli¹, Christine Bläuer², Patrick Cassitti³, Giovanni Cavallo¹, Irka Hajdas⁴, Sophie

Hueglin³, Hans Neukom³, Albert Jornet¹

(1) University of Applied Arts and Sciences of Southern Switzerland (SUPSI), Institute of Material and Construction (IMC) marta.caroselli@supsi.ch

(2) Conservation Science Consulting Sàrl, Fribourg, Switzerland.

(3) Foundation Pro Monastery of St. John, Müstair, Switzerland.

(4) Laboratory of Ion Beam Physics, ETH, Zurich, Switzerland

Abstract

During decades of archaeological investigations at the monastery of St. John in Müstair, a World Heritage site located in the canton of Grisons, Switzerland, more than 5000 mortar samples dated between about AD 775 and AD 1800 have been recovered. The site also features the remains of five mechanical mortar mixers dating from the 8th to the 10th century. This monastery acts as a case study to recount materials and methods in medieval and early modern construction sites. The proposed paper will focus on the earliest construction phase, which has been dated by dendrochronology between AD 775 and 788. A large number of archaeological features can be attributed to the Carolingian construction site: trenches, post-holes, fills, deposits of lime and plaster, as well as imprints on soil and mortar. They offer insights into the organization of the building site and the progression of the work. The petrographic analyses of mortars and raw materials further complement and expand our knowledge of Carolingian building techniques, so that different mortar groups have been identified with different petrographic characteristics.

1. Introduction

Building technology in general and mortar production in particular have been identified as key elements to understand and scientifically date materials, methods, movements and motivations of builders and patrons, especially for periods and sites with little evidence to draw on [1]. Building materials reflect natural resources as well as cultural choices. Methods of preparation and construction vary with period and purpose, but can tell also of skills and working conditions. With the movement of men, animals and materials also technologies and ideas are transported and create connections between sites far apart.

The above-mentioned aspects of the history of construction are being studied as part of the project "Mortar technology and construction history at Müstair Monastery".⁸ The focus of the project lies on the study of mortar fragments from the UNESCO World Heritage site of the Monastery of St John at Müstair. The monastery is amongst the best preserved monastic sites in Europe and since 1969 has been systematically investigated archaeologically below ground [2]. It is exceptionally well suited to a study of the development of stone building technology because it has a history of almost continuous construction activity for over a thousand years.

Moreover, the monastery boasts about 5000 samples of mortar from all periods, which allows us to correlate certain mortar types with period and function, as well as specific preparation and application methods. The importance of the study of mortars concerns their technical process of production. The scientific study of the material has implications in historical, archaeological and technological contexts [3].

The aims of this paper are: i) to study the mortar of all the buildings attributed to the Carolingian phase (church, convent, loggia building and Holy Cross Chapel); ii) to study the archaeological documentation of the excavation to identify particular construction techniques of the Carolingian phase; iii) to understand whether there are any similarities or differences (type of binder, type of aggregate, texture) in mortars with different functions: bedding mortar, floor mortar, plaster, painted plaster; iv) to extend our knowledge about the relationship between the archaeological findings and the results of the analytical studies of building materials.

Situation of the monastery in the Carolingian period

The Monastery of Müstair has been a very important religious, political and economic centre for many centuries. The largest surviving fresco paintings cycle of Carolingian Europe dated to the early 9th century, which decorates the church of St. John the Baptist, is evidence of its importance at the time of Charlemagne [4].

The monastery has been excavated almost in its entirety. The general chronological sequence is well understood in its main phases. Since then, as research at the site has progressed, our knowledge of the history and architectural development of the monastery has increased and some of the originally proposed dates have been corrected or further refined [5].

Dated to the year 775 by dendrochronology, the abbey church is one of only two surviving Carolingian churches in Switzerland. Archaeological investigations have established that the church was the first part of the monastery to be built [6]. The Carolingian complex consisted of a large, regular, two storeyed quadrilateral structure, with a large central courtyard

⁸ Funded by the Swiss National Fund (SNSF), the Foundation Pro Monastery of St. John and the Biosfera Val Müstair. <http://www.supsi.ch/imc/istituto/progetti/dettaglio.5797.backLink.76c387dc-d6bb-47ae-8c06-3b4678190667.html>.

surrounded on all four sides by open corridors and convent buildings, here called north, east, south and west wing respectively [2]. After the completion of the monastery, several additions and changes were made to the buildings. These additions have been subsumed under the term “second Carolingian construction phase”. Therefore, in the Carolingian period, buildings can be attributed to one of two phases: Phase I comprises the abbey church, the convent buildings and the Holy Cross-chapel, and dates between 774 and 788; phase II mainly describes an internal addition to the convent south corridor (the so-called “loggia building”) as well as water basins and cellars in the same courtyard. These additions were constructed at some time between the late 8th and the early 10th century (Figure 1).

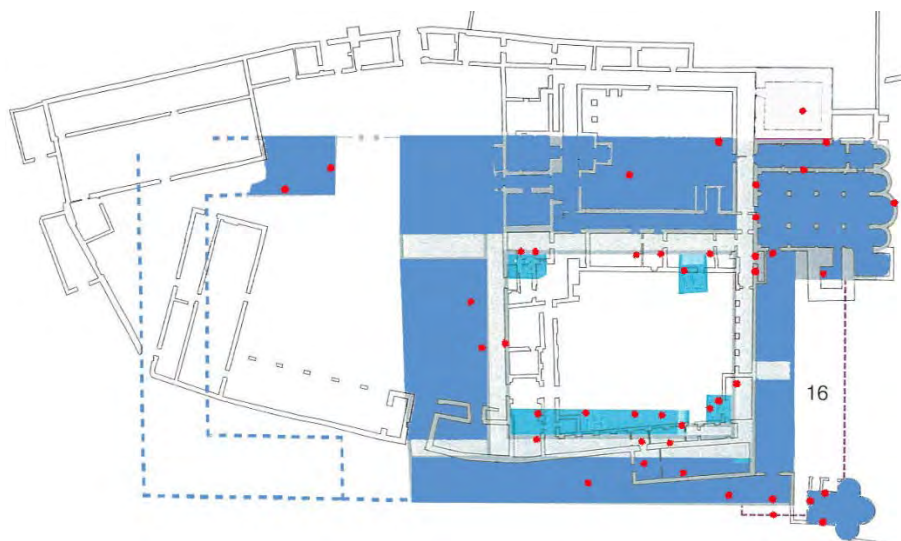


Figure 1: Reconstruction plan of the monastery during the Carolingian phases I and II [7, modified]. Main Church, convent (with corridors and wings around an open courtyard) and Holy Cross Chapel of phase I are coloured dark blue, the “loggia building” and other phase II buildings are light blue. Red dots represent the position of the mortar samples.

The monastery of St. John is one of the oldest examples of a church with cloister in Europe [8]. Its size is comparable to the largest monasteries of the time, such as the Reichenau [9] or San Vincenzo al Volturno [10]. This oldest part of the monumental complex with its two Carolingian phases was followed by at least eight major construction phases across 1200 years, which demonstrate the continuing importance of the site.

2. Material and methods

2.1 Archaeological research

Uniquely, at the monastery of St. John, conservation work has gone hand in hand with scientific research both above and below ground since 1969. The results led to a new understanding of the history and structural development of the monastery. Münstair monastery was one of the first archaeological sites in Central Europe, where the study of the remnants above as well as below ground was carried out. The stratigraphic study of the layers of soil and other characteristics was accompanied by a meticulous study of the walls and other features, which were still standing above ground. The archaeological layers could

thus be paralleled with extant structures. Since many of the monastery buildings can be precisely dated through dendrochronology, most archaeological features below ground are also chronologically well understood.

At present, only a small part of the archaeological results has been published. Most of it still awaits detailed evaluation. As part of the present project, the documentation regarding the construction layers which can be attributed to the various building phases of the monastery is being evaluated in detail. The investigation into the archaeological layers and features which can be attributed to the construction of the Carolingian convent has been completed only recently. They provide important insights into the organization of the building site for the Carolingian construction.

2.2 Selection of Carolingian fragments

In order to better understand the construction sequence and techniques of the two Carolingian construction phases, 120 mortar fragments attributed by archaeologists to these two first phases, have been chosen for characterization and comparison. Close attention was paid to the selection of samples from all major buildings and – when possible – only from primary (in situ) contexts. Sometimes, in the case of very long walls, it was necessary to take several samples. Furthermore, the samples cover different mortar types, the major categories being: bedding mortars, plasters and painted plasters (Table 1). Currently the floor mortars and the mortar from mortar mixers have not yet been analysed. In many cases the plasters were found to be composed of different layers: when present, we called *arriccio* the ground layer with coarse aggregate and *intonaco* the one beneath the painted layer and with finer aggregate.

Table 1: Carolingian samples selected and analysed. The table indicates the description of the source area (Figure 1), the sample ID, the mortar function and the research question connected with the sample.

Source area	Sample(s)	Mortar function	Research question
Church	23288, 23289, 6577, 11902	Bedding mortar	Common characteristics?
Church	11970	Bedding mortar	Compare with 8589 and 11902
Church Carolingian?	15439	Bedding mortar	Carolingian phase II?
Church	15783	Bedding mortar	Mud lime mortar?
Church	25005, 8589, 12593	Plaster	Similar to other Carolingian inside plasters of church or convent?
Church	24150-1B, 24150-3, 24150-4B, 24150-19, 24150-20	Painted plaster	Similar to other painted plaster from church?
Carolingian W-wing E-wall/W-corridor W-	957	Bedding mortar	Similar to other bedding mortars Carolingian phase I NESW-wings and -corridors?

Source area	Sample(s)	Mortar function	Research question
Carolingian N-wing N-wall N001	5410	Bedding mortar	Similar to other bedding mortars Carolingian phase I NESW-wings and -corridors?
Carolingian phase II NE	8154	Bedding mortar	Compare with 8647 from same well
Carolingian N- corridor S-wall foundation zone	8700	Bedding mortar	Similar to all bedding mortars Carolingian NESW-wings and - corridors, e.g. 9096 and 10637?
Carolingian N- corridor S-wall	10637	Bedding mortar (Sample with two different mortar varieties)	Similar to other bedding mortars of Carolingian NESW-wings and - corridors, e.g. 8700) and 9096
Carolingian outbuilding S-wall	3219	Bedding mortar	Similar to Carolingian outbuilding E-wall?
Carolingian S- corridor N-wall E- part	3769	Bedding mortar (with brick fragments)	Similar to other bedding mortars of Carolingian NESW-wings and – corridors, e.g. 3136?
Carolingian S-wing internal N-S-wall	12480	Bedding mortar	Similar to 12780 and to 12781?
Carolingian phase II Carolingian S-wing internal N-S-wall	12610	Bedding mortar	Compare with bedding mortar and plaster from Loggia building
Carolingian S-wing internal N-S-wall	12781	Bedding mortar	Compare with 12480 and 12780
Carolingian E-wing E-wall	14480	Bedding mortar	Compare with bedding mortars Carolingian phase I Carolingian NESW-wings and –corridors
Carolingian E- corridor E- wall/Carolingian E- wing W-wall	14977	Bedding mortar	Compare with bedding mortars Carolingian phase I Carolingian NESW-wings and –corridors.
W-wing (remains of) fireplace (open chimney) adjacent to E-wall W-front	315	Bedding mortar (in context with fireplace)	Different from bedding mortar 957 and from 494 floor mortar from underneath fireplace?
E-corridor W-wall E- front	12941	Mud-lime plaster	Similar to 13015?
N-corridor S-wall N- front	10402	Plaster	Similar to other bedding mortars Carolingian NESW-wings and - corridors, e.g. 9096 and 10637?
Doorway in Carolingian S- corridor S-wall	13023	Plaster	Similar to 3137, 3676 and 13018?
Carolingian S- corridor N-wall W- part	3136	Bedding mortar	Similar to other bedding mortars Carolingian NESW-wings and - corridors?
Loggia building	10127, 1260	Bedding mortar	Similar to bedding mortar 10126 from cellar 718 and 10134 from loggia building?

Source area	Sample(s)	Mortar function	Research question
Carolingian S-corridor N-wall	3137, 3676	Plaster	Similar to other bedding mortars Carolingian NESW-wings and -corridors, e.g. 3676?
Loggia building	9105-4B	Painted plaster	Difference to painted plasters from Carolingian phase I? Similar to other samples from 9105, 12180 and 12855?
Holy Cross Chapel	24965, 24966	Bedding mortar	Reference layer, compare to plaster 24608
Holy Cross Chapel	24967, 24969, 24972	Bedding mortar	Compare to other bedding mortars
Holy Cross Chapel	24608, 24970, 24979, 24980, 24609, 24978, 24650	Plaster	Compare to other plasters
Holy Cross Chapel	13/15;LIII1.02, 13/16;AEIII1.02	Plaster	Reference layer, compare to other plasters

2.3 Analytical studies of mortars

The mortar samples were first described using a binocular lens allowing up to 70x magnification. This description recorded the following features: a) binder colour and structure; b) the presence or not of lime lumps and their size; c) the overall colour, grain size and shape of the aggregate and the maximum grain size; d) the presence of additions like fibres, charcoal, brick, etc.; e) the macroscopically visible porosity and finally e) some notion on the overall hardness of the mortar and an estimation of the binder to aggregate ratio.

After this first selection, from 52 samples (listed in Table 1) thin polished petrographic sections were prepared by a specialized laboratory. On these, the following features were observed by means of polarized light microscopy [11]: binder: structure, colour, birefringence, homogeneity; lime lump types, e.g. internal structures, and their size; aggregate grains: grain sizes, grain shapes, mineral and rock types present; estimation of the grain size distribution and minimal and maximal grain sizes; additions and special features like e.g. brick grains or grains of partly melted binder material, etc.; macro-porosity: like retraction fissures, air pockets and water voids.

The thin sections of the mortars from the Holy Cross Chapel have been analysed by point counting [12]. The binder to aggregate ratio (B/A) was calculated to represent the volumes of the dolomitic lime putty versus the volume of sand, as it was mixed in the initial recipe. It was considered that the binder volume used as a putty neither expanded nor shrank much during setting, hence that the volume of the binder determined by point counting represents approximately the volume of the lime putty used. The volume of sand used for mixing a mortar is measured as numbers of shovels or buckets, hence this volume does contain, apart

from rock fragments, grains, i.e. the actual sand grains, also the voids in between them. In an average sand the voids make up about 45% of the total volume and only 55% of the volume are the sand grains. By point counting however only the rock fragments can be counted, hence the value determined for the aggregate only represents 55% of the actual volume of sand used initially. For the B/A ratios reported here, the point counted volumes of aggregate were therefore multiplied by 1.82.

Particles of the separated mortar binders have been systematically analysed by Fourier-transform infrared spectroscopy [13]. The equipment used was a Bruker ALPHA-P; preparation technique: Diamond ATR; measuring range: 4000 - 375 cm⁻¹, number of scans 24, resolution 4 cm⁻¹. The detection limit for a mineral phase in a mixture is around 2% by weight.

3. Results

3.1 Archaeological findings

The study of the archaeological remains allowed to understand the construction procedures followed at the monastery building site. First, the ground was prepared. The excavations showed that strata dated to the centuries before the Carolingian building activities are completely missing in the entire area of the Carolingian convent buildings. This came as a surprise because such strata could clearly be identified in the excavations in the later west courtyard of the monastery [14]. It is very unlikely that this is based on natural causes. It rather indicates that this is the result of flattening the ground in the entire construction area by the Carolingian workmen. However, the site was not entirely levelled into a horizontal plane, but rather left with a slight southward slope which followed the natural topography of the terrain.

The reason for leaving the site with a slight slope might be seen in the fact that the amount of material that had to be removed was considerably less than if the whole site had been completely levelled to a horizontal plane. Furthermore, water was naturally drained from the site during heavy rain and therefore prevented the site from being waterlogged. The construction work proper took place on the surface which had thus been obtained. These activities resulted in the deposition of layers containing charcoal, mortar and lime as well as fine chippings of stone, marble and brick.

After the construction area had been prepared, the position of the foundation trenches was laid out on the ground. The southern wing of the convent is the only place where foundation trenches were found that were misplaced (by about 1 m to the north) and filled in again, before the proper foundation trenches were dug. The foundation trenches were dug through 60 to 100 cm of underlying clay down to natural soil in order to find stable ground to support the massive walls of the two storied convent buildings [15].

The Carolingian foundations were constructed with two different layers. The bottom layer was built with two courses of rounded stones bound with clay which filled the foundation trench completely. The top layer was then built with one or several courses of stones bound with mortar on which then the wall proper was built [15].

The impressions of small square wooden pegs in the mortar of the foundations were found in the inner corners of the rooms. The impressions show that the pegs were sitting on the bottom course of the foundation stones. They probably served to hold strings that marked the planned location of the inner sides of the walls. This would have allowed a greater precision when erecting the walls on top of the more irregular foundations. No such impressions, however, were found on the outer side of walls which means that the thickness was probably determined by using measuring rods.

The remains of a Carolingian mortar mixer lie north of abbey church and convent. The pit of the mixer is ca. 3.20 -3.40 m in diameter and at least 40 cm deep; in the middle of the pit is a posthole filled with vertical stones which used to hold a now lost wooden post, originally acting as pivot for the rotating part of the device.

Several features show the importance of water on the construction site. Water channels crossed the construction site, and were filled in after the completion of the building.

After the construction was complete, the surface was flattened again by spreading a layer of soil which covered all the features related to the building of the monastery. On top of this layer of soil the mortar floors and ovens of the monastery were then constructed.

3.2 Characterization of mortars

Abbey Church. The petrographic analyses of the bedding mortars from the abbey church show common characteristics: rich in binder ($B/A > 1$), the grain size of the sand varies from medium to coarse (up to 8 mm), and is not well sorted (Figure 2A). The peculiarity of the aggregate composition is the absence of carbonate phases. The only one that contains dolomite fragments is sample 11902 taken at a height of 2.85 m in the facade. The pores are roundish and/or irregular in shape. The observation of thin sections of plasters allowed to discriminate 5 layers: 1) external painted layer, 2) whitewash layer; 3) *intonaco* with a well-sorted sand of fine grain size from silica metamorphic rocks (carbonate also present); 4) whitewash layer; 5) The *arriccio* is made of unsorted sand of coarse grain size up to 1 cm, from metamorphic rocks and some fragments of different carbonates (Figure 2B).

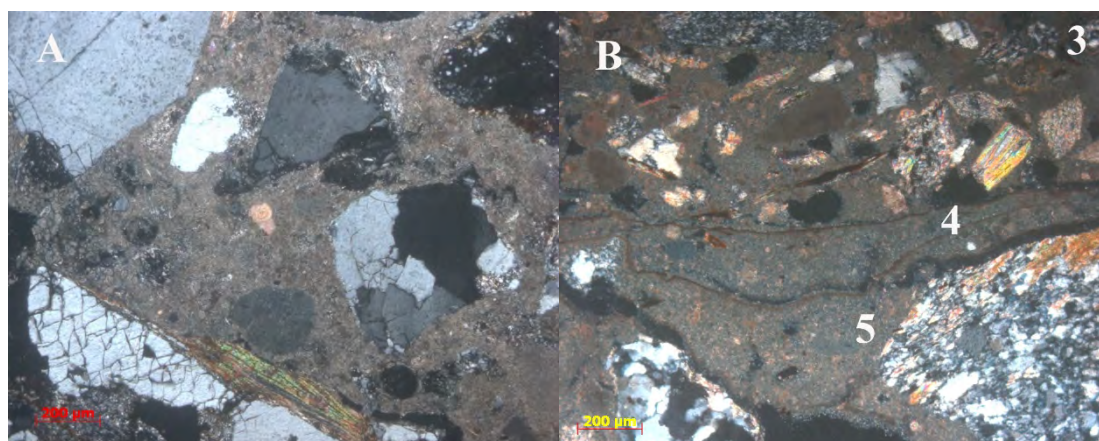


Figure 2: thin section images 5x, XPOL: A) Sample 23288, bedding mortar from the main church with $B/A > 1$, aggregate without carbonates and grain size from medium to coarse. B) Sample 24150-19: layers of plaster: 3-intonaco with a well sorted sand of fine grain size; 4- whitewash layer; 5- *arriccio* with unsorted sand of coarse grain size.

Convent. The bedding mortars collected from the convent were much poorer in binder (B/A 1:1). They also differ from the mortars from the church in the aggregate because here the finer grain size is also present together with medium and coarse sands (up to 1 cm). The aggregate also contains carbonate rock fragments (Figure 3A). The plasters are characterized by a high amount of binder when compared with the bedding mortars from the same areas. The plasters consist of a single layer of *arriccio* made of unsorted sand with a grain size from fine to coarse. The aggregate is mainly composed of fragments from metamorphic rocks (gneiss, schist), quartz in single crystals, dolomite, limestone and micas (Figure 3B).



Figure 3: thin section images 5x, XPOL. A) Sample 12781, bedding mortar from the convent. An unsorted sand with carbonate phases is visible. B) Sample 315, the plaster consists of a single layer of *arriccio* covered by a whitewash layer.

Loggia building. The bedding mortars of the “loggia building” and the convent are very similar: even if a higher presence of micas seems to be present in mortars from the former (Figure 4A). The painted plaster of all the fragments of the “loggia building” is characterised by a light brown colour due to high presence of very fine crystals of (possible) clay minerals that gives it its strong yellowish colour. The painted plaster consists of a single layer of *arriccio* with Mg-lime binder and a not sorted sand. The aggregate is mainly composed of

fragments from metamorphic rocks (gneiss, schist), quartz in single crystals and micas. In these painted plasters there are no carbonate rock fragments in the sand (Figure 4B).

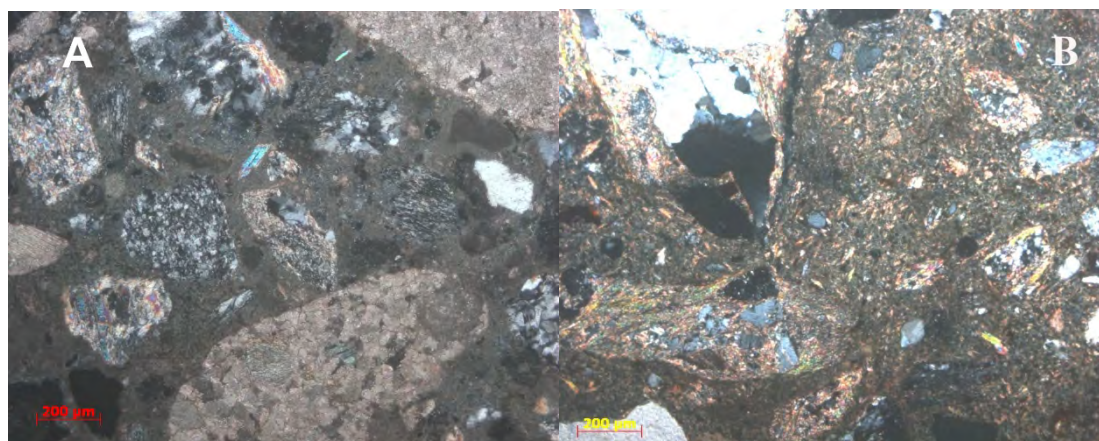


Figure 4: thin section images 5x, XPOL. A) Sample 10127 bedding mortar of the “loggia building” similar to those of the convent; B) sample 9105, painted plaster of the loggia building characterized by high presence of very fine crystals of (possible) clay minerals.

Holy Cross Chapel. The analysis shows that the intonaci of the Chapel of the Holy Cross are very rich (Figure 5) in binder: binder to aggregate ratios near between 1:0.5 (3 samples) and 1:1.5 (one sample) volume ratios. All but one bedding mortar and all plasters and the analysed arriccio were much poorer in binder showing binder to aggregate ratios of 1: 2 to 1:3.5.

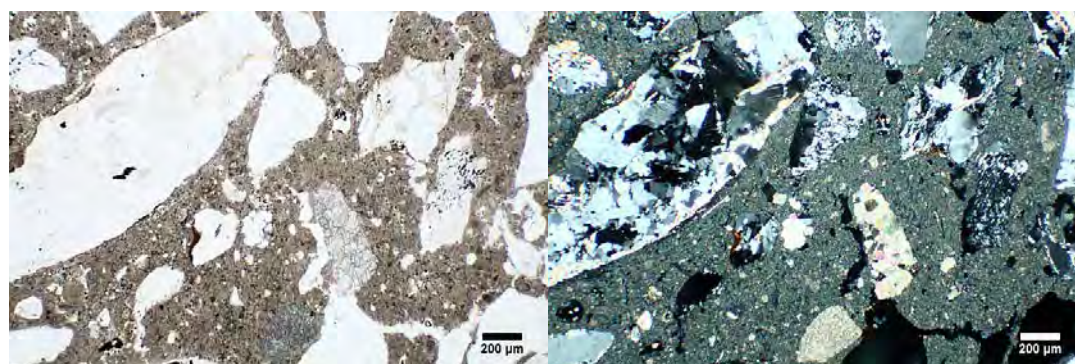


Figure 5: Thin section from *intonaco* of the Holy Cross Chapel, with a high B/A and mainly crystalline rock fragments as aggregate. Sample 24980: Left PPol, right XPOL.

The maximal grain size of the aggregate is 2 mm for all intonaci except one where grains up to 4 mm could be observed. This sample is the same, showing a less binder-rich mixture than the others. The bedding mortars do contain sand grains of up to 10 mm in size and probably even larger (only small samples of maximally a few cm in diameter were available for the laboratory analysis). An exception from this is the bedding mortar from the choir screen and one from the north wall of the nave, which both show a maximum grain size of only 2 mm.

All aggregates in the mortars are mixtures of carbonates, usually dolomites, and carbonate-free rocks, with the carbonate-free rock fragments being much more abundant. The carbonate fragment content of the 15 samples analysed lie between 3% and just below 20%

by volume of the total aggregate. Further investigations will show whether this observation can be correlated with specific proveniences of the sands. The majority of the aggregates of the mortars from the Holy Cross Chapel are rock fragments rich in quartz, feldspar and muscovite (Figure 5). More rarely rock fragments containing biotite or two mica gneisses can be found. Accessorily rock fragments containing minerals like black or blue tourmaline, amphiboles, epidotes or rutile can be found.

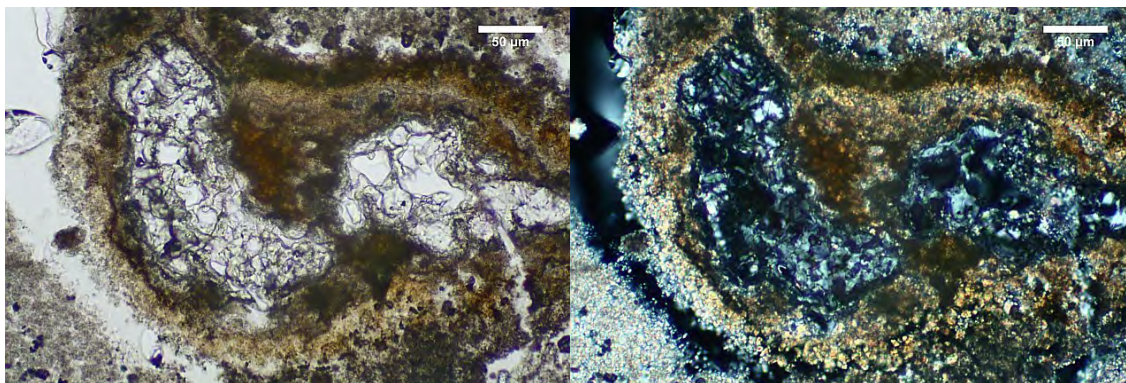


Figure 6: Siliceous, melted phases in a plaster (intonaco) of the Holy Cross Chapel, Scale bar 50µm. Sample 24'978. Left PPOL, right XPOL

The binder in all samples consists exclusively of dolomitic lime and in most samples some siliceous phases belonging to the binder could be observed either through microscopy (Figure 6) or in the FTIR spectra. The mineralogy determined through FTIR spectroscopy showed that the binders of all Carolingian samples contained calcite as well as dolomitic lime-related phases, usually magnesite or hydromagnesite (Figure 7). In one plaster sample some residual brucite ($Mg(OH)_2$) was analysed, in five samples the presence of aragonite could be assumed.

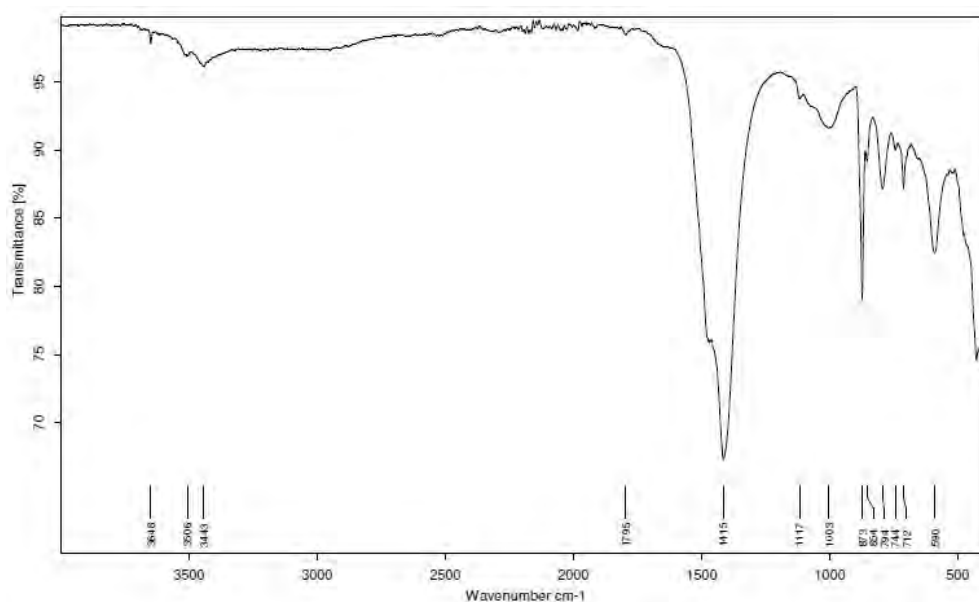


Figure 7: FTIR spectrum of the sample 24972. Peaks of calcite are: 1796, (peak at around 1396 cm^{-1} is covered by carbonate double peaks of hydromagnesite), 873, 712 cm^{-1} . Peaks identifying hydromagnesite are: 3648, 3506, 3443, shoulder at 1473, 1415, 854, 794, 744, 590 cm^{-1} .

4. Discussion

The binder of all the mortar and plaster samples from the monastery analysed so far is made from dolomitic lime and it can be assumed that they have been produced from local dolomitic rocks, as the geology of the valley of Müstair is strongly dominated by dolomites but limestones are very rare [16]. Which dolomite was used in which period to produce the binder materials for the mortars is at the moment under investigation as part of the same research project: preliminary results are reported in another paper in this volume [17].

Two different groups of bedding mortar have been identified with different petrographic characteristics: one comes from the main church and one from the large adjacent building complex to the west, which consists of the convent, the “loggia building” and the Holy Cross Chapel.

The mortars and plasters of the church are very rich in binder and the plasters are characterized by four layers as preparation of the surfaces to be painted. This indicates execution by specialized workers and a very accurate realization for the most important building of the monumental complex. The interposition of the whitewash between the *arriccio* and the *intonaco* probably means that the church was not decorated at first, confirming more recent archaeological hypotheses [18]. Sample 11902, the only one that contains dolomite fragments, was taken from a heavily disturbed part of the wall, into which windows were inserted in the 15th and 18th century. It could therefore belong to a later phase.

The archaeological investigations have shown that the church was completed before work on the cloister started. This is shown by the fact that the walls of the church do not interlock with those of the convent. This, together with the fact that there are clear differences between the mortars used in the construction of the church and those used for the convent, seems to indicate that two different workshops were involved in the construction of the monastery. Considering that the church is architecturally more complex than the rest of the monastery, with higher walls, five apses and two annexes, this result could indicate that specialists were called for its construction, while the convent was constructed by another workshop.

There are marked differences between the plasters in the different Carolingian buildings. Like those in the church, the pictorial surfaces of Holy Cross Chapel consist of several layers, *arriccio* and *intonaco*, both rich in binder. On the contrary the painted plaster fragments recovered from the convent, which stem from the Carolingian convent and the “loggia building”, consisted of a single layer. In some cases, a layer of whitewash was applied before the surface was painted, probably to homogenize the surface and make it smoother. The plaster of the “loggia building” is peculiar, as it contains a substantial fraction of clay minerals that may indicate the use of unwashed sand. From all plaster samples of the Carolingian monastery, only the plaster samples from the loggia building contain such very

fine aggregates. This choice could have been made on purpose, to take advantage of the better workability or to obtain a smoother surface due to the presence of the clayey fraction. On the other hand, the use of unwashed sand could have been fortuitous, due to an accidental change of the raw material.

Based on these observations, different groupings of the analysed plasters can be proposed, based on different characteristics. If grouped according to the number of layers of plaster, the church and the Holy Cross chapel show clear similarities, as in both buildings the interior surfaces possess an *arriccio* and an *intonaco* layer, on which the painting was applied. The painted layer from the convent, on the other hand, has been applied directly onto the first layer of plaster after it was covered with a layer of whitewash. If grouped according to the characteristics of the plaster, then the fragments belonging to the “loggia building” stand out because of the presence of a clayey fraction. It seems that a clear distinction exists between the painted plasters from the two religious buildings and from the convent buildings. This could be due to a difference in status or in function of the decorated interiors. Possibly they also indicate the work of different groups of people. The very peculiar character of the plaster from the “loggia building” sets it apart from all the others. As it is the youngest Carolingian building, which was added sometime after the work on the monastery had been completed, this difference might be due to yet another group of craftsmen being in charge of the interior decoration.

From their mineralogical composition, it can be assumed that the sands used as aggregates for the diverse mortars came from a local source. The exact provenience of the sand is still under investigation as part of this project, but different supply sources for sands can be assumed: the mortars of the church and the plaster of the “loggia building” do not have a carbonate fraction, unlike all the other samples. This characteristic is typical of the sands of the north-eastern side of the Val Müstair, while the main watercourse which runs through the valley, the river Rom, carries sands with important carbonate fractions. The use of sand collected from different areas could be a further proof of the non-contemporaneity of the construction of these buildings.

5. Conclusion

This preliminary report of an interdisciplinary project shows the contribution that each individual discipline can provide. Only by combining the results of all research areas can an almost complete picture be drawn of how construction works were done in historic times at Müstair monastery. In particular, the use of different techniques and materials (B/A ratio, sand composition, significant presence of clay minerals) found in the different buildings (church, Holy Cross Chapel, convent and “loggia building”) could indicate consecutive construction phases of the monastery, the presence of more than one team of builders, or different construction techniques chosen on purpose to differentiate between buildings with different functions and status. The usefulness of the approach followed by the project is shown by the fact that the observations from the petrographic study of the Carolingian

mortar fragments and the results of the archaeological investigations into the Carolingian construction phases so far fit very well, and do therefore complement and validate each other.

Acknowledgments

The authors would like to thank Richard Sadleir for the English language revision of the text. We are grateful to the anonymous reviewer for the suggestions that improved the paper. The authors wish to acknowledge the financial support of this research provided by SNSF (Swiss National Science Foundation, Switzerland – Grant project number 105211_169411) and Biosfera Val Muestair (<https://www.biosfera.ch/de>).

References

1. Elsen J, Brutsaert A, Deckers M, Brulet R (2004) Microscopical study of ancient mortars from Tournai (Belgium), *Materials Characterization* 53, 289–295.
2. Sennhauser H R (1996) *Müstair Kloster St. Johann 1*. vdf, Zürich.
3. Lugli S, Marchetti Dori S, Caroselli M. (2013) Petrography of mortars and plasters as a tool to distinguish construction phases for the history buildings of the Modena area (Northern Italy). *Proceedings of the 3rd Historic Mortar Conferences 11-14 September 2013, Glasgow, Scotland*.
4. Exner M (2007) Das Bildprogramm der Klosterkirche im historischen Kontext. In: Goll J, Exner M, Hirsch S (eds) *Müstair: Die mittelalterlichen Wandbilder in der Klosterkirche*. NZZ Libro, Zürich, 83-114.
5. Hurni JP, Orcel C, Tercier J (2007) Zu den dendrochronologischen Untersuchungen von Hölzern aus St. Johann in Müstair. H. R. Sennhauser (Red.), *Müstair, Kloster St. Johann 4*. Zürich: vdf, 99-116.
6. Goll J (2007) Das Kloster St. Johann in Müstair seit Karl dem Grossen. In: Goll J, Exner M, Hirsch S (eds) *Müstair: Die mittelalterlichen Wandbilder in der Klosterkirche*. NZZ Libro, Zürich, 27-42.
7. Courvoisier HR (1996) *Müstair, Kloster St. Johann*, edited by Sennhauser H.R, vdf Hochschulverlag, ETH Zürich, 57-65.
8. Legler R (1996) Probleme mit einem Phantom oder: Seit wann gibt es einen Kreuzgang in der abendländischen Klosterarchitektur? In: Sennhauser H R (ed) *Wohn- und Wirtschaftsbauten frühmittelalterlicher Klöster*. vdf, Zürich.
9. Zettler A (1988) *Die frühen Klosterbauten der Reichenau*. Thorbecke, Sigmaringen.
10. Hodges R (1995) *San Vincenzo al Volturmo 2*. British School at Rome, London.

11. Norma Uni 11176:2006, Descrizione petrografica di una malta.
12. Roduit N (2007) JMicroVision: un logiciel d'analyse d'images pétrographiques polyvalent. PhD-thesis, faculté des sciences de l'Université de Genève.
13. Derrick M, Stulik D, Landry JM (1999) Infrared Spectroscopy in conservation science. The Getty Conservation Institute Los Angeles.
14. Neukom H (2019) Der Westhof im Kloster St. Johann in Müstair: Archäologische Befunde im Wirtschaftshof bis 1500. Müstair Studien 1. Schnell & Steiner, Regensburg.
15. Goll J (2016) Müstair, Kloster St. Johann. In: Papajanni K, Ley J (eds.) Karolingerzeitliche Mauertechnik in Deutschland und in der Schweiz. Schnell & Steiner, Regensburg.
16. Trümpy R (2007) Zur Geologie des Münstertals (Val Müstair). In: Sennhauser HR (ed) Müstair, Kloster St. Johann. 4 Naturwissenschaftliche Beiträge, vdf Hochschulverlag AG ETH Zürich, p. 11-22.
17. Cavallo G, Caroselli M, Jornet A, Cassitti P (2019) Preliminary research on potential raw material sources for dolomitic lime mortars at St John convent at Müstair, Switzerland. HMC Proceedings, Pamplona, Spain, 2019.
18. Goll J (2008) Müstair, Ausgrabung und Bauuntersuchung im Kloster St. Johann. Jahresberichte des Archäologischen Dienstes Graubünden und der Denkmalpflege Graubünden 2006:23-36

Animal, Vegetable or Mineral? Characterising shell-lime, maerl-lime and limestone-lime mortar evidence from the Late Norse and Medieval site of Tuquoy, Orkney

Mark Thacker¹, John Hughes², Nic Odling³

(1) University of Stirling, mark.thacker@stir.ac.uk

(2) University of the West of Scotland, john.hughes@UWS.ac.uk

(3) University of Edinburgh, nicholas.odling@ed.ac.uk

Abstract

Recent examination of an extensive curated assemblage of mortar samples, recovered from the Late Norse and Medieval site of Tuquoy (Orkney) during excavation in the 1980s, suggested the collection was associated with distinct groups of compositionally contrasting materials related to discrete constructional events. Subsequent petrographic analysis supported this early interpretation and presented evidence for a remarkable series of phase-specific mortars, bound with a range of different biogenic and geogenic lime source materials - including marine shell, coralline algae (*maerl*) and limestone. Wider landscape survey highlighted the broad range of exposed calcareous materials in the coastal and sedimentary environments dominating the Northern Isles of Scotland today, and that many of these different potential lime sources were exploited by craftspeople at different times in the Medieval and later period is now clear.

Given the high significance of the Tuquoy mortar study for our understanding of the development of this culturally important site, and as a prelude to more general publication of the wider archaeological project, a further investigation of selected samples from the mortar assemblage is now being undertaken through a range of geoscientific techniques. This paper presents emerging evidence from a comparative petrographic, SEM-EDS and XRD study designed to further characterise these various mortar materials, and challenge those previous interpretations of contrasting building lime sources. Like most environmental archaeological investigations, this study is essentially concerned with interpreting the depositional histories of surviving materials, but with a particular focus on establishing the distinction between (anthropogenic) kiln relict and (natural) added temper mixtures when both contain biogenic and geogenic clasts.

Introduction

The Late Norse and Medieval settlement site of Tuquoy is located on the south-west coast of Westray, Orkney, in the Northern Isles of Scotland. The upstanding archaeology of Westray from this period is rich and includes the remains of two Medieval and later parish churches, a large late Medieval castle and a Medieval and later multiperiod farmstead, all of which are

situated on the more fertile coastal fringes of the island. Indeed, the former parish church of Cross Kirk at Tuquoy is located within a burial ground which is now situated at the shore edge, just above high tide.



Figure 1a (above) – Crosskirk Tuquoy from the south-east. Note the putlog socket between nave doorway and window. Scale 500mm; photograph Mark Thacker.



Figure 1b (above) – 50m east of the upstanding church. The eroding cliff-section containing Tuquoy hall and settlement from the south. Scale 500mm; photograph Mark Thacker.

The ruinous remains of Cross Kirk present a bicameral architectural form, wherein a smaller narrower chancel (in this case barrel-vaulted) is situated at the east end of a wider but coeval nave (see Figure 1a). This planform is widely distributed at Late Norse sites throughout Scandinavia, Scotland and Ireland, and most of these buildings have been ascribed to the 11th-13th-century on planform alone [1-3]. The multiphase form of the church at Tuquoy, however, has had increased significance for North Atlantic scholars since

Clouston suggested that the extension of the building's nave (to provide room for a larger congregation) provided physical evidence for the emergence of a parish system in the Northern Isles, and for an earlier pre-parochial network of 'ounceland' chapels closely associated with high status farms [4, 5]. One of the classic site-types for this binary Late Norse farm/church configuration in Orkney survives on the very small island of Wyre, where the upstanding remains of a masonry tower and nave-and-chancel chapel are located very close to one another. Moreover, a reference in *Orkneyinga Saga* attributing construction of this tower to Kolbein Hróga ('Cubbe Roo') before 1150 [6], suggests this may be the earliest masonry castle building surviving in Scotland.

Despite the importance of the Tuquoy church to Orcadian archaeology, however, the form and location of the secular settlement associated with this site remained unknown until the 20th century when 'massive stone walls' began eroding out of a coastal cliff-section approximately 50m west of the upstanding bicameral church [7] (see Figure 1b). Moreover, one of these walls was described as 'bearing the same shelly lime render as occurs on high-status medieval buildings such as Cubbe Roo's Castle and The Wirk', and this newly identified site was then subject to a multi-season programme of excavation and environmental sampling in the 1980s [7]. This ultimately revealed the remains of a small multiphase masonry hall and other structures, and excavated deposits from the hall returned a series of radiocarbon dates suggesting occupation in the 12th century [8, <https://canmore.org.uk/c14index/2822>]. Significantly for this paper, the sampling strategy associated with that excavation also included the careful recovery and curation of an extensive assemblage of lime mortar samples.

The mortar assemblage from Tuquoy has now been subject to two programmes of investigation. An initial study was undertaken during a wider research project investigating the Medieval and later masonry mortars of North Atlantic Europe [3], and those initial interpretations are now being re-assessed, challenged and refined as a prelude to publication of the wider archaeology of the Tuquoy site. Both mortar studies will be summarised below.

The Initial Study

Methods 1

The initial study of the Tuquoy mortar materials included: hand sample analysis of the mortar assemblage curated from the hall excavation; field survey of the mortars displayed in the neighbouring church; and thin-section petrographic analysis of selected samples from both sites. Hand sample analysis of all fragments identified as mortar or plaster within the curated assemblage was undertaken by non-intrusive examination of sample surfaces with the unaided eye, a x10 hand lens and a x40 field scope. Subsequent fieldwork in Westray included non-intrusive survey of the upstanding ruined bicameral church at Tuquoy and

walkover survey of the adjacent shoreline, with the collection of a variety of loose material samples.

A representative range of mortar samples from both building sites was then selected for thin section preparation, to enable petrographic analysis. These selected fragments were sawn in a variety of planes (relative to wall faces), and dried, before one sawn surface was consolidated with 'epothin' epoxy resin. The consolidated surface was then ground on a horizontal lap to form a flat surface and mounted on a 75 x 26mm slide. Excess material was cut off the mounted sample to allow the material to be lapped, hand polished to a standard 30µm thick, and coverslipped. These prepared thin sections were subject to microscopic examination in plane and polarised light, using a Leica DMLM polarising microscope with image capture by LAS V4.0 software.

XRD analysis was undertaken on two biocarbonate inclusions, hand-picked from selected mortar samples. These materials were ground down by hand in a mortar and pestle to achieve a <50-micron grain size, then scanned in a Bruker D8 Advance x-ray diffractometer using Cu K-alpha radiation filtered to remove the Cu K-alpha 2 peak. The samples were scanned from 2 to 70 degrees 2-theta at a step size of 0.025 degrees and a dwell time of 1.5 seconds per step. The resultant scans were analysed using the Bruker EVA software coupled with the current issue of the ICDD PDF-4 database, with modal analysis carried out using TOPAS 3.0 Reitveld analysis software calibrated and checked against several representative synthetic mineral mixtures.

Hand Sample Analysis

Surface examination of mortar fragments from the excavation assemblage suggested each sample represented a compositionally consistent single-phase material, without layering or stratigraphic horizons. The overall assemblage was clearly comprised of at least three different mortar types, however, and these were characterised according to the following typology:

- **Type A** – A fine, hard and buff-coloured lime mortar included with a high concentration of coralline algae fragments (hereafter *maerl*) which displayed a spectrum of altered colours and textures. These samples generally presented a planar face, with surviving mortar 'tails' on the reverse which had been moulded to the jointing in the face of the underlying rubble wall (see Figure 2a).
- **Type B** – A very lime-rich, fine, soft and white-coloured lime mortar containing a low concentration of discoloured *C. edule* shell fragments with distinctively ribbed morphologies. Also presenting a planar face, with surviving mortar 'tails' on the reverse which had been moulded to the jointing in the face of the underlying rubble wall (see Figure 2b).

- **Type C** – A fine light-buff lime mortar without visible geogenic or biogenic inclusions but containing a widespread distribution of very fine black grains. These samples presented very thin (6-7mm only) coating profiles and no moulded mortar ‘tails’.



Figure 2a. Thick section mortar Type A x 2. Note: thin mortar ‘tails’ (with coherent rounded ends which may have abutted underlying constructional clay mortar in the masonry joint) and the more planar face of the former mortar surface. Field of view approx. 120mm; Photograph M. Thacker



Figure 2b. Thick section mortar Type B. Note very wide mortar tail suggesting much coarser underlying rubble wall; planar face of previous coating surface; high concentration of discoloured bioclasts including probable *maerl* and shell in this particular section. Field of view approx. 100mm; Photograph M. Thacker

The planar surface displayed by many of the mortar fragments within the curated assemblage suggested the collection was dominated by ‘coating’ fragments, which had been deposited in a plastic state upon and/or within the surface of a masonry wall. Moreover, the smooth texture of the moulded tails and other surfaces suggested that these mortar fragments had been in direct contact with bare rubble stone and were not underlain by earlier mortars in these particular wall face contexts. Most of the mortar samples collected during the 1982-3 excavations were found in stratified deposits and labelled by context, and when mortar was found adhering to a wall this was recorded in the sample labelling (O. Owen pers. com.). Indeed, some of the labels associated with the Type A samples characterised above clearly referred to the ‘hall’ building from which they had been removed, and some labels gave a valuable hint of phasing. Type A sample TWO.04, for instance, was described as “plaster from 1 after removing 2”, with Wall 1 referring to the external face of the hall and Wall 2 part of a substantial workshop immediately adjacent. Although also displaying a mortar tail indicating initial deposition within the surface of a masonry wall, the building from which Type B sample TWO.08 had derived was not immediately clear from its label description of ‘shaped plaster’; the lack of reference to a particular building in this instance probably therefore indicating retrieval from a secondary depositional context. Both Type C sample labels clearly indicated they had been removed from the neighbouring Cross Kirk, however, and the lack of mortar tails in these coating fragments was therefore of some interest.

It is important to note that two of the three mortar types characterised in the above typology displayed biogenic inclusions whose character suggested the lime matrix had been

manufactured from biocarbonate lime sources; with Type A samples included with altered skeletal *maerl* fragments with some similarities to the assemblage from Cubbie Roo's site on Wyre [9], and Type B samples included with altered *C. edule* shell fragments (similar to those from *Eaglais na h'Aoidhe* on Lewis for instance [10]). The lack of visible (potentially kiln relict) carbonates in the Type C samples, therefore, presented a compositional contrast in addition to the morphological differences noted above.

Field Survey

The Tuquoy settlement buildings themselves could not be re-evaluated during this study, as the site had been carefully back-filled after the 1980s excavations, but subsequent fieldwork in Orkney did include a walkover of the adjacent foreshore and a preliminary survey of the neighbouring bicameral church [3].

The ruinous remains of the church at Tuquoy still clearly displayed two distinct phases of construction on the date of survey, although heavy consolidation of the wall faces and some wallhead re-construction effectively precluded comprehensive in-situ characterisation of the structure's mortar archaeology (particularly in the secondary west end of the nave). Various fragmentary patches of mortar indicated the church building had previously been externally coated, however, and more extensive evidence for a very fine mortar coating survived on internal wall faces throughout the primary east end of the building - in both nave and chancel. Three superimposed layers of compositionally contrasting mortars were noted at the east end of the south nave wall, however, and the distinctive brown-coloured and shell-included mortar which underlay this stratigraphic sequence was also visible in the wall core to 280mm deep (within a putlog socket). Acknowledging the limited exposure (resulting from widespread consolidation), limited visibility (the internal coating was obscured by organic growth whilst the external coating was very fragmentary), and general lack of continuity between core and coating (resulting from re-pointing), the evidence was regarded as sufficient to suggest these mortars were constructional materials and a single loose sample of the brown-coloured shell-included mortar was collected from within the core of the south nave wall (adjacent to the putlog). This sample was characterised in hand sample as follows:

- **Type D¹** – Sample TWO.09 is hard brown-coloured lime mortar included with a fine mixture of lustrous shell fragments (grading to 2-3mm), but without any clearly identifiable relict limekiln evidence.

Petrographic Analysis 1

Petrographic analysis was undertaken on mounted thin sections prepared from nine selected mortar samples. This included at least one section from each putative mortar type but, with a particular concern to further investigate the potential use of *maerl* as a lime

source, the sub-assembly was dominated by samples previously characterised as Type A materials.

The main characteristics of each sample Type in polarised light are summarised below:

- **Type A** samples (TWO.01, TWO.02, TWO.04, TWO.06 and TWO.07) generally display a bimodal matrix-supported texture², with a coarse fraction containing *maerl* and marine shell fragments grading to 8mm diameter (see Figure 3a). These biogenic clasts present a spectrum of altered textures, including increased micritisation, loss of internal microstructure, loss of grain boundary coherence, and increased optical continuity with the supporting carbonate matrix, such that any distinction between the bioclast and matrix is often ambiguous. The carbonate matrix is generally cryptocrystalline to microcrystalline with more dense areas often resolving to concentric and/or cellular relict biogenic forms consistent with skeletal *maerl*. A low concentration of highly altered quartz-rich geogenic clasts are also evident in these sections, with clasts displaying distinct grain boundaries but also isotropic properties, high vesicle concentrations and some spiniflex textures. Possible relict fuel inclusions are very rare in these thin sections, but some opaque and irregular possible relict peat evidence was noted. These mortars have generally been tempered with a well-sorted submillimetric mixture of subangular monocrystalline quartz and marine shell (grading to 0.25mm) with rare feldspar and larger subrounded quartzose grains included.
- **Type B** sample (TWO.08) is also bimodal, but with an extraordinary high volume of very fine ('cloudy') cryptocrystalline carbonate matrix supporting a very low concentration of poorly-sorted clasts grading to 5mm (see Figure 3b). This coarse fraction is dominated by a mixture of altered marine shell fragments (including *C. edule*) with a lower concentration of altered geogenic clasts with some spiniflex textures. The section includes a moderate concentration of opaque probable peat fuel relicts, and a lithic/shell temper mixture dominated by fine (submillimetric) marine shell fragments.
- **Type C** sample (TWO.03) is a well-sorted and very fine mortar material which displays a remarkably high concentration of altered quartz-included geogenic clasts forming an interconnected network of 'globular', vesicular and isotropic reaction products (with indistinct grain boundaries) which are closely associated with widespread evidence for very fine altered biogenic clasts (see Figure 3c). The mortar displays a low concentration of fine, irregular and opaque probable peat fuel relicts and is tempered with a fine mixture of monocrystalline quartz and marine shell.
- **Type D** mortar sample (TWO.09) presented a matrix-supported poorly-sorted mixture of biogenic and geogenic grains grading to 3mm (see Figure 3d). Identifying relict lime-source carbonates within these sections was challenging, but two large rounded areas of amorphous carbonate and localised scatters of fine quartz (interpreted as intraclasts released from a quartz-included lime-source 'protolith') were regarded as probable evidence for a geogenic lime-source which was tentatively identified as a micritic

limestone/mudstone. These sections did also contain a very low concentration of micritic and fractured *maerl* fragments, although these did not appear to have a textural relationship with the supporting carbonate matrix, whilst the fine shell within the temper mixture appeared largely unaltered. A low concentration of fine probable relict peat fuel inclusions was also noted.

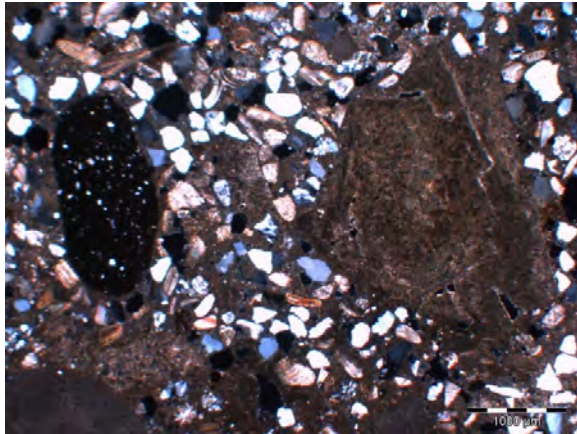


Figure 3a. Subrounded kiln relict maerl fragment close to optical continuity with general mortar matrix in mortar Type A sample TWO.02, with adjacent rounded and isotropic sandstone clast. XPL; Scale bar 1000µm; photomicrograph M Thacker.

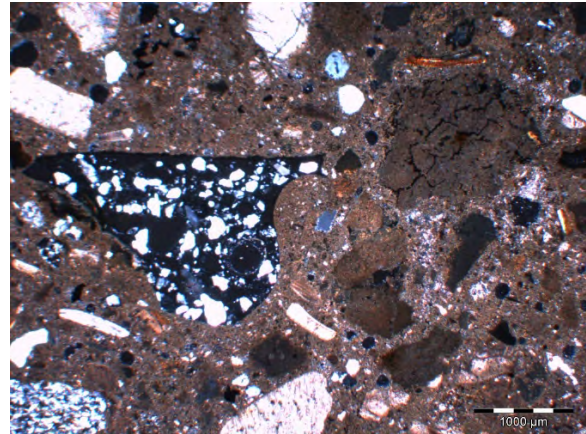


Figure 3b. Well developed broken slag fragment and highly altered shell fragments in bimodal Type B mortar sample TWO.08. XPL; 1000µm; photomicrograph M Thacker.

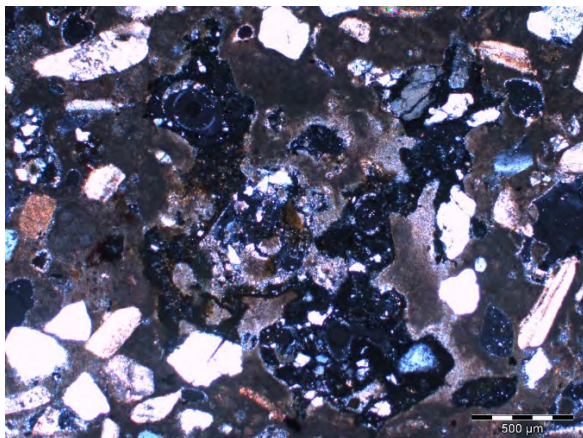


Figure 3c. Delicate network of calc-silica reaction products and altered biogenic grains in well-sorted mortar Type C sample TWO.03. XPL; Scale bar 500µm; photomicrograph M Thacker.

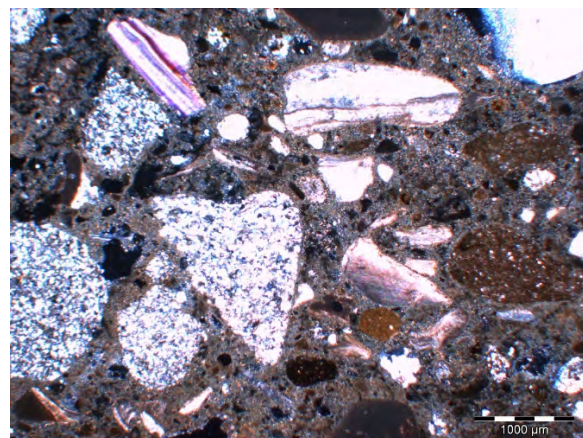


Figure 3d. Poorly-sorted mixture of lustrous marine shell and calc-arenite in mortar Type D sample TWO.09. XPL; Scale bar 1000µm; photomicrograph M Thacker.

XRD Analysis 1

To further characterise the biocarbonate inclusions within the mortars of the curated assemblage, multiple *maerl* (TQ2) and *C. edule* shell (TQ8) inclusions were picked out from Type A sample TWO.02 and Type B sample TWO.08 and submitted for XRD analysis. These analyses returned similar ratios of different carbonate polymorphs - dominated by high

calcium calcite (59-71%), with significant magnesium calcite (24-32%) and almost trace (1.2-1.3%) aragonite fractions. Unlike TQ8, however, *maerl* sample TQ2 also returned very minor levels of periclase (1.3%) (see Table 1 below).

Summary of the Initial Study

The initial study of mortar samples retrieved from the excavated settlement and upstanding church at Tuquoy highlighted evidence suggesting the combined assemblage was comprised of four compositionally contrasting mortar materials. Within this typology, mortar Types A and B (from the settlement excavation) included high concentrations of altered biogenic (*maerl* and marine shell) grains, with lower concentrations of altered quartz-rich geogenic clasts. The altered micritic/cryptocrystalline texture of these biogenic clasts, and their intimate textural and optical relationship with their supporting (lime mortar) carbonate matrices, was interpreted as evidence that these Type A and Type B materials were *maerl*-lime and shell-lime mortars respectively. Mortar Types C and D (from the upstanding church) were both more tentatively interpreted as geogenic-lime mortars, largely on the basis of various altered quartz-rich clasts which in Type C were in remarkably high concentration.

In-situ evidence suggesting that *maerl* had been exploited as a building lime-source at Cubbie Roo's castle and chapel on Wyre, had already been identified when the curated assemblage from the Tuquoy excavation became available for examination [9]. The *maerl*-lime mortar evidence reported during this initial study of the Tuquoy hall mortars, therefore, is consistent with Lamb's observation that these structures were coated with similar materials [7] (see above) and parallels the broad contemporaneity of these various Orcadian buildings. The compositional contrasts upon which the Tuquoy mortar typology was based, however, suggest that this Westray site is associated with at least three separate lime-bonded constructional events, and that (unlike the Wyre buildings) the church and hall at Tuquoy had been constructed at different times [3]. Since accepting this interpretation would have significant implications for our understanding of the development of the site, further geoscientific study of these complex materials was commissioned to reassess those interpretations.

A Materials Reassessment

Methods 2

A reassessment of the Tuquoy mortar evidence was undertaken on samples selected from the initial study, and included SEM-EDS, further XRD, and further petrography analysis. For the SEM-EDS analysis, polished thin sections of Type A sample TWO.04, Type B sample TWO.08, and Type D sample TWO.09 were prepared and carbon-coated. These slides were analysed using a Hitachi S4100 Field Emission Scanning Electron Microscope (FESEM) using Backscattered Electron Imaging at 20kV accelerating voltage, with chemical analysis performed using an Oxford Instruments Energy Dispersive Spectrometer (EDS). The second

round of XRD employed the same methods as the initial study, but examined various different materials including: fine <63µm fractions of three selected mortar fragments which had been crushed in a mechanical jaw crusher then sieved to remove the coarser fractions; further selected mortar inclusions picked-out from the surface of mortar fragments using a sharp point; and loose fragments of detrital materials collected during walkover of the Tuquoy shoreline. These latter materials included a small sample of aeolianite, from which another 30µm thin section was also prepared. Finally, armed with evidence reported from the SEM-EDS and XRD analyses, a further round of petrographic analysis was undertaken at the University of Stirling, using an Olympus BX51 polarising microscope and analySIS pro imaging software.

SEM-EDS Analysis

Samples from each of the three main constructional mortar types (so excluding Type C coating samples) were subject to SEM-EDS analysis, to further examine the relationships between various (biogenic and geogenic) inclusions and the supporting carbonate matrices.

With reference to Figures 4a-e, the results of this study and a summary of interpretations are presented below:

- **Type A** sample TWO.04 presents a matrix-supported mixture of high Ca *maerl* and shell fragments, whilst a porous fragment of material containing both Ca and P suggests some bone fragments may also be present. Notably, the general carbonate matrix also presents a high Ca composition, often with a small P and S signature but with no appreciable Mg content. The section contains some sedimentary sandstone, but elemental mapping suggests this lithology has no Ca-bearing phase.

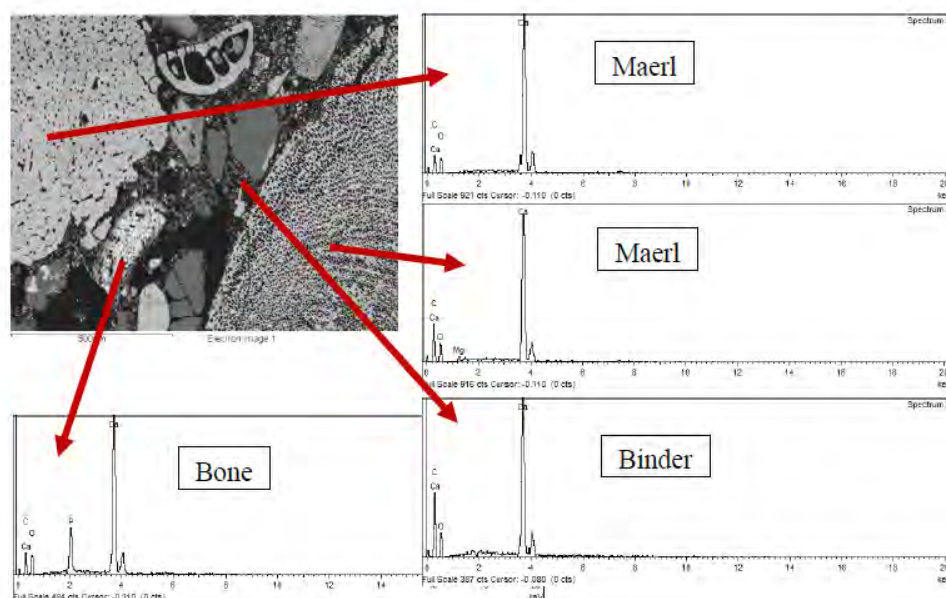


Figure 4a. SEM image of an area of Type A mortar sample TWO.04, with associated EDS spectra for two *maerl* fragments of varying textures, one probable bone fragment and the supporting matrix. Scale bar 500µm; SEM Image John Hughes.

- **Type B** (sample TWO.08) presents a nearly pure high-Ca matrix, supporting shell fragments with a similar chemistry and porous texture. This section also contains some remnant bone fragments (here with some altered halos) and widespread evidence for highly altered subangular fragments of quartz-included slag, with well-developed (spherical) vesicles and some spinaflex textures.

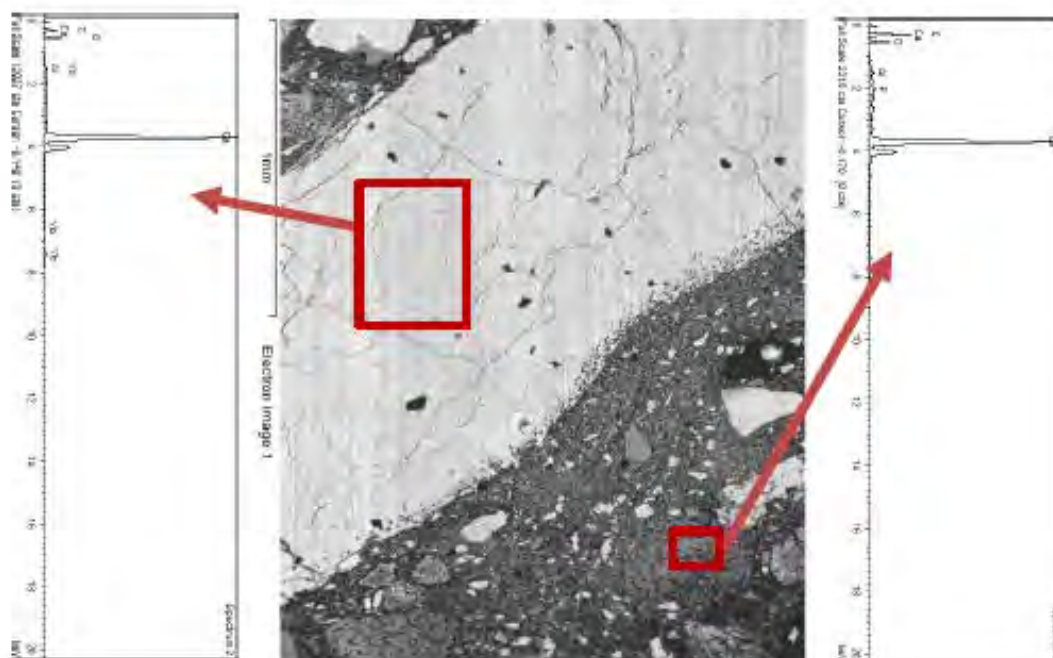
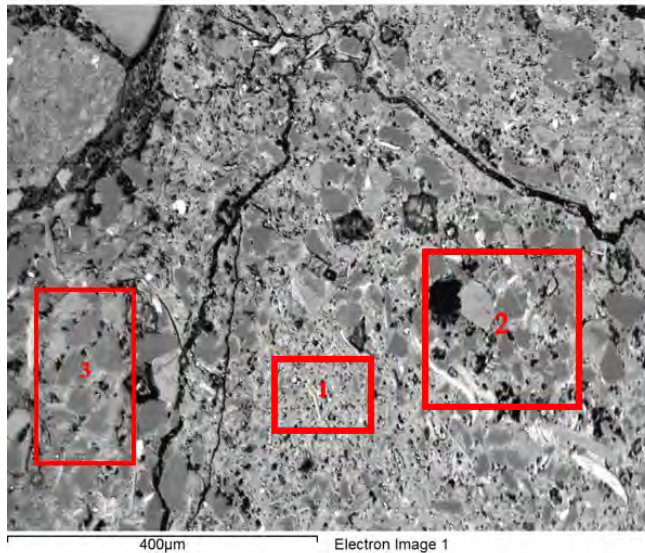


Figure 4b. SEM image of an area of Type B mortar sample TWO.08, with associated EDS spectra for an area of shell and supporting carbonate matrix. Scale bar 1mm; SEM image John Hughes

- **Type D** (sample TWO.09) presents a more heterogeneous calcareous matrix with an appreciable Si, Mg and Al content consistent with a fine included aggregate or possibly a hydraulic phase. A quartz grain with a halo of Si-Ca, Al and Mg, and another quartz-included Ca-Si slag with a diffuse grain boundary, was also noted. The section also contains large subangular siltstone fragments with a well-sorted and calcareous composition (characterised here as a calc-arenite), as well as high calcium shell fragments.

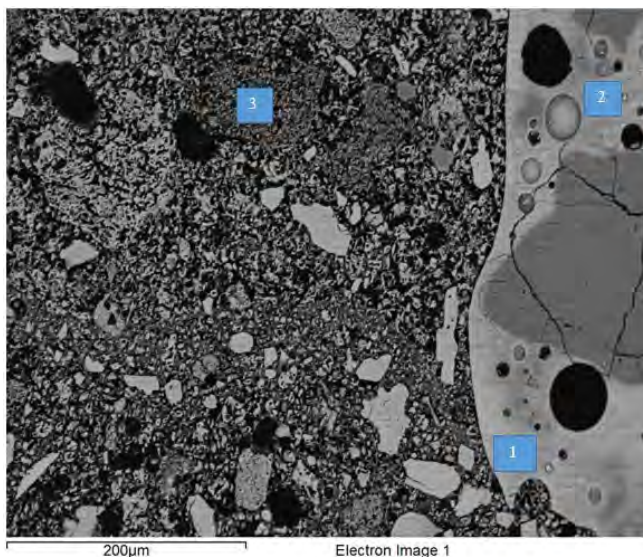
In summary, SEM-EDS analysis indicates that the mortar matrix in both the Type A (TWO.04) and Type B (TWO.08) samples was composed of a high Ca-carbonate with only minor evidence for other elements such as Mg, S and Fe, and this is indicative of a carbonate source comparable to the biogenic clasts which are widely distributed throughout these sections. This interpretation is consistent with the pseudomorphic features visible in calcined lime inclusions of similar dimensions to neighbouring biogenic clasts, although it was not initially clear how this evidence relates to the abundant Ca-Si slag fragments in Type B sample TWO.08 since these clearly suggest the raw material contained a high proportion of silicates (see summary and discussion below).

In contrast to these Type A and B mortars, the supporting carbonate matrix in Type D sample TWO.09 presented a consistently higher Si and Al content. The abundant grains of calcarenite in this section were not noted in previously considered sections and might be considered as a possible lime-source material, although, except for the apparently rare grains of reacted quartz, there is a lack of obvious clinker phases in the section.



Spectrum Area	Compd%		
	1	2	3
Na ₂ O	3.67	3.49	3.9
MgO	5.57	5.58	1.85
Al ₂ O ₃	14.42	15.25	13.08
SiO ₂	46.53	46.04	64.48
P ₂ O ₅	0.64	1.03	-0.02
SO ₃	0.27	0.26	0.37
K ₂ O	6.76	6.78	5.29
CaO	5.51	6.13	3.92
TiO ₂	2.74	2.18	0.79
FeO	13.88	13.25	6.34
Normalised	99.99	99.99	100

Figure 4c. SEM image of large rounded sedimentary grain in Type A mortar sample TWO.04. Numbered areas relate to EDS analyses in adjacent table. Scale bar 400µm; SEM image John Hughes.



Spectrum Area	Compd%		
	Slag 1	Slag 2	Binder 3
Na ₂ O	6.91	6.77	0.24
MgO	2.39	1.59	0.24
Al ₂ O ₃	9.86	12.65	1.04
SiO ₂	57.54	63.51	0.7
P ₂ O ₅	2.18	1.58	2.29
SO ₃	0.04	0.17	0.91
K ₂ O	4.74	5.55	0.02
CaO	7.13	3.94	94.56
TiO ₂	2.02	-	-
FeO	7.19	4.24	-
Normalised to	100	100	100

Figure 4d. SEM image of Type B mortar sample TWO.08. Numbered areas relate to EDS analyses in adjacent table. Scale bar 200µm; SEM image John Hughes.

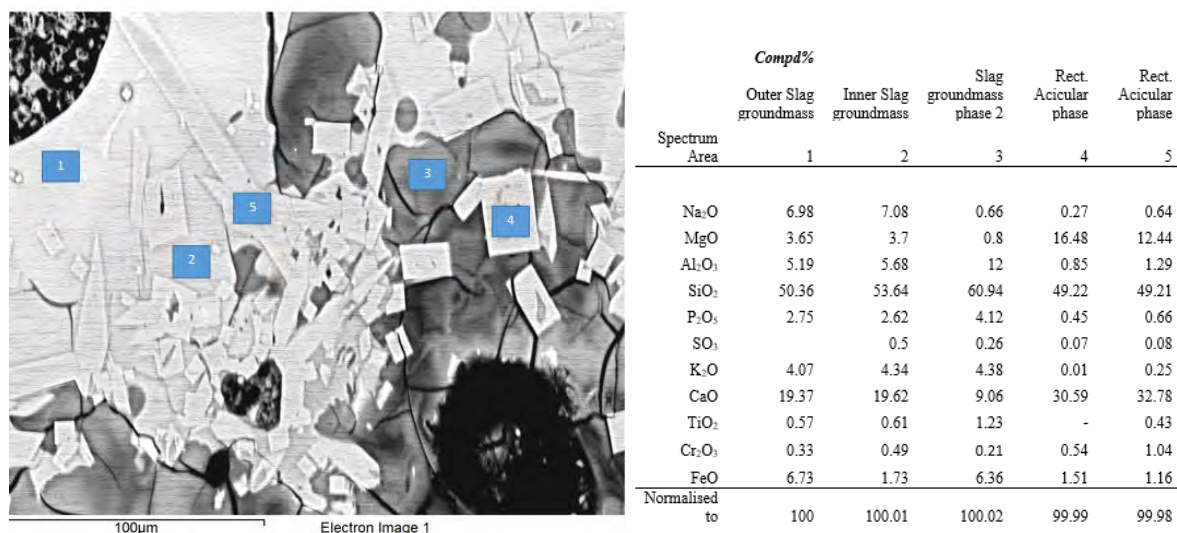


Figure 4e. SEM image of part of a slag grain in Type B mortar sample TWO.08. Numbered areas relate to EDS analyses in adjacent table. Scale bar 100µm; SEM image John Hughes.

XRD Analysis 2

Further investigations of selected materials from the Tuquoy assemblage was undertaken using XRD, with a particular concern to examine the polymorphic mineralogy of various calcareous materials, including mortar inclusions, mortar matrices and some environmental materials. The background to this study was provided by recent experimental work which had demonstrated that Orcadian *maerl* gravels are dominated by high-magnesium calcite, which undergoes a predictable series of mineral phase changes with increasing temperature, whilst *C. edule* shells undergo parallel changes from aragonite to (low-Mg) calcite [3]. The polymorphic profile of these biogenic inclusions from historic mortars can then be used to characterise thermal histories, as had been previously done during the Cubbie Roo's Castle study [3]. Essentially, this same approach was being adopted to establish whether selected inclusions within the Tuquoy Type A mortar had undergone heating (so were a probable lime source) by comparison with (presumably unheated) detrital samples from the adjacent foreshore.

Including the investigations undertaken during the initial study (see above), XRD analysis was undertaken on the following materials:

- (i) fine sieved fractions (<63µm) from jaw-crushed fragments of Type A (TWO.06), Type B (TWO.08) and Type D (TWO.09) mortar samples;
- (ii) maerl inclusions (TQ2 & TQ4) removed by hand from the surface of two different Type A mortars (TWO.02 & TWO.04);
- (iii) *C. edule* shell (TQ8) inclusions removed by hand from the surface of a Type B mortar (TWO.08);
- (iv) a maerl inclusion (TQ3) collected from the foreshore close to the Tuquoy settlement site; and
- (v) a loose fragment of aeolianite (TQ10) collected from beneath an exposure close to the Tuquoy settlement.

Table 1. Sample compositions by XRD analysis.

Sample	Mg-Calcite	Calcite	Periclase	Dolomite	Aragonite	Trace + Silicates
Maerl						
TQ2	24	71	1.3	-	1.3	2.4
TQ3	11	86	-	-	-	3
TQ4	-	94	-	-	-	6 ¹
Shell						
TQ8	32	59	-	-	1.2	7.8
Aeolianite						
TQ10	6	56	-	4.1	8.7	25.2 ²
Mortar						
TWO.06	-	76	-	-	4	20 ³
TWO.08	-	96	-	-	-	4 ⁴
TWO.09	1.5	78	-	-	2.3	18.2 ⁵

All figures are percentages of total composition; all figures less than 1% are regarded as 'trace'; all carbonate polymorph figures are rounded up to nearest integer; Trace + Silicates: 6¹ in TQ 4 includes 3% quartz & 1% microcline; 25.2² includes 12% albite, 9.7% microcline & 3.4 muscovite; 20³ in TWO.06 includes 7.4% quartz, 5.5% mullite & 3.5% microcline; 4⁴ in TWO.08 includes 1% quartz & 1% albite; 18.2⁵ in TWO.09 includes 10% quartz, 4.3% albite, 1% microcline & 1% muscovite.

The results indicate that the polymorphic profile of all three mortar fine fractions is dominated by (low-Mg) calcite, although small metastable polymorph concentrations are evident in Type D sample TWO.09 (see table 1). The relative concentration of silicates in the fine fraction data from all three mortars appears to correlate with the relative concentrations of fine temper noted during thin section analysis, however, and this is supported by the relatively high concentrations of quartz within Type A sample TWO.06 and Type D sample TWO.09. The most notable detail within this data, therefore, is the continued evidence for very low temper (and low quartz) concentrations in Type B mortar sample TWO.08.

All biocarbonate materials, including the mortar inclusions and the detrital foreshore *maerl* sample TQ3, are dominated by (low-Mg, high-Ca) calcite. The complete lack of high-Mg calcite in mortar inclusion TQ4, and the relatively low fraction of this same polymorph in detrital sample TQ3 are notable.

Petrographic Analysis 2 & Reassessment Summary

With reference to the emerging SEM-EDS and XRD reports, a petrographic re-evaluation of the Tuquoy thin section assemblage (with the addition of a recently prepared thin section of aeolianite sample TQ10) was undertaken to inform final interpretations. This re-assessment also prompted a further round of analysis on the SEM-EDS geochemical data as the reflexive cycles of this investigation continued.

The very close optical and textural relationship between included bioclasts and supporting carbonate matrices in Type A and Type B mortars (noted in the initial study) is striking. The

evidence for altered shell material in Type A mortars is perhaps more salient than previously reported, but the heterogeneity in the temper profiles of these Type A sections² lends further support for the *maerl*-lime and shell-lime interpretations of these Type A and B materials. SEM-EDS analysis indicates that these (biogenic and anthropogenic) Type A and B materials also have very similar high-Ca compositions with no appreciable Si content (see Figure 4a & 4b). This high-Ca evidence is consistent with the XRD data from *maerl* inclusion TQ4, removed from this same SEM-EDS analysed mortar sample (TWO.04), and with the fine fraction from Type A mortar sample TWO.06. There is a lack of evidence within the current XRD data to suggest a correlation between *maerl* mineralogy and depositional context in the Tuquoy assemblage, as the foreshore *maerl* clast TQ3 displays much less high-Mg calcite than expected from previous analyses of Orcadian materials, and even presented a lower concentration of this polymorph than the *maerl* mortar inclusion TQ2 from Type A sample TWO.02. The low levels of high-Mg calcite in the mortar inclusions of TQ2 and TQ4, and the low level of aragonite in the *C. edule* mortar inclusions of TQ8, however, are both consistent with the polymorphic inversion associated with heated kiln relicts of these types [3]. The lack of aragonite and high-Mg calcite in the fine fraction from sample TWO.08 is also consistent with the high-Ca chemistry of the matrix of this same mortar sample, suggested by the EDS data, and with the XRD results returned by shell-lime mortar fine fractions from other sites [3]. The mineralogy and geochemistry of these materials in a naturally deposited environmental context therefore clearly requires more work (only a single *maerl* fragment was analysed here), but the textural, optical and geochemical characteristics of these bioclastic materials in the mortars themselves presents convincing positive evidence for a biogenic lime-source in these Type A and Type B mortar fragments.

Whilst there is an apparent lack of part-calcined geogenic calcareous lime source materials in all the Tuquoy mortar samples examined in these studies (such as those described in [11] for example), these mortars are often clearly associated with evidence for altered geogenic clasts of some sort, and these present a range of forms. Indeed, petrographic analysis suggests that at least some of the altered geogenic clasts visible in the Type A mortar thin sections have been formed from very rounded (detrital) sandstone clasts which display a spectrum of altered textures - including irregular clast boundaries and isotropic phases but no very significant calcareous component (see for example Figures 2a and 3a). These clasts often appear to be at an early stage of alteration, with vesicular and isotropic glassy materials sometimes limited to narrow areas and 'blisters' around clast rims. Importantly, the apparent lack of a significant calcareous component within these altered rounded clasts is consistent with the EDS data from a similarly red-coloured ferruginous grain in TWO.04, wherein normalised spectra analysis indicates a CaO fraction of 3.92-6.13% only (see Figure 4c). More highly altered geogenic textures are visible in Type B sample TWO.08, in broken angular fragments of well-developed previously liquid phase glassy materials with abundant well-formed crystals and some spinaflex textures (see Figure 3b), and EDS analysis indicates these 'slags' contain a CaO fraction ranging from 3.94-19.62% (see Figure 4d & 4e). The low

calcareous fraction within these altered silica-rich geogenic clasts suggests they are incidental relicts of the limekiln charge, and not lime-source materials.

Type C sample TWO.03 was not subject to SEM or XRD analysis, but a better interpretation of this material has been informed by comparative microscopic analysis of an aeolianite sample collected during walkover of the Tuquoy foreshore. TWO.03 is a fine well-sorted mortar of very similar texture to the aeolianite thin section TQ10 but contains an extraordinarily high concentration of slaggy clasts which are not apparent within this latter naturally deposited material. Moreover, unlike in thin section TWO.04 (Type A) and TWO.08 (Type B), the slags in thin section TWO.03 are not fragmented but appear to have derived from very fine geogenic protoclasts which have a close association with neighbouring fine altered bioclasts (see Figure 3c). It is this material which accounts for the distinctive fine black specks seen in the Type C hand samples during the initial study (and not noted in other mortars in the assemblage), and on this basis an aeolianite lime-source is suspected.

The initial study suggested that Type D sample TWO.09 had been manufactured from a geogenic lime source on the basis of both negative and positive evidence. The marine shell fraction within TWO.09 displays an unaltered range of colours and variously lustrous textures in hand sample, and this is consistent with the high birefringence, surviving microstructural integrity and lack of relationship with the supporting carbonate matrix associated with these grains in thin section. Overall, the evidence suggests that this mortar was not manufactured from a biogenic lime source. The initial study identified various subangular clasts of a fine-grained calc-sediment as a probable lime-source, and the SEM-EDS evidence identified a Ca-bearing lithology (characterised as a calc-arenite in sample TWO.09) as a possible lime-source also. It has not been possible to identify clearly part-calcined lime-source relicts in this reassessment of this material, but the identification of localised scatters of fine quartz within TWO.09 in the initial study, and their characterisation as intraclasts released during calcination of the geogenic parent lime-source, is consistent with the evidence for reacted quartz grains reported during the SEM work. The identification of Si, Al and Mg in the cryptocrystalline carbonate matrix of this material also clearly supports a geogenic lime provenance, with some Mg also evident in the XRD data from the TWO.09 fine fraction. This evidence for a Si, Al and Mg bearing carbonate matrix in TWO.09 presents a clear contrast with the biogenic mortar Types A and B described above, as does the lack of evidence for large isotropic/vesicular slags which were so clearly evident in the biogenic-lime materials.

A comparative summary of these various compositional criteria for mortar Types A, B, C and D, is presented in Table 2.

Table 2. Summary of Mortar Compositions by Type

Mortar Type	Grain Distribution	Carbonate Relicts	Slag Relicts	Fuel Relicts	Matrix Composition	Added Temper
A	Bimodal	Maerl/Shell	Poorly developed	Peat	High-Ca	High concn. Sub-mm shell & quartz
B	Bimodal	Shell/Maerl	Well-developed	Peat	High Ca	Low concn. Sub-mm shell & quartz
C	Well-sorted	Aeolianite	Complex	Peat	Unknown	Low concn. Sub-mm shell & quartz
D	Poorly-sorted	Limestone	Minimal	Peat	Ca with Si, Al & Mg.	Mod. concn. shell & quartzose

Conclusion

A reflexive programme of hand sample examination, petrographic thin section analysis, SEM-EDS analysis and XRD analysis of a mortar assemblage from Tuquoy in Westray (Orkney) has presented a consistent suite of evidence suggesting that the assemblage curated from the excavated settlement is dominated by biogenic-lime mortars (Type A and B), manufactured from *maerl* and marine shells, whilst the materials collected from the upstanding church are geogenic-lime mortars (Type C and D). Compositional variations and contrasts within this binary interpretation suggest that four different mortar types (A-D) are represented in the overall assemblage.

Discussion

Evidence for phase-specific lime-source contrasts in single multiphase sites is widespread across the north and west of Scotland and, at least in part, the broad range of different biogenic and geogenic lime-source materials used in the Northern Isles throughout the Medieval and later periods reflects the wide range of calcareous resources available in this coastal sedimentary environment [3]. This wide distribution of calcareous materials, however, also often results historic mortars in which both kiln-relicts and added-tempers are composed of various mixtures of altered geogenic and biogenic materials with complex depositional histories, and this can make lime provenance interpretations challenging. In the case of the Tuquoy assemblage, this complexity is heightened by the high geogenic/biogenic variability in foreshore compositions noted during walkover survey, and the close proximity of aeolianite outcrops which are also composed of carbonate cemented biogenic and geogenic grains. Indeed, detached and eroded fragments of aeolianite also currently contribute to the detrital materials covering the Tuquoy foreshore, adding even further cycles of complexity to the depositional profile of this environment.

The Tuquoy mortar materials are essentially composed of complex mixtures of closely associated biogenic, geogenic and anthropogenic materials, with altered characteristics resulting from primary, secondary and often tertiary depositional processes. A robust interpretation of these complex materials has required a reflexive interdisciplinary approach

to materials analysis, with a particular focus on examining the relationships between these various altered inclusions and the supporting carbonate matrix. All four mortar types characterised in this study display evidence for altered biogenic and geogenic materials, and these appear closely associated in mortar types A, B and C. Elsewhere, an apparent correlation between altered biocarbonate and non-calcareous geogenic clasts has now been reported in several shell-lime mortars across North Atlantic Europe [3], suggesting that both materials are relicts of the limekiln charge [13]. This re-assessment of the Tuquoy assemblage has effectively demonstrated the potential for SEM-EDS analysis to usefully inform that discourse, through the comparative analysis of binder, lime-source and slag geochemistry.

The emergence of slags in limestone-lime mortars is often interpreted as the result of ‘over-burning’ or impurities in the limestone lime source, but the vitreous materials in the Tuquoy assemblage are not consistent with this interpretation. A detailed study of slag inclusions within limestone-lime mortars manufactured at Charlestown (Fife, Scotland), for example, demonstrated that these materials retained a mineral composition dominated by Ca-rich silicate minerals, with a CaO fraction of between 40.8 and 56.2% [12]. The slag inclusions in Type A and B mortars from the Tuquoy assemblage, in contrast, often appear to have formed from silicate-rich sandstone materials with a range of low calcareous compositions. There is no convincing petrographic evidence for a textural relationship between these altered geogenic clasts and the supporting carbonate matrix in either mortar type, and the lack of evidence for Si phases in the SEM-EDS data from these mortar matrices also appears inconsistent with a high-silicate lime-source material (see Figures 4d & 4e). These glassy vesicular fragments require further work, but do not appear to be the product of a geogenic lime source material which has differentiated into calc-silicate slag fragments and Ca-rich binder. As above, it appears more likely that these belong to a class of vitreous fragments noted within historic and experimental materials elsewhere across Scotland, where they have been interpreted as evidence for the incidental inclusion of foreshore gravels within a limekiln charge dominated by a biogenic lime-source [13, 3]. Ultimately, therefore, the altered geogenic evidence in these materials actually lends further support to a biogenic lime source interpretation for mortar Types A and B.

The compositional contrasts observed across the combined Tuquoy mortar assemblage suggest that each of the mortar types characterised in the above investigation is associated with a separate constructional event, and on this basis the initial study suggested that (unlike at the Wyre site of Cubbie Roo’s Castle) the hall and church at Tuquoy had been constructed at different times [9, 3]. The recent reassessment of these mortars presented above has supported the materials interpretations which emerged from that initial study, and this effectively turns attention back to the contexts from which these samples were retrieved. With further evidence for the development of these remarkable buildings emerging from other research undertaken for the wider Tuquoy project, the contexts from which these mortar samples were retrieved will be reconsidered in the forthcoming monograph publication [14].

Further Work

The XRD results from the *maerl* analysis highlight a requirement for much more representative sampling and analysis of environmental materials, and at Tuquoy this comparative approach should be extended to include petrographic analysis of locally available temper sands. The interpretation that mortar Type C sample TWO.03 has been manufactured from aeolianite should be followed up by a comparative study of the shell evidence, since initial examination suggests neither the aeolianite nor TWO.03 contain evidence for larger shells such as *C. edule*. Further analysis should also re-consider the bone evidence apparent in Type A and B mortars, since some evidence for P in the carbonate matrix was noted. A further mortar survey of the chapel would be very useful and, although currently precluded by extensive consolidation, future work should aim to retrieve multiple mortar samples from fixed primary constructional core contexts.

Acknowledgements

Many thanks to Olwyn Owen, director of the Tuquoy project, for commissioning this reassessment and for commenting on an earlier draft of this paper; to Tommy Pottinger of Tuquoy Farm and Allan Rutherford of Historic Environment Scotland for permission to work at the church site; to Julie Gibson, Orkney Archaeologist, for general support in Orkney; to Mike Hall of the University of Edinburgh for thin section preparation, and to Geoff Bromiley of the University of Edinburgh who supervised the doctoral research within which the initial study featured. The Tuquoy project is funded by Historic Environment Scotland and administered by the Archaeology Institute, Orkney College, University of the Highlands and Islands. Mark Thacker undertook the reassessment of the Tuquoy materials discussed in this paper within his work for the Scottish Medieval Castles & Chapels C14 Project (SMCCCP) which is funded by Historic Environment Scotland (Archaeology Programme and Cultural Resources Team) and the University of Stirling.

Endnotes

1 – Although clearly recognised as contrasting materials, the church samples TWO.03 and TWO.09 were both labelled Type C in the initial study. Mortar Type D has been introduced here for greater clarity.

2 – TWO.06 and TWO.07 are less clearly bimodal.

References

1. Fleming A, Woolf A (1992) Cille Donnain: a Late Norse church in South Uist. PSAS 122: 329-350.

2. Thacker M (2015) Cille Donnain Revisited: negotiating with lime across Atlantic Scotland from the 12th-century. *Journal of the North Atlantic* 9: 45-66.
3. Thacker M (2016) Constructing Lordship in North Atlantic Europe: the archaeology of masonry mortars in the Medieval and later buildings of the Scottish North Atlantic. 3 vols. Unpublished PhD thesis, University of Edinburgh.
4. Clouston J (1932) A history of Orkney. MacKintosh, Kirkwall.
5. Gibbon S (2007) Medieval parish formation in Orkney. In B Ballin Smith, S Taylor, G Williams (eds.) *West over Sea. Studies in Scandinavian sea-borne expansion and settlement before 1300*. Brill, Leiden. Pp. 235-250.
6. Pálsson H, Edwards P (1978) *Orkneyinga Saga. The History of the Earls of Orkney*. Penguin. Middlesex. P. 155.
7. Lamb R (1993) Tuquoy: The Norse Magnate Farmstead. In C Morris (ed.) *Congress Diary*. pp. 1-101. In C Batey, J Jesch & C Morris (eds.) *The Viking Age in Caithness, Orkney & the North Atlantic*. Edinburgh University Press, Edinburgh. P. 82.
8. Owen O (1993) Tuquoy, Westray, Orkney: a challenge for the future? In C Batey, J Jesch, C Morris (eds.). *The Viking Age in Caithness, Orkney & the North Atlantic*. Edinburgh. Pp. 318-339.
9. Thacker M (2013) The Late Norse 'coral' or maerl-limes of Orkney: an on-site mortar archaeology of Cubbie Roo's castle and chapel. *Proceedings of the 3rd Historic Mortars Conference, Glasgow 2013*. Rilem, Glasgow.
10. Thacker M (2011) The lime and shell-lime mortars of the Western Isles. Unpublished MA thesis, University of York.
11. Hughes J, Cuthbert S (2000) The petrography and microstructure of medieval lime mortars from the west of Scotland: implications for the formulation of repair and replacement mortars. *Materials & Structures* 33: 594-600.
12. Leslie A, Hughes J (2004) High-temperature slag formation in historic Scottish mortars: evidence for production dynamics in 18th-19th century lime production from Charlestown. *Materials Characterisation* 53: 181-186.
13. Thacker M (2013) Making lime at the edge of the world. *Proceedings of the 3rd Historic Mortars Conference, Glasgow 2013*. Rilem, Glasgow.
14. Owen O (in prep.). Tuquoy: Investigations at a Norse manorial farm in Westray, Orkney.

Topic 8: Dating of historic mortars



An Ecology of Castle Construction: geoarchaeology, archaeobotany & radiocarbon analysis in the ecotone of Lochindorb Castle

Mark Thacker¹

(1) University of Stirling, Scotland, U.K., mark.thacker@stir.ac.uk

Abstract

A multidisciplinary study of the landscape, buildings and materials associated with the medieval castle of Lochindorb is presented, as part of the Scottish Medieval Castles & Chapels C-14 Project. The paper will begin by highlighting the position of the castle on an important routeway through NE Scotland, before describing various contrasts in the bedrock geology, vegetational history and climate of neighbouring districts. Briefly summarising previous interpretations of the standing building, an account of the current investigation will be presented which includes petrographic, archaeobotanical and radiocarbon analysis of various building materials. The paper will conclude with an interim summary of the study results, before a final discussion returns to the surrounding landscape, with a focus on boundaries, administration and transport. Along the way, the paper will highlight significant issues relating to the radiocarbon dating of mortar-entrapped relict limekiln fuels and present the first independent evidence relating to the chronology and phasing of this important medieval site.

Introduction

Lochindorb Castle is located on a small windswept island in a freshwater loch high in the Grampian mountains of north-east Scotland (Figure 1). The site is surrounded by a wide moorland from which rounded hilltops rising to around 500m and shallow fast flowing streams provide limited relief. Indeed, this area has recently been granted Special Landscape Area status on the basis of its ‘homogeneity...sense of spaciousness...wide views...sparse human presence...[and the]...almost complete absence of built structures’ [1]. Despite this apparently remote location, however, Lochindorb Castle occupies a very prominent place in the history of medieval Scotland. Constructed by the powerful Clan Comyn in the 13th-century, and subsequently occupied by King Edward I of England and various regional overlords, this building was recognised as such a potent instrument of seignorial power that the Scottish Crown finally ordered its ruination in the mid-15th-century.

Landscape Analysis

Lochindorb Castle is located on high ground close to the watershed between the Spey and Findhorn rivers. Both watercourses rise in the Monadhliath Mountains, approximately 80km



Figure 1 – Lochindorb Castle in its largely treeless mountain setting. Looking to the south, with the higher ground of the Spey-Findhorn watershed rising behind the loch.

SW of the castle site, and describe roughly parallel NE courses across the country before discharging into the sea at the Moray Firth. By the time they pass beneath Lochindorb the Spey and Findhorn are powerful rivers with very few crossing points, but the narrow strip of high ground in-between provides the context for an important SW-NE routeway across Highland Scotland (see Figure 2). That Lochindorb Castle was a significant landmark along that track is clearly evident in this surviving 17th-century account:

‘Badenoch and Elgyn ar distant the nearest way 36 myl. the way is by Creig-Elachy, whilk is fornent Rothimurcus throw Bulladren, by the kirk of Duthel to Lochenduyrb, holding the south syd therof, to the castell off Dunfale then throw the glen of Pluscardie” [2]



Figure 2 – Detail of a topographical map of northern Scotland, showing the locations of Lochindorb & Inverlochy castles (marked with red balloons), adjacent river systems, and routeway (dotted line). Map annotated using Edina Digimap; © Crown Copyright & Database Right 2019. Ordnance Survey

The Spey-Findhorn watershed follows a ridgetop to the south of Lochindorb, and all the smaller watercourses surrounding the castle site flow north toward the lower Findhorn.

From the reverse perspective, the land rises more gently from this northerly direction, and drops more steeply to the south - to Duthel and the Spey.

This SW-NE topography broadly reflects the bedrock geology of this mountainous region, which is dominated by NE-trending Dalradian metamorphosed sediments with large intrusive granite outcrops. Although generally comprised of metamorphosed sandstones (amphibolite facies, micaceous to quartzose psammities and semipelites) this Group does also include some metalimestones, and a locally high concentration of small quarries around Grantown-on-Spey (10km south) present the closest reported calcareous outcrops to the castle site [3]. The metamorphic geology of the region's interior, however, presents a striking contrast with the fertile *Laich* of Moray coastal plain to the north, which is characterised by sedimentary sequences of Permian, Triassic and Jurassic age with widespread sandstone outcrops [3]. This coastal area also contains some small calcareous deposits, however, including a bioclastic limestone across the Findhorn near Ardclach and the well-known limestone quarry and kiln complex at Cothall, on the banks of the lower Findhorn 20km to the north [4]. Several reports indicate both these outcrops were quarried for lime manufacture during the 18th and 19th centuries [5, 6, 7, 8, 9]. SMCCCP work in Strathspey demonstrates that the Grantown metalimestones have been exploited from the 12th/13th century, whilst an early 19th-century account reports that “the lime used in the building of...[Lochindorb]... castle was brought in the state of stone in creels on horses' backs from the quarries near to Grantown, and burned at limekilns on the opposite side of the hill from the loch” [10]. Given the apparent lack of calcareous outcrops in the immediate surroundings of the castle site, this might explain why the prominent hilltop overlooking Lochindorb from the east is named ‘Limekiln Hill’ (gaelic: ‘*Carn na Uil*’ or ‘*Càrn na h-Ath-aoil*’), and map evidence would suggest this place-name has been in continuous use since at least the late 16th-century and is probably medieval [4, 11, 12]. The adjacent settlement is also known as ‘*Lymkills*’ (later Easter and Wester), and this is unlikely to relate to the 3 kilns depicted around the settlement on 19th-century maps [4].

The bedrock geology around Lochindorb, however, is largely obscured by superficial deposits of infertile peat and acidic soils colonised by coarse grasses and *Calluna*. With the exception of various enclosed 19th-21st century plantations and a few stands of pine and birch woodland which may be semi-natural (eg. *Chorrycharcle* and *Tiribeg* [13]) very few trees survive within the viewshed of the castle site. Several commentators have highlighted evidence for peat-buried stumps of oak and fir [9, 10] and suggested Lochindorb forest was heavily wooded during the middle ages [14, 15, 16], but radiocarbon and isotope evidence from higher altitudes suggests these may be sub-fossil relicts of woodland communities which perished during pluvial periods of increased rainfall and peat formation thousands of years ago [17]. Indeed, the Spey-Findhorn watershed site of *Allt na Feithe Sheilich* (on the *Monadhliath* plateau 595m high & 16km SW of Lochindorb) has presented the earliest evidence for blanket bog development in Britain, with an open pine-birch woodland dating to around 6,900 BP still surviving here in sub-fossil tree layers [18]. It is notable that bog-wood survival at lower altitudes is much rarer [17], and interpreting areas without depicted

trees on historic maps can be problematic [13]. But the continued lack of woodland around Lochindorb in the post-medieval cartographic evidence down to the late 16th-century is consistent with 18th-century written accounts, and presents a striking contrast with the ‘deep forests of pine, larch, oak, &c.’ lining the River Spey throughout this same period in both sources [4, 8, 11, 12, 13, 19].

The dearth of refined chronological evidence for the development of open moorland around Lochindorb is problematic, but two of the best known semi-natural woodlands in Scotland do still survive in reasonable proximity to the castle site, and these present important taxonomic comparanda. Indeed, the forests of Abernethy and Darnaway display remarkably contrasting pine/birch and oak-rich arboreal populations and, although the ecosystems of both sites have been modified by human agency in recent periods, historical and palynological evidence suggests these contrasts have persisted since trees first began to colonise the wider region after the last glacial maximum [18]. In this regard, the distinctive mixed pine/birch (with very little oak) community of Abernethy Forest still strongly reflects the vegetational history of its higher-altitude/poorer-soils/inland/continental mid-Strathspey environment to the south of Lochindorb [17, 20], whilst the more thermophilous, taxonomically-varied and oak-rich woodland of the royal Forest of Darnaway reflects the vegetational history of its richer-soils/lower-altitude/coastal lower Findhorn environment to the north of the castle site.

Previous Evidence - The Castle Building

Repeated architectural surveys of the ruinous remains of Lochindorb Castle have reported that the surviving fabric displays evidence for two main constructional events. The primary phase is characterised by the substantial remains of a large quadrilateral enclosure surrounded by high masonry curtain walls, with rounded towers protruding from each angle containing distinctive fish-tailed arrow-slits (see Figure 3). A later 13th-century date has been confidently assigned to this primary structure based on the typological form of these architectural details, with the building interpreted as a recent development from earlier 13th-century enclosures without angle towers, and regarded as broadly coeval with a similarly configured castle (commissioned by the same Comyn overlords) on the west coast of Scotland at Inverlochy (see Figure 2) [21, 22]. Indeed, although the primary work at Lochindorb clearly displays much narrower masonry walls than the Inverlochy structure, and the towers have less projection, it has been suggested that the similarities between these two buildings are so close that they are likely to have been constructed by the same team of masons [22, 23].

A late 13th-century ascription for Lochindorb, however, is also consistent with various strands of indirect historical evidence relating to the site. This includes: a report that John II Comyn (one time ‘Guardian of the Realm’ and brother in law to the Scottish king John Balliol) died at Lochindorb in 1302; an account describing occupation by the English king Edward I during his 1303 campaign; and a document referring to ‘Robert of Lochindorb’ which

suggests that some kind of seigniorial caput was in place here by 1279 [24]. Although this evidence is circumstantial, and it is important to recognise that there is no direct supporting evidence for this interpretation, these late 13th and early 14th-century documents are very likely to be associated with the upstanding primary enclosure castle visible today. Indeed, assuming John I Comyn was the patron, the evidence supports a very narrowly defined 1258-78 date range for the construction of the primary curtain-walled building [24].

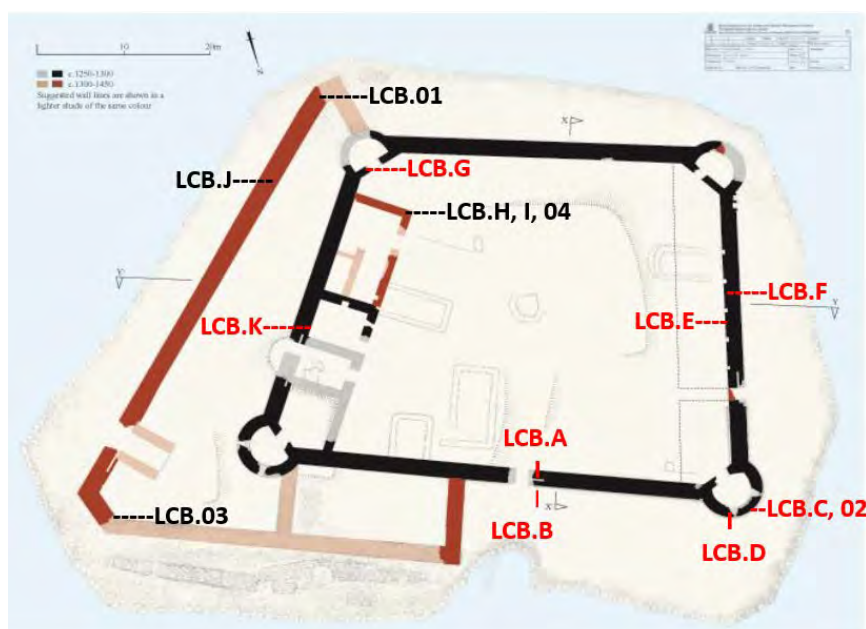


Figure 3 – RCAHMS ground-floor plan of Lochindorb castle showing two main phases (GV004942 © Historic Environment Scotland), annotated to illustrate SMCCCP sample contexts. Scale bar 20m.

Secondary work at Lochindorb includes the so-called ‘outer-works’, which describes another curtain wall enclosing the island to the east and north-east surrounding the main entrance, and a masonry east range constructed within the primary enclosure (see Figure 3 below). Both of these structures reportedly abut the upstanding fabric of the primary east curtain wall, so have been associated with a later constructional event, and both are likely to have been built before the Scottish Crown ordered the castle’s ruination in 1458. In contrast to the primary enclosure, however, it is difficult to ascribe a more refined constructional chronology within that wide (200 year) medieval window, and previous interpretations are speculative. Cruden [22], for example, suggested that the ‘distinctly superior work’ of the outer-works indicated it had been built by Edward I during his 1303 campaign, and this was supported by the RCAHMS whose 1300-1335 ascription was initially predicated on the apparently ‘near impenetrable’ character of the castle (suggested by the failure of a 1335 siege) and the resemblance of the pointed arch-head in the east gate to features at nearby Rait [23]. The RCAHMS also ascribed the south end of the east range to this same phase, although Gifford [16] had previously related this range to the upper courses of the E curtain and NE tower and suggested this work may be ascribed to the 15th-century. The evidential basis for this latter chronological interpretation is unclear, although there is documentary evidence to suggest the castle was ‘strengthened’ in 1455, during the Douglas occupation of

the site which ultimately prompted the Crown order [21]. This may, therefore, provide a historical context.

Buildings Analysis

Lochindorb Castle was visited twice by this author during 2017, and on each occasion the fabric was examined from ground-level only. The upstanding walls of the primary phase enclosure were found to present an almost complete quadrilateral ground plan and generally survive to around 5m high, although corner towers are often more ruined. Importantly for our research, however, the surviving monument presents a good mixture of visible masonry contexts including: largely complete wall faces; deep core rubble where facing stone has been lost; and full face-core-face cross-sections of masonry in upstanding wall sections adjacent to collapse. Except for an external basal plinth with a battered profile, the primary phase curtain walls display vertical internal and external faces, dominated by a poorly sorted mixture of angular to subangular schistose rubble with minor concentrations of red granite, and sandstone dressings in contrasting (red and buff) colours. The rubble face stones are generally flat-laid and 'naturally-bedded' in rough courses of approximately 500mm high, with only occasional large edge-bedded face stones evident. The masonry is fully lime-bonded in all visible upstanding sections, and very large volumes of mortar have been used in the castle's primary construction; with very wide bed joints and particularly large volumes of core mortar visible. This constructional mortar is generally very hard and appears compositionally consistent and continuous in all examined primary phase core and bed contexts. Secondary (leached) calcite obscures surface compositions in some areas (particularly in the south), but apart from some recent limited consolidation of interstitial joints in the south-east wall there is little to suggest multi-periodicity at lower levels in the primary curtain walls and towers.

Ultimately, the in-situ surface composition of the surviving primary constructional mortar of Lochindorb Castle was characterised as follows:

General description: Buff-brown coloured, coarse lime mortar.

Carbonate kiln relicts: Probable limestone-lime mortar, exhibiting a low concentration of rounded orange-brown probable heated limestone kiln-relicts, generally grading to 10mm.

Added temper: Tempered with a coarse mixture of quartz-rich sands and rounded to subrounded gravels to 15mm.

Fuel kiln-relicts: Wood-fired with low surface concentrations of wood-charcoal probable kiln-relict fragments. Long blocky longitudinal fibres (LCB.B), and some ring porosity visible with a hand lens in transverse view (LCB.G) suggests the assemblage includes *Quercus* sp.

The secondary outer-works and east range at Lochindorb Castle have been constructed in rubble stone of similar geological character to the primary phase work, although neither of

these later structures display an external basal plinth. The survey confirmed that both of these structures do clearly abut the primary curtain wall although, significantly for chronological interpretation, no direct stratigraphical relationship between them was noted. Constructional mortar materials are most clearly visible in wall breaches in the south-east facet of the outer-works, where a full face-core-face cross-section is exposed, and in the core of the south wall of the east range where some external face stone had been lost. In-situ examination initially suggested that these materials are tempered with a finer aggregate material than was evident in primary curtain wall contexts. Accepting that these different taphonomic environments can result in contrasting textures, these materials were characterised in-situ as follows:

General description: Buff-coloured fine-textured lime mortars.

Carbonate kiln-relicts: Limestone-limes containing locally high concentrations of grey subangular geogenic carbonate kiln-relicts to 25mm diameter.

Added temper: Lithic-temper dominated by a fine buff-coloured quartz-rich aggregate, generally grading to 1mm with occasional larger clasts to 10mm.

Fuel kiln-relicts: Wood-fired with locally high concentrations of wood-charcoal probable fuel kiln-relicts in the south range, but a dearth of evidence in the outer-works.

In summary, the evidence for widely distributed constructional core mortar exposures, phase-specific contrasting mortar compositions, and some (albeit limited) visibility of mortar-entrapped relict limekiln fuel fragments, suggested that further investigation of the masonry materials at Lochindorb Castle might usefully inform our understanding of the site. With the support of Historic Environment Scotland and the castle's owner, therefore, the building was subject to a limited programme of materials sampling, specifically targeting the three main upstanding structural contexts of the primary curtain wall/towers, secondary outer-works, and the south end of the secondary east range.

Sample contexts are annotated onto a plan of the castle in Figure 3 above. Ultimately, the assemblage included: 3 core mortar fragments, with a single sample removed from each of the main three contexts (LCB.02, LCB.01 & LCB.04); 1 probable relict limestone clast included within the core mortar of the outer-works (LCB.03); 1 loose sandstone fragment from inside the castle enclosure (LCB.05); a single sample of sand/gravel aggregate from the north bank of the surrounding loch (LCB.06); and 13 probable relict fuel fragments from wall core contexts in all three main structures (LCB.A-K). This relict fuel assemblage was clearly dominated by wood-charcoal fragments and included: 8 fixed (in-situ) mortar-entrapped relict limekiln fuel fragments from well distributed wall core contexts around the primary curtain walls and towers; 4 fixed (in-situ) mortar-entrapped relict limekiln fuel fragments from a small area of exposed core rubble in the south wall of the east range (3 of which were removed from a single mortar sample); and 1 loose (ex-situ) probable relict limekiln fuel fragment from a core context within the east wall of the outer-works.

Materials Analysis

In common with all SMCCCP studies, the various materials included in the Lochindorb assemblage were subject to a suite of geoarchaeological, archaeobotanical and radiocarbon analyses, and the results of these investigations will be summarised below:

(i) Geoarchaeological Analysis

The mortar, limestone, aggregate and sandstone samples were each subject to a two-stage preparation and analysis procedure adopted from previous research [25]. This involved: the initial preparation of two opaque 1-2mm thick mounted and polished ‘thick sections’ from each sample, which were scanned and examined by light microscopy in reflected light; and the subsequent preparation of a single standard 30µm thin section from each sample (re-mounted from the most interesting thick section slide to present the same surface) which was investigated microscopically in polarised light.

Microscopic analysis in thick and thin section identified that all constructional mortar samples had been manufactured from geogenic (rather than biogenic) carbonate sources, and both approaches highlighted differences between the coarsely crystalline limestone relicts in LCB.04 (from the east range) and the finer limestone kiln relicts within LCB.01, 02 and 03 (from the primary enclosure and outer-works). Indeed, the coarsely crystalline relict limestone evidence in LCB.04 was so texturally distinctive and in such high concentration, that this material could be identified as a probable metalimestone in reflected light at very low magnification, and that initial interpretation was subsequently confirmed by petrographic analysis in polarised light. The much finer texture and lower concentration of the relict limestone evidence in LCB.01 and 02, however, made interpretation more challenging and precluded refined characterisation in thick section. The lime-source materials within these two mortars were clearly very similar, however, and petrographic analysis subsequently suggested these clasts (and relict limestone sample LCB.03) were probably sedimentary and should be characterised as texturally heterogeneous microcrystalline limestones.

The quartzofeldspathic and quartz-rich mineralogy of the temper mixtures was similar in all three mortar samples, and consistent with the sand sample from the loch (LCB.06), although each of these samples did betray textural contrasts relating to differences in material grading. The sections prepared from LCB.02 (from the NW angle-tower) clearly presented a much coarser and more poorly-sorted temper profile than LCB.01 or LCB.04 and this is consistent with contrasts noted during building survey (see above). Only very limited concentrations of fuel evidence was visible in these section slides, but it is notable that one of the LCB.01 thick sections and the LCB.04 thin section contained wood-charcoal fragments with biostructural characteristics (ring porosity in transverse section and long narrow fibres with blocky terminals in longitudinal section) consistent with *Quercus* sp.

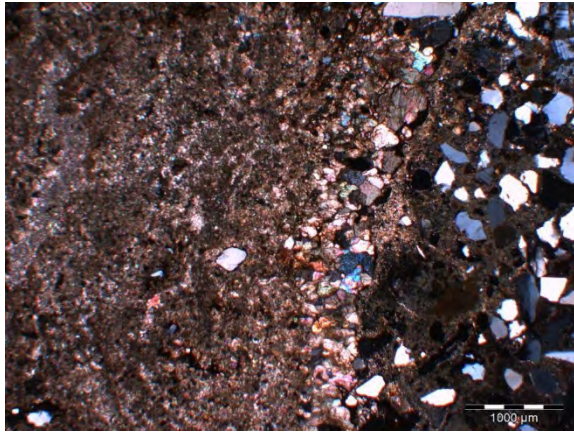


Figure 4a – Relict limestone in LCB.01a. XPL.

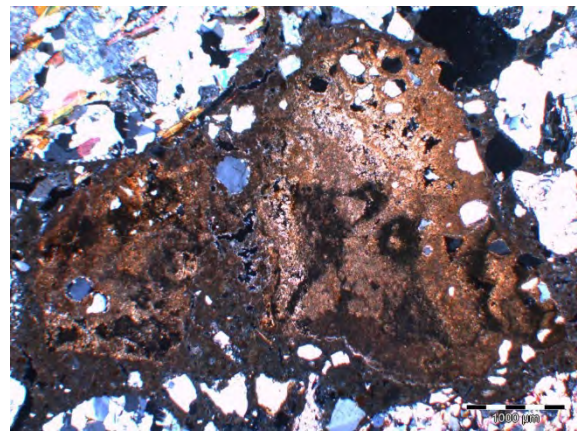


Figure 4b - Relict limestone in LCB.02a. XPL

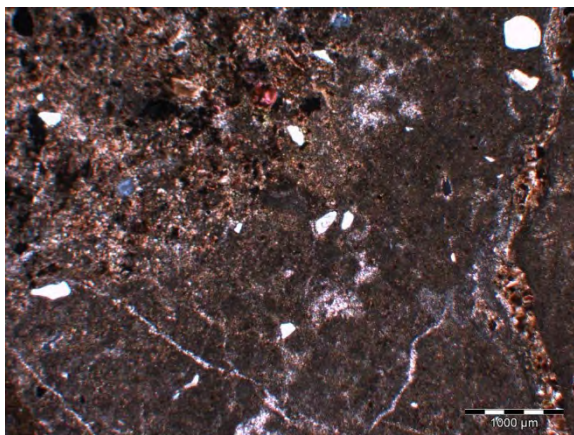


Figure 4c – Relict limestone in LCB.03. XPL.

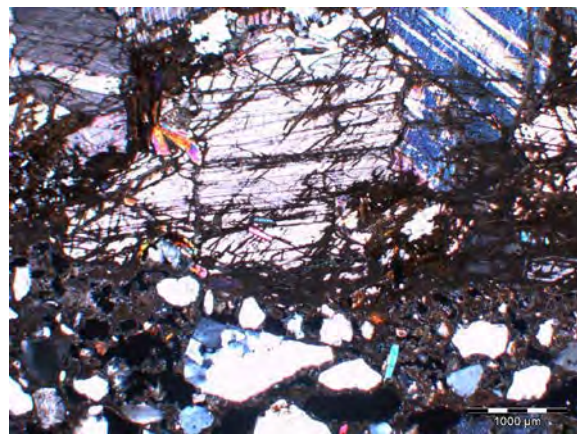


Figure 4d – Relict metalimestone in LCB.04a. XPL.

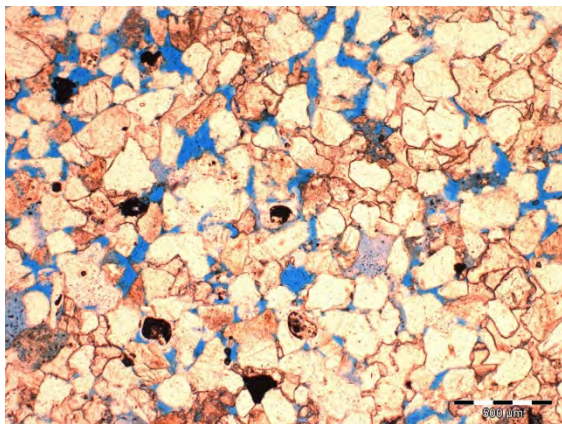


Figure 4e – Porous sandstone texture in PPL.

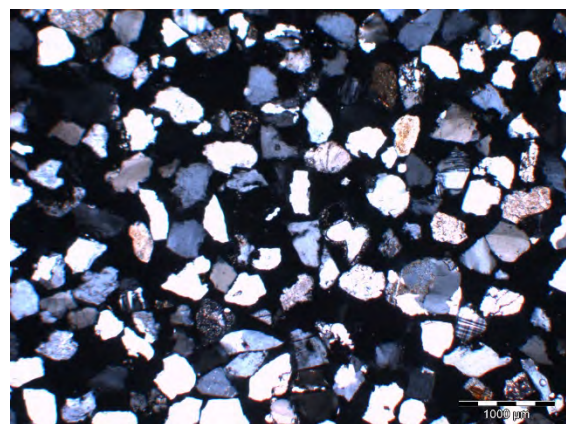


Figure 4f – Cast sample of aggregate. XPL.

In summary, therefore, the Lochindorb Castle assemblage presents compositional evidence for three different mortar types, including two geologically-contrasting limestone sources, and contrasting temper grades. LCB.01 (outer-works) and LCB.04 (east range) present somewhat similar temper profiles, but these materials can be separated on their respective geogenic lime-source materials; and although LCB.01/LCB.03 (outer-works) and LCB.02 (primary angle tower) present similar limestone sources, these mortars can be separated by

their contrasting temper profiles. Comparative analysis of these relict limestones with samples from regional outcrops is ongoing, but in interim the texture of the meta-limestone kiln relicts visible in mortar sample LCB.04 (east range) appears broadly consistent with samples previously collected by the SMCCCP from Grantown Marble Formation outcrops in Strathspey, whilst the limestone kiln relicts visible in samples LCB.01 (outer-works), LCB.02 (primary tower) and LCB.03 (outer-works) appear texturally consistent with samples previously collected by the SMCCCP from Stotfield Cherty Rock outcrops close to the Moray coast. Further fieldwork and lab-work is required here, particularly since this latter material also displays some characteristics consistent with descriptions of the ‘calcrete’ limestones from the Cothall outcrop on the lower Findhorn and elsewhere [26, 27], and further comparative analysis is also required to identify possible sources of the Lochindorb sandstone (LCB.06) from the well-known and widely distributed quarried outcrops of the Moray coast.

(ii) Archaeobotanical Analysis

All 13 single-entity relict fuel samples within the Lochindorb Castle assemblage were recognised as wood-charcoal fragments during buildings analysis, and this was confirmed during lab-based microscopic examination. Transverse sections of these fragments were examined in reflected light and interpreted with reference to standard botanical literature [28], initially to characterise taxonomy (to genus level) and morphology (bark, curvature, age-span etc). The character of each sample could then be assessed against the wider assemblage in order to select individual samples for radiocarbon analysis.

These analyses indicated that the assemblage was almost completely dominated by *Quercus* sp. Indeed, 12 of the 13 wood-charcoal fragments were characterised as such, including all the samples removed from fixed masonry contexts. This is also consistent with the evidence reported during geoarchaeological analysis of the mortar thick and thin sections (see above), and the only taxonomically contrasting sample was a fragment of *Pinus* sp. collected from a loose (ex-situ) context in the core of the east wall of the outer-works. The *Quercus*-dominated wood-charcoal assemblage from Lochindorb was also dominated by amorphous morphologies, however, and no surviving evidence for bark, cambium, sapwood/heartwood boundaries, or very high curvature biostructural profiles was noted. The tendency for *Quercus* to split longitudinally along its wide rays often results in very narrow samples which can make curvature characterisation challenging, but the lack of visible biostructural curvature suggested that at least 8 of these samples are unlikely to derive from contexts close to the centre of the parent stem, although the 5 fragments which did display some moderate biostructural curvature might. In general, however, the relict fuel assemblage from Lochindorb Castle is dominated by amorphous fragments of oak, whose position relative to the growing edge of the branch or tree trunk from which they derived (and so chronological relationship with the time of death of the wood) is unknown.

(iii) Radiocarbon Analysis

8 single-entity mortar-entrapped relict limekiln fuel fragments, from fixed primary enclosure and east range contexts at Lochindorb were selected for radiocarbon analysis. The *Pinus* sp. sample from the outer-works was not submitted in this initial round due to the loose context in which it was found. All submitted samples had been identified as *Quercus* sp., but the selected group did include a range of biostructural curvatures, as listed in table 1 below.

Table 1. Site context, archaeobotanical character and radiocarbon ages of selected fuel samples.

Site Context			Sample Character			¹⁴ C Results		
Phase	Structure	Code	Taxa	Curve	Rings	Lab.Code	BP*	Cal.AD**
1	N. Curtain	LCB.A	Quercus	Mod.	10+	GU45348	835	1155-1266
1	NW. Tower	LCB.C	Quercus	Low-Mod.	10	GU45349	862	1048-1255
1	W. Curtain	LCB.E	Quercus	Low	6	GU45351	932	1025-1165
1	SE. Tower	LCB.G	Quercus	None	8	GU45352	940	1025-1160
3	E. Range	LCB.la	Quercus	None	18	GU45353	842	1058-1263
3	E. Range	LCB.lb	Quercus	None.	7	GU45354	891	1040-1217
3	E. Range	LCB.lc	Quercus	None.	8	GU45355	848	1053-1262

All samples are from constructional wall core contexts; * BP ages are +/- 31 years; **Cal.AD ages are at 95.4% probability; Calibrated using OXCAL v.4,3.2 [29] and Intcal. 13 atmospheric curve [30].

Without wishing to place undue emphasis on such raw data and small sample numbers, there are two important aspects to these results which require consideration. Firstly, an inversely proportional relationship between sample age (calibrated and uncalibrated) and curvature is evident in the phase 1 data, with higher curvature samples returning younger radiocarbon dates. And secondly, almost all of the calibrated results from the phase 1 samples are earlier than the generally accepted (1258-1278AD) constructional date of the monument. The phase 3 results also appear very early and these two aspects of the raw data are probably related.

Although there are a number of possible reasons for these early dates (including use of standing dead wood), the data highlights the lack of demonstrably short-lived material in the assemblage and suggests that a significant quantity of outer rings had been lost from the submitted samples. These relict fuel fragments presented narrow time-widths (only two samples displayed more than 10 annual rings), indicating that significant wood-charcoal fragmentation had taken place. But the striking relationship between radiocarbon age and biostructural curvature evident here is not consistent with samples derived from the same tree limbs, and suggests that a variety of different diameter tree trunks and/or branches were harvested for inclusion within the limekiln charge. The relatively narrow range of radiocarbon ages in each phase indicates that all samples had stopped exchanging carbon with the environment within a reasonably short period, but this data also suggests that this period of wood formation was significantly earlier than the two constructional events in question.

These early dates have important implications for previous relict kiln fuel studies, where interpretations have been predicated on unmodelled, uncharacterised or bulk-charcoal radiocarbon dates [31]. Clearly, the fuel used to charge a limekiln is always going to have stopped exchanging carbon with the atmosphere before building construction has been completed, and so early dates are likely. Given that the documentary evidence describing the existence of a building is also often inherently late, however, such early radiocarbon data can represent a useful *terminus post quem* (TPQ) with which to bracket the constructional event [25; 31; 32]. Where the sample assemblage is not demonstrably short-lived, however, and/or there is a significant gap between the C-14 data and the documentary evidence, a statistical model is required which accepts that the individual results are all outliers, down-grades the effect of the older material on final interpretations, and privileges younger dates [33].

A multiple plot of the Bayesian model constructed to interpret the Lochindorb Castle data is appended to this paper (appendix 1. Fig 5c). This outlier model constrains the radiocarbon results into phases 1 and 3, but also includes the 15th-century crown order for the destruction of the castle and the 1279 reference to Robert of Lochindorb. A ‘Span’ function was also included within each of the two model phases, and these returned similar time-depths of 164 years for the phase 1 and 167 years for the phase 3 assemblages (appendix 1, Figures 5d & 5e). Within this model, the End Boundary distribution following each of these assemblage ‘phases’ represents the associated constructional event [31], indicating a date range for the primary phase enclosure castle of 1155-1281AD @ 94.6% (1186-1254AD @ 68.2%), and for the east range of 1202-1442AD @ 95.4% (1213-1336AD @ 68.2%). Single plots of these constructional End Boundary distributions are presented below (see Figures 5a & 5b).

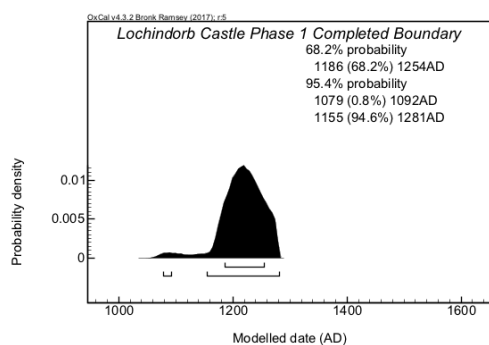


Figure 5a – Bayesian plot of Phase 1 boundary.

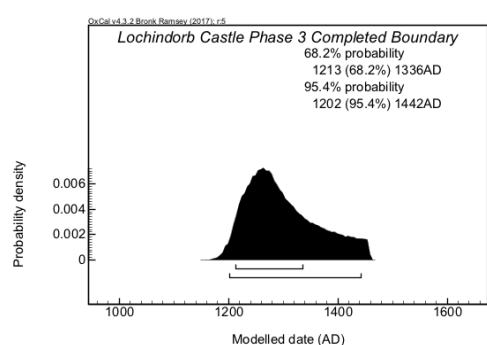


Figure 5b – Bayesian plot of Phase 3 boundary.

Conclusions

This SMCCCP study of Lochindorb Castle has presented several strands of original evidence relating to the development of the site. Buildings and geoarchaeological analyses indicate that the monument has generally been constructed with locally sourced schistose and granite rubble blocks, with sandstone dressings probably transported from quarries near the

Moray Firth. The monument contains evidence for three contrasting lime mortars, and this suggests that the primary enclosure, outer-works and south end of the east range are associated with three different constructional events. Whilst the contrast in temper profile between the primary enclosure and outer-works mortars usefully informs this phasing interpretation, the apparent similarities in lime sources of these mortars and the contrast with the sample from the east range is probably more significant. These results appear consistent with previous interpretations suggesting the outer-works and primary enclosure are reasonably close in date, whilst the contrasting meta-lime source lends some support to Gifford's suggestion that the east range (or at least the south of it) is significantly later [16]. This study also provides an objective criterion to investigate this hypothesis in other castle contexts, including further examination of the suggested multiperiodicity in the E range, E curtain and NE tower [16, 23].

In terms of the regional exploitation of materials, it is notable that the contrasting lime-sources highlighted by petrographic analysis have been sourced from different lithostratigraphic contexts, and landscape analysis currently suggests these source outcrops were located at significant distances from the castle site. The study is based on limited sample quantities and further work is required, but the sedimentary character of the lime-source evident in the primary enclosure and outer-works appears particularly striking in this regard, since these two early phases also betray surviving evidence for dressed sandstone which is likely to have been sourced from outcrops close to the Moray coast. This suite of evidence for the exploitation of materials transported from north of the castle is also consistent with the oak dominated relict fuel assemblage removed from this primary phase enclosure - given the more thermophilous woodland populations associated with the Findhorn/Moray coast and the relative lack of this genus in the mid-Speyside/Cairngorm populations.

Radiocarbon analysis of mortar-entrapped relict limekiln fuel fragments during the above study has presented the first independent dating evidence relating to the construction of Lochindorb Castle. This has enabled a multidisciplinary Bayesian model for the castle's construction to be formulated, which includes the archaeological (phasing) and documentary evidence, but also allows for the potentially long-lived character of the submitted fuel assemblage. This model presents an end boundary distribution which is consistent with the architectural style of the primary phase structure.

Discussion – Toward an Ecology of Castle Construction

The SMCCCP study presented above has highlighted evidence which suggests that Lochindorb Castle was constructed within an ecotone – a boundary zone between the sedimentary, fertile, low altitude, coastal and warm biome of the Moray coast, and the metamorphic, infertile, higher altitude, continental and colder biome of the Grampian Mountains. Asynchronicities in vegetational histories and distinctive localised contexts add

complexity to this simple distinction, but the dichotomy provides an effective general environmental model for further comparative work on the medieval buildings of the region.

More paleoenvironmental work is urgently required to inform our interpretations of the vegetational history of the moorland around Lochindorb, but 18th-century reports of ‘great quantities of oak and fir, found in the mosses of this parish’ [9] are a vivid reminder that the environment here has been subject to significant change during the Holocene Period. From this wider perspective it is important to note that NW Europe was still enjoying the benefits associated with the ‘medieval warm epoch’ when the primary phase enclosure of Lochindorb was constructed [34], as this climatic cycle may have mitigated the regional environmental contrasts highlighted above - blurring the ecotone character of the locality somewhat. By the mid-19th-century, however, the minister for Edenkillic parish reported that:

“The climate is very different in the two opposite extremities of north and south of this parish...[At] Darnaway...[in the coastal north]...the atmosphere is remarkably dry, mild and salubrious. But leaving the forestry, and ascending towards the southern extremity of the parish, [toward Lochindorb] the difference of climate is very perceptible. Here, from the entire destitution of wood, and from the proximity to the lofty mountains on the southwest...boisterous winds...the snow is frequently covering the whole surface to the depth of several inches...frost considerably intense...More rain, too, falls here than on the low grounds of Morayshire...” [6].

Whilst the antiquity of the parish name Edenkillic (Gaelic: *Aodincoillie*) is unknown, its accepted translation ‘the face of the woods’ [6, 9] effectively signifies an ecological boundary.

Just as changes in the physical environment can be an important factor in the availability of materials, interrelated changes in the cultural, political and economic context of a building often affect the pattern or scale of resource exploitation strategies in ways which are reflected in phase-specific material contrasts. Indeed, whilst Lochindorb Castle is located close to a boundary between marble or limestone, rubble or freestone and pine or oak, it is clear from the above study that the patrons and/or builders of the primary enclosure and outer-works could surpass the architectural limitations of the castle’s immediate environment and exploit resources on a regional scale. Crucially, this would also have demanded the sourcing and transport of materials from across administrative boundaries.

A recent re-interpretation of administrative boundaries in Moray has suggested that Lochindorb’s 18th-century position within the Strathspey parish of Inverallan has a medieval origin [35]. This is consistent with the wider pattern of parochial administration, since Edenkillic is very likely to have been centred on Dunphail Castle (close to the lower reaches of the Findhorn), and Lochindorb was clearly associated with the supra-parochial lordship of Badenoch from the 13th and 14th centuries [24, 35]. From a landscape perspective, however, we should have expected the parish boundary between Edenkillic and Inverallan to follow the clearly defined watershed between the Findhorn and Spey, to the south Lochindorb, and

the location of the castle within the tributaries of the Findhorn would normally situate the building well within the parish of Edenkillie. The process by which this Badenoch land unit came to be situated to the north of this watershed remains obscure, but this has clearly distorted the parochial landscape, whilst the post-medieval position of the parish boundary (across the loch of Lochindorb but just north of the island) is also remarkable.

This northern extension of the Badenoch lordship into ‘Stathfindhorn’ might present a physical context for the exploitation of materials from the Moray coastal biome, but this is also curious from an administrative context when later medieval and early modern documentary records indicate constructional materials for important seigniorial buildings were often supplied as rent or services by the tenants of the lordship concerned [31]. Whilst it is possible that the quarried schistose rubble evident in all buildings and the metalimestone lime-source of the east range may be associated with such practices, construction of the earliest phases of Lochindorb Castle was also probably associated with materials sourced from outside the (essentially metamorphic) lordship of Badenoch. Indeed, I would suggest that if the documentary evidence for Lochindorb hadn’t survived, we probably wouldn’t associate this building with Badenoch, Inverallan or Speyside at all.

The surviving materials at Lochindorb present evidence for interrelated processes of political and environmental change. The castle fabric is dominated by the primary phase exploitation of a range of materials from the wider region, assembled at a remote location, modified by itinerant craftspeople, and patronised by a powerful noble family administering land across 13th-century Scotland during a period of warm climate, stable government and economic growth. The secondary east range, in contrast, presents a limited volume of masonry fabric, bound with mortar materials from the nearby Strathspey biome. If further work can confirm a mid-15th-century constructional chronology for this fabric, then this might coincide with a short period of renewed warming, but by the time of the 1548 Crown order for the ruination of Lochindorb Castle, the climate of NW Europe was fast declining into the so-called ‘Little Ice Age’ [34]. Gilbert reports that the Scottish Crown continued to use the surrounding forest for grazing horses and cattle into the later 15th-century [36], and it is possible that the fragmentary turf-covered buildings noted by the RCAHMS [23] are associated with this activity. This late medieval reference to grazing doesn’t demonstrate a lack of woodland, but a 1606 grant in favour of the Campbells of Cawdor does include ‘...the loch of Lochindorb, with the houses in it, and the neighbouring Sheilings’ [37]. By this 17th-century period of increasing climatic instability, therefore, Lochindorb is associated with seasonal occupation during summer months (from Inverallan?) and travellers passing on the nearby road.

As a final note, it is striking that none of the surviving constructional mortars at Lochindorb Castle appear to have been manufactured in limekilns charged with peat or bog-wood from the surrounding moors, although such materials may have been used in the agricultural kilns of the adjacent settlement of ‘Limekills’ in a later period. It remains possible, therefore, that these building limes were sometimes manufactured at the outcropping limestone source, and this would certainly explain the striking combination of *Quercus* sp. and limestone in the

mortars of the primary phase masonry. The evidence for Quercus and metalimestone in the east range and Pinus in the outer-works suggests this is not a simple correlation, however, whilst the oak, birch and alder recorded in the parish of Cromdale, Inverallan and Advie in the late 18th-century does highlight the possibility of a semi-natural Speyside source [13]. The transport of quicklime from distant sources, however, would also not explain the *Càrn na h-Ath-aoil* place-name for the high hill overlooking the Lochindorb site. Indeed, although the source of Lauder's information is unknown, the materials evidence in the south of the east range is remarkably consistent with his suggestion that "the lime used in the building of the castle was brought in the state of stone in creels on horses' backs from the quarries near to Grantown, and burned at limekilns on the opposite side of the hill from the loch" [10]. Evidence reported elsewhere suggests the reasons for such lime place-names are often now ambiguous [36] and Lauder may have been imposing 19th-century practices onto a past narrative, but the antiquity of the place-name and its proximity to the castle site lend the suggestion some credence. The provenance of the early limestone and sandstone evidence at Lochindorb very clearly requires more work, with the wide distribution of dressed sandstone in medieval buildings across the largely metamorphic and igneous landscapes of NE Scotland prompting numerous questions about how the coastal quarries in Moray and elsewhere were patronised, administered and worked in different periods. In the absence of navigable rivers, however, it is certain that these materials would have been transported along roads similar to those described between Grantown and Lochindorb by Lauder, and between Badenoch and Elgin by the 'Gentlemen of that Country' from an earlier period [2].

Acknowledgements

Many thanks to: Angelika Cawdor for permission to undertake sampling at the site; Keith Duncan for discussion of the site's environmental status; Sharon Morris for boat transport; Iain Anderson for discussion of the RCAHMS survey; Mike Hall for thin section preparation; Mike Cressey for archaeobotanical mentoring and Alex Bayliss for discussion and feedback on the Bayesian modelling. Richard Oram commented on an early draft of this paper as did the anonymous peer reviewer. The SMCCCP is funded by Historic Environment Scotland (APG and CRT), and the University of Stirling.

References

1. Highland Council with SNH (2011) Assessment of Highland Special Landscape Areas. 132-137.
2. Anon (1644) Noats of distances for Badenoch. Pont's Texts. Can be viewed at <https://maps.nls.uk/pont/texts/transcripts/ponttext139v-140r.html>
3. Stephenson D, Gould D (1995) The Grampian Highlands. British Regional Geology. HMSO, London.

4. OS (1874) Ordnance Survey Six-inch 1st Edition 1843-1882 map. Elgin Sheet XXIX (includes Cromdale, Inverallan and Ardvie), survey date 1868-71. Can be viewed at www.nls.uk.
5. MacBean H (1842) Parish of Ardclach. NSA 13: 26-43
6. Farries P (1842) Parish of Edenkillie. NSA 13: 178-194.
7. Grant L. (1793). Parish of Cromdale. OSA 8: 251-260. Page 255.
8. Grant J. (1841). Parish of Cromdale, NSA 14: 432-443. Page 433.
9. MacDonnel J (1793) Parish of Edenkeillie. OSA 13: 553-566.
10. Cumming A (1911) Loch-in-Dorb, An Ancient Royal Fortress. PSAS 46: 357-364.
11. Pont T (1583-96) Pont 8, Moray and Nairn. Can be viewed at www.nls.uk.
12. Roy W (1747-55) Military Survey of Scotland. British Library Maps C.9.b 27/3d. Can be viewed at www.nls.uk.
13. Dunlop B (1994) The native woodlands of Strathspey. Scottish Natural Heritage Research, Survey & Monitoring Report No. 33.
14. Bain G (1893) History of Nairnshire. Telegraph Office, Nairn. Page 112
15. Lauder (1830) in Barrow G (1967) The Wood of Stronkalter, A Note on the Relief of Lochindorb Castle by Edward III in 1336. The Scottish Historical Review 46, 141, Part 1, pp. 77-79
16. Gifford J (1992). Highlands and Islands. Buildings of Scotland. Penguin, London.
17. Dubois A, Ferguson D (1985) The Climatic History of Pine in the Cairngorms based on Radiocarbon Dates and Stable Isotope Analysis, with an Account of the Events leading up to its Colonization. Review of Palaeobotany and Palynology 46: 55—80.
18. Birks H (1980-2007) Allt na Feithe Sheilich. JNCC Quaternary of Scotland.
19. Bleau J (1654) Moravia Scotiae provincia, ex Timothei Pont/scedis descripta et aucta per Robert Gordonium a Strathloch. Can be viewed at <https://maps.nls.uk/atlas/bleau/browse/110>
20. O' Sullivan P (1975) Vegetation history and the native pinewoods. In R Bunce, J Jeffers eds Native Pinewoods of Scotland. Proceedings of Aviemore Symposium, 1975, 60-69.
21. MacGibbon D, Ross T (1887) The Castellated and domestic architecture of Scotland from the twelfth to the eighteenth century 1. David Douglas, Edinburgh.
22. Cruden S 1960 The Scottish Castle. Nelson. Edinburgh.

23. Anderson I, Dixon P (2011) Inverlochy and Lochindorb Castles – A Comparative Study. *Architectural Heritage* 22: 1-17.
24. Barrow G (1988) Badenoch and Strathspey 1130-1312. Part 1: Secular and political. *Northern Scotland* 8 (1): 1-15.
25. Thacker M 2016 Constructing Lordship in North Atlantic Europe: the archaeology of masonry mortars in the medieval and later buildings of the Scottish North Atlantic. 3 vols Unpublished PhD Thesis University of Edinburgh.
26. Parnell J (1983) The Cothall Limestone. *Scottish Journal of Geology* 19 2: 215-218.
27. Tandon S, Friend P (1989) Near surface shrinkage and carbonate replacement processes, Arran Cornstone Formation, Scotland. *Sedimentology* 36 1113-1126.
28. Schweingruber F (1990) Microscopic Wood Anatomy. Structural variability of stems and twigs in recent and subfossil woods from Central Europe. Swiss Federal Institute for Forest, Snow and Landscape Research Switzerland.
29. Bronk Ramsey C (2009a) Bayesian Analysis of Radiocarbon Dates. *Radiocarbon* 51: 337-60.
30. Reimer P, Bard E, Bayliss A, Beck J, Blackwell P, Bronk Ramsey C, Grootes P, Guilderson T, Haflidason H, Hajdas I, HattĚ C, Heaton T, Hoffmann D, Hogg A, Hughen K, Kaiser K, Kromer B, Manning S, Niu M, Reimer R, Richards D, Scott E, Southon J, Staff R, Turney C, & van der Plicht J. (2013). IntCal13 and Marine13 Radiocarbon Age Calibration Curves 0-50,000 Years cal BP. *Radiocarbon*, 55(4): 1869-87.
31. Thacker M (in prep) Dating Medieval Buildings by Radiocarbon Analysis of Mortar-Entrapped Relict Limekiln Fuels.
32. Thacker M (2017) MacGillechrist's Castle: An environmental Study in Medieval Buildings Archaeology from Argyll. In P Martin (ed.) *Galleys and Castles*. IBT, Laxay.
33. Bronk Ramsey C (2009b) Dealing with outliers and offsets in radiocarbon dating. *Radiocarbon* 51 (3): 1023-1045.
34. Lamb H (1977) *Climate: past, present and future*. Volume 2, Climatic history and the future. Routledge, Oxon.
35. Ross A 2015 Land assessment and Lordship in Medieval Northern Scotland. 97, 253
36. Gilbert J (1979) Hunting and Hunting reserves in medieval Scotland. John Donald, Edinburgh. 249
37. Shaw L (1775) *History of the Province of Moray*. 254

38. Thacker M (2011) The lime and shell-lime mortars of the Western Isles. Unpublished MA thesis, University of York.

Appendix 1

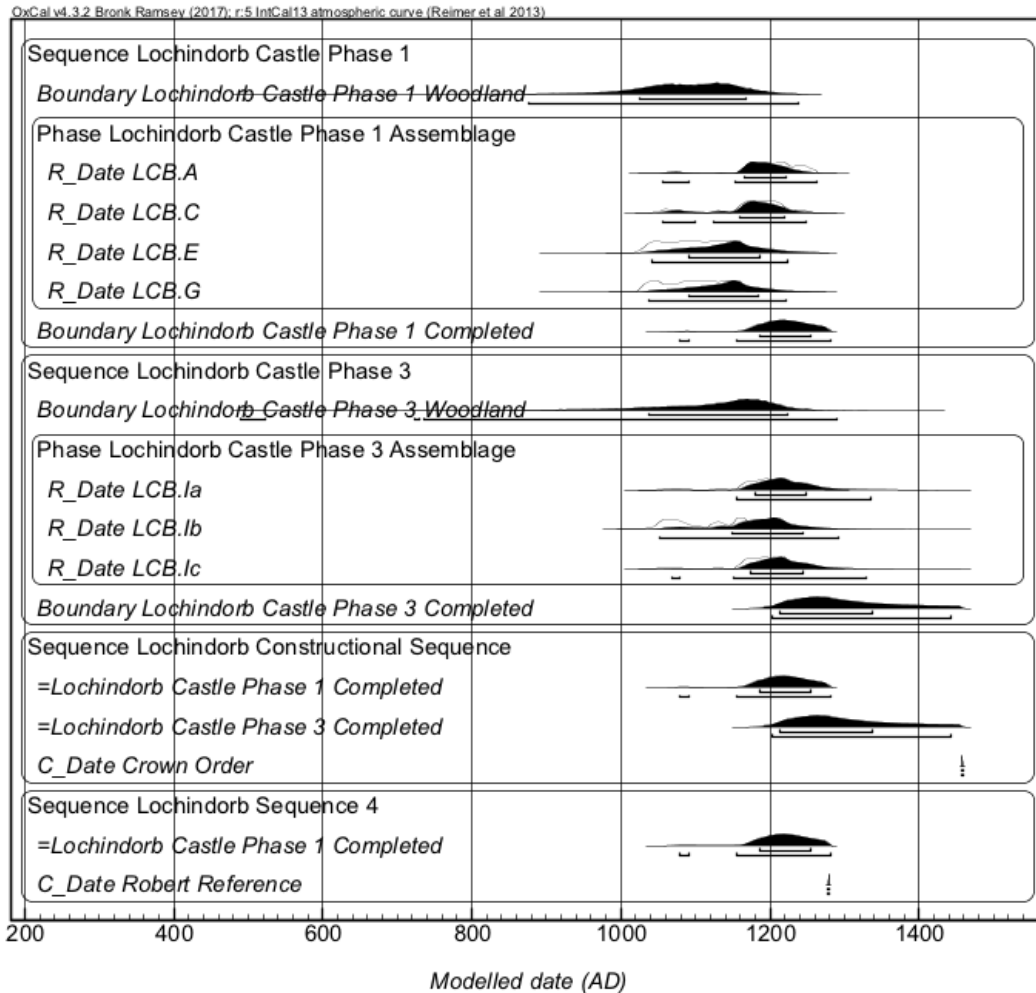


Figure 5c (above) - Multiple Plot from a multidisciplinary Bayesian model of the Lochindorb Castle evidence.

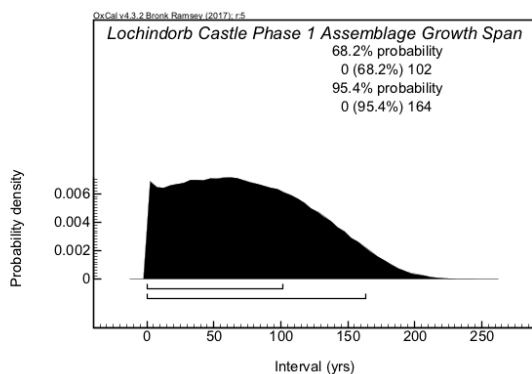


Figure 5d (above) – Phase 1 assemblage span.

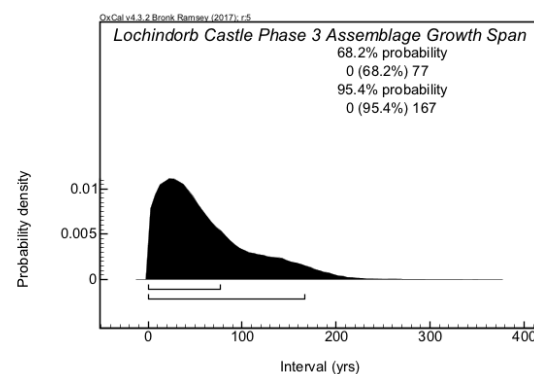


Figure 5e (above) – Phase 3 assemblage span.

Characterization of historic mortars: techniques used to establish a construction chronology. Case study: “Aragoneses’ Mill” as it belongs to popular architectural heritage

Esther Moreno Fernández¹, Javier Pinilla Melo¹, Francisco González Yunta², Alberto Sepulcre Aguilar², Ignacio Lombillo Vozmediano³, Yosbel Boffill Orama³

(1) Departamento de Construcción y Tecnología Arquitectónica, Escuela Técnica Superior de Arquitectura de la Universidad Politécnica de Madrid. Esther.moreno@upm.es, Javier.pinilla@upm.es

(2) Departamento de Construcciones Arquitectónicas y Departamento de Tecnología. Escuela Técnica Superior de Edificación, Universidad Politécnica de Madrid. Francisco.gonzalez.yunta@upm.es, Alberto.sepulcre@upm.es

(3) Departamento de Ingeniería Estructural y Mecánica. Universidad de Cantabria. Escuela Superior de Ingeniería Civil, Santander, España. ignacio.lombillo@unican.es, Yosbel.bofill@unican.es

Abstract

Restoration actions in building construction require complete preliminary studies. It is essential to perform tests for the characterization and identification of materials.

In this work, mortars and bricks characterization as a method of dating constructive techniques have been used. A case study for the “House of Aragoneses”, an ancient watermill sited in Monachil, Granada, is presented.

According to the building historical studies, there was an oil mill on that place that worked due to the Huenes River waterflow from the 15th to the 16th centuries. It may have disappeared because of the ravages of the Monachil Moorish properties in the riots prior to 1570. But from the documentary information existing in the archives, the construction works from XV to XVI century are not clear. The building underwent changes throughout history but there is not any documentation related to these interventions. By means of different tests and characterization techniques, dating and identification of existing masonry works at the “House of Aragoneses” has been accomplished.

Introduction

The term "popular architecture" is related to societies of agricultural and livestock producers. These primitive, popular and vernacular constructions move around parameters related to functionality, constructive techniques and the language of the materials used.

The popular construction starts from the establishment of functional needs and some pre-established conditions such as the environment, the bioclimatic characteristics and the available materials. In this way, architecture can be understood and interpreted not only as the complex of transformations carried out by man, but also as the direct translation of the

physical forms of a certain culture that manifests in the built heritage [1]. The popular architectural heritage is a witness of the life and history of the communities. It shapes the identity of the cities, and constitutes a community heritage that various generations, from distant times, have been creating in several ways. Such as their needs, the materials around them and the peculiarities of the surrounding landscape where they have to live in. However, there is a part of the built heritage that, a priori, is not classified as interesting or as a historic asset to be preserved, but it represents an enormous value for the inhabitants of this certain population. It may be due to the fact that "it has always been there" and buildings presence is closely and sentimentally linked to the most distant memories. An example of this is the mill of the Aragonese located in the village of Monachil, Granada. It constitutes a sample of *Hacienda de Olivar*, whose greater development takes place in the 18th century, during which the productive and agriculture economy in Lower Andalusia is redefined, representing a highlight of the increase of the olive cultivation [2, 3].

Monachil, is located in a fertile valley of the Sierra Nevada massif, just 8 km far from Granada and includes places as relevant as the Veleta peak or the ski resort of Sierra Nevada. The contextualization and understanding of the property are directly conditioned by three historical stages [4].

Medieval Period. With the consolidation of the Nazarí Kingdom, the settlement of Monachil originates like a farmhouse. *Quayat al-Munastal* - the Arabic name that will derive in Monachil - will stand out within the Granada's "Comarca de la Vega" region for its high agricultural productivity. The location of the building at this time is difficult to determine. However, it would be within the space or environment of the main mosque, which was located where the current parish church stands.

Modern Period. The economic and social reorganization of Monachil, after the reconquest of the Catholic Kings, are the keys that establish and promote the new development and urban growth. The foundation of the church of La Encarnación in 1501 establishes the origin of a new neighbourhood; La Rambla, whose arrangement is established from the so-called Plaza Alta or High Square. This space will structure the way of implantation of the popular hamlet, and also the productive and supply equipment as oil and flour mills...

Contemporary Period. The current shape of the building responds to different phases of construction rearrangements, which will have a turning point in the last third of the eighteenth century. The urban location of the Casa del Molino begins to be defined from the sixteenth century. From then on, a complex network of historical processes will define the resulting land structure. In 1834, Monachil acquires the condition of town. This implies its consolidation as an urban, administrative and civil unit. The channelling works of the Monachil and Huenes rivers, already in the second half of the 20th century, directly influenced the current configuration of the site of the building.

The first known graphic source of the municipality of Monachil is the iconographic representation contained in the Catastro de la Ensenada (1752), where the house of the

Aragoneses is represented. It is a manor house located on an isolated plot surrounded by gardens (Figure 1).



Figure 1. Iconographic representation of the real estate, Catastro de la Ensenada (1752).

The current architectural configuration presents a two-storeys building with an irregular surface per plant of 1050 m², divided in three buildings around two courtyards. It responds to the typology of "Hacienda de olivar" or olive farmhouses. It is a functional model that reached its peak in the eighteenth century, when the demand for oil increased by the Spanish colonies of the New World before the failure of the implantation of the oil in American territories. The olive farm is an architectural type in which the production of olive oil conditions the spatial planning of the dependencies dedicated to it. It means a productive area or mill and a differentiated residential area of the owner or manor.

The smallest and oldest farmhouse of this type comes from the year 1450, rebuilt later in the sixteenth century by its owner Alonso de Venegas and his wife Brianda. A wealthy couple of converts, whose names are among the first settlers of Monachil after the fall of the Nazari Kingdom. They are, without doubt, the most important family of the town before the expulsion of 1568. As a curiosity, a member of the Venegas family was in Mexico and returned with a daughter of Moctezuma, a surname that would later be incorporated into the family coat of arms located in the main altarpiece of the church.

According to the existing historical studies on the building in the XV and XVI centuries, there was an oil mill on the site that took advantage of the waters of the Huenes River, and that could have disappeared during the damage caused to the Moorish properties of Monachil throughout of the revolts prior to 1570 [4].

Around 1780, a noble residential space with columned patio and fountain is added to the pre-existing building (mill with a house above). In later works, the mill and the house is transformed into a productive oil space with a loading yard. The old courtyard with a rectangular floor plan and Mudejar architecture, has a lower paved floor, with octagonal stone pillars, surrounded by a corridor covered with wooden ceilings. The upper floor closed with glass glazing and posts with bolsters. The exterior stands out for its main façade and the

nobiliary coat of arms above the jamb of the door that is the only element that has patrimonial protection (Figure. 2).



Figure. 2 Patio with fountain in noble residential area. Main facade

Through the patio you can access the area of the olive mill that has been preserved to this day (Figure 3).



Figure 3. Water mill and presses with steam engine, all of them from 19th century

At the end of the 19th century, the water mill was modernized with an attached double-height room housing new hydraulic presses and a steam engine. They will replace the 18th century ones with “counterbalance tower” and “press beam” function.

At the beginning of the 20th century the house became the property of the Aragón family, popularly known as the “señoricos de Aragón”⁹. Later, his heirs sold it to the municipality of Monachil.

In the most recent period, the productive activity was abandoned and the noble residential space was converted into a multi-family dwelling in an unfortunate way. Because it caused serious damage in some points: creating and closing openings, attaching cantilevers and hanging volumes, making defective bathroom installations, replacing structural floors and pavements, building new stairs, etc.

⁹ Masters of Aragon in a slightly derogatory sense.

Of the stately mansions that should have existed in Monachil, this is the only one that is still preserved today.

As it has been described, the building complex is a result of transformations and/ or aggregations over the centuries. This makes it difficult to verify the chronological dating of all the elements. The walls of the building are all mixed brick masonry with lime and pebble square inserts, regardless of the time of construction (Figure 4).



Figure 4. Mixed masonry walls

Constructions carried out between 15th and 18th centuries are not clear in the existing archives documentary information.

Characterization of the construction materials is a technique that helps to situate the different construction elements over time. Mainly, in the case of buildings whose execution process has not been sufficiently documented in the past. The constituent materials of the old masonries present incompatibilities with some materials that are currently used nowadays. So, their precise identification is a very important tool when establishing the criteria for intervention in a building like this [5].

There are numerous studies on historical materials where different analysis techniques are used [6-15]. Most of the studies consulted have used a combination of different conventional techniques such as mineralogical, thermogravimetric analysis and optical and electronic microscopy.

The objective of the current building renovation project that is going to be carried out, is to give a cultural and public use to the Casa del Molino (Mill House). It is promoted by the Junta de Andalucía and the municipality of Monachil. This study focuses on characterizing the constituent materials of masonry walls. On one hand, to confirm the conclusions of the historical studies and, on the other hand, to help establish the intervention criteria in the building renovation. With that aim, XRD, Thermogravimetry and microscopic observation techniques have been used. In addition, physical and mechanical tests on mortars have been carried out.

Materials and methods

Samples of mortar and brick from the different walls were taken. In the Figure 5 diagram, both places where materials were obtained from and in situ tests were performed are show.

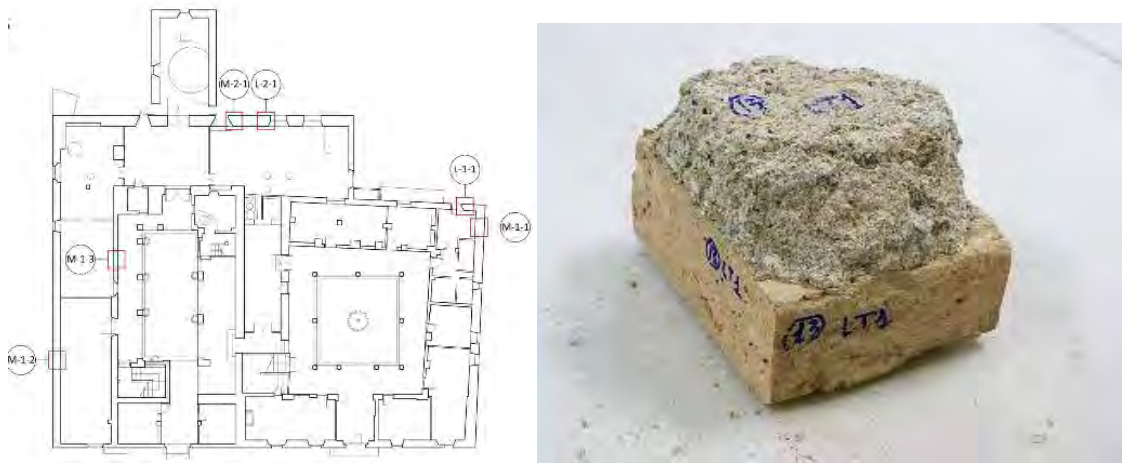


Figure 5. Plan of the building with marked areas where the samples were obtained from.

Hydraulic tests have been carried out to determine the physical properties of mortars (Figure 6).



Figure 6. Hydraulic tests on mortars

In order to know the crystal structure, an X-ray diffraction (XRD) analysis was carried out with a Bruker D8 Advance powder diffractometer equipped with a high-stability copper-anode X-ray source and a SOL-X energy dispersion detector and large active area for X-ray diffraction (Figure 7).



Figure 7. Finely grinded mortar samples for analysis by XRD.

In order to obtain information on the studied samples mineralogy, thin sheets have been prepared for observation by Optical Polarization Microscopy (OPM) with a Kyowa polarized and transmitted light petrographic microscope, mod. BIO-POL (Figure 8).



Figure 8. Polished binder samples up to thin section.

Samples were observed by Scanning Electron Microscopy (SEM) with a Jeol JSM-820 microscope operating at 20kV and equipped with Oxford EDX analysis (Figure 9).

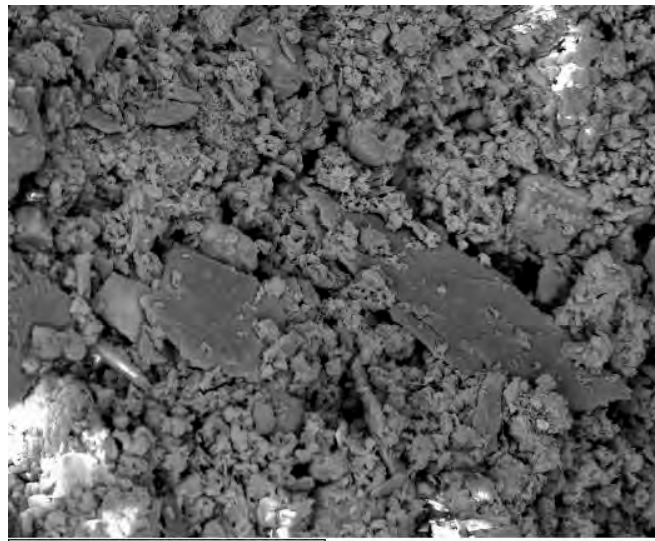


Figure 9. mortar MT2 x1000 picture

Thermogravimetric Analysis (TG / DTA) was used for chemical characterization. A Thermal Analysis Instruments brand, mod. SDT Q600 was used, integrated by a differential scanning calorimeter (DSC) and a thermo-gravimetric analyser (TGA), with platinum-rhodium thermocouples to know each component proportion.

Additionally, and to estimate the mechanical properties in order to perform calculations to determine the strength of the walls, non-destructive (NDT) sclerometer and penetrometer tests have been performed in situ.

Sclerometer and penetrometer tests on mortars

The use of a pendulum sclerometer provides a rapid qualitative indication of the quality of mortar through the correlation with the energy absorbed by the mortar during the impact [16,17]. It is considered as a low-impact test for monitoring the quality of mortars through

the evaluation of its surface hardness. The equipment utilized in this study was a SCHMIDT PM-type pendulum hammer.

Another test used for the in-situ characterization of mortars was the penetrometer technique, for which a portable PNT-G penetrometer was utilized. The penetrometry of mortars used, based on the PNT-G method developed by Natale Gucci [18,19], provides a rapid qualitative indication of the compressive strength of the material through the correlation with the energy necessary for performing a standardized perforation. The procedures followed to carry out the previous tests are included in the RILEM MS-D.7 [20] and RILEM MDT. D.1 [21] recommendations, respectively.

The tests were carried out in areas signed by figure10. In each test multiple repetitions were performed to, as far as possible, reduce the uncertainty of the average value obtained.



Figure 10 Localization of tests on mortars. (a) 19th-20th century construction; (b) 15th century construction remodelled in the 18th century.

Results and discussion

Samples of bricks and mortars of different masonry walls have been tested. Table 1 shows the average values of physical properties of the samples extracted in construction phase 1 from the 15th to the 18th century and 2 for those from the 19th to the 20th century. It shows that the properties are very different according to the construction phases, with lower apparent densities in the first construction phase.

Table 1: Physical properties such as bulk density (Da), absorption coefficient (Ca), porosity (Pa) and volumetric mass density (Dr) of the mortar samples.

Specimen	Da (g/cm ³)	Ca (%)	Pa (%)	Dr (g/cm ³)
M-1	1.6	19.3	30.7	2.73
M-2	1.97	14.5	21.89	2.69

Dolomite, Plagioclase, Quartz, Calcite and Phyllosilicates presence has been detected in all mortar samples through X-ray diffraction (Figure 11).

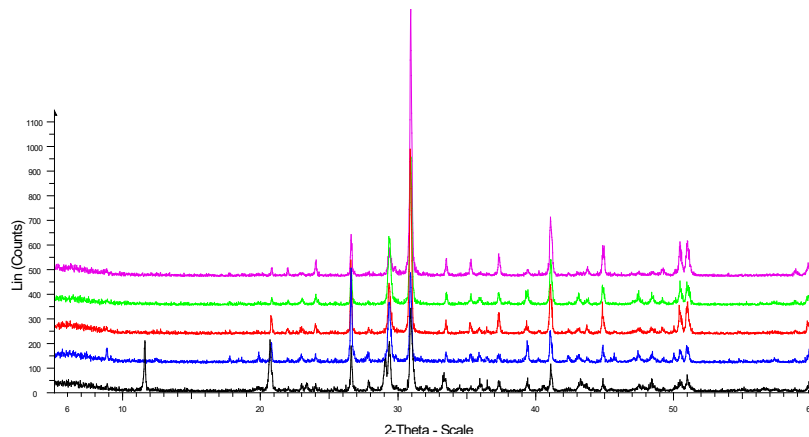


Figure 11. XRD of all tested mortars

In the SEM images, neither any presence of CSH gel nor any Ca(OH)_2 has been observed, indicating that all the lime has been carbonated. Crystals of silicic aggregate in a calcite matrix is observed (Figure 12).

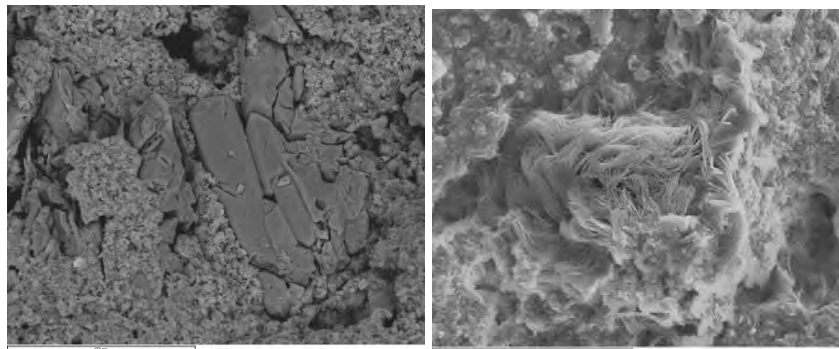


Figure 12. SEM images of binder and aggregate of a mortar sample

Mortar components ratios have been determined by thermogravimetric tests. These results confirmed that all the tested mortars have lime binders and dolomitic and / or silicic aggregates (Quartz and Feldspar). Figure 13 shows two thermograms of the tested mortars. Up to 420 °C, weight loss due to absorbed water and salt crystallization are observed. At 720 °C decomposition of Dolomite is produced and from 800 °C on Calcite decomposition happens.

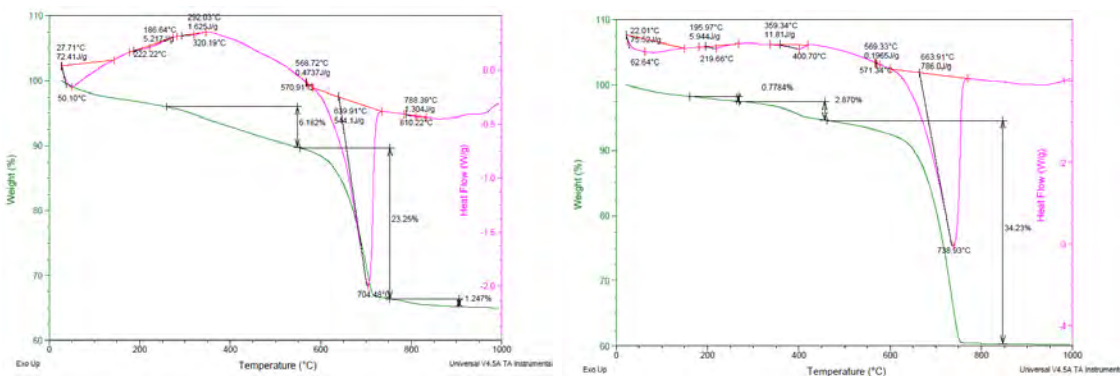


Figure 13. Thermograms resulting from thermogravimetric analysis

Historical studies hypothesis are confirmed [4], there are 2 types of mortars clearly differentiated. Some poorer, with lime: aggregate, between 1: 2 to 1: 2.5 and densities around 1.23 g/cm^3 , corresponding to the 15th -18th century walls, and richer ones, with a 1: 1.3 ratio and a bulk density of around 1.78 g/cm^3 , from the 19th -20th century walls.

No presence of CSH gel or CAH compounds has been observed, so the presence of Portland cement or natural cements is totally dismissed, what places these masonries in the 19th or early 20th century. The cement industry was developed in Spain 50 years after European industry. The first natural cement factories in Spain opened in the region of Lower Urola, Basque Country, in 1835 and shortly after Catalonia did. The first Spanish cement Portland factory opened in Tudela Veguin, Asturias, in 1898 [22]. In Andalusia natural cements were not developed, since they need the presence of marl limes, so the first Portland cement factory in Andalusia region to open was the Financial and Mining Company of La Caleta de Málaga in 1921, and that of Inocencio Romero de la Cruz, in Atarfe, Granada, also in 1921 [23].

Bricks TDA tests show a weight loss due to the evaporation of water up to 100°C, indicating a higher humidity and therefore, porosity in the first period sample, 15th-18th century, respecting to the second period, 19th-20th century. Calcium carbonated deposits (caliche) are indicated by a loss of weight at 800°C. First period sample showed a greater presence of caliche compared to that of the second period. Greater number of endothermic peaks in the first period brick are observed. That indicates the presence of a greater quantity of clays that have not been fully fired, due to lower temperatures in their manufacture.

Penetrometric and sclerometric tests on mortars

The values registered are shown in Table 2. In the penetrometric test cases, the table includes the compressive strength value of the mortar, R_c , determined from Gucci's relationship, $R_c=(PI+22)/134$ [19], which proposes a relationship between the values of the penetrometric index (PI) and the compressive strength of the mortar, in the case of mortars with a compressive strength less than 4MPa.

In each test multiple repetitions were performed to, as far as possible, reduce the uncertainty of the average value obtained. The values registered are shown in Table 2.

In the penetrometric test cases, the table includes the compressive strength value of the mortar, R_c , determined from Gucci's relationship, $R_c=(PI+22)/134$ [29], which proposes a relationship between the values of the penetrometric index (PI) and the compressive strength of the mortar, in the case of mortars with a compressive strength less than 4MPa.

As for the mechanical characterization NDTs on the mortar of the masonries under study (penetrometric and sclerometric), the dispersion of the results in the two test zones should be highlighted. Generally, it was found that the 19th-20th century mortar was of better quality than that the 15th-18th century one. In this respect, the correspondence with the

results for the samples of mortar tested in the laboratory to compression should be noted, where clearly different behavior was found in the two masonries.

Table 2: Penetrometric Index (PI) and surface hardness values obtained.

Position	DFJ-01 (19 th -20 th century)				DFJ-02 (15 th -18 th century)			
	Penetrometric Index (PI)	267	1115	1441	1399	96	124	68
814		1139	2383	2093	60	54	20	12
887		2040	680	1069	193	61	39	291
763		2297	582	890	183	60	86	106
1038		1441	1226	1636	31	26	149	37
Average (PI)	1260.00				90.05			
Rc (MPa)	9.57 *				0.83			
Rebound index (RI)	26	17	20	15	14	18	12	14
	25	12	15	42	16	24	14	18
	25	35	25	40	18	20	22	17
	25	35	23	22	17	15	16	19
Average (RI)	25.13				17.13			
Class	B – Moderate (25-35)				A – Weak (15-25)			

*It should be commented that the value of Rc in this area must be considered questionable, since it is above 4 MPa, the maximum value established by Gucci for the use of his correlation equation.

The compressive strength of the mortars (Rc) obtained in the penetrometric test using Gucci's equation, Table 2, was 0.83 MPa for the 15th-18th century mortars (a value close to the one obtained in the laboratory, 0.96 MPa) and 9.57 MPa for the 19th-20th century mortars. In this latter case, given the estimated strength through the above-mentioned equation is greater than 4 MPa, the maximum value established by Gucci for its use, this value should be treated cautiously.

Regarding to obtained results from sclerometric tests, they behave in a similar way to those obtained in the penetrometric test. Better classification of the mortars is obtained in the case of 19th-20th century masonries with Class B – Moderate, compared to the 15th-18th century masonries with Class A – Weak.

Conclusions

The tests carried out on the existing building materials in the Casa de los Aragonés from Monachil, have helped to place in time different construction elements of the building.

Current historical studies on this building, stated that the building was built in several phases. Including a significant growth in the 19th-20th century and a 21st century refurbishment, not knowing exactly the construction process between the 15th and the 18th centuries.

From this investigation two masonry types, corresponding to a two unique phases construction can be concluded. Therefore, considering historical studies and the materials tests results, it is concluded that in the building there are the following masonries, corresponding to two unique construction periods:

18th century. Brick masonries with lime and pebble square inserts, with low temperature fired bricks and lime mortars between 1:2 and 1:2.5 lime-aggregate ratios and around 1.23 g/cm³ densities.

That means a first construction phase, on 18th century, made of mixed masonry with natural stone and low temperature burnt clay bricks and lime mortars with low lime/aggregate ratios and densities.

19th to early 20th century. Same brick masonries with lime and pebbles inserts, including higher firing temperatures bricks, lime mortars with 1:1.3 lime aggregate ratios and around 1.78 g/cm³ bulk density.

A second construction phase, from the 19th or early 20th century, with the same type of masonry work, but bricks burnt at higher temperature and lime mortars with a richer proportion of binder.

Regarding building materials, all tested mortars were made of lime as a binder and dolomitic and/or silicic aggregates (Quartz and Feldspar). According to their time of construction, the following materials have been identified and characterized:

18th century lime Mortar. A dolomitic lime mortar, with 44% of Dolomite and Quartz composition can be identified from the XRD tests. Two types of mortars with very different properties and state of preservation have been found:

- One mortar mostly converted into sand with 1.23 g/cm³ bulk density and 1: 2.5 lime-aggregate ratio.
- Another type of mortar in good preservation state, less disaggregated and with an bulk density between 1.78-1.97 g/cm³, 1:2 lime-aggregate ratio and compressive strength of 1.21-3.16 MPa. In the thin section, fine to very fine grain size was observed. By means of the SEM a mortar rich in lime with enough presence of clay can be confirmed. Clays mineralogy were identified with XRD analysis. Resulting in Mica/ Paragonite: 60%, Smectite: 28% and Chlorite: 12%. The angular morphology of the dolomite grains indicates that it was used as a crushed aggregate for the mortar, probably to provide whiteness to the sample. Observation by SEM reveals smaller Quartz and Feldspar crystals in a homogeneous matrix of well-crystallized Calcite.

19th century lime mortar. From the XRD tests a well-carbonated and rich lime mortar with dolomitic aggregates (20%) can be concluded. In SEM images exam, Magnesium that can have dissolved and recrystallized, is detected. In the thin sections, quite large dolomitic

crystals with a closed structure are observed. This mortar presents a good preservation state, and a 1: 1.3 lime-aggregate ratio.

18th century brick. They were made of a lean clay with a high content of siliceous sand and a high presence of caliche. Due to a high content of unburnt clay and high porosity a low temperature firing is concluded. The estimated properties are the following:

- Bulk density: 1.79 g/cm³- Compressive strength. 15.88-20.94 MPa

19th century brick. They were made with a lean clay with some siliceous sand content, and low presence of caliche. Less porosity and less presence of unburnt clays permit conclude a higher temperature of firing. The estimated properties are the following:

- Bulk density. 1.59 g/cm³- Compressive strength. 13.78-14.19 MPa

Hydraulic binders presence is dismissed, so masonries actuations should have to be made with aerial mortars. It is necessary that new mortars do not have a greater rigidity than the existing binders, which could produce breakages in coatings and grouting.

From all the above it is clear that the bricks have all been manufactured with the same type of lean clay and siliceous sand, however different cooking temperatures have been observed, corresponding to the two different construction moments identified. The bricks of the areas executed in the 15th-18th century present a less refined raw material, with a high content of caliche, a high content of unburnt clay and a high porosity. However, bricks used in 19th-20th century show lower caliche content, lower unburnt clay content and lower porosity, indicating a higher firing temperature.

Until the 20th century, clay firing furnaces used wood and coal as fuels. However, in the 19th century, the design of furnaces in Europe improved, with the furnaces of lower draft or inverted flame [24]. In them, the heat flow crosses the load from top to bottom to evacuate through the chimney at the bottom of the oven. This type of oven reaches higher and more uniform firing temperatures, and therefore, produce a lower porosity, which has been detected in the different types of bricks tested

Regarding to the NDTs applied to the characterization of the mortars, the dispersion of the results should be highlighted. However, both with the sclerometric tests, and with the penetrometric ones, it was demonstrated that the mortars of the 19th-20th century were of higher quality than those of the 15th-18th century, which is in line with the clearly different behavior of the two masonries.

The building called Molino de los Aragoneses, Casa Grande or Casa Molino, of Monachil, holds both historical heritage values (witness of the population evolution and testimony of the transitional architecture from Baroque to Neoclassicism) and typological ones. It is an example of *Hacienda de Olivar*, almost unique in the province of Granada.

Mortars analysis has helped to establish a construction chronology differentiating ancient and modern phases of the mill architecture. It has also allowed for a better interpretation and understanding of the remains of this building adding value to popular heritage. Also it has served to make decisions related to the building renovation determining which zones have to be conserved and recovered to avoid their destruction.

Acknowledgements

The authors wish to thank “Organismo Autónomo de Parques Naturales” and “Cátedra Proiescon Universidad-Empresa” for the partial financing of this work through the Project “Study of Casa de los Aragoneses to assess the state of the structure and materials”.

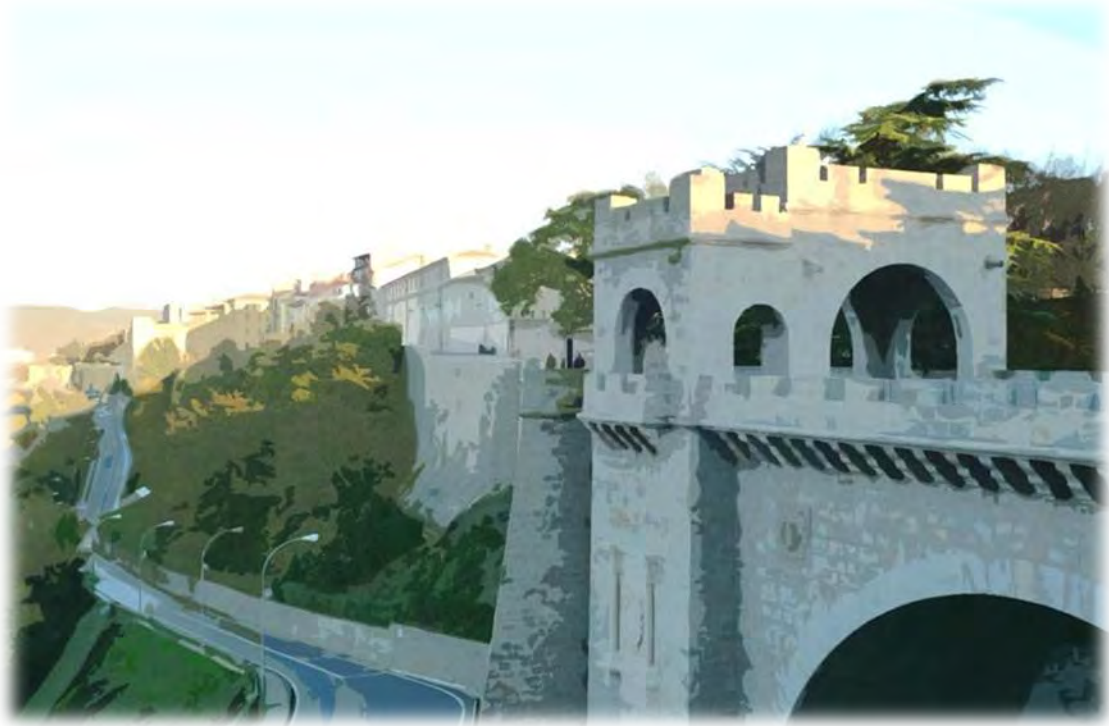
References

1. Maldonado L, Vela F. De arquitectura y arqueología (1998) Ediciones Munilla-Lería.
2. Bonet, A. Andalucía Barroca: Arquitectura y Urbanismo, Biblioteca de Arte Hispánico Barcelona: Polígrafa, (1978), pp. 302 -310.
3. Torices N., Zurita E. Cortijos, haciendas y lagares: arquitectura de las grandes explotaciones agrarias de Andalucía. Provincia de Granada. Sevilla: Dirección General de Arquitectura y Vivienda, (2003) pp.87.
4. Torices N, Gómez J.J, López P. Informe histórico-artístico y arquitectónico del Molinode los Aragoneses en Monachil, Granada (2014) Consejería de Vivienda y Ordenación del Territorio de la Junta de Andalucía.
5. Moreno E, González F, Pinilla J, Corrochano C. (2017). Materials identification methodologies for intervention in architectural heritage. Dyna Ingeniería e Industria. doi.org/10.6036/8200
6. Moropoulou A, Bakolas A, Bisbikou K, (1995) Characterization of ancient, byzantine and later historic mortars by thermal and X-ray diffraction techniques. Termochimica Acta. 270: 779-795.
7. Moropoulou A, Bakolas A, Bisbikou K, (2000). Investigation of the technology of historic mortars, Journal of Cultural Heritage. 1: 45-58
8. Bakolasa A, Biscontina G, Moropoulou A, Zendri E, (1998) Characterization of structural byzantine mortars by thermogravimetric analysis. Termochimica Acta 321:151-160
9. Adriano P, Santos Silva A, Veiga R, Mirao J, Candeia A.E, (2009) Microscopic characterisation of old mortars from the Santa Maria Church in Évora. Mat. Charact. doi: 10.1016/j.matchar.2008.11.008.

10. Middendorf B, Hughes J.J, Callebaut K, Baronio G, Papayianni I. 2005 Investigative methods for the characterisation of historic mortars- Mineralogical characterization. Chemical characterization. Materials and Structures. Vol 38, 8
11. Isen, J. (2006) Microscopy of historic mortars-a review. Cem. And Concr. Res. 36: 1416-1424
12. Válek J, Hughes J. J, Caspar J. W. P. Groot. (2012) Historic mortars, characterisation, assessment and repair. Springer
13. Pires J, Cruz A.J, Techniques of Thermal analysis applied to the study of cultural heritage (2007), Journal of Thermal Analysis and Calorimetric, 87: 411-415.
14. Bartz W, Rogo J, Rogal R, Cupa A, Szroeder P. (2012)- Characterization of historical lime plasters by combined non-destructive and destructive tests: The case of the sgraffito in Bo_żnow (SW Poland). Const. & Build. Mat. 30: 439-446.
15. Starinieri V, Papayianni I, Stefanidou M. Study of materials and technology of ancient floor mosaics' substrate. 1ar Historical Mortars Conference, Lisbon, Portugal 2008
16. Tavares M, Magalhães AC, Veiga MR, Velosa A, Aguiar A (2008) Repair mortars for a maritime fortress of the 17th century. In: Medachs – Construction Heritage in Coastal and Marine Environments: damage, diagnostics, maintenance and rehabilitation, Lisbon, LNEC.
17. Tavares M, Veiga MR (2007) A Conservação de Rebocos Antigos - Restituir a Coesão Perdida através da Consolidação com Materiais Tradicionais e Sustentáveis. In: VII SBTA – Seminário Brasileiro de Tecnologia de Argamassas, Recife – Pe, ANTAC.
18. Gucci N, Barsotti R (1995) A non-destructive technique for the determination of mortar load capacity in situ. Materials and Structures vol. 28(5): 276-283.
19. Gucci N, Sassu M (2002) Resistenza delle murature: valutazione con metodi non distruttivi, il Penetrometro PNT-G. L'Edilizia 16(2):36-40.
20. RILEM Recommendation MS-D.7 (1997) Determination of pointing hardness by pendulum hammer. RILEM TC 127-MS: 'Tests for masonry materials and structures'. Materials and Structures 30:323-328.
21. RILEM Recommendation MDT. D.1 (2004) Indirect determination of the surface strength of unweathered hydraulic cement mortar by the drill energy method. RILEM TC 177-MDT: 'Masonry durability and on-site testing'. Materials and Structures 37:485-487.
22. Varas M.J., Alvarez de Buergo M., Fort R. The origin and development of natural cements: The Spanish experience. Constr. Build. Mat. (2007) Volume 21, Issue 2, February, pp. 436-445.

23. Puche O., Mazadiego L. F.. Las canteras históricas de Morata de Tajuña y la cementera Portland Valderribas. Primer Simposio Ibérico sobre Geología, Patrimonio y Sociedad, Tarazona (Aragón) (2000) 13, pp. 109-123.
24. Rhodes D. Hornos para ceramistas. Ediciones CEAC 2004.

Topic 9: Natural and Roman cement mortars



From marlstone to rotary kilns – the early development of Portland cements in Central Europe

Farkas Pintér¹, Christophe Gosselin², Thomas Köberle³, István Vidovszky⁴, Johannes Weber⁵

(1) Scientific laboratory, Federal Monuments Authority Austria, Arsenal 15/4 1030 Vienna, Austria, farkas.pinter@bda.gv.at

(2) Geotest SA, En Budron E7, CH-1052 Le Mont sur Lausanne, Switzerland, christophe.gosselin@geotest.ch

(3) Technische Universität Dresden, Institute of Geotechnical Engineering, D-01062 Dresden, thomas.koeberle@tu-dresden.de

(4) Budapest Department of Construction Technology and Management, Budapest University of Technology and Economics, 1111 Budapest, Műegyetem rkp. 1-3. Hungary; e-mail: ividovszky@ekt.bme.hu

(5) Institute of Arts and Technology/Conservation Sciences, University of Applied Arts Vienna, Austria, Salzburg 14/1, 1010 Vienna, johannes.weber@uni-ak.ac.at

Abstract

Based on the optical and electron microscopic investigations of Portland cement structures from nine Central European historic objects built between the 1860s and 1908, the present paper discusses the phase composition, microstructural properties of unhydrated residues and hydrated cement phases as well as fingerprints of the main milestones of the development of early Portland cement production. The early cements of the 1860s were characterized by their coarse grain size and very heterogeneous composition containing, besides C_3S , C_2S , C_3A and ferrite, a wide range of under and over burned components. Although the Portland cements produced in the following decades were less heterogeneous, cement phases suggest the absence of accurate control of the raw mix and the use of different types of shaft kilns and ring kilns. Finally, Portland cements produced in the early 1900s show features characteristic of clinker burned in early rotary kilns. Despite the slight increase in cement fineness, analyses suggest that the evolution of milling technique could not keep up with the calcination technologies. The compositional differences of hydration products between the samples produced in different periods were mostly due to the addition of calcium sulfate which presumably started in the last decades of the 19th century.

Introduction

The history of modern hydraulic binders started with the invention of natural hydraulic lime, NHL (1756) which was followed by James Parker's Roman cement (RC) in 1796 [1]. Realizing the advantages of cementitious binders, the early 19th century was characterized by intensive experiments, especially in England and France, to achieve hydraulic binders with enhanced properties. In 1824 the product name Portland cement (PC) was introduced by Joseph Aspdin. Nevertheless, this so-called "proto PC" showed more similarities with Smeaton's NHL than those of PCs produced in the second half of the 19th century [1]. Two decades later, in 1844 William Aspdin and Isaac Johnson succeeded in burning cement

clinker above the sintering temperature (i.e. >1300°C) for the first time [1]. Nevertheless, the PCs of the second half of the 19th century were characterized by very inhomogeneous mineral compositions. Despite the technological progress the cement heterogeneity was a consequence of a simple shaft kiln technology and the lack of exact adjustment of the raw materials. Especially in the Alpine regions (i.e. South Germany, Austria and Switzerland), but also in Hungary a few cement plants used the local natural rocks (i.e. marlstone, clayey limestone) to produce, similarly to RC, so-called natural PC [2], [3], [4], [5]. Consequently, the PCs of the “early years” (i.e. 1850 to 1900) frequently had variable qualities and achieved lower strengths compared to their 20th century followers [1]. The establishment and evolution of European cement plants strongly depended on the economical development of the countries. In the early years (i.e. 1850s) English PC was exported to the western part of the Continent, but shortly after (1855) the first German PC plants started also supplying their products [6]. One year later Austria (i.e. the Austro-Hungarian Empire) also launched its first PC plant in Kirchbichl, Tyrol [7]. In the following decades Germany and Austria were the two biggest PC producers in Central Europe. These countries not only dominated the market, but also hindered the development of the cement industry in the surrounding territories, particularly in Switzerland (establishment of the first PC plant in 1871, [8] and Hungary (establishment of the first PC plant in 1878 [4]). The 1880-90s were characterized by the abrupt growth of cement plants and technological investments especially in the Austro-Hungarian Empire and Germany. In this period three main type of kilns existed; discontinuous and continuous shaft kilns [7] and ring kilns (in Germany since 1864 [9]). The most important technological development of PC production took place around the turn of the 20th century with the adoption of rotary kilns [1] followed by the development of clinker coolers. Germany was among the first countries that started operating rotary kilns (1899 [10]). Some years later also Switzerland (1904), Hungary (1904) and Austria (1906) [4], [7], [8] introduced the rotary kiln technology. However, it has to be mentioned that the dissemination of rotary kilns took slowly place and even in the first decade of the 20th century the lion’s share of the Central European PCs was produced in continuous and automatic shaft kilns as well as in ring kilns [4], [10], [11].

Although ball mills were already in operation in the second half of the 19th century, the milling technology was mainly restricted to the use of edge mills. The wider dissemination of ball mills can be dated back to the early 20th century. Table 1 summarizes the most significant development in PC production in the countries of this study.

Presently, there is an increasing interest and importance in investigating historical PC-based construction materials due to their use in a large number of heritage buildings. The insight into the material characteristics of PC-based historic objects supports the understanding of early cement production techniques and the often good to excellent performance of these materials after more than a century. Consequently, the information obtained may contribute to gain more data for conservation, preservation and maintenance of PC-based historic structures. The present study attempts to outline the main characteristics of early PCs based

on the investigation of concretes, artificial stones and mortars originated from the former Austro-Hungarian Empire, Germany and Switzerland between the 1860s and 1908.

Table 1. Milestones in the development of PC production in Austria, Hungary, Germany and Switzerland between the late 1850s and early 1900s

Age	Austria	Hungary	Germany/ S-Germany	Switzerland
1850-60	1856: start of (natural) PC production in Kirchbichl, Tyrol	-	1855: start of (artificial) PC production in Stettin (today in PL)	-
	Kiln technology: shaft kilns			
1860-80	Establishment of approx. 25 cement plants all-over Austria	1878: start of (artificial) PC production in Lábatlan	1864-1883: <i>production of natural PC in Blautal (S-Germany)</i> 1864: introduction of ring kilns 1878: first German standard to test PC	1871: start of (artificial) PC production in Luterbach/Soleure; until 1880 four cement plants in CH
	Kiln technology: shaft kilns, continuous shaft kilns and ring kilns Milling technology: edge mills and double pendulum rapid mills with built-in sieves, ancillary ball mills			
1880-1900	1888: Austrian standard to test PC 1894: Association of Austrian Cement Producers		1899: first commercial use of a rotary kiln in Niedersachsen	1880: creation of the Federal Laboratory of Materials Testing (EMPA)
	1890s: beginning of the use of calcium sulfate as a retarding agent?			
1900->	1906: first rotary Kiln (Mannersdorf)	1903: auto-matic shaft kiln (Beocsin) 1904: first rotary Kiln (Lábatlan) 1912: introduction of ball mill technology	<i>1929: introduction of first rotary kilns in Blautal, S-Germany</i>	1904: start of (artificial) PC production; first rotary kiln
	Spread and development of rotary kilns, clinker coolers and ball mills			

Sampling and analytical methods

A total of 20 samples from 9 objects (Table 2) constructed in Austria, Hungary, Germany and Switzerland between the 1860s and 1908 were taken and analyzed by optical and electron microscopy. To assure the originality of the materials historical sources have been

thoroughly investigated prior to sampling. Samples were embedded in epoxy resin and thin sections of standard 30 μm thickness as well as polished sections were prepared. Thin sections were analyzed in the optical microscope (Zeiss AXIOScope A1) using transmitted plain (PPL) and cross-polarized (XPL) in order to determine the mineral composition of the unhydrated cement residues and secondary phases in the binders. Prior to analysis polished sections were etched with Nital (1.5 ml of HNO_3 in 100 ml of isopropyl alcohol for 6 to 8 seconds), and the residue of the etchant was removed by ethanol [12] in order to highlight unhydrated cement grains and their microstructure by reflected light (RL) in the optical microscope. The distribution of the average and maximal grain sizes of residual cement was estimated in the optical microscope by the counting and measuring of 50 to 80 single grains in each sample. The etched surface was then re-polished and coated with carbon to be analyzed by scanning electron microscope (Zeiss EVO15, acceleration voltage 15kV) coupled with an energy dispersive X-ray spectrometer (Oxford DryCool). A large number of analysis points and atomic ratio plots were used to characterize unhydrated residual cement grains and hydration products. Cement chemistry notation is used throughout this document with the following abbreviations: A= Al_2O_3 , C= CaO , F= Fe_2O_3 , H= H_2O S= SiO_2 and $\text{\$}$ = SO_3 .

Table 2. Samples of the study

Sample	Object	Year	Sample	Analyses
G-1860s	Cathedral of Freiburg, Germany	1860s(?)	joint mortar	cement residues
A-1869	Collegiate church Admont, Austria	1869-70	mortar, artificial stone	cement residues, hydration products
G-1879	Federal Fortress Ulm, Germany	1879	joint mortar	cement residues, hydration products
A-1893	Collegiate church, Weißenbach/Triesting, Austria	1891-93	artificial stone	cement residues, hydration products
A-1899	House Anderhalden, Bregenz, Austria	1899	cement mortar	cement residues
CH-1900	Aventicum (archaeological site), Switzerland	1897-1900	cement restoriartion mortar	cement residues, hydration products
A-1903	Former slaughterhouse, Vienna 11 th distr., Austria	1903	artificial stone, mortar	cement residues
A-1907	Depot, Vienna 20 th distr., Austria	1907	artificial stone	cement residues
H-1908	Budapest University of Technology and Economics, Budapest, Hungary	1906-08	concrete, cement mortar	cement residues, hydration products

Results

Composition and evolution of cement clinker

Historical PCs are characterized by large amounts of coarse residual cement grains [12], [13]. Their evaluation (Figure 1) indicates a slight decrease of the average grain sizes, however in the cements of the early 20th century oversize particles of up to 1 mm were also detected. Further characteristic of early PCs, which can be attributed to the development of kiln technology, is that the cements became more homogenous in their mineralogical composition. The following section discusses the above properties in detail.

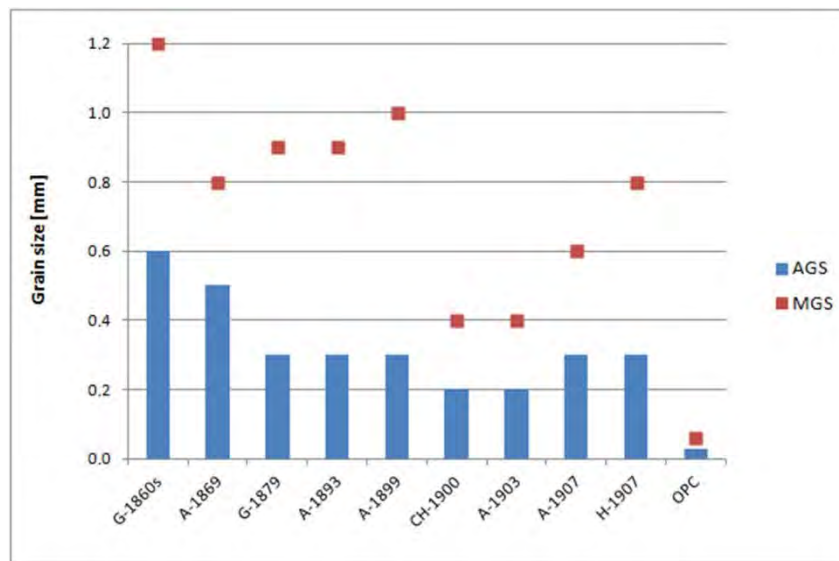


Figure 1. Distribution of average (AGS) and maximum (MGS) grain sizes of residual cement grains in the samples compared to that of modern Ordinary Portland cement (OPC)

Samples from the 1860s to the early 1870s

The cements of “early ages” (samples G-1860s and A-1869) are characterized by very coarse (Figure 1) and mineralogically very heterogeneous materials. Although all four PC clinker minerals (i.e. C_3S , C_2S , C_3A and ferrite) are present, C_2S dominates over C_3S and their crystal sizes, shape and inner structure indicate not only inhomogeneous firing (i.e. presumable temperature differences of up to 700°C within one batch and existence of hot spots >1400°C) and slow cooling conditions, but also heterogeneous raw materials in terms of composition and grain size distribution [5]. The combination of these factors resulted not only in the above described properties of the PC clinker minerals, but also in the formation of mineral phases atypical for modern PCs [13], [14], [15], on the other hand frequently reported in historical RCs [16]. Glassy residues containing tabular gehlenite laths (C_2AS), wollastonite (CS), Ca-pyroxene and silica residues with rims of calcium diffusion and formation of calcium silicates, such as CS , C_3S_2 etc, are the most frequently detected phases formed in the low temperature regimes of the kiln [16].

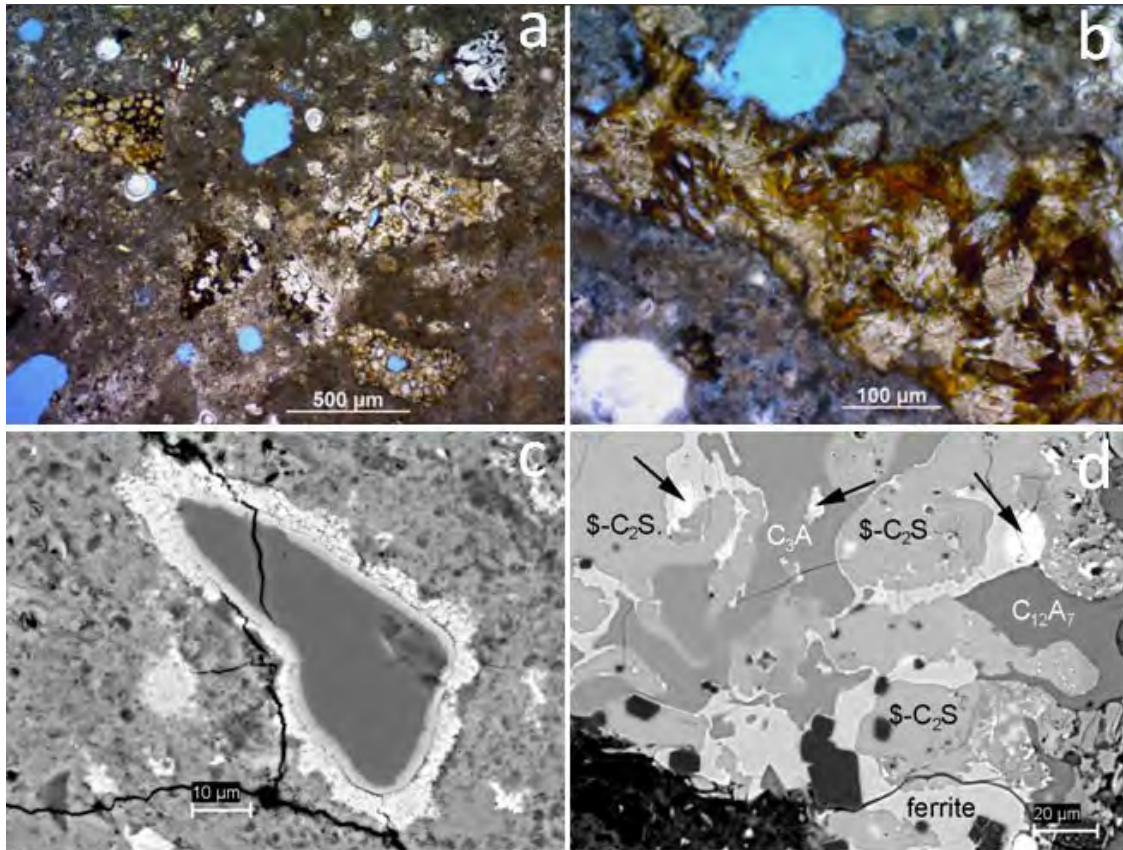


Figure 2 Typical residues in the samples from the 1860s; a: large unhydrated cement grains in a completely carbonated binder (G-1860s, PPL), b: large residue containing C_2S with finger-like extensions into brown ferrite (G-1860s, PPL), c: silica residue with traces of calcium diffusion (outer rim of C_2S ; A-1869, SEM-BSD), d: heterogeneous residue containing different type of sulfur-bearing cement phases (CaS is indicated by arrows). Coarse crystal sizes indicate slow cooling rates (A-1869, SEM-BSD).

Flux phases typically form large crystals which are indicative for very slow cooling rates and besides C_3A also $C_{12}A_7$ can be found suggesting high amounts of alumina-rich phases (i.e. clay minerals and feldspars) in the raw material [5], [14]. The samples from Admont (A-1869) represent a specific type of PC produced from a natural marlstone source rock [5]. In this cement under burned particles similar to the characteristic cement lumps of RC [17] are indicative for the original source rock. The sulfate content of solid fuel (e.g. brown coal) or the raw material (i.e. pyrite in the marlstone) used for cement burning could also contribute to the formation of sulfur-bearing cement clinker phases [5]. Although they occur only in minor amounts, $\$-C_2S$ (sulfo-belite), $C_5S_2\$$, $C_4A_3\$$ and calcium sulfide in the samples A-1869 could have also a slight influence on the formation of hydration products (see below). Figure 2 shows some typical examples of cement clinker phases observed in the mortars from the 1860s.

Samples from 1879 to 1900

Despite a few inventions in the field of cement kiln technology (e.g. introduction of continuous shaft kiln, etc.) the examples from the second half and the late 19th century (G-1879, A-1893, A-1899, CH-1900) show many similarities (Figure 3) with that of early PCs of

the 1860s. The cements are ground coarsely; structures contain lots of unhydrated cement grains and components formed at lower temperature are still present along with the PC clinker phases. Furthermore, the features of C_2S and aluminite phases clearly indicate long residence time of burning, slow cooling rates and the presumable existence of hot spots in the shaft kilns. Nevertheless, some features, such as the slightly increased ratio of C_3S to C_2S , the decrease of the amount of low temperature phases and the slight decrease of cement grain sizes can be interpreted as fingerprints of the technological improvements of the late 19th century [13], [18], [19].

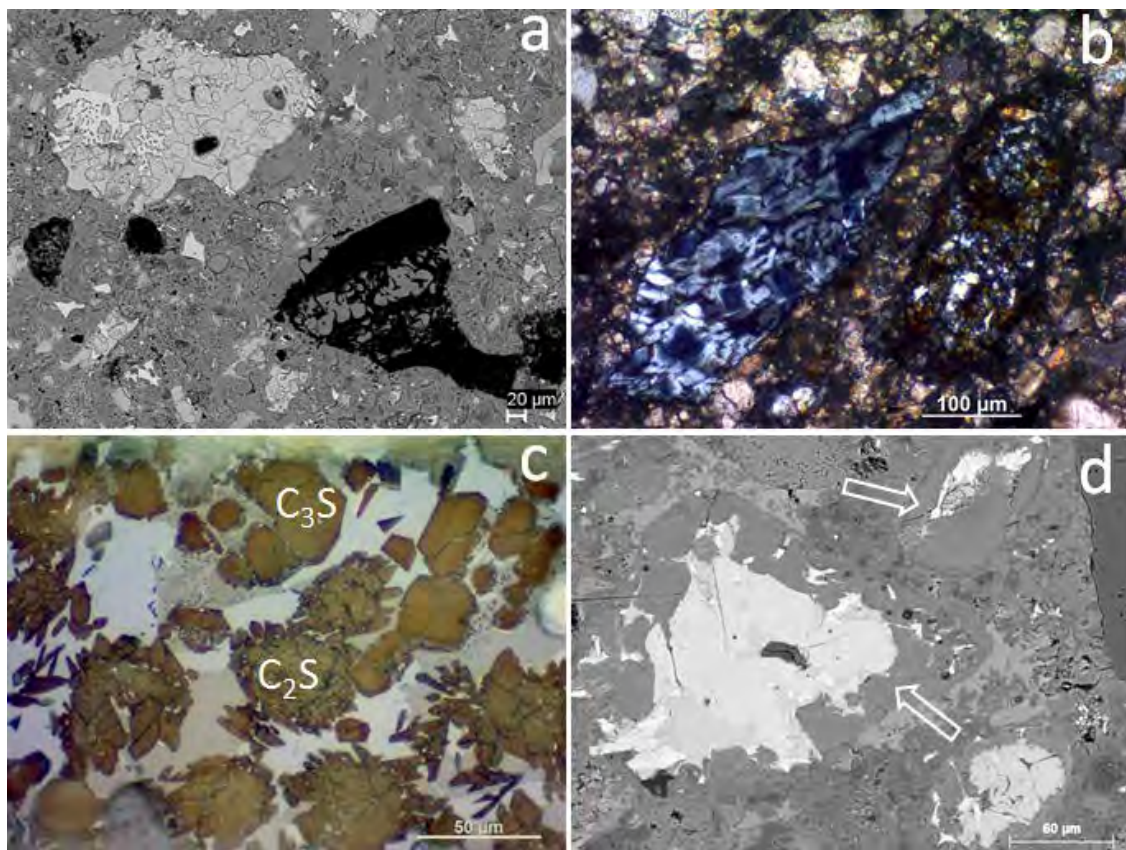


Figure 3 Typical residues in the samples between 1879 and 1900; a: unhydrated cement grains (top left) and brow coal residue from the fuel (black, G-1879, SEM-BSD), b: large residue containing tabular C_2S in a glassy matrix (left) and anhydrous cement (right; A-1893, XPL), c: cement residue with coarse aluminite (grey) and ferrite (white), C_3S (brown angular grains) and dismembered C_2S indicating slow cooling (A-1899, RL, Nital etch), d: cement grains exhibiting thick hydration rims (arrows, CH-1900, SEM-BSD).

Samples from 1900 to 1908

The above described trends can also be followed in the samples of the early 20th century (A-1903, A-1907 and H-1907, Figure 4); C_3S dominates over C_2S , under burned, low temperature components are rare or, in some cases, completely missing. Nevertheless, due to the co-existence of different kiln technologies, differences can also be found between PC-based

structures of this period. This is well-visible when comparing the cement mortars of two Viennese objects constructed in 1903 (A-1903) and 1907 (A-1907).

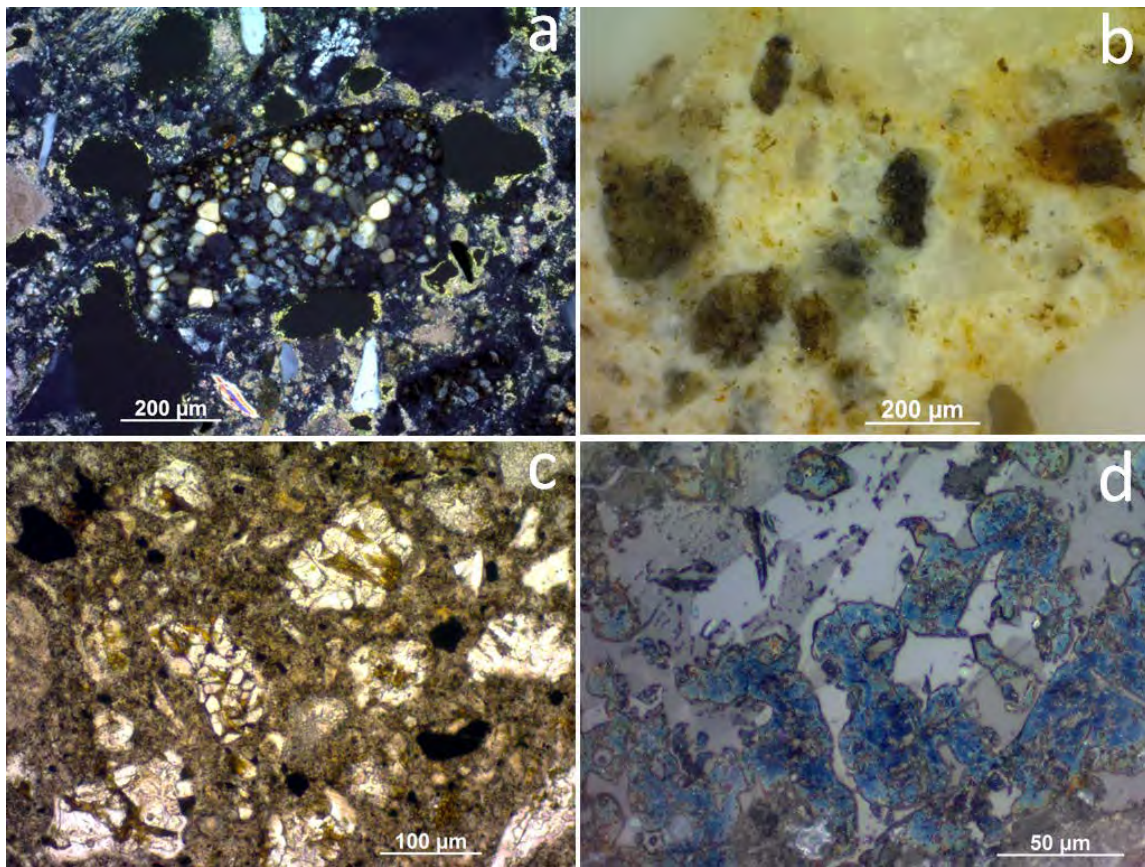


Figure 4 Typical residues in the samples between 1900 and 1908; a: large unhydrated cement grain consisting predominantly of C_2S with few C_3S crystals (A-1903, XPL), b: unhydrated cement grains in sample A-1907 matrix (IL/DF), c: cement residues in a terrazzo sample (H-1908, PPL), d: cement residue with coarse aluminates (grey), prismatic ferrite (white) and partially hydrated C_3S and C_2S (blue; H-1908, RL, Nital etch).

While the older cements clearly bear the properties of a heterogeneous product burned most probably in a shaft kiln, the different appearance of the residual cement grains of the other sample indicates a homogenous firing technique suggesting that the cement was probably calcined in an early rotary kiln (1906: first rotary kiln in Austria). In addition, finer prismatic interstitial aluminates and ferrite phases also indicate faster cooling rates compared to the slowly-cooled PC products of the 19th century and suggest the use of early clinker coolers [20]. Furthermore, residues of solid fuel are also missing in these later samples. However, despite the progress in kiln technology certain parameters also indicate the differences between the PCs of the early 20th and modern OPC. First, based on the crystal grain sizes of the flux phases it is assumed that the cements were cooled by using a simple clinker cooler (e.g. rotary or vertical drum cooler [21]). Although there is only very sporadic information available about the development of clinker coolers, the quenching of clinker, typical for modern OPC, can certainly be excluded. Secondly, cement fineness was comparable to that of the late 19th century products assuming that the grinding technology could not keep up with the calcination technologies. Consequently, both properties are not

only indicative for the early PCs of the 20th century, but they could also significantly affect the hydration and strength development of mortars and concrete.

Properties and development of hydrate phases

While most historical PC structures contain high amounts of unhydrated residues allowing the extensive analysis of the original cement, the hydrate matrix frequently bears the imprints of secondary processes such as carbonation or infiltration of sulfate. Therefore, and also because of the often restricted sampling possibilities, only a few samples containing uncarbonated binder portions could be analyzed. Based on extensive SEM-EDX measurements on hydrate phases of mortar and concrete samples from five objects (see Table 2) significant differences could be detected between the cements produced around the late 1860s and that of after the 1880s.

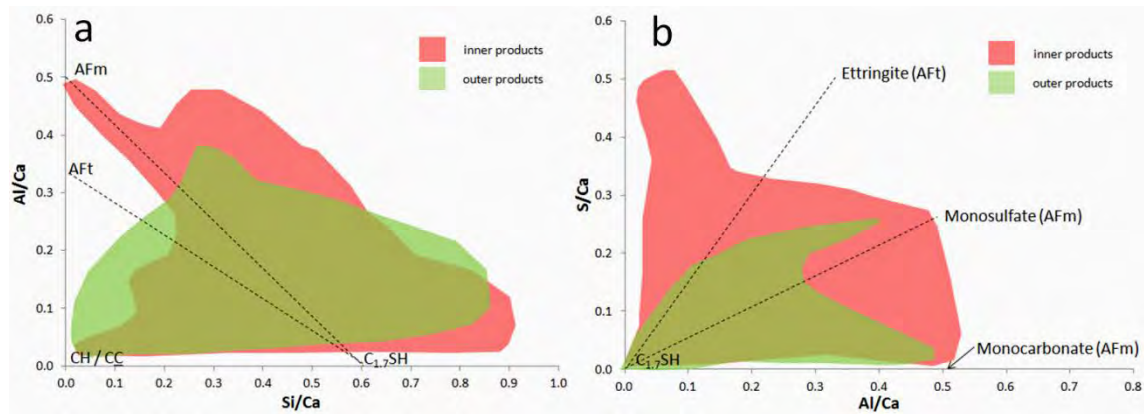


Figure 5 Atomic ratio plots showing the distribution of hydrate phases formed in the inner (red) and outer (green) products (sample A-1869; for explanation see text).

The hydrates phases in the mortars made out of natural PC from Admont, Austria (A-1869) exhibit heterogeneous appearance and a high microporosity. Similarly to OPC, some dense inner products are predominantly related to the hydration of grains rich in C₃S. The outer hydration products form a mixture of compact clusters and platy AFm phases. Figure 5 shows the distribution of the atomic ratios of the inner products (hydrate phases formed at the surface of the larger cement grains) and outer hydration products (hydrate phases formed in the water-filled space) [22]. The composition of the inner products partly overlaps with that of the outer products and the data are very scattered and make the exact intermixing difficult to identify. The inner products are composed of a mixture of C-S-H and AFm (monosulfoaluminat and monocarboaluminat), in which AFt (ettringite) is detected in insubstantial amounts [5]. The outer products contain less sulfo-AFm/AFt than the inner products, contrary to the usual observations made on modern OPC [22].

On the contrary, the distribution pattern of hydration products (Figure 6) of the samples from Germany (1879) and the period of the last decade of the 19th until the early 20th

century show very similar patterns to that of modern OPC. Well-developed inner hydration products are predominantly connected to C_3S in the samples and composed of C-S-H and partly CH. Depending on the existence or lack of secondary processes (i.e. carbonation and/or sulfate ingress) outer products are either composed of a mixture of C-S-H, AFm phases (monosulfoaluminate and/or monocarboaluminate) or AFt (ettringite). If the dominating AFm phase is monocarboaluminate and also ettringite appears, the sulfo-AFm was decomposed and converted into AFt due to subsequent carbonation and/or infiltration of excess sulfate [23].

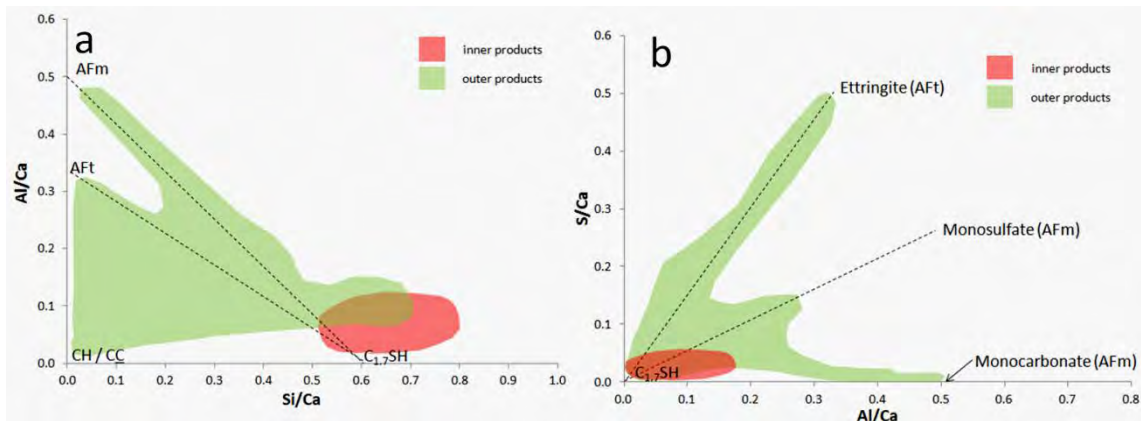


Figure 6 Atomic ratio plots showing the distribution of hydrate phases formed in the inner (red) and outer (green) products (data based on samples G-1879, A-1899 and H-1908; for explanation see text).

On the other hand, the dominance of monosulfoaluminate and the limited amount of ettringite suggest either that the hydrate matrix did not undergo any severe transformation or the amount of sulfate-bearing phases in the cement was low [22].

The main difference between the hydrate phases of the natural PC samples and those from the turn of the century can be found in the distribution of sulfate-bearing components. While sulfo-AFm and AFt concentrate in the outer products in the younger cements and show a similar distribution pattern to that of modern OPC [19], [22] in the older cements monosulfoaluminate and ettringite are predominantly found in the inner hydration products [5]. The later distribution pattern suggests that in the early stage of hydration the amount of sulfate ions was limited in the system which indicates the lack of calcium sulfate as a retarding agent. In practice, the setting time was probably regulated in the “early ages” by a technique described in historical sources [2]; before milling the clinker was stored in a hut for several days, where atmospheric humidity reacted and deactivated to some extent the reactive aluminate phases responsible for prompt setting (i.e. C_3A and probably also amorphous aluminates). The concentration of sulfate-bearing phases in the inner hydration products can be attributed to the dissolution of sulfur-rich cement clinker phases in the later stages of hydration [5]. On the contrary, the enrichment of sulfo-AFm and/or AFt in the outer products detected in German cements from the late 1870s and the samples produced since the 1890s shows a very similar distribution pattern to modern OPC and thus the appearance of calcium sulfate as a retarding agent can be suggested. Around 1880 the

Association of German Cement Plants defined the use of by-mixed calcium sulfate in PC [24], followed by the Association of Austrian Cement Plants in the late 1880s which also allowed the use of a maximum gypsum content of 2% as retarding agent [11]. Nevertheless, it has to be mentioned that many Central European cement producers advertised their products even in the early 1900s as being free of gypsum and thus offering a pure cement binder free of any “contamination” [4]. Furthermore, sulfur content in the fuel (brown coal, coke) could also influence the amount of sulfate in the cements and thus the formation of hydrate phases. Therefore, the use of calcium sulfate as a retarding agent is presumable, but its overall use cannot be verified for that period.

Conclusions

The comprehensive investigation of 20 samples from 9 objects constructed in Central Europe between the 1860s and the early 1900s enabled to get insights into material characteristics, production techniques and hydration mechanisms of historical PCs. Due to the limited amount of examples our study is not intended to completely reconstruct the development of PC in this period, nevertheless results correlate with known technological improvements and in some cases also provided new insights into the characteristics of early PCs. Based on our research following statements can be made:

- large amount of coarse unhydrated cement residues is one of the typical features of early PCs allowing their unambiguous identification, characterization and differentiation from modern PC products;
- there is a slight, but traceable decrease in the average particle size distribution of the cements in the decades following the onset of PC production. However, the maximum grain sizes vary within a wide range and residual cements up to 0.9 mm in diameter were observed even in the youngest binders;
- the comparatively slow increase of cement fineness leads to the assumption that the development of grinding technology could not keep up with the new calcination technologies;
- the oldest cements (1860s) exhibit extremely inhomogeneous compositions which indicates a very heterogeneous heat distribution, long burning and slow cooling rates, typical for (early) shaft kilns. Residues of organic matter are suggestive for the use of solid fuels (e.g. brown coal);
- cements produced between the 1870s and 1890s were still heterogeneous and comparable to those produced some decades earlier, however, they were also slightly finer and the amount of under burned particles decreased as well. Yet all cements of the study originated from this period were produced in shaft kilns;

- cements burned around and shortly after the turn of the century show either similarities with their precursors suggesting that they were calcined in shaft kilns, or they exhibit the features similar to OPC. Later samples suggest the use of early rotary kilns, nevertheless cement residues still indicate relatively slow cooling rates and a less advanced grinding technique;
- the cement hydration products in the samples from the 1860s are characterized by outer products poor in sulfo-AFm and/or AFt suggesting that during the early-age hydration no or only very limited amount of sulfate was available. Therefore, the use of calcium sulfate as a retarding agent can be excluded;
- on the contrary, samples from the turn of the century suggest the application of calcium sulfate as a setting retarder. Therefore, the hydration process was very similar to that of modern OPC even though many of the investigated examples were burned in shaft kilns;
- the results suggest that the introduction of calcium sulfate as a setting retarder took place ten to twenty years before the spread of the rotary kilns indicating that many of the PCs produced in shaft kilns were probably deactivated by gypsum. Nevertheless, its overall use in PCs around the turn of the century cannot be verified;
- many of the objects and cement structures were in good to excellent state of preservation after more than 100 to 140 years of exposure and service life indicating the durability of the cements produced that time. Although not all aspects of this behavior are clearly explainable so far, the grain size distribution of the cements could have a significant impact on the fresh mortar properties (i.e. control of w/c ratio and workability, etc.), the development of macro- and microporosity and thus the durability of the structures.

Acknowledgements

The authors would like to thank Karl Stingl, Áron Németh and Alexandra Sagmeister for their support in sampling and providing data about the objects.

References

1. Blezard RG (1998) History of Calcareous Cements. In: Hewlett PC (ed) *Lea's Chemistry of Cement and Concrete*, 4th ed. Elsevier-Butterworth-Heinemann, Oxford
2. Pierus T (1900) *Ueber die Fabrikation von Roman- und Portland-Cement*. Pierus Verlag, Wien
3. Leube H (1969) *Ein Pionier in der Zementindustrie / Gustav Ernst Leube (1808 - 1881)*. Unpublished doctoral thesis, University of Vienna

4. Berecky E, Reichard E (1970) A magyar cementipar története. Műszaki Könyvkiadó, Budapest
5. Pintér F, Gosselin C (2018) The origin, composition and early age hydration mechanisms of Austrian natural Portland cement. *Cem Concr Res* 110: 1–12
6. Albrecht H (1991) Kalk und Zement in Württemberg / Industriegeschichte am Südrand der Schwäbischen Alb. Landesmuseum für Technik und Arbeit in Mannheim, Verlag Regionalkultur
7. Huber F (1994) 1894-1994, 100 Jahre Vereinigung der österreichischen Zementindustrie. Zement + Beton Handels- und Werbeges.m.b.H.
8. Spicher G, Marfurt H, Stoll N (2013) Ohne Zement geht nichts: Geschichte der schweizerischen Zementindustrie, NZZ Libro, Zürich
9. Haegermann G (1964) Vom Caementum zum Zement - Vom Caementum zum Spannbeton, Beiträge zur Geschichte des Betons. Vol. 1, Bauverlag GmbH, Wiesbaden
10. Stark, J. & Wicht, B. (1998): Geschichte der Baustoffe - Bauverlag GmbH, Wiesbaden und Berlin, S. 1-205
11. Riepl F (2008) Die wirtschaftliche und technologische Entwicklung der Zementindustrie unter besonderer Berücksichtigung der Verdienste von Hans Hauenschild. Unpublished doctoral thesis, University of Vienna
12. Campbell, DH (1999) Microscopical Examination and Interpretation of Portland cement and Clinker. Skokie: Portland Cement Association
13. Pintér F, Köberle T, Weber J (2013) Composition and properties of a historic Portland cement mortar from 1879: a microscopic study. In: Proceedings of the 14th EMABM Conference, Helsingør, Denmark, June 10-14
14. Ando Y, Hirono S, Sawaki D et al (2014) Microscopy to evaluate the properties of cement and alterations in historic mortar/concrete of old Nobiru Port project, Northeast Japan. In: Proceedings of the 36th ICMA Conference, Milan, Italy, April 13-17
15. Katayama T, Ando Y, Hirono S et al (2014) Relicts of unhydrated cement clinker in a historic concrete from the 19th century – microscopy with EDS analysis of old training dyke at Yokohama Port, Japan. In: Proceedings of the 36th ICMA Conference, Milan, Italy, April 13-17
16. Weber J, Bayer K, Pintér F (2012) 19th century ‘novel’ building materials: examples of various historic mortars under the microscope. In: Válek J, Hughes JJ, Groot CJWP (eds) *Historic mortars: Characterization, Assessment and Repair*, Springer Science & Business Media, Dordrecht, Heidelberg, New York, London

17. Weber J, Gadermayr N, Kozłowski R et al (2007) Microstructure and mineral composition of Roman cements produced at defined calcination conditions. *Mater Charact* 58: 1217–1228
18. Pintér F, Gosselin C (2015) Material characteristics of prefabricated concrete elements from a late 19th century church in Lower Austria. In: Proceedings of the 15th EMABM Conference, Delft, The Netherlands, June 17-19
19. Gosselin C, Pintér F (2016) Examples of early age Portland cements applied in historical masonries. In: Proceedings of the 4th Historic Mortars Conference, Santorini, Greece, October 10-12
20. Vidovszky I, Pintér F (2018) An Investigation of the Application and Material Characteristics of Early 20th-Century Portland Cement-Based Structures from the Historical Campus of the Budapest University of Technology and Economics. *Int J Arch Her.* doi:10.1080/15583058.2018.1545059
21. Moore D (2011) Clinker coolers. In: *Cement Plants and Kilns in Britain and Ireland*. https://www.cementkilns.co.uk/ck_coolers.html
22. Taylor HFW (1990) *Cement Chemistry*. 2nd ed, Academic Press, London
23. Matschei T, Lothenbach B, Glasser FP (2007) The AFm phase in Portland cement. *Cem Concr Res*: 37: 118–130
24. Kehm O (1907) Die Entwicklung der oberschwäbischen Zementindustrie. In: Bücher K (ed) *Zeitschrift für die gesamte Staatswissenschaft* 63, Tübingen

European natural cements - their key technical properties under standardised conditions

David Hughes¹, Johannes Weber², Vincenzo Starinieri³, Farkas Pinter⁴, Christophe Gosselin⁵,

Steven Feldman⁶, Cecilia Pesce²

(1) University of Bradford, Bradford, UK, d.c.hughes@bradford.ac.uk

(2) University of Applied Arts, Vienna, Austria, johannes.weber@uni-ak.ac; cecilia.pesce@northumbria.ac.uk

(3) Sheffield Hallam University, Sheffield, UK, v.starinieri@shu.ac.uk

(4) Federal Monuments Authority Austria, Vienna, Austria farkas.pinter@bda.gv.at

(5) Geotest SA, Le Mont sur Lausanne, Switzerland, christ.gosselin@gmail.com

(6) National Institute of Standards and Technology, Gaithersburg, USA, steven.feldman@nist.gov

Abstract

The first comparative study on 7 commercially available Roman cements has been undertaken. In the absence of a European Standard, the testing procedures have followed a protocol proposed by the EU FP7 funded ROCARE project, which itself is based upon various ENs for cement and building limes. Evaluation has been made of mineralogy, particle size distribution, setting time, strength, water absorption, pore size distribution and mortar microstructure. Five of the cements required retardation and citric acid was used. The use of a pre-hydration technique was also investigated to extend the workable life of mortars to some 2 hours. The results confirm the view that the term Roman cement refers to a broad family of cements with a diverse range of properties which will need to be accounted for in future work to produce an all-encompassing Standard.

Introduction

Roman, or Natural, cement was a major material in the architecture of 19th C Europe [1]. However, its use declined as Portland cement came to dominate each national market in turn. There has been a gradual increase in interest in these cements in recent years but the market is only supplied by relatively few producers. Calcined from marlstones at temperatures below sintering, Roman cements reveal compositions and properties which differ significantly from those of Portland cements. Whilst they are presumed to have a number of features in common, such as: rapid setting, delayed development of the final strength, high capillary porosity, and mostly good resistance against sulphate attack, an inherent feature is the variability in their performance dependant on the nature of the source marl, calcination conditions and any post-production processing.

Despite the small number of producers there is no single approach to specifying each cement and National Standards are not consistent [2, 3]. The aim of this paper is to assess

key features of the cements available to the European market place using common methodologies based upon protocols developed during the EU FP7 funded ROCARE project 226898 [4]. This document modifies the procedures specified within EN 196-1 to adjust for the rapid set and the high water demand of typical Roman cements. The cements included in this programme are Prompt (Vicat, France), Folwark (Institute of Ceramics and Building Materials, Poland), Marfil (Cementos Collet, Spain), Cemento Rapido Figueres (Ciments Figueres, Spain), Tigre Rapido (Cemento Natural Tigre, Spain), Cemento Mallorquin (Sa Cimentara, Spain) and Natural Roman Cement, hereafter abbreviated to NRC (Roman Products, UK).

Methods

Mineralogy of each cement was determined by XRD powder analysis carried out with an X'Pert Pro PANALytical diffractometer (Cu tube, $\lambda=1.54 \text{ \AA}$). The phase quantification by Rietveld analysis used an external standard (rutile) for the non-crystalline products. Particle size distribution was determined by laser diffraction using a Mastersizer 3000 from Malvern Panalytical using isopropanol as a dispersant; refractive index = 1.680. Three measurements per sample were taken. Examination was undertaken of final setting time of pastes produced at w/c = 0.65 and early age hydration pathway of pastes, produced at w/c = 0.6 (by XRD according to the same protocol as above).

Mortars were produced as per EN 196-1 using CEN sand, aggregate:cement ratio of 3:1 by weight and a w/c = 0.6. In order to produce mortars possessing a workable life suitable for sample production (~10 minutes) citric acid was incorporated into the mix water to provide suitable retardation (see Table 1). Cements NRC and Mallorquin did not require retardation.

Table 1. Modifications to mortars

Cement	Citric acid*	w/c
NRC	-	0.63
Mallorquin	-	0.68
Tigre Rapido	0.15%	0.62
Marfil	0.1%	0.67
Prompt	0.05%	0.60
Figueres	0.05%	0.70
Folwark	0.1%	0.60

* expressed as % by weight of the cement

Samples were produced for strength testing (EN 1015-11) at ages of 3 hours, 1, 7, 28, 91 & 270 days and water absorption coefficient (EN 15801) at ages of 28 and 91 days. These mortars were also observed using scanning electron microscopy (SEM). Vacuum impregnated polished thin sections prepared at mortar ages of 28 days were used to obtain detailed information on mortar fabrics and unhydrated residues, while the hydrated binders in respect to their morphological characteristics and pore structure were studied on fracture surfaces at ages of 28 and 91 days. The instrument used for SEM work was a FEG Quanta 250

SEM (FEI, U.S.A.) coupled with a Pegasus APEX energy-dispersive X-ray spectroscope (Ametek EDAX, U.S.A.) equipped with the Genesis SEM Quant software (SEM-EDX). Images were taken at high vacuum, for which the sections were coated with carbon while the fracture surfaces were gold sputtered. The acceleration voltage was 20 kV, using the backscattered electron mode (BSE) in all of the applications. In addition, the pore size distribution was determined by mercury intrusion porosimetry at an age of 91 days. The tests were carried out by means of a Pascal 140/240 mercury intrusion porosimeter from Thermofisher. The test specimens consisted of mortar fragments measuring approximately 5x5x10 mm collected from the core of each mortar beam. The samples were dried in a fan-assisted oven at 60 °C until constant weight prior to testing. The mercury contact angle was taken to be 140°.

During the production of these mortars the expected variation in workability – hence, water demand – was observed. Additional mortars were produced to a constant flow (EN 1015-3) of 17 ± 0.5 cm and tested for strength at ages of 7 and 91 days (the w/c ratio required to produce this flow is also shown in Table 1 and illustrates the varying water demand of the mortars). In order to produce these mortars a common citric acid content of 0.5 % was used where necessary, this being to allow the measurement of the flow unimpeded by any loss of workability due to rapid setting.

An alternative retardation approach has been previously reported [5] in which the cement is pre-hydrated by producing a damp sand and cement mixture and stored for specified time prior to final mortar production. The term De-Activated Roman Cement (DARC) has been adopted. Values of de-activation water of 10 % and 15 % (by weight of the dry cement) were used to prepare the “damp” mixtures which were then stored for 30 minutes. The mixing of the final mortar (w/c = 0.6) was the same as specified in EN 196-1 except that a prolonged high speed mixing time of 5 minutes after the “scraping of the bowl” phase was adopted. Workable Life was assessed according to EN 1015-9 with a target time of approximately 2 hours suitable for working with renders.

Data on anhydrous cements

Mineralogy

The composition of each cement is shown in Table 2 and three features are immediately apparent. By XRD each cement comprises both crystalline and amorphous phases; the latter of unknown composition but believed to be mainly calcium aluminates [4] and calcium-alumino-silicates [6].

Di-calcium silicate is the dominant phase, being present in four variants. Belite (C_2S) is observed in two polymorphs i.e. low temperature α' - C_2S and higher temperature β - C_2S . It has been previously confirmed that these phases co-exist with the proportion of α' - C_2S decreasing as the calcination temperature increases [7]. For the current cements the ratio of

α' -C₂S to β -C₂S lies within the range 0.17 to 0.37; in contrast the ratio for “optimum” cements produced in a laboratory kiln, where the temperature gradients were kept to a minimum, is in excess of unity [7]. Carbonation of C₂S during calcination is evidenced by the production of both spurrite - Ca₅(SiO₄)₂(CO₃) - and tilleyite - Ca₅Si₂O₇(CO₃)₂. The ratio of carbonated to un-carbonated C₂S generally lies in the range 0.3 – 0.5 with the exception of *Prompt* which registers 0.8. Previous data [6] shows a value similar to the other cements which suggests that the batch of *Prompt* from which the current sample was obtained may have undergone more carbonation within the kiln than usual.

Table 2. Composition of cements (% by weight)

Phase	NRC	Mallorquin	Tigre	Marfil	Prompt	Figueres	Folwark
β -C ₂ S	23	27	22	22	16	23	26
α' -C ₂ S	6	6	7	8	5	4	10
C ₄ AF	4	3	3	4	6	5	6
Lime	--	--	1	--	--	--	--
Periclase	4	1	3	1	3	1	1
Anhydrite	1	1	tr	2	1	1	--
Portlandite	5	2	6	3	5	8	5
Quartz	3	5	3	3	2	4	3
Calcite	20	19	17	18	19	15	11
Spurrite	8	6	11	9	13	10	10
Tilleyite	3	4	2	3	4	4	4
Gehlenite	4	7	5	11	7	7	8
Ye'elimite	--	--	--	1	2	2	--
Muscovite	2	--	2	--	--	1	--
Amorphous	20	20	19	16	18	17	17

Additionally, all cements show evidence of incomplete calcination as evidenced by residual quartz and surprisingly high amounts of calcite from low temperature areas of the kilns (Figure 1a).

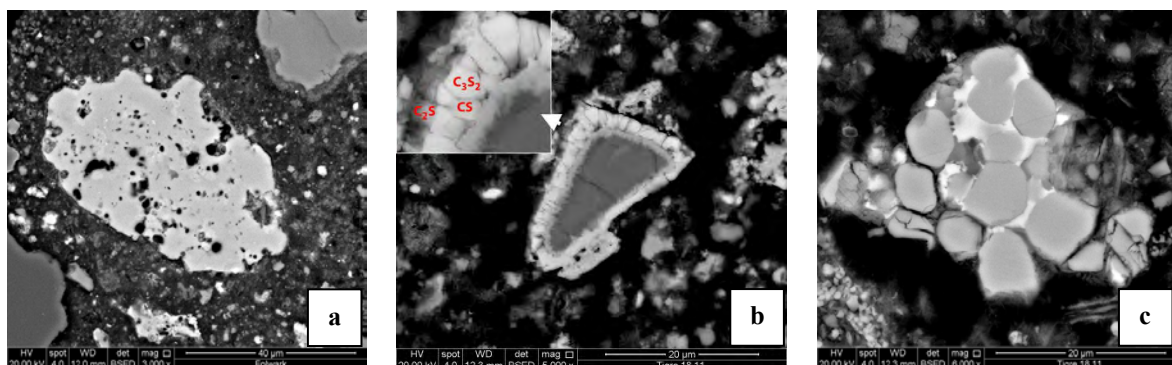


Figure 1. Characteristic constituents of natural cements, here observed as unhydrated residues in 28 days mortars; (a) calcite from the raw feed with thermally induced alterations as part of the underburned portion, (b) quartz with reaction rim containing increasing amounts of calcium towards the margin where crystals of CS, C₃S₂ and C₂S can be identified by EDX, see detail, (c) belite clusters with interstitial phase indicating initial melt formation as part of the overburned portion of the cement

The quartz is commonly observed as unreacted cores surrounded by calcium silicates (Figure 1b). Evidence of high temperature phases such as ye'elimite ($\text{Ca}_4\text{Al}_6(\text{SO}_4)\text{O}_{12}$) and substantial quantities of gehlenite ($\text{Ca}_2\text{Al}_2\text{SiO}_7$) and belite clusters associated with melt formation (Figure 1c) completes the picture of heterogeneous calcination conditions within many kilns. Free lime (CaO) is notable by its absence having been rapidly converted to portlandite ($\text{Ca}(\text{OH})_2$).

Granulometry

The particle size data is shown in Figure 2. All cements have a similar maximum particle size although there are differences in the size distribution as shown by both D_{50} and surface area measurements. *Folwark* is clearly the finest cement and it is known that in the grinding process all oversize particles are re-ground until no residue remains. *Tigre* and *Marfil* only differ in the coarser regions whilst the remaining cements are similar except with differences in the coarser region, especially *Figueres*.

A comparison of the w/c ratios necessary to obtain mortars of common flow (Table 1) with the physical parameters (Figure 2) reveals that there is no relationship between the data sets. This is not surprising since it does not account for the hydration occurring in these highly reactive cements during the time taken to mix the mortars and conduct the consistency test. Such an investigation is beyond the scope of the current study.

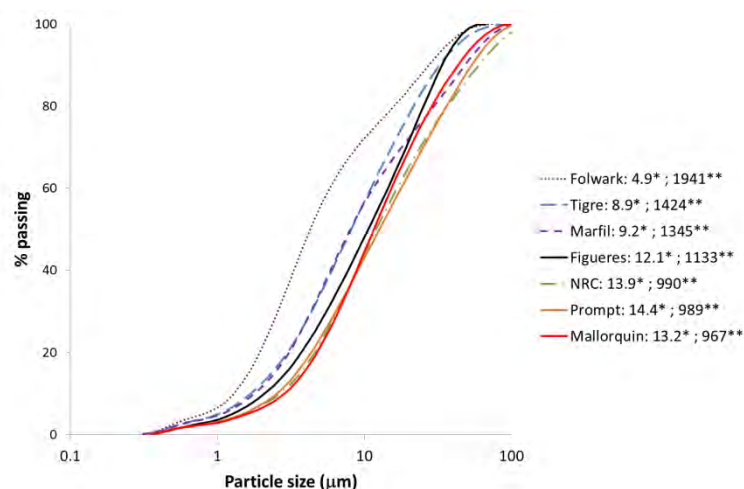


Figure 2. Particle size distribution * D_{50} (mm); ** Specific surface area (m^2/kg)

Final setting

Table 3 reveals a wide range of final setting times with *Figueres*, *Marfil*, *Folwark* and *Tigre* showing the rapid setting which is a common feature of Roman cements. It is understood that NRC undergoes a period of air-slaking of the calcined marl fragments before they are ground. As such, this is a commercial version of the DARC process previously described and has historical precedent [8] and the extended setting time is a consequence. However, the

mineralogical analysis (Table 2) does not show the presence of early hydrated phases such as monocarboaluminate which was observed in de-activated *Gartenau* cement investigated in a previous project [5]. This may be a reflection of the *Gartenau* cement having been ground prior to de-activation whilst the NRC was exposed in much coarser fragments. In addition, *Gartenau* cement was exposed to surface water on the wet sand whereas NRC would have been exposed to atmospheric humidity.

In contrast to the extended setting time measured for *Mallorquin* the manufacturer quotes a value of 19 minutes [9]; the reason for the difference is unexplained and is currently being investigated. Similarly, the setting time of *Prompt* is greater than we have previously measured.

Table 3. Final setting of pastes with no retarder (w/c = 0.65)

Sample	Setting time
Mallorquin	133 min
NRC	90 min
Prompt	30 min 30sec
Figueres	5 min 30 sec
Marfil	4 min 15 sec
Folwark	3 min 15 sec
Tigre	2 min 45 sec

Data on hydrated cements

Mineralogy

The compositions of pastes hydrated for 1 day are shown in Table 4. XRD shows the early age reactions to be dominated by alumina bearing phases with or without the inclusion of sulphate; note that all anhydrite has been consumed within 24 hours. As previously observed [6] *Prompt* yields a high content of ettringite with the raw cement having a high SO₃ content. In contrast, *Folwark*, with a low SO₃ content [10], produces no ettringite, but rather, the highest AFm content.

Any hydration of the belite phases is not readily shown by XRD since reaction is likely to be limited and any hydrates included within the amorphous phase, itself a contributor of alumina to the earlier reactions. Thus, any reaction can only be inferred from small decreases in belite content which may itself be masked by dilution of the cement content by the incorporation of hydrate water. Such early hydration has been previously reported by Hong and Young [11] and related to crystal size rather than to a particular polymorph. They showed that α'_L -C₂S with a surface area of some 40 m²/g was fully hydrated within 7 days. In a previous study [4] 2-day old pastes of different cements were observed in the SEM. Despite the limitations of the small spatial resolution of the EDX point analysing system preventing quantifiable analysis of single phases, evidence of C-A-S-H phases was apparent.

Table 4. Composition of pastes hydrated for 1 day (% by weight)

Phase	NRC	Mallorquin	Tigre	Marfil	Prompt	Figueres	Folwark
β -C ₂ S	20	24	19	19	16	20	25
α' _H -C ₂ S	3	5	4	5	4	3	5
C ₄ AF	3	2	3	2	3	3	2
Periclase	3	1	2	1	2	1	1
Portlandite	3	1	3	--	1	4	2
Quartz	3	5	3	3	2	3	3
Calcite	20	18	19	18	17	14	9
Spurrite	6	5	7	5	9	7	6
Tilleyite	3	5	1	1	2	3	4
Gehlenite	5	9	4	12	6	10	10
Muscovite	2	1	2	1	--	--	--
Ettringite	7	6	4	7	11	7	--
Monocarbonate	5	1	8	2	3	6	10
Hemicarbonate	2	1	4	--	6	3	5
Monosulfate	--	--	--	1	--	--	--
Solid solution AFm (8.47Å)	--	--	--	5	--	--	--
Wollastonite	--	4	--	--	--	--	4
Amorphous	17	14	19	20	20	16	15

Properties of mortars

Microscopy

While polarising microscopy on thin sections, an important tool to characterise mortars and identify natural cement binders, is not presented in this contribution (examples are given e.g. by Weber et al. [12]), SEM studies on fractures of 28 and 91 days mortars illustrate the microstructural evolution of the hydrated matrix in terms of the shape and size of hydrates and the continuous though not complete closing of early age capillary pores (Figure 3 shows the extremes of WAC data; see Table 6).

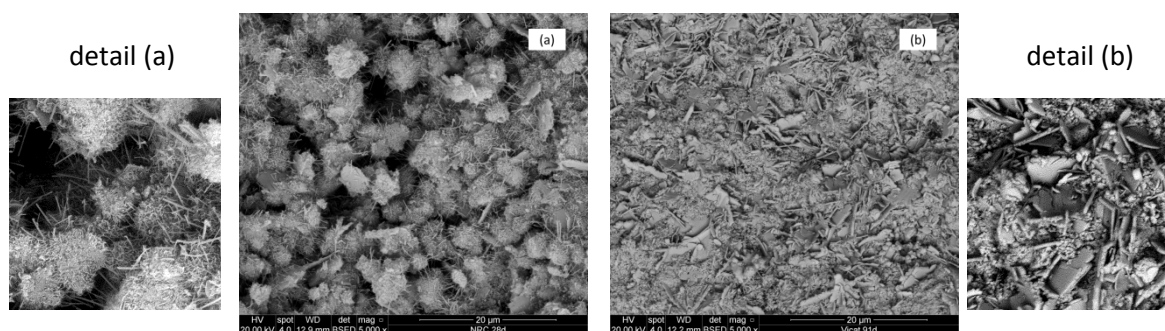


Figure 3. SEM micrographs of (a) NRC at 28 days and (b) Prompt at 91 days

Pore size distribution

Figure 4 shows the pore size distributions of all mortars at an age of 91 days. The uni-modal distribution typical of mature Roman cements [e.g. 13] is exhibited. Of all cements *Prompt* and *Mallorquin* show the most restricted distribution in the 0.1 μm range; in contrast, *Marfil* exhibits the widest distribution.

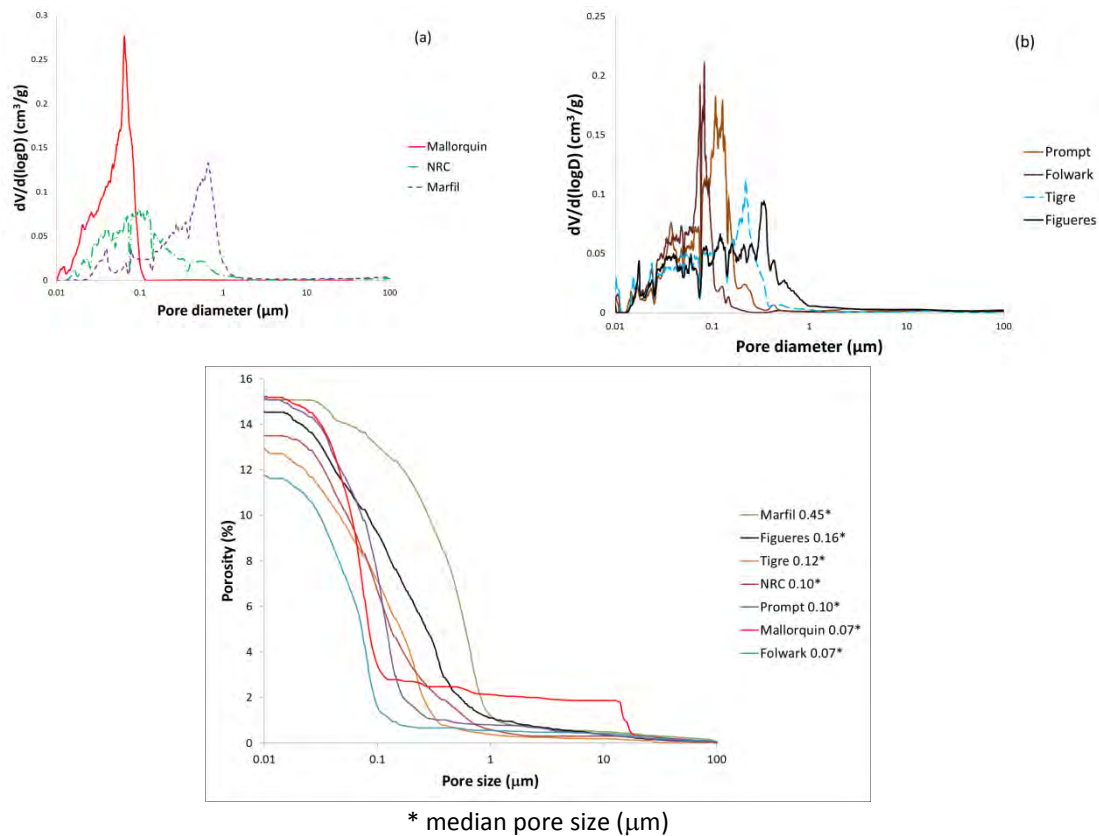


Figure 4. Pore size distributions of mortars; (a) & (b) - derivative, (c) - cumulative

Strength

Compressive strength development of mortars made at a fixed $w/c = 0.6$ is shown in Figure 5 for ages between 3 hours and 270 days; *Mallorquin* was too weak to demould for testing at 3 hours. The commonly observed profile of the initial very early age strength being maintained through a “dormant” period until a phase of rapid strength development is apparent for all cements; the onset of the latter phase is cement dependent and may not occur until an age of at least 28 days. All cements, with the possible exception of *Folwark*, suggest the potential for significant strength increase after 270 days, the last test age in this programme. The differing profiles illustrate the challenge faced by trying to select a single age at which to specify the strength of Roman cements for classification purposes. This may be illustrated by considering *Folwark* and *Marfil* cements; whilst *Marfil* shows the lowest strength of all cements at 28 days and *Folwark* the highest, there is no statistical difference between the two cements at 270 days. As a consequence of both long setting times and low

strength, *Mallorquin* and NRC would not generally be considered ideal for the rapid production of cast elements.

In light of the potential hydration of the C_2S phases observed at 1 day it would have been expected that strength would have increased at early ages rather than be static. However, it is possible that changes to the chemistry of the pore solution reduce the solubility of the C_2S phases to the extent that its hydration is temporarily suppressed. The concentrations of lime and Al in solution may have this effect although their impact has only been previously studied in relation to the hydration of Portland cements [14].

The porosity of the mortars at 91 days generally lies in the range 12 – 19% by volume (Figure 4) whilst the commensurate strength is in the range 7 - 21 MPa. There is no correlation between strength and porosity, whether total porosity or by excluding the finest pores. During an earlier EU funded project (ROCEM EVK4-CT-2002-00084) many cements were calcined under controlled kiln conditions in the laboratory and the development of pore structure of pastes of 3 of them over a period of 26 weeks have been previously reported [14]. Re-analysis of this data, taking an arbitrary measure of coarse porosity being that in pores $>0.03 \mu\text{m}$, and correlating with their strengths shows an interesting behaviour (Figure 6). At high values of porosity ($>0.3 \text{ cm}^3/\text{g}$) there is a good relationship between strength and porosity; however, at lower values of porosity, as found in more mature pastes, much more scatter is observed. Whilst the porosity of the current mortars (Figure 7) is less than that of the pastes due to the presence of the sand, the porosity of their paste fraction is likely to be in the similar range of low porosity and high scatter, which may offer an explanation for the lack of correlation obtained in the current study.

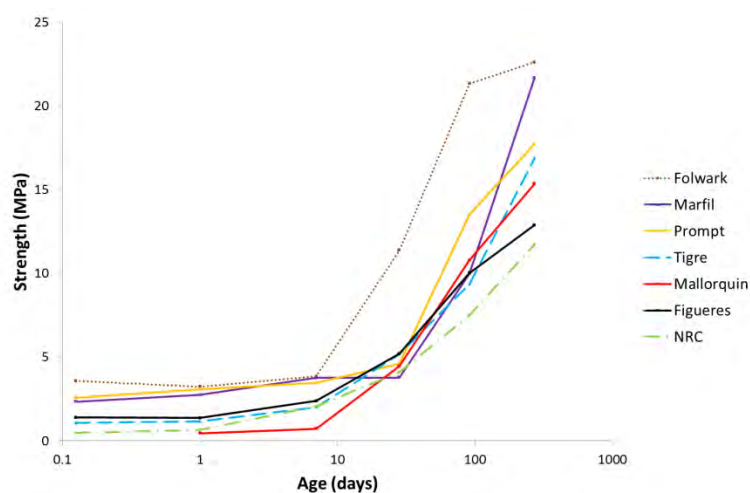


Figure 5. Compressive strength development of mortars produced at $w/c = 0.6$.

It is often said that production of mortars to a constant workability yields more practical information than the standard mortars produced at a constant w/c . Thus, a small programme was undertaken as previously described (see Table 1).

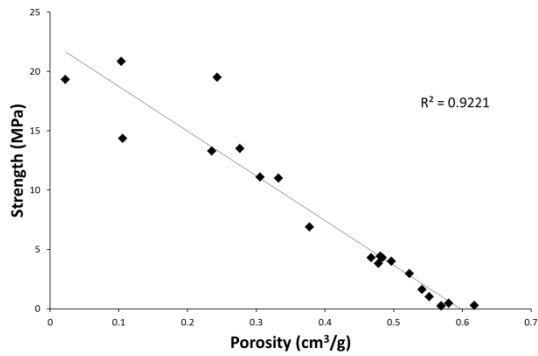


Figure 6. Strength – porosity >0.03 μm relationship of ROCEM pastes.

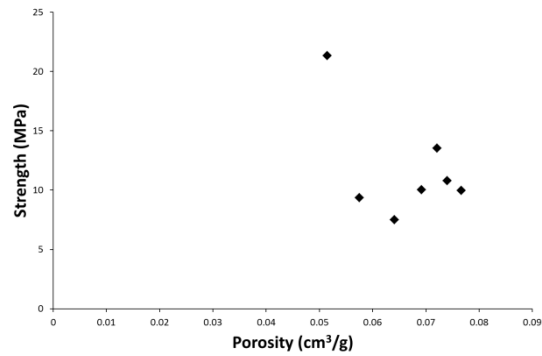


Figure 7. Strength – porosity >0.03 μm relationships of ROCEM mortars.

Figure 8 shows the comparison of strengths at ages of 7 and 91 days; the values in parentheses are the w/c ratios for the mortars of constant workability which were produced with a citric acid content of 0.5 % with the exception of NRC and *Mallorquin*. The effect of the differences in concentration of citric acid between the two series is apparent by considering *Folwark* and *Prompt* cements which have the same w/c in both series. At an age of 7 days the additional citric acid has had no significant effect on the strength of *Prompt*, whilst it has reduced the strength of *Folwark*; however, at 91 days the increased retarder has reduced the strength of *Prompt* but increased the strength of *Folwark*. Such behaviour has been previously observed during the ROCARE project.

Neither *Mallorquin* nor NRC required the retarder but did require additional water to deliver the required flow. However, the strengths of these mortars are higher at 91 days than the original set at w/c = 0.6. It may be that the additional workability permitted better compaction.

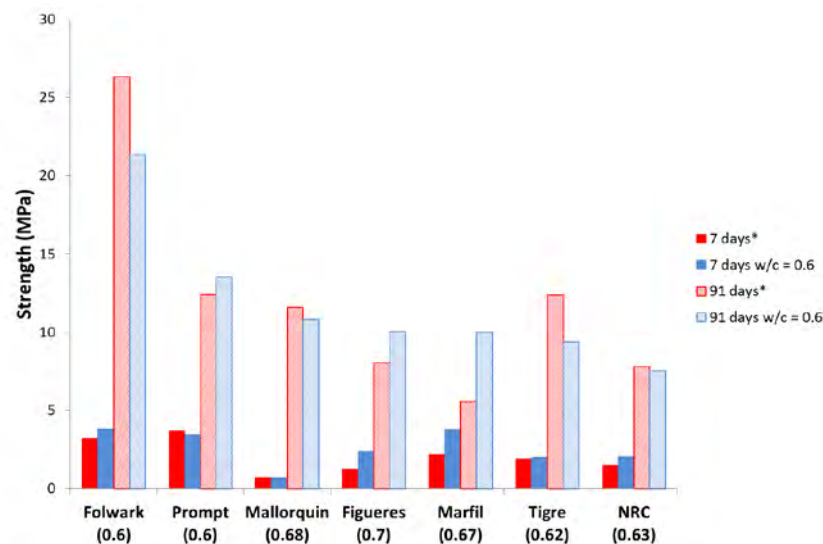


Figure 8. Comparison of strength for mortars produced at constant w/c and constant workability*.

Of the remaining cements both *Figueres* and *Marfil* exhibited expected behaviour with the highest strengths at each age aligning with the lower w/c ratio. However, *Tigre* performed

similarly to *Folwark* in that the strength at 91 days was higher for the slightly higher w/c again suggesting a beneficial influence of the additional retarder.

Given the observed potential for citric acid to influence strength in a variety of ways it is not possible to reliably classify each cement when mortars are produced to a constant workability when retarded by 0.5 % citric acid and further study is required.

Water Absorption Coefficient

The WAC data at ages of 28 and 91 days is shown in Table 6 and it can be seen that, with the exception of *Folwark*, the WAC has reduced with age. A feature of enhanced curing of *Folwark* is the appearance of microcracks which are visible in thin sections (not included within this paper). These may account for the small increase in WAC between 28 and 91 days but not sufficiently extensive to substantially impact on strength development. It is generally the case that the two slow setting cements, NRC and *Mallorquin*, possess the highest values of WAC. No correlation between WAC and pore structure as determined by MIP has been established; probably as a result of the well-known limitations of the MIP technique. However, a qualitative interpretation of the micrographs in Figure 3 generally shows a densification of the microstructure as the WAC reduces (Table 6).

Table 6. Results of Water Absorption Coefficient ($\text{kg/m}^2/\text{h}^{0.5}$).

WAC ($\text{kg/m}^2/\text{h}^{0.5}$)	NRC	Mallorquin	Tigre	Marfil	Figueres	Prompt	Folwark
28 days	4.57	3.57	4.04	2.81	3.40	2.50	1.31
91 days	3.20	2.91	2.29	1.97	1.87	1.28	1.41

Figure 9 shows the poor correlation between WAC and strength, further emphasising the limitations of relying on the specification of strength, despite its simplicity, to fully describe the in-situ performance of cements.

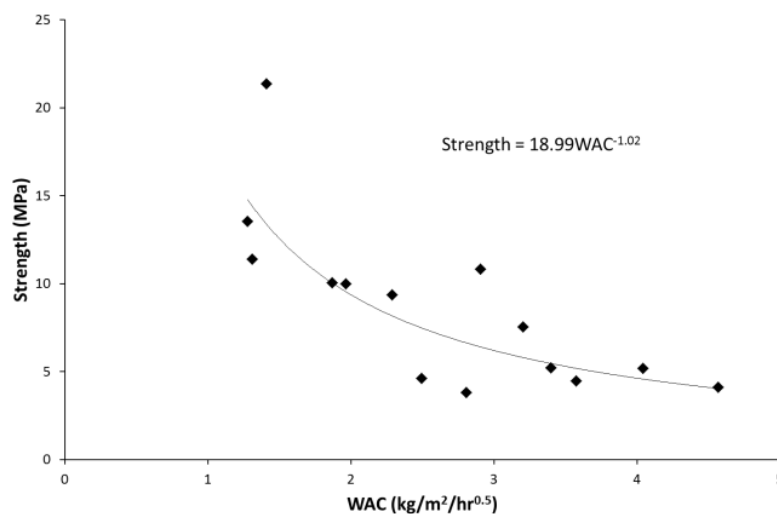


Figure 9. Correlation between strength and water absorption coefficient at 28 and 91 days.

De-activation as a method of retardation

It has been previously reported that this process might not be universally appropriate to all Roman cements [5]; thus, the opportunity was taken to assess the technique for the 5 rapid setting cements. The intention was not to determine optimum processing conditions such that more detailed study may be required before embarking upon its exploitation. The factors which have been used to control workable life were (1) the de-activation water (%), (2) the storage time before the final mortar was produced (mins) and (3) remixing the mortar upon the first reduction in workability. Thus, a mortar might typically be expressed as 10 %/30 mins.

As has previously been observed *Prompt* does not respond to this treatment, possibly as a result of the high ettringite production in early hydration. Indeed, a 10 %/30 mins mortar actually lost workability more rapidly than the control whilst having the same workable life.

The workable life is determined as the time when the penetration load reaches 1500 g; at this stage the mortars were re-mixed. As has been previously observed [5] after re-mixing whilst the workability is restored the rate of workability loss is reduced. In both cases the final workable life has exceeded the target life of 2 hours. It is apparent that, despite requiring more de-activation water, *Figueres* mortar loses workability at a faster rate than does *Tigre* (Fig 10). *Marfil* shows a similar performance to *Figueres* in the first phase but after re-mixing loses workability at a slightly faster rate. Thus, these 3 cements have the potential to be suitably retarded by the DARC process without the use of chemical retarders.

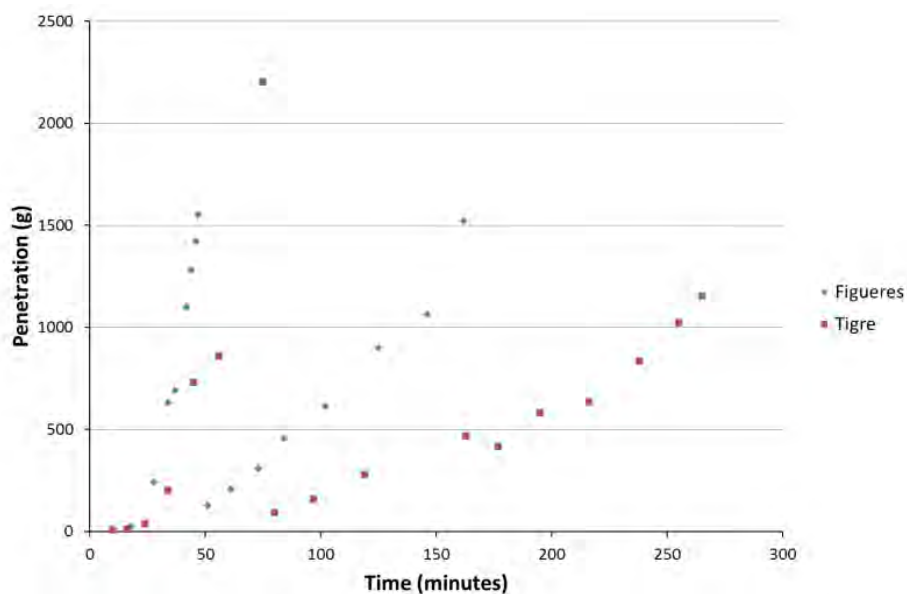


Figure 10. Raw data from Workable Life test for *Figueres* (15 %/30 min) and *Tigre* (10 %/30 min).

Samples for strength testing were made at the outset of the Workable Life test (A) and immediately after re-mixing (B). Strengths at 7 and 42 days are shown in Table 7 together with 7 day strength and an estimate of 42 day strength from the earlier reported

programme. All strength differences between A and B occurrences are statistically significant. Thus, it can be seen that at 7 days 2 of the cements show a small decrease in strength following re-mixing whilst only a single cement shows the same at 42 days. Using *Gartenau* cement it has been previously shown that re-mixing has little or no impact on strength at ages between 7 and 91 days. Table 7 also shows that in comparison with the 3:1 mortars at w/c = 0.6 their DARC companions are weaker at both ages. In part this is a consequence of the DARC process; whilst also having been produced at the same w/c ratio they had previously been de-activated with water which if accounted for would raise the w/c ratio to at least 0.7. Even at an age of 42 days the strength of DARC *Marfil* is much below that of the “control”; this may be a reflection of the longer “dormant” period shown by this cement (see Fig 5).

A DARC *Folwark* mortar (15 %/30 min) was produced. Upon mixing the mortar had a “crumbly” texture; however, immediately upon mixing after the “scraping” phase it turned into a very “creamy” consistency. It recorded a workable life of some 21 hours. An additional mix was made with the inclusion of 0.2 % citric acid with the intention of overcoming the crumbly texture phase. Not only did this fail but the workable life was in excess of 2 days. The strength of the first mortar was 1.3 and 10.3 MPa at 7 and 42 days respectively in comparison with 3.9 and 13.6 MPa for the “control” samples. Much further work should be undertaken before any recommendation can be made on the applicability of DARC with *Folwark*; a training programme for prospective renderers is considered essential.

Table 7. Strengths of DARC mortars at ages of 7 and 42 days.

	7d (A)	7d (B)	7d	42d (A)	42d (B)	42d est
Tigre	1.36	0.89	2.01	5.10	4.56	6.10
Marfil	0.36	0.40	3.75	0.67	0.93	5.16
Figueres	1.63	1.42	2.38	4.61	4.96	6.27

Conclusions

This study has shown that:

- All cements possess a mineralogical composition including both low and high temperature compounds indicating a range of calcination conditions within each kiln. With the exception of *Folwark*, the particle size distributions are broadly similar. There is no correlation with variations in mortar workability and early age reactions should be accounted for.

- Two cements are slow setting, one is moderate and four set rapidly. The early age hydration is influenced by the sulphate content in each cement, producing both ettringite and AFm phases.
- The pore size distribution at 91 days is typical of mature Roman cements, being uni-modal but with the median pore size varying by nearly one order of magnitude. Porosity is in the range 12 – 19 %.
- Strength development follows a commonly observed path of the 3 hour strength being maintained for up to 28 days before a period of rapid strength gain occurs. Most of the cements suggest the potential for further strength gain at ages beyond 270 days.
- The use of citric acid has a complex and inconsistent influence on strength development.
- The WAC reduces between 28 and 91 days and shows poor correlation with strength. There is also no simple correlation with pore size distribution as measured by MIP; the same holds for strength and porosity.
- Whilst *Tigre*, *Figueres* and *Marfil* respond beneficially to pre-hydration in order to extend workable life the latter is still weak at an age of 42 days.

Acknowledgements

The cement companies for supply of materials. Renata Tislova for the MIP data used in Figure 6. Paul Prucker at TPA, Vienna for the use of laboratory facilities. Anthony Baragona for assistance with strength measurement.

References

1. Kozłowski R, Hughes D, Weber J (2010) Roman cements: key materials of the built heritage of the 19th century. In: Bostenaru Dan M, Poikryl R, Torok A (eds) *Materials, Technologies and Practice in Historic Heritage Structures*, Springer, Netherlands pp. 259-277
2. NF P15-314:1993 Liants hydrauliques: Ciment prompt naturel. AFNOR, Paris
3. UNE 80309:2006 Cementos naturales: Definiciones, clasificación y especificaciones de los cementos naturales. AENOR, Madrid
4. Gurtner C, Hilbert G, Hughes D, Kozłowski R, Weber J (Eds), *Manual on Best Practice in the Application of Roman Cements*, Version 2, November 2012, downloadable from <http://www.rocare.eu>
5. Starinieri V, Hughes D, Gosselin C, Wilk D (2013) Pre-hydration as a technique for the retardation of Roman cement mortars. *Cem Concr Res* 46: 1-13

6. Gosselin C (2013) Composition and hydration of some Roman (Natural) cements. Inst Concr Tech Year Book 2013-2014:64-72
7. Hughes D, Jaglin D, Kozłowski R, Mucha D (2009) Roman cements – Belite cements calcined at low temperature. Cem Concr Res 39: 77-89
8. Chateau T (1863) Technologie du Batiment, Tome premier, Librairie D'Architecture de B. Bance, Paris
9. Salom J (2018) Private Communication
10. Strasser W (2018) Private Communication; acid soluble SO₃ measured as 0.7%
11. Hong S-Y, Young JF (1999) Hydration kinetics and phase stability of dicalcium silicate synthesized by the Pechini Process. J Am Ceram Soc 82 [7]: 1681-1686
12. Weber J, Bayer K, Hughes D, Köberle T, Pintér F, Strasser W (2017) Natural cements on the European market—their microstructural features and mortar properties. Proc. 16th Euroseminar on Microscopy Applied to Building Materials, 14-17 May 2017, Les Diablerets (CH): 140-143
13. Tišlova R, Kozłowska A, Kozłowski R, Hughes DC (2009) Porosity and specific surface area of Roman cement pastes. Cem Concr Res 39:950-956
14. Scrivener KL, Nonat A (2011) Hydration of cementitious materials, present and future. Cem Concr Res 41: 651-665

Restoration techniques using 1930's Portland cements at Porte de l'Est in the Roman city-wall of Aventicum, Switzerland

Christophe Gosselin¹, Noé Terrapon²

(1) Geotest SA, En Budron E7, Le Mont sur Lausanne, Switzerland, christophe.gosselin@geotest.ch

(2) Site et Musée Romains d'Avenches Laboratoire de conservation-restauration, Avenches, Switzerland, noe.terrapon@vd.ch

Abstract

Historic masonries using hydraulic cements were extensively used for construction and restoration at the turn of the 20th century. Different cements such as Roman (or natural) cements, natural Portland cements or dolomitic cements, were used according to their local availability and the choice or experience of architects and workers. The Roman city Aventicum (now Avenches) was built at the beginning of the 1st century AD. Unique in Switzerland and classified as of national importance, the Roman wall of Aventicum was built during the second half of the 1st century AD. 5.5 kilometres long, this vast perimeter crowned the capital of the Helvetians and showed the power of Rome. Subsequent to a large campaign of archaeological and restoration works initiated from 1845, the Porte de l'Est, one of the four original main entrances of the city, was restored in the 1930s with the construction of a protection wall above the Roman vestiges. The walls were made of artificial and joined stones composed of concrete and finishing mortar imitating local natural stones. This study presents first the technological details of the artificial stones made of different natural Portland cements. Although the cements differ in the sulfate content, the microscopy exams show very good compatibility properties within the successive layers with a strong interface and no internal sulfate reaction leading to degradation.

Introduction

The use of Portland cement is controversial because of reversibility issues in conservation and restoration of cultural heritage objects. The incompatibility issues of Portland-type cement materials applied on stones or joints are usually stated by conservators and the scientific community [1-5]. Cement concrete and mortars are identified in many objects built and restored between 1850-1950, during which they were preferentially used for economical (rapid production compared to stone art) and technical (strength, presumable resistance to freezing and aggressive environments) purposes. The durability of Portland cement-based materials is illustrated in many historic structures [6-8] or stone imitation works [9]. This article presents the case of Porte de l'Est in Avenches (CH), where the 1930's conservation strategy of Roman vestiges mostly used Portland cement to produce protection walls and aesthetic mortars. The article details the techniques used and the characterization of concrete and mortars based on microscopy.

Historical context

During the 1st century AD, the colony of Aventicum manifested its status as a city by acquiring a wall more than 5.5 km long, 7 m high, including battlements, and 2.4 m wide. The structure was equipped with seventy-three towers, a round path with several entrances, including two monumental gates. It still defines the territory occupied by the former capital of the Helvetians [10]. With its impressive dimensions and its layout still visible in many places, the wall is one of the most important Roman buildings in Switzerland. The monument has recently been the subject of an in-depth study to consider its restoration [9].

In 1885, the Pro Aventico Association was founded to highlight Roman monuments and monitor archaeological excavations. Three architects followed one another in different stages of wall restoration (1898 Mayor, 1907 Naef, 1916 Bosset). From 1899, particular care was taken to preserve the original wall (the restorations should not be confused with Roman masonry). The joints were distinguished by a different treatment and the boundaries were marked by a mortar tinted "red ochre" [11]. The execution and reconstruction of successive cement screeds protecting the wall heads were also widely discussed by the protagonists [11-14]. After several tests, regulations were developed requiring that the walls must keep their ruined appearance and the roof, while playing its protective role, must be limited to representing a horizontal section of the wall while remaining aesthetic. At Porte de l'Est, the elevations were first restored in natural stone rubble -Jura limestone rubble for the smaller elevation and Jura limestone with shell sandstone blocks for the larger- before being raised with artificial stone. The distinction between the original part and restitution was then ensured by the distinction between the building materials.

In 1916, a systematic phase of raising the walls of Porte de l'Est began under the direction of L. Bosset. The first mention of artificial stone was made in his diary from June 6 to 14, 1916¹⁰. A first imitation stone vault was cast on a semi-circular formwork in 1917 [14]. Its raw surfaces were then cut, and false joints were carved to give it the appearance of the original stone apparatus (Figure 1a). From 1925 to 1929, the first major works using exclusively artificial stone were carried out. The documents describing these interventions best are the archival photographs in which we can see the construction of the buttresses in large apparatus of the corridors of the door (1925) imitating shell sandstone (Figure 1b) and the pillars of the tower (1926) imitating Jura limestone (Figure 1c and 1d), as well as the laying of imitations of yellow limestone rubble for the small apparatus.

The use of artificial stone having then become relevant (cast vaults, rubble imitating Jura limestone, large blocks imitating shell sandstone or Jura limestone), all masonry was therefore restored and enhanced with this material. Only the protective screeds were still made of natural stones. 1935 marked the end of the reconstruction work on Porte de l'Est. No information is given on the origin of the binders and aggregates used during the work. The restoration work on the Roman theatre in Aventicum was also carried out by the same

¹⁰ « On prépare des moellons de parement et on en fabrique en pierre artificielle »[14]

company, Righetti, under Bosset's direction in 1926-1930. The techniques used on these two sites were different, but it is believed that the same cement suppliers, mentioned in [6], may have been used for Porte de l'Est. The technique of artificial stone casting is well documented.

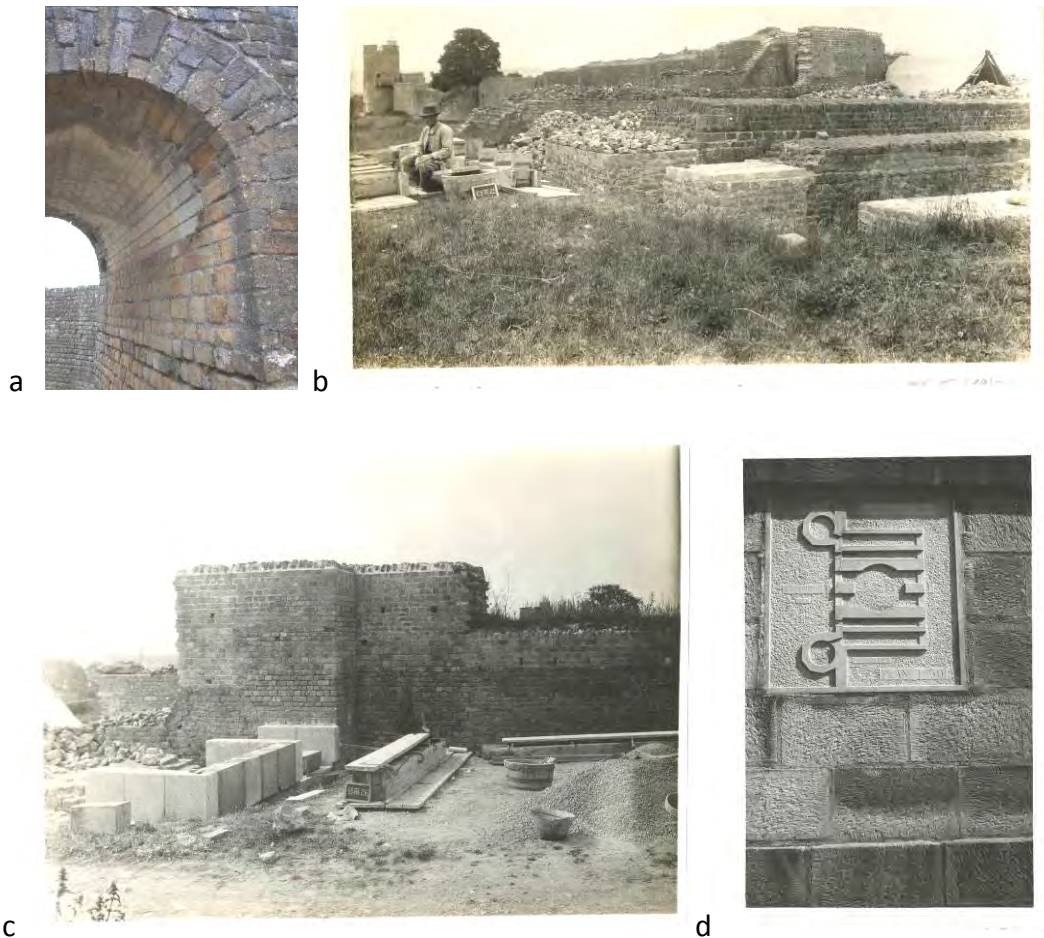


Figure 1. Application of artificial stones in Aventicum, a: stone vault (1917), b: large apparatus buttresses imitating shell sandstone (1925), c: pillars of the tower imitating Jura limestone (1926), d: artificial stone imitating Jura limestone (1935)

The procedure consisted in vigorously compacting a thin and fairly dry mortar against one or more of the vertical walls of a formwork, depending on whether ashlar stones (Figure 2a) or corner stones (Figure 2b) were produced. This 2-3 cm thick compact layer of surface mortar was tinted in the mass so that it could be cut to give it the appearance and relief of the original stones (Figure 1d and Figure 2b). A layer of coarse concrete was then poured into the mould, which tightens the surface cement and holds it in place during setting (Figure 1b, Figure 1c, Figure 2). Modules were manufactured to clamp up to six blocks of the correct size. The photographs from 1925-1926 illustrate the process of making large masonry blocks imitating shell sandstone (Figure 1b) and Jura limestone (Figure 1c); in Figure 1c, the restitution of one of the pedestals is illustrated by the blocks of its base, ready to receive the second level: the simultaneous formwork of six blocks covered with a board and the

aggregates with screens. A large formwork allowing the manufacture of at least ten blocks at a time is also observed in the background.

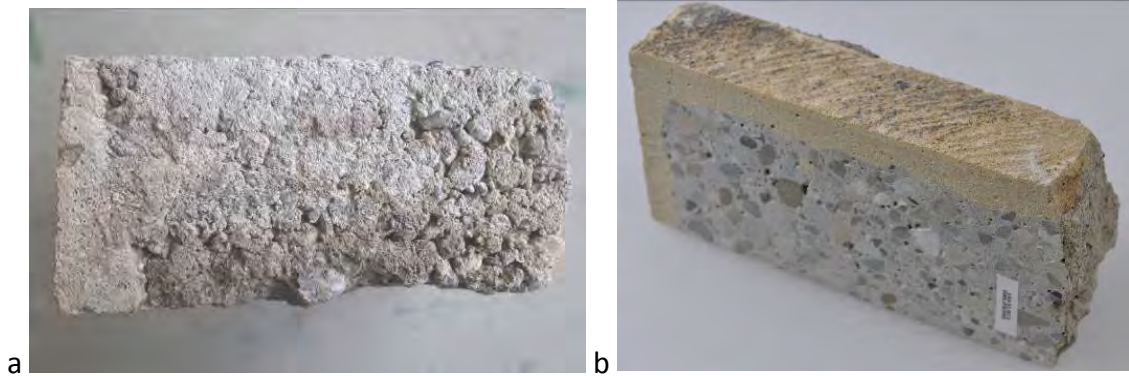


Figure 2. a: ashlar stone, b: corner stone

Samples and methods

In 2012, four cores (35 mm diameter and approx. 130 mm long), labelled M1 to M4, were sampled from different artificial stones. Figure 3 shows the cross section of the cut cores where the sections prepared for microscopy are marked by red dashed lines. The four samples present two or three different layers, each with a distinct texture (grain size, colour), between which interface appears more or less clearly. The areas of interest, shown by red squares in Figure 3, were sampled and impregnated with epoxy resin to create polished sections for microscopic analyses. A Philips Quanta 200 microscope was used for structural analysis of mortars. EDX microanalyses were performed by a Bruker AXS Quantax spectrometer, for chemical identification (point and elementary distribution) of the main phases observed. No analysis was performed on the core of M4, its composition having been considered comparable to that of M1 and M2.

Microscopy results

The analysis focused on the porosity, the nature of cement and the hydration products of the two or three presentative layers and interfaces of the samples M1 to M3.

Sample M1 and M2

Figure 5 shows the difference of porosity observed through the samples M1 and M2. The porosity progressively decreases from the core of concrete (layer 3) to the finishing layer (layer 1). The latter appears relatively porous, with many compaction voids related to casting and poorly dense hydration products.

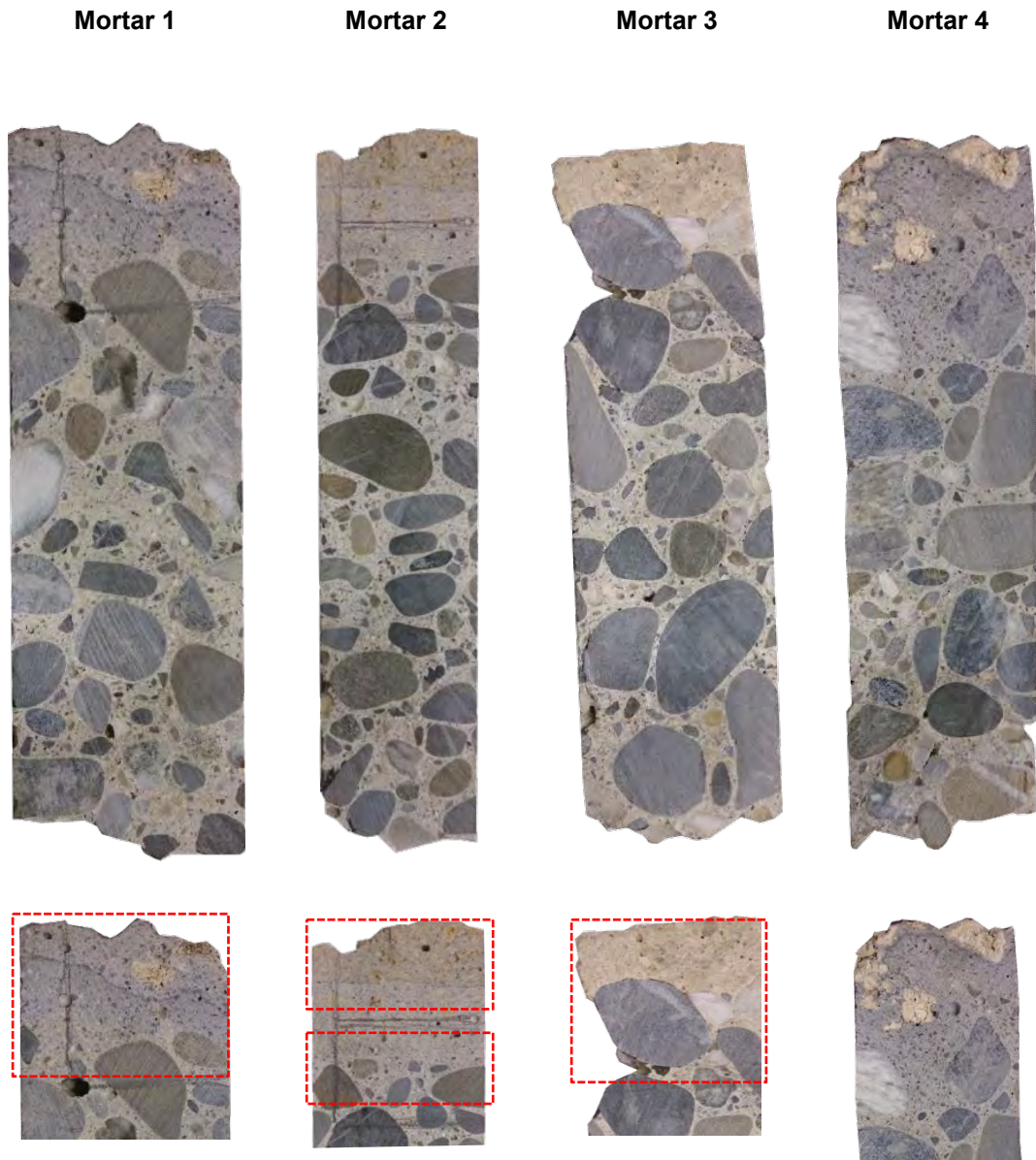


Figure 3. Cross section of samples M1 to M4

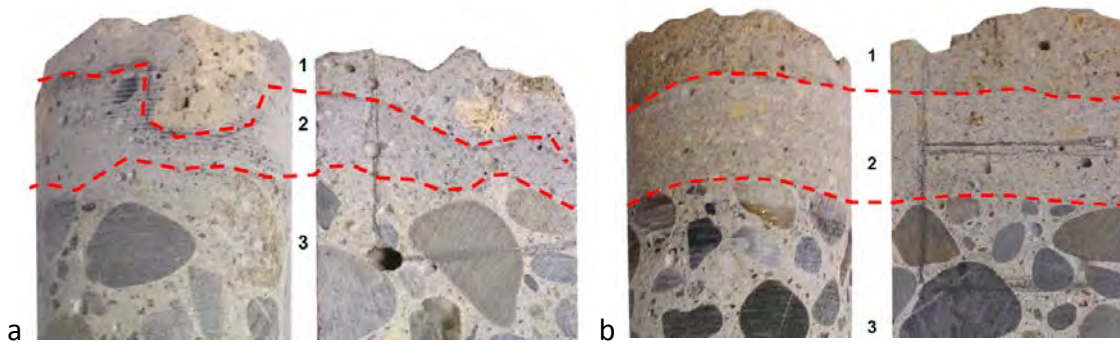
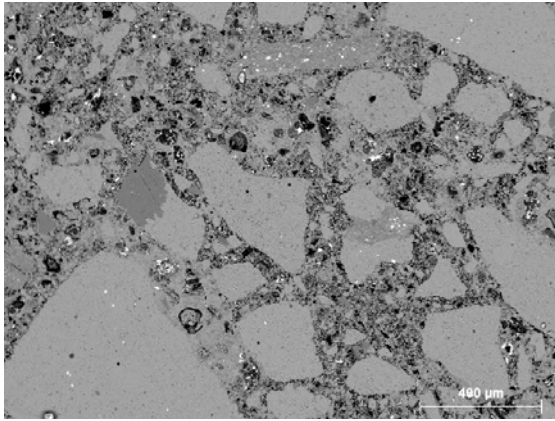
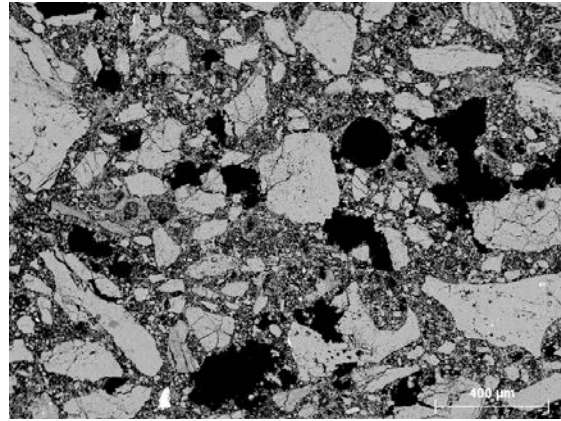


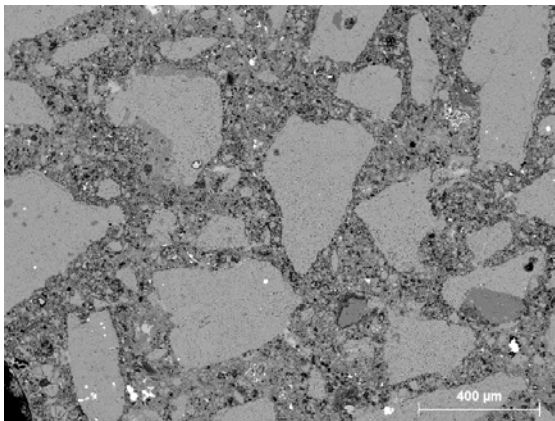
Figure 4. Finishing mortar (1), bonding mortar (2) core (3), a: sample M1, b: sample M2



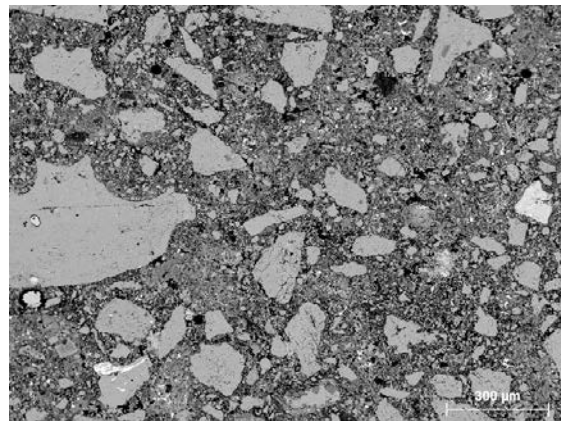
Layer1: finishing mortar M1



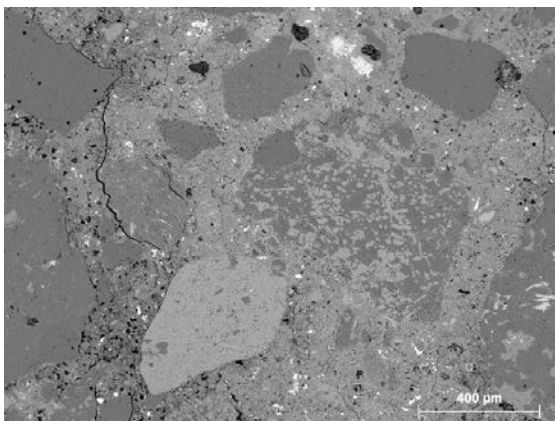
Layer1: finishing mortar M2



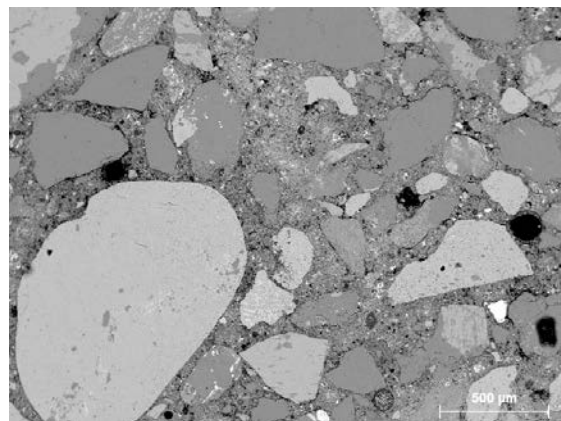
Layer 2: bonding layer M1



Layer 2: bonding layer M2



Layer 3: core in concrete M1

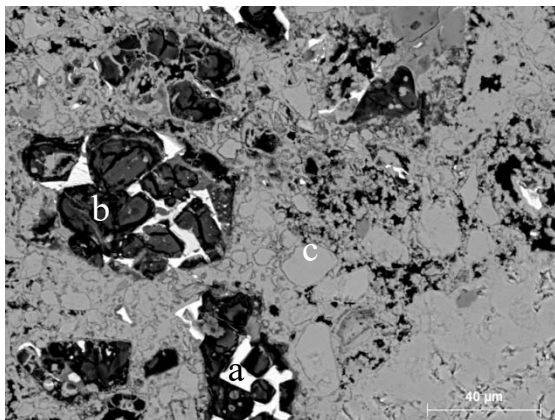


Layer 3: core in concrete M2

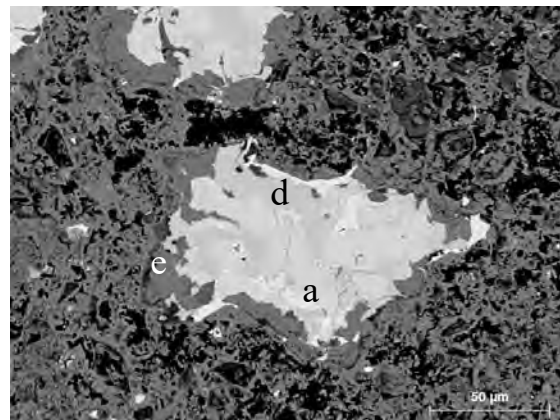
Figure 4. Microstructure and porosity of the different layers, sample M1 and M2

Figure 6 details presentative cement grains observed in the different layers of samples M1 and M2. Results are interpreted for each layer in the dedicated section of the article. The distribution of calcium, silica, aluminium and sulfur on both sides of the interfaces (marked by the red dashed line) between the different layers are given in the elemental mapping for sample M1 and M2 (Figure 7 and Figure 8, respectively). The mappings mainly illustrate the difference in the sulfur content between the finishing and the bonding mortars. The latter

contains the highest sulfur content among the three materials. The difference in Ca, Si and Al distribution mainly originates from the nature of the aggregates.

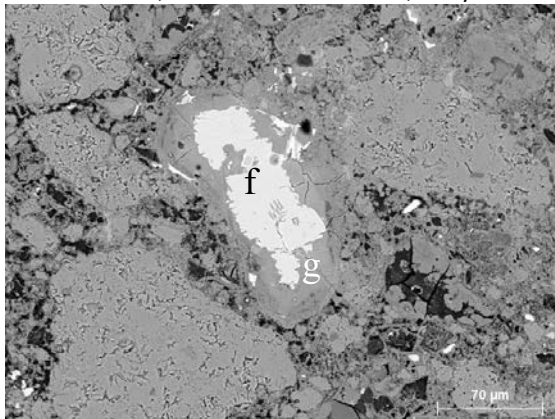


Layer 1: finishing mortar M1

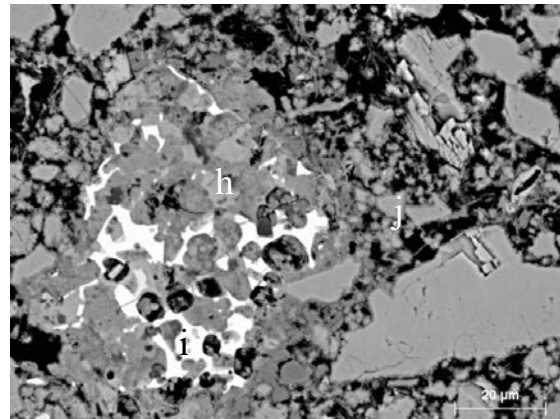


Layer 1: finishing mortar M2

a : unhydrated ferrite, b: silica gel subsequent to decalcified calcium silicates, c: powder from addition of crushed stone, d: calcium aluminates, e: hydration products C-S-H

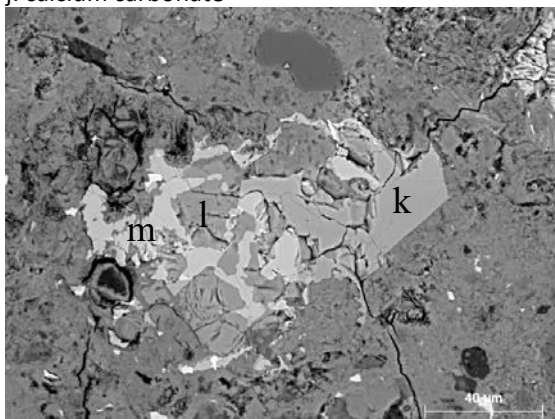


Layer 2: bonding mortar M1

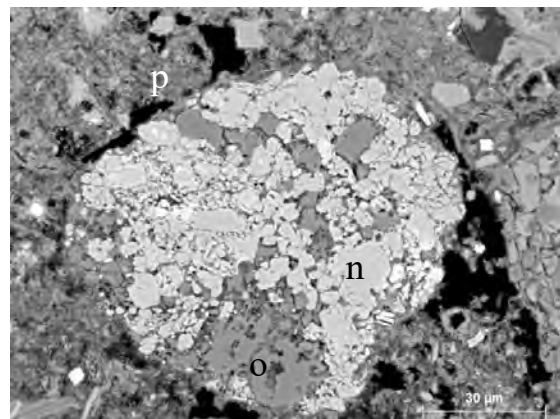


Layer 2: bonding mortar M2

F: tricalcium silicates C_3S , g: hydration products C-S-H, h: anhydrous phase Ca-Al-Si, i: unhydrated ferrite, j: calcium carbonate



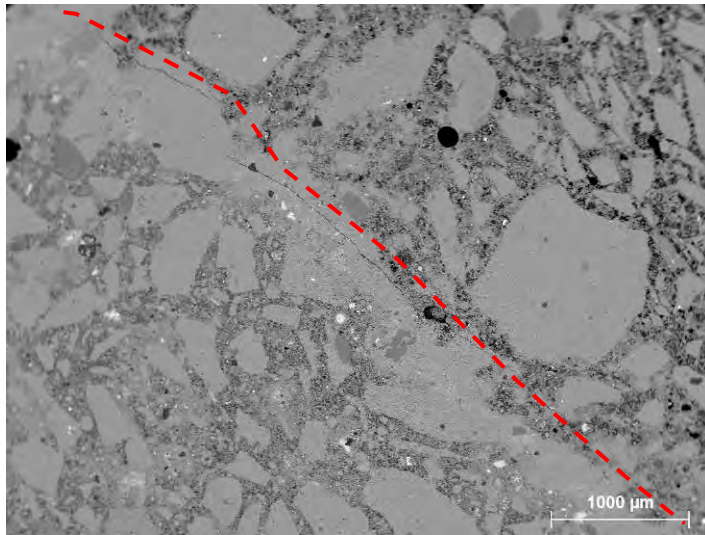
Layer 3: core in concrete M1



Layer 3: core in concrete M2

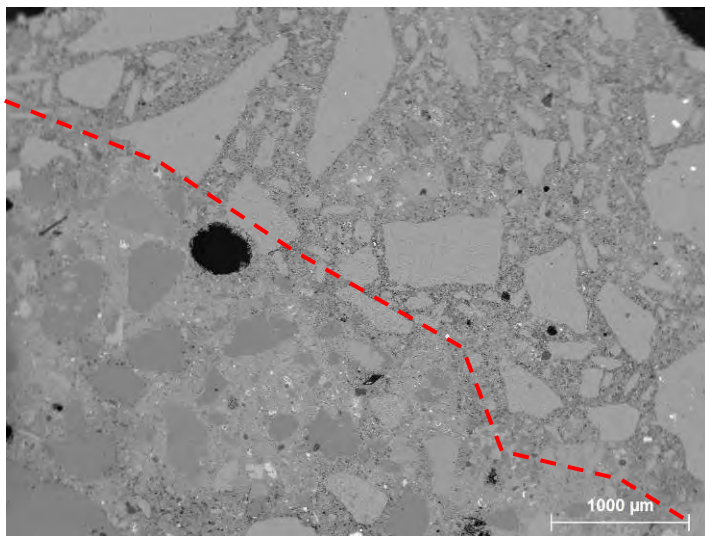
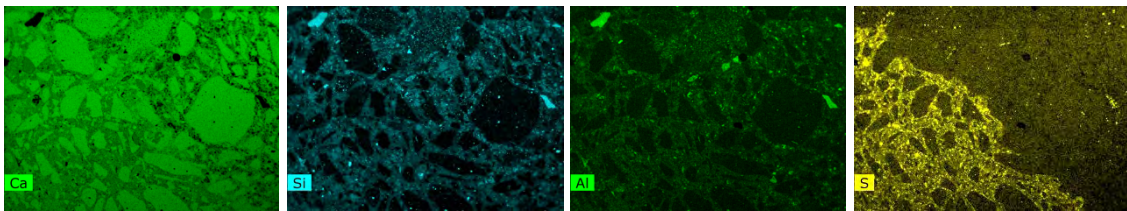
k: phase from the melilites group (possibly alumino-akermanite from the chemical analysis), l: calcined clay with wt% composition $K_{26}Si_{17}Al_{17}O_{41}$, m: tricalcium silicates C_3S , n: phases with wt% composition $Ca_{18}Si_{17}Al_{13}Fe_9O_{43}$, o: non calcined albite, p: C-S-H

Figure 6. Details on cement grains of the different layers, sample M1 and M2



Sample M1

Interface
finishing/bonding



Interface
bonding/concrete

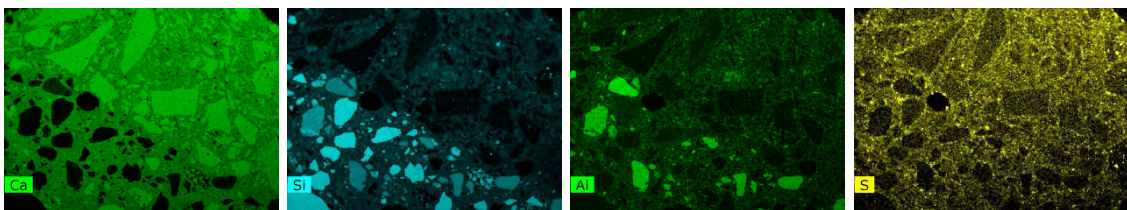
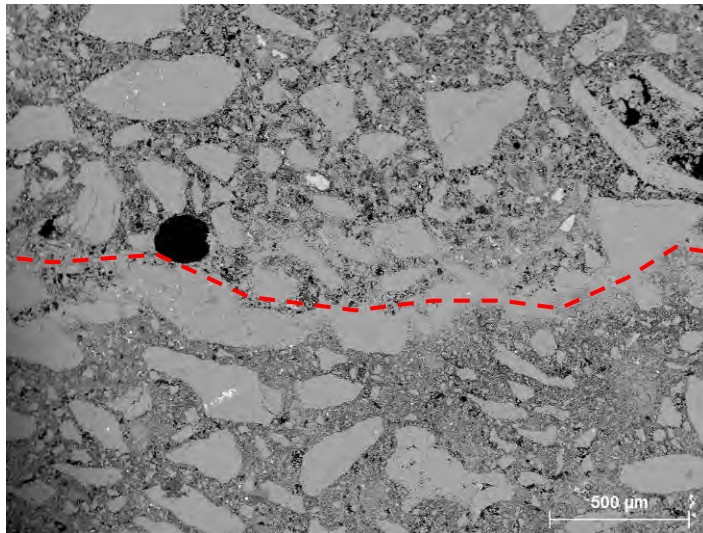
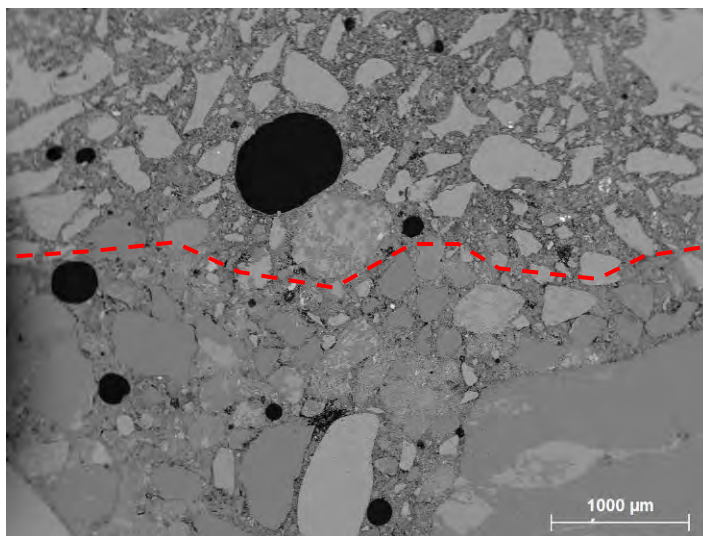
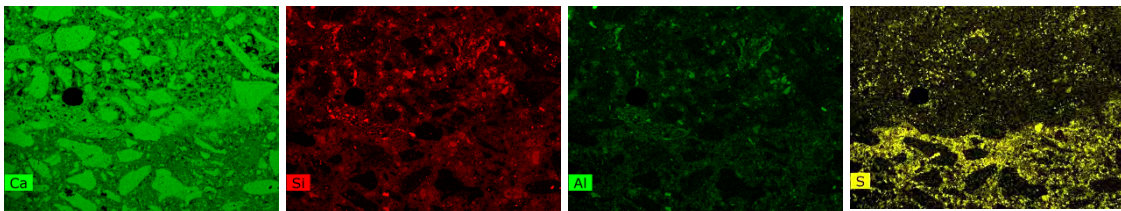


Figure 7. Interface between the different layers, including elemental mapping (Ca, Si, Al, S), sample M1



Sample M2

Interface
finishing/bonding



Interface
bonding/concrete

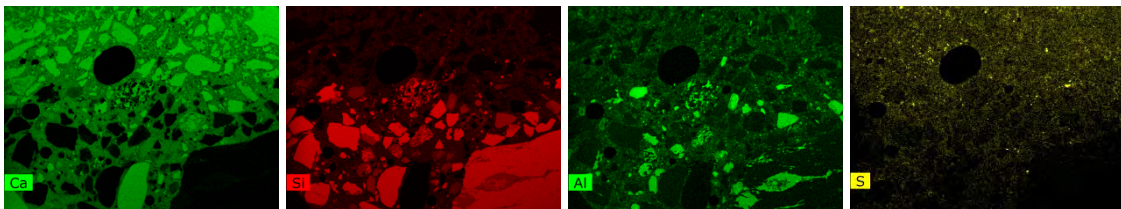


Figure 8. Interface between the different layers, including elemental mapping (Ca, Si, Al, S), sample M2

The analysis only focused on the finishing mortars, assuming that the concrete core is comparable to that of samples M1 and M2. A difference of porosity is observed within the finishing layer (Figure 10). This results from the presence of an existing crack at the interface with concrete, leading to strong leaching and carbonation of hydration products and

remnants of anhydrous cement grains, in which the calcium silicates decalcified to form an amorphous silica gel (Figure 11, caption d).

Sample M3

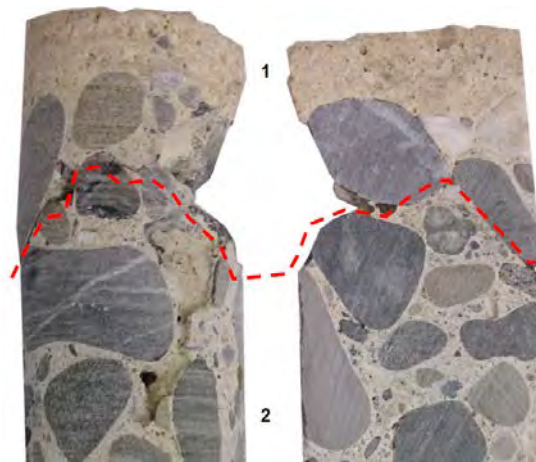


Figure 9. Finishing layer (1) and core (2), sample M3

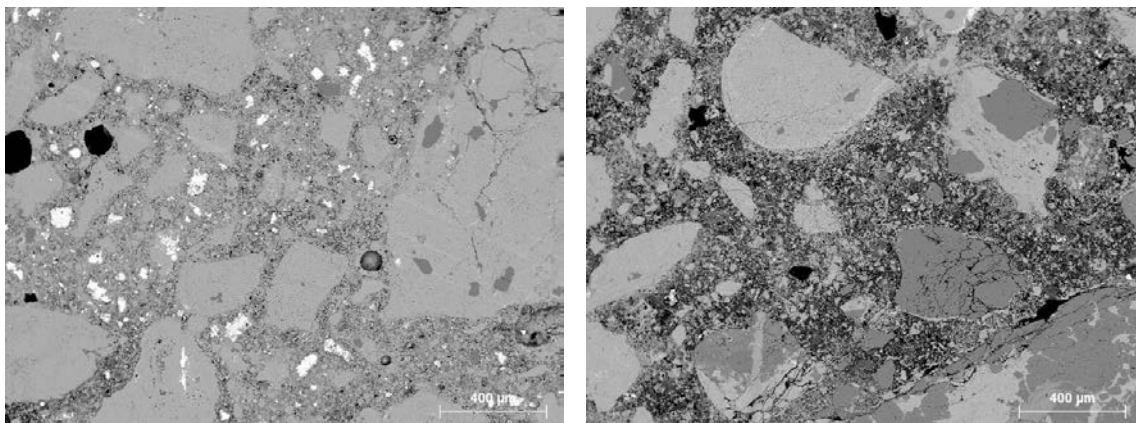
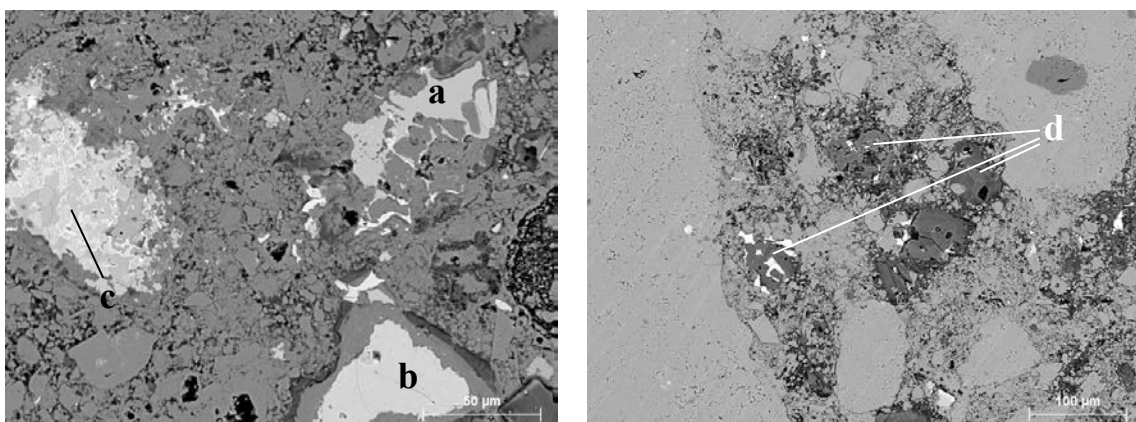


Figure 10. Microstructure and porosity within the finishing layer, sample M3, left: external area, right: near cracked interface with concrete



a: calcium aluminium C_4A type, b: calcium silicate C_2S , c: grain with C_2A , C-A-(S) and ferrite, d: decalcified C_2S in a cement grains

Figure 11. Details on cement grains within the finishing mortar, sample M3. Left: external area, right: near-cracked interface with concrete

Interpretations

Based on the microscopic observations, the cementitious materials used to produce artificial stones are interpreted below.

The inner core is composed of a concrete with a grain size of 0-2 cm, composed of Portland-type cement and mainly siliceous aggregates. This concrete has a sound and dense microstructure, without any sign of degradation. Many anhydrous cement grains are still present in the matrix. The cement has a mineralogy comparable to that of modern Portland cements, with calcium silicate phases (remaining C_2S) included in solid solutions of the calcium aluminate type (C_3A , C_2A , C_4AF) and the presence of thick and dense inner C-S-H at the boundary.

The intermediate bonding mortar is observed in samples M1 and M2. This mortar remains fairly porous despite the high degree of cement hydration. Finely ground residue (shred from shell sandstone with a calcareous matrix) is evenly distributed in the mortar. The cement is referred to as Portland type because of the high temperatures ($>1300^\circ\text{C}$) identified. The composition of the cement grains is identical to that of the cement used for micro-concrete and finishing mortar. However, the elementary mapping of sulfur (Figure 7 and Figure 8 clearly indicates a sulfate-bearing cement, comparable to modern Portland cements. Within the bonding mortar, sulfur is homogeneously distributed, incorporated into the hydrated phases of the cement (in the form of calcium mono-sulfo-aluminate and calcium tri-sulfo-aluminate ettringite) covering the inner walls of the trapped air pores. The elementary mapping indicates a clear interface, without any diffusion of sulfur through the different layers.

A tinted finishing mortar, including stone powder to imitate local natural materials, covers the bonding mortar (samples M1 and M2) or is directly applied on the concrete (sample M3). In the three samples, the finishing mortar is made of Portland cement. Unlike the concrete and the bonding mortar, this cement is free of sulfates (clear interface without diffusion of sulfur, highlighted by elemental mapping). The microstructure of the finishing mortar is more porous in comparison with the subsurface layers. A large reserve of cement grains is visible and decalcified under the effect of atmospheric carbonation and ambient humidity. The decalcification of calcium silicates yields to a silica gel and a ferrite phase skeleton. Such carbonation level can result from the low compactness of the mortar. The granular filler of the mortar is composed of siliceous limestone sand and the same crushed limestone as that of the bonding mortar.

Portland cement phases predominate in the three different layers. Seldom cement grains with remnants of calcium carbonate, non-calcined clay materials, or albite, possibly indicate a single source of marl calcined in a shaft kiln although rotary kilns were introduced in 1904 in the Swiss production of artificial Portland cements [16].

Figure 5 indicates a porosity progressively decreasing from the core (concrete) to the finishing mortar (except for sample M3, subject to leaching and carbonation subsequent to cracking at the interface). This difference probably originates from the casting and finishing techniques. The finishing mortar was first cast as thin layers in the formworks. A dry composition of this mortar, strongly compacted against the formwork walls, can explain the nature and shape of pores observed in the samples. The three layers (micro-concrete, bonding, finishing) are compatible and adhere to each other. The presence of progressively porous mortars on a denser concrete structure contributes to the stability of the interfaces and protects the masonry structure [1]. The mortars and concrete are chemically compatible, even though the presence of sulfates is detected and confined to the intermediate bonding mortar only. No diffusion of sulfates through the inner micro-concrete or the outer finishing mortar is observed. Similarly, no degradation related to an internal sulfate reaction between the different layers is identified.

Conclusions

This study presents a consistent application of the first "Portland" cements for the 1930's conservation of Roman vestiges of the Porte de l'Est in Avenches. The restoration ethics of Jacques Mayor and his successors Albert Naef and Louis Bosset is remarkable for the end of the 19th century, a period when national and international charters and conventions have not yet been established. There is early implementation of the principles of the Venice Charter (1963), in particular Articles 9 and 12 on authenticity. The technique of artificial stones was systematically used to imitate local sandstone and limestone and recreate parts of walls designed on the basis of archaeological works. The overall durability of the walls is good despite local degradations due to rising dampness. At least two types of Portland cements were used and differentiated by the initial sulfate content. Sulfate is predominantly present in the bonding mortars and in lesser amounts in the core made of concrete. The choice of cement could have been motivated by the setting regulation required for the cast of concrete and the bonding layer. In contrast, the finishing layer contains no sulfate, suggesting the use of rapid cement to produce the finishing render imitating stone. The physical and chemical compatibility criteria are verified between the different concrete and mortars. The microscopy analysis reveals both a sound microstructure of each layer of the wall (core and external mortars) and compatibility at their interface, with good physical adherence and no diffusion of sulfate. Local masonry works are planned to restore local surfaces of walls suffering from rising dampness. Roman cement mortar with addition of tuff-stone is suggested to create a new finishing mortar.

References

1. Isebaert A, Van Parys L and Cnudde V (2014) Composition and compatibility requirements of mineral repair mortars for stone – A review. *Construction and Building Materials*, 2014, vol. 59, p. 39-50.

2. Varas-Muriel M J, Pérez-Monserrat EM, Vázquez-Calvo C et al (2015). Effect of conservation treatments on heritage stone. Characterisation of decay processes in a case study. *Construction and Building Materials*, 95, 611-622.
3. Pacheco-Torgal F, Faria J and Jalali S (2012). Some considerations about the use of lime–cement mortars for building conservation purposes in Portugal: A reprehensible option or a lesser evil?. *Construction and Building Materials*, 30, 488-494.
4. Moropoulou A, Polikreti K, Ruf V et al (2003). San Francisco Monastery, Quito, Ecuador: characterisation of building materials, damage assessment and conservation considerations. *Journal of Cultural Heritage*, 4(2), 101-108.
5. Gosselin C, Girardet F and Feldman SB (2012). Compatibility of Roman cement mortars with gypsum stones and anhydrite mortars: The example of Valère Castle (Sion, Switzerland). In *Proceedings of the 12th International Congress on the Deterioration and Conservation of Stone, New York* (pp. 22-26).
6. Gosselin C, Pintér F (2016) Examples of early age Portland cements applied in historical masonries. In: *Proceedings of the 4th Historic Mortars Conference, Santorini, Greece, October 10-12*.
7. Pintér F, Gosselin C (2018) The origin, composition and early age hydration mechanisms of Austrian natural Portland cement. *Cem Concr Res* 110: 1–12
8. Pintér F, Gosselin C (2015) Material characteristics of prefabricated concrete elements from a late 19th century church in Lower Austria. In: *Proceedings of the 15th EMABM Conference, Delft, The Netherlands, June 17-19*
9. Flück M (2019) *Le mur d'enceinte romain d'Avenches-Aventicum, Lausanne*.
10. Castella D (2015) *Aventicum. A Roman Capital City*
11. Mayor J (1899) *Lettre au président de la commission romaine de la société des monuments historiques suisses*.
12. Mayor J (1900) *Lettre au président de la société romaine de la comission des monuments historiques suisses*.
13. Naef A (1907) *Rapport sur les travaux de 1907 à la porte de l'Est et la tour de la Tornallaz à Avenches*.
14. Bosset L (1916) *Enceinte romaine d'Avenches. Porte de l'Est. Journal des travaux dès le 1er janvier 1916*.
15. Lollini F, Carsana M and Bertolini L (2017). A study on the cement-based decorative materials in the San Fedele Church in Milan. *Case studies in construction materials*, 7, 36-44.

16. Spicher G, Marfurt H, Stoll N (2012) Ohne Zement geht nichts. Neue Zürcher Zeitung, Zurich

Drying Shrinkage of Historic Portland Cements: Factors to be Considered for Successful Repair

Simeon Wilkie¹, Thomas Dyer²,

(1) Getty Conservation Institute, swilkie@getty.edu

(2) University of Dundee, t.d.dyer@dundee.ac.uk

Abstract

Drying shrinkage of building materials containing Portland cement is a key concern in their conservation. While drying shrinkage can lead to cracking of hardened cementitious materials, it is also an important consideration for repair materials, as failure to match the shrinkage of the original and new materials can result in a repair that is poor. However, this is a complicated issue, as changes in manufacturing technology and processes, available raw materials, and the introduction and development of material standards, have all had an effect on the physical and chemical properties of cementitious building materials. As such, historic materials vary considerably from those that are manufactured today, and there is limited understanding of how to address drying shrinkage.

In order to better understand this issue, a study of the reversible drying shrinkage of materials containing historic Portland cements, taken from structures *in-situ*, was undertaken. Statistical analyses of the results were then performed in order to determine which physical and chemical properties have the most influence on drying shrinkage, and the implications posed for the conservation of historically-significant structures.

Introduction

The number of historically-significant concrete structures which require conservation work is ever increasing, and, in many cases, patch repairs are a part of this. However, there are conflicting perspectives on the way this should be approached; on one side it is argued that the performance of the repair is the key factor, on the other, that historical authenticity of the material is most important and that repairs should be a 'like-for-like' replacement. Both of these approaches have issues. Modern 'performance based' repair mortars are usually pre-batched proprietary products which are designed to be compatible with modern concrete, and are significantly different from the historic material which they are to repair. This not only has the potential to result in repairs which are mechanically incompatible, but, as they vary in colour, texture and porosity, they can also be unsightly, weather differently and damage the historic aesthetic of the structure. However, as previously reported [1], we do not currently possess the means to accurately determine the w/c ratio or the original mix proportions of historic concrete due to the physical and chemical changes which occur over time, and this makes truly 'like-for-like' replacements unrealistic.

In any case, the current long-term success rate for patch repairs is low. In a survey of 230 concrete repairs, 60% of which involved patching, Tilly and Jacobs [2] found that only 45% of cementitious patches and 50% of polymer modified patches successfully met their guaranteed life expectancy, with most having failed within 10 years. In many cases, these patches were applied in tandem with a coating (such as a barrier or hydrophobic treatment) which was applied on top, and this appears to yield a higher success rate. When only solo patch repairs were considered, the average success rate of patch repairs was only 30%. Given that the global concrete repair mortar market is forecast to be worth USD 2.62 billion by 2021 [3], this high failure rate clearly has serious financial implications. However, there are wider implications for historic structures, as it is not always appropriate to use coatings and there are uncertainties regarding the impact of carrying out multiple repair actions simultaneously.

The key material property which affects the success of a patch repair is shrinkage. Shrinkage occurs in cement pastes as they dry during and after hardening, and can lead to significant contraction, which in turn can result in cracking. When attempting repairs, it is essential that each repair situation is considered individually with a comparison of the original material – which has already completed shrinkage cycles – with the new material that will undergo shrinkage in the future [4]. This is important because the bond between the repair layer and the old material acts as a restraint [5] potentially causing curling and delamination of adjacent layers with different shrinkage properties [6].

There are several factors which affect shrinkage properties. These include the aggregate characteristics, aggregate content, water content, cementitious materials, curing conditions, environmental conditions and the element size and shape [7]. While most of the shrinkage movement is due to the cement paste, some aggregates are also prone to shrinkage – with dense aggregate generally undergoing less shrinkage than lightweight aggregate [8].

While there are different types of shrinkage, drying shrinkage is of primary concern. It can be defined as volumetric change due to drying, and is related to the volume of water lost [9] from the hardened material stored in unsaturated air [10]. Drying shrinkage involves two different types of movement; reversible and irreversible. The irreversible movement represents a large proportion of the maximum shrinkage and occurs during the first drying period, with further wetting and drying cycles producing largely reversible movement [11]. During the first drying period, the water lost is the excess from the mix which does not react with the cement, but is required to aid compaction and workability, and becomes trapped in the pores of the hardened cement paste [12].

The reversible moisture movement, or wetting expansion, occurs once the paste has hardened and will typically represent between 40 and 70 percent of drying shrinkage, with the effects of prolonged periods of dry weather usually reversed by a relatively short period of rain [10]. However, the change in volume of the hardened material is not equal to the volume of total water removed, as water is removed from both gel and capillary pores, and

the loss of easily evaporable water which is only loosely held in relatively large capillary pores (>10 nm) causes little or no shrinkage [13,14].

Typically, drying shrinkage develops more quickly near the drying surface than in the centre of an element [15] and occurs to a smaller degree in concrete than in neat cement paste, as the aggregate restrains shrinkage of the cement matrix, thus reducing overall shrinkage [11,16]. Volumetric changes occur due to several factors, including temperature fluctuations, self-desiccation (internal drying), and loss of water from the gel pores and the various cement hydrates (external drying) [17], which consequently cause the cement paste to contract [10]. This contraction is normally hindered by external or internal restraints, which induce tensile stresses that can exceed the tensile strength of the material and result in cracking [5]

While both the initial irreversible, and the ongoing cycles of reversible drying shrinkage are both important considerations for repair materials, it is the reversible movement which is the focus of this study.

Methodology

Following a thorough review of literature, a set of variables which were deemed most likely to influence drying shrinkage were selected for further study. These variables were: ultimate drying shrinkage, mass loss during drying, maximum aggregate size, fineness modulus of the aggregate (FM), surface area to volume ratio (SA/V), volume of the sample, the oven-dried density (OD Density) and porosity.

Reversible drying shrinkage was monitored on 23 concrete samples obtained from structures located across Scotland, the oldest of which dated to 1858 and the youngest to 1978. The samples were a variety of cores and irregular masses removed from structures *in-situ*, which varied in mass from 1.0 – 3.8 kg and in volume from 440 – 1656 cm³. The measurements were carried out following the recommendations for mechanical measurement found in BS 1881-206 [18]. Sets of two DEMEC studs were secured with a two-part epoxy resin, approximately 100 mm (4 inches) apart, on opposite faces on one axis of solid concrete samples. In the case of concrete cores, sets of two studs were secured across three axes. After the resin had set, the solid concrete specimens were placed in water for 72 hours, to allow them to become fully saturated. These were then removed and the mass and distance between the DEMEC studs recorded. The samples were stored in an environmental chamber – which controlled relative humidity (50-60%) and temperature (21 ± 1°C) – and were monitored for 85 days, with the mass, distance between DEMEC points and environmental conditions recorded. After 85 days the samples were placed in an oven and dried for 5 days at 105°C, after which they were allowed to cool to room temperature in a desiccator before measuring the mass and distance between DEMEC points. The distance between DEMEC studs was measured mechanically using a lever linkage with the movement magnified by a sensitive dial gauge, which was calibrated using an invar steel reference bar.

The strain was then calculated by multiplying the difference between the saturated and daily readings by the strain represented by each division of the dial gauge. The ultimate drying shrinkage was considered to be that calculated from the final reading – taken after oven-drying.

The density of each hardened concrete sample was determined in accordance with BS EN 12390-7:2009 [19], and weighed in the ‘oven-dried’ and ‘fully saturated’ states. The porosity was determined to be the volume, as a percentage, filled with water when the concrete was fully saturated, but empty when the concrete was oven-dried.

The aggregate content was calculated in accordance with the BS 1881-124 [20] method for calculating insoluble residue. However, as no reference samples of aggregate were available, it was assumed that none of the aggregates were acid-digestible. Aggregate for grading was removed from the bulk concrete specimens in accordance with BS 1881-124 [20] and the grading of the aggregate was then measured following the dry sieving procedure described in BS EN 933-1 [21] and using standard sieves conforming to BS EN 933-2 [22]. In order to include the results of the sieve analyses in later factor analysis, each aggregate grading was defined in terms of a single factor, known as the ‘fineness modulus.’ The fineness modulus (FM) is defined as the sum of the cumulative percentages retained on the sieves of the standard series divided by 100; with increasing FM values representing coarser grading [10].

The bulk oxide contents were determined using a PANalytical Zetium X-ray fluorescence spectrometer (XRF) with RhK α radiation source. First XRF analysis was carried out on powdered concrete samples, and then on the insoluble residue obtained by acid digestion. A Siemens D5000 X-ray Diffractometer (XRD) with monochromatic CuK α radiation source and curved graphite, single crystal chronometer (30 mA, 40 kV) was used to analyse the mineralogical composition of the insoluble residue, and the Rietveld refinement method was used for quantification. The chemical and mineralogical compositions of the insoluble residue were then compared at an elemental level in order to estimate the chemical composition of any amorphous component of the insoluble residue. The aggregate composition could then be calculated by subtracting the corrected composition of the amorphous material from the insoluble residue. Finally, the chemical composition of the binder could then be calculated by subtracting the composition of the aggregate from the previously determined chemical composition of the concrete sample.

Statistical Analysis

Statistical analysis software Minitab 13 was used to help establish the weighting of each variable. The selected set of variables were fed into the program which created regression models containing subsets of these variables. The outputs from Minitab – ‘ R^2 ’, ‘ R^2 adjusted’, ‘*Mallows’ Cp*’, and ‘*S*’ – were then used to identify the best-fitting regression model and, therefore, the variables most likely to influence ultimate drying shrinkage.

Factor analysis, which attempts to account for the variation in a number of original variables using a smaller number of index variables, known as ‘factors’ [23], was also carried out. The results of this analysis were then plotted and the loading patterns adjusted through various orthogonal rotations of the axes to assist their interpretation. These factors have a loading between -1 and 1, which indicates how strongly that particular factor affects the variable. The closer the loading is to -1 or 1, the stronger the effect of the factor – with loadings closer to zero, indicating a weaker effect. The locations of the plotted variables can also be used to establish relationships between them. For example, the closer the angle of separation between two variables is to 0° the stronger the correlation, an angle of separation close to 90° suggests very little or no correlation, and an angle of separation closer to 180° shows a strong anti-correlation.

Results and Discussion

From the results of the first best subset regression (Table 2), it would appear that the individual variable which most influences the ultimate shrinkage (oven-dried), is the density of the samples. However, this model is fairly inaccurate and a more accurate model for predicting the ultimate shrinkage can be determined by examining the subset models which contain more variables.

Table 1. Results of first ‘best subset regression’ for response ‘ultimate shrinkage’

Subset	Variables	R ²	R ² (Adj.)	Cp	S	Mass Loss	Max. Agg. Size	FM	Agg. Content	SA/V	Volume	OD Density	Porosity
1A	1	55.6	53.5	5.6	0.0153							x	
1B	1	34.0	30.8	17.6	0.0187		x						
1C	2	63.2	59.5	3.4	0.0143				x			x	
1D	2	61.6	57.7	4.3	0.0146						x	x	
1E	3	69.4	64.5	2.0	0.0134		x		x			x	
1F	3	68.6	63.6	2.4	0.0136				x		x	x	
1G	4	73.2	67.2	1.8	0.0129		x		x		x	x	
1H	4	72.1	65.9	2.4	0.0131		x		x	x		x	
1I	5	74.1	66.5	3.3	0.0130	x	x		x		x	x	
1J	5	74.0	66.3	3.4	0.0131		x		x		x	x	x
1K	6	74.5	65.0	5.1	0.0133	x	x		x	x	x	x	
1L	6	74.4	64.8	5.2	0.0133	x	x		x		x	x	x
1M	7	74.7	62.9	7.0	0.0137	x	x	x	x		x	x	x
1N	7	74.6	62.8	7.0	0.0137	x	x		x	x	x	x	x
1O	8	74.7	60.3	9.0	0.0142	x	x	x	x	x	x	x	x

Taking into consideration the R² adjusted (the coefficient of determination adjusted for the number of variables in the model) values only, it would appear that subset 1G best explains the variation of ultimate drying shrinkage. Subset 1G also has the lowest S (standard error) value – indicating that it is also the most accurate of the models. However, the Mallows’ Cp

value (which helps identify the precision) is relatively low in comparison to the number of parameters considered, which indicates it may not be as precise as other models, when compared to the full model.

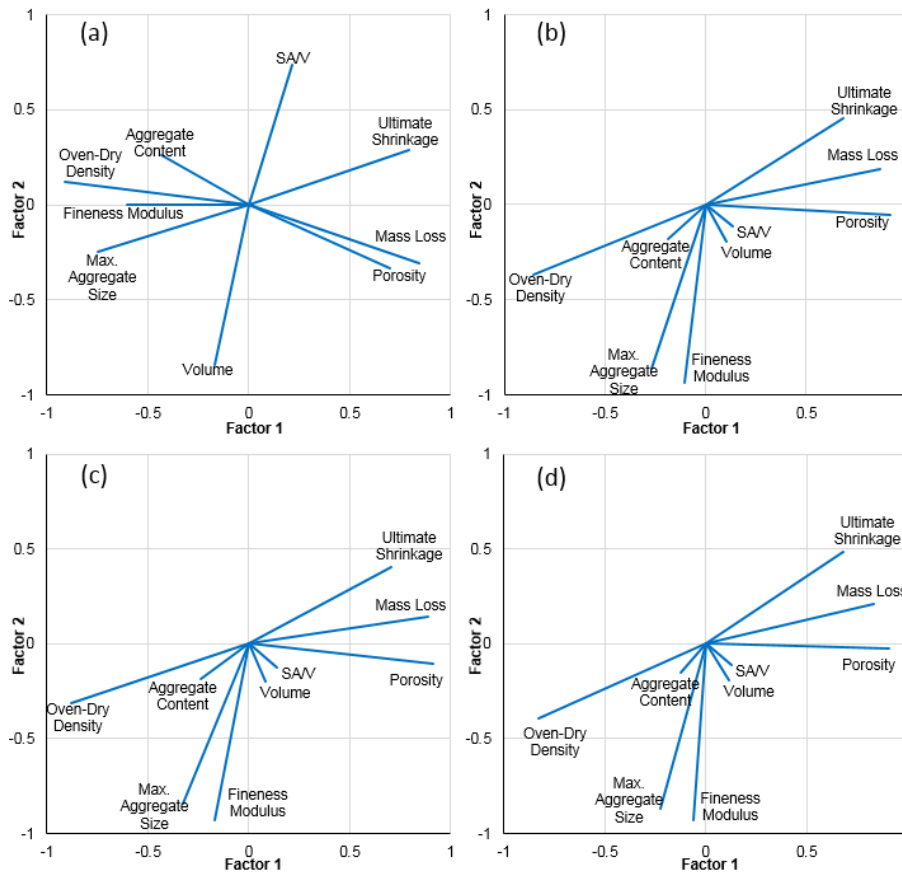


Figure 1. Factor loading plots for analysis 1, (a) no rotation, (b) Equimax rotation, (c) Varimax rotation, (d) Quartimax rotation.

In consideration of R^2 adjusted, subsets 1I and 1J have the next highest values – and also have relatively low S values. However, they each consider 5 out of the 8 possible variables, and so the possibility of overfitting needs to be considered. Overfitting occurs when the regression considers traits that are unique to the samples considered in the regression as being valid predictors for all future responses.

In this case, the variable ‘volume’ stands out as a source of overfitting. Only a limited number of samples provided for this project were suitable for use in the drying shrinkage study due to their physical dimensions, and several of those that were suitable came from the same source and had the same dimensions. For example, samples 1-6 were cores (80×150 mm) from the same structure, and samples 7-9 were cores (120×150 mm) from the same structure. As such, it is possible that the regression model is incorrectly considering a correlation between specimen volume and other variables which are inherent to the source of the concrete.

Table 2. Results of second ‘best subset regression’ for response ‘ultimate shrinkage’.

Subset	Variables	R ²	R ² (Adj.)	Cp	S	Agg. Content	Density	OD	Max. Agg. Size	Al ₂ O ₃	CaO	Fe ₂ O ₃	MgO	SiO ₂	SO ₃
2A	1	55.6	53.5	24.0	0.0153		X								
2B	1	34.0	30.8	44.9	0.0187				X						
2C	2	64.7	61.1	17.2	0.0140		X			X					
2D	2	63.4	59.7	18.4	0.0143		X				X				
2E	3	72.8	68.5	11.3	0.0126		X	X			X				
2F	3	69.4	64.5	14.7	0.0134	X	X	X							
2G	4	80.2	75.7	6.2	0.0111		X	X			X		X		
2H	4	76.1	70.8	10.1	0.0122		X	X		X	X				
2I	5	85.3	81.0	3.2	0.0098		X	X			X	X	X		
2J	5	85.0	80.6	3.5	0.0099	X	X	X					X	X	
2K	6	86.4	81.3	4.1	0.0097	X	X	X				X	X	X	
2L	6	85.9	80.6	4.7	0.0099	X	X	X			X		X	X	
2M	7	86.5	80.2	6.1	0.0100	X	X	X	X	X	X		X	X	
2N	7	86.5	80.1	6.1	0.0100	X	X	X			X	X	X	X	
2O	8	86.6	78.9	8.0	0.0103	X	X	X	X	X	X		X	X	X
2P	8	86.5	78.8	8.0	0.0104	X	X	X	X	X	X	X	X	X	
2Q	9	86.6	77.3	10.0	0.0107	X	X	X	X	X	X	X	X	X	X

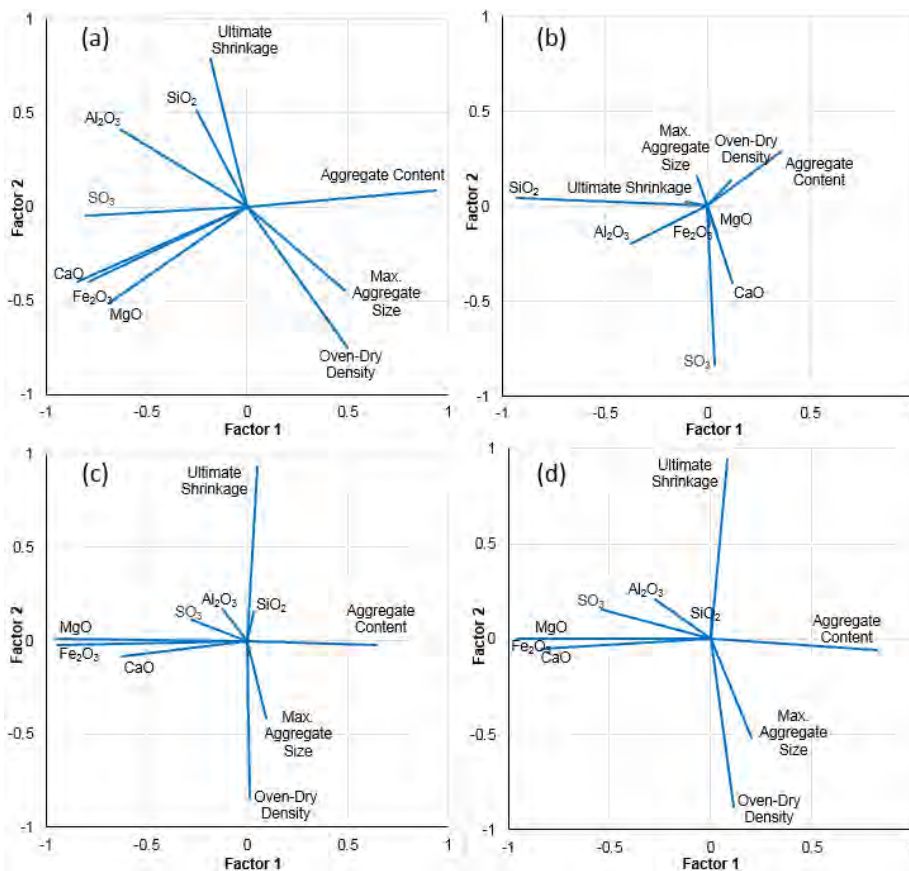


Figure 2. Factor loading plots for analysis 2, (a) no rotation, (b) Equimax rotation, (c) Varimax rotation, (d) Quartimax rotation.

This hypothesis can be considered further by examining the results of the factor analysis. In all four of the factor loading diagrams, 'ultimate strain' and 'volume' are close to 90° apart from each other which suggests no correlation between the ultimate shrinkage and the volume of the specimen – supporting the theory that the inclusion of volume in the best subset regression models may be a result of overfitting. Similarly, the variable 'SA/V' appears to show very little correlation to ultimate strain in any of the rotated loading plots, and so its inclusion in best subset models in response to ultimate strain is also probably a result of overfitting – although, while SA/V does not appear to affect ultimate shrinkage, it did have a significant effect on the rate of drying shrinkage due to an increase in the rate of moisture loss.

Furthermore, the lack of correlation between either of these variables and ultimate strain also concurs with research carried out by Almudaiheem & Hansen [24], which suggested that ultimate drying shrinkage of concrete, mortar and cement paste was independent of specimen size and shape.

This method of analysis can also be applied to other variables considered in the best subset regression. For example, the relatively small angles between 'mass loss' and 'ultimate shrinkage' in each of the rotated loading plots suggests a moderately strong correlation between these two variables. The variables 'oven-dry density' and 'aggregate content' similarly are separated by a relatively small angle, and so a strong correlation between these two variables is also implied. Furthermore, both of these variables are separated from 'ultimate shrinkage' by almost 180°, which in turn suggests a strong anti-correlation between each of these two variables and ultimate shrinkage – i.e. as either oven-dry density or aggregate content increases, the ultimate shrinkage decreases.

Each factor loading plot also suggests a strong correlation between 'maximum aggregate size' and 'fineness modulus'. This is to be expected as the fineness modulus (FM) is the sum of the cumulative percentages *retained* on the sieves of the standard series divided by 100, and, therefore, samples containing larger aggregate size have a higher FM value. Furthermore, the factor loading plot with no rotation suggest a very strong anti-correlation between each of the variables, 'maximum aggregate size' and 'fineness modulus', with 'ultimate shrinkage'. However, this anti-correlation, whilst still present, is less pronounced in each of the various rotated loadings.

Taking into account the results from the factor analysis, the results of the best subset regression need to be reconsidered and, if ultimate shrinkage is considered independent of both SA/V and volume, then subset models including these terms should be considered to be the result of overfitting and disregarded. As such, it would appear that the best subset model is 1E which indicates that the most important variables affecting ultimate shrinkage are oven-dry density, maximum aggregate size and aggregate content – variables which all have a strong anti-correlation with ultimate shrinkage according to the factor analysis.

While the use of certain types of aggregate can result in an increase in shrinkage [25], the majority of drying shrinkage is attributed to the cement paste and the effect of aggregate content is twofold: Firstly, as aggregate is generally more dense and has a lower shrinkage capacity, increasing the aggregate content results in a decrease in the overall shrinkage of concrete, and also results in an increase in density – thus explaining the relationship between aggregate content, oven-dried density and ultimate shrinkage. Secondly, the use of aggregate reduces the shrinkage of concrete by providing internal restraint [16], and it would seem from this analysis that the size of the aggregate has an effect on the extent of this – with larger aggregates providing greater restraint.

If best subset model is considered to be 1E – with the most important variables affecting ultimate shrinkage being oven-dry density, maximum aggregate size and aggregate content – the regression equation for ultimate shrinkage, with standard error of 0.0134, is:

$$US = 0.213 + 0.000832 \times AC - 0.000094 \times ODD - 0.000470 \times MAS \quad (1)$$

where:

- US is ultimate shrinkage, as a percentage;
- AC is aggregate content, as a percentage;
- ODD is oven-dry density, in kg/m³;
- MAS is maximum aggregate size, in mm.

Using this equation, a prediction of ultimate shrinkage was calculated for each sample and compared to the actual ultimate shrinkage observed during the experimental procedure. The error between these two is shown in Figure 3.

However, these predictions of ultimate shrinkage do not take into consideration the effects that the chemical composition of the binder will have on the shrinkage properties of the concrete. As the chemical composition of cement determines the nature of hydration products formed – which, in turn, affects the porosity of the hardened cement paste and so influences shrinkage – it is also necessary to consider its effect on shrinkage.

In order to do this, a second analysis was carried out which included the variables identified by the previous analysis, and also the major oxide composition of the binder. The results of the best subset regression are shown in Table 2 and the factor loading plots in Figure 2.

Taking into consideration the R² adjusted values only, it would appear that subset 2K best explains the variation of ultimate drying shrinkage. Subset 2K also has the lowest standard error, which suggests that it is also the most accurate of the models. However, the Mallows' Cp value is relatively low in comparison to the number of parameters considered, and so the model may lack precision.

Taking the factor analysis into consideration, in all rotations, the SiO₂ content and ultimate shrinkage are shown to be the most closely correlated. In three of the four rotations, the previously identified variables 'oven-dry density' and 'maximum aggregate size' are both

shown to have strong anti-correlations to ultimate shrinkage. As subset 2K includes these three factors, this is further support for the selection of 2K as the subset which best explains ultimate shrinkage. As such, the regression equation for ultimate shrinkage, with standard error of 0.009716, is:

$$US = 0.0747 + 0.00212 \times AC - 0.000090 \times ODD - 0.000736 \times MAS - 0.00445 \times Fe_2O_3 + 0.0239 \times MgO + 0.00299 \times SiO_2 \quad (2)$$

where:

Fe_2O_3 is the Fe_2O_3 content attributed to the binder, as a % by total mass of concrete;

MgO is the MgO content attributed to the binder, as a % by total mass of concrete;

SiO_2 is the SiO_2 content attributed to the binder, as a % by total mass of concrete;

Using this equation, a second prediction of ultimate shrinkage was calculated for each sample and compared to the actual ultimate shrinkage observed during the experimental procedure, as shown in Figure 3. These plots show that the second model, which incorporates both physical and chemical characteristics, is both more accurate and more precise.

However, these results should be considered with caution due to the potential for errors in the chemical composition data. Furthermore, these analyses were conducted on the results from only 23 samples. As such, additional studies on a much larger size and range of samples with known chemical composition are required to fully determine the influence of these variable on drying shrinkage, and enable the conception of a model which can make more accurate and precise predictions.

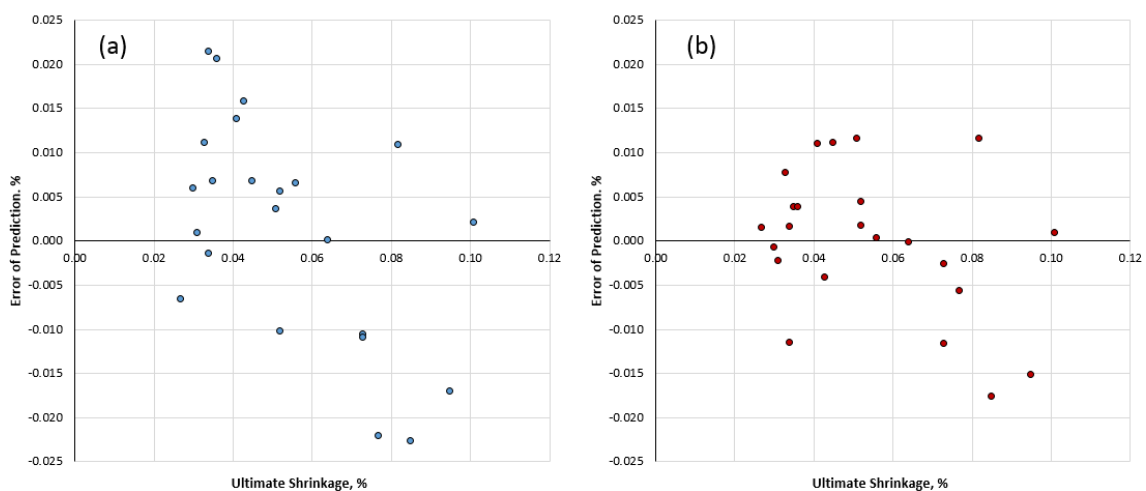


Figure 3. Error of predicted shrinkage using regression Equation 1 (a) and Equation 2 (b) plotted against actual ultimate shrinkage observed

Variables Not Considered In Analysis

There are some variables known to influence drying shrinkage that were not considered in this analysis. While aggregate content, grading (FM) and maximum size were all included,

the type and shrinkage capacity of the aggregate were not. As previously mentioned, the use of aggregate prone to shrinkage results in increased shrinkage of concrete [25], and this is likely to have had an effect on the ultimate shrinkage. In particular, one sample, which was made using an artificial lightweight aggregate, exhibited extremely high ultimate shrinkage and this may have been incorrectly attributed to other variables in the statistical analysis.

While the porosity of the samples was considered in the analysis, w/c and original curing conditions were not, and both of these variables have a significant impact on the formation of the cement paste microstructure, and, therefore, can also significantly impact its shrinkage.

This analysis also does not take into consideration the irreversible drying shrinkage which takes place during the initial period of drying, as the samples used in the study were from historic structures. As any new material which will be used for repair will undergo both initial irreversible shrinkage, as well as long-term cyclic shrinkage, it is important that both of these movements are taken into consideration during their design. While the factors impacting both irreversible and reversible movement are the same, no statistical analysis of their effects on irreversible movement was carried out during this study. It is, therefore, not possible to draw any conclusions about the extent of the relationship between these factors and the irreversible drying shrinkage which occurs during the initial drying period.

Finally, this analysis does not consider the effects of external restraints, such as steel reinforcement, and these will ultimately have an effect on the amount of shrinkage that concrete will undergo *in-situ*.

Implications for Historically-Significant Structures

The results of this study pose implications to the conservation of historically-significant structures in two regards:

The first of these is in respect to the design of drying shrinkage properties for repair materials. The results of the statistical analysis suggest that the key variables influencing ultimate shrinkage are oven-dry density, maximum aggregate size and aggregate content, and, as a result, any purpose made like-for-like repair material would need to replicate these in order to have matching shrinkage properties.

However, there are significant challenges in accurately determining concrete properties [1] such as density and aggregate content, when there is a limited amount of original material on which to undertake analysis. Furthermore, it is clear from the second statistical analysis that the chemical composition of the binder is also a significant factor which affects drying shrinkage, and there are still challenges in accurately determining this.

Accurately designing and manufacturing *identical* like-for-like replacements with matching shrinkage properties is impractical in most cases. However, the relationships between

particular variables and ultimate drying shrinkage established in this study suggest that it should be relatively easy to formulate repair materials with appropriate shrinkage characteristics, which can also be manufactured to match the aesthetic of the original material without taking away from the historic character of a structure. However, for some conservators, there may be concern over the ‘historical authenticity’ of anything other than an *exact* replacement.

The second implication of these results is in respect to climate change. In all cases, the samples reached a state of equilibrium at controlled temperature and relative humidity, where drying shrinkage did not progress any further. However, when the samples were oven-dried – resulting in severe change in temperature and relative humidity – drying shrinkage progressed much further. On average, oven-drying resulted in an increase of shrinkage strain from the maximum observed after air-drying for 85 days in the controlled environment, by a factor of 2.06 (105% increase). It should be noted that the increase for each sample was dependent on the SA/V and volume of the samples, which affected the proportion of ultimate shrinkage which was observed after air-drying for 85 days in the controlled environment.

This presents the possibility that, as climate change occurs, the drying shrinkage cycles of concrete structures will change. While the estimates of the extent to which global temperatures will change vary significantly, it is clear that climate change is inevitable, and this may affect concrete structures in two ways.

Firstly, an increase in the drying shrinkage of existing structures could result in both the formation of new cracks and widening of existing cracks. This, in turn, increases the risk of other durability related issues which will require remedial action to be taken. Secondly, if repair materials are designed to have specific shrinkage properties based on the behaviour of original material, and these change as a result of climate changes, this could result in an increase in the failure rate of concrete repairs if the shrinkage properties of the repair material do not change similarly.

Conclusion

In this study, the reversible drying shrinkage of concrete samples taken from historic structures was monitored, and statistical analyses of the results were then carried out in order to determine which variables have the most impact. The results of this study suggest that the key variables influencing ultimate shrinkage are oven-dry density, maximum aggregate size and aggregate content, with the chemical composition of the binder also having an influence. A model taking these variables into consideration was formulated, but further research is required to expand on this and produce a model which can more accurately predict the shrinkage of the repair material. While a predictive model should allow repair materials with appropriate shrinkage characteristics to be formulated, there are concerns about how accurately the variables from the original material can be determined

using current methods. As such, the approach of creating like-for-like replacements which are authentic replicas of the original material is likely to be very challenging.

Given the effects of other factors, such as curing conditions and the degree of hydration, on the microstructure and mechanical properties of hardened concrete, it may, in reality, be more effective to undertake a more in-depth study of the *in-situ* material, and to try and replicate its physical properties as closely as possible through a series of trials. For example, DEMEC studs like the ones used in this study could easily be applied to strategic positions on a structure *in-situ*, and the strain measured over the course of a year to take into account the key variations that occur as a result of the change in environmental conditions. The data obtained would allow a shrinkage profile of the material to be developed, which would inform conservators on the range of shrinkage parameters which need to be met by a repair material.

Furthermore, the issue of climate change is one which needs to be considered in relation to the conservation of historically-significant concrete structures and the use of repair materials. As changes in temperature and precipitation levels occur, it is possible that the drying shrinkage cycles of concrete structures will alter in response to these and may result in both the formation of new cracks and widening of existing cracks. As such, the need for concrete repairs may increase with climate change and any repair materials which are designed with drying shrinkage in mind will also need to respond accordingly.

References

1. Wilkie S, Dyer T (2016) Can we accurately evaluate cement and other constituents in historically-significant concrete structures? Proceedings of the 4th Historic Mortars Conference: 240-247
2. Tilly GP, Jacobs J (2007) Concrete Repairs: Performance in service and current practice. IHS BRE Press, Bracknell
3. Markets and Markets (2016) Concrete Repair Mortars Market by Type (Polymer-Modified Cementitious Mortar and Epoxy-Based Mortar), Application Method (Manual, Spraying, and Pouring), End-use Industry - Global Forecast to 2021 Market Research Report. Markets and Markets
4. The Concrete Society (2009) Technical Report No. 69: Repair of concrete structures with reference to BS EN 1504. The Concrete Society, Camberley
5. Bissonnette BPP, Pigeon M (1999) Influence of key parameters on drying shrinkage of cementitious materials. Cement and Concrete Research 29: 1655–1662.
6. Day K (2010) Construction processes for improved durability. In: Soutsos M (ed) Concrete Durability: A practical guide to the design of durable concrete structures: 315-342. Thomas Telford, London

7. Kwan AKH, Fung WWS, Wong HHC (2010) Reducing drying shrinkage of concrete by treatment of aggregate. *Magazine of Concrete Research* 62:435-442.
8. Building Research Establishment (1991) Digest 361: Why do buildings crack? Building Research Establishment, Watford
9. Zhang W, Zakaria M, Hama Y (2013) Influence of aggregate materials characteristics on the drying shrinkage properties of mortar and concrete. *Construction and Building Materials* 49: 500-510.
10. Neville AM, Brooks JJ (2010) *Concrete Technology*. 2nd edn. Pearson Education Limited, Harlow
11. Domone PLJ (2001) Concrete. In: Illston JM, Domone PLJ (ed). *Construction Materials: Their nature and behaviour*: 89-224. Spon Press, London
12. The Concrete Society (2000) Technical Report No. 54: Diagnosis of deterioration in concrete structures - identification of defects, evaluation and development of remedial action. The Concrete Society, Crowthorne
13. Neville AM (2011) *Properties of Concrete*. 5th edn. Pearson Education Limited, Harlow
14. Bye GC (1999) *Portland Cement*. 2nd edn. Thomas Telford, London
15. Ayano T, Wittmann FT (2002) Drying, moisture distribution, and shrinkage of cement-based materials. *Materials and Structures* 35:134-140.
16. Imamoto K, Masanao A (2008) Specific surface area of aggregate and its relation to concrete drying shrinkage. *Materials and Structures* 41:323-333.
17. Saliba J, Rozière E, Grondin F, Loukili A (2011) Influence of shrinkage-reducing admixtures on plastic and long-term shrinkage. *Cement & Concrete Composites* 33:209–217.
18. British Standards Institution (1986) BS 1881-206:1986, *Testing Concrete, Part 206: Recommendations for determination of strain in concrete*. BSI, London
19. British Standards Institution (2009) BS EN 12390-7:2009, *Testing Hardened Concrete, Part 7: Density of hardened concrete*. BSI, London
20. British Standards Institution (2015) BS 1881-124:2015, *Testing Concrete, Part 124: Methods for analysis of hardened concrete*. BSI, London
21. British Standards Institution (2012) BS EN 933-1:2012, *Tests for Geometrical Properties of Aggregates, Part 1: Determination of Particle size distribution - Sieving method*. BSI, London

22. British Standards Institution (1996) BS EN 933-2:1996, Tests for Geometrical Properties of Aggregates, Part 2: Determination of particle size distribution - Test sieves, nominal size of apertures. BSI, London
23. Chatfield C, Collins AJ (1980) Introduction to Multivariate Analysis. 1st edn. Chapman and Hall, London
24. Almudaiheem JA, Hansen W (1987) Effect of Specimen Size and Shape on Drying Shrinkage. ACI Materials Journal, March-April:130-135.
25. Building Research Establishment (1991) Digest 357: Shrinkage of natural aggregates in concrete. Building Research Establishment, Watford

Repairs to Historic Concrete Pavement at Jacob Riis Park Utilizing Natural, Roman and Portland Cements

Michael P. Edison

Society for the Preservation of Historic Cements, Inc., sphc2011@gmail.com

Abstract

In the wake of Hurricane Sandy in October, 2012, debris from the devastated adjacent community of Breezy Point, New York was deposited on Jacob Riis Park's concrete parking field by the US Federal Emergency Management Agency (FEMA). Damage to the pavement resulted from both the debris-handling operations and the direct impact of the storm itself. Repairs to the historic concrete specified by the US Army of Corps of Engineers (USACE) were to utilize concrete based on natural cement which conformed to the requirements of ASTM C10 to match the original pavement. At the same time, USACE performance requirements specified a minimum compressive strength of 31 MPa at 28 days, well beyond the typical properties of natural cement.

Through development and testing a compromise repair mix was formulated based on a combination of natural cement, Roman cement and portland cement binders. The mix met the Corps of Engineers performance requirements while maintaining ASTM C10 cement as 50% of the binder.



Figure 1. 1956 aerial view of Riis Park and the Marine Parkway Bridge. [1]



Figure 2. Fire destroyed 130 homes in Breezy Point during Hurricane Sandy [2]

Hurricane Sandy

Jacob Riis Park (Figure 1) is a seaside beach, bathhouse, park and golf course located on the Rockaway Peninsula in New York City's Borough of Queens. The entire park, including buildings, pavements, playgrounds and landscaping is a designated National Historic District due to its relatively unaltered 1930's construction, of which it is considered a good example [3]. It was originally operated as a New York City Park and is currently managed by the US National Park Service as part of the Gateway National Recreation Area.

On October 29, 2012, a storm surge of 2.7 m (8.94 ft) inundated the Rockaway Peninsula and the village of Breezy Point that sits at the narrow peninsula's western edge [4]. On October 30, fire broke out destroying 130 homes and damaging 50 more. (Figure 2)

Natural Cement Concrete

In the wake of the storm and fire, emergency operations directed by FEMA cleared debris from Breezy Point and deposited it on the adjacent Riis Park parking field. The heavy loading of the debris itself as well as of the equipment used to move it, created multiple areas of damage to the concrete pavement (Figure 3).

Natural cement concrete was referenced as having been used in the original construction by the Historic Preservation Officer of the New York City Department of Parks. In 2014, USACE issued a repair contract which included replacement of 917 m³ (1200 yd³) of natural cement concrete. The specifications required the contractor to submit samples of the original pavement for petrographic and chemical analysis and final mix designs were to be based on the results of that analysis.

The natural cement was specified to conform to the requirements of ASTM C10/10M-2010, Standard Specification for Natural Cement and was also required to attain a minimum compressive strength of 31 MPa (4500 psi) in 28 days. ASTM C10-conforming cements and the concretes made from them are generally incapable of developing the specified strength in the specified 28-day interval.



Figure 3. Typical damaged pavement areas, resulting from placement and removal of Hurricane Sandy debris.
Photo by the author, 2014.

While natural cement was the predominant hydraulic binder used in the United States in the 19th Century [5], it was quickly overtaken by portland cement in the early 20th Century [6]. Yet natural cement did not disappear during that period, and through most of the 20th Century it was commonly used as a component in both masonry cements and in concrete mixtures as a blend with portland cement. [7]

Discussions of the conflicting requirements led to a compromise requirement that natural cement would comprise 50% by volume of the repair mix binder. The project specifications were effectively changing from an historic replication mix to a performance specification based on materials appropriate to the original construction period. In the early to mid-20th Century tradition of usage, blending of natural and portland cements would be permitted in order to achieve the target strength. At that point, analysis and replication of the existing pavement was no longer relevant to the execution of the work and no petrographic analysis was pursued.

The contractor for the project was required to identify and propose matching coarse and fine aggregates. Cow Bay sand conforming to ASTM C33 was identified as a matching fine aggregate and a blend of equal proportions of ¾" Delaware River Stone and ¾" Bluestone was identified as a good match to the coarse aggregate.

The binder matrix was composed of equal volumes of portland cements and natural cements, supplemented with trace amounts of iron oxide colorants conforming to ASTM C979 to better match the original concrete matrix color. The portland cements conformed to ASTM C150 Type I and Type I/II. A blend of Lehigh White Portland Cement (19.4%), Federal White Portland Cement (7.8%) and Essroc Grey Portland Cement (31.9%) was used to closely approximate the existing pavement matrix color when blended with natural cement. All percentages are by mass on the basis of total binder. The higher density of portland cement as opposed to natural cement accounts for the higher percentage by mass (59.1%) of the portland component.

In order to meet a short construction schedule of just a few months and to minimize costs, natural cements utilized were a blend of Rosendale 10C Natural Cement and Marfil Roman Cement. Both cements meet the definition of natural cement, a hydraulic cement produced by calcining argillaceous limestone at a temperature below the sintering point and grinding to a fine powder [8]. Roman cements do not typically meet the specific chemical and physical requirements of ASTM C10 due to excessive SO₃ content and excessively rapid time of initial setting.

It was determined through testing that blending Marfil Roman Cement with Rosendale 10C American Natural Cement could result in SO₃ content within the standard's 3% maximum restriction while producing set times surpassing the minimum 10-minute requirement for quick-setting natural cement as specified in ASTM C10. Mixtures of 50% Marfil and 50% Rosendale 10C were found to reliably comply with these requirements while allowing for some natural variations in raw materials composition. Even mixtures of 80% Marfil / 20% Rosendale 10C were found to comply. The challenge of meeting the ASTM C10 requirement for SO₃ (3.0% max.) is complicated by the addition of calcium sulphate as a set regulating additive in natural cement production.

Tests results listed in Table 1 for the various natural cements and blends of Rosendale 10C with Marfil are based on the test methods specified in ASTM C10/10M-14. Specifically, the standard specifies use of a blend of 75% natural cement and 25% portland cement conforming to the requirements of ASTM C150 Type II in the autoclave expansion test, representing a modification to the standard ASTM C151 test method. The standard's compressive strength test requirements specify use of a 1:1 mix by mass of natural cement and ASTM C778 20-30 test sand, representing a modification to the ASTM C109/109M compressive strength test method. The modifications have been part of earlier versions of the ASTM C10 standard as well, and represent adaptations of test methods originally designed for testing of portland cements so that they may be used with natural cements.

Mixture of the blended natural and Roman cements with portland cement effectively retarded initial setting of the natural cement blend further, allowing the mixes to be placed without undue haste. Given the revised specification of equal volumes of natural and portland cements as a binder, the testing matrix became a simple exercise in evaluating

compressive strength test results for concretes incorporating varying amounts of the blended cementitious component. Initially a mix containing 550 lbs. of cement per cubic yard was tested, followed by a mix containing 600 lbs. per cubic yard. While the 600 lb. mix met the minimum strength requirements, the contractor opted for a higher strength mix containing 660 lbs. of cement per cubic yard on the assumption that field results would tend to be lower than those obtained in the laboratory under more ideal conditions using more accurately batched mixtures.

Table 1. Properties of Roman and American Natural Cements vs. ASTM C10 Requirements

Property	Test Method	ASTM C10 Requirement	Rosendale 10C*	Marfil	1:1 Marfil: 10C [11]	4:1 Marfil: 10C [12]
SO ₃ %	ASTM C114	3% Max.	2.23 - 2.80%	3.2 – 3.4%	2.5%	3.0%
Loss on Ignition, %		12% Max.	8.77- 11.92%		7.78%	7.0%
Insoluble Residue, %		2% Min.	8.15 - 8.77%		7.39%	6.0%
Autoclave Length Change, %	ASTM C151 (Modified)	0.80% Max.	0.34 -0.70%		0.62%	0.23%
Air Content, %	ASTM C185	12% Max.	5.0 - 7.0%		7.0%	7.0%
Time of Setting, minimum	ASTM C191	10 minutes (Quick-Setting) 30 minutes (Regular)	42 – 84 minutes	2 - 5 min.	47 minutes	25 minutes
Compressive Strength, Mpa (psi)	ASTM C109/109M (Modified)	3.5 (510) at 7 days	5.8 – 6.6 (840-960)		15.6 (2260)	12.8 (1860)
		7.0 (1020) at 28 days	15.2 – 18.3 (2200-2660)		19.8 (2870)	12.8 (1850)

* Rosendale 10C data represents range reported for three separate test series [10]

The final mix design used for the work consisted of:

- 300 kg (660 lbs) Natural/Roman/Portland blend with pigments ASTM C10, C150, C979
- 554 kg (1219 lbs) Fine Aggregate ASTM C33/33M
- 795 kg (1750 lbs) Coarse Aggregate ASTM C33/33M

The blended cements with pigments were prepared at the natural cement producer's plant and packaged in supersacks. This allowed precise control of color and mass of each bag, to improve consistency of results on site. A spectrophotometer and color quality control software were used to measure and record color data for every mix. Overall color differences, dE, were below 1.0 for all of the mixes, an extremely consistent result for cementitious mixes. (Paint color tolerances, which are more easily controlled, are typically

held to the dE <1.0 standard.) Each pallet was weighed and a printed batch ticket was archived. A small sample of each mix was retained for quality control purposes.

Admixtures

Air entraining admixture conforming to the requirements of ASTM C260 was added by the contractor on site, to achieve the specified air content of 5.0%, plus or minus 1.5%. A water reducing admixture conforming to the requirements of ASTM C494 was also used. Specifications called for slump of 1 to 3 inches. In addition, due to ASR instability of one of the selected coarse aggregates, a lithium admixture conforming to ASTM C494 was added to prevent alkali silica reaction.

Execution of Repairs

All concrete mixing was performed on site using a Zim mobile volumetric mixer. Aggregates were delivered to the site in bulk and were stored in separate piles (Figure 4). The blend of cements and pigments was delivered in supersacks with polyethylene pallet covers (Figure 5) and were stored on site under an impermeable tarp.



Figure 4. Onsite storage of fine and coarse aggregates. Photo by the author.



Figure 5. A truckload of pigmented Natural/Roman/Portland cement supersacks departs the Edison Coatings factory for delivery to Riis Park. Photo by the author.



Figure 6. Typical prepared repair area, with welded wire mesh placed for reinforcement. Photo by the author.



Figure 7. Typical completed Repairs. Photo by the author.

Repair areas were sawcut and welded wire mesh was placed for reinforcement (Figure 6). Following placement, repairs were moist-cured for several days. Typical completed repairs are shown in Figure 7.

Over the course of the Summer of 2014, some 917 m³ (1200 yd³) of Natural/Roman/Portland cement concrete were placed. This represented a small portion of the overall mass of the historic concrete parking field.

Variations in properties were reported in the tests of site mixes. Slumps were measured at 4" to 5.75" for various tested mixes, exceeding the specified 1" to 3" slump per ASTM C143. Air contents ranged from 4.5% to 7.1%, generally within the specified 3.5% to 6.5% range. Compressive strengths at 28 days ranged from 21.65 Mpa to 30.83 MPa (3140 psi to 4470 psi), the equivalent of 70% to 99% of design strength. Strengths of 90% or higher are deemed acceptable. The lower strengths of some mixes are likely to have resulted from higher water addition levels in those mixes. Over time, the strengths of all mixes are expected to increase significantly.

Figure 8 is an aerial photo of Riis Park and the Marine Parkway bridge (Renamed the Gil Hodges Memorial Bridge) taken roughly one year after repairs were completed.



Figure 8. Aerial photograph of Riis Park and the Gil Hodges Memorial Bridge, approximately one year after completion of repairs. Photo by the author.

Conclusions

The project demonstrated how traditional Natural, Roman and Portland cements could successfully be combined to meet contemporary engineering requirements. The effectiveness of modern commercial admixtures for concrete, including air entrainment, water reduction and ASR-preventative materials was also demonstrated for this combination of traditional and contemporary cements. Ultimately, only time will confirm the durability and long-term performance of the mixtures employed and the project will come to represent a significant demonstration of both the potential and the limitations of these mixtures in a severe coastal service exposure.

From a preservation viewpoint, a parking field may not be the most inspirational subject for a case study. The process of balancing performance and durability with the desire to maintain at least a portion of the historic authenticity of original components may be instructive, however.

References

1. https://en.wikipedia.org/wiki/Jacob_Riis_Park
2. https://upload.wikimedia.org/wikipedia/commons/c/c6/Breezy_Point_Sandy_fire.jpg
3. "Development Concept Plan, Environmental Assessment: Jacob Riis Park, Gateway National Recreation Area, New York-New Jersey". Internet Archive. United States Department of the Interior, National Park Service. June 1989. Accessed February 2019

4. US Geological Survey, <https://www.weather.gov/okx/HurricaneSandy>, Accessed February 2019
5. Cummings, Uriah,(1898) American Cements, Rogers and Manson, NY pp. 288-289
6. Hahn, Thomas and Kemp, Emory (1994), Cement Mills Along the Potomac River, p.16, Institute for the History of Technology and Industrial Archaeology Vol. 2, Number 1, West Virginia
7. Edison, Michael P, (2006) The American Natural Cement Revival; Reintroducing a Historic Masonry Material and One of ASTM's Oldest Standards, ASTM Standardization News, January 2006 https://www.astm.org/SNEWS/JANUARY_2006/edison_jan06.html
8. ASTM C219-14, Standard Terminology Relating to Hydraulic Cement, ASTM International
9. TEC Services, (2015-17), Reports of Natural Cement Testing, unpublished
10. TEC Services (2014) Report of Natural Cement Testing #14-095, unpublished
11. TEC Services (2014) Report of Natural Cement Testing #14-397, unpublished

Methodology of identification of natural and historic Portland cements. Application and study in mortars of Madrid and Barcelona

Cristina Mayo Corrochano¹, Judith Ramírez-Casas², David Sanz Arauz³, Antonia Navarro

Ezquerro², Juan Ramon Rosell Amigo²

(1) AIPA (Analysis and Intervention in Architectural Heritage) research group, Polytechnic University of Madrid, Spain, cristina@estudiomayo.com

(2) Department of Technology of Architecture, Polytechnic School of Building of Barcelona (EPSEB), GICITED group, judith.ramirez@upc.edu, antonia.navarro@upc.edu, joan.ramon.rosell@upc.edu

(3) Department of Construction and Architectural Technologies of the School of Architecture of Madrid. AIPA research Group, Polytechnic University of Madrid, Spain, david.sanz.arauz@upm.es

Abstract

Natural cement was patented in England in 1796, but did not arrive in Spain until 1835. Its arrival supposed a natural coexistence with the rest of traditional mortars that had been used (lime, hydraulic limes and gypsum). However, its use was not extended in time, and soon it was replaced by the use of artificial Portland cements.

Although in Spain the natural cement came later, it was massively used in the decorations of historicist and modernist facades during the 19th and 20th century. Nowadays, after more than 100 years since its construction, it's necessary to conserve all this heritage. In order to achieve a good restoration, it is essential to correctly identify the binders originally used. The restoration of these mortars with incompatible materials can cause irreparable damage to the original elements of the buildings.

The aim of this research is the development of a simple, practical and economical method for the identification of natural cements and historic Portland cements mortars. We have used petrographic microscopy techniques in laboratory samples to establish the identification patterns of these cements. Then, this methodology has been applied in samples of buildings of Madrid and Barcelona where it is documented the use of historical cement mortars.

The differences in the formation of alite and belite crystals between Portland and natural cements have been analyzed, as well as the differences in the petrographic textures between the cements of Madrid and Barcelona.

Introduction

The present research is focused on the study of natural cement, the precursor of Portland cement. It was extensively used in the construction of many civil works and to decorate

historical buildings during the nineteenth and beginning of twentieth century in Madrid and Barcelona.

Natural cement was highly demanded in various sectors of civil engineering: sewerage, water supply, canals, ports and tunnels. In the construction sector, the use of natural cement was initially limited to the foundation of buildings and masonry mortars, and occasionally also used as render mortar and even stucco imitating stone ashlar.

This new material was highly valued for its good response to the effects of fresh or salty water [1]. Natural cements are produced calcining limestone (with clays containing between 25~40%) at low temperatures, 800 ~ 1200 ° C, below the sintering temperature [2]. However, natural cements was quickly eclipsed by the arrival of Aspdin Portland cement.

We have analyzed unhydrated modern Portland and Natural cements [3] in DRX to see the mineralogical composition differences. We observe that the main difference between both materials lies in the calcination temperature. Since natural cement is produced at temperatures below 1200 °C, its main phase is belite. While in the case of Portland cement, whose calcination temperature is higher than 1200°C, its main phase is the alite.

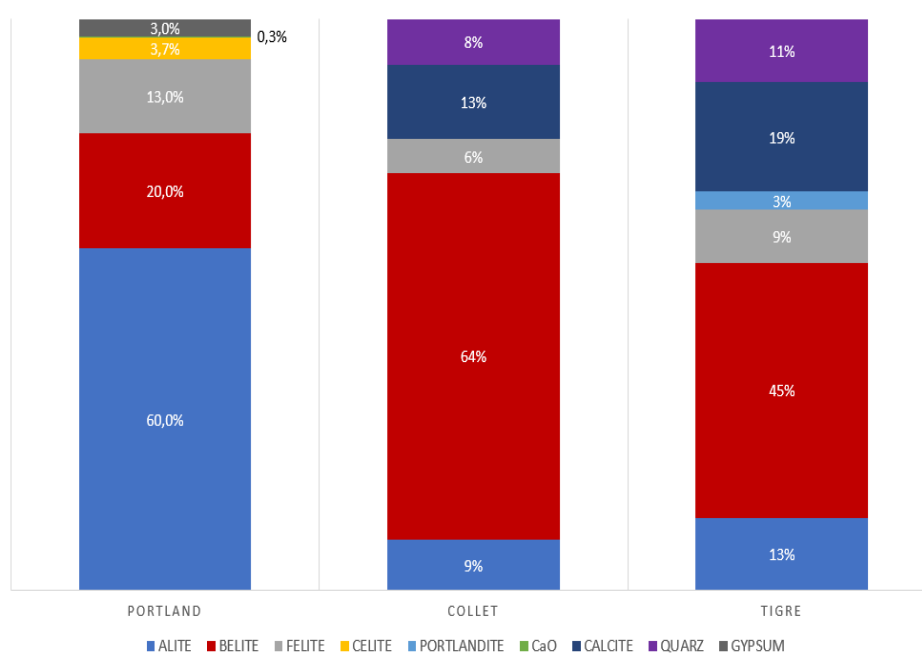


Figure 1. Mineralogical composition of unhydrated Portland and Natural cements .

Background study

In Spain natural cement industrial production began simultaneously in the Basque Country and Catalonia during the 1850s (Figure 1). In the Basque country the first industrial factory was founded in Arona (Bajo Urola, Gipuzkoa) in 1858 and was called "Nuestra Señora de los Dolores" (1858-1930). In the same year in Girona (Catalonia) the Pérez Torruella y Cia company was founded and began to produce natural cement and hydraulic limes [2, 3].



Figure 2. Location of the first natural cement factories in Spain [4].

The historical documentation proves that the production of natural cement in Spain did not finish after the Spanish civil war (1936-1939), in fact it continued after the year 1968 (Figure 2) to the present residual production of four factories in the Catalan territory. After the Spanish civil war there was an increase on the demand of this kind of cement, responding to a need of rebuild a country destroyed by the war and because of the lack of a suitable coal to produce Portland cement and the problems for the transport. Due to this, many small factories appeared all over Spain to supply locally the need of each area. So much so, that it is known that in 1945 there were four natural cement factories in Madrid [5] and twenty in Catalonia, which coexisted with one and seven Portland cement factories respectively. We find this coexistence interesting due to one of the aims of this study is to distinguish between natural cement and historical Portland cement.

Nevertheless, Portland cement industry expanded in the market disproportionately and make that many natural cement plants had to close. Despite of this, some natural cement plants continued to produce fast natural cement to this day. Actually there are four natural cement factories in Spain: Cementos Collet, Cementos Figueres, Cementos Tigre and Lafac, all in Catalonia.

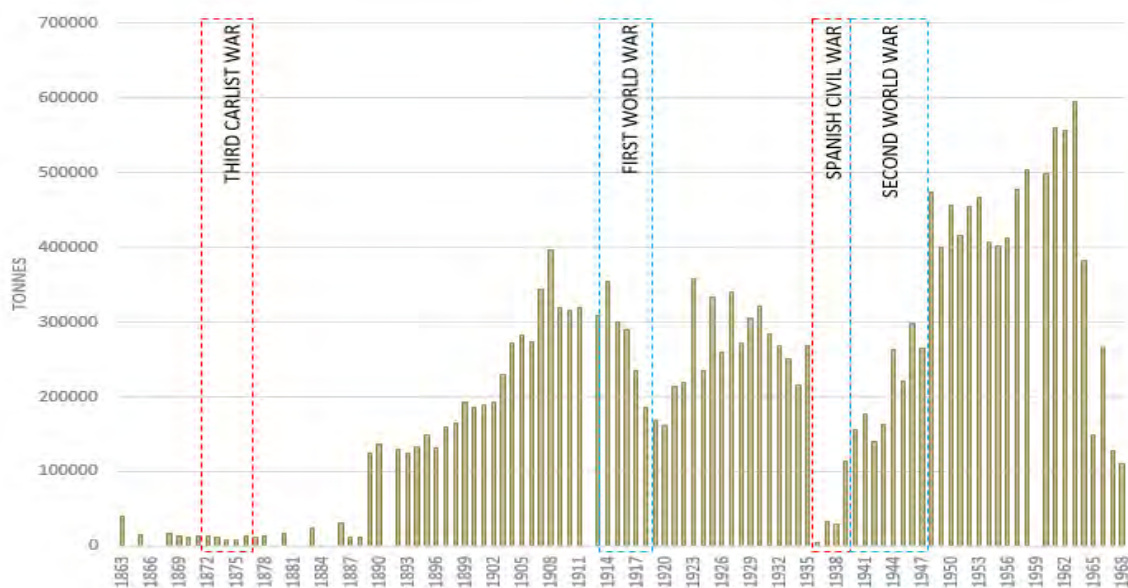


Figure 3. Annual production of natural cement in Spain [6].

Natural cement identification methodology

The main problem we faced in this research is the visual identification of the historic mortar used during this period of time. This is because the line between a natural cement and an historic Portland cement is very thin.

Due to this, and with the aim of establishing the right methodology to differentiate natural and Portland cements coexisting in those days, polished thin sections are done from the laboratory modern cement test pieces (Collet, Tigre and Portland cement) in order to establish natural cement identification patterns [6, 7]. We analyze the samples and established the patterns (Figure 3):

1. Natural cements have a color between ochre and light brown.
2. Presence of lumps of calcined marls in the natural cement samples. The existence of these lumps is due to the cooking itself and to the deficient milling technology of the time.
3. Due to the difference in the calcination temperature in the production of both materials, we can observe different unhydrated phases in their polished thin section with an optical polarized microscopy. In the case of natural cements we observe the presence of unhydrated belite crystals and absence of unhydrated alite crystals, while in Portland cements we can observe both unhydrated phases. We can also confirm the presence of belite or alite crystals, with a chemical analysis in the SEM. The poor quality of the grinding technology of the natural cements allows fragments of calcined marl to remain unhydrated in the setting process, making easy to identify unhydrated belite crystals inside the lumps. On the other hand, in the production of the historic Portland cements, the continuous vertical kilns used in the production of natural cement were reused. The calcination process in this kind of kilns was longer than in a modern horizontal kiln and it allowed the belite and alite crystals to acquire a larger size than in modern Portland cement. The large size of the unhydrated alite crystals present in historic Portland cements greatly facilitates their identification by petrographic microscopy.

After we have established this identification patterns, we apply a working methodology for the identification of natural cement in samples taken from representative buildings build between 1850 and 1965 in Madrid and Barcelona, which their historical documentation mentions the use of natural or Portland cement and have no suffered restorations, so they still have the original materials:

1. Analyze the color of the polished thin section sample in the stereomicroscope.
2. Analyze the presence or not of lumps of calcined marls in a petrographic microscope.
3. Analyze the presence or absence of unhydrated alite and belite crystals in a petrographic microscope.

4. Confirm the chemical composition of the unhydrated crystals in the SEM.

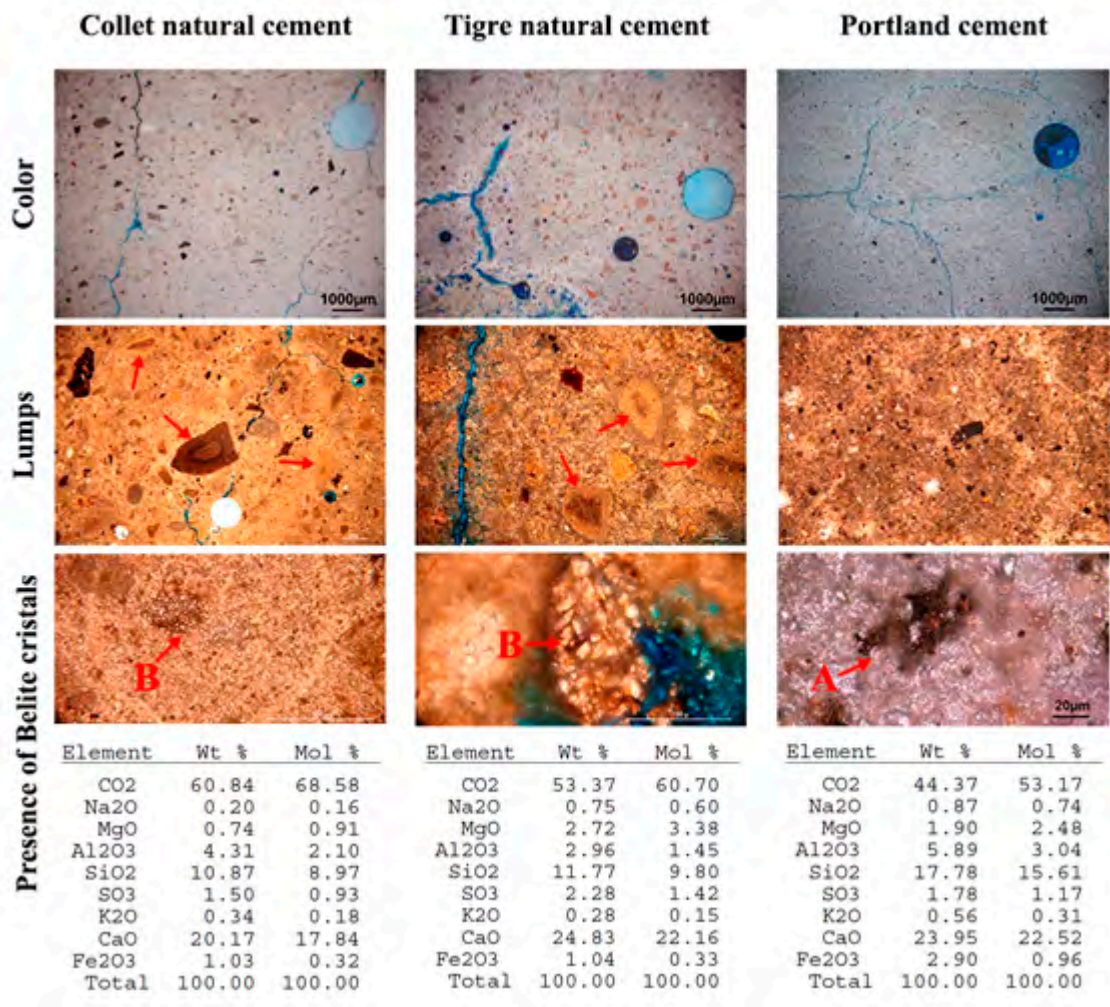


Figure 4. Analysis of Collet, Tigre and Portland cement samples. Alite (A), belite (B). [7]

Results. Application of the Natural cement identification methodology

After we have established a working methodology for the identification of natural cement, we use it with samples taken from representative buildings build between 1850 and 1965 in Madrid and Barcelona, which their historical documentation mentions the use of natural or Portland cement. We have tried to ensure that the samples collected are representative of the time of construction of the buildings, even though they have undergone subsequent restorations.

Thereby we can test this methodology for the identification of natural cements.

Table 1. Summary table of samples, Madrid (M) and Barcelona (B)

Sample number	Name	Building	Location (sample)	Year	Type of mortar
M1	Velazquez Palace	Museum building	Facade	1883	In situ run profile
M2	Apartments Recoleta's Street	Residential building	Interior patio	1863	Render
M3	Music Palace	Concert hall	Column	1924	Column of the original ballroom of the basements
M4	Cerralbo museum	*Museum building	Garden pavilion	1884	Balustrade. Cast decorative elements
B1	Villarroel	Residential building	Facade	1900	Cast decorative elements
B2	Hivernacle (greenhouse)	Greenhouse	Cladding metal structure	1887	Cast decorative elements
B3	Bellesguard Tower	*Museum building	Tower needle	1909	Masonry mortar

* The building was originally a single-family dwelling

Sample M1

The Velazquez Palace was built by Ricardo Velázquez Bosco between years 1881 and 1883 for the national mining exhibition in the Retiro Park. The sample was taken from a run profile decoration of the facade.



Figure 5. Main facade of the Velazquez Palace. Detail of the run profile decoration where the sample was taken.

In this case it is confirmed the use of natural cement on the facade decorations. With the use of petrographic microscope we can observe the characteristic lumps of over fired, well fired and under fired marls, typical of this kind of cement. This and the lack of alite crystals in the incompletely hydrated grains of cement confirm the use of natural cement in this building.

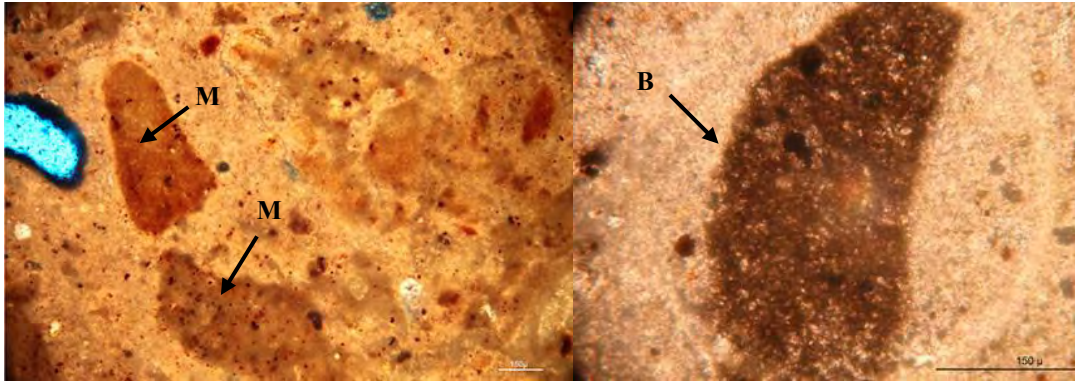


Figure 6. Thin section photomicrograph. Transmitted light. Detail of a lump of calcined marls (M) and the unhydrated belite crystals (B).

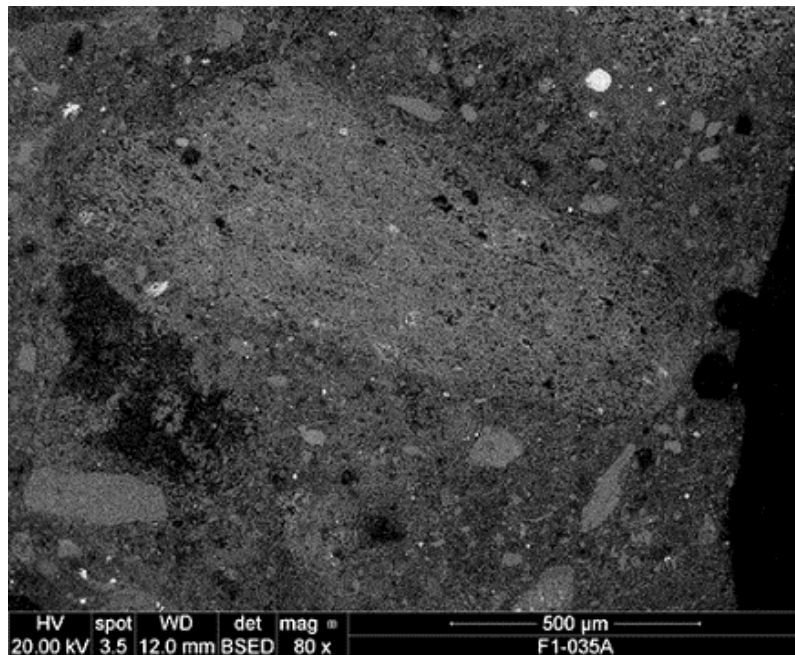


Figure 7. Microphotography by SEM. Detail of a lump of calcined marl.

Sample M2

The apartments' building was built between 1863 and 1872 in 13th Recoleta's Street promoted by Pascual Madoz. However, the building was restored in the beginning of the XX century.



Figure 8. Facade of the building. Thin section photomicrograph. Incident light. Absence of lumps of calcined marls.

A sample was taken from the render of an interior patio. In this case Portland cement was used for the mortar. It can be seen clearly with a petrographic microscope the presence of non-hydrated belite and alite crystals (Figure 8 and 9) and the absence of lumps of calcined marls (Figure 7).



Figure 9. Thin section photomicrograph. Trasmited light. Detail of unhidrated belite (B) and alite (A) crystals.

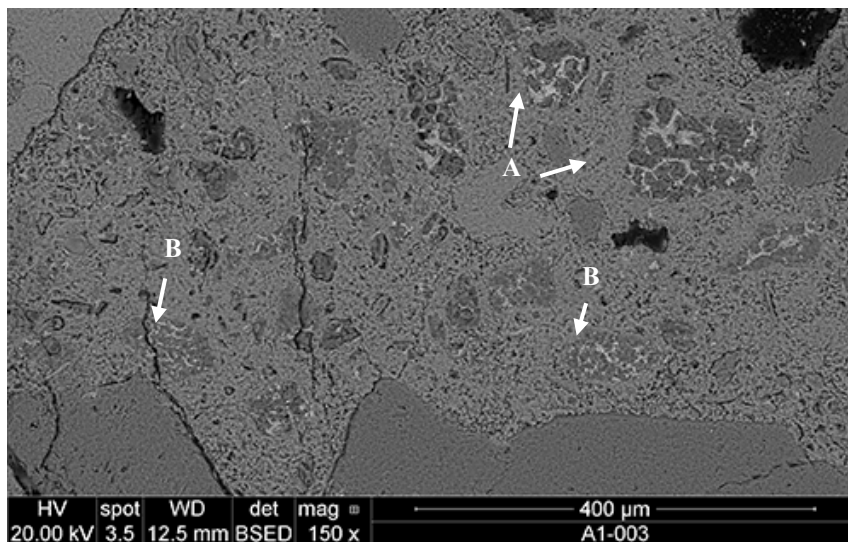


Figure 10. Microphotography by SEM. Identification of unhydrated belite (B) and alite (A) crystals.

Sample M3

The Music Palace was built in 1925 by Secundino de Zuazo Ugalde. This sample was taken from a column of the original ballroom of the basements. In this case Portland cement was use for the building structure. As in the case of sample M2 it can be clearly seeing in the petrographic microscope unhydrated belite and alite cristals and the absence of lumps of calcined marls.

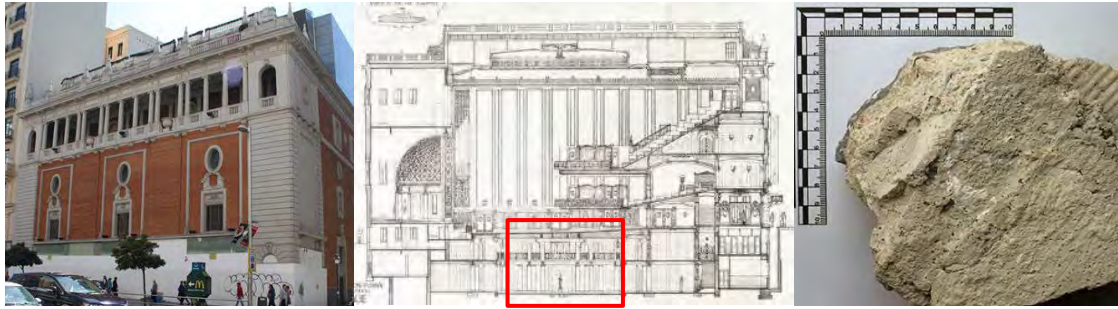


Figure 11. Main facade of the building. Location of the column of the original ballroom, where the sample was taken.

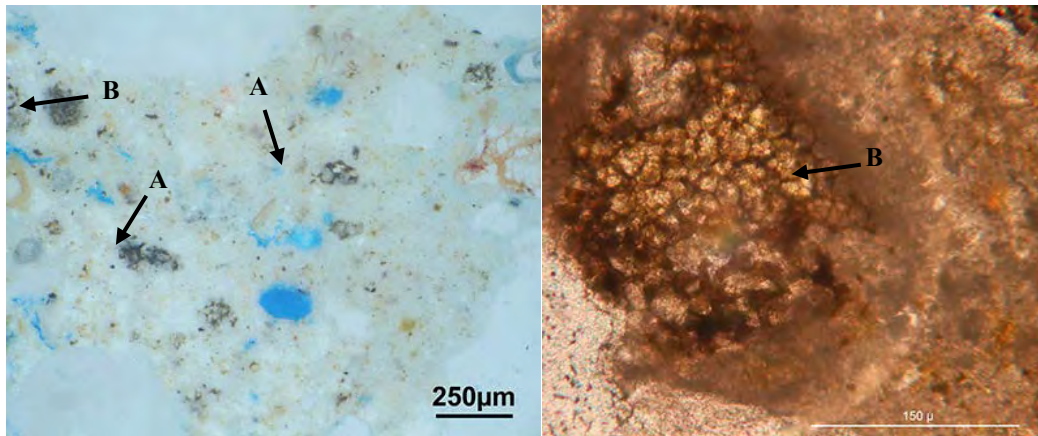


Figure 12. Thin section photomicrograph. Incident light. Alite crystals (A) and large belite crystals (B)..
Trasmitted light. Detail of unhydrated belite crystals (B).

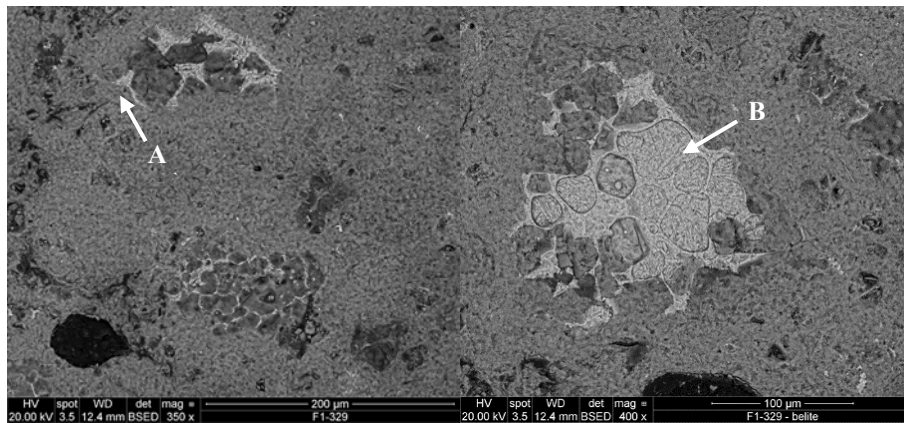


Figure 13. Microphotography by SEM. Identification of unhydrated belite (B) and alite (A) crystals.

Sample M4

Cerralbo museum was built in 1884 by the architect Alejandro Sureda, but its pavilion garden was built years later in 1891 by Luis Cabello y Asó. During the Spanish civil war, a bomb fell on the pavilion destroying part of the structure and decorations. The architect Manuel Martinez Chumillas was commissioned to restore it in 1940.



Figure 14.: Exterior view of the Cerralbo Palace. Garden pavilion. Detail of the damage of the balustrades of artificial stone.

The sample was taken from one of the balustrades of the garden pavilion. The sample have a light brownish "natural cement" typical color.

However, although grains on non-hydrated cement with exclusive belite crystals presence were found, the total lack of the characteristic lumps of calcined marls reveals that this is not a natural cement. We can say that this is a belitic cement calcined at low temperature.

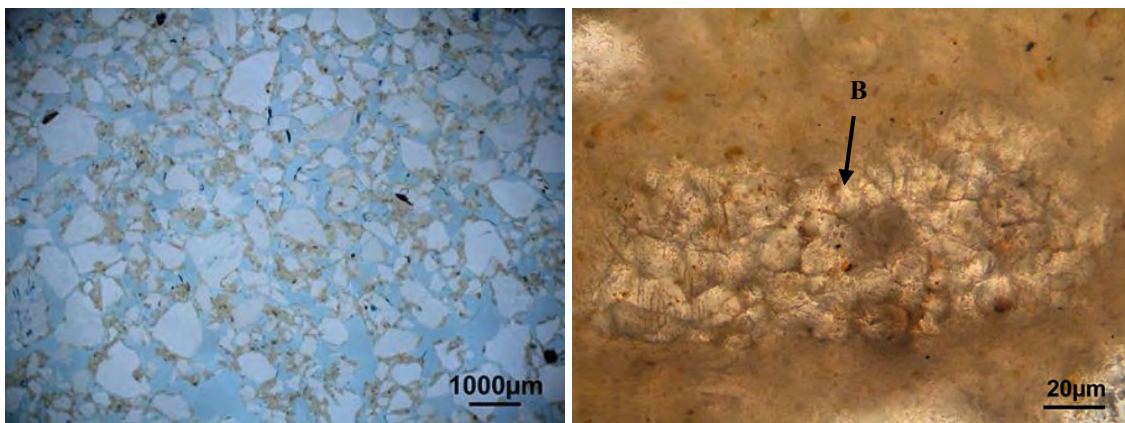


Figure 15. Thin section photomicroscograph. Incident light. The absence of lumps of calcined marls are observed. Thin section photomicroscograph; Trasmited light. Detail of unhydrated belite crystals (B).

Sample B1

The building it's located in the "Eixample of Barcelona" and presents the typical constructive characteristics designed by Idelfons Cerdà.

It was built in 1900, years after the beginning of the constitution of the expansion of the city (1859-1867). This was a period of massive use of natural cement in Catalonia, and de facade have artificial stone ornamental elements that usually use this new material.



Figure 16. Facade photography of the building in 1959. Detail of the ornamental elements of the Villarroel street facade. Sample detail.

A sample is taken of one of these ornamental elements. The mortar presents a light brownish natural cement typical color. We can also see lumps of calcined marls with unhydrated belite crystals inside in the petrographic microscope. This and the absence of alite crystals or lime nodes in the mortar indicate that is a natural cement.

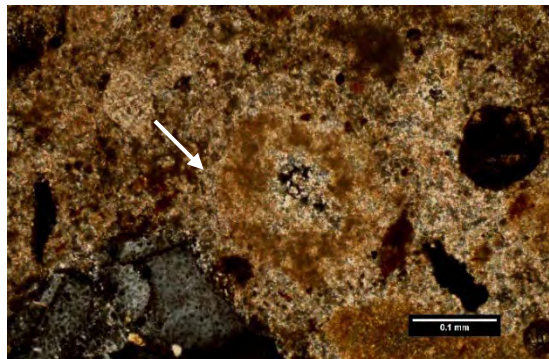


Figure 17. Thin section photomicrograph. Transmitted light, crossed nicols. Detail of a lump of calcined marls with unhydrated belite crystals inside.

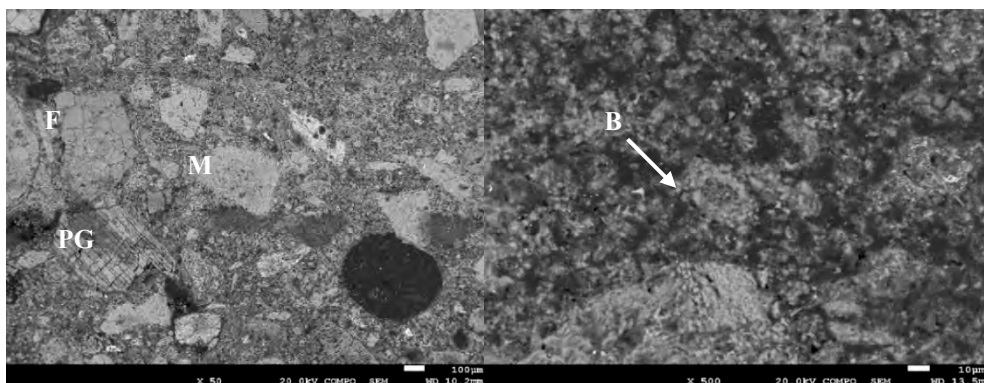


Figure 18. Microphotography by SEM. Identification of Feldspars (F), plagioclase (PG) and a lump of calcined marl (M). We can also see unhydrated belite crystals (B) inside a lump of calcined marl.

Sample B2

L'Hivernacle was built by Josep Fontserè in 1887 in the Ciutadella Park. This building is an example of the influence of the crystal Palaces of the universal exhibitions of the 19th century in Barcelona architecture. Nowadays the building is under restoration.

The structure of the building is made of steel frames, brick structure walls and a crystal roof. All of vertical structure is surrounded by artificial stone decorations.



Figure 19. Indoor photographs of the greenhouse. Detail of the artificial stone decorations. Sample detail

A sample is taken in one of these decorative cash elements. In the optical microscope we can see the light brownish color of the sample and the presence of lumps of calcined marls with unhydrated belite crystals inside that indicate that is a natural cement.

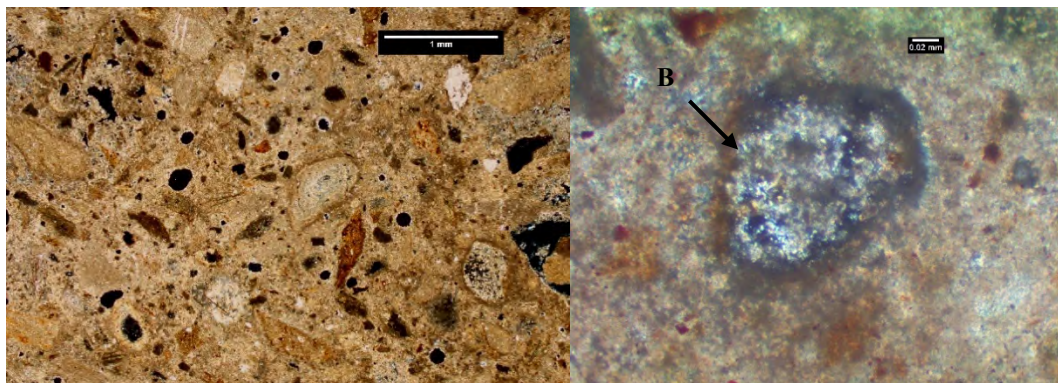


Figure 20. Thin section photomicrograph transmitted light, crossed nicols. Detail of the lumps of calcined marls. Detail of the unhydrated belite crystals inside of a lump (B).

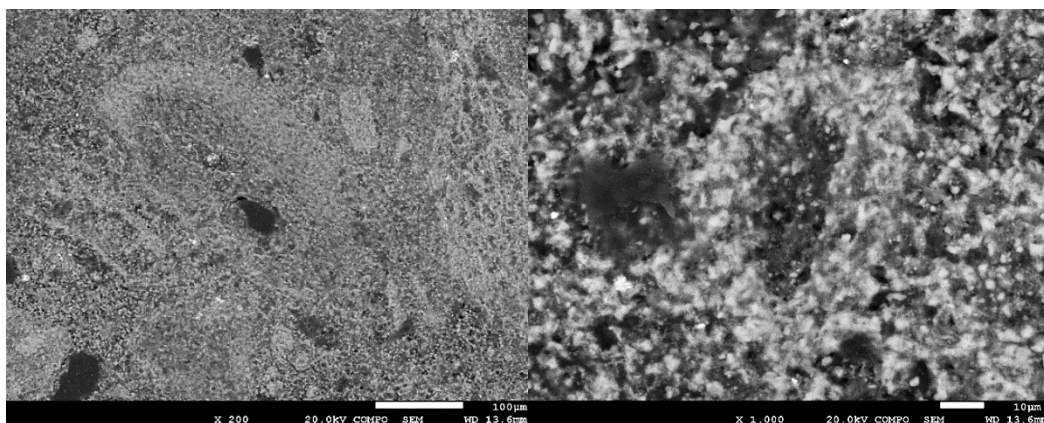


Figure 21. Microphotography by SEM. Detail of a lump of calcined marl with unhydrated belite crystals inside.

Sample B3

The Bellesguard tower was building and designed by Antonio Gaudí between 1900 and 1909. This project and the Colonia Güell Crypt, are part of Gaudí's "testing workshop", where he puts into practice innovative architectural solutions that he will later use in the Sagrada Familia. Because Gaudi was one of precursors of the use of natural cement in Spain, is interesting to analyze the type of mortar used in the building.



Figure 22. Fasade of Bellesguard tower and a detail of the masonry of the tower needle.

A sample is taken of the masonry mortar of the tower needle. The mortar has the characteristic brownish natural cement color. But if we analyze it closer in the petrographic microscope, we can see a completely different structure than in a natural cement sample. This characteristic color is due to the presence of ceramic fragments in the arid of the mortar that give it the hydraulic properties. This, and the presence of calcite nodules, which are currently carbonated, confirm that is a lime mortar.

We also can observe that some of the ceramic fragments have a reaction edges with the conglomerate.

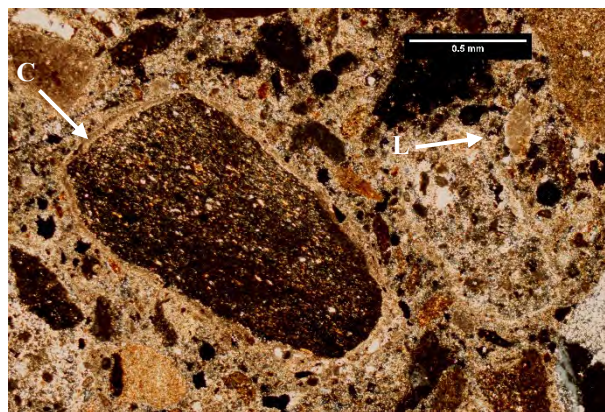


Figure 23. Sample B3. Trasmited light, crossed nicols. Presence of a large number of ceramic fragments (C). Presence of calcite nodels (L).

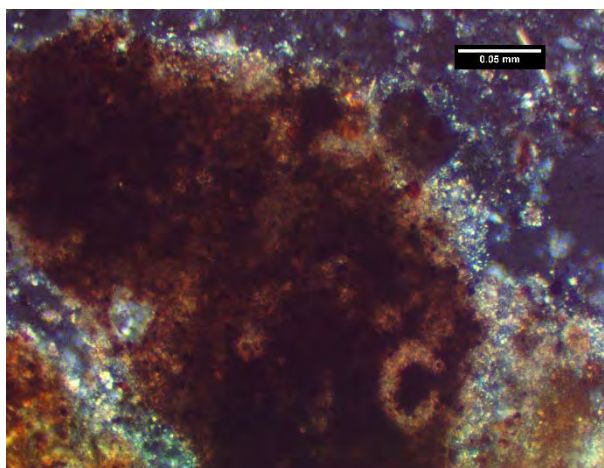


Figure 24. Sample B3. Transmitted light, crossed nicols. Visible reaction rim around a ceramic fragment.

Table 2 : Summary table of results

Sample number	Year	Type of mortar	Type of binder
M1	1883	In situ run profile	Natural cement
M2	1863	Render	Portland cement
M3	1924	Column of the original ballroom of the basements	Portland cement
M4	1884	Balustrade. Cast decorative elements	Belitic cement
B1	1900	Cast decorative elements	Natural cement
B2	1887	Cast decorative elements	Natural cement
B3	1909	Masonry mortar	Lime with fired crushed ceramics

Conclusions

Three different types of conglomerates have been identified in the seven buildings studied. Because there is more than 60 years that separated their construction dates, the coexistence of the different conglomerates is confirmed.

The methodology used allows us to identify the type of binder. The peculiarities of the unhydrated phases visualized have allowed us to make the distinction between the natural cement and the Portland cement.

This methodology has also allowed us to detect the mortars originally considered as originals and that the identification allowed us to date it after the construction of the building and therefore attribute it to a restoration.

Acknowledgements

The authors would like to express their thanks to Mr. Johannes Weber for his invaluable help in learning how to interpret the samples and for his warm welcome at his University.

A part of this study has been financed by the Generalitat de Catalunya (Spain), as part of the 2009 SGR 878 project, GICITED Research Group.

References

1. J. Ramírez-Casas, J. Rosell Amigó, J. Rosell Colomina, *Ciment natural a Catalunya: Història, producció i usos*, in: Publisher EPSEB (Ed.), *Libr. Actas La 1a Jorn. Dr. TAEU 2018*, Barcelona, 2018: pp. 10–15. <http://hdl.handle.net/2117/127779>.
2. C. Gurtner, G. Hilbert, D. Hughes, R. Kozłowski, J. Weber, *Manual on best practice in the application of roman cements. Roman cement, past and present. Conservation theory and practice*, (2012) 113. [http://www.rocare.eu/page/imgt/file/rocare-manual_low-res\(2b\).pdf](http://www.rocare.eu/page/imgt/file/rocare-manual_low-res(2b).pdf).
3. J. Mayo, C.; Sanz, D.; Pineda, *Metodología simplificada de identificación mediante MOP de las cales hidráulicas y los cementos naturales*, in: U. de Navarra (Ed.), *Tradic. Versatilidad e Innovación En La Cal Un Mater. Excel.*, VI Jornadas FICAL, Pamplona, 2018: pp. 188–199.
4. C. Barahona Rodríguez, *Técnicas para revestir fachadas. Arquitectura y teconología I.*, Madrid, 1999.
5. M.J. Varas, M.A. de Buergo, R. Fort, *The origin and development of natural cements: The Spanish experience*, *Constr. Build. Mater.* 21 (2007) 436–445. doi:10.1016/j.conbuildmat.2005.07.011.
6. Ministerio de Fomento, *Datos estadísticos correspondientes al año económico de 1945*, Junta superior facultativa de minería, Madrid, 1946.
7. C. Mayo Corrochano, *El cemento natural en el Madrid de los siglos XIX y XX. Identificación de sus aplicaciones, estado de conservación y compatibilidad con los cementos actuales.*, Universidad Politécnica de Madrid, 2015.

The use of mortars in Palau Güell by Antoni Gaudi

Ricardo Gomez-Val¹, Judith Ramirez-Casas¹, Antonia Navarro-Ezquerria¹

(1) Universitat Politècnica de Catalunya, ricardo.jose.gomez@upc.edu, judith.ramirez@upc.edu, antonia.navarro@upc.edu

Abstract

In Catalonia during 19th century there was a process of industrialization following the Llobregat river. One of the traditional materials used historically in building had been lime mortar. Natural cement began to be used from the middle of the 19th century in order to improve quality and characteristics of mortar elements. Barcelona experimented a huge urban expansion during the second half of 19th century. In order to do new buildings it was necessary to develop new techniques and materials.

Antoni Gaudi finished his studies in 1876 and he began working in Barcelona since then. He had learned from traditional materials and techniques at his father workshop in his hometown. He also learned from new technologies at School of Architecture in Barcelona.

Güell family were a wealthy family who owned different industries around Catalonia, following Llobregat river. They were the founders of a Portland factory in Spain, at Castellar de N'Hug in 1904. Before that date some Portland cement shipments had arrived and had been used in Barcelona's buildings imported from France.

They asked to a young architect, Antoni Gaudi to build their family house in the centre of Barcelona, near the harbour. Palau Güell built from 1886 to 1890 was the first important project done by Antoni Gaudi. In this building, Gaudi was able of studying and experimenting different technologies and materials that he would later use in other buildings as Mila's House or Sagrada Familia.

Palau Güell is built during a period of confluence between traditional and industrial techniques. There are some traditional techniques as paintings or plaster coatings with other more industrialised as the use of pavements and finishing which they answer to a will of seriation and standardizing. There is a neat debate between technique and art and the relationship between production and design. Gaudi was focused in order to introduce new technologies to buildings and to enhance traditional ones.

In Palau Güell different mortars are used as binder materials and as fastening material for façades and pavements. This different way of using mortars lead us to do research in some areas of Palau Güell obtaining interesting results in the use of natural cements.

This lab research has allowed us to understand the development of mortars by Antoni Gaudi. This research proves how Gaudi was an architect related to traditional techniques but looking to its development through research and experimentation.

Introduction

Palau Güell is one of the masterpieces by Antoni Gaudi, nevertheless quite unknown until now. It is situated near Barcelona's harbour in one of the streets that crosses gothic district from Montjuich hill until Ramblas. As its name says it's a Catalan palace built to be the manor of Güell family. They were a wealthy family who had several industries around Catalonia. Palau Güell was built in the city centre of Barcelona in order to be the cultural and main centre for improving the social life of the family.

It was begun to be built on 1886 and finished on 1890. The parcel where it is situated it's a ground between other buildings in a quite narrow although important street. This kind of construction takes profit of patio as an architectonic element, creating the hall of the building inside. This palace should host a whole single family plus servants and it should be suitable for social parties and meetings. We can find important meeting spaces as halls and living-rooms. It has different floors from ground floor where it's the entrance until the roof. It has a total of 2.850 m² divided in five different floors.

Antoni Gaudi travelled to Barcelona on 1869 in order to study architecture. In this recently created school of architecture he could learn from the best architects. He got an important knowledge on building techniques, drawing, physics and mathematics.

Gaudi was really attracted by Gothic architecture although he knew its lacks and he wanted to overcome it. He considered Gothic architecture had been an important challenge in the evolution of the architectonic techniques. He wanted to solve some of the technical problems experimented by this architecture that had not been solved yet. Gaudi was attracted from the Gothic architecture as a Christian artistic movement that had developed techniques and materials until its final step. He was interested by the improving solutions gotten by the Gothic architecture and its development towards perfection.

In order to improve building techniques, Gaudi knew he had to develop new technologies or to use the new ones that were being developed amongst Europe. Gaudi is an architect very interested in all the new technologies and materials developed by the industry. Although he was totally against serial production he wanted to improve traditional techniques. This is one of the reasons why Gaudi was never linked to a material not to a technology. He was using different materials and techniques getting the best of them and putting them to the limit. He used in his buildings timber, stone, iron, ceramics and all the different material and techniques he could. It's in the centre of this way of working that we can understand the use of mortars and cements by Antoni Gaudi.

The use of binders in Catalonia

The use of binders throughout history has always been linked to different aspects. It is not the same a façade coating, a supporting wall, an element subject to the effects of seawater or the need for a fast supporting when making a brick vault (Catalan vault). Each use implies that the properties of the binder to make mortar must be different. Therefore it is logical that the choice of the binder is based on the use that is given to him. Another aspect to consider is the availability of the raw materials and the distance between the production site and the market.

The XIXth century was a crucial period for these aspects. First, transport changed substantially thanks to the appearance and expansion of railway lines. This new transport mean allowed having materials manufactured at different points in the territory. Especially important were the train lines linking the north of Catalonia with Barcelona. The other aspect was the development of technology together with the advances that were being produced since the eighteenth century on the science and use of different kind of binders. This development was carried out especially in France and England. In Catalonia arrived at their peak during the nineteenth century, with the beginning of the making of a new binder, the natural cement. It was used at the same time that other ones as lime and gypsum, and even later with the Portland cement. Portland cement would be mainly used for a new constructive system, reinforced concrete, which it would prevail on all kind of constructions.

At the end of the nineteenth century there was an important inherited knowledge from the previous century in the use of the binders. In Spain, P. Madoz, in its *Diccionario geográfico-estadístico-histórico de España*, publishes in one of the volumes in 1847 a detailed study of engineer PL Espinosa. It gives an explanation of the properties of the limestone from the quarries of the province of Vizcaya, with a careful classification of lime and natural cements, depending on the content of clays [1].

On one hand there was gypsum, used for very specific works, especially for coatings and interior decorations. In some areas where it was common to find deposits of gypsum (Pallars, Solsonès, etc.), it was common to use gypsum as mortar, for a variety of constructive elements, facade enclosures, pavements and others. In other territories where limestone was more abundant, the most used conglomerate was lime, aerial but also hydraulic one. It must be said that until hydraulic binders were not available, these were replaced by the addition of pozzolanic ash to the mortars. By this mean it was obtained a hydraulic mortar with an aerial binder, which supposed a faster support.

The other binder that would begin to be made in Spain in the mid-nineteenth century, it is the natural cement or also known in Europe as Roman cement. The knowledge of natural cement in Spain was initially brought by the English soldiers in 1837 in San Sebastián (Guipúzcoa). Some years later the first factories were established in Iraeta and Zumaya [2] and almost simultaneously in Catalonia, in the area of Girona (1858).

The natural cement sometimes was confused with the hydraulic lime due to its similarity. It is a hydraulic binder that proceeds from the burning of marls (limestone containing a significant amount of clay). Unlike lime, it has not to be extinguished before using it. It gets strong much faster and it has also more mechanical strength.

Finally, the last binder to appear in building technology was the artificial Portland cement. In Spain, the first Portland cement production, as we know it now, was in 1898 in Tudela Veguín, Oviedo. In Catalonia it was a little later, in 1903. This cement was an evolution and somehow an improvement of the natural cement. In the natural cement its hydraulic behaviour and its quality depended one hundred per cent of the marls rock and nothing more. Nevertheless in the Portland cement, since it is made from a mixture of limestone and clays (hence the name of artificial) their properties could be controlled. Even so we have to understand that the evolution from one binder to another was gradual. At the end of nineteenth century we can speak of the natural Portland cement that would be on between the natural and the artificial cement [9].

Antoni Gaudi was one of the first architects on using Portland cement on its works, as it has been widely reported on Sagrada Familia church [5] The use of this special cement it was due in part of its aim of researching for new materials and its better properties than traditional materials.

Thus, in the years that Palau Güell was built, Eusebi Güell, a manufacturer of Portland cement since 1904 at his factory ASLAND in Castellar de N'Hug, this cement could still not be used. It only could be used if it was imported, since some Portland cement shiploads are known at the port of Barcelona, from Newcastle (England) and others [9].

Therefore, the types of binders used by Antoni Gaudi at the Palau Güell could be different. He would probably took into account the benefits and properties of the different mortars. With the range of products that there were in the market, natural cement was an innovative material of the moment that could be found in this monumental complex.

Previous works carried out in Palau Güell

During the works on the Palau Güell between 1886 and 1890 it was the ideal moment to test different solutions. Palau Güell had different technical problems to be solved. Also the use of various building materials allowed Gaudi to try different mortars and compositions in order to check the benefit of them.

On recent years as the restoration of the building was going on, some studies on the mortars used in Palau Güell have been done. It is very interesting the research carried out by the lab of heritage research from University of Barcelona [7]. In a report of this lab done on July 27th 2002 they tested one piece of mortar from the ceiling of the noble room. This test was done taking profit of the falling down of one of the pieces of crystalline lime that are coating the ceiling of the noble floor (Figure 1). In this test they considered that it was not Portland

cement but they didn't conclude which binder it was. In order to advance in the characterization of the mortars used on Palau Güell the following research has been carried out.

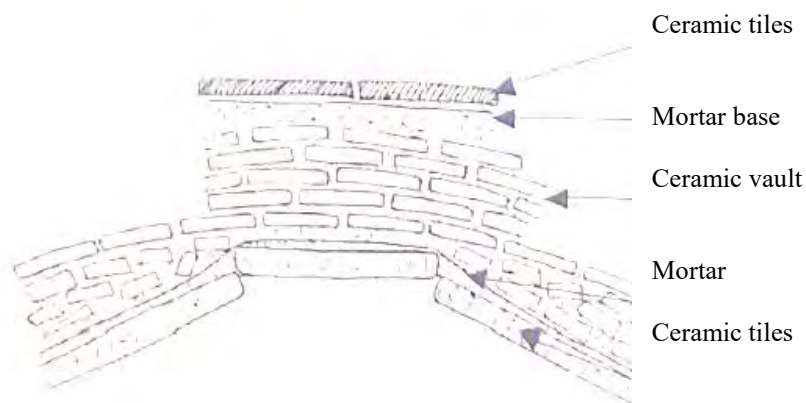


Figure 1. Detail extracted from this report [7] “Section of the disposition of different materials forming the vault in the studied area”

Methodology of study

In order to do a right research on this building a plan of visits was held. The first goal was to recognize the different kind of mortars being used in Palau Güell. After doing different research visits they were identified approximately 30 mortars in the building.

We should be especially careful with the mortars used in different elements on the roof. During the restoration held between 2004 and 2011 lots of these elements were affected and part of the original mortars removed and changed for some other modern ones.

In order to begin the research we chose two different elements in the same area of the building, the noble floor where it was the living room of the building. We took one sample from the mortar used in the ceiling (Figure 3) and another from the mortar used in on the ground in this area (Figure 4). We chose two small areas that we were sure they hadn't been restored, the ground of the inner part of the chimney and the ceiling of a small staircase that begins in the living room.

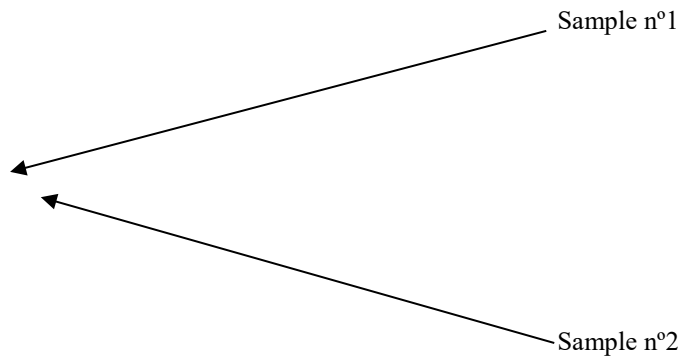


Figure 2. Plan of the noble floor drawn by Joan Alsina Arús on 1910.



Figure 3. Collection area sample 1



Figure 4. Collection area sample 2

We decided to try different methods to test these samples. We took different samples with a measure of 2 cm per 5 cm approximately. The goal of these two samples was to find amongst them some rests of natural cement that could prove our initial thesis.

The following tests were realized to these samples:

- Visual observation
- Thin section study with polarizing petrographic microscope (Optika microscope with 4X, 10X, 20X and 40X lenses) and image capture
- Binder elemental composition determination with electronic microscope (Scanning electron microscope SEM Brand JEOL Model JSM-7001F, Energy Dispersive X-ray spectroscopy EDX)
- Mineralogical composition of the binders (fraction size under 0,063 mm) with a powder diffractometer (PANalytical X'Pert PRO MPD Alpha) with copper radiation.
- Binder hydraulic properties with Differential Thermal Analysis (TG)

Lab research carried out

Sample n°1: Main floor ceiling mortar

The mortar found is grey-brown colour and it's very cohesive. The maximum size of aggregate is 3 mm and they are mainly of silica composition (polycrystalline and monocrystalline quartz grains, orthoclase feldspar- some of them altered with sericite-fragments of metamorphic rocks tipus schist) and with subangular form (Figure 5). Also there are some limestone grains (fragments of limestone rocks and marble rocks) with subrounded form.

In the fine fraction (size under 0,063 mm) there is also clay (phyllosilicate minerals of the kaolinite, illite and biotite type) and belite crystals non-hydrated at the grains of slaked lime or at the large grains of overburnt cement stones were found (Figure 6).[1]

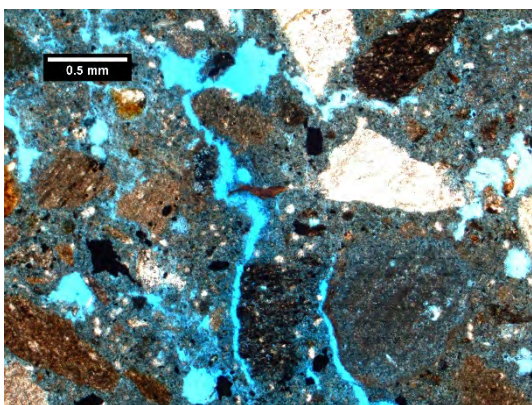


Figure 5. Microphotography with plain light where it can be seen quartz grains, fragments of metamorphic rocks and limestone grains. Also there can be seen retraction cracks and rounded pores.

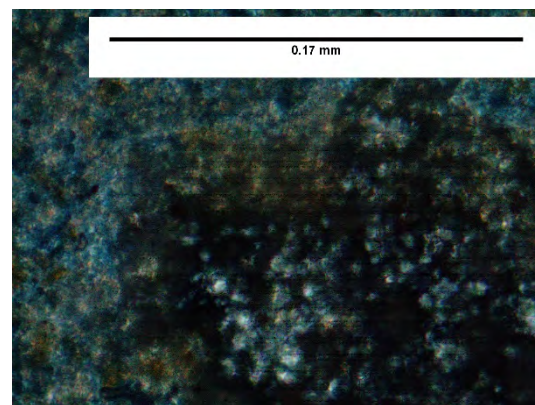


Figure 6. Microphotography with crossed-polarized light of a burnt limestone grain where it can be seen belite crystals.

The elemental composition of the binder has been obtained by electronic microscope and EDX elemental analysis (Table 1). The presence of silicon oxide and calcium oxide is

noteworthy, although the presence of alumina oxide has also been detected in percentages higher than 4%. Sodium, magnesium, chlorine and potassium oxides were detected as minor components.

The mineralogical composition of the binder was established using X-ray diffraction analysis (Figure 7). The following components were identified:

- The quartz, the anorthite and the orthoclase are due to the thin section arid size (size under 0,063 mm)
- The calcite is due to the carbonated part of the binder.
- The gehlenite and the calcium aluminium silicate are the definite elements to show that the cement used is natural cement. There are still some non-hydrated areas.

Observing the conglomerate with electron microscopy, hydrated grains have been detected with an unhydrated central nucleus (Figure 8).

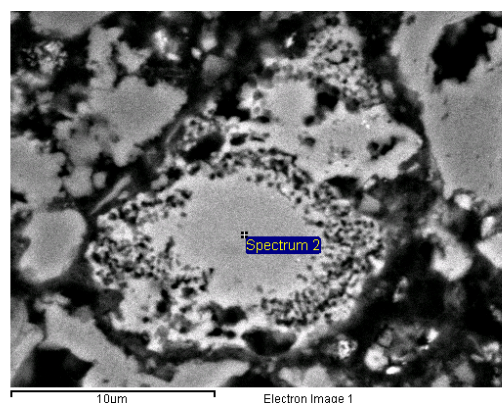
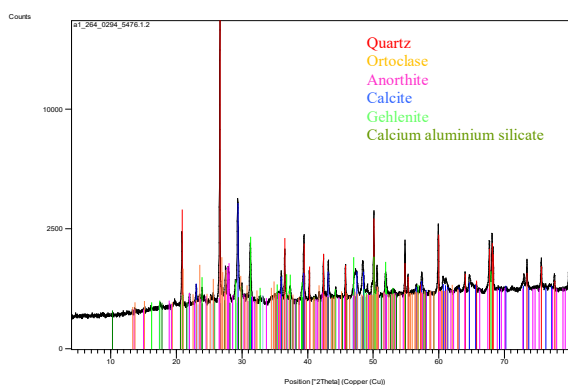


Figure 7. DRX spectrum of the binder

Figure 8. Grain of the original binder showing a hydrated ring around an unhydrated core (image with back scattered electrons)

Table 1. Elemental composition

Element	O	Na	Mg	Al	Si	Cl	K	Ca
%	56.86	0.64	0.84	4.80	21.10	0.47	1.69	13.60

Differential Thermal Analysis allows checking that with a difference of temperatures of 950°C a 28% of the sample is lost. This fact means that there are few composites that are decomposed in this range of temperatures (Figure 9). The highest peaks are found at 300°C, which it fits with the loss of water of some clay and at 800°C matches with the calcite decomposition.

If we compare the loss of weight produced by the decomposition of calcium carbonates (decomposition of CO₂) at more than 600°C and the quotient between this loss and the water that decomposes between 200 and 600°C, we can determine the degree of hydraulicity of the analysed mortar [8] (Figure 10). So we can conclude that it is a mortar

with hydraulic binder, of the type of the roman cement totally carbonated. There are nodules of gehlenite hydrate, and silicic aggregate, maximum size of 3 mm.

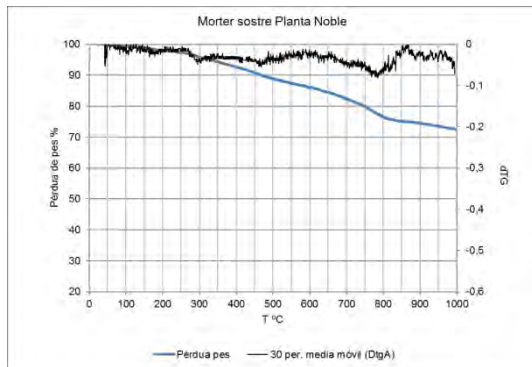


Figure 9. Shows the termogravimètric line in blue and black represents derivation of termogravimètric.

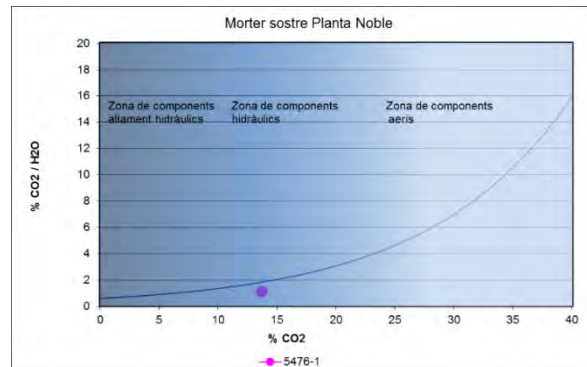


Figure 10. CO₂ to structurally bound water ratio in relation to % CO₂

Sample nº2: Main floor pavement mortar

The mortar found is grey-brown colour and it's very cohesive. Maximum size of aggregate is 2 mm and they are mainly of silica composition (fragments of metamorphic rocks tipus phyllite) and with subangled form (Figure 11). Also there are some limestone grains (fragments of limestone rocks) with subrounded form. There are some limestone fragments not enough burnt. In the inner parts we can find belite crystals non-hydrated (Figure 12).

In this sample we cannot find so much porosity associated with fissure systems and there are more spherical pores, due to the gasification during the setting of the mortar.

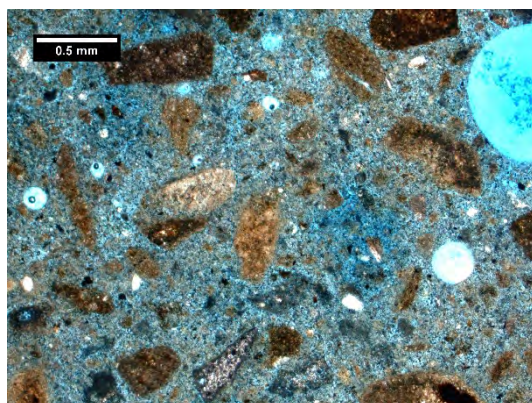


Figure 11. Microphotography with plain light where it can be seen fragments of metamorphic rocks and limestone grains. Also there can be seen rounded pores.

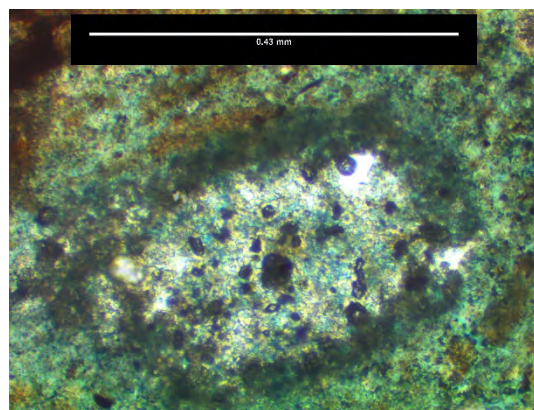


Figure 12. Microphotography with crossed-polarized light of a burnt limestone grain where it can be seen belite crystals.

The elemental composition of the binder has been obtained by electronic microscope and EDX elemental analysis. (Table 2). The presence of silicon oxide, iron oxide and calcium oxide is noteworthy, although the presence of alumina oxide has also been detected in percentages higher than 2%. Magnesium, sulphur and potassium oxides were detected as minor components.

The mineralogical composition of the binder was established using X-ray diffraction analysis (Figure 13). The following components were identified:

- The quartz is due to the thin section arid size (size under 0,063 mm)
- The calcite and the vaterite are due to the carbonated part of the binder
- The gehlenite and the calcium aluminium silicate are the definite elements to show that the cement used is natural cement. There are still some non-hydrated areas.

Observing the conglomerate with electron microscopy, hydrated grains have been detected with an unhydrated central nucleus (Figure 14).

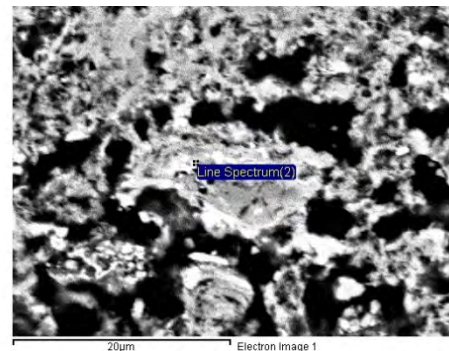
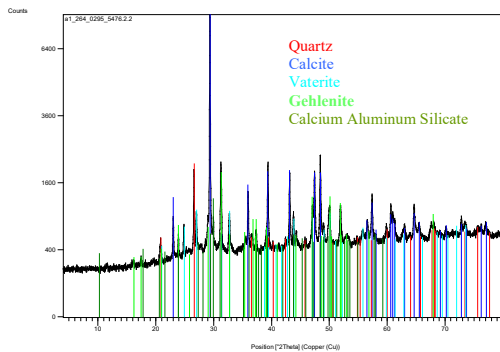


Figure 13. DRX spectrum of th binder

Figure 14. Grain of the original binder showing a hidrated ring around an unhydrated core (image with back scattered electrons)

Table 2. Elemental composition

Element	O	Mg	Al	Si	S	Fe	K	Ca
%	44.05	1.22	2.11	7.37	0.5	12.33	0.53	31.89

Differential Thermal Analysis allows checking that with a difference of temperatures of 950°C a 38% of the sample is lost. This fact means that there are more composites that are decomposed in this range of temperatures than in the ceiling one (sample nº1) (Figure 14). The highest peaks are found at 300°C, which it fits with the loss of water of some clay and between 750°C and 800°C that matches with the vaterite decomposition (first peak) and calcite.

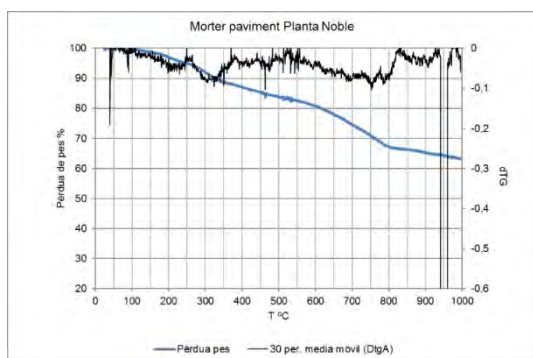


Figure 14. Shows the termogravimètric line in blue and black represents derivation of termogravimètric.

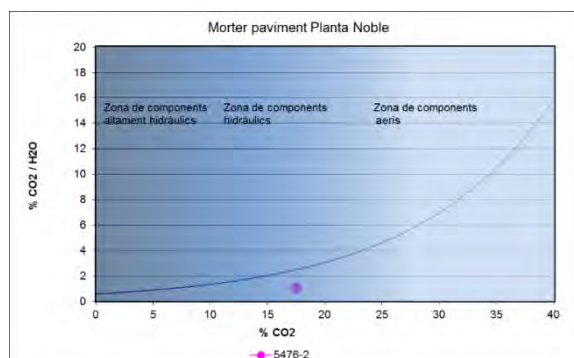


Figure 15. CO₂ to structurally bound water ratio in relation to % CO₂

If we compare the loss of weight produced by the decomposition of calcium carbonates (decomposition of CO₂) at more than 600°C and the quotient between this loss and the water that decomposes between 200 and 600°C, we can determine the degree of hydraulicity of the analysed mortar (Figure 15). So we can conclude that it is a hydraulic binder mortar, cement type naturally carbonated by now, but no nodules gehlenite hydrate, and silicic acid, maximum size of 2 mm.

Conclusions

The two samples studied are just the beginning of a more wide research about the use of materials and innovative building technology by Antoni Gaudi. These studies carried out in the materials laboratory of the EPSEB in UPC are the beginning of a more wide research. These first examples that we have been able to analyse thanks to the Servei de Patrimoni Arquitectònic of the Diputació de Barcelona are showing us the way to continue in our research. The two selected samples are an interesting selection of the noble floor of Palau Guell, one of the ceiling and one from the floor. These samples were selected as we were totally sure they were non-altered areas. The one of the ceiling it was under one small staircase and the one on the floor under the original pavement, never touched until now. Also these two samples they belong to two different building techniques, as one it is coating (ceiling) and the other has a supporting goal (floor). As we already knew from other studies carried out about Antoni Gaudi [3], he was an architect with an important knowledge of the traditional techniques but with also a highly innovative look. His innovation aims were focused on the improvement of his architecture and the technology he needed to improve it.

In this goal it is where we can find its innovation in building materials. Along his career he was using different and innovative building techniques and materials as other studies have already demonstrated with the use of reinforced concrete [4]. But it has not been yet studied his evolution in order to get to these materials from the traditional materials he had learnt and used until then. Palau Güell was the building in which he could try and search different methods and materials.

The use of natural cement in different areas of Palau Güell as it has been already shown in our study it's an important step in this knowledge about the evolution of the technical knowledge by Gaudi. What we have found proves how Gaudi was trying different new materials that were beginning to be used at this time at Catalonia in order to test its properties and behaviour. The use of natural cement is a clear explanation of this evolution from Gaudi. As he was innovative in his designs and forms, he was innovative in his building techniques trying to get the best materials he could in order to carry out his projects.

References

1. Cristina Mayo Corrochano, David Sanz Arauz, and José Ignacio Pineda Enebra. 2018. "Metodología Simplificada de Identificación Mediante MOP de Las Cales Hidráulicas y Los Cementos Naturales." In , 188–99. Grupo de Investigación MIMED-Servicio de Publicaciones de la Universidad de Navarra.
<http://dadun.unav.edu/handle/10171/52333>.
2. *Datos Estadísticos Correspondientes Al Año Económico de 1867*. 1869. Madrid.
3. García Gabarró, Gustavo. 1994. *Leyes de La Naturaleza y Composición Arquitectónica : El Ejemplo de Antonio Gaudí / Tesis Doctoral Presentada Por Gustavo García Gabarró ; Tutoría: Juan Bassegoda Nonell*.
[https://discovery.upc.edu/iii/encore/record/C__Rb1093451__Sgustavo garcia gabarro__Orightresult__U__X4?lang=cat&suite=def](https://discovery.upc.edu/iii/encore/record/C__Rb1093451__Sgustavo%20garcia%20gabarro__Orightresult__U__X4?lang=cat&suite=def).
4. Grima López, Rosa, Antonio Aguado de Cea, and Josep Gómez Serrano. 2013. "Gaudí and Reinforced Concrete in Construction." *International Journal of Architectural Heritage* 7 (4): 375–402. <https://doi.org/10.1080/15583058.2011.632470>.
5. Grima, R., J. Gómez Serrano, and A. Aguado. 2007. "The Use of Concrete in Gaudí's Sagrada Familia." *International Journal of Architectural Heritage* 1 (4): 366–79. <https://doi.org/10.1080/15583050701476630>.
6. Johannes Weber, Farkas Pintér, and Thomas Köberle. 2016. "Microscopic Techniques to Study Mineral Materials in Cultural Heritage: A Workshop for the Optimal Use of Polarized Light Microscopy and SEM to Better Understand Building Materials and Their Defects." Vienna. http://www.icvbc.cnr.it/invitation_MWS_2016.pdf.
7. Madoz, Pascual, 1806-1870. 1845. *Diccionario Geográfico-Estadístico-Histórico de España y Sus Posesiones de Ultramar / Por Pascual Madoz*. Madrid : Est. Literario-Tipográfico de P. Madoz y L. Sagasti,.
[https://discovery.upc.edu/iii/encore/record/C__Rb1152416__Spascual madoz__Orightresult__U__X4?lang=cat](https://discovery.upc.edu/iii/encore/record/C__Rb1152416__Spascual%20madoz__Orightresult__U__X4?lang=cat).
8. Megias, Laura, and Marius Vendrell. 2002. "Estudi Analític Dels Morters i Disposició d'aquests En La Cala Efectuada." Barcelona.

9. Moropoulou, A., A. Bakolas, and K. Bisbikou. 1995. "Characterization of Ancient, Byzantine and Later Historic Mortars by Thermal and X-Ray Diffraction Techniques." *Thermochimica Acta* 269–270 (December): 779–95. [https://doi.org/10.1016/0040-6031\(95\)02571-5](https://doi.org/10.1016/0040-6031(95)02571-5).
10. Ramírez Casas, Judith. 2018. "Ciment Natural a Catalunya : Història, Producció i Usos." *Jornada de Doctorado Del Programa de Tecnología de La Arquitectura, de La Edificación y Del Urbanismo: Libro de Actas 2018*, 10–15. <https://upcommons.upc.edu/handle/2117/127779>.

When Portland cement meets natural cement

Elisabeth Marie-Victoire¹, Myriam Bouichou¹

(1) Laboratoire de Recherche des Monuments Historiques (LRMH), Ministère de la Culture - Centre de Recherche sur la Conservation (CRC), MNHN, CNRS - France, elisabeth.marie-victoire@culture.gouv.fr, myriam.bouichou@culture.gouv.fr

Abstract

The development of the Portland cement industry gradually replaced natural cement production by the end of the 19th century. But in the pivotal period in between, in some constructions, natural cement – which was still used for ornaments – could neighbour Portland cement used for the structural elements. In this paper, a critical combination of both types of cements in one of the first reinforced concrete buildings of Paris will be presented. In 2016, a restoration of the façades of François Hennebique’s headquarters built in the late 19th in Paris city centre was planned. After removal of the thick layers of paint accumulated over time, locally serious cracking was observed leading to a deeper diagnosis. Optical microscope observations and SEM examinations combined with EDS analysis evidenced a massive sulphate reaction in the Portland cement structural elements, probably due to the vicinity of high sulphate content natural cement. Combined with carbonation-induced corrosion, these two decay mechanisms strongly impacted the final restoration protocol.

Introduction

The story of cements as we know them today [1] began in 1756 with John Smeaton’s experiments for the construction of the Eddystone lighthouse on the Plymouth waterfront in England. Smeaton discovered that some of the local stone with high clay content, after calcination, could set under water. In 1796, James Parker, after similar trials on Sheppey’s island pebbles, patented the first “roman cement”, produced by burning these clayey limestones at 900°C. At the same period in France, a “plaster-cement” was patented after the discovery of analogous marlstone pebbles in Boulogne-sur-Mer. These findings stimulated chemists’ research all over Europe and especially in France, with the work of Louis Vicat, who, after understanding the mechanisms leading to hydraulicity, clearly established the suitable proportion of quicklime and clay required [3]. From that moment [2], the production of natural cement boomed all over the world (England, Poland, Russia, Canada, etc.), with, for example, Pouilly or Vassy cements in France which were used for Troyes and Angers cathedral restorations, and Rosendale cement in the United states which is renowned for having been used in New York for the construction of the Brooklyn bridge and for the pedestal of the statue of Liberty [4]. In conjunction with the evolution of the industrial process, a vast panel of natural cements was commercialized, from rapid to slow

or semi-slow setting. But the location of the natural cement plants was imposed by the existence of cement stone deposits [5], and the quality of the production could be variable. So rapidly after the work of Vicat came the first production of artificial cement, this new cement being produced by mixing suitable proportions of limestone and clay, separately quarried. Thus in 1824, Joseph Aspdin, former brick producer, patented the fabrication of a new artificial “Portland cement”, based on the mixing and kilning of limestone and clay, which after setting did look like the stone of Portland’s Island in the Dorset. The techniques of production of Portland cements then continuously improved, notably with the increase of kilning temperature almost until vitrification, after Isaac Johnson’s experiments, or with the introduction of rotary kilns. As the industrial processing of these artificial cements was also eased by the separate extraction of the raw material, Portland cements gradually replaced natural cements and the production of the latter ended. It stopped in England in 1950 and in 1971 in the United States [3], France being the only country conserving its production up to today near Grenoble, but with a limited catalogue, as only the production of “Prompt cement”, which is fast-setting cement, was maintained.

The end of the 19th century was a turning point in cement production and at that period, Portland cement began to overwhelm the market, together with the emergence of new architectural concepts. But natural cements were still used for specific applications such as sealing, sewage pipes or ornaments, due to their specific rapid setting, their resistance to aggressive water and to the fineness of the ornamental elements that could be cast. So it was not rare by the end of the 19th to encounter in the same building structural elements made of Portland cement and ornaments made of concrete.

The purpose of the present study was to evaluate the potential impact of this vicinity, knowing that the composition of the natural cements was strongly linked to the local cement stone available, and that it could highly vary from one production site to another, and from one country to another so that contrary to Polish or English cements, French natural cements are known to contain high sulphate content [6][7][8][9][10]. Therefore, the compatibility between an early Portland cement and a sulphate-rich natural cement could be questioned. This issue was explored in the context of a restoration operation on the headquarters of Hennebique in Paris city centre.

Construction of the headquarters of Hennebique in Paris city centre

In 1898, François Hennebique, one of the inventors of reinforced concrete, asked the architect Edouard Arnaud to build his headquarters in Paris city centre, using his newly patented reinforcing system (Figure 1a). In 1900, a splendid 36 metre-high building (Figure 1b) exhibiting arches, balusters bow-windows and cast decorations (Figure 2a), was achieved, with additional ornamental flamed stoneware sculptures from Alexandre Bigot (Figure 2b) in a pure Art Nouveau style. It was one of the first reinforced concrete building constructed in Paris, and a kind of Hennebique manifesto, as it was achieved just before the universal exhibition of 1900.

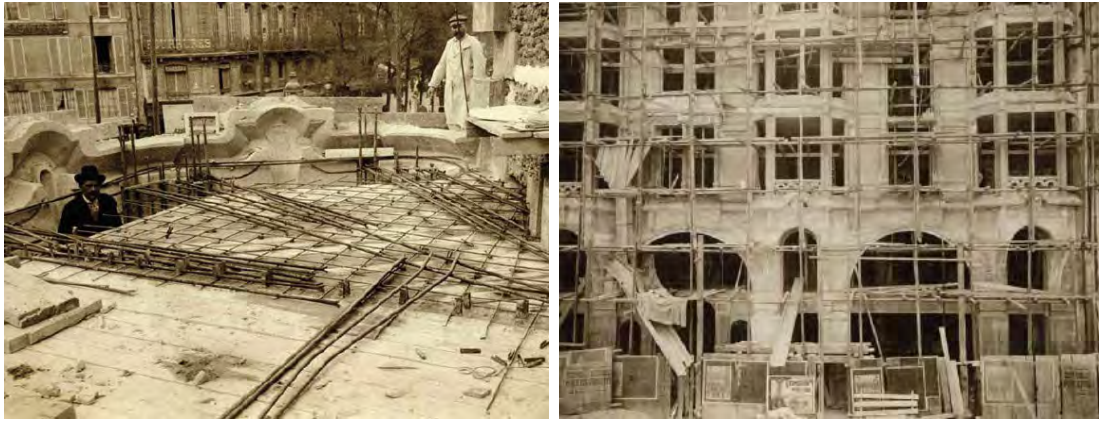


Figure 1. Pictures by Clément Maurice [11] [12]. a) The newly patented Hennebique reinforced concrete was employed. b) Overview of the worksite.



Figure 2. Art Nouveau style façade ornaments. a) Cast cement elements [7][8], b) Flamed stoneware from Alexandre Bigot.

Restoration: initial project

In 2016, a soft restoration operation was planned under the direction of the architect company A.C. Perrot and F. Richard. Concerning the concrete, the aim was mainly to clean the façades, eliminate the thick layers of paint accumulated over time (Figure 3) and repair a few cracks and spalls linked to rebar corrosion in protrusive architectural elements such as balconies.

The protocol initially adopted by the architect was to remove the paint layers (ice projection and chemicals), to repair the spalls and to apply a water repellent.



Figure 3. General view of the building. a) in 1900 [7][8], b) in 2016.

When the paint removal operation was finished, incredibly detailed finishing of the concrete emerged with light tool marks (Figure 4a) and a mixture of ochre and grey concretes. Locally serious cracking (Figure 5a and 6a), but also thick black crusts (Figure 4b), and spalls (Figure 5b and 6b) more massive than expected could be observed. It was also noticed that the structural elements were made of greyish concrete, while the finishing renders and the ornaments were made of ochre mortars.



Figure 4. Detailed view of the façades. a) Chiselled finishing, b) Black crust under the paint.



Figure 5. Detailed view of the façades. a) Shrinkage cracks of the natural cement mortars, b) Spall revealing a highly corroded rebar.



Figure 6. Detailed view of the façades. a) Shrinkage cracks of the natural cement mortars, b) Spall revealing a highly corroded rebar.

Secondary phase of diagnosis

Prior to the further steps of the restoration, a secondary step of diagnosis was conducted in order to better understand the decay mechanisms initially hidden by the paint. The experimental protocol included two phases performed in parallel:

1. Cement identification which was performed through cross section microscopy observation and XRD.
2. Decay comprehension which was carried out combining fractures and cross section microscopy and SEM observation associated with EDS analysis, carbonation depth measurements and sulphate concentration profiles.

Optical microscope observations and XRD

Samples were taken from both the structural greyish concrete and from the ochre mortar used respectively for the finishing render and for the cast ornaments. Sampling was performed by cutting and coring in both sound and degraded areas, and at several levels of the building (level 2 to 10).

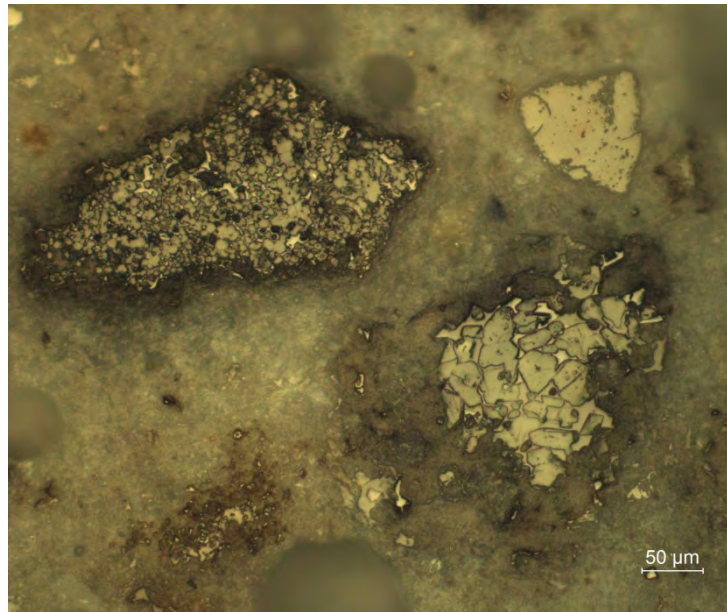


Figure 9. Combination of large crystallized grains filled either with small C2S or large C3S. Optical microscope view (G=X20) of the greyish concrete.

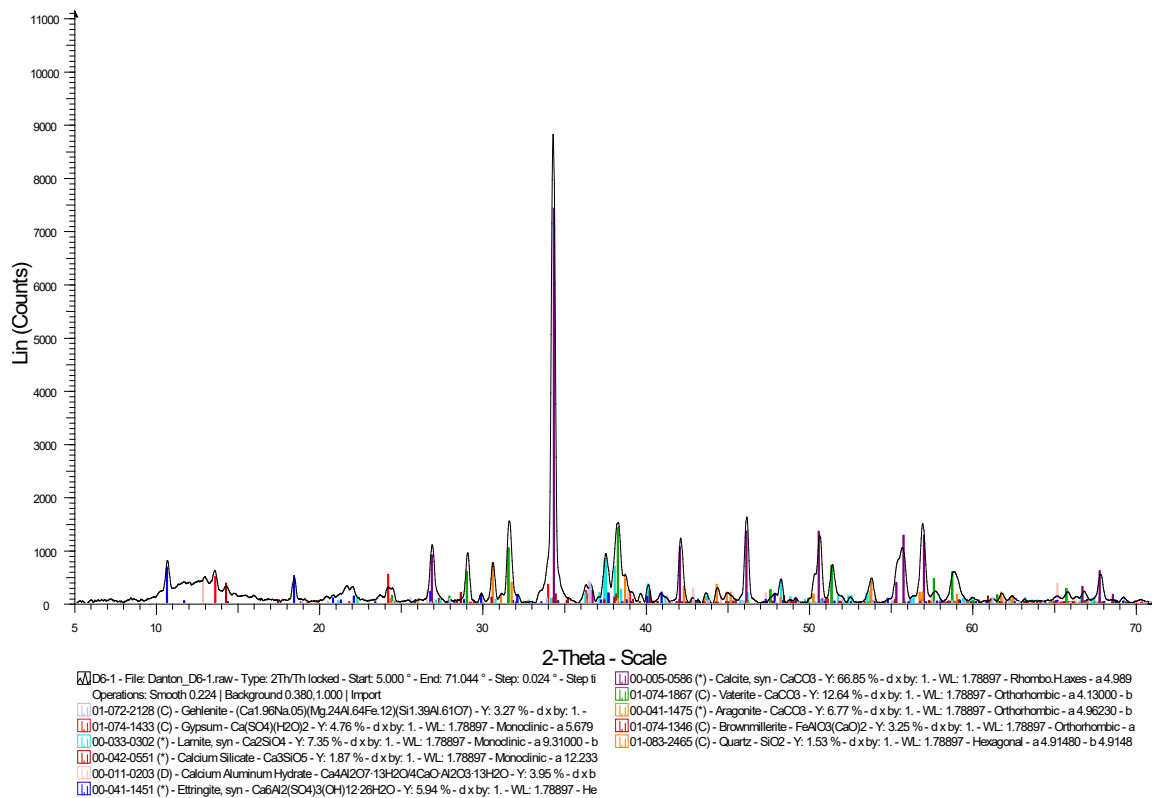


Figure 10. XRD analysis of a carbonated ochre render sample.



Figure 11. Large well crystallized clinker grain filled with small round beige C2S. Optical microscope view (G=X20) of the ochre render.

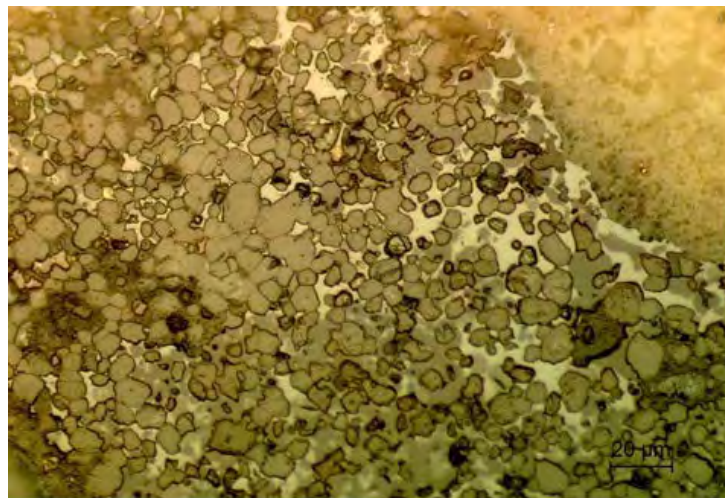


Figure 12. Detailed view of a clinker grain filled with small round beige C2S crystals showing parallel striations for some of them. Optical microscope view (G=X20) of the ochre render.

Carbonation depth

Carbonation depths were measured after phenolphthalein tests and compared to concrete covers evaluated by electromagnetic detection. The results showed a surprisingly low average carbonation depth for a more than centennial concrete (Table 1), as it was systematically lower than 20mm. Consequently, carbonation had only reached the less covered rebars, and only in one of the 6 zones (Z1-Z6) examined.

Table 1. Concrete cover vs. carbonation depth [13].

Testing Area	Average concrete cover (mm)	Minimum concrete cover (mm)	Carbonation depth (mm)
Zone 1 Level 2 (Z1R2)	72	31	15
Zone 2 Level 2 (Z2R2)	54	10	20
Zone 3 Level 4 (Z3R4)	53	27	15
Zone 4 Level 4 (Z4R4)	48	24	7
Zone 5 Level 10 (Z5R10)	55	34	5
Zone 6 Level 10 (Z6R10)	53	29	20

Sulphate profiles concentration

Sulphate concentrations were obtained by ionic chromatography after acid attack, according to EN 196-2 [14]. The results clearly revealed exogenous sulphate contamination (Fig. 13), probably connected to the Parisian urban pollution, but also to the use of natural cement in the finishing mortar, as already observed on French cements [7]. The threshold of 4% per weight of cement, known to be deleterious for Portland cement, was systematically exceeded in the first centimetre of concrete, and almost in all cases in the second centimetre too. But no correlation with the elevation on the façade could be evidenced.

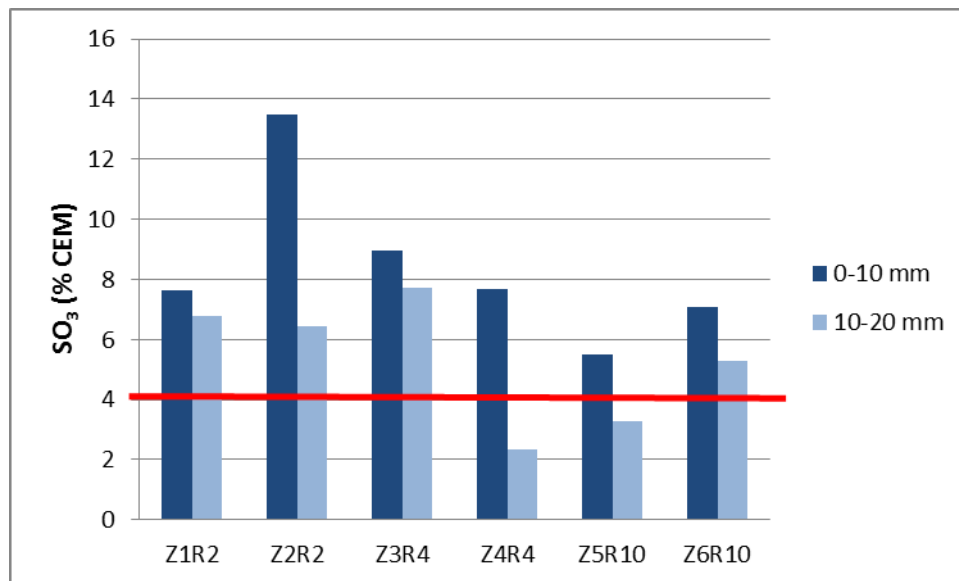


Figure 13. Sulphate concentration (% CEM) per zone elevation on the façade (R2 = 2nd floor, R10 = 10th floor) and depth. [10]

Scanning Electron Microscope observations

SEM observations of cross sections revealed a noticeable sulphate reaction in the structural concrete at the interface with the natural cement. Thus, massive ettringite could be observed both in the pores, often totally filled, and in the cement matrix (Figure 14 and Figure 15).

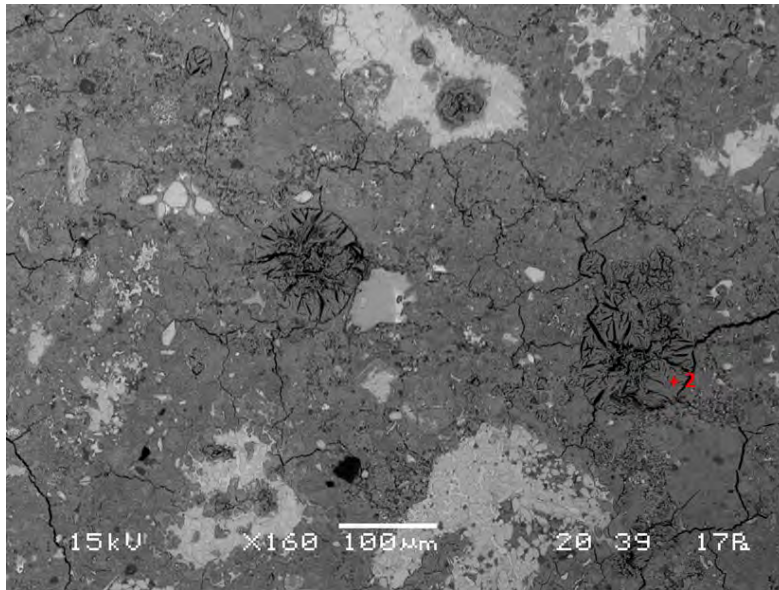


Figure 14. SEM view of the structural concrete revealing the presence of massive ettringite in the pores and in the cement matrix (G=X160).

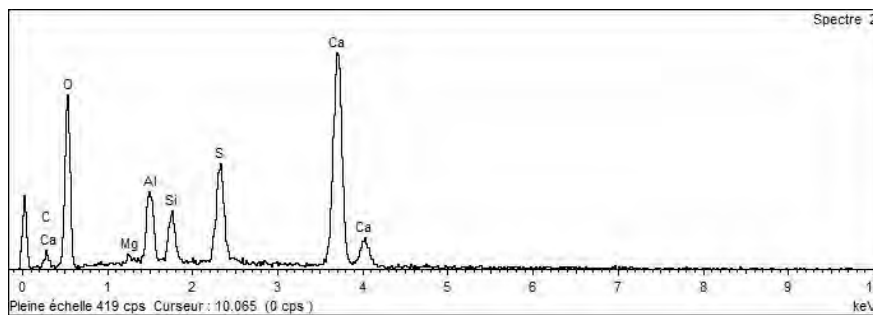


Figure 15. EDS analysis of point 2 identified on Figure 13 confirming the presence of ettringite.

Synthesis of the secondary phase of diagnosis

This secondary phase of diagnosis, performed after paint removal, revealed the use of distinct binders depending on the location in the building. Thus, if the structural concrete was Portland cement-based, natural cement was used for the finishing render and the cast elements.

Chemical analysis evidenced very high sulphate concentration (up to 13.5% by weight of cement), both on the surface and subsurface of the concrete. These results were consistent with the black crusts observed on the façade, but also with the use of natural cement as binder of the finishing render, as the French natural cements are known to be rather sulphate-rich [6][7][8][9][10]. But while natural cements are quite resistant to sulphate reactions – mainly due to the absence of portlandite in their hydrated phases – Portland cements are much more sensitive to sulphates. Consequently, massive ettringite could be observed both in the pores and in the cement matrix of the structural concrete made of early Portland cement. As this sulphate reaction was specially noticeable at the interface

between the structural concrete and the render, and as the structural concrete was not in direct contact with atmospheric sulphates – because it was systematically covered with a thick layer of natural cement render (1 to 4cm as a minimum) – it can be assumed that the vicinity of the natural cement was deleterious to the Portland cement concrete.

Another surprise in this diagnosis is the surprisingly low average rate of carbonation measured for a concrete dating back to 1900 (20mm as a maximum). Nevertheless, as the concrete was quite fractured, it can be suspected that carbonation could have progressed deeper locally in conjunction with the cracks. This could explain the important spalls associated with rebar corrosion observed on the structural concrete which was generally covered with a thick layer of render. But for some of the cast elements, where the concrete cover was really low, carbonation depth was sufficient to generate carbonation induced corrosion.

Final restoration protocol

After cleaning, the initial restoration protocol was to plan a standard repair of the spalls and the application of a hydrophobic product.

But the second step of diagnosis evidenced that the two main mechanisms affecting the reinforced concrete façades were carbonation induced corrosion and sulphate reactions. As there is currently no cure-all treatment for both types of decay and as both mechanisms are driven by the presence of water, it appeared that the best solution was to try to stop rainwater penetration. But the substantial presence of salts was not favourable to the use of a water-repellent, as they might produce deep degradation behind the treated depth. The multi-layered composition of the façade, which could affect their migration, was also a contrary argument. Finally, the combined lack of durability depending on the shape of the façade and the lack of reversibility of such treatment on porous materials, led to abandoning the water-repellent solution.

But there was still a need for waterproofing of the façades. As a consequence, the final restoration protocol did include the repair of the cracks and spalls with natural cement-based slurries and mortars (Fig. 15), and the application of a 3 layered water-based polyurethane coating, specifically designed to be sulphate-resistant and able to bridge the active cracks.

Unfortunately, the splendid grey and ochre shades of the façades, and the incredibly detailed handmade tool marks disappeared under the coating (Fig. 16). But without such a treatment, they might also have disappeared due to spalling and cracking. So, as the paint is removable, it is to be hoped that new treatments will allow conservation of both the material and the aspect in the future.



Figure 15. Cracks and spalls were repaired using slurries and natural cement-based mortars. Picture by Dominique Bouchardon



Figure 16. The water-based polyurethane coating dedicated to preserving the concrete unfortunately did mask the incredibly detailed surface of the façade. Picture by Dominique Bouchardon.

Conclusion

In 1900, at the turning point of the production of natural cement vs. artificial cement, François Hennebique, one of the inventors of reinforced concrete, built his headquarters in the city centre of Paris. 116 years after its construction, a restoration operation was decided with the aim of recovering the shades and the detailed finishing of the concrete typical of that period. But the cracks and spalls observed after the removal of the thick layers of paint accumulated with time led to a second diagnosis step. This evidenced the use of two types of binders: early Portland cement for the structural concrete and natural cement for the finishing render and the cast ornaments. The diagnosis also showed that the concrete was affected both by a carbonation-induced corrosion and by noticeable sulphate reaction in the

structural concrete, the latter probably being due to the vicinity of the natural cement-based mortars. To avoid further decay due to this conjunction of decay mechanisms, a final waterproofing coating had to be applied, with an unfortunate aesthetic impact.

Acknowledgements

The authors would like to thank the architect company A.C. Perrot and F. Richard and specially E. Le Gouvello who conducted the restoration of the building.

References

1. Bosc J L, Chauveau J M, Clement J, Degenne J, Marrey B, Paulin M (2001) Joseph Monier et la naissance du ciment armé. 180 p.
2. Cornier N (1904) Notice sur les ciments de Grenoble, 23^{ème} session de l'association française pour l'avancement des sciences. Grenoble. 29 p.
3. Vicat L (1818) Recherches expérimentales sur les chaux de construction, les bétons et les mortiers ordinaires, Editions Goujon. Paris. 97p.
4. Hadley T (1999) Natural cement. Concrete. pp. 39-41.
5. Baron J, Sauteret R (1982) Le béton hydraulique connaissances et pratique, Presse de l'école nationale des ponts et chaussées. 560 p.
6. Gurtner C, Hughes D, Weber J (2012), Manual on best practice in the application of roman cements. Roman cement, past and present - Conservation theory and practice, ROCARE FP7-ENV-2008-1 EU-project, 113p.
7. Bouichou M., Marie-Victoire E., Texier A., Blondiaux T. (2019) How to Identify a Natural Cement: Case Study of the Vassy Church, France. In: Hughes J., Válek J., Groot C. (eds) Historic Mortars. Springer, Cham
8. Cailleux, E., Marie-Victoire, E., Sommain, D., (2005) Microstructural and weathering mechanisms of natural cements used in the 19th century in the French Rhône-Alpes region. Proceedings on the international workshop on: Repair mortars for historic masonry, Delft, 26th-28th January 2005
9. Cailleux, E., Marie-Victoire, E., Sommain, D., (2006) Study of natural cements from the French Rhône-Alpes region, Proceedings of the international conference on Heritage, Weathering and conservation, Madrid, 21-24 June 2006, vol. I, p. 77-84
10. Gosselin, C., Martinet, G., Royer, A. et Vergès-Belmin V., "Natural cement and monumental restoration: the case of Bourges cathedral", in: Materials and Structures, 2009, n°42, p. 749-763

11. Arnaud E (1899-1900), Immeuble du bureau central Hennebique, 1 rue Danton, Paris 6^e. IFA Archives on reinforced concrete - Hennebique (BAH): Bureau Technique Central, GESTION1 1/1 (doc. 1-A-004-006).
12. Perrot A C, Richard F (2016), Paris VIème arrondissement, Immeuble dit Maison Hennebique, 1 rue Danton, Place St André des Arts - Restauration des façades et des toitures - Notice de présentation, 18p.
13. Logel S (2016), Caractérisation de matériaux et évaluation de leur état sanitaire – Immeuble Hennebique – Paris (75), Rapport BPE N°PMH161193V1, 29p.
14. Logel S (2016), Dosage en sulfates – Etude comparative – Immeuble Hennebique – Paris (75), Rapport BPE N°PMH161273V1, 5p.

Topic 10: Conservation issues concerning mortars, plasters, renders and grouts. Diagnosis. Decay and damage mechanisms. Case studies



Decorative renders simulating stone of middle 20th century in the region of Lisbon

Maria do Rosário Veiga¹, António Santos Silva², Cláudia Martinho³, Paulina Faria⁴

(1) Buildings Department, National Laboratory for Civil Engineering, rveiga@lnec.pt

(2) Materials Department, National Laboratory for Civil Engineering, ssilva@lnec.pt

(3) Dep. Civil Engineering, FCT, NOVA University of Lisbon, cm.martinho@campus.fct.unl.pt

(4) CERIS and Dep. Civil Engineering, FCT, NOVA University of Lisbon, paulina.faria@fct.unl.pt

Abstract

Housing and public urban buildings of the middle 20th century period, in Portugal, are characterized by a sober, rather severe, architectural and constructive design, known as “Estado Novo” period. In the region of Lisbon, the façades of many of those buildings are covered with a very durable unpainted decorative type of render, called “marmorite”. Considering that cementitious binders were already often used in that period, both in structural elements and in coatings, and due to the darkening effect of fungus, soiling and pollution, there was a generalized belief that *marmorite* renders were cement-based mortars. As a consequence, repair interventions used materials and techniques chosen for cementitious renders. However, the characterization of the *marmorite* render of the National Laboratory for Civil Engineering main building, in Lisbon, revealed that the render was composed by air lime, limestone and marble. Later, an experimental characterization campaign of samples of *marmorite* renders of 20 other buildings in the region of Lisbon revealed that they were generally composed by air lime, sometimes coloured with an inorganic pigment, and mainly limestone and marble aggregates of different colours selected to obtain an aesthetic effect.

Introduction

Housing and public urban buildings of the middle 20th century period, in Portugal, are characterized by a sober, rather severe, architectural and constructive design. It is the so-called Estado Novo Portuguese style, that integrates the late modernism period. In the region of Lisbon, many of those buildings were covered with very durable unpainted decorative renders, simulating stone, known as “marmorite” renders, expression that could be translated as something like “marbled” renders or “marmoreal” renders (Figures 1-3).

A special application technique was used to obtain the stone effect, consisting on: application of a common regularization render layer; application of a finishing render layer with a mineral binder and aggregates selected to obtain an aesthetic effect, usually of limestone or marble nature; short drying period for partial hardening; washing of the superficial skin of the binder in order to let the aggregates visible; very careful curing to

avoid cracking of the render, which was rich in binder to provide a good key for the aggregates.

These *marmorite* renders were used both in public buildings of some importance, such as Lisbon University (1961) and National Laboratory for Civil Engineering – LNEC (1952) (Figure 1), and in housing urban buildings of the same period for medium and medium-high classes (Figures 2 and 3). They have also been used to retrofit older housing urban buildings, some for rent.

Being a very durable kind of render, after more than 5 decades, they show few anomalies, such as some cracks, stains and fungi and punctual erosion and lacunae (Figure 3).



Figure 1 – Façade of LNEC main building covered with *marmorite* render: a) General view; b) Detail of *marmorite*

In Institutional buildings, neutral colours were used (combinations of grey and cream colours) (Figure 1), while in housing buildings several colours, such as red-pink, green and yellow, were adopted by adding inorganic pigments to the binder and choosing marble and limestone aggregates of matching colorations (Figures 2-3).

This finishing technique for these façades is thought to be based in techniques of the same type used in Central Europe in the period between wars [1, 2]. However, the mortars were artisanal, produced in situ, opposite to most of the Central European ready-mixed mortars reported in literature.

Considering the period – middle 20th century – in which cementitious binders were already often used, both in structural elements and in coatings, and due to the darkening effect of fungi, soiling and pollution, there was a generalized belief in the technical milieu that these decorative renders were cement-based mortars. This belief was enhanced by the existence of an official specification document referring the use of a cement mix [3].



Figure 2 – Façades covered with colourful *marmorite* renders of Av. De Roma, Lisbon

As a consequence, repair interventions on those building façades used materials and techniques chosen for cementitious renders.

In 2006 a restoration of the main building of the National Laboratory for Civil Engineering, in Lisbon, was planned. It is a building of the late modernism period in Portugal, constructed between 1950 and 1952, designed by a team coordinated by the architect Porfírio Pardal Monteiro, one of the most reputed building designers of that period [4, 5]. The façade is rendered with a cream/light grey coloured *marmorite* (Figure 1), which presented dark stains and some cracks. To guarantee a suitable restoration, the original render has been analysed, from the points of view of material, performance and technique. It was then verified that the *marmorite* render had been applied with a thickness variable between 5 and 8 mm, on a first coat of hydraulic render and was composed at 95 % by calcium carbonate [6] meaning that the binder was air lime, opposite to expectations.



Figure 3 – Pink-red traditional *marmorite* render in Lisbon: a) General view during cleaning; b) Detail of red/pink *marmorite*

Was this building an exception? It was possible to identify and interview some retired old masons that applied *marmorite* in the past and the majority also referred that cement was

the binder used. But they also explained that the formulation of the *marmorite* mortar was generally kept secret by the expert professionals [7].

A large experimental campaign was later accomplished to clarify the composition of *marmorite* renders of that period, in the Lisbon region. Samples of 20 buildings from 3 different districts (Lisbon, Santarém and Setúbal) were collected and characterized from the chemical, mineralogical, microstructural, physical and mechanical points of view [8].

Revealing the materials and compositions used and highlighting the employed technique, this study aims at gathering information in order to allow the planning of suitable, compatible interventions and in this way contributing for the preservation of this characteristic decorative render.

Materials

Samples of *marmorite* renders were collected in the districts of Lisbon, Santarém and Setúbal (within the region marked by the red circle in the map of Portugal mainland - Figure 4), in LNEC's main building, located in a heavy car and plane traffic, and in housing buildings mainly of the decades 1950-1960, with different colours. It should be noticed that the collection of samples was generally only allowed by the owners in the case of renders with anomalies and in limited quantity and dimensions. Such low quantities permitted chemical, mineralogical and microstructural tests, but in many cases were not enough for physical and mechanical testing (Figure 5).

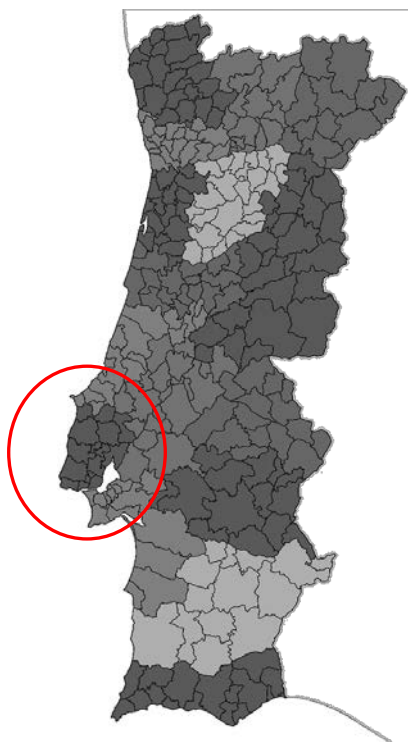


Figure 4. Map of Portugal mainland signaling the region where the samples were collected



Figure 5. Samples of differently coloured *marmorites* collected

Methods

The tests used for the characterization of the samples were [6, 7]:

a) Mineralogical, chemical, petrographical and microstructural tests:

- X-ray diffraction analysis (XRD) in a *Philips PW3710 X-ray diffractometer*, with 35 kV and 45 mA, using Fe-filtered Co K α radiation of wavelength $\lambda = 1.7903 \text{ \AA}$;
- Thermogravimetric and differential thermal analysis (TGA/DTA) performed in a *Setaram TGA92 analyser*, under argon atmosphere (3 L/h) and using platinum-rhodium crucible of 50 μl capacity, with heating rate of 10 $^{\circ}\text{C}/\text{min}$, from room temperature to 1000 $^{\circ}\text{C}$;
- Soluble silica, sulphates and alkalis content evaluation was made by gravimetric and atomic absorption spectrometry analysis;
- Granulometric analysis of the sand (separated from the binder by a controlled acid digestion according to a LNEC internal protocol for mortar samples with limestone aggregates) and stereozoom observation of the obtained granulometric fractions;
- Observation of vacuum impregnated polished and thin sections by optical microscopy (OM), using *Olympus PMG3 and BX50* microscopes;
- Scanning electron microscope (SEM) coupled with an energy dispersive X-ray microanalysis system (EDS). The SEM used was a JEOL JSM-6400, and the EDS is an INCA X'Sight detector from Oxford Instruments. Samples were gold sputtered, and the acceleration voltage used was 15 kV using the backscattered electron image mode (BSE).

b) Physical tests:

- Open porosity by the method of hydrostatic weighing based on EN 1936 [9];
- Mercury intrusion porosimetry (only one case);
- Water absorption by capillarity by a method based on EN 15801 [10] and adapted for irregular samples [11] (Figure 6 a);

- Compressive strength using a method based on EN 1015-11 [12] and adapted for irregular samples [11] (Figure 6 b), using a Hoytom S.L., model HM-S equipment, with load cells of 200 kN and 2 kN.



Figure 6. Physical and mechanical testing: a) Water absorption by capillarity; b) Compressive strength

Results and Discussion

LNEC main building

The results of the characterization of the *marmorite* of LNEC's façade are presented in tables 1 and 2 and in Figure 7.

The results of the characterization tests, presented in table 1, allowed to establish the composition of the LNEC's *marmorite* render as mainly constituted by about 95 % calcite and small proportions of quartz and hematite, as well as some contamination with sulphates, probably from the environmental pollution. The very low alkalis and soluble silica contents indicated that there are no hydraulic compounds. The aggregates, of limestone and marble, are constituted by subangular grains from under 0.075 - 2.5 mm with predominance of the fraction 1.25 – 2.5 mm.

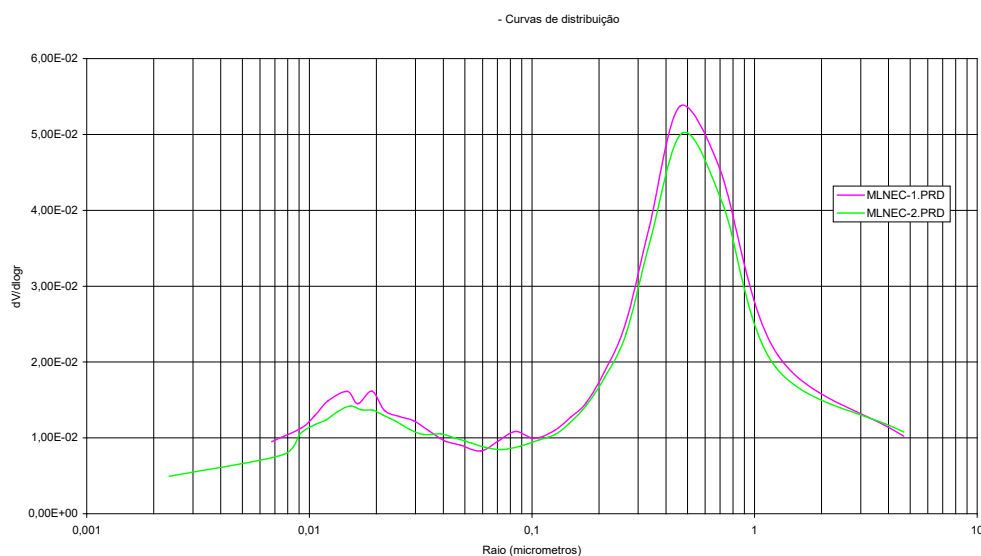
Table 1 – Chemical, mineralogical and granulometric results of LNEC's *marmorite* samples [6, 4]

Sample	XRD	TGA/DTA	IR and grain size distribution	Chemical analysis (wt. %)	b/a (wt.)
LNEC's main building	Mainly calcite, some quartz and traces of hematite	95 % calcium carbonate	IR: 2.5%; Soluble fraction: 2.5%; Grain size distribution mainly 1.25 to 2.5 mm	Sodium: 0.02; Potassium: 0.03; Sulphates: 0.36; Soluble silica: 0.50	1:1

IR – Insoluble residue in acid; b/a – binder/aggregate ratio

Table 2 – Physical results of LNEC's marmorite samples [4, 8]

Sample	Bulk density (kg/m ³)	Porosity (%)	MIP	Coefficient of capilarity (kg/(m ² .min ^{1/2}))
Façade of LNEC's main building – tests in 2006	2330	12 (MIP technique)	Bimodal structure with the following peaks: 0.02 and 0.5 µm	0.48
Façade of LNEC's main building – tests in 2017	2056	20 (hydrostatic weighing technique)	-	0.56

Figure 7. Pore size distribution of the *marmorite* of LNEC's façade [4]

The main physical characteristics, presented in table 2, indicate relatively low porosity with a bimodal structure with critical pore size of 0.5 µm and capillary coefficient considered low when compared with other air lime mortars [11, 13, 14].

Housing buildings

The analysis of 20 samples of *marmorite* renders extracted from building façades of 3 districts in the Lisbon region showed thicknesses varying between 2 and 8 mm, applied on a thicker coat of render. The results of the samples, distributed by colour, in order to highlight the pigments used, are summarized in table 3 and allow to conclude that the samples are mostly composed by air lime as a binder and mainly calcitic aggregate, in some cases with also dolomitic and siliceous grains and sometimes including glass residues.

The composition data also confirm that the colours of the binder were obtained with oxides: hematite for red, goethite for yellow and chromium oxide for green, which were the colours commonly used. The aggregate was chosen in order to match these colours.

The proportions binder:aggregate, in weight, are very variable, from about 1:1 (PN8, PN6, PN11) to about 1:6 (PS4, RM4). However, for those with low content of binder, it is possible

that, for such thin samples, surface washing and erosion may have influenced some reduction of the binder content.

Table 3 – Compositional results of *marmorite* samples

District / Local	Sample	Colour	Calcite	Calcitic Agg.	G	Glass	H, Go, Cr	D, F	Q	Cem	b/a (wt)
Lisbon / Campo de Ourique 1951	LX1	Pink / Red	94.30	63.88	-	-	1.00 H	4.70 Q	4.70	-	1:3.0
Lisbon / Moscavide 1950-1956	M1		93.25	71.36	-	-	-	1.00 F	5.75	-	1:4.8
Setúbal /Setúbal 1948	S4		94.73	40.91	-	-	-	1.00 D	4.27	-	1:1.1
Setúbal / Pinhal Novo <1951	PN11P		80.09	30.03	1.8 6	5.00	1.00 H	-	12.05	-	1:1.2
Setúbal / Pinhal Novo <1951	PN5P		77.84	37.72	-	5.00	1.50 H	-	15.66	-	1:2.0
Setúbal / Pinhal Novo	PN12		63.02	59.87	-	-	2.00 H	-	5.00	25.7	1:2.5
Lisbon / Mem Martins <1953	MM3		89.05	68.15	-	-	-	-	5.00	-	1:4.7
Santarém / Rio Maior 1971	RM6		33.93	10.18	-	32.79	0.50 H	-	32.79	-	1:4.3
Santarém / Rio Maior	RM7R		28.50	5.70	-	21.15	-	1.00 F	49.35	-	1:4.6
Setúbal / Pinhal Novo 1948	PN1R		95.05	64.39				1.00	3.95		1:3.0
Setúbal / Pinhal Novo <1951	PN5R		93.16	71.29	2.9 6				3.88	-	1:3.9
Lisbon / Sintra (1956?)	PS4	Dark grey	90.93	77.15	2.2 5	-	-	1.00	2.00	-	1:6.4
Setúbal / Pinhal Novo <1951	PN11R		83.75	48.85	-	5.00	-	-	11.25	-	1:2.5
Setúbal / Pinhal Novo 1948	PN1P	Yellow	94.23	63.83	1.7 7	-	1.00 Go	1.00	2.00	-	1:2.7
Setúbal / Pinhal Novo	PN2V		40.93	12.28	-	-	-	-	59.07	-	1:3.4

Table 3 (Continued)– Compositional results of *marmorite* samples

District / Local	Sample	Colour	Calcite	Calcitic Agg.	G	Glass	H, Go, Cr	D, F	Q	Cem	b/a (wt)
Santarém / Rio Maior	RM7P	Green	30.57	9.17	-	62.93	1.50 Cr	-	5.00	-	1:4.9
Santarém / Rio Maior	RM4		27.59	8.28	-	66.41	1.50 Cr	-	5.00	-	1:5.5
Setúbal / Pinhal Novo	PN8		78.95	23.69	2.10	14.05	1.00 Cr	1.00	5.00	-	1:1.0
Setúbal / Pinhal Novo	PN6		78.30	23.49	-	14.70	1.00 Cr	1.00	5.00	-	1:1.1
Setúbal / Pinhal Novo	PN2P		27.64	8.29	1.48	23.29	1.00 Cr	-	23.29	-	1:4.9

G – Gypsum; H – Hematite; Go – Goethite; Cr – Chromium; D – Dolomite; F – Feldspar; Q – Quartz; P – Portlandite; Cem – Cement; Si – Silica; b/a – binder / aggregate ratio

A synthesis of the composition, together with the results of physical and mechanical characterization, are presented in table 4, for the samples now organized by district and not by colour, in order to investigate local influences.

Table 4 – Composition and physical and mechanical results of *marmorite* samples

District / local / const date	Sample	Composition	b/a (wt)	Bulk density (kg/m ³)	Porosity (%)	Coefficient of capilarity (kg/(m ² .min ^{1/2}))	Compressive strength (MPa)
Lisbon / C.Ourique / 1951	LX1	Air lime : Calcitic and silic agg	1 : 3	2159	18	0.33	-
Lisbon / Moscavide 1950-1956	M1	Air lime : Calcitic and silic agg	1 : 4.8	-	-	-	-
Lisbon / Mem Martins < 1953	MM3	Air lime : Calcitic, dolomitic and silic agg	1 : 4.7	2088	18	0.18	1.33
Lisbon / Sintra Aprox. 1956	PS4	Air lime : Calcitic, dolomitic and silic agg	1 : 6.4	2245	10	0.25	-
Santarém / Rio Maior 1967	RM4	Air lime : Calcitic, silic and glass agg	1 : 5.5	-	-	-	-
Santarém / Rio Maior 1967	RM6	Air lime : Calcitic, silic and glass agg	1 : 4.3	-	-	-	-
Santarém / Rio Maior 1971	RM7P	Air lime : Calcitic, silic and glass agg	1 : 4.9	2006	16	0.73	4.43
	RM7R	Air lime : Calcitic, silic and glass agg	1 : 4.6	-	-	-	-

Table 4 (Continued)– Composition and physical and mechanical results of *marmorite* samples

District / local / const date	Sample	Composition	b/a (wt)	Bulk density (kg/m ³)	Porosity (%)	Coefficient of capilarity (kg/(m ² .min ^{1/2}))	Compressive strength (MPa)
Setúbal / Pinhal Novo / 1948	PN1P	Air lime : Calcitic, dolomitic and silic agg	1 : 2.7	2249	14	0.51	-
	PN1R	Air lime : Calcitic, dolomitic and silic agg	1 : 3	-	-	-	-
Setúbal / Pinhal Novo	PN2P	Air lime : Calcitic, silic, glass and ceramic agg	1 : 4.9	-	-	-	-
	PN2V	Air lime : Calcitic and silic agg	1 : 3.4	-	-	-	-
Setúbal / Pinhal Novo < 1951	PN5P	Air lime : Calcitic, silic and glass agg	1 : 2	-	-	-	-
	PN5R	Air lime : Calcitic, silic and glass agg	1 : 3.9	-	-	-	-
Setúbal / Pinhal Novo < 1951	PN11P	Air lime : Calcitic, silic and glass agg	1 : 1.2	2118	13	0.17	-
	PN11R	Air lime : Calcitic, silic and glass agg	1 : 2.5	2254	13	0.47	-
Setúbal / Pinhal Novo	PN6	Air lime : Calcitic, dolomitic, silic and glass agg	1 : 1.1	-	-	-	-
Setúbal / Pinhal Novo	PN8	Air lime : Calcitic, dolomitic, silic and glass agg	1 : 1	1983	21	0.88	-
Setúbal / Pinhal Novo	PN12	Cement : Calcitic, and silic agg	1 : 2.5	2205	21	0.04	31.03
Setúbal / Setúbal / 1948	S4	Air lime : Calcitic, dolomitic and silic agg	1 : 1.1	-	-	-	-

As referred before, only part of the samples could be tested for bulk density, porosity and water absorption by capilarity and only 3 could be subjected to the determination of compressive strength (Figure 6), due to size limitations.

All the cases present air lime as a binder, with the exception of PN12 (in Setúbal / Pinhal Novo), which is a cementitious render. As it is the only case, it is possible that it is a substitution render applied in an intervention.

The aggregates vary depending on local geology and on vogue/fashion. The aggregates of the Lisbon cases are mainly calcitic, namely of limestone and marble origin, sometimes also dolomitic, with small proportions of quartz. The case studies of Santarém, which are the most recent of the analysed group, all have calcitic and siliceous aggregates and include glass residues as a part of the aggregates. In Setúbal the case studies are the oldest and have a more heterogeneous mix of aggregates, including glass and ceramic pieces in one case, besides calcitic, dolomitic and small proportions of quartzitic aggregates.

The physical characteristics, synthetized in table 4, evidence that porosity is also very variable, between 10 % (PS4) and 18 % (LX1 e MM3), nevertheless lower than the usual values for air lime mortars [15] which are generally in the order of 20-30 %. Capillary coefficients obtained are of the same order of magnitude as those obtained for LNEC's *marmorite*: between 0.18 to 0.73 kg/(m².min^½). Porosity, capillary absorption and also bulk density point out to vary compact mortars, which is consistent with the artisanal technique used of squeezing against the substrate, followed by washing to remove superficial binder and by careful curing conditions. The few results of compressive strength obtained (only three samples included pieces with the dimensions needed for this test) show moderate results for air lime *marmorite* mortars (1.33 and 4.43) and a very high value for the cement *marmorite* render (31 MPa for PN12).

With the short sampling that was possible to test, it is not possible to find a pattern of correlation between binder:aggregate ratio and porosity, capillary coefficient or compressive strength. Nevertheless, this lack of correspondence is common in air lime renders, as there are many other factors with overlapping influence, such as the technique of application (namely the squeezing against the substrate and the application and curing conditions), the water absorption of the aggregates and of the substrate, and the packing of the aggregates.

Conclusions

In the decades of 1940-1960, in the region of Lisbon, a decorative type of render with a finishing thin layer simulating stone, with visible aggregates, known as *marmorite* render, was commonly used.

Although most of those buildings already had a structure of concrete, or at least partially of concrete (for example concrete slabs between floors supported by structural masonry walls), it was verified that *marmorite* render was an air lime render with mainly carbonate aggregates of marble and limestone. That was not in accordance with what was gathered in interviews to old masons different that could be explained both by the secrecy that involved the *marmorite* mortars formulation and by the fact that those old masons consider cement as the “new” building material that presented a revolution on their old way of building, therefore, they prefer to remember and to talk about building with cement.

In Institutional buildings, the renders presented neutral colours, obtained by the selection of the raw materials (white calcitic air lime and chosen aggregates) while in housing buildings

different colours were used, obtained by the addition of inorganic pigments and selection of matching marble aggregates. The pigments found were hematite, goethite and chromium oxide, according to the typical façade colours: red/pink, yellow and green. Those coloured façades originated picturesque quarters, typical of the modernist zones of Lisbon. In some areas, usually out of the centre of towns, more open colouring was chosen, through the use of glass and ceramic residues, clearly showing the joyful individual taste of their owners.

Marmorite renders that still protect and decorate many façades in the region of Lisbon are now aged of more than fifty years. Most of them never had any maintenance operations in this period and they still present efficient conditions, with suitable cohesion and adhesion, due to well-chosen materials and a careful and efficient application technique. Therefore, apart from effective technical characteristics, one can say they have a low embodied energy because the environmental impact is divided by a long period without maintenance and repair materials. In the last decade many of them started decaying, partly due to traffic pollution that attack carbonate materials and to the corrosion of reinforcing steel bars of some of the concrete substrates. Due to lack of knowledge about their composition and their particular application technique, the interventions were directed to the painting of the façades, hiding the *marmorite* render sometimes in an irreversible way and completely changing the brightness, the typical colour tonalities and the whole image of those quarters.

Therefore, revealing the materials and compositions used, this study intends to generate data to allow the planning of suitable, compatible interventions and the preservation of these durable and specific render.

Acknowledgements

Acknowledgements are due to Portuguese Foundation for Science and Technology for supporting project DB-Heritage - Database of building materials with historical and heritage interest (PTDC/EPH-PAT/4684/2014), to LNEC through the project PRESERVE - – Preservation of renders and plasters of the Built Heritage with Cultural Value, and to the old masons that were possible to interview.

References

1. Govaerts Y, Verdonck A, Meulebroeck W, De Bouw M (2015) Development of artificial stone imitations at the turn of the 20th century through patent analysis in a Belgian context. Proc. of 5th Int. Cong. on Construction History, Vol. 2, 229-236.
2. Dekeyser L, Verdonck A, De Clercq H (2015), Belgian Craftsmanship in the interwar period: formulas and application techniques of decorative cement-based wall finishes. Int J Archit Herit 11:621-635.
3. Laboratório Nacional de Engenharia Civil (1952) – Execução de marmorites. LNEC, Lisboa: 1952. Especificações. E 5 – 1952.

4. Veiga R, Tavares M, Magalhães AC, Santos Silva A, et. al. (2006) Reparação das fachadas de marmorite do Edifício Principal do LNEC. Relatório /2006 NRI.
5. Veiga R, Tavares M, Magalhães A C (2007), Restauro da fachada em marmorite de cal do Laboratório Nacional de Engenharia Civil, em Lisboa. Materiais, métodos e resultados. In Proc. VII Simpósio Brasileiro de Tecnologia de Argamassas (STBA), Recife, Brasil.
6. Martinho C (2007), Marmorite: caracterização e contributo para a sua conservação. Master Thesis presented at NOVA University of Lisbon.
7. CEN (2006) Natural stone test methods. Determination of real density and apparent density, and of total and open porosity. CEN, EN 1936-2006.
8. CEN (2009) Conservation of cultural property. Test methods. Determination of water absorption by capillarity. CEN, EN 15801.
9. Magalhães A, Veiga, M R (2009) Physical and mechanical characterisation of ancient mortars. Application to the evaluation of the state of conservation. Mater Construcc 59(295): 61-77. DOI: 10.3989/mc.2009.41907.
10. CEN (1999) Methods of test for mortar for masonry. Determination of flexural and compressive strength of hardened mortar. CEN, EN 1015-11.
11. Veiga M R, Fragata A, Velosa A L, Magalhães A C, Margalha M G (2010) Lime-based mortars: viability for use as substitution renders in historical buildings. Int J Archit Herit 4 (2): 177-195.
12. Damas A L, Veiga M R, Faria P, Santos Silva A (2018) Characterisation of old azulejos setting mortars: a contribution to the conservation of this type of coatings. Constr Build Mat 171: 128-139.
13. Veiga M R (2017), Air lime mortars: what else do we need to know to apply them in conservation and rehabilitation interventions? A review. Constr Build Mat 157:132–140.

The analysis of the proportion of mortar for Japanese roof tile (Ibushikawara) in Taiwan by applying of Taguchi Method

Mei-Tsu Hsu¹, Bing-Sheng Yu²

(1) Master Student, Institute of Mineral Resources Engineering, National Taipei University of Technology, matt85208@gmail.com

(2) Associate Professor, Institute of Mineral Resources Engineering, National Taipei University of Technology, Bing@ntut.edu.tw

Abstract

In recent years, cultural heritage preservation and rehabilitation have been gradually emphasized in Taiwan. Although the amounts of literature and studies, buildings and materials have increased substantially, studies of mortar application in old Japanese roof tiles (Ibushikawara) are still scarce. Also, reasonable importance has yet been credited to partial application or the mortar, such as its application to the Ibushikawara. Since typhoons occur frequently in Taiwan, the adhesive bond strength of lime mortars for jointing the Japanese roof tiles needs to be strong enough in order to prevent any damages that may occur to the roof-tile due to strong winds. On the other hand, during roof repairmen and roof-tile replacement, the mortar needs to be removed easily from the old roof-tiles in order to repurpose the tiles.

Due to the lack of knowledge in tile mortar, cement was used in some restoration works to repair old Japanese roof tile in Taiwan. Due to its overpowering mechanical strength, cement would damage the tile surface and cause the tiles to lose its repurposing ability. Therefore, this study aims to discover the optimal proportion of the mortars that has sufficient adhesive bond strength to comply with Taiwan's strong wind resistance regulations and can be easily removed from the roof-tile.

This study adopts the Taguchi method with references to literatures and mortar proportions used by traditional craftsmen. A total of eight factors are used optimize the results, including lime-sand ratio, fiber ratio, and the types of lime, etc.. The preliminary results revealed that the adhesive bond strength of all groups of mortar in this study meet the Taiwanese standard of 0.09 kg/cm², and some of them can be removed completely from the old Japanese roof-tiles.

Introduction

Japanese roof-tile is called “いぶしかわら” (ibushikawara) in Japanese, and “爇瓦” in Chinese. As the Japanese government had to construct various institutions and official dormitories in the period of Japanese occupation of Taiwan (1895-1945), Japanese roof-tiles were a requisite building material in Taiwan [1-2]. According to field research, hundreds of

Japanese-styles old buildings with Japanese roof-tiles are still be used and resided in 2018 [2]. In order to make the Japanese roof-tiles more affixed on the roof, some Japanese documents mentioned the use of lime mortar materials for ridge roof-tile fixing [3]. In the case of Japanese-style historic buildings in Taiwan, lime mortars are also used to fill in the overlap between the roof-tiles (see Figures 1b and 1c). Due to the unique climate in Taiwan, monsoons and typhoons often generate strong winds or lead to windstorms [4, 5]. It is an important topic to make old Japanese roof-tiles more affixed on the roof to avoid wind damages.

However, tile damages may still occur sometimes due to poor quality or impact against heavy objects blown by the strong wind, which may require old roof-tiles to be repaired and replaced. According to the traditional architects, when roof-tiles are damaged in the early days, all roof-tiles (both good and damaged ones) were removed from the roof and separated. Lime mortar was also shaved from the old roof-tiles. Then, the intact old roof-tiles would be re-led on the roof with new ones. Mortar would again be used to re-plaster the overlaps. Since the early 2000's, there has been a steady growth in public awareness of cultural heritage preservation and demand for conservation of old building [5]. Although many scientific studies have been carried out on various applications of lime mortars for the old building in Taiwan, such as its use as jointing bricks in structural masonry walls [6] and protecting bamboo and wood lath-made walls against water and erosion [7]. But there is still a lack of research on mortar knowledge for old Japanese roof-tiles.

Unfortunately, due to the lack of research and knowledge of craftsmanship specialization, it was discovered in recent cases of Taiwan that cement was used to repair the Japanese-roof-tile to achieve wind protection [8]. As a result, Japanese roof-tiles are damaged and must be discarded without being repurposed. (Figure 1a) Cement-based mortars contain high stiffness and mechanical strength, while low in water vapor permeability and production of soluble salts. Due to these reasons, mortars have been disapproved for application in the conservation of cultural heritage [9]. Numerous studies on the adequacy to be used in historical building have established that lime mortars are more suitable for conservation of old building compared to cement. These studies include the analysis of mechanical strength and physical and mechanical characteristics of different types of lime mortar and other additives that are used in historical buildings [10]. Most of these studies discuss the compressive strength and tensile strength of lime mortars, while a few discuss the adhesion strength of lime mortar and the background materials in restoration for historic monument, mainly for wall [11-12] or stone adhesion [13]. However, the adhesion strength of the lime mortar to roof-tiles has not been explored to ensure its wind resistance. It has also yet been discussed whether the application of lime mortar to roof-tile requires the ability to be removed from substrate without damage, in order for roof-tiles to be repurposed.

Therefore, this paper focuses on the effect and optimization of using different types of lime mortars as adhesive bond on Japanese roof-tile interfaces and the ability to remove lime mortars from Japanese roof-tiles. The collection of mortar proportions data is based on

craftsmanship, historical documents [14] and related research [5-7, 15-16]. The main materials are slaked lime, sand, fiber material (hemp) and seaweed paste. Due to the wide variety of proportioning materials, such as types of slaked limes or sand with different particle sizes, this study will use the Taguchi experimental design method to set eight control factors in order to plan the most suitable mortar proportion to be used on old Japanese roof-tile.



Figure 1a. The old Japanese roof-tiles with cement



Figure 1b. Plastering the lime mortar on old Japanese roof-tiles



Figure 1c. The old Japanese roof-tiles with lime mortar [22]

Experimental

Experimental design by Taguchi method

The Taguchi method is a statistical method to determine the unknown properties of the different parameters and proportions in the experiment process and to analyze the interaction among the factors [17]. The Taguchi method also allows control of variations caused by the uncontrollable factors, and minimizes the effect of those uncontrollable factors [1]. Since this experiment has multiple ratios and different amounts, the L18 orthogonal array of the Taguchi method was used in this study. Eight matches can be placed in the L18 array (also called the control factors), and one of the matches can program two levels (levels are different ratios), while the other seven] can program three levels. In this way, 18 groups of lime mortars with different proportions were programmed, and the S/N ratio and average value of the experimental result and data were analyzed to understand the impact of the designated eight factors on the mortar.

Materials

This section will introduce the setting of each of the eight factors. The proportions and ratios of all 18 experiment groups are shown in Table 1. The factors and levels of L18 orthogonal array. All proportions are measured in weight ratio.

Factor A: According to the craftsmen, a small amount of cement is added to monument repair to help the mixing of the lime mortar. This factor is intended to explore the impact of adding cement. Therefore, factor A is the cement-lime ratio, and the ratio of the two levels is designed. One is to add cement (when the lime weighs 1g, the cement is 0.03g), and the other is does not add cement.

Factor B is the lime-sand ratio. This study refers to relevant research and literatures [5-7,14-16] to design three levels of ratios, namely 1:1, 1:2 and 1:3.

Factor C is the ratio of two types of sand. One is the yellow coarse sand from China with a particle size of 2~0.07mm, and the other is grey fine sand from Taiwan with a particle size of 0.3~0.07mm. According to the craftsmen, the coarse sand in lime mortar has a higher strength than the fine sand, but it is undetermined if the same effect applies to roof-tiles. Therefore, three levels (proportions) were set in this experiment to understand the impact that sand properties impose on mortar. The first level is only includes the coarse sand, the second level includes half of coarse sand and half of fine sand, and the third level only includes fine sand.

Factor D is the various types of lime. Three types of limes were used in this experiment. The first level adopts oyster ash. Previous studies have indicated that its viscosity is better than other limes [5]. Oyster Shell Lime is almost no longer produced and is currently rare in Taiwan. The Oyster Shell Lime used in this study is provided by the Cultural Affairs Bureau of Kinmen County. The second level is the slaked lime of the Tainan Guanziling brand, which is the type of lime that is commonly used in the restoration of monuments in Taiwan. The third level is slaked lime that is produced by Chu-shin Chemical Co., Ltd., which was used in the restoration of old houses in Hsinchu.

Factor E is the length of the fiberglass. The 6mm fiberglass was used in the restoration of the Taiwan National Convention and Historic Site in Tainan. Since the craftsmen said that the longer the fiberglass, the stronger the mortar, this study set the length as 6mm, 25mm and 41mm to investigate whether different fiberglass length impose an impact on the mortar.

Factor F is the ratio of lime to total fiber, and the reference is the same as factor B. The three levels of the factor are set to 1:0.03, 1:0.04 and 1:0.05.

Factor G is the the glass fiber-hemp ratio in all the fiber materials. Study has found that the combination of hemp and glass fiber mixed in the equal amount can give different effects [16]. Three different levels are programmed, in proportion to hemp to fiberglass. The first level includes only hemp in the fiber material, expressed as 1:0. The second level is 1:1, which is half fiberglass and half hemp. The third level is 0:1, which only includes fiberglass.

Factor H is the lime-seaweed powder ratio. Seaweed powder provides the function of retarding admixtures in lime mortar [7,16]. In the early days, it was directly added as a seaweed paste. As it is rather difficult to produce and store now, seaweed powder made by Nanxing Company has been used based on craftsmen experience and research. Three levels

are set. The first level is 1:0 (that is, no seaweed powder is added), the second level is 1:0.0125, and the third level is 1:0.0167.

Table 1. The factors and levels of L18 orthogonal array.

No.	Factor	Level 1	Level 2	Level 3
A	Ratio of lime: cement	1:0	1:0.033	
B	lime: sand	1:1	1:2	1:3
C	Coarse sand : fine sand	1:0	1:1	0:1
D	Types of limes	Oyster Shell Lime	Guanziling lime	Chu Shin Co. Lime
E	Fiberglass length	6mm	25mm	41mm
F	lime : fiber	1:0.03	1:0.04	1:0.05
G	Hemp :Fiberglass	1:0	1:1	0:1
H	Lime:Seaweed powder	1:0	1:0.0125	1:0.0167

Specimen preparation

The ratios of the experimental samples of all 18 experimental groups were based on the L18 orthogonal array of the Taguchi experimental method (see Table 2).

Table 2. L18 orthogonal array

No	A	B	C	D	E	F	G	H
1	1	1	1	1	1	1	1	1
2	1	1	2	2	2	2	2	2
3	1	1	3	3	3	3	3	3
4	1	2	1	1	2	2	3	3
5	1	2	2	2	3	3	1	1
6	1	2	3	3	1	1	2	2
7	1	3	1	2	1	3	2	3
8	1	3	2	3	2	1	3	1
9	1	3	3	1	3	2	1	2
10	2	1	1	3	3	2	2	1
11	2	1	2	1	1	3	3	2
12	2	1	3	2	2	1	1	3
13	2	2	1	2	3	1	3	2
14	2	2	2	3	1	2	1	3
15	2	2	3	1	2	3	2	1
16	2	3	1	3	2	3	1	2
17	2	3	2	1	3	1	2	3
18	2	3	3	2	1	2	3	1

Mortar samples of Group 1 all measured level 1 in Factors A-H. The ratios of each factor of the first group are shown below. Factor A, the lime-cement ratio, is 1:0, which shows that there no cement in this group of mortar. Factor B is 1:1. Factor C is 1:0, which means that all the sand added is coarse. Factor D is Oyster Shell Lime. Factor E is 6mm. Factor F lime-fiber

ratio is 1:0.03. Factor G Fiberglass-Hemp ratio is 1:0, which indicates that only hemp was used in the fiber material of Group 1 and no fiberglass was added. Factor H ratio is 1:0, which indicates that the seaweed powder was not added to the lime mortar in Group 1. Other group ratios are also determined based on the above-mentioned method used in Group 1 with reference to the information in Tables 1 and 2.

The water consumption and mixture process of lime mortars are based on the information provided by traditional craftsmen. According to Taiwan standard CNS 12611 [18], stirred lime mortar was applied to a slice of Japanese roof-tiles measuring 7 cm *5 cm *2 cm, and the application area was 5 cm * 5 cm. The lime mortar connects the original piece to another piece as a test unit. The piece of old Japanese roof-tiles that was used for test sampling was the undamaged portion of the roof-tile that cannot be repurposed. The craftsmen determines the of the roof-tiles. Yongfeng tile kiln is the producer of old Japanese roof-tiles. One experimental group conducted 3 samples for each test. The sample curing condition was for 28 days in outdoors to approximate the true climate of northern Taiwan.

Pull-off testing

Pull-off testing is used to measure the direct tensile strength or adhesive bond strength of an interface. Since strong winds often occur in Taiwan, detachment and displacement of roof tiles are the most common type of damages that occur to old building roof in Taiwan. The use of lime mortars in Japanese roof-tiles for the purpose of adhesion strength has become an important topic for discussion. In this study, the sample underwent to a pull-off test to detect the adhesive strength of the mortar in the roof-tiles. The pull-off test conducted refers to CNS Standard 12611 [18] as illustrated in Figure 2(a), and the use of Universal Testing Machine (UTM) by Comotech Testing Machines equipped with 500 kN load.

Analysis of the ability of mortar to be removed from the roof-tile

The purpose of removing the mortar smoothly from the tile is to allow the tile to be undamaged and reused. In this study, shear bond strength test was first performed to simulate the action of removing mortar from the roof-tile, and the goal was the discovering the minimum shear strength. The smaller the shear strength, the easier it is for the craftsman to remove the mortar. The shear bond strength test is illustrated in Figure 2(b), and the test method referenced study [16, 20-21].

After performing the shear bond strength test, the sample is analyzed in two ways. The first method is to analyze the type of fracture of the sample interface. The fracture mode is divided into two types according to the definition of Taiwan research [15-16, namely adhesive (fracture at the interface between the mortar and the roof-tile) and cohesive (fracture in the roof-tile) types. Since the surface of the old Japanese roof-tile has a layer of black-coating that is smoked, unlike the gray of the base of the roof-tile itself [2], the color can be used to determine whether the types of fracture are cohesive or adhesive.

The second method is to study the ratio of the residual area of the adhesive fracture that the base of roof-tile did not damage. The goal is to minimize the residual area. The ratio of the residual area is calculated by the ratio of the area of the adhered mortar to the area of the adhesive surface in a multiple of 10%. The measurement is recorded as 0.1 if there was no residual area on the roof-tiles to suffice the Taguchi method.

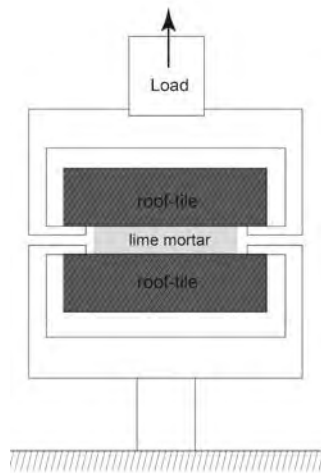


Figure 2a. Demonstration of samples on Pull-off testing.

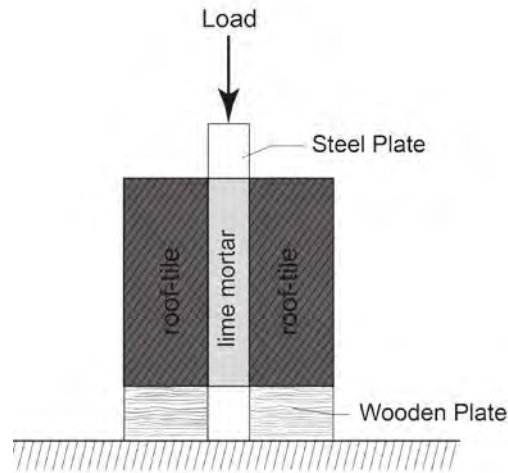


Figure 2b. Demonstration of samples on Shear bond strength test

Results and Discussion

Results from the pull-off testing and mortar removal ability analysis for the 18 groups are summarized in Appendix 1, Appendix 2 and Appendix 3. The response table of L18 factors is shown in Table 3. These data indicate that the average adhesive bond strength of all experimental groups exceeds 0.09 kg/cm^2 , which meets the minimum limit strength of wind resistance design specifications in Taiwan. The average adhesive bond strength in all 18 groups ranges between a minimum of 0.1 kg/cm^2 and a maximum of 1.77 kg/cm^2 . The difference is 17.7 times. This demonstrates that the different level of the factors has a substantial impact on the adhesive bond strength of the lime mortar.

After the shear bond strength test was conducted on the 18 groups of samples, it was found that the type of fractures were all adhesive. This shows that removing the mortar does not damage the tiles. Moreover, among the 18 groups, four groups of lime mortar (1st, 2nd, 7th and 12th groups) could be removed from the roof tiles completely, which is in line with traditional application of lime mortar technology in Taiwan.

Due to the fact that the results of the average adhesive bond strength meet the standard, the optimal parameters selection is focused on the removal ability of the mortar from the roof-tile. Because the types of fracture of the 18 groups were all adhesive, the ratio of the residual area of the lime mortar can directly determine the results of the shear bond strength test. Based on Table 3, Figure 3 and Figure 4 that are calculated using the Taguchi method, an optimal proportion of lime mortar is programmed. The experimental optimal condition for residual area ratio and shear adhesive strength were determined by the “the-

smaller-the-better” approach. The impact of each factor on the removal ability of lime mortar from the old Japanese roof-tile is discussed below.

Table 3. The response table of L18 factors for the average value (AVG) and S/N ratios of adhesive bond strength, shear strength of adhesives and ratio of residual area.

Adhesive bond strength AVG (%)								
	A	B	C	D	E	F	G	H
Level 1	0.72	0.62	0.87	0.97	0.88	0.74	0.76	0.76
Level 2	0.60	0.72	0.53	0.53	0.53	0.57	0.75	0.50
Level 3		0.65	0.60	0.49	0.59	0.69	0.48	0.74
Adhesive bond strength S/N ratio (%)								
	A	B	C	D	E	F	G	H
Level 1	-6.48	-8.50	-3.00	-2.10	-2.72	-6.21	-4.04	-5.79
Level 2	-6.01	-4.19	-9.16	-7.99	-9.69	-6.88	-5.17	-8.64
Level 3		-6.04	-6.58	-8.64	-6.32	-5.65	-9.52	-4.30
Shear strength of adhesives AVG (%)								
	A	B	C	D	E	F	G	H
Level 1	2.10	1.47	2.15	2.43	2.39	1.90	1.82	2.03
Level 2	2.04	2.15	2.20	1.66	1.86	2.21	2.47	1.59
Level 3		2.59	1.86	2.12	1.96	2.10	1.92	2.59
Shear strength of adhesives S/N ratio (%)								
	A	B	C	D	E	F	G	H
Level 1	-6.09	-3.41	-6.38	-7.79	-7.49	-4.84	-4.84	-6.31
Level 2	-5.89	-6.40	-6.36	-3.61	-4.97	-6.81	-7.51	-4.08
Level 3		-8.15	-5.23	-6.56	-5.50	-6.31	-5.62	-7.58
Ratio of residual area AVG (%)								
	A	B	C	D	E	F	G	H
Level 1	24.50	16.73	21.72	41.69	12.28	24.50	14.51	21.15
Level 2	21.16	18.37	27.82	3.41	20.61	33.92	25.60	24.49
Level 3		33.37	18.93	23.38	35.58	10.06	28.37	22.83
Ratio of residual area S/N ratio (%)								
	A	B	C	D	E	F	G	H
Level 1	-12.67	-4.04	-11.40	-23.92	-9.52	-14.05	-7.75	-17.68
Level 2	-19.35	-23.26	-20.08	0.38	-11.06	-20.53	-13.38	-19.65
Level 3		-20.74	-16.56	-24.49	-27.45	-13.46	-26.91	-10.69

The contribution rate of Factor A in the residual area ratio and shear strength is less than 1%, which indicates that the cement does not need to be added to the lime mortar. The lime mortar can achieve its purpose without cement, which can also reduce material cost. Therefore, Factor A selects A1 (A1 representing the first level of Factor A, which will be expressed later, like B1, C2, etc.) to be the optimal proportion of lime mortar.

It can be seen from Figure 2 that factor B has the smallest result in B1 in both the ratio of the residual area and the shear bond strength. This indicates that B1 works best, so the 1:1 ratio of B1 is selected. This ratio will be able to reduce the shear bond strength and the residual area ratio when it is applied to the mortar used on traditional Taiwanese roof-tile. However, this study in lime mortar used for the Taiwanese roof-tile did not take into consideration the

factors of adding seaweed powder and fiberglass, and nor did it discuss the proportion of sand produced in different sizes. [15]

For Factor C, the results indicate that the use of coarse sand in mortar (C1) can obtain the maximum adhesive bond strength, which is comparable to the craftsmen experience that the use of pure coarse sand is better than fine sand. However, since the selection of the optimal ratio mainly considers the minimum residual area ratio and shear bond strength, the optimum level is C3 (all used fine sand).

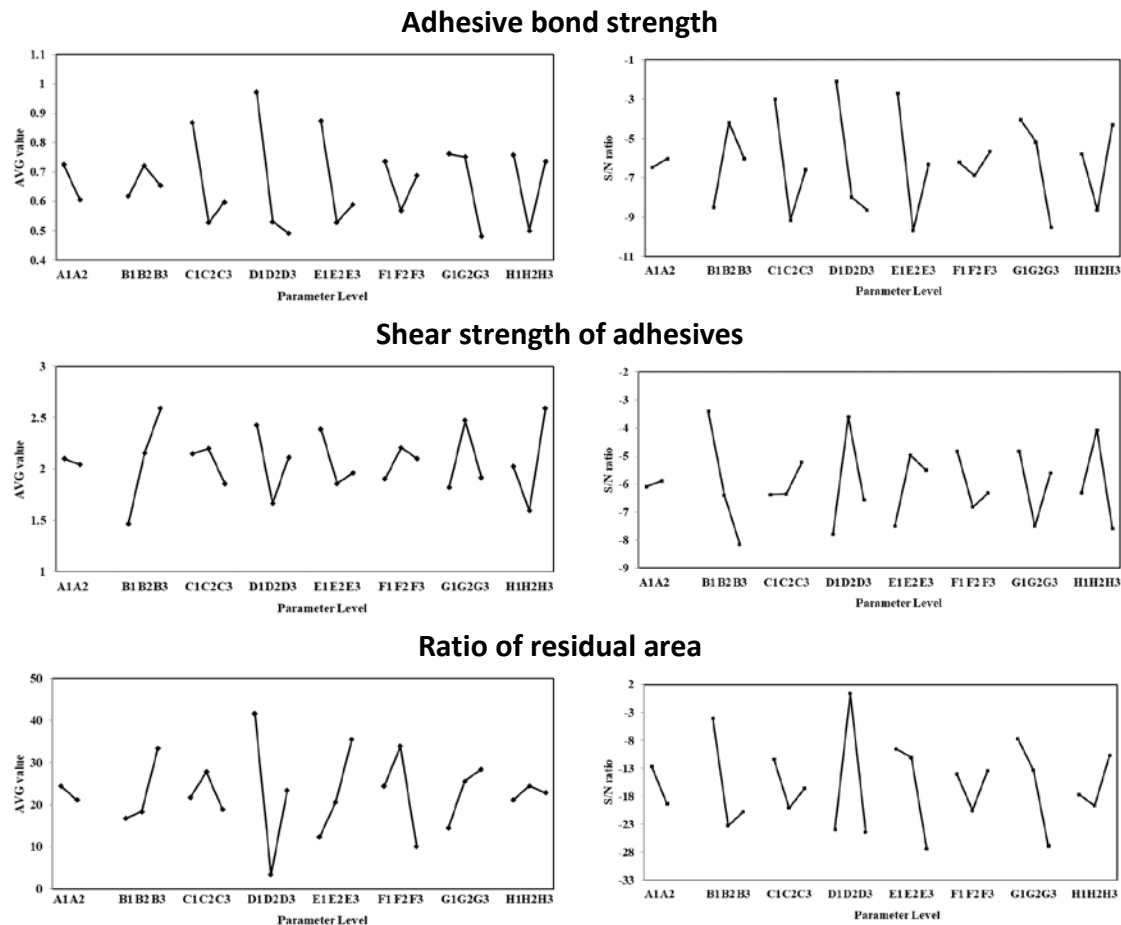


Figure 2. Factor response graph for average(AVG) values and the signal-to-noise (s/n) ratios for the adhesive bond strength, shear strength of adhesives and ratio of residual area

In Factor D, the results of adhesive bond strength and shear bond strength in Oyster Shell Lime (ie D1) are the highest. Previous studies have also mentioned that the adhesion of Oyster Shell Lime is the best among other types of lime, while Guanziling lime has the worst [1]. This study did not conduct comparison against the lime produced by Chu Shin Company. The results in residual area ratio and shear bond strength of Guanziling lime are also the smallest, and the adhesive bond strength is much smaller than that of Oyster Shell Lime. Although all substrates and methods of pull-off test in previous study were different, similar results were obtained.

The effects of Factor E are highly correlated with Factor G since Factor G determines whether fiberglass was added to the mortar. In particular, G1 has the best effect for all conditions (maximum adhesive bond strength, minimum residual area ratio and shear bond strength). This indicates that with only the addition of hemp and without fiberglass can the mortar achieve the purpose of this study and attain better adhesive bond strength.

Factor F is the smallest ratio of residual area of F3, and the best effect. Since the contribution of the F factor is low in the shear bond strength and the difference between the F1 and F3 values is small (as shown in Figure 3), F3 is selected as the optimum proportion.

Factor H is very unique in that its impact on shear bond strength is substantial, but its effect on the residual area ratio is minimal. The effect of seaweed powder is a kind of retarding admixtures in lime mortar [7, 16]. There is limited research on the seaweed powder in the mortar, this phenomenon needs to be further clarified. Since H2 has the lowest shear strength, it was chosen as the optimization parameter.

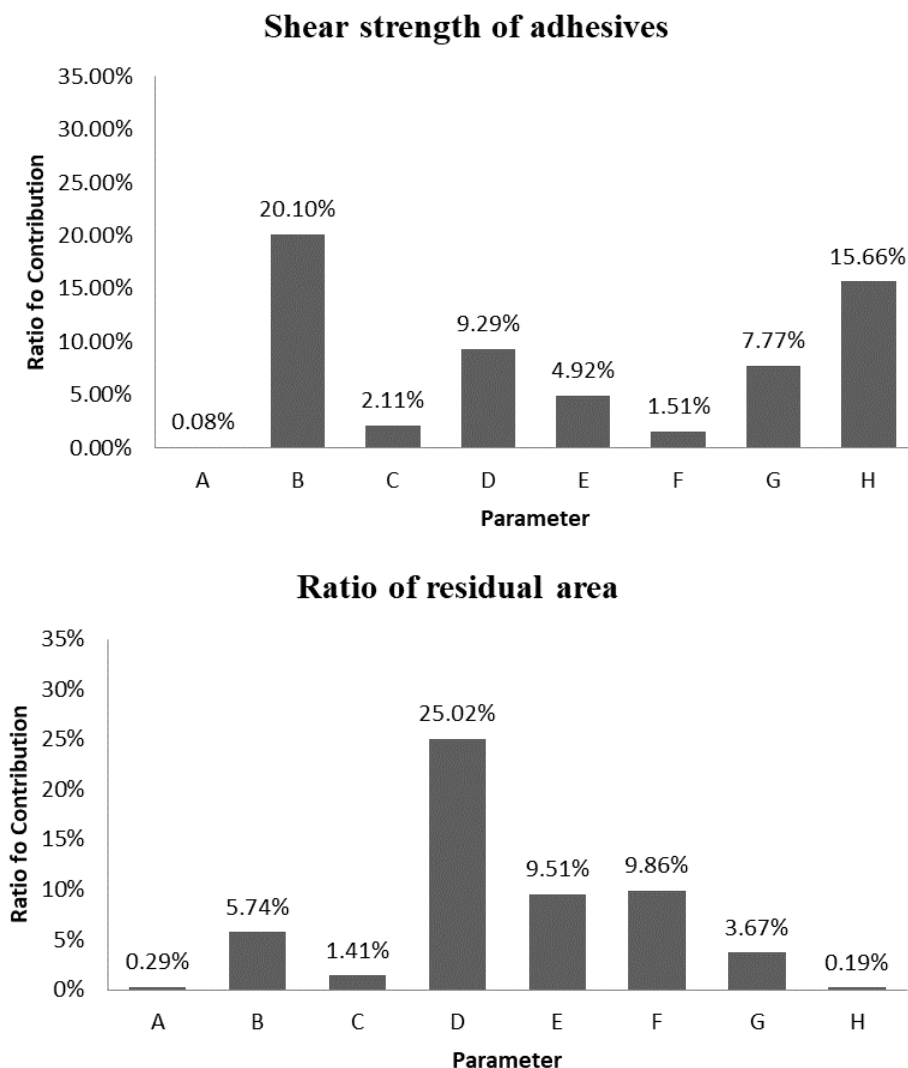


Figure 3. The response graph of L18 contribution in AVG for shear strength of adhesives and ratio of residual area

In summary, the optimal parameters in residual area ratio and shear adhesive strength are A1, B1, C3, D2, F3, G1, and H2. This indicates that the lime-cement ratio is selected from A1 is without the addition of cement. The lime-sand ratio is 1:1 (B1). Fine sand (C3) for the proportion of sand with different particle sizes. The type of lime in mortar is Guanziling lime (D2). The ratio of lime to fiber material is 1:0.05 (F3). The proportion of hemp and fiberglass in the fiber material is selected as G1, which indicates that the optimal lime mortar only had the addition of hemp. The lime-seaweed powder ratio is chosen as 1:0.0125 (H2).

Conclusion

It is an important issue to fix the Japanese historic roof-tiles in Taiwan. The restoration work requires a type of lime mortar that has sufficient adhesive bond strength but can also be easily removed from the roof-tiles. In this study, the Taguchi experiment method was used to set eight factors to discover the optimal parameters. Taguchi method was used to analyze the impact of various proportions and factors in lime mortar, optimize the ability for adhesive bond strength of interface on Japanese roof-tiles, and the initial removal ability lime mortars from Japanese roof-tiles.

The average adhesive bond strength of all experimental groups exceeds 0.09 kg/cm², which meet the minimum limit strength of wind resistance design specifications in Taiwan. This shows that the mortar can be applied to the roof of the restored monuments and also complies with Taiwan's regulations. Four groups of lime mortars can be removed from old Japanese roof-tiles samples completely and did not impose any damage to the roof-tiles. This reveals that the proportion of mortar in this study can represent traditional mortar technology and is in line with Taiwan's traditional roof restoration method. The lime mortars in four groups can remove from the old Japanese roof-tiles samples completely and didn't damage to the roof-tiles, this reveal that lime mortars are suitable for conservation of cultural assets with old Japanese roof-tiles.

In conclusion, the optimal parameters are A1, B1, C3, D2, F3, G1, and H2. This result indicates that the lime-cement ratio is selected from A1, which is without the addition of cement. The lime-sand ratio is 1:1 (B1). Fine sand (C3) for the proportion of sand with different particle sizes. The type of lime in mortar is Guanziling lime(D2). The ratio of lime to fiber material is 1:0.05 (F3) The proportion of hemp and fiberglass in the fiber material is selected as G1, which incidates that the optimal lime mortar only had the addition of hemp. The lime-seaweed powder ratio is chosen as 1:0.0125 (H2).

References

1. Shiu C (2000) Report of Japanese-style Dormitory research in Taipei city. Department of Civil Affairs, Taipei, p.5-13

2. Chang Y (2018) A Study on the Japanese Roof tile in North Taiwan-Take Ibushikawara as Study. Master's Thesis of Graduate Institute of Cultural Heritage. Taipei National University of the Arts, Taipei.
3. Kenchiku Shiryo Kenkyusha (1997) Roof, sheet metal, plastering work. Kenchiku Shiryo Kenkyusha, Tokyo, p.13
4. Cheng, C. M., & Chang, C. H. (2005). Specifications on Building Wind Resistance Design and Wind Environmental Issues in Taiwan. In Workshop on Regional Harmonization of Wind Loading and Wind Environmental Specifications in Asia-Pacific Economies.
5. Yeh R, Shiue C, Chang C, Chan I (2003) The Technology of Historic Buildings Restoration—A Research for the Property of Materials and the Methods of Restoration in Lime Work. Architecture and Building Research Institute, Taipei
6. Wang X (2003) Study on the characteristic of mortar materials in Taiwan traditional brick buildings. Master's Thesis of Department of Cultural Heritage Conservation. National Yunlin University of Science and Technology, Yunlin
7. Huang M (2006) The Research on the Craftsmanship of Bamboo lath and Wood lath During the Japanese Occupation in Taiwan. Master's Thesis of Graduate Institute of Cultural Heritage. Chung Yuan Christian University, Taoyuan
8. Lee Q (2013) Restoration and Re-use Planning of Japanese-style Police officers 'quarters of New Taipei City Historic Buildings in Tamsui. Culture Affairs Department, New Taipei
9. Veiga, M. do Rosário, Fragata, A., Velosa, A. L., Magalhães, A. C., & Margalha, G. (2010). Lime-based mortars: viability for use as substitution renders in historical buildings. *International Journal of Architectural Heritage*, 4(2), 177-195
10. Veiga, R. (2017). Air lime mortars: What else do we need to know to apply them in conservation and rehabilitation interventions? A review. *Construction and Building Materials*, 157, 132-140.
11. Andrejkovičová, S., Velosa, A. L., & Rocha, F. (2013). Air lime–metakaolin–sepiolite mortars for earth-based walls. *Construction and Building Materials*, 44, 133-141.
12. Veiga, M. R., Velosa, A., & Magalhães, A. (2009). Experimental applications of mortars with pozzolanic additions: characterization and performance evaluation. *Construction and building materials*, 23(1), 318-327.
13. Bromblet, P. (2000). Evaluation of the durability and compatibility of traditional repair lime-based mortars on three limestones/Bestimmung der Beständigkeit und der Verträglichkeit traditioneller Reparaturmörtel mit Kalk als Bindemittel auf drei unterschiedlichen Kalksteinen. *Restoration of Buildings and Monuments*, 6(5), 513-528.
14. Susuki C (1892) Kenchiku Gaku Teiyo. Fuchi ten dō, *Hiroshima*, p.115

15. Feng C (2003) Study on Fundamental Characters of the Traditional Roof Mortar in Taiwan. Master's Thesis of Department of Architectur. National Cheng-Kung University, Tainan.
16. Chou C (2006) A Study on Fundamental Characters of the Stucco Mortar on the construction Walls Built in the Japanese Rule Period. Master's Thesis of Department of Architecture. National Cheng-Kung University, Tainan.
17. Taguchi G., Chowdhury S., Wu Y. (2005), Taguchi's Quality Engineering Handbook. John Wiley & Sons Inc., New Jersey, p.57-59
18. Günay, M., & Yücel, E. (2013). Application of Taguchi method for determining optimum surface roughness in turning of high-alloy white cast iron. *Measurement*, 46(2), 913-919.
19. CNS Standards 12611 (2017) Organic adhesives for ceramic tiles, Bureau of Standards, Metrology and Inspection, MOEA, Taiwan
20. Lee D, Chang S, Wu J (2011) Preliminary Study on the Reversibility of the Traditional Mortar. *Journal of Cultural Property Conservation: Bureau of Cultural Heritage in Taiwan* ,15, 63-76.
21. Singh, S. B., & Munjal, P. (2017). Bond strength and compressive stress-strain characteristics of brick masonry. *Journal of Building Engineering*, 9, 10-16.
22. Chen T, Chang J, Lin Y. (2013) Site manager training course materials for restoration of historic building. Bureau of Cultural Heritage, Ministry of Culture (BOCH), Taiwan.

Appendix 1. Adhesive bond strength

adhesive bond strength (kg/cm ²)	Data1	Data2	Data3	AVG	S	S/N
1	1.48	1.76	2.08	1.77	1.1406	24.60
2	0.132	0.076	0.42	0.21	1.0853	25.62
3	0.706	0.286	0.162	0.38	1.2288	25.68
4	1.06	0.99	0.9	0.98	1.6455	25.72
5	0.754	0.774	0.53	0.69	1.3868	25.56
6	0.64	1.01	0.684	0.78	1.2566	25.26
7	1.066	1.004	1.028	1.03	1.2129	25.56
8	0.104	0.09	0.114	0.10	1.0185	25.42
9	0.61	0.42	0.68	0.57	1.5940	25.38
10	0.418	0.492	0.544	0.48	1.4667	24.35
11	0.254	0.722	0.526	0.50	1.9432	25.37
12	0.416	0.33	0.294	0.35	1.0636	24.86
13	0.356	0.458	0.222	0.35	1.2342	25.43
14	0.656	0.566	0.58	0.60	1.1886	25.87
15	1.21	0.42	1.19	0.94	0.8211	24.52
16	0.634	0.772	0.364	0.59	1.8187	25.00
17	0.99	1.186	1.024	1.07	1.2068	26.08
18	0.418	0.76	0.516	0.56	1.7466	24.48
AVG				0.6644	1.3366	25.26

Appendix 2. Shear strength of adhesives

shear strength adhesives (kg/cm ²)	Data1	Data2	Data3	AVG	S	S/N
1	1.48	1.76	2.08	1.77	0.3002	-5.06
2	1.36	1.12	0.68	1.05	0.3449	-0.75
3	2	1.44	1.36	1.60	0.3487	-4.22
4	2.68	3.96	1.76	2.80	1.1049	-9.37
5	1.8	1.16	1.28	1.41	0.3402	-3.17
6	2.24	1.84	1.84	1.97	0.2309	-5.94
7	2.96	2.96	5.2	3.71	1.2933	-11.72
8	2.16	2.6	2.32	2.36	0.2227	-7.48
9	2.76	1.64	2.24	2.21	0.5605	-7.08
10	1.24	1.52	3.16	1.97	1.0372	-6.64
11	0.64	2.32	2.04	1.67	0.9001	-5.21
12	1.32	0.28	0.6	0.73	0.5327	1.39
13	0.56	1.52	0.96	1.01	0.4822	-0.73
14	3.04	4.36	2.04	3.15	1.1637	-10.34
15	2.4	3.88	1.44	2.57	1.2292	-8.82
16	2.4	1.16	1.36	1.64	0.6657	-4.75
17	4.32	2.64	3.72	3.56	0.8514	-11.19
18	2.32	1.2	2.68	2.07	0.7718	-6.69
AVG				2.07	0.687	-6

Appendix 3. Ratio of residual area

	Data1	Data2	Data3	AVG	S	S/N
1	0.1	0.1	0.1	0.10	0.0000	20.00
2	0.1	0.1	0.1	0.10	0.0000	20.00
3	0.1	0.1	10	3.40	5.7158	-15.23
4	50	100	40	63.33	32.1455	-36.72
5	10	10	0.1	6.70	5.7158	-18.24
6	20	50	0.1	23.37	25.1198	-29.85
7	0.1	0.1	0.1	0.10	0.0000	20.00
8	50	0.1	100	50.03	49.9500	-36.20
9	40	100	80	73.33	30.5505	-37.78
10	50	70	50	56.67	11.5470	-35.19
11	0.1	60	60	40.03	34.5833	-33.80
12	0.1	0.1	0.1	0.10	0.0000	20.00
13	0.1	20	0.1	6.73	11.4893	-21.25
14	10	0.1	0.1	3.40	5.7158	-15.23
15	10	0.1	10	6.70	5.7158	-18.24
16	0.1	10	0.1	3.40	5.7158	-15.23
17	50	100	50	66.67	28.8675	-36.99
18	10	0.1	10	6.70	5.7158	-18.24
AVG				22.825	14.363	-16

Evolution of mortars composition and characteristics during the 20th century– Study of Portuguese buildings awarded with Architecture Valmor Prize

Luís Almeida¹, António Santos Silva², José Mirão³, Maria do Rosário Veiga⁴

(1) National Laboratory for Civil Engineering, HERCULES Laboratory and University of Évora, Geosciences Department, Portugal, lalmeida@lnec.pt

(2) National Laboratory for Civil Engineering (LNEC), Materials Department, Portugal, ssilva@lnec.pt

(3) HERCULES Laboratory and Geosciences Department, University of Évora, Portugal, jmirao@uevora.pt

(4) National Laboratory for Civil Engineering (LNEC), Buildings Department, Portugal, rveiga@lnec.pt

Abstract

20th century is most known for the changes that have led to a new paradigm of construction techniques and the increasing use of new materials on the verge of modernity. Reinforced concrete has become the wide spread new construction material, letting behind traditional lime mortars that were used massively throughout the past centuries. Thus, Portland cement gradually substituted lime-based mortar's binders, both aerial and hydraulic, and quickly bestowed an unmatched material to all construction agents, however almost incompatible with the traditional ones.

The Valmor Prize, one of the most prestigious prizes for Architecture in Portugal, was established in the beginning of 20th century to distinguish the most architectural striking buildings in Lisbon. In this paper the results of physical, mechanical, chemical and mineralogical characterization of renders and plasters collected in several Valmor awarded case studies will be presented. Their study aims to understand the evolution of composition and physical and mechanical characteristics of wall renders and plasters over the 20th century, since this knowledge and the evaluation of conservation state will have a huge contribution for valorisation and preservation of built heritage.

Introduction

The Valmor Prize for architecture was established in 1902. Since then eighty buildings were awarded. Throughout more than a century its attribution remains the responsibility of the Lisbon City Council, which continues to privilege and stimulate the social function of architecture through a regulation that has undergone successive changes [1]. The knowledge of building materials, rendering mortars and plasters, their formulation and evolution of their characteristics over time allow a more informed assessment of their state of conservation and of the constructive techniques used during the 20th century.

From the middle of the 20th century Portland cement was used in a massive way in the construction structures. Therefore, the use of aerial binders decreased. In fact, the demand

for new and quicker construction solutions led to the abandonment of the application of these materials.

The purpose of this paper is to present a preliminary characterization of the evolution of the physical, mechanical and mineralogical characteristics of rendering mortars and plasters in seven case studies of award-winning buildings during the first five decades. The results obtained are expected to contribute to a better knowledge on this historical and architectural heritage and will contribute to the development of safeguard measures that will possibly be required in the future.

Methodology

Case Studies

Sampling was carried out on masonry mortars and plasters from both the interior and exterior walls.

Most of the collected samples are made up of several layers, comprising different thickness and composition (Figure 1), being the outermost layers thinner. Excluding *Bernardo da Maia* House all the buildings were in use; hence sampling was a challenging task and the number of samples per case study was restricted. It was always carried out with the consent of the owners in discrete places or in walls where detachments were identified.

In *Ventura Terra* House, *Luiz Rau* Building and *Bernardo da Maia* House, respectively samples CVT 3, AR49 15 and CBP 4, the finishing layers were composed by a gypsum plaster. Those layers will only be referred in this work concerning mechanical and physical tests as part of each complete sample set. Sample identification, typology, location and award year (usually coeval with the year of construction) are shown in Table 1. Figure 2 shows the places where sampling was carried out.

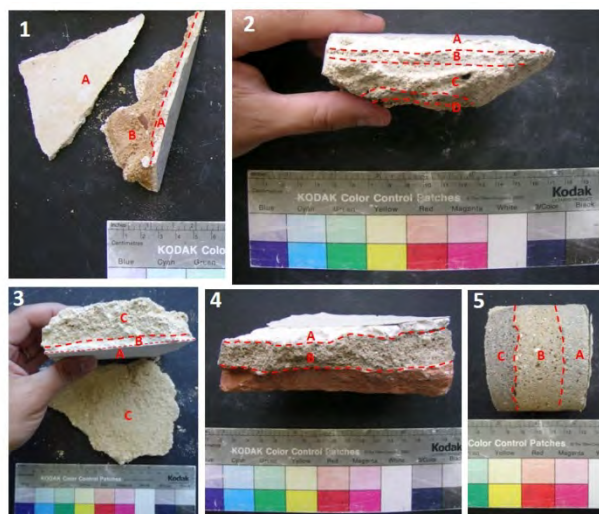


Figure 1. Multilayer samples: 1 – CVT 3; 2 – CMAG 11; 3 – AR49 15; 4 – CBP 4; 5 – DN 12

Table 1. Samples identification, typology, location and remarkable features

Case studies	Award year	Samples identification	Typology/location	Relevant macroscopic features	
Ventura Terra House	1903	CVT 3B	Plaster. Room wall	Yellowish to red coloured mortar with lime lumps and siliceous aggregate	
<i>Malhoa</i> House	1905	CMAG 11*	A	Non-original rendering mortars (most likely from 1970's/1980's restoration works) External South-East wall.	Grey to white layer with fine siliceous aggregate
			B		Greyish layers with siliceous aggregate
			C		
			D		
<i>Luiz Rau</i> Building	1923	AR49 15*	B	Plasters from a window opening. Stairs. 4 th Floor	Grey to white layer with fine siliceous aggregate
			C		Yellowish to red coloured mortar with lime lumps and siliceous aggregate
Rosário de Fátima Church	1938	IRF 1	Plaster. Sacristy wall	Yellowish to red coloured mortar with lime lumps and siliceous aggregate	
		IRF 4A	Plaster. Bell tower wall	Yellowish to red coloured mortar with lime lumps and siliceous aggregate	
Bernardo da Maia House	1939	CBP 1	Plaster. Basement room wall	Whitish to grey mortar with lime lumps and siliceous aggregates	
		CBP 4B	Plaster. North-east Bathroom wall	Greyish to brown coloured mortar with siliceous and ceramic aggregates	
Diário de Notícias Building	1940	DN 12*	A	Basement. Storage room	Greyish coloured mortar with siliceous aggregate
			B		Brownish coloured mortar with siliceous aggregate and lime lumps
			C		Greyish coloured mortar with siliceous aggregate
Laboratories of Pasteur Institute of Lisbon	1958	LIP 1	Rendering mortar. Chimney wall	Greyish mortar with siliceous aggregate	

* Multilayer sample. Sorted by alphabetic order – A is the most superficial layer. Mechanical and physical characterization (except open porosity evaluation) was carried out over the sample set

Methods

Mineralogical composition was determined by X-ray diffraction (XRD) that was carried out using Cu K α radiation, scan speed of 0.05°/s and 2 θ ranging from 3° to 75°. Two types of fractions were analysed, the fraction corresponding to the mortar as collected, designated as overall fraction and obtained by grinding the disaggregated mortar, and a binder rich fraction, which was obtained from the fines of the disaggregated material. Both fractions

were ground to pass a 106 µm sieve. The overall fraction was also used for thermogravimetric and differential thermal analysis (TGA-DTA).



Figure 2. Sampling places: 1 - *Ventura Terra* House; 2 - *Malhoa* House; 3 - *Luiz Rau* Building; 4,5 - *Rosário de Fátima* Church; 6, 7 - *Bernardo da Maia* House; 8 - *Diário de Notícias* Building; 9 - Laboratories of Pasteur Institute of Lisbon

The TGA-DTA analysis was performed under an argon atmosphere (3 L h^{-1}) and a heating rate of 10 °C/min from room temperature to 1000 °C . The carbonates content (expressed in % CaCO_3) was calculated as follows:

$$\% \text{CaCO}_3 = [P(\text{CO}_2) \cdot \text{MM}(\text{CaCO}_3)] / \text{MM}(\text{CO}_2)$$

$P(\text{CO}_2)$ is the mass loss obtained in the temperature range $500\text{--}900 \text{ °C}$ (corresponding to decarbonation of calcium carbonate), $\text{MM}(\text{CaCO}_3)$ is the molar mass of calcite and $\text{MM}(\text{CO}_2)$ the molar mass of carbon dioxide.

While these methods contributed to assess the relationship between chemical and mineralogical composition, physical and mechanical characterizations, namely water absorption, compressive strength, open porosity and ultrasonic pulse velocity were carried out to evaluate the quality and strength of the mortars.

To evaluate the water absorption by capillary uptake [2, 3] the external face of the specimen was placed in contact with water using a wire basket and wet geotextile gauze. The specimen, which is in contact with water through the wet textile, is weighed periodically to determine the water absorption. The capillarity coefficient is determined as the slope of the initial straight part of the absorption curve in function of the square root of time.

For compressive strength test, the samples were placed in a compression equipment used on standardised method of EN 1015-11 [4]. For ultrasonic pulse velocity an indirect method was applied [5]. In order to calculate the pulse velocity, transducers were kept on the same sample face and placed at a known distance (1 cm interval). After going through the material, the pulse of vibrations is reconverted into an electrical signal. After recording in a graphic the pairs of values (distance, time) it is possible to estimate an approximation of the velocity by computing the inverse of a trend line slope.

The open porosity was determined by hydrostatic weighing after vacuum immersion [6, 7]. This method combines the results of dry sample, immersion and water-saturated weighing. Porosity was calculated as the volume of pores in percentage.

Results and discussion

Mineralogical characterization by XRD

Figures 3 and 4 illustrate the XRD mineralogical composition of the mortar's binder rich fractions. It should be mentioned that the analysis of the overall fractions indicates quartz and alkali feldspars as the main components of the mortars, associated with calcite, whereas kaolinite and muscovite are accessory minerals.

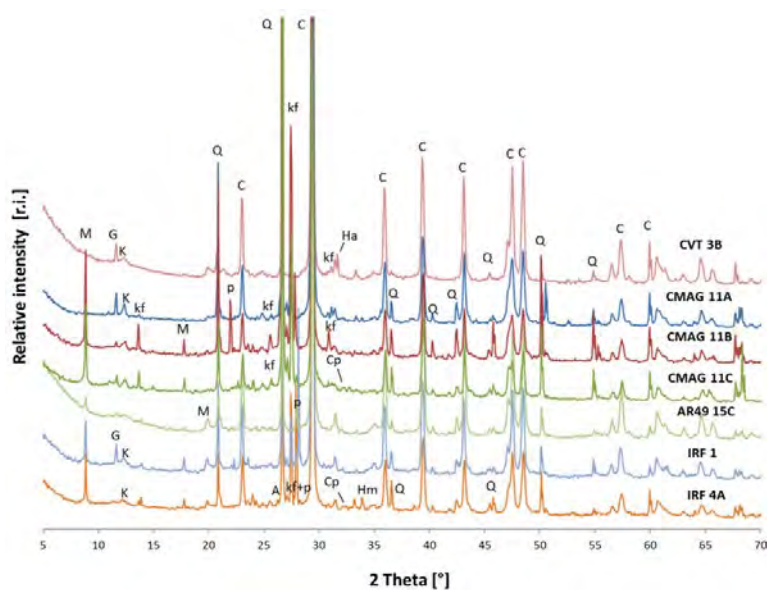


Figure 3. Binder rich fraction diffractograms for samples belonging to awarded buildings from 1903 (CVT3-B) to 1938 (IRF1, IRF4A). Notation: C- Calcite; Q- Quartz; M- Muscovite; G- Gypsum/Calcium carboaluminate; K- Kaolinite; Kf- K-feldspar; Cp – Clinker Portland; p- Plagioclase; Ha- Halite; Hm- Hematite; A – Aragonite

Results clearly show that samples CVT 3B, AR49 15C, IRF 1, and CBP 1 present a calcitic air lime binder. In samples IRF 4A, CBP 4B, LIP 1 and in multilayer samples sets DN 12 and CMAG 11 compounds typically associated to Portland cement mineral phases were identified (e.g. ettringite, portlandite and calcium silicate hydrates).

The presence of clay minerals (e.g. kaolinite) in these mortars can be damaging, since they favour the penetration of water and/or reduce the porosity of the matrix, leading to mechanical microtensions in combination with salts crystallization [8, 9]. This evidence could be stated in sample CVT 3B by the presence of kaolinite and halite. Sample CBP 4B present traces of vaterite, a polymorph of calcium carbonate normally attributed to dissolution and re-crystallization phenomena of the calcitic binder [10, 11]. Most of the samples presents a peak at approximately 7.6 Å, attributed to hydrated compounds (e.g. gypsum and/or calcium carboaluminate).

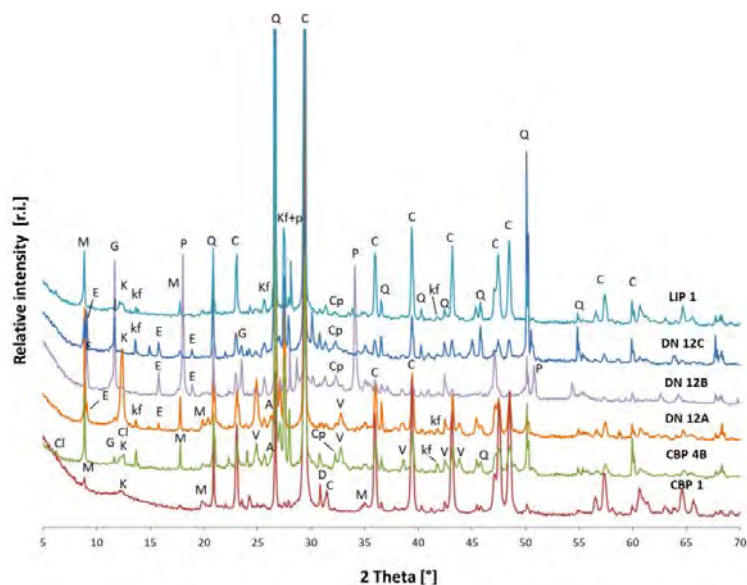


Figure 4. Binder rich fraction diffractograms for samples belonging to awarded buildings from 1939 (CBP1, CBP4B) to 1958 (LIP1). Notation: C- Calcite; Q-Quartz; M-Muscovite; G-Gypsum/Calcium carboaluminate; K-Kaolinite; Kf- K-feldspar; Cp - Clinker Portland; V-Vaterite; E-Ettringite; p-Plagioclase; D-Dolomite; A – Aragonite; P – Portlandite; Cl - Chlorite

TGA-DTA analysis

The analysis of TGA-DTA curves, combined with XRD data, allowed the selection of the temperature ranges associated to weight loss. The temperature ranges vary depending on the presence of certain compounds. Although the intervals are not uniform, the following can be generically considered: 25–100 °C, 100–200 °C, 200–500 °C and 500–900 °C. The weight loss in the temperature range from 25 to 100 °C is related to dehydration of hygroscopic or adsorbed water, while the weight loss in the temperature range from 100 to 200 °C is due to the loss of crystallization water of hydrated salts (e.g. gypsum). The weight loss between 200 and 500 °C occurs mainly due to the loss of chemically bound water (dehydroxylation) of clay minerals [11] (e.g. kaolinite) and hydraulic compounds. The last weight loss temperature interval considered is between 500 and 900 °C that corresponds to the loss of CO₂ due to the decomposition of calcium carbonate [13].

Non-hydraulic mortars are considered to have less than 3 % of chemically bound water of hydraulic compounds and a high content of CO₂.

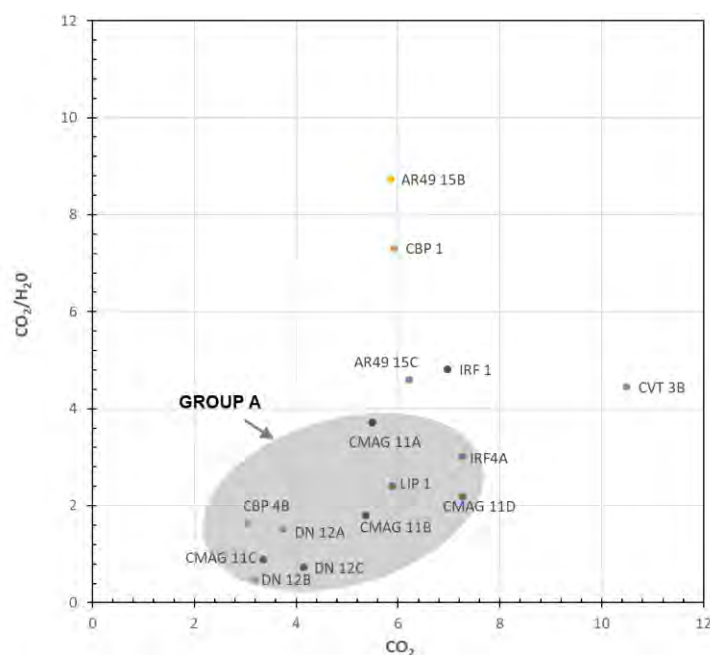


Figure 5. CO₂ to structurally bound water ratio in relation to % CO₂

Though, mortars with higher quantity of bound water and proportionally small quantities of CO₂ are considered hydraulic [14-17]. Figure 5 illustrates the relation between the weight loss due to total H₂O and CO₂ amounts shown in Table 2. A cluster of samples with CO₂ content varying between 3.04 % (sample CBP 4B) and 7.26 % (sample CMAG 11D) and CO₂/H₂O ratio varying between 0.47 (sample DN 12B) and a value below 4.0 (sample CMAG 11A=3.72), possibly define a group of samples (group A) that carry hydraulic feature. The remaining samples possibly represent a group of aerial calcitic binder.

Table 2. Amounts of CO₂, LOI, H₂O, CaCO₃ and CO₂/H₂O ratio obtained by TGA

Samples identification	Award year	CO ₂ (%)	LOI ⁺ (%)	H ₂ O ⁺⁺ (%)	CaCO ₃ (%)	CO ₂ /H ₂ O
CVT 3B	1903	10.49	12.98	2.36	23.84	4.44
CMAG 11A*	1905	5.50	7.99	1.48	14.77	3.72
CMAG 11B*		5.37	8.46	2.99	12.20	1.80
CMAG 11C*		3.35	7.33	3.78	7.61	0.89
CMAG 11D*		7.26	10.75	3.32	16.50	2.19
AR49 15B		1923	5.85	6.64	0.67	13.30
AR49 15C	1923	6.21	7.65	1.35	14.11	4.60
IRF 1	1938	6.97	8.42	1.45	15.84	4.81
IRF 4A		7.27	10.72	2.41	18.80	3.02
CBP 1	1939	5.92	6.73	0.81	13.45	7.31
CBP 4B		3.04	4.92	1.85	6.91	1.64
DN 12A	1940	2.75	6.28	2.47	8.52	1.11
DN 12B		3.20	10.21	6.83	7.27	0.47
DN 12C		4.14	10.04	5.66	9.41	0.73
LIP 1	1958	5.89	8.36	2.45	13.39	2.40

⁺ loss of ignition, obtained from the weight loss between 25 and 1000 °C; ⁺⁺ Total water, obtained from the weight loss between 25 and 500 °C; *Non-original renders

The higher calcium carbonate content in CVT 3B should not be explained by the use of carbonated aggregates since they have not been detected so far. Thus, it should be rich in calcitic binder. The determination of insoluble residue should confirm this hypothesis.

Physical and mechanical characterization

The capillarity coefficient by contact represents the slope of the tangent line to the first section of the water absorption plot. This section is defined until there is a sudden change in the graph's progress, where the slope of the trend line becomes less pronounced, reflecting the cessation of rapid absorption and initiating slow absorption in which the water transport mechanism occurs by diffusion [18]. Nevertheless, in the case of set of samples DN 12 and AR49 15 a resumption of the initial behaviour with a sudden change in the graph's progress seems to occur as shown by the arrows in the Figure 6. This behaviour may be related to the transition of samples interface as they were tested assembled as part of the same set.

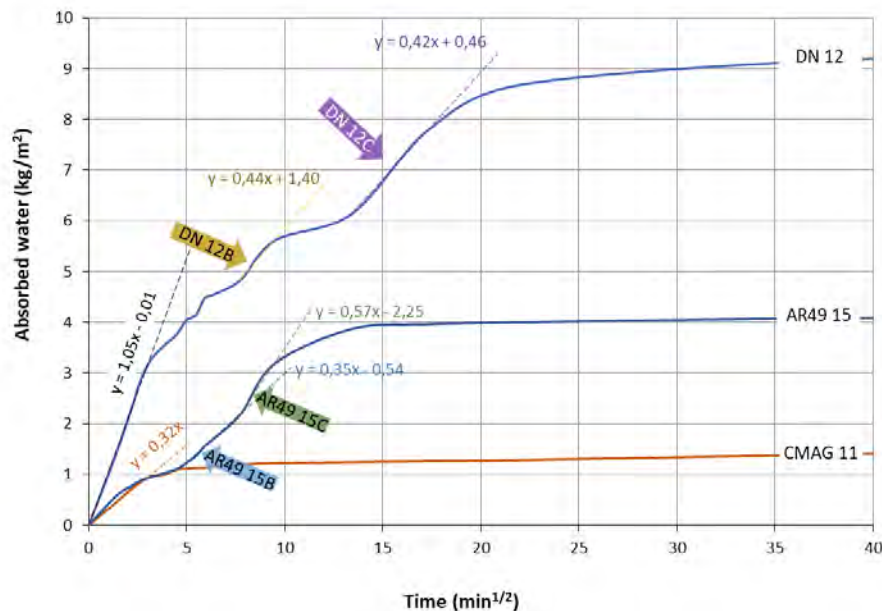


Figure 6. Absorbed water during time in multilayer samples

Water absorption coefficient for the single layer samples is shown in the Figure 7. The highest absorption coefficient values were obtained in the samples CVT 3B and CBP 4B whilst samples CMAG 11 and AR49 15B recorded the lowest values. Table 3 shows the compilation of physical and mechanical characterization, namely open porosity, compressive strength and ultrasonic pulse velocity. Multilayer samples were tested assembled as a set due to the reduced quantity of material considering the large number of tests that was carried out and to the mechanical difficulty in separating each layer.

Results of characterization for single layer samples should not be directly related with those obtained for multilayer samples which were tested as a whole set. Nevertheless, multilayer samples results should be indicative of physical and mechanical properties for the whole set.

As it would be expected samples with higher water absorption coefficients ($> 1.50 \text{ kg/m}^2 \cdot \text{min}^{1/2}$), namely CVT 3B, IRF 1, CBP 1 and CBP 4B present a higher open porosity ($> 25 \%$).

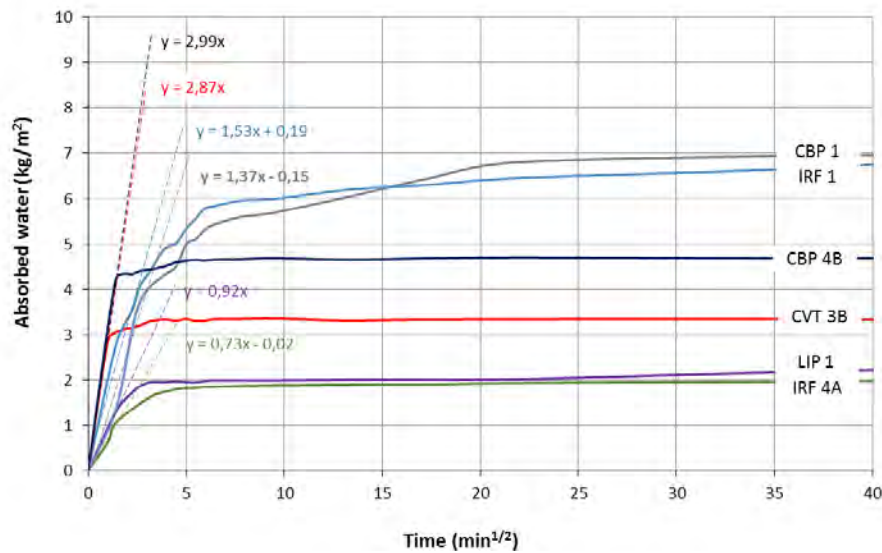


Figure 7. Absorbed water during time in single layer samples

Table 3. Results of physical and mechanical characterization

Sample s	Awar d year	Binder type ¹	Water absorption coefficient ($\text{kg/m}^2 \cdot \text{min}^{1/2}$)	Water absorptio n at 24h (kg/m^2)	Open porositi y (%)	Compressiv e strength (MPa)	Ultrasoni c pulse velocity (m/s)
CVT 3B	1903	aerial	2.87	3.33	27.1	2.57	1074
CMAG	1905	hydrauli	0.32 ³	1.40 ³	17.2 ³	18.70 ³	3175 ³
CMAG		hydrauli					
CMAG		hydrauli					
CMAG		hydrauli					
AR49	1923	aerial ²	0.35	4.09 ³	30.0 ³	1.77 ³	1477 ³
AR49		aerial	0.57				
IRF 1	1938	aerial	1.53	6.95	30.8	2.09	2290
IRF 4A		hydrauli	0.73	1.97	22.7	⁴	1044
CBP 1	1939	aerial	1.37	6.70	27.8	2.27	1049
CBP 4B		hydrauli	2.99	4.68	25.8	5.48 ⁵	2143
DN 12A	1940	hydrauli	1.05	9.18 ³	23.7	2.34 ³	1398 ³
DN 12B		hydrauli	0.44		23.1		
DN 12C		hydrauli	0.42		17.6		
LIP 1	1958	hydrauli	0.92	2.19	22.6	16.58	1321

¹ – most likely binder type according to TGA-DTA analysis and XRD data; ² – only according to TGA-DTA analysis. No XRD data available for the binder rich fraction; ³ -Results obtained for the set of the multilayer samples; ⁴ – Not tested; ⁵ – Result obtained for the set CBP 4A and CBP 4B; *Non-original renders

Figure 8 presents open porosity in relation to water absorption coefficient. Except for AR49 and CBP 4B samples, the higher water absorption coefficient indicates larger capillary pore diameters, thereby increasing the likelihood of being air lime mortars.

Samples AR49 15B and AR49 15C show high porosity values and relatively low mechanical characteristics, consistent with air lime mortars, but lower capillarity coefficients not confirming the tendency above stated. This may be due to perturbations of the porous structure, which take place when salts or neo-forming products are present or formed. The last can be exemplified by CaCO₃ polymorphs which are formed by recrystallization processes. However, the presence of these type of products was not confirmed so far.

The assessment of aggregate/binder ratio and grain size distribution would be helpful to understand this behaviour as it would influence the water uptake, especially for CBP 4B, which has the highest water absorption coefficient.

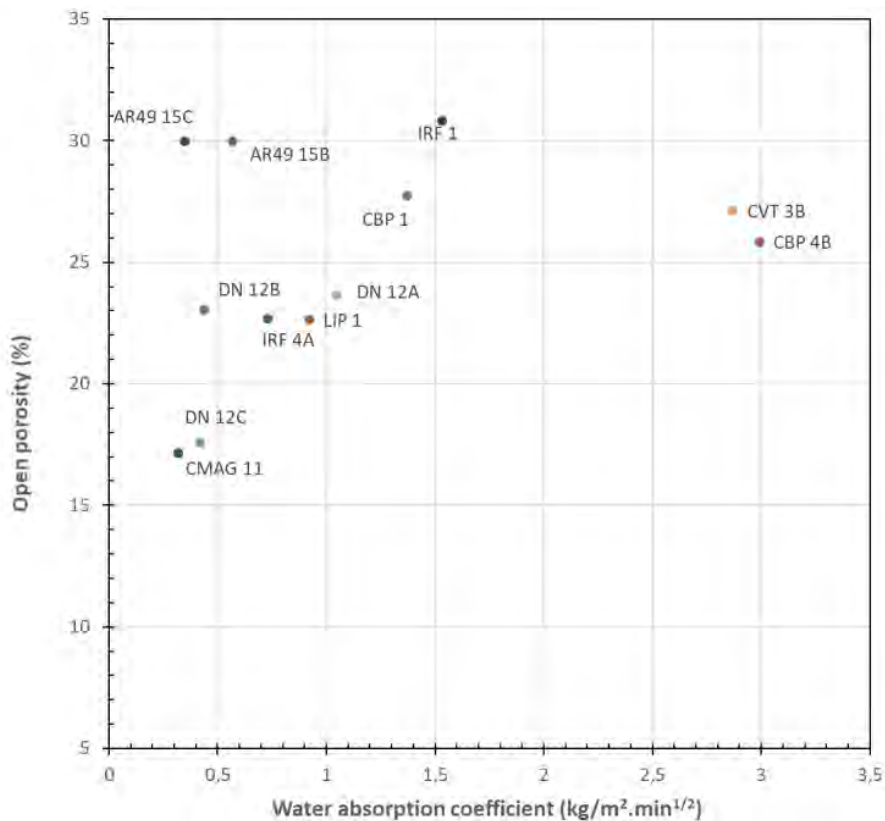


Figure 8. Open porosity in relation to water absorption coefficient

Concerning compacity (Figure 9), which is dependent on the porous structure and affects the compressive strength, in comparison to other multi-layered samples it is observed that the sample set CMAG 11 stands out with the highest ultrasonic velocity propagation and the highest compressive strength resulting in the highest compacity. On the other hand, DN 12 sample set shows an inferior strength, compatible to air lime mortars.

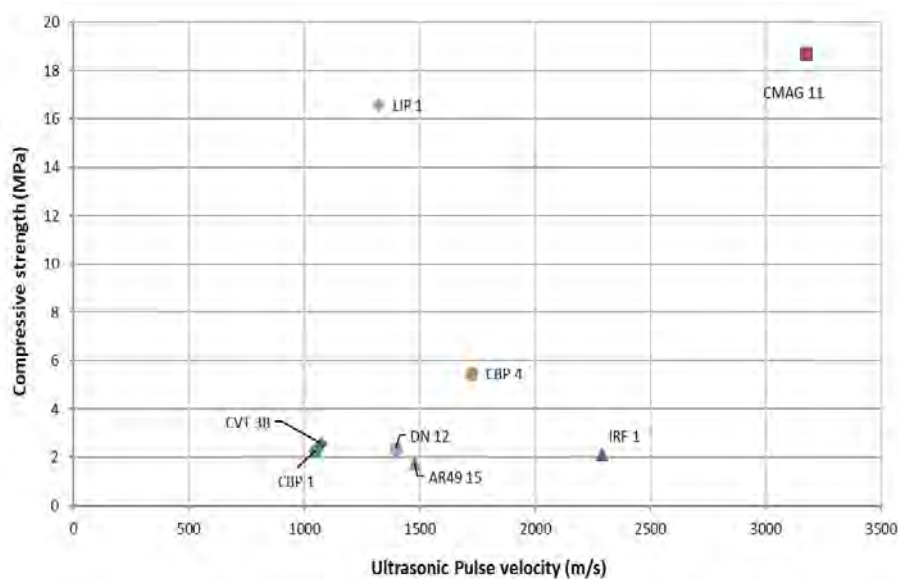


Figure 9. Compressive strength in relation to ultrasonic pulse velocity

Another sample that stands out is LIP 1. It also has a high compressive strength value, however its compacity is in-between the range of velocities for single layer samples. Although high values of compressive strength indicate the use of hydraulic binders, it would be useful to know the aggregate/binder ratio for it would contribute to better understand the mechanical characteristics.

Conclusions

Almost all mortars from the buildings awarded in 1903, 1923, 1938 and 1939 share the same mineral assemblage, namely in terms of binder, only varying their proportions. The first awarded building studied presents the mortar with the highest binder content.

Based on the similarity of the mineral composition of the binder paste of the *Diário de Notícias* building from 1940 (samples DN 12A, DN 12B and DN 12C), it is assumed the binder has cementitious compounds due to the presence of common Portland cement phases (C_3S , β - C_2S and C_4AF). However, the possibility that these mortars have also a second binder, such as air lime, is not excluded, since in the sample DN 12B lime lumps were detected by macroscopic observation. Thus, the combined results of water absorption by capillary uptake, compressive resistance and compacity support the hypothesis that these mortars are not completely cementitious. If they are, they would disclose higher values for compression strength and compacity.

The analysis conducted on *Casa Malhoa* samples (CMAG 11A to CMAG 11D), which are not the original mortars, revealed that they must be hydraulic mortars. Their porous structure does not allow a high absorption of water by capillary uptake, furthermore a high level of compacity and a high compression strength were verified.

Samples IRF 4A (yr. 1938), CBP 4B (yr. 1939) and LIP 1 (yr. 1958) complete the range of hydraulic mortars, as shown by the mineralogical composition.

Regarding the evolution of the constituents of the mortars used during the five decades analyzed and based on the considered sample universe it is not possible to conclude on the employability of the main binders and their decline over time. However, air lime may be used until the 1940s, at least mixed with cementitious binders. The use of air lime will have declined, and the hydraulic binders will soon have begun to take their place.

This work is part of an ongoing research and it is extremely important to use complementary analytical techniques to settle the difficulties of interpretation imposed so far. Those are meant to be the study of mortars microstructure and the assessment to the binder/aggregate ratio.

Acknowledgments

Authors would like to thank the Portuguese Science and Technology Foundation (FCT) for their support through SFRH/BD/112809/2015 PhD grant and through PTDC/EPH-PAT/4684/2014 project: DB-HERITAGE – Heritage database on historical construction materials and acknowledge National Laboratory for Civil Engineering (LNEC) for its support through the projects DUR-HERITAGE – Durability and characterization of historical interest construction materials and PRESERVE – Preservation of renders from built heritage with cultural value: identification of risks and contribution of traditional knowledge and new materials for conservation and protection. Finally, the authors would like to thank the buildings' owners for having authorized the inclusion of the buildings as case studies.

References

1. Almeida L, Santos Silva A, Rosário Veiga M, Mirão J (2017) Characterization of renders from buildings awarded with Lisbon's Valmor prize of architecture (1902 – 2002). State of conservation and contributions for preservation. In: Mazzolani FM et al (ed) Proceedings of 3rd International Conference on Protection of historical constructions. Lisbon, Portugal, 12 – 15 July, 2017.
2. Rosário Veiga M, Magalhães A, Bosilikov V (2004) Capillarity tests on Historic mortar samples extracted from site. Methodology and compared results. In 13th International Masonry Conference, Amsterdam, July 2004.
3. Santos D, Rosário Veiga M (2004) Ficha de Ensaio de revestimentos de paredes FE Pa 40. Revestimentos de paredes. Ensaio de absorção de água por capilaridade para amostras irregulares e friáveis. Lisbon: LNEC.
4. EN 1015-11 (1999) Methods of test for mortar for masonry Part 11: Determination of flexural and compressive strength of hardened mortar. Jul.1999

5. CEN (1999) Natural stone test methods. Determination of real density and apparent density, and of total and open porosity. EN 1936:1999, Brussels, Belgium.
6. RILEM Technical Committee 25 PEM (1980) Recommended tests to measure the deterioration of stone and to assess the effectiveness of treatment methods. *Mater. Struct.* 13(75): 175-253
7. Veniale F, Setti M, Rodriguez-Navarro C, Lodola S (2001) Role of clay constituents in stone decay processes, *Mater. Constr.* 51: 163–182.
8. Borsoi G et al (2019) Analytical characterization of ancient mortars from the archaeological roman site of Pisões (Beja, Portugal). *Const. Build. Mat.* doi:10.1016/j.conbuildmat.2019.01.233
9. Santos Silva A, Cruz T, Paiva MJ, Candeias A, Adriano P, Schiavon N, Mirão J (2011) Mineralogical and chemical characterization of historical mortars from military fortifications in Lisbon harbour (Portugal). *Environ. Earth Sci.* 63: 1641–1650.
10. Bakolas A, Biscontin A, Zendri AE (1998) Characterization of structural byzantine mortars by thermogravimetric analysis. *Thermochim. Acta* 321: 151–160.
11. Miriello D, Barca D, Bloise A et al (2010) Characterisation of archaeological mortars from Pompei (Campania, Italy) and identification of construction phases by compositional data analysis. *J. Archaeol. Sci.* 37: 2207–2223.
12. Guerra García P, Sanz Arauz D, Vela Cossío F (2013) Microscopy and techniques of characterization applied to archaeological work: a proposal of study in hydraulic Roman mortars analysed in Cuenca province (Spain). *Proceedings of 3rd Historic Mortar Conference HMC13, Glasgow.*
13. Cardoso I, Macedo MF, Vermeulen F, Corsi C, Santos Silva A, Rosado L, Candeias A, Mirão J (2014) A multidisciplinary approach to the study of archaeological mortars from the Town of Ammaia in the Roman Province of Lusitania (Portugal), *Archaeometry* 56 (1): 1–24.
14. Genestar C, Pons C, Más A (2006) Analytical characterisation of ancient mortars from the archaeological Roman city of Pollentia (Balearic Islands, Spain), *Anal. Chim. Acta* 557: 373–379.
15. Maravelaki-Kalaitazaki P, Bakolas A, Moropoulou A (2003) Physico-chemical study of Cretan ancient mortars, *Cem. Concr. Res.* 33: 651–661.
16. Moropoulou A, Bakolas A, Bisbikou K, (2000) Investigation of the technologies of historic mortars, *J. Cult. Heritage* 1: 45–58.

17. Brown WC, Dietrich M, Latimer M (2004) Assessing the impact of thickness on the performance of stucco cladding. Technical Series 04-123. Research Highlight. Ottawa: Canada Mortgage and Housing Corporation.

Practical application of lime-pozzolan mortars to damp masonry

Dita Frankeová¹, Dana Janotová¹, Zuzana Slížková¹

(1) Institute of Theoretical and Applied Mechanics of the Czech Academy of Sciences, frankeova@itam.cas.cz, janotova@itam.cas.cz, slizkova@itam.cas.cz

Abstract

The purpose of this study was to evaluate the performance of experimental lime-metakaolin renders in real conditions. For in situ testing, a cemetery fencing wall was chosen which, as demonstrated by a previous survey, was loaded with a high degree of moisture and water-soluble salts. This paper is focused on the visual and chemical-mineralogical characterization of the renders two years after application. Samples were taken from both the upper and lower parts of the wall. The analyses showed low concentrations of water-soluble salts (0.01-0.03 wt.%) in the samples collected in the lower parts, while in contrast, the upper parts contained high concentrations up to 2.5 wt.% of salts. TGA and XRD analyses revealed that the high water content in the stained areas did not allow the carbonation reaction to take place to its full extent, while the pozzolanic reaction between the lime and the metakaolin was supported in these conditions. Lime-metakaolin renders are highly prone to colour change (moisture retention) due to the presence of pores in the 0.01-0.1 μm size range.

Introduction

The Cultural Heritage Fund of the Czech Republic contains important objects, as well as many small structures of local significance, which are supposed to be protected and maintained in good condition for future generations. Many of these objects suffer from water penetrating into the masonry construction, and this would require a comprehensive solution which, however, often cannot be realised for financial reasons. In recent decades, lime-cement renders have often been used to repair such walls for higher durability compared to pure lime renders. From the current perspective, cement-based repair mortars are considered to be incompatible with old masonry due to their excessive strength and stiffness, low permeability and release of soluble salts [1-4].

The presented study focused on the application of selected laboratory-tested pozzolanic mortars, developed as compatible and durable renders for application in severe weathering environments, in real conditions on historical structures. A cemetery fencing wall in Krchleby (about 100 km from Prague), as an example of a non-roofed cultural heritage structure exposed to severe atmospheric conditions (wind-driven rain, rising moisture, hygroscopic salts, and freezing-thawing cycles), was chosen for the application. This construction was to be rendered according to a request from the cultural heritage authorities. This paper describes the behaviour of various lime mortars after application to the historical wall.

Experimental procedure

Location

The fencing cemetery wall in Krchleby was built in 1865 during extension work on the cemetery area and reconstruction of the adjacent renaissance church. The fence frames are made of fired-clay bricks, and the pillars dividing the wall are made of bricks and stones. The wall is built upon stone foundations. Prior to this intervention, the structure was covered with cement-lime based renders that showed several degradation patterns leading to loss of material, e.g. cracks, delamination, spalling, and chalking. The wall was covered from the interior side up to half of its height by earth, constituting the main source of moisture and salts. Damage to the brick wall developed mainly due to ground moisture rising from the earth behind the construction and inadequate rainfall drainage, but also due to the effects of salt (de-icing salts, neighbouring cemetery, and agricultural activity). As depicted in Figure 1, the area in height from 150 to 170 cm, where moisture evaporation and crystallization of salts occur, was the most damaged. A more detailed brick-masonry survey prior to the application of the test mortars revealed a very high moisture content in the masonry up to one meter in height (roughly equivalent to the level of elevated terrain on the cemetery side). Chlorides were found in the lower parts of the masonry in elevated to very high amounts; at a height of about 1-1.75 m a very high degree of nitrates and chlorides was determined. Sulphates were present in the elevated range in all analysed samples. The old plaster was removed before application of the studied repair mortars.



Figure 1. Cemetery fencing wall in Krchleby (Czech Republic)

Materials

The raw materials employed in the production of the mortars are listed in Table 1. Lime putty, lime hydrate and metakaolin (burnt clay shale) as a pozzolan admixture, were used as binding materials. The aggregate material was natural river sand.

Air-entraining agents Berolan LP 50 (sodium lauryl sulphate basis) and Ligaphob N90 (sodium oleate basis) were dosed at 0.5% of the total dry weight of the mixture.

The chosen weight ratio of binder:aggregate was 1:5, while the binder:pozzolanic additive ratio was 3:1. The characteristics of the above materials are reported in Table 1. Table 2 shows the weight and volume ratios of the various components employed in manufacturing the mortars.

The mortar mixtures were applied on a cleaned section of the cemetery wall (approx. 2 x 5 m) in one-layer thick, 50cm-wide, vertical strips (Figure 2).

Table 1. Characterisation of materials

Material	Code	Specification/Supplier
Lime putty	Lp	prepared in an experimental kiln, matured for 2 months, density 1200 kg.m ⁻³
Lime hydrate	Lh	air lime CL90 Čerták® ($\leq 98\%$ Ca(OH) ₂), Vápenka Čertovy schody, a.s.
Metakaolin	M	metakaolin Mefisto L05 (granulometry 0-0.02 mm), České lupkové závody, s.r.o
Sand	S	siliceous river sand Straškov 0/4 mm, EUROVIA Kamenolomy, a.s.
Air-entraining agent	ls	Berolan LP50 (sodium lauryl sulphate basis), Berolan® Vertriebs-Ges.m.b.H
	ol	Ligaphob N90 (sodium oleate basis), Peter Greven

Table 2. Mix proportions of the tested mortars

Mortar code	Composition	Weight ratio
Lh	Lh: S	1:5
LhM	(Lh : M) : S	(0.75:0.25):5
LpM	(Lp : M) : S	(0.88:0.11):3
LhM_ls	(Lh : M) : S + 0,5% Berolan LP50	(0.75:0.25):5
LhM_ol	(Lh : M) : S + 0,5% Ligaphob N90	(0.75:0.25):5

Methods

Moisture distribution and moisture content

The moisture distribution of the renders applied to the cemetery wall (South-facing) was first assessed using a microwave-based measuring device designed for the non-destructive measurement of moisture in porous materials, MOIST 210. A probe with a signal penetration depth of 3 cm was used. Readings were taken in a regular grid of approximately 400 × 200 cm (width × height).

Another five samples of the mortars were collected by hammer and chisel to gravimetrically determine their moisture content to calibrate more precisely the microwave values as proposed by Válek et al. [5].

The moisture content was determined gravimetrically after drying the samples in an oven at a temperature of $100\pm 5^\circ\text{C}$. The moisture content was expressed as a percentage in respect to the dry weight of the sample, and was evaluated according to ČSN P 730610 [6].

Ion chromatography

The concentration of water-soluble salts (anions) in the solutions prepared from the collected samples was quantified by ion chromatography with a Dionex ISC-5000. The mobile phase used was composed of a mixture of 4.5 mM sodium carbonate and 1.4 mM sodium bicarbonate.

Thermogravimetric analysis

Thermogravimetric analysis (TGA/DTG) was used to follow the progress of the carbonation and hydration in the binders. The mortars were gently crushed in a porcelain bowl, and the finest fraction, containing grains below 0.063 mm in size, was used for a thermal analysis. The thermal analysis was carried out on the SDT Q600 instrument (TA Instruments) in the range of temperatures between 25-1000°C. For the analysis, volumes of approx. 20 mg in mass were placed in ceramic pans and heated in an N₂ atmosphere at a rate of 20°C per minute.

X-Ray diffraction

The mineralogical composition of the binder-rich fraction was studied by means of X-ray diffraction (XRD) using the D8 Advance X-ray diffractometer from Bruker with generator settings: CuK α radiation ($\lambda=1.5405 \text{ \AA}$), 40 kV voltage and 40 mA current intensity.

Electron microscopy

The microstructure of the specimens was analysed with a scanning electron microscope (SEM). SEM analysis (SEM: MIRA II LMU, Tescan Corporation, EDX detector: Bruker Corporation) was performed on polished cross-sections of the mortar samples. A thin layer of carbon was applied to the sample to ensure conductivity.

Mercury porosimetry and BET

Open porosity (Po %) and pore-size distribution (in the range of $0.001 < r < 100 \mu\text{m}$), were determined using a Micromeritics AutoPore IV 9500 V1.09 porosimeter (mercury injection porosimetry, MIP). Mortar fragments of cca. 2.5 cm³ were oven-dried for 24 h at 60°C before analysis.

The specific surface area of the samples was calculated according to the Brunauer–Emmett–Teller procedure using gas (N₂) physisorption on a Micromeritics ASAP 2020. Before the analysis the specimens were degassed for 16 h at 35 °C.

Results

One month after the application of the experimental renders, stains with a significantly darker colour appeared on the metakaolin lime mortars (LhM, LpM). These dark spots reached from the base up to three quarters of the height of the wall and corresponded to areas with a significantly higher moisture content. The pure lime mortar did not show such darkening.

The renders were exposed to the influence of rising damp, rain water and frost over a 2-year period. All these factors influenced the course of hydration and carbonation of the binder. After 12 months (LhM_ls and LhM_ol) and 24 months (Lh, LhM and LpM), samples were taken from both the upper and lower parts of the wall and analysed in terms of water content, water-soluble salts content, thermal analysis (TGA), X-ray diffraction (XRD) and electron microscopy (SEM).

Moisture and soluble salts distribution

The samples were taken from the lower and upper portions of the experimental panels, from heights of approximately 30 to 60 cm and 165 to 175 cm respectively. The positions of the samples collected can be seen in Figure 2. Moisture content was determined by the gravimetric method and evaluated according to the Czech technical standard [6]. The concentration of anions of the water soluble salts was evaluated according to the EUREKA EU - 1270 classification, which defines the possible risks and degree of degradation caused by the salts. All the collected data is summarized in Table 3.

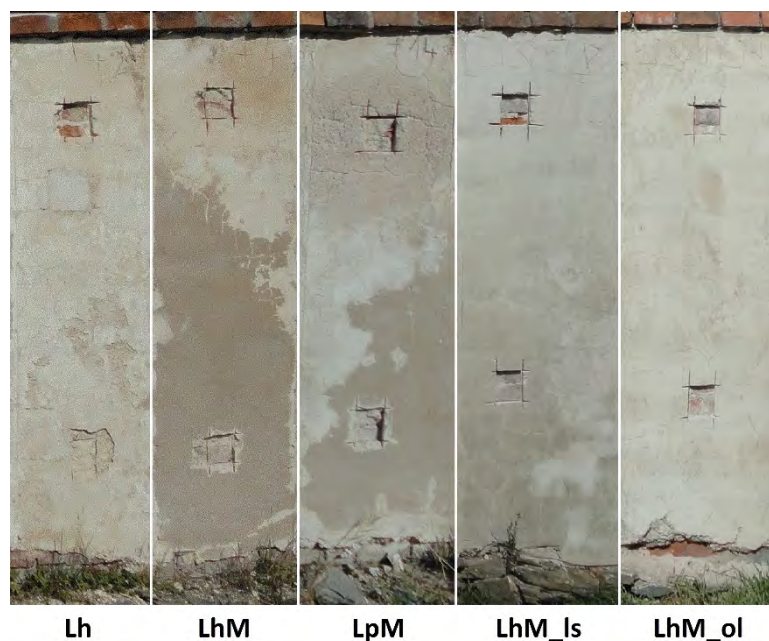


Figure 2. Experimental renders 12 months after application (LhM_ls and LhM_ol) and 24 months after application (Lh, LhM and LpM).

Table 1. Moisture content (gravimetry) and salinity (IEC) in samples collected from the upper (U) and lower (L) parts of the wall.

Sample		Moisture content (wt %)	Salt content (wt. %)			EUREKA classification*		
			Cl ⁻	NO ₃ ⁻	SO ₄ ²⁻	Cl ⁻	NO ₃ ⁻	SO ₄ ²⁻
Lh	U	1.4	0.27	0.76	0.04	3	4	1
	L	2.6	0.02	0	0.07	1	0	1
LhM	U	4.5	1.04	2.46	0.07	4	4	1
	L	14.0	0.02	0	0	1	0	0
LpM	U	3.8	1.42	1.74	<0.02	4	4	0
	L	10.9	0.02	0.03	0.02	1	1	1
LhM_Is	U	0.5	0.08	0.11	0.02	2	2	2
	L	2.8	0.02	0.01	0.03	1	1	1
LhM_ol	U	0.6	0.10	0.10	0.01	3	2	0
	L	1.0	0.01	0.00	0.00	1	0	0

*EUREKA classification [7]: Class 0 – trace amount, Class 1 – very low salinity, Class 2 – medium salinity, Class 3 – high salinity, Class 4 – extremely high salinity

The moisture distribution in the surface layer of the renders (to a depth of 3 cm) was assessed by the microwave probe. The moisture distribution map is presented in Figure 3.

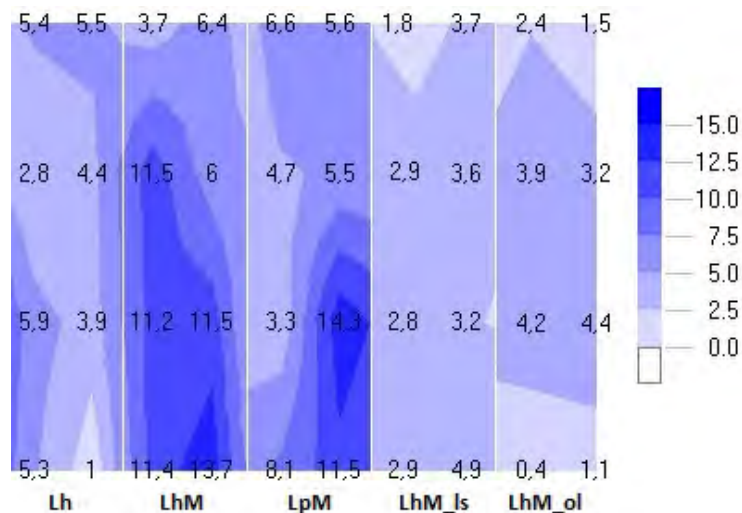


Figure 3. Moisture distribution in wt. % assessed by microwave probe.

In this figure it can be seen that a high degree of moisture was detected in the lower parts of the masonry, especially in the LhM and LpM samples, which were fully saturated with water (14 wt. %). Water was present due to capillary rise transporting it to the upper parts of the masonry where evaporation took place and salt crystallization occurred.

The LhM_Is and LhM_ol renders were applied to the wall in places where the terrain height behind the wall was lower compared to other sections and the maximum water rise height

(the so-called ‘equilibrium line’, separating the dark, damp zone from the dry one) was much lower. The moisture content of the samples did not exceed 4 wt.% (a very low content according to ČSN P 730610).

Concerning the distribution of chloride and nitrate ions in mortars with metakaolin (LhM and LpM) very small concentrations were found in the samples collected in the lower parts. These ions, due to their high solubility, were transported to the upper level [8] where the moisture vapor from the masonry evaporated and subsequent crystallization caused damage. Chloride ions were present in the form of NaCl as determined by XRD (Table 3.) and SEM/EDS (Figure 4). It probably originated from de-icing salts used for road maintenance. The high level of nitrates could be attributed to nearby agricultural activity and/or decomposition of organic matter (human activity, cemetery) [9].

The addition of an air-entraining additive to the lime-metakaolin mortar – samples LhM_ol and LhM_Is – caused a decrease in chloride and nitrate content by one order in the upper parts of the wall. This phenomenon can be explained by the larger pore size of aerated mortars in which capillary absorption is reduced.

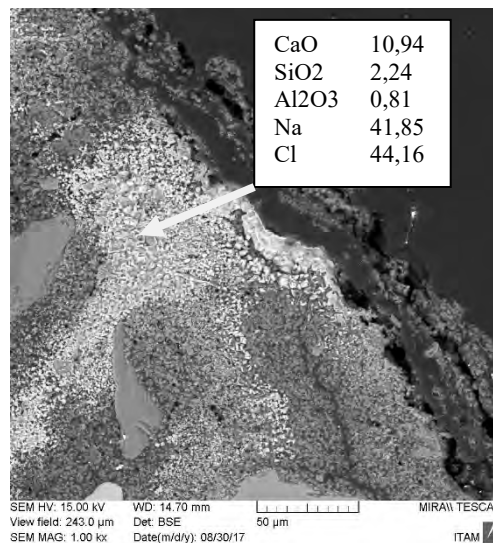


Figure 4. SEM micrograph – detail of NaCl deposits in the microstructure of the sample LpM (upper part), arrow points to area of EDS analysis

Mineralogical composition

The TGA analysis of lime mortar Lh showed that the samples taken from the upper and lower parts of the wall vary significantly in the degree of carbonation. While at the bottom there is only a trace (approximately 1.5%) of calcium hydroxide in the binder, its proportion in the binder in the upper wall sample is 62%, which is probably due to a water content insufficient for the carbonation reaction. The presence of salts in the upper part manifests as deformation of the calcium carbonate decomposition peak, specifically by splitting it into several bands in the temperature range of 500-1000°C [10]. This phenomenon is even more apparent in the LhM and LpM mortars, where CaCO₃ decomposes in 4 steps (560°C, 635°C,

745°C and 940°C) probably due to the presence of NaCl. Contrary to the Lh lime mortar, the LhM and LpM metakaolin mortars are uncarbonated in the lower portion of the wall. In this section the moisture content reaches 14% by weight, i.e. the plaster pores are filled with water, and the penetration of carbon dioxide is significantly limited. These conditions, on the other hand, are favourable for the course of the pozzolan reaction between Ca(OH)₂ and metakaolin, the products of which are hydrated calcium silicates CSH (peak 100-150°C) and hydrated calcium aluminates CAH – hydrogarnet, hydrocalumite and hydrotalcite (peaks 200-400°C). CAHs have been identified by XRD, but with CSH it is not possible due to its non-crystalline nature.

The addition of an air-entraining additive to the lime-metakaolin mortar – samples LhM_ol and LhM_ls – unified the mineralogical composition between the upper and lower parts of the experimental wall. In the thermograms of these samples, one dominant band of calcium carbonate decomposition with a maximum of 750-800°C, indicates that all samples have a carbonated binder. In the area of dehydration of CSH and CAH (100-400°C), a gradual weight loss occurs with a single more pronounced band of 240°C. Samples of LhM_ol which contain sodium oleate exhibit a negligible peak in the 300-350°C range associated with the burning of this organic additive.

The results of the XRD analysis summarised in Table 4 revealed good agreement with the thermal analysis results.

Table 4. Mineralogical composition of samples from the upper (U) and lower (L) parts of the wall.

Analyte	Lh		LhM		LpM		LhM_ls		LhM_ol	
	U	L	U	L	U	L	U	L	U	L
Portlandite	70.1	1.8		34.0		26.3				1.0
Quartz	2.2	9.7	7.9	6.1	6.9	14.0	3.6	3.3	3.6	2.9
Calcite	23.4	85.2	72.7	13.5	81.0	29.9	95.0	93.8	81.8	80.8
Muscovite	1.5	1.8	0.2	2.7	0.7		0.9	0.6		
Feldspars	2.2	1.6	16.1	0.3	4.3	6.9	0.5	2.4	2.3	2.5
Hydrotalcite	0.7		0.5	2.3		3.5				
Halite			2.7		6.6					
Hydrogarnet				29.5	0.5	9.8				
Hydrocalumite				11.6		9.7				
Vaterite									12.3	12.8

The XRD analysis shows that the sample also contained some fine aggregates such as quartz, muscovite and feldspar. The occurrence of halite (NaCl) in the upper portions of the LhM and LpM mortars confirms the results determined for water-soluble salts. In addition to the portlandite and calcite, the hydrated phases hydrotalcite, hydrocalumite and hydrogarnet can also be included in the binder components. While hydrogarnet is a common product of the pozzolanic reaction of lime with metakaolin [11,12], the formation of hydrotalcite and

hydrocalumite may be caused by the presence of Cl^- ion. These minerals can be assigned to the group of layered double hydroxides (LDHs) – complex compounds containing AFm phases which are able to bind chloride ion to their structure [13,14]. In the samples of LhM_ol mortar modified with sodium oleate, vaterite, a less stable polymorph of CaCO_3 , was found. The formation of this polymorph is associated with the presence of an organic compound (derived from oleic acid) [15,16].

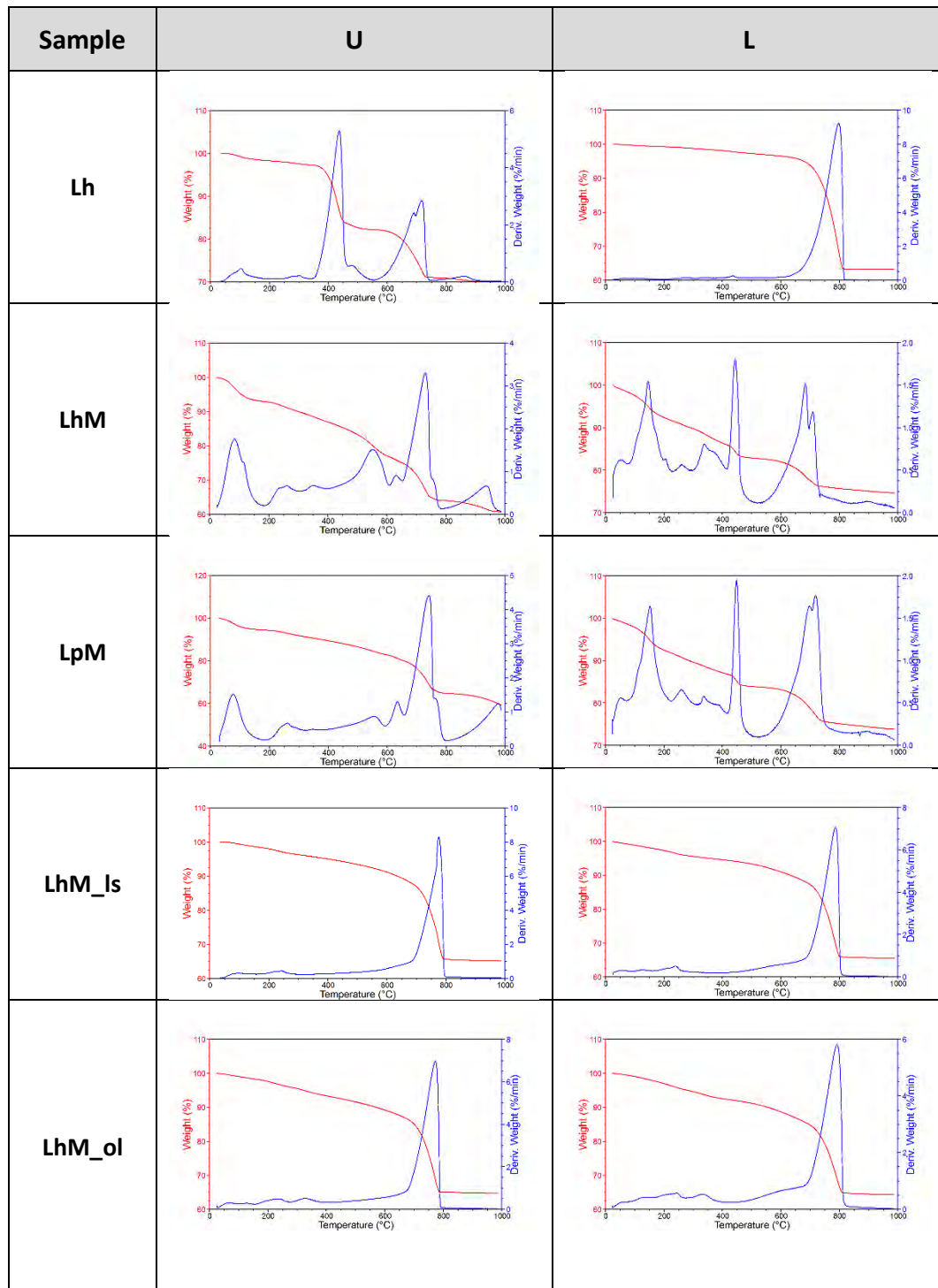


Figure 5. TGA/DTG (red/blue) curves of the binder fraction of samples extracted from upper (U-left) and lower (L-right) parts of the experimental wall.

Characterisation of the pore system

The mercury intrusion porosity and specific surface area of the mortars taken from the upper and lower portions of the wall are given in Table 5. Differential pore radius distributions are plotted in Figure 6.

Table 5. Mercury intrusion porosity and specific surface area determined for samples collected from the upper (U) and lower (L) parts of the wall.

Mortar		Specific surface S_{BET} (m^2/g)	Mercury intrusion porosity (%)
Lh	U	2.84	29.0
	L	1.60	21.0
LhM	U	3.65	24.0
	L	6.63	26.5
LpM	U	3.92	25.8
	L	5.98	27.8
LhM_Is	U	4.08	27.6
	L	5.04	30.8
LhM_ol	U	2.53	28.9
	L	2.71	28.1

The lower Lh sample has a lower porosity and specific surface than the upper one, because the carbonation of the lime binder resulted in refining and filling in the porous structure [17,18].

The addition of metakaolin to the lime binder had a significant effect on pore size distribution: the pore volume in the region between 0.1 and 1 μm was shifted to 0.01–0.1 μm . The lower sample has a higher S_{BET} compared to the upper sample and a slightly higher porosity. The pozzolanic reaction, which prevailed over carbonation in the lower parts of the masonry due to sufficient moisture, produces CSH and CAH products that have a larger S_{BET} and a porous structure with higher porosity [18].

The LhM_Is and LhM_ol samples showed a reduced hydration rate due to aeration additives, and hence the number of pores exhibiting 0.01–0.1 μm compared to LhM and LpM. In contrast, there is an increase in the number of pores of 0.1–1 μm corresponding to the air lime component of the binder.

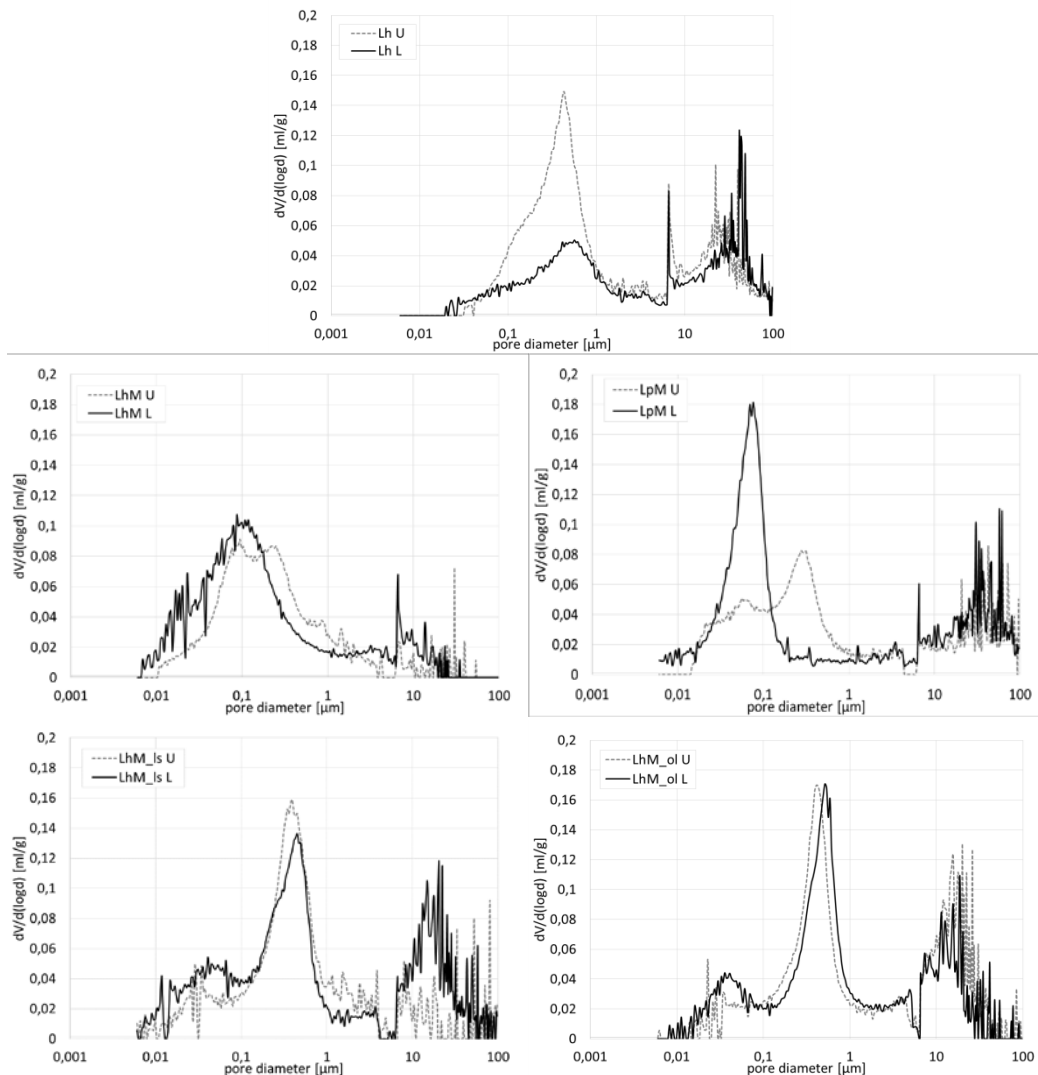


Figure 6. Pore size distribution curves for mortars taken from the upper and lower parts of the wall.

Conclusions

The purpose of the study was to evaluate the performance of experimental lime-metakaolin renders in real conditions. For in situ testing, a cemetery fencing wall was chosen which, as demonstrated by the previous survey, was loaded with a high degree of moisture and water-soluble salts.

The main conclusions from this study are:

- Lime-metakaolin renders are highly prone to colour change (noticeable darkness) due to wetting of the render. If this render is applied to a substrate with non-homogeneously distributed moisture content, this fact will manifest in the inconsistent appearance of the render (staining). The colour stains are probably stronger the higher the differences in moisture content.

- Low concentrations of water-soluble salts (0.01-0.03 wt.%) were determined in the samples collected in the lower parts, while in contrast, the upper parts contained high concentrations up to 2.5 wt.% of salts.
- Two years after application, the mineralogical composition of the samples from highly damp (stained) areas differs significantly from those with lower moisture. The TGA and XRD analyses revealed that the high water content in the stained areas did not allow the carbonation reaction to take place to its full extent, while the pozzolanic reaction between the lime and the metakaolin was supported in these conditions.
- Depending on whether the carbonation or the pozzolanic reaction prevails, a certain microstructure of the binder is formed. In the pure lime and lime-metakaolin mortars from the upper drier parts, 0.1-1 μm pores are predominant, while at the stains the majority of the pores are in the range of 0.01 to 0.1 μm .
- The addition of an air-entraining agent into the lime-metakaolin mortars led to a more equal distribution of the moisture content, mineralogical composition and pore system in both the upper and lower parts of the experimental wall, resulting in a satisfactory appearance without visual signs of moisture and decorative defects.
- Although the visual signs of dampness and decorative spoiling were at the bottom of the wall, greater salt contamination was determined at the top. This may indicate the presence of hygroscopic salts that attract moisture from the air at a certain relative humidity and prevent the mortar from drying. However, the decisive factor in moisture retention is the presence of pores in the 0.01-0.1 μm size range.

Acknowledgements

This study was supported by the grant 18-28142S from the Czech Science Foundation. We thank Alberto Viani for carrying out the XRD measurements and Milan Svoboda for the MIP and BET measurements. We also thank Marek Eisler for proofreading the text.

References

1. Elert K, Rodriguez-Navarro C, Pardo ES (2002) Lime mortars for the conservation of buildings. *Studies in Conservation* 47:62-75
2. Silva BA, Ferreira Pinto AP, Gomes A (2015) Natural hydraulic lime versus cement for blended lime mortars for restoration works. *Constr Build Mater* 94:346-360.
3. Ashurst J, Ashurst N (1998) Practical building conservation. English Heritage Technical Handbook. Mortars, Plasters and Renders. Ashgate
4. Veiga MR, Velosa A, Magalhaes A (2009) Experimental applications of mortars with pozzolanic additions: characterization and performance evaluation. *Constr Build Mater* 23:318–27

5. Válek J, Kruschwitz S, Wöstmann J et al (2010) Non-destructive investigation of wet building materials: multi-methodical approach. *J Pref Constr Fac* 24: 462-472
6. ČSN P 73 0610 (2000) Hydroizolace staveb - Sanace vlhkého zdiva - Základní ustanovení. The Czech technical standard.
7. Pavlikova M, Pavlik Z, Keppert M et al (2011) Salt transport and storage parameters of renovation plasters and their possible effects on restored buildings' walls. *Constr Build Mater* 25:1205–1212
8. Lubelli B, van Hees RPJ, Groot CJWP (2004) The role of sea-salts in the occurrence of different damage mechanisms and decay patterns of brick masonry, *Constr Build Mater* 18:119-124
9. Bläuer C, Rousset B (2014) Salt sources revisited. In 3rd Int, Conf. Salt weathering of buildings and stone statues. Brussels: KIK-IRPA 305-18
10. Biscontin G, Birelli MP, Zendri E (2002) Characterization of binders employed in the manufacture of Venetian historical mortars. *J Cult Herit* 3:31-37
11. Cabrera J, Rojas MF (2001) Mechanism of hydration of the metakaolin–lime–water system, *Cem Concr Res*, 31(2), 177-182
12. Siddique R, Klaus J (2009) Influence of metakaolin on the properties of mortar and concrete: A review. *App Clay Sci* 43:392-400
13. Machner A, Zajac M, Haha MB et al (2018) Chloride-binding capacity of hydrotalcite in cement pastes containing dolomite and Metakaolin. *Cem Concr Res* 107:163-181
14. Shi X, Xie N, Fortune K et al (2012) Durability of steel reinforced concrete in chloride environments: An overview. *Constr Build Mater* 30:125-138
15. Fiori C, Vandini M, Prati S et al (2009) Vaterite in the mortars of a mosaic in the Saint Peter Basilica, Vatican (Rome). *J Cult Herit* 10:248-257
16. Nunes C, Slížková Z (2016) Freezing and thawing resistance of aerial lime mortar with metakaolin and a traditional water-repellent admixture. *Constr Build Mater* 114:896-905
17. Lawrence RM, Mays TJ, Rigby SP et al (2007) Effects of carbonation on the pore structure of non-hydraulic lime mortars. *Cem Concr Res* 37:1059–1069
18. Arandigoyen A, Bicer-Simsir B, Alvarez JI et al (2006) Variation of microstructure with carbonation in lime and blended pastes. *App Surf Sci* 252:7562-7571

The use of dolomitic lime in mortar samples from a 15th-century buttress of York Minster (York, UK)

Cecilia Pesce¹, Alick Leslie², Alison Henry², John David³, Giovanni Pesce¹

(1) Department of Architecture and Built Environment, Northumbria University, Newcastle upon Tyne, UK, cecilia.pesce@northumbria.ac.uk, giovanni.pesce@northumbria.ac.uk

(2) Building Conservation & Research Team, Conservation Department - Historic England, Swindon, UK, Alick.Leslie@HistoricEngland.org.uk, Alison.Henry@HistoricEngland.org.uk

(3) York Minster, York, UK, johnd@yorkminster.org

Abstract

This paper describes the results of a series of analyses carried out on mortar samples from a 15th-century buttress of York Minster (York, UK). The aim of these analyses was to investigate the materials and technologies used in the late Middle-Ages for the construction of one of the most important religious places in Northern England. The limited knowledge currently available on the past use of locally-sourced construction materials represent an important limitation to the design of the new conservation works, since the choice of appropriate compatible materials can only be achieved through a detailed knowledge of the materials and technology used in the past. To provide an initial insight on the construction materials and technologies used at York Minster in the late Middle-Ages, mortar samples from one of the buttresses under restoration were collected and analysed using a variety of techniques such as optical and electron microscopy, X-ray diffraction analysis and Fourier Transform Infrared spectroscopy. The results suggest that the binder in this mortar was produced using locally available dolomitic limestone. The quicklime produced, a mixed oxide of calcium and magnesium, was directly mixed with locally-sourced river sand in a ratio 1:2.5 using a technology currently known as 'hot mixed' lime.

Introduction

York Minster is one of the most important religious places in Northern England and has been a centre of Christianity since the 7th Century CE. Its architecture shows the development of the Gothic style in England over a timespan of almost three centuries and is still nowadays a major destination of great religious and artistic interest.

The Cathedral lies at the top of a slight hill at the very centre of Roman York and its present architecture is the result of several building campaigns through the centuries [1]. The original Norman building, probably completed in c-1100, underwent several modifications during the 12th Century after a fire damaged the eastern arm [2, 3]. For this work, which involved the apse, the central tower and the transepts, magnesian limestone was newly quarried [2]. From the second half of 14th Century further modifications have been made to the eastern arm of the church, which entailed the reconstruction of the old choir and the

creation of two new Chapels in a Flamboyant and Perpendicular Gothic style. The mortar sample investigated in this study comes from a buttress located in the southern wall, which is part of the 5 western bays (the choir and presbytery) added at the beginning of the 15th Century [3].

Despite its vast cultural and artistic relevance, the knowledge regarding the building materials and techniques used in the past centuries for the construction of York Minster is far from complete. It is general knowledge that in the past, construction skills, knowledge and expertise were developed empirically and passed orally between members of the same guild, with a high risk of being lost if not properly recorded when the related materials and technology changed.

The limited knowledge currently available on the use, in the past centuries, of locally available construction materials (e.g. lime, and sand) is an important limitation to the design and execution of current conservation works because the production of new, compatible repair mortars can only be achieved through an accurate understanding of the materials and techniques used in the past centuries in the construction of the church.

Materials and methods

Samples of mortar were collected by York Minster's stonemasons during the restoration work of a 15th-century buttress, on the external face of the south wall of the choir. The samples were carefully packed and sent to Northumbria University for analyses. On arrival the samples were removed from the packaging and observed as received with the naked eye and using a stereo optical microscope at low magnification (10x-50x).

To investigate the binder-to-aggregate ratio and the mineralogical and petrographic characteristics of the aggregate, petrographic analyses in thin sections were carried out. Four representative mortar samples from the same block were vacuum impregnated with resin (no dye added) at Department of Earth Sciences, Durham University, and mounted on 76x26 mm glass slide before being polished. The sections were examined under low and medium magnification on a Leitz 12 Pol petrographic microscope in both plain polarised and crossed polarised light. Photomicrographs of the samples were taken through one of the eyepiece tubes using a Canon Powershot G5 digital camera.

To investigate the chemical characteristics of the lime, two different kind of white lumps commonly embedded in historic mortars were selected and used: lumps of un-burned pieces of limestone (the same stone used to produce the lime), and lumps of carbonated lime that did not mix with the aggregate. Lumps embedded in historic mortars can have various origin [4]. Hard white lumps are thought to be the un-decomposed remains of the limestone that was fired in the kiln. These lumps have characteristics similar to those of the limestone used to produce the lime [5, 6]. Soft white lumps are thought to originate from poor mixing of the lime with the aggregate [6, 7]. The lime contained in the lump undergoes the same carbonation process as the rest of the binder and any microstructural and crystalline

structure of the original stone is lost. Extraction and preparation of the lumps was carried out using a MZ6 Leica stereo microscope, according to the description provided by Pesce [8]. The micro-morphological characterisation of the lumps (up to 20 mm diameter) was carried out using a Tescan Mira 3 Scanning Electron Microscope (SEM) in high vacuum mode, coupled with an Energy-Dispersive X-ray spectrometer (EDX), for elemental analysis. Prior to the analysis, the samples were coated with a 5 nm thick Platinum layer.

Mineralogical characteristics of the lumps were investigated using a Siemens D5000 diffractometer with Cu-K α radiation, in the 2θ range 2-70° with an increment of 0.02/step and scan speed of 1 sec/step, at 40 KV and 40 mA. Prior to analysis the lumps were ground using an agate mortar and pestle and sieved to obtain a granular material with particles of <106 μm diameter. To identify the mineralogical phases in the XRD spectra, a search/match approach with software DIFFRACPlus EVA was used by comparing experimental peaks with reference patterns contained in the Bruker EVA software database.

Fourier-Transform Infrared Spectroscopy (FT-IR) was used to investigate the nature of the carbonate. According to some literature, biogenic calcite can be differentiated from anthropogenic by means of FT-IR exploiting the difference in the structural order. Infrared spectrum of calcite shows three absorption peaks corresponding to the vibrational modes of carbonate ions: asymmetric stretch (ν_3 , 1420 cm^{-1}), out-of-plane bending ($\nu_2 = 874 \text{ cm}^{-1}$) and in-plane bending ($\nu_4 = 713 \text{ cm}^{-1}$) [9, 10]. It has been observed that during transformation of amorphous calcium carbonate into crystalline calcite in a biological system, ν_4 peak becomes sharper while ν_2 remains constant and the intensity ratio ν_2/ν_4 decreases from 8 to 3, which is the typical geological value [10, 11]. Gueta *et al.* [12] demonstrated that the distortion of crystalline calcite lattice causes broadening, i.e. smaller height, of ν_4 peak whereas ν_2 peak remains constant. To carry out the FT-IR analysis of York Minster samples, the same powder used for the XRD were analysed using a Perkin Elmer spectrometer in Attenuated Total Reflectance (ATR) mode. The instrument was equipped with germanium crystal, in the 4000-380 cm^{-1} spectral range, 4 cm^{-1} resolution and accumulations of 12 scans. Powder samples were chosen over the lumps' fresh surface because of the typical improved sharpness of their resulting peaks [10]. The collected spectra were elaborated using the ThermoFisher Scientific software Omnic.

Results

Observation at low magnification

Under the stereo optical microscope at low magnification (10x-50x), the sample showed a white binder and very abundant, sub-rounded grey-brownish aggregate fragments (0.1-1 mm diameter). Very abundant white lumps of various diameter (2-10 mm) were embedded in the mortar sample.

Petrographic analyses

Results of the mineralogical and petrographic analyses highlighted the presence of several circular areas of less than 0.2 mm diameter and of lighter colour in the matrix. These showed a radiating pattern of acicular crystals that were ascribed to recrystallised concretionary regions where a primary mineral was dissolved in wetting episodes and re-precipitated with a radial sphaerulitic structure upon drying.

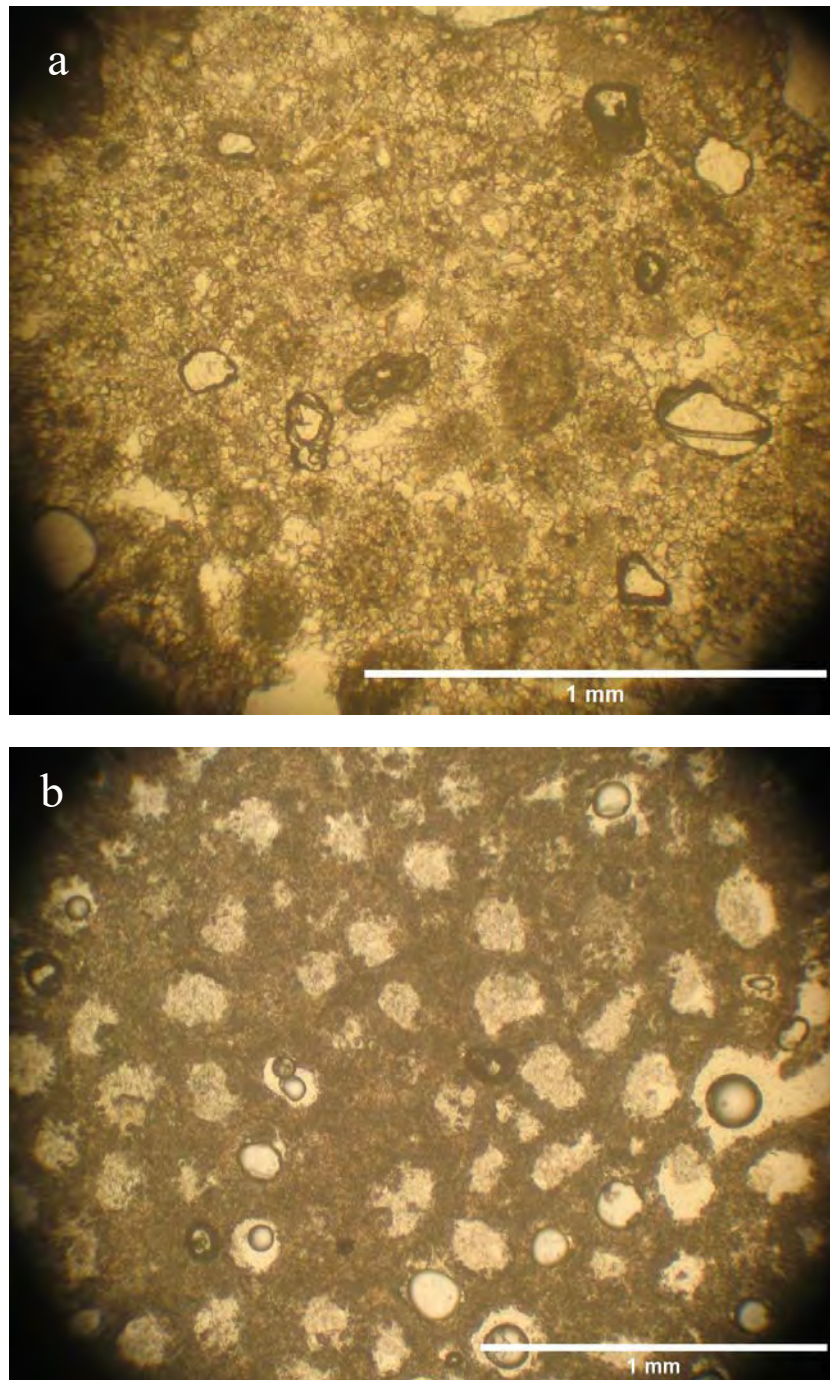


Figure 1. Optical microscope images of (a) crystalline oolitic dolostone and (b) part-burned dolostone showing oomoldic porosity.

The aggregate was found to be a medium grade silicate river sand with grains in the size range of 0.1–1 mm diameter. Grain shape was found to be angular to sub-round. Most grains consisted of single macro-quartz crystals, whereas some were clusters of small grains cemented by iron hydroxides, probably limonite.

The spacing of the sand grains suggested a binder-to-aggregate ratio of about 1:2.5. However, this ratio does not take into account the presence of particles of un-burned and over-burned limestone within the quicklime used to produce the mortar. Mixed in with the quartz aggregate were flakes of carbonate with diameters $1 \text{ mm} < \phi < 10 \text{ mm}$. There were 3 main types: i) pure crystalline limestone or dolostone; ii) fragments of oolitic dolomite; and iii) part-burned fragments of the same material (Figure 1-a and 1-b).

SEM-EDX Analyses

Results of the analyses at the SEM of a fresh section of an un-burned lump (Figure 2-a) showed a porous structure characterised by circular or elliptical cavities 40-90 μm across, tightly distributed on the lump section. At higher magnification (Figure 2-c) these rims showed the presence of large (up to 5 μm length) rhombohedral crystals with well-defined edges. EDX analysis, performed on one of the rims, in the area highlighted in Figure 2-a, showed the relative abundance of the various elements in the lump. The average values for 8 analysed points (4 nm spot size) are reported in Table 1. According to this result, the most abundant elements were O, Ca, Mg, and C, which together made up to 90%w/w of total counts. Traces elements (<1%w/w) were Si, Al, S, Cl, Fe, which come from mineral inclusions of aggregate fragments. The average w/w ratio of Ca:Mg was 1.47. This w/w ratio can be converted to an atomic ratio by using a conversion factor of 0.6, i.e. the atomic weights ratio of magnesium and calcium - 21.31 and 40.08 respectively – resulting in a Ca:Mg atomic ratio of 0.89. This value is close to that of dolomite, a mineral characterised by a typical Ca:Mg atomic ratio of 1, and is in agreement with the rhombohedral shape of the crystals found in Figure 2-c [13]. The lumps of pure carbonated lime showed a different texture compared to the un-burned lump, made of sub-micrometer-sized crystals (Figure 2-b).

XRD Analyses

The XRD spectrum of a hard lump (Figure 3-a) showed peaks of calcite and magnesite. Calcite was more abundant than magnesite in a ratio of 3:1 circa, estimated by comparing respective principal peaks' heights. Magnesite peaks were all shifted of +0.3 degrees 2-Theta with respect to those of the reference pattern of magnesite, suggesting a distortion of the crystal lattice [14].

An XRD spectrum of a soft lump is reported in Figure 3-b. The spectrum showed peaks of calcite, magnesite and quartz in a ratio of 5:1:1 circa.

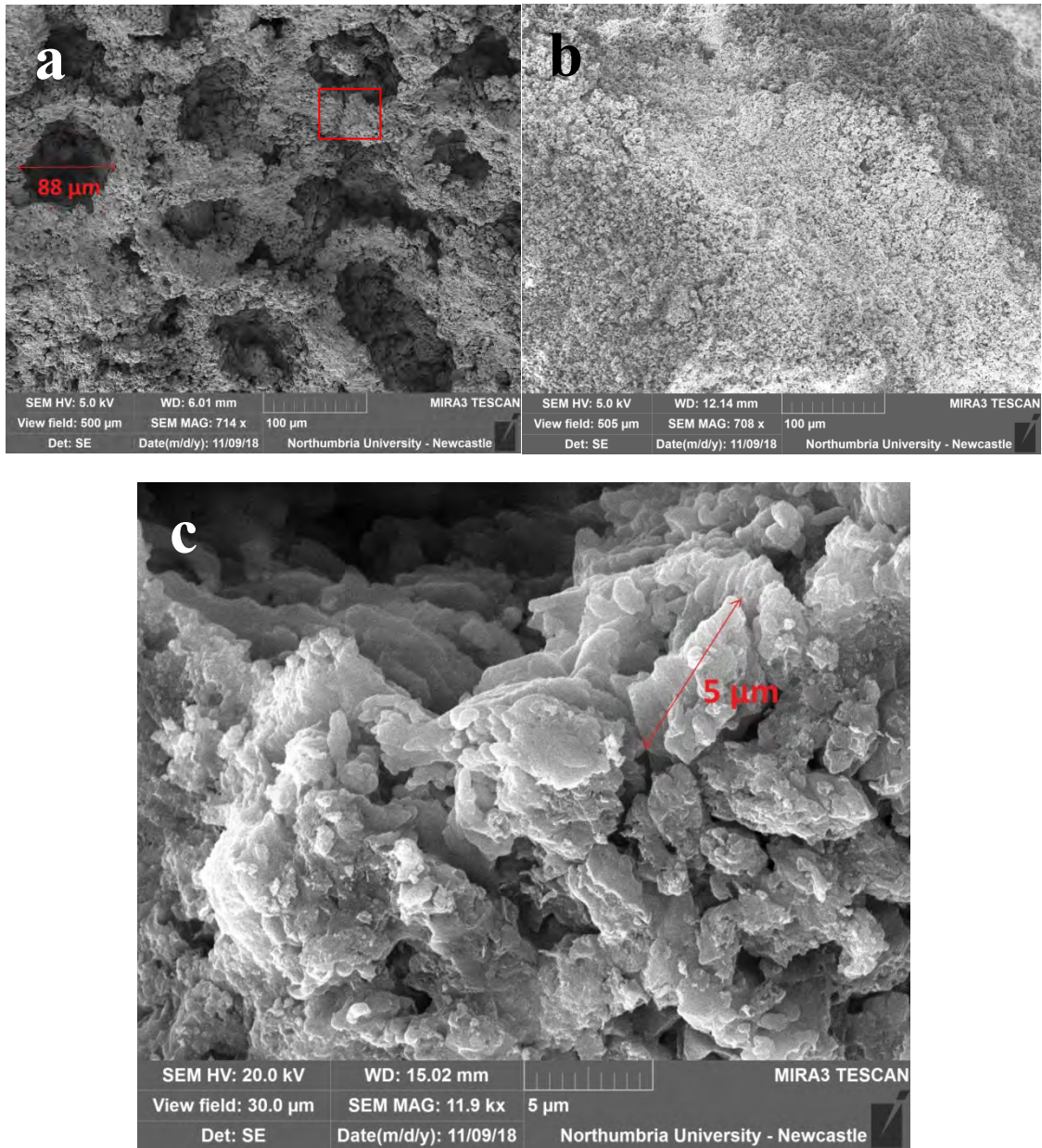


Figure 2. SEM photomicrograph of broken surface of a hard lump contained in the mortar.

Table 1. Relative abundances of elements in a hard lump

Element	Average Relative Abundance (%W)
C	13.94
O	49.38
Ca	17.55
Mg	11.91
Al	0.16
Si	0.15
S	0.23
Cl	0.11
Fe	0.24
Pt	7.88

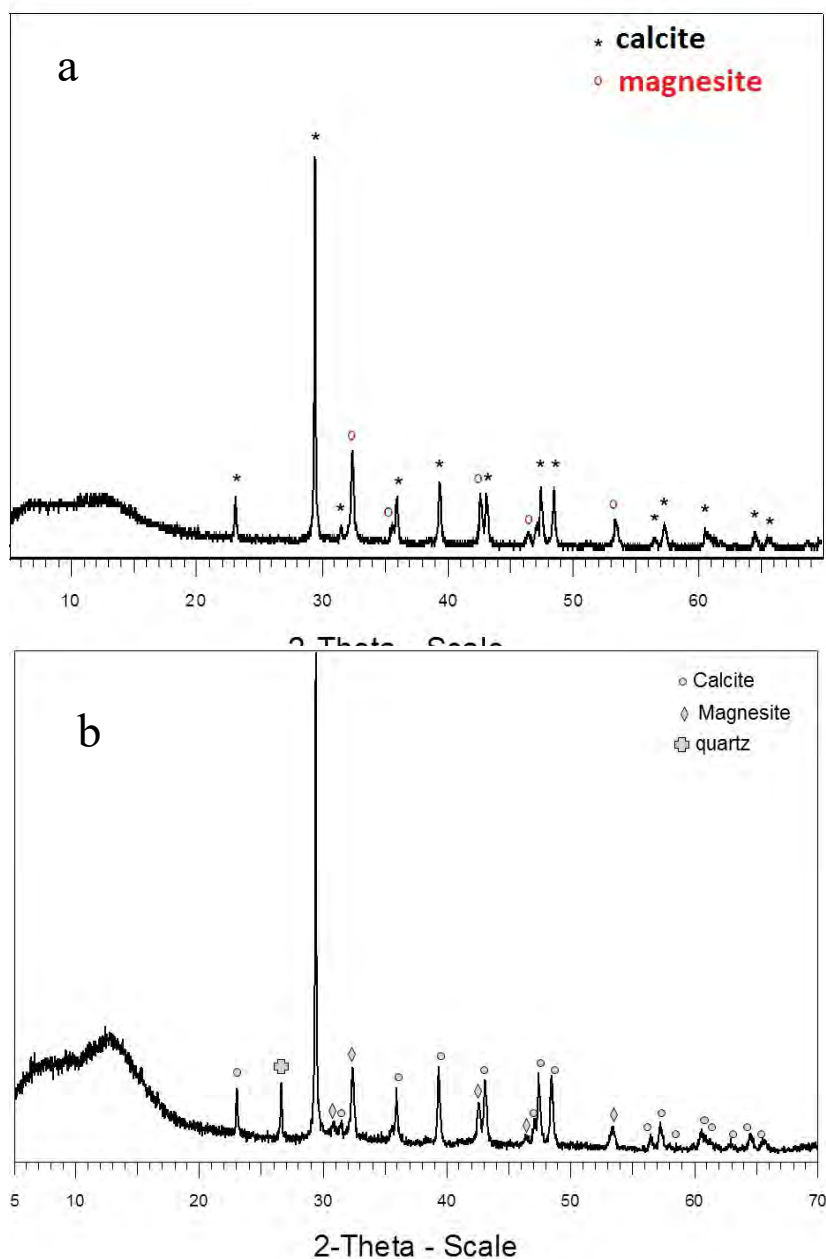


Figure 3. XRD spectra of (a) a hard lump and (b) a soft lump.

ATR/FT-IR Analysis

The infrared spectrum of a hard lump (Figure 4) showed typical peaks of calcite corresponding to vibrational modes of carbonate ions ν_3 , ν_2 and ν_4 respectively at 1405, 872 and 713 cm^{-1} . Presence of magnesite was confirmed by the ν_4 peak at 745 cm^{-1} , in agreement with the XRD and EDX results. The broad band centred at about 600 cm^{-1} was also found in magnesite spectra [15]. No peaks of hydrate forms of magnesium carbonate were detected.

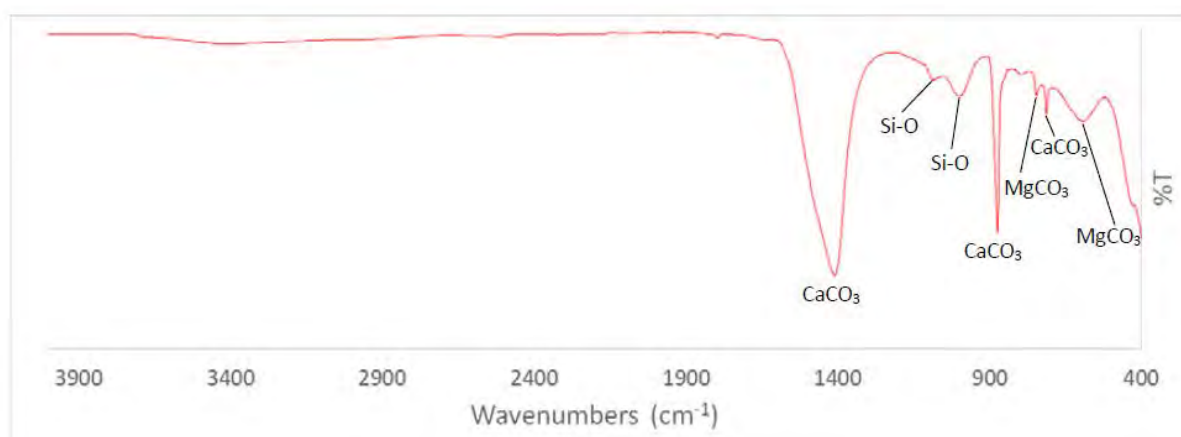


Figure 4. Infrared spectrum of a hard lump.

The infrared spectrum of a soft lump (Figure 5) showed peaks of calcite at 1408, 872, and 712 cm^{-1} corresponding respectively to ions ν_3 , ν_2 and ν_4 vibrational modes of carbonate ions. Two broad bands in the Si-O stretching vibration range ($\nu_{\text{Si-O}}$, 1200-800 cm^{-1} , [16]) and Si-O-Si stretching (weak broad band at 790 cm^{-1}) suggested the presence of silicate minerals, in agreement with XRD analyses.

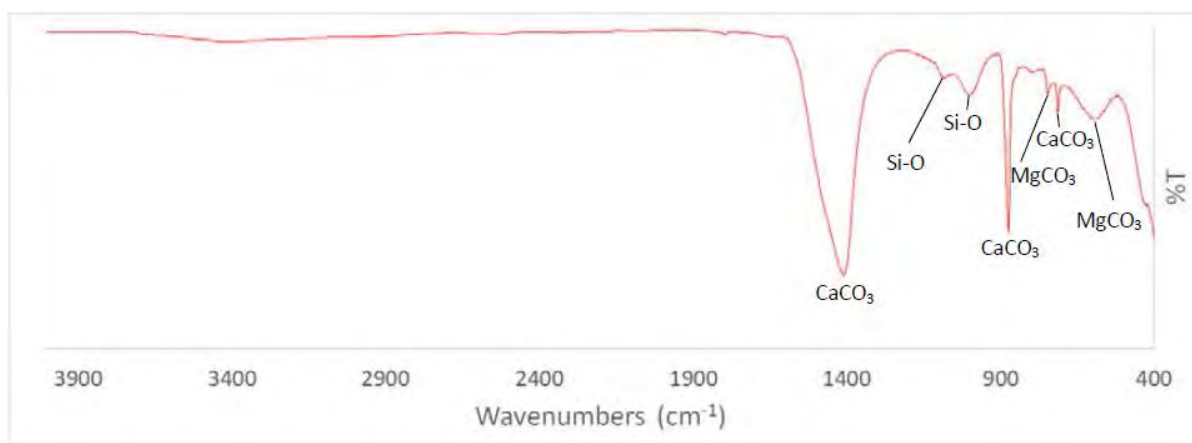


Figure 5. Infrared spectrum of a soft lump.

The heights of FT-IR peaks corresponding to the ν_2 (874 cm^{-1}) and ν_4 (713 cm^{-1}) bending modes of carbonate ion in calcite were measured for calculation of ν_2/ν_4 ratio. The baselines were drawn between the closest minima on both sides of the measured peak as suggested by Chu *et al.* [10]. However, the presence of magnesite in the sample must be considered as it influences ν_2/ν_4 ratio as the ν_2 vibration frequencies of magnesite and calcite overlap. Hence the obtained ratios are likely to be overestimated since the peak at 874 cm^{-1} corresponds to the vibration of carbonate ions of both calcite and magnesite. The results suggest the following ratios for the hard and soft lump, respectively:

$$(\nu_2/\nu_4)_{\text{hard}} = 5.78$$

$$(\nu_2/\nu_4)_{\text{soft}} = 6.00$$

Values of both samples are far from those of geological origin and suggest a low structural order of the analysed calcite lattice [10, 11]. This could be due to the fact that calcination process partially destroyed or modified the original mineral structure.

Discussion

The high amount of white lumps observed within the sample matrix with both the naked eye and under an optical microscope at low magnification are supposed to be linked with a particular production technique of the mortar. This entailed the slaking of quicklime directly into the sand while adding a sufficient amount of water to reach optimal workability, according to the current so-called technique of ‘hot mixing’ [17-20]. Slaking of lime occurs during the mixing and if the mortar is placed before all the lime has slaked and broken down to fine material (that can be more readily integrated with the aggregate), the late-slaking material remains as small lumps in the mortar. However, a straightforward correlation between the presence of several lumps and the use of ‘hot mixing’ technology has not been demonstrated yet, and it is beyond the scopes of this paper.

The observation of a hard lump at the SEM showed an internal, regular pattern of round structures (Figure 1-b and Figure 2-a) that can be related to the oolites. Because of the white colour and the powdery texture of the lump and as confirmed by the low structural order of calcite found by FT-IR analyses, these have obviously been subject to a thermal treatment in the kiln, but the cellular structure of these spherical grains has not been destroyed by the heat. This oolitic structure is very similar to the structure of a local magnesian limestone, referred to as ‘Highmoor’ stone, which is frequently encountered in petrographic studies of building stones used in historic buildings in Yorkshire [21, 22]. The results suggest that magnesian limestone was used for lime production. Concentration of various elements as emerged from the EDX analysis of the same sample confirm this hypothesis by highlighting a mixed composition of Ca and Mg carbonates, possibly a combination of minerals such as calcite and dolomite, both of them sharing a similar rhombohedral crystal habit, and most probably formed during diagenesis of the original limestone [21, 23]. The amount of magnesite found by XRD and FT-IR analyses corroborated the possibility that Mg-lime was used in the mortar. In the hard lump magnesite was found at approximately 1:1 ratio with respect to calcite, whereas in the soft lump it was found at approximately 1:3 ratio. Magnesite is commonly found in magnesian limestones along with calcite and dolomite and for this reason lumps rich in magnesite are likely to be un-burnt remains of the original rock used for lime production [24].

Conclusions

This paper describes the results of a series of analyses carried out on mortar samples from a 15th-century buttress of York Minster (York, UK) with the aim of investigating the materials and technologies used in the late Middle-Ages in the construction of one of the most important religious places in Northern England.

Overall the results suggest that to produce the bulk mortar used in the buttress, dolomitic lime was used together with fine river sand in a ratio 1:2.5. Both materials were sourced locally. In particular the lime was produced by firing magnesian limestone, possibly the same 'Highmoor' stone still quarried today (as a building material, not for producing lime), about 10 miles west of York.

The presence of numerous soft and hard lumps suggest that the lime was not previously slaked in excess of water and used as lime putty. On the contrary, it is likely that the quicklime and the aggregate were mixed first, with only a small addition of water, using a process similar to the one currently known as 'hot mixing'.

Acknowledgment

The authors are grateful to Dr Timothy Palmer for the analysis of the thin sections and to Dr Charis Theodorakopoulos and Valentina Risdonne from the Department of Arts at Northumbria University for assisting with FT-IR analyses. The authors would like to thank the masons at York Minster for their support during the visits at the building and at the yard. This work was supported by Historic England.

References

1. Vv Aa (1977) A history of York Minster. Clarendon Press, Oxford
2. Gee EA (1977) Architectural History until 1290. In: Alymer GE, Cant R (ed) A history of York Minster, 1st edn. Clarendon Press, Oxford
3. Harvey JH (1977) Architectural History from 1291 to 1558. In: Alymer GE, Cant R (ed) A history of York Minster, 1st edn. Clarendon Press, Oxford
4. Pesce GLA, Ball RJ, Quarta G et al (1999) Identification, Extraction, and Preparation of Reliable Lime Samples for 14C Dating of Plasters and Mortars with the 'Pure Lime Lumps' Technique. Radiocarbon 54:933–942
5. Elsen J (2006) Microscopy of historic mortars — a review. Cement and Concrete Research 36:1416–1424.
6. Leslie AB, Hughes JJ (2002) Binder microstructure in lime mortars: implications for the interpretation of analysis results. Q J Eng Geol Hydrogeol 35:257–263
7. Bakolas A, Biscontin G, Moropoulou A et al (1995) Characterization of the lumps in the mortars of historic masonry. Thermochim Acta 269–270:809–816
8. Pesce GLA (2010) Radiocarbon Dating of Lumps of not Completely Mixed Lime Contained in Old Constructions: the Sampling Problem. In: 2nd Historic Mortars Conference HMC2010 and RILEM TC 203-RHM Final Workshop

9. White WB (1974) The carbonate minerals. In: Farmer VC (ed) *The Infrared Spectra of Minerals*, 1st edn. Mineralogical Society of Great Britain and Ireland
10. Chu V, Regev L, Weiner S et al (2008) Differentiating between anthropogenic calcite in plaster, ash and natural calcite using infrared spectroscopy: implications in archaeology. *J Archaeol Sci* 35:905–911
11. Beniash E, Aizenberg J, Addadi L et al (1997) Amorphous calcium carbonate transforms into calcite during sea urchin larval spicule growth. *Proc R Soc B Biol Sci* 264:461–465
12. Gueta R, Natan A, Addadi L et al (2007) Local atomic order and infrared spectra of biogenic calcite. *Angew Chemie - Int Ed* 46:291–294
13. Moyce EBA, Rochelle C, Morris K et al (2014) Rock alteration in alkaline cement waters over 15 years and its relevance to the geological disposal of nuclear waste. *Appl Geochemistry* 50:91–105
14. Cullity BD (1956) *Elements Of X Ray Diffraction*. Addison-Wesley Publishing Company Inc
15. RRUFF Database. Magnesite R040114.
<http://rruff.info/magnesite/display=default/R040114>. Accessed 11 December 2018
16. Chukanov NV (2014) *Infrared spectra of mineral species*. Springer, Netherlands
17. Brown A (2017) Hot-mixed mortars Advantages and limitations. *The Building Conservation Directory* 37–38
18. Copsey N (2017) Hot Limewashes and Sheltercoats. *The Building Conservation Directory* 37–38
19. Artis R (2018) *Specifying Hot-Mixed lime mortars - Technical Paper 28*
20. Copsey N, Gourley B (2013) Hot-Mixed Lime Mortars. In: 3rd Historic Mortars Conference
21. Lott GK, Cooper AH (2005) The building limestones of the Upper Permian, Cadeby Formation (Magnesian Limestone) of Yorkshire. *British Geological Survey Internal Report IR/05/048*
22. Ingham JP (2011) *Geomaterials Under the Microscope*. Manson Publishing
23. Barber DJ, Wenk HR (1979) Deformation twinning in calcite, dolomite, and other rhombohedral carbonates. *Phys Chem Miner* 5:141–165
24. Chever L, Pavía S, Howard R (2010) Physical properties of magnesian lime mortars. *Mater Struct Constr* 43:283–296

The Restoration of the church of Our Lady of the Assumption, Dauis, Bohol, Philippines

Engr. Jim Franklin O. Kalaw¹, Engr. Raul Y. Naguit Jr.¹

(1) National Historical Commission of the Philippines, jim_kalaw@yahoo.com, raul_naguit@yahoo.com

Abstract

The study presents the history of Our Lady of Assumption Church of Dauis, Bohol, the timeline of its construction, the damage it sustained after the 7.2 magnitude earthquake of October 2013, the roles of the Philippine cultural agencies and formation of the Heritage Task Force, and its restoration Detailed Engineering and Architectural Studies (DEAS) conducted and Material Investigation using Elemental Analysis, Surface Strength, Binder analysis of mortar, Porosity Analysis and Water absorption capacity (WAC) determination, and Compressive strength of sillars was conducted to achieve the conservation plan for the structure. The study also highlighted on the restoration phase and the study alternative compatible materials. The restoration of Dauis Church lasted for four (4) years from the pre-restoration phase, restoration proper and the rehabilitation of church components. With the restoration of Bohol and Cebu churches, it promotes awareness in conservation of the heritage structures in the country.

Introduction

History of Dauis Church

Bohol island is one of the most significant area for the Spaniards, the famous blood compact happened in the island. The first town established by the Spaniards is in Mariveles now called Dauis. The word Dauis came from the local word “*Lawis*” meaning sandbar or cape described by the terrain of the town. Two religious orders managed Dauis church; the Jesuits was the first and established the “*visita*”. The Recollects then took over management in 1768 [1]. The first church structure in the Philippines was made of light materials: posts of hardwood, roofs of thatch and walls of wood or bamboo [2]. Lightweight materials like wood has two major disadvantages, highly combustible to fire and it cannot withstand strong calamities like typhoons [2]. In 1774, the wooden church was replaced with stone. Due to the continuous invasion of the Moros, a watchtower was also constructed. Only the watchtower remained up to date with minor renovations through time [1]. The construction of the existing structure started in 1863 and completed in 1879 [1]. The structure was built with “*mamposteria*”, a mixture of lime and other available materials near the structure and the “*sillar*” used was coral stones [2]. As time passed by, numerous alterations and interventions were done which includes a new façade and a portico. The materials for these

new additions were made of cement, roofing was replaced with galvanized iron and cement plaster in some parts of the church [1].



Figure 1. Our Lady of Assumption Church, Dauis, Bohol before the 7.2 magnitude earthquake [3].

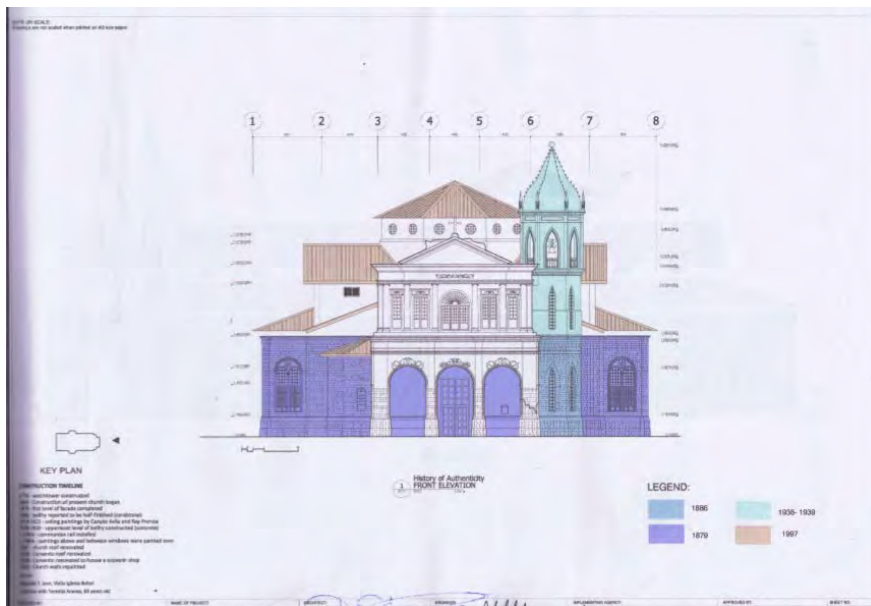


Figure 2. As-built façade of the church showing the construction timeline.

7.2 Magnitude Earthquake of 2013

In the morning of October 15, 2013, a 7.2 magnitude earthquake hit the province of Bohol approximately 1.2 miles east of the town of Carmen that resulted in damages of various commercial and industrial infrastructures [3]. Heritage structures declared as World Heritage Sites, National Cultural Treasures, National Historical Landmarks, and Important Cultural Properties within this region were not immune to destruction.



Source:

<https://www.gmanetwork.com/news/news/photo/46607/daus-church-in-bohol-badly-damaged-by-quake/photo/>

Source:

<https://newsinfo.inquirer.net/507169/6-dead-power-down-as-7-2-quake-hits-bohol>

Figure 3. Epicenter of Earthquake and Façade Daus Church after the 7.2 magnitude earthquake
Heritage Task Force

Upon news of the earthquake, Cultural Government agencies headed by the National Commission for Culture and the Arts (NCCA) met to construct a plan of action with regards to the massive damage on cultural properties. Through this meeting, a heritage task force was formed to initially assess, document and propose a conservation plan. With the National Museum (NM) and the National Historical Commission of the Philippines (NHCP) as the implementing agencies, teams of cultural workers proceeded to affected areas.

Results of the assessment revealed that twenty-two (22) heritage structures from Bohol and Cebu were prioritized due to the need of immediate action. The responsibility on the conservation of these structures was distributed to the two implementing agencies. The gravely damaged Daus church was assigned to NHCP.

Dislodged sillars were collected, sorted, and marked according to its location. These were stored in a secured area with near ideal storage conditions to prevent further deterioration to the stones.

National Historical Commission of the Philippines (NHCP)

Researchers, Engineers, Architects, and Scientists took part in the material characterization of Daus church. The team who undertook the investigation were faced with challenges brought about by the urgency of the results and the extent of damage. Limited equipment, manpower and experience were some of the hindrances in executing the most comprehensive investigations. Despite of the limitations, the NHCP was able to produce a method of conservation and conservation management plan of Daus church.

NHCP divided the responsibility to study the heritage structures onto its two departments: Historic Preservation Division (HPD) and Materials Research Conservation Division (MRCD). HPD, which is composed of architects and engineers, as the personnel in-charge for the detailed engineering and architectural study and estimates for the cost in restoration. MRCD, which is composed of engineers, scientists and conservators, are responsible for the material investigation of building components. Through scientific analysis from the results of the material investigation, MRCD recommends materials to be used.

Detailed Engineering and Architectural Study (DEAS)

Conservation decisions on heritage preservation and restoration are made with the knowledge of its significance, history, past interventions, and current condition of the physical resources available. DEAS consists of the architectural and engineering records, as-built plans using computer aided tools and complete photo documentation. Soil boring tests and geological survey analysis are also part of the DEAS which is necessary in the structural analysis and design of the restoration project. Due to lack of surveying equipment, technical staff and manpower, the NHCP opted to collaborate with a third-party contractor to provide the DEAS.

The DEAS started with the Soil testing using Borehole with standard penetration following ASTM D1586. The collected samples were brought to laboratory for the further analysis. The soil testing done was as follows: A. Grain Size Analysis following ASTM D422, B. Moisture Content following ASTM D2216, C. Atterberg Limit Test following ASTM D4318, D. Soil Classification Test following ASTM D2487, and E. Unconfined Compression Test Following ASTM D2938. The Structure's elevation (front, rear, right and left), electrical design, historical records of the structure, floor plan, and as-built plans was also drawn using computer aided tools.

Material Investigation

Material Investigation is defined as the scientific analysis of the material components of building materials through careful examination and interpretation of quantitative and qualitative data collected from a combination of destructive and non-destructive testing techniques [4]. This became the reference for materials to be used in the formulation of the restoration proposal.

Since the Daus Church was constructed using unreinforced masonry, the material investigation of its mortar, rubble core, sillars and plaster were the immediate focus of the tests. Analysis of materials includes methodologies that determine its mechanical and physical properties and chemical composition. Phases of the investigation are as follows: A. Elemental Analysis, B. Surface Strength C. Binder analysis of mortar, D. Porosity Analysis and Water absorption capacity (WAC) determination, and E. Compressive strength of sillars.

Elemental Analysis

In situ elemental analysis of varying location points interior and exterior to the church was carried out. The Handheld Element analyzer Olympus Delta Professional X-Ray Fluorescence (XRF) with silver (Ag) anode was used as a form of non-destructive testing to determine the elemental composition of paint, metal alloys, exposed concrete and other component materials semi-quantitatively. Testing is done on the surface of the material.

The XRF reading is the elemental composition of mortars, plaster and coral stones were done. Each testing was set to 60 seconds, following the Geochem standard of the equipment. This test is a gives a quantitative result that would only provide an elemental analysis.

Table A. X-Ray Fluorescence Results of Component Materials

Elements	Coral Stone	Mortar	Plaster
	Composition (%)		
Aluminum (Al)			0.38
Silicon(Si)	1.7692	0.9427	2.4199
Sulfur (S)	0.2033	0.3773	0.2921
Chlorine (Cl)	0.0621	0.066	0.5117
Calcium (Ca)	37.61	31.53	34.53
Titanium (Ti)	0.0755	-	0.0791
Manganese (Mn)	-	-	0.0249
Iron (Fe)	0.2175	0.4169	1.1888
Zinc (Zn)	0.0036	0.0033	0.0048
Arsenic (As)	-	-	0.0011
Rubidium (Rb)	-	-	0.0015
Strontium (Sr)	0.577	0.416	0.154
Zirconium (Zr)	-	0.0105	0.0048
Thorium (Th)	0.0062	0.0078	0.0031
Light Elements	59.46	66.23	60.8

Result shows signs of soiling in the samples tested because traces of Sulfur and other elements. Coral stones, porous in nature, must have the capacity to absorb and release moisture to prevent deterioration [5]. However, due to excessive soiling, the pores of the stone get clogged up and disrupt the wetting and drying cycle. There are many factors affecting the rate of deterioration, but one major cause is acid rain which is brought by the pollution in the environment. The acid rain reacts with the calcite on a stone which causes dissolution and alteration therefore causing decay and loss of material.

Surface Strength

Rebound hammer test was done on-site using a Proceq Silver Schmidt type N test hammer as a form of non-destructive testing to identify areas of erosion and detachment. Forty-four location points were conducted for the entire structure.

Results indicate that there were no detachment and erosion on the sillars. However, pulverization of the mortars and rubble core was observed in some areas. Loss of adhesion was observed on the interior plastered walls due to incompatible thermal expansion of materials.

Binder analysis of Mortars

Binder proportion analysis is done to determine the ratio of three basic components of historic building materials especially mortars. Acid digestion is used to separate the binder component (acid soluble, usually calcium carbonate), the fines (finely-textured impurities such as clay) and the sand or aggregate [6]. This is important in providing information regarding the preparation of repair materials compatible with the original.

Table 2. Binder Analysis of mortars

Location	Dissolved Binder (%)	Fines (%)	Aggregates (%)
Exterior	94.041	5.308	0.561
Interior	74.547	24.899	0.553

Collected Mortars consisted primarily of binder. However, it is possible through the technique of acid digestion, the calcium rich aggregates may be dissolved in the process. The results of the analysis carried out are just an approximation of the sample's material composition and is basically depended on the nature of the sample taken and the effect of carbonaceous and calcareous impurities present in the sample. These impurities can present a misleading binder/fines/aggregates proportions. It should be taken into consideration since in practice, it is often sufficient to make a relative measurement to compare one material with another.

Porosity Analysis and Water absorption capacity (WAC) determination

Porosity represents a fraction of the accumulated volume of a particular solid occupied by empty spaces within solids, or pores. Determination of total porosity of stone is important in the deterioration, durability assessment, behavior and effectiveness of treatment, hence essential in the overall material characterization of a structure ^[5]. Total porosity of collected solid building materials were measured through indirect measurement by water absorption to provide an estimate of the percent porosity.

Table C. Porosity and Water absorption capacity of Mortar and Coral Stone

Location	Porosity (%)	WAC (%)
Exterior (Mortar)	35.82	25.60
Interior (Mortar)	33.61	22.99
Coral Stone	33.78	24.78

Comparison between the water absorption of the mortar and the facework is essential in the restoration process. Results indicates that the purpose of these mortars was to regulate moisture movements on the masonry wall. These mortars facilitate the evaporation of moisture through them rather than through the sillars.

Compressive Strength of Sillars

Dauis church was built with Coral stones. These materials are commonly used during the Spanish occupation in the Philippines because of its availability and abundance especially on structures near shores. Massive coral stones were formed to smooth squared stones forming ashlar masonry. Collected loose coral stone samples was tested to measure its compressive strength using Floor type Shimadzu Universal testing machine (UTM) UH-A-C Series was used in this procedure to determine the compressive strength in terms of Megapascal.

The average compressive strength of the coral stone collected in Dauis church is 11.293 MPa. This information was used to evaluate the proposed alternative materials to be introduced especially for the missing parts. Although heritage structures within this region comprises of coral stones, it cannot be considered that they are of the same strength.

Restoration Plan

The protection of the country's-built heritage is mandated by the Republic Act 10066 "National Cultural Heritage Act of 2009" [7]. Still in its early stages of implementation, the law has many discernable flaws. Restoration of unreinforced masonry heritage structures has yet to be regulated and guidelines are still to be put in place. In this regard, the NHCP has conducted two international conferences with foreign experts on conservation to discuss possible and appropriate methods of restoration for the damaged structures. Learnings retrieved from these conferences were applied in the creation of a conservation master plan. The plan was guided by international charters in conservation, in which two guidelines were considered, i) replace the component with the same material taking into consideration strengthening the original material to prevent the occurrence of another failure of the structure and ii) replace the missing components with compatible materials taking into consideration appearance, physical and mechanical properties. Also, the replacement material must be reversible and will not damage the original material. The combination of results of the studies, architectural plans and structural analysis served as the scientific evidences for the methods and materials to be used in the plan [8].

Restoration Phase

The restoration started with the return of coral stones its proper location ensuring its bond to the rubble core stone wall, then was stabilized. During the process, all of the sillars were cleaned properly removing all of the vegetation and soiling. Following this, the rehabilitation of the roofing system commenced, removing the existing roofing and replacing it with a

lighter material ensuring its stability to calamities. Anastylis was the method used for the portico and pediment. The doors, mouldings, windows, choirloft and electrical wiring was also included in the restoration phase of the church.

Evaluation of replacement materials

Corals used in the construction of the built heritage are now inaccessible due to environmental constraints. With the initiative of heritage advocates, alternative materials were assessed to see if it is compatible with the original material. Due to this, a comparison of the material properties of limestone gathered from a quarry near the town of Daus and coral stone collected from the walls was done. Results show a significant difference in porosity, WAC, density, and maximum stress. Although they are similar aesthetically, limestone would not be compatible because of its higher physical and mechanical properties.

Table E. Physical and Mechanical properties of Coral Stone versus Limestone

Material	Porosity, %	WAC, %	Density, g/mL	Max Stress, MPa
Coral Stone	33.78	24.78	1.38	11.293
Limestone	9.76	4.34	2.23	24.787

The data shows that there is a significant difference in the physical and mechanical properties between coral stone and limestone. The highly porous coral stone compared to the compact limestone would affect the moisture transport within the walls. The difference in density would cause significant stress on the coral causing loss of material.

In line with this, NHCP is currently collaborating with Mines and Geosciences Bureau (MGB) for the research study on the identification of indigenous materials and rock sites as alternative compatible materials in the restoration of heritage structures in the Philippines.

Broken and damaged coral stones were used as aggregates to slurry lime for repointing and mortar. Various mixtures were evaluated for their compatibility in terms of strength and appearance.

Table F. Fabricated Blocks Physical and Mechanical Results

Sample Code	Percent Calcium (%)	Compressive strength (MPa)
3 Lime : 1 Coral	38.68	0.87
1 Lime : 3 Coral	39.63	0.84
1 Cement : 2 Lime : 6 Coral powder	9.88	1.76
1 Cement : 3 Lime : 9 Coral powder	24.55	1.54

It is noted that the material used for the repair of mortar in the unreinforced structure is not a load bearing material thus high strength is not expected. The result shows that there is a minimal strength on all fabricated materials. The mixture of 1 Lime : 3 Coral powder was selected as most compatible for restoration. This was also chosen to complement the appearance of the original coral stones.

Consolidation of Rubble Core

Consolidation is a process in which a consolidant is applied to the rubble core to strengthen the weakened surface and slow the rate of material loss. Also, the method penetrated through the pores of the weakened material at a certain depth, strengthening the bond. The consolidation process initially used lime water to the exposed rubble for weeks followed by application of slurry lime. Calibrated epoxy was then applied to fill loss of volume of the rubble core.

Application of Repointing

With the use of appropriate materials and methods, this will also serve as a protection and sacrificial material to the facework. The Repointing must be softer and makes the wall assembly watertight. [Benjie]. Following the specifications gathered in the binder analysis, the conservation team tested the various mixtures on the wall to evaluate its applicability.

Restoration of East and West Transept

There are parts in Daus church that the wall completely collapsed in which there are no usable materials. One option was to rebuild the wall using the same materials and method of construction. However, this method must address the following issue: what if the same intensity of earthquake strikes the Philippines, will it survive? Taking this issue into consideration, the team opted to use acceptable modern material in rebuilding the collapsed wall but ensuring that it is true to the original wall. A deeper foundation complying with the existing structural code in the Philippines was built using cement material and the remaining coral blocks were cut and then cladded on the cement wall securing the connection.

Application of Protective Coating

The high humidity of the area has accelerated the rate of deterioration of the structure. Biological growth is abundant on the walls making it continuously damp. Due to the high concentration of moisture, the surface will weaken. Application of protective coating is one of the options for its prevention, however it risks disrupting effective water transport.

All walls to be coated must be clean from any substrate that might give a negative effect to the structure like mosses and other biological growths. Nippon Water Repellant solution for masonry was used. It is a solvent-based primer of silane/siloxane mixture. It reduces the capillary absorption of the walls without blocking the pores and does not affect the diffusion

permeability. It also allows the walls to breathe letting the water vapor escape [9]. The application of water repellent is also taken into consideration, areas where water is trapped like ledges, more layers of coating was applied. Its protection is for three years from the application but these may vary depending on the extent of water passing through the walls.

Maintenance Program

Philippines is divided into several islands, in which monitoring by concerned government agencies (NHCP, NM and NCCA) is a challenge. An effective maintenance program is more cost effective compared to intervention works. For sustainability, the NHCP provided trainings and conferences to locals to give consciousness on the importance of the restoration and preservation of their built heritage. Since the earthquake, the stakeholders are now taking an active role in its preservation. The decision makers are now conscious of the effects of consulting conservation professionals rather doing it on their own.

Conclusion

The restoration of Daus Church took four years to complete. The restoration works were distributed to three phases, the first phase was the pre-restoration wherein certain parts of the structure were protected using shoring in order to prevent collapse. The second phase was the restoration proper wherein the rubble core was consolidated, collapsed walls were rebuilt and the roofing system was replaced. The last phase was the site development, which includes the remaining work was done, including the rehabilitation of the interior walls, ceiling painting, retablos, lightings, pews and landscaping.

The restoration of Bohol and Cebu damaged by the 7.2 magnitude earthquake was a breakthrough in the awareness in conservation of the heritage structures in the country. Plenty of stakeholders are now active in promoting the protection of it. It is recommended to conduct continuous study and research on the effect of the restoration materials.

References

1. Galende P G. (2007). Philippine Church Façade. Vibal Publishing House, Inc., Philippines
2. Jose R T. (1991). Simbahan Church Art in Colonial Philippines 1565 – 1898. Ayala Foundation, Inc., Philippines
3. <https://www.gmanetwork.com/news/lifestyle/artandculture/330979/from-treasure-to-rubble-heritage-churches-before-and-after-the-bohol-quake/story/>
4. Weaver G., et al (1992). Science for Conservator Volume 1, an introduction to Materials. Routledge, London and New York
5. Forsyth M. (2013). Materials & Skills for Historic Building Conservation. Wiley-Blackwell Publishing Ltd., United Kingdom

6. Teutonico M. T. (1988). ARC A Laboratory Manual for Architectural Conservators. ICCROM, Rome
7. Implementing Rules and Regulations of Republic Act No. 10066 National Cultural Heritage Act of 2009
8. International Charter for the Conservation and Restoration of Monuments and Sites (The Venice Charter 1964). ICOMOS 1964
9. Technical Data Sheet, Nippon Paint Water Repellant Solution, August 2018

Digital image analysis as basis for the evaluation of repair mortars in architectural conservation

C. Kaiser^{1*}, L. Oetinger^{1*}, R. Killian²

(1) Department of Inorganic materials & Recycling, Fraunhofer Institute for Building Physics IBP, christian.kaiser@ibp.fraunhofer.de, lea.maria.oetinger@ibp.fraunhofer.de

(2) Research section for cultural heriatge preservation, Fraunhofer Institute for Building Physics IBP, ralf.kilian@ibp.fraunhofer.de

**Contributed equaliy*

Abstract

This study examines whether it is possible to evaluate earlier restoration interventions through the analysis of historical repair mortars. The data source for this approach originates from the project Pompeii Arch&Lab, which understands Pompeii as an archive and exposition laboratory for conservation-restoration treatments. Several historical repair mortars from Pompeii were investigated to check their performance and assessing whether the mortars can be reproduced for the purpose of material investigation through digital image analysis (DIA) of thin sections. In addition, this gives the opportunity to gain new perspectives on historical restoration measures. To determine the error susceptibility of this method, the procedure was compared with other analysis methods (SEM, EDS, XRD, XRF, LDS, μ CT) in the laboratory. The promising results and the technically simple procedures that were used may make this approach interesting for future applications.

1. Background and Introduction

Repair mortars play a central role for the preservation of architectural heritage. They are therefore often tested extensively in the context of any restoration project to the end of finding the best possible material [1]. In general, the new material should not have any negative effect on the original one in a long term perspective. A rough distinction is made between different objectives, namely whether the mortar is used for fillings, plasters, edge repairs or grouting compounds for securing detached plasters. The use therefore influences the composition of the mortar. Our observations, however, show that the character of the material and the type of intervention are only one side of the picture. Obviously, the current conservation-restoration theory plays a decisive role especially when treatments impact the overall appearance of the object. Earlier restorations are therefore usually evaluated from an aesthetic point of view. Accordingly, we can assume that every conservation-restoration concept is not only influenced by the current state of knowledge but also by the taste of the time. This aspect can be understood as a time-dependent mixture between the prevailing restoration ethics and the practical implementation of conservation measures.

The history of repair mortars usually receives little attention. As a result, traces of previous restorations are often removed without documentation or justification. But this lies in the nature of things, because any intervention is aimed at maintaining or optimising the existing condition. Thus each generation of “conservators” tries to meet this challenge in its own way, leaving behind its own ideas and notions. In order to assess how successful historical measures to preserve cultural heritage have been, we need to look at these traces. The prerequisite for tracing a good overall picture is to find places that have always been open to international discussion and have a long history of conservation. The ancient city of Pompeii meets these requirements and, if we consider the archaeological site as an exposure laboratory for earlier conservation materials, its significance for this study becomes apparent. Since its first excavation in the 17th century, the preservation of Pompeii represents a special challenge [2], not least because of its extension. This, along with its “completeness”, makes ancient Pompeii special. Since restoration measures were carried out in different areas of the site at different times, a history of repair mortars has become legible. These historic tracks can be followed. To find answers to the question of how successful and durable the conservation materials actually are, a chronological classification is required. We solved this problem through extensive archive research and by comparing excavation reports, historical photographs and paintings with the on-site situation. However, this also restricts the applicability of the method, because it can only be used on “visible” mortars. Grouting material, for example, can only be dated indirectly. Be that as it may, this approach allows to identify correlations between used materials and durability as well as to classify the restoration measures over time. Moreover, the advantage of this classification method is that it is non-destructive. In the second step, the investigation focuses primarily on edge repairs, because these had noticeably changed their materiality over time, as well as their form, shape and surface structure. This type of mortar secures the edges of wall paintings and plasters so that no large quantity of water can penetrate into the structure, which can lead to deformations thus causing loss of substance (Figure 1).



Figure 1. Reddish repair mortar No. 2002 in the Casa del Labirinto. (Fraunhofer IBP, 2017)



Figure 2. Cross-section of No. 2002, composed of a preparatory and a top layer. (Fraunhofer IBP, 2017)

For this study, samples were taken from pre-selected mortars from two houses: the Casa di Sallustio (CdS) in Regio VI Insula 2 [3] and the Casa del Labirinto (CdL) in Regio VI Insula 11 [4]. Both houses were excavated in the 19th century. We are thus dealing with mortars from the 19th and the beginning of 20th centuries. Since our concept for material adjustment is mainly based on the analysis of thin sections, the sample size of 2x2x2cm seems sufficient (Figure 2). To react to the heterogeneity of each mortar, three samples were taken from different positions. Information about the exact location, exposure and condition of each mortar was recorded and stored in a database. This data basis provides the key for the correlation-analysis for the classification of these historic mortars, which generally are not described or documented in the archives of the site. For an evaluation, however, it is necessary to determine the raw materials used, the chemical reactions between components (e.g. pozzolanic reactions), the dimensions of the aggregates, microstructure, binder/aggregate ratio or percentage of pores [5]. Thanks to this characterization, it will be possible to reconstruct mortar mixtures by reverse engineering with properties similar and compatible with the original restoration mortars [1]. Furthermore, these reconstructions can be used for extensive analysis in the laboratory.

2. Experimental Setup and Digital Image Analysis

After analysing the historical context, samples of repair mortars from the 19th and 20th century are taken from different, selected position in the CdS and the CdL. The selected, historic edge repairs show a good state of preservation and still fulfil their function of stabilising plasters. The 17 samples from the CdS and the 12 samples from the CdL were selected to allow a comparison between internal and external exposure. To demonstrate the method with all its limitations and difficulties, three samples are presented in the following text. Two samples can be dated via archive material while the third's chronology is delimited in a time-phase by correlation analysis. Only two samples of the mortar-type 1000 exist. Detailed information on the mortars will be published separately and in the final report of the Arch&Lab project. In brief, the microscopic analysis of the mortars shows a very heterogeneous size and material distribution of the aggregates. The volcanic origin is apparent with volcanic sand, pyroxene, plagioclase/feldspar, mica and fine/coarse calcite [5]. Also a percentage of 21-% magnesium could be determined in the matrix of mortar 1000. This could indicate a dolomitic lime as binder [6]. In our case, we are dealing also with a kind of foamed aggregates. These affect the mortar by making it lighter but cause some issues in the DIA. In addition, many mortars have a two-layer structure (Figure 2). Currently, for the recreation of the historic mortar, we focus on the preparatory layer, as we assume that it is mainly responsible for the functional fulfilment (e.g. absorb occurring forces). The top mortar is therefore to be understood as a protective layer for the preparatory mortar.

Table 1. Overview of the presented samples. AQ stands for “ante quem”, meaning the sample dates before the mentioned time.

Mortar-ID_ Sample-No.	Origin (House)	Exposition	Date
1000_1	CdS	Internal North	AQ ca. 1880
1000_2	CdS	Internal North	AQ ca. 1880
1008_1	CdS	Internal East	n.a.
1008_2	CdS	Internal East	n.a.
1008_3	CdS	Internal East	n.a.
2002_1	CdL	External West	AQ 1920
2002_2	CdL	External West	AQ 1920
2002_3	CdL	External West	AQ 1920

Several factors must be considered before performing DIA of mortars, because the results are also directly related to the quality of the image. Since the method is based in particular on segmentation of colour-values, even a non-uniform illumination can impact greatly the precision of the measurement [7]. Thus, one of the main limitations of DIA is that segmentation features cannot be effective if the colour difference between the mortar components is not measurable. Dyeing methods can be of help here, but in this experiment, they have not yet been applied. Instead, other investigation methods are used in parallel. The resin has been dyed blue, which makes it easier to separate the background and pores from the matrix and the aggregates. To minimize the subjective interventions by the operator and to guarantee traceability, all parameters have been defined.

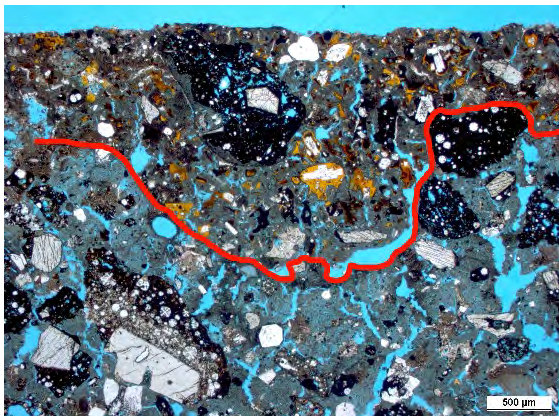


Figure 3. Thin section of mortar 1000 with the two layers. (Fraunhofer IBP/F. Schlütter, 2017)

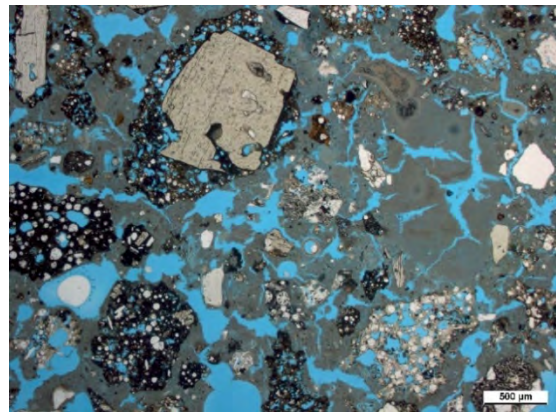


Figure 4. Detail of mortar 2002. (Fraunhofer IBP/F. Schlütter, 2017)

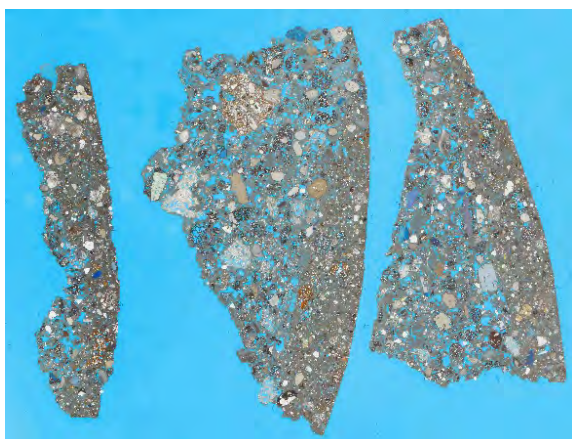


Figure 5. Thin sections pol II 2002_1/2/3. (Fraunhofer IBP, 2018)

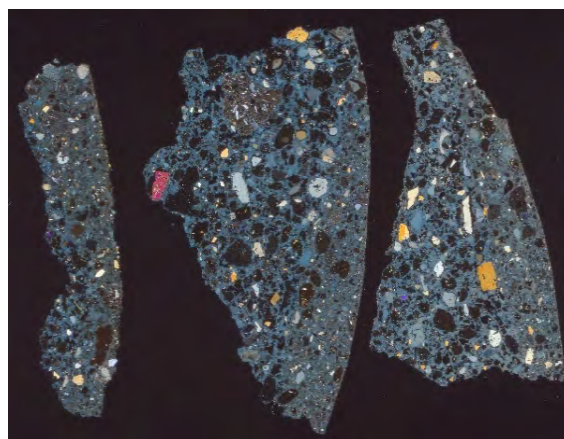


Figure 6. Thin sections pol ⊗ 2002_1/2/3. (Fraunhofer IBP, 2018)



Figure 7. Thin sections inverted 2002_1/2/3. (Fraunhofer IBP, 2018)

Digital image analysis also depends on the resolution of the image material. There are two possibilities, either a scan via a flatbed scanner or the thin section is scanned step by step with the microscope at high magnification and then combined to one HD-image [7-11]. The latter would allow to capture more details but would also significantly increase the amount of data to analyse. After considering both procedures, we chose a hybrid solution. For larger aggregates (>50 μm) a scan with a flatbed scanner with 4800dpi suffices (Figure 5 - 7). For the particles below 50 μm , microscope images are evaluated, statistically weighted according to their area and fed to the entire analysis. The same approach was used for measuring the pore sizes. The size of each particle in the thin section will also depend on a random intersection of the sample [12] and this will also influence the results of the grain size distribution. Furthermore, we have to consider weathering processes, which might change the matrix and the pores.

The analysis of thin sections has a long tradition in the field of conservation and many data is already available. This can provide extensive information about the material with the use of modest analysis equipment. For our research, the key question is whether the information contained in 2D images of thin sections can be reconstructed into an approximately faithful 3D material representation [13]. This approach has been repeatedly used in the literature,

even though today new and more complex techniques such as μ CT are available [14–23]. This is done for a good reason, because, despite the latest developments in 3D imaging, the availability of the necessary equipment, sample size and preparation, the amount of data to be evaluated and the ensuing costs are important issues. For our research we use the open source software ImageJ (<https://imagej.nih.gov/ij/>). Finally, deep- and machine learning can obviate a frequently mentioned limitation of the DIA, the ineffective automatic segmentation processes. Pattern recognition [7] can extend the standard segmentation based on colour differences to provide statistical information of higher order [24]. The purpose of this statistic data is to help the reconstruction method to evolve, in order to determine the 3D volume of the individual aggregates. According to the fact that a thin-section also has a volume of approximately $25\mu\text{m}$, the following assumptions are made for our model. If I_0 denotes an image set of $M \times N$ and $\vec{A}=(R,G,B)$ is the colour level of (m,n) pixel in I_0 . For example, for the distribution of the aggregates we scan the image, focusing on the sum of that represents the aggregates as area [13].

$$C_3 = \sum_{x=0}^m \sum_{y=0}^n D(x+i, y+j) \text{ AND } \vec{A} = (R_r, G_g, B_b)$$

To compare the three thin sections of each mortar we have to normalize the results and consider a statistical weighting. The thin section with the largest mortar profile is then given the highest weighting, since it can be assumed that this one represents the best grain size distribution. For the grain size classification the feret diameter (min & max) is used, which correlates in practice with the sieve-classes [7]. In order to reconstruct the corresponding volumes from the measured areas, we assume that: First, the smaller the grain, the more spherical the reconstruction. Secondly, if the grains are undirected, it can be assumed that the grain size distribution in $M \times N$ is valid not only in XY but also in XZ and YZ directions. Thirdly, it follows that feret-diameter-min represents approximately the depth especially of crystalline materials. If the aggregates show a discernible direction, the latter assumption becomes even more relevant. However, this does not necessarily apply to the amorphous aggregates and therefore larger deviations are to be expected in the 3D reconstruction. In other words, it is a packaging problem, i.e. how tightly objects can fill a volume [25], with the difference that, depending on the rheology, the binder is to be regarded as a kind of expanding medium.

To verify our model (Figure 8-9), we also analysed the mortar 1008_1 by computer tomography (μ CT). This step enabled us to calculate the possible deviation between percentage area proportions and percentage volume proportions of the aggregates. These results were then compared with the results of the particle size distributions determined by laser diffraction spectroscopy (LDS). As expected, at DIA the quality of segmentation plays a key role in the proposed procedure (Figure 10). In addition, as it was shown in our case, certain aggregates can make the segmentation considerably more difficult: since these aggregates represent a kind of foamed isotropic material with enclaves of different minerals,

they possess intra-grain pores [26]. Therefore, the extraction-procedure uses the physical properties visible in transmitted cross-polarized light illumination and bright field illumination.

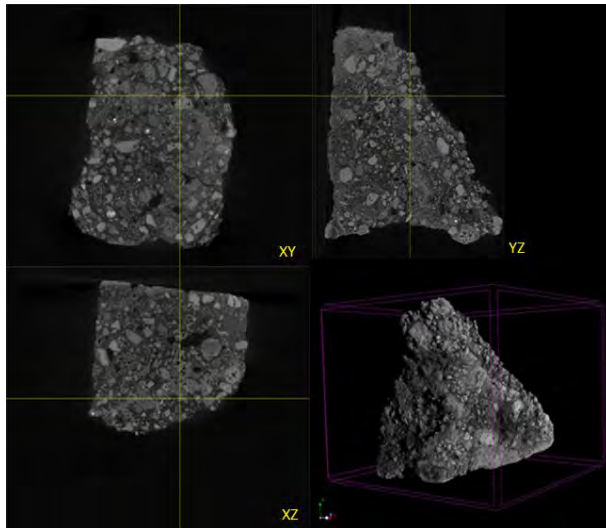


Figure 8. μ CT of Mortar 1008_1. (Fraunhofer IBP, 2019)

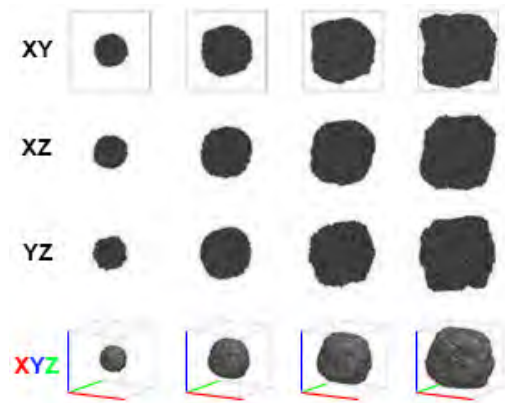


Figure 9. 3D reconstruction from 2D image of thin sections. (Fraunhofer IBP, 2019)

This allows to select the aggregates and count the intra-grain pores. In addition, the procedure shows that the inverted bright field image is also useful for the segmentation, because the inverted colours make it easier for the operator to differentiate between the components and to optimize each selection. In summary, we combine the selections from each of these 3 images, which represent the starting point for the analysis (Figure 5-7). Furthermore, the use of some sub-processes to separate stacked grains and to fill “holes” in the selection has also been well-established. For separating we use simple operations like Erosion and Dilation, with a range of <5 pixel. The proportions and the distribution of pores, matrix and aggregates can be statistically determined in this way. It is, however, necessary to stress that every operation may contain errors, which have to be statistically taken into account. The result obtained by a single operator may vary by ca. 2.5%. But considering that the mortars are all hand-mixed and have also variations in the composition, this error is negligible. Thus the examined thin sections of each mortar varied in their area, for example the range of mortar 1000 lies between 109 mm² to 134 mm², the loading-value of the one with the larger area is higher and represents the composition of the mortar more accurately.

3. Results

In summary, the historic repair mortars provide with a ratio of about 1:0.9 in the CdS and 1:0.8 in the CdL a higher amount of binder. After carbonization the porosity varies between 11% and 14%. This almost 1:1 composition could have been chosen because of its good workability and plasticity, which allows a vertical and horizontal application. Furthermore

the high percentage of binder could be related to the slight hydraulicity of the mortar 1000 [6], caused by the use of hydraulic aggregates, called Puzzolana a local source in the Vesuvius region. In combination with calcium hydrate it forms calcium-silicate and calcium-aluminate-hydrate phases, which changes the mechanic and physical properties of the mortar. Another component that influences the pattern and the properties of the mortars are accumulations of binder, acting as aggregate after carbonization. The reason for this accumulations lies in an imperfect mixing process of a highly viscous lime with “sand”. Their occurrence illustrates the on-site (often handcrafted) production of the mortar. Due to the optical similarity to the binder, the segmentation of these “aggregates” include some handicaps.

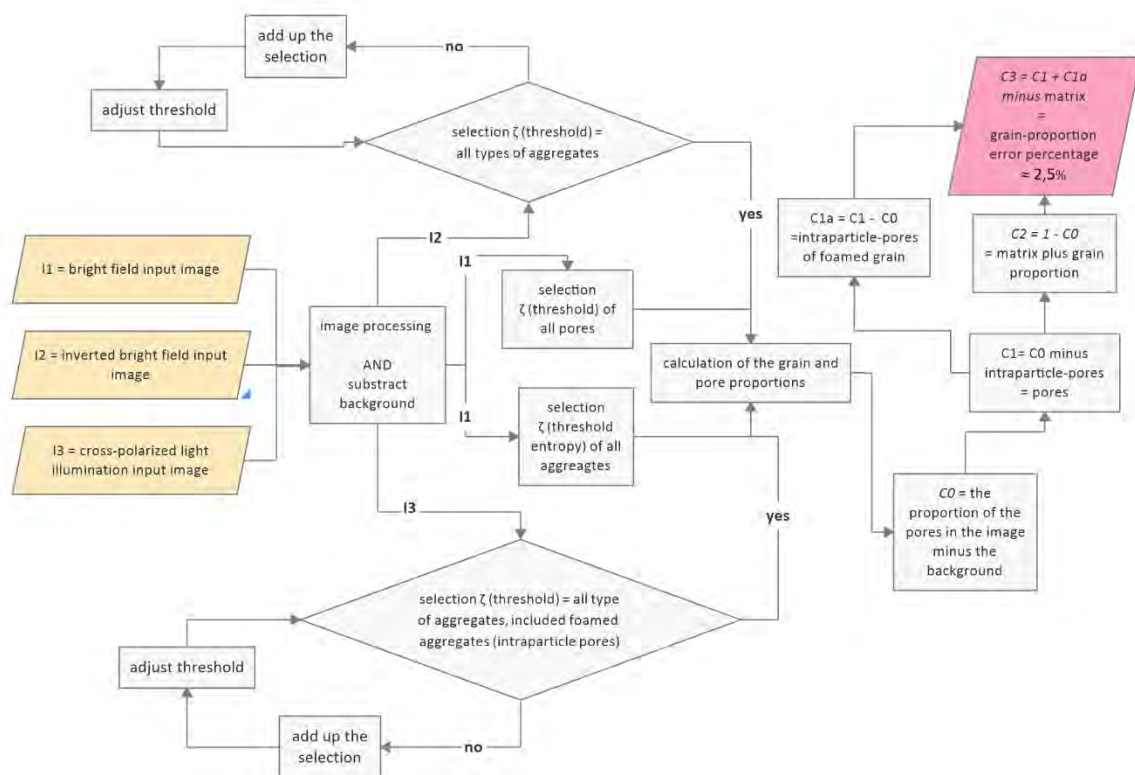


Figure 10. Procedure of the DIA. (Fraunhofer IBP, 2019)

The foamed aggregates with a percentage of ca. 25 % in the CdS and ca. 38 % in the CdL reduce the weight of the mortars and change their consistency, which allows to apply them in a convex profile with a thickness of some centimetres and a width of 10–30 cm (Figure 11). This shape of the historic repair-mortar include both good adhesion forces to the masonry and cohesion forces within the mortar structure. Also an important feature for the properties of mortars is the grain size distribution. The repair mortars have a wide variety of

distribution from the reconstruction with the original repair mortar proves the concept (Figure 15).

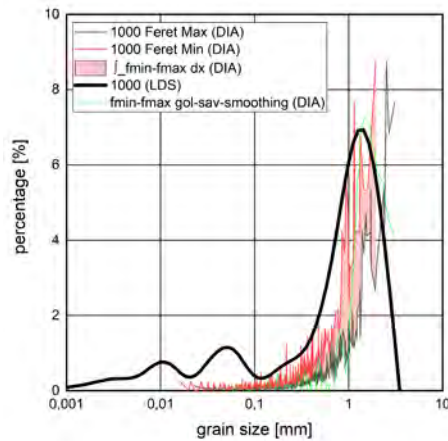


Figure 12. Comparison the results of the grain size distribution between DIA and LDS (Fraunhofer IBP, 2019)

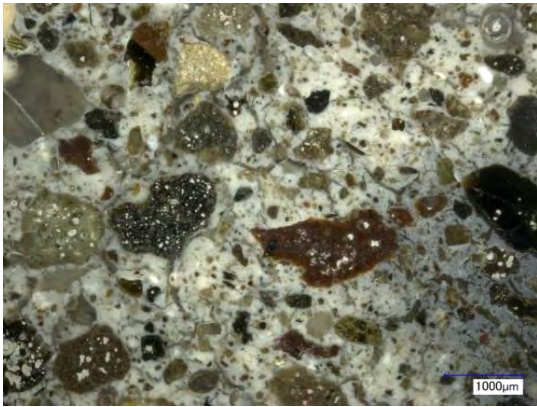


Figure 13. Cross section of the recreated mortar. (Fraunhofer IBP, 2018)

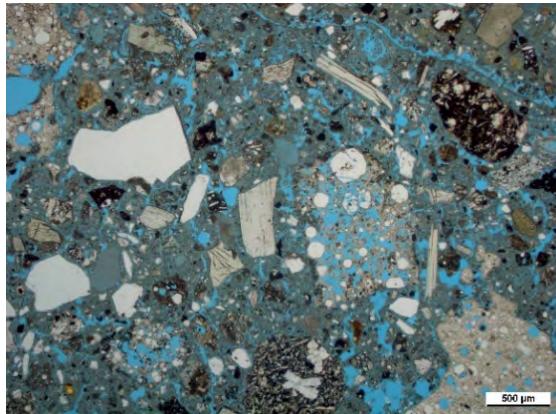


Figure 14. Thin section of the original repair mortar (Fraunhofer IBP/F. Schlütter, 2017)

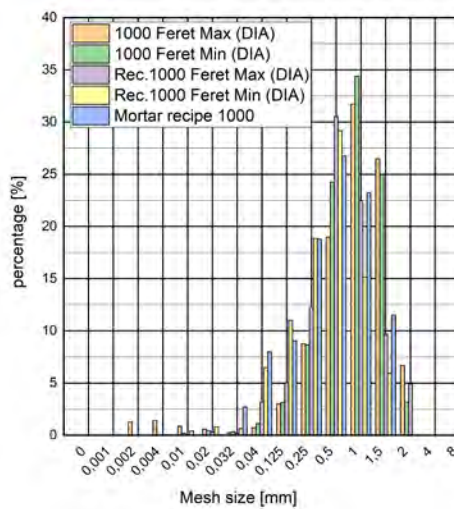


Figure 15. Comparison between the recipe and the reconstructed mortar. (Fraunhofer IBP, 2019)

4. Conclusion

This research shows that it is possible to recreate a historic conservation mortar based on DIA. Of course, potential errors must be taken into account and the results must be critically questioned. However, the combination of different analysis methods help to determine the error-value and confirm the concept. The sequence of different analysis-steps results in an examination process-pipeline that anyone can use due to its low technical complexity. It starts with a microscopic analysis on thin section, which allows to determine a mineral and chemical characterisation. Furthermore, DIA is capable to analyse the proportion of the components as well as the grain size distribution. Obviously, because of the factor of time and the weathering history of the mortar, there will always be a gap between the historic and the recreated mortar. Furthermore, the question arise, how accurately the mortar has to be reconstructed and how the craftsmanship and the shape of the edge repairs affects the durability of the intervention. Since repair mortars are still applied today for the same reason, namely to preserve wall paintings and plasters in situ, the evaluation of historic repair mortars are going to play an important role in the field of conservation. One advantage of the DIA method is that with the new machine- and deep-learning tools there is space for improvement, especially in case of image analysis. It also became clear that craftsmanship is an extremely important factor for a successful and sustainable conservation intervention. However, an evaluation of historic treatment would open up the possibility of checking both the ageing behaviour and the long-term durability of the material. Finally the analysis of repair mortars offers new discussions about preserving-methods and also the opportunity to obtain new perspectives on historical restoration interventions.

5. Acknowledgement

The fruitful collaboration of different disciplines like art history, archaeology, conservation-restoration as well as mineralogy was a key factor in this project. By combining different scientific fields, new approaches to the restoration research were created. We wish to express our gratitude to Dr. Katrin Wilhelm, Dr. Pia Kastenmeier, Dr. Frank Schlütter, Dr. Sara Saba, Edith Aichinger, Clara Friedl as well as the entire Arch&Lab Team, who supports this research. Furthermore we would also like to thank to the Parco Archeologico di Pompei and its director Massimo Osanna for the cooperation.

References

1. A. Moropoulou, A. Bakolas, P. Moundoulas, E. Aggelakopoulou (2008) Reverse engineering: a proper methodology for compatible restoration of mortars. In: RILEM (ed) Repairs Mortars for Historic Masonry: Proceedings pro067. RILEM, Delft
2. Caro S de (2015) Excavation and Conservation at Pompeii: a Conflicted History. <http://www.fastionline.org/docs/FOLDER-con-2015-3.pdf>

3. Laidlaw A, Stella MS, Collins-Clinton J (2014) The House of Sallust in Pompeii (VI 2, 4). *Journal of Roman archaeology Supplementary series*, vol 98. *Journal of Roman Archaeology*, Portsmouth, RI
4. Strocka VM (1991) Casa del Labirinto (VI 11, 8-10). *Häuser in Pompeji*, vol 4. Hirmer Verl., München
5. Casadio F, Chiari G, Simon S (2005) Evaluation of binder/aggregate ratios in archaeological lime mortars with carbonate aggregate: A comparative assessment of chemical, mechanical and microscopic approaches. *Archaeometry* 47(4): 671–689. doi: 10.1111/j.1475-4754.2005.00226.x
6. Schlütter F Untersuchungsbericht 6010-17: Mikroskopische Charakterisierung von Mörtelproben aus Pompeji. nicht veröffentlicht 2017
7. Carò F, Di Giulio A (2004) Reliability of textural analysis of ancient plasters and mortars through automated image analysis. *Materials Characterization* 53(2-4): 243–257. doi: 10.1016/j.matchar.2004.06.014
8. Marinoni N, Pavese A, Foi M et al. (2005) Characterisation of mortar morphology in thin sections by digital image processing. *Cement and Concrete Research* 35(8): 1613–1619. doi: 10.1016/j.cemconres.2004.09.015
9. Mertens G, Elsen J (2006) Use of computer assisted image analysis for the determination of the grain-size distribution of sands used in mortars. *Cement and Concrete Research* 36(8): 1453–1459. doi: 10.1016/j.cemconres.2006.03.004
10. Miriello D, Crisci GM (2006) Image analysis and flatbed scanners. A visual procedure in order to study the macro-porosity of the archaeological and historical mortars. *Journal of Cultural Heritage* 7(3): 186–192. doi: 10.1016/j.culher.2006.03.003
11. Tarquini S, Armienti P (2003) QUICK DETERMINATION OF CRYSTAL SIZE DISTRIBUTIONS OF ROCKS BY MEANS OF A COLOR SCANNER. *Image Anal Stereol* 22(1): 27. doi: 10.5566/ias.v22.p27-34
12. Sandström M (1995) Determination of the size distribution of aggregates by computer assisted image analysis: Nordtest, project 1218-95. SP rapport, 1995:52. Swedish National Testing and Research Institute (SP), Borås
13. Tahmasebi P, Sahimi M (2012) Reconstruction of three-dimensional porous media using a single thin section. *Phys Rev E Stat Nonlin Soft Matter Phys* 85(6 Pt 2): 66709. doi: 10.1103/PhysRevE.85.066709
14. Feng J, Teng Q, He X et al. (2018) Reconstruction of three-dimensional heterogeneous media from a single two-dimensional section via co-occurrence correlation function. *Computational Materials Science* 144: 181–192. doi: 10.1016/j.commatsci.2017.11.030
15. Bodla KK, Garimella SV, Murthy JY (2014) 3D reconstruction and design of porous media from thin sections. *International Journal of Heat and Mass Transfer* 73: 250–264. doi: 10.1016/j.ijheatmasstransfer.2014.02.006

16. Izadi H, Baniassadi M, Hasanabadi A et al. (2017) Application of full set of two point correlation functions from a pair of 2D cut sections for 3D porous media reconstruction. *Journal of Petroleum Science and Engineering* 149: 789–800. doi: 10.1016/j.petrol.2016.10.065
17. Wu Y, Lin C, Ren L et al. (2018) Reconstruction of 3D porous media using multiple-point statistics based on a 3D training image. *Journal of Natural Gas Science and Engineering* 51: 129–140. doi: 10.1016/j.jngse.2017.12.032
18. Li DS, Tschopp MA, Khaleel M et al. (2012) Comparison of reconstructed spatial microstructure images using different statistical descriptors. *Computational Materials Science* 51(1): 437–444. doi: 10.1016/j.commatsci.2011.07.056
19. Karimpouli S, Tahmasebi P, Saenger EH (2018) Estimating 3D elastic moduli of rock from 2D thin-section images using differential effective medium theory. *GEOPHYSICS* 83(4): MR211-MR219. doi: 10.1190/geo2017-0504.1
20. Hajizadeh A, Farhadpour Z (2012) An Algorithm for 3D Pore Space Reconstruction from a 2D Image Using Sequential Simulation and Gradual Deformation with the Probability Perturbation Sampler. *Transp Porous Med* 94(3): 859–881. doi: 10.1007/s11242-012-0028-7
21. Keehm Y (2004) Permeability prediction from thin sections: 3D reconstruction and Lattice-Boltzmann flow simulation. *Geophys. Res. Lett.* 31(4): 691. doi: 10.1029/2003GL018761
22. Quiblier JA (1984) A new three-dimensional modeling technique for studying porous media. *Journal of Colloid and Interface Science* 98(1): 84–102. doi: 10.1016/0021-9797(84)90481-8
23. Yves Rémond, Saïd Ahzi, Majid Baniassadi and Hamid Garmestani Applied RVE Reconstruction and Homogenization of Heterogeneous Materials
24. Jähne B (2002) *Digitale Bildverarbeitung, 5., überarbeitete und erweiterte Auflage.* Springer Berlin Heidelberg, Berlin, Heidelberg, s.l.
25. Donev A, Cisse I, Sachs D et al. (2004) Improving the density of jammed disordered packings using ellipsoids. *Science* 303(5660): 990–993. doi: 10.1126/science.1093010
26. Lacaze J, Arnal A, Dupuy J-L et al. (2002) SEPARATION OF THE INTER- AND INTRA-PARTICLE POROSITY IN IMAGES OF POWDER COMPACTS. *Image Anal Stereol* 21(3): 183. doi: 10.5566/ias.v21.p183-189

Topic 11: Preservation. Consolidation materials and techniques. Development of new products. Preventive conservation



Frost resistance of reproduced mosaic mortars

Pavla Bauerová^{1,2}, Pavel Reiterman^{1,3}, Eva Vejmelková², Martin Keppert^{1,2}

(1) University Centre for Energy Efficient Buildings of Czech Technical University in Prague, pavlabau@centrum.cz, pavel.reiterman@fsv.cvut.cz, martin.keppert@fsv.cvut.cz

(2) Department of Materials Engineering and Chemistry, Faculty of Civil Engineering, Czech Technical University in Prague, eva.vejmelkova@fsv.cvut.cz

(3) Experimental Centre, Faculty of Civil Engineering, Czech Technical University in Prague

Abstract

Flax oil has been used as mortar-improving admixture since ancient times. The present paper aimed to quantify the effect of flax oil on engineering properties of aerial lime based mortar, which composition was inspired by mortars collected from several Czech and Austrian mosaics from the end of 19th and beginning of 20th century. The oil increased the air content of mortar, its porosity and water repelling ability, but reduced the rate of carbonation and strength. On the other hand, the mortar's frost resistance was significantly improved by flax oil. The optimum dosage of flax oil was determined to be 1% by weight of lime hydrate; at this dose the negative and positive effect of flax oil are balanced resulting in the best durability performance of the mortar.

Introduction

Mortars and plasters are fundamental construction materials since ancient times and thus they are widely characterized in order to understand their technology and determine proper conservation and restoration practices [1-3]. One of numerous application fields of mortars is production of mosaics, which dates back to Hellenistic Greece [4] and continued over the following periods [5-7]. In context of Central Europe, mosaics have become a popular decorative element in architectural design since the late 19th century. In the course of time the status of these modern mosaics (e.g. late 19th and 20th century) is shifting from contemporary artworks to historic monuments. Since they have not been considered "enough historic" so far, quite low attention has been drawn to them and their conservation. Knowledge of materials composition and properties of mosaics to be conserved is of crucial importance. The material substance of historic mosaic mortars varied a lot; as an example may be used results of research done on mosaic of the Grotta Buontalenti, Florence, from 16th century [7]: four types of mosaic mortar were identified; all of them contained calcitic binder but differed largely in binder aggregate ratio (from 1/3 to 2/1) and nature of aggregates – quartz sand, grinded marble and limestone and feldspar were identified. Another type of binder used frequently "Roman stucco" – mixture of lime, travertine powder, linseed oil and herbs [8]– or "cocciopesto" – mixture of lime and grinded red-clay ceramic providing a hydraulic binder [6, 9].

The present paper is based on current research performed on several mosaics found in Czech Republic and made between 1880-1910. Again range of binders (aerial lime, hydraulic lime, cocchiopesto) and aggregates (calcite, quartz) were identified; presence of flax oil was detected by FTIR in some samples [10]. The aim of this study is to evaluate engineering properties of mosaic mortar based on aerial lime, quartz sand, limestone flour and flax oil as variable admixture. The studied mortar composition was inspired by composition of the real mortars, but the used content of aggregates (two types of quartz sand, limestone flour) was not exactly the same as in authentic samples. The reason is that precise determination of aggregates amount in lime mortar is difficult due to limited amount of authentic material available for analysis and further, the specification of calcite-based filler in calcitic binder is complicated by its equal chemical nature (CaCO_3)

Experimental

The study of reproduced mosaic mortars was performed on set of mortars (Table 1) with varying content of flax seed oil. Lime hydrate (CL 90 S, by Lhoist Czech Republic) was used as binder. Two fractions of quartz sand (0-0.5 mm and 0.5-1 mm) and fine limestone flour (d_{50} 9.5 μm) were used as filler. Food-grade flax oil was dosed from 0.5 to 2% by mass of lime hydrate. The mixing procedure [11] consisted in mixing of all dry components; the oil was dispersed separately in small amount of dry mix and then this suspension was mixed with the rest of dry components and finally water was added.

Table 1. Composition of mortars with flax oil (in g)

	Lime	Sand 0-0.5	Sand 0.5-1	Limestone	Oil
MC	1000	750	250	500	0
M05	1000	750	250	500	5
M10	1000	750	250	500	10
M15	1000	750	250	500	15
M20	1000	750	250	500	20

The consistency and entrained air content of mortar was measured by standard procedures (EN 1015-3 and 7) by help of flow table test and pressure type air content meter. The specimens for hardened mortar testing were prepared by help of standard 40 x 40 x 160 mm moulds; the prisms were stored in laboratory condition and kept moist in order to prevent fast drying and to ensure the carbonation course. The compressive and flexural strength was determined after 14, 28 and 62 days of curing by MTS Criterion 43 machine. A set of auxiliary cubic specimens (without limestone flour and with reduced amount of sand) was prepared in order to monitor the influence of flax oil on the carbonation course. These auxiliary specimens were prepared and stored in same way as the “main” samples; the carbonation course was examined by X-ray diffraction (XRD) analysis. Samples were collected from the surface of specimens and stored, until the analysis, in sealed containers in desiccator. The XRD was performed by help of PANalytical Aeris diffractometer, equipped by $\text{Co}_{K\alpha}$ tube (40

kV, 7.5 mA). The diffractograms were collected between 8-85 ° 2 θ , step size 0.0027 °, counting time 97.92 s. The Soller slits (0.04 rad.) were used in incident and diffracted beam, divergence (0.5 °) and antiscatter (9 mm) slits were used in incident and diffracted beam respectively. The data were evaluated by help of Profex 3.12.1 software and quantified by Rietveld method. The rate of carbonation was evaluated in terms of degree of conversion (α) of portlandite (Ca(OH)₂) defined as Eq. 1 where w^0 is initial content of portlandite, w is actual content of portlandite in given time. The auxiliary samples contained 66.7% of lime hydrate in time zero (the used lime hydrated was stored properly and any spontaneous carbonation was not detected by XRD), the rest was quartz.

$$\alpha = 100 \frac{w^0 - w}{w^0} [\%] \quad (\text{Eq. 1})$$

$$i = At^{1/2} \quad (\text{Eq. 2})$$

The cured samples (62 days) were further subjected to pore size distribution measurement (mercury intrusion porosimetry by devices Pascal 140 and 440); the rate of liquid water transport in mortars was characterized by help of absorption coefficient A [$\text{kg m}^{-2} \text{s}^{-1/2}$] determined by help of automated imbibition experiment with laterally insulated cubic samples. In this experiment, the amount of soaked water i [kg m^{-2}] is measured in time t (Eq. 2). The frost resistance of mortars was tested by cycling of prismatic specimens according to temperature/time program shown in Figure 1.

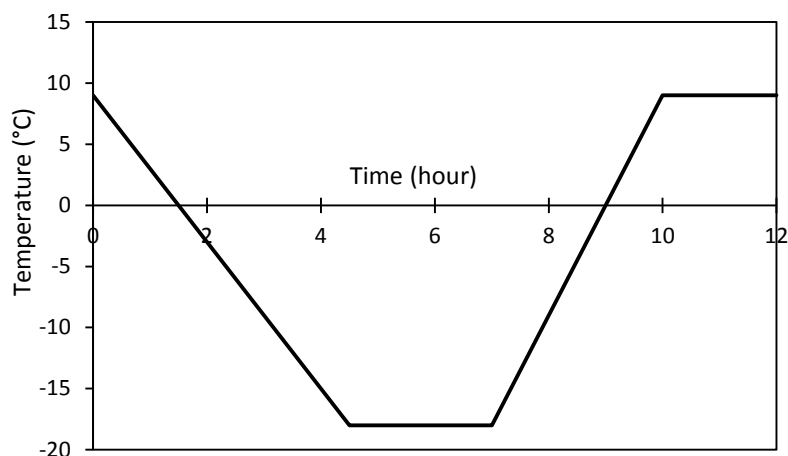


Figure 1. Time/temperature program for a single freeze/thaw cycle.

The samples were first let to soak by water for twice 24 hours (from both lateral sides, depth of water pool 1 cm), then sealed to a plastic bag and subjected to cycling; the samples were sealed for the whole test period in order to keep the moisture content constant. Such experimental arrangement was chosen in order to simulate real conditions – mosaics are frequently placed in exterior, subjected to the rain fall and capillary moisture elevation. The frost resistance of concrete is standardly tested by freezing-thawing of samples being repeatedly fully immersed in water. Mortars (not only the mosaic ones) are not in real

conditions fully saturated, but their moisture content is controlled by intake and outtake (evaporation) of water. The compressive and flexural strength were measured after 50, 100 and 150 cycles. The experiment was evaluated in term of index of frost resistance – i.e. ratio of flexural strength after given number of cycles and initial flexural strength of the material.

Results

The tested mortars differed in content of flax oil; its presence influenced already the properties of fresh mortar mix (Figure 2). The consistency of control mortar MC was 130 mm, the admixing of oil caused it to increase, i.e. the oil acted as plasticizer. Even a very low dosage (0.5%) of oil nearly doubled the entrained air content of the mortar; further higher doses did not have such distinct effect and air content remained constant (4%).

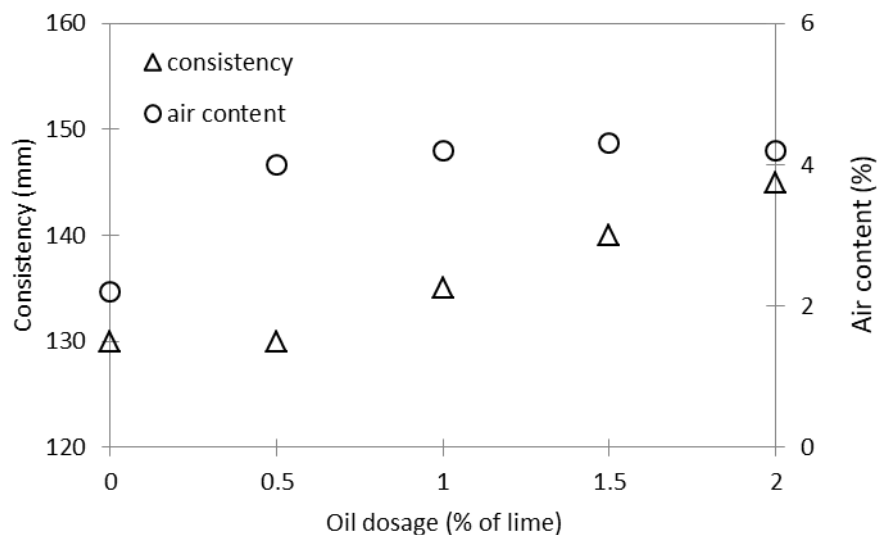


Figure 2. Influence of flax oil on consistency and air content of fresh mortar mix.

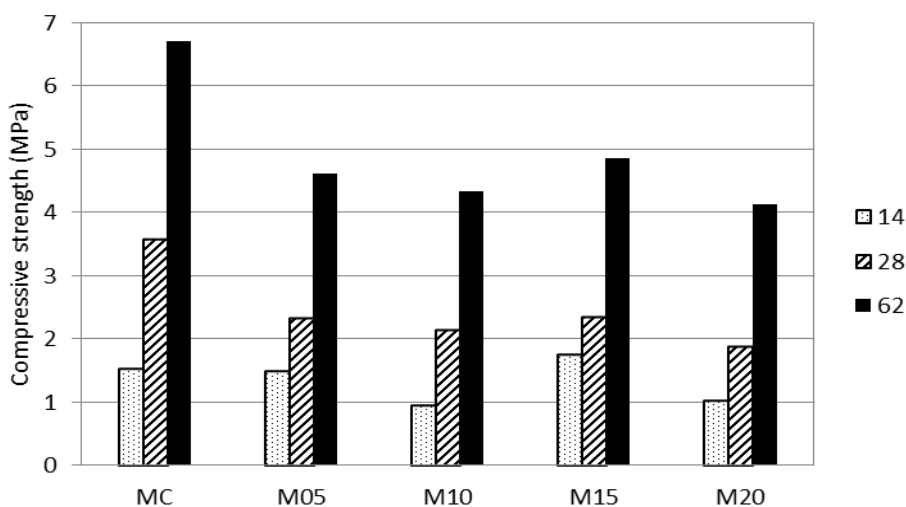


Figure 3. Evolution of compressive strength of mortars in time.

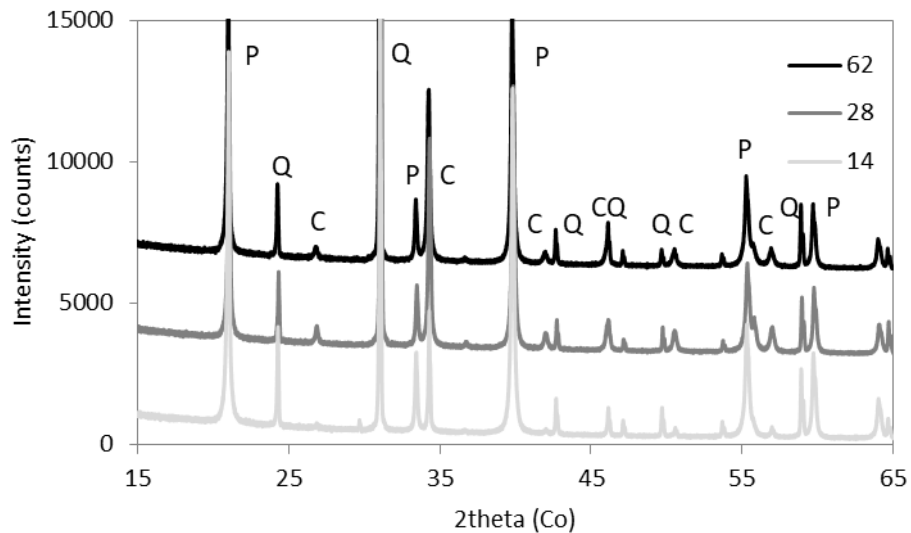


Figure 4. Diffractograms recorded in auxiliary mortars (without limestone flour as filler) containing 1% of flax oil. P = portlandite, Q = quartz, C = calcite.

The compressive strength of all mortars obviously grew in time (Figure 3). The presence of flax oil reduced the strength and its growth rate. Similarly to the entrained air content, the 0.5% oil dose had similar effect as 2%. The carbonation process (Eq. 3) is responsible for the strength growth in air-lime based systems. The conversion of portlandite (Ca(OH)_2) to calcite (CaCO_3) was observed by XRD; example of diffractograms recorded in mortar with 1% of flax oil (Figure 4) illustrates qualitatively the increase of calcite (C) diffractions and decrease of portlandite (P) diffractions. The Rietveld refinement of diffractograms was performed, providing the content of the present phases. The evolution of degree of portlandite conversion (Eq. 1) in time (Figure 5) revealed that the fastest portlandite conversion to calcite occurred in MC mortar, while the presence of oil gradually reduced the rate of carbonation.

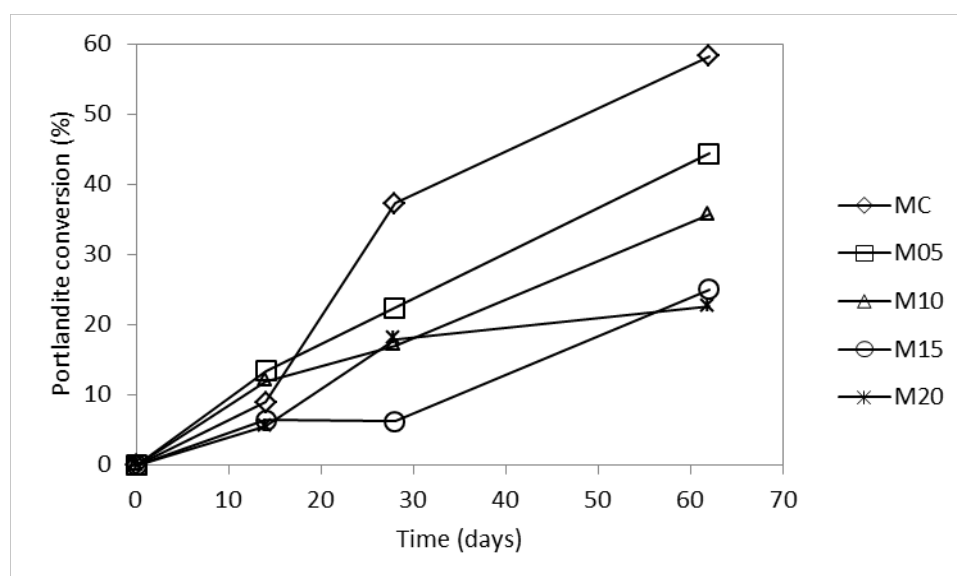


Figure 5. Degree of conversion of portlandite to calcite in time.

Pore size distribution is important factor controlling both mechanical and durability properties of (not only) mortars. The control mortar reached total porosity 38.5% (Figure 6.), the increasing dose of flax oil gradually increased total porosity up to 45%. Moreover, the presence of oil doubled the average pore size (from 0.25 μm to 0.54 μm).

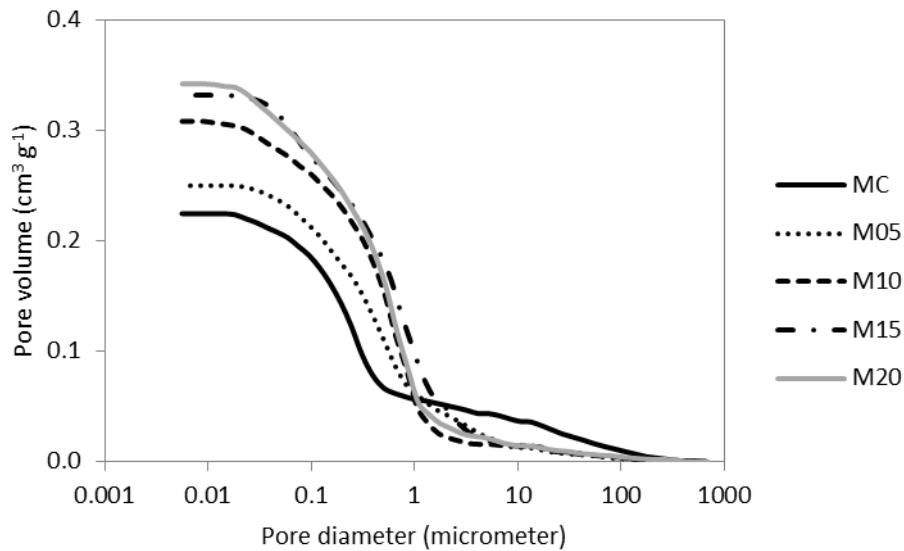


Figure 6. Pore size distribution of flax oil containing mortars.

Finally, the oil somewhat reduced the volume of pores 5-100 μm . Rate of liquid water transport by capillary action (Table 2.) was expressed by water absorption coefficient (Table 2.); the flax oil reduced the water absorption coefficient by nearly two orders of magnitude. This measurement clearly confirmed the water repelling ability of flax oil.

Table 2. Water absorption coefficient of mortars.

Material	A [$\text{kg}/\text{m}^2\text{s}^{1/2}$]
MC	0.0981
M05	0.0607
M10	0.0217
M15	0.00309
M20	0.00224

The freezing/thawing resistance (Figure 7.) of control mortar was very poor, even 50 cycles caused significant reduction of strength. The best performance featured mixture M10 with 1% of flax oil – the strength loss was rather low and nearly independent on number of cycles.

Discussion

The obtained results provided a better insight on flax oil performance in aerial lime based mortar. The flax oil increased the flowability and entrained air content of mortar. The positive effect of an oil on plasticity is something what one would expect since its generally

lubricating nature, but triglycerides are not used nor studied as concrete/mortar plasticizers due to detrimental effect on strength [12]. Such negative effect on strength, and its growth

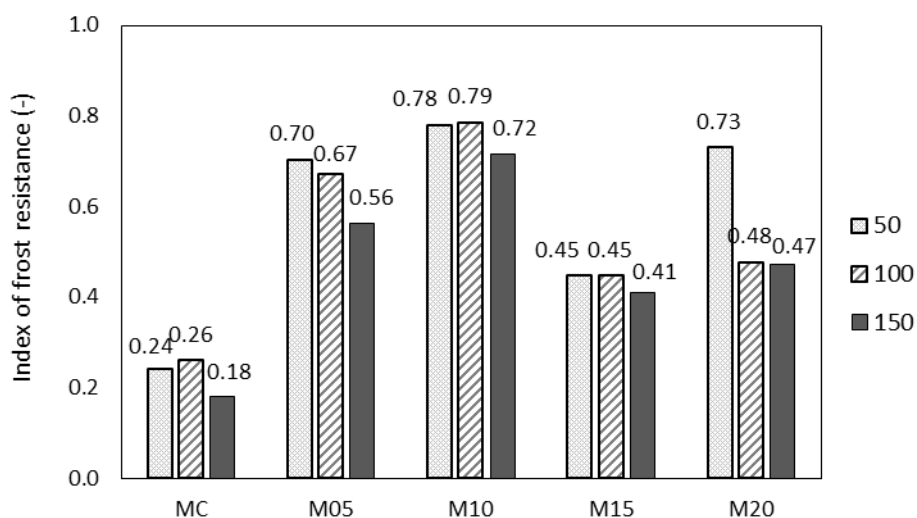


Figure 7. Index of frost resistance (ratio of final and initial flexural strength) of mortars after 50, 100 and 150 freezing cycles.

rate, was observed also in this lime-based mortar. There could be two reasons for the observed strength reduction – firstly the oil increased the porosity and secondly, its presence reduced the rate of carbonation. The lime carbonation is known to be positively dependent on the relative humidity [13], it indicates that carbonation is proceeding in solution present in pores of material. The results of water absorption test (Table 2) indicated that flax oil is very efficient water repellent, thus the reduced rate of carbonation is due to lower content of liquid water in the material. Even though the negative effect of oil on the rate of carbonation was dependent on the oil dose, the strength of all oil-containing mortars (M05 to M20) was practically equal. It indicates that their lower strength was not caused just by slower carbonation, but the presence of oil affects negatively the particles consolidation in the material.

The ability of flax oil to reduce the water absorption is comparable with zinc stearate, commercially used water repellent [14]. The porosity increase due to the oil had two reasons (or two contributing effects) – content of entrained air was doubled by oil (2 to 4%) and also the amount of sub-micron pores, detected by mercury intrusion porosimetry (MIP), was increased by oil MIP porosity (38.5 to 45%). The higher air content was observed in similar system with 1.5% of flax oil [15]; likewise common water repellents (stearates, oleates) are increasing the air content [16]. Opposite, olive oil was reported to reduce significantly the MIP porosity [17]. Besides the higher porosity, oil caused also certain enlargement of pores (Figure 6), what could improve the rate of water transport [18]; nevertheless this possible effect was outweighed by the oil-water repellent effect. Both reduced water absorption and higher air content are responsible for outstanding positive effect of flax oil on frost resistance of mortars; the optimum content was identified as 1% by weight of lime hydrate –

this dosage has sufficient water repellent and air-entraining ability, but the strength reduction due to slower carbonation and higher porosity, is not critical yet.

Conclusions

The engineering properties of reproduced mosaic mortars, based on aerial lime, were highly dependent on flax oil dosage. This admixture increased the air content of the mortar and also its flowability. The rate of carbonation was negatively influenced by oil due to its water-repellence; the liquid water presence in pores of lime-based material is crucial for its carbonation. The oil also increased the porosity of mortars, what again contributed to the lower strength. Nevertheless these negative impacts were outweighed by the mentioned excellent water repellent ability of flax oil. This property is responsible for significant improvement of the frost resistance of mortars. The optimum dosage of flax oil was determined to be 1% by weight of lime hydrate; at this dose the negative and positive effect of flax oil are balanced resulting to good performance of the mortar.

Acknowledgement

The work has been supported by Czech Science Foundation project Nr. 18-13525S “Modern mosaic mortars in a microscope – methods for their materials characterization and degradation studies”.

References

1. Elsen J (2006) Microscopy of historic mortars—a review. *Cem Conc Res.* doi:10.1016/j.cemconres.2005.12.006
2. Yaseen IAB, Al-Amoush H, Al-Farajat M, Mayyas A (2013) Petrography and mineralogy of Roman mortars from buildings of the ancient city of Jerash, Jordan. *Con Build Mat.* doi:10.1016/j.conbuildmat.2012.08.022
3. Leone G, DeVita A, Magnani A, Rossi C (2016) Characterization of archaeological mortars from Herculaneum. *Thermochim Acta.* doi: 10.1016/j.tca.2015.12.003
4. Guimiersorbets AM, Nenna MD (1992) The use of glass, faience and painting in the mosaics of Delos. *Bull Correspondance Hellenique.* doi:10.3406/bch.1992.4669
5. Puertas F, Blancivarela MT, Palomo A, Ortega-Calvo JJ, Arino X, Saizjimenez C. Decay of Roman and repair mortars in mosaics from Italica, Spain (1994) *Sci Tot Environ.* doi:10.1016/0048-9697(94)90109-0
6. Izzo F, Arizzi A, Cappelletti P, Cultrone G, De Bonis A, Germinario C, Graziano SF, Grifa C, Guarino V, Mercurio M, Morra V, Langella V (2016) The art of building in the Roman period (89 B.C. – 79 A.D.): Mortars, plasters and mosaic floors from ancient Stabiae (Naples, Italy). *Con Build Mat.* doi:10.1016/j.conbuildmat.2016.04.101

7. Costagliola P, Baldi G, Cipriani C, Pecchioni E, Buccianti A (2000) Mineralogical and chemical characterisation of the Medicean glass mosaic tesserae and mortars of the Grotta del Buontalenti, Giardino di Boboli, Florence, Italy. *J Cult Heritage*. doi:10.1016/S1296-2074(00)01085-2
8. Fiori C, Vandini M, Prati S, Chiavari G. Vaterite in the mortars of a mosaic in the Saint Peter basilica, Vatican (Rome) (2009) *J Cult Heritage*. doi:10.1016/j.culher.2008.07.011
9. Perná I, Hanzlíček T, Kracík Štorkánová M (2014) Characterization of historic mosaic at Pfeiffer-Kral sepiulcher, jablonec nad Nisou: a study of the mortar and tesserae origin. *Ceramics Silikáty* 58:308-313
10. Bauerová P., Reiterman P, Pavlíková M., Kracík Štorkánová M, Keppert M (2019) Fresh state properties of lime mortars with flax oil admixture. *Acta Polytechnica CTU Proceedings* Vol. 21. In Press
11. Nunes C., Slížková Z (2014) Hydrophobic lime based mortars with linseed oil: Characterization and durability assessment. *Cem Conc Res*. doi:10.1016/j.cemconres.2014.03.011
12. Hamad BS, Rteil AA, El-Fadel M (2003) Effect of used engine oil on properties of fresh and hardened concrete. *Con Build Mat*. doi:10.1016/S0950-0618(03)00002-3
13. Pavlík V, Užáková M (2016) Effect of curing conditions on the properties of lime, lime–metakaolin and lime–zeolite mortars. *Con Build Mat*. doi:10.1016/j.conbuildmat.2015.10.128
14. Vejmelková E, Koňáková D, Čáchová M, Keppert M, Černý R (2012) Effect of hydrophobization on the properties of lime–metakaolin plasters. *Con Build Mat*. doi:10.1016/j.conbuildmat.2012.07.097
15. Nunes C, Slížková Z (2016) Freezing and thawing resistance of aerial lime mortar with metakaolin and a traditional water-repellent admixture. *Con Build Mat*. doi:10.1016/j.conbuildmat.2016.04.029
16. Izaguirre A, Lanas J, Álvarez JI (2010) Ageing of lime mortars with admixtures: Durability and strength assessment. *Cem Conc Res*. doi:10.1016/j.cemconres.2010.02.013
17. Ventolà L, Vendrell M, Giraldez P, Merino L (2011) Traditional organic additives improve lime mortars: New old materials for restoration and building natural stone fabrics. *Con Build Mat*. doi:10.1016/j.conbuildmat.2011.03.020
18. Keppert M, Čáchová M, Koňáková D (2015) Transport of liquids in porous rocks. *Mat Sci Forum*. doi: 10.4028/www.scientific.net/MSF.824.117

Preliminary results on the use of ammonium phosphate solutions for the consolidation of lime-based mortars

Enrico Sassoni¹, Cesare Pizzigatti¹, Elisa Franzoni¹

(1) Department of Civil, Chemical, Environmental & Materials Engineering (DICAM), University of Bologna, Italy, enrico.sassoni2@unibo.it, cesare.pizzigatti2@unibo.it, elisa.franzoni@unibo.it

Abstract

In this study, a preliminary evaluation of the effectiveness of aqueous solutions of diammonium hydrogen phosphate (DAP) for the consolidation of lime-based mortars is reported. Four types of mortars were considered: 2 lime-based mortars (containing either siliceous or calcareous aggregates), 1 lime-based mortar also containing brick powder as a pozzolanic addition (so-called “*cocciopesto*” mortar) and 1 mortar based on natural hydraulic lime. Two different formulations of the DAP solution were considered, differing in terms of DAP concentration, CaCl₂ addition as a calcium source and ethanol addition to boost formation of calcium phosphate (CaP) phases. First, for the various types of mortar, the nature and the morphology of the new CaP phases were investigated by FT-IR and SEM. Then, the mechanical benefit resulting from the new CaP was evaluated, in terms of increase in dynamic elastic modulus and compressive strength. The microstructural compatibility of the treatments was also evaluated, by determining the alterations in pore size distribution. The results of the study indicate that new CaP phases are formed after 24 hours for both DAP concentrations, the amount of new phases and the mechanical improvement being higher for the more concentrated solution. In no case did dramatic pore occlusion and alteration in the pore size distribution take place, which allows expecting no dramatic alteration in the mortar ability to exchange water and water vapour with the environment. The more concentrated solution caused some visible colour change in the case of mortars not originally white (“*cocciopesto*” and NHL mortars), which makes the use of less concentrated solutions advisable on those substrates.

Introduction

This study reports some preliminary results on the use of ammonium phosphate solutions for the consolidation of lime-based mortars.

Research on innovative consolidants for lime mortars is needed, because to find a treatment that is effective, compatible and durable at the same time is still an open challenge [1]. In fact, lime-based consolidants are compatible with lime-based mortars, but their effectiveness is not always as high as hoped: in the case of lime-based mortars consolidated by nanolimes, promising mechanical strengthening has been reported [2,3], but research is still in progress to increase the nanolime penetration depth into the porous substrate [3].

Silicate consolidants are effective when applied onto substrates containing siliceous fractions, but their performance is lower on mortars made of lime binder and calcareous aggregate. Polymeric consolidants have shown many durability issues in the past, so they should be selected with care.

The idea to use ammonium phosphate solutions for consolidation of lime-based mortars came from the very encouraging results obtained in the last few years on their use for consolidation of calcareous stones, especially marble [4,5]. Indeed, when applied onto carbonate stones, ammonium phosphate solutions have shown a significant ability to bond loose grains, thus improving mechanical properties, without significantly altering the stone colour, water and water vapour transport properties [5]. This is possible because the reaction between the ammonium phosphate solution (providing PO_4^{3-} ions) and the substrate (providing Ca^{2+} ions) produces calcium phosphates (CaP), ideally hydroxyapatite (HAP), inside the pores [4]. The grain boundaries are bonded by the newly formed HAP, even though pores are not occluded by the reaction product.

To evaluate the suitability of using ammonium phosphate solutions also for the consolidation of lime-based mortars, in this study some preliminary tests were performed. Specimens of four different types of mortars were produced, differing in terms of binder and aggregate. After curing, the samples were treated by two different formulations of the phosphate solution, applied for increasing time. The newly formed phases were analysed by FT-IR and SEM/EDS and the changes in mechanical properties, open porosity and pore size distribution were evaluated.

Materials and methods

Samples

Four types of mortar were produced: (1) air lime + siliceous aggregate (quartz), (2) air lime + calcareous aggregate (calcite), (3) air lime + brick dust (*“cocciopesto”*) + siliceous aggregate, (4) natural hydraulic lime + siliceous aggregate. For each type, the label and formulation are reported in Table 1.

Table 1. Mix design of the four different mortars (parts by volume)

Mortar	Lime	NHL	Cocciopesto	Siliceous sand	Calcareous sand	Water
LIME+SIL	1	-	-	2	-	1
LIME+CALC	1	-	-	-	2	1
COCCIO	1	-	1	2	-	1
NHL	-	1	-	3	-	1

Prismatic specimens ($4 \times 4 \times 16 \text{ cm}^3$) were produced, demoulded after 1 week and then cured in laboratory conditions ($\text{RH} = 50 \pm 5\%$, $T = 21 \pm 2 \text{ }^\circ\text{C}$) for 7 years before testing. For preliminary tests aimed at evaluating the nature of the new CaP phases formed after

treatment, for each condition two samples with size approximately $2 \times 2 \times 1 \text{ cm}^3$ were obtained from the prisms by sawing.

Treatments

Two formulations of the phosphate treatment were considered, based on previous results obtained on marble [5]: (1) aqueous solution containing 0.1 M DAP + 0.1 mM CaCl_2 in 30 vol% ethanol (labelled “0.1 M DAP”); (2) aqueous solution containing 2 M DAP + 2 mM CaCl_2 in 10 vol% ethanol (labelled “2 M DAP”). In the case of the “COCCIO” samples, not enough specimens were available for testing both solutions, so only the 2 M DAP formulation was tested.

All the reagents were purchased from Sigma-Aldrich. The solutions were applied by poultice (cellulose pulp:solution mass ratio of 1:4) onto the $4 \times 4 \times 16 \text{ cm}^3$ prismatic specimens and the $2 \times 2 \times 1 \text{ cm}^3$ samples. In both cases, samples were covered with a sheet of Japanese paper to avoid sticking and a 1 cm-thick layer of poultice imbued with the solutions, then samples were wrapped with a plastic film to prevent evaporation and left to react for 24 hours. Afterwards, samples were unwrapped, rinsed with deionized water and left to dry in laboratory conditions. Samples were then tested as described in the following.

Characterization

To determine the nature of the new CaP phases, one of the $2 \times 2 \times 1 \text{ cm}^3$ samples was manually ground to separate the binder and the aggregate. Then, the binder (i.e., the finer fraction) was analysed by Fourier Transform Infrared Spectrometry (FT-IR), using a Perkin Elmer Spectrum One spectrometer.

To evaluate the morphology of the new CaP phases, the other $2 \times 2 \times 1 \text{ cm}^3$ sample was analysed by scanning electron microscopy (SEM), using a Philips XL20 SEM. The samples were made conductive by preliminary coating with aluminium.

To assess the increase in mechanical properties after treatment, the dynamic elastic modulus (E_d) was determined on the prismatic samples, before and after treatment. E_d was calculated according to the formula $E_d = \rho \times \text{UPV}^2$, where ρ is the density and UPV is the ultrasonic pulse velocity. A Matest instrument with 55 kHz transducers was used to measure the UPV, adopting the transmission method.

Mechanical consolidation was also assessed in terms of increase in compressive strength (R_c), determined by subjecting the prismatic specimens to compressive test, according to EN 196-1 [6]. An Amsler-Wolpert loading machine was used.

To evaluate the alteration in pore size distribution caused by new CaP phases, mercury intrusion porosimetry (MIP) was performed on samples obtained by chisel from the prisms subjected to mechanical testing. Samples for MIP included one of the original external surfaces of the prisms, so that alterations in pore size distribution (expectedly more

pronounced near the treated surface) would be more likely to be detected. A Porosimeter 2000 Carlo Erba with Fisons Macropore Unit 120 was used.

Results and discussion

For all types of mortar, formation of new CaP phases after reaction for 24 hours is confirmed by SEM observation (Figure 1) and FT-IR analysis (Figure 2).

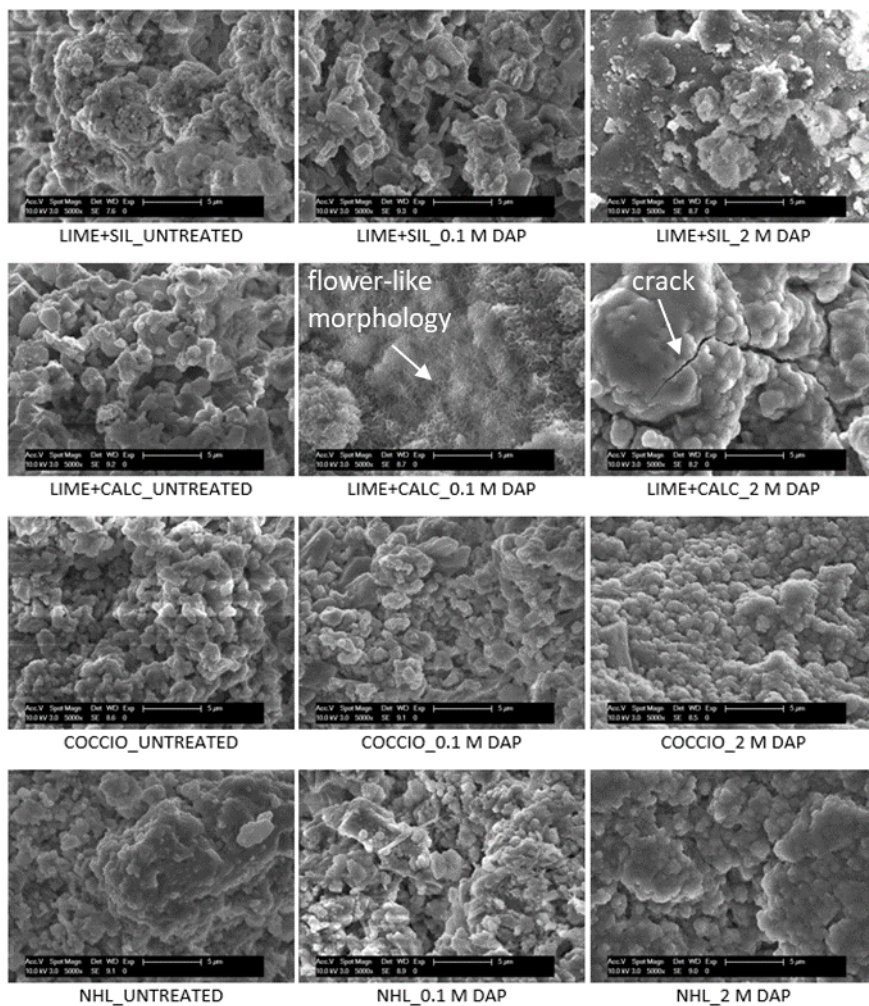


Figure 1. SEM images of untreated and treated samples (scale bar = 5 µm).

In Figure 1, formation of new CaP phases is clearly visible in the case of the LIME+CALC sample, where a new flower-like morphology is present after treatment with the less concentrated solution and a cracked coating is formed after treatment with the more concentrated one. In the other samples, the formation of new CaP is less evident from SEM images, but still confirmed by the FT-IR spectra (Figure 2). In fact, new bands are present, which are compatible with formation of HAP (having bands at 1031, 604, 563 cm^{-1} [7]), even though formation of octacalcium phosphate (OCP, having bands at 1038, 602, 560 cm^{-1} [7]) cannot be completely excluded. Being much less soluble than calcite, formation of OCP is anyway not undesired [5]. In all the samples, formation of new CaP phases is also indicated by the presence of P in the SEM-EDS spectra (not reported for brevity's sake).

In all cases, new phases formation was more pronounced in samples treated with the more concentrated solution: in Figure 2, the zone where HAP bands are expected is highlighted in red; in the case of the more concentrated solution, new bands in this zone are clearly visible, while in the case of the less concentrated solution new bands are much less pronounced.

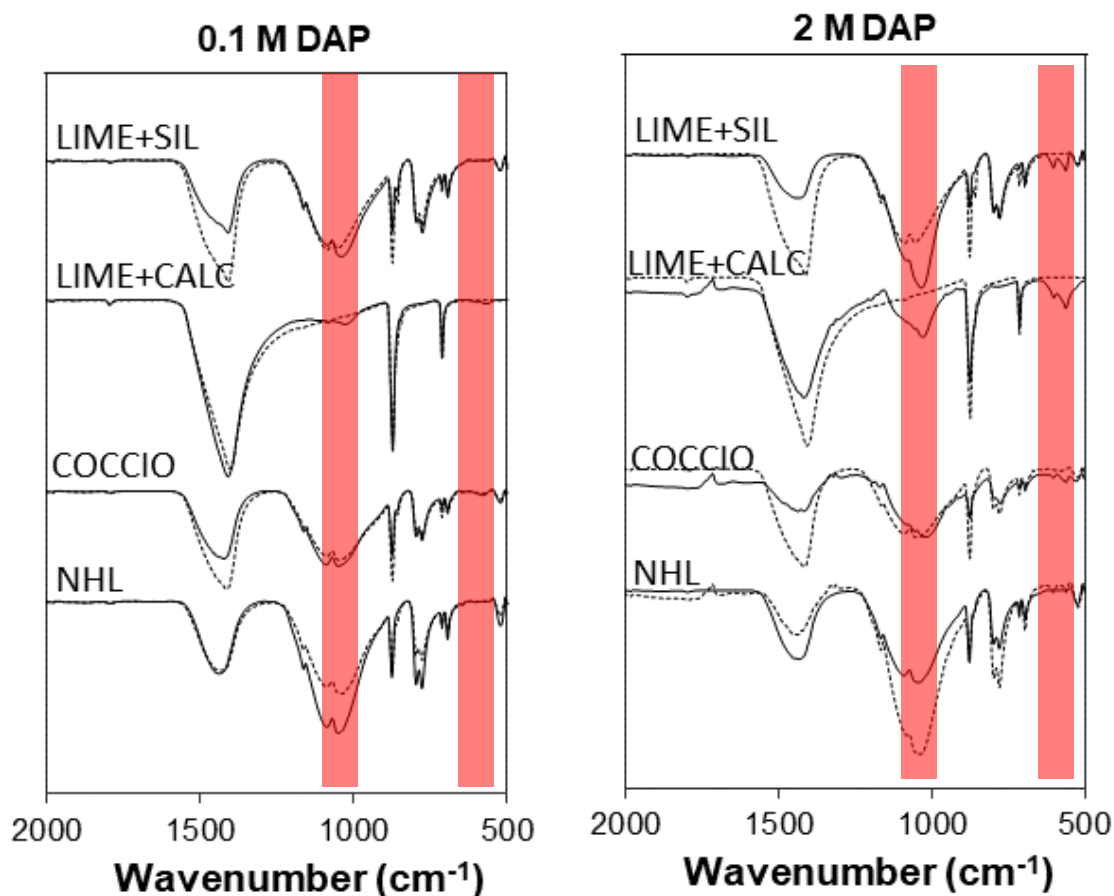


Figure 2. FT-IR spectra of untreated samples (dashed lines) and samples treated for 24 hours (solid lines). The position where HAP bands are expected is highlighted in red.

As a result of new CaP formation, significant mechanical improvement was found after treatment, as reported in Table 2 for the less concentrated solution (0.1 M DAP) and in Table 3 for the more concentrated one (2 M DAP). This was possible because the newly formed CaP phases acted as bridges, improving the bonding between the aggregates in the mortar. For both formulations, the mechanical improvement was higher for the two mortars based on air lime (LIME+SIL and LIME+CALC), compared to the “*cocciopesto*” and NHL mortars. This is thought to be a consequence of the fact that, in the former mortars, the binder is calcite (highly reactive to form HAP upon reaction with the phosphate solutions), while in the latter case the binding fraction is mostly calcium silicate hydrates. No major difference was found between air lime mortars containing either siliceous or calcareous aggregate, thus confirming that conversion of the binding fraction plays the most important role. This is thought to be a consequence of the different size and reactivity of calcite crystals in the binding fraction (smaller crystals, higher specific surface area, higher reactivity) and in the aggregate fraction (bigger crystals, lower specific surface area, lower reactivity), so that the

difference between the LIME+SIL and LIME+CALC becomes secondary. Further tests are in progress to fully elucidate this point. In all cases, the good mechanical improvement was made possible by the high penetration depth of the consolidating solutions. Indeed, preliminary tests indicated that both consolidating solutions are able to saturate by capillarity samples with 4 cm-height in about 1 hour.

Table 2. Mechanical improvement after consolidation with a solution containing 0.1 M DAP + 0.1 mM CaCl₂ in 30 vol% ethanol

Mortar	Untreated		Treated		Improvement	
	E _d (GPa)	R _c (MPa)	E _d (GPa)	R _c (MPa)	ΔE _d (%)	ΔR _c (%)
LIME+SIL	5.6	2.2	6.3	2.6	+12%	+16%
LIME+CALC	5.9	1.9	6.4	2.2	+8%	+16%
COCCIO	-	-	-	-	-	-
NHL	3.7	1.6	3.8	1.5	+2%	0%

Table 3. Mechanical improvement after consolidation with a solution containing 2 M DAP + 2 mM CaCl₂ in 10 vol% ethanol

Mortar	Untreated		Treated		Improvement	
	E _d (GPa)	R _c (MPa)	E _d (GPa)	R _c (MPa)	ΔE _d (%)	ΔR _c (%)
LIME+SIL	5.6	2.2	9.3	5.5	+66%	+150%
LIME+CALC	5.9	1.9	9.4	4.2	+59%	+121%
COCCIO	7.2	3.8	9.3	7.1	+29%	+87%
NHL	3.7	1.6	5.8	2.8	+57%	+75%

Table 4. Variations in open porosity (OP) and average pore radius (r_{av}) after treatment.

Mortar	Untreated		0.1 M DAP		2 M DAP	
	OP (%)	r _{av} (μm)	OP (%)	r _{av} (μm)	OP (%)	r _{av} (μm)
LIME+SIL	24.7	1.36	31.8	1.48	25.7	1.36
LIME+CALC	26.2	1.04	27.7	7.60	25.2	6.95
COCCIO	23.6	6.72	-	-	24.7	7.57
NHL	21.6	7.72	20.3	6.99	23.1	7.30

Notwithstanding the increase in cohesion and compressive strength, in no case did dramatic pore occlusion take place. As reported in Table 4, some reduction in total open porosity and average pore radius occurred after treatment, but in all cases the changes were minor (some variability is intrinsic to the heterogeneity of the mortar samples). The lack of dramatic alterations in pore size distribution can be considered as a positive outcome of the treatment, because strong alterations in the pore system, and consequently in the water and water vapour transport properties, might have negative consequences on the durability of the treated mortar [8]. Because no dramatic increase in the amount of smaller pores was found after treatment, no increase in the risk connected to freeze-thaw and salt crystallization cycles is expected. However, specific durability tests should be carried out to confirm this.

Finally, it should be mentioned that the solution with the lower concentration did not cause any visible colour change in any of the treated specimens. On the contrary, in the case of the solution with the higher concentration, no visible change was observed in the lime-based specimens (originally white), but some whitening occurred in the case of the lime-brick dust mortar (originally pink) and in the case of the NHL-based mortar (originally grey).

Conclusions

In the present study some preliminary results were reported on the use of ammonium phosphate solutions for the consolidation of lime-based mortars. Based on the obtained results, the following conclusions can be derived:

- in all the investigated mortars (air lime + siliceous aggregate, air lime + calcareous aggregate, air lime + brick dust + siliceous aggregate, natural hydraulic lime + siliceous aggregate), formation of new calcium phosphate phases was found after treatment with ammonium phosphate solutions for 24 hours.
- the presence of new CaP phases was found in the mortars treated with both solutions, their amount being higher for the more concentrated solution (2 M DAP + 2 mM CaCl₂ in 10 vol% ethanol), compared to the less concentrated one (0.1 M DAP + 0.1 mM CaCl₂ in 30 vol% ethanol), as expected. Clear but limited mechanical improvement was provided by the less concentrated solution, while the more concentrated one caused very significant strengthening, especially of the air lime-based mortars (independently of the composition of the aggregate).
- In no case did dramatic pore occlusion and alteration in the pore size distribution take place, owing to the low thickness of the CaP layer deposited inside the pore walls, as suggested by the SEM observation. This allows expecting no dramatic alteration in the mortar ability to exchange water and water vapour with the environment.
- The more concentrated solution caused some visible colour change in the case of mortars not originally white (COCCIO and NHL mortars), so on those substrates the use of less concentrated phosphate solutions is advisable.

Acknowledgments

M.Eng Sofia Fantini is gratefully acknowledged for collaboration to experimental tests.

References

1. Toniolo L, Paradisi A, Goidanich S, Pennati G (2011) Mechanical behaviour of lime based mortars after surface consolidation. *Constr Building Mater* 25:1553–1559
2. Borsoi G, Lubelli B, van Hees R, Veiga R, Santos A (2017) Evaluation of the effectiveness and compatibility of nanolime. *Constr Building Mater* 142:385–394

3. Rodriguez-Navarro C, Ruiz-Agudo E (2018) Nanolimes: from synthesis to application Pure Appl. Chem. 90:523–550
4. Sassoni E, Naidu S, Scherer GW (2011) The use of hydroxyapatite as a new inorganic consolidant for damaged carbonate stones. J Cultur Herit 12:346-355
5. Sassoni E (2018) Hydroxyapatite and Other Calcium Phosphates for the Conservation of Cultural Heritage: A Review. Materials 11 (2018) 557
6. European standard EN 196-1, Methods of testing cement - Part 1: Determination of strength, 2005
7. Karampas IA, Kontoyannis CG (2013) Characterization of calcium phosphates mixtures. Vib Spectrosc 64:126– 133
8. Scherer GW, Wheeler GS (2009) Silicate consolidants for stone. Key Eng Mater 391:1-25

Comparative study of ethyl silicate versus acrylic resin consolidation of wall painting with high water and salts contents: a case study at the Chapter Hall of Chartres cathedral

Laura Normand^{1,2}, Stéphanie Duchêne^{1,2}, Véronique Vergès-Belmin^{1,2}, Claire Dandrel³,

David Giovannacci^{1,2}, Witold Nowik^{1,2}

(1) Laboratoire de Recherche des Monuments Historiques (LRMH), Ministère de la Culture, 29 rue de Paris, 77420 Champs-sur-Marne, France. laura.normand.ext@culture.gouv.fr, stephanie.duchene@culture.gouv.fr, veronique.verges-belmin@culture.gouv.fr, david.giovannacci@culture.gouv.fr, witold.nowik@culture.gouv.fr

(2) Sorbonne Universités, Centre de Recherche sur la Conservation (CRC, USR 3224), MNHN, Ministère de la Culture, CNRS; CP21, 36 rue Geoffroy-Saint-Hilaire, 75005 Paris, France.

(3) Conservator-restorer of wall painting, 5 rue A. Fleming, 92260 Fontenay-aux-Roses, France. claire.dandrel@gmail.com

Abstract

The consolidation of wall paintings is particularly challenging when high contents of water and hygroscopic salts contaminate the masonry. Many wall paintings are in this situation, but only a few of them offer the possibility of easy access and long-term monitoring. The 14th century wall painting located on the east wall of the Chapter Hall of Chartres cathedral (France) is one of these. The aim of this study was to assess the compatibility, efficacy and long-term behaviour of ethyl silicate Silres BS OH 100 and acrylic resin Primal E330S for the consolidation of such wall paintings. Observations and tests were performed before, three and nine months after the treatments. Temperature and relative humidity were monitored next to the tested areas during the whole period of the study. Nine months after application, ethyl silicate did not show any measurable consolidating effect and kept its initial hydrophobicity. On the other hand, despite the apparition of some rare and scarce white spots, a significant consolidating effect was achieved with the acrylic resin without considerable changes of water absorption and repellency.

Introduction

The conservation of wall paintings is a complex operation, which becomes challenging when high water and salts contents are present in the masonry, especially when combined with uncontrolled climatic conditions; variations in temperature and humidity can produce cycles of crystallisation/dissolution of hygroscopic salts and generate stresses leading to substrate alteration [1,2]. On wall paintings, these stresses induce a loss of cohesion and adherence of the paint layers [3,4]. When climate conditions cannot be stabilised and desalination of paintings is not possible, a cohesion increase can be achieved by consolidation using various dedicated products. Unfortunately, many consolidation treatments have resulted in accelerated deterioration of paintings on over a short or longer term [5,6].

Consolidating products used in wall painting conservation are either organic, organo-mineral or inorganic. We will not focus here on the inorganic products such as: nanolimes, ammonium oxalate and di-ammonium phosphate or barium hydroxide, which have been intensively studied in the last decade [7,8]. In this study, we will focus our attention on organic and organo-mineral products.

Synthetic acrylic or vinyl polymer adhesives have been widely used since the 1960s to increase superficial cohesion and provide a protective coating [9,10]. According to several authors, the main problems in the use of organic products are their incompatibility with lime-based painting leading to damage and their significant contribution to the alteration of capillary transport and wettability [10,11]. Moreover, the shrinkage of the polymeric film during its ageing may create cracks, loss of cohesion and detachment of the paint layer [7,8]. Aesthetic changes such as yellowing have also been observed [12,13]. In the context of salt contamination, the presence of the polymeric film may induce salt crystallisation in deeper layers, leading in some cases to the detachment of the paint layer [7].

Organo-mineral products, such as tetraethoxysilanes, are an alternative to synthetic polymers. The hydrolysis of these silicon-based products induces the formation of an amorphous silica gel [15,16]. The characteristics and stability of this gel are correlated both with the conditions of the solvent evaporation process [17], which can be disturbed by temperature and relative humidity conditions [18], and with the type and amount of catalyst [19]. The main drawbacks to the use of such products are: the formation of a rigid and brittle network [18,20], an excessive modification of capillary transport, an insufficient penetration depth and excessive colour changes [6].

As far as we know, no publication has been focused on the consolidation of both wet and salt contaminated *affresco* wall paintings *in-situ* in western countries. Wall paintings contaminated with salts have apparently been successfully consolidated in sub-tropical conditions [7] and the consolidation of salt-bearing laboratory samples conditioned under various relative humidity conditions has been tested [21]. The present article is a contribution to research and understanding on consolidation performed on *affresco* powdery wall paintings with high water and salt content.

Context

The Chapter Hall and its paintings

The Chapter Hall of Chartres cathedral (France) is located behind the apse of the monument, at ground level, below the Saint-Piat chapel (Figure 1). It is a rectangular room with vault arches eight metres high and stained-glass windows. The walls were decorated in the 14th century with paintings covering the walls starting from two meters above the floor up to the top of the arches. Wall paintings have been covered with several whitewashes over time. The painting was done with the *affresco* technique, using lime with pigments such as

yellow, red and brown ochre, carbon black and azurite [22-24]. The Chapter Hall is currently closed to visitors, but a project for a permanent exhibition is in preparation.

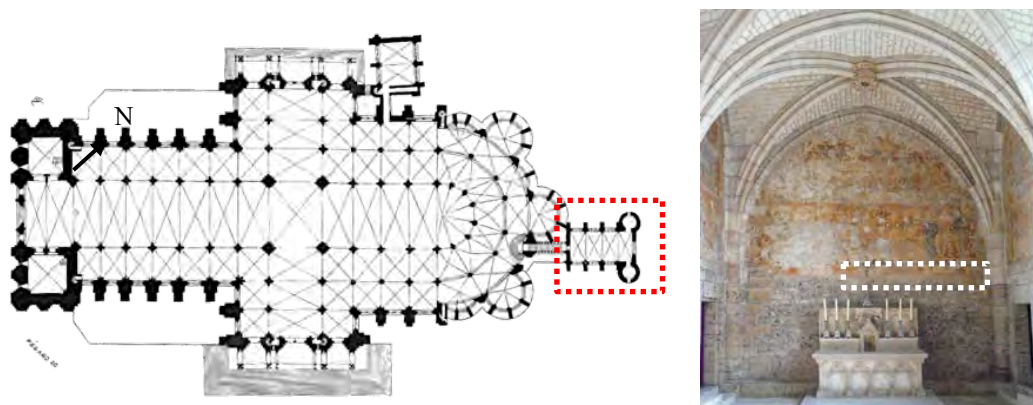


Figure 1. Floor plan of the Chartres cathedral with location of the Chapter Hall in the red dotted rectangle (on the left), and view of the east wall 14th century painting with test area in the white dotted rectangle (on the right)

East wall

On the east wall, historiated and religious decor is incomplete (Figure1), but some scenes and figures are still visible, such as Christ in the act of blessing surrounded by angels [25]. The crystallisation of gypsum produced lifting, flaking and powdering of the paint layer. Prior to the study, whitewashes and salt crystallisations were mechanically removed with a scalpel, and the paint layer was flattened and stuck to the mortar by a brush application of isopropanol through Japanese paper. Up to now, the paint layer has remained flat but still powdery, but no salt crystallisation has reappeared.

The long term conservation of these wall paintings is very uncertain because a large amount of water and salt are present in the masonry, particularly on the east wall. Indeed, water content reaches high values from 25 to 38% in mass, according to measurements performed two years before our study, in 2015 [26]. The salt concentrations expressed as chlorides (0.13% to 0.65%), nitrates (0.69% to 5.49%) and sulphates (0.11% to 15.67%) were far higher than accepted limit values, $\leq 0.1\%$, $\leq 0.5\%$ and $\leq 0.1\%$ respectively [27]. The wetness of the east wall appears to be due to both: capillary rise for the lower part of the wall and the presence of hygroscopic salts, probably introduced by previous seepage, for the rest of the wall [28]. In these conditions, any microclimate changes or potential variation in water uptake may accelerate the degradation of the wall paintings. The future opening of the hall to visitors will certainly change the environmental conditions, raising the risk of salt crystallisation and hence accelerating the destruction of the remaining paint layer. In order to avoid or at least to slow down the damage process, consolidation of the wall painting had to be considered.

Materials

Consolidating products and their application

The study initially included seven consolidating products which can be used for consolidating wall paintings [29]: two nano-limes (CaLoSil IP5 and CaLoSil Grey), a mixture of nano-lime and nano-barium hydroxide, an ethyl silicate (Silres BS OH 100) and three acrylic resins (Paraloid B72, Primal E330S and Carboset 525). This article focuses on only two consolidating products, displaying contrasting behaviours: Silres BS OH 100 and Primal E330S. A further publication will describe the results obtained for the whole set of tested products.

The solventless ethyl silicate Silres BS OH 100 (Wacker Chemie AG) was diluted in ethanol in ratio 2:1 (v/v). As the spraying of this product was ineffective, it was applied by brush in one pass. A white veil appeared less than one hour after the treatment, so it was decided not to repeat the application. The fresh product uptake was 1.5 L/m².

The commercial water suspension of acrylic resin Primal E330S (C.T.S. France) was diluted in ethanol at 2% (v/v), and then applied by spraying. Application was performed in a single pass and repeated two times one month apart. The total fresh product uptake was about 0.8 L/m².

Test areas

A part of the east wall painting was granted for consolidation tests. Nine test areas were selected and included a frieze with three main areas of orange, yellow and dark red ochre pigments (Figure 2). The first test area was the reference zone on which no consolidating product was applied. The other eight were dedicated for the application of a series of consolidation tests. Silres BS OH 100 and Primal E330S were applied respectively in areas No.3 and No.5.



Figure 2. The nine test areas on the east wall with orange, yellow and dark red parts

Assessment methods

Dry matter

The amount of dry product remaining after setting was evaluated for each product with their respective ready-to-apply dilutions. Each product was poured into a 9 cm diameter pre-

weighed petri dish and weighed (initial weight W_i), then allowed to dry to constant weight in laboratory conditions. The final weight W_f was recorded and the dry matter was calculated: $D_m (\%) = (W_f * 100) / W_i$.

Microclimate conditions monitoring

Climate was monitored by three thermo-hygrometric sensors (Rotronic HydroLog HL20/21) fixed on the east wall just below the paintings: one on the north side, one on the centre, and one on the south side. One other sensor was installed outside, just above the front door of the Chapter Hall. Temperature and relative humidity were recorded once an hour for one year.

Moisture and hygroscopic moisture contents

Moisture and hygroscopic moisture contents (resp. MC and HMC) of the wall painting were assessed with samples collected by drilling at different depths in the east wall, in areas without paintings, then put in distinct pre-weighed airtight glass vials. Samples were weighed just after collection (initial weigh W_i), then after drying to constant weight (dry weigh W_d) in an oven at 65°C, and finally after 5 weeks in a sealed chamber at 97% of relative humidity (wet weight W_w) using K_2SO_4 saturated saline solution. Values of MC and HMC are calculated as follows: $MC = (W_i - W_d) * 100 / W_d$, and $HMC = (W_w - W_d) * 100 / W_d$ [29].

Optical microscopy

A digital microscope AM4013MZT Dino-Lite Universal was used to take micro-pictures of the paint surface in the test areas for a follow-up of potential salt crystal bursts or colour changes. Pictures were taken under two magnifications (x50 and x250) in each part (orange, yellow and dark red) of the test areas at each step of the survey.

Spectrophotocolorimetry

Colour changes were assessed using a Minolta 2300D spectrophotocolorimeter equipped with a circular window of 8mm diameter using a D65 standard light source. Results are presented according to the CIE $L^*a^*b^*$ system. To limit the measurement error due to the positioning of the device, the initial position of the window of the apparatus was photographed and the measurements were performed in a series of three independent positionings. Colour measurements were performed on the orange part of all test areas, selecting a location as smooth and homogeneous as possible. Several values were calculated: average and standard deviation of measurements as well as the colour change $\Delta E^* = \sqrt{(\Delta L^*)^2 + (\Delta a^*)^2 + (\Delta b^*)^2}$, with the lightness coordinate change $\Delta L^* = L^*_2 - L^*_1$ and the colour coordinates change $\Delta a^* = a^*_2 - a^*_1$ and $\Delta b^* = b^*_2 - b^*_1$.

Cotton swab and scotch tape tests

The cotton swab test allows the assessment of the superficial cohesion of a surface before and after consolidation [11]. A cotton swab was lightly rubbed against the painted surface and observed with the naked eye. Superficial cohesion was then assessed according to the quantity of powdery layer remaining on the cotton swab. If the cotton swab can still trap powdery material from the tested surface after consolidation, this means that there is no increase in superficial cohesion. This test is easy to carry out, but the result depends on the force applied to the cotton swab. The test was performed on the orange, yellow and red parts of each tested area by the same operator, familiar with the test.

A scotch tape test or peeling test was also performed to assess the superficial cohesion. It was carried out in this study following the protocol of Drdácý for an *in-situ* test [30] using 3M Scotch tape. However, during the scotch tape test, the adhesive did not stick to the test surface, probably due to the high moisture content present at the paint surface. As a result, the scotch tape tests provided non-interpretable results.

Water drop test

The water drop test provides information on the water repellency of a surface by recording the time of absorption of the drop. The longer the absorption time and the more spherical the drops shape, the higher the repellence [31]. A small drop of water was gently applied to the surface with a 5 µl Eppendorf pipette. A stopwatch was activated as soon as the drop touched the surface, and stopped when the drop was fully absorbed and the wet surface lost its glossy aspect. On the orange part of each test area, 10 drops were applied next to each other on a small area as smooth and homogeneous as possible.

Sponge test

A water absorption test was carried out by the sponge method. It consisted of a contact-plate containing a slightly humid sponge of 5.5 cm in diameter (from C.T.S. S.R.L., Italy). The sponge was soaked with 5ml of water and weighed (initial weigh W_i). The contact-plate containing the sponge was gently pressed against the surface until the edges of the contact-plate touched the wall. After 120 seconds, the sponge was removed and weighed again (final weight W_f). The amount of water absorbed by the wall painting per unit surface area and per unit of time was calculated: $W_a = (W_i - W_f) / (A \cdot t)$ with A the surface contact of the sponge in m^2 (i.e. $2.376 \cdot 10^{-3} m^2$) and t the application time in seconds (i.e. 120 seconds). The test was performed only once before and after consolidation in the same place for each test area, on a surface as smooth and homogeneous as possible in the orange part.

Results

Dry matter

Silres BS OH 100 solution leaves a high amount of dry matter (25.2%). The product initially forms a transparent film, which cracks and shrinks after 6 weeks, resulting in the formation of flakes (Figure 3). Diluted Primal E330S produces a low amount of dry matter (1.5%) and forms a stable, homogeneous, smooth and transparent film in the petri dish after drying.

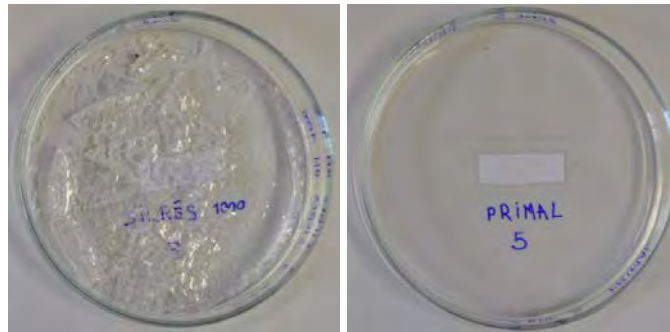


Figure 3. Silres BS OH 100 on the left and Primal E330S on the right after drying in a petri dish

Microclimate

Temperature (T) and relative humidity (RH) were recorded during the whole study, from October 2017 for 12 months (Figure 4). The indoor temperature varied between 2°C and 25°C while outdoors, it fluctuated between -6°C and 30°C. Daily fluctuations of the T were far larger outdoors than inside the hall. RH varied indoors in the range 62-98% and outdoors 30-99%. The RH inside the Chapter Hall is rather high and most of the time higher than the average daily RH outside, which could be explained by the high water content in walls combined with infrequent opening of the room.

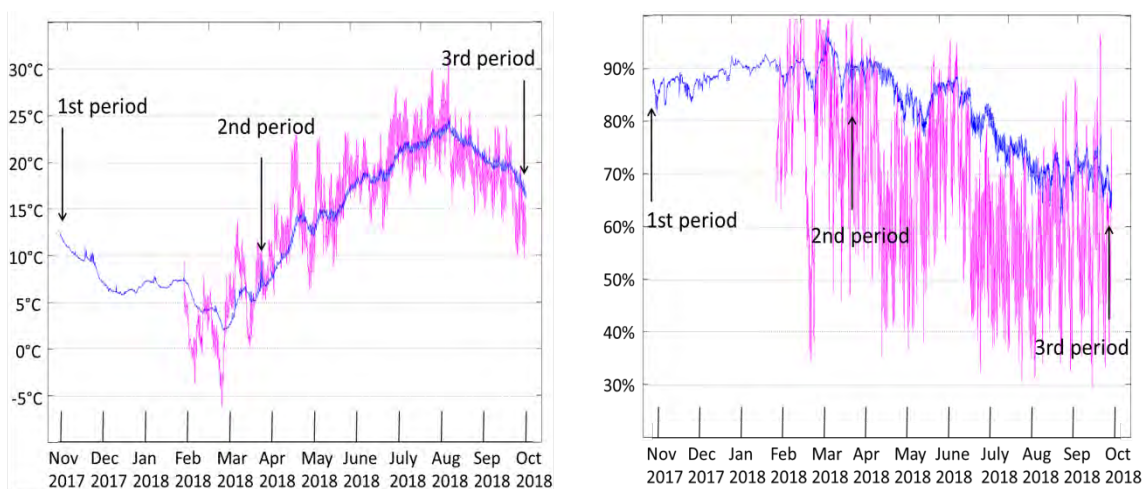


Figure 4. Temperature (on the left) and relative humidity (on the right) recorded during 13 months from October 2017 inside the Chapter Hall (blue line) and outdoors (magenta line)

The first period (October 24-25, 2017) corresponds to tests performed before consolidation, the second period (March 27-28, 2018) to tests performed three months after consolidation and the third period (October 01-02, 2018) to tests performed nine months after consolidation. Ideally T and RH have to be relatively similar in order to make comparisons of tests relevant. The T ranges during the first and the third period are close to each other (respectively about 15°C and 17°C), but T for the second period is noticeably lower (about 7°C). The RH ranges are similar for the first and second period (between 84% and 93%) and clearly higher than those of the third test period (around 67%). Such differences are liable to introduce a bias into our tests results and have to be taken into account in their interpretation.

Moisture and hygroscopic moisture contents

The location of samples for the calculation of the MC and HMC is shown in Figure 5 and the corresponding values are indicated in Table 1. On the day when the sampling was performed, the wall was quite wet with MC values between 13.3-16.1%. This value is far higher than the limit of 5% below which a sample is considered dry. It can be attributed to the presence of hygroscopic salts, as the HMC ranges from 17.8 to 32.6%.

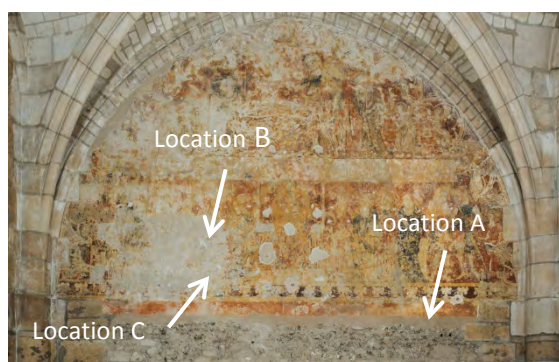


Figure 5. Location of samples

Table 1. Moisture content (MC) and hygroscopic moisture content (HMC) of collected samples

	Depth	MC %	HMC %
Location	0-3 cm	15.5	22.1
A	7-10 cm	13.3	17.8
Location	0-1 cm	14.0	31.8
B			
Location	0-1 cm	15.0	30.2
C	1-3 cm	16.1	32.6
	3-4 cm	13.9	23.1

Saline contamination

The sequence of crystallisation of salts as a function of T and HR was simulated using the ECOS/RUNSALT software [32,33] on the basis of quantitative analysis of salts done in 2015 [26]. One sample located near location B and taken from 3 to 4 cm in depth was chosen for its particularly high salt concentrations in nitrate, sulphate and chloride ions (Figure 6).

According to Figure 6, gypsum is the only salt able to crystallise when the RH is higher than 60%, either at 5°C or 20°C. Between 50% and 60% RH, sodium nitrate can possibly crystallise too. As the T and RH recorded during the study fluctuated respectively in the range 5-20°C and 60-95% RH there should not be any crystallised salts except gypsum on the east wall. Below 60% RH, the risk of crystallisation of different salts would become higher.

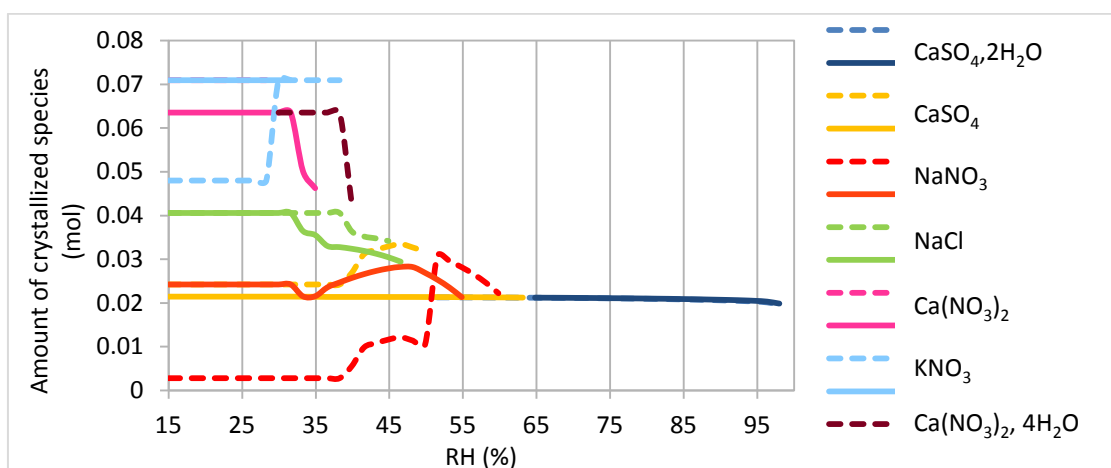


Figure 6: *In silico* simulation of the crystallisation of different salts species in function of RH, at 5°C (dotted line) and 20°C (full line)

Naked eye and digital microscope observations

Two parameters were assessed: whitening and gloss. On the reference area no change was observed at three and nine months. A slight white haze appeared on the dark red part less than one hour after the application of the ethyl silicate. This area did not show any gloss change. Three and nine months after consolidation, no further change of the surface was observed: the slight white haze was still observed on the dark red part. Primal E330S did not induce any white haze or gloss change. However, very small and rare white “spots” were visible in the dark red part nine months after the last application of the Primal E330S, without any lifting of the paint layer.

Colour

The results are based on two sets of measurements carried out in the orange part of each test area three months and nine months after the consolidation. Calculated ΔL^* , Δa^* , Δb^* and ΔE^* values are presented in Table 2. The reference and ethyl silicate areas show a ΔL^* lower than 2 six months after the second test period, while the acrylic resin shows a change of 3.5. For the total change ΔE^* , the reference area shows an almost imperceptible change of 2 units. Ethyl silicate does not lead to perceptible colour changes ($\Delta E^* = 0.5$) after its quite immediate colour shift due to haze formation, while Primal E330S treated zone shows a delayed shift ($\Delta E^* = 5.7$) resulting in a lighter, less yellow and less red colour according ΔL^* , Δa^* and Δb^* values.

Table 2. Calculated shifts of colorimetric coordinates

	Δa^*	Δb^*	ΔL^*	ΔE^*
Reference area	-0.6	-1.9	-0.4	2.0
Silres BS OH 100	0.3	0.1	-0.3	0.5
Primal E330S	-2.5	-3.7	3.5	5.7

Superficial cohesion of the paint layer

The cohesion of the paint layer was poor in the reference area: a large amount of powdery material was collected on the cotton swab. In the Silres BS OH 100 treated area, a slight improvement in the superficial cohesion was observed in the orange part, but no significant change was noticed on the yellow and red parts. Primal E330S offers a good improvement in the superficial cohesion in the three parts, with a very small amount of pigment adhering to the cotton after consolidation.

Hydrophobicity

The absorption time of the water drop is shown in Figure 7. A variation in the absorption time between the 10 water drops for the same test area and test period appears, particularly for the Silres BS OH 100. Before consolidation, these variations highlight the heterogeneity of the test areas. More significant variation after consolidation than before consolidation might attest either to a heterogeneous distribution of the product or to different behaviour of the product, depending on the zone. For the reference area, the average absorption time of a water drop increased over time from 18s to 37s and 40s. The average absorption time three months after consolidation with Silres BS OH 100 is 46 times higher than before consolidation, rising from 11s to 511s. A spherical shape of the water drop (Figure 8) indicates high water repellence. However, after nine months, the water absorption time decreased slightly to 364s. The average absorption time for Primal E330S three months after consolidation is 26 times higher than before consolidation, going from 4s to 104s, which indicates that the acrylic resin also increases the absorption time of the surface considerably but to a lower extent than ethyl silicate. This behaviour remains constant even after nine months.

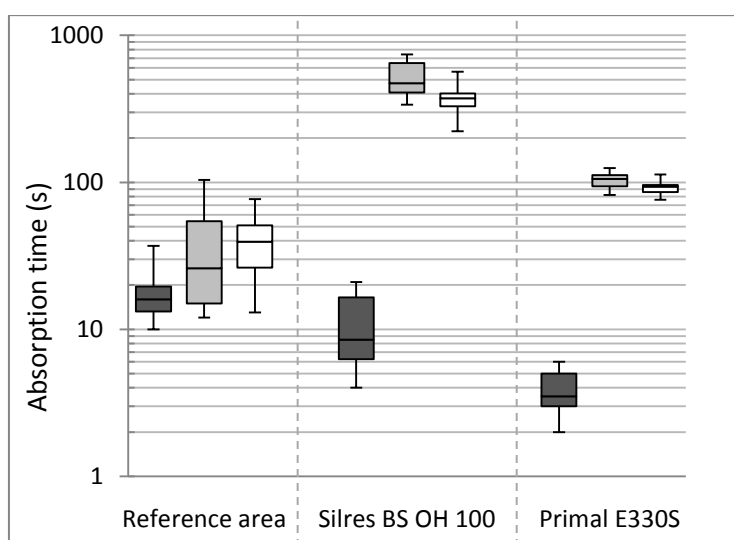


Figure 7. Ranges of absorption times of 10 water drops before consolidation (dark grey), three months (light grey) and nine months after consolidation (white)



Figure 8. Water drop deposited nine months after consolidation for the test area consolidated with Silres BS OH 100

Water absorption

Before the application of the consolidating products, the absorption coefficient W_a was not the same in the three test areas, thus indicating the variability and the heterogeneity of water surface absorption properties from one area to another (Figure 9). This variation might be due to different moisture contents, different porosities and/or salt clogging. Both consolidated areas show a decrease in the W_a value three months after application of the products: 33% decrease for Primal E330S, and 94% decrease for Silres BS OH 100 which is maintained even nine months after consolidation. The W_a value in the reference area is the same for the first two test periods but increases for the third test period (+43%). The increase in the W_a value for the third test period is also observed for the two treated areas. This behaviour is probably due to a drier state of the investigated area; for the third period, the T was $\sim 2^\circ\text{C}$ higher and the HR $\sim 15\%$ lower. These climatic conditions probably led to a lower moisture uptake of the salts contaminating the porous network.

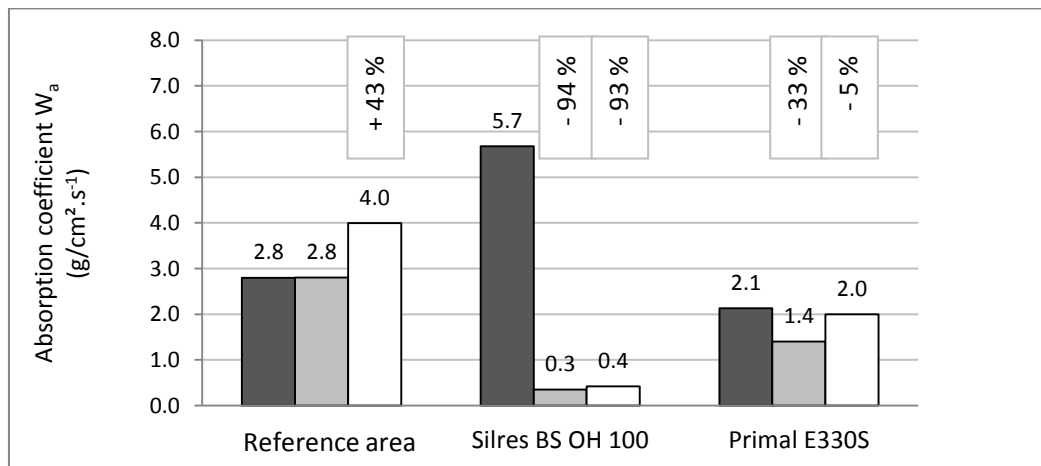


Figure 9. Water absorption coefficient W_a before consolidation (dark grey), 3 months (light grey) and 9 months after consolidation (white). Top bar chart - relative W_a change in comparison with W_a before consolidation.

Discussion

A suitable consolidation treatment must fulfil three main requirements [34-36]: efficiency, compatibility or chemical inertness and durability. Other requirements such as reversibility, non-toxicity and environmental safety are also important to comply with. Our study did not allow investigating all these criteria, but at least the overall efficiency, compatibility and to a certain extent, durability were evaluated. However, some of our evaluations like colour and water absorption measurements may be affected by microclimate conditions. That has brought us to cautious interpretations.

A product dedicated to consolidation has to improve the cohesion and/or the adherence of the paint layer to the support. The superficial cohesion of the paint layer was slightly improved only in the orange part of the area consolidated with Silres BS OH 100 according to

the cotton-swab test. This poor and only local improvement of the superficial cohesion suggests that the expected compact superficial layer [17] did probably not form. Additionally, the observed high hydrophobicity suggests that the ethyl silicate did not polymerize completely, probably because of high water content in the wall [37]. On the contrary, the cotton swab test shown that Primal E330S induced a good improvement of the superficial cohesion for all parts of the test area. Unfortunately, the observations made with cotton-swab cannot be supported by scotch test results because of the high moisture content in the wall preventing the adherence of the scotch to the surface.

Products used for conservation purposes should not lead to any colour or gloss changes, or chemical reaction with the paint layer, or significant changes in the capillary transport. None of the two evaluated products give excellent results with respect to all these criteria, but the acrylic resin appears more satisfactory than ethyl silicate. Silres BS OH 100 was judged unsatisfactory from aesthetic point of view, because of the appearance of a slight white haze right after application, which remained unchanged nine months later. The phenomenon was particularly visible on the dark red part, but it was not possible to say if it was also present on the other brighter colours. This haze could be due to a chemical reaction of the ethyl silicate with pigments or with the salts present in the wall painting. Primal E330S gave quite satisfactory results and did not induce any colour change or gloss visible with the naked eyes even three months after application. Yet, the treated area showed a slight colour change nine months after consolidation, either due to lower water content in the wall or drier microclimate conditions, or to ageing. Moreover, rare and small white “spots” appeared nine months after consolidation. They could either be the result of a slow reaction between the acrylic resin and salts or pigments, or gypsum crystallisations as suggested by ECOS/RUNSALT simulation.

The water absorption was very different from one treated area to the other. Application of the ethyl silicate caused poor absorption of water. It might be due either to a significant hydrophobicity or to a plugging of the porous network produced by high amounts of the product. The results of the drop test tend to prove that the very low absorption of water is rather linked to the hydrophobicity. This is a major drawback, able to induce future salt crystallisation underneath the consolidated layer and thus a risk of subsequent paint layer detachment. Primal E330S induced a lower decrease of water absorption than the ethyl silicate, probably because of a small quantity of the applied acrylic resin or a moderate hydrophobicity of the treated surface. The drop test also indicated a different water repellence of the surface consolidated with the ethyl silicate in different zones of the test area, which could be the result of a non-homogeneous distribution of the product, while the acrylic resin seems to have been applied uniformly.

An overall evaluation regarding our tests indicates that Primal E330S seems to be more suitable than Silres BS OH 100 for our application, even if results obtained in this study stand in contrast to the literature for the acrylic resin [9] which report poor durability and colour

changes after a longer period of time than nine months. This study will be continued for a better view of studied parameters change over time.

Conclusion

The results of our study stress the differences in behaviour of Silres BS OH 100 and Primal E330S applied for the consolidation of wall painting in terms of efficiency and compatibility. However, it is important to keep in mind that microclimatic conditions, as well as water and salts contents, were particularly critical in this work. Ideally, consolidation should improve the cohesion of the paint layer without disturbing other physical properties. The application of ethyl silicate in the presence of high water content appears to be problematic. A significant consolidating effect appeared with the acrylic resin without large changes in water absorption and with reasonable water repellency as opposed to the ethyl silicate treatment. Despite a good behaviour in an aesthetic point of view of the acrylic resin, the appearance of rare and small white “spots” nine months after application could be a future issue. This will be investigated further.

The larger work is in progress and will allow to compare the results obtained with seven consolidating product including Silres BS OH 100 and Primal E330S in larger period of time, in order to determine the most adapted product to consolidate the east wall paintings in the Chapter Hall of the Chartres cathedral.

References

1. Arnold A, Zehnder K (1990) Salt weathering on monuments. In: Grafo Edizioni (ed) The conservation of monuments in the Mediterranean Basin: the influence of coastal environment and salt spray on limestone and marble, Proceedings of the 1st International Symposium, Bari, Italy 31-58
2. Snethlage R, Wendler E (1997) Moisture cycles and sandstone degradation. Environmental Sciences Research Report ES 20:7-24
3. Zehnder K, Arnold A (1989) Crystal growth in salt efflorescence. Journal of Crystal Growth 97.2:513–521
4. Piqué F, Dei L, Ferroni E (1992) Physicochemical aspects of the deliquescence of calcium nitrate and its implications for wall painting conservation. Studies in Conservation 37.4:217–227
5. Charola AE, Laurenzi Tabasso M, Santamaria U (1985) The effect of water on the hydrophobic properties of an acrylic resin. In: Presses polytechniques romandes (ed) Vth international congress on deterioration and conservation of stone, Proceedings, Lausanne, Switzerland 739-747

6. Ferreira Pinto AP, Delgado Rodrigues J (2014) Impacts of consolidation procedures on colour and absorption kinetics of carbonate stones. *Studies in Conservation* 59.2:79–90
7. Giorgi R, Ambrosi M, Toccafondi N, Baglioni P (2010) Nanoparticles for cultural heritage conservation: calcium and barium hydroxide nanoparticles for wall painting consolidation. *Chemistry - A European Journal* 16.31:9374–9382.
8. Otero J, Charola AE, Grissom CA, Starinieri V (2017) An overview of nanolime as a consolidation method for calcareous substrates. *Ge-conservación* 1.11:71–78
9. Carretti E, Dei L (2004) Physicochemical characterization of acrylic polymeric resins coating porous materials of artistic interest. *Progress in Organic Coatings* 49.3:282–289.
10. Chelazzi D, Poggi G, Jaidar Y, et al (2013) Hydroxide nanoparticles for cultural heritage: consolidation and protection of wall paintings and carbonate materials. *Journal of colloid and interface science* 392:42–49
11. Baglioni P, Chelazzi D, Giorgi R, et al (2014) Commercial Ca(OH)₂ nanoparticles for the consolidation of immovable works of art. *Applied Physics A* 114.3:723–732
12. Favaro M, Mendichi R, Ossola F, et al (2006) Evaluation of polymers for conservation treatments of outdoor exposed stone monuments. Part I: Photo-oxidative weathering. *Polymer Degradation and Stability* 91.12:3083–3096
13. Milanesi C, Baldi F, Borin S, et al (2009) Deterioration of medieval painting in the chapel of the Holy Nail, Siena (Italy) partially treated with Paraloid B72. *International Biodeterioration & Biodegradation* 63.7:844–850
14. Dei L, Baglioni P, Mauro M (1999) Materials for wall paintings conservation: change of physicochemical properties, ageing effects, and reversibility. Oddy A, Carroll S (1999), *Reversibility: does it exist*
15. Borsoi G, Tavares M, Veiga R, Silva AS (2012) Microstructural Characterization of Consolidant products for historical renders: an innovative nanostructured lime dispersion and a more traditional ethyl silicate limewater solution. *Microscopy and Microanalysis* 18.5:1181–1189
16. Darwish SS (2013) Evaluation of the effectiveness of some consolidants used for the treatment of the XIXth century egyptian cemetery wall painting. *International Journal of Conservation Science* 4.4:413–422
17. Zendri E, Biscontin G, Nardini I, Riato S (2007) Characterization and reactivity of silicatic consolidants. *Construction and Building Materials* 21.5:1098–1106
18. Bigas JP, Martinet G, Perrot AC, et al (2009) *Pierre et patrimoine: Connaissance et conservation*. Actes sud

19. Brus J, Kotlik P (1996) Cracking of organosilicone stone consolidants in gel form. *Studies in conservation* 41.1:55–59
20. Grissom CA, Charola AE, Boulton A, Mecklenburg MF (1999) Evaluation over time of an ethyl silicate consolidant applied to ancient lime plaster. *Studies in Conservation* 44.2:113–120
21. Gregorio SD (2010) Nanorestore® for the consolidation of wall paintings. Influence of the thermohygro-metric parameters and the presence of saline contamination on the efficacy of the treatment. In: CeROArt. Conservation, exposition, Restauration d'Objets d'Art. Association CeROArt asbl
22. Duboscq B (2015) Étude de deux prélèvements de polychromie de la salle capitulaire, cathédrale de Chartres. Laboratoire M.S.M.A.P. SARL, rapport MSMA P 15-060 MH, Pessac, France
23. Ramirez-Martin S (2015) Étude stratigraphique de décor peint, salle capitulaire de la cathédrale de Chartres. Études Recherches Matériaux secteur Monuments Historiques, rapport ERM 15 099 SR 160, Poitiers, France
24. Trichereau B, Martos-Levif D (2016) Chartres, salle capitulaire, Caractérisation et analyses physico-chimiques. LRMH Laboratoire de Recherche des Monuments Historiques, rapport n°1261D, Champs-sur-Marne, France
25. Dandrel C (2017) Rapport d'étude et intervention, Chartres, salle capitulaire de la cathédrale, peintures murales. Rapport interne, Fontenay-aux-Roses, France
26. Ramirez-Martin S (2015) Étude de la contamination saline et de l'humidité de la maçonnerie, Mur Est de la salle capitulaire de la cathédrale Notre-Dame de Chartres. Études Recherches Matériaux secteur Monuments Historiques, rapport ERM 15 211 SR 306, Poitiers, France
27. Ouvrage collectif (2006) Ouvrages de maçonnerie. Ministère de la culture et de la communication, Département communication et documentation, Paris, France
28. Normand L, Vergès-Belmin V (2016) Cathédrale Notre-Dame de Chartres, salle capitulaire, décor peint du mur intérieur est, Mesure des propriétés de sorption d'eau et analyses MEB-EDS de prélèvements effectués par forage et d'un évaporat. LRMH Laboratoire de Recherche des Monuments Historiques, rapport n°1261E, Champs-sur-Marne, France
29. Normand L, Duchêne S, Vergès-Belmin V, et al (2019) Étude de la consolidation de peintures murales en présence de forte teneur en eau et en sels solubles : essais de consolidants sur le mur est de la salle capitulaire de la cathédrale de Chartres. LRMH Laboratoire de Recherche des Monuments Historiques, rapport n°1453A, Champs-sur-Marne, France

30. Drdácý M, Lesák J, Rescic S, et al (2012) Standardization of peeling tests for assessing the cohesion and consolidation characteristics of historic stone surfaces. *Materials and structures* 45.4:505–520
31. Bläuer C, Franzen C, Vergès-Belmin V (2012) Simple field tests in stone conservation. In: *Proceedings of the 12th International Congress on the Deterioration and Conservation of Stone*, New York, USA: Columbia University
32. Bionda D, Storemyr P (2002) Modeling the behavior of salt mixtures in walls: a case study from Tenaille von Fersen, Suomenlinna, Finland. In: Von Konow T (ed) *The study of salt deterioration mechanisms. Decay of brick walls influenced by interior climate changes*, Helsinki: Suomenlinnan Hoitokunta, 95-101
33. Price C A (2000) An expert chemical model for determining the environmental conditions needed to prevent salt damage in porous materials. In: Archetype Publications (ed) *European Commission Research Report No 11, Protection and Conservation of European Cultural Heritage*, London
34. Mora P, Mora L, Philippot P (1984) *Conservation of wall paintings*, Butter Worths. London, Boston
35. Giorgi R, Dei L, Baglioni P (2000) A new method for consolidating wall paintings based on dispersions of lime in alcohol. *Studies in conservation* 45.3:154–161
36. Baglioni P, Giorgi R, Chen C (2003) Nanoparticle technology saves cultural relics: Potential for a multimedia digital library. In: *Online Proceedings of DELOS/NSF Workshop on Multimedia Contents in Digital Libraries*, Chania, Crete, Greece
37. Sassoni E, Graziani G, Franzoni E (2016) An innovative phosphate-based consolidant for limestone. Part 1: Effectiveness and compatibility in comparison with ethyl silicate. *Construction and Building Materials* 102:918–930

Comparative analysis of permeability values of traditional aerial lime mortars for preventive conservation

Ana González-Serrano¹, Reyes Rodríguez-García¹, Esther Ontiveros-Ortega²

(1) Department of Architectural Constructions I, University of Seville, gserrano@us.es, rgarcia@us.es

(2) Laboratory of Geology, Andalusian Historical Heritage Institute, esther.ontiveros@juntadeandalucia.es

Abstract

The suitable materials defined the influence of aerial lime characteristics in water vapour permeability capacity in pre-dosed mortars of powder and in putty lime as traditional construction permeable material for its application in render and plaster mortars in Cultural Heritage conservation. In this study have been elaborated selected mortars sample following UNE-EN 1015-19 that determines the water vapour permeability to these mortars. The influence of the porosity and the carbonation process in the permeability coefficient measured in different periods of time, until 180 days, addition to considering the importance of the type of aggregate and relation binder/water in its properties. This study establishes the values that coincide and significant variations in the characterization for every mortar. Tests results determined the water vapour exchanges, allow for analysed the singular circumstances and indicated the permeability behaviours of the different mortars selected. After 90 days, all the mortars reach equilibrium in terms of this permeability values and it is the SPL mortars that retain the most water. It is possible to conclude that these aerial limes guarantee the renders and plaster mortars breathability with a controlled dosing.

Introduction

The intervention in the render mortar of the building wall implies consider a series of previous decision making. Any action should be served to improve the quality of the building and its surroundings. Most of the time, the plaster of the wall intervention is done for aesthetic reasons other than for technical needs. The correct determination of the mortar properties to be repaired is a fundamental and essential aspect, in order to guarantee that a correct intervention is made. The new render mortar should be designed compatible with the pre-existing coatings to avoid any chemical reaction that compromises the adhesion [1, 2, 3] between both and these with the wall.

It is important that the mixtures of render and plaster mortars are homogeneous and that the manufacturer has a statistical monitoring of the final product dosages so that its production corresponds to the mixture designed. There should be a rigorous control in the proportion of mixing water to obtain a mortars homogeneous quality and to avoid segregation. The time and proportion of water required should be established to have a uniform distribution of its components which this may involve the mortar can be discarded if

it does not meet these requirements. The control of raw materials documentation, the manufacturing processes and the quality of the final product should be manufacturer responsibility and the rigorous application in building should be specialized technical assistance responsibility in accordance with these requirements. Therefore, in relation to quality control at work, should be used products labelled and with technical sheet to define their characteristics, composition and manufacturer application instructions; but above all, they should be required not to apply products that have not been previously tested in wall building [4].

In some buildings, it is necessary to apply a specific mortar when producing moisture by capillary action with the presence of salts, and in other circumstances predesigned mortars should be used to give a very specific response; these mortars can usually be found in the construction market. In built heritage, the cause for interventions may also be problems of compatibility between the materials and the decision of which product to use is important; surely it is required to reproduce a historical mortar, it is not possible to resort to industrial mortars [5]. There are traditional pre-dosed mortars that can be suitable products to be applied in these circumstances. As mentioned above, it is required and necessary to know the information of mortars characteristics, the water vapour permeability and mechanical resistance values, colour, etc. to ensure if they can satisfy the requirements of the project.

The suitable materials should always be used in historic building and this compatibility is defined in relation to the substrate and the existing mortars on historic renders and plasters mortars. This study refers to the influence of traditional aerial lime characteristics in water vapour permeability capacity in pre-dosed mortars of powder and in putty lime. It is interesting to define this behaviour as traditional construction permeable material for its application in render mortar and plaster mortar in Cultural Heritage conservation. In summary, the composition and dosage of the mortar influence its characteristics and define its porosity. Several studies propose the analysis of the relationship between porosity and carbonation of the limes that compose the renders and plaster mortars and relate the macro structure of the pores with their properties [6, 7]

One of the principal advantages of the aerials lime mortars use resides in the aptitude to regulate moisture content of environmental humidity. However, sometimes it is not possible to obtain enough data about old materials, especially concerning masonry which is more difficult to test than render or plaster mortars. The mortars characteristics to use can be established, based on the results obtained, in order to ensure functionality and compatibility with wall. Capillary rising damp is a cause that often affects the walls of old and modern buildings, causing damage to render mortar and brickwork. This process is caused by the capillary absorption of porous building materials in contact with subsoil water. The accumulation of soluble salts at the plaster-substrate interface with subsequent crystallization and dissolution cycles can lead to loss of adhesion and detachment of the render or plaster mortar [7, 8, 9]. The coatings must guarantee the breathability of the wall

to prevent its deterioration and to avoid efflorescence or subflorescence deposited on the surface of masonry.

Therefore, there are resources to measure the size distribution of empty spaces and evaluate the material porosity, to establish the value of water vapour permeability that allows for characterizing the behaviour of the mortar against wall moisture. These data permit to evaluate the response of the mortar against the transpiration capacity from the walls. The correct coating application also conditions the response of the water vapour permeability of a mortar. In particular, the unskilled labour may distort the internal structure of the product since it can make mistakes in the apply process.

Material and Methods

It used for this study lime from Moron de la Frontera City (Seville, Spain), which currently has two forms of quicklime production, traditional and industrial. This unique case allows greater control of variables involved in the production process such as the nature of the limestone, as reflected in previous works, kiln type and its technological implications [10]; such as the effect of calcination temperature and heating rate. The exceptional production conditions of such lime have made it an object of study for application in restoration works of Cultural Heritage demonstrating its high quality as a building material. In November 2011, declared Intangible Heritage of Humanity, in the category of Best Practices by UNESCO [6]. A suitable characterization of coatings mortars is the basis for maintain their value and usefulness in Cultural Heritage conservation.

The pre-dosed mortars are studied, elaborated with this traditional lime in its two varieties: CL-90 powder lime (hereinafter mCL) and CL-90-SPL putty lime (hereinafter mSPL). The pre-dosed aerials lime mortars are dosed for fabricant to apply directly in building with its instructions and specific conditions to use. These two mortars are selected and applied in different layers on coating: as render base mortars (hereinafter B) and plaster mortars (hereinafter F) for fine finish. Their denominations are: mCLB, mCLF, mSPLB and mSPLF.

The mortars reaction to water from can be specified with capillary water absorption tests to quantify the porosity of the mortar, but it is the capacity of water vapour transmission that allows studying the product permeability as a function of curing time. To realize this study have been elaborated selected mortars sample following UNE-EN 1015-19:1999/A1:2005 standard [11] that determines the degree of permeability to the mortars water vapour in render mortar and plaster mortar.

The water vapour flow $\Delta G/\Delta t$ (Kg/s) is determinate with the straight line which define three points from the hygroscopic intervals. The water vapour permeance (Λ) is calculated with the following formula:

$$\Lambda = \frac{1}{A\Delta_p/(\Delta G/\Delta t) - R_A}, \text{ in kg/m}^2 \cdot \text{s} \cdot \text{Pa}$$

Reference by [11]: A: surface of top of the recipient where the sample is based (m²); Δp : water vapour pressure difference between ambient air and saline solution (Pa); $\Delta G/\Delta t$: water vapour flow (kg/s); RA: cold air water vapour flow resistance between sample base and saline solution (0,048.109 Pa m² s/kg by 10 mm of cold air). The water vapour permeability value is obtained from the average value of water vapour permeance multiplied by the medium value of sample thickness. This average value of the water vapour permeability is obtained from the values of five test sample.

The mortar permeability is directly related to the porosity of the product which, in turn, is determined by the granulometry; therefore it is considered important to measure the ascending flow of water vapour across the material and in the opposite direction. This analysis allows checking the influence of the carbonation process in the permeability coefficient measured in different periods of time: 28, 90 and 180 days, addition to considering the importance of the type of aggregate (composition and granulometry) and relation binder/water in mortars properties.

Experimental description

The water vapour permeability test of a product or constructive element allows evaluate the liquid ability to let water vapour pass through the pores it contains. The watertightness, the superficial or interior condensation of the walls define very important properties such as the capacity of breathability or water vapour evaporation in that material compose them.

In this case, to quantify the mortar water vapour permeability, it should take account that water vapour has ability to pass through the solids, like most gases; the amount of water vapour that pass through depends directly on the pressure to which the gas is subjected against the solid, on the surface through which it passes and the application time, in turn, inversely proportional to the solid thickness that flowing through [12]. The test is made with samples to 10 mm maximum thicknesses, whereas there is maximum thickness recommended for the layers of render mortar in a wall.

The lime mortars have the property of regulating the relative air humidity and the ambient temperature, the interest is focused in knowing the time margin in which the stabilization or saturation time occurs, which can be correlated with the moment in which the different mortars could reach total carbonation. The moisture absorb ability may differ depending on the apply technique and the material composition used in the mortar dosage and even may depend on the additives that include into the mass as stabilizers.

It is important to control the condition in the mortars that are studied since they only differ in the granulometry. In this way, is isolated the effect of the mortar aggregates and can be established parameters that be used for the comparison between the different types of dosages with aerial lime and others that contain additives or hydraulic binders.

Samples

In this case, the tests samples were made according to the indications of the UNE-EN 1015-19:1999/A1:2005 standard. The ten circular samples for each type of mortar have 160 mm in diameter y 10 mm total thickness. They were obtained after designed specific circular methacrylate test mould in order to get the piece that is described in the reference prescriptions (see Figure 1). The mortars samples are prepared with the kneading water content is shown in Table 1 [13].

Table 1. Fresh mortars properties by [13]

Mortar Type	H ₂ O (%)	Consistency (mm)
mCLB	22.0	150.0
mCLF	22.2	142.0
mSPLB	17.5	172.8
mSPLF	17.0	166.0

In the case of putty lime mortars (mSPL) the water content is determined after drying the mortar paste in the stove. The mSPL are the pastes most fluid and with less water content. The consistence of the fresh mortars depends on the B/W ratio, type of lime, content in fine aggregates, roundness of the grains and his composition. This explains the greater flow of the mSPL mortars, related to the type of lime, and the mCLB due to its less content in fines less capacity to retain water [13]. The samples are conserved to reproduce the conditions of humidity, curing and unmold period that indicates the UNE-EN 1015-11:2000 standard [14] until the 28 days have elapsed to complete the water vapour permeability test.

Resistance to the water vapour permeability test

The specifications of the UNE-EN 1015-19:199/A1:2005 standard, which is applicable to mortars in exterior use, is implement as a reference to perform the test to determine the water vapour permeability, considering that the air lime mortars are products with proven ability to regulate the exchange of water vapour with the environment and to quantify how it affects the variations of humidity and temperature of any room within a building.

As mentioned earlier, ten circular samples are made with each type of mortar, which half (five samples) are placed in circular plastic recipients containing saturated potassium nitrate solutions (KNO₃) which provides a relative humidity (RH) of 93.2%; and to control the water vapour pressure for lower relative humidity, the other half of containers (with other five samples) contain a saturated solution of lithium chloride (LiCl) that generates a RH of 12.4% (Figure 1).

With different partial vapour pressure, in order to generate a constant water vapour flow, through the sample. In that way, the effect of the up and down water vapour flow through the thickness of the samples (10 mm) can be evaluated, keeping the mould containers inside

a chamber that provides a constant temperature of $20^{\circ}\text{C} \pm 2^{\circ}\text{C}$ and relative humidity (RH) constant of $50\% \pm 5\%$ [11]. Control periods are established in three time stages: at 28 days, as required by standard regulations, extending the test to two other periods at 90 and 180 days.

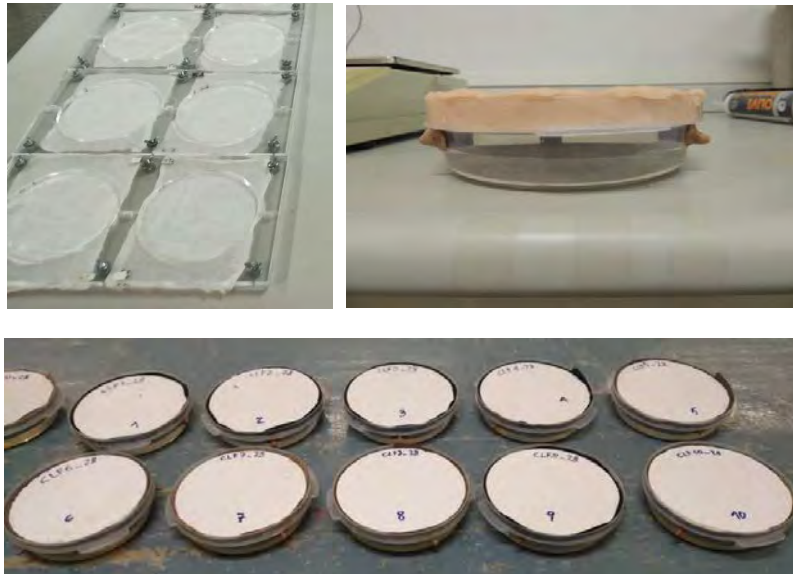


Figure 1. Samples in their test specimen recipients by UNE-EN 1015-19 [11]

Results and Discussion

This study establishes the water vapour permeability values that coincide and those which demonstrate significant variations due to the characteristics of the materials used for every mortar, mCLB, mCLF, mSPLB and mSPLF. Through the weight variations of the samples containers, the balance that generate in the exchange of water vapour flows can be deduced and how the different types of mortars respond. The test results analysis allows establish that, under the temperature and humidity conditions established by UNE-EN 1015-19: 1999 / A1: 2005 standard reference, the values obtained at 28, 90 and 180 days are important to analyse.

As indicated in Figure 2, 3 and 5, the water vapour permeability values obtained to each type of mortars are included in the reference range of 5 to 11μ (indicated by dashed lines), both for the analysis of the ascending water vapour flow (NKO_3) and the descending (LiCl) in all the dosages of mortars. These values of water vapour permeability are considered acceptable since they guarantee the mortars breathability, therefore also its correct functionality and adhesion to any type of masonry. The porosity of lime mortars decreases during the first month, the period in which the carbonation process is faster leading to a 12% increase in volume caused by the transformation of portlandite into calcite [15].

The Figure 2 show the water vapour permeability values expressed as inflow and outflow exchanges respectively. In initial 28 days, the water vapour flow is similar in all mortars although SPLB result in lower values.

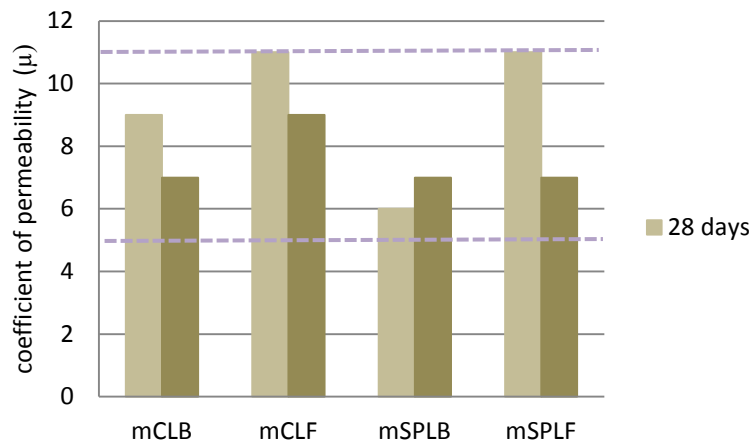


Figure 2. Variation of water vapour inflow and outflow at 28 days

Greater flow exchange value is produced in fine mortars; the mortars mCLF and mSPLF present the highest values of water vapour permeability which could be correlated with its porosity and granulometry [6, 7]. These results not differ from other traditional air lime mortars tests also where mCL and mSPL lime are used [13, 16].

At 28 days, in all mortars, the water vapour inflow is greater than the outflow except the mSPLB; it is highlighted that fine mortars (F) have the highest coefficient of permeability. This effect may be a consequence of the drying process, the samples are still losing water by drying and carbonation has not advanced because the water vapour outflow is slower. In the tests results are defined the values obtained to determine the degree of symmetry in water vapour data and exchanges. The mCL tendency is that the water vapour outflow increases with time up to 90 days, due to effect of lime type, from this time all their values fall.

After 90 days (see Figure 3), when all the mortars are supposed already carbonated [6, 7, 15], the differences are observed between mCL mortars. It is detected that mCLB stabilize the water vapour inflow and outflow values that considered optimal to avoid efflorescence and guarantee mortar breathing, while mCLF reduces the outflow values.

In contrast, mSPLB regulates the flow exchange in a similar way to the rest of fine mortars, registering a greater water vapour absorption capacity, increasing the value of the permeability coefficient in the downward flow. In general, fine mortars (F) have higher coefficient of permeability values. On the contrary, the tendency in mSPL is the outflow reduces the coefficient of permeability with time except the mSPLB that increases it.

The fine mortars, both mCLF and mSPLF, follow the same initial regulation tendency although they reduce the difference between the water vapour they transmit to the environment and the one they are able to retain. The render mortars (B) have a pore size dominant around 1 μm at 90 days and this size evolves towards pores of size 2 μm and a new

group of 5 mm pores appears at 180 days; this is observed in the mCLB values. In the case of plaster mortars, the pore size changes little from 90 to 180 days. Figure 4 shows the comparative study of this progression with mCLB and mCLF between 90 and 180 days [13].

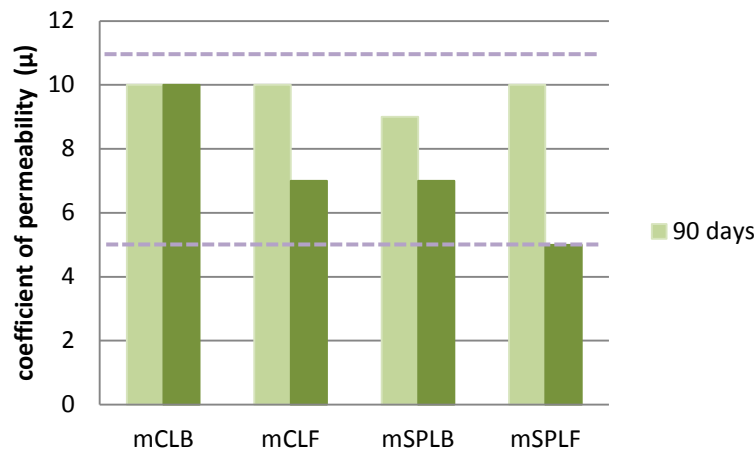


Figure 3. Variation of water vapour inflow and outflow at 90 days

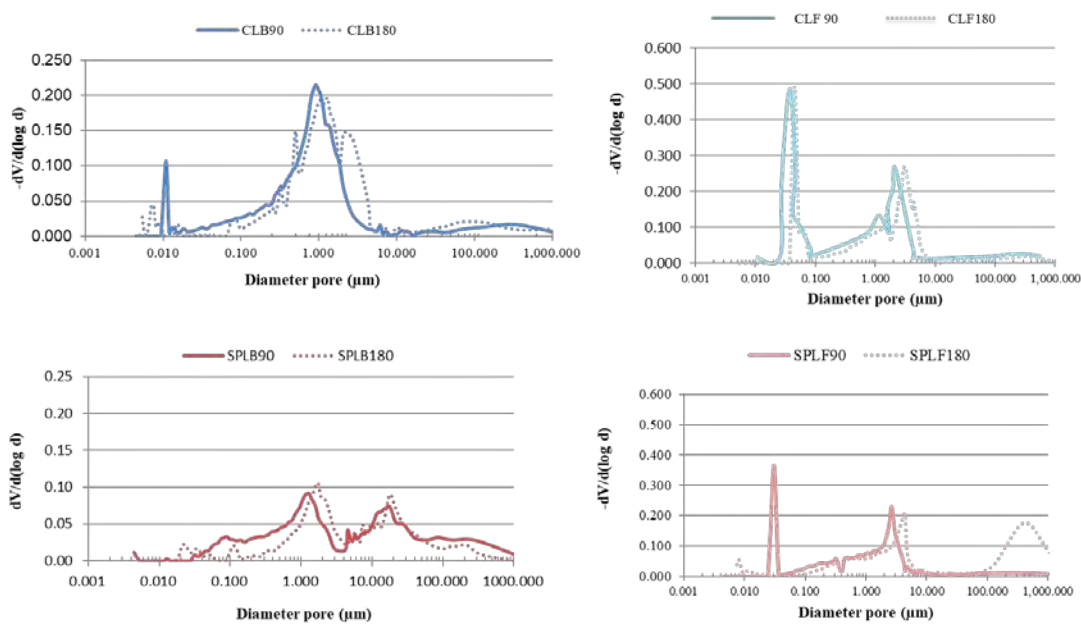


Figure 4. Pore size distribution of the different mortars at 90 and 180 of curing time by [13].

If it compared with the values of the mechanical strengths of this same type of mortars obtained in previous studies, the stable water vapour regulation coincides with the values of flexibility over time of the mortar cured. The microstructure of the binder has an important role in the compactness of material; the homogenization is appear at 90 days in most of the mortars studied, which indicates that most of the modifications of the binder take place at 90 days [13].

After 180 days, (see Figure 5) the equilibrium between the water vapour outflow and inflow in mCLB, mCLF and mSPLB occurs; it is mSPLF that presents the most differences between the inflow and outflow of water vapour. This mortar is the one with the largest pore size due

to carbonation. As expected, the highest values of water vapour resistance factor refer to fine mortars and among fine and base mortars, the ones with mCLB y mCLF appear to register better behaviour, because the drying is faster in the mCL mortars[13]. As long as the water vapour permeability values are preserved in equilibrium, both to absorb and to evaporate moisture to the environment, it will be more difficult induced efflorescence salt marks on coating.

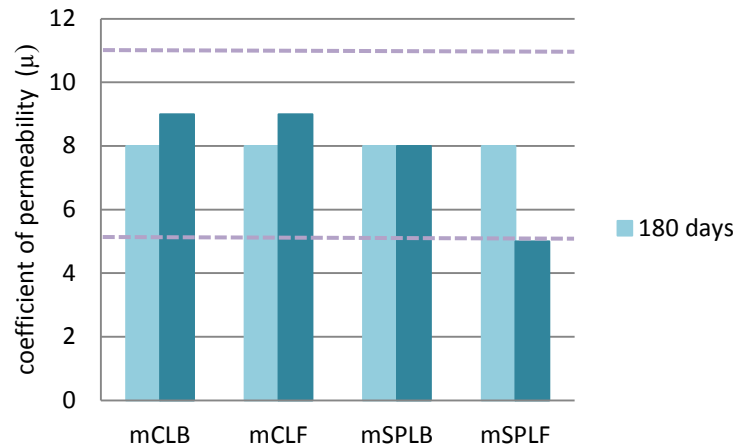


Figure 5. Variation of water vapour inflow and outflow at 180 days

In the samples group, it is verified that water vapour permeability is stabilized with the increment macro porous proportion. In fine mortars for plasters, mCLF and mSPLF, is more irregular this water vapour exchange. At 90 and 180 days all the mortars tested tend to decrease the water vapour permeability through time and consequently its water vapour resistance factor tends to increase, with the exception of the mSPLF mortar.

It is at 180 days when there is a significant balance between the mortars mCLB, mCLF and mSPLB, their water vapour flow exchange values are stables, both downward and upward, until being the same for the three mortars practically (see Figure 5). This coincides with data obtained in porosity tests where these types of mortars have a similar size at 90 and 180 days. Only mSPLF not change its exchange trend since 28 days, in the three time periods studied, although it should be noted that the exchange flow values are progressively reduced over time. The mSPLF mortar has the largest pore size in the micropores and macropores range [17], therefore it is a less breathable mortar than the others.

To characterize this type of products, in addition to analyzing the values of the permeability coefficient, other aspects related to the flow of water vapour can be studied. In 180 days most values are almost constant then it should be analyzed the singular circumstances such us room temperature, humidity, etc. and indicated the permeability behaviours of the different dosages.

In addition, it should be noted that the water vapour diffusion coefficient (μ), that is, the coefficient of permeability indicator of mortars for render mortar and plasters, should be provided by the manufacturer, who is responsible for ensuring that this data are supported

by certified tests. With Traditional products is difficult this data to appear normally in technical specifications of the data sheet.

In the specifications documents for AFAM coating mortars [18] the manufacturer conditions required to facilitate the product characteristics are reflected. In this regard, there is little organized information that could be useful as data reference. The requirements only apply in the Spanish standards to exterior use or monolayers mortars; there are no specific requirements for the application in interior use mortars. For this reason, it is interesting to evaluate these pre-doses mortars characteristics, that these reference values are defined to use in architectural heritage.

Conclusion

Experimental data, according to the dimensions of the test, permit discussed water vapour permeability properties of two types of aerials lime mortars. These properties are altered over time, registering the stable permeable capacity of all mortars since the 90 days and almost completely at 180 days. After 90 days, it is the SPL mortars that retain the most water.

From the evaluation of the resultants, it observed that this test method applied should be change the time control periods of water vapour flow exchange, considering the time required for each material, in this case the aerials lime mortars, because coefficient of permeability is critical to evaluate the respirability of the wall.

The values obtained with these products, high quality and purity air lime mortars, verify the quality of their components and confirm their ability to eliminate water vapour by themselves and through the layers of the wall coating; these characteristics improve stability and durability of mortars as products used to the rehabilitation and restoration of the architectural heritage.

References

1. Myrin M and Balksten K (2006) Lime-based repair mortars - influence by surface working methods on behaviour and durability of mortar". International Conference on Heritage, Weathering and Conservation, pp. 763-769. Madrid, España.
2. Pacheco-Torgal F, Faria J and Jalali S (2012) Some considerations about the use of lime-cement mortars for building conservation purposes in Portugal: A reprehensible option or a lesser evil. *Construction and Building Materials*, vol. 30 pp. 488-494. <https://doi.org/10.1016/j.conbuildmat.2011.12.003>
3. Budak M, Akkurt S and Boke H (2010) Evaluation of heat treated clay for potential use in intervention mortars. *Applied Clay Science*, vol. 49, nº 4, pp. 414-419. <https://doi.org/10.1016/j.clay.2009.11.031>

4. Corroto M, Sabador E, Medina C, Frías M, Sánchez-de Rojas M (2012) Reparación de revocos de morteros. Nuevos documentos normativos de AENOR. Informes de la Construcción. Vol. 64, Nº EXTRA, 141-151. ISSN: 0020-0883. eISSN: 1988-3234. doi: 10.3989/ic.11.052
5. Rosell Amigó JR (2012). Algunas consideraciones sobre la cal y sus morteros. II Jornadas FICAL. Barcelona: Universitat Politècnica de Catalunya. Grup de Recerca GICITED, pp. 6-16. Access in <http://hdl.handle.net/2099/11616>
6. Ontiveros-Ortega E, M.Ruiz-Agudo E, Ontiveros-Ortega A (2018) Thermal decomposition of the CaO in traditional lime kilns. Applications in cultural heritage conservation. Construction and Building Materials, Volume 190, Pages 349-362. <https://doi.org/10.1016/j.conbuildmat.2018.09.059>
7. Stefanidou, Maria (2010) Methods for porosity measurement in lime-based mortars. Construction and Building Materials. Volume 24, Issue 12, Pages 2572-2578 <https://doi.org/10.1016/j.conbuildmat.2010.05.019>
8. Elert K, Rodríguez-Navarro C, Sebastian Pardo E, Hansen E, Cazalla O (2002) Lime Mortars for the Conservation of Historic Buildings. Journal Studies in Conservation. Volume 47, 2002 - Issue 1 <https://doi.org/10.1179/sic.2002.47.1.62>
9. Marinowitz C., Neuwald-Burg C., Pfeifer M. (2012) Historic Documents in Understanding and Evaluation of Historic Lime Mortars. Historic Mortars. RILEM Bookseries, vol7. Springer, Dordrecht. https://doi.org/10.1007/978-94-007-4635-0_2
10. Carrera Díaz G. Cal de Morón, (2015) Ser calero en Morón de la Frontera, Sevilla, España. Ejemplo de Buenas Prácticas Salvaguarda del Patrimonio Inmaterial de la Humanidad, En Cal viva. Asociación Cultural de Hornos de la Cal de Morón, pp.111. ISBN: 978-84-606-5983-9.
11. UNE EN 1015-19:1999/A1: 2005. Métodos de ensayo de morteros de albañilería. Parte 19: Determinación de la permeabilidad al vapor de agua de los morteros endurecidos de revoco y enlucido.
12. Sastre Sastre R, Muñoz Salinas F (2010) Propiedades de los materiales y elementos de construcción. Edita Universidad Politècnica de Catalunya, SL. Barcelona. España.
13. Ontiveros-Ortega E, Rodríguez-García R, González-Serrano A, Molina L (2018) Evolution of mechanical properties in aerial lime mortars of traditional manufacturing, the relationship between putty and powder lime. Construction and Building Materials, Volume 191, Pages 575-589 <https://doi.org/10.1016/j.conbuildmat.2018.10.053>
14. UNE-EN 1015-11:2000/A1:2007. Métodos de ensayo de los morteros para albañilería. Parte 11: Determinación de la resistencia a flexión y a compresión del mortero endurecido.

15. Arizzi A, Cultrone G (2013) The influence of aggregate texture, morphology and grading on the carbonation of non-hydraulic (aerial) lime-based mortars. *Quarterly Journal of Engineering Geology and Hydrogeology*. 46(4) pp. 507-520.
16. González-Serrano A, Rodríguez-García R, Molina-Sanz L, Ponce-Ortiz M (2017) Natural clay plasters: Checking regulations to characterizations tests. *Vernacular and earthen Architecture: Conservation and Sustainability. Conference: Sostierra 2017, 3rd Restapia, 3rd Versus*. pp. 379 - 382. doi: 10.1201/9781315267739-67
17. Ontiveros-Ortega E, Ontiveros-Ortega A, Moleon JA, Ruiz-Agudo E (2017) Electrokinetic and thermodynamic characterization of lime-water interface: Physical and rheological properties of lime mortar. *Construction and Building Materials*. Volume 151, ELSEVIER. Pages 809-818 <https://doi.org/10.1016/j.conbuildmat.2017.06.147>
18. Asociación Nacional de Fabricantes de Mortero (AFAM) (2012) *Recomendaciones y Pliego de Condiciones para Revestimientos de Mortero. Código Técnico de la Edificación*. ISBN: 978-84-613-2654-9 Access in www.afam.es

Challenges and strategies of preventive conservation in places of worship – Church of Nossa Senhora de Guadalupe case study

Alexandra Marco^{1,2,3}, Manuela Pintado³, Patrícia R. Moreira^{1,2,3}, Eduarda Vieira^{1,2}

(1) *Escola das Artes, Universidade Católica Portuguesa, Porto, Portugal, alexandra.marco.ma@gmail.com*

(2) *CITAR – Centro de Investigação para a Ciência e a Tecnologia das Artes, Universidade Católica Portuguesa, Porto, Portugal, prmoreira@porto.ucp.pt, evieira@porto.ucp.pt*

(3) *CBQF – Centro de Biotecnologia e Química Fina, Universidade Católica Portuguesa, Porto, Portugal, mpintado@porto.ucp.pt*

Abstract

Romanesque granitic churches with 15th–16th century fresco mural paintings presenting black stains that tarnish both support and chromatic layer and the solutions for their removal, are the primarily focus of our on-going investigation. One of its unique case studies, Nossa Senhora de Guadalupe Church, is addressed here for the identification of its main environmental risks aiming to develop a preventive conservation plan that improves the preservation of the monument's value, ultimately more cost-effective. One of its main problems has to do with the excavation site with a partially buried main chapel and unexcavated blocks in some facades. The sunken part of the building as water capillarity in its floor, water percolation in the south facade, and roof infiltrations (in the past and present). Apart from the high content of water, other environmental factors such as chromatic alteration, biological growth, wind erosion and particle deposition contributed to its degradation. Solutions were suggested for the more urgent and curative ones, but the long-term maintenance measures will only be possible to recommend after a thorough examination of the monument's conditions.

1. Introduction

In general churches undergo numerous and varied reforms and transformations throughout their history, either due to cult changes or aesthetics at the time. They are comprised of different materials (original or additions) with different tensions, which may or may not be compatible amongst each other, and with different degrees of decay/weathering. As such, it is essential to know the characteristics of the building under study (construction materials, construction system, topographic implantation, incidence of meteoric elements, solarisation, among others), to understand its behaviour. Depending on where the monument is established, there are different factors such as climate, geographical location and terrain characteristics, which should be considered [1]. Since mural paintings live entwined with the architectural structure, it is therefore necessary to have a global view of the problem when regarding their degradation and conservation. Physical, chemical and biological factors are responsible for the deterioration of monuments [2-4] with many of these elements acting in

synergistic or antagonistic associations [1, 5]. Several granite churches on northern Portugal show a problem of dark stains that appear both on the support and on the 15th–16th fresco mural paintings. Solutions for what seems to be caused by a succession of factors, both biological and chemical, yet to be encountered are under survey [6-9].

The existence of guidelines, norms, and guiding principles [10-15] is designed to assess risks and, consequently, to manage those risks. Risks to cultural heritage depend on natural threats caused by meteoric agents that are continuous, with slow, cumulative and irreversible effects [16] while anthropogenic ones result from various human actions including inadequate management, lack of maintenance, neglect or inadequate restorations. Risk assessment should be an integral part of conservation practices and conservation and management plans. When (or if) threats and causes of deterioration are identified, evaluated and prioritized, their effects can be minimized or mitigated based on a management plan [17]. The technical teams involved in the architectural heritage must be multidisciplinary, consisting of professionals with different expertise, such as Civil Engineering, Architecture or Conservation [18].

1.1 Mural paintings in N. Portugal: the case of Nossa Senhora de Guadalupe Church

The fresco painting was of common use in the 15th and 16th century in religious buildings from north to south of Portugal [19]. Later, the aesthetic changes and the novelty of other decoration styles, such as tiles, or the use of gold leaf, to gild the wooded altars were responsible for many of these paintings being destroyed or covered. Due to recent restorations of those altars, a considerable number of paintings are being rediscovered, some of them with urgent need for conservation.

Built in the second half of the 15th century, the Church of Nossa Senhora de Guadalupe is still unchanged preserving the primitive feature. The church was possibly commissioned by D. Fernão de Brito, due to the similarities of style with other cultural heritage in Vila Real that are attributed to him [20]. It is of Romanesque style with the exception of the lancet arch portal in the main façade and the triumphal arch that are Gothic. The exterior decoration is sparse [21]. The lateral facades are traversed in the upper part by numerous carved stones of humans and animals. The back facade corresponding to the main chapel exhibits a coat of arms, the same one depicted on the altar table [22] presumably later added to the construction [21] (Figures 1a, 1b, 1c, 1d). The interior is also plain, composed by a single nave, main chapel and a sacristy on its left. The south portal is one meter above ground, so a stairwell of four semi-round steps helps reaching it (Figure 2). The granite slab floor preserves graves, some of them engraved from the 16th and 17th century (Figure 3). The only decoration of some refinement is the 16th century frescoes on the bottom wall of the main chapel or presbytery dated from 1529 and signed **AM.DRA** [21]. It is a composition organized in 3 frames – in the central area is represented the Tree of Jesse, with 11 royal male characters being portrayed from the waist up, upon open flowers. All of them hold a phylactery that identifies them by name. At the centre, the Virgin Mary holds the child in her

right hand [22]. The background of this main composition is an imitation of a brocade textile [23]. Two columns frame the central composition of the frescoes from the grotesque drawings at the sides with red background and grey and white figures [24], and on a lower level a geometric composition. The altar table has a representation of an episcopal coat of arms attributed to D. Pedro de Castro, who commissioned the mural paintings [23], encased by a laurel wreath and flanked by two hybrid figures in a grotesque style [22] (Figure 4).



Figure 1. (A) Romanesque church with gothic portal. (B) Coat of arms on the exterior facade of the main chapel. (C) Arch portal with fitomorphic decoration. (D) Carved ornates of humans and animals in the upper part of the building on the lateral facades. (C) and (D) © João Sandes.



Figure 2. Semi-round stairwell leading to the exit of the South portal

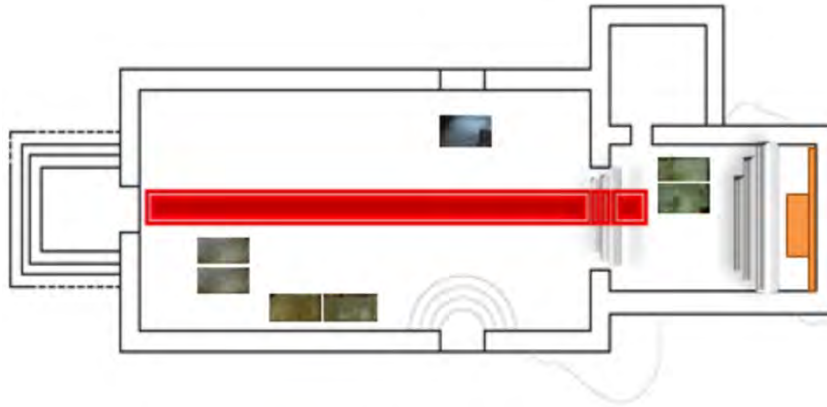


Figure 3. Plant with the location of the tombs: five on the nave and two on the main chapel



Figure 4. Fresco mural painting from the 16th Century representing the Tree of Jesse on the bottom wall and an episcopal coat of arms attributed to D. Pedro de Castro who commissioned the mural paintings on the altar table of the main chapel

According to Joaquim Caetano [24] the murals are attributed to the painting centre “Oficina III”, operating also in S. Salvador de Travanca Monastery (Amarante), Sta. Marinha Church (Vila Real), S. Brás Chapel (Vila Real), S. Miguel de Tresminas Church (Vila Pouca de Aguiar), Sta. Leocádia Church (Chaves), and S. João Baptista Church (Chaves) [24, 25] (Figure 5).

2. Risk assessment

2.1 Interior/exterior surroundings

The Church of Nossa Senhora de Guadalupe oriented west–east is allocated on a rural area, isolated on a small elevation of land at the end of a path, with no traffic. In the vicinity of the back of the churchyard there are two private constructions. From the lateral view of the

monument it is perceived that the church was excavated on site, in an inclined terrain with a lower height on the east facade and downhill to the main entrance (Figure 6). Three granite blocks unexcavated are embedded on the north and south facades (Figures 7a, 7b). The graves on the floor of the nave still have the bones of the deceased accordingly to the clerical who oversees Vila Real church's heritage for 30 years. In the vicinity of the church, to south, there is a water course for irrigation at 10 meters and a stream at 500 meters west. The church is surrounded by not very dense vegetation, constituted essentially of undergrowth and some bushes leaning on the facades, with fewer trees on the outer perimeter.



Figure 5. Map with the location of the 6 churches with mural painting belonging to the same painting centre “Oficina III”: S. Salvador de Travanca Monastery (Amarante), Sta. Marinha Church (Vila Real), S. Brás Chapel (Vila Real), S. Miguel de Tresminas Church (Vila Pouca de Aguiar), Sta. Leocádia Church (Chaves), and S. João Baptista Church (Chaves). ©Google Maps

2.2 Interventions review

The interventions on Guadalupe church were requested by DGEMN (General Directorate of National Buildings and Monuments) and only the more relevant were listed here.

Between 1969 and 1992 the ceilings of the sacristy and the nave were repaired because of poor conditions and risk of collapsing, consolidated and waterproofing the latter. Cement mortar joints were removed in 1996 from the granite floor, main chapel, its leading stairs, and the outer pavement. Some new stones were applied where the original ones were too degraded or missing [22]. In the same year a polychrome wooden panel representing the Tree of Jesse covering the bottom wall of the main chapel was removed (no indication where it went), and frescoes were found with identical theme [20]. Mural da História (conservation-restoration company with mural painting expertise) did the mural restoration comprising of the bottom wall with the Tree of Jesse and an altar table. In 2004 the risk chart of the

monument was elaborated by DGEMN/DREM Norte (Northern Regional Directorate of National Buildings and Monuments) [22].

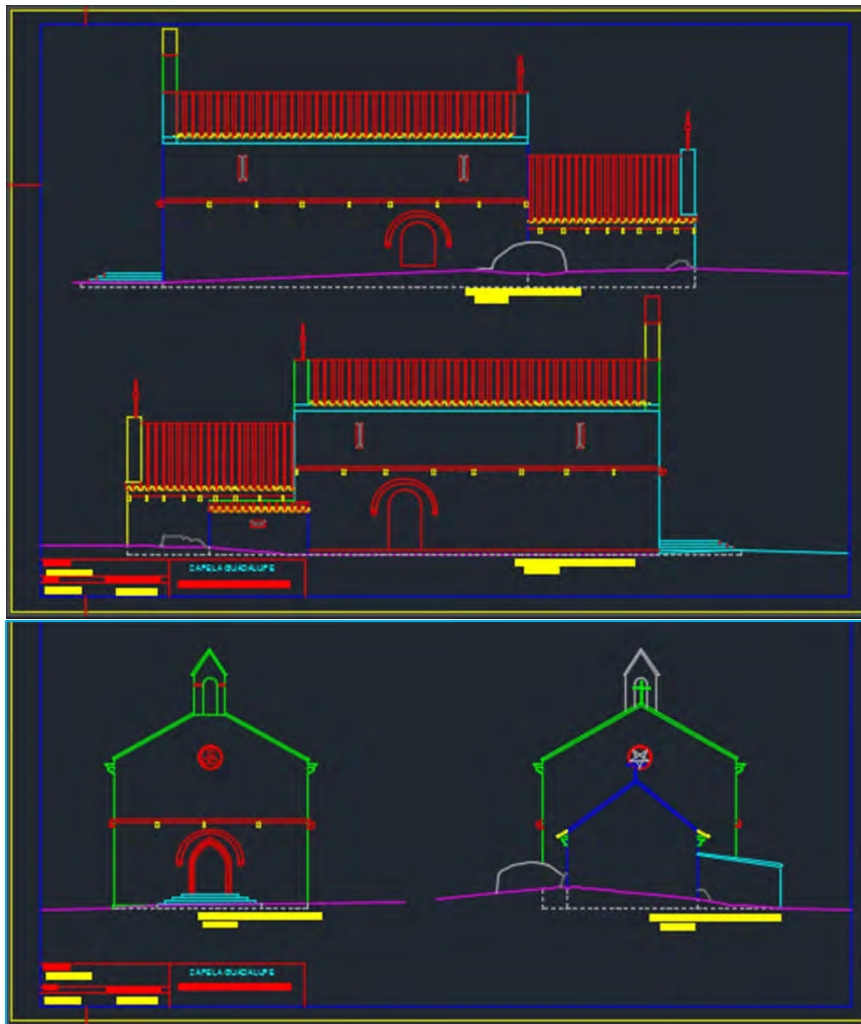


Figure 6. Architectural plants of the 4 facades of Guadalupe Church demonstrating different terrain elevations with lower height on the chapel than on the main entrance. ©João Sandes



Figure 7. Granite blocks unexcavated, part of the walls: (A) Approximately with three meters on the North façade of the main chapel. (B) One small and the other with a length of approximately three meters on the South facades of the main chapel and nave.

Although these interventions exist for consultation, others occurred without being historically processed on file. One of those interventions was the substitution on a date not specified and by unknown persons of the granite joints by Portland cement mortars. Another intervention refers to the two 18th (?) century altars transferred from the Vila Real Cathedral to the nave of Guadalupe church, one on each side of the triumphal arch, replacing the painted wooden panels that hanged on the walls. These paintings are now facing each other in the north and south facades of the nave. This information came to us from testimony by the elderly caretakers of the church.

2.3 Conservation conditions. Deterioration agents mapping

The mapping of deterioration is a methodology that allows to relate the location of the alteration products with the causes of the alterations, namely the various climatic, architectural and lithological aspects involved and to monitor their development [26]. The building and its movable heritage shows different types and levels of deterioration.

2.3.1 Granite

Granite can show various forms of alterations, frequently present in our monuments, contradicting the idea that these rocks are of resistant material and, therefore, with long durability [3]. Some of those forms of alterations are present in this church stones such as granular disintegration, loss of material, efflorescence, percolation, chemical degradation, biocolonization, open joints, and also deposits of mortar leakages and water capilarity, exemplified by Figures 8a–8e. The majority of the granite joints either on the walls or on the floor are missing with some being replaced by Portland cement mortar (Figure 8f). Both lateral walls of the nave have dark stains at about a meter high with some green biocolonization (photosynthetic microorganisms such as algae).

2.3.2 Integrated heritage

The ceilings of the main chapel and the sacristy have infiltration problems (Figure 9a). The integrated heritage such as two wooden altars, the stairways and floor of the choir and a full half size figure sculpture are infested by wood-decay insects (Figure 9b). Candlesticks are placed on the stairs to the main chapel and the wax pours onto the granite floor (Figures 9c, 9d). There is still organic matter on the soil of the church beneath the granite slabs belonging to the dead buried in the graves at the nave and main chapel. The switchboard as some precarious connections and is also employed to storage utensils and liquid bottles. There are some procedures in place establishing a climate of comfort for worshipping such as a gas heater and a butane gas cylinder (Figures 9e, 9f). The mural paintings were restored in 1996. However since that date, and although the cohesion of the layers appear solid, a whitish veil is now covering them, presumably salt efflorescence. The dark stains that conceal the paintings, almost to the point of not being able to identify what lies beneath (the Virgin

Mary), couldn't be cleaned in the restoration process, and still exists with the same intensity (see Figure 4).

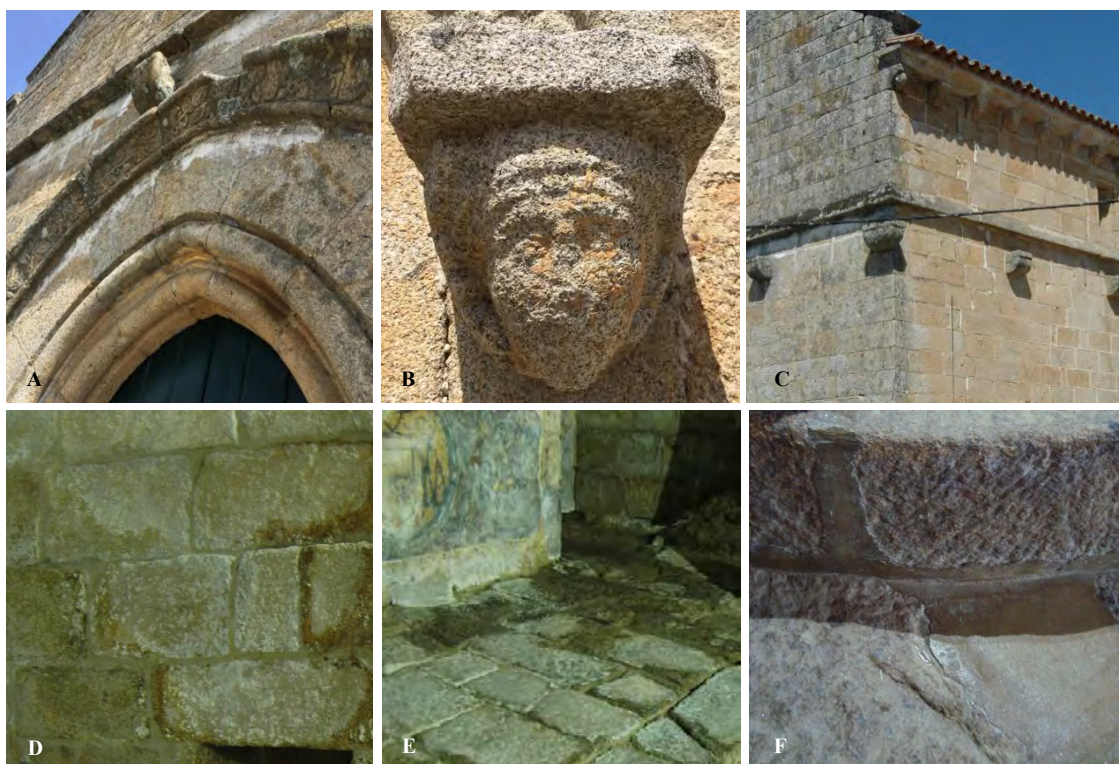


Figure 8. (A) Whitish deposits of mortar leakages probably due to rainwater infiltrations, loss of decorated stone fragment, and biocolonization by different species of lichens (colouring the facades in whitish-grey, yellow, orange, and dark green). (B) Granular disintegration of the granite stone by erosion of the wind and pluvial activity. ©João Sandes. (C) Extremely yellow granite on the South façade of the nave probably a result of a chemical process, and oxidation of some of the minerals that constitute the granite blocks releasing iron oxides. (D) Salt efflorescences and water percolation in the church interior walls. (E) Groundwater capillarity due to open joints. (F) Application of cement mortars in some previous undocumented intervention.

2.4 Risk factors

Water is one of the most aggressive agents and causes the main structural damages. Degradation can be caused by a physical mechanism or the combination of a physical and chemical process [27]. Humidity can be conveyed by air, capillarity, condensation or infiltration [28]. Rainwater infiltrates the building through open joints or fractures of the masonry and bad roof insulation. The capillarity moisture increase is the result of groundwater capillarity rise through the foundations. Water is also a vehicle for transporting other alteration agents, such as soluble salts [29]. The greater destructive action of soluble salt minerals is when solubility, hygroscopicity and the crystallization of forces developed in their growth process is higher, as well as increased occurrences of crystallization/dissolution cycles [30].

The indoors environment depends heavily on the outside climate, the building's structure and size, building materials, soil hydrogeology [18] and topography. The surface materials are affected by sudden changes in environmental temperature and humidity, as these two

parameters govern the most common forms of deterioration, such as wet-dry cycles [16], thermal shocks [31], dissolution-crystallization of surface or substrate salts [32, 33, 34], and the materials stress or fatigue, which induces fracture, blisters, peeling, disintegration and detachment of the stone surface [16].

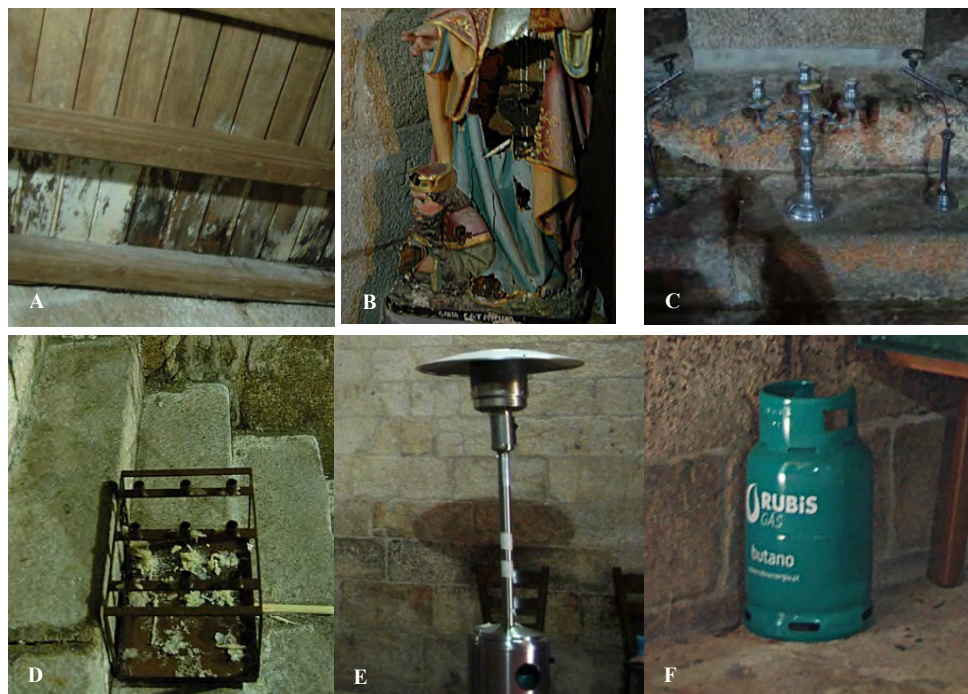


Figure 9. (A) Actual state of the ceiling in the sacristy with water infiltrations. (B) Wooden polychromed sculpture hollowed by insects infestation. (C) and (D) Candlesticks placed on the stairs of the main chapel and when litten, the hot wax pours onto the granite floor. (E) Gas heater. (F) Butane gas cylinder

2.5 Risks. Levels and measures

There are ten agents of biodeterioration or risk factors. Nine agents were defined by Stefan Michalski for the CCI [35] and published by ICOM in 2004 [12] – direct physical forces, theft and vandalism, fire, water, plagues, contaminants, lighting/radiation, temperature, and relative humidity. A tenth agent – negligent procedure – was later added to Michalski's table, proposed by Robert Waller. However, in this present study, only the risks with greater impact were taken into consideration.

Among these agents, water exists in abundance on the walls and especially the floor of Nossa Senhora de Guadalupe Church either by infiltration through the roof in the past and currently or by infiltration through the walls, condensation or capillarity, being responsible for salts perceived in the superficial accumulation of white powder on the walls and floor, and for biocolonization. Rain carries contaminants that degrade materials on the outdoor [36], and water percolation is responsible for the granite stone hydrolysis process by altering its elemental alumina-silicate minerals. The wind carries dust and solid particles responsible for the abrasion and erosion of stone blocks. Considering the location of the dark stains, this case study also differs from others in the vicinity and presenting the same problems. While usually encountered in the areas that visually seem to be damper, at one to two meters

high, in this present church the tarnished area is located near the roof and at the centre of the wall. There are several hypotheses for the materialization of these stains, yet to be conclusive in our studies, such as the rainwater infiltration through the poor ceiling insulation, the product of chromophore microorganisms, or a symbiosis of several factors.

There are plagues such as lichens, mosses and plants on the outdoor facades. The profusion of lichens denotes high levels of humidity and low atmospheric pollution indicating that the church isn't located in an urban or industrial area [30, 37] as does the absence of black crusts in its facades [37]. There is also an insect's infestation on the wooden elements, and a very likely possibility of the existence of bacteria and fungi that, although not visible to the naked eye, dwell on every microclimate. Lichens and mosses are responsible for the degradation and staining of the granite blocks, while bacteria, fungi and lichens may excrete acids that solubilize materials, produce pigments (like the dark stains in the mural painting), and cause fissures and cracks by the establishment of hyphae inward layers.

Negligent procedure is characterized by the lack of proper cleaning and building maintenance. The cleaning of the church is weekly, prior to the religious service that varies in schedule according to the time of the year, but is restricted to one day per week (Wednesday). The insufficient cleaning cause deposition and concentration of dust, dirt and debris on the surfaces, besides the negative aesthetic impact that they represent, they cause retention of humidity and alteration of temperatures, and consists of a significant source of nutrients, generating successive biological colonization [38]. Other negligent procedures may be the bad course of actions such as applying products to eradicate the wooden insect infestation without training, supervision, or the use of specialized help (as conveyed by the custodians of the monument), or the filling of some joints with Portland cement mortar (not specified when or by whom) that arise compatibility problems. The cement-based mortars applied in ancient architectural structures with traditional technologies may damage the original because of their significant differences in physical and mechanical properties. They create different and higher tensions, fractures on the less resistant or older of the two materials – granite, and restraining water evaporation on the granite blocks, produce some soluble salts that promote its migration to the more porous materials [39]. Ultimately, impacts the building's thermal inertia.

Temperature (T) and relative humidity (RH) were not monitored at this stage. However, the church is located in a region with large thermal amplitudes (day-night and winter-summer). Substantial variations of T and RH are responsible for infiltrations, condensation, pitting, efflorescence, detachment, fractures, stains, biocolonization and biodegradation, among others.

2.6 Preventive conservation strategy

Portugal does not have a preventive conservation policy for historical buildings. The only maintenance plan, regarded more as a theoretical proposal, was established for one of our major monuments and Lisbon's most visited, and the result of a Ph.D. thesis in 2007 [40] based on British and Italian methodology [41]. However, the concern regarding maintenance plans for heritage buildings is not new. Since the 1970's The Netherlands implemented "Monument Watch" a preventive conservation of built heritage, closely followed by northern Europe (although not responsible for the execution of the maintenance actions only their planning) [42], and in 2009 in Belgium was founded the UNESCO PRECOM³OS Chair, established at Ku Leuven (Leuven Catholic University) (<https://set.kuleuven.be/rlicc/research/precomos>). In Portugal, because of the lack of budget, knowledge, and support tools to help planning, there is a more reactive maintenance strategy instead of a more preventive one [41]. To fill this gap, it was created in 2018 the HeritageCARE project – Monitoring and preventive conservation of historical and cultural heritage (<http://heritagecare.eu/>), partner of DGPC (General Directorate of Cultural Heritage) to work as a risk management tool in response to the need for an integrated methodology for the preventive conservation of historic buildings in Southwest Europe.

Facing that difficulty, we based our work upon the three PRECOM³OS (Preventive Conservation, Maintenance, and Monitoring of Monuments and Sites) [17] preventive conservation levels: (i) primary prevention – means to avoid the causes of unwanted effects (degradation); (ii) secondary prevention – means that allow early detection monitoring of the symptoms caused by unwanted effects; and finally (iii) tertiary prevention – means that allow avoiding further spread or the generation of new unwanted (side) effects [43].

The existence of monitoring, maintenance and diagnosis methods mitigates deterioration, avoids the unnecessary use of curative treatments to prolong the life of cultural heritage, and induces a reduction in intervention costs if and when that is required. The maintenance plan is the primary intervention and a necessary tool to uphold the monuments (churches) good conditions, while assuring its proper use [44].

The secondary intervention is monitoring as a diagnostic tool. Monitoring and examination methods to be developed this current year, will allow for a more suitable Preventive Conservation Plan to devise a tertiary intervention in a sustainable approach by rationalizing and optimizing if possible the available resources [41]. The tasks developed are the assessment of climate monitoring (to be evaluated monthly) and examination methods. The examination methods of the granite structure and mural painting layers will start by an extensive photographic documentation; characterization of the type and origin of the granite; characterization of paint and mortar layers by different analysis; identification of the type of salts present; characterization of mineral components of the water; characterization of water content on the surfaces; identification of the microorganisms present;

characterization of the dark stains on mural painting and the elaboration of deterioration maps.

The alteration factors are usually treated through curative interventions, while the causes of those alterations are addressed with preventive interventions [29]. Although it is preferable to preserve than cure, there are some aspects of this monument that demand a hands-on approach. The humidity resulting of roof infiltrations (in the sacristy and main chapel) must be solved with the necessary repairs for a good insulation and the isolation or filling of mortar joints. For moisture originating from the soil and surface waters, it is possible to use different procedures depending on the degree of water infiltration such as execution of drainage, and execution of hydric section cuts [45]. The perimeter drainage system is the most common and most effective with several types of solutions: porous draining pipes; perimeter air chamber; among others. Waterproofing products for application on the walls are a solution when drainage is not possible. Also, the electro-physical barriers is one of the methods with better results, only it is intrusive, for it is necessary to make a cut on the wall to insert a metallic tube and needs periodic monitoring and maintenance [46]. Moreover, the wooden altars are in an urgent need of disinfestation. These interventions are costly and should be conducted by specialized companies. In the end, it is the responsibility of the historical building tutelage, in this case the DGPC to decide how and when should they be carried out as well as the available budget for such treatments.

Conclusion

To prolong the life span of historic buildings and its integrated heritage, and to reduce costs, it is essential to devise an effective management strategy and maintenance plan.

Having taken the case study of Nossa Senhora de Guadalupe Church as a starting point, it allowed us to understand that the management model of conservation approach is to prevent risk factors, with a methodology of risk assessment. Although our research is still in an early stage, a preliminary qualitative assessment of the main environmental risks for the conservation of the mural paintings in this monument was performed. Once the risk factors responsible for the more significant damages are identified and prioritized, several actions can be recommended, and will then enable us to replicate and implement the methodology in other cases with identical features. It could be a key to a sustainable conservation insofar as there are monuments that are not guarded by the DGPC, nor have tutelage, and are in rural and isolated locations with cessation or decrease of cult duties in several of them. As such, only well-structured preventive conservation plans with the involvement of the local stakeholders will guarantee conserving instead of restoring, which occur when levels of degradation are severe, in the case of mural painting often amounting to total loss.

Acknowledgments

Funding: This work was supported by Fundação para a Ciência e Tecnologia (FCT) through POCH – Operational Human Capital Program, co-participated by the Social European Fund (FSE) and MCTES National Fund [Ph.D. grant number SFRH/BD/125596/2016]; the BIO4MURAL – Soluções inovadoras de biotecnologia para remoção de pigmentação e conservação preventiva de pintura mural cultural e historicamente relevante supported by FCT,IP and Programa Operacional Competitividade e Internacionalização (FEDER) [grant number PTDC/HAR-ARQ/29157/2017] and FCT for funding through the Strategic Projects CITAR [grant number UID/EAT/0622/2016] and CBQF [grant number UID/Multi/50016/2013]. We also thank João Sandes, Master student of Conservation-restoration at the Universidade Católica Portuguesa (Porto), for the architectural plants and some of the church photography.

References

1. Crispim C A, Gaylarde C C (2005) Cyanobacteria and biodeterioration of cultural heritage: A review. *Microb Ecol* 49(1): 1–9. doi: 10.1007/s00248-003-1052-5
2. Blazquez A B et al (2000) Evaluation of the effect of some biocides against organisms isolated from historic monuments. *Aerobiologia* 16(3–4):423–428
3. Costa D, Delgado Rodrigues J (2011) Conservação de materiais graníticos. Um contributo do LNEC para a preservação do património. In: Actas do simpósio Património em Construção. Laboratório Nacional de Engenharia Civil (LNEC), Lisboa. http://repositorio.lnec.pt:8080/bitstream/123456789/1003038/1/doria_costa_paper_final.pdf
4. Eckhardt F E W (1985) Solubilization, transport, and deposition of mineral cations by microorganisms – efficient rock weathering agents. In: Drever J I (ed) *The Chemistry of Weathering*. D. Reidel Publishing Company, Kiel: 161–173. doi: 10.1007/978-94-009-5333-8_10
5. Warscheid T, Braams J (2000) Biodeterioration of stone: a review. *Int Biodeter Biodegrad* 46(4):343–368. doi: 10.1016/S0964-8305(00)00109-8
6. Marco A et al (2015) Effect of different biocides on the growth of fungi responsible for black stains in mural paintings. In: *Congress of Microbiology and Biotechnology, 2015*. Évora University, Évora
7. Marco A (2016) *Caracterização da Colonização Microbiana da Pintura Mural de Três Igrejas (N. Portugal): Estudo Preliminar do Crescimento Microbiano, Avaliação da Actividade de Biocidas e Proposta de Intervenção Futura, Vol I*. Universidade Católica Portuguesa

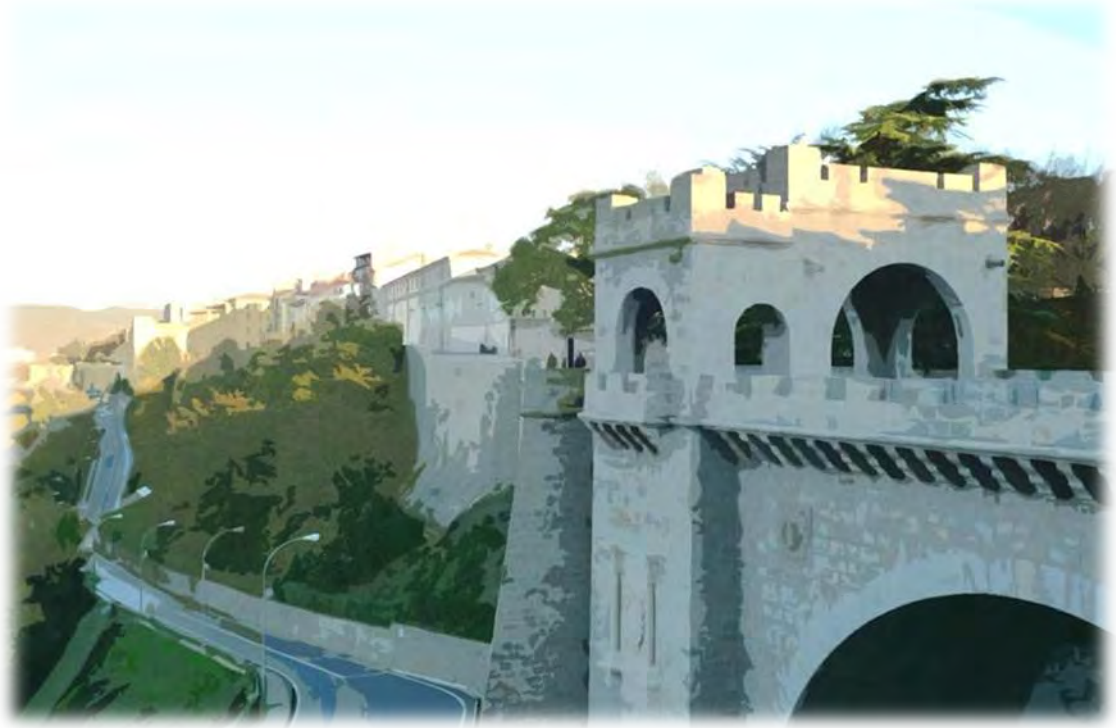
8. Marco A (2016) Caracterização da Colonização Microbiana da Pintura Mural de Três Igrejas (N. Portugal): Estudo Preliminar do Crescimento Microbiano, Avaliação da Actividade de Biocidas e Proposta de Intervenção Futura, Vol II. Universidade Católica Portuguesa
9. Marco A et al (2017) Innovative biotechnology solutions for black stain removal and preventive conservation of historical and culturally important mural paintings. In *Ciência 2017 – Encontro com a Ciência e Tecnologia em Portugal*. Centro de Congressos de Lisboa. http://www.encontrociencia.pt/files/Poster_Ciência2017.pdf
10. Camacho C (coord) (2007) *Temas de Museologia. Plano de conservação preventiva. Bases orientadoras, normas e procedimentos*, 1st edn. IMC, Lisboa. <http://www.patrimoniocultural.gov.pt/static/data/ljf/ipmplanoconservacaopreventiva.pdf>
11. Michalski S (1994) A systematic approach to preservation: description and integration with other museum activities. *Stud Conserv* 39(sup2):8–11. doi: 10.1179/sic.1994.39.Supplement-2.8
12. Michalski S (2004) *Conservação e preservação do acervo*. In: Boylan P J (ed). *Como gerir um museu: manual prático*. ICOM, Paris. <https://unesdoc.unesco.org/ark:/48223/pf0000184713>. Accessed 05 February 2019
13. Michalski S, Pedersoli Jr J L (2016) A guide to risk management of cultural heritage. In: Aslan Z, Sabik A (ed). *CCI/ICCROM, Sharjah*. https://www.iccrom.org/sites/default/files/2017-12/risk_management_guide_english_web.pdf. Accessed 16 May 2019
14. Waller R (1994) Conservation risk assessment: a strategy for managing resources for preventive conservation. *Stud Conserv*. doi: 10.1179/sic.1994.39.Supplement-2.12
15. Waller R, Michalski S (2005) A paradigm shift for preventive conservation, and a software tool to facilitate the transition. In: *ICOM Committee for Conservation, 14th Triennial Meeting The Hague Preprints: 733–738*. ICOM, London
16. Camuffo D (2013) *Microclimate for cultural heritage. Conservation, restoration, and maintenance of indoor and outdoor monuments*, 2nd edn. Elsevier Science B V, USA
17. PRECOM3OS (no date) *What is Preventive Conservation?* <http://precomos.org> Accessed 24 June 2014
18. Ferreira T M, Vicente R, Silva J A R M da (2013) Estratégias e processos de inspeção para avaliação e diagnóstico do património edificado. *Conservar Património* 18:21–33. doi: 10.14568/cp2013007

19. Correia V (1921) A pintura a fresco em Portugal nos séculos XV e XVI (ensaio). Imprensa Libanio da Silva, Lisboa
20. Parente J (no date) Roteiro arqueológico e artístico do concelho de Vila Real, 4th edn. Mediana – Sociedade Gestora de Imagem e Comunicação, SA, Porto
21. Parente J (2014) Idade Média no distrito de Vila Real. Tomo IV. Monumentos e outros testemunhos medievais, 1st edn. Âncora Editora, Lisboa
22. SIPA (1996) Igreja Paroquial de Mouços/Igreja de Nossa Senhora de Guadalupe, DGPC. http://www.monumentos.gov.pt/Site/APP_PagesUser/SIPA.aspx?id=5729. Accessed 10 April 2019
23. Bessa P V de A (2007) Pintura mural no fim da Idade Média e início da Idade Moderna no norte de Portugal. Universidade do Minho
24. Caetano J I (2001) O Marão e as oficinas de pintura mural nos séculos XV e XVI. In: Gonçalves C. V. (ed). Estudos de Património Cultural, 1st edn. Editora Aparição, Lisboa
25. Afonso L U (2009) A pintura mural portuguesa entre o Gótico Internacional e o fim do Renascimento: Formas, significados, funções, Vol I. Fundação Calouste Gulbenkian e Fundação para a Ciência e a Tecnologia, Lisboa
26. Alves C A S et al (2002) Estudo da distribuição espacial de patologias em elementos graníticos do Mosteiro de São Martinho de Tibães, Braga. Estudos/Património – Ciências e Técnicas Aplicadas ao Património: 30–36. <http://www.patrimoniocultural.gov.pt/media/uploads/revistaestudospatrimonio/n3/Estudospatrimonio3.pdf#page=30>. Accessed 27 February 2014
27. Camuffo D (1995) Physical weathering of stones. *Sci Total Environ* 167(1–3):1–14. doi: 10.1016/0048-9697(95)04565-I
28. Karaca Z (2010) Water absorption and dehydration of natural stones versus time. *Constr Build Mater* 24(5):786–790. doi: 10.1016/j.conbuildmat.2009.10.029
29. Pamplona M et al (2007) Documentar para melhor conservar: O uso de produtos consolidantes e hidrófugos em intervenções de conservação em monumentos portugueses construídos em pedra. *Conservar Património*. doi: 10.14568/cp6_2
30. Cardoso F S (2008) Estudo da deterioração da pedra na Igreja de Paço de Sousa – proposta de tratamento. Faculdade de Engenharia da Universidade do Porto. <http://hdl.handle.net/10216/59348>.
31. Schellen H L (2002) Heating monumental churches: indoor climate and preservation of cultural heritage. Technische Universiteit Eindhoven, The Netherlands

32. López-Arce P et al (2009) Deterioration of dolostone by magnesium sulphate salt: An example of incompatible building materials at Bonaval Monastery, Spain. *Constr Build Mater* 23(2):846–855. doi: 10.1016/j.conbuildmat.2008.04.001
33. López-Arce P et al (2011) Preservation strategies for avoidance of salt crystallisation in El Paular Monastery cloister, Madrid, Spain. *Environ. Earth Sci.* 63(7–8):1487–1509. doi: 10.1007/s12665-010-0733-x
34. Price C A (2007) Predicting environmental conditions to minimise salt damage at the Tower of London: a comparison of two approaches. *Environ Geol* 52(2):369–374. doi: 10.1007/s00254-006-0477-9
35. CCI (2016) Preventive conservation and risks. Agents of deterioration. <https://www.canada.ca/en/conservation-institute/services/agents-deterioration.html>. Accessed 5 June 2017
36. UNESCO (1969) La conservación de los bienes culturales, Museos y monumentos XI. ONU, Paris. https://unesdoc.unesco.org/in/documentViewer.xhtml?v=2.1.196&id=p::usmarcdef_0000135545&file=/in/rest/annotationSVC/DownloadWatermarkedAttachment/attach_import_474827ff-9133-45fd-9168-db996b76f83f%3F_%3D135545spao.pdf&locale=en&multi=true&ark=/ark:/48223/ Accessed 22 May 2019
37. Lobo, J M V (2008) Diagnóstico da deterioração do granito no Farol de São Miguel-O-Anjo (Foz do Douro – Porto) e medidas de conservação. Faculdade de Ciências da Universidade do Porto. <https://hdl.handle.net/10216/64155>. Accessed 12 March 2015
38. Lacerda M (2002) Na perspectiva do tempo. *Estudos/Património*: 5–7. <http://www.igespar.pt/media/uploads/revistaestudospatrimonio/n3/Estudospatrimonio3.pdf>. Accessed 14 September 2016
39. Torraca G (2009) Lectures on materials science for architectural conservation. Escobar A (ed). The Getty Conservation Institute, Los Angeles. http://www.getty.edu/conservation/publications_resources/pdf_publications/pdf/torraca.pdf. Accessed 21 May 2019
40. Lobo de Carvalho J (2009) Conservação do Património – Políticas de Sustentabilidade Económica. Instituto Superior Técnico de Lisboa
41. Hutsebaut-Buyse V (2016) Maintenance in historic buildings in Belgium and Portugal Civil Engineering. Instituto Superior Técnico de Lisboa. https://fenix.tecnico.ulisboa.pt/downloadFile/281870113703462/Dissertation_HutsebautBuyse.pdf. Accessed 21 May 2019

42. Čebroň Lipovec N, Van Balen K (2008) Preventive conservation and maintenance of architectural heritage as means of preservation of the spirit of place, in 16th ICOMOS General Assembly and International Symposium: Finding the spirit of place – between the tangible and the intangible. ICOMOS 1–8, Quebec. https://www.icomos.org/quebec2008/cd/toindex/77_pdf/77-oKQk-292.pdf.
43. Van Balen K (2015) Preventive Conservation of Historic Buildings. Restoration of Buildings and Monuments 21(2–3):99–104. doi: 10.1515/rbm-2015-0008
44. Della Torre S (2010) Critical reflection document on the draft European standard CEN/TC 346 WI 346013 Conservation of cultural property – condition survey of immovable heritage. In: Seminar on condition reporting systems for the built cultural heritage. Monumentenwacht Vlaanderen. Unpublished discussion document, Antwerp
45. Freitas V, Gonçalves P (2003) Humidade na construção. Feup: 1–56. http://paginas.fe.up.pt/~vpfreita/6_PC2005.pdf. Accessed 21 May 2019
46. Díaz C del P (2004) Pintura mural. Conservación y restauración, 1st edn. Cie Inversiones Editoriales Dossat 2000, S.L., Madrid

Topic 12: Repair mortars and grouts. Requirements and design. Compatibility issues. Durability and effectiveness. Repair mortars: Adequacy of testing procedures



Effects of natural zeolite addition to lime based render layers for restoration of historical buildings

Marina Aškračić¹, Dimitrije Zakić¹, Aleksandar Savić¹, Ljiljana Miličić²

(1) Faculty of Civil Engineering, University of Belgrade, amarina@grf.bg.ac.rs; dimmy@grf.bg.ac.rs; savic.alexandar@gmail.com

(2) Laboratory for binders, chemistry and mortars, IMS Institute, Belgrade, ljiljana.milicic@institutims.rs

Abstract

Renders, as the most exposed elements of historical buildings, have limited durability therefore their periodical inspection and replacements are necessary. Various studies have been made with a purpose to develop renders with improved resistance to environmental conditions, yet compatible with originally used materials (mortars and masonry). Although traditional renders were applied in several layers with different properties, most of the studies are based on only one layer production and testing. Natural zeolites are crystalline hydrated aluminosilicates with a specific three-dimensional framework structure. They have been used as a pozzolanic addition in lime mortars since ancient times. This paper presents the effects of natural zeolite addition on physical and mechanical properties of lime-based historical mortars, representing both base and superficial layer of traditional renders. Only locally available materials were used in the mix design. Capillary water absorption coefficient, water absorption after 48 hours, open porosity, flexural and compressive strength were measured on prismatic samples after 14, 28 and 60 days, and compared with the recommended properties for each render layer. The results demonstrate positive effects of zeolite addition to lime based render layers for restoration of historical buildings.

Keywords: natural zeolite, lime renders, compatibility, historical mortars

Introduction

In the case of historical buildings renders as the outer coats are continuously exposed to environmental conditions and therefore demand constant care and repair. Historical circumstances in many parts of the world caused periods of complete neglect of these buildings and sometimes even complete loss of original coatings. Information about technology of their production and placing, as well as their functionality are based on existing literature and investigations performed on preserved renders.

They were usually placed in three layers, each of them having different design and properties. The first (base) layer was used for homogenization of the surface and creation of the bond with the support [1]. It was usually made of a coarse mortar with binder:aggregate volumetric proportions of 1:2-3 and well-graded sand with particle size up to 4-5 mm. Type of the applied aggregate usually differed depending on local availability [2]. The

intermediate layer corrected the defects of the base layer and finishing layers [1]. It usually had the similar composition to the base layer, with possible increase in binder content, sometimes containing sand of finer gradation [2]. The third (outer) layer had both aesthetic and preservation function. It defined the colour and the finishing of the surface and decreased weathering of the whole system [1]. It was usually designed with higher binder content (binder:aggregate ratio equalled 1:1-2) with fine sand (particle size below 0.5 mm). White sand or powdered marble or chalk were often used to achieve a light colour of this layer [2].

In order to accomplish the best performance of a multilayer system described above it is recommended that the strength of the render layers should be unchanged or to be decreasing from inner to the outer layers, while water vapour permeability should be as high as possible, and it should increase towards the outer layers. Capillary water absorption should also follow the same trend, and increase towards the outer layers.

If the renders were exposed to high relative humidity conditions, different materials had been used in order to improve properties of lime based system. In these cases natural hydraulic limes or pozzolans or even brick dust had been applied [3]. A number of investigations in different countries was conducted focusing on application of locally available natural or artificial pozzolanic materials and exploring their possible use in production of lime based mortars, renders and plasters. These include: metakaolin, crushed brick, enamel glass, Cabo Verde and Acores pozzolans, clays calcinated at different temperatures, Czech clay shell, different clay minerals, natural and artificial zeolite, etc. [4-8].

Natural zeolites, used as pozzolanic addition in the study described within this paper, are microporous, hydrated alumina-silicate minerals with open three-dimensional crystal lattice. Zeolites from different locations have different crystalline structure. Use of zeolite as a pozzolanic addition has been investigated in several papers, but the connection between its reactivity and composition has not yet been explained in details. Ince et al. [7] investigated influence of partial replacement of lime with zeolite and Bayburt stone by mass in amount of 2.5, 5, 10, 20, 30, 40 and 50%. Researchers concluded that the addition of these materials increased compressive strength of lime mortars and influenced the decrease of porosity by improving the rate of water loss at the early stages of mortar production. Optimum amount of replacement, based on the results of this study, was 30%. Pavlík and Užáková [6] also investigated lime based mortars with 50% of lime replacement with natural zeolite. These authors also varied the curing conditions of the prepared mixtures. The highest values of compressive strength were achieved for the humid conditions. When samples were exposed to combined curing conditions (three months in humid and then in laboratory conditions) loss of compressive strength was noticed, although reached values still exceeded values achieved in the mixtures constantly exposed to laboratory conditions. Liguori et al. [9] investigated zeolite addition in fiber reinforced natural hydraulic lime mortars. The highest increase in strength and the lowest porosity were achieved by 20% replacement.

This paper presents study of influence of partial mass replacement of lime with locally available natural zeolite (in Serbia) on the physical and mechanical properties of lime mortar mixtures, intended for both inner and outer render layers applied for restoration of historical buildings.

Materials and mixtures

In order to produce render system that would be compatible with the historically used materials, six mixtures intended for both inner and outer render layers were designed. Two mixtures containing only lime putty as a binder and sand of different gradations were used as reference. Other four mixtures were made with partial replacement of 20% and 40% of lime by natural zeolite.

Materials

Lime putty produced by “Javor”, Veternik (Serbia) was used as a binder in all of the mixtures. This putty was produced by slaking of quicklime from “Jelen Do” quarry, Požega (Serbia) with water in excess. At the time of mixing the lime putty was one year old (preserved for 6 months by the producer, and then 6 months in sealed plastic containers). The chemical composition of the putty, determined by chemical analysis, is presented in Table 1. Bulk density of the putty was 1390 kg/m³, while bulk density of lime was 600 kg/m³.

Table 1. Chemical composition of lime putty

Component	Percent
Free water	19.90
CaO	58.69
SiO ₂	0.30
Fe ₂ O ₃ +Al ₂ O ₃	0.80
MgO	0.84
SO ₃	0
CO ₂	1.32
Chemically bound water	18.17

Table 2. Chemical composition of natural zeolite

Component	Percent
Loss on ignition:	14.13
SiO ₂	64.16
Al ₂ O ₃	10.95
Fe ₂ O ₃	2.82
CaO	4.25
MgO	1.01
SO ₃	0.15
P ₂ O ₅	0.13
Na ₂ O	0.18
K ₂ O	2.05
MnO	0.13
Cl ⁻	0.001

Natural zeolite excavated in Igroš, near Brus (Serbia) was used in this study as a partial replacement for lime. Before application zeolite was grounded to fineness of 10% residue on 45 µm sieve. Chemical composition of zeolite, determined by chemical analysis, presented in Table 2, specifies that it contains 77.9% of SiO₂+ Al₂O₃+ Fe₂O₃. The mineralogical composition of zeolite, determined by XRD analysis, is shown in Figure 1.

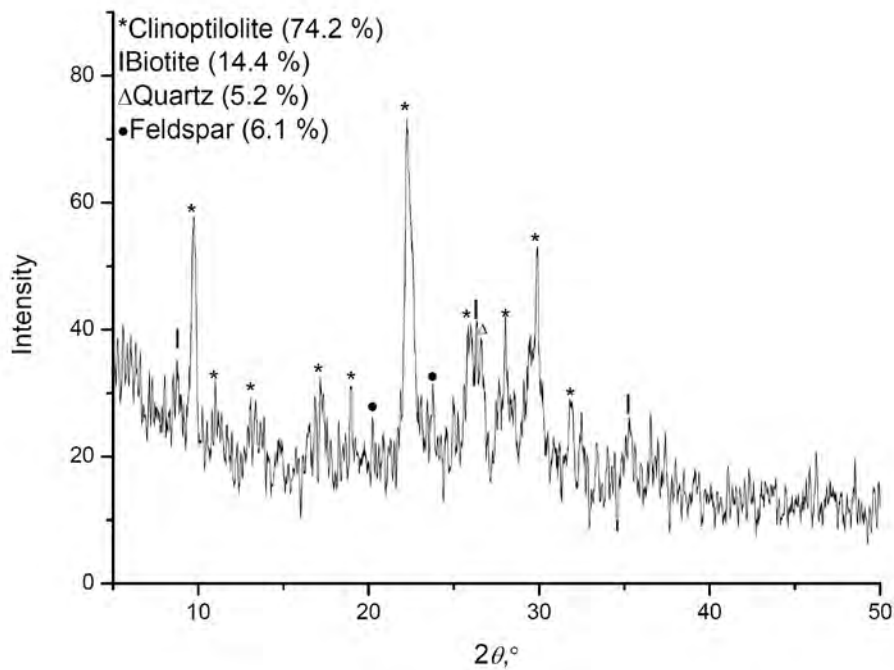


Figure 1. Mineralogical composition of zeolite (XRD analysis)

Natural river aggregate originating from Danube river (Serbia) in two different gradations 0/4 mm and 0/0.5 mm was used, designated as C and F, respectively. Bulk density of aggregate F amounted to 1400 kg/m³ and of aggregate C to 1610 kg/m³. The photos of aggregates and zeolite used are presented in Figure 2.



Figure 2. Component materials: a) aggregate F, b) aggregate C, c) natural zeolite

Chemical composition of two types of sand was determined through chemical analysis and presented in Table 3. Both of the sands were mostly of silicate origin, with aggregate F had higher carbonate content than aggregate C.

Mixtures

The reference mixture for inner render layers (1/3) was designed with lime to aggregate volumetric ratio of 1:3, using aggregate C and lime putty as a binder. Similarly, the reference mixture for the outer render layer (1/1) was designed with lime to aggregate ratio of 1:1, using aggregate F and lime putty as a binder. Water content for both mixtures was adopted in order to fulfill consistency and flowability conditions for these types of renders.

Consistency of the mixtures was tested using the flow table test. Measured diameter was 140 mm for mixture 1/3 and 170 mm for mixture 1/1. Mixtures containing natural zeolite were produced by replacing of lime in both reference mixtures by 20% and 40% (by mass). The mixture design is presented in Table 4.

Table 3. Chemical composition of aggregate

Component	Aggregate F (%)	Aggregate C (%)
SiO ₂	69.57	80.49
Al ₂ O ₃	4.20	3.90
TiO ₂	0.52	0.21
Fe ₂ O ₃	5.17	4.32
CaO	8.02	4.21
MgO	2.15	1.38
Na ₂ O	1.30	1.09
K ₂ O	1.18	1.10
Cl ⁻	0.05	0.05
Sulfats that desolve in water	0.02	0.02
Sulfats that desolve in acid	0.03	0.02

Table 4. Mixture design

Mixture	Lime (kg/m ³)	Lime putty (kg/m ³)	Zeolite (kg/m ³)	Aggregate C (kg/m ³)	Aggregate F (kg/m ³)	Additional water (kg/m ³)	Water/ binder ratio
1/3	200	250	-	1610	-	230	1.4
1/3-20	160	200	40	1610	-	240	1.4
1/3-40	120	150	80	1610	-	250	1.4
1/1	435	544	-	-	1015	239	0.8
1/1-20	348	435	87	-	1015	261	0.8
1/1-40	261	326	174	-	1015	283	0.8

The masses of binder and sand needed to produce required mix proportions by volume were calculated using previously determined density values of component materials. Adopted volumetric proportions were used for calculation of mass of dry lime (marked as lime in Table 4). Lime putty mass was determined by dividing mass of lime with 0.8, in accordance with the measured free water content within the putty. Total amount of water in the mix presents the sum of free water found within lime putty and additional water added to the mixture.

Preparation of the samples

All the mixtures were prepared in the same way using Pail mixer type Beckel EM 20. Firstly, lime putty was mixed with additional water for 1 min and then together with zeolite for

another minute. At the following stage, the aggregate was added during next 60 s, without stopping the mixer. Mixing was then continued for 7 min, with the 1 min pause that was made in order to remove the remained material from the paddle and the sides of the bucket. Preparation of mortar was finalized after 2 additional minutes of mixing, giving a total mixing time of 13 min. Prismatic samples (4×4×16 cm) were placed in two layers using manual compaction method.

Mixtures containing zeolite were stored in containers in humid environment (RH=100%) for two days. After demolding, the samples were stored in plastic bags above water surface at relative humidity (RH = 100%). At the age of 28 days, samples were divided in two groups. First group of samples for each mixture with zeolite continued to be exposed to the same conditions as previously described. Second group of samples was taken out of the plastic bags and cured in laboratory conditions with temperature (T) of 20±2°C and relative humidity RH=50±10%, up to the age of 60 days. These conditions were chosen as representatives of two possible applications of the renders: in constantly humid environment (RH=100%) or in normal conditions, with prolonged curing until the age of 28 days (RH=100/50%).

The reference mixtures were cured during first five days in closed containers in humid environment, and then two more days in molds in the laboratory conditions (RH=50%, T=20±2°C). After total period of seven days, samples marked 1/3 were removed from molds and cured in the laboratory conditions (T=20±2°C, RH=50±10%) until testing. Due to the low mechanical properties, samples of reference mixture 1/1 could not be removed from molds after only 2 days of curing in laboratory conditions, and they remained in molds for three more days (10 days in total).

Results and analysis

Testing methods

After reaching the testing age (14, 28 or 60 days) six samples of each mixture were dried in the oven for 72 hours at 60°C. One group of three samples was used for determination of flexural and compressive strength of the mixtures. The second group of samples was coated with a paraffin layer after which each sample was split in two halves. Five halves were used for capillary water absorption test, while one half was used for determination of open porosity.

Compressive and flexural strength

Testing of mechanical properties was conducted according to the standard EN 1015-11:2008. Flexural strength was determined as an average value of three measurements, while compressive strength represents the average value of five measurements. Flexural and

compressive strength of all mixtures at different ages and different curing conditions, with indicated standard deviations on the average values, are presented in the Figures 3 and 4.

Development of both properties was influenced by: sand gradation, binder content, percentage of zeolite addition and curing conditions. Flexural strength of mixtures containing zeolite was lower than flexural strength of reference mixtures, at all ages.

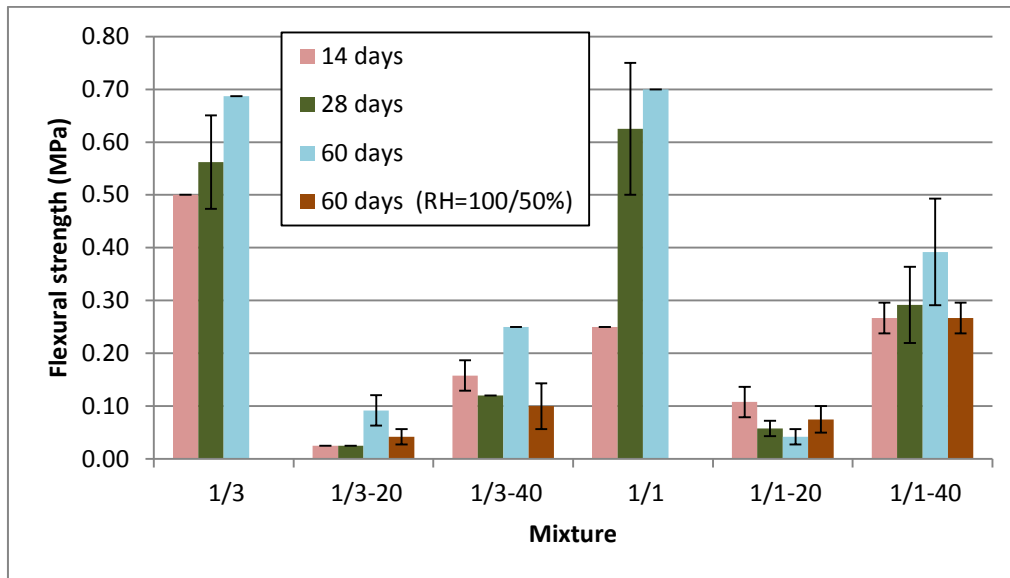


Figure 3. Development of flexural strength of samples through time

Use of zeolite as a partial replacement of lime led to an increase of compressive strength values for all mixtures during all development stages, except for the inner layer mixture with 20% of zeolite. Mixtures containing finer aggregate and increased binder content reached the highest values of compressive strength. These mixtures were made with higher content of zeolite that can participate in pozzolanic reaction and have reduced transition zone, owing to the smaller particle size of aggregates.

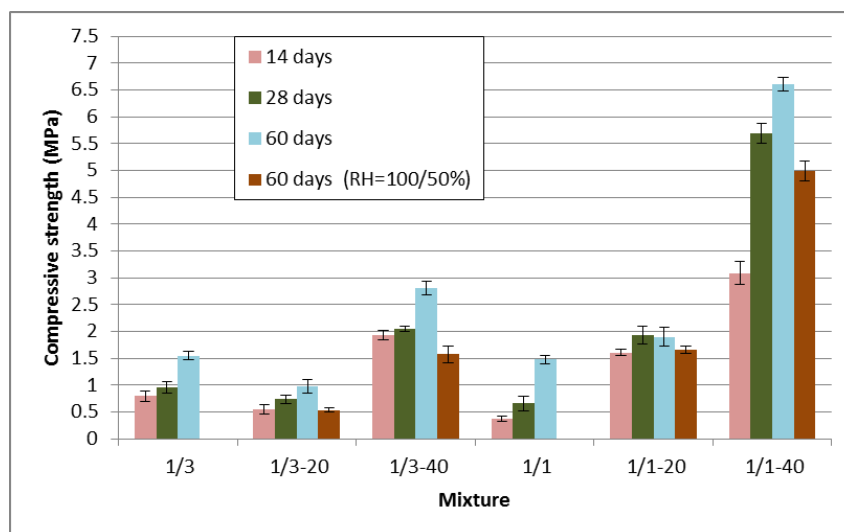


Figure 4. Development of compressive strength of samples through time

Combined curing conditions led to a decrease in compressive strength values for all the mixtures. This behaviour has already been described in literature as a consequence of instability of calcium aluminate hydrates or C-S-H phases due to their dehydration or transformation [6].

When the development of compressive strength through time is observed it can be noticed that mixtures with 20% of partial replacement of lime have reached maximum possible values by the age of 60 days in humid environment, while compressive strength of mixtures containing 40% of zeolite would probably continue to grow until the age of 90 days.

Open porosity

Testing was carried out following the recommendations of the standard for determination of open porosity of natural stone (EN 1936:2006). Previously dried samples were placed in a vacuum desiccator, after measurement of mass (m_d), at the pressure of 5 kPa (the lowest pressure that could have been achieved) in duration of two hours. After this period the water was introduced in the system in the way that the samples were totally immersed in water after 15 min, when the pressure was equalled with the atmospheric pressure. Samples were held in water for another 24 hours, after which the mass of surface dry samples (m_s) and their mass under water (m_h) were measured. Open porosity (p_o) was calculated according to the following expression:

$$p_o = \frac{m_s - m_d}{m_s - m_h} \cdot 100$$

Open porosity values for all mixtures are presented in Figure 5.

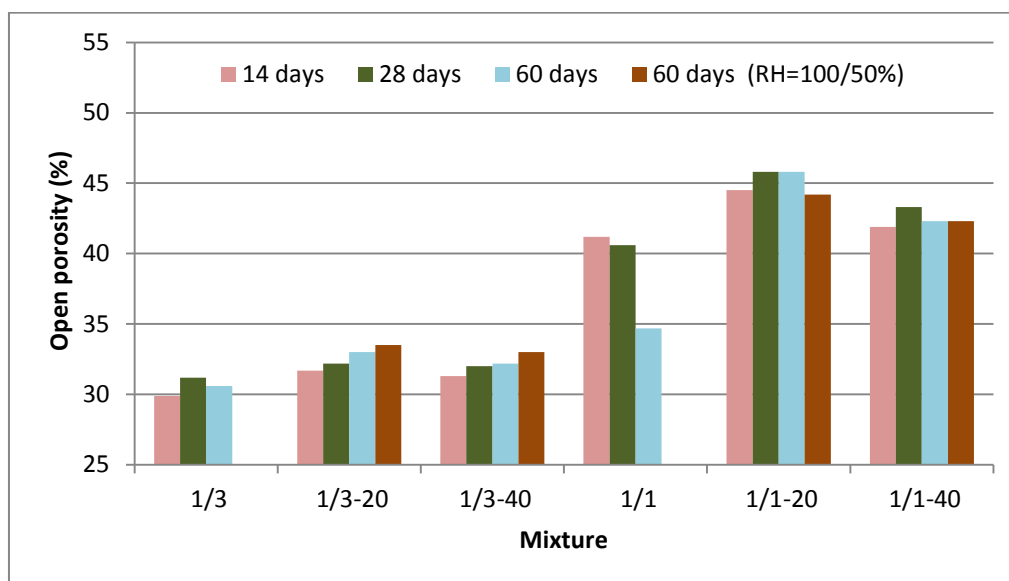


Figure 5. Open porosity of mixtures at different ages

According to the presented results, zeolite addition did not affect the values of open porosity of the mixtures in higher extent. There is a noticeable difference between mixtures

intended for inner and outer layers, which is a consequence of different binder:aggregate ratio and amount of binder in the mixtures.

Capillary water absorption

Samples for the test were prepared according to the standard EN 1015-18:2008. After drying and cooling, the samples were covered with paraffin layer over all lateral sides and then split into two halves (app. 4×4×8 cm each). Prepared samples were then positioned in the box in the way that the broken surface was in contact with the water. Water level was held constant at 10 mm above the sample surface. Since the addition of zeolite was expected to increase the water absorption of the mixtures, the mass of the samples was measured in shorter intervals than stated in the standard. Measurement was conducted after 2, 5, 10, 20, 30, 60 and 90 minutes, and also 48 hours after the beginning of the test. Capillary water absorption coefficient was determined as a slope of the first part of the diagram presenting dependence of the absorbed water per surface unit from square root of time (Figure 6). Measured values (A) are presented in Table 5 together with the period of time necessary for the water to reach the top of the samples (t) and water absorption after 48 hours (U).

It is commonly observed that the addition of pozzolanic admixtures influences an increase of total porosity, but also a decrease in mean pore size, and consequently a decrease in capillary water absorption. This kind of behaviour could only be related to mixture designated 1/1-40 that showed similar or lower capillary water absorption coefficient than reference mixture. All the other results show great increase in water absorption rate for mixtures containing zeolite. This increase is the highest in mixtures with lower percentage of zeolite addition, especially in the case of samples cured in combined conditions. Partially, this could be explained by the specific structure of zeolite due to which it can absorb molecules of water that can take up to 50% of its volume.

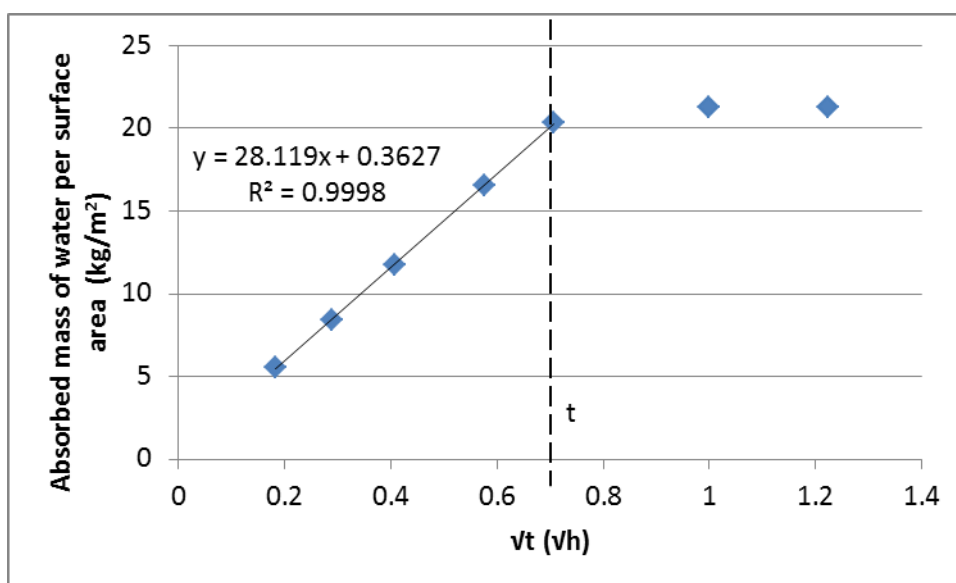


Figure 6. Principle of determining capillary water absorption coefficient presented on an example of mixture designated 1/3-40 at the age of 60 days (RH=100%)

Table 5. Capillary water absorption test results

Mixture	14 days			28 days			60 days		
	A (kg/(m ² √h))	t (min)	U (%)	A (kg/(m ² √h))	t (min)	U (%)	A (kg/(m ² √h))	t (min)	U (%)
1/3	18.87	30	11.0	20.90	26	10.8	16.80	30	10.5
1/3-20 *	37.19	13	14.0	38.07	15	14.3	38.75	20	14.1
1/3-20 **							39.27	10	14.2
1/3-40 *	31.76	23	14.8	30.67	23	13.7	28.12	30	15.4
1/3-40 **							31.82	30	15.1
1/1	20.50	53	19.7	24.19	35	18.9	18.09	30	18.7
1/1-20 *	31.60	40	28.8	32.35	35	30.2	32.57	44	30.4
1/1-20 **							43.84	20	26.9
1/1-40 *	18.60	>90	23.4	18.50	>90	26.8	18.56	>90	27.3
1/1-40 **							14.51	>90	26.6

* RH=100%; ** RH=100/50%

This kind of behaviour could explain the increase of water absorption values after 48 h for all mixtures with addition of zeolite. Similarly, as in the case of open porosity, values increased with the binder content increase. The highest values within renders for inner and outer layers were reached by the mixtures 1/3-40 and 1/1-20, respectively, at the age of 60 days.

The rise of water level in the samples was the fastest for the mixture 1/3-20, followed by the mixture 1/1-20 both containing 20% of zeolite.

Analysis of technical recommendations

Complementary to the previous investigations, tested properties were compared with recommended technical requirements for the replacement rendering mortars, whose overview is presented by Nogueira et al. [2].

The recommended values for bulk density range between 1.5 and 1.8 g/cm³, which was accomplished for all mixtures with coarser aggregate whose bulk densities ranged between 1.68 and 1.8 g/cm³. Mixtures with finer aggregate reached lower values of bulk density, between 1.31 and 1.45 g/cm³.

Porosity of mortars used for replacement of rendering mortars should be between 20 and 40% according to Papayianni [10] and between 30 and 45% according to Moropoulou et al. [11]. Open porosity of presented mixtures varied between 29.9 and 45.8%, satisfying the second recommendation.

Optimal compressive strength values are different according to different authors. Veiga et al. [4], as a conclusion of Oldrenders project, recommend the range between 0.4 and 2.5 MPa at 90 days as most appropriate for renders, while Papayianni [10] set higher values of

strength between 3 and 6 MPa. At the age of 60 days tested mortars reached compressive strength between 0.98 and 6.61 MPa for humid curing conditions and between 0.54 and 4.99 MPa for combined curing conditions. According to Veiga et al. the mixture 1/1-40 reached compressive strength values that are above the upper limit for this type of material. On the other hand, only mixture 1/3-40 cured in humid conditions came close to the values recommended by Papayianni (2.8 MPa at the age of 60 days).

The capillary water coefficient of all mixtures was higher than the recommended values of the stated authors.

Prepared mixtures were also analyzed regarding the requirements for different render layers and their compatibility. Mixture 1/3-40 within inner layers and mixture 1/1-20 within outer layers reached similar values of compressive strength at the age of 28 days (app. 2 MPa) and 60 days in combined curing conditions (app. 1.5 MPa). During humid curing conditions the mixture 1/3-40 reached higher value of compressive strength, which fulfills the requirements for decrease of strength towards the outer layers of the render system. Open porosity, capillary water absorption coefficient and water absorption were all higher for mixture 1/1-20, which is also adequate since these properties should increase towards the outer layers of the system.

Conclusions

Influence of zeolite as a partial replacement of lime in two types of mortar render mixtures is presented in the paper. Investigated parameters were: flexural and compressive strength, open porosity, capillary water coefficient and water absorption.

Overall results show that mixtures containing zeolite, with exception of mixture 1/3-20, have a potential in application as renders for historical buildings, in both curing regimes.

Zeolite addition led to a decrease in flexural strength, and an increase in compressive strength, excluding mixture 1/3-20. Although, there was a noticeable decrease in compressive strength values of the samples cured in combined conditions (RH=100/50%) they were still higher or similar to the values measured for the reference mixtures.

Zeolite addition did not have a strong influence on the open porosity values of the mixtures, but it led to an increase of capillary water absorption coefficient and water absorption after 48 hours.

Bulk density and compressive strength of the mixtures were mostly within recommended boundaries. Capillary water absorption coefficient was higher than recommended values for all of the mixtures.

When presented results are compared with recommendations for different layer render properties and with the technical requirements described above, it can be concluded that mixtures 1/3-40 and 1/1-20 are potential candidates for inner and outer layers respectively.

Testing of the system consisting of these two mixtures, as well as determination of physical and mechanical properties of all mortar mixtures at different ages is planned as a continuation of the presented research.

References

1. Barbero-Barrera M, Maldonado-Ramos L, Van Balen K, García-Santos A, and Neila-González F (2014) Lime Render Layers: An Overview of Their Properties *J Cult Herit* 15 (3):326–30.
2. Nogueira R, Ferreira Pinto A, Gomes A (2018) Design and Behavior of Traditional Lime-Based Plasters and Renders. Review and Critical Appraisal of Strengths and Weaknesses *Cement Concrete Comp* 89:192–204.
3. Moropoulou A, Bakolas A, Anagnostopoulou S (2005) Composite Materials in Ancient Structures *Cement Concrete Comp* 27(2):295–300.
4. Veiga R, Do Fragata M, Velosa A, Magalhães A, and Margalha G (2010) Lime-Based Mortars: Viability for Use as Substitution Renders in Historical Buildings *Int J Archit Herit* 4 (2):177–95.
5. Arizzi A, Cultrone G. (2012) Aerial Lime-Based Mortars Blended with a Pozzolanic Additive and Different Admixtures: A Mineralogical, Textural and Physical-Mechanical Study *Constr Build Mater* 31:135–43.
6. Pavlík V, Užáková M. (2016) Effect of Curing Conditions on the Properties of Lime, Lime-Metakaolin and Lime-Zeolite Mortars *Constr Build Mater* 102:14–25
7. Ince C, Derogar S, Tiryakiođlu N Y, Cengiz Toklu Y. (2015) The Influence of Zeolite and Powdered Bayburt Stones on the Water Transport Kinetics and Mechanical Properties of Hydrated Lime Mortars *Constr Build Mater* 98:345–52.
8. Aškračić M, Zakić D, Savić A, Jevtić D, Mušović E, Stanimirović S (2018) Lime Renders with Addition of Recycled Crushed Brick for Restoration of Historical Buildings, 15th Congress of Association of Structural Engineers of Serbia Proceedings, 180-189, ISBN 978-86-6022-069-3
9. Liguori B, Caputo D, Iucolano F. (2015) Fiber-Reinforced Lime-Based Mortars: Effect of Zeolite Addition *Constr Build Mater* 77:455–60.
10. Papayianni I (2006), The longevity of old mortars, *Appl. Phys. A* 83:685-688.
11. Moropoulou A, Bakolas A, Moundoulas P, Aggelakopoulou E (2009) Reverse engineering: a proper methodology for compatible restoration of mortars, in: *Workshop Repair Mortars for Historic Masonry*, RILEM Publications, 278:291.

Use of ultrafine mafic rocks for the enhancement of carbonation reaction in lime renders

Loucas Kyriakou¹, Ioannis Rigopoulos¹, Ioannis Ioannou¹

(1) Department of Civil and Environmental Engineering, University of Cyprus, 1678 Nicosia, Cyprus, kyriakou.loucas@ucy.ac.cy, rigopoulos.ioannis@ucy.ac.cy, ioannis@ucy.ac.cy

Abstract

Lime renders have been used as building materials since the earliest periods of antiquity. These composites set and harden through carbonation; the latter is a rather slow chemical reaction between calcium hydroxide and atmospheric carbon dioxide (CO₂) to form calcium carbonate. In view of the slow rate of carbonation, which is considered a major drawback for the use of lime renders in vernacular and contemporary architecture today, several studies in the literature focus on the mechanism and kinetics of the aforementioned setting/hardening reaction, as well as on the factors affecting its rate. The present study focuses on lime-based renders that have been modified through the addition of ball-milled olivine basalt and dolerite quarry waste material. Both ultrafine rock additives were added to the mixtures at a percentage of 15% (w/w in partial replacement to the lime binder). Thermogravimetric (DTA/TG) and XRD analyses, as well as the phenolphthalein test, demonstrated an increase in the carbonation rate of the lime renders containing the aforementioned additives. The nano-modified end-products could potentially be used not only in restoration projects, but also in contemporary architecture.

Introduction

Carbonation in lime composites is a chemical process that proceeds gradually towards the inner layers of the material [1] and entails the transformation of calcium hydroxide (Ca(OH)₂) into calcium carbonate (CaCO₃). The aforementioned reaction is considered to be of great importance due to its direct effect on the physical and mechanical properties of hardened hydrated lime mortars. This mechanism generally results in an increase in density and strength, as well as in a modification of the pore structure of the mortars [2]. Nevertheless, the carbonation process is relatively slow under ambient conditions due to the low carbon dioxide (CO₂) content in the atmosphere (i.e., ~400 ppm). This is considered to be a major drawback for the setting and hardening of hydrated lime mortars.

Carbonation in lime mortars is highly controlled by the diffusivity of CO₂ through their pore system [3]. However, the conversion of calcium hydroxide into calcium carbonate crystals also implicates the reduction of the pore size, thus obstructing the accessibility of CO₂ to the inner layers of the material [4]. The kinetics of lime carbonation are also controlled by different environmental parameters, such as temperature, relative humidity, drying and

wetting processes and atmospheric CO₂ concentration [2, 5-7], as well as by different characteristics of the material under study, such as its composition, particle size gradation and morphology [8-10].

Several studies refer to the mineralization of CO₂ using basaltic rocks [11-13] and their efficacy in storing CO₂ through mineral carbonation [14, 15]. Although in-situ mineral carbonation offers the potential for permanent CO₂ storage in the form of carbonate minerals, this approach has only been rarely investigated on a pilot scale [16]. Other studies insinuate that waste materials, such as mine waste, can also be classified as a source of mineral carbonation. According to Li and Hitch [17, 18], ultramafic mine waste rock shows high CO₂ uptake potential; hence, the reduction of its particle size to the nanoscale range through the ball milling technique can definitely increase its CO₂ uptake. The development of nano-sized rock powders with enhanced CO₂ uptake has in fact been thoroughly investigated using a variety of lithologies [19].

Even though a significant number of research efforts have focused on the mineralization of ophiolitic rocks, the use of the latter as additives in lime-based renders is a relatively new research field. Nevertheless, according to Westgate et al. [20], the use of olivine aggregates in lime mortars can enhance the carbonation reactions and subsequently the CO₂ adsorption capacity of the end-products. According to the aforementioned researchers, the dolomite (CaMg(CO₃)₂) formed from the reaction of olivine with lime and CO₂ further promotes a greater compressive strength in these composites.

In this study, an olivine basalt and a dolerite quarry waste material have been used as additives in lime-based renders at a percentage of 15% (w/w in partial replacement to the lime binder). These specific mafic rock samples were selected due to their high CO₂ storage potential. In order to further increase their CO₂ uptake, ball milling was carried out prior to their use as additives, using a planetary ball mill, based on the results acquired by Rigopoulos et al. [21, 22, 23]. In the new renders, the carbonation process was experimentally evaluated using thermogravimetric (DTA/TG) and X-ray diffraction (XRD) analyses, as well as the phenolphthalein test. The evolution of the microstructural features and of the carbonation reactions was also studied through Scanning Electron Microscopy (SEM) in combination with energy dispersive X-ray spectroscopy (EDXS).

A deep understanding of the parameters affecting the carbonation of lime composites could result in the development of building materials with enhanced physico-mechanical properties and CO₂ sequestration capacity; these could be suitable for applications not only in contemporary architecture but also in restoration projects.

Materials and Methods

Raw materials and sample preparation

Three lime-based renders were designed and produced in the laboratory; one reference mixture and two optimized ones with the addition of olivine basalt and dolerite waste material at a percentage of 15% w/w in partial replacement to the binder. The binder in the reference mixture consisted of 100% CL80 hydrated lime supplied by Hellenic Mining Public Co., while the aggregate fraction in all three mixtures was a local calcareous sand with 0-2 mm particle size. XRD semi-quantitative analysis of these aggregates indicated calcite (up to 60%), albite (25%), quartz (15%) and chlorite (traces) [24, 25]. The selected binder/aggregate ratio was 1:3 w/w, based on the positive results of previous studies [26] and the commonness of this proportion in old lime composites from Cyprus [27].

The olivine basalt (BAS) used in the studied mixtures was collected from the Troodos ophiolite that is considered to be the most well preserved ophiolite complex in the world. The dolerite (DOL) was a representative sample of waste material (quarry fines) that was collected from a quarry located in Sia village, Nicosia District. Polarized microscopy and powder XRD analysis of the olivine basalt indicated the presence of forsteritic olivine, tremolite, actinolite, augite, talc, chlorite, magnetite and basaltic glass [21]. XRD analysis of the dolerite indicated that its mineralogical composition includes augite, anorthite, chlorite, actinolite, epidote, albite, quartz, calcite and magnetite [28]. Both the olivine basalt and the dolerite quarry waste were sieved to acquire the 104-150 μm fraction range prior to the ball milling process. The materials were subsequently subjected to wet ball milling in a tungsten carbide bowl using 30 tungsten carbide balls with a diameter of 10 mm and ethanol as process control agent (i.e., milling liquid). The ball to powder mass ratio was 20:1 w/w, the fluid to powder mass ratio 1:2 and the rotation speed 300 rpm. The ball milling process was interrupted every 5 min with 5 min stay, in order to avoid heating of the samples. The ball-milled samples were dried overnight under ambient conditions. Based on the experimental results of previous studies [21-23, 28], the optimum ball milling parameters for each sample were applied in terms of their CO₂ uptake (Table 1).

Table 1. Ball milling conditions, textural properties and CO₂ uptake of nano-additives (data from Rigopoulos et al., [21, 28])

Sample	Ball milling conditions	Textural properties			CO ₂ uptake ($\mu\text{mol g}^{-1}$)
	Milling time (h)	BET ($\text{m}^2 \text{g}^{-1}$)	Pore volume ($\text{cm}^3 \text{g}^{-1}$)	Average pore diameter (nm)	
BAS	4	58.9	0.106	6.2	222.1
DOL	20	32.9	0.151	16.0	96.9

The reduction of the particle size of the olivine basalt and dolerite samples down to the nanoscale range after ball milling has been confirmed by Rigopoulos et al. [21, 28]; these studies used conventional and high resolution transmission electron microscopy (TEM, HRTEM) to prove that the majority of the particle sizes in the milled basalt and dolerite ranged between 20-35 nm and 30-50 nm, respectively.

The water demand of each mixture was subsequently estimated after achieving a constant workability in the range of 165 ± 5 mm according to [EN 1015-3] [29]. The water to binder ratio (W/B), along with all other mix design parameters are given in Table 2.

Table 2. Mix design of laboratory composites. All quantities are measured by mass.

Mixture	Aggregates	Binder + Additive	Water/Binder	Workability (mm)	Additive*	
					Basalt	Dolerite
REF	3	1	0.850	167.53	-	-
DOL15	3	1	1.026	162.20	-	15
BAS15	3	1	0.980	162.61	15	-

* % w/w in partial replacement to binder

The ultrafine rock powders were added to the mixtures in an aqueous suspension, after a 15 min sonication. The fresh mortars were cast in standardized prismatic 40 x 40 x 160 mm and cubic 50 x 50 x 50 mm metallic molds and then stored in a room with constant temperature (23 ± 5 °C) and relatively humidity ($50 \pm 5\%$). The specimens were demolded 3 days after casting and cured in the same room mentioned above. Their physico-mechanical properties were determined after 28 and 90 days of curing.

Experimental tests

The vacuum saturation method using water as the wetting liquid was used in order to assess the open porosity of the mixtures. Additional information regarding the average pore size and pore size distribution of the samples was provided using a Micrometrics Mercury Intrusion Porosimeter (MIP) (Autopore IV 9520) with low pressure upper limit 50 psia and high pressure up to 60,000 psia.

Capillary absorption measurements were carried out on cubic specimens (50 x 50 x 50 mm) using water as the wetting liquid, following the method described by Hall and Hoff [30]. The capillary absorption coefficient was determined from the gradient of the plot of the first section of the graph of liquid absorbed per unit area of inflow surface [g/m^2] against the square root of time [$\text{s}^{1/2}$].

Three prismatic specimens (40 x 40 x 160 mm) were used for testing the materials under flexural load (three-point bending), in accordance with the procedure described in EN 1015-11 [31]. The mean uniaxial compressive strength of each mixture was determined using the six half prisms acquired from the three-point bending test.

Differential Thermal and Thermogravimetric Analyses (DTA/TG) were also carried out on powder samples taken from the surface of each specimen in order to investigate the presence of portlandite and subsequently the progress of carbonation as a function of time. The analyses were performed using a Shimadzu DTG-60H from 35 °C to 1200 °C, at a heating rate of 5 °C/min.

The microstructural characteristics of the studied renders in relation to the evolution of the carbonation reactions were investigated using a JEOL, JSM-6610 LV scanning electron microscope (SEM), equipped with a BRUKER type QUANTAX 200 energy dispersive X-ray spectrometer (EDXS). All the analyses were carried out on gold-coated samples under high vacuum conditions.

The potential mineralogical transformations that have occurred in the studied samples were investigated through powder XRD analysis using a Bruker D8 Advance system. The analyses were carried out using a step scan of 1°/min within the 3-80° 2θ angle range, with a continuously rotating sample.

For the determination of the evolution of the carbonation front over time, the phenolphthalein staining method was used. Phenolphthalein indicator was evenly applied on fresh broken surfaces of the specimens. A change in deep pink color indicated the presence of highly alkaline portlandite, whereas colourless areas showed that portlandite had been transformed into calcite [32]. All the samples were promptly photographed within the first minute following the phenolphthalein application.

Results and Discussion

Figure 1 summarizes the qualitative results of the phenolphthalein stain test carried out 28 and 90 days after casting. The nano-modified composites (DOL15, BAS15) showed an evident increase of the carbonation depth compared to the reference (REF) sample. Furthermore, the composite containing ball-milled olivine basalt showed a further increase of the carbonation depth, compared to the composite with ultrafine dolerite. It is worth noting that the composite with ball-milled basalt seemed to be fully carbonated after 90 days. This may be attributed to the fact that the olivine basalt has a considerably higher specific surface area (BET, $\text{m}^2 \text{g}^{-1}$) and CO_2 uptake compared to the dolerite (see Table 1). The higher CO_2 uptake of the basaltic sample is, in turn, attributed to its high content in forsteritic olivine [21], which is one of the most promising minerals for the sequestration of CO_2 . However, it should be underlined that the conversion of olivine into magnesite is not favored at ambient conditions. On the other hand, the dissolution of olivine can considerably increase the pH and in turn the solubility of CO_2 in aqueous solutions [33]. Thus, in the nano-modified mortar with ultrafine olivine basalt, similar changes in the pore solution chemistry could potentially accelerate the CaCO_3 precipitation rates.

The results confirm the positive effect of both nano-additives on the carbonation of lime mixtures; this is also in line with other researches [20]. As expected, an evolution of the

carbonation front over time was also observed (Figure 1). This indicates an enhancement of the carbonation reaction, which proceeds from the surface into the core of the nano-modified specimens. However, it should be highlighted that the phenolphthalein stain method is only a simple empirical method for estimating the progress of carbonation. This is due to the fact that the phenolphthalein indicator changes color over a narrow range of alkaline environments and not sharply at a specific pH [34].

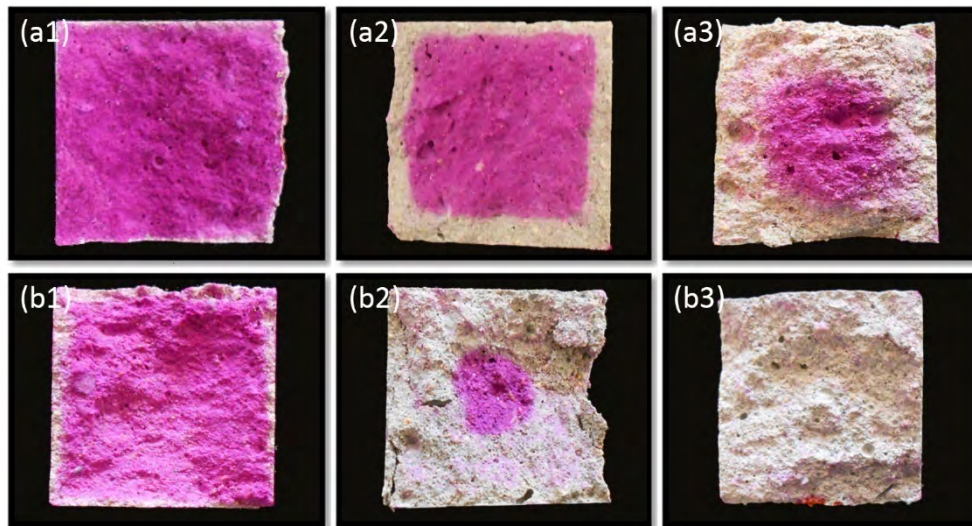


Figure 1: Illustration of the carbonation front over time (days) in prismatic specimens (cross section dimensions 40 x 40 mm) as measured with the phenolphthalein stain method: (a1, b1) REF; (a2, b2) DOL15; (a3, b3) BAS15. Top row: samples at 28 days after casting; bottom row: samples at 90 days after casting. Each individual sample is representative of the average state of all samples tested.

Powder XRD was used in order to identify the mineral phases of the initial rock materials [21, 28]. Silicate minerals, such as olivine, augite and anorthite, have high proportions of calcium, magnesium and iron cations, which are the necessary components for binding CO_2 , hence promoting mineral carbonation [35]. Additional XRD analyses were performed on superficial powder samples collected from the reference and nano-modified mixtures at 28 and 90 days after casting. The results demonstrate that the content of portlandite decreases with the addition of the studied nano-additives, as shown in Figure 2a. Although this reduction in the main portlandite peak intensity could be attributed to the partial replacement of lime by ultrafine mafic rocks, it may also provide information on the different effect of each nano-additive on the carbonation of air lime renders. Figure 2a shows that the reduction in the main portlandite peak intensity is more obvious in the composite with ultrafine basalt compared to that with ultrafine dolerite, which is in line with the results of the phenolphthalein indicator test (see Figure 1).

Thermal analyses of material collected from the surface of the specimens indicated enhanced carbonation in the nano-modified composites (BAS15, DOL15), compared to the reference sample (REF). This is confirmed through a comparison of the endothermic reaction at temperature ca. 400-500 °C, which corresponds to the dehydroxylation of portlandite (Figure 2b). In fact, this figure shows the complete absence of portlandite in the nano-

modified specimens, thereby indicating the enhancement of the carbonation reaction in the latter.

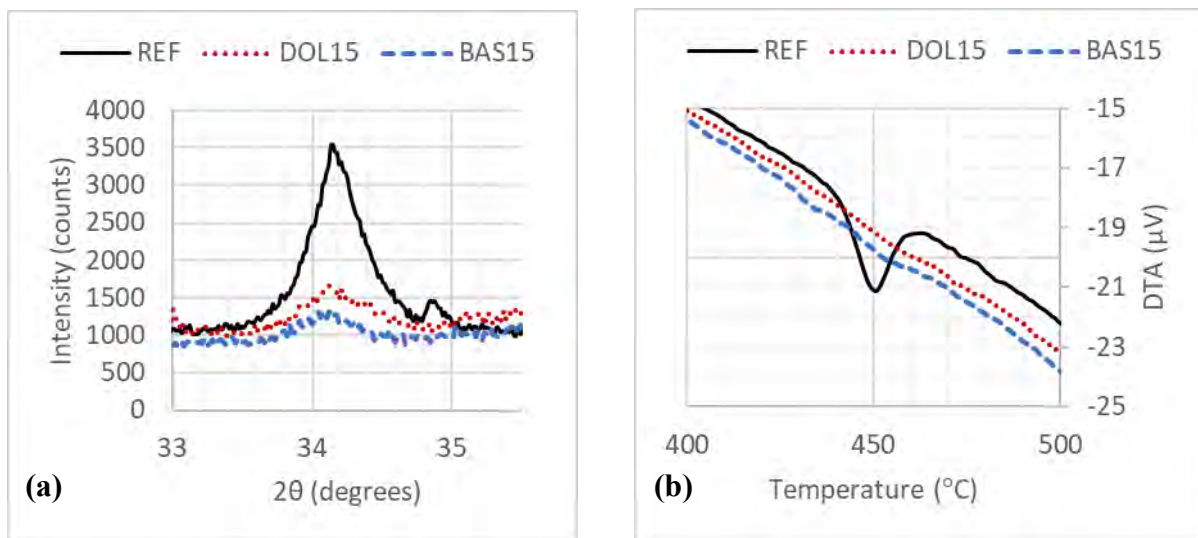


Figure 2: (a) XRD patterns of all mixtures showing the decrease in the intensity of the main portlandite peak ($2\theta = 34.09^\circ$) with olivine basalt and dolerite addition; (b) DTA curves of all mixtures showing the elimination of portlandite (endothermic reaction at temperature ca. 400-500 °C) with olivine basalt and dolerite addition. All measurements shown were carried out 90 days after casting.

SEM images from the surface of the specimens showed a denser matrix for the nano-modified composites compared to the reference one (Figure 3). This is mainly attributed to the nano-filler effect, as well as to the enhancement of the carbonation kinetics in the former, thereby highlighting the potential of olivine basalt and dolerite waste material in accelerating carbonation.

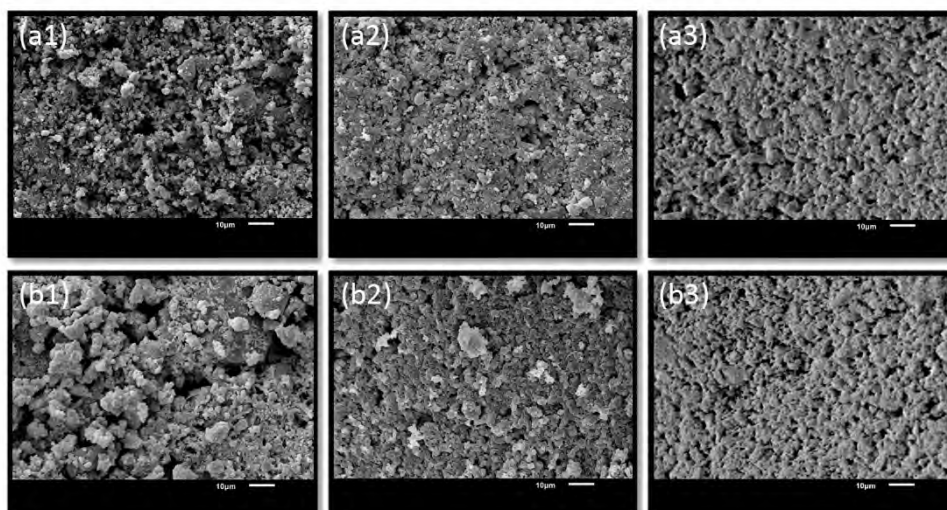


Figure 3: SEM images from the surface of the studied renders, showing their microstructural features: (a1, b1) REF; (a2, b2) DOL15; (a3, b3) BAS15. Top row: samples at 28 days after casting; bottom row: samples at 90 days after casting. Each individual sample is representative of the average state of all samples tested.

Table 3 presents the physical properties of the laboratory composites at 28 and 90 days after casting. Slightly higher values were observed for the porosity of the nano-modified

composites, whilst their capillary absorption was also increased. This is mainly attributed to the presence of microcracks in the nano-modified mixtures, as confirmed by SEM. The formation these microcracks is probably attributed to the increased water/binder ratios (Table 2), incited by the higher specific surface area of the nano-additives.

Table 3. Physical properties of laboratory composites measured at 28 and 90 days after casting.

Sample	Curing Days	Open porosity (%)	Average pore diameter (nm)	Capillary Absorption Coefficient (mm/min ^{1/2})
REF	28	30.0	295	1.40
	90	27.0	297	1.34
DOL15	28	30.6	209	1.66
	90	27.9	196	1.58
BAS15	28	31.5	220	2.00
	90	29.9	244	1.87

The average pore diameter values recorded by MIP (Table 3) show that the addition of either ultrafine olivine basalt or dolerite resulted in a decrease of the average pore diameter of the end-products compared to the reference sample. This decrease is more evident in the composite with ultrafine dolerite. MIP also verified a shift of the main peak of the pore size towards smaller pore sizes in the nano-modified composites; this is noticeable even from the age of 28 days (see Figure 4). This is in line with other researches [36] that documented the alteration of the pore distribution of lime composites when nano-additives were added, due to their proven behavior as nano-fillers.

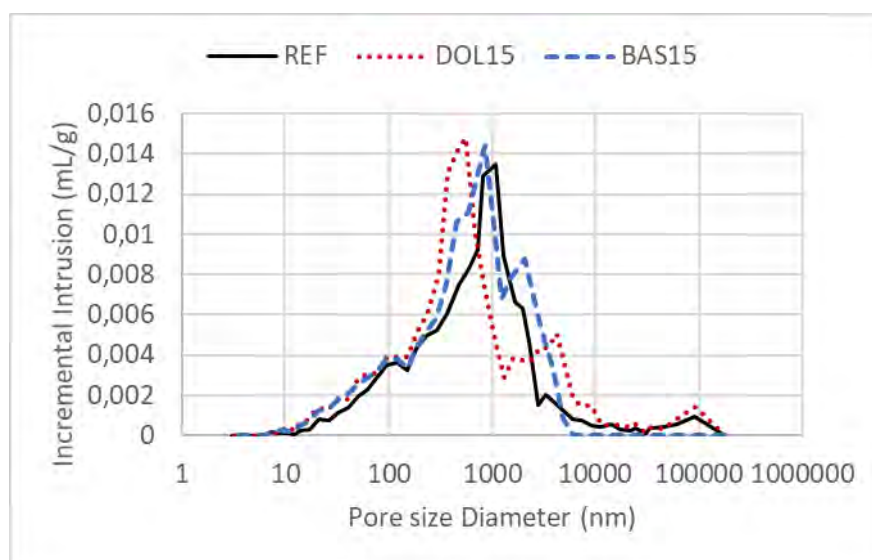


Figure 4: MIP pore size distribution for laboratory composites at 28 days of curing.

Table 4 summarizes the mechanical properties of the laboratory mixtures at 28 and 90 days after casting. Regarding the flexural strength, there are no significant differences among the nano-modified composites and the reference one in the longer term. The absence of any significant improvement in the flexural strength at 90 days after casting could be attributed

to the fact that the use of both nano-additives resulted in an increased water/binder ratio during mixing, as shown in Table 2. Nevertheless, the use of both nano-additives (especially BAS) resulted in an increase in the early term (28-day) composite flexural strength; this is important in practice.

Table 4. Mechanical properties of laboratory composites measured at 28 and 90 days after casting. Standard deviation values in parentheses.

Sample	Curing Days	Flexural Strength (MPa)	Compressive Strength (MPa)
REF	28	0.71	1.45
		(0.01)	(0.09)
	90	1.17	2.26
		(0.04)	(0.17)
DOL15	28	0.77	2.93
		(0.03)	(0.23)
	90	1.05	3.10
		(0.10)	(0.18)
BAS15	28	1.05	1.42
		(0.15)	(0.05)
	90	1.19	1.72
		(0.05)	(0.06)

A significant enhancement of the compressive strength is evident only in the nano-modified composite with ultrafine dolerite (Table 4). On the contrary, this mechanical parameter is adversely affected due to the addition of ultrafine basalt. This is probably attributed to the significant amount of volcanic glass (~30%) in the basaltic sample, which has been devitrified into secondary hydrous minerals (mainly chlorite). Chlorite is a soft mineral, which belongs to the phyllosilicate subclass of minerals. It absorbs water within the layers of its structure and generally lowers the coherence of rocks [37].

Conclusions

This paper investigated the effect of ball-milled olivine basalt and dolerite quarry waste material used as nano-additives in hydrated lime composites (at 15% w/w in partial replacement to the binder). Qualitative results through the phenolphthalein stain test, indicated a notable increase of the carbonation depth in the nano-modified composites compared to the reference one. This enhancement of the carbonation process was more evident in the composite with ultrafine basalt; this is attributed to the abundance of forsteritic olivine in this rock sample, which probably changed the pore solution chemistry, thereby accelerating the precipitation of carbonate minerals. The carbonation process was further studied by XRD and thermal analyses, which indicated a significant reduction (or even elimination) of the portlandite content due to the presence of the aforementioned nano-additives. Additionally, SEM observations showed a denser microstructure in the nano-modified composites, which is mainly attributed to the nano-filler effect. The denser

microstructure is also probably linked to the enhancement of the carbonation process in the nano-modified renders.

The microcracks in the nano-modified mixtures, the formation of which is related to the increased water/binder ratios due to the presence of the nano-additives, may be responsible for the slightly higher open porosity values, as well as for the increase in capillary absorption observed. In addition, the presence of ultrafine olivine basalt and dolerite waste material resulted in a decrease of the average pore diameter of the nano-modified composites, compared to the reference sample. The flexural strength did not show any significant improvement in the longer term due to the use of the nano-additives; nevertheless, the early term flexural strength of the composites was improved in the case of both nano-additives. On the contrary, the compressive strength was considerably improved only in the composite with ultrafine dolerite, while the ultrafine olivine basalt had an adverse effect on this mechanical parameter. The latter is probably related to the presence of the soft secondary mineral chlorite in the basaltic sample, which can have an unfavorable effect on the compressive strength of hardened composites.

The results clearly demonstrated the potential of ultrafine olivine basalt and dolerite waste material in accelerating the carbonation kinetics when added to hydrated lime composites. It should also be emphasized that the incorporation of both nano-additives into lime render mixtures may benefit the reduction of CO₂ emissions associated with the production of lime, thereby contributing to the strategy for the mitigation of greenhouse gas emissions.

Acknowledgements

The authors would like to acknowledge financial support from the Republic of Cyprus and the European Committee through the Cyprus Research Promotion Foundation (Project KOINA/M-ERA.NET/0316/04). LK would also like to acknowledge financial support from the University of Cyprus.

References

1. Elsen J (2006) Microscopy of historic mortars - a review. *Cem Concr Res* 36:1416-1424
2. Oliveira MA, Azenha M, Lourenço PB et al (2017) Experimental analysis of the carbonation and humidity diffusion processes in aerial lime mortar. *Constr Build Mater* 148:38-48
3. Sánchez-Moral S, García-Guinea J, Luque L et al (2004) Carbonation kinetic in Roman-like lime mortars. *Mater Constr* 54:23-37
4. Ferretti D, Bažant ZP (2006) Stability of ancient masonry towers: Moisture diffusion, carbonation and size effect. *Cem Concr Res* 36:1379-1388

5. Van Balen K (2005) Carbonation reaction of lime, kinetics at ambient temperature. *Cem Concr Res* 35:647-657
6. Ergenç D, Fort R (2018) Accelerating carbonation in lime-based mortar in high CO₂ environments. *Constr Build Mater* 188:314-325
7. Cizer Ö, Van Balen K, Elsen J et al (2008) Carbonation reaction kinetics of lime binders measured using XRD. International Conference on Accelerated Carbonation for Environmental and Materials Engineering, Rome, Italy
8. Lanas J, Sirera R, Alvarez JI (2005) Compositional changes in lime-based mortars exposed. *Thermochim Acta* 429:219-226
9. Cizer Ö, Van Balen K, Elsen J et al (2012) Real-time investigation of reaction rate and mineral phase modifications. *Constr Build Mater* 35:741-751
10. Lawrence RM, Mays TJ, Walker P et al (2006) Determination of carbonation profiles in non-hydraulic lime mortars using thermogravimetric analysis. *Thermochim Acta* 444:179-189
11. Schaefer HT, McGrail BP, Owen AT (2010) Carbonate mineralization of volcanic province basalts. *Int J Greenhouse Gas Control* 4:249-261
12. Schaefer HT, Horner JA, Owen AT et al (2014) Mineralization of Basalts in the CO₂-H₂O-SO₂-O₂ System. *Environ Sci Technol* 48:5298-5302
13. Schaefer HT, McGrail BP, Owen AT (2009) Basalt-CO₂-H₂O Interactions and Variability in Carbonate Mineralization Rates. *Energy Procedia* 1:4899-4906
14. Snæbjörnsdóttir SO, Wiese F, Fridriksson T et al (2014) CO₂ storage potential of basaltic rocks in Iceland and the oceanic ridges. *Energy Procedia* 63:4585-4600
15. Snæbjörnsdóttir SO, Gislason SR (2016) CO₂ Storage Potential of Basaltic Rocks Offshore Iceland. *Energy Procedia* 86:371-380
16. Matter JM, Broecker WS, Gislason SR (2011) The CarbFix Pilot Project - Storing Carbon Dioxide in Basalt. *Energy Procedia* 4:5579-5585
17. Li J, Hitch M (2018) Ultra-fine grinding and mechanical activation of mine waste rock using a planetary mill for mineral carbonation. *Int J Miner Process* 158:18-26
18. Li J, Hitch M (2015) Ultra-fine grinding and mechanical activation of mine waste rock using a high-speed stirred mill for mineral carbonation. *Int J Miner Metall Mater* 22:1005-1016
19. Rigopoulos I, Ioannou I, Delimitis A, Efstathiou AM, Kyratsi T (2018) Ball milling effect on the CO₂ uptake of mafic and ultramafic rocks: a review. *Geosciences* 8:406

20. Westgate P, Ball RJ, Paine K (2019) Olivine as a reactive aggregate in lime mortars. *Constr Build Mater* 195:115-126
21. Rigopoulos I, Petalidou KC, Vasiliades MA et al (2015) Carbon dioxide storage in olivine basalts: effect on ball milling process. *Powder Technol* 273:220-229
22. Rigopoulos I, Vasiliades MA, Petalidou KC et al (2015) A method to enhance the CO₂ storage capacity of pyroxenitic rocks. *Greenhouse Gases Sci Technol* 5:1-14
23. Rigopoulos I, Vasiliades MA, Ioannou I et al (2016) Enhancing the rate of ex situ mineral carbonation in dunites via ball milling. *Adv Powder Technol* 27:360-371
24. Fournari R, Ioannou I, Vatyliotis D (2015) A study of fine aggregate properties and their effect on the quality of cementitious composite materials. In: Lollino G, Manconi A, Guzzetti F et al (eds) *Engineering Geology for Society and Territory – Volume 5*. Springer, Cham
25. Fournari R, Ioannou I (2019) Correlations between the Properties of Crushed Fine Aggregates. *Minerals* 9:86
26. Lanas J, Alvarez-Galindo J (2003) Masonry repair lime-based mortars: factors affecting the mechanical behavior. *Cem Concr Res* 33:1867-1879
27. Theodoridou M, Ioannou I, Phylokyprou M (2013) New evidence of early use of artificial pozzolanic material in mortars. *J Archaeolog Sci* 40:3263-3269
28. Rigopoulos I, Petalidou KC, Vasiliades MA et al (2016) On the potential use of quarry waste material for CO₂ sequestration. *J CO₂ Util* 16:361-370
29. European Committee of Standardization (1999) *Methods of test for mortar masonry – Part 3: Determination of consistence of fresh mortar (by flow table)*, EN 1015-3
30. Hall C, Hoff W (2012) *Water Transport in Brick, Stone, Concrete*. Taylor and Francis, London and New York
31. European Committee for Standardization (1999) *Methods of test for mortar for masonry. Determination of flexural and compressive strength of hardened mortar*, EN 1015-11
32. Despotou E, Schlegel T, Shtiza A et al (2014) Literature study on the rate and mechanism of carbonation of lime mortars. 9th Internations Masonry Conference, Guimarães, Portugal
33. Oelkers EH, Declercq J, Saldi GD, Gislason SR, Schott J (2018) Olivine dissolution rates: A critical review. *Chem Geol* 500:1-19
34. Lawrence R (2006) *A study of carbonation in non-hydraulic lime mortars*. University of Bath, Bath, UK

35. Kelemen PB, Matter J (2008) In situ carbonation of peridotite for CO₂ storage. *Proc Natl Acad Sci USA* 105: 17295-17300
36. Alvarez JI, Fernández JM, Navarro-Blasco I et al (2013) Microstructural consequences of nanosilica addition on aerial lime building materials: Influence of different drying conditions. *Mater Char* 80:36-49
37. Rigopoulos I, Tsikouras B, Pomonis P et al (2010) The influence of alteration on the engineering properties of dolerites: The examples from the Pindos and Vourinos ophiolites (northern Greece). *Int J Rock Mech Min Sci* 47:69-80

Microstructure of lime pastes with the addition of vegetable oils

Cristiana Nunes¹, Alberto Viani¹, Kateřina Mlsnová¹, Dita Frankeová¹, Petra Mácová¹

(1) Institute of Theoretical and Applied Mechanics of the Czech Academy of Sciences, nunes@itam.cas.cz; viani@itam.cas.cz; mlsnova@itam.cas.cz; frankeova@itam.cas.cz; macova@itam.cas.cz

Abstract

Vegetable oils can be used as water-repellent additives for mortars and coatings for improving their durability when applied in the protection of structures exposed to severe weathering conditions involving water ingress. Previous studies have shown that, besides imparting water-repellence, vegetable oils can significantly affect the microstructure of the lime paste. The influence of the addition of different amounts (0.5 and 1.5 wt%) of linseed, stand, and rapeseed oil on the microstructure of lime pastes has been investigated with thermogravimetry, Fourier transform infrared spectroscopy, X-ray powder diffraction, and scanning electron microscopy, up to 180 days of age. The wettability of the pastes was analysed by measuring the contact angle of water drops on the pastes' surface. The overall results indicate that linseed and rapeseed oil are more reactive with lime than stand oil, thus, affecting the microstructure of the paste more significantly. The lower reactivity of stand oil is assigned to the considerably lower amount of carbon-carbon double bonds as compared with the other oils. A higher amount of stand oil may be required to achieve water-repellence in the lime paste.

Introduction

The current demand for sustainable development has drawn attention to the use of materials from renewable natural products. Regarding the design of construction materials with improved durability, there is an increasing interest for the utilization of vegetable oils as water-repellent additives for mortars [1] and coatings, in the latter case either used alone or as a component in paints [2]. Several types of vegetable oils have been recently studied as water-repellent additives for lime-based mortars to be used in the restoration of traditional constructions with promising results [e.g., 3-5]. Besides imparting water-repellence, vegetable oils can significantly affect the microstructure of the lime paste [6].

Vegetable oils are mainly composed of glycerides, i.e., esters of glycerol and fatty acids. Fatty acids are straight-chain compounds with an even number of carbon atoms in their molecules. Chain lengths are most commonly between C₁₂ and C₂₂ [7]. The type of fatty acids present in an oil determines its physical and chemical character. The fatty acid composition of vegetable oils varies depending on several factors, like the type of plant, quality of the seeds, the climate and soil in which the plant grows and also on the methods of extraction [8]. Hence, results from studies using the same type of oil may vary considerably.

In this study, three types of oil were selected to be used as additives for preparing lime pastes and compare their effect on the microstructure of the paste: linseed oil, stand oil from linseed oil, and rapeseed oil. In a previous study [9], linseed and stand oils added to lime mortar attained comparable results as synthetic water-repellents (e.g., metal soaps, silanes), so, they can be considered as eco-friendly alternatives. In this study, rapeseed oil was included because of its worldwide availability, low-cost, and promising results obtained when added to Portland cement [1].

Linseed oil has a long tradition of use as a coating and as an additive for mortars [10] thanks to its high content of fatty acids with carbon-carbon double bonds like linolenic acid (45-60%) which make it highly chemically reactive [11]. Linseed is grown in Russia, North America, India, and Argentina and is becoming more popular in Europe [7]. Stand oil is obtained by thermal polymerization, a process in which the oil is heated at high temperature (>270°C) in the absence of oxygen, leading to the polymerization of fatty acids' double bonds and crosslinking of triglycerides [12]. Rapeseed oil is the only vegetable oil cultivated on a large scale in northern Europe, China, India, and Canada. Edible rapeseed is rich in oleic acid (50-65%) but also contains a relevant amount of linoleic (20-30%) and linolenic acid (6-14%) and has a lower level of saturated acids than any other commercially available oil [7].

Experimental

Materials and sample preparation

The pastes were prepared with pure hydrated lime powder (class CL90). The linseed and rapeseed oils used are of edible quality. According to the producer, the stand oil purchased is pure, i.e., does not contain any additives, and is commonly used in the restoration of wooden objects. Each oil was added in 0.5 and 1.5 wt.% with respect to the weight of lime. The oil was mixed with the lime powder according to the procedure detailed in [6], which consists in mixing the oil with an increasing amount of binder. The lime and oil mix is then blended with water to achieve a fresh paste with a consistency of 20 ± 3 mm determined according to ASTM C110 [13]. The paste code assigned to each mix (henceforth used to designate each paste) and the values of the water/binder ratio and consistency obtained for each paste, are given in Table 1.

Table 1. Values of water/binder ratio and consistency for each paste.

Paste code	Oil	Amount of oil (wt.%)	Water/binder ratio	Consistency (mm)*
L	-	-	1.02	20
LO/0.5	Linseed	0.5	1.05	18
LO/1.5	Linseed	1.5	1.13	17
LS/0.5	Stand	0.5	1.05	17
LS/1.5	Stand	1.5	1.08	20
LR/0.5	Rapeseed	0.5	1.11	18
LR/1.5	Rapeseed	1.5	1.20	19

* Determined according to the modified Vicat apparatus [13]

The addition of oils to lime increases the water demand because oil decreases the adsorption of water to the lime particles covered with oil, leading to an increase of the cohesion of the paste and a reduced workability. The increment of kneading water with the addition of oils to reach the same workability as the reference, is in agreement with previous studies in mortars [3, 4, 6].

The fresh pastes were spread over a tile using a frame to obtain a tablet with an even thickness of 6mm (Figure 1.a). The fresh plates were then stored at 90% RH for 2 days at room temperature ($20 \pm 5^\circ\text{C}$) to allow a small portion of water to evaporate, hence facilitating cutting out samples from the tablets. The fresh tablets were cut with a metallic ring of 30mm inner diameter (Figure 1.b) and stored in a room with $60 \pm 10\%$ RH, $20 \pm 5^\circ\text{C}$, and 500 ± 50 ppm of CO_2 (atm). After one day, the circular tablets (30mm diameter and 6mm thickness) were transferred from the tile to grid-lined shelves to allow carbonation from both sides. The samples were analysed after 7, 14, 28, 90 and 180 days of curing. Before each of the analysis, described in the next section, the samples were dried for 24h inside a desiccator with silica gel at room temperature.

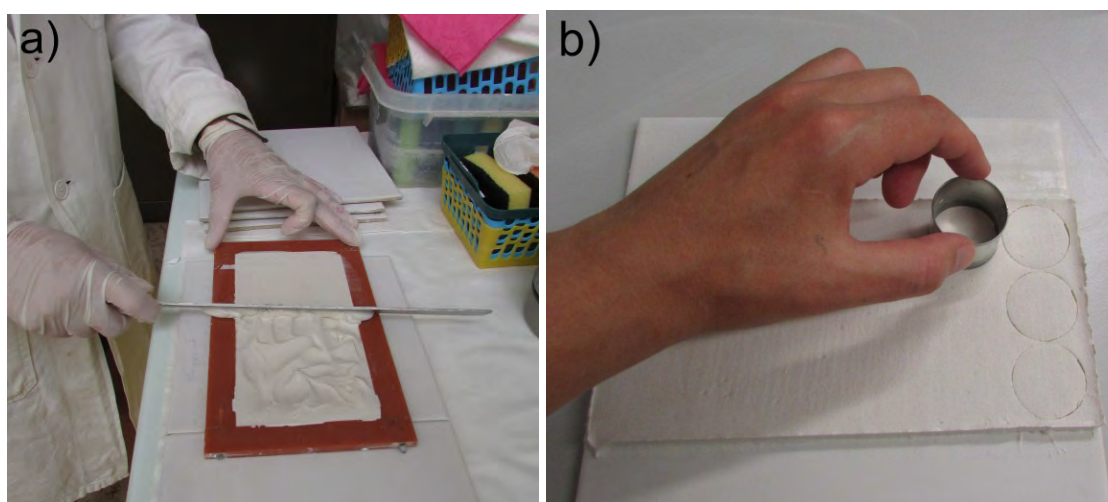


Figure 1. Preparation of the samples: a) spreading of the paste using a frame to obtain an even thickness; b) cutting of the fresh paste with a ring to obtain circular tablets.

Analytical techniques

The oils were analyzed with gas chromatography (GC) to determine the component acids and its respective amount in each oil. The oils were prepared for GC analysis according to the method described in ISO 12966-2 [14]. The gas chromatograph used was an Agilent 6890N with flame ionization detection with an SP-2560 (Supelco) column.

The contact angle of the pastes with water drops was used to measure the wettability of the pastes. A drop of $0.20 \pm 0.05 \mu\text{l}$ of water was poured from ca. 5 cm distance from the surface and a photograph was taken within 10 s after the drop touched the surface. The angle of the drop of water in relation to the surface was then calculated using image analysis. The

contact angle was measured after 14, 28, and 90 days of curing on 3 specimens from each paste; the contact angle was measured in triplicate for each specimen.

The carbonation reaction in the pastes was studied with thermogravimetric analysis (TG) with a TA instrument in a static nitrogen atmosphere at a T range of 20–1000 °C and at a heating rate of 20 °C/min. The pastes were analyzed with TG after 7, 14, 28, 90, and 180 days of curing. The mineralogical composition of the samples was studied by X-ray powder diffraction (XRPD). XRPD data were collected with a Bragg–Brentano θ - θ diffractometer; quantitative phase analysis (QPA) was performed with the Rietveld method. Fourier transform infrared (FTIR) spectroscopy measurements with the attenuated total reflection technique were performed using an external module iZ10 of Nicolet iN10 equipped with diamond crystal. The spectra were collected at 4 cm⁻¹ resolution and 64 scans in the range 4000–525 cm⁻¹. The pastes were analyzed with XRPD and FTIR after 7 and 90 days of curing. The analysis with TG, XRPD, and FTIR was performed in the same specimen from each paste. Prior to the analysis, the specimens were crushed in an agate mortar to obtain a powder.

Photomicrographs of the freshly fractured surface of each paste specimen with 90 days of age were taken with a scanning electron microscope (SEM) to investigate the effect of oil on the morphology of the pastes. The photomicrographs were taken under high vacuum at 15 kV voltage and at a working distance of 15 mm.

Results and discussion

The main component fatty acids detected in the oils with GC are given in Table 2. Linseed oil contains the highest number of unsaturated centres (C-C double bonds) which is mainly attributed to the high content of linolenic acid (49%). Rapeseed oil also contains a relevant amount of unsaturated fatty acids which is mainly attributed to the high content of oleic acid (62%). The main difference between rapeseed and linseed oils is that rapeseed is mainly composed of mono-unsaturated fatty acids, whereas linseed oil is mainly composed of poly-unsaturated fatty acids. Stand oil shows the lowest amount of unsaturated fatty acids as a result of the thermal polymerization process.

Table 2. Main component fatty acids of the oils (wt. %) determined with GC.

Oil	Palmitic 16:0*	Stearic 18:0*	Oleic 18:1*	Linoleic 18:2*	Linolenic 18:3*
Linseed oil	6	4	19	16	49
Stand oil	10	6	29	8	1
Rapeseed oil	5	2	62	19	7

* Number of carbon atoms: Number of unsaturated centres.

The results of the contact angle measurements revealed that only the pastes with 1.5% of linseed and rapeseed oil attained hydrophobic properties. The hydrophobicity evolved with time: up to 14 days of curing the pastes were hydrophilic, but after 28 days, LO/1.5 registered a contact angle of 129° (± 13), and after 90 days an angle of 134° (± 6). The paste

LR/1.5 showed similar contact angles after 28 and 90 days: $152^\circ (\pm 6)$ and $154^\circ (\pm 4)$, respectively.

Thermogravimetry can give precise data on the quantities of $\text{Ca}(\text{OH})_2$ and CaCO_3 present in a specimen since their thermal breakdown is well differentiated. Figure 2 shows the CaCO_3 content of each paste determined up to 180 days of age. Up to 28 days of age, the amount of CaCO_3 in all the pastes with oil is similar or higher than the reference. After 90 days of curing, all pastes with oil show a lower amount of CaCO_3 than the pure lime paste. The results indicate that the presence of oil in the early stages of curing accelerates carbonation, but afterward the tendency is reverted. After 180 days of curing, all pastes show similar calcium carbonate content as determined after 90 days. The decrease in carbonation rate with time has also been observed in a previous study with pastes [6] and is attributed to the development of a less porous (carbonated) layer on the exposed surface which hinders CO_2 diffusion into the centre of the paste. The pastes with oil have lower carbonation rate than the reference due to their water-repellence that hampers CO_2 access to the lime particles through the pore water.

The higher rate of carbonation in the early ages of the pastes with oil in comparison with the reference can be assigned to the air bubbles formed at the surface of the fresh paste during mixing (observed with the naked eye during sample preparation). The macropores formed at the surface increase the specific surface area of the specimens hence giving access to CO_2 diffusion into the matrix during the first stage of curing. The air bubbles formed are assigned to the saponification reaction that occurs when mixing an alkaline substance (lime) with oil. Other authors [15] consider that the presence of carbohydrates in organic additives can constitute a source of carbon for the formation of CaCO_3 .

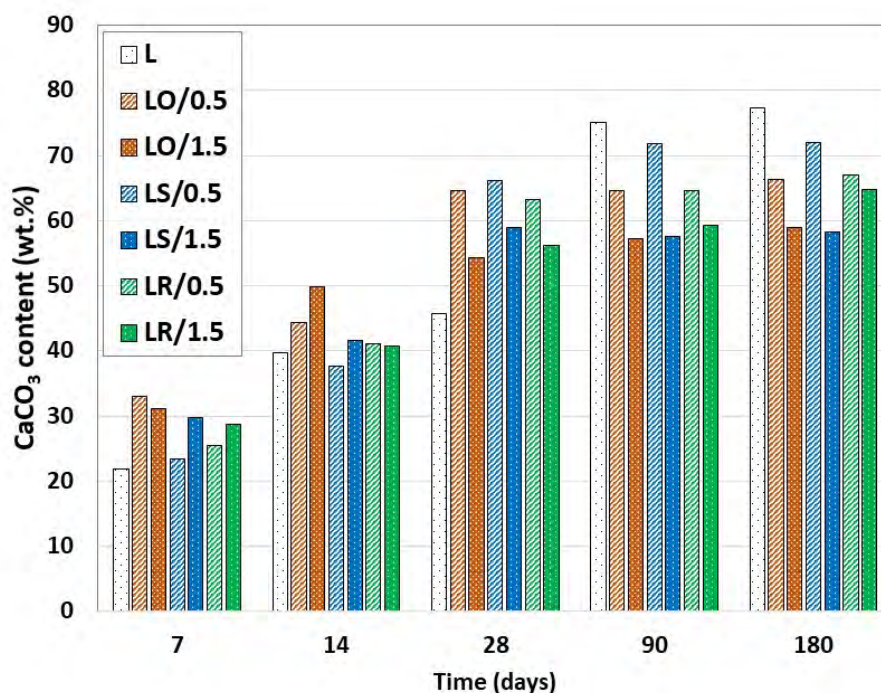


Figure 2. Evolution of the calcium carbonate content in the pastes measured with TG up to 180 days.

The results of XRPD analysis of the pastes with 7 and 90 days of age are shown in Figure 3.

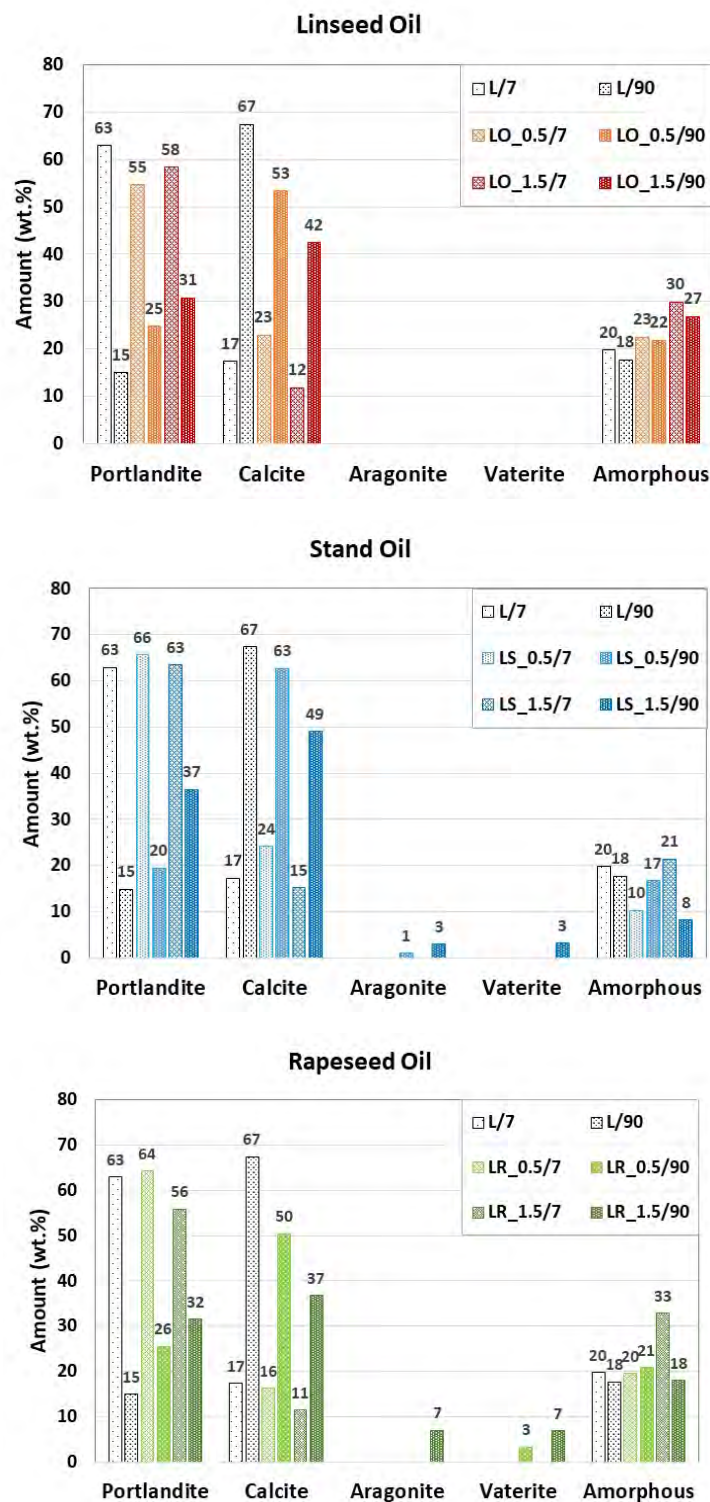


Figure 3. Results of the XRPD-QPA of the samples after 7 and 90 days of curing.

All pastes with 7 days of age and with 0.5% of oil have a higher calcite content than the reference (except LR/0.5), but after 90 days this is reverted and all samples containing oil have a lower calcite content in comparison with the pure lime paste, confirming the TG results. LR/1.5 shows the lowest calcite content whereas LS/0.5 contains almost the same amount as the reference. Stand oil added in 1.5% also had the least effect from all oils in the

precipitation of calcite. Increasing the amount of any oil delays calcite precipitation at a later age, which is in line with the TG results. After 7 days, all samples with oil contain a higher or similar amount of amorphous phase with respect to L, except LS/0.5 which shows significantly lower content. After 90 days, the amorphous content is generally reduced, except in the case of LS/0.5 (7% increment) and LR/0.5 (1% increment). The reduction is most significant in the case of LR/1.5. Linseed and rapeseed oils increase the amount of amorphous phases whereas stand oil seems to reduce the amount of amorphous phases with respect to the reference. Aragonite and vaterite were detected in a small amount in samples containing stand oil. A higher amount of both these phases was detected in samples with rapeseed oil.

The FTIR technique enables the detection of both organic substances and CaCO_3 polymorphs [16]. The FTIR spectra of each paste with 90 days of age is depicted in Figure 4. The FTIR analysis confirmed the XRPD results regarding the detection of CaCO_3 polymorphs: presence of portlandite and calcite in all samples, low intensity peak of vaterite ($\sim 745 \text{ cm}^{-1}$) in LR/0.5, LR/1.5, and LS/1.5, and relevant peak of aragonite ($\sim 858 \text{ cm}^{-1}$ and 700 cm^{-1}) in LR/0.5, LR/1.5 and LS/1.5. The FTIR spectra did not detect bands assigned to the presence of oil in the specimens because the amount of oil added is likely too low.

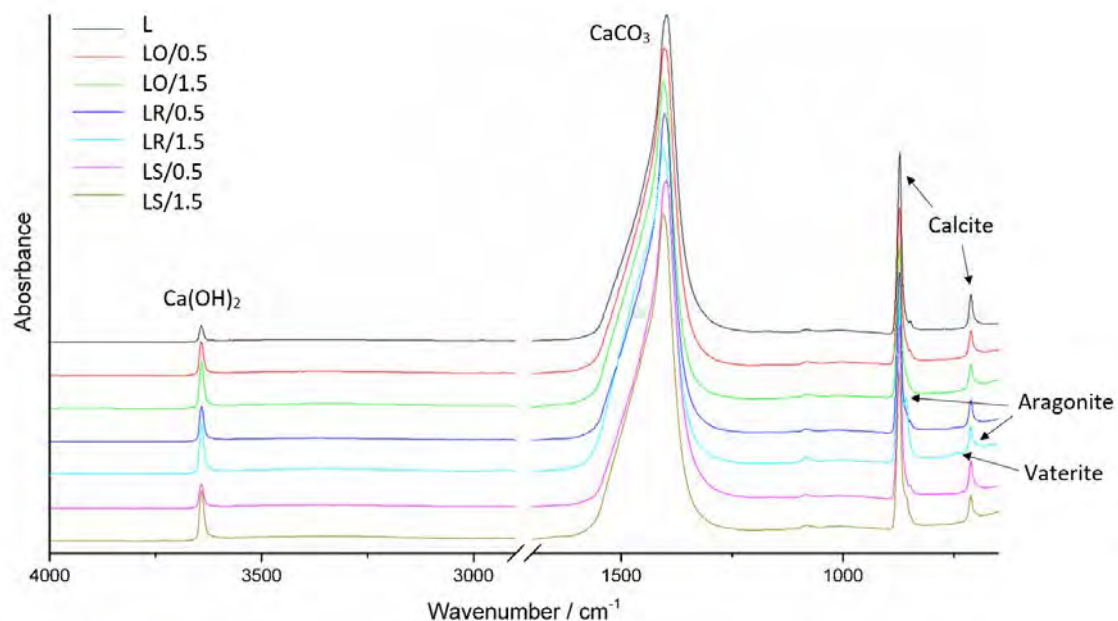


Figure 4. FTIR spectra of the samples with 90 days of age.

Figures 5, 6, 7, and 8 show the typical morphology of the pastes as observed under SEM, both close to the exposed surface (edge) and in the centre of the specimen. In general, all pastes show a denser structure close to the exposed surface and a more porous structure in the centre of the specimen. In L paste (Figure 5) scalenohedral CaCO_3 crystals are observed close to the surface, whereas the centre of the specimen is composed of polyhedral-shaped crystals and hexagonal plate-like portlandite crystals. According to Jung et al [17], the scalenohedral habit precipitates under non-stoichiometric conditions assigned to low CO_2

concentration and has been observed by Cizer [18] on the exposed surface of lime pastes carbonated under similar conditions.

The morphology, shape, and size of the precipitates are influenced by the type and amount of oil added to the lime paste. In the case of LO (Figure 6), the matrix is more amorphous and denser close to the surface; increasing the amount of oil results in a more porous structure; less scalenohedral crystals precipitate close to the surface, and some portlandite hexagonal-shaped crystals can be observed. This seems in general agreement with the amorphous content detected with XRPD in these samples (Figure 3). The centre of the pastes with linseed oil shows hexagonal portlandite crystals, sometimes with corroded edges, in higher number and thickness than the platelets observed in L paste.

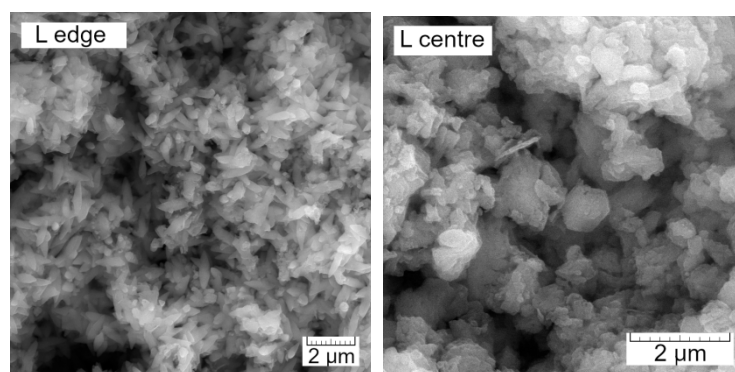


Figure 5. SEM photomicrographs of L paste with 90 days of age taken close to the exposed surface (edge) and in the centre of the specimen.

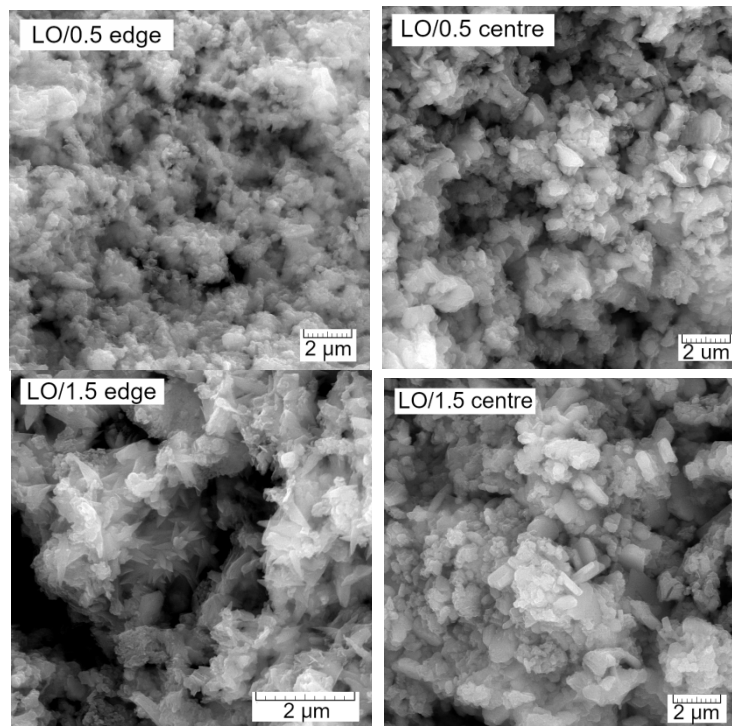


Figure 6. SEM photomicrographs of LO paste with 90 days of age taken close to the exposed surface (edge) and in the centre of the specimen.

The aspect of LS paste (Figure 7) close to the surface is similar to that of the reference, but the centre is composed of portlandite crystals in higher amount and size. Increasing the amount of oil leads to an amorphous aspect at the surface and an increment of portlandite hexagonal crystals in the centre of the specimen.

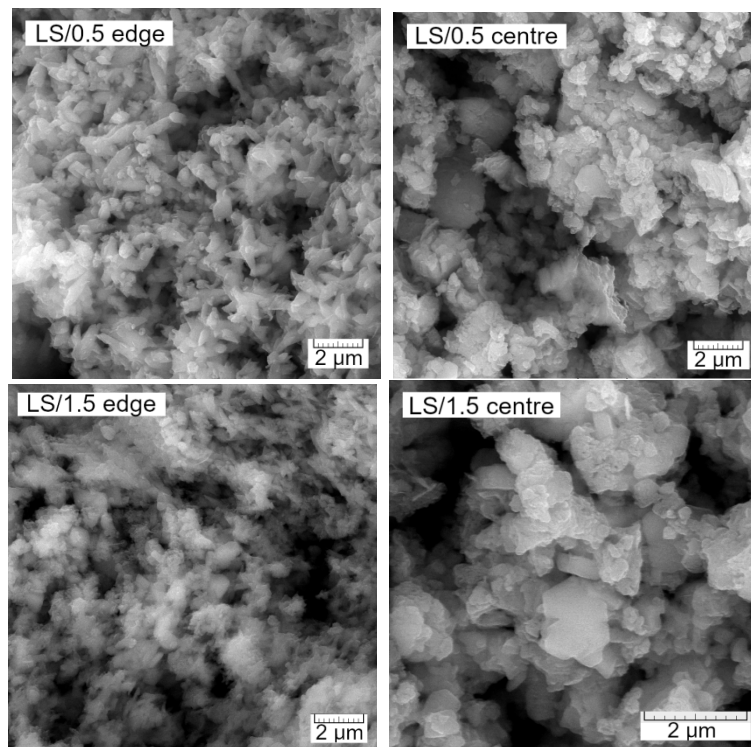


Figure 7. SEM photomicrographs of LS paste with 90 days of age taken close to the exposed surface (edge) and in the centre of the specimen.

The aspect of LR paste (Figure 8) close to the surface is also similar to that of L paste. As in the case of LO, increasing the amount of oil leads to a carbonation delay also close to the surface as indicated by the presence of some portlandite hexagonal crystals along with scalenohedral crystals. Plate-like crystals with corroded edges were observed in the centre of the paste, which probably corresponds to portlandite.

Figure 9 shows the texture of the pastes as observed under SEM at low magnification. The striking difference between the pastes with oil and the pure lime paste is mainly assigned to air bubbles formed during mixing of the fresh paste as a result of the saponification reaction between lime and oil, resulting in rounded macropores with a mean size of ca. 50 µm. Rapeseed oil had the highest influence on the development of macropores whereas stand oil had the least effect.

In general, the SEM observations are in line with the results obtained with TG, XRPD and FTIR: (i) denser structure close to the surface which probably hinders the diffusion of CO₂ to the centre of the specimen; (ii) presence of scalenohedral calcite indicating lack of CO₂ thus further contributing to the carbonation delay; (iii) presence of portlandite in higher amount in the pastes with oil as compared to the reference; (iv) increment of portlandite with

increasing amount of oil, indicating carbonation delay. Vaterite and aragonite typical morphologies (detected with XRPD and FTIR) were not observed in the pastes, probably due to their rare occurrence in the matrix of the pastes.

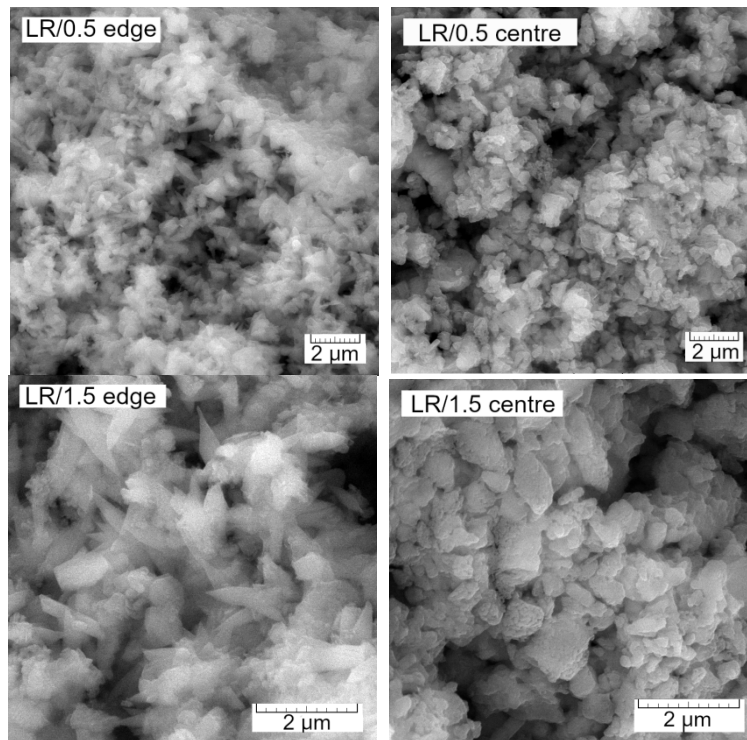


Figure 8. SEM photomicrographs of LR paste with 90 days of age taken close to the exposed surface (edge) and in the centre of the specimen.

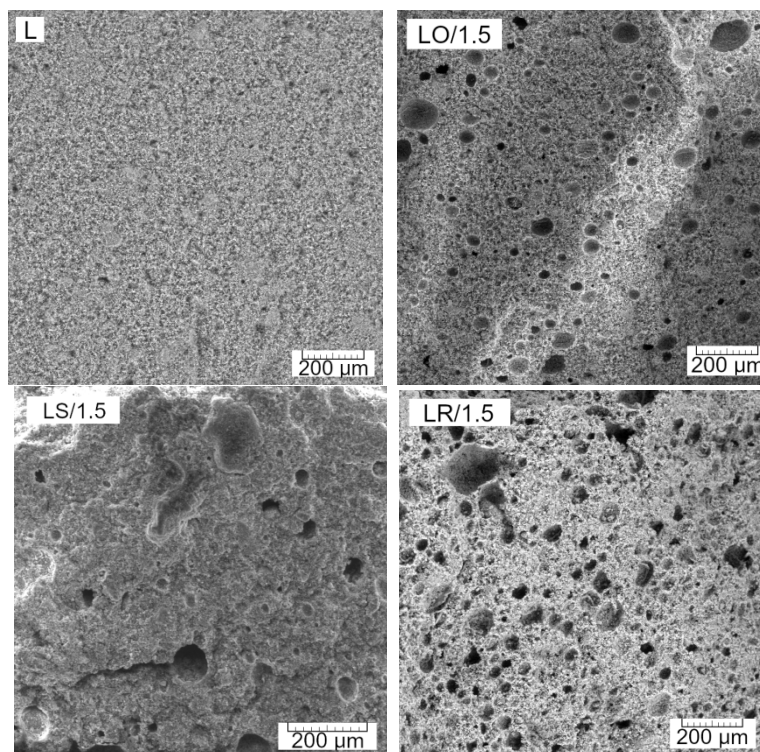


Figure 9. SEM photomicrographs of the pastes with 90 days showing the typical aspect of their texture at low magnification.

The influence of organic additives on the morphology (shape and size) of calcium carbonate precipitation from calcium hydroxide is well reported in the literature [e.g. 19, 20, 21]. The effect that each oil has on the microstructure of the lime paste is mainly assigned to the fatty acid components of the oil. Interestingly, fatty acids have been found to mediate crystallization of calcium carbonate through the formation of amorphous intermediate [22]. A similar mechanism might have produced the higher content of amorphous phase in the samples with linseed oil, because of its high content in fatty acids. Linseed and rapeseed oil are more reactive than stand oil because they contain a higher number of unsaturated centres. In the present study, rapeseed oil imparted higher water-repellency to the lime paste, which is in line with the results obtained by Justnes et al [1] who compared the effect of several vegetable oils (including linseed and rapeseed) on the properties of Portland cement. The higher degree of hydrophobicity granted by rapeseed in comparison with linseed oil is probably related to its higher content of mono-unsaturated acids that react more easily with lime than the poly-unsaturated fatty acids present in linseed oil. However, rapeseed oil affected more significantly the microstructure of the paste as observed by the amount of macropores formed, reduction of calcite content, and presence of CaCO₃ polymorphs. Hence, lime mortars prepared with rapeseed oil are likely to have lower mechanical strength.

Conclusions

Vegetable oils can be used as water-repellent additives for mortars and coatings for improving their durability when applied in the protection of structures exposed to severe weathering conditions involving water ingress. Previous studies have shown that, besides imparting water-repellence, vegetable oils can significantly affect the microstructure of the lime paste. The influence of the addition of different doses (0.5 and 1.5 wt%) of linseed, stand, and rapeseed oil on the microstructure of lime pastes has been investigated in this study.

The results of TG showed that up to 28 days of curing, samples with oil were more carbonated than the reference, but after 90 days the calcium carbonate content was lower, namely in the specimens with 1.5 wt% of oil. Stand oil added in the lowest amount had the least effect on the delay of the carbonation reaction. A small amount of aragonite and vaterite was identified with XRPD and FTIR in specimens containing stand and rapeseed oil. Linseed and rapeseed oil added in 1.5 wt.% promoted the development of amorphous phases, which were reduced over time down to a similar amount to that of the pure lime paste.

SEM analysis indicated that the pastes with linseed oil exhibited a larger crystal size and a more amorphous and porous structure in relation to the reference. Rounded macropores with a mean diameter of 50 µm were observed. The texture of the pastes with stand oil was very similar to that of the reference, apart from the higher number of bubble-like pores. The paste with rapeseed oil showed a higher number of macropores in comparison with the

linseed paste. The matrix was also more porous and amorphous than that of pure lime. Only the pastes with 1.5 wt% of linseed and rapeseed oil exhibited hydrophobicity.

The overall results indicate that linseed and rapeseed oil are more reactive with lime than stand oil, thus affecting the microstructure of the paste more significantly. The lower reactivity of stand oil is assigned to the significantly lower amount of C-C double bonds as compared with the other oils. A higher amount of stand oil may be required to achieve water-repellence in the lime paste.

Acknowledgements

This study was supported by the grant 18-28142S from the Czech Science Foundation. We are thankful to Veronika Koudelková for taking the SEM microphotographs.

References

1. Justnes H, Ostnor TA, Vila B (2004) Vegetable oils as water-repellents for mortars. In: Proc. 1st Int. Conf. Asian Concrete Federation, Chiang Mai, 689– 698
2. Alam M, Akram D, Sharmin E et al (2014) Vegetable Oil Based Eco-Friendly Coating Materials: A Review Article. *Arabian J Chem.* doi:10.1016/j.arabjc.2013.12.023
3. Pahlavan P, Manzi S, Sansonetti A, Bignozzi MC (2018) Valorization of organic additions in restorative lime mortars: Spent cooking oil and albumen. *Constr Build Mater.* doi: 10.1016/j.conbuildmat.2018.06.089
4. Nunes C, Slížková Z (2016) Freezing and Thawing Resistance of Aerial Lime Mortar with Metakaolin and a Traditional Water-Repellent Admixture. *Constr Build Mater.* doi:10.1016/j.conbuildmat.2016.04.029
5. Fang S, Zhang H, Zhang B, Li G (2014) A Study of Tung-Oil–lime putty—A Traditional Lime Based Mortar. *Int J Adhesion and Adhesives.* doi:10.1016/j.ijadhadh.2013.09.034
6. Nunes C, Mácová P, Frankeová D et al (2018) Influence of Linseed Oil on the Microstructure and Composition of Lime and Lime-Metakaolin Pastes after a Long Curing Time. *Constr Build Mater.* doi:10.1016/j.conbuildmat.2018.09.054
7. Gunstone FD (1996) *Fatty Acid and Lipid Chemistry.* Aspen Publishers, Maryland
8. Kasote DM, Badhe YS, Hegde MV (2013) Effect of Mechanical Press Oil Extraction Processing on Quality of Linseed Oil. *Industrial Crops and Products.* doi:10.1016/j.indcrop.2012.05.015
9. Nunes C, Slížková Z (2015) Lime-based repair mortars with water-repellent admixtures: laboratory durability assessment. In: Proc. 2nd Int. Conf. Preservation, Maintenance and Rehabilitation of Historical Structures. GLI, Barcelos, 851–860

10. Vitruvius (1999) *Ten Books on Architecture* (trans. Ingrid D. Rowland) Cambridge University Press, Cambridge
11. Masschelein-Kleiner L (1995) *Ancient Binding Media, Varnishes and Adhesives*. ICCROM, Rome
12. Zovi O, Lecamp L, Loutelier-Bourhis C et al (2011) Stand Reaction of Linseed Oil. *Eur J Lipid Sci Tech*. doi:10.1002/ejlt.201000414
13. ASTM C110 – 16e1: Standard Test Methods for Physical Testing of Quicklime, Hydrated Lime, and Limestone, Chapter 5: Standard consistency of lime putty (Modified Vicat Apparatus)
14. ISO 12966-2:2017 Animal and vegetable fats and oils - Gas chromatography of fatty acid methyl esters - Part 2: Preparation of methyl esters of fatty acids
15. Ravi R, Rajesh M, Thirumalini S (2018) Mechanical and Physical Properties of Natural Additive Dispersed Lime. *J Build Eng*. doi:10.1016/j.job.2017.10.009
16. Vagenas N (2003) Quantitative Analysis of Synthetic Calcium Carbonate Polymorphs Using FT-IR Spectroscopy. *Talanta*. doi:10.1016/s0039-9140(02)00638-0
17. Jung WM, Kang SH, Kim WS, Choi CK (2000) Particle Morphology of Calcium Carbonate Precipitated by Gas-liquid Reaction in a Couette-Taylor Reactor. *Chem Eng Sci*. doi:10.1016/s0009-2509(99)00395-4
18. Cizer O (2009) Competition between carbonation and hydration on the hardening of calcium hydroxide and calcium silicate binders (PhD thesis) KU, Leuven
19. Zhang K, Corti C, Grimoldi A et al (2018) Application of Different Fourier Transform Infrared (FT-IR) Methods in the Characterization of Lime-Based Mortars with Oxblood. *Appl Spectroscopy* doi:10.1177/0003702818815693
20. Loste E, Díaz-Martí E, Zarbakhsh A, Meldrum FC (2003) Study of Calcium Carbonate Precipitation Under a Series of Fatty Acid Langmuir Monolayers Using Brewster Angle Microscopy. *Langmuir*. doi:10.1021/la026837k
21. Wada N, Kanamura K, Umegaki T (2001) Effects of Carboxylic Acids on the Crystallization of Calcium Carbonate. *J Colloid & Interface Sci*. doi:10.1006/jcis.2000.7215
22. DiMasi E, Patel VM, Sivakumar M, et al (2002) Polymer-Controlled Growth Rate of an Amorphous Mineral Film Nucleated at a Fatty Acid Monolayer. *Langmuir*. doi:10.1021/la0260032.

Improvements to Water, Salt-Scaling and Freeze-Thaw Resistances Of Historic Mortar Replication Mixes

Michael P. Edison¹, Chad Lausberg¹

(1) Edison Coatings, Inc., edison@edisoncoatings.com, chad@edisoncoatings.com

Abstract

While the long-term destructive potential of liquid water in masonry assemblies is well known, the potential for disruption of saturated mortars exposed to freezing conditions can represent a more challenging and immediate problem. Highly porous and permeable mortars, valued in historic preservation work, also have the potential to become rapidly saturated. In horizontal traffic surfaces such as pavements and stairways, damages related to water ponding and saturation prior to freezing may be further exacerbated by the presence of de-icing salts whose crystallization may cause exfoliation, delamination and disruption of substrates.

Testing was undertaken to evaluate mortar admixtures in various historic mortar replication mixes incorporating Natural Cement, Natural Hydraulic Lime 3.5, Roman Cement and Portland Cement-Lime binders. Testing was based on a modified ASTM C672/C672M-12: Standard Test Method for Scaling Resistance of Concrete Surfaces Exposed to Deicing Chemicals. The most effective treatment for improving freeze-thaw, water and salt-scaling resistances while maintaining high moisture vapour permeability was a proprietary cationic acrylic latex admixture at 75% concentration.

Introduction

Freeze-thaw resistance of mortar is commonly improved in one of three ways: air entrainment, use of water repellents, or polymer modification. Harder portland cement-lime mortars, such as ASTM C270-14a [1]. Types S and M by proportions, have been found to exhibit good freeze-thaw resistance both with and without air entrainment [2]. Mortars whose hardness, density, and/or modulus of elasticity are significantly higher than those of the original mortar are known to be incompatible with many types of historic masonry construction, however. The objective of this study was to provide practical guidance to promising approaches for improving performance of historic masonry mortars of various compositions.

Air entrainment is achieved by incorporating additives conforming to ASTM C226-12, Standard Specification for Air-Entraining Additions for Use in the Manufacture of Air-Entraining Hydraulic Cement, which create micro bubbles in the mortar. While it is commonly believed that the bubbles create void spaces into which ice or salt crystals can expand without disruption to the mortar, the effects of air entrainment are more complex

and have been the subject of extensive research [3]. The size, distribution, and percentage of air voids are critical. Excessive air-void volume can negatively affect compressive strength, bond strength, and water absorption; inadequate air-void volume may prove ineffective in overcoming ice and salt-crystal expansion stresses.

Water repellents can effectively reduce water absorption into mortar from exterior exposure. As disruption will result only when freezing occurs while mortar is saturated, significant reductions in water absorption can improve freeze-thaw resistance. While a variety of water-repellent chemistries have been employed commercially, the most common types in use today are based on organosilane and siloxane prepolymers. Proprietary high-solids silane-cream water repellents are claimed to offer improved performance due to their heavier application and reduced volatility, allowing higher amounts of active treatment to be deposited more deeply within the mortar [4,5].

Polymer modification improves multiple key properties of mortar including bond strength, shrinkage, water absorption, and flexural strength [6]. At moderate polymer-binder ratios, they do not significantly reduce moisture-vapour permeability. Polymer additives increase freeze-thaw resistance by forming hydrophobic polymer-binder co-matrices. Many different polymer modifiers are commercially available, but the most effective ones do not substantially degrade when saturated with water or in long-term exposure to ultraviolet radiation in sunlight.

Of the available polymer modification chemistries, 100% acrylic admixtures are favoured for both their mechanical and colour stability. Most 100% acrylic admixtures are described by their manufacturers as being based on non-ionic polymer chemistry. In the early 1990s, a unique acrylic polymer, described by its manufacturer as being based on cationic polymer chemistry, became commercially available and was promoted as offering superior chemical and water resistance. While it was not disclosed how cationic chemistry related to the claimed performance improvements, internal testing confirmed the claim of superior water-resistance. This proprietary polymer was a component used in this study because of those properties [7].

Though primarily focused on polymer modification, the evaluations performed within this study included all three approaches to some extent. Although not intended to be an exhaustive academic examination of the many variables associated with each approach, the study's comparisons of relative performance of representative examples were valuable in ranking the relative potential benefits of air entrainment, water repellents, and polymer modification in improving the freeze-thaw resistance of historic mortar replication mixes. Correlation with real-world experience was also a central focus in selecting methods and mortar formulations, and in evaluating results.

East Block: Parliament Hill, Ottawa, and St. Patrick’s Basilica, Montréal

The initial impetus to undertake the study of polymer modification of masonry mortar was the premature freeze-thaw failure in early 2013, during the first winter after application, of an air-entrained ASTM C270 Type O repointing mortar on projecting elements of the northwest tower of the East Block on Parliament Hill in Ottawa (Figure 1). The mortar had been proportioned at 1 part ASTM C150 portland cement Type 1, 2.5 parts ASTM C207 hydrated Type SA air-entrained lime, and 8 parts ASTM C144 sand by volume (1:2.5:8). Air content was 12 to 15%. Failures did not occur on vertical surfaces.



Figure 1. East Block Parliament Hill, Ottawa, Ontario, built 1859-1866, the sloped elements (below the windows) of the northwest tower four years after repointing of the freeze-thaw damaged areas with polymer modified repointing mortar, 2017. Photo by Michael Edison.

Architect Fernando Pellicer of DFS Architecture in Montréal had previously undertaken more than 12 years of in situ comparative observations using polymer-modified and -unmodified mortars at St Patrick’s Basilica in Montréal. In 2001 Pellicer wrote that “water infiltration and saturation of mortar joints in solid masonry walls has always been a concern, especially in northern climates where the action of freeze-thaw cycles is very destructive.” He referred to “the potential benefits of polymer modified re-pointing mortars: Improved bond, flexural and compressive strengths, reduced water absorption and greater freeze-thaw resistance” as “a few of the positive points.” He recognized, however, that “the challenge is to develop a polymer modified re-pointing mortar in which the positive aspects are retained to a sufficient degree and yet maintain an acceptable level of vapour transmission” [8].

In light of his observations over time at St. Patrick’s Basilica, Pellicer concluded that the polymer-modified mortars generally remained in better condition than their unmodified counterparts and elected to consider use of polymer-modified mortar for repointing the

damaged areas of the East Block tower. He chose a 50% dilution with water of a commercially available acrylic-latex modifier, Restoration Latex #1. The admixture was used with the same Type O mortar mix that had been employed for all the repointing work performed during the previous season.

In April 2013 DFS Architecture engaged the laboratory services of Edison Coatings, manufacturer of the polymer modifier, to evaluate the effects of polymer modification on the air-entrained Type O restoration mortar. Edison Coatings' lab tested modified mortar against an unmodified control, focusing on three key performance properties: compressive strength, water-vapour transmission, and cold-water absorption.

Mortars were mixed to a typical repointing Vicat consistency of 25±2 mm penetration, per ASTM C780-00, Standard Test Method for Preconstruction and Construction Evaluation of Mortars for Plain and Reinforced Unit Masonry. Mortar cubes (50-mm) for compression testing were prepared and tested per ASTM C109/C109M-08, Standard Test Method for Compressive Strength of Hydraulic Cement Mortars (Using 2-in. or [50-mm] Cube Specimens). Unmodified mortar cubes were cured in a humidity chamber at 95 to 100% relative humidity for 18 days. Modified mortars were dry-cured in ambient laboratory air for 7 days to allow film formation, followed by 11 days curing in the humidity chamber. Dry-curing is aging without misting or further addition of water. The polymer modifier slows the rate of drying, retaining sufficient water in the mortar to promote cement hydration during the critical initial days of curing [9].

Results of compression testing indicated approximately 12% higher compressive strength for the polymer-modified mortar (Table 1). This difference can reasonably be attributed to the water-reducing effects of latex modifiers, whose surfactants allowed the 25 mm Vicat consistency to be achieved at a lower water-binder ratio.

Table 1. Compressive Strength results for polymer-modified vs. unmodified Type O mortars

Mortar Mix	Sample	Cure Method	Compressive Strength (psi)	Average (psi)
1:2.5:8 Non-Modified (cement:lime:sand)	4	18-Day Damp	800	758
	5	18-Day Damp	700	
	6	18-Day Damp	778	
1:2.5:8 Latex Modified (cement:lime:sand)	4	7 Air + 11 Damp	850	850
	5	7 Air + 11 Damp	850	

The purpose of this test was to determine whether polymer modification would lead to excessive strength increases, compromising the desire for low to moderate strength mortar. While compressive strength is not the only property of interest in evaluating mechanical performance, it is a convenient benchmark for other properties, such as flexural strength and modulus of elasticity, which tend to develop in proportion to compressive strength.

The 12% differential in compressive strength was deemed insignificant. Practical experience in reviewing tests of field-mixed mortars suggests variations greater than 12% from batch to batch are to be expected, even when using the same carefully measured mix design. Results for both mortars were also well within the range of typical strengths observed for cement-lime-sand mortars specified and prepared by proportions [10].

Water-vapour transmission testing was performed in accordance with ASTM E96-90, Standard Test Method for Water Vapor Transmission of Materials, Method B, Wet Cup. Mortar discs of uniform thickness were cast and cured in the manner appropriate to each mortar. Results indicated approximately 75% retention of water-vapour transmission rates in the modified mortar compared to the unmodified control (Table 2).

Table 2. Water Vapour Transmission Rates, polymer-modified vs. unmodified Type O mortars

Mortar Mix	Sample	Vapour Transmission (g/in ² /h)
1:2.5:8 Unmodified	1	0.0939
	2	0.1080
	3	0.0920
	Average	0.0979
1:2.5:8 Polymer Modified	1	0.0745
	2	0.0731
	3	0.0716
	Average	0.0730

This was considered more than adequate. Beyond the practical impact of inherent variability in mortar properties, precision of the ASTM E96 method is limited and significant coefficients of variation are reported in the standard for reproducibility and repeatability. Accordingly, it is impractical to closely specify or control mortar-water vapour permeability to the degree of precision that would make a 25% reduction the critical tipping point between compatibility. Mix designs should target larger differences between mortar and masonry unit or stone water vapour permeabilities to assure that the mortar is always more permeable.

Water absorption was evaluated in accordance with ASTM C67-12, Standard Test Methods for Sampling and Testing Brick and Structural Clay Tile, Part 8 Absorption. 50 mm cubes were cast and cured as per the compression-testing regimen above, and were then immersed them in room-temperature water for 24 hours. Results indicated an approximate 80% reduction in water absorption for the modified mortar compared with the unmodified control (Table 3).

These results were taken as confirmation of Pellicer's hypothesis. At the moderate polymer-binder ratio tested, polymer-modified mortar had the potential to improve freeze-thaw resistance without significant changes in mortar strength or permeability.

Subsequent to the presentation of these findings, the damaged areas of the East Block tower were repointed with the same polymer-modified air-entrained Type O mortar tested. The

work was performed in spring 2013. To date, some six years later, there has been no reoccurrence of the freeze-thaw-related damage observed after the first year with the unmodified mortar that was otherwise of the same composition.

Table 3. Cold water absorption of polymer-modified vs. unmodified Type O mortars

Mortar Mix	Time, min	Cure Method	Water Absorption g/100 cm ²	Water Absorption, %
1:2.5:8 Unmodified (cement:lime:sand)	0	18-Day Damp	0	0
	15		31.56	3.37
	60		61.20	6.53
	120		81.44	8.69
	240		111.84	11.93
	360		132.48	14.13
	1440		138.20	14.74
1:2.5:8 Latex Modified (cement:lime:sand)	0	7 Air + 11 Damp	0	0
	15		3.32	0.38
	60		6.24	0.72
	120		8.20	0.94
	240		11.08	1.27
	360		13.84	1.59
	1440		15.96	2.87

Foley Courthouse, Albany, New York

Repointing mix design for the granite pavement at Foley Courthouse in Albany, New York, was initially based on a blend of ASTM C10 natural cement and ASTM C207 Type S lime. Although the original mix was placed in late fall and improperly cured, its immediate failure led to reconsideration of mix design and selection of a more robustly hydraulic mortar with proportions of 1:2 by volume of ASTM C10 natural cement and ASTM C144 aggregate. The failure in the first winter of this second pavement mortar led to initiation of a study by the authors of freeze-thaw resistance of historic mortar-replication mixes in pavement applications. Typical damages are shown in Figure 2.

The impermeable, poorly graded granite pavement system was susceptible to water ponding, mortar saturation, and consequential freeze-thaw damage. Initial research focused on trying to determine why the 1:2 mix design was vulnerable to freeze-thaw failure and to identify alternative mix designs that could potentially perform better.

A laboratory study was initiated based on a modified ASTM C666-03, Resistance of Concrete to Rapid Freezing and Thawing. The modification involved substitution of brick assemblies for the concrete prisms used as test specimens in the ASTM standard.

Three sets of brick and mortar assemblies were made, in which the mortar to be tested was placed between two common red bricks. The assemblies were believed to be more representative of the geometry and moisture dynamics for masonry mortar applications. The

goal was to gauge relative freeze-thaw resistance properties of the mortars themselves, rather than focusing on the specifics of the Foley Courthouse pavement, granite pavement applications in general, or the more variable range of potential interactions with other substrates.



Figure 2. Foley Courthouse, Albany, New York, built 1932 to 1934. Some pavement mortar failures manifested themselves as a thin layer of dry, hardened mortar above a layer of wet, disaggregated mortar, presumably corresponding with the depth within the joint at which mortar was frozen while saturated. Photos by Chad Lausberg

Three mix designs were tested in volume proportions of 1:1, 1:1.5 and 1:2 ASTM C10 natural cement to ASTM C144 sand, respectively. All of the mortars were mixed in accordance with ASTM C305-11, Standard Practice for Mechanical Mixing of Hydraulic Cement Pastes and Mortars of Plastic Consistency. All were mixed to a typical consistency for setting mortar, 45 mm \pm 2 according to the Vicat cone penetrometer per ASTM C780-08, Standard Test Method for Preconstruction and Construction Evaluation of Mortars for Plain and Reinforced Unit Masonry. The brick and mortar assemblies were cured in a curing chamber for 28 days at 95 to 100% relative humidity. After curing, the brick and mortar assemblies were placed in a shallow pan with 6.35 mm (1/4 inch) of water and subjected to 50 freeze-thaw cycles of 16 hours at -18°C (0°F) and 8 hours at 22°C (72°F).

When the 50 freeze-thaw cycles were complete, all of the mortars were found to be in perfect condition, exhibiting no scaling or other damage. Even the 1:2 mix that had failed in one season at Foley Courthouse was in perfect condition. These observations led us to conclude that ASTM C666 did not correlate well with real-world observations and that an alternative, more aggressive testing procedure was required. Although laboratory conditions were not a direct reproduction of the failed assemblies and exposures at Foley, a portion of each assembly was completely saturated when frozen and some degree of failure was expected. A meaningful test would not only reproduce some failure but would also exhibit some differentiation between different mortars.

More Stringent Testing Based on ASTM C672 (Modified)

A new study was then initiated utilizing a modified ASTM C672/C672M-12, Scaling Resistance of Concrete Surfaces Exposed to Deicing Chemicals. Concrete paver and mortar

assemblies were substituted for mortar prisms to more accurately represent geometry and moisture dynamics of the mortar joints in a pavement assembly. Assemblies were 330 mm x 330 mm (13 x 13 inches), creating 813 mm (32 lineal inches) of mortar joints. Edge dams were created with vinyl tile and polyurethane sealant to produce a ponded water condition. All of the mortars were mixed using the ASTM C305 procedure and adjusted to the same 45 mm \pm 2 Vicat consistency. Joint widths were controlled at 1.26 cm (1/2 inch).

A wide range of mix designs was tested to obtain freeze-thaw performance trend information for potential restoration mortars (Table 4). Common binders like portland cement/hydrated lime, American natural cement, Roman cement, and natural hydraulic lime were proportioned with aggregates conforming to the requirements of ASTM C144-04, Standard Specification for Aggregate for Masonry Mortar at commonly used ratios. Portland cement conformed to the requirements of ASTM C150-07, Standard Specification for Portland Cement Type I. Hydrated lime conformed to the requirements of ASTM C207-06, Standard Specification for Hydrated Lime for Masonry Purposes Type S. Natural cement conformed to the requirements of ASTM C10-06, Standard Specification for Natural Cement. Natural hydraulic lime 3.5 conformed to the requirements of EN-459 1:2010 for natural hydraulic lime 3.5. These mix designs were then modified with different additives and treatments as noted, to determine whether and how they influenced freeze-thaw resistance.

Table 4. Mix Designs Tested for Freeze-Thaw Resistance, ASTM C672-Modified

Binder	Proportions (Type)	Modification	Cure Time (days)
Portland/Lime	1:0.25:3.75 (M)	None	7
Portland/Lime	1:0.25:3.75 (M)	100% Liquid Polymer	7
Portland/Lime	1:1:6 (N)	None	7
Portland/Lime	1:1:6 (N)	88C Silane Cream	7
Portland/Lime	1:1:6 (N)	75% Liquid Polymer	7
Portland/Lime	1:2.5:8 (O)	50% Liquid Polymer	7
Portland/Lime	1:2.5:8 (O)	75% Liquid Polymer	7
Portland/Lime	1:2.5:8 (O)	100% Liquid Polymer	7
American Natural Cement	1:1	None	56
American Natural Cement	1:1	89W Siloxane	56
American Natural Cement	1:1	12% Air	28
American Natural Cement	1:1	100% Liquid Polymer	28
American Natural Cement	1:2	100% Dry Polymer	28
American Natural Cement	1:2	50% Liquid Polymer	28
American Natural Cement	1:2	100% Liquid Polymer	28
Roman Cement	1:1	100% Liquid Polymer	28
NHL 3.5	1:2.5	None	28
NHL 3.5	1:2.5	88C Silane Cream	28
NHL 3.5	1:2.5	100% Liquid Polymer	28

The liquid polymer used in the study is a proprietary commercial cationic acrylic-latex modifier, the same as used in the East Block tower mortar evaluations. It is supplied by the manufacturer at 28% solids by mass. Test specimens designated as “100% Liquid Polymer” (Table 4) indicate use of undiluted, full-strength admixture with no additional water; 75% indicates dilution of 3 parts admixture and 1 part water; 50% indicates 1:1 dilution with water. All dilution rates are by mass. These dilutions were used to allow the optimum level of modification to be determined, the minimum amount needed to substantially improve performance without significantly reducing vapour permeability.

Unmodified control mixes for comparison were simply mixed with water as required to achieve the target Vicat consistency. Cure times were selected based on binder composition and characteristics. Because portland cement/lime-based mixes are known to cure and reach nominal full strength faster than natural cement and natural hydraulic lime, the portland cement/lime-mix designs were cured for 7 days, while the natural cement and natural hydraulic lime mixes were cured for 28 to 56 days.

All polymer-modified mortars were dry-cured, while unmodified mortars were cured in a humidity chamber at 95 to 100% relative humidity. After curing, the assemblies were flooded with 6.35 mm (1/4 inch) of 4% calcium-chloride solution and freeze-thaw cycles of 16 hours (ponded condition) at -18°C (0°F), followed by 6 hours at 22°C (72°F) and then 2 hours at 0°F (-18°C) wet, but without ponding. High permeability of the unfrozen assemblies causes the calcium-chloride solution to drain prematurely, so wet assemblies were frozen for 2 hours at -18°C (0°F) before ponding for the 16-hour cycle.

Salt scaling is defined as damage caused by freezing a saline solution on the surface of a concrete body [11]. ASTM C672 specifies scaling ratings from 0 to 5 (Table 5).

Table 5. ASTM C672 Scaling Ratings

Rating	Observations
0	No Scaling
1	Very Slight Scaling (3 mm [1/8 in] depth, max, no coarse aggregate visible)
2	Slight to Moderate Scaling
3	Moderate Scaling (some coarse aggregate visible)
4	Moderate to Severe Scaling
5	Severe Scaling (coarse aggregate visible over entire surface)

According to the standard, observations must be made every five freeze-thaw cycles or when a change has occurred. The standard also mandates that the surface be flushed

thoroughly every five cycles and the calcium-chloride solution replaced, but this was done every cycle because of the highly permeable assembly design. One person made all observations and assigned ratings for every test sample as ratings are somewhat subjective and likely to vary between technicians. Testing continued for 50 cycles or until a Severe Scaling rating of 5 was reached, whichever occurred first.

Observations for mixes based on portland cement and hydrated lime binders are plotted in Figure 3. The poorer performing mixtures display curves that are more horizontal, indicating rapid progression toward a rating of 5, Severe Scaling. The better-performing mixtures display curves that are more vertical, many of them never reaching the 5 rating at the end of the 50-cycle testing regimen.

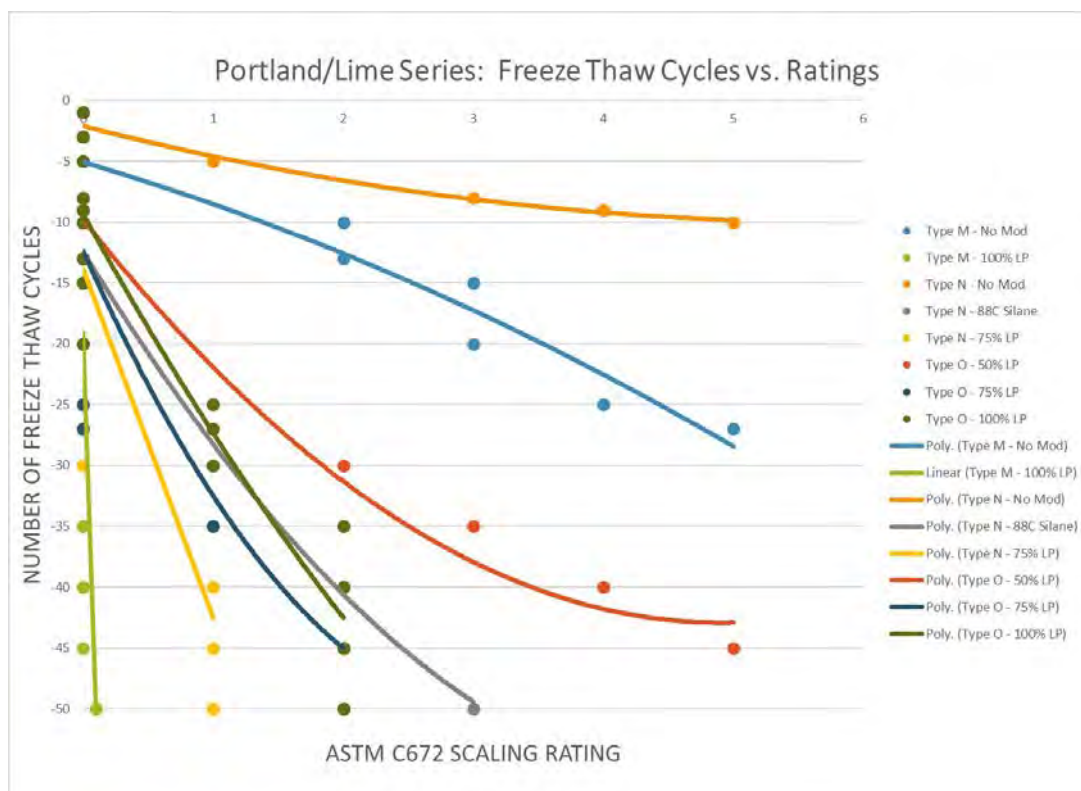


Figure 3. Portland cement/lime series: freeze-thaw cycles vs. scaling ratings

The results of testing showed a strong correlation between polymer modification and freeze-thaw scaling resistance. All of the polymer-modified mortars performed significantly better than the unmodified mortars. For Type O (1:2.5:8) mortars, the optimum level of polymer modification was achieved at 75% concentration, producing the same high degree of scaling resistance as the 100% (undiluted) specimen. Relatively high compressive-strength mortars with and without polymer modification generally performed better than lower strength mortars, as may be expected, but even Type M mortar performance improved significantly when polymer-modified.

One half of the unmodified Type N mortar panel was treated with a proprietary commercial high-solids silane-cream water repellent, Silan-Treat 88C. The performance improvement

was significant, with the untreated side reaching failure with a scaling rating of 5 after just 10 cycles. The treated side of the same panel completed the full 50 cycles with only moderate scaling, a rating of 3.

Observations for mixes based on natural cement and hydrated lime binders are similarly plotted in Figure 4. Observations for the mixes based on natural hydraulic lime 3.5 are plotted in Figure 5.

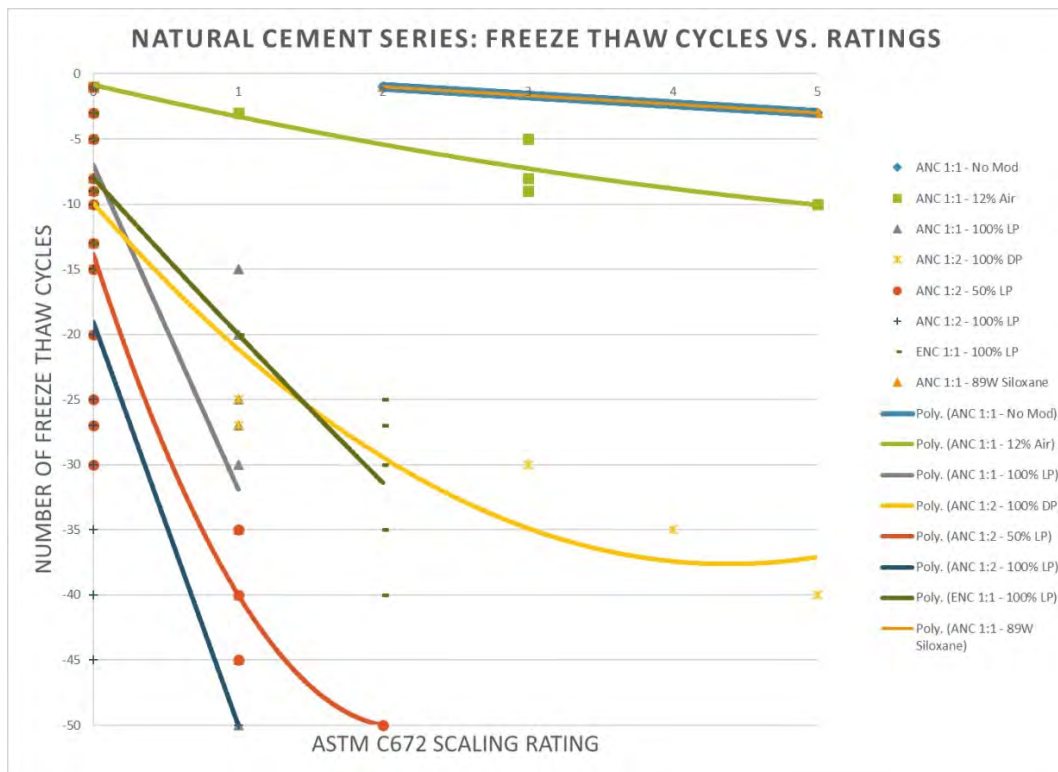


Figure 4. Natural-cement series: freeze-thaw cycles vs. scaling ratings

Similar to the results for portland cement/lime mortars, polymer-modified natural cement and natural hydraulic lime mixes were observed to perform significantly better than unmodified mixes. An air-entrained 1:1 natural cement-sand mix was found to perform only slightly better than the same mix without air entrainment. The non-air-entrained mix failed after 3 cycles, while the air-entrained mix endured 10 cycles. All polymer-modified mixes, regardless of composition or mix proportions, endured the full 50 cycles without reaching a scaling rating of 5.

One half of one of the natural-cement specimens was treated with a commercial 10% siloxane water-repellent treatment, Silox-Treat 89W. No improvement was observed with this treatment.

Half of one of the NHL 3.5 panels was treated with the high-solids silane-cream water repellent, Silan-Treat 88C. The untreated side failed in 13 cycles, while the treated side endured the full 50 cycles with a final rating of 4 (Figure 6).

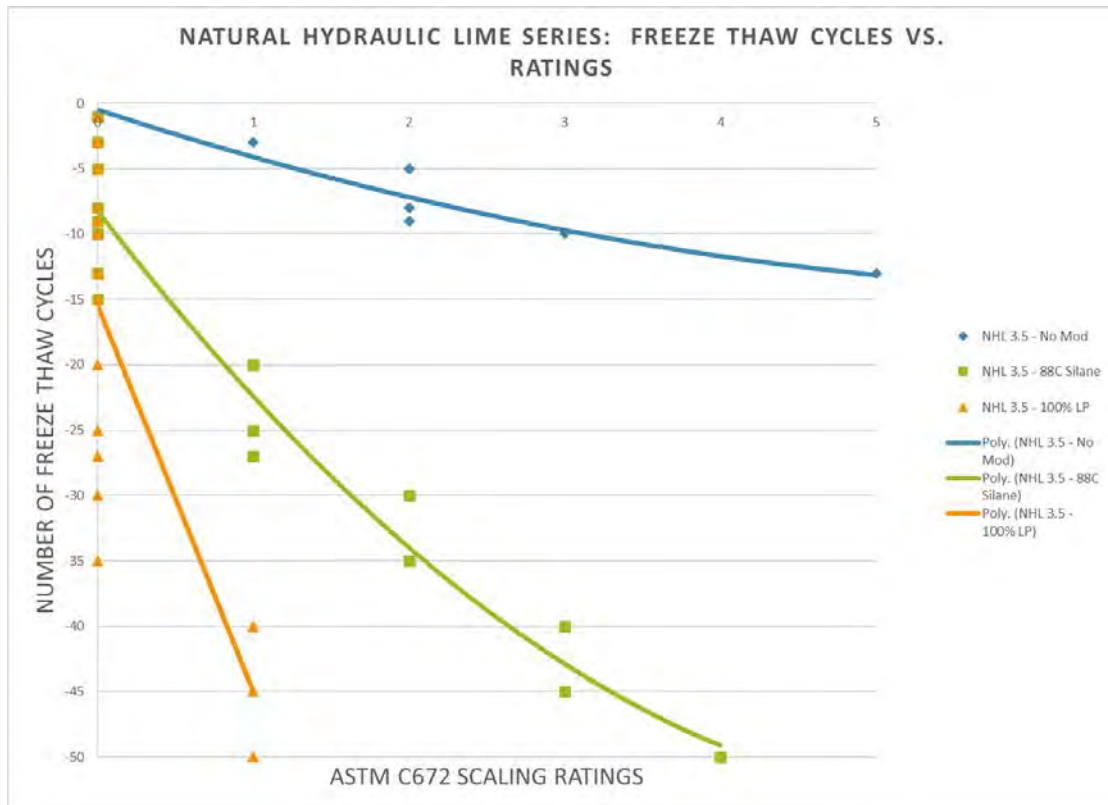


Figure 5. Natural hydraulic lime series: freeze-thaw cycles vs. scaling ratings



Figure 6. NHL 3.5 mortar with and without silane cream water repellent, after testing of 50 freeze-thaw cycles. The left side is treated with silane cream, the right side is untreated, 2017. Photograph by Chad Lausberg

A proprietary redispersible dry acrylic copolymer modifier was added to one of the natural-cement mixes. While scaling resistance improved significantly compared with the unmodified mix, it did not perform as well as the liquid polymer modifier tested at various

concentrations. The dry polymer-modified mortar failed at 40 cycles, while even the 50% diluted liquid polymer version of the same mix endured the full 50 cycles with a final scaling rating of just 2. The 100% liquid polymer completed the 50-cycle test with a final scaling rating of just 1.

Effect of Polymer Modification on Mortar Density

In polymer-modified concrete applications, a primary objective is to reduce permeability to water and dissolved deicing salts. This is done to protect embedded reinforcing steel from corrosion. Reduced permeability is achieved by incorporating a defoaming agent, which has the effect of reducing air content and increasing density. Specifications typically require air content not to exceed 6.5% [12].

The improvements in water resistance observed in this study were not the result of increased mortar density caused by air reduction, however. Modification with the optimized polymer in this study actually resulted in significant density reductions.

For Type O mortar (1:2.5:8), based on portland cement and hydrated lime, density when mixed with water was 2.047. The same mortar, mixed with 75% polymer, had a density of 1.285, a reduction of roughly 37%. For 1:1 natural-cement mortar graded aggregate, density was 2.014 when mixed with water and 1.239 when mixed with 75% polymer, a reduction of roughly 38%. The changes are a result of higher air content.

Saturation Coefficients

All of the mortars tested for freeze-thaw resistance were also tested according to ASTM C67-12, Standard Test Methods for Sampling and Testing Brick and Structural Clay Tile, Part 8 Absorption. All mortars were mixed using ASTM C305. Five mortar cubes for each mix design were prepared in accordance with ASTM C109/C109M-08, Standard Test Method for Compressive Strength of Hydraulic Cement Mortars (Using 2-in. or [50-mm] Cube Specimens). The cubes were cured using the same procedure as for the freeze-thaw testing. After curing, cubes were oven dried at 65.5°C (150°F) for 4 hours and weighed to obtain the initial dry weight. The cubes were then submerged in cold water at 22.2°C (72°F) for 24 hours and reweighed to obtain cold weight. The cubes were then submerged in boiling water for 1 hour at 100°C (212°F), allowed to cool to 22.2°C (72°F), and reweighed to obtain boiling weight. Saturation coefficient was then calculated based on the average values obtained for the quintuplicate samples, using the following formula:

$$\text{Saturation coefficient} = \frac{(\text{cold weight} - \text{dry weight})}{(\text{boiling weight} - \text{dry weight})}$$

Saturation coefficient is a value between 0 and 1 and relates to the absorption rate of water into a porous material. Values close to 1 correspond to a fast absorption rate, and values

close to 0 correspond to a slow absorption rate. If the cold weight is close to the dry weight, the absorption rate is relatively slow, and the saturation coefficient will be low. If the cold weight is close to the boiling weight, the absorption rate is relatively fast, and the saturation coefficient will be high. High saturation coefficients indicate potential poor freeze-thaw resistance, as materials that are quickly saturated are more vulnerable to disruption upon freezing. For brick, a coefficient greater than 0.8 indicates unsuitability for exposure to severe weather.

Table 6 correlates the saturation-coefficient results obtained in the ASTM C67 absorption testing with the freeze-thaw performance results obtained in the ASTM C672 freeze-thaw testing.

Table 6. Saturation Coefficient (SC) Compared to Freeze Thaw Performance (Scaling Rating)

Mortar	Modification	SC	Cycles	Scaling Rating ASTM C672
Type M (1:0.25:3.75)	None	0.95	27	5
	100% LP	0.45	50	0
Type N (1:1:6)	None	0.90	10	5
	75% LP	0.27	50	1
Type O (1:2.5:8)	50% LP	0.28	45	5
	75% LP	0.18	50	2
	100% LP	0.09	50	2
ANC (1:1)	None	0.96	3	5
	12% Air	0.85	10	5
	100% LP	0.16	50	1
ENC (1:1)	100% LP	0.27	40	2
ANC (1:2)	100% DP	0.74	40	5
	50% LP	0.57	50	2
	100% LP	0.49	50	1
NHL 3.5 (1:2.5)	None	0.78	13	5
	100% LP	0.33	50	1

A red rating was assigned to mortars that failed (scaling rating of 5) before 15 cycles indicating poor freeze-thaw resistance. Red ratings correlate well with high saturation coefficients.

Yellow was assigned to mortars that failed before 50 cycles, representing mortars with freeze-thaw resistance that was superior to the poorest performing mortars but inferior to the best performing mortars. These results do not correlate particularly well with saturation coefficient. In the case of unmodified Type M mortar, the mid-range performance in spite of high saturation coefficients may be attributable to the generally better freeze-thaw resistance associated with relatively high compressive-strength mortars. The failure at 45 cycles of the Type O mortar modified with 50% diluted liquid polymer is an indication of sub-optimal modifier concentration, as the same mortar modified at higher levels of polymer concentration performed extremely well. The failure at 40 cycles of the mortar modified with dry polymer is an indication that the dry polymer is not as effective in improving scaling resistance as even the 50% diluted liquid polymer.

Green was assigned to mortars that remained intact after 50 cycles, indicating good freeze-thaw resistance. These correlated well with low saturation coefficients.

All of these mortars were polymer-modified, supporting the general indication that polymer-modified mortars exhibit superior freeze-thaw resistance by virtue of reduced saturation coefficient.

Conclusions

The goal of the program was to identify, rather than quantify with great accuracy, promising approaches to improving freeze-thaw resistance of various replication mixes for historic mortars. The ultimate proof of merit can come only through significant numbers of real-world applications and evaluation of their performance over time.

The ASTM C666 freeze-thaw resistance test, modified using masonry assemblies in place of mortar prisms, was found to correlate poorly with the real-world observations that led to initiation of these studies. Modified ASTM C672 scaling-resistance tests, on the other hand, correlated well with those observations.

Mortars modified with a proprietary liquid acrylic copolymer exhibited significantly better resistance to scaling and freeze-thaw exposures than their unmodified counterparts. This result was consistently observed across the full range of mortars tested, whether based on portland cement and hydrated lime, natural cement, or natural hydraulic lime. Non-hydraulic binders were not tested.

Compared with the levels of improvement achieved through liquid polymer modification, use of relatively high compressive-strength mix designs, air entrainment, dry polymer modification, and treatment with a 10% siloxane water repellent were relatively ineffective. A proprietary high-solids silane-cream water repellent produced significant improvements, however.

The optimum level of polymer modification for Type O portland cement-lime-sand mortar to significantly increase freeze-thaw resistance while maintaining other properties compatible with historic masonry was determined to be a dilution of 3 parts modifier to 1 part water by mass. This was the minimum level at which the full benefits of modification were obtained.

A number of in situ applications have been implemented over the past five years utilizing polymer modification and silane-cream treatment of various mortars in various cold weather locations. Future work will continue to track these applications and their performance.

References

1. ASTM C270-14a Standard Specification for Mortar for Unit Masonry, ASTM International
2. Tate, Michael J. and Thomson, Margaret L. (2001) "Effect of Air Entrainment on Freeze-Thaw Durability of Type S Portland Cement-Lime Masonry Mortars" (Fredericton, N.B.: 9th Canadian Masonry Symposium, June),
https://canadamasonrydesigncentre.com/download/9th_symposium/MORTAR04.pdf
3. Scherer, George W. (2008) "Modeling Damage from Ice and Salt," in CONMOD '08: International RILEM Symposium on Concrete Modelling; Delft, The Netherlands, Pages 13-23, <http://demo.webdefy.com/rilem-new/wp-content/uploads/2016/10/pro058-002.pdf>.
4. Wacker Chemie AG, Concrete Protection for Concrete Advantages (Munich, Germany, n.d.) https://www.wacker.com/cms/media/publications/downloads/6527_EN.pdf.
5. Edison Coatings Inc., Silan-Treat 88C (Plainville, Conn.: Edison Coatings, Inc., Jan. 2018), Page 1, edisoncoatings.com/88C.pdf.
6. Lavelle, Joseph A. (1988), "Acrylic Latex-Modified Portland Cement," ACI Materials Journal 85, no. 1 144–48.
7. Edison Coatings laboratory, internal studies, 1981–2018, unpublished.
8. Pellicer, Fernando (2001) "Potential Uses for Polymer-Modified Repointing Mortars," (Fredericton, N.Br.: 9th Canadian Masonry Symposium, June 2001), https://canadamasonrydesigncentre.com/download/9th_symposium/MORTAR01.pdf
9. Dow Construction Chemicals, (2010) "Polymer-Modified Mortars," Concrete Construction, https://www.concreteconstruction.net/how-to/polymer-modified-mortars_o.
10. SUNYAB-Amherst Campus Ellicott Complex Mortar Cube Breaks, (1999) unpublished

11. Valenza II, John J. and Scherer, George W. (2007) "A Review of Salt Scaling: I. Phenomenology," *Cement and Concrete Research* 37, 1007–1021, http://www.iust.ac.ir/files/crc/yekta_program/forum/f0a6ed6c3f.pdf.
12. 548.4-93: Standard Specification for Latex-Modified Concrete (LMC) Overlays (Reapproved 1998), American Concrete Institute Technical Documents (1993), 6.

Formulated lime mortars as a sustainable practice for Built Heritage conservation in Mexico

Marlene Sámano Chong

National School of Conservation, Restoration and Museography of the National Institute of Anthropology and History, marlene_samano_c@encrym.edu.mx

Abstract

In Mexico, the restoration of lime mortars is developed with regional materials and mostly prepared and evaluated on site. To assure the effectiveness of the local pozzolanic material, qualitative, economic and brief tests can be developed *in situ*. The measurement of properties such as setting time, water absorption, resistance to compression and resistance to salt attack can provide tools to analyze compatibility with historic mortars and the correct operation of restoration procedures. In contrast to usual practices of Built Cultural Heritage restoration in Mexico, where traditionally a minimum of 10% cement is added to achieve some of these properties, formulated lime mortars (air lime + pozzolans) are a compatible option for historic mortars, generating sustainable practice, reducing environmental impact, promoting local consumption and safeguarding traditional constructive culture.

Introduction

In the restoration of Mexican historic buildings, an addition of cement (usually at least 10%) in the air lime and aggregate mortar is common. This promotes an increase in the mortar strength, reduces setting time, sets in reduced CO₂ or high humidity environment, and helps to solve lime technology deficiency. However, this practice leads to a range of subsequent complications, e.g. presence of soluble salts that break down the historic material, a hardness greater than that of the historic fabric and the irreversibility / untreatability of interventions, inevitably causing damage to the original stone and/or lime mortar systems.

In contrast, formulated lime mortars are more compatible with the original lime systems, in terms of physical and chemical properties, because they confer the desired properties of setting in humid environments or low presence of CO₂, reduced setting time and increased strength without adverse effects.

The term of formulated limes is established in the European Standards of Building Lime EN 459-1:2010 and it refers to lime with hydraulic properties mainly consisting of air lime and/or natural hydraulic lime with added hydraulic and/or pozzolanic material [1]. Pozzolans are aggregates for mortars of siliceous or alumino-siliceous origin, which by themselves have little or no cementing value, but when they have been finely divided and in the presence of water they react chemically with the hydroxide of calcium Ca (OH)₂ at room temperature to form compounds with cementing properties [2].

The study of mineralogical, physical and chemical characterization of lime mortars and the pozzolanic effect has a long history, beginning in the first century BC. with the work of Marco Vitrubio Polión in his work "De architectura" [3]. In Mexico, the use of lime as a construction material has been common since the pre-Hispanic era, manifested in monumental buildings in different cultures such as Teotihuacan, Olmec, Mayan, Zapotec and Aztec. Lime was used to give cohesion to the structural constructive systems, as well as for plasters and the elaboration of decorative elements. Characterization of historic mortars in archaeological elements has confirmed the use (either of impurities or additions) of pozzolanic materials, due to the presence of particles with high silica content [4]. In the study of Mexican historic mortars from the Vice-regal era, a meeting of knowledge and exchange of technologies in lime is recognized. The Spanish tradition that inherited from Roman technology the use of pozzolans was combined with local pre-hispanic comprehension of materials [4] syncretising the knowledge on the production of lime mortars.



Figure 1. Mayan building. El Palacio from Archaeological site of Palenque, Chiapas. Construction made with limestone, lime mortars, lime plasters and lime decorative elements. STROM 2007.

Modern practices for mortars in conservation of historical buildings have been developed [5] and deepened in the nature, origins, design, application and assessment of lime materials [6] [7]. Comparative studies of lime mortar properties with other prepared with different percentages of white and Portland cement showed that additions of cement to lime and sand mortars affect their properties considerably. Thus in restoration procedures cement should be avoided due to the unacceptable alteration of properties in terms of hardness and water vapour permeability [8].

As to material characterization and properties measurement there are some manuals such as the "Laboratory Manual for Architectural Conservators" [9] with a compendium of diverse standard tests (ASTM, RILEM, etc.) that were adapted for the purposes of architectural conservation. Although it is not an exclusive manual for mortars assessment, this document presents useful recommendations for simple and applicable methods for material studies.

Methodological approaches for evaluating properties of injection mortars such as volume change, porosity, expansion coefficient, strength, adhesiveness, setting conditions and the influence of particle size are available [10]. However, the proposed analysis cannot be used

for the evaluation of lime mortars, as it is a study of injection mortars with a fluid state and specific purposes different from those of a paste. It represents an interesting methodology because it adapts standards (ASTM) into conservation practices and proposes analyzing classifying them among those that can be performed *in situ* or in the laboratory. Also, the effect of pozzolanic additions as a sustainable alternative to cement mortars and the percentages of additions needed to modify lime mortar properties, have been analyzed [11].

In Mexico, in the field of conservation and restoration of historical buildings, the systematic study of the influence of additions with pozzolanic behaviour in lime mortars is incipient. As a start, a bachelor thesis in restoration, in which a comparative study between different pozzolanic used as aggregates, is done [12]. It is necessary to continue with research to propose a clear methodology for the evaluation of the properties of lime mortars linked with the on-site conditions and the performance needed of the restoration mortars in Mexican conditions such as the restriction of the accessibility of standardized materials and limited resources for testing materials for each conservation project. In the Seminar of Mural Painting Restoration of the National School of Conservation (ENCRyM), comparative studies have been carried out among diverse additions that could result in a pozzolanic mortar; teachers and students have dedicated several decades to recover and use lime technology, and this study derives from this interest.

The main objective of this research is to offer alternatives for the assessment of formulated lime mortars as a substitute to cement, recuperate qualitative tests to evaluate pozzolanic effectiveness in local materials and utilize scientific assessment based on the adaptation of standardized procedures for sustainable conservation practice to reduce environmental impact, promote local consumption and safeguard traditional constructive culture.

Formulated lime mortars as a sustainable alternative to cement additions

To understand the phenomena of incompatibility between lime mortars and those of cement or lime/cement mixed mortars, it is necessary to recognize the particular properties of lime mortars such as high vapour permeability that allows moisture absorption and evaporation, regulating the humidity inside a building; the flexible nature of lime assimilates structural movements without cracking. It is environmentally friendly because it doesn't contain volatile organic compounds or other contaminants and the alkalinity of lime suppresses the growth of pathogens; and aesthetically, lime mortars show a shiny surface due to the light scattering properties of the calcium carbonate crystals [13].

Restoration mortars must function as a sacrificial material and cement additions increase mortar's strength creating a mechanical incompatibility. This addition also lowers the permeability, promoting moisture to be trapped inside the materials, causing the decay of historic lime mortars before the intervention ones. In addition, clinker additives such as sodium hydroxide, sodium silicate, sodium sulphate and calcium sulphate, that accelerate the setting time, are soluble or partially soluble compounds which in presence of humidity

dissolve and migrate in historic material, promoting its disintegration by the pressure of the recrystallization process inside the pores of materials. Finally, restorations executed with Portland cement contrast in colour and brilliance with the original lime because of its gray colour [7].



Figure 2. Aztec altar of skulls with restoration joints made of lime/cement mortar. STROM/ INAH 2009.



Figure 3. Detail of the Aztec altar of skulls, where original plaster is lost and stone presents decay because of the presence of soluble salts from the lime/cement joints. STROM/INAH 2009.

In addition to the material and cultural incompatibility, cement production has an environmental impact; this industry produces about 4.3 billion tons of cement per year [14], which means 10% of the CO₂ emissions emitted by humans [11]. That means that the cement industry contributes substantially to greenhouse effect leading to global warming. It has been determined that in the lime burning process there is an emission of CO₂ in a range of 0.1 to 0.8 tons per tonne of lime produced but it has the quality of recarbonation, absorbing environmental CO₂ in a range of approximately 70 to 80% of that issued at the time of burning; unlike cement that absorbs only between 20 and 25% of the CO₂ emitted in its production [11].

Methods to evaluate pozzolan reactivity *in situ*

Pozzolans have a variable chemical composition but they mainly consist of amorphous silica and probably also amorphous alumina; the vitreous particles react with water and lime to form hydrated calcium silicates and aluminates [15]. Not only the siliceous composition is important for the pozzolan effect, but also other circumstances have to be considered, such as the molecular structure reactive with lime in the presence of moisture, an amorphous vitreous state and a high specific surface [16]. The reactive nature of pozzolans is accentuated by the degree of fineness as the physical surface of the particles increases, influencing reaction speed [16]. To comply with the specification "ASTM C432-59T", pozzolans must have finesse: retained in 30 mesh (ASTM) 2% max. (590µm mesh) and retained in 200 mesh (ASTM) 10% max. (74µm mesh) [17].

Evaluation of pozzolanic reactivity- PH change test

Several tests have been developed to evaluate the pozzolanic reactivity in order to study the feasibility of using an accessible deposit as an addition into mortars. Many tests specified in literature and standards require sophisticated and expensive laboratory equipment and installations. For some projects, this type of analysis is out of reach because of its complexity, high cost and required time [18]. However, there are some simple tests that can be done in the field or in a simple laboratory to determine if a material has pozzolanic activity.

One test to determine the pozzolanic activity is through the contrast of the pH change in a control solution of limewater and another of limewater with pozzolanic additions. The principle of the qualitative test is that reactive silica (in a pozzolan) will be combined with the lime in a saturated solution and will reduce the alkalinity of the solution. By testing the pH of the solution at regular intervals, the rate of pH reduction and, therefore, the speed of pozzolanic activity can be controlled [19]. This test requires greater refinement, but has allowed comparisons of pozzolanic activity. The results have shown a decrease in pH in an average of 3 points from the day 14 measure.



Figure 4. Pozzolan in limewater. Day 1 pH measure 12/13. TECTRAD/ INAH 2019



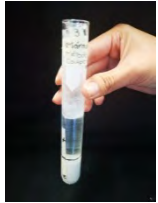
Figure 5. Pozzolan in limewater. Day 7 pH measure 11/12. TECTRAD/ INAH 2019

Evaluation of pozzolanic reactivity - the Cowper Method

This method was proposed by A. D. Cowper in 1927 and its objective is to determine the volume increase of a mixture sample of slaked lime and pozzolanic additions. Samples of materials with possible hydraulic action can be tested, the hydraulicity reaction will produce aluminium silicate hydrates in colloidal form that will increase the volume of the sample. This increase after seven days of the material is a qualitative indication of the hydraulicity [20]. Hydrated calcium aluminosilicates formed by the reaction are much more bulky than pozzolan or lime, so at the end of the test the volume of solid matter should be greater than that of the freshly made mixture and should settle more slowly [6].



Day 1



Day 7



Day 14

Figure 6 Calcium carbonate in limewater where there is no increased volume. Days 1, 7 & 14. TECTRAD INAH 2019



Day 1



Day 7



Day 14

Figure 7 Volcanic rock Tezontle in 200 mesh in limewater where there is an increased volume in days 7 & 14. TECTRAD INAH 2019



Day 1



Day 7



Day 14

Figure 8 Diatomaceous in 200 mesh in limewater where there is an increased volume in days 7 & 14. TECTRAD INAH 2019

Property evaluation of formulated lime mortars

Preparation of the test cubes and curing

The characteristics and behaviour of lime mortars are not only influenced by their components but also by the techniques of preparation, application and curing. For the design and elaboration of the mortars, the following must be taken into consideration:

- Lime: texture and hydration time
- Aggregates: Texture, size distribution, cleaning
- Mortar: Preparation of the mortar through obtaining the vacuum index
- Pozzolans: particle size, percentage of the dosage of $\frac{1}{4}$ of the mortar mass [21], mixed with water before adding to the mortar, understand pozzolans role in mortar not as an aggregate but as an addition.



Figure 9 Lime paste test to verify correct texture for mortar mixture. TECTRAD INAH 2019



Figure 10 Aggregates selection with different size distribution. TECTRAD INAH 2019



Figure 11 Mortar preparation through the vacuum index. TECTRAD INAH 2019



Figure 12 Dosage of pozzolanic additions into mortar. TECTRAD INAH 2019

The preparation procedure for test cubes for laboratory analysis includes steps of molding and compaction, demolding [6] and the curing conditions for setting mortars with pozzolanic material according to the standard ASTM C 1707 Standard Specification for Pozzolanic Hydraulic Lime for Structural Purposes.

To set mortars they can be stored in metal molds that contain two parts that are assembled and fixed with screws [22]; it is also possible to use plywood molds that have been soaked in water [6]. It is necessary to consider making a triad of specimens for each test performed. For tests of lime mortars containing pozzolans, it is recommended that the molding is done by hand and the mortars in the mold must be stored for 60 ± 12 hours in sealed plastic bags before demolding. Once this time has elapsed, the test pieces are demolded and must be stored in an environment (wet room or cabin) that is not less than 95% RH [22]. The time in which the specimens are allowed to set depend on each of the tests; some of them are made with fresh mortar and others with set mortar. In case of set mortar tests, the ASTM C1713-12 Standard specification for mortars for the repair of historic masonry, establishes that curing times for air or hydraulic lime should be 128 days [23]. The formulated lime is not specified, however, it is a material with very similar qualities. Mortars made with formulated lime are very resistant, durable and reach their structurally acceptable resistance in a period between 28 and 90 days [11].

Properties of fresh mortar: Stiffness range

Stiffness refers to the gradual transformation of fresh / plastic mortar. Quick stiffness will affect the mortar's workability since the operator may not have enough time to use the mortar before it hardens. In addition, an excessively slow stiffness rate will reduce the pace of work [11]. In the use of formulated lime mortars, the evaluation of this property is important, since, due to the presence of pozzolans, the stiffing process is more accelerated. The ASTM C 359 Standard test method for early hardening of Portland cement, tests a mortar using a Vicat apparatus to measure the depth of penetration of a needle 10 seconds after the mortar is released [24], however, the evaluation times of the norm is too brief and

the results are not significant for the evaluation of a formulated lime mortar. Other studies suggest pozzolan should be added immediately before the use of the mortar and that there is a margin of approximately two hours for its application [6]. Taking this time as a reference, penetration readings with Vicat apparatus of the original standard (3, 5, 8 and 11 minutes after batch processing) can be adapted spacing the measurements at 30, 60, 90 and 120 minutes. The purpose of this test method is to determine the degree to which a formulated lime mortar develops rigidity that modifies the workability of the mortar. In this way it is possible to establish the working time once the pozzolans have been mixed with the lime mortar.



Figure 13 Metal molds for mortars in accordance with ASTM C 1707. TECTRAD INAH 2019



Figure 14 Plywood molds for mortars. TECTRAD INAH 2019



Figure 15 Formulated lime mortars stored in sealed bags before demolding in accordance with ASTM C 1707. TECTRAD INAH 2019



Figure 16 Formulated lime mortars in setting process under a high RH environment in accordance with ASTM C 1707. TECTRAD INAH 2019



Figure 17 Stiffness range to measure lime mortar period of workability once pozzolans have been added. TECTRAD INAH 2019

Properties of set mortar: Compression Test

According to the ASTM C311, Standard Test Methods for Sampling and Testing Fly Ash or Natural Pozzolans for Use in Portland-Cement Concrete, the most common criterion to

determine the pozzolanic activity is the compressive strength test in a mixture containing pozzolanic materials to verify their changes into the capacity to withstand a load per unit area. This test does not provide direct information about the pozzolanic material itself but about the results related to the physicochemical characteristics that these materials promote in a mortar [25]. When doing a comparative test between an air lime mortar and another one with pozzolans additions (formulated lime mortar), it is possible to verify the reactivity of the material, noticing a difference in the compressive strength between both mortars, where the one that contains the pozzolans, has a greater resistance.

It is necessary to make some adjustments of the standard ASTM C109 Standard Test Method for Compressive Strength of Hydraulic Cement Mortars, since it is designed to evaluate cement mortars and not formulated lime mortars [26]. The adaptations consist mainly in allowing a longer setting time. The time ranges are taken from previous lime mortar studies, where compression tests are established at 28, 56 and 90 days [11].



Figures 18 & 19. Compression strength tests as an indicator between lime and formulated lime mortars. TECTRAD INAH 2017.

Properties of set mortar: Determination of water absorption by the pipette method (Karsten tube)

The standard UNE-EN 16302: 2013 specifies a method to determine the absorption of water by the pipette method (Karsten tube) of porous inorganic materials used in the cultural heritage [27]. The test consists of measuring the volume of water (ml) transferred from the pipette through a certain test area (cm²) after a set time, expressed in ml/cm².

The permeability of a material is the ability it has to transmit a fluid, in this case water. A material will be more permeable when it is porous and the pores are large and connected. The use of pozzolan additions decrease the porosity [28] creating a less permeable mortar. It

is possible to execute comparative evaluation between air lime mortar with air lime mortar with pozzolans (formulated mortar) to compare the changes in water absorption.



Figure 20. Water absorption test with Karsten tube. TECTRAD / INAH 2018

Properties of set mortar: Determination of the resistance to salts crystallization

The standard UNE-EN 12370 evaluates the relative resistance of mortars to the alterations caused by the crystallization of the salts [29]. After drying to constant mass, the test piece is immersed in a sodium sulphate solution, then dried and allowed to cool to room temperature. This cycle is repeated 15 times and the variation of the mass in percentage is determined. The use of pozzolan additions lessens the probability of salts efflorescence at reducing the porosity in the mortar [28], so comparative tests can be held between air lime mortars and formulated lime mortars, to verify the pozzolanic effectiveness.



Figure 21. Salts crystallization resistance. Carmona TECTRAD INAH 2018

Discussion

The methods and studies proposed here are adequate for the reality of restoration works in Mexico, that is, with limited resources of time and economy. These enhance the virtues of

the discipline in this country, such as the use of material resources available in the region, which promotes a possible compatibility between the materials. The methods proposed here offer alternatives to evaluate and use formulated lime mortars as an alternative to the use of cement in the restoration materials without the contraindications or negative effects that this material implies for the conservation of historical factories. The aim of this research is to prove and adapt tests and their requirements to provide affordable methodologies to evaluate formulated lime mortars properties.

Mortar design is linked to the understanding of the characteristic and properties of the constitutive materials, of their function within the construction system, of the substrate properties on which it will be applied, of the environmental conditions to which it will be exposed and of the appropriate application technique. The results of the tests carried out in the laboratory should be understood more as a reference than as a total projection of the operation of the mortar.

Characterizing mortar properties is just one step for the development of technical specifications. A conservation project should be the result of the heritage values recognition and of a proposal that comprehensively preserves them, under the understanding of the historic building deteriorating agents and performing under discipline foundations and principles. Conservation must bring together sciences (with their rationality and scientific method) with the humanities and with experience to link into an applied approach; this can be done through research, technological experimentation and restoration actions, under a framework of experience and access to technology [30].

Conclusion

The use of formulated lime mortar, although it is not a measure of immense proportions to reduce carbon dioxide emissions is a possible alternative to conduct sustainable actions for the conservation of cultural heritage.

In addition to this, it is possible to recycle material by using pozzolans derived from bio products of industrial processes, or waste from the brick industry; this promotes the reuse of materials considered useless and that would otherwise be polluting waste and thus avoids the use and exploitation of new natural resources.

Also, by using pozzolanic materials from the region, the local economy is strengthened either by purchasing materials or by employing labour from the surrounding populations. The expensive transportation of materials is avoided, making it a more economical and a less polluting process.

The most important point of the sustainable character of these actions is considering the communities' participation. In this way, restoration transcends to the culture preservation where not only the material is conserved, but also traditional practices are strengthened, preserving this intangible heritage.

In this way, technological recognition can be transferred, not only as a memory, but as a sustainable catalyst for the generation of new buildings with qualities such as being appropriate for environmental conditions, provide comfort to its users, cause a minimum ecological impact, have a low cost and strengthen the character of traditional architecture as an element of identity at the local level. This means, dignifying the constructive culture through the recognition of its technological, documentary, economic, social and aesthetic values.

Sustainability can't be considered the framework of conservation, but it can be understood as a tool to relate with society and the environment [31]. Heritage conservation, is a discipline that does not affect the planet's resources and that does not compromise future generations, using processes to achieve the interaction of society, environment and culture in order to achieve a future where these dimensions are balanced for a better quality of life [32].

References

1. Foster S (2010). The new Standard for Building Lime. http://www.kulturarvbornholm.dk/uploads/1/1/2/5/11258347/norm_459.pdf accessed 28 February 2019.
2. ASTM C-618-17a (2017) Standard Specification for Coal Fly As and Raw or Calcined Natural Pozzolan for Use in Concrete, ASTM International, West Conshohocken, PA.
3. Polión M V (1992). Los diez libros de arquitectura. Ediciones Akal. España
4. Barba L, Villaseñor I (2013) La cal: historia, propiedades y uso. Universidad Nacional Autónoma de México, México
5. Ashurst J (1983). Mortars, plasters and renders in conservation (Vol. 3). Ecclesiastical Architects' and Surveyors' Association.
6. Henry A, Stewart J (2011) Mortars, Renders & Plasters. Ashgate Publishing Limited, USA
7. Brocklebank I (2012) Building Limes in Conservation. Donhead, Michigan
8. Teutonico J M, McCaig I, Burns C, Ashurst J (1994). "The Smeaton Project: Factors Affecting the Properties of Lime-Based Mortars.". APT Bulletin, 25.
9. Teutonico J M (1988). A laboratory manual for Architectural Conservators. Italia. http://www.iccrom.org/ifrcdn/pdf/ICCROM_11_LabManual_en.pdf accessed 28 February 2019
10. Biçer-Simsir B, Rainer L (2013). Evaluation of Lime-Based Hydraulic Injection Grouts for the Conservation of Architectural Surfaces: A Manual of Laboratory and Field Test Methods. GCI, Los Angeles

https://www.getty.edu/conservation/publications_resources/pdf_publications/pdf/evaluation_grouts.pdf accessed 28 February 2019

11. Ahmed A, Davies Mac-Eteli (2016). Sustainable High-Performance Lime Mortar using Pozzolans. Lambert Academic Publishing, Germany
12. Villalvazo V (2017). Estudio y caracterización de morteros puzolánicos para su uso en la restauración de patrimonio cultural edificado. (Tesis de pregrado). ENCRyM INAH, México
13. Snow J, Torney C (2014). Lime mortars in Traditional buildings. Historic Scotland, Scotland
14. Tokyay M (2016) Cement and Concrete Mineral Admixtures. CRC Press, Ankara
15. Torraca G (2009). Lectures on Materials Science for Architectural Conservation. The Getty Conservation Institute. ISBN 978-0-9827668-3-5, Los Angeles
16. Sepulcre A, (2005). Influencia de las adiciones puzolánicas en los morteros de Restauración de fábricas de interés histórico-artístico (Tesis doctoral). Escuela Técnica Superior de Arquitectura, Madrid
17. Costafreda JL (2011). Granulometría y reacción puzolánica in: IV Convención Cubana de Ciencias de la Tierra-Geociencias 2011 Cuba. http://www.redciencia.cu/geobiblio/paper/2011_Costafreda_MIN6-PCD55.pdf accessed 28 February 2019
18. Boffery G, Hirst E, Livesey P (2012). The use of Pozzolans in Lime Mortars in Brocklebank I (ed) Building Limes in Conservation. Donhead. Michigan
19. Testing Methods For Pozzolans. (s.f.). Practical Action, The Schumacher Centre for Technology & Development. <https://solucionespracticas.org.pe/Descargar/620/5322> accessed 28 February 2018
20. Torres L (2013). Recomendaciones para la caracterización de la cal y otros materiales calcáreos in Barba L (ed) La cal: historia, propiedades y uso. 1ra Edición. Universidad Nacional Autónoma de México. México
21. Bryce y wisemann ASTM C1707-11 (2011) Standard Specification for Pozzolanic Hydraulic Lime for Structural Purposes, ASTM International, West Conshohocken, PA
22. ASTM C1707-11 (2011) Standard Specification for Pozzolanic Hydraulic Lime for Structural Purposes, ASTM International, West Conshohocken, PA
23. ASTM C1713-17 (2017) Standard Specification for Mortars for the Repair of Historic Masonry, ASTM International, West Conshohocken, PA

24. Concrete property Test (2008). National Concrete Pavement Technology Center <http://www.cptechcenter.org/technical-library/documents/mco/summaries/concrete-property/concrete-slump.pdf> accessed 28 February 2018
25. Quarcioni V, Chotol F, Coelho A, Cincotto M (2015). Indirect and direct Chapelle's methods for the determination of lime consumption in pozzolanic materials. *Revista IBRACON de Estruturas e Materiais*, 8(1), <https://dx.doi.org/10.1590/S1983-41952015000100002> accessed 28 February 2018
26. ASTM C109 / C109M-16a (2016). Standard Test Method for Compressive Strength of Hydraulic Cement Mortars (Using 2-in. or [50-mm] Cube Specimens), ASTM International, West Conshohocken, PA
27. UNE-EN 16302:2016 (2016) Conservación del patrimonio cultural. Métodos de ensayo. Medición de la absorción de agua por el método de la pipeta.
28. Salazar, A. (2006). Puzolanas. www.ecoingenieria.org/docs/Puzolanas.pdf accessed 28 February 2018
29. UNE-EN 12370:1999 (1999) Métodos de ensayo para piedra natural. Determinación de la resistencia a la cristalización de las sales.
30. Torraca G (1996) The scientist's role in historic preservation with reference to stone conservation in Historical and philosophical issues in the conservation of cultural heritage. Getty Conservation Institute, Los Angeles
31. Avrami E C (2012) A systems approach to historic preservation in an era of sustainability planning. Graduate Program in Planning and Public Policy, The State University of New Jersey, USA
32. Desarrollo sostenible (s.f.) UNESCO. <http://www.unesco.org/new/es/education/themes/leading-the-international-agenda/education-for-sustainable-development/sustainable-development/> accessed 22 November 2017.

The impact of elevated temperatures on the properties of lime-based mortars

Vasiliki Pachta¹, Sofia Triantafyllaki¹, Maria Stefanidou¹

(1) Laboratory of Building Materials, School of Civil Engineering, Aristotle University of Thessaloniki, vpachta@civil.auth.gr, sofiatriad@hotmail.com, stefan@civil.auth.gr

Abstract

Although exposure to fire and elevated temperatures seems to be a significant decay factor of structures and building materials, the impact of elevated temperatures at the properties of traditional mortars used in historic structures has not been yet adequately studied. In the present study, two series of mortar mixtures based on lime-pozzolan and lime-pozzolan-brick dust were manufactured and tested. In the first series the aggregates were natural, of siliceous origin (gradation 0-8mm), while in the second one 40% of the natural aggregates were substituted by crushed brick of the same gradation. At the age of 28 and 90 days, two specimens of each mortar composition were subjected to elevated temperatures (200°C, 400°C, 600°C, 800°C and 1000°C), under a specific heating procedure. Subsequently, their physical (volume change, ap. specific gravity, porosity) and mechanical (dynamic modulus of elasticity, flexural, compressive strength) properties were recorded. According to the results, lime-based mortars presented high performance until 800°C, while at 1000°C they still maintained their volume stability. The presence of brick dust and crushed brick in their matrix significantly enhanced their resistance.

Introduction

The preservation state of historic mortars is closely related to a synergy of factors regarding their type and consistency, their properties, the environmental conditions of each area, as well as accidental actions that may occur during their service life (i.e. earthquakes, floods, landslides and fire) [1-3]. Although nowadays exposure to fire and elevated temperatures seems to be a significant decay factor of structures and building materials, the topic is not adequately studied up to now [4-5].

Despite the fact, that many monuments have been subjected to fire, as identified by archaeological remnants or historic sources, limited survey has been made on the performance of traditional mortars to elevated temperatures [4]. Experimental results showed that lime-based mortars, especially regarding the binding system lime-pozzolan, are generally resistant at elevated temperatures, maintaining their structure and properties even at the temperature of 1000°C [4].

In addition, the adaptation of fire safety criteria on the restoration of monuments is a critical aspect that should be taken into account, in order to determine the post-fire residual

strength of historic masonries or to apply effective repair materials, resistant to elevated temperatures (specific applications i.e. churches, buildings of public use) [6]. Besides that, the results deriving could be taken into account in constituting relevant regulations.

On the other hand, exposure to fire and elevated temperatures in cement-based materials (mortars, concrete), launched at the beginning of the 20th century (1922) [7] and is induced during the last decades [8-12]. According to literature [8-9], specific properties of building materials are influenced due to fire (i.e. physico- mechanical and chemical characteristics, microstructure etc). The deterioration may vary according to the characteristics of the fire (i.e. maximum temperature, fire duration) and the properties of the building materials.

According to the temperature/time development standard curves (Figure 1), the maximum temperature attained during a fire, is around 1100-1200°C, while the temperature development rate may vary [5]. It is considered that during the first 30 minutes of the action, temperature is rising up at 822°C. However, due to the difficulty of simulating such a high development rate in a laboratory level, researchers usually propose a rate of 5-10°C/min, in order to study the performance of building materials at elevated temperatures [4] [9-11].

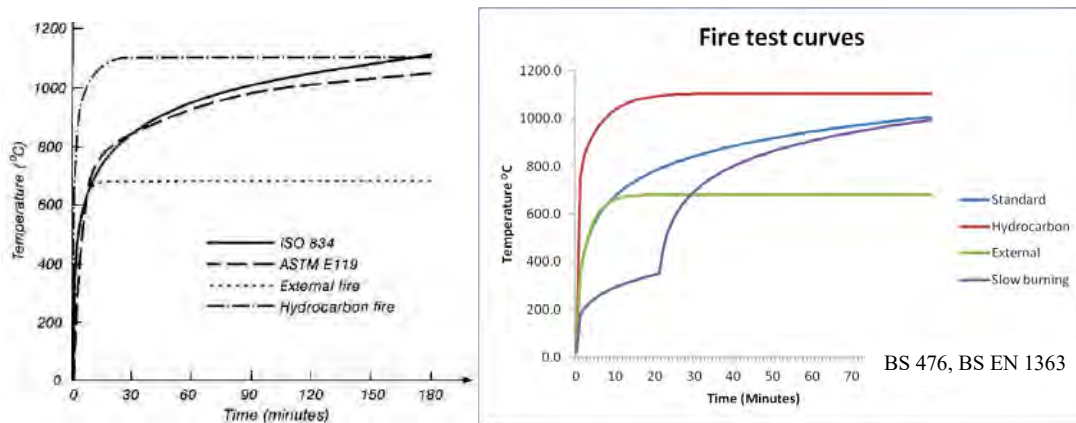


Figure 1. Temperature / time development standard curves during fire action [5]

Regarding the performance of cement-based materials at elevated temperatures, between 100-200°C, the materials' free moisture evaporates, while above 250°C the dehydration or loss of the bonded water begins [8]. The silicate hydrates of the cement paste (C-S-H gel) decompose above 300°C and portlandite decomposes above 500°C, influencing the stability of the cement matrix [12]. Aggregates perform in a different way according to their origin, but generally siliceous aggregates are more resistant than calcareous [12].

Concerning the mechanical behaviour of cement-based materials, up to 300°C their strength is not significantly reduced, whereas between 300-500°C it decreases around 15-40% [8, 12]. Above 550-600°C, strength is minimized, while after 800°C complete degradation of the matrix launches [8-11].

The present study focuses on evaluating the performance of lime-based mortars at elevated temperatures. To this direction two series of mortar mixtures based on lime-pozzolan and lime-pozzolan-brick dust were manufactured and subjected to elevated temperatures (200°C, 400°C, 600°C, 800°C and 1000°C). Subsequently, their physical (volume change, ap. specific gravity) and mechanical (flexural, compressive strength) properties were recorded. The test results were comparatively evaluated, in order to determine the performance of the compositions to elevated temperatures, as well as to define the parameters that have to be taken into account when the mortars' resistance at high temperatures has to be studied.

Materials and methods

According to former research, historic mortars were diachronically based on lime, while pozzolan and crushed brick also participated in the binding system [2. 4. 13-14]. Aggregates were usually natural, of siliceous origin, while crushed brick was also added [2. 4. 13-14]. Their gradation was mainly 0-8mm, while the B/A ratio ranged from 1/2 to 1/3 [4].

In an effort to simulate the characteristics and constituents of historic mortars two mortar series were manufactured and tested. According to Table 1, both series were based on lime and pozzolan, while brick dust was also added, in a proportion of 10% w/w of binders. The aggregates used were of gradation 0-8mm, while their origin varied. In the first series they were natural, of siliceous origin, while in the second one 40% of the natural aggregates were substituted by crushed brick of the same gradation. The Binder/Aggregate (B/A) ratio was kept 1/2.5 for all mixtures.

A sulphate free, polycarboxylate superplasticizer at proportion of 1% w/w of binders was added (Table 1), in order to reduce the water demand [13-14]. The Water/Binder (W/B) ratio was adjusted for achieving workability of 15±1cm, according to EN1015-3. The manufacture and curing of the mortar specimens was according to EN1015-11, while totally 16 specimens (dimensions 4x4x16cm) of each mortar series were manufactured and tested.

Table 1. Constituents and proportions of the mortar series

Raw materials	Mortar series				
	Parts of weight	LP	LPB	LP-b	LPB-b
Hydrated lime	1.0	1.0	1.0	1.0	1.0
Natural Pozzolan fine grained	1.0	0.8	1.0	0.8	0.8
Brick dust	-	0.2	-	0.2	0.2
Sand of siliceous origin, pale colour (0-4mm)	3.0	3.0	1.8	1.8	1.8
Gravel of siliceous origin (4-8mm)	2.0	2.0	0.2	0.2	0.2
Crushed brick (0-4mm)	-	-	1.2	1.2	1.2
Crushed brick (4-8mm)	-	-	0.8	0.8	0.8
Super plasticizer (% w/w of binders)	1%	1%	1%	1%	1%
W/B ratio	0.57	0.68	0.7	0.68	0.68
Workability (cm) (according to EN1015-3:1999)	15.5	15.3	16.0	15.3	15.3

Twenty-eight and ninety days after their manufacture, the physico-mechanical properties of the mortar compositions were recorded, regarding porosity and apparent specific gravity [15], dynamic modulus of elasticity [16], flexural and compressive strength [17]. Subsequently, two specimens of each mortar composition were subjected to elevated temperatures (200°C, 400°C, 600°C, 800°C and 1000°C). This was performed in order to identify the most representative testing age of the mortar specimens, taking into account that the cement-based mortars are usually tested at the age of 28 days [10-11], while the strength development rate of lime-based mortars is generally low [14].

For the experiment, an electric furnace was used, where the temperature rate and duration time could be manually set. The heating scheme followed (maximum temperature, heating rate, exposure time and cooling rate) was based on former research work and was aligned with the contemporary research on cement-mortars and concrete [4. 8-13]. The methodology concerned testing at 200°C, 400°C, 600°C, 800°C and 1000°C, heating rate 5°C/min, exposure duration to the maximum temperature 2h and cooling rate 2°C/min. In Figure 2 the heating exposure scheme is presented.

After each exposure, the specimens maintained for 24h at laboratory conditions, while for every specimen the weight and dimensions were recorded, in order to estimate their weight and volume changes. Additionally, their mechanical characteristics were tested, regarding dynamic modulus of elasticity [16], flexural and compressive strength [17]. Finally, all the results were comparatively evaluated in order to identify the performance of lime-based mortars in the tested temperatures and document the parameters that influence their behaviour.

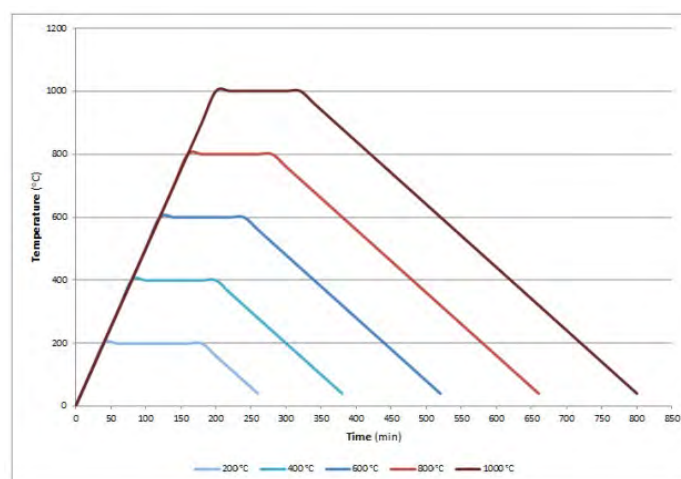


Figure 2. Heating scheme of the mortar specimens (rate, exposure time, cooling rate)

Results and discussion

The physico-mechanical properties of the mortars at the age of 28 and 90 days are presented in Table 2, regarding porosity, apparent specific gravity, dynamic modulus of elasticity, flexural and compressive strength.

From the evaluation of the results, it was concluded that at the age of 28 days the LP composition (lime-pozzolan, comp. strength: 4.2MPa) presented higher mechanical strength compared to the LPB one (lime-pozzolan-brick dust: 3.15MPa). At 90 days the compressive strength of LP was 6.59MPa (increase 57%), while that of LPB was 6.53MPa (increase 107%). This phenomenon maybe related to the lower early strength development rate of the LPB composition.

When crushed brick was added in both mixtures (LP-b, LPB-b), the compressive strength of 28d was almost at the same level, while at 90d LP-b showed a significant increase (8.09MPa). Flexural strength and Dynamic Modulus of Elasticity values were corresponding to the compressive strength. Regarding the physical properties of the compositions, the addition of brick dust and crushed brick to all mixtures resulted, as expected, in an increase of porosity and decrease of the apparent specific gravity.

Table 2. Physico-mechanical properties of the mortars at the age of 28 and 90 days.

Mortar series	Porosity (%)		Ap. Spec. Gravity		Dyn. Mod. of Elasticity (GPa)		Flexural strength (MPa)		Compressive strength (MPa)	
	28d	90d	28d	90d	28d	90d	28d	90d	28d	90d
LP	16.15	21.02	1.84	1.88	16.22	16.88	1.70	2.18	4.20	6.59
LPB	16.66	22.78	1.90	1.84	13.32	15.58	1.12	2.00	3.15	6.53
LP-b	19.92	22.08	1.78	1.76	13.88	15.36	1.56	2.20	4.01	8.09
LPB-b	18.58	25.53	1.81	1.73	14.48	15.33	1.21	2.07	3.44	6.06

Regarding the performance of the mortar series at the elevated temperatures, it was observed that they all retained their volume and structure at all temperatures (Figure 3). Up to 400°C no significant alterations were recorded, while above 600°C limited surface decay was observed (limited and edges' mitigation). At 1000°C loosening of material was more intense, however the specimens maintained their volume stability.

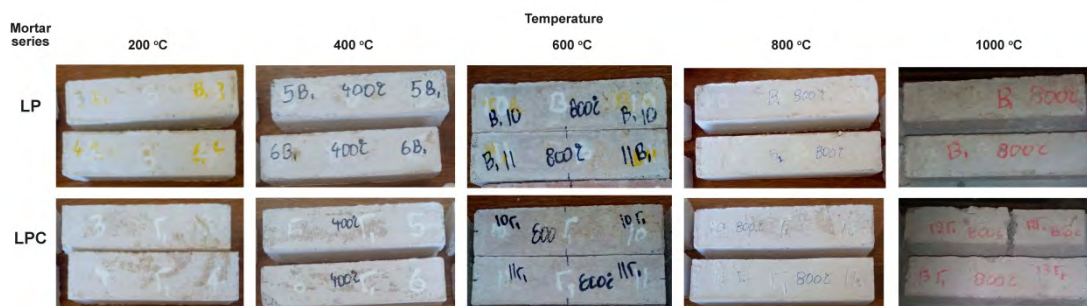


Figure 3. Macroscopic images of series LP and LPC at the elevated temperatures

In Figures 4-5 the volume and mass changes of the 28d specimens after their exposure at elevated temperatures are presented, while at Table 3 and Figures 5-7 their mechanical properties (at the age of 28 and 90 days) are shown.

Regarding the weight loss (Figure4), it was shown that the greater loss for all specimens was recorded at 200°C (10-12%), probably due to free moisture evaporation. It was gradually increased up to 800°C and was maximized at 1000°C (14-23%). The performance of all specimens was similar, however the more intense weight loss was attained when crushed brick was used (LP-b, LPB-b).

Regarding volume change (Figure5), again the specimens presented similar performance, with the more extreme alterations to be seen for LP and LP-b compositions. Generally, at 200°C the volume was slightly increased or decreased, while at 400°C it was increased for all specimens (0.7-1.8%). At 800°C it was reduced (1-3%) and remained at the same level at 1000°C.

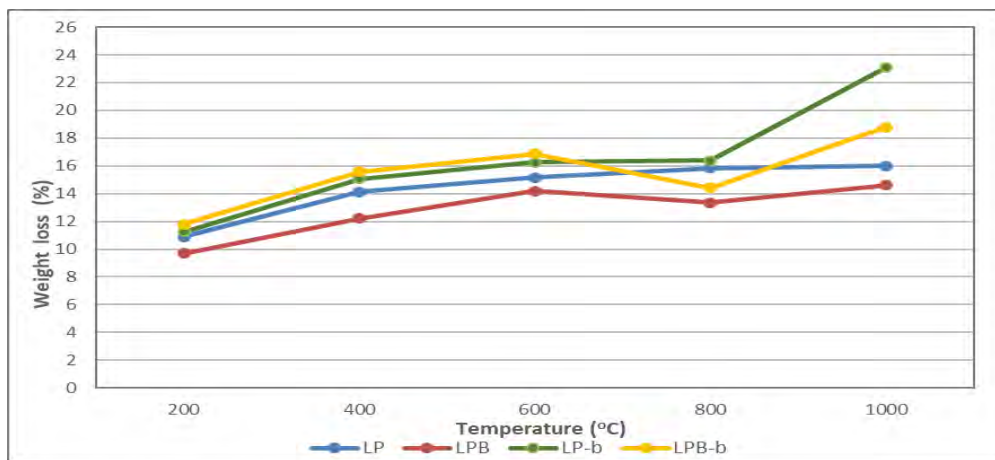


Figure 4. Weight loss of the mortar specimens at elevated temperatures (28d)

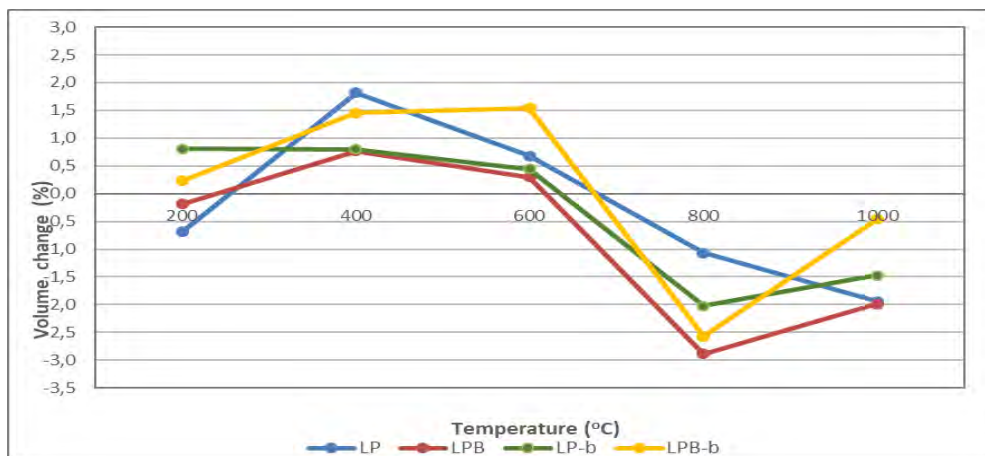


Figure 5. Volume change of the mortar specimens at elevated temperatures (28d)

Concerning the mechanical characteristics of the specimens after their exposure (Table 3, Figures 6-8), it can be firstly asserted that at the age of 90 days there was a significant increase of strength (flexural and compressive), compared to the 28d values.

Regarding flexural strength (Figure 6), the performance of all compositions was similar at the age of 28 and 90 days, while the 90d values were increased. At 200°C strength was increased

around 20-40%, for all specimens, with the highest values to be seen for composition LP-b at 28d (2.3MPa) and LP at 90d (2.8MPa). At 400°C it was significantly decreased (around 40-50%) and was further reduced at 600°C (around 50-90%). The more intense decrease at 600°C was shown in the 90d specimens, while at 800°C the flexural strength was minimized. Negligible values were recorded at 1000°C. Comparing the performance of all compositions, LP-b presented the highest resistance, when tested at the age of 28d, while at 90d LP showed a better performance.

Compressive strength presented fluctuations on the specimens' values, according to their age of testing. At 28d (Figure 7) there was a strength increase at 200°C for all compositions, from 20 to 100%, with the higher increase to be observed when brick dust was added in the mixtures (LPB, LPB-b). At 400°C a further increase was seen for compositions LP and LP-b, while at 600°C the strength was still maintained at high levels (50-100% from the initial values). At 800°C a significant strength decrease was observed for all specimens (around 50% from the initial values), while at 1000°C their strength was minimized (0.4-0.6MPa).

At 90d age (Figure 8) the strength level of all specimens was significantly increased at all exposed temperatures, while the performance of each composition presented some differences compared to the one given at 28d. Specifically, the main strength increase was recorded at 200°C (40-100%), with the higher rate to be given for LP and LPB series. At 400°C the strength was decreased, but was still higher than the initial values (around 25-30%) and maintained at the same level at 600°C. At 800°C there was a significant reduce around 40-50% from the initial values, while at 1000°C it was minimized up to 0.5-0.9MPa.

Table 3. Compressive strength of the mortar specimens at elevated temperatures (at the age of 28 and 90 days).

Mortar series	Compressive strength (MPa)									
	200°C		400°C		600°C		800°C		1000°C	
	28d	90d	28d	90d	28d	90d	28d	90d	28d	90d
LP	5.53	13.26	8.55	8.79	6.94	7.92	1.86	4.18	0.43	0.69
LPB	6.58	11.86	6.25	8.91	5.93	8.43	1.33	3.00	0.60	0.54
LP-b	6.37	12.22	8.04	9.97	6.27	8.99	2.00	4.18	0.52	0.92
LPB-b	6.06	8.72	6.80	8.68	6.46	7.18	1.41	2.06	0.45	0.89

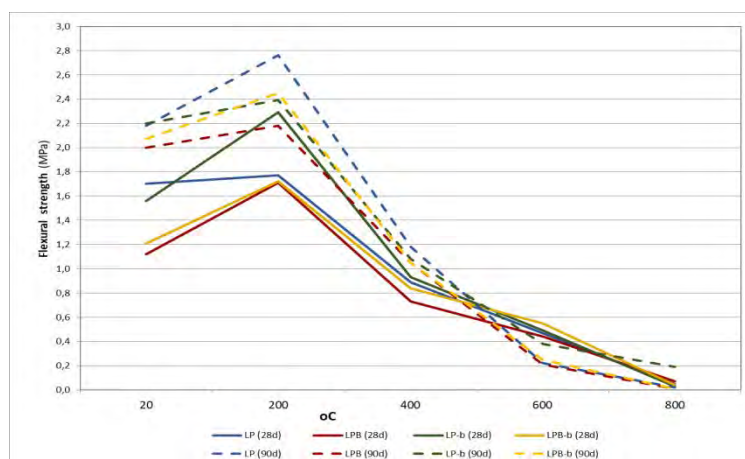


Figure 6. Flexural strength of the mortar compositions at elevated temperatures (28 and 90d)

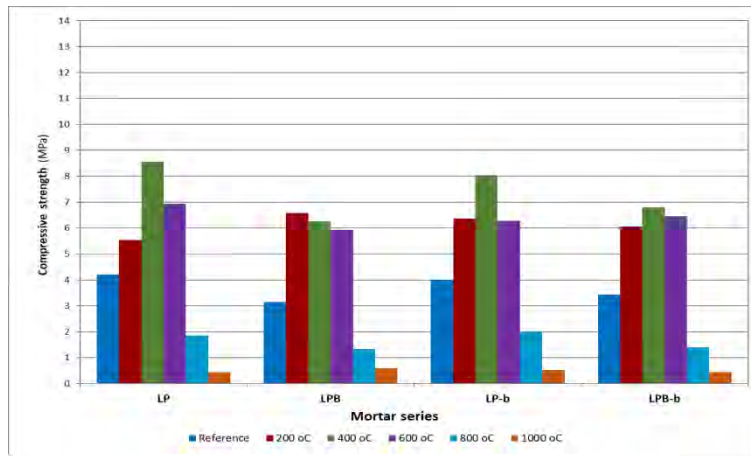


Figure 7. Compressive strength of the mortar compositions at elevated temperatures (28d)

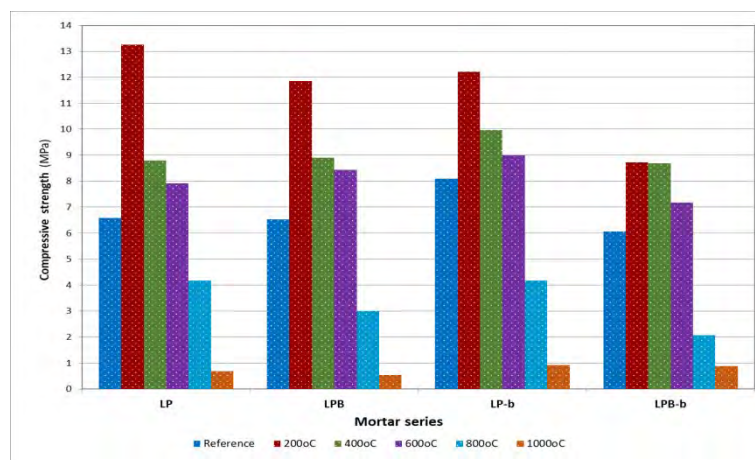


Figure 8. Compressive strength of the mortar compositions at elevated temperatures (90d)

Conclusions

From the comparative evaluation of the results, it can be concluded that all series of lime-based mortars presented a good performance throughout their testing at elevated temperatures. Their structural, physical and mechanical properties were maintained up to 800°C, while at 1000°C they still preserved their mass and volume, exhibiting however reduced strength. It was also shown that the addition of brick dust and crushed brick, enhanced the resistance of mortars at elevated temperatures.

It was generally observed that there were significant fluctuations at the testing values of all compositions between the ages of 28 and 90 days. Taking also into account that the strength of lime-based mortars is significantly enhanced until the age of 90 days, this age may be proposed for testing their resistance at elevated temperatures.

Taking into account all the above remarks, it can be concluded that the study of traditional mortars at elevated temperatures, is a field that should be further investigated, since it can be related with the service-ability and maintenance of historic structures. Although cement-

based materials present generally a reduced resistance to fire action, it is shown that lime-based mortars exhibit a good performance up to 800°C and preserve their structure up to 1000°C. However, the microstructure and mineralogical alterations occurring during high temperatures should further be envisaged, especially in the case of brick dust and crushed brick addition in the lime-pozzolan matrix. On the other hand, the significance of rendering fire-safety codes in historic structures that have been rehabilitated is emphasized.

References

1. Van Hees R.P.J. Binda L. Papayianni I. Toubakari E. (2004) Characterisation and damage analysis of old mortars. *Mat and Str* 37:644-648
2. Pachta V. Papayianni I. (2017) The Study of the Historic Buildings of Eclecticism in Thessaloniki Under the Prism of Sustainability. *Proc Env Sc* 38:283-289
3. Baronio G. Binda L. Tedeschi C. Tiraboschi C. (2003) Characterisation of the materials used in the construction of the Noto Cathedral. *Constr and Build Mat* 17: 557-571
4. Pachta V. Triantafyllaki S. Stefanidou M. (2018) Performance of lime-based mortars at elevated temperatures. *Constr and Build Mat* 189:576–584
5. Russo S. Sciarretta F. (2013) Masonry exposed to high temperatures: Mechanical behaviour and properties - An overview. *Fire Safety Journal* 55:69-86
6. Naziris I.A. Lagaros N.D. Papaioannou K. (2016) Optimized fire protection of cultural heritage structures based on the analytic hierarchy process. *J of Build Eng* 8:292-304
7. Lea F. Stradling R. (1922) The resistance to fire of concrete and reinforced concrete. *Engineering* 114:2959
8. Georgali B. Tsakiridis P.E. (2005) Microstructure of fire-damaged concrete. *Cem and Concr Comp* 27:255–259
9. Khoury G.A. (2000) Effect of fire on concrete and concrete structures. *Progr in Struct Eng Mat* 2:429-437
10. Wang W. Xiao J. Xu S. Wang C. (2017) Experimental study on behavior of mortar-aggregate interface after elevated temperatures. *Front of Struct and Civ Eng*, 11(2):158-168
11. Irshidat M.R. Al-Saleh M.H. (2018) Thermal performance and fire resistance of nanoclay modified cementitious materials. *Constr and Build Mat* 159:213-219
12. Ingham J.P. (2009) Application of petrographic examination techniques to the assessment of fire-damaged concrete and masonry structures. *Materials Characterization* 60:700-709

13. Papayianni I. Pacht V. Stefanidou M. (2013) Analysis of ancient mortars and design of compatible repair mortars: the case study of Odeion of the Archaeological site of Dion. *Constr and Build Mat* 40:84-92
14. Papayianni I. Stefanidou M. (2006) Strength-porosity relationships in Lime- Pozzolan mortars. *Constr and Build Mat* 20(9):700-705
15. RILEM CPC 11.3, Absorption of water with immersion under vacuum, *Materiaux et Constructions* 17, 101 (1984) 391-394.
16. BS 1881-203:1986, Testing concrete, Part 203: Recommendations for measurement of velocity of ultrasonic pulses in concrete.
17. BS EN1015-11:1999, Methods of test for mortar for masonry, Part 11: Determination of flexural and compressive strength of hardened mortar.

Characterization and compatibility assessment of commercial stone repair mortars

Barbara Lubelli¹, Timo G. Nijland², Rob P.J. van Hees¹

(1) Delft University of Technology, Delft, The Netherlands, b.lubelli@tudelft.nl, r.p.j.vanHees@tudelft.nl

(2) TNO, Delft, timo.nijland@tno.nl

Abstract

Commercial, ready mix stone repair mortars have often been applied in conservation practice for the restoration of natural stone, brick and terracotta, over the last decades with varying success in terms of durability of the repair mortar itself and compatibility with the substrate. In this research, four commercial stone repair mortars, commonly used in conservation practice in the Netherlands, have been characterized in laboratory. The composition of the repair mortars was studied by means of microscopy on thin sections. The effect of curing was assessed by comparing specimens cured in laboratory (28 days) and under outdoor conditions (28 days and 1 year). The porosity and pore size distribution of the mortars were determined by Mercury Intrusion Porosimetry and related to the measured capillary water absorption and drying behaviour. The hygric dilation both at different RHs and after saturation with water was measured. The flexural and compressive strength of the mortars were assessed, as well as their pull-off strength. Finally, based on the measured properties an attempt was made to evaluate the compatibility of the mortars with two limestone substrates of different total porosity and pore size.

Introduction

Repair mortars are mortars used in the conservation practice to replace or to model a missing parts in brick or stone units, concrete or decoration elements in natural stone or terracotta. The scope of the repair can be aesthetic (improvement of the appearance) and/or functional (prevention of further decay). As for any conservation intervention, one of the main requirements for repair mortar is its compatibility with the existing fabric, i.e. the repair should not cause any damage to the original material and be, at the same time, as durable as possible [1, 2]. For a repair mortar to be compatible, it is a well-accepted criterion that the mortar properties should be similar to those of the substrate on which it is applied. Next to this general criterion, some researchers have specified a range of values for some properties of the mortar, relevant for the assessment of compatibility [3-5]; in some cases a weight has been attributed to each property, based on its relevance for the overall compatibility [6]. Despite the fact that these criteria and specifications provide a valuable support in the choice of a compatible repair mortar, their application in conservation practice is generally limited [7]. One of the reasons of their limited use, is the need to carry out several measurements on both the mortar and the substrate. The use of ready mix

mortars with known properties, could contribute to reduce the necessary measurements. Unfortunately, information sheets of commercial repair mortars do not always provide the relevant properties of the product, making a substantiated choice difficult for the user. Besides, different producers are using different methods to assess these properties, which complicates the comparison [8].

In order to get more insight in the properties of ready mix repair mortars, in this research four commercial stone repair mortars, commonly used in conservation practice in the Netherlands, have been characterized in laboratory. Based on the results, an attempt has been made to evaluate their compatibility with two limestone substrates of different total porosity and pore size.

The research described in this paper is part of a broader investigation on repair mortars, which has as main aim the set-up of a methodology for supporting practitioners in the choice of a compatible repair mortar in the field.

Materials and methods

Materials

Four ready mix mortars were selected among those commonly used in conservation practice in the Netherlands, as resulted from an on-line questionnaire among architects, conservators and other practitioners and from inspections of case-studies [7]. The description of the products reported below is based on the information provided in the technical sheets:

- Repair mortar R: mortar with mineral binder and natural stone aggregate.
- Repair Mortar J: mortar with mineral binder especially developed for the repair of natural stone.
- Repair mortar MT: mortar with mineral binder and natural stone aggregate. The mineral binder is an inorganic polymer resulting, after mixing, from a reaction between the liquid and the solid components.
- Repair mortar MS: mortar with mineral binder.

These mortars are available in a range of colours and grain size distributions, to adapt to different substrates. In this research we selected for all mortars a maximum size of the aggregate of 0.5 mm and a neutral (beige) colour, in order to facilitate the comparison.

Specimens preparation and curing

The mortars were prepared according to the indications of the producers. Mortars R, J and MS were prepared adding tap water in an amount sufficient to obtain a workability between

160 and 170 mm, measured according to NEN-EN 413-2:2016 [9] (Table 1). Mortar MT was prepared using the reaction liquid provided with the dry mortar, in the amount suggested by the producer; it was not possible to measure the workability of mortar MT due to its very quick hardening.

Table 1. Water content and workability of the fresh mortars

Repair mortar	Water content (ml/kg dry product)	Workability (mm)
R	210	160
J	262	157
MT	226*	-
MS	163	156

* instead of water, the reaction liquid provided by the producer was used.

All mortar specimens, with the exception of those used for the determination of the mechanical strength, were prepared on a stone substrate; in fact, it is known that the properties of a mortar prepared in a mould of non-absorbing material (such as metal or polystyrene) may differ from those of the same mortar when applied on a realistic substrate, and be therefore less representative of the properties of the mortar in the field [10]. Depending on the test to be carried out, some of the specimens were detached from the substrate after a few days, before complete hardening. In order to facilitate the detachment, a paper tissue was used between the substrate and the mortar. The specimens for the measurement of the adhesion were prepared on two limestone substrates having very different porosity and pore size, and thus different suction and roughness of the surface: Maastricht and Migné limestone. Maastricht limestone has an open porosity of about 50 vol% and an unimodal pore diameter size of about 45 μm ; Migné limestone has an open porosity of ca. 30 vol% and pore diameter in the range of 0,5-2 μm [11]. As most of the investigated repair mortars are cement based (§?), curing was done either in laboratory at 20°C /95% RH or outdoors, in a place protected from rain. The different types and the size of the specimens are summarized in Table 2.

Characterization methods

Several properties of the mortar were investigated. Properties were selected among those considered most relevant for the assessment of the compatibility of a repair mortar. These included: composition (type of binder and aggregate), porosity, pore size distribution and moisture transport properties, hygric dilation and some mechanical properties, including pull-off strength.

Microscopy observation on thin sections

Polarizing and fluorescent microscopy (PFM) observations have been carried out on thin sections of the mortars, according to the procedure and the technique described in [12]. For

each mortar type, three specimens, cured at different conditions, were studied: cured under lab conditions (20°C / 95% RH) for 28 days, cured outdoors for 28 days and for one year.

Table 2. Type of specimen, size, curing conditions and investigations carried out

Specimen	Material	Size [mm]	Curing	Investigation
Type A	Mortar only	160 x 40 x 40	Few days under plastic sheets, after at 20 °C 95%RH	Mechanical strength
Type B	Mortar, prepared on a brick substrate and detached after few days	210 x 100 x 20	Few days under plastic sheets, after some specimen at 20 °C 95%RH, other outdoors	Moisture transport properties, porosity & pore size distribution, microscopy study on thin sections
Type C1	Mortar prepared on Maastricht and Migné substrates and detached from the substrate after few days	160 x 40 x 20	Few days under plastic sheets, after outdoors	Hygric dilation
Type C2	Mortar prepared on Maastricht and Migné substrates	160 x 80 x 20	Few days under plastic sheets, after outdoors	Adhesion

Porosity and pore size distribution

The porosity and the pore size distribution of the mortars were measured with the use of Mercury Intrusion Porosimeter (Micrometrics Autopore IV9500) in twofold on samples of about 1 cm³ collected from specimens of type A.

Moisture transport properties

The capillary water absorption of the mortars was measured in threefold on 50 x 50 x 20 mm specimens cut from mortar slabs of type A after 28 days of curing. The specimens were dried at 40 °C and sealed on the lateral sides with epoxy resin; absorption took place from the 50 x 50 mm surface originally in contact with the substrate. The test was carried out at 20°C / 50% RH. The weight of the specimens was recorded at regular intervals. The Water Absorption Coefficient (WAC) was calculated as the slope of the first, linear part of the water absorption curve. After saturation with water, the bottom of the specimens was sealed with impermeable tape, the specimens were stored at 20 °C / 50% RH and their weight was recorded at regular intervals to assess their drying rate.

Hygric dilation

The hygric dilation of the mortar was measured on specimens of type C1 by means of a dilatometer (precision 0.001 mm). For each mortar type/substrate combination, 3 specimens were tested. After conditioning of the specimens at 20 °C / 30 % RH, the RH was increased stepwise to 50, 65, 80 and 95% RH, while keeping the temperature constant; at the end the specimen were immersed in water. Each condition was kept constant for at least 24 hours. At the end of each period, the length and weight of the specimens of the specimens were recorded and the hygric dilation coefficient calculated as follows:

$$eh_{h_1-h_0} = [1000 * (L_{h_1} - L_{h_0})] / L_{h_0}$$

where:

$eh_{h_1-h_0}$ hygric dilation coefficient between initial condition h_0 and condition h_1 , in $\mu\text{m mm}^{-1}$

L_{h_1} length of the specimen in μm at condition h_1

L_{h_0} length of the specimen in μm at condition h_0

Mechanical properties

The flexural and compressive strength of the mortars at 28 days were determined on 5 specimens of type A for each mortar type, according to NEN-EN 196-1:2016 [13] [13]; the specimens were saturated in water before testing. At first the flexural strength was determined; then the compressive strength was measured on the two resulting half specimens.

Pull-off test

The adhesion of the repair mortar to the substrate was measured on specimens of type C1 after 1 and 3 months of outdoor exposure. The test dollies (50 x 50 mm surface) were glued to the mortar surface by the use of a two-components glue and incisions around the dollies were made in the mortar prior to the test. The pull force was applied with the rate of 25N/sec until the dolly detached. At least two tests for each type of mortar were carried out.

The results of the test were evaluated taking into account the location of the detachment (in the mortar, in the substrate or at the interface) and the force at which the detachment occurred.

Results

Petrographic characterization of the repair mortars

Mortar R is composed of a Portland cement binder with the addition of limestone powder and rounded quartz sand (Figure 1). The porosity is estimated to be about 15 vol%. Large

voids are present, most probably due to the limited compaction during application; no significant presence of air bubbles, as would have resulted from the presence of an air entraining agent, is observed (Figure 1). After 1 year of curing outdoor, carbonation is still limited to the exterior surface (less than a few mm).

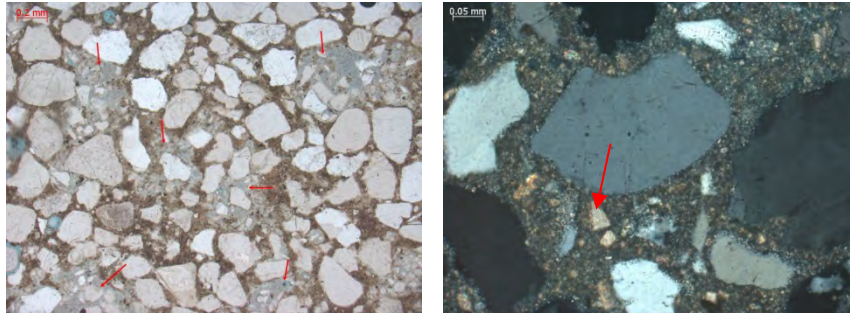


Figure 1. Left: Microphotograph of the microstructure of repair mortar R, showing the presence of large voids and locally lack of compactness (after 28 days of curing in outdoor conditions; parallel polarized light). Right: Microphotograph of a detail of the binder of mortar R, showing the presence of limestone powder (after 28 days of curing in outdoor conditions; crossed polarized light).

Mortar J shows the presence of a lime binder with some hydraulic components, C_2S (Figure 2) and possibly C_3S ; based on these observations it can be concluded that the binder is a mix of air lime with some Portland cement or hydraulic lime. The aggregate is constituted by light weight aggregate (expanded clay), broken marble pieces and rounded quartz sand (Figure 2). The mortar is fully carbonated already after 28 days of outdoor exposure. Also in this case air bubbles are scarce, but several large voids are present, due to lack of sufficient compaction. The open porosity visible by microscopy can be estimated to be about 5 vol%; additionally, there is about 10 vol% of mostly closed porosity constituted by the hollow lightweight aggregate.

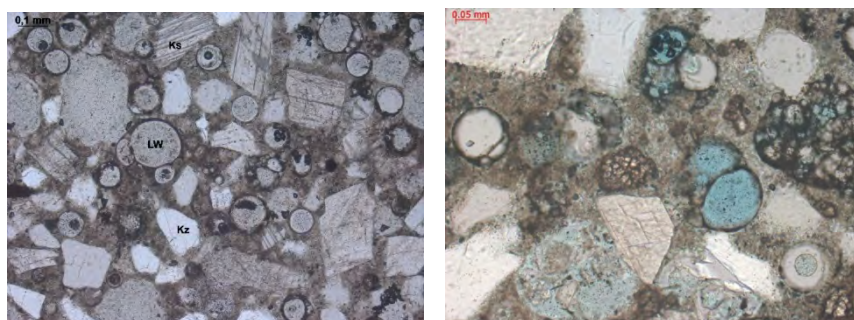


Figure 2. Left: Microphotograph of the aggregate (Ks= marble, Kz = quartz sand, LW = lightweight aggregate) in mortar J (parallel polarized light). Right: Microphotograph of mortar J showing a C_2S cluster (after 28 days of curing under outdoor conditions; parallel polarized light).

Mortar MT has a non-traditional binder, probably originating from the reaction between zinc oxide powder and the reaction liquid, a water solution of zinc chloride [14]. There is no experience with the microscopic investigation of this type of binder. The aggregate is rounded limestone sand. The porosity of this mortar visible by microscopy is about 1 vol% (Figure 3).

The thin section of mortar MS shows the presence of a binder containing both C_2S and C_3S , probably Portland cement (Figure 4); the aggregate is constituted by round quartz sand. Large voids, due to lack of compaction, are present. The porosity visible by optical microscopy is estimated to be about 30 vol%. The mortar was already fully carbonated after 28 days of curing.

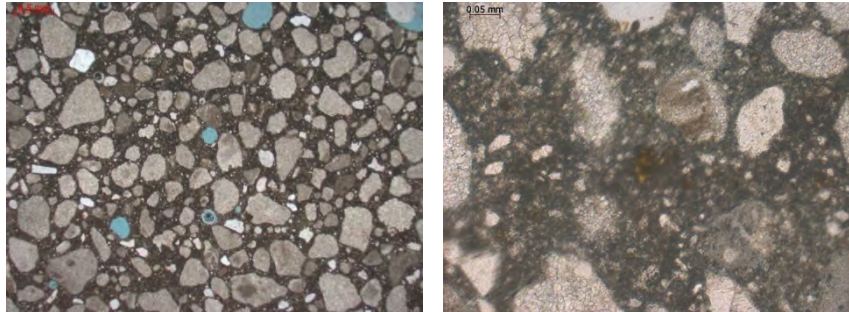


Figure 3. Microphotograph of mortar MT (after 28 days curing in laboratory conditions; parallel polarized light)



Figure 4. Left: Microphotograph of the aggregate (Kz = quartz sand) in mortar MS (after 28 days curing under outdoor conditions; parallel polarized light). Right: Microphotograph of a detail of mortar MS: in the binder C_2S and C_3S can be identified (after 28 days curing under outdoor conditions; parallel polarized light).

Porosity and pore size distribution

The open porosity and pore size distribution of the repair mortars, as resulting from MIP measurements, are reported in Figure 5. For readability reason, only one curve for each mortar is reported in the graph (replicates gave very similar results).

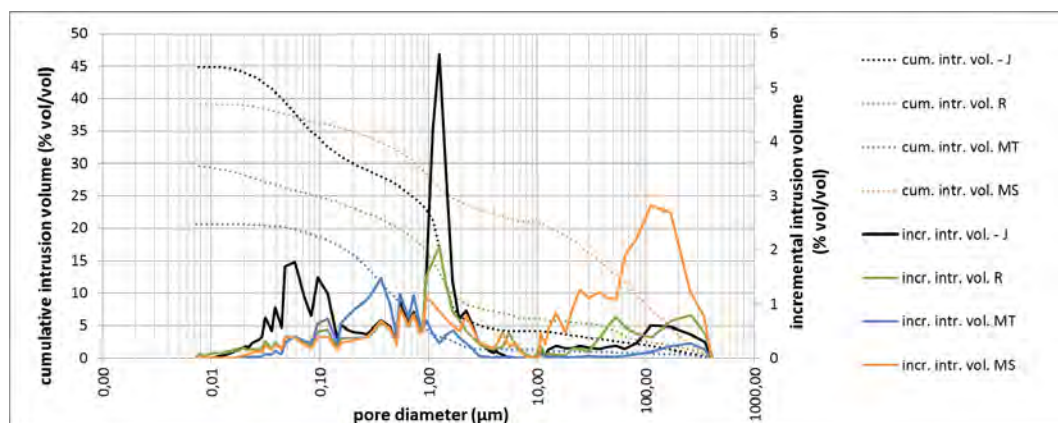


Figure 5. Pore size distribution (dotted line) and open porosity (continuous line) of the repair mortars as measured by MIP'

Repair mortar J shows the highest porosity (45 vol%), with a majority of pores between 0.02 and 0.1 μm and between 1 and 2 μm diameter. The fine porosity is due to the porosity in the binder and, most probably, also to the (closed) porosity in the hollow lightweight aggregate. Possibly, the thin walls of the lightweight aggregate broke at high intruding pressures, allowing for intrusion of mercury in the (relatively large) hollow aggregate; this resulted in the large intrusion volume measured in the high pressure range. Because of this reason the open porosity measured by MIP might be overestimated.

Repair mortar MS has an open porosity of 39 vol%, with pores in a wide size range and a large volume of pores larger than 10 μm .

Repair mortar R has an open porosity of 30.5 vol%, with most pores in the range between 1 and 2 μm ; smaller and coarser (between 50 and 300 μm) pores are present as well. The very large pores are probably the voids observed in the thin section and can be attributed to the scarce compaction of the mortar during preparation.

Repair mortar MT shows the lowest open porosity among the investigated mortars (20.5 vol%). Its pore size is unimodal, with most pores between 0.1 and 1 μm . In this case, the large voids ($> 100 \mu\text{m}$) observed in the thin sections were not measured by MIP: this can be due to the fact that the small samples used for the MIP measurements (about 1 cm^3) and these might not contain voids or have voids of sizes exceeding the range measurable by this technique.

Moisture transport properties

The capillary water absorption of the repair mortars is shown in Figure 6. The water absorption coefficients (WAC), density and porosity as measured by immersion are reported in Table 3.

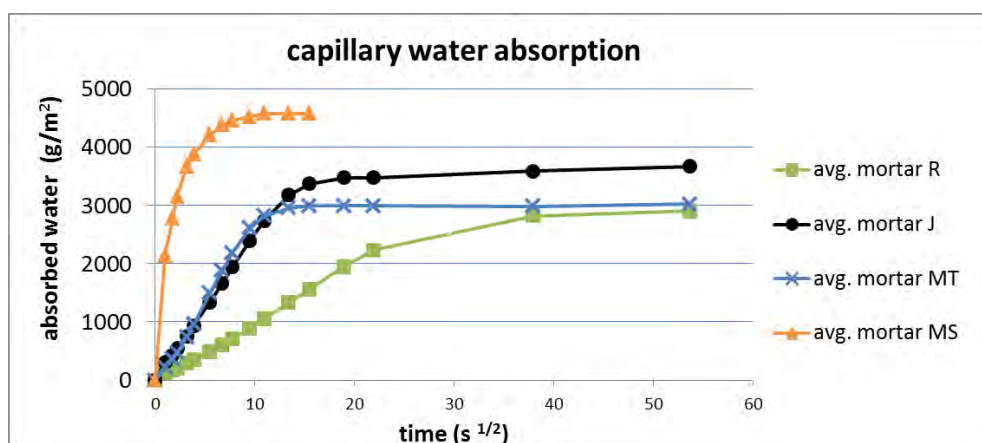


Figure 6. Capillary water absorption of the repair mortars (each point in the curve is the average value of 3 specimens)

Table 3. WAC, capillary water content, density and porosity of the repair mortars

Repair mortar	WAC [g/(m ² sec ^{0.5})]	Capillary water content [% of dry weight]	Density [kg/m ³]	Porosity (by immersion) [vol%]	Porosity (by MIP) [vol %]
R	102	8.9	1714	35.3	30.5
J	217	13.7	1350	49.1	45
MT	275	6.3	2303	13.1	20.5
MS	1412	17.6	1386	47.7	39

Repair mortar MS shows the fastest capillary absorption, (WAC 1412 g m⁻² sec⁻¹). This behaviour can be explained by its high volume of capillary pores (radius between 10 and 100 µm), which contributes to quick and high water suction. Repair mortars MT and J have a comparable WAC (275 and 217 g m⁻² sec^{-0.5} respectively). Mortar R has the slowest capillary absorption (WAC = 102 g m⁻² sec^{-0.5}) among the investigated mortars. The reason for the slower capillary absorption of the mortar R cannot be directly deduced based on the MIP results. The connectivity and tortuosity of the pore network, or the use of additives (not detectable with the used investigation methods) might be the reasons of these differences.

The density of the mortars varies between 1350 kg/m³ (mortar J, with lightweight aggregate) and 2303 kg/m³ (mortar MT). The porosity measured by immersion is, with the exception of mortar MT, always higher than the porosity measured by MIP. This is probably due to the presence of large voids, visible in the thin sections, which fall often outside the measuring range of the MIP.

The drying curves of the mortars are reported in Figure 7. Repair mortar MS and J show a similar drying rate: both have an initially almost linear drying phase (liquid moisture transport) followed by a slower drying phase (water vapour transport). In repair mortars R and MT, which dry slower, this difference is less evident. When comparing the capillary absorption and the drying curves, it can be concluded that mortar MT absorbs relatively fast but it dries slowly. This might have negative consequences for its durability.

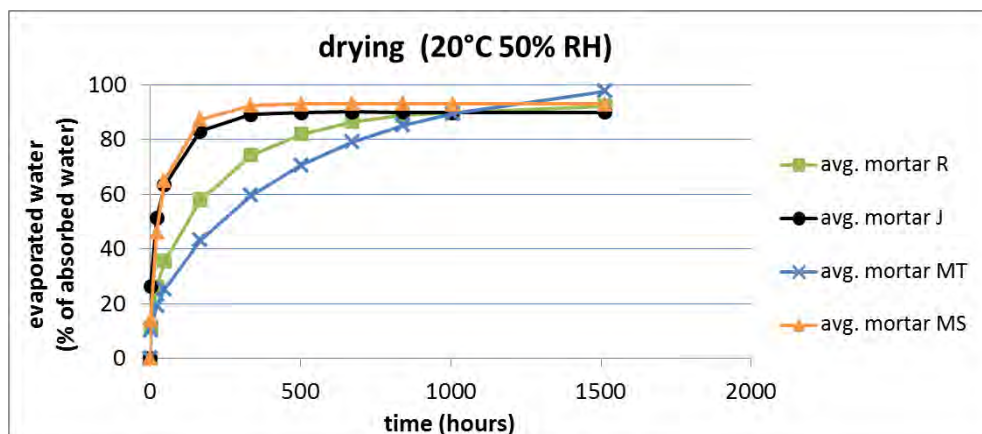


Figure 7. Drying curves of the repair mortars

Hygic dilation

The hygic dilation of the repair mortars, prepared on Maastricht and Migné limestone, is reported in Figure 8. There is a large scattering of the data; no clear difference in hygic dilation has been found for the same mortar applied on two substrates. As expected, the dilation increased with increasing RH and, even more, after saturation in water.

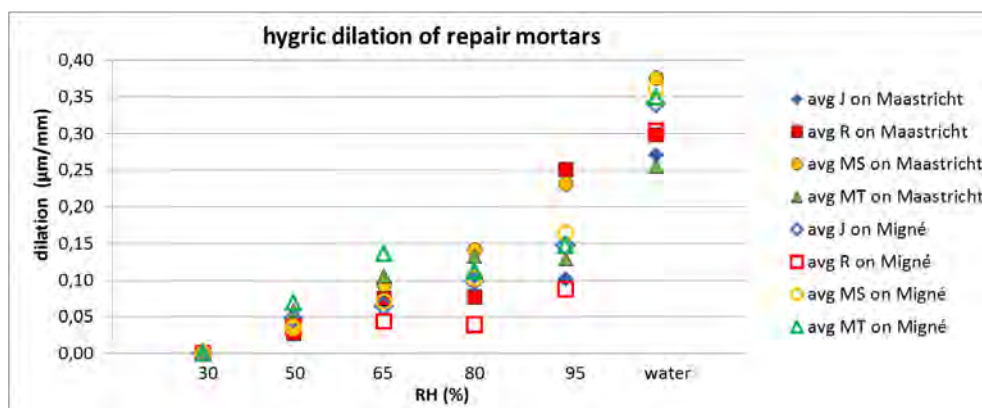


Figure 8. Hygic dilation of repair mortars prepared on Maastricht and Migné limestone)

Mechanical properties

The average flexural and compressive strength values of the mortars (in saturated conditions) are reported in Table 4. Mortar MT shows the highest strength: its compressive strength is up to 4 times higher that of the other mortars. Repair mortars J and MS have the lowest mechanical strength. MT and R were found to be stiffer than J and MS.

Table 4. Flexural and compressive strength of the mortars

Mortar	Average flexural strength (<i>standard deviation</i>) [N/mm ²]	Average compressive strength (<i>standard deviation</i>) [N/mm ²]
J	2.30 (0.15)	5.45 (0.04)
R	3.38 (0.08)	7.37 (0.15)
MT	5.56 (0.52)	19.54 (1.05)
MS	2.49 (0.24)	4.67 (0.64)

Pull-off test

The results of the pull-off test are summarized in Table 5. It should be mentioned that not all prepared specimens could be tested, as some of the mortars detached from the substrate during preparation of the specimen for the test. A large scattering of the results has been observed, even in the case of tests carried out on the same mortar/substrate combination. This suggests that a larger number of replicates would be necessary to draw more definitive conclusions. In general, it can be observed that repair mortars applied on Migné show a low

adhesion, due probably to the fine structure of the stone and to its smooth surface (Figure 9).

Table 5. Results of the pull-off test

Age of specimen	Substrate	Mortar	F max (N)	Fracture
1 month	Maastricht limestone	R	112	At interface and in substrate
		J	> 155	In substrate
		J	263	At interface
		MS	85	In substrate
		MS	101	In substrate
		MT	37	At interface and in substrate
	Migné limestone	MT	134	In substrate
		J	86	At interface
		R	24	At interface
		MS	151	At interface
		MS	95	At interface
		MT	> 970	At interface
3 months	Maastricht limestone	MT	497	At interface and in substrate
		J	101	At interface and in substrate
		J	52	At interface
		J	200	In substrate
		MS	222	In substrate
		MS	21	In substrate
		MS	227	In substrate
		MS	145	At interface and in substrate
	Migné limestone	MT	145	At interface and in substrate
		MT	239	At interface and in substrate
		J	148	At interface
		J	169	At interface
		MS	68	At interface
		MS	124	At interface
Migné limestone	MT	637	In substrate	
	MT	279	At interface and in substrate	

These results are not necessarily negative; however, the detachment of the mortar by the application of a very low force is not desirable. Repair mortar MT is the only mortar showing a (too) strong adhesion on Migné limestone: in this case failure occurred in the substrate. In the case of mortars applied on Maastricht limestone, failure often occurred in the substrate, even for very low applied forces (Figure 9). This is probably due to the rough surface of this very coarse stone and to its low mechanical strength. No significant differences in adhesion were observed between specimen tested one and three months after application.

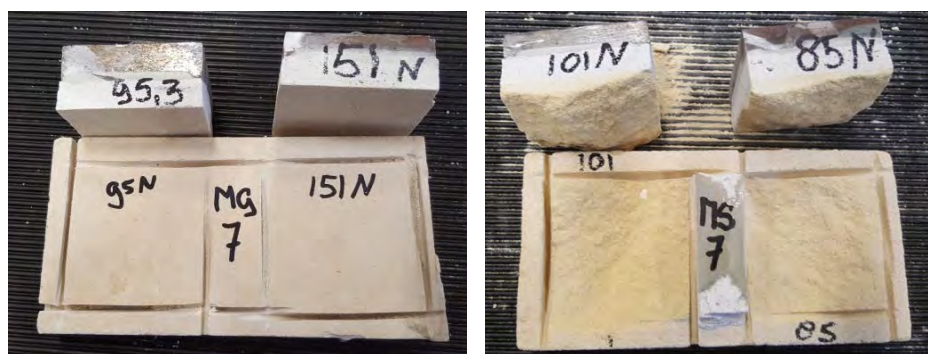


Figure 9. Left: Mortar MS applied on Migné limestone, after pull-off test (mortar tested 1 month after application): fracture at substrate/mortar interface; Right: Mortar MS applied on Maastricht limestone, after pull-off test (mortar tested 1 month from application): fracture in the substrate.

Discussion and conclusions

First of all, from the technical sheets of the products, it became clear that these do not provide sufficient information on the composition and on the properties of the products; when properties are mentioned, the (standard) test procedure used of their determination is generally not reported and the terminology used sometimes differs from what is common in test standards and scientific literature. Besides, often a large range of values is provided for some properties, meant to include all possible variations for the selected product. Actually, the characterization tests showed that the studied repair mortars have quite different properties in terms of moisture transport and mechanical behaviour, although their technical sheets would suggest they to be very similar. They were found to have different binders and aggregate types.

When considering the expected effect of the physical properties of the mortar on its durability, it can be supposed that repair mortars having a high water absorption and a slow drying, such as mortar MT, may remain wet for a longer period and therefore run a higher risk of frost decay and biological growth; also in the case of the presence of salts in the substrate, these properties would be undesirable.

All mortars have a sufficient mechanical strength, but some mortars are stiffer than others. A too stiff mortar might not be compatible with substrates having a large hygric dilation. Mortars MT and, to a lower extent, mortar R, are stiffer than mortars J and MS. This confirms that the binder type (cement in mortar R and a blend of different binders in mortar J and MS) plays an important role in the resulting strength and stiffness of the mortar [15]. Regarding the adhesion to the substrate, mortar MT showed a too strong adhesion to both the tested substrates. This would be a disadvantage in the practice, as it might lead, in the case of failure of the repair, to damage to the original substrate.

As an exercise, an attempt has been made to evaluate the compatibility of these repair mortars with two substrates, based on compatibility requirements established in literature. In this process, some difficulties became immediately clear. Some properties, such as drying rate and pore size distribution cannot be easily expressed by one single value; therefore, it is

not always easy to define what is more or less similar. If the behaviour of the mortar is compared to that of the substrates, it becomes clear that some requirements might be hard to be fulfilled and/or not all requirements can be fulfilled at the same time; for example in the case of Maastricht limestone, it will be difficult to find a ready mix mortar which satisfies the requirements related to the WAC; in fact the presence of a percentage of small pores, unavoidable in a mortar, will slow down the capillary absorption. Besides, it became clear that, in order to carry out all laboratory tests and measurements, considerable time and budget would be needed, which are often not available in the conservation practice. The question left is whether it would be possible to prioritize the relevance of the mentioned requirements and relative properties/ tests depending on their relevance for the assessment of the compatibility and define simple methods to assess these properties, preferably on site.

Acknowledgments

This research was carried out in the framework of the programmatic collaboration *MonumentenKennis* between TNO, TU Delft and the Dutch Cultural Heritage Agency (RCE). The authors wish to thank Arjan Thijssen (TU Delft) for carrying out the MIP measurements and Ron van Zwet (TNO) for support in the laboratory work.

References

1. Van Balen K, Papayianni I, R. Van Hees R et al (2005) Introduction to requirements for and functions and properties of repair mortars. *Mater. Struct. Constr.*, 38:781–785
2. van Hees RPJ (2012) RILEM TC 203-RHM: Repair mortars for historic masonry *Mater. Struct.* 45:1287–1294
3. Sasse H, Snethlage R (1997) Methods for the evaluation of stone conservation treatments. In Baer NS, Snethlage R (eds) *Saving our architectural heritage: the conservation of historic stone*, Wiley New York
4. Siegesmund S, Snethlage R, (2011) *Stone conservation*. in Siegesmund S, Snethlage R (eds) *Stone in Architecture: Properties, Durability*, 4th edn. Springer
5. Isebaert A, Van Parys L, Cnudde V (2014) Composition and compatibility requirements of mineral repair mortars for stone - A review, *Constr. Build. Mater.* 59:39–50
6. Rodrigues JD, Grossi A (2007) Indicators and ratings for the compatibility assessment of conservation actions, *J. Cult. Herit.*, 8:32–43
7. Lubelli B, Van Hees R, Van Hunen M et al (2018) *Steenreparatiemortels - Onderzoek naar het gedrag en de duurzaamheid van reparatiemortels in het lab en in de praktijk*, TUDelft report

8. van Hees RPJ, Lubelli B (2016) Keuze van steenreparatiemortels in historische gebouwen: geen eenvoudige zaak, in Nijland TG (ed) Kennis van de Gevel, TNO, Delft, 47-57.
9. CEN (2018) EN 413-2 -Masonry cement - part 2: Test methods
10. Wijffels T, van Hees R (2000) The influence of the loss of water of the fresh mortar to the substrate on the hygric characteristics of so-called restoration plaster. In Verhoef LGW, Wittmann FH (eds) Proceeding of the Int. Workshop on Urban Heritage and Building maintenance, Aedificatio Publishers, Freiburg
11. Borsoi G, Lubelli B, van Hees RPJ, (2016) Effect of solvent on nanolime transport within limestone: How to improve in-depth deposition, Colloids Surfaces A Physicochem. Eng. Asp., 497
12. Nijland TG, Larbi JA, (2010) Microscopic examination of deteriorated concrete,” in: Maierhofer C, Reinhardt HW, Dobmann G eds) Non-destructive evaluation of reinforced concrete structures, Woodhead, Oxford, pp. 137–179.
13. “NEN-EN 196-1 Methods of testing cement - Part 1: determination of strength.” 2018.
14. Tennent NH, Calcutt L, Oliveira TP et al, (2014) The evaluation of zinc hydroxychloride cement pastes for the conservation of damaged tiles. In ICOM-CC 17th Trienn. Conf.
15. Válek J, Hughes HH, Pique F, et al (2017) Functional Requirements for Surface Repair Mortars for Historic buildings, draft RILEM publication, RILEM TC 243-SGM 2017 unpublished

Impact of aggregates on fresh mortars' properties

Ana Rita Santos¹, Maria do Rosário Veiga¹, António Santos Silva¹, Jorge de Brito²

(1) National Laboratory for Civil Engineering, arsantos@lnec.pt, rveiga@lnec.pt, ssilva@lnec.pt

(2) Instituto Superior Técnico, jb@civil.ist.utl.pt

Abstract

The workability of a mortar largely depends on its water content, water retentivity and internal friction of the particles. Since these properties are closely related to properties such as porosity, size, shape and amount of aggregate, and type and amount of binder, it is expected that the use of different aggregates changes the water/binder (w/b) ratio in order to keep the target flow consistency.

In order to evaluate the influence of aggregates' mineralogy, shape and grain size distribution on fresh mortars' properties (such as workability, flow ability, water content and water retentivity), several mixes were prepared using three different binders, five aggregates of different mineralogy and two size distribution curves. The results indicate that, in general, a greater specific surface area (SSA) of the mix constituents will increase the amount of water required to lubricate the surface of the particles and will also enhance the water retentivity. However, a large SSA can be obtained for a significant range of fine grains, which leads to an optimization of the packing density of solid materials, thus offsetting the effect of the SSA through their own lubricating mechanism.

Introduction

The preparation of a mortar mix with high plasticity is important to facilitate the mason's work, since mortars must be easy to place and spread, but this must be achieved with the minimum water content necessary to have a workable mortar, since water in excess eventually evaporates, increasing the porosity and weaken the mortars in the hardened state.

During mixing of the raw materials, the workability of the fresh mortars is controlled by the interaction between the aggregates' particles and the binder and is closely related to the amount of binder (binder/aggregate ratio - b/a) and the water content (water/binder ratio - w/b) of the initial mix [1, 2, 3].

Concerning the effect of binder, it is known that the use of lime mortars improves the workability and water retentivity, by comparison with hydraulic mortars [4, 5], giving the mason more time to apply the mortar, as well as improve the compatible criteria with the pre-existing elements. Portland cement mortars, on the other hand, set too fast and thus make the task of the mason more difficult; therefore, it contributes to poorer workability. Additionally, this mortar has low

water retentivity, a high soluble salts content, and excessive stiffness, which are undesirable characteristics in a well-balanced mortar [6].

Aggregates are, by weight or by volume, the major component of mortars and their characteristics can influence the mortars' consistence in two main ways: (1) by modifying the rheological properties, largely due to the particle size distribution and geometry, and (2) by affecting the lubricant water content, necessary to achieve a required level of workability, again largely because of the particle characteristics and also their absorptivity [7].

The study of Amenta *et al.* [8], about the effect of the physical and geometrical characteristics of the aggregates, on the properties of the fresh and hardened NHL5 mortars, concluded that, for the same consistence, an enhancement of packing density resulted in a beneficial reduction in the w/b ratio, since the same amount of binder will lubricate more effectively a mix with aggregate of higher packing density [9, 10], as any excess of fines above the optimum amount increases the distance between the aggregate particles and, therefore, reduces the interaction between them [11]. Concomitantly, Yahia *et al.* [12] reported that filling voids in a packed system may improve the arrangement of particles in the system, ensuring a better contribution of the mixing water to achieve adequate plasticity in the mix.

Regarding the effect of the morphological properties of the aggregates (shape and surface texture), it is known that the use of aggregates with an angular shape and rough surface increases the water content, when compared with rounded and smooth particles aggregates, due to the increase of friction between the angular grains, thus requiring more water to act as lubricant, reducing the friction between aggregate particles, to improve the workability [8, 13]. However, the effect of particle shape and surface texture is apparently more pronounced for fine aggregates, *i.e.* less than 4 mm [14, 15]. Thus, the factor "shape", in general, is offset by the high amount of fines, often found in crushed sand [9].

Another important factor of the aggregates characteristics that affect the water content and consequently the workability is their mineralogy. Amenta *et al.* [8] compared the workability of the fresh NHL5 mortars using two sands of the same gradation and different mineralogy, observing that the use of crushed limestone sand increases the water content of mortar mixes, when compared with siliceous sand, due to its higher angularity and water absorption. Also Arizzi and Cultrone [16] reported that mortars with limestone sand require more water in their composition. However, the authors attribute this behaviour to the higher specific surface area of the limestone aggregate.

Clays also have a deep effect on the workability of the mortars and this characteristic depends both on their mineralogy, grain size distribution and on particle shape and, presumably, also on the surface properties. Clay particles lead to a higher water requirement for a given consistence, due to its higher SSA. However, the increase of the amount of mixing water does not lead to a decrease of the water retentivity capacity, due to the water retaining properties of the clay minerals [17]. Furthermore, the increase in water content varies with the type of clay,

decreasing with kaolinite and increasing with smectite (where the most common mineral is montmorillonite) [7]. It is also known that high amounts of flaky minerals, as phyllosilicate minerals that break into thin sheets or flakes, increase the water demand and have a negative effect on the workability [15].

Other parameters of the aggregates can also influence the water content, such as the bulk density and absorptiveness of the aggregates, which, in turn are related with particle shape and fineness [18].

In this investigation, the use of different aggregates on the performance of fresh rendering mortars is presented. The aggregates have been analysed in terms of their mineralogy, particle shape and grading proprieties and their effects on fresh mortars' properties were assessed by using very simple parameters but highly relevant in field condition and for practitioners: workability, flow, water content and water retentivity.

Materials and Methods

Materials and mortars mix

Thirty mortars compositions were prepared with the following binders: calcium hydrated lime powder (*Ca*), class CL90-S [19], natural hydraulic lime (*Ch*), class NHL3.5 [19], and Portland cement (*Ci*), CEM II/B-L 32.5N [20]. Five sands of different mineralogy (two siliceous sands, different in shape, a natural - *A* and a crushed one - *Sb*; a limestone crushed sand - *C*; a crushed basaltic sand - *B*; and a crushed granite sand - *G*) were used as aggregates.

To study separately the grain size and the mineralogy effects, the five sands were calibrated in two different grain size ranges. The first one was named *standard grain size (CP)* and was defined by standard NP EN 196-1 [21]; the second one was referred as *optimized grain size (CO)*, and was established according to the Fuller's distribution, assuming a *Fuller* exponential number of 0.50 [22], in order to obtain a well-graded sand, with a better packing of the grains.

All mortars compositions were designed using a binder/aggregate (*b/a*) ratio of 1:3 by volume. However, owing to the different percentages of each size fraction of the sands, and due to the rearranging of particles, the final volume proportion of the total curve resulted in 1:2.5 in the preparation of mortars with standard sands (*CP*) and 1:2.3 for the mortars with optimized sands (*CO*). All mortars were prepared based on European standard EN 1015-2 [23].

Methodology

Characterization of binders and aggregates

The particle size distribution of the materials employed in the mortars' formulation and their geometrical particle properties were determined with a laser diffraction analyser *Coulter LS 230*. The loose bulk density of the binders and sands, as well as the water absorption of the aggregates, were determined according to the EN 1097-3 [24] and EN 1097-6 [25] respectively.

The mineralogical composition of the sands was determined by X-ray powder diffraction (XRD) in a Philips PW3710 X-ray diffractometer, with 35 kV and 45 mA, using Fe-filtered CoK α radiation of wavelength $\lambda = 1.7903 \text{ \AA}$. Diffractograms were recorded from 3° to $74^\circ 2\theta$, at an angular speed of $0.05^\circ 2\theta/s$. The crystalline phases were identified by comparison with the International Centre for Diffraction Data Powder Diffraction Files (ICDD PDF).

Microscopic observations of the aggregates were carried out using an *Olympus SZH* stereo-zoom microscope with a video camera *Olympus DP20* to analyse the textural differences existing between the aggregates.

Fresh mortars' characterization

Due to the complexity of factors that affect the mortars workability, a reliable way to ensure the correct amount of water that needs to be added to a mortar, is to specify an optimum flow (consistence), thus taking into account the various variables affecting workability such as porosity, size and shape of aggregate, type of binder and relative proportions binder/aggregate.

In order to ensure that all mortars include the correct amount of water that would ensure a good workability for rendering mortars, the amount of mixing water was adjusted, in order to achieve similar flow diameter (consistence), assessed by the flow table test [26]. The water content is reported as water/binder ratio (w/b).

Water retentivity is an important parameter in fresh mortars, not only to enhance workability (plasticity), but also to ensure that adequate water is available to hydrate the hydraulic components of the mortars. It also limits the absorption of the mixing water by the substrate, and thus provides good mechanical and adhesive properties to the mortars. In this study, the water retentivity was assessed for various mortars mixes, adopting the guidelines of prEN 1015-8 [27].

The bulk density of the fresh mortars was determined according to EN 1015-6 [28].

Results and discussion

Aggregates and binders

The particle size distribution (PSD) of the binders and sands, determined with a laser diffraction analyser, is present in Figure 1.

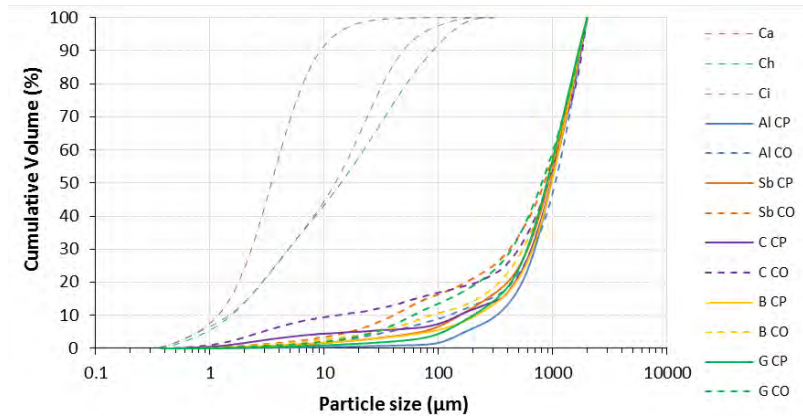


Figure 1. Particle size distribution of the raw materials.

The PSD of the calcium hydrated lime (*Ca*), with at least 90 % of the particle diameter (D_{90}) under 9 μm , shows a mean peak around 3 μm , while the natural hydraulic lime (*Ch*) is the coarser used binder, with median particle diameter (D_{50}) of approximately 14 μm and a D_{90} of 89 μm . Portland cement (*Ci*) present similar, but lower, particle properties than *Ch*.

Considering the sands, as expected, the grain size distribution of *CO* sands has, in comparison with *CP* sands, a more significant fine fraction. It can also be seen that limestone sands contain a higher volume of fines, than the other sands, for both grain size curves, as a consequence of breaking during the process due to preferential fracture surfaces of this aggregate.

Table 1 present some physical characteristics of the binders and aggregates. Table 2 includes the mineralogy and the morphology of the aggregates determined respectively by X-ray diffraction (XRD) and optical microscopy.

Table 1. Physical properties of the raw materials.

Charact.	Grain size	Aggregates					Binders		
		Al	Sb	C	B	G	Ca	Ch	Ci
SSA (m^2/g)	CP	0.21 ± 0.01	0.57 ± 0.10	1.54 ± 0.16	0.58 ± 0.03	0.36 ± 0.05	7.39 ± 0.05	2.18 ± 0.01	1.81 ± 0.01
	CO	0.58 ± 0.12	1.16 ± 0.17	2.89 ± 0.46	0.92 ± 0.10	0.79 ± 0.04			
ρ (kg/m^3)	CP	1491 ± 1.0	1476 ± 1.1	1461 ± 4.6	1638 ± 1.3	1429 ± 6.4	340 ± 3.1	660 ± 2.3	870 ± 3.8
	CO	1575 ± 11.2	1504 ± 11.1	1431 ± 15.0	1635 ± 3.6	1488 ± 3.4			
W (%)	-	0.35 ± 0.02	0.38 ± 0.01	1.87 ± 0.08	1.21 ± 0.06	0.72 ± 0.04	-	-	-

SSA - Specific surface area; ρ - Loose bulk density; W - Water absorption.

Table 2. Morphological and mineralogical characterization of the aggregates.

Aggregate	Morphology and mineralogy
 <p style="text-align: center;">Al</p>	<ul style="list-style-type: none"> - The grains of the natural siliceous sand (<i>Al</i>) have a homogeneous and sub-rounded shape, medium sphericity and smooth surfaces; - Quartz, feldspar (mainly microcline) and mica (mainly muscovite), with traces of kaolinite.
 <p style="text-align: center;">Sb</p>	<ul style="list-style-type: none"> - The crushed siliceous grains (<i>Sb</i>) have a heterogeneous and sub-angular shape, low sphericity and very rough texture; - Quartz, feldspar (mainly microcline) and mica (mainly muscovite), with traces of kaolinite.
 <p style="text-align: center;">C</p>	<ul style="list-style-type: none"> - The limestone grains (<i>C</i>) have angular shape and low sphericity and present smooth surface with a few fractures; - Calcite with low proportion of dolomite and some traces of kaolinite and quartz. In the filler fraction, traces of feldspar and mica (mainly muscovite).
 <p style="text-align: center;">B</p>	<ul style="list-style-type: none"> - The basaltic grains (<i>B</i>) have very angular to sub-angular shape and show medium sphericity and rough surface; - Quartz, feldspar (plagioclase), mica (namely biotite), pyroxene, olivine and vermiculite. Also, calcite and montmorillonite was detected.
 <p style="text-align: center;">G</p>	<ul style="list-style-type: none"> - The granitic grains (<i>G</i>) are sub-angular in shape and show medium sphericity and rough surface. - Quartz, feldspar (albite and microcline) and mica (muscovite and biotite). Also chlorite and some traces of hematite.

Fresh mortars' characterization

Workability and consistence

Table 3 presents the relationship between the water content of the mortars, expressed by water/binder ratio (*w/b*), the flow diameter and a qualitative assessment of the mortars' workability.

Table 3. Properties of the fresh mortars

Characteristics	Binder	Samples identification									
		Al		Sb		C		B		G	
		CP	CO	CP	CO	CP	CO	CP	CO	CP	CO
w/b ratio (by weight)	Ca	2.4	2.2	2.3	2.2	2.2	2.1	2.3	1.9	2.4	2.1
	Ch	1.2	1.2	1.2	1.2	1.1	1.1	1.2	1.1	1.2	1.2
	Ci	0.9	0.9	0.9	0.9	0.8	0.8	0.9	0.8	0.9	0.9
Flow diameter (mm)	Ca	150 ± 2	151 ± 1	150 ± 2	153 ± 5	149 ± 2	146 ± 2	149 ± 2	147 ± 1	149 ± 1	152 ± 3
	Ch	150 ± 3	149 ± 3	149 ± 1	153 ± 4	152 ± 4	153 ± 2	150 ± 1	154 ± 5	151 ± 2	152 ± 3
	Ci	162 ± 4	164 ± 1	167 ± 4	168 ± 4	165 ± 3	166 ± 2	169 ± 5	169 ± 4	166 ± 2	165 ± 4
Qualitative assessment of workability	Ca	Good	Good	Good	Good	Good	Good, but hard to spread	Good	Good	Good	Good
	Ch	Good	Very good	Good	Good	Good	Good, but hard to spread	Good	Good, but dry very fast	Good	Very good
	Ci	Good	Good	Good	Good	Good	Very good	Good, but heavy	Good, but heavy	Good, but slight exudati on	Good, but slight exudati on

According to the experimental results, the ideal water content to obtain “good workability” was achieved by ensuring that all lime-based mortars (*Ca* and *Ch*) had a flow diameter of 150 ± 5 mm and 165 ± 5 mm for the cement mortars (*Ci*), measured according to the flow table test [26].

In general, mortars with natural siliceous sand (*Al*) and with granitic sand (*G*) improve the workability. The basaltic sand (*B*) ensures good plasticity to mortars but they dry faster and are heavier thus making the mason’s work harder. Moreover, limestone with optimized sand (*C CO*), due to the high fines content (Figure 1), although having good consistency, the mortars stick to the trowel thus making them difficult to apply. Besides the good workability, the use of granitic sand with Portland cement (*Ci G*) leads to a slight exudation of the mortar, probably due to the high water content that was used to achieve the same flow diameter.

The data also show that the water content is strongly affected by the type of binder used in the mortars: the lower the binder hydraulicity, the higher the amount of water required in order to reach a given flow. The greater capacity of air lime to absorb water, when compared with the hydraulic binders, results of having finer particles and therefore a greater specific surface area (*SSA*), as shown in Table 1.

Regarding the effect of the grain size of the aggregate on the fresh mortars’ behaviour, it is possible to observe two distinct behaviours in the w/b ratio, dependent of type of binder used:

- In natural hydraulic lime (*Ch*) and Portland cement (*Ci*) mortars, the w/b ratio does not generally change with the variation of the grain size distribution of the sand. However, even for the same w/b ratio, the increase in binder content in the optimized mortars (*CO*) slightly increases the water content in the mix, which is caused by the higher SSA of the *CO* sands (Table 1).
- In air-lime mortars (*Ca*), the use of standard grain size distributions (*CP*) leads to an increase in the w/b ratio, when compared with the *CO*. The reduction of the water content in air-lime mortars with *CO* sands is ascribed to a physical effect where the increase of the packing density of these mixes overlaps the effect of the larger SSA of the used sands. In fact, the smaller diameter of the air-lime binder particles, when compared with the other binders (Figure 1), fills fewer voids of the *CO* sand and covers the aggregate particles, acting as lubricant, decreasing the friction between aggregate particles and thus enhancing the plasticity and workability of the mix [4].

Concerning the mineralogy of sand, in general the use of limestone aggregates leads to the lowest w/b ratio, notwithstanding the highest SSA and water absorption of this aggregate (Table 1). This behaviour is in disagreement with other studies, which report that the use of limestone in the mortars increases the water demand of the mix, when compared to siliceous sands [8, 16]. However, in this investigation, the used limestone sand presents a higher percentage of fines when compared with the other sands. The fine content of sand could contribute to fill the voids among coarse particles, so that excess fine particles act to provide lubricant effect, which can facilitate the movement of coarse particles, as reported by Yahia *et al.* [12] about the addition of limestone filler.

Also the mortars with *B CO* sand with all binders, present low w/b ratio and a great plasticity, which could be attributed to the presence of vermiculite in the constitution of this sand (Table 2), that could enhance the flow diameter for low water content [29].

Unlike limestone and basalt aggregates, the used granitic and siliceous sands lead to the increase of the w/b ratio, namely on the *Ca* mortars. These aggregates have in their constitution the presence of muscovite (Table 2) that, in general, is associated with a decrease of the slump flow of the concrete [30]. Thus, to achieve a given consistence in mortars that have muscovite in their composition, it is necessary to increase the water content in the mix due to the high specific surface area of the mica mineral and its lamellar shape. Moreover, according to De Schutter and Poppe [9], the use of aggregates with low bulk density, as the granitic sand in this work (Table 1), tends to increase the water content.

Comparing the two sands with similar mineralogical composition and gradation, *i.e.* *A1* and *Sb*, but with different shape, few differences on the w/b ratio of the mixes were detected, for a given consistence. A slight increase in fines content of the crushed siliceous sand (*Sb*) could mask the effect of the shape, decreasing the friction between the angular grains.

Bulk density

Figure 2 presents the average of bulk density values of the fresh mortars.

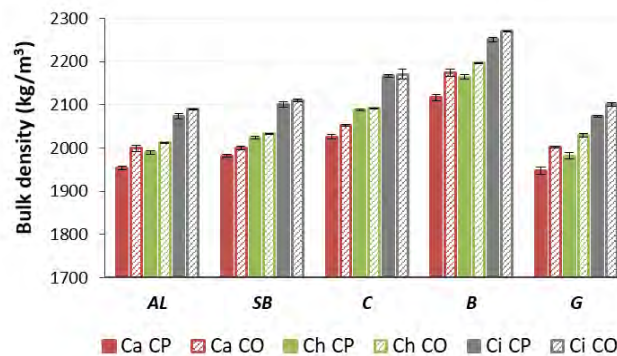


Figure 2. Bulk density of the fresh mortars.

Figure 2 shows that the bulk density of the optimized fresh mortars (CO) are slightly higher than standard mortars (CP), being the most marked difference in *Ca* mortars, less than 3%. This behaviour is in the agreement with the data of the bulk density of sands, in which CO sands have a higher loose bulk density and a lower voids content than the CP sands, evidencing the higher compactness of these sands.

Concerning the mineralogy of the sand, the use of basaltic aggregate, followed by limestone aggregate, increases the bulk density of the fresh mortars, for all used binders, thus making the application harder than other mixes, because of their weight, which required more energy from the mason. In general, the results obtained are linked to the bulk density of aggregate. However, some contradiction is observed, namely in mortars with limestone sand. Limestone sand presents low values of bulk density and high voids content (Table 1) when compared with the other sands, but mortars with limestone sand show high values of bulk density in the fresh state (Figure 2). This is linked to the filler effect, since the existing voids between the sand grains are very small and filled with fine binder material, which is responsible for increased compactness, and subsequently, higher density.

Furthermore, for each type of binder, a slight decrease in w/b ratio leads to a slight increase of the values of bulk density of the fresh mortars, namely in *Ca* mortars, which could be associated to the enhancement of packing density which resulted in a beneficial reduction in the w/b ratio [8].

Water retentivity

The effects of the different binders on the water retentivity of the fresh mortars, as well as the effect of the mineralogy of the aggregates, were assessed by using different aggregates and similar grain size distribution (CP). The results are presented in Figure 3. The data presented in Figure 3 show that, as expected, air lime mortars have higher water retentivity than mortars with the other used binders, which is closely related to the SSA of the binder system. In fact, hydrated lime (*Ca*), has the highest SSA of all binders ($7.4 \text{ m}^2/\text{g}$) when compared with

Portland cement (*Cl*), which has SSA ($1.8 \text{ m}^2/\text{g}$) lower than the *Ca* binder. This trend is in agreement with Tate [31], which reports that the fine particle size of the hydrated lime enhances the ability of the plastic mortar to retain water, when applied to an absorptive base. In addition, Pavía and Hanley [5] reported that an increase of water retentivity is related to an increase of the free lime content in the mix. This trend was also observed in this investigation for the different types of the binder used.

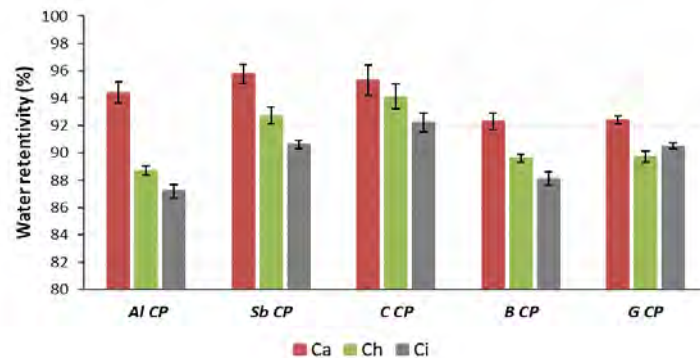


Figure 3. Water retentivity of the fresh mortar with the standard grain size distribution (*CP*).

Regarding the mineralogy of the used sand in the composition of the fresh mortars, under the same proportions, limestone sand generally enhances the water retention. On the other hand, the use of basaltic and natural round siliceous sands worsens the water-retentivity of the fresh mortars. Similar to binders, this behaviour can be related to the SSA of the aggregates, since, in general, the water retentivity capacity increases with the increase of the SSA of the aggregates (Table 1).

However, it is observed that basaltic aggregate has high SSA and shows low water retentivity, which may suggest that water retentivity characteristics of the mortar are influenced by aggregate size but also by the state of packing of the fresh mortar (indirectly assessed by the bulk density in this study). In fact, changes in bulk density affect water retentivity due to the differences in the pore size distribution: with increased bulk density, the aggregates are packed more closely and hence the pores between aggregates are smaller than at lower bulk densities.

Comparing the two sands with similar mineralogical composition but different shape, *Al* and *Sb*, it is observed that the use of angular aggregates enhances the water retentivity for all used binders. The use of crushed angular aggregates leads, in general, to high filler content, which increases the SSA and enhances the packing density, thus helps to reduce the voids content which improves the water retentivity.

Figure 4 shows the results of the water retentivity of three specimens with two different grain sizes distribution (standard - *CP* and optimized - *CO*). In general, the water retentivity capacity is higher in *CO* mortars, for all types of binder, which can also be related with the SSA of the used sand, but also to the enhancement of the packing density.

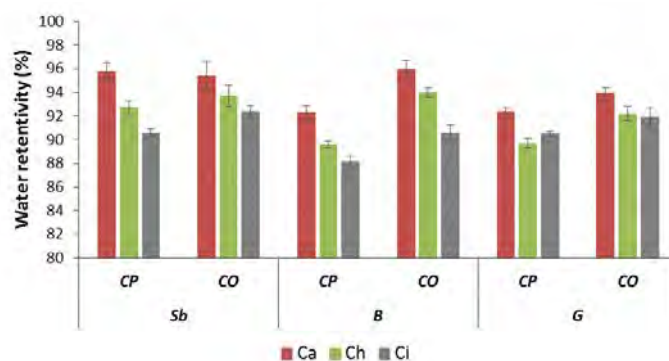


Figure 4. Water retentivity of the fresh mortars with different grain size distributions.

Furthermore, the use of clays in the *CO* mortars, besides the increase in the SSA of the sand, also contributes to an increase of the water retentivity, due to their water binding ability [17]. In fact, a substantial increase on the water retentivity with the use of *B CO* sand is observed, when compared to *B CP*, which is attributed to the presence of vermiculite in their constitutions (Table 2), which has a great capacity to absorb water and hold it in the interlayer space, thus generating the high water retentivity capacity presented in Figure 4.

On the other hand, the slight increase of the amount of mixing water in the *CO* mortars, in the hydraulic mortars (*Ch* and *Ci*), does not lead to a decrease of the water retentivity capacity, due to the water retaining properties of the clay minerals.

Conclusions

Considering the effect of the aggregates on the fresh mortars' properties, the following conclusions can be drawn:

- Workability:

With the exception of the mortars with limestone sand, the use of optimized sand with fuller distribution enhanced the plasticity and the workability of the mix, namely on the natural hydraulic lime and Portland cement mortars.

In general, mortars with natural siliceous sand (*A*) and with granitic sand (*G*) have better workability. On the other hand, the use of limestone (*C*) with optimized sand (*CO*), even though leading to good consistency, sticks to the trowel, making them difficult to apply.

Although the effect of particles' shape is expressed indirectly by the packing density, it was observed for two sands, with similar mineralogical composition, but different shape, that the use of angular aggregates slightly improves the workability.

- Water content:

In air lime mortars, the use of optimized sands (*CO*) reduces the water required to achieve the same plastic consistence of the standard sands (*CP*), due to the enhancement of the

packing density caused by the low particle sizes of the lime binder, where the small voids between the particles of *CO* sands are filled with the binder. Therefore, the binder acts as lubricant, decreasing the friction between aggregate particles, by increasing the distance between them, and thus enhancing the plasticity and workability of this mix. On the opposite, in hydraulic mortars with the main diameter of particle size greater than the air lime binder's, the use of *CO* sand leads to an increase of binder content, which, for a similar w/b ratio, slightly increases the water demand, due to the greater surface area of this sand.

The use of limestone sand decreases the amount of the water used in the preparation of the mortar, for the same consistence. Increasing the very fine particles beyond the optimum amount, reducing the interaction among them, and thus increasing the flow. On the other hand, the presence of large content of muscovite in the aggregates' constitutions, leads to an increase of the water demand.

- Water retentivity and bulk density:

The use of *CO* mortars, for all types of binder, enhances the water retentivity and bulk density, which can be related to the SSA and loose bulk density of the used sand, but also to the enhancing of the packing density.

Moreover, the use of limestone sand as well as the presence of vermiculite clay minerals seem to improve the plasticity and the water retentivity of the fresh mortars.

The use of angular aggregates increases the bulk density (indirectly the packing density) and enhances the water retentivity; however, few differences on the water demand of the mixes were detected.

In summary, there are two main characteristics of the aggregates that affect the water content of a mix: total specific surface area (SSA) and the packing density. The greater SSA of the mix constituents will increase the amount of water required to lubricate the surface of the particles and enhances the water retentivity. However, a large surface area can be obtained either by having a fine grain size distribution or a large proportion of sharp, angular particles, which also leads to an optimization of the packing density of solid materials, thus offsetting the effect of the surface area through their own lubricating mechanism. Furthermore, the presence of clay minerals, could increase the water demand and enhance the water retentivity.

Moreover, all mortars achieved good workability ensuring flow diameters of 150 ± 5 mm for the lime-based mortars and 165 ± 5 mm for the cement mortars.

References

1. Lanás J, Pérez-Bernal JL, Bello MA et al (2004) Mechanical properties of natural hydraulic lime-based mortars. *Cement and Concrete Research* 34 (12):2191-2201.

2. Haach V, Vasconcelos G, Lourenço P (2011) Influence of aggregates grading and water/cement ratio in workability and hardened properties of mortars. *Construction and Building Materials* 25 (6): 2980-2987.
3. Romano R, Torres D, Pileggi R (2015) Impact of aggregate grading and air-entrainment on the properties of fresh and hardened mortars. *Construction and Building Materials* 82: 219-226.
4. Westerholm M, Lagerblad B, Silfwerbrand J et al (2008) Influence of fine aggregate characteristics on the rheological properties of mortars. *Cement and Concrete Composites* 30 (4): 274-282.
5. Pavía S, Hanley R (2010) Flexural bond strength of natural hydraulic lime mortar and clay brick. *Materials and Structures* 43 (7): 913-922.
6. Tougelidis G, Providakis C (1995) Effects of lime mortars on masonry construction. *Transactions on the Built Environment* 15: 215-222.
7. Sims I, Brown B (1998) Concrete aggregates. In Lea's chemistry of cement and concrete. Arnold, New York. ISBN: 0-340-56589-6.
8. Amenta M, Karatasios I, Maravelaki-Kalaitzaki P et al (2017) The role of aggregates characteristics on the performance optimization of high hydraulicity restoration mortars. *Construction and Building Materials* 153: 527-534.
9. De Schutter G, Poppe A (2004) Quantification of the water demand of sand in mortar. *Construction and Building Materials* 18 (7): 517-521.
10. Erdoğan ST, Fowler DW (2005) Determination of aggregate shape properties using x-ray tomographic methods and the effect of shape on concrete rheology. Research Report ICAR-106-1. University of Texas.
11. Mehdipour I, Khayat K (2018) Understanding the role of particle packing characteristics in rheophysical properties of cementitious suspensions: A literature review. *Construction and Building Materials* 161: 340-353.
12. Yahia A, Tanimura M, Shimoyama Y (2005) Rheological properties of highly flowable mortar containing limestone filler-effect of powder content and W/C ratio. *Cement and Concrete Research* 35 (3): 532-539.
13. Kazmierczak C, Arnold D (2012) Influência da forma dos grãos e do teor de filler na trabalhabilidade de argamassas de revestimento. *Proceedings of 4^o Congresso de Argamassas e ETICS*. Portugal, Coimbra.
14. Wills M (1967) How aggregate particle shape influences concrete mixing water requirement and strength. *Journal of Materials* 2 (4): 843-865.

15. Lagerblad B, Gram H, Westerholm M (2013) Quality of fine materials from crushed rocks in sustainable concrete production. Proceedings of the 3rd International Conference on Sustainable Construction Materials and Technologies (SCMT3). Japan, Kyoto.
16. Arizzi A, Cultrone G (2013) The influence of aggregate texture, morphology and grading on the carbonation of non-hydraulic (aerial) lime-based mortars. Quarterly Journal of Engineering Geology and Hydrogeology 46 (4): 507-520.
17. Winnefeld F, Böttger KG (2006) How clayey fines in aggregates influence the properties of lime mortars. Materials and Structures 39 (4): 433-444.
18. Gonçalves JP, Tavares LM, Toledo Filho RD et al (2007) Comparison of natural and manufactured fine aggregates in cement mortars. Cement and Concrete Research 37 (6): 924-932.
19. Instituto Português da Qualidade (IPQ) NP EN 459-1:2015, Building lime; Part 1: Definitions, specifications and conformity criteria.
20. Instituto Português da Qualidade (IPQ) NP EN 197-1:2012, Cement; Part 1: Composition, specifications and conformity criteria for common cements.
21. Instituto Português da Qualidade (IPQ) NP EN 196-1:2017, Methods of testing cement; Part 1: Determination of strength.
22. Fuller W, Thompson S (1907) The laws of proportioning concrete. Transactions of the American Society of Civil Engineers 57 (2): 67-143.
23. European Committee for Standardization (CEN) EN 1015-2:1998, Methods of test for mortar for masonry; Part 2: Bulk sampling of mortars and preparation of test mortars.
24. Instituto Português da Qualidade (IPQ) NP EN 1097-3:2002, Tests for mechanical and physical properties of aggregates; Part 3: Determination of loose bulk density and voids.
25. Instituto Português da Qualidade (IPQ) NP EN 1097-6:2016, Tests for mechanical and physical properties of aggregates; Part 6: Determination of particle density and water absorption.
26. European Committee for Standardization (CEN) EN 1015-3:1999, Methods of test for mortar for masonry; Part 3: Determination of consistence of fresh mortar (by flow table).
27. European Committee for Standardization (CEN) pr EN 1015-8:1999, Methods of test for mortar for masonry; Part 8: Determination of water retentivity of fresh mortar.
28. European Committee for Standardization (CEN) EN 1015-6:1998, Methods of test for mortar for masonry; Part 6: Determination of bulk density of fresh mortar.

29. Mo K, Lee H, Liu M et al (2018) Incorporation of expanded vermiculite lightweight aggregate in cement mortar. *Construction and Building Materials* 179: 302-306.
30. Leemann A, Holzer L (2001) Influence of mica on the properties of mortar and concrete. *Proceedings of the 8th Euroseminar on Microscopy Applied to Building Materials (EMABM)*. Greece, Athens.
31. Tate M (2005) The most important property of cement-lime mortar in masonry construction is *Proceedings of International Building Lime Symposium*: Orlando, Florida.

NHL-based plasters and renders – Assessing the influence of mixing method on workability and hardened mortar properties

Frowin Ruegenberg¹, Martin Schidlowski¹, Tobias Bader¹, Anja Diekamp¹

(1) Unit of Material Technology, University of Innsbruck, Frowin.Ruegenberg@uibk.ac.at, Martin.Schidlowski@uibk.ac.at, Tobias.Bader@uibk.ac.at, Anja.Diekamp@uibk.ac.at

Abstract

The term “workability” summarizes essential properties of plaster mortars that underlie subjective interpretation resulting in different approaches for its basic description. Generally, workability is influenced by composition and treatment of mortar, which affect the fresh mortar properties. A comprehensive overview of fresh and hardened mortar characteristics allows generating data, which can be used to predict durability qualities. Thus, within the present study two NHL-based recipes were evaluated with regard to the influence of different mixing methods. Varying the mixing time aims at simulating different workmanship methods on the building site. The properties that were investigated within this study cover mechanical and transport properties of NHL-based plaster mortars in order to estimate the influence of mixing method and water content, respectively, on fresh and hardened mortar characteristics. First results revealed that the interaction between mixing time, water content as well as type of hydrated lime affect the mentioned properties. The gained insights into the interaction between “workability” and resulting durability properties of NHL plaster mortars is beneficial for the understanding of modern and traditional NHL-based systems.

1 Introduction

NHL is the abbreviation of “natural hydraulic lime” and describes an inorganic binder, which has been used since early medieval times in Tyrol and South Tyrol for plaster and masonry mortars [10]. As a matter of fact, the appropriate materials show an outstanding durability, which is often attributed to the unique pore space properties of NHL-based materials [4]. Historic and currently available NHL contain hydrated lime (portlandite) and hydraulic acting components (mainly C₂S, C₃A). Hence, the hardening of the material is characterized by the combination of carbonation and hydraulic/ pozzolanic reactions, respectively. This hardening mechanism results in a heterogeneous composition of reaction products containing calcite, C-S-H phases, Afm-phases and alteration products such as silica gels, whose effects on durability are not investigated ultimately [9]. Today, NHL is commonly used for cultural heritage and reconstruction, as well as for new construction applications.

Previous studies focused on the combined reaction, porosity and mechanical properties of NHL and NHL-related materials [1, 2, 5, 6, 18] and on applied requirements for repair

mortars for historic masonry [15, 17, 23]. “Workability” as main characterization factor for the behavior of the material on building site is used in literature frequently as synonym for fresh mortar consistency. Beside instructions of accurate workmanship of plasters and renders on building site (e.g. [12, 20]) only a small amount of publications attempt to describe the mostly subjective used term “workability” as combination of measurable parameters and the sum of macroscopic properties, respectively (e.g. [3]). Nevertheless, Hanley et al. [14] examined the workability of NHL based mortars in the proper sense in relation to fresh mortar parameters, such as water content, initial flow as well as its subsequent influence on strength.

The present study focuses on the application of different mixing methods, derived from factual practice in workmanship of plasters on building sites, on NHL-based mortar recipes as illustrated in Figure 1. As expected, considering practical aspects and as recognized in the course of the present investigations, the mixing time affects the properties of mortar [11]. Understandably, the mixing time modifies the properties more fundamentally, that could be characterized through the flow diameter at a given water content as single sum parameter. Hence, additional fresh mortar lab parameters like air content and bulk density were implemented in the present study. Currently, dry mortar industry in Austria classifies plaster mortars according to ÖNORM EN 998-1 [35], which is linked to testing standard series for mortar [25-30]. Hence, the required 28 days (strength) parameter were determined in course of this study.

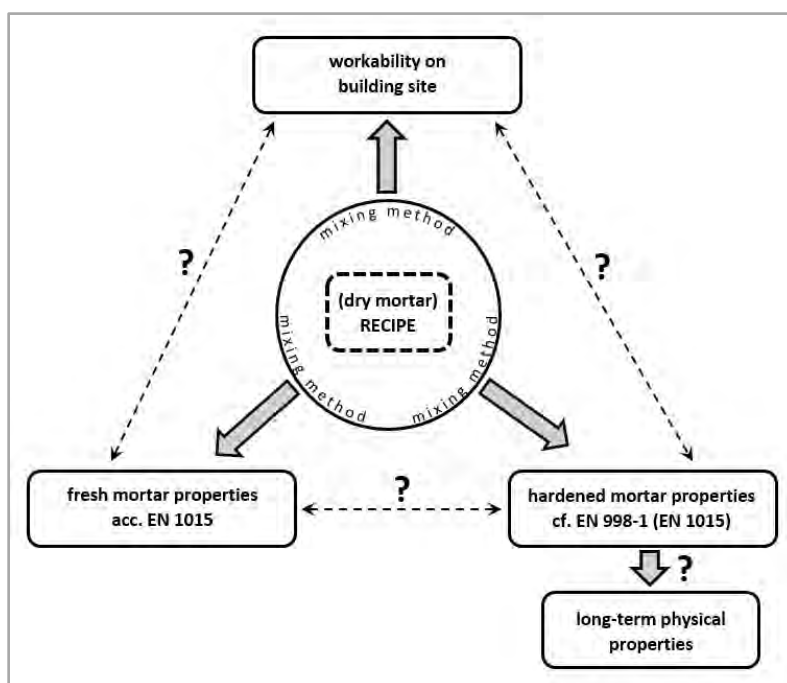


Figure 1. Interaction that will be investigated within the present study.

The objective of this experimental study is to assess the influence of mixing method on the short and longtime properties of the NHL based plaster mortars in order to give recommendations for the proper handling. Accordingly, this examination believed to be

beneficial for adapting materials and methodology on building sites to specific conditions. Additionally, the workability related factors, which are influencing the durability of NHL mortars, will be presented.

2 Methods and materials

2.1 Raw materials

The following dry components, which have been homogenized by using a Collomix hand-held mixer with a mixing paddle type “WK” for 5 minutes, were used for the tested mortar recipes:

- Natural hydraulic lime NHL 5 (according to ÖNORM EN 459-1: 2015 [33])
- Dry hydrated lime (calcium hydrate; CL 90-S according to [33])
- Lime putty, aged for more than 3 months (CL 90 according to [33], added as “Lime Putty PreMix” like described in section 2.2)
- Local dolomitic filler (0.0-0.09 mm)
- Graded, crushed calcareous sand “KS-VM” as aggregate (max. grain size 1.2 mm)

The water content of the lime putts material has been determined by drying under 105 °C, the results are given in Table 1.

Table 1. Water and Ca(OH)₂ content of Lime putty and the “Lime Putty PreMix”.

Material	Water content	Ca(OH) ₂ -content
Lime Putty*	53.51 wt.-%	47.49 wt.-%
Lime Putty PreMix**	78.68 wt.-%	21.32 wt.-%

* Total residuum as Ca(OH)₂; ** ratio calculated from results determining humidity under 105 °C and mixing ratio with water, see section 2.2

2.2 Dry mortar recipes

For the present study, two different concepts of materials, which are commonly used in the preservation of cultural heritage, were tested.

- Dry mortar **material A** bases on commercial NHL based plaster recipes, which are designed for manual workmanship, containing NHL 5, hydrated lime (“HL”), local dolomite filler and natural calcareous sand (“KS-VM”). It was decided for the present experiment, that influences of (varying) quality of the natural sand should be avoided, furthermore, there should have been assured the comparableness with other ongoing testing series. Therefore, instead of the natural sand we used three graded fractions of crushed and classified lime-sand, which were re-combined receiving a grain-size

distribution curve with a maximum grain size of 1.2 mm (KS-VM). Furthermore, it was avoided using standard quartz sand (according to ÖNORM EN 196-1), because its spherical grain shape does not allow applicable trials as a plaster mortar.

- Mortar **material B** contains only NHL 5, dolomite filler and calcareous sand (KS-VM). Comparable to the traditional practice on cultural heritage building sites, the lime component was added in form of lime putty. For practicability it was pre-mixed for three minutes with tap water in the mixer according to [32], forming a highly fluid lime hydrate-suspension (“Lime Putty PreMix”). The mixing ratio of 55 wt.-% water and 45 wt.-% putty was determined in the course of pretests on building site with comparable materials. Hence, instead of pure water the suspension was used to adapt the consistence like described in section 2.3.

The mixing ratio of the dry components for material A and B are shown in Table 2.

Table 2. Mixing ratios of dry materials A and B.

Dry raw material*	Material A	Material B
NHL 5 (acc. to [33])	130 kg	130 kg
Crushed calcareous sand KS-VM	730 kg	730 kg
Local Dolomite filler (0.0-0.09 mm)	100 kg	100 kg
Hydrated lime (CL 90-S, acc. to [33])	40 kg	-**
Total:	1000 kg	960 kg

* see section 2.1; ** added later with water as “Lime Putty PreMix”, see below.

2.3 Fresh mortar mixing

The fresh mortars has been mixed with a mixer according to European standard [32]. Primarily, the water or the lime putty water-suspension/pre mix, respectively, have been added to the mixing bowl before the mixer has been switched on. The dry mortar blendings have been added within the first seconds of the mixing process.

Mixing of mortar at the building sites occurs with lots of different mixing machines and techniques, so it is difficult to specify clearly and hardly to translate the processes into the laboratory. Anyway, the transmission of the influence of mixing time on quantifiable lab parameters of fresh and hardened mortar, thus on the sum of properties, was the aim of the present investigation.

- **Mixing method 1)** occurred with a total mixing time of 15 seconds, which is technically oriented on the treatment time of plaster material in commercial mixing pumps like PFT type G4/G5 or MAI type g4 business of about 15 sec. [11].
- **Mixing method 2)** with a total mixing time of 60 seconds is referring approximately to [25], where a mixing time of 30 plus 60 seconds (total 90 seconds) is recommended. However, the standard allows an aberration of the denoted mixing time, if it becomes

declared separately. Upon the experience, that after 60 seconds the homogenization of mortars in manual and mechanical mixing is adequate, and to have a clear differentiation from mixing method 3), it was decided to reduce the total mixing time to one minute.

- **Mixing method 3)** has been operated with a mixing time of 180 seconds. This time (or longer) is used usually on building sites, when natural hydraulic lime premix products for cultural heritage become homogenized with water [11]. Furthermore, in European standard [25] a mixing time of 180 seconds is proposed for the mixing of lime containing mortars and lightweight mortars in the compulsory mixer.

2.4 Fresh mortar characterization

As described in section 2.5, water content is the variable factor at the building site, that will be adjusted to get a constant consistence with an adequate workability, using a specific mixing method (e.g. working with a certain mixing pump).

Therefore, consequently the water factor has been adapted in the lab testing series to achieve a nearly constant consistence, controlled by the flow table. This methodology was carried out in other studies (e.g. [5]). However, we indicate the water factor as ratio of water to mortar by mass (according to [34]), and not the water to binder factor W/B.

In case of material B, water has been added in form of the premix containing lime putty as described in section 2.2 to regulate the consistence. The proper **water content** has been calculated afterwards on base of the data obtained by drying of the lime putty (see Table 1) and the mixing ratio with the water (described in section 3.1). Cizer [7] followed this procedure as well.

The slump test according to [26] has been used to determine the **initial flow** diameter as quantifiable value for the consistence of the incurring fresh mortars. As described in section 2.5, it was decided to regulate the consistence on an initial flow (spread) of 165 ± 5 mm by adapting the water content.

In order to characterize the effect of the different mixing methods on the mortar fresh state, the **air void content** by volume was determined according to European standard [28]. Additionally, the bulk density of the fresh mortar (**fresh mortar raw density**), following the procedure described in [27] was measured.

The **water retention** is an important parameter for the practical use of a plaster. It quantifies the property of a fresh mortar, to avoid the water extraction by a highly absorbing substrate like porous bricks. The European standard for building lime [34] provides a testing method for the determination of the water retention in wt. %, which was used within the present study.

The following abbreviations are being used in the following descriptions:

- Water content (factor): WF [%]
- Initial flow diameter: IFD [mm]
- Fresh mortar raw density: FMRD [g/dm³]
- Air content: AC [%]
- Water retention: WR [%]

2.5 Workability

As described by Hanley [14], the water content is a main factor, that influences the workability of a mortar, although many other factors affect it as well. Moreover, he postulated the initial flow as a reliable way, to identify the correct amount of water for an appropriate workability of a mortar. This approach is similar to the procedure of treatment of a mortar on the construction site. Additionally to the characterization of initial flow, water content and other laboratory parameters, generated by a certain mixing method (see section 2.3), workability testing by two qualified skilled craftsmen will be operated.

The ideal consistency, represented through the initial flow, was figured out by preliminary tests, where the water content at the different mixing times was varied. Hence, the target initial flow was defined with a value of 165 ± 5 mm. This value is also mentioned in [14] as ideal consistency for mortars based on NHL 2, whereat slightly higher values for NHL 3.5 are stated. A flow diameter of 185 mm for NHL 5, which corresponds to the European standards' specification, emerged as to thin fluid and runny for our plaster validation on the vertical test surfaces. Possible reasons for this discrepancies could be the difference in the sieve line (1.2 mm vs. over 5 mm in [14], another binder quality (loose bulk density of circa 550 vs. 750 g/cm³ for NHL 5) and different approaches by recipes and mixing methodology.

The following workability trials were done as blank testing, whereat the fresh plasters were applied manually with a layer thickness of 10-20 mm on vertical brick sheeting's of 50x30 cm², which previously were coated halfway with an impervious primer to simulate a crystalline rock substrate. Divergent from the common used, standardized practice [20], it was resigned to wet the highly absorbing bricks with water before application. This should lead to two total different substrates relating to its water absorption properties – highly absorbing brick and impervious primer surface.

During the plastering several crucial criterions regarding to the handling of the material and its properties on the small test surfaces were evaluated:

- **Consistence:** evaluation of the rigidity of the material in the manual processing (ok; ⊕: viscous/⊖: thin fluid);
- **Performance** (Plastering/Sharpening): describes, how smooth it was to lay on the mortar and to create a flat plane (1 – easy; 5 – stiff);

- **Stability:** tendency of the fresh material to slide down on the vertical surface (1 – stable; 5 – strong disposition to flow off);
- **Cracking:** tendency of crack formation (within the first hour after application); This Parameter is to handle with care in the present context, because the renunciation of wetting the highly absorbing substrate leads inevitably to a desiccation of the fresh plaster and sequentially to the forming of cracks. Lime and NHL mortars as well need a humid environment in the first stage of hardening to avoid the formation of shrinkage and stress cracks [20]; This, is usually achieved by manual wetting of the plastered walls for a few days or by suitable weather conditions. Furthermore, a quantification of crack formation is very difficult on small areas, usually a few square meters and a longer observation time are needed for clear crack diagnosis.

2.6 Preparing and curing of the test specimen

For preparation of the subsequent hardened mortar testing series, sample prisms according to [32] were prepared. The fresh mortar has been mixed like described in section 2.3 and placed in two layers into molds with the dimension of 40x40x160 mm³. The consolidation occurred by “shocking” referring to the shock table method, described as well in [32].

The curing conditions were selected according to [29]. For the first 7 days the prisms were cured under high humidity (relative humidity of >95 %) and 20 ± 2 °C, whereat the stripping of the forms was conducted already after 5 days. The further sample conditioning up to 28 days occurred under 65 ± 5 % relative humidity and 20 ± 2 °C.

Overall, there has been made one sets of sample prisms per mortar recipe and per mixing method. Two samples were used for the nondestructive and destructive strength tests and the check of water content and carbonation grade. The remaining prism was used for the measurement of the open porosity and the water absorption properties.

2.7 Hardened mortar characterization

The strength properties tests were conducted as described in [29] ÖNORM EN 1015-11: 2007. Between the determination of bending tensile (**flexural strength** “R_F” and **compressive strength** “R_C” ([N/mm²] or [MPa]) the **carbonation depth** was estimated on the fresh fracture surface by the phenolphthalein testing method (0.5 % phenolphthalein in methanol solution), which is described in [19]. The residual water content was quantified by drying the residual of the strength sample at 105 °C.

The **open porosity** by volume of the test specimen was determined in reference on procedure described in [31]. Moreover, **water absorption** by covering the samples with water under atmospheric pressure and a temperature of 20 ± 2 °C until constant weight was determined by weight measuring. Afterwards, the **drying behavior** under 65 % relative humidity and 20 ± 2 °C was diagnosed [19]. Additionally, the **capillary water absorption**,

following the procedure described in [30], was measured. The quantification occurred through the water absorption coefficient “ C_w ” [$\text{kg}/(\text{m}^2/\text{min}^{0.5})$], calculated differing to the standard out of the values 10 and 20 min. values (saturation before 90 min.). Drying of the samples was conducted at 105 ± 5 °C and not at 60 °C (as designated in the standard).

3 Results and discussion

3.1 Materials, mixing and fresh mortar properties

As mentioned previous, the dry mixing of the materials A and B occurred by mass ratios, as intended in European standards and as established in industrial scale dry mortar mixing. However, homogenization of the raw materials on cultural heritage construction sites is executed typically by volume. The effectively mixing ratios by mass, in addition to the measured initial flow and water contents at the different mixing times are shown in Table 3.

Table 3. Calculated mixing ratios of materials A and B (by using 2000 g and 1900 g dry material) on a total mass of 1000 kg; specified fresh mortar parameters (full descriptions of raw materials and abbreviations are described in section 2.4).

	Material A			Material B		
NHL 5	130 kg			127.0 kg	128.0 kg	128.3 kg
KS-VM	730 kg			712.9 kg	718.9 kg	720.4 kg
Filler	100 kg			97.7 kg	98.5 kg	98.7 kg
Hydrated lime	40 kg			62.5 kg	54.6 kg	52.6 kg
Mixing time [sec]	15	60	180	15	60	180
WF [wt. %]	18.0	18.0	16.5	22.25	19.44	18.73
IFD [mm] *	166.5	168.0	165.0	166.5	165.0	166.0
FMRD [g/dm^3]	2119	2141	2161	2072	2117	2118*
AC [vol. %]	5.5	4.5	4.0	4.0	3.5	4.75*
WR [wt. %] *	83.8	85.5	88.6	89.1	88.4	91.4

* arithmetic mean of at least two measurements.

The described approach of mixing the dry material B with the lime putty water premix instead of pure water as with material A, follows consequently to different mixing ratios of the hydrated lime component and the other ingredients in material B. As already observed by Hanley [13, 14], the different mixing ratio affects workability as well as fresh and hardened mortar properties.

In the course of the testing series, it was found out that the mixing intensity of the mixer according to [32] depends strongly on the used amount of dry mortar: the overall best outcome (high initial flow diameter at constant water content) was reached by utilizing 1800 – 2000 g of dry mortar. Moreover, this quantity emerged as practicable for executing several testing methods. The short mixing method of 15 seconds shaped up as the most sensitive on slight discontinuities in the frame conditions.

Researching the fresh mortar parameters, determined on a similar consistence (initial flow diameters), several relationships can be identified: using a shorter mixing time follows,

probably due to an minor homogenization grade and less wetting of the dry particles, to a higher requirement of water (WF) compared to the longer mixing method. This relationship is even more distinct at material B than A, where consequently short mixing implies higher amounts of lime hydrate. The fresh mortar raw density (FMRD) as well depends on mixing time and water content: longer homogenization with a smaller amount of water leads to a higher fresh mortar density.

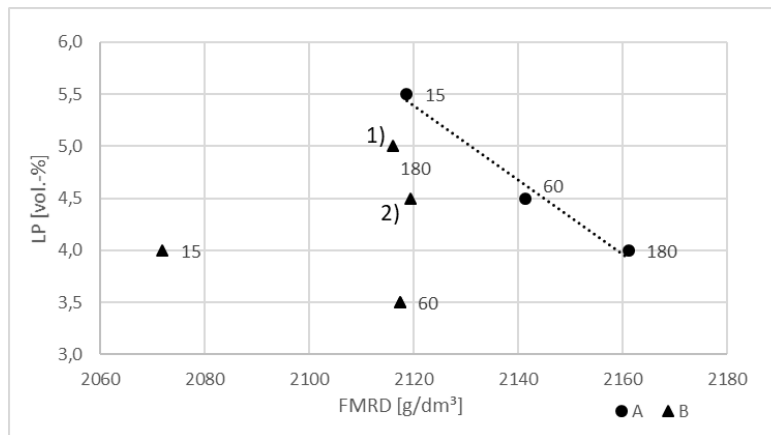


Figure 2. Plot of fresh mortar bulk density against air content for materials A and B at the different mixing times (repeat determination: measuring points 1) and 2)).

Conventional cement-lime mortar for machined application usually contains air entraining additives, which get activated while melding it with water. This materials show in fresh mortar state an air content of over 10 vol. % and, understandably, a clear negative correlation of fresh mortar bulk density and air content [11]. Air content measurements on our samples showed a notably lower content of pores within 3.5 and 5.5 vol. %, what complicates to the postulation of a significant variability of the single values within this narrow range. As shown in Figure 2, the adverse correlation could be found by testing mat. A. However, material B did not shows no correlation between air content and raw density, neither by repeat determination using 180 seconds of mixing.

The water retention shows a dependency of mixing time and, consequently affected by the method of calculation according to [34], the water content: longer mixing and/or a reduced water factor leads to a higher amount of water in the fresh mortar matrix when it is exposed to water absorption conditions. Again, the dependence is more pronounced at material A.

Water retention of commercial dry mortar plasters, blended with water retention additives as methyl cellulose, achieve values of about 92 wt. % at short mixing times (corresponding to machined building site mixing with water) on to 99 wt. % at long mixing times. This effect can be explained due to progressing swelling of the additive in contact with water during melding [11].

As figured out through comparison tests, OPC based materials with comparable recipe and without containing the relevant additives, reach values of about 85 wt. % at a mixing time of 60 seconds, at identical consistence. Thus, the NHL based plaster material shows similar

water retention values at comparable conditions. However, the water content of the cementitious systems is lower than the water contents of NHL systems, on the other hand fresh mortar density aims values over 2200 g/dm³. In comparison to our material, this leads probably to a hard workable material (see also section 3.2).

3.2 Workability

As shown in Table 3, every material was modulated to receive a usable initial flow by modifying the water content for the workability testing. As just described in section 2.5, a flow diameter of 165±5 mm emerged itself as ideal target value. Trials with higher water content and therefore a higher flow value were conducted as well, but they turned out as not practicable because the mortar was too thin fluid and runny for the application on the vertical surfaces.

Generally, workability evaluation is controlled widely by subjective assessment of the involved artisans. Even just the interpretation of the given estimation parameters can be construed in different ways. Nevertheless, it was aimed to generate a meaningful data set, so the abovementioned workability weighting of the two craftsmen was averaged – the values on the relative scale had a maximum variation of 1. The maintained data is shown in Table 4 among other already presented parameters, which should help to guide to a comprehensive understanding of the present system.

Table 4. Workability data in combination with already presented mixing and fresh mortar parameters. The two listed values at line “stability” and “performance” are the arithmetic mean of the two single grades (one for each craftsmen); The upper parameter represents the estimation on strong absorbing substrate, below the value for the impervious primer surface.

	Material A			Material B		
Hydrated Lime	40 kg			62.5 kg	54.6 kg	52.6 kg
Mixing time [sec]	15	60	180	15	60	180
WF [wt. %]	18.0	18.0	16.5	22.25	19.44	18.73
IFD [mm]	166.5	168.0	165.0	166.5	165.0	166.0
FMRD [g/dm ³]	2119	2141	2161	2072	2117	2118
AC [vol. %]	5.5	4.5	4.0	4.0	3.5	4.75
Consistence (ok/+/-)	+*	ok	ok	ok	+	ok
Stability (1 -stable; 5 - flowing off)	1.5	2.5	2.5	1.0	2.0	2.0
	2.5	3.5	3.5	3.5	4.0	2.5
Performance (1 - easy; 5 - stiff)	2.0	2.5	2.5	1.5	2.0	2.0
	2.0	3.5	3.5	1.5	3.5	3.5
Annotation	performance ok	appears as “poor” mixture	hard to work with, runny	best workability	workability ok	quite hard to work with

* repeated mixing with higher water contents (19 wt.-%, 20 wt.-%) led to not workable material.

The overall best workability properties appeared during testing of material B, mixed for 15 seconds. This material was very stable and showed a good adhesion on the brick surface, but tended to flow off at the primer. The tendency to show a good adhesion at the strong absorbing surface and an explicit lower stability against off-flowing at the impermeable substrate was observed strongly as well at a mixing time of 60 seconds, and minor relevant at 180 seconds. Material B showed at all mixing methods a moderate higher adhesion on the brick.

Probably, the described effect of adhesion force change on different substrates using different mixing times can be explained through the different homogenization grade of the lime hydrate component and the remaining dry materials in fresh mortar: material A is adequate homogenized already when adding the water, material B needs to be homogenized 60 – 180 seconds to reach a sufficient intermixture. Absolute amounts of lime hydrate and water, which are linked at material B due to the adding of the lime putty- water premix may be another explanation. In this hypothesis, higher quantities would affect a higher difference of stability on variable water absorbing surfaces and generally a lower adhesion at the primer.

Both materials A and B showed the phenomenon of better workability - performance and stability – at shorter mixing times. As aforementioned the short mixing goes along with higher amounts of water (and at material B more lime hydrate as well) and a reduced fresh mortar density at the same consistency. Accordingly, a decreased mortar density could be interpreted as indicator for better workability.

At the same mixing time, material B achieved higher grades for the performance and higher stability on the brick substrate – this factor can be correlated positively with higher water and hydrated lime content, therefore diminished mortar density. It can be assumed, that the different type of calcium hydrate (dry powder in material A; lime putty, suspension in material B) could also have a substantial impact on workability.

Benchmarking the grade of cracking formation of the different compounds on such small testing surfaces is very difficult. Every plaster showed more or less strong cracks on the highly absorbing brick surface due to fast aspiration of the batching water in the plaster. Hence, fast shrinkage occurs and leads to contraction and crack forming. Therefore, we see that pre-wetting of the subsequent coated surface is essential for a high plaster quality, particularly on substrates like bricks. A rudimental tendency of less cracking was noted with increasing water retention values, which appeared mainly at longer mixing times. Generally, we noted a subsidiary developing on cracks on the primer surface. Plasters with high lime content (as the present materials) have the advantage, that contraction cracks can be closed afterwards by actively moistening the surfaces [20].

3.3 Strength (28 d) and hardened mortar properties

The evolution of (early) strength properties, which in NHL based mortars are mainly induced by hydration of the containing calcium silicates and aluminates (mainly C_2S , C_3A) at a sufficient moisture content [8], without responding here to the complex hydration kinetics behavior of the binder system. Furthermore, the water quantity controls strongly the strength development in cementitious systems: As shown in Table 5, higher water factors require an increasing of capillary pore volume and therefore at a decreasing of strength [22]. This effect can be transferred also on (hydraulic) lime based rendering mortars. According to this, we noted an inverse correlation between water- and pore volume denominated factors as water content, water-to-binder ratio, sum of air content and water content, and stability describing properties as flexural- and compressive strength.

Table 5. Selection of porosity influencing/describing parameters and strength properties (28 d).

	Material A			Material B		
	40 kg			62.5 kg	54.6 kg	52.6 kg
Hydrated Lime	40 kg			62.5 kg	54.6 kg	52.6 kg
Mixing time [sec]	15	60	180	15	60	180
WF [wt. %]	18.0	18.0	16.5	22.3	19.4	18.7
W/B	1.06	1.06	0.97	1.17	1.06	1.04
IFD [mm]	166.5	168.0	165.0	166.5	165.0	166.0
FMRD [g/dm ³]	2119	2141	2161	2072	2117	2118
Sum WF+AC [vol. %]	23.5	22.5	20.5	26.3	22.9	23.5
WR [wt. %]	83.8	85.5	88.6	89.1	88.4	91.4
E_D [GPa]	3.8	3.5	5.7	2.3	4.1	4.3
R_F [N/mm ²] (SD)	0.54 (0.08)	0.63 (0.15)	0.70 (0.04)	0.41 (0.02)	0.50 (0.01)	0.49 (0.13)
R_C [N/mm ²] (SD)	0.98 (0.14)	1.22 (0.20)	1.81 (0.25)	0.60 (0.13)	0.81 (0.03)	0.85 (0.28)
Bulk density ρ_{28d} [kg/dm ³]	1.86	1.83	1.91	1.72	1.79	1.83
Open porosity 28d [vol. %]	32.1	31.8	30.0	35.2	33.5	32.3
Carbonation 28d grade [%]	≈30	≈20	≈13	≈13	≈15	≈13

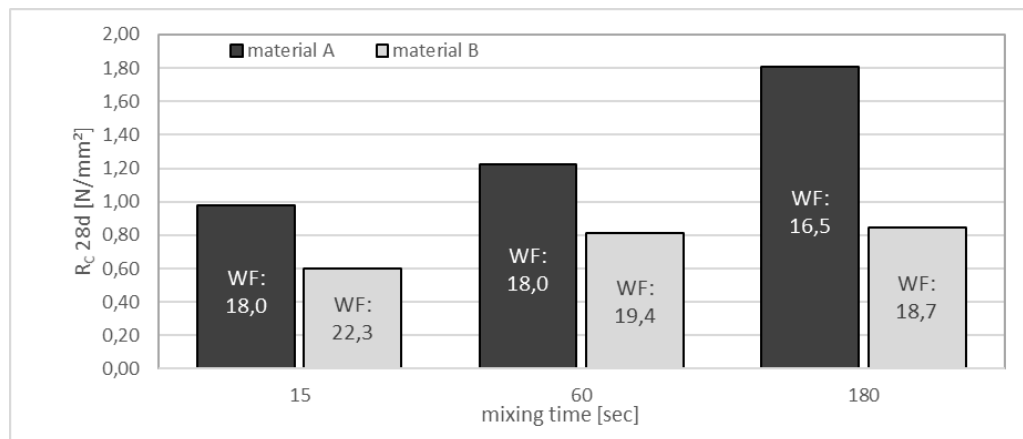


Figure 3. Compressive strength R_C after 28 d curing as a function of mixing time and water content [%] (water values inside the bars, standard deviation of strength see Table 5).

Thus, also the used mixing time has an input on mechanical properties: as shown in Figure 3, longer mixing times, which requires less water, favor the development of higher compressive and flexural strength. Hence, we observed that the short mixed plasters with a lower fresh mortar density and better workability properties show a slower development of mechanical properties, but correspondingly higher open porosity. The variability of strength is higher at material A, this could be based on the general higher water and lime hydrate content in material B, which affects a commonly retarded setting and a narrower distribution of compressive (early) strength values closer to the plastic state. Moreover, we do not register a relation between strength and carbonation depth after 28 days, which leads to the interpretation that the impact of hydraulic reaction is still dominant over the carbonation for formation of solid phases. This finding is comparable to the literature [2].

Table 6. Evolution of bulk density and selected 28 d parameters.

	Material A			Material B		
	15	60	180	15	60	180
Mixing time [sec]	15	60	180	15	60	180
WF [wt. %]	18.0	18.0	16.5	22.3	19.4	18.7
FMRD [kg/dm ³]	2.12	2.14	2.16	2.10	2.12	2.12
Bulk density ρ_{7d} [kg/dm ³]	2.12	2.11	2.18	2.05	2.09	2.12
Bulk density ρ_{14d} [kg/dm ³]	1.85	1.86	1.97	1.82	1.87	1.89
Bulk density ρ_{28d} [kg/dm ³]	1.86	1.83	1.91	1.72	1.79	1.83
$\Delta\rho_{28-14d}$ [kg/dm ³]	0.01	-0.03	-0.06	-0.10	-0.08	-0.06
Open porosity 28d [vol. %]	32.1	31.8	30.0	35.2	33.5	32.3
Carbonation 28 d grade [%]	30	20	13	13	15	13
Residual moisture 28d [wt. %]	0.7	0.9	1.2	1.0	1.0	1.1

Taking a view at the raw densities (fresh mortar bulk density, bulk densities after 7, 14 and 28 days), we see after the change of curing humidity from 95 % to 65 % RH after 7 days a general reduction in bulk densities due to desiccation of free water. Between 14 and 28 d, this process continues on, material B at any mixing time and material A at longer mixing times of 60 and 180 seconds, register still a loss of mass. An anomaly is denoted at material A, which was mixed by only 15 seconds: its raw density increases slightly between 14 and 28 days. Researching the carbonation grade and residual moisture after 28 days, we see that the mentioned sample shows the highest carbonation at the lowest moisture contents. Accordingly, the water retention shows the lowest values at this sample (see Table 5). Hence, we can assume that the mass increase is induced by the reaction of portlandite to calcite through CO₂ incorporation.

3.4 Porosity and water transport properties

As shown in Table 5 and mentioned in section 3.3 we found a dependency of the mixing time, water content and open porosity. The interrelationships between the relevant parameters and specific values, which describe the water transport at selected conditions (water absorption at vacuum and at atmosphere pressure, drying under 20 °C and 65 % RH), are shown in Table 6.

Obviously, a higher mixing water content leads to a higher porosity, the air content at fresh mortar state as result of mixing technique and mortar composition seems to influence the porosity secondary. The open porosity of dry mortar (mat. A) with a mean value of 32.1 vol. % at short mixing/higher water contents is slightly higher than 30.0% at long mixing times. Mat. B was generally mixed with higher water factors and reaches values of 35.2-32.3 vol. %. The observed positive correlation between water retention and open porosity is also mentioned in the literature [1].

Table 6. Selection of true porosity influencing and describing parameters and water transport describing parameters (28 d samples).

	Material A			Material B		
	40 kg			62.5 kg	54.6 kg	52.6 kg
Hydrated Lime	40 kg			62.5 kg	54.6 kg	52.6 kg
Mixing time [sec]	15	60	180	15	60	180
WF [wt. %]	18.0	18.0	16.5	22.3	19.4	18.7
AC [vol. %]	5.5	4.5	4.0	4.0	3.5	4.75
Sum WF+AC [vol. %]	23.5	22.5	20.5	26.3	22.9	23.5
Open porosity (vacuum) [vol. %]	32.1	31.8	30.0	35.2	33.5	32.3
Water absorption at atm. pressure for 10 min. [vol. %]	14.3	14.4	13.3	17.1	15.6	15.1
Water absorption at atm. pressure for 24 h [vol. %]	14.4	14.8	13.8	17.3	16.1	15.5
Ratio water abs. under atm. pressure / open porosity	0.45	0.47	0.46	0.49	0.48	0.48
Water absorption coeff. C_w 10-20 min [kg/(m ² /min ^{0.5})]	1.32	1.03	0.79	0.98	0.97	0.91
Residual moisture 28 d [wt. %]	0.7	0.9	1.2	1.0	1.0	1.1

The water absorption at atmospheric pressure represents the influence, which occurs, when a building is exposed to weathering. After 24 hours, we reach a water absorption of 45-49 % relating to the open porosity. Additionally we see, that after 10 minutes over 95 % of the available porosity (compared with abs. after 24 h) is already filled with water, which corresponds to a very fast water absorption. The water absorption coefficient C_w correlates with open porosity and supports the fast water absorption. Here we do not recognize anomalies between the samples/mixing times.

As shown in Figure 4, drying under 20 °C and 65 % RH shows a quite slow progress within the first 6 hours due to loss of surface moisture, with is represented by a flat curve in the

diagram at the beginning. After 6-24 hours, we denote the transition to capillary water transport under humid conditions, which goes along with an increasing slope of mass loss [21]. Conspicuously, the sample of material A and short mixing times shows a faster weight loss compared to the other samples, whose trends are equal until this period. Therefore, we can assume a higher capillary water transport in material A (short mixing) and faster reaching of diffusive vapor transport (flattening of the curve) and “dry” conditions. Additionally, the present material shows the lowest contents of residual moisture after 28 days, which supports the diagnosis of highest water transport, but is also probably connected to the carbonization process (see section 3.3). After about 2 days of drying sample material B with long mixing time shows the tendency of acceleration of water desorption in respect to the other samples. Therefore, we note the anomaly at the sample with the lowest open porosity, whereas at material A the material with the highest open porosity showed the fastened mass loss. This leads to the suggestion that the particular consideration at the porosity under vacuum does not lead to a sufficient explanation of water transport properties.

Samples showed a volume of over 50 % of capillary pores in the system (relating to open porosity), that do not transport and incorporate water under normal conditions. The samples with faster mass loss show relatively low ratios of water absorption under atmospheric pressure to open porosity. In the literature, this ratio is labeled as “saturation value S ” (for natural stone; e.g. [16, 24]), which can be used as simplified parameter to characterize the long-term durability against atmospheric impacts as freeze-thaw exposure, because the harmful water becomes desorbed rapidly [12]. Additionally, the volume of under normal conditions not with water filled pores is high in relation to the total porosity, this volume is gettable for volume expanding processes (ice formation, crystallization of salt).

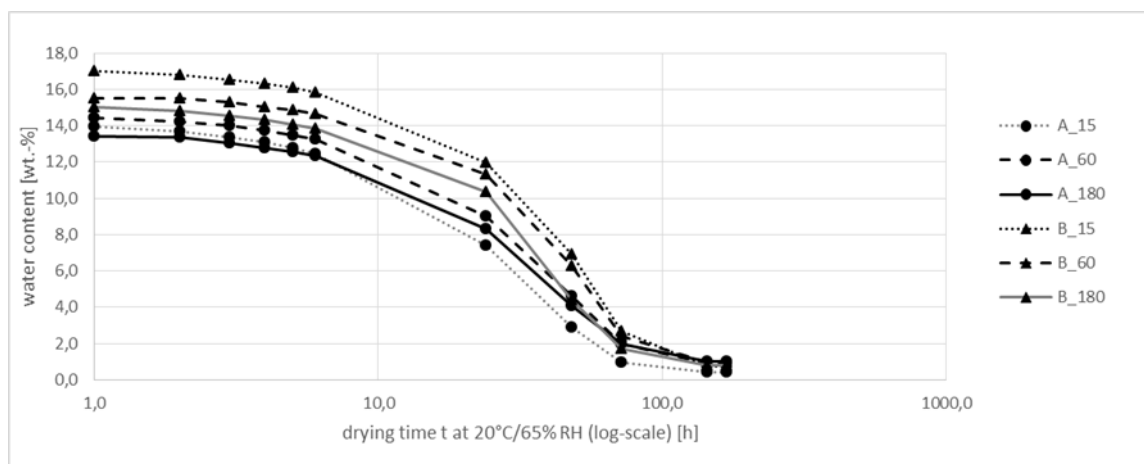


Figure 4. Drying properties (weight loss due to water release) under 20 °C and 65 % RH.

4 Conclusions

Within the current study, the influence of mixing method on workability and hardened mortar properties of two NHL-based plaster recipes was investigated. The investigated recipes called Material A and Material B differ with regard to the added type and content of hydrated lime.

In summary, we observed a considerable influence of plaster recipe type as well as mixing time on workability, fresh and hardened mortar properties and mechanical strength. Hence, implementing of additional fresh mortar parameters such as air content and bulk density as well as the declaration of the mixing method are recommended (see also [23]). The choice of material type and processing technology on building site should occur under consideration of the present conditions. Thus, it implies that the processor has several options as modifying the mixing time and/or water content, to adapt the mortar properties according to specific situations. Nevertheless, it is important in every case using NHL based (and not with additives, as methyl cellulose modified) materials to follow the generally accepted presetting as wetting the substrate before the application of the plaster.

Dry mortar material A (characterized by fixed content of dry hydrated lime) reaches generally higher early strengths and a faster onset of carbonation process. Furthermore, it achieves the requirements according to standardization, which is based primarily on 28-day (compressive strength) properties, in a reliable way. Accordingly, using long mixing times and small amounts of water, makes material A the only material in the testing series that can be classified into strength class “CS II” according to [35] ($R_{C28d} > 1.5 \text{ N/mm}^2$), therefore it is comparable with cementitious-lime-plaster and allows a comparatively rapid continuing with subsequent working steps [11]. Workability and long-term stability is expected to be enhanced at short mixing times, using a higher water content and reaching lower densities.

Mortar material B (characterized by a variable content of lime putty) shows a slow strength evolution, due it does not allows a quick subsequent processing, but offers more possibilities to adapt the material specifically. Therefore, it is the suitable material type for the purpose in cultural heritage and the treatment through highly skilled craftsmen. The mixing time influences the properties as well as at material A, shorter mixing leads to a good performance. Accordingly, a decreased mortar density could be seen as indicator for better workability. Moreover, we revealed an inverse correlation between mixing time and water content, witch consequently leads to a higher porosity. Disparities between the 28 d strength parameters and water transport properties (absorption and desorption) are less pronounced as in material A.

Comparing the open porosity values with literature [7, 18], we note a good accordance with the stated values of comparable materials (about 25-40 vol. %) in consideration of the differing components (e.g. type of NHL), mixture ratios and workability parameters. Strength properties showed lower values as in the cited publications [14, 18], which is interpreted as

result of the lower NHL content in our mixtures. The compressive strengths obtained in our study are similar to the results obtained by Allen et al. [1].

The results can be summarized as good qualitative base data for establishing the workability, short and long-term properties of generalized NHL based plaster mortars. Studies about durability, such as freeze-thaw-resistance, also at totally carbonated samples will be part of the further research. Moreover, examination of pore space properties with more refined methods (e.g. 3D X-ray microscopy and microstructural analysis) should provide insights for an extensive understanding of the present system.

Acknowledgments

This study was carried out within the K-Regio project “NHL - Natürlich hydraulische Kalke - Verstehen des Systems NHL”. The funding for the project is provided by the European Regional Development Fund (ERDF), which is gratefully acknowledged. The authors are grateful for fruitful collaboration with the project partners and the input given in the course of present research.

References

1. Allen G, Ball R (2012): Mechanical Properties of Hydraulic Lime Mortars. 4th Portuguese Congress on Mortars and ETICS 2012, Coimbra, Portugal
2. Arizzi A, Martinez-Huerta G, Sebastian-Pardo E, Cultrone G (2015): Mineralogical, textural and physical-mechanical study of hydraulic lime mortars cured under different moisture conditions. *Mater Construcc* 65: 318
3. Balksten K (2007): Traditional Lime Mortar and Plaster - Reconstruction with Emphasis on Durability. Thesis for degree of Doctor of technology, Chalmers University of Technology, Göteborg
4. Bidner T (2007): Welches Material und warum? – Überlegungen zur Praxis der Restaurierung. In: Diekamp A (ed) *Naturwissenschaft & Denkmalpflege*, 1st edn. University Press Innsbruck
5. Cizer O, Van Balen K, Van Gemert D (2007): Carbonation and hydration of mortars with calcium hydroxide and calcium silicate binders. *International Conference on Sustainable Construction Materials and Technologies 2007* Coventry: 611 - 621
6. Cizer O, Van Balen K, Elsen J, Van Gemert D (2008a): Crystal morphology of precipitated calcite crystals from carbonation of lime binders. *ACEME08, 2nd International Conference on Accelerated Carbonation for Environmental and Materials Engineering 2008* Rome: 149-158

7. Cizer O, Van Balen K, Van Gemert D (2008b): Blended lime-cement mortars for conservation purposes. In: D’Ayala D (ed), Fodde E (ed) *Structural Analysis of Historic Construction*, Taylor & Francis Group, London
8. Cizer O, Van Balen K, Van Gemert D (2010) Competition between hydration and carbonation in hydraulic lime and lime-pozzolana mortars. *Adv Mater Res* 133-134: 241-246
9. Diekamp A, Stalder R, Konzett J, Mirwald PW (2012): Lime Mortar with Natural Hydraulic Components: Characterisation of Reaction Rims with FTIR Imaging in ATR-Mode. In: Válek J (ed), Hughes J (ed), Groot C (ed): *Historic Mortars, Characterisation, Assessment and Repair*. RILEM Bookseries 7 part 1: 105-113
10. Diekamp A (2014): *Bindemitteluntersuchungen an historischen Putzen und Mörteln aus Tirol und Südtirol*. Dissertation University of Innsbruck
11. Dry mortar industry, pers comm (2018)
12. Groot C, Hughes J, Van Balen K, Bicer-Simsir B, Binda L, Elsen J, Hees, RPJ, Von Konow T, Lindqvist, JE, Maurenbrecher P, Papayianni I, Subercaseaux M, Tedeschi C, Toumbakari EE, Thompson M, Valek J, Veiga MR (2012): RILEM TC 203-RHM: Repair mortars for historic masonry: Performance requirements for renders and plasters. *Mater Struct* 45: 1277-1285
13. Hanley R (2006): *The relationship between workability and bond strength of lime mortars*. MSc Thesis, University of Dublin, Trinity College Dublin
14. Hanley R, Pavia S (2008): *A study of the workability of natural hydraulic lime mortars and its influence on strength*. *Mater Struct* 41: 373–381
15. Hees R, Veiga MR, Slížková Z (2017): Consolidation of renders and plasters. In: *Mater Struct* 50: 50-65
16. Hirschwald J (1912). *Handbuch der bautechnischen Gesteinsprüfung – Borotraeger Verlag, Berlin*
17. Hughes J, Groot C, Van Balen K, Bicer-Simsir B, Binda L, Elsen J, Hees RPJ, Von Konow T, Lindqvist JE, Maurenbrecher P, Papayianni I, Subercaseaux M, Tedeschi C, Toumbakari EE, Thompson M, Valek J, Veiga, MR (2012): RILEM TC 203-RHM: Repair mortars for historic masonry The role of mortar in masonry: an introduction to the requirements for the design of repair mortars. *Mater Struct* 45: 1287-1294
18. Isebaert A, De Boever W, Descamps F, Dils J, Dumon M, De Schutter G, Van Ranst E, Cnudde V, Van Parys L (2016): Pore-related properties of natural hydraulic lime mortars: an experimental study. *Mater Struct* 49: 2767-2780

19. Knöfel D, Schubert P (1993): Mörtel und Steinerfüllungsstoffe in der Denkmalpflege. Verlag Ernst & Sohn, Berlin
20. Krebs R (2018): Kalkputz – Eine Anleitung für die Praxis. In: Spiro A (ed), Gönül P (ed), Göhler H (ed) Über Putz. Oberflächen entwickeln und realisieren, 5th edn. GTA Verlag, Zürich
21. Krus M (1995): Feuchtetransport- und Speicherkoeffizienten poröser mineralischer Baustoffe. Theoretische Grundlagen und neue Meßtechniken. Dissertation Fakultät für Bauingenieur- und Vermessungswesen, Universität Stuttgart
22. Locher FW (2000): Zement – Grundlagen der Herstellung und Verwendung. Verl Bau und Technik, Düsseldorf
23. Marenbrecher P, Groot C, Hughes J, Van Balen K, Bicer-Simsir B, Binda L, Elsen J, Hees RPJ, Von Konow T, Lindqvist JE, Papayianni I, Subercaseaux M, Tedeschi C, Toumbakari EE, Thompson M, Valek J, Veiga, MR (2012): RILEM TC 203-RHM: Repair mortars for historic masonry. Requirements for repointing mortars for historic masonry. Mater Struct 45: 1303-1309.
24. Mirwald P (1997): Physikalische Eigenschaften von Gesteinen. In: Berufsbildungswerk des Steinmetz- und Bildhauerhandwerks EV (ed): Naturwerkstein und Umweltschutz in der Denkmalpflege, Ebner Media Group GmbH & Co KG, Ulm
25. ÖNORM EN 1015-2 (2007): Methods of test for mortar for masonry. Part 2: Bulk sampling of mortars and preparation of test mortars
26. ÖNORM EN 1015-3 (2007): Methods of test for mortar for masonry. Part 3: Determination of consistence of fresh mortar (by flow table)
27. ÖNORM EN 1015-6 (2007): Methods of test for mortar for masonry. Part 6: Determination of bulk density of fresh mortar
28. ÖNORM EN 1015-7 (1999): Prüfverfahren für Mörtel für Mauerwerk. Teil 7: Bestimmung des Luftgehaltes von Frischmörtel
29. ÖNORM EN 1015-11 (2018): Methods of test for mortar for masonry. Part 11: Determination of flexural and compressive strength of hardened mortar
30. ÖNORM EN 1015-18 (2003): Prüfverfahren für Mörtel für Mauerwerk. Teil 18: Bestimmung der kapillaren Wasseraufnahme von erhärtetem Mörtel (Festmörtel)
31. ÖNORM EN 1936 (2007): Natural stone test methods — Determination of real density and apparent density, and of total and open porosity
32. ÖNORM EN 196-1 (2016): Methods of testing cement. Part 1: Determination of strength

33. ÖNORM EN 459-1 (2015): Building lime Part 1: Definitions, specifications and conformity criteria
34. ÖNORM EN 459-2 (2010): Building lime. Part 2: Test methods
35. ÖNORM EN 998-1 (2017): Specification for mortar for masonry Part 1: Rendering and plastering mortar

Lime-based grouts for architectural surface repair. Comparison of their performance by using laboratory and field test methods

Vasiliki Pachta¹, Ioanna Papayianni¹, Thomas Spyriiotis¹

(1) Laboratory of Building Materials, School of Civil Engineering, Aristotle University of Thessaloniki, vpachta@civil.auth.gr, papayian@civil.auth.gr, skthomas869@gmail.com

Abstract

Lime-based grouts are usually applied for the consolidation and strengthening of historic masonries and architectural surfaces (renders, plasters, murals' substrates). Regarding architectural surfaces' repair, the selection and application of grouts, implies the implementation of a series of test methods. In the present study, three often used compositions of lime-based grouts, containing lime-pozzolan (L:P - 1:1 by mass), lime-pozzolan-white cement (L:P:WC - 1:0.8:0.2 by mass) and hydraulic lime NHL 3.5 were tested, by using laboratory and field test methods. The properties tested were fluidity, penetrability, volume stability and shrinkage tendency, as well as compressive and flexural strength of the grout mixtures at the age of 28, 90 and 180 days. The results from the laboratory and field tests were compared and found to be in agreement with the good performance of grouts. From the evaluation of the three types of grouts, it was concluded that all of them were acceptable, in relation to the LP performance at fresh and hardened state. The early strength (28d) was slightly higher in the composition with 10% WC and NHL3.5, but the long-term one (180d) was highest in the LP composition. Field tests seemed to be indicative of the good performance of grouts.

Introduction

Grouting is a widely used irreversible technique that focuses on filling discontinuities, strengthening masonries, or consolidating architectural surfaces [1-6]. The second case, usually refers to multilayer mortar systems, such as renders, plasters, murals' and wall mosaics' substrates, as well as other decorative elements (i.e. mortar cast reliefs) [5-9]. They are usually characterized by a stratigraphy of 2 to 4 well-compacted mortar layers the thickness of which is decreased to the surface [6-9]. Other characteristics related may be the decrease of the aggregates' granulometry to the surface, with a corresponding increase of the Binder/Aggregate (B/A) ratio, as well as a decrease of porosity [9].

The most often pathology symptoms that may be encountered in the architectural elements' substrate can be related to lacunas, discontinuities, as well as cracks or detachments (Figure 1) [9-10]. These can be either detected in the interface of the mortar layers or between the mortar layers and the masonry subground (Figure 2). The degradation rate may vary, according to a synergy of factors, such as differential movements due to accidental loads,

accumulation of moisture and salts, failures during layers' application, use of incompatible repair materials [9-11].



Figure 1. Detachments and loosening of the mortar layers from murals' substrate

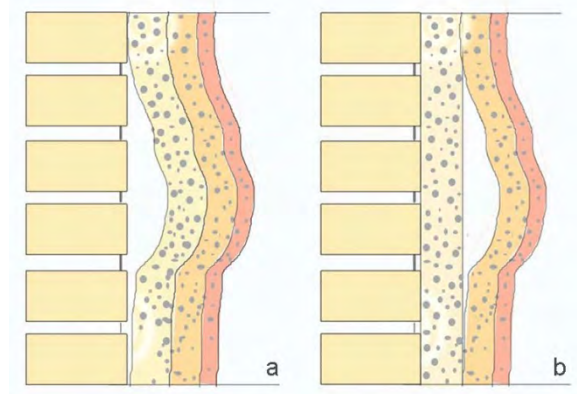


Figure 2. Schematic design of the mortar substrate's detachments. a. detachment between the mortar layers and the masonry, b. detachment in the interface of the mortar layers

The common method for repairing the discontinuities of the mortar layers is by inserting lime-based grouts [6-9]. To test the performance and efficacy of this type of grouts, several studies have been made, including laboratory and field test methods [6-9]. In the present study, three types of lime-based grouts, containing lime-pozzolan (L-P: 1:1 by mass), lime-pozzolan-white cement (L-P-WC: 1:0.8:0.2 by mass) and hydraulic lime NHL 3.5 were tested, by using laboratory and field test methods. The results were comparatively evaluated in order to assess the efficacy of the tested grouts, as well as of the methodologies followed.

Materials and methods

Three compositions of lime-based grouts, containing lime-pozzolan, lime-pozzolan-white cement and hydraulic lime NHL 3.5 were manufactured and tested. The characteristics of the binders used are given in Table 1, while the constituents and proportions of the grout mixtures in Table 2. A polycarboxylate superplasticizer (1% by mass of binders), was added to all mixtures, in order to reduce the water demand, which has a negative effect on the fresh and hardened state properties of the grouts [4. 9. 12].

Table 1. Characteristics of the binding agents used in the grout mixtures

Raw materials	App. Specific density	Pozzolanicity index ASTM C311:77 (MPa)	Particle size analysis (laser granulometry) Grain diameter (μm) of volume fractions (%)	
			d50	d90
Hydrated lime	2.471	-	3.09	10.80
Milos pozzolan	2.403	10.50	4.30	11.60
Natural Hydraulic lime (NHL 3.5)	2.741	-	9.60	128.00
White Cement CEM II/A-LL42.5N	3.100	-	17.00	57.90

Table 2. Constituents and proportions of the grout compositions

Raw materials	Grout series			
	Parts of weight	LP	LPWC	NHL
Hydrated lime		1.0	1.0	-
Natural Pozzolan, fine grained		1.0	0.8	-
White cement (CEM II/A-LL42.5N)		-	0.2	1.0
Natural Hydraulic lime, NHL 3.5		-	-	
Superplasticizer 1% w/w of binders		v	v	v
W/B ratio		1.05	0.98	1.01

For the manufacture of the grout mixtures, a high-speed mixer was used, with increased speed up to 7000 rpms (for a total period of 5 minutes). The binding agents were firstly hand-mixed, while the water quantity was gradually added. Superplasticizer of carboxylic acid basis, was firstly mixed in a limited water quantity (part of the total amount) and was afterwards put in the mixture.

The grout specimens, dimensioned 4x4x16cm, were cured at a chamber of 90% RH and 20°C, up to the testing dates (28, 90 and 180 days). In order to evaluate their performance, their properties at fresh and hardened state were determined. Regarding their fresh state, both laboratory and field tests methods were applied, as following:

Laboratory tests

- Flow time (Figure 3), according to ASTM C939-02 and EN 445: 2007 Marsh cones. The water quantity was adjusted to keep the flow time for the ASTM cone at 10 ± 1 sec, which according to previous research work [4. 9. 12], influences positively both the fresh and hardened state properties of the grouts. Flow time was afterwards tested by using the EN cone, in order to compare the test results, while all measurements were repeated 1h after, to estimate the applicability of grouts with time, or the fluidity loss with time.

- Penetrability (Figure 3), according to the sand-column test (EN 1771:2004). Plexiglas cylinders were filled with natural, siliceous sand (2-4 mm).

- Volume stability, according to ASTM C 940-98A (with reduced grout volume). The grout was put in a graduated glass cylinder (500 mL) and was covered. Twenty four hours later, the volume change and bleeding were calculated. The upper limit of 5%, as defined by the relevant studies [4. 9. 12], was taken into consideration.

Field tests

- Injectability of the grout with the syringe test [13], in order to evaluate the ability of the grout to penetrate into an aggregate system (Figure 3). A limited quantity of grout (20ml) was poured into a vertically held syringe (60 mL), partially filled (20ml) with crushed sand (2-4mm). Therefore the injectability of the grout was classified as easy (E), feasible (F), difficult (D), according to the difficulty of the grout to pass the sand volume by pressing the syringe plunger.

- Drying shrinkage [13] with the use of mortar cups (dimensions 4x8cm), made of a lime-pozzolan mortar with natural sand of 0-4mm (Figure 3). A cylindrical cavity of dimensions 5x3 cm, was made in their center, in which 20ml of the grout was inserted. The cavity was pre-wetted before the grout application. The cracking tendency of the grout was recorded for a period of 12 days and was classified as following [13]:

NS: no drying shrinkage (when no cracks were observed)

MS: medium drying shrinkage (cracks ranging less than 0.5mm)

HS: high drying shrinkage (cracks ranging more than 0.5mm).



Figure 3. Fresh state properties of the grouts. Marsh cones, column sand test, syringe test, drying shrinkage with mortar cups (from the left to the right)

At hardened state, the grout specimens were measured for determining shrinkage deformations (through weight and volume change of specimens cured at a chamber with 60% RH and 20°C temperature), Dynamic Modulus of Elasticity (BS 1881-209:1990), flexural and compressive strength (BS EN1015-11:1999).

Results and discussion

The results of the fresh state properties of the grout mixtures are presented in Tables 3-5, as well as in Figure 4. From the evaluation of the laboratory testing results (Table 3), it was firstly asserted that all grout mixtures presented good performance, in accordance to the limitations provided by former research work [4. 9. 12]. In all cases, the flow time 1h after their manufacture was slightly increased and maintained in the ASTM limit of 10 ± 1 sec, showing that all tested grouts could be applicable throughout working time. A slightest increase was remarked for LP mixture. Regarding the correlation of ASTM and EN cones' values, the latter presented a reduction of around 35%.

Penetrability (Table 3, Figure 4) was in all cases around 3-5 s, while LP mixture presented the lower time (2.93 s). Volume reduction was below the 5% limit for all compositions, as well as bleeding. The lowest values were attained for LPWC composition (vol. reduction: 2.8%, bleeding: 0.5%).

Table 3. Fresh state properties of the grouts

Grout type	Flow time (s)				Penetrability (s) EN1771:2004	Volume stability (%)	
	ASTM C 939		EN 445: 2007			Volume reduction	Bleeding
	0h	1h	0h	1h			
LP	10.95	10.98	6.94	6.86	2.93	4.5	1.5
LPWC	10.27	10.54	6.74	6.80	4.85	2.8	0.5
NHL	10.41	10.62	6.65	6.87	3.34	5.0	3.0

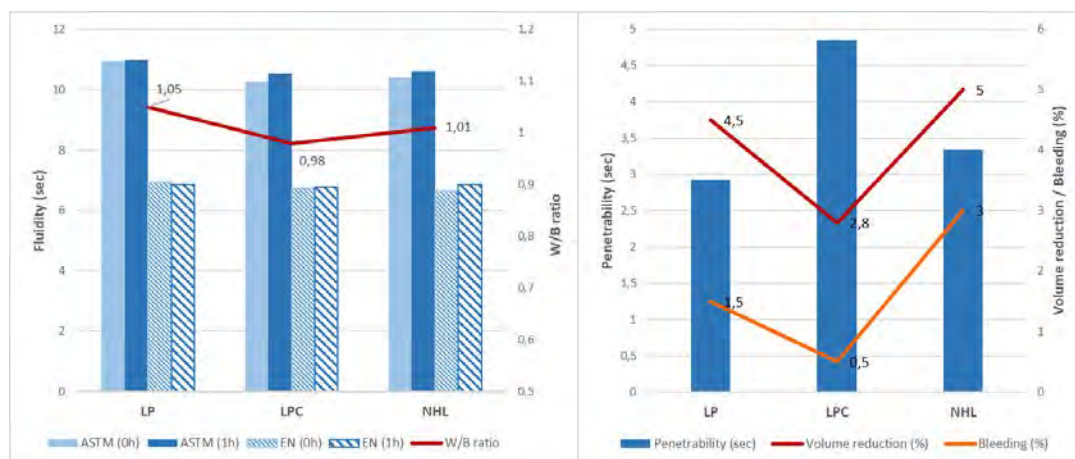


Figure 4. Fresh state properties of the grouts. Fluidity compared to W/B ratio (left), penetrability compared to volume change (right)

Regarding the field testing results, these were generally in accordance with the laboratory ones (Table 4). All grout mixtures, characterized as acceptable according to the sand column laboratory test, presented a good behaviour under the flow syringe test. As expected, LP showed better fluidity and penetrability in comparison to the other two types of grouts. Syringe test results followed in general those of laboratory tests for penetrability (Table 4).

Table 4. Fresh state properties of the grouts (laboratory and on site testing)

Grout type	Grout flow Syringe Test*	Flow time (s)		Penetrability (s)
		0h	1h	
LP	Easy (E)	10.95	10.98	2.93
LPWC	Easy (E), near to (F)	10.27	10.54	4.85
NHL	Feasible (F)	10.41	10.62	3.34

* easy (E): grout flows out of the syringe when pressure is applied; feasible (F): grout does not flow out of the syringe when pressure is applied; difficult (DL): grout does not reach the tip of the syringe when pressure is applied.

** no drying shrinkage (NS): when no cracks were observed; medium drying shrinkage (MS): cracks ranging less than 0.5mm; high drying shrinkage (HS): cracks ranging more than 0.5mm.

Regarding the drying shrinkage test (Table 5, Figure 5) all mixtures showed a low or medium level of shrinkage, during the 12 days of the experiment. Comparing the on site measurement with the shrinkage measurements of 4x4x16cm specimens at laboratory, the following remarks could be asserted:

The volume changes of the grout specimens began to be measured 7 days after their moulding. On the opposite, the field test of the volume change in the mortar cups was measured from the first day of their casting, showing a more realistic behaviour of the inserted grout. Therefore, the qualitative results of the mortar cups' observation for the first 5 days were important and showed that in the case of the LP grout, an evaporation of extra water occurred, without any cracking in the internal or in the perimeter of the grout. In LPWC grouts, a semi-circular crack in the internal and perimeter of the grout appeared, while in NHL3.5 a superficial film was formed retaining the evaporation of water below the film, without any cracking. The visual record of the above remarks are presented in Figure 5.

At the age of 12 days there were measurements of the volume change of the specimens at laboratory and visual estimation of the mortar cups filled with grouts, as indicated in Table 5.

Table 5. Volume changes of the grout mixtures (measurements and visual estimation)

Grout type	Volume change (%) 12d after casting	Characterization according to cracks in the perimeter / internal*
LP	-0.14	MS / NS
LPWC	-0.98	MS / MS
NHL	-1.10	MS / NS

* Characterization of the behavior [13]: NS: no drying shrinkage, MS: medium drying shrinkage (cracks <0.5mm), HS: high drying shrinkage (cracks >0.5mm).

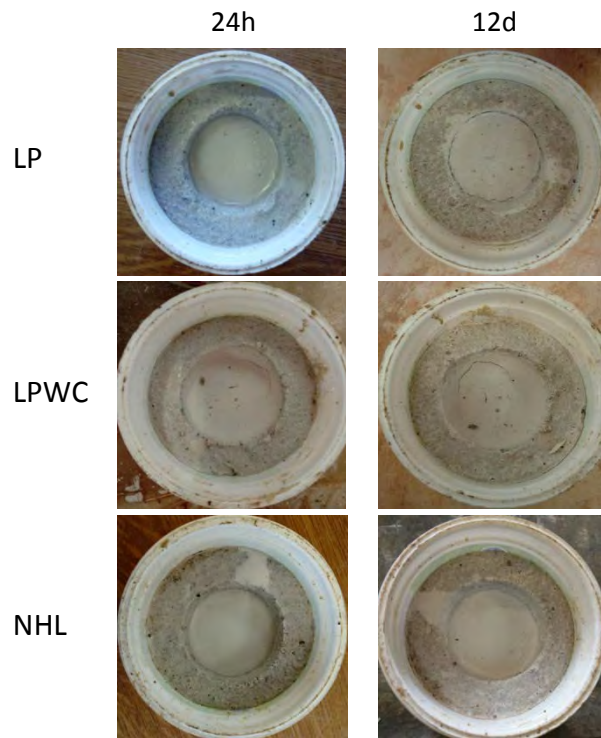


Figure 5 Drying shrinkage of the grout mixtures 24h and 12 days after their manufacture

Regarding the shrinkage tendency of the grout mixtures, recorded through their volume and weight change (Figure 6), it was concluded that all compositions had the same trend in the weight loss diagram, which was finally around 40%. LPWC presented the better performance. In the volume loss diagram (Figure 6) NHL presented significant fluctuations, while LP and LPWC showed the same tendency. Again, LPWC presented the better performance with a final volume loss around 6%.

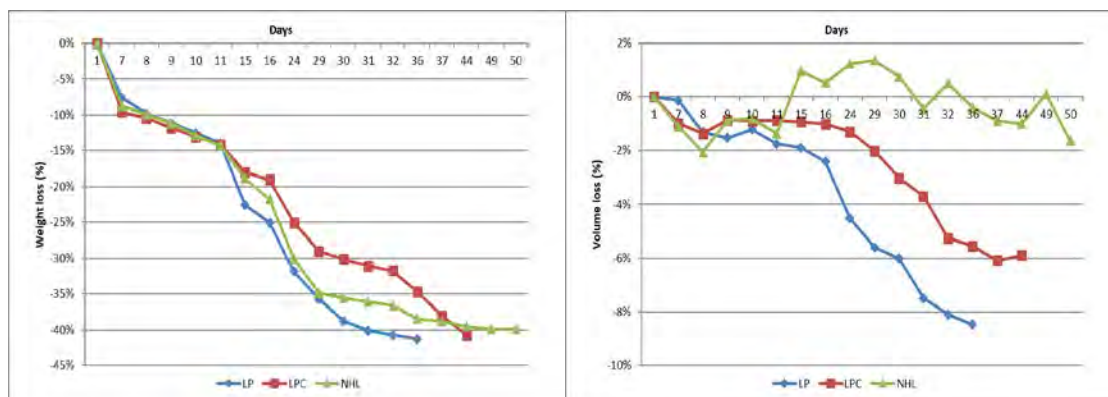


Figure 6. Weight (left) and volume change (right) of the grout compositions

In general, it could be said that the early volume changes were low and in accordance with the observations from the field tests, showing that the field test was indicative of the behavior of the grouts. However, by overviewing the shrinkage measurements of the three series of the grout mixtures exposed to RH 60%, temperature 20°C, it is obvious that the essential volume changes happened after 14-15 days of the specimens' exposition to the low

RH 60% environment and ranged from 1.5 to 8%. The lowest volume change was recorded for the NHL3.5 grout type. Perhaps, longer time observation of the mortar cups with the grouts could be useful for an overall estimation of their behavior.

The mechanical properties of the grout compositions, are presented in Figure 7. From the evaluation of the results, it was firstly concluded that the mechanical characteristics were significantly enhanced from 28 to 180d for all mixtures. The Dynamic Modulus of Elasticity was in the same level for all mixtures at the age of 28d (1.8-2GPa) and 90d (2.5-3GPa), while at 180d it was increased from 3.2 to 3.75 GPa.

Flexural strength (Figure 7) was also at the same level at 28d for all mixtures (~0.6MPa) and was significantly increased at 90 and 180d, in particular for the compositions LPWC and NHL (1-1.2MPa). On the other hand, although compressive strength was almost at the same level for all compositions at 28d (1-1.2MPa) and 90d (2.2-2.3MPa), 180d strength values increased, reaching 3.0MPa.

Generally, it was concluded that the LP composition presented a slight lower strength development rate, but at the age of 180d the strength achievement was 3MPa and obviously contributed more to the long-term strength.

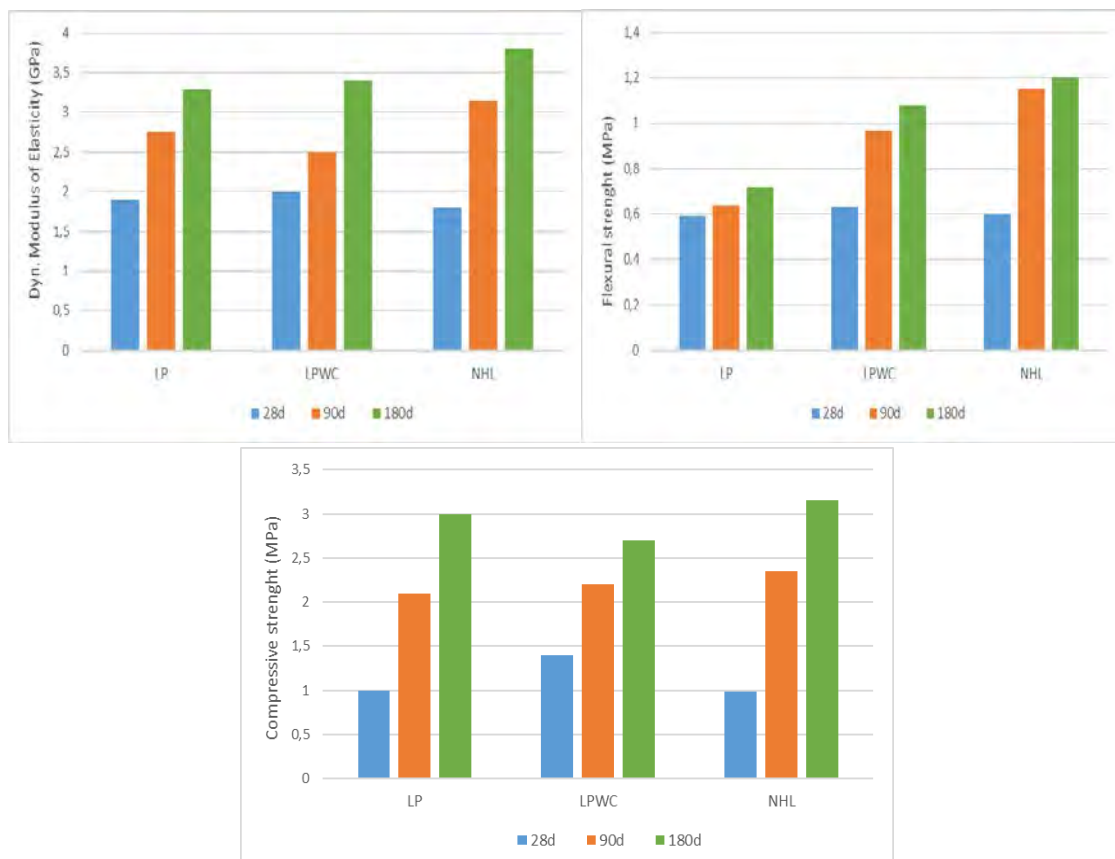


Figure 7. Mechanical properties of the grout compositions at the age of 28, 90 and 180 days

Conclusions

The aim of this research work focused on finding the reliability of both laboratory and field test methods, regarding the fresh state properties of specific lime-based grouts, as well as documenting their performance in terms of fresh and hardened state properties.

From the evaluation of the results, it was firstly concluded that field test results were in accordance with the corresponding laboratory ones, concerning the properties of the grouts in fresh state. Fluidity, measured both with the ASTM and EN Marsh cones, as well as through the syringe test, provided similar results. A correlation of the measured values by using ASTM and EN Marsh cones was given. All grout mixtures, had a good performance during the tests, whereas LP composition (lime:pozzolan) exhibited the utmost maintenance of fluidity throughout time. Penetrability measured with the sand column and the syringe test, also provided relevant results. On the other hand, volume stability measured by the ASTM standard showed acceptable values for all grout mixtures, while the best behaviour was attributed to LPWC grout mixtures.

Regarding the hardened state properties of the grouts, tested in a wide period from 28 to 180 days, a significant increase of the mechanical properties was shown at the age of 180 days. The highest final values were attained for NHL3.5 and LP mixtures, but the early strength was benefited from white cement addition and NHL binder.

Concluding, it may be said that the performance of lime-based grouts at early age could be evaluated through laboratory and field test methods, which provide respectively quantitative and qualitative data, very useful for their applicability. For long-term efficiency of grouts further tests should be adopted, concerning measurements at laboratory and on site scale.

References

1. Binda L. Modena C. Baronio G. Gelmi A. (1994) Experimental qualification of Injection Admixtures used for Repair and Strengthening of Stone Masonry Walls. In: Proc. of the 10th International Brick and Block Masonry Conference. Calgary. 539-548
2. Vintzileou E. Miltiadou-Fezans A. (2008) Mechanical properties of three-leaf stone masonry grouted with ternary or hydraulic lime-based grouts. *Engineering Structures* 30:2265-2276
3. Bras A. Henriques F.M.A. (2012) Natural hydraulic lime based grouts - The selection of grout injection parameters for masonry consolidation. *Construction and Building Materials* 26:135-144
4. Papayianni I. Pachta V. (2015) Experimental study on the performance of lime-based grouts used in consolidating Historic Masonries. *Mat and str* 48:2111-2121

5. Ferragni D. Forti M. Malliet J. Teutonico JM. Torraca G. (1985) In situ consolidation of wall and floor mosaics by means of injection grouting techniques. *Conservation in Situ Mosaics*, ICCROM, 3:83-101
6. Bicer-Simsir B. Griffin I. Palazzo-Bertholon B. Rainer L. (2010) Lime-based injection grouts for the conservation of architectural surfaces. *Stud in Cons* 55(1):3-17
7. Azeiteiro L.C. Velosa A. Paiva H. Mantas P.Q. Ferreira V.M. Veiga R. (2014) Development of grouts for consolidation of old renders. *Constr and Build Mat* 50:352–360
8. Padovnik A. Piqué F. Jornet A. Bokan-Bosiljkov V. (2016) Injection Grouts for the Re-Attachment of Architectural Surfaces with Historic Value - Measures to Improve the Properties of Hydrated Lime Grouts in Slovenia. *Int J of Arch Her* 10(8):993-1007
9. Pachta V. Papayianni I. (2017) Influence of resins on the properties of lime-pozzolan grouts for surface consolidation, In: Papayianni I, Stefanidou M, Pachta V (Eds.) *Proc. of the 4th Historic Mortars Conference, HMC2016, Santorini, Greece*, ISBN 978-960-99922-3-7, pp. 588-597
10. Calicchia P. Bosco Cannelli G. (2005) Detecting and mapping detachments in mural paintings by non-invasive acoustic technique: measurements in antique sites in Rome and Florence. *Journal of Cultural Heritage* 6:115-124
11. Petkovic J. Huinink HP. Pel L. Kopinga K. van Hees RPJ. (2010) Moisture and salt transport in three-layer plaster/substrate systems. *Construction and Building Materials* 24:118–127
12. Papayianni I. Stefanidou M. Pachta V. (2013) Grouts for injection of historical masonries: Influence of the binding system and other additions on the properties of the matrix. In: Valek J Hughes J Groot C (Eds.) *Historic Mortars: Characterization, Assessment and Repair*, RILEM Bookseries, Springer, pp. 383-392
13. Simsir B.B. Rainer L. (2013) Evaluation of lime-based hydraulic injection grouts for the conservation of architectural surfaces. *A manual of laboratory and field test Methods* p. 69-71, 83-86. The Getty Conservation Institute.

Evaluation of the fresh state properties of lime-based grouts through inter-laboratory comparative testing

Vasiliki Pachta¹, Davide Gulotta², Jan Valek³, Ioanna Papayianni¹

(1) Laboratory of Building Materials, School of Civil Engineering, Aristotle University of Thessaloniki, vpachta@civil.auth.gr, papayian@civil.auth.gr

(2) Dept. of Chemistry, Materials and Chemical Engineering "Giulio Natta", Politecnico di Milano and Getty Conservation Institute, Science Department, Los Angeles, dgulotta@getty.edu

(3) Institute of Theoretical and Applied Mechanics, Czech Academy of Sciences, valek@itam.cas.cz

Abstract

The need for evaluating the efficacy of the fresh state properties testing of lime-based grouts emerged during the activities of RILEM TC SGM and continued in the frame of RILEM TC 277 LHS. To this direction, a collaboration of three laboratories was achieved (AUTH, POLIMI, ITAM) to perform a protocol of testing grouts. The first question confronted was the influence of the binding system on the fresh state properties. Six types of grout mixtures were prepared (repeated 2 to 8 times) and tested. The binders used were Ledan TB1, PLM-A, NHL 3.5, finely milled NHL 3.5 quicklime, Roman cement : air lime (4:6) + 0.3% citric acid and lime : pozzolan (1:1) + 1% w.w. superplasticizer. The fresh state properties measured were fluidity (ASTM C939-02, EN 445: 2007), penetrability (EN 1771:2004) and volume stability (ASTM C 940-98A). The type of mixer (Hobart or high speed), the time of mixing, as well as the grout and the room temperature were recorded. From the evaluation of the results, it was concluded that different types of grout performed differently in mixing and testing procedures, while the mixing time and the room temperature also affected the grouts' properties.

Introduction

The consolidation of historic structures with grouts is a widely used restoration technique either for strengthening the masonry [1-5], or for improving the cohesion of the building materials themselves (mortar to stone or brick, successive mortar layers) [6-8]. In many past cases, incompatible repair materials were used without preliminary analysis and evaluation of the existing building materials' properties. This often resulted in secondary problems that aggravated the preservation state of the structures [5. 9]. Gradually, research started focusing on more compatible solutions [2-5]. Such research is still in progress, since no specific regulations regarding the control of the performance and effectiveness of such kind of grouts exist.

On the other hand, there is a variety of testing methodologies regarding the fresh state properties of lime-based grouts, which are either focusing on specific standards, or have been developed by Researchers' experience [3-8]. In most cases, researchers proceed to

adaptations of the existing standards, since these mainly focus on cement-based grouts [3-9].

The need for evaluating the suitability of the laboratory testing methods concerning the fresh state properties of lime-based grouts, was identified during the activities of the RILEM Technical Committee SGM 'Specifications for non-structural grouting of historic architectural surfaces'. To this direction, a collaboration of three laboratories was achieved (Aristotle University of Thessaloniki, AUTH; Politecnico di Milano, POLIMI; Institute of Theoretical and Applied Mechanics, ITAM), in order to perform a round robin testing protocol of grouts. The experimental study is still in progress in the framework of the current RILEM Technical Committee 277 LHS 'Specifications for testing and evaluation of lime-based repair materials for historic Structures TC'.

The aim of the study was to identify the parameters influencing the fresh state properties of different types of grouts and to preliminary evaluate the reliability and applicability of the methods proposed for testing them. Six types of grout mixtures were manufactured, including both custom-made and commercial ready-mixed grouts. Different mixing procedures were applied, while the properties measured concerned fluidity (according to ASTM C939-02 and EN 445: 2007 flow cones), penetrability (EN 1771:2004) and volume stability (ASTM C 940-98A).

Materials and methods

As it has been described, the experimental study concerned a comparative testing of the fresh properties of lime-based grouts, implemented in the three participating Laboratories (AUTH, POLIMI, ITAM). Six types of mixtures were prepared, concerning both commercial ready-mixed and custom-made grouts usually applied for the consolidation of historic masonries. These referred to Ledan TB1 (supplied by Tecno Edile Toscana), PLM-A (supplied by CTS), NHL 3.5, a lime-pozzolan grout (proportion w/w 1:1) with the addition of 1% w/w superplasticizer, finely milled NHL 3.5 quicklime with ~40 wt% of unslakable residue and Roman cement (Prompt by Vicat) : air lime (proportion w/w 42.2:57.8) + 0.3‰ citric acid. All grout mixtures were reproduced 2 to 8 times in order to assess the repeatability of the measurements. In all cases, the room, as well as the grout temperature after mixing were recorded. In Table 1 the characteristics of the binders used in the custom-made grouts are presented.

Two different mixing procedures were applied, concerning the use of a high-speed mixer (up to 8000 rpms) and a three speed Hobart mixer (Figure1). In the first case (implemented by AUTH), the grouts were firstly hand mixed with an adequate quantity of water for a period of 2 minutes, in order to become homogenized. Then, the high-speed mixer was used for a period of 4 to 10 min, with a gradual increase of the velocity. Water was gradually added, in order to keep the flow time for ASTM C939-02 flow cone at 10±1 sec. According to previous

research work [5, 9], this limitation influences positively both the fresh and hardened state properties of the grouts.

Table 1. Characteristics of the binding agents used in the grout mixtures

Raw materials	App. Specific density	Pozzolanicity index ASTMC311:77 (MPa)	Particle size analysis (laser granulometry) Grain diameter (μm) of volume fractions (%)	
			d50	d90
Air lime	2.471	-	3.09	10.80
Milos pozzolan	2.403	10.50	4.30	11.60
Natural Hydraulic lime (NHL 3.5)	2.741	-	9.60	128.00

In the second case (implemented by POLIMI and ITAM), a premeasured amount of water was put into the Hobart mixer and the commercial ready-mixed grouts (TB1 and PLM-A) were gradually added within 1 minute while mixing at speed level 1 (140 rpm). The speed was then increased to level 2 (285 rpm) for a period of 5 to 6 minutes.

Two additional grouts were implemented by ITAM. Roman cement: air lime and citric acid were premixed dry in a mixing bowl and a premeasured amount of water was added during 30s while mixing. The mixing then continued at the speed level 1 (125 rpm) for a period of 4 minutes. Experimentally, also a grout made of finely milled unslaked NHL 3.5 was prepared. The binder was mixed with 3/5 of earlier predetermined total amount of water needed for slaking and achieving the right consistency. After the first minute, the rest of water (2/5) was added gradually while continuously mixing at the speed lever 1 (125 rpm) for another 10 minutes.



Figure 1. Mixing apparatus of grouts. High-speed mixer (left), Hobart mixer (right).

Regarding the fresh state properties of the grouts, the following properties were measured:

- Flow time, according to ASTM C939-02 and EN 445: 2007 Flow cones (Figure 2). Measurements were performed with the standard grout quantity and with a reduced grout volume adjusted to fill a final volume of 500 ml. Test were conducted immediately after mixing and then repeated 1 hour after the grout manufacture, in order to estimate the loss

of fluidity and applicability of grouts in practice. In the case of the Hobart mixer, the grout mixtures were passed through a 1mm sieve before testing. Orifice diameter was 10 mm except some tests carried out by ITAM where 8 mm orifice was also used (Table 6).

- Penetrability, according to the sand-column test (EN 1771:2004) (Figure 2). Plexiglas cylinders (height: 39 cm, diameter: 2.22 cm), filled with natural, siliceous sand of granulometry 2-4 mm were used. Such gradation simulates voids and discontinuities of approximate width 0.3-0.6 mm, as has been pointed out at literature [3, 5, 6].

- Volume stability, according to ASTM C 940-98A (adjusted to a reduced grout volume of 500 ml) (Figure 2). The grout was put in a graduated glass cylinder and covered to prevent evaporation. Twenty-four hours later, the volume of the grout as well as of the bleed water was measured, and the volume change (expansion or reduction) and bleeding were calculated (according to the equations mentioned in the Standard method). The upper limit of 5%, as defined by the relevant studies [5, 9], was taken into consideration.



Figure 2. Fresh state properties testing. ASTM and EN flow cones (left), sand column test (middle), volume stability test (right).

In Table 2, the grout mixtures prepared by each laboratory, as well as the testing techniques followed, are comparatively presented.

Table 2. Grout mixtures prepared and tested by each laboratory

Grout mixtures	Mixing		Flow time			Volume stability (reduced)	Penetrability
	High ²	Hobart	ASTM	EN	EN (reduced)		
NHL 3.5	AUTH	-	AUTH	AUTH	-	AUTH	AUTH
LP ¹	AUTH	-	AUTH	AUTH	-	AUTH	AUTH
Ledan TB1	AUTH	POLIMI ITAM	AUTH	AUTH POLIMI ITAM	POLIMI ITAM	AUTH POLIMI ITAM	AUTH ITAM
PLM-A	-	POLIMI ITAM	-	-	POLIMI ITAM	POLIMI ITAM	ITAM
RCL	-	ITAM	-	ITAM	-	ITAM	ITAM
NHLQ	-	ITAM	-	ITAM	-	ITAM	ITAM

¹ Lime:Pozzolan (1:1) + superplasticizer 1%ww

² High speed mixer

Results and discussion

In order to facilitate the comparative evaluation of the testing outcomes, the experimental results of each laboratory are presented in different tables. Therefore, in Tables 3-4 the test results of AUTH are shown, in Tables 5-6 the results of POLIMI and in Tables 7-8 the results of ITAM. In the tables, the coding of the grouts is referred, in order to better correspond the individual characteristics of each mixture.

In the preliminary phase of testing, not all standard testing were performed by all laboratories (except for fluidity) (Table 2). The results are discussed accordingly. Moreover, the lack of information about the composition and fineness of the commercial grouts (LEDAN TB1, PLM-A) made the comparison more difficult.

Table 3. Constituents and mixing procedure of the grouts (tested by AUTH)

Code No.	Temperature (°C)		Mixing apparatus	Mixing time (min)	Binding Agents	W/B ratio
	Lab	Mixture				
1A	19.4	19.0	High speed mixer (8000rpm)	3.5 (hand) - 10 (mixer)	NHL 3.5	1.18
1B	20.5	19.6		2 (hand) - 4 (mixer)		1.03
1C	20.7	19.8		2 (hand) - 7 (mixer)		1.08
1D	20.0	19.6		2 (hand) - 5 (mixer)		1.05
1E	20.3	19.6		2 (hand) - 5 (mixer)		1.05
1F	20.5	19.6		2 (hand) - 5 (mixer)		1.05
1G	20.9	19.7		2 (hand) - 5 (mixer)		1.08
1H	20.9	19.7		2 (hand) - 5 (mixer)		1.05
2A	24.0	28.0	High speed mixer (8000rpm)	2 (hand) - 7 (mixer)	Ledan TB1	1.75
2A				2 (hand) - 6 (mixer)		1.50
2A				2 (hand) - 5 (mixer)		1.25
2A				2 (hand) - 4 (mixer)		1.00
2B	24.5	28		2 (hand) - 7 (mixer)		1.75
2B				2 (hand) - 6 (mixer)		1.50
2B				2 (hand) - 5 (mixer)		1.25
2B				2 (hand) - 4 (mixer)		1.00
3A	21.7	20.4	High speed mixer (8000rpm)	2 (hand) - 8 (mixer)	Lime:Pozzolan 1:1 superplasticizer 1%ww	1.33
3B	21.5	20.3		2 (hand) - 5 (mixer)		1.45
3C	21.8	20.4		2 (hand) - 5 (mixer)		1.45
3D	21.6	20.2		2 (hand) - 5 (mixer)		1.45

From the evaluation of the results, it was observed that all test methods applied were reliable (Table 4). However commercial grouts (such as Ledan TB1) probably require adjustments of the mixing procedure, which affect the rheology and volume changes of the mixtures.

Table 4. Fresh state properties of the grouts mixtures (tested by AUTH)

Code No.	Flow time (s)				Penetrability (s) EN1771:2004	Volume stability (24h %) (reduced volume)		
	ASTM C 39		EN 445: 007			Volume reduction	Bleeding	Expansion
	0h	1h	0h	1h				
1A	10.10	10.97	6.34	6.45	3.20	2.00	1.60	0.00
1B	10.69	11.75	6.74	7.07	3.23	2.00	0.60	0.00
1C	10.50	10.78	6.77	7.08	4.12	2.00	0.70	0.00
1D	10.44	10.75	6.77	6.95	4.13	1.00	1.20	0.00
1E	10.59	11.72	6.98	7.14	5.03	1.00	1.00	0.00
1F	10.72	11.29	6.60	6.63	4.22	1.00	0.80	0.00
1G	10.70	11.16	6.60	7.09	4.12	2.00	1.00	0.00
1H	10.80	10.90	6.73	6.90	4.15	2.00	1.00	0.00
STDEV	0.22	0.40	0.19	0.25	0.59	0.52	0.31	0.00
2A	12.41	17.40	8.27	10.50	2.38	0.00	0.00	3.30
2A	13.50		8.31					
2A	15.00		9.47					
2A	18.50		13.14					
2B	11.38	17.84	7.05	10.87	3.50	0.00	0.00	3.30
2B	14.50		8.98					
2B	16.44		10.15					
2B	18.09		13.50					
STDEV	0.73	0.31	0.86	0.26	0.79	0.00	0.00	0.00
3A	10.78	11.72	6.84	7.33	4.22	0.20	0.20	0.00
3B	10.37	11.36	6.50	6.90	2.98	1.40	1.00	0.00
3C	10.37	11.78	6.41	7.01	2.88	2.00	1.80	0.00
3D	10.44	11.60	6.41	7.07	2.78	0.20	1.00	0.00
STDEV	0.20	0.19	0.20	0.18	0.67	0.90	0.65	0.00

Table 5. Constituents and mixing procedure of the grouts (tested by POLIMI)

Code No.	Grout type	Temperature (°C)		Mixing apparatus	Mixing time (min)	Mixture quantity	Grout (g)	Water (g)	W/B ratio	Grout mix volume (cm ³)
		Room	Mixture							
2C	LEDAN TB1	20±2°C	21±0.4	Hobart mixer	1 + 6	Standard	1350	1080	0.8	1787
2D			24.5±0.7		1 + 6	Reduced	675	540	0.8	893
4A	PLM-A		24.5±0.7		1 + 6	Reduced	900	720	0.8	1013

Table 6. Fresh state properties of the grouts mixtures (tested by POLIMI)

Code No.	Grout type	Mixture quantity	Flow time (s) EN 445: 2007 (10 mm outlet)	Volume stability (24h %)	
				Bleeding	Expansion
2C	LEDAN TB1	Standard	114.0	0	0
2D		Reduced	42.7±0.6	0	0
4A	PLM-A	Reduced	37.6±0.8	0	0

Table 7. Constituents and mixing procedure of the grouts (tested by ITAM) (n.r. not relevant)

Code No.	Grout type	Temperature (°C) RH (%)		Mixing apparatus /max. speed	Mixing time (min)	Mixture quantity	Grout (g)	Water (g)	W/B ratio	Grout mix volume (cm ³)
		Room	Mixture							
2E	Ledan TB1	22.7 45%	20.3 20.2	Hobart mixer 285 RPM	1+6	Reduced	900	720	0.8	1200
2F	Ledan TB1	24.4 38%	21.0			Standard	1350	1080	0.8	1787
2G	Ledan TB1		21.1			Reduced	675	540	0.8	893
4B	PLM-A	21.7	20.2	Hobart mixer 285 RPM	1+5	Reduced	900	720	0.8	1013
4B	PLM-A	48%	20.4			Reduced	900	720	0.8	1013
5A	RCL	22.7 45%	22.3	Hobart mixer 125 RPM	0.5+4	Standard	1015	1200	1.2	1550
5A	RCL									
6A	NHLQ	22.7	46.5	Hobart mixer 125 RPM	1+10	Standard	600	1300	n.r.	1300
6A	NHLQ	45%	48.2			Standard				
6B	NHLQ	24.4	54.7			Standard	900	1730		1900
6B	NHLQ	38%	48.6			Standard	600	1300		1300

Table 8. Fresh state properties of the grouts mixtures (tested by ITAM) (n.d. not determined)

Code No.	Grout type	Mixture quantity	Flow time (s) EN 445: 2007		Volume stability (24h%)		Penetrability (s) EN1771:2004
			8 mm	10 mm	Bleeding	Expansion	
2E	Ledan TB1	Reduced (1 L)	1510	n.d.	0	0	n.d.
			753	n.d.	0	0	189
2F	Ledan TB1	Standard (1 L)	n.d.	148	0	0	282
2G	Ledan TB1	Reduced (500mL)	n.d.	93	0	0	334
4B	PLM-A	Reduced (400 mL)	n.d.	50	0.25	0	n.d.
4B	PLM-A	Reduced (400 mL)	n.d.	49	0.25	0	n.d.
5A	RCL	Standard (1 L)	12.9	n.d.	0	0	n.d.
5A	RCL	Standard (1 L)	13.4	n.d.	0	0	21 stopped at 200 mm
6A	NHLQ	Standard (1 L)	31.5	n.d.	0	0	n.d.
6A	NHLQ	Standard (1 L)	24.3	n.d.	0	0	38
6B	NHLQ	Standard (1 L)	n.d.	55	0	0	17
6B	NHLQ	Standard (1 L)	n.d.	14	0	0	45

Generally, it was observed that different types of grout, perform better under different mixing procedures. Custom-made mixtures, such as lime-pozzolan and NHL 3.5 required high speed mixing (up to 8000rpm), in order to become homogenized and avoid segregation (Table 3). The measurements were repeated for eight batches of the same grout mixture for NHL3.5 and Ledan TB1 and for four batches for the same lime-pozzolan grout mixture. The

proposed mixing time was 2min of hand mixing and 5min of gradual rpm increase. The use of low speed mixing for the binders composed of fine particles such were the RCL (5A) and NHLQ (6A, 6B) grouts (Table 7), showed higher values of flow time, compared with the aforementioned custom made grouts, but sufficient for some case studies. It is obvious that the upper limits of the measured values should be well defined in the round robin protocol.

On the other hand, commercial grouts (i.e. Ledan TB1) seemed to performed better at low mixing speed that could be achieved by the Hobart mixer and commonly 1+6min mixing time. When they were mixed with high speed mixer, extreme foaming was observed (i.e. Ledan) (Figure 3), which led to extreme water evaporation (W/B increase) and difficulty in applying the flow cone test. The quantity of grout also influenced the mixing results, as significant foaming was observed also during Hobart mixing of Ledan TB1 when standard amounts were employed (Figure 3). Mixing a reduced quantity of the grout following the same mixing procedure provided a more homogenous and foam-free result compared to the full amount. It was noticed that the technical guidelines of the relevant products do not give much details regarding the type and time of mixing, referring only to hand mixing.



Figure 3. Extreme foaming of ready-mixed grouts (Ledan TB1) in the high speed mixer (left and middle image) and after Hobart mixing of standard grout quantity (image on the right).

Regarding the fluidity testing through the flow cones and since this property is directly linked to the W/B ratio, flow time limits should be further defined in the round robin protocol and be correlated with the grout type (structural, surface), as well as the characteristics of each case study (i.e. voids size).

The results concerning the performance of different grouts for which high speed mixer was used and long-time mixing (7-10min) are presented in Tables 3-4. The W/B ratio was above 1.0 for all mixtures and the low standard deviation (SDEV<1) of the measurements performed by AUTH (Table 4) indicated adequate reliability of the testing method followed. The lower coefficient of variation was presented by the NHL 3.5 and lime-pozzolan mixtures (STDEV: 0.20-0.22).

Concerning the ability of grouts to maintain their fluidity 1h after their manufacture (Table 4), it was observed that custom-made grouts presented a better performance with an increase of flow time around 3-8%, while commercial ones (Ledan) showed an increase

around 40%. This parameter is closely related to the performability of grouts during application and should be further taken into account [5]. In Figure 4 a correspondence of the values of fluidity measured by ASTM C939 and EN 445:2007 for NHL 3.5 and lime-pozzolan is presented.

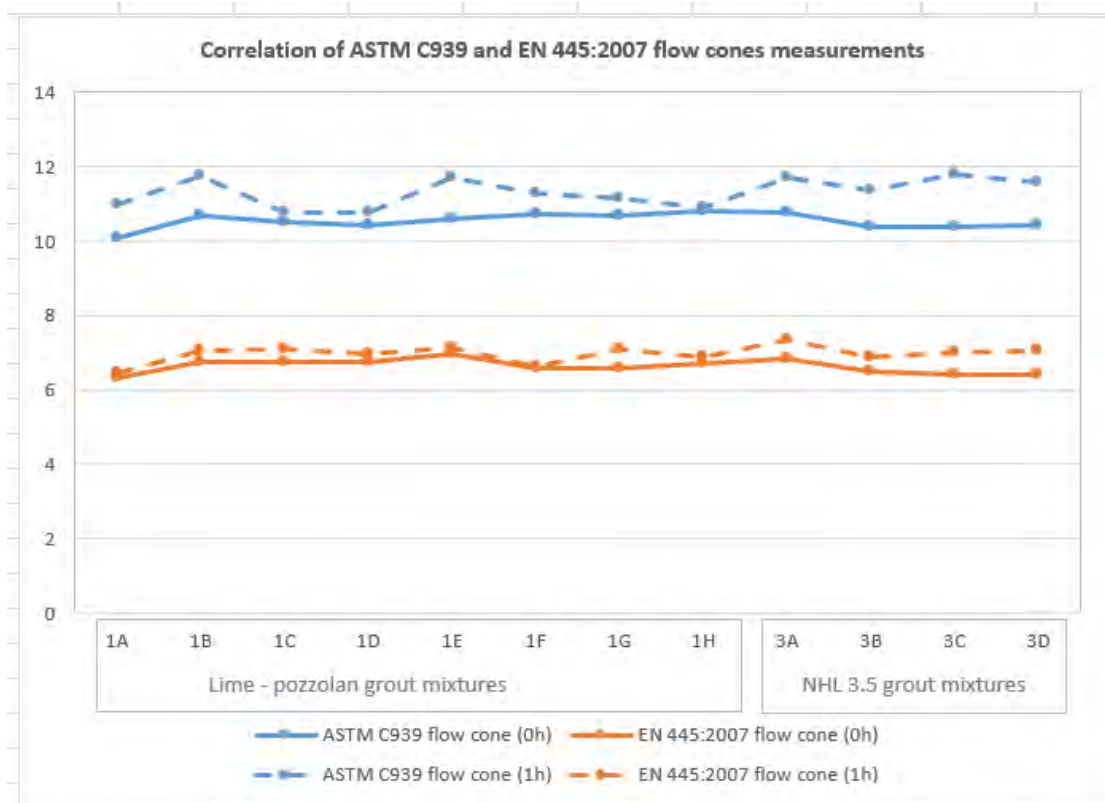


Figure 4. Correlation of ASTM C939 and EN 445:2007 flow cones measurements in the lime-pozzolan and NHL 3.5 grout mixtures.

The fluidity results of LEDAN TB1 prepared with Hobart mixer are not consistent between different laboratories (Table 4, 6, 8). In Figure 5, a correlation between the flow time and the W/B ratio of the grout mixtures prepared by the three Laboratories is presented, indicating the wide range of results.

Considering the results of Tables 5-8, where the commercial Ledan TB1 and PLM-A grouts were mixed with the Hobart mixer (low speed) following the indications of the suppliers, the W/B ratio was low (0.8). Fluidity was measured by EN 445 flow cone, by using standard quantity and reduced one for economy of the material. It seemed that the reduced quantity did not influence the measured time of the flow immediately after mixing. However, compared with the time of flow of the Ledan TB1 grout manufactured with the high-speed mixer (Table 4) the time was much higher, due to the significantly lower W/B ratio (Figure 5). In particular, POLIMI results (Table 6) generally showed a slightly higher fluidity of the grout with respect to the ITAM ones (Table 8) using both standard and reduced grouts quantities. The same applies to the fluidity results of the commercial PLM-A grout. The sensitivity of the flow test to the speed of mixing, amount and diameter of outlet orifice is demonstrated by values obtained on the Ledan TB1 2E and 2F mixtures at ITAM's laboratory. The select orifice

of 8 mm was not adequate to the fluidity of the grout made of Ledan TB1 in the first set of tests. The flow values obtained with 10 mm orifice were comparable between ITAM and POLIMI with respect that the speed of mixing was slighter lower at ITAM (125rpm v. 140rpm).

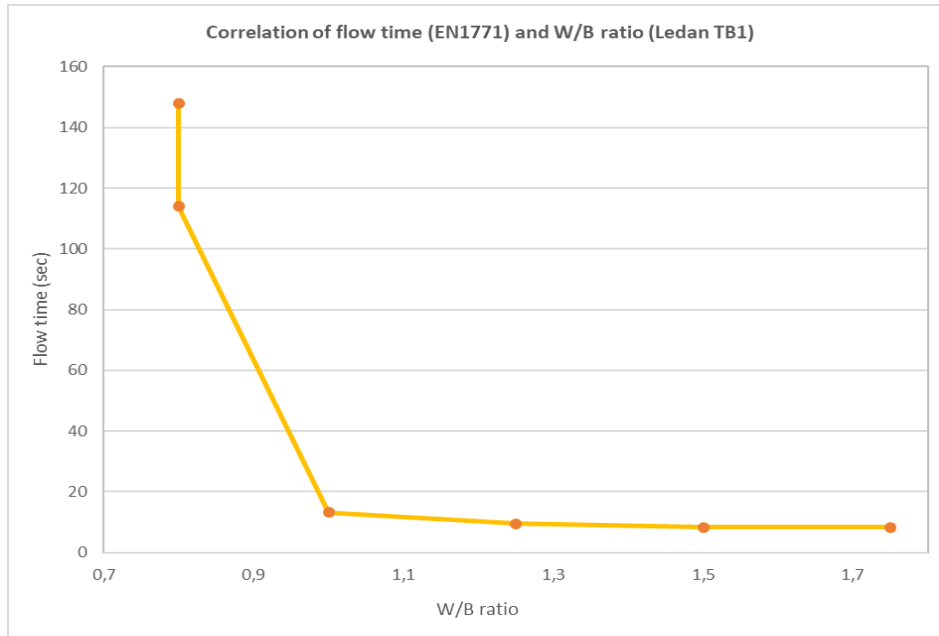


Figure 5. Correlation of flow time according to EN 445:2007 and W/B ratio of Ledan TB1 mixtures, prepared by the three Laboratories.

Regarding penetrability, the testing procedure according to EN 1771:2004, seemed to be adequate and reliable for all grout mixtures tested at AUTH. For maintaining flow time at the level of 9-11 s (ASTM C939-02), the corresponding penetration time values ranged in all compositions from 2.5 to 5 s (Table 4). This is considered to be an acceptable time according to former research work [5, 9]. Among the different types of grouts penetrability seemed to be slightly better in the case of lime-pozzolan (perhaps because of the higher fineness), while for the other mixtures it ranged from 3 to 4 seconds (Table 4). However, the selected type and granulometry of the aggregates in the sand column is the main parameter, in order to define the performance of grouts and has to be well defined in the round robin protocol.

Testing volume stability according to ASTM C 940-98A, in the reduced volume of 500 mL (the Standard proposes 1000 mL) seems to be adequate reliable for all grout mixtures. According to ASTM C940-98A volume change refers only to expansion and bleeding. Through the experimental process, it was observed that Ledan TB1 grouts presented expansion after 24 hours when prepared with a high-speed mixer, while NHL 3.5 and lime+pozzolan presented reduction of volume (Table 4). Therefore, the volume stability definition should comprise both expansion and also reduction.

As for the commercial grouts prepared with Hobart mixers, the volume stability results of ITAM and POLIMI laboratory were comparable. LEDAN TB1 showed no volume change in all test. PLM-A was observed to be stable after POLIMI testing, while a slight bleeding (+0.25%)

was measured by ITAM. Both grouts made of unslaked lime NHL3.5 and roman cement showed a very good volume stability, however they also both started to set much earlier than the other ones.

Considering the work done up to now by the three involved laboratories, only for one type of grout, that of Ledan TB1 measurements were made for fluidity (by the three Labs), volume stability (by the two Labs) and penetrability (by two Labs). The fluidity of the above mentioned grout with W/B ratio 0.8 and low speed mixing was much lower (flow time more than double) of that of the high speed mixing). However, the mixing with high speed mixer seemed to be problematic for Ledan TB1, since extreme foaming was created. The lack of analytical technical description of the characteristics of this commercial material made impossible an explanation of this behavior.

It is therefore concluded, that there are still several issues that have to be experimentally documented, regarding the fresh state properties testing of lime-based grouts. The correlation (ratio) between ASTM C939-02 and EN 445: 2007 flow cones results could be found, through an adequate number of experimental tests. It is significant to define limitations of the flow time according to the grout use (consolidation of masonry elements, or architectural surfaces). In addition, the correlation among different types of sand (origin, granulometry) used in the sand column test is of great importance. Finally, the influence of other parameters (i.e. differences in room temperature) on the fresh state properties of grouts is of interest.

Conclusions

The aim of the experimental study was to identify the reliability and applicability of the test methods concerning the fresh state properties of different type lime-based grouts. Through the evaluation of the inter-laboratory testing results it was observed that the applied methods were generally reliable for measuring the grouts' performance. The tests yielded the best results when comparing the rheological properties of grouts of the same composition and prepared under the same conditions (the same lab, equipment, ambient temperature, and operator). The grouts' performance was significantly affected by the mixing procedure and also by the testing procedure.

Specifically, the custom-made grouts (i.e. lime+pozzolan, NHL 3.5) performed better at high speed mixing (up to 8000rps), while commercial ones (i.e. Ledan TB1) required low mixing speed (Hobart mixer) and time. In all cases, fluidity of low-speed mixed commercial grouts provided results of low comparability between different laboratories, whereas the results of the volume change were more consistent. Penetration time measured according to EN 1771:2004, was reliable for all grout mixtures determined within one laboratory (AUTH). The type and granulometry of the aggregates in the sand column has to be defined. Testing volume stability according to ASTM C 940-98A however with the reduced quantity of 500ml, was reliable for all grout types. However, the terminology should be clarified in the

standards to incorporate also the volume reduction. It was noted that other parameters such as the mixing time and the room temperature differences affected the performance of grouts.

Considering that grouts are generally prepared on site in lower amount than those required by the standard testing, the reliability of reduced quantity testing should be further experimentally examined. Such approach can be more suitable for real site condition and, ultimately, more sustainable. The adjustment of selected testing procedures to the field conditions are one of the objective of the ongoing round robin activity of the RILEM TC 277 LHS.

Technical data sheets of commercial grouts, which are extensively used on site, generally do not provide accurate instructions about the preparation and mixing procedures. The results of the inter-laboratory testing showed that mixing procedures, testing conditions and, possibly, the role of the operator may affect the measurements of some fresh state properties. It is therefore necessary to define detailed specification and upper limits for the preparation of the grouts and testing, to obtain more robust and repeatable results (a detailed protocol of round robin testing). The testing of the fresh state properties of lime-based grouts is a process that still needs further consideration and research, since different types of grouts require different methodological approach.

References

1. Binda L. Modena C. Baronio G. Gelmi A. (1994) Experimental qualification of Injection Admixtures used for Repair and Strengthening of Stone Masonry Walls. In: Proc. of the 10th International Brick and Block Masonry Conference. Calgary. 539-548
2. Vintzileou E. Miltiadou-Fezans A. (2008) Mechanical properties of three-leaf stone masonry grouted with ternary or hydraulic lime-based grouts. *Engineering Structures* 30:2265-2276
3. Bras A. Henriques F.M.A. (2012) Natural hydraulic lime based grouts - The selection of grout injection parameters for masonry consolidation. *Construction and Building Materials* 26:135-144
4. Van Gemert D. Ignoul, S. Brosens K. Toumbakari E.E. (2015) Consolidation and strengthening of historical masonry by means of mineral grouts: Grout Development. *Int Journal for Restoration of Buildings and Monuments* 21(1): 29-45
5. Papayianni I. Pachta V. (2015) Experimental study on the performance of lime-based grouts used in consolidating Historic Masonries. *Mat and str* 48:2111-2121
6. Bicer-Simsir B. Griffin I. Palazzo-Bertholon B. Rainer L. (2010) Lime-based injection grouts for the conservation of architectural surfaces. *Stud in Cons* 55(1):3-17

7. Azeiteiro L.C. Velosa A. Paiva H. Mantas P.Q. Ferreira V.M. Veiga R. (2014) Development of grouts for consolidation of old renders. *Constr and Build Mat* 50:352–360
8. Padovnik A. Piqué F. Jornet A. Bokan-Bosiljkov V. (2016) Injection Grouts for the Re-Attachment of Architectural Surfaces with Historic Value - Measures to Improve the Properties of Hydrated Lime Grouts in Slovenia. *Int J of Arch Her* 10(8):993-1007
9. Papayianni I. Stefanidou M. Pachta V. (2013) Grouts for injection of historical masonries: Influence of the binding system and other additions on the properties of the matrix. In: Valek J Hughes J Groot C (Eds.) *Historic Mortars: Characterization, Assessment and Repair*, RILEM Bookseries, Springer, pp. 383-392

Lime-pozzolan injection grouts with ovalbumin and ethanol added as water-reducing agents: grout design and assessment of the mineralogical evolution

Chiara Pasian¹, Michele Secco^{2,3}, Francesca Piqué⁴, Gilberto Artioli^{3,5}, Sharon Cather⁶

(1) Department of Conservation and Built Heritage, University of Malta, chiara.pasian@um.edu.mt

(2) Department of Civil, Environmental and Architectural Engineering (ICEA), University of Padua, Italy, michele.secco@unipd.it

(3) Inter-Departmental Research Center for the Study of Cement Materials and Hydraulic Binders (CIRCe), University of Padua, Italy

(4) Institute of Materials and Constructions (IMC), University of Applied Sciences and Arts of Southern Switzerland (SUPSI), Lugano, Switzerland, francesca.pique@supsi.ch

(5) Department of Geosciences, University of Padua, Italy, gilberto.artioli@unipd.it

(6) Professor Emerita of The Courtauld Institute of Art, London, UK

Abstract

Non-structural lime-pozzolan injection grouts with water-reducing agents were designed for the stabilisation of delaminated historic plasters in water-sensitive situations, such as plasters contaminated with soluble salts. Water used as suspension medium in a grout can activate and mobilise salts, potentially jeopardising the original materials. Two water-reducing components were considered for the fluid mixture: (i) ethanol, as a partial substitute for water, is a less effective solvent for soluble salts; (ii) ovalbumin is a protein found in egg white, which has been studied as a water-reducer. The evolution of the chemical reactions in grout samples was assessed by X-ray powder diffraction (XRPD) coupled with quantitative phase analysis (QPA) by means of the Rietveld method. Microstructural and microchemical analyses were performed by scanning electron microscopy-energy dispersive microanalysis (SEM-EDS) on cross-sections of grouts aged 150 days, to characterise the packing geometry of the material and the microchemical profile. The influence of both ethanol and ovalbumin in the formation of mineral phases and on the material internal structure is here discussed, as well as how this affects other properties of the grouts.

Introduction and objectives

Injection grouting is a stabilisation intervention which aims to re-establish adhesion between delaminated plaster layers (or between support and plaster layer), introducing a bulked fluid material with adhesive properties –the injection grout [1]. To ensure compatibility with lime-based original materials such as historic plasters, typically lime-based or hydraulic lime-based injection grouts are employed for such intervention. Lime-based injection grouts are composed of binder, fillers, additives and a suspension medium which is typically water [2].

Water is required for the grout setting and to improve injectability, but it may lead to excessive shrinkage, grout segregation [1] and it may solubilise salts present in the porous layered structure, which can potentially cause disaggregation problems in the original materials related to their re-crystallisation. Injection grouting often entails the introduction of large amounts of water, both during the pre-wetting phase and with the injection of the grout [3]. Studies have been carried out involving the introduction of superplasticisers in the grout mixture to reduce the amount of water required and retain a good injectability [3; 4; 5; 6; 7]. Superplasticisers, however, may lead to soluble salts formation [4] and to low porosity of the hardened material [8], which in turn may potentially reduce the water vapour permeability and the capillary absorption capacity of the grout. In the present research, non-structural lime-pozzolan-based injection grouts have been designed in the laboratory with a reduced water content to limit the risks related to a high water content. This was pursued without the use of superplasticisers, but with two water-reducing agents: ethanol and ovalbumin. The evolution of the chemical reactions in grouts containing such water-reducing agents has been followed in samples at different stages of ageing, and microstructural and microchemical analyses have been performed to characterise the overall packing geometry of the hardened material and the microchemical profile of the binder matrices. Such results are linked to the mechanical properties of the hardened grouts.

Materials and mixtures design

Lime-pozzolan grouts with reduced water content for non-structural injection grouting have been designed in the laboratory. The two water-reducing agents have been used for the following reasons:

- Ethanol has been used as a partial substitute for water in the suspension medium of the grout, being a less effective solvent for salts compared to water [9, 10]; pre-mixed commercial grouts and a grout prepared in the laboratory with water-ethanol as suspension medium have proved to have adequate properties for their potential use on site [3];
- Ovalbumin has been used as a water-reducing additive; it is a water-soluble protein present in egg white, which was employed in previous studies in the whisked form to reduce the amount of water in injection grouts, improving their rheological properties and acting as an air-entrainer [11]. Ovalbumin was used whisked, into the consistence of a foam, adding 1 g protein (in powder) to 7 mL of deionised water.

Fixed components were employed for all the grouts considered in the present paper:

- Slaked lime putty as a binder; the putty is composed of portlandite (solid component) and water in volume ratio 1:1;
- Pozzolana: pumice powder, 0-90 μm , reactive with lime due to the Si-rich amorphous constituent of pumice [12];

- Pozzolanic filler: Soda-lime-borosilicate hollow glass micro-spheres as lightweight pozzolanic filler [13] (Scotchlite K1[®], 30–120 μm granulometry; XRPD analyses showed that the material is entirely amorphous).

Reduction of water

Commercial pre-mixed injection grouts (hydraulic lime-based) prepared with up to 25% water : 75% ethanol (in volume) proved to have adequate injectability, shrinkage, porosity, cohesion and adhesion, and to be therefore potentially usable on site [3, 14]. Nevertheless, in [3] it was not possible to fully assess the influence of ethanol in the mixture, since the commercial formulas were not fully disclosed. In the present research components with known composition were used as constituents for the grout design. Starting from the previous studies [3], the amount of ethanol in the suspension medium was further increased to 15% water : 85% ethanol¹¹ (in volume), with a final water to binder ratio of about 0.4 (see Table 2), which is around the minimum suggested in hydraulic systems for complete chemical reactions to occur [15]. Such proportion of water-ethanol was empirically determined, and it involved the minimum amount of water to obtain grouts with good cohesion and adhesion and injectability. The binder used was a slaked lime putty (Ca(OH)₂ + water); when preparing the grout, just the solid paste of the putty was selected, draining the water in excess. In the solid paste of slaked lime putty, particularly in an aged one, water molecules are adsorbed onto Ca(OH)₂ particles [16]. Therefore, considering the grout in its fresh state, the water making part of the suspension medium of the grout migrates in the porosity of the building materials, while the water adsorbed onto the slaked lime putty particles is not 'free' and tends not to migrate. The choice of such binder also allows to reduce the amount of water in the grout, given the better working properties of an aged slaked lime putty compared to those, for instance, of hydrated lime in powder mixed with water [16].

In order to reduce the shrinkage, potentially increased by the relatively fast alcohol evaporation, quartz sand (100-250 μm) was added to the water-alcohol mixture; the aggregate was added also to the control mixture with only water for consistency (see Table A).

Extensive previous unpublished research by the Conservation of Wall Painting Department of the Courtauld Institute, from the late 90s, assessed properties of whisked egg white as an additive for injection grouts for the stabilisation of lime-based decorated plasters. Such additive has proved to improve injectability, to decrease water release and sedimentation, and to act as an air-entrainer. The present research considers whisked ovalbumin (which is the main protein in egg white –over 50% of its proteins by weight– and has foaming properties [17]) instead of egg white for reproducibility and consistency. The air-entraining properties of the whisked albumin affect porosity, which in turn may affect other physical

¹¹ Absolute ethanol.

mechanical properties of the grout [18]. The grout with ovalbumin was compared to the control mixture without albumin (see Table A).

A third grout with reduced water content was formulated combining the use of water-ethanol as suspension medium and ovalbumin. It was verified that the presence of ethanol determines the collapse of the albumin foam, which is due to the breaking of the bubbles in the foam in presence of alcohol. This is determined by an increased solubility in the non-polar group of the protein which leads to the disruption of hydrophobic interactions in the whisked ovalbumin [19]. Nonetheless, since the suspension medium is added at the end in the grout preparation, the mixture retains suitable working properties. In order to prevent shrinkage, quartz sand was added as in the case of the water-alcohol grout. The control mixture contains ovalbumin and only water as the suspension medium, and quartz sand for consistency (see Table 1).

Grout mixtures

All the grouts contain:

- 125 g slaked lime putty (just the solid paste, drained; corresponding to 100 mL in volume); of these, 62.5 g ca. is $\text{Ca}[\text{OH}]_2$ and 62.5 g ca. is water. The actual binder, used to calculate water to binder ratio (see Table 2), is therefore $\text{Ca}(\text{OH})_2 = 62.5 \text{ g}$
- 90 g pumice (corresponding to 100 mL in volume)
- 20 g Scotchlite K1© (corresponding to 300 mL in volume)

The variables in the grouts are: presence of albumin; presence of quartz sand; and suspension medium (15% water : 85% ethanol or 100% water). Table 1 reports the variables for each mixture tested in this research. In the nomenclature, AL indicates the presence of ovalbumin, EA of ethanol, Q of quartz sand; C indicates that the grout is the control. Every grout with reduced water content is compared to the corresponding control (AL vs. C; EA_Q vs. C_Q; AL_EA_Q vs. AL_C_Q). In the grouts with ethanol and the corresponding controls, there are 150 g of quartz sand (corresponding to 100 mL in volume); in grouts with ovalbumin, there are 2.5 g of protein (to whisk it to the consistence of a foam, 7 mL of deionised water per ovalbumin gram was added). Table 2 reports the amount of suspension medium in the grout and the water to binder ratio of each mixture.

Table 1. Grout mixtures: variables present

Grout	Ovalbumin	Quartz sand	15% H ₂ O : 85% EtOH	100% H ₂ O
AL	√	-	-	√
C	-	-	-	√
EA	-	√	√	-
C_Q	-	√	-	√
AL_EA_Q	√	√	√	-
AL_C_Q	√	√	-	√

Where √ is present and – is absent

Table 2. Grout mixtures: suspension medium and water/binder

Grout	15% H ₂ O : 85% EtOH	100% H ₂ O	Water/binder
AL	-	120 mL	1.92
C	-	120 mL	1.92
EA	170 mL	-	0.41
C_Q	-	170 mL	2.72
AL_EA_Q	180 mL	-	0.43
AL_C_Q	-	180 mL	2.88

Experimental methods

Assessment of the mineralogical evolution

In the lime-pozzolan-based grouts considered, both hydraulic reactions and carbonation take place [20]. The presence of both ethanol and ovalbumin may have an influence on such chemical reactions. Ovalbumin is a water retainer [11] and can therefore slow reactions down; ethanol has been reported to delay hydraulic reactions [21]. Mineralogical quantitative phase analyses (QPA) were performed through X-rays powder diffraction (XRPD) on samples of grouts after 7, 28 and 150 days from their preparation, in order to follow their mineralogical evolution. In order to simplify the results of the mineralogical data, quartz sand was excluded from the formulations analysed with XRPD. Analyses were carried out with a Bragg-Brentano θ - θ diffractometer (Panalytical X'Pert PRO, Cu K α radiation, 40 kV and 40 mA) equipped with a real time multiple strip (RTMS) detector (X'Celerator by Panalytical). The grout samples were micronised with ethanol 99%. Interpretation of the diffraction patterns was carried out with the software X'PertHighScore Plus 3.0 by PANalytical, comparing the mineral profiles with the database from the International Centre for Diffraction Data (ICDD). The Rietveld method [22] was employed to perform the QPAs, with refinements carried out with TOPAS software (version 4.1) by Bruker AXS. 20 wt% of zincite was added to the samples in powder as internal standard, and the crystalline and amorphous content was calculated with the combined Rietveld-RIR method [23]. The PONCKS method [24] was used in order to quantify the pozzolanic raw materials, such as pumice and Scotchlite K1[®] glass microspheres, distinguishing them from the non-crystalline components in the grouts (ovalbumin, water and pozzolanic reaction products). Pumice and Scotchlite K1[®] (mixed in the same proportions used in the grouts; such mixture will be called PUM-SK1 in this paper) were mixed with 10 wt% of standard NIST Al₂O₃ to create a peak phase, and therefore to allow their quantification. A pseudo-Voigt function was used to model the Bragg peaks in the samples patterns, fitting the background by a 12 coefficients Chebyshev polynomial. The lattice parameters, Lorentzian crystal sizes and scale factors were refined for each phase. The March Dollase algorithm [25] was used to model any residual preferred orientation effect.

Results and discussion

The progression of pozzolanic reactions and carbonation over time (at 7, 28, 150 days of curing) was monitored with QPA. In particular, the progression of the pozzolanic reactions was followed calculating the ratio between the pozzolanic raw materials at the different curing times and the starting amount of these materials (PUM-SK1/PUM-SK1⁽⁰⁾). Carbonation was followed calculating the ratio between secondary carbonates at the different curing times and the starting amount of portlandite ($\text{CaCO}_3/\text{Ca}(\text{OH})_2^{(0)}$). Figure 1 shows the variation of such ratios overtime, comparing the grout with the water-reducing agent to its corresponding control.

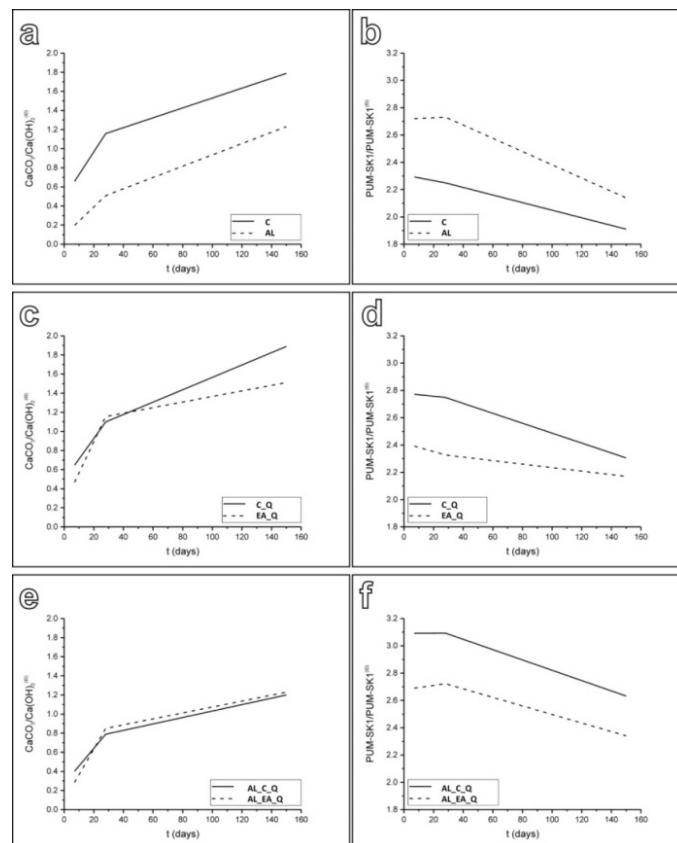


Figure 1. $\text{CaCO}_3/\text{Ca}(\text{OH})_2^{(0)}$ and PUM-SK1/PUM-SK1⁽⁰⁾ ratios over time for each pair of grouts. Degree of carbonation of grouts (a) AL and C, (c) EA_Q and C_Q, (e) AL_EA_Q & AL_C_Q; decrease of the PUM-SK1 fraction of grouts (b) AL and C, (d) EA_Q and C_Q, (f) AL_EA_Q and AL_C_Q

The following can be observed:

- Grout AL with albumin vs. control C without albumin:

Grout AL shows a much lower $\text{CaCO}_3/\text{Ca}(\text{OH})_2^{(0)}$ ratio at each analysed curing time compared to the control; this indicates a reduction in the rate of carbonation due to ovalbumin (Figure 1a). The protein also seems to slow pozzolanic reactions down at short curing time (7 and 28 days), while at 150 days the difference in terms of reaction degree between the grout with ovalbumin and the control is lower (Figure 1b). This behaviour is probably linked to the

water retention imparted to the grout by ovalbumin, particularly in the first days from the preparation of the grout.

- Grout EA_Q with ethanol vs. control C_Q with water:

A comparable degree of carbonation is observed in the two grouts during the first 28 days, while at 150 days of curing grout EA_Q with alcohol has a lower degree of carbonation (Figure 1c). Ethanol slows carbonation down because an overall lower amount of water leads to a lower amount of $\text{Ca}(\text{OH})_2$ dissolved for the reaction to occur. Pozzolanic reactions, on the other hand, seem to progress to higher extent in grout EA_Q with ethanol in the first 28 days, while at 150 days the difference between the two mixtures is less marked (Figure 1d). Therefore, the addition of ethanol does not significantly influence the pozzolanic reactions; this is due to the fact that the minimum amount of water for the reactions to occur is present (ethanol acts as a substitute to water to ensure the injectability of the mixture).

- Grout AL_EA_Q with ovalbumin and ethanol vs. control AL_C_Q with ovalbumin and only water:

The two grouts show a very similar degree of carbonation over time. On the other hand, the degree of pozzolanic reactions is significantly higher in the grout with ethanol compared to the control.

Characterisation of the internal microstructure

Samples of the grouts were analysed with SEM-EDS after 150 days from their preparation, both cross-sections and broken-sections. The scanning electron microscope used was a CamScan MX2500 equipped with a LaB_6 cathode and a four quadrant solid state BSE detector for imaging. The analytical conditions were the following: accelerating voltage 20 kV; filament current 1.80 A; emission current 20 μA ; aperture current 300 nA; working distance 20–30 mm. For the chemical microanalysis, an EDAX-EDS energy dispersive X-rays fluorescence spectrometer was employed, with a Sapphire Detector composed by a LEAP+ Si(Li) crystal and a Super Ultra Thin Window.

Results and discussion

EDS microanalyses of the samples in cross section showed for all grouts the microchemical profile of the binder matrices typical of pozzolanic binders, containing both carbonation and pozzolanic products (with occurrence of Ca and Si, with a dominance of Si). The concentration of reaction products close to smaller pumice particles confirms their pozzolanic reactivity. Figure 2 includes a number of representative backscattered electrons images (BSI), showing the microstructural features of the different mixtures in broken section. The results obtained with the mineralogical analysis of the samples at 150 days reflect what observed at the SEM-EDS in terms of microstructure.

- Grout AL with albumin vs. control C without albumin:

Grout AL shows a lower amount of reacted binder matrix compared to grout C, which is characterised by a denser matrix packing and lower degree of porosity (Figures 2a and b). The surface of Scotchlite K1® microspheres appear neat in grout AL with ovalbumin, while in grout C without ovalbumin dissolution areas are present, with deposition on the surface of reaction products. Such features show a different degree of reaction in the two grouts according to the presence or absence of ovalbumin, confirming the decrease in carbonation and hydration reaction rate in presence of ovalbumin observed with XRPD.

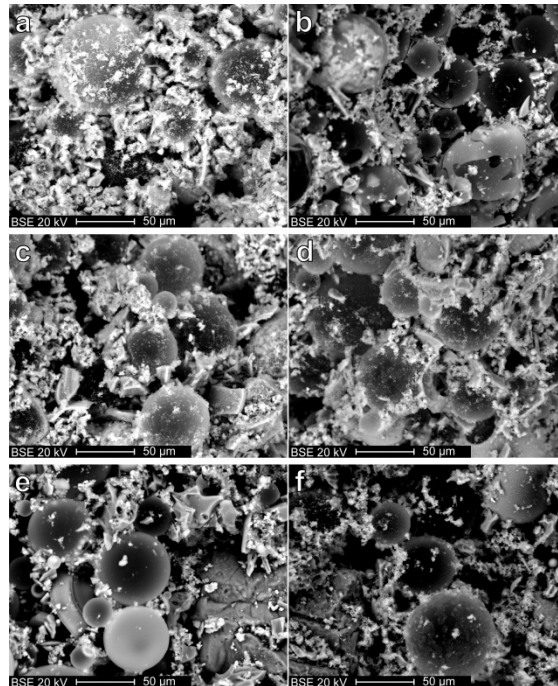


Figure 2. Broken section; backscattered electron image (BSI) of grout (a) C, (b) AL, (c) C_Q, (d) EA_Q, (e) AL_C_Q, (f) AL_EA_Q

- Grout EA_Q with ethanol vs. control C_Q with water:

The grout with ethanol and the one with only water have a denser packing geometry compared to grouts AL and C because quartz sand is added in their formulation. Grouts EA_Q and C_Q seem to have a comparable amount of reaction products and similar microstructure.

- Grout AL_EA_Q with ovalbumin and ethanol vs. control AL_C_Q with ovalbumin and only water:

These two grouts, although containing quartz sand like grouts EA_Q and C_Q, show a less dense packing geometry, and a higher degree of porosity because of the presence of whisked ovalbumin in the formulation. The lower amount of reaction products confirms the lower degree of reactions observed with XRPD, particularly regarding pozzolanic reactions. The sample prepared with water (AL_C_Q) shows a lower degree of pozzolanic reaction compared to AL_EA_Q prepared with alcohol; in the grout with ovalbumin and water, the

surface of microspheres looks intact, while in the grout with ovalbumin and ethanol dissolution of the microspheres surface is observed, indicating that the degree of chemical reactions is higher. Ethanol determined the collapse of the ovalbumin foam; it can be deduced that this limits the inhibition effect of ovalbumin in the extent and rate of chemical reactions.

Influence of internal microstructure and mineralogical phases on mechanical properties

Internal microstructure and mineralogical phases together with porosity have an influence on the mechanical strength of grouts. Direct tensile strength is typically related to the phases formation and how they interlock in the 3D packing geometry, and it is interesting to compare such results to the XRPD and SEM-EDS data. Direct tensile strength refers to the cohesion of the hardened mixture.

Results and discussion

Compressive strength and direct tensile strength were tested on the grout samples 150 day-aged. Results are reported in Table 3.

Table 3. Compressive strength (σ_c) and tensile strength (σ_t) of grouts

Grout	Compressive Strength σ_c (N/mm²)	Direct tensile strength σ_t (N/mm²)
AL	1.83	0.25
C	3.07	0.35
EA	3.08	0.29
C_Q	3.01	0.31
AL_EA_Q	1.15	0.23
AL_C_Q	1.39	0.18

- Grout AL with albumin vs. control C without albumin:

Grout C is less porous, has a higher degree of reactions and mineralogical phases formed and a denser 3D structure, and therefore both its compressive and direct tensile strength are higher than those of grout AL with ovalbumin.

- Grout EA_Q with ethanol vs. control C_Q with water:

The grout with ethanol and the grout with only water have a comparable mechanical strength; they indeed show a comparable microstructure and presence of reacted mineral phases, confirmed also in the XRPD analyses.

- Grout AL_EA_Q with ovalbumin and ethanol vs. control AL_C_Q with ovalbumin and only water:

Grout AL_EA_Q has a slightly lower compressive strength compared to the control, while it has a higher direct tensile strength, probably related to the higher degree of pozzolanic reactions, observed also with XRPD.

Final discussion and conclusions

Two water-reducing agents were used in the formulation of lime-pozzolan grouts for the stabilisation of historic plasters: ethanol as a partial substitute to water and ovalbumin. Mineralogical analyses of the phases formed and microstructural analyses allowed to identify the following patterns:

- The presence of ovalbumin reduced the extent and speed of carbonation and hydraulic reactions in grouts prepared with only water;
- Ethanol reduced and slowed down carbonation, but did not seem to affect significantly pozzolanic reactions (the minimum water content needed to complete the hydraulic reactions was present);
- The presence of both ovalbumin and ethanol determines a higher degree of chemical reactions compared to when ovalbumin is present in grouts prepared with just water;

In addition to this, the mineralogical and microstructural data were confirmed by data regarding mechanical strength.

Overall, ovalbumin has shown to reduce and slow down chemical reactions (when used in presence of just water); however, the grout tested has adequate cohesion to be used on site. Ovalbumin does not allow a high reduction in water, but provides the mixture with enhanced working properties [11, 26] and determines a very high porosity of the hardened grout, which determines in turn an adequate water vapour permeability and capillary water absorption [18]. Its low dry density may be useful when a light material is required on site.

In previous research [3] the use of ethanol as a substitute to water for some pre-mixed commercial grout led to grouts with suitable working properties and performance in the hardened state; however, its role in chemical reactions was not entirely understood, due to the non-fully disclosed formulation of the commercial products. The present research proves that the presence of ethanol slightly reduces carbonation, but it does not significantly affect pozzolanic reactions, as long as the minimum water amount for the hydraulic reactions to occur is kept. Therefore, ethanol allows a significant reduction in water in grouts preparation, useful in water-sensitive situations on site such as in presence of plasters highly contaminated with soluble salts. For the grouts tested in this research, the water reduction was up to 85%; such water reduction led to grouts with adequate mechanical strength (comparable to that of the grouts with just water) and still with a high porosity [18], which is fundamental for the stabilisation of highly porous building materials such as historic plasters and wall paintings.

In conclusion, the water-reducing agents studied may be used in the formulation of site-specific injection grouts. Injection grouts need to tailor the specific case under consideration. In particular, in the design of water-alcohol injection grouts one needs to consider not just the original materials of the plaster or wall painting to stabilise, but also their performance characteristics (such as porosity, capillary water absorption, mechanical strength) and the environmental conditions in which the grouting intervention takes place, as they may have an influence during the intervention and in the performance of the grout.

List of materials

Slaked lime – Grassello di Calce Candor, 48-months-aged. Production batch: L0211-E,

Lime deposit: IT-BR-003-FASANO. Calce Viva. Adriatica Legnami s.r.l. S.S. 16 – Km

855,500 IT 72015 Fasano di Brindisi (IT)

Pumice – Powdered Pumice 7/0 (FF), 0-90 .m. CTS s.r.l., C.T.S. Suisse SA,

Via Carvarina, 1, 6807 Taverne, TI (CH)

Quartz sand – Milled quartz sand, 100-250 .m. Taiana SA, Via Pobiette, 1, 6928 Manno

(CH)

Scotchlite SK1 – Soda lime borosilicate glass microspheres, 3MTM Scotchlite™ K1R.

THYMOS AG, Militarstrasse 34, 3014 Bern (CH)

Ethyl alcohol – Ethyl alcohol. Emanuele Centonze SA, Via Luigi Favre 16, 6828 Balerna,

Chiasso (CH)

Albumin – Albumin ex egg, 80%, Alfa AesarR. Johnson Matthey & Brandenberger AG,

Glattalstrasse 18, Postfach 485, 8052 Zurich (CH)

Acknowledgements

We would like to thank Dr Christian Paglia, Director of Istituto Materiali e Costruzioni (IMC, SUPSI), for access to the SUPSI-IMC laboratory to carry out the physical and mechanical tests. Prof Albert Jornet (IMC, SUPSI) is acknowledged for his invaluable advice.

References

1. Biçer-Şimşir B, Rainer L (2013) Evaluation of Lime-Based Hydraulic Injection Grouts for the Conservation of Architectural Surfaces. The Getty Conservation Institute
2. Biçer-Şimşir B, Griffin I, Palazzo-Bertholon B, Rainer L (2009) Lime-based injection grouts for the conservation of architectural surfaces. *Rev Conserv* 10:3–17

3. Pasian C, Piqué F, Jornet A (2017) Non-structural injection grouts with reduced water content: changes induced by the partial substitution of water with alcohol. *Stud. Conserv.* 62(1):43–54
4. Flatt RJ, Girardet FJ (2000) Injectable slurries for the in situ conservation of pavement mosaics. In: *Proceedings of the 9th International Congress on Deterioration and Conservation of Stone, Venice, June 19–24 2000*, Elsevier Science B.V., pp.297–305
5. Papayianni I, Pachta V, Stefanidou M (2012) Experimental study of nano-modified lime based grouts. *World J Eng* 9(6):501-508
6. Papayianni I, Pachta V (2015) Experimental study on the performance of lime-based grouts used in consolidating historic masonries. *Mater Struct* 48: 2111-2121
7. Padovnik A, Piqué F, Jornet A, Bokan-Bosiljkov V (2016) Injection grouts for the re-attachment of architectural surfaces with historic value – Measures to improve the properties of hydrated lime grouts in Slovenia. *Int J Archit Herit* 10(8):993-1007
8. Flatt RJ (2002) Polymeric Dispersants in Concrete. In: *Polymers in Particulate Systems – Properties and Applications*, Marcel Dekker Inc., pp. 247–294
9. Kolker A, de Pablo J (1996) Thermodynamic modelling of the solubility of salts in mixed aqueous-organic solvents. *Ind. Eng. Chem. Res.* 35:228–233
10. Pinho SP, Macedo EA (2005) Solubility of NaCl, NaBr, and KCl in water, methanol, ethanol, and their mixed solvents. *J. Chem. Eng. Data* 50:29–32
11. Rickerby S, Shekede L, Zaixuan F, Wei T, Hai Q, Jinjian Y, Piqué F (2010) Development and testing of the grouting and soluble salts reduction treatments of Cave 85 wall paintings. In: N. Agnew (Ed.), *Conservation of Ancient Sites on the SilkRoad. Proceedings of the Second International Conference on the Conservation of Grotto Sites, Mogao Grottoes, Dunhuang, People’s Republic of China, June 28–July 3 2004*, Getty Conservation Institute, Los Angeles, pp. 471–479
12. Massazza F (2002) Properties and applications of natural pozzolanas. In: *Structure and Performance of Cements*, Bensted J, Barnes P (Eds.), Spon Press, London, pp. 326–352
13. Shayan A, Xu A (2004) Value-added utilisation of waste glass in concrete. *Cem. Concrete Res.* 34:81–89
14. Pasian C, Piqué F, Riminesi C, Jornet A (2017) How not to bother salts while grouting. In: *Proceedings of the Fourth International Conference on Salt Weathering of Buildings and Stone Sculptures, Potsdam, September 20-22 2017*, pp. 158–167
15. Taylor HFW (1997) *Cement Chemistry*. 2nd ed., Thomas Telford Publishing

16. Hansen EF, Rodríguez-Navarro C, Van Balen K (2008) Lime putties and mortars, insights into fundamental properties. *Stud. Conserv.* 53:9–23
17. Mine Y (1995) Recent advances in the understanding of egg white protein functionality. *Trends Food Sci. Technol.* 6(7):225–232
18. Pasion C, Secco M, Piqué F, Rickerby S, Artioli G, Cather S (2016) Performance of grouts with reduced water content: the importance of porosity and related properties. In: *Proceedings of the 4th Historic Mortars Conference, October 10–12 2016, Santorini, Greece*, pp. 639-646
19. Calandrini V, Fioretto D, Onori G, Santucci A (2000) Role of hydrophobic interactions on the stabilisation of native state of globular proteins. *Chem. Phys. Lett.* 324:344–348
20. Cizer Ö, Van Balen K, Elsen J, Van Gemert D (2012) Real-time investigation of reaction rate and mineral phase modifications of lime carbonation. *Construct. Build. Mater.* 35:741–751
21. Muhua T, Roy DM (1987) An investigation of the effect of organic solvent on the rheological properties and hydration of cement paste. *Cem. Concrete Res.* 17:983–994
22. Rietveld H (1969) A profile refinement method for nuclear and magnetic structures. *J. Appl. Crystallogr.* 2(2):65–71
23. Gualtieri AF (2000) Accuracy of XRPD QPA using the combined Rietveld–RIR method. *J. Appl. Crystallogr.* 33(2):267–278
24. Scarlett NV, Madsen IC (2006) Quantification of phases with partial or no known crystal structures. *Powder Diffr.* 21(4):278–284
25. Dollase WA (1986) Correction of intensities for preferred orientation in powder diffractometry: application of the March model. *J. Appl. Crystallogr.* 19(4):267–272
26. Pasion C (2017) Non-structural lime-based injection grouts with reduced water content for decorated surfaces. PhD thesis, The Courtauld Institute of Art, London

Limestone-filled, hydraulic-lime mortars for historic and traditional fabrics

Marwa Aly¹, Sara Pavía¹

(1) Department of Civil Engineering, Trinity College Dublin, Ireland. alym@tcd.ie; pavias@tcd.ie

Abstract

Hydraulic lime (HL) mortars are considered compatible with historic fabrics and used in repairs. They consist of lime and clinkers (mainly belite). As belite hydrates slowly, some HLs develop strength for up to a year. This has raised concerns with conservationists. This paper partially replaces natural HL (NHL5) with limestone to lower ultimate strengths that can damage for some fabrics. It investigates the hydration of NHL5 in the presence of limestone and the impact on mortar properties.

Despite the NHL's low aluminate content, limestone reaction is evident. Limestone-triggered hydrates appear in the matrix and at interfaces, likely strengthening the transition zone. The limestone fineness and permeability, and the significant specific surface area of its microcrystalline carbonate may have enhanced reactivity.

The 10-20% limestone replacements increased the 28-day strength. However, they lowered the NHL5 strength after 90 days (flexural) and 180 days (compressive). In contrast, the NHL5 mortar keeps developing compressive strength, increasing by c.14 between 90 and 180 days and c. 10% between 180 days and 1 year. The strength raise did not significantly affect the hygric properties. When NHL5 is replaced with 10-30% limestone, the finest mortar pores are preserved (water vapour permeability varies insignificantly). Contrary to Portland cement (PC), the limestone lowers the water demand of the NHL5 mortars. To achieve a proper workability using less water has benefits relevant for those involved in mortar design.

Introduction

Limestone is considered an active addition in PC and currently, the European Standards [1] include four limestone cements with limestone content ranging from 6 to 35%. In the cement industry, limestone has been linked to lower costs, enhanced performance, energy saving and reduction of CO₂ emissions on cement production [2-4]. Hydraulic limes (HLs) contain silicate and aluminate clinkers identical to those in PC however, limestone is not added to HL. Natural hydraulic limes (NHLs) have been used since antiquity. Today NHL mortars are considered masonry-compatible due to their hygric and mechanical properties [5-14] and are used in new building and masonry repair. They are regaining popularity as a more sustainable alternative to PC because they require lower production energy and absorb part of their CO₂ emissions during hardening. Their chemical and physical compatibility relies on the fact that they contain a mixture of free lime and aluminate and

silicate clinkers (of which belite-C2S- is the most abundant). The free lime provides workability and sustained plasticity due to its high water retention, while the belite delivers hydraulic cements that contribute to strength gain and enhance durability. This results in materials of high water vapour permeability, lower strength and a greater plasticity than cement-based materials which have been favoured in restoration for decades. It is known that NHL mortars display bond strengths and structural behaviour compatible with masonry units; and that the hydraulic set of NHLs leads to earlier strength development and a greater ultimate strength, a lower shrinkage and a superior durability than hydrated limes [5-14]. European designation HL5/NHL5 (with the greatest hydraulic content) is used when a fast set and hardening and a greater durability are required (strong exposure or presence of water). Per standard requirement, HL5/NHL5 must reach over 7 N/mm² at 28 days [15], however, there is no long-term strength requirement in the standards. Belite hydrates so slowly that the strength of NHL5-based materials will keep rising after 28 days and well after the material has been set into the fabric. This has raised concerns within conservationists as, in practice, a HL5/NHL5 mortar can develop strength for up to a year and after. This paper reviews the effect of limestone in PC and experimentally investigates limestone impact in HL using a NHL5 complying with EN459-1 [15], including 15-22% available lime and significant (43%) belite.

Limestone in PC

Influence of limestone on PC hydration

By 1938, Bessey [16] had already suggested that ground limestone takes part in reactions with PC aluminates. Later, other authors evidenced that carbonate ions (CO_3^{2-}) replace sulfate ions (SO_4^{2-}) in cement hydrates so that calcium carboaluminate forms in place of monosulfate – AFm phases- [17-21]. According to these authors, C_3A hydrates into $\text{C}_3\text{A} \cdot 1/2\text{CO}_2 \cdot 12\text{H}_2\text{O}$ which reacts with CO_3^{2-} resulting from limestone dissolution to form calcium carboaluminate hydrate ($\text{C}_3\text{A} \cdot \text{CaCO}_3 \cdot 11\text{H}_2\text{O}$). This phase, growing epitaxially on CaCO_3 , was observed by Barriochini and Murat [22] and others. The reaction of alite with CaCO_3 to form calcium carboaluminate which leads to an early strength increase has been reported by Pera et al. [23]. Authors also report that limestone (CaCO_3) accelerates PC hydration [23-27], in particular the hydration of alite. The acceleration is attributed to CaCO_3 particles acting as nuclei for the formation and growth of more abundant C-S-H and CH which causes a drop in the concentration of Ca and Si ions in the interstitial solution that speeds up clinker dissolution.

Impact of limestone on PC properties

In PC, limestone increases water demand [23] and increases early strength. The early strength increase has been attributed to speeding up hydration and to the resulting calcium carboaluminate and calcium carboaluminate hydrates improving density. Low level limestone replacements (5-10%) either not reduce or increase strength but a dilution effect exists at

higher dosages unless the cement is ground finer to compensate [23-26]. Livesey [28] reports that 5% limestone replacement accelerates strength gain at early ages. Vuk et al.[29] report early strength increase with 5% limestone however, later strength either remained the same or decreased depending on the clinker fineness and chemistry. At higher limestone replacements (15-25% and over) strengths are lower than for comparable PC mixes [30-31]. The greater packing of the granular skeleton caused by fillers that lifts strength is well known [25]. This effect is apparent at early ages but does not produce additional ultimate strength [32]. Most authors claim that the calcium carbo-silicate hydrates (resulting from the limestone/ alite reaction) increase strength however, there is no agreement on the strength increase by the calcium carboaluminate hydrates (from the limestone/C₃A reaction). Some authors [23-25] state that they barely increase strength while others [2, 33-34] claim that they contribute to the early strength, because they are stiffer and have greater molar volume than the corresponding sulfoaluminates (AFm) and final cubic hydrates (C₃AH₆) that would result from the hydration of C₃A alone.

Materials and methods

The limestone qualifies as a filler (both in composition and grading). It consists of 95.8% CaCO₃ and practically no clay (Al₂O₃=0.3% by weight) -Table 1- therefore, it qualifies as a filler [35-36]. According to the particle size distribution (Figure 1), c.63% of the limestone is graded under 0.063 mm thus qualifying as a filler according to EN 933-10 [37]. It is widely acknowledged that fine limestone filler (with a greater specific surface area) enhances formation and growth of C-S-H and the dissolution of CaCO₃ to generate CO₃²⁻ thus accelerating and amplifying silicate and aluminate reactions.

Table 1. Composition (% by mass) and properties of the Portland stone base bed [36].

Ca CO ₃	Mg carbonates	Alumino silicates	Fe ₂ O ₃	SiO ₂	Water+ other	Porosity%	Capillary suction g/m ² .s ^{0/5}	%Water absorption
95.8	1.2	0.3	0.3	1.3	1.4	15.40	82.16	7.19

The limestone filler was chosen with a view to enhance the compatibility of the NHL repair mortars with the substrate. The limestone used to make the filler features in many, 18th century buildings in Dublin including the Four Courts (1775) (Figure 2) which often show old mortar repairs made with crushed Portland stone (Figure 3). It is an oolitic limestone consisting of calcite (CaCO₃) with traces of silica in the form of quartz (SiO₂). It contains abundant microcrystalline CaCO₃, with a higher specific surface and a greater reactivity than coarser, crystalline carbonates. It has a grain supported fabric of ooids (Figure 4), with substantial inter-particular space which results in significant porosity and permeability (Table 1). Macropores (10–100µm) dominate the pore system and c. 20% micropores (0.01-0.20 µm) are also present [36].

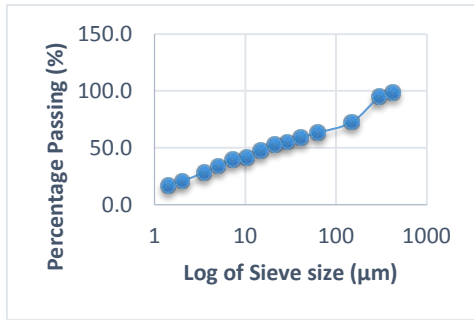


Figure 1. Particle size distribution of the limestone filler.



Figure 2. Portland stone at The Four Courts showing old mortar repairs made with crushed Portland stone - Figure 3.

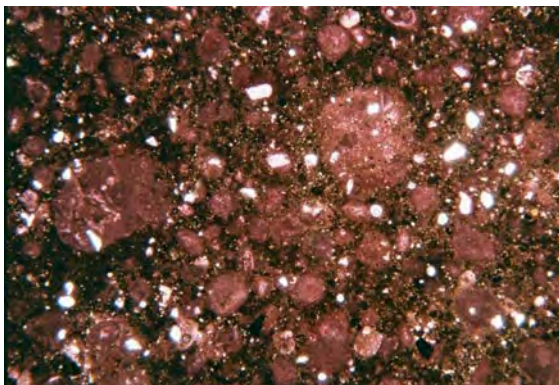


Figure 3. Petrographic photograph of an early 20th century repair mortar made with crushed Portland stone and fine quartz sand set in a PC binder. 2X natural light. Field of view c. 7 mm.



Figure 4. Petrographic image of the Portland stone consisting of ooliths and shells of microcrystalline carbonate cemented with coarser crystalline carbonate. 2X polarised light. Field of view c. 7 mm

The NHL5 contains available lime – $\text{Ca}(\text{OH})_2$ - (15-22% after slaking), residual unburnt CaCO_3 (23%) and significant belite (43% - C_2S) -Table 2. Some C_3S -alite- can be present due to “high-temperature spots” during burning. The NHL5 has no impurities relevant to classification and labelling and a minimal presence of Al_2O_3 (up to c. 2%) sulphates and alkalis, which are very low in the parent limestone (Table 2). The XRD analysis evidenced significant CH (Portlandite – $\text{Ca}(\text{OH})_2$), silicates (alite/belite) and some carbonate (CaCO_3), silica (SiO_2) and lime (CaO). The peaks identified as alite (Ca_3SiO_5) correspond to both belite and alite. It was not possible to tell them apart as the most intense peaks of belite are overlapped by alite and the alite content is likely under the detection limit. The surface area of the NHL5 is 8000 cm^2 per gram [38].

Table 2. Chemical and mineral composition of the NHL5 in % by mass [38].

Chemical composition									
CaO	SiO ₂	Al ₂ O ₃	Fe ₂ O ₃	SO ₃	MgO	K ₂ O/Na ₂ O	LOI	CaO ₂ - calcimetry	Insoluble
59	15	1.92	0.57	0.41	1.01	0.28	16	10	5.6
Mineral composition									
Ca(OH) ₂	CaCO ₃	C ₂ S	C ₃ A	C ₂ AS	C ₄ AF	CaSO ₄			
22	23	43	0.7	1.3	0.7	0.7			

Mortar composition and curing. Mortars with NHL5 binder replaced with limestone (10, 20 and 30% by weight) were produced with a binder/aggregate ratio of 1:3 by weight. The aggregate is a siliceous sand similar to the CEN standard sand-Table 3. Workability and aggregate content were kept constant to attribute the variation of properties to the limestone content. All mortars were mixed to a 165 ± 5 mm initial flow in order to measure how the limestone filler affects workability and the mortar's water demand to reach a specific flow. The 165 ± 5 mm flow was selected because it provided the best workability by trial [39]. The results evidenced that, despite the considerable porosity of the limestone filler, increasing limestone content lowered the water demand of the NHL5 mortars -Table 3. On the contrary limestone replacement increases the water demand of PC composites [23]. The mortars were moulded and compacted on a vibration Table according to EN 459-2 [39]. They were cured for 25 days at 90% humidity and $20 \pm 2^\circ\text{C}$ temperature. After 28 days, some specimens were tested and the rest kept in standard conditions for testing at 90 and 180 days. Each property measured is the arithmetic mean of six specimens.

Table 3. Composition and water content of the mortars.

Designation	% NHL5	% Limestone	W/B
100% NHL5	100	0	0.73
10% L	90	10	0.69
20% L	80	20	0.64
30% L	70	30	0.60

Testing methods. The microstructure and hydration of the limestone-filled pastes were studied with a scanning electron microscope (SEM). Energy dispersive X-ray microanalysis (EDXA) was carried out to determine the elemental composition of the mineral phases in the matrix and at interfaces. Specimen fragments were taken from the curing chamber at 7, 28 and 35 days. EDXA analysis was carried out using a detector at 20KV. The images were captured between 2 and 10KV. The mineralogical composition of the NHL5 was analysed by X-Ray Diffraction (XRD), using a Phillips PW1720 XRD with a PW1050/80 goniometer and a PW3313/20 Cu k-alpha anode tube at 40kV and 20mA. All measurements were taken between 3 and 60 degrees (2θ) at a step size of 0.02 degrees/second. The porosity was tested according to RILEM recommendations [40]. The water absorption was measured according to UNE [41] and the capillary suction estimated with the EN 1925 procedure [42]. The water vapour permeability was measured with the wet cup method in EN 1015-19 [43]. The test lasted for 8 weeks and the samples were weighted at weekly intervals. The weight stabilised during the first week and the subsequent 7 weeks of readings allowed to determine the water vapour coefficient. The compressive and flexural strengths were measured according to EN 1015-11 [43]. The flexural test was performed on 40x40x160 mm specimens using rates of loading of 1 mm/min. The compressive strength was measured on the half prisms at the same loading rate.

Results and discussion

The limestone / hydraulic lime system

While limestone reactions are well documented in PC, the system limestone-HL has not yet been investigated in detail. NHL5 typically contains more free lime and residual CaCO_3 than PC [38, 44, 45] (Table 4). Furthermore, due to the different production temperature (<1200°C for NHL5 vs >1300°C in PC), the calcium silicate, aluminate and ferrite contents are different. In PC, alite is the most abundant component and aluminates and aluminoferrites are usually present (c.10%) while in NHL5, belite is the most abundant and aluminate and ferrites are very low (Table 4). Alite hydrates quickly, being the main contributor to early strength and partially responsible for the early set but belite hydrates late (after c. 18 hours [46]) and contributes little to strength [47]. When alite hydrates C-S-H forms together with a supersaturated solution from which CH crystals subsequently precipitate. Belite progresses likewise, however at a slower pace and producing 2/3rd less CH [48-49].

Table 4. Comparison of mineral composition of NHL5 and cement [38, 44, 45].

Compounds	NHL5- % by mass	CEM I- % by mass
Insoluble content	4 - 5.6	trace
Free lime - Ca(OH)_2	21 - 22	2
Unburnt Ca CO_3	23	0
Alite – C_3S	Trace - 2	58
Belite - C_2S	43 - 45	13
Tricalcium aluminate - C_3A	0.7 - 2	9
Gehlenite - C_2AS	1.3 - 2	0
Ca aluminoferrite - C_4AF	0.7 - 2	8
Gypsum - $\text{CaSO}_{4x} 2\text{H}_2\text{O}$	Trace - 0.7	5

The reactions between limestone and alite/aluminates are widely acknowledged in PC however, rather than alite, the NHL5 contains significant belite (43%) and little aluminate (0.7-2%) - Table 2. In spite of this, given their similar composition and hydration kinetics of alite and belite, it is likely limestone also affects belite hydration. Furthermore, limestone is reported to react with cement containing no aluminates: Monteiro and Meht [50] observed the formation of a $\text{CaCO}_3 / \text{Ca(OH)}_2$ compound at interfaces that strengthens the transition zone due to the substitution of the large and highly oriented CH crystals with the CaCO_3 - Ca(OH)_2 compound of lower crystallinity.

Effect of limestone filler on the strength of NHL5 mortar

All the limestone-filled mortars reached their maximum compressive strength at 90 days to later drop while the NHL5 mortar continued to develop strength, increasing by c.14 between 90 and 180 days (Figure 5). This strength will further grow up to one or two years. The compressive strength of standard NHL5 mixes usually multiplies by 4-5 times between 28

days and one year and keeps growing by c. 10% between 1 and 2 years [13, 38, 51]. The 10 and 20% limestone replacements enhanced the 28-day compressive strength of the NHL5 by 36 and 20% respectively while the 30% limestone lowers it considerably (Figure 5). The 10% limestone mortar's strength remains superior up to 180 days. After this, the NHL5 mortar starts to become stronger. The strength of the 20% limestone mortar remains superior up to 125 days; later (180 days) is c.14% lower than the NHL5. The 30% replacement decreased the compressive strength of the NHL5 mortar at all ages (by 25-59%). PC authors report strength loses for 15-25% limestone replacement and over [30-31]. The early strength increase caused by the limestone is attributed to the lower water demand of the limestone-filled mortars; the increase of early hydrates and their placement.

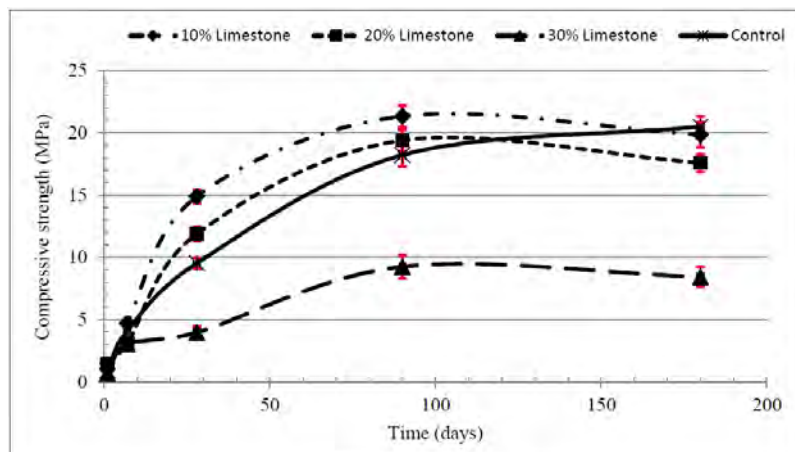


Figure 5. Compressive strength of NHL5 and NHL5-limestone-filled mortars over 180 days. COV 10% limestone=3-15%; 20% limestone=3-8%; 30% limestone 1-12%; 100%NHL5=4-14.

The mortars reached their maximum flexural strength at 90 days to later drop. This drop is usually attributed to the transformation of early hydrates into more stable, weaker phases [34]. The 10% replacement significantly increased the flexural strength of the NHL5 by 56% at 28 days (Figure 6). It enhanced the NHL5 flexural strength up to c.100 days, after this time, it begins to drop (Figure 6). The flexural strength of the 20% limestone mortar is marginally superior up to 28 days however, at 90 and 180 days, it is 20 and 34% lower (respectively) than the NHL5 mortar. These differences will become more pronounced as the flexural strength of the NHL5 will rise by c.16% or over between 180 days and 1 year [51]. The 30% limestone replacement reduced the NHL5 flexural strength at all ages however much less than the compressive strength.

Effect of limestone filler on NHL5 hydration

The SEM/EDXA analyses evidenced that the limestone particles are active on hydration, as they are often covered with hydrates even after 7 days of curing. The limestone changes the microstructure of the hydraulic lime paste and the nature of some of the hydration phases. The NHL5 paste shows more uniformly distributed C-S-H fibrils and gels (Figure 7) whereas in the limestone-filled pastes, particles covered with hydrate fibrils (probably C-S-H) are abundant (Figure 8).

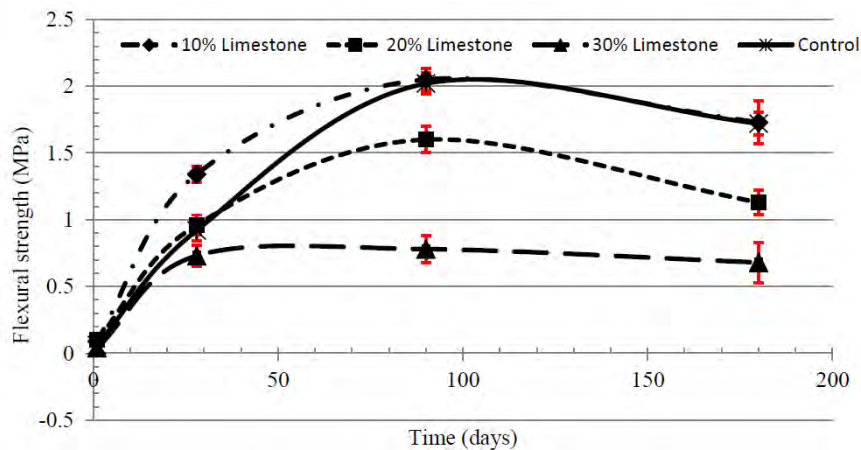


Figure 6. Flexural strength development of NHL5 and NHL5-limestone-filled mortars. COV 10% limestone=4-12%; 20% limestone=4-7%; 30% limestone 0-15%; 100%NHL5=0-7%.

The 10% limestone filled pastes at 7 days show limestone particles and occasional hydrates (fibrils-probably C-S-H) and hexagonal plates). At 28 days, extensive fibrous hydrates alternating with occasional plates cover most particles (Figure 8). The 30% limestone pastes, at 7 and 28 days, show plentiful products of hydration similar to those in the 10% pastes, with abundant hexagonal plates and fibril-coated particles. Figure 9 shows a calcium silicate, possibly belite (Figure 10) covered with hydrates including plates and smaller crystals. The elemental analysis of the larger plates (Figure 11), often hexagonal, suggest that they are CaCO_3 / $\text{Ca}(\text{OH})_2$ compounds formed by the reaction between the limestone (CaCO_3) and the C_2S –belite. As aforementioned, Monteiro and Meht [50] observed the formation of a CaCO_3 / $\text{Ca}(\text{OH})_2$ compound at interfaces leading to the strengthening of the transition zone. In the limestone-filled pastes, hexagonal and planar plates, similar in morphology to CH but often of lower-crystallinity often appear as products of hydration (Figures 8-9) on particle interfaces and in the paste. Their spectra always show Si, Al and a raised C peak suggesting that they can be hydrates resulting from the limestone reaction.

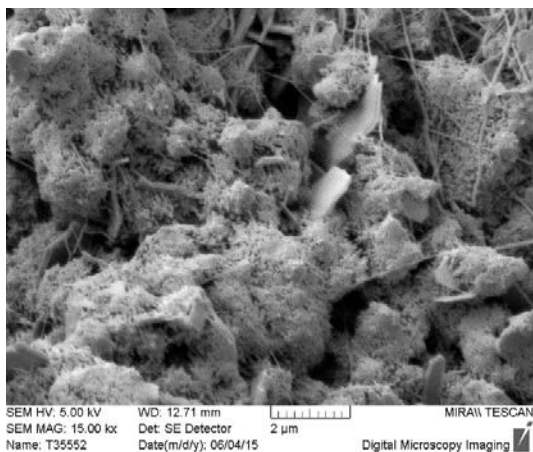


Figure 7. NHL5 paste at 28 days shows C-S-H evenly spread and hexagonal aluminosilicate hydrates.

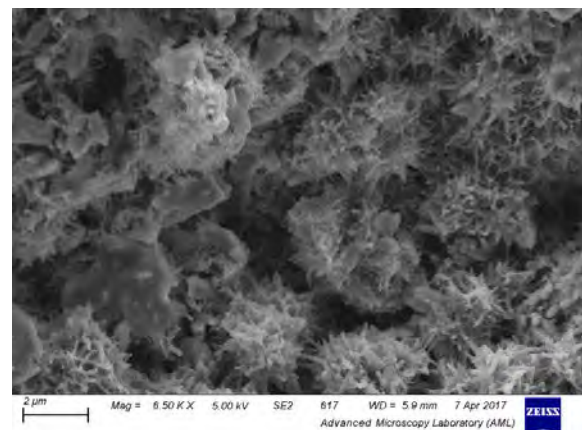


Figure 8. 10% limestone-filled paste at 28 days showing hydrates covering most particles.

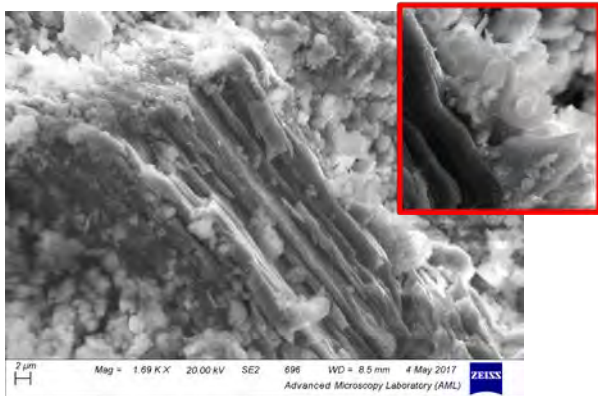


Figure 9. Calcium silicate clinker in a 30% limestone-filled paste with abundant plates (tending to hexagonal) and lower crystallinity phases at the interface.

Insert: Detail of interface with hydrate plates. Field of view c. 8 μm.

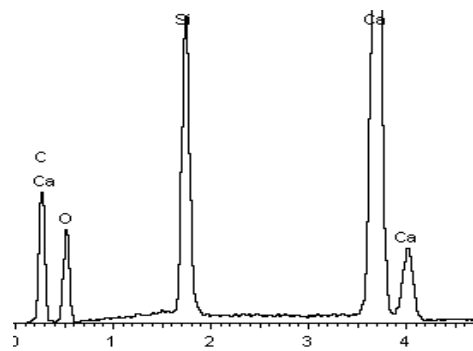
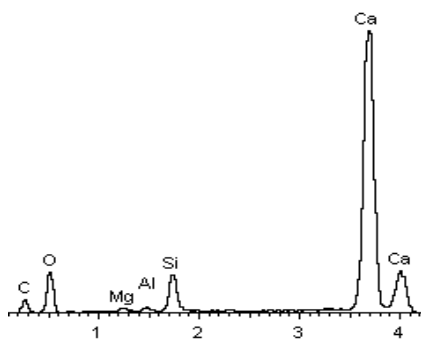


Figure 10. Elemental composition of the calcium silicate in Figure 9- probably belite.

Figure 11. The elemental composition of the larger plates at the interface (figure 9) suggest that they are $\text{CaCO}_3 / \text{Ca}(\text{OH})_2$ compounds formed by the reaction between the limestone (CaCO_3) and the C_2S –belite.

Effect of limestone filler on the hygric properties of NHL5 mortar

The 10 and 20% limestone replacements slightly reduced the porosity of the NHL 5 mortar by c. 8 and 5% respectively while the 30% replacement increased it by 12%. A similar trend was observed for water absorption (Figure 12), as this property strongly relates to the open porosity. The 10 and 20% limestone replacements decreased water absorption by 9 and 7% respectively while the 30% replacement raised it by c.14%.

The results agree with PC authors: Cussino and Negro [34] experimentally confirmed a decrease in porosity as calcium carboaluminate hydrate was formed. Similarly, according to Tsvilis et al. [52, 53], 10% limestone (at 0.50 w/c and 3:1 sand:cement) decreased the porosity of PC materials while replacements over 20% increased it. PC authors usually attribute this reduction to the additional nucleation sites (provided by the limestone particles) which result in a further distribution of C-S-H blocking capillary pores. A refinement of the pore structure due to the limestone reaction has even been reported in low aluminate and ferrite cement [54]. The porosity decrease can also relate to the well-known physical effect of fillers increasing packing and enhancing density.

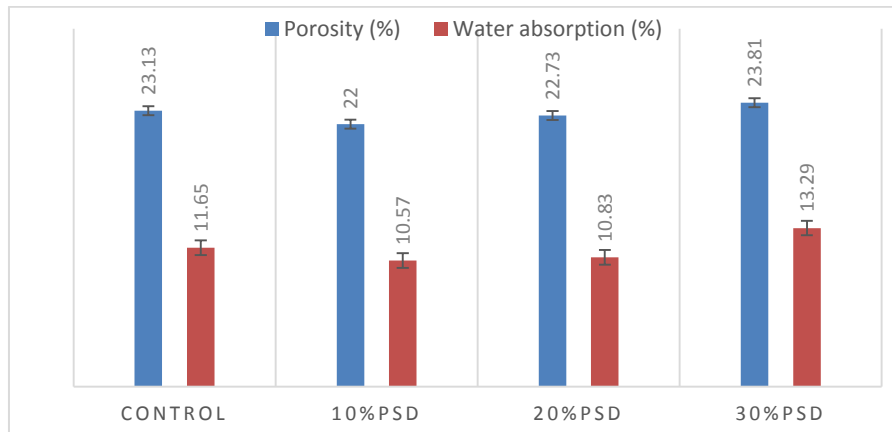


Figure 12. Porosity and water absorption of NHL5 and NHL5/limestone mortars at 90 days. $COV_s=0.10-3.20$.
PSD= Portland Stone dust.

Capillary suction followed a similar trend. The suction of the 10% limestone mortar is the lowest (30% lower than the NHL5 mortar-Figure 13). The 20% limestone shows a 9% decrease in suction while the 30% mortar shows the highest capillarity, 73% over the NHL5 despite having similar porosity. Suction is determined by pore size and interconnection, it seems that beyond the 20% replacement, limestone significantly increases capillary suction which may be due to the more abundant interfaces rising the quantity of suction-active pores. The slightly lower hygric properties of the 10 and 20% limestone replacements can be partly due to their lower water demand however, the water content of the 30% replacement is even lower ($W/B=0.6$ vs $W/B=0.7$ for the 10% replacement) and yet, the composites show greater porosity and permeability which may be due to the presence of more abundant interfaces. The coefficient of variation (COV) indicates reliable values.

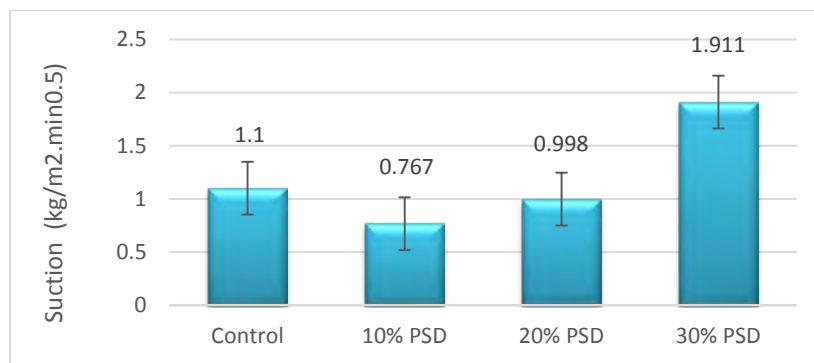


Figure 13. Capillary suction of NHL5 and NHL5/limestone mortars at 90 days.
 $COV=1.14$ (control); $COV=6.40$ (10-20%); $COV=8.19$ (30%).

The 10 and 20% limestone replacements slightly lowered the water vapour permeability of the NHL5 mortars while the 30% replacement slightly enhanced it (Figure 14) however, the variation is not significant. Water vapour permeability is determined by the finest pores (<75 μ m in rocks [55]). Therefore, the limestone replacement preserves the finest pores in the mortars while lowering the water-transport active pores.

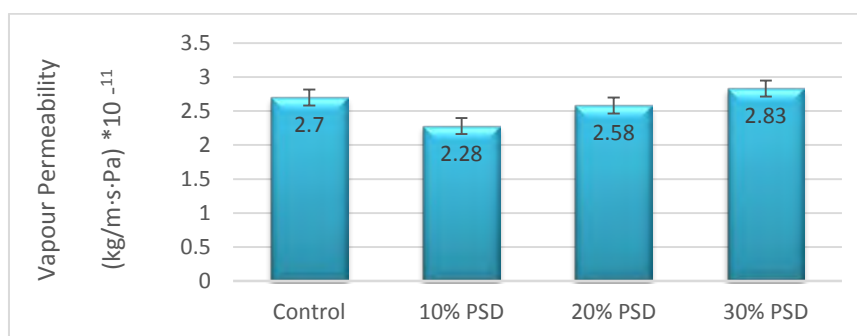


Figure 14. Water vapour permeability of NHL5 and NHL5/limestone mortars at 90 days. COV=8 (control); COV=3-8 (10-20%); COV=6 (30%).

Conclusion

This paper replaces NHL5 mortar binder with limestone in an effort to lower high ultimate strengths that can be detrimental for certain fabrics. The hydration of NHL5 in the presence of limestone and the impact on mortar properties are studied.

Despite the lime's low aluminate content, limestone reaction is evident. The limestone changes the microstructure of the NHL5 paste and the nature of some hydrates. Limestone particles covered with C-S-H fibrils are abundant at early stages. Hydrate plates (probably $\text{CaCO}_3/\text{Ca}(\text{OH})_2$ compounds formed by limestone-belite reaction) strengthen transition zones. Calcium carbo-silicate and carboaluminates hydrates were evidenced in the matrix as plates, similar to CH but often of lower-crystallinity. The limestone fineness ($63\% < 63 \mu\text{m}$), its permeability and the significant specific surface area of its microcrystalline carbonate components have probably enhanced reactivity.

When NHL5 is replaced with 10-30% limestone, the finest mortar pores are preserved (water vapour permeability varies insignificantly) whereas the water-transport active pores tend to slightly decrease (with <20% limestone) or increase (at 30% replacement). The 10% replacement reduced porosity, water absorption and capillary suction by 8, 9 and 30% respectively; and the 20% replacement by 5, 7 and 9%. In contrast, the 30% replacement increased the properties by 12, 14 and 73% respectively. The strong capillary suction rise is likely due to the more abundant interfaces of the 30% replacement rising the quantity of suction-active pores. The reduction of hygric properties at 10-20% replacement is likely due to additional, limestone-induced hydrates.

The 10-20% limestone replacements increased the 28-day strength. However, the limestone lowered strength after 90 days (flexural) or 180 days (compressive) while the NHL5 mortar continued to develop compressive strength, increasing by c.14 between 90 and 180 days and a further c. 10% between 180 days and 1 year. The reduction of the late strength caused by the limestone can be due to transformation (e.g. carbonation) of some limestone-induced hydrates such as the $\text{CaCO}_3/\text{Ca}(\text{OH})_2$ compounds or even the calcium carbo-silicate and carboaluminates hydrates.

Contrary to PC, the limestone lowers the water demand of the NHL5 mortars increasing 28-day strength but lowering the final strength without a major effect on moisture transport and vapour permeability. To achieve a proper workability using less water in mortars has benefits relevant for those involved in mortar design.

A NHL mortar's water content can be lowered by partially replacing the binder with limestone. This would increase strength for up to 125-180 days however, after this, the limestone would lower the strength of the NHL5. The limestone can lower the strength of NHL5 so that they do not become overly strong over long time periods and damage some historic fabrics.

Acknowledgment

This research was funded by the Irish Research Council. Testing was carried out in the Dept. of Civil Engineering, Trinity College Dublin. We thank Chief Technician D. McAuley for facilitating our work and M. Grimes and E. Dunne for their assistance. Thanks to Dr R. Goodhue of the ICRAAG (Irish Centre for Research in Applied Geosciences) for his help with the XRD analysis and to D. Simpson and C. Dooley of the ICRAAG and the Advanced Microscopy Laboratory (SFI supported centre at the AMBER, CRANN Institute) respectively for their help with the SEM.

References

1. EN 197-1:2011. Part 1: Composition, specifications and conformity criteria.
2. Voglis N, Kakali G, Chaniotakis E, Tsvivilis S, (2005) Portland-limestone cements. Properties and hydration compared to other composite cements. *Cem. Concr. Comp.* 27(2) 191-196.
3. Moir G.K (2003) Limestone Cements: Gaining Acceptance. *Int. Cem. Rev.*, 67-70.
4. Hooton R D, Nokken M and Thomas M D A Portland-limestone cement: state-of-the-art and gap analysis. (2007) *Cem. Ass. Canada. Univ. of Toronto.*
5. Ashurst J and Ashurst N (1998) *Practical Building Conservation, Volume 3: Mortars, Plasters and Renders.* Gower Technical Press, Aldershot.
6. Banfill P.F.G, Forster A.M (1999) A relationship between hydraulicity and permeability of hydraulic lime. *Proc. Int. RILEM workshop (PRO 12), Historic Mortars: Characteristics and tests*, 173-183.
7. Pavía S., Bolton J. (2000) *Stone, Brick and Mortar.* Wordwell. Bray.
8. Livesey P (2002) Succeeding with Hydraulic Lime Mortars. *J of Arch. Cons.*, 8:2, 23-37. DOI: 10.1080/13556207.2002.10785317

9. Livesey P, Holmes S, Farey M. (2003) Hydraulic Lime Mortar for Stone, Brick and Block Masonry: A Best Practice Guide. Donhead UK.
10. Lanas J., Perez Bernal J.L., Bello M.A., Alvarez Galindo J.I. (2004) Mechanical properties of NHL-based mortars. *Cem Concr Res* 34: 2191–2201
11. Henriques F.M, Charola A.E, Groot, C, Forster AM, Auras M. (2004) Formulating mortars and renders for historic buildings. *Int. J. Rest.* (10) 6: 583-591
12. Pavía S. and Hanley R. (2010) Flexural bond strength of natural hydraulic lime mortar and clay brick. *Mat and Str*, 43 (7): 913 – 926
13. Costigan A. and Pavía S. (2010) Mechanical properties of clay brick masonry bound with hydraulic limes and hydrated calcium lime. *Proc of 8th Int. Masonry Conf.*, Dresden, Jäger, Haseltine, Fried eds.: 903 - 914
14. Groot C., Hughes J.J. et al. (2012) RILEM TC 203-RHM: Repair mortars for historic masonry: Performance requirements for renders and plasters. *Mat and Str* 45:1277–1285. DOI 10.1617/s11527-012-9916-0
15. EN 459-1: 2010 Building limes. Specification and Conforming Criteria.
16. Bessey G.E. (1938) *Procd. Symp. Chem. Cements*, Stockholm: 186.
17. Grandet J. and Ollivier J. P. (1980) Etude de la formation du monocarboaluminate de calcium hydrate au contact d'un granulat calcaire dans une pate de ciment portland. *Cem and Concr Res.* vol. I: 759-770.
18. Feldman R. F., Ramachandran V. S. and Sereda P. J. (1965) Influence of CaCO₃ on the hydration of 3CaO.Al₂O₃. *J. Am. Ceram. Soc.* 48 (i): 25-30.
19. Bachiorrini A., Guilhot B., Murat M., Negro A., Soustelle M., Fournier A.A.(1986) Influence de la calcite sur l'hydratation de l'aluminate moncalciq. Correlation entre les resultants experimentaux et la thermodynamique du système. 8th ICCS, Rio de Janeiro, Brazil. Vol.IV: 376-380.
20. Vernet C. (1986) Sequence et cinétique des reactions d'hydratation de l'aluminate tricalciq en presence de gypse, de chaux et de fillers calcaires. 8th ICCS, Rio de Janeiro, Brazil. Vol.III: 70-74.
21. Ramachandran V. S. (1988) Thermal analysis of cement components hydrated in the presence of Calcium carbonate, *Termochemica Acta* 127: 385-394.
22. Bachiorrini A. and Murat M. (1987) Evolution microstructurale des composites du système ciment alumineux-granulat calcaire. I. Mode de propagation de la fissure. *Cem. Conc. Res.* 17: 242-248.

23. Péra J., Husson S., and Guilhot B. (1999) Influence of finely ground limestone on cement hydration. *Cem. Concr. Comp.* 21(2): 99-105.
24. Soroka I. and Stern N. (1976) Calcareous Fillers and the Compressive Strength of Portland Cement. *Cem. Concr. Res.* Vol. 6: 367-376.
25. Soroka I. and Setter N. (1977) The effect of fillers on strength of cement mortars. *Cem. Concr. Res.* 7(4): 449–56.
26. Ramachandran V. S. and Zhang C. M. (1986) Hydration kinetics and microstructural development in the $3 \text{ CaO} \cdot \text{Al}_2\text{O}_3 - \text{CaSO}_4 \cdot 2\text{H}_2\text{O} - \text{CaCO}_3 - \text{H}_2\text{O}$ system. *Mat. and Str.*, 19, 114 (1986) 437-444
27. Kurdowski W. (2014) *Cement and Concrete Chemistry*. Springer. Netherlands.
28. Livesey P.(1991) Strength Characteristics of Portland-Limestone Cements, *Cons. & Buil. Mat.*, vol. 5, no. 3: 147-150.
29. Vuk T., Tinta V., Gabrovšek R. and Kaučič V. (2001) Effect of limestone addition, clinker type and fineness on properties of PC. *Cem. Conc. Res.* 31: 135-139.
30. Matthews J.D. (1994) Performance of limestone filler cement concrete. In *Euro-Cements –Impact of ENV 197 on Concrete Construction*, (Dhir and Jones Eds.), E&FN Spon, London: 113-147.
31. Dhir R.K., Limbachiya M.C., McCarthy M.J., Chaipanich A. (2007) Evaluation of portland limestone cements for concrete construction. *Mat. Str.*40:459-473.
32. Sprung S. and Siebel E.(1991) Assessment of the suitability of limestone for producing Portland limestone cement. *ZKG International, Edition B*, 44(1): 1-11.
33. Jambor J. (1980) Influence of $3\text{CaO} \cdot \text{Al}_2\text{O}_3 \cdot \text{CaCO}_3 \cdot n\text{H}_2\text{O}$ on the structure of cement paste. 7th ICCO, Paris, France Vol.IV: 487-492.
34. Cussino L. and Negro A. (1980) Hydratation du ciment alumineux en presence d'agrégat siliceux et calcaire, 7th ICCO, Paris, France. Vol.V: 62-67.
35. De Weerdt K. (2007) Ternary Blended Cements with Fly Ash and Limestone. Part II: Limestone powder. SINTEF report.
36. Pavía S. and Aly M. (2016) Influence of aggregate and supplementary cementitious materials on the properties of hydrated lime (CL90s) mortars. *Mat. de Constr.* (66) 324 e104 <http://dx.doi.org/10.3989/mc.2016.01716>
37. *EN 933-10:2001 Tests for geometrical properties of aggregates. Assessment of fines. Grading of fillers (air-jet sieving)*

38. Saint Astier/CESA (2015) *Natural Hydraulic Limes (NHL). Technical data sheet. Conforming to European Regulations (CE) n°1907/2006. NHL 5.* <http://www.stastier.co.uk/nhl/health-safety/nhl5-hs.htm>. -accessed 2016.
39. EN 459-2: 2010 *Building lime. Test methods.*
40. RILEM (1980) Tests to measure the deterioration of stone and assess the effectiveness of treatment methods. *Mat. and Str.* 13: 175– 253.
41. UNE 67-027-84 *Determinacion de la absorcion de agua. Ladrillos.*
42. EN 1925: 1999 *Natural stone test methods. Determination of water absorption coefficient by capillarity.*
43. EN 1015-11/19: 1999 *Methods of test for mortar for masonry. Determination of water vapour permeability of hardened rendering and plastering mortars/Determination of strength.*
44. Grist E.R., Paine K. A., Heath A., Norman J., Pinder H.(2015) *The environmental credentials of hydraulic lime-pozzolan concretes*, *J. Cleaner Prod.* <http://dx.doi.org/10.1016/j.jclepro.2015.01.047>
45. Mertens G., Madau P., Durinck D., Blanpain B. & Elsen J. (2007) *Quantitative mineralogical analysis of hydraulic limes by X-ray diffraction.* *Cement and Concrete Res.* 37(11): 1524-1530.
46. Taylor H. F. (1997). *Cement chemistry.* Thomas Telford.
47. Bogue R.H. and Lerch W. (1934) *Heat of hydration of portland cement pastes*, Bureau of Standards *J. of Res.*, Vol. 12, No. 5 p. 645. Res. Paper 684 (RP684)
48. Odler I. (2007) *Hydration, setting and hardening of Portland cement*, in *Lea's chemistry of cement and concrete*, Hewlett P.C. Ed (UK: Elsevier): 241-289.
49. Pavia S. (2008) *A petrographic study of mortar hydraulicity*, in HMC08, 1st Historic Mortar Conference, Lisbon, Portugal: LNEC.
50. Monteiro P.J.M and Meht P.K. (1986) *Interaction between carbonate rock and cement paste.* *Cem. Concr. Res.* 16: 127-134.
51. Costigan A., Pavia S., Kinnane O. (2015) *An experimental evaluation of prediction models for the mechanical behaviour of unreinforced, lime-mortar masonry under compression*, *J. of Build. Eng.*, 4: 283 – 294
52. S. Tsivilis, G. Batis, E. Chaniotakis, G. Grigoriadis and D.Theodossis, “*Properties and behavior of limestone cement concrete and mortar*”, *Cem Concr Res* 30, 10, (2000): 1679-1683.

53. S. Tsivilis E. Chaniotakis, E. Badogiannis, G. Pahoulasa and A. Ilias, A study on the parameters affecting the properties of Portland limestone cements, *Cem Concr Comp* 21, (1999): 107-116.
54. Sellevold E. J, Bager D. H., Klitgaard-Jensen E. and Knudsen T. (1982) Silica Fume-Cement Pastes: Hydration and Pore Structure, Condensed Silica Fume in Concrete, Institutt for Bygningsmateriallære, Norges Tekniske Høgskole, Universitetet i Trondheim, Trondheim, Norway, BML 82.610: 19-50.
55. D. Hoffmann, K. Niesel K. and R. Plagge, Relationship between pore structure and other physical-technical characteristics of stone, 8th Int. Congress on Deterioration and Conservation of Stone, ed. J. Rieder, Berlin (1996): 461-472.

Comparing the moisture permeability of limecrete and concrete floor slabs

Grace A. Phillips¹, Kevin Briggs¹, Iain McCaig², Richard J. Ball¹

(1) University of Bath, gap37@bath.ac.uk, ORCID ID : 0000-0001-5858-6508; ab2kb@bath.ac.uk, ORCID ID: 0000-0003-1738-9692; easrjb@bath.ac.uk, ORCID ID : 0000-0002-7413-3944

(2) Historic England, iain.mccaig@historicengland.org.uk

Abstract

Retrofitting impermeable ground-bearing floor slabs to an old building is thought to ‘drive’ soil moisture up adjoining walls. Historic England has commissioned the University of Bath to conduct research into water vapour and liquid permeation through typical floor slab materials, and their influence on local soil moisture. The project comprises computer modelling to examine the response of soil moisture to slab installation, laboratory tests to analyse moisture movement rates through slab materials, and field monitoring to measure the effect of different slab materials *in situ*. Initial laboratory tests on two materials, concrete and NHL5-based limecrete, used a bespoke modular soil-slab-air apparatus developed to establish evaporation rates through slab materials. Subsequent material characterisation tests were conducted to compare their microstructural properties and moisture transfer characteristics including mercury intrusion porosimetry (MIP), sorptivity tests, and scanning electron microscopy (SEM). Preliminary results showed the NHL5-based limecrete slab was only marginally more permeable than the concrete slab, suggesting that a NHL5-based limecrete slab might be more effective than a concrete slab in reducing water rise in a wall. Further testing of limecrete mixes and *in situ* monitoring is proposed to verify these results.

Introduction

Moisture is a major cause of deterioration of historic building fabric. It drives many deleterious processes including biological growth, the actions of soluble salts, chemical attack and freeze-thaw damage [1, 2]. Therefore, understanding moisture movement and the factors affecting it are important considerations in building conservation. The sketch in Figure 1 shows the main sources and pathways of moisture in and around a building of traditional construction. Internal sources, such as condensation and leaks, can be controlled by regular maintenance, adequate heating, and ventilation [3]. External water sources including precipitation and wind driven rain can be controlled by creating a water shedding building envelope. But a more discreet and equally important external water source is soil moisture. Although soil moisture levels are influenced by the hydrological characteristics of the site, defective drains and inadequate surface water disposal arrangements often prove to be significant sources. In modern buildings damp proof courses (DPCs) are used to control

the capillary rise of moisture in walls, but historic buildings rely on the ability of permeable building fabric to absorb and readily allow evaporation of moisture [4]. Therefore, any alterations that might affect the ‘hygric balance’ (water in = water out) of the building, such as the introduction of a concrete ground-bearing floor slab, require careful consideration.

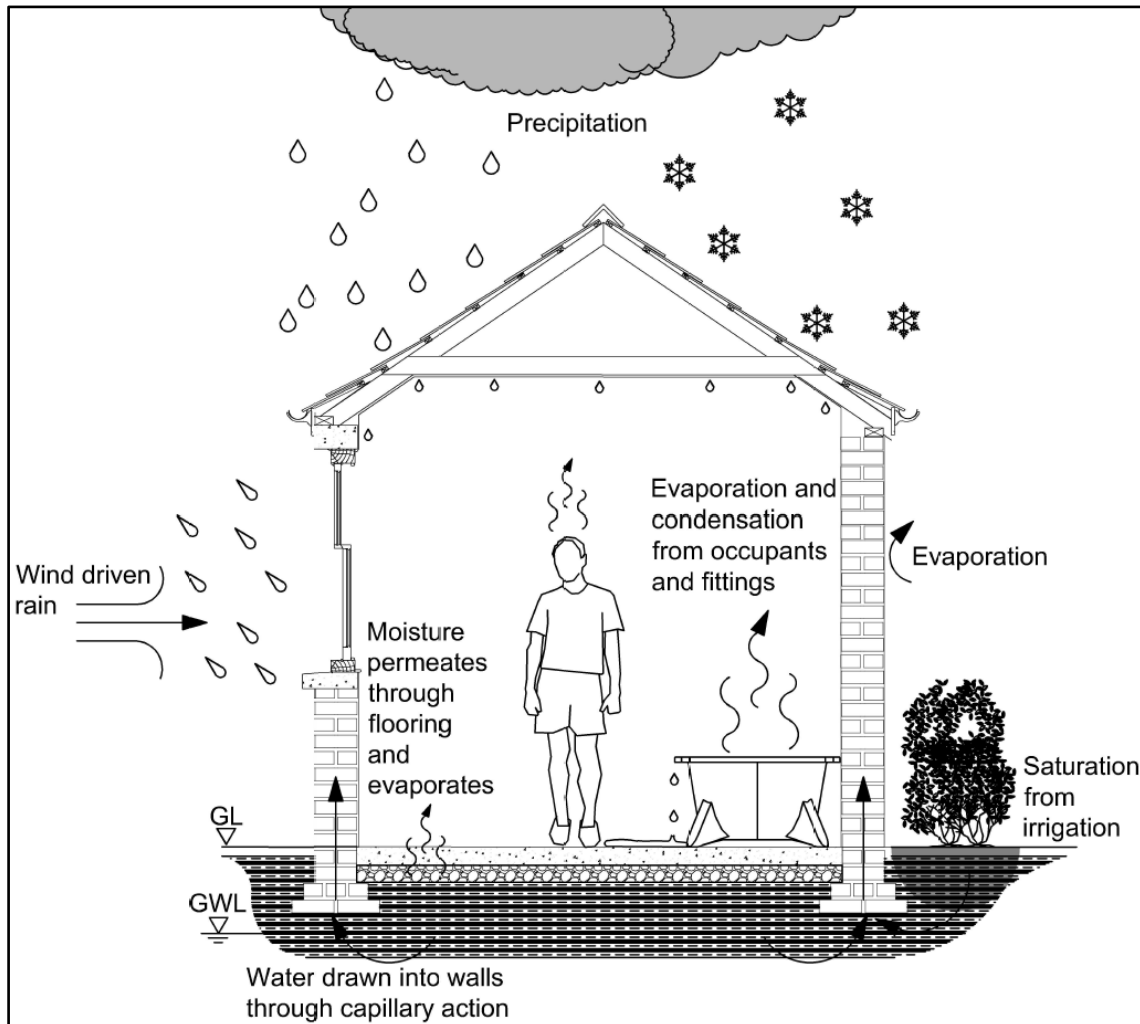


Figure 1. Moisture movement in and around buildings.

Research is being carried out at the University of Bath in collaboration with Historic England to understand the influence of floor slab material (concrete or limecrete) on soil moisture and dampness within the walls of historic buildings. Firstly, modelling was used to explore how the permeability of floor slab materials influenced local ground water flow in the liquid and vapour phases. Secondly, a suite of laboratory tests were carried out to determine the material properties of concrete and limecrete slabs and measure their comparative moisture permeation rates. Lastly, long term field measurements have been taken at two properties to investigate the in situ response of both soil and wall moisture levels to changes in floor materials [5]. These measurements are ongoing. This paper focuses on the initial findings from the laboratory element of the project, outlining the experiments and comparing concrete and limecrete slabs with respect to their moisture transport properties. The laboratory tests included a modular soil-slab-air experiment and a range of material

characterisation tests. The modular soil-slab-air experiment was developed for the project and was run for a period of at least four weeks per slab in order to measure moisture transfer rates. Subsequent characterisation tests were carried out in order to correlate the slab properties with the observed water movement. These tests included imaging using a scanning electron microscope (SEM), mercury intrusion porosimetry (MIP), sorptivity testing, and mechanical characterisation by compression testing.

Materials

Two materials have been tested in the modular system; concrete and limecrete. The limecrete slab was manufactured using the highest strength classification of commercially available natural hydraulic lime (NHL5). The slab mix designs are shown in Table 1.

Table 1. Material designs for concrete and limecrete slabs tested

	Limecrete	Concrete
Components	NHL (Roundtower NHL5) 6mm to dust aggregate Gravel	Cement 6mm to dust aggregate Gravel
Coarse:fine ratio	0.54	0.4
Binder:aggregate ratio	0.33	0.2
Water ratio	0.50	0.625
Binder:fine aggregate:coarse aggregate ratio	1.00 : 1.95 : 1.05	1.00 : 3.57 : 1.43

The concrete and limecrete were cast as circular slabs, as shown in Figure 2, to fit the modular set-up. Two bolts were cast into the slab to facilitate installation and removal. The concrete and limecrete slabs were of thickness 84mm and 86mm \pm 2mm respectively. They were cast to fit the apparatus, which had an internal diameter of 355mm \pm 1mm with a gap around the perimeter of approximately 10mm. Slabs were installed within 2-4 weeks of casting and had not completely cured.



Figure 2. Cast concrete slab prior to use in the modular slab experiment.

Experimental Set-up and Procedure

Modular Slab Experiment

The set-up for the modular slab experiment is shown in Figure 3. A galvanised steel cylinder was filled with 50mm of gravel, then 80mm of clay soil. The clay was saturated with water. Water evaporating from within the cylinder was replaced by water supplied at a constant pressure head through the use of a Mariotte bottle. The Mariotte bottle was set on scales to log the change in mass with time. A Tinytag temperature and relative humidity (RH) probe was installed at the top of the cylinder to monitor the environment at the surface. The experiment was run for a minimum of four weeks with no soil to determine the free water conditions and then with a bare soil layer for four weeks, as shown in Figure 4, to establish the evaporation rate for a bare soil condition.

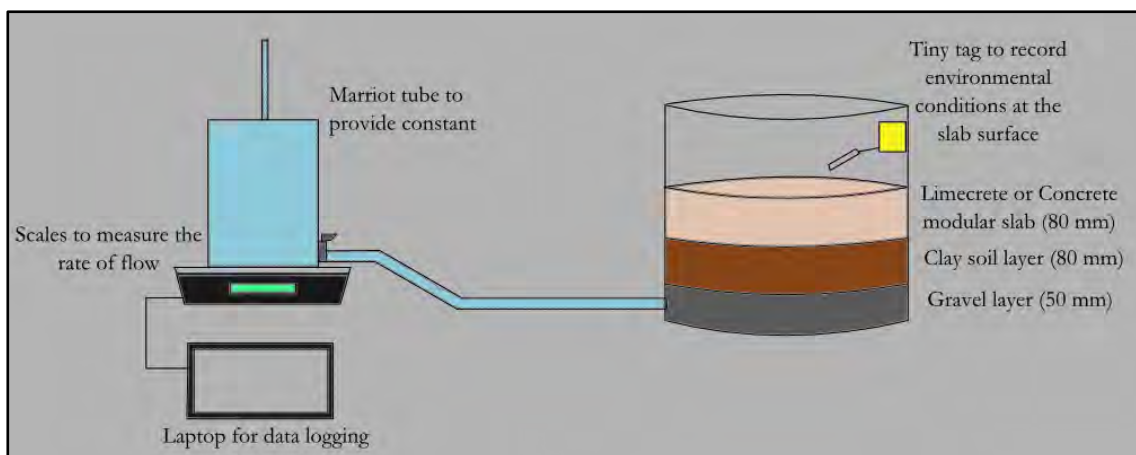


Figure 3. A diagram of the modular soil-slab-air experiment set-up.



Figure 4. Initial saturation of the bare soil surface.

The cast slabs were inserted into the cylinder directly onto the clay soil surface and sealed with silicon rubber around their perimeter. This setup excluded additional elements such as damp proof membranes (DPMs) and so does not directly replicate typical floor systems. However this enables a direct comparison of slab materials to be made without inhibiting moisture transfer to the underside of the slab. Each stage of the test was monitored for a duration of at least four weeks. The limecrete was monitored for the first 12 weeks followed by bare soil for 4 weeks and then the concrete slab for 9 weeks. Following extraction from the apparatus both slabs underwent further analysis.

SEM Imaging

Scanning electron microscopy (SEM) imaging was carried out using a JEOL SEM6480LV to reveal the microstructure and nature of the porosity. The SEM scans a focused beam of electrons on the surface which interact with the sample producing secondary electrons which are detected and the resulting signal used to produce an image. Fracture surfaces from slab samples were coated in gold prior to imaging to prevent surface charging, enabling clearer images to be taken and at higher levels of magnification. Images were taken at x100, x500, x1k, x2k, x4k, x5k, and x10k magnification.

Mercury Intrusion Porosimetry (MIP)

MIP tests provided a quantitative measure of the size distribution of the internal pores. The Pascal 140 and Pascal 440 from Thermo Scientific were both used to carry out the test. The sample is first inserted into the low pressure Pascal 140 which pressurises the mercury, forcing it into the accessible pores. As the pressure increases, the mercury enters into smaller pores. The Pascal 140 increases the pressure up to 400kPa and once the test is completed in the Pascal 140 the sample is transferred to the high pressure Pascal 440. The Pascal 440 increases the pressure up to 400MPa. The results from the 140 and 440 are then combined providing data over the entire pressure range. Plotting the pore diameter against intruded pore volume is a tool for establishing the critical length of a material. The critical length, ' R_c ', is the pore diameter that corresponds to the sample's breakthrough pressure. It is considered the largest particle size that can percolate through a sample.

Compression Tests

Compression tests, carried out to BS 1015-11, elucidated the mechanical properties of the slab material. Blocks of approximate size 40mm x 40mm x 40mm (± 4 mm) were cut from the slab following testing and the exact measurements to the nearest mm recorded. Six samples cut from each slab were tested to failure using either the 50kN Instron 3369 or the 2000kN Autamax 5 concrete compression equipment and the peak load was recorded. The peak load and applied area were then used to calculate the ultimate compressive strength of the sample. This characteristic is important as slabs require a minimum compressive strength to be suitable for use as a floor slab [6].

Sorptivity Tests

Sorptivity tests enabled the material's capacity to absorb water to be ascertained. This property is important as the absorption provides a supply of water to be transferred and evaporated. The tests were carried out to BS 1015-18. Samples were cut to 40mm x 40mm (± 4 mm) x approximately 80mm. The samples were dried in a 50°C oven until constant mass was achieved. Samples were then placed within a tray of water on supports such that the sample was immersed in approximately 10mm of water. Samples were weighed and the water height on the sample surface was measured at 10, 40, 90, 160, and 250 minutes.

Results

Water Transfer Rates

The change in mass of the mariotte bottle was recorded at one minute intervals, allowing the water (vapour) transfer rate through the slabs to be easily calculated in gmin^{-1} or gday^{-1} . The water transfer rate represents the actual evaporation rate from the slab or soil surface, which is less than the potential evaporation rate from a free water surface [7]. The rate can be converted to ms^{-1} using equation 1,

$$E \left(\text{ms}^{-1} \right) = \frac{E(\text{gday}^{-1})}{86400 \times 10^3 \times \rho \times A} \quad \text{Equation 1}$$

where 'E' is the water transfer rate, ' ρ ' is water density for the average air temperature, and 'A' is the area of the slab at 0.088 m^2 . The resulting rates are in Table 2.

Table 2. Actual evaporation rates for each testing configuration

Surface	Average E (gmin^{-1})	Average E (gday^{-1})	Average Temp. ($^{\circ}\text{C}$)	ρ (kg/m^3)	Average E (ms^{-1})
Free water (gravel)	0.1708	246.0	18.1	998.6	32.39×10^{-9}
Bare clay surface	0.0754	108.6	19.4	998.3	14.31×10^{-9}
Limecrete (NHL5) slab	0.0063	9.018	20.1	998.2	1.188×10^{-9}
Concrete slab	0.0041	5.966	20.9	998.0	0.786×10^{-9}

The gravel surface had the greatest water transfer rate and had more than double the water transfer rate of the bare clay surface; this is because the clay restricted the supply of water to the surface for evaporation. The addition of a slab further restricted the supply. The limecrete slab was only marginally less restrictive than the concrete slab. For the limecrete and concrete slabs water transfer rates were smaller than the bare clay soil by 12 and 18 times respectively.

SEM Imaging

The x10k SEM images of the limecrete and concrete are presented in Figure 5 and 6, respectively. Calcium Silicate Hydrate (C-S-H) can be seen in both samples with a greater number of larger needle-like structures in the NHL5 limecrete sample.

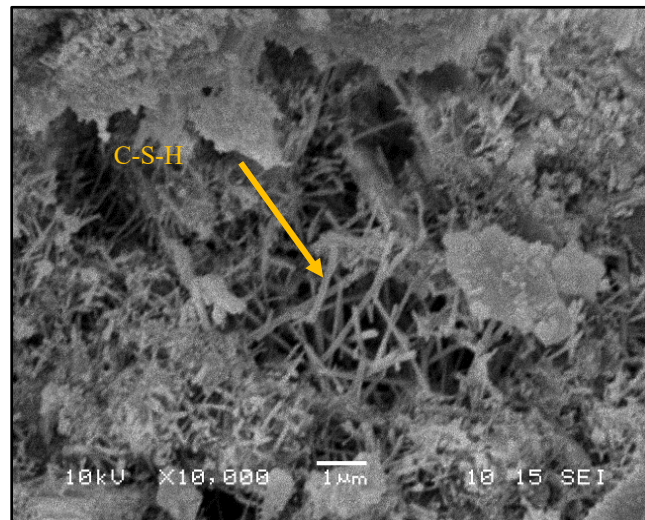


Figure 5. SEM image of the NHL5 limecrete sample showing signs of formed calcium silicate hydrate (C-S-H).

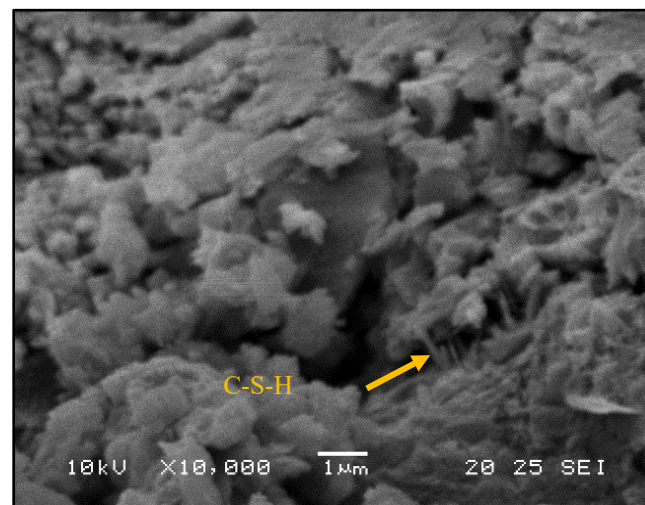


Figure 6. SEM image of the concrete sample showing signs of formed C-S-H.

Mercury Intrusion Porosimetry (MIP)

MIP results are provided in Table 3 and Figure 7. The critical length ' R_c ' for both materials lie within the capillary region; for limecrete it was circa 50nm and the concrete had a bimodal distribution with two peaks at around 75nm and 300nm. For concrete the largest pore diameter of 300nm is the critical length and represents the largest size particle that can percolate through the sample. Through comparing the limecrete and concrete plots in

Figure 7. it can be seen that the limecrete had a greater pore volume, as is confirmed by the total pore volume values given in Table 3.

Table 3. MIP results for limecrete and concrete

Case	Bulk Density (g/cm ³)	Total Pore Volume (cm ³ /g)	Total Pore Area (m ² /g)	Porosity by Hg Intrusion (%)	Average Pore Diameter (nm)
Limecrete	2.1319	0.0915	10.236	19.51	35.75
Concrete	2.2096	0.0665	6.716	14.68	39.58

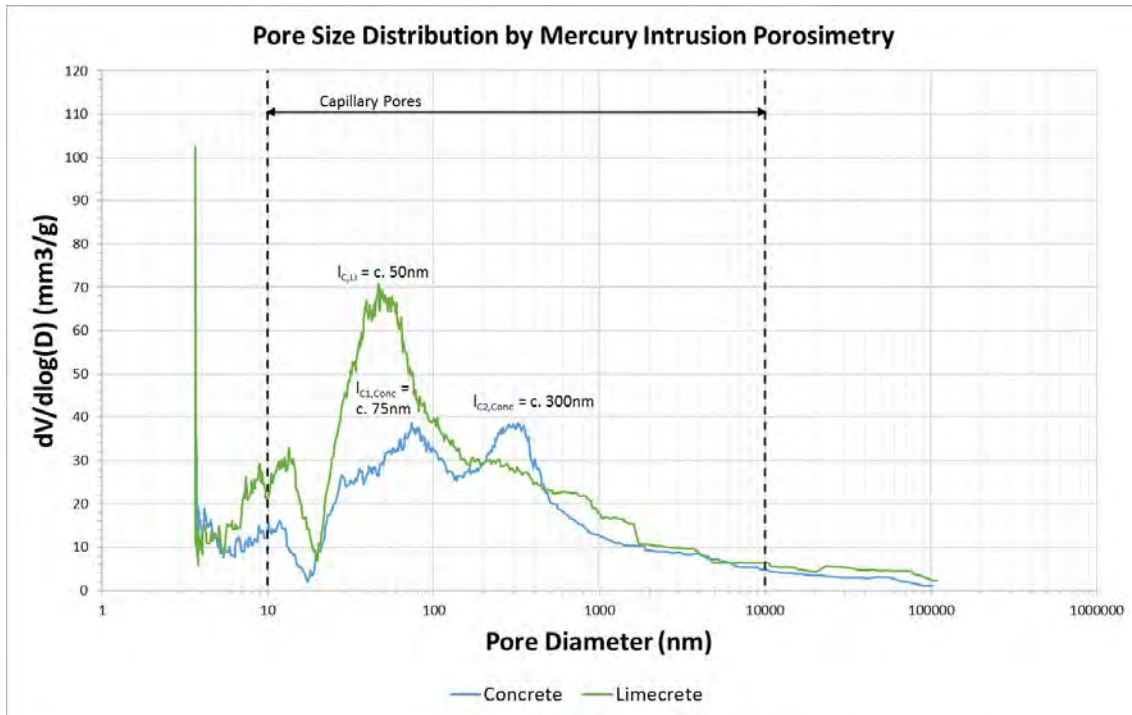


Figure 7. Plot of pore volume measured by MIP, with pore diameter for the limecrete and concrete samples.

Compressive Strength

The results for the compressive tests are given in Table 4. The Limecrete had an average compressive strength of 14.56MPa. The concrete samples exhibited a greater compressive strength of 25.18MPa, however the concrete samples were less consistent, as demonstrated by the larger standard deviation. Any samples that exceeded the 50kN load capacity of the Instron 3369 were tested using the Automax 5.

Sorptivity

The coefficient of water absorption was calculated for each sample using the equation

$$C = 0.1 \frac{m_{90} - m_{10}}{A\sqrt{t}} \quad \text{Equation 2}$$

where 'C' is the coefficient of water absorption in kgm⁻²min^{0.5}, 'm₉₀' is the sample mass at 90 minutes in kg, 'm₁₀' is the sample mass at 10 minutes in kg, 'A' is the cross-sectional area in

m^2 , and 't' is the time in minutes. Table 5 shows the sorptivity results for two samples of concrete and one sample of limecrete.

Table 4. Compressive strengths for limecrete and concrete samples

Material	Sample	Instrument Capacity	Ultimate Compressive Strength σ_{ULT} (MPa)	Mean Compressive Strength (MPa)	Standard Deviation (MPa)
Limecrete	L1	50kN	15.22	14.56	1.15
	L2a	50kN	13.13		
	L3	50kN	15.51		
	L4	50kN	15.04		
	L5	50kN	12.80		
	L6	50kN	15.69		
Concrete	C1a	2000kN	24.02	25.18	4.90
	C2	2000kN	21.05		
	C3	2000kN	21.86		
	C4	50kN	20.32		
	C5	50kN	31.99		
	C6	50kN	31.85		

Table 5. Sorptivity coefficients for limecrete and concrete

Sample	Material	Mass at 10s, m_{10} (g)	Mass at 90s, m_{90} (g)	Coefficient of water absorption ($\text{kgm}^{-2}\text{min}^{0.5}$)
L3	Limecrete	290.51	294.06	0.023
C2	Concrete	269.60	271.36	0.013
C3	Concrete	299.38	300.93	0.010

Discussion

Water Transfer Rate

Models of ground and wall moisture flow have been developed at the University of Bath. These suggest that the floor slab material will affect the supply of water to the wall base and hence the water available for transfer through the wall. The initial laboratory results showed that the clay had an influence on the rate of water transfer and evaporation and that the presence of a slab further impeded water transfer. The two slab materials tested to date, NHL5-based limecrete and concrete, exhibited similar water transfer rates with limecrete being marginally more effective at moisture transfer. Further testing including alternative slab compositions and capillary breaks is proposed to ascertain whether the modular slab experiment supports the findings from the model. The authors are also undertaking *in situ* long term monitoring of full scale trials at two historic properties to assess what impact slabs have on wall and soil moisture.

SEM Imaging

The needle-like structures shown in Figure 5 and 6 are calcium-silicate-hydrate (C-S-H) formed from hydrated silicates in both the NHL and cement. In NHLs they grow during the initial hydration phase of hardening, enhancing the material's strength. The morphology of the C-S-H structures in the concrete sample are more consolidated compared to that in the NHL resulting in a denser structure. This is demonstrated by the smaller number of voids visible in Figure 6 than in Figure 5 and the higher bulk density and lower pore volume values for concrete in Table 3.

Mercury Intrusion Porosimetry (MIP)

The bulk density and pore volume values for the concrete showed that it is more dense than the limecrete. Whilst the concrete had a larger critical length and a greater average pore diameter, the limecrete had a greater pore volume, most of which lies within the capillary region. It is this accessible interconnected pore structure that contributes to greater water transfer rates through the limecrete.

Compressive Strength

The compressive strength for the concrete was almost double that of the limecrete. The minimum compressive strength of the limecrete was 12.80MPa which is adequate for classification as a GEN 1 concrete. GEN 1 concrete typically has a compressive strength of 10MPa and the NHBC class this as suitable for use in unreinforced house floors with permanent finishes [6, 8 n.d., 9 n.d.]. Floor slab compressive strength is only one indication of appropriateness for use and further testing is required before slab mixes are adopted. For example durability testing is required to assess the slab resistance to abrasion, freeze-thaw, and chemical and salt attack.

Sorptivity

The sorptivity of the limecrete was approximately double the concrete's sorptivity. This suggests that the limecrete uptakes water quicker than the concrete, providing more water supply for evaporation at the surface, enabling higher water transfer rates. Further sorptivity testing is proposed to validate these results and compare these slab materials with those used in future tests.

Conclusions

The water transfer rates derived from the bespoke modular soil-slab-air apparatus showed that soil restricts the water supply to the surface for evaporation, and the addition of a slab restricts the supply further. The water transfer rate of the sample slabs was affected by the sorptivity of the material and the presence of an interconnected pore structure. The NHL5

limecrete slab was found to have a greater sorptivity and pore volume than the concrete slab, and hence it had a greater water transfer rate when tested in the soil-slab-air apparatus. Preliminary results obtained from modelling and laboratory tests suggest that NHL5-based limecrete was marginally more effective than a concrete slab in transferring moisture. However, this has yet to be verified with further testing of different slab compositions, by the long-term monitoring of *in situ* installations, and through representative slab tests including typical construction details such as capillary breaks. Following the successful demonstration of the apparatus detailed in this article, further floor slab systems will be tested to provide a representative range of moisture transport characteristics. Additional studies will explore construction variations such as the inclusion of cracks and construction joints.

Acknowledgements

This study was supported by Historic England and the EPSRC Centre for Decarbonisation of the Built Environment (dCarb) [grant number EB-AR1218]. The authors wish to extend their thanks to David Muddle and David Surgenor for their assistance in the project.

References

1. Cultrone, G., Sebastián, E., and Huertas, M.O., 2007. Durability of masonry systems: A laboratory study. *Construction and Building Materials*, 21(1), pp.40–51.
2. Feilden, B.M. (Bernard M., 2003. Botanical, biological and microbiological causes of decay. In: *Conservation of Historic Buildings*. Abingdon: Architectural Press, pp.133–138.
3. Feilden, B.M. (Bernard M., 2003. Internal environment of historic buildings. In: *Conservation of Historic Buildings*. Abingdon: Architectural Press, pp.173–185.
4. Douglas, J., 1998. The development of ground floor constructions: part IV (damp proofing methods). *Structural Survey*, 16(2), pp.76–80.
5. Briggs, K., 2017. Do some floor slab retrofit solutions increase wall damp in historic buildings?
6. NHCB, 2018. Concrete and its reinforcement. In: *NHBC Standards 2018*. pp.11–22. Available from: <http://www.nhbc.co.uk/Builders/ProductsandServices/Standardsplus2018/#14> [Accessed 18 April 2018].
7. Penman, H.L., 1948. Natural evaporation from open water, bare soil and grass. [Online]. *Proceedings of the Royal Society of London. Series A, Mathematical and physical sciences*, 193(1032), pp.120–45. Available from: <http://www.ncbi.nlm.nih.gov/pubmed/18865817> [Accessed 19 April 2018].

8. Mister Concrete, *Concrete types and their strengths* / *Mister Concrete* [Online]. Available from: <http://www.misterconcrete.co.uk/concrete-types-and-their-strengths> [Accessed 18 April 2018].
9. EasyMix Concrete UK Ltd, *Types Of Concrete And Their Strengths - EasyMix Concrete UK Ltd* [Online]. Available from: <https://www.easymixconcrete.com/news/types-of-concrete-and-their-strengths/> [Accessed 18 April 2018].

Impact of guar gum and chitosan ethers on physico-mechanical properties and durability of natural hydraulic lime mortars

Tomáš Žížlavský^{1*}, Martin Vyšvařil¹, Patrik Bayer¹, Pavla Rovnaníková¹

(1) Faculty of civil engineering, Brno University of Technology, Veveří 331/95 Brno 602 00 Czech Republic, zizlavsky.t@fce.vutbr.cz, vysvaril.m@fce.vutbr.cz, bayer.p@fce.vutbr.cz, rovnanikova.p@fce.vutbr.cz

Abstract

The addition of guar gum derivatives and chitosan ethers has been studied in the natural hydraulic lime (NHL) mortars. These types of polysaccharides can be possibly used as viscosity enhancing admixtures or water retaining agents for the mortars instead of cellulose ethers. The water retention capacity is an essential property of the mortars to enhance the hydration of NHL and mortar adhesion to the substrate. The main part of this study is addressed to the physico-mechanical properties, microstructure, and durability of NHL mortars. The hydroxypropyl- derivatives showed air-entraining function, which is beneficial for the durability of mortars and affects porosity of mortars, as well as water absorption coefficient. The biopolymer addition slightly improved initial flexural strength with the increasing difference for later ages, the only exception being hydroxypropyl guar, which showed slight decrease of flexural strength. Compressive strength decreased by the addition of biopolymeric admixture in all cases; the degree of decrease was dependent on the type and dosage of the admixture.

Introduction

Lime is one of the oldest and most versatile binders used since the ancient times. The natural hydraulic lime (NHL), obtained by burning limestone containing clay impurities, expresses improved physico-mechanical properties such as higher strength and increased durability compared to the aerial-lime based mortar. The NHL has been therefore used for the constructions of greater importance. In the modern times the importance of the limestone quality on the properties of lime has been re-discovered by the British pioneer John Smeaton, whom purposefully used NHL-based mortar during the construction of Eddystone lighthouse in 1750s, which was taken down in 1870s due to the erosion of the underlying rock [1] and not the condition of the building itself. This case shows nicely the benefits and durability of the constructions made from NHL.

During the 20th century the NHL was mostly replaced by cement in the building industry, but thanks to the amount of historical buildings, the need of the NHL for the repairs is still present. In the modern world, industrially prepared, pre-mixed, mixtures are widely used not only in the building industry, but also due to the easiness of the preparation for the end-user. These dry-mix mixtures usually contain viscosity enhancing admixture (VEA), commonly

some of the cellulose ethers, which improves the workability, water retention, and overall the fresh-state properties of the prepared mortar. Due to the nature of cellulose manufacturing [2] the alternative biopolymers are lately being studied, one of them is guar gum and its derivatives. Main advantage of the guar gum is the elimination of the chemical processing while obtaining the polysaccharide from the raw material, namely, beans of *Cyamopsis tetragonoloba* plant. Guar gum derivatives, hydroxypropyl guar (HPG) and carboxymethylhydroxypropyl guar (CMHPG) are widely used derivatives, chiefly in the textile industry, the drilling industry, or in explosives and paper production [3, 4]. In the building industry they are mostly used to improve self-consolidating concrete characteristics, especially bleeding and segregation [5–7]. HPG added to cementitious mixture increases the water-retention capacity of fresh mortar [8] but it is not as effective as hydroxyethylmethyl cellulose [9]. HPG is a non-ionic derivative, while added in lime mortar showed air-entraining function, which affects also durability, water absorption capacity through capillarity, whereas the strength of the specimens has been also positively influenced [10–13]. On the other hand, the addition of ionic CMHPG, do not impact the amount of air entrained in the air lime mortar and the strength of the samples are comparable to the non-admixed mortar, but the workability is affected the same way as in the case of HPG [12, 13].

Chitosan is a linear biopolymer produced by deacetylation of chitin. Chitin is one of the most common biopolymer on the Earth along with cellulose. Its chemical structure is similar to the one of the cellulose only differing by the substitution of one hydroxyl group by the acetyl amine group. Chitosan is obtained by deacetylation of chitin (e.g. treating the shells of shrimp and other crustaceans by sodium hydroxide), its poor solubility in alkaline solution is improved by etherification, resulting in multiple chitosan derivatives (e.g. carboxymethyl chitosan (CMCH) or hydroxypropyl chitosan (HPCH)) [14–16]. Chitosan derivatives added to cementitious material decrease the flow value of the mortar and improve the water retention value of the fresh mortar; in both cases CMCH is more effective than the HPCH [17, 18]. Chitosan addition has a slightly retarding effect on the cementitious mortar due to its polysaccharidic structure, but shows slight improvement for compressive strength [17–19]. While added to aerial lime-based mortar, the disparity in effectiveness of the derivatives on fresh state properties is not observed with exception of air-entraining function of HP derivative [20]. CMCH shows more positive influence on the mechanical properties slightly improving both, flexural and compressive strength with growing dosage-dependency, whilst the HPCH mildly decreases even the flexural strength of the specimens up until the 90 days of age [21]. The decrease of compressive strength of materials with biopolymeric admixture has been spotted by several authors [10–12, 22].

Differences in the impact of biopolymeric addition on the properties of aerial-lime and hydraulic binder based mortar have been spotted [23–25], so it can be assumed that there will be difference also between properties of NHL and any of the above-mentioned binders. Therefore the aim of this study is to improve the knowledge on the behaviour of guar gum and chitosan derivatives modified NHL mortars by investigating the influence of admixture

type on the physico-mechanical properties of mortar with emphasis on the differences between the binders.

Materials and methods

Materials and sample preparation

The samples were prepared from the NHL 3.5 lime (Otterbein Calcidur) according to EN 459-1, and siliceous sand of fraction 0–4 mm (Českomoravský štěrk a.s., Hulín, Czech Republic) the materials were mixed in a 1:1 volumetric ratio (1:2 by weight). The biopolymers were added in the doses of 0.1%, 0.5% and 1% of the weight of binder. The admixtures used were products of Lamberti s.p.a. (guar gum derivatives (HPG and CMHPG)) and Kraeber & co GmbH (chitosan derivatives (HPCH and CMCH)). These materials were well-mixed to prepare homogenous dry mixture, which was introduced into water using constant water:binder ratio of 0.7. The samples were then cast into 40×40×160 mm prismatic moulds and demoulded after 48 hours. The beams were stored in the laboratory conditions (20 °C, 50% relative humidity) until the day of testing.

Methods

After the mixing the following fresh-state properties were tested: flow value (EN 1015-3), water retention value (EN 459-2), bulk density of fresh mortar (EN 1015-6), and air content of fresh mortar (EN 1015-7). On the hardened samples of the age of 7, 28, and 90 days the bulk density by weighting and measuring the beams, and flexural and compressive strength (EN 1015-11) were determined. The 28 days old specimens were also used to specify porosity using high pressure mercury intrusion porosimetry, water absorption coefficient due to capillarity action (EN 1015-18), and frost resistance test according to ČSN 72 2452. It was chosen to define the durability coefficient after 15 cycles, 1 cycle consisting of freezing fully saturated sample for at least 4 hours at -20 ± 3 °C followed by thawing in water bath for at least 2 hours. The frost resistance coefficient is a ratio between the strength of tested mortar and strength of reference mortar (in our case stored under water for the duration of durability test).

Results and discussion

Fresh state properties

Fresh state properties of the NHL based mortars are summarized in Figure 1. All the admixtures with exception of CMHPG had notable impact on the flow value (Figure 1C), CMCH having more linear dosage-dependency then the other two admixtures. The HPCH increases the flow value of cementitious mortar up until the 0.3% dosage, while in NHL-based mortar it decreased the value even in lower doses [17]. Contrary to aerial lime-based mortar, the CMHPG did not affect the flow value [13]. The air-entraining function observed

on lime mortars [13, 20] was proven for HPCH in highest dose only and also HPG (Figure 1B). The air content increase for the other two admixtures correlates with the workability change, the effect observed also for other different biopolymers addition to lime mortar [23, 25]. Density of fresh mortar (Figure 1A) is closely-linked with the air content in the fresh mortar, because besides the type of admixture, the air entrapped during mixing is the only variable in the mortar composition. The admixtures showed water-retaining function (Figure 1D) observed also in lime [10, 11, 13, 20] and cementitious [8, 9, 17, 18] mortars. The HPCH performance was better in the NHL mortars than in the cementitious mixture [17].

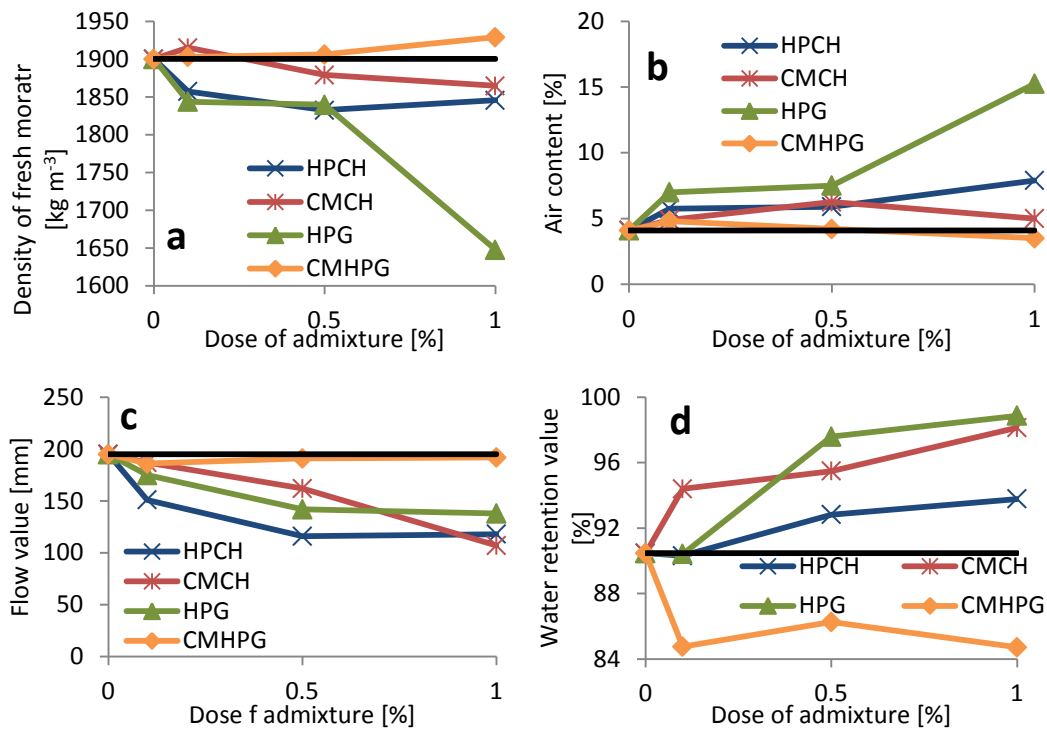


Figure 1. Fresh state properties of the NHL 3.5 mortars with admixtures.

Physico-mechanical properties

Bulk density

The bulk densities of the 90 days old specimens are compared in Figure 2. The average density of the mortars is around 1620 kg m^{-3} . The correlation with the air content in fresh mortar is obvious, for the density of HPG 1 mortar is notably lower (about 90% of density of reference mortar).

The flexural strength results in different ages are shown on Figure 3. The lower strength of the 7 days old specimens with highest dose of admixture, especially the chitosan ethers, may be caused by two different causes: by the increased humidity and water retained in the specimens similar to the sodium alginate in lime mortar [23], or more likely, due to a slightly retarding effect of chitosan derivatives on the hydraulic reactions [17]. The increase of flexural strength in comparison with reference mortar is probably caused by the water-

binding function of the derivatives used, which thereby slightly decreases the water:binder ratio, which in turn increases strength of hydraulic binders [26–28]. The addition of low dose of HPG decreased long-term flexural strength by almost 30%, this corresponds with the effect of low doses of biopolymer observed within both, hydraulic [25], and non-hydraulic [12, 21, 23] binders.

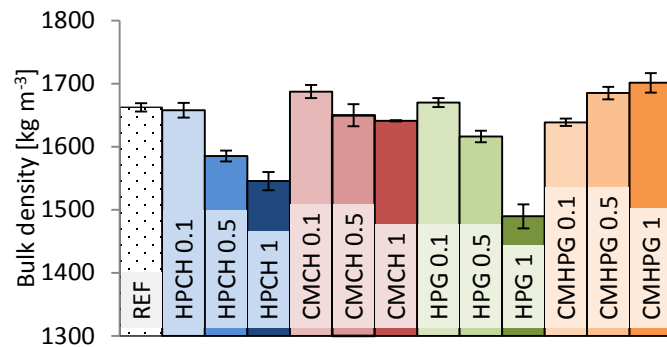


Figure 2. Bulk densities of the specimens 90 days old. Flexural and compressive strength

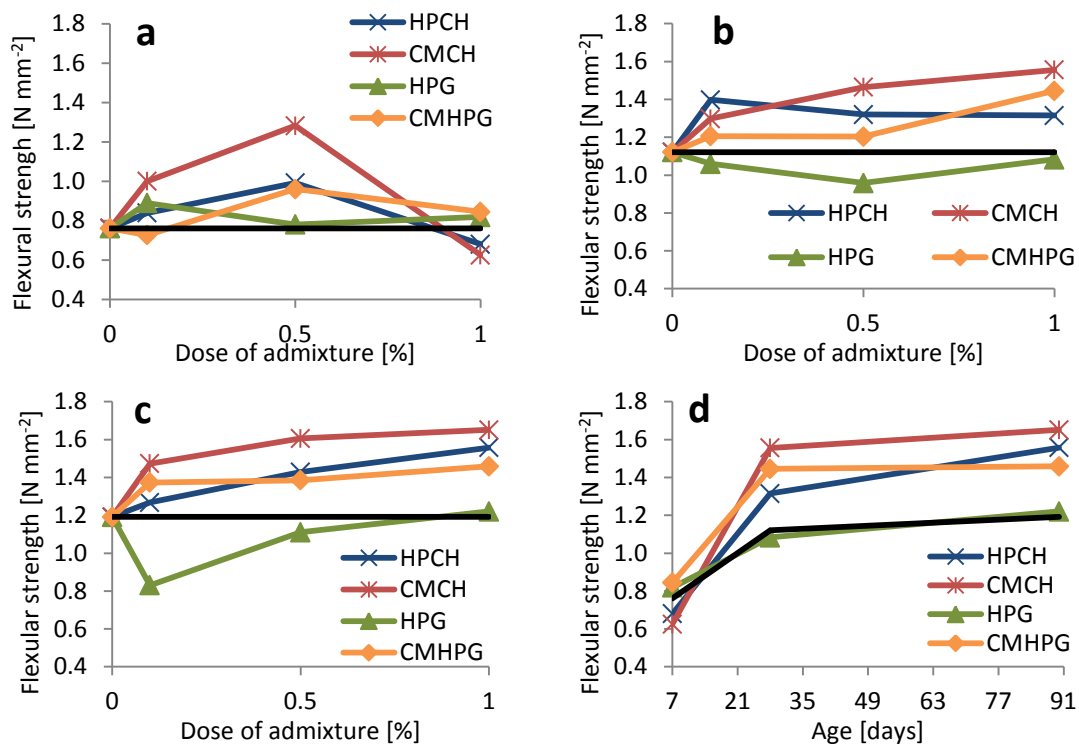


Figure 3. Flexural strength of studied specimens in the age of 7 days (a), 28 days (b), and 90 days (c) and time evolution of strength of samples with 1% of admixture (d).

Contrary to other biopolymers [25] the guar gum and chitosan derivatives diminished the compressive strength of tested mortars. The most notable decrease of strength was observed in the case of addition of HPG. This is in accordance with Paiva et al [29], who used methylhydroxypropyl cellulose, a water-retaining cellulose ether with air-entraining function – similarly to HPG, in white Portland cement-based render mortars. The authors suggest that the strength reduction is mainly caused by the increasing amount of pores, which weakens

the material. Considering the fresh-state properties results (Figure 1) the cases are similar. The strength decrease in the case of HPG is more significant than in aerial lime-based mortars [10, 12] due to the nature of connection between the porosity and strength of the binders. The strength growth of the CMCH-modified mortar asks for the future research of long-term properties of mortars for it suggests similar trend as while used in aerial lime based mortars, where the CMCH surpassed HPCH regarding long-term strengths [21].

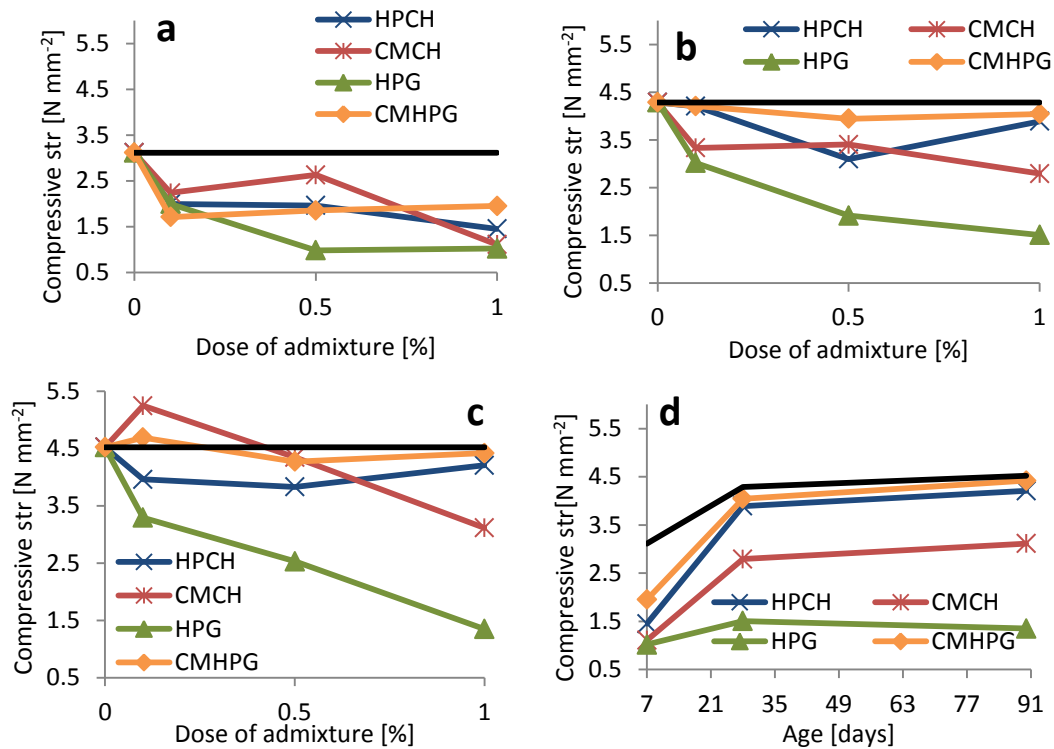


Figure 4. Compressive strength of studied specimens in the age of 7 days (a), 28 days (b), and 90 days (c) and time evolution of strength of samples with 1% of admixture (d).

Porosity

In Figures 5 and 6, the curves of cumulative pore volume are illustrated. The shape of the curves is similar for all of the studied samples and is typical for lime and cement mortars where most of the pore volume is made up of pores of diameter around 1 μm [10–12, 18, 21]. On the Figure 5, the air-entraining function of HP derivatives is represented by the increased volume of large pores around 12 μm . The HP derivative modified samples contain larger pores in the area of main pore volume than the CM derivative or the reference one. The prevalence of larger pores leads to the increase of total porosity as indicated by the increase of cumulative pore volume. The CMCH 1 mortar contained large volume of pores larger than 1 μm . The diametrically different curve shape of the CMCH 1 mortar indicates evenly distributed pores in the mixture and may be the reason for the improvement of the physico-mechanical properties of the specimens. Same effect of CMCH addition was reported by Lasheras-Zubiarte et al [18] on cementitious materials in lower dose (0.4%),

whereas in lime mortar, a different porosity, developed over longer period of time, was distinguishable for same dosage, as in our case (1%) after 365 days of curing time [21].

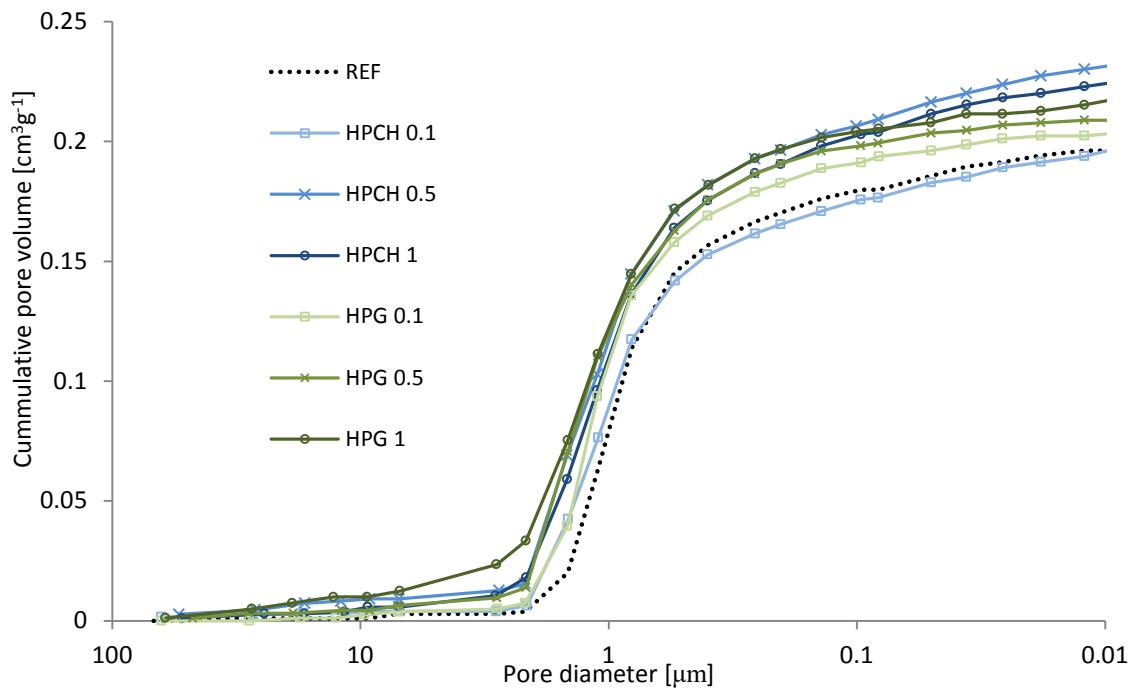


Figure 5. Cumulative pore volume curves of 28 days old specimens with HP derivative.

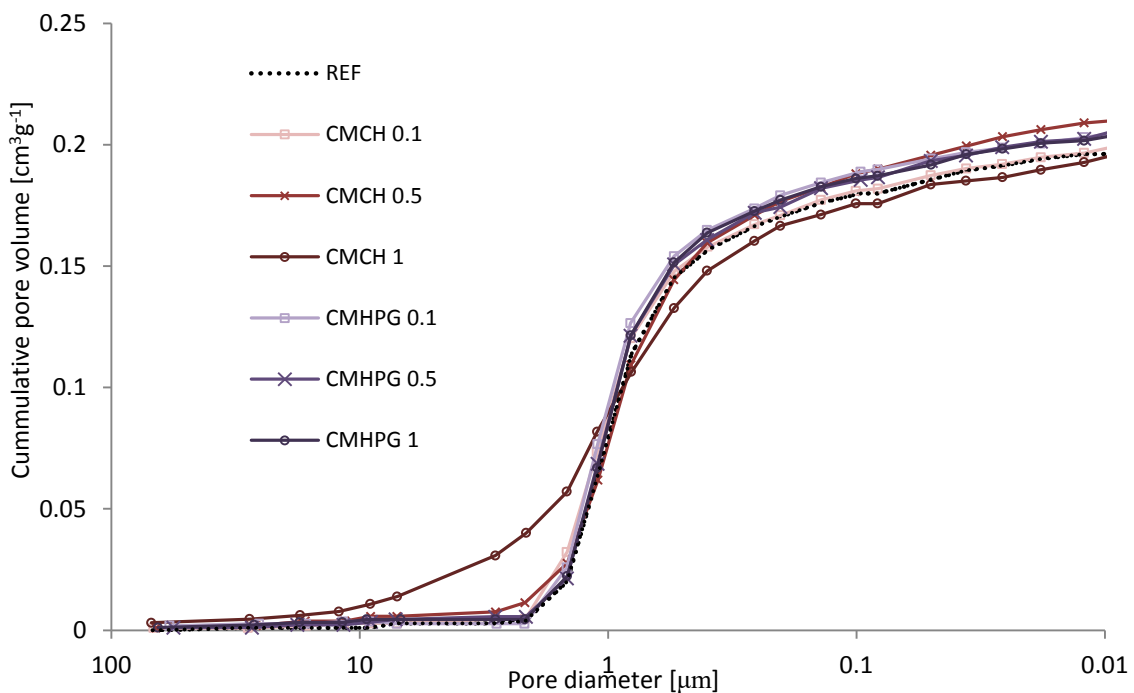


Figure 6. Cumulative pore volume curves of 28 days old specimens with CM derivative.

Water absorption due to capillarity action

The humidity transport in the mortars modified by the admixture is expressed as the capillary water coefficient C according to EN 1015-18 and apparent moisture diffusivity D_w

and the values are summarized in Table 1. HP derivatives in lower doses and CM derivatives increase the capillary water coefficient, since the water intake due to suction is faster than in the mortar without admixtures. The value of capillary water coefficient decreases in the high dose of HP derivative. This is, according to Paiva et al [29], due to an air-entraining function of the admixtures. The results obtained on fresh mortar (Figure 1) and the porosity study (Figures 5 and 6) support the hypothesis of interruption of capillary network by the aerial pores in the mixture. The difference in efficiency if chitosan and guar gum HP derivatives is also in correlation with the air content and porosity results. The similar results were obtained on aerial lime-based mortars in several studies [10–12, 21].

Table 1. Capillary water coefficient (C) and apparent moisture diffusivity (D_w) of the mortars.

	REF	HPCH 0.1	HPCH 0.5	HPCH 1	CMCH 0.1	CMCH 0.5	CMCH 1	HPG 0.1	HPG 0.5	HPG 1	CMHPG 0.1	CMHPG 0.5	CMHPG 1
C [kg m^{-2} $\text{min}^{-1/2}$]	1.98	2.35	1.94	1.40	3.13	2.29	2.20	2.77	0.43	0.95	3.12	3.11	2.81
$D_w \times 10^{-6}$ [$\text{m}^2 \text{s}^{-1}$]	0.68	1.23	0.79	0.45	1.79	1.00	1.06	1.39	0.06	0.19	2.41	1.75	1.52

Frost resistance

Frost resistance of mortars is presented as frost resistance coefficient for the flexural strength after 15 freezing-thawing cycles of fully saturated samples. The coefficient shown in Table 2 is the ratio of strength of tested specimens with the strength of the samples stored under water upon the duration of the experiment. The admixtures increased the C_f with the exception of CMHPG.

Table 2. Frost resistance coefficient (C_f) and flexural strength (R_{ff}) after 15 freezing-thawing cycles of tested mortars.

	REF	HPCH 0.1	HPCH 0.5	HPCH 1	CMCH 0.1	CMCH 0.5	CMCH 1	HPG 0.1	HPG 0.5	HPG 1	CMHPG 0.1	CMHPG 0.5	CMHPG 1
C_f [-]	0.19	0.38	0.85	0.69	0.32	0.91	0.64	0.83	0.81	0.61	0.14	0.22	0.07
R_{ff} [N mm^{-2}]	0.28	0.59	1.32	1.08	0.46	1.75	1.87	0.98	1.02	0.98	0.18	0.28	0.09

The highly decayed samples with CMHPG are shown in the Figure 7 alongside with HPG 1 samples, which showed some longitudinal cracks, and in one case, about 1 mm of surface layer had been separated. Other samples, except for the reference ones, were in same or better conditions than the HPG 1 samples, with some longitudinal cracks and several smaller defects predominantly seen on the edges. The best performing admixture was HPG, which notably increased durability even in the lowest dose, but further addition did not lead to improvement. The durability of the mortars is improved by the air pores in the matrix, which

occurred due to air-entraining function of HP derivatives (Figure 1b). The HPG addition also increased the durability of the aerial lime mortar [10]. The dosage-dependant effect is different to other biopolymers [25], where biopolymers in the highest dosage were the best performing. The durability decrease in the highest doses of the admixtures is partially caused by the highly beneficial effect of water immersion on the strength of the reference mortars, where the reference samples reached high strengths, thus affecting negatively the durability coefficient (see CMCH and HPG 0.5 and 1 in Table 2). According to the Czech standard (ČSN 72 2452) the specimens are considered durable to the specified amount of cycles if the durability coefficient $C_d \geq 0.75$, so the mortars with addition of 0.5% of HPCH, CMCH, and HPG and with the addition of 0.1% of HPG are durable for 15 freezing-thawing cycles.



Figure 7. Highly altered samples after 15 freezing-thawing cycles (numbers represent admixture dosage in %).

Conclusions

The impact of addition of derivatives of two different biopolymers, guar gum and chitosan, has been studied. The efficiency of the admixture depends mainly on the type of biopolymer and additionally on the substituent group.

Hydroxypropyl derivatives, especially in higher doses, showed air-entraining function, therefore, besides the air content in the fresh mortar, most other properties studied were also influenced. The guar gum derivative improved the fresh state properties, such as air content in the fresh mortar, water retention value, and flow value reduction more efficiently than the chitosan ether. However, the plasticizing effect of aerial pores should be taken into account while interpreting the flow table test results. On the other hand, the carboxymethyl derivatives without the air entraining function, decreased flow value and increased the water retention value in similar way as the hydroxypropyl derivatives; furthermore, the carboxymethylhydroxypropyl guaran had no effect on workability, decreased air content and, therefore, notably decreased the water retention value of fresh mortar.

The addition of biopolymers improves the flexural strength with exception of hydroxypropyl guar, which reached similar values to the reference mortar. Carboxymethyl chitosan is the most effective. Biopolymer addition decreased notably the initial compressive strength, with difference diminishing during ageing. Carboxymethyl chitosan had less negative effect on the compressive strength than other three admixtures.

The water transport represented by capillary water coefficient and apparent moisture diffusivity is increased by the addition of biopolymer. With growing dosage, the hydroxypropyl derivatives, thanks to their air-entraining function, decreased both variables rapidly impeding the humidity advance.

The admixture efficiency depending on the type and dosage improved the durability of mortars, with exception for carboxymethylhydroxypropyl guar, being the hydroxypropyl guaran the most effective admixture in lowest dose.

Hydroxypropyl guaran was overall the best performing admixture for the natural hydraulic lime mortar. It improved all the properties studied with the exception of compressive strength. Therefore, in cases of applications of mortars with higher compressive strength required, the use of chitosan derivatives could be considered as an appropriate solution. Carboxymethylhydroxypropyl guaran did not improve any of the studied attributes of mortars for their further utility as a building material.

Acknowledgement

This work has been financially supported by BUT specific research project FAST-J-19-5803. The authors gratefully acknowledge Kreaber & Co GmbH and Lamberti s.p.a. for the all products provided for the study.

References

1. Douglass J N (1878) Note on the Eddystone lighthouse. Minutes of proceedings of the Institution of Civil Engineers. 53(3):247–248.
2. Thomas B B (1958) The production of chemical cellulose from wood. J Chem Edu 35(10):493–498
3. Gross R A, Scholz C (2001) Biopolymers from polysaccharides and agropoteins. American Chemical Society, Washington.
4. Zhang H, Zhou J, Zhou Y, Zhang Y (2013). Research and application of carboxymethyl hydroxypropyl guar (CMHPG) fracturing fluid. Complex hydrocarbon reservoirs. (02)
5. Plank J (2004) Application of biopolymers and other biotechnological products in building materials. Appl Microbiol Biotechnol. 66(1):1–9
6. Khayat K H (1998) Viscosity-enhancing Admixtures for Cement-based Materials – an overview. Cem Concr Compos. 20(2–3):171–188
7. Lachemi M, Hossain K M A, Lambros V, Nkinamubanzi P-C, Bouzoubaa N (2004) Performance of new viscosity modifying admixtures in enhancing the rheological properties of cement paste. Cem Cocr Res. 34(2):185–193

8. Govin A, Bartholin M-C, Biasotti B, Giudici M, Langella V, Grosseau P (2016) Modification of water retention and rheological properties of fresh state cement-based mortars by guar gum derivatives. *Constr Build Mater.* 122:772–780
9. Medić V (2013) Influence of hydroxypropyl guar on water retention of cement based renders. *Glas. hem. tehnol. Bosne Herceg.* 40:57–60
10. Izaguirre A, Lanás A, Álvarez J I (2010) Ageing of mortars with admixtures: Durability and strength assessment. *Cem Concr Res.* 40(7): 1081–1095
11. Izaguirre A, Lanás A, Álvarez J I (2011) Characterization of aerial lime-based mortars modified by the addition of two different water-retaining agents. *Cem Concr Compos.* 33(2):309-318
12. Žižlavský T, Vyšvařil M, Bayer P, Rovnaníková P (2018) Influence of guar gum derivatives on hardened properties of aerial lime-based mortars. *Key eng mater.* 760:22–29
13. Vyšvařil M, Hegrová M, Žižlavský T (2018) Rheological properties of lime mortars with guar gum derivatives. *Key Eng Mater.* 760:257–265
14. Rinaudo M (2006) Chitin and chitosan: Properties and applications. *Prog Polym Sci.* 31(7):603–632
15. Mourya V K, Inamdar N N (2008) Chitosan-modifications and applications: Opportunities galore. *React Funct Polym.* 68(8):1013–1051
16. Pillai C K S, Paul W, Sharma C P (2009) Chitin and chitosan polymers: Chemistry, solubility and fiber formation. *Prog Polym Sci.* 34(7):641–678
17. Lasheras-Zubiate M, Navarro-Blasco I, Fernández J M, Álvarez J I (2012) Effect of the addition of chitosan ethers on the fresh state properties of cement mortars. *Cem Concr Compos.* 34(8):964–973
18. Lasheras-Zubiate M, Navarro-Blasco I, Álvarez J I, Fernández J M (2011) Interaction of carboxymethylchitosan and heavy metals in cement media. *J Hazard Mater.* 194:223–231
19. Ustinova Y V, Nikiforova T P (2016) Cement compositions with the chitosan additive. *Procedia Eng.* 153(8):810–815
20. Vyšvařil M, Žižlavský T (2017) Effect of chitosan ethers in fresh state properties of lime mortars. *IOP Conf Ser: Mater Sci Eng.* 251:012039
21. Žižlavský T, Vyšvařil M, Bayer P, Rovnaníková P (2018) Properties of aerial lime-based mortars with chitosan ethers. *Solid State Phenom.* 276:75–82
22. Singh N K, Mishra P C, Singh V K, Narang K K (2003) Effects of hydroxyethyl cellulose and oxalic acid on the properties of cement. *Cem Concr Res.* 33(9):1319–1329

23. Žižlavský T, Vyšvařil M, Rovnaníková P (2018) Characterization of aerial lime-based mortars with addition of biopolymers. IOP Conf Ser: Mater Sci Eng. 379:012006
24. Olivia M, Jingga H, Toni N, Wibisono G (2018) Biopolymers to improve physical properties and leaching characteristics of mortar and concrete: A review. IOP Conf Ser: Mater Sci Eng. 345:012028
25. Žižlavský T, Vyšvařil M, Rovnaníková P (2019) Physical-mechanical properties and durability of hydraulic lime-based mortars with non-traditional biopolymers. Acta Polytechnica in print
26. Lawrence R M H, Walker P (2008) The impact of the water/lime ratio on the structural characteristics of air lime mortars. In: D'Ayala D, Fodde E (eds) Structural analysis of historic construction, Taylor & Francis Group, London.
27. Schulze J (1999) Influence of water-cement ratio and cement content on the properties of polymer-modified mortars. Cem Concr Res. 29(6):909–915
28. Costigan A, Pavia S (2010) Influence of mortar water content on the strength of lime mortar masonry. Proc of BRI. <http://hdl.handle.net/2262/57403>. Accessed 17 December 2018
29. Paiva H, Esteves L P, Cachim P B, Ferreira V M (2009) Rheology and hardened properties of single-coat render mortars with different types of water retaining agents. Constr Build Mater. 23(2):1141–1146

Diethyl oxalate-based microgrouts in calcium carbonate systems: formulation, field testing and mineralogical characterization

J. Herrick Porter¹, C. Pasion¹, M. Secco^{2,3}, M. Salameh⁴, N. Debono⁵

(1) *Department of Conservation & Built Heritage, University of Malta, jennifer.porter@um.edu.mt, chiara.pasion@um.edu.mt*

(2) *Department of Civil, Environmental and Architectural Engineering (ICEA), University of Padua, Italy, michele.secco@unipd.it*

(3) *Inter-Departmental Research Center for the Study of Cement Materials and Hydraulic Binders (CIRCe), University of Padua, Italy*

(4) *RIWAQ, michel.sal@gmail.com*

(5) *Conservator in private practice, nathalie_debono@hotmail.com*

Abstract

A microgrout based on diethyl oxalate binder and limestone aggregate was developed for the conservation of painted lime plasters detached from a limestone substrate, after formulations based on nanolime dispersions failed to perform as expected. Microgrouts bound with nanolime, nanosilica, ammonium oxalate and diethyl oxalate were developed and tested in the field, and diethyl oxalate formulations demonstrated the best working properties and performance characteristics. The diethyl oxalate microgrouts were further subjected to laboratory testing to determine the rate and products of binder and aggregate reaction. This article describes the results of the field development and testing of these microgrouts, and the characterization of the mineralogical phases formed in the set diethyl oxalate microgrout via X-ray powder diffraction (XRPD) coupled with quantitative phase analysis (QPA).

Introduction

In wall paintings and historic plasters, delamination between plaster layers (or between support and plaster) may vary from a few millimetres to several centimetres. Such delamination, resulting in lack of adhesion of the layers involved, is typically addressed by injection grouting. The grouting of narrow delaminations (≤ 2 mm wide), often referred to in the conservation field as *microgrouting* [1], poses particular challenges: it requires the introduction of a thin, fluid material which can flow into narrow cavities (≤ 2 mm wide) but must also have bulking properties and contain sufficient binder and aggregate to create a well-adhered and cohesive solid upon setting. These requirements are often contradictory and demand a high degree of performance from these materials. However, while the development and testing of thicker grouts for larger voids (2 mm or more) have been extensively studied [e.g. 1, 2, 3, 4], microgrouts have never been the subject of systematic study, in large part because they are materials designed to perform only in small quantities. Formulations often cannot be up-scaled to conform to standardized-testing sample size

requirements without significant alteration of their performance and properties. Microgrouts therefore remain materials which are widely-used in conservation, but prepared *ad hoc* in the field, with little information available about their development and testing.

The Department of Conservation and Built Heritage of the University of Malta was recently faced with the challenge of developing an appropriate microgrout system for the stabilization of lime plasters detached from a limestone substrate while conserving a cycle of 18th C C.E. domestic wall paintings in the Chapel of Palazzo de la Salle in Valletta, Malta. Initially these detachments were treated with a microgrout bound with a nanolime dispersion, but the performance of the material was unsatisfactory. This paper describes the development of a better-performing microgrout based on diethyl oxalate and limestone aggregate, and its testing alongside nanolime, nanosilica, and ammonium oxalate-bound formulations. In addition, the consolidation of limestone using diethyl oxalate has been studied in the laboratory [5, 6] but to the best of the authors' knowledge it has not yet been applied in the field. XRPD analysis was therefore carried out to characterize the rate and products of reaction between diethyl oxalate and limestone aggregate. This article describes the treatment criteria used to design and evaluate the various microgrouts, the selection of the binders and their characteristics, and the results of field and laboratory testing of the different systems.

Wall paintings in the Chapel at Palazzo de la Salle: materials & conservation issues

In 2016, the Department of Conservation and Built Heritage of the University of Malta began a project to conserve a cycle of early 18th C CE wall paintings in the chapel of Palazzo de la Salle, a residence of Knights of the Order of St John from the 16th-18th C CE located in Valletta, Malta's capital city. The painting cycle consists of illusionistic architectural features, garlands and floral motifs, with central narrative roundels and coats of arms supported by reclining figures (Figure 1). The cycle is one of the few domestic Baroque wall paintings to survive in Malta relatively intact and uncompromised by heavy-handed past restorations.

The Palazzo and its chapel are entirely constructed of Globigerina limestone ashlar. Globigerina, a soft, porous, pale-yellow stone, is the most commonly-used construction material in the Maltese islands, now and in the past [7]. As is typical of Maltese construction to this day, the Globigerina ashlar were joined using fine-grained (aggregate ≤ 1 mm) pale-yellow mortars made of lime and powdered Globigerina (*xax* in Maltese). Because of their fine granulometry and narrow particle-size distribution, and the porous nature of the aggregates and stone substrate to which they are applied, these mortars are often prepared with a high water-content and applied in fine, thin layers to the smooth Globigerina support. These characteristics were exploited to mask the joints between ashlar when preparing a wall for painting, by feathering excess pointing mortar out from the joint and onto the ashlar faces, resulting in patches of thin lime plaster (2-4 mm thick) lining the surface of the ashlar blocks adjacent to the joints. As is common in the Maltese Baroque period [8], the paintings

in the Chapel are bound in linseed oil and applied directly to this mixed plaster and limestone support.

Unsurprisingly, adhesion between the fine-grained and relatively smooth stone substrate and the fine lime-and-stone-dust plaster often fails, resulting in detachment of the painted plaster along the ashlar joins, and characteristic patterns of loss in the painted surface (Figure 1). These detachments can be relatively wide (>5 mm), but narrow detachments (≤ 2 mm) are more common and can extend to depths of 2-3 cm behind the surface of the plaster (Figure 2).

Reattachment of these narrowly-delaminated plaster patches required a grouting material capable of entering very narrow openings, flowing extensively and filling relatively large volumes with low release of liquid; a material which would set with minimal shrinkage, good cohesion and adhesion, and without forming a film. Grouts prepared with lime (slaked lime putty or hydrated lime) and aggregates (even ≤ 75 μm) proved to be too viscous to flow within such thin delaminations, and thus a microgrout had to be developed.

Microgrout development

Lime is commonly used as a binder for grouts designed for calcium carbonate wall painting systems, mainly for reasons of chemical and physical-mechanical compatibility [1]. Microgrouts for the re-adhesion of micro-detachments in the wall paintings at Palazzo de la Salle were initially prepared using CaLoSiL E50, a nano-dispersion of lime in ethanol, but demonstrated unsatisfactory performance: it was difficult to prepare microgrouts with lime content and binder:aggregate ratios high enough to allow the mixtures to flow behind detachments, but low enough to prevent shrinkage, cracking and powdering of the set microgrout. CaLoSiL E50 contains only 0.05 g/mL lime, and to achieve sufficient flow and thinness the CaLoSiL had to be diluted 60-75% before combining with aggregates. Therefore, only small quantities of lime and aggregates were deposited within detachments during each injection and repeat injections were required to fill voids. Even so, the CaLoSiL-based microgrouts failed, leaving poorly-bound, powdering material in the voids, and the introduction of excess of liquid into the painting system was not considered acceptable. Alternative microgrout formulations were therefore prepared and tested in the field using a selection of inorganic binders.

Intervention criteria & materials selection

Microgrouts have three components: binder, aggregates and suspension medium. In order to select and combine these into a microgrout appropriate for treating the Chapel wall paintings, site-specific intervention criteria were established, defining the working properties and performance characteristics of the ideal material for the intervention (Table 1).

Table 1. Intervention criteria for microgrouts for the Chapel at Palazzo de la Salle

Working properties required	Performance characteristics required
<ul style="list-style-type: none"> ▪ Good injectability – must pass through a 0.6 mm needle ▪ Minimal separation / rate of separation slow enough to allow good working times ▪ Good flow – able to enter openings ≤ 2 mm wide, and travel 1-2 cm within a crack 	<ul style="list-style-type: none"> ▪ Good adhesion ▪ Good cohesion ▪ Sufficient bulking to fill space between substrate and detachment ▪ Minimal shrinkage ▪ No film formation ▪ Porosity similar to that of plaster and stone

Selection of aggregates & suspension media

Lightweight aggregates were selected to minimize the weight of the grout, increase flow during injection and produce a porous set material. The properties of the chosen aggregates, Poraver[®] microspheres, Scotchlite S22[®] microspheres and *χαῆx* (Globigerina dust), are described in Table 2.

Table 2: Aggregates selected for use

Aggregate	Composition	Reason for selection	Disadvantages
Poraver Expanded Glass [®] (Sieved $\leq 75 \mu\text{m}$)	Porous glass spheres; SiO_2 with some Na_2O , CaO , Al_2O_3 [23]	Lightweight; round particles increase flow; porosity allows physical interlock with grout matrix, contributing to cohesion and reducing shrinkage	Because porous, require more suspension medium to be added to the mixture; tend to clump on injection
Scotchlite S22 [®] (average grain size $29 \mu\text{m}$)	Hollow glass microspheres; Si with some Ca [24]	Very lightweight; round particles increase flow	Smooth microspheres provide no physical interlock with other grout components; tend to separate out of grout mixture
<i>Χαῆx</i> (sieved to $\leq 75 \mu\text{m}$)	Globigerina limestone dust, CaCO_3 (product of the cutting of Globigerina)	Very fine-grained; component of original plaster and stone materials; rough and irregular particles contribute to good packing geometry	Because fine-grained and porous, requires additional suspension medium

Water and/or ethanol were used as suspension media due to inherent properties of the binders (solubility) or because the dispersants were already present in their formulation, e.g. ethanol for CaLoSiL E50 (see Table 3).

Binder selection

Four inorganic binders were selected based on their compatibility with calcium carbonate systems and their previous testing for use in conservation as binders and/or consolidants for plasters, stone and/or grouts: nanolime (CaLoSiL E50) [9], nanosilica (Nano Estel) [10],

ammonium oxalate [11, 12] and diethyl oxalate [5, 6]. The source, composition and working principles of each of these materials are summarized in Table 3.

Table 3: Composition & setting reactions of selected microgrout binders

Binder*	Solvent/ Dispersant	Comments	Setting mechanism	Product
CaLoSiL E50	Ethanol	Ca(OH) ₂ nano-particles dispersed in ethanol, 50 g/L	Ca(OH) ₂ reacts with CO ₂ in the air to form CaCO ₃ . Ethanol evaporates	Calcium carbonate
NanoEstel	Water	SiO ₂ nano-particles dispersed in water, 30% w/v	Water evaporates, and silica particles coalesce and bind	Silica
Ammonium oxalate, (NH ₄) ₂ C ₂ O ₄	Water	Soluble in water up to 5% w/v	Reacts with CaCO ₃ to form calcium oxalate. Water evaporates	Calcium oxalate
Diethyl oxalate, (C ₂ H ₅) ₂ C ₂ O ₄	Water	Soluble in water up to up to 3% v/v	Reacts with water and CaCO ₃ to form calcium oxalate. Excess water evaporates	Calcium oxalate

* CaLoSiL E50: IBZ-Salzchemie GmbH & Co.KG. NanoEstel: CTS Europe. Ammonium oxalate: Sigma Aldrich. Diethyl oxalate: Alfa Aesar, 99%.

While nanolimes are a common choice of grout binder for the reattachment of lime plasters to a limestone support and have been widely used in the field for this purpose [13], silica and oxalate materials are less commonly used as grout binders. Nano/colloidal silica and ammonium oxalate have been explored as a consolidants for plaster and stone surfaces [e.g. 10, 11, 12], and as binders for repair plasters [e.g. 14]; ethyl silicates have been tested for use in stone conservation grouts [15]; but no published sources thus far report on the use of ammonium oxalate in grout systems.

On the other hand, diethyl oxalate (referred to hereafter as DiOx) is a relatively new chemical in the field of conservation. It was nonetheless tested for comparison with ammonium oxalate, since it is reported to achieve better penetration than ammonium oxalate [5, 6], a characteristic which was felt to be advantageous in the microgrouting treatment since it might improve adhesion between the grout material and the surfaces under treatment.

Experimentation with DiOx for conservation applications has only been undertaken recently by a single research group, who was searching for a consolidation product with better penetration characteristics than ammonium oxalate [5, 6]. Like ammonium oxalate (hereafter AmOx), DiOx reacts with calcium carbonate to form calcium oxalates, which are very stable mineral products, less soluble in water over a much wider pH range than calcium carbonate [11].

Preliminary studies show that hydrolysis of DiOx takes place alongside a reaction with CaCO₃ to produce ethanol and a range of calcium oxalate products, including whewellite, weddellite and caoxite, the latter never having been detected in nature, nor as a product of

AmOx reactions [5, 6]. In the study by Conti et al. [5,6], after 3 days 84% of the DiOx had reacted, with a simultaneous increase in ethanol. Calcium carbonate remained present throughout testing, indicating that it did not react completely. Conti et al. hypothesized that an intermediary product may have formed which interfered with the reaction with CaCO₃.

The Conti group also hypothesized that because DiOx is less polar than AmOx, it should have fewer ionic interactions with the substrate matrix and impurities such as salts, thus allowing it to penetrate deeper into the substrate and result in more effective consolidation. While the study did find that the DiOx reaction is significantly slower than AmOx, which they hypothesize should also favour greater penetration, the group has not published any further findings which support this hypothesis.

Both AmOx and DiOx have low solubility in water (AmOx: max ~5% w/v [5, 11, 16]; DiOx: max ~3% v/v [5, 6, 17]), limiting the concentration of either which can be added to a microgrout. Despite this limitation, the reaction of AmOx and DiOx with calcium carbonate sets them apart from CaLoSiL and Nano Estel: the oxalate binders can react with the limestone substrate and the detached lime plaster, but also with the *xahx* aggregate of the microgrout, which may result in better cohesion of the grout and adhesion to treated surfaces. DiOx also reacts with water (water is necessary for the reaction between DiOx and CaCO₃ to go forward). This means that both oxalate binders would begin to react with the other components of the microgrout even before injection into the painting system, giving these microgrouts limited working times, though the DiOx reaction is slower [5, 6].

Microgrout design & field testing

Various combinations of the selected binders, suspension media and aggregates were designed and tested, generally in proportions of 2 liquid (binder + suspension medium):1 aggregate. Over 30 combinations using the different binders were tested before a few mixtures with acceptable working properties were found. These mixtures were then subjected to the field-testing program summarized in Tables 4 and 5.

Table 4: Field tests used to evaluate microgrouts

Working property	Testing procedure	Figure
Good injectability	Injection of the microgrout through a 0.6 mm needle	/
Minimal separation	Microgrout observed in mixing container and in the syringe before injection to assess rate of solid-liquid separation	3
Good flow	Distance of microgrout flow down the face of a smooth Globigerina block measured; quality of the extruded microgrout drip observed	4

Table 5: Field tests used to evaluate microgrouts

Performance characteristic	Testing procedure	Figure
Good adhesion	Ease of removing dried sample of microgrout from the surface of Globigerina assessed by lifting with metal spatula	/
Good cohesion	Surface of dried microgrout pressed and scratched with tip of a pointed metal spatula	/
Minimal shrinkage	Sample of microgrouts applied in uniformly-sized Globigerina moulds assessed for shrinkage and cracking after drying	5
No film formation	Samples used for shrinkage tests evaluated by eye	/
Similar porosity (microgrout/Globigerina)	Uniformly sized and wetted pieces of sponge were placed on the surface of dried microgrout samples. Amount and rate of water diffusion into the grout and stone measured	6

Results of field testing

While the testing program did not follow standard procedures, it adapted field testing methods [18] which allowed an assessment of the properties and some of the performance characteristics of the various mixtures, and a comparison of the different preparations. Results (Table 6) clearly indicated that CaLoSiL E50 and Nano Estel were not acceptable binders for the microgrout systems, and that DiOx performed the best out of the four.

Table 6: Summary of field test results

Performance	Microgrout binders			
	DiOx	CaLoSiL E50	AmOx	Nano Estel
Separation	Separation was fast in all mixtures where the microgrout was able to flow into cracks ≤ 2 mm			
Injectability	Good in most tests	Fair - clumping dependent on binder	Good in most tests	Good in most tests
Flow	Good - thin microgrout but bulking, even distribution	Good - thin microgrout slightly less bulking than DiOx	Bad - often thick & clumping	Fair - sometimes thick and clumping
Film formation	None	None	None	Yes
Shrinkage	None	Cracking observed	None	Surface film cracked
Cohesion	Good	Poor	Good	Poor below surface crust
Adhesion	Good	Poor	Good	Fair
Liquid water absorption	Similar to stone	<i>Not tested because failed previous tests</i>	<i>Not tested because failed previous tests</i>	<i>Not tested because failed previous tests</i>

While the microgrout prepared with the other binders demonstrated unacceptable characteristics such as a tendency to clump during injection, separation during drying,

cracking/shrinkage and/or surface film formation, DiOx and AmOx formulations could enter openings ≤ 2 mm wide and flowed well; did not shrink or crack; did not separate during drying; adhered well to stone; were cohesive; and did not form surface films of binder. They also appeared to absorb liquid water at a rate comparable to the substrate, i.e. Globigerina limestone.

AmOx- and DiOx-based microgrouts performed similarly overall, except in one fundamental respect: the reaction time of AmOx was much shorter than that of DiOx, which reduced the working time of the preparation. While a DiOx-based microgrout retained similar working properties over a 7-hour period, AmOx-based microgrouts showed increased clumping during injection within a few hours of the preparation of the mixture. This fits with the findings of Conti et al., who demonstrated that the reaction of an aqueous solution of DiOx with CaCO_3 is much slower than the AmOx reaction, taking about 4 days to complete [5, 6].

Poraver[®] and Scotchlite[®] aggregates were eliminated over the course of testing because they tended to separate out of the mixture in the syringe and during drying (Poraver[®] sank while Scotchlite[®] floated), and they reduced the cohesion of the microgrouts due to poor packing geometry. Poraver[®] contributed to clumping, even when sieved ≤ 75 μm . *xañx* generally performed well, and, being composed of CaCO_3 , had the added advantage of reacting with DiOx, which contributed to the cohesion of the set microgrout. Rapid separation between liquid and solid components was an unavoidable characteristic of all the microgrout formulations, largely attributable to the performance of the Poraver[®] and Scotchlite[®] aggregates. However, separation during application and setting was less of a problem in formulations containing only *xañx* aggregate. It was sufficient to shake the container/syringe before using these microgrouts to put the aggregates in suspension, and the DiOx/*xañx* microgrouts did not demonstrate any significant separation after injection and setting between porous layers.

The testing led to the refinement of a microgrout with DiOx binder and *xañx* aggregates, using the maximum soluble concentration of 3% DiOx in water (v/v). The final formulation was composed of 1 part *xañx* by volume and two parts 3% DiOx solution by volume. This formulation was tested on site by injecting the microgrout in delaminations between non-historic lime washes and a Globigerina substrate, to verify injectability, adhesion and cohesion of the mixture in a real case. The microgrout easily entered narrow gaps ≤ 2 mm and flowed 3-4 cm behind the delaminations, providing good adhesion and cohesion.

The final microgrout formulation is composed of 3% DiOx in water (v/v) and *xañx* in the proportion of 2:1 solution:filler ratio in volume. This corresponds to 3% DiOx in water (1.5 mL DiOx in 48.5 mL water) mixed with 24.6 g *xañx*.

Laboratory characterisation of DiOx microgrout: reaction rates and products

While field testing indicated that the DiOx microgrout had good working properties, and the performance characteristics which could be tested also were generally good, the reaction

process, the possibility of intermediate products being formed and the products of the completed reaction needed to be determined. X-ray powder diffraction (XRPD) coupled with quantitative phase analysis (QPA) by means of the Rietveld method was employed to assess the evolution of the chemical reactions in the microgrout samples 7, 14, 30 and 180 days after their preparation. Samples were analysed at the Inter-departmental Research Center for the Study of Cement Materials and Hydraulic Binders (CIRCe) of the University of Padova, Italy.

Sample preparation

The DiOx-based microgrout was prepared in the formulation described above. Sample moulds 40 mm high x 50 mm diameter were prepared from PVC tubing. Each mould was sliced along its length to facilitate opening and demoulding of dried samples. The moulds were placed on the surface of a Globigerina limestone slab and their edges sealed with oil-based plastilene. The surface of the stone within the tube was pre-wet with 0.5 mL of 50% ethanol/water solution, to simulate the pre-wetting of detachments before the microgrouting treatment. The pre-wetting solution was allowed to absorb into the stone before adding the microgrout to the moulds.

The microgrout preparation was shaken to suspend its solid components and 5 mL were immediately measured out by syringe and injected into the mould. Four samples were prepared, one for each curing time analysed.

Analytical strategy

The microgrout samples were left to set at 15-20°C and ca. 70% RH, since the presence of water is necessary for the reaction between DiOx and CaCO₃ to occur, meaning that reaction products could continue to form over time, upon exposure to high relative humidity after the microgrout sample had dried.

Samples of the microgrout were analysed at intervals of 7, 14, 30 and 180 days from their preparation to assess the rate of reaction and identify final reaction products.

Mineralogical analyses were performed through X-ray powder diffraction (XRPD). The analyses were carried out after micronization of the materials through a McCrone micronizing mill, using a plastic jar with agate grinding elements and ethanol 99% as micronizing fluid. Data were collected using a Bragg–Brentano θ - θ diffractometer (PANalytical X'Pert PRO, Co K α radiation, 40 kV and 40 mA) equipped with a real time multiple strip (RTMS) detector (X'Celerator by Panalytical). Data acquisition was performed by operating a continuous scan in the range 3-85 [$^{\circ}2\theta$], with a virtual step scan of 0.02 [$^{\circ}2\theta$]. Diffraction patterns were interpreted with X'Pert HighScore Plus 3.0 software by PANalytical, qualitatively reconstructing mineral profiles of the compounds by comparison with PDF databases from the International Centre for Diffraction Data (ICDD). Then, quantitative phase analysis (QPA) was performed on the sole bulk samples using the Rietveld method

[19]. Refinements were accomplished with TOPAS software (version 4.1) by Bruker AXS. The determination of both crystalline and amorphous content was calculated on most samples by means of the internal standard method, with the addition of 20 wt% of zincite to the powders as internal standard. The observed Bragg peaks in the powder patterns have been modelled through a pseudo-Voigt function, fitting the background by a 12 coefficients Chebyshev polynomial. For each phase, the lattice parameters, Lorentzian crystal sizes and scale factors have been refined. Although samples were prepared with the back loading technique to minimize preferred orientation of crystallites a priori, during the refinement, any residual preferred orientation effect was modelled with the March Dollase algorithm [20]. The starting structural models for the refinements were taken from the International Crystal Structure Database (ICSD).

XRPD Results

Results are reported in Table G. Presence of weddellite ($\text{CaC}_2\text{O}_4 \cdot (2 + x)\text{H}_2\text{O}$) indicates that calcium oxalate formed as a result of the reaction, though only in very small quantities (between 0.5 and 0.8%). There appears to be a slight increase in the concentration of weddellite after 30 days, but this apparent trend is attributable more to statistical variation and to small compositional heterogeneities than to a progression of the reaction. Overall, no definite kinetic evolution was observed over time, suggesting that the reactions were complete before the first analysis after 7 days. Calcite was present in all samples throughout the test period, with very little change in concentration, indicating that much of the CaCO_3 from the $\text{x}\alpha\text{h}\text{x}$ remains unreacted. The presence of smectite, a clay mineral present in $\text{x}\alpha\text{h}\text{x}$, should also be noted, since it undoubtedly plays a role in the binding of the microgrout.

Table G: XRPD results

Material detected	Testing interval			
	After 7 days (%)	After 14 days (%)	After 30 days (%)	After 180 days (%)
Calcite	43.4	43.9	43.1	43.9
Mg-Calcite	33.7	30	31	35
Magnesite	0.6	0.6	0.7	0.5
Weddellite	0.5	0.5	0.8	0.7
Quartz	2.5	1.6	2	1.9
Microcline	0.2	0.5	1	0
Hematite	0.3	0.2	0.3	0.3
Smectite	3.3	4.4	4.5	3.8
Amorphous	15.5	18.2	16.7	13.9

Final discussion & conclusions

The XRPD results correlate with Conti et al., who found that 84% of the diethyl oxalate had reacted after 3 days and that unreacted calcite remained present throughout testing [5, 6]. Only weddellite could be detected as a reaction product in the samples of the present

research, while Conti et al. detected whewellite, caoxite and other forms of calcium oxalate through μ -Raman analysis [5, 6].

Considering the small quantity of weddellite detected, this mineral may not be the sole binder of the microgrout; the clay mineral smectite, though also present in only small quantities, may also play a binding role. Smectite is a swelling clay and therefore could have very negative impact on microgrout properties (shrinkage, cohesion, adhesion) [21], however this behaviour was not observed in the microgrout, possibly because of its low concentration. Relative humidity in Malta generally remains consistently high throughout the year (50-90%), particularly on the interior of historic constructions, which reduces the risk of significant smectite swelling/shrinking activity [19]. Nonetheless, the microgrout should be tested further to better understand the role of DiOx and clay in binding and its long-term stability when exposed to cycles of wetting and drying [22]. A source of non-smectite containing *xahx* should also be explored.

Despite the remaining questions surrounding the DiOx reaction, analysis undertaken during this study and the work by Conti et al. indicate that calcium oxalate is the main product of the reaction of DiOx and CaCO_3 , and is formed within a few days of microgrout preparation and application. Calcium oxalates have low solubility in water and are extremely stable materials [5, 11]. Furthermore, oxalate-forming materials have been in use in conservation for many years and undergone extensive testing, so the performance of calcium oxalate treatments over time is well-characterised [5, 11, 12]. In light of this and the superior performance of the DiOx microgrout as compared with other inorganically-bound microgrouts in this study, DiOx can be considered a promising material for conservation applications such as microgrouting. Testing of variants of the microgrout formulation is ongoing.

Illustrations



Figure 1. Detail of Baroque painting on east wall of the Chapel at Palazzo de la Salle. Note the characteristic pattern of painted plaster detachment and loss along the joints between ashlar support (Department of Conservation and Built Heritage, University of Malta, 2018).

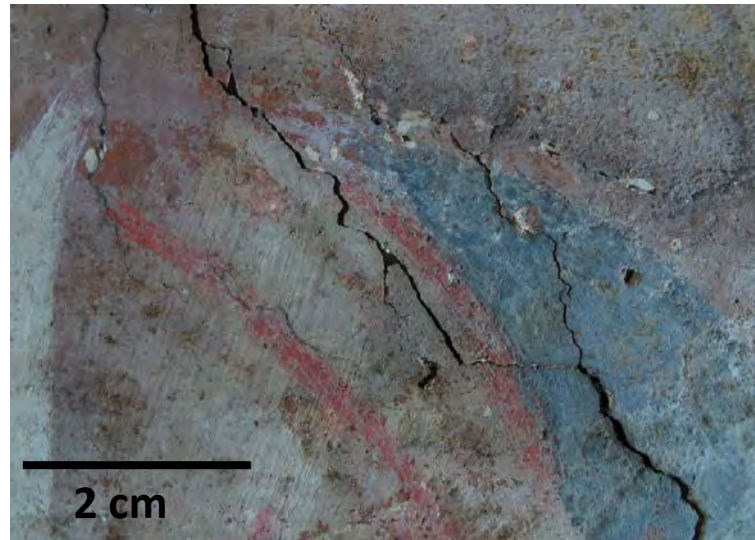


Figure 2: Detail of detached painted plaster in the wall painting at Palazzo de la Salle. The detachment between plaster and wall is ~1-2 mm wide (Department of Conservation and Built Heritage, University of Malta, 2016).



Figure 3: Separation of solid and liquid microgrout components after mixing (Department of Conservation and Built Heritage, University of Malta, 2017).



Figure 4: Flow testing (Department of Conservation and Built Heritage, University of Malta, 2017).



Figure 5: Shrinkage testing. A CaLoSiL-based microgrout exhibiting cracking after application and setting in a Globigerina cup (Department of Conservation and Built Heritage, University of Malta, 2017).



Figure 6: Comparison of DiOx microgrout and Globigerina liquid water absorption. The DiOx sample was applied and set in a Globigerina cup (Department of Conservation and Built Heritage, University of Malta, 2017).

References

1. Biçer-Şimşir B, Griffin I, Palazzo-Bertholon B et al (2009) Lime-based injection grouts for the conservation of architectural surfaces. *Rev Conserv* 10:3–17
2. Pasian C, Piqué F, Jornet A (2017) Non-structural injection grouts with reduced water content: changes induced by the partial substitution of water with alcohol. *Stud Conserv* 62(1):43–54
3. Padovnik A, Piqué F, Jornet A et al (2016) Injection grouts for the re-attachment of architectural surfaces with historic value – measures to improve the properties of hydrated lime grouts in Slovenia. *Int J Archit Herit* 10(8):993-1007
4. Papayianni I, Pachta V 2015. Experimental study on the performance of lime-based grouts used in consolidating historic masonries. *Materials and Structures* 48(7): 2111–2121
5. Conti C, Aliatis I, Casati M et al (2014) Diethyl oxalate as a new potential conservation product for decayed carbonatic substrates. *Journal of Cultural Heritage* 15:336–338
6. Conti C, Aliatis I, Casati M et al (2013) First results on diethyl oxalate as a new product for the conservation of carbonatic substrates. In: Toniolo L, Boriani M, Guidi G (eds) *Built Heritage 2013: Monitoring Conservation Management*. Springer International Publishing, Switzerland
7. Cassar J, Torpiano A, Zammit T et al (2017) Proposal for the nomination of Lower Globigerina Limestone of the Maltese Islands as a "Global Heritage Stone Resource". *EPISODES* 40(3):221-31
8. Mantella G, Guido S, Santamaria U et al (2014) La chiesa di Santa Caterina a la Valletta e la pittura a olio su muro. Il restauro come caso di studio sulla tecnica pittorica di Mattia Preti a Malta. XII Congresso Nazionale IGIC – Lo stato dell'arte – Accademia Di Belle Arti di Brera – Milano 23/24 ottobre 2014
9. Daehne A, Herm C (2013) Calcium hydroxide nanosols for the consolidation of porous building materials - results from EU-STONECORE. *Heritage Science* 1:11
10. Borsoi G, Veiga R, Santos Silva A (2013) Effect of nanostructured lime-based and silica-based products on the consolidation of historical renders. *HMC13: Proceedings of the 3rd Historic Mortars Conference, Glasgow, UK, 11-14 September 2013*. University of the West of Scotland
11. Matteini M, Moles A, Giovannoni S (1994) Calcium oxalate as a protective mineral system for wall paintings: Methodology and analyses. In: Fassina V, Ott H, Zezza F (eds), *Conservation of monuments in the Mediterranean basin: stone monuments, methodologies for the analysis of weathering and conservation*. Proceedings of the 3rd

International Symposium, Venice, 22–25 June 1994. Soprintendenza di Beni Artistici e Storici di Venezia, Venice

12. Dreyfuss T, Cassar C (2017) Onsite testing of ammonium oxalate treatment applied to historical salt-infested limestone. *Journal of Civil Engineering and Architecture* 11:175-183
13. Maryniak-Piaszczyński E, Ziegenbalg G (2010) Nano-lime as a binder for injection grouts and repair mortars. 2nd Conference on Historic Mortars-HMC 2010 and RILEM TC 203-RHM final workshop 2010. RILEM Publications SARL
14. Kühnlenthal M, Kaiser E, Fischer H (2000) Testergebnisse und verfahrensweisen bei der einstellung des reparaturmörtels. In: Kühnlenthal M, Fischer H, Akasheh TS (eds), *Petra: die restaurierung der grabfassaden; Deutsch-Jordanisches Projekt zum Aufbau eines Konservierungszentrums für Petra*. ICOMOS-Hefte des Deutschen Nationalkomitees 34/Arbeitshefte des Bayerischen Landesamtes für Denkmalpflege 105. Bayerisches Landesamt für Denkmalpflege, Munich
15. Rousset B, Gentile S, James J et al (2005) Injection grouts for molasse sandstones: preliminary assessments. *Proceedings of RILEM workshop: repair mortars for historic masonry*, Delft. RILEM
16. National Center for Biotechnology Information. PubChem Compound Database CID=14213. <https://pubchem.ncbi.nlm.nih.gov/compound/14213>. Accessed 2 February 2019
17. National Center for Biotechnology Information. PubChem Compound Database CID=7268. <https://pubchem.ncbi.nlm.nih.gov/compound/7268>. Accessed 2 February 2019
18. Biçer-Şimşir B, Rainer LH (2013) Evaluation of lime-based hydraulic injection grouts for the conservation of architectural surfaces: a manual of laboratory and field test methods. Getty Conservation Institute, Los Angeles
19. Rietveld H (1969) A profile refinement method for nuclear and magnetic structures. *Journal of Applied Crystallography* 2
20. Dollase W (1986) Correction of intensities for preferred orientation in powder diffractometry: application of the March model. *Journal of Applied Crystallography* 19
21. Velde B (2008) Clay minerals. In: Avrami A, Guillaud H, Hardy M (eds), *Terra Literature Review: An Overview of Research in Earthen Architecture Conservation*. Getty Conservation Institute, Los Angeles

22. Scherer GW, Gonzalez IJ (2005) Characterization of swelling in clay-bearing stone. In: Turkington AV (ed) Stone decay in the architectural environment, Geological Society of America Special Paper 390. Geological Society of America, Washington, DC
23. Poraver© Product Safety Information sheet. 2016-01-08
24. Pasian C, Secco M, Piqué F et al (2018) Lime-based injection grouts with reduced water content: an assessment of the effects of the water-reducing agents ovalbumin and ethanol on the mineralogical evolution and properties of grouts. *Journal of Cultural Heritage* 30:70–80

Influence of the substrate on the mechanical characteristics of the applied mortars

Isabel Torres¹, Dora Silveira², Inês Flores-Colen³, Rafael Pinto⁴, Gina Matias²

(1) DECivil, University of Coimbra/ADAI-LAETA/ITeCons, itorres@dec.uc.pt

(2) ITeCons, dora.silveira@itecons.uc.pt, ginamatias@itecons.uc.pt

(3) CERIS, DECivil, IST, University of Lisbon, ines.flores.colen@tecnico.ulisboa.pt

(4) PhD student, DECivil, University of Coimbra Research fellow, IST, rafaeltravincas@gmail.com

Abstract

The facades of historic buildings are mostly coated with mortars, usually based on air or hydraulic lime, or they are left uncoated. As these mortars are the most external elements of these constructions, they are also the most exposed and the first to undergo degradation and, therefore, the first to require conservation/replacement. The choice of these replacement/repair mortars requires very special care. According to the available standards, the performance of these mortars is evaluated based on laboratory-produced test samples, with standard specimen dimensions and under standard curing conditions. The behaviour of the mortar, over time, will be influenced by the characteristics of the substrate and by the interface that will be created between substrate and mortar. The present study is part of a broader investigation within the scope of the IF Mortar project, which aims to analyse the influence of the characteristics of several substrates on the characteristics of different mortar types. In this paper, results obtained during previous experimental campaigns, related to the mechanical characteristics of several mortars applied to different substrates, will be presented.

1. Introduction

Exterior wall coatings are fundamental for the good performance of buildings, since these elements are the first layer of protection against the wear caused by external agents, such as climate actions, mechanical actions and pollution [1, 2]. Since rendering mortars are the most common type of coatings in Portugal, both in new and in historical constructions, their detailed and rigorous characterization is of great importance. These renders may consist of cement-based mortars, for new constructions, and lime-based mortars, for historical constructions, and may be traditional and produced in-situ or pre-dosed.

The study of mortars and their characteristics is fundamental to prolong the lifespan of facades. In general, service performance of mortars is influenced by the characteristics of the substrate, the application conditions, the curing conditions and the characteristics of the mortars themselves [3-8]. The characterization of mortars is normally carried out in laboratory, in accordance with the applicable standards, i.e. the necessary tests are carried

out on specimens of standard dimensions, made for that purpose and hardened under standard curing conditions. However, the behaviour of the mortar, after application on the substrate, will not be exactly the same [9] and depends on other factors such as the characteristics of the substrate, the environmental conditions during the application, among others [10].

After application of the mortar in the substrate, an interface is formed, and the interactions that occur after contact between the two materials change over time due to hydration kinetics and substrate absorption [11, 12]. The behaviour of the mortar is thus influenced by the characteristics of the substrate and of the interface that will be formed between these two materials [10].

Several authors have focused on the study of the mortar- substrate interface and the factors that influence the adhesion between these two elements [13-15]. However, there is still little research regarding the change in the characteristics of mortars after application to substrates.

The present work is a part of a broader research project that is being developed within the scope of the IF MORTAR project. This project aims to analyse the influence of substrates on the characteristics of mortars, to more rigorously predict the behaviour of mortars after their application, based on the characterization carried out in the laboratory. In accordance with the available standards, the characteristics of the mortars are evaluated on laboratory test specimens, with dimensions, cure conditions and tests procedures according to the prescribed. However, when we apply these mortars on the real supports, their behaviour will not be exactly the same. Thus, with this project, it is intended to analyse the influence of the characteristics of several substrates on the characteristics of several mortars, so that when choosing the type of mortar coating to be applied, we can, based on the characteristics indicated by the manufacturer, estimate what will be its real behaviour when applied on the support.

This paper presents a comparative analysis of results obtained in experimental campaigns focusing specifically on the analysis of the mechanical characteristics of several mortars applied to various substrates.

2. Experimental campaigns

2.1 Objectives

The main objective of the experimental campaigns developed [16-20] was to analyse the influence of the characteristics of different substrates, curing and application conditions on the characteristics of different type of mortars. Application conditions studied included preparation of the substrate, number of mortar layers and thickness of mortar layer(s). In one study, the tests were carried out after standard curing conditions and also after accelerated aging [18].

2.2 Materials

The substrates and mortars to be studied were selected considering those that are the most commonly used in Portugal. The selected materials and their preparation and application conditions are presented in Table 1.

Table 1 – Materials and application conditions

		Experimental Campaigns				
		C1 ⁽¹⁶⁾	C2 ⁽¹⁷⁾	C3 ^(18,19)	C4 ⁽²⁰⁾	
Substrates	Type	Concrete	X	X	X	X
		Hollow brick	X	X	X	X
	Preparation	Without previous treatment		X	X	
		Previous wetting	X	X	X	X
		Previous immersion in water		X		
		Application of a previous layer of mortar (roughcast)				X
Mortars	Type	Cement (traditional)	X	X	X	X
		Hydraulic lime (traditional)				X
		Air lime (pre-dosed)			X	
	Layers and thickness	Cement (pre-dosed)	X	X	X	
		1 layer	X	X	X	X
		2 layers	X			
		3 layers	X			
		Total thickness (cm)	1.5/3	2	1.5	1.5
	Curing conditions	Standard cure	X ^a	X ^b	X ^b	X ^b
Accelerated aging				X ^c		

^a For 7 days, in a sealed polyethylene bag, in a room at 25°C and 65% RH; during the remaining days until the first test date, in a room at 25°C and 65% RH (tests at 28 and 60 days for the mortars hardened in the moulds; tests at 28, 60 and 90 days for the mortars hardened in the substrates).

^b For 7 days, in a sealed polyethylene bag, in a room at 20° C and 65% RH; during the remaining days until the first test date, in a room at 20°C and 65% RH (tests at 28, 60 and 90 days).

^c After the normal curing, the samples were submitted to accelerated aging during 8 days and subjected to two series of conditioning of four cycles each one: 1st series: 60±2°C during 8h±15min; 20±2°C/65±5% RH during 30±2min; -15±1°C during 15h±15min; 20±2°C/65±5% RH during 30±2min; 2nd series: partial emersion in water (5mm) at 60±2°C during 8h±15min; 20±2°C/65±5% RH during 30±2min; -15±1°C during 15h±15min; 20±2°C/65±5% RH during 30±2min.).

Regarding the choice of the substrates, it should be noted that concrete and hollow ceramic bricks were chosen in all studies because they are commonly used substrates.

Traditional cement mortars (1:3 cement to aggregate volume ratio, by volume, for C3; 1:4 cement to aggregate volume ratio, by volume, for the other works) were used in all the experimental campaigns and pre-dosed cement mortars were used in three campaigns, given that these types of mortar are commonly used in new constructions. Two lime

mortars, which are used for the rehabilitation of old/historic constructions, were also selected, namely, a traditional hydraulic lime mortar (1:3 lime to aggregate volume ratio, by volume) and a pre-dosed air lime mortar.

2.3 Specimen preparation

Mortar specimens were prepared according to all the applicable standards. Prismatic specimens (40x40x160 mm³) were prepared for mechanical characterization, namely for the determination of mechanical strengths and modulus of elasticity.

Afterwards, the different mortars were applied to the different substrates, as indicated in Table 1. In three campaigns (C2, C3, C4), to facilitate the subsequent detachment of the mortar layer, a plastic or fiberglass mesh was applied between the substrate and the mortar. In campaigns C2, C3 and C4, the mortars were applied in a single layer, with a thickness of 2 cm, 1.5 cm and 1.5 cm, respectively. In campaign C1, the traditional cement mortar was applied in one (thickness of 3 cm), two (thickness of 1.5 each), or three layers (thickness of 1 cm each) with a total thickness of 3 cm, and the pre-dosed cement mortar was applied in one layer with two different thicknesses (1.5 cm and 3 cm). All the campaigns followed the curing conditions as indicated in Table 1 and campaign C3 also considered accelerated aging conditions (according to EN 1015-21) [21].

After the curing time, in some selected models, the mortars were detached from the substrates, and specimens were cut for mechanical characterization.

2.4 Mechanical characterization tests

Mechanical strength and dynamic modulus of elasticity tests of the mortars hardened in the moulds were carried out, according to the applicable standards, as given in Table 2.

Different methodologies were used for the mechanical characterization of the mortars applied to the substrates:

- For campaigns C1 and C2, the analysis was performed without detachment of the mortars from the substrates. For this purpose, the pendulum rebound hammer index and the apparent ultrasonic pulse velocity — parameters that give indications about the mechanical strength and modulus of elasticity of the mortars — were determined.
- For campaigns C3 and C4, the mortars were detached from the substrates and their compressive strength and dynamic modulus of elasticity were determined. Since the specimens hardened in the moulds have different dimensions from those detached from the substrates (the former 40x40x80 mm³, and the latter 40x40x15 mm³), additional specimens with 40x40x15 mm³ were cut from the specimens hardened in the moulds and their compressive strength was also determined.

In campaigns C2, C3 and C4, the tensile adhesive strength of the mortars to the substrates was also determined.

The characteristics evaluated in the different works and the standards followed are indicated in Table 2.

Table 2 – Mechanical characterization

Mortars	Characterization	Standards	Experimental Campaigns			
			C1	C2	C3	C4
Hardened in the moulds	Compressive strength	EN 1015-11 [22]	X	X	X	X
	Flexural tensile strength	EN 1015-11 [22]	X	X	X	X
	Dynamic Modulus of elasticity	NF B10-511 [23]	X	X	X	
Applied to the substrates	Adhesion to the substrate	EN 1015-12 [24]		X	X	X
	Dynamic Modulus of elasticity	NF B10-511 [23]	X	X		
	Pendulum rebound hammer index	...	X	X		
	Propagation ultrasonic waves pulse velocity	NP EN 12504-4 [25]	X	X		
Detached from the substrates	Compressive strength	EN 1015-11 [22]			X	X
	Dynamic Modulus of elasticity	NF B10-511 [23]			X	X

3. Results

3.1 Comparison between mortars hardened in the moulds and mortars applied to the substrates

3.1.1 Compressive strength

As for the compressive strength of the mortars hardened in the moulds, it was observed that the mortars with the highest values are the traditional cement mortars, followed by the manufactured pre-dosed cement mortars and, finally, by the hydraulic lime and air lime mortars. When comparing these values with those obtained for the mortars detached from the substrates (campaigns C3 and C4), it is verified that the compressive strength is always higher for the detached mortars. In fact, when the mortars are applied to the substrates, the substrates absorb some of their mixing water and thus the mortars have their porosity reduced and strength increased. As the substrates have different water absorption capacities, their influence in this parameter is different. In fact, there was a greater strength

increase for the mortars applied to the brick substrate, which is the most absorbent substrate.

For the mortars that were not detached from the substrates (campaigns C1 and C2), higher values of the pendulum rebound hammer index were registered for traditional cement mortars, when compared to industrialized mortars. It was also observed that, for the same type of mortar, this index is higher when the mortar is applied to the brick substrate, when compared to the concrete substrate.

3.1.2 Dynamic modulus of elasticity

As expected, for the mortars hardened in the moulds, the cement mortars displayed the highest dynamic modulus of elasticity and the lime mortars the lowest. It was also possible to observe that, generally, there was an increase of the dynamic modulus of elasticity with the application to the substrates.

3.2 Influence of curing conditions

3.2.1 Compressive strength

This analysis was only possible in campaign C3, in which two different types of curing conditions were performed: standard curing and accelerated aging. For traditional cement mortar and pre-dosed air lime mortar, a similar tendency was observed: when applied on the concrete substrates, the compressive strength increased with accelerated aging, while when applied on brick substrates the opposite occurred. In the case of the pre-dosed cement mortar, strength increased when it was applied on both substrates.

3.3 Influence of substrate preparation

3.3.1 Compressive strength

Based on the results obtained in campaign C3, in which mortars were applied to substrates without any previous preparation and to substrates that were previously wet, it can be concluded that the compressive strength of the traditional cement mortar applied on brick and concrete decreases with wetting, while for the pre-dosed air lime mortar applied on both substrates the opposite occurs, i.e. strength increases. For the pre-dosed cement mortar, there is no clear trend.

In campaign C4, mortars were applied to wet substrates as well as to substrates with a roughcast. In this case, it was found that the compressive strength obtained for the mortars applied to substrates with roughcast was always lower than that obtained for mortars applied to substrates that were simply wet.

3.3.2 Adhesion to the substrate

This parameter was analysed in campaigns C2, C3 and C4. As previously mentioned, in campaign C3, the behaviour of mortars applied to substrates without previous preparation and previously wet was compared. In campaign C4, the behaviour of mortars applied to previously wet substrates and to substrates with a roughcast was compared. It was verified, in both situations, that the surface conditions of the substrates influence the adhesion of the mortars.

In campaign C2, it was not possible to obtain a direct relation between the results obtained for the two types of substrates. A great variability of values of the adhesion tensions, for the two types of mortars, was verified.

In campaign C3, for mortars applied on substrates without previous treatment, it was only possible to obtain valid results for the brick substrate. For wet substrates, valid results were obtained for both substrates, and it was possible to conclude that wetting the substrate increases mortar adhesion.

In campaign C4, it was observed that, for the brick substrate, the application of the roughcast increased the adhesion to the substrate, whereas for the concrete substrate the opposite occurred.

4. Conclusions

The characterization of rendering mortars is usually performed in the laboratory, with standard tests, for which the specimens are produced in non-porous moulds. When the mortar is applied to real substrates, some of the mixing water, together with some of the fines, is absorbed by the substrate and can alter the properties of the hardened mortar.

The results obtained during four experimental campaigns allowed confirming that, in fact, the properties of the substrates, the application conditions and the curing conditions influence the characteristics of the applied mortars. The main conclusions reached are:

- Generally, the compressive strength of mortars increases with the application to the substrates, and this increase is more significant for more porous and absorbent substrates; this behavior occurs when there is a good adhesion;
- For the dynamic modulus of elasticity, the trends are similar to those observed for the compressive strength, as expected;
- The condition of the substrate at the moment of mortar application, namely its previous wetting and the eventual application of a roughcast, is also a parameter that influences mortar behavior, mainly its adhesive strength. Previous wetting and application of a roughcast increase adhesive strength.

5. Acknowledgements

The work presented was carried out within the framework of the IF MORTAR project (POCI-01-0145-FEDER-032223), within the scope of the Portugal 2020 program, financed by FEDER through the POCI program. The funding provided is kindly acknowledged. The authors also thank CERIS/IST.

References

1. Veiga, M. R. (1998); “Behavior of Wall rendering mortars - Contribution to the study of their resistance to cracking (in portuguese)”, PhD Thesis, FEUP, 458 p.
2. Magalhães, A. (2002) – “Pathology of old plasters”. *Cadernos Edifícios*, n.o 2, Lisboa: LNEC, pp. 69- 84.
3. Veiga, M. R. (2001); “Wallcovering: functions and requirements” (in portuguese) *Arquitectura e Vida*; Ano I. 12.
4. Freitas, V. P.; Corvacho, H.; Sá, A.; Quintela, M. A. (2008) - "Discussing the durability assessment of cement mortars - a contribution for a prediction model". In: 11DBMC - International Conference on Durability of Building Materials and Components. Istanbul: Istanbul Technical University. N. Turkeri (ed.), CD.
5. Flores-Colen, I; Brito, J. de; Branco, F. (2009) - “In situ adherence evaluation of coating materials”, *Experimental Techniques*, Volume 33 Issue 3, May/June, 51-60.
6. Malva, M. (2009); “Rendering mortars for old buildings contribute to the evaluation of their performance through in situ and laboratory test techniques” (in portuguese), Msc Thesis, Instituto Superior Técnico, Lisboa, Fevereiro, 212 p.
7. Silva, L.; Ferreira, V. M.; Vera, F. (2003) - "Influence of parameters associated with the mixing and application of a monolayer coating, with air introducer, on the properties of paste mortar and hardened ". In: 2o Simpósio Internacional sobre Patologia, Durabilidade e Reabilitação de Edifícios. Lisboa: GECORPA, CIB W86, LNEC, pp. 547-556.
8. Romano, C.; Schreurs H.; Silva, F.; Cardoso, F.; Barros, M.; Pileggi, R.; John, V. (2010) – “Effect of the mixing procedure on the characteristics of industrialized coating mortars (in portuguese)”. In: 3o Congresso Português de Argamassas de Construção, sob a Égide da energia. Laboratório Nacional de Engenharia Civil, 18-19 de Março.
9. Moropoulou, A., Bakolas, A., Bisbikou, K. Physico-chemical adhesion and cohesion bonds in joint mortars imparting durability to the historic structures. *Construction and Building Materials*, v. 14, n. 1, p. 35-46, feb. 2000.
10. Silva CM, Flores-Colen I, Gaspar S, Numerical analysis of renders’ adhesion using an interface model, *Constr Build Mater*, 38 (2013) 292–305

11. Nicot, P. Interactions mortier-support: éléments déterminants des performances et de l'adhérence d'un mortier. 2008. Tese (Doutoramento em Engenharia Civil) – Université de Toulouse, Toulouse, 2008.
12. Costa, E. B. C.; John, V. M. "Adhesion cement-substrate - state of the art" (in portuguese). In: IX SIMPÓSIO BRASILEIRO DE TECNOLOGIA DE ARGAMASSAS, Belo Horizonte: GT Argamassas, 2011.
13. Palmer, L. A.; Parsons, D. A. A study of the properties of mortars and bricks and their relation to bond. Bureau of Standards Journal of Research, v. 12, n. 5, p. 609-644, may 1934.
14. Aguiar, J. B.; Cruz, M. D. A study of the adhesion between hydraulic mortars and concrete. Journal of Adhesion Science and Technology, v. 12, n. 11, p. 1243-1251, 1998.
15. Carvalho, A. N. Evaluation of the adhesion of mortar coatings: A contribution to the identification of the mechanical adhesion system. 2005. Tese (Doutoramento em Engenharia) – Universidade Federal de Minas Gerais, Belo Horizonte, 2005.
16. Gonçalves, A. "Study of the influence of the application factors on the performance of coating mortars using in situ test techniques" (in portuguese). Msc Thesis, 2010. Instituto Superior Técnico, Lisboa, 2010.
17. Arromba, J. "Influence of support on the performance of plasters applied to brick and concrete supports using in-situ test techniques" (in portuguese). 2011. Msc Thesis, Instituto Superior Técnico, Lisboa, 2011.
18. Torres, I. "Influence of the absorption of the support in the coating mortar". (in portuguese) (Pos Doc Report), FEUP, Porto, 2014.
19. Torres, I.; Veiga, R.; Freitas, V. Influence of substrate characteristics on behavior of applied mortar. Journal of Materials in Civil Engineering, v. 30, n. 10, oct. 2018.
20. Torres, I.; Matias, G.; Paulo, D. "Influence of the presence of roughcast in the characteristics of applied mortars". (in portuguese) In: 3^o Simpósio de argamassas e soluções térmicas de revestimentos, Coimbra: ITeCons, 2018.
21. Comité Européen de Normalisation (CEN). EN 1015-21: Methods of test for mortar for masonry - Part 21: Determination of the compatibility of one-coat rendering mortars with substrates. Bruxelles, 2002.
22. CEN. "Methods of test for mortar for masonry – Part 11: Determination of flexural and compressive strength of hardened mortar". Brussels: EN 1015-11:1999
23. AFNOR – "Mesure du module d'élasticité dynamique" Norme Française Homologué, Paris, abril 1975. NF B 10-511.

24. CEN. “Methods of test for mortar for masonry - Part 12: Determination of adhesive strength of hardened rendering and plastering mortars on substrates”. EN 1015-12:2000b. Brussels: Comité Européen de Normalisation.
25. CEN. “Testing concrete - Part 4: Determination of ultrasonic pulse velocity”. EN 12504-4:2004. Brussels: Comité Européen de Normalisation.

Lime Based Mortars. Relationships between Composition Parameters and Mechanical Strength

Ioanna Papayianni¹, Dimitris Papadimitriou¹

(1) Aristotle University of Thessaloniki, Greece, papayian@civil.auth.gr, dpapajim@gmail.com

Abstract

Lime based mortars are used for repairing Heritage Structures (HS), since they are considered more compatible to old mortars compared with cement based ones. Apart from hydrated lime they often contain a hydraulic component such as pozzolan, brick dust or small percentage of cement (usually $\leq 30\%$ by mass of the binder content). Hydraulic lime such as NHL3.5 is also used for repairing HS. Lime based mortars are characterized by low strength potential and slow strength development rate. The main parameters influencing the mechanical strength are the type of binder or binding agent, the water to binder ratio (W/B) and the binder to aggregate ratio (B/A). Furthermore, the curing regime analogous to the binder type as well as compaction or workmanship applied to mortar play also an important role in mortar's strength development.

Trying to find interrelationships between mechanical strength and composition parameters, a peer review of literature made and 123 different mortar compositions were listed and categorized according to aforementioned influential parameters. The relevant regulative frames were kept for the curing conditions and compaction. The water content was the required for workability 15 ± 2 cm expansion measured with flow table (according to EN1015-3).

The data concerned the compressive and flexural strength of 4x4x16cm mortar specimens at 28-d and 90-d ages. The influential composition parameters were the binding system, W/B and B/A ratios. The binding systems compared were hydrated lime CL90 (EN 459), hydraulic lime NHL3.5, lime:pozzolan (1:1), lime:pozzolan:brick dust (10-20% by mass of binder), lime:cement (10-20% by mass of binder). The evaluation of the results showed that: The strength development depends mainly on the type of binding systems and W/B ratio. The stronger the hydraulic content the higher the strength development. The effect of B/A is relatively low in these mortars which have been cured properly up to testing the mechanical strength. The rate of strength development (f_{c28}/f_{c90}) ranges from 45-70%, that means the 28-d strength is not representative of the final strength capacity of these mortars. The 28-d flexural strength of these mortars constitutes the 30-40% of their compressive strength.

The paper contributes to design of lime-based mortars on a scientific basis since diagrams of strength-W/B have been plotted for each of the studied binding systems.

Keywords: compressive and flexural strength, W/B ratio, B/A ratio, binding systems, strength development rate

Introduction

Having experienced the bad consequences from the use of strong cement-based repair mortars in restoration of Historic Structures (HS), lime-based mortars are preferred in repairing masonry HS. They often contain apart from hydrated lime a hydraulic component such as pozzolan, calcined clays, brick dust or small percentage (commonly $\leq 30\%$ by mass of binder content). Natural Hydraulic Lime NHL3.5 is also used in repairing HS. Mortars based on above mentioned binding systems are in general “soft”, of relatively low strength capacity and slow rate of strength development. They are of higher porosity in comparison to cement based mortars. The last 25 years research has focused on the science, technology and performance in practice of lime based mortars all over the world and particularly in Europe.

The reports and publications of RILEM TC 203 RHM (2003) [1][2][3] were very helpful in promoting knowledge of lime based repair mortars. However, much experimental work is needed to put the topic of designing lime-based mortars on a scientific basis. The paper contributes to this direction by providing diagrams of relationships of main parameters influencing the mechanical strength such as Water/Binder ratio and compressive strength of different binding systems.

The main parameters that affect the mechanical strength and other characteristics (such as porosity and long term performance) of lime-based mortars repair are the binding system, the water to binder ratio (W/B), the Binder/Aggregate ratio (B/A) as well as adequate workability, proper application and curing analogous to binder and the functional role of repair mortar in masonry structure. However, for the selection of these parameters to design the mortars, environmental conditions or other durability aspects should be also taken into account [4].

Although there is an effective regulative frame for cement-based products (mortars and concretes) there is not a specified one for the lime based mortars. Besides, the trade of many ingredients used in mortar mixtures is not accompanied by quality ratification. Therefore, relevant research results are not easily compared. However, it's necessary to find an area in which most of experimental results are included. To this direction, a survey of literature made as well as an experimental research on the relationship of basic parameters of lime-based mortar's composition and its mechanical strength.

Literature Survey

An effort made to find data from literature concerning composition parameters of lime-based mortars and mechanical strength so as to investigate the relationships between them. About 50 publications in magazines and Proceedings from 8 relevant Conferences were reviewed covering a period from 90's to 2016. A number of 123 different lime mortars' compositions were selected and their characteristics were recorded in Tables such as the

indicative Table 1 (the relevant literature is included in Table 1). It was decided to include only lime-based mortars containing hydrated lime $\geq 50\%$ by mass of the binding system. Some basic parameters were only considered for comparing mortars such as: the binding system, the Water/Binder (W/B) ratio and the Binder/Aggregate (B/A) ratio while other parameters such as compaction during casting and curing up to the age of crushing were denoted that were according to regulation. Furthermore, a categorization of the binding systems described in literature was made such as: hydrated lime, hydraulic lime, hydrated lime + pozzolan, hydrated lime + pozzolan + brick dust (20-30% by mass of the binder content), hydrated lime + pozzolan + white Portland cement (10-20% by mass of binder). The W/B ratios corresponded to a workability expansion 15 ± 1 cm (measured according to EN 1015-3). The B/A ratio were separated to 1:1.5, 1:2.5 and 1:3 found commonly in plasters and bedding mortars.

The relationship of the different aforementioned parameters with the mechanical strength (compressive strength) was plotted after regression analysis in Figures 1 to 6.

Reviewing the published papers on lime based repair mortars a lot of remarks could be made regarding the variability of the binding agents available at the market, the lack of regulative frame for the design of lime based repair mortars, the missing pieces of information about the characteristics of ingredients and mortar mixtures in fresh or hardened state. For example, in the case of natural pozzolan the origin and fineness of it play an important role to strength development of the mortar containing it. It is often described in papers that the mortars showed adequate workability without a measurable value about it. The W/B ratio or the use of superplasticizer are not always mentioned.

Table 1. Characteristics of different mortars' compositions

Binders	Mixture	B/A (by mass)	W/B	Workability (cm)	Compressive Strength (MPa)				Flexural Strength (MPa)				Title	Authors	Source
					28	90	180	360	28	90	180	360			
Hydrated lime	1	1/2.5			0.3 2	0.6 2	1.2	1.8					Mortars for intervention in monuments and historical buildings	Ioanna Papayanni, Maria Stefanidou	STREMAH 2003 (57-64)
Hydrated lime+pozzolan	2	1/2.5			2.4 7	2.8 0	3.8	5.0							
Hydrated lime+pozzolan+white cement 20%	13	1/2.5			3.3 1	5.0 2	4.9	5.8							
Hydrated lime	LPo.A.	1/1.5				1.2			0.5				Optimization of Compatible Restoration Mortars for The Protection of Hagia Sophia	A. Moropoulou, A. Bakolas, P. Moundoulas, E. Aggelakopoulou, S. Anagnostopoulou	2nd International Congress on Studies in Ancient Structures
Hydraulic lime	NHL.A.	1/2.3				3.3			0.7						
Hydrated lime	NHL.A.	1/2.3				3.5			0.7						
Hydraulic lime	NHLA	1/2.3	0.54	15.5	3.4 8	5.6 7							Hydraulic lime mortars for the restoration of historic masonry in Crete	P. Maravelaki-Kalaitzaki, A. Bakolas, I. Karatasios, V.	Cement and Concrete Research 35,2005(1577-1586)
Hydraulic lime	NHLA	1/2.5	0.66	15.5	3.4 8	5.6 7									

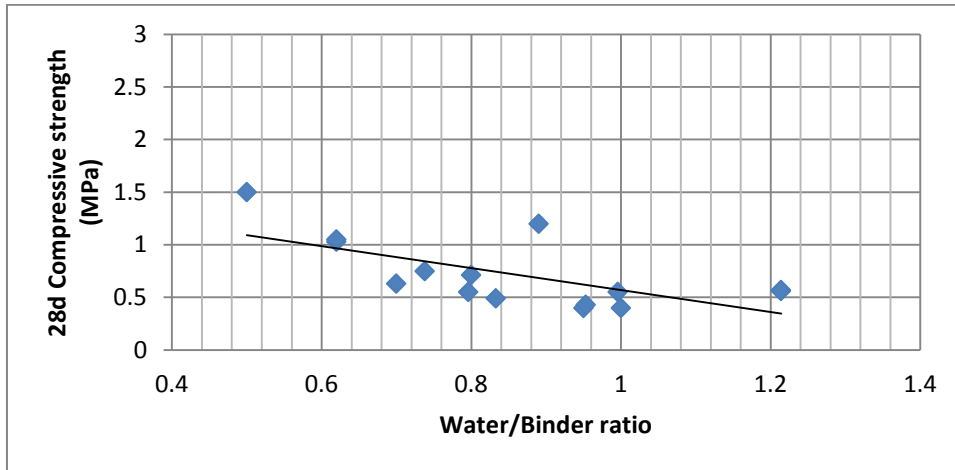


Figure1. Relationship of 28-d compressive strength to Water/Binder ratio, Binding system= Hydrated lime CL90, Binder/Aggregate ratio (B/A)=1:2.5-3.0

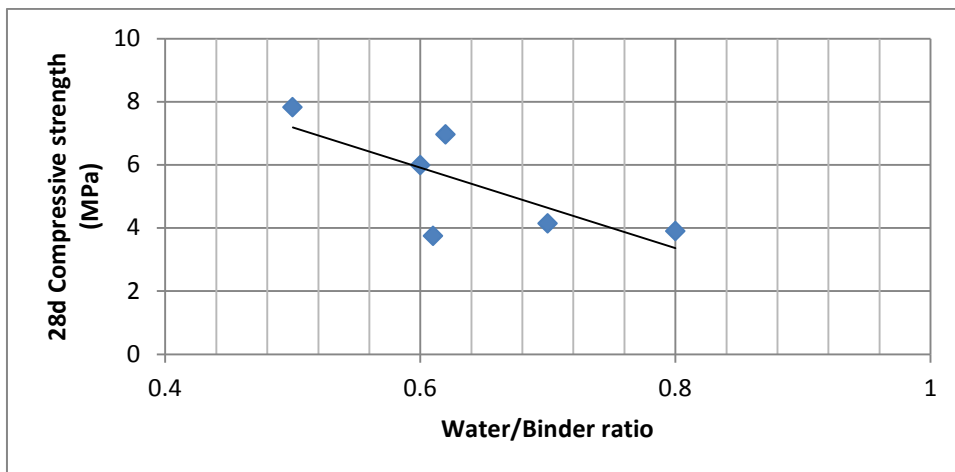


Figure2. Relationship of 28-d compressive strength to Water/Binder ratio, Binding system= Hydraulic lime NHL3.5, Binder/Aggregate ratio (B/A)=1:2.5-3.0

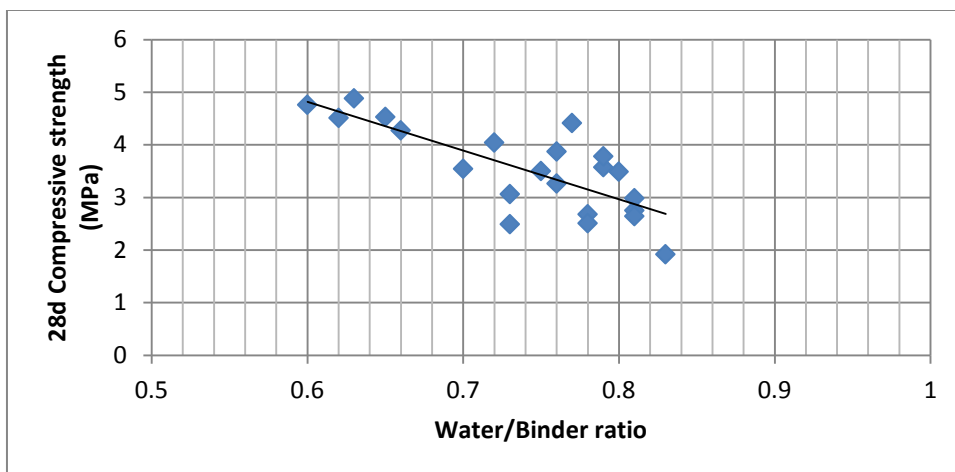


Figure3. Relationship of 28-d compressive strength to Water/Binder ratio, Binding system= Hydrated lime + pozzolan, Binder/Aggregate ratio (B/A)=1:2.5-3.0

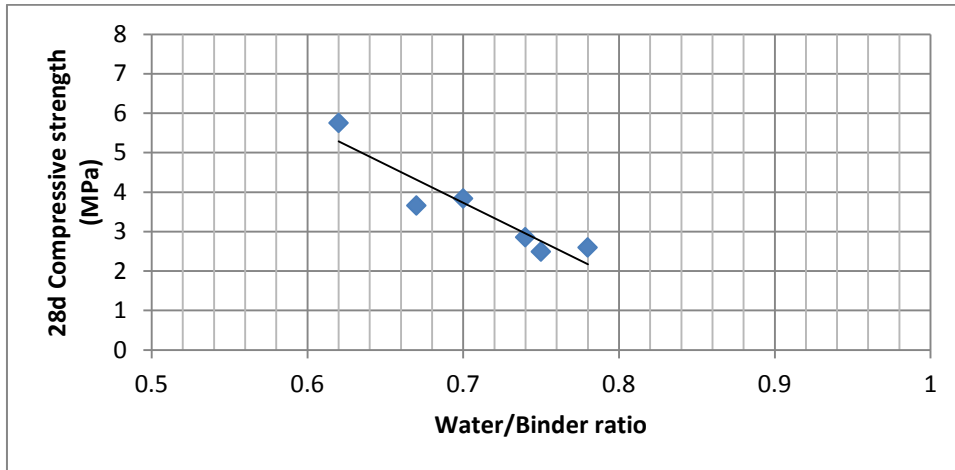


Figure4. Relationship of 28-d compressive strength to Water/Binder ratio, Binding system= Hydrated lime + pozzolan + brick dust (10-15% w/w of total binder), Binder/Aggregate ratio (B/A)=1:2.5-3.0

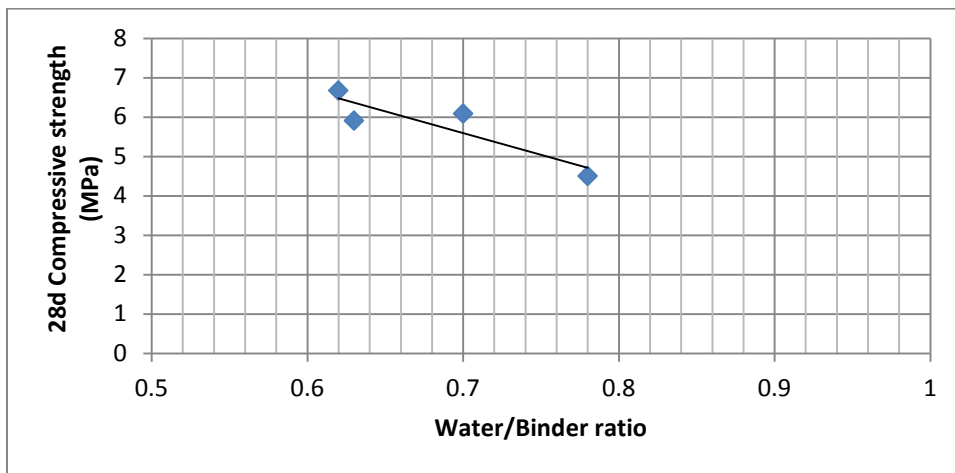


Figure5. Relationship of 28-d compressive strength to Water/Binder ratio, Binding system= Hydrated lime + pozzolan + white portland cement (10% w/w of total binder), Binder/Aggregate ratio (B/A)=1:2.5-3.0

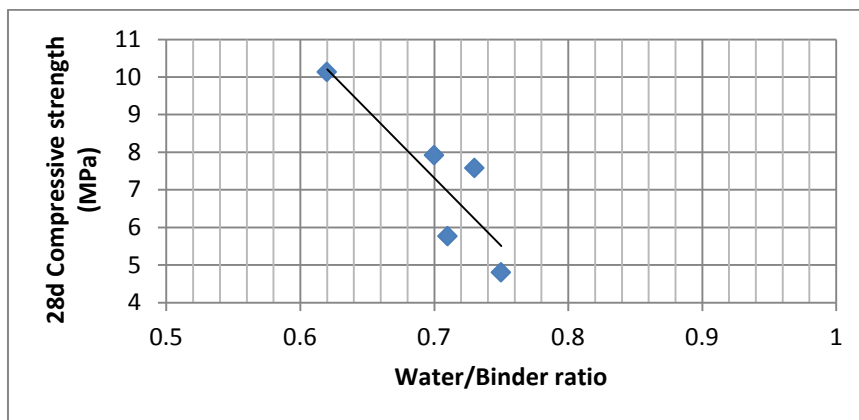


Figure6. Relationship of 28-d compressive strength to Water/Binder ratio, Binding system= Hydrated lime + pozzolan + white portland cement (20% w/w of total binder), Binder/Aggregate ratio (B/A)=1:2.5-3.0

Experimental Part

To validate somehow the relationships taken from the processing of literature data, an experimental work has been done by keeping the same parameters for proportioning of mortar mixtures. The characteristics of the ingredients used are given in Table 2 and the mortars' composition and mechanical strength in Table 3. For the mixing, workability and mechanical characteristics, the relevant EN 1015 were followed for each case. The expansion of flow table was kept $15\pm 1\text{cm}$ for all mixtures.

Table 2. Properties of raw materials

Raw materials	App. Specific density	Pozzolanicity index ASTM C311:77 (MPa)	Particle size analysis (laser granulometry) Grain diameter (μm) of volume fractions (%)	
			d50	d90
Air lime	2.471	-	3.09	10.80
Volcanic pozzolan	2.403	10.50	4.30	11.60
Natural Hydraulic lime (NHL 3.5)	2.741	-	9.60	128.00

The rate of strength is shown in Figure 7.

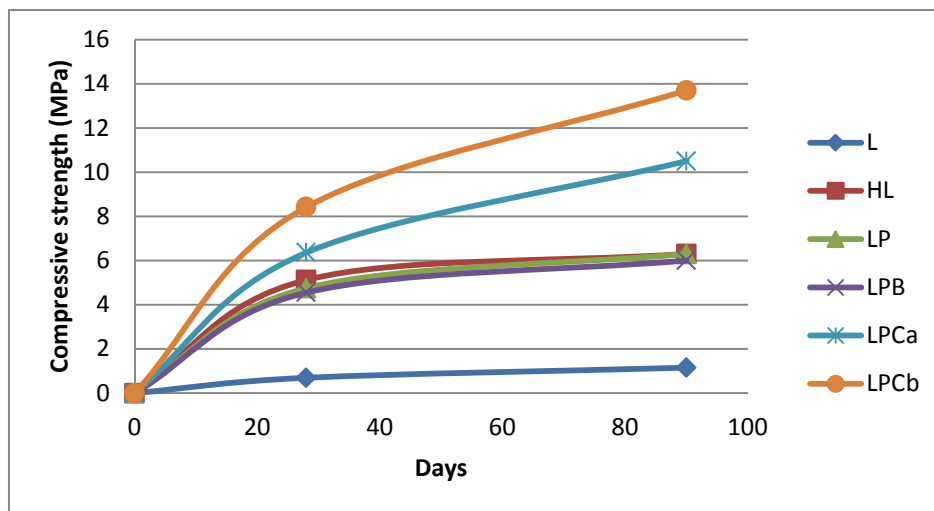


Figure 7. Rate of strength development of experimentally studied mortars (B/A=1:2.5-1:3)

Table 3. Composition of the mixtures and mechanical strength at 28 days

Mixture	Binding System	B/A	W/B	Dynamic Modulus of Elasticity (GPa)	Average Compressive strength (MPa)		Average Flexural strength (MPa) 28d
					28d	90d	
L – 1	Hydrated lime	1/1.5	0.62	3.157	0.5	0.9	0.04
L – 2		1/1.5	0.70	2.886			
L – 3		1/2.5	0.62	5.822	0.694	1.15	0.11
L – 4		1/2.5	0.62	8.073			
L – 5		1/2.5	0.70	5.300			
HL – 1	Hydraulic lime	1/1.5	0.60	14.712	4.8	8.0	1.48
HL – 2		1/2.5	0.60	20.222	5.12	6.3	1.5
HL – 3		1/3	0.70	18.877			
HL – 4		1/3	0.62				
LP – 1	Lime+poz zolan	1/1.5	0.62	13.409	5.65	-	1.44
LP – 2		1/1.5	0.70	13.628			
LP – 3		1/2.5	0.62	12.667	4.75	6.3	1.64
LP – 4		1/2.5	0.70	15.441			
LPB – 1	Lime+ pozzolan+ brick dust	1/1.5	0.60	15.109	4.5	-	1.51
LPB – 2		1/1.5	0.70	15.921			
LPB – 3		1/2.5	0.62	18.203	4.55	6.0	1.61
LPB – 4		1/2.5	0.70	17.742			
LPCa – 1	Lime+ pozzolan+ white cement 10%	1/1.5	0.62	15.855	6.01	-	1.64
LPCa – 2		1/1.5	0.70	14.766			
LPCa – 3		1/2.5	0.62	19.110	6.36	10.5	1.53
LPCa – 4		1/2.5	0.70	17.086			
LPCb – 1	Lime+ pozzolan+ white cement 20%	1/1.5	0.60	17.672	-	-	2.23
LPCb – 2		1/1.5	0.70	15.521			
LPCb – 3		1/2.5	0.62	17.295	8.42	13.7	2.23
LPCb – 4		1/2.5	0.70	19.179			

Results and Discussion

Regarding the data (28d compressive strength, W/B ratio) taken from literature after processing in Figures 1-6, it could be said that the gradient of the regression line expressing strength – W/B relationship is obviously lower in the case of pure hydrated lime than that of lines corresponding to lime + hydraulic components. The higher the hydraulicity of the component, the steeper the slope of the strength – W/B regression line. The most often recorded W/B ratios for lime-based mortars with hydraulic components ranged between 0.6 to 0.8. A continuous effort to enrich the list of data will help in increase reliability of plotted strength- W/B relationships for each binding system.

Based on experimental results it could be said that:

- Mortars of hydrated lime CL90 (EN459) showed 90-d strength 1.45MPa. At 28-d age only 65-70% of 90-d compressive strength is developed. The 28-d flexural strength constitutes 30-40% of the respective compressive strength.
- Mortars of hydraulic lime NHL3.5 (EN459) showed 90-d strength 6.3MPa. At 28-d age only 53-56% of the respective 90-d compressive strength is developed. The 28-d flexural strength is around 28-35% of the respective compressive one.
- Mortars of lime + pozzolan (1:1) showed 90-d compressive strength 6MPa. At 28-d age only the 55-63% of 90-d strength is developed. The 28-d flexural corresponds to 33-46% of the respective compressive strength.
- Mortars of lime + pozzolan + brick dust (10 – 20% w/w of binders) showed at 90-d compressive strength 6MPa. At 28-d age only 48-50% of the 90-d strength is developed. The 28-d flexural strength constitutes the 35% of the respective compressive strength.

Mortars with lime + pozzolan + cement (10% by mass of binder content) developed 90-d strength is around 50% lower than that of 90-d strength and 28-d flexural strength is > 25% of the respective compressive strength.

According to experimental, in lime based mortars with a hydraulic component the 90-d strength is 6-11MPa except for the case of lime + pozzolan + cement (20% by mass) where the 90-d compressive amounts 14MPa. The 28-d strength is 40-50% lower than 90-d strength. The flexural strength is $\geq 25\%$ of the compressive one. The effect of B/A on the strength development does not seem to be so influential as the W/B, if the mortar mixtures have been cured properly up to testing.

References

1. Maurenbrecher P, Groot C (2016) Repair mortars for historic masonry. State of the art report of RILEM TC 203 RHM, RILEM Report. Paris, France
2. Hughes JJ and members of RILEM TC 203 RHM (2012) The role of mortar in masonry: an introduction to requirements for the design of repair mortars. *Mat Str* 45:1287-1294
3. Veiga MR Conservation of historic renders and plasters from laboratory to site 2nd Int Conf on Historic Mortars. Prague. September 2010, RILEM TC 203 RHM:1241-1256
4. Papayianni I, Hughes J Testing properties governing the durability of lime based repair mortars (2018) *RILEM Tech Letters* 3:135-139

Investigating differences in the performance of lime-based mortars

Ioanna Papayianni¹, Vasiliki Pachtta¹, Emmanouela Berberidou¹, Maria Kalogirou¹

(1) Laboratory of Building Materials, School of Civil Engineering, Aristotle University of Thessaloniki, papayian@civil.auth.gr vpachtta@civil.auth.gr

Abstract

Lime based mortars in general, are commonly considered more suitable mortars for repairing historic structures, in which hydrated lime dominates in the binding system. They are of low strength capacity (lime:cement 1:1 is not commonly included) and consist of hydrated lime (CL) or CL plus a hydraulic component, such as cement, pozzolan, calcined clays or combination of them. Natural hydraulic lime (NHL) could also be considered as lime-based binder since it contains hydraulic constituents, such as dicalcium silicate compounds. It is well known that two mechanisms of setting and hardening go in parallel in these mixed-type binding systems. In the paper a number of lime based mortars, such as pure CL 90, NHL 3.5 (according to EN 459), CL90-natural volcanic pozzolan (Poz.) (1:1) and CL90-Pozz-cement (1:0.7:0.3) are monitored by implementing tests in fresh and hardened state. Physico-chemical properties, mechanical and elastic characteristics have been recorded up to the age of 180 days. Remarks concerning the behavior of them such as the capillary elevation, the rate of strength development, shrinkage deformation are made. Generally, it seems that in spite of some differences the test results of the properties of lime mortars with a hydraulic component form a separate bundle from that of the pure CL 90 mortars. This shows that many alternative compositions of lime-based mortars can lead to mortars of similar performance.

Keywords: lime-based mortars, pozzolan, white cement, physical-mechanical properties

Introduction

Lime-based mortars are commonly characterized as ‘soft’ mortars of relatively low strength capacity, slow rate of strength development and high porosity. They maybe factory made mortars, semi-factory or site-made mortars [1] and are used for repairing Historic Structures (HS). Since earth HS constitute a separate case study tailored to HS repair mortars (site made), they are often designed by using traditional and locally available raw materials as well as hydraulic components , such as natural pozzolan [2], brick dust [3], trass [4], calcined clays (metakaolin) [5, 6], Portland cement [7, 8] and many other materials (zeolite), forming mixed-type systems. In these systems two parallel mechanisms of setting-hardening occur at the same time [9]. There are adequate references about the factors influencing the process of these competitive mechanisms [10, 11, 12].

The behaviour of lime-based mortars with hydraulic components is clearly distinguished from the pure lime mortars. The question is that among a great variety of combinations of hydraulic components which are the acceptable lower and upper limits in strength and if each hydraulic component differentiates and how much the properties and behaviour of lime-based mortars. A comparison with NHL3.5 [13] mortars (often used in repair masonry) could also be useful.

To this direction, the presented paper contrivbutes by comparing long-term physical and mechanical characteristics of lime-based mortars containing the following binding systems: **1** / Pure lime CL90, **2** / lime+volcanic pozzolan (1:1), **3** / lime+volcanic pozzolan (1:1)+coarse river aggregates, **4** / NHL3.5, **5** / lime+volcanic pozzolan+white cement (1:0.7:0.3).

Experimental part

Four series of lime-based mortars were prepared and tested by using four different binding systems: pure lime CL90 (according to EN459), Natural Hydraulic Lime NHL3.5 (according to EN459), Hydrated Lime + Volcanic Pozzolan 1:1 (CL90-Poz) and Hydrated Lime+ Volcanic Pozzolan + White Cement 1:0.7:0.3 (CL90-Poz-Cem). Some of the characteristics of the constituents are given in Table 1.

For mortar mixtures, siliceous coarse sand (0-8mm) was used at B/A ratio 1:2.5. An extra CL90-Poz mixture was prepared with aggregates of granulometry 0-16mm at B/A ratio 1:2.5. After sieve analysis the granulometric curves selected were for sand grain size 0-8mm: 60% 0-4mm + 40% 4-8mm and for aggregates size 0-16mm: 50% 0-4mm + 40% 4-8mm + 10% 8-16mm.

Table 1. Characteristics of the constituents of lime-based mortars

Raw materials	App. Specific density	Pozzolanicity index ASTM C311:77 (MPa)	Particle size analysis (laser granulometry) Grain diameter (µm) of volume fractions (%)	
			d50	d90
CL90	2.471	-	3.09	10.80
Poz	2.403	10.50	4.30	11.60
NHL 3.5	2.741	-	9.60	128.00
White Cement CEM I52.5N	3.100	-	17.00	57.90

For the preparation of all mixtures, the same procedure was followed. The raw materials after drying were mixed and water was added gradually with superplasticizer (1% by mass of the total binder content). The mixing was 2 minutes at low velocity and 2 minutes at high velocity. The workability was checked according to EN1015-3. The required value for an acceptable mixture was 15±1cm expansion in flow table. Compaction of mortars inside

4x4x16cm moulds was achieved by vibration on a special table. The composition of the five mortar mixtures are shown in Table 2. The mortar specimens were cured at proper environmental conditions according to EN1015-11.

Table 2. Constituents and proportions of the mortar compositions

Constituents	Mortar compositions (parts by weight)				
	1	2	3	4	5
Hydrated lime	1	1	1	-	1
Volcanic Pozzolan, fine grained	-	1	1	-	0.7
Natural Hydraulic lime, NHL 3.5	-	-	-	1	-
White cement (CEM II/A-LL42.5N)	-	-	-	1	0.3
Sand aggregates (0-8mm)	2.5	5	-	5	5
River aggregates (0-16mm)	-	-	5	-	-
Superplasticizer 1% w/w of binders	1%	1%	1%	1%	1%
W/B ratio	0.93	0.58	0.6	0.53	0.59

The apparent specific gravity, the natural absorption and open porosity were measured according to RILEM CPC 11.3, at 90d and 180d ages. The results are shown in Table 3.

Table 3. Physical properties of the mortar compositions

Mortar composition	Ap. Spec. gravity		Absorption (%)		Open porosity (%)	
	90d	180d	90d	180d	90d	180d
1	1.74	1.75	16.66	16.11	28.94	28.26
2	1.82	1.87	12.77	12.61	23.20	23.58
3	1.85	1.88	13.38	13.09	24.74	24.62
4	1.90	1.97	11.97	11.01	22.75	21.68
5	1.80	1.87	14.00	13.40	25.25	25.03

The water hair elevation of the hardened mortars was measured at 28d, 90d and 180d ages, according to EN1015-18. In Figures 1-3 the results for the five compositions are shown.

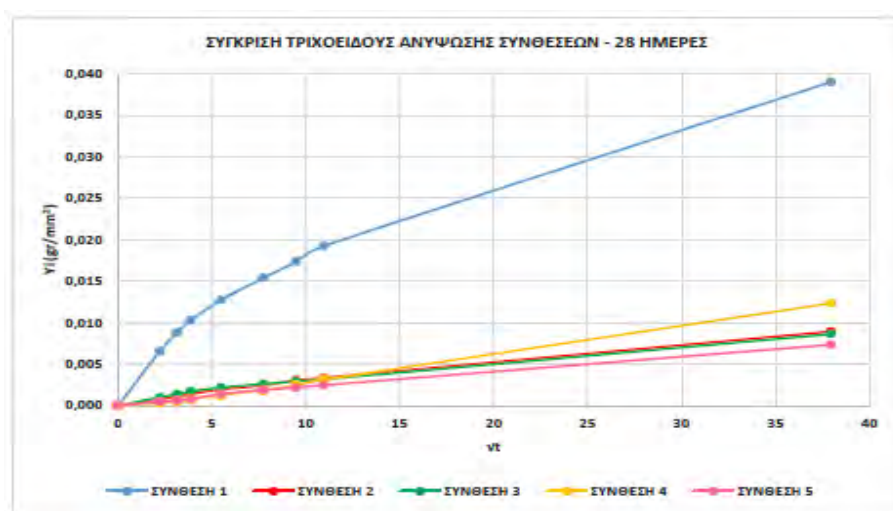


Figure 1 Capillary absorption of the mortar specimens at 28d age

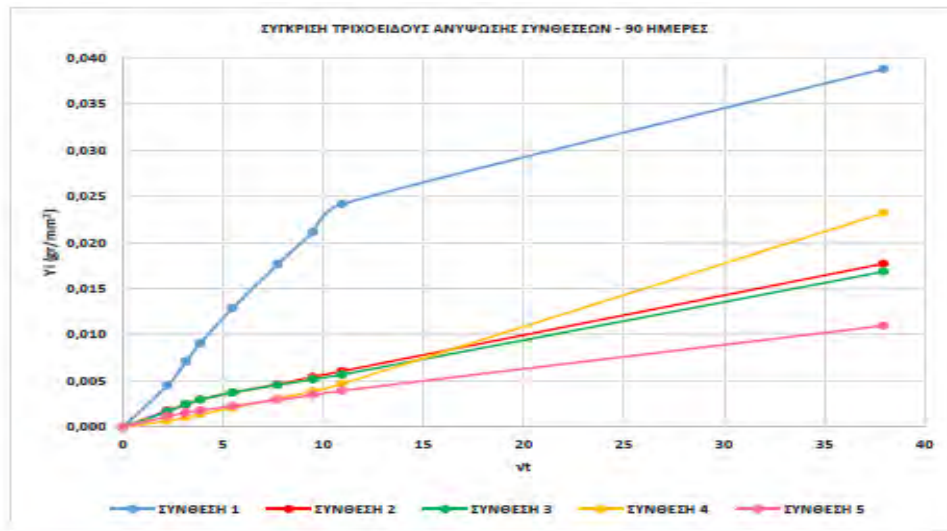


Figure 2 Capillary absorption of the mortar specimens at 90d age

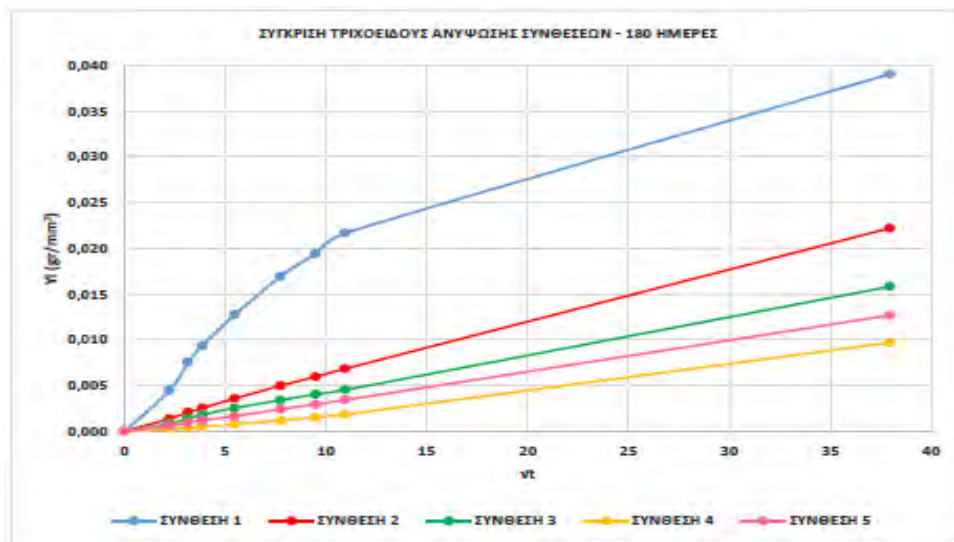


Figure 3 Capillary absorption of the mortar specimens at 180d age

The volume changes of the mortar specimens with time were measured from the age of 10 days up to 200 days. The mortar specimens were placed in a climatic chamber of 20 ± 2 °C and RH $65 \pm 5\%$. In Figure 4 the curves of the volume changes for each composition are depicted.

Regarding the mechanical characteristics, the flexural and compressive strength of the specimens (4x4x16cm) at 28d, 90d and 180d age are shown in Table 4, as well as the dynamic modulus of elasticity. In Figure 5 the rate of compressive strength development for each type of binding system is obvious.

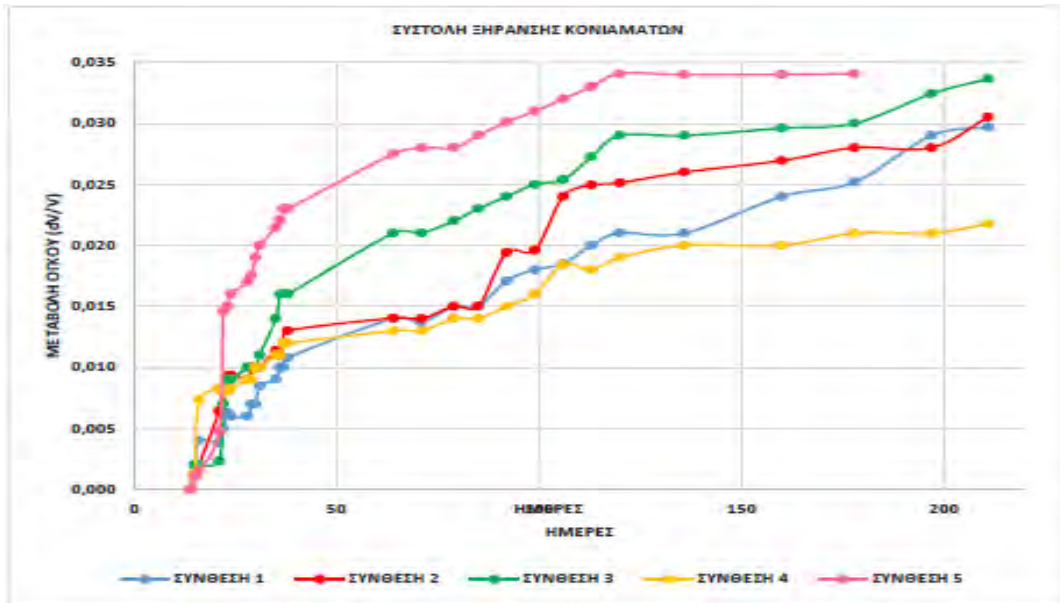


Figure 4 Volume changes of the mortar mixtures

Table 4. Mechanical properties of the mortar compositions

Mortar composition	Dyn. Modulus of Elasticity (GPa)			Flexural strength (MPa)			Compressive strength (MPa)		
	28d	90d	180d	28d	90d	180d	28d	90d	180d
1	-	-	-	-	-	-	0.31	0.85	0.90
2	12.06	12.72	12.90	1.05	1.63	1.65	3.60	7.19	7.85
3	13.16	17.50	17.68	1.15	2.43	2.89	4.47	9.87	11.18
4	15.15	19.04	19.32	1.05	3.04	3.13	4.14	8.63	8.76
5	20.48	21.22	21.53	2.44	3.12	3.34	5.63	10.69	12.60

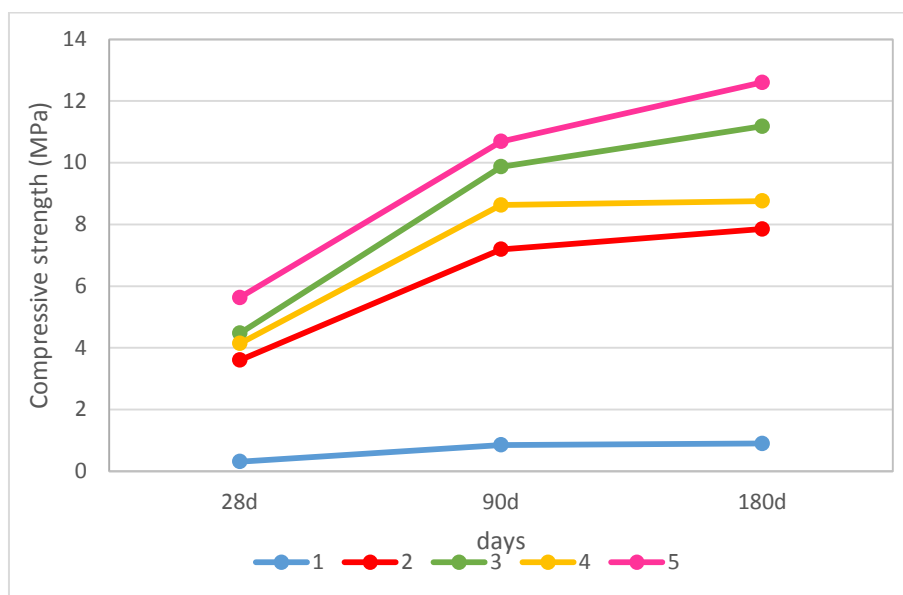


Figure 5 Rate of compressive strength development

Results and Discussion

Regarding the physical characteristics of the mortars of Table 3 and Figures 1-3, it could be said that the apparent specific gravity of lime+hydraulic component mortars (code Nr 2, 3, 4, 5) was slight higher than that of pure lime. The mortar with cement presented the higher value (1.80) but below the value 2.0, which was the upper one for lightweight mortar/concrete. The value for No 3 mortar with coarser aggregate was slight higher than that of the respective mortar No2 with sand. The absorption and porosity of the mortars (No 2, 3, 4, 5) were obviously lower than that of the pure lime mortar. The 90d and 180d values for each mortar composition did not differ much that means the 90d values were near the final ones.

At 28d the capillary absorption of the mortars (No 2, 3, 4, 5) was very low, 0.010g/mm², while that absorption of pure lime mortar (No1) was 0.040g/mm², four times higher. At 90d the capillary absorption of No1 was 0.039g/mm², while for mortars (No2, 3, 4, 5) ranged from 0.010-0.017g/mm². At 180d the capillary absorption for mortar No1 remained 0.039g/mm², while for those No 2, 3, 4, 5 ranged from 0.010-0.022g/mm². The higher with time capillary absorption of mortars with hydraulic components could be attributed to micro-cracking because of shrinkage, but of course it was lower than that of the pure lime mortar.

As shown in Figure 4, the higher and of great rate volume shrinkage has been showed by the mortar No5 with cement. It was 0.034% of the volume after 200 days monitoring. The lowest volume shrinkage was developed by mortars No 4 with NHL3.5. The 200d volume shrinkage of the other mortars (No 1, 2, 3) was 0.030-0.033%. It seems that the deformation of pure lime mortar was slower and it could be said that at 50 days (after 40 days exposition to RH 65±5%) more than 50% of the 200d shrinkage has been developed apart from lime mortar that showed 40% of the 200d shrinkage.

Comparing the mechanical characteristics of the mortars, it seems that the mortars with hydraulic components developed a 28d compressive strength from 3.6MPa to 5.63MPa. The stronger the hydraulic component the higher the 28d strength. The mortar No3 with coarse aggregates developed higher than that of No3 with sand. At 90 days the compressive strength of mortars No 2, 3, 4, 5 ranged from 7.19-10.69MPa, while for the pure lime mortar the respective strength was 0.85MPa. At 90 days the compressive strength of the mortars No 2, 3, 4, 5 ranged from 7.85-12.60Mpa, while the corresponding strength for pure lime was 0.90MPa.

As is obvious in Figure5 of the compressive strength development at 90 days, a percentage 84-98% of the 180d strength was developed while at 287 days the compressive strength was generally 50% of the corresponding 90d strength. That means that 90d compressive strength represented better the final strength of the lime-based mortars.

In general, it could be said that there are many alternative compositions of lime-based mortars with hydraulic components which present similar performance with small differences analogous the hydraulic capacity and content of the component in the mortar mixture.

References

1. EN998-1 (2010) Specifications for mortar for masonry. Part 1: Rendering and Plastering mortars.
2. Papayianni I. (2005) Design and manufacture of repair mortars for interventions on monuments and historic buildings. RILEM 2nd Workshop on Repair Mortars for Historic Masonries. RILEM TC RMHM2, Delft.
3. Gina M., Faria P., Torres I. (2008) Lime Mortars with brick dust and grounded particles for ancient masonry development and evaluation. Proc. of HMC08.
4. Groot C. (2016) Repair mortars for historic masonry. Effects of the binder choice on durability. HEROV, Vol. 61, No1.
5. Santos Silva A., Garneiro A., Grilo J., Veiga R., Velosa A. (2013) Long-term behaviour of lime-metakaolin pastes at ambient temperature. Applied Clay Science, 88-89: 49-55.
6. Pavlik V., Uzakova . (2016) Effect of curing conditions on the properties of lime, lime-metakaoline and lime-zeolite mortars. Construction and Building Materials, 102:14-25.
7. Pozo A. (2015) Evolution of mechanical properties and drying shrinkage in lime based and lime-cement based mortars with pure limestone aggregates. Construction and Building Materials, 77:472-478.
8. Arandigoyen M., Alvarez J.I. (2006) Blended pastes of cement and lime. Pore structure and capillary porosity. Applied Surface Science, 252:8077-8085.
9. Alvarez J.I. et al. (2019) Mechanisms of setting and hardening of lime based binding systems. RILEM TC 277 LHSdoc (under publication).
10. Lanas S., Sirera R., Alvarez J.I. (2006) Study of the mechanical behaviour of masonry repair lime-based mortars cured and exposed under different conditions. Cement and Concrete Research, 36:967-970.
11. Cizer O., Van Balen K., Van Gemert D. (2010) Competition between hydration and carbonation in hydraulic lime and lime-pozzolan mortars. Advanced Materials Research, 133-134:241-246.

12. Cultrone G., Sebastian E., Ortega Huertas M. (2004) Forced and natural carbonation of lime-based mortars with and without additives. Mineralogical and textural changes. *Cement and Concrete Research*, 35:2278-2280.
13. EN459-1 (2015) Building limes. Part 1 Definitions, Specifications and Conforming Criteria.
14. Maravelaki-Kalaitzaki P., Bakolas A., Karatasios I. (2005) Hydraulic lime mortars for the restoration of Historic Masonry in Crete. *Cement and Concrete Research*, 35:1577-1586.

A grout and mortar system for fine cracks and shallow surface fills in Carrara marble

Andrew Thorn

Fine Art Conservator, ARTCARE, Australia, Andrew.Thorn@artcare.cc

1. Introduction

Filling fine cracks and shallow losses in stone is a particularly demanding challenge, particularly where the object is an outdoor dense marble sculpture. Three sculptures at the one site are discussed to demonstrate the binding properties of lithium silicate to formulate grouts and mortars, to provide durable and stable repair materials.

There are many examples of marble repair, where the losses are broad and deep, for example the Arch of Septimus Severus [1] in Rome required fills as much as 50cm deep, and hence could be successfully completed using traditional lime fills. Indoor marbles have been filled using a range of synthetic materials [2] but such materials are unstable in outdoor exposure, either breaking down, discolouring or changing the biological regime. These two cited papers have been chosen simply because they represent two divergent approaches presented contemporaneously more than 30 years ago, illustrating how the argument has unfolded since, but more importantly how such approaches do not successfully apply to the issues of exposed shallow fills and fine cracks.

The three sculptures discussed in this paper present the challenges of providing stable shallow fills to inherent pits in the Carrara marble of two portrait figures of “*Queen Victoria*” and her consort “*Prince Albert*” (Charles Summers, 1876). The third sculpture “*Young Bull and Herdsman*” (Sir Joseph Boehm, 1888) consists of a three-quarters life-size bull and male attendant carved from a solid piece of Carrara marble, (henceforth referred to as the bull). This work has developed a series of fine deep fissures across its upper section that increase water penetration into the marble. Water penetration not only perpetuates the mechanical failure but increases dissolution of the marble. At this stage in the deterioration there is no fracturing, granulation or loss, other than through human interference, but a deep crack at the neck of the bull has raised concerns about allowing the process to continue. A deeper discussion of the crack formation is currently in preparation.

The bull started life as the centrepiece of the new works in the then National Gallery and most likely remained there until the gallery relocated in 1968. When first studied by the conservator in 1999, the bull was still in a protective structure but one of recent construction at its relocated site. It is concluded that the severe cracking had developed in less than 40 years of outdoor exposure. There has been no further development of cracks since 1999, although observations are confined to photographic comparison rather than precise measurement.

The shallow losses, most disfiguring in the face of Queen Victoria, are the result of pits in the marble prior to quarrying. They were most likely present at completion. Carrara marble has a reputation for declining in quality the further the purchase is made from the quarry, and while the two portraits were carved in London they are symptomatic of much of Australia's outdoor Carrara statuary, that arrives on the assumption that return postage is prohibitive. Even carvers working in Carrara are cautious when carving faces, ensuring that the details and often the polished final face is completed before undercutting to form the rear of the head. Both pits and veins can disfigure a work, but in this case they are prolifically distributed across the figure.

Earlier attempts to fill marble using lime-based fills had all failed, despite the conservator having success with such approaches on deeper fills in other contexts. The challenge is to retain a fill at such shallow depth and most importantly, not to have the feathered edge of the fill dis-aggregate. Attempts to fill the fine cracks in the bull had all failed due to the narrow dimensions of the crack. Measurements taken on some of the more visible fissures showed them to be no more than 0.35 mm wide at the outer opening (Figure 1). Lime based mortars simply do not have the cohesive strength to form in such narrow voids.

A system for the treatment of all three sculptures is described whereby the one system has been applied initially as a liquid consolidant adhesive, to the fine cracks and as a pre-bonding agent for the shallow fills. This is followed by a grout and then a mortar system of carefully graded aggregates, colour matched to the surface of the marble.

Questions have been asked of the conservator as to whether the marble should be placed indoors, and while this was its original location, its presence at the RASV has always been as an outdoor work. Prior to accepting indoor relocation a system of water-repellency is being trialled where lithium silicate, due to its ability to adhere to calcitic substrates has been used as a coupling agent for the application of water dispersed silane/siloxane hydrophobic treatments.

2. History of the three works

All three sculptures started life indoors, being part of the combined Victorian Library, Museum and National Gallery collection, formed by Act of Parliament in 1869. These were new works to augment a fine collection of plaster casts of the great masters aimed at uplifting the aspirations of a fledgling colony.

Summers was commissioned to carve a group of four royal portraits in around 1876. Three of the works survive. Boehm carved his bull in London some time before its arrival at the Great Exhibition of 1888, at which time it was snapped up by the local Gallery, keen to acquire modern art of reliable taste.

As the three institutions grew, the National Gallery swarmed to a new site a century after the opening of the first museum, in 1968. At that time academic royal figures and bulls were

no longer required to maintain the sense of achievement then prevailing in the arts and wider world, and hence the Gallery's collection of recent antiquities were bequeathed to all takers. Victoria and Albert were two of a set of four royal portraits, a third, Alexandra, was offered to the town of Alexandria, and so it is no surprise that the bull ended up at the Royal Agricultural Society of Victoria. Early images of the bull show it as a centrepiece in the Art Gallery, surrounded by paintings and, given the location of the relevant room, it is unlikely that it was moved outdoors earlier than the 1960s when the Gallery vacated the site. The conservator first encountered the bull in 1999 at which time it was still under cover but the structure appeared quite recent. The crack pattern across the upper back of the bull was apparent at that time, which suggests that it either formed while indoors or, more plausibly, in the less than 40 years that it had been set in outdoor exposure.

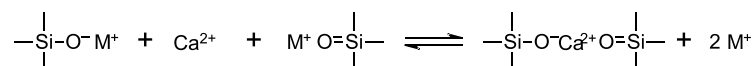
3. Lithium silicate binder for calcitic substrates

Lithium silicate has unique properties in being able to form strong adhesive bonds to both silicates and carbonates, due largely in the latter instance to its dual formation of silicon dioxide and lithium carbonate as shown in equation 1.



Equation 1. Reaction of lithium silicate solution to form lithium silicate/oxide and lithium carbonate [3]

Ca^{++} can participate in the reaction with lithium silicate as follows:



M^+ being the positively charged alkali cation.

Equation 2. Reaction of Ca^{++} with lithium silicate (from personal communication with Eq1 author 2019).

Lithium silicate has been sourced from Woellner as Betolin¹² and earlier, from PQ Corporation¹³. The PQ product presented orange staining issues but with greater solvent tolerance. Trial applications of liquid lithium silicate (Betolin Li22) to the Prince Albert figure resulted in a noticeable white film, readily removable but not ideal. The manufacturer's representative pointed out that this problem could be avoided if the lower solids grade Li20 is selected. Both Li22 and Li24, significantly, deposit lithium silicate in the container, whereas Li20 remains stable. Li22 makes a superior mortar but the white veil issue over-rides any benefits in workability and short-term rheology.

¹² <https://www.woellner-familienstiftung.eu/files/downloads/TDS/TDS-Betolin-Li20-GB.pdf>

¹³ https://www.pqcorp.com/docs/default-source/recommended-literature/pq-corporation/lithium-silicate/bulletin17-110alithiumslicate.pdf?sfvrsn=65897963_3

The mortar applied to the marble has been achieved by the simple addition of lithium silicate to marble flour and 5% quartz flour, cognisant of the grain size of Carrara marble (300-500 microns). The addition of phosphoric acid, discussed in the next section, was not adopted for these treatments but is considered a benefit. For purposes of rapid build for deep fills, the first layers may be applied using coarser particles up to 2 mm, on the observation that a layer can be about five times as thick as its maximum grain size without developing cracks.

4. Lithium phosphate formation

Lithium carbonate, formed as a secondary mineral in the reaction, is a moderately soluble mineral, relative to both calcite and gypsum. Table 1 summarizes the solubility of these minerals together with less soluble homologues. The incorporation of phosphoric acid into lithium-based mortars has shown improved strength, particularly wet strength at early cure. The choice of phosphoric acid has been based entirely on the insolubility of lithium phosphate but does find common ground with the work of Sassoni and colleagues [4, 5] in their use of hydroxyl apatite for the consolidation of friable marble. In the current trials, liquid phosphoric acid has been more amenable than tri-ammonium phosphate as it can make contact with the lithium silicate liquid in a more dilute and compatible manner. Up to 1% w/w Phosphoric acid remains stable in a 50% aqueous lithium silicate dilution and has been successfully incorporated into trial mortars and grouts at the ratio of approximately 0.5% total mortar mass. Table 1 includes the solubility data for lithium phosphate, showing it to be significantly less soluble than lithium carbonate, less soluble than gypsum but still substantially more soluble than calcite.

Table 1. Solubility of lithium carbonate, compared to calcite and gypsum, and to lithium phosphate, a sparingly soluble lithium salt (various sources).

Lithium species g/L	Formula	0°C	10°C	20°C	30°C	40°C
Lithium carbonate	Li ₂ CO ₃	15.4	14.3	13.3	12.6	11.7
Calcium carbonate	Ca CO ₃			0.006		
Calcium sulphate	CaSO ₄ .2H ₂ O	2.23	2.44	2.55	2.64	2.65
Lithium fluoride	LiF			2.7	1.35	
Lithium phosphate	Li ₃ PO ₄			0.39		
Calcium phosphate	Ca ₃ (PO ₄) ₂			0.02		

Given the difficulty in modifying lithium silicate in any way, including its intolerance to pH adjustment and organic solvent addition, various approaches have been tried to modify the grout and mortar formulations. It should be pointed out however that both grout and mortar can be formulated perfectly well without modification and that after seven years of in-situ observation there has been no leaching or detachment as a result of lithium carbonate dissolution. Equally there have been no instances of white bloom when using Lithisil 20 and no deposition in storage containers for grades below Li22. Never-the-less the presence of a soluble mineral is undesirable in the long term, whereby separation may

develop at the interface, particularly between a mortar and its attachment substrate simply through the loss of lithium carbonate crystals.

While the addition of phosphoric acid improves mortar strength, it remains to be confirmed whether it provides better attachment to the calcitic surface. Pre-wetting the marble break surface with a 1% phosphoric acid adjusted lithium silicate is being studied currently.

5. Consolidation requirements

None of the three sculptures under discussion have required consolidation although the surface of the Bull has a far more granular upper surface than either of the royal portraits, but not such that consolidation has been considered an essential treatment. Testing on various granular marbles has confirmed that lithium silicate can perform well as a consolidant, as verified in tests of which Figure 3 shows the results of consolidating crushed marble passed through a 3 mm sieve with no bottom cut off. Sieved marble particles in the range 1.1-2mm provided a more demanding test with the resultant mortar having markedly less cohesion to a point where it would not qualify as a suitably strong mortar. These tests on lithium silicate binding, while conducted in the pursuit of achieving well bound mortars through aggregate size selection have also demonstrated the ability of lithium silicate to bond to large marble particles. Lithium silicate in liquid form is used as a surface wetting agent to ensure good attachment of mortars and in the case of the bull, has been applied in two cycles to penetrate the narrowest parts of all cracks.

6. Injection grout considerations

The first and most obvious consideration with grouts is that they are normally not visible on the surface, and hence issues of texture and colour become less significant. Stable and strong porous grouts have previously been formulated using quartz flour in the general size range up to 150 μm with 98% passing 106 μm , with similar results achieved with marble powders sieved to below 106 μm .

Cracks on the bull have been measured to be no greater than 350 μm wide, requiring a very fine aggregate. Crack depth has not been established although Sassoni has established crack depth in some Carrara marble to be contained to the upper 2 cm [6]. Figure 1 compares the measured cracks to a simulated cavity where controlled particle size grouts have flowed into a wedge opening at 2mm and closing at the bottom at less than 0.1 mm. It can be seen that with the chosen aggregate distribution grout is deposited well into the crack size range of the bull.

The study of grout behaviour into fine cavities [7] has demonstrated that lithium silicate grout phase separates at around 0.3 mm cavity width, whereby the free head liquid is absorbed into finer voids below the grout. This is argued to be a benefit in allowing a degree of void filling and adhesion at spacings finer than those which particles could reach but which are critical in crack stabilization.

Filling of the sub 0.35mm voids was considered an essential requirement of the cracks on the bull, regardless of whether that material contained aggregate or not, as will be described further on.

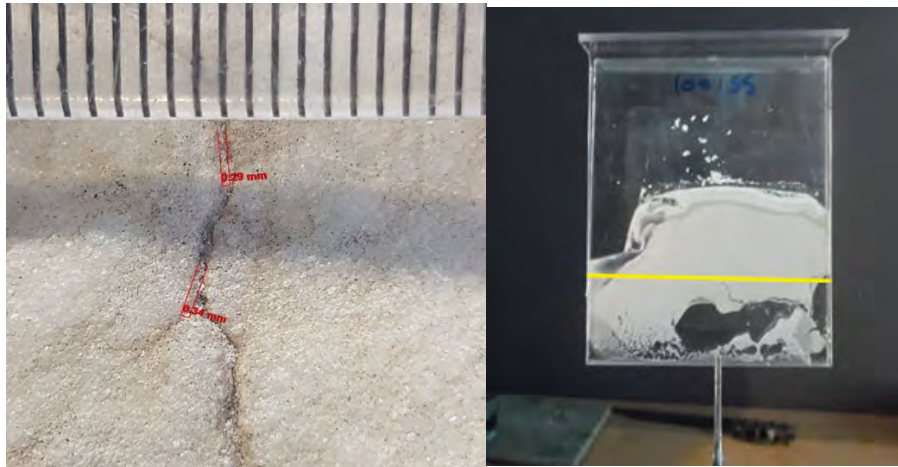


Figure 1. The more visible cracks on the bull, measured using Zeiss Axiovision software, shows the cracks to be no greater than 0.34mm in this image. On the right a tapered cavity simulation opens at 2 mm at the top, tapering to less than 0.1 mm at the bottom. In this instance particles in the range 1-150 microns have been able to reach to below the crack sizes measured on the bull. The 0.34mm void cavity width has been indicated with a yellow line.

7. Mortar requirements

When the first research began on developing a siliceous grout for sandstone, in addition to the various design criteria established for mortars in general [8], a further eight were considered for outdoor sandstone [9]. Of these eight, two are of critical consideration for outdoor stone:

1. The repair must remain colour compatible in both wet and dry conditions.
2. The repair mortar must match the bio-nutrient balance of the parent material.

Colour stability is achieved not only by the mortar deriving its colour substantially from the larger aggregates with minimal addition of fine pigments, but to achieve wet and dry compatibility the repair must be as porous as the parent surface. Hand in hand with this the repair must provide a nutrient suite similar to that of the parent. No matter how well matched a repair is upon completion, its ultimate colour stability will be determined by how closely it tracks the bio-colonization of the parent stone through changing seasons (Figure 2). Portland cement repairs on outdoor sandstones literally bristle with mosses and other higher species due to the very high nutrient supply in the Portland cement. The same can be said for the use of lime mortars on non-calcareous stones. Calcitic stones provide the same challenges but in this case the presence of calcium carbonate is desirable, as is a reasonable matching of surface texture.



Figure 2. Ethyl silicate mortar repairs carried out to a broken stone in 1996. This image, taken 23 years later in 2019, shows the stone still wet after rain. The mortar repair, now detaching due to movements in the joined stone, achieves both requirements of having good wet colour and a balanced recolonization of biota, in this case two forms of crustose lichen.



Figure 3. Three views of a mortar composed of marble passed through a 3 mm sieve (not intended to match Carrara marble). Left - the surface as applied off the spatula with rudimentary levelling. Centre – the same batch with all but the upper left corner polished. Right – the underside of one sample showing the coarse texture. It is noted that Carrara marble has grains in the range 300-500 microns, not those used here. No quartz flour was added to these mortars.

One of the features of lithium silicate mortars, more relevant to recent works, is the ability to polish the surface after set. This allows for very precise gloss matching. The central sample of Figure 3 has been polished to a low sheen and in other recent works, highly polished black marble and grey granites have been gloss matched through a combination of polishing and lithium silicate glazing (paper in preparation).

While there may be other methods of achieving a durable fill that can be wet and dry colour matched, as well as gloss matched, the lithium silicate marble mortar is capable of achieving all design criteria. Figure 3 shows three views of an entirely marble chip filled mortar. Marble chips were crushed sufficiently to pass through a 3mm opening sieve. While there was no specific particle size grading this type of manual crushing produces a substantial fraction

finer than 0.5 mm with no more than 10% above 1 mm. The crushed marble was mixed with lithium silicate alone with no modification and no measurement other than to produce a moderately workable mortar. A further test restricting the particles to 0.5-1.18 mm produced a totally unworkable mortar but was achieved by saturating the particles and allowing the excess liquid to drain away. This product also produced a well bound cohesive material. The third test in the range 1.18-3 mm had very poor cohesion.

Water absorption has been evaluated for this work in relative terms only. The aim has been to ensure that the mortar allows the passage of water equal to or greater than the parent material. In the case of Carrara marble, metamorphism of the grains of Carrara marble ensures very slow water transport but high absorption in the fine contact boundaries [10]. The mortar is more open porous and while there is a degree of control over this it has been considered desirable to have a more porous and absorptive mortar system. Matching gloss levels imposes other bounds on granulometry that may produce a more dense material but still not approaching that of a metamorphic stone. Porosity can be reduced though the application of further lithium silicate washes, with or without siloxane emulsion additions.

The incorporation of phosphoric acid at 0.5% total solids mass has been achieved by the order in which the acid is introduced to the other components. Reverse migration is controlled by gelling the lithium silicate prior to its incorporation.

The density of the mortar can be controlled by incorporating glass microspheres, which also make the finishing of the fill easier but with some sacrifice to gloss options where these matter. A lighter more porous mortar has been achieved by incorporating microspheres and diluting the lithium silicate in equal parts with water. The aim of this evaluation was not so much to make weaker mortars but to ensure that where others might desire this it remains within the design capabilities of the product.

Executive properties form an important part of the design process as a perfect mortar can only be considered such if it can be applied in an uncomplicated manner. The working life of the mortar is almost infinite if kept active during working times and excess material stored in sealed containers with sufficient liquid buffer. One of the short-comings of earlier ethyl silicate based mortars was the difficulty in keeping the mortar on the spatula during application. Lithium silicate is both strongly adhesive and tacky when in the wet formulated state.

Viscosity can be adjusted in minor ways to maintain workable consistency and, importantly, the ratio of lithium silicate to aggregate has quite wide tolerances such that continued additions of either lithium silicate or water maintain a uniform final product.

8. Treatment of Victoria and Albert

Both of these sculptures present the same range of issues, with Victoria being the more disfigured of the two.

When first encountered both figures were situated under Moreton Bay fig trees, a particularly polluting species that drops sticky residues and attracts a myriad of fruit devouring birds, most of whom depart the trees weighing roughly the same as when they arrived. The depth and extent of the pitting on the face of Victoria became fully apparent when the sculpture was first cleaned in 2006. The first sight was of a heavily graffitied face, and this together with the accumulations from the trees and birds were removed with ammonium bicarbonate poultice cleaning. The cleaned face, typical of many parts of both figures, fully exposed the disfiguring pits that were clearly inherent defects in the marble, together with some additional impact damages such as the bridge of the nose in Figure 4.



Figure 4. Victoria And Albert at left. A detail of the disfiguring pitting on Victoria's face after cleaning and just prior to lithium silicate mortar repairs in 2012, centre, and the filled surface after 6 years in 2018.

At that time the surface was rebuilt using slaked lime, quartz flour and marble dust with 5% acrylic emulsion used as the diluent. The fill began to fail within 18 months in a typical fashion for weak mortars; friable loss around the contact edges before complete separation. The inability of lime to form strong adhesive bonds is well known and masons prefer to cut a deep sharp edge for any form of plastic repair. The previously quoted treatment of the Arch of Septimus Severus¹ required the filling of very large losses but does not describe instances of shallow filling requirements. Nardi does describe the incorporation of acrylic emulsion for fine crack filling and it is assumed that a transition between straight lime and acrylic addition was made. This author has also used acrylic augmented lime fills to repair highly decorative marble that remain effective after 21 years. Acrylic is not a natural partner for lime mortars as it causes stretching and cracking not encountered in straight lime putty fills.

Both RASV portraits were conserved further in situ in 2012, at which time remnant lime fills were removed and the lithium silicate mortar system applied. A critical observation during the application of lithium mortars is the fact that large loose grains, when deposited on the marble surface, become firmly attached if left for an hour. Tools left uncleaned for 30 minutes also become very difficult to clean.

The lithium silicate based mortar, comprising ground marble and 5% quartz flour has been in place for seven years at time of writing. In that time there have been some losses from very shallow pointing marks, some of which were filled due to their colour rather than surface impression. The larger fills remain intact, particularly around their contact edges where the first signs of failure appear. Feathered edges where shallow divots merge into the sound surface also remain largely intact, and have survived for five times longer than the lime fills. Importantly the face of Victoria remains more or less blemish free.

9. Young Bull and Herdsman

The bull has been in an outdoor exposure since 2006 when it was relocated from a protective shelter subject to high vandalism due to its remote location. It is unclear how long the bull spent in full exposure before being protected by the shelter demolished in 2006 but it is estimated that it was no longer than 30 years. When first inspected in the shelter in 1999 the bull already displayed all of the crack pattern that shows today. Photographic comparisons are difficult on such fine cracks as the surface was not recorded in sufficient detail in the period 1999-2006. The cracks seen today are all evident in 2006 images however it cannot be stated with certainty that they have increased through gradual erosion of the openings. A study of the cracks and their origins is in preparation but the more urgent considerations have centred around whether the bull should be returned to an indoor environment and whether if left outdoors its inevitable rate of erosion can be modified.

The pattern of fine cracks in the upper marble (Figure 1, Figure 5) are not considered a structural issue, despite the deepest and most visible one appearing to suggest the head may detach at any moment.



Figure 5. Young Bull and Handler, showing a detail of the overall crack pattern across the upper back of the bull.

Two approaches have been adopted for this sculpture, both involving lithium silicate. The first is the filling of the extensive crack network and the second, not described in great detail here, is the application of a siloxane emulsion coupled with lithium silicate to provide adequate attachment to the marble without requiring any form of surface modification (in preparation).

Lithium silicate has been added to marble powder sifted through a 106 micron sieve and 10% quartz flour, to make a workable grout with good flow. The typical ratio of lithium to

aggregate is 65:100 to produce a grout that can be administered through a 0.9 mm pipette tip. This grout applied to a 2 mm cavity between Plexiglass walls has flowed freely to more than 1.5 metres. Greater flow can be achieved by increasing the ratio to 130:100 while still producing a hard setting grout with satisfactory cohesive strength. The cracks in the bull were first treated with pure liquid lithium silicate Li 20, followed by progressively more viscous mixes applied 24 hours apart. On each occasion the crack was allowed to fill.



Figure 6. Detail of the filling process on left with the upper crack over-filled prior to finishing. The completed surface on right after 18 months.



Figure 7. The drapery above the Handler's wrist required extensive mortar repairs, testing the modelling abilities of the mortar.

The final application of 65:100 liquid:aggregate was allowed to over-fill the surface. This over-fill was removed with diamond discs attached to a Dremel drill. The ability to work the cured mortar in this manner is critical to achieving a gloss match but also serves as testament to the cohesive strength of the grout. The ground surface was dense but more water absorptive than the parent marble, thus lithium silicate has been applied during all stages of the application, including the final grinding. Further application of lithium silicate

allows for the densification of the surface after grout cure, less porous than the final mortar application and in pigmented washes to match the adjacent natural surface patination.

While the application of lithium silicate to the cracks has reduced their ability to absorb water there remains a desire to make them, and the surface of the marble itself, less impacted by rain. Australia does not yet suffer the damaging levels of acid rain of the northern hemisphere but all rain is well below the equilibrium pH of calcite. Early trials using hydrogen functional siloxane, both directly to the marble surface and following application of lithium silicate, acting as a coupling agent, failed to provide hydrophobicity for more than 12 months. The siloxane is water immiscible and thus had to be applied after the lithium silicate had fully reacted.

Current research has successfully combined a siloxane emulsion, Dow Corning IE 6683, with Litisil 20 at 15% w/w for both components. IE 6683 is described by the manufacturer as an emulsion containing Silicic acid-diethoxyoctylsilyl trimethylsilyl ester, Triethoxy(octyl) silane, hydroxy terminated dimethyl siloxane, Dimethyl siloxane with aminoethylaminopropyl oxane, and solvents including acetic acid. One assumes there is good reason for this blend of silanes. The critical point is that the lithium silicate is stable upon addition of the IE6683 at concentrations avoiding an altered surface appearance and that the mixture imparts hydrophobicity.

Early trials have focussed on treatment of a 19th century Portland cement object giving preliminary indications of durability in a partially calcitic substrate. While short term water repellency can be achieved on marble the screening process will resolve whether this system can perform over a suitable treatment cycle of at least five years.

10. Conclusion

The treatments described in this paper are considered by the curator as maintenance procedures and, as in the case of the previous lime repairs, deterioration of the repairs has been determined to be non-damaging to the object. Improving on existing repair systems is considered the main imperative and this has been achieved in the case of mortars lasting at least five times longer than previous repairs.

Lithium silicate has been able to effectively consolidate granular marble surfaces, and on this basis has also proven capable of binding free flowing grout formulations and viscous mortars. It has been used in the current case studies as a grout to fill narrow voids, thus reducing water entry into a cracked marble surface. Lithium silicate and marble powder mortars have been applied to very shallow losses and perform well after three years. Earlier attempts using lime techniques failed rapidly and hence the current system is more durable and more amenable to achieving a marble like finish.

References

1. Nardi R. 1987. The conservation intervention on the arch of Septimus Severus in the Roman Forum. In 8th Triennial Meeting of the International Council of Museums, Conservation Committee. 493-502
2. Larson J.H. 1986. The conservation of a marble group of Neptune and Triton by Gian Lorenzo Bernini. In International Institute for the Conservation of Historic and Artistic Works, Bologna Preprints – Conservation of Stone and Wallpaintings. Brommelle N.S. and Smith P. (eds) 22-26.
3. Thomas, A. 2008. Waterborne silicates in coatings and construction chemicals. In Surface Coatings Australia, March 2009, 10-18
4. Sassoni E, Graziani G, Franzoni E. 2015 Repair of sugaring marble by ammonium phosphate: comparison with ethyl silicate and ammonium oxalate and pilot application to historic artifact. Mater. Design 88:1145-1157.2015.
5. Sassoni E., Graziani G., Franzoni E., Scherer G.W., Consolidation of sugaring marble by hydroxyapatite: some recent developments on producing and treating decayed samples, In: Hughes J. & Howind T. (Eds) Science and Art: A Future for Stone: Proceedings of the 13th International Congress on the Deterioration and Conservation of Stone, Volume 2. Paisley: University of the West of Scotland, 6-10 September 2016, 947-954
6. Sassoni, E. 2015 crack depth, awaiting from author
7. Thorn, A. 2016 Injection grouts based on Lithium Silicate binder: A simulated cavity test. In Preprints of the 4th Historic Mortars Conference, Santorini, Greece.
8. Ferragni, D., Forti, M., Malliet, J., Mora, P., Teutonico, J.M., and Torraca, G. 1984. Injection grouting of mural paintings and mosaics. In International Institute for the Conservation of Historic and Artistic Works Paris Preprints – Adhesives and Consolidants Brommelle N.S., Pye E.M., Smith P. and Thomson (eds) 110-116.
9. Thorn, A. 2010 Two siliceous grouts for the preservation of stone. In Preprints of the 2nd Historic Mortars Conference and RILEM TC 203 Final Workshop 2010. Prague, Czech Republic. IV.39
10. Meng, B. 1992 Moisture-transport-relevant characterization of pore structure. 7th International Congress on Deterioration and Conservation of Stone. Delgado Rodrigues J., Henriques F. and Telmo Jeremias F. (eds) 387-396.

Evaluation of the rheological behaviour of a natural additive of vegetal origin in restoration lime mortars as an ecological and sustainable alternative

N. Guasch-Ferré¹, M.R. Veiga², T. Díaz Gonçalves², M. T. Doménech-Carbó³, J.L. Prada⁴, X.

Mas i Barberà³, M.P. de Luxán Gómez del Campillo⁵

(1). *Departament d'Arts i Conservació-Restauració. Facultat de Belles Arts, Universitat de Barcelona, Barcelona*

(2). *Laboratório Nacional de Engenharia Civil (LNEC), Lisboa*

(3). *Institut de Restauració del Patrimoni, Universitat Politècnica de València (IRP-UPV), València*

(4). *Escola Superior de Conservació i Restauració de Béns Culturals de Catalunya, Barcelona*

(5). *Instituto de Ciencias de la Construcción Eduardo Torroja (IETcc-CSIC), Madrid*

1. Introduction

Recent investigations reinforce the idea of incorporating organic components to historic mortars into the binding matrix. There exists debate about the possibility of these additives modifying the properties of the fresh mortar or about them improving the properties of the hardened mortar. This study has tested how the incorporation of tragacanth gum into the binder matrix of slaked lime putty mortars, in variable percentages, modifies the rheological behaviour.

Tragacanth gum is an additive of natural origin, exuded from the *Astragalus gummifer* tree. It has been known since remote times. In the 3rd century B.C., Theophrastus mentioned Crete, the Peloponnese and Media as places where it is produced. During the Middle Ages it came to Europe through trading vilages in Italy, according to the Pisa institutes in 1308. Pierre Belon, a famous French naturalist, observed and described in 1550 the tragacanth gum crops in northern Minor Asia. In 1700 Tournefort observed in Mount Ida in Candia the special way in which the gum oozes from the plant [1].

Halfway through the 20th century, authors such as Neuburger and Hodges [2, 3], who were pioneers in the study of modern mortars, prove the use of tragacanth gum since old age as an adhesive for mortars and essential ingredient in the making of compatible mortars for the conservation and restoration of historical buildings of the time. In this sense, this mixture was used in restoration projects during the first half of the 20th century [4].

On the other hand, consulting the relationship between historical additives and their properties published by Sickels in 1981, it can be summarized that sugar¹⁴, as a generic term has been used to: accelerate setting and increase resistance, emulsify or stabilise producing

¹⁴ The name sugar is used to refer to different monosaccharides and disaccharides, although by extension it refers to all carbohydrates (monosaccharides, disaccharides, oligosaccharides and polysaccharides).

in more hardness and stability of the mixture; withstand frost; modify plasticity to improve workability of the mortars; water retaining agent; delay, solidify and harden mixtures and as a strengthener and binder [5, 6].

However, it is worth mentioning that Sickels's list of additives only shows the use of sugars extracted from exudates of vegetal origin to: emulsify or stabilise producing higher hardness and stability of the mixture; modify the plasticity to improve the workability of the mortars and as a strengthener and binder. The use of tragacanth gum is only shown as a strengthener and is also shown as a thickener when mixed with water.

Next, two tables of organic additives are presented [7]: the first one enumerates the organic materials, grouping sugars as a general term, traditional lime mortars regarding the developed functions through history (Table 1); the second enumerates organic materials, grouping sugars as a generic term, used as additives in traditional lime mortars, in ancient Egypt, the roman times and in the construction of some European buildings according to some documents [5, 6] (Table 2).

Table 1. Table of organic additives (sugars as a generic term) in lime mortars regarding developed functions through history. Acronyms: 1. cotton; 2. fig juice; 3. fruit juice; 4. arabic gum; 5. molasses; 6. sugar; 7. starch; 8. glucose; 9. tragacanth gum; 10. tragacanth gum diluted in water

FUNCTIONS THAT DEVELOP	1	2	3	4	5	6	7	8	9	10
acceleration of curing and increase in resistance		x				x	x			
emulsifiers or stabilisers (obtaining a mixture with higher hardness and stability)			x	x		x				
resistance to frost						x				
enhancers of plasticity to improve workability of mortars		x				x		x		
retarders						x				
reducers of water need						x				
solidifiers, rigidifiers, hardeners					x	x				
strengtheners, binders	x	x		x		x			x	
thickeners										x

Regarding other investigators which refer to sugar as an organic additive in traditional lime mortars, Hiscox, D. and Hopkins, A. (1994) [12] are worthy of mention. Their *Recetario Industrial* describes a mortar called sugar mortar. The authors elaborate on the making of the mortar, with two equal parts of lime and brown sugar with water, resulting in a mortar comparable to a portland cement in terms of resistance. Today, sugar is related to concrete curing. Lapiente, R. (2008) [13], states that sugar is a retarder in concrete curing, so it can be used for this purpose.

Table 2. Table of organic additives (sugars as a generic term) utilised in traditional lime mortars. Acronyms: 1. cotton; 2. fig juice; 3. fruit juice; 4. arabic gum; 5. molasses; 6. sugar; 7. elm bark

BUILDING DOCUMENTS	1	2	3	4	5	6	7
Egypt, 150 BC [8]		x		x			
Vitruvian time, 46 BC		x					
Pliny, 23 AD		x					x
Middle Ages, 13 th c.			x			x	
Middle Ages 16 th c.			x			x	
Plat, 1653 [9]				x			
halfway through 18 th c.		x	x				
Vicat and Smit, 1837 [10]					x	x	
Burnelly, papers of the time, 1850 [11]	x			x			

Nowadays, tragacanth gum is utilised mostly in hide treatment, as a polishing compound and is occasionally used as a fabric strengthener. It has also been used as mucilage or paste for the topic treatment for burns. It is also used in pharmacy products and as an emulsifier, thickener and stabiliser in foods. Within the textile industry, it is used in the making of several tint inks; in ceramic industry it is used as a filler and suspending agent for pigments. Moreover, it is the traditional binder used in the manufacture of pastel paints for artists, since it does not adhere to itself when dried, unlike other gums [14-17].

However, there are no current references about the use of this gum as a strengthener or thickener in lime mortars. Regarding the use of sugars extracted from exudates of vegetal origin as strengtheners, there are current investigations regarding the use of nopal gum as strengthener in indoor adobe architecture in Mexico. Based on different experimental tests carried out both in laboratory and in the field with nopal gum, the study concludes that the polysaccharide strengthens the clay in adobe, providing firmness and solidity [18]. These studies part from the investigations by Hansen about the effect of organic additives, such as nopal, in lime mortars [19] and from the revision performed by the researchers team in Getty Conservation Institute in collaboration with English Heritage and Universidad de Granada [20] regarding inorganic strengtheners and the protection treatments to be applied to limestone stones as well as lime plasters [21].

In this sense, and considering suggested precedents and taking into account Mexican literature from mid to late 19th century where it is stated that “nopal produces the tragacanth gum in the country” [22, 23] and their similar physical and chemical features, this study suggests the incorporation of tragacanth gum into the binding matrix in lime mortars to study its effect and to evaluate its possible use as additive in lime mortars as an ecological and sustainable alternative to synthetic, non-biodegradable and irreversible resins, and to ensure a higher compatibility with the original materials in the restoration of monumental constructions of patrimonial interest.

2. Materials

The materials chosen for the preparation of mortars were a slaked lime putty from St. Astier (class CL 90-S in paste, slaked in mass and with a minimum aging of 6 months [24] supplied by the company NATURCAL, S.L. (Bilbao) and crushed white marble sand from Macael, of metamorphic origin, composed basically by calcite (up to a 99% in the majority of cases) supplied by LAFAC, S.L. products (Barcelona) with a distribution of a grain size (by sifting) of 0.063 mm to 1 mm [25] (Figure 1).

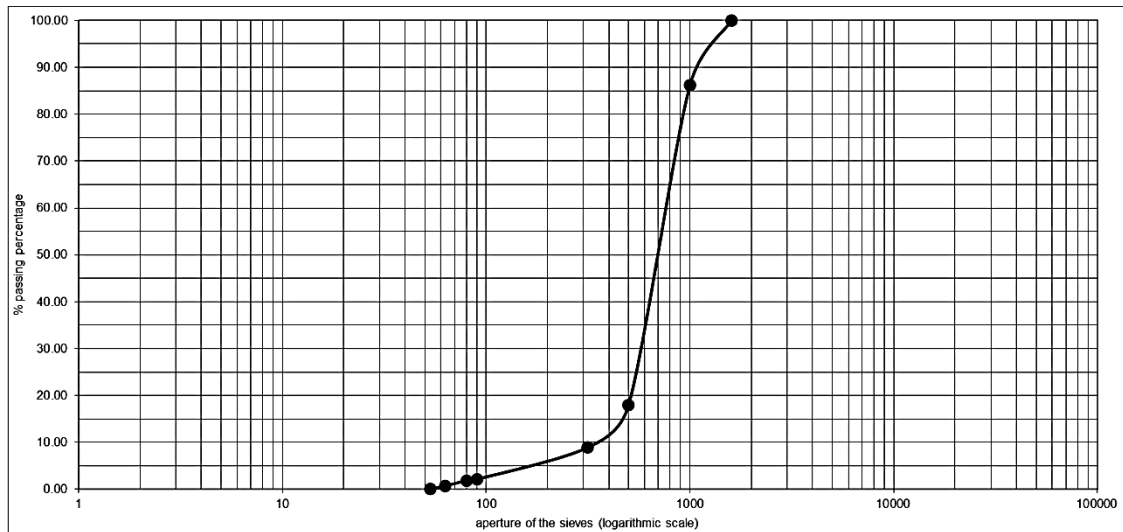


Figure 1. Granulometric curve of aggregate (the marble sand from Macael)

The tested additive was tragacanth gum (reference code in food industry E-413) by the company KREMER Pigment (product number: K63400). It is the dry exudate of the tree *Astragalus gummifer* bark, forming irregular ribbons and flakes, present in Iran and the Middle East. Fisically, tragacanth gum can be presented as white-slightly yellowish powder. Chemically it is characterised for being a polysaccharide formed by two main fractions, known as tragacanthin and basorin. Tragacanthin represents around 30% of the total and is soluble in water forming colloidal solutions. Basorin is insoluble, but it swells and forms a colloidal gel. Both are formed basically by arabinogalactans [17, 26]: Xyl (14.9%), Ara (34.7%), Ramo (3.4%), Fuc (7.4%), GalU (13.8%), GluU (3.5%), Glu (11.5%), Gal (10.8%) [27]

The materials are mixed in a relation in weight 1:2; that means the mortars are prepared mixing 500 g of slaked lime putty and 1000 g of aggregate. According to the norm [28] the percentages of additives in mortars will be inferior to 5% of the binder weight. Following this rule, a total of five mortars are prepared for each test: four of them with an additive (test mortar) and one of them without additives (reference mortar). The number of replicates for each test is three. The dosages tested are 0.5, 1, 1.5 and 2% relative to the total binder weight. The coding of the samples is as follows: T (reference mortar); 0.5TG (test mortar with an addition of 0.5% of tragacanth gum); 1TG (test mortar with an addition of 1%

tragacanth gum); 1.5TG (test mortar with an addition of 1.5% tragacanth gum) and 2TG (test mortar with the addition of 2% tragacanth gum) (Table 3).

Table 3. Admixtures and dosages of the tested mortars

Binder	Aggregate	Dosage (in weight)	Additive (powder)	Additive percentage (% in binder weight)	
Slaked lime putty CL 90-S (UNE-EN 459-1) Provider: NATURCAL, S.L.	Crushed white marble sand from Macael Granulometry: 0.063 mm Φ 1.00 mm Provider: LAFAC, S.L.	1:2	Tragacanth gum Provider: KREMER	0%	T
				0.5%	0.5TG
				1%	1TG
				1.5%	1.5TG
				2%	2TG

3. Methods

3.1. Mortars preparation

The preparation of the test mortars is performed according to the specifications in regulations [29,30]. To facilitate the handling of slaked lime putty, it is put in a drum and it is mixed automatically and manually until an homogeneous mixture is obtained. The slaked lime putty itself has enough water for an optimal hydrated lime ready to use. First, the homogenised paste and the powder additive are weighed respectively in the percentages mentioned before. After that, the admixtures are mixed with an automatic mixer (Manufactured by TESTIMONIS Milano-Italy) [31] at a slow speed (speed 1 in the device) during 2 minutes and 30 seconds. The automatic mixing is halted and the mixing is manually finished for the last 30 seconds to ensure that there is no material left at the bottom without mixing. Then, the aggregate is added for 15 seconds while the device continues to function and the mixing is allowed to continue with the three admixtures for 2 minutes and 30 seconds. The process is stopped and continued by hand, once again to ensure that all the material is thoroughly mixture. To ensure an homogeneous mixture, the mixer is activated for a final 30 seconds.

3.2. Rheological properties

For the fresh state, several properties were studied: consistency [32]; density [33]; air content [34]; water-retention capacity [35] and setting time [36].

3.2.1. Consistency

The slump value is determined by measuring the medium diameter, in mm, of a fresh mortar sample which has been put, with the help of a specific mould, on a flow table, where the mortar, after 15 seconds of being put inside the mould, is slowly removed. Then, the mortar

under goes 15 knocks, lifting the flow table and dropping freely from a given height, with a constant frequency of approximately one knock per second.

It is worth mentioning that given that this study aims to determine how the incorporation of an additive into the binder matrix of slaked lime putty mortars modifies their rheological properties, this test does not add more water than the amount contained by default. This way, it is possible to assess the consistency of the fresh state mortar is affected.

3.2.2. Density

It is determined by dividing weight (g) of the tested mortar by its volume (dm^3) which occupies when introduced, as prescribed, in a recipient of a given capacity (cylindric glass with a capacity of 0.5 l (0.5 dm^3)). It should be noted that this test is performed immediately after the test of the determination of consistency of the fresh state mortar, and therefore the mixture of the mortar used is the same. This way, the mortar is characterized in a general and continuous way.

3.2.3. Air content

It is determined through method A (pressure method) described by the norm, since previous tests are performed, to check that the studied mortars have a value of less than 20% of air inside the mortar. To perform this method, a normalised aerometer is used (FORM+TEST. Prüfsysteme, Riedlingen). This apparatus has a pressure chamber where certain pressure is applied. The discharging valve of aperture allows the pressure between the pressurised chamber and the recipient containing the mortar sample to balance, thus achieving stable pressure. The reading of the calibration manometer is the measure of air contained of the fresh state mortar, which corresponds to the decrease in pressure.

3.2.4. Water-retention capacity

It is determined by measuring the quantity of water retained in the mortar after the normalized suction treatment, expressed in the absorbed percentage compared to the original water content. In our case, the original water content is unknown since the used binder for the tested mortars is a slaked lime putty which, as mentioned before, already contains water. For this reason, the first step is to determine the original water content in the slaked lime putty with the regulated test [37], which consists in calculating the humidity of the material after being dried, through 12 h cycles in a 60°C heater, until constant weight is achieved. The results obtained from the test determine that the water/lime ratio of the slaked lime putty used is 60/40 (values in %).

3.2.5. Setting time

It is determined by measuring the time, in minutes, since resistance to penetration ($0.5\text{N}/\text{mm}^2$) by a normalised bradawl is achieved. The result is obtained by immediately inserting the data obtained above and below the defined limit.

4. Results and discussion

4.1. Rheological properties

From the summary of the results of the tests of the characterisation of the rheological properties of the fresh state mortar, it can be determined, in general terms, that the tested gum, tragacanth gum (TG), modifies all rheological properties tested: consistency, density, air content, water-retention capacity and setting time (Table 4). The behaviour depends on the chemical nature of the polysaccharide and the percentage of gum that has been added into the mortar (0.5%, 1%, 1.5% and 2%) as shown:

Table 4. Rheological properties of tested mortars

	Slump (mm)	Density (g/L)	Air content (%)	Water-retention capacity (%)	Setting time (min)
T	156.7	1894	4.6	80.10	5760
0.5TG	142.5	1838	7.3	94.68	5970
1TG	131.0	1845	7.0	91.51	5437
1.5TG	120.0	1843	6.5	88.70	3046
2TG	110.5	1833	5.9	94.29	-

4.1.1. Consistency

As it can be observed in Figure 2, mortar T presents a slump within normal parameters set by the norm (156.7 mm slump). Therefore, as it is expected, the slaked lime putty mortar has optimal plasticity. Regarding the addition of TG to the mortar, it behaves differently depending on the percentages (0.5%, 1%, 1.5% and 2%). The slump of the mortar decreases as more percentage of gum is added, but when 1% or more gum is added, the slump values are no longer within the margin of what constitutes a plastic mortar (140 and 200 mm slump by the norm). Therefore, it can be determined that without the modification the water in the mixture, the consistency of the mortar decreases. This effect means TG works as a thickener. That is to say, in all tested cases, an additional water incorporation would be required if one wanted to obtain the same consistency found in T mortar.

4.1.2. Density

As it can be observed, the addition of the TG substantially modifies the density of the mortar in fresh state regarding the density of the T mortar. The density values obtained show two

inflection points (Figure 3): the first one in the 0.5% percentage of the gum, where the density value decreases significantly regarding the value of density of the T mortar. Next, the mortar with the addition of 1% of gum experiments a slight recovery of density; the second point of inflection in the percentage of 1.5% of gum, where the density value decreases once again until the 2% gum percentage. From the obtained results after the determination of the density of the tested mortars, it can be determined that the TG substantially reduces the density of the mortar, especially in a percentage of 0.5% gum regarding T mortar.

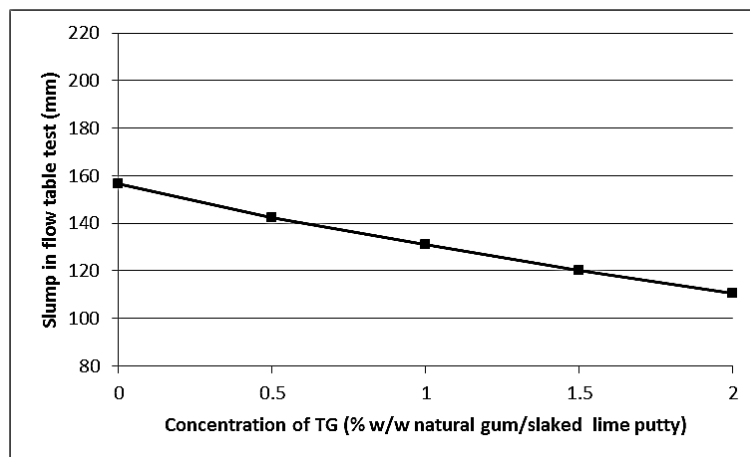


Figure 2. Slump results in flow table test vs. concentration of tragacanth gum (TG)

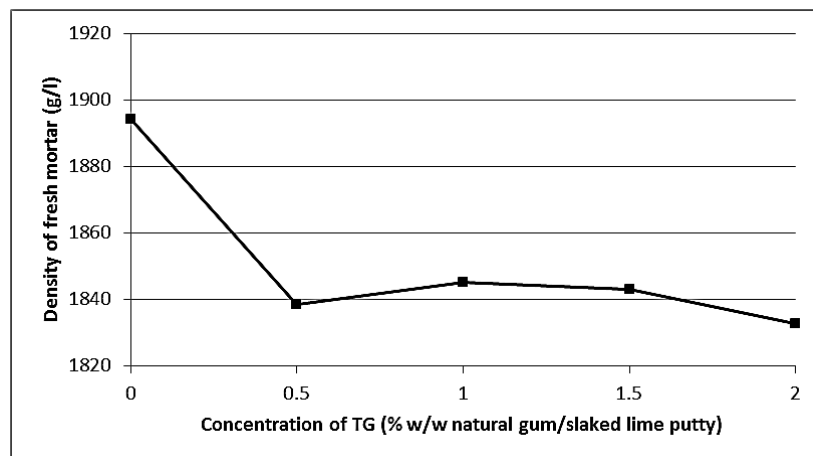


Figure 3. Density of the fresh mixtures vs. concentration of tragacanth gum (TG)

4.1.3. Air content

Before anything else, it is determined that T mortar is within the normed set by the norm [30] as optimal air content, since it specifies that the air content of the reference mortar without additives should not exceed 5% in volume and the obtained value in T mortar is 4.6% (Figure 4). The obtained values in the determination of the air content in mortars with the addition of TG show a great increase in air volume inside the mortar structure. More specifically, the addition of 0.5% of TG in the mortar is the value which shows the biggest

difference compared to other percentages (1%, 1.5% and 2%), which decrease progressively, but always above the levels of air seen in T mortar. Therefore, it can be concluded that TG, as an additive in mortars of slaked lime putty, behaves as an air entraining agent (AEA). In this sense, there exist other studies about this issue which determine that natural organic polymers have inherent tensioactive properties which lower superficial tension of the aqueous base of the paste of the mortar, allowing for the entrance of air bubbles into the mortar structure [38, 39, 40]. Therefore, given the spherical shape of the air bubbles, these work as lubricants for the fresh state mortar, improving its docility [41].

Moreover, the obtained results about the determination of air content in the mortar can be correlated with the results obtained about the determination of density of the mortar, since the incorporation of air into the mortar structure translates into a decrease of density.

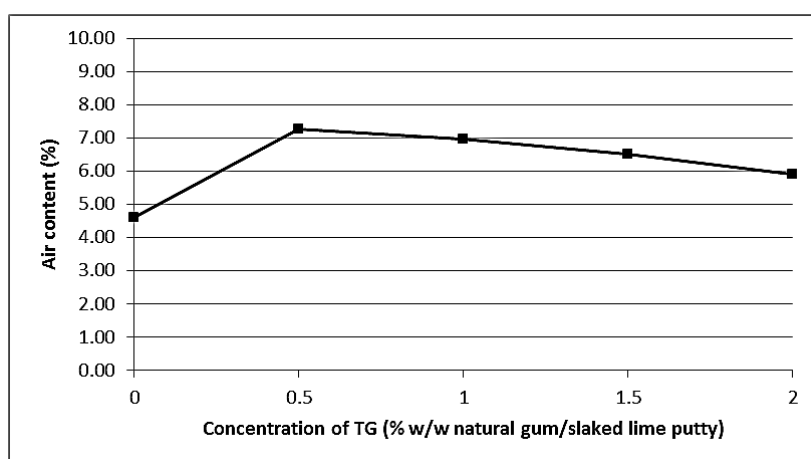


Figure 4. Air content of mortars vs. concentration of tragacanth gum (TG)

4.1.4. Water-retention capacity

At a general level, it can be observed that the addition of TG increases the water retention capacity of the mortar. Specifically, in general terms, mortars with the addition of TG increase their water retention capacity by 11 and 15%. Also, the percentages which increase the water retention capacity by a largest amount are 0.5% and 2% (Figure 5). Therefore, it can be concluded that TG as an additive for slaked lime putty mortars behaves as a water retaining agent.

4.1.5. Setting time

From the obtained results about the determination of setting time, it can be firstly concluded that mortars with an addition of TG in a 0.5% percentage increase the setting time in relation T mortar; secondly, mortars with an addition of 1% of TG decrease the setting time in relation with T mortar. Lastly, with an addition of 1.5% and above of TG the setting time significantly decreases in comparison with other obtained data from different

amounts of TG and T mortar (Figure 6). Therefore, the mortar with an addition of TG only increases the setting time with an addition of 0.5% of gum. At higher percentages than indicated, the tested mortars with the addition of TG decrease its setting time substantially.

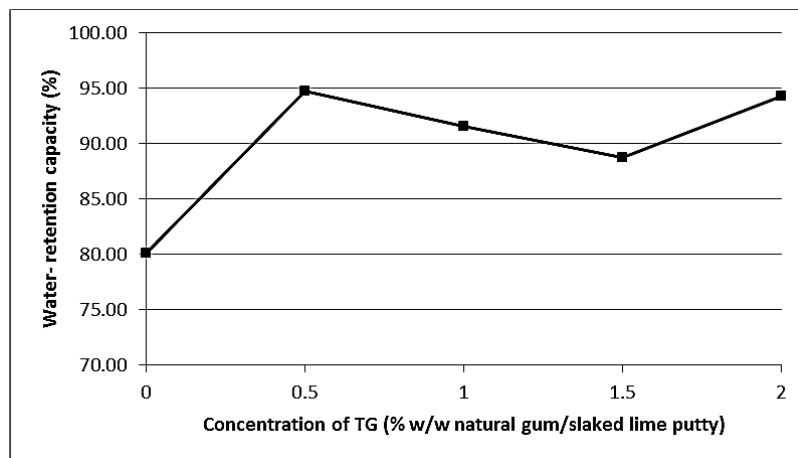


Figure 5. Water-retention capacity of the mortars vs. concentration of tragacanth gum (TG)

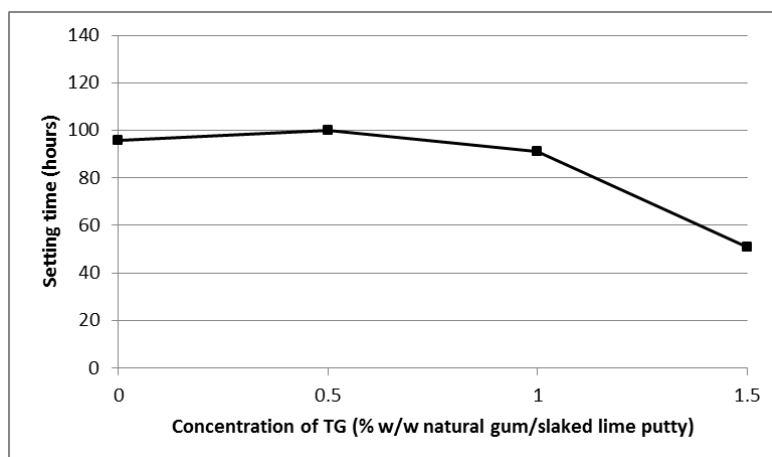


Figure 6. Setting time of mortars vs. concentration of tragacanth gum (TG)

5. Conclusions

The physical behaviour of a mortar depends on a number of factors. Fundamentally, it firstly depends on the type of binder used, in this study the slaked lime putty and secondly the type of aggregate chosen, that is, its composition, granulometry and shape. Finally, the dosage of the mortar. The obtained result, after the mixing of the admixtures, with or without addition of additives, is a mixture which shows uniform and porous texture. However, it must be noted that the initial structure transforms physically and chemically due to the carbonation which evolves in time. This happens due to the reaction of hydrated lime with carbon dioxide in the atmosphere, that entails a hardening and a cohesion that give the whole a new properties, both physical and mechanical, as well as behaviour against water and durability.

That being considered, in the different types of tested mortars, the main variation among them has been the amount of added gum (0.5TG, 1TG, 1.5TG and 2TG). The rest of intrinsic parameters, such as the type of lime, the aggregate and the mortar dosage, have been kept constant. This variable has only been necessary since the evolution in time and the properties acquired by the different tested mortar families that have been very different, as determined the results exposed in this study. These have been conditioned mainly by two factors: firstly, the interaction of the TG with lime particles and its distribution on the mortar texture. Secondly, the incorporation of air with the consequent formation of bubbles.

In this sense, it can be concluded that the determined rheological properties of the mortar with the addition of TG show adequate application possibilities: ease of application due to the docility obtained thanks to the spherical shape of the air bubbles incorporated in the mortar structure and the high setting time which allow for a better finish. On the other hand, the added TG shows a high water retention capacity which will be kept in the mortar for a long period of time. This property is of special importance when a cladding is performed under different humidity and temperature conditions [42], since it avoids a rapid evaporation of the mortar and the consequent generation of shrinkage cracks. Therefore, the TG would be a natural organic additive of vegetable origin that could be utilised, for example, in slaked lime putty mortars applied to stucco restoration.

But it has to be added that, to make the TG the ideal additive, the percentages used must be first optimised. In our case, it has been determined that the most effective percentage in all performed tests is 0.5% gum. The other higher percentages decrease benefits. Therefore, future investigations should try to determine and characterise the mortar benefits, both fresh and in hardened state, with the addition of the gum, between 0.1% and 0.5% percentages to better assess if the 0.5% percentage would be the maximum recommended in slaked lime putty mortars.

Last, it is worth noting that this natural gum of vegetal origin could be an alternative to the different types of additives which are available commercially nowadays, which include cellulose derivatives for the most part: ethylcellulose (EC), hydroxyethylcellulose (HEC), hydroxypropylcellulose (HPC), carboxymethylcellulose (CMC), methylcellulose (MC) and ether mixtures of cellulose: hydroxypropylmethylcellulose (HPMC) and methylhydroxyethylcellulose (HEMC). The percentages of these additives do not normally surpass 0.7% [42]. But, notwithstanding each case of application, the field of restoration asks for a personalised diagnose of the situation and previous studies to determine which of all the existing additives is the most adequate and compatible with the original materials.

Acknowledgements

The analytical study carried out in this research has been funded through the Projects CTQ2014-53736-C3-1-P and CTQ2014-53736-C3-2-P, which are supported with Ministerio de Economía, Industria y Competitividad (MINECO) and Fondo Europeo de Desarrollo Regional

(ERDF) funds, as well as project CTQ2017-85317-C2-1-P supported with funds from, MINECO, ERDF and Agencia Estatal de Investigación (AEI) are gratefully acknowledged.

Also, the analytical study carried out in this research has been funded through the Projects PIP 2009-2012: “Degradação e conservação de materiais porosos artificiais” (proc 0205/11/17685) and “Técnicas e materiais de conservação e restauro de revestimentos históricos” (proc 0803/11/17798).

References

1. Noriega JM (1902) Curso de Historia de Drogas. Edición de los Anales del Instituto Médico. Oficina Tipográfica de la Secretaría de Fomento, México
2. Neuburger A (1930) The Technical Arts and Sciences of the Ancients, London, UK, 51
3. Hodges H (1964) Artifacts, London, UK
4. Bedolla Arroyo JA et al (2009) Aditivos orgánicos en morteros de cal apagada en la edificación histórica. Ciencia Nicolaita 51: 153-166
5. Sickels LB (1981) Organic additives in mortars. EAR 8:7-20
6. Sickels LB (1982) Organics vs. Synthetics: their use as Additives in Mortars. Mortars, Cements and Grouts used in the Conservation of Historic Buildings, Symposium. ICCROM, Roma 38-45
7. Cečov E (2009) The effect of linseed oil on the properties of lime-based restoration mortars. Tesi doctoral. Universit di Bologna, Italia
8. Janot F (2008) Momies. Rituels d’immortalit dans l’Egypte ancienne. Editions White Star, Pars 178-215
9. Plat SH (1653) The Jewel House of Art and Nature. Elisabeth Alsop, London
10. Vicat LJ (1837) A Practical and Scientific Treatise on Calcareous Mortars and Cements, artificial and natural, trans Colonel J.T. Smith, R.E. John Weals, Architectural Library, London 84
11. Burnell GR (1850) Rudimentary Treatise on Limes, Cements, Mortars, Concretes, Mastics, Plastering, etc. John Weals, London
12. Hiscox GD, Hopkins AA (1994) El recetario industrial. Enciclopedia de frmulas, secretos, recetas, prcticas de taller, manipulacions, mtodos de laboratorio, conocimientos tiles. Trabajos lucrativos para pequeas y grandes industrias. Gustavo Gili, Barcelona.

13. Lapuente Aragón R (2008) Conglomerantes. Tema 13. Temas de química (II). Presentaciones adaptadas al texto del libro para alumnos de ITOP el CCP. Departamento de Ingeniería de la Construcción. Universidad de Alicante, Valencia
14. Whistler R (1973) Industrial Gums. Academic Press.
15. Glicksman M (1980) Food hydrocolloids. CRC Press.
16. Aspinall GO (1985) The polysaccharides. Academic Press
17. Cottrell IW, Baird JK (1998) Gomas. In: Enciclopedia de tecnología Química Kirk-Othmer, Limusa. Kirk-Othmer Concise Encyclopedia of Chemical Technology, New York
18. Torres-Acosta AA, Cano-Barrita PF de J (2007) Las bondades del nopal. Construcción y Tecnología 233:44-49
19. Hansen EF, Rodríguez C (2002) Los comienzos de la tecnología de la cal en el mundo maya: innovación y continuidad desde el Preclásico Medio al Clásico Tardío en Nakbé, Petén, Guatemala. In: Laporte, J.P. Escobedo, H. XV Simposio de Investigaciones Arqueológicas en Guatemala. Museo de Arqueología y Etnología de Guatemala, Guatemala 203-206
20. Hansen EF et al (2003) Lime Mortars and Plasters Bibliography: Sorted by General Category. Getty Conservation-Institute, Los Ángeles
21. Barbero Barrera MM (2011) Mejora del comportamiento térmico de los morteros de cal aditivados y su empleo en la rehabilitación de inmuebles. Tesis Doctoral. Escuela Técnica Superior de Arquitectura. UPM, Madrid
22. Alzate Ramírez JA (1831) Gacetas de Literatura de México. Tomo tercero, Puebla.
23. Espinosa RA (1897) Ligeros apuntes para la Geografía y Estadística del Estado de Aguascalientes. In: Edición de El Republicano, Aguascalientes.
24. UNE-EN 459-1:2011 Cales para la construcción. Parte 1: Definiciones, especificaciones y criterios de conformidad
25. UNE-EN 1015-1:1999, UNE-EN 1015-1:1999/A1:2007 Métodos de ensayo de los morteros para albañilería. Parte 1: Determinación de la distribución granulométrica (por tamizado)
26. Calvo M (2004) La Ciencia y la Tecnología de los Alimentos. Algunas notas sobre su desarrollo histórico. Alimentaria 41 359:19-34
27. Bonaduce I et al (2007) Gas chromatographic–mass spectrometric characterisation of plant gums in samples from painted works of art. Journal of Chromatography 1175:275–282

28. UNE-EN 934-3:2010+A1:2012 Aditivos para hormigones, morteros y pastas. Parte 3: Aditivos para morteros para albañilería. Definiciones, requisitos, conformidad, marcado y etiquetado
29. UNE-EN 1015-2:1999, UNE-EN 1015-2:1999/A1:2007 Métodos de ensayo de los morteros para albañilería. Parte 2: Toma de muestra total de morteros y preparación de los morteros para ensayo
30. UNE-EN 480-13:2010+A1:2011 Aditivos para hormigones, morteros y pastas. Métodos de ensayo. Parte 13: Mortero de referencia para albañilería para ensayos de aditivos para morteros
31. UNE-EN 196-1:2005 Métodos de ensayo de cementos. Parte 1: Determinación de resistencias mecánicas
32. UNE-EN 1015-3:2000, UNE-EN 1015-3:2000/A1:2005 Métodos de ensayo para morteros de albañilería. Parte 3: Determinación de la consistencia del mortero fresco (por la mesa de sacudidas)
33. UNE-EN 1015-6:1999, UNE-EN 1015-6:1999/A1:2007 Métodos de ensayo de los morteros para albañilería. Parte 6: Determinación de la densidad aparente del mortero fresco
34. UNE-EN 1015-7:1999 Métodos de ensayo de los morteros para albañilería. Parte 7: Determinación del contenido en aire en el mortero fresco
35. prEN 1015-8:1999 Methods of test for masonry. Part 8: Determination of water retentivity of fresh mortar.
36. UNE-EN 1015-9:2000, UNE-EN 1015-9:2000/A1:2007 Métodos de ensayo de los morteros para albañilería. Parte 9: Determinación del periodo de trabajabilidad y del tiempo abierto del mortero fresco
37. UNE 103300:1993 Determinación de la humedad de un suelo mediante secado en estufa.
38. Izaguirre AA, Lanas J, Alvarez JI (2011) Characterization of aerial lime-based mortars modified by the addition of two different water-retaining agents. Cem. And Concr. Res. 33:309-318
39. Rixom R, Mailvaganam N (1999) Chemical admixtures for concrete. E&FN Spon, London 214-215
40. Seabra MP *et al.* (2009) Admixtures effect on fresh state properties of aerial lime based mortars. Construction and Building Materials 23:1147-1153
41. Rodriguez-Mora O (2003) Morteros. In: Guía general in Asociación Nacional de Fabricantes de Mortero (AFAM), Madrid

42. Sychala E (2015) The effect of lime and cellulose ether on selected properties of plastering mortar. *Procedia Engineering* 108:324-331

The initial reactions of lime-pozzolan pastes for conservation of masonry

Tuğçe Büşra Su¹, Richard J Ball¹, Juliana Calabria Holley¹

(1) University of Bath, tbs31@bath.ac.uk, easrjb@bath.ac.uk, jch51@bath.ac.uk

Abstract

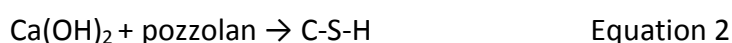
Throughout the lifetime of historic buildings the masonry will often undergo at least one conservation intervention. The need for conservation arises from the different elements of the building and to this end mortars have a very important role to play. Historic lime mortars and the various components from which they are made including the type of lime, pozzolan and aggregates have been extensively studied. They have received attention concerning their degree of reactivity and how they interact with the masonry units which are commonly stone or brick. The pozzolan-lime reactions, and the hydration and carbonation processes are important factors that influence the final properties of any lime-pozzolan mortars. In this study lime-pozzolan paste combinations are defined as a combination of calcium lime (CL 90) with a pozzolanic additive. The pozzolanic materials; wood ash, brick dust and Argical M1000 have been investigated in this study. To understand the role of the different pozzolans on the initial hydration reactions of the lime in pozzolan-lime pastes, the rheology and hydration kinetics were evaluated using a TA Hybrid Rheometer DHR – 2 and a Calmetrix I-Cal 4000 calorimeter respectively. In terms of kinetics evolution, Argical M1000, a type of metakaolin exhibited greater pozzolanic activity than wood ash and brick dust. Calorimetry and rheology tests have shown corroborative results regarding the initial hydration reactions of the pozzolan-lime pastes, different effects were observed for each type of pozzolan.

1 Introduction

With age materials are expected to fail, this failure of the macrostructure is very likely to have been caused by changes at the nano and microstructural level [1]. It has been demonstrated that there is a correlation between the chemical and physical properties of pozzolans and the performance at the micro scale within historic buildings [2]. The longevity of a repair made using these materials can be influenced by these interactions. It therefore follows that to be able to understand the behaviour and properties of historic mortars, it is important to understand the behaviour of the types of binder, aggregates and additives that have been used. In this study, a number of representative pozzolans were chosen to investigate their effects on mortar performance. Within the test mixes the proportions of CL90 hydrated lime, fine sand and water were kept constant.

Pozzolanic materials are siliceous or siliceous and aluminous in nature as defined in the ASTM C618 Standard [3]. They have no binding ability by themselves to form calcium silicate

hydrate (C-S-H) and calcium aluminate hydrate (C-A-H). To produce C-S-H or C-A-H pozzolanic materials require mixing with calcium hydroxide and water (Equation 1) [4]. Limes are classified as hydraulic and non-hydraulic (also called hydrated lime). Hydraulic limes can gain strength in the short term since they contain hydraulic phases which form calcium silicate hydrate (C-S-H) phases upon contact with water. These (hydraulic) phases originate from the reaction of lime with impurities containing silica, alumina and iron during the burning process at specific temperatures [5]. Non-hydraulic limes can be used in the form of lime putty, produced from quick or pure lime, or as a dry hydrated powder. However since non-hydraulic lime does not have any siliceous or alumina siliceous constituents, they require additives such as pozzolans to allow the formation of C-S-H phases during setting. Long term strength in limes is gained through carbonation as described by Equation 1 [6]. In this process carbon dioxide will dissolve in water forming carbonic acid which subsequently reacts with the lime forming calcium carbonate which leads to hardening (Equation 1). The pozzolanic reaction (Equation 2), hydration and carbonation processes (Equation 1) play a key role in determining the compatibility and durability factors for pozzolan-lime mortars used in conservation.



Previous studies have been carried out on the characterisation and standardization of mortars. In 1993 ICCROM (International Centre for the Study of the Preservation and Restoration of Cultural Property) and English Heritage carried out a joint study of the Smeaton Project and between 1997 and 2004, a study on pozzolanicity with cement was carried out by the British Standards Institute [7]. Any standardization for pozzolan-lime for use in renovation interventions has not been carried out since this time. This study provides new information on the behaviour of pozzolans. There are many studies [8-11] which investigate the physical characteristics of pozzolans such as surface area, particle size, fineness on the reactivity of lime-pozzolan pastes.

In this study we have investigated the physical and chemical characteristics of the pozzolans. The first step was the characterisation of raw pozzolanic materials. For the elemental analysis Energy Dispersive X-ray Spectroscopy (EDX) was carried out. X-ray Powder Diffraction (XRD) was used to identify the crystalline phases. The rheometer and calorimetry tests were performed to obtain information about the mechanisms of hydrated lime early hydration in the presence of pozzolanic materials. This study will investigate the effect of different pozzolan-lime combinations. The rheology of the pastes coupled with the oscillation tests provided information about how the behaviour of the different pastes change under the stress over time. This paper will look to correlate the kinetics of reactions with the changes in rheological behaviour. Together the hydration / pozzolanic kinetics and the monitoring of the setting behaviour of the pastes via the rheology studies will provide

information about the effect of the different pozzolans on the properties of the pozzolan-limes pastes.

2 Experimental Methodology

2.1 Materials

The lime selected for this study was Limbux CL90 hydrated lime supplied by Tarmac. It has low levels of impurities and does not contain any aluminate and silicate phases and therefore, does not have inherent pozzolanic activity. In this study three different pozzolanic materials have been investigated; wood ash, brick dust, and metakaolin (Argical M1000) supplied by Cornish Lime, Bodmin, UK. The pozzolan-lime paste mix proportions are presented in Table 1.

Table 1: Pozzolan-lime pastes mix proportions.

	% Pozzolan in Paste	Total mass (g)	Lime (g)	Pozzolan (g)	Water (g)	P/L* Ratio	B/W** Ratio
Mix 1	10%	50	5	20	25	0.25	1
Mix 2	18%	50	16	9	25	0.56	1
Mix 3	25%	50	12.5	12.5	25	1	1
Mix 4	34%	50	17	8	25	2.15	1

*P/L: Ratio of Pozzolan/Lime **B/W: Ratio of Binder (Lime + Pozzolan)/Water

Within the literature the pozzolan to lime (P:L) ratio of typical mixes range from 2.125 to 0.25. The most effective P:L was found to be 0.56 [12]. The ratios studied before such as 0.25, 0.56, 1, 2.15 for P/L ratio are chosen for this study as well.

2.2 Instrumentation

A Calmetrix I-Cal 4000 Calorimeter was used to obtain information about the kinetics of the reaction between the pozzolans and lime. The hydration reactions were analysed for a period of 120 hours to investigate the effects of the different pozzolans with the CL90 lime.

Microscopic analysis was carried out using a Joel JSM 6301F field emission scanning electron microscope with Energy Dispersive X-ray Spectroscopy (EDX) to obtain the elemental composition of the different raw materials. All samples were left under vacuum for 24 hours prior to testing to reduce moisture levels.

TA Hybrid Rheometer DHR-2 was used for the rheology studies. Changes in the paste rheology were analysed with viscosity when the stress is applied by time. A geometry gap of 1mm was utilised for all experiments. The upper and lower plates were disposable and had diameters of 25 and 60 mm respectively. The mixes were hand- stirred for 3mins before

placing on the lower plate. To reduce water loss via evaporation, the plate area was covered by a plastic lid, after the geometry gap is applied.

Characterisation of the crystalline phases present in the specimens was carried out using a WinXPOW PKS_2.01 Version X-ray diffractometer. $\text{CuK}\alpha$, X-rays of wavelength 1.540598\AA were used in combination with a Multi-MYTHEN detector. Scans were carried out over a 2-theta range from 17° to 75° with a step size of 0.015° and a time per step of 300.0 Ms.

3 Results and Discussion

3.1 Characterisation of raw materials

Argical M1000, Wood ash and brick dust are produced at temperatures of $600\text{--}800^\circ\text{C}$, above 850°C and above 1000°C respectively. The elemental analysis (EDX) confirmed that CL90 is a pure hydrated lime which does not contain silicon (Si), aluminium (Al) or magnesium (Mg). The highest quantity of Si was observed in Argical M1000 which was 23.12% by weight. Cornish Lime brick dust (21.01%) had a comparatively lower Si weight percentage than Argical M1000. Wood ash showed the lowest Si and Al content which are important for promoting pozzolanic reactions with lime (CL90). The amount of aluminium oxide impacts the strength, setting characteristics, microstructure, acid resistance of the properties and metakaolin includes 40% aluminum oxide while other pozzolan, slag has 10% aluminum oxide content [13]. Walker and Pavia reported that the initial setting time of pozzolan-lime pastes are increased by the presence of silica and alumina phases, while the content of calcium and magnesium oxides decrease it [14]. Contrarily, $\text{Mg}(\text{OH})_2$ is not associated with the strength of samples in terms of the studies of Edwards [15]. In terms of this study, Argical M1000 has the highest initial setting time while wood ash has the lowest regarding their silica and alumina contents. This is shown in Figure 6 where the lowest initial reaction delayed Argical M1000 and brick dust initiated. The presence of Ca as not detected for Argical M1000 while Cornish Lime brick dust and wood ash had levels of 18.15% and 21.65% respectively. Quantities of chlorine (Cl) were detected in the wood ash along with a high proportion of potassium (K). Small amounts of K and sodium (Na) were detected in the wood ash and brick dust, Figure 1.

The X-ray Diffraction Patterns (XRD) of the pozzolans, shown in Figure 2, were used to identify the crystalline phases present in the specimens. Quartz which was identified in the Argical M1000, brick dust and wood ash by peaks at 2-theta values of 20.85° , 26.63° , 36.49° , 50.17° and 68.18° [16]. In the wood ash, wollastonite was identified by peaks at 2-theta values of 28.07° , 34.58° , 36.49° , 42.46° , 59.95° [17], and potassium chloride through peaks at 28.414° , 40.618° , 58.792° , 66.568° [18], sodium chloride peaks at 31.569° , 45.155° , 56.098° [18].



Figure 1: Elemental composition of the raw materials (Weight %)

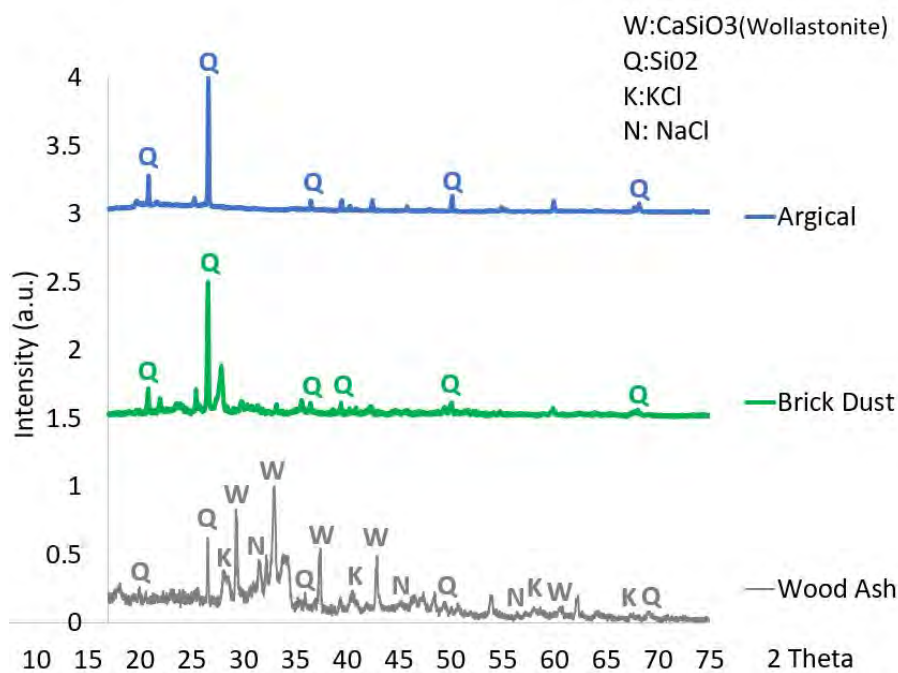


Figure 2: Representative Diffraction Patterns of raw materials

With the SiO₂ + Al₂O₃ content, the pozzolans are rated since they are associated with the hydraulic components in limes [14]. Therefore, the type of pozzolan used in a mortar will have its own characteristic pozzolanic activity and acceleration period associated with hydration. The dissolution and hydration reaction are likely to occur earlier than the pozzolanic reactions. However the separation of these effects on the kinetics are not straightforward [19]. This study investigates the early kinetics within pozzolan-lime pastes.

3.2 Isothermal Heat Evolution Calorimetry

Since the correlation between the first day reactions and 28-day strength was found, the isothermal calorimetry test is studied to analyse the initial reactions [20]. The reaction kinetics were evaluated using isothermal calorimetry. The pozzolan-lime pastes (lime, pozzolan and water) were mixed for 3 minutes in plastic cups prior to loading into the chamber of the calorimeter. Measurements were recorded for 120 hours using a temperature of 40 ° C. Previous studies by Chaudhari et which compared results at temperatures of 25°C and 40°C indicated that better results we achieved at 40°C [20, 21].

The power (mW/g) and time(h) curves of mixtures showed endothermic and exothermic peaks (Figure 3, 5 and 6). The curves of lime with brick dust and lime with metakaolin-Argical M1000 showed small exothermic peaks (approximately 15.7mW), while the endothermic reaction is seen by the curves of lime with wood ash (-7.2mW) (Figure 6). The heat evolution for the initial hydration reactions (1.5 h) are shown in Figures 3 and 4. Any new phases are seen in the graphics. The difference between lime-gypsum-metakaolin and lime and metakaolin was studied by Tydlitat et al [22]. This showed that lime with pozzolanic pastes exhibited a very small peak in the power versus time plots while gypsum additions accelerated the heat evolution two or three times more and produced another phases.

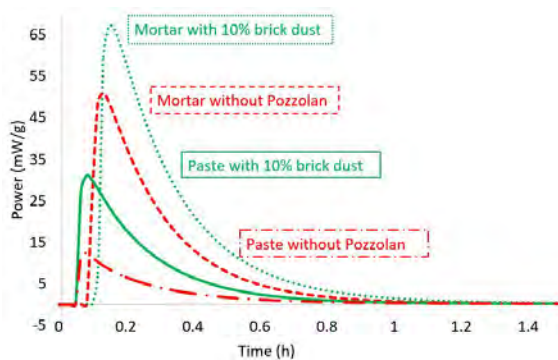


Figure 3: Power graph for lime mortars and pastes with and without brick dust (pozzolan). Measurements taken at 40 ° C

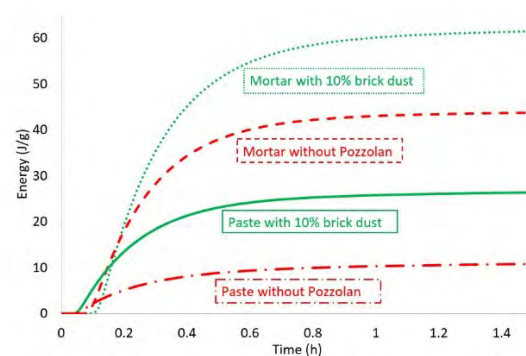


Figure 4: Energy graph for lime mortars and pastes with and without brick dust. Measurements taken at 40 ° C

The curves in Figure 3 show the differences power output between mortar and paste with and without brick dust for experiments performed at 40 ° C, while the curves in Figure 4 show energy differences between mortar and paste. As shown in Figure 3 and Figure 4 the power output and heat evolution are not as high for the pastes as they are for the mortars with the same pozzolan (brick dust). It is expected that pozzolanic materials would enhance the paste and mortar, however it was also observed that the addition of the sand increased the rate of heat evolution. Therefore, suggesting that sand could be improving the particles' dispersion in the mix, exposing the surface area of all the constituents and therefore allowing more reactions to take place (Figure 4). The peaks in Figure 3 and Figure 4 might be accelerated by the physical effects with unreactive components such as sand.

In Figure 5 it can be seen that the mix with the higher percentage (34%) of Argical M1000 delivered the highest power output. For the lime paste without Argical M1000, it is clearly seen that after the first energy peak around 0.2 hours, the power output decreases for all the samples. However, Argical M1000 contents of 25% and 34% presented slight increases. This suggests that more reactions take place with the increase in the Argical M1000 content and at 40°C, the rates of heat evolution are directly proportional with the quantity of pozzolans (Figure 5). Any new phase within 5 days was seen after the first peak but there was a wide shoulder shape which may be explained by formation of a new phase for 34% Argical M1000 content of paste.

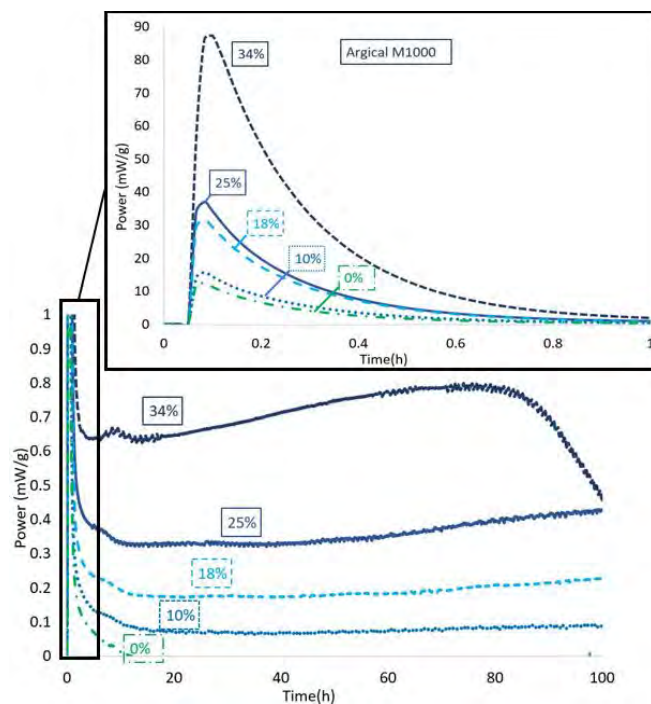


Figure 5: The reaction kinetics of CL90 lime pastes containing 0, 10, 18, 25 and 34% Argical M1000 at 40 °C

Figure 6 shows a comparison of the power output of different types of the pozzolan at the same percentage within the typical water and lime quantity as binder water ratio (B/W) is 1. Different kinetics concerning the dissolutions and reactions are shown. Argical M1000 showed a highest energy output, suggesting a high pozzolanic activity while wood ash showed the lowest energy output. Therefore, the heat evolution of the different pozzolan-lime pastes highlighted the significant effect that the type of pozzolan can have on the kinetics.

EDX analysis of the ash indicated 0.41% chlorine and the alkali metals sodium and potassium. Peaks for potassium chloride and sodium chloride were also observed in the XRD pattern (Figure 2). As the dissolution of these salts is endothermic their presence could be an explanation for the negative power values recorded for the wood ash compared to the Argical M1000 and brick dust which showed exothermic reactions.

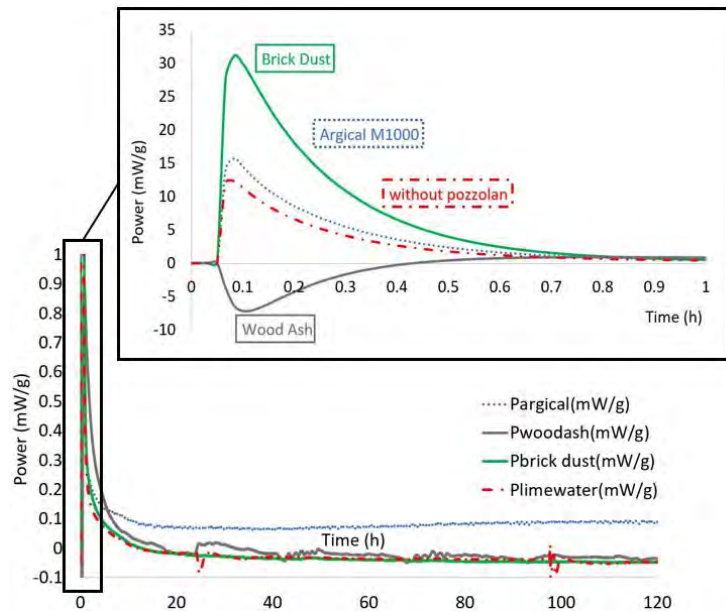


Figure 6: The kinetics evolutions of the pastes with different Pozzolans 10% at 40 °C

For example, even though the evolution of brick dust is the highest for the first 40 hours, Argical M1000 accelerated the energy evolved to a greater extent compared to the other pozzolans (wood ash and brick dust) after the 40 hours mark (Figure 7).

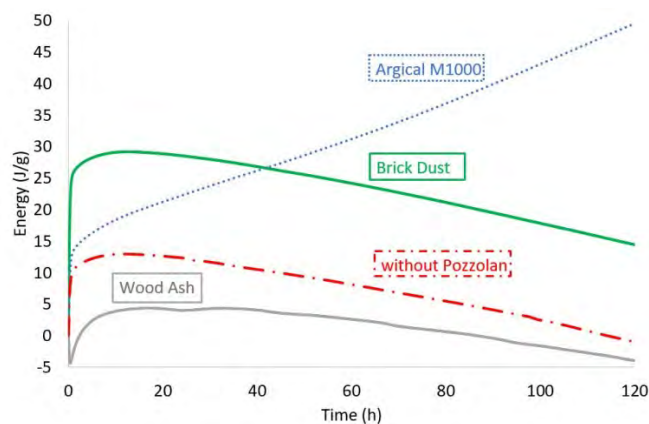


Figure 7: The energy kinetics evolutions of the pastes with different pozzolans 10% at 40 °C

The heat evolutions between 0.2 h to 1 h of all mixtures shows similar decreasing behaviour. Some pozzolanic materials appear to show activity later on. Therefore, more research is required to monitor the pozzolan-lime pastes for a longer period of time.

3.2.2 Rheology of the pozzolan-lime paste

The Rheology gives information about the compositions in terms of their flowability, behaviours under pressure, shear rate, resting times which are necessitated indirectly for conservation. The pozzolan–lime mixes were studied using a rheometer which applies a force to materials over time to provide information on the flow and deformation behaviour.

The shear stress and shear rate proportions are calculated to measure viscosity of the materials to define the characterisation with flow curve. The results presented in Figures 8 to 11 show that all pastes have exhibited a pseudoplastic behaviour (non-Newtonian) because of the shear thinning characteristics exhibited. For the mortar application, high viscosity and plasticity are sought to be achieved [23] since the viscosity of pozzolans shows the workability. The pozzolans used in this study are listed as their workability respectively; Argical M1000, wood ash and brick dust (Figure 13). Viscosity of all samples is increased over time in Figure 10 as it is observed to be changing from liquid like behaviour to solid like behaviour. The increase of yield stress of Argical M1000 separated from others is related to the workability of the paste [24, 25] (Figure 11). However, it is not correlated with the kinetics of energy evolution of the hydration reactions, which showed a higher early energy out for brick dust.

The graphics between Figures 11 to 13 show oscillation tests of three pozzolans at 40 °C. Due to Argical M1000 consisted paste being more structured than the other pozzolans a more elastic behaviour with the higher internal structure is shown. The storage and loss modulus of Argical M1000 pastes show behaviour changes from an initial elastic and liquid like behaviour then stiffening and changing to a solid like behaviour over time. Figure 10 shows that the materials with 90° phase angles at the beginning are showing more liquid like behaviour. The more solid like behaviours characteristic of 0° angles are observed later. This behaviour is expected when the loss of water and hydration reaction in 1.5 hours are considered. However, Argical M1000 paste is becoming a more structured form with less oscillation force compared to the past containing brick dust.

However, the tests show promise that the rheology measurements can be used to study the initial changes in stiffness when the pozzolans are first mixed with lime. This could be due to pozzolanic reaction, dissolution and water absorption into porous particles, such as the brick dust.

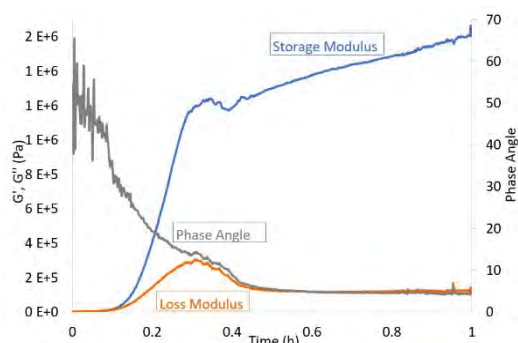


Figure 8: Storage modulus, loss modulus and phase angle against time for 10% Argical M1000 at 40 °C

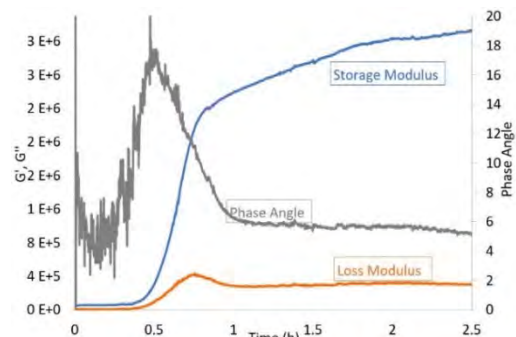


Figure 9: Storage modulus, loss modulus and phase angle against time for 10% Brick Dust at 40 °C

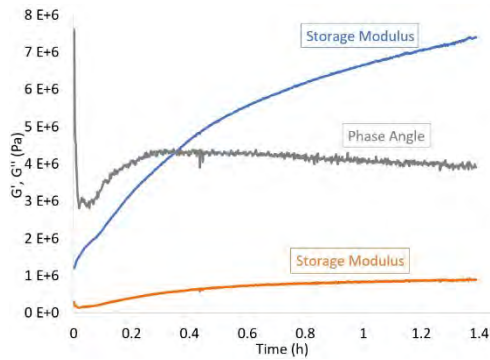


Figure 10: Storage modulus, loss modulus and phase angle against time for 10% Wood Ash at 40°C

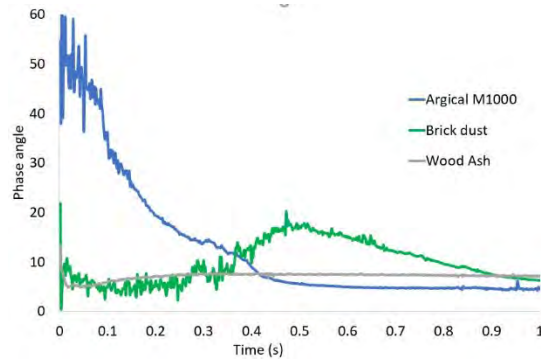


Figure 11: Phase angle against time for Argical M1000, brick dust and wood ash

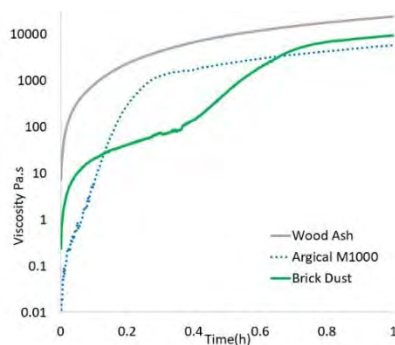


Figure 12: Viscosity against time for Argical M1000, brick dust and wood ash

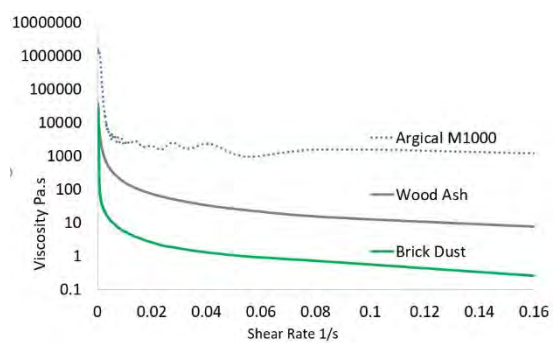


Figure 13: Viscosity against shear rate for Argical M1000, brick dust and wood ash

4 Conclusions

The early reactions between lime and Argical M1000, wood ash and brick dust were studied using calorimetry and rheology. Since Natural Hydraulic Limes from different manufacturers can exhibit varying properties, even within the same classification as defined by standard EN459, there is a growing interest in alternative mortar systems.

Calcium lime – pozzolan mortars offer an alternative and here we evaluate the performance of such mortars through the study of rheological and calorimetry properties [26]. When pozzolanic limes are used in conservation the rheological properties are important as they are related to properties such as workability which is important for practitioners. The study helps in conservation applications in terms of understanding the materials and their reactions.

The following conclusions have been drawn:

- The heat of reactions evolved when Argical M1000 was mixed with lime increased with the amount of Argical M1000 within the first 1 hour after mixing. The evolution of all heat peaks was completed within 1.5h.
- After the first peak between 0.1 to 0.6h, the mixture consisting of 34% and 25% Argical M1000 showed little changes which can be new phases in progress.

- The peaks of the kinetics evolution ascended directly proportionally with the amount of Argical M1000 (34%, 25%, 18%, 10%) in the mixtures. Hence, it can be claimed that the pozzolan effected the heat evolution of mixtures in terms of both acceleration and increase.
- After 1 hour the heat generated from the reaction between lime, pozzolan and water was not detectible. No further heat was detected by the calorimeter during a further 120h of monitoring.
- The reaction rate of CL90 lime paste with the pozzolans; brick dust and Argical M1000 is accelerated compared to the reference sample lime pastes without pozzolan.
- The ability of sand to accelerate the pozzolanic reaction can be observed by comparing the mortars with and without pozzolan where the heat evolution was increased by the presence of sand. It is also noteworthy that the hydration reaction was delayed.
- Energy dissipation and viscosity of material behaviour are seen corresponded with the kinetics evolution of the pozzolanic paste in isothermal calorimetry. When the hydration reaction is decelerated (0.2-0.6h), the viscosity and stiffnesses are changed for Argical M1000. For brick dust the changes of rheology are started after the hydration reaction. However, for wood ash, the time of the kinetic changes on calorimetry was approximately at the same arrangement (0.1-0.6h) with the rheology.

5 Future work

Future work will involve correlating the minerology of the pozzolans with the calorimetry and rheology data. We intend to investigate how the dissolution of minerals in the pozzolans affects the reactions.

The physical parameters such as surface area, fineness and particle size distribution will then be determined and fixed for all materials to enable a more accurate comparison of the chemical parameters.

6 References

1. P. S. Das *et al.*, "Failure and deformation mechanisms at macro- and nano-scales of alkali activated clay," *J. Phys. D. Appl. Phys.*, vol. 49, no. 23, 2016.
2. R. Walker and S. Pavía, "Physical properties and reactivity of pozzolans, and their influence on the properties of lime-pozzolan pastes," *Mater. Struct. Constr.*, vol. 44, no. 6, pp. 1139–1150, 2011.
3. R. Talero *et al.*, "Comparative and semi-quantitative XRD analysis of Friedel's salt originating from pozzolan and Portland cement," *Constr. Build. Mater.*, vol. 25, no. 5, pp. 2370–2380, 2011.

4. E. Navrátilová and P. Rovnaníková, “Pozzolanic properties of brick powders and their effect on the properties of modified lime mortars,” *Construction and Building Materials*, 2016.
5. J. Elsen, K. Van Balen, and G. Mertens, “Historic Mortars,” *Hist. Mortars*, no. January, 2018.
6. J. Setina, A. Gabrene, and I. Juhneviča, “Effect of pozzolanic additives on structure and chemical durability of concrete,” *Procedia Eng.*, vol. 57, pp. 1005–1012, 2013.
7. C. Heritage, *ICCROM and the Conservation Of Cultural Heritage a hIstORy Of the ORganizatIOn’s fIRst 50 yeaRs, 1959-2009*. 2009.
8. M. Jerman, V. Tydlitát, M. Keppert, M. Čáchová, and R. Černý, “Characterization of early-age hydration processes in lime-ceramic binders using isothermal calorimetry, X-ray diffraction and scanning electron microscopy,” *Thermochim. Acta*, vol. 633, pp. 108–115, 2016.
9. E. Navrátilová and P. Rovnaníková, “Pozzolanic properties of brick powders and their effect on the properties of modified lime mortars,” *Construction and Building Materials*, vol. 120. pp. 530–539, 2016.
10. J. M. Teutonico, I. McCaig, C. Burns, and J. Ashurst, “The Smeaton Project: Factors Affecting the Properties of Lime-Based Mortars,” *APT Bull.*, vol. 25, no. 3/4, p. 32, 2006.
11. R. Idir, M. Cyr, and A. Tagnit-Hamou, “Use of fine glass as ASR inhibitor in glass aggregate mortars,” *Constr. Build. Mater.*, 2010.
12. E. Vejmelková, M. Keppert, P. Rovnaníková, Z. Keršner, and R. Černý, “Properties of lime composites containing a new type of pozzolana for the improvement of strength and durability,” *Compos. Part B Eng.*, vol. 43, no. 8, pp. 3534–3540, 2012.
13. C. Li, H. Sun, and L. Li, “A review: The comparison between alkali-activated slag (Si + Ca) and metakaolin (Si + Al) cements,” *Cem. Concr. Res.*, vol. 40, no. 9, pp. 1341–1349, 2010.
14. R. Walker and S. Pavía, “Behaviour and Properties of Lime-Pozzolan Pastes,” *8th Int. Mason. Conf. Dresden, July 2010*, pp. 353–362, 2010.
15. D. D. Edwards, “Sustainable Lime Mortars,” no. May, 2009.
16. H. Paiva, A. Velosa, P. Cachim, and V. M. Ferreira, “Effect of pozzolans with different physical and chemical characteristics on concrete properties,” *Mater. Construcción*, vol. 66, no. 322, p. e083, 2016.
17. D. Bajare and G. Bumanis, “Obtaining composition of geopolymers (alkali activated binders) from local industrial wastes,” *Civ. Eng. ...*, no. June, pp. 50–56, 2011.

18. M. Li *et al.*, “The Electrochemical Co-reduction of Mg-Al-Y Alloys in the LiCl-NaCl-MgCl₂-AlF₃-YCl₃ Melts,” *Metall. Mater. Trans. B Process Metall. Mater. Process. Sci.*, vol. 46, no. 2, pp. 644–652, 2015.
19. G. D. S. (UGent) and N. D. B. (UGent) Gert Baert (UGent) , Isabel Van Driessche (UGent) , Serge Hoste (UGent), “Magnel Laboratory for Concrete Research, Ghent University, Ghent, Belgium; 2 Laboratory for Inorganic and Physical Chemistry, Ghent University, Ghent, Belgium,” *Concrete*, p. 12 pages, 2007.
20. X. Li *et al.*, “Reactivity tests for supplementary cementitious materials: RILEM TC 267-TRM phase 1,” *Mater. Struct. Constr.*, vol. 51, no. 6, 2018.
21. O. a. Chaudhari and J. J. Biernacki, “Leaching Behavior of Hazardous Heavy Metals from Lime Fly Ash Cements,” *J. Environ. Eng.*, no. May, p. 120802053312003, 2012.
22. V. Tydlitát, A. Trník, L. Scheinherrová, R. Podoba, and R. Černý, “Application of isothermal calorimetry and thermal analysis for the investigation of calcined gypsum-lime-metakaolin-water system,” *J. Therm. Anal. Calorim.*, vol. 122, no. 1, pp. 115–122, 2015.
23. M. Frías, M. I. S. De Rojas, and J. Cabrera, “Effect that the pozzolanic reaction of metakaolin has on the heat evolution in metakaolin-cement mortars,” *Cem. Concr. Res.*, vol. 30, no. 2, pp. 209–216, 2000.
24. I. Janotka, F. Puertas, M. Palacios, M. Kuliffayová, and C. Varga, “Metakaolin sand-blended-cement pastes: Rheology, hydration process and mechanical properties,” *Constr. Build. Mater.*, vol. 24, no. 5, pp. 791–802, 2010.
25. A. F. N. De Azerêdo, G. Azeredo, and A. M. P. Carneiro, “Study of Rheological Parameters of Lime-Metakaolin Paste Made of Kaolin Wastes and Lime paste,” *Key Eng. Mater.*, vol. 668, no. 16th NOCMAT, pp. 419–432, 2015.
26. C. Diogo and P. Figueiredo, “Properties and performance of lime mortars for conservation : the role of binder chemistry and curing regime A thesis submitted by Cristiano Diogo Pinho Figueiredo,” 2018.

Efficiency of field test methods for evaluation of non-structural injection grouts in Slovenian conservation practice

Andreja Padovnik¹, Violeta Bokan Bosiljkov¹

(1) Faculty of Civil and Geodetic Engineering, University of Ljubljana, Slovenia andreja.padovnik@fgg.uni-lj.si, violeta.bokan-bosiljkov@fgg.uni-lj.si

Abstract

Simple field test methods are designed for quick quality control of non-structural injection grouts in fresh state and after drying. The field tests adapt to conditions at the conservation site, which decrease their accuracy and reproducibility.

The aim of research reported in this paper was to assess the efficiency of selected field test methods based on results provided by Slovenian conservators during the workshop. The results show that in most cases the same test performed by different conservators gives comparable data. Higher variation of test results was observed for the methods where viscosity of the grout and content of the air considerably influence the test results. The Slovenian conservators selected injectability with a syringe, expansion and bleeding, wet density, water retention and realise and drying shrinkage with mortar cup, as tests that enable efficient evaluation of properties at the conservation site. However, adequate training is needed for Slovenian conservators to acquire required skills to properly use selected field test methods. Otherwise they can be misguided by obtained test results.

Introduction

Field test methods for the in-situ evaluation of properties of non-structural injection grouts were designed for conservators. In 2011 the Getty Conservation Institute (GCI) published a manual with adapted standard laboratory test procedures and field methods aimed at testing injection grouts intended for the conservation of architectural surfaces [1]. The field test methods were later used for the comparative evaluation of lime-based hydraulic injection grouts [2].

The main aim of the field methods is fast and easy quality control of the grout's properties at the particular conservation site. The grout was previously designed and tested in laboratory conditions. The field tests are aimed at evaluating the working properties of the grouts and their performance during setting and/or hardening in a realistic environment.

The main advantage of the field tests is their adaptability to conditions at the site and application of simple and inexpensive test equipment. On the other hand, the field tests are not as precise as the laboratory tests and are rarely reproducible, due to fluctuating

environmental conditions and varying substrates. Therefore, they cannot be applied in the design process of a new grout or modification process of existing grout composition.

The aim of research reported in this paper is to assess efficiency of the field test methods based on results provided by different groups of Slovenian conservators that attended a workshop organised by the University of Ljubljana, Faculty of Civil and Geodetic Engineering. A custom-mixed grout and a commercial grout were used in the study. Tests carried out at the workshop were injectability and flow with a syringe, flow on plastered tile, expansion and bleeding, wet density, water retention and release and drying shrinkage with a mortar cup [1]. Due to Slovenian conservators' considerable interest, three sessions of the workshop were carried out, with 15 participants at each workshop day. These 15 conservators were further divided into 3 groups of 5 conservators, meaning that a total of 9 groups of conservators participated in the study. Each group prepared two grout mixtures and tested them with selected procedures, with only one execution. However, three groups decided to work with their own mixtures for which they provided all materials. These results were omitted from the study and thus number of particular test repetitions was reduced accordingly.

Quantitatively, efficiency of a particular test method was assessed separately for each of the two tested mixtures. Reference mean value and standard deviation/ coefficient of variation were provided by Andreja Padovnik, who performed each test three times. She has had many years of experience with the execution of the laboratory and field test methods that evaluate properties of injection grouts [3, 4]. Reference values were compared to the mean value and standard deviation/ coefficient of variation calculated from results provided by the conservators attending the workshop.

During the workshop the Slovenian conservators evaluated each test based on their testing experiences, by filling in a prepared questionnaire. In this way qualitative assessment of field test methods' efficiency was obtained.

Materials and methods

Grout formulation and preparation

One commercial and one custom grout compositions were selected for the field testing (Table 1).

Ledan TB 1 is a commercial grout mixture based on natural lime and hydraulic binder, inert silica, slate, pozzolan, plasticizer and air-entraining admixtures [5]. The amount of water specified by the manufacturer of the Ledan TB 1 was used to prepare this grout.

The custom-mixed grout LS was developed in the framework of Padovnik's doctoral thesis [3, 4] and contained hydrated lime, limestone filler, superplasticizer and water.

Table 1. Compositions of commercial and custom mixed grouts.

Sample	Composition
TB	250 g Ledan TB1 228 g water
LS	145 g hydrated lime 515 g limestone filler 3.3 g PCE-SP 270 g water

Commercially available dry hydrated lime belongs to class CL 90-S according to the EN 459-1:2010 standard and the filler contains 99.6% of CaCO₃ in the form of calcite and 0.4% of quartz (SiO₂). The grain size distribution of the limestone filler is shown in Figure 1. As a chemical admixture, a polycarboxylate ether-based superplasticizer (PCE-SP) was used. The dosage of the PCE superplasticizer (0.5 %) was calculated as a percentage by weight of all the solid materials, i.e. the binder and the filler.

The materials were stored in a room at a controlled temperature of 19°C ± 1°C and a relative humidity of 60 ± 5% until the grout mixtures were prepared, using tap water at a temperature of 19°C ± 1°C.

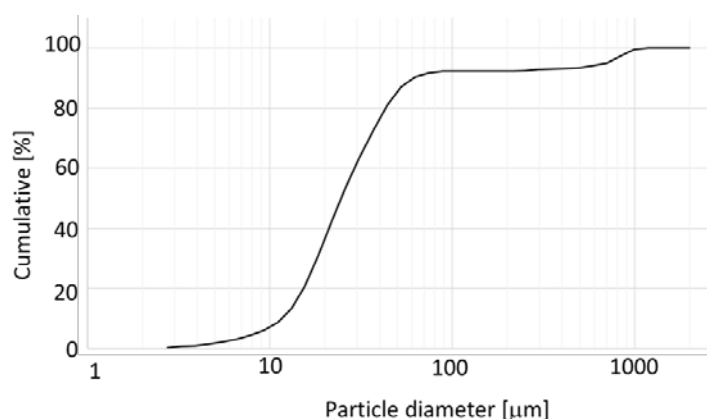


Figure 1. Grain size distribution of the limestone filler.

Mixture TB was mixed by hand. Pre-measured amount of water was added into dry ingredients and mixed for 3 minutes, in accordance with the manufacturer's instructions [5].

Mixture LS was prepared with a simple kitchen mixer. The binder and the filler were dry mixed by hand. After that, 70% of total water was added and mixing was carried out for 2 min at low speed (540 rpm). During the last 15 sec of the mixing, the PCE superplasticizer and the remaining 30% of the water were added to the mixture. Then the mixer was switched to the medium speed (1200 rpm) where mixing was carried out for further 3 min.

The simple kitchen mixer and mixing by hand were chosen to simulate the preparation of grout mixtures on the conservation site. The mixer is a small handheld electric whisk with

300W power and five drive positions for optimum power transmission. The metal whisk is 8.5 cm long and has a diameter of 4.6 cm.

Field test methods

Field test procedures that were evaluated at the workshop for Slovenian conservators are predominantly modified or non-modified tests proposed by Biçer-Şimşir and Rainer [1]: wet density, expansion and bleeding, injectability and flow with a syringe, flow on plastered tile and drying shrinkage with a mortar cup. Brief description of the tests procedures is given below.

Seven groups of conservators carried out the test procedures on the grout mixture LS, and six groups on the mixture TB. As stated earlier, every group performed each particular test only once, and reference values were obtained through three repetitions of each particular test.

To obtain qualitative assessment of selected field test methods' efficiency during the workshop, the conservators evaluated each procedure on their own practical experiences.

Wet density: The grout mixture was weighted in a 10-mL syringe, and the density was calculated by dividing the weight of the grout by its volume.

Expansion and bleeding test was used to determine the amount of water that separates from freshly mixed grout and accumulates on its surface. Graduate cylinder of 100 mL was filled with fresh grout of 80 mL. The change in the total volume and the accumulation rate of the bleed water on the surface of the grout were observed over a period of time.

Water retention and release test was used to determine the ability of the fresh grout to retain water when subjected to suction. Water retention capacity was determined by the adapted standard procedure prEN 1015-8:1999. The grout is placed in a standard mould, with the upper diameter of 150 mm, lower diameter of 140 mm and a height of 15 mm. The grout surface is covered with a thin sheet of a nonwoven tissue and filter paper plates and immediately inverted onto a smooth levelled non-absorbent surface. A 2 kg weight is placed on the back of the mould and the grout is subjected to suction for 5 minutes. After 5 minutes, the filled mould is inverted again and the filter papers at the top of the grout surface are removed. The thickness of compact grout layer in contact with the filter papers is checked by cutting the grout with a knife or spatula (Figure 2). The water retentivity of the grout is classified as: good (G_D) – if the thickness of the compact layer is less than or equal to 5 mm and the grout is still fluid under the compact layer; medium (M_D) – if the thickness of the compact layer is between 5 and 10 mm and the grout is still fluid under the compact layer; or bad (B) – if the thickness of the compact layer is more than 10 mm. The thickness of the compact layer, measured from the top of the grout layer, is recorded as D in millimetres.



Figure 2. Checking the thickness of compact layer.

Injectability test with a syringe was used to determine the ability of the grout to fill a capillary network of dry granular materials under pressure. 20 mL of grout were poured into a vertically held syringe that was partially filled with 20 mL of granular material. After that, pressure is applied on the grout with a plunger. Siliceous sand was used as granular material, with grain size between 2 and 4 mm, which simulates an approximately 0.3-0.6 mm large crack or void width. The injectability of the grout was classified as [1]: easy (E) – if the grout flows through the granular material and out of the syringe tip when pressure is applied; feasible (F) – if the grout flows through the granular material and reaches the tip but does not flow through it; or difficult (D_L) – if the grout stops in the granular material before reaching the tip. The penetration distance, measured from the top of the granular material to the level the grout has reached, is recorded as L in millimetres.

Flow with a syringe was used to evaluate the ability of the grout to fill the capillary network of dry granular materials under gravitational force.

The grout is poured into a vertically held syringe that is partially filled with 20 mL of siliceous sand. The penetration of the grout into the capillary network is observed after 5 min. The grain size of siliceous sand is between 2 and 4 millimetres. The flow of the grout is classified as [1]: easy (E) – if the grout flows through the granular material and the tip of the syringe in 5 minutes or less; feasible (F) – if the grout reaches the tip but does not flow through it in 5 minutes; difficult (D_L) – if the grout halts in the granular material after 5 minutes. The penetration distance, measured from the top of the granular material to the level the grout has reached, is recorded as L in millimetres.

Flow on a plastered tile was used to compare the ability of the grout to flow within open and closed vertical V-shaped channels in plaster (Figure 3). 10 mL of grout were injected into a vertical crevice and the distance to which the grout was able to flow was recorded. The flow of the grout was classified as [1]: low (L)—if the grout flows a distance less than 100 mm; medium (M)—if the grout flows a distance less than 200 mm; or high (H)—if the grout flows a distance more than 200 mm. Plaster for the plastered tile was made from 1 part of calcium lime putty, 0.5 part of white cement and 3 parts of limestone sand. The procedure for preparing the vertical crevices described in Biçer-Şimşir and Rainer [1] was followed.

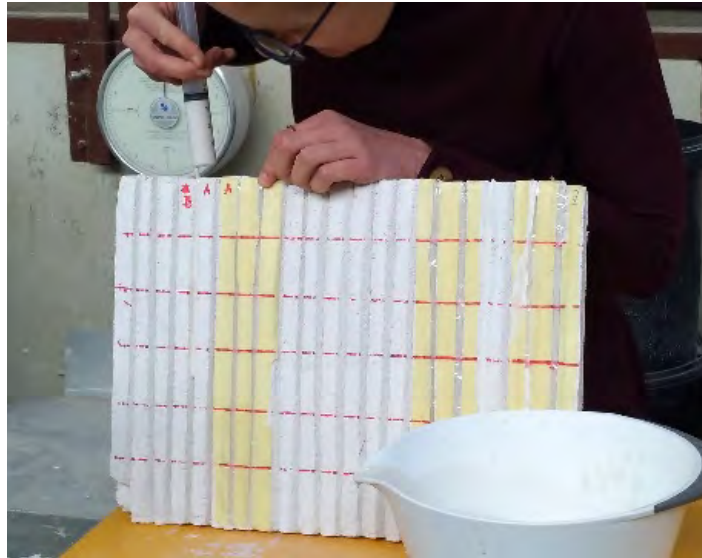


Figure 3. Flow on plastered tile with open and closed V-shaped channels.

Drying shrinkage with a mortar cup was used for the observation of dimensional changes and formation of cracks in the grout. A constant grout volume of 20 mL was injected into two types of dry mortar cups (LL and LSC). The LL mortar was prepared with 1 volume part of calcium lime putty and 2 volume parts of fine calcite sand (0/1mm), while the LSC mortar was prepared with 1 volume part of the lime putty, 0.5 volume part of white cement and 3 volume parts of fine silicate sand (0/1 mm). The mortar cups were prepared by following the procedure given in Biçer-Şimşir and Rainer [1]. The water absorption coefficient for the LL mortar was equal to $6.0 \text{ kg}/(\text{m}^2 \cdot \text{min}^{1/2})$, and for the LSC mortar it was equal to $2.3 \text{ kg}/(\text{m}^2 \cdot \text{min}^{1/2})$, after 10 min.

The drying shrinkage of the grout was classified as [1]: no drying shrinkage (NS)—no visible separation between the grout and the mortar and no visible cracking in the grout; medium drying shrinkage (MS)— a separation of less than 0.5 mm between the grout and the mortar and/or a maximum crack size of less than 0.5 mm in the grout; or high drying shrinkage (HS)—a separation of more than 0.5 mm between the grout and the mortar and/or a maximum crack of more than 0.5 mm. These observations were made 24 hours after the injection of the grout into the mortar cup.

Results and discussion

Single results of wet density, bleeding and water retentivity of the grout mixtures LS and TB are given in Table 2. Mean values, standard deviations and coefficients of variation for groups of conservators (denotation groups) and for the reference results (denotation reference), are given in Table 3.

Table 2. Wet density, bleeding, and water retention and release test results of the LS and TB mixtures tested with field test methods.

Sample	Wet density (g/cm ³)	Bleeding (%)	Water retention and release (%)
LS (reference)	1.78	3.1	G ₆
	1.75	3.7	G ₅
	1.75	4.4	G ₅
LS1	n.d.	5.0	M ₈
LS2	1.71	n.d.	B ₁₅
LS3	n.d.	3.7	G ₃
LS4	1.74	n.d.	M ₉
LS5	1.73	n.d.	M ₁₀
LS6	1.80	2.5	G ₅
LS7	n.d.	3.7	B ₁₅
TB (reference)	1.50	1.23	G ₀
	1.43	2.47	G ₀
	1.46	1.82	G ₀
TB1	1.43	1.23	G ₀
TB2	1.27	0.0	G ₀
TB3	1.37	n.d.	G ₀
TB4	1.26	0.0	G ₀
TB5	0.78*	0.63	G ₀
TB6	1.48	0.0	G ₀

Note: G – good; M – medium; B – bad. Subscript number indicates the thickness of the compact layer.

* result was excluded from calculation of the mean value and standard deviation

The reference mean value and standard deviation of the LS mixture wet density was 1.76 g/cm³ and 0.02 g/cm³, respectively. The results obtained by conservators for the same mixture were between 1.80 and 1.71 g/cm³, with a mean value of 1.75 g/cm³ and standard deviation of 0.04 g/cm³. We can see that, for the LS mixture, the mean density measured by conservators is the same as the reference value. For the TB mixture there is important difference between the two mean densities, with the reference mean density of 1.46 g/cm³ and the groups' mean density of 1.36 g/cm³. The groups' standard deviation of 0.10 g/cm³ is 2.5-times higher compared to the reference standard deviation (0.04 g/cm³). Results of the wet density test indicate that the method with a syringe is operator sensitive, since standard deviation and coefficient of variation are considerably higher for the groups' results, compared to the reference results for the two mixtures. However, the mixing method seems to be the most important influencing parameter, since result variation is considerably higher for the TB mixture, which was prepared by hand mixing. Lower groups' mean density (for 7 %) compared to the reference value can be thus explained with lower homogeneity of particular mixture and/or possible presence of entrapped air that was not removed during the tapping operation [1]. Recent study [6] shows that mixing procedure influences viscosity of the fresh grout, estimated by the Marsh cone method (EN 445: 2008), considerably. Hand

mixing provided much higher viscosity (3 min 07 sec) compared to mixing with the kitchen mixer (2 min 05 sec). Higher viscosity is a plausible reason for higher content of air in the tested sample.

Table 3. Mean value, standard deviation and coefficient of variation for the LS and TB mixtures – reference and groups test results of wet density, bleeding and water retention and release.

Sample	Wet density			Bleeding			Water retention and release		
	(g/cm ³)	std	cov	(%)	sd	cov	(%)	std	cov
LS-reference	1.76	0.02	0.98	3.7	0.4	12.4	G ₅	1	22
LS-groups	1.75	0.04	2.22	3.7	1.0	27.4	M ₉	5	49
TB-reference	1.46	0.04	2.40	1.8	0.6	33.7	G ₀	0	0
TB-groups	1.36	0.10	7.11	0.5	0.6	126.9	G ₀	0	0

Results of the expansion and bleeding test, where the separation of water and solids indicates the extent of the grout segregation, show for the LS mixture a similar relation between the reference and the groups' results, compared to the wet density test. The bleeding reference mean value is the same as the groups' mean value (3.7 %), with the groups providing a higher standard deviation (1.0 %). For the TB mixture, on the other hand, mean values of bleeding differ considerably, with the reference mean value of 1.8 % and the groups' mean value of 0.47 %, but obtained standard deviation is the same for the reference and group test results. We can conclude that operator and mixing method are the main parameters that influence the bleeding test results, which is supported by results in [6].

The water retention and release test method showed high differences in the test results when the LS mixtures were tested. Only two samples, LS3 and LS6, showed the same results as the reference grout, with an approximately 3 to 5 mm thick layer in contact with the filter papers, which classified them as good (G). The ability of the rest of the LS mixtures to retain water when subjected to short term suction was considerably reduced and they were classified as M (medium; LS1, LS4, LS5) or B (bad; LS2, LS7). On the other hand, all samples of the TB grout had good water retention (G) with no compact layer in contact with the filter papers, the same as the reference mixtures. This can be due to the higher viscosity of the grout.

During the workshop it was observed that some groups of conservators did not follow the mixing instructions for the grout mixture LS, which can be the main reason for decreased stability of some grouts and their ability to retain water. One group put all ingredients of the mixture LS into a mixing container and mixed them for 5 min at low speed (540 rpm). Another group mixed the TB mixture with the kitchen mixer. We were not informed why they did not follow the instruction.

Based on this observation and the presented results we can conclude that the main reason for the tests' results variation is the grout mixing procedure and the accuracy with which the group carried out the test and read the obtained results.

Table 4. Injectability and flow with syringe, and flow on plastered tile with open and closed channels test results of the LS and TB mixtures.

Sample	Injectability with syringe	Flow with syringe	Flow on plastered tile	
			Open channel	Closed channel
LS (reference)	E _{>30}	D ₃	H _{>200}	L ₈₅
	E _{>30}	D ₂	H _{>200}	L ₈₅
	E _{>30}	D ₂	H _{>200}	H _{>200}
LS1	E _{>30}	D ₀	H _{>200}	L ₁₀₀
LS2	E _{>30}	D ₂	L ₃₀	L ₃₅
LS3	E _{>30}	D ₉	L ₅₀	H _{>200}
LS4	n.d.	D ₁₅	H _{>200}	H _{>200}
LS5	E _{>30}	D ₃	n.d.	n.d.
LS6	E _{>30}	n.d.	H _{>200}	H _{>200}
LS7	n.d.	D ₈	H _{>200}	H _{>200}
TB (reference)	E _{>30}	E _{>30}	H _{>200}	H _{>200}
	E _{>30}	E _{>30}	H _{>200}	H _{>200}
	E _{>30}	E _{>30}	H _{>200}	H _{>200}
TB1	E _{>30}	E _{>30}	H _{>200}	H _{>200}
TB2	E _{>30}	D ₂₅	H _{>200}	H _{>200}
TB3	E _{>30}	D ₃₀	H _{>200}	H _{>200}
TB4	E _{>30}	D ₂₇	H _{>200}	H _{>200}
TB5	n.d.	D ₂₀	H _{>200}	H _{>200}
TB6	n.d.	n.d.	H _{>200}	H _{>200}

Note: E – Easy; F – Feasible; D – difficult; L – low; M – medium; H – high. Subscript number indicates the penetration distance.

Single results of the injectability and flow with the syringe tests, as well as the results of flow on the plastered tile with open and closed channels, are given in Table 4. Mean values, standard deviations and coefficients of variations, for groups of conservators and for the reference results, are given in Table 5.

Table 5. Mean value, standard deviation and coefficient of variation for the LS and TB mixtures– reference and groups test results.

	LS-reference	LS-groups	TB-reference	TB-groups
Injectability with syringe (mean)	E _{>30}	E _{>30}	E _{>30}	E _{>30}
Flow with syringe (mean)	D ₃	D ₆	E _{>30}	D ₂₆
std	2	6	0	4
cov	77	90	0	16
Flow on plastered tile				
Open channel (mean)	H _{>200}	M ₁₄₇	H _{>200}	H _{>200}
std	0	83	0	0
cov	0	56	0	0
Closed channel (mean)	M ₁₆₈	M ₁₅₆	H _{>200}	H _{>200}
std	59	71	0	0
cov	57	46	0	0

From the injectability test results it can be seen that all samples had the ability to flow through the dry siliceous sand and out of the syringe tip when pressure was applied. According to these results, the injectability of the LS and TB mixtures can be classified as E (easy) [1] and the reproducibility of the test can be evaluated as excellent.

Situation is different, when the flow of the grout due to gravity was tested. All samples tested under gravity showed reduced ability to penetrate into the dry siliceous sand, compared to the injectability test, where additional pressure was applied to the grout. All LS samples, as well as TB2, TB3, TB4 and TB5 samples reached the distance between 0 and 27 mm under the gravitational force and the flow was classified as difficult (D). On the other hand, all reference results of the TB mixture and only a single groups' sample TB1 had the ability to pass through the dry capillary network of the granular material under gravity and were classified as easy (E). Because each group filled the syringe with the granular material, there were probably differences in the siliceous sand particle packing between the groups, which can influence the test results considerably. Moreover, the procedure of pouring the grout into the syringe can be an influencing parameter. This shows that the operator, in addition to the mixing procedure, has an important influence on the flow test results.

The results of flow on the plastered tile showed differences between the test results only in case of the LS mixtures. Closing of the vertical channels changed flowability of the grout through the channels for a majority of test repetitions. However, observed changes are not consistent - better, the same or poorer flowability was observed, when changing the method from open to closed channels test. We estimate that the observed changes are consistent with repeatability of the test method, a statement which is supported by the same mean value and standard deviation obtained in the reference and groups tests when the closed channel test method was used. On the other hand, the reference and groups TB samples prepared at the workshops reached the flow distance exceeding 200 mm, for the open and closed channels, and were classified as high (H). The result of this test is influenced by the way how the grout is injected into the channel and by the water retention capacity of the grout, since porous nature of the channels' surface can suck water from the grout. Therefore, grout TB with higher water retentivity, compared to the LS grout, exhibited better results and excellent reproducibility of the test.

Table 6 shows the results of the drying shrinkage tests inside the mortar cups made of lime (LL) and lime-cement (LSC) mortar. The change in the volume of the reference mixtures LS and TB after drying in the LL and LSC mortar cups can be seen in Figure 2. Although water absorption coefficient of the LL mortar is much higher than that of the LSC mortar, there is no visible difference between the drying shrinkage test results for the two mortar composition.

All reference and groups LS samples show an approximately 0.10 mm thick separation ring close to the mortar cup's inner surface and, as a rule, no cracks inside the samples, for the LL and LSC mortar cups. The only exceptions are samples LS6 and LS7, where cracks of 0.1 mm

in width were observed, when the LL cups were used. Therefore, all LS samples were classified as grout with medium drying shrinkage (MS).

Table 6. Drying shrinkage in mortar cup test results of the LS and TB mixtures.

Sample	Lime mortar cup			Lime-cement mortar cup		
	Separation size (mm)	Crack size (mm)	Class	Separation size (mm)	Crack size (mm)	Class
LS (reference)	0.10	0.00	MS	0.10	0.00	MS
	0.10	0.00	MS	0.10	0.00	MS
	0.10	0.00	MS	0.10	0.00	MS
LS1	0.10	0.00	MS	0.10	0.00	MS
LS2	0.10	0.00	MS	0.10	0.00	MS
LS3	0.10	0.00	MS	0.10	0.00	MS
LS4	0.10	0.00	MS	0.10	0.00	MS
LS5	0.10	0.00	MS	0.10	0.00	MS
LS6	0.10	0.10	MS	0.10	0.00	MS
LS7	0.10	0.10	MS	0.20	0.00	MS
TB (reference)	1.00	0.50	HS	0.50	0.60	HS
	0.35	0.20	HS	0.25	0.25	HS
	0.50	0.25	HS	0.25	0.25	HS
TB1	0.85	0.10	HS	0.50	1.50	HS
TB2	0.75	1.50	HS	0.60	1.50	HS
TB3	0.70	0.15	HS	1.00	0.10	HS
TB4	0.65	0.15	HS	0.50	0.75	HS
TB5	0.30	0.90	HS	0.40	2.00	HS
TB6	0.50	0.10	MS	0.50	0.20	MS

Note: NS - No drying shrinkage; MS - Medium drying shrinkage; HS - High drying shrinkage.

Situation is quite different for the TB grout, where different thicknesses of separation rings were observed in tested samples, ranging from 0.30 to 1.00 mm for the LL mortar cups, and from 0.40 to 1.00 for the LSC mortar cups. At the same time, cracks were formed also inside of each sample, with thicknesses between 0.10 to 1.5 mm for the LL and LSC mortar cups. Therefore, all but one TB samples can be classified as grout with high drying shrinkage (HS). The only exception is sample TB6 with the MS classification.

The mortar cups simulate the absorptive effect of porous plaster and demonstrate the extent of the grout volume stability when exposed to drying. Low volume stability of the grout leads to the formation of cracks inside the grout. By comparing the behaviour of the grouts in mortar cups, it is possible to obtain information about long term (24 hour or more) ability of particular grout to retain moisture inside its structure. We can see that the LS grout behaved much better, compared to the TB grout. Separation ring between mortar cup and grout and/or cracks inside the grout can also indicate excessive water content in the grout mixture, which could reduce the strength of the grout mixture [1].



Figure 4. Reference mixtures LS and TB after drying in lime (LL) and lime-cement (LSC) mortar cups.

We can see (Table 2) that the TB grout with good water retentivity in the fresh state showed poor volume stability when exposed to the long term drying (Table 6), which resulted in relatively thick separation rings and cracks inside the grout. There are also significant differences between results of different groups, which indicate that hand mixing could influence properties of the grout. However, in general the results of drying shrinkage test belonging to individual groups are comparable, since they are inside the same class. We believe that main reason for such results is the use of mortar cups with the same properties at the workshop. Preparation of the mortar cups by each conservator/group of conservators would reduce reproducibility of the drying shrinkage test method considerably.

Conclusions

The field test methods, which were evaluated in the framework of the workshops, are relatively easy, quick and effective in quality control of non-structural grouts on conservation site. The Slovenian conservators recognised the advantages of these methods and the possibility of adjusting them to the individual situations and problems related to re-attachment of decorative plasters. They selected the following field methods as the most efficient: injectability with a syringe, expansion and bleeding, wet density, water retention and release and drying shrinkage with mortar cup.

The field test methods presented in this study can be very useful for the grout property evaluation, but they have also some limitations. The tests are not as precise as the laboratory tests and the results can depend on skills and/or accuracy of conservator/restorer, who performs the field methods. The obtained results show that the same test performed by different groups of operators gives in most cases comparable data.

Although the wet density test is a simple method, attention should be paid to the procedure of filling the syringe with the injection grout. The differences in the results between groups can be due to different contents of air in the fresh mixture. Differences are bigger in mixtures of higher viscosity, which makes it more difficult to fill the syringe.

The mixing procedure and the time of mixing were precisely defined and were the same for all groups, but some of the workshop participants did not follow the procedure. This could lead to differences in the test results, because different samples of the same grout could have different viscosity and different content of entrained and/or entrapped air.

Different mixing and filling procedures are most probably the reason for significant differences between results of the grout's wet density, especially for the TB grout, and of the grout's bleeding for the mixture LS. To evaluate the ability of the fresh grout to retain water on conservation site, during the grouting procedure, the adapted standard procedure proved to provide useful information to conservators. Reproducibility for the TB grout was excellent. On the other hand, in case of the LS grout, water retentivity was classified from good to bad. This could be the result of lower viscosity of the LS grout, due to its composition and mixing procedure.

The reproducibility of the injectability with the syringe method is excellent, for the LS and TB grout, which indicates that pressure transferred to the grout by the operator in order to provoke flow of the grout through granular material is the prevailing influencing parameter of this test method. Situation is considerably different, with poor reproducibility of the method, where only gravity was used to provoke flow of the grout through the granular material. The same influencing parameters as for the wet density are the most probable reason for the observed differences in the results of the flow with syringe, along with the differences in the granular material packing density inside the syringe.

Flow of the grout on the plastered tiles showed good reproducibility of the method for the TB grout. Different results obtained by three groups when testing the LS grout are the consequence of different technique for emptying the grout into the channels. Non-continuous injection of the grout into the channel reduces the flow distance, while continuous injection with constant velocity increases the flow distance of the grout.

The drying shrinkage test with the mortar cups showed good reproducibility, with all samples of the LS grout and all but one samples of the TB grout resulting in the same shrinkage class of MS and HS. The same properties of the mortar cups that were used in the study could be the main reason for good reproducibility of the method.

Finally, the obtained results show that the test operator had prevailing influence on the test results' variation, along with the mixing procedure. Since majority of conservators that attended the workshop carried out the selected test procedure for the first time and without repetition, lack of training can be the main reason for poor reproducibility of some test methods. Therefore, adequate training is needed for the Slovenian conservators to acquire

required skills to properly use proposed field test methods, so they are not misguided by the test results.

Acknowledgments

This research was undertaken in a framework of the project C3330-17-529030 "Raziskovalci-2.0-UL-FGG-529030". Ministry of Education, Science and Sport of the Republic of Slovenia has approved the project. The investment is co-financed by the Republic of Slovenia and the European Union under the European Regional Development Fund. The authors acknowledge also the financial support from the Slovenian Research Agency through the research core funding No. P2-0185.

References

1. Biçer-Şimşir B, Rainer HL (2013) Evaluation of lime-based hydraulic injection grouts for the conservation of architectural surfaces: A manual of laboratory and field test methods. Los Angeles, The Getty Conservation Institute. http://hdl.handle.net/10020/gci_pubs/evaluation_grouts
2. Biçer-Şimşir B, Rainer L (2014) Field test methods for comparative evaluation of lime-based hydraulic injection grouts for the conservation of architectural surfaces. In ICOM-CC 17th Triennial Conference Preprints, Melbourne, 15–19 September 2014, ed. J. Bridgland, art. 1102, 10 pp. Paris: International Council of Museums.
3. Padovnik A (2016) Consolidation of detached plaster layers of mural paintings with non-structural grouting: doctoral thesis. Ljubljana: 218 p., (in Slovenian) <http://drugg.fgg.uni-lj.si/5511/>
4. Padovnik A, Piqué F, Jornet A, Bokan-Bosiljkov B (2016) Injection Grouts for the Re-Attachment of Architectural Surfaces with Historic Value—Measures to Improve the Properties of Hydrated Lime Grouts in Slovenia. *Int J Archit Herit* 10 (8):993-1007 doi: 10.1080/15583058.2016.1177747
5. Ledan TB1 (2018) <https://shop.kremerpigments.com/media/pdf/31000e.pdf>
6. Predovnik N (2017) The influence of different mixer types on the properties of injection grouts : graduation thesis. Ljubljana, 49 p., (in Slovenian) <https://repozitorij.uni-lj.si/IzpisGradiva.php?id=98383>

5th Historic Mortars Conference – 19-21 June 2019 – Pamplona, Spain

Edited by José Ignacio Álvarez, José María Fernández, Íñigo Navarro, Adrián Durán,
Rafael Sirera

RILEM Proceedings PRO 130

ISBN: 978-2-35158-221-3

e-ISBN: 978-2-35158-222-0

2019 Edition

HMC's are fully consolidated as a one-of-a kind forum to deal with historic mortars, renders and grouts, the variety of their compositions and raw materials, diverse methodologies of study, archeological sites, dating, preservation, durability, obtaining of repair materials and testing methods, consolidation, and even the upgrade of the repair mortars by nano-technology. This HMC 2019 gathers 140 scientific and technical high-levelled contributions of participants from the five continents. Up to twelve different topics are displayed in the Conference Programme, thus emphasising the wide range of approaches that enrich the final outcome of the event. The profitable exchange between the science advances and the practice taking place during the Conference is supported by contributions focused on a more theoretical scientific point of view combined with those works more oriented towards real applications, including case studies, assessment of the state of conservation of some ancient materials or monitoring of the effectiveness of some rehabilitation procedures and repair materials.

RILEM Publications S.a.r.l.
4 avenue du Recteur Poincaré
75016 Paris - FRANCE
Tel: + 33 1 42 24 64 46 Fax: + 33 9 70 29 51 20
E-mail : dg@rilem.net